Eur J Nucl Med Mol Imaging (2015) 42 (Suppl 1):S1–S924
DOI 10.1007/s00259-015-3198-z

EANM'15

Annual Congress of the European Association of Nuclear Medicine

October 10 - 14, 2015
Hamburg, Germany

Abstracts

European Journal of Nuclear Medicine and Molecular Imaging
Volume 42, Supplement 1
10.1007/s00259-015-3198-z

This supplement was not sponsored by outside commercial interests. It was funded entirely by the association's own resources.

Springer

Welcome to the EANM Congress 2015 in Hamburg

With great pleasure the European Association of Nuclear Medicine welcomes you to its 28th Annual Congress in Hamburg, Germany.

During the EANM Congress you will be able to discuss the state-of-the-art that clinical, translational and fundamental nuclear medicine has to offer in the usual multidisciplinary setting that is so typical for our profession. From all over the world physicians, scientists and technologists will travel to Hamburg for EANM'15 to attend plenary lectures, scientific sessions and the state of the art in nuclear medicine and molecular imaging presented in Continuing Medical Education (CME).

This year's plenary sessions will focus on Clinical Molecular Imaging on Sunday, October 11 (including the Marie Curie Lecture by Prof. Stefano Fanti from Bologna, Italy on the role of nuclear medicine in prostate cancer), and on Therapeutic Nuclear Medicine on Monday, October 12. As part of the M2M - Molecule to Man track, which this year is featured over three days of the Congress, the plenary session on Tuesday, October 13 will focus on Targets and Probes. We are very pleased that Prof. Paul Workman, President and CEO of The Institute of Cancer Research, London, UK will address target discovery and probe identification in oncology, to be followed by lectures of Dr. Matthias Friebe and Prof. Guus van Dongen on probe selection and development for molecular imaging and therapy from the perspective of industry and academia, respectively. Of course the traditional Highlights Lecture on Wednesday, October 14 is scheduled, this year presented by Prof. Andreas Buck and Prof. Clemens Decristoforo.

This year we again feature special tracks. Last year's very successful Biology track has been renamed to the M2M - Molecule to Man track. Thanks to the efforts of the EANM Translational Molecular Imaging, Drug Development and Radiopharmacy Committees, you will find a wealth of events on basic and translational research in molecular imaging and therapy on Monday, Tuesday and Wednesday, including Tuesday's plenary session. As a sequel to "ISTARD", the collaborative efforts of the EANM Dosimetry and Radionuclide Therapy Committees resulted in an annual track now named Dosimetry and Molecular Radiotherapy (Do.MoRe) which will run throughout the Congress.

The Scientific Programme Committee, representing all EANM Committees, received a total of 1.916 abstracts, of which 1.710 were accepted for oral sessions (500 presentations) or poster sessions (1.210 presentations). In the pre-congress and joint symposia, a large number of experts from disciplines outside nuclear medicine together with experts from the EANM Committees will provide new data and will share with you how nuclear medicine contributes to better science and enhanced patient care throughout the areas in which nuclear medicine is utilised.

In collaboration with the European School of Nuclear Medicine, the EANM Committees organised a full track of CME sessions, including the highly appreciated interactive sessions. Education in cross-sectional imaging has been expanded to meet the needs of nuclear medicine physicians for performing state-of-the-art hybrid imaging. The Young EANM organised activities focussed on the career perspective of young professionals in nuclear medicine. Serving the nuclear medicine technologists, the EANM Technologist Committee again designed a full parallel programme of oral and poster sessions as well as Continuing Technologist Education (CTE) sessions and courses.

Organisation of the EANM'15 Congress has been the work of many members of the EANM Committees, strongly supported by the staff of the EANM Executive Office. During the meeting the speakers and presenters will share their data with you. I thank all those who contributed their time and effort into presenting a five-day meeting for you to learn, discuss and enjoy.

On behalf of the EANM Board, the EANM Scientific Programme Committee, the Local Organising Committee and the staff of the EANM Executive Office in Vienna, I welcome you to the EANM Congress 2015 and I hope you will experience a scientific, educational and successful meeting that meets your expectations and offers you a pleasant stay in Hamburg.

Prof. Dr. Wim J.G. Oyen
EANM Congress Chair 2014-2016

Saturday, October 10, 2015

Time/Room	Hall 1	Hall 16	Hall 7	Hall 6	Hall G	Hall 18/19	Hall 8	Hall E	Hall D	Hall F	Hall 3 - Poster Exhibition
Capacity	3000	30	60	370	150	50	260	260	230	260	
08:00 - 19:00		EANM Advisory Council Meeting (11:00 - 13:00)	EANM Delegates Assembly (13:45 - 16:00)	EANM Members Assembly (16:00 - 18:00)			Pre-Symposium 1: Current Trends in Diagnosis and Therapy of Prostate Cancer (09:00 - 16:00)	Pre-Symposium 2: New Imaging Techniques and Impact on Clinical Care: Balance between Quality and Dose Reduction (09:00 - 12:30) ----- Pre-Symposium 3: Neuroinflammation (13:30 - 17:00)	Pre-Symposium 4: Meeting with Industry (09:00 - 12:30) ----- Pre-Symposium 5: Translation of Radiopharmaceuticals from Molecule to Man (13:30 - 17:00)	Pre-Symposium 6: Pharmacokinetic Modelling and Dosimetry (09:00 - 12:30) ----- Pre-Symposium 7: Translational Molecular Imaging to Support Drug Development (13:30 - 17:00)	Poster Setup (08:00 - 18:00)
19:00 - 20:00	OPENING CEREMONY (19:00 - 20:00) & WELCOME RECEPTION (20:00 - 22:30)										

Sunday, October 11, 2015

Time/Room	Hall 1	Hall 2	Hall 4	Hall G1	Hall G2	Hall 6	Hall F	Hall E	Hall 8	Hall D	Hall 3 - Poster Exhibition
Capacity	3000	1100	800	580	560	370	260	260	260	230	
08:00 - 09:30	101 CME 1 - Interactive Bone & Joint Bone Planar and Hybrid Scintigraphy: Patterns, Pearls, Pitfalls	102 Joint Symposium 1: EANM/EACVI: Cost-effectiveness in Cardiac Imaging: From Theory to Practice	103 Technologists 08:00 - 08:12 Opening Ceremony 08:15 - 09:45 CTE 1: Brain Imaging (Tech Guide Book Launch)		105 Do.MoRe: PRRT Treatment Planning			108 Pitfalls & Artefacts & Physiology - Interactive: Clinical Consequences of Neuroimaging			Poster Walks PW01, PW04, PW07, PW10 (08:30 - 09:30)
10:00 - 11:15	201 Plenary 1 incl. Marie Curie Lecture Clinical Molecular Imaging		203 In Hall 1: Plenary 1 incl. Marie Curie Lecture Clinical Molecular Imaging								
11:30 - 13:00	301 CME 2 Oncology & Paediatrics & Bone and Joint Sarcomas	302 Joint Symposium 2: EANM/ETA-CRN: What the Doctor Tells and the Patient Understands - Update on Thyroid Cancer Communication	303 Technologists CTE 2 - Interactive: Multiprofessional Discussion on Extended Competencies for Nuclear Medicine Technologists	304 Special Symposium: Evidence-based Medicine - Implications for Imaging	305 Do.MoRe: Novel Therapies	306 Physics & Instrumentation & Data Analysis: PET/MR	307 Neurosciences: Basic Neuroscience		309 Clinical Oncology: Gastroesophageal & Colorectal Cancer	310 Cardiovascular System: Cardiac Innervation Imaging	
13:00 - 14:30					GE Healthcare: Diagnostic Confidence in Molecular Imaging Through Consistent Quantification Today & Tomorrow	Bayer HealthCare Pharmaceuticals: The Pivotal and Evolving Role of the Nuclear Medicine Specialist in mCRPC		BTG: TheraSphere in Personalised Medicine - The Achievable Goal	Young EANM Daily Forum		
14:30 - 16:00	401 CME 3 Paediatrics & Cardiovascular Paediatric Heart and Lung Disease	402 Joint Symposium 3: EANM/ESSO: Radioguided Surgery	Technologists 403a 14:30 - 15:30 Mini Course 1 - Interactive: Signs in Nuclear Medicine Imaging	404 Clinical Oncology - Featured: Prostate (PSMA)	405 Do.MoRe - Featured: Endocrine & Neuroendocrine Tumours	406 Teaching Session: Anatomy Refresher and Cross-sectional Imaging: Thorax	407 Radiopharmaceuticals & Radiochemistry: Radiochemistry - Methods	408 Conventional & Specialised Nuclear Medicine: Infection & Inflammation	409 Physics & Instrumentation & Data Analysis: Data Analysis & Management I	410 Cardiovascular System: PET Perfusion Imaging	Poster Sessions P01 - P19 (16:00 - 16:30)
16:30 - 18:00	501 CME 4 Inflammation & Infection Imaging Infection in the Immunocompromised Patient	502 Joint Symposium 4: EANM/EORTC: Hypoxia Imaging: A Powerful Tool to Better Understand Tumour Biology and Guide Cancer Therapy	********* 403b 15:45 - 16:45 Mini Course 2 - Interactive: PET/CT Artefacts ********* 403c 17:00 - 18:00 Mini Course 3 - Interactive: SPECT/CT Artefacts		505 Do.MoRe: Treatment of Bone Metastases	506 Teaching Session: Anatomy Refresher and Cross-sectional Imaging: Abdomen & Pelvis	507 Clinical Oncology: Lung	508 Conventional & Specialised Nuclear Medicine: Thyroid & Parathyroid	509 Physics & Instrumentation & Data Analysis: Data Analysis & Management II	510 Cardiovascular System: SPECT & PET Perfusion Imaging	

Monday, October 12, 2015

Time/Room	Hall 1	Hall 2	Hall 4	Hall G1	Hall G2	Hall 6	Hall F	Hall E	Hall 8	Hall D	Hall 3 - Poster Exhibition
Capacity	3000	1100	800	580	560	370	260	260	260	230	
08:00 - 09:30	601 CME 5 Interactive PET with Choline Tracers	602 Joint Symposium 5: EANM/MDS: Dopamine Transporter Imaging: Current Topics	603 Technologists Oral Presentations 1		605 Do.MoRe: PRRT Dose Response	606 M2M: SPECT Translational Studies		608 Pitfalls & Artefacts & Physiology - Interactive: Imaging in Inflammation and Infection		610 UEMS/CANMD Session: Practical Quality Management in Nuclear Medicine	Poster Walks PW02, PW05, PW08, PW11 (08:30 - 09:30)
10:00 - 11:15	701 Plenary 2 Therapeutic Nuclear Medicine		703 In Hall 1: Plenary 2 Therapeutic Nuclear Medicine								
11:30 - 13:00	801 CME 6 Neuroimaging Brain Tumours - PET vs. MRI: Therapy Planning and Response Assessment	802 Joint Symposium 6: EANM/ESTRO: Molecular PET Imaging in Adaptive Radiotherapy: Focus on Current Trends, Challenges and Solutions	803 Technologists Oral Presentations 2	804 Clinical Oncology - Featured: Image Guided Surgery	805 Do.MoRe - Featured: Prostate Cancer Therapy	806 M2M: Radiopharmaceuticals & Radiochemistry: Macromolecules I	807 Teaching Session: Anatomy Refresher and Hybrid Imaging of the Foot and Ankle		809 Clinical Oncology: Prostate I - Choline	810 Conventional & Specialised Nuclear Medicine: Bone & Joint	
13:00 - 14:30					Genzyme: New Trends in the Management of Thyroid Cancer	Sirtex: SIRFLOX - A New Option for Colorectal Liver Metastases		Eli Lilly and Company: Who Should Be Considered for an Amyloid Scan? Real World Experiences Partnering in a Dementia Multi-disciplinary Team (MDT)	Young EANM Daily Forum		
14:30 - 16:00	901 CME 7 Physics & Paediatrics Radiation Protection	902 Joint Symposium 7: EANM/EACVI/ESC: New Clinical Guidelines on Infectious Endocarditis and CIED Infections	903 Technologists CTE 3 - Interactive: Comprehensive PET/MRI Practice	904 Committee Symposium - Neuroimaging Counteracting Dementia: Imaging Evidence for Cognitive and Brain Reserve	905 Do.MoRe: Radiobiology - Molecular Radiotherapy	906 M2M: Radiopharmaceuticals & Radiochemistry: Radiotracers - Brain	907 Teaching Session: The Spine: Anatomy, Pathology and Correlative Imaging	908 Clinical Oncology: Prostate II - Beyond Choline		910 Clinical Oncology: Rapid Fire Session	Poster Sessions P20 - P38 (16:00 - 16:30)
16:30 - 18:00	1001 CME 8 Cardiovascular EANM/EACVI Joint Session: Imaging in Heart Failure: Focus on Nuclear Medicine Techniques and Clinical Implications	1002 Joint Symposium 8: EANM/EAU: PET Imaging of Genito-urinary Malignancies beyond Prostate	1003 Technologists CTE 4: Infection Imaging in Nuclear Medicine	1004 Neurosciences - Featured: Dementia	1005 Do.MoRe: 90Y SIRT Treatment Planning	1006 M2M: Radiopharmaceuticals & Radiochemistry: Peptides	1007 DGN-Sponsored Symposium: PET/MRI	1008 Conventional & Specialised Nuclear Medicine: General & Miscellaneous	1009 Physics & Instrumentation & Data Analysis: Image Reconstruction, Quantification & PET/MR	1010 Clinical Oncology: Melanoma & Lymphoma	

Tuesday, October 13, 2015

Time/Room	Hall 1	Hall 2	Hall 4	Hall G1	Hall G2	Hall 6	Hall F	Hall E	Hall 8	Hall D	Hall 3 - Poster Exhibition
Capacity	3000	1100	800	580	560	370	260	260	260	230	
08:00 - 09:30	1101 CME 9 Radionuclide Therapy & Thyroid & Translational Molecular Imaging Theranostics: What We Have and What We Can Achieve	1102 Joint Symposium 9: EANM/ESSR/ESSKA: Evaluation of the Painful Knee Arthroplasty	Technologists In Hall 3 - Poster Exhibition: Poster Sessions TP01, TP02, TP03, TP04		1105 Do.MoRe: Quantitative Molecular Imaging	1106 M2M: Molecular & Multimodality Imaging: Tumour Biology & Optical Imaging	1107 SNMMI Symposium: Hepatobiliary Scintigraphy in Abdominal Pain	1108 Pitfalls & Artefacts & Physiology (Cardiovascular) - Interactive: MPS, SPECT-CT, PET, Newer Techniques such as CZT and IQ SPECT			Technologist Poster Sessions TP01, TP02, TP03, TP04 (08:00 - 09:30) Poster Walks PW03, PW06, PW09, PW12 (08:30 - 09:30)
10:00 - 11:15	1201 Plenary 3 (M2M - Molecule to Man Track) Targets and Probes		1203 In Hall 1: Plenary 3 (M2M - Molecule to Man Track) Targets and Probes								
11:30 - 13:00	1301 CME 10 Dosimetry & Translational Molecular Imaging Preclinical Quantitative Imaging and Dosimetry	1302 Joint Symposium 10: EANM/ELI: Lymphoma and PET/CT Update	1303 Technologists Oral Presentations 3		1305 Do.MoRe - Featured: Therapy - Miscellaneous	1306 M2M - Featured: Molecular & Multimodality Imaging: PSMA	1307 Cardiovascular System: Myocarditis, Amyloidosis, Sarcoidosis & Vasculitis	1308 Conventional & Specialised Nuclear Medicine: Paediatric - General	1309 Physics & Instrumentation & Data Analysis: Quality Control, Performance, Standardisation	1310 Clinical Oncology: Miscellaneous	
13:00 - 14:30									Young EANM Daily Forum		
14:30 - 16:00	1401 CME 11 Radiopharmacy New Protein Deposition Tracers	1402 Joint Symposium 11: EANM/ENETS: Management of Neuroendocrine Tumours	1403 Technologists CTE 5: Lean Principles and Improved Departmental Management	1404 Cardiovascular System - Featured: Imaging of Plaques, Angiogenesis & Ischaemic Memory	1405 M2M: Radiopharmaceuticals & Radiochemistry: Radiochemistry & Instrumentation	1406 M2M: Molecular & Multimodality Imaging: Therapy - Preclinical Studies, α & β Radiation	1407 Teaching Session: Interactive Quiz: Radiology and Cross- sectional Imaging	1408 Clinical Oncology: Paediatric Oncology	1409 Physics & Instrumentation & Data Analysis: Instrumentation	1410 Neurosciences: Psychiatry	Poster Sessions P39 - P63 (16:00 - 16:30)
16:30 - 18:00	1501 CME 12 Drug Development & Radiopharmacy Radiopharmaceutical Design	1502 Joint Symposium 12: (M2M - Molecule to Man Track) EANM/ESMI/COST: Lead Compounds in Theranostics			1505 Do.MoRe: Thyroid	1506 M2M: Molecular & Multimodality Imaging: PET - Translational & Clinical Studies	1507 Teaching Session: Interactive Quiz: Nuclear Medicine with Correlative Imaging	1508 Cardiovascular System: Miscellaneous	1509 Clinical Oncology: Neuroendocrine	1510 Neurosciences: Neuroimaging - Data Analysis	

Wednesday, October 14, 2015

Time/Room	Hall 1	Hall 2	Hall 4	Hall G1	Hall G2	Hall 6	Hall F	Hall E	Hall 8	Hall D	Hall 3 - Poster Exhibition
Capacity	3000	1100	800	580	560	370	260	260	260	230	
08:00 - 09:30	1601 CME 13 Translational Molecular Imaging & Radiopharmacy Image Guided Surgery in Urological Malignancies	1602 Joint Symposium 13: EANM/ESPGHAN: Paediatric Gastrointestinal Nuclear Medicine	1603 Technologists 09:30 - 10:45 CTE 6: Imaging Protocols in Radionuclide Therapy		1605 Do.MoRe: 90Y SIRT Dose Effects	1606 M2M: Radiopharmaceuticals & Radiochemistry: Macromolecules II		1608 Clinical Oncology: Breast & Gynaecology		1610 Clinical Oncology: Brain, Head & Neck	
10:00 - 11:30	1701 CME 14 Drug Development & Translational Molecular Imaging Multimodal Imaging Agents (Probes, Techniques & Applications)				1705 Do.MoRe: Miscellaneous	1706 M2M: Molecular & Multimodality Imaging: PET Tracers - Preclinical Studies		1708 Clinical Oncology: Therapy Response & External Beam RT	1709 Physics & Instrumentation & Data Analysis: Radiation Exposure & Protection	1710 Neurosciences: Movement Disorders	
11:45 - 13:20	1801 11:45 - 12:15: Awards Ceremony 12:15 - 13:15: Highlights Lecture 13:15 - 13:20: Closing Ceremony		1180 KW In Hall 1: 11:45 - 12:15: Awards Ceremony 12:15 - 13:15: Highlights Lecture 13:15 - 13:20: Closing Ceremony								

Pre-Congress Meetings/Sessions
Plenary Sessions
Continuing Medical Education Sessions
Scientific Symposia
Technologist Sessions
Featured Sessions
Special Features
Industry Sponsored Symposia
Poster Sessions
Parallel Sessions

101 - Sunday, October 11, 2015, 8:00 AM - 9:30 AM, Hall 1
CME 1 - Bone & Joint (Interactive): Bone Planar & Hybrid Scintigraphy: Patterns, Pearls, and Pitfalls

OP001
Patterns
G. Gnanasegaran, UK

OP002
Pearls
F. Paycha, FRANCE

OP003
Pitfalls
K. Strobel, SWITZERLAND

102 - Sunday, October 11, 2015, 8:00 AM - 9:30 AM, Hall 2
Joint Symposium 1: EANM/EACVI: Cost-effectiveness in Cardiac Imaging: From Theory to Practice

OP004
What is Cost-effectiveness: Theory and Implications/Implementation
S. S. Tan, NETHERLANDS

OP005
Cost-effectiveness of the Different Myocardial (Perfusion) Imaging Techniques
S. E. Petersen, UK

103 - Sunday, October 11, 2015, 8:15 AM - 9:45 AM, Hall 4
CTE 1: Brain Imaging (Tech Guide Book Launch)

OP006
Imaging in Oncological Brain Diseases (PET/CT)
G. Testanera, ITALY

OP007
Tracers for Brain Imaging
A. Socan, SLOVENIA

OP008
Principles of Functional Brain Imaging with Radiotracers
A. Signore, ITALY

105 - Sunday, October 11, 2015, 8:00 AM - 9:30 AM, Hall G2
Do.MoRe: PRRT Treatment Planning

OP009
Investigation on the number of PET measurements needed for accurate prediction of therapeutic biodistribution in PRRT

D. Hardiansyah[1,2], W. Guo[1], P. Kletting[3], B. Müller[4], F. Mottaghy[4], G. Glatting[1]; [1]Medical Radiation Physics/Radiation Protection, Universitätsmedizin Mannheim, Medical Faculty Mannheim, Heidelberg University, Mannheim, GERMANY, [2]Department of Radiation Oncology, Universitätsmedizin Mannheim, Medical Faculty Mannheim, Heidelberg University, Mannheim, GERMANY, [3]Klinik für Nuklearmedizin, Universität Ulm, Ulm, GERMANY, [4]Klinik für Nuklearmedizin, University Hospital, RWTH Aachen University, Aachen, GERMANY.

Aim: Aim of this study was to investigate the variability of individual time-integrated activity coefficient (TIAC) prediction for different positron emission tomography (PET) measurement protocols in peptide-receptor radionuclide therapy (PRRT).Material and Methods: Assumed true model parameters were derived using "Simulation, Analysis and Modeling II" software by fitting the physiology based pharmacokinetic (PBPK) model parameters to the data of 15 patients (^{111}In-DTPAOC, serum and organ activity data). Predicted model parameters based on the simulation of PET measurements were derived as follows: first, a PET measurement after bolus injection of 150 MBq of ^{68}Ga-DOTATATE was simulated using the assumed true model parameters; second, different PET sampling protocols (PSPs) were implemented to take organ activity data from the simulated time activity curve of ^{68}Ga-DOTATATE. Six PET sampling protocols were investigated: 30 min (PSP1), 60 min (PSP2), 240 min (PSP3), 30 min plus 60 min (PSP4), 30 min and 240 min (PSP5), 60 min and 240 min (PSP6); third step, random noise was added to the simulated organ activity data with fractional standard deviation (FSD) of 10^{-3} using the "PopKinetics" software; fourth, the PBPK model was fitted to these noisy data to derive predicted model parameters. The therapeutic biodistribution was simulated for the model with true parameters and the model with predicted parameters assuming an infusion over 30 min of 3.3 GBq ^{90}Y-DOTATATE. Time integrated-activity coefficients (TIACs) of tumour and kidneys were calculated for both models. The variability between predicted TIACs and true TIACs were compared for tumor and kidneys. Results: Protocols with simulated PET measurement (PSP 1 to 3) showed high values for both kidneys and tumour variabilities. In these 3 protocols PSP 3 sampling at 240 min showed the lowest variability for kidneys (10±7) % and tumour (28±24) %. Variabilities obtained using two time-point PET data (PSP 3 to 6) were much smaller than those of one time-point PET data. The best results were found at PSP6 which were (2±) % for kidneys and (7±1) % for tumour. Conclusion: The PET

measurement protocol at 240 min post injection is important for predicting the therapeutic biodistribution. Protocols with two time-point PET measurements showed higher accuracy than those with one PET measurement. The protocol with PET measurements at 60 min and 240 min post injection is recommended for further investigations.

OP010

The prediction accuracy of therapeutic biodistribution in PET-based treatment planning of PRRT with different Bayesian parameter estimation methods

W. Guo[1], D. Hardiansyah[1,2], A. A. Attarwala[1,2], C. Maaß[1], G. Glatting[1]; [1]Medical Radiation Physics/Radiation Protection, Universitätsmedizin Mannheim, Medical Faculty Mannheim, Heidelberg University, Mannheim, GERMANY, [2]Department of Radiation Oncology, Universitätsmedizin Mannheim, Medical Faculty Mannheim, Heidelberg University, Mannheim, GERMANY.

Aim: The aim of this study was to compare the prediction accuracy of therapeutic biodistributions in PET-based treatment planning of peptide-receptor radionuclide therapy (PRRT) with two Bayesian parameter estimation methods. Materials and Methods: A recently developed physiologically based pharmacokinetic (PBPK) model was fitted to the biokinetic data of patients (SAAM II, The Epsilon Group, Charlottesville, USA) using two different methods: Standard Two-Stage (STS) and Iterative Two-Stage (ITS). The two methods yield assumed true parameters (TPs) and Bayesian parameters. Biokinetic data of 14 patients were obtained after the bolus injection of 152±15 MBq of ^{111}In-DTPAOC from the serum activity and the organ activity taken by a Gammacamera. Based on assumed true parameters PET measurements were simulated after bolus injection of ^{68}Ga-DOTATATE of 150 MBq. Organ activity data from simulated time activity curves were taken at 30 min, 60 min and 240 min post injection. A PET noise model with related coefficient c of 3 and 30 which simulates typical error in PET measurements was included to simulate the organ activity data for used time points. The PBPK model was fitted to the simulated noisy PET data with Bayesian parameters obtained by STS and ITS to derive predicted parameters (PPs). Therapy was simulated for TPs and PPs assuming an infusion of 3.3 GBq of ^{90}Y-DOTATATE over 30 min. Area under the curves (AUCs) of simulated time activity curves in kidneys and tumour were calculated for therapeutic biodistribution using TP (AUC_{TP}) and PP (AUC_{PP}). Variability between AUC_{TP} and AUC_{PP} was calculated and analysed. Result: For noise level of c = 3 using Bayesian parameter from ITS the variabilities were (9 ±7) % for tumour and (2±1) % for kidney, while they were (14 ±9) % for tumour and (2±3) % for kidneys using the Bayesian parameters from STS. The highest variabilities were (18±11) % for tumour and (3±2) % for kidneys for c=30 using Bayesian parameters from STS and it was (12±9) % for tumour and (2±1) % for kidneys using ITS. Within the same coefficient of noise level the variability of AUCs with the ITS method showed lower values for both tumour and kidneys than using the STS method. However, no significant ($p<0.05$, Student's t test) difference was found. Conclusion: The ITS fitting method seems better suited for deriving the Bayesian parameters and predicting the therapy. Further investigation based on a larger population size and with improved sampling schedule is however needed.

OP011

Fractional contribution of extrapolations after 96 h in absorbed dose calculation to kidneys in 450 patients with neuroendocrine tumours receiving ^{177}Lu-DOTATATE therapy

M. Sandstrom, U. Garske-Román, D. Granberg, A. Sundin, M. Lubberink; Nuclear medicine & PET, Uppsala University, SWEDEN.

Aim: As in all therapies using ionizing radiation, a patient-specific optimization of the delivered radiation should be performed in therapy with ^{177}Lu-DOTA-D-Phe1-Tyr3-octreotate (^{177}Lu-DOTATATE). To determine the total time-integrated activity concentration in an organ, extrapolation from the first measurement to time of injection and extrapolations from the last measurement to infinity are needed. It is stated in EANM guidelines that the fractional contribution from the extrapolations should be less than 20% for bone marrow and whole-body dosimetry [1]. The main aim of the present work was to study the fractional contribution after 96 h to the time-integrated activity in kidney in therapy with ^{177}Lu-DOTATATE. Secondary aim was to investigate the influence on the absorbed dose calculation. Materials and Methods: Four hundred fifty patients (219 female and 231 male) with neuroendocrine tumors with high somatostatin receptor expression were included. SPECT/CT over the abdomen were acquired at 24, 96 and 168 h after start of infusion of ^{177}Lu-DOTATATE. In two patients one kidney was excluded due to adjacent tumours. For the kidneys the fractional contribution was calculated for a single therapy cycle of 7.4 GBy from 96 h to infinity. Ratios between absorbed dose calculations performed using only 24 and 96 h measurements AD(24-96) versus absorbed dose calculations performed using 24, 96 and 168 h measurements AD(24-96-168) was performed. Results and discussion: In the right kidney the extrapolated fractional contribution after 96 h

was 29% (Median; Min - Max 12-60) while the absorbed dose ratio was 0.97 (0.67-1.64). The fractional contribution after 96 h was higher than the recommended 20%, not including the time before the first measurement. For the majority of the patients the AD(24-96) estimation gave a value close to the AD(24-96-168) but overestimations of up to 60% and underestimations of up to 30% of the absorbed dose were also seen. No significant differences between left and right kidneys were found. Conclusions: To meet the EANM dosimetry committee recommendation of at most 20% extrapolated fractional contribution in the determination of kidney doses and to get a reliable absorbed dose estimation, it is not sufficient to have the last measurement point at 96 h p.i., and later measurements are needed. 1. Hindorf C, Glatting G, Chiesa C, Linden O, Flux G. EANM Dosimetry Committee guidelines for bone marrow and whole-body dosimetry. Eur J Nucl Med Mol Imaging. 2010;37:1238-50. doi:10.1007/s00259-010-1422-4.

OP012

Preliminary results of a Dosimetry-Based peptide receptor radionuclide therapy in patients with advanced neuroendocrine tumors

A. Filice[1], F. Fioroni[2], E. Grassi[2], V. Ferri[2], M. Casali[1], M. Roncali[1], M. Sollini[3], A. Frasoldati[4], A. Versari[1]; [1]Department of Nuclear Medicine IRCCS-Arcispedale Santa Maria Nuova, Reggio Emilia, ITALY, [2]Medical Physics Unit, IRCCS-Arcispedale Santa Maria Nuova, Reggio Emilia, ITALY, [3]IRCCS MultiMedica, Sesto San Giovanni, Reggio Emilia, ITALY, [4]Endocrinology Unit IRCCS-Arcispedale Santa Maria Nuova, Reggio Emilia, ITALY.

Purpose: Peptide Receptor Radionuclide Therapy (PRRT) has an important role in the treatment of advanced neuroendocrine tumors (NETs). Dosimetry allows to personalize this therapy. The aim of this study is to create a strategy of treatment balancing renal protection and tumor treatment, using both ^{177}Lu-DOTATOC and ^{90}Y-DOTATOC to obtain the best ratio. Methods: The PRRT protocol that we are using in our center is a monocenter, rospective, non-randomized, phase II study. It is a dosimetry-based study in which the dosimetric evaluation (kidney, bone marrow, tumor) is performed at the first cycle of ^{177}Lu-DOTATOC. According to these data we calculate the projected adsorbed dose for kidneys, bone marrow and tumor tissues (max 5 lesions). A cohort of 12 patients who underwent more than 2 PRRT administrations and 2 68Ga-DOTATOC PET-CT scans (PET1: baseline and PET2: after the second cycle) were selected. Up to 5 target lesions/patient (volume range 2.3-243 ml) were analysed. Lesions analysed were grouped based on the localisation: liver (28), lymph node (7), and bone (8). The dose to the lesions was calculated at organ level through multiple SPECT-CT scans with the OLINDA/EXM sphere model. Maximum SUV value was evaluated for each lesion and the percentage difference (PD%) between PET1 and PET2 values was calculated. Results: Mean, standard deviation (SD), and range values for PD% were: liver (2.2, 31, -49-75); lymph node (25, 62, -45-117); bone (8, 16, -6-45). Absorbed doses were: liver 41±26 Gy, lymph node 19±29 Gy, bone 13±13 Gy. We found higher correlation between absorbed doses and SUV max at PET1 for all lesions (liver, lymph node, bone), than between absorbed doses and lesions volume. We didn't find a good correlation between absorbed doses and PD%. Conclusions: These preliminary results suggest that a dosimetric evaluation at the first cycle of PRRT allows to obtain a good personalization of the treatment approach. The range of lesion adsorbed doses and PD% values is very broad but probably the second cycle is not adequate to investigate the correlation between tumor response and site of disease because is too early in this clinical setting.

OP013

Pre-treatment intensity of DOTATOC uptake for prediction of response to selective intravascular radionuclide therapy

T. D. Poeppel[1], H. V. Ngo[1], I. Binse[1], H. Lahner[1], N. Unger[1], A. Bellendorf[1], S. Ezziddin[2], A. Bockisch[1], A. Sabet[1]; [1]Universitaetsklinikum Essen, Essen, GERMANY, [2]Universitaetsklinikum des Saarlandes, Homburg, GERMANY.

Aim: DOTATOC PET/CT is known to depict somatostatin receptor expression of neuroendocrine tumour (NET) lesions. Yet, DOTATOC uptake is also related to the perfusion of a lesion. There is a strong connection between the perfusion of a lesion and treatment response in selective intravascular radionuclide therapy (SIRT). Yet, it is unclear if DOTATOC uptake may serve as a parameter to predict treatment response in SIRT. This study assesses the value of baseline line DOTATOC PET in predicting the response to SIRT with Y-90-microspheres in patients with hepatic metastatic NET. Methods: 25 patients with hepatic metastatic gastroenteropancreatic (GEP) NET who were treated with SIRT were retrospectively analysed. Ga-68-DOTATOC-PET/CT was performed at baseline and three months after the treatment. The maximum standardised

uptake value (SUVmax) was determined as a measure of DOTATOC uptake. In each patient a maximum of three clearly delineated tumour lesions was selected as target. SUVmax and tumour-to-spleen ratios (SUVmaxT/s) of target tumour lesions were calculated. Response of each tumour lesion was evaluated according to the relative change in SUVmaxT/s (%Δ SUVmaxT/s). The association of baseline SUV parameters and functional response was tested using Spearman's rank correlation analysis. Results: 69 lesions were included into the analysis. Mean tumour and splenic SUVmax at baseline were 19.9 ±1.7 and 23.4 ±1.7, respectively. 50 lesions showed a reduction in SUVmax three months after SIRT. Mean post-SIRT SUVmax was 10.8±1.7. Relative change in SUVmaxT/s was 26.7±12.8 %. Baseline SUVmax showed a moderate (r=0.132) and SUVmaxT/s a slightly better correlation with lesion-based response (r=0.441). Conclusions: Pre-treatment intensity of DOTATOC uptake in terms of SUV parameters is only moderately related to lesion-based functional response to SIRT in GEP NET patients.

OP014

An image based method for bone marrow dosimetry in 177Lu-DOTATATE therapy

J. Svensson[1], J. Söderström[2], T. Magnander[2], E. Wikberg[2], B. Wängberg[3], P. Bernhardt[2]; [1]Department of Oncology, The Sahlgrenska Academy, Sahlgrenska University Hospital, Göteborg, SWEDEN, [2]Department of Radiation Physics, The Sahlgrenska Academy, Sahlgrenska University Hospital, Göteborg, SWEDEN, [3]Department of Surgery, The Sahlgrenska Academy, Sahlgrenska University Hospital, Göteborg, SWEDEN.

Aim: Treatment with 177Lu-DOTATATE for advanced neuroendocrine tumours expressing somatostatin receptors has proven efficient and safe. Organs at risk are mainly the kidneys and the bone marrow. Though well tolerated in general, bone marrow toxicity might become dose limiting. The aim of this study was to evaluate an image based method to estimate the absorbed dose to the bone marrow during 177Lu-DOTATATE treatment. Materials and methods: 51 patients with advanced neuroendocrine tumours were treated with 177Lu-DOTATATE on 1-6 occasions. The patients were evaluated according to the mean absorbed dose to the bone marrow using the 4 planar images collected at 2, 24, 48 and 168 hour after injection. By using a segmentation tool in the in-house made software RONSO, the high uptake area in the images was separated from the low uptake area. The high uptake area consisted of the tissue related activity in tumours and organs, and the low uptake area contained the blood related activity in the images. Absorbed dose to the bone marrow was calculated as sum of; the self-dose from charges particles in the bone marrow, the cross-dose from the tissue related area (solely γ-radiation contribution) and the cross-dose from the blood related area. Results: The median of the mean absorbed dose to the bone marrow was 0.17 Gy (range 0.08 - 0.49 Gy) for the first therapy cycle; where an average amount of 7.5 GBq (range 4.2 - 8.3 GBq) 177Lu-DOTATATE was administered to the patients. For all the treatment cycles (in average 3 occasions) the median of the mean absorbed dose was 0.51 Gy (range 0.16 - 1.35 Gy). The self-dose made the largest contribution to the mean absorbed dose to the bone marrow. Conclusion: The image based method developed in this work might be useful for bone marrow dosimetry. The mean absorbed doses varied considerably between patients which illustrates the need for individual dosimetry, especially when the total amount of 177Lu-DOTATATE in on-going studies tend to increase, and also when other treatment options make it necessary to preserve bone marrow function. The method requires to be validated for a more patient specific purpose, which can be done by blood dosimetry from blood sampling.

OP015

Prediction accuracy of therapeutic biodistribution in peptide receptor radionuclide therapy: Role of patient-based treatment planning

D. Hardiansyah[1,2], C. Maaß[1], A. Attarwala[1,2], P. Kletting[3], B. Müller[4], F. Mottaghy[4], G. Glatting[1]; [1]Medical Radiation Physics/Radiation Protection, Universitätsmedizin Mannheim, Medical Faculty Mannheim, Heidelberg University, Mannheim, GERMANY, [2]Department of Radiation Oncology, Universitätsmedizin Mannheim, Medical Faculty Mannheim, Heidelberg University, Mannheim, GERMANY, [3]Klinik für Nuklearmedizin, Universität Ulm, Ulm, GERMANY, [4]Klinik für Nuklearmedizin, University Hospital, RWTH Aachen University, Aachen, GERMANY.

Aim: An accurate treatment planning is needed in peptide-receptor radionuclide therapy (PRRT) for ensuring the optimal tumor irradiation while diminishing the toxicity for the kidneys. The aim of this study was therefore to show the prediction accuracy of the therapeutic biodistribution in peptide receptor radionuclide therapy (PRRT) for different degrees of individualization when using physiologically based pharmacokinetic modelling (PBPK).Material and Methods: The parameter of a recent PBPK model of PRRT were fitted to the biokinetic data of 15 patients with metastasized neuroendocrine tumors (NETs): serum and

planar gamma camera data after the injection of ^{111}In-DTPAOC to derive the assumed true model parameters. Four mathematical phantom patients (MPP) were defined with increasing amount of patient-specific information: MPP_{true} is the PBPK model with 15 sets of all assumed true model parameters; MPP_{mean} is the PBPK model with all model parameters fixed to the mean values of the 15 patients; $MPP_{specific}$ uses additional individual patient data: physical parameters (body weight, body surface area, age, gender), hematocrit, volume of the tumor, glomerular filtration rate and flow to the tumor; MPP_{PET} is $MPP_{specific}$ with one simulated positron emission tomography (PET) data set at t=60 min after injection of ^{68}GA-DOTATATE to fit the model parameters. Therapy was simulated as an infusion of 3.3 GBq of ^{90}Y-DOTATATE over 30 min for all MPPs. Area under the curve (AUC) of time activity curve in tumor and kidneys were calculated for total simulation duration of 14 d. The relative differences (RD) of AUCs of MPP_{mean}, $MPP_{specific}$ and MPP_{PET} to MPP_{true} were analyzed. Results: RDs of MPP_{mean} were RD_{tumor} = (625±1266) % and $RD_{kidneys}$ = (11±38) %, demonstrating that patient individual data are needed for treatment planning. Inclusion of patient individual data in $MPP_{specific}$ lead to significantly lower RD in the tumor: RD_{tumor} = (-2±27) % and $RD_{kidneys}$ = (16±43) %. RD in MPP_{PET} showed a major improvement for the kidneys due to the inclusion of simulated PET data: RD_{tumor} = (-2±22) % and $RD_{kidneys}$ = (-0.1±0.5) %. Summary: Individual biokinetics are needed to predict the biodistribution in PRRT using theses somatostation analogs. Additional use of a single PET measurement together with the PBPK model significantly improved the prediction.

OP016

The variability of predicted area under the curves for different degrees of noise in PET measurements for treatment planning in peptide-receptor radionuclide therapy

D. Hardiansyah[1,2], W. Guo[1], P. Kletting[3], B. Müller[4], F. Mottaghy[4], G. Glatting[1]; [1]Medical Radiation Physics/Radiation Protection, Universitätsmedizin Mannheim, Medical Faculty Mannheim, Heidelberg University, Mannheim, GERMANY, [2]Department of Radiation Oncology, Universitätsmedizin Mannheim, Medical Faculty Mannheim, Heidelberg University, Mannheim, GERMANY, [3]Klinik für Nuklearmedizin, Universität Ulm, Ulm, GERMANY, [4]Klinik für Nuklearmedizin, University Hospital, RWTH Aachen University, Aachen, GERMANY.

Aim: Accuracy of treatment planning in peptide-receptor radionuclide therapy (PRRT) depends on the variability of the individually predicted biodistribution. The aim of this study was to investigate the variability of the area under the curves (AUCs) for different degrees of noise in simulated positron emission tomography (PET) measurements for PRRT.Material and Methods: A physiologically based pharmacokinetic (PBPK) model of PRRT was used in this study. Assumed true model parameters for 15 patients were derived using "Simulation, Analysis and Modeling II" software by fitting the PBPK model parameters to their biokinetic data (^{111}In-DTPAOC, serum and organ activity data). Predicted model parameters based on the PET simulation were derived as follows: first, a PET measurement after bolus injection of 150 MBq of ^{68}Ga-DOTATATE was simulated using the assumed true model parameters; second, the organ activity data of kidneys, tumour, spleen and liver at 60 min and 240 min post injection were taken; third, random noise was added to the simulated organ activity data with fractional standard deviations (FSD) of 10^{-1}, 10^{-2}, 10^{-3}, and 10^{-4} using the "PopKinetics" software; fourth, the PBPK model was fitted to these noisy data to derive predicted model parameters for the patients. Two mathematical patient phantoms (MPPs) were built: true MPP (PBPK model with assumed true model parameters) and predicted MPP (PBPK model with predicted model parameters). Therapeutic biodistribution was simulated for true and predicted MPPs assuming an infusion over 30 min of 3.3 GBq ^{90}Y-DOTATATE. AUCs of tumour and kidneys were calculated for both MPPs. The variability V between predicted AUCs and true AUCs were calculated for tumour and kidneys. Results: The variabilities for FSD = 10^{-1} and 10^{-2} showed low accuracy for the prediction of the therapeutic biodistribution: FSD = 10^{-1} yielded V_{tumor} = (27±23) % and V_{kidney} = (13±5) %; FSD = 10^{-2} yielded V_{tumor} = (23±10) %, V_{kidney} = (7±3) %. FSD 10^{-3} and FSD 10^{-4} showed acceptable variabilities for the prediction (V_{tumor} = (8±2) %, V_{kidney} = (2±1) % and V_{tumor} = (1±1) %, V_{kidney} = (0.3±0.3) % for FSD = 10^{-3} and 10^{-4}, respectively. Conclusion: Organ activity measured from two time points by PET could possibly be used to reliably predict the individual therapeutic biodistribution. Typical PET measurements have noise equal or lower than FSD=10^{-3} and thus could possibly lead to an acceptable prediction of therapeutic biodistribution.

108 - Sunday, October 11, 2015, 8:00 AM - 9:30 AM, Hall E
Pitfalls & Artefacts & Physiology - Interactive: Clinical Consequences of Neuroimaging

OP017
Value and Pitfalls of Neuroimaging in a Memory Clinic
B. N. M. van Berckel, NETHERLANDS

OP018
Value and Pitfalls of Neuroimaging in a Primary Care SettingA. Fellgiebel, GERMANY

OP019
Value and Pitfalls of Neuroimaging in Preclinical Stages of Dementia
F. Jessen, GERMANY

201/203 - Sunday, October 11, 2015, 10:00 AM - 11:15 AM, Hall 1
Plenary 1: Clinical Molecular Imaging (incl. Marie Curie Lecture)

OP020
Marie Curie Lecture: Prostate Cancer
S. Fanti, ITALY

OP021
Imaging of Atherosclerosis: Translation from Research to Practice
J. H. F. Rudd, UK

OP022
Neuroimaging - Mandatory Biomarker in Dementia Assessment?
P. Scheltens, NETHERLANDS

301 - Sunday, October 11, 2015, 11:30 AM – 01:00 PM, Hall 1
CME 2 - Oncology & Paediatrics & Bone and Joint: Sarcomas

OP023
Molecular Imaging in Bone Sarcomas: Implementing the Role of PET/CT
E. Lopci, ITALY

OP024
Enchondroma, Osteochondroma, Chondrosarcoma: A Multimodality Imaging Challenge
F. Paycha, FRANCE

OP025
Soft Tissue Sarcomas, Role of PET/MR
F. Giammarile, FRANCE

302 - Sunday, October 11, 2015, 11:30 AM – 01:00 PM, Hall 2
Joint Symposium 2: EANM/ETA-CRN: What the Doctor Tells and the Patient Understands - Update on Thyroid Cancer Communication

OP026
The New American Thyroid Association Guidelines on the Diagnosis and Management of Thyroid Nodules and Differentiated Thyroid Cancer: a Summary of the European Perspective and Commentaries
M. Hoffmann, AUSTRIA

OP027
Patient Information in Thyroid Cancer
J. Taylor, UK

OP028
Patient Information in General Oncology
W. T. van der Graaf, NETHERLANDS

303 - Sunday, October 11, 2015, 11:30 AM – 01:00 PM, Hall 4
CTE 2 - Interactive: Multi-Professional Discussion on Extended Competencies for Nuclear Medicine Technologists

OP029
How It All Began: 1999 Competencies
J. A. Jorge, SWITZERLAND

OP030
How It All Developed: Advance Practice and Interaction with External Societies
G. Testanera, ITALY

OP031
Adapting to the Future: EANM-TC Document on Competencies
P. Fragoso Costa, GERMANY

304 - Sunday, October 11, 2015, 11:30 AM – 01:00 PM, Hall G1
Special Symposium: Evidence-based Medicine - Implications for Imaging Communication

OP032
Evidence-based Imaging - The Editor's View
D. Delbeke, USA

OP033
Evidence for Advanced Imaging in Radiotherapy Practice - The Clinician's View
U. Nestle, GERMANY

OP034
Beyond RECIST: Progressing Advanced MRI Applications into Clinical Practice
D. M. Koh, UK

305 - Sunday, October 11, 2015, 11:30 AM - 12:45 PM, Hall G2
Do.MoRe: Novel Therapies

OP035
First-in-man experience of CXCR4-directed endoradiotherapy with ^{177}Lu- and ^{90}Y-labelled pentixather in heavily pretreated multiple myeloma with extensive intra- and extramedullary disease

K. Herrmann[1], M. Schottelius[2], C. Lapa[1], A. Poschenrieder[2], H. Hänscheid[1], U. Keller[2], A. Schirbel[1], S. Kropf[3], A. K. Buck[1], S. Knop[1], H. Einsele[1], H. Wester[2]; [1]Universitätsklinikum Würzburg, Würzburg, GERMANY, [2]Technische Universität München, München, GERMANY, [3]Scintomics GmbH, Fürstenfeldbruck, GERMANY.

Aim: The chemokine receptor CXCR4 is a key factor for tumor growth and metastasis in several types of human cancer. Based on our promising experiences with a radio-labelled CXCR4 ligand ([68Ga]pentixafor) for diagnostic receptor targeting, [177Lu]- and [90Y]pentixather were recently developed as endoradiotherapeutic vectors. Here, we summarize the first-in-man experience with CXCR4-directed therapy with these radiolabelled receptor ligands. Materials and Methods: Three patients with intra- and extensive extramedullary manifestations of multiple myeloma were included. All had exhausted all available treatment options including stem cell transplant (SCT). CXCR4-target expression was demonstrated by baseline [68Ga]pentixafor-PET. Each treatment was approved by the clinical ethics committee. Pre-therapeutic [177Lu]pentixather dosimetry was performed prior to treatment with 15.2 and 23.5 GBq [177Lu]pentixather, and 6.3 GBq [90Y]pentixather, respectively. Subsequently, patients underwent additional chemotherapy and autologous SCT for bone marrow rescue. Early treatment response was monitored by conventional criteria and [18F]FDG-PET/CT. Results: Pentixather-radionuclide therapy was well tolerated in all 3 patients. Two patients underwent response assessment with [18F]FDG-PET/CT showing significant therapeutic effect with one partial and one complete metabolic response. Conclusion: In combination with cytotoxic chemotherapy and autologous SCT, CXCR4-targeted radiotherapy with pentixather appears to be a promising novel treatment option for patients with advanced multiple myeloma, especially in patients with extramedullary manifestations.

OP036
Radionuclide treatment with 64Cu-Cl2 in patients with progressive malignant gliomass

E. Capasso, Jr.[1], M. C. Valentini[2], S. Mirzaei[3], P. Knoll[3], C. Meleddu[1]; [1]U.O.C. Nuclear Medicine, Cagliari, ITALY, [2]S.C. Neuroradiology, C.T.O., Turin, ITALY, [3]Department of Nuclear Medicine with PET-Center, Wilhelminenspital, Vienna, AUSTRIA.

Background: Gliomas are the most common type of brain tumor, of which malignant astrocytomas (MA), also defined as glioblastoma multiforme (GBM) and anaplastic astrocytoma (AA) have a poor survival rate. The standard care is based on cyto-reductive surgery followed by radiotherapy and adjuvant chemotherapy (CHT). Several trials have been performed with i.e. combination of temozolomide, thalidomide with antiangiogenetic drugs, but the impact on survival remains limited. Further, many types of cancers typically show high levels of

copper, including gliomas. Beaucase of its ß- emission the copper isotope 64Cu has been discussed for therapeutic applications. AIM: The aim of this case study was to evaluate the possible impact of treatment with 64Cu-Cl2 in patients with progressive GBM and AA despite previous standard treatment. MATERIALS AND METHODS: A 51y female patient affected by GBM with primary localization in left thalamus with progressive disease (PD) after surgery and radiochemetherapy was enrolled. She received twice intravenously a dose of 3300 and 2590 MBq of 64CuCl2 in alternating days. The treatment was well tolerated, without clinical side effects. The patient underwent to a PET/CT scan, from vertex to thorax, 1 hour after the tracer administration. RESULTS: The 64CuCl2 PET scan showed a high uptake in left thalamic and frontal lesions, in correlation to the known morphologic target lesions. One month later the patient underwent to a control MRI which showed remarkable volume reduction of the lesions with disappearance of the previously peritumoral edema and readjustement of the brain midline structure. CONCLUSIONS: Radinuclide treatment with 64CuCl2 is very well tolerated and could be of potential benefit in malignant glioma patients with PD despite standard treatment.

OP037

Clinical Feasibility and Effectiveness of Intraperitoneal Radionuclide Therapy with Lu-177 3BP-227 in Metastatic Adenocarcinoma of Pancreas

A. Singh[1], H. Kulkarni[1], C. Schuchardt[1], S. Wiessalla[1], M. Sayeg[1], I. Klette[1], F. Osterkamp[2], U. Reineke[2], C. Smerling[2], R. P. Baum[1]; [1]Zentralklinik Bad Berka, THERANOSTICS Center for Molecular Radiotherapy and Molecular Imaging (PET/CT), Bad Berka, GERMANY, [2]3B Pharmaceuticals GmbH, Berlin, GERMANY.

Aim: Metastatic pancreatic adenocarcinoma (mPaCa) has a very poor prognosis. Following our experience on dosimetry and intravenous (i.v.) radiopeptide therapy with Lu-177 3BP-227 (a neurotensin antagonist targeting NTR-1), we report the feasibility and effectiveness of serial intraperitoneal administrations of Lu-177 3BP-227 for the treatment of mPaCa.Materials and Methods:A 59-year old female with inoperable mPaCa (vascular infiltration, lymph node, liver, peritoneal metastases) and massive ascites was referred with progressive disease after 7 cycles of chemotherapy for radiopeptide therapy. Following initial feasibility and dosimetry using 1400 MBq of i.v. Lu-177 3BP-227, the patient received 6400, 7500, and 5300 MBq Lu-177 3BP-227 over a period of six months. Dosimetry (MIRD) was performed using OLINDA/EXM software. Feasibility was assessed by dosimetry, patient tolerance, side-effects, and toxicity profile (hematological, renal, liver) based on serial determination of laboratory tests and renal scintigraphy. Effectiveness was assessed by monitoring clinical outcome, tumor markers, and by imaging (PET/CT) pre- and post-therapy.Results:Clinical feasibility was confirmed by tolerance of therapy without any significant side effects. Liver parameters remained within normal limits during therapy. Serial whole-body scintigraphy and SPECT/CT demonstrated excellent tracer uptake in the primary tumor and in the widespread metastases. On dosimetry, whole-body uptake showed a bi-exponential decline, the tumor uptake followed an exponential decline, and the kidneys showed an exponential clearance with more prolonged kinetics compared to i.v. application. Mild and reversible hematotoxicity (Hb 5.9 mmol/L) was observed after the second dose (anemia existed before therapy). No renal toxicity was observed (despite there was only a single functioning kidney).Therapeutic effectiveness was confirmed by clinical assessment (significant improvement in quality of life and functional status), and severe reduction in ascites formation (drainage from twice daily to once every 3 days). Partial Remission (PR) was achieved according to RECIST (regression in size of the primary tumor and the hepatic metastases on MRI and CT) and by PERCIST (reduction of uptake in primary tumor and metastatic lesions on F-18 FDG PET/CT). Finally, a persistent fall of the tumor marker CA 19-9 (from 1423 to 192 U/ml) occurred. The patient is still alive 8 months after start of PRLT. Conclusion: Intraperitoneal peptide radioligand therapy using Lu-177 3BP-227 was clinically feasible and effective for the management of metastatic pancreatic adenocarcinoma. The excellent results obtained in this patient warrant the need of further studies and possibly earlier application of Lu-177 3BP-227 for the therapy of peritoneal carcinomatosis and associated ascites.

OP038

Nanovectorized radiotherapy by convection-enhanced delivery (CED), a promising strategy that demonstrates high efficacy in a murine model of human endometrial adenocarcinoma.

A. Genin[1,2,3], C. Lefebvre-Lacoeuille[1,3,2], J. Rousseau[4,5], N. Chouin[4,5], P. Fosse[6], D. Dabli[6], F. Bouchet[6], N. Lepareur[7], P. Descamps[1,3], F. Hindré[1,8,2], O. F. Couturier[1,6,2], **F. Lacoeuille**[1,2,6]; [1]LUNAM Université, Angers, FRANCE, [2]Inserm UMRS_1066 MINT, Angers, FRANCE, [3]Department of Obstetrics and Gynaecology, CHU Angers, Angers, FRANCE, [4]LUNAM Université, Nantes, FRANCE, [5]AMaROC, ONIRIS, Nantes, FRANCE, [6]Nuclear Medicine Department, CHU Angers, Angers, FRANCE, [7]Department of Nuclear Medicine, Centre Eugène Marquis, Rennes, FRANCE, [8]PRIMEX Plateforme de Radiobiologie et d'Imagerie Expérimentale, Angers, FRANCE.

Aim: To evaluate the biodistribution, the toxicity, the dosimetry and the antitumor efficacy of intra-tumoral injection of rhenium-188 loaded nanoparticles (LNC-188Re-SSS) by

CED. Materials and methods: Ishikawa endometrial carcinoma cell lines were implanted subcutaneously in nude mice (n=70). For biodistribution and efficacy studies CED procedure was realized at D28 after tumour implantation. CED was performed using an osmotic pump (0.5μL/min for 20 minutes) after immobilisation of anaesthetized mice on a stereotactic frame. For biodistribution studies, animals (n=30) were injected by CED either with 3MBq of 188ReO4- (n=15) or LNC-188Re-SSS (n=15) and sacrificed at 1h (n=10), 24h (n=10) or 72h (n=10). For efficacy studies, control group mice were injected by CED with saline (n=8) or blank LNC (n=8) and treated group mice were injected with escalating dose of LNC-188Re-SSS: 3MBq (n=8), 6 MBq (n=8) or 12 MBq (n=8). Efficacy on tumour growth was assessed by clinical palpation and μMRI. The time for the tumour volume doubling was chosen as endpoint, leading to the euthanasia of the animal. The physical dose deposited in the tumour for each treated animal was estimated by Monte Carlo simulation (Geant4) using measured biodistribution and μMRI tumour volumes,. Haematological toxicity in mice was evaluated using blood sampling of 50μL (retro-orbital sinus) at D2, D7, D14 and D21 after treatment with saline (n=4) and after treatment with LNC-188Re-SSS, 3MBq (n=4), 6MBq (n=4) or 12 MBq (n=4). Results: Nanovectorization of 188Re combined with CED allowed the confinement of more than 30 % of ID in the tumour limiting therefore urinary excretion of 188Re since 0,1% versus 81,9% of ID were excreted in urine 24h after CED of LNC-188Re-SSS and 188ReO4- respectively (p=0.016). Nanovectorized radiotherapy has drastically increased the median survival time compared with control group. Animals whose tumor received a dose higher than 69 Gy (69-340 Gy) showed an ISTmedian of + 933%, whereas animals whose tumor received a dose lower than 69 Gy (21-67Gy) showed an ISTmedian of + 391%. Complete response with eradication of the tumor was observed in 4/12 (33.3%) animals of the former group. Depletion of platelets was observed following LNC-188Re-SSS injection with a time to nadir between D14-D21 whereas transient lymphocyte depletion was only observed at D7 for the highest administered activities (12MBq). Conclusion: CED of LNC-188Re-SSS demonstrates interesting biodistribution properties and high efficacy in a model of human endometrial carcinoma.

OP039

Tumour-Absorbed Dose for Patients in a Phase I study undergoing antibody-radionuclide-conjugate (ARC) therapy with ^{177}Lu-DOTA-HH1

C. Stokke[1], A. Løndalen[2], J. Blakkisrud[1], J. Dahle[3], T. Bach-Gansmo[2], J. Holtedahl[1], A. Martinsen[1], B. Bolstad[3], H. Holte[4], A. Kolstad[4]; [1]The Intervention Centre, Oslo University Hospital, Oslo, NORWAY, [2]Department of Radiology and Nuclear Medicine, Oslo University Hospital, Oslo, NORWAY, [3]Nordic Nanovector ASA, Oslo, NORWAY, [4]Department of Oncology, Radiumhospitalet, Oslo University Hospital, Oslo, NORWAY.

Aim: ^{177}Lu-DOTA-HH1 (Betalutin™) is a novel anti-CD37 antibody-radionuclide-conjugate (ARC) currently under investigation. Betalutin™ is developed by Nordic Nanovector ASA and consists of lutetium-177 which is chelated to the DOTA-conjugated antibody HH1. Oslo University Hospital is participating in a phase I/II study where Non-Hodgkin Lymphoma patients are treated with ^{177}Lu-DOTA-HH1. In the current work, we estimate tumour-absorbed doses and aim to investigate dose-response relationships at the lesion level. Material and methods: Patients with relapsed CD37+ indolent B-cell NHL were eligible for inclusion in the 3x3 dose escalation study. Three dose levels have been tested (10 MBq/kg, 15 MBq/kg, 20 MBq/kg). Eleven patients were assessed for distribution of radioactivity by SPECT/CT at the time-points 96 and 168 hours post administration, of whom 4 also underwent planar whole-body (WB) imaging at additional time points. Clinical response assessment included 18F-FDG PET/CT. PET/CT scans were performed at baseline and at 3 months and 6 months follow-up. In this work, response was assessed by the change in SUV_{max} value for each individual lesion. For 2 patients at each dose level, i.e. a total of 6 patients, we have calculated mean tumour-absorbed dose for 2 or 3 separate lesions. The SPECT/CT images were analyzed, and tumour uptake and volume at the different time points determined. Cumulative activities were calculated from mono-exponential fits, as verified by co-registered conjugate view WB images when available. Results: The mean overall tumour-absorbed dose was 2,13 mGy/MBq (range 0,42 - 4,77 mGy/MBq). For patients in the 10 MBq/kg group, the 15 MBq/kg group (MTD) and the 20 MBq/kg group the median dose was 138 cGy, 297 cGy and 310 cGy, respectively. Interpatient and, to some degree, also intrapatient variances were observed. Dose-rate maps at the voxel level and dose-volume histograms for each tumour were also investigated. Only 3 of the 14 tumours studied showed a less than complete SUV_{max} response at 3 months, thus establishing meaningful correlations between tumour-absorbed dose and response was difficult. However, all 3 lesions with an incomplete response received a dose below the overall mean dose of 286 cGy. This suggested dose-response trend requires investigation of more patients. Conclusion: Tumour-absorbed doses for patients undergoing antibody-radionuclide-conjugate (ARC)

therapy with ^{177}Lu-DOTA-HH1 were determined. Although preliminary results are too limited to establish valid correlations, lesions with an incomplete response received a dose below the overall mean dose. Further evaluation of dose-response relationships will require a larger data material.

OP040

Preliminary Dosimetry Results from a Phase II Study Evaluating the Efficacy and Safety of Ultratrace® Iobenguane I 131 in Patients with Relapsed/Refractory Malignant Pheochromocytoma/Paraganglioma

D. A. Pryma[1], C. Jimenez[2], B. Chin[3], J. R. Olsen[4], M. H. Pampaloni[5], L. B. Solnes[6], J. Stubbs[7], T. Armor[8], J. D. Jensen[8], V. Wong[8]; [1]Hospital of the University of Pennsylvania, Philadelphia, PA, UNITED STATES, [2]University of Texas M.D. Anderson Cancer Center, Houston, TX, UNITED STATES, [3]Duke University Medical Center, Durham, NC, UNITED STATES, [4]Washington University School of Medicine, St. Louis, MO, UNITED STATES, [5]University of California, San Francisco, San Francisco, CA, UNITED STATES, [6]Johns Hopkins University, Baltimore, MD, UNITED STATES, [7]Radiation Dosimetry Systems, Inc., Milton, GA, UNITED STATES, [8]Progenics Pharmaceuticals, Inc, Tarrytown, NY, UNITED STATES.

Aim: Radioiodinated meta-iodobenzylguanidine (MIBG) is used for diagnosis and treatment of neuroendocrine tumors, such as pheochromocytomas and paragangliomas (pheo/para). Azedra™ (Ultratrace®iobenguane I131) is a high specific activity form of MIBG developed from a solid phase radiolabeling technology that dramatically reduces cold iobenguane carrier in the final product. Clinical studies with Azedra suggest this may result in reduced toxicity, increased tumor uptake, and anti-tumor activity. The aim of this study is to evaluate the efficacy and safety of two therapeutic doses of Azedra up to 18.5 GBq each (≤296 MBq/kg) given 3 months apart in patients with iobenguane-avid metastatic and/or recurrent pheo/para. Patient-specific dosimetry was employed for treatment planning to confirm the protocol-specified administered activity did not exceed pre-specified absorbed dose levels. Methods: The absorbed radiation dose was estimated after a single IV administration of 111-222 MBq of Azedra. Serial anterior/posterior scintigraphic images were obtained over 3-6 days. Count data was extracted from the whole body scans and CT-based volumes were used to estimate radiation absorbed dose to normal organs and tissues per the MIRD schema. Radiation dose estimates for a planned cumulative therapeutic administration of 37 GBq were performed using OLINDA/EXM software (version 1.1) and reduced when necessary to limit radiation dose under pre-specified limits for the kidneys (<23 Gy), liver (<30 Gy) and lungs (<17.5 Gy). Results: Results are available for 44 patients who underwent dosimetric evaluation. Of these, 41 (93.2 %) demonstrated tumor avidity and 38 (86.4%) were eligible to receive up to 37 GBq based on dosimetry while 6 (13.6%) were eligible with dose reduction. 34 (77.3%) patients received two therapeutic administrations ranging from 32-38 GBq. Mean radiation doses (±SD) were: kidneys, 12±5.1 Gy; liver, 14±4.2 Gy; lungs, 10±3.4 Gy. Mean dose to non-source organs ranged from 2-6 Gy. Mean total body radiation dose was 3.7±0.9 Gy (range 2.4-7.3 Gy). Azedra was generally well tolerated with gastrointestinal and hematologic toxicity most frequently reported. Conclusion: This prospective treatment planning paradigm for high dose therapy is an important safety check-point to estimate potential risks to tissue distribution in critical organs such as kidneys, liver and lungs. Patient-specific treatment planning provides a means of optimizing each patient's therapeutic administration (in this case, activity reduction), regardless of the uniqueness of an individual's specific biodistribution or biokinetics/clearance patterns.

OP041

Lu-177-Trastuzumab as a potential radiopharmaceutical for targeted radionuclide therapy of HER2/neu expressing metastatic breast cancer patients: feasibility study

J. Shukla, P. Bhusari, R. Vatsa, M. Parmar, G. Singh, B. R. Mittal; Post Graduate Institute of Medical Education & Research, Chandigarh, INDIA.

Introduction:Her2/neu expressing breast cancers are the most aggressive type of breast cancers. Trastuzumab is a humanized monoclonal antibody approved by FDA for the treatment of Her2 breast cancer. Radiolabeled antibodies have emerged as promising vehicles for targeted radio-immuno therapy of recurrent and metastatic disease. The aim of the study is to evaluate the feasibility of Lu-177-Trastuzumab for the treatment of Her2/neu expressing metastatic breast cancer. Methods:DOTA-Trastuzumab conjugates were developed using different molar excess of DOTA (5 to 40). The conjugates were purified using gel filtration chromatography. Characterization of the conjugates was done using SDS-PAGE and MALDI/TOF mass spectrometry. Radiolabeling of the conjugated Trastuzumab (0.5-3 mg) (dissolved in acetate buffer;pH=5) was done using Lu-177 chloride(750-850MBq) at 42oC for 2 hours. Post labeling purification of Lu-177-Trastuzumab from free Lu-177 was done

using gel filtration chromatography. The quality control of the purified Lu-177-Trastuzumab was done by radio-ITLC. Sterility and Endotoxin testing was performed. In vitro stability of the Lu-177-Trastuzumab was assessed up to 20 hours post labelling.The ethical clearance was obtained from the Institute's ethics committee. The patients were selected on the basis of [F-18] FDG scan. Immunohistochemistry (IHC) proven Her2 positive (n=3) and Her2 negative (n=3) were enrolled after getting informed written consent. Thewhole-body and SPECT/CT images were acquired at day 1 and day 7/8 post intravenous injection of 185-370MBq of Lu-177-Trastuzumab. The uptake of the radiopharmaceutical in the lesions was correlated with IHC and [F-18]FDG reports. Results:Conjugated trastuzumab with 2.5-8 molecules of DOTA per molecule of antibody was used for clinical grade preparation of Lu-177-Trastuzumab. The conjugated antibody showed two distinct bands of heavy and light chains on SDS-PAGE gel electrophoresis. No peak except corresponding to conjugated antibody was observed in MALDI mass spectra indicated the presence of intact antibody. Radiolabeling yield obtained was 70-91%. The product was stability upto 12 hours post preparation in vitro. The preparations were sterile and endotoxin content was <100 EU/V. The physiological tracer uptake was visible in heart, liver,spleen and nasopharynx. The blood pool activity was very high at 2 hr and was decreased after 7 days.Uptake of Lu-177-Trastuzumab was observed in all Her2 positive breast cancer and its metastatic lesions. No uptake of Lu-177-Trastuzumab was noted in any of the Her2 negative patients on IHC. Conclusion: Lu-177-Trastuzumab SPECT/CT imaging indicated that the radiopharmaceutical may hold great potential for radioimmunotherapy of Her2 overexpressing metastatic breast cancer.

306 - Sunday, October 11, 2015, 11:30 AM - 12:45 PM, Hall 6
Physics & Instrumentation & Data Analysis: PET/MR

OP042

Multiparametric characterization of early tumour response using PET/MR in patients with lung cancer using a voxelwise analysis.

A. M. E. Engberg, A. E. Hansen, S. W. Langer, H. H. Johannesen, N. H. Langer, M. Nørgaard, J. Löfgren, S. H. Keller, L. Højgaard, A. Kjær, B. M. Fischer; Rigshospitalet, Copenhagen, DENMARK.

Aim: In this study we explore if multiparametric imaging with simultaneous FDG-PET and Diffusion Weighted (DW) MRI can improve our understanding of tumour response and flare during chemotherapy and reveal patterns enabling us to early and accurately predict therapy response. Material: Eight patients were recruited from an ongoing, prospective study including patients with histologically or cytologically confirmed lung cancer referred for standard chemotherapy with carboplatin and vinorelbine. The patients underwent simultaneous FDG-PET/MRI (Siemens mMR) prior to (day 0), during (day 2, 7 and/or 12), and after (day 21) the first or second cycle of chemotherapy. Four patients completed 5 PET/MR scans and 4 patients 4 PET/MR scans. Methods: PET/MR was performed one hour after injection of 18F-FDG over 2 bed positions covering thorax. MRI included VIBE-DIXON (for attenuation correction), T1, T2, and DWI (b-values 0, 150, and 1,000). An experienced radiologist and nuclear medicine physician defined tumour volumes on all scans and the following parameters were extracted: SUVmax and SUVmean (maximum and mean standardized uptake value), and ADCmin and ADCmean (minimum and mean apparent diffusion coefficients). A spatial analysis was performed identifying the centre of mass (CM) for the PET and ADC tumour volumes. A multivariate Gaussian Mixture Model (GMM) was applied on the joint ADC and PET data using the Expectation-Maximization algorithm and limiting the number of clusters to 5. Results: All scans were of an acceptable image quality and the CM analysis suggests no significant offset between PET and ADC tumour volumes. Regarding primary tumour two patterns of FDG-uptake were identified: A) Responding pattern, where SUV drops immediately after the first administration of chemotherapy (day 2) and remains largely unchanged on the following scans. B) Non-responding pattern: SUV is unchanged during and after chemotherapy. Regarding ADC values the results are less clear. However, both responding and non-responding patients showed a trend towards an initial decrease after the first dose of chemotherapy followed by an increase. The voxelwise analysis of the joint ADC and PET data indicated a pattern of decreased tumour heterogeneity and identified clusters with apparent anatomical features. Conclusion: Multiparametric imaging with simultaneous FDG-PET and DW-MRI in lung cancer patients is feasible. These preliminary data indicates that it is possible to identify a responding pattern by voxelwise GMM analysis already 24 hours after chemotherapy; potentially enabling a rapid shift to a more efficient therapy in non-responding patients.

OP043

Yttrium-90 PET/MRI is superior to Bremsstrahlungs-SPECT/CT in treatment verification after selective internal radiotherapy - initial results

A. P. Bellendorf[1], B. Gomez[1], J. Schelhorn[2], A. Sabet[1], S. P. Müller[1], H. V. Ngo[1], A. Bockisch[1], T. D. Poeppel[1]; [1]University Hospital Essen, Department of Nuclear Medicine, Essen, GERMANY, [2]University Hospital Essen, Germany, Institute for Diagnostic and Interventional Radiology and Neuroradiology, Essen, GERMANY.

Aim: Bremsstrahlung-(BS) SPECT/CT is currently the preferred imaging modality for assessment of microsphere distribution after selective internal radiotherapy (SIRT). Yet, bremsstrahlung imaging is limited in spatial resolution. With a low decay probability of approx. 1:30 million, positron emission is observed in Y-90 decay which allows assessment of treatment microsphere distribution by positron emission tomography (PET). This study aims to evaluate Y-90 PET/MR for treatment verification after SIRT in comparison with BS-SPECT/CT and pre-treatment Tc-99m HSA-Microspheres SPECT/CT. METHODS: 16 patients with primary and secondary hepatic malignancies underwent pre-treatment Tc-99m HSA-Microspheres SPECT/CT (within 6 weeks before SIRT) and post-SIRT BS-SPECT/CT (both Siemens Symbia T2, acquisition time[AT] 35 min.) as well as Y-90 PET/MRI (Siemens mMR, AT 20min) within 48 hours after SIRT. 3 readers with experience in hybrid imaging and MRI reviewed all datasets. A total of 247 lesions was analysed with regard to the following criteria: 1) number and lesion-to-liver contrast (3-point ordinal scale (OS):1=low-3=good) of focal intrahepatic nuclide depositions including morphological correlation(4-p. OS: 1=no corr.- 4=excellent corr.). 2) Delineation of extrahepatic depositions and quality of anatomical localisation (1=no local.-3=good corr.). 3) Overall image quality (1=non-diagn.-4=good). 4) Correlation with pre-SIRT Tc-99m HSA-SPECT/CT. RESULTS: 1)Y-90 PET/MRI showed more focal deposition than BS-SPECT (82 vs. 74, mean lesions per patient 5,3 vs. 4,6) with higher lesion-to-liver contrast (median contrast 3 vs. 2, p=0.003). 2) More extrahepatic depositions were found in Y-90 PET/MRI with better mean localisation quality (6 vs. 1 lesions, mean quality 1 vs. 3). 3) Overall image quality (IQ) and quality of co-registration (CR) showed no significant difference between PET/MRI and BS-SPECT/CT (mean IQ: 3 vs. 3, CR: 3,5 vs. 4). 4) pre-SIRT HSA-SPECT/CT (5.9 lesions per pt., 91 total) showed a higher congruence with Y-90 PET/MR (5.2 lesions per pt., 82 total) than with BS-SPECT/CT (4.6 lesions per patient, 74 tot.) CONCLUSION: Y-90 PET/MRI showed a higher detection rate and superior image quality of intra- and extrahepatic nuclide depositions after SIRT compared to BS-SPECT. Moreover, there was a higher congruence between pre-treatment Tc-99m HSA-SPECT/CT and Y-90 PET/MR in comparison with BS-SPECT/CT.

OP044

Lean body mass estimation from standard, Dixon-based attenuation correction in combined PET/MRI

I. Rausch[1], P. Rust[2], M. D. DiFranco[1], M. Lassen[1], A. Stadlbauer[3], M. E. Mayerhöfer[3], M. Hartenbach[4], T. Beyer[1]; [1]Center for Medical Physics and Biomedical Engineering, Medical University of Vienna,, Vienna, AUSTRIA, [2]Department of Nutritional Sciences, University of Vienna,, Vienna, AUSTRIA, [3]Department of Biomedical Imaging and Image-guided Therapy, Medical University of Vienna, Vienna, AUSTRIA, [4]Division of Nuclear Medicine, Department of Biomedical Imaging and Image-guided Therapy, Medical University of Vienna, Vienna, AUSTRIA.

Aim: Standardized Uptake Values (SUV) normalized to lean body mass (LBM) may correlate better with the metabolic activity as SUVs normalized to body weight (BW). However, patient-specific LBM calculations are based on general assumptions. Here, we evaluate if the information obtained in PET/MR imaging from standard, MR-based attenuation correction (MR-AC) can be used to predict LBM for each patient more accurately. Method: 10 volunteers (5m, 5f) who underwent a body composition measurement using a BODPOD system (Life Measurement) were included in this study. Subjects were scanned within ±3 days in a PET/MR system (mMR, Siemens Healthcare) from head to toe using MR head and surface coils. Three consecutive multi-bed acquisitions of the MR-AC image data were acquired in free breathing, except for the thorax (full-inspiration breath-hold) using the standard DIXON MR-AC protocol. For each subject and MR-AC map, the following compartmental volumes were calculated using Matlab (MathWorks): whole-body (WB), soft tissue (ST), fat (F), and intermediate tissue (IM), with the latter comprising voxels interpolated between (F) and (ST). We report intra-subject differences in WB and sub-compartmental volumes (ST, F and IM) relative to the WB volume by means of coefficients of variation (CV). The LBM was calculated from the MR-AC by the formula: $LBM\text{-}AC=(ST*\rho ST+IM*\rho IM*1/2)/(ST*\rho ST+F*\rho F+IM*\rho IM)*BW$, were ρ is the tissue-dependent density ($\rho ST=1.1$ kg/L, $\rho F=0.9$ kg/L, $\rho IM=1$ kg/L). Pearson's correlation was calculated between LBM-BODPOD, LBM-AC and LBM estimated by an estimation formula (Sugawara 1999) (LBM-Formula). Linear regression

(avoiding intercept) was used to scale LBM-AC to LBM-BODPOD. Results: Mean CV for all 30 scans was 2.1±1.9% (WB). When excluding the AC-maps with missing tissue artifacts (MT) the CV was reduced to 0.3±0.2% (WB). Mean CV for sub-compartments (all maps, maps without (MT) and tissue swap artifacts (TS)) were: ST (0.9±1.1, 0.7±0.7%), F (2.9 ±4.1, 1.3±1.0%), and IM (3.6±3.7, 1.3±0.7%). Correlation analysis showed better correlation between LBM-AC and LBM-BODPOD ($r=0.99$, $p<0.001$ / excluding MT&TS: $r=0.99$, $p<0.001$) than between LBM-BODPOD and LBM-Formula ($r=0.89$, $p<0.001$ / excluding MT&TS: $r=0.91$, $p<0.001$). Linear regression of data excluding MT&TS results in a scaling factor of 1.08 for LBM-AC . Conclusion: LBM estimation from DIXON MR-AC maps correlates well with standard LBM measurements and, thus, offers routine SUV-LBM-based quantification in PET/MR.

OP045

Semi-quantitative assessment of 18F FDG uptake in the normal skeleton using simultaneous PET/MRI: initial comparison to PET/CT in 50 patients

G. Xu, R. Minamimoto, A. Quon, E. Mittra, **A. Iagaru**; Stanford University School of Medicine, STANFORD, CA, UNITED STATES.

Introduction: Differences in the attenuation correction methods between clinical PET/CT scanners and newly introduced whole-body simultaneous PET/MRI systems could affect the estimated specific uptake values in normal and pathologic structures. Here we evaluated the semi-quantitative 18F-FDG measurements on PET/MRI vs. PET/CT. Materials and methods: Fifty consecutive cancer patients were enrolled in a PET/MRI vs. PET/CT comparison research protocol. First, a PET/CT scan (GE Discovery 600 or 690) was acquired at mean±SD: 73±16 min after FDG injection, followed by PET/MRI scan at 161±31 min after FDG injection. Ten regions of interest (ROIs) in representative areas of the axial and proximal appendicular skeleton were measured from PET in PET/MRI and PET/CT for every patient. In addition, another dataset from 30 patients who had dual time PET/CT was used for comparison. The latter had similar delays between scans as from PET/CT to PET/MRI. SUVmax and SUVmean from the selected ROIs were used for an analysis using Pearson correlation coefficients (CCs). Results: SUVmax values for the normal skeleton obtained from PET/MRI and PET/CT showed good agreement (CC=0.84), similar to the values from the dual time point PET/CT study (CC=0.85). However, the SUVmean values were significantly more variable by PET/MRI compared with PET/CT (CC 0.88 vs. 0.94, $P = 0.006$). No significant differences were noted in either the SUVmax or SUVmean values across all ROIs between PET/MRI and PET/CT exams. Conclusion: Our data demonstrate reliable quantification in the normal skeleton for the simultaneous PET/MRI studies in comparison with PET/CT. The SUVmax is less variable than SUVmean in this cohort. Evaluation of semi-quantitative measurements in malignant bone lesions should also be done.

OP046

Evaluation of the influence of truncation artifacts using in-vivo based quantification accuracy methods in combined PET/MRI

J. Maus[1], G. Schramm[2,1], F. Hofheinz[1], L. Oehme[3], A. Lougovski[1], J. Petr[1], I. Platzek[4], B. Beuthien-Baumann[3], J. Steinbach[1], J. Kotzerke[3], J. van den Hoff[1,3]; [1]PET Center, Helmholtz-Zentrum Dresden-Rossendorf, Dresden, GERMANY, [2]Medical Imaging Research Center, KU Leuven, Leuven, BELGIUM, [3]Department of Nuclear Medicine, University Hospital Carl Gustav Carus, Technische Universität Dresden, Dresden, GERMANY, [4]Department of Radiology, University Hospital Carl Gustav Carus, Technische Universität Dresden, Dresden, GERMANY.

Aim: Quantitative accuracy of standardized uptake values (SUV) and tracer kinetic uptake parameters in patient investigations requires determination of regional activity concentrations in PET data. This determination rests on the assumption that the scanner calibration is valid in-vivo. In a recent study we introduced a method to test this assumption. For 3 different PET and PET/CT systems the activity concentration of urine samples measured in a well-counter were compared to those derived from PET images of the bladder. The study demonstrated a low but systematic underestimation of 7-12% of PET relative to a cross-calibrated well-counter for 56 subjects. In the present study we have applied this method to the Philips Ingenuity-TF PET/MR to evalute the impact of MR-based truncation artifcats on the overall quantitative accuracy of this system. Methods: 21 clinical whole-body F18-FDG scans were included in this study. The bladder region was imaged as the last bed position and urine samples were collected afterwards. PET images were reconstructed including MR-based attenuation correction with and without truncation compensation and 3D region-of-interests (ROI) of the bladder were delineated by 3 observers. Activity concentrations were determined in the PET images for the bladder as well as for the urine by measuring the samples in a well-counter. Results: The in-vivo activity concentrations of the bladder were significantly lower in PET/MR than in the well-counter with a ratio of the former to the latter of 0.756±0.060 (mean±std.dev.) and a range of

[0.604-0.858]. Linearity scans revealed a systematic error of 8-11 % (avg. 9 %). After correcting for this systematic bias caused by shortcomings of the manufacturer's calibration procedure the PET to well-counter ratio increased to 0.832±0.064 [0.668-0.941]. After applying compensation for truncation of the upper extremities in the MR-based attenuation maps the ratio further increased to 0.871±0.069 [0.693-0.992]. Conclusions: Our results show, that the Ingenuity-TF PET/MR underestimates activity concentrations in the bladder by 17% which is 7 percentage points larger than in the previously investigated PET/CT systems. This difference in behavior can be attributed to remaining limitations of MR-based attenuation correction as our results on truncation compensation related influences suggest - leaving only a 2 pp. larger underestimation of activity concentrations if corrected. Thus, quantification accuracy of the Ingenuity-TF PET/MR can be considered acceptable for clinical purposes. The comparison of PET images from the bladder region with urine samples has proven a useful method to evaluate quantification accuracy of different PET systems in-vivo.

OP047

Improvements in PET Image quality from TOF PET/MRI

R. Minamimoto, M. Jamali, A. Barkhodari, D. Holley, G. Zaharchuk, C. Levin, **A. Iagaru**; Stanford University, STANFORD, CA, UNITED STATES.

Purpose: A completely novel integrated PET/MRI scanner with TOF technology has been recently introduced. Here we evaluated the potential of TOF PET/MRI to reduce various PET image artifacts, by comparing the images to non-TOF PET/MRI, TOF PET/CT and non-TOF PET/CT. Materials and methods: All patients underwent a single-injection of FDG, followed first by PET-CT and subsequently by PET-MRI scan. The standard of care PET/CT exams were performed using a GE Discovery 690 PET/CT scanner. The research PET/MRI images were acquired on a GE Signa PET/MRI scanner. All PET images were reconstructed with and without the TOF data, resulting in 4 series of PET images (TOF PET/MRI, non-TOF PE/MRI, TOF PET/CT and non-TOF PET/CT). Visual analysis of these series was performed for 1) dental metal artifacts, 2) breathing artifacts, and 3) scatter artifacts caused by high excretion of FDG in the bladder. PET image quality was evaluated using a 3-point scale (1 - clinically significant artifact; 2 - non clinically-significant artifact; and 3 - no artifact). Results: Data from 25 oncologic patients (mean ± SD age: 56 ± 13 years; female 10, male 15) were used. The average scores of TOF PET/MRI, non-TOF PET/MRI, TOF PET/CT and non-TOF PET/CT for dental artifacts were 2.8, 2.5, 2.4 and 2.3, respectively; for breathing artifacts were 2.8, 2.5, 2.2 and 1.9, respectively; and for pelvic artifacts were 2.7, 1.7, 2.0 and 1.3, respectively. TOF PET/MRI images had the highest image quality scores among the 4 series of PET data analyzed for these types of artifacts. Conclusion: TOF PET/MRI showed promising results in reduction of various PET artifacts in this cohort, when compared to non-TOF PET/MRI, TOF PET/CT and non-TOF PET/CT.

307 - Sunday, October 11, 2015, 11:30 AM - 1:00 PM, Hall F
Neurosciences: Basic Neuroscience

OP048

In vivo evaluation of [^{11}C]preladenant for imaging of adenosine A_{2A} receptors in the conscious monkey

X. Zhou[1], E. de Vries[1], K. Ishiwata[2], R. Dierckx[1], S. Nishiyama[3], H. Tsukada[3], P. Elsinga[1]; [1]University Medical Center Groningen, Groningen, NETHERLANDS, [2]Research Team for Neuroimaging, Tokyo Metropolitan Institute of Gerontology, Tokyo, JAPAN, [3]Central Research Laboratory, Hamamatsu Photonics K.K., Hamamatsu, JAPAN.

Aims: The adenosine A_{2A} receptor ($A_{2A}R$) is studied as a therapeutic target in several neurologic and psychiatric disorders. Recently, we have synthesized [^{11}C]preladenant, a PET ligand with high affinity and selectivity for the $A_{2A}R$. The present study aims to evaluate [^{11}C]preladenant in conscious monkey brain. Materials and methods: Conscious monkeys (n=6) were *i.v.* injected with [^{11}C]preladenant and a 90 min dynamic scan was started. Arterial blood samples with metabolite analysis were obtained during the scan to provide the input function for kinetic modelling. Distribution volume (V_T) was obtained by modelling with the Logan graphical analysis with t* set to 22 min post injection. Simplified reference tissue model (SRTM) and multilinear reference tissue model (MRTM) were used to estimate binding potential (BP_{ND}) in striatum. Cerebellum, cingulate, parental cortex and occipital cortex were tested as reference regions. The values of BP_{ND} obtained from reference tissue-based models were compared with the BP_{ND} calculated from Logan analysis using the formula $V_{T,\ target}/V_{T,\ reference}$-1. The best reference tissue was selected based on high BP_{ND} in striatum with low intra-individual variance. Results: Regional uptake of [^{11}C]preladenant was consistent with the distribution of $A_{2A}Rs$ in the monkey brain, with the highest uptake in putamen, followed by caudate, and the lowest uptake in cerebellum. The tracer kinetics was well fitted with the Logan plot. V_T estimates ranged from 0.89±0.31 in cerebellum to 5.86±2.10 in putamen. BP_{ND} values estimated from SRTM and MRTM were comparable, with slightly higher (1-3%) values predicted

by MRTM. Striatal BP_{ND} predictions with SRTM (5.05±1.01 and 4.02±1.06, for putamen and caudate, respectively) and MRTM (5.11±1.00 and 4.10±1.05, for putamen and caudate, respectively) were in agreement with BP_{ND} calculated from Logan analysis (5.64±1.54 and 4.12±1.26, for putamen and caudate, respectively), but with a small negative and significant ($p<0.05$) bias of <10%, when cerebellum was used as the reference region. As a trade-off between bias and noise, coefficient of variance (COV) of BP_{ND} predicted by SRTM and MRTM (~20%) was smaller compared with BP_{ND} estimate from Logan analysis (~28%). Other reference regions showed an increased (7-20%) negative bias of BP_{ND} prediction, compared with cerebellum prediction. Compared to V_T, BP_{ND} seemed to be a more stable parameter with smaller COV in striatum (~20% BP_{ND} COV vs. ~35% V_T COV in striatum). Conclusions: [^{11}C]Preladenant PET is suitable to non-invasively quantify A_{2A}Rs in monkey brain. MRTM and SRTM using cerebellum as the reference tissue are applicable models for A_{2A}R quantification.

OP049

Sigma-1 and dopamine D2 receptor occupancy of the dopamine stabilizer pridopidine in the brain of living rats

K. Sahlholm[1], J. W. A. Sijbesma[2], B. Maas[2], C. Kwizera[2], N. K. Ramakrishnan[2], R. A. J. O. Dierckx[2], P. H. Elsinga[2], A. Van Waarde[2]; [1]Department of Neuroscience, Karolinska Institute, Stockholm, SWEDEN, [2]University of Groningen, University Medical Center Groningen, Department of Nuclear Medicine and Molecular Imaging, Groningen, NETHERLANDS.

Objectives: Dopamine stabilizers have stimulatory actions under low dopamine tone and inhibitory actions under high dopamine tone without eliciting catalepsy. Pro-mnemonic and neuroprotective effects have also been attributed to these compounds, which are either neutral antagonists or partial agonists at the dopamine D2 receptor. The mechanism underlying their stimulatory and neuroprotective actions is unknown but could involve sigma-1 agonism, since these drugs have shown nanomolar in vitro affinity to sigma-1 receptors. In order to test this hypothesis, we examined the dose-dependent D2R and sigma1R occupancy of the dopamine stabilizer pridopidine (ACR16) in living rats. Methods: Male Wistar rats were treated with various doses of pridopidine (0, 3, or 15 mg/kg, s.c.), one hour before injection of the sigma1R ligand [11C]SA4503 or the dopamine D2R ligand [11C]raclopride. Some animals received 60 mg/kg pridopidine and were only scanned with [11C]raclopride. Dynamic microPET scans were made with a Siemens/Concorde Focus220 camera. Cerebral [11C]SA4503 binding was quantified using plasma input data acquired by arterial sampling and distribution volume (VT) calculated by Logan graphical analysis. Striatal [11C]raclopride binding was quantified using target-to-cerebellum ratios and binding potentials calculated with a simplified reference tissue model. RESULTS: Pridopidine dose-dependently reduced the VT of [11C]SA4503 in all examined areas of the rat brain. Particularly at the 15 mg/kg dose, pridopidine reduced the clearance of radioactivity from plasma and increased the metabolic degradation of [11C]SA4503 (parent fraction at 60 min 33% vs 55% at baseline). Cunningham-Lassen plots based on regional VT and metabolite-corrected plasma input data indicated sigma-1 receptor occupancies of 57 ± 2% and 85 ± 2% after pretreatment of animals with 3 and 15 mg/kg pridopidine. These drug doses did not reduce [11C]raclopride binding in the striatum, but at 60 mg/kg, pridopidine caused a significant reduction of the target-to-nontarget ratio of the D2 ligand (from 3.85 ± 0.48 to 1.96 ± 0.10), reflecting 66% D2R occupancy. Conclusions: At therapeutically effective doses, pridopidine occupied a high fraction of the sigma1R population and a negligible fraction of the dopamine D2R population in rat brain. Significant occupancy of dopamine D2 receptors was only observed at a dose of pridopidine 20-fold higher than was required for occupancy of sigma-1 receptors. The characteristic actions of dopamine stabilizers may result from the combination of high sigma-1 affinity (possibly sigma-1 agonism) with low-affinity dopamine D2 antagonism.

OP050

PET/MR hybrid scanner imaging of cerebral blood flow using 15O-water positron emission tomography and arterial spin labeling magnetic resonance imaging in newborn piglets

J. B. Andersen[1], W. Henning[1], U. Lindberg[2], C. N. Ladefoged[1], L. Højgaard[1], G. Greisen[3], I. Law[1]; [1]Department of Clinical Physiology, Nuclear Medicine and PET, Rigshospitalet, University of Copenhagen, Denmark, København Ø, DENMARK, [2]Functional Imaging Unit, Rigshospitalet, Glostrup Hospital, University of Copenhagen, Denmark, København Ø, DENMARK, [3]Department of Neonatology, Rigshospitalet, University of Copenhagen, Denmark, København Ø, DENMARK.

Aim: Abnormality in cerebral blood flow (CBF) distribution can lead to hypoxic-ischemic damage in newborn infants and is a major cause of later neurocognitive impairment. Thus, a clinically useful, robust and accurate method for measuring CBF in newborn infants is needed. The aim of the study was to investigate minimally invasive approaches to measure CBF by comparing simultaneous 15O-water positron emission tomography (PET) and single-TI pulsed arterial spin labeling (ASL) magnetic resonance imaging (MR) on a hybrid PET/

MR system in seven newborn piglets. Materials and methods: The experimental protocol for the study was approved by the Danish Animal Experiments Inspectorate and conducted in accordance with the Animal Ethics Policy at the University of Copenhagen. On each piglet, four scans at baseline and four scans after acetazolamide stimulus were performed. Positron emission tomography was performed with repeated IV injections of 20 and 100 MBq 15O-water to test CBF reliability at low activity injections. Cerebral blood flow was quantified using a 1-tissue-compartment model employing two different input functions: either an arterial input function (AIF) or an alternative image derived input function (IDIF) generated from the dynamic PET scan using a VOI in the left ventricle of the heart. Results: The mean global CBF(95%CI) PET-AIF, PET-IDIF and ASL at baseline were 27(23;32), 34(31;37) and 27(22;32) mL/100g/min, respectively. At acetazolamide stimulus PET-AIF, PET-IDIF and ASL were 64(55;74), 76(70;83) and 79(67;92) mL/100g/min, respectively. At baseline the differences between PET-AIF, PET-IDIF and ASL were 22%($p<0.0001$) and -0.7%($p=0.9$). At acetazolamide the differences between PET-AIF, PET-IDIF and ASL were 19%($p=0.001$) and 24%($p=0.0003$). ASL CBF showed the largest variance when accounting for dose and acetazolamide effect ($p=0.01$). There was no significant difference in variation between the 20 MBq PET CBF scans compared to the 100 MBq PET CBF scans ($p=0.06$). On visual presentation the distribution of regional CBF showed that the variation across voxels was greater in ASL CBF images with both very high and negative value voxels. Conclusion: In conclusion, PET-IDIF overestimated global CBF. An injected activity of 20 MBq 15O-water had acceptable concordance with 100 MBq, and may be used clinically without compromising image quality. Global ASL CBF and PET CBF were congruent during baseline but not during hyperperfusion. Single-TI ASL was questionable for regional CBF measurements. Further evaluation of the regional accuracy of ASL CBF and PET CBF is needed in newborn infants with low absolute rates of flow.

OP051

PET Imaging of Tau Pathology in two Transgenic Mouse Models using [^{18}F]-THK-5117

M. Brendel[1], A. Jaworska[2], F. Probst[1], F. Overhoff[1], J. Carlsen[1], S. Lindner[1], J. Herms[2], P. Bartenstein[1], N. Okamura[3], **A. Rominger**[1]; [1]University of Munich, Munich, GERMANY, [2]DZNE, Munich, GERMANY, [3]Tohoku University, Sendai, JAPAN.

Aims: Abnormal accumulation of tau aggregates in brain is one of the hallmarks of Alzheimer's disease (AD). To visualize the tau deposition in vivo, a previously developed 2-arylquinoline derivative [^{18}F]-THK-5117 was evaluated in two transgenic tau mouse models using μPET in combination with autoradiography and histopathology. Methods: μPET scans were performed in P301S (N=11) and BiGT animals (N=16) of different age groups. For control groups age- and background-matched wild-type (WT) littermates were used. After i.v. application of 16 ± 2 MBq [^{18}F]-THK-5117 a dynamic 90 min (20-50 min for BiGT) emission recording was initiated followed by a 15 min transmission scan using the Siemens Inveon DPET. After coregistration to an MRI atlas and cerebellar scaling, volume-of-interest based analysis (SUVR) and statistical parametric mapping (SPM) were performed. PET results were compared with ex vivo and in vitro autoradiography and validated with AT8 staining for neurofibrillary tangles. Results: Emission time from 20-50 min showed suitability for static economized PET recordings and test-retest analyses revealed robust SUVR values ($r=0.9$). SUVR increases were detected in the brainstem of P301S mice (+11%; $p < 0.001$) compared to WT animals. In BiGT animals significant increases in SUVR were found in entorhinal/amygdaloidal areas (+15%; $p < 0.001$) when compared to WT. Histologically assessed tau loads correlated well with PET-SUVR for P301S ($r=0.8$; $p<0.001$) and BiGT ($r=0.7$; $p<0.001$) mice while distribution patterns of AT8 positive tau were reflected by SPM analyses. In vivo PET findings could be verified by autoradiography where blocking with cold tracer proved the specificity to tau depostitions. Conclusions: [^{18}F]-THK-5117 is a promising PET tracer and suitable for preclinical tau imaging in the mouse brain. Pathology-related effects could be successfully imaged in vivo in two transgenic tau models, where in vivo assessment of the given inter-animal heterogeneity can potentially improve subsequent treatment studies in the future.

OP052

Altered brain serotoninergic neurotransmission and glucose metabolism in an original mouse model of synucleinopathy

E. LEVIGOUREUX[1], C. BOUILLOT[2], T. BARON[3], **L. ZIMMER**[1], S. LANCELOT[1]; [1]Université Claude Bernard Lyon 1, Lyon, FRANCE, [2]CERMEP-Imaging Platform, Lyon, FRANCE, [3]ANSES, Lyon, FRANCE.

Aim: Alpha-synuclein (α-syn) aggregation is a neuropathological hallmark of neurodegenerative diseases called synucleinopathies, including Parkinson's disease, dementia with Lewy bodies and multiple system atrophy. The purpose of this study was to evaluate serotoninergic and metabolic disorders in an original mouse model of synucleinopathy. Materials and methods: This study used a model of transgenic mouse (TgM83) expressing in an accelerated manner the

human A53T mutated α-syn. Control animals were C57Bl/6S mice presenting a deletion of the α-syn locus (KO α-syn) and C57Bl/6S mice (wild type). MicroPET acquisitions were performed with [18F]MPPF, a serotonin 5HT1A receptor radiopharmaceutical, [11C]DASB, a serotonin transporter radiopharmaceutical and [18F]FDG. Regions of interest were drawn manually according to the stereotaxic atlas and anatomical MRI acquisitions. Regional standardized uptake value ratio (SUVR)s were calculated and normalized to cerebellar cortices for [11C]DASB and to temporal cortices for [18F]FDG. For [18F]MPPF, images were analyzed with Logan BP and normalized to cerebellar cortices. Results: MicroPET images showed an increased uptake of [18F]MPPF in this mouse model of synucleinopathy. In TgM83 mice BP were 0.96, 0.76 and 0.96 in the hippocampus, cingulate cortex and frontal cortex, respectively, versus 0.54 ($p<0.0001$), 0.45 ($p=0.0001$) and 0.65 ($p=0.0002$) in WT mice and 0.44 ($p<0.0001$), 0.39 ($p=0.0001$) and 0.73 ($p=0.0133$) in KO α-syn mice. Conversely, a hypometabolism of glucose was observed in TgM83 mice in the same regions: SUVR were 1.26, 1.26, 1.22 in hippocampus, cingulate cortices and frontal cortices, respectively, versus 1.35 ($p=0.0001$), 1.46 ($p<0.0001$) and 1.33 ($p=0.0136$) in WT mice and 1.39 ($p=0.04$), 1.52 ($p=0.0003$) and 1.34 ($p=0.05$) in KO α-syn mice. No significant differences were observed between the three groups for [11C]DASB uptake. Conclusion: Our results demonstrated in a mouse model of synucleinopathy a regional overexpression of 5HT1A receptors, without serotonin transporter modifications and with a carbohydrate hypometabolism. This study revealed for the first time that an overexpression of α-syn modifies the serotonin neurotransmission. Brain serotonin concentrations will be determined to propose a pathophysiological mechanism.

OP053

Longitudinal Imaging of Acute Neuroinflammation with [11C]PBR28 in an Ischemic Stroke Rat Model

M. Tóth[1], P. Little[1,2], F. Arnberg[1,2,3], J. Häggkvist[1], J. Mulder[4], A. Varrone[1], C. Halldin[1,5], B. Gulyás[1,5], S. Holmin[1,2]; [1]Karolinska Institutet, Department of Clinical Neuroscience, Stockholm, SWEDEN, [2]Karolinska University Hospital, Department of Neuroradiology, Stockholm, SWEDEN, [3]Karolinska University Hospital, Department of Radiology, Stockholm, SWEDEN, [4]Karolinska Institutet, Department of Neuroscience, Stockholm, SWEDEN, [5]Imperial College-NTU, Lee Kong Chian School of Medicine, Singapore, SINGAPORE.

Aim: Adequate estimation of neuroinflammatory processes following ischemic stroke is essential for better understanding of disease mechanisms, and for the development of treatment strategies. With [11C]PBR28, we have monitored the inflammatory response after transient cerebral ischemia in rats longitudinally, using a recently developed rat stroke model with isolated focal cortical infarcts. Our aim was to compare the suitability of BPND as an outcome measure compared to %SUV, in this novel animal model. Matherials and Methods: Six Sprague-Dawley rats (300-400g) were anaesthetized with isoflurane in 100% O2. Occlusion of the M2 segment of the middle cerebral artery (M2CAO) was maintained for 90 min, and animals were imaged at 1, 4, 7 and 14 days after reperfusion (one animal missing day 14) with a bolus injection of [11C]PBR28 through tail vein cannulation in nanoScan PET/MRI and PET/CT systems (Mediso Ltd, Budapest Hungary). PET scans were co-registered to individual T1-weighted MRI images in PMOD 3.3 (Zurich, Switzerland). As a primary outcome BPND was estimated with SRTM, using the contralateral cortex as reference region. Results: [11C]PBR28 showed high uptake in the Infarct region from day 4 with gradual decrease at later time points. The following average %SUV values were obtained from the Infarct region on day 1: 67.21 ± 3.68 (n = 6), day 4: 151.16 ± 41.59 (n = 6), day 7: 141.02 ± 51.56 (n = 6) and day 14: 124.59 ± 33.29 (n = 5). At day 4, 7 and 14 there was a significantly increased uptake of [11C]PBR28 compared to day 1, while have found no significant change in the uptake of Contralateral Cortex during the 14 days of imaging. BPND in the Infarct region was 0.22 ± 0.19 (n = 6) on day 1 and similarly to %SUV there was a significant increase in BPND on day 4: 1.73 ± 0.78 (n = 6), day 7: 1.59 ± 0.96 (n = 6) and day 14: 0.86 ± 0.64 (n = 5) compared to day 1. Conclusion: The longitudinal follow up of inflammatory response with the TSPO radioligand [11C]PBR28 in rats after cerebral ischemia showed significantly up-regulated TSPO binding in the Infarct region from day 4, with both %SUV and BPND. This activation gradually decreased between day 4 and day 14. The present model (M2CAO) appears to be well suited for studies on neuroinflammation with a more rapid response compared to the MCAO model.

OP054

Evaluation of the effect of radiotherapy on neuronal integrity in rats using [11C]flumazenil PET

A. Parente, D. Vallez Garcia, P. van Luijk, J. A. Langendijk, R. A. J. O. Dierckx, J. Doorduin, E. F. J. de Vries; RUG, Groningen, NETHERLANDS.

Aim: Whole brain radiotherapy is frequently used in the treatment of primary and metastatic brain tumors. Unfortunately, radiotherapy also damages normal brain tissue, which can lead to serious and debilitating cognitive dysfunction. The exact mechanisms behind the radiotherapy-induced cognitive dysfunction remain elusive, but it may, in part, be explained by

neuronal damage and neuronal loss. The aim of this study was therefore to evaluate if whole brain radiotherapy induced neuronal loss in healthy rats, using PET with the GABAA receptor antagonist [11C]flumazenil as a marker for neuronal loss. Material and methods: Male Wistar rats (n=24, age 8-9 weeks) were divided in 3 groups of 8 rats: control, sham irradiated, and whole brain irradiated. Whole brain irradiation was performed by the delivery of 25 Gy of X-rays in a single dose, under anesthesia, using an in-house developed rat brain collimator so that only the brain was exposed. Sham irradiated rats underwent the same procedure, but were not irradiated. [11C]Flumazenil PET scans were performed 3 months after (sham-)irradiation. Control rats were scanned at an age of 8-9 weeks to assess the effect of aging on [11C]flumazenil PET. [11C]Flumazenil was injected intravenously at a constant flow of 1 ml/min (62±26MBq) and a dynamic PET scan of 60 minutes was acquired. The PET scan was accompanied by arterial blood sampling and metabolite analysis. One-tissue compartment modeling was used to calculate the volume of distribution (VT) in different brain regions, using blood and metabolite corrected plasma as input. Results: In control rats, the highest VT was found in the frontal cortex (12.0±2.0) and hippocampus (11.0±1.8) and the lowest in the pons (4.9±0.8) and medulla (4.2±0.7). No statistical significant differences in the VT were found between control and sham irradiated rats, showing that aging did not affect [11C]flumazenil binding. However, the VT in rats irradiated with 25 Gy was statistically significantly lower in all brain regions ($p<0.05$), including frontal cortex (33%), hippocampus (32%), pons (33%), and medulla (35%), when compared to sham irradiated rats. Conclusion: Whole brain irradiation resulted in statistically significantly decreased binding of [11C]flumazenil to GABAA receptor. This finding suggests that radiotherapy-induced cognitive dysfunction could be related to neuronal loss.

OP055

Inverse translation of PET auditory system activation studies to rats using F-18-FDG PET

M. Mamach[1,2], G. Berding[1,2], J. P. Bankstahl[1], F. Wilke[1], L. Geworski[1], F. M. Bengel[1], S. Kurt[1,2]; [1]Medical School, Hannover, GERMANY, [2]Cluster of Excellence "Hearing4All", Oldenburg, GERMANY.

Aim:Functionality assessments of the auditory system using statistical parametric mapping (SPM) with multiple PET activation studies of a patient with moderate auditory stimuli are standard in humans. We performed an adapted inverse translation of this method to healthy, auditory unimpaired rats and assessed its functionality and magnitude.Methods:Scans were performed in 12 female Sprague Dawley rats using F-18-fluorodeoxyglucose (FDG, 16-20 MBq) PET (Inveon, Siemens). The tracer was always injected via tail vein in awake animals placed into a motion restricting tube within a sound attenuated box. Three sets of separate scans were acquired for each animal, each under the following conditions: (i) 55 dB background noise (BG55), (ii) 65 dB continuous white noise (WN65) and (iii) 95 dB pulsed rippled noise (RN95). All sound conditions started 1 min before tracer injection and lasted for 41 min. Scanning was performed across 30 min starting 1 h after injection. Data were reconstructed iteratively including 57Co-transmission-source-based attenuation correction. Spatial normalization and brain activity normalization were performed using a FDG template and mask provided by PMOD3.6 software. Mean normalized counts were extracted for auditory regions (inferior colliculus (IC), mediate geniculate body (MGB) and auditory cortex (AC)) using Schwarz's VOI atlas. Pairwise comparisons across conditions assessed differences of relative activities in VOIs and SPM8 based voxel-wise extent and T-value.Results:RN95-vs-BG55 and WN65-vs-BG55 comparisons revealed significant increased uptake by 15.5% and 12.5% in the IC based on VOI analysis ($p<0.001$). Correspondingly, SPM analysis showed suprathreshold voxels in 97% and 77% of this VOI ($p<0.001$), with T-max value of 9.9 and 8.3, respectively. RN95-vs-WN65 and RN95-vs-BG55 showed increased uptake ($p<0.001$) of 6.5% and 5.6% in the MGB - encompassing 35% and 21% of this VOI ($p<0.001$) with a T-max value of 5.0 and 4.3. Comparing RN95-vs-WN65 resulted in an increased uptake ($p<0.05$) in the auditory cortex by 2.8%, corresponding to 1% of this VOI (T-max=3.9, $p<0.001$). Finally, WN65-vs-BG55 revealed decreased uptake ($p<0.001$) in the AC (-2.8%) corresponding to 5% of this VOI (T-max=5.3, $p<0.001$).Conclusions:In contrast to humans, activation in the AC of rats was lower compared to peripheral structures (e.g. IC). A deactivation of the AC was observed with louder continuous stimulus compared to background. Our data demonstrate the ability of FDG PET to detect activations in all observed auditory areas and to differentiate between auditory conditions. This technique may be used to characterize animal models for hearing disorders.

309 - Sunday, October 11, 2015, 11:30 AM - 1:00 PM, Hall 8
Clinical Oncology: Gastroesophageal & Colorectal Cancer

OP056

18F-FDG PET/CT as Predictive of Response after Chemoradiation in Esophageal Cancer Patients

E. Elimova, X. Wang, **E. C. Etchebehere**, Y. Shimodaira, H. Shiozaki, R. Wadhwa, V. Planjery, N. Charalampakis, M. A. Blum, W. Hofstetter, J. Lee, B. R. Weston, M. S. Bhutani, H. A. Macapinlac, J. A. Ajani; The University of Texas MD Anderson Cancer Center, Houston, TX, UNITED STATES.

Introduction: The purpose of this study was to evaluate if a baseline, an interim or a post-chemoradiation (CTRT) 18F-FDGPET/CT studies could provide information on pathologic response to CTRT and overall survival (OS). Materials and Methods: Thirty-one patients with histologically proven adenocarcinoma or squamous cell carcinoma of the esophagus, fit for trimodality therapy were prospectively enrolled. Most were men (93.5%), and had a stage III cancer (74.2%). Chemotherapy consisted of oxaliplatin/5-fluorouracil (45.2%) and taxane/5-fluorouracil (54.8%). All patients underwent a baseline, an interim (performed 12+/-2 days after onset of CTRT) and a post-CTRT 18F-FDGPET/CT study. The 18F-FDGPET/CT variables evaluated were at baseline, interim and post-CTRT studies maximum standardized uptake value (SUVmax) and total lesion glycolysis (TLG). Clinical and 18F-FDGPET/CT parameters were correlated with pathologic complete response (pathCR) and OS. Results: Among the 31 patients studied, 61.3% achieved a clinical complete response (cCR) and 87.1% had surgery. The median OS was 35.1 months (95% CI: 19.9 - NA). PathCR rate was 22.2%. There was only a marginal association between cCR and pathCR (p=0.06). None of the other variables was predictive of pCR. There was association between OS and baseline TLG (p=0.03) at the optimal cutoff TLG value of 75.15. Additionally, TLG and αTLG post-CTRT were also associated with OS (p = 0.01 and 0.03, respectively). Conclusion: None of the PET parameters are predictive of pCR but TLG at baseline and post-CTRT are prognostic of OS.

OP057

Diagnostic performance of 18F-fluorothymidine PET/CT for primary gastric cancer and its lymph node metastasis: Comparison with 18F-fluorodeoxyglucose PET/CT

M. Nakajo[1], Y. Kajiya[2], A. Tani[2], M. Jinguji[1], Y. Nakabeppu[1], M. Nakajo[2], S. Shimaoka[3], T. Nihara[3], S. Tanaka[4], T. Yoshiura[1]; [1]Department of Radiology, Kagoshima University, Graduate School of Medical and Dental Sciences, Kagoshima, JAPAN, [2]Department of Radiology, Nanpuh Hospital, Kagoshima, JAPAN, [3]Department of Gastroentenology, Nanpuh Hospital, Kagoshima, JAPAN, [4]Department of Pathology, Nanpuh Hospital, Kagoshima, JAPAN.

Aim: To examine the diagnostic performance of 18F-fluorothymidine (FLT) PET/CT for primary and metastatic lymph node gastric cancer foci by comparing with 18F-fluorodeoxyglucose (FDG) PET/CT. Materials and Methods: The enrolled study population comprised 17 patients with 17 newly diagnosed gastric cancers who underwent surgical resection of primary cancers and regional lymph nodes after both FLT and FDG PET/CT. The SUVmax of primary gastric cancer was compared between FLT PET/CT and FDG PET/CT studies using Wilcoxon signed-rank test. Associations of SUVmax levels with pathological factors were examined using the Mann-Whitney U or the Spearman rank correlation test. Diagnostic indices for detecting nodal metastasis were compared between the two tracers using the McNemar exact. Results: Fourteen of 17 primary cancers were visualized by both FLT and FDG PET/CT studies, and the residual 3 pathologically T1b cancers were not visualized by either method. FLT SUVmax was significantly lower than FDG SUVmax in all of the 14 visible primary cancers (7.1 ± 4.0 vs. 10.2 ± 5.0, p=0.003). The SUVmax was significantly correlated with tumor size for both FLT and FDG (FLT: ρ=0.56, p=0.036, FDG: ρ=0.59, p=0.025), but were not associated with the depth of invasion, nodal metastasis and differentiation. The sensitivity, specificity and accuracy for detecting nodal metastasis were 31.0% (9/29), 100% (166/166) and 89.7% (175/195) for FLT PET/CT, and 44.8% (13/29), 98.7% (164/166) and 90.8% (177/195) for FDG PET/CT, respectively. The sensitivity (p=0.13), specificity (p=0.48) and accuracy (p=1.00) were not significantly different between the two modalities. SUVmax was not significantly different between FLT (4.6 ± 3.1) and FDG (4.2 ± 1.0) (p=0.91) in the 9 concordant true positive nodes. Conclusions: FLT PET/CT has a comparable potential with FDG PET/CT in diagnosing primary and nodal foci of gastric cancer despite significantly lower FLT uptake in the primary foci.

OP058

Role of 18F-FDG PET/CT in predicting pathologic response to neoadjuvant chemo-radiotherapy and survival in patients of non-metastatic esophageal and gastro-esophageal junction carcinoma

A. Pruthi[1], S. Taywade[2], P. S. Choudhury[2]; [1]Sir Ganga Ram Hospital and Research Centre, New Delhi, INDIA, [2]Rajiv Gandhi Cancer Institute & Research Centre, New Delhi, INDIA.

Objective: To assess the role of 18F-FDG PET/CT in predicting the pathologic response and survival of patients with non-metastatic esophageal carcinoma treated with neoadjuvant chemo-radiation (CRT) and esophagectomy. Methods: 32 patients (18 males, 14 females; mean age 56.7 years, median age 58 years) with locally advanced (stage II/ III) esophageal carcinoma who underwent neoadjuvant chemo-radiation (CRT) followed by total esophagectomy at our institute during 2010-13 were analysed. Their pre-treatment staging and post neoadjuvant chemo-radiation 18F-FDG PET/CT studies were re-evaluated by an experienced nuclear medicine physician.

Response to neoadjuvant chemo-radiation on PET/CT images was compared to pathologic response. Follow-up information was obtained after careful evaluation of patient's electronic medical records. Disease free survival was calculated from the day of surgery till the first evidence of recurrence. Various PET/CT findings like SUV max, presence of lymph nodal abnormalities were correlated with pathologic response, incidence of recurrence and disease free survival using appropriate statistical tests. Results: Most tumours were squamous cell carcinomas (29 out of 32; 90.6%) and involved mid-thoracic esophagus (17 out of 32; 53.1%). Post-CRT 18F-FDG PET/CT study identified pathologic response with 76.2% sensitivity, 70% specificity and 74.2% accuracy. However, negative predictive value was only 41.7%. Patients were followed up for median duration of 10.8 months (interquartile range 6.3- 17.7 months). PET/CT parameters like SUVmax and presence of lymph nodal abnormalities in pre-treatment scan didn't show significant correlation with disease free survival. Pathologic response was found to correlate with the post-CRT FDG PET/CT maximal standardized uptake value (SUVmax) ($p<0.05$) and a post-CRT FDG PET SUVmax of >= 4 was found to be the only factor which correlated with reduced disease free survival (1 year survival rate of 25% vs. 68.1%; p value = 0.026). Conclusion: Post chemo-radiation PET/CT was found to be predictive of pathologic response and disease free survival. In view of low negative predictive value, surgery should still be considered even if the post-CRT FDG-PET/CT scan is normal because microscopic residual disease cannot be ruled out.

OP059

Recurrence Detection in Pancreatic Cancer: The Value of Quantitative FDG-PET/CT

J. T. Friis[1], O. S. Bjerring[2], M. G. Hildebrandt[1], S. Hess[1], O. Gerke[1], P. F. Høilund-Carlsen[1]; [1]Dept. of Nuclear Medicine, Odense University Hospital, Odense C, DENMARK, [2]Dept. of Surgery, Odense University Hospital, Odense C, DENMARK.

Aim: FDG-PET/CT is relatively unexplored in pancreatic cancer. The aim of this project was to investigate whether SUV-based semi-quantitative measures obtained by FDG-PET/CT could help differentiate cancer recurrence from non-specific lesions in patients with suspected recurrence of pancreatic cancer.Materials and Methods: As part of an ongoing prospective clinical trial, 25 patients with resectable pancreatic cancer were recruited postoperatively. FDG-PET/CT was performed, as part of protocolled follow-up, 3, 6, 9, 12, 18, and 24 months after surgery; if recurrence occurred, the patients dropped out of the study. The reference standard was a composite decision at a multidisciplinary team conference based on all available data, including follow-up scans and biopsies, when available. FDG-PET/CT scans were as-sessed visually by experienced nuclear medicine physicians and dichotomized into 'recurrence' or 'no recurrence'. In patients with recurrence, only the last scan leading to the diagnosis was included in the analysis. In patients without recurrence, any scan with a positive lesion was registered, and the one with the most FDG-avid lesion was included in the analysis. The FDG-uptake in suspicious lesions was characterized by the SUVmax value and the partial volume corrected SUVmean (cSUVmean) value. If a scan had no lesions suspicious of malignancy (true or false negatives), a value of '0' was imputed. Outcome measures were sensitivity and specificity and receiver operating characteristic (ROC) analysis of SUV measures with values of area under the curve (AUC).Results: Of the 25 patients, 16 were diagnosed with recurrence during the study period, while 9 remained disease free. Sensitivity and specificity were 0.88 (95% CI: 0.62-0.98) and 0.33 (0.07-0.70), respectively. Median SUVmax values in false positive and true positive lesions were 4.1 (3.3-16.8) and 7.0 (4.7-20.5), respectively ($p<0.04$). Median cSUVmean values in false positive and true positive lesions were 3.8 (range 3.6-10.7) and 6.6 (3.5-20.4), respectively ($p<0.04$). ROC analysis of cSUVmean values had an AUC of 0.75 (0.53-0.97) and a sensitivity and specificity of 0.81 and 0.78 with an optimal cSUVmean cut-off set at 4.4.Conclusion: Visual assessment of FDG-PET/CT imaging for recurrent pancreatic cancer had a high sensitivity, but a low specificity and, therefore, seems not suited for the detection of recurrent pancreatic cancer. Mean SUVmax and cSUVmean were significantly higher in malignant than benign lesions, albeit with wide ranges. Quantification seemed to increase specificity and may, thus, be considered helpful for differentiating malignant from benign lesions.

OP060

Contribution of 18F-FDG PET/CT in patients suspected for colorectal cancer recurrence, with normal or increased CEA.

H. Balink[1], E. van der Zee[1], J. P. E. N. Pierie[1], R. J. Bennink[2], H. J. Verberne[1]; [1]Medical Center Leeuwarden, Leeuwarden, NETHERLANDS, [2]Academic Medical Center, University of Amsterdam, Amsterdam, NETHERLANDS.

Objective: Colorectal cancer (CRC) is an increasing health problem, in particular in developed countries. Patients with a history of primary CRC surgically treated with the intention of curation benefit from an optimal postoperative follow-up. The current Dutch guidelines recommend computed tomography (CT) as the imaging modality of choice, whether or not indicated by an elevated carcinoembryonic antigen (CEA) level.

However, ^{18}F-fluorodeoxyglucose (^{18}F-FDG) positron emission tomography (PET)/CT, seems to have a better diagnostic precision than CT in detecting CRC recurrence. The objective of this retrospective study was to evaluate the diagnostic precision of ^{18}F-FDG PET/CT in detecting CRC recurrence during follow-up, after the primary CRC was surgically treated with curative intention. Patients were included with either a normal CEA level (and with equivocal radiology findings), or elevated CEA levels. Methods: In total 124 were included. All patients with suspected recurrence of CRC during follow-up were subjected to ^{18}F-FDG PET/CT imaging. A total of 124 ^{18}F-FDG PET/CT scans were assessed and the ^{18}F-FDG PET/CT outcome was subsequently verified based on the findings during the follow-up period after ^{18}F-FDG PET/CT. Results: In the overall population, with a proven CRC recurrence prevalence of 68,6% (n = 85), ^{18}F-FDG PET/CT had an overall sensitivity, specificity, and accuracy of 94,1% , 82,1% and 90, 3% respectively. As expected patients with a normal CEA level (n = 25) had a lower CRC recurrence prevalence compared to those with an elevated CEA level (n = 94) (48% vs. 72%, p = 0.021). ^{18}F-FDG PET/CT in CEA normal patients had a sensitivity, specificity, and accuracy of 91.7%, 84.6% and 88%, and for those patients with an elevated CEA level these values were 94,1%, 80,8% and 90,4%, respectively.Conclusions: ^{18}F-FDG PET/CT showed, irrespective of CEA levels, a high diagnostic accuracy in detecting or excluding CRC recurrence during postoperative follow-up. However these retrospective data should be regarded as preliminary and the role of ^{18}F-FDG PET/CT as the imaging modality of choice in patients suspected for CRC recurrence needs to be confirmed in prospective trials.

OP061

Evaluating Quantitative Measures in Incidental Colorectal PET Findings

T. Nguyen, S. Hess, H. Petersen, P. F. Hoeilund-Carlsen; Dept. of Nuclear Medicine, Odense University Hospital, Odense, DENMARK.

Aim: In oncologic PET, SUV_{max} and SUV cutoff values to distinguish malignant from benign lesions are often reported. However, studies have repeatedly questioned their validity as their reliability and comparability are influenced by many factors. We investigated such measures of common quantitative analysis in incidental colorectal (ICR) findings using dedicated software.**Materials and Methods**: FDG-PET studies in 24 patients with ICR uptake and 28 lesions (8 colorectal cancers, 12 polyps, and 8 with only benign findings) were retrospectively analyzed. To test analysis method variability, two lesion delineation techniques were applied with dedicated software (ROVER, ABX, Radeberg, Germany) using background corrected lesion-based threshold (LT) and voxel-based threshold (VT). A built-in partial-volume correction (PVC) was also employed and lesion measures of SUV_{max}, SUV_{mean}, $SUV_{mean, PVC}$, metabolically active volume (MAV), and mean metabolic volumetric product ($MVP_{mean} = SUV_{mean}$ MAV) were extracted.**Results**: In all lesions, $SUV_{max} > 5$ and $SUV_{mean} \geqq 3$. Measured SUV_{max} values were reproducible and malignant measures (16.5 ± 6.1) were higher than benign (10.2 ± 3.7) levels (p = 0.04), but none of them deviated (p = 0.3-0.7) from those of polyps (15.1 ± 7.5). SUV_{mean} values in malignant (LT: 10.2 ± 3.4, VT: 8.8 ± 2.8) compared to benign (LT: 6.5 ± 2.3, VT: 6.2 ±2.2) findings were also higher (p = 0.03-0.07) and both were indistinctive (p = 0.3-1) from those of polyps (LT: 10 ± 5.2, VT: 9.5 ± 5). The differences between VT and LT methods (p = 0.4-1) did not alter overall relations. Some malignant MAV and MVP_{mean} peaks were well above those of polyps and benign findings, both of which were at similar levels. PVC generally increased values by a factor of 1.3-2.7 ($p < 0.01$) at preserved relative levels. Inter-group relations for all measures, however, were insignificant (p = 0.1-0.3) due to value fluctuations.**Conclusion**: Quantitative analysis of ICR findings with common approaches showed that lesion etiology (i.e., malignant, polyp, or benign) cannot be differentiated by SUV_{max} or SUV_{mean} alone, nor can any useful cutoff value be set. MVP_{mean} might indicate distinctions better by incorporating lesion extent (MAV), but also lacks generally distinctive levels. Variations with different segmentations and PVC contribute to estimate variability, but affected overall relations less. It remains to be assessed whether more optimal data analysis methods and corrections can yield measures, e.g. $MVP_{mean, PVC}$, that better reflect the disease severity and extent than SUV_{max} values.

OP062

18F-FDG PET/CT versus CT evaluation of treatment response in patients with metastatic colorectal cancer receiving chemotherapy with a monoclonal antibody (bevacizumab or cetuximab)

Z. Nemeth[1], Z. Lengyel[2], K. Boér[1], E. Hitre[3], K. Borbély[3]; [1]Szent Margit Hospital, Budapest, HUNGARY, [2]Pozitron-Diagnosztika Kft, Budapest, HUNGARY, [3]National Institute of Oncology, Budapest, HUNGARY.

The study aim was to compare the effectiveness of evaluation of tumour response by positron emission tomography with 18F-fluorodeoxyglucose (18F-FDG PET/CT) and computed tomography (CT scan) in patients with metastatic colorectal cancer receiving combination treatment with chemotherapy and cetuximab or bevacizumab. A total of eleven patients who were candidate first line systemic treatment for metastatic colorectal cancer were enrolled in our study from April to

November 2014. All patients (pts) were evaluated by both 18F-FDG PET/CT and CT scan before and after systemic treatment. 18F-FDG PET/CT evaluation was performed after the second treatment, while the CT scan after the third therapy in every case. Systemic treatment consisted of chemotherapy with 5-fluorouracil, leucovorin, irinotecan (FOLFIRI) in combination with a monoclonal antibody bevacizumab or cetuximab (FOLFIRI+cetuximab: 3 pts and FOLFIRI+ bevacizumab: 8 pts). The primary tumours were histologically proven and all patients had at least one > 2 cm liver metastasis on axial imaging (CT). The maximum standardized uptake value (SUVmax) was measured at baseline and after chemotherapy. The relative FDG uptake changes in liver metastases were calculated (dSUV) as well. Our results were evaluated by European Organisation for Research and Treatment of Cancer (EORTC) FDG response criteria. A total of eleven patients were eligible for response evaluation. Regarding PET/CT with EORTC criteria 8 pts. (72.7%) had partial metabolic response (PMR), 3 pts. (27.3%) had progressive (27.3%) disease (PMD). Patient were classified in two by two tables according to RECIST responders (CR, PR, SD), non responders (PD) based on CT scans, ad classified based on SUVmax responders (> 25% decrease from baseline) and non-responders (< 25% decrease from baseline). Results showed an almost 100% match between the two classification methods (RECIST, EORCT criteria). SUVmax predicted all eight RECIST-responders correctly the only mismatch occured to the fact that progressive disease was not recognised by CT scan, but was reported by PET/CT scan. As regards CT scans there were no significant changes in those 8 pts. who had PMR at PET/CT assessment and in these cases CT showed stable disease. In one case a new lesion was detected only by PET/CT. Based on our preliminary results morphological and metabolic imaging indicates in some cases a differential therapeutic decisions in metastatic colorectal cancer. Moreover the change of SUVmax appears to be a usefull tool for evaluating tumour response. The patient recruitement is open, more data is being collected.

OP063

Comparison of 18F-FDG PET-CT to conventional CT imaging in providing optimal pre-treatment staging in patients with incidentally diagnosed gall bladder cancer.

N. Jain, J. Bal, C. Nagpal, B. Rajashekharrao, A. Velumani; Nueclear Healthcare Limited, Delhi, INDIA.

Introduction: After a cholecystectomy, incidental gallbladder cancer (IGC) requires accurate imaging studies to determine the actual extent of the disease to properly tailor subsequent treatment. Aim: To compare 18F-fluorodeoxyglucose positron emission tomography-computed tomography (18FDG PET-CT) to conventional imaging (CT Abdomen and Chest) to provide optimal pre-treatment staging in patients with IGC. Patients and Methods: Between January 2014 and April 2015, all patients with IGC and at least T1b stage on histopathology underwent 18F-FDG whole body PET-CT. The PET/CT findings were grouped as locoregional disease (operable) and disseminated disease (inoperable). Results of PET/CT were compared with conventional CT imaging. Results: The series included 41 patients, 32 women and 9 men, with a median age of 50 years (range 35-72 years). The Whole body PET CT imaging was performed at a median time of 6 weeks after cholecystectomy (range 4-24 weeks). 18FDG PET-CT findings were negative in 10 patients and positive in 31 patients. Of these 31 patients 7 were with localized potentially resectable disease (PRD) and 24 with disseminated disease (inoperable). Conventional CT imaging observations were negative in 21 patients and positive in 20 patients. Amongst these 20 patients, 3 with localized potentially resectable disease (PRD) and 17 were with disseminated disease. In comparison to CT, PET CT changed management in additional 31.7% cases and thus was superior to conventional imaging ($p=0.02$, $p<0.05$). PET CT also identified more number of lesions in cases with disseminated disease. Conclusions: For patients presenting with stage T1b or greater IGC, the use of 18FDG PET-CT imaging will help reduce the number of patients undergoing non-therapeutic re-exploration and avoid radical surgeries thus tailoring subsequent disease management.

310 - Sunday, October 11, 2015, 11:30 AM - 1:00 PM, Hall D
Cardiovascular System: Cardiac Innervation Imaging

OP064

Variation in haplotypes of the norepinephrine transporter is not associated with sympathetic activity as measured by cardiac 123I-mIBG scintigraphy

D. O. Verschure[1,2], F. Baas[1], B. L. F. van Eck - Smit[1], G. A. Somsen[3], H. J. Verberne[1]; [1]Academic Medical Center, Amsterdam, NETHERLANDS, [2]Medisch Centrum Alkmaar, Alkmaar, NETHERLANDS, [3]Cardiology Centers of the Netherlands, Amsterdam, Amsterdam, NETHERLANDS.

Aim^{123}I-*meta*-iodobenzylguanidine (^{123}I-*m*IBG) scintigraphy has been extensively validated and clinically used to evaluate cardiac sympathetic function in cardiac diseases. The semi-quantitative outcome (i.e. heart mediastinal ratio (H/M)) is an independent prognostic parameter in patients with chronic heart failure (CHF). ^{123}I-*m*IBG is a radiolabelled norepinephrine (NE) analog that has the same presynaptic uptake, storage and release mechanism as NE. The norepinephrine transporter (NET), encoded by the solute carrier family 6 (SLC6A2), is responsible

for reuptake of NE into presynaptic nerve terminals and is a regulator of norepinephrine homeostasis. It has been demonstrate that polymorphism of SLC6A2 correlates with blood pressure, but it is unknown if polymorphism of SLC6A2 influence the H/M. Therefore we investigated if SLC6A2 polymorphism influences ^{123}I-*m*IBG results. Materials and Methods: Forty-nine adults with CHF (age 66.5±8.1 years, LVEF 22,3±6.4 and functional class NYHA 2,3±0.4) referred for ^{123}I-*m*IBG scintigraphy were enrolled. 15 minutes (early H/M) and 4 hours (late H/M) after administration of 185 MBq ^{123}I-*m*IBG anterior planar thoracic images were acquired with medium energy collimators. H/M was calculated based on the mean count densities from the manually drawn regions of interest (ROI) over the left ventricle and a predefined fixed ROI placed in the upper mediastinum. DNA of the subjects was extracted from whole-blood samples. Twelve exons of the SLC6A2 gene were analysed.Results The mean early H/M was 2.10±0.39, late H/M 1.81±0.39 and WO 13.7±11.2. Genotyping of the SLC6A2 gene resulted in 6 different genotypes. Between the 2 largest haplotype groups C-T-C-A-T (n=22) vs. C-T-C-A/G-C-G/T (n=18) there was only a significant difference in early H/M (respectively 2.07±0.30 and 2.11 ±0.50, $p = 0.027$). However, multivariate regression analyse using haplotype, LVEF and NYHA class possible explanatory factors, showed only LVEF as an independent predictor of early H/M (adjusted $R^2 = 0.063$, $p = 0.05$). Increased H/M was associated with increased LVEF. For late H/M similar results were obtained where only the LVEF was an independent predictor (adjusted $R^2 = 0.116$, $p = 0.01$). For WO the LVEF and NHYA were independent predictors (adjusted $R^2 = 0.105$, $p = 0.03$). Conclusion: This is the first study that investigated the association between NET polymorphism and cardiac ^{123}I-*m*IBG scintigraphically derived parameters. Despite a small difference in early H/M between the two most common haplotypes, variation in NET haplotype could not explain a significant part of the variation in the ^{123}I-*m*IBG scintigraphically derived parameters.

OP065

Effect of standardization of I-123 MIBG heart-to-mediastinum ratio on the prognostic threshold: application to multicenter database of chronic heart failure

K. Nakajima[1], K. Okuda[2], S. Matsuo[1], T. Nakata[3], S. Kinuya[1]; [1]Kanazawa University Hospital, Kanazawa, JAPAN, [2]Kanazawa Medical University, Uchinada, JAPAN, [3]Hakodate Gryoukaku Hospital, Hakodate, JAPAN.

Purpose. As I-123 metaiodobenzulguanidine (MIBG) has been used for the assessment of prognosis in patients with chronic heart failure (CHF), we have proposed to unify the MIBG heart-to-mediastinum ratio (HMR) to overcome differences in camera-collimator systems. The aim of this study was to evaluate the effect of the standardization on prognostic variables and thresholds for mortality risks. Methods. A total of 225 phantom experiments were performed in 84 hospitals to determine conversion coefficients (K) to the mathematically calculated reference values. For example, the K value of low-energy high-resolution (LEHR) collimator was 0.55, LE general purpose (GP) 0.65, and medium-energy (ME) GP 0.88. Using the collimator-specific K values, all HMRs could be standardized to those of the commonest ME types (ME88). Japanese pooled databases (n=933) from 6 cohort studies, in which at least 5-year prognosis was known, was used for validation. Mean age was 61±13 years, time of follow-up 7.7 ±4.3 years (range 0.08-14.6 years), and ejection fraction 36±13%. Late HMR in the anterior image was used for the analysis in this study. Cardiac death due to pump-failure, acute myocardial infarction and sudden cardiac death was used as a single endpoint. Since 4 hospitals used LEGP and 2 used LEHR collimators, they were unified to HMRs comparable to the ME88 condition. Multivariate analysis and receiver operating curve analysis were applied to compare the original and standardized HMRs. The optimal thresholds for predicting cardiac death were also determined. Results. The original mean HMR of 1.71±0.33 (95% range 1.18-2.41) increased to 2.00±0.44 (95% range 1.25-3.01) as the standardized HMR. The best cutoff values for predicting cardiac death was HMR=1.66 (ROC AUC=0.694) and 1.89 (ROC AUC=0.698) for the original and standardized HMRs, respectively. Multivariate proportional hazard analysis for all the follow-up period selected the same 5 variables of age, male sex, left ventricular ejection fraction, NYHA functional class and MIBG late HMR. Chi-square values of the logistic analysis for the 5-year survival and death using the same variables were 164.9 (ROC AUC 0.780) and 167.2 (ROC AUC 0.781) for original and standardized HMR groups, respectively ($p<0.0001$ for both). Conclusion. Using the calibration phantom method to unify HMRs, all HMRs were successfully converted to the ME88 condition. An optimal threshold for stratifying prognosis became increased (HMR=1.9) with keeping the statistical power to precisely predict cardiac death. The standardization method could further effectively function when both LE and ME collimators are used in a multicenter study.

OP066

Proposal for a standardized method to evaluate 123I-MIBG SPECT in HF patients: importance in decision making of ICD implantation.

V. Frantellizzi, A. Farcomeni, P. Scarpato, G. A. Follacchio, S. Sollaku, N. Salvi, P. Scarparo, M. Liberatore, F. Monteleone, F. Fedele, G. De Vincentis; Sapienza University of Rome, Rome, ITALY.

Patients (pts) with Heart Failure (HF) have high risk of fatal

malignant ventricular arrhythmias. Implantable cardioverter-defibrillator (ICD) is the therapy of choice but ICD implant should be reserved to high risk pts, considering also inappropriate shocks and costs. Aim of the study was to assess if 123I-MIBG scan is useful in decision making for ICD implantation. 170 pts were prospectively evaluated in term of occurrence of arrhythmic events (AE) with mean 19,7 month follow up. The average value of left ventricular ejection fraction (LVEF) was 31,1% +/- 9,4% and among these 69 had idiopathic disease and 101 had post-ischemic disease. At 20 and 240 minutes after MIBG administration, planar and SPECT cardiac images were obtained. Planar images were analyzed as Early and Late Heart-to-Mediastinum (HM) ratio and Washout Rate (WR). SPECT studies were processed with Myovation software (GE Healthcare) and row data for each of 17 segments of a standard polar map were obtained. Using a 5-point visual scoring model , data were semi-quantified and Late Summed Scores (LSS) was obtained. We evaluated area under the ROC curve (AUC) for each diagnostic test and thresholds by means of sensitivity and specificity. Optimal thresholds were chosen by Youden's index. Optimal weights for separate segments were estimated by means of logistic regression, with zero weights fixed by minimization of the Akaike information criterion through forward selection. The HM ratio value of 1.6 showed a 0.64 sensitivity (SE) and 0.415 specificity (SP), whereas a 1,4 cut-off value showed 0.588 SE and 0.809 SP. When examining the WR we obtained for a cut-off value of 20% , 91% SE and 28% SP. More accurate results were obtained with a reference cut-off of 30% , with 73% SE and 53% SP. Taking into account LSS, using a cut off value of 26 we obtained 0.795 SE and 0.274 SP, whereas a cut off value of 43 had a SE of 0.625 and a SP of 0.804. Has, in our opinion, to be underlined how studies conducted with SPECT technique generally have provided very interesting results in the clinical setting, but did not provide technical details on how to achieve and interpret the parameters obtained. In our patients series, the best result in terms of accuracy in predicting AE was achieved by LSS scoring, in spite of a number of criticisms and doubts about the real usefulness and reproducibility of SPECT data by several authors.

OP067

Role of Myocardial Perfusion, Sympathetic Denervation, and Scar Size in Predicting Inducibility of Ventricular Arrhythmia in Ischemic Cardiomyopathy

M. T. Rijnierse, C. P. Allaart, S. De Haan, H. J. Harms, M. C. Huisman, A. M. Beek, A. A. Lammertsma, A. C. Van Rossum, P. Knaapen; VU University Medical Center, Amsterdam, NETHERLANDS.

Introduction: Myocardial perfusion, scar size, sympathetic denervation and innervation-perfusion mismatch, obtained from positron emission tomography (PET) and late gadolinium enhanced cardiovascular magnetic resonance imaging (LGE-CMR), may all contribute to enhanced risk prediction of ventricular arrhythmias (VA). There may, however, be overlap between some of these risk markers, as they are based on similar pathophysiology. The aim of this study was to assess the role of PET and LGE-CMR derived risk markers in predicting VA inducibility in the same patient population.Methods: 52 patients (66 ± 9 years, 90% male, LVEF 29 ± 6%) with ischemic cardiomyopathy and left ventricular ejection fraction (LVEF) ≤35% who were referred for primary prevention implantable cardioverter-defibrillator (ICD) implantation were included. LGE-CMR was performed to assess LV volumes, function, and scar size. [^{15}O]H_2O PET and [^{11}C]hydroxyephedrine PET were performed to assess both resting and hyperemic myocardial blood flow (MBF), and sympathetic innervation. Innervation and perfusion defect size, and innervation-perfusion mismatch size were calculated. After ICD implantation, an electrophysiological study (EPS) was performed and was considered positive in case of sustained VA.Results: Patients with positive EPS (n=25) showed more severely impaired hyperemic MBF (1.36 ± 0.39 vs. 1.71 ± 0.39 mL min^{-1} g^{-1}, *P*=0.003), larger sympathetic denervation size (28 ± 12 vs. 21 ± 13%, *P*=0.048), and tended to have larger scar size (24 ± 13 vs. 18 ± 9 g, *P*=0.07) and perfusion defect size (22 ± 13 vs. 15 ± 11%, *P*=0.06) compared with EPS negative patients (n=27). No differences were observed in LV volumes, LVEF, and innervation-perfusion mismatch size. Multivariable analysis revealed that impaired hyperemic MBF was the single best independent predictor for VA inducibility (OR 0.78, 95% CI 0.65-0.94, *P*=0.007). A combination of risk markers did not yield incremental predictive value over hyperemic MBF alone.Conclusion: Of all previously validated approaches to evaluate the arrhythmic substrate, impaired hyperemic MBF was the only independent predictor of VA inducibility. Moreover, a combined approach of different imaging variables did not have incremental value. These results suggest that quantitative PET perfusion imaging may be promising in risk prediction of VA.

OP068

Prognostic value of myocardial I-123 metaiodobenzylguanidine imaging in patients with atrial fibrillation

Y. Saushkina[1], Y. Lishmanov[1,2], I. Kisteneva[1], S. Popov[1]; [1]RI Cardiology, Tomsk, RUSSIAN FEDERATION, [2]National Research Tomsk Polytechnic University, Tomsk, RUSSIAN FEDERATION.

Purpose. The problem of diagnostic and treatment of cardiac arrhythmias is one of the most actual in modern medicine. To date, the mechanisms underlying the majority of cardiac arrhythmias are unclear. The disturbance of sympathetic innervation of the heart may be the cause of atrial fibrillation and reason of myocardial dysfunction of the left ventricle. In the 1950s the relationship between the occurrence of AF and the autonomic nervous system has been described. Cardiac autonomic nervous system have been shown to play an important role in the initiation, persistence and termination of AF. In addition, there is actual a question evaluate the effectiveness of the treatment of this arrhythmia. Thus, the purpose of this study was to detect the correlations between the cardiac autonomic innervation and the clinical course of AF after radiofrequency catheter ablation (RFCA). Methods. In this study were enrolled 15 patients with essential hypertension (EH) (the duration of EH was 5-20 years) and persistent AF. All patients underwent single-photon emission computer tomography (SPECT) with I-123 metaiodobenzylguanidine (123I-MIBG) to evaluate cardiac sympathetic nervous system activity before and 12 months after RFCA. SPECT with 123I-MIBG was performed at 20 min (early phase) and 4 h (delayed phase) after intravenous injection. The early and delayed heart-to-mediastinum ratio (HMR) and the washout rate (WR) were performed. Local denervation was evaluated on polar map images using the 17-segment model of left ventricle (LV). Results. A year later after RFCA in 7 patients arrhythmia paroxysms were not observed without antiarrhythmic therapy (AAT). Atrial fibrillation with frequency up to 1 times per month was observed in four patients with AAT. One patient had a repeat RFCA. In all patients the early HMR and delayed HMR was significantly higher vs baseline (1,58±0,15 vs 1,91±0,20; $p<0,05$ and 1,69 ±0,22 vs 1,96±0,42; $p<0,05$). There was no correlation between 123I-MIBG parameters and the duration of EH, the duration of AF and the frequency of AF episodes. However, the delayed HMR before RFCA was strongly correlated with the presence of arrhythmia recurrence a year later after RFCA ($r=-0,878$, $p=0.001$). Also we conducted ROC-analysis and identified the main scintigraphic predictors of the effectiveness of interventional treatment of atrial fibrillation. The most significant indicator in predicting the efficacy of RFCA was delayed HMR=1,7 (AUC=0,99; p=0,0001; sensitivity - 100%; specificity - 71%). Conclusions. Thus, delayed heart-to-mediastinum ratio may be an independent scintigraphic predictor of the effectiveness of interventional treatment of atrial fibrillation.

OP069
Cardiac sympathetic activity in 22q11 deletion syndrome

D. O. Verschure[1,2], E. Boot[1,3], T. A. van Amelsvoort[4], J. Booij[1], B. L. F. van Eck - Smit[1], G. A. Somsen[5], H. J. Verberne[1]; [1]Academic Medical Center, Amsterdam, NETHERLANDS, [2]Medisch Centrum Alkmaar, Alkmaar, NETHERLANDS, [3]The Dalglish Family Hearts and Minds Clinic for Adults with 22q11.2 Deletion Syndrome, Toronto, ON, CANADA, [4]University of Maastricht, Maastricht, NETHERLANDS, [5]Cardiology Centers of the Netherlands, Amsterdam, NETHERLANDS.

Aim: 22q11 Deletion syndrome (22q11DS) is a relatively common genetic condition caused by a microdeletion on the long arm of chromosome 22. The deleted region spans more than 40 genes, one of which is the gene that encodes for the enzyme catechol-O-methyl-transferase (COMT). COMT enzyme is involved in the degradation of catecholamines, including norepinephrine (NE). Indeed, reduced COMT enzyme activity and impaired catecholamine turnover have been reported in 22q11DS.Clinically, adults with 22q11DS are at increased risk for sudden unexpected death. Although the causes are likely multifactorial, increased cardiac sympathetic activity with subsequent fatal arrhythmia, due to increased levels of NE, should be considered as a possible mechanism predisposing to premature death in 22q11DS. The purpose of this study was, therefore, to determine whether cardiac sympathetic activity is increased in adults with 22q11DS compared to healthy controls. Materials and Methods: All study participants underwent 123I-mIBG scintigraphy. Planar 123I-mIBG images were analysed by one experienced observer blinded to patient data. Heart-to-mediastinum ratios (H/M) were calculated from the 123I-mIBG images using a region-of-interest over the heart and the upper part of the mediastinum fifteen minutes (early images) and 4 hours (late images) after administration of 123I-mIBG intravenously. Washout (WO), as an indicator or adrenergic drive, was calculated as a ratio of early and late H/M.ResultsFive adults with 22q11DS (mean age 28.6 ±4.8 years) without any congenital heart disease and five age- and sex-matched healthy controls (mean age 28.0±7.9 years) were enrolled. There were 3 males and 2 females in both groups. There were no significant differences in early and late H/M between the 22q11DS and the control group. However, there was a significant difference in WO between the 22q11DS and the control group (-4.92±2.8 and -10.44±7.2, respectively; p=0.027). Conclusion: This preliminary study for the first time suggests increased adrenergic drive in adults with 22q11DS using 123I-mIBG scintigraphy. This

increased adrenergic drive might explain one possible mechanism predisposing to premature death in 22q11DS.

OP070

Assessment of right ventricular sympathetic dysfunction in patients with Arrhythmogenic Right Ventricular Cardiomyopathy using 123I-Metaiodbenzylguanidin

A. Todica[1], J. Siebermair[2], J. Schiller[1], M. Zacherl[1], W. Fendler[1], P. Bartenstein[1], R. Wakili[2], M. Hacker[3], S. Lehner[1]; [1]Department of Nuclear Medicine - University of Munich, Munich, GERMANY, [2]Medical Department I - University of Munich, Munich, GERMANY, [3]Division of Nuclear Medicine - Medical University Vienna, Vienna, AUSTRIA.

Aim: Arrhythmogenic right ventricular cardiomyopathy (ARVC) is a mainly inherited heart-muscle disease, which is characterized by a progressive replacement of contractile heart muscle by fibrotic and fat tissue primarily in the right ventricle, ultimately resulting in heart failure. The regional reduction of left ventricular myocardial 123I-MIBG-uptake is associated with higher risk of future recurrent life-threatening events in patients with ARVC. Therefore, we prospectively evaluated the sympathetic function using 123I-MIBG SPECT/CT in patients diagnosed with ARVC and in patients with idiopathic ventricular fibrillation (IVF). The objective of this study was to institute a novel approach by using the additional morphological information from the low-dose CT. Methods: Sympathetic innervation of the heart was assessed using 123I-MIBG SPECT/low-dose CT in 13 patients diagnosed with ARVC according to the modified task force criterions, and 10 patients diagnosed with IVF. Late planar H/M ratio was calculated for both groups. The 123I-MIBG uptake in the left (LV/M) and right ventricle (RV/M) was evaluated separately based on the morphological information available from the CT scan and set in relation to the uptake in the mediastinum. Results: The mean planar H/M ratio in the ARVC group was slightly lower as compared to the IVF group but did not reach statistical significance (1.5±03 vs. 1.7±0.2, p=0.068). The optimal cut-off value to discriminate between ARVC and IVF was 1.66 with a sensitivity of 75%, a specificity of 60% and an AUC of 0.73. There was a significant difference between the ARVC and the IVF group for the LV/M ratio (3.2±0.5 vs. 3.9±0.8, p=0.014). The ideal cut-off value was 3.41 (sensitivity 77%, specificity 80%, AUC 0.78). The RV/M ratio was able to distinguish best between ARVC and IVF resulting in a higher significance (1.6 ±0.3 vs. 2.0±0.2, p=0.001). Hereby the best cut-off value was 1.88 (sensitivity 88%, specificity 90%, AUC 0.93). Conclusion: The separate assessment of the left and right ventricle could be reliably performed with the help of the low-dose CT. The RV/M ratio was significantly lower in patients with diagnosed ARVC and the RV/M ratio could distinguish with the highest sensitivity and specificity between ARVC patients and our reference collective.

OP071

Sleep-disordered breathing is associated with impaired cardiac sympathetic innervation and predict prognosis in patients with heart failure

T. Pellegrino[1], S. Paolillo[2], V. Piscopo[2], A. Boemio[2], R. Carotenuto[2], B. Russo[2], S. Pellegrino[2], G. De Matteis[2], P. Perrone Filardi[2], A. Cuocolo[2]; [1]Institute of Biostructures and Bioimages, Naples, ITALY, [2]University of Naples - Federico II, Naples, ITALY.

Background: Unfavorable effects of sleep-disordered breathing (SDB) in heart failure (HF) are mainly mediated by impaired sympathetic activity. However, few data are available on SDB and cardiac adrenergic impairment evaluated at myocardial level. The aim of the present study was to assess the relationship between SDB, cardiac sympathetic innervation and prognosis in HF patients. Methods: Ninety-four patients (66.1±9.8 years) with systolic HF (median left ventricular ejection fraction 32±7%) underwent nocturnal cardiorespiratory monitoring to assess presence and type of SDB by Apnea/Hypopnea Index (AHI), and 123I-MIBG myocardial scintigraphy to calculate heart-to-mediastinum (H/M) ratios and 123I-MIBG washout rate. Patients were prospectively followed for 29±18 months for the combined endpoint of cardiovascular death and HF hospitalization. Results: Of 94 patients, 72 (77%) showed SDB and, compared to non-SDB, had significantly reduced early (1.67±0.22 vs. 1.77 ±0.13; $p<0.02$) and late (1.50±0.22 vs. 1.61±0.23; $p<0.04$) H/M ratios. At multiple linear regression analysis, early and late H/M ratios remained independent predictors of AHI ($\beta=-0.749$; $p<0.001$; $\beta=-0.830$; $p=0.001$, respectively). Similarly, AHI was the only predictor of early ($\beta=-0.643$; $p<0.001$) and late ($\beta=-0.453$; $p<0.002$) H/M ratios. Patients with AHI above the median showed significantly higher event rates and worse survival compared to patients with AHI below the median (35% vs. 9%, respectively; $p<0.01$). Similarly, patients with moderate to severe disorder showed significantly increased incidence of the combined endpoint and worse survival compared to patients with mild or no disorder (35% vs. 11.7%; $p<0.01$). Adding SDB variables to the already known prognostic role of 123I-MIBG imaging, we observed an incremental prognostic discrimination with the

worst survival in patients with both SDB and H/M impairment. Conclusions: Patients with systolic HF and SDB show more impaired cardiac adrenergic innervation and more adverse prognosis compared to HF patients without SDB.

YE1- Sunday, October 11, 2015, 1:00 PM - 2:30 PM, Hall 8
Young EANM Daily Forum 1: Leadership Skills

OP071b
Welcome to Hamburg
R. Freudenberg, GERMANY

OP071c
Building a Successful Nuclear Medicine Department
S. Fanti, ITALY

OP071d
Become the Leaders of Tomorrow
I. Carrio, SPAIN

OP071e
Dealing with Stress at Work
J. Buscombe, UNITED KINGDOM

OP071f
Closing Remarks

401 - Sunday, October 11, 2015, 2:30 PM - 4:00 PM, Hall 1
CME 3 - Paediatrics & Cardiovascular: Paediatric Heart and Lung Diseases

OP072
Paediatric Cardiology and Nuclear Medicine
O. Milanesi, ITALY

OP073
Paediatric Lung Scintigraphy
L. Drubach, USA

OP074
Myocardial Molecular Imaging in Paediatrics
P. Zucchetta, ITALY

402 - Sunday, October 11, 2015, 2:30 PM - 4:00 PM, Hall 2
Joint Symposium 3: EANM/ESSO: Radioguided Surgery

OP075
Sentinel Lymph Node in Breast Cancer: Why Surgeons need Isotopes
R. Audisio, UK

OP076
Sentinel Lymph Node in Breast Cancer: Imaging or not Imaging: That is the Question?
F: Giammarile, FRANCE

OP077
Sentinel Lymph Node in Melanoma: What a Clinician Expects
O. Zoras, GREECE

OP078
Sentinel Lymph Node in Melanoma: The EANM Guideline
C. Bluemel, GERMANY

403a - Sunday, October 11, 2015, 2:30 PM - 3:30 PM, Hall 4
Mini Course 1 - Interactive: Signs in Nuclear Medicine Imaging

OP079
Signs in Nuclear Medicine Imaging
G. Gnanasegaran, UK

403b - Sunday, October 11, 2015, 3:45 PM - 4:45 PM, Hall 4
Mini Course 2 - Interactive: PET/CT Artefacts

OP080
PET/CT Artefacts
L. Lezaic, SLOVENIA

403c - Sunday, October 11, 2015, 5:00 PM - 6:00 PM, Hall 4
Mini Course 3 - Interactive: SPECT/CT Artefacts

OP082
SPECT/CT Artefacts
A. C. Geão, PORTUGAL

404 - Sunday, October 11, 2015, 2:30 PM - 4:00 PM, Hall G1
Clinical Oncology - Featured: Prostate (PSMA)

OP083
Upgrading and downgrading of prostate biopsy results in a phase 2 study of MIP-1404 SPECT/CT in men undergoing radical prostatectomy

K. Goffin[1], S. Joniau[1], P. Tenke[2], G. Dabasi[3], K. Slawin[4], W. Ellis[5], B. Alekseev[6], I. Buzogány[7], S. Mishugin[8], E. Klein[9], J. Stolz[10], V. Student[11], P. Koranda[12], V. Matveev[13], T. Armor[14]; [1]University Hospitals Leuven, Leuven, BELGIUM, [2]Jahn Ferenc South Pest Hospital, Budapest, HUNGARY, [3]Semmelweis University, Budapest, HUNGARY, [4]Vanguard Urologic Institute, Houston, TX, UNITED STATES, [5]University of Washington, Seattle, WA, UNITED STATES, [6]Moscow Research Oncological Institute, Moscow, RUSSIAN FEDERATION, [7]Peterfy Sandor Street Hospital, Budapest, HUNGARY, [8]City Clinical Hospital # 57, Moscow, RUSSIAN FEDERATION, [9]Cleveland Clinic, Cleveland, OH, UNITED STATES, [10]University Hospital Motol, Prague, CZECH REPUBLIC, [11]11University Hospital Olomouc, Olomouc, CZECH REPUBLIC, [12]University Hospital Olomouc, Olomouc, Olomouc, CZECH REPUBLIC, [13]Russian Oncology Research Center, Moscow, RUSSIAN FEDERATION, [14]Progenics Pharmaceuticals, Inc., Tarrytown, NY, UNITED STATES.

Aim: MIP-1404 is a technetium-99m labeled small molecule to image PSMA expression in prostate cancer. The objective of this analysis was to explore the relationship between MIP-1404 uptake in the prostate gland and the incidence of upgrading and downgrading of prostate needle biopsies following radical prostatectomy (RP) in the phase 2 clinical trial MIP-1404-201 (NCT01667536). Materials / Methods: Prostate needle biopsy Gleason scores recorded in case report forms of 104 patients prior to surgery were compared to the final histopathologic Gleason score of the RP specimen, assessed by the site pathologist, to determine the rate of upgrading and downgrading in evaluable patients with pre-surgical biopsy and post-surgery pathology results. ^{99m}Tc-MIP-1404 SPECT/CT of the pelvis was acquired prior to surgery. Quantitative results of MIP-1404 uptake were obtained by calculating the maximal tumor to background ratio (TBR) for the prostate gland of each patient. A one-sided Student's t-test was performed to test for significant increase in TBR between patients with upgraded or downgraded final histopathologic Gleason score ≤7 and >7. Results: 31% (25/81) of evaluable patients had their biopsy Gleason score upgraded to >7 or downgraded to ≤7 by histopathologic assessment of the prostatectomy specimen. 79% (11/14) of patients upgraded to a Gleason score > 7 including one downgraded (Gleason 9 to 8) demonstrated high MIP-1404 lesion uptake (TBR >30:1) with a mean TBR of 47:1 [95% CI (30-63:1)]. 91% (10/11) of patients downgraded to Gleason score ≤7 had significantly (P<0.001) lower lesion uptake (TBR <30:1) with a mean TBR of 16:1 [95% CI (10-22:1)]. Conclusion: MIP-1404 uptake in the prostate gland is significantly higher in prostate cancer patients upgraded at RP from those who are downgraded at RP. MIP-1404 may be useful to indicate if a needle biopsy has under- or overestimated the severity of disease.

OP084
Differences in biodistribution of Lu-177-DKFZ-PSMA-617 and Ga-68-DKFZ-PSMA-11 in the same patient group

O. E. SAHIN[1], J. NEMATYAZAR[1], B. RAZAVI[1], N. YEYIN[1], A. AYGUN[1], M. OCAK[2], E. DEMIRCI[3], L. KABASAKAL[1]; [1]Istanbul University,Cerrahpasa Medical Faculty,Department of Nuclear Medicine, İstanbul, TURKEY, [2]Istanbul University,Pharmacy Faculty,Department of Pharmaceutical Technology, İstanbul, TURKEY, [3]Sisli Etfal Training and Research Hospital,Department of Nuclear Medicine, İstanbul, TURKEY.

Aim: PSMA is an excellent target for prostate cancer imaging and therapy using Ga-68 and Lu-177 labeled ligands. Human biodistribution studies of Ga-68-PSMA ligand have demonstrated that highest uptake of radiotracer is observed on kidneys and salivary glands and moderate uptake in lacrimal glands, liver and spleen. However, Lu-177-PSMA-ligand is a different compound and there is no information about its biodistribution. Therefore the aim of the study was to evaluate the biodistribution of these two compounds. Material and Method: For this purpose, 17 patients (mean age 68.8±6.7 years) who had PSMA PET/CT imaging and who underwent Lu-177-PSMA therapy were included. PSMA PET imaging was not longer then 1 month at the time of therapy. SUVmax values of parotid glands, kidneys, liver, spleen and primary

tumour (n=6), metastatic lymph nodes (n=8) and bone metastases (n=9) were obtained from PET images. From the SPECT/CT images obtained 24 h after Lu-177-PSMA administration ROIs were drawn over the same areas and background corrected maximum counts are calculated. Results: Highest uptake is observed in kidneys (45.0±18.9) followed by lymph nodes (23.2±24.8), bone metastases (15.9±6.0), primary tumor (12.8±15.9), parotid gland (12.2±3.1) and lowest in lacrimal glands (7.5±4.3) in PSMA PET images. The biodistribution of Lu-177-PSMA was completely different giving the highest uptake in parotid glands (678.7±352.2) followed by bone metastases (651.7±498.8) lymph nodes (561.3±322.8), lacrimal glands (342.4±231.0) kidneys (249.0±146.8) and primary tumor (102.5±78.2). Conclusion: It seems that biodistribution of Lu-177-PSMA is different then Ga-68-PSMA and highest radiation absorbed doses are given to parotid gland and to the metastatic tissues during the therapy of Lu-177-PSMA. Kidneys are getting significantly lower radiation doses as compared to that of Ga-68-PSMA due to lower uptake.

OP085

(68)Ga-labelled PSMA in prostate cancer: its diagnostic value in patients with biochemical recurrence of prostate cancer

S. Vöö, A. van Kroonenburgh, F. M. Mottaghy; Maastricht University Medical Center, Maastricht, NETHERLANDS.

Background: There is an ongoing need for an accurate imaging modality which can be used for staging, metastatic evaluation, predicting biologic aggressiveness, and investigating recurrent disease in prostate cancer. Prostate specific membrane antigen (PSMA) displays an increased expression in prostate tumor cells and is regarded as an ideal target for prostate cancer. Its biodistribution is favourable in comparison to choline or acetate. Recently, a new anti-PSMA-HBED ligand [(68)Ga-PSMA] has been introduced for PET imaging of prostate cancer. Goal. The aim of this evaluation was to analyse the diagnostic value of (68)Ga-PSMA PET/CT in patients with suspected recurrent prostate cancer and a possible association between different clinical variables and the imaging results. Methodology. We performed a retrospective analysis on 30 consecutive patients (median age 68 years) with suspected biochemical recurrence of prostate cancer who underwent (68)Ga-PSMA PET/CT between January 2013-December 2014. Other clinical factors such as prostate-specific antigen (PSA) level, PSA doubling time (PSA-DT), Gleason score (GSC), age, and amount of injected tracer were evaluated in correlation with the imaging results. Furthermore, multifocal prostate biopsies or clinical follow-up were performed in all patients following the (68)Ga-PSMA PET/CT. Results. In 83.3% of the patients at least one lesion indicative of prostate cancer recurrence was detected. A total of 45 focal prostatic lesions were considered positive on (68)Ga-PSMA PET with an average maximum standardized uptake value (SUVmax) of 12 ± 8 (1.1-25), compared to a low background SUV (median SUV 0.7). All PET-positive lesions were confirmed as true-positive on histology and/or clinical follow-up. However, of all prostate biopsy samples taken for verification, 3 samples proved to be positive on histology but false-negative on PET (Gleason 4). Tumor detection was positively associated with the PSA levels (>2.5 ng/ml). Other clinical parameters, such as GSC, PSA-DT, age, and dose of injected tracer, showed no association with the PSMA PET findings. A lesion-based analysis revealed a sensitivity, specificity, negative predictive value (NPV), and positive predictive value (PPV) of 93%, 100%, 92%, and 100%, respectively. A patient-based analysis revealed a sensitivity of 96%. Conclusion. (68)Ga-PSMA PET/CT shows a high sensitivity and, importantly, a high specificity in detecting prostate cancer, even in patients with low PSA levels. Therefore, PSMA(-HBED) PET/CT is a promising imaging approach that could guide the therapy management in patients with suspected recurrence of the disease.

OP086

Pelvic Dynamic Imaging with Pixel-Based Analysis of Ga-68 PSMA PET/CT

E. Hsiao, G. P. Schembri, D. L. Bailey, E. A. Bailey, P. J. Roach; Royal North Shore Hospital, St Leonards, AUSTRALIA.

Aims:Ga-68 PSMA is a relatively new PET tracer for prostate carcinoma. Little in vivo data are available in humans on its uptake kinetics in normal and pathologic sites. The study aims to assess the uptake rates in normal tissues and to investigate the timing of tracer uptake in pathologic sites compared to physiologic bladder or ureteric activity.Materials and Methods:Ten patients referred for PSMA PET/CT (3 for staging and 7 for biochemical recurrence) underwent a 30-minute dynamic scan of the pelvis on a Siemens Biograph mCT following administration of 127-158MBq of Ga-68 PSMA (HBED) as well as a 1-hr post-injection whole body scan. Time-activity data were obtained and Patlak-Rutland analysis was performed using in- house software. K_i (influx rate constant) and V_d (volume of distribution) maps were generated from the regression curves fitted pixel-by-pixel. Uptake rate of PSMA avid lesions and normal sites were assessed.Results:Five patients had local PSMA-avid disease, while 7 pathologic nodes were evident in 2 patients and 4 bone sites of uptake were evident in 3 patients. Two patients had no

PSMA-avid disease in the field of view. Normal sites for correlation were defined as the sites without focal PSMA uptake on conventional 1-hr delay imaging. There were 9 bone sites, 4 prostate sites and 7 pelvic nodes. Time-activity curves were so far obtained in 3 patients comparing the pathological sites to ureters and bladders. Conclusion: Both primary and metastatic prostate carcinomas show rapid and early uptake of Ga-68 PSMA within minutes of injection and markedly higher uptake rates compared to normal tissues. The bladder and ureteric activities begin to rise after 15 minutes. Early imaging of PSMA may offer improved depiction of disease burden with less confounding bladder or ureteric activity..

OP087

Cervical lymph node metastases is not an uncommon finding in Ga-68-DKFZ-PSMA-11 PET/CT imaging in patients with prostate cancer

J. Nematyazar[1], O. E. SAHIN[1], B. RAZAVI[1], E. DEMIRCI[2], A. AYGUN[1], M. OCAK[3], C. OBEK[4], A. R. KURAL[5], L. KABASAKAL[1]; [1]Department of Nuclear Medicine, Cerrahpasa Medical Faculty, Istanbul University, Istanbul, TURKEY, [2]Department of Nuclear Medicine, Sisli Etfal Training and Research Hospital, Istanbul, TURKEY, [3]Department of Pharmaceutical Technology, Pharmacy Faculty, Istanbul University, Istanbul, TURKEY, [4]Department of Urology, Cerrahpasa Medical Faculty, Istanbul University, Istanbul, TURKEY, [5]Department of Urology, Acibadem University Medical Faculty, Istanbul, TURKEY.

Aim: Prostate cancer is the most common solid cancer in men and it is the second most common cause of death. The type of therapy in prostate cancer is mainly influenced by the presence of metastases. Recently, it has been shown that PSMA PET imaging with Ga-68 labeled small molecule inhibitors are highly sensitive and specific for detection of prostate cancer and its metastases. Whole body imaging feature of PET imaging makes it possible to detect metastases at unexpected sites of the body. The aim of the present study was to evaluate the distribution of metastatic sites in prostate cancer patients who underwent PSMA PET imaging. Material and method: We retrospectively evaluated the files of patients who underwent Ga-68-PSMA PET imaging in our institution between October 2013 and February 2015. There were 391 PSMA PET imaging studies performed for the indication of staging, restaging and therapy monitoring. Mean age was 66.7 ±8.1 years and mean PSA level was 22.1±69.0 ranging from 0.01 to 700. Results: In PSMA PET imaging there was a positive lesion in 315 (80%) patients. Among these patients, primary tumor was detected in 215 (68%) patients. Bone, lymph node and organ metastases were detected in 117 (37%), 130 (41%) and 15 (5%) patients, respectively. Bone or lymph node metastases were detected in 186 (60%) patients. Among them 54 (30%) patients had only bone and 68 (37 %) patients had only lymph node metastases. In patients who had lymph node metastases 108 (82%) had pelvic, 46 (%35) had abdominal and 22 (17%) had cervical lymph node metastases. Conclusion: The distribution of metastatic sites in PSMA PET imaging suggested that cervical lymph node metastases is not an uncommon finding even with low PSA levels. Also these findings suggested that prostate cancer may have different biological features, some of them may have osteophilic and some of them may have lymphophilic behavior

OP088

Prospective Comparison of the detection rate of 18F-Fluoromethylcholine and 68Ga-PSMA-HBED PET/CT in men with prostate cancer with rising PSA post curative intent therapy, being considered for targeted therapy

J. Morigi[1,2], P. Stricker[3,4], P. van Leeuwen[3,4], R. Tang[2,5], B. Ho[2], Q. Nguyen[3,4], A. Hickey[2], D. Stark[2], A. Young[2], S. Fanti[1], L. Tarlinton[2], L. Emmett[2,5]; [1]Nuclear Medicine OU, Policlinico S.Orsola-Malpighi / University of Bologna, Bologna, ITALY, [2]Department of Diagnostic Imaging, St Vincent's Public Hospital, Sydney, NSW, AUSTRALIA, [3]St Vincent's Prostate Cancer Centre, St Vincent's Clinic, Sydney, NSW, AUSTRALIA, [4]Australian Prostate Cancer Research Centre – New South Wales, The Garvan Institute of Medical Research/The Kinghorn Cancer Centre, Sydney, NSW, AUSTRALIA, [5]University of New South Wales (UNSW), Sydney, NSW, AUSTRALIA.

Aim: In men with prostate cancer (PCa) and biochemical failure following therapy, current imaging techniques have a low detection rate at PSA levels at which targeted salvage therapy is effective. 11C-Choline or 18F-Fluoromethylcholine (FMC), though widely used, have poor sensitivity at low PSA levels. 68Ga-PSMA-HBED (PSMA) has shown promising results in retrospective trials. The aim of this study is to prospectively compare detection rates of PSMA versus FMC PET/CT in men initially managed with either radical prostatectomy (RP) or radiation treatment (RT), being considered for targeted therapy.Methods: A referred sample of men with rising PSA following treatment, eligible for targeted treatment, was prospectively included. Patients on hormonal or chemotherapy treatment were excluded. PSMA, FMC PET/CT and diagnostic CT were

undertaken in all patients sequentially, and assessed by blinded experienced readers. Scan results and management impact change was documented. Results: 38 patients (pts) were enrolled. 34/38 (89%) pts were post-RP, 4/38 (11%) pts were post-RT. 12/38 (32%) pts underwent initial RP and subsequent salvage RT. Mean PSA at imaging was 1.74 ± 2.54 ng/ml. Overall, 68% (26/38) of pts had a positive scan indicating at least one lesion suspicious for PCa recurrence. Of these, 14/26 (54%) were positive on PSMA alone, 42% (11/26) were positive on both FMC and PSMA, 1/26 on FMC alone (false positive on biopsy). Histopathology was available at time of submission for 6 PSMA lesions, all true positive (6/6). Diagnostic CT was inconclusive in all men. With PSA 2.0, 86% PSMA vs. 57% FMC. On lesion-based analysis, PSMA detected more lesions than FMC (59 vs. 29, $p < 0.001$). There was a 63% (24/38) overall management impact, 54% (13/24) due to PSMA imaging alone. The primary limitation is absence of histopathology in some lesions due to small lesion size/accessibility. Conclusion: In patients with rising PSA evaluated for targeted treatment , PSMA demonstrated a significantly higher detection rate at low PSA levels, resulting in a significant overall management impact.

405 - Sunday, October 11, 2015, 2:30 PM - 4:00 PM, Hall G2
Do.MoRe - Featured: Endocrine & Neuroendocrine Tumours

OP089

Ac-225-DOTATOC - dose finding for alpha particle emitter based radionuclide therapy of neuroendocrine tumors

C. Kratochwil[1], F. Bruchertseifert[2], F. L. Giesel[1], C. Apostolidis[2], U. Haberkorn[1], A. Morgenstern[2]; [1]University Hospital Heidelberg, Heidelberg, GERMANY, [2]European Commission - Joint Research Centre, Institute for Transuranium Elements, Karlsruhe, GERMANY.

Objectives: There are no established dosimetry tools to predict toxicity of "targeted alpha-therapy" (TAT), yet. We conducted an dose escalation to find the maximum tolerable dose (MDT) of single cycle and fractionation concepts for Ac-225-DOTATOC radionuclide therapy. Methods: According to Declaration of Helsinki's "Unproven interventions in Clinical Practice" we performed 48 treatment cycles in 36 patients with progressive neuroendocrine tumors (NET). After each cycle acute hematotoxicity was documented according to CTCAE criteria. First observations are also available for chronic kidney toxicity as the follow up for the first 17 patients has now reached 2 years. Results: The MTD of a single cycle Ac-225-DOTATOC was considered to be 40 MBq. Multiple fractions were tolerated with 25 MBq every 4 months or 18.5 MBq every 2 months. Cumulative activities of 75 MBq were found tolerable in regard to delayed toxicity. The radiologic treatment response that was observed in some patients is without clear preference of a particular fractionation concept until now. Conclusions: We present a well tolerable treatment protocol for TAT with Ac-225-DOTATOC in NET patients that also demonstrated promising Treatment efficacy in various patients. If TAT provides general advantages in comparison to beta emitter based radionuclide therapy cannot be derived from the available data, yet. Comparative trials are needed in the future.

OP090

Optimal sampling schedule: accurate estimation of time-integrated activity coefficients in peptide receptor radionuclide therapy (PRRT)

C. Maaß[1], J. Sachs[1], D. Hardiansyah[1], P. Kletting[2], F. M. Mottaghy[3], G. Glatting[1]; [1]Medical Radiation Physics/Radiation Protection, Medical Faculty Mannheim, Heidelberg University, Mannheim, GERMANY, [2]Department of Nuclear Medicine, Ulm, GERMANY, [3]Department of Nuclear Medicine, Aachen, GERMANY.

Aim: The aim of this study was (1) to determine population parameter values and using these parameter values (2) to quantify the effect of sampling schedules with differing sizes on the estimation of time-integrated activity coefficients in PRRT with 111In DTPAOC in 15 patients.Materials and Methods: Fifteen patients with proven neuroendocrine tumours (NETs) were investigated. Planar whole-body scans using a double-head γ-camera (ECAM, Siemens, Erlangen, Germany) were performed at 45 min, 4 h, 1, 2 and 3 or 5 d and serum measurements were taken at 5 min, 0.5, 1, 2, 4 h and 1, 2, 3 or 5 d after injection of 111In-DTPAOC [1].A physiologically based pharmacokinetic (PBPK) model [1] was implemented using SAAMII software (version 2.2, The Epsilon Group, Charlottesville, USA). Population parameter values were determined using an iterative two stage (ITS) algorithm.Using both individual and population based parameter values and sampling schedules with different sizes in the model, the relative difference (RD) between actual and estimated time-integrated activity coefficients for tumour, kidneys, liver, spleen, serum and whole body was quantified.Sampling schedules were modified as follows: (1) one and (2) two measurement points (5 and 10 cases/patient) omitted once for each organ and the serum measurements. Mean and standard deviation of the RD were calculated and averaged over all cases and all

patients.Results: Using the individual parameter values the mean RDs were for tumour, kidneys, liver, spleen, serum and whole body (1) (0±4)%, (0±2)%, (3±11)%, (3±9)%, (5 ±14)%, (1±3)% and (2) (13±35)%, (0±2)%, (4±11)%, (3 ±8)%, (4±15)%, (1±3)%.Using the population based parameter values the mean RDs were for tumour, kidney, liver, spleen, serum and whole body (1) (0±1)%, (0±0)%, (0±3)%, (0±1)%, (-1±4)%, (0±1)% and (2) (13±37)%, (0±1)%, (1±2)%, (0 ±1)%, (-1±6)%, (0±2)%.Conclusion: The application of Bayes parameters in physiologically based pharmacokinetic modelling allowed for an accurate estimation of time-integrated activity coefficients even in case less information (measurement data) is available. In this patient group, omitting one measurement point leads only to a small error.Literature1.Kletting P, Müller B, Erentok B, Schmaljohann Jr, Behrendt FF, Reske SN, et al. Differences in predicted and actually absorbed doses in peptide receptor radionuclide therapy. Med Phys. 2012;39(9):5708.

OP091

The intensity of 18FDG uptake is not a surrogate marker of morphological tumor progression in patients with metastatic differentiated thyroid cancer.

M. Terroir, I. Borget, F. Bidault, D. Deandreis, A. Al Ghuzlan, D. Hartl, M. Ricard, A. Berdelou, L. Dercle, J. Lumbroso, E. Baudin, M. Schlumberger, S. Leboulleux; Gustave Roussy, Villejuif, FRANCE.

Aim: In patients with metastatic differentiated thyroid carcinoma (DTC), thyroglobulin doubling time (TgDT) and fluorodeoxyglucose (FDG) uptake as well as age, tumor size and iodine uptake are prognostic factors for survival. High FDG uptake is a poor prognostic factor. Consequently, lesions with high FDG uptake are often considered aggressive and may be monitored and treated with local modalities.The aims of this retrospective single center study were to determine whether the intensity of FDG uptake was correlated to tumor progression or tumor growth rate (TGR) expressed as the percentage of increase in tumor size during a one year-period (TGR) and to TgDT.Materials and methods: Fifty five patients with DTC were included between July 2012 and May 2014 with the following criteria: (i) at least one distant metastasis measuring ≥ 1 cm in diameter (ii) evaluation by FDG-positron emission tomography/computed tomography (PET/CT) performed at our center (iii) at least one CT or another FDG-PET/CT performed more than 3 months after the reference FDG-PET/CT (iv) absence of systemic or local treatment between the two imaging procedures.Results: At the patient level, DTC were papillary (33), follicular (8) or poorly differentiated (14). Forty-seven patients were refractory to radioactive iodine (RAI). Their mean TgDT when available was 101 days with TgDT <1 year in 20 patients and >1 year in 12 patients. The median higher SUV max of each patient was 13.2 (range 3.6-66.2). The two-year survival was 100% for patients with SUV max <5 and 68% for patients with SUV max >5. The TgDT was 258 days for patients with SUV max <5 and 101 days for patients with SUV max >5. At the lesion level, one hundred fifty six metastatic lesions located in the lung (63), neck lymph nodes (28), chest lymph nodes (42), bone (11), liver (2) and other sites (10) were studied. The median size was 16 mm, median SUV max: 8.7; median metabolic volume: 3.7 cm^3. The median one-year TGR by lesion was 16% (range 0->100%). SUV max and metabolic volume of each lesion were not correlated to their one-year TGR (p=0.28 and p=0.77 respectively). SUV max of each lesion was not correlated to tumor size.Conclusion: The intensity of FDG uptake is not correlated to morphological tumor progression assessed by one-year TGR and cannot be used as a surrogate marker of morphological progression.

OP092

Assessment of lesion response in differentiated thyroid cancer patients undergoing radioiodine treatment using 124I PET/CT

R. Wierts[1], B. Brans[1], B. Havekes[1], S. G. E. A. Halders[1], F. M. Mottaghy[1,2], W. Jentzen[3]; [1]Maastricht University Medical Center, Maastricht, NETHERLANDS, [2]University Hospital RWTH Aachen University, Aachen, GERMANY, [3]Klinik für Nuklearmedizin, Universität Duisburg-Essen,, Essen, GERMANY.

Aim: This study assesses the lesion response in patients with differentiated thyroid cancer (DTC) undergoing radioiodine therapy by means of 124I PET/CT, 18F-FDG PET/CT, and/or 131I SPECT(/CT) imaging. Materials and methods: Pretherapeutic 124I PET/CT images of 41 DTC patients undergoing radioiodine therapy were retrospectively analyzed. 124I PET/CT images were acquired 24 and ≥96 hours after oral administration of approximately 28 MBq. Using an automated iterative thresholding algorithm, each lesion was segmented on the PET images to determine the volume and residence time used to predict the therapy-delivered absorbed radiation dose (TAD). The lower volume limit of determinability was 0.15 mL; following a previous study, the minimum TAD was determined for smaller lesions. Lesions were identified as thyroid remnants or metastatic tissue (lymph node, pulmonary, mediastinal, bone). Lesion response was determined based on 124I PET/CT, 18F-FDG PET/CT and/or 131I SPECT(/CT) follow-up images performed in the first year after treatment. A lesion not evident on any of the follow-up images was considered a completely responding lesion; otherwise assigned as an incompletely responding lesion. Significant

differences in TADs and lesion volumes were evaluated by Mann-Whitney U test. Results: Of 161 lesions included, 113 (70.2%) were identified as thyroid remnants and 48 as metastases (29.8%). 69 (61.1%) thyroid remnants and 26 metastases (54.1%) were smaller than 0.15 mL. Complete response was observed for 96 thyroid remnants (85.0%) and 30 metastases (62.5%). For thyroid remnants and metastases, the median TAD of the completely responding group was significantly higher (remnants: 200 Gy, metastases: 62 Gy) than the median TAD of the incompletely responding group (remnants: 54 Gy, metastases: 15 Gy); the significance levels (P) were 0.046 for the thyroid remnants and 0.018 for the metastases. For metastases, the lesion volumes were significantly smaller for the completely responding lesions than that of the incompletely responding lesions (P=0.001) but not for the thyroid remnants (P=0.168). Conclusion: 124I PET/CT-based lesion dosimetry in combination with 18F-FDG PET/CT and/or 131I SPECT(/CT) follow-up images can be used for the assessment of lesion response in DTC patients undergoing RAIT.

OP093

Bone marrow dosimetry assessed with quantitative SPECT/CT is predictive of subacute thrombocytopenia following ^{177}Lu-octreotate PRRT

M. E. Marcotte, M. Del Prete, E. O. Gaudin, F. A. Buteau, P. Després, **J. M. Beauregard**; Université Laval, Quebec City, QC, CANADA.

Aim: Along with the kidney, the bone marrow (BM) is a critical organ in ^{177}Lu-octreotate peptide receptor radionuclide therapy (PRRT). Traditionally, BM dosimetry has been assessed using serial blood sampling, which is cumbersome and also inaccurate when a large tumor burden results in a significant cross-dose to the BM. Quantitative SPECT (QSPECT) can overcome these limitations. Our aim was to correlate QSPECT-derived BM dose estimates with the short-term platelet (PLT) count variation following ^{177}Lu PRRT. Materials and Methods: 29 ^{177}Lu-octreotate cycles (median: 7.4, range: 5.6 to 8.3 GBq) in 8 patients suffering from neuroendocrine tumour were studied. Patients underwent serial QSPECT/CT at 4, 24 and 72 h. Self-dose to the BM was derived from activity concentration sampling using a volume of interest over L4 vertebral body, while the cross-dose to the BM was estimated from total activity retention in the QSPECT field of view. For each individual cycle, the total BM dose was correlated to absolute and relative PLT count variation from baseline (lowest count between 2 and 4 weeks post-PRRT). Results: Median BM dose per cycle was 148 (62 to 370) mGy, and the cross-dose accounted for a median of 7.7 (2.8 to 47.7) % of the total BM dose. Median absolute and relative PLT count variations were -17 (-100 to 64) x10^9/L and -7.5 (-32 to 59) %, respectively. There was a significant, moderate inverse correlation between the absolute or relative PLT variation and BM dose, with Spearman *r* values of -0.47 (*P*=0.01) and -0.39 (*P*=0.04), respectively. Thrombocytopenia occurred following every cycles where >150 mGy were delivered to the BM, and was more pronounced than where <150 mGy were delivered (median of -8 vs. -43 x10^9/L, respectively; *P*=0.005). Conclusion: Our results provide an initial clinical validation of the accuracy of QSPECT-based BM dosimetry, which appears to be predictive of subacute BM toxicity, i.e. transient thrombocytopenia. QPSECT has the potential to become a non-invasive and practical approach for simultaneous tumour, kidney and BM dosimetry in ^{177}Lu radionuclide therapy, hence facilitating the implementation of personalized PRRT.

OP094

Comparison of quantitative ^{177}Lu measurements in European hospitals

A. Fenwick[1], J. Merrett[2,1,3], L. Johansson[1]; [1]National Physical Laboratory, Teddington, UNITED KINGDOM, [2]University of Surrey, Guildford, UNITED KINGDOM, [3]Royal Surrey County Hospital, Guildford, UNITED KINGDOM.

The accuracy of quantitative imaging in SPECT is critical when determining doses delivered during PRRT therapies with ^{177}Lu. In order to determine the measurement capability of a representative subset of hospitals within Europe, a comparison exercise was developed to test both the inter-clinic variability and to assess which methods for activity determination were most effective. An elliptical Jaszczak phantom containing an anthropomorphic insert with lung and bone-equivalent materials and an exterior set of body contour rings was used to compare the ability of leading clinics in the UK, Netherlands, Germany, Sweden, Italy and the Czech Republic. The phantom was used in conjunction with a set of well-characterised, traceable ^{177}Lu sources consisting of an inner hot spherical core surrounded by an outer warm background at an activity concentration ratio of approximately 1:15. The total activity in the spheres ranged from 60-100 MBq at the time of measurement. The sources were designed to mimic a relatively large tumour with homogeneous uptake of ^{177}Lu labelled peptides within a liver which also had partial homogeneous uptake. Although this setup could only be described as partly representative of a real patient, the principles regarding the ability of the camera to recover the activity (although simplified) are largely the same. SPECT/CT Images were taken with both a standard set of acquisition parameters and those used clinically at each site (if different). A total of 6 sources were used in the exercise, all of which were made at NPL and produced in a manner traceable to national standards. The results show that

large deviations were observed at some sites, however, the majority of clinical centres were able to determine the activity to within ±20%. In conclusion, improved calibration protocols should be developed and harmonised in order to improve accuracy and guidance on methods for making standard calibration phantoms should be given at a European level.

406- Sunday, October 11, 2015, 2:30 PM - 4:00 PM, Hall 6
Teaching Session: Anatomy Refresher and Cross-sectional Imaging: Thorax

OP095

Anatomy Refresher and Cross-sectional Imaging: Thorax

C. Fowler, **UNITED KINGDOM**

407 - Sunday, October 11, 2015, 2:30 PM - 4:00 PM, Hall F
Radiopharmaceuticals & Radiochemistry: Radiochemistry - Methods

OP096

Enabling Research on Epilepsy through a New and Efficient Synthesis of [18F]UCB-H, a PET Tracer for the Imaging of SV2A

C. Warnier[1,2], C. Lemaire[1,2], J. Aerts[1,2], J. Mercier[3], A. Plenevaux[1,2], A. Luxen[1,2]; [1]University of Liege, Liege, BELGIUM, [2]Cyclotron Research Centre, Liege, BELGIUM, [3]UCB Pharma, Braine-L'Alleud, BELGIUM.

IntroductionEpilepsy is a neurological condition that affects an estimated 50 million people throughout the world. Although a number of treatments are available for that disease, the cellular mechanisms at the origin of epilepsy remain largely unknown. From that perspective, considerable effort was put into the development of [18F]UCB-H, which recently proved to be a very promising PET tracer for the exploration of neurotransmission processes, and the diseases related to their malfunction, such as epilepsy[1-4]. [18F]UCB-H binds specifically, and with nanomolar affinity to the Synaptic Vesicle Protein 2A (SV2A), which is also the binding site of the anti-epileptic drug Levetiracetam (Keppra®, UCB Pharma). Until now, [18F]UCB-H was only available through a long, multi-step radiosynthesis that is technically complex to implement and affords a limited yield of radiotracer.[5]MethodsIn this work, we present a new short, simple and efficient single-step radiosynthesis of [18F]UCB-H. We successfully synthesized a N-heteroaryliodonium precursor of the radiotracer. The direct labelling of the iodonium using the classical Kryptofix/K18F fluorination method afforded good RCY's of nca[18F]UCB-H (RCY's > 50%). An automation sequence for this straightforward radiosynthesis was therefore developed.ResultsThe fully automated radiosynthesis, from [18F]fluoride trapping on QMA to the end of the automated distribution of the injectable [18F]UCB-H, lasts 60 min and affords 32±2% RCY (n=6, 50<A(StartOfSynthesis)<240 GBq), non-corrected for decay. High specific activities of 500-1000GBq/μmol at the end of the synthesis were obtained, as determined by radio-UPLC analysis. Moreover, data concerning the stability of the precursor, radiochemical & chemical purity of [18F]UCB-H, as well as solvent trace analysis and stability of the tracer in the final formulation, confirm that this production method shall fulfill the standard GMP requirements.ConclusionWe designed a new production method for [18F]UCB-H that is short and easy to implement on any automation system. To the best of our knowledge, this is the first diaryliodonium 18F-labelling that has been adapted for the production of high activites (up to 95GBq) of a radiotracer fit for clinical trials.AcknowledgementsWe gratefully acknowledge the FRS-FNRS (FRIA) for funding this work and UCB Pharma SA Belgium for collaborationReferences[1] Warnock, G. I. et al., J Nucl Med 2014, 55(8), 1336; [2] Bretin, F. et al., EJNMMI research 2013, 3(1), 35; [3] Lynch, B. A. et al. Proc Natl Acad Sci USA 2004, 101(26), 9861; [4] Mercier, J. et al. ChemMedChem 2014; [5] Aerts, J. et al., EJNMMI, EANM abstracts 2013, 40(2), 89

OP097

Radiolabeling of proteins using radiofluorinated nitrile oxides

P. Krapf[1,2], **B. D. Zlatopolskiy**[1,2], R. Kandler[2], B. Neumaier[3,2,1]; [1]University Clinic of Cologne, Cologne, GERMANY, [2]Max-Planck-Institute for metabolism research, Cologne, GERMANY, [3]Forschungzentrum Jülich GmbH, Jülich, GERMANY.

Objectives: ^{18}F-Labeling using azide alkyne "click" cycloaddition became a popular method of PET chemistry. Recently, several novel ^{18}F-labeled 1,3-dipoles (other than azides) were applied for the preparation of ^{18}F-labeled small molecules via 1,3-dipolar cycloadditions. Especially, reactions of highly reactive radiofluorinated nitrile oxides could be an attractive alternative to azide "click" labeling. The aim of this work was the development of a novel procedure for protein labeling using nitrile oxide chemistry. Methods: The reaction of *o*- and *p*-[^{18}F]fluorobenzaldehydes ([^{18}F]**1a**,**b**) with hydroxylamine afforded *o*-, *p*- [^{18}F]fuorobenzaldoximes ([^{18}F]**2a**,**b**). *o*- and *p*-[^{18}F]fluorobenzimidoyl chlorides ([^{18}F]**3a**,**b**) - more stable precursors for the generation of nitrile oxides in situ - were obtained via chlorination of [^{18}F]**2a**,**b** using *IODO-GEN precoated reaction vials*. The solutions of the labeling synthons

were added to the corresponding derivatized and native proteins to yield ^{18}F-labeled conjugates. The conjugations were optimized with respect to protein amount. Purification of labeled biopolymers was performed using PD10-column. Results: [^{18}F]**3a**,**b** were obtained in RCY of up to 90% under optimized reaction conditions (1 M HCl, 15 min, 50 °C). [^{18}F]**3a**,**b** were highly stable under strongly acidic conditions (> 5h). Application of water insoluble oxidant allowed to avoid undesirable oxidation and/or denaturation of the proteins. The reaction of [^{18}F]**3a**,**b** with BCN-derivatized BSA as well as with native BSA and Annexin V led to the corresponding radiolabeled isoxazole as well as amidoxime conjugates, respectively, in RCCs of 30-90% within 10 min (pH=7.5-9.0; RT-37°C). Reasonable RCCs (60%) were obtained already with 0.5-5 nmol of proteins. Labeled proteins were isolated in RCPs > 95 after simple gel filtration. Conclusion:The novel radiolabeling procedure allows a fast and efficient radiofluorination of proteins and, consequently, represents an attractive alternative to conventional methods for protein ^{18}F-labeling.

OP098

Synthesis of PET tracers via SN2 radiofluorination under “minimalist” conditions

M. A. Omrane, B. D. Zlatopolskiy, E. A. Urusova, R. Richarz, P. Krapf, B. Neumaier; Institute of Radiochemistry and Experimental Molecular Imaging, Cologne, GERMANY.

Objective: Recently we developed a novel procedure for the preparation of ^{18}F-labeled arenes under “minimalist” conditions using only onium salts as radiolabeling precursors and [^{18}F]fluoride. Neither azeotropic drying, nor base or any other additives were necessary. The aim of this work was to extend this method to the preparation of radiofluorinated aliphatic compounds via SN_2 radiofluorination. Methodology: [^{18}F]Fluoride was eluted from a QMA cartridge with appropriately protected precursors of 5-[^{18}F]FDR, 6-[^{18}F]FDGal and [^{18}F]FET in MeOH. MeOH was evaporated at 65-70 C within 2-3 min, MeCN was added and the resulting solutions were heated to give the corresponding ^{18}F-labeled intermediates. The latter were purified by SPE and thereafter deprotected under acidic conditions. If necessary radiolabeled products were purified by SPE or HPLC. Conjugation of 5-[^{18}F]FDR with the model aminnoxy-substituted compound, methyl 6-aminooxyhexanoate, was optimized with respect to reaction conditions and precursor amount. Results: [^{18}F]F$^-$ was eluted from an anion exchange resin almost quantitatively. Under optimized conditions the appropriately protected 5-[^{18}F]FDR, 6-[^{18}F]FDGal and [^{18}F]FET were prepared from the corresponding 3-*N*,*N*,*N*-trimethylammoniumalkyl(aryl)sulfonyl precursors in RCCs up to >92%, 6% and 71%, respectively. After SPE purification of the radiolabeled intermediate followed by the deprotection step with 1 M HCl (110 °C, 10 min) 5-[^{18}F]FDR was prepared in 48% RCY (EOB) and excellent RCP. No additional purification was needed. The content of D-Ribose (60-80 μg/batch) was sufficiently low to allow an efficient conjugation with methyl 6-aminooxyhexanoate. The corresponding oxime was prepared in RCCs up to 93% and RCPs >96%. *N*-Boc-[^{18}F]FET-OtBu was quantitatively deprotected with DCE/TFA (10 min; 80°C) to give radiofluorinated amino acid in 70% RCC over two steps. Conclusion: The SN_2 aliphatic radiofluorination under “minimalist” conditions is suitable for fast and simple preparation of ^{18}F-labeled compounds. An important additional advantage of this methode is the cationic trimethylammonium tag, which in many cases allows an efficient SPE separation of the radiolabeled compound from the labeling precursor.

OP099

Carbonylation via Conversion of [11C]CO2 into [11C]CO Mediated by [11C]Silane Derivatives

C. Taddei, S. Bongarzone, A. Haji Dheere, A. D. Gee; The Rayne Institute, London, UNITED KINGDOM.

Introduction and AimCarbon monoxide (CO) can be used to synthesise biologically active molecules, such as amides, esters and ketones.[1] [11C]CO is traditionally produced by the gas phase reduction of [11C]CO2 at elevated temperatures[2] or by chemical conversion of CO2 to CO. The chemical conversion of CO2 to CO can be obtained using silane derivatives in two steps: i) CO2 insertion in a silane derivative leading to a silane intermediate followed by ii) CO release triggered by an activator.[3] The produced CO can be transferred in a second vial and coupled with an amine and an organic halide yielding the desired carbonylation product. Herein, this CO2 to CO methodology is applied to carbon-11 labelling by converting [11C]CO2 to [11C]CO and subsequently used to yield [11C]amide-containing molecules. This represents the first carbonylation methodology mediated by a silane derivative reported to date. Moreover, the fully automated synthesis was performed utilising an Eckert & Ziegler Modular-Lab.Method and ResultsThe carbonylation reaction was developed using a simple two-vial reaction setup. In the first vial, [11C]CO2 to [11C]CO conversion was achieved by coupling [11C]CO2 and a silane derivative at room temperature. Following the addition of a decarbonylating agent (activator) with heating, [11C]CO was produced. The release of [11C]CO from the first vial and transfer of

[11C]CO into a second vial was time-monitored. The transfer of [11C]CO to a second vial containing an amine and an organic halide led to the production of the relative [11C]amide derivative. As model reaction, [11C]N-benzylbenzamide was obtained in a high radiochemical purity (>98%) and short synthesis time (~15 min from EOB).ConclusionA novel carbonylation method mediated by a [11C]silane derivative has been successfully developed. This method is an attractive route to produce [11C]carbonyl-containing molecules, obviating the need of gas phase reduction infrastructure. Furthermore, the deigned automated synthesis will be applied to generate new carbon-11 PET tracers.Research SupportThis work was supported by European Commission, FP7-PEOPLE-2012-ITN (316882, RADIOMI), Medical Research Council (MRC, MR/K022733/1) and Biomedical Research Centre award to Guy's & St Thomas' NHS Foundation Trust.References[1] C. F. J. Barnard (2008) Organometallics, 27, 5402; A. Brennfuhrer, et al (2009) Angew. Chem. Int. Ed. Engl., 48, 4114. [2] S. K. Zeisler, et al (1997) Appl. Radiat. Isot., 48, 1091. [3] S. D. Friis, et al (2011) J. Am. Chem. Soc., 133, 18114; C. Lescot, et al (2014) J. Am. Chem. Soc., 136, 6142.

OP100

Synthesis and in vivo evaluation of a novel peptide-based N3S1 chelator for 99mTc-labeled radiotracer with enhanced renal clearance

D. Lee, K. Choi; Korea Atomic Energy Research Institute, Jeongeup, KOREA, REPUBLIC OF.

Objectives: Peptide-based N3S1 chelator PXC, which are comprised of amino acids (Pro-X-Cys backbone, X are designated for some amino acids) for radiolabeling with 99mTc has been designed and evaluated for development of radiopharmaceuticals. However, the lipophilicity of the first core structure, Pro-Gly-Cys (PGC) in its RGD complex (PGC-RGD) has resulted in substantial hepatobiliary excretion when administered in tumor-bearing mice. In this study, to improve biological behavior in the biodistribution with the intention of enhancing renal clearance, a novel tripeptide chelating sequence, PKC and its RGD conjugate(PKC-RGD) were synthesized and evaluated in normal mice to explore the effect of chelator on the pharmacokinetic properties. Methods: we have synthesized Pro-Lys-Cys (PKC) by substitution of L-glycine by L-lysine for the preparation of PKC-c(RGDyK) (thus N3S1 chelator-RGD conjugate with L-lysine on the PXC backbone). After preparation of the synthesized chelators-RGD conjugates, the properties of the radiolabeling and a comparison of biodistribution for 99mTc-PGC-c(RGDyK) and 99mTc-PKC-c(RGDyK) were evaluated in vitro and in normal mice, respectively. Results: The target specificity of the resulting PKC-RGD was similar to that of PGC-RGD as determined by a cell binding assay and a competition binding assay. The 99mTc radiolabeling of PKC-RGD resulted in radiochemical yields of 98% under mild conditions at high specific activities. Biodistribution data in normal mice clearly showed a significant decrease in intestinal uptake at 2h postinjection for the 99mTc-PKC-c(RGDyK) compared to the 99mTc-PGC-c(RGDyK) (from 24.35% ID/g to 8.49% ID/g for the GI tract). The 99mTc-PKC-c(RGDyK) biodistribution was also showed by a higher retention of radioactivity in the whole body, but with kidney accumulation over 8-fold higher than observed with 99mTc-PGC-c(RGDyK) at 2h (12.62%ID/g for PKC-RGD and 1.54%ID/g for PGC-RGD, respectively). Conclusions: These results show that the biodistribution may be altered especially concerning lipophilicity resulting in renal rather hepatobiliary excretion. This comparative study make it possible to explore the effects of lipophilicity on the biodistribution of 99mTc-labeled c(RGDyK) through the using different tripeptide N3S1 chelators. Therefore, 99mTc-PKC-RGD may be an attractive alternative for the in vivo imaging of integrin receptors.

OP101

Influence of a novel, versatile bifunctional chelator on radiolabelling, pharmacological and targeting properties of a minigastrin analogue for molecular imaging and therapy applications

J. Pfister[1], D. Summer[1], C. Rangger[1], M. Petrik[2], E. von Guggenberg[1], P. Minazzi[3], G. B. Giovenzana[4], C. Decristoforo[1]; [1]Medical University Innsbruck, Innsbruck, AUSTRIA, [2]Institute of molecular and translational medicine, Faculty of medicine and dentistry, Palacky University, Olomouc, CZECH REPUBLIC, [3]CAGE Chemicals srl, Novara, ITALY, [4]DSF, Università del Piemonte Orientale "A. Avogadro", Novara, ITALY.

Aim: AAZTA (6-[bis(carboxymethyl)amino]-1,4-bis(carboxymethyl)-6-methyl-1,4-diazepane) is a promising chelator with potential advantages over DOTA for radiopharmaceutical applications. Its mesocyclic structure enables fast radiolabelling under mild conditions with trivalent metals including 68Ga for PET, but also 177Lu for radionuclide therapy. Here we describe the conjugation of a bifunctional AAZTA derivative on a model minigastrin derivative as a potential theranostic agent. Materials and Methods: An AAZTA derivative with an aliphatic C9 chain as linker was coupled to a minigastrin [AAZTA0, D-Glu1, desGlu2-6]-minigastrin (AAZTA-MG) and labelled for the experiments with 68Ga and 177Lu using standard labelling protocols. The characterization in vitro included stability studies in different media as well as the determination of the partition coefficient in octanol/PBS (log D). Affinity determination (IC50) and cell uptake studies were performed in A431-CCK2R cells

expressing the human cholecystokinin-2 receptor. Using the same cell lines μPET/CT and ex vivo biodistribution studies were performed in tumour xenograft bearing nude mice for 68Ga labelled compound and normal biodistribution for [177Lu]-AAZTA-MG. Results and Conclusion: AAZTA-MG showed a high radiochemical yields for labelling with 68Ga (>95%),177Lu (>98%) and 111In (>98%) at high SA. The log D value of -3.7 for [68Ga]-AAZTA-MG and [177Lu]-AAZTA-MG indicates a highly hydrophilic character of the complexes. Stability test showed overall high stability in solution with some decomposition in human plasma for 68Ga labelled compound and transchelation towards DTPA for 177Lu. IC50 value of 10.0 nM was determined for AAZTA-MG, which indicates a high affinity binding for the CCK2 receptor with no significant differens for the corresponding natGa and natLucomplexes. Specific cell uptake after 60 min incubation resulted to be >7.5% for [68Ga]-AAZTA-MG in A431-CCK2R cells and >9.5% for the 177Lu labelled counterpart, comparable to other DOTA-MG-analogs. μPET studies in nude mice xenografts revealed high selective accumulation in A431-CCK2R positive tumours of 68Ga-labelled AAZTA-MG (2.5 % ID/g in 1 h post injection), but also comparably higher blood levels as corresponding DOTA-analogs. Biodistribution in normal nude mice for 177Lu labelled compound showed a considerable intestinal (7.3% ID/g) and liver (1.5 % ID/g) uptake. Overall, AAZTA showed interesting properties as bifunctional chelator for peptides providing mild radiolabelling conditions for both 68Ga and trivalent metals having advantages of currently used DOTA. Studies are ongoing to further investigate in vivo targeting properties and stability issues and influence of spacer length on biodistribution.

OP102

Evaluation of configurationally restricted copper-64 labelled bis tetraazamacrocyclic as potential PET agents for CXCR4 expression in oncology imaging

G. S. Clemente, B. P. Burke, S. Nigam, C. Cawthorne, S. J. Archibald; University of Hull, Hull, UNITED KINGDOM.

Introduction: Chemokines are signalling proteins responsible for inducing cell migration. One of their receptors, CXCR4, is commonly over-expressed in several lines of cancer.(1) CXCR4 positive tumours generally have a higher degree of metastatic potential, triggering interest in this receptor as target for drug development and molecular imaging.(2) Following on from previous results published by our group showing the synthesis of novel configurationally restricted bis tetraazamacrocycles that act as CXCR4 antagonists, in which metal complexation enhances both binding affinity and receptor residence time, the radiolabelling with a positron-emitting isotope was attempted to evaluate prospective applications in PET.(3,4) Aim: The main goal of this work is to optimise the radiolabelling of the previously synthesised bis tetraazamacrocyclic with copper-64 (t1/2=12.7h) without the need of structural changes and achieving a radiotracer chemically identical to its characterised cold analogue. Full evaluation of the in vivo characteristics in wild type and CXCR4 over-expressing tumour-bearing mice is currently ongoing. Methods: Mono- and bis-copper versions of the bis tetraazamacrocyclic complex were synthesised by converting 64CuCl2, obtained in cyclotron through 64Ni(p,n)64Cu nuclear reaction, into 64Cu(OAc)2, pH 5.5, followed by complexation of the ligand using a range of temperatures, solvents and reaction times. Formation of the radiolabelled mono-copper complex was attempted by two different approaches: direct chelation of the macrocycle and transchelation with previously coordinated zinc, using stoichiometrically controlled reactions. Bis copper radiotracer was achieved via direct chelation of the non-radioactive mono-copper species. Reactions were followed by radioTLC/HPLC, reformulated and intravenously injected in both normal and CXCR4 over-expressing tumour bearing mice. In vivo competitive blocking studies are being carried out using the clinically licensed CXCR4 antagonist plerixafor (AMD3100). Results: After optimisation of the several radiolabelling approaches, yields above 95% and specific activities up to 9.5 GBq/μmol were achieved. In vivo μPET showed the expected affinity for the CXCR4 receptor.Conclusion: 64Cu radiolabelling of bis tetraazamacrocyclic was successfully achieved to perform in vivo biodistribution studies in CXCR4 over-expressing tumour-bearing mice. The long half-life of 64Cu and receptor residence time could offer improved tumour/background ratios, making it a potential candidate for CXCR4 mapping through PET imaging. Further studies are currently ongoing to fully validate and optimise in vivo properties. M. Palacios-Arreola et al., J Immunol Res, 2014, 2014, 1-8. 2. E. Roussos et al., Nat Rev Cancer, 2011, 11, 573-587. 3. A. Khan et al., J Am Chem Soc, 2009, 131, 3416-3417. 4. R. Smith et al., Dalton Trans, 2012, 41, 11369-11377.

OP103

Efficient production of PET tracers on a preparative scale via copper-mediated radiofluorination under "minimalist" conditions

J. Zischler[1,2,3], B. D. Zlatopolskiy[1,3], P. Krapf[1,3], F. Zarrad[1,2,3], E. A. Urusova[1,3], E. Kordys[1,3], H. Endepols[1,3], B. Neumaier[1,2,3]; [1]University Clinic Cologne, Cologne, GERMANY, [2]Forschungszentrum Jülich GmbH, Jülich, GERMANY, [3]Max-Planck Institute for Metabolism Research, Cologne, GERMANY.

Objectives: Recently two novel methods for the copper-mediated aromatic nucleophilic radiofluorination of (mesityl)(aryl)iodonium salts (MAI) and aryl pinacol boronates (ArBPin) were published. Evaluation of these methods revealed that although both showed high efficacy in small scale experiments, they were inoperative for PET tracer production on a clinical scale. The aim of this work was the development of a versatile and practical procedure for the preparation of PET tracers in a practical scale via Cu-mediated radiofluorination. Methods: Cu catalysts were unstable under conventional strongly basic radiofluorination conditions. Therefore, $^{18}F^-$ was eluted from an anion exchange resin with only 0.06-0.1 mg K_2CO_3 in MeOH ("low base" conditions). After removal of MeOH the residual [^{18}F]KF/K_{222} or 18-crown-6 complex was redissolved in a solution of the appropriate Cu-salt and the corresponding ArBPin or iodonium salt precursor. The reaction mixture was heated for 20 min. Furthermore, the radiofluorination of iodonium salts under "minimalist" conditions (no addition of base and cryptand, no azeotropic drying) was examined. [^{18}F]Fluoride was eluted from the anion exchange resin with the corresponding (mesityl)(aryl)iodonium salt precursor in MeOH. The solvent was evaporated, the residue taken up in a solution of $(MeCN)_4CuOTf$ in DMF and heated. Results: [^{18}F]Fluorobenzene, 4-[^{18}F]fluoroanisole and 3-[^{18}F]fluorobenzaldehyde were obtained under "low base" conditions in RCCs of 26-56% (from MAI) and 41-64% (from ArBPin), respectively. Under "minimalist" conditions, the model compounds were prepared from MAI in RCCs of 78-90%. Protected 6-[^{18}F]fluorodopamine and 4-[^{18}F]fluorophenylalanine were obtained in 71-94% RCCs. Subsequent hydrolysis of the protected intermediates and HPLC isolation afforded the clinically relevant PET tracers in RCYs of 46 and 66%, respectively. Additionally, [^{18}F]DAA1106, a promising tracer for visualization of neuroinflammation, was efficiently prepared in 60% RCY. The specific activity of 4-[^{18}F]FPhe and [^{18}F]DAA1106 amounted to 109 GBq/μmol and 66 GBq/μmol starting from 49.5 and 2.4 GBq, respectively. Conclusion: A robust "low base" protocol for the efficient copper-mediated preparation of [^{18}F]arenes from diaryliodonium salts and aryl pinacol boronates was established. Furthermore, we developed a novel radiofluorination method that combines the advantages of "minimalist" approach to radiolabeling with the exceptional capabilities of copper mediated aromatic nucleophilic radiofluorination.

408 - Sunday, October 11, 2015, 2:30 PM - 4:00 PM, Hall E
Conventional & Specialised Nuclear Medicine: Infection & Inflammation

OP104

[18F]DPA-714 as a biomarker for an early detection with PET imaging of synovium inflammation in osteoarthritis model

S. Pesnel[1], F. Gimié[1], V. Meneyrol[1], G. Pottier[2], S. Bénard[1], R. Boisgard[2], F. Dollé[2], E. Jestin[1,3,4]; [1]GIP CYROI - RIPA, Sainte Clotilde, RÉUNION, [2]CEA, I2BM,SHFJ, IMIV UMR 1023 Inserm/CEA/Université Paris Sud /CNRS, Orsay, FRANCE, [3]INSERM, UMR1188 DéTROI, Sainte Clotilde, RÉUNION, [4]Université de la Réunion, Sainte Clotilde, RÉUNION.

Aim: The purpose of this study was to assess the [18F]DPA-714 as novel candidate PET tracer in osteoarthritis model. DPA-714 is a translocator protein (TSPO) ligand. TSPO has been recognized as a biomarker for inflammatory diseases. It has been already shown that TSPO ligands were promising radioligands for targeting arthritis in an mBSA-induced arthritis model in rats. Materials & Methods: Female Wistar rats received a single intra-articular injection of monoiodoacetate (MIA) in the right knee to induce osteoarthritis (OA) lesions and sterile saline in the left knee joint. The animals were scanned in vivo by microPET/CT at 7, 14, 21 and 28 days post-injection to assess the uptake of the tracer in the different stages of the disease. For PET imaging, animals were injected with 38 ± 5 MBq of [18F]DPA-714 and imaging started 45 minutes post-injection. In order to compare this tracer to the current tracers used in clinic: [18F]FDG and [99mTc]oxidronate, the same study was repeated with these 2 tracers. Histology study was performed to correlate the uptake of [18F]DPA-714 to the presence of TSPO and to assess the inflammatory process. Results: The OA lesions were clearly visible on the CT images from day 7 post-injection of MIA. For the 3 tracers the uptake was more important in the right knee compared to the left knee (control). An average increase in activity of 40% for the [18F]DPA-714, 8% for the [99mTc]oxidronate and 7% for the [18F]FDG at day 7 was observed. This uptake increased with the severity of the disease. The increase in activity was higher with the [18F]DPA-714 than with the [99mTc]oxidronate and [18F]FDG from day 7 to day 21. Conclusion: These preliminary results demonstrate that [18F]DPA-714 can be used to follow-up the inflammation in our OA model. Compared to the tracers used in clinic, this tracer allows a better visualization of the disease in the early stages of the disease. Currently a similar study is performed on another model of arthritis (rupture of anterior cruciate ligament in rats).

OP105

Liposomal corticosteroid treatment of experimental arthritis can be monitored non-invasively with radiolabeled anti-FAP antibodies

T. van der Geest[1], D. Gerrits[1], J. M. Metselaar[2,3], G. Storm[2,4], T. K. Nayak[5], A. Freimoser-Grundschober[6], C. Klein[6], B. Walgreen[7], M. M. Helsen[7], M. I. Koenders[7], P. Laverman[1], O. C. Boerman[1]; [1]Department of Radiology and Nuclear Medicine, Radboud university medical center, Nijmegen, NETHERLANDS, [2]Department of Targeted Therapeutics, MIRA Institute, University of Twente, Enschede, NETHERLANDS, [3]Department of Experimental Molecular Imaging, University Clinic and Helmholtz Institute for Biomedical Engineering, RWTH-Aachen University, Aachen, GERMANY, [4]Department of Pharmaceutics, Utrecht Institute for Pharmaceutical Sciences, Utrecht University, Utrecht, NETHERLANDS, [5]Roche Pharmaceutical Research and Early development, Innovation Center Basel, Basel, SWITZERLAND, [6]Roche Pharmaceutical Research and Early development, Innovation Center Zurich, Schlieren, SWITZERLAND, [7]Department of Experimental Rheumatology, Radboud university medical center, Nijmegen, NETHERLANDS.

Aim: Rheumatoid arthritis is a chronic autoimmune disorder involving joint inflammation eventually leading to cartilage destruction. Fibroblast activation protein (FAP) is highly expressed by fibroblast-like synoviocytes in arthritic joints. Therefore radioimmunoimaging with anti-FAP antibodies might be an attractive non-invasive imaging tool to monitor therapeutic interventions. Since treatment of arthritis often includes systemic or intra-articular administration of corticosteroids, we treated mice with collagen-induced arthritis (CIA) with prednisolone containing long-circulating liposomes (PLP-LCL) and investigated whether the efficacy of this treatment could be monitored with radiolabeled anti-FAP antibodies. Methods: CIA was induced in male DBA/1J mice. Mice were treated with a single injection of 10 mg/kg PLP-LCL, while the control group received empty LCL. To monitor the therapeutic effect, SPECT/CT images were acquired 24 h after injection of ^{99m}Tc-labeled HYNIC-conjugated anti-FAP antibody, 28H1, at 1, 4 and 9 days after treatment. After image acquisition, mice were dissected to determine radioactivity uptake in joints and uptake was correlated with the macroscopic arthritis score. Results. Treatment of CIA with PLP-LCL suppressed joint swelling. Already at one day after treatment the macroscopic arthritis scores were decreased with 50%. Scores further decreased to only 10% of the initial scores at 4 and 8 days post treatment. In contrast, macroscopic scores increased up to 600% in untreated mice at 8 days. ^{99m}Tc-HYNIC-28H1 showed strongly increased uptake in inflamed joints as compared to non-inflamed joints. Uptake of ^{99m}Tc-HYNIC-28H1 ranged from 1.5 %ID/g in non-inflamed joints to 22.6 %ID/g in severely inflamed joints. Most importantly, uptake of radiolabeled 28H1 in inflamed joints correlated with arthritis score (Spearman's ρ 0.67, $p<0.0001$) and increased with severity of arthritis. Conclusions. SPECT/CT imaging with the anti-FAP antibody specifically visualized arthritic joints and tracer accumulation correlated with the severity of the inflammation. We conclude that SPECT/CT with ^{99m}Tc-HYNIC-28H1 can be used to accurately and noninvasively, monitor the course of CIA in mice.

OP106

Tc-99m-CXCL8 SPECT to image disease activity in inflammatory bowel disease

E. Aarntzen, D. De Jong, R. Hermsen, J. Drenth, O. Boerman, W. Oyen; Radboudumc, Nijmegen, NETHERLANDS.

Aim: Inflammatory bowel diseases (IBD) are defined as chronic relapsing immune-mediated disorders of the gastrointestinal tract. IBD exacerbations are characterized by an extensive recruitment of immune cells into the intestinal wall, which may lead to severe tissue damage. The majority of activated neutrophils are CXCL8-receptor positive. Considering the chronic relapsing character of IBD, accurate and timely diagnosis of an exacerbation is pivotal for early adaptation of the treatment and reduction of the disease burden. The gold standard is endoscopic evaluation, but is invasive and associated with complications. We previously developed a Tc-99m-labeled CXCL8 preparation with good imaging characteristics of inflammation in preclinical models including colitis [Rennen et al. JNM, 2003] and a clinical study [Bleeker-Rovers et al. JNM, 2007]. Materials and methods: In this study, we investigate the accuracy of Tc-99m-CXCL8 SPECT to detect and localize disease activity in a prospective series of patients with IBD. A total of 30 patients (17 Crohn's disease, 14 Ulcerative colitis); disease episodes participated. Ninety-two matched segmental Tc-99m-CXCL8/histology pairs and 72 matched segmental endoscopy/histology pairs were studied. Imaging was performed after injection of 400 MBq Tc-99m-CXCL8 (protein dose: 5 μg/patient). Planar and SPECT acquisitions of the abdomen were performed at 30 min and 4 h after the injection. Results: Uptake of Tc-99m-CXCL8 in intestinal lesions was significantly increased during exacerbations, as compared to scans performed during follow-up, whereas uptake in bone marrow, spleen or liver remained constant. On a per patient basis, sensitivity was 95% (95%CI 77-99%) and 44% (95%CI 14-79. The positive predictive value (PPV) and negative predictive value (NPV) was 81% (95%CI 61-93%) and 80% (95%CI 28-99%). The sensitivity and specificity on a per segment basis for the detection of colitis inflammation was 82% (95%CI 68-92%) and 72% (95%CI 57-

84%), using histology as gold standard. The PPV and NPV was 74% (95%CI 60-85%) and 81% (95%CI 66-91%). False positive segments included 'faint uptake' in the ascending colon (4 patients), pseudopolyps in the transverse colon (1 patient) and terminal ileum that could not be confirmed by histology or endoscopy (1 patient). Conclusion: Tc-99m-CXCL8 SPECT provides a novel imaging technique to target neutrophil recruitment to the intestinal wall, which may be helpful to assess moderate to severe exacerbations of IBD. Further validation studies are warranted to potentiate Tc-99m-CXCL8 SPECT as a biomarker to scale up or step down treatment with immune modulating drugs in a personalized fashion.

OP107

Role of 18F-FDG PET/CT in the evaluation of response to antibiotic therapy in patients affected by infectious spondilodiscitis

F. Simone, **A. Niccoli Asabella**, D. Rubini, A. Notaristefano, F. Iuele, G. Rubini; Nuclear Medicine Unit, D.I.M., University of Bari "Aldo Moro", Bari, Italy, Bari, ITALY.

Aim: to evaluate the usefulness of 18F-FDG PET/CT to detect the early response to antibiotic therapy in patients affected by infectious spondilodiscitis and to compare the role of 18F-FDG PET/CT and MRI in post-treatment evaluation.Materials and Methods: 15 patients (12 M, 3 F), with mean age 65±13 years old, with typical clinical symptoms of Infectious Spondilodiscitis (pain, fever and increase of inflammatory indexes) and confirmed by blood culture or vertebral biopsy underwent within three day-interval a 18F-FDG PET/CT and Magnetic Resonance (MR) at "baseline" and after antibiotic therapy with Teicoplanine, Levofloxacine and Rifampicine. Semiquantitative parameters at 18F-FDG PET/CT "baseline" SUV max1, MTV1 and TLG1 and after therapy SUV max2, MTV2 and TLG2 of involved vertebrae were calculated. Follow-up period of at least three months was available for all patients.T-student test for paired groups was performed to compare baseline and after therapy 18F-FDG PET/CT semiquantitative parameters.Results: According to 18F-FDG PET/CT parameters all patients showed a response to antibiotic therapy. All patients were positive at "baseline" MR of the spine, while at follow-up, 7/15 patients showed MR signs of infection and were considered "positive", and 8/15 showed resolution of infectious condition and, therefore they were considered "negative". A statistical significant difference between 18F-FDG PET/CT "baseline" and after antibiotic therapy was found for all semiquantitative parameters: SUV max (t=5.8, p=0); MTV (t=2.66, p=0.02); TLG (t=4.53, p=0). The comparison between the "baseline" and "after treatment" 18F-FDG semiquantitative parameters showed a significative reduction of all parameters. This reduction was relevant also in patients with positive post-treatment MR. This bias is probably due to the tissue remodelling in the very immediate phase post-treatment, resulted positive at MR and negative at 18F-FDG PET/CT. Clinical follow-up of at least three months confirmed these results.Conclusions: 18F-FDG PET/CT is useful to detect the early response to antibiotic therapy in patients affected by infectious spondilodiscitis. 18F-FDG PET/CT semiquantitative parameters provide critical diagnostic information of the infectious process. 18F-FDG PET/CT should be considered as first-line exam in the diagnosis of spondilodiscitis while MR should be preferred for delayed evaluation.

OP108

The role of 18FDG-PET/CT for interim evaluation of therapy response in spondylodiscitis

P. Ghedini[1], C. Nanni[1], I. Petri[1], L. Zanoni[1], I. Grassi[1], S. Cambioli[1], D. Fiorenzo[2], S. Fanti[1]; [1]Nuclear Medicine, University Hospital S. Orsola-Malpighi, Bologna, ITALY, [2]Department of Diagnostic Imaging, University Hospital S. Orsola-Malpighi, Bologna, ITALY.

Aim: The aim of this study is to examine the role of the 18F-FDG-PET/CT in patients affected by spondylodiscitis and analyzing new possible parameters to early evaluate therapy response. Materials and Methods: We retrospectively enrolled 61 patients (21 female, mean-age 61) with diagnosis of spondylodiscitis. Among the 61 patients, 11 had tubercular, 1 fungal and 49 pyogenic spondylodiscitis. All patients underwent 18F-FDG-PET/CT baseline scan with determination of C-reactive protein (CRP) value and a second scan after 2-4 weeks of therapy. We analyzed SUV of both scans, delta-SUV (SUV1-SUV2/SUV1) in comparison with CRP levels during therapy. Furthermore we evaluated the volume of the infection, that we named "metabolic infection volume" (MIV) in the first and second scan. We selected a threshold of 50% of Lesion SUV1-2 for MIV definition. Delta-MIV (MIV1-MIV2/MIV1) were calculated and compared with SUV changes. Lesion-to-liver (LLR) ratio, lesion-to-mediastinal ratio (LBR), delta-LLR and delta- LBR after therapy were evaluated in every patients. Relationship between these different SUV and MIV parameters with therapy response and clinical outcome were investigated. Results: The mean SUV at diagnosis was 9,7+/-3,3. The mean CRP level at diagnosis was 2,9+/-2,8 mg/dl. SUV1 was not correlated with the CRP1 level at diagnosis (p=0.6) and SUV2 was not correlated with CRP2 (p=0.71). In responders patients, SUV2 and CRP2 were significantly lower than SUV1 and CRP1 ($p<0.001$ and $p<0.0001$ respectively). MIV2, LLR2 and LBR2 were also significantly lower than MIV1, LLR1 and LBR1 ($p<0.003$). ROC curves for delta-SUV showed a sensitivity of 87 % and a specificity of 82% with a cut-off of 33%. ROC curves for SUV2 showed a

sensitivity of 83% and a specificity of 46% with a cut-off of 5.0. ROC curves for CRP2 showed a sensitivity of 47% and a specificity of 82% with a cut-off of 0.71 mg/dl. ROC curves for delta-CRP showed a sensitivity of 82% and a specificity of 55% with a cut-off of 70%. OC curves for delta-LLR showed a sensitivity of 88% and a specificity of 87% with a cut-off of 30%. Delta-MIV correlate with delta-SUV. Conclusions: Delta-SUV provided a higher sensitivity and specificity in responders patients. SUV2 provided significantly lower specificity. SUVparameters performed better than CRP level. MIV, despite difficuties in its delineation, represented a possible useful parameter in infection with high metabolism grade. Finally, LLR provided a significantly higher specificity, with comparable sensitivity.

OP109

A Direct Comparison of 18F-FDG and 68Ga-DOTANOC PET/CT for Detection of Cardiac Sarcoidosis: Diagnostic Accuracy and Inter-observer Variability

L. C. Gormsen, A. Haraldsen, S. Kramer, W. Kim, P. Borghammer; Aarhus University Hospital, AARHUS C, DENMARK.

Aim: Cardiac sarcoidosis (CS) is a potentially fatal condition resulting in increased risk of sudden cardiac death. Overall survival in CS patients is substantially increased by corticosteroid therapy and correct diagnosis is therefore important. Unfortunately, no single test or imaging modality has acceptable diagnostic accuracy and the CS diagnosis is still based on insufficient clinical criteria. 18F-FDG PET/CT has previously shown some diagnostic promise, but is hampered by physiological glucose uptake in the myocardium. 68Ga-DOTANOC binds to somatostatin receptors on inflammatory cells in sarcoid granulomas. We compared the diagnostic accuracy of 68Ga-DOTANOC and 18F-FDG for diagnosing CS, and assessed inter-rater agreement among three readers. Materials and methods: 19 patients (7 female) with suspected CS were prospectively recruited in the trial. 18F-FDG (5 MBq/kg) and 68-Ga-DOTANOC (3 MBq/kg) scans were performed 60 and 90 minutes post injection, respectively, on a Siemens Biograph 64 scanner with <7 days between scans. Prior to 18F-FDG PET, participants were instructed to fast for >12 hours. PET/CT images were reviewed by three experienced nuclear medicine physicians. Studies were categorized as positive, negative, or inconclusive. In case of reviewer disagreement, final PET diagnosis was based on majority decision. To assess diagnostic accuracy of both PET tracers, we used the established reference standard based on CS criteria laid out by the Japanese ministry of Health and Welfare combined with clinical follow up. Inter-observer variability for both tracers was calculated using Fleiss kappa for multiple observers and trichotomous outcome. Results: Based on the reference standard, 3/19 patients suffered from CS, which was in line with the expected proportion. 10/19 18F-FDG scans were rated as inconclusive by consensus diagnosis rendering calculations of diagnostic accuracy impossible. In contrast, accuracy was 100 % for 68Ga-DOTANOC based on the consensus diagnosis among readers. Interestingly, Fleiss kappa was extremely poor for 18F-FDG PET (combined kappa 0.11, NS) showing that reviewers disagreed greatly in interpreting the images. Fleiss kappa was somewhat better for 68Ga-DOTANOC (0.36, p=0.001), which is fair agreement - but still demonstrates significant inter-rater disagreement. Conclusion: Despite relevant and recommended patient preparations, 18F-FDG PET/CT images of the heart were extremely hard to interpret for signs of CS resulting in disappointingly low concordance rates among reviewers and correspondingly poor diagnostic accuracy. By contrast, 68Ga-DOTANOC PET/CT had excellent diagnostic accuracy with the caveat, that inter-observer variability was significant. 68Ga-DOTANOC PET/CT looks promising as an alternative CS PET tracer with images preferably reviewed by multiple readers.

OP110

Comparison between ^{18}F-FDG PET/CT and ^{99m}Tc-HMPAO-labelled leukocyte SPECT/CT in 50 patients with suspected osteomyelitis

P. Ferro[1], G. Cusato[1], S. Fiorino[1], M. Spallino[1], C. E. Popescu[2], R. Sara[2], L. Conversano[2], M. Milella[2], C. Rossetti[2]; [1]Università Milano-Bicocca, Milano, ITALY, [2]Ospedale Niguarda, Milano, ITALY.

Aim:Early diagnosis is crucial for the management of bone infections and surrounding tissue involvement in suspected osteomyelitis. Several diagnostic tools are currently available , such as x-ray, CT, microbiological cultures, and serological tests. Nuclear Medicine could be useful, with ^{99m}Tc-HMPAO labelled leukocyte SPECT/CT (HMPAO-SPECT/CT) and ^{18}F-FDG PET/CT (FDG-PET/CT) scan.The aim of our preliminary study was to evaluate and compare the clinical value of HMPAO-SPECT/CT and FDG-PET/CT in the diagnosis of bone infections.Methods:We retrospectively analysed 50 patients (29 males, 21 females, age range 24-84 years) with suspected osteomyelitis who underwent both FDG-PET/CT and HMPAO-SPECT/CT.Clinical symptoms, serological tests (PCR values), CT scans and ongoing antibiotic therapy at the time of the studies were analysed.FDG-PET/CT and HMPAO-SPECT/CT were considered “positive” or “negative” on agreement of 3 independent observers on qualitative analysis of the images; SUV max was measured in each detected lesion and correlated to PCR levels.Final diagnosis of infection was based on microbiological culture, serological tests (PCR) and clinical

follow-up. HMPAO-SPECT/CT and FDG-PET/CT were compared with each other considering separately bone and soft tissue.Results:FDG-PET/CT showed higher values of sensibility (90 vs 44% in bone and 94 vs 59% in soft tissue), negative predictive values (NPV) (83 vs 53% in bone, and 85 vs 52% in soft tissue) and accuracy (88 vs 64% in bone and 88 vs 70% in soft tissue) than HMPAO-SPECT/CT. On the contrary HMPAO-SPECT/CT exams demonstrated better specificity (95 vs 83% in bone and 94% vs 73% in soft tissue) and positive predictive value (PPV) (93 vs 90% in bone tissue and 95 vs 89% in soft tissue) (p<0,006).In 14/50 patients (28%) FDG-PET/CT was positive whereas HMPAO-SPECT/CT was negative. All these 14 patients were under antibiotic therapy during investigations and their clinical history suggested a chronic process.We observed a correlation between SUV max and PCR values: SUV max was higher in patients with positive PCR levels (SUV max 2,45-12,72 corresponding to PCR 2,3-17,6 mg/dl).Conclusion:18F-FDG-PET/CT and 99mTc-HMPAO-SPECT/CT scans are a reliable support tool for clinical and serological data in the evaluation of patients with suspected osteomyelitis, providing additional information on anatomic localization and extent of the infection processes. Either in bone and soft tissue, FDG-PET/CT has proven to have higher sensibility, accuracy and NPV while HMPAO-SPECT/CT shows relatively higher specificity. 99mTC-HMPAO-SPECT/CT could be less effective in patients with chronic disease and suffered from the ongoing antibiotic therapy.

OP111

The added value of 18F-FDG PET for the staging of patients with invasive fungal infections

A. O. Ankrah[1,2], A. W. J. M. Glaudemans[1], E. F. J. de Vries[1], R. H. J. A. Slart[1,3], R. A. J. O. Dierrckx[1], M. M. Sathekge[2], H. C. Klein[4]; [1]Department of Nuclear Medicine and Molecular Imaging, University Medical Center Groningen, Groningen, NETHERLANDS, [2]Department of Nuclear Medicine, University of Pretoria, Pretoria, SOUTH AFRICA, [3]Biomedical Photonic Imaging Group, University of Twente, Enschede, NETHERLANDS, [4]Department of Psychiatry, University Medical Center Groningen, Groningen, NETHERLANDS.

^{18}F-FDG PET has proven added value in many malignant diseases, but its role in infectious diseases still has to be defined. It is important to correctly stage invasive fungal infections at an early time point to make proper clinical decisions, since fungal infections often occur in immunosuppressed patients, to whom the infection may be life-threatening.The aim of this study was therefore to determine the added value of ^{18}F-FDG PET compared with conventional imaging for the staging of patients with fungal infections.Materials and methods- All patients with a proven fungal infection who underwent a ^{18}F-FDG-PET/CT between October 2009 and December 2014 were retrospectively included. Fungal infection was proven by histology or cultures. All patient dossiers were checked for infection parameters, clinical history, and imaging procedures. All ^{18}F-FDG-PET/CT scans were performed on a Biograph mCT TOF system (Siemens) according to the EARL guidelines. All PET findings were compared to the findings based on all other imaging modalities combined in order to determine if ^{18}F-FDG -PET/CT could provide more information. The ^{18}F-FDG-PET findings were also correlated to the infection markers in the blood.Results- 9 males (32%) and 19 females (68%) between the ages of 6 months up to 75 years were included. All the patients were immunocompromised, mainly due to treatment of an underlying haematological malignancy (64%) or organ transplantation (21%). Indications for the scans included unexplained fever, determining the absence of fungal infections before proceeding with stem cell transplant and in some cases to determine other sites of fungal infections.In total, ^{18}F-FDG-PET revealed 107 fungal infection lesions, compared to 60 lesions detected by conventional imaging. The SUVmax of all lesions was heterogeneous, varying from 1.14 To 17.86 (mean 5.36) ^{18}F-FDG PET detected more lesions than conventional imaging in 19 (68%) patients. The majority of these patients had extra-thoracic disease. In 4 (14.2%) cases, ^{18}F-FDG-PET/CT noted disease activity where findings on other modalities were equivocal. In total, ^{18}F-FDG-PET/CT added diagnostic information in 23 patients (82%) which potentially could influence clinical decisions. No correlation was found between the infection parameters and ^{18}F-FDG-PET/CT findings.Conclusion- ^{18}F-FDG-PET/CT has significant added-value over conventional imaging in the initial evaluation of patients with invasive fungal infections. The main added value is in finding lesions outside the thoracic region. To our opinion, whole body ^{18}F-FDG-PET/CT accompanied by high-resolution CT scan of the chest should be the imaging modality of choice in (suspected) fungal infections.

409 - Sunday, October 11, 2015, 2:30 PM - 4:00 PM, Hall 8
Physics & Instrumentation & Data Analysis: Data Analysis & Management I

OP112

Pixel-based Source Depth Measurement for Cerenkov Luminescence Imaging

L. Altabella[1], C. R. Gigliotti[1], F. Boschi[2], A. E. Spinelli[1]; [1]San Raffaele Scientific Institute, Milano, ITALY, [2]University of Verona, Verona, ITALY.

Aim: Optical tomography represents a challenging problem in optical imaging because of the intrinsically ill-posed inverse problem due to photon diffusion. Cerenkov luminescence

tomography (CLT) for optical photons produced in tissues by several radionuclides (i.e.: 32P, 18F, 90Y), has been investigated using both 3D multispectral approach and multiviews methods. Difficult in convergence of 3D algorithms can discourage to use this technique to have information of depth and intensity of source. For these reasons, we developed a faster 2D corrected approach based on multispectral acquisitions, to reconstruct source depth and its intensity. Methods: Monte Carlo simulations were developed using GAMOS plug-in for GEANT4, validated for Cerenkov optical photon production as well as optical photon transport. Experimental data were acquired using IVIS SpectrumCT (Perkin Elmert, USA). We scanned a capillary (1.0 mm diameter) filled with 0.5 MBq of 32P-ATP. Capillary was placed inside slices of chicken breast to simulate tissue scattering. We considered three thickness of chicken breast: 6, 9 and 11 mm. According to Beer Lambert law we can derive the unknown source depth, using a pixel-wise fit of several images acquired using different spectral filters from 560 nm to 660 nm with a pass of 20 nm. More precisely we fit radiance (p/sec/cm2/sr) in each location for all the images as function of different μeff that depends on the filter wavelength. Considering a two parameters linear fit of the intensity logarithm, corrected both for theoretical Cerenkov emission spectrum and for diffusive optical transport as implemented by Coquoz, we derived a pixel-based depth source map and a 2D depth corrected intensity source map. Results and conclusion: We obtained a pixel-based source depth reconstruction with a maximum error in source region of 10% for 6 mm source, and less than 3% for the deeper sources. Combining depth information and source intensity, we can recognize and discriminate source characteristics in terms of intensity. This is particularly interesting in animal model with several tumor masses. In these cases image acquired from animal surface can mislead for example in presence of deeper but more intense tumor. This work demonstrates that it is possible to obtain reliable information concerning the Cerenkov optical source using a 2D multispectral imaging approach. Further developments of this work consist of applying this method on in vivo studies.

OP113

Correcting for Patient Motion on a Solid State Multiple Pinhole Dedicated Cardiac Camera

S. Redgate[1], D. C. Barber[2], J. W. Fenner[2], A. Al-Mohammad[3], J. C. Taylor[1], M. B. Hanney[1], W. B. Tindale[1]; [1]Nuclear Medicine, Sheffield Teaching Hospitals NHS Foundation Trust, Sheffield, UNITED KINGDOM, [2]Medical Physics Group (Cardiovascular Science), University of Sheffield, Sheffield, UNITED KINGDOM, [3]Cardiothoracic Directorate, Sheffield Teaching Hospitals NHS Foundation Trust, Sheffield, UNITED KINGDOM.

Aim: Patient motion ≥13mm introduces artefacts into myocardial perfusion images[1]. Procedure guidelines recommend correction, which involves alignment of the projections prior to reconstruction. Multiple pinhole cardiac cameras acquire data at all angles simultaneously, presenting the potential for 3D motion correction. The aim of this study was twofold: a) to perform simulations to determine the magnitude and duration of motion that introduces significant motion artefacts on this system and b) to develop a technique for 3D motion correction and test this on patient studies. Materials and Methods: Phantom images were acquired in the centre of the field of view and offset in the X, Y and Z directions. These were used to simulate 5-20mm creep and step motion, with step durations of 30, 60, 90 and 180s. Qualitative assessment, through blinded reporting and quantitative assessment through calculation of the total perfusion defect (TPD) was performed to identify motion artefacts (TPD ≥5.5%). Motion correction was performed by reframing the list mode data into a series of 30s images, reconstructing each frame and then registering and summing these to produce a corrected image. This was validated on images with simulated motion and applied to images with no motion. Additionally, forty patient studies were assessed for motion and the motion correction algorithm was applied to studies with significant motion. Results: Qualitative analysis identified motion artefacts for ≥10mm motion. Quantitative analysis identified artefacts for ≥11mm 180s step motion and >15mm creep motion. No artefacts were identified for step motion with a 30s duration, confirming that this is a suitable reframing duration for motion correction. Motion correction visually removed 9/10 motion artefacts on the phantom simulations and reduced all the TPD values to ≤4%. When applied to images with no motion there was no difference between the original and motion corrected images or TPD values. Two patients (5%) were identified as having significant superior-inferior patient motion and motion correction improved the appearance of the anterior and inferior walls on these studies. This is a retrospective analysis, but arguably it might have changed patient management in a couple of cases. Conclusion: Patient motion ≥10mm magnitude and >30s in duration introduces significant motion artefacts into myocardial perfusion images acquired on a multiple pinhole cardiac camera. Motion correction, as described, successfully corrects for patient motion artefacts in this study. Correction of patient motion on this system has been shown to be technically feasible and accurate. 1. J Nucl Med,42(5) 4687-694

OP114

Partial volume correction of Image Derived Input Functions using a novel Single Target Correction Technique

J. C. Dickson[1], K. Erlandsson[2], H. Sari[2], S. Wan[1], A. Groves[2]; [1]University College London Hospital NHS Foundation Trust, London, UNITED KINGDOM, [2]University College London, London, UNITED KINGDOM.

Introduction: The move to non-invasive image derived input functions (IDIF) in PET has been hampered by difficulties correcting for partial volume effects (PVE) in the volumes of interest used to produce the input functions. We have previously attempted to use Rubidium-82 PET to quantify perfusion in colorectal cancer tumours [1]. In this paper we introduce a novel single target correction (STC) technique [2], and apply it to IDIF derived from dynamic Rubidium-82 PET images of the femoral arteries. Methods: Six patients with suspected colorectal cancer were involved in this study. Each had a dynamic Rubidium-82 PET scan and CT perfusion to assess tumour perfusion. To define a volume of interest for the IDIF and for partial volume correction, the femoral artery was segmented from the CT perfusion scan. The dynamic PET data was then registered to this VOI using a registration between the CT perfusion scan and the CT scan for attenuation correction that was acquired for PET. With segmented vessel and PET data in the same space, the STC partial volume correction (PVC) technique was applied to the PET data. In essence, the technique is an evolution of the Müller-Gartner method, which uses true volume extent and an estimate of the Point Spread Function (PSF) to correct the PET data. In this study we used an experimentally derived PSF of 11.4mm (FWHM). Changes to IDIF pre and post correction were assessed by measuring the change at peak, where spill-out factors are greatest; and in final PET frame where spill-in factors play a larger role. The effect on values of tumour K1 was also assessed. Results: The peak IDIF uptake went up on average by a multiple of 2.80 [Range: 2.12-3.43] when partial volume correction was applied. This is not unexpected given the PSF of Rubidium PET and the typical diameter of femoral arteries. In comparison, in the last frame where spill-in factors to the IDIF become more of an issue the uptake increased on average by a multiple of 1.40 (Range: 1.22-1.62] with corrections applied. As a consequence, K1 is reduced on average by 65.43% [Range: 34.37-79.67] after correction. Conclusions: PVC using a single target technique make substantial changes to the IDIF and estimated kinetic parameters. References: 1. Dickson J et al J Nucl Med. 2014; 55 (Supplement 1):507 2.Erlandsson K, Hutton B, J Nucl Med. 2014; 55 (Supplement 1):2123

OP115

Voxel-level dosimetry with a grid-based Boltzmann solver for patient-specific nuclear medicine dosimetry

J. Mikell[1,2], F. Mourtada[3], T. Wareing[4], **S. C. Kappadath**[1,2]; [1]UT MD Anderson Cancer Center, Houston, TX, UNITED STATES, [2]UT Graduate School of Biomedical Sciences, Houston, TX, UNITED STATES, [3]Christiana Care Health System, Newark, DE, UNITED STATES, [4]Varian Medical Systems, Pala Alto, CA, UNITED STATES.

Aim: MIRD assumes uniform uptake at the organ level and patient geometry based on anthropomorphic phantom geometry. Voxel-level dosimetry models are able to overcome these shortcomings and provide patient-specific dosimetry. Full radiation transport solutions that solve the linear Boltzmann transport equation (LBTE) under patient-specific conditions are considered to be more accurate. Deterministic grid-based Boltzmann solvers (GBBS) are full transport solutions to the LBTE in addition to Monte Carlo (MC) approaches. We have validated GBBS Attila v8.0.0 with MC DOSXYZnrc for beta and gamma sources in both homogeneous and heterogeneous medium with clinically acceptable uncertainties. The aim of this work is to implement GBBS for patient-specific voxel-level nuclear medicine dosimetry and compare its performance against MC. Materials and Methods: We investigated GBBS using single time-point quantitative SPECT/CT for 90Y-glass-microsphere HCC patient and 131I-NaI thyroid cancer patient with lung metastases. The gold standard for voxel-level dosimetry was MC. Tissue material and density were obtained from CT while activity distribution was from SPECT. For 90Y we calculated absorbed doses from only the 90Y beta spectra. For 131I we simulated the auger+conversion electrons, beta particle spectra, and gamma+x-ray spectra. To perform patient-specific GBBS, the required tetrahedral mesh geometry was generated adaptively using tetgen v1.5.0. To control the adaptation, a mesh-sizing function was generated based on the activity, material, and gradient of the material distribution. Mapping of material, density, and activity to tetrahedrons was done using the nearest voxel centroid to the tetrahedron centroid. The electron energy cutoff was 100 keV for 131I (200 keV for 90Y) while the photon energy cutoff was 1 keV. Quantitatively, we compared mean, minimum, maximum absorbed dose to tumors and normal tissues. Qualitatively, we compared dose-volume histograms (DVH) and line profiles through tumors. Results: GBBS for 90Y took 38s, while the I131 took 606s (208s for auger+conversion electrons, 94s for beta, and 304s for gamma+x-ray component). For 90Y the GBBS mean and maximum absorbed dose to tumor and normal liver were within 2.3% of MC. For total I131 the mean and maximum absorbed dose to tumors were within 4.3%; mean and maximum doses to left and right lung were within 3% and 7.6%, respectively. Line profiles of voxel-doses through

tumors and DVHs visually agreed well between GBBS and MC. Conclusion: GBBS with adaptive meshing provides patient-specific nuclear medicine dosimetry with accuracy comparable to MC and computation speeds suitable for routine clinical practice. Grant support NIH/NCI R01 CA138986.

OP116

FDG-PET/CT of Bronchial Carcinoma Under Neoadjuvant Chemotherapy: Background Based Adaptive Volume Metrics Outperform TLG and MTV in Predicting Therapy Response

I. A. Burger[1], R. Casanova[1], S. Steiger[1], P. Stolzmann[1], M. W. Huellner[1], P. Veit-Haibach[1], A. Soltermann[1], C. R. Schmidtlein[2]; [1]University of Zurich, Zurich, SWITZERLAND, [2]Memorial Sloan Kettering Cancer Center, New York, NY, UNITED STATES.

Purpose: Tumor response assessment to chemotherapy using FDG PET metrics is gaining acceptance. The most common PET metric is maximum standardized uptake value (SUV_{max}). However, several studies have suggested that the metabolically active tumor volume (MTV) or the total lesion glycolysis (TLG) are superior for assessing tumor burden and probably also response to therapy. The optimal method for defining MTV and TLG is still controversial; initially all voxels with FDG activity above 42% of SUV_{max} were used. Recently we have suggested a method that adapts to the local background to determine the background subtracted lesion activity (BSL) and the background subtracted volume (BSV). It was the aim of our study to investigate the correlation between PET metrics and therapy response in non-small cell lung carcinoma (NSCLC). Patients and Methods: Forty-six NSCLC patients were retrospectively identified, the PET/CT data before and after neo-adjuvant chemotherapy were analyzed regarding SUV_{max}, MTV, TLG, BSL and BSV on both scans and the relative changes were calculated. The tumor regression grade (TRG) as an indicator of tumor response was assessed on H&E stained sections of the corresponding surgical specimens using a 4-tiered scale. TRG was correlated with the relative change of all PET metrics using Spearman rank test. Results: Both the change in tumor size and SUV_{max} did correlated with the TRG with $p = 0.038$ and $p < 0.001$, respectively. The PET volume metrics based on a fixed threshold of SUV_{max} did not correlate with TRG (TLG: $p = 0.389$ and MTV: $p = 0.420$). However, both background activity based PET volume metrics BSL and BSV significantly correlated with TRG ($p = 0.001$ for both). Conclusion: Volume based PET metrics using a fixed threshold (42% SUV_{max}) for delineation did not correlate with TRG. However tumor regression correlated well with SUV_{max} and both background based PET volume metrics BSL and BSV.

OP117

Automated organ segmentation in pre-clinical 4D PET/CT images

C. Maaß[1], J. Avelar Rivas[1], A. A. Attarwala[1], B. Abualhaj[1], S. Niedermoser[2], C. Wängler[3], G. Glatting[1]; [1]Medical Radiation Physics/Radiation Protection, Medical Faculty Mannheim, Heidelberg University, Mannheim, GERMANY, [2]Molecular Imaging and Radiochemistry, Department of Clinical Radiology and Nuclear Medicine, Medical Faculty Mannheim, Heidelberg University, Mannheim, GERMANY, [3]Biomedical Chemistry, Department of Clinical Radiology and Nuclear Medicine, Medical Faculty Mannheim, Heidelberg University, Mannheim, GERMANY.

Aim: Treatment planning in molecular radiotherapy relies on the estimation of time-activity curves [1]. To provide an optimal therapy, this estimation needs to be accurate and reproducible (observer independent).The aim of this work was (1) to implement an algorithm for the automated segmentation of relevant structures (tumour, organs at risk) in pre-clinical 4D PET/CT images and (2) to determine the optimal number of clusters.Materials and Methods: Biodistribution of 18F-SiFalin-PEG1-TATE [2] in six AR42J tumour bearing mice was obtained from a preclinical PET/CT (Bruker BioSpin MRI GmbH, Ettlingen, Germany). This tracer binds specifically to the somatostatin receptor subtype 2, which is overexpressed in neuroendocrine tumours.An in-house software for automated organ segmentation of 4D PET/CT images was implemented in MATLAB (R2014b, MathWorks, Natick, Massachusetts, USA). This algorithm clusters time-activity curves voxelwise using k-means. The optimal number of clusters depends on the region and was determined by minimising (1) the Calinski-Harabasz-criterion (ratio of within to outer cluster variances) and (2) the relative deviation (RD) between clustered and actual organ volumes. Clustered organ volumes were calculated by summing up all clusters within an organ.Reproducibility of the algorithm was tested by determining both the optimal number of clusters and the time-activity curves five times for tumour and kidneys (averaged over six mice).Accuracy of the algorithm was evaluated by comparing clustered organ volumes and manually drawn volumes to actual organ weights.Results: The mean numbers of optimal clusters were (1) 10±2 and 4±1 and (2) 7±3 and 9±2 for tumour and kidneys, respectively.RDs of the manually drawn and actual tumour and kidney volumes were (-1 ±54)% and (-17±14)%. RD of the clustered and actual volumes was for tumour and kidney (1) (-37±38)% and (-10 ±19)%, (2) (0±6)% and (3±4)%.Conclusion:Automated organ segmentation of 4D pre-clinical images is reproducible and observer independent. The optimal number of clusters is crucial and can be determined using the presented method (2). Thus, an accurate and automated determination of time-

activity curves is possible.Literatur:1.Glatting G, Bardies M, Lassmann M. Treatment planning in molecular radiotherapy. Z Med Phys. 2013;23(4):262-9.2.Wängler C, Niedermoser S, Chin J, Orchowski K, Schirrmacher E, Jurkschat K, et al. One-step 18F-labeling of peptides for positron emission tomography imaging using the SiFA methodology Nature Protocols. 2012;7:1946-55.

OP118

Does Reducing Reconstruction Voxel Volume / Increasing Matrix Size Improve Lesion Detectability? A phantom and clinical feasibility demonstration using next generation digital PET/CT

J. Zhang[1], K. Binzel[1], C. Wright[1], V. Nagar[1], P. Bardos[1], P. Maniawski[2], M. V. Knopp[1]; [1]The Ohio State University, Columbus, OH, UNITED STATES, [2]Philips Healthcare, Cleveland, OH, UNITED STATES.

Aim: The replacement of the photomultiplier with a solid state, digital photon counting detector is a technological leap that leads to higher photon counting rates, less dead time and improved dose response linearity. PET has traditionally used comparatively to CT and MRI smaller reconstruction matrix and thus larger voxel volumes. This study investigates if lesion detectability can be improved by larger matrix reconstruction of phantoms and in clinical oncologic PET/CT.Materials and methods: A Philips Vereos TF 64 digital PET/CT (Cleveland, OH) was used for NEMA and Jaszczak phantom acquisitions as well as in 20 clinical patients referred with suspected malignancies. Clinical whole body PET scans were acquired after average injection of 480 MBq 18F-FDG with 90s per bed position, 40% overlap and a 576mm FOV. Images were reconstructed in 144x144 matrix with voxel volume of 4 x 4 x 4 (64) mm3, 288x288 matrix with voxel volume of 2 x 2 x 2 (8) mm3 voxel volume, and 576x576 matrix with voxel volume of 1 x 1 x 1 (1) mm3. All three reconstructed image data sets were assessed by comparative analysis using two independent readers. Lesion detectability as well as confidence of diagnostic relevance was assessed, however only lesions of >2cm in unidimensional diameter on CT included. The phantoms were evaluated against the known parameters and the recovery coefficients calculated.Results: Image quality of all data sets and reconstruction volumes was classified as satisfactory. 48 lesions are included in this evaluation, all of them visualized on the largest reconstruction matrix. 11 lesions were only confidently detected on the 1 mm3 voxel reconstructed images. 13 lesions were first visualized on the 2 mm3 voxel and also seen on the 1 mm3 but not on the 4 mm3 voxel reconstructed images. Overall, readers consistently rated the 288 matrix images to be preferable over the 144 matrix images. The 576 matrix images were rated on average 38% more preferable than the 288 matrix images and equivalent to the 288 matrix in all remaining cases. The 1 mm3 voxel reconstructed phantom data presented consistently the best recovery coefficient.Conclusion: Larger matrix size / reduced voxel volume reconstruction substantially improved clinical lesion detectability and on phantom scans calculated recovery coefficients. The improved counting capabilities of the digital detector system appears to enable a consistent utilization of larger reconstruction matrix that was shown to improve lesion detection by substantially reducing partial volume effects.

OP119

A New Statistical Model For Quantifying Tumor Heterogeneity in Emission Tomography

J. Varga[1], A. Forgács[2,1]; [1]University of Debrecen, Debrecen, HUNGARY, [2]ScanoMed Ltd., Debrecen, HUNGARY.

Beside biological heterogeneity, the scatter of voxel values in a tumor volume is also influenced by partial volume effect (PVE) and noise. The smaller the object, the contribution of PVE is more significant. We propose a procedure to separately access the significance of biological heterogeneity. Methods: We estimate a homogeneous tumor volume that - after convolution with the PSF - would best approximate the observed distribution in a neighborhood of the tumor. We alternatingly estimate the tumor mask, and the tumor and background levels. We statistically test the null hypothesis that the variance inside the tumor volume in the difference image (observed - homogeneous distribution blurred) is fully explained by noise. An F-test is applied to the ratio of observed and expected variances (based on a reference area), with corrected degrees of freedom taking into account that neighboring pixels are correlated. First we tested the algorithm on 2-dimensional slices of simulated and phantom data. Our *simulation* data consisted of rings with 2 to 16 pixels external radius (4 mm/pixel), and internal radius half of that. Ring to background activity ratio was 4. Poissonian random noise with variation coefficient of 0.3, 1, 3, 10, and 30% was added to each, resulting in 40 simulated images. For the *phantom* PET studies we used (a) the IEC body phantom containing 6 fillable spheres (diameters: 10, 13, 17, 22, 28 and 37 mm). The sphere-to-neighborhood activity ratio was 10. (b) A special heterogeneous phantom consisted of seven 2 mL syringes, 2-3-2 of them filled with different concentrations of C-11, immersed in F-18-labeled water. 12 images were acquired through 60 min, resulting in “tumor” max / background ratios from 16 to 8. Results: The method failed to identify heterogeneity at 30% error level in case of the 4 smallest simulated rings (r=2⋯8 pixels), and at 10% error level just the smallest one; the rest showed significant departure from homogeneity. All but the smallest sphere resulted in p>0.05 (keeping the

hypothesis of homogeneity). The tumor-to-background ratio from the model showed degraded contrast recovery only for the 2 smallest spheres. The heterogeneous phantom showed strongly significant heterogeneity at all contrast levels. Discussion: Our model tests object heterogeneity separately from partial volume effect and noise; thus it should be applicable to smaller objects than direct measures of region variance. An additional benefit is a robust estimation of tumor activity level, offering an objective parameter for follow-up studies.

410 - Sunday, October 11, 2015, 2:30 PM - 4:00 PM, Hall D
Cardiovascular System: PET Perfusion Imaging

OP120

Relationship Between Coronary Artery Calcium Score and Coronary Flow Reserve in Patients Evaluated for Coronary Artery Disease: a Hybrid Rb-82 PET/CT Imaging Study

E. Zampella[1], P. Arumugam[2], R. Assante[1], D. Tout[2], V. Gaudieri[1], C. Nappi[1], T. Mannarino[1], M. Panico[3], S. Daniele[3], W. Acampa[3], M. Petretta[4], C. Tonge[2], A. Cuocolo[1]; [1]Department of Advanced Biomedical Sciences, University of Naples Federico II, Naples, ITALY, [2]Nuclear Medicine Centre, Central Manchester University Teaching Hospitals, Manchester, UNITED KINGDOM, [3]Institute of Biostructure and Bioimaging, National Council of Research, Naples, ITALY, [4]Department of Translational Medical Sciences, University of Naples 'Federico II', Naples, ITALY.

Aim: Limited data are available on the value of coronary artery calcium (CAC) to predict myocardial blood flow (MBF) impairment and coronary vasodilator dysfunction. We assessed the relationship between CAC score, hyperemic MBF and coronary flow reserve (CFR) in patients without known coronary artery disease (CAD) undergoing hybrid Rb-82 PET/CT imaging. Materials and Methods: We evaluated 637 (age 58±13 years) consecutive patients without a documented history of CAD referred to myocardial perfusion imaging due to presence of multiple cardiac risk factors or risk assessment before general surgery. All patients were studied by vasodilator stress Rb-82 PET/CT and CAC scoring. The CAC score was measured according to the Agatston method. Resting and hyperemic MBF and CFR were automatically quantified. Patients were stratified into four groups based on their CAC score (0, 0.01-99.9, 100-399.9 and ≥400). Perfusion measurements were compared across levels of CAC score using one-way analysis of variance (ANOVA). The Spearman correlation coefficient was assessed between continuous CAC score and MBF or CFR. Univariable and multivariable logistic regression analyses were used to determine the variables associated with reduced (<2) CFR. Results: Patients had a global resting MBF of 1.18±0.39 ml/min/g. During hyperemia, MBF increased to 2.74±0.80 ml/min/g ($p<0.001$ vs. resting). CFR averaged 2.46 ±0.73. CAC score was 0 in 305 (46%) patients. Of those with CAC >0, the score was 0.01-99.9, 100-399.9 and ≥400 in 21%, 15% and 18% of patients, respectively. Global CAC score showed significant inverse correlation with hyperemic MBF and CFR (both $p<0.001$). No correlation was found between CAC score and baseline MBF ($p=0.611$). At ANOVA, among the four CAC groups, hyperemic MBF (2.97, 2.69, 2.74 and 2.23 ml/min/g) and CFR (2.67, 2.44, 2.38 and 2.00) significantly decreased (both $p<0.001$) with increasing CAC levels. Differently, a comparable global resting MBF among the four CAC groups was observed ($p=0.287$). At univariable analysis age ($p<0.001$), diabetes ($p<0.001$), family history of CAD ($p<0.05$), hypertension ($p<0.05$) and CAC score ($p<0.001$) displayed an inverse relationship with CFR. At multivariable analysis only age ($p<0.001$), diabetes ($p<0.001$) and CAC score ($p<0.05$) were independently associated with reduced CFR. Conclusions: In patients without known CAD there is a significant relationship between hyperemic MBF and CFR, and the extent of CAC. Noteworthy, diabetes and CAC score independently predict a CFR reduction. These results suggest that CAC score provides incremental information about CFR over established CAD risk factors in patients with suspected CAD.

OP121

Low-dose relative and quantitative myocardial blood flow imaging using 82Rb-PET

C. M. Hoff, E. Dul, L. P. Tolbod, H. J. Harms, K. Bouchelouche, J. Frøkiær, J. Sørensen; Aarhus University Hospital, Department of Nuclear Medicine & PET-Centre, Aarhus, DENMARK.

Aim: Relative and absolute measures of myocardial blood flow (MBF) are derived from a single 82Rb PET/CT scan using list mode data to extract static, gated and dynamic PET series. However, due to the short half-life of 82Rb (76s), high doses of 82Rb (>1100 MBq) are used in order to maximize image quality of the static images. Such high doses challenge scanner dead time performance and require a large eluate volume (20-40 mL) to be infused into the patient. The aim of the current study was to examine MBF with a low dose (LD) 82Rb protocol compared to the institution's standard

higher dose (HD) protocol.Methods: Nineteen patients referred to 82Rb PET were included in the study. Patients were examined during rest and stress with repeated LD and HD dose Rb-PET. We excluded four patients due to motion artifacts. Mean HD dose was 1137 MBq (range 1065-1187 MBq) and mean LD dose 347 MBq (range 269-449 MBq). Regional and global rest and stress MBF values, total perfusion deficit (TPD), ejection fraction (EF) and %-perfusion using the 5-segment model were calculated using commercially available software QPET (Cedars Sinai).Results: Mean segmental MBF (±SD) at rest was 1.09±0.32 and 1.18±0.30 mL/g/min, p=0.001 at LD and HD, respectively. At stress MBF was 2.30±1.00 and 2.48±1.17 mL/g/min, p=0.0007 at LD and HD, respectively. There was good correlation between LD and HD segmental MBF (LD=0.85xHD+0.14, R2=0.9, p<0.001). Mean global MBF at rest was 1.09±0.29 and 1.18±0.28 mL/g/min, p=0.14 at LD and HD, and at stress 2.26±0.96 and 2.43±1.14 mL/g/min, p=0.08 at LD and HD, respectively. Again good correlation between LD and HD global MBF. (LD=0.86xHD+ 0.13, R^2=0.9, p=0.02).Mean TPD with HD patients was 1.86±2.57% and 2.44±2.71% with LD patients. Correlation between LD and HD TPD was LD=0.92xHD+0.73, R2=0.77, p=<0.0001. Mean percentage perfusion with HD was 75.4±7% and 71.7±7.6% with LD patients. Correlation between LD and HD %-perfusion was LD=0.90xHD+3.79, R^2=0.69, p<0.0001. Mean EF with HD patients was 65±10% and 61±11% in LD patients with a good correlation. (LD=0.93xHD+0.85, R2=0,76, p=0,001).Conclusion: Excellent correlation between reduced dose and standard dose was found for absolute MBF. Correlation was still good for EF, TPD and %perfusion with LD being roughly 1/3 of the institutions standard dose. However, due to the increased image noise at LD, relative measures exhibited more scatter, potentially decreasing sensitivity.

OP122

Attenuated Coronary Flow Reserve Early after Implantation of a Bioresorbable Vascular Scaffold: one-month results of the VANISH-trial

W. Stuijfzand, R. Driessen, P. Raijmakers, A. Lammertsma, A. van Rossum, Y. Appelman, J. Lemkes, M. van Leeuwen, N. van Royen, P. Knaapen; VU University Medical Center, Amsterdam, NETHERLANDS.

Background: The bioresorbable vascular scaffold (BVS) may facilitate restoration of normal coronary physiology after resorption of the scaffold. Conversely, early after BVS implantation the mean luminal area is decreased in comparison with conventional metal stents due to bigger strut thickness which may impact coronary flow reserve (CFR). Therefore, a randomised clinical trial of BVS vs. metal drug eluting stent (DES) was initiated, utilizing positron emission tomography (PET) perfusion imaging to assess (hyperemic) myocardial blood flow (MBF) and CFR over a three year period (VANISH-trial). These are the one-month results of the ongoing VANISH-trial to investigate MBF and CFR early after BVS vs. DES implantation. Methods: Sixty patients (45 men (75%), 55 ± 7 years) with a documented single vessel type A or B1 lesion, either stable or unstable angina without biochemical signs of myocardial infarction, were included in this single blind randomized clinical trial. Patients were randomized to implantation of a DES or BVS (Xience Prime or ABSORB, respectively) in a one-to-one fashion. Approximately 1 month after percutaneous coronary intervention patients underwent $H_2{}^{15}O$ PET to assess (hyperemic) MBF and CFR. Results: Lesions were predominantly located in the LAD (n=36, 60%) and less frequently in the RCA (n=14, 23%) or Cx (n=10, 17%). One patient refused PET perfusion at 1 month follow-up (DES arm). Mean rest and hyperemic MBF of the treated vascular territory were 0.99 ± 0.26 and 3.18 ± 0.79 $mL{\cdot}min^{-1}{\cdot}g^{-1}$, respectively. MBF of the treated myocardial territory during rest and hyperemia of DES was comparable with the BVS arm (0.96 ± 0.24 vs. 1.02 ± 0.28 $mL{\cdot}min^{-1}{\cdot}g^{-1}$, p=0.38, and 3.33 ± 0.77 vs. 3.04 ± 0.80 $mL{\cdot}min^{-1}{\cdot}g^{-1}$, p=0.16, respectively). CFR of the treated territory was significantly lower in the BVS arm compared to DES (3.09 ± 0.94 vs. 3.57 ± 0.85, p<0.05). No differences in (hyperemic) MBF and CFR were documented in remote areas between treatment arms. Conclusions: CFR is slightly attenuated one month after implantation of a BVS compared with a DES, which may be related to the increased dimensions of bioresorbable scaffold material as compared with metal.

OP123

Measurement of left ventricular volumes and function using oxygen-15 labelled water gated positron emission tomography: comparison with cardiovascular magnetic resonance imaging

R. S. Driessen, J. Van Timmeren, W. J. Stuijfzand, M. T. Rijnierse, I. Danad, P. G. Raijmakers, A. M. Beek, A. C. Van Rossum, A. A. Lammertsma, H. J. Harms, M. C. Huisman, P. Knaapen; VU University Medical Center, Amsterdam, NETHERLANDS.

Measurement of left ventricular volumes and function using oxygen-15 labelled water gated positron emission tomography: comparison with cardiovascular magnetic resonance

imagingBackground: Positron emission tomography (PET) myocardial perfusion imaging is used for the diagnosis of coronary artery disease (CAD). Diagnostic and prognostic information, however, benefits from an assessment of left ventricular (LV) volumes and function. Recent developments in PET technology have fulfilled the prerequisites for [^{15}O]H_2O PET-derived LV function and dimensions. The aim of this study was to explore the feasibility of evaluating LV function by [^{15}O]H_2O PET using cardiovascular magnetic resonance imaging (CMR) as the reference technique.Materials and methods: Fifty-seven subjects with a varying degree of LV volumes and function were studied. LV end-diastolic volume (LVEDV), LV end-systolic volume (LVESV), and LV ejection fraction (LVEF) were assessed using both ECG-gated first-pass dynamic [^{15}O]H_2O PET and CMR. Intraclass correlation coefficients (ICC) were determined for intraobserver and interobserver variabilities.Results: PET derived LVEDV was comparable with CMR (206 ± 71 vs. 212 ± 68 mL, respectively; P = 0.13). However, LVESV was lower for PET (113 ± 67 vs. 127 ± 70 mL; P < 0.01), resulting in a higher LVEF (49 ± 14 vs. 44 ± 14%; P < 0.01). Correlations between PET and CMR for LVEDV, LVESV, and LVEF were 0.93, 0.91, and 0.87, respectively (P < 0.01 for all). Interobserver ICC for LVEDV, LVESV and LVEF was 0.97, 0.97 and 0.91, respectively. Intraobserver ICC was 0.99, 0.98 and 0.85 for LVEDV, LVESV and LVEF, respectively.Conclusion: It is feasible to assess cardiac functional data using gated dynamic [^{15}O]H_2O PET within the context of a routine quantitative myocardial perfusion study, without increasing radiation exposure or study duration. Good correlations with CMR and excellent reproducibility were found across a widerange of LV volumes and functions. However, PET slightly underestimated LVESV, yielding an augmented LVEF as compared with CMR.

OP124

Gated PET-measured cardiac synchrony correlates with QRS duration.

L. Juárez-Orozco[1], R. H. J. A. Slart[1], R. A. Tio[1], H. Boersma[1], R. A. Dierckx[1], A. Gonzalez-Monroy[1], F. Iñarra-Talboy[2], E. Alexanderson[2]; [1]University Medical Center Groningen, Groningen, NETHERLANDS, [2]Instituto Nacional de Cardiología "Ignacio Chávez", Mexico City, MEXICO.

BACKGROUND: Gated PET myocardial perfusion represents a modern technique with state-of-the-art software for assessment of stress myocardial blood flow (sMBF) and perfusion reserve (MPR). Additionally, it offers the possibility to evaluate ventricular mechanical synchrony of contraction through the Entropy (E) measurement. Interestingly, synchrony has been previously studied although no current gold standard technique is available. The standard 12-derivation EKG is considered useful to assess ventricular electrical synchrony through the evaluation of the QRS complex. Its prolongation (>120ms) has been considered in as criteria for guiding resynchronization therapy. The present study aims to evaluate the relationship between PET-derived ventricular E and the EKG-measured QRS duration when sMBF and traditional cardiovascular risk factors are taken into account. METHODS: We retrospectively included 70 patients (54% males) who underwent a rest and adenosine stress dynamic and 8-frame gated 13N-ammonia PET scan without prior history of myocardial infarction. A standard 12-lead resting EKG was acquired for every patient at the time of the scan. Demographic variables included gender, age, hypertension, type 2 diabetes mellitus, dyslipidemia and smoking. MPR was calculated as the ratio between sMBF and rest myocardial blood flow. Entropy was expressed as a percentage inversely proportional to the uniformity of the ventricular contraction. The QRS complex duration as the dependent variable was dichotomized as normal or prolonged (cutoff 120 ms) and analyzed with a multiple stepwise binary logistic regression model. Statistical analysis was performed using SPSSv.20. RESULTS: Our population had a mean age of 63±10 years. There were 68% of patients with hypertension, 60% with dyslipidemia, 14% with diabetes mellitus and 54% with family history of cardiovascular disease. We documented a mean sMBF=2.09±0.64, mean MPR=2.65±0.83 and mean E=43.8±8.9%. The logistic regression showed Entropy as a significant predictor for an enlarged QRS complex (b=0.116 SE=0.050, OR=1.123 95% [1.018, 1.239], p=0.020). CONCLUSION: Gated PET derived phase Entropy, as a measure for ventricular synchrony, is related to the finding of a prolonged QRS complex in the standard EKG when sMBF and coronary risk factors are taken into account. This suggests that PET derived mechanical synchrony assessment may be useful in further risk stratification. Further research into its role for therapeutic is selection needed.

OP125

Stress-induced Systolic Dysfunction and Subendocardial Ischemia in Left Ventricular Hypertrophy Patients With Preserved Maximal Blood Flow in Ammonia PET

R. Sciagra, H. Castagnoli, F. Cipollini, R. Calabretta, S. Passantino, I. Olivotto; University of Florence, FLORENCE, ITALY.

Aim: Left ventricular (LV) ejection fraction (EF) decrease in stress gated PET reveals ischemia. Patients with hypertrophic cardiomyopathy (HCM) have abnormalities in myocardial blood flow (MBF) due to microvascular dysfunction, but whether these cause ischemia is uncertain. Owing to increased wall thickness, subendocardial ischemia has been suspected, but this could remain undetected if epicardial MBF is

maintained. We assessed whether there is a relationship between LVEF decrease and abnormalities in subendocardial MBF despite preserved maximal MBF in LV hypertrophy patients.Materials and Methods: We studied 15 LV hypertrophy (maximum wall thickness 17 ± 5 mm) patients undergoing rest and stress (dipyridamole) 13NH3 gated PET because of suspected HCM. Gated PET images were analyzed using QGS, MBF was assessed using the PCARD module of PMOD software and a 17 segments scheme. Segmental endocardial and epicardial MBF were evaluated using 13NH3 parametric mapping. Transmural perfusion gradient (TPG) was defined as endocardial MBF/epicardial MBF.Results: In all patients stress MBF was > 1.85 mL/min/g tissue and myocardial flow reserve > 2.5. There were 10 patients with unchanged or increased LVEF after stress (G 1), and 5 with LVEF decrease (G 2). Entire wall resting and stress MBF were not different between the two groups (rest G 1: 0.85 ± 0.22 vs. rest G 2: 0.89 ± 0.11; stress G 1: 2.72 ± 0.46 vs. stress G 2: 2.65 ± 0.54; all NS), so resting endocardial (G 1: 0.83 ± 0.23 vs. G 2: 0.80 ± 0.11; NS) and epicardial MBF (G 1: 0.67 ± 0.24 vs. G 2: 0.64 ± 0.17; NS), and resting TPG (G 1: 1.31 ± 0.26 vs. G 2: 1.32 ± 0.28; NS). Under stress, epicardial MBF remained comparable (G 1: 1.79 ± 0.56 vs. G 2: 1.82 ± 0.59, NS), but endocardial MBF was lower in G 2 (G 1: 2.26 ± 0.66 vs. G 2: 2.03 ± 0.40, $p < 0.0001$) and TPG became significantly different: G1: 1.36 ± 0.36 vs. G 2: 1.22 ± 0.42, $p < 0.02$. The proportion of segments with lower endocardial than epicardial MBF under stress was significantly higher within G 2 than within G 1 patients (36% vs. 16%, $p< 0.001$).Conclusion: In patients with LV hypertrophy suspected of HCM, but with apparently preserved stress MBF, an abnormal LVEF response in stress gated PET was accompanied by decreased stress endocardial MBF, a finding that supports the notion of isolated subendocardial ischemia.

OP126

AQUA-5: Four Software Tools for 15O-Water PET Myocardial Perfusion Quantification Exhibit Good Intraobserver Reproducibility

S. V. Nesterov[1,2], K. Yoshinaga[3], Y. Tomiyama[3], C. Han[1], R. Sciagrà[4], V. Berti[4], P. Knappen[5], I. Danad[5], J. M. Knuuti[1]; [1]Turku PET Centre, Turku, FINLAND, [2]Institute of Evolutionary Biochemistry and Physiology, RAS, St. Petersburg, RUSSIAN FEDERATION, [3]Hokkaido University Graduate School of Medicine, Sapporo, JAPAN, [4]Nuclear Medicine Unit of the University of Florence, Florence, ITALY, [5]Departments of Nuclear Medicine and PET Research, of VU University Medical Center, Amsterdam, NETHERLANDS.

AIM. 15O-labelled water is considered the gold standard for myocardial blood flow (MBF) quantification with PET. Several software tools (SW) enable the quantification; however, there are still no exhaustive cross-comparison studies for these SW, needed to standardize the approach. In the AQUA-5 project, we aimed to investigate several clinically important issues, and as an initial step, we aimed to evaluate the intraobserver reproducibility of MBF and myocardial flow reserve (MFR) using existing SW. METHODS. Five tools-Carimas, CardiacVUer, HOQUTO, PMOD, and Siemens In-House Software-were studied using dynamic PET scans (a hybrid 64-row Discovery VCT PET/CT scanner) from 91 clinical patients. 15O-labelled water (900-1100 MBq) was injected at rest; a stress scan was performed using adenosine (140μg/kg/min). Experts used one of the tools each to analyze global and regional (LAD, LCx and RCA) MBF and MFR twice with at least one week interval. We applied a custom linear mixed model for the repeated measures to produce the two agreement metrics-intraclass correlation coefficient (ICC) and difference between the values from the models-calculated pairwise. Differences below 20% of median values with corresponding ICCs above 0.75 witnessed to good reproducibility. RESULTS. MBF-rest and stress-was measured in mL/min/g, MFR and ICC were unitless. CARIMAS. Global rest MBF (rMBF) - 0.00±0.07, ICC=0.95; stress MBF (sMBF) - 0.04±0.37, ICC=0.94; MFR - 0.05±0.38, ICC=0.91. Regional rMBF values ranged from 0.01±0.06 to 0.01±0.12, ICC: 0.90-0.97; regional sMBF: 0.01±0.45-0.13±0.41, ICC: 0.92-0.94. Regional MFR: 0.01±0.47-0.10±0.39, ICC: 0.85-0.93. CARDIAC VUER. Global rMBF - 0.00±0.05, ICC=0.97; sMBF - 0.01±0.15, ICC=0.98; MFR - 0.00 ±0.21, ICC=0.96. Regional rMBF: 0.00±0.06-0.01±0.05, all ICC values were 0.97; regional sMBF: 0.00±0.19-0.02±0.17, ICC: 0.97-0.98. Regional MFR: 0.00±0.21-0.01±0.24, ICC: 0.95-0.96. HOQUTO: Global rMBF - 0.05±0.31, ICC=0.66; sMBF - 0.18±0.97, ICC=0.58; MFR - 0.01±0.95, ICC=0.96. Regional rMBF: 0.05 ±0.34-0.96±8.56, ICC: 0.00-0.69; regional sMBF: 0.04 ±1.33-0.18±1.27, ICC: 0.56-0.67. Regional MFR: 0.02 ±1.10-0.15± 1.38, ICC: 0.46-0.54. PMOD: Global rMBF - 0.00±0.07, ICC=0.97; sMBF - 0.09±0.46, ICC=0.83; MFR - 0.04±0.38, ICC=0.90. Regional rMBF: 0.00 ±0.08-0.01±0.09, ICC: 0.94-0.98; regional sMBF: 0.06 ±0.43-0.11±0.55, ICC: 0.81-0.89. Regional MFR: 0.00 ±0.40-0.06± 0.45, ICC: 0.88-0.90. SIEMENS IN-HOUSE SW: Global rMBF - 0.09±0.15, ICC=0.85; sMBF - 0.02±0.29, ICC=0.94; MFR - 0.15±0.36, ICC=0.93. Regional rMBF: 0.04±0.08-0.11±0.18, ICC: 0.81-0.95; regional sMBF: 0.01±0.32-0.03±0.32, ICC: 0.93-0.96. Regional MFR: 0.10±0.36-0.17± 0.40, ICC: 0.93-0.94. CONCLUSION. The intraobserver reproducibility was good in four out of the five studied tools for measuring MBF with 15O-water PET.

OP127

Spill-over effect of radioactivity from right ventricular cavity on septum in cardiac PET ^{15}O-water study

C. Han; Turku University Central Hospital and University of Turku, TURKU, FINLAND.

Purpose: In heart, ventricular septum separates the left and right ventricles(LV and RV), implying that the spill-over effects from both sides should be considered in PET studies. However, in cardiac PET perfusion analysis, the effect from right ventricular radioactivity is not always corrected, leading the loss of accuracy of modelling results in septum. This study investigates the bias in perfusion estimation without RV spill-over correction, based on human 15O-water studies and simulated data.Methods: Two 1-tissue compartment models for ^{15}O-water study(Iida et al. 1989), with and without RV spill-over correction (LV Model and LV_RV Model), have been implemented in Carimas (a PET data analysis package developed in Turku PET Centre, Finland http://www.turkupetcentre.fi/carimas). In simulation study, time-active curves (TAC) from left (LV) and right ventricular cavities were taken from typical ^{15}O-labelled water clinical studies. In LV_RV Model, the myocardial ROI TAC was expressed as: ROI(t)=Va_lv*LV(t)+Va_rv*RV(t)+alpha*C(t), where Va_lv and Va_rv are spill-over fractions from LV and RV, respectively, and alpha is perfusable tissue fraction. 100 ^{15}O-water PET perfusion patient data were analyzed using two models.Results: In patient data, septal perfusion was found to be reduced 17.3% without RV spill-over correction, meanwhile, lateral segments had very slight effect by RV radioactivity (0.9%). In simulation study, RV was found to affect significantly the perfusion estimation and this effect becomes bigger for higher perfusion values and larger Va_rv. When ground values of Va_rv=0.1, 0.15, 0.2, 0.25ml/ml, for ground flow value of 0.98 ml/g/min (as rest condition), estimated flow values with LVModel were 0.94(-13%), 0.85(-20%), 0.78(-27%) and 0.72(-33%) ml/g/min, respectively; for ground flow value of 3.2 ml/g/min (as stress condition), estimated values with LVModel were 2.66(-17%), 2.34(-27%), 2.07(-36%) and 1.84(-43%) ml/g/min, respectively. Meanwhile, estimated flow values from LV_RVModel were very close to ground values (error<2%).Conclusions: Based on patient data and simulation, this study confirms that spill-over effect from RV leads to severe underestimation of perfusion in septum, unless correction is applied in the analysis tool.

501 - Sunday, October 11, 2015, 4:30 PM - 6:00 PM, Hall 1

CME 4 - Inflammation and Infection: Imaging Infection in the Immunocompromised Patient

OP128

Imaging Infection in the HIV Positive

M. M. Sathegke, **SOUTH AFRICA**

OP129

Imaging Infection in the Immunosuppressed Patient

C. Bleeker-Rovers, **NETHERLANDS**

OP130

Imaging Infection in the Post-Transplant Patient

J. Buscombe, **UK**

502 - Sunday, October 11, 2015, 4:30 PM - 6:00 PM, Hall 2

Joint Symposium 4: EANM/EORTC: Hypoxia Imaging: A Powerful Tool to Better Understand Tumour Biology and Guide Cancer Therapy

OP131

Hypoxia as Target for Cancer Therapy

K. Williams, **UK**

OP132

Imaging Hypoxia: Facts and Pitfalls

M. R. Horsman, **DENMARK**

OP133

Experience using Hypoxia Imaging in Clinical Trials

P. Lambin, **NETHERLANDS**

505 - Sunday, October 11, 2015, 4:30 PM - 6:00 PM, Hall G2

Do.MoRe: Treatment of Bone Metastases

OP134

Optimization of imaging following 223Ra administration in targeted alpha-emitting radionuclide therapy of bone metastases.

N. Benabdallah[1], M. Bernardini[2], C. de Labriolle Vaylet[3], D. Franck[1], A. Desbrée[1]; [1]IRSN, Fontenay aux Roses, FRANCE, [2]Hôpital Européen George Pompidou, Paris, FRANCE, [3]Hôpital Trousseau, Paris, FRANCE.

Purpose: With a growing demand of alpha-emitting radiopharmaceuticals, especially Xofigo® (223RaCl2) which is used in the treatment of metastatic bone disease, the optimization of dosimetry becomes necessary.

Indeed, in Europe, as stated on the council directive 2013/59/euratom, exposures of target volumes for radiotherapeutic purposes shall be individually planned taking into account that doses to non-target volumes and tissues shall be as low as reasonably achievable. To personalize the dosimetry, patient images shall be used. Nevertheless, less than 2% of the 223Ra emissions are from photons. Therefore, the purpose of this study was then to investigate the possibility of imaging 223Ra. Methods: The experiments were conducted at the Hopital Européen Georges Pompidou with an Infinia Hawkeye 4 gamma camera, equipped with a medium-energy collimator. Imaging parameters, such as sensibility, spatial resolution and energy spectrum, were determined using several physical phantoms with a source of 6 MBq of 223Ra. Bone metastases were modeled with a NEMA Body Phantom to investigate image degradation based on the concentration of 223Ra. Results: The acquired energy spectrum allowed to visualize several photon peaks: at 85, 154 and 270 keV. Camera sensitivity measured from the phantom study was 102.3 cps/MBq for the 85 keV ± 20 %, 89.9 cps/MBq for the 154 ± 20 % window and 65.4 cps/MBq for the 270 ± 10 % window. The spatial resolution (full-width at half-maximum) was respectively 1.7, 1.9 and 1.8 cm for the three energy windows. SPECT/CT images of NEMA Body Phantom without and with attenuation have permitted to determine the best reconstruction parameters. Conclusion: This study has demonstrated that it is possible to obtain clinically relevant information from images of 223Ra. All these results will be valuable to analyze biodistribution imaging of the radiopharmaceutical in the patient body and go further in the reconstruction of patient images in order to personalize the dosimetry.

OP135

Progress of blood capacity under Radium-223 treatment

C. Körber, N. Körber-Hafner; Nuclear Medicine Fulda, Fulda, GERMANY.

AIM OF STUDY: Since some months Radium-223 (Xofigo, Bayer Pharma AG, Berlin, Germany) is a rationale for the treatment of castration-resistent metastatic prostate cancer (1) The relevance of the irradiation on blood building is not yet well investigated and could be a reason for the decline of blood cells. We therefore investigated this effect on the blood levels under therapy. METHOD: We have treated 10 patients so far and investigated the blood levels of erythyrocytes, leucocytes and thrombocytes under therapy, at the beginning and the end of Radium-223 infusion as well as in all cycles of injection. We compared the blood levels according to the level at the start point. Furthermore other possible side effects we evaluated. Statistical analyses were conducted with Statistica 10.0 (StatSoft). Two-tailed P values of less than 0,05 were considered to indicate statistical significance. RESULTS: The time interval of investigation was between February 2014 and February 2015. No severe side effects as nausea or vomiting could be ruled out. The levels of leucocytes reduced between injection 1 and 2 (mean ± SD) 5,6 to 4,6 ($p<0,08$), between injection 1 and 3 $p<0,1$, between injection 1 and 4 $p<0,01$, between injection 1 and 5 $p<0,13$, between injection 1 and 6 $p<0,3$. Similar results were found for the parameters of erythrocytes and thrombocytes, revealing a significant decline of blood cells between injection 1 and 4, but no significant reduction of the blood building capacity regarding injection 1 and 6. DISCUSSION: The treatment of castration-resistent metastatic prostate cancer is a save treatment option without severe side effects as shown. The reduction of the blood building regarding erythrocytes, leucocytes and thrombocytes are only significant between the injection 1 and 4, but the blood levels from start and end point after 6 injections show no significant reduction. No participant of the treatment group had to be excluded. Literature: Parker C. et al., Alpha Emitter Radium-223 and survival in metastatic prostate caner, N Engl J Med 2013;369:213-223.

OP136

Feasibility and efficacy of 223Ra-dichloride in treatment of bone metastases in patients with castration-refractory prostate cancer (mCRPC)

s. mazzarri[1], G. Boni[1], E. Borsò[2], L. Galli[3], A. Farnesi[4], F. Betti[1], L. Antonacci[1], A. Traino[5], S. Ricci[4], D. Volterrani[1]; [1]Regional Center Of Nuclear Medicine, University Hospital Of Pisa, pisa, ITALY, [2]Division of Nuclear Medicine, Sant'Andrea Hospital of La Spezia, La Spezia, ITALY, [3]Oncology Division, University Hospital of Pisa, pisa, ITALY, [4]Oncology Division,University Hospital of Pisa, pisa, ITALY, [5]Health Physics Unit, Section of Medical Physics, University Hospital, Pisa, Italy, pisa, ITALY.

Aim: To present the Tuscany single-centre experience about the employing of the novel therapeutic radiopharmaceutical 223Ra-dichloride in the treatment planning of patients with mCRPC. Method:Thirteen patients were treated from August 2013 to date. Five patients have been enrolled in the Bayer Clinical Study 16216 and 8 have been treated as routine application. Patients (age 67±8.4 yrs, median PSA 149.5 ng/mL, excluding one case of neuroendocrine differentiation) received 223Ra-dichloride 50 kBq/kg i.v. on day 1 every 28 days for a maximum of 6 cycles. Pre-treatment evaluations were made using CT in order to exclude visceral metastases, and bone scan. Patients have been evaluated at every cycle with

complete blood chemistry (including serum ALP, PSA and LDH), pain VAS score, quality of life questionnaire (FACT-p), and analgesic consumption. The last group of patients started the cure in March 2015. Results: At the current time-point 13 patients received 72 cycles of 223Ra-dichloride. No problems in vial manipulation, dose preparation and administration occurred. A multidisciplinary team has followed patients during both screening and treatment period. Only 3 cycles have been delayed (2 due to blood toxicity, 1 due to drug's manufacturing hitches) and 3 patients discontinued the treatment (2 because of non reversible blood toxicity and anorexia, and 1 because of hepatic disease progression). Regarding valuable clinical data, bone marrow toxicity resulted in G3 anemia in 2 patients, G2 neutropenia in 2 patients, and G1 thrombocytopenia in 1 patient. Anorexia G3 occurred in 3 patients, while no case of diarrhoea was observed. Biomarkers response showed median ALP decline of -50% and median LDH decline of -5%. We observed mean PSA decline of -15%. One patient who presented with superscan at baseline received 223Ra-dichloride 5 cycles before hepatic progression, showing ALP levels decline of -89%, LDH -44% and PSA -48%. According to VAS score and FACT-p, most of patients had bone pain relief and reduced pain drugs intake. Conclusion: Single-centre experience shows the feasibility and efficacy of radiometabolic therapy with 223Radium-dichloride in patients with mCRPC. Multidisciplinary careful evaluation of bone marrow toxicity and gastrointestinal adverse events must be carried out to optimize individual compliance. Palliative effect allows decreasing pain drugs consume. The mild toxicity could permit the use of 223Ra- dichloride in combination with other treatments.

OP137

Metastatic control probability in patients with prostate cancer metastatic to bone treated ^{186}Re-HEDP

A. M. Denis-Bacelar[1], A. Divoli[2], S. Chittenden[2], Y. Du[2], G. D. Flux[2]; [1]Institute of Cancer Research, London, UNITED KINGDOM, [2]Royal Marsden Hospital, London, UNITED KINGDOM.

Aim: The metastatic control probability model can be used to estimate the impact of relevant factors on response to treatment. Disease burden is of particular interest in patients with castration-resistant prostate cancer (CRPC) metastatic to bone, where the number and volume of bone lesions varies for each patient. The aim of this study was to determine the metastatic absorbed dose necessary to obtain a metastatic control probability of 0.9 in patients treated with molecular radiotherapy. Materials and Methods: A cohort of 22 patients treated with 5 GBq of ^{186}Re-HEDP from a phase II clinical trial was considered. Absorbed dose distributions were obtained using the Qrius^{TM} dosimetry toolkit from quantified co-registered sequential SPECT scans of the thorax and pelvis. Bone lesions were outlined using volume-dependent thresholds obtained from phantom studies. Tumour control probabilities (TCP) and biological effective doses (BED) were calculated for each lesion using the linear-quadratic model. Radiobiological parameters for prostate cancer cells of α=0.12, α/β=1.5, clonogenic cell density of 10^7 cm^{-3} and a repair half-time of 1.5 h were assumed for all patients. The metastatic control probability (MCP) was determined as the product of the TCP to each lesion. The metastatic absorbed dose (the mean of the absorbed doses delivered to all lesions) necessary to achieve an MCP of 0.9 was then determined from the delivered absorbed dose distribution. Results: A total of 379 metastatic bone lesions were outlined, with a median of 11 per patient. The mean total volume of lesions was 228 ml (range 17 - 913 ml). The mean lesion volume per patient ranged from 6 ml to 57 ml. The range of metastatic absorbed doses delivered was 8 - 32 Gy. The metastatic absorbed dose to obtain an MCP of 0.9 ranged from 93 Gy to 589 Gy (mean 219 Gy). Conclusion: Preliminary results show that the metastatic absorbed doses required to achieve a high metastatic cure probability changes significantly within the patient cohort studied. This indicates the effect of the heterogeneous distribution of absorbed doses delivered to multiple lesions, whereby the MCP is heavily influenced by lesions with the lowest uptake.

OP138

A DOTA conjugated Zoledronic acid derivative: A novel bone targeting theranostic compound

M. Meckel[1], R. Bergmann[2], W. Mohnike[3], M. Miederer[4], F. Roesch[1]; [1]University of Mainz, Mainz, GERMANY, [2]Helmholtz Zentrum, Dresden-Rossendorf, GERMANY, [3]Diagnostisch Therapeutisches Zentrum, Berlin, GERMANY, [4]University Hospital, Mainz, GERMANY.

Aim of the study: Zoledronic acid proofed to have a high affinity to calcified tissues and is commonly used in the treatment of osteoporosis and bone metastases. A conjugate of zoledronic acid with a macrocyclic chelator, labeled with ^{68}Ga and ^{177}Lu, opens new possibilities in bone targeted radionuclide imaging and therapy. Endoradiotheraphy with ^{177}Lu-labelled macrocyclic bisphosphonates could have great potential subsequent to PET examinations utilized with ^{68}Ga-labelled analogous in the treatment of painful skeletal metastases, following the *theranostics* concept. Methods: We synthesized a DOTA zoledronic acid conjugate (DOTAM^{ZOL}) and labelled it with the PET-nuclide ^{68}Ga, and the therapy nuclide ^{177}Lu. The new bone targeting compound was evaluated in *in vivo* small animal PET and SPECT and in *ex vivo* organ distribution studies against [^{18}F]NaF, ^{223}RaCl$_2$ and other

DOTA bisphosphonates in healthy Wistar rats, followed by first human applications in metastatic patients. Results: The new ligands reached a RCY of 80 to 90% in 15 min with ^{68}Ga. After resin purification the purity of the [^{68}Ga]DOTAM^{ZOL} was higher than 98%. The tracers showed low uptake in soft tissue, a fast renal clearance and a high accumulation in bone (SUV_{Femur} = 5.4±0.6). Labelling with ^{177}Lu resulted in quantitative yields. [^{177}Lu]DOTAM^{ZOL} showed a superior target to background ratio compared to $^{223}RaCl_2$. First applications in bone metastatic patients revealed high accumulation in metastatic lesions. Conclusions: The novel bone targeting compound DOTAM^{ZOL} showed a promising uptake profile and a high target to background ratio. The *theranostic* approach seems to be a promising concept for the management of bone metastases in future.

OP139

Dosimetry Results of Lu-177-DKFZ-PSMA-617 Treatment in Castration Resistant Prostate Cancer Patients

N. Yeyin[1], A. Mohammad[1], **L. Kabasakal**[1], E. Demirci[2], A. Aygun[1], M. Ocak[3], T. Toklu[4], H. Tanyildizi[1], N. Selcuk[4]; [1]Department of Nuclear Medicine, Cerrahpasa Medical Faculty, Istanbul University, istanbul, TURKEY, [2]Department of Nuclear Medicine, Sisli Etfal Training and Research Hospital, istanbul, TURKEY, [3]Department of Pharmaceutical Technology, Pharmacy Faculty, Istanbul University, istanbul, TURKEY, [4]Department of Nuclear Medicine, Yeditepe University Medical School, istanbul, TURKEY.

Aim: The unique expression of PSMA provides an excellent target for prostate cancer imaging and therapy using Ga-68 and Lu-177 labeled PSMA ligands. Lu-177-DKFZ-617 PSMA ligand seems to be a promising tracer for radionuclide therapy in patients with progressive prostate cancer. However, there are no published data regarding the radiation dose given to the normal tissues for the systemic therapy of Lu-177-DKFZ-617 PSMA ligand. The aim of the present study was to estimate the radiation doses in patients who underwent radiomethabolic therapy. Methods and materials : The study composed of 9 patients with progressive disease who underwent Lu-177 PSMA therapy with a mean age of 62 ±5.7 years. All patients had prior PSMA PET imaging and had intense tracer uptake at the lesions. Patients received a mean of 5.4±1.5 GBq, ranged from 3.3 GBq to 7.4 GBq Lu-177-PSMA. To evaluate bone marrow absorbed dose 2 cc blood samples were withdrawn in short variable times (3, 15, 30, 60, 180. minutes and 24, 48, 120. hours) after injection. Further more whole body images were obtained at 4, 24, 48 and 120 hour after injection and in order to quantify the activity taken up in the body, kidneys, liver, right parotid and left parotid, and over lesions. The geometric mean of anterior and posterior counts were determined through ROI analysis, after that background subtraction and attenuation correction were applied using patients Ga-68-PSMA PET/CT images taking into account. Organ thickness, body thickness and Hounsfield unites from Computed Tomography scan. OLINDA/EXM dosimetry program was used for curve fitting, residence time calculation and absorbed dose calculations. Results: Calculated absorbed dose of bone marrow, left kidney, right kidney, left parotid, right parotid and total body were 0.08±0.0.03, 2.12 ±0.66, 1.95±0.78, 2.88±1.83, 2.79±1.32, (Gy/3.7GBq) respectively. For the liver, left and right lacrimal glands and whole body radiation doses were 0.6±0.2, 6.2±3.9, 6.4±3.4 and 0.1 ±0.04 (Gy/3.7 GBq) respectively. The estimated lesion doses were ranged from 3.05 to 47.7 GY/3.7 GBq with a mean of 12.6±12.8 Gy/3.7GBq. Conclusions : Our first results suggested that Lu-177 DKFZ-PSMA-617 therapy is a safe method, which can be given in 3 to 4 cycles of 7.4 GBq. The target organ seems to be the parotid glands rather than kidneys and bone marrow. The lesion radiation doses are within acceptable ranges however there is a substantial individual variance so patient dosimetry seems to be mandatory.

OP140

Peptide Radioligand Therapy (PRLT) Using Lu-177 Labeled DOTAGA-PSMA Inhibitor Yields Objective Responses in Metastatic Castrate-resistant Prostate Cancer

H. R. Kulkarni[1], A. Singh[1], C. Schuchardt[1], I. Klette[1], H. J. Wester[2], R. P. Baum[1]; [1]THERANOSTICS Center for Molecular Radiotherapy and Molecular Imaging, Bad Berka, GERMANY, [2]Pharmaceutical Radiochemistry, Technical University Munich, Munich, GERMANY.

Aim: We present the first clinical results assessing objective response after therapy with Lu-177 DOTAGA-PSMA inhibitor (Lu-177 PSMA) in patients with metastatic castrate-resistant prostate cancer (mCRPC).Methods: Peptide radioligand therapy (PRLT) with Lu-177 PSMA was performed in 56 patients, administering a total of 131 cycles. Ga-68 PSMA PET/CT (contrast-enhanced CT scan) was used for patient selection as well as follow-up after 2 and 4 therapy cycles. The mean administered activity of Lu-177 PSMA per cycle was 5.7±0.8 GBq, median 5.8 GBq. Post-therapy response after 2 or 4 cycles could be assessed until now in 31 patients. The results were analyzed using a prospective patient database (338 items/patient).Results: According to molecular imaging criteria, partial remission was observed in 14 (44 %) patients, correlating with the fall in PSA after therapy. The disease remained stable in 7 (22 %) patients. Progressive disease after initial response was noted in 3 (9.6 %) patients.

Median time to progression after the first PRLT in initial responders was 13 months (range 4 - 11). Thus, the number of responders was 24/31 patients (78 %). 7 patients (22 %) with extensive metastastes did not respond to therapy and died with a median time of 10 months after the first therapy cycle. Morphological response (partial remission according to RECIST) was observed in 6 patients, and stable disease in 15 patients. All symptomatic patients reported significant improvement in pain and quality of life after therapy. The treatment was well tolerated by all patients without any significant adverse effects (especially no dry-eye-dry-mouth syndrome) or alterations in any of the laboratory parameters or of renal function (as determined by Tc-99m MAG3/TER and serial creatine and GFR measurements).Conclusion: Peptide radioligand therapy (PRLT) utilizing the small molecule Lu-177 DOTAGA-PSMA inhibitor is efficacious, not only in terms of symptomatic improvement, but also for reducing the tumor burden. PRLT was well tolerated in all patients, i.e., without hematological, salivary or renal toxicity.

OP141

Quantifying the Effect of Peptide Amount on the Biologically Effective Dose for Therapy using Lu-177 Labeled PSMA Ligands

P. Kletting[1], C. Schuchardt[2], H. Kulkarni[2], M. Sayeg[2], S. Wiesalla[2], G. Winter[1], A. Singh[2], R. Baum[2], A. Beer[1]; [1]Ulm University, Deparment of Nuclear Medicine, Ulm, GERMANY, [2]Zentralklinik Bad Berka, THERANOSTICS Center for Molecular Radiotherapy and Molecular Imaging (PET/CT), ENETS Center of Excellence, Bad Berka, GERMANY.

Peptide radioligand therapy (PRLT) using Lu-177 labeled PSMA ligands is a promising therapy option for patients with prostate cancer. The effect of peptide amount on the biodistribution and absorbed dose has been observed in animal studies and in patients [1-2] for PRLT, but was never systematically investigated and quantified for PSMA ligands. The aim of this work is to quantify the impact of PSMA peptide amount on the biologically effective dose (BED) for critical organs and the tumor using a physiologically based pharmacokinetic model. Methods: Included were 5 patients suffering from metastasized prostate cancer. The administered activity was 5.7±1.3 GBq (labelled with 160±16 μg) Lu-177 PSMA ligand. Based on 4-6 [0.5, 3, 24, 48, (72), 120 h] conjugated planar whole-body scans, time-dependent whole-body, organ and tumor activities were determined. A physiologically based pharmacokinetic (PBPK) model was developed using SAAM 2. Relevant biological mechanisms such as blood flow, transport in the interstitial space, specific binding, internalization, release of activity from cell and renal clearance were included in the model. The model parameters were fitted to the time activity data of the patients or were taken from the literature. For the simulation study the model was implemented in Matlab/Simulink. The degree of binding sites saturation and the BED of the tumor and critical organs were calculated using the estimated model parameters for different amounts of peptide. Results: The model describes the data well. Standard deviations and correlation matrixes are adequate. The estimated values for tumor perfusions (0.01-8 ml/g/min) and receptor concentrations (18-2200 nmol/L) showed high variation. However, kidney receptor concentrations (21±12 nmol/L) were in the same order of magnitude for all patiens. The simulation study using these parameters showed that for moderately or poorly perfused tumors small amounts of peptide led to considerably lower saturation of binding sites compared to kidney and salivary glands. Therefore, the BED for a moderately perfused tumor for a limiting kidney dose of 10 Gy was 2.3 -fold higher when increasing the amount from 16 nmol to 256 nmol. Conclusions: Saturation of binding sites in kidney and salivary glands is reached with considerably lower amounts of peptide than in many tumors. Therefore, optimizing the amount of peptide (or preloading) with PSMA ligands might considerably improve the ratio of tumor-to-salivary and tumor-to-kidney BED. [1] Kletting et al. 2012 Med. Phys. [2] Sabet et al. 2013 EJNMMI Res#

506 - Sunday, October 11, 2015, 4:30 PM - 6:00 PM, Hall 6
Teaching Session: Anatomy Refresher and Cross-sectional Imaging: Abdomen & Pelvis

OP142

Anatomy Refresher and Cross-sectional Imaging: Abdomen & Pelvis

C. Fowler, **UNITED KINGDOM**

507 - Sunday, October 11, 2015, 4:30 PM - 6:00 PM, Hall F
Clinical Oncology: Lung

OP143

18F-fluorodeoxyglucose PET/CT and Dynamic Contrast-Enhanced MRI as prognostic indicators in Malignant Pleural Mesothelioma (the SWAMP trial)

D. O. Hall[1], I. D. Lyburn[1], J. Searle[1], C. E. Hooper[2], N. A. Maskell[3]; [1]Cobalt Health, Cheltenham, UNITED KINGDOM, [2]Worcester Royal Hospital, Worcester, UNITED KINGDOM, [3]University of Bristol, Bristol, UNITED KINGDOM.

Aims: The South West Area Mesothelioma and Pemetrexed (SWAMP) trial was carried out to assess the role of various

biomarkers in monitoring treatment in Malignant Pleural Mesothelioma (MPM). This included ^{18}F-fluorodeoxyglucose positron emission tomography with computed tomography (FDG PET/CT) and dynamic contrast-enhanced magnetic resonance imaging (DCE-MRI). This paper assesses the prognostic ability of baseline volumetric PET/CT and DCE-MRI. Materials and Methods: 73 patients were recruited, 58 received chemotherapy, 15 were included in the comparator arm. Patients had FDG PET/CT and DCE-MRI on the same day at a single institution. PET/CT studies were carried out on a Philips Gemini system, and DCE-MRI was carried out on a Philips Open MRI scanner. Follow up was for at least 12 months. The PET studies were assessed using volumetric analysis including all areas with SUV > 2.5. Metabolic Tumour Volume (MTV) was calculated. The DCE-MRI enhancement images were assessed, and an ROI was drawn at over a central tumour slice. The integrated area under the enhancement-time curve in the first 90s was calculated (IAUC90). Kaplan-Meier analysis was carried out for PET MTV and DCE-MRI IAUC90. Results and conclusions: Overall Survival (OS) was significantly longer for MTV below median than above ($p<0.001$), 481 days (IQR 266-709 days), compared with 266 days (IQR 177-456 days). OS was generally longer for IAUC90 below median than above, 458 days (IQR 233-689 days) compared with 274 days (IQR 204-498 days) though the difference wasn't significant at the 5% level ($p=0.08$). Adding IAUC90 to MTV gave no significant change in prognosis. Baseline FDG PET/CT was predictive of OS. Baseline DCE-MRI (iAUC90) was not predictive of OS. However, DCE-MRI results were promising, and would be worth further study.

OP144

Respiratory-gated FMISO-PET/CT detects tumor hypoxia with higher sensitivity in non-small cell lung cancer

S. Watanabe[1], **S. Okamoto**[1], T. Shiga[1], T. Inoue[2], K. Hirata[1], K. Magota[1], K. Nishijima[3], Y. Kuge[3], H. Shirato[2], N. Tamaki[1]; [1]Department of Nuclear Medicine, Hokkaido University Graduate School of Medicine, Sapporo, JAPAN, [2]Department of Radiation Medicine, Hokkaido University Graduate School of Medicine, Sapporo, JAPAN, [3]Central Institute of Isotope Science, Hokkaido University, Sapporo, JAPAN.

Objective: More appropriate therapeutic strategies are required for the tumor hypoxia evaluated by PET. However, respiratory motion during PET imaging introduces quantitative inaccuracies in non-small cell lung cancer (NSCLC). For the exact targeting to hypoxic area in NSCLC in radiation therapy, respiratory gating (RG) on the hypoxic PET may be a good tool. The aim of this study was to investigate the usefulness of RG on 18F-fluoromisonidazole (FMISO) PET image quantification for hypoxia. Methods: FMISO-PET/CT was performed in 13 patients with pretreatment NSCLC. PET images were scanned by integrated PET/CT scanner at 4 hours after FMISO injection. The respiratory signal was obtained using a pressure sensor integrated in an elastic belt placed around the patient's abdomen. The respiratory cycle was divided into 5 phases, corresponding to about 6 minute/phase accumulation in our protocol. We used the 3rd phase for analysis which is equivalent to expiration phase. Non-gating images (NG) were reconstructed with median 6 minutes of acquired PET data, adapting to RG images. Differences in SUVmax, tumor to muscle ratio (TMR), tumor to blood ratio (TBR) and hypoxic volume (HV) between RG and NG images were analyzed. We defined hypoxia as the area with TBR ≥ 1.50. Results: In RG images, SUVmax, TMR and TBR increased in 10 patients comparing to those in NG images. RG images analysis demonstrated significant increase comparing to NG images for SUVmax (RG: Median 1.90, Range 0.72 - 4.89), (NG: 1.71, 0.64 - 4.92), ($p = 0.008$), TMR (RG: 1.58, 0.53 - 3.54) (NG: 1.43, 0.46 - 3.65) ($p = 0.011$), and TBR (RG: 1.39, 0.50 - 3.90) (NG: 1.31, 0.45 - 3.92) ($p = 0.006$). Measurements in RG images showed increase of up to 22.0% in SUVmax, 23.7% in TMR and 22.0% in TBR from NG images. The hypoxia was observed in 3 patients with NG images, and increased to 5 patients with RG images. HV in RG was also significantly larger than that in NG (RG: 9.9 mL, 0.1 - 53.1 mL) (NG: 9.2 mL, 0.0 - 52.5 mL) ($p = 0.022$). HV increased in all 5 patients from NG images to RG images. Conclusions: FMISO-PET with RG demonstrated higher sensitivity of hypoxic evaluation. RG might be useful tool for the exact targeting to hypoxic area in NSCLC for the radiation therapy.

OP145

Predictive value of intratumoral metabolic heterogeneity features for early treatment failure of tyrosine kinase inhibitor in patients with EGFR mutated NSCLC

S. Ha, S. Park, S. Lee, J. Paeng, B. Keam, T. Kim, D. Kim, D. Heo; Seoul National University Hospital, Seoul, KOREA, REPUBLIC OF.

Aim: Intratumoral heterogeneity has been associated to treatment failure and patient prognosis. We hypothesized that intratumoral metabolic heterogenetiy measured by textural analysis on pretreatment [F-18] fluoro-deoxyglucose positron emission tomography/computed tomography has predictive value in targeted therapy in patients with non-small cell lung cancer (NSCLC)Materials and methods: NSCLC cases with activating EGFR mutation treated with tyrosin kinase inhibitor (TKI) were retrospectively reviewed. Eight selected textural features (TFs) were explored for predictive value in test set

(n=161) and applied in validation set (n=21) for survival analysis. Recursive partitioning method was used to find the optimal cutoff value and Harrell's C index was used to calculated predictive value.Results; All the 8 TFs had significantly increased harzard ratio (HR) for progression free survival (PFS) in univariate analysis (e.g. local entropy: HR 6.41, 95% confidential interval [CI] 2.80-14.68). Multivariate analysis with initial stage, performance status (PS), and metabolic volume showed independent predictive value of TFs (HR 4.86, 95% CI 1.97-11.98 by local entropy). TFs had incremental predictive value of early TKI failure compared to stage and PS (C-index 0.596 vs. 0.662, P=0.024, by local entropy).Conclusion: TFs for intratumoral metabolic heterogeneity are significant predictive factors for TKI treatment in EGFR mutant NSCLC patients. These TFs could be used for companion diagnostic markers for identification of a risky population of early EGFR TKI failure. Correlation study to genomic alteration should be needed in future.

OP146

Correlation of metabolic information on PET/CT and tissue expression of HIF-1α and CD68$^+$ macrophages in surgically treated NSCLC

E. Lopci[1,2], F. Grizzi[1], L. Toschi[1], D. Rahal[1], L. Olivari[3], F. Marchesi[1], D. Qehajaj[1], N. Cortese[1], G. Finocchiaro[1], S. Mattioli[2], M. Roncalli[1], S. Fanti[4], A. Santoro[1], A. Chiti[1]; [1]Humanitas Clinical and Research Hospital, Rozzano (Milano), ITALY, [2]Alma Mater Studiorum University, Bologna, ITALY, [3]University of Milan, Milano, ITALY, [4]University Hospital S. Orsola-Malpighi, Bologna, ITALY.

Purpose: It is largely recognized that tumour hypoxia hampers the efficacy of chemo- and radio-therapy, and negatively affects the outcome of different cancers. Herein we investigate the role of FDG-PET parameters in surgical treated Non-Small Cell Lung Cancer (NSCLC), by comparing the imaging findings with the tissue expression of hypoxia inducible factor (HIF-1α) and the amount of CD68$^+$ macrophages. Materials and Methods: A series of 29 patients with up-front resectable NSCLC (stage IA-IIIA; M:F=22:7), who underwent FDG-PET examination prior to surgery, was enrolled consecutively in the study. PET images were visualized on a GE Advanced 4.6 workstation and used to define semi-quantitative and quantitative parameters: SUV_{max}, SUV_{mean}, metabolic tumour volume (MTV) and total lesion glycolysis (TLG=MTV*SUVmean). Surgical histological specimens were analyzed and for each patient two consecutive 2μm-thick sections were treated with antibodies raised against HIF-1α (R&D Systems, Milan, Italy) and CD68 (Dako, Milan, Italy) following a standardized immunohistochemical protocol. The immunoreactivity was semi-quantitatively evaluated and the obtained scores compared with imaging findings. Results: Immunohistochemical staining on NSCLC demonstrated an up-regulated expression of HIF-1α in 17 out of 29 (60%) specimens. The intensity of immunoreactivity was categorized as follows: weak (score 1) in 8 cases, moderate (score 2) in 5 cases, and high (score 3) in 4 cases. When compared to PET data, SUV_{max}, SUV_{mean} and TLG resulted significantly correlated to the intensity of HIF-1α expression ($p<0.05$). More specifically, score 2 demonstrated the highest semi-quantitative and quantitative values compared to score 1, consistent with low hypoxia level, but also to score 3: this latter result appears more likely related to the increased presence of tumour necrosis and expression pattern heterogeneity associated to higher levels of hypoxia. CD68$^+$ macrophages were consistently present in all of the investigated specimens, confirming their functional role in tumour hypoxia. Conclusions: Although our findings need to be extended in a larger series of NSCLCs, the present study shows a direct association between FDG-PET parameters and the tumor expression of HIF-1α . Moreover, macrophages are found as the most representative immune cell population, being present at high densities in all the investigated specimens.

OP147

Correlation between circulating tumor biomarkers and positron-emission tomography in advanced non-small cell lung cancer

G. Ferrarazzo[1], F. Bongioanni[1], C. Genova[2], M. Massollo[3], G. Karalis[4], E. Rijavec[2], F. Biello[2], G. Barletta[2], S. Coco[2], A. Alama[2], A. Truini[2], I. Vanni[2], G. Sambuceti[1], F. Grossi[2], **S. Morbelli**[1]; [1]Nuclear Medicine Unit, IRCCS San Martino - IST, University of Genoa, Genoa, ITALY, [2]Lung Cancer Unit, IRCCS San Martino - IST, Genoa, ITALY, [3]Nuclear Medicine Unit, Galliera Hospital, Genoa, ITALY, [4]PET/CT Alliance Medical, Istituto Salus, Genoa, ITALY.

Background: Circulating tumor cells (CTCs) and plasma circulating-free DNA (cfDNA) are promising candidates as non-invasive prognostic markers in malignant diseases. 18-fluorodeoxyglucose positron emission tomography/computed tomography (18FDG-PET/TC) has a well-recognized diagnostic and prognostic value in non-small cell lung cancer (NSCLC). Very little is known about the mutual relationship between circulating biomarkers (CTCs and cfDNA) and 18FDG-PET/CT indicators in NSCLC. Methods: Peripheral blood samples from 28 patients affected by advanced/metastatic NSCLC were collected before starting first-line chemotherapy. CTCs were isolated by size using a filtration-based device (ScreenCell) and then identified and enumerated; cfDNA was isolated from plasma (QIAamp DNA Blood Mini Kit, Qiagen) and quantified by qPCR method using human

telomerase reverse transcriptase (hTERT). All patients underwent 18FDG-PET/TC (Biograph 16 Siemens) at baseline. Maximum diameter (dmax) of the primary lesion (T), dmax of the greater lymph nodal (N), and metastatic (M) lesions were measured. Similarly, maximum and mean standardized uptake value (SUVmax, SUVmean) and size-incorporated SUVmax (SIMaxSUV) were computed for T, N and M, respectively; SIMaxSUV was calculated with the following formula for T, N, and M: SIMaxSUV= SUVMax*dmax. Presence (B+) and absence (B-) of metabolically active bone lesions (bone mets) were recorded. The association among CTCs, cfDNA and 18FDG-PET/CT-derived parameters was evaluated through multivariate analysis. T-test was performed to evaluate the difference in CTCs and cfDNA in B+ and B- groups, respectively. Results: Twenty-eight patients were evaluated; median age was 66 years (range: 51-80); male/female ratio was 18/10; 15 patients were current smokers, while 11 were former-smokers and 2 were never-smokers. Histo-types were grouped as it follows: adenocarcinoma= 22; squamous cell carcinoma= 5; not otherwise specified NSCLC= 1. Nine patients out of 28 had metabolically active bone lesions. Median CTC count was 7 CTCs/3ml (range: 0-47 CTCs/3ml), while median HTERT copy number was 109.0 (range: 16.7-1405-5). At multivariate analysis, SUVmax of T was the only variable independently associated with cfDNA (p=0.036). No correlations were highlighted between CTCs and all the other PET-derived parameters. A trend towards significance between high HTERT and the presence of metabolically active bone lesions was observed (p=0.058). Conclusions: Our data demonstrate that the expression of cfDNA is correlated with the metabolic activity of the primary tumor lesion. Since SIMaxSUV was not correlated with HTERT, it appears that the expression of cfDNA depends from tumor metabolism rather than its burden. Further analyses on 18FDG-PET/TC-derived metabolic tumor volume are ongoing.

OP148

Density cut off value for metastatic mediastinal and hilar lymph nodes in lung cancer patients

P. Flechsig, P. Frank, D. Rath, C. Kratochwil, H. Kauczor, U. Haberkorn, F. Giesel; University Hospital Heidelberg, Heidelberg, GERMANY.

Purpose:Lung cancer often co-exits with chronic lung diseases such as COPD, and mediastinal lymph nodes may be positive with FDG-PET due to inflammatory disease alone. Nevertheless, FDG-PET is the primary imaging modality used for staging patients with lung cancer, including nodal status. The purpose of this study is to evaluate if density measurements by means of Volumetric CT histogram analysis can improve the characterization of lymph nodes in staging of patients with lung cancer.Materials and Methods:248 lymph nodes of 159 patients aged 41-78 years (87 male, median age 57) diagnosed with lung cancer were investigated. Native FDG-PET/CT (Biograph 6 PET/CT) was performed prior to surgery/biopsy as part of clinical staging. Analysis of lymph nodes was done on the basis of FDG-uptake (SUVmax) and Volumetric CT histogram analysis. These findings were correlated to the gold standard of histopathology.Results:130 positive and 118 negative histological proven lymph nodes were successfully analyzed by Volumetric CT histogram. Histological positive lymph nodes presented a significantly higher median CT HU value ($p < 0.05$, Fig. 1). The incidence of malignancy was 82% above a cut off value of 20HU, the incidence of benign findings was 91% below a cut off value of 20HU. In subgroup analyses, density analyses failed to differentiate between different malignant tumour entities (Adeno CA, Adenosquamous CA, NET, SCLC, other).Conclusion:As an additive value for the preoperative N-staging in lung cancer patients a possible cut off value of 20HU might divide mediastinal lymph nodes of FDG-equivocal patients into affected and not-affected ones. Nevertheless, density analyses cannot differentiate between different tumour entities.

OP149

Comparison of predicted FEV1 and observed FEV1 post lung surgery Using lung Perfusion scintigraphy

V. Rangarajan, N. Purandare, A. Agrawal, S. Shah, S. Nag, P. Ranganathan, C. S. Pramesh; Tata Memorial centre, Mumbai, INDIA.

Aim: To study the correlation between predicted FEV1evaluated by lung perfusion and actual post -operative values of FEV1 in patients undergoing surgery for lung cancer. Materials & Method: This was IRB approved prospective study of patients undergoing lung surgery(lobectomy/pneumonectomy) who were referred for pre-operative prediction of post-operative pulmonary function by lung perfusion scintigraphy using 99mTc MAA. All patients underwent surgery within 2 weeks of the 99m Tc MAA study. Post-operative spirometry study was conducted 4-6 months after surgery. A sample size of 50 was estimated and data collected over 18 months. The estimation of post-operative FEV1 was calculated using actual preoperative FEV1 and percentage perfused lung using a software that divides both lungs into 3 equal zones - anterior and posterior and counting using geometric mean. On the basis of type of planned surgery popFEV1 was calculated as percentage and absolute value. Pearson's correlation coefficient was used to evaluated the relationship between the popFEV1 by lung perfusion scintigraphy and post-operative actual FEV1 measured by spirometry. Agreement

between the 2 methods was analyzed by Bland -Altman method. Results - 50 patients were included in the study. The age range was 32-77 years, males were 39 and 11 were females.50% had upper lobe, 26% had lower lobe, 6% had middle lobe, 12% had main bronchus involvement and 4% others. Histologically 42% were adenocarcinoma, 16% NET, 36% squamous carcinoma and others 6%. The correlation between PPOFEV1 lung perfusion scintigraphy and measured actual post-operative FEV1 by spirometry showed a statistically significant correlation, R=0.847. The correlation coefficient was higher at 0.930 for pneumonectomy patients against 0.792 for lobectomy. The Pearson's correlation coefficient is significant at the 0.01 level (2-tailed). The agreement analysis using Bland-Altman method showed a mean difference between the 2 methods of evaluation of pulmonary function was 0.0558 (mean) with standard deviation 0.284. Conclusion - The current method of quantification using geometric mean and planar method is exceptionally good for predicting lung function after pneumonectomy, however post - lobectomy the planar method is just optimal for prediction. SPECT and CT based segmentation improves the prediction post lobectomy as well. Preoperative FEV1 estimation using lung perfusion is a reasonably good predictor of actual post operative FEV1 in patients undergoing surgery for lung cancer.

OP150

The Relationship between Staging and SUVmax in Non-Small Cell Lung Cancer

H. KAYA[1], **T. Balci**[2], H. KOMEK[3], M. CENGIZ[4]; [1]DicleUniversity Medical Faculty, DIYARBAKIR, TURKEY, [2]Firat University Medical Faculty, ELAZIG, TURKEY, [3]Diyarbakir State Hospital, DIYARBAKIR, TURKEY, [4]Dicle University Medical Faculty, DIYARBAKIR, TURKEY.

Introduction: In this study, we aimed to determine the relationship between the stage of the disease and the maximum standard uptake value (SUVmax), one of the most important quantitative parameters of PET imaging for tumors, in non-small cell lung cancer (NSCLC).Materials and Methods: Seventy three patients with histopathological diagnosis of NSCLC (27 adenocarcinomas, 29 squamous cell lung carcinoma, 17 unclassified subtypes) to whom PET/CT scan was performed between July 2009 to July 2011, were evaluated retrospectively.F-18 fluoro-2-deoxy-D-glucose (FDG) of 370-555 MBq (10-15 mCi) was injected via a peripheral vein of the patients at least 4 hours fasting period and blood glucose levels under the 150 mg/dl and 45-60 minutes following injection PET/CT imaging was performed of the body areas between the vertex and the third upper part of the thigh.In addition to the visual evaluation of the PET/CT images, SUVmax in the tumor tissue and mediastinal lymph nodes was determined. FDG uptake of the lymph nodes, distant metastasis and tumor were assessed by the PET / Ct and they were recorded to make staging according to tumor, node, metastasis (TNM) staging system (Phase I, II, III, IV). The cut-off value for SUVmax was considered as 2.5.The relationship between the NSCLC subtypes and SUVmax were determined by Spearman's correlation test.Results: The patients with an average age of 61.36 ± 9.6 years (32 to 83 years old), 10 women (13.7%) of them, included in the study.Distribution of patients according to the stage was as follows; stage I: 14 patients (19.2%), stage II: 12 patients (16.4%), stage III: 20 patients (27.4%), Stage IV: 27 patients (37%).SUVmax values according to the stage was determined as; Stage I: 11.6 ± 4.6, Stage II: 13.5 ± 6.4, Stage III: 12.6 ± 4.8, Phase IV: 17.5 ± 8.6.In NSCLC subtypes, a significant correlation between SUVmax and the stage was revealed ($r = 0.319$, $p = 0.006$).Conclusion: Due to positive relationship between the increase in SUVmax and tumor stage, we believe that it could help clinicians in order to make a prediction about the patient's prognosis.

508 - Sunday, October 11, 2015, 4:30 PM - 6:00 PM, Hall E
Conventional & Specialised Nuclear Medicine: Thyroid & Parathyroid

OP151

Size doesn't matter: predictive value of new quantitative analysis for differential diagnosis of primary hyperparathyroidism lesions vs. thyroid nodular disease in parathyroid scintigraphy

A. V. Koljevic Markovic[1,2], M. Jankovic, G. Pupić[1], R. Džodić[1]; [1]National Cancer Research Center Serbia, Belgrade, SERBIA, [2]Faculty of Electrical Engineering, University of Belgrade, Belgrade, SERBIA.

Aim: The problem of segmentation and recognition of parathyroid lesions in the presence of concomitant thyroid nodular disease is present in conventional SPECT/CT investigations as well as in gamma camera imaging. Aiming to improve specificity of parathyroid scintigraphy in concomitant thyroid nodular disease, we developed a new processing method in ROI time/activity data analysis. MM: Total of 53 patients, median age of 57(19-80) years, with clinical diagnosis hyperparathyroidism (PHPT) and ultrasound positive report of nodular or multinodular goiter, underwent preoperative, dual- tracer: 99m Tc-pertecnetat and 99mTc-MIBI, double- phase scintigraphy by EANM guidelines (2009). Specially designed software we developed examined ROI time/activity changes in the form of grid with different, optional sizes, up to maximal resolution (1, 5mm). We correlated our findings with PTH levels, histology

results and conventional scintigraphic findings: subtraction and visual interpretation of planar images of neck and mediastinum in oblique sections, according to ultrasound PTA localization and delayed scans in one hour interval. Results: Parathormone (PTH) was increased in the group: median 120,2 pg/ml (range 70- 658pg/ml).Following histopathology: a) thyroid - benign: adenoma folliculare, colloides and cystica: 45(83%)pts ; malignancy: 8 (10%)pts- papillary 7 pts and one for medullary; b) parathyroid - autonomy (PTA) 53(70,2%): solitary: 44 patients, hyperplasia: 8 pts- 7/8 patients with two lesion and 1/7 had all four lesions and one PT carcinoma;.c.) median PTA volume was 760(55-6125)mm^3. Standard findings (subtraction, oblique planar scans and delayed phase) in total of 63 lesion (in 53 pts) had 10 FN (mostly in hypeplasia PTA), and PPV was 81%. Using specially designed software, thyroid TACs represented, as expected, exponentially declining curves but parathyroid lesions had typical uptake pattern in the form of late phase peak, independent to PTA volume and/or PTH levels. The thyroid gland washout was up to 28% in normal, adenoma or thyroid carcinoma tissue. A new processing method for a PTA had PPV 97%. Conclusion: Application of new imaging data quantification, we developed, was effective in small parathyroid lesions concomitant to thyroid nodular disease, complementary used with standard protocols. This novelty could be implemented in various nuclear medicine hybrid imaging investigations, following pathological metabolism, in ROI sizes up to maximal resolution.

OP152

A prospective comparative study of parathyroid dual-phase scintigraphy, dual-isotope subtraction scintigraphy, 4D CT, and ultrasonography in primary hyperparathyroidism

M. Krakauer[1], B. Wieslander[1], P. S. Myschetzky[1], A. Lundstrøm[1], T. Backer[1], C. H. Sørensen[2], W. Trolle[2], B. Nygaard[3], F. N. Bennedbæk[3]; [1]Gentofte Hospital, Helleup, DENMARK, [2]Rigshospitalet, Copenhagen, DENMARK, [3]Herlev Hospital, Herlev, DENMARK.

Purpose: Preoperative localization of the diseased parathyroid gland(s) in primary hyperparathyroidism (PHP) allows for minimally invasive surgery. This study was designed to establish the optimal first-line preoperative imaging modality. Methods: 91 patients were studied consecutively in a prospective head-to-head comparison of dual isotope (Tc-99m Sestamibi vs. I-123) subtraction parathyroid scintigraphy (PS), dual-phase PS, 4D CT, and ultrasonography (US). Surgery, histological confirmation, and postoperative normalization of Ca^{++} and PTH was the reference standard. Results: Ninety-seven hyperfunctioning parathyroid glands (HPG) were identified by the reference standard. Sensitivity and specificity for subtraction PS, dual-phase PS, 4D CT, and US was 93%, 65%, 58%, 57% and 99%, 99.6%, 86%, 95%, respectively. Inter-rater agreement was excellent for subtraction PS (κ=0.96) while only fair for 4D CT (κ=0.34). Pinhole imaging and subtraction of late images (the latter especially in case of a nodular thyroid gland) increased the sensitivity of subtraction PS. SPECT/low-dose CT did not increase sensitivity but aided in the exact localization of the HPGs. Of 7 negative subtraction PS studies 4D CT and US was able to locate 3 and 1 additional HPGs, respectively. Conclusions: Dual isotope pinhole subtraction PS has higher diagnostic accuracy compared to dual-phase PS, 4D CT, and US as a first-line imaging study in PHP. In case of a negative scintigraphy or suspicion of multiglandular disease 4D CT and/or US is recommended as a second-line modality. However, diagnostic algorithms should be adapted in accordance with local availability and expertise.

OP153

Comparison of 99mTc-sestamibi/123I subtraction SPECT/CT and combined 99mTc-sestamibi/123I sub-traction SPECT/CT with planar pinhole image in hyperparathyroidism

V. Tunninen[1], P. Varjo[1], M. Seppänen[2]; [1]Satakunta Central Hospital, PORI, FINLAND, [2]Turku University Hospital, Turku, FINLAND.

Introduction. ^{99m}Tc-sestamibi/^{123}I subtraction SPECT/CT is a valuable tool for localization of parathyroid adenomas. The aim of this study was to evaluate whether the review of additional planar pinhole image improves the outcome of ^{123}I/^{99m}Tc -sestamibi subtraction SPECT/CT in parathyroid scintigraphy. Subjects and Methods: Parathyroid scintigraphy with ^{99m}Tc (750MBq) and ^{123}I (20MBq) was performed for 59 patients with hyperparathyroidism (55 pHPT, 4 sHPT). Two simultaneous ^{99m}Tc /^{123}I acquisitions were performed (SPECT/CT and anterior planar pinhole imaging). Two anonymized image sets were generated to compare SPECT/CT and combined SPECT/CT+Pinhole planar images (^{99m}Tc-sestamibi,^{123}I, and subtraction images). Each quadrant in relation to the thyroid gland (and other, referring to ectopic localization) was classified as negative or positive with the confirmation of histologic analysis as the reference standard. A McNemar test was performed to compare the sensitivities and specificities between the image sets. Results. There were 68 adenomas confirmed by histology in 59 patients. Fifty-two patients had solitary adenomas, six patients had double adenoma, and one patient had four hyperplastic glands. Sixty-two and sixty-six adenomas were correctly visualized by SPECT/CT (six false positive) and SPECT/CT+Pinhole (four false positive), respectively. The sensitivity and specificity were

slightly higher with SPECT/CT+Pinhole than with SPECT/CT (97,06% vs. 91,18% and 98,24% vs. 97,36%, respectively. p = 0,7237). False-positive rate was 8,82% with SPECT/CT, and decreased to 5,71% with SPECT/CT+Pinhole.Conclusion. This study indicates that the use of additional pinhole image with ^{99m}Tc-sestamibi/^{123}I subtraction SPECT/CT increases both sensitivity and specificity of parathyroid scintigraphy. Although the difference was not statistically significant, the use of additional pinhole imaging is useful especially in cases where SPECT/CT remains negative. The use of additional planar pinhole image with ^{99m}Tc-sestamibi/^{123}I subtraction SPECT/CT is thus recommended in selected cases.

OP154

Value of 18F-Choline PET-CT in the assessment of primary hyperparathyroidism comparing with 99mTC-Sestamibi SPECT-CT

M. Beheshti[1], **L. Imamovic**[1], G. Spaun[2], M. Steinmair[1], K. Emmanuel[2], V. Alibegovic[3], C. Pirich[4], W. Langsteger[1]; [1]PET-CT Center Linz, St. Vincent's Hospital, Linz, AUSTRIA, [2]Department of Surgery, St. Vincent's Hospital, Linz, AUSTRIA, [3]Department of Clinical Pathology, St. Vincent's Hospital, Linz, AUSTRIA, [4]Nuclear Medicine & Endocrinology, Parcelsus Medical University, Salzburg, AUSTRIA.

Aim: In this prospective study we compared the accuracy of 18F-Choline (FCH) PET-CT with 99mTC-Sestamibi SPECT-CT for preoperative detection of parathyroid adenoma in patients with primary hyperparathyroidism. METHODS: Both 99mTC-Sestamibi SPECT-CT and FCH PET-CT were performed in 25 consecutive patients with biochemical evidence of primary hyperparathyroidism. At least one abnormal 99mTc-Sestamibi and FCH focus corresponding to a parathyroid gland or ectopic parathyroid tissue in each imaging modality was considered as positive finding. Twenty patients with positive findings in at least one imaging modality underwent surgical exploration and the results of imaging modalities were verified with histopathologic findings as the standard of truth. RESULTS: All patients showed biochemical evidence of primary hyperparathyroidism with a mean serum calcium level of 2.7 ± 0.4 mmol/l and parathormone (PTH) level of 178.5 ± 165.8 pg/ml. Intraoperative PTH monitoring showed significant drop in PTH level in all patients. In patient-based analysis, FCH PET-CT was able to detect parathyroid adenoma in 84% of patients (21/25) while 99mTC-Sestamibi SPECT-CT was positive in 52% of patients (13/25). The mean serum calcium and PTH levels of patients with negative imaging modalities were 2.66 ± 0.05 mmol/l and 123.05 ± 18.0 pg/ml. In a lesion-based analysis in 20 patients who underwent surgical exploration, the detection rate of FCH PET-CT was 87% (21/24) comparing with 50% (12/24) detected by 99mTC-Sestamibi SPECT-CT. CONCLUSION: In this prospective study, FCH PET-CT showed promising results to be a potential functional imaging modality - clearly superior to 99mTC-Sestamibi SPECT-CT - in the detection and localization of parathyroid adenoma in patients with primary hyperparathyroidism.

OP155

Tc-99m MIBI-scintigraphy for malignancy risk assessment of hypofunctionning thyroid nodules

K. Rösel, C. Schneider, C. Kobe, M. Dietlein, A. Drzezga, **M. C. Schmidt**; University Hospital of Cologne, Department of Nuclear Medicine, GERMANY.

Aim: In Germany with its borderline iodine supply patients with hypofunctionning thyroid nodules (HTN) as assessed by pertechnetate scintigraphy have a malignancy risk of about 1.7 - 3 %. Fine needle aspiration cytology is used for futher evaluation being inconclusive in about 20%. Tc-99m-MIBI scintigraphy can be used for malignancy risk assessement of HTN. We wanted to test its clinical usefulness.Methods: Between 2007 and 2010 108 patients with one HTN were retrospectively identified from our institutional database who had undergone Tc-99m-MIBI-scintigraphy and subsequent surgery. Histopathology served as golden standard. Tc-99m-MIBI images were grades as following: Match = HTN and MIBI with a concordant lower uptake as the surrounding thyroid tissue; Isointense Uptake = MIBI uptake in the HTN equal to surrounding thyroid tissue; Mismatch = MIBI uptake higher than surrounding thyroid tissue. Results: 98 patients had a benign and 10 a malignant histology. Patients with benign nodules had 34 Match, 11 isointense and 51 Mismatch findings. Patients with malignant nodules had 8 Mismatch and 2 isointense findings the latter being explained by papillary microcarcinomas. The negative predictive value of Tc-99m-MIBI scintigraphy was 96% and the positive predictive value 14%. Fine needle aspiration biopsy being performed in 77 patients missed 6 malignant nodules. Conclusions: Tc-99m-MIBI scintigraphy can serve as an additional technique for malignancy risk assessment of hypofunctionning thyroid nodules. Though the majority of Mismatch findigs represent benign thyroid nodules the likelihood of malignancy increases in this group. A negative Tc-99m-MIBI scintigraphy has a high likelihood of a benign finding justifying a conservative

management. Though small in number, Tc-99m-MIBI may miss papillary microcarcinomas.

OP156

Role of real time ultrasound elastography in diagnosing hyper functional thyroid nodules and predicting treatment response

V. Stebner[1], M. Ruhlmann[1], R. Görges[1], J. Farahati[1], D. Simon[2], A. Bockisch[1], S. Rosenbaum-Krumme[1], J. Nagarajah[3]; [1]Department of Nuclear Medicine, Medical Faculty, University Duisburg-Essen, Essen, GERMANY, [2]Department of General and Visceral Surgery, Bethesda Hospital, Duisburg, GERMANY, [3]Department of Radiology, Memorial Sloan Kettering Cancer Center, New York, NY, UNITED STATES.

Background/AimUltrasound based real-time elastography (USE) is increasingly studied in clinical setting primarily for detection of suspicious thyroid nodules with controversy results. However, the role of USE for diagnosis of scintigraphically hyper functional thyroid nodules is still unclear. In this study we investigated the detection capability of USE for benign thyroid nodules and analyzed additionally, if USE is able to predict radio-iodine treatment (RIT) response in those patients.The first part of the study included 134 hyper functional thyroid nodules of 101 consecutive patients. The following attributes of the nodules were analyzed: stiffness with the USE using scores of Rago (3 item score) or Asteria (5 item score) and ultrasound criteria using TIRADS. The second part of the study included 73 hyper functional thyroid nodules (51 unifocal, 7 bifocal, 15 multifocal) of 73 consecutive patients prior to RIT. The following attributes of the nodules were analyzed before RIT: stiffness with the USE using scores of Rago (1 = soft, 2 = medium, 3 = hard), classical ultrasound criteria like echogenicity and perfusion, thyroid scintigraphy and TSH level in blood. Approximately four months after RIT the therapy response was evaluated by thyroid scintigraphy and TSH level in blood. Therapy response was defined as normalized TSH level and thyroid scintigraphy without hyper functional nodules.94 of the exmined thyroid nodules (70%) were rated as hard (suspicious for malignancy) and 41 nodules (30%) as soft (not suspicious) with a specificity of 30%. The scoring systems of Rago and Asteria showed no significant difference. Applying the TIRADS criteria 44 nodules (33%) had a higher risk for malignancy (33 nodules TIRADS 4a, 11 nodules TIRADS 4b). Combining USE and TIRADS 32 nodules (24%) were categorized as suspicious (intersection of hard nodules that are categorized as TIRADS 4a or 4b).RIT was successful in 66 nodules (responder) and not successful in 7 nodules (non-responder). In the group of responders 21 nodules were rated as “soft”, 12 nodules as “medium” and 33 nodules as “hard”. Regarding the non-responder 4 nodules were rated soft and 3 nodules hard. There was no statistic significant correlation between USE score and therapy response.ConclusionUSE cannot reliably identify scintigraphically hyperfunctional thyroid nodules as benign nodules. Its accuracy in the assessment of at least “hot” thyroid nodules is to be questioned. USE cannot predict therapy (non-) response of RIT of hyper functional thyroid nodules and has therefore no influence on therapy planning.

OP157

Cancer Risk After Medical Exposure to 131I in Benign Thyroid Diseases

I. CILLERO ETXEBESTE, A. MENDIOLA, P. SANTESTEBAN, M. MITXELENA, I. ARIAS-CAMISON, G. RIOS, F. RODRIGUEZ; FUNDACIÓN ONKOLOGIKOA, SAN SEBASTIAN, SPAIN.

OBJECTIVE: The objective of this study was to evaluate the incidence of cancer in patients treated with ^{131}I for benign thyroid disease. MATERIAL AND METHODS: This is a retrospective study in which a total of 1511 patients , residents in Guipúzcoa (Spain), were included from 1995 to 2011. All of them had received a radioiodine treatment (RAI) for Grave’s disease, autonomously functioning nodules (AFN), multinodular goiter (MNG) or treatment refractory hyperthyroidism. The administered ^{131}I dose was calculated on the basis of the thyroid’s volume, 24h uptake of ^{131}I and clinical examination. The dose range was 185-740 MBq. The observed variables were: reason for ^{131}I treatment, administered activity of ^{131}I, thyroid absorbed dose, other organ groups that concentrate ^{131}I, time since exposure and pathological anatomy examination. We reviewed the most sensitive organs for radiation-induced oncogenesis including salivary glands, breast, kidney, bladder, pancreas, stomach and thyroid. Lymphoma and leukemia’s incidence in these patients was also studied. Incident cancer cases were identified from Guipúzcoa’s Cancer Registry. Standardized incidence rate (SIR) was estimated as an approach to cancer risk. RESULTS: This study included 1217 women and 294 men. The median age was 58.37. The follow-up period of these patients ranged from 1 to 16 years. Thyroid cancer was diagnosed in 10 patients during the follow-up period. .All patients who developed a thyroid cancer were men. Among these 10 patients, the average ^{131}I was 573.5Mbq. Five of these patients were treated for AFN whereas the other five patients suffered from MNG. None of these patients were treated for Grave’s disease. Pathological examination revealed a prevalence of papillary tumour (6/10) two patients presented follicular tumour, one present medullary thyroid carcinoma and one leiomyosarcoma. Three patients died of thyroid cancer. Among these 3 tumours one was a papillary tumour, one was leiomyosarcoma and one

was medullary carcinoma. SIR was 4.3 (CI: 0.86-0.71) which is similar to Gipúuzcoa's general population. CONCLUSION: The incidence of thyroid cancer in these series was not significantly different from its incidence in the general population. There is no demonstrable increase of risk overall after ^{131}I administration in our study.

OP158

Contribution of SPECT/CT in extrathyroid radioiodine uptake in patients with differenciated thyroid cancer.

J. Villanueva Curto, A. Sainz-Esteban, A. Cobo Rodríguez, C. Gamazo Laherrán, M. Ruíz Gómez, M. Gónzalez Selma, M. Alonso Rodríguez, R. Olmos García; HOSPITAL CLÍNICO UNIVERSITARIO DE VALLADOLID, Valladolid, SPAIN.

Aim:To asses the contribution of SPECT/CT performed after treatment with 131I in patients with differentiated thyroid cancer (DTC) in the localization and characterization of extrathyroid uptakes detected in the whole body scintigraphy (WBS).Methods:We include 40 patients (31 women, mean age: 57±18 years) with DTC (35 papillary, 2 follicular and 3 indiferentiated). After an hipoiodine diet, a WBS and a SPECT/CT were performed 6-9 days after the administration of a therapeutic dose of 131I (mean dose: 4.2 ± 0.8 GBq) and 4 weeks after withdrawal of hormonal replacement treatment (21) or stimulation with recombinant TSH (19). Scintigraphy findings were correlated with radiology, histology or follow-up.Results:In 11 patients, WBS and SPECT/CT did not show any extrathyroidal uptake. In the remaining 29 patients, 44 foci were detected. Three foci were only detected in SPECT/CT, 2 of them were metastases in cervical adenopathies and one a bronchiectasis. Of the 41 foci detected in both techniques, 12 were metastases (9 cervical adenopathies and 3 distant metastases), and 29 were false positives. SPECT/CT improved the localization of all of them, dismissing 26 false positives in salivary glands (3), bowel (7), kidney (1), thymus (5), breast (1), bronchiectasis (4), and contamination (5). In 3 patients, in spite of the improvement of localization, SPECT/CT did not correctly characterize three foci that were at final diagnosis a bronchiectasis, a renal and an ovaric cysts.Conclusions:SPECT/CT improved the localization and characterization of extra thyroid uptakes detected in WBS, dismissing false positives. In a small percentage of patients, new focus were detected in SPECT/CT, with no changes in the staging of patients.

509 - Sunday, October 11, 2015, 4:30 PM - 6:00 PM, Hall 8
Physics & Instrumentation & Data Analysis: Data Analysis & Management II

OP159

18F-FDG PET/CT: Is SUV reliable to evaluate the adrenal glands normal metabolic behavior?

I. Rodrigues, A. Martins, J. Pereira, R. Domingos, S. Carmona, L. Oliveira; Joaquim Chaves Saúde – Nuclear Medicine Department, Lisbon, PORTUGAL.

Aim: To compare normal adrenal glands (AG) SUVmax obtained in two different time points, using two reconstruction methods, in order to evaluate SUV reliability to evaluate AG normal metabolic pattern.Materials and methods: This retrospective study included 56 AG of 28 patients [13M/15F; mean age: 61,4 ± 12,9 years] with glycemic values below 120mg/mL and without adrenal disease (excluded by clinical history, recent image and laboratory tests). The technical procedure consisted of the administration of 18F-FDG followed by a rest period and hydration. Two PET/CT studies were performed [Biograph 6 TrueView PET/CT, Siemens]: a whole body study from the base of the skull to the mid-thigh (WB) (Δinjection-acquisition= 94,4 ± 15,9 minutes) and a delayed abdominal image (DAI) (Δinjection-acquisition= 180,6 ± 24,1 minutes). The CT study was acquired with low dose protocol for attenuation correction and anatomical localization. The processing included the visual analysis of the tomographic studies and the calculation of SUVmax in AG in the WB and in DAI by two different iterative reconstruction methods: 1) SUVmax_2D [8 subsets, 4 iterations, matriz 168x168] SUVmax_3D [21 subsets, 3 iterations, matriz 336x336]. Statistical analysis was performed using paired t-Student test.Results: In initial images, the mean SUVmax_2D (2,00 ± 0,40) are not statistically different (p=0,168). In DAI SUVmax_3D (2,20 ± 0,48) is higher than SUVmax_2D (1, 96 ± 0,52) (p=0,001). Comparing the mean SUVmax_2D of AG in initial and delayed images, the differences found with both reconstruction methods were not statistically different, although both reconstruction methods showed a different tendency: there is a slight mean SUVmax decrease (-2,48 %) for SUVmax_2D and a slight SUVmax increase (5,26 %) for SUVmax_3D.Conclusion: Small differences in reconstruction methods can happen when hardware and/or software is upgraded and this can significantly change the normal AG SUV calculation. This change can be non-homogeneous as verified in this work - we have documented no significant AG SUV change in the initial WB images and a significant SUV change on the DAI, using two reconstruction methods. This aspect conducted to an apparent different metabolic behavior of normal AG during time - although the differences were not statistically significant, a slight increase or slight decrease in AG SUV was documented during time as different reconstruction methods were used.

OP160

Partial Volume Correction of Amyvid and FDG PET data using the discrete iterative Yang technique

J. C. Dickson[1], K. Erlandsson[2], M. Lehmann[2], M. Modat[2], N. Burgos[2], A. Groves[2], J. Schott[2]; [1]University College London Hospital NHS Foundation Trust, London, UNITED KINGDOM, [2]University College London, London, UNITED KINGDOM.

Introduction: Partial volume effects can severely compromise both visual and quantitative PET, particularly in the populations referred for dementia PET imaging. Atrophy and cortical thinning can lead to apparent reductions in tracer uptake that are purely an effect of anatomical features, which compromises the ability of the PET study to accurately map underlying physiological processes. To overcome these issues, partial volume correction (PVC) techniques can be applied. In this study we introduce the "discrete iterative Yang" (diY) technique, and look at the improvement in tracer uptake in a cohort of Amyloid and FDG PET studies. Methods: A mix of twenty-two patients and age-matched controls were involved in this study. All subjects had Amyvid PET, FDG PET, and a recent T1 weighted MR study. T1 data were co-registered to FDG PET and 18F-Amyvid data before being segmented and parcellated into volumes using the Niftyseg algorithm [1]. PET data were then up-sampled to the MR voxel size before PVC was applied using the diY technique. In essence the technique involves the PET image being represented as a piecewise constant image, which is convolved with the system point spread function. The ratio of the original and convolved images is used as correction factors that are applied to the PET image. The regional mean values are estimated iteratively. After a few iterations of this process, the PET image can be considered to be partial volume corrected. Once the correction had been applied, the visual and quantitative changes to the PET distributions were assessed pre and post correction. Results: Of the 22 subjects, 13 had a scan negative for amyloid deposits. After PVC, global grey-matter SUVr in these subjects decreased by an average of 12.2% (95%CI: 8.7-15.7) due to a reduction of spill-in from non-specific white matter uptake. In Amyloid positive patients, SUVr increased by 26.7% (95%CI: 22.17-31.26%) by reducing spill-out from cortical grey matter. Similarly in control FDG studies SUVr in cortical grey matter increased by 26.3% (95%CI: 25.22-27.41) after the application of the PVC. Visually there was better contrast between grey and white matter areas on Amyloid PET, and FDG PET with abnormalities better differentiated with diY PVC applied. Conclusions: Partial volume correction using diY improves quantitative accuracy, and offers better differentiation between normal and abnormal studies.

Reference: [1] Cardoso MJ et al 2012. Geodesic Information Flows in Med. Image Comput. Comput Assist. Interv. : MICCAI 2012;7511:262-270 2012.

OP161

Prognostic and predictive values of initial 18FDG PET features using random forest classifier: Application to patients after chemo-radiotherapy for oesophageal cancer

P. Desbordes[1,2], R. Modzelewski[3,1], S. Vauclin[2], P. Vera[3,1], I. Gardin[3,1]; [1]QuantIF LITIS - EA4108, University of Rouen, Rouen, FRANCE, [2]Dosisoft, Cachan, FRANCE, [3]Henri Becquerel Center, Rouen, FRANCE.

Aim: Many features can be extracted from 18FDG PET images to describe cancer. We propose a machine learning technique based on a Random Forest (RF) classifier to select features having a prognostic or predictive value among a large amount of different characteristics.Materials and methods: 65 features are extracted from medical records (age, stage ⋯) and PET images: classical features (SUV, Metabolically Tumor Volume (MTV) ⋯), 1st order features (skewness, entropy ⋯) and texture parameters from texture matrices: Gray Level Cooccurrence Matrix (GLCM), Gray Level Zone Length Matrix (GLZLM) and Gray Level Difference Matrix (GLDM). Patient classification is performed using RF algorithm with 2000 decision trees, firstly without any Feature Selection (FS), and secondly with a FS. The selection is performed in 2 steps. First, a correlation analysis is done using the Spearman method to keep uncorrelated features. They are compared two by two and are considered as correlated if the Spearman coefficient (sp) verified $|sp| \geq 0.8$ and $p < 0.05$. Next, the RF algorithm is applied on the remaining features to find the most relevant features using the importance index. The RF classifier has been applied to a database of 66 patients with an oesophageal cancer treated by radio-chemotherapy (CRT). The classification accuracy has been evaluated using the Out-Of-Bag (OOB) error.Results: When the RF classifier is applied to the 65 initial features, OOB error reaches 33.3% and 25.8% for prognostic and predictive studies respectively. The FS strategy improves the classification accuracy, to reach an OOB error of 22.7% and 22.7% respectively. The Spearman analysis revealed that none of the clinical data are correlated with PET characteristics, neither for correlation (GLCM), Cluster Shade (CS, GLCM) Busyness (GLDM) and Zone Percentage (ZP, GLZLM). Twelve groups of correlated features can be created leading to 31/65 features selected. The best 3 prognostic features are MTV, correlation (GLCM) and the Nutritional Risk Index (NRI), whereas the best 3 predictive features are MTV, ZP and correlation (GLCM).Conclusion: ML technique, such as random forest classifier, is an interesting tool to find the

most relevant among a large amount of features, to classify patients. A FS is mandatory to improve the classification accuracy. In case of oesophageal cancer, MTV and texture parameters appear as relevant feature and improve predictions.

OP162

Biomathematical modeling approach to predict clinical SUVR in amyloid PET imaging towards efficient radioligand discovery and development

Y. Arakawa[1], M. Shidahara[1], Y. Nai[2], S. Furumoto[2], C. Seki[3], N. Okamura[1], M. Tashiro[2], M. Tashiro[2], Y. Kudo[1], K. Yanai[1], K. Gonda[1], H. Watabe[2]; [1]Tohoku University School of Medicine, Sendai, JAPAN, [2]CYRIC, Tohoku University, Sendai, JAPAN, [3]National Institute of Radiological Sciences, Chiba, JAPAN.

Aim: Purpose of the study is to develop a new methodology to predict clinical SUVR of amyloid PET radioligands by extending biomathematical modeling, which was previously proposed by Guo et al. [1]. Methods: 6 amyloid radioligands, [11C]PIB, [11C]BF-227, [11C]AZD2184, [18F]FACT, [18F]Flobetapir and [18F]AZD4694 were explored in this study. For each tracers, time-activity curves (TACs) were generated using one-tissue compartment model with arterial plasma input function and calculated kinetic parameters (K1, k2 and BPND). By biomathematical modeling simulation, K1, k2 and BPND values were derived using lipophilicity (logP), apparent volume (Vx), free fraction in plasma (fP), free fraction in tissue (fND), dissociation constant (KD) and density of Amyloid β (Bavail) [1]. Lipophilicity was using ClogP (chemoffice ver. 2012, Hulinks Inc.), moriguchi logP, MlogP (dproperties, Affinity Science corp.). Vx was also computed using dproperties. Both fP and fND were calculated by relational expressions among logP, fND and fP. Regression lines of logP vs. fND and fND vs. fP. were derived from three publications, Guo et al. [1], Summerfield et al. [2] and Wan et al.[3]. KD was obteined from publications. Bavail was fixed at 3nM for healthy control (HC) and 50nM for severe Alzheimer Disease (AD) patient. Predicted SUVRs of HC and AD were then obtained by dividing the summed TACs of the target region over that of the reference region. The predicted SUVRs of HC and AD for each tracer were then compared with previously reported in vivo SUVRs of HC and AD groups respectively. The correlations between predicted and reported SUVRs were compared for 6 combinations of logP and regression line (ClogP-Guo, ClogP-Summerfield, ClogP-Wan, MlogP-Guo, MlogP-summerfield and MlogP-Wan). Results: Good correlations between predicted SUVR(y) and in vivo SUVR(x) were observed in the case of MlogP-Summerfield ($y = 1.05 x + 0.04$, $r2 = 0.70$) and MlogP-Wan ($y = 2.67 x - 1.42$, $r2 = 0.70$). On the other hand, poor correlation was observed in case of ClogP-Guo ($y=0.59x+0.36$, $r2=0.38$). Conclusion:Proposed methodologies (MlogP-Summerfield and MlogP-Wan) were able to predict SUVR with good correlation against in vivo SUVRs for 6 amyloid tracers, showing potential to be applied to other amyloid radioligands. Reference: [1] J Nucl Med. 2009, 50(10):1715-23. [2] J Pharmacol Exp Ther, 2006; 316:1282-90 [3] J. Med. Chem. 2007, 50:4606-15

OP163

Correlation of SUV and tumor to blood standard uptake ratio (SUR) with the metabolic uptake rate derived from quantitative dual time point measurements.

F. Hofheinz[1], J. van den Hoff[1], A. Lougovski[1], K. Ego[2], H. Amthauer[2], I. Apostolova[2]; [1]Helmholtz-Zentrum Dresden-Rossendorf, Dresden, GERMANY, [2]Clinic of Radiology and Nuclear Medicine, University Hospital, Magdeburg, GERMANY.

Aim: Determination of tumor SUV is widely used for quantitative assessment of tumor metabolism in FDG-PET. However, the SUV approach has several well known limitations compromising its ability to act as a surrogate parameter of glucose consumption. Recently, we have shown that SUR overcomes most of these limitations as long as FDG kinetics in the target structure can be considered irreversible [1,2]. Excellent linear correlation of SUR and Km from Patlak analysis was found using dynamic imaging of liver metastases. However, due to the perfectly standardized uptake period used for SUR determination and the comparatively short uptake period these results are not directly applicable to clinical whole body examinations, in which the uptake periods often vary considerably. Therefore, the aim of this work was to investigate the correlation of SUR and Km in clinical whole body scans, where Km was approximated by Ks derived from dual time point (DTP) measurements [3]. Methods: DTP FDG-PET/CT was performed in 76 consecutive patients with histologically proven NSCLC. In the PET images the primary tumor was delineated with an adaptive threshold method. For determination of the blood SUV the aorta was delineated manually in the attenuation CT. The aorta ROI was transferred to the PET image. Blood SUV was computed as the mean value of the aorta ROI. SUR values were computed as ratio of tumor SUV and blood SUV. SUR values were scan-time-corrected to 60 min p.i. as described in [2]. Metabolic uptake rate Ks was computed similar to the procedure in [3]. The correlation of SUV and SUR with Ks was investigated. Results: There was highly significant correlation of SUR and Ks (R^2=0.9). However, the correlation coefficient appeared somewhat lower than previous results obtained from dynamic imaging and standardized uptake times (R^2=0.96 [1]). As expected, SUV showed

markedly lower correlation with Ks than SUR (R^2=0.76). Conclusion: Our results show that in clinical whole body PET the correlation of uptake values with the metabolic trapping rate can be improved notably by blood normalization and scan-time-correction. Furthermore, the high correlation of SUR with Ks indicates that for histologically unambigous tumor lesions DTP do not provide added value in comparison to the SUR approach. Literature: [1] EJNMMI Res 2013,3:77 [2] EJNMMI Res 2014,4:18 [3] EJNMMI Res 2012,3:16

OP164

Impact of Use of Fanbeam Collimator in Interpretation of 99mTc-TRODAT Scans and Comparison of Image Quality with Low Energy High Resolution Collimator by Inter-observer Agreement Using Kappa Statistics

H. Rathore[1], T. Bharadwaj[1], H. Shah[1], P. Aland[1], B. Jois KS[1], S. Ghosh[1], L. Reddy[1], P. Chandrak[2], M. Prabhu[3], P. Kumar[1], P. Chaudhuri[1], C. Sekhar[1], S. Shraddha[1], V. Lele[1]; [1]Jaslok Hospital and Research centre, Mumbai, INDIA, [2]Tata Memorial Hospital, Mumbai, INDIA, [3]Narayana Hrudayalaya, Bangalore, INDIA.

Introduction: 99mTc Trodat Brain SPECT is a powerful tool in diagnosis and evaluation of patients with Parkinsonism. However the unavailability of finite resolution and lack of anatomic details makes the interpretation of scans difficult. With the advent of the Fanbeam ultra high resolution collimator (FBUHR), the resolution and sensitivity has increased multifold. Aim: 1. To prove if use of Fanbeam Collimator improves inter-observer agreement within Nuclear Medicine Physicians in regards to interpretation of ^{99m}Tc-TRODAT scans. 2. To compare image quality of FBUHR and Low Energy High Resolution (LEHR) collimator in ^{99m}Tc-TRODAT imaging. Materials and Methods:-^{99m}Tc Trodat scans acquired over a period from January 2014 to April 2015 were included in the study. • 40 scans - 20 from each FanBeam and LEHR were made anonymous, randomised and were given to three nuclear medicine physicians A, B, C, who interpreted them individually as normal and abnormal, the scan quality was interpreted as good and average or poor.• The data was analysed between 3 groups, Group I included A and B, II included B and C, III included A and C. Using Kappa(k) analysis in terms of agreement, <0 suggesting that less than chance agreement, 0.01-0.20slight, 0.21-0.40fair, 0.41-0.60moderate, 0.61-0.80substantial, and 0.81-0.99 almost perfect agreement, 1 is perfect agreement and 0 is exactly what would be expected by chance. Result: Our data indicate that the imaging outcome expressed by the inter-observer agreements and quality of scans has an excellent test reproducibility and correlates with imaging quality and disease severity. In overall evaluation, we found Moderate Agreement in all 3 groups I, II, III with kappa 0.46, 0.525, 0.421 respectively for scan quality and Moderate agreement in group I and III, and Substantial Agreement in the group II for diagnosis of Parkinsonism. Individually, the FBUHR shows kappa value of 0.48, 0.49, 0.56 and LEHR shows -0.041, 0.062, -0.086 in groups I, II, III respectively for Scan Quality which shows moderate agreement in all 3 IOA groups for FBUHR, and less than chance agreement or slight agreement for LEHR Collimator. These findings suggest that ^{99m}Tc-TRODAT BRAIN SPECT imaging using FBUHR is useful and feasible for imaging Parkinsonism with more accuracy than LEHR. Conclusion: The image quality was consistently rated better with the use of FBUHR as compared to the LEHR collimator. This translated in an improved interobserver agreement across scans with the use of FBUHR, resulting in better scan interpretation.

OP165

Standardized uptake values of 99mTc-MDP SPECT bone scans - a novel method for absolute SPECT/CT quantification

W. He, W. Zhai, W. Yu; Huadong Hospital, Shanghai, CHINA.

Objectives : To investigate the variation of SUV values in 99mTc-MDP bone scans using SUV SPECT hybrid reconstruction based quantitative methods. Methods: 535 patients (mean age 63.07) without bone metastasis which has been diagnosed by CT and MRI were enrolled in this study ,and they were divided into four groups : 100 cervical vertebra cases , 161 thoracic vertebra cases, 172 lumbar vertebra cases and 102 pelvis cases. To generate SUV-calibrated images, the raw SPECT data was reconstructed using the software 'SUV-SPECT' (HERMES MEDICAL SOLUTIONS). Corrections were applied for CT attenuation, Monte Carlo-modeled scatter correction, resolution recovery, scaling for injected dose and radioactive decay. The units of counts-per-voxel were scaled to activity per unit volume (Bq/cc) based on previously performed phantom calibration work to allow for SUV measurements. The reconstructed images were analyzed using a constrained threshold-based volume of interest approach to automatically calculate the uptake in the bony structures. SUVmax by body weight was recorded in the derived volume. All the values were measured twice to verify consistency.95% medical reference range SUV was generated .Results : The mean SUVmax of cervical vertebra group was 9.78±3.07 (ranging from 5.00 to 17.27), thoracic vertebra8.81 ±2.17(ranging from 5.11 to 12.82),lumbar vertebra 9.64 ±2.48 (ranging from 5.81 to 15.58)and pelvis(ranging from 5.72 to 16.99). The repeated results were consistent.Conclusions : This method is accurate, easy-to-use and robust, providing absolute quantification in SPECT/CT,

which promises to be widely used in primary diagnosis and evaluation of therapy response.

OP166
Development of Motion Correction Methods for Cardiac PET Imaging

T. Noponen[1,2], R. Klén[1,3], T. Kokki[1,2], J. Teuho[1], K. Thielemans[4], J. Koikkalainen[5], E. Hoppela[1], H. Sipilä[1], J. Lötjönen[5], M. Teräs[1], J. Knuuti[1]; [1]Turku PET Centre, Turku University Hospital and University of Turku, FINLAND, [2]Department of Nuclear Medicine, Turku University Hospital, FINLAND, [3]Department of Mathematics and Statistics, University of Turku, FINLAND, [4]University College London, London, UNITED KINGDOM, [5]Knowledge Intensive Services, VTT Technical Research Centre of Finland, FINLAND.

Introduction: In cardiac PET, pulsatile and respiratory motion may cause severe artifacts. Especially when imaging few millimeter targets such as coronary plaques, cardiac tumors or focal inflammations without any motion correction, a few centimeter physical movement of the heart can impair an image quality significantly. In this project, dual gating and motion correction methods for cardiac PET were developed and their technical features were studied. Material and methods: Respiratory gating methods based on spirometry and impedance measurements were developed and tested with cardiac MR and PET imaging. Additionally, three motion correction methods were implemented for cardiac PET/CT imaging. In the first method, dual-gated data from PET images were only used to compensate respiratory and pulsatile motion. In the second method, the respiratory motion correction was implemented by using respiratory gated CT images and pulsatile motion by using solely PET data (CT-PET based method). In the third method, dual-motion correction was carried out by using CT based motion models (CT only method). These techniques were tested using phantom and patient data. Furthermore, the optimal number of dual-gates for cardiac PET was studied. Results: Spirometry based respiratory gating method was found to be feasible in both cardiac MRI and PET studies. The amplitude of spirometry signal correlated well with the respiratory induced movement of heart. Impedance based respiratory gating method worked well especially in time-based gating. The motion correction did not succeed, when only PET data were used for motion modeling. However, CT-PET based and CT-only methods were able to correct respiratory and pulsatile motion efficiently in both phantom and patient studies. The motion was reduced in the patient study from 19 to 9 mm and in the phantom study from 15 to 5 mm. Additionally, the optimal number of dual gates for cardiac PET was found to be 24. Conclusions: Using our dual-gating approach and motion-correction methods, both respiratory and pulsatile motions can be reduced significantly in cardiac PET imaging.

510 - Sunday, October 11, 2015, 4:30 PM - 6:00 PM, Hall D
Cardiovascular System: SPECT & PET Perfusion Imaging

OP167
Long-term Prognostic Value of Stress Myocardial Perfusion Imaging and Coronary Computed Tomography Angiography: a Meta-analysis

V. Cantoni[1], R. Green[1], W. Acampa[2], M. Petretta[3], G. De Matteis[1], B. Russo[1], T. Mannarino[1], M. Salvatore[4], A. Cuocolo[1]; [1]Department of Advanced Biomedical Sciences, University of Naples Federico II, Naples, ITALY, [2]Institute of Biostructure and Bioimaging, National Council of Research, Naples, ITALY, [3]Department of Translational Medical Sciences, University of Naples 'Federico II', Naples, ITALY, [4]IRCCS SDN, Naples, ITALY.

Aim: Although stress myocardial perfusion imaging (MPI) by single photon emission computed tomography and coronary computed tomography angiography (CCTA) should be considered complementary, as the anatomical data provided by CCTA differ from the functional information obtained by stress MPI, in clinical these two imaging modalities are alternatively used. Thus, we performed a meta-analysis of published studies, including patients with suspected or known coronary artery disease (CAD), to compare the long-term predictive value for adverse cardiac events of stress MPI and CCTA.Material and methods: An English literature search was performed using the PubMed, Cochrane, Web of Science, and Scopus database to identify articles published between January 2000 and June 2014. To harmonize the predictors of interest, a study was included if all of the following criteria were met: 1) reported a prospective or retrospective analysis of subjects with suspected or known CAD referred for stress MPI to search inducible ischemia or CCTA to detect significant stenosis; 2) provided the unadjusted and/or adjusted hazard ratio (HR) at Cox regression analyses of dichotomous abnormal versus normal perfusion at MPI or coronary stenosis ≥50% luminal narrowing at CCTA; 3) provided primary data on clinical outcomes for adverse events with a follow-up ≥2.5 years; 4) included ≥100 patients.Results: Total of 20 articles (10 MPI and 10 CCTA) were finally included, recruiting 22, 280 patients (13,484 in MPI and 8,796 in CCTA studies). The pooled HR for the occurrence of the primary end point was lower (P=0.04) for MPI (HR 2.60, 95% confidence interval, CI, 2.06-3.29) compared to CCTA (HR 5.70, 95% CI 2.68-12.1). Among the included publications, 4 MPI and 4 CCTA

studies reported the HR for the occurrence of hard events (nonfatal myocardial infarction or cardiac death). The pooled HR was comparable (P=0.11) for MPI (HR 2.75, 95% CI 2.11-3.59) and CCTA (HR 5.34, 95% CI 2.46-11.60) studies. The HR for the occurrence of a combined end point including revascularization was reported in 5 MPI and 6 CCTA studies. The pooled HR was higher (P=0.002) for CCTA (HR 8.27, 95% 3.77-18.14) compared to MPI (HR 2.84, 95% CI 1.68-4.79).Conclusion: CCTA appears more predictive than MPI when coronary revascularization is included in the end point. On the other hand, no differences exist in the prognostic effectiveness of MPI and CCTA for the occurrence of hard events.

OP168

Clinical utilization of submillisievert stress only myocardial perfusion imaging and concurrent coronary artery calcium score: A single institutional experience of a novel cardiac SPECT camera using cadmium zinc telluride (CZT) semiconductor technology

J. Liu, E. Hasche, J. Kilian, H. Dixson, B. Elison, C. Bui, H. Tie, R. Dunn, C. Smillie, Q. Chiam, K. Lee; Bankstown-Lidcombe Hospital, Bankstown, AUSTRALIA.

Aim: To investigate the clinical impact of ultralow dose stress only myocardial perfusion imaging (ULDSO-MPI) and concurrent coronary artery calcium score (CACS) on patients with low pre-test probability for ischaemic heart disease while achieving submillisievert radiation exposures. Material and methods: 120 consecutive patient referrals for ULDSO-MPI with concurrent CACS on the Discovery NM/CT 570c camera (GE Healthcare) were studied. ULDSO-MPI was performed using 100MBq (0.8mSv) Tc-99m sestamibi and 10 minute cadmium zinc telluride (CZT) - SPECT acquisition. CACS was performed using low dose (0.8mSv) prospective ECG gated CT acquisition and adaptive statistical iterative reconstruction (ASIR). CACS CT was synergistically used for SPECT attenuation correction. Outcomes were obtained in 103/120 patients based on cardiology outpatient clinic letters. Results: Technically satisfactory studies were obtained in all patients. Total (ULDSO-MPI+CACS) radiation dose was 1.61±0.11mSv (mean ±SD). All 47 patients with zero CACS had a normal MPI result, and 94 %(44/47) were subsequently discharged from COPCs (defined as no scheduled COPC appointment within the next 12 months). 38/103 patients were started on more aggressive medical therapy. Statistical analysis using Wilcoxon rank sum (Mann-Whitney U) test demonstrated that the patient group started on more aggressive medical therapy was associated with significantly higher CACS (mean CACS = 253) when compared with the group of no change to medications (mean CACS = 28, $p < 0.0001$). Meanwhile, the patient group with ongoing follow up was associated with significantly higher CACS when compared with the discharge from clinic group ($p < 0.001$). Conclusion: Ultralow dose stress only imaging with calcium score is clinically useful and is associated with a very low total radiation dose (1.6 mSv). MPI assesses the short term while the CACS assesses the long term risk for developing ischaemic heart disease. Concurrent zero CACS and normal MPI aid subsequent patient discharge from the COPCs (94% discharge rate). Abnormal CACS leads to more aggressive medical therapy, particularly as the calcium score risk level rises.

OP169

Detection of myocardial ischemia using artificial neural network: different characteristics from conventional defect scoring methods

K. Nakajima[1], S. Matsuo[1], K. Okuda[2], K. Yokoyama[3], H. Bunko[4], S. Kinuya[1], L. Edenbrandt[5]; [1]Kanazawa University Hospital, Kanazawa, JAPAN, [2]Kanazawa Medical University, Uchinada, JAPAN, [3]Matto Ishikawa Central Hospital, Hakusan, JAPAN, [4]Kanazawa Cardiovascular Hospital, Kanazawa, JAPAN, [5]University of Gothenburg, Gothenburg, SWEDEN.

Purpose. Although induced ischemia has been evaluated using stress myocardial perfusion imaging with visual and quantitative scoring methods, a new approach using artificial neural network (ANN) to detect ischemia was developed and its characteristics to identify abnormality were examined. Methods. Patients with coronary artery diseases were selected from 3 hospitals. Mean age was 70±10 years (male 61%) and all patients underwent coronary angiography (0-, 1-, multi-vessel disease (MVD): 25, 29, 52 cases). Patients with old myocardial infarction (OMI, 27%) and coronary revascularization (30%) were included. The training database for the ANN system included normal and perfusion defects, and was classified by experienced physicians, in which 1051 patients (M/F=498/553) were included. Quantification of defects by summed stress/rest/difference scores (SSS, SRS, SDS) were used as a reference, and the normal database using Japanese Society of Nuclear Medicine working group was installed (cardioREPO software). The gold standards were expert consensus of well-experienced nuclear physicians and coronary stenosis of ≥75% or ≥50%. ANN identified abnormal areas and probability (ANN values) in the stress map (ANN stress defect) and difference map between rest and stress (ANN ischemia). Diagnostic accuracy of ANN was compared to conventional visual consensus and scoring methods. Results. The ANN stress

defect value was higher in the consensus defect group than in the no-defect group (0.92±0.11 vs. 0.25±0.32, P<0.0001), and the ANN ischemia was higher in the ischemia group than in the no-ischemia group (0.70±0.40 vs. 0.004±0.032, P<0.0001). Area under the curve with receiver-operating characteristics curve analysis (AUC-ROC) showed comparable diagnostic accuracy between ANN and the scoring methods (0.97 vs. 0.98 for stress defect, and 0.88 vs. 0.94 for ischemia, both P=NS). When diagnostic accuracy was examined with neither OMI nor revascularization they were also comparable (ROC-AUC: ANN ischemia 0.93, ANN stress defect 0.97). The relationship between ANN and scores were not linear, and the ANN increased in the range of SSS and SDS of 0 to 6 rapidly, reaching plateau (nearly 1.00) in the higher score level. Even when coronary stenosis was used as the gold standard of abnormality in patients with neither OMI nor revascularization, sensitivity, specificity and accuracy did not differ significantly among visual consensus, scoring method and ANN methods. Conclusion. ANN provided comparable diagnostic accuracy to the expert interpretation for detection of ischemia even including patients with MVD, OMI and revascularization. The different characteristics from the scoring could provide good adjunctive diagnostic suggestions in clinical practice.

OP170

Nuclear Cardiac Imaging Versus Fractional Flow Reserve in Diagonal Side Branch Ostial Stenosis After Left Anterior Descending Crossover Stenting

S. Fukuzawa, S. Okino, J. Maekawa, S. Ichikawa, N. Kuroiwa, K. Yamanaka, T. Igarashi, M. Inagaki; Funabashi Municipal Medical Center, FUNABASHI, JAPAN.

Background: Although angiographic stenosis of a side branch ostium is frequently observed after stent implantation in a main vessel, the clinical advantages of treating these lesions using complex interventional strategies remain unclear, and such interventions may increase the subsequent risk of adverse clinical events. In addition, these lesions cannot be properly evaluated by conventional coronary angiograms. Objectives: The aim of this study was to compare fractional flow reserve (FFR) and ischemic burden with nuclear cardiac imaging in jailed ostial diagonal lesions after main left anterior descending artery (LAD) crossover stenting. Methods: 38 patients with LAD lesions treated by main LAD crossover single stenting were consecutively enrolled. After successful stenting, FFR was measured at the jailed diagonal side branch. Additional interventions were not performed at the same procedure except TIMI 3 flow of side branch. Intracoronary pressure measurements to determine FFR of the jailed side branch are increasingly performed during coronary angioplasty. Furthermore, one-day stress-rest Tc-99m sestamibi nuclear imaging protocol was used for all patients after procedure within 2 weeks. Results: Among 18 side branches with > 75% diameter stenosis, 6 (33%) had FFR ≤ 0.75, and among 20 side branches with ≤ 75% diameter stenosis, one (5%) had FFR ≤ 0.75 after stent implantation in main vessels. Nuclear study demonstrated inducible ischemic burden (>10%) in only one case of all patients. On the other hand, 26 (68%) patients showed no ischemic area. Clinical follow-up was performed in all patients. Mean duration was 28±9 months. During the follow-up period, one patient of the inducible ischemia underwent side branch stenting and 2 patients underwent TLR because of main stent restenosis. No stent thrombosis was observed in these patients. Conclusion: The finding of the current study is that there is a discrepancy between angiographic percent diameter stenosis and FFR in jailed side branch lesions. Furthermore, nuclear imaging demonstrated that almost of the patients with inadequate FFR of side branch had mild (<10%) ischemic burden and good prognosis.

OP171

In vivo validation of gated myocardial SPECT imaging for quantification of small hearts: comparison with cardiac MRI

C. Kondo, E. Watanabe, M. Momose, K. Fukushima, K. Abe, N. Hagiwara, S. Sakai; Tokyo Women's Medical University, Tokyo, JAPAN.

Aim:In patients with small hearts, defined as an end-systolic volume (ESV) of ≤20 ml calculated using the Quantitative Gated SPECT (QGS) program for gated myocardial perfusion imaging, underestimation of ESV and overestimation of ejection fraction (EF) are frequent and have limited reliability. A newly developed cardiac software, cardioREPO (cREPO, previously named EXINI heart), using novel active shape modeling and volume-dependent edge correction algorithm for left ventricular (LV) delineation, effectively reduces the effects on ESV and EF of a small heart documented on digital phantom experiments (Nakajima K, EJNMMI 2013). The aim of this study was to validate cREPO in vivo for measuring LV volumes and EFs of both small and normal-sized hearts compared with cardiac MRI (CMR). Materials and Methods: We performed stress 99mTc-MIBI SPECT and gated CMR within 30 days interval for 33 patients (mean age, 66 yrs; 19 male) with known or suspected coronary artery disease. Post-processing of resting SPECT data using both QGS and cREPO

provided EF, end-diastolic volume (EDV) and ESV. These results were compared with corresponding data from CMR measured independently by experts in a totally blinded fashion. The following data are expressed as mean±SD (range). Results:The study subjects had body surface area of 1.67±0.17 m2 (1.32-1.98 m2) and consisted of 15 small and 18 normal-sized hearts. CMR gave EFs, EDVs and ESVs of 61%±4% (52%-70%), 127±27 ml (85-191 ml) and 52±17 ml (27-91 ml). QGS gave these values of 68%±10% (43%-86%, p<0.0001 vs CMR), 72±20 ml (42-119 ml, p<0.0001 vs CMR) and 25 ±14 ml (8-66 ml, p<0.0001 vs CMR). cREPO also gave values of 70%±4% (61%-77%, p<0.0001 vs CMR), 87±21 ml (50-131 ml, p<0.0001 vs both CMR and QGS) and 26±8 ml (12-55 ml, p<0.0001 vs CMR). Bland Altman plots showed the deviations (mean±1.96SD) of QGS from CMR of EF, EDV and ESV were 7%±16%, -55±28 ml and -27±23 ml, respectively, and the values of cREPO from CMR were 9%±10%, -41±29 ml and -26±26 ml, respectively. The magnitude of the overestimation of EF by QGS compared with CMR strongly correlated with given EF values (r=0.80, p<0.0001), but no significant correlation was seen with cREPO (r=-0.09, p=0.62). Thus, cREPO provided relatively constant overestimation of EFs by 9% from CMR within the range of EFs in both small and normal-sized hearts. Conclusion:The active shape modeling and volume-dependent edge correction program effectively reduced overestimation of EF of a small heart in vivo.

OP172

Diabetes Mellitus independently determines PET-derived systolic function

L. Juárez-Orozco[1], R. J. J. Knol[2], R. A. Tio[3], S. Lazarenko[2], R. H. J. A. Slart[3], F. M. van der Zant[2]; [1]Rijksuniversiteit Groningen, Groningen, NETHERLANDS, [2]Medical Center Alkmaar, Alkmaar, NETHERLANDS, [3]University Medical Center Groningen, Groningen, NETHERLANDS.

Type 2 diabetes mellitus (DM) has an important role in the development of coronary artery disease (CAD) and may influence systolic function by disturbance of coronary vasculature dilatory capacity. Myocardial perfusion PET is the current reference technique for quantitative evaluation of myocardial blood flow (MBF) and for assessment of the myocardial perfusion reserve (MPR). Moreover, PET can accurately determine systolic function through the left ventricle ejection fraction (LVEF). The present study aimed to evaluate a suspected relationship between DM and systolic function when accounting for MPR and additional cardiovascular risk factors. METHODS: We retrospectively included, with a prospective analysis, 591 patients without previous myocardial infarction, referred for dynamic and gated rest and adenosine stress 13NH3 myocardial perfusion PET between 2012 and 2014. Six patients were excluded for incomplete quantitative perfusion, expressed by MPR, or systolic function expressed by resting LVEF. Clinical records were retrieved for demographic data. MBF and MPR were obtained from the PET data using the SyngoMBF software package. DM was operationalized as a dichotomous variable for presence or absence of the disease. After distribution evaluation of the continuous predictors we performed a bootstrapped multiple linear regression analysis for gender, age, hypercholesterolemia, hypertension, smoking habit, DM and MPR as independent variables and LVEF (expressed as a percentage) as the dependent variable for the model. The statistical analysis was performed using SPSSv.21. P-values ≤ 0.05 were considered statistically significant. RESULTS: Our population (mean age of 66.3±10 years) was composed by 293 males and 297 females. Of these, 16% (94) were smokers, 57.1% (336) had hypertension, 37.6% (221) had hypercholesterolemia, 33.8% (199) had a positive family history for CAD and 15.2% (83) were known with DM. A mean global MPR of 2.17±0.57 and mean LVEF 65.7%±12.2 was measured. Consecutively, multiple linear regression analysis showed a statistically significant relation for age B=6.986 S.E.=1.013 95%CI [5.115, 8.929], p=0.001, MPR B=2.081 S.E.=0.908 95%CI [0.442, 3.713], p=0.021, and the presence of DM B=-3.108 S.E.=1.288 95%CI [-5.674, -0-668], p=0.016. CONCLUSION: There is a significant relationship between DM and PET-derived systolic function in patients without a previous myocardial infarction which persists when accounting for the significant relationship that age and global MPR (along with clinically relevant risk factors) have with LVEF. Our study underlines the importance of DM as a risk factor for deteriorating systolic function. This warrants the need for further research into elucidating the integration of DM and MPR in early clinical decision-making.

OP173

Are myocardial perfusion reserve and LVEF modified by diabetes mellitus? A cardiac PET study.

L. Juárez-Orozco[1], R. H. J. A. Slart[1], R. A. Tio[1], H. H. Boersma[1], A. Ayala-German[2], L. Walls-Laguarda[2], R. A. Dierckx[1], E. Alexanderson[3]; [1]University Medical Center Groningen, Groningen, NETHERLANDS, [2]Universidad Nacional Autónoma de México, Mexico City, MEXICO, [3]Instituto Nacional de Cardiología “Ignacio Chávez”, Mexico City, MEXICO.

Diabetes mellitus (DM) constitutes a chronic degenerative disease with an elevated risk of cardiovascular events. State-of-the-art techniques such as PET myocardial perfusion scanning have

demonstrated that myocardial perfusion reserve (MPR), as well as the left ventricle ejection fraction (LVEF), offer predictive value for adverse cardiovascular events in the setting of coronary artery disease (CAD). Moreover, MPR in spared myocardium (MPR-sm) has shown to be related to systolic function in CAD patients. The present study aimed to evaluate whether the relationship between quantitative perfusion assessed by MPR-sm and LVEF is modified by the presence of diagnosed DM. Methods. We retrospectively included, with prospective analysis, 178 patients (124/54 men/women) who were referred to a PET perfusion scan for known or suspected CAD. There were 60 patients with previously diagnosed DM who were matched to non-diabetic controls (118 patients) according to age, gender, BMI, and size of previous infarction (when present). Other cardiovascular risk factors were comparable. All of the patients underwent a 2-phase (rest and adenosine stress) [13N] Ammonia gated myocardial PET scan. SyngoMBF and QPS-QGS software were utilized for reconstruction and interpretation of the scans. The areas of previous infarction were excluded manually to account for the MPR-sm. After the univariate analysis, we performed a linear regression analysis utilizing the general linear model for LVEF using MPR-sm, DM, and pairing variables. An interaction considering MPR-sm and DM was manually entered in a second step. A p-value<0.05 was considered significant for derived coefficients. Results. Mean age for the diabetic and non-diabetic groups was 66±9 and 65±9 respectively. There was cumulative frequency of 93 (57.8%) with dyslipidemia, 104 (64.6%) with hypertension, 71 (44.1%) of smokers, and 77 (43%) with a previous MI. The univariate analysis for LVEF as the dependent variable revealed a trend towards significance for DM (p=0.06) and a high significance for the MPR-sm (p=0.001). MPR-sm was found to be significant predictor variable for LVEF (p=0.001) while DM resulted not to be significant (p=0.49). The interaction for predictors was performed manually without yielding significance. Conclusion. The presence of DM in patients with known or suspected CAD is not a modifier for the strong relationship between MPR-sm and LVEF. The independent correlation between DM and MPR-sm with LVEF suggest that a possible direct effect of DM on LVEF is outweighed by the effect of MPR-sm. Further studies for gaining insight on the impact of DM in the perfusion-function relationship are warranted.

OP174

Coronary Artery Calcium and Coronary Flow Reserve by Hybrid Rb-82 PET/CT Imaging in Non-diabetic and Diabetic Patients With Normal Myocardial Perfusion

R. Assante[1], P. Arumugam[2], E. Zampella[1], V. Gaudieri[1], C. Nappi[1], T. Mannarino[1], D. Tout[2], M. Larobina[3], B. Russo[1], W. Acampa[3], M. Petretta[4], C. Tonge[2], A. Cuocolo[1]; [1]Department of Advanced Biomedical Sciences, University of Naples Federico II, Naples, ITALY, [2]Nuclear Medicine Centre, Central Manchester University Teaching Hospitals, Manchester, UNITED KINGDOM, [3]Institute of Biostructure and Bioimaging, National Council of Research, Naples, ITALY, [4]Department of Translational Medical Sciences, University of Naples 'Federico II', Naples, ITALY.

Aim: We assessed the relationship between coronary artery calcium (CAC) and coronary flow reserve (CFR) in non-diabetic and diabetic patients with normal stress myocardial perfusion imaging.Materials and Methods: We evaluated 541 consecutive patients (441 non-diabetic and 100 diabetic patients) without a documented history of CAD and normal myocardial perfusion imaging at vasodilator stress Rb-82 PET/CT imaging. The CAC score was measured according to the Agatston method. Resting and hyperemic myocardial blood flow (MBF) and CFR were automatically quantified. Patients were stratified into two groups based on their CAC score (0-99.9 and ≥100). The Spearman correlation coefficient was assessed between continuous CAC score and MBF or CFR values. Univariable and multivariable logistic regression analyses were used to determine the variables associated with reduced (<2) CFR.Results: Among non-diabetic patients, 330 (75%) had CAC <100 and 111 (25%) ≥100, while in diabetic patients 65 (65%) had CAC <100 and 35 (35%) ≥100 ($p<0.05$). CFR was reduced in 54 (16%) non-diabetic patients and in 19 (29%) diabetic patients with CAC <100 ($p<0.05$). In both non-diabetic and diabetic patients, CAC score was inversely correlated with hyperemic MBF ($r=-0.15$ and $r=-0.26$, respectively, $p<0.05$) and CFR (r -0.19 and $r=-0.23$, respectively, $p<0.05$). On the contrary, there was no correlation between CAC and baseline MBF in both non-diabetic and diabetic patients. In non-diabetic patients, univariable analysis demonstrated that age ($p<0.001$), hypertension ($p=0.05$) and CAC score ($p<0.001$) displayed an inverse relationship with CFR, while multivariable analysis indicated that age ($p<0.05$) and CAC score ($p<0.05$) were independently correlated with reduced CFR. In diabetic patients, age ($p<0.05$) and CAC score ($p<0.05$) displayed an inverse relationship with CFR. However, at multivariate analysis only CAC score ($p<0.05$) resulted as independent predictor of reduced CFR in diabetic patients.Conclusions: In diabetic and non-diabetic patients with normal stress myocardial perfusion there is an inverse correlation between CAC score and both hyperemic MBF and CFR that remain also after adjusting for age and conventional cardiovascular risk factors. In diabetic patients without known CAD a reduced CFR could help to identify early structural alterations of the arterial wall.

601 - Monday, October 12, 2015, 8:00 AM - 9:30 AM, Hall 1
CME 5 - Interactive: PET with Choline Tracers

OP175
Basic Premises to Imaging with 11C or 18F Choline
L. Mansi, ITALY

OP176
11C or 18F Choline in Diagnosing, Staging, Re-Staging and Detecting Occult Recurrences of Prostate Cancer
P: Castellucci, ITALY

OP177
18F-Fluorocholine in Castration-Resistant Prostate Cancer and in other Malignancies
S. Balogova, SLOWAKIA

OP178
18F-Fluorocholine in the Management of Non-Malignant Pathologies
J.-N. Talbot, FRANCE

602 - Monday, October 12, 2015, 8:00 AM - 9:30 AM, Hall 2
Joint Symposium 5: EANM/MDS: Dopamine Transporter Imaging: Current Topics

OP179
Quantification Approaches to DAT Imaging
L. Tossici, UK

OP180
DAT Normal Values: Results from the ENC-DAT Study
A. Varrone, SWEDEN

OP181
Is DAT in Essential Tremor Really Normal?
A. Antonini, ITALY

OP182
DAT Imaging and Cognition in Early PD
D. Aarsland, NORWAY

603 - Monday, October 12, 2015, 8:00 AM - 9:30 AM, Hall 4
Technologist Oral Presentations 1

OP183
^{18}F-FDG PET-CT and Radiotherapy Planning in Lung Cancer - Technical aspects and benefits from metabolic radiotherapy planning

J. Pinto[1], L. Vieira[1], D. Faria[2], J. Vale[3], G. Fonseca[3]; [1]Lisbon School of Health Technology, Lisbon, PORTUGAL, [2]Hospital Lusíadas Porto, Oporto, PORTUGAL, [3]Júlio Teixeira S.A – Radioterapia, Oporto, PORTUGAL.

Introduction:18F-FDG positron emission tomography/ computed tomography (PET-CT) has become an integral component of lung cancer staging because it improves the detection of nodal and distant metastases and significantly alters patient man¬agement. PET is more sensitive than computed tomography (CT) for staging, delineation of the extent of malignancy and for the identifi¬cation of distant metastatic disease. The use of Positron Emission Tomography - Computer Tomography (PET-CT) for target volume delineation in radiation treatment planning allows the combination of the anatomical features of CT with the metabolic evaluation provided by PET.The aim of this study is to compare the definition of planning target volume (PTV) using CT versus 18-FDG PET-CT, the impact on the radiotherapy planning and technical implications on daily routine PET-CT procedures in a Nuclear Medicine Department.Material and methods: A total of 20 patients diagnosed with lung cancer of both genders, with ages between 35-85 years old, underwent three-dimensional conformal radiotherapy (3D CRT). In all the patients a CT scan and an 18-FDG Whole Body PET/TC, complemented with additional segmental late images for radiotherapy planning were performed. The delineation of the GTVs was performed by independent observers based on CT only vs PET-CT images. The PTV was created using the same margins for both GTV volumes. PTV was chosen because is the volume used for radiotherapy treatment planning and that influences the patient treatment. Both volumes were compared.Results: Our preliminary results show larger CT-based PTVs, compared with the PET-CT-based PTVs. The average total PTV from the CT and PET-CT scans was 129.87 cm3 and 66,39 cm3 respectively ($p < 0.05$). An average reduction of 38% in size was observed when PET-CT-based PTVs were used.Conclusion: The use of 18-FDG PET-CT allows a better identification of the metabolic disease in Lung cancer patients. In the CT scan radiooncologist while delineating planning volumes tend to include tissue non metabolic active increasing the GTV and as consequence, the PTV. An increase of planning volume may lead to alterations in the treatment schemes and increase in patient comorbidities.

OP184

Influence of attenuation correction methods in the renal scintigraphy with 99mTc-DMSA

A. I. Santos[1], **A. Amaro**[2], E. Carolino[2], H. Silva[2], L. Vieira[3], T. F. Vaz[2]; [1]Hospital Garcia de Orta, Almada, PORTUGAL, [2]Escola Superior de Tecnologia da Saúde de Lisboa, Lisbon, PORTUGAL, [3]Escola Superior de Tecnologia da Saúde de Lisboa & Instituto de Biofísica e Engenharia Biomédica, Faculdade de Ciências, Universidade de Lisboa, Lisbon, PORTUGAL.

Introduction: The estimate of relative renal function (RRF) through scintigraphy with dimercaptosuccinic acid labelled with Technetium-99 metastable (99mTc-DMSA) may be influenced by kidney depth (KD), due to attenuation by surrounding soft tissue. The KD is rarely determined and considered for RRF estimate, so other methods are applied to circumvent this problem, namely through calculation of the geometric mean (GM) or by application of empirical formulae. Aim: Identify the influence of different attenuation correction (AC) methods on RRF estimate determined by scintigraphy with 99mTc-DMSA. Materials and methods: Thirty-one patients underwent the same acquisition protocol of 99mTc-DMSA scintigraphy. Two independent Technologists performed the image processing, changing the method applied for RRF determination, namely: Raynaud method, Taylor method, Tonnesen method, GM and without any method of AC (WAC). Each exam was processed three times in the same conditions. To identify the influence of the different AC methods on RRF estimate was applied the Friedman test and to evaluate the association and significance between KD and the variables age, weight and height was used Pearson correlation test. Results: Statistically significant differences were found between the different methods ($p<0.001$), except the comparisons between WAC/Raynaud, Tonnesen/GM and Taylor/GM ($p=1.000$), for both kidneys. A strong positive correlation was found between weight and all the methods of KD estimation. Conclusion: Regarding the three methods of KD calculation (Raynaud, Taylor, Tonnesen), the Taylor method is the closest to the GM. The choice of the AC method influences significantly the quantitative parameters of RRF, that way the method selected should be used wisely and standardized for each department in order to allow comparisons throughout time.

OP185

The role of the Nuclear Medicine Technologists in Cyclotron related Research & Development

P. Costa[1], L. Cunha[2], L. F. Metello[2]; [1]Nuclear Medicine Department, ESTSP.IPP & CADCTR, Vila Nova de Gaia, PORTUGAL, [2]Nuclear Medicine Department, ESTSP.IPP & CADCTR & IsoPor SA, Vila Nova de Gaia, PORTUGAL.

Introduction: Nuclear Medicine is a highly dynamic field, based on synergies between several different scientific fields such as Physics, Chemistry, Biology and Engineering, among others. Over the last decade, several areas of Nuclear Medicine have been particularly active in terms of research. Some examples are developments made in Instrumentation, Image Processing, Therapeutic Applications, Radiopharmacy and Radionuclide Production. It is undeniable that modern research requires multidisciplinary cooperation and collaboration. In this context, advanced practice adequately based on proper education and training of Nuclear Medicine Technologists (NMT) should involve active participation in R&D applied projects. Aim: Using as example one of the fields already mentioned (Radiopharmacy and Radionuclide Production) this paper aims to describe and exemplify the possible role of the Nuclear Medicine Technologist in cyclotron-centered R&D processes. Methods: Examples of research & development projects on Radiopharmacy and Radionuclide Production will be shown, describing the role of the NMT, but also analyzing the interactions with other professionals from the different fields of scientific knowledge needed for the specific requisites of projects being mentioned. Results/Conclusions: Based on our own experience and activity in the field of cyclotron-centered research for Radiopharmacy and Radionuclide Production (including activities at distinct levels in different projects regarding, but not limited to, the development of targetry applied solutions - concerning the targets themselves and all that it is related - the practical methods and solutions to transport the produced activity and/or the recovery, the synthesis and/or purification and distinct processing of radiopharmaceutical products and sub-products, etc.) we consider that multidisciplinarity is indeed a mandatory aspect in research & development processes, at the same time that only highly-educated NMTs might play a "real role" in this specific field essentially due to its versatility and "natural" capacity to integrate basic and applied research, always without losing the focus on the practical questions to be solved/answered and the final applicability of research results, while permanently complying with all the best practices and measures concerning radiation protection, so assuring a safe environmental conditions for themselves as for the remaining health professionals, the members of the public eventually around and the environment itself.

OP186

Occurrence and Characterisation of Perfusion Defects on $^{13}NH_3$ Myocardial PET/CT Due to Side Branch Occlusion After Ramus Descendens Anterior Stenting

H. Kan, R. J. J. Knol, S. V. Lazarenko, M. Wondergem, N. J. Hoogvorst, F. M. van der Zant; MCA, Alkmaar, NETHERLANDS.

Aim: Coronary stenting is frequently accompanied by occlusion of side branches of the targeted coronary artery. This has been shown to induce small reversible or persistent perfusion defects on myocardial perfusion SPECT studies. Data from $^{13}NH_3$ PET/CT studies concerning such perfusion abnormalities after ramus descendens anterior (RDA) stent placement is lacking, and thus this study aimed to analyze the effect of RDA stents on myocardial perfusion as measured by $^{13}NH_3$ PET/CT. Patients and methods: From September 10th 2013 till August 29th 2014, 581 consecutive patients that underwent $^{13}NH_3$ myocardial perfusion PET/CT were prospectively entered in a database. All patients gave written informed consent for usage of their anonymous data. Baseline characteristics and cardiac risk factors were collected. The datasets of patients with a stent in the RDA were evaluated by two experienced readers for the existence of reversible or persisting perfusion defects within the RDA flow territory and subsequently categorized as normal, infarction, ischemia, small persisting defect after stent placement or small amount of ischemia after stent placement. Results: 581 patients {66±10 years (mean±SD), male:female 311(53.5%):270(46.5%)} were included in the database. Of these, 195(34%) had family history of heart disease, 93(16%) were smokers, 125(22%) were diabetic patients, 238(41%) had hypercholesterolemia, 333(57%) had hypertension and 110(19%) had a history of myocardial infarction. A stent in the RDA was present in 53 patients {65±10 years, male:female 33(62%):20(38%)}, of which 29 patients had a stent in the proximal RDA, 18 in the mid-RDA and 6 in both the proximal and mid-RDA. $^{13}NH_3$ myocardial perfusion was scored as normal in 26 (49%), as infarction in 5 (9%), and as ischemia in 2 patients (4%). 6 patients (11%) showed a small persisting defect within the RDA flow territory whereas 14 patients (26%) showed a small area of ischemia in the RDA territory. Conclusion: RDA stents cause small $^{13}NH_3$ myocardial perfusion defects in 38% of the patients of which 70% are reversible.

OP187

Usefulness of simultaneous intermediate-level exercise for dobutamine stress myocardial perfusion imaging.

T. Kasai[1], M. Aiga[1], Y. Iwasaki[2], K. Oshima[1], Y. Fujita[1], Y. Sasaki[1], N. Tanaka[1], A. Yamashina[2]; [1]Tokyo Medical University Hachioji Medical Center, Tokyo, JAPAN, [2]Tokyo Medical University, Tokyo, JAPAN.

Aim: Although dobutamine stress testing is selected when a patient cannot exercise sufficiently, and adenosine is contra indication, not a few cases cannot achieve their target heart rate, resulting in insufficient stress testing. We developed a novel stress method of simultaneous intermediate-level exercise for dobutamine stress myocardial perfusion imaging and assessed the usefulness of this new stress method. Materials and methods: We retrospectively extracted consecutive 44 patients who underwent dobutamine stress myocardial perfusion imaging between September, 2010 and March, 2015. The patients were divided into 2 groups, dobutamine only (22 patients, DOB group) and dobutamine + exercise (22 patients, DOB+EX group). DOB was continuously administered up to 40μg/kg/min. Exercise was performed on a bicycle ergometer up to 75watts as adjusted for each patient tolerance. We investigated the frequency of insufficient stress testing, adverse effects, image quality, hemodynamic kinetics, cumulative administered DOB dose, consumed time for stress testing and compared them between the 2 groups. Results: There was no difference in image quality between 2 groups. Adverse events were occurred 4 cases (18%) in the DOB+EX group during early recovery phase as vasovagal hyperactivity; however, no severe events were demonstrated. Insufficient stress testing were frequent in the DOB group than that in the DOB+EX group (16 (72.7%) vs. 0 (0%); $p<0.001$). Although heart rate was higher in the DOB+EX group (140.5±8.2bpm vs. 117.5 ±17.5bpm, $p<0.001$), there was no difference in peak systolic blood pressure (193.8±22.6mmHg vs. 177.1±30.8mmHg, n.s.). Cumulative DOB dose was higher in the DOB group than that in the DOB+EX group (13.8±6.2mg vs. 6.5 ±3.8mg, $p<0.001$). Heart rate reduction at 2 minutes after termination of stress testing was greater in the DOB+EX group (24.2±9.6% vs. 2.7±6.4%, $p<0.001$). Consumed time for stress testing was shorter in the DOB+EX group than that in the DOB group (586.0±164.3sec. vs. 1240.5±297.0sec, $p<0.001$). Conclusion: DOB+EX reduces insufficient stress testing and contributes to improve the sensitivity of the stress perfusion imaging. In addition, DOB+EX is safe and useful method to improve laboratory throughput.

OP188

Low-dose hybrid CCTA/SPECT image acquisition based on BMI : a case report

V. Weichselbaumer, J. Trinckauf, E. Müller, D. Benz; University hospital Zurich, Zurich, SWITZERLAND.

Aim: In recent years there was a growing interest in the reduction of radiation exposure to patients in diagnostic imaging. The combination of low-dose SPECT myocardial perfusion imaging (MPI) with ultra-low-dose coronary CT angiography (CCTA) allows a comprehensive diagnostic assessment of coronary artery disease (CAD) with low radiation burden. Based on a BMI (body mass index) scale developed at our institution, we have adjusted our scanning protocols, in order to decrease radiation exposure and maintain diagnostic image quality. The aim of this case report is to demonstrate the feasibility of such a low-dose protocol using the BMI scale. Materials and

methods: A 74-year-old female with a BMI of 30.8 presented with new onset of palpitations and an asymptomatic ST-depression during exercise test was referred to our institut for ruling out CAD. The diagnostic work-up started with the acquisition of a CT to measure the calcium score (CT Revolution, GE Healthcare) for risk stratification. Subsequently, an ultra-low-dose CCTA with prospective ECG-triggering was acquired. Technologists at our institution are responsible for selecting BMI adjusted scanning parameters such as kV, mA, contrast agent volume and flow rate. Immediately after the injection of 45ml of Visipaque 320, the CCTA was acquired. Due to calcifications in the right coronar artery (RCA), a low-dose 1-day 99mTc-tetrofosmine stress/rest imaging exam was acquired to exclude a possible hemodynamic relevance of this lesion. Pharmacological stress was done with adenosine, and 163 MBq 99mTc-tetrofosmine was injected at stress midpoint. The99mTc-tetrofosmine dose was prepared by technologists and the acquisition time was calculated using the BMI scale. After a one-hour break stress MPI acquisition (Discovery NM530c, GE Healthcare) was acquired during 912 seconds. Rest MPI was acquired immediately after stress MPI, using 523 MBq 99mTc-tetrofosmine (912 seconds). Results: The total effective radiation dose to the patient was 6.06 mSv, (calcium score: 0.57mSv, CCTA: 0.89mSv, stress/rest SPECT MPI: 1.09 mSv / 3.5 mSv). Image quality was rated as excellent with sharp endocardial and epicardial edge definition, high myocardial count density and uniformity, and without any extracardial background noise. Conclusions: The low-dose SPECT and CCTA protocols provides excellent image quality at low radiation exposure. The BMI scale was developed to optimize work-flow for technologists concerning the calculation of scanning parameters for low-dose hybrid CCTA/SPECT imaging.

OP189

Impact of dynamic acquisition in dual-phase ^{18}flurorocholine PET-CT on radiation exposure of staff and patients

J. BARBIAUX, C. CHNINA, C. HASBROUCQ, S. PETIT, M. THELU, A. BAILLIEZ, T. BLAIRE; GIE HumaniTEP - Hôpital Saint Philibert, LOMME, FRANCE.

Purpose: A dual phase acquisition is usually performed in 18-fluorocholine (FCHOL) PET-CT to assess the prostatic cancer: anearly phase (dynamic acquisition on the pelvis) and a whole body scan (starting 60 minutes after the injection). With recent technological improvements to PET imaging equipment, this study assessed the impact of early phase in patient's irradiation and in staff's exposure. Materials and Methods: Fifty consecutives patients referred for a prostatic cancer in our department were retrospectively included.After injection of 3MBq/kg of FCHOL, the dual-phases acquisitions were performed using a Siemens Biograph mCT Flow 20: the early phase (an 6 minutes early dynamic acquisition on the pelvis, to avoid the bother of the prostatic bed's study before bladder's filing) and the classical whole body acquisition (a study from head to thighs with increased acquisition time on the pelvis and reconstruction in a finer matrix 400 * 400). The CT radiation's exposures (mGy.cm) ofthe patients on both phases were reported and compared. The expositions of the technologists (μSv) for carrying the patients on both acquisitions were measured using an operational dosimetry (APVL, EPD MK2+). Results: For the patients, 263±47 MBq of FCHOL were injected. The mean weight was 85±15 kg. The mean age was 69±7 years. The mean size was 175±7 cm. The mean radiation's exposure was 171±39 mGy.cm and 657±196 mGy.cm for the early and the classical phases respectively. For the technologists, the mean operational dosimetry was 1.55 ±0.22μSv (0.85±0.12μSv in the early phases and 0.70±0.10 μSv in the classical acquisitions). The radiation's exposure of the early phases represented 21% for the patients and 55% for the technologists.Conclusion: The early phases acquisitions represented 21% of the total irradiation for the patients and 55% of the technologists' exposure. It might be interesting to discuss with the medical staff to reduce the systematic realization of the early acquisitions.

OP190

Radiation Dose to the Eye Lens: Does Positioning Really Matter?

C. Baun[1], K. Falch[1], K. D. Nielsen[2], S. Shanmuganathan[1], O. Gerke[1], P. Hoeilund-Carlsen[1]; [1]Odense University Hospital, Odense, DENMARK, [2]University College Lillebaelt, Odense, DENMARK.

Aim: The scan field in oncology patients undergoing eyes-to-thighs PET/CT must always include the base of the scull according to department guidelines. The eye lens is sensitive to radiation exposure and if possible it should be avoided to scan the eye. If the patient's head is kipped backwards during the scan one might avoid including the eye in the CT scan without losing sufficient visualization of the scull base. The aim of this study was to evaluate the possibility of decreasing the radiation dose to the eye lens, simply by changing the head position, when doing PET/CT from the base of the scull to the thigh. Methods and materials: The study was performed using a human like whole body phantom with electronic dosimetry units placed upon each eye to detect the exact radiation dose to the eye lens during each scan. The phantom's head was placed in two different positions, (a) elevated with a pillow below the head (standard), and (b) kipped backwards with the pillow below the neck (kipped). For each head position, CT scans

were repeated 5 times with both a low dose and a high dose CT protocol; in this way, a total of 20 CT scans were performed. Robust standard errors were used in order to account for intragroup correlation due to repeated measurements. Results: Overall, position 'kipped' reduced the radiation dose to the lens, on average by 42.9% or in mean by 1.15 mSv (95% CI: 0.45-1.85; p=0.001) compared to 'standard', i.e., from 2.68 mSv (range 0.67 - 4.68) to 1.53 mSv (range 0.69 - 4.46). With the high dose protocol and position 'kipped', the radiation dose to the lens decreased by 41.5%, on average by 1.52 mSv (95% CI: 0.39-2.64; p=0.008) compared to 'standard', i.e., from 3.66 mSv (range 1.62 - 4.68) to 2.14 mSv (range 1.12 - 4.46). With the low dose protocol and position 'kipped', the decrease was comparable in relative terms: by 45.6% or, in absolute terms on average, 0.78 mSv, (95% CI: -0.05 to 1.61; p=0.07, i.e., from 1.71 mSv (range 0.67 - 2.97) to 0.93 mSv (range 0.69 - 1.66). Not in a single case had position 'kip' the effect that one could not overlook the skull base.Conclusion: These results indicate that it is possible to reduce the radiation dose to the eye lens without loss of diagnostic information in the scan by optimizing positioning of the head.

605 - Monday, October 12, 2015, 8:00 AM - 9:30 AM, Hall G2
Do.MoRe: PRRT Dose Response

OP191
PRRT toxicity: DOTATOC versus DOTATATE

M. Sollini[1], E. Grassi[2], F. Fioroni[2], A. Filice[2], V. Ferri[2], A. Frasoldati[2], A. Versari[2]; [1]IRCCS MultiMedica, Sesto San Giovanni, ITALY, [2]Santa Maria Nuova Hospital IRCCS, Reggio Emilia, Reggio Emilia, ITALY.

Aim: Many radiolabeled somatostatin analogues with different affinity profiles for somatostatin receptor subtypes and different biological half-time (63 hours for DOTATOC and 81 hours for DOTATATE) have been employed in Peptide Receptor Radionuclide Therapy (PPRT). We aim to compare PRRT toxicity profiles of DOTATOC and DOTATATE radiolabeled with 90Y or 177Lu in patients with neuroendocrine tumors (NET). Materials and methods: we retrospectively evaluated 16 NET patients of whom 8 treated with 90Y/177Lu-DOTATOC (group 1) and 8 treated with 90Y/177Lu-DOTATATE (group 2) with comparable characteristics (risk factors, number of cycles, cumulative administered activity). Patients were blinded selected (independently from acute and chronic/long term toxicities as well as outcome). Risk factors for PRRT were recorded. 3D-dosimetry of each patient was calculated at organ-level with OLINDA/EXM software. Both BED of kidneys and adsorbed dose of bone marrow were calculated. Haematological parameters including WBC, Hb, PLT and creatinine were recorded to assess acute and chronic toxicity according to CTAE v4.0. Results: Hypertension and/or diabetes were present in 3 patients of each group. Patients of both groups received a median of 4 administrations (range 3-6). The mean cumulative administered activities were 4847 ±4366 MBq and 5365±4107 MBq for 90Y-DOTATOC and 90Y-DOTATATE, respectively (p=0.8) and 12506 ±8362 MBq and 10545±4551 MBq for 177Lu-DOTATOC and 177Lu-DOTATATE, respectively (p=0.5). At least one adverse event (leukopenia, anemia, thrombocytopenia, renal failure) was observed in 7/8 and 8/8 patients, in group 1 and 2 respectively. Overall, in group 1 25 adverse events (grade 1-2) occurred and in 12/25 (48%) adverse events were chronic/long term (G1-2 leukopenia=3, G1 anemia=4, G1 thrombocytopenia=2, G1-2 renal failure=3). Overall, in group 2 52 adverse events (grade 1-4) occurred and in 9/52 (17%) adverse events were chronic/long term (G1 leukopenia=1, G1-G2 anemia=5, G1 thrombocytopenia=1, G1-4 renal failure=2). In group 2 transient acute toxicity between administrations occurred more frequent compared to group 1 (43 versus 13 adverse events, p=0.0046). BED of kidney resulted 32±20 Gy in group 1 and 49±23 Gy in group 2 (p=0.14) while bone marrow adsorbed dose was 0.177±0.113 Gy in group 1 and 0.411 ±0.183 Gy in group 2 (p=0.008). Conclusion: our results suggest a major number of adverse events during PRRT using DOTATATE than DOTATOC although in case of DOTATOC we observed a more frequent chronicity/long term mild toxicity (48% versus 17%). No cases of severe haematological disease (i.e. myelodysplasia) were observed while chronic renal failure requiring dialysis occurred in one patient of group 2.

OP192
[^{177}Lu-DOTA]-D-Phe$_1$-Tyr$_3$-Octreotide (^{177}Lu-DOTATOC) for Peptide Receptor Radiotherapy in Patients with Advanced Neuroendocrine Tumours: A Retrospective Phase II Study of Efficacy and Safety

H. R. Kulkarni[1], R. P. Baum[1], A. W. Kluge[2], M. Sayeg[1], U. Schorr-Neufing[2], K. Niepsch[1], N. Biterlich[2], C. van Echteld[3]; [1]Zentralklinik Bad Berka, THERANOSTICS Center for Molecular Radiotherapy and Molecular Imaging (PET/CT), Bad Berka, GERMANY, [2]ABX-CRO GmbH, Dresden, GERMANY, [3]ABX-CRO, Dresden, GERMANY.

Background: To evaluate efficacy and safety of ^{177}Lu-DOTATOC as agent for peptide receptor radiotherapy (PRRT) of advanced neuroendocrine tumours (NET). Material and methods: Fifty-six subjects with metastasized and progressive NET (50% midgut, 26.8% pancreatic, 23.2% other primaries) were included in prospective database and retrospective analysis was performed. Subjects received on average 2.1 (range 1 - 4)

cycles of ^{177}Lu-DOTATOC (median administered activity 7.0 GBq) at three-monthly intervals. Efficacy was analyzed based on RECIST and by number of treatment cycles and histology. Results: In the total population, median progression-free and overall survival was 17.4 and 34.2 months, respectively. Repeatedly treated patients had an Overall progression free survival of 30.2 months. Objective response rate (complete or partial) was 33.9%, while disease control rate was 66.1%. A high number of complete responses (16.1%) was observed, 78% of which were ongoing at the end of the Observation period. 14% of subjects required more than one cycle to induce an Initial response. In 32% of responders, it took four to eight months from the first PRRT cycle, before an initial response could be documented. After initial response, morphological outcome may improve for up to 20 months after the last PRRT. In 47% of subjects it took more than 9 months from start of PRRT until an objective response occurred. No SAE, and only a single case (1.8%) of self-limiting grade 3 hematotoxicity was observed. No renal toxicity was found, although 19.6% of subjects had mild renal insufficiency at baseline. Conclusions: ^{177}Lu-DOTATOC is a novel agent for PRRT with unusual potential to induce objective response in progressive neuroendocrine tumours and long lasting disease control, even when administered at moderate activity doses. Efficacy was highest when the agent was administered in repetitive cycles, indicating that efficacy should be established only after Administration of the prescribed dose. With only 6.2% non-responders, the overall disease control rate (DCR) was 93.8%, compared to 80.3-85.0% reported for ^{177}Lu-octreotate. This difference in DCR between the peptides is accounted for by an about ten-fold higher rate of subjects experiencing a complete response following ^{177}Lu-DOTATOC. In the subgroup of patients with GEP-NET, the proportion of complete responders was 25%, which is the highest value ever reported to date. A particularly high therapeutic index is suggested by the observed safety profile, also in subjects with a priori reduced bone marrow or renal function, which reflects a uniquely low uptake of ^{177}Lu-DOTATOC by normal organs.

OP193

Long term survival analysis after i.a. 90Y-DOTATATE PRRT, in patients with non-resectable, advance progressive liver dominant neuroendocrine neoplasms.

M. L. Nowicki[1], S. J. Konsek[2], L. Jaskiewicz[2], M. Mol[3], A. Sankowski[1], J. R. Buscombe[4], L. Bodei[5], R. Mikolajczak[6], **J. B. Cwikla**[2]; [1]Department of Radiology and Diagnostic Imaging, Hospital Ministry of Internal Affairs & Administration, Warsaw, POLAND, [2]Department of Radiology, Faculty of Medical Sciences, University of Warmia and Mazury, Olsztyn, POLAND, [3]Radiology and Diagnostic Imaging, Medical Center for Postgraduate Education, Warsaw, POLAND, [4]Department of Nuclear Medicine, Addenbrooke's Hospital, Cambridge, UNITED KINGDOM, [5]Division of Nuclear Medicine, European Institute of Oncology, Milan, ITALY, [6]Centre POLATOM, National Centre for Nuclear Research Radioisotope, Otwock, POLAND.

Purpose: To evaluate long term survival in group of patients with non-resectable, liver dominant and progressive neuroendocrine neoplasms after i.a. 90Y DOTATATE peptide receptor radionuclide therapy (PRRT) in gastroenteropancreatic neuroendocrine tumours (GEP-NET). Patients and Methods: The study group: 38 patients, 17 female, mean age 56.2. All with histological proven extensive non-resectable GEP-NET. Half of them with secretor tumours. All had documented DP (RECIST and/or clinical in case or secretor tumours) with relapse on previous therapy. 22 pts with initial i.a. PRRT after relapse of chemo and somatostatin analogues (SST) therapy, others 16 pts had previous i.v. PRRT. Overall 104 therapy session using i.a. 90Y-DOTATATE performed. Initial clinical tumour responses assessed, 6W after therapy and then after each of the 3M intervals of follow-up. The objective tumour response was classified according to RECIST, initially 6W and then after each of the 6M. Adverse Events (AE) of therapy were evaluated using CTCAE NCI (ver. 4.0). Overall survival (OS) and progression free survival (PFS) were evaluated using Kaplan Meier methods. Results: The median OS and PFS for all pts were 39.0M and 24.5M, in group with initial i.a. PRRT were 50.0 and 28.5M in those with previous i.v. PRRT were 20.5 and 12.0M. The clinical response including performance status (PS), initial and 6W after PRRT were significant improved consider all pts and in both groups. ($P<0.05$). Clinical response at 6W seen as PR 29, SD 7 and 2 had DP. At 6M after treatment 27 had PR, 6 SD and 4 DP. After 12M 24 had PR 4 SD and 6 DP. After 24M 11 had PR, 9 SD and rest 6 developed DP. Radiological response (RECIST) at 6W after PRRT was noted in 3 subjects, 33 pts had SD, after 6 M of follow-up 8 had PR, 28 had SD and rest 4 developed DP. After 12M 8 pts had PR, 23 pts had SD and 4 had DP. After 24M, PR was noted in 4, 16 SD and 3 DP. Conclusion: Intra-arterial PRRT using 90Y-DOTATATE seems to be effective in patients with extensive, liver dominant, non-resectable and progressive GEP-NET. Especially as initial therapy after relapse of other therapy options. Could be used as alternative therapy approach in those after i.v. PRRT, who relapse and whom i.v. PRRT could be cause of AE (kidney and bone marrow). Objective response of PRRT, base on RECIST, underestimate benefits of this type of therapy.

OP194

Early assessment of renal impairment in patients undergoing Peptide Receptor Radionuclide Therapy evaluated by MAG3 renal scintigraphy

R. A. Werner[1,2], S. Beykan[1], C. Lapa[1], C. Bluemel[1], U. Eberlein[1], T. Higuchi[1,2], H. Wakabayashi[1], K. Herrmann[1,3], A. K. Buck[1], M. Lassmann[1], H. Hänscheid[1]; [1]Department of Nuclear Medicine, University Hospital Würzburg, Würzburg, GERMANY, [2]Comprehensive Heart Failure Center, University Hospital Würzburg, Würzburg, GERMANY, [3]Department of Molecular and Medical Pharmacology, David Geffen School of Medicine at UCLA, Los Angeles, CA, UNITED STATES.

Objectives: Due to the potential nephrotoxicity of Peptide Receptor Radionuclide Therapy (PRRT), pre-therapeutic assessment of kidney function is mandatory. Radiation damage of irradiation is the proximal tubuli reabsorbing the radionuclide and the interstitium retaining the radioactivity. Therefore, kidney function test measuring tubular extraction, like mercaptoacetyltriglycine (^{99m}Tc-MAG3), provides additional information in early stages of suspicious renal failure. The aim of this study was an early assessment of renal impairment after treatment with ^{177}Lu-octreotide to investigate the potential loss of kidney function as a function of the administered activity. Materials and Methods: From March 2011 to December 2014, renal impairment was analyzed prior to 136 treatments (32 patients) using ^{99m}Tc-MAG3 clearance (mean follow-up, 366 ± 201 days). Subsequently, PRRT was performed with a mean cumulative activity of 32.2 GBq ^{177}Lu-octreotide (3-7 cycles, standard intervals of 3 months). The ratio of the MAG3 tubular extraction rate (TER) to TER of lower limit (RaTER) was calculated and analyzed as a function of the cumulative administered activity by linear regression analysis. Results: Prior to PRRT, 12 patients showed impaired renal function and 20 patients demonstrated normal kidney function, as indicated by ^{99m}Tc-MAG3 renal scintigraphy (mean TER, 233.5 ± 52.6 ml/min/1.73 m^2). RaTER was 131 ± 0.25 %. Linear regression analysis revealed a median shift of renal function of -0.03% per administered GBq (quartile, -0.34%/GBq, +0.14%/GBq). The following equation was utilized: (relative change in TER per GBq of ^{177}Lu) = 0.0088 - 0.0106 x (initial TER/TER$_{lower\ limit}$). Furthermore, negative gradients showing a high loss of TER per administered activity were observed in patients with a good kidney function whereas in the cohort with initial renal impairment the TER remained almost constant. To illustrate this, we found in 13 patients having an initial TER of <1.3*TER of lower limit that the worst reduction of kidney function was only 0.21% per administered GBq. Conclusion: Only patients with an appropriate kidney function prior to the start of PRRT seem to be at risk of developing renal impairment in the course of therapy. On the other hand, an initially reduced ^{99m}Tc-MAG3- clearance prior to the first treatment cycle seems not to be an exclusion criteria for PRRT. In this study investigating the early assessment of renal function by ^{99m}Tc-MAG3 renal scintigraphy, a low risk of PRRT related renal damage was demonstrated even in a long-term follow-up over one year.

OP195

Super-selective Hepatic Arterial Infusions of n.c.a. Lu-177-Dotatoc in Inoperable Neuroendocrine Liver Metastases of Gastro-Entero-Pancreatic (GEP) Tumors; Preliminary Results

G. S. Limouris[1], N. Trompoukis[1], V. Poulantzas[1], I. Karfis[2], A. Chatzioannou[1], M. Lyra[1], V. Michalaki[3], N. Triantaphyllou[4], G. Nikou[5], M. Paphiti[6], V. R. McCready[6], L. Moulopoulou[1]; [1]Nucl Med Div-1st Radiology Dept , "Aretaieion" Hospital, Athens University Medical Faculty, Athens, GREECE, [2]Nuclear Medicine Dept, Institute "Bordet", Brussels, BELGIUM, [3]Department of Surgical Oncology, "Aretaieion" Hospital, Athens University Medical Faculty, Athens, GREECE, [4]Neurology Dept, 'Aeginiteion" Hosp, Athens Univ Medical Faculty, Athens, GREECE, [5]Gastrointestinal Div, I Dept of Propedeutic Internal Medicine "Laikon" Hospital, Athens, GREECE, [6]Nuclear Medicine Dept, Royal Sussex County Hosp, Brighton, UNITED KINGDOM.

Aim: To evaluate the effectiveness of non carrier added (n.c.a.) Lu-177 DOTA-TOC in inoperable liver metastases, positive for sst2 receptor overexpression (verified by Octreoscan and confirmed by biopsy) due to neuro-endocrine gastro-enteropancreatic (GEP) tumours. Lu-177 DOTA-TOC has been infused after selective catheterization of the hepatic artery ('ARETAIEION' PROTOCOL), minimising in parallel the toxicity of non-target tissues.Materials and Methods: The average dose per session to each patient (9 pts so far in total) was 7.3±2.3 GBq. Repetitions did not exceed 6-fold with treatment intervals of 8-11 weeks, to avoid stunning effect. Response assessment was classified according to the therapeutic benefit. Absorbed doses delivered to metastases, kidneys and red marrow was calculated according to MIRD scheme and perfoermed using OLINDA 1.1 software. The derived values were correlated to the Response Evaluating Criteria in Solid Tumours (RECIST). CT/ MRI scans were performed as baseline before, during and after the end of treatment and monthly ultrasound images for follow-up estimation and measurements. Toxicity (World Health Organization criteria) was measured using blood and urine tests of renal, hepatic and bone marrow function.Results: None of the patients resulted complete response (0.0%); partial response was assessed in 6 (66.0%) and disease stabilization in 3 (34.0%). An 8-month median survival time was estimated for all patients, so far. Six

of 9 (66.0%) showed a mean target diameter shrinkage ranging from 32% to 46%. The organ average radiation dose estimation was found as follows: (a) Liver Tumor 3.0-9.9mGy/MBq, (b) Liver 0.03-0.1 mGy/MBq, (c) Kidneys 0.03-0.4 mGy/MBq, (d) Spleen 0.02-1.2 mGy/MBq and (f) Bone marrow 0.008-0.05 mGy/MBq. The average absorbed dose per session to a tumor for a spherical mass of 20 gr was estimated to be 9.3 mGy/MBq, depending on the histotype of the tumor. WHO toxicity grade 2 erythro-, leuko- and thrombo-cytopenia occurred in 2 (22.0%) cases observed about after the 3rd session.Conclusion: In unresectable metastatic liver lesions positive for somatostatin receptors repeated, trans-hepatic high doses of n.c.a. Lu-177 DOTA-TOC resulted in a more than promising therapeutic outcome with a partial response in approx 66% of the treated patients. Given the loco-regional modality character of the administration technique, no nephrotoxicity has been so far observed.

OP196

Relationship between baseline GFR, [Lu-177] -DOTATATE Clearance and Radiation Dose to Kidneys During Radionuclide Therapy for Somatostatin-Expressing Tumours

D. L. Bailey[1], T. M. Hennessy[2], K. P. Willowson[2], D. L. Chan[1], G. P. Schembri[1], A. Aslani[1], N. Pavlakis[1]; [1]Royal North Shore Hospital, Sydney, AUSTRALIA, [2]University of Sydney, Sydney, AUSTRALIA.

AIM: To examine the relationship between glomerular filtration rate (GFR) and clearance of therapeutic non-carrier added [Lu-177]-DOTATATE (nca-LuTATE) for treatment of neuroendocrine tumours (NETs) and meningiomas expressing somatostatin receptors, and to examine the impact on radiation dosimetry to the kidneys.MATERIALS AND METHODS: All data were acquired on SPECT/CT cameras (Siemens Symbia.T6 and Intevo) using medium-energy collimation and a single photopeak (208 keV ±10%). The accuracy of our whole body (WB) planar imaging and quantitative SPECT/CT (qSPECT) data have previously been validated to within ±10%. Images were acquired immediately after injection of the nca-LuTATE (ITG/ANSTO and Auspep) and at 4, 24 and 96 or 120 hrs post-injection. Whole body clearance was assessed with planar imaging and kidney uptake was measured with qSPECT. The qSPECT data were input to OLINDA/EXM 1.1 for estimation of kidney dosimetry. A total of 36 treatments in 12 subjects were evaluated with this protocol. Subjects were administered a mean of 7.8 GBq (range 6.2 - 8.7 GBq) of nca-LuTATE.RESULTS: A bi-exponential fit to the WB data demonstrated a fast component of clearance of 2.1±0.6 hrs and a slow component of 58.1±7.2 hrs. Baseline GFR showed a good correlation with the fast component when fitted with an exponential curve (R^2=0.74) but was unrelated to the slow component. Radiation dose estimated to the kidneys from qSPECT likewise demonstrated a significant dependence on GFR with slower clearance rates corresponding to higher kidney dosimetry.CONCLUSION: Baseline GFR affects the fast component of clearance of nca-LuTATE and impacts on the radiation dose received by the kidneys. Radiation dose to the kidneys can almost double when GFR is < 60 ml/min/1.73m^2 compared to a GFR of > 100. Individualisation of patient treatments should consider this when aiming to maximise therapeutic efficacy

OP197

Recurrent glioblastoma multiforme - local alpha emiters targeted therapy with 213Bi-DOTA-substance P

L. Królicki[1], A. Morgenstern[2], **J. Kunikowska**[1], H. Koziara[3], B. Królicki[3], M. Jakuciński[4], D. Pawlak[5], C. Apostolidis[2], F. Bruchertseifer[2]; [1]Nuclear Medicine Department, Medical University of Warsaw, Warsaw, POLAND, [2]European Commission, Joint Research Centre, Institute for Transuranium Elements, Karlsruhe, GERMANY, [3]Department of Neurosurgery, Institute of Psychiatry and Neurology, Warsaw, POLAND, [4]Department of Nuclear Medicine, Brodnowski Hospital, Warsaw, POLAND, [5]Radioisotope Centre POLATOM, National Centre for Nuclear Research, Otwock, POLAND.

Glioblastoma multiforme (GBM) is the most common and malignant primary brain tumor. The median survival time is 14.6 months from time of diagnosis, in spite of aggressive surgery, radiation therapy and chemotherapy. Only 3 to 5% of patients survive more than three years. Recurrence of GBM is nearly universal, confers a dismal prognosis with a 6-months progression free survival (6M-PFS) rate of 15% to 21% and a median survival of 6.2 months. Advancements in the past decades have not significantly increased the overall survival of patients with this disease. GBM has been demonstrated NK-1 receptor system and substance P can be used as a ligand for targeted therapy. Alpha emitter, like 213Bi offers the new potential for selective irradiation of tumors, with minimizing damage to adjacent tissue.Material and methods:21 patients with primary recurrent glia tumor IV after standard therapy were included in the study during two years. Following intracavitary or intratumoral insertion of 1-2 catheter systems, patients were treated with 1-8 doses of 2 GBq 213Bi-DOTA-Substance P (213Bi-SP) in intervals of 2 months. 68Ga-DOTA-Substance P (68Ga-SP) was co-injected with the therapeutic doses to assess biodistribution using PET/CT. Therapeutic response was monitored with MRI. Study was approved by the ethical committee of the Medical University of Warsaw.Results:Treatment with activity up to 13 GBq 213Bi-SP was tolerated well with only mild transient adverse

reactions: in 1 patient transient increase of focal neurological symptoms and in 3 patients episodes of epileptic seizures several days after treatment. PET/CT imaging showed high retention of the radiolabeled peptide at the tumor site.Out of 21 evaluable patients, 17 progressed within the follow-up period, 5 of them are alive at the end of follow-up. Four patients were excluded from evaluation due to lack of data. Median progression free survival was 3.7 months, with a 6 months progression free survival rate of 19% . The median overall survival from the first diagnosis was 25.2 months, and from the start of 213Bi-SP was 6.5 months. Follow up of therapeutic responses and toxicity is continued and patient recruitment is ongoing.Conclusions:Treatment of recurrent GBM with 213Bi-SP is safe and well tolerated. Targeted alpha therapy with 213Bi-SP may evolve as a promising novel option for treatment of recurrent GBM.

606 - Monday, October 12, 2015, 8:00 AM - 9:30 AM, Hall 6
M2M: SPECT Translational Studies

OP198

Non-invasive determination of the Beta Bell Mass with ^{111}In-exendin-3 in a Rat Model of spontaneous Type 1 Diabetes

L. Joosten[1], M. Brom[1], D. Bos[1], C. Frielink[1], P. Hanneke[2], O. Boerman[1], M. Gotthardt[1]; [1]Radboud university medical center, Nijmegen, NETHERLANDS, [2]GROW mumc, Maastricht, NETHERLANDS.

Aim Thebeta cell mass (BCM) plays a key role in the development and progression ofdiabetes, but the onset of beta cell loss and the relationship between loss ofbeta cell mass and beta cell function still needs to be unraveled. Anon-invasive method to determine the BCM *invivo* would allow measurement of the BCM during the development andprogression of type 1 and 2 diabetes. Exendin-3 is a stable glucagon-likepeptide 1 (GLP-1) analogue with high affinity for the glucagon-like peptide-1receptor specifically expressed on beta cells. In this study we investigatedthe potential of ^{111}In-exendin-3 to determine the BCM *in vivo* in a rat model that closelymimics the development of type 1 diabetes in humans: BioBreeding Diabetes Prone(BBDP) rats. In this model the potential of SPECT, the relationship between theBCM, exendin uptake in the pancreas and inflammation of the islets ofLangerhans (insulitis) were investigated.Materials and Methods BBDPrats (n = 45) of 4-18 weeks of age were injected intravenously with 15 MBq ^{111}In-exendin-3.SPECT/CT images were acquired 1 h p.i. and the animals were euthanized afterSPECT/CT acquisition. The biodistribution of the tracer was determined and thepancreas was used to determine the BCM by morphometric analysis and degree of insulitis.Results WithSPECT the pancreas in rats was visualized. In healthy rats (4 weeks) efficientaccumulation of ^{111}In-exendin in the pancreas was observed (0.29 ±0.03 %ID/g). In severely diabetic rats (18 weeks) pancreatic tracer uptake wassignificantly reduced with more than ninety percent ($p=0.0004$). The uptake ofthe tracer correlated with BCM (mg) (Pearson $r = 0.80$, $p < 0.0001$). *Ex vivo* autoradiography showed high accumulationof ^{111}In-exendin-3 in the islets of Langerhans in healthy rats andvery low accumulation in the exocrine pancreas. The accumulation in theendocrine pancreas was reduced in rats with beta cell loss and in severelydiabetic rats, with no insulin-positive cells, tracer uptake in the pancreas wasundetectable by autoradiography. Furthermore, insulitis did not have an influenceon the uptake of exendin in the pancreas.Conclusion Inconclusion, in a rat model of type 1 diabetes, closely mimicking the humandevelopment of type 1 diabetes, the BCM can be monitored with ^{111}In-exendin-3SPECT. These results indicate that ^{111}In-exendin-3 is a promising tracerto determine the BCM during the development of type 1 diabetes in patients,without interference of severe insulitis.

OP199

Preclinical imaging of the co-stimulatory ligands CD80/CD86 with 111In-DOTA-Belatacept in oncology and atherosclerosis

A. Müller Herde[1], R. Meletta[1], P. Dennler[2], E. Fischer[2], R. Schibli[1], S. D. Krämer[1]; [1]ETH Zurich, Zurich, SWITZERLAND, [2]Paul Scherrer Institute, PSI-Villigen, SWITZERLAND.

Aim: The co-stimulatory ligands CD80 and CD86 play a crucial role in the initiation and maintenance of an immune response and are found on activated antigen presenting cells (APCs). The human derived Raji cell cell line, originated from Burkitt's lymphoma, is associated with a frequent expression of CD80 and CD86. In the context of atherosclerosis, we identified CD80 and CD86 on APCs with significant higher levels in vulnerable plaques [1]. We propose, CD80 and CD86 as promising targets for imaging inflammation. In a proof-of-principle study, the fusion protein Belatacept (Nulojix®), containing the extracellular portion of CTLA-4 as binding motif, was labeled with indium-111. We analyzed the in vitro stability of this radiotracer and evaluated it in mice bearing CD80/CD86-positive Raji xenografts and in a mouse model of atherosclerosis (ApoE KO). Material and methods: Commercially available Belatacept was conjugated with p-SCN-Bn-DOTA, radiolabeled with In-111 and purified by size-exclusion chromatography (SEC). Stability was investigated after incubation in human or mouse plasma at 37 °C up to 72 h by SEC. CD1 nude mice bearing Raji xenografts and ApoE

KO mice were injected i.v. with 10 MBq 111In-DOTA-Belatacept (25 μg, baseline). Blockade animals simultaneously received unlabeled Belatacept (500 μg). In vivo and ex vivo SPECT/CT scans or biodistribution studies were performed 48 h post injection. Oil red o staining was performed with excised blood vessels to visualize plaque lipids. Results: 111In-DOTA-Belatacept was successfully produced in 73-78% radiochemical yield. 82% of labeled fusion protein remained intact after 72 h of incubation in plasma. In vivo, 111In-DOTA-Belatacept accumulated in Raji xenografts and a reduced accumulation was determined under blockade conditions. These results were confirmed by biodistribution revealing a significant reduction in blockade animals. Ex vivo SPECT scans of the aortic arch and the carotids of ApoE KO mice showed a high accumulation in atherosclerotic plaques and a reduced signal under blockade conditions. Tracer accumulation and plaque localization determined by oil red o staining were consistent. Conclusion: The co-stimulatory ligands CD80 and CD86 are promising targets for the non-invasive imaging of activated immune cells.111In-DOTA-Belatacept accumulates specifically in human derived Raji lymphoma xenografts in vivo and binds to inflammatory plaques in a mouse model of atherosclerosis. Reference: [1] Müller A., et al. (2014) Int J Cardiol, 174, 503-15.

OP200

Initial experiences with the Mediso nanoSCAN preclinical SPECT/MR

M. Segbers[1], J. C. Haeck[1], I. L. Bakker[1], J. de Swart[1], M. Kovács[2], M. R. Bernsen[1], M. de Jong[1]; [1]Erasmus Medical Center, Rotterdam, NETHERLANDS, [2]Mediso Medical Imaging Systems, Budapest, HUNGARY.

Aim: SPECT and MR imaging are for the first time combined in a single hybrid platform: the Mediso nanoScan SPECT/MRI (Mediso, Budapest Hungary). Combining MRI and SPECT could improve localization of the radioactivity in small animals and aid in organ delineation for biodistribution in vivo and pharmacokinetic analysis, as MRI is well known for its superior soft tissue image contrast compared to CT. In this study the first in vivo images were acquired using different tracers. Materials and methods: System specifications: A 1 Tesla horizontal bore permanent magnet with 500mT/M gradients has been coupled in line with a multi-pinhole SPECT subsystem with four rotating 9.5mm NaI detectors. For MR image acquisition a 35mm-diameter solenoid coil was used. Collimators with 64 pinholes of 1.7mm diameter were used and all SPECT acquisitions covered in approximately 7cm the entire body using spiral scanning with step and shoot (rotation in steps of 12.9 degrees). Images of C7Bl/6 mice were acquired after injection with 42MB 99mTc-MDP and 23MBq 99mTc-DMSA. MRIs were acquired with a T2-weighted Fast Spin Echo (FSE) using TR/TE=4377/88.5, 0.27x0.27x0.8mm voxels in 7 minutes and a T1-weighted Gradient Echo using TR/TE=15/3, 0.15x0.15x0.6mm voxels in 11 minutes. The acquired MR images covered the SPECT FOV. PC3 tumor bearing mice were scanned ex vivo 24hours after injection with 25MBq 111In-JMV4168; a gastrin-releasing peptide receptor (GRPR) antagonist that binds to the GRP receptors of the PC3 tumor. SPECT was combined with a T2-weighted FSE using TR/TE=4000/25 and 0.27x0.27x1mm voxels acquired in 10 minutes. Basic MR image quality was determined by signal to noise ratios (SNR) of various tissues. Results: The 99mTc-MDP scan clearly showed the expected tracer uptake in the bones in excellent detail. 99mTc DMSA showed the expected high tracer uptake in the kidneys that could be clearly localized to the renal cortex on the T2-weighted MRI overlay. The 111In-JMV4168 scan showed expected high tracer uptake in the tumor and much lower uptake in the kidneys. Overall, MRI SNR was tissue dependent and varied between 7.2 for muscle and 28 for tumor. Conclusion: The Mediso nanoScan SPECT/MRI is capable of generating visually qualitative and well interpretable SPECT/MR images. The MR images show detailed anatomy within soft tissues and aid tremendously in localization of radioactive tracer uptake.

OP201

Noninvasive visualization of microRNA by Tc-99m radiolabeled anti-microRNA oligonucleotide in tumor xenografts

L. KANG; PEKING UNIVERSITY FIRST HOSPITAL, BEIJING, CHINA.

Introduction: MicroRNAs have been considered as important biomarkers for malignant tumors. Although various optical imaging methods have been developed for the noninvasive detection of microRNAs, they were generally limited in penetrated ability, genetic modification, and potential toxicity. In this study, we firstly used a radionuclide-based imaging method for the noninvasive visualization of overexpressed miR-21 in tumor bearing mice. Methods: MiR-21 targeted anti-miRNA oligonucleotide (AMO) with partial 2'-O-methyl and phosphorothioate modification was designed and synthesized. Technetium-99m (99mTc) labeled AMO was prepared via the conjugation with NHS-MAG3. 99mTc-AMO was evaluated for its stability, inhibitory ability and cellular uptake in vitro, and further in vivo distribution and imaging in multiple kinds of tumor xenografts. Results: 99mTc-AMO was prepared with high labeling efficiency and specific activity. 99mTc-AMO inhibited miR-21 and up-regulated the expression of PTEN. Fluorescence labeled AMO displayed specific and durable distribution in tumor cells. Further, in tumor

bearing mice, 99mTc-AMO showed significant more accumulation in miR-21 overexpressed tumors than control probe, which suggested the effective delivery of 99mTc-AMO in miR-21 over-expressed tumors. Conclusions: This study supports the effectiveness of 99mTc radiolabeled AMO in the noninvasive visualization of miR-21 in malignant tumors and suggests a potential candidate for tumor imaging.

OP202

Quantitative and longitudinal SPECT imaging of intramuscular transplanted islets of Langerhans using [123I]IBZM

S. M. A. Willekens, I. van der Kroon, D. Bos, L. Joosten, C. Frielink, O. C. Boerman, M. Brom, M. Gotthardt; Radboud university medical center, Nijmegen, NETHERLANDS.

Aims: Besides insulin therapy, pancreatic islet transplantation is considered one of the most promising therapies for type 1 diabetes. Despite improved immunosuppressive therapy, islet transplantation still results in short term insulin independence. A non-invasive imaging method to monitor the viable transplanted islets might provide insight in the faith of the islets after transplantation. Moreover, it could offer the possibility to evaluate therapeutic interventions that might improve long term transplantation outcome. Dopamine 2 (D2) receptors are expressed on beta cells and are therefore a suitable target to monitor islet grafts. Here, we investigated the use of the D2 receptor antagonist [123I]Iodobenzamide ([123I]IBZM) for quantification of viable graft volume and longitudinal grafts analysis. Methods: Six weeks after transplantation of 1000, 2000 or 3000 islets intramuscularly, rats received 50 MBq [123I]IBZM intravenously and one hour post injection SPECT images were acquired. Afterwards, animals used for ex vivo autoradiography were injected with [125I]IBZM, euthanized 1h post-injection, and the graft containing muscles were dissected for ex vivo SPECT, autoradiography and histological analysis. Viable graft volume was calculated histologically by multiplying insulin-positive area by interslice distance of the analyzed slides. For longitudinal graft analysis, rats were transplanted with 1500 islets and monitored for 10 weeks. Results: Six weeks after transplantation, a clear signal of all grafts was observed by SPECT. Moreover, SPECT signal correlated linearly with viable graft volume (Pearson r = 0,73). The SPECT signal in the calf muscle detected ex vivo correlated with the signal in the calf muscle in vivo. Furthermore, ex vivo autoradiography confirmed specific tracer accumulation and co-localization with the grafts location, as determined histologically. Longitudinal graft analysis showed a gradual increase in SPECT signal with a peak around five weeks after and signal stabilization afterwards. Conclusion: In conclusion, [123I]IBZM can successfully be applied for non-invasive quantitative and longitudinal graft monitoring in vivo. Especially in combination with other beta cell specific tracers, such as exendin, it might provide a strong tool to obtain detailed complementary information by non-invasive molecular imaging and to predict islet graft metabolic state and transplantation outcome.

OP203

Radioimmunoimaging of targeting CD133 antigen for colorectal cancer stem cells, a preliminary study

R. An, X. Jin, J. Lang, D. Weng, **X. Lan**; Union Hospital, Tongji Medical College, Huazhong University of Science and Technology, Wuhan, CHINA.

Objective: Cancer stem cells (CSC) provide a new approach for the diagnosis of malignant tumors. CD133 is the one of the most intensively studied biomarkers. The aim of this study was to target the colorectal CSC marker CD133 with 131I-labeled specific monoclonal antibody (AC133 mAb). Methods: The expression level of CD133 in three different colon cancer cells (HT29, HCT116 and DLD-1 cell) were detected by flow cytometry. 131I-AC133 mAb was prepared and identified. Cellular uptake studies were performed, and its relationship with the CD133 expression levels was analyzed. The tumor xenografts models were prepared for SPECT imaging and biodistribution experiments at different time points after 131I-AC133 mAb injected. Autoradiography and immunofluorescence studies were preformed to verify the CD133 expression in vivo. Results: The expression levels of CD133 molecules in HT29 and HCT116 cells were 91.33%±1.66% and 90.83%±2.47%, respectively, which were significantly higher than that in DLD-1 cells (3.87 ±0.57%). The radiochemical yield and radiochemical purity of 131I-AC133 mAb were 68.37% ± 2.45% and 91.18% ± 3.41% (n=3), respectively. Cellular uptakes of 131I-AC133 mAb in HT29 and HCT116 cells were 29.63% ± 3.92% and 33.99% ± 6.65% at 4 h, respectively, which showed significantly higher than that in DLD-1 cells (2.89% ± 0.90%, $P < 0.01$). After incubation with non-labeled AC133 mAb as a blocking group, the cellular uptakes were dramatically decreased to 3.22% ± 0.18% and 3.67% ± 0.56% in HT29 and HCT116 cells, respectively, which suggested specific binding. In vivo SPECT images, clear tumor signals were seen on the tumor sites of HT29 and HCT116 tumor-bearing mice at 7 d after injected 131I-AC133 mAb, and the tumor uptakes in biodistribution study were 5.49% ± 0.42% ID/g and 5.04% ± 0.05% ID/g (n=5), respectively, which were significantly higher than that in the DLD-1 tumor bearing mice (1.20±0.11% ID/g, $P < 0.05$). The ratios of tumor-to-muscle (T/B) at 7 d were 11.34±0.09 (HT29), 11.31±1.05 (HCT116) and 3.43±0.53(DLD-1), respectively.

The immunofluorescence and autoradiography studies showed the radioactivity distribution was consistent with the expression of the CD133 in vivo. Conclusions: 131I-AC133 mAb could target CD133 antigen in colorectal cancer cells specifically, and the uptakes of the tracers were correlate with the CD133 expression. These suggested that 131I-AC133 mAb was feasible as a radioimmunoimaging agent for targeting CD133-positive cancer stem cells. This work was supported by NSFC 81371599.

OP204

SPECT/CT Imaging of Programmed-Death Ligand 1 Expression of Tumors and Antigen-Presenting Cells

S. Heskamp[1], W. Hobo[1], J. D. M. Molkenboer-Kuenen[1], D. Olive[2], W. J. G. Oyen[1], H. Dolstra[1], O. C. Boerman[1]; [1]Radboud University Medical Center, Nijmegen, NETHERLANDS, [2]CRCM, Immunity and Cancer, Inserm, Marseille, FRANCE.

Introduction: Antibodies that block the interaction between the inhibitory signaling molecules programmed death-ligand 1 (PD-L1) and PD-1 have shown impressive anti-tumor activity. Patients with PD-L1 expressing tumors are most likely to respond to this type of treatment. Therefore, imaging of PD-L1 expression may aid in selecting patients for PD-1/PD-L1 targeting therapy. Previously we have shown the feasibility to image PD-L1 expressing human xenografts in mice. However, in patients, PD-L1 is also expressed on activated antigen presenting cells (APCs), such as dendritic cells and macrophages. This may hamper tumor visualization. The aim of our study is to determine what the effect of PD-L1 expressing APCs is on the tumor uptake of radiolabeled anti-PD-L1 antibodies. Material and methods: The anti-PD-L1 monoclonal antibody, PD-L1.3.1, was radiolabeled with Indium-111 (^{111}In). Two groups of immunodeficient NOD/SCID/IL2Rg(null) mice were irradiated (2.5 Gy whole body), followed by intrafemural transplantation of human CD34+ hematopoietic stem cells (HSCs). A control group was not irradiated nor transplanted. At day 54, mice were inoculated s.c. with MDA-MB-231 cells. Three weeks later, one HSC-transplanted group was injected i.p. with 0.6 mg/kg LPS in order to activate APCs and upregulate PD-L1 expression. One day later, all groups were injected i.v. with 13 MBq ^{111}In-PD-L1.3.1. Three days later, mice underwent SPECT/CT imaging and tissues were collected for ex vivo biodistribution. Results:SPECT/CT imaging clearly visualized MDA-MB-231 xenografts in all groups. In LPS-treated mice, ^{111}In-PD-L1.3.1 clearly visualized the activated cells in spleen and lymph nodes. Ex vivo biodistribution showed that tumor uptake was not significantly different between the groups (Control: 42.7 ± 8.1 %ID/g, HSC transplantation: 57.3 ± 12.0 %ID/g, HSC transplantation + LPS stimulation: 34.8 ± 18.2 %ID/g). Strikingly, spleen uptake was significantly increased in LPS-treated mice (Control: 16.7 ± 3.9 %ID/g, HSC transplantation: 25.9 ± 9.1 %ID/g, HSC transplantation + LPS stimulation: 85.1 ± 30.9 %ID/g, $p = 0.004$). Within the LPS-stimulated group, there was a significant correlation between spleen uptake and tumor uptake ($r=0.91$). Mice with the highest spleen uptake showed the lowest tumor uptake. Conclusion: This study showed the feasibility to image tumor PD-L1 expression, even in the presence of human PD-L1 expressing APCs. Upon LPS injection, APCs were activated and up-regulated PD-L1. This resulted in enhanced uptake of ^{111}In-PD-L1.3.1 in spleen and lymph nodes, as was visualized by SPECT/CT imaging. This did not hamper the visualization of PD-L1 expressing tumors.

OP205

Radiolabelled superagonist rhTSH analogues TR1401 and TR1402 for in vivo imaging of poorly differentiated thyroid cancer

F. Galli[1,2], I. Manni[3], G. Piaggio[3], L. Balogh[4], B. D. Weintraub[5], M. W. Skudlinski[5], R. A. J. O. Dierckx[2], A. Signore[1,2]; [1]Nuclear Medicine Unit, Department of Medical-Surgical Sciences and of Translational Medicine, Faculty of Medicine and Psychology, "Sapienza" University of Rome, Rome, ITALY, [2]Department of Nuclear Medicine and Molecular Imaging, University Medical Centre Groningen, University of Groningen, Groningen, NETHERLANDS, [3]Molecular Oncogenesis Laboratory, Experimental Oncology Department, Regina Elena National Cancer Institute, Rome, Italy, Rome, ITALY, [4]National "Frederic Joliot Curie" Research Institute for Radiobiology and Radiohygiene, Budapest, HUNGARY, [5]Trophogen Inc.,, Rockville, MD, UNITED STATES.

Introduction: Patients affected by poorly differentiated thyroid cancer (PDTC) may show a negative 131I scintigraphy because of the loss of the iodine symporter (NIS). However, expression of TSH receptor (TSHR) is usually preserved. Therefore, the aim of our study was to compare two new radiolabelled superagonist rhTSH analogues for imaging PDTC. Methods: Analogues (namely TR1401 and TR1402), with a TSHR binding affinity ten times higher than Thyrogen®, were radiolabelled with 99mTc using an indirect method via HYNIC conjugation. In vitro quality controls were performed to evaluate the stability of the labelling and the retained affinity for the receptor. These included SDS-PAGE, cysteine challenge and cell binding assay on TSHR positive cell lines lacking NIS. In vitro assays were also performed with radiolabelled human recombinant TSH (Thyrogen®) to compare affinity for the TSHR of each radiopharmaceutical. In vivo studies were

performed in 40 athymic nude CD-1 mice bearing either TSHR+ or TSHR- xenografts from human thyroid cancer cell lines. Furthermore, 4 dogs with spontaneous thyroid cancer were studied by 99mTc-TR1401 SPECT/CT, 99mTc-TR1402 SPECT/CT, 131I SPECT/CT and 18F-FDG PET/CT in different days within 2 weeks. Results: Suepragonist rhTSH TR1401 and TR1402 analogues were labelled with high labelling efficiency (>95%), high stability and retention of both biological activity and structural integrity. Analogues showed high affinity for the TSHR with dissociation constants (Kd) of 2.7 nM for 99mTc-TR1401, 0.5 nM for 99mTc-TR1402 and 8.4 nM for 99mTc-Thyrogen. In tumor targeting experiments, a focal uptake of radiolabelled analogues was observed in TSHR+ cells with a target-to-background ratio up to 3 at 3 h p.i., whereas no significant uptake was observed in mice bearing TSHR- cells. Similar observations were made in dogs with spontaneous intra-glandular papillary thyroid cancer, in which TSHR expression was confirmed by immunohistochemistry. Conclusions: We were able to efficiently radiolabel new superagonist rhTSH analogues with 99mTc with retention of in-vitro and in-vivo binding affinity with TSHR. 99mTc-TR1402 proved a high superiority than 99mTc-TR1401 and 99mTc-Thyrogen. This new radiopharmaceutical opens new perspectives for pre-surgical TSHR-based staging of thyroid cancer, for diagnosis of radioiodine negative cancer remnants, local relapses and/or distant metastases.

608 - Monday, October 12, 2015, 8:00 AM - 9:30 AM, Hall E
Pitfalls & Artefacts & Physiology - Interactive: Imaging in Inflammation and Infection

OP206
Pitfalls and Artefacts in Imaging Inflammation and Infection: Radiopharmaceuticals
N. Hartman, UK

OP207
Pitfalls and Artefacts in Imaging Inflammation and Infection: Labelled Leucocytes
E. Lazzeri, ITALY

OP208
Pitfalls and Artefacts in Imaging Inflammation and Infection: PET
A. Glaudemans, NETHERLANDS

610 - Monday, October 12, 2015, 8:00 AM - 9:30 AM, Hall D
UEMS/CANMD Session: Practical Quality Management in Nuclear Medicine

OP209
Welcome by the Committee Chair
S. Mirzaei, AUSTRIA

OP209b
Request to Different Levels of a Radiopharmacy Laboratory
K. Solanki, UNITED KINGDOM

OP209c
Good Clinical Practice for Pulmonary SPECT
M. Bajc, SWEDEN

OP209d
Good Medical Practice of Hybrid Imaging in Neurology
A. Ciarmiello, ITALY

OP209e
Quality Check in Hot Lab. State of the Art in Italy
M. Riondato, ITALY

OP209f
Importance of a QM in a NM Department
E. Bombardieri, ITALY

OP209g
PET/CT Audit in the UK
W-L. Wong, UNITED KINGDOM

701/703 - Monday, October 12, 2015, 10:00 AM – 11:15 AM, Hall 1
Plenary 2: Therapeutic Nuclear Medicine

OP210
Paediatric Radionuclide Therapy
M. Gaze, UK

OP211
Radiosynoviorthesis - State of the Art after 60 Years of Experience
W. U. Kampen, GERMANY

OP212
Radioembolisation of Liver Metastases and HCC
E. Garin, FRANCE

801 - Monday, October 12, 2015, 11:30 AM – 01:00 AM, Hall 1
CME 6 - Neuroimaging: Brain Tumours - PET vs MRI: Therapy Planning and Response Assessment

OP213
Molecular Aspects of Brain Tumours and Specific PET Radiotracers
K. Herholz, **UK**

OP214
Neurosurgery Planning
R. Díez-Valle, **SPAIN**

OP215
Radiotherapy Planning
A. Grosu, **GERMANY**

OP216
Treatment Response Assessment and Treatment Monitoring
N, **Galldiks**, **GERMANY**

802 - Monday, October 12, 2015, 11:30 AM – 01:00 AM, Hall 2
Joint Symposium 6: EANM/ESTRO: Molecular PET Imaging in Adaptive Radiotherapy: Focus on Current Trends, Challenges and Solutions

OP217
Lung Cancer: The Radiation Oncologist's Point of View
B. Dubray, **FRANCE**

OP218
Lung Cancer: The Nuclear Medicine Physician's Point of View
P. Vera, **FRANCE**

OP219
Head and Neck Cancer: The Radiation Oncologist's Point of View
V. Grégoire, **BELGIUM**

OP220
Head and Neck Cancer: The Nuclear Medicine Physician's Point of View
W.J.G. Oyen, **NETHERLANDS**

803 - Monday, October 12, 2015, 11:30 AM - 1:00 PM, Hall 4
Technologist Oral Presentations 2

OP221
Investigation of kidney function with a dynamic FDG-PET/MR

B. K. Geist, A. Staudenherz; Medical University of Vienna, Vienna, AUSTRIA.

Aim: To study kidney function with FDG PET would be of clinical relevance for cancer patients undergoing staging before nephrotoxic chemotherapy will be applied. But investigation of kidney function with PET is a little explored field in nuclear medicine. The MR modality is suited for examine kidney, since the high-resolution morphological information of the MR allows a detailed discrimination of the FDG behavior in various regions in the organ. Our aim is to extract kidney function parameters (e.g. glomerular filtration rate, split kidney function, extraction function, etc.) from a single dynamic PET/MR scan. Methods: At the General Hospital in Vienna we started to acquire the time activity curves of the routine PET tracer F-18-FDG directly after injection separately for each kidney region, using MR images for kidney segmentation. From the temporal behavior of the tracer concentration in the different kidney regions as well as from the results from kinetic modeling, conclusions to the kidney function parameters are drawn. The obtained values are then compared to the results from MAG 3 renography and GFR-measurement. Results: So far the time activity curves from the FDG PET studies revealed a good correlation with the renal split function from MAG 3 renography. The preliminary results will be presented in detail. Conclusion: In order to facilitate the examination protocol for the determination of kidney functions, a PET/MR scan of the kidney is studied in comparison with routinely used kidney examinations in nuclear medicine and MR renography.

OP222
Wholebody Blood Pool in Bone Scintigraphy: Usefulness in the differential diagnosis of inflammatory arthritis - Preliminary Results

M. Casanova Martins, B. Patel, C. Humphreys, P. Ali; ABMU HB, Swansea, UNITED KINGDOM.

Introduction: To establish a differential diagnosis of inflammatory arthropathy (IA) it is important to assess the presence of hyperemia and increased relative tissue vascularity in bone scintigraphy. However, limiting early blood flow (BF) and blood pool (BP) imaging to a single symptomatic anatomic region might not entirely reveal the nature/extent of a multifocal systemic pathology. Instead, a global approach to the early imaging stages could be useful. This approach does not allow the

acquisition of the quick BF study to assess local hyperaemia yet allowing performing a wholebody blood pool (WB BP) study and therefore gathering systemic information on the tissue vascularity surrounding most joints. Aim: The aim of this work is to evaluate the usefulness of dual-phase wholebody skeletal scintigraphy in the assessment of IA. Materials and Methods: Between January 2014 and April 2015, 46 bone scans were performed for the assessment of IA. Patients underwent either triple-phase (n=40) or dual-phase bone scintigraphy (WB BP and delayed imaging) (n=6). Images and reports were retrospectively analysed. Results: In the triple-phase group, 60%(n=24) cases presented changes in all stages of the triple-phase scintigraphy, with accurate localization of active disease in the targeted joint. 100%(n=24) of these studies however, also presented increased uptake in other joints on delayed imaging. In 40%(n=16) studies there were no changes in the early imaging stages. Of these, only 25%(n=4) were completely normal in the delayed stage. In the remaining 75%(n=12) cases, the early imaging stages were normal, with marked increased uptake in other joints in the delayed stage, leading to inconclusive reports. In the dual-phase group, the report issued was conclusive in all cases. Of these, 67%(n=4) were positive, with matching changes in several joints in both stages of the study and 33%(n=2) had normal WB BP and increased multifocal uptake in the delayed WB scan. Discussion: The dual-phase WB protocol has increased the frequency of conclusive reports to 100% in the assessment of IA. Acquisition of early WB images increases the diagnostic accuracy whilst only adding 2-3 minutes to the study time. Hyperaemia is not assessed in dual-phase scintigraphy but this does not seem to affect the interpretation of these examinations. In addition, early WB imaging provides a systemic joint assessment allowing the evaluation of the extent of disease. Conclusion: Dual-phase wholebody skeletal scintigraphy is a simple but useful technique for the detection and characterization of widespread joint abnormalities and its routine use is recommended.

OP223

Comparison of Ga-68-DOTATATE PET/CT and In-111-octreotide SPECT/CT for the detection of neuroendocrine tumors

M. Kieft, E. A. Aalbersberg, M. P. M. Stokkel; NKI-AVL, Amsterdam, NETHERLANDS.

AIMIn our hospital, Ga-68-DOTATATE was implemented in Augustus 2011, and thereafter the number of Ga-68-DOTATATE PET/CTs is increasing rapidly at the expense of In-111-octreotide SPECT/CT. The aim of this study is to compare the detectability of neuroendocrine tumors (NET) between both techniques.MATERIALS & METHODSBetween August 2011 and February 2015 209 Ga-68-DOTATATE PET/CT scans were performed in 187 neuroendocrine tumor patients. In 111 cases the patients underwent an In-111-octreotide SPECT/CT and PET/CT; in 28 cases the scans took place within a maximum interval of 12 months.Based on the PET/CT reports, 12 cases showed one or more lesions, eight showed none and in eight cases the images were inconclusive. For the 12 cases with tumor lesions we scored the PET/CT, the SPECT/CT, and the planar images for total number of lesions and quantified the images. The lesions were divided in three categories: liver, skeletal, and other. The quantitative analysis of the PET/CT was based on SUVmax. On planar imaging and SPECT/CT lesions were scored visually (0= no uptake, 1= equivocal, 2≤ liver, 3> liver, 4= intense). Eight patients received somatostatin analogues between the scans. One lesion was resected and this lesion is removed from the analysis.RESULTSPET/CT depicted 149 lesions, SPECT/CT 41 lesions, and planar imaging 31 lesions. All lesions visible on SPECT/CT were found on PET/CT except for one. In the liver, 64 lesions were found with PET/CT, 19 with SPECT/CT and 16 with planar imaging. Of the 25 skeletal lesions on PET/CT, 3 were also seen on SPECT/CT and none on planar imaging. Sixty additional lesions were identified with PET/CT in other parts of the body, of which only 19 were visible on SPECT/CT and 15 on planar imaging. The discrepancy between PET/CT and SPECT/CT can be partially explained by the fact that whole-body SPECT/CT is not regularly performed, however in most cases Ga-68-DOTATATE PET/CT is more sensitive for NET then In-111-octreotide SPECT/CT.No correlation was found between SUVmax on PET/CT and visibility of the same lesion on SPECT/CT or the planar image.CONCLUSIONThese preliminary results show that Ga-68-DOTATE PET/CT has a higher detectability of lesions in comparison to In-111-octreotide imaging. Due to the ongoing application of Ga-68-DOTATATE more data will become available in the next months, which will also be analyzed. Based on these results, it can be concluded that In-111-octreotide scintigraphy alone is not standard clinical practice anymore.

OP224

Phase analysis using ECG-gated myocardial FDG PET in the rat in comparison with speckle tracking echocardiography

A. Mizutani[1], I. Matsunari[2], M. Kobayashi[3], K. Nishi[4], W. Fujita[5], S. G. Nekolla[6], K. Kawai[7], K. Fukuchi[1]; [1]Osaka University, Osaka, JAPAN, [2]Saitama Medical University Hospital, Saitama, JAPAN, [3]Kanazawa University, Kanazawa, JAPAN, [4]Nagasaki University, Nagasaki, JAPAN, [5]Kanazawa Medical University, Ishikawa, JAPAN, [6]Technical University Munich, Munich, JAPAN, [7]Osaka UniversityKanazawa University, Kanazawa, JAPAN.

Aim: Clinical studies have shown that phase analysis using ECG-gated myocardial SPECT/PET is useful for assessing left ventricular dyssynchrony. However, its feasibility has not yet been validated in small animals such as rats, where small heart size and high heart rate pose a technical challenge. The aim of this study was to assess the feasibility of phase analysis using ECG-gated myocardial FDG PET in rats with myocardial infarct in comparison with speckle tracking echocardiography as a reference standard for dyssynchrony. Methods: Twenty-nine Wister rats with myocardial infarct underwent ECG-gated FDG PET in list-mode for 20 minutes using a dedicated small animal PET scanner (Triumph II/LabPET8, TriFoil Imaging). Image reconstruction was performed using ordered-subset expectation maximization (OSEM) in 16 frames per cardiac cycle. All the rats also underwent speckle tracking echocardiography using Vivid7 (GE Healthcare) with a small and high-frequency (~14 MHz) linear transducer (i13L, GE Healthcare). For PET, standard deviation of time to peak thickening (PET_SD) was calculated as an index of dyssynchrony using AHA 17 segment model. For speckle tracking echocardiography, standard deviation of time to peak radial strain on a mid-ventricular short-axial image (echo_SD) was obtained as an echocardiographic index of dyssynchrony. Results: PET_SD measured by ECG-gated PET showed a significant positive correlation with echo_SD ($R=0.597$, $p<0.001$). In addition, PET_SD showed significant correlations with measures of disease severity such as left ventricular ejection fraction ($R=-0.575$, $p<0.001$) and infract size ($R=0.614$, $p<0.001$). Conclusion: Our results indicate that phase analysis using ECG-gated myocardial FDG PET is feasible in the rat model of myocardial infarct, and thus may provide a measure of left ventricular dyssynchrony.

OP225

Eye Spy: An Investigation into Tc-99m Pertechnetate Lacrimal Scitigraphy for Protocol Optimization

E. Souza, **V. Janse van Rensburg**, P. Sandhu, L. Perry, H. Tam, Z. Win; Imperial College Healthcare NHS Trust, London, UNITED KINGDOM.

Aim: To assess the change in diagnosis between three different lengths of acquisition (0-15mins, 0-23mins, 0-31mins) and post-rinse static to determine if a shorter acquisition will yield the same clinical result for lacrimal scintigraphy studies using Tc-99m pertechnetate. Our local protocol uses a 31minute dynamic (eighteen 10-seconds frames, then 60-second frames), followed by a 60second, post rinse static view. The aim of this study was to evaluate the clinical utility of extra data collected after the initial 15minutes dynamic acquisition. Materials and Methods: Data was retrospectively collected from 40 patients referred to our department for lacrimal scintigraphy, over a period of 6 months. The right side and left side of each patient were considered as separate systems, thus a total of 80 lacrimal systems were evaluated. Anonymised printscreens were produced showing data acquired 0-15mins, 0-23mins, 0-31mins post administration and the post-rinse static. Two radiologists reviewed the images recording their diagnosis based on 0-15mins, 0-23mins and 0-31mins of data post administration. The diagnosis reached when the post rinse image was reviewed was also recorded. Diagnosis was categorised as no obstruction, partial obstruction or total obstruction, pre and post sac. We calculated the percentage of lacrimal systems where there was a change in diagnosis between the 0-15mins vs 0-23mins and 0-23mins vs 0-31mins datasets. We also calculated the change between each separate dataset and the post-rinse diagnosis eg 0-15mins vs post-rinse. Results: The percentage of lacrimal systems where there was a change in diagnosis changed was 14.4% between the 0-15mins vs 0-23mins and 7.5% between the 0-23mins vs 0-31mins. When the diagnosis reached from the post-rinse static image was compared to the diagnosis reached from the other time-frames: 31.3% was changed vs 0-15mins; 21.9% was changed vs 0-23mins diagnosis; 16.3% was changed vs 0-31mins diagnosis. Conclusion: This study demonstrates that although there is still a substantial amount of information after a 15minute dynamic phase, as the duration of the initial dynamic phase of lacrimal scintigraphy increases the impact on diagnosis is reduced. However we found there was a significant change in diagnosis after the post-rinse images. Therefore we would suggest that a shorter acquisition protocol could be adopted clinically as long as the post-rinse image is included. We suggest a shorter dynamic acquisition of 23minutes followed by a post-rinse image would increase patient throughput and comfort whilst maintaining diagnostic accuracy.

OP226

Radionuclide therapy of metastatic melanoma with benzamide derivate I-131-BA100 after patient stratification with F-18-DOPA

F. O. Spohn, K. Kunze, F. Giesel, W. Mier, U. Haberkorn, C. Kratochwil; Heidelberg University Hospital, Heidelberg, GERMANY.

Aim:Benzamide derivates have been shown to selectively accumulate in melanotic melanoma. Some patients with metastatic melanoma show therapeutically promising accumulation of the benzamide derivate I-131-BA100.L-DOPA is a precursor to the biological pigment melanin.We evaluated if it's possible to select which patient could benefit from a radioligand therapy with I-131-BA100 using F-18-DOPA for prediagnostic.Methods:15 patients with metastatic melanoma were examined. In line with the propagation diagnostic and

staging a F-18-FDG PET/CT was acquired.With regard to a radionuclide therapy both I-131-BA100 whole body scan and PET/CT with the melanin precursor F-18-DOPA were done at intervals of few days.48 hours after intravenous injection of 230 +/- 35 MBq I-131-BA100 planar whole body scans and tomographic images in SPECT technique were acquired.In the best case the F-18-DOPA examination was done on the very same day of benzamide imaging. After intravenous injection of 215 +/- 55 MBq F-18-DOPA 15 minutes p.i. an emission scan of the trunk and a low-dose CT for attenuation correction was processed.Results:Benzamide- and DOPA-examination showed no pathological retention in known multiple metastases in 4 patients. 10 patients showed congruent findings with both tracers. On the contrary there was found a discrepant case. This patient had moderate to intensive DOPA-positive lesions which showed no retention with the benzamide-derivate.Conclusion:The correlation of F-18-DOPA- and I-131-BA100-uptake is sufficiently enough to preselect patients who could benefit from this type of therapy. Because of the individual case of missing correlation between benzamide- and DOPA-uptake diagnostic imaging with I-131-BA100 is still advisable.

OP227

Impact of syringe residual activity in SUV measurement

P. Felício[1], J. Hunter[2], N. G. Dowell[2], T. Vaz[1], F. Lucena[1]; [1]Lisbon School of Health Technology, Lisbon, PORTUGAL, [2]Clinical Imaging Sciences Centre, Brighton and Sussex Medical School, University of Sussex, Brighton, UNITED KINGDOM.

The use of the semi-quantification standard uptake value (SUV) in PET/CT image has an important role in the evaluation of individual response to therapy however many factors may interfere with the calculation of SUV. One factor is the residual activity in the syringe after injection. The aim of this research is to assess the influence of the syringe residual activity in the SUV, in PET/CT images with ^{18}F-FDG. Forty-eight patients with clinical indication for performing PET/CT with ^{18}F-FDG were included. Inclusion criteria were: avid ^{18}F-FDG tumour uptake in the PET/CT images and blood glucose level between 4 and 8 mmol/L. Images were acquired 1 hour after the radiopharmaceutical injection (400 MBq) according to departmental procedure. Reconstruction and processing of the images were performed with ordered subset expectation maximization (OSEM) algorithm (4 iterations; 8 subsets; 5 mm Gaussian filter), 168x168 image matrix; zoom 1; voxel size 5 mm^3. A dose modulated CT scan was acquired prior to the PET scan for attenuation correction (120 KV; 50 mAs (ref); 5 mm slice thickness). Maximum SUV (SUV_{max}) based on patient weight was obtained, with (SUV_{max}-C) and without correction (SUV_{max}-NC) for the injected activity, keeping the same procedure (ROI area, slice and lesion). Descriptive and inferential statistics (t-test for paired-samples and person-correlation) were applied (IBM SPSS software, version 22). Significance was considered for p-value<0.05. After the data collecting, mean values were obtained: ^{18}F-FDG activity (393±21 MBq), syringe residual activity (3.38±2.43 MBq), ROI area (1.69±0.65 pixels), SUV_{max}-C (12.33±6.37), SUV_{max}-NC (11.95±6.18). As it was expected a strong linear positive correlation (r=0.99, p-value=0.00) was found between the two SUV_{max}. However, the comparison of means showed statistically significant differences (p-value=0.00), associated with an increase of SUV_{max} after correction. These results are in agreement with the SUV empirical formula, which takes into account the activity concentration in the ROI and the injected activity. This way, the corrected activity will produce an increase in the SUV_{max} obtained. No correlation was shown between SUV_{max}-NC and SUV_{max}-C, with regard to the injected activity, the syringe residual activity or patient weight. The correction for syringe residual activity increases the SUV_{max} and further research should be performed in order to identify the clinical impact of this difference. It is recommended that the same method for SUV_{max} measurement is applied, especially in the evaluation of individual response to therapy.

OP228

Protocol Optimisation of [^{68}Ga]-PSMA PET/CT Imaging on a High Sensitivity Time-of-Flight Pet Scanner

E. A. Bailey, E. Hsiao, G. Schembri; Royal North Shore Hospital, Sydney, AUSTRALIA.

AIM: The use of [^{68}Ga]-PSMA PET/CT in the staging and response to therapy of patients with prostate cancer is increasing. There are limited guidelines suggesting the ideal parameters to ensure high image quality using a Time of Flight (ToF) PET/CT system. We used external triggered gating to investigate the optimal scanning parameters (dose injected, time per bed position) for whole body PSMA PET scanning on a Siemens Biograph mCT with extended axial field of view (FoV), time-of-flight scanner with resolution recovery (HD).METHODS: Patients referred for a PSMA PET scan with a rising PSA were injected with 150MBq of [^{68}Ga]-PSMA (HBED). An externally triggered gated (ETG) WB PET scans were acquired at 60 minutes on a ToF PET/CT (Siemens Biograph mCT64x64). Data were reframed into 30 sec time bins (6 gates) using ToF 3D-OSEM with CT-based AC, SC and PSF recovery and then combined using in-house software to give different total acquisition times (30 secs, 60secs, *etc* up to 180 secs). ROIs are defined over areas of assumed homogeneity (*e.g.*, liver and salivary glands), lesions, bladder and blood pool across all reformatted studies. Image

coefficient of variation (CoV%), SUV_{max} and visual assessment were used to quantify the relationship between dose injected and time per bed position.RESULTS: A total of 6 studies were included for analysis with an average injected dose of 141MBq (125-165MBq), weight 81kg (71-88kg) and PSA range 3 to 56ng/mL. Based on a PSMA injected dose of 141MBq, the scanning time per bed position appears to plateau based on CoV% in liver, nodes and salivary glands at around 120 secs per frame. The SUV_{max} was reproducible from 60secs to 180secs acquisition time with a maximum deviation in the shortest time frames of <15%.CONCLUSION: The use of ETG acquired data to assess varying parameters such as different acquisition times and injected doses allows the assessment of the impact on image quality between injected dose and scanning duration. In this analysis, the image quality and reliability of quantitative measures such as SUV_{max} appears to be achieved at 120secs per bed position with an injected dose administered of 141MBq. This approach is now being used to assess optimal parameters for PSMA PET delayed imaging acquired between 120 and 180 minutes post injection.

804 - Monday, October 12, 2015, 11:30 AM - 1:00 PM, Hall G1
Clinical Oncology - Featured: Image Guided Surgery

OP229
SPECT/CT for Anatomical Mapping of Lymphatic Drainage in Vulvar Cancer: Possible Implications for the Extent of Inguinal Lymph Node Dissection

A. Collarino[1,2], M. L. Donswijk[2], W. J. van Driel[3], M. P. Stokkel[2], R. A. Valdés Olmos[2,4]; [1]Institute of Nuclear Medicine, Università Cattolica del Sacro Cuore, Roma, ITALY, [2]Department of Nuclear Medicine, The Netherlands Cancer Institute – Antoni van Leeuwenhoek Hospital, Amsterdam, NETHERLANDS, [3]Department of Gynaecological Oncology, The Netherlands Cancer Institute – Antoni van Leeuwenhoek Hospital, Amsterdam, NETHERLANDS, [4]Interventional Molecular Imaging Laboratory and Nuclear Medicine Section, Department of Radiology, Leiden University Medical Center, Leiden, NETHERLANDS.

Aim: to assess the lymphatic drainage pattern using SPECT/CT in clinically node-negative (cN0) patients with vulvar cancer, and to evaluate the possible implications for the extent of inguinal lymph node dissection.Material and Methods: Lymphoscintigraphy and SPECT/CT were performed in 83 patients (mean age 67.8, range 25-93y) vulvar cancer patients scheduled for sentinel node (SN) biopsy after four peritumoral injections of 99mTc-nanocolloid. Using SPECT/CT SN and higher-echelon nodes were identified and were anatomically localized in the groin according to Daseler's five zones: four zones obtained by drawing two perpendicular lines over the saphenofemoral junction and one zone directly overlying this junction. Lymph nodes into the pelvis were classified into three zones: external iliac/obturator, the common iliac and the para-aortic zones.Results: A total of 217 SNs and 202 higher-echelon nodes were localized using SPECT/CT. All SNs were located in the groin and were classified in one of the five zones according to Daseler: 149 (69%) in the medial superior region, 31 (14%) in the medial inferior region, 22 (10%) in the central region, 14 (6.5%) in the lateral superior region and only 1 (0.5%) in the lateral inferior region. The higher-echelon nodes were located both in the groin (15%) and in the pelvic region (85%).Conclusion: In cN0 vulvar cancer patients scheduled for the SN procedure, lymphatic drainage occurs predominantly to the medial regions of the groin. Drainage to the lateral inferior region of the groin is only incidental, and in SN positive patients this zone might be spared for subsequent extended lymph node dissection; this may lead to a decrease of the morbidity associated with this procedure. SPECT/CT is able to personalize lymphatic mapping, providing detailed information about the number and anatomical location of SNs for adequate surgical planning in the groin.

OP230
3D freehand-SPECT navigation for intraoperative radioactive seed localisation using single or multiple 125I seeds in breast-conserving cancer surgery

B. Pouw, L. J. de Wit-van der Veen, F. van Duijnhoven, E. J. T. Rutgers, R. A. Valdés Olmos, M. P. M. Stokkel, M. T. F. D. Vrancken Peeters; Netherlands Cancer Institute, Amsterdam, NETHERLANDS.

Background: The use of mammographic screening has led to the identification of more women with non-palpable breast cancer. For subsequent treatment adequate localisation techniques are required for radical excisions. For radioactive seed localisation (RSL) a radioactive Iodine-125 seed (125I-seed) is implanted in the centre of the tumour and intraoperatively localised using a gamma probe. In case of extensive ductal carcinoma in situ (DCIS) or multifocal carcinoma, multiple 125I-seeds can be used to delineate the borders of the involved area. For localisation control of the seed, preoperative imaging is not performed in the surgical position and therefore the exact 125I-seed depth remains unknown during surgery. For this purpose, we evaluated freehand-SPECT (fh-SPECT), which facilitates 3D navigation towards the 125I-seed. Methods: Fourteen female patients (Mean age 56 years) with 21 implanted 125I-seeds scheduled for RSL were included. Eleven patients had 1 125I-seed implanted in the primary lesion, 2

patients 2, 1 patient 3. In 3 patients, an additional 125I-seed was implanted as a marker for an up-front systemically treated tumour-positive axillary lymph node. Fh-SPECT localised 125I-seeds by measuring gamma counts from different directions all registered by an optical tracking system. A reconstruction and visualisation algorithm enabled 3D navigation towards the 125I-seeds. Surgeons estimated the depth of 125I-seeds after excision and compared this with the depth indicated by fh-SPECT. Results: Fh-SPECT visualised all 125I-seeds in the primary tumours and provided pre-incision depth information. The deviation between the fh-SPECT depth and the surgical depth estimation was 2.7 mm (SD 2.1mm, Range 0-7mm). 3D fh-SPECT was especially useful identifying multiple implanted 125I-seeds where the conventional gamma-probe has more difficulty to discriminate 125I-seeds by transcutaneous measurements. In two patients the excision was irradical and tumour was detected at the resection border; for 1 patient a DCIS component was detected at the resection margin and another patient had invasive ductal carcinoma in the resection border. In one patient a diagnostic excision of three lesions was performed of which one contained tubular carcinoma. Conclusion: Fh-SPECT with 3D navigation is feasible in RSL based on single or multiple implanted 125I-seeds. The modality is able to provide real-time 3D information about the depth and location of the 125I-seeds, contributing to adequate excision of non-palpable breast cancer. 3D navigation may become important in breast-preserving cancer surgery.

OP231

Intraoperative evaluation of a true hybrid modality for combined radio- and fluorescence guided sentinel node biopsy

N. S. van den Berg[1,2], H. Simon[3], G. H. KleinJan[1,2], J. Chambron[3], B. M. Tijink[2], S. Horenblas[2], F. W. B. van Leeuwen[1,2]; [1]LUMC, Leiden, NETHERLANDS, [2]AVL-NKI, Amsterdam, NETHERLANDS, [3]Eurorad, Strassbourg, FRANCE.

Introduction:The clinical implementation the hybrid tracer ICG-99mTc-nanocolloid, that is composed of a near-infrared fluorescence component (ICG; indocyanine green) and a radioactive component (99mTc-nanocolloid), has stimulated the generation of sophisticated imaging modalities that allow consecutive detection of the two signatures. In the current study, we report on the first-in-human use of a true hybrid opto-nuclear modality for image-guided surgery.Materials and Methods:Nine patients scheduled for sentinel node biopsy of penile (n=7) or head and neck cancer (n=2) were included after obtaining written informed consent. The number and location of the sentinel node(s) were determined after hybrid tracer injection and subsequently lymphoscintigraphy (15min and 2hours post-injection) and SPECT-CT imaging (2.5hours post-injection). Intraoperatively, sentinel nodes were pursued using the hybrid opto-nuclear modality (prototype; Eurorad, Strassbourg, France). After initial localization of the gamma signal, the probe was switched to the fluorescence mode. Fluorescence tracing was performed under ambient light condition. First in the high sensitivity mode (0.9V) first, and after confirming the location of the node the settings were switched to a low sensitivity mode (0.7V). Post-excision, the measurements were repeated on the surgical specimens. 5-Second count rates were noted for both gamma and fluorescence tracing. Obtained fluorescence tracing results were compared to the results obtained with the conventional fluorescence camera (PDE; Hamamatsu Photonics, Hamamatsu, Japan).Results:In the nine patients included in this trial, intraoperatively 20 sentinel nodes were pursued. All SNs could be gamma traced. In the high sensitivity mode, all sentinel nodes were detected via fluorescence tracing (20/20). In the low sensitivity mode, however, only 7/20 nodes could be traced (35%). Presence of the fluorescence signal in the node was confirmed in all cases using the fluorescence camera. Surgeons that were used to gamma tracing considered fluorescence tracing with the opto/nuclear-probe technology intuitive and the ability to trace this signature in ambient light was considered valuable for surgical logistics.Discussion:The hybrid surgical guidance modality that allows for combined gamma and fluorescence tracing proved to be feasible and was considered a valuable addition during sentinel node biopsy procedures that use the hybrid tracer ICG-99mTc-nanocolloid.

OP232

Role of Robotic assisted PET-CT guided biopsy in 18F-FDG/Ga68 DOTANOC avid suspicious lesions

S. Gambhir, A. Prashanth, S. Barai, H. Lal, A. Nath, G. Sankar, N. Kumar, M. Ravina; Sanjay Gandhi Post Graduate Institute of Medical Sciences, Lucknow, Uttar Pradesh, INDIA.

Aim: To evaluate the role Robotic guided PET-CT biopsy in terms of histopathological yield and complication rate. Introduction: CT guided biopsy of lesions with high necrotic content is unfruitful in most circumstances. So PET-CT guided biopsy will alleviate the flaws of both CT guided biopsy and PET-CT as standalone modalities. Robotic systems can enhance surgical and interventional procedures through improved precision, stability, and dexterity. The high precision of registration, planning, and movement of the robotic arm enables an effective biopsy in all cases, with a high accuracy for even relatively small targets. Materials and methods: 20 patients were referred for PET-CT guided biopsy in our center for the following indications, Unknown primary with likely

primary detected from PET-CT, suspicious lesions identified from PET-CT in a known primary disease and FNAC or CT guided biopsy negative lesions which are high index of suspicion for malignancy. Procedure was done on an outpatient basis with written informed consent after appropriate investigations. PET CT along with contrast was done in order to locate the larger vascular structures near the lesion. Biopsy procedure was done on a separate day planned using the already acquired PET-CT images. 3 cases which were excluded due to the following reasons lesion resolved completely on check scan, severe dyspnoea which prevented stable positioning of the patient, procedure abandoned because of needle in dangerously close proximity to aorta. Results: Tissue was adequate and histo-pathological diagnosis was achieved in all patients except one in whom a repeat procedure yielded positive results. The locations of lesion were thoracic in 88%, spine in 6% and pelvis in the rest 6% of patients. Out of the 17 lesions biopsied 11% (2 lesions) were benign and 89% (15 lesions) turned out to be malignant. Tissue yield from the procedure was 100%. The only complication (1 out of 17 patients - 6%) which arose was self limiting pneumo-thorax. Conclusion: In sharp contrast to the CT guided manual procedure which requires multiple check CT scans robotic procedures inherently need lesser manipulation by user. Robotic assisted PET-CT procedures have lesser complications better histo-pathological yield. It also results in lesser radiation dose to the patient and short learning curve.

OP233
FDG PET/CT Guided Biopsy

C. NANNI[1], A. CAPPELLI[1], T. BALBI[1], F. MANGIACOTTI[1], A. GASBARRINI[2], T. GRAZIANI[1], I. SANDLER[1], R. GOLFIERI[1], S. FANTI[1]; [1]AOU S.ORSOLA-MALPIGHI, BOLOGNA, ITALY, [2]IOR, BOLOGNA, ITALY.

Biopsy of suspect tissues is required to reach a definitive diagnosis. Open incisional biopsy (OIB) is traditionally the method of choice, providing an accuracy of approximately 100%. OIB is very expensive and is associated with several drawbacks (morbidity, surgical complications, tumor contamination of surrounding tissues). The development of imaging-guided biopsies (ultrasound, computed tomography) has almost overcome these disadvantages. However, in recent literature a variable amount of non-diagnostic procedures is reported, leading to an accuracy ranging between 70%-90%. FDG PET/CT is a functional imaging technique highlighting areas of active malignancy/infection with a very high sensitivity in comparison to conventional imaging. It detects abnormal signals even before cancer-related morphological changes occur, and can accurately discriminate between fibrous residual tissue after therapy and disease persistence or relapse. It can potentially be used to drive the biopsy to the most active lymph node or to the most active area within a suspect mass. Aim of this study is to preliminary assess FDG PET/CT guided biopsy feasibility and accuracy in the diagnosis of malignancy/infection.So far 7 patients with unclear hypermetabolic findings were enrolled (5F,2M, mean age 50). 5/7 had a suspect malignancy relapse (3 anorectal, 1 ovarian, 1 NHL) and 2/7 did not have a significant clinical history. 4/7 had a previous non diagnostic CT-guided biopsy. They underwent a FDG PET/CT guided biopsy performed by experienced personnel (interventional radiologist, nuclear medicine doctor, orthopedic). 5/7 pts underwent also contrast media injection to depict vessels surrounding the lesion used to help in drawing the most appropriate needle route. The needle was tracked by driving its progression into the area with the highest SUVmax through repeated PET/CT acquisition (1bed/position; acquisition time 1 min). On average, the procedure lasted approximately 1h per patient. The sample was laid down on adhesive glass slide to obtain cytological extemporaneous exam to test its adequacy and, in some cases, for an immediate diagnosis. 6/7 pts had a definitive pathological diagnosis after PET/CT biopsy (1TBC, 1sacral chordoma, 2 rectal ca relapse, 1 serous papillary ovarian ca, 1 intermediate lymphoma) while in 1 pt histopathology demonstrated post RT scar tissue. This pt is currently in follow-up. No pts had complications. These preliminary results prove that FDG PET/CT guided biopsy is feasible in the clinical practice. Furthermore it positively impacted on the time to treatment onset in those pts who presented with a previous non diagnostic biopsy.

OP234
MRI based identification of lymph nodes and nerves, the next step in sentinel node procedures for head and neck cancer?

T. Buckle[1], B. M. Verbist[1], G. H. KleinJan[1], M. de Ruiter[1], M. A. van Buchem[1], A. J. Balm[2], F. W. B. van Leeuwen[1]; [1]LUMC, Leiden, NETHERLANDS, [2]NKI-AvL, Amsterdam, NETHERLANDS.

Background: Sentinel node (SN) procedures in the head-and-neck area are challenging due to the many critical anatomical structures located in the five dissection regions (Level I-V). Preoperative SN identification, based on SPECT/CT, and radioguided dissections are limited in their ability to identify clustered SNs. Nor do these imaging technologies provide insight in the location of peripheral nerves adjacent to the SNs. In search of methods that allow more detailed lymph node (LN) identification and visualization of peripheral nerves, a new MRI-based imaging technology was evaluated. The locations of the visualized LNs were compared to the SN

visualization-rate in a historic cohort of patients. Methods and Patients: Retrospective analysis of a database containing pre-operative imaging results (SPECT/CT) and pathology reports from 100 head-and-neck melanoma and 40 oral cavity cancer patients was used to evaluate the incidence of SN visualization and occurrence of metastasis per dissection level. Nerve imaging was performed on a Philips 3T Ingenia MRI scanner in fifteen healthy volunteers using a D-prep MRN sequence (scanning-time: 2-5 minutes) and a standard head coil. Anatomical reference images were acquired using a standard T1-3D TSE sequence. An Overlay of both MR images was used to place the LNs and nerves in their anatomical context. Results: Retrospective assessment of SPECT/CT-based preoperative visualization of SNs revealed that 61% of were visualized in levels I-III (61%), and herein 54% contained micrometastases. With D-prep MRN LNs could be detected with a significant improvement in the level of detail as compared to low-dose CT. The highest density of LNs was seen in dissection level I - III and discrimination could be made between single nodes and clusters of 3-5 nodes. Next to allowing the identification of LNs, this MRI technology also improved the insight in the location of the facial nerve including its mandibular, zygomatic and cervical branches (diameter: 0.19 ± 0.04, 0.17 ± 0.03 and 0.19 ± 0.03 mm respectively). Variation in the course of the visualized nerves, in relation to the submandibular salivary gland, as well as variation in the location, amount (27 ± 10 LNs per subject) and size (range 21-1085 mm3) of the LNs was seen between volunteers. Conclusion: D-prep MRN enabled detailed visualization of single LNs located in clusters and facial nerve branches, which contributes to improved pre-operative assessment of sentinel node procedures.

805 - Monday, October 12, 2015, 11:30 AM - 12:45 PM, Hall G2
Do.MoRe - Featured: Prostate Cancer Therapy

OP235

The potential of F-18 Fluoride PET as a surrogate for Radium-223 chloride lesion dosimetry in hormone refractory prostate cancer patients

I. Murray, S. J. Chittenden, C. C. Parker, G. Flux; Royal Marsden NHS Foundation Trust, Sutton, UNITED KINGDOM.

Aim: The aim of this investigation was to assess the response of castration-refractory prostate cancer bone metastases to 223Ra-chloride treatment using sequential 18F-Fluoride PET imaging. Additionally we hypothesised that since 18F-Fluoride and 223Ra share a common biological target, a single 18F-Fluoride scan at baseline could serve as a surrogate for 223Ra-chloride dosimetry. Methods: Five patients received two intravenous injections of 223Ra chloride, 6 weeks apart, at 100 kBq per kg whole-body weight. The pharmacokinetics and biodistribution of 223Ra-chloride as a function of time were determined. In addition PET/CT imaging using 18F-Fluoride was carried out immediately prior to treatment, prior to the second treatment at week 6, and subsequently at 12 weeks after baseline. Changes in both the SUVpeak and the percentage injected activity per kilogram of each lesion were measured and plotted against baseline 18F-Fluoride uptake on a lesion by lesion basis. Results: A total of 33 lesions were identified. Relatively small changes were observed in the uptake of lesions between baseline and 6 weeks. More significant changes were observed between baseline and 12 weeks. There was a clear correlation between baseline uptake of 18F-Fluoride and the subsequent decrease in 18F-Fluoride uptake at 12 weeks (r2 = 0.88). The hypothesis that 18F-Fluoride uptake could predict the effect of 223Ra-chloride treatment was further supported by the demonstration of a correlation (r2 = 0.79) between 223Ra and 18F-Fluoride uptake in metastatic bone lesions as well as the observation that the effective half-life of 223Ra-chloride in metastatic lesions was close to the physical half-life. Conclusion: Analysis of this small group of patients suggest that uptake of 18F-Fluoride has the potential to predict subsequent response to 223Ra-cloride therapy and serve as a surrogate measure of tumour dose.

OP236

Feasibility of 223Ra quantitative imaging for lesion dosimetry

G. A. Follacchio[1], V. Frantellizzi[1], R. Pellegrini[1], R. Pani[1], M. Pacilio[2], B. Cassano[2], M. Liberatore[1], F. Monteleone[1], T. Garkavaya[1], G. Ventroni[2], L. Mango[2], G. De Vincentis[1]; [1]Policlinico Umberto I - Sapienza University, Rome, ITALY, [2]A.O. San Camillo-Forlanini, Rome, ITALY.

223Ra-chloride is a novel bone-targeting radiopharmaceutical effective on bone pain in patients with metastatic castration-resistant prostate cancer. In 223Ra complex decay spectrum, α particles account for nearly 95% of emissions while photons represent less than 2% of total decay energy. Aim of this study was to evaluate feasibility of an imaging procedure based on 223Ra γ-emitting component in order to acquire significant data for personalized dosimetric evaluation. Nine male patients receiving 223Ra-chloride treatment (50 kBq/kg every 4 weeks for 6 injections) were enrolled. On the basis of 99mTc-MDP bone scan, we selected a single area of interest (thorax or pelvis) characterized by relevant bone metastasis. Gamma-camera calibration measurements with a source of 223Ra were carried out including sensitivity test and transmission curves. For each patient we performed serial planar static images of the chosen district on the 3rd-7th-14th-21st day after

first 223Ra injection (double-peak acquisitions with energy window centred at 82 and 158 keV, each 20% wide, MEGP collimator, 256x256 matrix, acquisition time 40'). In 3 patients we could perform early acquisitions at 4 and 24 h. For most of the patients, transmissive images were also acquired. Bone lesions were manually delineated on 99mTc-MDP bone scan, then ROIs were superimposed to 223Ra serial images after spatial co-registration with bone scan performed by a MATLAB tool. Activity quantification was performed correcting by attenuation, scatter and partial background subtraction. Absorbed dose to lesions was assessed by MIRD approach deriving S-values from OLINDA/EXM tabulations, estimating lesion volume by CT contouring. 99mTc percent uptake was evaluated on bone scan images. Over nine patients, twenty-four lesions were delineated at bone scan. Twelve lesions showed a wash-in phase, so biokinetics was assumed bi-exponential; mono-exponential biokinetics was assumed for remaining lesions. 223Ra effective half-life showed a median value of 7.8 days. Median absorbed dose to lesion for a single injection resulted 0.6 Gy (range 0.2-1.9 Gy); considering Relative Biological Effectiveness for α particles (RBE=5), DRBE /Aadm to lesions ranged from 340 to 2450 mGy/MBq. 99mTc and 223Ra percent uptake resulted significantly related on linear regression analysis. Our experience confirmed feasibility of quantitative imaging in patients treated with 223Ra-chloride. Collected data were useful to perform biokinetics studies and bone lesion dosimetry. Optimal timing for serial acquisitions resulted at 4, 24, 48 and 168 h. Absorbed dose to lesions was remarkable compared to β-emitting bone-seeking radiopharmaceuticals. Significant correlation between 99mTc-MDP and 223Ra percent uptake could allow dosimetry-based treatment.

OP237

A Monte Carlo study of small-scale dosimetry in capillary vessels during internal radionuclide therapies with 223Ra, 111In, 131I and 177Lu

S. Leotta[1], **E. Amato**[1], A. Italiano[2], L. Auditore[1], R. Gentile[1], S. Baldari[1]; [1]University of Messina, MESSINA, ITALY, [2]Istituto Nazionale di Fisica Nucleare, MESSINA, ITALY.

This study was aimed to evaluate the combined effects of radiopharmaceutical diffusion and range of the emitted radiation in a model of tumour capillary vessels. We developed a computational model representing a blood capillary vessel surrounded by solid tumour tisssue, and we simulated the transport of radiation emitted by by 223Ra, 111In, 131I and 177Lu nuclides using two different Monte Carlo codes: Geant4 and MCNPX. In particular, we simulated a cylindrical vessel having 10 um of inner radius and 10 um of thickness filled by blood and surrounded by cylindrical layers of soft tissue, 10 um thick each. For each nuclide, several models of radiopharmaceutical outflow through the capillary vessel were considered: in blood only, representative of radio-embolization procedures, in capillary cells, representative of an anti-angiogenic radiopharmaceutical accumulating in them, and several models of extra-vascular dispersion. Radial dose profiles around the capillary vessel were obtained and compared between codes and between the physics models available. The results for beta and Auger emitters demonstrate that the photon dose is at least four orders of magnitude lower with respect to the one deposited by electrons. For which concerns 223Ra, the beta emissions of the daughters give a contribution three orders of magnitude lower with respect to the alpha particles, even if with a much longer range. For each nuclide and for every diffusion model, the Endothelial Cell Mean Dose (ECMD) and the Tumour Edge Mean Dose (TEMD) per unit cumulated activity were computed and represented in tabular form, together with the initial radioactivity (IR) necessary to deposit 100 Gy of dose at the edge of the viable tumour. Such results may help to characterize the dose inhomogeneities in solid tumour therapies with radiopharmaceuticals, taking into accunt the interplay between drug diffusion from vasculature and range of ionizing radiations.

OP238

Factors Affecting RADIUM-223 Therapy

E. Etchebehere, J. Araujo, D. Milton, N. Swanston, H. Macapinlac, E. Rohren; The University of Texas MD Anderson Cancer Center, Houston, TX, UNITED STATES.

AIM: The purpose of this study was to evaluate the factors that may affect Radium-223 therapy (Ra-223). MATERIALS AND METHODS: We retrospectively reviewed 110 histologically confirmed hormone-refractory prostate cancer patients (42-88 y old; mean 69yrs.) with bone metastases, with or without visceral and nodal metastases. End points were overall survival (OS), progression-free survival (PFS), time to progression (TTP), bone event-free survival (BeFS), and bone marrow failure (BMF). The following parameters were evaluated prior to the 1st Ra-223 cycle: hemoglobin ($Hb_{Initial}$) levels (<10 vs >10g/dl), PSA levels ($PSA_{Initial}$<10 vs >10ng/ml), ALP levels ($ALP_{Initial}$<147 vs >147IU/L), ECOG status ($ECOG_{Initial}$), pain score ($pain_{Initial}$), use of chemotherapy ($Chemo_{Prior}$) and external beam radiation therapy ($EBRT_{Prior}$). Additionally, the total number of radium cycles (Ra_{Tot}) were evaluated. During/after Ra-223 the following parameters were evaluated: PSA doubling time (PSA_{Dt}), use of chemotherapy ($Chemo_{During/After}$), $EBRT_{During/After}$, $Abriaterone_{During/After}$ and $Enzalutamide_{During/After}$.RESULTS: The median follow-up time was 8.3 months (0.4-18.4 months). Fifty-eight (53%) patients received all 6 Ra-223 cycles. Fifty (45%) patients

died, 85 (77%) progressed and 24 (22%) had a bone event. The median OS was 11.7 months, PFS was 4.3 months, TTP was 4.4 months, BeFS was 8.6 months and BMF was 8.6 months.A significant reduction of ALP levels ($p<0.001$) and pain score ($p=0.041$) occurred throughout the Ra-223 cycles. A significant risk of progression was associated with declining ECOG status (HR=3.79; $p<0.001$) and increase in PSA_{DT} (HR=15.82; $p<0.001$).Univariable analysis demonstrated that Ra_{Tot}, $ALP_{Initial}$, $ECOG_{Initial}$, $pain_{Initial}$ and $Abriaterone_{During/After}$ were significantly associated with OS ($p\leq0.008$), PFS ($p\leq0.003$) and BeFS ($p\leq0.020$). Additionally, Ra_{Tot}, $Hb_{Initial}$, $ALP_{Initial}$, $ECOG_{Initial}$, $pain_{Initial}$ and $EBRT_{During/After}$ were associated with BMF ($p\leq0.002$).When adjusting for all covariates, however, only Ra_{Tot} and $Abriaterone_{During/After}$ remained significantly associated with OS (HR=0.56; $p<0.001$; and HR=0.32; $p=0.033$, respectively), PFS (HR=0.67; $p<0.001$; and HR=0.52; $p=0.041$, respectively) and BeFS (HR=0.62; $p<0.001$; and HR=0.32; $p=0.019$, respectively). Additionally, only Ra_{Tot} (HR=0.73; $p=0.025$), $ALP_{Initial}$ (HR=3.11; $p=0.043$) and $EBRT_{During/After}$ (HR=3.62; $p=0.053$) remained significantly associated with BMF. CONCLUSIONS: More Ra-223 cycles were beneficial and reduced the risk of death, progression and the risk of a bone event. The risk of progression was increased 3 times with a declining ECOG status and 15 times with rise in PSA_{DT}. During Ra-223 cycles, the concomitant use of Abriaterone seems to have a beneficial effect while the EBRT increased the risk of BMF.

OP239

Therapy of Metastasized Prostate Cancer Using a Lu-177 Labeled PSMA Inhibitor (I&T): First Dosimetric Results in Patients

C. Schuchardt[1], S. Wiessalla[1], A. Özkan[2], H. R. Kulkarni[1], M. Shahinfar[1], M. Sayeg[1], M. Weineisen[3], H. J. Wester[3], R. P. Baum[1]; [1]THERANOSTICS Center for Molecular Radiotherapy and Molecular Imaging, BAD BERKA, GERMANY, [2]Yildiz Technical University, Department of Physics, Istanbul, TURKEY, [3]Technical University Munich, Pharmaceutical Radiochemistry, Faculties of Chemistry and Medicine, Munich, GERMANY.

Aim: The prostate-specific membrane antigen (PSMA) is significantly over-expressed in prostate cancer cells compared to normal prostate tissue. The aim of our study was to determine the kinetics and dosimetry in patients undergoing peptide radioligand therapy (PRLT) of metastasized prostate cancer using the Lu-177 labeled PSMA inhibitor (I&T: imaging and therapy). Methods: 20 patients with progressive, castrate resistant metastatic prostate cancer (aged 73+/-7 years) were included in the analysis. High PSMA expression was verified before treatment by Ga-68 PSMA PET/CT. The administered activity ranged from 3.6 to 8.6 GBq Lu-177 PSMA. Based on five conjugated planar whole-body scans, time-dependent organ and tumor activities were determined and dosimetric calculations were performed according to the MIRD scheme using OLINDA/EXM software. To analyse the kinetics, we used the following parameters: effective half-life in hours (representing the slower beta-phase) and uptake in %IA (fraction of injected activity), which were calculated using the fit of the time-dependent activity curve to a mono- or bi-exponential function. Blood samples were drawn to determine the blood kinetics and to estimate the absorbed dose to red marrow. Results: Very intense uptake in the tumour lesions as well as significant uptake in the kidneys and the salivary glands was observed in all patients. Blood sampling revealed fast clearance from blood with half-lives of 12min (alpha-phase) up to 42hours (beta-phase). There was rapid clearance of tracer from whole body with a half-life of 12-91hours. The maximum renal uptake was 12%IA and showed a fast wash-out with half-lives of 19-82hours. Parotid glands demonstrated high uptake up to 1.2%IA with half-lives of 32+/-20hours (maximum 118hours). Concerning malignant lesions we distinguished between bone (30) and lymph node (12) metastases. The maximum uptake was 1.6% IA for bone and 1.8%IA for lymph node metastases. All tumour lesions followed an exponential decline with a mean half-life of 60hours. The following organ- and tumour doses were calculated: Whole body 0.03+/-0.02mGy/MBq (0.01-0.07mGy/MBq); kidneys 0.7+/-0.4mGy/MBq (0.2-1.5mGy/MBq); parotid glands 1.4+/-1.3mGy/MBq (0.1-4.8mGy/MBq); bone lesions 0.2-28mGy/MBq; lymph node lesions 0.1-78mGy/MBq. Clinically, no adverse effects were observed in any of the patients concerning renal function (serial follow-up up to 24months) or salivary glands. Conclusions: Despite high uptake in the kidneys and salivary glands, the high tumor uptake, fast renal wash-out and rapid blood clearance confirm the efficacy and safety of PRLT using the Lu-177 labeled PSMA inhibitor PSMA I&T in patients with metastasized prostate cancer.

OP240

Radiation Sensitivity of Prostate Cancer Cells for Beta- or Auger-Electron, Alpha-Particle, or Photon Irradiation.

J. Elgqvist, K. Claesson, E. Larsson, S. Oredsson, O. Vilhelmsson-Timmermand, T. Tran, S. Strand; Institute for Clinical Sciences, LUND, SWEDEN.

Aim. Radioimmunotherapy against prostate cancer is an evolving research area due to the absence of a curative therapy of the metastatic disease. The purpose of this study is to investigate radiation sensitivity of prostate cancer cell lines DU145, LNCaP, and PC3 irradiated with 177-Lu, 111-In, alpha-particles from 241-Am, or 137-Cs. Materials and Methods. The three cell lines DU145, LNCaP and PC3 were irradiated

using an unspecific IgG1 antibody labeled with 177-Lu or 111-In, by external photon irradiation using 137-Cs, or by using an external 241-Am alpha-particle irradiator. The cells were subjected to absorbed doses equal to 0, 0.5, 1, 2, 4, 6, 8, or 10 Gy. For evaluation of cell survival; colony forming and tetrazolium-based assays were used. Regarding the tetrazolium-based assay; after irradiation in 96- or 24-well plates tetrazolium solution was added to each well, incubated, and then measured for level of absorbance at 450 nm, indicating the amount of live/viable cells. Results. For DU145 the SF at 2.0 Gy (SF2Gy) was 0.58 ± 0.06, and 0.40 ± 0.08 (mean ± SEM) after irradiation by 177-Lu or from photons from the LINAC, respectively. Irradiations using 111-In are on-going for DU145. For LNCaP the SF2Gy was 0.62 ± 0.03 for the 177-Lu irradiation. Irradiations using 111-In for the LNCaP cells are on-going. Irradiations of the PC3 cells are also on-going. Irradiations using 241-Am shows a significantly reduced cell survival already at an absorbed dose equal to 2 Gy. Compared to 137-Cs photon irradiations, a preliminary RBE equal to 4-5 is observed for the alpha-particle irradiations of the LNCaP and DU145 cells, at 37% cell survival. Conclusions. A significantly lower SF2Gy value after irradiation with 111-In in DU145 cells, compared to irradiation with 177-Lu or 137-Cs/LINAC is observed. Irradiation using 241-Am show a high level of cell killing efficacy, indicating a potential use of alpha-particle emitters labeled to specific antibodies for the treatment of microscopic prostate cancer. The results indicate that the inherent radiosensitivity of prostate cancer cell lines might vary greatly and that it therefore is very important to consider which type of irradiation to use in targeted radionuclide therapies.

806 - Monday, October 12, 2015, 11:30 AM - 12:45 PM, Hall 6
M2M: Radiopharmaceuticals & Radiochemistry: Macromolecules I

OP242

Influence of Histidine-Containing Tags on Biodistribution of Radiolabelled ADAPT-Based Imaging Probes

S. Lindbo[1], J. Garousi[2], M. Åstrand[1], H. Honarvar[2], A. Orlova[2], S. Hober[1], **V. Tolmachev**[2]; [1]Royal Institute of Technology-KTH, Stockholm, SWEDEN, [2]Uppsala University, UPPSALA, SWEDEN.

Aim. ADAPTs are a class of small (~5 kDa) robust scaffold proteins suitable as probes for radionuclide molecular imaging in vivo. The attachment of a histidine-containing tags to the scaffold proteins allows efficient purification by immobilized metal ion affinity chromatography (IMAC) and permits labelling with $^{99m}Tc(CO)_3$. Earlier, we have demonstrated that replacement of the hexahistidine (H_6)-tag with the negatively charged histidine-glutamate-histidine-glutamate-histidine-glutamate (HE_3)-tag reduces hepatic uptake of radiolabelled affibody molecules. The same effect has been confirmed for other scaffold proteins, DARPins, and short peptides. The aim of this study was to evaluate effect of histidine-containing tag composition on biodistribution of ADAPTs. Material and methods. A series of anti-HER2 ADAPT6 probes having DEAVDANS lead sequence and H_6- or HE_3-tags at N-termini has been prepared. In two variants, maleimido derivative of DOTA was conjugated to a unique cysteine was incorporated at N-terminus. DOTA-C-HE_3-ADAPT6 and DOTA-C-H_6-ADAPT6 were labelled with ^{111}In. HE_3-ADAPT6 and H_6-ADAPT6 were labelled with $^{99m}Tc(CO)_3$ using IsoLink kit. Binding specificity, affinity, and cellular processing of new conjugates was evaluated using HER2-expressing SKOV-3 ovarian carcinoma cells. Biodistribution at 1,4 and 24 h p.i. was evaluated in normal NMRI mice. Tumour-targeting properties of the best $^{99m}Tc(CO)_3$-labelled variant, $^{99m}Tc(CO)_3$-H_6-ADAPT6 were evaluated in BALB/C nu/nu mice bearing SKOV-3 xenografts. Results. All radiolabeled ADAPTs demonstrated specific binding to SKOV-3 cells with affinities in the range of 1.1-2.8 nM. The internalization by SKOV-3 cells was slow. In vivo, all conjugates cleared rapidly from blood via kidneys with subsequent renal re-absorption. The hepatic uptake of ^{111}In-DOTA-C-H_6-ADAPT6 was slightly but significantly ($p<0.05$) higher that the uptake of ^{111}In-DOTA-C-HE_3-ADAPT6 at 1 h pi, but biodistribution was very similar at later time points. Surprisingly, the uptake of $^{99m}Tc(CO)_3$-HE_3-ADAPT6 was significantly ($p<0.05$) higher than uptake of $^{99m}Tc(CO)_3$-H_6-ADAPT6 in liver, blood, and bone at 1h p.i. At 4 h p.i., hepatic uptakes were equal, but $^{99m}Tc(CO)_3$-H_6-ADAPT6 provided lower uptake in blood and bone. $^{99m}Tc(CO)_3$-H_6-ADAPT6 demonstrated high (19± 3 %ID/g at 4 h p.i.) and specific tumour uptake. Tumour-to-blood and tumour-to-liver ratios were 102± 29 and 12± 3, respectively. Conclusion. Influence of histidine-containing tag on biodistribution of scaffold proteins depends on composition of a scaffold protein and might differ appreciably. This should be take into account in molecular design of imaging probes based on engineered scaffold proteins.

OP243

Preclinical development of a novel combination therapy against ovarian carcinoma: Combination of anti-L1CAM Lutetium-177 radioimmunotherapy and clinically relevant protein kinase inhibitors

D. Lindenblatt[1], G. Pellegrini[2], S. Cohrs[1], P. R. Spycher[1], D. Vukovic[1], E. Fischer[1], R. Schibli[1,3], **J. Grünberg**[1]; [1]Paul Scherrer Institut, Villigen PSI, SWITZERLAND, [2]Univerity of Zurich, Institut für Veterinärpathologie, SWITZERLAND, [3]Department of Chemistry and Applied Biosciences, ETH Zurich, SWITZERLAND.

Aim: Previously we have shown that paclitaxel improved anti-L1CAM lutetium-177 radioimmunotherapy in an ovarian cancer xenograft model (EJNMMI Research 2014, 4:54). Based on this finding we asked whether the addition of modern and clinical relevant protein kinase inhibitors (PKIs) offers also a therapeutic possibility to improve RIT against ovarian carcinoma. Five PKIs for cytotoxicity screenings were chosen based on their current clinical relevance (clinical phase II-III, ovarian cancer) and their influence on cell cycle regulation and DNA damage repair pathways. We combined selected PKIs with anti-L1CAM monoclonal antibody chCE7 labelled with lutetium-177 for our investigations. Material and methods: PKIs cytotoxicities were determined via cell colony-forming assays. Biomarker of double-strand-breaks (dsDNA breaks; pH2A.X) was analysed by Western blot after single or combined treatments. Levels of histone phosphorylation were quantified by fluorescence microscopy. Flow cytometry analysis was performed to evaluate levels of apoptosis based on combination- or monotreatments. For immunohistochemistry, nude mice (n = 3) were subcutaneously injected with SKOV3ip human ovarian carcinoma cells and treated with 2 MBq ^{177}Lu-DOTA-chCE7 alone or in combination with 60 mg/kg MK1775 administered 72h post radioimmunotherapy. PKI dosages were applied daily for 4 consecutive days. Accordantly, untreated controls received PBS. 6 days post treatment start tumours samples were collected and stained against pH2A.X. Results: *In vitro c*ytotoxicity studies demonstrated that the IC_{50} values of the different PKIs ranging from nanomolar to micromolar concentrations indicating varying sensitivities of ovarian cancer cell lines. Western blot analysis of IGROV1 cell lysates revealed that combination of ^{177}Lu-DOTA-chCE7 (5 MBq/ml) and PKI MK1775 (300 nM) induced higher levels of histone phosphorylation (pH2A.X) compared to either monotreatment. This observation was confirmed and quantified by florescence microscopy demonstrating a significant increase in pH2A.X positive cells (^{177}Lu-DOTA-chCE7 + MK1775: 91.1% vs. ^{177}Lu-DOTA-chCE7: 71.7% and MK1775: 55.5%; $p < 0.05$). Increased amounts of present dsDNA breaks resulted in a significant higher number of early apoptotic tumour cells after combined treatment compared to monotreatments (^{177}Lu-DOTA-chCE7: 7.9%, MK1775: 28.6%, ^{177}Lu-DOTA-chCE7 + MK1775: 40.1%; $p < 0.05$). Pretreated tumour xenografts showed positive stainings for pH2A.X foci indicating present dsDNA breaks in tumour tissue. *Ex vivo* quantification of pH2A.X foci is currently under investigation. Conclusion: The combination of ^{177}Lu-DOTA-chCE7 and protein kinase WEE1-inhibiting MK1775 is a promising treatment strategy against ovarian carcinoma. The amount of induced dsDNA lesions and apoptosis early post treatment start is significantly increased compared to either monotreatment.

OP244

Feasibility of Affibody molecule-based PNA-mediated pretargeting.

H. Honarvar[1], K. Westerlund[2], M. Altai[3], M. Sandström[4], A. Orlova[5], V. Tolmachev[3], A. Eriksson Karlström[2]; [1]Institute for Immunology, Genetics and Pathology, Uppsala University, Uppsala, SWEDEN, [2]School of Biotechnology, Division of Protein Technology, KTH Royal Institute of Technology, Stockholm, SWEDEN, [3]Rudbeck Laboratoriet, Uppsala, SWEDEN, [4]Uppsala University Hospital, Uppsala, SWEDEN, [5]Preclinical PET Platform, Department of Medicinal Chemistry, Uppsala University, Uppsala, SWEDEN.

Aim. Affibody molecules are small (7 kDa) non-immunoglobulin scaffold proteins, which enable high contrast visualization of cancer-associated molecular targets. However, their renal clearance is followed by high renal re-absorption, which prevents their use for radionuclide therapy with residualizing radiometals. To overcome this problem, we tested hypothesis that the use of Affibody-based peptide nucleic acids (PNA)-mediated pretargeting would enable higher accumulation of radiometals in tumors than in kidneys. The aim of this study was to provide a proof-of-principle for Affibody based PNA-mediated pre-targeting. Material and methods. We designed an anti-HER2 Affibody-PNA chimera ZHER2:342-SR-HP1containing 15-mer HP1 PNA recognition tag, and a complementary HP2 hybridization probe. Presence of a tyrosine residue at N-terminus and DOTA-chelator at C-terminus of HP2 permitted labeling with both 125I and 111In. DOTA-chelator conjugated to the N-terminus of ZHER2:342-SR-HP1provided radiolabeling of the chimera with 111In. In vitro binding specificity, affinity, and cellular processing properties of constructs were studied using HER2 -expressing SKOV-3 and BT474 cell-lines. The in vivo targeting specificity and biodistribution profile of ZHER2:342-SR-HP1 and 111In/125I-HP2 were studied in mice bearing SKOV-3 xenografts. Results. 111In-ZHER2:342-SR-HP1 demonstrated specific-binding to HER2-expressing BT474 and SKOV-3 cancer cells in vitro with affinity of 6±2 pM. The binding of radiolabeled complementary PNA probe 111In/125I-HP2 to ZHER2:342-SR-HP1 pre-treated cells was specific with affinity of 200-400 pM. 111In-ZHER2:342-SR-HP1showed specific accumulation in SKOV-3 xenografts in BALB/C nu/nu mice and a rapid clearance from blood. Pre-saturation of SKOV-3 with non-labeled anti-HER2 Affibody or the use of HER2-negative Ramos xenografts resulted in significantly lower tumor uptake of 111In-ZHER2:342-SR-HP1. The complementary PNA probe 111In/125I-HP2 accumulated in SKOV-3 xenografts only in presence of ZHER2:342-SR-HP1, injected 4 h earlier. The tumor accumulation of 111In/125I-HP2 was very low (at the same level as in muscles) without ZHER2:342-SR-HP1 pre-

injection. The uptake of 111In-HP2 in SKOV-3 xenografts was 19±2 %ID/g at 1 h after injection. The uptake in blood and kidneys were ca. 50- and 2-fold lower, respectively. Conclusion. We have shown that the use of Affibody-based PNA-mediated pretargeting enables specific delivery of radionuclides to tumors and provides higher radiometal concentration in tumors than in the kidneys. This opens a way for investigation of such promising therapeutic radionuclides as low energy beta emitter 177Lu, or alpha emitters 212Bi, 213Bi, and 227Th, for Affibody-mediated therapy.

OP245

An Anti-HER2 Nanobody Labeled with 18F Using a Residualizing Label for Assessing HER2 Status

G. Vaidyanathan[1], D. McDougald[1], J. Choi[1], E. Koumarianou[1], M. Pruszynski[2], T. Osada[1], H. Lyerly[1], T. Lahoutte[3], M. R. Zalutsky[1]; [1]Duke University Medical Center, Durham, NC, UNITED STATES, [2]Institute of Nuclear Chemistry and Technology, Warsaw, POLAND, [3]Free University of Brussels, Brussels, BELGIUM.

Aim. A PET imaging method for determination of HER2 status in breast cancer (bc) patients would be highly desirable. Nanobodies (Nbs) are single domain antibodies derived from *Camelidae*. Their small size (~15 kDa), nM-range affinity, low immunogenicity and other properties are very attractive for PET imaging. The goal of this study was to develop an anti-HER2 Nb labeled with ^{18}F using a novel residualizing labeling (RL) strategy as a potential tracer for assessing HER2 status in bc patients. Methods. *N*-succinimidyl 3-((4-(4-[^{18}F]fluorobutyl)-1H-1,2,3-triazol-1-yl)methyl)-5-(Boc_2-guanidinomethyl)benzoate) (Boc_2-[^{18}F]SFBTMGMB) was synthesized by the click reaction of an azido precursor and [^{18}F]fluorohexyne, and treated with TFA to generate the RL [^{18}F]SFBTMGMB. The anti-HER2 Nb 5F7 was conjugated with [^{18}F]SFBTMGMB, and for comparison, with [^{18}F]SFB (non RL) and the previously validated RL, [^{125}I]SGMIB. The labeled nanobodies were evaluated by TCA precipitation, ITLC, and gel electrophoresis. Binding affinity was determined using HER2-expressing BT474M1 bc cells and immunoreactive fraction (IF) by the Lindmo method. Paired-label internalization of [^{18}F]SFBTMGMB-5F7 versus [^{125}I]SGMIB-5F7, and [^{18}F]SFB-5F7 versus [^{125}I]SGMIB-5F7, was evaluated using BT474M1 cells in vitro. Paired-label biodistribution of [^{18}F]SFBTMGMB-5F7 and [^{125}I]SGMIB-5F7 was determined in SCID mice bearing BT474M1 xenografts. Results. Nb 5F7 was labeled with [^{18}F]SFBTMGMB with a conjugation efficiency of 33.4 ± 5.2% (n = 4). TCA precipitation, SDS-PAGE, and ITLC indicated >95% of radioactivity was protein-associated. [^{18}F]SFBTMGMB-5F7 bound specifically to HER2 with 62-84% IF and a Kd of 4.65 ± 0.88 nM. Comparable results were obatined with [^{18}F]SFB-5F7 and [^{125}I]SGMIB-5F7. Paired-label internalization indicated about 50% of initially bound radioactivity was trapped intracellularly for [^{18}F]SFBTMGMB-5F7 and [^{125}I]SGMIB-5F7 over 1-4 h. In contrast, only 39.9 ± 0.3% of [^{18}F]SFB-5F7 was internalized at 1 h and intracellular activity decreased to 24.5 ± 1.1% at 4 h. Tumour uptake of [^{18}F]SFBTMGMB-5F7 in vivo was 29.0 ± 3.9% ID/g and 36.3 ± 14.1% ID/g compared to 26.3 ± 3.1% ID/g and 32.5 ± 12.1% ID/g for [^{125}I]SGMIB-5F7 at 1 h and 2 h, respectively, with tumor:blood ratio for the ^{18}F conjugate increasing from 16.6 ± 5.0 at 1 h to 47.4 ± 13.1 at 4 h . Conclusions. [^{18}F]SFBTMGMB is perhaps the first ^{18}F agent specifically designed for RL properties and shows advantages for this purpose both in tumour cells and xenograft models. Moreover, the [^{18}F]SFBTMGMB-5F7 Nb conjugate is a promising agent that warrants further evaluation for PET imaging of HER2-expressing malignancies.

OP246

DOTAGA vs DOTA: an extra negative charge reduces hepatic uptake of Affibody molecules labelled with 111In and 68Ga

J. Strand[1], H. Honarvar[1], K. Westerlund[2], B. Mitran[3], A. Orlova[3], A. Eriksson Karlström[4], V. Tolmachev[1]; [1]Department of Immunology, Genetics and Pathology, Uppsala, SWEDEN, [2]Division of protein technology, Stockholm, SWEDEN, [3]Preclinical PET Platform, Uppsala, SWEDEN, [4]Division of protein technology, Uppsala, SWEDEN.

Aim: Affibody molecules are small (7kDa) scaffold proteins. Earlier, we investigated the impact of charge, lipophilicity and positioning of different amino acid tags on Affibody targeting properties. We found that the negatively charged variant of tags at N-terminus provide the lowest hepatic uptake. We hypothesize that the N-terminal placement of a chelator providing increased negative charge of a complex with a radionuclide might be used for reduction of liver uptake. To test this hypothesis, we compared targeting properties of anti-HER2 affibody molecules labelled with 111In- and 68Ga using DOTAGA and DOTA chelators. In complexes with trivalent metals, DOTAGA provides an extra negative charge compared with DOTA. Methods: DOTA and DOTAGA were conjugated to N-terminus of synthetic ZHER2:2891 via amide bond. The conjugates were labelled with 68Ga and 111In. In vitro binding specificity and internalization assays were performed using high HER2-expressing SKOV-3 and low HER2 expressing LS174T cells. The tumour targeting and biodistribution properties of 111In- and 68Ga-labelled conjugates were compared in nude mice bearing SKOV-3 xenografts at 2 hours post injection. PET imaging of SKOV-3 xenograft bearing mice

was preformed 2 h after injection of 68Ga-DOTAGA-ZHER2:2891. Results: DOTAGA-ZHER2:2891 and DOTA-ZHER2:2891 were stably labelled with 68Ga and 111In. The radiolabelled conjugates showed preserved binding specificity to HER2-expressing cells in vitro. All conjugates demonstrated slow internalization rates after binding to both SKOV-3 and LS174T cells. In vivo, the tumour uptake was similar, 22±2, 19 ±2, 25±2, and 23±5 %ID/g for 111In-DOTAGA-ZHER2:2891, 68Ga-DOTAGA-ZHER2:2891, 111In-DOTA-ZHER2:2891, and 68Ga-DOTA-ZHER2:2891, respectively. In vivo blocking assay confirmed specificity of tumour targeting. A combination of a nuclide and a chelator had clear influence in biodistribution in normal tissues.111In-labeled conjugates cleared significantly rapider from blood than 68Ga-labelled variants. The use of DOTAGA provided significantly lower hepatic uptake and blood radioactivity concentration for both radionuclides. The most pronounced difference between chelators was in the case of 68Ga. The use of DOTAGA provided appreciably higher tumour-to-blood (61 ±6 vs 23±5, $p<0.05$) and tumour-to-liver (10.4±0.6 vs 4.5±0.5, $p<0.05$) ratios that the use of DOTA. MicroPET/CT imaging confirmed that 68Ga-DOTAGA-ZHER2:2891 can visualize HER2-expressing xenografts with high contrast. Conclusion: This study demonstrated that chelators may be used for modification of uptake of Affibody molecules in normal tissues and improvement of imaging contrast. The use of DOTAGA for labelling with 68Ga resulted in a much better biodistribution profile for Affibody molecules compared with DOTA.

OP247

Generalized syntheses of tumor targeted yolk/shell structured multifunctional nanosystems

F. Chen, H. Hong, S. Shi, H. F. Valdovinos, T. E. Barnhart, W. Cai; University of Wisconsin-Madison, MADISON, WI, UNITED STATES.

Aim: To develop a generally applicable protocol for yolk/shell structured multifunctional nanosystems, to be used for tumor targeted PET image-guided drug delivery. Materials and Methods: Upconversion nanoparticle (UCNP, with NIR-in-NIR-out upconversion luminescence) was used as the initial example. UCNP was first coated with a dense silica ($dSiO_2$) shell, forming UCNP@$dSiO_2$, followed by re-growth of a shell-thickness controllable mesoporous silica nanoshell (MSN) to form UCNP@$dSiO_2$@MSN. A Na_2CO_3 etching protocol was then used to selectively etch away dSiO2, leaving behind yolk/shell structured nanoparticles denoted as UCNP@HMSN. A step-by-step surface engineering process was then adopted to conjugate (or label) NOTA, polyethylene glycol (PEG) linkers, TRC105 (an anti-CD105 antibody), and ^{64}Cu to form ^{64}Cu-UCNP@HMSN-PEGTRC105. Both hydrophobic (i.e. Sunitinib) and hydrophilic (i.e. Doxorubicin) drugs could be loaded inside UCNP@HMSN. Systematic in vivo PET imaging and biodistribution studies were performed in 4T1 tumor-bearing mice to evaluate and confirm tumor targeting capability, validated by in vitro/ex vivo studies. Results: TEM confirmed successful synthesis of UCNP@HMSN. By changing the "yolk" to superparamagnetic iron oxide nanoparticle (SPION) or quantum dot (QD), we confirmed the general applicability of this protocol. In vitro CD105 targeting in HUVEC (CD105+) and MCF-7 (CD105-) cells showed strong/specific binding of FITC-conjugated UCNP@HMSN-PEG-TRC105 to CD105+ cells with negligible non-specific binding. In vivo tumor targeting and PET imaging demonstrated CD105-specific targeting of ^{64}Cu-UCNP@HMSN-PEG-TRC105 in 4T1 tumor-bearing mice, with peak tumor uptake of ~6.5 %ID/g at 6 h post-injection. CD105 specificity was confirmed by blocking and ex vivo histology studies. Conclusion: We report the generalized syntheses of yolk/shell structured nanosystems for tumor targeted PET imaging and drug delivery. With UCNP, QD, SPION, or other nanocrystals inside each yolk/shell structure, this nanoplatform is highly versatile for future tumor targeted multimodality image-guided drug delivery.

807 - Monday, October 12, 2015, 11:30 AM - 1:00 PM, Hall F
Teaching Session: Anatomy Refresher and Hybrid Imaging of the Foot and Ankle

OP248

Anatomy Refresher and Hybrid Imaging of the Foot and Ankle

C. Fowler, **UNITED KINGDOM**

809 - Monday, October 12, 2015, 11:30 AM - 1:00 PM, Hall 8
Clinical Oncology: Prostate I - Choline

OP249

Role of [11C]choline PET/CT in tailored Cyberknife stereotactic Therapy in patients with prostate recurrent isolated lymph node.

P. Gandolfo[1], **F. Ria**[2], A. Bergantin[2], A. S. Martinotti[2], I. Redaelli[2], M. Invernizzi[2], A. Vai[2], I. Bossi Zanetti[2], L. C. Bianchi[2], G. Beltramo[2]; [1]Nuclear Medicine Unit - Centro Diagnostico Italiano, Milan, ITALY, [2]Cyberknife Unit - Centro Diagnostico Italiano, Milan, ITALY.

Aim: [11C]choline PET/CT has been established as a diagnostic tool in re-staging patients with biochemical failure after radical treatment for prostate cancer in particular for its capability to detect the presence of lymph node and bone metastases. The knowledge of the anatomical site of recurrence may be useful to refer patients to the specific tailored therapy, in addition to the conventional anti-hormonal therapy. We investigated the role of [^{11}C]choline PET/CT as an image method to select patients for Cyberknife stereotactic tailored therapy. Methods and Materials: Between March 2009 and march 2013 a cohort of 30 patients with up to 3 synchronous lymph node prostate metastases staged with [11C]choline PET/CT (47 lesions, median volume 12,92 cc, range 0,39 -111,67), following biochemical recurrence after local curative treatment were treated with Cyberknife Stereotactic Body Radiotherapy (SBRT) in our Center. In all patients [11C]choline PET/CT images was used to select and delineated target volumes at lymph node recurrent sites. The mean age of patients population at the time of the Cyberknife treatment was 68 years (range 55-84). Cyberknife prescription doses were 3000-3600 cGy delivered in 3 consecutive fractions of 1000-1200 cGy. In 14 lesions (37%) SBRT was performed as re-irradiation (the recurrent lesion was situated in the previously irradiated volume). Results: The Cyberknife treatment was well tolerated without any acute or late toxicity at all. There were no in field recurrence, resulting in a local control of 100%. Eleven and 3 patients, respectively required a second and third salvage treatment for metachronous metastatic disease. The median time to clinical progression was 14 months (range 3-54). After a median follow up of 33 months (range 13-73) 16 patients started with Androgen Deprivation Therapy (ADT) because of polymetastatic disease resulting in an ADT-FS of 80% at 1 year and 65% at 2 years. The median time ADT was deferred resulted of 26 months (range 4-56). Conclusions: The recent evidence of the potential toxic nature of ADT suggest that effective local therapy might reduce the burden of systemic therapies usually given to patients with metastatic prostate cancer. Although there are not literature data that support the use of [11C]choline PET/CT to plan target volume at lymph nodal level our preliminary results are promising, showing that the treatment is well tolerated with excellent rate of local control and suggest a potential role of [11C]choline PET/CT to select and refer patients to specific treatment strategies.

OP250

Comparison of [18F] choline PET/CT with integrated [18F] choline PET/MRI in patients with suspected recurrent prostate cancer.

A. Wetter[1], B. M. Schaarschmidt[2], M. Schenck[3], H. Rübben[3], S. Lütje[4], T. Pöppel[4], M. Forsting[1], T. Lauenstein[1]; [1]University Hospital Essen, Dept. of Radiology and Neuroradiology, Essen, GERMANY, [2]University Hospital Düsseldorf, Dept. of Radiology, Düsseldorf, GERMANY, [3]University Hospital Essen, Department of Urology, Essen, GERMANY, [4]University Hospital Essen, Department of Nuclear Medicine, Essen, GERMANY.

Purpose: To prospectively compare diagnostic performance of [18F] choline PET/CT with [18F] choline PET/MRI in patients with suspected recurrent prostate cancer. Methods: 68 patients were assigned for a clinically indicated [18F] choline PET/CT because of a rising PSA-level after radical prostatectomy. After PET/CT was completed, patients were transferred to the PET/MRI unit and simultaneous [18F] choline PET/MRI examinations were conducted on an integrated PET/MR scanner. Sequence protocol consisted of one pelvic PET scan with an acquisition time of 20 minutes and simultaneous acquisition of T2 and T1-weighted MR images before and after administration of a paramagnetic contrast agent. PET/CT and PET/MR image analysis was prospectively performed by different groups of nuclear medicine physicians and radiologists with respect to the detection of lymph node metastases, bone metastases and local recurrence of the tumor. Results: Simultaneous PET/MRI examinations were successfully accomplished in all patients with diagnostic image quality. [18F] choline PET/CT diagnosed pelvic tumor lesions in 52 patients (76.5%), PET/MRI revealed pelvic tumor lesions in 55 patients (80.9 %). Concordant diagnoses of PET/CT and PET/MRI were achieved in 60 patients, whereas PET/MRI led to a discordant diagnosis in 8 patients (11.8 %). In three patients where no suspicious lesion was detected with PET/CT, PET/MRI led to the diagnosis of a local recurrence in 1 patient and suspected bone metastases in two patients. In the remaining five patients, PET/MRI found additional lymph node metastases in one patient and additional bone metastases in four patients. From a clinical point of view, PET/MRI led to a change of management in 2 patients (2.9 %) Conclusion: Simultaneous [18F] choline PET/MRI is a robust method for clinical use and provides additional information as compared to PET/CT in patients with suspected recurrent prostate cancer. However, a significant change of diagnosis with following change of treatment is observed only in a small percentage of patients.

OP251

Prognostic value of FCH PET/CT in response to radical radiotherapy in patients with localized prostate cancer

M. Sepulcri, A. Negri, E. Agostini, S. Galuppo, A. Cervino, G. Saladini, A. Scaggion, M. Paiusco, L. Evangelista; Istituto Oncologico Veneto I.R.C.C.S., PADOVA, ITALY.

Aim: the aim of this study was to assess the value of FCH PET/CT in predicting the outcome of patients with localized prostate cancer treated by radical radiotherapy.Materials and methods:

from a mono-centric PET/CT database, we retrospectively revised pre-treatment FCH PET/CT scans of 11 patients who underwent radiotherapy (dosage: 78 Gy/39 fractions) for the treatment of localized prostate cancer. For each study, SUVmax, SUVavg and metabolic tumor volume (MTV) were evaluated. Moreover, the value of PSA before radiotherapy (PSAp) was recovered. A follow-up period after PET/CT scan, of at least one-year, was required. In accordance with the observational period, patients were classified as disease free (DF) if the increase of PSA value after radiotherapy was less than 2 ng/mL respect to PSA nadir value, conversely with an increase of PSA higher than 2 ng/ml they were classified as recurrent (not disease free, NDF). A Kolgomorov-Smirnov test was used to compare the distribution of semi-quantitative PET and PSA data of the two patient groups.Results: mean, minimum and maximum values of SUVmax, SUVavg, MTV and PSAp were 9.6 (3.2-22.7), 5.1 (3.0-9.4), 11.1 (0.1-49.1) and 19.5 ng/mL (2.0-73.5 ng/mL), respectively. After one year of follow-up, 7 patients were considered as DF and 4 patients were considered as NDF. The values of DF patients were 6.2 (3.2-12.6), 3.6 (3.0-4.2), 6.0 (0.1-25.8) and 15.6 ng/mL (2.0-54.8 ng/mL) respectively for SUVmax. SUVavg, MTV and PSAp. For NDF patients the corresponding obtained values were 15.5 (10.4-22.7), 7.9 (5.6-9.4), 22.6 (7.1-49.1) and 26.2 ng/mL (5.0-73.5 ng/mL). In NDF patients, the mean values of SUVmax and SUVavg were significantly higher than in DF group ($p<0.05$ and $p<0.01$, respectively) while MTV and PSAp were not statistically different between the two groups.Conclusion: high values of FCH SUVs in prostate cancer of patients who are candidates to radiotherapy result predictive of poor outcome after one year of follow-up. Therefore, the SUV values could be useful to identify those patients who could benefit from a boosted radiotherapy dose to the dominant intraprostatic tumour lesion.

OP252

Predictive role of 11C-Choline PET/CT on the lymph nodal relapse in prostate cancer patients treated by salvage radiotherapy

E. Incerti[1], A. Fodor[2], P. Mapelli[1], C. Fiorino[3], P. Alongi[4], M. Kirienko[4], G. Giovacchini[5], E. Busnardo[1], G. Berardi[2], R. Calandrino[3], L. Gianolli[1], N. Di Muzio[2], M. Picchio[1]; [1]Nuclear Medicine Department, IRCCS San Raffaele Scientific Institute, Milan, ITALY, [2]Radiotherapy Department, IRCCS San Raffaele Scientific Institute, Milan, ITALY, [3]Medical Physics Department, IRCCS San Raffaele Scientific Institute, Milan, ITALY, [4]University of Milano-Bicocca, Milan, ITALY, [5]Department of Radiology and Nuclear Medicine, Stadtspital Waid, Zurich, SWITZERLAND.

Aim: The aim was to investigate the possible association between imaging parameters of 11C-Choline PET/CT (Choline-PET/CT) with survival outcomes: overall survival (OS), loco regional relapse free survival (lRFS), clinical relapse free survival (cRFS) and biochemical relapse free survival (bRFS) in patients with prostate cancer (PCa) treated with helical tomotherapy (HTT) on lymph node (LN) recurrence.Materials and Methods: This retrospective study include 68 patients with PCa (mean age: 68 yrs; range: 51-81 yrs) with biochemical recurrence after primary treatment (median PSA: 2.42 ng/ml; range: 0.61-27.56 ng/ml) who underwent Choline-PET/CT from January 2005 to January 2013. PCa patients presented Choline-PET/CT pathological uptake at LN site, were treated with salvage HTT. Positive pelvic and/or abdominal LNs were treated with a median dose of 65.8 Gy (range: 50.0-74.2) in 28 fractions. PET derived parameters such as SUVmax of the most active lesion, SUVmean of all metabolically active lesions and MTV with a threshold of 40%-50%-60% were calculated. Best cut-off values of PET derived parameters discriminating between patients with/without relapses were assesed by ROC analysis: OS, LRFS, CRFS and BRFS were considered. Univariate and multivariate Cox regression analysis including the most predictive PET derived parameters were performed. Results: Choline-PET/CT showed pathologic LNs in 4 patients at pelvic level, in 5 at abdominal level, in 13 at both pelvic and abdominal, in 46 at abdominal and/or pelvic and/or other sites. With a median follow-up of 20 months (range: 3-97 months). The 2-year OS, LRFS, CRFS, BRFS were 86.7%, 91.4%, 51.5% and 40.0% respectively. Significant best cut-off values could be found for both CRFS/BRFS for MTVs threshold. The most discriminative cut-off, based on the AUC of the ROC curves, was MTV60>0.64cc that also confirmed its independent predictive role in multivariate analysis. No significant cut-off values were found for both SUVmax and SUVmean. A two variable model including MTV60 and PET positive LNs site (pelvic vs extra-pelvic disease) well predicts the risk of relapse (2-year CRFS with 0, 1, 2 risk factors equal to $100 \pm 10.0\%$, $62.1 \pm 11.4\%$ and $11.4 \pm 9.7\%$ respectively, $p<0.0001$). Conclusion: PET derived parameters are predictive of tumor response in PCa patients treated with moderately hypo-fractionated HTT. In particular, MTV60 and extra-pelvic disease are predictive of relapse in PCa patients with LNs recurrent. This information may be useful in assessing the comparative effectiveness of various conventional and emerging treatment strategies, and to determine their ability to stratify patients in clinical trials.

OP253

Dynamic 11C-Choline PET/CT in biochemical relapse of prostate cancer: feasibility, clinical role and potential impact in guiding radiotherapy

P. Alongi[1], M. Spallino[2], E. Incerti[1], L. Gianolli[1], M. Picchio[1]; [1]IRCCS San Raffaele Scientific Institute, Milano, ITALY, [2]University of Milano-Bicocca, Milano, ITALY.

Aim : The real utility of Dynamic-11C-Choline-PET/CT (D-PET) in evaluation of local relapse and pelvic lymph-nodes has not been demonstrated yet. Despite an unconfirmed role, association of D-PET with standard PET/CT acquisition is largely used by several PET centre. The aim of this retrospective study was to assess the clinical use of D-PET in patients (pts) with rising PSA after prostatectomy candidates to radiotherapy (RT). Matherials and Methods : 30 pts with rising PSA (range 0.94-6.5 ng/ml) after prostatectomy who underwent to RT on suspicious local or lymph-nodal disease revealed by 11C-Choline PET/CT, were identified retrospectively in our database. In addition to standard PET/CT acquisition (from vertex to mid-thigh), a post-injection D-PET study was performed focusing on the pelvis. Asymmetry and abnormal 11C-Choline uptake at prostate bed and/or lymph-nodes stations were used to define D-PET positivity. PSA levels and clinical outcome were available for all pts. Results : D-PET showed tracer uptake on the prostate bed confirmed by standard PET/CT acquisition in 7/30 pts; 4/7 showed tracer uptake also on the pelvic lymph-nodes. All these 7/30 pts received RT at the site of suspicious local relapse and/or simultaneous integrated boost on the avid lymph-nodes following reduction of PSA (range 0-0.68ng/ml) and good control of disease (median PFS: 30,5 months). In 15/23 pts D-PET revealed 11C-Choline avid pelvic lymph-nodes that were treated by RT using PET/CT in the planning treatment obtaining sensible reduction of PSA levels and good clinical outcome. Only 4/15 pts had biochemical relapse after long time (PFS >24months). Mimicking a clinical scenario, D-PET was useful in the decision making to discriminate lymph-nodes uptake to urethral urine activity in 3/30 pts and to distinguish inflammatory lymph-nodes in 6/30 pts. These 9/30 pts did not received any local treatment showing no progression of disease during the follow-up. Overall, use of D-PET associated to standard PET/CT did not increase significantly the total time of examination (Mean 21 minutes), showing any difference in radiation exposure. Conclusion : the additional use of 11C-Choline D-PET, demonstrated to be a valuable tool allowing an improved evaluation of relapsing prostate cancer and providing crucial information in guiding radiotherapy.

OP254

11C-choline PET/CT in castrate-resistant prostate cancer patients treated with Docetaxel

F. Ceci[1], P. Castellucci[1], T. Graziani[1], R. Renzi[1], J. J. Morigi[1], G. M. Lima[1], F. Lodi[1], R. Schiavina[2], A. Ardizzoni[3], S. Fanti[1]; [1]Nuclear Medicine - S.Orsola-Malpighi Hospital - University of Bologna, Bologna, ITALY, [2]Department of Urology - S.Orsola-Malpighi Hospital - University of Bologna, Bologna, ITALY, [3]Department of Oncology - S.Orsola-Malpighi Hospital - University of Bologna, Bologna, ITALY.

Aim: to investigate the role of ^{11}C-choline PET/CT in the evaluation of the response to treatment in patients with metastatic castration-resistant prostate cancer (mCRPC) treated with Docetaxel in comparison with PSA response. Material and Methods: inclusion criteria were a) mCRPC with rising PSA levels b) Docetaxel as first line of chemotherapy (Docetaxel=75mg/m2 + prednisone=5mg); c) ^{11}C-choline-PET/CT and PSA values assessments performed before and after Docetaxel administration. 60 patients were retrospectively enrolled (age mean/range=68.9/57-84 years-old). ^{11}C-choline PET/CT (PET1) was performed as baseline before Docetaxel (mean value=2.4 months) and after (PET2) the end of treatment (mean value=3 months). PSA values were measured before (PSA1) (mean value=2.7 months) and after the end of treatment (PSA2) (mean value=2.8 months). PET2 was reported as complete (CR) or partial response (PR) or stable disease (SD). The appearance of a new PET-positive lesion was considered progression disease (PD). PSA-trend was calculated considering absolute values variations between PSA1 and PSA2. PSA-response was considered as a decrease ≥50% between PSA1 and PSA2. Clinical, radiological and laboratory follow-up were: range from 6- to 53 months (mean 13.5 months). Results: the 65%(39/60) of patients showed PD at PET2; 23.3% (14/60) showed a SD, while 11.7% (7/60) showed PR or CR. The 48.3% (29/60) of patients showed increasing PSA trend, while the 51.7% showed decreasing PSA-trend. A PSA-response ≥50% was observed in 41,7% (25/60). Considering the 29 patients with increasing PSA-trend, the 79.3% (23/29) showed PD, while the 20.7 (6/29) showed SD. Considering the 31 patients with decreasing PSA-trend, the 48.4% (15/31) showed PD, the 29% (9/31) showed SD while the 22.6% (7/31) showed CR or PR. Considering the 25 patients with PSA-response ≥50%, the 44% (11/25) showed PD at PET2. All patients with PD at PET2 were confirmed by clinical or radiological follow-up. Conclusion: Our data suggest that the increase in PSA values (increasing PSA-trend) measured after the end of Docetaxel is predictive of PD. In case of decreasing PSA values after therapy (decreasing PSA-trend and PSA-response ≥50%), ^{11}C-choline PET/CT may be useful to identify those patients with PET progression despite PSA response. In our patient series, this event occurred in the 44% of the patients showing PSA response.

OP255

Usefulness of 18F-fluorocholine positron emission tomography - computed tomography in occult biochemical recurrence of prostate cancer. A prospective multicentre study

Q. Gillebert[1], V. Huchet[1], C. Rousseau[2], A. Cochet[3], P. Olivier[4], F. Courbon[5], V. Nataf[1], J. Talbot[1]; [1]Department of Nuclear Medicine, Hôpital Tenon, Assistance Publique-Hôpitaux de Paris, Paris, FRANCE, [2]Nuclear Medicine Department,

Institut de Cancérologie de l'Ouest René Gauducheau, Nantes, FRANCE, [3]Department of Nuclear Medicine, Centre Georges-François Leclerc, Dijon, FRANCE, [4]Department of Nuclear Medicine, Hôpital de Brabois, Nancy, FRANCE, [5]Department of Nuclear Medicine, IUCT-Oncopole/Institut Claudius Regaud, Toulouse, FRANCE.

Introduction: The aim of the study was to evaluate the clinical impact of 18F-fluorocholine (FCH) PET/CT on management of patients with occult biochemical recurrence of prostate cancer (rPCa) after initial radical treatment. Methods: 177 patients with occult biochemical rPCa (mean PSA serum level: 7.5 ng/mL, range 0.5-244) after initial radical treatment were included in this multicentre prospective study, due to negative or inconclusive results of MRI of the pelvis and of bone scintigraphy. All patients underwent FCH PET/CT. To determine its impact on patient management, the referring physicians prospectively filled-in a 1st questionnaire before FCH PET/CT concerning the scheduled patient management and then a 2nd questionnaire about the actual management decided after PET/CT. On basis of data of 6 month post-PET follow-up, an independent panel determined the adequacy of the management decision and, if adequate information was available, site-based and patient-based standard of truth (SOT). If SOT could be obtained, centralised masked reading was performed, to determine diagnostic performance. Results: The positivity rate was 58% (103/177 positive FCH PET/CT). A change in patient management was induced in 98 cases (55%). In 38 patients, physicians changed a palliative treatment for a curative treatment with 23 salvage radiotherapies (S-RT), 8 surgical procedures, 7 high intensity focalised ultrasounds (HIFU). In 5 patients, physicians added a curative treatment (2 S-RT, 2 surgical procedures, and 1 brachytherapy) to androgen deprivation therapy (ADT). ADT was begun after FCH PET/CT in 24 patients. In 10 patients, curative treatment was changed for a palliative treatment. In 12 patients, physicians chose to defer the scheduled treatment (10 ADT and 2 S-RT). Finally, the therapeutic protocol has been modified after FCH PET/CT in 9 patients (6 ADT protocols, 2 S-RT and 1 surgical procedure). After FCH PET/CT, 10 CT scans, 17 MRI and 30 biopsies have been performed. The agreement between FCH PET/CT and the tests was 77%. Of the 177 FCH PET/CT, the induced management decisions were inadequate in 8% (15/177). The SOT could be determined for 70 patients and 72 sites. The patient-based detection rate of recurrence was 73%. The reproducibility between on-site and masked readings of PET was substantial with a Cohen's kappa coefficient of 0.67 (95% CI = 0.50-0.83). Conclusion: FCH PET/CT was a powerful tool to detect biochemical recurrence of PCa, even after negative pelvis MRI or bone scintigraphy. It could increase the effectiveness of therapeutic strategy.

OP256

Helical tomotherapy and bone metastases in prostate cancer patients: role of Choline-PET/CT

P. Mapelli[1], V. Gangemi[2], E. Incerti[1], G. Giovaccchini[3], C. Deantoni[4], A. Fodor[4], S. Baldari[2], L. Gianolli[1], N. Di Muzio[4], M. Picchio[1]; [1]Nuclear Medicine Unit, IRCCS San Raffaele Scientific Institute, Milano, ITALY, [2]Nuclear Medicine Unit, Department of Biomedical Sciences and of Morphologic and Functional Images, University of Messina, Messina, ITALY, [3]Department of Nuclear Medicine and Radio-Oncology, Stadtspital Triemli, Zurich, SWITZERLAND, [4]Radiation Oncology Department, IRCCS San Raffaele Scientific Institute, Milano, ITALY.

Aim. The number of metastases may reflect the biological aggressiveness of the tumor and may determining the possibility of curative potential interventions such as surgery or high-dose targeted radiotherapy (RT). The aim of the present study is to evaluate the efficacy of Choline-PET/CT based helical tomotherapy (HTT) as an innovative therapeutic approach on bone metastases, in a cohort of prostate cancer (PCa) patients with a limited number of metastases. Materials and methods. This retrospective study included 20 PCa patients presenting biochemical relapse of disease (value of the PSA > 0,2 ng/mL) after primary treatment who underwent Choline-PET/CT and to HTT treatment, from 2007 to 2014. Radiotherapy treatment was delivered with a median dose of 71±5 Gy (range: 60-76) and 51 Gy (range: 30-60) on prostatic bed, LN and bone metastases respectively. All patients underwent to androgen deprivation therapy (ADT) and this treatment was not discontinued for the whole duration of the study. The effectiveness of the treatment was assessed with biochemical response at 3/6/12 months, biochemical relapse-free survival (bRFS) and overall survival (OS) at 1-2 years. Results. The median age at Choline-PET/CT was 67 (range: 51-79). Nine/20 (45%) patients had only bone disease while 11/20 (55%) had disease at bone and lymph nodes (LN). Nineteen/20 patients underwent HTT on prostatic bed, pelvic LNs and bone metastases and 1/20 patient was subjected HTT only on bone. Treatment on the prostatic bed and pelvic lymph node was performed regardless the Choline-PET/CT findings in those sites. In addition, 6/20 patients who presented extra-pelvic LNs detected on Choline- PET/CT, HTT was performed on these sites. The mean follow-up from primary treatment was 56 months (range: 6-179 months) with median of 38 months. At 3 months the biochemical complete or partial response was 82%, at 6 months was 82% and at 12 months was 63%; bRFS at 1-2 year was 55-30% respectively; OS at 1-2 year was 100% and 92% respectively. Conclusion. Choline-PET/CT based HTT is a valid therapeutic approach in PCa patients with a low volume of metastases after primary treatment and biochemical relapse of disease. Further studies are

needed to confirm our results and to stratify PCa patients that may have benefit from this therapeutic approach based on specific clinical and imaging features.

810 - Monday, October 12, 2015, 11:30 AM - 1:00 PM, Hall D
Conventional & Specialised Nuclear Medicine: Bone & Joint

OP257

The Clinical Impact of Tc-99m HDP SPECT-CT in the diagnosis and management of complex foot and ankle pathology

C. Tang[1], K. Alsey[2], H. Zaw[2], M. Nathan[1]; [1]Royal Free Hospital, London, UNITED KINGDOM, [2]Hillingdon Hospital, London, UNITED KINGDOM.

Aims: Complex foot and ankle pathology can pose a diagnostic challenge to the clinician. SPECT-CT imaging is being increasingly used as a problem solving tool in these challenging cases, usually when other imaging modalities have been inconclusive.The aims of this study were:1.To evaluate the diagnostic utility of SPECT-CT in identifying potential pain generating pathology2.To determine the influence of SPECT-CT in directing subsequent patient management3.To evaluate patients' clinical outcomes where management was directed by SPECT-CT. Materials and Methods: Between June 2012 and December 2014, 61 consecutive patients (39 females and 22 males, age range 17-85) who were assessed by specialist foot and ankle surgeons and who were subsequently referred for Tc-99m HDP SPECT-CT were included. In total, 65 SPECT-CT scans were identified. Patients were divided into subgroups depending on the scan indication:1. Localisation of probable symptomatic site (43 scans)2. Non-union of fusion (14 scans)3. Metalwork related problems (5 scans)4. Infection (3 scans). The diagnostic utility SPECT-CT, impact on subsequent management and patient outcomes were assessed through correlation of SPECT-CT reports with serial post imaging clinic letters and discussion of individual cases with the orthopaedic surgeons. Results: SPECT-CT was considered diagnostically useful in 86% (56/65) scans : 79% (34/43) of localisation of symptomatic site scans and 100% in all other categories.SPECT-CT influenced subsequent patient management in 57/65 scans: 37% (24/65) further surgery, 8% (5/65) planned surgery, 22% (14/65) therapeutic steroid inject0ions and 22% (14/65) conservative treatment.Of 36 patients who had active intervention, 11/36 (31%) had successful outcomes following surgery, 10/36 (28%) following steroid injections. 14 patients who had conservative treatment were all considered to have had successful outcomes as they were not re-referred to orthopaedics. Conclusion: SPECT-CT was considered diagnostically useful in the majority of cases, particularly for non-union, metalwork problems and infection. SPECT-CT was also clinically useful in subsequent patient management by directing patients towards active surgical intervention or conservative management. Patient outcomes following surgical intervention were mixed, the reasons for which are multifactorial. Nevertheless, this study demonstrates that SPECT-CT has an important role as problem solving tool in the investigation of complex foot and ankle pain.

OP258

Altered bone metabolism of the spine in ankylosing spondylitis demonstrated by ^{18}F-fluoride PET/CT - A novel evaluation tool in patients with relatively low modified Stoke Ankylosing Spondylitis Spine Scores

J. Kim, Y. Choi, S. Lee, Y. Joo, T. Kim; Hanyang University Medical Center, Seoul, KOREA, REPUBLIC OF.

Objectives: The purpose of this study was to identify alterations of bone metabolism of the spine in patients with ankylosing spondylitis (AS) by ^{18}F-fluoride PET/CT and to consider its potential role in the assessment of AS. Methods: Thirty-three consecutive AS patients with inflammatory back pain were included in this prospective study. Clinical disease activity was assessed using the Bath AS Disease Activity Index (BASDAI) and the Korean version of the Bath Ankylosing Spondylitis Functional Index (KBASFI). The presence of altered bone metabolism activity on ^{18}F-fluoride PET/CT was assessed in posterior structures of the spine [cervical, thoracic and lumbar facet joints (FJs), costovertebral joints (CVJs), costotransverse joints (CTJs)] and anterior discovertebral units (DVUs) of vertebral body. Clinical disease activity parameters and ^{18}F-fluoride PET/CT findings were compared in patients with different extents of spinal structural changes on radiography as assessed by the modified Stoke AS Spinal Score (mSASSS) [low change : mSASSS (≤9); high change: mSASSS (>9)]. Results: Altered bone metabolism in the posterior structures of the spine on ^{18}F-fluoride PET/CT were found in most of the patients (27/33, 81.8%) and there was no difference between the two subgroups [low mSASSS, 10/12, 83.3% vs. high mSASSS, 16/18, 88.9%, respectively]. Altered bone metabolism in the anterior DVUs was frequently detected in the mid-thoracic spine, especially T4/T5 level, and differed between the subgroups [low mSASSS, 1/12, 8.3% vs. high mSASSS, 11/18, 66.1%]. In the low mSASSS subgroup, the presence of alterations of bone metabolism in posterior structures, especially FJs, was associated with clinical disease activity scores on the BASDAI and/or KBASFI. Conclusions: ^{18}F-fluoride PET/CT provides additional information about

alterations of bone metabolism in the spine compared with currently used methods of identifying anatomical structural changes. Altered bone metabolism on ^{18}F-fluoride PET/CT is frequently seen in posterior structures of the spine even in the patient with low mSASSS. Moreover, in these patients, metabolic abnormality of the FJs is associated with daily clinical problems. In a single session, ^{18}F-fluoride PET/CT could be used to investigate alterations of posterior structures of the spine, including T-spines, which are underestimated by the mSASSS system. We suggest that popularization of ^{18}F-fluoride PET/CT might contribute to the early diagnosis and evaluation of disease activity, especially in AS patients with low mSASSS.

OP259

99mTc-labelled D-Glucosamine Uptake Reflects Disease Activity in Patients with Ankylosing Spondylitis and Rheumatoid Arthritis

S. Angelides, A. Markewycz, N. Manolios, M. Ali, K. Pavic, R. de Costa, B. Camden; Westmead Hospital, Westmead, AUSTRALIA.

Background: Currently, assessment of disease activity in inflammatory arthritic conditions such as rheumatoid arthritis (RA) and ankylosing spondylitis (AS) is suboptimal. Subclinical disease is not infrequently under-estimated. This study evaluated the clinical utility of a novel radiotracer, 99mTc-Glucosamine, in the assessment of disease activity for both RA and AS.Methods: 30 RA patients (11 male, 19 female) and 12 patients with AS (all male) of various stages of disease were recruited into the study. 99mTc-Glucosamine was prepared in-house and patients received 600 MBq intravenously. Whole body and static images were acquired at 15 min and 3 hr later, using a dual-head Siemens Symbia SPECT/CT gamma camera. Images were analysed by a nuclear physician and each joint given a score (0-5) based on the tracer uptake. A similar scoring system was used for bone scans. A clinical score (0-3) was given, based on the number of tender and swollen joints present, by a rheumatologist. An MRI score of 0-5 was given for each imaged joint that was screened. Glucosamine scans were then compared to other routinely used tests, including haematological, biochemical and autoimmune serological parameters, MRI, and bone scans, and correlated with clinical activity.Results: Optimal images were obtained at 3 hr post-injection in all patients. 99mTc-Glucosamine scans were more adept at identifying active disease and differentiating inflammatory manifestations of disease from non-inflammatory causes. In AS patients, active sacro-iliitis was observed in three patients on the 99mTc-Glucosamine scans. In RA, 99mTc-Glucosamine accumulated at all known sites of disease involvement, and was most pronounced in patients with active untreated disease. Using Spearman's correlation co-efficient, there was a positive correlation between glucosamine scan scores, CRP ($p=0.048$) and clinical assessment ($p=0.003$) that was not noted with bone scans.Conclusion. The radiotracer was well tolerated with no adverse events. 99mTc-Glucosamine imaging can detect spinal inflammation in AS, while plain X-rays and MRI were useful in the detection of chronic related changes. Bone scan changes in the SI joints persist longer than those seen on 99mTc-Glucosamine imaging, and thus were less sensitive in tracking changes in the clinical course. With respect to RA, 99mTc-Glucosamine scans correlated well with the clinical evaluation of patients and were superior to bone scans for imaging inflamed joints. Unlike MRI, which is excellent for imaging specific joints, 99mTc-Glucosamine imaging gives a good overall clinical picture of the patient and correlates well with the clinical activity warranting further evaluation.

OP260

Bone SPECT-CT in the diagnosis and management of facial asymmetry due to mandibular condylar hyperplasia

L. Mohamed Salem, **Sr.**, M. Ibañez Ibañez, V. Godoy Bravo, L. Álvarez Nieto, R. Reyes Marles, D. Segarra Fenoll, M. Castellón Sanchez, P. Nicolas Ruiz, L. Frutos Esteban, J. Navarro Fernandez, M. Murcia Durendez, A. Montellano Fenoy, M. Claver Valderas, M. Roldan Rubio, A. Abella Tarazona; Hospital Clínico Universitario Virgen de la Arrixaca, Murcia, SPAIN.

Aim:To assess the value of Bone SPECT-CT, in the diagnosis and management of facial asymmetry, due to mandibular condylar hyperplasia.Materials and methods:Together with the Oral and Maxillofacial Surgery Department of our hospital, we study retrospectively 99 studies belonging to 73 patients with mean age 24.2 years, who underwent a Bone SPECT-CT with Differential Condylar Quantification (DCQ), considering a DCQ $\geq$ 55% suggestive of active condylar hyperplasia (CH), 46 patients had a normal study and 27 had abnormal one, 10 patients of 27 with abnormal study had several follow-up studies with at least a 6 month-interval, and 8 patients of 46 patients with normal studies.Patients with normal study (inactive CH) and with abnormal study who had a normal follow-up study were referred for mandibular osteotomy for the correction of facial asymmetry.Patients with abnormal study and signs of progression of the disease were referred for condylar shave first, then for mandibular osteotomy in a second time.Results:7 of 10 patients with a first abnormal study had a normal follow-up study a second, third or forth study, until

Differential Condylar Quantification drop down to values considered as normal.3 of 10 patients with a first abnormal study had progression of the disease.8 patients with a first normal study had normal follow-up study.3 patients of 10 were referred for condylar shave (30% of patients with abnormal study who had follow-up).Conclusion:Bone SPECT-CT with Differential Condylar Quantification is a sensitive method to exclude active condylar hyperplasia in patients with facial asymmetry.Practicing follow-up Bone SPECT-CT can avoid unnecessary condylar shave in 70% of the patients with active condylar hyperplasia.

OP261

Optimising Quantitative SPECT in Condylar Hyperplasia

D. O. Hall, A. Demmery, J. Kabala; UH Bristol NHS FT, Bristol, UNITED KINGDOM.

Aims: The intensity of uptake in the abnormal condyle in bone SPECT of condylar hyperplasia can be used as a biomarker for disease progression. In our institution, SPECT/CT is used for older teenagers and adults, and SPECT only for younger patients.Studies can be quantified to give additional information. Methods suggested have included % uptake on abnormal side, ratio to clivus, and ratio of abnormal to normal side; previous studies have used 2D analysis and SPECT only, whereas in this study we have considered 3D analysis and SPECT/CT. This study was carried out to determine whether 3D quantification of SPECT bone studies in condylar hyperplasia is affected by using CT Attenuation Correction (CTAC) and by peak or mean count over each condyle.Materials and methods: 13 clinical studies using Tc-99m HMDP SPECT and SPECT/CT carried out in a single institution in 2014 for unilateral condylar hyperplasia were analysed. 10 were SPECT/CT and 3 paediatric studies were SPECT only. All studies were acquired on a Siemens Symbia T16 system. Volumes of Interest at 40% of maximum count were drawn over both condyles and over the Clivus in 3D using Siemens Syngo Volumetric Analysis, and the peak and mean count were recorded. Results were expressed as % of uptake on abnormal side compared with abnormal, ratio to clivus, and ratio of abnormal to unaffected side. Results were compared between CTAC and Non-AC and peak versus mean count.Results and Conclusions: The ratio of peak or mean condylar count to clivus was significantly affected ($p<0.05$) by use of CTAC, so different normal ranges would be needed in each case; this also suggests that this method would not be good for SPECT-only, as the ratio would vary from patient to patient. Measurements of % uptake on each side and ratio of abnormal to normal were not significantly affected by CTAC or use of peak or mean count. However, there were individual differences which might affect results in a particular case, so methods used should be standardised.

OP262

Clinical value of SPECT/CT in the 'unhappy' total knee arthroplasty (TKA)- a prospective study in a consecutive series of 100 painful knees after TKA

M. T. Hirschmann[1,2], H. Rasch[3]; [1]Kantonsspital Baselland (Bruderholz, Liestal, Laufen), Department of Orthopaedic Surgery and Traumatology, Bruderholz, SWITZERLAND, [2]University, Basel, SWITZERLAND, [3]Kantonsspital Baselland (Bruderholz, Liestal, Laufen), Institute of Radiology and Nuclear Medicine, Bruderholz, SWITZERLAND.

Bone SPECT/CT is considered as beneficial in unhappy patients with pain, stiffness or swelling after total knee arthroplasty (TKA). The purpose of this study was to identify typical pattern of bone tracer uptake (BTU) distribution and intensity values in patients after TKA. The above findings were correlated with the type and fixation of TKA, the time from TKA and intraoperative findings at revision surgery. A total of 100 knees of 84 consecutive patients (mean age±SD 70 ±11 years) after TKA with persistent knee pain were prospectively included. All patients underwent clinical examination, standardized radiographs and Tc-99m-HDP-SPECT/CT as part of a routine diagnostic algorithm. The diagnosis before and after SPECT/CT and final treatment were recorded. TKA component position was determined on 3D reconstructed images. Intensity and anatomical distribution of BTU was determined. Maximum intensity values were recorded as well as ratios in relation to the proximal mid-shaft of the femur. Univariate analyses (Chi square test, Pearson correlation, t-test for independent samples) were performed ($p<0.05$). SPECT/CT changed the clinical diagnosis and final treatment in 85/100 (85%) knees. Intraoperative findings confirmed the preoperative SPECT/CT diagnosis in 32/33 knees (97%). TKA loosening as well as progression of patellofemoral OA was correctly diagnosed in 100% of knees. Typical patterns of BTU for specific pathologies were identified. Loose femoral TKA components significantly correlated with increased BTU at the lateral femoral regions ($p<0.05$). Loose tibial TKA components significantly correlated with increased BTU at all tibial regions ($p<0.05$) and around the tibial peg ($p>0.01$). In conclusion, the diagnostic benefits of SPECT/CT in patients after TKA have been proven. Typical pathology related BTU patterns were identified, which will improve reporting quality. Due to the benefits in establishing the correct diagnosis SPECT/CT it should be part of the routine diagnostic algorithm for patients with pain after TKA.

OP263

Multimodality work-up of patients with suspected infected hip prosthesis: radiography, ESR/CRP testing, joint aspiration, and 18F-FDG PET/CT

W. Broos, R. Kwee, J. Geurts, S. Vöö, B. Brans, R. Weijers; Maastricht UMC, Maastricht, NETHERLANDS.

Objective. To investigate the relative contributions of radiography, ESR/CRP testing, hip joint aspiration, and 18F-FDG PET/CT in the work-up of suspected infected hip prosthesis.Methods. In 45 hips of 45 consecutive patients (58% males, mean age 67 years, range 35-82), the relative contributions of radiography, ESR/CRP testing, synovial fluid culture and white blood cell (WBC) count after joint aspiration, and 18F-FDG PET/CT to the diagnosis of periprosthetic joint infection (PJI) were assessed using stepwise multiple regression analysis. Cultures of synovial fluid and periimplant tissues after revision surgery or clinical follow-up ≥6 months served as reference standard.Results. Synovial fluid culture (B=0.4553, standard error (SE)=0.1241, P=0.0011) and 18F-FDG PET/CT (B=0.5340, SE=0.1523, P=0.0017) were independent tests associated with the diagnosis of PJI. Radiography, ESR, serum CRP, and WBC count of synovial fluid were not independent distinguishing tests. When either a positive synovial fluid culture or positive 18F-FDG PET/CT result were considered positive for PJI, a sensitivity of 96.2% (95% confidence interval [CI] 81.1-99.3%) and specificity of 33.3% (95% CI 13.8-60.9%) were yielded. When the combination of both a positive synovial fluid culture and positive 18F-FDG PET/CT result were considered positive for PJI, a sensitivity of 69.6% (95% CI 49.1-84.4%) and specificity of 100% (95% CI 70.1-100%) were yielded.Conclusion. Synovial fluid culture and 18F-FDG PET/CT were found to be the only independent tests associated with the diagnosis of infected hip prosthesis. PJI is very likely when both tests are positive and very unlikely when both tests are negative.

OP264

The evolution of radiologically occult bone metastases detected on FDG-PET/CT

P. Martineau, M. Pelletier-Galarneau, X. Pham, A. Sheikh; The Ottawa Hospital, Ottawa, ON, CANADA.

Background: FDG-PET/CT is widely used for the staging of malignancies. Occasionally, focal FDG uptake within bone or bone marrow is present on the PET component of the exam without corroborative findings on the co-registered CT. Such findings often requires biopsy, further characterization with MRI, or followup imaging to elucidate their true significance.Methods: We reviewed all FDG-PET/CT reports from our institution dated between 9/1/2012 and 4/2/2015 (N=4280) and identified all patients with focal bone uptake without corroborative findings on the co-registered CT (N=75, 1.8%). For these patients, follow-up imaging was reviewed in order to determine the nature of the PET finding.Results: A total of 89 lesions in 75 patients were identified as 'suspicious for early osseous metastases' due to focal FDG uptake and absence of corroborative findings on the co-registered CT. The mean SUV of these lesions was 4.6 (range 1.5-22.5). 32 (43%) of these patients had followup imaging allowing for reassessment of the lesion site at multiple time points. Of these, 20 (63%) subsequently developed osseous metastases visible on conventional imaging, with aggressive lesions visible on CT (n=11), MRI (n=7), PET-CT (n=1), and plain film (n=1) an average of 160, 88, 39, 812, and 88 days, respectively, following the initial staging PET-CT. The mean SUV of these lesions was 5.6 (range 2.2-22.5). Of the remaining 12 patients, no aggressive osseous lesions were visible on followup MRI (n=1) at 75 days or on CT (n=11) an average of 417 days (range 229-597) following the PET. The mean SUV of these lesions was 3.6 (range 1.5-6.4).Conclusion:Our results show that the majority (63%) of our patients with suspected early osseous metastases developed disease which eventually became visible on conventional imaging; however, a significant portion (37%) of patients with suspected osseous lesions failed to develop radiologically apparent disease. Whether this was due to false-positive PET, false-negative CT/MRI findings, response to treatment or a combination of these factors is unclear. Lesions which became apparent on followup imaging generally had higher SUVs; however, significant overlap in the range of SUVs of those lesions which become apparent and those that remain occult limits the predictive power of SUV in this context. Our findings are of particular significance to those institutions which use PET for initial staging, but perform follow-up with conventional imaging. Our results suggest that, in cases of 'early osseous metastases', corroboration with MRI or biopsy is strongly recommended to ensure proper staging.

YE2 - Monday, October 12, 2015, 1:00 PM - 2:30 PM, Hall 8
Young EANM Daily Forum 2: Career Speed Date

OP264b
Meet the Experts

C. Decristoforo, **AUSTRIA**
M. Hofman, **AUSTRALIA**
D. Delbeke, **USA**
F. Jamar, **BELGIUM**

901 - Monday, October 12, 2015, 2:30 PM - 4:00 PM, Hall 1
CME 7 - Physics & Paediatrics: Radiation Protection

OP265
The New European BSS and its Implications in Nuclear Medicine
G. O'Reilly, IRELAND

OP266
Individual Justification in Paediatrics – from Concepts to Practice
A. I. Santos, PORTUGAL

OP267
Dose Optimisation in Paediatric Nuclear Medicine
F. Fahey, USA

OP268
Radiation Protection Issues in Therapy with Lu-177, Y-90 and Ra-223
S. Holm, DENMARK

902 - Monday, October 12, 2015, 2:30 PM - 4:00 PM, Hall 2
Joint Symposium 7: EANM/EACVI/ESC: New Clinical Guidelines on Infectious Endocarditis and CIED Infections

OP269
Infective Endocarditis; the Clinical Problem and Needs
J. M. Miro, SPAIN

OP270
Imaging Infective Endocarditis: How Molecular Imaging got into our Clinical Guidelines
P.A. Erba, ITALY

OP271
New Guidelines on the Management of Infective Endocarditis
G. Habib, FRANCE

903 - Monday, October 12, 2015, 2:30 PM - 4:00 PM, Hall 4
CTE 3 - Interactive: Comprehensive PET/MRI Practice

OP272
MR Basics and Clinical Applications
J. Graessner, GERMANY

OP273
MR/PET: Technical Challenges and Clinical Applications
V. Diehl, GERMANY

OP274
Clinical PET/MR – Where Are We after Five Years?
A. Beer, GERMANY

904 - Monday, October 12, 2015, 2:30 PM - 4:00 PM, Hall G1
Committee Symposium - Neuroimaging: Counteracting Dementia: Imaging Evidence for Cognitive and Brain Reserve

OP274b
Relevance of Brain Reserve for Clinical Nuclear Neurology
S. Morbelli, ITALY

OP274c
Brain Structural and Functional Correlates of Reserve Across Different Dementias
R. Pernecky, UK

OP274d
Multimodal Neuroimaging Correlates of Reserve from Cognitively Normal Older Adults to Alhzheimer's Disease
E.M. Arenaza-Urquijo

905 - Monday, October 905 - Monday, October 12, 2015, 2:30 PM - 4:00 PM, Hall G2

Do.MoRe: Radiobiology - Molecular Radiotherapy

OP275

Novel treatment strategy for glioblastomas using Auger-electron therapy and concomitant chemotherapy - in vitro studies

A. Therkelsen[1], B. B. Olsen[1], B. Halle[2], P. Høilund-Carlsen[1], H. Thisgaard[1]; [1]Department of Nuclear Medicine, Odense University Hospital, Odense, DENMARK, [2]Department of Neurosurgery, Odense University Hospital, Odense, DENMARK.

Introduction: Glioblastomas (GBM) remains non-curable by conventional treatment strategies. Due to their infiltrative growth, complete resection is not possible and chemo- and radiotherapy are dose limited. A promising treatment strategy is convection-enhanced delivery of the Auger-electron-emitting thymidine analog [125I]5-Iodo-2'-deoxyuridine (125I-UdR) into the tumor site of the brain. By combining this therapeutic approach with concomitant thymidylate synthetase-inhibition of the GBM cells, a further increase of the therapeutic effect can be expected due to an increased DNA-incorporation of 125I in the tumor cells (1). Using viability- and radioactivity uptake assays to analyze a patient-derived GBM cell line in vitro we aimed to elucidate the individual and combined effects of exposure to the therapeutic components: Thymidylate synthetase-inhibition using methotrexate (MTX) or 5-fluoro-2'-deoxyuridine (F-UdR), Auger-electron-therapy using 125I-UdR, and the currently clinically used first-line chemotherapeutic agent temozolomide (TMZ).Material and methods: The human derived cell line T87 was used in all assays and cultured as spheroids in serum free medium. Cellular 125I-UdR uptake assays were performed after a 4 hour co-incubation with 18.5 kBq/mL 125I-UdR and various concentrations of MTX or F-UdR. CellTiter-Blue assays were used to determine cell viability after incubation with 125I-UdR, MTX/F-UdR, and TMZ for 7 days.Results: Radioactivity uptake assays showed that F-UdR was more potent than MTX to increase the uptake of 125I-UdR in the GBM cells. Cells treated with 1 nM F-UdR incorporated 1.8-fold more 125I-UdR than cells treated with 1 nM MTX and cells treated with 125I-UdR alone. A 1000 fold higher MTX concentration, i.e., 1 μM was required to achieve the same increase in 125I-UdR uptake as found using F-UdR. Viability assays showed no viable GBM cells after exposure to 0.01 μM or more MTX/F-UdR for 7 days, demonstrating the toxic effects of these compounds. Exposure to TMZ and 125I-UdR alone showed therapeutic effects with IC50 values of 206 μM (198-214 μM) and 109 Bq/mL (99-120 Bq/mL), respectively. By combining TMZ and 125I-UdR a further decrease in GBM cell viability was found, but no sign of synergy between the two compounds was observed.Conclusion: Concomitant F-UdR resulted in a high increase of 125I-UdR uptake in the GBM cells and at much lower doses than MTX. Exposure to TMZ and 125I-UdR showed strong therapeutic effects, albeit without signs of synergy between the two compounds.References: (1) Kassis et al: Acta Oncol. 2000;39(6):731-7.

OP276

The effects of dose-rate on radiation induced platelet toxicity in internal radiotherapy.

J. Rousseau[1], S. Becavin[1], F. Nguyen[1], N. Sas[1], M. Magnen[1], M. Bourgeois[2,3,4], M. Meckel[5], F. Roesch[5], N. Chouin[6,4]; [1]LUNAM Université, Oniris, "AMaROC", Nantes, FRANCE, [2]CRCNA, INSERM, Université de Nantes, UMR_S 892, Nantes, FRANCE, [3]ARRONAX cyclotron, Saint Herblain, FRANCE, [4]CHU Nantes, Nuclear medicine department, Nantes, FRANCE, [5]Institute of Nuclear Chemistry, Johannes-Gutenberg-University Mainz, Mainz, GERMANY, [6]LUNAM Université, Oniris,, Nantes, FRANCE.

Aim: We investigated the impact of bone marrow (BM) dose-rate variations on mouse thrombopoïesis in a context of internal radiotherapy. Material and Methods: Mice were injected with osteotropic agents: 18F-Na (37-60MBq) or bisphosphonates (BP) labelled either with 64Cu (15-50MBq) or 90Y (0.8-4.9MBq). Biodistributions were determined by counter measurements and cumulated activities within bones were calculated. Dosimetry was performed using a representative mouse CT image integrated into GATE. Absorbed doses were determined for the entire BM or the femur one. Hematological toxicity was monitored via platelet counts over time after injection. BM toxicity was assessed by femur histology and via progenitor colony assays. Experimental data were compared to simulations of a thrombopoïesis compartmental model previously published. It is based on the linear-quadradric model and considers kinetics of BM cell proliferation, differentiation and radiosensitivities.Results: For each radiopharmaceutical, dose-effect relationships on depletion and recovery were demonstrated for BM cells and platelets. Irradiation dose-rates were different for the three radionuclides as 98% of the absorbed dose was deposited in 0.5, 3 and 15 days for 18F-Na, 64Cu-BP and 90Y-BP. A same absorbed dose to the BM of 4.3±0.3 Gy lead to depletions of 65% for 18F-Na and 64Cu-BP versus 40% for 90Y-BP between 7 and 10 days post-injection. Platelet kinetics and depletions were very similar for mean absorbed doses around 4.5±0.3 Gy of 18F-Na or 64Cu-BP and 14.2±2.7 Gy of 90Y-BP.Same dose-rate effects were noticed for the BM cells and the hematopoietic progenitor depletions. Similar progenitor depletions (86-88%) were observed following absorbed doses delivered to the BM of 1.6±0.3 Gy for 18F-Na or 64Cu-BP and 5.5±0.5 Gy for 90Y-BP. Progenitor kinetics were also different: a faster but incomplete recovery (even at

day 46) was observed following a 90Y-BP irradiation whereas the recovery was complete at day 21 for 18F-Na and 64Cu-BP.The compartmental model predicted platelet kinetics and depletions for the three radiopharmaceuticals except for higher doses of 90Y-BP. Despite the simulated decrease of progenitors radiosensitivity in the case of the protracted 90Y irradiation, the model was still unable to accurately predict platelet kinetics or the fastest progenitor recovery. These results highlighted the possibility of a radiobiological process which is not considered in the compartmental model in addition to dose-rate effects.ConclusionWe experimentally demonstrated a significant impact of the dose-rate on BM cells and platelets. A potential adaptive biological process during the Y90 long-lasted irradiation could be involved in this effect.

OP277

Different DNA Damage Repair Rates in Blood Lymphocytes after Peptide Receptor Radionuclide Therapy and Radioiodine Therapy of Thyroid Cancer

U. Eberlein[1], C. Nowak[2], C. Lapa[1], C. Bluemel[1], M. Peper[2], R. A. Werner[1], A. K. Buck[1], H. Scherthan[2], M. Lassmann[1]; [1]Department of Nuclear Medicine, University of Würzburg, Würzburg, GERMANY, [2]Bundeswehr Institute of Radiobiology affil. to the Univ. of Ulm, Munich, GERMANY.

Objectives: Radiation-induced DNA double strand breaks (DSBs) cause, in their vicinity, the phosphorylation of the histone H2AX (then called γ-H2AX) and the accumulation of the 53BP1 protein that binds to and signals damaged chromatin at a DSB site. This leads to the formation of microscopically visible nuclear foci containing both markers, which thus mark radiation-induced DSBs. The aim of the study is to describe the time course of DNA damage in blood lymphocytes in molecular radiotherapy after internal irradiation with I-131 and Lu-177. Methods: We investigated blood samples of patients either after their first peptide receptor radionuclide therapy (PRRT) or their first radioiodine therapy (RIT) of differentiated thyroid cancer (DTC). The average frequencies of radiation-induced foci (RIF) containing both γ-H2AX and 53BP1 fluorescence were determined in the nuclei of two-colour immunostained γ-H2AX/53BP1 lymphocytes isolated from peripheral blood samples of patients before and after molecular radiotherapy (MRT). The foci containing both DSB markers were scored manually in a fluorescence microscope equipped with a red/green double-band-pass filter by an experienced observer. The individual background focus rate was determined in a sample taken prior to therapy. The EANM SOP for DTC was followed to determine the absorbed dose to the blood. The number of RIF as a function of time was described by combining a linear dose-dependent increase with a multi-exponential function characterizing different rates of DNA repair. Results: 283 blood samples (at least 6 per patient) of 36 patients (PRRT: 16, RIT: 20) up to 168h after therapy were evaluated. At late time points (10-12h) after therapy the decay of the average RIF number per cell is best described by a mono-exponential decay function with a decay constant of 0.04h-1. When the absorbed dose to the blood exceeded 20mGy in the first hour, only seen in patients with DTC, we observed the on-set of a fast repair component with a fast decay rate of 0.33h-1 resulting in a bi-exponential decay function. Conclusions: This analysis provides a comprehensive description of the time course of the number of radiation-induced DNA damage foci after molecular radiotherapy of beta emitters. It furthermore reveals a threshold dose for the induction of a fast repair component after in vivo DSB induction by incorporated I-131.

OP278

Impact of Bi-Exponential Repair Kinetics of Sub-lethal Damage on the Relative Effectiveness in Molecular Radiotherapy

A. Malaroda[1], A. J. Green[2], A. B. Rosenfeld[1]; [1]University of Wollongong, Wollongong, AUSTRALIA, [2]National Physical Laboratory, Teddington, UNITED KINGDOM.

AIMS: In Molecular Radiotherapy, the rate of production of sub-lethal lesions competes with the rate of their repair, moreover each type of lesion is characterised by their specific production and repair rates. For example, there is evidence that the repair kinetics in mouse kidney cells is at least bi-exponential, with a fast (<1 h) and a slow (>2h) component. The aim of this study was to compare the impact on the Relative Effectiveness, and by extension on the Biologically Equivalent Dose (BED), of bi-exponential repair kinetics with respect to the widely accepted mono-exponential repair rate. METHODS: The Linear Quadratic model takes the repair rate of sub-lethal lesions into account through the Lea-Catcheside time protraction factor. Thus, Lea-Catcheside factor (G) and Relative Effectiveness (RE) were calculated for a bi-exponential repair rate of constants 0.15 h (fast) and 5.03 h (slow), data published in the literature for mouse kidney cells. Partition coefficients, for the fast and slow components respectively, of [0.5,0.5], [0.25,0.75], [0.75, 0.25], [0.9,0.1], [0.1,0.9] were considered. Mono-exponential dose-rate was assumed with effective decay rates ranging between 0.001 and 5 h^{-1} (i.e. $0.13 < T_{1/2} < 693$ h). Effective Lea-Catchised factors (G_{eff}) and Relative Effectiveness (RE_{eff}), explicitly accounting for the bi-exponential repair rates, were calculated. These were then compared to G_{mean} and RE_{mean} factors calculated using a mean repair rate for each pair of partition coefficients; the mean repair rate representing the global

repair rate used when a mono-exponential repair rate kinetic is assumed. Comparison was carried out by calculating the percentage difference between G_{eff} and G_{mean} and between RE_{eff} and RE_{mean}. RESULTS: The mean repair constants ranged between 0.17 and 1.18 h, depending on the partition coefficients. When the percentage differences were considered, these were equivalent for the Lea-Catcheside factors and the Relative Effectiveness and depended only on the repair rates, their partition coefficients and the effective half-lives: for all the partition coefficients, a percentage difference greater than 50% was observed for effective half-lives greater than 5 h. As a function of the effective decay rate, the lowest percentage difference was observed when the fast repair constant was dominant (partition coefficient [0.9, 0.1]). CONCLUSIONS: Under the assumptions of this study, the mean value of the individual repair constants of each sub-lethal lesions repair mechanism led to an underestimation of the RE, and therefore of the BED, up to 50% for clinically relevant effective half-lives ($T_{1/2}$ > 5 h).

OP279

Terbium-161 a Promising Radionuclide for the Irradiation of Tumor Cells and Micrometastases: Monte Carlo Dose Assessment using CELLDOSE

E. Hindie[1], M. A. Quinto[2], P. Zanotti-Fregonara[1], C. Morgat[1], C. Champion[2]; [1]CHU Bordeaux - University of Bordeaux - UMR 5287, Bordeaux, FRANCE, [2]Université de Bordeaux, CNRS/IN2P3, Centre d'Etudes Nucléaires de Bordeaux Gradignan (CENBG), Gradignan, FRANCE.

AIM: Radiopharmaceutical therapy, traditionally limited to the treatment of advanced metastatic disease, is now being considered in earlier settings to destroy minimal residual disease or occult micrometastases. The current study compares the effectiveness of ^{161}Tb, ^{177}Lu and ^{111}In to irradiate micrometastases. ^{161}Tb and ^{177}Lu associate a medium-energy β^- emission with various conversion and Auger electrons. They also have a small photon component which allows imaging. By contrast, ^{111}In is a γ-isotope for imaging that emits conversion and Auger electrons potentially helpful for therapy. METHODS: Electron dose was assessed in spheres of various sizes (from a 10-mm metastasis to a 10-μm single cell) with the Monte Carlo code CELLDOSE. The spheres were uniformly labeled with ^{161}Tb, ^{177}Lu or ^{111}In. Doses were compared for a fixed amount of energy released per unit volume (1 MeV per μm^3). The dose contribution from photons was neglected. RESULTS: In a 10-mm metastasis, the three isotopes exhibited equivalent dose deposit after normalization (1 MeV released per μm^3). This dose was 154 Gy for ^{161}Tb, 152 Gy for ^{177}Lu and 155 Gy for ^{111}In. However, for smaller micrometastases (<500μm), ^{161}Tb and ^{111}In were more effective than ^{177}Lu. For instance, in a 50-μm micrometastasis, the dose was 31 Gy for both ^{161}Tb and ^{111}In *vs*. 13.6 Gy for ^{177}Lu. In this 50-μm metastasis, conversion and Auger electrons were responsible for 75% of the dose from ^{161}Tb and for 20% of the dose from ^{177}Lu. A specific advantage of ^{111}In emerged only for single cells. In a cell of 10-μm diameter, doses from ^{111}In, ^{161}Tb and ^{177}Lu were 20.7 Gy, 11.5 Gy and 3.5 Gy, respectively. CONCLUSION: Choosing the appropriate isotope is fundamental to achieve an effective irradiation of micrometastases. Our study shows a selective advantage of ^{161}Tb over ^{177}Lu, especially for metastases <500μm, resulting from an emission spectrum rich in low-energy conversion and Auger electrons. ^{111}In appears advantageous for killing single-cells, but has the drawback of having a larger fraction of photon emission compared to ^{161}Tb.

OP280

Alpha radioimmunotherapy using 213Bi-anti MISRII mAb in ovarian cancer

R. LADJOHOUNLOU, Jr.[1,2,3], A. PICHARD[1,2,3], V. BOUDOUSQ[1,2,3], N. CHOUIN[4], F. BRUCHERTSEIFER[5], A. MORGENSTERN[5], I. Navarro-Teulon[1,2,3], J. Pouget[1,2,3]; [1]Inserm U1194, MONTPELLIER, FRANCE, [2]IRCM, Institut de Recherche en Cancérologie de Montpellier, Montpellier, FRANCE, [3]Université de Montpellier, Montpellier, F-34090,, Montpellier, FRANCE, [4]AMAROC, ONIRIS, NANTES, FRANCE, [5]European Commission, Joint Research Centre, Institute for Transuranium Elements, Karlsruhe, GERMANY.

Hypothesis: We assessed in vitro the therapeutic efficacy of the newly developed anti-MISRII mAbs (16F12 and 12G4) labeled with 213Bi in the therapy of ovarian cancer. In vivo, we explored their potential use during brief intraperitoneal radioimmunoptherapy (BIP-RIT). Methods: In vitro, clonogenic survival of SK-OV-3 cells expressing MISRII receptor were evaluated. Briefly, SK-OV-3 cells (donor cells) were incubated for 90 min with increasing activities (0-0.5MBq/mL) of anti MISRII 213Bi-16F12, 213Bi-12G4 mAbs or irrelevant 213Bi-Rituximab. We used the standard medium transfer protocol between donor cells and recipient cells (grown in non-radioactive medium previously incubated for 2h with donor cells) to evaluate bystander cytotoxic effects.

Uptake of radioactivity per cell together with appropriate cellular S-values were determined for absorbed dose assessment. Radiation-induced biological effects were measured in both donor and recipient cells as the yield of DNA double strand breaks (DSBs) through immunofluorescent detection of gamma-H2AX and 53BP1. In vivo we assessed in nude mice bearing intraperitoneal 2-3 mm SK-OV-3 MSIRII tumors nodules the biodistribution of radiolabeled antibodies (IP-RIT, 0-2.96MBq; 37MBq/mg) or BIP-RIT (5.5-12.9MBq; 37MBq/mg). BIP-RIT consisted of intraperitoneal injection of radiolabeled mAbs followed by washing of the peritoneal xenograft cavity with saline solution. After, the biodistribution of radiolabeled antibodies was investigated after IP and BIP-RIT. Results: In vitro we showed the strong efficacy of 213Bi-12G4 and 213Bi-16F12 mAbs. Bystander cytotoxicity was measured in all recipient cells for the three radiolabeled mAbs. In agreement with DNA DSBs formation, uptake of radioactivity by donor cells was shown to be higher for 213Bi-16F12 than for 213Bi-12G4. DNA DSBs yield was lower in recipient cells and preliminary results indicate that their complexity might be lower than the one measured in donor cells. In vivo, maximum tolerated activity of 213Bi-16F12 was about 2.9MBq and 12.9MBq after IP-RIT and BIP-RIT, respectively. Moderate hematological toxicity was observed in groups treated with the highest amount of activity. Biodistribution studies indicated that the tumor-blood uptake ratio was 1.4 and 6.3 one hour after IP and BIP-RIT, respectively. This ratio was decreased to 0.2 and 3.7, three hours post treatment, respectively. Therapeutic efficacy of 213Bi-12G4 and 213Bi-16F12 mAbs after IP-RIT and BIP-RIT is ongoing. Conclusions: In vitro, we showed the strong therapeutic efficacy of anti-MISRII 213Bi-16F12 mAb against ovarian cancer cells. We also showed that bystander effects were involved. In vivo, the feasibility of BIP-RIT using high activities of 213Bi-mAbs was demonstrated. We are now assessing its therapeutic efficacy using 213Bi-16F12.

OP281

Monte Carlo evaluation of Auger-electron emitting radionuclides in 3-D cellular models

N. Falzone[1,2], S. Able[1], S. Terry[1], J. M. Fernández-Varea[3], K. A. Vallis[1]; [1]University of Oxford, Oxford, UNITED KINGDOM, [2]Tshwane University of Technology, Department of Biomedical Science, Pretoria, SOUTH AFRICA, [3]Universitat de Barcelona, Facultat de Física (ECM and ICC), Barcelona, SPAIN.

Aim Auger-electron emitting radionuclides are ideal molecularly targeted radiotherapeutic (mTRT) agents when treating disseminated cancer cells and micro-metastasis. In the present study we evaluate the spatial distribution as well as clonogenic survival (SF) of two mTRT strategies in an in-vitro based 3-D tumour spheroid model; ^{111}In-DTPA-hEGF (a peptide targeting the epidermal growth factor-EGF) and ^{111}In-Trastuzumab (an antibody directed against the human epidermal growth factor receptor-2, HER2/neu). This information is then used to validate Monte Carlo (MC) simulations of a close packed 3-D cellular model in predicting tumour control probability (TCP). Materials and Methods Spheroids were formed from three tumour cell lines, MDA-MB-468 and MDA-MB-231/H2N breast cancer and SQ20B head/neck cancer cells, using a hanging droplet method. Spheroids were treated with ^{111}In-DTPA-hEGF (8 MBq/μg, 40 nM), and ^{111}In-Trastuzumab (6 MBq/μg; 10 nM) and evaluated 1 h and 24 h after treatment. SF was determined using a clonogenic assay and distribution was evaluated by cellular fractionation and micro-autoradiographic (MAR) staining of spheroid sections. The 3-D spheroid models were generated by a closed packed algorithm and MC software, PENELOPE was used to model radiation transport. Results Clonogenic survival correlated with radionuclide penetration, with the smallest SF noted in cell lines expressing the highest number of receptors; for EGFR targeting with ^{111}In-DTPA-EGF, the least survival was noted in MDA-MB-468 spheroids, while the lowest SF was noted in MDA-MB-231/H2N spheroids treated with ^{111}In-Trastuzumab. SQ20B form very tightly packed spheroids and although expressing a high number of EGFR, it showed little radionuclide penetration and corresponding greater survival. MAR staining showed two distinct spatial distribution patterns, i.e. outer rim of activity (1 h post treatment) or uniform distribution (24 h post treatment). TCP depended strongly on spatial distribution of the radionuclides, with uniformly distributed radionuclides achieving TCP1. Conclusion Tumour spheroids offer a viable model for investigating the penetration and spatial distribution of radiolabelled probes in tumour cells. Data was employed to inform mathematical modelling, in order to be able to use in silico methods to simulate drug distribution in tumour cells.

OP282

Potential radioprotectors and radiosensitizers in neuroendocrine tumor cells

S. Exner[1], S. Poenick[1], V. Prasad[2], **C. Grötzinger**[1]; [1]Charité - Universitätsmedizin Berlin, Gastroenterology, Berlin, GERMANY, [2]Charité - Universitätsmedizin Berlin, Nuclear Medicine, Berlin, GERMANY.

Aim: Neuroendocrine tumors (NETs) express somatostatin receptors that are currently utilized for diagnostic and therapeutic approaches. For peptide receptor radionuclide therapy (PRRT), somatostatin analogs like octreotide, are coupled to radionuclids like yttrium 90 or lutetium 177,

which after injection are bound and taken up specifically by NETs. PRRT can deliver radiation doses of up to 250 Gy to the tumors. Nevertheless, complete remission is extremely rare, compared to similar radiotherapies for thyroid cancer and non-Hodgkin lymphoma. One hypothesis potentially explaining the discrepancies between expected result and observed outcome of PRRT might be that somatostatin analogs induce a G1 arrest in NET cells, thereby making them radioresistant. Materials and Methods: To investigate this, NET cell lines were incubated with or without agonists and exposed to different radiation doses from a 137Cs source between 0 and 50 Gy. Cells were harvested at distinct timepoints, stained with propidium iodine and the cell cycle distribution was assessed by FACS analysis. Results: Initially, the somatostatin receptor expression (SSTR1-5) of five neuroendocrine tumour cell lines (BON, H727, QGP-1, LCC18, UMC11) was analyzed by quantitative real time PCR to assess the cell specific expression patterns of the different receptor subtypes. In radiation experiments all of five tested NET cell lines showed a radiation-induced decline in G1 cells as well as a G2/M arrest. Also, the percentage of apoptotic cells in sub-G1 phase increased time- and dose-dependently. Pretreatment with a potential G1 inhibitor resulted not only in an expected G1 arrest but also in a decrease of radiation-induced G2/M arrest. Moreover, a reduction of cells in sub-G1 was observed in two of five cell lines. In contrast, the combination of octreotide treatment with radiation showed no difference compared to radiation alone, not supporting the initial hypothesis. Conclusion: Further experiments are needed to better understand the influence of somatostatin agonists and other intrinsic or extrinsic factors on neuroendocrine tumor cells to pave the way for a significant increase in the overall therapeutic efficacy of PRRT.

906 - Monday, October 12, 2015, 2:30 PM - 4:00 PM, Hall 6
M2M: Radiopharmaceuticals & Radiochemistry: Radiotracers - Brain

OP283

Pharmacokinetic analysis of [11C]PBR28 in the rat model of herpes encephalitis: comparison with (R)-[11C]PK11195 for pre-clinical imaging

P. Kopschina Feltes[1], A. Parente[1], D. Vállez Garcia[1], J. W. A. Sijbesma[1], C. M. Moriguchi Jeckel[2], R. A. J. O. Dierckx[1], E. F. J. de Vries[1], J. Doorduin[1]; [1]University of Groningen, Groningen, NETHERLANDS, [2]Pontifícia Universidade Católica do Rio Grande do Sul, Porto Alegre, BRAZIL.

Aim: [^{11}C]PBR28 is a second generation translocator protein (TSPO) ligand with supposedly better imaging characteristics than the most commonly used tracer [^{11}C]PK11195. Surprisingly, only limited studies have evaluated the pharmacokinetic and binding profile of [^{11}C]PBR28 in neuroinflammatory models in rodents. For this reason, [^{11}C]PBR28 was evaluated and compared to [^{11}C]PK11195 for the detection and quantification of neuroinflammation for pre-clinical research. Materials and methods: Herpes simplex encephalitis (HSE) was induced in male Wistar rats by intranasal inoculation of the herpes simplex type-1 virus, resulting in neuroinflammation. At 6-7 days post inoculation, 60-min dynamic [^{11}C]PBR28 or [^{11}C]PK11195 PET scans were performed. During the scans arterial blood samples were taken to generate blood and metabolite-corrected plasma input curves for pharmacokinetic modeling. Differences between control and HSE rats were assessed by voxel-based analysis, using standardized uptake values, and volume-of-interest analysis, using the reversible two-tissue compartment model to determine the binding potential (BP_{ND}). Results: Voxel-based analysis showed that [^{11}C]PBR28 was able to detect overexpression of TSPO in brain areas that are known to be affected in the HSE rat model. [^{11}C]PBR28 had a faster metabolism than [^{11}C]PK11195, with 50% of metabolites in plasma present at 5 min and 21 min, respectively. [^{11}C]PBR28 demonstrated a higher sensitivity than [^{11}C]PK11195 in the detection of neuroinflammation. The BP_{ND} of [^{11}C]PBR28 was significantly higher ($p<0.05$) in the medulla (150%), pons (121%), midbrain (94%), thalamus (76%), hippocampus (65%), hypothalamus (44%) and cerebellum (37%) of HSE rats when compared to control rats, while a higher BP_{ND} of [^{11}C]PK11195 was only found in the medulla (59%). Comparison of BP_{ND} between control groups showed no statistical difference, suggesting that non-specific binding of both tracers is similar. Conclusion: [^{11}C]PBR28 performed better than [^{11}C]PK11195 in the detection of TSPO overexpression in the HSE rat model, as the BP_{ND} was found to be increased in more brain regions. The results of this study suggest that [^{11}C]PBR28 is a better tool for pre-clinical research of neuroinflammation.

OP284

Radiosynthesis and fundamental evaluation of (R)-[11C] emopamil as a novel tracer for imaging enhanced P-glycoprotein function in the brain

J. Toyohara[1], M. Okamoto[1,2], H. Aramaki[2], Y. Zaitsu[2], I. Shimizu[2], S. Hosokawa[2], K. Ishiwata[1]; [1]Tokyo Metropolitan Institute of Gerontology, Tokyo, JAPAN, [2]Waseda University, Tokyo, JAPAN.

Aim: A number of substrate for P-glycoprotein (P-gp), such as [11C]verapamil ([11C]VER), was developed for imaging P-gp function with positron emission tomography (PET). These substrates can measure decreased function of P-gp as an increased uptake of tissue radioactivity. However, it would likely not be able to measure enhanced P-gp function, because base-line tissue radioactivity is already at most immeasurable. Emopamil (EMP) is a calcium channel blocker of the phenylalkylamine class, having high blood-brain barrier permeability and weak substrate properties for P-gp. These properties would be suitable for measuring enhanced P-gp function in the brain. The purpose of this study is to synthesize (R)- and (S)-[11C]EMP and to characterize their properties as a P-gp tracer. Materials and Methods: The EMP includes a chiral quaternary carbon centre, and a previous research has indicated that the optical isomers differ significantly in their biological effects. Therefore, we first synthesized (R)- and (S)-[11C]EMP and compared their biodistribution, peripheral metabolism, and effects of P-gp inhibitor cyclosporine A (CysA). Then, we compared the brain pharmacokinetics of (R)-[11C]EMP and (R)-[11C]VER in base line and CysA pre-treatment with small animal PET. Results and conclusion: (R)- and (S)-[11C]EMP were synthesized from (R)- and (S)-noremopamil, respectively, by methylation with [11C]methyl triflate in the presence of NaOH at room temperature. The yield of (R)- and (S)-[11C]EMP was approximately 30%. The specific activity of (R)- and (S)-[11C]EMP was >74 GBq/μmol and radiochemical purity was >99%. The biodistribution of (R)- and (S)-[11C]EMP in ddY mice demonstrated a significantly higher uptake of (R)-[11C]EMP in the brain. The regional brain distribution of (R)- and (S)-[11C]EMP were homogeneous and no stereo-selective. (R)- and (S)-[11C]EMP were rapidly metabolized to hydrophilic metabolite. Unchanged form of (S)-[11C]EMP (39%) was significantly lower than that of (R)-[11C]EMP (46%) at 15 min after injection in plasma. In contrast, over 88% of radioactivity in the brain was intact and no stereo-selective. CysA pre-treatment increased brain activity approximately 3-fold, however, no stereo-selective. Since (R)-[11C]EMP was metabolized less than that of (S)-[11C]EMP, (R)-enantiomer was further evaluated with small animal PET. The base line area-under-the-curve (AUC) of brain radioactivity (0-60 min) of (R)-[11C]EMP was 2-fold higher than that of (R)-[11C]VER, but its AUC after CysA pre-treatment was comparable to that of CysA pre-treated (R)-[11C]VER. In conclusion, (R)-[11C]EMP can be used as a novel tracer for imaging P-gp function with a higher base line uptake than (R)-[11C]VER.

OP285

Discovery of a Fluorinated 4-Oxo-Quinoline Derivative as a Potential PET Radiotracer for Targeting CB2 Receptor

L. Mu[1], R. Slavik[2], A. Herde Müller[2], S. D. Krämer[2], M. Weber[3], R. Schibli[2], S. Ametamey[2]; [1]UniversitätsSpital Zürich, ZURICH, SWITZERLAND, [2]ETH Zurich, ZURICH, SWITZERLAND, [3]Kantonsspital St. Gallen, ZURICH, SWITZERLAND.

Objectives: The cannabinoid receptor type 2 (CB2) is part of the endocannabinoid system and has gained growing attention in recent years due to its important role in neuroinflammatory/neurodegenerative diseases [1, 2].The PET imaging of CB2 has so far been unsuccessful. Recently, we reported on a carbon-11 labeled 4-oxo-quinoline derivative, designated RS-016 [3], as a promising radiotracer for imaging CB2. In this report, three fluorinated analogues of RS-016 were designed, synthesized and evaluated for their utility as imaging agents for the CB2. Methods: Three fluorinated analogues of RS-016 namely RS-030, RS-122 and RS-126 were synthesized using a multi-step reaction sequence and their binding affinities towards CB2 were determined using [^{3}H]-CP-55, 940. The most potent compound, RS-126 ((N-(1-adamantyl)-1-(2-(2-fluoroethoxy)ethyl)-8-methoxy-4-oxo-1,4-dihydroquinoline-3-carboxamide), was radiolabeled with fluorine-18 and further evaluated in autoradiographic studies, biodistribution experiments and metabolic studies. Results: The syntheses of RS-030, RS-122 and RS-126 were accomplished in overall chemical yields of 30%, 16% and 6%, respectively and their binding affinities (Ki values) towards CB2 ranged from 72-1.2 nM. RS-126 exhibited the highest binding affinity and selectivity towards CB2. [^{18}F]RS-126 was obtained in ≥ 99% radiochemical purity with a specific radioactivity of 98 ± 44 GBq/μmol (n = 15) at the end of synthesis. The logD7.4 value was 1.99 and in vitro autoradiographic studies with CB2-positive rat spleen tissue revealed high and displaceable binding. [^{18}F]RS-126 was stable in vitro in rat and human plasma over 120 min, whereas 55% intact parent compound was found in vivo in rat blood plasma at 15 min p.i.. Biodistribution studies confirmed accumulation of [^{18}F]RS-126 in rat spleen with a specificity of 79% under blocking conditions. Conclusion: The fluorinated CB2 radioligand, [^{18}F]RS-126, demonstrated high specificity towards CB2 receptor in vitro and in vivo and is potentially a promising ligand for imaging CB2 receptor expression. References: 1. Di Marzo, V. (2009). *Pharmacological Research* 60:77-84 2. Pertwee, R.G. (2009). *Br J Pharmacol* 156:397-411 3. Slavik, R., Herde, A.M., Bieri, D., Weber, M., Schibli, R., Krämer, S.D., Ametamey, S.M., and Mu, L. (2015). *Eur J Med Chem* 92:554-64

OP286

PET imaging of P-glycoprotein function at the rodent BBB: Diurnal fluctuations and impact of sleep deprivation

H. Savolainen[1], P. Meerlo[1], A. van Waarde[1], P. Elsinga[1], A. D. Windhorst[2], N. Colabufo[3,4], G. Luurtsema[1]; [1]University of Groningen, University Medical Center Groningen, Groningen, NETHERLANDS, [2]VU University Medical Center, Amsterdam, NETHERLANDS, [3]Università degli Studi di Bari, Bari, ITALY, [4]Biofordrug, Bari, ITALY.

Aim: Blood-brain barrier (BBB) contributes to brain homeostasis by protecting the brain from harmful compounds. P-glycoprotein (P-gp) is one of the major efflux transporters at the BBB. P-gp function can be modulated by endogenous and exogenous factors. Yet, little is known about fluctuations in P-gp function across the sleep-wake cycle. Recent studies suggest that substances accumulating during wakefulness may be cleared from the brain during sleep, a process that is impaired after sleep deprivation [1]. Therefore our research questions were: Is P-gp function constant or does it fluctuate across the day? Is P-gp function stronger during sleep and is it negatively affected by sleep deprivation? Materials and methods: Four groups of male Sprague-Dawley rats (n=6-8) were scanned at different moments of the 12 h light - 12 h dark cycle to study diurnal variations: early light phase (ZT 3, group 1), late light phase (ZT 9, group 2), early dark phase (ZT 15, group 3) and late dark phase (ZT 21, group 4). In two additional groups (n=7), controls were allowed to sleep normally while the experimental animals were sleep-deprived for 10 h in a slowly rotating drum during the light phase, which represents the normal sleep period. All rats were scanned with a new P-gp substrate tracer, [^{18}F]MC225 ((5-(1-(2-fluoroethoxy))-[3-(6,7-dimethoxy-3,4-dihydro-1H-isoquinolin-2-yl)-propyl]-5,6,7,8-tetrahydronaphthalen). Arterial blood samples were drawn during a 60 min scan. Afterwards, rats were terminated and peripheral organs and brain regions were collected for biodistribution analysis. Results: Distribution volumes (V_T) were calculated by a one-tissue-compartment model fit using whole blood and metabolite-corrected plasma data as input function. In all brain regions, group 3 had 1.2-1.8 fold higher V_T than other groups. Groups 1, 2 and 4 showed no significant differences. In the biodistribution study, some peripheral organs (e.g. testes) showed similar diurnal variation. Distribution volumes in sleep-deprived animals and controls were not significantly different. Conclusion: P-gp function in rats displays a daily rhythm with reduced function at the beginning of the dark phase or active phase. This rhythm is not dependent on sleep since sleep deprivation had no effect. It may be that P-gp function is modulated by the endogenous circadian clock via other processes than sleep, such as rhythms in neurotransmitters or cytokines. References: 1 He et al, J Neurosci 2014, 34, 14697-14706

OP287

Comparative Evaluation of Two PET Radioligands for PDE10A, [11C]T-773 and [18F]FM-T-773-d2 in Nonhuman Primates

A. Takano[1], V. Stepanov[1], R. Nakao[1], N. Amini[1], H. Kimura[2], C. Halldin[1]; [1]Karolinska Institutet, STOCKHOLM, SWEDEN, [2]Takeda Pharmaceutical Company, Limited., FUJISAWA, JAPAN.

Aim: Since PDE10A is distributed mainly in striatal regions, it may be involved in psychiatric and neurodegenerative diseases such as schizophrenia and Huntington's disease. Here we evaluated and compared two recently developed radioligands for PDE10A [1], [11C]T-773, [1-[2-fluoro-4-(tetrahydro-2H-pyran-4-yl)phenyl]-5-methoxy-3-(1-phenyl-1H-pyrazol-5-yl)pyridazin-4(1H)-one] and a fluoromethyl analog, [18F]FM-T-773-d2, in nonhuman primates. Materials and methods: PET measurements (123 min) were performed four times for each PET radioligand using six female rhesus monkeys. Two monkeys had both radioligands and other four had one radioligand. Arterial blood sampling was performed to obtain the plasma input function. Protein binding was measured, and radio-metabolite analysis was performed for each PET measurement. The putamen and caudate as the target regions, and the cerebellum as a reference region, were delineated on coregistered PET/MRI. Total distribution volume (VT) was calculated by a two-tissue-compartment model (2TC). Binding potential (BPND) was calculated as a ratio of the VT between the target region and the reference region minus one. BPND was also calculated with simplified reference tissue model (SRTM). The stability of the outcome measures was investigated using the truncated PET data. Results: The whole brain uptake at peak was higher with [18F]FM-T-773-d2 than with [11C]T-773 (4.5%ID vs 3.4%ID). Average fractions of the parent compounds at 30 min were 57.3 ± 6.1% with [11C]T-773 and 63.7 ± 1.6% with [18F]FM-T-773-d2. No radio-metabolites more lipophilic than the parent compounds were detected. Protein binding was higher with [18F]FM-T-773-d2 than with [11C]T-773 (78.9 ± 3.1% and 56.7 ± 7.3%). VT of the cerebellum and putamen was 3.9 ± 0.5 and 11.9 ± 3.3 for [11C]T-773 and 4.8 ± 1.0 and 11.1 ± 0.8 for [18F]FM-T-773-d2, respectively. The BPND of the putamen obtained with 2TC and SRTM was 2.0 ± 0.4 and 1.9 ± 0.4 for [11C]T-773, and 1.4 ± 0.3 and 1.3 ± 0.3 for [18F]FM-T-773-d2. The duration of PET measurements was shortened stably to 39 min for [11C]T-773 and 33 min for [18F]FM-T-773-d2 for VT obtained with 2TC while it was shortened stably to 63 min for [11C]T-773 and 75 min for [18F]FM-T-773-d2 for BPND obtained with SRTM. Conclusion: Both [11C]T-773 and [18F]FM-T-773-d2 have good characteristics as PET radioligands for PDE10A. Although the whole brain uptake at peak was higher for [18F]FM-T-773-d2, BPND was higher for

[11C]T-773. The duration of PET measurement can be shortened to 39 min for both radioligands if the VT of the striatal regions obtained with 2TC is the outcome measure.

OP288

Quantification of Available NMDA (GluN) Receptor NTD Drug Binding Sites with the GluN2B-targeting PET Tracer [^{11}C]NB1

S. D. Krämer[1], T. Betzel[1], L. Mu[2], B. Tewes[3], B. Frehland[3], D. Schepmann[3], R. Schibli[1], B. Wünsch[3], S. M. Ametamey[1]; [1]ETH, Zurich, SWITZERLAND, [2]University Hospital Zurich, Zurich, SWITZERLAND, [3]Westfälische Wilhelms-Universität, Münster, GERMANY.

Aim: NMDA receptors (GluN) are key regulators of CNS plasticity and higher cognitive functions. We aimed at evaluating the potential of our novel GluN2B-targeting PET tracer [^{11}C]NB1 (7-[^{11}C]methoxy-3-(4-phenylbutyl)-2,3,4,5-tetrahydro-1H-benzo[d]azepin-1-ol) for quantitative PET and receptor occupancy studies. [^{11}C]NB1 is structurally related to drug candidates, such as ifenprodil, eliprodil and Ro-25-6981 that selectively bind to the GluN2 N-terminal domain (NTD).Materials and Methods: [^{11}C]NB1 was synthesized from its phenolic precursor by [^{11}C]methylation with [^{11}C]CH3I. Time-activity curves (TAC) for rat brain regions were recorded by PET after intravenous injection of 20 to 67 MBq [^{11}C]NB1. The blood TAC was simultaneously measured from a minimally invasive arterio-venous shunt. Data were fit to compartment models and input-function independent quantification methods were evaluated. To investigate the influence of cerebral glutamate on [^{11}C]NB1 PET, ketamine (25 mg/kg) was injected intraperitoneally 15-20 min before tracer injection. Receptor occupancy by eliprodil was characterized after intravenous injection of various doses of eliprodil 1 minute before the tracer (n=14).Results:For experiments with blood TAC recording (n=6; 1 blood TAC failed), [^{11}C]NB1 specific activity was 254-368 GBq/μmol (0.4-0.8 ng/kg injected dose). Data followed a 2-tissue compartment model with scan-time independent VT from 10 min onwards. Extraction from plasma to brain was close to 100%. At distribution equilibrium, tracer concentration in the first, non-specific compartment, was similar to the plasma concentration, resulting in VND ~1. Under baseline conditions (n=3), average VT was between ≤ 4.8 for olfactory cortex and cerebellum grey matter and ≥ 6.0 for midbrain and thalamus. The integrated standardized uptake value from 0 to 60 min (SUV0-60min) was evaluated for quantification in the absence of an input function. The comparison with VT revealed a Pearson's r for the 5 animals and 13 brain regions each, of 0.840. VT values after ketamine challenge (n=2) were similar to baseline values and values for SUV0-60min were not significantly affected (n=3). Whole brain SUV0-60min after eliprodil injection followed a saturation function. The fit dose at 50% receptor occupancy was 1.5 μg/kg (4.2 nmol/kg). Maximal blocking by an excess of eliprodil, NB1 and Ro-25-6981 was 47% (fit), 46% (n=1) and 55% (n=1), respectively, in agreement with ex vivo biodistribution results.Conclusion: [^{11}C]NB1 allows to quantify the availability of GluN2B NTD binding sites in rat brain. Whole brain specific binding is ~47% of total binding. Quantification is possible with and without an input function. Receptor occupancy by GluN2B NTD-targeting drugs can be quantified with [^{11}C]NB1.

OP289

Autoradiography and microPET rodent evaluation of the [18F]MCL-524 - an 18F-labelled dopamine D2/D3 receptor agonist

V. Stepanov[1], J. Häggkvist[1], M. Svedberg[1], R. Krasikova[2], S. J. Finnema[1], A. W. Sromek[3], J. L. Neumeyer[3], C. Halldin[1]; [1]Karolinska Institutet, Stockholm, SWEDEN, [2]N.P. Bechtereva Institute of Human Brain, St.-Petersburg, RUSSIAN FEDERATION, [3]McLean Hospital/Harvard Medical School, Belmont, MA, UNITED STATES.

AIM: Carbon-11 labeled dopamine D_2/D_3 receptor agonist radioligands have been shown to be sensitive to amphetamine-induced elevations in extracellular dopamine concentration across species. Labeling with fluorine-18 further increases usefulness of such radioligands for long duration imaging scenarios. In view of this, a novel fluorine-18 radiolabeled dopamine D_2/D_3 receptor agonist - [^{18}F]MCL-524 - was recently developed and evaluated successfully in non-human primates (NHP) (Finnema *et al*., J Nucl Med. 2014, 55:1164-70). We here evaluated scope of usefulness of [^{18}F]MCL-524 for autoradiography, using post-mortem tissue, as well as its potential for rodent PET imaging. METHODS: [^{18}F]MCL-524 was synthesized as described previously (Finnema *at al*. 2014). For autoradiography evaluation, rat and mouse brain slices (coronal sections, 14 μm thick) were incubated with 0.02 and 0.2 MBq/ml of [^{18}F]MCL-524 for 55 minutes in the absence and presence of 10 μM butaclamol, washed and imaged on a Fujifilm BAS-5000. Rodent PET imaging was conducted using rats with Mediso nanoScan® PET/MRI and nanoScan® PET/CT cameras (imaging time of 63 minutes, average injection of 17±1 MBq [^{18}F]MCL-524). Striatal BP_{ND} values were estimated with SRTM, using cerebellum as a reference region. RESULTS: In autoradiography studies accumulation of [^{18}F]MCL-524 was observed in most regions of the brain, including cortex and striatum, with little to none of the binding being displaceable by butaclamol. The result is in-line with other attempts to use carbon-11/fluorine-18 labeled D_2/

D_3 receptor agonists for the purpose. In the rodent baseline PET studies, average striatal BP_{ND} values were low, 0.29±0.23 (n=3), and a large variability between individual animals was observed. Pre-treatment with 1mg/kg of raclopride decreased striatal BP_{ND} by ~70% (n=3). CONCLUSIONS: The low BP_{ND} and high variability in [^{18}F]MCL-524 binding across animals limits its usefulness as an imaging tool for small animal PET. Comparison of the NHP and rodent imaging results indicates that the kinetic behavior of dopamine D_2/D_3 receptor agonist ligands *in vivo* differs significantly across species. Great care should be taken when assessing PET radioligands suitability for dopamine D_2/D_3 receptor imaging using different species.

OP290

Comparative evaluation of (R)-[11C]verapamil and [11C]-N-desmethyl-loperamide to assess P-glycoprotein function at the mouse blood-brain barrier

T. Wanek[1], S. Mairinger[1], J. Stanek[1,2], M. Sauberer[1], T. Filip[1], A. Traxl[1], C. Kuntner[1], J. Pahnke[3], M. Müller[2], O. Langer[1,2]; [1]AIT Austrian Institute of Technology, Seibersdorf, AUSTRIA, [2]Medical University of Vienna, Vienna, AUSTRIA, [3]University of Oslo (UiO) and Oslo University Hospital (OUS), Oslo, NORWAY.

Aim: Brain distribution of many drugs can be restricted by efflux transport at the blood-brain barrier (BBB) mediated by the adenosine triphosphate-binding cassette transporter P-glycoprotein (Pgp). Pgp function has been shown to be altered in neurological diseases such as epilepsy and Alzheimer's disease. Positron emission tomography (PET) with the Pgp substrates (*R*)-[^{11}C]verapamil ([^{11}C]VPM) and [^{11}C]-*N*-desmethyl-loperamide ([^{11}C]dLop) has been used to assess Pgp function at the rodent and human blood-brain barrier (BBB). Aim of this study was to directly compare [^{11}C]VPM and [^{11}C]dLop for assessment of Pgp function at the mouse BBB. Material and Methods: Imaging experiments were performed in groups of isoflurane-anesthetized, female C57BL/6N mice and homo- and heterozygous Pgp-knockout mice which were pretreated 2 h prior start of PET with different doses of the Pgp inhibitor tariquidar or vehicle solution. Dynamic (0-60-min) PET scans were initiated at the start of injection of either [^{11}C]VPM or [^{11}C]dLop. Brain uptake of [^{11}C]VPM or [^{11}C]dLop, was expressed as the brain to plasma ratio of radioactivityin the last PET frame (50-60 min after injection). In separate groups of mice radiolabelled metabolites of both radiotracers were analyzed in plasma and brain by radio-TLC.ResultsFollowing injection, radioactivity in whole brain reached an approximately 3-4 times higher peak concentration for [^{11}C]VPM than for [^{11}C]dLop. [^{11}C]VPM washed out from brain whereas [^{11}C]dLop appeared to be trapped in brain tissue. In Pgp knockout mice, brain uptake of [^{11}C]VPM and [^{11}C]dLop was 3.9- and 2.8-fold higher, respectively, as compared with wild-type mice. In heterozygous mice, which have 50% lower Pgp expression levels at the BBB than wild-type mice, brain uptake of [^{11}C]VPM and [^{11}C]dLop was increased by only 1.5- and 1.1-fold, respectively, as compared with wild-type mice. Both radiotracers showed tariquidar dose dependent increases in brain distribution. Whereas brain distribution of [^{11}C]VPM reached in tariquidar-treated mice similar levels as in Pgp knockout mice, this was not the case for [^{11}C]dLop. For both radiotracers, radiolabelled metabolites were detected in plasma and brain with a higher percentage of radiolabelled metabolites for [^{11}C]dLop than for [^{11}C]VPM. Conclusion: Both [^{11}C]VPM and [^{11}C]dLop can be used to assess Pgp function at the mouse BBB. However, both radiotracers displayed limited sensitivity to assess small (<50%) variations of Pgp function at the mouse BBB, with [^{11}C]dLop being less sensitive than [^{11}C]VPM. Use of both radiotracers is compromised in mice by significant peripheral metabolism and brain uptake of radiolabelled metabolites.

---

907 - Monday, October 12, 2015, 2:30 PM - 4:00 PM, Hall F
Teaching Session: The Spine: Anatomy, Pathology and Correlative Imaging

---

OP291

The Spine: Anatomy, Pathology and Correlative Imaging

I. Pressney, UNITED KINGDOM

---

908 - Monday, October 12, 2015, 2:30 PM - 4:00 PM, Hall E
Clinical Oncology: Prostate II - Beyond Choline

OP292

Noninvasive Quantification of Tumor Blood Flow in Prostate Cancer using 82Rb PET/CT

L. P. Tolbod[1], M. M. Nielsen[1], H. J. Harms[1], B. G. Pedersen[2], P. Borghammer[1], M. Borre[3], K. Bouchelouche[1], J. Frøkiær[1], J. Sørensen[1]; [1]Dept. Nuclear Medicine & PET-Centre, Aarhus University Hospital, Aarhus N, DENMARK, [2]Department of Radiology, MR-Centre, Aarhus University Hospital, Aarhus N, DENMARK, [3]Dept. Urology, Aarhus University Hospital, Aarhus N, DENMARK.

Objective: Tumor Blood Flow (TBF) is an indicator of tumor aggressiveness in a variety of cancers and may aid in identifying

aggressive prostate cancer and in monitoring treatment. The gold standard for measuring TBF is 15O-H2O PET combined with arterial blood sampling (BSIF). This is, however, logistically challenging and requires an on-site cyclotron. We investigated the accuracy of simplified TBF measurements using with image derived input functions (IDIF) with 15O-H2O and the more widely accessible tracer 82Rb. Method: 9 patients with prostate cancer were included. Dynamic PET scans of the heart (for IDIF extraction) and pelvis were performed with both 15O-H2O and 82Rb. During the 15O-H2O scans arterial blood sampling was performed. On the same day, T2w and DWI MRI were acquired. IDIFs were automatically extracted using cluster analysis. ROIs of tumor, peripheral zone and transition zone were drawn on MRI images coregistered to the PET series. TBF was calculated using BSIF or IDIF data from either the aorta, as obtained from the separate heart scan, or the iliac arteries. Results: Automatic extraction of IDIFs derived from the aorta/left ventricle (heart scans) and the iliac arteries (pelvis scans) was successful in all cases. Excellent correlations were found between TBF obtained using blood sampler input and each IDIF (TBF(heart IDIF)=1.11xTBF(BSIF)+0.004, R2=0.96 and TBF(Iliac IDIF)=5.23xTBF(BSIF)-0.16, R2=0.93) for the 15O-H2O scans. Correcting for the flow-dependent extraction of 82Rb using the Renkin-Crone model, a good correlation was found between 82Rb K1 and 15O-H2O TBF (R2=0.96). Furthermore, high correlation was found between 82Rb K1 and 82Rb SUV (SUV=7.82xK1(82Rb)+0.47, R2=0.83). In 5 patients, TBF was elevated relative to the peripheral zone. However, in 4 patients elevated blood flow was also seen in the transition zone, most likely due to benign prostatic hyperplasia. Conclusion: Both 15O-H2O and 82Rb can be used for quantitative imaging of tumor blood flow in prostate cancer without catheter-based arterial blood sampling. Full pharmacokinetic analysis can be performed without the need for arterial blood sampling by using the automatically extracted IDIFs from either the iliac arteries or a separate scan of the heart. In the former case, a scanner dependent recovery factor is needed. Further simplification is possible by using SUV values obtained from static images.

OP293

Phase I Safety and Biodistribution Study of 124I-PEG-AVP0458 Diabody in Patients with TAG-72 Positive Ovarian and Prostate Cancer

A. M. Scott[1,2], T. Akhurst[3], F. Lee[2], M. Ciprotti[1], I. Davis[1], A. Weickhardt[1], H. Gan[1], P. Kocovski[2], N. Guo[2], D. Murphy[3], R. Hicks[3], S. Lee[1], G. O'Keefe[1], S. Gong[1], P. Hudson[4]; [1]Austin Health, Melbourne, AUSTRALIA, [2]Olivia Newton-John Cancer Research Institute, Melbourne, AUSTRALIA, [3]Peter MacCallum Cancer Centre, Melbourne, AUSTRALIA, [4]Avipep Pty Ltd, Melbourne, AUSTRALIA.

Background: The development of antibody therapeutics for imaging and payload delivery is complex, and intact IgG have long half-lives that impact on tumor:blood ratios and tumor penetrance. Smaller molecular weight antibody constructs (eg diabodies) have been developed for improved penetrance into tumor, faster blood clearance, and enhanced tumor: normal tissue uptake, however renal uptake may impact on imaging and therapeutic effects. Through a novel pegylation strategy, a diabody to TAG-72 (AVP0458) has been generated, and produced under cGMP for a first-in-human clinical trial.Materials and Methods: We have conducted a Phase I, open label, first-in-human trial of PEG-AVP0458. The primary study objective was the safety of single dose of I-124 PEG-AVP0458 in patients (pts) with TAG-72 +ve relapsed / metastatic prostate or ovarian cancer. Secondary study objectives were evaluation of the biodistribution, tumor targeting, pharmacokinetics (PK) and immunogenicity of I-124 PEG-AVP0458. Pts were infused with I-124 PEG-AVP0458 (3-5mCi) at one of two dose levels (1mg/m2 and 10mg/m2), and imaged sequentially over a one week period. Safety, PK, and immunogenicity were assessed up to 30 days post infusion.Results: Six pts (1F:5M; age range 62-85yrs; 1 ovarian cancer, 5 prostate cancer) were entered into the study, 3 at each dose level. I-124 PEG-AVP0458 was well tolerated, with no infusion-related adverse events, and no serious adverse events observed. There was consistent biodistribution on PET imaging of I-124 PEGAVP0458, with no normal tissue uptake. High tumor uptake was evident in metastatic disease in liver and lymph nodes, with lesion uptake seen within 1-2 days post infusion. PK analysis showed a T½β of 46.8 ± 12.4 hrs. There was no impact of protein dose on biodistribution, tumor uptake or PK. No immunogenicity to PEG-AVP0458 was evident.Conclusions: I-124 PEG-AVP0458 is safe, and demonstrates excellent, rapid targeting of tumor in-vivo, with no normal organ uptake, and high tumor: blood ratios. This data demonstrates the feasibility of using pegylated diabodies for imaging and for payload delivery of radionuclides (RIT) or cytotoxic drugs (ADC) in cancer patients.ANZCTR Number: ACTRN12612000802808

OP294

Parasympathetic Imaging of Prostate Cancer using 11C-Donepezil PET.

M. Stokholm[1], S. Høyer[2], S. Jakobsen[1], D. Bender[1], M. Borre[3], J. Frøkiær[1], **P. Borghammer**[1]; [1]Department of Nuclear Medicine & PET Centre, Aarhus University Hospital, Aarhus, DENMARK, [2]Department of Pathology, Aarhus University Hospital, Aarhus, DENMARK, [3]Department of Urology, Aarhus University Hospital, Aarhus, DENMARK.

Background It was recently shown that high-grade prostate

cancer (PC) is characterized by parasympathetic neuroneogenesis, which promotes cancer dissemination, and is associated with decreased survival. We have previously validated 11C-donepezil PET as a marker of parasympathetic innervation. 11C-donepezil PET could therefore have utility in risk-stratification of PC patients, and may facilitate targeted biopsies or focal therapyObjectivesTo investigate 11C-donepezil uptake in low- and high-grade PC as a marker of parasympathetic neuro-neogenesis.MethodsThe 11C-donepezil uptake in PC was investigated using autoradiography of prostatectomy tissue from 13 patients and correlated to Gleason scores (GS). In pilot PET-studies we aim to perform in vivo 11C-donepezil PET imaging in two groups of 12 PC patients with low- and high-risk PC based on biochemical and biopsy risk-stratification.ResultsIn prostatectomy tissue, 11C-donepzil exhibited increased uptake in high-grade PC compared to low-grade and benign hyperplasia. The mean uptake ranged from 56% (GS3+3) to 409% (GS4+4). Preliminary in vivo 11C-donepezil PET studies in five PC patients with low-grade PC (GS≤7) demonstrated only slight uptake in the prostate (SUVmax<4.6), whereas two patients with high-grade PC (GS≥8) showed high focal uptake in the prostate (SUVmax >7.5). Interestingly, high uptake was also seen in bone metastases (SUVmax 7-12) and enlarged pelvic lymph nodes (SUVmax 7-11) in two patients with disseminated PC.ConclusionsIn autoradiography studies, the uptake in tumor tissue of the cholinergic PET ligand 11C-donepezil correlated with GS. Preliminary PET studies suggest that 11C-donepezil may be able to predict the GS in vivo. Parasympathetic PET imaging may therefore have utility for targeted biopsies in PC patients, and may aid in selecting patients for radical prostatectomy.

OP295

Effect of androgen deprivation therapy on the results of PET/CT with [18F]fluciclovine in patients with prostate cancer

T. Bach-Gansmo[1], H. Sletten[2], M. C. Småstuen[2], A. M. Løndalen[1], T. V. Bogsrud[1]; [1]Oslo University Hospital, Oslo, NORWAY, [2]Oslo and Akershus University College, Oslo, NORWAY.

Purpose: Anti-androgenic hormonal treatment seems to reduce the sensitivity of 11C- and 18F-Choline PET (1). [18F]-fluciclovine (FACBC) is a new radiopharmaceutical for positron emission tomography (PET) of prostate cancer. We wanted to find out to which extent androgen deprivation therapy (ADT) would influence the sensitivity of FACBC PET in patients with metastatic disease. Methods: This was a retrospective register trial performed in 350 patients with prostate cancer examined with FACBC, of whom 76 received ADT. Informed consent was obtained from all patients. The sensitivity of FACBC PET/CT in patients on ADT was compared with the sensitivity for the total material, 350 patients with primary or recurrent prostate cancer with or without metastatic disease. Results: The number of PET positive cases in the total material was 59%. The sensitivity was 71%, higher but not statistically significant, in the subgroup receiving ADT, and this whether the PSA was stable/declining (65% positive PET) or rising (77% positive PET). Discussion/ Conclusion: Invitro studies have shown that anti-androgen treatment causes downregulation of the LAT3 receptor, which in turn is responsible for an upregulation of LAT1 and ASCT transporters (2), responsible for the uptake of amino acids such as fluciclovine. ADT does not render FACBC PET examinations negative, and as a result FACBC may be particularly useful in this patient group. Additionally FACBC may be less suitable for monitoring the response to ADT. References: 1.Giovacchini G, Picchio M, Coradeschi E, Scattoni V, et al. [11C]Choline uptake with PET/CT for the initial diagnosis of prostate cancer: relation to PSA levels, tumour stage and anti-androgenic therapy. Eur J Nucl Med Mole Imaging 2008;35:1065-1073. 2. Wang Q, Tiffen J, Bailey CG, Lehman ML, et al. Targeting amino acid transport in metastatic castration-resistant prostate cancer: effects on cell cycle, cell growth, and tumor development. J Natl Cancer Inst. 2013;105(19):1463-73.

OP296

68Ga-DOTATATE compared with11C-Choline PET/CT in patients with hormone-resistant prostate cancer at biochemical relapse.

O. Alonso[1,2], G. Dos Santos[1,2], E. Savio[1], M. Garcia-Fontes[1], H. Engler[1]; [1]Uruguayan Centre of Molecular Imaging (CUDIM), Montevideo, URUGUAY, [2]Clinical Hospital, University of Uruguay, Montevideo, URUGUAY.

In hormone resistant prostate cancer (HRPC), neuroendocrine differentiation has been associated with up to 85% of patients. These cells express somatostatin receptors (SSTR) that can be targeted with 68Ga-DOTATATE. Therefore, we present the preliminary results of a prospective trial aiming to compare the diagnostic values of 68Ga-DOTATATE and 11C-Choline PET/CT in patients with HRPC at biochemical recurrence. The study involved 64 prostate cancer patients (median age: 65, range: 47-85 years) with PSA relapse under androgen deprivation therapy, with a median trigger PSA level of 4.25 ng/mL (range: 0.22-291 ng/mL). Within 1-2 weeks, a PET/CT study was performed with 68Ga-DOTATATE and 11C-

Choline with an approximately dose of 100 MBq and 400 MBq, respectively, using a 64-slice PET/CT with time-of-flight correction. Correlative imaging, histopathology and/or clinical follow-up (median follow-up time: 19 months, range: 9-31 months), were considered as reference standard. Both techniques showed positive local, regional lymph node and distant findings in 31 patients. Results were concordant in 57 cases (89%), with discordant findings observed in patients with bone (n=2) and regional lymph nodes lesions (n=5). On a per patient basis, sensitivity, specificity, positive and negative predictive values with their 95% confidence intervals were the same for both techniques: 0.82 (0.65-0.93), 0.90 (0.73-0.98), 0.90 (0.73-0.98) and 0.81 (0.65-0.93), respectively. Although a trend toward a lower sensitivity was observed for patients with lower PSA levels, the difference was not statistically significant: 0.63 vs. 0.89, P=0.13, same values for both tracers, for patients with PSA < 4.25 and ≥ 4.25 ng/mL, respectively. False-positive lesions (n=5) were found, for both tracers, in 3 patients and were located in the prostate bed (n=1) and regional lymph nodes (n=4), being 3 discordant. In all cases, pathology revealed non-specific inflammatory lesions. 68Ga-DOTATATE and 11C-Choline PET/CT seem to have complementary value for the evaluation of HRPC patients with biochemical relapse. Further studies are needed to confirm these findings.

OP297

Two-phase 68Ga-PSMA-HBED-PET/CT in patients with high-risk prostate carcinoma or PSA-relapse

C. Bouter, B. Meller, C. O. Ritter, J. Lotz, J. Meller, S. Hijazi, C. O. Sahlmann; UMG Göttingen, Göttingen, GERMANY.

Aim: Current preclinical studies show increasing uptake of Ga-68-PSMA over time indicating a better lesion/background ratio in Ga-68-PSMA-PET/CT. The aim of this study was the evaluation of the clinical value of two-phase Ga-68-PSMA PET/CT in patients with high risk prostate carcinomas (PC) or suspected recurrence of disease. Methods: A retrospective study of 35 PC patients (aged 48-76, median 71) that underwent two-phase Ga-68-PSMA-PET/CT was performed. Acquisition was done 1h and 3h after injection of 140-392 MBq (median 301 MBq) Ga-68-PSMA with 10-11 bed positions on a Philips Gemini TF16. Maximum standard uptake values (SUVmax) of lesions were measured in both scans and lesions were correlated with histology and / or diagnostic findings of other imaging modalities. Results: Primary tumor showed high SUVmax values 1h p.i. (range 4,3-64,4; median 10, 85) with significantly increased values after 3h p.i. (range 5,3-107,6; median 18,15). Histologically proven lymph node (LN) metastases also showed high SUVmax values 1h p.i. (range 2-37,3; median 9,8) rising up to 3h p.i. (range 3,7-52,7; median 15,2) whereas no correlation between size and SUVmax was detected. Radiologically proven bone metastasis also featured significantly higher SUVmax values in scans up to 3h p.i. (median 1h p.i.: 4,8; median 3h p.i. 7,15). However, benign LN showed lower SUVmax values 1h p.i. (range 0,8-2,5; median 1,4) with decreasing values 3h p.i. (range 0,7-1,5; median 1,05). Conclusions: Uptake of PC lesions in Ga-68-PSMA-PET/CT increases significantly over time in vivo. Two-phase Ga-68-PSMA-PET/CT may help to differentiate between benign lesions and PSMA-expressing PC-relapses or -metastases.

OP298

A Direct Comparison Study of Ga-68-NODAGA-MJ9 (MJ9, Bombesin) to F-18-FCH (FCH) in Recurrent Prostate Cancer

P. Mitsakis[1], T. Zilli[2], M. Kosinski[3], J. Delage[1], H. Maecke[4], R. Mansi[4], J. Bourhis[5], F. Buchegger[1], R. Miralbell[2,6], J. O. Prior[1]; [1]Department of Nuclear Medicine, Lausanne University Hospital, Lausanne, SWITZERLAND, [2]Department of Radiation Oncology, University Hospital of Geneva, Geneva, SWITZERLAND, [3]Institute of Radiation Physics, Lausanne, SWITZERLAND, [4]Department of Nuclear Medicine, University Hospital of Freiburg, Freiburg, GERMANY, [5]Department of Radiation Oncology, Lausanne University Hospital, Lausanne, SWITZERLAND, [6]Institut Oncològic Teknon, Barcelona, SPAIN.

Purpose: We aimed to compare the diagnostic accuracy of 68Ga-NODAGA-MJ9 (MJ9, a novel radiopharmaceutical targeting the gastrin releasing peptide receptor) PET/CT with 18F-FCH (FCH) in recurrent prostatic cancer (PC).Materials and Methods: MJ9 was radiolabelled with the eluate of a 68Ge→68Ga generator using an automatic processor unit (PharmTracer). FCH PET/CT was performed with 18F-labelled fluoromethycholine. We included 33 PC patients (age 68±6y [53-82y]) treated by prostatectomy (27/33=82%) or radiation therapy without prostatectomy (6/33=18%) with biochemical PC relapse (PSA 4.7 ±4.1ng/mL [range 0.3-18.1]) and mean Gleason score 7.2 ±0.9 [5-9]. They underwent within a 10-day period both 68Ga-NODAGA-MJ9 (200MBq) and 18F-FCH (200 MBq) PET/CT imaging at 70 min p.i. Lesions were classified of local, lymph node [LN] and osseous origins and corresponding SUVbw_max (SUV) was recorded in each lesions.Results: In total, 81 lesions (14 local, 39 LN, 24 bone) were detected in 29 patients using 68Ga-NODAGA-MJ9 or 18F-FCH. In 4 patients (4/33=12%)

no lesion was found with both tracers (n=4; PSA=1.2±1.0 [0.3-2.4]). Of the 77 remainder lesions, SUV was similar in local lesions (n=14; MJ9=6.2±3, FCH=5.9±3.2, p=0.8), while it was significantly higher for MJ9 in LN (n=39; MJ9=9.3±8.3; FCH=5.7±4.8; p=0.004) and significantly lower for MJ9 in bone lesions (n=24; MJ9=2.2±1.8; FCH=6.1±3.6; p<0.0001). As compared to FCH, MJ9 missed 18/24 (75%) lesions in bone, 7/39 (18%) lesions in LN, but detected 5/39 (13%) more lesions in LN. When excluding bone lesions, MJ9 had +46% higher SUV than FCH (n=53; MJ9=8.5±7.4; FCH=5.8±4.4; p=0.005).Conclusion: 68Ga-NODAGA-MJ9 uptake was greater than 18F-FCH PET/CT in local and lymph node lesions, while 18F-FCH seemed better for bone lesions in biochemical relapse of prostate cancer patients.

OP299

A Novel Gallium-68-Labelled GRP Receptor Antagonist, [68Ga]Sarabesin 3, for Prostate Cancer Imaging: First Results in Therapy Naïve Primary Patients

I. L. Bakker[1], A. C. Fröberg[1], M. Busstra[1], G. J. L. H. van Leenders[1], E. de Blois[1], I. Schoots[1], J. Veenland[1], T. Maina[2], W. M. van Weerden[1], B. Nock[2], M. de Jong[1]; [1]Erasmus MC, Rotterdam, NETHERLANDS, [2]National Center for Scientific Research "Demokritos", Athens, GREECE.

AIM: There is an unmet demand for more sensitive diagnostic tools in patients with prostate cancer (PC), to improve staging as well as tumour localisation in case of increased tumour markers after treatment. Gastrin releasing peptide receptors (GRPr), being overexpressed in PC but not in normal prostate tissue or benign hyperplasia, could provide an excellent target in PC. [68Ga]Sarabesin 3, a GRPr antagonist, was selected for clinical translation after promising preclinical results in mouse PC models, including high tumour uptake and favourable tumour-to-background ratios. The aim of this trial is to validate GRPr PET-CT imaging in patients with primary PC who are scheduled for surgery. MATERIALS AND METHODS: As yet, three patients with PC confined to the prostate have been included; patients were imaged over a period of 3.5 h after administration of [68Ga]Sarabesin 3 (147±14 MBq, 40±5 μg). PET-CT imaging included dynamic scanning, multiple local images, and two total-body scans. The bladder was continually flushed, enabling optimal imaging of the prostatic region. PET-CT images were matched with the most recent MR scans. Radiotracer stability, activity curves in blood and urine as well as gastrin levels were measured. After prostatectomy, the pathologist examined the tissue confirm tumour localisations and autoradiography was performed to confirm GRPr overexpression. RESULTS: [68Ga]Sarabesin 3 PET-CT-scans showed focal uptake in the prostate first at 45 min p.i.. At earlier time points blood pool activity was too high to distinguish from focal accumulation. In all patients increased uptake was seen corresponding to localisations of PC as determined by pathology. One patient had a tiny tumour, which could only be confirmed by a special biopsy procedure including 40 biopsies; PC was found in only one needle core. Still, persistent uptake was corresponding to this tiny lesion. In another patient the MR identified unilateral tumour presence, while histology confirmed results of the GRPr scan, showing tumour on both sides. The GRPr-expressing pancreas showed high physiological uptake. Diffuse and low uptake was seen in the whole gastrointestinal tract and lower oesophageal and rectal sphincters. The liver showed almost no activity. Serial images and urine specimens showed fast renal excretion. The compound was very stable in blood and urine. Apart from some discomfort by the flush catheter, patients did not report any side effects. CONCLUSION: These first findings suggest [68Ga]Sarabesin 3 PET-CT to have great potential as an imaging tool in patients therapy naïve primary suffering from PC.

910 - Monday, October 12, 2015, 2:30 PM - 4:00 PM, Hall D
Clinical Oncology: Rapid Fire Session

OP300

Use of 18FDG-PET/CT to predict outcome in patient with locally advanced pancreatic cancer

L. Locantore[1], P. Mapelli[1], E. Incerti[1], P. Alongi[2], V. Gangemi[3], P. Passoni[4], N. Slim[4], N. Di Muzio[4], L. Gianolli[1], M. Picchio[1]; [1]Nuclear Medicine Department, IRCCS San Raffaele Scientific Institute, Milan, ITALY, [2]University of Milano-Bicocca, Milan, ITALY, [3]Nuclear Medicine Unit, Department of Biomedical Sciences and of Morphologic and Functional Images, University of Messina, Messina, ITALY, [4]Radiotherapy Department, IRCCS San Raffaele Scientific Institute, Milan, ITALY.

Aim. Despite the routinary use of chemotherapy (CH) in combination with radiotherapy, patients with locally advanced pancreatic cancer (LAPC) have a poor prognosis. Helical tomotherapy (HTT) is a promising option for local control, allowing a highly conformed radiation dose to the lesion, sparing non-target organs. We investigated if routinary use of 18FDG-PET/CT (PET) could predict progression free survival (PFS) in patients with LAPC. Materials and methods. Fifteen patients with a mean age of 63 years (range: 45-81 years) were enrolled and underwent to PET at basal time, after CH and HTT treatment, for a total of 45 scans. Results were interpreted in both a qualitative (visual examination) and semiquantitative way (maximum and delta standard uptake value - SUVmax and ΔSUV%). PET results were compared to clinical and

radiological follow-up data (12 months). PFS using Kaplan-Meier method and relative risk of progression (RRP) with Cox regression analysis were estimated for all patients. A ΔSUV cut-off of positivity for survival analysis was derived from ROC curve analysis. Results. PET was positive in all patients at basal time, in 10/15 after CH and in 11/15 after HTT. SUVmax ranged from 2.3-13.4 (mean: 7.0) at basal time, 1.5-14.8 (mean: 5.0) after CH and 1.8-17.3 (mean: 4.9) after HTT. ΔSUV values ranged from 31-88% (mean: 53%) after CH and 11-79% (mean: 50%) after HTT. Twelve months follow-up data showed stable disease in 8/15 and progression of disease in 7/15 patients. On the basis of ROC analysis results, a ΔSUV cut-off of threshold of 30% (ΔSUV30) was chosen. PFS rates over 1-year in the PET group with ΔSUV<30 after CH versus the PET group with ΔSUV>30 were 45% versus 53% (p= 0.360). PFS rates over 1-year in the PET group with ΔSUV<30 after HTT versus the PET group with ΔSUV>30 were 25% versus 75% (p= 0.075). Cox regression analysis showed a high RRP for PET group with ΔSUV<30 after HTT (HR 5.9; p= 0.064). Conversely, no significant results was found on risk analysis for PET group with ΔSUV<30 after CH. Conclusions. The routinary use of PET after combined treatment demonstrated a predictive role for therapy response assessment. ΔSUV% cut-off approach might provide efficient risk stratification after HTT. Our results suggest a high prognostic value of PET using a ΔSUV30 for HTT response assessment in prediction of RRP and PFS.

OP301

Predictive value of 18F-FDG PET/CT in patients after primary radio-chemotherapy of head and nack cancers.

I. SANDLER[1], P. Castellucci[1], R. Frakulli[2], U. Caliceti[3], G. M. Lima[1], J. J. Morigi[1], A. Bellusci[3], S. Cammelli[2], S. Fanti[1]; [1]Università di Bologna, Nuclear Medicine Unit, S.Orsola-Malpighi Hospital, Bologna, ITALY, [2]Università di Bologna, Radiotherapy Unit, S. Orsola-Malpighi Hospital, Bologna, ITALY, [3]Università di Bologna, Head and Neck Unit , S. Orsola-Malpighi Hospital, Bologna, ITALY.

Aims: The purpose of this retrospective study is to assess the prognostic value of ^{18}F-FDG PET/CT performed as treatment response evaluation after primary concomitant radio-chemotherapy (RT-CT) for locoregional advanced Head and Neck squamous cell carcinoma (HNSCC). Methods: 151 patients, (108 males and 43 females, mean age 59 yo) underwent ^{18}F-FDG PET/CT after RT-CT for HNSCC, between 2006-2013 to assess response treatment. The sites of HNSCC were oral cavity (10%), nasopharynx (14%), oropharynx (53%), hypopharynx (7%), larynx (7%), salivary glands (5%) and paranasal sinuses (4%). ^{18}F-FDG PET/CT has been preformed from 6 to 36 weeks (median 21 weeks) after the end of RT-CT. Patients were divided in three groups: ^{18}F-FDG PET/CT performed from 6 to 14 weeks after the end of RT-CT (group-A; 31 patients), from 15 to 23 weeks (group-B; 89 patients) and from 24-36 weeks (group-C; 31 patient). ^{18}F-FDG PET/CT scans were performed according to standard procedure then were visually analyzed by two expert physicians and categorized as negative ("score-1"), doubt negative ("score-2"), doubt positive ("score-3") and positive ("score-4"). Patients were followed-up, based on clinic and radiological and/or histological findings, up to 60 months and for at least 12 months after end of therapy (median 38 months). ^{18}F-FDG PET/CT results were classified as true positive (TP), true negative (TN), false positive (FP) and false negative (FN). Results: - Group A: showed "score-1" 14 patients, "score-4" 12 patients, therefore ^{18}F-FDG PET/CT sensitivity 69%, specificity 77%, VPP 75%, VPN 71%, accuracy 0.73. This group showed five doubt scans (16%) as "score-2": two negatives and three positives. No "score-3" - Group B: showed "score-1" 55 patients, "score-4" 27 patients, therefore ^{18}F-FDG PET/CT sensitivity 84%, specificity 98%, VPP 96%, VPN 91%, accuracy 0.93. This group showed total seven (8%) doubt scans: three scans (3,5%) as "score-2" (one negative and two positives) and four scans (4, 5%) as "score-3" (two negatives and two positives). - Group C: showed "score-1" 24 patients, "score-4" 6 patients, therefore ^{18}F-FDG PET/CT sensitivity 100%, specificity 100%, VPP 100%, VPN 100%, accuracy 1. This group showed only one doubt scan (3%) as "score-2" that was find out to be negative. Conclusions: According to our data, PET/CT with ^{18}F-FDG showed an excellent prognostic value of treatment response to primary concomitant RT-CT if performed at least after fourteen weeks following the end of RT-CT. We observed also that the numbers of "doubt scans" significantly decrease after fourteen weeks following the end of RT-CT.

OP302

Predictive value of 18F-FDG PET/CT in restaging patients affected by ovarian cancer: a multicenter study.

F. Caobelli[1], P. Alongi[2], L. Evangelista[3], M. Rensi[4], A. Castello[5], I. Laghai[5], C. E. Popescu[6], C. Dolci[6], S. Seghezzi[7], Young AIMN Working Group; [1]Hannover Medical School, Hannover, GERMANY, [2]University of Milano Bicocca,, Milan, ITALY, [3]Istituto Oncologico Veneto, Padua, ITALY, [4]Hospital of Udine, Udine, ITALY, [5]University of Florence, Florence, ITALY, [6]Niguarda Hospital, Milan, ITALY, [7]Hospital of Treviglio, Treviglio (BG), ITALY.

Purpose: ovarian cancer is the eighth most common malignancy among women and has a high mortality rate. Prognostic factors able to drive an effective therapy are essential. 18F-FDG PET/CT has been investigated in patients with epithelial ovarian cancer and showed promise in diagnosing, staging,

detecting recurrent lesions and monitoring treatment response. Conversely, its prognostic role remains unclear. We aimed at assessing the prognostic value of 18F-FDG PET/CT performed in the restaging process in a multicentre study. Methods: We evaluated 168 patients affected by ovarian carcinoma, who underwent a restaging 18F-FDG PET/CT. The presence of local recurrences, nodal involvement and distant metastasis was recorded as well as lesion dimensions, maximum and mean standardized uptake values (SUVmax and SUVmean, respectively). Progression Free Survival (PFS) and Overall Survival (OS) at 3 and 4 years were computed by using Kaplan-Meier curves. Increased odds ratio was assessed using Cox regression analysis testing all lesion parameters measured by PET/CT. Results: PFS was significantly longer in patients with a negative than a positive restaging PET/CT study (3- and 4-years PFS 64% and 53% vs. 23% and 12%, respectively; $p<0.001$). Similarly, a negative study was associated with a significantly higher OS rate after 4 years of follow-up (67% vs. 25% in negative and positive group, respectively; $p<0.001$). Nodal or distant involvement were also independently associated with an increased risk of disease progression (HR 1.6 and 2.2, respectively, $p=0.003$). Moreover, PET/CT showed an incremental prognostic value compared to FIGO staging system, able to further stratify patient risk within the same staging assignment. At ROC analysis, no thresholds for semiquantitative parameters were predictive of a worse outcome. Conclusion: 18F-FDG PET/CT has an important prognostic value in assessing the risk of disease progression and mortality rate. An effective therapy planning might therefore effectively rely on 18F-FDG PET/CT findings. Semi-quantitative data were not proven to be an effective tool to predict disease progression.

OP303

Early 18F-FDG uptake as a reliable imaging biomarker of T790M-mediated resistance but not MET amplification in NSCLC

V. De Rosa[1], F. Iommelli[1], M. Monti[2], C. Mainolfi[2], R. Fonti[1], S. Del Vecchio[2]; [1]Institute of Biostructures and Bioimages, National Research Council, Naples, ITALY, [2]Department of Advanced Biomedical Sciences, University of Naples "Federico II", Naples, ITALY.

Aim: The two main mechanisms of resistance to EGFR tyrosine kinase inhibitors (TKI) in non-small cell lung cancer (NSCLC) are the occurrence of T790M secondary mutation in the kinase domain of EGFR and MET amplification. We previously showed that ^{18}F-FLT uptake is a reliable imaging biomarker of tumor response in refractory NSCLC due to both mechanisms of resistance. Here we tested whether ^{18}F-FDG PET/CT is able to detect the T790M- or MET-mediated resistance and to monitor the reversal of such resistance by EGFR T790M or MET inhibitors in tumor-bearing animals. Materials and Methods: Erlotinib-resistant NSCLC cell lines (H1975 and H1993) were treated with WZ4002, an EGFR T790M inhibitor, or the MET-inhibitor crizotinib depending on the mechanism of resistance. The levels and phosphorylation status of key proteins in the glycolytic cascade and oxidative phosphorylation were tested in response to treatment along with ^{18}F-FDG uptake. Then nude mice bearing H1975 and H1993 xenografts were subjected to ^{18}F-FDG PET/CT scan before and after treatment (50 mg/kg p.o. for 3 days) with erlotinib, WZ4002, crizotinib or vehicle. Three-dimensional region of interest analysis was performed to determine the percent change of ^{18}F-FDG uptake in response to treatment. At the end of imaging studies, tumors were removed, counted and analysed for glycolytic and mitochondrial proteins as well as signaling mediators. Results: H1975 cells showed a statistically significant reduction of ^{18}F-FDG uptake in response to treatment with WZ4002 (-61% ± 10%, $p=0.02$) whereas tracer uptake remained unchanged in response to erlotinib. H1993 cells, despite their known MET-mediated resistance, showed a decrease of ^{18}F-FDG uptake in response to erlotinib that became even stronger after treatment with the MET inhibitor (-70% ± 11%, $p=0.04$). Western blot analysis of glycolytic and mitochondrial proteins confirmed the different metabolic response of resistant H1975 and H1993 cells to erlotinib. In agreement with *in vitro* findings, imaging studies with ^{18}F-FDG PET/CT in H1975 tumor-bearing mice showed a strong reduction of ^{18}F-FDG uptake after treatment with WZ4002 whereas an increase of ^{18}F-FDG uptake was observed after treatment with erlotinib. Conversely, H1993 tumors bearing MET amplification showed a reduction of ^{18}F-FDG uptake after treatment with both crizotinib and erlotinib. The reduction of *in vivo* ^{18}F-FDG uptake was always associated with downregulation of key glycolytic proteins and upregulation of mitochondrial complexes in excised tumors. Conclusion: ^{18}F-FDG uptake is a reliable imaging biomarker of T790M-mediated resistance and its reversal in NSCLC whereas it fails to detect MET-mediated resistance.

OP304

Integrated 18F-FDG PET/MR imaging in the assessment of soft tissue sarcoma: initial experience with surgical and histopathological correlation

S. Vöö, D. Loeffen, R. Weijers, F. Mottaghy; Maastricht University Medical Center, Maastricht, NETHERLANDS.

Background. PET/MRI is an evolving hybrid imaging modality which combines the inherent strengths of MR with a high soft-

tissue contrast resolution and PET's functional metabolic capabilities.Goal. The objective of the present study was to evaluate whether integrated (18)F-FDG PET/MR imaging could improve the diagnostic workup in patients with soft-tissue sarcoma (STS) and its role in characterization and pre-operative staging of STS in comparison to MR.Material and Methods. Eleven patients (age range 42-72 years) with biopsy-proven STS who were referred for surgery were included in this prospective study. Preoperative FDG PET/MR was carried out in all patients with acquisition of T1W, T2W, short tau inversion recovery (STIR), and contrast-enhanced (ce) MR sequences. PET data were acquired simultaneously with the MR scan after injection of 199±58 MBq of (18)F-FDG. In addition, a skull-to-knee PET/MR (DIXON sequence) was acquired. Imaging results were correlated with the surgical and histologic findings.Results. The most common STS histologic type was malignant fibrous histiocytoma (30%). With regard to tumor grading, MR-based findings were in agreement with the PET findings in most of the cases (9/11, 81%). In 2 cases (19%) the metabolic findings on PET accurately indicated a low-grade STS, in agreement with histology and in contrast to the high-grade tumor suggested on MR images (T2W, ceMR). Tumor extent/invasiveness, as delineated on MR and PET, corresponded to surgical and histopathologic findings in majority of cases (7/11). However, in 4/11 cases the FDG-uptake on PET extended beyond the tumor delineation on MR. Histologic analysis confirmed a larger gross tumor volume and a deeper tumor invasiveness in the surrounding tissue in three cases, but reactive inflammatory changes in one case. These yielded an overall staging accuracy of 64% for MR and 91% for the hybrid PET/MR. In addition, PET/MR imaging revealed the presence of unexpected distant metastases in 18% of cases.Conclusion. MR alone is a robust modality in staging of STSs. However, combining (18)F-FDG PET with MR imaging on a hybrid PET/MR system results in greater accuracy with regard to overall staging and tumor delineation. Therefore, the combined modality of simultaneous PET/MRI is a valuable noninvasive diagnosis tool that could improve the clinical (pre-operative) decision in STS.

OP305

Evaluation of tumor hypoxia prior to and during radiotherapy in intermediate-risk prostate cancer using ^{18}F-Misonidazole PET/CT

M. Dore[1,2], S. Supiot[1,2], C. Cheze-Le-Rest[3], L. Ferrer[1,2], G. Delpon[1,2], M. Hatt[4], S. Guerif[3], D. Visvikis[4], **C. Rousseau**[1,2]; [1]Institut de Cancerologie de l'ouest Nantes, Saint Herblain, FRANCE, [2]INSERM UMR 892 CRCNA, Nantes, FRANCE, [3]University Hospital, Poitiers, FRANCE, [4]INSERM UMR 1101 LaTIM, Brest, FRANCE.

Aim: Since hypoxia is a major factor of radioresistance of prostate cancer (PC), we prospectively assessed hypoxia prior to and during radiotherapy treatment using ^{18}F-Misonidazole (FMISO) PET/CT.Method: Inclusion criteria were intermediate-risk PC patients planned to receive high-dose (>74 Gy) radiotherapy to the prostate without hormonal treatment. Prior to radiotherapy, all patients underwent a $FMISO_1$ PET/CT (45 min dynamic imaging, and late static imaging at 2,5h and 3,5h post-injection of 4 MBq/kg), as well as a trans-pelvic coil 1.5 T MRI and 18FCholine-PET. All images were co-registered using iPLANNET (Brainlab®). In $FMISO_1$-positive patients, a second $FMISO_2$ PET/CT was acquired after a minimal delivered dose of 18 Gy. FCholine and FMISO-positive volumes were segmented by the automated Fuzzy Locally Adaptive Bayesian (FLAB) method. In $FMISO_1$-positive patients, a dynamic analysis of early tumor uptake was performed. Results: Out of the 27 patients (median age 76 [65-81]), 7 and 9 patients were considered positive at 2.5h $FMISO_1$ PET/CT and 3.5h $FMISO_1$ PET/CT respectively. Median SUV_{max} and SUV_{max} tumor to muscle (T/M) ratio were respectively 3.4, 3.6 [1.9-8.2] for 2.5h $FMISO_1$ PET and 3.2, 4.4 [2.2-15.6] for 3.5h $FMISO_1$ PET/CT. Median $FMISO_1$-positive volume was 1.1 ml [0.4-2.4]. Time-activity curves extracted from dynamic images allowed to differentiate hypoxic volume from urine artifacts in 3 patients who had underwent transurethral resection of the prostate due to an abrupt rise of the curve at 20 min. During radiotherapy, $FMISO_2$-positive volumes were no longer detected in 5/9 patients, and $FMISO_2$-positive volume significantly decreased in the remaining 4 patients (median volume 0.7 ml [0.3-1.8]). A weak correlation was observed between $FMISO_1$-positive and MRI-, FCholine-positive areas (median Dice's coefficient=0.03 and 0.01 respectively). Conclusion: To the best of our knowledge, this is the first study showing that a small FMISO-positive volume can be detected in one third of intermediate-risk PC patients. Dynamic analyses could eliminate false positive areas related to urine excretion. Decreased hypoxic volumes were observed in all FMISO-positive patients, which suggests that fractionated radiotherapy induces tumor reoxygenation.

OP306

Multimodal imaging agents for sentinel node mapping as a means to (re)connect nuclear medicine to advances made in robot assisted surgery.

G. H. KleinJan[1,2], N. S. Van den Berg[1,2], E. Wit[2], E. Vegt[2], F. W. B. Van Leeuwen[1], H. G. Van der Poel[2]; [1]Leiden University Medical Centre, Leiden, NETHERLANDS, [2]NKI-AVL, Amsterdam, NETHERLANDS.

Introduction: Prostatectomies and complementary extended

pelvic lymph node dissection (ePLND) of (sentinel) lymph nodes (LN) at risk of containing metastases are increasingly being performed using high-tech robotic approaches. Although this technological evolution has clear surgical advantages, the physical nature robotic systems limits integrated use of routine radioguided surgery technologies. This limitation has driven robotic engineering efforts towards the integration of fluorescence rather than radioguidance. We here present an attempt to reconnect the robotic developments to nuclear medicine, by making use of a hybrid tracer (radioactive and fluorescent) that allows for fully integrated preoperative nuclear imaging and intraoperative fluorescence guidance towards sentinel nodes (SN). Methods: Fifty patients with a Briganti nomogram-based risk >10% of lymph node (LN) metastases were included. After indocyanine green (ICG)- 99mTc-nanocolloid injection, nuclear imaging was performed to locate the SN(s). The 3D information of the SPECT-CT was used by the surgeon to plan the operation with a da Vinci Si robotic system equipped with a Firefly near-infrared fluorescence endoscope. Intraoperatively, fluorescence guidance was used to optically identify the preoperatively defined SN(s); fluorescence imaging (FI) could be conveniently (dis)activated during the resection using a simple hand-switch. The number and location of the intraoperatively identified SNs, the in vivo and ex vivo fluorescence-based SN identification rate and radioactivity measurements, and the tumor status of SNs and LNs removed with ePLND were recorded and analyzed. Results: Based on SPECT-CT imaging a total 201 SNs (median 4) were identified of which 54 (26.9%; median 1) were located outside the standard ePLND. During surgery, 34 SNs could not be resected based on their location (e.g mesorectal fascia) and/or the risk of complications. FI was integrated into the surgical process and thereby helped to identify 15 additional SNs not previously identified on preoperative imaging. In total, 182 SNs were intraoperatively excised of which 82% were identified with the Firefly in vivo (ex vivo: 98%) could be identified with FI. All excised SNs were radioactive. With ePLND an additional 589 LNs were removed (median 10). Histopathological evaluation revealed tumor-positive SNs in 26% of patients (n=13). In 11 of these, the SN(s) was the only tumor-positive node. In two patients besides a tumor-positive SN, additional tumor-positive LNs were found. In one node positive patient, the SN was negative (false positive rate 7%). Conclusion: With the hybrid tracer preoperative SPECT/CT imaging information can be integrated into state-of-the-art surgical robotics, where it complements fluorescence-based SN identification.

OP307

68Ga-OPS202/177Lu-OPS201, a high performance theranostic pair of radiolabelled somatostatin antagonists for PET imaging and radionuclide therapy: translational aspects

G. P. Nicolas[1], R. Mansi[1], F. Kaul[1], S. Vomstein[1], J. Kaufmann[2], H. Bouterfa[2], D. Wild[1], M. Fani[1]; [1]University Hospital Basel, BASEL, SWITZERLAND, [2]OctreoPharm Sciences GmbH, BERLIN, GERMANY.

Aim: To evaluate the somatostatin receptor (sst2)-antagonist Cpa-c(DCys-Aph(Hor)-DAph(Cbm)-Lys-Thr-Cys)-DTyr-NH_2 (JR11), for PET imaging and peptide receptor radionuclide therapy (PRRT) of neuroendocrine tumours (NETs) and address translational aspects related to clinical applications. Materials and Methods: Comprehensive *in vivo* evaluation of ^{177}Lu-OPS201 (^{177}Lu-DOTA-JR11) was performed in HEK-hsst2 xenografts comparatively to ^{177}Lu-DOTA-TATE. The influence of the peptide mass was assessed by a mass escalation study in HEK-hsst2 and AR42J xenografts. Various biodistribution modifiers were tested, including kidney protection agents and i.v. injections of octreotide. In parallel, a phase I/II clinical trial was initiated, comparing two microdoses (15 and 50 μg) of ^{68}Ga-OPS202 (^{68}Ga-NODAGA-JR11) PET/CT with ^{68}Ga-DOTA-TOC in the same 12 patients with NETs (ClinicalTrials.gov NCT02162446). Results: ^{177}Lu-OPS201 showed 2.6-times higher tumour dose and 1.8-fold higher kidney dose, resulting in 34% more favourable tumour-to-kidney dose ratio compared to ^{177}Lu-DOTA-TATE. Biodistribution and nanoSPECT/CT showed that escalating the injected peptide mass of ^{177}Lu-OPS201 from 10 to 200 pmol drastically improved the tumour-to-background uptake ratios in HEK-hsst2 and AR42J xenografts: tumour-to-liver increased from 16 to 52 and from 30 to 54, respectively and tumour-to-bone-marrow from 25 to 97 and from 23 to 93, respectively, 4h p.i. However, tumour-to-kidney ratios remained mostly unchanged. Pre-injection of lysine, gelofusin or combination of both decreased the kidney uptake of ^{177}Lu-OPS201 about 40%. Interestingly, 200-fold excess of octreotide seemed to have no influence on the distribution of the antagonist, including the tumour uptake. In patients, both ^{68}Ga-OPS202 doses showed improved tumour-to-background ratios compared to ^{68}Ga-DOTA-TOC PET/CT. Especially, matched liver metastases (visible on all 3 scans) showed a factor of 2 increase in tumour-to-liver-background uptake ratios (mean±σ) 4.4±3.5 (15 μg)/4.9±3.9 (50 μg) vs 2.1±1.5 for ^{68}Ga-DOTA-TOC. The 50 μg dose seemed to further decrease the uptake of ^{68}Ga-OPS202 in the sst2-positive organs compared to 15 μg, e.g. in the spleen (11.5±5.1/10.3±3.0), pancreas (2.7±1.1/2.3 ±0.7) and intestine (3.6±1.5/3.0±0.9), compared to ^{68}Ga-DOTA-TOC (27.9±11.5, 4.1±1.5 and 5.5±1.2, respectively). Conclusion: Increased image contrast of ^{68}Ga-OPS202, along

with an advantageous tumour-to-kidney dose ratio of ^{177}Lu-OPS201, is expected to improve sensitivity and diagnostic accuracy of PET/CT imaging and safety window of PRRT in NET patients, compared to the agonists. An optimized peptide mass of the radiolabelled antagonist is likely to further enhance the performance of this promising theranostic pair. First *in vivo* pre-clinical data indicated that, when using sst2 antagonists for PRRT, octreotide treatment may not be interrupted.

OP308

First results with Lu-177-PSMA617 in targeted radionuclide therapy of patients with metastatic hormone-refractory prostate cancer

C. Kratochwil[1], F. L. Giesel[1], A. Afshar-Oromieh[1], M. Benešová[2], W. Mier[1], M. Eder[2], K. Kopka[2], U. Haberkorn[1]; [1]University Hospital Heidelberg, Heidelberg, GERMANY, [2]Division of Radiopharmaceutical Chemistry, German Cancer Research Center (DKFZ), Heidelberg, GERMANY.

Objectives:We report our clinical experience with PSMA targeted radionuclide therapy of patients with metastatic hormone-refractory prostate cancer in regard to toxicity and treatment effects using Lu-177-PSMA617, a PSMA ligand consisting of a DOTA-chelate tagged to the Glu-urea-Lys motif via an aromatic linker which further improves tumor accumulation while reducing kidney uptake.Methods:We retrospectively evaluate 35 patients that received therapy with Lu-177-PSMA617 in our department. All patients were hormone- and taxan-refractory or taxanes were contraindicated and the oncological status was progressive. A PSMA-positive tumor phenotype was previousely validated with PSMA-PET/CT (Ga-68-PSMA-11, Glu-urea-Lys-Ahx-HBED-CC), respectively. Acute hematotoxicity was evaluated with lab tests and clinical exam according to CTCEA criteria and response was evaluated with PSA sampling and radiologic follow-up.Results:In patients with multifocal bone lesions but no bone marrow-carcinosis (no superscan in bone scintigraphy) 6 GBq Lu-177-PSMA617 every 2 months was found to be tolerable in regard to hematotoxicity. Other common side effects were xerostomia, less common fatigue and seldom unspecific intestinal disorders. Dosimetry presents kidney doses of less than 1 Gy per 1 GBq Lu-177-PSMA617 and no renal toxicity was observed, yet. Five patients, who were in end-stage situation when receiving the therapy, died before follow-up imaging. PSA-response was observed in the majority of the patients. After 3 cycles (6-9 months) PSA progression re-occurred in ca. 50% of the patients. In the other 50% sustainable biochemical and radiologic response was observed including one patient with complete remission in PSMA-PET.Conclusions:Radionuclide therapy with Lu-177-PSMA617 demonstratesa favorable therapeutic range and can induce biochemical as well as radiologic responses with moderate acute toxicity. Clinical trials evaluating PFS and OS are encouraged.

OP309

Baseline 18F-FDG PET/CT Predicts Progression-Free Survival After Radium-223

E. Etchebehere, J. Araujo, G. Ray, D. Milton, N. Swanston, H. Macapinlac, E. Rohren; The University of Texas MD Anderson Cancer Center, Houston, TX, UNITED STATES.

AIM: The purpose of this study was to evaluate if whole-body ^{18}F-FDG PET/CT is able to predict which patients will benefit from Radium-223 therapy (Ra-223). MATERIALS AND METHODS: We retrospectively reviewed 26 histologically confirmed hormone-refractory prostate cancer patients (52-84 y old; mean 69 ± 9 yrs.) with bone metastases (without visceral metastases). The patients were submitted to an 18F-FDG PET/CT scan prior to Ra-223. Overall survival (OS) was the primary end point. Secondary end points were progression-free survival (PFS) and bone event-free survival (BeFS). We evaluated the presence of nodal metastases, the total number of radium cycles (Ra_{Tot}) and the following 18F-FDG PET/CT parameters: the highest SUVmax of a bone metastasis (*h*-SUVmax), the TLG of bone metastases (TLG_{Bone}) and TLG of bone and nodal metastases (TLG_{All}). RESULTS: The median follow-up time was 6.14 months (0.36-9.72 months). Eight (31%) patients presented nodal metastases prior to Ra-223. Fourteen (54%) patients received all 6 Ra-223 cycles, three (12%) were still in progress and 9 (35%) discontinued Ra-223. Reasons for withdrawal from Ra-223 were: progression (n=6), hematologic toxicity (n=1), declining ECOG status (n=1) and/or a bone event (n=1). During Ra-223, four patients died, 11 (42%) progressed and six (23%) had a bone event. The median OS was not reached (less than 50% of the patients died), the median PFS was 5.91 months and the BeFS was 8.61 months. In a univariate model, Ra_{TOT} was associated with OS (HR=0.38; p=0.018), PFS (HR=0.55; p<0.001) and BeFS (HR=0.45; p=0.001). Each additional cycle of Ra-223 was associated with a 62% reduction in the risk of death, a 45% reduction in risk of progression or death and a 55% reduction in risk of experiencing a bone event or death. PFS was significantly associated with *h*SUVmax (HR=1.39; p=0.002) and marginally associated with TLG_{Bone} (HR=1.69; p=0.0520) and TLG_{All} (HR=1.70; p=0.051). A *h*SUVmax cutoff ≥ 5.6 (p=0.003) and a TLG_{Bone} cutoff ≥ 240 (p=0.006) separated patients with a shorter PFS. BeFS was not associated with any of the FDG-PET/CT parameters nor with the presence of nodal metastases. CONCLUSIONS: Baseline 18F-FDG PET/CT is able to predict PFS during Ra-223. A one-unit increase in *h*SUVmax was associated with a 39% increase in risk of

progression or death. Patients with hSUVmax below 5.6 had a longer progression-free survival. More Ra-223 cycles were beneficial and reduced the risk of death, progression and the risk of a bone event.

OP310

64Cu-ATSM PET/CT in solid tumours: *a prognostic evaluation for disease outcome*

E. Lopci[1,2], I. Grassi[3], S. Cambioli[3], A. Gamboni[4], F. Salvi[5], G. Cicoria[3], F. Lodi[3], C. Dazzi[6], S. Mattioli[7], S. Fanti[3]; [1]Humanitas Clinical and Research Hospital, Milano, ITALY, [2]Alma Mater Studiorum University, Bologna, ITALY, [3]University Hospital S. Orsola-Malpighi, Bologna, ITALY, [4]Ospedale degli Infermi, Faenza, ITALY, [5]Ospedale Bellaria, Bologna, ITALY, [6]Istituto Oncologico Romagnolo, Ravenna, ITALY, [7]Alma Mater Studiorum, Bologna, ITALY.

Purpose: 64Cu-ATSM is a well-known PET radiopharmaceutical applied for tumour imaging of hypoxia. One of the advantages of this compound compared to other hypoxia-avid tracers is the high tumour-to-background signal offered, which guaranties a facilitated tumour delineation. The current study aimed at analyzing optimal semi-quantitative and quantitative parameters obtained by 64Cu-ATSM PET/CT in the same cohort of patients with special focus on their correlation to disease outcome. Materials and Methods: A prospective recruitment of 18 consecutive patients (M:F=13:5; mean age 60.7 years) with locally advanced NSLCL (n=7) or head and neck cancer (HNC) was performed. Each participant received 105-500MBq of tracer according to body size and was scanned in a 3D-mode on a PET/CT tomograph 60 minutes after tracer injection. PET images were reconstructed and visualized on a GE Advanced 4.6 workstation for the definition of semi-quantitative and quantitative parameters: SUV_{max}, $SUV_{ratio\text{-}to\text{-}muscle}$, SUV_{mean}, hypoxic volume (HV) and hypoxic burden ($HB=HV*SUV_{mean}$). These data were subsequently correlated to disease outcome, expressed in terms of progression-free survival (PFS) calculated on a follow-up period of median 14.6 months. Results: All patients showed a moderately to highly increased uptake of 64Cu-ATSM in tumour lesions, with a mean SUV_{max} of 5.2 (range 1.9-8.3), mean SUV_{ratio} of 4.4 (range 1.6-6.8) and SUV_{mean} of 2.8 (range 1.0-6.8). Also a broad range of HV and HB was defined, with as mean values 99.3cm^3 (range 2.5-453.7) and 301 (4.2-1134), respectively. The ROC analysis identified as reference cut-offs with respect to disease outcome the following values: SUV_{max} >2.5 (AUC 0.57; sens. 88.9%; spec.50%), SUV_{ratio} ≤4.4 (AUC 0.60; sens. 50; spec. 83.3%), SUVmean >1.5 (AUC 0.61; sens. 88.9%; spec. 50%), HV >160.7cm^3 (AUC 0.61; sens. 55.6%; spec. 75%), HB >160.7 (AUC 0.67; sens. 58.3%; spec.83.3%). In our cohort, tumour hypoxic burden (HB) showed a statistically significant difference in terms of mean values on the ANOVA test with respect to disease progression (p=0,038). On univariate analysis, the Cox regression confirmed these findings and showed a significant correlation to PFS for HB (p=0.05) and tumour hypoxic volume (p=0.019). Conclusions: In our cohort, the definition of optimal semi-quantitative and quantitative parameters on 64Cu-ATSM PET/CT appears feasible and in line with previously published data. However, when considering the prognostic role with respect to disease outcome, the more robust parameters are represented by hypoxic tumour volume (HV) and hypoxic burden (HB).

1001 - Monday, October 12, 2015, 4:30 PM - 6:00 PM, Hall 1
CME 8 - Cardiovascular & EACVI: Imaging in Heart Failure: Focus on Nuclear Medicine Techniques and Clinical Implications

---

OP311
Clinical Perspective: Therapeutic Options
A. J. H. A. Scholte, NETHERLANDS

OP312
Selecting Patients for Revascularisation
O. Gaemperli, SWITZERLAND

OP313
Selecting Patients: CRT
C. Uebleis, GERMANY

OP314
Selecting Patients for ICD
H. J. Verberne, NETHERLANDS

1002 - Monday, October 12, 2015, 4:30 PM - 6:00 PM, Hall 2
Joint Symposium 8: EANM/EAU: PET Imaging of Genito-urinary Malignancies beyond Prostate

OP315
Clinicians Needs for Kidney and Bladder Cancer Imaging
J. Walz, FRANCE

OP316
PET Imaging of Kidney and Bladder
C- Divgi, USA

OP317
Clinical Needs for Testis Cancer and other Malignancies
J. Walz, FRANCE

OP318
PET Imaging of Testis Cancer and other Malignancies
K. Herrmann, GERMANY

1003 - Monday, October 12, 2015, 4:30 PM - 6:00 PM, Hall 4
CTE 4 - Joint Session with Inflammation & Infection Committee: Infection Imaging in Nuclear Medicine

OP319
Overview on Infection Imaging by SPECT and PET
O. Gheysens, BELGIUM

OP320
Overview on Inflammation/Infection and Standardised Cell Labelling Procedure
E. Lazzeri, ITALY

OP321
Image Acquisition and Interpretation Parmaeters for Planar, SPECT and PET
A. Signore, ITALY

1004 - Monday, October 12, 2015, 4:30 PM - 6:00 PM, Hall G1
Neurosciences - Featured: Dementia

OP322
GLP-1 analogue liraglutide prevents decline of brain glucose metabolism in Alzheimer's Disease: Randomized, placebo-controlled double-blinded clinical trial

M. Gejl[1], L. Egejord[2], A. Møller[1], S. B. Hansen[1], K. Vang[1], A. Rodell[1], H. Brændgaard[1], H. Gottrup[1], A. Schacht[1], N. Møller[1], B. Brock[1], J. Rungby[2], A. Gjedde[3]; [1]Aarhus University Hospital, Aarhus, DENMARK, [2]Aarhus University, Aarhus, DENMARK, [3]University of Copenhagen, Copenhagen, DENMARK.

Introduction: Type 2 Diabetes Mellitus (T2D) increases the risk of Alzheimer's disease (AD) and vice versa. Suggested common pathophysiological mechanisms include deficient insulin and glucagon-like-peptide-1 (GLP-1) signalling. In rodent models of AD, the GLP-1 receptor agonist liraglutide limits amyloid (Aβ) deposition and inflammation, blocks memory deterioration, and may normalize glucose consumption. As a surrogate marker of synaptic dysfunction and neuronal activity, [18F]fluorodeoxyglucose ([18F]FDG) uptake in brain is sensitive to disease progression. The decline of the cerebral metabolic rate of glucose (CMRglc) is closely related to cognitive impairment. We predicted that treatment with liraglutide would reduce the accumulation of Aβ and improve CMRglc measured with positron emission tomography (PET) of AD patients. Materials and methods: In this 26-week, randomized, double-blind, placebo-controlled trial, we randomized 38 patients with moderately advanced AD to treatment either with liraglutide (n=18) or with placebo (n=20) as add-on medication. We mapped the changes of regional Aβ loads and cerebral blood flow (CBF) values in brain from the early and late phases of tracer Pittsburgh compound B ([11C]PIB) uptake and retention in brain, and the changes of CMRglc from the uptake of FDG, both with PET. We also monitored changes of cognition by means of the WMS-IV scale. Results: During the 26 weeks, the [11C]PIB retention increased significantly in the temporal lobes of both placebo ($P = 0.04$) and liraglutide groups ($P = 0.04$), and in the occipital lobe of the liraglutide-treated group ($P = 0.04$), but the increases did not differ between the two groups ($P \geq 0.38$). The expected correlation between values of CMRglc and CBF, confirmed at baseline and in the placebo-treated patients, was absent in patients treated with liraglutide. The CMRglc declined significantly in the placebo group ($P<0.05$) in precuneus ($P = 0.009$), and the parietal ($P = 0.04$), temporal ($P = 0.046$), and occipital lobes ($P = 0.009$), and in cerebellum ($P = 0.04$). In contrast, patients treated with liraglutide had a numerical, albeit insignificant, increase of CMRglc after the six months of treatment. Cognition was unchanged during the trial in both groups. Conclusion: In AD

patients, liraglutide treatment prevented the decline of CMRglc seen in placebo-treated patients where it signifies cognitive impairment, synaptic dysfunction, and disease evolution. We tentatively ascribe the loss of CBF-CMRglc coupling by liraglutide to altered lactate signalling in the neurovascular unit.

OP323

A randomized, controlled, multicenter, international study of the impact of florbetapir (18F) PET amyloid imaging on patient management and outcome

M. Pontecorvo[1], M. Grundman[2], B. Dubois[3], F. Nobili[4], C. Sadowsky[5], A. McGeehan[1], M. Lowrey[1], A. Dudek[1], M. Flitter[1], G. Dell'Agnello[6], A. Chevrette[7], W. Deberdt[7], A. Arora[1], M. D. Devous Sr[1], M. Mintun[1]; [1]Avid Radiopharmaceuticals, Philadelphia, PA, UNITED STATES, [2]Global R&D Partners, LLC and University of California, San Diego, San Diego, CA, UNITED STATES, [3]Salpêtrière Hospital, Paris, FRANCE, [4]University of Genoa (DINOGMI), Genoa, ITALY, [5]Nova SE University, Fort Lauderdale, FL, UNITED STATES, [6]Eli Lilly Italia, Sesto Fiorentino, ITALY, [7]Eli Lilly France, Paris, FRANCE.

Aim: The study evaluated the impact of amyloid PET on patient management and outcomes in a multicenter, randomized, controlled study.M ethods: Physicians in France, Italy and the US identified patients seeking diagnosis for MCI or dementia, where AD was considered a possible (<85% certain) cause. They recorded a working diagnosis and management plan including any plans for diagnostic and neuropsychological testing, follow-up and referral visits, and any medications planned to improve cognition. Patients underwent a florbetapir PET scan and were then randomized to either immediate or delayed (1 year) feedback regarding amyloid status (positive: Aβ+, negative: Aβ-). Patients returned after 3 months and the physician updated the diagnosis and constructed a summary of actual management, including neuropsychological and diagnostic testing actually performed, followup/referral visits that occurred and medications actually used to treat cognitive impairment since the post-scan visit. Patients returned to the center one year post-baseline for assessment of patient and caregiver outcome. Change in patient cognitive status was assessed with the ADAScog (investigators were blinded to the baseline ADAScog). Patient and caregiver health outcomes and quality of life were assessed at both 3 months and one-year with the RUD, EQ-5D, Geriatric Depression, QoL-AD, Zarit Burden and the Self Efficacy for Managing Dementia scales. It was hypothesized that outcomes would be worse for Aβ+ than for Aβ- patients (i.e., reflecting the impact of Alzheimer's disease) and that this effect might be mitigated for Aβ+ subjects in the immediate feedback group. Results: A total of 618 subjects were randomized to the immediate (308) or to the delayed (310) PET feedback arms, including 174 subjects in France, 221 in Italy and 223 in the US. 599 completed the 3 month and 560 completed the one-year follow-up visits, with the last visit conducted in April 2015. Analyses are ongoing. Preliminary results indicate that the percentage of patients for whom the actual management composite observed at 3 months was different from the baseline management plan (the protocol specified primary outcome) was significantly greater for the group that received immediate feedback regarding amyloid status than for those with delayed feedback. Three month and 1 year results will be presented for both the study as a whole and for individual European countries. Conclusions: This is the first large multicenter randomized controlled study of the clinical impact of amyloid PET and may help guide the use of amyloid PET imaging at both the global and country level.

OP324

18F-Florbetaben PET Imaging of Morphologically Distinct Amyloid β Deposits

O. Sabri[1], A. M. Catafau[2], H. Barthel[1], J. Seibyl[3], B. Ghetti[4], J. Leverenz[5], J. W. Ironside[6], S. Bullich[2], W. Schulz-Schaeffer[7], A. Hoffmann[8]; [1]Leipzig University, Leipzig, GERMANY, [2]Piramal Imaging, Berlin, GERMANY, [3]IND, New Haven, CT, UNITED STATES, [4]Indiana University School of Medicine, Indianapolis, IN, UNITED STATES, [5]Cleveland Lou Ruvo Center for Brain Health, Cleveland, OH, UNITED STATES, [6]University of Edinburgh, Edinburgh, UNITED KINGDOM, [7]Georg August University Göttingen, Göttingen, GERMANY, [8]Bayer Pharma, Berlin, GERMANY.

Aim: Post mortem histopathology is still regarded as gold standard to diagnose Alzheimer's disease (AD). Morphologically distinct amyloid β(Aβ) deposits, such as diffuse or neuritic Aβ plaques (DIFF, NEUR), and vascular Aβ (VASC) may be present in this disorder. Aβ PET imaging recently emerged as a promising alternative to potentially shift the gold standard AD diagnosis to in vivo. 18F-Florbetaben (FBB) has been validated as a biomarker of NEUR. It was the aim of this project to investigate the impact of the different forms of Aβ deposits on FBB PET scans. Materials and methods: Brain tissue was collected from 87 end-of-life patients (age 80 ±10yrs; 64 AD, 14 other dementia, 9 non-demented) who underwent a FBB PET scan before death. Aβ immunohistochemistry (IHC) was used for assessment of VASC. Aβ IHC and Bielschowsky silver stain were used for assessment of NEUR and DIFF in frontal, occipital, anterior cingulate and posterior cingulate cortices. From the total of 87x4=348 samples, 329 were finally assessed, and classified as Aβ absent (none or sparse) or present (moderate or frequent). Cortical standardized uptake value ratios (SUVRs) were obtained in all regions of interest (ROIs) using cerebellar grey matter as reference region. A linear regression model was fitted for each

ROI as: SUVR=a0+an×n+ad×d+av×v, where a0, an, ad, av are constants, and n=NEUR, d=DIFF and v=VASC. n, d, and v were assigned two values: 0=Aβ absent; 1=Aβ present. Results: In ROIs with high frequency of Aβ (frontal, posterior cingulate cortex), both DIFF (ad=0.32 and 0.42) and NEUR (an=0.27 and 0.21) contributed significantly to the SUVR. In ROIs with low frequency of Aβ (occipital, anterior cingulate cortex), only DIFF contributed significantly to the SUVR (ad=0.24 and 0.55). The presence of VASC contributed significantly to the SUVR only in the occipital ROI (av=0.13). Conclusion: There was a significant impact of DIFF on FBB SUVRs in brain regions with low Aβ load, supporting the use of FBB in detecting early stages of Aβ deposition. The impact of VASC on FBB SUVRs was only significant in the occipital cortex. These results underline the importance of measuring the topographic distribution of Aβ aggregates, and suggest potential utility of FBB in detecting cerebral Aβ angiopathy. Research support: Piramal Imaging, Berlin, Germany

OP325

18F-Florbetaben beta-amyloid PET scan quantification: Do cerebellar plaques influence SUVR?

A. M. Catafau[1], S. Bullich[1], J. Seibyl[2], H. Barthel[3], B. Ghetti[4], J. B. Leverenz[5], J. W. Ironside[6], W. J. Schulz-Schaeffer[7], A. Hoffmann[8], O. Sabri[3]; [1]Piramal Imaging GmbH, Berlin, GERMANY, [2]Molecular Neuroimaging, New Haven, CT, UNITED STATES, [3]Leipzig University, Leipzig, GERMANY, [4]Indiana University School of Medicine, Indianapolis, IN, UNITED STATES, [5]Puget Sound Health Care System and University of Washington, Seattle, WA, UNITED STATES, [6]University of Edinburgh, Edinburgh, UNITED KINGDOM, [7]Georg-August University Göttingen, Göttingen, GERMANY, [8]Bayer Pharma AG, Berlin, GERMANY.

Aim: Standardized uptake value ratios (SUVR) using cerebellar grey matter as the reference region are commonly used for quantification of 18F-Florbetaben (FBB) scans. However, cerebellar plaques may be present in Alzheimer disease (AD). The aim of this study was to assess the influence of cerebellar plaques in FBB SUVR, when using cerebellar grey matter as the reference region. Materials and methods: Cerebral (frontal, occipital, anterior and posterior cingulate) cortex and cerebellar cortex tissue from 87 end of life patients (64 AD, 14 other dementia, 9 non-demented aged volunteers; 80.4±10.2 yrs) who underwent a FBB PET before death was neuropathologically assessed using the Bielschowsky silver stain and Amyloid β (Aβ) immunohistochemistry. Neuritic/cored and diffuse plaques were rated as absent, sparse, moderate and frequent. Cerebral cortical SUVRs were compared among brains with different cerebellar plaque loads. Results: None from the 83 evaluable cerebellar samples showed frequent plaques. Sparse diffuse plaques were found in 33 samples, and moderate diffuse plaques in 5. Only 1 sample showed both sparse neuritic/cored and sparse diffuse plaques. Subjects with higher cerebellar plaque loads showed higher cerebral cortical Aβ loads and higher cerebral cortical standardized uptake values. Thus, cerebral cortical SUVRs significantly increased with cerebellar plaque load (range from 1.36 (cerebellar plaques absent) to 1.86 (cerebellar plaques moderate) across regions, all p values <0.004). However, in cerebral cortical regions with moderate or frequent Aβ plaques no significant SUVR differences were found among brains showing different cerebellar plaque loads (all p values >0.39). Conclusions: In brains with higher cerebral cortical Aβ loads, cerebellar plaques were found in 47% of cases, mostly as sparse diffuse plaques (40%). The presence of cerebellar plaques did not influence the SUVRs in subjects with moderate or frequent cortical Aβ. Therefore, the effect of cerebellar plaques in FBB SUVR appears to be negligible even in advanced stages of AD with a high cortical Aβ load.

OP326

Clinical [^{18}F]Florbetaben-PET Imaging - Benefit of Early Acquisition

S. Daerr[1], M. Brendel[1], C. Zach[1], A. Danek[1], H. Barthel[2], O. Sabri[2], P. Bartenstein[1], **A. Rominger**[1]; [1]University of Munich, Munich, GERMANY, [2]University of Leipzig, Leipzig, GERMANY.

Objectives: In the last few years [^{18}F]-labelled amyloid PET radiotracers have been developed and recently received clinical approval. We now report on our experience with a heterogenous patient cohort using [^{18}F]Florbetaben (FBB) PET. A major goal was to investigate the benefit of an additionally performed early post injection acquisition of the FBB-PET. Methods: All subjects for amyloid imaging were recruited in a clinical setting. Aside from undergoing a detailed neuropsychiatric test battery, collection of biomarkers (MRI, CSF, FDG-PET) was performed as well. Furthermore 300 MBq [^{18}F]Florbetaben were injected i.v. and PET scans were routinely acquired 90 min p.i., and an early acquisition starting just after injection was performed in a subset of patients. Visual comparison and semiquantitative correlation analyses were performed between FDG- and early FBB uptake. Results: A total of 105 patients (mean age 70.3±9.5y) were scanned. In a subset of 44 patients an early acquisition of the FBB-PET could be performed, in 35/44 patients the individual FDG-PET was available. In 16/35 cases the regularly acquired amyloid PET was read negative, 19/35 cases were amyloid-positive. When the early acquisition of FBB was processed in

Neurostat and compared to a normative database, the visual interpretation resembled the pattern of the individual FDG-PETs, irrespective of the amyloid-status in the late FBB-scans. The semiquantitative correlation analyses ranged from R=0.78 to R=0.94 ($p<0.01$) in different brain regions assessed, altogether resembling good-to excellent correlation features between early FBB and FDG-metabolism. Conclusions: We report on the clinical use of Florbetaben-PET in a non-selected patient cohort. Early [^{18}F]Florbetaben acquisitions as a perfusion-like marker closely resembled FDG-PET findings. These findings need to be further investigated in a larger patient cohort, but could potentially substitute an additional FDG-PET scan in the future.

OP327

Resveratrol in Alzheimer's disease: a PIB positron emission tomography/computed tomography study

A. Damian[1], A. de la Fuente[2], G. Castellano[3], E. Savio[2], P. Buccino[2], B. Aguiar[4], A. Quagliata[1], F. Cano[3], M. Gonzalez[2], S. Dansilio[4], A. Kmaid[5], I. Savio[5], H. Engler[2]; [1]Uruguayan Centre of Molecular Imaging (CUDIM); Nuclear Medicine Centre, University of the Republic, Montevideo, URUGUAY, [2]Uruguayan Centre of Molecular Imaging (CUDIM), Montevideo, URUGUAY, [3]Department of Social and Preventive Medicine, University of the Republic, Montevideo, URUGUAY, [4]Department of Neuropsychology, University of the Republic, Montevideo, URUGUAY, [5]Department of Geriatrics, University of the Republic, Montevideo, URUGUAY.

Resveratrol (trans-3,5,40-trihydroxystilbene) is a polyphenol that has shown potential beneficial effects in cardiovascular and neurodegenerative disorders. Although it has been proved that resveratrol promotes vasodilatation, the regional changes in cerebral blood flow (CBF) induced by this polyphenol have not been fully assessed yet. Pittsburgh Compound B (PIB) is a lipophilic thioflavin derivative PET tracer used to detect amyloid depositions, for example in patients with Alzheimer's Disease (AD). The molecules of resveratrol and PIB have structural similarities, which can indicate possible similar interactions with amyloid depositions. Additionally, it has been published that early images of the PIB scans can be used as an indicator of CBF.Aim: To assess the possible effect of a short treatment with resveratrol on the amyloid deposition images with PIB PET and on a rough index of CBF.Materials and methods: Prospective study that included twelve PIB positive AD patients (58-85 years old, 5 men) that underwent clinical and extensive neuropsychological examination. The mean progression time from diagnosis was 2.6±2.2 (SD) years, with a mean Mini-mental state examination score of 22.5±3. After the first PIB positive scan, the patients were treated with oral administration of 1 g trans-resveratrol daily during 8 days. A second PIB scan was performed the last day of treatment. Parametric images of the first 6 min (eSUV and ePIB normalized to the cerebellum) and the last 20 min (tSUV and tPIB) of the PIB scans were obtained and analyzed using predefined Volumes of Interest (VOIs) and a voxel based approach with the software Statistical Parametric Mapping (SPM8). Results: The analysis of changes in amyloid depositions (tPIB and tSUV) did not reveal significant differences before and after the treatment with Resveratrol in any region of the cortex. Voxel based analysis of the early images (eSUV) of the PIB scans showed an increased uptake in the occipital cortex bilaterally after the treatment with Resveratrol ($p<0.001$, uncorrected for multiple comparisons, 100 voxels extent threshold) with a minor extension to the left inferior parietal lobe. We couldn't find a significant correlation between eSUV and ePIB.Conclusions: There were not changes in amyloid depositions after a week of treatment with Resveratrol. Changes in the early distribution of PIB, interpreted as an increased CBF, were observed in the occipital and inferior parietal cortex. Further studies with specific CBF tracers are needed to study the regional effect of resveratrol in brain perfusion.

1005 - Monday, October 12, 2015, 4:30 PM - 6:00 PM, Hall G2
Do.MoRe: 90Y SIRT Treatment Planning

OP328

Partition model absorbed dose biases and variability due to tumor-to-normal-liver ratios following 90Y microsphere therapy

J. Mikell[1,2], A. Mahvash[1], W. Siman[1,2], F. Mourtada[3], **S. C. Kappadath**[1,2]; [1]UT MD Anderson Cancer Center, Houston, TX, UNITED STATES, [2]UT Graduate School of Biomedical Sciences, Houston, TX, UNITED STATES, [3]Christiana Care Health System, Newark, DE, UNITED STATES.

Aim: Partition model (PM) assumes uniform distribution of 90Y microspheres within tumors (T) and non-tumoral (NT) compartments. In addition, it assumes a single scalar (TNR) to describe the relative activity concentration (AC) of 90Y microspheres between T and NT. However, clinical reality presents multiple tumors that have different uptake and non-uniform AC. Monte Carlo (MC) provides voxel-based absorbed dose distributions throughout T and NT volumes. Only in the ideal case of uniform uptake to a single T and uniform uptake to NT will the mean absorbed dose estimates from PM equal MC. In this work we calculate 1) the differences between PM and MC for mean absorbed doses to T and NT, and 2) the variability of PM doses on estimates of TNR. Various TNR were calculated using 1) mean tumor AC (meanT), 2) maximum tumor AC (maxT), and 3) four estimates of mean NT AC. Materials and Methods: We analyzed

21 90Y glass-microsphere cases; 7 were single tumor cases. MC absorbed doses were calculated from quantitative 90Y SPECT/CT. Tumors and livers were segmented by radiologist. PM tumor uptake was characterized by meanT and maxT; volume-weighting was used for multiple tumors. PM NT uptake was characterized by mean AC of the entire NT VOI (meanNT) and mean AC of three spheres (D=2.5cm) placed in different locations within NT by radiologist. We generated eight estimates of TNR and consequently eight estimates of absorbed dose to T and NT. We assessed the differences (%Δ) of PM absorbed dose estimates relative to MC and the variability (coefficient of variation, COV) of PM absorbed doses due to TNR. Results: For single tumors using TNR=meanT/meanNT, the average %Δ and (range) was 70%±24% (31% to 99%) for T and 71%±26% (23% to 90%) for NT. For multiple tumors using TNR=volume-weighted-meanT/meanNT, the average %Δ and (range) was 103%±119% (-28% to 476%) for T and 54%±21% (20% to 99%) for NT. For single tumors using TNR=maxT/meanNT, the average %Δ was 192%±89% (53% to 295%) for T and 2%±58% (-65% to 65%) for NT. The PM absorbed dose COV due to TNR variability for single (multiple) tumors was 0.32±0.17 (0.32±0.16) for T and 0.42 ±0.29 (0.23±0.29) for NT. Conclusion: There are large biases and high variability in PM absorbed dose estimates for T and NT stemming from the uncertainties in the TNR that hold true even in the best case scenario of single tumors. Grant support NIH/NCI R01 CA138986.

OP329

99mTc-MAA SPECT/CT lung shunt estimations are more accurate than those obtained from planar scintigraphy

J. Prince, A. F. van den Hoven, G. C. Krijger, N. de Wit, B. J. van Nierop, M. N. G. J. Braat, M. A. A. J. van den Bosch, H. M. Verkooijen, M. G. E. H. Lam; UMC Utrecht, Utrecht, NETHERLANDS.

Aim: Shunting of yttrium-90 microspheres to the lungs can preclude radioembolization if the estimated absorbed lung dose after treatment is >30 Gy on ^{99m}Tc-MAA planar scintigraphy. The objective of this study was to investigate the validity of planar scintigraphy lung shunt after ^{99m}Tc-MAA compared with SPECT/CT and to identify risk factors for a high lung shunt. Materials and methods: Between March 2011 and November 2013 patients eligible for radioembolization were included in this retrospective, cross-sectional, single-center study. The lung shunt fraction after ^{99m}Tc-MAA injection was measured by dividing the counts in the lungs by the counts in the lungs and liver. The absorbed dose (Gy) on SPECT/CT was based on the estimated MBq/mL in the basal lung assuming a homogeneous density and distribution. Univariable analyses were used to test for association ($p<0.05$) between the occurrence of lung shunting on planar scintigraphy or SPECT/CT and the following risk factors: tumor type, tumor burden in the target volume (in %), angioinvasion, extrahepatic disease, and time between ^{99m}Tc-MAA injection and imaging (in minutes). Results: A total of 139 ^{99m}Tc-MAA injections were performed in 112 patients. A median lung shunt fraction on planar scintigraphy of 5.5% (range 0.3-39%) was found. The ability of both measurements to differentiate between patients (the reliability) was moderate, as the intraclass correlation coefficient, $ICC_{consistency}$ (ignoring systematic error), was 0.72; the $ICC_{agreement}$ was 0.59. Planar scintigraphy overestimated the absorbed dose by a median of 1.4 Gy / GBq yttrium-90 (range -2.2 - 14.9 Gy) compared to SPECT/CT. On planar scintigraphy 4 cases exceeded the 30 Gy threshold. However, SPECT/CT did not agree in 1 case and identified 4 extra cases ineligible for treatment. Univariable analyses identified the following risk factors both on planar scintigraphy and SPECT/CT: angioinvasion, tumor burden, and time between ^{99m}Tc-MAA injection and imaging. Only planar scintigraphy showed an association between lung shunt and hypervascularity and extrahepatic disease. Conclusion: Planar scintigraphy overestimates lung shunting compared to SPECT/CT. A clinical significant threshold for lung shunting should be defined for SPECT/CT and may be used in combination with risk factors for accurate patient selection.

OP330

Previsional dosimetry based on 99mTc-MAA SPECT for radioembolization of liver lesions with 90Y-loaded microspheres: impact of attenuation correction, scatter correction and calibration

M. Pacilio[1], C. Chiesa[2], **M. E. Ferrari**[3], F. Botta[3], L. Lorenzon[1], M. Mira[2], M. Ljungberg[4], M. Cremonesi[3]; [1]Azienda Ospedaliera San Camillo Forlanini, Roma, ITALY, [2]Istituto Nazionale dei Tumori, Milano, ITALY, [3]European Institute of Oncology, Milano, ITALY, [4]Lund University, Lund, SWEDEN.

Background and aim: Therapy optimization in radioembolization (RE) with 90Y-loaded microspheres should be pursued through treatment planning based on 99mTc-MAA-SPECT image. The accuracy of the quantification depends on differen issues. The aim of this study was to evaluate the influence of attenuation and scatter corrections in the 99mTc-MAA-SPECT images for RE dosimetry of simulated patients and clinical cases. Methods: Simulated and real 99mTc-MAA-SPECT images were reconstructed by OSEM algorithm without corrections (NoAC_NoSC) or with scatter (NoAC_SC), attenuation (AC_NoSC), scatter and attenuation (AC_SC) corrections. Monte Carlo (MC) simulations (SIMIND code) were performed for three different body size

and different activity distribution (uniform activity in the whole liver, or in a liver lobe, or with hot lesions with lesions/normal liver ratio=5). 36 clinical cases were also studied with a relative calibration method. Lesions and healthy parenchyma were manually contoured on the co-registered CT-SPECT images. The absorbed dose distributions were calculated at dose level from the activity maps, comparing results obtained from different correction methods in terms of DVHs and dose profiles. For simulated cases, the dose image derived from the input activity map was the Gold Standard (GS) while for clinical cases, the dose map from AC_SC was considered as reference. Results: For simulated cases, differences vs. GS decrease implementing AC and SC in the tomographic reconstruction. Deviations from GS of D95%, D70%, D50% for lesion and healthy parenchyma are lower for AC_NoSC, than for NoAC_SC.In the clinical cases, deviations from GS of D90%, D70%, D50%, are lower for AC_NoSC, than NoAC_SC for lesions, while for healthy parenchyma the absence of attenuation correction is less critical than the absence of scatter correction.Conclusions:All corrections are needed to improve dosimetric accuracy.The difference in the results of the healthy parenchyma between simulations and real patients, as regards the influence of separate AC and SC, could be due to the influence of patient motion (respiration, not present in simulations) or variability of activity distributions in real patients.However, for the most important side of the planning strategy (safety=parenchyma dosimetry) the absence of attenuation correction (not available in all SPECT system) seems less critical than the absence of scatter correction (available on all system). Despite inaccuracies, the dosimetry approach provides a much safer (lower toxicity) and efficient (higher tumour irradiation) approach showing therefore a better RE optimization than using others empirical methods indicated by producers (BSA, tumor involvement, mean dose to lobe).

OP331

Effect of Data-Driven Respiratory Gating on Radioactivity Quantification in Liver Lesions for Pre-Radioembolization Tc-99m-MAA SPECT/CT

J. C. Sanders[1,2], A. H. Vija[3], T. Kuwert[1], P. Ritt[1]; [1]Clinic of Nuclear Medicine, University Hospital Erlangen, Erlangen, GERMANY, [2]Pattern Recognition Lab, University of Erlangen-Nuremberg, Erlangen, GERMANY, [3]Siemens Molecular Imaging, Hoffman Estates, IL, UNITED STATES.

Aims: In single photon emission-computed tomography (SPECT), comparatively long acquisition times may lead to blurring and underestimation of radioactivity in foci moved by respiration. This can be mitigated by respiratory gating, whereby a surrogate signal representing the patient's respiratory state is used to subdivide the data into gates, within which motion is assumed negligible. Individual gates can then be analyzed separately. The aim of this study was to examine the extent to which radioactivity in liver lesions varies after respiratory gating is applied. Methods: After granting informed consent to participate in the study, 7 patients (5M/2F) aged 64.9±5.8 Y were injected intraarterially with 143.7±43.5 MBq Tc-99m-MAA (microaggregated albulin) as part of our clinic's standard Y-90 radioembolization planning protocol. A SPECT/CT acquisition was then performed using a Symbia T2 (Siemens Molecular Imaging) with 60 views (15 sec each). List-mode data was acquired, and, using a fully-automated, data-driven gating method, a respiratory-gated dataset with 5 gates was generated in addition to the standard ungated dataset. Reconstruction was carried out with a research version of xSPECT Quant (20 iterations/1 subset). CT attenuation and scatter correction, but no post-smoothing, was performed. Magnetic resonance (MR) images were selected for each patient and co-registered with SPECT reconstructions. Using the MRs, volumes of interest (VOIs) were defined for each patient around lesions exhibiting tracer uptake. Within each VOI, the ratio R of activity in each gated reconstruction to that in the ungated reconstruction was then computed. Results: For 13 of the 16 VOIs assessed, R>1 for at least one gate, indicating underestimation of activity in the ungated reconstruction. Taking the maximum R for each lesion, the mean across all VOIs was 1.15±0.22. Taking the minimum, the mean was 0.82±0.10. For each lesion, the average deviation across all gates was 0.09±0.09. Conclusion: In this study, 81.3% of examined lesions showed underestimation in the ungated dataset, the average magnitude of which was 15%. This implies that blurring due to respiratory motion incurs a bias on ungated SPECT images. Variation across gates for each lesion was due to activity passing in and out of the static VOI as the patients breathed. Although not affecting the lung/liver shunt currently used for radioembolization planning, underestimation of tumor activity may have implications on future efforts to personalize therapy to maximize tumor dose. One limitation of the study is the small number of patients analyzed, which must be increased to reach a definite conclusion.

OP332

Feasibility and safety of selective internal radiation therapy (SIRT) procedure in one day

A. Dieudonné[1], A. Siebert[2], M. Abdel-Rehim[2], S. Legendre[1], S. Sebahoun[1], M. Ben-Reguiga[1], V. Vilgrain[2], R. Lebtahi[1]; [1]Department of Nuclear Medicine, Beaujon Hospital, Assistance Publique-Hôpitaux de Paris (APHP), Clichy, FRANCE, [2]Department of Radiology, Beaujon Hospital, Assistance Publique-Hôpitaux de Paris (APHP), Clichy, FRANCE.

SIRT procedures are usually performed in two steps separated by 7 to 14 days. Here we study the feasibility of performing the procedure in day. Methods: From a 5 years experience of SIRT, with 80 procedures, we had 4 cases for which a second pre-therapeutic angiogram was performed the same day than the therapeutic injection, followed by Tc-99m-labelled-macro-agregated-albumin-particles (MAA) injection. For these patients a second pre-therapeutic angiogram was programmed and new gastric arteries were identified and embolized. This was followed by the injection of MAA to re-evaluate the lung-shunt fraction, extra-hepatic uptake, the perfusion of the liver and the dosimetry of the tumor and non-tumoral tissues. Due to specific circumstances, this procedure was programmed the same day than the therapeutic injection. After 185 MBq intra-arterial injection of MAA, the patients were transferred to the nuclear medicine department for a SPECT/CT acquisition with the catheter in place. The images were analyzed during the transfer of the patient back in the interventional room for the microspheres injection that took 15 minutes. The microspheres (resin, SIRSPHERE, SIRTEX) were prepared and injected. The quality control of the microspheres injection by bremsstrahlung SPECT/CT (50-150 keV, MELP) was done the day after to avoid contamination of the Tc-99m peak. Results: For all 4 patients, no complication related to the transfer back and forth to the nuclear medicine department occurred. The time between the MAA and microspheres injection varied from 1 to 1,5 hours. The comparison of MAA and microspheres showed a very good agreement between MAA and microspheres, meaning that the presence of MAA in the micro-vessels does not perturb the perfusion of the microspheres and the injection of microspheres can be done 1 to 1,5 hours after the MAA injection.Conclusion: The “one day” SIRT procedure, done under specific circumstances, highlights the feasibility and safety of the process in term of patient management and the very good agreement between microspheres and MAA perfusion.

OP333

Regularized reconstruction results in a major improvement of Y-90 PET/CT image quality after SIRT with Y-90 microspheres

K. Tatsch[1], J. Touati[2], M. Leicht[1], C. Puskas[1], L. Maron[1], H. Arques Aguilo[2]; [1]Municipal Hospital Karlsruhe Inc, Dept. of Nuclear Medicine, Karlsruhe, GERMANY, [2]GE Healthcare, Buc, FRANCE.

Due to the physical properties of Y-90, Bremsstrahlung SPECT/CT images after SIRT are hampered by low quality. PET/CT scans might enhance image quality, however, due to the low count statistics based on the Y-90 inherent low positron emission decay, images acquired at reasonable scanning times for the patient are generally hampered by high noise levels. This study investigates whether an advanced reconstruction algorithm (regularized reconstruction aiming for full convergence; Q.Clear) can significantly improve image quality of Y-90 PET/CT scans following Y-90 SIRT therapy. So far we investigated the PET/CT (GE Discovery 710) Y-90 TOF-scans of 14 patients after radioembolization of liver tumors and metastases with Y-90 SIR-Spheres. Six different iterative reconstructions were performed: Standard (Std) with routine parameters for FDG scans (3 it, 24 sub, filter 6.4 mm, 256 matrix), 2 data sets reconstructed in a 192 matrix (8 it, 16 sub, filter 9 (V1) and 17 mm (V2)) and 3 data sets using Q.Clear (Q) with different beta values (750; 1000; 2000). All images were visually assessed by 4 readers (2 experts and 2 non-experts) with respect to 3 parameters: visual image quality, noise level and lesion detectability. Rating was based on a numeric scale from 1 (worst) to 5 (best). Rating for Image Quality was 1.4±0.3 for Std, 1.6±0.3 for V1, 2.4±0.3 for V2, 3.5±0.3 for Q.750, 4.0±0.3 for Q.1000 and 4.3±0.2 for Q.2000. Rating for Noise Level was 1.3±0.3 for Std, 1.6±0.3 for V1, 3.5±0.4 for V2, 3.0 ±0.3 for Q.750, 3.7±0.3 for Q.1000 and 4.6±0.4 for Q.2000. Rating for Lesion Detectability was 1.4±0.4 for Std, 1.6±0.3 for V1, 2.4±0.5 for V2, 3.6±0.4 for Q.750, 4.0±0.4 for Q.1000 and 3.9±0.4 for Q.2000. There was no statistical difference between expert and non-expert reads. Thus, in all three categories best results were obtained for Q.Clear reconstructions. Q.Clear data using a beta value of 2000 delivered the best trade off. Image quality of Y-90 PET/CT scans after SIRT can be dramatically improved by using Q.Clear, a regularized reconstruction algorithm aiming for full convergence. The very low noise levels achieved allow for an excellent delineation of the regional deposition of SIR-Spheres within the treated liver lobes or segments, which is a prerequisite for using such data for improved dosimetric calculations and comparisons with pre-therapeutic FDG and MAA scans. Currently patients are followed to additionally address whether these high quality scans may have impact on a better prediction of treatment response.

OP334

A branching artery tree model in concordance with microscopy observations of microsphere distribution in liver following radioembolisation

J. Högberg[1], M. Rizell[1,2], R. Hultborn[1,2], J. Svensson[1,2], O. Henrikson[1,2], J. Mölne[1,2], P. Gjertsson[2], P. Bernhardt[1,2]; [1]The Sahlgrenska Academy at The University of Gothenburg, Gothenburg, SWEDEN, [2]Sahlgrenska University Hospital, Gothenburg, SWEDEN.

Aim: Our previous investigations have demonstrated that large clusters of resin microspheres are common in normal liver tissue arteries after radioembolisation, causing more heterogeneity in the absorbed dose distribution than can be explained by depositions limited to the final arterioles. In order to reproduce microsphere-clustering findings, we constructed a hepatic artery branching tree

model. Materials and Methods: The virtual hepatic branching artery tree model consisted of a dichotomous (one vessel always branching into two vessels) branching artery of 20 generations. The inner artery diameter exponentially decreased from the lowest to the highest generation. Three variable parameters were optimised to obtain concordance between simulations and measured microsphere distributions: a combined artery coefficient of variation (ACV) for the inner diameter of all artery generations and the microsphere flow distribution at the nodes; a hepatic tree distribution volume (HDV); and an embolisation (EMB) parameter that reduces the artery diameters. The model was tested against previously measured activity concentrations in 16 biopsies, where the microsphere distribution was determined via light microscopy of 15 30-μm sections per biopsy (mean concentration, 14 microspheres/mg; distributions were divided into three groups with mean microsphere concentrations of 4.6, 14, and 28 microspheres/mg). Results: Optimisation of the simulations, by increasing microsphere concentrations and simultaneously increasing ACV and EMB and decreasing HDV (from 130 to 22 cm^3), demonstrated increasing cluster sizes in wider vessels with increasing microsphere concentration. Conclusion: Simulations revealed that microsphere clusters are larger and more common in volumes with high microsphere concentrations, thereby able to reproduce the distributions found in our previous microscopy investigations, the latter demonstrating that the absorbed dose distribution is more non-uniform for resin microspheres than what has been hypothesized or demonstrated by others. The non-uniform absorbed dose pattern for glass spheres is expected to depend mostly on high activity per microsphere, whereas microsphere clusters, caused by embolisation effects, are expected to be much more common for resin sphere treatments. The always relatively small and yet decreasing HDV with increasing microsphere concentration shows that our dichotomous branching model is a simplified model of a native hepatic branching artery tree, the latter demonstrated by anatomy studies to be much more complex than our model. Our model could be useful, though, when limited to small-scale analysis of specific liver segments where the mean absorbed dose within the segment is detected with Single-Photon Emission Computed Tomography (SPECT) or Positron Emission Tomography (PET).

OP335

Reconstruction, volumetry and dosimetry optimisation for 99mTc-SPECT and 90Y-PET images: towards reliable DVH for SIRT treatments

M. Bernardini[1], H. Thevenet[1], C. Berthold[2], A. Fischer[3], A. Petitguillaume[4], A. Desbrée[5], C. Smadja[1], P. Weinmann[1], N. Ghazzar[1]; [1]European Hospital Georges Pompidou, PARIS, FRANCE, [2]Gustave Roussy Institut, Villejuif, FRANCE, [3]Philips GmbH Innovative Technologies, Aachen, GERMANY, [4]Cancéropole Grand Sud Ouest, Toulouse, FRANCE, [5]LEDI, IRSN, Fontanay aux Roses, FRANCE.

Aim: Our purpose was to optimise image reconstruction and volumetric delineation on MAA-99mTc-SPECT/CT and 90Y-PET/CT images, in liver treatment with Selective Internal Radiation Therapy (SIRT), in order to improve dosimetry calculations. The prediction power of MAA-99mTc for 90Y-spheres treatments was also investigated as well as dose-effect relationship relating DVHs with patients follow-up. Materials and methods: To minimise errors in volumes delineation and quantification, 2 NEMA phantom studies were performed. 99mTc-MAA-SPECT/CT images were acquired with a hybrid gamma camera Infinia-Hawkeye (GE) and 90Y-PET/CT images with a Discovery 690 VCT-TOF (GE). Phantom optimisation results were applied to images of 10 patients treated with 90Y-SIR-spheres® (SIRTEX): treatment planning (99mTc-SPECT/CT), post-dosimetry (90Y-PET/CT) and dose-effect relationship (ceCT, 18F-PET/CT) were investigated via DVHs and isodoses. Dosimetry was based on kernel convolution (Imalytics, Philips). Results: 90Y and 99mTc phantom studies enabled to establish the reconstruction parameters that minimise errors in volumes and quantification for PET and SPECT images: optimised reconstruction and adaptive thresholding, allow decreasing average error in volumes from -64.3% to 2.2%. Using the "best volumes" on the "best quantification", here called "cross volumes" technique, allows decreasing error of mean concentration from -64.4% to -52.2% in average. Partial volume effect correction (PVC) decrease quantification error to -17.4% in average. For 90Y-PET images, optimising reconstruction parameters increase mean absorbed dose of +88.1% in average (from +21.0% to +235.9%, depending on volume). Applying PVC, mean absorbed dose increases of +70.9% in average (from +48.6% to 100.4% depending on volume). For 99mTc-SPECT images, optimising reconstruction parameters does not increase significantly quantification (maximum dose difference is -4,0%). With PVC correction, mean absorbed dose increase of +110% in average (from +74.2% to 162.8% depending on volume). These results were applied to analyse patient's images. Differences between lesions delineate on ceCT (pre-therapeutic image reference) and volumes threshold on 99mTc-SPECT and 90Y-PET, reach 320%. Intersections between volumes show important discrepancies too. Absorbed doses in 90Y-PET and 99mTc-SPECT volumes are higher than in ceCT lesions, pointing out the problem of targeting in SIRT. DVH establish a relationship between volume and dose, overtaking the inadequate information of mean absorbed dose. Conclusion: As mean absorbed dose does not represent the irradiation and radiobiological effects on lesions and organs at risk (parallel organs), DVH is essential to optimise treatment planning and to evaluate dose-response effect. To obtain reliable DVH, optimisation of volumes delineation is mandatory as errors in volumes can be important and the impact on dosimetry huge.

1006 - Monday, October 12, 2015, 4:30 PM - 6:00 PM, Hall 6
M2M: Radiopharmaceuticals & Radiochemistry: Peptides

OP336

Assessing the impact of clinically certified NEP and/or ACE inhibitors on the in vivo profile of [111In-DOTA] MG11: A comparative study in mice

A. Kaloudi[1], E. Lymperis[1], E. P. Krenning[2], M. de Jong[2,3], B. A. Nock[1], **T. Maina**[1]; [1]Molecular Radiopharmacy, INRASTES, NCSR Demokritos, ATHENS, GREECE, [2]Institute of Nuclear Medicine, Erasmus MC, ROTTERDAM, NETHERLANDS, [3]Insitute of Radiology, Erasmus MC, Rotterdam, NETHERLANDS.

Aim: We have recently shown that treatment of mice with the neutral endopeptidase (NEP)-inhibitor phosphoramidon (PA) improves the bioavailability and tumor uptake of several radiopeptides. For the truncated gastrin radiotracer [^{111}In-DOTA]MG11 ([(DOTA)DGlu^{10}]gastrin(10-17)) this method led to impressively high tumor-to-kidney ratios. Translation of this concept in the clinic requires the use of clinically certified NEP inhibitors, such as thiorphan (TO) and its orally administered prodrug racecadotril (Race). On the other hand, both NEP and angiotensin converting enzyme (ACE) have been shown to participate in the catabolism of gastrin analogs. In the present study, we first compare the effects induced on the biological profile of [^{111}In-DOTA]MG11 during NEP inhibition by: i) PA (reference), ii) TO, or iii) Race. Furthermore, we investigated the role of ACE in the catabolism of the radiotracer employing the established ACE-inhibitor lisinopril (Lis). Materials and Methods: [^{111}In-DOTA]MG11 was co-injected with vehicle, or with PA (300 μg), or TO (150 μg), or Lis (100 μg), or Race (2 mg; 30-40 min in advance via ip injection). Mouse blood collected 5 min post-injection (pi) was analyzed by HPLC to assess catabolism rates. Biodistribution was performed at 4 h pi in SCID mice bearing AR42J xenografts after co-injection of [^{111}In-DOTA]MG11 with vehicle, or with PA, or TO, or Lis, or PA+Lis, or Race (ip pre-injected). Results: Treatment of mice with PA, TO or Race increased the levels of circulating [^{111}In-DOTA]MG11 from 5% to 70-75% at 5 min pi. During NEP-inhibition, tumor uptake impressively increased from 1.8 ±1.0%ID/g (controls) to 15.3±4.7%ID/g (PA) and 12.3 ±3.6%ID/g (TO), while with Race tumor values reached 6.8 ±2.8%ID/g. Conversely, Lis had no effect on tumor uptake and no additive effect when co-injected with PA. In all cases renal accumulation remained low and unaffected by any of the above inhibitors. Conclusions: This study has shown that ACE is not involved in the in vivo degradation of [^{111}In-DOTA]MG11, confirming NEP as the predominant degrading enzyme of the radiotracer. NEP inhibition with the clinically tested NEP inhibitors TO and Race resulted in significant enhancement of tumor-to-kidney ratios versus controls. The fact that TO, unlike its ip-administered prodrug Race, produced comparable effects with PA highlights the importance of sufficient NEP-inhibition for maximizing tumor targeting. Further studies, to optimize doses, administration routes and inhibitor-combinations, are currently in progress to advance translation of this concept into the clinic.

OP337

A phage display derived stabilised bicyclic peptide targeting MMP-14 shows high imaging contrast in small animal PET imaging

M. Eder[1], S. Pavan[2], U. Bauder-Wüst[1], K. van Rietschoten[2], L. Baldassarre[2], U. Schierbaum[3], O. Seibert[3], K. Leotta[3], S. Campbell[2], H. Harrison[2], C. Stace[2], E. Walker[2], U. Haberkorn[3], K. Kopka[1], D. P. Teufel[2]; [1]Radiopharmaceutical Chemistry, German Cancer Research Center, HEIDELBERG, GERMANY, [2]Bicycle Therapeutics Limited, Cambridge, UNITED KINGDOM, [3]CCU Nuclear Medicine, German Cancer Research Center, HEIDELBERG, GERMANY.

Aim: Radiolabeled bicyclic peptide scaffolds represent highly attractive molecules for PET imaging of various oncological entities and for therapeutic applications due to their low molecular weight, high affinity and specificity. In the present work, bicyclic peptides directed against the tumor associated matrix metalloproteinase 14 (MMP-14, MT1-MMP) were identified, preclinically characterized and further optimized with regard to their in vivo stability and their clinical potential as PET imaging agent. Materials and Methods: Thio-ether formation via the three reactive cysteines of a randomized amino acid sequence and fusion to the phage gene-3-protein generated a library of bicyclic peptides [1]. An affinity selection process yielded several binders with variants showing single digit nanomolar affinity and high specificity for MMP-14. The selected Bicycle structure offers the ability to alter properties through chemical modification and the addition of functional groups via linkers without affecting the affinity, for example a site-specific labelling with the radiochelator DOTA. This construct was radiolabelled with Ga-68 or Lu-177, respectively, and analyzed preclinically according to its cell binding and in vivo tumor-targeting properties. In order to further improve the pharmacokinetic and tumor targeting properties the Bicyclic peptide sequence was stabilized by chemical modification. Results: The initially selected compound DOTA-N144 already revealed high specificity and affinity (KD= 0.5 nM) as determined by fluorescence polarization competition assays. MALDI-TOF analysis of wild-type N144 in mouse plasma however indicated loop-opening potentially causing in vivo instabilities. Several targeted chemical modifications of the amino acid sequence led to a stabilised variant with retained

affinity and specificity. Organ distribution at 1 h p.i. of the optimal dose showed a significantly higher MMP14-specific tumor uptake of 12.02 ± 2.37 %ID/g (0.12 ± 0.06 %ID/g for non-binding scrambled variant) as compared to the non-stabilised compound (2.75 ± 0.88 %ID/g). Both compounds showed fast background clearance (<1 %ID/g for all organs except the kidneys) resulting in high imaging contrast in the μPET studies. Conclusions: The phage display selection of bicyclic peptides was shown to be a highly flexible and attractive strategy for generating and developing peptidic drug leads. The stabilised bicyclic DOTA-lead compound revealed MMP-14-selective tumor uptake in the xenograft model and rapid clearance from non-target crucial organs resulting in high imaging contrasts. The compound represents a highly promising radiotracer which could be used as radiopharmaceutical for future clinical PET imaging and radioendotherapy of MMP14-expressing tumors. References: [1] Heinis C, et al (2009) Nat Chem Biol, 5(7), 502-07.

OP338

Sometimes, Less is More: Specific Activity of Radiopharmaceuticals and its Impact on Biodistribution and Imaging Contrast

J. Notni[1], D. Reich[1], J. Pollmann[1], F. Hofmann[1], M. Weineisen[1], T. Kapp[2], F. Rechenmacher[1], H. Kessler[2], H. Wester[1]; [1]Pharmaceutical Radiochemistry, Garching, GERMANY, [2]Center for Integrated Protein Research, Garching, GERMANY.

For a fixed dose of a radiopharmaceutical (given in MBq), the specific activity A_S (e.g. in GBq/μmol), defined as radioactivity (A) divided by the total molar amount (n) of labelled and unlabelled precursor, is determining the overall injected dose of pharmacologically active compound (e.g., in mg/kg). Particularly for radiopharmaceuticals with saturable targets, such as receptors, the latter can have a pronounced effect on both target accumulation and general biodistribution, and therefore on imaging results. While this is a known and well-described phenomenon, its extent is often underestimated. Here, its manifestation is illustrated on examples of current PET-tracer development. TRAP-based trimers of a) cyclo(RGDfK), targeting αvβ3 integrins, b) an acyclic pseudopeptide, targeting α5β1 integrins, and c) a EuK-based ligand, targeting PSMA, were synthesized from the alkyne-functionalized monomers by one-pot click-chemistry (CuAAC) conjugation to a tris-azide-functionalized TRAP chelator. Affinities (IC50) were determined by ELISA on vitronectin/fibronectin (αvβ3/α5β1), or displacement assays on LNCaP cells (PSMA). Following fully-automated ^{68}Ga labelling, the compounds were administered to mice bearing M21 (integrins) or LNCaP (PSMA) xenografts, with specific activities ranging from 0.5 to 1500 GBq/μmol (approx. 35 nmol to 13 pmol for a 20 MBq injection), which underwent PET and ex-vivo biodistribution studies. Trimerization of the receptor ligands resulted in substantially increased target affinities (αvβ3: 220 pM, α5β1: 80 pM, PSMA: 2 nM) compared to the monomers (5, 2.3, and 36 nM, respectively). For all investigated tracers, variation of A_S resulted in dramatic changes in biodistribution and thus, tumor/organ and tumor/"background" ratios. For example, increasing the total dose of the α5β1-targeting TRAP-trimer Ga-Aquibeprin from 16 pmol to 6 nmol resulted in improved PET tumor/muscle ratio from 5.3 to 12.4. Likewise, for 20 MBq of the ^{68}Ga-labelled EuK trimer, lowering A_S from 540 to 20 GBq/μmol resulted in strongly declining kidney uptake from 28.7 to 3.2 %ID/mL, respectively, while LNCaP tumor uptake was just slightly decreased from 1.5 to 1.3 %ID/mL.Specific activity is an important factor in tuning the in-vivo properties of radiopharmaceuticals, allowing to improve tumor contrast and to manage specific uptake in other tissues. As such, it deserves more attention, particularly in view of substantial evidence for the fact that lower A_S (i.e., higher amounts of pharmacologically active compound) can improve addressing of tumors, while higher A_S can result in more detailed physiological target visualisation. Thus, we advocate for a more detailed investigation of this parameter in radiopharmaceutical studies.

OP339

Assessment of the specificity of 99mTc-duramycin in a mouse model of colorectal cancer

F. Elvas[1,2], C. Vangestel[1,2], K. Y. Pak[3], S. Stroobants[1,2], S. Staelens[1], L. wyffels[1,2]; [1]University of Antwerp - Molecular Imaging Center Antwerp, Wilrijk, BELGIUM, [2]University Hospital Antwerp - Department of Nuclear Medicine, Edegem, BELGIUM, [3]Molecular Targeting Technologies, Inc., West Chester, PA, UNITED STATES.

Aim: As most cancer therapies available have a pro-apoptotic and necrotic effect, the use of specific radiotracers allows for molecular imaging of cell death. Duramycin is a small peptide (MW~2kDa) that recognizes cell death by binding to the head group of phosphatidylethanolamine (PE) with high affinity. Recently, we showed the ability to image therapy-induced cell death in a mouse model of colorectal cancer using 99mTc-labeled duramycin(1). In the current study we aimed at assessing the specificity of 99mTc-duramycin for imaging cell death in chemotherapy treated tumor-bearing mice by performing a blocking study. Materials and Methods: Human colorectal cancer cells (Colo205) were subcutaneously inoculated in both hind legs of athymic nude mice. After the tumors reached 217 mm^3, baseline

static SPECT-CT scans were performed 4 h after injection of 99mTc-duramycin (36.0 ± 1.8 MBq). Chemotherapy consisted of a combination of 80 mg/kg irinotecan plus 5 mg/kg oxaliplatin (q.d. in alternate days during one week) or the corresponding vehicles for control mice (n=6 tumors/group). 99mTc-duramycin (35.0 ± 4.7 MBq) was intravenously injected 24 h after the last course of treatment, and following a 4 h radiotracer uptake-period animals underwent static SPECT-CT imaging. For blocking, duramycin (2 mg/kg as 0.8 mg/mL solution in saline) was injected 30 min before the radiotracer. Radiotracer uptake in the tumors was evaluated by SPECT (%ID/g/kg) and by γ-counting of the tumors (%ID/g). Cleaved caspase-3 (CC3) and TUNEL staining of the tumors will allow assessing cell death in the tumor. Results: On the SPECT images, tumors showed an increased accumulation of 99mTc-duramycin following combination chemotherapy (144.2 ± 19.1%ID/g/kg; $p<0.001$), compared to control (40.6 ± 2.8%ID/g/kg). The binding of 99mTc-duramycin was blocked by preinjection of nonlabeled duramycin (32.9 ± 9.7%ID/g/kg; $p<0.001$). In treated tumors the radioactivity in the tumors positively correlated to CC3 ($r=0.85$, $p<0.001$) and TUNEL ($r=0.81$, $p<0.001$) stainings. For the blocking, regional distribution of radioactivity in the tumors will be determined by autoradiography, and correlated to CC3 and TUNEL staining. Conclusion: Our results show that 99mTc-duramycin specifically accumulates in apoptotic tumors in response to therapy. 99mTc-duramycin holds promise as a radiotracer for early treatment evaluation with potential clinical usefulness in the setting of oncology. 1. Elvas F, et al. Characterization of [99mTc]Duramycin as a SPECT Imaging Agent for Early Assessment of Tumor Apoptosis. Molecular imaging and biology : MIB. Apr 21 2015. DOI: 10.1007/s11307-015-0852-6

OP340

Development of radiocobalt-labeled GRPR antagonist NOTA-PEG2-RM26.

B. Mitran[1], Z. Varasteh[1], U. Rosenström[2], V. Tolmachev[3], G. Lindeberg[2], M. Larhed[4], A. Orlova[1]; [1]Preclinical PET Platform, Department of Medicinal Chemistry, Uppsala University, Uppsala, SWEDEN, [2]Organic Pharmaceutical Chemistry, Department of Medicinal Chemistry, Uppsala University, Uppsala, SWEDEN, [3]Biomedical Radiation Sciences, Immunology, Genetics and Pathology, Uppsala University, Uppsala, SWEDEN, [4]Science for Life Laboratory, Department of Medicinal Chemistry, Uppsala University, Uppsala, SWEDEN.

Aim: High GRPR expression is associated with numerous cancers including those of the prostate and breast. Bombesin (BN) analogues bind with high affinity to GRPR, having significant potential for radionuclide imaging and therapy of GRPR-expressing tumors. We have recently investigated a high-affinity antagonistic analog of bombesin (RM26) conjugated to NOTA chelator via a diethylene glycol (PEG2) spacer (NOTA-PEG2-RM26), labeled with 68Ga, 111In and Al18F. 68Ga-labeled NOTA-PEG2-RM26 showed favorable pharmacokinetic properties. However, as seen for 111In-NOTA-PEG2-RM26, the clearance of radioactivity from blood and receptor positive organs, combined with long retention in tumors resulted in higher tumor-to-background ratios at later time-points. The aim of the current study was to develop a 55Co-labeled PET agent to visualize GRPR. 55Co is a promising β+ emitting radioisotope, the 17.5 h half-life allowing transport to distant scanning centers and imaging at later time-points, when better contrast can be achieved. Materials and methods: The initial preclinical characterization of NOTA-PEG2-RM26 was performed using 57Co as a surrogate nuclide. Stability, in vitro binding specificity and cellular processing were analyzed. In vivo binding specificity and biodistribution were studied in NMRI mice. Results: NOTA-PEG2-RM26 was successfully radiolabeled with 57Co with yields exceeding 99% and demonstrated high stability under EDTA challenge. The radiopeptide showed retained binding specificity to GRPR in vitro. The internalization rate was very slow, internalized radioactivity fraction reaching 12% of cell associated radioactivity 24 h after incubation start. 57Co-NOTA-PEG2-RM26 biodistribution in mice was characterized by rapid clearance of radioactivity from blood (1.3±0.2% IA/g) and normal non-GRPR expressing organs and low liver uptake (0.65 ±0.05 % IA/g), 30 minutes after injection. The clearance was predominantly renal, with low degree of radioactivity reabsorption (6.4±1.9 %IA/g, 30 minutes p.i.). In vivo binding specificity studies showed a significant reduction of radioactivity uptake in GRPR expressing organs (pancreas, small intestines, and stomach) for mice co-injected with excess non-labeled peptide. Conclusions: The initial biological results suggest that radiocobalt-labeled-NOTA-PEG2-RM26 is a promising tracer for the visualization of GRPR-expressing tumors. The use of 55Co as label might provide a probe for PET imaging.

OP341

^{68}Ga-RM2 for imaging of prostate cancer - Successful implementation of Synthesizer- and Kit-based production methods

M. Zerna, A. Müller, **M. Berndt**; Piramal Imaging, Berlin, GERMANY.

Aim: Prostate cancer (PCa) is the most common cancer in men and the second most common cause in cancer-related deaths. Current diagnostic methods are limited in the accurate detection of primary prostate cancer. ^{68}Ga-RM2 is a nona-peptide with optimized binding sequence for Gastrin Releasing Peptide receptor (GRPr) which is overexpressed in prostate cancer. ^{68}Ga-RM2 has been identified from initial clinical studies as a potential imaging agent for detection of primary prostate cancer with high

specificity due to its low uptake in normal prostate and in benign hyperplasia. In order to support the ongoing systematic clinical exploration of ^{68}Ga-RM2 and its ability to improve pre-treatment risk-assessment and therapy-planning, robust GMP compliant manufacturing methods are needed using automated synthesizers and "ready-to-use" lyophilized kits. Herein, we report on our work in establishing a robust automated synthesis of ^{68}Ga-RM2 which could be further simplified to a "shake-and-bake" method. Materials and Methods: ^{68}Ga was obtained from an IGG100 generator (Eckert&Ziegler). Automated production was performed on a PharmTracer module (Eckert&Ziegler) using sterile cassettes, pre-filled RM2-precursor vials (ABX) and a Ga-labeling reagent kit (ABX/Eckert&Ziegler). The ^{68}Ga-generator eluate was trapped on a cation exchange cartridge. This cartridge was eluted with 5M NaCl + 5.5M HCl into the reaction vial, filled with RM2-precursor, sodium acetate solution and scavenger. After labeling at 100-110°C, buffered saline was added and the mixture was passed through a C18 cartridge. After washing the cartridge with buffered saline, ^{68}Ga-RM2 was eluted with ethanol (50%) and diluted with buffered saline. The influence of scavengers was investigated, as well as a process without the C18 cartridge purification. In a second approach, a "shake-and-bake" kit preparation was established. The ^{68}Ga-generator eluate was added directly into a vial containing RM2-precursor, sodium acetate and scavenger. The vial was heated and optionally buffer was added for pH-adjustment. Results: The automated synthesis provided up to 850 MBq of ^{68}Ga-RM2 in >70% uncorrected yield in 20min including purification and formulation. The radiochemical purity was >97% (HPLC and TLC) if ascorbic acid was used as scavenger. Without C18 cartridge purification, ^{68}Ga-RM2 was obtained in 14min in >76% uncorrected yield and purity of >95%. The simple and easy to use "shake-and-bake" kit approach provided ^{68}Ga-RM2 in 90% uncorrected yield and purity of >95%. Conclusion: ^{68}Ga-RM2 can be reliably manufactured on automated synthesizers as well as by a simple "shake-and-bake" kit strategy. Both methods provided ^{68}Ga-RM2 in high yields and high radiochemical purity.

OP342

Kit formulation, preclinical evaluation and experimental radionuclide therapy using CCK2 receptor targeting cyclic minigastrin

E. von Guggenberg[1], C. Rangger[1], L. Balogh[2], Z. Pöstényi[2], D. Pawlak[3], R. Mikołajczak[3]; [1]Department of Nuclear Medicine, Innsbruck Medical University, Innsbruck, AUSTRIA, [2]"Frédéric Joliot-Curie" National Research Institute for Radiobiology and Radiohygiene (NRIRR), Budapest, HUNGARY, [3]Radioisotope Centre POLATOM, National Centre for Nuclear Research, Otwock, POLAND.

Aim: Radiolabelled cyclic minigastrin analogues belong to the most promising candidates for possible clinical application in diagnosis and therapy of cholecystokinin-2 receptor (CCK2R) expressing tumours, mainly medullary thyroid cancer (MTC) and small cell lung cancer. Within an international collaboration of the IAEA we have developed and preclinically evaluated specific kit formulations for Tc-99m and Lu-177 labelling of two cyclic minigastrin analogues, HYNIC/DOTA-cyclo[γ-D-Glu-Ala-Tyr-D-Lys]-Trp-Met-Asp-Phe-NH2 (HYNIC/DOTA-cyclo-MG1) and HYNIC/DOTA-cyclo[γ-D-Glu-Ala-Tyr-D-Lys]-Trp-Nle-Asp-Phe-NH2 (HYNIC/DOTA-cyclo-MG2). Materials and methods: Two different lyophilized kit formulations were prepared for HYNIC- and DOTA-peptides. The stability during storage and after radiolabelling was examined at different time points. Cell uptake studies were performed in A431 human epidermoid carcinoma cells stably transfected with the human CCK2R (A431-CCK2R) and mock transfected cells (A431-mock). The biodistribution in xenografted mice (5 animals per group) was studied up to 24 hours (Tc-99m) and 7 days (Lu-177). An experimental radionuclide therapy (6 animals per group) was carried out with 177Lu-DOTA-cyclo-MG1 and 177Lu-DOTA-cyclo-MG2 at the dose level of 15 and 30 MBq. A dog with histologically confirmed MTC underwent diagnostic imaging and radionuclide therapy with HYNIC/DOTA-cyclo-MG1. Results and conclusion: The kit formulations displayed a high stability during storage. The radiochemical purity (RCP) at a specific activity >100 GBq/μmol resulted to be >90% for both 99mTc-labelled HYNIC-peptides, >93% for 177Lu-DOTA-cyclo-MG1 and >98% for 177Lu-DOTA-cyclo-MG2. The RCP of the 99mTc- and 177Lu-labelled peptides remained stable for 4 h and declined to ~95% (177Lu-DOTA-cyclo-MG2) and ~90% (177Lu-DOTA-cyclo-MG1) at 24 h after preparation. Cell uptake studies in A431-CCK2R cells confirmed a high receptor-specific cell internalization (>20% at 2 h after incubation). Biodistribution studies in xenografted mice revealed a tumour uptake of >3% ID/g for Lu-177 (4 h p.i.) and Tc-99m (1 h p.i.) and a tumour to kidney ratio of ~2 (Tc-99m) and ~3 (Lu-177). In the 15 MBq-group the mean tumour volume doubling time was 1.8 (A431-CCK2R) and 1.2 (A431-mock) times higher than in the untreated control group. For the 30 MBq-group these values resulted to be 2.6 (A431-CCK2R) and 1.7 (A431-mock). SPECT/CT imaging with 99mTc-HYNIC-cyclo-MG1 in a dog confirmed local recurrence of MTC. The first treatment with 177Lu-DOTA-cyclo-MG1 was well tolerated. All together the obtained results are promising for a potential clinical application in patients.

OP343

Development & application of an [18F] anti-amyloid peptide radiotracer

O. Morris[1], J. Gregory[1], A. Blykers[2], D. Allsop[3], M. Taylor[3], S. Allan[1], A. McMahon[1], H. Boutin[1], C. Prenant[1]; [1]The University of Manchester, Manchester, UNITED KINGDOM, [2]Vrije Universiteit Brussel, Brussels, BELGIUM, [3]The University of Lancaster, Lancaster, UNITED KINGDOM.

Aim: Development and automation of novel [18F] radiochemistry and its application in site-specifically radiolabelling an amino(oxy)-functionalised anti-amyloid peptide (RI-OR2) for use as an early-stage Alzheimer's Disease (AD) radiotracer.AD is a neurodegenerative disorder characterised by a progressive decline in cognitive function. AD pathology is identified by the formation of plaques, abnormal peptide clusters, mainly comprising fibrillar β-amyloid (Aβ). Plaques deposition leads to impaired synaptic transmission giving rise to the expression of the recognised cognitive symptoms.RI-OR2 is a novel brain-penetrant retro-inverso peptide inhibitor of an Aβ oligomer sequence. It has been reported to reduce amyloid deposition, associated oxidation and inflammation whilst also having a marked stimulatory effect on neurogenesis. This thereby demonstrates its potential therapeutic application. The retro-inverso D-amino-acid sequence confers high resistance to proteolysis and in-vivo stability to the RI-OR2. Unlike currently used AD radiotracers, RI-OR2, presents as an interesting PET probe owing to its ability to bind to early-, rather than late-, stage amyloid aggregates. In so doing, this might permit detection of AD early in disease onset, allowing more effective therapeutic intervention.RI-OR2 has been functionalised with an amino(oxy) functional group, permitting site-specific radiolabelling with the water-soluble prosthetic group, 2-[18F]fluoro-3-pyridinecarboxaldehyde.Materials & Methods: 2-[18F]Fluoro-3-pyridinecarboxaldehyde was produced by [18F]fluorination of 3-carboxaldehyde-N,N,N-trimethylpyridine-2-aminium bromide, obtained from 2-bromopyridine-3-carboxaldehyde. The 18F-prosthetic group was purified using SPE and reacted with amino(oxy)-RI-OR2, in aqueous conditions. The chemical identity of 2-[18F]Fluoro-3-pyridinecarboxaldehyde was determined by comparing its chromatographic properties with those of the standard 2-Fluoro-3-pyridinecarboxaldehyde.Results: 2-[18F]Fluoro-3-pyridinecarboxaldehyde was produced on a GE-Tracerlab FXFN within 40 min. achieving RCY of 80% ± 5% (n=5). Preliminary results show incorporation of the prosthetic group into the RI-OR2 achieving RCY of 40% ± 5% (n=3) within 30 min., as confirmed by SE-HPLC. 18F-labelled peptide was purified using SE-HPLC, RCP of >95% was obtained. In-vitro stability tests have been performed and preliminary study of the in-vivo biodistribution of this radiotracer has been performed in wild type pre-clinical models. Conclusion: We hereby present a novel [18F] radiolabelling technique of RI-OR2 using an [18F] water-soluble prosthetic group. Site-specific radiolabelling of RI-OR2 with 2-[18F] Fluoro-3-pyridinecarboxaldehyde is efficient, high yielding and proceeds under mild conditions. Optimisation of RI-OR2 radiolabelling and pre-clinical investigation of the 18F-labelled peptide in AD animal models (APPswe/PS1ΔE9 transgenic mice) is in progress and results will be shown.

1007 - Monday, October 12, 2015, 4:30 PM - 6:00 PM, Hall F

DGN-Sponsored Symposium: PET/MRI

OP344

Welcome

S. Klutmann, **GERMANY**

OP345

PET/MRI - Methodology, Standardisation and Challenges

B. Sattler GERMANY

OP346

PET/MRI in Oncology

A. J. Beer, **GERMANY**

OP347

PET/MRI - Applications in Cardiology

M. Schwaiger, **GERMANY**

OP348

Brain Imaging with PET/MRI

O. Sabri, **GERMANY**

1008 - Monday, October 12, 2015, 4:30 PM - 6:00 PM, Hall E
Conventional & Specialised Nuclear Medicine: General & Miscellaneous

OP351

Ga-68 macroaggregated albumin (MAA) Perfusion PET/CT for lobar pulmonary function quantification: comparison with anatomic method, volumetric CT and planar scintigraphy.

P. Le Roux, T. Leong, S. A. Barnett, R. J. Hicks, P. Eu, J. Callahan, R. Manser, M. S. Hofman; Peter MacCallum Cancer Centre, Melbourne, AUSTRALIA.

Aim: Patients with lung cancer and borderline pulmonary function should have preoperative evaluation of predicted postoperative residual lung function according to the European clinical guidelines (ERS and ESTS) to determine suitability for radical therapy. Several methods are currently used including anatomic estimation based on counting the number of segments to be removed, planar perfusion scintigraphy or volumetric CT. Pulmonary perfusion PET/CT can be performed by substituting labeling of macroaggregated albumin (MAA) with Ga-68 for Tc-99m. The aim of this study was to compare lobar function computed with PET-CT and the conventional methods. Materials and methods: Twenty two patients with lung malignancy and lung function impairment (mean FEV1 1.93L ± 0.67, mean DLCO 73 ± 21% predicted) underwent respiratory gated (4D) PET-CT lung perfusion scans after injection of approximately 50MBq of Ga-68 MAA. Lobes were delineated on CT images and segmentation was subsequently applied to the PET images to determine lobar perfusion (MIM version 6.3 software). Bland-Altman statistic was used to calculate agreement between the lobar lung function in the lobe with tumour using PET compared to anatomic estimation based on counting the number of segments (anatomic method), volumetric CT, and planar perfusion scintigraphy. Scintigraphy was not available in 6 patients. Results: Bland-Altman bias of PET compared to the anatomic method, volumetric CT and planar scintigraphy was -2.3 ± 7.3, -2.9 ± 4.6 and -1.6 ± 9.0, respectively. For some patients with tumors resulting in distal vascular obstruction or severe emphysematous change, there was major disagreement between anatomic and functional methods. The absolute difference between PET versus anatomic method, volumetric CT and planar scintigraphy was higher than 5% of global lung function in 11/22 patients, 8/22 and 13/16 patients, respectively. The difference was greater than 10% in 5, 1 and 6 patients, respectively. Conclusions: Lobar lung function computed with Ga-68 MAA PET lung perfusion imaging differs significantly in some patients from anatomical, CT and planar scintigraphy methods. Further studies are needed to assess if perfusion PET allows better prediction of postoperative lung function and may influence management of lung surgery patients.

OP352

The Importance Of Scintigraphic Pattern in the Suspected Diagnosis Of Sjögren's Syndrome.

B. Garcia-Garcia, M. J. Ribelles, E. F. Guillén, L. Sancho, M. Rodriguez, M. J. García-Velloso, P. DeCastro, E. Ornilla, J. Á. Richter; Clinica Universidad de Navarra, Pamplona, SPAIN.

AIM: To estimate the diagnostic contribution of Technetium 99m pertechnetate salivary gland scintigraphy (SGS) in referred patients due to suspicion of Sjögren's Syndrome (SS). The association among the degree of involvement shown by SGS, antibodies, biopsy result, and final diagnosis, was evaluated. MATERIALS AND METHODS: 87 SGS were performed in 84 subjects, who were sent from different specialty physicians (Neurology, Internal Medicine, and Rheumatology). All the patients underwent scintigraphy using a standardized protocol that included a sequential acquisition of images (1 minute/frame) and a salivary stimulation with citric acid 30 minutes later. Curves and glandular uptake were assessed qualitatively. Regarding the number of affected glands (n), four scintigraphic patterns were stablished: P-I (n=0), P-II (n=1), P-III (n=2), and P-IV (n≥3). Salivary gland biopsy was made in 19 patients, and ANA/ENA antibodies in 75. SS final diagnosis was confirmed in 23 cases, as stated in the American-European Consensus Criteria (AECC). RESULTS: Gland biopsy was positive in 9 patients (7 of which showed an altered uptake in SGS) and negative in 4 patients. Nevertheless, 6 samples got inconclusive results. ANA/ENA antibodies were detected in 42 cases, and negative in 33. Normal scintigraphic uptake was pointed out in 20 subjects, and abnormal patterns were reported in 67: 13 P-II, 26 P-III, and 28 P-IV. In relation to the final diagnosis, SGS globally depicted 84.6% sensitivity, 26.2% specificity, 32.8% positive predictive value (PPV), and 80% negative predictive value. These results were respectively modified by the four aforementioned uptake patterns. P-II: 33.34%, 66.67%, 20%, and 80%. P-III: 63.6%, 42.1%, 24.14%, and 80%. P-IV: 76.5%, 51.6%, 46.4%, and 80%. Assuming the antibodies presence as reference value, SGS result showed coincidence in 39 subjects, supporting or discarding SS diagnosis. There were discordant results in 36 patients: 21 of them were considered false-positive scintigraphy, 14 of which maintained antisialogogue therapy; 9 were false-negative scintigraphic cases, 3 referred previous sialoadenitis, 2 got a false-negative result for antibodies, and there was 1 patient lost. CONCLUSION: SGS is a useful diagnostic tool for the diagnosis of SS. Its performance improves significantly according to the number of affected glands. When interpretating SGS results in suspected SS, we may need to consider the coexistence of other

circumstances which could modify salivary secretion, particularly the concurrence with antisialogogue drugs.

OP353

Surgical planning issues of radio-guided sentinel node biopsy (SNB) in patients (pts) with second primary ipsilateral breast cancer (SPIBC)

C. Peterle, C. Cittanti, P. Carcoforo, M. Portinari, V. de Cristoforo, I. Santi, S. Panareo, L. Feggi; S. Anna University Hospital, Cona (FE), ITALY.

Background: Widespread of breast-conserving surgery and the boost of life expectancy in these pts contribute in increasing the number of women with SPIBC who have to undergo second radio-guided SNB.The aim of this retrospective study was to assess incidence and sites of possible altered lymphatic drainage in pts who underwent SNB for SPIBC and its impact in the increasing percentage of due conversion of the surgical treatment from local anaesthesia to general anaesthesia.MethodsWe re-evaluated all data about pts who underwent lymphoscintygraphy(LS)for detection of SNB since October 2012 to March 2015, dealing separately with pts with SPIBC:all of them had previous breast-conserving surgery,with either SNB or SNB followed by axillary lymph-node dissection(ALND).The day before surgery we injected the tracer(Nanocoll® 70MBq)with periareolar intradermal technique(PA)if the surgeon was planning to remove SN only in local anaesthesia,whereas intra and peritumoral injection(IPT)was used if the surgeon was planning to remove simultaneously SN and breast cancer.We considered SN in abnormal lymphatic drainage basin all the SN located in sites other than ipsilateral axilla.We dealt separately with non-identified SN.ResultsIn our NM Unit SN lymphoscintigraphy was performed on 745 pts:722 to detect SN for primary breast cancer;23 because affected by SPIBC(3.09%).No SN was visualized in 8/722 pts(1.11%),while in 1 pt SN was not in the ipsilateral axilla(1/722;0.14%).Among the 23 pts with SPIBC,in 6 pts(26.1%)SN was not found neither by LS nor during surgery by gammaprobe(all these pts previously underwent ipsilateral complete ALND);at least one SN was removed in 17/23 pts.The SN was found in ipsilateral axilla in 10/17 pts(58.82%:1 IPT;9 PA);in abnormal site in 7/17 pts(41.18%):contralateral axilla 3/17 pts(17.65%: 1 IPT, 2 PA);internal mammary 3/17 pts(17.65%:1 IPT,2 PA);anterior subcostal site 1/17 pts(5.88% PA).19/23 pts underwent surgery in local anaesthesia(82.6% PA),while 4/23 pts in general anaesthesia(17.4% IPT).In 3/17 pts(17.6%),in order to remove the LS-located SN in deep sites,it became necessary to delay surgery to convert from local to general anaesthesia.In one case (anterior subcostal site) SPECT-CT was necessary to locate SN during preoperative LS. Conclusions: This preliminary study shows that surgical planning(based on LS and SPECT-CT results)is critical in SPIBC pts(compared to not previously operated pts),being higher the percentage of SN non-visualized or in abnormal site,which require general anaesthesia(26.1% vs 1.11%;41.18% vs 0.14%:p<0,01).In pts who already underwent ALND,as expected,the rate of SN detection is significantly reduced,thus leading to ineffective surgery.

OP354

Factors influencing brown fat activation in FDG PET/CT: a retrospective analysis of 21,000+ cases

J. Steinberg, E. Vegt; Netherlands Cancer Institute, Amsterdam, NETHERLANDS.

Aim: Brown fat, or brown adipose tissue (BAT), is known to exhibit high uptake of ^{18}F-fluorodeoxyglucose (FDG) on positron emission tomography (PET), and can either be mistaken for malignancy or obscure underlying malignancy. BAT activation is associated with age, body mass index, gender, and ambient temperature. Nuclear medicine physicians have sought ways to reduce BAT activation, such as the administration of diazepam prior to injection of FDG, which is thought to decrease BAT activation via a reduction in sympathetic activity. The goal of this study was to gain further insight into the relative contribution of factors that may influence the activation of BAT. Materials and methods: A retrospective study of FDG PET/CT scans was performed using a database of PET/CT reports of 21,326 patients through the years of 2007-2014. The report contains information regarding the date and time of the scan, the age and gender of the patient, observed BAT activation, and the administration of diazepam. The date of the scan was used to determine average outdoor temperatures using data from that National Climatic Data Center (Asheville, North Carolina, United States). The data were analyzed using software developed in-house. Results: The number of patients with BAT activation was 864 (4.1%). BAT activation was observed to be higher in women than in men (6.2% vs. 1.6%, $p < 0.0001$), higher in patients under 60 years old than over 60 years old (6.6% vs. 1.9%, $p < 0.0001$), higher when average outdoor temperatures were below 10°C than above 10°C (4.8% vs. 3.4%, $p < 0.0001$), and higher for FDG injections in the morning than in the afternoon (4.6% vs. 3.3%, $p < 0.0001$). Diazepam usage was associated with much higher BAT activation (14.1% vs. 2.7%, $p < 0.0001$), among both genders, all ages, and outdoor temperatures. Conclusion: This large retrospective study provides more insight into the relative importance of several factors known to influence BAT activation. Using this information, additional measures can be taken to reduce BAT activation among high-risk individuals during FDG PET examinations. However, contradictory to

our expectation, we observed much higher BAT activation in patients who had received diazepam before the scan. This suggests that diazepam increases the likelihood of BAT activation, but it may also be due to the fact that patients at increased risk of BAT activation were selected to receive diazepam. More prospective studies are warranted to elucidate this finding.

OP355

Role of HIF-1 in Hypoxia Stimulated Glucose Metabolism in Human Endothelial Cells

J. Paik[1], j. Park[2], K. Jung[3], K. Lee[4]; [1]samsung medical center, seoul, KOREA, REPUBLIC OF, [2]samsung medical center, sungkyunkwan university, seoul, KOREA, REPUBLIC OF, [3]Samsung medical center, Sungkyunhwan University, seoul, KOREA, REPUBLIC OF, [4]samsung medical center, Samsung medical center, Sungkyunhwan University, seoul, KOREA, REPUBLIC OF.

Aim-Hypoxia is a common denominator of many vascular disorders and can profoundly affect endothelial function and metabolism. In this study, we evaluated the effect of oxygen depletion on endothelial 18F-FDG uptake, GLUT1expression and hexokinase activity, and investigated the role of HIF-1α in this response. Methods and Results— Human umbilical vein endothelial (HUVE) cells under normoxia, hypoxia, and reoxygenation were evaluated for 18F-FDG uptake, hexokinase activity, and Western blot analysis of GLUT1 and HIF-1α protein. The role of HIF-1α in hypoxia-stimulated 18F-FDG uptake was assessed by stabilization with a HIF-1α inhibitor. In addition, the effect of HIF-1α in hypoxia-stimulated HUVE cells was measured by 18F-FDG uptake and HIF-1α expression level with HIF-1α siRNA transfection and HIF-1α inhibitor. Furthermore, HIF-1α activation in hypoxic HUVE cells was assessed by HIF-1α transcription factor assay. Involvement of potential signaling pathways was investigated with respective protein kinase inhibitors. Exposure to hypoxia for 6 and 16 hr increased HUVEC 18F-FDG uptake to 181.0 ± 9.1% and 196.4 ± 1.1% of controls, respectively. Reoxygenation after 16 hr hypoxia gradually recovered 18F-FDG uptake to 4 hr. Hypoxia also induced a 3.9 ± 0.7 fold elevation of hexokinase activity, and a significant increase in GLUT1 and HIF-1α levels. HIF-1α stabilization with DMOG was sufficient to sustain hypoxia-stimulated 18F-FDG uptake during reoxygenation and to increase 18F-FDG uptake in normoxic conditions. Hypoxic HUVE cells significantly increased HIF-1α activation using transcription factor assay to 2.51 ± 0.02 fold elevation of controls. HIF-1α was activated by hypoxia and inhibition of the protein with HIF-1α siRNA and HIF-1α inhibitor completely abrogated the ability of hypoxia to increase HIF-1α and FDG uptake. Cycloheximide, tyrosine kinase inhibition with genistein, and protein kinase C (PKC) inhibition with staurosporine completely abolished hypoxia-stimulated FDG uptake by inhibiting HIF-1α increase. PI3 kinase inhibition with wortmannin blocked hypoxia-stimulated FDG uptake, not by inhibiting HIF-1α increase but by attenuating HIF-1α transcription activity. Conclusions— Hypoxia enhances endothelial cell glucose uptake by upregulating hexokinase activity and GLUT1 expression. The findings further indicate that HIF-1α plays a central role in this metabolic response with dependence of its increase on PKC and transcription activity on PI3K activities. Our findings provide a molecular basis for the mechanism in which ECs respond to acute hypoxia. The results of this study suggest that cross-talk between AMPK and Akt is essential for angiogenesis under conditions of hypoxic stress, but dispensable for angiogenic cellular responses in normoxic endothelial cells.

OP356

Initial Experience with PET/MRI in the Evaluation of Diabetic Foot

D. Franceschi, K. Yaddanapudi, R. Matthews, V. Brunetti, B. Martin; SUNY at Stony Brook, StonyBrook, NY, UNITED STATES.

INTRODUCTION: Osteomyelitis is a common complication of diabetic foot Infections. Accurate diagnosis of bone involvement in the setting of complicated diabetic foot is a diagnostic challenge. We present our initial experience with FDG PET/MRI to determine bone involvement in diabetic patients with chronic foot infection. MATERIAL AND METHODS: Seven patients with chronic foot infection and clinical suspicion of osteomyelitis underwent PET-MRI of the foot. The MR imaging findings were graded as Grade 0 – normal signal, Grade I - hazy reticulated, T1 hypointense signal, Grade II - confluent T1 hypointense signal. Grade II, confluent signal was considered diagnostic of osteomyelitis. Reticulated signal was believed to reflect edema on MRI. Abnormal focal increased FDG uptake localizing to the bone on fused PET-MRI images was considered as osteomyelitis. Five of the seven patients subsequently underwent surgery. Two patients diagnosed with osteomyelitis refused surgery and opted for conservative therapy. RESULTS: All seven patients had osteomyelitis according to PET- MRI findings. Five patients had osteomyelitis on histopathology and 2 patients according to secondary clinical end points. Three cases with FDG

uptake involving the bone on fused images had negative MRI patterns (Grade I reticulated T1 hypointense signal or no signal change). All the cases positive on MRI were positive on FDG-PET. The sensitivity of PET-MRI to diagnose osteomyelitis was 100% in this small series of diabetic patients with chronic foot infection. CONCLUSIONS: PET-MR proved to be highly sensitive modality with high reader confidence for diagnosis of osteomyelitis in diabetic foot infections, reflecting complimentary nature of these modalities.

1009 - Monday, October 12, 2015, 4:30 PM - 6:00 PM, Hall 8
Physics & Instrumentation & Data Analysis: Image Reconstruction, Quantification & PET/MR

OP357

Scatter correction requirements for quantitative I-131 SPECT: Triple Energy Window and full Monte Carlo correction compared in phantom acquisitions

C. A. J. van Gils[1,2], R. van Rooij[1], C. Beijst[1], H. W. A. M. de Jong[1]; [1]University Medical Center Utrecht, Utrecht, NETHERLANDS, [2]St. Antonius Ziekenhuis, Nieuwegein, NETHERLANDS.

Aim: For accurate dosimetry in I-131 therapy, reliable quantitative SPECT reconstructions are essential. However, due to the complex emission spectrum of this isotope, accurate scatter correction is not trivial. Especially downscatter from higher energetic 606 keV gamma emissions in the 364 keV photopeak energy window poses a challenge. The goal of this research is to compare the effectiveness of two different scatter correction methods, namely triple energy window (TEW) and full Monte Carlo scatter correction. By doing this, scatter correction requirements for performing quantitative I-131 SPECT can be derived. Materials and methods: A NEMA IEC body phantom is used in which the two largest of the six fillable spheres contain non-radioactive water, whereas the other spheres contain I-131 solution in an activity concentration ratio of approximately 10:1 compared to the background compartment. Acquisitions are performed using a Siemens Symbia T16 utilizing the HE collimator over 120 angles. Total acquisition duration is varied to investigate the influence of noise and activity on the scatter correction performance. Using the in house developed and validated reconstruction software Utrecht Monte Carlo System (UMCS), reconstructions are generated without scatter correction, with TEW scatter correction and with full Monte Carlo-based scatter correction. All methods use OSEM reconstruction with 8 subsets with varying number of iterations (1-40). The resulting data is analyzed along the NEMA NU 2-2007 guidelines, calculating hot- and cold-sphere contrast, as well as the percentage of background variability and the residual count error in the lung insert. Results: As expected, applying no scatter correction yields the poorest results in all measured parameters. The TEW correction method results in overestimation of scatter contribution in the photopeak window, leading to erroneous quantification and unrealistically high recovery coefficients. Monte Carlo scatter calculations on the other hand provided validated, accurate scatter corrections, regardless of object geometry and scan duration and resulted in a significant improvement of all measured parameters over no scatter correction. Conclusion: Scatter correction is important in accurate I-131 quantification. Conventional TEW correction can yield overestimations of scatter, potentially leading to consequent underestimation of total uptake and apparent increase in hotspot uptake in clinical scans. Therefore, extra caution should be exercised when using TEW correction for quantification purposes. Full Monte Carlo calculations provide object-specific scatter corrections leading to the most accurate quantification. Therefore, it is considered the method of choice for quantitative I-131 SPECT.

OP358

Absolute quantification in SPECT - a phantom study

J. Kupferschlaeger, J. Lott, L. Kuenzel, H. Dittmann, C. la Fougère; University Hospital Tuebingen/Department of Radiology/ Division of Nuclear Medicine, Tuebingen, GERMANY.

Aim: New software solutions like Q.Metrix® (GE Healthcare) promise absolute quantification of SPECT data using attenuation-, scatter correction and resolution recovery. Aim of this study was to investigate the accuracy of quantification as well as scatter correction, the determination of recovery coefficients (RC) for partial volume correction (PVC), the influence of CT high voltage (HV) and tube current on quantification. Material and methods: IEC-Phantom with Hot-Sphere-Insert (6 hollow spheres with diameters 10-37mm) and lung insert was filled with 99m-Tc for three lesion to background ratios (LBR): LBRinf (1:0), LBR4 (4:1), LBR8 (8:1). All measurements were performed on a Discovery 670 NM/CT PRO® (GE) SPECT/CT system. For each LBR we performed CTs with 3 HV-settings (140kVp, 120kVp, 100kVp) and for each HV three tube-current settings (10mA, 30mA and 75mA, rotation time 0.8 sec). Reconstruction was performed with OSEM algorithm (2i10s, no pre- and postfiltering) including scatter-, CT-based attenuation correction and resolution recovery. For quantification we used the following VOIs: 2 VOIs in the phantom background, 6 VOIs for the spheres using threshold segmentation, 2 cylindrical VOIs in the (cold) lung insert and a VOI for the whole phantom. For each VOI we determined

average and maximum activity concentration in Bq/ml. Results: CT HV and tube current has minor influence on quantification: we observed a maximum deviation less than 1.6% from the activity concentrations using a reference CT (120kVp, 75mA) for attenuation correction. The total activity in the phantom as well as the activity concentration in the background could be reproduced excellently with a maximum error of 5%. Resolution recovery improves the recovery for volumes larger than 5 ml by approx. 20% but was limited for volumes smaller than 5 ml. Maximum values from the VOIs tend to be overestimated (RC-range 1.0 to 1.5 for large volumes) depending on iteration parameters and the LBR. Average values depended on VOI type and accurate VOI-placement. The smallest two spheres (10mm, 13mm) could hardly be quantified or detected for LBR8 and LBR4. Scatter correction underestimates the scatter fraction: about 50% of the background activity concentration was found in the cold lung insert. Conclusions/Discussion: Absolute quantification of SPECT data using the Q.Metrix® software is possible if all corrections are applied. This is valid for large structures like organs but PVC should be applied for quantification of small lesions. Further improvement of scatter correction is needed.

OP359

Absolute quantification in a commercial SPECT/CT: Tc-99m Activity recovery in NEMA/IEC and anthropomorphic phantoms.

S. Gnesin[1], P. Leite Ferreira[2], J. Malterre[2], J. Prior[2], F. Verdun[1]; [1]Institute of Radiation Physics, Lausanne University Hospital, Lausanne, SWITZERLAND, [2]Department of Nuclear Medicine, Lausanne University Hospital, Lausanne, SWITZERLAND.

Aim: Similar to PET, absolute quantitative image modality is becoming available in commercial SPECT/CT devices. The goal of this study was to assess the quantitative accuracy of activity concentration recovery as a function of image reconstruction parameters using a NEMA/IEC and an anthropomorphic abdominal phantom. Materials and methods: We performed quantitative ^{99m}Tc-SPECT/CT acquisitions (Siemens Symbia Intevo) of a NEMA/IEC phantom (6 hot spheres, 10:1 sphere to background activity ratio, 1 lung insert) and an anthropomorphic abdominal phantom (commercial Kyoto Liver/Kidney phantom) including a liver insert (volume=1.8L) with 3 hot-spheres (20-30-40mm diameter, 5:1 hot-sphere to liver activity concentration ratio). Background activity concentration (AC_{bg}) was 33/104 kBq/mL in the NEMA/abdominal phantom respectively. SPECT acquisitions used 120 projections (20s/projection). Reconstructions were performed with the proprietary iterative conjugate gradient algorithm. Reconstruction parameters such as iteration number (It range: 4-48, 6 subsets) and gaussian smoothing (FWHM range: 0-10 mm) were varied. Recovery coefficients (RC, mean and max), relative lung error (only for the NEMA phantom) and image noise (COV) on the background were assessed. Results: On the NEMA phantom, measured AC_{bg} was <6% from the expected true value for all tested cases. RC increased less than linearly with iterations. RC relative increment (mean/max) was 13/18%, 8.5/12%, 4/7.5% when varying from It=4 to 8, 12 to 24 and 24 to 48 respectively. It=20 and gaussian smoothing of 7.5mm limited the COV to ≤20%. In these conditions RC (mean/max) were 0.8/1.2 for lesion size > 5 mL and 0.42/0.55 at 1 mL. Lung relative error was fairly sensitive to It changes and ranged from 8 to 12% with increasing smoothing levels. Comparable AC_{bg} accuracy and RC values were found for the abdominal phantom. In this specific case, the higher activity concentration resulted in reduced background variability (COV=10% at It=20, FWHM = 7.5mm). Conclusions: Absolute quantification in commercial SPECT/CT is becoming available. The tested device provided a good accuracy in background activity recovery. Relative lung error was comparable to PET levels assessing the efficient integration of attenuation and scatter corrections with adequate detector modeling. Reliable SPECT quantification has the potential to improve clinical outcome and radiation dosimetry assessments. Reconstruction parameters influence RC (and thus SUV), and optimization is recommended in accordance with clinical requirements.

OP360

Comparison of Image Reconstruction Techniques for Single Photon Emission Computed Tomography (SPECT)

M. Dimcheva, S. Sergieva, A. Jovanovska; Sofia Cancer Center, Sofia, BULGARIA.

The aim of this study was to compare the performance of filtered backprojection (FBP) and iterative reconstruction algorithms available in clinical SPECT software. Materials and Methods: SPECT images of a Jaszczak phantom with cold rod inserts, hot and cold spheres and capillary line sources were acquired on a dual-head SPECT-CT system Symbia T2, Siemens. Image acquisition was performed using a 180° non circular orbit for each detector, with 120 projection angles, 500 000 counts per projections 128 × 128 matrix size, zoom = 1 and pixel size of 4.8mm. A symmetrical 15% wide energy window for the acquisition was centered at 140 keV. The phantom studies were acquired for 30 sec per projection angle. FBP reconstructions were performed by use of the ramp filter limited at the Nyquist frequency (0.5 cycle per pixel). The different type of filter using FBP reconstructions was also considered. The images reconstructed with OSEM were filtered with

a symmetric 3-D Gaussian function having a full width at half maximum of 1 pixel (4.8 mm). Iterative reconstruction of these images was halted after 12 iterations using 4 subsets. Each combination of subsets and iterations was applied to the same set of noisy projection data. The linear attenuation correction was set to μ = 0.15 cm -1. Results: The effect of image smoothing with the use of Gauss filter with different FWHM = mm are shown. Application of Gauss post-filtering degrades the contrast but did not affect the high quality of images. However, this result applies only if Gauss filter's FWHM coefficient does not exceed a double value of the pixel size. Generally, iterative technique (OSEM algorithm) gives better outcomes for both the qualitative and quantitative assessment of SPECT studies in comparison to FBP method. Conclusion: The quality of the image depends on several factors such as spatial resolution, contrast and noise. Proper filter selection is significant for the improvement of the image quality and therefore for the diagnostic evaluation.

OP361

Quantitative Yttrium-90 PET/CT acquisition and reconstruction optimization: An anthropomorphic phantom validation.

S. Gnesin[1], L. Paterne[1], A. Boubaker[2], S. Adib[2], M. Pappon[2], M. Kosinski[1], J. Prior[2], S. Baechler[1], F. Verdun[1]; [1]Institute of Radiation Physics, Lausanne University Hospital, Lausanne, SWITZERLAND, [2]Department of Nuclear Medicine, Lausanne University Hospital, Lausanne, SWITZERLAND.

Aim: Post-radioembolization ^{90}Y spatial distribution and radiation dosimetry can be obtained from clinical quantitative ^{90}Y-PET/CT and used to evaluate treatment outcome and validate predictive dosimetry based on ^{99m}Tc-MAA SPECT/CT. We aimed at determining optimal reconstruction parameters for quantitative ^{90}Y-PET/CT acquisition of an anthropomorphic abdominal phantom. Materials and methods: We performed 10 sequential (1 per day) PET/CT scans (Discovery 690, GE-Healthcare) of an anthropomorphic abdominal phantom including a liver insert (volume=1.8L) with 3 hot-spheres (20-30-40mm diameter). Hot-sphere to liver ^{90}Y activity concentration (AC_{bg}) ratio was 5:1. Initial liver background activity concentration was 1MBq/mL. The rest of the phantom being water filled. AC_{bg} linearity as a function of time was assessed in the liver background. At each time point, recovery coefficients (RC, mean and max) and contrast-to-noise ratio (CNR) in hot spheres and image noise (COV) in the liver background were assessed as a function of different reconstruction parameters: OSEM iterations (It=1, 2, 3, subsets=24), frame duration (F_d=20, 30, 45 min). The impact of Time-of-flight (TOF) information and point-spread-function (PSF) recovery where also assessed. Results: TOF-based reconstructions provided AC_{bg} and RC convergence in 1 and 2 iterations respectively, while 2/3 iterations where required for AC_{bg}/RC to converge to a stable value otherwise. Furthermore, TOF reconstructions minimized spurious signal in regions without activity concentration. Higher RCs were obtained for combined TOF+PSF reconstructions regardless other reconstruction parameter combinations (RC_{mean} from 0.45 in 20-mm spheres; 0.5 in 30-mm spheres; 0.65 in 40mm spheres). Measured AC_{bg} in TOF+PSF reconstructions was <8% from the expected true value down to 300 kBq/ml where no-TOF reconstructions resulted in up to 20% AC_{bg} underestimation. PSF-based reconstructions (It=2, F_d=30 min) displayed COV≥40% for AC_{bg}<300kBq/mL; the same level of noise was found for AC_{bg}<450kBq/mL when no PSF recovery was applied. When using TOF+PSF reconstructions (It=2, F_d=30 min), lesions detectability (CNR>4) was possible down to 1000/800/600 kBq/mL on the 20/30/40mm sphere respectively. Conclusions: Combination of TOF and PSF improves quantitative assessment in intrinsically low-statistic ^{90}Y-PET acquisitions. TOF+PSF based reconstruction significantly reduced correlated noise and improved activity recovery convergence and detectability at matched frame duration.

OP362

FDG uptake quantification: a new approach using tumour delineation on maximum intensity projections

A. de Jong[1], B. A. Blomberg[1], R. A. Nievelstein[1], V. Frings[1], G. Kramer[2], A. J. de Langen[2], O. S. Hoekstra[2], R. Boellaard[2]; [1]UMC Utrecht, Utrecht, NETHERLANDS, [2]VU Medical Center, Amsterdam, NETHERLANDS.

Aim: To study the performance of a new approach for FDG uptake quantification using tumour delineation on PET maximum intensity projections (MIPs). The tool is designed to allow faster tumour delineation by minimizing user interaction (i.e. it is not required to delineate each lesion in all PET image slices). The tool specifically enhances workflow in case the patient has a large number of lesions. Materials and methods: A new tool was developed that generates FDG whole-body PET/CT MIPs at 0 (coronal), 45, 90 (sagittal) and 135 degrees (MIP tool). Next, tumours can be delineated manually with or without intensity thresholds on these MIPs. These MIP delineations are then back-projected to the FDG PET/CT images to obtain an initial tumour mask per lesion. Final tumour delineations are then derived by performing a region growing method starting at the maximum intensity voxel per lesion (within these masks), using a background corrected 50% of maximum threshold (A50%). From the final delineation SUVmax, SUVmean, metabolic active tumor volume (MATV) and total lesion glycolysis (TLG) are derived. The performance of the method was tested using the NEMA NU 2 Image Quality

phantom, and in eight FDG whole-body PET/CT scans of therapy-naïve non-small-cell lung cancer patients. The phantom study was performed according to EARL specifications and the patients were examined following the EANM FDG PET/CT guidelines (Boellaard et al EJNMMI 2015; 42: 328-54). Phantom data will be compared using the expected uptake parameters, and both phantom and clinical data will be compared using an image based A50% method (Cheebsumon et al EJNMMI 2012; 2: 56) to delineate tumours (VOI tool). Results: For the phantom study MIP tool SUVmax approached real SUV by 96%. MIP tool SUVmean approached real SUV by 77%. MIP tool MATV and TLG approached real volume and real TLG by 83% and 65% respectively. For the phantom study SUVmax and SUVmean were identical for both tools. MATV as well as TLG differences were within 1% between both tools. In the clinical studies, SUVmax as well as SUVmean were identical between both tools. MATV and TLG differences ranged between 0-4% and 0-3% respectively. Conclusion: The MIP based delineation approach provided comparable (<4%) results to those obtained using the image based delineation approach. The method may require less user interaction in case of multiple lesions and could be an interesting alternative for assessing total tumour burden quickly.

OP363

The influence of ignoring higher bone attenuation on pelvic and spinal lesions in [18F]NaF PET/MRI examinations.

G. Schramm[1,2], L. Oehme[3], J. Maus[2], F. Hofheinz[2], J. Petr[2], A. Lougovski[2], B. Beuthien-Baumann[3], J. van den Hoff[2]; [1]KU Leuven, Leuven, BELGIUM, [2]Helmholtz-Zentrum Dresden-Rossendorf, Dresden, GERMANY, [3]Universitaetsklinikum Carl Gustav Carus, Dresden, GERMANY.

Aim: MRI-based attenuation correction (MRAC) in clinical whole-body PET/MRI imaging routinely is based on tissue type segmentation. Due to lack of MRI signal in cortical bone and the varying signal of spongeous bone, standard whole-body segmentation-based MRAC neglects the difference between the attenuation coefficient of soft tissue and the (higher) one of bone (MRAC-nobone). In the present work we have quantified the bias caused by MRAC-nobone in spinal and pelvic lesions in 20 PET/MRI examinations with [18F]NaF using the reconstructed PET standard uptake value (SUV) as the relevant measure. Methods: We reconstructed 20 PET/MRI [18F]NaF patient data sets acquired with a Philips Ingenuity TF PET/MRI. First, we used the vendor-provided MRAC-nobone algorithm to reconstruct PET-nobone. Second, we used a threshold-based algorithm developed in our group to automatically segment bone structures in the [18F]NaF PET images. Subsequently, an attenuation coefficient of 0.11 1/cm was assigned to the segmented bone regions in the MRI-based attenuation image (MRAC-bone) which was used to reconstruct PET-bone. The automatic bone segmentation algorithm was validated in 6 PET/CT [18F]NaF examinations. Finally, relative SUVmean and SUVmax differences between PET-bone and PET-nobone of 8 pelvic and 41 spinal lesions, and of other regions such as lung, liver, and bladder were calculated. Results: The comparison of [18F]NaF-based and CT-based bone segmentation in the 6 PET/CT patients showed a Dice similarity of 0.7 with a true positive fraction of 0.72 and a false positive fraction of 0.35. The [18F]NaF-based bone segmentation worked well in the pelvis and spine. However, it showed artifacts in the skull and in the extremities. The analysis of the 20 [18F]NaF PET/MRI examinations revealed relative SUVmax differences between PET-nobone and PET-bone of (-8.7% ± 2.7%, p = 0.01) and (-8.1% ± 1.9%, p = 2.4e-8) in pelvic and spinal lesions, respectively. A maximum SUVmax underestimation of -13.7% was found in lesion in the third cervical spine. The averaged SUVmean differences in volumes of interests in lung, liver and bladder were below 3%. Conclusion: Neglecting higher bone attenuation in MRAC leads to a systematic moderate SUV underestimation in spinal and pelvic lesions. The developed automatic [18F]NaF PET-based bone segmentation allows to include higher bone attenuation in whole-body MRAC and thus improves quantification accuracy for pelvic and spinal lesions in [18F]NaF PET/MRI examinations enabling direct comparisons to PET/CT examinations.

OP364

Evaluation of Siemens SMART Neuro AC Calculated Attenuation Correction for FET PET

P. Ritt, T. Kuwert, C. von Gall; Clinic of Nuclear Medicine, University Hospital, Erlangen, GERMANY.

Aim: Correction for photon attenuation (AC) in PET is essential for quantitative imaging. Before hybrid PET/CT scanners were available, emission-based, calculated AC was common. It is generally accepted that for PET examinations of the brain, hybrid PET/CT often adds little benefit beyond AC. For this reason, enhanced calculated AC methods have been (re-)introduced into hybrid PET/CT and PET/MRI scanners. We aimed for evaluating the accuracy of one of these calculated AC methods, namely Siemens' SMART Neuro AC, which has recently become available. Materials and MethodsFET PET/CTs were acquired for 17 patients (6 male, 11 female, mean age 36±15 y), suspected of recurrent cerebral malignancies. The average injected dose was 200±50 MBq at 73±18 kg. The PET images were reconstructed from the counts acquired between 30 and 60 min p.i. The reconstruction was carried out with OSEM3D at 12 subsets, 4 iteration, and 5.0 mm Gaussian smoothing. AC images were obtained using the CT data (CTAC), as well as by applying the SMART Neuro calculated attenuation correction (calcAC).

Images that represent the difference between both AC strategies were generated and non-rigidly registered to an MRI atlas. By this, the differences between calcAC and CTAC were evaluated in 19 MRI-defined brain regions. Additionally, the differences for FET-positive lesions were assessed in terms of change of the ratio of the lesion's SUVmax to the SUVmean of a non-affected, contralateral region. Results: CalcAC leads, on average, to an underestimation of activity concentration when compared to CTAC. Subsequently, the activity of calcAC images in the parietal, occipital, frontal, temporal lobes, and in the cerebellum were 90.0: 84.4: 94.6: 89.5: 87.9% of the CTAC images' values respectively. However, the differences were symmetrical in left-right direction. Consequently, the deviations for the quotient SUVmax/SUVmean were smaller, on average 2.8 percent and ranging from 0.1 to 9.9%. This deviation did not lead to any reclassification of the lesions as either benign or malignant when a threshold of x was used for this purpose. Conclusion: Although finding slightly higher deviations between CTAC and calcAC reconstructed images than reported by the manufacturer (99% of brain pixels below 10% error), the bias will most likely not influence diagnoses based on SUV ratios. This fact may be attributed to the left-right symmetry of the bias. Nevertheless, one has to keep in mind the potentially lower measured activity and should be especially cautious when comparing to data obtained with CTAC in prior examinations.

1010 - Tuesday, October 13, 2015, 8:00 AM - 9:30 AM, Hall D
Clinical Oncology: Melanoma & Lymphoma

OP365

Interim [18F]-FDG-PET in MALT lymphoma patients treated with immunotherapy: which Deauville score is the best predictor of end-of-treatment outcome?

T. Traub-Weidinger, M. Raderer, B. Kiesewetter, M. Weber, G. Karanikas, M. Mitterhauser, M. Hacker, M. E. Mayerhoefer; Medical University of Vienna, Vienna, AUSTRIA.

Aim: To determine, which score of the 5-point Deauville treatment response scale, as assessed by interim [18F]-FDG-PET, is the best predictor of end-of-treatment outcome in patients with FDG-avid MALT lymphoma undergoing immunotherapy. Method: Our prospective study included patients with histologically verified MALT lymphoma scheduled to receive rituximab-based immunotherapy and to undergo whole-body [18F]-FDG-PET/CT before treatment, after three therapy cycles (interim), and after six therapy cycles (end-of-treatment). Patients without FDG avidity at pre-treatment [18F]-FDG-PET were excluded. In the remaining patients, treatment response of all nodal and extranodal lymphoma lesions visible on pre-treatment [18F]-FDG-PET was assessed on interim [18F]-FDG-PET, separately for four different cut-off scores of the Deauville scale: score 2 = uptake higher than the background activity, score 3 = uptake higher than the mediastinal blood pool, but lower than the liver; score 4 = uptake comparable to, or slightly higher than the liver, score 5 = uptake clearly higher than the liver. For each of the four lesion-based cut-off scores, the ICML/Lugano classification was used for assigning each patient to an outcome class: complete remission (CR), partial remission (PR), stable disease (SD), or progressive disease (PD). These interim outcomes were then compared to the end-of-treatment outcomes according to the ICML/Lugano classification using kappa coefficients. Results: Fifteen patients with 35 lesions met our participation criteria. Using a Deauville cut-off score of 2, five patients were rated as CR, six patients as PR and four as SD at interim restaging. Using a Deauville cut-off score of 3, seven patients were rated as CR, four patients as PR and four as SD at interim restaging. Using a Deauville cut-off score of 4, eight patients were rated as CR, three patients as PR and four as SD at interim restaging. Using a Deauville cut-off score of 5, ten patients were rated as CR, two patients as PR, and three as SD at interim restaging. The Deauville scores 2, 3, 4, and 5 showed agreement with end-of-treatment outcomes (nine CR, three PR, three SD, and no PD) in 66.7%, 80%, 86.7%, and 86.7%, with kappa values of 0.5, 0.67, 0.77, and 0.75, respectively. Conclusion: Interim [18F]-FDG-PET after three cycles of immunotherapy can predict the end-of-treatment outcome in patients with FDG avid MALT lymphoma using a Deauville cut-off score of 4.

OP366

The Deauville Criteria and Metabolic Parameters as Prognostic Factors in Interim PET in Hodgkin Lymphoma: a Single Centre Experience

M. Cuzzocrea[1], L. Guerra[2], F. Elisei[2], C. Crivellaro[1,2,3], E. De Ponti[4], S. Bolis[5], L. Baratto[1], S. Pacella[1], M. Arosio[2], C. Landoni[1]; [1]Department of Nuclear Medicine, University of Milan-Bicocca, Milan, ITALY, [2]Department of Nuclear Medicine, San Gerardo Hospital, Monza, ITALY, [3]Tecnomed Foundation, University of Milan-Bicocca, Milan, ITALY, [4]Department of Medical Physics, San Gerardo Hospital, Monza, ITALY, [5]Department of Haematology, San Gerardo Hospital, Monza, ITALY.

BACKGROUND AND AIM OF THE STUDY: 18-Fluorodeoxyglucose (FDG) positron emission tomography/computed tomography (PET/CT) is the most accurate tool for staging, treatment monitoring, and response evaluation in Hodgkin lymphoma (HL). The interim-PET (i-PET) is considered predictive of final response and prognosis; early determination of treatment sensitivity by i-PET is the best tool to guide

individualized, response-adapted treatment. This study aimed to explore the prognostic role of i-PET in patients with HL: Deauville criteria, SUVmax and SUVpeak were respectively correlated to disease free survival (DFS) and overall survival (OS). METHODS: We retrospectively evaluated 83 patients (47 men, 36 women; mean age 40±14 years, range 20-73) with newly diagnosed HL, stage I-IV disease (5 stage I, 39 stage II, 18 stage III and 21 stage IV). All patients were studied with 18F-FDG PET/CT prior to treatment (baseline PET), after two cycles of chemotherapy (i-PET) and at the end of the treatment. Treatment was not changed according to the results of the i-PET. i-PET were qualitatively interpreted by two observers using the Deauville five-point scale. A score of 1-3 was regarded as "negative" and 4 or 5 as "positive". Lesions with the highest FDG uptake on i-PET was selected as "reference lesion" and SUVmax and SUVpeak were calculated. All datasets were correlated with DFS and OS. ROC curves were analysed to find best SUVmax and SUVpeak thresholds predictive for complete response and OS. Kaplan-Meier method was used to evaluate DFS and OS. RESULTS: The median follow-up was 36 months for DFS and 50 months for OS. i-PET scan resulted negative for 66 patients (79.5%) and positive for 17 patients (20.5%). The positive and negative predictive values of i-PET for predicting treatment outcome were 47,0% and 93,9%, respectively. The DFS and OS for positive i-PET and negative i-PET were 58.2% and 96.7% ($p<0.0001$), and 70.6% and 98.5% (p 3 were relevant on OS ($p=0.014$ and $p=0.022$, respectively); no significant differences were found in DFS. CONCLUSIONS: Early interim PET/CT is a good predictor of outcome in patients with HL. Deauville criteria using a cut off between 3 and 4 was reliable to discriminate patients with poor from good prognosis. Similarly, metabolic features of reference lesion (SUVmax ≤ 3 and SUVpeak < 3) are predictors of good prognosis.

OP367

PET/FDG and Interleukin-10 as prognostic indicators in Diffuse Large Type B-Cell Lymphoma

L. Tagliabue[1], L. Ottobrini[2], C. B. Colombo[2], S. Seghezzi[3], I. Libani[2], A. Moro[1], M. Violati[1], L. De Fazio[4], A. Bertolini[5], P. Foa[2], G. Lucignani[2]; [1]AO San Paolo, Milano, ITALY, [2]University of Milan, Milano, ITALY, [3]AO Treviglio-Caravaggio, Treviglio, ITALY, [4]AO Lodi, Lodi, ITALY, [5]AO Valtellina e Chiavenna, Sondrio, ITALY.

AIM: Diffuse large B-cell lymphoma (DLBCL) is the most common non-Hodgkin's lymphoma. In these patients, FDG/PET has been reported to be a good prognostic indicator when performed during therapy (interim-PET/FDG) and more so at the end-of-therapy. However, because of the still limited prognostic accuracy of interim-PET/FDG and, to some extent, also of end-of-therapy-FDG/PET, given the evidence of IL-10 involvement in DLBCL genesis and progression, we aimed to evaluate the prognostic role of combined IL-10 serum assay and PET/FDG. Patiens and methods: Twenty-four drug-naive patients with DLBCL Ann Arbor stage > I underwent both IL-10 serum assay and PET/FDG evaluation three times: at the time of diagnosis, after 2 cycles of R-CHOP (interim), and again at the end-of-therapy. PERCIST criteria were used for the assessment of PET/FDG studies. Results: Interim-PET/FDG allowed us to discriminate two patient populations: one with a complete metabolic response, i.e. PET/FDG-negative (15/24 patients), and another with either partial metabolic response or progressive disease, i.e. PET/FDG-positive (9/24 patients). At end-of-therapy, PET/FDG scan was negative in 19/24 and positive in 5/24 patients, as PET/FDG became negative in 4 patients that were PET/FDG-positive at interim. A disease relapse was observed within 36 months after therapy completion in 2/19 patients and in 4/5 patients that were FDG/PET-negative and FDG/PET-positive, respectively, at the end-of-therapy. IL-10 serum levels, detectable in serum at staging but not after therapy, did not appear to be significantly related to metabolic response. The results of IL-10 assay and PET/FDG analyzed together conveyed these novel findings: A) High IL-10 levels (> than 10pg/ml) at staging were recorded among all the relapsing patients (i.e. 4/5 PET/FDG-positive and 2/19 PET/FDG-negative at the end-of-therapy). B) When values of IL-10 measured at staging are combined with either interim- or EOT-PET/FDG results, it is possible to stratify patients with high/low probability of relapse with the same accuracy. C) Low levels of IL-10 appear to characterize a population of "slow responders with favorable prognosis", i.e. patients PET/FDG-positive at interim and PET/FDG-negative at end-of-therapy, that do not relapse. Conclusions: In DLBCL patients, following 2 cycles of R-CHOP, the combination of IL-10 assays and PET/FDG increases the prognostic accuracy by decreasing both false negative and false positive prognoses, and, at the end-of-therapy, allows to identify patients at high risk for relapsing disease among both PET/FDG-positive and PET/FDG-negative subjects. IL-10 could be routinely used along with FDG/PET for the prognostic assessment of DLBCL patients.

OP368

Assessing Bone Marrow Involvement in DLBCL: Comparison of FDG PET and Bone Marrow Biopsy

V. Ptacnik, K. Benesova, E. Cmunt, J. Kubinyi, M. Trneny; Charles University Prague, Prague, CZECH REPUBLIC.

Aim: FDG PET/CT is important imaging method for clinical stage determination of DLBCL. According to new guidelines (Cheson et. al., J Clin Oncol 2014) FDG PET can in majority of cases substitute bone marrow biopsy for possible bone marrow involvement evaluation. Methods: Retrospective analyze

of 217 consecutive patients was done. The group consists of 112 men and 105 women (median age 65 years) with newly diagnosed DLBCL. All had available staging bone marrow biopsy (BMB) and FDG PET. We compared results of PET and BMB to establish the differences between positivity rates of each method. Evaluation of PET was done visually, increased FDG uptake was considered positive. Focal and diffuse FDG hyperaccumulation was distinguished. BMB was evaluated histologically to determine type of involvement and percentage of malignant cells. The confrontation of findings was done; impact to clinical stage (CS) and outcome of treatment were compared. Results: Comparing PET and BMB findings, 82% were congruent, 71.9% of them were negative and 10.1% positive; 17.9% findings were contradictory: 13.4% were PET only positive and 4.6% BMB only positive. Out of 10 BMB only positive patients 8 had discordant histological finding and 2 had concordant finding with low level of bone marrow infiltration. Analyzing PET only, 23.5% patients were positive, BMB positive were 14.7% findings and positive finding according to at least one method had 28.1% patients. Seven patients had diffusely increased FDG uptake in bone marrow, 4 of them had positive BMB finding, 3 had negative bone marrow biopsy - these were considered as false positive. PET driven clinical stage was downgraded from stage IV to localized by BMB in 2 cases and upgraded from localized to stage IV in 1 patient. 30 of 32 patients with initial bone marrow involvement had BMB after treatment, 2 (6.7%) remained BMB+. 46 of 51 initially PET positive patients had restaging PET after therapy, 4 (8.7%) remained positive. Two of 22 initially PET+/BMB+ patients lingered PET+/BMB+ after therapy, none remained positive only with one method. Conclusions: PET compared with BMB increases finding of bone marrow involvement from 14.7% to 23.5%, combining the methods we get on 26.7% positive findings. PET misses BM involvement in 4.6% of patients. Almost half of the diffuse PET+ cases are false positive, therefore we recommend bone marrow biopsy performance in these cases.

OP369

Prolonged overall survival in metastatic melanoma with low tumor burden at anti-PD1 initiation: CT-scan, 18-FDG-PET and blood samples

L. Dercle, S. Ammari, M. Texier, E. Lanoy, S. Champiat, D. Deandreis, M. Terroir, A. Marabelle, M. Schlumberger; Gustave Roussy, Villejuif, FRANCE.

PURPOSE: Immunotherapies targeting the pathway of the programmed death-1 ("anti-PD1") receptor lead to a delayed clinical response that is sustained in only a fraction of patients with metastatic melanoma. The rationalization of the use of this costly drug requires identifying patients with demonstrated clinical benefit. Patients with serum LDH>250 (biologic tumor burden [TB], blood sample) are considered at high risk by the AJCC M-staging system. Our group demonstrate that a TB_{3D}>202cm3 (anatomic TB, CT-scan) is classified high risk. The primary objective was to characterize if biomarkers extracted from the whole metastatic tumor volume by ^{18}F-FDG PET at anti-PD1 initiation predict overall survival [OS]. METHODS: Patients with metastatic melanoma prospectively included in phase I trials were eligible. All the lesions measurable at baseline within the whole tumor volume were measured on CT-scan (anatomic TB: TB_{1D}, TB_{2D}, TB_{3D}), on FDG-PET (metabolic TB: MTV; glycolysis: TLG, SUV_{max}, SUV_{mean} and HISUV). The respective effect on OS and PFS was evaluated and derived from Cox proportional hazard models. RESULTS: Data were available in 28 patients with a median follow-up of 13.2 months. A significant correlation of biomarkers of TB (p<.05) was demonstrated for anatomic TB (TB_{3D} vs TB_{1D}: r=.78), metabolic TB (MTV vs TLG: r=.93), MTV/TLG vs TB_{3D} (r=.61/.62) and MTV/TLG vs LDH (r=.37/.40). Patients with lower TB showed a prolonged survival: TB_{1D} <113 (p.0008), LDH<250 (p.01), MTV<21 cm3 (p.02) and TLG<171 (p.13). Hazard ratio of death for one SD increase were: 2.07 [1.31; 3.27] for LDH (p<.01), 2.64 [1.57; 4.45] (p<.01) for TB_{1D}, 2.09 [1.33;3.30] (p<.01) for TB_{2D}, 2.32 [1.45; 3.72] (p<.01) for TB_{3D}, 1.41 [0.87;2.26] (p=.16) for MTV, 1.08 [0.67;1.75] (p=0.76) for TLG, .87 [.47;1.59] (p=.21) for SUVmax, 1.10 [.37;3.32] (p=.86) for SUVmean and 0.81 [.45;1.43] (p=0.46) for HISUV. CONCLUSION: Proof of concept that a screening of good candidate for immunotherapy is achievable by medical imaging: low TB (anatomic, metabolic and biologic) at the initiation of anti-PD1 show prolonged survival. An increased TB on CT-scan (TB3D>202cm3, TB2D>113mm), and/or 18F-FDG-PET (MTV) and/or blood samples (LDH>250) might identify high risk patients and the most accurate imaging modality might depend on the dominant site of the metastases (e.g.: FDG-PET for bone, CT-scan for liver). Biomarkers estimating the intensity of the glycolytic activity within the tumor volume (SUVmax, SUVmean, HISUV) are not prognostic of OS.

OP370

Cost-effectiveness analysis of sentinel node biopsy in patients with primary cutaneous melanoma

P. Serra-Arbeloa[1,2], Á. O. Rabines-Juárez[1], S. Álvarez-Ruiz[3], F. Guillén-Grima[2]; [1]Complejo Hospitalario de Navarra, Pamplona, SPAIN, [2]Universidad Pública de Navarra, Pamplona, SPAIN, [3]Hospital Universitario Miguel Servet, Zaragoza, SPAIN.

Aim: To develop a cost-effectiveness analysis of the role of the sentinel node biopsy (SNB) in patients with different Breslow thickness primary cutaneous melanomas (CM) over a 10 year time horizon, using the health care system perspective. Methods: A decision tree model was used to compare two different

strategies of management of patients diagnosed with CM, wide excision with SNB followed by complete lymph node dissection (SNB) and wide excision only (WE). The economic and clinical outcomes, measured as mean total cost per patient, cost effectiveness ratio (CER), incremental cost effectiveness ratio (ICER), life years saved (LYSs) and quality-adjusted life years (QALYs), were calculated from the model. Transition probabilities of disease progression and survival rates were obtained from the published literature after a systematic review, and the costs from government official publications. A sensitivity analysis was performed to test the robustness of the model, analysing the changes in different variables of every branch of the tree. Results: Base case analyses suggested that the mean total cost per patient with intermediate thickness CM receiving the SNB strategy was 25,822 € with 0.84 LYSs, 0.69 QALYs, and a CER of 30,812 €/LYS and 37,125 €/QALY; being of 22,683 € with 0.81 LYSs, 0.67 QALYs, 28,143 €/LYS and 33,780 €/QALY when the patient received the WE only. The ICER for SNB was 97,849 €/LYS and 130,508 €/QALY. In a patient with thick CM the mean total cost of the SNB was 36,101 € with 0.63 LYSs and 0.46 QALYs, and a CER of 57,263 €/LYS and 77,896 €/QALY. For a WE patient was 18,185 € with 0.67 LYSs, 0.49 QALYs, 27,264 €/LYS and 37,162 €/QALY. The ICER for SNB was -490,202 €/LYS and -692,074 €/QALY (Northwest quadrant; SNB dominated by WE). The mean cost of the patient with thin CM was 25,980 € with 0.92 LYSs, 0.72 QALYs, 28,897 €/LYS and 35,943 €/QALY for the first strategy, and 7,800 € with 0.92 LYSs, 0.83 QALYs, 8,877 €/LYS and 9,365 €/QALY for the second one. The ICER was -9,217,203 €/LYS and -165,191 €/QALY (Northwest quadrant). The sensitivity analysis showed no significant differences in the results. Conclusion: SNB appears not to offer an improvement in health outcomes in terms of LYSs and QALYs for patients with thick and thin CM, and a slight benefit for those with intermediate CM. SNB seems not to be cost-effective compared with WE in any CM thickness.

OP371

The role of preoperative lymph node ultrasound in patients with primary cutaneous melanoma: a meta-analysis

P. Serra-Arbeloa[1,2], Á. O. Rabines-Juárez[1], S. Álvarez-Ruiz[3], F. Guillén-Grima[2]; [1]Complejo Hospitalario de Navarra, Pamplona, SPAIN, [2]Universidad Pública de Navarra, Pamplona, SPAIN, [3]Hospital Universitario Miguel Servet, Zaragoza, SPAIN.

Aim: The objective of the study was to evaluate the diagnostic accuracy of high-resolution ultrasound (US) in detecting nodal involvement before performing the sentinel node biopsy (SNB) in patients with primary cutaneous melanoma (CM). Methods: A systematic review was conducted following the Preferred Reporting Items for Systematic reviews and Meta-Analyses (PRISMA) guidelines criteria. An electronic search using the terms “melanoma” and “sentinel node” was performed in MEDLINE, Scopus and Web of Knowledge (WoK) databases. Studies were considered if they reported data on preoperative lymph node US accuracy that allowed creating a 2x2 table, excluding those with high risk of bias (QUADAS-2 criteria). A meta-analysis was used to calculate the pooled sensitivity and specificity with their 95% confidence intervals (95%CI) and to test heterogeneity. Sensitivity and subgroup analyses were performed to search the articles that provided more heterogeneity. After the study, a level of recommendation for the use of the technique, according to the Scottish Intercollegiate Guidelines Network (SIGN) criteria, was established. Results: Seven articles were included. Two of them reported accuracy data per patient, 2 per node and 3 per patient and node. A total of 1,229 patients and 2,270 nodes were considered, with a mean SN positivity rate of 11.9% and a mean of false negative rate of 16,4%. In the results per patient, the weighted sensitivity was 33% (95%CI=24-36%) and the weighted specificity 93% (95%CI=91-94%). When the results were obtained per node, the weighted sensitivity and specificity were respectively 16% (95%CI=13-20%) and 97% (95%CI=96-97%). In both cases, a high heterogeneity between the studies was found. After sensitivity and subgroup analysis, the heterogeneity persisted and when the articles that provided more heterogeneity were excluded, the sensitivity of the preoperative US per patient decreased up to 25%. Conclusions: Preoperative ultrasonography to detect lymph node involvement in patients with CM presents a very low sensitivity; a negative ultrasonographic result does not exclude lymph node metastases. US cannot replace SNB in the detection of lymph node metastases. The maximum level of recommendation of US for this indication is C (being A the highest and D the lowest).

OP372

Lymphoscintigraphy and Sentinel Lymph Node Biopsy in Cutaneous Melanoma: Analysis of 201 Patients From a Single Institution

L. Jaukovic, M. .Rajović, M. Radulovic, L. Kandolf-Sekulovic; Military Medical Academy, Belgrade, SERBIA.

AIM: Sentinel lymph node biopsy (SLNB) is widely accepted method in the management of clinically localized cutaneous melanoma. The aim of this study was to report the results on patients scheduled for preoperative lymphoscintigraphy and SLNB. METHODS: At Medical Military Academy, Belgrade, 250 patients were identified for SLNB between 2010-2014. Out of them, retrospective review of 201 patients with cutaneous melanoma was performed. Lymphoscintigraphy was used

in all the patients and dual labeling method (blue dye/ nanocolloid) in less than one half of them. To delineate the relation of patients', tumors' and scintigraphic characteristics with positive SLN status, we examined all variables by univariate logistic regression with odds ratios representing effect size. RESULTS: Overall identification rate of SLN was 98.5%. Positive SLN (metastatic, one or more) was seen in 47 (23.4 %) patients. Drainage to one regional basin was seen in 176 (87.6 %) and multiple drainage regions (up to three) - in 24 patients (11.9%). In transit lymph nodes were detected in 20 patients. Univariate regression analysis with 201 cases included in model revealed Breslow thickness, nodular melanoma histological subtype and acral localization- to be significant independent predictors of SLN status ($p<0.05$). CONCLUSION: Beside the well established primary tumor thickness as the predictor of SLN positivity, we observed acral body site location and nodular melanoma to significantly enhance the risk for regional metastases. Our data confirm that multidisciplinary approach of SLNB is relevant as a diagnostic and staging procedure in cutaneous melanoma patients.

1101 - Tuesday, October 13, 2015, 8:00 AM - 9:30 AM, Hall 1
CME 9 - Radionuclide Therapy & Thyroid & Translational Molecular Imaging: Theranostics: What We Have and What We Can Achieve

OP373
Established and Innovative Applications for Diagnosis
W. Weber, USA

OP374
Theranostics in Clinical Experience: From Nets to Prostate Cancer
S. Ezzeddin, GERMANY

OP375
Theranostic Targeting Vectors and Nanoparticles
F. Kiessling, GERMANY

1102 - Tuesday, October 13, 2015, 8:00 AM - 9:30 AM, Hall 2
Joint Symposium 9: EANM/ESSR/ESSKA: Evaluation of the Painful Knee Arthroplasty

OP376
Normal Knee Joint Biomechanics and Surgical Techniques of Knee Arthroplasty
R. Nizard, FRANCE

OP377
What the Surgeon Wants to Know from Imaging in Painful Knee Arthroplasty
M. T. Hirschmann, SWITZERLAND

OP378
Radiologic Imaging
A. Hirschmann, SWITZERLAND

OP379
Hybrid Imaging in the Painful Knee Arthroplasty: Role and Limits
H. K. Mohan, UK

1105 - Tuesday, October 13, 2015, 8:00 AM - 9:30 AM, Hall G2
Do.MoRe: Quantitative Molecular Imaging

OP380
Y-90 imaging for dosimetry in radioembolization: comparison between scatter corrected bremsstrahlung SPECT/CT and time-of-flight PET/CT

Y. K. Dewaraja[1], P. M. Novelli[1], J. A. Fessler[1], M. U. Feng[1], R. Nelson[1], J. Rothley[1], M. Ljungberg[2], P. L. Roberson[1], S. J. Wilderman[1]; [1]University of Michigan, Ann Arbor, MI, UNITED STATES, [2]Lund University, Lund, SWEDEN.

Aim: To compare quantitative imaging of Y-90 by scatter-corrected bremsstrahlung SPECT (SPECT+SC) and PET with time-of-flight (PET+TOF) for dosimetry applications. Methods: A torso phantom with 0.74 GBq of Y-90 in liver and 60 mL tumor (5:1 tumor-to-liver) was imaged with a Siemens Symbia SPECT/CT and Biograph mCT PET/CT using a prolonged acquisition (90 min in both) such that the total counts were similar to a 20 min patient scan with 4 times the activity, which is typical for imaging following radioembolization with glass microspheres. A high-energy collimator and 105-165 keV window was used for SPECT. The in-house 3-D OSEM SPECT reconstruction used an analytical projector coupled with object-specific scatter estimates from Monte Carlo (MC) updated after 10 iterations. 3-D OSEM PET reconstruction was performed with 1 - 5

iterations (21 subsets) with resolution recovery and TOF. The tumor and healthy liver activity was quantified using a self-calibration based on the known liver activity. For PET, activity was also quantified directly using the image Bq/mL values provided by the system. Post-radioembolization SPECT/CT and PET/CT for 2 patients were also reconstructed as above and quantified using a calibration from the phantom experiment. 3-D dosimetry was performed using a previously developed MC algorithm. Results: Tumor contrast, background noise, tumor quantification error and healthy liver quantification errors were 56%, 14%, 30%, -8% respectively for SPECT without scatter correction, but improved to 94%, 12%, 4, -1% respectively for SPECT+SC after just 3 updates of the scatter estimate. The corresponding results for PET+TOF (1 iteration, 21 subsets) were 100%, 24%, -0.5%, 0.1%, without substantial improvement with more iterations. At equivalent noise, SPECT+SC had better contrast and quantification than PET+TOF. Using the direct PET quantification, activities were underestimated by up to 19%. In patients, the estimated liver activity compared to 'truth' (total administered activity accounting for lung shunt) was within 14% for SPECT without SC, 6% for SPECT+SC and 9% for PET+TOF. Using the direct PET quantification, patient liver activity was underestimated by up to 27%. There was good agreement between SPECT and PET based tumor and liver dose volume histograms only when SC was included (mean doses agreed to within 12%). Conclusions: For relatively large targets, quantitative accuracy and contrast of bremsstrahlung SPECT+SC approaches that of PET+TOF, but with less noise. Similarly in patients, dose estimates based on SPECT+SC agreed well with estimates based on PET+TOF. Further studies with small targets are needed to compare resolution.

OP381

Study of the impact of PSF and Noise on Dose Volume Histograms (DVH) for the dosimetry of Y-90

H. Levillain, **M. Sanchez-Garcia**, A. Dieudonné; Department of Nuclear Medicine, Beaujon Hospital, Assistance Publique-Hôpitaux de Paris (APHP) & INSERM U1149, Clichy, FRANCE.

Our aim was to evaluate the degradation of dose-volume histograms (DVH) induced by partial volume effect (PVE) and noise independently and for simulated SPECT and PET. Methods: First, we have analytically modelled uniform spheres (contrast=10) with different diameters: 1 cm, 5 cm and 10 cm (S1, S2, S3 respectively). We have analytically simulated the effects of PVE and noise. PVE was simulated with the convolution of a Gaussian point spread function (PSF) characterised by full width at half maximum (FWHM). The noise was simulated by a log-normal distribution characterised by relative standard-deviation (RSD). For the 3 spheres, PVE and noise were applied separately for distinct analysis, with 2 PVE: FWHM=5mm and 10mm, and 2 noises levels: RSD=0.10 and 0.3, representative of the clinical routine. Then we have simulated the degradation of SPECT and PET devices, according to what is observed in clinical routine, with respectively (FWHM=10 mm, RSD=0.10) and (FWHM=5 mm, RSD=0.3). The DVHs were computed from absorbed dose calculation using dose-point kernels (DPK) in each generated activity map, including the non-degraded one, with a homogenous water medium. Finally, DVHs were compared to theoretical ones, for the following absorbed dose criteria: D80, D50, Dmean and D20. Results: PVE decreased D80, D50 and had no impact on the other absorbed dose criteria, except for S1 for which D20 was underestimated of 66%. The more PSF was close to sphere's size, the more the effect of PVE was important. As an example, for all spheres, D80 (for which one PVE had a major impact) was underestimated between 38% and 8.1% and between 61% and 20% for FWHM of 5mm and 10mm respectively. Noise decreased D80 and increased D20 and had no influences on D50 and Dmean. For the most degrading noise level RSD=0.1, D80 was underestimated between 0.4% and 9.5%, D20 was overestimated for all spheres, between 6.4% and 12.2%. The simulated SPECT underestimated D80 up to 80%, D50 up to 82%, Dmean up to 79%, and D20 up to 78%. The simulated PET underestimated D80 up to 21%, D50 up to 17%, Dmean up to 12%, and D20 up to 4%. Conclusion: This study highlights the impact of PVE and noise on the DVHs, showing the importance of controlling and evaluating these effects to set-up absorbed dose protocols.

OP382

An inter-operator study of the accuracy of Y-90/In-111 DOTATATE dosimetry using an anthropomorphic phantom

T. Sanderson, **J. Gear**, A. Divoli, A. Craig, M. Gray, I. Murray, G. Flux; The Royal Marsden NHSFT, Sutton, UNITED KINGDOM.

Aim: To determine the accuracy and inter-operator variability of dosimetry performed on patients undergoing Y-90/In-111 DOTATATE radiopeptide therapy using a 3D printed anthropomorphic phantom. Method: The 3D printed phantom was based on a cohort of neuroendocrine patients and contained liver, spleen, kidney and spherical hepatic lesions. Organs and lesions were filled with a representative concentration of Y-90 and In-111

to that observed clinically. SPECT/CT imaging was performed using the clinical dosimetry imaging protocol and processed by 4 independent operators. Post therapy SPECT imaging was performed on a Siemens Symbia Intevo SPECT/CT system at 24, 48 and 72 hours post administration with 15% energy windows over the 171 and 245 keV In-111 peaks and 6% windows either side of the peaks to enable triple energy window scatter correction. Siemens Flash 3D reconstruction was performed using a CT attenuation correction. 6 subsets and 8 iterations were sufficient for reasonable image quality without over amplifying image noise or generating excess resolution recovery artefacts. Scatter data was smoothed using a 12 mm Gaussian kernel and corrected during reconstruction. Organ and lesion segmentation was carried out using the CT image. VOI counts were converted to activity using a pre-acquired calibration dataset. Time-activity curves were plotted and cumulated activity was determined from the integral of a single exponential fit. Y-90 organ S-factors for the standard reference man were scaled for organ mass and lesion S-factors were interpolated from unit-density sphere S-factors from Olinda. In addition a digitally segmented image of the phantom was inputted into the OEDIPE Monte Carlo dosimetry tool to provide organ specific S-factors. Results: Absorbed doses measured by different operators was consistent for all VOIs with a coefficient of variation below 20%. Mean percentage errors in activity quantification across all VOIs ranged from 4% to 21% with an average deviation of 10%. Absorbed dose accuracy ranged from 4% for lesions and organs greater than 4 cm in diameter to 22% for lesions 2 cm in diameter. The Percentage differences when using mass scaled S-factors to that calculated using Monte Carlo varied from 3 to 10%. Inaccuracies due to not considering organ cross-dose were less than 1%. Conclusions: The accuracy and reproducibility of dosimetry calculations should be determined to enable dose-response relationships to be investigated. The results from this study compare favourably with absorbed dose calculation accuracies suggested in the literature of 30-100% and are sufficient to validate the dosimetry methodology employed.

OP383

Modelling of a Patient-Specific ^{177}Lu-Dotatate Therapy Renal Dosimetry Process for Investigation of Uncertainties

J. Gustafsson[1], G. Brolin[1], M. Cox[2], M. Ljungberg[1], L. Johansson[2], K. Sjögreen Gleisner[1]; [1]Department of Medical Radiation Physics, Clinical Sciences Lund, Lund University, Lund, SWEDEN, [2]National Physical Laboratory, Teddington, UNITED KINGDOM.

AIM: The aim was to investigate the uncertainties in kidney absorbed dose and biologically effective dose (BED) for SPECT/CT-based patient-specific dosimetry in ^{177}Lu-Dotatate therapy. MATERIAL AND METHODS: A Monte Carlo method for uncertainty propagation was applied to a computer model of the dosimetry process. As basic tools, simulated SPECT images of three anthropomorphic computer phantoms coupled to pharmacokinetic models of ^{177}Lu-Dotatate were used. The phantoms had well-defined absorbed-dose rate curves for every structure and hence reference values, corresponding to "true values", of renal absorbed doses and BED. From the reconstructed SPECT images (60 projections, 45 s/projection, OSEM with compensation for attenuation, scatter and distance-dependent resolution) the renal absorbed-dose rate was determined at four time-points (0.5 h, 24 h, 96 h and 168 h) post injection. Curve fitting yielded estimates of the absorbed dose and BED (α/β = 2.6 Gy, T_{rep} = 2.8 h). Uncertainties were introduced in different steps of the process, in particular in the *a*) estimation of system sensitivity, *b*) variability in imaging time-points, *c*) SPECT projection noise, *d*) CT-derived density map used for attenuation and scatter correction and for absorbed-dose rate determination, *e*) ^{177}Lu emission spectrum, *f*) kidney VOI delineation, and *g*) recovery coefficient. The kidney absorbed dose and BED were then quantified in 256 Monte Carlo realisations from which the mean and standard deviation (SD) were derived. By sequential replacement of the individual variable parameters by fixed values, the decrease in dispersion was analysed as a measure of the parameter's influence on the combined uncertainty in absorbed dose. RESULTS: The kidney absorbed dose SDs were approximately 6 % for all phantom kidneys, with the variability in kidney recovery coefficient and the camera sensitivity being the most influential contributors. The derived deviations between mean and reference absorbed dose were between -0.4 % and 6.7 %. The BED results were similar to the absorbed dose results. CONCLUSIONS: Using the dosimetry process model with assumed but plausible standard uncertainties in input parameters, the standard uncertainty in kidney absorbed dose was approximately 6 %. The most important contributors were effects which are correlated between imaging time-points, e.g. the recovery coefficient and the system sensitivity, while uncorrelated effects, like SPECT projection noise and kidney VOI delineation variability, had marginal influence on the absorbed dose estimations. The BED was not appreciably affected by variations in the absorbed-dose rate curve beyond the associated uncertainty in absorbed dose.

OP384

Dosimetry of Lu-177 DKFZ-PSMA-617 for the treatment of metastatic prostate cancer using quantitative SPECT/CT

A. Delker, W. Fendler, A. Brunegraf, A. Gosewisch, F. Gildehaus, P. Bartenstein, G. Böning; University of Munich, München, GERMANY.

Aim: Estimation of radiation dose helps to determine the optimal activity to achieve best therapeutic effect in combination with limited side effects. Our aim was to perform first image based dose calculations for tumor tissue and critical organs after application of Lu-177 DKFZ-PSMA-617 for the treatment of metastatic prostate cancer. Methods: Whole-body planar images and SPECT/CT of the abdomen data were acquired in 10 patients (mean age 70 years) at approximately 1h, 24h, 48h and 72h after administration of 3.7 GBq Lu-177 DKFZ-PSMA-617 on a Siemens Symbia SPECT/CT. Quantitative 3D SPECT OSEM reconstruction was performed with corrections for photon scatter, photon attenuation and detector blurring. A camera specific calibration factor derived from phantom measurements was applied. Total activity in the kidneys, liver, spleen, salivary glands and 4 tumor lesions in each patient were calculated using a combination of linear approximation, exponential fit, and target-specific S values according the MIRD concept. Results: The average estimated dose ± SD was 2.4 Gy ± 0.6 Gy in the kidneys, (0.7 Gy/GBq), 0.4 Gy ± 0.2 Gy in the liver, 0.4 Gy ± 0.1 Gy in the spleen and 5.1 Gy ± 2.0 Gy in the salivary glands (1.4 Gy/GBq). Critical dose limit for the kidneys was not reached in any of the patients. Doses for tumor lesions up to 35.7 Gy were observed. An increased uptake in the intestine was observed after approx. 24h with overlap to the kidneys by about 50-75% for planar images. Conclusions: Critical organs are the salivary glands and the kidneys. Kidneys, based on their vital function, are the dose limiting organ in analogy to other Lu-177 based therapies. Quantitative 3D SPECT improves accuracy of kidney dose estimation due to reduced overlap by activity on the colon on late images. Our results further suggest that the activity administered for each cycle could be increased to optimally exploit the tumor dose.

OP385

Accuracy of Triple Energy Window vs. Analytical Photon Distribution Scatter Corrections in Lu-177 Studies

C. F. Uribe[1,2], L. Frauenstein[3,1], P. L. Esquinas[1,2], J. Tanguay[1], M. Gonzalez[4], A. Celler[1]; [1]Medical Imaging Research Group, University of British Columbia, Vancouver, BC, CANADA, [2]Department of Physics and Astronomy, University of British Columbia, Vancouver, BC, CANADA, [3]Department of Computer Science, Otto von Guericke University of Magdeburg, Magdeburg, GERMANY, [4]Vancouver Coastal Health, Vancouver, BC, CANADA.

Aim: Accuracy of absorbed dose calculations in personalized radionuclide therapy is directly related to the accuracy of activity estimates obtained at each of imaging time-points. Our objective was to compare the accuracy of ^{177}Lu quantification achieved using two scatter correction (SC) methods: 1)triple energy window (TEW) and 2)analytical photon distribution interpolated (APDI). Materials and Methods: Four series of experiments were performed using objects filled with ^{177}Lu: (a) seven spheres [0.5-113mL] were scanned in air, and in a cylinder filled with cold and hot water; (b) six bottles [8.5-34mL] in air and hot water, (c) four bottles [33.9mL] in a Thorax phantom filled with water (lungs and spine inserts, and additional beef bone created non-uniform density distribution), (d) four bottles [34-200mL] in air and between four 2L water bags. SPECT/CT SymbiaT (Siemens-Healthcare) camera with MELP collimator, and three energy windows were used (208keV photopeak and two scatter windows). OSEM reconstruction included attenuation correction (AC) and resolution recovery (RR), and either TEW or APDI. Segmentations for objects in air and in cold water used fixed thresholds of 0.1% and 1%, respectively, while for hot background, a fixed 40% threshold and our iterative adaptive dual thresholding (IADT) method were used. Four additional scans (six objects [17-200mL] placed in a cylinder with four different backgrounds) were performed to create an IADT calibration curve. Results: For objects placed in cold uniform-density backgrounds (air, water) the accuracy of activity quantification was similar for both SC methods. Depending on object size and shape the errors ranged from 3-6% in air to 10-12% in water. Although in scans of objects placed in hot background the accuracy of total activity reconstruction was about 6%, the quantification of individual objects was highly dependent on their sizes and segmentation method. When using IADT segmentation the errors ranged from 3% for large objects to over 30% for small spheres, using 40% fixed threshold resulted in larger errors. For objects placed in non-uniform-density background the APDI method outperformed TEW by a factor of three. Conclusion: For areas with uniform density (majority of clinical situations), similar levels of activity quantification of ^{177}Lu can be achieved when using TEW or APDI scatter correction (SC). Phantom experiments showed that for objects ≥34ml, activity can be reconstructed to within 10%. APDI outperforms TEW in non-uniform-density areas (e.g. a tumor close to the spine), but is more complex and requires more computer time than TEW.

OP386

Towards a quality assurance for dosimetry in peptide receptor radionuclide therapy (PRRT) with 177Lu-DOTATATE

G. Marin, B. Vanderlinden, Z. Wimana, T. Guiot, I. Karfis, P. Flamen; Institut Jules Bordet, Bruxelles, BELGIUM.

Aim177Lu-DOTATATE is the most commonly used radiopeptide for PRRT. In order to establish a reliable dose-response/toxicity correlation it is necessary to achieve a good

precision on all measurements. The aim of this work was to evaluate the precision of the dosimetric procedure.Materials and methodsEight patients with neuroendocrine tumors received 4 to 5 cycles of 177Lu-DOTATATE. Three SPECT/CT (4, 24, 168h post-injection) and five blood samples (0, 1, 4, 24, 168h post-injection) were performed after each administration. Organs activities were calculated by multiplying the volumic activities by the manually delineated CT volumes. Time-activity curves (TAC) were obtained by fitting measured activities with biexponential functions. Residence times (RTs) were obtained by integrating the TACs.To avoid inter-patient variability, RTs and volumes were normalized by the respective mean value of each organ for all cycles for each patient (mean normalized value = 1).The precision of RTs and volumes was evaluated with the standard deviations of the normalized RTs (nRTSDs) and normalized volumes (nVSDs) for each organ. As those SDs still contain both stochastic quantification errors and intra-patient inter-cycle variability, their analysis will help discriminate between the two.ResultsFor kidneys, nRTSDs of 0.14 and 0.10 were found respectively for the right and left. A linear correlation (R^2 = 0.78) was found between the nRTSDs of each pair, suggesting that nRTSDs are not completely explained by quantification errors.For the spleen, a higher nRTSD of 0.18 was found, partly due to diurnal volume modification because of the dynamical status of splenic blood supply, as highlighted by a nVSD of 0.14 for spleen versus 0.04 for kidneys.For the liver, nRTSD was 0.22. Two patients showed a systematic RT decrease over therapy cycles (corresponding to decreasing lesion uptake). When they were discarded from the evaluation, the liver nRTSD decreased to 0.08.For the total body, the higher nRTSD (0.21) may come from low image statistic.For the bone marrow, a different quantification procedure based on blood samples lead to a nRTSD of 0.19.ConclusionOrgans nRTSDs allowed estimation of the maximum stochastic errors on dose quantification in PRRT. Intra-patient variability was shown to be a source of overestimation, but can be reduced with a quality assurance program driven by error analysis. This will help identify methodological sources of error requiring additional quality control, leading to better precision on dose-response/toxicity correlations.

OP387

International Multicentre Evaluation of Absolute Quantification in Planar and SPECT Imaging

B. E. Zimmerman[1], I. Buvat[2], E. C. Frey[3], A. J. Green[4], D. Grošev[5], M. Lassmann[6], M. Ljungberg[7], **G. Poli**[8]; [1]National Institute of Standards and Technology, Gaithersburg, MD, UNITED STATES, [2]Service Hospitalier Frédéric Joliot, Paris, FRANCE, [3]Johns Hopkins Medical Institutions, Baltimore, MD, UNITED STATES, [4]National Physical Laboratory, Teddington, UNITED KINGDOM, [5]University Hospital Centre Zagreb, Zagreb, CROATIA, [6]Universitatsklinik Wurzburg, Würzburg, GERMANY, [7]Lund University, Lund, SWEDEN, [8]International Atomic Energy Agency, Vienna, AUSTRIA.

Aim: Accurate quantitation of activity provides the basis for internal dosimetry of targeted radionuclide therapies. The International Atomic Energy Agency has recently conducted a Coordinated Research Project entitled “Development of Quantitative Nuclear Medicine Imaging for Patient Specific Dosimetry”. The main purposes of this project were to investigate the quantitative imaging capabilities at sites with a variety of experience and equipment and to assess the levels of errors in activity quantitation resulting from the use of SPECT and planar imaging. Materials and methods: Participants from 10 countries took part in the intercomparison by quantifying activities using planar, SPECT and SPECT/CT imaging. Participants were provided with four epoxy-filled cylinders containing 133Ba, chosen as a surrogate for 131I. The 133Ba sources, with nominal volumes of 2, 4, 6 and 23 mL, were calibrated by the U.S. National Institute of Standards and Technology, with the activity unknown to the participants. The sources were imaged in a cylindrical phantom filled with water. In a first trial, participants estimated the activities using local protocols. In the second trial, participants repeated the measurements using a standardized protocol, with acquisition and processing methods more rigorously defined. Finally, processing and analysis of the data from the second trial was repeated centrally. Results: In the first trial, true activities were underestimated by 15-20% with planar imaging, after rejection of outlying data. SPECT with Chang’s attenuation correction data showed the highest variability and the true activity was underestimated by 5-10%. SPECT/CT gave the best accuracy and reproducibility in all trials. The second trial showed some improvements in accuracy, variability and outlying results. Planar imaging was subject to methodological errors, e.g., in the use of a transmission scan for attenuation correction. The use of Chang attenuation correction (AC) was essential for SPECT without CT-based AC, and variability resulted from definition of phantom contours.Conclusion: The project demonstrated the need for training and standardized protocols to achieve good levels of quantitative accuracy and repeatability in a multicentre setting. Absolute quantification of simple objects with no background activity was possible with errors of +8 % with planar imaging, -7 % with SPECT (with Chang-AC) and better than 6 % for SPECT/CT. CT-based AC was the best, and in a clinical scenario would handle uniform and non-uniform attenuation distributions. Processing for SPECT/CT was more

standardized and less subject to errors and therefore seems the best option for quantitative nuclear medicine imaging.

1106 - Tuesday, October 13, 2015, 11:30 AM - 1:00 PM, Hall 6
M2M: Molecular & Multimodality Imaging: Tumour Biology & Optical Imaging

OP388

Insights into the DNA damage response can improve peptide receptor radionuclide therapy outcomes

J. Nonnekens, C. Beerens, M. van Kranenburg, D. C. van Gent, M. de Jong; Erasmus MC, Rotterdam, NETHERLANDS.

Aim: The targeted treatment of neuroendocrine tumors (NET) with lutetium-labeled somatostatin analogues (peptide receptor radionuclide therapy, PRRT) is successfully applied in clinical trials, while similar approaches may also be feasible for many other tumor types. PRRT of metastasized NETs is very promising with improved patient outcome compared to other treatments, but cure is reached only in very low percentages. To achieve an even better tumor response, the administrated dose cannot simply be increased because of dose limiting toxicity in bone marrow and kidneys. Therefore, in order to improve the current treatment outcome, we investigated the DNA damaging effects of PRRT with the final aim to enhance these effects through modulation of the DNA damage response. We aim specifically to sensitize the (fast replicating) tumor cells without further damage to healthy tissues using PARP inhibitors. Materials and methods: All experiments were performed with rat pancreatic CA20948 tumor cells expressing the somatostatin receptor subtype 2 or human tumor cells lines stably transfected with this receptor subtype. Cells were incubated for 4 hours with increasing doses of ^{177}Lu-[DOTA, Tyr^3]octreotate (DOTA-TATE), followed by non-radioactive chases for different periods until 5 days post treatment. Cells were fixed and fluorescently stained with different antibodies (53BP1, gamma-H2AX) to visualize the accumulation of DNA repair proteins to the produced DNA double strand breaks. Cell proliferation was measured using EdU incorporation and Click-iT labeling technology. Simultaneously, cells were incubated during the chase period with the PARP inhibitor Olaparib. Furthermore, cells were subjected to different doses of ^{177}Lu-DOTA-TATE in the absence or presence of Olaparib and cellular survival was measured using colony assay and sulforhodamine B colorimetric assay. Results: Cells treated with ^{177}Lu-DOTA-TATE showed accumulation of 53BP1 and gamma-H2AX in so-called foci, indicating the production and repair of DNA double strand breaks. Foci were visible up to 3 days after treatment. Interestingly, addition of Olaparib led to increased and prolonged DNA damage, specifically in replicating cells. ^{177}Lu-DOTA-TATE eradicated cells in a dose dependent manner and cell killing was enhanced by Olaparib. Conclusions: PRRT produced DNA single and double strand breaks and triggered the DNA damage response in our in vitro models. Through modulation of the DNA damage response with Olaparib, we were able to enhance the DNA-damaging effects of PRRT, specifically in replicating cells. We expect that our results will eventually improve the current PRRT outcome, leading to increased patient survival rates.

OP389

Blocking DNA repair mechanism - the way to improve alpha targeted therapy of glioblastoma multiforme ?

E. Rosiak[1], H. Koziara[2], R. Matyskiel[1], B. Królicki[2], L. Królicki[1]; [1]Department of Nuclear Medicine, Medical University of Warsaw, Warsaw, POLAND, [2]Department of Neurosurgery, Maria Skłodowska-Curie Memorial Cancer Center and Institute of Oncology, Warsaw, POLAND.

AIM: Recently the alpha targeted therapies using intracranial delivery of 225Ac or 213Bi-labeled Substance P (SP) have been developed. Our aim was to investigate the radiobiological effects of alpha-particles from 213 Bi and 225Ac- on cell survival, cell cycle progression and DNA ploidy in glioblastoma multiforme (GBM) cells cultured in vitro under hypoxia and normoxia condition.MATERIALS: Cultured cells in vitro were obtained from tumor samples from 43 patients with histologically confirmed of GBM. They were treated with 1 dose of 1,2MBq 213 Bi-SP/1ml medium or 1 dose of 180kBq 225Ac-SP/ 1ml medium under normoxia and hypoxia (0,7-0, 8% O2). Non-irradiated cancer cells cultured under normoxic and hypoxic condition were used as a control. METHODS: The level of apoptosis and necrosis, measurement of cellular DNA content and the analysis of the cell cycle we performed by flow cytometry under aerobic and hypoxic conditions. Experimental data was obtained at 1 h, 3 h, 6 h, 12 h, 24 h, 48 h, 72 hours and 10 days after application of isotopes for cell cultures. RESULTS: Alpha radiation induced cell cycle alterations. Between 24 - 72 hr after the treatment with 213 Bi-SP and 225Ac-SP under normoxia during S-phase cycle were 100%± 0.0% and 99.9%±0.12 % cells; under hypoxia during S-phase were 99.88 %± 0.29% cells and 100%± 0% cells respectively. 72 hours after treatment with 213 Bi-SP and 225Ac-SP under hypoxia and normoxia we observed enhanced self-renewal of cancer cells, DNA repair and significantly decreased the population of cells in S phase with accumulation of cells in G2/ M phase as well as radiation-induced chromosomal damage, alterations in the structure and number of chromosomes with high levels of tetraploidy or

aneuploidy.10 days after treatment with 213 Bi-SP and 225Ac-SP the ratio of G2/G1 cells increased significantly compared to control cells: under normoxia ratio of G2/ G1 was 8.13%±4.38% and 9.33%±5.0%; under hypoxia ratio of G2/ G1 was 10.72%±2.90% and 11.02% ±3.10% respectively ($p<0.05$)CONCLUSION: These results suggest that alpha therapy induces DNA damage that are reflected in transient arrest in S-phase up to 72 hours under hypoxic and normoxic condition. This response can however be reduced by the activities of DNA repair pathways observed after 72 hours. Alpha targeted therapy combined with blocking DNA repair mechanisms could be therefore offer as a therapeutic strategy for glioblastoma multiforme and further research will be needed.

OP390

Radiation-Induced Media-Transferred Bystander Effect in Breast Cancer Cells

K. L. Madsen, P. F. Høilund-Carlsen, B. B. Olsen; Odense University Hospital, Odense, DENMARK.

Aim: In radiation biology, the term *bystander effect* refers to the phenomenon that non-irradiated cells exhibit similar changes as nearby irradiated cells, e.g., DNA double strand breaks (DSBs), chromosomal instability, and cell death. The aim was to investigate if this bystander effect could be media-transferred to non-irradiated cells by incubation in irradiated cell conditioned medium (ICCM). Material and methods: Human breast cancer MCF-7 cells in medium were irradiated with 0, 1, 2, 4 or 8 Gy of external ionizing radiation. After 24 h, the ICCM was transferred to a new series of non-irradiated MCF-7 cells to examine for a potential medium-transferred bystander effect using three different endpoints: i) DSBs visualized by γH2AX-foci after 18 h incubation with ICCM, ii) number of micronuclei in binuclear cells as a marker of chromosomal instability after 48 h of incubation with ICCM, and iii) the effect on cell death after 7 days of incubation with ICCM as judged by the CellTiter-Blue Viability Assay, which measures metabolic activity. Results: Re i: DSBs were induced in the non-irradiated cells since the average number of γH2AX-foci pr. cell was significantly increased independent of radiation dose; 0 Gy 0,5±0,8, 1 Gy 1,7±1,6 ($P < 0,001$), 2 Gy 1,3±1,4 ($P < 0,01$), 4 Gy 2,7±2,7 ($P < 0,0001$) and 8 Gy 3,9±3,5 ($P < 0,0001$). Re ii: The number of micronuclei in binuclear cells was negligible with only a small and insignificant increase upon incubation with ICCM, suggesting the absence of chromosomal instability. Re iii: There was no cell death upon incubation with ICCM; on the contrary, stimulating effects were observed on the metabolic activity independent of radiation dose; 0 Gy 100%±3,1, 1 Gy 111%±2,0 ($P < 0,01$), 2 Gy 117%±1,0 ($P < 0,001$), 4 Gy 117%±1,4 ($P < 0,001$) and 8 Gy 108%±2,6 (not significant). Conclusion: There was a significant radiation-induced medium-transferred bystander effect with respect to DSBs, but chromosomal instability was not significant in non-irradiated cells incubated in ICCM. In addition, a somewhat surprising and significant increase in metabolic activity was observed. This apparently paradoxical increase warrants further experiments.

OP391

Ex vivo tumor tissue culture to mechanistically examine DNA-damage after peptide receptor radionuclide therapy

J. Nonnekens, C. Beerens, D. C. van Gent, M. de Jong; Erasmus MC, Rotterdam, NETHERLANDS.

Aim: Many studies to explore cellular mechanisms of anticancer therapies are performed on cell lines. However, morphology, complexity and key parameters of actual tumors differ considerably from cell lines grown in 2D culture. Moreover, tumors from different patients differ in their response to therapy, necessitating personalized treatment. To take analysis of anticancer therapies to the next level, we have developed a novel system to examine human tumor tissue *ex vivo*. Specifically, we examined patient neuroendocrine tumors (NETs) that will be treated with lutetium-labeled somatostatin analogues (peptide receptor radionuclide therapy, PRRT). This approach allows for detailed analysis of the cellular responses, such as the DNA damage response, over prolonged periods of time in the relevant tumor context. Materials and methods: Fresh human tumor tissue derived from surgery or biopsies was cut in thin slices (300 μm) with a Leica vibrotome. Culturing of NET-slices was performed at 37°C on a rotating platform (60rpm). Besides using human tumor tissue, xenografted neuroendocrine tumors grown on mice were used. These slices were grown on cell strainer inserts at 37°C. Slices were incubated for 4 hours with various doses of ^{177}Lu-[DOTA,Tyr^3]octreotate (DOTA-TATE), followed by non-radioactive chases for different periods. Slices were formalin fixed and paraffin embedded. 4m paraffin sections were subjected to immunohistochemical stainings: hematoxylin and eosin staining for morphology and fluorescent staining with different antibodies (53BP1, gamma-H2AX) to visualize the accumulation of DNA repair proteins to the produced DNA double strand breaks. Cell proliferation was measured using EdU incorporation and Click-iT labeling technology. Cell death was measured using apoptotic TUNEL labeling. Results: In the current settings, the tissue slices could be kept alive for approximately 1 week after dissection. Cells of slices treated with ^{177}Lu-DOTA-TATE showed foci formation of 53BP1 and gamma-H2AX, indicating the production of DNA double strand breaks, up to for several days after

treatment. Furthermore, the treatment reduced replication and induced apoptosis. Conclusions: PRRT produced DNA double strand breaks and triggered the DNA damage response in NET tumor slices. These results give mechanistic insights into the effectiveness of PRRT. We will apply this knowledge to improve the current PRRT-protocols and increase patient survival rates. Furthermore, looking from an animal welfare aspect; the use of tissue slices as an intermediate step between *in vitro* cell assays and *in vivo* mouse experiments will tremendously reduce the amount of laboratory animals needed.

OP392

Clinical Relevance of Targeting SSTR2, GRPR and CXCR4 with Radioligands for Imaging and Therapy in Breast Cancer

S. Dalm, A. Sieuwerts, M. Look, M. Melis, C. van Deurzen, J. Foekens, M. de Jong, J. Martens; Erasmus MC, Rotterdam, NETHERLANDS.

Introduction: Imaging and therapy using radioligands targeting receptors expressed on cancer cells is successfully being used in patients with neuroendocrine tumors. Previous studies have demonstrated expression of the somatostatin receptor subtype 2 (SSTR2), the gastrin releasing peptide receptor (GRPR) and C-X-C chemokine receptor 4 (CXCR4) on breast cancer (BC). Since GMP-compliant radioligands targeting the SSTR2, GRPR and CXCR4 are available, targeting these receptors on BC might offer new imaging and therapy options. BC is a heterogeneous disease consisting of multiple molecular subtypes, which influence treatment and prognosis. We investigated the SSTR2, GRPR and CXCR4 mRNA levels of 915 BC patients and correlated this with important clinico-pathological factors and prognosis. Materials and Methods: SSTR2 and GRPR expression of 13 clinical BC specimens was analyzed by in vitro autoradiography using ^{111}In-Octreotate and ^{111}In-AMBA, respectively, and correlated with corresponding mRNA levels. Moreover, SSTR2, GRPR and CXCR4 mRNA levels of 915 BC specimens (from lymph node negative (LNN) and lymph node positive (LNP) patients) were determined using RT-qPCR and associated with known clinico-pathological factors (total patient group) and prognosis (LNN patients). Results: A significant positive correlation was found between binding of ^{111}In-Octreotate and ^{111}In-AMBA to the BC specimens and SSTR2 (Rs=0.7348, P=0.0042) and GRPR mRNA levels (Rs=0.9352, P<0.0001), respectively. Furthermore, in the total patient group high SSTR2 and high GRPR mRNA levels were both associated with estrogen receptor (ER) positive (P<0.0001) and progesterone receptor (PR) positive tumors (P<0.0001). On the contrary, high CXCR4 mRNA levels were associated with ER negative tumors (P<0.0001). No association was found between SSTR2 and GRPR expression and prognosis in the untreated LNN patients. Contrary to what expected, higher CXCR4 expression was associated with better prognosis in the LNN patient group (Hazard ratio metastasis free survival=0.76 (0.64-0.90), P=0.001). Conclusion: SSTR2 and GRPR mediated imaging can be applied in ER and PR positive tumors, while CXCR4 mediated imaging is best suited for ER negative tumors. Thus, ER positive patients resistant to current standard lines of therapy might benefit from radioligands targeting SSTR2 or GRPR, while in progressing ER negative patients CXCR4 therapy might be considered, particularly those patients whose lesions are demonstrated positive based on imaging using the respective ligands.

OP393

Increase of PSMA Expression by Androgen Deprivation

B. Meller, C. O. Sahlmann, S. Hijazi, C. Bouter, L. Trojan, J. Meller, P. Thelen; Georg-August-University Göttingen, Göttingen, GERMANY.

Aim: PSMA is novel and promising target for diagnostics and therapy of prostate carcinoma (PC). The aim of this investigation was to increase PSMA-expression for improved detection of recurrent PC and its metastases in diagnostics as well as better targeting for radiopeptide-therapy by use of standard PC drugs. Material & Methods: Radiolabeling of 5 μg PSMA-HEBD-CC (ABX) were performed with M = 1200 MBq $^{68}GaCl_3$ (iThemba Labs) in a GRP Module (Scintomics). The human castration resistant cell line VCaP (CRPC) was obtained from ATCC. Parallel cultures were treated with 1 nM testosterone and with 5 μM abiraterone over 48 h. The androgen sensitive cell line (revCRPC) was long-term sub-cultured with 1 nM testosterone. Parallel cultures were incubated without testosterone or received additionally 5 μM abiraterone acetate for 48 h. To assess the capacity of cells for the labeled compounds, 0.3 nM ^{68}Ga-labeled peptide (100-300 kBq/ml) was simultaneously applied to 3 parallel cells cultures for each interval (1 - 3 hours) and each cell line. Experiments were repeated for three times. Cells were harvested and measured activity was correlated to the cell count. Additionally, PSMA-mRNA expression was investigated by qPCR. Results were statistically evaluated by non-parametric tests. Results: Androgen sensitive cells (revCRPC) accumulated the tracer significantly higher than the castration resistant subtype (CRPC, p<0.05). ^{68}Ga-PSMA-HEBD-CC uptake almost doubled during 3 h in all cell lines (p<0.01). Compared to non-treated cells in parallel cultures the pre-incubation with abiraterone over 48 h resulted in a significant increased uptake in CRPC (p<0.001). In revCRPC pre-incubation with abiraterone resulted in an eight-fold higher uptake after 3h. Withdrawal of medium supplementation testosterone additionally increased the uptake up to ten-fold (p<0.01). The influence of abiraterone on PSMA-expression was confirmed by PCR

data in both cell lines. Conclusions: We found an increasing uptake of ^{68}Ga-PSMA-HEBD-CC over time, probably based on an increasing internalization rate. Our investigations verify an increase of PSMA-mediated uptake by androgen deprivation in CRPC and androgen sensitive cell lines. These results might be useful in the early detection of PC recurrence as well as for PSMA-mediated therapy. These results may contribute to the development of improved protocols in PSMA-mediated imaging and therapy sequencing.

OP394

Detrimental Effects of Radiation on the Fluorescence of Fluorophores: Implications for Dual-Modality Imaging

R. Hernandez[1], S. Heskamp[2], M. Rijpkema[2], D. M. Goldenberg[3], W. McBride[3], A. Morgenstern[4], F. Bruchertseifer[4], W. Cai[1], O. Boerman[2]; [1]University of Wisconsin-Madison, Madison, WI, UNITED STATES, [2]Radboud University Medical Center, Nijmegen, NETHERLANDS, [3]Immunomedics Inc., Morris Plains, NJ, UNITED STATES, [4]Institute of Transuranium Elements, Karlsruhe, GERMANY.

Aim: Despite the large interest on nuclear/optical multimodality imaging, the effect of radiation on the fluorescence properties of fluorophores remains unknown. Herein we determined the radiosensitivity of the near infrared dye IRDye800CW, and devised a strategy to ameliorate its negative impact for multimodality imaging. Materials and Methods: Buffered aqueous solutions of IRDye800CW were incubated in the presence of increasing activities of ^{111}In, ^{68}Ga, or ^{213}Bi (γ, β, and α emitter, respectively) and its normalized fluorescence (λ_{ex}=740 nm and λ_{em}=796 nm) was determined at different radiation exposure times. The radioprotective effect of three hydroxyl radical scavengers (ethanol, gentisic acid, and ascorbic acid (AA)), was examined. The impact of other factors such as activity concentration, temperature, type of buffer, and pH on the fluorescence properties of IRDye800CW was also determined. Similar experiments were conducted on RDC018, a DOTA-conjugated IRDye800CW-derivative used as multimodality imaging probe in pretargeting. Results: A significant decrease of the fluorescence of IRDye800CW was observed upon incubation with escalating activities of ^{111}In, ^{68}Ga or ^{213}Bi. The effect was dependent on the amount of activity as well as the type of radiation, which supported our hypothesis of a free radical mediated mechanism. ^{68}Ga showed the largest radiolytic effect - the fluorescence signal of the fluorophore was reduced to background levels within 30 min incubation with 20 MBq of ^{68}Ga-, followed by ^{111}In and ^{213}Bi. IRDye800CW and RDC018 presented similar radiosensitivity except for ^{213}Bi-labelled RDC018, which exhibited enhanced radiolysis, presumably due to direct radiation damage induced by α particles. The addition of scavengers provided a concentration dependent radioprotective effect. Among all scavengers, AA provided the most robust protection over a wide range of concentrations and preserved RDC018 fluorescence at much higher activity levels. Interestingly, AA afforded only partial radioprotection of ^{213}Bi-RDC018, which further supported our hypothesis of α particle-fluorophore direct interaction. Conclusion: Herein we provide the first report on the radiosensitivity of fluorophores, and outline a set of conditions that minimize the deleterious effects of radiation damage on nuclear/optical multimodality imaging probes.

OP395

Characterisation and quantification of fluorescently labeled Exendin for beta cell targeting and comparison with radiolabeled Exendin

S. Ekim, D. Bos, M. Brom, M. Gotthardt; Radboud University Medical Centre, Nijmegen, NETHERLANDS.

Background and aims: Exendin can specifically bind to the glucagon-like peptide 1 receptor (GLP-1R) which is expressed on the beta cells in the pancreas. By targeting GLP-1R with radiolabeled Exendin, it is possible to determine the beta cell mass. However, the resolution of PET and SPECT is not sufficient to examine tracer accumulation at the cellular level, which could provide vital information about the specificity of the tracer for beta cells. By using fluorescent labeled tracers, it is possible to study the kinetics of radiotracer accumulation at the cellular level. But quantification of the fluorescently labeled tracers is difficult because of the limited penetration depth of the fluorescent label and attenuation/absorption and autofluorescence of organs. The aim of the study is developing a sensitive and quantitative technique to measure accumulation of fluorescently labeled tracers, comparing the biodistribution of fluorescent labeled Exendin with radiolabeled Exendin and evaluation of the effect of peptide dose for both tracer.Materials and methods: GLP-1R over-expressing CHL cells were used in experiments. For in vitro experiments 30nM Exendin-3-Cy5.5(Ex-Cy5.5) was incubated at 37°C degrees for 4 hours, and blocking experiment with an 30 fold molar excess unlabeled Exendin-3 was performed in 3 separate wells. The cell-bound fluorescence was measured with ELISA-plate reader.Ex-Cy5.5 and Exendin-3-DTPA-^{111}In(Ex-DTPA-^{111}In) biodistribution studies were performed in BALB/c nude mice with a subcutaneous CHL-GLP1R tumor. Mice were injected with 0,3-1-3-10μg of Ex-Cy5.5 or Ex-DTPA-^{111}In and after 4 hours the organs were dissected and homogenized for fluorescence measurements. Samples are measured in ELISA plate reader with organ

specific standards.Results: Binding assay performed on CHL-GLPl R(+) cells showed that Ex-Cy5.5 can specifically bind to GLP1R at a percentage of 17% which is similar to Ex-DTPA-^{111}In. The uptake of Ex-3-Cy5.5 in the tumor was 8, 49±3,99 %lD/g when 0,3μg was injected and maximum relative uptake was observed at 1μg (21,04±6,35 %lD/g). With higher doses lower tumor accumulation was observed.Conclusion: A very sensitive and quantitative technique for biodistribition studies of fluorescently labeled peptides was developed.By preparing organ specific standard curves, fluorescence signal detected from the organs could be accurately quantified. The results showed that the optimal dose for in vivo targeting of the GLP-1R with Ex-Cy5.5 and Ex-DTPA-^{111}In is different. This should be taken into account while using the fluorescently labeled tracers to study the kinetics of radiotracer accumulation. ln vivo optimal dose for Ex-Cy5.5 is observed as 1μg, while for Ex-DTPA-^{111}In it is observed as 0,3μg.

1107 - Tuesday, October 13, 2015, 8:00 AM - 9:30 AM, Hall F
SNMMI Symposium: Hepatobiliary Scintigraphy in Abdominal Pain

OP396
Hepatobiliary Scintigraphy - Diagnosis of Abdominal Pain
H. A. Ziessman, **USA**

OP397
Development of Appropriate Use Criteria for Hepatobiliary Scintigraphy of Abdominal Pain
H. Jadvar, **USA**

1108 - Tuesday, October 13, 2015, 8:00 AM - 9:30 AM, Hall F
Pitfalls & Artefacts & Physiology (Cardiovascular) - Interactive: MPS, SPECT-CT, PET, Newer Techniques such as CZT and IQ SPECT

OP398
SPECT
J. Bucerius, **NETHERLANDS**

OP399
SPECT-CT
R. Buechel, **SWITZERLAND**

OP400
PET
W. Burchert, **GERMANY**

OP401
Newer Technologies
D. Agostini, **FRANCE**

1201/1203 - Tuesday, October 13, 2015, 10:00 AM - 11:15 AM, Hall 1
Plenary 3: Targets and Probes

OP402
Target Discovery and Probe Identification in Oncology
P. Workman, **UK**

OP403
Probe Selection and Development for Molecular Imaging and Therapy, the Perspective of Industry
M. Friebe, **GERMANY**

OP404
Probe Selection and Development for Molecular Imaging and Therapy, the Perspective of Academia
G. A. M. S. van Dongen, **NETHERLANDS**

1301 - Tuesday, October 13, 2015, 11:30 AM - 01:00 PM, Hall 1
CME 10 - Dosimetry & Translational Molecular Imaging: Preclinical Quantitative Imaging and Dosimetry

OP405
Preclinical Quantitative Imaging for Dose Assessments
E. Visser, **NETHERLANDS**

OP406
Dosimetric Models in Preclinical Studies
M. Bardiés, **FRANCE**

OP407
PK Model Based Dose Calculations and Dose-effect Relations in Preclinical Studies
N. Chouin, **FRANCE**

1302 - Tuesday, October 13, 2015, 11:30 AM - 01:00 PM, Hall 2
Joint Symposium 10: EANM/ELI: Lymphoma and PET/CT Update

OP408
FDG for Assessment of Lymphoma Subtypes other than HL, DLBCL and FL
S. Barrington, **UK**

OP409
Response Assessment for New Targeted Agents, What is known?
M. Meignan, **FRANCE**

OP410
How is PET-CT Impacting on Radiotherapy Planning in Lymphoma
L. Specht, **DENMARK**

1303 - Tuesday, October 13, 2015, 11:30 AM - 12:45 PM, Hall 4
Technologist Oral Presentations 3

OP411
Adaptation of 13N-NH3 and 18F-FDG Imaging Protocols for sarcoidosis for new scanner technology

C. Abreu[1], J. O'Doherty[1], S. Barrington[1], S. Pereira[1], L. Alves[1], J. John[1], P. Schleyer[2]; [1]PET Imaging Centre, King's College London, King's Health Partners, St Thomas' Hospital, London, UNITED KINGDOM, [2]PET Imaging Centre, King's College London, London, UNITED KINGDOM.

Background. Perfusion 13N-NH3 and 18F-FDG viability studies are performed as combined investigations to assess for possible cardiac sarcoidosis. At our centre we perform a 1-day protocol beginning with a dynamic rest 13N-NH3 (550 MBq) scan using quantitative Patlak analysis and visual analysis followed by an 18F-FDG cardiac scan at 30 minutes and a half body scan at 60 minutes post injection. Recently we have installed 2 new GE Discovery 710 PET CT scanners, and have subsequently adapted our imaging protocol to capitalise on the new techniques available on these scanners. Methods. We performed 14 patient scans for suspected cardiac sarcoidosis on a Discovery 710 PET/CT scanner. The new imaging protocol was compared with that from our previous scanner (GE Discovery VCT). The D-710 is different in terms of crystal material (LYSO vs BGO), acquisition mode (3D only), image reconstruction and ultra low dose CT for attenuation correction (Q.AC). ECG gating was performed on all 18F-FDG images, and respiratory motion correction was also evaluated. Average cine CT images were used for attenuation correction to reduce respiratory motion induced by PET/CT misalignment. Further manual alignment was also required for some patients. Results. Patient radiation exposure for the cine CT was reduced using the Q.AC CT reconstruction algorithm by a factor of 2.18 in both DLP (103.59 to 47.56) and CTDIvol. (6.47 to 2.97). Image quality was felt to be improved compared to the D-VCT. Radiation dose due to CT attenuation correction is markedly reduced using the new scanning technology. Further improvements to flow quantitation may be made by using compartmental modelling instead of Patlak analysis. Conclusion. Installation of new PET/CT scanners enabled a significant change in cardiac acquisition protocol, which improves image quality, reduces radiation dose and can provide a more accurate CT registration for attenuation correction. It may be possible to further reduce patient dose by lowering the administered 13N-NH3 activity without compromising image quality due to the increased sensitivity of the D-710 compared to the D-VCT.

OP412
Benign Iodine-131 Treatment - Passing tasks from physician to technologist

H. C. Larsen, L. F. Grønnemark, P. C. Holdgaard, MD; Department of Nuclearmedicine, Vejle Hospital - Part of Lillebaelt Hospital, Vejle, DENMARK.

AIM: In Departments of Nuclear Medicine in Denmark the benign Iodine-131 treatment is most often given by a physician. Furthermore the physician gives the information about the treatment to the patients. Previously at our department the physician gave the information about the benign Iodine-131 treatment to

each patient individually, including the precautions and possible side effects. The physician used an entire working day performing this procedure. The purpose of this project was to pass some of the tasks from the physician to the technologists, and thereby save physician time and give more responsibility and new skills to the technologists. Methods and materials: In a period of 2 months the task of giving information to the patients was handed over from the physicians to 2 technologists. We also changed it to a common information session held by the technologist for all the patients scheduled that day instead of the physician gave the information individually to each patient. The first common session were held by the physician and 2 technologists observed. After a while, it was one of the technologists who did the common session, observed by the physician. Finally when the technologists were familiar with the common session, one of the 2 technologists did the session alone. Results: Now the common information session is held by the technologist about the precautions and possible side effects to the benign Iodine-131 treatment and other practical information. The session lasts 20 minutes and often includes 8 patients. Doing the information session the patients are allowed to ask questions and this might benefits the other patients. The physician has a short individual conversation with each patient after the common session. The physician still makes palpate the thyroid gland and decides the Iodine-131 dose. The individual conversation takes 5-10 minutes per patient. Before the setup was changed the physician spend an entire working day giving information to the Iodine-131 patients. Now the physician only spends 2-3 hours talking with the Iodine-131 patients. Conclusion: By doing a common information session and by passing some of the tasks in benign Iodine-131 treatment from the physician to the technologist it is possible to considerably reduce the use of physician time, which then can be allocated to other tasks. Additionally it gives the two technologists more responsibility and additionally skills, better understanding of this patient group and thereby a more meaningful workday.

OP414

Methods for preparing and acquiring PET/CT exams with 18F-Fluorodeoxyglucose and 18F-Fluoromethycholine

R. Sanco, M. Zappalà, V. Arnoldo, L. Memo, E. Zaramella, A. Carraro, L. Evangelista; Istituto Oncologico Veneto I.R.C.C.S., PADOVA, ITALY.

Introduction. To date, the standardization of protocol for preparation and acquisition of PET/CT images with 18F-Fluorodeoxyglucose (FDG) and 18F-Fluoromethylcholine (FCH) are missed. Because both the examinations are functional, the patient preparation is critical. The aim of the present prospective study was to determine the effect of patient preparation on PET image quality, both visually and semiquantitatively. Materials e methods. We collected data from 87 patients: 60 underwent FDG PET/CT and 27 performed a FCH PET/CT. Each patient was asked to compile a questionnaire that was based on food information, such as the type and the amount. Moreover, technician data (i.e. true, random and single coincidence, tracer dose, injection and acquisition time) and semiquantitative features (such as maximum and mean Standardized Uptake Value-SUVmax and SUVmean-, and Standardized Uptake Lean Value-SUL) were collected and correlated with clinical and demographic parameters. T-Student test and ANOVA test were used for the statistical analysis. Results. In 60 patients undergoing FDG PET/CT, a higher singles coincidence rate was found in case of a fasting >10h as compared to a fasting ranged between 5-10h (43.8 ±5.7 x105 vs. 37.8±6.7x105; p=0.028). Moreover, the rate of random and true coincidences was higher in patients with a body weight (BW)>60 kg and in those who had a water consumption >1liter before scan. At semiquantitative analysis, patients with a body mass index (BMI) >25 showed a significantly higher liver SUVmax and SUVmean than those with a BMI60kg than those with a BW<60kg, although not statistically significant. None of clinical parameters was associated with semiquantitative data (SUVmax and SUVmean of liver and kidney). Finally, we found that the bowel FCH uptake was visually inferior in patients with a BMI<25 than those with a BMI>25 (p=0.025). Conclusions. To improve the quality of FDG and FCH PET images seems necessary to prepare the patient as following: 1) to prolong the fasting time (>10 hours) before the examination; 2) to avoid the assumption of carbohydrate the evening before PET exams (to improve cardiac evaluation; especially in case of thoracic disease) and 3) to invite to drink at least 1 liter of water before the examination.

OP415

SPECT Myocardial Perfusion Imaging Quantification in Obese Subjects: Influence of Attenuation Correction with Computed Tomography Attenuation Maps

O. Stakhiv[1], M. Clarke[2], M. Aplin[2], N. Singh[2], K. Day[2], S. Dizdarevic[2], M. Jessop[2], E. Sousa[1]; [1]Escola Superior de Tecnologia da Saúde de Lisboa, Instituto Politécnico de Lisboa, Lisbon, PORTUGAL, [2]Nuclear Medicine, Department of Imaging, Brighton and Sussex University Hospital NHS Trust, Brighton, UNITED KINGDOM.

Introduction: Myocardial Perfusion Imaging (MPI) is a well implemented technique for assessment of Coronary artery disease (CAD. Obese subjects have a larger volume of soft tissue and organs that attenuate gamma causing false positive results due to attenuation artefacts. Aim: To evaluate the Influence of attenuation correction with Computed Tomography Attenuation Maps

(CTAM) in perfusion quantification for subjects with Body Mass Index (BMI) between 30 and 35, and above 35. Methods: Four groups of 72 subjects 47 with BMI between 30 and 35 Kg/m2 (27 male (GMI) and 20 female (GFI)) and and 24 (13 male (GMII) and 11 female (GFII)) with BMI between 30 and 35 Kg/m2 above 35 Kg/m2 who underwent stress-rest, SPECT MPI of a two days protocol, by EANM guidelines protocol with activity adjusted to subject's mass (400 MBq for subjects 110 kg), with 99mTc-tetrafosmin, for suspected CAD, were analysed with and without the incorporation of CTAM, for stress and rest studies, the studies were reconstructed by OSEM/MLEM. All images segmentation and quantification was done by myocardial walls regions for perfusion: Anterior (Ant), Inferior (Inf), Lateral (Lat), Septal (Sep) and Apical (Api), recurring to QGS/QPS. Each study was processed three times by one operator, and average value was used. For statistical evaluation it was used Friedman test for nom parametrical pared samples. Results: Statistically significant differences were found in comparison of studies with and without attenuation correction for: GFI group of stress and rest studies respectively for Lat ($p=0.006$, and $p=0.034$), Inf ($p=0.000$, and $p=0.000$) and Sep ($p=0.074$, and $p=0.044$); GFII group in stress study in Lat ($p=0.073$) and in stress and rest studies respectively for inferior wall ($p=0.001$, and $p=0.008$); GMI group of stress and rest studies respectively for Lat ($p=0.000$, and $p=0.000$), Inf ($p=0.000$, and $p=0.000$), Sep ($p=0.003$, and $p=0.001$) and for rest study in Api ($p=0.045$). GMII group of stress and rest studies respectively for Lat ($p=0.020$, and $p=0.014$), Inf ($p=0.000$, and $p=0.000$), Sep ($P=0.003$ and $p=0.075$). A significance level of 5% was used. Discussion: The influence of attenuation correction with CTAM is bigger within the groups with BMI between 30 and 35 Kg/m2, for male and female. This influence is also seen more markedly in the male groups. Conclusion: Differences between the male and female sets, agree with the ones described in literature.

OP416

[18F]-FDG SUV of reference regions in PET/MRI following standard MR-based attenuation correction

I. Haidinger[1], I. Rausch[1], M. Mayerhöfer[2], M. Hartenbach[3], T. Beyer[1]; [1]Centre for Medical Physics and Biomedical Engineering, Medical University of Vienna, Vienna, AUSTRIA, [2]Division of Radiology, Department of Biomedical Imaging and Image-guided Therapy, Medical University of Vienna, Vienna, AUSTRIA, [3]Division of Nuclear Medicine, Department of Biomedical Imaging and Image-guided Therapy, Medical University of Vienna, Vienna, AUSTRIA.

Aim: Standard MR-based attenuation correction (AC) in PET/MRI is based on dedicated MR images and thus, not intrinsically representative of measured attenuation coefficients. This may lead to a bias in the reconstructed PET activity values. Here, we evaluate standardized uptake values (SUV) of reference regions in FDG-PET/MRI whole-body (WB) imaging in dual-time point examinations.Material and Methods: SUV of reference regions (LI: liver, MD: mediastinum and MU: muscle) were defined in two patient groups: single-injection, dual-scan (SI-DS) PET/CT-PET/MR or single-injection, single-scan (SI-SS) PET/MR examination.SI-DS group: WB-imaging of 77 patients was performed 77±28min pi of 250MBq FDG on a Siemens Biograph-TPTV and repeated 133±30min pi on a Biograph mMR PET/MR. Standard acquisition, AC and reconstruction protocols were used. For each patient volumes of interest (VOI) were defined manually on the PET/CT images for LI (14mL), MD (4.5mL) and MU (4.5mL). VOIs were transferred manually to co-registered PET/MR image data.SI-SS group: WB-imaging of 30 patients was performed 93±19min pi of 250MBq FDG on a Siemens Biograph mMR. Similar size VOIs were defined manually on AC-PET images for LI (14mL), MD (4.3mL) and MU (4.2mL). Mean and maximum SUV were calculated for all scans and regions. Paired and non-paired Willcoxon tests ($p<0.05$) were used to test differences in SUV for significance of PET/CT versus PET/MR in SI-DS and PET/MR in SI-DS versus SI-SS, respectively.Results: In SI-DS SUVmax in PET/CT and PET/MR was 4.1(±0.8) and 2.4(±0.7) for LI, 3.1(±0.7) and 1.9(±0.7) for MD and 1.6(±0.5) and 1.1(±0.5) for MU, respectively. Corresponding SUVmean values were: 2.6(±0.5) and 1.6(±0.4) for LI, 2.0(±0.4) and 1.2(±0.4) for MD and 0.9(±0.3) and 0.6(±0.3) for MU, respectively. Differences were statistically significant ($p<0.001$).In SI-SS SUVmax was 2.2(±0.4) for LI, 2.0(±0.5) for MD and 0.9(±0.3) for MU. Corresponding SUVmean values were: 1.6(±0.3), 1.4(±0.3) and 0.6(±0.1), respectively. Differences to the corresponding SUV in the PET/MR data SI-DS group were not statistically significant in the liver ($p>0.05$), but statistical significance was found in MD (SUVmean) and MU (SUVmax).Absolute SUV differences between PET/MR in SI-SS and SI-DS examinations were similar to pi-time-dependent differences reported in Cheng et al. (MIB 2013) and Laffon et al. (JNMT 2011). Absolute differences between PET/CT and PET/MR were larger, most likely due to differences in the AC methods.Conclusion: Group-wise comparison of PET/CT and PET/MR data indicates a systematic underestimation of SUVs in reference regions of PET/MR images following standard MR-AC compared to PET/CT.

OP417

Do Metal Objects in the Topogram Influence the Patient Dose?

K. Falch[1], C. Baun[1], S. Shanmuganathan[1], M. Nikolajsen[2], O. Gerke[1], P. Hoeilund-Carlsen[1]; [1]Odense University Hospital, Odense, DENMARK, [2]University College Lillebaelt, Odense, DENMARK.

Aim: Patients scheduled for PET/CT are always requested to remove metal objects if possible from their clothes and body before the scan. However, quite often the planning CT topogram reveals forgotten items such as dentures, jewelry, keys, or coins. If these objects are removed before the diagnostic CT scan without performing a new topogram, the dose modulation software miscalculates the mA, and the radiation dose to the patient will increase.The aim of this study was to assess the impact of metal objects in the topogram upon the radiation dose to the patient if a new topogram is not performed after removal of these high attenuation objects. Methods and materials: The study was performed using an Alderson phantom with a metal object present during the topogram in a diagnostic CT protocol. Three objects were used: a belt in the pelvic area, a key at the right thorax, and a cell phone at the right thigh. For each object, 10 scans were performed removing the object between the topogram and the CT scan, thus, a total of 30 'with-object-scans' were performed. The results of these were compared to 10 scans performed without any metal objects present during the topogram. The CT dose for each scan was estimated by the dose length product (DLP). An exploratory linear regression model was applied on the dose-length product (DLP) using the different circumstances as explanatory factor ('without object' (reference) vs. 'with belt' vs. 'with key' vs. 'with cellphone'). Results: *Preliminary results based on the first 20 scans*: Compared to scout without object, mean DLP was increased by 2.26 mGy-cm (95% CI: 1.68-2.84; $p<0.0001$) in phantoms with belt and decreased by 0.65 mGy-cm (95% CI: 0.07-1.23; $p=0.03$) in phantoms with key. With cellphone, DLP was increased by 1.26 mGy-cm, but not to a statistically significant degree (95% CI: 0.68-1.84)). Adjusted R squared was 0.87. Conclusion: These preliminary data show that the dose to the patient is increased when a larger metal object is present during the topogram and no new topogram is performed after removal prior to the diagnostic CT scan. This should encourage technologists to perform a new topogram, whenever changes of the scanning circumstances have been made.

OP418

The Effect of Type of Collimation, Duration of Image Acquisition and Scatter Correction in Heart-to-Mediastinum Ratio of I-123-MIBG Scintigraphy

S. Chaves, T. Vieira, A. Sá Pinto, V. Alves, A. Fernandes, J. G. Pereira; Centro Hospitalar de São João, Porto, PORTUGAL.

Aim: Heart-to-mediastinum ratio (H/M) has been commonly utilized as an indicator of myocardial 123I-Metaiodobenzylguanide (123I-MIBG) uptake.However, estimates of the H/M vary depending on the choice of acquisition parameters and the application of corrections to physical phenomena such as scattering.The purpose of this study was to analyze how the choice of different acquisition times, collimator types and scatter correction (SC) influences the H/M calculation.Materials and MethodsWe randomly selected 6 patients that were sent to our Nuclear Medicine Department for oncological evaluation. Images acquisition began 3 hours post-injection of 123I-MIBG (185-370 MBq). First, were acquired 2 sequential thoracic static (TS) images of 5 minutes (5M) each, (LEHR collimators; 256x256 matrix; 20% energy window was set on 159 keV); this step was repeated, in sequence, using ME collimators. After this, a whole body (WB) scanning (LEHR collimators; 256x1024 matrix; speed of 10 cm/min) was acquired. SC was applied defining a second window (130 keV +/- 10%) during the acquisition of TS and WB imaging, when using LEHR collimators. Ten minutes images (10M) were obtained by the sum of the counts in the sequential 5 minute images. An irregular ROI was manually drawn over the left ventricle (H) and a rectangular ROI (120 pixels) was placed in the upper mediastinum (M). The H/M was defined as the ratio of the average counts in the heart and mediastinum ROI's. H/M ratios were calculated for the eight images for each patient: 10M/LEHR, 10M/LEHR/SC, 5M/LEHR, 5M/LEHR/SC, 10M/ME, 5M/ME, WB, WB/SC. The correlations of the H/M ratios of the eight images were determined.Results and ConclusionMean H/M ratios for WB, 5M/LEHR, 10M/LEHR, 5M/ME, 10M/ME, WB/SC, 5M/LEHR/SC, 10M/LEHR/SC, were 1.75 ± 0.25, 1.82 ± 0.30, 1.82 ± 0.30, 2.43 ± 0.48, 2.46 ± 0.49, 3.24 ± 0.95 3.46 ± 0.97, 3.92 ± 1.24, respectively.There were no significant correlations of H/M ratios of SC images with non-SC images.There were significant correlations of H/M ratios obtained in images with 5M and 10M, for both type of collimators studied (rLEHR = 0.99, errorLEHR = 0,01 and rME = 0.98, errorME = 0,09), with 10M/LEHR and WB (rWB = 0.91, erroWB = 0,15), with 10M/LEHR and 10M/ME (r10M = 0.97, error10M = 0,09) and with 5M/LEHR and 5M/ME (r5M = 0.96, error5M= 0, 11).This research suggests that H/M ratios may be obtained from images with smaller acquisition times, across different types of collimators and administered activities.

1305 - Tuesday, October 13, 2015, 11:30 AM - 12:45 PM, Hall G2

Do.MoRe - Featured: Therapy - Miscellaneous

OP419

An automatic delineation method for bone marrow absorbed dose estimations of 89Zr PET/CT studies

N. E. MAKRIS, R. Boellaard, C. W. Menke-van der Houven van Oordt, A. A. Lammertsma, M. C. Huisman; VU University Medical Center, Amsterdam, NETHERLANDS.

Purpose: To develop and validate an automatic delineation method for estimating red marrow (RM) activity concentrations and absorbed doses in positron emission tomography/computed tomography (PET/CT) studies using ^{89}Zr labelled tracers. Methods: Five patients with advanced colorectal cancer received 37.1 ± 0.9 MBq [^{89}Zr]cetuximab, 2 hours after administration of a therapeutic dose of 500 mg m^{-2} unlabelled cetuximab. For each patient, five PET/CT scans (1, 24, 48, 96 and 144 h post injection) were acquired using a Gemini TF-64 PET/CT scanner. Low dose CT data were used to manually generate volumes of interest (VOI) in the lumbar vertebrae (LV). In addition, LV VOI were generated automatically using an active contour method applied to the low dose CT. This method first identifies the outer bone structure of the LV, based on local intensity information in the low dose CT image, and subsequently partitions the LV between compact bone and bone marrow. RM activity was then determined by mapping the low dose CT derived RM VOI onto the corresponding PET scans. Finally, these activities were used to derive residence times and, subsequently, the self and total RM absorbed doses using OLINDA/EXM 1.1. Results: High correlations (r^2>0.85) between manual and automated VOI methods were obtained for both RM activity concentrations and total absorbed doses. On average, the automatic method provided values that were less than 5% lower than those obtained with the manual method. Conclusions: An automated and efficient VOI method, based on an active contour approach, was developed, enabling accurate estimates of RM activity concentrations and total absorbed doses.

OP420

Phase II Study of Lutetium-177-labeled Anti Carbonic Anhydrase IX Monoclonal Antibody Girentuximab in Patients with Advanced Renal Cell Carcinoma.

C. H. J. Muselaers[1], M. J. Boers-Sonderen[2], T. J. van Oostenbrugge[1], O. C. Boerman[3], I. M. E. Desar[2], A. B. Stillebroer[4], S. F. Mulder[2], C. M. L. van Herpen[2], J. F. Langenhuijsen[4], E. Oosterwijk[4], P. F. A. Mulders[4], W. J. G. Oyen[3]; [1]Radboudumc, Dept. of Urology, Dept. of Radiology and Nuclear Medicine, Nijmegen, NETHERLANDS, [2]Radboudumc, Dept. of Medical Oncology, Nijmegen, NETHERLANDS, [3]Radboudumc, Dept. of Radiology and Nuclear Medicine, Nijmegen, NETHERLANDS, [4]Radboudumc, Dept. of Urology, Nijmegen, NETHERLANDS.

Aim: Despite recent advances in treatment of metastatic clear cell renal cell carcinoma (ccRCC), the search for alternative treatment modalities which induce durable response with milder toxicity profiles continues. A phase II radioimmunotherapy (RIT) trial with ^{177}Lutetium (^{177}Lu)-girentuximab was initiated based on the encouraging results of a phase I to evaluate the efficacy of this RIT approach in patients with advanced ccRCC. Materials and methods: In this uncontrolled, non-randomized phase II trial, patients with progressive metastatic ccRCC who met the inclusion criteria received RIT with ^{177}Lu labeled girentuximab if targeting of the antibody was observed after a diagnostic injection with ^{111}Indium labeled girentuximab. Patients were eligible for another treatment cycle if no prolonged grade 4 hematological toxicity and at least stable disease (SD) according to RECIST v1.1 was observed on evaluation after 3 months. Retreatment was at 75% of the previous activity dose with a maximum of 3 treatment cycles. Results: Between August 2011 and April 2014, 14 patients enrolled in the study and received at least one infusion with ^{177}Lu-girentuximab. SD after the first RIT was observed in 8 patients (57%), partial regression (PR) was seen in 1 patient (7%), whereas progressive disease (PD) was seen in the other 5 (36%) patients. Of the 8 patients with SD and 1 with PR, 3 patients were not eligible for retreatment due to prolonged hematological toxicity. After the second treatment cycle, PD was observed in 1 out of 6 patients. The treatment was generally well tolerated, but resulted in transient grade 3-4 hematological toxicity in all but 1 patient. Conclusion: RIT with ^{177}Lu-girentuximab resulted in disease stabilization in the majority of patients with progressive ccRCC. Apart from transient myelotoxicity, RIT was well tolerated.

OP421

Preliminary experience in treating high-risk neuroblastoma using tandem high dose dosimetry-guided 131I-MIBG treatment combined with chemotherapy

G. Boni[1], s. mazzarri[1], M. Menconi[2], A. C. Traino[3], E. Borsò[4], S. Bernasconi[2], G. Casazza[2], C. Favre[5], D. Volterrani[1]; [1]Regional Center Of Nuclear Medicine, University Hospital Of Pisa, pisa, ITALY, [2]Division of Pediatric Onco-hematology, University Hospital, Pisa, Italy, pisa, ITALY, [3]Health Physics Unit, Section of Medical Physics, University Hospital, Pisa, Italy, pisa, ITALY, [4]Nuclear Medicine Division, Sant'Andrea Hospital of La Spezia, La Spezia, ITALY, [5]Division of Pediatric Onco-hematology, Meyer Pediatric Hospital, Florance, Florance, ITALY.

Aim: To evaluate the feasibily and safety data of tandem high dose dosimetry-guided 131I-MIBG infusions combined with chemotherapy in patients with refractory neuroblastoma. Method: Patients (age 8.5±4.4 yrs) with high-risk neuroblastoma refractory to multiple chemotherapy schedules and evidence of MIBG-avid disease by 123I-MIBG scan received two "tandem" high-dose 131I-MIBG treatments within 15 day. During the first infusion of 131I- MIBG, the patients received 12 mCi/Kg (mean 259 mCi, range 230-320 mCi). A contemporary dosimetric study was performed to calculate the absorbed dose by patient to estimate the

activity require for the second 131I-MIBG treatment (the target is to deliver a combined whole body radiation dose of 4 Gy). During day 1-5 by the first administration, patients received Topotecan iv 0.7 mg/m2 daily as cytotoxic drug and also as radiosensitiser. After 15 days patients were retreated with 131I-MIBG, and between Day 15-19 Topotecan 0.7 mg/m2 daily was administered again. Peripheral blood stem cells (PBSC) were available for transplantation in all the patients.Post-treatment evaluations were performed every 6-8 weeks after the infusion, including a diagnostic 123I-MIBG scan, tumor imaging studies (CT or MRI) as well as urine catecholamines, and a bone marrow aspirate and biopsy.ResultsFour patients with evidence of MIBG-avid disease were treated from December 2013 to date.All the patients completed the protocol receving a second infusion of 131I-MIBG (mean activity 283 mCi, range 100-353 mCi) to deliver a total whole body absorbed dose of 4 Gy The median time to second infusion was 16 days (range 14-19 days). No important adverse events were observed during both combined treatments. Expected bone marrow toxicity reached grade 4 neutropenia in 3 patients, grade 3 thrombocytopenia in 2 patients - which were treated with platelet transfusions - and grade 1 anemia in 2 patients. Bone marrow suppression completely recovered two months after second cycle in all the patients, without requiring PBSC transplantation. We observed a response rate (CR+PR) in 2/4 patients 3 months after the completion of the combined therapeutic regimen. Regarding other two patients, one case of stability and one of progression disease occurred. Conclusion. Single-centre preliminary experience show the feasibility of radiometabolic therapy with tandem high-dose dosimetry-guided of 131I-MIBG combined with chemotherapy. This therapy seems to be a safe and effective treatment modality for high-risk neuroblastoma with compromised organ functions. However, this was a small and heterogeneous cohort and further studies are needed.

OP422

Compared therapeutic efficacy of 177Lu-HH1 and 177Lu-rituximab in non-Hodgkin B-cell lymphoma

A. Pichard, **Jr**.[1,2,3], S. Marcatili[4,5], A. Courteau[4,5], R. Ladjohounlou[1,2,3], G. Cartron[6], I. Navarro-Teulon[1,2,3], A. Repetto-Llamazares[7], H. Heyerdahl[7], M. Bardiès[4,5], J. Dahle[7], J. Pouget[1,2,3]; [1]Inserm U1194, Montpellier, FRANCE, [2]IRCM, Institut de Recherche en Cancérologie de Montpellier, Montpellier, FRANCE, [3]Université de Montpellier, Montpellier, FRANCE, [4]UMR 1037 INSERM, Toulouse, FRANCE, [5]Centre de Recherche en Cancérologie de Toulouse, Toulouse, FRANCE, [6]6Département d'Hématologie, Unités Mixtes de Recherche–Centre National de la Recherche Scientifique 5235, Centre Hospitalier Universitaire de Montpellier, Montpellier, FRANCE, [7]Nordic Nanovector ASA, Kjelsåsveien 168 B, Oslo, NORWAY.

Aims. We compared in vitro and in vivo the therapeutic efficacy of a new antibody radionuclide conjugate (ARC), namely Betalutin™ and of 177Lu-labeled rituximab. Betalutin™ consists of the HH1 monoclonal antibody (mAb) radiolabeled with 177Lu and is directed against the CD37 receptor expressed by B-lymphoma cells. Materials and methods. In vitro, the therapeutic efficacy of 177Lu-rituximab, Betalutin™ and of the non-specific 177Lu-cetuximab was assessed in three different lymphoma cell lines (Ramos, DOHH2 and Rec-1) exposed for 18 hours to increasing activities (0, 0.5, 1, 2, 4 and 6 MBq/mL) of radiolabeled mAbs or to unlabelled mAbs (0-40μg/mL). Clonogenic survival was then measured and the mean absorbed dose to the nucleus was calculated using the MIRD formalism. Therapeutic efficacy and toxicities were also determined in mice subcutaneously xenografted with Ramos cells after intravenous administration of the three ARCs. SPECT-CT imaging and conventional biodistribution studies were performed and used for further tumour and organ absorbed dose assessment. Results. The highest cytotoxicity was observed for 177Lu-rituximab, followed by 177Lu-HH1 and the lowest for 177Lu-cetuximab. The highest sensitivity to ARC was observed in human follicular lymphoma cells (DOHH2) and the lowest for Burkitt lymphoma cells (Ramos), with mantel cell lymphoma cells (Rec-1) in between. Unlabelled rituximab was more efficient in killing cells than HH1 mAb mainly through apoptosis induction. The efficacies of the unlabelled mAbs were subtracted from the therapeutic efficacies of the ARCs to find the efficacies of the radiation only. In DOHH2, 177Lu-HH1 was more toxic per Gy than 177Lu-rituximab, 177Lu-cetuximab being in between. No linear nor linear-quadratic model fitted the data. The interpretation for Ramos survival curves was less obvious and depended on the chosen regression model: no differences in therapeutic efficacy of 177Lu-rituximab, 177Lu-HH1 and 177Lu-cetuximab were observed after linear-quadratic fitting (dose-effect relationship) while significant differences were observed when linear models were used (no dose-effect relationship). A linear relationship could be established between survival and the mean nucleus absorbed dose in both DOHH2 and Ramos cells exposed to 177Lu-cetuximab. In vivo, SPECT-CT study confirmed specific tumor targeting of Betalutin™. Preliminary results highlight the therapeutic efficacy of BetalutinTM associated with a lower toxicity than for 177Lu-rituximab. Conclusion. Our results show that the nature of absorbed dose-effect relationship associated with RIT of lymphoma depend on the nature of both ARC and cell line. Lack of absorbed dose-effect relationship may be explained by uncertainties inherent to absorbed dose assessment or to bystander effects.

OP423

Efficacy of radioembolization with holmium-166 microspheres; primary outcome of the phase II HEPAR trial

J. Prince, B. A. Zonnenberg, J. F. W. Nijsen, M. L. J. Smits, A. F. van den Hoven, F. J. Wessels, R. C. G. Bruijnen, M. N. G. J. Braat, G. C. Krijger, M. G. E. H. Lam, M. A. A. J. van den Bosch; UMC Utrecht, Utrecht, NETHERLANDS.

Aim: Microspheres containing holmium-166 in a poly L-lactic acid matrix (^{166}Ho) have been developed for radioembolization. In a phase 1 dose-escalation study, the maximum tolerated dose to the liver was found to be 60 Gy. The aim of this phase II trial was to evaluate the efficacy in patients with liver metastases. Materials and Methods: Patients were included in this single-center, single-arm study if they had liver-dominant metastases on baseline ^{18}F-FDG-PET with triphasic liver CT which were irresectable and refractory to systemic therapy. Patients received whole liver treatment (aimed absorbed dose 60 Gy, equal to 3.8 GBq/kg liver tissue). The study had a sequential design with an interim analysis after 30 patients, and every 6 patients, until a maximum of 48 patients. The primary objective was tumor response of two pre-specified target lesions on triphasic liver CT at 3 months, per RECIST 1.1. The response was calculated using evaluable patients (available case analysis) and with missing data imputed as progressive disease (imputed case analysis). Toxicity was scored using CTCAE version 4.03. Follow up continued until disease progression, or up to 12 months. Results: From May 2012 until March 2015, 56 patients with various primary tumors were included of whom 38 patients were treated. Four patients' outcomes were not evaluable due to: no response consensus among 3 raters, no contrast enhanced CT for evaluation, use of concomitant chemotherapy and death prior to imaging due to extrahepatic disease recurrence. Four others have not reached 3 months follow up. Stable disease or partial response in the liver after 3 months was detected in 20/30 patients (67%, 95% CI 49 – 81%) for the available case analysis and 20/34 (59%, 95% CI 42 – 74%) for the imputed case analysis; both proportions were above the pre-specified stopping boundary for treatment effect (40%), so the inclusion was closed. Median survival was estimated at 14 months (95% CI 8 – ∞ months). Clinical toxicity of grade 3 or 4 at any time after treatment consisted of: abdominal pain (18% of patients), nausea (9%), liver abscesses (3%), paroxysmal atrial tachycardia (3%), vomiting (3%), ascites (3%), gastric stenosis (3%), thoracic pain (3%), and upper gastrointestinal hemorrhage (3%). Laboratory examination after treatment showed grade 3 or 4 toxicities in levels of alkaline phosphatase (70%), gamma-GT (78%), lymphocytes (11%), and ALAT (4%).ConclusionRadioembolization with holmium-166 microspheres induces a tumor response in the liver with an acceptable toxicity profile.

OP424

Prolonged overall survival after 99mTc-MAA SPECT personalized treatment planning in radioembolization of hepatocarcinoma with 90Y glass microspheres: preliminary results of a 2 cohort study.

M. Maccauro[1], C. Chiesa[1], A. Facciorusso[2], M. Mira[3], C. Spreafico[4], R. Romito[1], C. Morosi[4], C. Sposito[2], S. Bhoori[2], M. Migliorisi[5], B. Padovano[1], E. Seregni[1], A. Marchiano'[4], F. Crippa[1], V. Mazzaferro[2]; [1]Nuclear Medicine, Foundation IRCCS Istituto Nazionale Tumori, Milan, ITALY, [2]Surgery 1, Foundation IRCCS Istituto Nazionale Tumori, Milan, ITALY, [3]Post graduate Health Physics School, University of Milan, Italy, Milan, ITALY, [4]Radiology 2, Foundation IRCCS Istituto Nazionale Tumori, Milan, ITALY, [5]Clinical engineering, Foundation IRCCS Istituto Nazionale Tumori, Milan, ITALY.

Aim: to estimate the clinical impact of 99mTc-MAA SPECT based personalized treatment planning in radioembolization (TARE) of hepatocarcinoma (HCC) with 90Y glass microspheres. Methods: 2 cohorts of intermediate/advanced HCC patients were treated. The cohort 1 of 52 patients was enrolled in a phase II prospective study (Mazzaferro 2013) with strict exclusion criteria: tumor burden > 50%, anti-tumor therapy including drug treatment within 30 days before TARE, previous TACE. Complete occlusion of the main trunk of portal vein affected few patients (4/29=14% PVT III, 1/29=3% PVT IV). Therapeutic activity was chosen according to the device pamphlet in order to deliver 120 Gy to the injected lobe. In Child A patients, a threshold for liver decompensation risk of 15% had been determined at 75 Gy (absorbed dose averaged on the whole parenchyma) with retrospective 99mTc-MAA SPECT dosimetry. For a tumor control probability of 50%, threshold was at 250 Gy for small lesions (10 gram) for larger lesions.189 sequential "real life" patients were enrolled in cohort 2, including any tumor mass, concomitant sorafenib, previous TACE and complete PVT. For a meaningful comparison, a subcohort of cohort 2 was selected applying retrospectively the exclusion criteria of cohort 1. The 90Y activity was personalized with prospective 99mTc-MAA SPECT dosimetric treatment planning and the previous thresholds. Liver decompensation within 6 months clearly attributable to progression was not attributed to the treatment. Results: treatment planning modified the activity in 73% of patients with respect to pamphlet indications. Activity was increased/decreased in 47%/25% of patients (mean +100%/-30%). The prescription coincided with the

device indication only in 28% of cases. The parenchyma absorbed dose standard deviation was strongly reduced in cohort 2 (30 Gy vs 16.5 Gy). Tumor absorbed doses did not differ. Treatment related liver decompensation incidence in Child A patients of subcohort 2 (11/71=15.5%) was maintained as in cohort 1 (6/43=14%), as programmed. Overall survival was prolonged: 15 m, 95% C.I [12 - 18] of cohort 1 versus 17 m, 95% C.I [13 - 19] in subcohort 2. The same is confirmed in the advanced patients with PVT: 13 m, 95% C.I. [9 - 17] versus 15 m, 95% C.I. [10 - 17]. Conclusion: in HCC patients without complete obstruction of portal vein, treatment planning resulted in fully personalized administrations, more homogeneous treatment conditions, identical toxicity incidence and prolonged survival with respect to the fixed dose of 120 Gy to lobe.

1306 - Tuesday, October 13, 2015, 11:30 AM - 1:00 PM, Hall 6

M2M - Featured: Molecular & Multimodality Imaging: PSMA

OP425

One-step radiosynthesis of 68Ga-DKFZ-PSMA at room temperature

Z. Wimana, C. Artigas, P. Flamen, G. Ghanem; Institut Jules Bordet, Université Libre de Bruxelles, Brussel, BELGIUM.

Germanium-68/Gallium-68 generator (68Ge/68Ga) has been under investigation and constant improvement since the late 1970s to reach GMP and pharmaceutical grades lately. Up-to-now, transchelation of 68Ga-cation at high temperatures has been the method of choice to prepare many tracers; however, more straight-forward radiosyntheses preferably at room temperature are now being developed as interesting alternatives to avoid the use of expensive equipment and lengthy procedures. This could allow a significant reduction in production cost and increase in the accessibility of Pet-based-molecular-imaging. We present here a one-step-labelling procedure of DKFZ-PSMA-11 ligand with 68Ga3+ at room temperature as a ready-to-use all-in-one kit and its successful use in prostate cancer patients.MATERIALS AND METHODS: A ready-to-use GMP kit (ANMI SA, Belgium) consisting in one vial containing lyophilized DKFZ-PSMA-11 (25μg), acetate buffer and excipients received up to 10ml of 0.1M HCL 68Ge/68Ga generator eluate directly and was allowed to incubate for 8-10 min at room temperature without any stirring. Radio-HPLC was used to compare radiochemical purity (RCP) as well as the stability of the tracer before and after SPE-C18 column purification. The same parameters were compared with preparations made with an automatic synthesizer with cassettes using Ga3+ purification/concentration on an ion exchanger, labeling at 95°C and C18 purification. RESULTS: The one-step method to prepare 68Ga-DKFZ-PSMA proved to be both highly efficient and reproducible. For the one step method we observed a labeling yield of 97.6±2.2%, a RCP of 99.7±0.3% and specific activity of 1.4±0.2 mCi/μg. In comparison, the tracer produced with the automated method showed similar RCP (>99.5%), specific activity (1.6±0.3 mCi/μg), but an important lower labeling yield (77.8±5.8%). The tracer produced with the one step method was stable in saline and serum over a course of 3h with a chemical purity above 99%. Purification over a SPE-C18 column did not result into substantial differences in RCP (99.9±0.1%) and stability (RCP at 3h>99%). No bacteriological burden or endotoxins were demonstrated. The C18-purified filter-sterilized end-product was administered to patients. CONCLUSION: We report here an original procedure to prepare 68Ga-DKFZ-PSMA and its successful use in metastatic prostate cancer patients for the first time.68Ga-DKFZ-PSMA is an example as the same procedure may be adaptable for other chelating groups and may considerably extend the variety of tracers by avoiding heat. With the introduction of pharmaceutical grade 68Ge/68Ga generators, would such methods mimic the success story of 99mTechnetium chemistry five decades ago is an open question.

OP426

Radiosyntheses and Preclinical Evaluation of Radiofluorinated PSMA-Ligands

J. Cardinale, M. Schäfer, M. Benesova, U. Bauder-Wüst, D. Komljenovic, M. Eder, M. E. Ladd, K. Kopka; German Cancer Research Center, Heidelberg, GERMANY.

Aim: Urea-based inhibitors of the prostate-specific membrane antigen (PSMA) are well known and promising candidates for the diagnosis (1,2) and therapy of prostate cancer. The aim of the project was the development of fine-tuned F-18 labelled PSMA-ligands affording an alternative ligand for the well-known 68Ga-PSMA-617 and 68Ga-PSMA-HBED-CC (68Ga-PSMA-11). Therefore the binding affinity and internalization characteristics have been determined for the selection of candidates for further in vivo biodistribution and PET experiments. Materials and Methods: The PSMA binding-motif Glu-NH-CO-NH-Lys was synthesized by a well-known method (3) on a solid phase (chlorotrityl-resin) and subsequently an amino acid linker was build up by fmoc-based solid phase peptide synthesis (SPPS). After separation from the resin and deprotection the peptidomimetics were conjugated using radiofluorinated prosthetic groups. The non-radioactive reference compounds were also prepared by SPPS. The Ki-values of all compounds were determined by competitive binding assays on LNCaP cells against 68Ga-PSMA-10 using the respective cold reference compounds. Subsequently the internalization of the radiofluorinated ligands was determined.

Moreover, two of the novel radiotracers were evaluated by dynamic PET experiments. Results: The no-carrier-added radiofluorination of the new PSMA-ligands with selected prosthetic groups was accomplished with good radiochemical yields. The Ki-values of the most promising compounds PSMA-1001, PSMA-1002 and PSMA-1003 were in the range of 1.5-3.0 nM. The internalized activity per 10e5 cells was approx. 3 % for PSMA-1001/1002 and approx. 7 % for PSMA-1003, respectively. During dynamic PET PSMA-positive LNCaP tumors could be visualized using radiofluorinated PSMA-1001 and PSMA-1003 as early as 1 h p.i.. However, both tracers showed significant uptake in the liver. Altogether PSMA-1003 led to the best results and the structure is currently modified for further optimization of the pharmacokinetics. Conclusions: The preparation of the precursors by SPPS enables the build-up of a huge library of diverse PSMA-targeted ligands. Based on PSMA-617, a series of promising radiofluorinated PSMA ligands was developed and evaluated in vitro and in vivo. After a further improvement of the pharmacokinetics the novel 18F-labelled tracers may lend themselves as promising compounds for first-in-man clinical studies. Literature: (1) A. Afshar-Oromieh et al., Eur J Nucl Med Mol Imaging. 2013, 40, 486-495. (Best Clinical Paper, EJNMMI Prize 2014) (2) Z. Szabo et al., Mol. Imaging Biol., Ahead of print, Doi.: 10.1007/s11307-015-0850-8 (3) M. Eder et al., Bioconjugate Chem. 2012, 23, 688-697.

OP427

NODA-GA-PSMA : A versatile probe for SPECT/PET imaging of PSMA-positive tumors.

E. Gourni[1,2,3], V. Goncalves[4], F. Denat[4], P. T. Meyer[2], H. R. Maecke[2]; [1]German Cancer Consortium (DKTK), Heidelberg, GERMANY, [2]Department of Nuclear Medicine, University Hospital Freiburg, Freiburg, GERMANY, [3]German Cancer Research Center (DKFZ), Heidelberg, GERMANY, [4]Institut de Chimie Moléculaire de l'Université de Bourgogne, Dijon, FRANCE.

Objectives: The type II integral membrane protein, prostate specific membrane antigen (PSMA), is overexpressed on prostate cancer as the stage and grade of the tumor progresses, especially in androgen-independent, advanced and metastatic disease. The ability to image PSMA by using ^{68}Ga-HBED-CC-PSMA was proven to be successful preclinically and clinically. The present study aims at developing and evaluating an urea-based PSMA inhibitor suitable for labeling with ^{111}In for SPECT as well as ^{68}Ga and ^{64}Cu for PET imaging. Methods: The urea-based PSMA inhibitor - lysine-urea-glutamate - coupled to the spacer Phe-Phe-D-Lys(suberoyl) and functionalized with the chelator 1,4,7-triazacyclononane, 1-glutaric acid-4,7 acetic acid (NODAGA), to obtain NODAGA-Phe-Phe-D-Lys(suberoyl)-Lys-urea-Glu (VG66). VG66 was radiolabeled with ^{111}In, ^{68}Ga and ^{64}Cu. The radioconjugates were further evaluated in vitro and in vivo in LNCaP xenografts by biodistribution and PET studies. Biodistribution studies were also performed with ^{68}Ga-HBED-CC-PSMA and ^{111}In-DKFZ-PSMA-617 for comparison. Results: ^{68}Ga-VG66, ^{64}Cu-VG66 and ^{111}In-VG66 were prepared in radiochemical purity >95% and specific activities 85, 30 and 10 MBq/nmol exhibiting a $\log D_{octanol/PBS}$ of -3.54±0.06, -3.33 ±0.09 and -3.32±0.05, respectively. $^{68/nat}$Ga-VG66, $^{64/nat}$Cu-VG66 and $^{111/nat}$In-VG66 exhibited high affinity for the LNCaP cells, with K_d values of 19.3±2.5 nM, 25.1±2.0 and 5.5±0.9 nM, respectively. They revealed comparable internalization profiles with approximately 75% of the total cell associated activity internalized after 3h of incubation with the cells. ^{68}Ga-VG66 showed very high stability after its administration in mice and metabolite analysis of the mouse-plasma 15 min p.i.. Tumor uptake of ^{68}Ga-VG66 (14.5±2.9% IA/g) in LNCaP xenografts at 1 h p.i is slightly lower than ^{68}Ga-HBED-CC-PSMA (15.8±1.4% IA/g) but statistically not significant (P=0.67). The tumor-to-normal tissue ratios at 1 and 2 h p.i of ^{68}Ga-VG66 are comparable to ^{68}Ga-HBED-CC-PSMA (P>0.05). Tumor uptake of ^{111}In-VG66 (28.5±2.6% IA/g) at 1 h p.i. is lower than ^{111}In-DKFZ-PSMA-617 (52.1±6.5% IA/g) (P=0.02). The tumor-to-normal tissue ratios of ^{111}In-DKFZ-PSMA-617 are significantly higher than ^{111}In-VG66 at all tested time points. Tumor uptake of ^{64}Cu-VG66 at 1 h p.i was 20.3±1.5% IA/g. Biodistribution studies at later time points showed increasing tumor-to-background ratios with time. This was also illustrated by the PET images. Conclusion: VG66 can efficiently be labeled with ^{68}Ga, ^{64}Cu and ^{111}In leading to radiotracers with high affinity towards PSMA. ^{68}Ga-VG66 is comparable to HBED-CC-PSMA in terms of tumor uptake (P=67) and tumor to normal tissue ratios (P>0.05) Their promising in vivo pharmacokinetic performance may contribute to the improvement of the diagnostic imaging of tumors overexpressing PSMA.

OP428

68Ga-PSMA11-PET/CT - a new technique with high potential for the radiotherapeutic management of prostate cancer patients

F. Giesel[1], H. Fiedler[1], M. Stefanova[1], C. Kratochwil[1], A. Afshar-Oromieh[1], K. Kopka[2], J. Debus[3], U. Haberkorn[1], F. Sterzing[3]; [1]Radiologische Klinik / Abt. für Nuklearmedizin, Heidelberg, GERMANY, [2]Deutsches Krebsforschungszentrum (DKFZ) / Abteilung für Radiopharmazeutische Chemie, Heidelberg, GERMANY, [3]Radiologische Klinik / Abt. für Strahlentherapie, Heidelberg, GERMANY.

AIM: Radiotherapy is the main therapeutic approach besides

surgery of localized prostate cancer. It relies on risk stratification and exact staging. This report analyses the potential of [68Ga]Glu-urea-Lys(Ahx)-HBED-CC (68Ga-PSMA11) a new PET-tracer targeting PSMA for prostate cancer staging and individualized radiotherapy planning. MATERIALS & METHODS: A cohort of 57 patients with prostate cancer scanned with 68Ga-PSMA11 PET-CT for radiotherapy planning was retrospectively reviewed. 15 patients were at initial diagnosis and 42 patients at time of biochemical recurrence. Staging results of conventional imaging, including bone scintigraphy, CT or MRI, were compared with 68Ga-PSMA Ligand PET-CT results and the influence for radiotherapeutic management was quantified. RESULTS: 68Ga-PSMA ligandPET-CT has had a dramatic impact on radiotherapy application in the presented cohort. In 50.8% of the cases therapy was changed. CONCLUSION: The presented Imaging technique of 68Ga-PSMA-PET-CT could be a key technology for individualized radiotherapy management in prostate cancer.

OP429

The novel theranostic PSMA-ligand PSMA-617 in the diagnosis of prostate cancer by PET/CT: biodistribution in humans, radiation dosimetry and first evaluation of tumor lesions

A. Afshar-Oromieh[1], H. Hetzheim[2], C. Kratochwil[1], M. Benesova[3], M. Eder[4], O. Neels[4], W. Kübler[5], F. L. Giesel[1], W. Mier[6], K. Kopka[4], U. Haberkorn[1]; [1]University Hospital of Heidelberg, Heidelberg, GERMANY, [2]Div. of Medical Physics in Radiology, German Cancer Research Center, Heidelberg, Germany, Heidelberg, GERMANY, [3]Div. of Radiopharmaceutical Chemistry, German Cancer Research Center, Heidelberg, GERMANY, [4]Div. of Radiopharmaceutical Chemistry, German Cancer Research Center, Heidelberg, Heidelberg, GERMANY, [5]Div. of Radiation Protection and Dosimetry, German Cancer Research Center, Heidelberg, Heidelberg, GERMANY, [6]Division of Radiochemistry, University Hospital of Heidelberg, Heidelberg, GERMANY.

Purpose: PET-imaging with the ligand of the prostate-specific membrane antigen 68Ga-PSMA-11 is regarded as a significant step forward in the diagnosis of prostate cancer (PCa). More recently, a PSMA-ligand was developed which can be labeled with 68Ga, 177Lu and 90Y. This ligand, named PSMA-617, therefore enables both, diagnosis and therapy of PCa. The aim of this evaluation was to investigate the distribution of PSMA-617 in normal tissues and in PCa lesions as well as the radiation exposure of PET-imaging with 68Ga-PSMA-617. Methods: Nineteen patients with recurrent PCa were referred to 68Ga-PSMA-617-PET/CT. Quantitative assessment of tracer uptake of several organs and 53 representative tumor lesions was performed in 15 patients 1h and 3h p.i. In four additional patients, the same procedure was conducted at 5min, 1h, 2h, 3h, 4h and 5h p.i. Based on the data of these four patients the radiation exposure of a 68Ga-PSMA-617-PET/CT was identified. Results: Intense tracer uptake was observed in kidneys and salivary glands. In 14 of 19 patients (73.7%) at least one tumor suspicious lesion was detected 3h p.i.. Of 53 representative tumor lesions selected at 3h p.i., 47 lesions were visible at 1h p.i. Mean tumor-to-background ratios for SUVmax were 20.4 ± 17.3 (2.3 - 84.0) at 1h p.i. and 38.2 ± 38.6 (3.6 - 154.3) at 3h p.i. Average radiation exposure (effective dose) is approximately 2.1E-2 mSv/MBq. Conclusion: Within healthy organs, kidneys and salivary glands demonstrated the highest 68Ga-PSMA-617 uptake. The radiation exposure is relatively low. 68Ga-PSMA-617 can show PCa-lesions with very high contrast. Images conducted at 3h p.i. detected more PCa-lesions compared to images at 1h p.i..

OP430

Value of Ga-68 PSMA PET/CT for Patient Selection and Follow-up of Metastasized Prostate Cancer Patients Undergoing Peptide Radioligand Therapy (PRLT) with Lu-177 DOTAGA-PSMA Inhibitor

H. R. Kulkarni[1], H. J. Wester[2], A. Singh[1], R. P. Baum[1]; [1]THERANOSTICS Center for Molecular Radiotherapy and Molecular Imaging, Bad Berka, GERMANY, [2]Pharmaceutical Radiochemistry, Technical University Munich, Munich, GERMANY.

Aim: Ga-68 PSMA-HBED-CC (Ga-68 PSMA) is a sensitive and specific PET tracer for the detection of prostate cancer recurrences and metastases. The aim of this study was to determine the role of Ga-68 PSMA PET/CT in patients with metastasized castrate resistant prostate cancer (mCRPC) undergoing peptide radioligand therapy (PRLT) using Lu-177 DOTAGA-PSMA inhibitor (Lu-177 PSMA). Methods: Ga-68 PSMA PET/CT (contrast-enhanced CT scan) was performed in 217 patients (mean Gleason score 7±1, mean age 63±11 years, median PSA 58.2, range 0.1-2223 ng/ml), and repeated in 31 patients for follow-up after 2-4 cycles of PRLT using Lu-177 PSMA. PET/CT findings were also correlated with post-therapy Lu-177 PSMA whole body scans and SPECT/CT studies performed during therapy. Retrospective analysis was performed using our prospective database of patients undergoing PRLT. Results: Metastatic disease with PSMA expression was noted in 40 patients, including bone (n=35), two or more lymph node sites (n=31), lung (n=5) and liver (n=5). All Lu-177 PSMA positive lesions (noted on post-therapeutic scans) were previously also identified on PET/CT. Molecular response to PRLT could be assessed after 2-4 cycles of PRLT by Ga-68 PSMA PET/CT in 31 patients. Molecular response (EORTC) was noted in 14 patients, demonstrating strong correlation

between change in SUVmax and change in serum PSA level (r=0.84). On the other hand, morphological criteria (RECIST) established objective response in 6 of 14 patients. Disease remained stable in 7 and 15 patients, according to EORTC and PERCIST, respectively, and progressed in 10 patients. Conclusions: Ga-68 PSMA PET/CT enables not only effective selection of metastasized prostate cancer patients for therapy with Lu-177 labeled DOTAGA-PSMA inhibitor, but also for the assessment of objective therapy response, correlating well with change in serum PSA. It may be useful for the early identification of responders and non-responders, since molecular response precedes morphological changes in tumors.

1307 - Tuesday, October 13, 2015, 11:30 AM - 12:45 PM, Hall F

Cardiovascular System: Myocarditis, Amyloidosis, Sarcoidosis & Vasculitis

OP431

FDG PET Imaging of a Rat Model of Autoimmune Myocarditis: Comparison with Histological Analysis

R. A. Werner[1,2], Y. Maya[1,3], V. Jahns[4], H. Wakabayashi[1], M. Nakajo[1], K. Fukushima[5], M. Javadi[6], T. Yanagisawa[7], R. Jahns[8], T. Higuchi[1,2]; [1]Department of Nuclear Medicine, Universitätsklinikum Würzburg, Würzburg, GERMANY, [2]Comprehensive Heart Failure Center, Würzburg, GERMANY, [3]Research Centre, Nihon Medi-Physics Co., Ltd., Chiba, JAPAN, [4]Department of Pharmacology, Universitätsklinikum Würzburg, Würzburg, GERMANY, [5]Hyogo College of Medicine, Hyogo, JAPAN, [6]Division of Nuclear Medicine, Johns Hopkins University, MD, UNITED STATES, [7]Department of Cardio-angiology, Kitazato University School of Medicine, Tokyo, JAPAN, [8]Department of Internal Medicine I, University of Würzburg, Würzburg, GERMANY.

Aim: Reliable non-invasive tools to diagnose inflammatory activity are clinically relevant in patients with myocarditis for optimization of therapeutic strategies. The aim of this study is to assess the feasibility of serial monitoring of the inflammatory activity in a rat model of acute myocarditis utilizing high resolution small animal PET system and F-18 fluorodeoxyglucose (FDG). Materials and Methods: Autoimmune myocarditis was induced in Lewis rats by immunizing twice at a week interval with 10mg/mL porcine cardiac myosin with Freund's complete adjuvant (n=12) or adjuvant alone as control (n=8). Rats received serial imaging at week 1, 2 and 3 after first immunization utilizing a micro PET system. At fasting condition (>12h), static 10min chest FDG PET scans were started 60min after tracer administration. F-18 fluorobenzyl triphenyl phosphonium (FBnTP) myocardial perfusion PET imaging was also performed to identify the localization of the FDG signal in subset of animals. For post-mortem ex-vivo analysis (week 3), the hearts were sliced into 20-μm short axis sections for autoradiography and histological analysis with HE staining. Region of interest (ROI) were set on the autoradiograms, and the uptake values of each ROI were calculated as the background-corrected quantum levels per unit area (QL/pixel). Results: Multiple focal cardiac inflammatory lesions with intense macrophage infiltration were histologically identified at week 3 after immunization in 10 of 12 animals and 0 of 8 adjuvant alone controls. FDG PET showed multiple high-contrast focal tracer accumulation in all histologically confirmed myocarditis hearts at week 3, while no focal accumulation in controls (%ID/cc: 1.62±0.93 vs 0.25 ±0.04, $p<0.05$). Serial FDG PET imaging provided time course of the uptake signals (%ID/cc: 0.25±0.10, 0.28±0.11, 1.62±0.93, $p<0.05$ at week 1, 2 and 3, respectively). Ex-vivo analysis confirmed co-localization of the area of FDG accumulation and inflammatory lesions. Mean FDG activity (QL/pixel) at the inflammatory lesions identified by histology (223±99) was significant higher than remote control area (53±30, $p<0.0001$) and control hearts (13±4, $p<0.0001$). Conclusion: Focal increased FDG PET signals in the heart was well correlated with histologically identified inflammatory lesions in a rat model of autoimmune myocarditis. This FDG-PET imaging might be a promising approach for serial monitoring of the inflammatory activity, and this experimental platform would be available for better understanding of the inflammation dynamics for the development of novel therapeutic strategies.

OP432

Assessment of radiolabeled methionine for imaging myocardial inflammation in a rat model of autoimmune myocarditis: Comparison with18F-FDG and histological findings

Y. Maya[1,2], R. A. Werner[1,3], V. Jahns[4], H. Wakabayashi[1], M. Nakajo[1], K. Fukushima[5], T. Yanagisawa[6], R. Jahns[7], T. Higuchi[1,3]; [1]Department of Nuclear Medicine, Universitätsklinikum Würzburg, Würzburg, GERMANY, [2]Research Centre, Nihon Medi-Physics Co., Ltd., Chiba, JAPAN, [3]Comprehensive Heart Failure Center, Würzburg, GERMANY, [4]Department of Pharmacology, Universitätsklinikum Würzburg, Würzburg, GERMANY, [5]Hyogo College of Medicine, Hyogo, JAPAN, [6]Department of Cardio-angiology, Kitazato University School of Medicine, Kanagawa, JAPAN, [7]Department of Internal Medicine I, University of Würzburg, Würzburg, GERMANY.

Objectives: Myocarditis is thought to be one of the major causes of heart failure and sudden cardiac death in young adults. Currently, the definitive non-invasive method to detect and monitor the cardiac inflammatory lesions is missing, and invasive endomyocardial biopsy is associated with inherent sampling error. In this study, we

investigated the potential of radiolabeled methionine to assess the inflammatory activity utilizing a rat model of autoimmune myocarditis. Methods: Autoimmune myocarditis was induced in Lewis rats (150-210g) by immunizing twice at a 7-day interval with 10-mg/mL porcine cardiac myosin with Freund's complete adjuvant (mycobacterium tuberculosis) (n=4) or adjuvant alone as controls (n=4). On day 21 after immunization, study was performed with dual-tracer autoradiography to assess distribution of 14C-methionine and 18F-FDG in the hearts. At fasting condition (>12h), both 18F-FDG (37MBq) and 14C-methionine (0.5MBq) were administrated 90 min and 20 min before euthanizing the rats, respectively. The hearts were removed, frozen, and sliced into 20-μm short axis sections for autoradiography and histological analysis with HE staining. Region of interests (ROI) were set on the autoradiograms, and calculated the uptake values of each ROI, as the background-corrected quantum levels per unit area (QL/pixel) for 14C-methionine and 18F-FDG. Results: Multiple focal cardiac inflammatory lesions were histologically identified in all hearts with myosin treatment group, while no lesions were seen in rats with adjuvant alone. The autoradiographic images clearly demonstrated high-density accumulation of 14C-methionine, corresponding to histologically confirmed inflammatory lesions and focal 18F-FDG accumulation. The 14C-methionine uptake (mean binding signal intensity, QL/pixel) in the inflammatory lesions was significantly higher than remote non-inflammatory area (2561 ± 894 vs 1068 ± 339, $p<0.0001$) and control hearts (2561 ± 894 vs 727 ± 97, $p<0.0001$). Excellent positive correlation between intensity of 14C-methionine and 18F-FDG accumulation was observed ($r2 = 0.93$, $p<0.0001$). Contrast between inflammatory lesion and non-inflammatory area was higher in 18F-FDG than in 14C-methionine (3.45 ± 0.68 vs 2.07 ± 0.21, $p<0.05$). Conclusions: Using rat model of autoimmune myocarditis, we confirmed focal increased of 14C-methionine accumulation, co-localizing cardiac inflammatory lesions and 18F-FDG uptake. Further experiments using 11C-methionine PET are warranted to investigate the feasibility and robustness of in-vivo imaging and advantages over 18F-FDG PET especially regarding physiological background uptake issue.

OP433

Imaging of myocardial inflammation with somatostatin receptor based PET/CT - a comparison to cardiac MRI

C. Lapa[1], T. Reiter[1], X. Li[2], R. Werner[1], S. Samnick[1], R. Jahns[1], A. K. Buck[1], G. Ertl[1], W. R. Bauer[1]; [1]Universitätsklinikum Würzburg, Würzburg, GERMANY, [2]AKH Wien, Wien, AUSTRIA.

Aims: Acute myocarditis as well as post-ischemic myocardial inflammation are associated with a profound activation of the immune system that plays a pivotal role in the further clinical course. Present non- invasive imaging modalities allow no direct visualization of the involved macrophage system.We aimed to investigate the feasibility of somatostatin receptor (SSTR)-based positron emission tomography / computed tomography (PET/CT) for detecting acute inflammatory lesions in patients after myocardial infarction or peri-/myocarditis.MethodsOn a compassionate use base, 12 patients (7 males, 5 females) with active peri-/myocarditis (n=6) or sub-acute myocardial infarction (n=6) underwent SSTR-PET/CT imaging with 68Ga-DOTA-TOC and cardiac MRI within 3-10 days after onset of symptoms (mean, 7±3 days; interval between PET/CT and MRI, 3±3 days). PET images were visually scored. The AHA 17-segment model of the left myocardium was used for localization and comparison of inflamed myocardium for both imaging modalities. Using semi-quantitative analysis, tracer uptake was calculated as mean and maximum standardized uptake value (SUVmean and SUVmax) and compared to infarcted/inflamed myocardium with both remote myocardium and left ventricular (LV) cavity. Results: SSTR-PET/CT revealed areas with mild or moderately increased tracer uptake in the myocardium or the pericardium in all patients. In the 17-segment model, PET/CT yielded 55 and MRI 47 positive segments. Overall concordance of the 2 modalities was 85.3% (174/204 segments analyzed). In 9.3% (19/204), more positive segments were identified by PET/CT, whereas in 5.4% (11/204), MRI detected more positive segments. SUVmean and SUVmax in infarcted/inflamed areas were 3.5±0.9 and 4.0±1.1, respectively. The lesion-to-remote myocardium and lesion-to-LV cavity ratios were 1.9±0.4 and 1.9±0.3 for SUVmean and 1.8±0.3 and 1.7±0.3 for SUVmax, respectively. Conclusions: The different imaging patterns of SSTR-directed radiotracers and MRI suggest a complementary role of PET/CT for detecting/imaging myocardial inflammation in the course of myocarditis and/or sub-acute infarction. Our data warrant further analysis in larger prospective clinical studies.

OP434

Disphosphonates Cardiac Uptake in Familial Amyloid Neuropathy: Comparison between DPD and HMDP

H. Regaieg[1], R. De Paola Chequer[1], R. Ben Azzouna[1], V. Algalarrondo[2], B. Mahida[1], M. Slama[2], D. Le Guludec[1], F. Rouzet[1]; [1]Department of nuclear medicine, Bichat-Claude Bernard university hospital, Paris, FRANCE, [2]Department of cardiology, Antoine Béclère university hospital, Clamart, FRANCE.

Aims: Familial amyloid polyneuropathy (FAP) is a severe hereditary disease, due to production by the liver of a genetic variant transthyretin (TTR) resulting in tissue amyloid deposits. Cardiac involvement is of major prognostic value. Diphosphonate scintigraphy has been proposed as a diagnostic tool for TTR-related cardiac amyloidosis, but there is no consensus on the optimal radiopharmaceutical. Consequently, we compared the cardiac uptake of two 99mTc-labelled tracers: diphosphono-propanedicarboxylic acid (DPD) and hydroxymethylene

diphosphonate (HMDP) in patients with TTR-FAP. Methods: 122 consecutive patients with TTR-FAP were prospectively included and received randomly DPD or HMDP. Acquisitions (whole-body (WB) and chest SPECT) were performed 3 hours after intravenous injection of the tracer. Quantification of myocardial uptake on WB acquisitions was performed by use of the ratio between the geometric mean of either total or average counts of a region of interest (ROI) drawn over the heart area and the WB total or average counts (H/WBtotal or H/WBaverage). Quantification on SPECT acquisitions was performed by the ratio between 3D isocount volume of interest generated over the myocardium and a standard volume in the right lung (H/L). Quantification of soft tissues uptake was performed by use of ratio between average counts of a ROI drawn over the lumbar spine and a ROI drawn over soft tissues of the lower limb (B/ST) on the WB acquisition. Results: the DPD and HMDP groups of patients had similar age (62±15 vs. 59±14 years respectively; p=0.3), sex (males: 67% vs. 58% respectively; p=0.4), TTR mutation (Val30Met: 70% vs. 80% respectively; p=0.3) and activity of the tracer (DPD: 713±86 MBq vs. HMDP: 709±124 MBq; p=0.9). Quantitative parameters derived from whole body acquisition were significantly greater with DPD compared to HMDP (H/WBtotal: 3.8±2.7 vs. 2.4±2.1 respectively; p=0.002 and H/WBaverage: 5.2±2.2 vs. 4.3±1.3 respectively; p=0.01) as well as H/L derived from SPECT acquisition (3.9±3.7 vs. 2.0±1.9 respectively; p=0.001). The uptake by soft tissues was also greater in the DPD compared to HMDP group (B/ST: 3.6±2.0 vs. 5.7±2.9 respectively; p<0.0001). Conclusions: The present study shows that in patients with TTR FAP, the uptake of DPD in heart and other soft tissues is superior to that of HMDP. This suggests that DPD should be prioritized for initial assessment of patients suspected of cardiac involvement of TTR-related amyloidosis. Further study is required to assess whether this difference impacts the diagnostic performance and whether DPD is more accurate for the assessment of therapy response.

OP435

Cardiac involvement in systemic sclerosis patients can be detected by dual single-photon emission computed tomography of thallium-201 and iodine-123-beta-methyl-p-iodophenyl-pentadecanoic acid scintigraphy

S. Matsuo, K. Nakajima, S. Kinuya, K. Takahara; Kanazawa University Hospital, Kanazawa, JAPAN.

Objective: Systemic Sclerosis (SSc) is a clinically heterogeneous connective tissue disorder. Heart involvements confer a poor prognosis in patients with systemic sclerosis. Nevertheless, the prevalence of cardiac involvement is not fully evaluated. The purpose of this study was to detect myocardial metabolic and perfusion abnormalities at rest using 123I-BMIPP and 201Tl imaging in patients with systemic sclerosis patients. Methods: We examined 82 patients of collagen disease (male/female=18/64, mean age 55±14) (71 systemic sclerosis (SSs) (8 limited cutaneous SSc), 4 systemic lupus erythematosus (SLE), 5 mixed connective tissue disease (MCTD), 2 others). All patients underwent both resting 123I-BMIPP imaging and 201Tl imaging. Total defect score (TDS) of 123I-BMIPP and perfusion were semi-quantitatively determined with SPECT imaging using a 17-segment 5-point model and Japanese normal database. Mismatch was defined the difference of the score more than 2 (123I-BMIPP>201Tl). Left ventricular functional analysis was performed by QGS software. Results: Thirty-three out of 82 (40.7%) patients with collagen disease had metabolic abnormalities (defect score>3). TDS of 123I-BMIPP were 4.8±2.7 in patients with sclerosis and 201Tl defect score was 2.4±2.8 in sclerosis. Mismatch between 123I-BMIPP and 201Tl was found in 11 out of 82 patients (13.4%). Left ventricular ejection fraction was 69±16%, and end-diastolic volume 57±19ml, end-systolic volume 18±14ml. There was no perfusion-metabolic mismatch in patients with limited cutaneous SSc (n=8). Conclusion: Cardiac manifestation occurs earlier and frequently in an early stage systemic sclerosis patients with normal systolic function. The 123I-BMIPP metabolic SPECT can be utilized on systemic sclerosis patients.

OP436

Value of FDG-PET/CT and cardiac MR for the diagnosis and therapy monitoring in cardiac sarcoidosis.

B. SGARD, S. DJELBANI, J. TORDJMANN, G. POP, H. NUNES, D. VALEYRE, V. EDER, M. SOUSSAN; University paris XIII, Bobigny, FRANCE

Objectives: Cardiac sarcoidosis (CS) is associated with a poor prognosis. There are currently no clear recommendations on imaging strategy. The objective of this study was to compare FDG-PET/CT (PET) and cardiac MR imaging (MR) for the diagnosis and therapy monitoring of CS. Materials and Methods: We conducted a single-center retrospective study including 53 patients with histologically proven sarcoidosis and a suspicion of CS. PET and MR were performed in all patients in a maximum time interval of two months. PET were all performed after a low carbohydrate-high fat diet. A subgroup of 16/53 patients (30%), were followed during therapy using both MR and PET. MR was considered as positive if there was a delayed gadolinium enhancement located in the subepicardial area. PET was considered as positive if there was a focal or multifocal FDG uptake. The findings of PET and MR, as well as the reversibility under treatment were compared. Results: 36% of patients (n = 19/53) had a MR (+) and 13% (n = 7/53) had a PET (+). All patients with PET (+) had also an MR (+), with myocardial lesions located in the

same locations in all cases. Among patients, 30% (n=16/53) had residual physiological FDG uptake under therapy (diffuse, basal, papillary muscle). Among patients having baseline MR (+) and PET (+), 86% (n=6/7) had improving lesions on MR and 100% (n=6/6) on PET. None of the lesions in patients with MR (+) and PET (-) had modifications on follow-up MR. Conclusion: PET should be identify inflammatory CS and potential reversibility under treatment. PET should be systematically associated with MR for improving lesion characterization.

OP437

Relationship between active inflammation and myocardial injury in patients with cardiac sarcoidosis as detected by non-invasive multi-modality imaging

S. Kataoka, M. Momose, K. Fukushima, N. Serizawa, A. Suzuki, C. Kondo, K. Abe, S. Sakai, N. Hagiwara; Tokyo women's medical university, Tokyo, JAPAN

Aim: 18F-FDG PET/CT (PET), cardiac magnetic resonance (CMR) imaging and 123I-BMIPP/201TlCl dual myocardial SPECT have been reported to be useful to diagnose as cardiac sarcoidosis (CS), but the relationship between them is still poorly understood. The aim of this study is to clarify the relationship between the three modalities for CS. Materials and methods: We evaluated 16 patients (10 male, mean age 55±13 year old) with CS before steroid therapy who underwent PET, CMR and dual gated SPECT. Left ventricular myocardium was divided into 17 segments. BMIPP and TL defects were scored in each segment visually using a 5-point grading system: 0-4 (0,normal; 4,absent). BMIPP and TL total defect score was also calculated as summed BMIPP defect (BMDS), summed TL defect (TLDS) and summed mismatch score (MS). Late gadolinium enhanced (LGE) CMR and PET images were fused using a syngo.via software. Segmental FDG-SUVmax in the 17 regions as well as whole heart SUVmax were measured, and segmental LGE were assessed according to a 3-grading system (LGE0, no LGE; LGE1, partly positive LGE; LGE2, transmural LGE) on the fused images. All SPECT segments (17segs x 16 patients) were classified into the 3 groups of LGE score. Segmental BMIPP, TL defect, mismatch score and SUVmax were compared between the 3 LGE score groups using one-way ANOVA. Results: Whole heart SUVmax in the 16 patients was 6.6±5.0 and summed BMDS, TLDS, MS were 18.6±12.6, 12.9±10.9, 5.7±3.1, respectively. Segmental based analysis revealed that BMDSs were 0.49±0.95, 1.63±1.51, 2.57±1.60 in LGE0(n=156), LGE1(n=81), LGE2(n=35) (LGE0 <LGE1 <LGE2, $p<0.001$), and TLDSs were 0.33±0.76, 1.15±1.28, 1.86±1.44 in the 3 groups (LGE0 <LGE1 <LGE2, $p<0.005$), respectively. MSs in LGE1 and LGE2 groups were significantly higher than that in LGE0 group (LGE1, $p<0.001$; LGE2, $p<0.001$), but there was no significant difference in MS between LGE1 and LGE2. SUVmax in LGE1 group was significantly higher than that in LGE0 ($p<0.025$), but there was no significant difference in SUVmax between LGE1 and LGE2 groups. Conclusion: Higher SUVmax showing active myocardial inflammation was mainly located in the LGE region, where BMIPP-TL mismatch was observed. BMIPP-TL mismatch with higher FDG uptake still exists in the transmural LGE induced by granuloma, which may reflect injured but viable myocardium in the transmural LGE region among CS patients. The combination of the three modalities makes it possible to evaluate the morphological and pathophysiological aspects of CS.

OP438

Impact of 18F-FDG PET/CT in the management of patients with large vessel vasculitis associated to polymyalgia rheumatica.

C. Lavado-Pérez, I. Martínez-Rodríguez, I. Banzo, R. Quirce, J. Jiménez-Bonilla, M. De Arcocha-Torres, Z. Bravo-Ferrer, M. Jiménez-Alonso, J. L. López-Defilló, F. Gómez de la Fuente, D. Meza-Escobar, J. M. Carril; Nuclear Medicine. Molecular Imaging Group (IDIVAL). Marqués de Valdecilla University Hospital. University of Cantabria., Santander, SPAIN

Aim: Polymyalgia rheumatica (PMR) may present associated to large vessel vasculitis (LVV) that is often overlooked due to non-specific signs and symptoms. These patients frequently had a poor treatment response and need increased doses of steroids or other immunosuppressive drugs. Our aim was to evaluate the impact of 18F-FDG PET/CT in the management of LVV associated to PMR.Materials and methods: A prospective study including 40 consecutive patients with PMR (27 women/13 men, 68.10±10.27 years) was performed. An 18F-FDG PET/CT scan was requested on suspicion of associated LVV. PET/CT scan was obtained 180' after 18F-FDG intravenous injection. Images were evaluated using a visual analysis and grading the intensity of the vascular uptake from 0 (no uptake) to 3 (intense uptake). Five vascular regions were evaluated: supra-aortic trunks (SAT), thoracic aorta (TA), abdominal aorta (AA), iliac arteries (IA) and femoral/tibioperoneal arteries (FTA). A final diagnosis of LVV was established in 26 out of the 40 patients (65%), 20 of them were under therapy at the time of PET/CT examination. Results: The most frequently vascular region involved in the 26 patients with LVV was the TA (100%) followed by the SAT (61.54%) and the FTA (53.85%). The highest intensity of 18F-FDG uptake was at the TA (grade 2 and 3 in 24 patients). No uptake was visualized in any vascular region in 4 of the 14

patients without LVV (28.57%) and in the other 10 patients (71.43%) only a grade 1 uptake was observed in 1 or to 2 regions.18F-FDG PET/CT led to a therapeutic change in 17 out of the 20 (85%) treated LVV patients.Regarding the outcome in the 26 patients with LVV, 19 (73.08%) had a good clinical and biochemical response and a follow-up PET/CT performed in 8 of them showed a decrease of uptake. Despite an increase of treatment, 6 patients (23.08%) had a clinical and biochemical worsening and the follow-up PET/CT performed in 3 showed an increase of uptake. Finally, one patient (3.84%) in whom the treatment was not changed suffered a worsening.Conclusion: Our results confirmed the usefulness of 18F-FDG PET/CT for the detection of LVV associated to PMR. The most frequently involved region was the TA. The detection of vascular inflammation using 18F-FDG PET/CT had an important impact and led to a treatment change in a high percentage of patients with LVV.

1308 - Tuesday, October 13, 2015, 11:30 AM - 1:00 PM, Hall E
Conventional & Specialised Nuclear Medicine: Paediatric - General

OP439

Initial experience of DMSA SPECT-CT in the assessment of paediatric renal calculi

Ashford1, E Joel1, G Heath1, N Smeulders2, M Easty1, **L Biassoni**1Departments of Radiology1 and Urology2, Great Ormond Street Hospital for Children NHS Foundation Trust, London (UK)

Aim: Renal calculi are uncommon in children but, when they occur, they represent a significant cause of renal damage. Today, they are usually removed by percutaneous nephrolithotomy (PCNL), uretero-renoscopy or extracorporeal shock wave lithotripsy (ESWL). An abdominal radiograph and an ultrasound are the usual initial investigations but the position of the calculus may be incompletely defined. Aim of the study is to present our initial experience on ^{99m}Tc-DMSA with SPECT-CT in children with renal calculi. Methods: We performed DMSA SPECT CT in 19 consecutive children (age range 2–16 years, mean 9 years; 6 males, 13 females) with renal calculi. Calculi were diagnosed with ultrasound and abdominal x-ray. DMSA planar images were followed by SPECT and a low-dose CT. The split renal function, the renal parenchymal integrity, the number and position of calculi, and the Hounsfield Unit (HU) value of each calculus were noted. Two patients were scanned under general anaesthesia (GA); no sedation or GA was required in the other patients. The injected activity was calculated in proportion to body weight, scaling from a maximum of 100 MBq. The CT was acquired with 50 mAs, 80 kVp, tube rotation 0.8, collimation 2 x 1.5 mm, pitch 1.3, scan slice thickness 2mm. A topogram covering the abdomen and pelvis to detect possible stones in the ureters and bladder was performed in 11/19 (58%) patients (110 kVp, 36 mAs).Results: Renal scarring was demonstrated in 7/19 kidneys (37%), whilst 8/19 kidneys (42%) showed reduced renal function. SPECT helped to assess the integrity of the renal parenchyma adjacent to the calculus and to identify patients with chronic irrecoverable damage. The CT aided the location of the calculus within the collecting system. The stone density was pivotal in planning management (if <1000HU the patient was considered for ESWL, if >1000HU for PCNL). The effective dose equivalent (EDE) from the CT component was low (mean 0.36 mSv, range 0.21-0.75). The EDE from the topogram ranged between 0.016 and 0.032 mSv (mean 0.023). Conclusion: DMSA SPECT CT in paediatric patients with renal calculi provides both anatomical and functional information with very little extra radiation dose. These preliminary results are promising and deserve further evaluation.

OP440

99mTc-DMSA in Biopsy Confirmed Paediatric Acute Tubulointerstitial Nephritis

P. Zucchetta[1], E. Miorin[2], L. Murer[2], F. Bui[1], D. Cecchin[1], E. Vidal[2]; [1]Nuclear Medicine Dept. - University Hospital - Padova, Padova, ITALY, [2]Paediatric nephrology, dialysis and transplant - University Hospital - Padova, Padova, ITALY.

Acute tubulointerstitial nephritis (aTIN) is a frequent cause of acute renale failure in adults and children, accounting for 15-20% of acute kidney injury cases. Inflammatory cells infiltrating kidney interstitium, probably as a consequence of an antigen-initiated cell-mediated response, characterize it. Exposition to drugs, mainly non-steroidal anti-inflammatory drugs and antibiotics, is the most frequent etiology (70%), followed by viral and bacterial infections. Tubular dysfunction and a progressive reduction in glomerular filtration rate lead to renal impairment, which is usually reversed by timely treatment (elimination of the offending drug and steroids). Nevertheless, a delay in diagnosis and treatment may result in chronic tubulointerstitial nephritis, which can be steroid refractory. The clinical presentation is aspecific (fever, asthenia, etc) and there are no validated biomarkers. Imaging studies offer little contribution, since ultrasounds findings are usually not specific (kidney volumetric increase and diffuse cortical hyperechogenity) and 67Ga-citrate scintigraphy suffers of low specifity (50-60%) and significant radiation exposure, combined with long scanning times (48-72 h after injection). We have studied 5 patients (M4, F1, age range 3-17 y, age mean 15 y) diagnosed with acute tubulointerstitial nephritis. All patients presented acute renal failure, persistent fever (2-4 wk) and weakness. Diuresis was reduced in only one case.

Inflammatory markers were raised in all cases, with clear signs of acute kidney injury (creatinine clearance 55 ml/min/1.73 sqm) and tubular damage (glycosuria, elvated alfa1-microglobulin and NAG). Three cases had no of detectable causes (drugs, infection, immune system distrubances) and were classified as "idiopathic". One case developed uveitis two months later and was therefore classified as tubulointestitial nephritis-uveitis syndrome (TINU syndrome), whereas an Adenovirus infection was detected in the last one. All patients underwent 99mTc-DMSA scintigraphy during the acute phase of the illness. The scan was performed following the EANM procedural guidelines.Patchy hypofixation was observed in all cases, similar to some acute pyelo-nephritis patterns, but with bilateral involvement and a more diffuse distribution.Kidney biopsy has been performed in 4/5 patients, with kidney injury lasting > 6 wk. Histopathologic findings showed in all cases a typical inflammatory infiltration of the kidney interstitium.99mTc-DMSA scintigraphy could play a role in the diagnosis of acute tubulointerstitial nephritis, shortening the diagnostic work up and leading to a faster treatment. Considering the minimal radiation exposure and lack of invasivity it has promising perspectives also in the follow up of this underdiagnosed illness.

OP441

Evaluation of Schwartz eGFR-Cr in comparison with GFR measured by Tc-99m-DTPA clearance in healthy and in children with urinary tract infection with and without vesicoureteral reflux

M. Vlajković[1], S. Ilić[2], M. Rajić[1], M. Stević[1], M. Božinović[1], V. Živković[3], M. Matović[4]; [1]Center of Nuclear Medicine,Clinical Center Niš, Niš, SERBIA, [2]Center of Nuclear Medicine, Clinical Center Niš, Niš, SERBIA, [3]Clinic for Physical Medicine,Rehabilitation and Prosthetic, Clinical center Niš, Niš, SERBIA, [4]Center of Nuclear Medicine,Clinical Center Kragujevac, Kragujevac, SERBIA.

Objective: The aim of this study was to asses diagnostic performance of estimated glomerular filtration rate (eGFR-Cr) based on creatinine and body high equation originally developed by Schwartz. The assessment was done by means of comparison between glomerular filtration rate (GFR) measured by Tc-99m-DTPA clearance in children with no nephro-urological diseases, children with urinary tract infection without vesicoureteral reflux (VUR), and with VUR using Bland-Altman analysis.Material and Methods: The study enrolled 451 pediatric patients (104 male and 347 female, mean age 7.07±3.02 yrs, range 2-15 yrs), who were included in a retrospective review of GFR measurement data from the single institution's database. Subgroups of patients were formed according to the diagnosis as follows: control group (CG, n=64), group with urinary tract infection without VUR (UTI, n=299), and group with VUR (VUR, n=88). GFR was measured by Tc-99m-DTPA clearance method from a single blood sample drawn 180 minutes after radiopharmeceutical administration. eGFR was based on creatinine and body high equation. Results: Compared with GFR, the mean bias for eGFR-Cr in the study groups was as follows: CG: 1.937ml/min/1.73m2 (95% limits of agreement [LOA]: -36.759 to 40.633 ml/min/1.73m2), UTI: -3.010ml/min/1.73m2 (LOA: -57.292 to 51.272 ml/min/1.73m2) and VUR: 2.183mL/min/1.73m2 (LOA:-64.019 to 68.385 mL/min/1.73m2). eGFR-Cr demonstrated comparable accuracy to GFR in CG and UTI with 95% and 82% of estimates within 30% of GFR, while the estimates in VUR were less accurate, amounting to 68% of values within 30% of GFR.Conclusion: eGFR-Cr was found to be a reliable alternative to GFR in healthy children, as well as in those with urinary tract infection. However, it was found to be less accurate in children with vesicoureteral reflux and renal impairment.

OP442

Is the Clinical Diagnosis of Chronic Immune Thrombocytopenic Purpura in Pediatric Population Always Correct?

M. Todorovic-Tirnanic, D. Sobic-Saranovic, V. Artiko; Faculty of Medicine, University of Belgrade and Center of Nuclear Medicine, Clinical Center of Serbia, Belgrade, SERBIA.

Aim: 1. to investigate patophysiological mechanism of thrombocytopenia with ^{111}In-oxinate labeled autologous platelets in children with clinical diagnosis of chronic immune thrombocytopenic purpura (ITP); 2. to verify the diagnosis; 3. to predict the efficacy of the planned splenectomy. Material: 69 children (44 girls and 25 boys) aged from 3.1 -18.0 yrs (median = 11 yrs), body height: 100 - 187 cm (mean = 147 cm), body weight: 15 - 98 kg (median = 34 kg) were investigated. Methods: 1) 69 autologous ^{111}In-oxinate platelet (Pt) labelings; 2) 69 quality controls: a) general yield of labelling (GYL), b) differential yields of labeling (DYL): Pt DYL, red and white blood cell DYL, plasma DYL, c) initial platelet accumulation in the liver (IPAL); 3) Pt lifespan (LS); 4) Pt production index (PI); 5) Pt sequestration site and index estimation were performed. Results: Mean Pt blood count was 23 G/l (range: 1-122 G/l); mean blood sample volume for Pt separation and labeling was 55 ml (30 - 75 ml); mean radioactivity used for Pt labelling was 11.1 MBq; mean injected radioactivity was 6.7 MBq (2,6 - 10.1 MBq); mean GYL = 65.9 % (33.9 - 90.2 %); mean Pt DYL = 92.6 % (55.7 - 99.6 %); mean RBC&WBC DYL = 1.6 % (0.0 - 41.5 %); mean plasma

DYL =0.7 (0.2 - 7.3 %); mean IPAL = 11.9 % (3.0 - 35.8 %). Mean Pt lifespan was 12 hours (0.7 - 216 h). In 63/69 children (91.3 %) diagnosis of ITP was confirmed. In this group of children mean Pt lifespan was 9.6 h (0.7 - 93.6 h); mean Pt PI=1.8 (0.2 - 23.4); Pt sequestration site was: the spleen in 26 (42%), predominantly spleen in 9 (14%), liver in 3 (5%), mixed (in liver and spleen equally) in 24 (39%). In 6/69 (8.7 %) children clinical diagnosis of ITP was excluded. All of them had normal Pt lifespan: two had normal quantity of separated platelets (pseudothrombocytopenia) and four had inadequate Pt production (Pt PI ranged from 0.1 - 0.2). Conclusion: 1) In 6/69 children initial clinical diagnosis of ITP was changed: 2/69 had pseudothrombocytopenia, 4/69 inadequate platelet production. 2) In 63/69 children clinical diagnosis of ITP was confirmed. 3) Help in decision whether to perform splenectomy or not was enabled in 61% of confirmed ITP patients (with splenic, predominantly splenic and hepatic Pt sequestration).

OP443

Impact of colonic transit scintigraphy on clinical decision making in severely constipated children

E. Medaer, I. Hoffman, W. Thimister; KU Leuven, Leuven, BELGIUM

Aim: The objective of this study was to evaluate the diagnostic yield and the impact on clinical decision making of colonic transit scintigraphy in children with severe chronic functional constipation. Materials and methods: From September 2014 to March 2015, 7 patients (mean age 6.2 years, 4 girls and 3 boys) with chronic treatment-resistant functional constipation received an ^{111}indium-labeled diethylene triamine pentaacetic acid (^{111}In-DTPA) colonic transit scintigraphy in our institution. The scintigraphy was performed as part of the diagnostic work-up, with the aim of providing information on gastric emptying, small bowel transit and segmental colonic transit. After an overnight fast, patients ingested a small amount of water that was radiolabeled with ^{111}In-DTPA. They underwent repeated imaging in supine position between the detectors of a gamma camera to obtain anterior- posterior abdominal scans of 4 minutes duration each. The scans were taken at 4 h, 24 h and 48 h post-ingestion. Five technetium position markers were placed on anatomic landmarks to create a reference frame. Processing of the images was performed using the Hermes Hybrid Viewer and geometric centers were calculated. Results: Colonic scintigraphy showed normal transit time in 4 patients (57%), delay in the distal colon in 2 patients (29%), and colonic inertia in 1 patient (14%). This led to a diagnostic adjustment for 4 patients and a differentiation of the diagnosis for the 3 others. The results of the scintigraphy had therapeutic consequences for all of the patients. In 3 children (43%) the pharmaceutical treatment could be optimized. For3 other patients (43%) the planned intervention was altered. In 1 patient (14%) an operation could be avoided. Conclusion: This preliminary study demonstrates the added value of colonic transit scintigraphy in the investigation of functional constipation in children and the high impact on clinical decision making. Scintigraphic transit studies provide a noninvasive and safe assessment of whole-colon and regional colonic transit. Because of the physiological design and the reliability of the examination, we were able to offer diagnostic differentiation for all patients.

OP444

Accuracy of 99mTcO4- Meckel's Scan and Other Diagnostic Indicators in Symptomatic Paediatric Meckel's Diverticulum

Mazin Al Janabi1, Madan Samuel2,Andrea Kahlenberg3, Sujith Kumar41,4Department of Nuclear Medicine, 2Department of Pediatric Surgery, 3Department of Anaesthesia, Mediclinic City Hospital, Dubai, UNITED ARAB EMIRATES

Purpose: To evaluate the diagnostic accuracy of ^{99m}Tc-pertechnetate scintigraphy in children with symptomatic Meckel's diverticulum. Methods: This was a prospective linear observational study of 73 children with the diagnosis of symptomatic Meckel's diverticulum. Meckel's diverticulum scintigraphy was performed using ^{99m}Tc pertechnetate to evaluate ectopic gastric mucosa in MD in 61 (84%) children. Dynamic imaging was carried out for 60 minutes. Pharmacological intervention was not adopted to enhance the result of ^{99m}Tc-pertechnetate. Independent variables assessed were age, gender, weight-for-age z scores, clinical presentation, complications of MD, laparoscopy findings, haematology and biochemistry results, radiology, and histology. The sensitivity, specificity, positive & negative predictive values and accuracy of ^{99m}Tc-pertechnetate scintigraphy was assessed. Results: The incidence of MD with complications was 44%. The prevalence of ectopic gastric mucosa in histology specimens was 84%. There was a good correlation between rectal bleeding and presence of ectopic gastric mucosa (r = 0.94). Hematochezia associated with drop in haemoglobin (>2 g/dL) was diagnostic of MD with ectopic gastric mucosa in children (n=42; 58%. p = 0.006). Bilious vomiting was diagnostic of complicated MD (n=12; 16%. p = 0.007). ^{99m}Tc-pertechnetate scintigraphy sensitivity was 84% and specificity 22%. Positive predictive value was 0.64 and negative predictive value was 0.22. The accuracy of ^{99m}Tc-pertechnetate scintigraphy varies from 46% to 90%. The sensitivity and specificity of ^{99m}Tc-pertechnetate scintigraphy was dependent on the quantity and functional quality of the heterotopic gastric mucosa. Preoperative median z-scores was - 1.4 and postoperative median z-

scores were - 1.2. Conclusions: ^{99m}Tc-pertechnetate scintigraphy had a truncated predictive value. Its contribution in clinical decision making was poor. Clinical suspicion of MD should be high in children presenting with hematochezia associated with drop in haemoglobin by >2 g/dL. Laparoscopy is an effective diagnostic tool.

OP445

Clinical Value of Cerebral Perfusion SPECT Imaging in Children with Acute Sydenham's Chorea

S. M. d. A. Giorgio[1], M. G. Caprio[1], A. Romano[2], E. Vergara[1], G. Russo[2], M. Alessio[2], A. Cuocolo[1]; [1]Department of Advanced Biomedical Sciences, Naples, ITALY, [2]Department of Translational Medical Sciences, Naples, ITALY

Aim: Sydenham's chorea is the most common form of acute chorea during childhood ant it may be associated with cerebral perfusion abnormalities at SPECT imaging, mainly hyperperfusion or, more rarely, hypoperfusion patterns. We evaluated whether a better definition of cerebral perfusion patterns of the cortical/subcortical structures by SPECT imaging improves differential diagnosis and prognosis in pediatric patients with acute autoimmune Sydenham chorea. Material and Methods: Fifteen children (6 boys, age range 6-14 years) with a diagnosis of acute autoimmune chorea seen between 1999 and 2011 at our department were studied. Inclusion criteria were: presence of choreic movements with acute autoimmune etiology and age from 1 to 18 years. All patients had first a full physical examination including a rheumatologic and neuropsychiatric assessment. All patients also underwent brain magnetic resonance imaging (MRI) and cerebral SPECT imaging. MRI scan was performed with spin-echo T1 weighted, T2 weighted and FLAIR sequences. T1 weighted sequences were also obtained after administration of intravenous paramagnetic contrast (gadolinium). SPECT imaging was performed after intravenous injection of Tc-99m ethyl cysteinate dimer (32 Mbq/Kg) using a dual-head gamma camera (E-cam, Siemens Medical Systems) equipped with general purpose, low energy, parallel-hole collimator. The analysis was performed by comparing tracer uptake in the basal ganglia with the uptake in a control region. Results: At presentation, chorea was generalized in 9 patients and localized (hemichorea) in 6 patients. In addition to chorea, 6 subjects showed decreased verbal fluency and personality changes and one a left hemiparesis. Tests of liver and kidney function, antinuclear antibody, and anti-deoxyribonucleic acid were normal in all patients. Brain MRI revealed normal findings in 13 and small foci of white matter gliosis in 2 patients, without relevant clinical value. Cerebral SPECT showed unilateral increased perfusion in the basal ganglia in all 9 children with generalized chorea, while the remaining 6 patients had normal perfusion pattern. No relationship between the severity of the symptoms and the side of increased perfusion was found. A follow-up SPECT, performed during the recovery phase in 5 of the 9 patients with perfusion abnormalities at the first study, showed normal perfusion in all. Conclusions: The evidence of increased basal ganglia perfusion in during the active phase of the disease suggests that this abnormality is a marker of inflammatory chorea. Cerebral SPECT perfusion imaging could be an accurate noninvasive tool to monitor the course of acute autoimmune chorea in childhood.

1309 - Tuesday, October 13, 2015, 11:30 AM - 1:00 PM, Hall 8
Physics & Instrumentation & Data Analysis: Quality Control, Performance, Standardisation

---

OP446

Investigation of Image Quality with Sodium Pertechnetate ^{99m}Tc Produced by Cyclotron

S. V. Selivanova[1,2], É. Lavallée[1], O. Sarrihni[1], B. Guérin[1,2], É. Turcotte[1,2], R. Lecomte[1,2]; [1]Sherbrooke Molecular Imaging Center, CRCHUS, Sherbrooke, QC, CANADA, [2]Université de Sherbrooke, Sherbrooke, QC, CANADA.

Aim: Cyclotron production of technetium-99m (^{99m}Tc) is a promising route to supply ^{99m}Tc-radiopharmaceuticals. The main difference of cyclotron-produced ^{99m}Tc from generator source is its intrinsic contamination with shorter half-life ^{93}Tc, ^{94}Tc and longer-lived ^{95}Tc, ^{95m}Tc, ^{96}Tc, and ^{97m}Tc, which may affect image resolution and contrast. This study investigated the contamination due to the high-energy radioisotopic impurities present in sodium pertechnetate ^{99m}Tc produced with a cyclotron. Methods: Capillary and Jaszczak phantom imaging was performed using cyclotron-produced ^{99m}Tc (E_{in} = 24 MeV, 2 h irradiation, 99.815% ^{100}Mo enrichment) and ^{99m}Tc obtained from a generator up to 16 h after the end of production/elution. Radionuclidic/radioisotopic purity of the formulation was determined using gamma-ray spectrometry with calibrated HPGe detector and decay corrected to the imaging time. Planar images were acquired on a Discovery NM/CT 670 SPECT/CT camera (GE) equipped with low-energy high-resolution collimators. The energy windows were 140.5 keV ±7.5% (standard for ^{99m}Tc), 117.0 keV ±10% (low energy), and 170.0 keV ±10% (high energy). Results: For the main energy window, for a capillary filled with ^{99m}Tc-pertechnetate eluted from a generator, planar image resolution at full width half-maximum (FWHM) was 4.15±0.05 mm at 0 cm and 6.82±0.04 mm at 10 cm from the gamma-camera collimator. The FWHM resolution of images with cyclotron-produced ^{99m}Tc was 4.21 ±0.06 mm at 0 cm and 6.83±0.09 mm at 10 cm from the collimator. The resolution remained stable in time within measurement error. Planar images of Jaszczak phantom were of

comparable quality without significant loss in spatial resolution. On average, the contrast of images acquired using cyclotron-produced ^{99m}Tc (n=7) was 1.16±0.02 with contrast-to-noise ratio (CNR) of 10.47±0.26, which compares favorably to the best of two values obtained for generator ^{99m}Tc: 1.14 (contrast) and 10.28 (CNR). The relative count rate in high-energy window for the cyclotron-produced ^{99m}Tc increased up to 5-fold as compared to the generator ^{99m}Tc due to increased proportion of energetic ^{94}Tc and ^{96}Tc but remained below 10% of the total counts over the entire imaging period. Only marginal increase was observed in the low-energy window. Visually, two side-by-side images acquired with ^{99m}Tc from generator and cyclotron in the main energy window were found to be equivalent. Conclusions: At tested conditions, the scatter effect due to high-energy radioisotopic impurities present in ^{99m}Tc-pertechnetate produced with cyclotron did not influence visual image quality in the standard for clinical applications energy window. Early results of an ongoing clinical study (NCT02307175) confirm these findings.

OP447

One Size Fits All? Assessment of the Use of a Simple Calibration Protocol for Quantitative SPECT/CT Imaging of 177Lu in European Hospitals

J. Merrett[1,2,3], A. Fenwick[2], J. Scuffham[1,3], L. Johansson[2], A. Nisbet[1,3]; [1]University of Surrey, Guildford, UNITED KINGDOM, [2]National Physical Laboratory, Teddington, UNITED KINGDOM, [3]Royal Surrey County Hospital, Guildford, UNITED KINGDOM

The accuracy of molecular radiotherapy dosimetry calculations is critically dependent on the accuracy with which the quantitative imaging of the patient can be performed. However, there is no single established protocol for performing quantitative imaging. Therefore, the aim of this work was to assess the ability of a simple calibration protocol to quantify the activity in an unknown comparison source, simulating a relatively large lesion located within a patient in an area of warm background activity, in a number of hospitals across Europe.Two 177Lu sources were used at each hospital for this work, ranging from 30MBq to 100MBq at the time of imaging. All sources were filled at the UK National Physical Laboratory so the activities and activity concentrations were accurately known. A 16ml sphere was used to perform the calibration measurements: SPECT/CT acquisitions were performed of the sphere in an elliptical Jaszczak phantom in air, in water at the centre and in water off-centre. The comparison source was a 26ml central sphere, surrounded by an 80ml outer shell. The activity concentration ratio between the inner sphere and outer shell was approximately 15:1, providing a warm background. For the comparison exercise, the SPECT/CT acquisitions were also performed with the source positioned within a water-filled elliptical Jaszczak phantom with the addition of an anthropomorphic lung and spine insert and body contour rings that were added to the outside of the phantom. All image reconstruction was performed on a single Hermes Gold workstation using an OSEM algorithm with 5 iterations and 10 subsets. Images were corrected for scatter, attenuation and collimator-detector response. No corrections were performed for deadtime or partial volume effects due to the low activities and relatively large volumes used. Spherical volumes of interest of the physical size of the sources were used to extract total counts in all the SPECT images. A calibration factor was derived from the mean value (cps/MBq) of the three calibration measurements. This calibration factor was subsequently used to determine the activity within the central sphere in the comparison exercise. The data from the majority of the hospitals enabled the activity within the comparison source to be determined to within ±10%. This work demonstrated the ability of a single calibration protocol to be used successfully at a number of different hospital sites across Europe. It paves the way for harmonised calibration protocols to be developed, ensuring consistent patient treatment across all European hospitals.

OP448

Standardised Time-Dose Regimen for Ga-DOTANOC PET Imaging

J. K. J. Archer, M. J. Carroll, S. Vinjamuri, E. Panagiotidis; Royal Liverpool University Hospital, Liverpool, UNITED KINGDOM

Aim: The Royal Liverpool University Hospital (RLUH) has been established as a European Neuroendocrine Tumour Society (ENETS) Centre of Excellence for the last 5 years. Recently the department becoming one of the first in the UK to perform Gallium 68 (Ga68) DOTANOC PET as part of the diagnosis, pre-PRRT workup and post PRRT evaluation of such tumours. Although the local diagnostic reference level (DRL) is set at 200MBq, the time intensive production process and the short half-life of Ga68-DOTONOC (68 minutes) result in this rarely being achieved. At the RLUH the scanning radiographer attempts to compensate for this by adjusting the bed position times, resulting in highly variable image quality. This is further compounded by more usual factors such as variation in patient size. The aim of this project was to retrospectively inspect the administered activities and subsequent image quality for these patients, and develop a formalised activity-bed position time regimen that would help to standardise image quality at a more consistent level. Materials and Methods: A group of Ga68-DOTANOC patients (n = 50) scanned on the GE Discovery 690 at the RLUH were used to retrospectively inspect the variation in: injected activity, activity at scan start time, image quality, bed position time and patient dependent size parameters. Image quality was assessed by the signal-to-

noise ratio (SNR) calculated from standardised uptake values (SUV) measured in the spleen, an organ expressing homogenous tracer uptake. Results: The average administered activity was seen to be 132.6 ± 22MBq, the minimum activity being as low as 90.3MBq and the maximum that of the local DRL. The time from injection to scan start was seen to extend to a maximum of 36 minutes past the 1 hour window prescribed in the current protocol, resulting in a loss of 30.7% of the activity expected. 45 out of 50 patients exhibited a constant time per bed position, whilst 5 exhibited different times per bed position to optimise imaging of previously seen tumours. The spleen SNR ranged from 3.55 to 15.85, with mean of 10.45. Conclusions: Linear correlations have been made with specific indices that take into account the patient activity at scan time, the time per bed position and patient dependent size parameters. These indices have been rearranged to provide an optimum bed position time based on all the aforementioned factors. These have been verified with retrospective list mode reconstructions aiming for a consistent spleen SNR.

OP449

Evaluation of the Performance of a Biograph mCT-Flow PET/CT System according to NEMA NU2-2012 standards

I. Rausch[1], J. Cal-Gonzalez[1], T. Beyer[1], G. Minear[2]; [1]Center for Medical Physics and Biomedical Engineering, Medical University of Vienna, Vienna, AUSTRIA, [2]Dept of Nuclear Medicine, Landesklinikum St. Pölten, St. Pölten, AUSTRIA

Aim: To evaluate the physical performance of a Biograph mCT Flow PET/CT system with sequential and continuous patient table motion. Methods: We evaluated the performance of the Biograph mCT Flow 64-4R PET/CT system (Siemens Medical Solutions USA, Inc.). Spatial resolution, system sensitivity, noise equivalent countrate (NEC) and physical image quality (IQ) were assessed according to the NEMA NU 2-2012 standards. Resolution measurements were performed using an 18F-point source inside a glass capillary tube (inner diameter: 0.9-1.0 mm; wall thickness 0.4 mm). Sensitivity tests were performed with a 70cm long polyethylene tube filled with 4.5 MBq of FDG. Scatter fraction and count rate measurements were performed using a 70cm long polyethylene cylinder with a diameter of 20 cm, with a line source (1.04 GBq of FDG) inserted axially into the cylinder at 4.5 cm off-center. The standard NEMA IQ phantom with 6 spheres (internal diameter (mm): 10, 13, 17, 22, 28 and 37) was used for the evaluation of the IQ in whole-body imaging mode. First, the phantom was scanned over a single bed (4 min) according to the NEMA protocol. Second, a 2-bed position scan of 4 min each of the phantom with the image plane containing the spheres centered in the overlap region followed by a scan of the same axial scan field with Continuous Table Motion (CTM) at a table speed of 0.6 mm/s was performed. Image contrast and covariance for the six spheres in sequential and CTM mode were compared according to NU2-2012 regions. Measurements were done with a sphere-to-background ratio 8 to 1 and 4 to 1. Results: Spatial resolution measured as Full-Width-Half-Maximum (FWHM) was 4.3mm (r=1cm) and 7.8 mm (r=20cm). Measured sensitivity was 9.4 kcps/MBq, both at the center of the FOV and 10 cm off-centered. Measured peak NEC was 185 kcps at 29.0 kBq/mL. Scatter fraction was 33.5%.Sphere contrast recovery values (sphere-to-background of 8:1) varied from 42% (10mm) to 78% (37mm) for the NEMA protocol. No difference in contrast recovery values was seen between sequential and CTM acquisition. Background variability was slightly higher in CTM (between 2.4 and 6.3) compared to sequential mode (between 2.1 and 4.9). Conclusion: Basic performance (resolution, sensitivity, scatter, NEC) of the mCT Flow was equivalent to the performance of the predecessor mCT system. Contrast recovery in sequential and CTM acquisitions was similar, however, background variability was elevated slightly in CTM acquisition.

OP450

The effect of image reconstruction parameters in Mediso NanoScan PC PET/CT images obtained by two different positron emitting tracers under NEMA standards NU 4-2008

A. Gaitanis[1], E. Vlastou[1], P. Bouziotis[2], G. Kastis[3], C. D. Anagnostopoulos[1]; [1]Biomedical Research Foundation of the Academy of Athens (BRFAA), Athens, GREECE, [2]Institute of Nuclear and Radiological Sciences, Technology, Energy and Safety (I.N.Ra.S.T.E.S.) N.C.S.R., Athens, GREECE, [3]Research Center of Mathematics, Academy of Athens, Athens, GREECE

Aim: The Mediso NanoScan PC with 8 detector modules is a new commercially available small animal PET/CT scanner, suitable for both mice and rats imaging. To identify the optimum reconstruction approaches, we have assessed different image reconstruction parameters, for two different positron-emitting tracers under NEMA standards NU 4-2008. Materials and Methods: The scanner provides various reconstruction algorithms, however, in preclinical imaging, 3D OSEM (including a regularization method) is the most commonly used option. In this study, the combination of subsets (1, 2 and 4) and iterations (2, 4, 6, 8, 10) and the level total variation regularization (None, Low and High) were examined. All other reconstruction parameters such as coincidence mode, energy window, correction methods (attenuation and scatter) and voxel size were kept constant. For the image quality evaluation, all requirements of the NEMA standards were followed. The IQ

phantom was filled with 3.7MBq of 18FDG and after IQ phantom's cleaning and checked for zero activity, it was filled with 5.4 MBq of 68Ga. The acquisition time was thirty minutes for both positron emitters. For the quantitation of image quality, the following parameters were calculated: i) Recovery Coefficient (RC), ii) image noise (%STD), iii) spillover ratio (SOR) and iv) Contrast-to-Noise ratio (CNR). Results: The results indicate that the selection of the number of subsets can affect the RC values. As this number increases, the RC values increase and after a number of iterations, they remain unchanged (i.e. 2subsets/8iterations: RC1mm=0.05, RC2mm=0.22, RC3mm=0.67, RC4mm=0.83, RC5mm=0.92, 4subsets/8iterations: RC1mm=0.07, RC2mm=0.43, RC3mm=0.73, RC4mm=0.92, RC5mm=0.93). Furthermore, the level of regularization does not affect the RC values. Lower image noise is achieved using high level of total regularization (i.e. 4subsets/4iterations: 17.6% (Low), 6.6% (High)). The SOR values are improved as the number of subsets and iteration increases (i.e. 2subsets/2iterations: SORair & SORwater>0.25 and 4sub/2iter: SORair & SORwater <0.10). The CNR values depend on the number of subsets and the level of regularization (i.e. Low Regularization, 2subsets/4iterations: CNR1mm=0.18, CNR2mm=3.94, CNR3mm=15.76, CNR4mm=22.42, CNR5mm=27.88, High Regularization, 4subsets/4iterations: CNR1mm=1.11, CNR2mm=11.60, CNR3mm=28, CNR4mm=32.8, CNR5mm=35.2). Conclusions: Our findings demonstrate that selection of reconstruction settings should be determined by imaging requirements. To increased sensitivity, a 3D OSEM image reconstruction should be performed with low regularization level, four subsets and eight iterations. On the other hand, if high contrast images in low noise level are required, 3D OSEM image reconstruction should be performed with high level of regularization, four subsets and four iterations.

OP451

Considerations for Interpreting SPECT SUVs: Image Noise, Post-filter and SUV Metric

N. A. Bebbington[1], L. C. Jenkins[2]; [1]Queen Elizabeth Hospital Birmingham, Birmingham, UNITED KINGDOM, [2]HERMES Medical Solutions, London, UNITED KINGDOM

AIM: SUVs are used in PET to improve confidence in diagnosis and SPECT SUVs are now an emerging tool. Special consideration should be given to image reconstruction and interpretation of SPECT SUVs, due to inherent differences in resolution and noise between PET and SPECT. The reporting metric of choice may differ between these modalities: SUVmax is favoured in PET, but may not be appropriate for SPECT. The aim was to assess the effects of image noise and reconstruction settings on SUV and determine the most appropriate reporting metric. MATERIALS AND METHODS: The NEMA-IEC PET image quality phantom was filled with Tc-99m with a 6.7:1 sphere:background ratio. SPECT-CT data were acquired using a Siemens SymbiaT16/LEHR collimator (120x30sec projections, step-and-shoot with auto-contouring). Full-count SPECT data contained 8.4M counts. Poisson resampling was performed for a range of clinically realistic count densities (full down 1/16 counts). Data were reconstructed in HERMES HybridRecon v1.1B (with attenuation correction, scatter correction and resolution recovery) with a range of equivalent iterations and post-filters. These were analysed in HERMES HybridViewer v2.5. Spherical VOIs of nominal size were assigned to SPECT spheres. Three spherical VOIs (diameter 2.7cm) were placed in background. SUVmax and SUVpeak (1cc) were measured for all datasets. RESULTS: The true SUV of spheres was 6.7. Convergence: without post-filter SUVpeak was consistent with >90 iterations (>90% counts returned) for all spheres. At 30 iterations 55% counts were returned. Without post-filter SUVmax was less consistent with >90 iterations (>90% counts returned) for all spheres. At 30 iterations only 55% counts were returned. Increasing iterations is required for convergence but this increases noise. Variability: For the largest sphere (37mm diameter), as counts reduce SUVmax and SUVpeak increase. For an 8mm Gaussian post-filter SUVpeak increases by 51% from full counts to 1/16 counts, compared with 63% for SUVmax. This difference is reduced to 16% for a heavily filtered image. SUVpeak is most robust to varying count densities. CONCLUSIONS: SPECT data is more subject to effects of image noise and partial volume than PET, both of which cause variability in SUV. SUVpeak was the most robust SUV metric to image noise and is preferred for SPECT. It is important that noise and resolution are considered in the choice of post-filter. For studies with a large range in expected noise level, smoother filters are preferred.

OP452

Accurate model of a Capintec activity meter with the Monte Carlo code Fluka

F. Zagni[1], A. Evandri[1], G. Cicoria[1], A. Infantino[2], S. Vichi[2], S. Costa[3], M. Marengo[1]; [1]Medical Physics Department, University Hospital "S.Orsola – Malpighi", Bologna, ITALY, [2]Montecuccolino Nuclear Engineering Laboratory, Department of Industrial Engineering, University of Bologna, Bologna, ITALY, [3]PET Radiopharmacy Unit, University Hospital "S.Orsola – Malpighi", Bologna, ITALY

Aim. In this work we developed and validated a Monte Carlo model of one of the world's most diffused

radionuclide activity meters, using Fluka. Materials and Methods. We modelled the Capintec CRC-15, a widely diffuse model of activity calibrator. To this end, we used Fluka, a general purpose simulation code for radiation physics, covering an extended range of applications such as accelerator shielding, dosimetry and detector design. The main geometrical elements and materials of the ionizing chamber were included in the model. Thickness and position of internal components was evaluated through both direct measurements of external dimensions and CT/X-ray imaging. The radioactive sources were carefully modelled and located in the detector well; in the validation a set of reference sources was used: ^{137}Cs (22.7±1.5% MBq at time of measure), ^{133}Ba (1.3±1.5% Mbq), ^{131}I (71.5 ±1.5%), ^{57}Co (74.4±3%), ^{68}Ge "mock ^{18}F" (7.5±1.65%) and others. The container of each source and the correct filling were suitably modelled and included in Fluka input file. Calibration factors could be evaluated based on the energy deposited in the Argon gas. The entire decay scheme of each radionuclide was included in the simulations, including low-energy X-ray emission and the energy spectrum of beta particles. The results of the simulations (statistical error below 1%) were normalized to the response of the modelled ^{137}Cs source. The dependence of the sensitivity versus position of the source was also assessed in a range of 15 cm. Results. An high accuracy energy-response curve for the activity meter was calculated, allowing for prediction of an initial calibration factor for new radionuclides. In the benchmark against known standards, the ratio between simulated and measured relative response was: ^{133}Ba 1.007±0.015, ^{68}Ge 1.016±0.018, ^{131}I 0.971±0.017, ^{57}Co 0.970±0.035. The sensitivity-position curve gave 4% as a maximum discrepancy. Conclusion. An accurate model of a widely diffuse activity meter has been validated for a variety of gamma-emitting nuclides, covering a wide range of energies and source positions, showing discrepancies below 3% for all the tested sources. The Fluka code proved to be a powerful tool for assessment of activity meter's calibration factors for radionuclides commonly used in radiopharmacy facilities as well as for non-conventional radionuclides, and for the easy assessment of geometrical correction factors.

OP453

Phase I Trial comparing a Digital Detector PET/CT System with current photomultiplier PET Technology in Diagnostic Oncology

M. V. Knopp[1], K. Binzel[1], C. L. Wright[1], V. Nagar[1], P. Bardos[1], P. Maniawski[2], J. Zhang[1]; [1]The Ohio State University, Columbus, OH, UNITED STATES, [2]Philips Healthcare, Cleveland, OH, UNITED STATES.

Objectives: The commercial introduction of a solid state, digital photon counting PET detector PET/CT system presents a potential next generation leap that requires objective assessment of clinical capabilities. This Phase I trial was performed to demonstrate the potential clinical capabilities for oncologic whole body imaging and to recommend acquisition approaches. Methods: 40 patients volunteered to participate in an intra-individual matched pair comparison study using a digital PET/CT (Vereos, Philips Healthcare Cleveland) while their standard of care PET/CT exam was performed on a conventional photomultiplier TOF PET/CT system (Gemini 64 TF) at 75 min p.i. PET imaging was performed using a standard of care 480 MBq FDG dose. Ultra-low dose CT attenuation scans were acquired on the digital PET/CT using 120 KV, 50 mAs using iterative iDose4 reconstruction. PET emission was acquired with 90s per bed position, 39% overlap and 164 mm z-axis FOV and reconstructed using TOF with default 4x4x4, 2x2x2 and 1x1x1 mm voxel volumes using PSF and Gaussian filtering. The digital PET/CT system has also an improved time of flight (TOF) timing resolution of 320 ps vs. 550 ps in the comparator conventional system. Blinded visual and clinical read assessment was performed by a three reader panel independently. Results: All 40 patient studies were rated to be of evaluable image quality. The digital PET comparator scan was classified preferable in regard to count intensity and tissue delineation detail in all case comparisons. The confidence of lesion detection increased on the DPET scans with increased reconstruction matrix size, with significantly ($p \leq 0.05$) improved lesion characterization between the 4 and 1 mm comparators. Most pronounced differences were noted in small and intense lesions such as lymphnode metastases and small pulmonary nodules. No increase in non-specific uptake of lesions was noted on the higher resolution reconstruction matrices. Faster and lower dose acquisition approaches appear feasible as dose reduction simulations of up to 70% did not impact diagnostic assessability. Conclusions: The digital detector PET/CT demonstrated consistently preferable imaging features in the intra-individual comparison with improved lesion characterization most notable in small, metabolically active lesions. Whole body PET imaging with higher resolution matrix size appear readily feasible with digital PET leading to substantially reduced partial volume effects, thus improving lesion detectability and characterization of heterogeneous lesions. The 2mm / 288 reconstruction matrix appears to be the recommended standard to be utilized with the 1mm / 576 available for high definition images.

1310 - Tuesday, October 13, 2015, 2:30 PM - 4:00 PM, Hall D
Clinical Oncology: Miscellaneous

OP454

The role of 18F-FDG PET/CT for the detection of recurrent Osteosarcoma

F. Ceci[1], A. Angelini[2], P. Castellucci[1], T. Graziani[1], M. Polverini[2], P. Ghedini[1], S. Israel[1], R. Bonfiglioli[1], P. Ruggieri[2], S. Fanti[1]; [1]Nuclear Medicine - S.Orsola-Malpighi Hospital - University of Bologna, Bologna, ITALY, [2]Department of Orthopedics, Istituto Ortopedico Rizzoli, University of Bologna, Bologna, ITALY.

Aim: To investigate the diagnostic accuracy of 18F-FDG-PET/CT in osteosarcoma patients, with suspicious of disease recurrence after radical therapies. Materials and Methods: Inclusion criteria were: a) radical surgical treatment for proven osteosarcoma and documented complete remission after therapy; b) 18F-FDG-PET/CT during follow-up for clinical/diagnostic suspicious of relapse; c) histological validation of 18F-FDG-PET/CT findings. Thirty-seven osteosarcoma patients were retrospectively enrolled (20 male, 17 female; mean/median/range age 21/18/7-72 years-old). The primary sites of tumours were: femur (n=15); tibia (n=13); humerus (n=3); soft tissue (n=3); pelvis (n=2); ulna (n=1). 18F-FDG-PET/CT performance was assessed with a per-patient and per-site evaluation of sensitivity, specificity, accuracy, positive predicting value (PPV) and negative predicting value (NPV). The sites of relapse were classified as local (local relapse in bone and/or soft tissue), lung, lymph-nodes (LNs) and distant (other skeletal segments and/or distant soft tissue). The disease free survival (DFS) and the overall survival (OS) after 18F-FDG-PET/CT were evaluated. Results: 18F-FDG-PET/CT was positive in 89.2% (33/37) of patients. Local uptake was observed in 35.1%patients (13/37); lung uptake in 18.9% (7/37); local and lung in 2.7% (1/37); local and LNs in 10.8% (4/37); local, LNs and distant 5.4% (2/37); LNs and distant in 2.7% (1/37); lung, LNs and distant in 2.7% (1/37); local, LNs, lung and distant in 5.4% (2/37); lung and distant in 2.7% (1/37); only distant in 1/37 (2.7%). The per-site mean-SUVmax analysis resulted in: local=10.2; LNs=8.2; lung=5.6; distant=9.8. In order to validate 18F-FDG-PET/CT findings, all patients underwent surgery on the basis of 18F-FDG-PET/CT results. Histology resulted positive in 92% (34/37) of patients. A total of 51 pathologic lesions were evaluated (22 local relapse, 11 lung metastasis, 10 metastatic LNs, 8 distant metastatic lesions). On a per-patient analysis 18F-FDG-PET/CT showed a sensitivity, specificity, accuracy, PPV and NPV of 91%, 75%, 89%, 97%, 50%. On a per-site analysis the performance for local recurrence was 96%, 100%, 97%, 100%, 93%, while for lung recurrence detection was 80%, 100%, 92%, 100%, 88%. The mean follow-up after 18F-FDG-PET/CT was 21.5 months (range 1-82). At the end of follow-up 19% (7/37) of patients were death, 35% (13/37) were alive with disease and 46% (17/37) had no evidence of disease. At 18 months after 18F-FDG-PET/CT the DFS was 46% and the OS was 81%. Conclusion: 18F-FDG-PET/CT showed promising results for the recurrence detection in osteosarcoma patients with suspicious of relapse after radical treatment, particularly in the detection of local relapse and lung metastasis.

OP455

Initial FDG PET/CT predicts survival in adults ewing sarcoma family of tumors.

J. B. Bastien; B Jamet1, T Carlier1,2, L Campion3, E Bompas3, M Colombié4, D Rusu4, D Goulon4, V Fleury4, F Kraeber-Bodéré1,2, C Rousseau2,4, 1Nuclear Medicine Unit, University Hospital, Nantes, France, 2INSERM U892, CRCNA, Nantes, France, 3Oncology Unit, ICO Cancer Center, Saint Herblain, France, 4Nuclear Medicine Unit, ICO Cancer Center, Saint Herblain, France

AIM: FDG PET/CT is a recommended tool for initial staging and restaging of Ewing Sarcoma Family of Tumors (ESFTs). However, the use of baseline FDG PET/CT as a tool for assessing survival outcome was not yet reported. We evaluated the benefit of using quantitative PET-based parameters to predict the survival outcome of ESFTs patients. MATERIALS AND METHODS: 20 adult patients (10 men and 10 women) with ESFTs, treated according to Euro-Ewing 99 protocol, were retrospectively included. The primitive lesion of each patient was analyzed using different quantitative parameters: SUV (maximum, peak and mean), metabolic tumor volume (MTV) and total lesion glycolysis (TLG) before treatment. Kaplan-Meier method, Logrank tests and univariate Cox analyses were used to calculate survival curves and to analyze whether imaging and usual clinical prognostics factors (metastatic disease at presentation, axial tumor location, tumor size>10cm, sex and age≥20 years) could predict progression free survival (PFS) and overall survival (OS). RESULTS: The median age was 23 years (range, 16 to 61). Twelve patients were initially metastatic (lungs or bone marrow). For 10 patients, the disease location was osseous and for 10 non osseous (4 of them were PNET). Parameters data of 19 patients were interpretable. Univariate analysis showed different imaging parameters as predictors of OS: SUVmax (HR: 1.16; 95% CI: 1.02-1.33; P=0.021), SUVpeak (HR: 1.27; CI: 1-1.61; P=0.047), SUVmean (HR: 1.31; CI: 1.04-1.66; 0.024). Three years OS was 53% for SUVmax< 17 vs 25% for SUVmax>17 (P= 0.021). SUVmax (P=0.044), SUVpeak (P=0.027) and SUVmean (P=0.027) were predictive of PFS for univariate analysis. MTV and TLG were not predictive for PFS and OS. For clinical parameters at baseline, metastatic disease (HR: 13.5; CI: 1.55-102.15; P<0.001) and male sex (HR: 6.01; CI: 1.24-29.14; P=0.026) shortened only PFS.

CONCLUSION: At baseline, FDG PET with SUVmax, SUVpeak and SUVmean measured on primitive lesion could be a useful tool to predict OS and PFS for adult ESFTs patients.

OP456

Soft tissue sarcomas: Comparison between visual assessment and metabolic parameters in FDG PET/CT

D. Lopez, A. Domenech, C. Achury, R. Jaller, J. Duch, M. Estorch, A. Flotats, I. Carrió; Nuclear Medicine department. Hospital de la Santa Creu i Sant Pau, Barcelona, SPAIN

PURPOSE: To compare metabolic tumor parameters (Maximum Standard Uptake Value [SUVmax], Mean Standard Uptake Value [SUVmean], Metabolic Tumor Volume [MTV] and Total Lesion Glycolisis [TLG]) derived from 18F-FDG PET/CT with visual assessment in order to correlate with the clinical course of soft tissue sarcoma. MATERIALS AND METHODS: Eleven patients (p) [8 males; mean=49 y/o, range 23-67] with soft tissue sarcoma, histopathologically confirmed (5 fusocellular, 1 leiomyosarcoma, 4 lyposarcoma and 1 myxofibrosarcoma), who underwent baseline (before chemotherapy, surgery and radiotherapy) and early (after treatment) follow-up 18F-FDG PET/CT were retrospectively reviewed. Visual and Quantitative analysis were done in baseline and early follow-up PET/CT comparing the results with the late follow-up scan visual analysis. Based on visual assessment of the early follow-up PET/CT patients were considered to be in local recurrence (LR), disease progression (DP), stable disease (SD) and partial response to treatment (PR). Quantitative measurements to track changes in tumor volume and metabolic activity were performed using Philips *Tumor Tracking Application*, determining the SUVmax, SUVmean, MTV and TLG. Late follow-up scans (PET/CT and/or MRI) performed in a period of no more than 6 months after the last PET/CT were reviewed in order to assess the clinical course of the tumor. RESULTS: In the visual analysis, 2p were considered in LR, 3 in DP, 3 in SD and 3 PR. In the quantitative analysis, 1p visually considered in LR and 2 of the 3 in DP presented an increase in SUVmax, SUVmean, MTV and TLG, while the remaining patients in LR and in DP presented an increase in SUV values and a decrease in MTV and TLG. In 2 of the 3p considered visually in SD, a decrease of all the metabolic parameters was observed and no changes were seen in 1p. Two of the 3p in PR presented a decrease in all values while 1 had a decrease in SUV values and a minimum increase in TLG. Late imaging follow-up scans in the 2p with SD and a decrease in metabolic tumor parameters showed PR while in the remaining 9p no changes were seen between scans. Overall, a correlation between metabolic tumor parameters in the baseline and early follow-up PET/CT with the late follow-up scan visual analysis was observed in 63% (7/11) of the patients. CONCLUSION: In addition to the visual analysis, the metabolic parameters could be a useful tool to evaluate with more accuracy the clinical course of soft tissue sarcomas.

OP457

Tumour heterogeneity for differentiation between tumour and normal liver tissue in FDG-PET imaging

L. Jaritz[1], H. Ahmadzadehfar[1], M. Essler[1], N. Zsoter[2], L. Papp[2], F. Gaertner[1], R. A. Bundschuh[1], L. Thomas[1]; [1]Department of Nuclear Medicine, Universitaetsklinikum Bonn, Bonn, GERMANY, [2]Mediso Medical Imaging Systems, Budapest, HUNGARY

Introduction: In process of planning internal/external radiation-therapy it is essential to determine tumour-volume as accurate as possible. Therefore it is essential to differentiate benign from malignant tissue best possible. FDG-PET/CT has the ability to distinguish between metabolic active tumour and surrounding tissue by means of measured activity-uptake. By use of textural analysis based on a image-analysis of FDG-PET/CT images, structural features can easily be extracted. We investigated, if these textural parameters, which reflect the heterogeneity, function as a tool for differentiation between benign and malignant tissue and analysed the variability of heterogeneity within a tissue. Methods: 43 patients with liver-metastasis of colorectal-carcinomas have been examined on baseline FDG-PET/CT-scans before their first selective internal radiotherapy. In FDG-PET images liver metastasis and normal liver tissue were analysed with InterviewFusion-software (Mediso). Three volumes-of-interest (VOIs) with a fixed diameter of 25mm were drawn in healthy liver tissue, whilst metastasis were manually delineated. For determination of the tumour heterogeneity within these VOIs we calculated 30 different textural parameters including Entropy, Homogeneity and Contrast. For better comparison we measured established parameters used in clinical routine (mean and max standardized uptake values (SUVmean/SUVmax)). For statistical analysis we compared the heterogeneity in terms of intra-patient-variability and inter-patient-variability. Students-T-test was used to compare the parameters for healthy and pathological tissue. Results: The mean relative standard-deviation as measure for intra-patient-variability was found to be lowest for Busyness (2.4%), Homogeneity (5.1%), Correlation (7.8%), and Entropy (8.0%). These values were comparable with the ones for routine parameters SUVmax (7.5%) and SUVmean (6.9%). The mean inter-patient-variability was found to be lowest for Busyness (3.8%), Correlation (6.1%), Short Zone Emphasis (9.1%), and Homogeneity (11.9%). These were lower than the variability for SUVmean (20.7%) and SUVmax (18.9%). For differentiation between healthy liver-tissue and tumour we found 26 of the 30 textural

parameters statistically significant ($p<0.05$), highest significance was found for Homogeneity, Short Run Emphasis, Intensity Variation, and Short Zone Emphasis. SUVmean and SUVmax also showed ability to differentiate but with a lower statistical significance. Conclusion: In healthy liver tissue we found a intra-patient-variability comparable to the conventional SUVmax and SUV mean while for inter-patient-variability some textural parameters showed even lower values than the routine parameters. Furthermore most of the textural parameters showed better ability to differentiate between malignant and healthy tissue than the SUVmean and SUVmax. Therefore textural parameters are promising for classification lesions as well as to delineate malignant tissue for treatment-planning or response-evaluation.

OP458

Factors of FDG uptake in the liver and blood pool on PET scans

K. Zhou, **Sr**.; West China Hospital of Sichuan University, Chengdu, CHINA

Factors of FDG uptake in the liver and blood pool on PET scansObjectives: It was reported that the standardized uptake value (SUV) of 18F-FDG in children was lower than that of in adults on PET. But the correlation between SUV and age was unknown. The objective of present study was to find is there a correlation between SUV and age. Methods: Three hundred and seventy-eight patients (male 210, female 168) who received whole body 18F-FDG PET scans were included based on inclusion and exclusion creteria. In which, 230 had malignancy(171 lymphoma), and the others were healthy but for cancer screening. The age of them were 2-40 years (3 and 5 cases for 2 and 3 years, 10 cases for the rest). The correlations between SUVmax and SUVmean from liver and blood and gender, age, body weight, serum glucose and administration dose were analyzed uni- and multivariately. Then the independent factors were correlated with SUVs using curve estimation regression. Results: Univariate analysis revealed that there were positive correlations between SUVs and age, body weight, serum glucose and administration dose ($p<0.05$). There was no correlation between gender and SUVs ($p=0.612$). But only body weight and age had positive impact on SUVs after multivaraite analysis ($p<0.05$). Curve estimation showed the SUVs increased along with the age before 25 years, then it reached a platform. And the SUVs increased along with body weight without a platform. Conclusion: Both Age and body weight are independent factors on FDG uptake. SUVs increase along with the age before 25 years, then it reach a platform. And the SUVs increase along with body weight without a platform.

OP459

18F-FDG PET/CT role in staging of gastric carcinomas: comparison with conventional Contrast Enhancement Computed Tomography.

C. Altini, **A. Niccoli Asabella**, A. Di Palo, M. Fanelli, D. Rubini, C. Ferrari, A. Notaristefano, G. Rubini; Nuclear Medicine Unit, D.I.M., University of Bari "Aldo Moro", Bari, Italy, Bari, ITALY.

Aim: to evaluate the role of 18F-FDG PET/CT in staging gastric carcinoma comparing it with Contrast Enhancement Computed Tomography (CECT) and if morphological and functional parameters might give a contribution. Materials and methods: This retrospective study included 45 patients who underwent whole body CECT and 18F-FDG PET/CT before any treatment. We calculated CECT and 18F-FDG PET/CT sensitivity, specificity, accuracy, positive and negative predictive values (PPV and NPV) for gastric, lymphnode and distant localizations; furthermore we compared the two techniques by McNemar test. Linear regression was performed to evaluate SUVmax and SUVmean in relation to gastric lesion size. The role of 18F-FDG PET/CT semiquantitative parameters in relation to histotype, grading and site of gastric lesions were evaluated by ANOVA test. Results: sensitivity, specificity, accuracy, PPV and NPV of CECT and 18F-FDG PET/CT for gastric lesion were respectively 92.11%, 57.14%, 86.66%, 92.11%, 57.14% and 81.58%, 85.71%, 82.22%, 96.88%, 46.15%. No differences were identified between the 2 techiques about sensitivity and specificity. No stastistical differences were observed between PET parameters and histotype, grading and site of gastric lesion. The mean value of the maximum diameter was 52.59 mm (range 4 - ≥100). Considering 30 mm, as a threshold value for maximum diameter we divided patients in 2 groups: size ≤ 30 mm and size > 30. In 15/45 pts size was ≤ 30 mm and 18F-FDG PET/CT sensitivity and specificity resulted respectively 33.33% (95%CI: 7.88% to 69.93%) and 83.33% (95%CI: 36.10% to 97.24%). In 30/45 pts size was > 30 mm and 18F-FDG PET/CT sensitivity and specificity resulted respectively 96.55% (95%CI: 82.17% to 99.42%) and 100% (95%CI: 16.55% to 100%). SUVmax and SUVmean resulted positively related to lesion dimension (SUV max=3.53+0.11*lesion size, F=8.91, p=0.005; SUV mean=1.99+0.06*lesion size, F=7.07 p=0.01) No stastistical differences were observed between PET parameters and histotype, grading and site of gastric lesion. The results of CECT and 18F-FDG PET/CT about lymphnode involvement were 70.83%, 61.90%, 66.66%, 68%, 65% and 58.33%, 95.24%, 75.55%, 93.33%, 66.67%. The results of CECT and 18F-FDG PET/CT about distant metastases were 80%, 62.86%, 66.66%, 38.10%, 91.67% and 60%, 88.57%, 82.22%, 60%, 88.57%. 18FDG PET/CT specificity was significantly higher both for lymphnode and distant metastases.

Conclusions: the 18F-FDG PET/CT is a useful tool for the evaluation of gastric carcinoma to detect primary lesion, lymphnode and distant metastases using one single image whole-body technique. Integration of CECT with 18F-FDG PET/CT permits a more valid staging in these patients.

OP460

Utility of 18F-FDG PET/CT in Patients with Advanced Squamous Carcinoma of Uterine Cervix Receiving Concurrent Chemoradiotherapy: A Parallel Study of a Prospective Randomized Trial

F. Liu[1], C. Lai[1], L. Yang[1], C. Wang[1], G. Lin[1], C. Chang[2], S. Huang[3], Y. Huang[4], N. Peng[5], J. Hong[1], A. Chao[1], H. Chou[1], Y. Chang[1], T. Yen[1]; [1]Chang Gung Memorial Hospital and Chang Gung University College of Medicine, Taoyuan, TAIWAN, [2]Chang Gung University, Taoyuan, TAIWAN, [3]Chang Gung Memorial Hospital and Chang Gung University College of Medicine, Kaohsiung, TAIWAN, [4]Chang Gung Memorial Hospital and Chang Gung University College of Medicine, Chiayi, TAIWAN, [5]Kaohsiung Veterans General Hospital, Kaohsiung, TAIWAN

Aim: This study aimed to evaluate the utility of pre- and during-treatment 18F-fluorodeoxyglucose (18F-FDG) PET/CT in predicting failure patterns in patients with advanced uterine cervical cancer receiving concurrent chemoradiotheray (CCRT). Materials and methods: Patients with cervical squamous carcinoma, FIGO stage III-IVA or pelvic/paraaortic lymph node (LN) metastasis without other distant metastasis defined by 18F-FDG PET/CT entering a randomized controlled trial of CCRT (AGOG09-001) were eligible for this parallel study. PET/CT scans were performed at baseline, during week 3 of CCRT and 2-3 months after CCRT. PET/CT parameters included maximal standardized uptake value (SUVmax), metabolic tumor volume (MTV), SUVnode (largest SUVmax of all positive LNs), SUVratio (during-treatment SUVmax / pre-treatment SUVmax * 100%), and MTVratio. The Mann-Whitney U test and receiver operating characteristic curves were used to evaluate the potential predictors, and another independent patient dataset was used for validation. Results: Early treatment failure (within 6 months) was noted in 9 of 55 (16.4%) patients eligible for analysis. Both pre- and during-treatment cervical tumor volumes ($P < .001$) were significant predictors of local failure ($n = 4$). During-treatment SUVnode ($P = .019$) and maximal SUVratio of LNs ($P = .024$) were significant predictors of regional failure ($n = 4$). Distant failure was present in 5 patients, with during-treatment SUVnode ($P = .027$) and MTVratio of the cervical tumor ($P = .033$) as significant predictors. Conclusion: Pre- and during-treatment PET/CT may be useful in predicting early treatment failure patterns, thus early therapeutic modifications (locoregional and systemic) can be applied accordingly in hope for outcome improvement.

OP461

Face-To-Face 18F-FDG-PET/CT and CA125 (Serums Levels and Kinetic Values) in Patients with Suspected Recurrence of Ovarian Cancer.

A. Palomar Muñoz, J. M. Cordero García, G. A. Jiménez Londoño, M. P. Talavera Rubio, M. E. Bellón Guardia, B. González García, V. M. Poblete García, Á. Soriano Castrejón; Hospital General Universitario de Ciudad Real, Ciudad Real, SPAIN

PURPOSE: The aim of this study was to evaluate the capability of 18F-FDG-PET/CT in the detection of recurrences in ovarian cancer, when compared with CA125 serum levels, as well as the diagnostic influence of CA125 velocity (CA125v) and CA125 doubling time (CA125dt) in the PET/CT results. METHODS: A total of 54 women with suspicion of relapse, studied with a standard 18F-FDG-PET/CT and CA125 serum level were retrospectively studied. Patients were grouped according to CA125 normal serum levels before the PET/CT in 2 groups (1: CA125<35 IU/ml, 2: CA125>35 IU/ml).The final diagnosis was obtained by histological analysis or clinical follow up greater than 6 months. A total of 37 patients had at least two determinations of CA125 levels, which allowed to calculate CA125v and CA125dt, that were independently analysed. These patients were compared with the FDG-PET/CT results, classified as positive (A) and negative (B). RESULTS: PET/CT detected relapse in 45/54 (83.33%) patients, and was negative in 9/54 (16.66%) women, with only 1 false negative result, reaching a sensitivity of 97.83% and specificity of 100%. In contrast, attending to the CA125 levels, 35/54 (64.81%) patients were included in the group 1, and 19/54 (35.18%) in the group 2, with a sensitivity of 73.33%, and a specificity of 77.78%. In the group 1 (median 10.9, 5.2-33.9 IU/ml) PET/CT classified correctly 18 patients (7 negative, 11 positive), and 1 false negative. In the group 2 (median 69.9, 35.5-1950.9 IU/ml) PET/CT detected disease in 33 patients, without misdiagnoses. Regarding to the kinetic values, the A group composed by 28 patients showed a median CA125v of 5.17 (-0.05-87.03) and a median CA125dt of 3.71 (-175.03-32.66). The nine women included in the B group had a median CA125v of 0.27 (-0.56-364.05) and a median CA125dt of 2 (-148.6-23.22). No statistical differences were found between both groups concerning to the kinetics parameters (CA125v p=0.2, CA125dt p=0.3). CONCLUSION: The 18F-FDG-PET/CT shows a high diagnostic performance in the suspicion of ovarian cancer recurrence, regardless the levels of CA125 and the kinetic values. Thus, in case of clinical suspicion of ovarian cancer relapse, seems to be essential to carry out an FDG-PETCT study in all cases.

YE3 - Tuesday, October 13, 2015, 01:00 PM - 02:30 PM, Hall 8
Young EANM Daily Forum 3: Young Investigator Meeting

OP461b
Welcome and Introduction
N. Ristevska, FYROM
A. Gee, UNITED KINGDOM
M. de Jong, NETHERLANDS

OP461c
YIM 2015 Winner Presentation
I. Bakker, NETHERLANDS

OP461d
Past YIM Experience and Outcome
G. Treglia, SWITZERLAND
L. Lezaic, SLOVENIA

OP461f
Become a Young EANM Committee Member - Oncology Committee
R. Delgado-Bolton, SPAIN

OP461g
Become a Young EANM Committee Member - Bone and Joint Committee
T. van den Wyngaert, BELGIUM

OP461e
Closing Remarks

1401 - Tuesday, October 13, 2015, 02:30 PM - 04:00 PM, Hall 1
CME 11 - Radiopharmacy: New Protein Deposition Tracers

OP462
Clinical View of Deposition Tracers
R. Ossenkoppele, USA

OP463
New Tracers in the Pipeline
A. Stephens, GERMANY

OP464
Deposit Tracers in the Preclinical Research
D. Guilloteau, FRANCE

1402 - Tuesday, October 13, 2015, 02:30 PM - 04:00 PM, Hall 2
Joint Symposium 11: EANM/ENETS: Management of Neuroendocrine Tumours

OP465
Therapeutic Management of Neuroendocrine Tumours Ms **E. Caplin, UK**

OP466
The Role of PRRT in the Therapeutic Algorithm of Neuroendocrine Tumours
L. Bodei, ITALY

OP467
Future Therapeutic Scenarios: Combination or Competition?
A. Rinke, GERMANY

1403 - Tuesday, October 13, 2015, 02:30 PM - 04:00 PM, Hall 4
CTE 5: Lean Principles and Improved Departmental Management

OP468
Making Your Department LEAN
D. Gilmore, USA

OP469
How to Implement the LEAN Concept
J. Löfgren, DENMARK

OP470
The Impact of LEAN in a PET Department
E. Sanchez Saxtoft, DENMARK

1404 - Tuesday, October 13, 2015, 2:30 PM - 4:00 PM, Hall G1
Cardiovascular System - Featured: Imaging of Plaques, Angiogenesis & Ischaemic Memory

OP471
Simultaneous PET/MR imaging with FDG for the evaluation of symptomatic patients with non-stenotic carotid atherosclerotic plaques

F. Hyafil[1], A. Schindler[2], D. Sepp[3], T. Obenhuber[2], S. Höhn[2], S. Nekolla[1], M. Dichgans[3], M. Schwaiger[1], T. Saam[2], H. Poppert[3]; [1]Department of Nuclear Medicine, Klinikum rechts der Isar, Munich, GERMANY, [2]Ludwig-Maximilians-University Hospital Munich, Institute for Clinical Radiology, Munich, GERMANY, [3]Department of Neurology, Klinikum rechts der Isar, Munich, GERMANY

Introduction. High-resolution magnetic resonance imaging (MRI) can assess atherosclerotic plaque composition in carotid arteries with good correlation to histopathology. 18Fluorodeoxyglucose (18F-FDG) is a positron emission tomography (PET) radiotracer that accumulates in inflammatory cells present in atherosclerotic plaques. The aim of this study was to investigate in 18 patients with ischemic stroke classified as cryptogenic and presenting non-stenotic carotid atherosclerotic plaques the morphological and biological aspects of these plaques with MRI and 18F-FDG-PET imaging. Methods. Carotid arteries were imaged 150 minutes after injection of 18F-FDG with a combined PET/MRI system. American Heart Association (AHA) lesion type and plaque composition were determined on consecutive MR axial sections (n = 460) in both carotid arteries. 18F-FDG uptake in carotid arteries was quantified using tissue-to-background ratio (TBR) on corresponding PET sections. Results. Prevalence of complicated atherosclerotic plaques (AHA lesion type VI) detected with high-resolution MRI was significantly higher in the carotid artery ipsilateral to the ischemic stroke as compared to the contralateral side (39% vs. 0 %; $p = 0.001$). For all other AHA lesion types, no significant differences were found between ipsilateral and contralateral sides. In addition, atherosclerotic plaques classified as high-risk lesions with MRI (AHA lesion type VI) were associated with higher 18F-FDG uptake in comparison with other AHA lesions (TBR = 3.43 ± 1.13 vs. 2.41 ± 0.84; respectively; $p < 0.001$). Furthermore, patients presenting at least one complicated lesion (AHA lesion type VI) with MRI showed significantly higher 18F-FDG uptake in both carotid arteries (ipsilateral and contralateral to the stroke) in comparison with carotid arteries of patients showing no complicated lesion with MRI (mean TBR = 3.18 ± 1.26 and 2.80 ± 0.94 vs. 2.19 ± 0.57; $p < 0.05$, respectively), in favor of the presence of a diffuse inflammatory process along both carotid arteries associated with complicated plaques. Conclusions. Morphological and biological features of high-risk plaques can be detected with high-resolution MRI and 18F-FDG-PET in non-stenotic atherosclerotic plaques ipsilateral to the stroke, suggesting a causal role for these plaques in stroke. Combined 18F-FDG-PET-MRI systems might help in the evaluation of patients with ischemic stroke classified as cryptogenic.

OP472
Atherosclerotic Plaque 18F-NaF Uptake Predicts its Subsequent Morphologic Evolution and Calcification Density

F. Fiz[1], M. Bauckneht[1], G. Ferrarazzo[1], A. Piccardo[2], E. Pestarino[2], I. Calamia[1], M. Cabria[2], G. Villavecchia[2], C. Marini[3], S. Morbelli[1], G. Sambuceti[1]; [1]Nuclear Medicine Unit, Department of Health Sciences, University of Genoa, Genoa, ITALY, [2]Nuclear Medicine Unit, Ente Ospedaliero Galliera, Genoa, ITALY, [3]CNR-IBFM, Milano, ITALY

Background and Aims: Evaluation of calcium deposition within arterial calcifications (AC) can be performed using 18F-NaF PET/CT; our previous experience demonstrated that AC density at CT inversely correlates with its 18F-NaF uptake. We planned the present study to investigate whether a higher tracer uptake, by signaling an active calcium deposition, predicts a subsequent AC evolution. Patients and Methods: We retrospectively included 50 patients (18 women, mean age 68±9 years, age range 41-86) who underwent at least two consecutive 18F-NaF PET/CT in the course of follow-up of bone metastases from breast or prostate cancer. Only scan spaced at least one year and at most two years were included. In each scan we drew a volume-of-interest (VOI) on each AC within the infrarenal aorta walls and we calculated its average Hounsfield density (HU), its blood-pool normalized average uptake (target-to-background ratio, TBR, obtained by

normalizing AC SUVmean with the one of a 10-slice-thick VOI, drawn within the inferior vena cava) and its Calcification Score (CS, using an Agaston-like algorithm). We stratified all AC in tertiles according to their baseline TBR in "cold" (lower tertile, CP), "warm" (middle tertile, WP) and "hot" (higher tertile, HP) plaques. We then calculated, on each consecutive scan and on a plaque-by-plaque basis the percent difference in mean HU e CS (defined as DHU% and DCS%, respectively). Results: 430 AC were identified. In CP there wasn't any significant increase neither in HU nor in CS at subsequent scans. Conversely, both parameters significantly increased in WP and HP ($p<0.01$ and $p<0.001$, respectively). Mean DHU% was progressively increasing from CP to HP (11±9%, 36±16% and 67±32%, $p<0.01$ for CP vs. WP and $p<0.05$ for WP vs. HP); average DCS% showed a similar pattern ($p<0.05$). As a consequence, there was a positive correlation between TBR and both DHU% ($R=0.75$, $p<0.01$) and DCS% ($R=0.69$, $p<0.01$). Conclusion: 18F-NaF uptake within the atherosclerotic plaque, by tracing mineral turnover, can be used as a hallmark of calcium deposition and can therefore predict whether any given plaque will subsequently evolve in size and density.

OP473

18F-FDG-PET-CT assessed subclinical arterial inflammation is positively associated with non-invasive markers of arterial stiffness in recently diagnosed type 2 diabetes patients

S. A. de Boer[1], M. C. Hovinga - de Boer[2], J. D. Lefrandt[1], H. J. Lambers Heerspink[3], A. W. J. M. Glaudemans[4], D. J. Mulder[1], R. H. J. A. Slart[4,5]; [1]Department of Vascular Medicine, University Medical Center Groningen, University of Groningen, Groningen, NETHERLANDS, [2]Department of Radiology & Nucleair Medicine, Meander Medical Center, Amersfoort, NETHERLANDS, [3]Department of Clinical Pharmacy and Pharmacology, University Medical Center Groningen, University of Groningen, Groningen, NETHERLANDS, [4]Department of Nucleair Medicine and Moleculair Imaging, University Medical Center Groningen, University of Groningen, Groningen, NETHERLANDS, [5]Universtity of Twente, Department of Biomedical Photoacustic Imaging (BMPI), Enschede, NETHERLANDS

Aim: Type 2 diabetes mellitus (T2DM) is accompanied by premature arterial stiffness. The underlying mechanisms are unclear. We investigated the possible relation between subclinical arterial inflammation, calcification, atherosclerotic risk factors, skin advanced glycation end products (AGEs)), and arterial stiffness in T2DM. Materials & methods: 34 patients with recently diagnosed T2DM (RELEASE study: NCT02015299), without a history of cardiovascular disease and not using glucose lowering drugs, were studied (age 63 (55-66) yrs, 65% male, HbA1c 46 ±4.3 mmol/mol (6.4±0.4%), 18% smokers). Arterial stiffness was non-invasively assessed by aortic systolic blood pressure (aSBP, mmHg) and aortic (carotid-femoral) pulse wave velocity (aPWV) using applanation tonometry. A whole body 18-Fluorodeoxyglucose positron emission tomography-(low dose) computed tomography (^{18}F-FDG-PET-CT) scan was performed to assess arterial inflammation (standard uptake value (SUV)max (according to EARL guidelines)) and CT-scored arterial calcification (AC): visual score: 0 (no) to 4(>50% calcified plaque). SUVmax and AC scores were calculated in 4 individual segments (carotid arteries, ascending aorta and aortic arch, descending and abdominal aorta, and iliac and femoral arteries) and for the total aortic tree (aSUVmax, mean of 4 segments). Skin AGEs were measured as skin autofluorescence (SAF). Results and conclusion: aSUVmax and AC were not associated. aSUVmax was associated with atherosclerotic risk factors: BMI ($r=0.64$, $P<0.001$), HbA_{1c} ($r=0.59$, $P<0.001$), waist circumference ($r=0.55$, $P<0.001$) but not with, age, gender, smoking, lipids, and SAF. aSUVmax was associated with non-invasive markers of arterial stiffness: aSBP ($r=0.55$, $P=0.001$) and tended to correlate with aPWV ($r=0.33$, $P=0.059$). After multivariate adjustment ($r^2=0.79$, $P<0.001$), only HbA_{1c}, ($\beta=0.36$, $P<0.001$), waist circumference ($\beta=0.49$, $P<0.001$), aSBP ($\beta=0.49$, $P<0.001$), and aPWV ($\beta=0.24$, $P=0.014$) remained significant. AC was associated with male gender ($r=0.48$, $P=0.004$), age ($r=0.51$, $P=0.002$), BMI ($r=-0.43$, $P=0.011$), and SAF ($r=0.37$, $P=0.036$) and not with other mentioned atherosclerotic risk factors. None of AC scores correlated with aPWV, aSBP, or any of the SUVmax segments. After multivariate adjustment ($r^2=0.39$, $P=0.001$) only male gender ($\beta=0.49$, $P=0.003$) and SAF ($\beta=0.34$, $P=0.033$) remained significant. These results show that in recently diagnosed T2DM patients 18F-FDG-PET-CT revealed subclinical arterial inflammation but not calcification, and is positively associated with determinants of arterial stiffness, glycemic control and central obesity. Interessingly, while the extent of arterial calcification did not show any relation with arterial inflammation, it was independently associated with skin AGEs, suggesting discordant pathways at different stages of atherosclerotic disease.

OP474

Evaluation of the radiotracer [68Ga]pentixafor targeting the CXCR4 receptor with PET-MRI in a rabbit model of atherosclerotic plaques

F. Hyafil[1], I. Laitinen[1], M. Schottelius[2], M. Mohring[1], A. Poschenrieder[2], J. Brandl[3], C. Baumgartner[3], J. Pelisek[4], S. Nekolla[1], H. Wester[5], M. Schwaiger[1]; [1]Department of Nuclear Medicine, Klinikum rechts der Isar, Munich, GERMANY, [2]Pharmaceutical Radiochemistry, Technische Universität München, Garching, GERMANY, [3]Centre of Preclinical Research, Klinikum rechts der Isar, Munich, GERMANY, [4]Department of Vascular Surgery, Klinikum rechts der Isar,

Munich, GERMANY, [5]Pharmaceutical Radiochemistry, Technische Universität München, Munich, GERMANY

Introduction: The CXCR4 receptor is expressed at the surface of lymphocytes, macrophages and neutrophils. [68Ga]Pentixafor is a PET radiotracer that binds with a nanomolar affinity to the CXCR4 receptor. The aim of this study was to test whether [68Ga]Pentixafor binds specifically to CXCR4-expressing tissues and allows for the detection of inflamed atherosclerotic plaques induced in rabbits. Methods: Atherosclerotic plaques were induced by endothelial abrasion of the right carotid artery and abdominal aorta of 7 New Zealand White rabbits fed an atherogenic diet. Three non injured rabbits fed a chow diet were used as controls. Rabbits were imaged on a combined PET-MRI system 1 hour after injection of 15 MBq/kg of [68Ga]Pentixafor. Tissue to background ratios (TBRs) were measured with PET-MRI along carotid arteries and in the abdominal aorta. After PET-imaging, biodistribution studies were performed one hour after injection of 7.5 MBq/kg of [125I]Pentixafor. Tracer uptake was quantified on 20 μm cryosections of arteries using autoradiography and normalized to muscle uptake. In addition, blocking studies were performed in two atherosclerotic rabbits with pre-injection of 2 mg of the CXCR4 inhibitor AMD3100. Results: Biodistribution studies showed significantly higher accumulation of [125I]Pentixafor in CXCR4-expressing tissues such as spleen (0.19 ± 0.07 % ID / g), adrenal glands (0.30 ± 0.13 % ID/g) and bone marrow (0.16 ± 0.06 % ID/g), than in other tissues such as muscle (0.02 ± 0.01 % ID/g) or heart (0.02 ± 0.01 % ID/g). [125I]Pentixafor binding in CXCR4-expressing tissues was strongly decreased after injection of the CXCR4 inhibitor AMD 3100. One hour after injection of [68Ga]pentixafor, a clear signal was detected in vivo with PET-MRI in atherosclerotic plaques of the abdominal aorta and right carotid artery as compared to normal control arteries (average TBR = 1.95 ± 0.51 vs. 1.22 ± 0.25 and TBR = 1.24 ± 0.38 vs. 0.96 ± 0.37 ; $p < 0.05$ for both). Consistently, higher tracer uptake was measured by autoradiography in cryosections of atherosclerotic plaques as compared to normal arteries. Conclusions: [68Ga]Pentixafor accumulates specifically in CXCR4-expressing tissues in rabbits. [68Ga]Pentixafor uptake was increased in inflamed atherosclerotic plaques compared to normal arteries. Hence, [68Ga]Pentixafor might emerge as a valuable tool for the detection of high-risk atherosclerotic plaques with PET.

OP475

Targeting Aminopeptidase N (CD13) for molecular imaging of cardiac wound healing using ^{68}Ga-NOTA-c(NGR) in experimental myocardial infarction

S. Samnick[1], M. Schneider[1], J. Tillmanns[2], D. Fraccarollo[2], J. Bauersachs[2], A. Buck[1]; [1]University of Wuerzburg, Wuerzburg, GERMANY, [2]Hannover Medical School, Hannover, GERMANY

Purpose: Aminopeptidase N (CD13) is a transmembrane protease involved in cell adhesion, migration, proliferation, differentiation and angiogenesis. In myocardium, CD13 is overexpressed in athophysiologic conditions such as acute myocardial infarction (MI), where it facilitates inflammatory cell infiltration. After MI, the wound healing phase is important for successful tissue repair and improved remodeling. Molecular imaging could help to understand activity and duration of the repair processes in individual patients, and potentially allows patient-specific administration of pharmacotherapy to improve outcome after MI. On the other hand, peptides containing the NGR (Asparagine-Glycine-Arginine) motif bind selectively to CD13. This study investigates the potential of the radiolabeled NGR-containing tracer ^{68}Ga-NOTA-NGR as an imaging probe for in vivo assessment of the early wound healing phase after MI using PET. Methods: Myocardial ischemia/reperfusion injury (MI/R) was induced in rats, and the uptake of the novel ^{68}Ga-labelled NGR peptide (^{68}Ga-NOTA-NGR) was evaluated in comparison with ^{68}Ga-NOTA-RGD and ^{18}F-FDG at day 3, 7 and 21 post infarction using μ-PET and autoradiography. Expression of CD13, the molecular target of NGR, and $\alpha_v\beta_3$, the molecular target of RGD, were assessed in fibroblasts, inflammatory cells and endothelial cells in rat hearts by immunohistochemistry, and correlated with radiotracer uptake. Results: Infarcted and surviving myocardium was identified by ^{18}F-FDG-PET in all animals. In the infarcted myocardium, uptake of ^{68}Ga-NOTA-NGR was maximal from day 3 to 7 after MI/R, and correlated with fibroblast and inflammatory cell infiltration as well as ^{68}Ga-NOTA-RGD uptake. Conclusions: This study demonstrates for the first time the feasibility of PET with ^{68}Ga-NOTA-NGR for noninvasive and sequential determination of CD13 expression in rat heart after MI/R. This will facilitate monitoring of CD13 in the individual wound healing processes, allowing patient-specific therapies to improve outcome after MI.

OP476

Retrospective detection of remote and brief experimental myocardial ischemia using 99mTc-Fucoidan SPECT

N. Mikail[1], N. Anizan[2], L. Louedec[2], F. Al Shoukr[1], J. Michel[2], D. Letourneur[2], C. Chauvierre[2], D. LE GULUDEC[1], F. Rouzet[1]; [1]Nuclear Medicine Department, Bichat-Claude Bernard Hospital, APHP, Paris, FRANCE, [2]INSERM, U1148, Cardiovascular Bioengineering, Paris, FRANCE

Aim: the retrospective identification of a remote acute coronary syndrome is a diagnostic challenge. Because adhesion molecules such as selectins persist on the endothelial surface after ischemia has resolved, they represent a tissue “imprint” of the prior ischemic event, referred to as ischemic memory. The aim of this study was to assess whether 99mTc-fucoidan

SPECT, a P-and E-selectin targeting agent, allows to detect myocardial ischemic memory in a rat model of ischemia-reperfusion. Methods: Transient myocardial ischemia was induced in male Wistar rats by coronary ligation. Ischemia duration ranged from 5 min to 20 min and reperfusion duration ranged from 2 to 24 hours. SPECT/CT acquisitions were performed 2 hours after injection of 70 MBq 99mTc-Fucoidan. Images were visually assessed for the presence of a focal tracer uptake in the cardiac area. The animals were then sacrificed and the heart explanted, frozen and cut in slices for autoradiography (quantified using the uptake ratio between the area at risk and remote myocardium) and histology/immunostaining (P-/E-selectin expression). Results: For a constant delay of 2 hours of reperfusion, myocardial uptake of 99mTc-Fucoidan was detected after ischemia duration ranging from 20 minutes (3/3 rats), 10 minutes (3/4 rats) and 5 minutes (5/14 rats). On autoradiography, the uptake ratio of 99mTc-Fucoidan was 7.6 [4.6-8.4] at 20 min, 5.6 [3.8-12.1] at 10 min and 4.6 [2.0-8.2] at 5 min. Areas of 99mTc-Fucoidan increased uptake matched with endothelial expression of P-selectin. After 6 hours of reperfusion duration, the 99mTc-Fucoidan uptake was detected in 4/4 rats (10 min ischemia) and 3/5 rats (5 min ischemia). After 24 hours of reperfusion duration, 99mTc-Fucoidan uptake was detected in 3/7 rats (10 min ischemia) and 4/9 rats (5 min ischemia). Conclusion: This preliminary study shows that brief coronary occlusions (5 minutes) followed by reperfusion durations up to 24 hours are associated with P- and E-selectin endothelial expression, detectable in vivo by 99mTc-Fucoidan SPECT. Therefore, 99mTc-Fucoidan is a promising agent that could be useful in the retrospective diagnosis of acute coronary syndromes.

1405 - Tuesday, October 13, 2015, 2:30 PM - 4:00 PM, Hall G2
Young EANM Daily Forum 3: Young Investigator Meeting

OP477

Preparation of Carrier Free Yttrium-90 for Medical Applications Using a Novel Home-Made Y-Imprinted Sorbent

M. Abedi[1], **S. Shirvani Arani**[2], A. Bahrami Samani[3], M. Nabid[1]; [1]Department of Chemistry, Faculty of Science, Shahid Beheshti University, Tehran, IRAN, ISLAMIC REPUBLIC OF, [2]Assistant Professor Radiopharmaceutical Research and Development Lab (RRDL), Tehran, IRAN, ISLAMIC REPUBLIC OF, [3]Radiopharmaceutical Research and Development Lab (RRDL), Tehran, IRAN, ISLAMIC REPUBLIC OF.

Aim: Synthesis and characterization of a novel acryl amide-based yttrium imprinted sorbent via the ATRP approach for the preparation of medical-grade 90Y. Materials and methods: 2,2-bis(2-bromo-2-methylpropanoate)propane-1,3-disuccinate (L), which was synthesized in three steps in our lab, was used as an excellent chelating agent and also as an initiator for the preparation of a novel acryl amide-based ion imprinted polymer (IIP) for selective sorption of radio-yttrium. The YIP was prepared via copolymerization of the (Y- L) complex with acryl amide as the functional monomer and N,N'-methylenebisacrylamide as a crosslinking agent using the ATRP approach. The synthesized compounds were characterized, and sorption/desorption examination was performed. The prepared Y-IIP was used as a sorbent for the selective separation of 90Y from a synthetic solution of 90Y/Sr(natural, stable)/Zr(natural, stable). To the best of our knowledge, this was the first ionic-imprinted sorbent used to prepare carrier free 90Y. Results: The data confirmed the perfect separation of Sr(II) and Zr(II) from 90Y, which was maintained successfully on the column and eluted afterwards. As a result, the prepared, highly yttrium-selective sorbent can be used for the separation of Y-90 from its long-lived parent, Sr-90. In addition, if there are any other impurities even in trace amounts, such as Zr(II) that is a decay product of Y-90, they can be removed effectively to prepare medical grade 90Y from a long-lived 90Sr source via the least facility. Conclusion: In this study, a new acryl amide-based sorbent was synthesized in order to prepare medical-grade 90-yttrium. The synthesis was conducted through atom transfer radical copolymerization of AAm and MBAAm in the presence of BMPPS as the initiator and chelator for Y(III) ion that is capable of extracting and preconcentrating traces of Y(III) ion. The effective parameters of the yttrium (III) preconcentration were investigated. Due to the high selectivity obtained by the aforementioned, new, acryl amide-based sorbent, it can be used effectively for the selective separation and pre-concentration of yttrium (III). In future studies, we plan to utilize the prepared sorbent to fabricate a set of serial columns for the preparation of a 90Sr/90Y column chromatographic generator to obtain carrier-free 90Y. The freshly eluted radionuclide then can be used for radiolabeling of the peptides and antibodies that are used in targeted therapy for various types of cancers and solid tumors.

OP478

Cyclotron production of 43Sc - new radionuclide for PET technique

A. Bilewicz[1], R. Walczak[2], K. Szkliniarz[3], M. Sitarz[4], S. Krajewski[2], K. Abbas[5], J. Choinski[4], I. Cydzik[5], A. Jakubowski[4], J. Jastrzębski[4], A. Stolarz[4], A. Trzcińska[4], W. Zipper[3]; [1]Institute of Nuclear Chemistry and Technology, WArsaw, POLAND, [2]Institute of Nuclear Chemistry and Technology, Warsaw, POLAND, [3]Department of Nuclear Physics, University of Silesia, Katowice, Poland, Katowice, POLAND, [4]Heavy Ion Laboratory, University of Warsaw, Warsaw, POLAND, [5]European Commission, Joint Research Centre, Institute for Health and Consumer Protection, Ispra, ITALY

Aim: The ^{43}Sc ($t_{1/2}$ = 3.89 h) is an ideal β^+-emitter in PET diagnosis. It can be used as an alternative to ^{68}Ga, because ^{43}Sc has longer half-life and forms stable radiobioconjugates with a structure similar to ^{90}Y and ^{177}Lu, that is important in planning radionuclide therapy. In comparison with ^{44}Sc -other proposed isotope of scandium - ^{43}Sc has half-life and beta plus radiation similar to ^{44}Sc, moreover gamma-ray energy emission and intensity is much lower (372 keV, 23%) than in case of ^{44}Sc (1157 keV, 99%) what is not negligible for patient and medical personnel. ^{43}Sc can be produced via the $^{nat}Ca(\alpha,x)^{43}Sc$ reaction in medium size cyclotrons or in reactions $^{43}Ca(p,n)^{43}Sc$ and $^{42}Ca(d,n)^{43}Sc$ carried in small medical cyclotrons. The aim of our work was to find optimal parameters for target irradiations in order to maximize the production of ^{43}Sc with minimal impurities and to develop a simple chemical procedure for separation of ^{44}Sc from the calcium target. Materials and methods: In the present work, we used either high purity natural $CaCO_3$ or enriched $^{42}CaCO_3$ and $^{43}CaCO_3$ targets (Isoflex, Russia). The irradiations have been performed with the Scanditronix MC 40 Cyclotron of the Joint Research Centre (Ispra, Italy), or U-200P and GE-PETtrace cyclotrons of the Heavy Ion Laboratory, University of Warsaw. Target materials for irradiation were compacted into the specially designed aluminum capsules or were pressed into a rectangular pellet wrapped in the pre-formed aluminum foil and fixed to a water cooled target holders. The activities of the samples were measured with high resolution γ-ray spectrometry. $CaCO_3$ targets were dissolved in 0.2 M HCl and an ion exchange resin Chelex 100 was used to separate ^{43}Sc from target material.^{43}Sc-DOTATATE was synthesised with different amounts of the peptide and at various pH. Results: The three proposed methods of ^{43}Sc production allow obtaining the high activity of the radionuclide. ^{43}Sc was separated from the targets on iminodiacetic resin with efficiency higher than 95% and eluted in volume of 0.3 ml. The recovery of the calcium material is also very high (~90 %). The level of Ca^{2+} in ^{43}Sc fraction is less than 3 μg/ml. Conclusions: The ^{43}Sc radionuclide can be produced in amount of several GBq. The proposed production procedures are simple and fast. The synthesis and purification procedure can be simplified using C18 Sep-Pak® columns.

OP479

Production of High Specific Activity 186Re for Cancer Therapy Using WO3 Targets in a Proton Beam

M. E. Fassbender[1], E. R. Birnbaum[1], J. W. Engle[1], M. D. Gott[2], K. D. John[1], J. R. Maassen[1], F. M. Nortier[1], J. W. Lenz[3], C. S. Cutler[4], A. R. Ketring[4], S. S. Jurisson[4], E. R. Balkin[5], D. S. W. Wilbur[5]; [1]Los Alamos National Laboratory, Los Alamos, NM, UNITED STATES, [2]University of Missouri, Columbia, MO, UNITED STATES, [3]John Lenz and Associates, East Lansing, MI, UNITED STATES, [4]Univeristy of Missouri, Columbia, MO, UNITED STATES, [5]Univeristy of Washington, Seattle, WA, UNITED STATES

Rhenium-186 is a β-γ emitter with a half-life of 90.64 h and a $\beta-$ end-point energy of 1.07 MeV. The isotope is suitable to treat cancers of small dimensions (mm range). Moreover, its γ-emission at 137.15 keV is in the energy range favorable for both γ-camera and SPECT imaging. Current production methods rely on the neutron capture induced reaction 185Re(n,γ) in a reactor and are associated with low specific activities (0.6 kCi/mmol), thereby limiting the application of the isotope to palliative treatments. Production via charged particle irradiation of enriched 186W results in a 186Re product with a much higher specific activity; allowing its use in therapeutic nuclear medicine. Test targets of both sintered and pressed natWO3 powder were proton irradiated at the Los Alamos Isotope Production Facility (LANL-IPF) to evaluate radionuclide product yields, impurities, irradiation parameters and wet chemical Re recovery for a bulk production. We demonstrated that 186gRe can be isolated in 97% yield from irradiated natWO3 targets within 12 h of end of bombardment (EOB) via an alkaline dissolution followed by anion exchange. Tungsten (VI) oxide can be easily recycled for recurrent irradiations. Using a sintered target, 186Re batch yields of 42.7 +/- 2.2 μCi/μAh (439 +/- 23 MBq/C) (with respect to 186W content) were obtained after 24 h of irradiation in proton beams. The target entrance energy of the proton beam was determined to be 15.6 MeV. The specific activity of 186gRe at EOB was measured to be 1.9 kCi (70.3 TBq)/mmol. Based upon our studies of natWO3, a target of enriched 186WO3 irradiated in a proton beam of 250 μA for 24h can provide batch volumes of roughly 250 mCi (9.25 GBq) of 186gRe at EOB with a specific activity approaching the theoretical value of 35kCi/mmol (1295 TBq/mmol).

OP480

Direct production of 99mTc-Technetium using low energy cyclotrons and radionuclidic purity: our results so far using natMo-Molybdenum

L. Metello[1,2], P. Costa[1], L. Cunha[1,2], R. Jonhson[3], L. Matei[3], W. Gelbart[4], J. Obermair[5], C. Artner[5], P. Lass[6], G. Currie[7], L. Craciun[8], D. Niculae[8], S. Carmo[9], F. Alves[9], M. Botello[10]; [1]Nuclear Medicine Department, ESTSP.IPP, Porto, PORTUGAL, [2]Nuclear Medicine Department, IsoPor SA, Porto, PORTUGAL, [3]BSCI - Best Cyclotron Systems Inc, Vancouver, DC, CANADA, [4]ASD - Advanced Systems Design Inc, Vancouver, DC, CANADA, [5]IASON GmbH, Graz, AUSTRIA, [6]Medical Faculty, University of Gdansk, Gdansk, POLAND, [7]School of Dentistry and Health Sciences, Charles Sturt University, Wagga Wagga, AUSTRALIA, [8]Horia Hulubei National Institute of Physics & Nuclear Engineering, Bucarest, ROMANIA, [9]ICNAS - Institute for Nuclear Sciences Applied to Health, University of Coimbra, Coimbra, PORTUGAL, [10]IBILI, Medical Faculty, University of Coimbra, Coimbra, PORTUGAL

Introduction: Despite the global crisis concerning 99mTc delivering to Nuclear Medicine Departments there isn't yet a reliable solution. The cyclotron direct production of 99mTc, using the 100Mo(p,2n)99mTc nuclear reaction is our attempt to approach the problem, aiming to become efficient, reliable and sustainable from points of view as reducing drastically the radioactive waste being produced and becoming beneficial for all the involved parts. Between several critical factors, radionuclidic purity of cyclotron-produced 99mTc is being pointed as an issue of concern. Aim: This paper aims to disseminate the results being obtained so far in what concerns radionuclidic purity of the 99mTc already produced from natMo and some extrapolation calculi for the use of high-level of purity 100Mo. Material and Methods: natMo foils were stacked into a solid target of aluminum and short irradiations (with ~1-2 to 20 μA proton beams, during 2 to 20 seconds) were performed, using our in-house developed targets and target holder systems, on three different cyclotrons (IBA Cyclone-18, ACSI TR19 and GE PETtrace). Beam energy degraders based on aluminum were developed in-house with thicknesses calculated using SRIM/TRIM, allowing irradiations with 15 MeV in the IBA and GE machines. Produced activity was quantified using HPGe gamma spectroscopy to obtain the overall amount of 99mTc produced, as well as the different contaminants (such as 93Tc, 93mTc, 94Tc, 94mTc, 95Tc, 95mTc, 96Tc, 96mTc, 99Mo and 96Nb) whose activity was analyzed in terms of ratios in order to 99mTc activity. Novel ratios were extrapolated from our experimental data to an ideal case of irradiations using 100Mo enriched targets (with purities of 97,42% and 99,5%). Results: It has been observed, that 19 and 18 MeV irradiations of natMo lead to an higher level of contaminants, with produced yields of some contaminants much higher than those of 99mTc being produced (e.g.: 93Tc, 94Tc and 95Tc), however, extrapolated contaminant ratios for enriched targets suffer a reduction, even considering values deserving attention (e.g.: 94Tc/99mTc ≥ 1% or 93Tc/99mTc ≥ 3%). On other hand, our results confirm our hypothesis that 15 MeV irradiations could maintain considerable production yields, with a significant decrease of contaminants, with almost all extrapolated ratios reaching values ≤ 1%. Conclusion: Radionuclidic purity is a critical issue for the implementation of alternative routes for 99mTc production and our actual data points that 15 MeV proton beams could be considered, since drastically reducing contaminants while easing production and purification processes.

OP481

Extremely rapid, kit-based biomolecule labelling and molecular imaging with gallium-68: tris(hydroxypyridinone) chelators

M. T. Ma[1], J. D. Young[1], C. Imberti[1], C. Cullinane[2], M. S. Cooper[1], L. Meszaros[1], S. Y. A. Terry[1], B. Paterson[1], G. E. D. Mullen[1], J. R. Ballinger[1], P. Roselt[2], R. J. Hicks[2], P. J. Blower[1]; [1]King's College London, London, UNITED KINGDOM, [2]Peter MacCallum Cancer Centre, Melbourne, AUSTRALIA

The gallium-68 (68Ga) generator offers PET molecular imaging to hospitals without a cyclotron if simple labelling methods are devised. Current 68Ga clinical radiopharmaceutical syntheses require high temperatures (greater than 90 °C), and extended reaction times (5 - 20 min). We have previously shown that tris(hydroxypyridinone) (THP) ligands rapidly label with 68Ga quantitatively under mild conditions (Chem Commun, 2011; 47:7068). We now report the development of one-step labelling methods equivalent to kit formulation protocols, and the ability of 68Ga-THP peptide conjugates to image expression of peptide receptors in tumours in vivo. The THP-Ac chelator was labelled with 68Ga-generator eluate under a range of THP-Ac concentrations (0.1-1000 μM), pH values (4 - 7), buffers, and trace metal concentrations (Mg(II), Fe(III), Zn(II)). At 10 μM, 20 °C and all pH values and times, labelling efficiency of THP-Ac reached greater than 95% in under 2 min, and was unaffected by contaminating Mg(II), Zn(II) and Fe(III) at 30, 20, 0.3 mg/L, respectively. Vials containing lyophilised THP-Ac and buffer salts gave quantitative radiolabelling with unprocessed eluate in less than 5 min. New bifunctional chelator isothiocyanate and carboxylate derivatives of THP were synthesised and conjugated to (i) cyclic(RGDfK) peptides for targeting αvβ3 integrin expression, (ii) Tyr3-octreotate (TATE) peptide for targeting SSTR2 expression in neuroendocrine tumours, (iii) a urea-containing peptide targeting PSMA receptors for prostate tumours, and (iv) the monoclonal antibody, trastuzumab for HER2 receptors. All conjugates were labelled with 68Ga in greater than 95% radiochemical yield and high specific activity (up to 80 MBq/nmol at the point of administration) at 25 °C and formulated to pH 6 - 7 in 2 - 5 min. Biodistribution of tested αvβ3- and SSTR-targeting conjugates showed tumour-specific uptake and retention of target receptor affinity. Excretion was rapid and predominantly renal. Serum stability and biodistribution experiments point to excellent in vivo stability of the new radiotracers with respect to the 68Ga-THP complex. Notably, in vivo tumour uptake and biodistribution of 68Ga-THP-TATE was comparable to that of the clinical radiopharmaceutical, 68Ga-DOTA-TATE.The new tris(hydroxypyridinone) chelator and its conjugates enable

rapid radiolabelling with 68Ga under mild conditions without subsequent purification. The simplicity of radiochemical syntheses based on such conjugates is conducive to translation to one-step kit-based radiosyntheses that would greatly facilitate the expansion and adoption of 68Ga PET in hospitals.

OP482

Microfluidics and Microwave Assisted Synthesis of 99mTc(CO)3-MIP-1505, a ligand for carbonic anhydrase IX (CAIX). Comparison to Conventional Heating

J. Kelly, A. Amor-Coarasa, J. W. Babich; Weill Cornell Medical College, New York, NY, UNITED STATES

AIM: To compare the formation of a $^{99m}Tc(CO)_3$ complex and the subsequent labeling of **MIP-1505**, a ligand for carbonic anhydrase IX, using a microfluidics system, a microwave reactor, and a conventional heating block. METHODS: The microfluidics labeling experiments were undertaken on a NanoTek LF system (Advion) with the reactor coil heated to 150°C. A 150 μg/mL solution of MIP-1505 in DMSO and a 3.7 GBq/mL solution of $^{99m}TcO_4^-$ in saline containing 6 mg $CH_3BNa_2O_2$, 2.9 mg $Na_2B_4O_7.10H_2O$, 8.5 mg $C_4H_4Na_2O_6.2H_2O$, 7.2 mg Na_2CO_3 ("Isolink kit") were passed through the reactor at a maximum combined flow rate of 30 μL/min. Reaction times varied from 1-3 minutes according to stoichiometry and flow rates. Labeling in the microwave reactor (Biotage) was undertaken at 100°C, 125°C, and 150°C. Formation kinetics of the $^{99m}Tc(CO)_3$ complex were evaluated in the absence of MIP-1505. A solution of 50 μg MIP-1505 in 0.5 mL saline was added to the tricarbonyl kit, and the reaction was heated for up to 20 minutes. Synthesis of $^{99m}Tc(CO)_3$-MIP-1505 on a heating block (ThermoFisher) was undertaken over 60 min at 100°C[1].RESULTSIn 1 minute, 3 μg MIP-1505 was labeled in 91.2±0.6% yield in the microfluidics system. When reaction time was 2 minutes, 2.2 μg MIP-1505 was labeled in a similar yield. In both cases, 6-8% of the unbound ^{99m}Tc was in the form of the $^{99m}Tc(CO)_3$ complex. Rapid and nearly quantitative tricarbonyl formation was observed after 1 minute of microwave heating at 125°C (98.9±0.16%) and 150°C (99.9±0.2%), and after 2 minutes at 100°C (98.5±0.46%). Labeling of MIP-1505 was most rapid at 150°C, reaching 58.5±4.1% after 5 minutes. At 125°C the maximum labeling was 67.6±0.4% (10 minutes), while at 100°C the labeling was 51.1±3.4% (20 minutes). By conventional heating, the labeling of MIP-1505 was 63±12% after 60 minutes. CONCLUSIONS: Synthesis by microfluidics provides $^{99m}Tc(CO)_3$-MIP-1505 in high specific activity and with the greatest yield, though there is no time advantage relative to microwave heating when a clinical dose (<185 MBq) is produced. Both microwave heating and microfluidics are significantly faster than conventional heating with no significant difference in labeling yield. This is advantageous in the planning of pre-clinical and/or clinical studies. Economy of time and reagents makes microfluidics an attractive approach for the production of $^{99m}Tc(CO)_3$-MIP-1505 for pre-clinical studies, while microwave heating appears to be the most promising route to a clinical dose.[1] Lu, et al. J. Med. Chem. 2013, 56, 510-520.

OP483

Microfluidics Assisted Labeling of 68Ga-DOTATOC: Advantages and Limitations.

A. Amor-Coarasa, J. M. Kelly, J. W. Babich; Weill Cornell Medical College, New York City, NY, UNITED STATES

Aim: To maximize 68Ga-DOTATOC specific activity (SA) and minimize reaction time by using microfluidics (MFs) assisted chelation chemistry. Materials and Methods: Gallium-68 (68Ga) was obtained by eluting with 4 ml 0.05M HCl a 1.85 GBq (50 mCi, at calibration) itG 68Ge/68Ga Generator. Labeling was performed in a NanoTek Microfluidic Flow-Chemistry System (Advion, USA). The eluate was buffered with 120 μl of 3N NaOAc (pH 4-5). DOTATOC was prepared as a 100 μg/ml solution in the same buffer. The effect of stoichiometry and temperature (95 or 150 °C) was studied. Labeling was also performed in a conventional heater (CH) for comparison. Radio-HPLC was used to determine radiochemical yield (RCY) and purity. Results: The RCY of 68Ga-DOTATOC using MFs was nearly 70% (68.3±2.4%) at 150°C as compared to 46.5±4.4% at 95°C. RCY was not significantly dependent on DOTATOC mass within the 60 ng (42.2 pmol) to 150 ng (105 pmol) range. At 95°C, MFs labeling of DOTATOC varied from 41.6±6.5% (60 ng) to 50.7 ±3.5% (150 ng). The variation was similarly low at 150°C, with RCYs of 65.7±2.1% (60 ng) and 70.3±1.8% (150 ng). When the mass of DOTATOC was decreased to 15 ng, labeling yields decreased to 3.2±0.7% at 150°C and no labeling was observed at 95°C. Despite the high labeling yields (≈70% with 100 ng of DOTATOC at 150°C vs. <1% with CH at 95°C) obtained in 1 minute with the microfluidics system, the critical parameter for radiopharmaceutical production is radionuclide concentration. The maximum activity that can be produced in one minute using the buffered generator elution is 25.9 MBq (0.7 mCi), such that over 7 minutes are necessary to produce a patient dose of 185 MBq (5 mCi). During this time greater dose (lower SA) can be produced with CH. Use of 68Ga pre-concentration systems[1] allows the same patient

dose in 3 min, however increased manipulation is needed. In contrast preclinical doses can be obtained within seconds. Conclusion: Microfluidics assisted reactions have great potential for preparation of high specific activity products minimizing precursor degradation at high temperatures. It shows clear advantages for discovery applications and preclinical testing. However clinical application is severely limited by low activity/time production and high equipment costs. High potential for flow interruption also reduces its reliability for everyday radiopharmaceutical production in a clinical setting. References: 1: Alejandro Amor-Coarasa; Seza Gulec; Anthony McGoron; Inexpensive and cGMP capable Ga-68 purification system; J Nucl Med. 2012; 53 (Supplement 1):1742

OP484

A Fast Optical Method for Radiochemical Purity Evaluation

A. E. Spinelli[1], C. R. Gigliotti[1], F. Boschi[2]; [1]San Raffaele Scientific Institute, Milano, ITALY, [2]University of Verona, Verona, ITALY

Aim: The standard technique to evaluate the radiochemical purity (RCP) is the thin-layer chromatography. RCP is an important index for the radiopharmaceutical QA because identify the percent of the total radioactivity present in the desired chemical form in a radiopharmaceutical. This value is commonly obtained from the activity distribution measured with a conventional radiation detector along the chromatographic strip (CS). We propose here an alternative CCD-based approach to quickly image the CSs.Methods: We use a system composed of cooled electron multiplied charge coupled device (EMCCD) coupled with lens mounted on a light-tight box and a high-resolution intensifying screen for radiation conversion. CSs with 7 kBq of 68Ga-DOTANOC and 5 kBq of 99mTc-HMDP were imaged. A photographic image is acquired and then the samples are covered with the screen. The emissive signal is acquired for 10s. In order to validate our approach, the same strips were imaged with the Cyclone Plus Storage Phosphor system (Perkin-Elmer) based on a conventional PSP, routinely used to analyse CSs.Results and conclusion: From the activity profile evaluated along the signal of the 68Ga-DOTANOC acquired with the commercial system and with our optical system, we measured a RCP equal to 97.9% and to 96.8%, respectively. The 1.1% difference between the measured RCP shows a good accuracy of the optical approach. The analysis of the images of two strips treated with 99mTc-HMDP obtained with the two systems confirms the efficiency of the optical method. We observe that a quantitative analysis of CSs can be done using 10 sec (or even less) of exposure time with an optical system For this reason, the optical approach provides a quicker method to evaluate RCP with respect to the conventional one that takes few minutes. Furthermore the fusion of photographic and emissive images allows spatially localizing signals, permitting a convenient simultaneous analysis of different samples that cannot be done using conventional methods. The results show that the intensifying screen, even if is optimized for low energy X rays, can be reliably used also for γ and β radiations conversion.

1406 - Tuesday, October 13, 2015, 2:30 PM - 4:00 PM, Hall 6
M2M: Molecular & Multimodality Imaging: Therapy - Preclinical Studies, a & ß Radiation

OP485

Alpha- versus beta-emitting particles for pretargeted radioimmunotherapy of CEA-expressing human colon cancer xenografts

S. Heskamp[1], R. Hernandez[2], J. D. M. Molkenboer-Kuenen[1], M. Essler[3], F. Bruchertseifer[4], A. Morgenstern[4], W. J. G. Oyen[1], C. Seidl[5], W. McBride[6], D. M. Goldenberg[6], O. C. Boerman[1]; [1]Radboud University Medical Center, NIJMEGEN, NETHERLANDS, [2]University of Wisconsin, Madison, WI, UNITED STATES, [3]University of Bonn, Bonn, GERMANY, [4]Joint Research Centre – Institute for Transuranium Elements, Karlsruhe, GERMANY, [5]Klinikum rechts der Isar der Technischen Universität München, Munchen, GERMANY, [6]Immunomedics, Morris Plains, NY, UNITED STATES

Aim: Pretargeted radioimmunotherapy (PRIT) with the anti-CEA x anti-HSG bispecific antibody TF2, and ^{177}Lu-labeled di-HSG-DOTA peptide IMP288, can delay growth of CEA-expressing xenografts. A phase I study has shown the safety and feasibility of PRIT in colorectal cancer patients. The therapeutic efficacy of PRIT may be improved by using alpha-emitting radionuclides. The aim of this study was to compare the therapeutic efficacy of ^{213}Bi and ^{177}Lu for PRIT of CEA-expressing xenografts. Material and methods: The vitro binding characteristics (IC_{50}, K_d, internalization) of ^{213}Bi-IMP288 were compared to ^{177}Lu-IMP288. Tumor targeting of ^{213}Bi-IMP288 and ^{177}Lu-IMP288 was studied in mice with s.c. LS174T tumors that were pretargeted with TF2. Finally, the effect of ^{213}Bi-IMP288 (6, 12, or 17 MBq) and ^{177}Lu-IMP288 (MTD: 60 MBq) on tumor growth and survival was assessed. Toxicity was determined by monitoring body weight and by analyzing blood samples for haematological toxicity (haemoglobin, leucocytes, platelets). Results: Binding characteristics of ^{213}Bi-IMP288 were similar to ^{177}Lu-IMP288 (K_d = 0.8 nM). Tumor uptake was observed as early as 15 min post injection (9.2 ± 2.0 %ID/g) and the peptide cleared rapidly from the circulation. At 30 min post injection the blood level of ^{213}Bi-IMP288 was 0.44 ± 0.28 %ID/g. Uptake of ^{213}Bi-IMP288 in normal tissues was very low, except for some

uptake in the kidneys (1.8 ± 1.1 %ID/g). The biodistribution was comparable to ^{177}Lu-IMP288. PRIT treated mice showed significant inhibition of tumor growth and prolonged survival. Mean tumor doubling time for the PBS, 6 MBq ^{213}Bi-IMP288, 12 MBq ^{213}Bi-IMP288, and 60 MBq ^{177}Lu-IMP288 group was 3.3 ± 0.3, 6.5 ± 1.2, 11.1 ± 3.2, and 11.8 ± 9.3 days. Median survival for the PBS and 6 MBq ^{213}Bi-IMP288 group was 22 and 31 days, respectively. The 12 MBq ^{213}Bi-IMP288 and 60 MBq ^{177}Lu-IMP288 groups did not yet reach the median survival at day 35. Mice receiving 17 MBq ^{213}Bi-IMP288 showed significant weight loss, resulting in a median survival of 24 days. Tumor doubling time could not be reliably estimated for this group. No changes in haemoglobin, platelets, and leucocytes were observed. Conclusion: This study showed that PRIT with ^{213}Bi-IMP288 is feasible and at least as effective as ^{177}Lu-IMP288. Haematological toxicity and survival of mice treated with 12 MBq ^{213}Bi-IMP288 and 60 MBq ^{177}Lu-IMP288 were comparable. Future experiments should study the effect of multiple cycles ^{213}Bi- and ^{177}Lu-IMP288 on tumor growth, survival, and haematological and renal toxicity.

OP486

Targeted Radionuclide Therapy using high-LET particle emitter-labeled vectors against alpha-v-beta6-expressing cancers

S. PAILLAS[1], A. DESAI[2], I. QUETIER[2], J. MARSHALL[2], J. POUGET[3], J. SOSABOWSKI[1]; [1]Centre for Molecular Oncology, Barts Cancer Institute, London, UNITED KINGDOM, [2]Centre for Tumor Biology, Barts Cancer Institute, London, UNITED KINGDOM, [3]Inserm U1194, Montpellier, FRANCE

Targeted radionuclide therapy (TRT) has emerged as an attractive approach in cancer therapy since it allows the specific irradiation of tumor cells while sparing healthy tissues. TRT of solid tumors has a limited efficacy mainly because these tumors have high radioresistance and take up limited amounts of radiolabeled vectors. Strategies to overcome this include the use of small peptides and radionuclides that emit highly cytotoxic particles, namely high linear energy transfer (LET) particles such as alpha particles and Auger electrons. The epithelial-specific integrin avb6 is weak or absent on normal tissues but is upregulated in many cancers and is strongly associated with reduced survival. We have previously shown in vivo tumour targeting using radiolabelled A20FMDV2 a 20-mer avb6-specific peptide. Aims: The aim of the study is to assess the efficacy and toxicity of TRT in mice using both an internalising radiolabeled peptide and non-internalising monoclonal antibody (mAb) against avb6. The second aim is to validate in vivo gamma-H2AX (through γ-H2AX-MDC1 interaction) measurement as an indicator of the efficacy or toxicity of TRT by a novel quantitative and noninvasive imaging approach. Materials and methods: The 20 mer high affinity avb6-targeting peptide, A20FMDV2 used in previous work has been derivatised to contain a trimethylstannyl benzamide moiety so that it can be radiolabelled with high LET particle emitters: Auger electron emitter 125I and alpha particle emitter 211At. The peptide has been radiolabelled with 125I and radioligand binding and internalization assays have been carried out in cells that overexpress avb6 and compared with that of the 111In-DTPA-A20FMDV2 studied previously. In addition, lentiviral vectors encoding the reporter genes (γ-H2AX/MDC1-Luc2) were made by molecular cloning and used to coinfect avb6 expressing cells. To verify that our γ-H2AX/MDC1-Luc2 reporter functions well in tissue culture, stably infected cells were exposed to varying degrees of stress and the activities of reporter genes was observed by bioluminescence imaging and by western blot analyses of phosphorylated H2AX or Nluc2-H2AX. Results and conclusions: The peptide could be radiolabelled with radiolabelling efficiencies of 80-90% and purified to 100 % using Sep-Pak. Radioligand saturation binding assays show Kd and internalization rate comparable with that of the 111In-DTPA construct. Robust reporter activation can be observed in cells coinfected with reporter genes γ-H2AX/MDC1-Luc2 by bioluminescence imaging and western blot. These cells will be xenografted in mice to evaluate double strand breaks in vivo after TRT.

OP487

Involvement of direct and indirect (bystander) cytotoxic effects in alpha-RIT of small volume peritoneal carcinomatosis using ^{212}Pb-labeled mAbs

J. Pouget[1], R. Ladjohounlou[1], A. Pichard[1], V. Boudousq[1], S. Paillas[1], M. Le Blay[1], C. Lozza[1], M. Bardies[2], S. Marcatili[2], N. Chouin[3], J. Torgue[4], I. Navarro-Teulon[1]; [1]IRCM/INSERMU1194, MONTPELLIER, FRANCE, [2]UMR 1037 INSERM/UPS, TOULOUSE, FRANCE, [3]AMAROC, ONIRIS, Nantes, FRANCE, [4]AREVA Med, BETHESDA, WI, UNITED STATES

Hypothesis: We investigated in vitro and in vivo the relative contribution of direct and indirect (bystander) effects in the therapeutic efficacy of 212Pb-labeled mAbs used for treating small volume peritoneal carcinomatosis.Methods: In vitro, we investigated in A-431 cells exposed to increasing activities (0-0.5 MBq/mL; 37 MBq/mg) of either 35A7 (anti-CEA), Trastuzumab (anti-HER2) or PX (non-specific) 212Pb-labeled mAbs the relative contribution to cell killing of direct and bystander effects using standard medium transfer protocol. Biological end points included clonogenic survival and oxidative DNA damage including DNA double strand breaks measured both in donor (direct effect) and in recipient cells (bystander effects). Mean absorbed dose to the nucleus of donor cells was also determined using MIRD formalism. In vivo,

nude mice with intraperitoneal (i.p.) 2-3 mm A-431 tumor cells xenografts were i.p. injected with increasing activities (370-1480 kBq; 37 MBq/mg) of the above mentioned anti-CEA, anti-HER2 or non-specific 212Pb-mAbs. Determination of radioactivity at the tissue level was done using digital micro-autoradiography (DAR) and absorbed doses were calculated. Biological markers including 53BP1, caspase 3 and Ki67 proteins were also determined in tissue by immunohistochemistry. Results: In vitro we showed in donor cells the strong efficacy of 212Pb-35A7 and 212Pb-trastuzumab mAbs and also to a lower extent of 212Pb-PX mAb. Significant bystander cytotoxicity was measured in all recipient cells with the three radiolabeled mAbs. The complexity of DNA damage (53BP1 foci) observed in donor cells confirmed the high LET cytotoxic effects of 212Pb-mAbs while less complex damage were observed in recipient cells. In vivo, dose distribution was calculated using DAR analysis and voxel dosimetry. Results showed a strong dose gradient for anti-CEA 212Pb-mAbs while it was much more homogeneous for anti-HER2 or for the non-specific 212Pb-mAbs. These results explain the relative higher therapeutic efficacy previously reported in vivo for anti-HER2 212Pb-mAbs compared with anti-CEA 212Pb-mAbs. However, we also observed a similar formation of DNA damage in tissue independently of tumour absorbed doses thereby indicating that bystander effects could also be involved. Conclusions: Our results showed in vitro and in vivo the strong direct effects of 212Pb-labeled mAbs in killing tumour cells. Heterogeneity in mAbs distribution would explain the relative lack of efficacy per Gy (to the whole tumour) of anti-CEA mAbs compared with anti-HER2 mAbs. However, our preliminary data indicate that bystander effects would participate to 212Pb-labeled mAbs efficacy.

OP488

Targeted Alpha Radionuclide Therapy of Prostate Cancer Using a Small Molecule Inhibitor of Prostate-specific Membrane Antigen (PSMA)

K. L. S. Chatalic[1,2,3], S. Heskamp[4], J. Nonnekens[1,5], J. D. M. Molkenboer-Kuenen[4], D. van Gent[5], F. Bruchertseifer[6], A. Morgenstern[6], M. Weineisen[7], H. Wester[7,8], W. M. van Weerden[3], O. C. Boerman[4], M. de Jong[1,2]; [1]Department of Nuclear Medicine, Erasmus MC, Rotterdam, NETHERLANDS, [2]Department of Radiology, Erasmus MC, Rotterdam, NETHERLANDS, [3]Department of Urology, Erasmus MC, Rotterdam, NETHERLANDS, [4]Department of Radiology and Nuclear Medicine, Radboud University Medical Centre, Nijmegen, NETHERLANDS, [5]Department of Genetics, Erasmus MC, Rotterdam, NETHERLANDS, [6]Joint Research Centre – Institute for Transuranium Elements, Karlsruhe, GERMANY, [7]Pharmaceutical Radiochemistry, Technische Universität München, Munich, GERMANY, [8]Scintomics GmbH, Fürstenfeldbruck, GERMANY

Objectives: PSMA is a well-recognized target for imaging and therapy of prostate cancer (PCa); it is expressed in a very high percentage of PCa lesions. Radiolabeled PSMA-inhibitors localize rapidly to tumor lesions, including soft-tissue and bone metastases, but show high uptake in kidneys and salivary glands. The aim of the present study was to evaluate the potential of the alpha emitter ^{213}Bi coupled to PSMA I&T, a DOTAGA-chelated urea-based PSMA inhibitor, for therapy in PSMA-expressing tumor cells *in vitro* and *in vivo* in mouse xenografts. Materials and Methods: PSMA I&T was labeled with ^{111}In or ^{213}Bi. Pharmacokinetics of ^{111}In-PSMA I&T were evaluated in mice bearing subcutaneous PSMA-expressing LNCaP tumors and PSMA-transfected LS174T tumors. Biodistribution was determined 2h after ^{111}In-PSMA I&T injection (0.1-10 nmol). Blocking of PSMA-specific binding to kidneys was investigated by co-injecting 2-(phosphonomethyl)pentane-1,5-dioic acid (PMPA). The therapeutic efficacy of ^{213}Bi-PSMA I&T was tested *in vitro* in LNCaP cells and *in vivo* in LNCaP-xenografted mice. Cells were incubated (20 min) with ^{213}Bi-PSMA I&T, ^{213}Bi-DTPA, or medium, and fixed at 1, 2, 4, 24, and 48h after treatment. Mice were injected with ^{213}Bi-PSMA I&T (0.2 nmol, 5 MBq). Biodistribution was determined at 1h after injection, whereas tumor and kidneys were dissected at 1h and 24h after injection to study the therapeutic DNA-damage response. Fixed tumor cells and dissected tissues were stained with anti-53BP1 and anti-GEMININ antibodies and a TUNEL detection kit. Results: ^{111}In-PSMA I&T showed dose-dependent uptake in LNCaP and LS174T-PSMA tumors (t), kidneys (k), spleen, adrenals, lung and salivary glands. Optimal doses for tumor targeting were 0.1-0.3 nmol. Co-injection of 10 nmol PMPA resulted in a decrease in renal and tumor uptake of 60% and 17%, respectively, improving t/k ratio. Treatment of LNCaP cells with ^{213}Bi-PSMA I&T caused a decrease in cellular proliferation, induction of DNA double-strand breaks and apoptosis. The biodistribution patterns of ^{213}Bi-PSMA I&T and ^{111}In-PSMA I&T were similar. ^{213}Bi-PSMA I&T induced DNA-double strand breaks in LNCaP tumors, from which a significant amount was not repaired at 24h after injection. Conclusion: PSMA I&T is a promising targeting agent for radionuclide therapy of PCa. In this study we showed renal accumulation of this tracer to be efficiently reduced by co-injection of PMPA, while tumor uptake was preserved. Our preliminary results reveal a good targeting and therapeutic effect of ^{213}Bi-PSMA I&T *in vitro* and *in vivo*.*K.L.S.C. and S.H. contributed equally to this work

OP489

The next step in increasing the efficacy of PRRT: Preclinical studies in vicvo and in vitro with ^{213}Bi-[DOTA^0,Tyr^3]-octreotate

H. S. Chan[1], **M. W. Konijnenberg**[1], E. de Blois[1], S. Koelewijn[1], T. Anderson[2], M. Nysus[2], W. A. P. Breeman[1], R. W. Atcher[3], A. Morgenstern[4], F. Bruchertseifer[4], J. P. Norenberg[2], M. de Jong[1]; [1]Nuclear Medicine and Radiology, Erasmus MC, ROTTERDAM, NETHERLANDS, [2]College of pharmacy, University of New Mexico, Albuquerque, NM, UNITED STATES, [3]Los Alamos National Laboratory, Los Alamos, NM, UNITED STATES, [4]European Commission, JRC, Institute for Transuranium Elements, Karlsruhe, GERMANY

Peptide Receptor RadioTherapy shows a reasonable objective response rate of 30-35% with the use of ^{177}Lu-[DOTA^0,Tyr^3]-octreotate (^{177}Lu-DOTATATE). Alpha-particle emitters can augment the therapeutic efficacy of PRRT and make it exceptional, especially in small tumours and metastasis cell clusters. In preclinical studies with alpha-emitter labeled peptides high specific activity is required, because of the high-affinity, but low-capacity of tumour cell receptors. The stability of -particle emitting radiopeptides should be maintained until receptor mediated uptake, both *in vivo* as *in vitro*, to minimize off-targeting effects. Also the radio-peptide should have rapid uptake, high retention in tumour tissue and it should show high clearance capacity from normal tissue. In this study we optimized the application of ^{213}Bi-DOTATATE for targeted alpha-particle therapy *in vitro* and *in vivo*. We investigated for various somatostatin receptor-positive tumour models in mice the therapeutic efficacy of ^{213}Bi-DOTATATE. The labeling procedure for ^{213}Bi-DOTATATE was chemically optimized for preclinical applications. Materials and methods: Therapeutic effects *in vitro* were compared between ^{213}Bi-DOTATATE and ^{177}Lu-DOTATATE, using CA20948 (rat pancreatic tumour) and BON (human carcinoid) cell lines. Uptake in AR42J-bearing nude mice was investigated. Specific peptide receptor binding versus peptide mass, reduction of renal uptake by L-lysine, and mitigation of renal damage after PRRT were determined for ^{213}Bi-DOTATATE. Therapeutic efficacy of ^{213}Bi-DOTATATE was also investigated in CA20948- and H69 (human small lung carcinoma)-bearing nude mice, bearing tumours of different volumes. All experiments were guided by dosimetry to estimate the dose limits in organs and tumours and the relative biological effect of ^{213}Bi-DOTATATE compared to ^{177}Lu-DOTATATE. Results: Labeling of ^{213}Bi-DOTATATE was optimized for preclinical applications under physiologically acceptable conditions. ^{213}Bi-DOTATATE showed more effective cell killing *in vitro* in comparison to ^{177}Lu-DOTATATE at comparable absorbed doses. Tumour uptake *in vivo* depends on the peptide amount and therefore on specific activity. Renal uptake and absorbed renal doses could be decreased by pre-administration of L-lysine, thereby leading to higher tolerated activities and longer survival in nude mice. The therapeutic responses of small and large tumours after ^{213}Bi-DOTATATE did not show differences; in both being highly efficacious. Tumour growth delays of 50 days and more could be achieved compared to 30 days after ^{177}Lu-DOTATATE.Conclusions:^{213}Bi-DOTATATE has proven to be promising and safe in tumours with somatostatin receptor expression over a range of tumour volumes in mice. Optimal labeling conditions were determined for preclinical therapy studies in mice and renal toxicity could be managed by addition of L-lysine.

OP490

Preclinical Comparison of Therapeutic response to Treatment with 177-Lutetium labelled Somatostatin Receptor Agonists and Antagonists

S. Dalm[1], G. Doeswijk[1], S. Koelewijn[1], H. Maecke[2], M. de Jong[1]; [1]Erasmus MC, Rotterdam, NETHERLANDS, [2]University of Basel, Basel, SWITZERLAND

Introduction: Somatostatin receptor (SSTR) agonists are successfully being used in the clinic for radionuclide-mediated imaging and therapy of neuroendocrine tumors. Recently, studies showed a higher tumor uptake of SSTR antagonists compared to SSTR agonists. Furthermore, first studies on the feasibility of imaging and therapy of patients with SSTR antagonist showed promising results. However, to date no studies have been performed to compare the differences in therapeutic effect between SSTR agonists and SSTR antagonists. The aim of this project was to determine differences in therapeutic response after treatment with ^{177}Lu-Octreotate, an SSTR agonist, and ^{177}Lu-JR11, an SSTR antagonist, in preclinical studies in an in vivo mouse model. Materials and Methods: Male balb c nu/nu mice were subcutaneously inoculated with the SSTR-positive H69 cell line. For biodistribution purposes mice were injected with ~30 MBq ^{177}Lu coupled to 0.5, 1.0 and 2.0 μg JR11. At 4 time points (4 h, 2 d, 4 d and 7 d) post injection, tumors and organs were collected and radioligand uptake was determined. Also, therapy studies were performed comparing the effect of ^{177}Lu-Octreotate and ^{177}Lu-JR11. Animals (n=6 each group) were injected with either 0.5 μg/~30MBq ^{177}Lu-JR11, ^{177}Lu-Octreotate, after injection of 4 mg Gelofusin to reduce renal uptake, or received a sham injection. Animals were euthanized when tumor size reached 2000 mm^3. Results: Biodistribution studies showed 0.5 μg/30 MBq ^{177}Lu-JR11 to result in the highest tumor radiation dose (1.8±0.7 Gy/MBq), with lowest variation. Data was compared to previously performed biodistribution studies using ^{177}Lu-Octreotate in the same

mouse model. ^{177}Lu-JR11 tumor radiation dose was significantly higher than the optimal tumor dose reported for ^{177}Lu-Octreotate (0.4±0.1 Gy/MBq). Tumor-to-kidney ratio of ^{177}Lu-JR11 stayed the same for all peptide concentrations tested, but was significantly higher for ^{177}Lu-JR11 compared to ^{177}Lu-Octreotate; 0.97±0.32 Gy/MBq vs. 0.14±0.05 Gy/MBq respectively, using 0.5 μg/~30 MBq of both radiotracers. Five weeks after injection of a therapeutic dose of ^{177}Lu-JR11 or ^{177}Lu-Octreotate, survival in the 2 groups was 80% and 17%, respectively, while none of the animals of the control group survived up to that time point. Growth delay time was superior for animals treated with ^{177}Lu-JR11 (68±5 d) compared to ^{177}Lu-Octreotate (57±5 d) and control animals (41±6 d). Conclusion: The SSTR antagonist, JR11, showed higher uptake and a better therapeutic effect compared to the SSTR agonist, Octreotate, in H69 xenografts. Therefore, we conclude that the SSTR antagonist, JR11, may positively contribute to SSTR mediated imaging and therapy.

OP491

[177Lu]-OPS201 targeting somatostatin receptors: In vivo biodistribution and dosimetry in a pig model

S. Beykan[1], J. S. Dam[2], U. Eberlein[1], J. Kaufmann[3], B. Kjærgaard[4], L. Jødal[2], H. Bouterfa[3], M. Lassmann[1], S. B. Jensen[5]; [1]Department of Nuclear Medicine, University of Würzburg, Würzburg, GERMANY, [2]Department of Nuclear Medicine, Aalborg University Hospital, Aalborg, DENMARK, [3]Octreopharm Science GmbH, Berlin, GERMANY, [4]Biomedical Research Laboratory, Aalborg University Hospital, Aalborg, DENMARK, [5]Department of Nuclear Medicine, Aalborg University Hospital, Department of Chemistry and Biochemistry, Aalborg University, Aalborg, DENMARK

Aim: OPS201 is a new somatostatin receptor antagonist with high affinity towards the somatostatin receptor subtype sst2. In combination with 177Lu it can potentially be used for peptide receptor radionuclide therapy (PRRT) in patients with neuroendocrine tumors. Here we present the in vivo bio distribution of 177Lu OPS201 in pigs as a model for human dosimetry. Materials and Methods: All procedures involving animals were performed after a written permission from the Danish Animal Experiments Inspectorate. [177Lu]-OPS201 was produced on an E&Z Modular lab PharmTracer system by reacting 24 nmol of OPS201 precursor with [177Lu]-Chloride n.c.a. (ITG) in a sodium acetate / ascorbate buffer (pH 4.5) at 80°C for 20 minutes. In vivo biodistribution and dosimetry studies with 100 MBq (+/-10 MBq) [177Lu]-OPS201 were performed in anesthetized Danish Landrace pigs (2 female and 3 male, age 3 months, weight: 28 kg (+/- 2 kg)). A series of SPECT/CT scans were conducted until 10 days after intravenous injection. The physiological parameters were monitored and if necessary, corrected during the scans. Blood samples were taken to determine the time-activity curves in blood. Time-activity curves and residence times were calculated for the organs showing visible uptake. Based on these data, the absorbed organ dose coefficients for a 70kg patient were calculated using the OLINDA/EXM software. Result: The applied radio labeling procedure yielded [177Lu]-OPS201 (62-88%, non-decay corrected, RCP>98%). After injection, the blood samples showed fast clearance of the compound from the blood. Less than 5% of the injected activity was observed in the blood 10 min after injection. There was no visible uptake in the spleen but measurable uptake in the spine. For humans after an injection of 5 GBq [177Lu]-OPS201, the highest calculated absorbed doses were registered in the kidneys (13.7Gy), the osteogenic cells (3.9Gy), the urinary bladder wall (1.8Gy), and the liver (1.0Gy). None of the absorbed doses exceed organ toxicity levels. No metabolites of [177Lu]-OPS201 were found by radio HPLC analysis. Conclusion: In vivo distributions and absorbed doses are generally comparable to those obtained for other therapeutic somatostatin receptor ligands. However for a human study the potential uptake to the spine and the spleen need to be analyzed carefully. The analysis shows no indication that a human study leads to an overexposure of patients after giving a normal treatment of 5-7 GBq with [177Lu]-OPS201.

OP492

Development and human absorbed dose estimation of 47Scandium-anti-CD20 for radioimmunotherapy

L. Moghaddam-Bnaem[1], A. Jalilian[2]; [1]Amirkabir Technical university, Tehran, IRAN, ISLAMIC REPUBLIC OF, [2]Nuclear Science and Technology Research Institute, Tehran, IRAN, ISLAMIC REPUBLIC OF

Aim: In this investigation a new radiopharmaceutical using ^{47}Scandium for labeling Anti-CD20 is performed. Rituximab monoclonal antibody is selectively binds with high affinity to CD20 antigen, a surface antigen common in B-cell of lymphoid tissue. Scandium-47 is a moderate energy β- emitter (T1/2 = 3.42d, Eβmax= 441 keV ,%68; Eβmax= 600 keV , %32). Because the availability of 47Sc isotope is currently extremely limited, we have performed preliminary studies using 46Sc which is chemically identical. The chemical procedure, biodistribution in wistar rats and the absorbed dose of radiation into human organs by using biodistribution data in rats, after an intravenous administration of ^{47}Scandium-labeled Rituximab, were estimated. Material and Methods: In this work, Sc-46 chloride was obtained by thermal neutron activation flux of natural metallic scandium sample followed by dissolution in acidic media (radionuclidic purity via beta and gamma ray spectroscopy, 99.9% ; radiochemical purity

via ITLC, >99%) and used in radiolabeling of rituximab after conjugation with DOTA-NHS-ester The radiochemical purity (ITLC), stability studies (ITLC and size exclusion chromatography), determination of average number of DOTA conjugated per mAb (chelate: antibody ratio, 5.8:1) were determined followed by biodistribution studies for 46Sc and [46Sc]Sc-DOTA-anti-CD20 in wild type rats up to 72h. The biodistribution data in rats were analyzed to estimate the human's organs uptake and source organ residence times and cumulated activities. The dose calculation and estimation was done for a certain group of organs of human following the MIRD technique. As the S-factor is relevant to the particle energy that emitted by radionuclide for dose calculation the dose S-factor of ^{47}Sc is used. Results and conclusion: The binding of the radiolabeled antibody was showed to be 60% on Raji cells. The final compound was stable in presence of PBS at 37 °C and room temperature. The accumulation of the radiolabeled antibody in liver, spleen, kidney, heart and other tissues demonstrates a pattern similar to the other radiolabeled anti-CD20 immunoconjugates. The accumulation of the radiolabeled antibody in liver, spleen, kidney, heart and other tissues demonstrates a pattern similar to the other radiolabeled anti-CD20 immunoconjugates.The absorbed dose of ^{47}Sc -Riruximab in human is also estimated. The absorbed dose in human by lung, stomach, S intestine, liver, spleen, kidney and bone are 0.09, 0.06, 0.02, 2.94, 0.79, 0.13 and 0.27mGy/MBq respectively. The present study shows the possibility of antibody labeling for future use in radioimmunotherapy by 47Sc.

1407 - Tuesday, October 13, 2015, 2:30 PM - 4:00 PM, Hall F
Teaching Session: Interactive Quiz: Radiology and Cross-sectional Imaging

OP493

Interactive Quiz: Radiology and Cross-sectional Imaging

T. Lynch, **UNITED KINGDOM**

1408 - Tuesday, October 13, 2015, 2:30 PM - 4:00 PM, Hall E
Clinical Oncology: Paediatric Oncology

OP494

Clinical Impact of simultanous ^{18}FET PET/MRI for Pediatric CNS-tumors

L. Marner[1], K. Nysom[1], A. Sehested[1], L. Borgwardt[1], R. Mathiasen[1], P. S. Wehner[2], M. Jørgensen[1], P. Munck af Rosenschöld[1], C. Thomsen[1], L. Bøgeskov[1], H. Broholm[1], D. Scheie[1], M. Juhler[1], L. Højgaard[1], I. Law[1]; [1]Copenhagen University Hospital, Rigshospitalet, Copenhagen O, DENMARK, [2]Odense University Hospital, Odense, DENMARK

Aim: We aim to investigate the diagnostic value of simultaneous ^{18}F-flouro-ethyl-tyrosine positron emission tomography and MRI (^{18}F-FET PET/MRI) in comparison to MRI alone for primary CNS-tumors in children and adolescents at the time of diagnosis, before and after surgery, and if relapse or progression is suspected.Material and Methods: We aim to include 100 consecutive children and adolescents diagnosed with a primary CNS-tumor before the age of 18, and have so far included 8 patients (3-15 years). All but two required anesthesia and in half of the cases, the ^{18}F-FET PET/MRI replaced a regular MRI. Simultaneous with MRI of the brain (+/- spinal canal), a 40 min dynamic PET recording was performed using a 3T Siemens Biograph mMR after injection of 3 MBq/kg ^{18}F-FET. The PET images were reconstructed using a low-dose CT for attenuation correction. A summed image of the last 20 min of the PET recording was evaluated as PET uptake in tumor relative to unaffected gray matter as described previously*. The clinical impact of the FET PET/MRI was evaluated at a multidisciplinary team meeting by first considering the MRI and deciding the future plan and subsequently considering the PET/MRI and evaluating the possible changes in plans. Results: For 10 of 14 eligible patients, the parents have given consent for participation; 8 have been scanned. The patients had pilocytic astrocytoma WHO grade I (n=3, 2 with FET uptake, 1 without tumor residue), pilomyxoid astrocytoma WHO grade II (FET uptake), DNET WHO grade I (no FET uptake), ependymoma WHO grade II (FET uptake), atypical teratoid/rhabdoid tumor WHO grade IV(FET uptake), unbiopsied lesion suspected of tumor (no FET uptake). In 2 out of 8 cases, FET PET/MRI had a major clinical impact or gave support to a difficult clinical decision: One case changed the operation procedure by including an extra tumor focus. In another case, FET PET/MRI supported interpreting spinal changes as being artifact and not indicative of dissemination, thus reducing the radiation field from craniospinal to focal. Conclusion: The use of simultaneous ^{18}F-FET PET/MRI instead of MRI only is feasible with minimal need for extra anesthesia. The preliminary results show a major clinical impact of ^{18}F-FET PET/MRI in 2 of 8 cases. If further data supports a high percentage of clinical impact, we suggest a more regular use of this modality in children and adolescents with primary CNS-tumors.*Dunkl et al. (2015) JNM 56:88-92.

OP495

Evaluation of Early Response to Neoadjuvant Chemotherapy with FDG PET/CT and MRI in Pediatric Patients with Bone Sarcoma

M. Caglar, B. Aydin, B. Ergen, E. Karabulut, C. Akyuz; Hacettepe University, Ankara, TURKEY

Objective: 18F-FDG-PET/CT and diffusion-weighted MRI were used for predicting response to treatment in patients with

bone sarcomas in this study. Correlation between PET and MRI parameters with histopathological response and clinical outcome was assessed. Materials - Method: Sixteen patients (5 osteosarcoma, 11 Ewing's sarcoma) aged between 5-16 years were included in study. All patients underwent 18F-FDG-PET/CT and diffusion MRI before (PET1 and MR1) and after preoperative chemotherapy (PET2 and MR2) to assess the radiological tumor response. The number and localization of 18F-FDG involvements, "maximum standardized uptake" value (SUVmax), metabolic tumor volume (MTV) and total lesion glycolysis (TLG) in 18F-FDG-PET/CT, and tumor volume and apparent diffusion coefficients (ADC) from three separate areas within tumor on MRI were measured. Changes in parameters before and after treatment were compared with histopathological tumor response. Results: PET/CT at diagnosis showed 18F-FDG uptake in 1-32 different anatomical regions. Median SUVmax1 and TLG1 values at baseline were 6.0 (ranged between 2.6-9.4) and 127.0 (ranged between 8.2-573.3), respectively. Eight patients with good histologic response had lower median post-chemotherapy FDG-PET/CT parameters compared to those with poor response (1.7 vs 3.0 for SUVmax2 and 5.0 vs 62.5 for TLG2, respectively). The correlation coefficients between tumor necrosis and SUVmax2 and TLG2 were -0,647 and -0,656 respectively, $p<0,05$). Based on ROC curve analysis, SUVmax2 and TLG2 predicted a good pathological response. The optimal cut-off values for SUVmax2 and TLG2 were 2,25 and 43,85 which yielded a sensitivity/specificity of 0,83/0,75 and 0,67/100 respectively. Median diffusion MRI ADC changes were found 27.6 and 46.9 in poor and good responders, respectively ($p>0.05$, 8 patients). Conclusion: PET/CT can be used for identification of metastasis in patients with bone tumors on diagnosis and can predict the histopathological response after neoadjuvant therapy.

OP496

Clinical impact of FDG PET-CT in pediatric soft tissue sarcomas

M. Tuncel[1], N. Kurucu[2], P. Ö. Kıratlı[1], B. Erbaş[1], C. Akyüz[2]; [1]Hacettepe University, Department of Nuclear Medicine, ANKARA, TURKEY, [2]Hacettepe University, Department of Pediatric Oncology, ANKARA, TURKEY

Aim: The use of positron emission tomography-computed tomography (PET-CT) for the evaluation of pediatric patients with rhabdomyosarcoma has increased steadily over the last decade. The management of these tumors needs multimodality approach with accurate detection of disease burden. The aim of this study was to evaluate the clinical impact of PET/CT in pediatric patients suffering from rhabdomyosarcoma other osft tissue sarcoma. Materials and Methods: Between December 2011 and March 2015, 23 consecutive patients [F/M: 10/13, age median: 16±6.1 (range:3-22)] with 17 rhabdomyosarcoma and 6 with other soft tissue sarcomas were referred for FDG PET-CT. There were 40 referrals from 23 patients (9 for staging, 7 for equivocal conventional imaging, 13 for restaging and 11 for therapy response). Patient management-follow-up data, conventional imaging (CI) (30 with MRI, 4 with CT and 6 with both CT and MRI) and PET-CT results were than interpreted with pediatric oncologist to determine the clinical impact of the FDG PET-CT over CI and clinical evaluation. Results: FDG PET-CT detected malign disease in 30 referrals in 18/23 (78%) patients with median SUV max of 6±5 (range:2.5-24). In 5 patients FDG PET-CT was interpreted as normal without active metabolic disease. When compared to CI, FDG PET-CT has no clinical impact on patient management in 25/40 (62,5%) referrals (4 for staging, 9 for restaging and 11 for therapy response). In 15/40 (37,5%) referrals FDG PET had a major clinical impact (5 for staging, 7 for equivocal conventional imaging, 3 for restaging).In 7/15 (47%) of the referrals; FDG PET-CT changed treatment approach by changing the patients' stage (6 upstaged and and 1 down-staged). Therapy was ended due to true negative FDG PET-CT results in 3/15 (20%) patients, in 2/15 (13%) patients true positive PET leaded to more aggressive chemotherapy with the addition of radiotherapy. In 2/15 (13%) patients FDG PET-CT prevented therapy change to more extensive therapy by showing true negative results and in 1/15 (7%) patient FDG-PET-CT guided biopsy by showing metabolically active lesions. Conclusions: FDG PET/CT has a significant impact on the management of pediatric patients suffering from soft tissue sarcomas. It leads to a clinical decision change in 37.5% of the referrals especialy those referred due to equivocal CI. More studies are required for identifying the subgroup of patients who might benefit from a PET/CT.

OP497

Utility of PET/CT in children with Langerhans cell histiocytosis.

R. Czepczyński, E. Jodłowska, O. Zając-Spychała, M. Ruchała, J. Wachowiak; Poznan University of Medical Sciences, Poznań, POLAND

Introduction: Langerhans cell histiocytosis (LCH) is a very rare condition that primarily affects children. Its symptoms are caused by single or multiple tumors composed of Langerhans cells. Standard imaging modalities involved in the management do not include PET/CT. Aim of the study: To assess the utility of PET/CT in the management of children with LCH.Materials and methods: The study included 15 pediatric patients with LCH (age at diagnosis: from 3 months to

17 yrs., mean 4.8 ± 5.6 yrs., median 5.1 yrs.). 5 children had single system LCH, 10 children had multiple system LCH. Patients were treated in accordance with the current guidelines of Histiocyte Society (LCH-2009) using prednisone, vinblastine and 6-mercaptopurine. PET/CT using 18F-FDG was performed 60 min after injection of 18F-FDG using a routine protocol with Discovery ST scanner (GE) and compared with clinical status and other imaging modalities (CT, ultrasonography, MRI). Results. PET/CT was performed for staging of the disease (6 pts.), for the evaluation of treatment response (5 pts.), for the evaluation of treatment effect (10 pts.). Most patients had more than one PET/CT scan. Altogether 33 PET/CT scans were retrospectively evaluated (max. 6 PET/CT scans per one patient). In 5/6 cases the scan performed for staging showed FDG-avid foci in the bones (5), orbita (2), subcutaneous tissue (2) and liver (1). Only in one patient, small subcutaneous lesions showed no uptake of FDG. In none of the 3 patients with lung involvement pulmonary FDG uptake was found. PET/CT performed during chemotherapy for response evaluation, slight FDG activity was visible in 3/5 patients. Complete metabolic response was reported in 2/5 patients. At the final treatment evaluation of these 5 patients complete metabolic response was found in 4 patients and persistent uptake in one patient (non-responder according to the early scan and progression was observed in the subsequent PET/CT). The late evaluation showed disease recurrence in 2/10 children. Comparison with other imaging modalities showed that the reduction of FDG uptake during treatment preceded morphological remission and was a predictor of treatment response. Conclusions: Despite the heterogeneity of this small group, our experience confirms the utility of PET/CT in the management of LCH. Prospective studies are warranted to evaluate prognostic significance of PET/CT, especially with regard to the interim and post-therapy scans.

OP498

Value of FDG PET-CT in the therapy evaluation of Hodgkin's lymphoma

M. Tuncel[1], T. M. Kutluk[2], P. Ö. Kıratlı[1], B. G. Aydın[2], B. Erbaş[1], C. Akyüz[2]; [1]Hacettepe University, Department of Nuclear Medicine, ANKARA, TURKEY, [2]Hacettepe University, Department of Pediatric Oncology, ANKARA, TURKEY

Aim: 18 FDG PET-CT is a validated tool for staging and therapy response evaluation of Hodgkin's lymphoma (HL). FDG PET-CT offers several quantitative and qualitative parameters for the evaluation of therapy response. However the optimal parameter for prediction of therapy response and prognosis is yet to be determined. In this study we aimed to share our experience with FDG PET-CT in the management of patients with HLMaterial and method:18 FDG PET-CT was performed in 45 pediatric Hodgkin's lymphoma (mean age: 12.6±4, range: 4-20 yrs) at baseline (1) and after 2-3rd cycles of chemotherapy (interim)(2). End of therapy imaging (3) was available in 30 patients. The median follow-up was 20 months (4-46). Images were interpreted according to the Deauville 5-point score (DS). In addition, SUVmax values of the dominant lesion, diameter (dia) of the lesion on CT was measured. Percentage change of SUVmax and diameter values were also measured. The ROC curves were obtained to determine the AUC values and the optimal cut-off of parameters to predict relapse. Results: Interim PET-CT was normal in 75% of patients. DS 4-5 was in 23% of group. Six patients had progression or relapse during follow-up. SUV2 [0.5 ± 1.1(0-4) vs 6.6 ± 7.9 (0-5.2), p=0.024], SUV3 [0.6 ±1.4 (0-5.2) vs 8.38 ±9.7 (2-25), p=0.001], CT3 [7.6 ±6.3 (0-23) vs 25.4 ±22 (10-61), p=0.022] values were different in remission and relapse sub-groups. The AUC values were 0.78 (p=0.025) for SUV2, 0.936 (p=0.02) for SUV3, and 0.82 (p=0.026) for Dia3, respectively. The best cut-off values were 2.7, 2.2, and 10.5 mm. with a sens., spec., PPV, NPV of 66.7%, 94.9%, 66.7%, 94.9 % for SUV2, 80%, 88%, 95.6%, %57.1 for SUV3, and 80%, 70.3%, 33%, 95% for Dia3., respectively. DS 4-5 had 83.3% sens., 66.7% spec., 36.4% PPV, 94.6% NPV. PFS (progression free survival) in patients with DS 1-3 was better than in patients with DS 4-5 (Log-rank, p=0.004). Patients with values below the cut-off of SUV2, SUV3 and Dia3, had longer PFS than patients with higher values (Log-rank, p=0.0001, p=0.001, p=0.032). Conclusion: FDG PET-CT was useful for the evaluation of pediatric patients with HL. Interim DS 4-5 and high SUV 3 were the best predictors of shorter PFS. Our results should be confirmed in studies with larger number of patients.

OP499

Pediatric Hodgkin Lymphoma: visual and semiquantitative analysis of interim 18FDG-PET/CT in predicting treatment response and outcome.

C. Ferrari[1], **A. Niccoli Asabella**[1], M. Fanelli[1], N. Merenda[1], T. Perrillo[2], P. Muggeo[2], F. De Leonardis[2], N. Santoro[2], G. Rubini[1]; [1]Nuclear Medicine Unit, D.I.M., University of Bari "Aldo Moro", Bari, Italy, Bari, ITALY, [2]Department of Pediatric Hematology and Oncology, University of Bari "Aldo Moro", Bari, Italy., Bari, ITALY.

Background and aim: Interim 18FDG-PET/CT (PET-2) helps

predict outcome and tailor treatment in adults with Hodgkin Lymphoma (HL). In contrast, PET-2 data on pediatric HL are rare, with discordant results. Visual analysis using Deauville Score (DS) was proposed to assess PET response. However a 5-point scale did not preclude inter-observer reproducibility issues. Alternative approaches were developed to improve the accuracy and reproducibility of PET-2, mainly based on PET semi-quantitative parameters. We investigated the clinical usefulness of PET-2, evaluating both visual and semiquantitative analysis, in pediatric HL patients referred to a single center study. Materials and Methods: 18FDG-PET/CT was performed in 27 HL patients (age ≤16; average age: 12.8; 15 male:12 female) at baseline (PET-0), after 2 cycles of chemotherapy (PET-2) and at the end of treatment. PET response assessment was carried visually according to the DS, as well as semiquantitatively by use of absolute decrease in semiquantitative parameters from PET-0 to PET-2 (ΔsumSUVmax0-2, Δ∑SUVmean0-2, Δ∑MTV0-2, Δ∑TLG0-2) and the corresponding Response Indexes (RI%∑SUVmax0-2, RI%∑SUVmean0-2, RI%∑MTV0-2, RI%∑TLG0-2). Clinical response assessment was performed according the Cheson's Revised Response Criteria considering patients as responders (R) or non-responders (NR). Mean follow up was 23.3 months. T-student test for unpaired groups was performed to compare PET semiquantitative parameters between R and NR. Chi-square and Fisher exact test were performed to evaluate the association among categorical variables. The prognostic capability of 18FDG-PET/CT was calculated by ROC analysis and expressed as area under curve (AUC).Results: 5/27 (18%) patients were NR at the end of therapy based on clinical outcome and, among them, 2 became R in follow-up; another one remained NR while other two died. Visual assessment was: DS=1 in 14/27 (52%), DS=2 in 1/27 (3%), DS=3 in 4/27 (15%), DS=4 in 8/27 (30%) patients. Differences between R and NR were statistically significant for Δ∑SUVmax0-2 (t=2.45, p=0.026) and almost statistically significant for Δ∑SUVmean0-2 (t=1.88, p=0.071). No significant difference was found for the other parameters. Any association among Deauville evaluation and outcome at the end of therapy was found (Fisher exact test p=0.136). The better AUCs resulted for Δ∑SUVmax0-2 (0.836; cut-off<12.5, sensitivity 80%, specificity 91%). Conclusions: Semiquantitative analysis seems to be more accurate than visual analysis to interpret PET-2 and predict outcome in pediatric HL patients. In particular, Δ∑SUVmax0-2 appears to be the best PET parameters in predicting therapy response assessment in pediatric HL patients. The integration of Δ∑SUVmax0-2 with DS, could achieve to the best PET-2 performance.

OP500

Prognostic Value Of Different F-18 FDG PET/CT Quantitative Analytical Methodologies In Pediatric Hodgkin's Lymphoma

A. A. Kandeel[1], O. M. Serry[1], M. A. Alhussieny[1], W. O. Soliman[2]; [1]Kasr Alaini center of Oncology and Nuclear Medicine NEMROCK, Cairo, EGYPT, [2]57357 Children cancer Hospital, Cairo, EGYPT.

Introduction and aim of work: Assessment of the individualized SUVs, PET-derived total metabolic tumor volume (TMTV) and the product of both parameters, termed total lesion glycolysis (TLG) in both initial and interim PET if it carries a better PPV in early assessment of response to therapy in pediatric Hodgkin's lymphoma (PHL) patients. Patients and Methods: Retrospective analysis of PET/CT results was performed on 60 patients (42 males and 18 females; mean age 8.7±4.2 years). To assess the prognostic value of initial and interim 18F-FDG PET/CT, different semi-quantitative parameters such as SUVmax, SUVmean, Total lesion glycolysis (TLG) and TMTV of all lesions using SUVmax & mean including SUV2.5 and 40% of SUVmax as cut-off values were calculated. Follow up for 24 months from initial treatment with calculation of Disease Specific Survival (DSS). According to the recommendations of Deauville criteria interim PET (PET2) results were identified into three groups; PET2-negative (PET2-ve), PET2-positive (PET2+ve), and PET2-minimal residual uptake (PET2-MRU), the cut-off between PET2+ve and PET2-MRU was 3-4 in the 5-point scale. Results: Out of the 60 interim-PET scans, 50 scans were considered as PET2-ve (83.3%), 5 scans as PET2+ve (8.3%) and 5 scans as PET2-MRU (8.3%). The risk of the disease and the visual scoring assessment were significantly correlated with patient's outcome (whether Negative or Residual/Relapse) (p <0.0001). Different results were obtained; the most important were TLGmax2.5 (cut-off 2.5), TLGmean2.5 (cut-off 2) and TMTV2.5 (cut-off 0.75 ccm) in interim PET showed the highest sensitivity, specificity, PPV and NPV (58.5%, 97.9%, 87.5% and 90.3% respectively for the 3 parameters). Conclusion: TLGmax2.5, TLGmean2.5 and TMTV2.5 are the most relevant parameters for predicting the outcome in patients with PHL, and can add a significant prognostic

insight to interim PET response assessment. This may guide clinicians in their choice of therapeutic strategy.

1409 - Tuesday, October 13, 2015, 2:30 PM - 4:00 PM, Hall 8
Physics & Instrumentation & Data Analysis: Instrumentation

OP501

G -SPECT-I: a full ring high sensitivity and ultra-fast clinical molecular imaging system with < 3mm resolution

F. J. Beekman[1], F. van der Have[2], M. C. Goorden[1], P. E. B. Vaissier[1], J. van Roosmalen[1], H. During[3], B. Vastenhouw[1]; [1]TU Delft, Delft, NETHERLANDS, [2]MIlabs, Utrecht, NETHERLANDS, [3]MILabs, Utrecht, NETHERLANDS

AIM: We developed G-SPECT-I, a full ring stationary clinical SPECT system designed to enable -for the first time- clinical imaging with isotropic resolution below 3 millimeter and with unique capabilities for low-dose studies and imaging of fast tracer dynamics. The aim of this paper is to present its initial results. METHODS & MATERIALS: G-SPECT-I is based on a stationary ring consisting of nine large field-of-view cameras with 595 × 472 mm NaI crystals, a 3D stage that allows optimal sampling during scanning, and an interchangeable nonagon-shaped collimator containing 54 pinhole apertures and with a bore diameter of 398 mm that makes the system suitable for brain, extremity or pediatric imaging. A proprietary graphical user interface (MILabs, Utrecht, The Netherlands) enables preselection of the field-of-view in three dimensions through optical images of the patient. This allows focusing the pinholes on the desired area of interest, thereby maximizing sensitivity and sampling density for the imaging task at hand. SPECT images are obtained from list-mode data using model-based 3D pixel-based OSEM reconstruction that utilizes PSF models of system blurring and position-dependent sensitivity to increase resolution. Using a Derenzo hot rod phantom containing 45MBq Tc-99m, G-SPECT-I was compared to a Siemens Symbia equipped with Low Energy High Resolution (LEHR) collimators and using Flash3D OSEM reconstruction with resolution recovery. Scan time on both systems was 15 minutes. RESULTS: The smallest hot rods resolved by G-SPECT-I had a diameter of 3 mm while the Siemens Symbia recovered only 7 mm rods. Peak sensitivity of G-SPECT-I was 415 cps/MBq compared to 182 cps/MBq for the Symbia. With G-SPECT-I dynamic imaging with time frames of <10s can be performed for focused scans and ~30s for imaging the entire brain. CONCLUSION: Initial G-SPECT-I images show a excellent isotropic resolution. Given the field-of-view available for this prototype and its unique potential for fast dynamic imaging first ground-breaking applications are expected in brain, bone and pediatric imaging, especially since -next to very high resolution- very fast imaging will be possible.

OP502

Double-Sided Readout with Digital Photon Counters Enables Millimeter Spatial Resolution and 150 ps Time Resolution in 32 mm x 32 mm x 22 mm Monolithic LYSO:Ce Crystals

B. J. Peet, G. Borghi, V. Tabacchini, **D. R. Schaart**; Delft University of Technology, Delft, NETHERLANDS

Reducing PET scanning times and radiation exposure while improving image quality and quantitative accuracy requires detectors with better detection efficiency, spatial resolution, and time resolution, all at the same time. Digital photon counter (DPC) arrays are fully digital, solid-state single-photon sensors. DPC arrays are almost transparent to 511 keV gamma quanta, opening up new degrees of freedom in PET detector design. This work demonstrates the improvement in spatial and time resolution that can be obtained by reading out a monolithic LYSO:Ce crystal by means of two DPC arrays, coupled to its front- and back surface in so-called dual-sided readout (DSR) configuration, in comparison to conventional back-side readout (BSR).DPC arrays consisting of 8 x 8 DPC pixels and having a total area of 32 mm x 32 mm were optically coupled to commercially available LYSO:Ce crystals having dimensions of 32 mm x 32 mm x 22 mm. Both BSR or DSR configurations were tested. The spatial-, time- and energy-resolutions of both configurations were measured. In conventional BSR configuration, a spatial resolution of ~1.5 mm FWHM and a DOI resolution of ~4 mm FWHM was obtained, averaged over the entire detector area. In DSR configuration, a spatial resolution close to 1 mm FWHM was achieved in combination with a depth-of-interaction (DOI) resolution of < 2.5 mm FWHM. The coincidence resolving time (CRT) in BSR and DSR configurations were ~225 ps FWHM and ~150 ps FWHM, respectively. Compared to BSR, the DSR configuration significantly improves the time-, spatial- and DOI resolutions of the detector. Monolithic scintillator detectors with dual-sided DPC readout appear particularly promising for PET applications in which high spatial resolution, high time resolution, and high detection efficiency all are crucial, such as in neurology and pediatric medicine. This work was supported in part by EU FP7

project SUBLIMA, Grant Agreement No 241711 (www.sublima-pet-mr.eu).

OP503

First measurements and Monte Carlo simulations of a BGO-PMTs blocks array intended for continuous energy spectrum tomography in bremsstrahlung imaging

M. Hesse[1], S. Walrand[1], R. Wojcik[2], R. Lhommel[1], F. Jamar[1]; [1]Université Catholique de Louvain, Brussels, BELGIUM, [2]Ray Visions, Inc, Yorktown, VA, UNITED STATES

Rationale: A conventional Anger camera is not adapted to bremsstrahlung imaging: high energy x-rays may fall into the acquisition energy window after scattering in the collimator septa and also in the PMTs after going through the NaI crystal. This increases noise, limits the contrast, and reduces the quantification accuracy. The aim of this study is to experimentally validate previous Monte Carlo (MC) simulations (GateGeant4) showing that using BGO-PMT blocks with a high energy pinhole collimator greatly reduces the scattering contamination and enables the use of an extended energy window ranging from 50 to 400 keV. This would allow the development of a continuous energy spectrum tomography (CET) system. Method: A simple readout board was developed to handle an array of 2x3 BGO-4PMTs blocks coming from a retired PET Exact HR+ (CTI, Knoxville, TN). The energy spectrum of a 137Cs (662 keV) point source was acquired with this simple setup (without collimator or lead shielding). The spectrum was compared to the one simulated by MC (GateGeant4), and to the one acquired using a Triad XLT20 (Trionix, Twinsburg, OH) without collimator, equipped with a ½"-thick NaI crystal. BGO blocks pixelization (4.3x4.0mm pixels, 0.4mm-thick reflecting TiO2 separators) was modelled in the MC simulation while the energy resolution of the BGO-4PMTs block was approximated by a convolution with the sum of 2 Gaussians with energy-dependent FWHM . Results: The readout board was able to clearly identify all the BGO pixels. The energy spectrum acquired with the BGO setup was well reproduced by the MC simulations and displayed a scatter contamination in the [50-400] keV energy window 5 times as low as that obtained with the NaI based conventional camera Triad XLT20. The energy resolution of the BGO setup was measured as 17% at 662 keV.Conclusion: First measurements of the energy spectrum of a 137Cs point source on a simple setup consisting of a 2x3 BGO-4PMTs blocks array, confirm the advantage of BGO crystals over conventional NaI based camera in bremsstrahlung imaging by strongly reducing the scatter contamination in the energy window of interest ([50-400] keV). A dual head mobile CET prototype using a front-plate pinhole collimator is under development. This dedicated bremsstrahlung CET system will enable the dose optimization directly inside the catheterization room during 90Y liver radio-embolization which should result in an improvement of patient outcome.

OP504

Gamma-cube and X-cube: A New Scanner Generation for Benchtop Small Animal SPECT/CT

R. Van Holen, K. Deprez, B. Vandeghinste, S. Vandenberghe; Ghent University, Gent, BELGIUM

The first generation small animal imaging systems offer molecular 3D imaging at sub millimetre spatial resolution with SPECT and sensitivities in the order of several percents using PET. These systems often have a large footprint because they are based on large to medium-size detector technology, adopted from clinical scanners. The next generation of systems aims at (i) improved image quality, (ii) flexibility regarding installation and (iii) ease of operation. Our group has been working on detector hardware and collimator designs to perform SPECT and CT imaging at a footprint of 1/4th of a square meter. Using additive manufacturing of tungsten, lofthole collimators and high-resolution detectors, we have designed and constructed a benchtop microSPECT system. On the other hand, using state-of-the-art CMOS X-ray detector technology, a micro-focal X-ray tube and iterative image reconstruction, we have designed and constructed a benchtop microCT system. SPECT benchmarking has been performed for the general-purpose mouse collimator using performance measurements previously used to objectively determine spatial resolution, sensitivity, uniformity and contrast-to-noise. CT quality control has determined spatial resolution, low-contrast detectability and whole-body mouse imaging time. Results show that SPECT spatial resolution is below 700um measured using a line source. Image reconstruction from a hot-rod resolution phantom separates all rods from 700 micron diameter and larger. Point source sensitivity is above 1200cps/MBq in a simultaneous cylindrical FOV of 3 cm diameter and 1 cm height. Differential uniformity is 23% while contrast to noise curves are in line with current commercial systems' performance. CT imaging at 80um is possible with a soft tissue contrast that outperforms current systems. Whole body imaging of a mouse is possible within 30 seconds, using compressive sensing for dose reduction. All electronics and reconstruction servers are within a cube of 54x54x54cm3 system and the systems can be easily controlled using a tablet or a laptop. The small animal bed supports anesthesia, ECG, respiratory monitoring and heating. It can easily be transferred between both systems to obtain multi-modal SPECT-CT

images. In conclusion, we have developed a SPECT/CT imaging system that is competitive with the state-of-the-art but that can be installed in any certified environment on a table top.

OP505

Left ventricular function assessment using 123I/99mTc dual isotope acquisition with two semi-conductor cadmium zinc telluride (CZT) cameras: a dynamic cardiac phantom study

T. Blaire[1,2], A. Bailliez[1,2], D. Legallois[3], D. Agostini[3], A. Manrique[1,3]; [1]EA 4650, Normandy University, Caen, FRANCE, [2]Nuclear Medicine Department, IRIS, Polyclinique du Bois, Lille, FRANCE, [3]Nuclear Medicine Department, CHU Cote de Nacre, Caen, FRANCE

Objectives: New Cadmium-zinc-telluride (CZT) cameras dramatically increased sensitivity and energy resolution. Combining the use of 123I-metaiodobenzylguanidine with 99mTc myocardial perfusion agents could allow simultaneous assessment of myocardial perfusion, function and sympathetic innervation in patients with dilated cardiomyopathy. This phantom study compared the evaluation of left ventricular function in dual isotope conditions using two CZT cameras (DNM 530c, GE Healthcare and DSPECT, Spectrum Dynamics). Materials and methods: The Amsterdam gated (AGATE) dynamic cardiac phantom (Vanderwilt techniques, Boxtel, The Netherlands) was successively filled with a solution of 123I alone, 99mTc alone, and a mixture of 123I and 99mTc. A total of 24 datasets on each CZT camera were acquired using both energy windows (99mTc or 123I), with the following parameters: 10-minute acquisition, contraction rate of successively 70 and 85 bpm and ejection fraction (EF) set to 33%, 45% and 60%. End-diastolic (EDV), end-systolic (ESV) volumes, ejection fraction (EF), regional wall thickening and motion (17-segment model) were assessed using QGS. A linear model analysis included the effect of camera, acquisition type (single vs. dual isotope) and isotope (123I vs. 99mTc) and the interaction between isotope and camera type. Results: Myocardial volumes using single (123I, 99mTc) and dual isotope (reconstructed using both 123I and 99mTc energy windows) acquisitions were respectively for EDV (mL): 89±24 vs. 89 ±25 vs.91±24 vs. 90±24 for DNM and 64±12 vs. 81±20 vs.73 ±17 vs. 77±18 for DSPECT, ESV (mL): 41±1 vs. 41±1 vs. 42 ±1 vs. 42±1 for DNM and 29±4 vs. 35±2 vs. 31±3 vs. 34±3 for DSPECT, EF (%): 52±12 vs. 51±11 vs. 51±12 vs. 51±11 (p= NS) for DNM and 53±13 vs. 54±12 vs. 55±13 vs. 54±13 (p= NS) for DSPECT, regional thickening (%): 48±21 vs. 46±20 vs. 46±21 vs. 45±20 for DNM and 38±19 vs. 43±19 vs. 43±20 vs. 42±19 for DSPECT, regional motion (mm): 6.8±2.5 vs. 6.6 ±2.4 vs. 6.7±2.5 vs. 6.6±2.4 for DNM and 6.3±2.6 vs. 6.9±2.6 vs. 7.0±2.8 vs. 6.8±2.7 for DSPECT. There was a significant difference between DSPECT and DNM for EDV (p<0,009) and ESV (p<0,001) but not for LVEF (NS), regional motion (NS) or regional thickening (NS). Using the DSPECT, there was a significant difference for ESV between 99mTc and 123I acquisitions (p<0,007). Conclusion: In this phantom study, the two CZT cameras (DNM 530c and DSPECT) yielded significant difference between single and simultaneous dual isotope acquisition for ESV and EDV but yielded no significant difference between LVEF, regional motion and thickening.

OP506

Is there mutual interference between preclinical APD-PET and 3T MR in a sequential configuration ?

J. M. VRIGNEAUD[1], P. M. WALKER[2], B. BARBIER[3], A. CAMACHO[4], A. OUDOT[1], B. COLLIN[1], F. BRUNOTTE[1,5]; [1]Centre Georges-François Leclerc, DIJON, FRANCE, [2]LE2i CNRS UMR 5158, Faculty of Medicine, DIJON, FRANCE, [3]Trifoil Imaging, DIJON, FRANCE, [4]MR Solutions, GUILDFORD, UNITED KINGDOM, [5]LE2i CNRS UMR 5158, Faculty of Medicine, Dijon, FRANCE

AIM: The LabPET®/MRI system is a new preclinical imager with sequentially-acquired PET/MR scans capabilities. The dual modality system is composed of the digital APD-based labPET4 subsystem (Trifoil Imaging), coupled with a cryogen-free superconducting 3.0T MRI subsystem (MR solutions). The objective of the study was to evaluate the performance characteristics of each subsystem to identify the presence of mutual interference between the two modalities. MATERIALS AND METHODS: For the PET subsystem, NEMA NU-4-2008 performance characteristics were conducted with static magnetic field switched on (ON) and off (OFF). The following tests were performed: spatial resolution, counting-rate performance, scatter fraction, sensitivity and image quality. A Jaszczak phantom was also acquired at three different activity levels. For the MR subsystem, machine performance was evaluated with the PET subsystem electronics ON and OFF, as well as a third configuration in which the two subsystems were uncoupled. Gadolinium-doped flood field and resolution phantoms were used, and tests were carried out using a standard T1-weighted sequence with TR/TE 1000/20ms, matrix 256x256, FoV 40mm, slice 1mm. SNR, non-uniformity, circularity, ghosting, spatial resolution and phase/frequency profiles were quantified. RESULTS: For the PET subsystem, no significant differences were identified between the ON and OFF configuration for the spatial resolution, Jaszczak phantom and counting rate performance tests. However, peak absolute sensitivity was found to be 0.87% in the ON configuration versus 0.93% in the OFF configuration and sensitivity performance was decreasing with increasing ambient

temperature. Using the NEMA phantom, image uniformity was 7.9%/7.5% and spill-over ratios of 13.1%/14.2% and 24.0%/24.3% were obtained in water and air (ON/OFF). For the MR subsystem, no significant differences were observed among the experimental conditions. SNR was 49.7±0.5, image signal non-uniformity 6.0±0.1%. and the ghosting coefficient 0.0025±0.0001. No differences in phase/frequency profiles were observed. CONCLUSION: Whereas APD are known to be insensitive to magnetic field variations, their gain factor exhibits a strong dependence with temperature. In the operating configuration of the LabPET®/MRI system (ON), there is a slight increase in ambient temperature (+1°C) compared to the LabPET in the OFF configuration. This slight difference might explain the observed PET sensitivity variation of up to 6% when the PET detectors are in the same calibration state. Irrespective of the experimental conditions, the performance of the MRI subsystem did not appear to be altered by the physical and electrical presence of the PET subsystem.

OP507

Design of an Optimized Multi-pinhole Collimator for Brain SPECT

L. Chen, **G. S. Mok**; University of Macau, Taipa, MACAO

Aim: SPECT imaging on dopaminergic system is a powerful tool for diagnosing and staging Parkinson's disease (PD). Since pinhole SPECT provides superior trade-off between resolution and detection efficiency as compared to conventional low energy high resolution (LEHR) parallel-hole collimator for imaging small field-of-view (FOV), we propose to develop and evaluate a multi-pinhole (MPH) collimator for PD brain imaging based on a clinical SPECT/CT scanner. Materials and methods: We set the target resolution to be 7.27 mm which is the same as the resolution of LEHR at imaging distance of 10.5 cm, and the FOV was set to be 12 cm which is large enough to cover the whole striatum and substantia nigra region. The constraints for system optimization include maximum and minimum detector to center-of-FOV (CFOV) distances for the scanner which were 34.5 cm and 13 cm respectively, and the maximum and minimal imaging distances which were 34 cm and 12.5 cm respectively. Based on the work from Nillius *et al*. and the system constraints, we optimized the detection efficiency and calculated the design parameters. All pinholes were knife-edge and tilted to the CFOV. We then evaluated the imaging performance of the MPH and standard LEHR collimators using the digital Human Brain Phantom and analytical simulations. One hundred and twenty-eight noise-free projections were generated using 3D MPH/LEHR projectors over 360 degrees and reconstructed using the 3D MPH/LEHR OS-EM method with up to 300 updates. Normalized mean square errors (NMSE) were measured over the putamen region on the reconstructed images as compared to the original phantom. Results: The optimized design parameters were 20 pinholes with aperture size of 3.6 mm, acceptance angle of 56.4 degrees, 14.8 cm collimator length and 12.7 cm imaging distance. The detection efficiency of the proposed 20 pinholes collimator had 663% improvement as compared to the LEHR collimator. Simulations showed that there were no substantial artifacts observed in the MPH images and the putamen region can be clearly delineated. The NMSE for the MPH noise-free reconstructed images was comparable to that of the LEHR. Conclusion: The MPH collimator can provide six-fold detection efficiency at the same resolution compared with LEHR collimator, which can be traded for reduced acquisition time or lower injection dose. MPH SPECT for brain imaging is feasible and has the potential to improve PD diagnosis.

OP508

Design of shields for counting Cr-51 EDTA plasma samples from patients having a Tc-99m imaging study on the same day

N. Bird, D. Gillett; Addenbrooke's Hospital, Cambridge, UNITED KINGDOM

Aim: Patients are often referred for both a GFR and either a MUGA or a DMSA study. Currently, if both studies are performed on the same day, either the 4 hour GFR test with Cr-51 EDTA is completed before injecting the Tc-99m radiopharmaceutical or the two studies are performed concurrently and the plasma samples for the GFR are left for a few days for the Tc-99m to decay before counting. This is because a high activity of Tc-99m in the samples causes pileup into the Cr-51 window. The aim of this study was to devise a method whereby the two studies can be performed concurrently and the plasma samples counted the same day. Methods: Plasma samples from patients were analysed to determine the maximum Tc-99m activity likely to be present in samples when counted. Shields were designed to surround the counting tubes to sufficiently attenuate the 140 keV gammas to prevent pileup and dead-time problems, whilst limiting the reduction in sensitivity for 320 keV gammas from Cr-51. When using the shields the counting time was optimised so there should be no increase in uncertainty from counting statistics. 12 Samples from patients containing both isotopes were counted with the shields and after allowing the Tc-99m to decay. Results: The maximum Tc-99m activity found in the plasma samples was 10 kBq. It was determined that optimally shields would be made from 1 - 1.5 mm of lead. A set of 1.5 mm thick lead shields were made, the transmission for Cr-51 is 44 % and for Tc-99m is less than 1.5 %. These were found to be sufficient to eradicate the problem of pileup from up to 40 kBq of Tc-99m.

There was no increase in uncertainty from counting statistics when using the shields when counting time was increased to 5000 seconds per sample from 1500 seconds. There was good agreement between the concentrations of Cr-51 measured with shields and after decay of the Tc-99m.ConclusionUsing the shields makes it possible to count plasma samples for Cr-51 EDTA containing Tc-99m from other imaging tests without compromising the GFR test results. This has the advantage of reducing the time that patients need to remain in the Nuclear Medicine department without compromising how soon results are available. This can be particularly important in cancer patients being worked up for chemotherapy.

1410 - Tuesday, October 13, 2015, 4:30 PM - 6:00 PM, Hall D
Neurosciences: Psychiatry

OP509

Blunted striatal dopamine release in cannabis dependence

E. van de Giessen[1,2], J. Weinstein[1], C. Cassidy[1], M. Haney[1], M. Slifstein[1], A. Abi-Dargham[1]; [1]Columbia University College of Physicians and Surgeons/New York State Psychiatric Institute, New York, NY, UNITED STATES, [2]Academic Medical Center, Amsterdam, NETHERLANDS

Aim: The active component of cannabis (THC) induces a dopamine release in the striatum. Dependence on other dopamine enhancing substances of abuse is associated with blunted striatal dopamine transmission. The aim of this study is to measure striatal dopamine release capacity in a carefully selected sample of severely cannabis dependent (CD) subjects, who did not use other substances of abuse (including nicotine) and had no other major psychiatric illnesses. Materials and Methods: Eleven CD subjects and twelve healthy control (HC) subjects completed two positron emission tomography scans with [^{11}C]-(+)-PHNO, before and after oral administration of d-amphetamine. Percent change in [^{11}C]-(+)-PHNO binding after amphetamine (change in nondisplaceable binding potential, ΔBP_{ND}) was compared between groups. CD subjects stayed inpatient for 5-7 days prior to the PET scans to control abstinence. Correlations with psychopathological and neurocognitive parameters were examined. Results: CD subjects used marijuana for 29.1 ± 3.6 days during the month prior to inpatient admission and used an estimated 79.2 ± 72.7 grams during this month. CD subjects had significantly lower ΔBP_{ND} in the striatum (CD: -18.4 ± 4.3%, HC: -24.9 ± 4.5%, p = 0.002, effect size 1.48), specifically in the associative striatum (CD: -14.6 ± 4.1%, HC: -21.1 ± 5.2%, p = 0.003) and sensorimotor striatum (CD: -24.9 ± 6.1%, HC: -32.3 ± 4.2%, p = 0.003), and in the globus pallidus (CD: -13.0 ± 6.8%, HC: -22.6 ± 9.5%, p = 0.012, effect size 1.16). Lower dopamine release in the associative striatum correlated with more negative symptoms and higher inattention scores in CD subjects and with poorer working memory and probabilistic category learning performance in both CD and HC subjects. Conclusion: Striatal dopamine release is lower in the associative striatum and sensorimotor striatum in severely cannabis dependent subjects with no psychiatric comorbidities including any other substance abuse. The lower dopamine release in the associative striatum is related to more psychopathology and reduced neurocognitive performance in cannabis dependence.

OP510

Effect of chronic social defeat on neuroinflammation in rats: a PET imaging study with [11C]PK11195

P. Kopschina Feltes[1], E. F. J. de Vries[1], C. M. Moriguchi Jeckel[2], E. Kurtys[1], P. Michel[1], R. A. J. O. Dierckx[1], J. Doorduin[1]; [1]University of Groningen, Groningen, NETHERLANDS, [2]Pontifícia Universidade Católica do Rio Grande do Sul, Porto Alegre, BRAZIL

Aim: Stressful life events are considered to be predisposing factors for the onset of psychopathologies such as anxiety and depression. Psychosocial distress may disrupt fundamental interactions between the immune system and the brain, ultimately leading to mood and behavior alterations. In this context, it is hypothesized that chronic stress might trigger neuroinflammation. The present study evaluated whether repeated social defeat leads to neuroinflammation, using PET imaging. Methods: From day 0-4 of the experiment, 8 weeks old male Wistar rats (intruders) were placed in the home cage of an aggressive dominant male Long Evans rat (resident) for a total of 60 minutes each day. The intruders were attacked and defeated by the residents as indicated by adopting a submissive posture for at least 3 seconds. For the remaining time after submission, the intruders were placed in a wire-mesh cage. Control rats were exposed to a new cage without a resident, considering the same time points as their experimental counterparts. Behavioral alterations were assessed through a sucrose preference test at a concentration of 1% and an open field test, on day -2 and 5. On the 11th experimental day, an i.v. injection of [^{11}C]PK11195 was performed, followed by a 30-min static small animal PET scan 45 min after injection. Differences between groups were tested using an independent samples t-test on the standardized uptake value obtained from volume of interest analysis. Within subject differences in behavioral tests were tested through a paired t-test. A p-value <0.05 was considered statistically significant. Results: On day 5, the percentage of preference for sucrose solution was significantly decreased (21%, p<0.001) in defeated rats, whereas no difference was found in control rats. In the open field test, defeated rats had a significantly lower total distance

moved (32%, p<0.001), while no statistical difference was found in the control group between day -2 and 5. An increase in uptake of [^{11}C]PK11195 was found in the orbitofrontal cortex (33%, p=0.006), cerebellum (26%, p=0.032), insular cortex (22%, p=0.016), medial/prefrontal cortex (21%, p=0.007) and hippocampus (21%, p=0.047) of defeated rats on day 11, when compared to control rats. Conclusion: Repeated social defeat resulted in depressive-like behavior. In addition, neuroinflammation, as shown with [^{11}C]PK11195 PET, was found in brain regions associated with depression. These results suggest that neuroinflammation can arise from chronic exposure to stress.

OP511

Dopamine transporter availability in alcohol-dependent patients before and after deep repetitive transcranial magnetic stimulation: a ^{123}I-FP-CIT Study

D. Di Giuda[1], F. Cocciolillo[1], I. Bruno[1], I. Marini[1], M. Zollino[1], A. Ferrulli[2], M. Antonelli[2], G. Vassallo[2], A. Mirijello[2], G. Addolorato[2], A. Giordano[1]; [1]Nuclear Medicine Institute, Università Cattolica del Sacro Cuore, Roma, ITALY, [2]Internal Medicine Institute, Università Cattolica del Sacro Cuore, Roma, ITALY

AIM: Experimental and neuroimaging studies suggest a striatal dopaminergic dysfunction in alcohol dependence. Repetitive transcranial magnetic stimulation (rTMS) is a new and promising treatment for substance addiction. Preliminary data in alcohol-dependent patients showed that rTMS of the dorsolateral prefrontal cortex increases dopamine release in the striatum, reducing craving. We assessed DAT availability in actively drinking alcoholics before and after deep rTMS by ^{123}I-FP-CIT SPECT, investigating changes in DAT levels and clinical parameters. MATERIALS & METHODS: We enrolled 14 untreated patients (12 M, mean age: 49 ± 10 years) with a DSM-IV diagnosis of alcohol dependence in an active drinking phase and without a major psychiatric disorder. After baseline SPECT scan, 11/14 patients were randomised to a real rTMS (n=5) or a sham stimulation (n=6). Each patient underwent 12 rTMS sessions for one month and a second SPECT scan was carried out at the end of treatment. Severity of alcohol dependence and craving were assessed before and after rTMS with the Alcohol Dependence Scale, Penn Alcohol Craving Scale and Obsessive Compulsive Drinking Scale. Anxiety and depression were evaluated by the State-Trait Anxiety Inventory and Zung Depression Self-Rating Scale. The alcohol Timeline Follow-back (TLFB) was used to estimate daily drinking. A ^{123}I-FP-CIT template was generated with images of 20 healthy subjects (HS, 12 M, mean age: 47±16 years). Patient scans were spatially normalised to the ^{123}I-FP-CIT template by SPM8. The analysis was performed using VOIs selected from a digital atlas; VOI mean activity concentration was obtained through the Marsbar toolbox and Specific Binding Ratios (SBRs) were calculated in the caudate nuclei and putamina. RESULTS: At baseline, alcoholics showed higher SBRs in the caudate nuclei and putamina (p<0.05) in comparison with HS. An inverse correlation was found between SBR in the left caudate and anxiety levels (p<0.05). After treatment, patients submitted to real rTMS had a reduction in SBRs and differences were no longer detected in comparison with HS. Conversely, patients undergoing sham stimulation showed higher SBRs compared with HS (p<0.05) also in the SPECT scan after treatment. When considering TLFB data, a significant reduction in alcohol intake (p<0.05) was detected only in patients submitted to real rTMS. CONCLUSION: Our preliminary data show that striatal DAT availability was increased in alcohol-dependent patients, supporting the assumption of a dysfunctional dopaminergic system. Notwithstanding the small sample, an SBR "normalization" and a reduction in alcohol intake after real rTMS could suggest clinical efficacy of deep rTMS.

OP512

Regional cerebral blood flow changes in acute and transient psychotic disorders

R. Petrovic[1], A. T. Golubic[1], M. Rojnic[2], T. Samardzic[1]; [1]Department of Nuclear Medicine and Radiation Protection, University Hospital Center Zagreb, Zagreb, CROATIA, [2]Clinical Department of Psychiatry, University Hospital Center Zagreb, Zagreb, CROATIA

Aim: The aim of this study was to assess and evaluate brain perfusion single-photon computerized tomography (SPECT), as part of a continuing effort to understand the pathophysiology of the brain in acute and transient psychotic disorders (ATPD) and to correlate any abnormalities in the regional blood flow with psychopathology of these disorders. They present as an acute psychosis associated with acute stress, with sudden onset and polymorphous symptomatology, including psychotic symptoms such as hallucinations and delusions. Method: Twenty (11 male, 55%) newly referred patients with an ATPD diagnosis underwent regional cerebral blood flow (rCBF) examination brain SPECT. Their mean age was 30.5 years, range 18-52. Brain rCBF SPECT data from age- and sex-matched healthy volunteers were used as controls. Patients were diagnosed following ICD-10 criteria and were off psychoactive medication. SPECT scans were started 30 minutes after administration of 740 MBq of 99mTc-HMPAO in resting state, eyes closed and with low ambient noise. Tomograms were normalized to the mean brain activity and analyzed visually by two independent observers, unaware of clinical diagnosis. Results: Majority of our patients, 85%, had brain

perfusion changes, from small regions of decreased perfusion to widespread global cortical hypoperfusion and disseminated cerebral blood flow defects. Seven patients had globally hypoperfused cerebral cortex. In four patients hypoperfusion was found exclusively in only one region, three left frontal, 1 right temporal. Thirteen patients (76%) had two or more hypoperfused areas, 11 in the prefrontal lobes (55%), mostly in the left lobe (n=6) and bilaterally (n=4). Seven patients had hypoperfusion reported in temporal lobes, four in the right hemisphere and two bitemporal. Additional, detailed neurologic and laboratory examinations, including EEG and CT, were within normal limits in all patients. Conclusions: Compared with the normals, majority of patients with ATPD were characterized by abnormal rCBF, predominantly affecting prefrontal cortex and the temporal lobes, and, in some cases, whole cerebral cortex. Different factors might explain areas of decreased rCBF, in part as the consequence of neurophysiological changes which reflects dysfunction in neuronal activity responsible for psychotic symptoms such as hallucinations and delusions, and/or the result of some associated symptoms such as associated acute stress. However, perfusion imaging findings may be used as an additional diagnostic tool to guide psychiatrists searching for a definite diagnosis.

OP513

Pedophilia and Child Sexual Abuse: Evidence for Altered Serotonergic Function in Pedophilic Offenders

G. Berding[1], G. Tenbergen[2], F. Wilke[3], F. Paesler[1], L. Geworski[3], F. M. Bengel[1], T. H. C. Kruger[2]; [1]Department of Nuclear Medicine, Hannover Medical School, Hannover, GERMANY, [2]Clinic of Psychiatry, Socialpsychiatry and Psychotherapy, Hannover Medical School, Hannover, GERMANY, [3]Department of Medical Physics and Radiation Protection, Hannover Medical School, Hannover, GERMANY

Aim: Altered serotonin transporter (SERT) function has been demonstrated in subjects with higher impulsivity [1,2]. Reduced SERT function has been described in anxiety and depression disorders [3,4], which are typically associated with risk avoidance. The purpose of this study was to test the hypothesis of altered SERT function and impulsivity in paedophilic patients with histories of Child Sexual Abuse (CSA). Materials and methods: In this study 26 paedophilic patients (11 with CSA, 15 without) and 17 age matched healthy control subjects were enrolled. In each patient anxious and depressive symptoms were rated with the Hamilton Anxiety Scale (HAM-A) and Hamilton Depression Scale (HAM-D). To assess impulsive decision-making, the Information Sampling Task (IST) from the Cambridge Neuropsychological Test Battery (CANTAB) was used. I-123-ß-CIT SPECT (using a dual head SPECT/CT) was performed 4 hours post injection for measurement of SERT. Data was spatially normalized based on a template in Talairach space. Volumes of interest from the WFU pick-atlas were used to extract counts in regions with specific binding (thalamus, hypothalamus, midbrain and pons) and a cortical reference region for calculation of binding ratios. Results: SERT binding ratios for the midbrain region in paedophilic patients with CSA (2.00±0.12) were significantly (p=0.0477) elevated compared to the control subjects (1.88±0.14). In patients without CSA none of the regions SERT binding ratios were significantly different compared to control subjects. In patients with CSA a significant negative correlation between SERT binding in the thalamus and HAM-A score (r=-0.90, p=0.0001) as well as HAM-D score (r=-0.82, p=0.0022) was observed. Furthermore, a significant positive correlation between SERT binding in the pons and errors in the IST was found (r=0.64, p=0.0343). Conclusion: Our data indicate that increased SERT binding might be a characteristic of paedophilic offenders against children. Increased SERT binding in these patients was especially associated with fewer anxiety symptoms on the HAM-A and more impulsive decision-making as measured by the IST. These findings underline the relevance of the serotonergic system in paedophilia and child sexual abuse. References[1] Lesch et al. (2000) Behavioral Sciences and the Law, 18:581-604. [2] Rylands et al. (2012) Biol Psychiatry, 72:1004-11. [3] Olivier et al. (2008) Neuroscience, 152:573-84. [4] Staley et al. (2006) Biol Psychiatry 59:40-7.

OP514

Altered Regional Cerebral Blood Flow in Chronic Whiplash Associated Disorder

D. Vállez Garcia[1], A. Otte[2], A. T. M. Willemsen[1], R. A. J. O. Dierckx[1], J. Doorduin[1], G. Hostege[3]; [1]University Medical Center Groningen, Groningen, NETHERLANDS, [2]Offenburg University of Applied Sciences, Offenburg, GERMANY, [3]University of Queensland, Brisbane, AUSTRALIA

Aim: Whiplash trauma in one of the most frequent consequences of motor vehicle accidents. While initial symptoms resolve within a few weeks in many cases, some patients develop persistent symptoms that include pain, headache, visual, and/or psychological disturbances, termed as Whiplash-associated disorder (WAD). Although there is evidence supporting tissue lesion and central hyperexcitability, the pathophysiology is not well understood. In the current study, possible alterations in the regional cerebral blood flow (rCBF) were explored with PET imaging. Material and Methods: Twelve female patients diagnosed with WAD grade I/II were included 5±2 years after the accident, in addition to eight healthy matched volunteers. PET scans (ECAT HR+, Siemens) were acquired after injection of 500 MBq [15O]H2O for rCBF measurement. During acquisitions the

volunteers received a non-painful electrical stimulation of the neck (DS7A, Digitimer). Sensitivity thresholds were individually determined. Four condition were used: rest state, placebo-like state (current was expected but not generated), stimulation above perception threshold, and stimulation below pain or muscular contraction. These conditions were repeated three times, resulting in twelve scans. All participants completed a neurological interview, the Hospital Anxiety and Depression Scale, the Neck Disability Index (NDI), the Whiplash Disability Questionnaire, and rated pain on the visual analogue scale. Voxel-based analysis was performed on the scans with SPM8 in combination with SwE toolbox to account for repeated measurements. Level of significance was set to $p<0.005$ uncorrected, with an extent threshold of 100 voxels. Correlations between the rCBF of WAD patients in the significant clusters and the scores from questionnaires were analyzed using the Generalized Estimating Equations model in SPSS, with $p<0.05$ considered significant (Bonferroni-Holm). Results: In all the questionnaires WAD patients scored higher ($p<0.001$) than healthy volunteers. No significant differences in rCBF were found between conditions. In WAD patients, compared with healthy controls, a significant increase in the rCBF was found in the right superior parietal gyrus (T=3.52±0.51). In addition, a decreased rCBF was found in the left insula (T=3.66±0.72), right insula (T=3.62 ±0.68), and right thalamus (T=3.54±0.47). Within the WAD group, a negative association ($p<0.02$) was found in these regions between NDI scores and rCBF. Conclusion: WAD symptoms might be the result of a mismatch between the proprioceptive information from the cervical spinal cord and the information integrated in regions such as mesencephalon, thalamus and insula. Further investigation of the functional brain alterations present in WAD patients must, however, be performed for a better understanding of the pathophysiology.

OP515

Genetic influences in FDG uptake in precuneus and posterior cingulate cortex: a PET study in non-demented twins

S. Watanabe[1], H. Kato[1], E. Shimosegawa[2], J. Hatazawa[1], Osaka Twin Research Group; [1]Department of Nuclear Medicine and Tracer Kinetics, Osaka University Graduate School of Medicine, Suita, Osaka, JAPAN, [2]Department of Molecular Imaging in Medicine, Osaka University Graduate School of Medicine, Suita, Osaka, JAPAN

Purpose: The Alzheimer disease (AD) is the most common dementia. It is known as a multifactor disease, and many factors including genetic and environmental factors have been reported to be concerned in the onset of the disease. FDG-PET studies have been revealed the characteristic glucose metabolic patterns; decreased metabolism especially in precuneus and posterior cingulate cortex, even in the early stage of the disease. Some previous FDG-PET studies targeting for discordant (demented and non-demented) twin pairs reported reduced glucose metabolism in the non-demented co-twins, suggesting preclinical pathogenesis or contribution of genetic factors. We investigated whether genetic influences were observed in glucose metabolism in precuneus and posterior cingulate cortex using clinically non-demented concordant twins including young and middle aged subjects, and attempted to quantify the genetic and/or environmental influences. Methods: This research was carried out as a part of the twin research of our institution. FDG uptake was studied in 59 pairs of right-handed volunteer twins (41 monozygotic pairs (mean age 60.4 ± 11.9 years, age range 35-88 years) and 18 dizygotic pairs (mean age 64.9 ± 15.4 years, age range 32-85 years)) aged 30 years or over. The brain PET images were analyzed by voxel-based statistical analysis with automated region-of-interest setting. The mean FDG uptake in precuneus and posterior cingulate cortex was semi-quantified. We first referred Mini Mental State Examination (MMSE) scores and compared the scores with the regional glucose metabolism. Next, structural equation modeling (SEM) was applied to investigate the degrees of genetic, shared environmental, and unique environmental influences on the regional FDG uptake. Results: Although all the subjects were independent in the daily life, the MMSE scores were ranged between 22 and 30. However, no apparent differences in FDG uptake in precuneus or posterior cingulate cortex were observed between low MMSE score subjects and high MMSE score subjects. The SEM estimated genetic contribution to regional FDG uptake as 0.39 (95%CI: 0.11-0.66) in left precuneus, 0.28 (however, 95%CI of genetic parameter estimate include 0) in right precuneus, and 0.30 (95%CI: 0.25-0.66) in right posterior cingulate cortex, while common environmental rather than genetic influences were indicated in left posterior cingulate cortex (the relative importance was estimated as 0.43 (95%CI: 0.19-0.78).). Conclusion: We demonstrated not only environmental but also genetic contributions to the FDG uptake in precuneus and posterior cingulate cortex even in younger non-demented subjects, suggesting the essential genetic influence in these regions.

OP516

Decreased frontotemporal cerebral blood flow in congestive heart failure.

C. Pascovich[1], R. García[2], A. Damian[1], M. Langhain[1], E. Angarita[2], R. Ferrando[1]; [1]Nuclear Medicine Centre, Clinical Hospital, University of the Republic, Montevideo, URUGUAY, [2]Fundación Cardiovascular de Colombia., Bucaramanga, COLOMBIA

Background: Congestive heart failure (CHF) is one of the major public health problems with great impact on mortality and morbidity. Studies have shown that patients with CHF have cognitive impairments. Cerebral hemodynamic changes resulting from decreases in left ventricular ejection fraction (LVEF) as well as brain microinfarctions secondary to microembolisms could be underlying mechanisms. Reduced oxygen levels may cause neurotoxicity, particularly in certain areas more vulnerable to hypoxia like hippocampus, amygdala, frontal lobes and cerebellum. Aim: To evaluate the presence of regional cerebral blood flow decreases in patients with CHF.Materials and methods60 patients with CHF (42-82 years, mean 65.4±9.8; 38 male; functional class I-IV; LVEF 10-68%, mean 33.7±15.7%) and 40 normal controls (32-89 years, mean 61.9±16.4, 18 male) were evaluated using brain SPECT with 99mTc-ECD. Groups did not differ significantly in age and gender. Previous neurological or psychiatric pathology was excluded. Image analysis was performed in SPM8. Clusters greater than 100 volxels with $p<0.01$ FWE corr at the voxel level were reported ($p<0.001$ uncorr was considered if no results were found). Subsequent comparisons were performed excluding patients with ischemic heart disease (39/60) and possible depression (antidepressant medication or elevated CES-D scores) (10/60). Possitive correlations with LVEF and negative correlations with duration of the CHF were also assessed. Results: Patients with HCF showed extensive bilateral frontal hypoperfusion. Anterior temporal poles, midbrain and pons were also affected. Frontal, temporal and pontine changes remained after excluding patients with ischemic heart disease and possible depression. LVEF correlated positively with bilateral superior frontal perfusion. Negative correlation with duration of CHF showed a trend to statistical significance in dorsal frontal and posterior parietal cortex ($p<0.01$ uncorr). Conclusions: Patients with CHF have extensive frontal hypoperfusion as well as anterior temporal and brain stem hypoperfusion. Frontal changes correlated positively with LVEF. These findings are probably the result of chronic brain hypoxia due to CHF and can not be explained only by depression or atherosclerotic cerebrovascular disease. The results provide a neural basis for the presence of cognitive impairment in CHF, as frontal and temporal function is crucial for memory, attention and executive performance.

1501 - Tuesday, October 13, 2015, 4:30 PM - 6:00 PM, Hall 1
CME 12 - Drug Development & Radiopharmacy: Radiopharmaceutical Design

OP517
Perspectives of Developing New Radiopharmaceuticals: Research vs Clinical Application
H. Kung, USA

OP518
Strategy for the Discovery of New PET Radioligands at Pfizer R&D
L. Zhang, USA

OP519
Development of Peptide-Based Radiopharmaceuticals: From Bench-To-Bedside and Beyond
M. Fani, SWITZERLAND

1502 - Tuesday, October 13, 2015, 4:30 PM - 6:00 PM, Hall 2
Joint Symposium 12: EANM/ESMI/COST: Lead Compounds in Theranostics

OP520
Radiopeptide-based Theranostics
M. de Jong, NETHERLANDS

OP521
Camelid Theranostics in Cancer
M. D'Huyvetter, BELGIUM

OP522
Gadolinium-based Multimodal Particles for Theranostic Applications in Oncology
O. Tillement, FRANCE

1505 - Tuesday, October 13, 2015, 4:30 PM - 6:00 PM, Hall G2
Do.MoRe: Thyroid

OP523

The so-called thyroid stunning effect: quantitative radiobiological analysis and prediction of the remnant control probability.

S. Walrand, M. Hesse, F. Jamar; Université Catholique de Louvain, Brussels, BELGIUM

Aim: The origin of the reduction in thyroid uptake after a low activity iodine scan, so-called stunning effect, is still controversial. Two explanations prevail: an individual cell stunning that reduces its capability to store iodine without altering its viability or a significant cell killing fraction that reduces the number of cells in the tissue still taking up iodine. Our aim is to analyze whether this last assumption could quantitatively explain the observed reduction. Methods: a general expression of the cell survival fraction as a function of the mean absorbed dose was derived from the dose volume histogram measured in thyroid metastases by ^{124}I PET. Afterwards, the survival fractions were computed for ^{124}I, ^{131}I and ^{123}I using the radiosensitivities of normal and tumor human thyroid cell assays reported in the literature. Results: the computed survival fractions were in line with the uptake reduction observed after a 2 mCi 131I scan by Lassmann et al. (2004) and observed after a 5 mCi ^{123}I scan by Hilditch et al. (2002), as well. Contrary to a commonly accepted opinion, small absorbed dose, about 15 times lower than those delivered for ablation, already kill a significant fraction of cell. This results from the Poisson statistics governing the tissue control probability (TCP) (Brahme and Agren 1987). As a result the control a few grams of tissue requires high absorbed dose providing survival fraction lower than 10^{-9}. This feature was experimentally observed in megacolony cell assay (Kappler et al. 2007). Furthermore, the computed TCP quantitatively explained the administered activity needed for thyroid remnant ablation. Conclusion: The quantitative radiobiological analysis, based on radiosensitivities measured in thyroid cell assays, shows that the uptake reduction effect can be purely explained by the cell killing fraction. This supports the non-existence of an individual cell stunning effect that, if present, should induce an additional uptake reduction resulting in much larger decreases than those observed. The study shows that the three radioiodines isotopes (i.e. ^{124}I, ^{131}I, ^{123}I) induce a significant uptake reduction after a low activity scan. As the β/α ratio is very low, this effective fractionation of the therapy should not impact the patient outcome in agreement with recent studies. As a result, a pretherapeutic dosimetry study makes sense in order to optimize the administered activity in function of the uptake of the thyroid remnants that is highly patient dependent.

OP524

Measuring the radiation dose to the thyroid with a simple collar detector system in patients with radionuclide therapy; A feasibility study

P. Brinks, D. B. M. Dickerscheid, E. Kranenborg, J. Lavalaye, J. B. A. Habraken; St. Antonius hospital, Nieuwegein, NETHERLANDS

An important parameter for successful treatment of thyroid diseases with I-131 radionuclide therapy is the radiation dose delivered to the thyroid. To obtain the desired radiation dose, the administered patient-activity is calculated using thyroid uptake values, determined from pre-therapeutic uptake measurements of I-123. The actual radiation dose to the thyroid with therapy can be determined by measuring the activity in the thyroid at various time intervals after administration of the therapeutic dose of I 131, using gamma camera imaging. Because transporting the patient to the nuclear medicine facility is challenging (from a radiation safety point of view) and repeated measurements are time-consuming, the actual radiation-dose is typically not determined. We present a simple device that consists of a collar with a special dosimeter placed around the patient's neck, designed to continuously measure the activity of I-131 in the thyroid. Uptake can be measured without transporting the patients and repeated use of expensive diagnostic setups is also not required, thereby enabling the possibility to measure the actual delivered radiation dose in a simple and effective manner. The collar therapy indicator (CoTI) device, fabricated by AG Medical, contains up to 4 independent gamma radiation detectors, of which two are placed in a collar that is positioned around the patient's neck. The detectors are based on single Silicon Photo-Multiplier devices with a CsI(Tl) scintillation crystal. Data are temporarily stored on a lightweight and portable control unit and sent via a wireless connection to a tablet for storage and display. We present a feasibility study of CoTI for measuring the delivered radiation dose to the thyroid for I-131 radionuclide therapy patients. To demonstrate the working principle of CoTI for thyroid uptake measurements a comparison study between CoTI and a Siemens ECAM camera was performed, involving 20 patients. The results provided a good correlation between the two different methods, as confirmed by the obtained R2 value of 0.87, which clearly demonstrates the working principle of CoTI for thyroid uptake measurements. Additionally, we will present measurements of the uptake curve during I-131 radionuclide therapy. These results can be used to calculate the effective half-life and the actual radiation dose, assisting in the evaluation of radionuclide therapy. In conclusion, a new measurement device that is embedded in a collar around the patient's neck is presented. This device can be used to continuously measure the thyroid iodine uptake and thereby the radiation dose delivered during I-131 radionuclide therapy.

OP525

Relationship between circulating anti-thyroglobulin antibody (TgAb) and tumor metabolism in patients with Differentiated Thyroid Cancer (DTC): diagnostic and prognostic implications

E. Pomposelli[1], F. Pupo[2], I. Calamia[1], G. Ferrarazzo[1], G. Pesce[2], F. Fiz[1], G. Bottoni[1], M. Giusti[3], G. Sambuceti[1], M. Bagnasco[2], S. Morbelli[1]; [1]Nuclear Medicine Unit, IRCCS San Martino - IST, University of Genoa, Genoa, ITALY, [2]Autoimmunity Unit, IRCCS San Martino - IST, University of Genoa, Genoa, ITALY, [3]Endocrinology Unit, IRCCS San Martino - IST, University of Genoa, Genoa, ITALY

TgAb concentrations respond to changes in the mass of Tg-secreting thyroid tissue. It has been suggested that TgAb concentration may have clinical value as surrogate DTC tumor-marker. Recent evidence suggest a link between TgAb titers and DTC aggressiveness. DTC metabolism as assessed by 18F-FDG PET is a well-recognized prognostic indicator. AIM: to evaluate the relationship between TgAb levels and tumor glucose metabolism in patients with DTC. Methods: 71 patients with DTC who underwent 18F-FDG PET/CT scan were included in the present study. Indications for PET were negative iodine-131 whole-body scan and elevated TgAb level or restaging in high risk patients for diagnostic and prognostic purposes. Radioiodine avidity of DTC lesions was established on the bases of recent patients' history (post-therapeutic 131I scan was available for all patients). TgAb levels were measured with ELISA within 15 days from FDG-PET scan. On the bases of the results of FDG-PET, post-therapy 131I scans and Tg levels, patients were divided in two groups according to the evidence (ED) or absence (NED) of disease. ED patients were further divided in three subgroups: 1. radioiodine avid with positive FDG PET (PET+/131I+). 2. Radioiodine refractory with positive FDG PET (PET+/131I-) 2. Radioiodine avid with negative FDG-PET (PET-/131I+). Mean standardize uptake values of all FDG-avid lesions was assessed and averaged for each patient. T-test was performed to assess the difference between TgAb levels in ED and NED patients as well as between NED patients and PET+/131I+, PET+/131I- and PET-/131I+ subgroups independently. Linear regression was performed to assess relationship between TgAb on one side and SUVmean in the three subgroup of ED patients on the other. Results: TgAb levels (IU/L) were: 33 (range 9-117) in NED and 37 (range 2-416) in ED patients (p=ns); however this value raised to 94 (range 79-416) in PET+/131I+ subgroup ($p<0.003$ with respect to NED) while was significantly lower in PET+/131I- subgroup (24 IU/L; $p<0.04$ versus NED). Only one patient belonged to PET-/131I+ subgroup (Tgab were 47 IU/L). Finally, only in PET+/131I+ subgroup, SUVmean was directly correlated with TgAb levels (R2=0.76). Conclusions: Significantly higher TgAb in radioiodine avid DTC with positive FDG-PET support the role of TgAb levels as surrogate tumor marker in DTC patients (at least when radioiodine avidity and thus Tg-secretion is preserved). The correlation with tumor metabolism suggests that increased TgAb level may also have prognostic implications in the follow-up of DTC patients.

OP526

The Survival and Outcome of Recurrent Differentiated Thyroid Carcinoma: Results of a Long-Term Follow-up Study

J. Mihailovic, E. Matovina, N. Klicov; Oncology Institute of Vojvodina, Sremska Kamenica, SERBIA

Aim: To analyze the survival and outcome of recurrent differentiated thyroid carcinoma (DTC) treated with I-131. Patients and methods: Among 351 DTC patients treated with I-131 between 1977-2000, we analyzed 99 patients with recurrent disease (RD)(74 females, 25 males; 41 patients <45 years, 58 patients ≥45 years); median follow-up=12 years (range,1-39yr); 27 follicular, 70 papillary carcinomas and 2 undetermined histology; TNM stage I, II, III and IV included 4, 7, 24 and 48 patients, respectively while 16 patients were not staged. Initial nodal metastases (N1), distant metastases (M1) and combined metastases (N1M1) were presented in: 39, 53 and 1 patients, retrospectively, while 58 patients initially had no metastases (N0M0). Disease specific survival was analyzed by Kaplan-Meier method. Results: Among 351 DTC, RD was detected in 99 (28.2%) patients, median time of appearance was 67 monhts (range, 6-272 months). Recurrences were treated by RAI in 31 pts; surgery (S) in 9 pts, S+RAI in 38 pts; chemotherapy (CH) was performed in 1 patient; S+CH+external beam radiotherapy (EBRT) in 2 pts; CH+RAI in 2 patients; EBRT+S+RAI was performed in 9 pts; EBRT+S in 2 patent and EBRT+RAI in 1 patient; in 4 patients recurrences were not treated. At last check up, out of 99 patients with RD 49 (49.5%) patients were alive, 41 (41.4%) patients died due to disease related deaths, and 9 (9.1%) patients died from other causes. The 5-, 10-, 20- and 39-year disease specific survival was: 0.904 ±0.30; 0.756±0.46; 00.525±0.62, and 0.287±0.126, respectively. Conclusion: Careful monitoring of DTC patients is necessary for detection and treatment of recurrence. Patients with recurrent disease have worse

prognosis than those without recurrence, but may be cured if treated on time and properly (surgery with additional RAI, if necessary).

OP527

The effect of post-ablation 131I SPECT/CT on the staging and initial risk-stratification of children with differentiated thyroid cancer

B. Liu, R. Tian; Department of Nuclear Medicine, West China Hospital, Sichuan University, Chengdu, CHINA.

Purposes: Over the past decade, there is emerging literature that attempts to address the role of radioiodine SPECT/CT in the evaluation of differentiated thyroid cancer (DTC). Most of these studies have studied adult patients and experience derived from children patients is still scarce. In this retrospective study, we attempted to investigate the utility of post-ablation 131I SPECT/CT on the impact of staging, and initial risk-stratification of children with DTC. Methods: Sixty-two children (45 female, 17 male; mean age, 14.5 ± 6.2y,range,6-21y) with DTC referred for initial postsurgical 131I ablation were retrospectively included. In addition to planar whole body scanning performed approximately 5 days after the therapeutic administration of 2,220-5,550 MBq (60-150 mCi) of 131I, SPECT/CT scanning of the neck and other suspected areas of abnormal radioactivity uptake noted on planar scans were acquired. Sites of uptake seen on planar and SPECT/CT images were categorized as thyroid remnants, cervical lymph nodes, and distant metastases. Each patient was initially staged using the 7th edition of the AJCC/UICC staging system (stage I, or II) and risk-stratified using the risk of recurrence stratification system proposed by the American Thyroid Association (low-, intermediate-, or high-risk), based on clinical and pathology information, and then re-classified, taking into account additional findings from post-ablation 131I SPECT/CT. Results: By addition of SPECT/CT, post-ablation 131I scans detected cervical lymph node metastases and distant metastases in 9 (14.5%) and 4 (6.5%) of 62 patients, respectively. Such additional findings noted from post-ablation 131I SPECT/CT helped to alter the staging and initial risk-stratification in 4 (6.5%) patient and 5 (8.1%) patients, respectively. Conclusion: Our study indicates that post-ablation 131I SPECT/CT scans have potential to identify regional and distant metastases, providing an important contribution to staging and initial risk-stratification in children with DTC. This work was supported by the National Natural Science Fund of China Grant No. 81401445, 81471693.

OP528

Red marrow and blood dosimetry in 131I treatment of metastatic differentiated thyroid carcinoma: comparison in patients with repeated treatments

E. Richetta, M. Pasquino, C. Cutaia, A. Giostra, R. Pellerito, M. Stasi; AO Ordine Mauriziano di Torino, Turin, ITALY

Aim. Radioiodine treatment of metastatic differentiated thyroid carcinoma is often limited by red marrow toxicity. In our institution 131I administered activity is individually planned: dosimetry to red marrow and blood is performed before therapy (PT) to determine the maximum tolerable activity (<2Gy) and after treatment (IT). In this study we compared the results of the dosimetries performed on patients with subsequent therapies to investigate the possibility of using the first dosimetry as a reference for the following treatments as well. Materials and Methods. For 32 metastatic patients PT and IT doses (d1) to red marrow and blood, evaluated according to AIFM protocol during a first 131I treatment, were compared with doses (d2) calculated in the later treatment (14 ± 7 months after). PT dosimetry was performed one week before radioiodine therapy by administering a 131I tracer-activity: 4 blood samples were acquired and AP-PA wholebody measurements were performed by using a NaI counter 2h, 24h, 48h and 96h after the administration. For IT dosimetry detectors placed on patients' beds providing wholebody AP counts (every 2h, from 8.00 a.m. to 22.00 p.m. during patient's hospitalization) and 4 blood samples were acquired with the same PT time scheduling. 64 couples of doses (30 PT and 34 IT) (Gy/GBq) were compared : percentage dose differences were calculated and a t-test for paired samples was applied.Results. Mean (±1Dev.St) percentage differences between d1 and d2 for the 30 PT paired data was -0.4%±14% [-19÷20] for red marrow and -5.2%±17% [-34÷25] for blood respectively. Good correlation coefficient r was found between d1 and d2, confirmed also by paired samples t-test (red marrow r=0.94, p=0.87 and blood r=0.83, p= 0.22). Similar results were found evaluating the 34 IT paired doses: red marrow mean difference 6%±11% [-14÷24], r = 0.95, p =0.15 and blood 4%±19% [-35÷39], r = 0.75, p =0.98. Conclusion. We performed a comparison between pre-treatment and in-therapy red marrow and blood doses evaluated in two subsequent treatments on 32 patients treated with 131I for metastatic differentiated thyroid carcinoma. The preliminary results show mean differences between the paired PT and IT doses not significantly different and percentage variations within the experimental error of the calculation method. The good correlation between the first calculate dose and the later result could confirm the possibility to use the first dosimetry as a reference for following treatment, avoid in such a way to repeat the very time expensive dosimetric procedure.

OP529

Pre-therapy Bone Marrow And Lesion Absorbed Dose Estimation Using Different Dosimetry Models In Metastatic Differentiated Thyroid Cancer

M. M. Abuqbeitah, H. Tanyildizi, I. Çavdar, M. Demir, N. Yeyin, B. Vatankulu, L. Kabasakal; Istanbul University, Istanbul, TURKEY

Aim: Dosimetry is an alternative strategy to the administration of fixed radioactive iodine in metastatic thyroid cancer therapy. Pretherapy dosimetry is increasingly recommended to calculate the maximum tolerable Activity for each patient in order to deliver absorbed dose not exceed 2 Gy for the red bone marrow and meanwhile optimization the response level of desired targeted lesions. Materials And Methods: 14 patients (10 female ,4 Male and Mean age 44±15.84 y ,TSH 65±43 μIU/ml,HTC 38.43±3.81 ng/ml) suffering from metastatic differentiated thyroid cancer were submitted to pretherapy maximum safe activity and lesion absorbed dose protocol to establish successive therapy using OLINDA/EXM Software and five different dosimetry Methods for comparison purposes. Dual head scintillation camera was utilized to measure whole body and lesions activities by drawing region of interest adjacent to whole body and lesion contours and performing attenuation correction Besides to Blood samples collection which were measured in Well-Gama Counter at several time points; 2.6.24.48.72.96.144hours after oral administration of Radioiodine tracer (2mCi).To verify normal background count rate, 1 minute acquisition was performed before each whole body scan and subtracted from the related scan's count. The necessary data were collected and modified according to the parameters of the dosimetry methods adopted by OLINDA/EXM, Wessels et *al*,Traino et *al*,Siegel et al,Shen et *al* ,and Keizer et *al* . Results: According to OLINDA/EXM software mean absorbed dose from tracer activity was 3.11±1.76mGy/mCi ,Wessels et *al* was 3.27±1.9mGy/mCi,Traino et *al* was 2.68±1.53 mGy/mCi,Kiezure et *al* was 2.2±1.16mGy/mCi,Siegal et *al* was 2.56±1.86 mGy/mCi , and Shen et *al* was 4.05±3.4 mGy/mCi. Mean absorbed dose to distal metastatic lesions was 6,31Gy/mCi. The deviation between the results of OLINDA/EXM software and the other dosimetry methods was variable 5.1%, -13.8%, 30%, -17%, and -29%. Conclusion: Absorbed dose and maximum safe activity determination by OLINDA/EXM software is non-invasive method and can be used in clinical routines easily. It seems that combination between red marrow absorbed dose and lesion absorbed dose in the dosimetry protocol is very advantageous to accomplish highly successive therapy and complete remission of the lesions.

OP530

111In-CP04 - A Novel CCK2/Gastrin Receptor-Localizing Radiolabelled Peptide Probe for management of Patients with Progressive/Metastatic Medullary Thyroid Carcinoma (MTC): Rationale, Study Design and the Initial Promising Results of a Multicentre First Phase Study.

A. Hubalewska-Dydejczyk[1], C. Decristoforo[2], P. Erba[3], R. Mikolajczak[4], H. Maecke[5], K. Zaletel[6], P. Kolenc-Peitl[6], T. Maina[7], P. Garnuszek[4], I. Virgollini[2], G. Geobel[2], M. Konijnenberg[8], M. Hendriks-deJong[8], L. Froberg[8], W.Lenda-Tracz1, C.Rangger2, A.Kunzmann5,A.Sowa-Staszczak1, M.Trofimiuk-Muldner1,M.Tomaszuk1; [1]Jagiellonian University Medical College, Krakow, POLAND, [2]Innsbruck Medical University, Innsbruck, AUSTRIA, [3]3Azienda Ospedaliero-Universitaria Pisana, Pisa, ITALY, [4]Radioisotope Centre POLATOM, National Centre for Nuclear Research, Otwock, POLAND, [5]University Hospital Freiburg, Freiburg, GERMANY, [6]University Medical Centre Ljubljana, Ljubljana, SLOVENIA, [7]INRASTES, NCSR "Demokritos", Athens, GREECE, [8]Erasmus University Medical Center, Rotterdam, NETHERLANDS

The prognosis for patients with MTC is relatively good, however nonoperable/recurrent disease develops in approximately 50% of patients. The diagnostic and therapeutic algorithms in MTC cases still need to be optimized, as imaging techniques will not show any disease until serum calcitonin approaches at least 150 pg/ml as well as patients with surgically unresectable disease are left with few therapeutic options with low efficacy. CCK2 receptor is overexpressed in MTC with high density and >90% incidence. Since 1990, a variety of CCK2 receptor related peptides were studied; the DOTA-(DGlu)6-Ala-Tyr-Gly-Trp-Met-Asp-Phe-NH2 (CP04) showed the most promising characteristics (high receptor affinity, high stability and low kidney retention) and was selected for further clinical evaluation.The aim of the project is to establish the multinational cooperation in the innovative field of targeted radionuclide therapy using a CCK-2/gastrin receptor-seeking ligand CP04 radiolabelled with Indium-111 as an imaging biomarker.Methods: The study consists of two stages: WP1-Radiopharmaceutical development and WP2-Clinical trial. The goal of WP1 was to establish a clinically useful formulation for the preparation of 111In-CP04 including radiolabelling and stability testing and the extended single dose toxicity study including haematology, blood chemistry and histopathology.Minimally 20 patients with progressive/metastatic nonoperable histologically proven MTC with positive 18F-FDG-PET-CT/CT/MRI or positive calcitonin doubling time will be enrolled in the clinical study.The objective is to establish the safety of i.v. administration of a therapeutic amount of 111In-CP04 and to assess the tracer's

biodistribution and dosimetry in MTC and normal tissues and to determine critical organs. The evaluation of the potential of CCK2 receptor scintigraphy to detect cancer lesions for diagnostic (10ug) and therapeutic peptide dose (50ug) and the decrease of kidney dose after co-administration of gelofusine (nephroprotective agent) are planned. Results: We demonstrated that radiolabelling of CP04 with 111In could be effectively translated into a clinically useful formulation based on a simple kit procedure. The planned peptide dose allows clinical administration based on preclinical toxicity data. Standard Operating procedures for radiolabelling and imaging methods as well as the Study Protocol and documents to obtain the ethics committee's approvals for all participating centres are being finalized. The study will recruit patients soon. Conclusion: The project may become the first step in establishing a more selective and efficient strategy for the diagnosis, early detection and therapy of recurrent/metastatic MTC patients leading to reduction of mortality as well as improvement in life quality. GRAN-T-MTC is the ERA-NET part (TRANSCAN, EC-FP7).

1506 - Tuesday, October 13, 2015, 4:30 PM - 6:00 PM, Hall 6
M2M: Molecular & Multimodality Imaging: PET - Translational & Clinical Studies

OP531

Measurement of sorafenib concentrations using PET imaging in patients with advanced solid malignancies

L. H. Mammatas, M. Yaqub, N. H. Hendrikse, O. S. Hoekstra, R. J. Honeywell, M. Meijerink, L. A. Schwarte, G. J. Peters, A. A. Lammertsma, H. M. W. Verheul, C. W. Menke-van der Houven van Oordt; VU University Medical Center, Amsterdam, NETHERLANDS

Aim: Sorafenib is an oral protein kinase inhibitor targeting VEGFR, PDGFR and Raf kinases. It is currently registered for the treatment of metastasized hepatocellular carcinoma, renal cell cancer and iodine-refractory differentiated thyroid cancer. However, sorafenib leads to a response in only a subgroup of patients, while all are exposed to potential toxicity. Positron emission tomography (PET) may provide a non-invasive technique to predict which patients will benefit from this treatment. We hypothesize that response to sorafenib is dependent on achieving pharmacological active drug levels in tumor tissue and that quantitative PET imaging using radiolabeled sorafenib can predict these tumor concentrations. Materials and methods: At our center the GMP-synthesis of [11C]sorafenib has been developed. In this single center, proof of concept study, adult patients with advanced, biopsy accessible malignancies are included for which standard palliative treatment with sorafenib is indicated. [11C]Sorafenib dynamic PET is performed before and after two weeks of standard treatment. Pharmacokinetic modeling is applied to describe the tissue distribution and tumor uptake of [11C]sorafenib. Moreover, the amount of tracer uptake in tumor and blood measured with PET imaging is compared to the actual pharmacological active drug concentrations in tumor biopsies and blood samples after 2 weeks of treatment measured with liquid chromatography-tandem mass spectrometry (LC-MS/MS). Results: Six patients have been included: 1 patient with metastasized hepatocellular carcinoma, 4 patients with metastasized renal cancer and 1 patient with metastasized iodine-refractory follicular thyroid cancer. There was high physiological uptake of [11C]sorafenib in liver, gallbladder and kidneys due to metabolism and excretion of sorafenib, respectively. [11C]sorafenib uptake in tumor lesions was observed in 2/6 patients. The correlation between PET uptake and tumor and blood concentrations of sorafenib after two weeks of treatment will be shown. Conclusion: This study is the first step necessary to assess the feasibility of [11C]sorafenib PET as a quantitative predictive tool in cancer treatment.

OP532

Early and late evaluation of solid tumours with 64Cu-ATSM PET/CT: *a computer-aided fractal analysis*

E. Lopci[1,2], F. Grizzi[1], I. Grasso[3], C. Russo[1], G. Cicoria[3], S. Cambioli[3], F. Lodi[3], A. Chiti[4], S. Mattioli[5], S. Fanti[5]; [1]Humanitas Clinical and Research Hospital, Milano, ITALY, [2]Alma Mater Studiorum University, Bologna, ITALY, [3]Ospedale S. Orsola-Malpighi, Bologna, ITALY, [4]Humanitas University, Milano, ITALY, [5]Alma Mater Studiorum Bologna University, Bologna, ITALY

Purpose: 64Cu-ATSM is a well-known PET radiopharmaceutical applied for tumour imaging of hypoxia. Due to the long half-life of the radionuclide, early and delayed images can be acquired. However, no real evidence exists on the consistency of these two point-in-time acquisitions. The current study aimed at analyzing early and delayed acquisition on 64Cu-ATSM PET/CT in the same cohort of patients by comparing the information obtained from parametrical and computer-aided fractal geometry based analysis of the DICOM images. Methods: Five patients with pathologically proven head and neck cancer (HNC) or locally advanced NSLCL were included in the study. Each participant received 105-500MBq of tracer according to body size and was scanned in a 3D-mode on a PET/CT tomograph 60 minutes (early) and 16 hours (late) after injection. PET images were reconstructed and visualized on a GE Advanced 4.6 workstation for the definition of semi-quantitative and quantitative parameters: SUV_{max}, $SUV_{ratio\text{-}to\text{-}muscle}$, SUV_{mean}, hypoxic volume (HV) and hypoxic burden

(HB=HV*SUV_{mean}). DICOM data retrieved from both scans were subsequently analyzed using an ad-hoc computer-aided software to determine the Mean Intensity Value (MIV), Standard Deviation (SD), Relative Dispersion (RD), 3D Histogram Fractal Dimension (3D HIST FR DIM) and 3D Fractal Dimension (3DFD). Differences in between the parameters were compared using the Student's t-test, by considering as statistically significant p-values <0.05. Results: All patients showed an increased uptake of 64Cu-ATSM in tumour lesions, with a $SUV_{ratio\text{-}to\text{-}muscle}$ at early imaging of median 4.42, median SUV_{max} of 5.3, median SUV_{mean} of 2.8. The HV and HB at early imaging resulted respectively of median 41.4cm^3 and 161.2cm^3. All these semi-quantitative and quantitative data obtained at 1 hour resulted consistent with the same data obtained on delayed imaging (p>0.05). However, a statistically significant difference was found when compared the SUV_{max} of the muscle (p=0.045). Fractal analysis demonstrated that all parameters considered at early and late acquisition showed no statistically significant differences (p>0.05). A borderline value was obtained for MIV (p=0.075). This latter finding is mainly attributable to the limited series of analyzed patients, and the difference reported on muscle SUV_{max} applied as reference tissue for tumour contouring. Conclusions: Our findings support the reliable and consistent use of 64Cu-ATSM PET/CT obtained at early and delayed acquisition for the assessment of tumour hypoxia. Some attention might be paid when utilizing the data for radiotherapy contouring, because reference tissue uptake such as muscle SUV_{max} can show some difference in between the two scans.

OP533

Molecular imaging of neuroendocrine tumors with Scandium-44: a novel tool for THERANOSTICS

A. Singh[1], R. P. Baum[1], I. Klette[1], N. P. van der Meulen[2], C. Mueller[3], A. Tuerler[2], R. Schibli[3]; [1]THERANOSTICS Center for Molecular Radiotherapy and Molecular Imaging, ENETS Center of Excellence, Zentralklinik Bad Berka, Bad Berka, GERMANY, [2]Laboratory for Radio- and Environmental Chemistry, Paul Scherrer Institute (PSI), Villigen, SWITZERLAND, [3]Center for Radiopharmaceutical Sciences, Paul Scherrer Institute (PSI), Villigen, SWITZERLAND

Aim: Scandium-44 (44Sc) is a novel β+-emitting radionuclide for PET imaging. Chemically, Sc3+ is similar to lanthanides and rare earth elements (90Y3+, 177Lu3+) in its ability to form DOTA complexes. Given the physical properties, it may complement the use of Galium-68 (68Ga; short-lived, t1/2 = 68 min) for molecular imaging of neuroendocrine tumors (NETs). We report molecular imaging data using 44Sc-DOTATOC PET/CT in three patients with metastatic NETs.Materials and Methods:44Sc (t1/2 = 3.97 h, Eβ+ 1475.4 keV, 94.34%) was cyclotron-produced at PSI Villigen (Switzerland), transported over 600 km by road to ZBB (Germany), and radiolabelled with the somatostatin analogue DOTATOC (DOTA0,Tyr3-octreotide) with a specificity of 10 MBq 44Sc/nmol DOTATOC, and a high radiolabelling efficacy (99% ± 1.6; pH range = 3-4.5). 44Sc-DOTATOC (78, 96, and 130 MBq) was administered to 3 male patients (age range 57-70 years) with GEP-NETs presenting for restaging. Whole-body PET/CT (Biograph mCT Flow 64) scans were performed at variable time intervals from 10 min to 24 h p.i. and target-to-non-target uptake ratios were determined. The total number of SSTR-positive lesions was counted and SUV were determined in normal organs and metastases. Imaging results were compared to US, MRI, and 68Ga-DOTATOC PET/CT.Results: Molecular imaging with PET/CT following injection of 44Sc-DOTATOC demonstrated high specific tracer uptake in liver and lymph node metastases, with best target-to-non-target ratios seen at 2 to 4 h p.i. Two patients were diagnosed with progressive disease (PD): five additional metastases were detected in one patient, and one new metastasis was revealed in the other patient, compared to the previous 68Ga-DOTATOC PET/CT study. One patient had a single new small metastasis, but overall regressive tumor burden. No adverse effects were observed in any of the patients. Conclusions:44Sc is a highly promising positron-emitting radioisotope for the molecular imaging of NETs. When produced centrally, several patient doses can be delivered to PET imaging centers at a distance of over 1,000 kilometers. In this series, 44Sc-DOTATOC was found safe for human use, exhibited high target-to-non-target ratios, and delayed imaging up to 24 h p.i was possible. 44Sc-DOTATOC provides high diagnostic sensitivity and excellent image quality for PET imaging, and also demonstrates significant prominence as a THERANOSTIC radionuclide, since pre-therapeutic imaging and dosimetry by 44Sc-DOTATOC may be followed by radiopeptide therapy using the β–emitting Scandium-47 (47Sc).

OP534

Determination of chemokine receptor CXCR4 by 68-Ga-Pentixafor PET in patients with adrenocortical carcinoma

C. Bluemel[1], S. Hahner[1], B. Heinze[1], A. Schirbel[1], M. Schottelius[2], C. Lapa[1], S. Kropf[3], K. Lückerath[1], B. Allolio[1], M. Fassnacht[1], H. Wester[2], A. K. Buck[1], K. Herrmann[1]; [1]Universitätsklinikum Würzburg, Würzburg, GERMANY, [2]Technische Universität München, München, GERMANY, [3]Scintomics GmbH, Fürstenfeldbruck, GERMANY.

Aim: The chemokine receptor CXCR4 and its chemokine ligand 12 are key factors for angioneogenesis, metastasis and tumour growth in several human cancers and also overexpressed in adrenocortical neoplasia. Recently, 68-Ga-Pentixafor PET for in vivo CXCR4- imaging was introduced. The aim of the present study was to evaluate 68-Ga-Pentixafor for in vivo determination of CXCR4-expression in patients with adrenocortical carcinoma (ACC) to select suitable patients for CXCR4-directed therapies in a theranostic concept. Methods: 22 consecutive patients with histopathological proven metastasized ACC were examined with 68-Ga-Pentixafor-PET/CT and 18-F-FDG-PET/CT. Results of both imaging methods were compared and patients were classified as suitable or unsuitable for CXCR4-directed therapy. Results: In all patients 18-F-FDG-PET/CT and 68-Ga-Pentixafor-PET/CT were rated positive (100%), 48% had a local recurrence, 52% peritoneal/mesenterial, 33% retroperitoneal tumour lesions, 29% had lymph node metastases and 86% haematogenous metastases. Visual comparison of both tracers resulted in comparable findings in 7 (32%) patients and 4 (18%) patients in complementary findings. In 9 patients (41%) 18-F-FDG-PET/CT identified more lesions with visually higher uptake compared to CXCR4-imaging, whereas in 2 patients (9%) 68-Ga-Pentixafor-PET/CT identified more metastatic lesions than 18-F-FDG. The corresponding mean SUVmax value for 18F-FDG was 12.28±8.35 (range, 2.17-47.04) and thus significantly higher than the SUVmax for 68Ga-Pentixafor (mean, 8.40±5.77; range, 1.75-34.18). Overall, 12 out of 22 patients (54%) were rated as suitable and 3 patients (14%) as potentially suitable CXCR4-directed therapy, e.g. 177-Lu/90-Y-labelled Pentixafor analogues. Conclusions: CXCR4 is overexpressed in a subgroup of ACC patients allowing for CXCR4-directed therapies in 67% of patients in the present cohort. 68-Ga-Pentixafor-PET/CT provides excellent imaging quality and allows for selection and therapy monitoring of patients suitable for CXCR4-directed therapy.

OP535

Diagnostic value of (68)Ga - PSMA PET/CT in biochemical recurrence of prostate carcinoma with low PSA levels

E. Demirci[1,2], J. Nematyazar[1], R. Akyel[1], B. Razavi[1], A. Aygun[1], M. Ocak[3], M. Halac[1], A. Araman[3], L. Kabasakal[1]; [1]Department of Nuclear Medicine, Cerrahpasa Medical Faculty, Istanbul University, Istanbul, TURKEY, [2]Department of Nuclear Medicine, Sisli Etfal Training and Research Hospital, Istanbul, TURKEY, [3]Department of Pharmaceutical Technology, Pharmacy Faculty, Istanbul University, istanbul, TURKEY.

Purpose: 68Ga-DKFZ-11 (68Ga-PSMA) has been suggested as a novel tracer for detecting of PCa relapses and metastases. However there is a limited number of publications about the timing of PSMA PET/CT scan. The aim of the study is to evaluate the diagnostic value of PSMA PET/BT in the diagnosis of recurrent prostate cancer with low PSA levels. Materials and Methods: We performed a retrospective analysis in patients who underwent PSMA PET/CT from November 2013 to December 2014 in our department. 53 out of 178 patients who had rising PSA levels (still lower than 5ng/ml), and did not have known metastasis were included in this study. Results: Patients had an average PSA of 1.41 ng/ml. A total of 31 patients (58%) showed at least one extraprostatic or prostatic lesions. Intense pathologic radiotracer uptake was observed in 15 patients (28%) at the site of primary tumor. Lymph node metastases were detected in 19 patients (36%) and bone metastases were detected in 8 patients (15%). A PET positivity rate of 31% (n=4), 54 % (n=13) and 88% (n=14) observed in patients with PSA level of <0.2, 0.2-2 and 2-5 ng/ml respectively. Those with PSA level PSA <0.2, 0.2-2and 2-5 ng/ml had 8% (n=1), 21% (n=5), 56% (n=9) local recurrence 15% (n=2), 42% (n=10), 44% (n=7) lymph node metastasis and %15 (n=2), 8% (n=2), 25% (n=4) bone metastasis. A positive correlation observed between positivity rate and gleason scores (%15 for Gleason 6, %55 for Gleason 7, 75% for Gleason 8 and 77% for Gleason 9). PSMA PET/CT positivity's confirmed with biopsy (n=3), follow-up (n=26) and conventional imaging studies at the time of the PET/CT (n=11) or during follow up (n=13). According to patient-based analysis of 44 cases %57(n=25) of patients had true positive, %23(n=10) of patients had true negative, %2(n=1) patient had false positive, %18(n=8) of patients had false negative findings which are leading to a sensitivity of 58.1% (95%CI:42.1-72.9%) specificity of 90% (%95CI:%48.6-98.5). Within the patients who had PSA levels from 0.2 to 5, the sensitivity was %79.3 (%95 CI: %60-91.9). Conclusion: PET/CT with 68Ga PSMA is a valuable tool for assessing recurrence of PCa with a high sensitivity (%79.3) within the patients who has PSA levels between 0.2-5 ng/ml. Additionally PSMA PET/CT can be used in patients with very low (<0.2 ng/ml) but increasing PSA levels, which in many cases may influence the further clinical management.

OP536

Preliminary comparison of PET/CT and PET/MRI hybrid systems using a Ga-68 labeled PSMA ligand for initial staging of prostate cancer

S. Lütje[1], B. Gomez[1], J. Cohnen[1], B. M. Schaarschmidt[2], R. Reichel[1], S. Rosenbaum-Krumme[1], A. Bockisch[1], T. D. Poeppel[1], A. Wetter[3]; [1]Clinic for Nuclear Medicine, University Hospital Essen, Essen, GERMANY, [2]Department of Diagnostic and Interventional Radiology, Medical Faculty, University Düsseldorf, Düsseldorf, GERMANY, [3]Department of Diagnostic and Interventional Radiology and Neuroradiology, University Hospital Essen, Essen, GERMANY.

Aim: Despite improvements in diagnostic and therapeutic approaches, prostate cancer remains one of the leading causes of cancer-related death in men in the Western world. ^{68}Ga-labeled HBED-CC-PSMA is a highly promising new tracer for imaging of PCa. The aim of this study was to evaluate the feasibility of PET/MRI with this tracer for detection and locoregional staging of PCa at initial diagnosis in comparison to PET/CT. Materials and methods: Ten high-risk patients (mean serum prostate-specific antigen 12.0 ± 9.2 ng/ml) among which seven were suspected with PCa in transrectal biopsy, underwent PET/CT 66 ± 17 min after injection of the ^{68}Ga-HBED-CC-PSMA ligand (mean 102 ± 18 MBq/patient) followed by PET/MRI at 153 ± 66 min postinjection. Data from the two investigations were analyzed separately and compared regarding tumor detection rate and radiotracer uptake in tumor lesions and muscle tissue. Uptake was quantified in terms of the maximal standardized uptake value (SUV_{max}) within a spheroidal volume of interest (VOI). SUVs of PET/CT and corresponding PET/MRI were compared to each other with paired t tests. Reference VOIs were drawn in the gluteal muscles on the right side. The native SUV_{max} of the lesions were normalized to the SUV_{max} in the reference region. Tumor lesions within the prostate visualized by both techniques were correlated to histopathological analyses. Results: With both techniques, 8 histologically proven tumor lesions were identified in 7 patients. In three patients with negative transrectal biopsy results, no tumor lesions were identified with PET/CT and PET/MRI. Even though SUVs in PET/CT were slightly higher (mean SUV_{max} 12.7 ± 9.1, n=8) compared to PET/MRI (mean SUV_{max} 9.6 ± 5.8, n=8), PET/MRI provided significantly higher tumor-to-muscle ratios compared to PET/CT (mean 15.8 ± 9.7 and 8.1 ± 5.1, respectively, p=0.0016). Conclusion: PET/MRI is as reliable as PET/CT for detection and locoregional staging of patients with PCa at initial diagnosis.

OP537

Evaluation of the role of F-18 FDG PET/CT in childhood rhabdomyosarcoma - preliminary results

R. K. Gupta, **Jr**., M. Tripathi, S. Bakshi, N. Damle, K. Kumar, R. Bhayana, C. Bal; All India Institute of Medical Sciences, New Delhi, INDIA.

INTRODUCTION: The management of rhabdomyosarcoma (RMS) depends on risk stratification at diagnosis & treatment response. The methods used for initial evaluation include histopathology (HP), magnetic resonance imaging (MRI), contrast enhanced computed tomography (CECT), chest X-ray (CXR), non-contrast computed tomography (NCCT) chest, Technetium-99m Methylenediphosphonate (Tc-99m MDP) bone scan (BS) and bone marrow biopsy. Fluorine-18 Fluorodeoxyglucose (FDG) PET/CT has emerged as a useful modality for staging malignancies. In this study we compared F-18 FDG PET/CT with conventional imaging (CI) modalities for the staging of RMS. MATERIALS AND METHOD: Twenty two children (16 males) with mean age 8.13 years (range 2 to 17 years) were prospectively enrolled in this study. All patients were biopsy proven RMS with positive desmin and myogenin. Each patient underwent CECT and/or MRI of the primary tumour site, CXR and/or NCCT chest and Tc-99m MDP BS. The disease was staged according to TNM Pretreatment Staging Classification[1]. Each patient also underwent F-18 FDG PET/CT within one week of the MRI/CECT and were restaged using the information obtained from PET/CT. Nodal status and metastases as obtained by conventional imaging and after PET/CT were compared. RESULTS: F-18 FDG PET/CT detected additional lesions in 59 %(13/22) patients. In comparison to CI, F-18 FDG PET/CT detected additional nodes in 13% (3/22)patients and ruled out nodal involvement in 4%(1/22) patients. Additional distant metastatic sites in lung and bone marrow were detected in 9 % (2/22) patients. N stage changed in 31 %(7/22) patients, M stage changed in 9% (2/22) patients. Overall TNM staging changed in 18 %(4/22) patients. CONCLUSION: This study suggests that F-18 FDG PET/CT has potential to increase initial staging accuracy, specifically detection of nodal involvement and distant metastatic spread. REFERENCE: 1. Lawrence W, Jr, Anderson JR, Gehan EA, et al. Pretreatment TNM staging of childhood rhabdomyosarcoma: A report of the Intergroup Rhabdomyosarcoma Study Group. Children's cancer study group. Pediatric oncology group. Cancer. 1997;80:1165-1170.

OP538

Impact of 18F-FDG PET/CT in the diagnosis and therapeutic response of histiocytosis

L. M. Vija[1], G. Bera[2], J. Haroche[2], F. Cohen[1], P. Chaumet-Riffaud[1], A. Prigent[1], P. Maksud[2]; [1]Paris Sud University, Le Kremlin-Bicetre, FRANCE, [2]Groupe Hospitalier La Pitié-Salpêtrière, Paris, FRANCE.

Objectives: Histiocytosis (with its heterogeneous group of Langerhans cell histiocytosis (LCH) and subtypes of non-LCH histiocytoses) is a rare inflammatory and systemic disorder of unknown origin, characterized by infiltration of histiocytes in the affected tissues. The objective of this study was to assess the impact of 18F-FDG PET/CT for the diagnosis and metabolic response to immunomodulatory treatments.Patients and methods:We retrospectively analyzed baseline and follow-up 18F FDG PET/CT exams as it follows: 406 exams in 85 patients with Erdheim-Chester disease (ECD), 15 exams in 5 patients with Rosai-Dorfman disease (RDD), 55 exams in 20 patients with LCH, 102 exams in 14 patients with combined forms of histiocytoses (LCH+ECD, LCH+RDD), as well as 6 exams in

3 patients with xanthogranulomatoses. As the gold standard (histological confirmation of all the metabolic localizations) cannot be achieved, 18F FDG PET/CT exams, were compared with organ/system based radiological (CT/MRI) findings (for example: thorax, abdomen and pelvis CT, brain MRI, cardiac MRI, bone MRI), specific for every patient. Metabolic responses to treatments (41 patients on interferon-α, 13 patients on vemurafenib and 7 patients on infliximab) were assessed by the ΔSUVmax (baseline-final)/baseline of the highest-uptake lesion. Concordances between 18F FDG PET/CT and CT/MRI were assessed by the kappa (κ) coefficient. Results: Besides a whole-body topographical characterization, 18F FDG PET/CT showed an overall sensitivity and specificity ranging from 33 to 100% and from 60 to 100% respectively, according to the organ or system explored. Highest rates of metabolic uptake detection by 18F FDG PET/CT in histiocytosis lesions of both ECD and mixed forms, compared with CT/MRI, concerned long bone lesions (80% vs 73% for ECD, 93% vs 86% for mixed forms), with an excellent concordance (κ=0,96 for ECD, κ=1 for mixed forms) between imagistic methods. 18F FDG PET/CT identified 17 metabolic responses (41%) on interferon-α (24-month median follow-up), one complete response and 8 (62%) partial responses on vemurafenib (12-month median-follow-up), as well as a partial response on infliximab (15-month median follow-up).Conclusions:The results of this large retrospective study suggest that whole-body 18F FDG PET/CT is informative at diagnosis for a better whole-body staging (rapid and more exhaustive identification of localisations) for each histiocytosis subtype and for the evaluation of the metabolic response to various immunomodulatory treatments.

1507 - Tuesday, October 13, 2015, 4:30 PM - 6:00 PM, Hall F
Teaching Session: Interactive Quiz: Nuclear Medicine with Correlative Imaging

OP539

Interactive Quiz: Nuclear Medicine with Correlative Imaging

T. Lynch, **UNITED KINGDOM**

1508 - Wednesday, October 14, 2015, 8:00 AM - 9:30 AM, Hall E
Cardiovascular System: Miscellaneous

OP540

Increased myocardial 18F-FDG uptake after doxorubicin-based chemotherapy in Hodgkin disease: an early predictor of cardiotoxicity?

M. Bauckneht[1], G. Ferrarazzo[1], F. Fiz[1], P. Ghione[2], F. Bongioanni[1], A. Nieri[1], M. Pennone[1], S. Morbelli[1], P. Spallarossa[2], C. Marini[3], G. Sambuceti[1]; [1]Nuclear Medicine, IRCCS AUO San Martino IST, Genova, ITALY, [2]Department of Internal Medicine, Chair of Cardiology, University of Genoa, Genova, ITALY, Genova, ITALY, [3]Institute of Bioimaging and Molecular Physiology, CNR, Milan, Genoa Section, Genova, ITALY, Genova, ITALY.

Aim. Doxorubicin-induced cardiotoxicity is related to many pathophysiological mechanisms, including oxidative stress and increased endothelin-1 serum levels. Previous in vitro studies documented that both these mechanism promote GLUT expression in cardiomyocite's sarcolemma. The aim of the present study was to verify whether this phenomenon can increase FDG uptake in the left ventricular myocardium of patients with Hodgkin disease (HD) treated with Doxorubicin-based chemotherapy scheme. Materials and Methods. We retrospectively analyzed FDG PET/CT scans of 24 patients with HD (mean age was 34±13) selected according to the following inclusion criteria: 1) absence of any history of cardiovascular disease; 2) full remission after two ABVD cycles; 3) availability of at least 4 consecutive PET/CT scan performed for staging (PET1), interim (PET2), post-therapy (PET3) and six month follow up (PET4) evaluation. Time points of PET/CT scan were thus at baseline and at 2, 6 and 12 months, respectively. Volumes of interest were manually drawn on the left ventricular myocardium and on skeletal muscle (paraspinal) to estimate mean (SUVmean) and maximum (SUVmax) standardized uptake values that were normalized for SUVmean determined by drawing a 1-cm oval region of interest in the aortic arch as an index of blood pool tracer concentration. Results. Normalized myocardial SUVmean was 2.08±1.29 at baseline and showed a progressive increase that became significant at PET3 (3.31±2.66, $p<0.05$) to remain stable in PET4 at 3.55±2.53 ($p<0.05$ vs PET1, p=ns vs PET3, respectively). Conversely, muscle SUVmean increased from PET1 (0.34±0.12) to PET3 (0.49±0.28, $p<0.05$); however, it returned to baseline values at PET4 (0.37±0.13) (p=ns vs PET1, $p<0.05$ vs PET3, respectively). Consequently, SUVmean increased from PET3 to PET4 in the myocardium, while it dropped in the skeletal muscle, as demonstrated comparing the PET4/PET3 ratio in these two tissues ($p<0.05$). The same results were obtained when compared myocardial and skeletal muscle normalized SUVmax. Conclusions. Present data demonstrate a divergent metabolic pattern between myocardium and skeletal muscle in young patients treated with a Doxorubicin-based chemotherapy for HD. Intriguingly, the

main difference between myocardial and skeletal muscle FDG uptake was detected at follow-up analysis when compared to staging and post-therapy evaluation. Although our protocol does not imply a sugar free diet in the days preceding the scans, the increased myocardial uptake trend and the divergent muscular metabolic performance could be at least partially explained by a Doxorubicin-induced myocardial GLUT overexpression.

OP541

Reverse mismatch in a patient cohort undergoing 18F-FDG/82Rb dual isotope PET for assessment of myocardial viability: Is it a significant clinical problem?

A. K. Hansen, M. Gejl, K. Bouchelouche, L. P. Tolbod, L. C. Gormsen; Aarhus University Hospital, Aarhus, DENMARK.

Background: Dual isotope myocardial positron emission tomography (PET) with perfusion (e.g. 82Rb PET) and metabolism tracers (18F-FDG viability PET) during hyperinsulinemia is currently widely used when myocardial viability is assessed. The technique is used to identify viable but underperfused myocardium (hibernating myocardium) in order to guide potential revascularization efforts. 18F-FDG viability PET relies on the assumption that all viable tissue takes up 18F-FDG when sufficiently stimulated by hyperinsulinemia. This may, however, not always be the case. It has thus been demonstrated that patients with type 2 diabetes (T2D), as well as patients with dilated cardiomyopathy, has severely depressed myocardial glucose uptake. In a clinical setting, this is highly unfortunate since 1) viable but non-FDG avid myocardium may appear hypometabolic , and 2) a large fraction of patients with heart failure suffer from either diabetes or dilated cardiomyopathy. Perfused but apparently hypometabolic myocardium is termed ”reverse mismatch”. Aim: To assess the fraction of patients with reverse mismatch in a mixed patient cohort undergoing 18F-FDG viability PET. Materials and methods: 92 heart failure patients (25 with diabetes) undergoing 18F-FDG viability were retrospectively reviewed. Resting perfusion was assessed by 82Rb PET (1110 MBq) followed by 18F-FDG PET scans (400 MBq) of the heart region. 18F-FDG uptake was stimulated by a total of 2 hours hyperinsulinemic-euglycemic (HE) clamp (1 mIE/kg/min). Percentage of hypoperfused and hypometabolic myocardium was calculated based on a 5-point score (17-segment model) divided by the maximum points obtainable. The difference between percentage hypoperfused and hypometabolic myocardium was calculated (DIF_PERF_MET) and interpreted as reverse mismatch if normal perfusion was observed with depressed metabolism. Coincident hypoperfusion and hypometabolism was considered scar whereas hypoperfusion with normal metabolism was considered hibernation. Results: In 31/92 patients hypometabolic myocardium significantly exceeded the percentage of hypoperfused myocardium (REVERSE PATIENTS) indicating reverse mismatch [DIF_PERF_MET (%): 30.7 +/- 13.5 (REVERSE PATIENTS) vs. 11.4 +/- 7.1 (SCAR AND HIBERNATION), $p<0.001$]. No correlation was observed between left ventricle volume and degree of reverse mismatch and no impact of diabetes status on reverse mismatch was observed. Hibernating myocardium was demonstrated in only one patient. Conclusion: In a mixed patient cohort undergoing HE-clamp and 18F-FDG viability PET, reverse mismatch was observed in 34 % of studies regardless of diabetes status. Since underestimated viability may severely impact the decision to revascularize patients, 18F-FDG PET viability studies should be interpreted cautiously and preferably in conjunction with results from other modalities (e.g. MRI).

OP542

Assessment of cardiac sympathetic nerve system in the rat heart using 11C-HED

Y. Maya[1,2], R. Werner[1,3], H. Wakabayashi[1], M. Nakajo[1], K. Fukushima[4], C. Lapa[1], K. Herrmann[1], T. Higuchi[1,3]; [1]Department of Nuclear Medicine, Universitätsklinikum Würzburg, Würzburg, GERMANY, [2]Research Centre, Nihon Medi-Physics Co., Ltd., Chiba, JAPAN, [3]Comprehensive Heart Failure Center, Würzburg, GERMANY, [4]Hyogo College of Medicine, Hyogo, JAPAN.

Objectives: The sympathetic nervous system of the heart plays a crucial role in various cardiac diseases including ischemic heart diseases and heart failure. High-resolution small-animal PET enables noninvasive and quantitative evaluation of the heart in rodent models of human diseases. In this study, we investigate the feasibility of assessing sympathetic nerve system activity with 11C-HED PET in rat hearts. Methods: To confirm the specificity of 11C-HED uptake in rat myocardium, 11C-HED with a wide range of specific activities was injected (48.7+/-9.7MBq, ranged 0.2-60.4μg/kg cold mass) into healthy rats (n = 14) via a tail vein. Dynamic 23-frame PET images were started just before the tracer administrations, and obtained over 30 min. Time activity curves were generated for myocardial tissue region of interest (ROI) at mid ventricular level and blood activity at left atrial cavity ROI. Cardiac 11C-HED retention index (%/min) was calculated as myocardial tissue activity at 20-30min divided by the integral of the blood activity curves. In rat model of transient ischemia (7 days after 20 min left coronary occlusion and reperfusion, n=2), 11C-HED PET and following 18F-FDG PET as a reference of myocardial viability was performed to evaluate the feasibility of assessing the local sympathetic nerve damage. Results: In healthy rat hearts, dynamic PET demonstrated stable, high contrast and homogeneous left ventricular myocardial uptake within 5 min after intravenous tracer injection. In different 11C-HED specific activities, the estimated retention index decreased as

loading cold mass increased. These data were well fitted by a dose-response model (r2=0.92), and the estimated IC50 value (95% confidence intervals) was 46.3 (34.6-62.0) μg/kg. In rat model of transient ischemia, PET imaging clearly visualized the 11C-HED uptake defect in the anterolateral wall, while 18F-FDG uptake was preserved throughout the ventricle at the 11C-HED defect area. Post mortem tissue analysis with HE staining and tyrosine hydroxylase nerve staining confirmed denervation but viable myocardium after transient coronary occlusion. Conclusions: Cold mass effect of cardiac 11C-HED uptake measured as retention index by PET showed specificity of the imaging signal in the rat heart. Furthermore, local impairment of 11C-HED uptake despite preserved 18F-FDG uptake indicates feasibility of regional assessment of sympathetic nerve damage in rat model of ischemia. A combination of serial 11C-HED PET imaging and rat model of cardiac disease would be one of the promising approaches to investigate further insight into the dynamic pathophysiology of sympathetic nervous system of the heart.

OP543

Value of attenuation correction in stress-only myocardial perfusion imaging using CZT-SPECT

J. D. van Dijk[1,2], M. Mouden[1], J. Ottervanger[1], J. A. van Dalen[1], S. Knollema[1], C. H. Slump[2], P. L. Jager[1]; [1]Isala hospital, Zwolle, NETHERLANDS, [2]MIRA: Institute for Biomedical Technology and Technical Medicine, University of Twente, Enschede, NETHERLANDS.

Purpose: Attenuation correction (AC) has been shown to enhance conventional stress-only SPECT myocardial perfusion imaging (MPI). However, it remains unknown whether the same holds true when using the newest generation cadmium zinc telluride (CZT)-based cameras. The aim of this study was to determine the value of attenuation correction on stress-only MPI using a CZT-SPECT camera. Methods: A retrospective analysis was performed including 107 consecutive stable, low to intermediate risk patients (age 60 ± 12 years, 43% male gender and BMI 28.1 ± 4.7 kg/m^2) who underwent clinically indicated MPI CZT-SPECT/CT (Discovery NM/CT 570c, GE healthcare). The stress scans were reconstructed with and without CT-based attenuation correction (AC). Three types of images were created for interpretation; only displaying reconstructed data without AC (NC), only with AC, and with both NC and AC (NC+AC). Next, two experienced physicians visually interpreted by consensus these 321 randomized images for diagnostic outcome (normal, equivocal, abnormal scan) without knowledge of patient's history or other clinical findings. We have recorded all relevant events, in example, late coronary revascularization (>60 days), non-fatal myocardial infarction and all-cause death, in a mean follow-up time of 47.7 ± 9.8 months. Results: The percentage of normally interpreted scans increased from 45% using the NC images to 72% and 67% using the AC and NC+AC images, respectively ($p<0.001$). The percentage of images interpreted as equivocal decreased when including attenuation correction from 43% to 20% and 24% for the AC and NC+AC images, respectively ($p<0.001$). In addition, comparable hazards ratios on the recorded events were observed between the normally interpreted NC and AC (1.16, p=0.86), or NC+AC (0.99, p=0.99). Conclusion: The use of AC decreases the need for rest imaging in CZT-based SPECT cameras. This has the potential to reduce the cumulative radiation dose and improves laboratory efficiency. Although we did not assess the direct diagnostic accuracy, patient outcome seems unaffected.

OP544

Characterization of a dedicated myocardial cardio-centric SPECT-TC System: a preliminary phantom study

E. Richetta, M. Pasquino, C. Cutaia, G. Brusasco, G. Santopolo, I. Trabucco, A. Guida, R. Pellerito, M. Stasi; AO Ordine Mauriziano di Torino, Turin, ITALY.

Aim: The increasing need of faster myocardial perfusion imaging and dose patient reduction are nowadays satisfied by a novel dedicated cardiac equipment. At our institution a SPECT-CT was recently installed: cardio-centric multifocal collimators combined with a dedicated reconstruction software increased sensitivity and allows shorter image acquisition times or lower patient dose. With the aim to define the best acquisition protocol, a cardiac phantom was scanned with different frames and times. Semi-quantitative analysis was performed and images were qualitatively evaluated by two experienced physicians. Materials and methods: A thoracic phantom (Biodex) with a cardiac insert, simulating a focal perfusion deficit in heart wall, was filled with 99mTc uniform activity (37 GBq, dose-rate 5-6 kcps); acquisition was performed with cardio-centric collimators (Siemens SMARTZoom, matrix 128x128, angle 59°-104°, zoom1), varying the number of views (#frame:32, 30, 28,26, 22, 20, 18,10) and acquisition time per view (20, 15, 10, 5 s). A CT thoracic scan was then executed to correct images for scatter and attenuation. Reconstruction was performed with dedicated myocardial algorithm (Siemens IQSPECT-Iterative Flash3D, 8iteration, 4subset). Images were qualitatively inspected by two experienced physicians. For a semiquantitative analysis, a 17-segments QPS-model was adopted to evaluate perfusion polar maps; perfusion index, deficit extent, TPD, stress score SS and S% were analyzed as function of number of views and time per view; results were correlated to acquisition time. Results: Qualitative analysis of images showed an improved uptake-to-background ratio for a 18 frame-20s acquisition; for acquisition time less

than 20 s a poor statistic was found. The 17-segment analysis showed no significant variations at varying the number of views from 32 to 18. Scores range showed minimal fluctuations when number of views was changed (extent [42-45], TPD [30-33], SS [23-25] S%[34-37]), confirming the qualitative analysis performed by physicians. Reducing time per views, the difference becomes higher (extent [42-50] , TPD [31-37], SS [23-28] S%[34-41]). Finally, reducing frames from 32 to 18, the acquisition time decreases up to 60% with a substantially equal image quality. Conclusions: The best acquisition protocol was defined to optimize the procedure (18 frame-20s), according to qualitative and quantitative analysis. This operating mode, feasible only with this dedicated myocardial cardio-centric SPECT-TC System, allows to reduce acquisition time (or dose to patients) up to 40%, compared to standard protocols with an improved image quality.

OP545

Gated Myocardial Imaging: The impact of FBP and OSEM Image Reconstruction and Filtering on values of Left Ventricle function calculated with a commercial program - QGS*

D. S. Rosário; Karolinska Institutet, Stockholm, SWEDEN.

Aim: MPI tomographic (GSPECT) images are acquired synchronized with a patient's ECG for both stress and rest phases. These are reconstructed, processed and compared to detect changes in myocardial perfusion and left ventricular (LV) function. MPI image quality is strongly affected by the filtering process executed in GSPECT reconstruction. The optimal choice and selection of filter parameters is still considered a problem in the reconstruction process. The aim of this study was to evaluate how the change of filter parameters in Filtered Back Projection (FBP) and Ordered Subset Expectation Maximization (OSEM) reconstruction techniques affect the LV functional values calculated by QGS, a commercial program and the accuracy of the values as compared to ultrasound measurements. Methods: Thirty patients were included in study. GSPECT images were acquired in the stress and rest phases. A two days protocol was used and the radiopharmaceutical for both phases was 99mTc-sestamibi. The LV functional values (ejection fraction (LVEF), end diastolic volume (EDV) and end systolic volume (ESV)) were calculated with the QGS program for 8 different reconstruction procedures: FBP reconstructions and a Butterworth filter, using the same order, equal to 5, but changing the cut-off frequencies, which were: 0.20, 0.30, 0.40 and 0.50. For OSEM, all reconstructions were made with 4 iterations with 8 subsets and a Gaussian filter with different FWHM (mm), which were: 4, 8, 14 and 20. Reference LVEF values were calculated from ultrasound studies using Simpson's method. Results: There was a good correlation between functional values for most of the filter functions between phases and for LVEF against ultrasound, irrespective of reconstruction method. For FBP with a Butterworth filter with cut-off frequency 0.20 and OSEM with a Gaussian filter with FWHM 20, however, all correlations were poor. Discussion and Conclusions: LV functional values were shown to fairly independent of reconstruction method and filter function unless a very low pass filter was used. The good correlation between stress and rest phases showed that values were reproducible provided the perfusion distribution and LVEF were similar for both phases. There was also a good correlation between LVEF values measured with GSPECT and ultrasound. The best correlation was obtained with filters that resulted in noisy images. Since there were individual variations in LV functional values that could have affected a diagnosis, it may be better to choose reconstruction parameters that produce images that can be qualitatively assessed to ensure that the calculated are reasonably correct.

OP546

Feasibility of an eighth-time gated myocardial perfusion SPECT functional imaging using IQ-SPECT system.

F. Caobelli[1], J. T. Thackeray[1], A. Soffientini[2], F. M. Bengel[1], C. Pizzocaro[2], U. P. Guerra[2]; [1]Hannover Medical School, Hannover, GERMANY, [2]Fondazione Poliambulanza, Brescia, ITALY.

Background: IQ-SPECT, an add-on to general purpose cameras based on multifocal collimation, can reduce scan acquisition time to one fourth of standard procedures (12s/view) in myocardial perfusion imaging (MPI). In a phantom study, a reduction to one eighth of standard acquisition time (6s/view) was demonstrated as feasible. It remains unclear whether such a reduction could be extended to clinical practice. Methods: Fifty patients with suspected or diagnosed CAD underwent a two-day stress/rest 99mTc-sestamibi MPI protocol. Two consecutive SPECT acquisitions (6 and 12s/view) were performed. Electrocardiogram-gated images were reconstructed with and without attenuation correction (AC).Polar maps were generated and visually scored by 2 blinded observers for image quality and perfusion in 17 segments. Global and regional summed stress (SSS), summed rest (SRS) and summed difference scores (SDS) were determined. Left ventricular volumes and ejection fraction were calculated based on automated contour detection. Results: Image quality was scored higher for 12s/view scans, both with and without AC. Summed scores were statistically comparable between 6 and 12s/view acquisitions, either globally or in individual coronary territories (e.g. in AC images 6s vs 12s/view: SSS 6.6±8.3 vs 6.2±8.2, p=0.10; SRS 3.9±5.6 vs.3.5±5.3, p=0.19; SDS 2.8±5.7 vs. 2.6±5.7, p=0.59). Both acquisitions allowed an MPI-based diagnosis

of CAD in 25/50 patients (AC). End diastolic and end-systolic calculated volumes were modestly higher from 6s/view acquisitions compared to 12s/view (EDV +4.8 ml at rest and + 3.7 ml after stress,p=0.003; ESV +4.1 ml at rest and +2.6 ml after stress,p=0.01), whereas ejection fraction did not differ (-1.2% at rest, p=0.20 and -0.9% after stress, p=0.27). Conclusion: Image quality and LV functional parameters acquired at one eighth time were statistically comparable to the previously validated one fourth time protocol using IQ-SPECT. Shorter acquisition times without loss of diagnostic accuracy provides for improved patient comfort and streamlined departmental efficiency.

OP547

Impact of Data-Driven Respiratory-Motion Correction on the Extent/Severity of Myocardial Perfusion Defects of MPI SPECT Acquired with Discovery NM 530c: REGAT Software

D. Daou[1,2], R. Sabbah[3], H. Bouladhour[3], C. Coaguila[4]; [1]Cochin Hospital, APHP, Paris, FRANCE, [2]EA 7334 REMES, Université Paris-Diderot, Sorbonne Paris-Cité, Paris, FRANCE, [3]CHU Jean Minjoz, Besançon, FRANCE, [4]Centre Hospitalier de Bigorre, Tarbes, FRANCE.

Aim: We previously developed a data-driven respiratory-motion (RM) correction method for conventional SPECT gamma-cameras (REGAT) and adapted it to CZT multi-pinhole detector gamma camera (Discovery NM 530c). We recently reported that REGAT is clinically feasible, easily applicable and presents interesting impact on image characteristics when applied to myocardial perfusion SPECT imaging (MPI) realized with Discovery NM 530c. In this preliminary evaluation, we aimed to study whether REGAT applied to MPI (Discovery NM 530c) impacts the extent/severity of MPI defects (MPD). Materials and Methods: Were included 25 patients addressed for stress/rest MPI. All patients had prone stress MPI (2 MBq/Kg 99mTc-Tetrofosmin) than prone rest MPI 3-hours later (n=24/25 pts, 6 MBq/Kg). All acquisitions were made on Discovery NM 530c. Each list mode acquisition was processed to generate a dynamic SPECT acquisition study of 500 msec duration. Each dynamic SPECT study was processed to generate its corresponding data-driven RM curve. This curve was used to generate a mean RM GSPECT study which was reconstructed on Xeleris workstation. The corresponding reconstructed RM gated volumes were summed either without realignment (nonR-SPECT) or after rigid realignment (R-SPECT). These nonR-SPECT and R-SPECT studies (49 = 25 stress+24 rest) were classified by an experienced observer as presenting an impact (G1) or no impact (G2) on severity/extent MPD: an impact was considered present if ≥ 1 LV segment presented a modification ≥ 1 score (LV: 17 segments; 5 point scoring). Were noted the maximal RM in the 3 axis of reoriented LV: anterior/inferior (A-I), septal/lateral (S-L) and basal-apical (B-A) axis. Was also calculated variation of LV myocardial counts (LV-Max, %) between both R-SPECT and nonR-SPECT LV-Max. Results: A_I movement was the dominant movement (n=49): A-I, S-L and B-A axis were 9.7±4.6 mm, 1.8±1.1 mm, 3±2.3 mm. Variation in LV-Max (n=49) was 2.75±3.61 %. G1 consisted of 7/49 studies (14%). In G1 vs G2, variations in LV-Max were 3.7±7.9 % vs 2.6±2.4% (NS), and A_I movement were 15.7±3.5 mm vs 8.7 ±4 mm respectively (P<0.01). The cumulative % studies presenting with a positive impact on MPD (Cum) was correlated to the A_I movement: Cum (%) = 0.0043*A_I2 - 0.0325*A_I + 0.2099 (r2=0.9725, P<0.0001). In 13/49 studies (27%) with A_I >12 mm, 6/13 (46%) presented an impact on MPD. Conclusion: Data-driven respiratory-motion correction of MPI with Discovery NM 530c appears to impact MPD in a substantial number of studies. Its incidence is related to the magnitude of RM.

1509 - Wednesday, October 14, 2015, 8:00 AM - 9:30 AM, Hall 8

Clinical Oncology: Neuroendocrine

OP548

The Influence of ^{68}Ga-DOTATATE PET/CT Imaging in the Management Decision of Patients with Neuroendocrine Tumors

E. Skoura[1], O. M. AlMukhalid[1], E. Panagiotidis[1], M. Al Harbi[1], I. Kayani[1], S. Michopoulou[1], R. Syed[1], P. J. Ell[1], M. E. Caplin[2], J. Bomanji[1]; [1]UCLH, London, UNITED KINGDOM, [2]Royal Free Hospital, London, UNITED KINGDOM.

Aim: ^{68}Ga-DOTATATE PET/CT scan is a widely accepted method for imaging of neuroendocrine tumors (NET). This study evaluates the role of ^{68}Ga-DOTATATE PET/CT scan to influence management decisions in patients with NETs and evaluates any possible correlation between ^{68}Ga-DOTATATE PET/CT findings and patients' survival data. Materials and methods: Clinical outcome, survival, and change in management after ^{68}Ga-DOTATATE PET/CT were evaluated. Data from NET multidisciplinary team (MDT) minutes, patient discharge summaries and correspondence was reviewed to evaluate the influence of ^{68}Ga-DOTATATE PET/CT scan on patients' treatment plan. Results: During eight year time, more than 1000 ^{68}Ga-DOTATATE PET/CT scans were performed in patients with confirmed or suspected NETs. The findings of ^{68}Ga-DOTATATE PET/CT scans changed the patients' treatment plan in about 41% of the cases. The change in therapeutic management consisted mainly of resection of a previously unknown primary tumor, initiation of chemotherapy or peptide receptor radionuclide treatment (PRRT) due to

recurrence, change to chemotherapy instead of surgery or change to PRRT instead of chemotherapy. The most frequent management change was observed in patients with lung NET and medullary thyroid carcinoma while in patients with unknown site of primary NET, the change in treatment plan was lower. Furthermore, Kaplan Meier analysis has shown that the survival rates at 3 and 5 years after the ^{68}Ga-DOTATATE PET/CT scan was significantly better in patients with negative scans compared to those with positive scans ($p<0.01$). Conclusion: This large study demonstrates that ^{68}Ga-DOTATATE PET/CT scan can change the treatment plan in a significant percentage of patients with NET. Also, it is shown that a negative ^{68}Ga-DOTATATE PET/CT scan is associated with significantly better survival

OP549

Do we need full-dose contrast-enhanced CT for extra-hepatic staging using Gallium-68-DOTATATE-PET/CT in patients with neuroendocrine tumors (NET)?

A. Heinzel[1], D. Albanus[1], F. Verburg[1], F. Behrendt[1], F. Mottaghy[1,2], Z. Erdem[3], O. Erdem[3], J. Apitzsch[4]; [1]UK Aachen, Aachen, GERMANY, [2]Maastricht University Medical Center, Masstricht, NETHERLANDS, [3]Bülent Ecevit University, Karaelmas, TURKEY, [4]UK Gießen and Marburg, Marburg, GERMANY.

Aims: Previous studies have demonstrated that PET/CT with 68Ga-labeled somatostatin analogues is helpful in the assessment of the presence of metastatic disease in in patients with neuroendocrine tumors (NET) especially with regard to extra-hepatic metastases such as bone and lymph node metastases. It has to be noted that the PET in combination with full-dose contrast-enhanced CT (ceCT) exposes the patients to a high dose of radiation (up to 25Smv) whereas the non-contrast-enhanced low-dose CT (ldCT) might reduce the radiation to about 10mSv and at the same time avoid potential side effects of the contrast agent. Thus, we aimed to determine whether ceCT can be omitted in the assessment of extra-hepatic metastases in patients with NET. Methods/Materials: We retrospectively compared the performance of PET/ldCT versus PET/ceCT in 54 patients (26 male, 28 female) who underwent a Gallium-68-DOTATATE-PET/CT in our clinic. Patients were selected according to following criteria: available ldCT and ceCT; histologically confirmed NET; available follow-up of at least 6 months (median 12.6 months; range 6.1-23.2). PET/ldCT and PET/ceCT images were analyzed separately. The review process focused on metastases to bones and lymph nodes. Afterwards, the PET/ldCT and PET/ceCT results were compared to the reference standard consisting of clinical follow-up data to evaluate the diagnostic performance. Results: In PET/ceCT 139 true positive bone-lesions were detected compared to 140 in PET/ldCT, 106 true positive lymph node metastases (PET/ceCT) vs. 90 (PET/ldCT). On a per patient basis ld and ce PET-CT achieved similar sensitivity (both 100%) however, specificity was lower for PET/ldCT (89% vs. 77%). For lymph nodes PET/ceCT showed superior sensitivity and specificity (sensitivity 92% vs. 80% and specificity 83% vs. 65%). The positive predictive value (PPV) and negative predictive value (NPV) of PET/ceCT were 81% and 100% for bone metastases as well as 82% vs. and 92% for lymph node metastases. In contrast, PET/ldCT showed 91% PPV and 100% NPV for bone metastases as well as 78% PPV and 68% NPV for lymph node metastases. Conclusions: We demonstrate that ceCT should not be omitted for extra-hepatic staging using Gallium-68-DOTATATE-PET/CT in patients with neuroendocrine tumors. With regard to the detection of lymph node metastases ceCT is helpful to minimize false positive lesions. However, if only bone metastases are considered PET/ceCT and PET/ldCT show similar diagnostic performance.

OP550

The clinical role of Ga-68 DOTATE PET-CT in patients with neuroendocrine tumors

M. Tuncel[1], S. Kılıçkap[2], E. Akdemir[1]; [1]Hacettepe University, Department of Nuclear Medicine, ANKARA, TURKEY, [2]Hacettepe University, Department of Medical Oncology, ANKARA, TURKEY.

AİM: The introduction of Ga-68DOTATE PET-CT for the evaluation of neuroendocrine tumors(NETs) has significantly improved the diagnostic work-up. However impact on patient management is yet to be determined. We aimed to evaluate the clinical impact of the Ga-68DOTATE PET-CT in our patients suffering from NETs. Material & METHODS: The clinical and imaging data of 61 consecutive patients (F/M:35/26; agemedian:56±14years,range:22-82) with diagnosis of NET (9 carcinoids,2 pheochromocytomas,3 paragangliomas,4 medullary thyroid carcinomas,2 poorly and 41 well-differentiated gastroenteropancreaticNETs) were studied. All patients underwent Ga-68DOTATE PET-CT imaging for staging(n=9), restaging-suspected reccurence(n=48) and therapy response evaluation(n=4). Both PET-CT and conventional imaging (CI) were than interpreted together with medical oncologist to determine the clinical impact of the Ga-68DOTATE PET-CT. As a standard of reference clinical and imaging follow-up data were used (median:14 mo; range:9-48 mo). RESULTS: In 11 patients, PET-CT detected additional lesion sites (15 lesion sites in 10 patients), that are not detected by CI(3 endobronchial,5 lymph node,2 intestinal,2 pancreas and 3 bone, medianSUVmax:7[3-16], lesion size:10mm[5-20]). SUVmax values of lesions were higher in patients in whom

more lesions were seen by PET-CT (SUVmaxmedian:5.5 vs 20p<0.0001). Thirteen (21%) patients were interpreted as no evidence of disease by both PET-CT and CI. In 18/61(30%)patients, although detected malign lesions, Ga-68DOTATE PET-CT had no clinical impact over CI. PET-CT changed clinical management in 30/61(49%) patients;peptide receptor radionuclide therapy(PRRT) was considered as a systemic therapy option other than chemotherapy in 12/30(40%) patients due to high (tumor/liver SUVmax>2.2) radiotracer uptake, PRRT was prevented in 8/30(27%) patients due to low radiotracer uptake. PRRT was decided in 3(10%) patients instead of surgery/local ablative therapy due to systemic disease detected by PET-CT, 4/30(13%) patients underwent surgery for recurrence detected by PET, instead of follow-up with somatostatin analogue, systemic chemotherapy was decided instead of local therapy in 2/30(7%) patients, and radiofrequency ablation was decided for equivocal liver lesion on CI due to positive PET findings in 1/30(3%) patient. Among these 61 patients 17 patients also had FDG PET-CT in 2 months of Ga-68DOTATE PET. There was a negative correlation between FDG PET-CT and Ga-68DOTATE PET-CT (Spearman correlation coefficient-0,372 p:0,156). CONCLUSION: Ga-68DOTATE PET-CT has a major clinical impact in 49% of pts with NETs. It has detected more lesions than CI especially in patients with high radiotracer uptake and negatively correlated with FDG-PET. Our results indicate Ga-68DOTATE PET-CT as a mandatory procedure to guide patient management

OP551

Validation of parametric net influx rate images of ^{68}Ga-DOTATOC and ^{68}Ga-DOTATATE

E. Ilan, M. Sandström, I. Velikyan, A. Sundin, M. Lubberink; Section of Nuclear Medicine and PET, Department of Surgical Sciences, Uppsala University, Uppsala, SWEDEN.

Objectives: ^{68}Ga-DOTATOC/^{68}Ga-DOTATATE are radiolabelled somatostatin analogues used for diagnosis of somatostatin receptor(SSTR)-expressing neuroendocrine tumours.In addition, their use in treatment follow-up has been proposed. However, for these tracers SUV does not correlate linearly with the net influx rate(Ki), assumed to reflect SSTR density. Changes in Ki may better reflect treatment effects than changes in SUV, and it would be desirable to be able to compute parametric images showing Ki at the voxel level. The aim of this study was to evaluate parametric methods for computation of Ki images, and to compare image contrast in terms of tumour to liver ratio for parametric Ki images and SUV images. Materials and methods: Ten patients with metastatic neuroendocrine tumors underwent a 45-min dynamic scan followed by a whole-body (WB) PET/CT scans at 1 h post injection of ^{68}Ga-DOTATOC and ^{68}Ga-DOTATATE on consecutive days.The Ki was determined by nonlinear regression of an irreversible two-tissue-model as well as the Patlak method, using a descending aorta input curve. Parametric Ki images were made using a basic function method (BFM) implementation of the two tissue irreversible compartment model and Patlak method, and mean tumor Ki values were determined for 50% isocontour VOIs. Liver VOIs were drawn over WB and Ki images and tumour to liver ratios were calculated. The relation between the ROI-based and parametric Ki values were evaluated by using linear regression. Results: The correlation (R^2) between the ROI based (irreversible two-tissue-model) and parametric based (BFM) Ki images were 0.83 and 0.97 for ^{68}Ga-DOTATOC and ^{68}Ga DOTATATE, respectively with a slope of 1.0 in the both fits. The correlation (R^2) between the ROI based (Patlak) and parametric based (Patlak) Ki images were 0.95 and 0.76 for ^{68}Ga-DOTATOC and ^{68}Ga DOTATATE respectively with a slope of 1.1 in the both fits. The contrast between tumour and liver is 1.7 and 1.8 times higher in the parametric Ki images based on BFM than in the 1h WB images for ^{68}Ga-DOTATOC and ^{68}Ga-DOTATATE respectively. For parametric Ki images based on Patlak method the contrast is 2.4 and 2.7 times higher for ^{68}Ga-DOTATOC and ^{68}Ga-DOTATATE respectively. Conclusion: A good correlation and agreement between the parametric and ROI-based Ki values was found, showing that parametric K_i images are quantitatively accurate. In addition, tumour to liver contrast was higher in the parametric Ki images than in the 1h WB images both for ^{68}Ga-DOTATOC and ^{68}Ga DOTATATE.

OP552

68Ga-DOTA-NOC PET/CT SUVmax in patients with pancreatic NET: is it prognostic?

V. Ambrosini[1], G. Polverari[1], D. Campana[2], G. Cacciari[2], C. Peterle[1], S. Diodato[1], C. Nanni[1], G. Montini[1], P. Tomassetti[2], S. Fanti[1]; [1]Nuclear Medicine, University of Bologna, S.Orsola-Malpighi Hospital, Bologna, ITALY, [2]Internal Medicine, University of Bologna, S.Orsola-Malpighi Hospital, Bologna, ITALY.

Aim: to investigate the role of SUVmax measured on 68Ga-DOTA-NOC PET/CT as a potential prognostic factor in patients (pts) with pancreatic NET (pNET) . Materials and methods: Among the pts who underwent 68Ga-DOTANOC PET/CT from September 2006 to October 2014, those with pathologic confirmation of well differentiated pNET (WHO 2010: G1 or G2), documented disease at both 68Ga-DOTA-NOC PET/CT and CT (performed within a month) and a minimum clinical-radiological follow-up of 6 months (mo) were included in the study. Radiological follow-up consisted of a CT scan every 3 mo during the first year and every 6 mo afterwards. Pts with MEN syndrome were excluded. To evaluate the potential role

of SUVmax on prognosis, we divided the pts on the basis of the disease status at 24 months follow-up: pts with progressive disease (PD) were compared to those with stable disease (SD) or partial response (PR). Results: Overall 43 pNET pts were included (male:female=22:21; mean age=61.0±11.7 [35-81] years). In 35/43 (81,4%) the tumour was non-functioning while 8/43 (16, 3%) presented a clinical syndrome. Ki67 was ≤5% in 22/43 pts and >5% in 21/43 pts. TNM stage was III in 7 pts (16,3%) and IV in 36 (83,7%). Overall 18 pts (41,8%) had SD/PR while in 20 (46,5%) the disease progressed. SUVmax values were significantly higher (p=0.022) in pts presenting SD/PR (median 49.8, IQR25-75%:44.9-78.8) as compared to those with PD (median 33.4, IQR25-75%:26.1-52.4). At univariate analysis, risk factors for disease progression during follow-up included ki67>5% (p=0.009), SUVmax <37.8 (p=0.003) and medical therapy alone (as compared to medical therapy associated with PRRT, p=0.018). Stage IV (p=0.026), ki67>5% (p=0.009), SUVmax<37.8 (p=0.043) and medical therapy alone (p=0.015) were also confirmed at multivariate analysis. Conclusions: Our data provide evidence of the role of SUVmax as an accurate non-invasive parameter of disease prognosis in pts with pNET. Although not an objective of our study, our data also confirm the role of PRRT in pts clinical management.

OP553

Head-to-head comparison of 68Ga-DOTA-NOC and 18F-FDG PET/CT in neuroendocrine tumours: correlation between maximum standard uptake values and Ki67 proliferation index

R. Ferreira[1], R. Silva[1], A. Moreira[1], P. Lapa[1], P. Lapa[1], G. Costa[1], G. Costa[1], J. Lima[2]; [1]Serviço de Medicina Nuclear do Centro Hospitalar e Universitário de Coimbra, Coimbra, PORTUGAL, [2]Instituto de Ciências Nucleares Aplicadas à Saúde, Coimbra, PORTUGAL.

Introduction: Neuroendocrine tumours (NETs) have a heterogeneous biological behaviour that poses many clinical challenges and may compromise accurate diagnostic management, with consequences in treatment decision and prognosis evaluation. It is usually accepted that 68Ga-DOTA-NOC PET/CT is more useful in tumours with Ki67≤20% and that 18F-FDG PET/CT is more accurate when Ki67>20%. Aim: To compare 68Ga-DOTA-NOC and 18F-FDG PET/CT maximum standard uptake values (SUVmax) and correlate them with Ki67-indexes, in both primary and metastatic target (most relevant) lesions, in NETs. Materials and methods: We retrospectively reviewed patients with NETs, subjected to PET/CT with both 68Ga-DOTA-NOC and 18F-FDG, between March/2013 and March/2015. Both studies were performed 2.3±2.0 months apart. The patient's management and disease condition did not change during that period. Sixteen patients [13 male, 3 female; mean-age 68.2±12.4years(39-92); 11 gastroenteropancreactic-NETs and 5 lung-NETs] were selected. In 12 patients (75%), both exams were performed during staging and in 4 cases (25%) during follow-up. Primary tumour was present in all staging cases and was absent in all follow-up studies. Metastases were detected in 9 patients (5 in staging; 4 in the follow-up). SUVmax was recorded in 33 lesions (12 primary and 21 target metastases). Primary lesions were divided into two groups regarding Ki67: Group-1 (Ki67≤20%;n=5) and Group-2 (Ki67>20%;n=7). The 21 target metastases were also divided into two groups regarding Ki67 of the primary tumour: Group-A (Ki67≤20%;n=9) and Group-B (Ki67>20%;n=12). Results: The mean±SD SUVmax for 68Ga-DOTA-NOC and 18F-FDG was, respectively, 14.5±10.2 and 4.8±5.5 in Group-1, and 4.6±1.6 and 25.0±8.0 in Group-2. When comparing SUVmax between the two groups, we found a statistically significant difference with 68Ga-DOTA-NOC (p<0.05), but not with 18F-FDG SUVmax (p=0.17). In both groups, no significant tendency for higher SUVmax values of either of the radiopharmaceutical was observed (p=0.23;p=0.13). For target metastatic lesions, we conducted a similar analysis and found a statistically significant difference for 68Ga-DOTA-NOC SUVmax between Groups A and B (p<0.05) but not with 18F-FDG SUVmax(p=0.06). In Group-1 patients with metastases (5 cases), no statistically significant differences were observed in SUVmax values (for both 68Ga-DOTA-NOC and 18F-FDG), between primary and metastatic target lesions. Conclusion: Our data are consistent with the well-documented functional heterogeneity of NETs. They suggest that there is no direct association between somatostatin-receptor expression and metabolic degree of activity in these tumours. Therefore, we may conclude that these patients might benefit, despite de Ki67 proliferation index, from a complementary evaluation of both 68Ga-DOTA-NOC and 18F-FDG PET/CT.

OP554

68Ga-DOTANOC PET/CT imaging in localizing the primary site in patients presenting with metastatic neuroendocrine tumors and its impact on clinical decision making: Experience from a tertiary care centre in India

A. Pruthi, P. Pankaj, R. Verma, A. Jain, E. S. Belho, H. Mahajan; Sir Ganga Ram Hospital and Research Centre, New Delhi, INDIA.

Neuroendocrine tumours (NETs) are rare, heterogeneous group of tumours originating from small, occult primary sites and are characterized by over-expression of somatostatin receptors (SSTRs).Purpose: To retrospectively evaluate the efficacy of 68Ga-DOTANOC PET/CT imaging

in detecting the primary site in patients with metastatic neuroendocrine tumours of unknown origin and its impact on clinical decision making in such patients. Methods: Between December 2011 and September 2014, a total of 263 patients underwent 68Ga-DOTANOC PET/CT study in our department for various indications. Out of them, 68 patients (45 males, 23 females, mean age 54.9 +/- 10.7 years, range 31-78 years) with histopathologically proven metastatic neuroendocrine tumours and unknown primary site on conventional imaging underwent 68Ga-DOTANOC PET/CT as part of their pre-treatment staging work-up. Histopathology (wherever available) and/or follow-up imaging with biochemical markers were taken as reference standard. Quantitative estimation of SSTR expression in the form of maximal standardized uptake value (SUVmax) of detected primary and metastatic sites was calculated. Follow-up data of individual patients was collected through careful survey of electronic medical records and telephonic interviews. Results: Maximum patients presented to our department with hepatic metastasis (50 out of 68 patients) and grade I neuroendocrine tumours (>50%). 68Ga-DOTANOC PET/CT scan identified primary sites in 40 out of these 68 patients i.e. in approximately 59% patients. Identified primary sites were: Small intestine (19), Rectum (8), Pancreas (7), Stomach (4), Lung (1) and one each in rare sites in Kidney and Prostate. In one patient, 2 primary sites were identified (one each in stomach and duodenum). Mean SUV max of the detected primary sites was 25.1 +/- 18.0 (median 16.25, range 2.1-150). Significant positive correlation was found between SUV max of primary tumor and histopathologically proven sites of metastasis ($r = 0.662$; $p < 0.0001$). Based on the findings of the 68Ga-DOTANOC PET/CT scan, 3 out of 40 patients underwent definitive treatment for their primary tumour (1 gastric, 1 ileal and 1 prostatic tumour). 1 patient was being planned for resection of primary rectal lesion. 32 / 68 patients were started on long acting somatostatin analogues or chemotherapy or targeted therapy. 1 patient underwent multiple cycles of peptide receptor radionuclide therapy (PRRT) using 90Y and 177Lu labeled somatostatin analogues. Conclusion: Our findings indicate that 68Ga-DOTANOC PET/CT is a promising imaging modality in patients with metastatic neuroendocrine tumours of unknown origin for detection of the primary site and in guiding their therapeutic management.

OP555

F-18 DOPA PET/CT in patients with neuroendocrine tumors

A. T. Golubic, D. Huic, A. Mutvar, M. Zuvic; Department of Nuclear Medicine and Radiation Protection, University Hospital Center Zagreb, Zagreb, CROATIA.

Aim: The aim of this study was to examine and study the impact of F-18 DOPA PET/CT imaging in patients with medullary carcinoma and other neuroendocrine tumors. Materials and Methods: Twenty patients were referred to our Department for staging or restaging neuroendocrine tumors. They were scanned with F-18 dihydroxyphenylalanine (DOPA) PET/CT from November of 2012 to January 2015. In 13 of our patients, medullary carcinoma was diagnosed at least 11 months earlier; mean period from diagnosis to PET/CT was 5 years. Other neuroendocrine tumors were diagnosed in 7 patients (three with insulinoma, two with paragangliomas, one had pheochromocytoma and in one patient undefined NET was suspected). Because of elevation of tumor markers and/or equivocal findings of morphological imaging methods (i.e. ultrasound, MSCT or MRI), functional diagnostic imaging was proposed. The mean follow up period was 11.3 months. Results: An increased abnormal F-18 DOPA uptake was found in 12 patients (60%). In 9 out of 13 medullary carcinoma patients, a positive finding was reported, mostly due to metabolically active metastases in neck and mediastinal lymph nodes. Mean SUV value was 5.5, ranging from 2.6 to 9.5. Three patients referred with other NET diagnoses had a positive DOPA PET/CT scans and were spared further diagnostic procedures and unnecessary treatments. Two patients benefited greatly from an F-18 DOPA scan, as they were completely cured after surgical resection (one with insulinoma and one more with paraganglioma). Comparing with other imaging modalities used in our patient population (CT, MR, bone scintigraphy, Octreoscan, or Tc-99m-DMSA V scintigraphy), F-18 DOPA was found to be the most sensitive in discovering various disease locations, especially for medullary carcinoma. After F-18-DOPA PET/CT scan, surgical extraction of metabolically active tissues was performed , in seven patients. Conclusions: F-18-DOPA PET/CT is a novel, still emerging molecular diagnostic imaging method for staging and restaging neuroendocrine tumors. Both positive and negative scan findings were of significant use in our patient's further management, modifying therapy options to better suit the needs of each patient individually.

1510 - Wednesday, October 14, 2015, 8:00 AM - 9:30 AM, Hall D
Neurosciences: Neuroimaging - Data Analysis

OP556

Maps of serotonin transporter distribution in the human brainstem obtained using high-resolution PET correlates with post-mortem autoradiography data (ARG).

P. Fazio[1], M. Schain[1], K. Varnäs[1], C. Halldin[1], L. Farde[1,2], A. Varrone[1]; [1]Karolinska Institutet, Department of Clinical Neuroscience, Centre for Psychiatry Research, Stockholm, SWEDEN, [2]AstraZeneca Translational Science Centre at Karolinska Institutet, Stockholm, SWEDEN.

Aim. The human brainstem is a complex structure with a multitude of small nuclei and neural pathways of interest in the pathophysiology of CNS-disorders. In common with other monoaminergic systems, serotoninergic neurons originate from a group of nuclei located in the brainstem. The present study was designed to validate a methodology for in vivo quantification of radioligand binding to the serotonin transporter (5-HTT) in the human brainstem using high-resolution PET (HRRT) by comparison with post-mortem autoradiography (ARG). Methods. 3T-MR images and parametric ^{11}C-MADAM binding potential (BP_{ND}) images from 10 control subjects were used to generate a functional PET template of 5- HTT availability. An automated MR based two-step normalization procedure using various tools of the FMRIB Software Library (FSL) was employed to obtain accurate brainstem normalization. ROIs for different brainstem nuclei were defined using a threshold-based ROI-delineation method based on anatomical references and on 5-HTT availability patterns. BP_{ND} estimates in sub-cortical regions (putamen, nucleus caudatus and amigdala) were obtained by applying the AAL template. The ROIs were then transformed and applied individually to BP_{ND} images of 16 healthy subjects (14M/2F, 20-64 y). The *in vivo* distribution of BP_{ND} values was compared with the *in vitro* binding data using autoradiography studies of the human brain post-mortem and ^{3}H-MADAM as radioligand. Similar ROIs as those used in the PET study were delineated on ARG sections. Pearson correlation analysis was used to evaluate the relationship between the *in vivo* and *in vitro* binding data obtained in brainstem and sub-cortical regions. Results. The template-based method provided reliable BP_{ND} estimates in different regions of the brainstem. The highest BP_{ND} was found in the dorsal raphe (2.48±0.43), followed by the median raphe (2.20±0.47), superior colliculi (2.05±0.44), ventral midbrain (1.85±0.34) and the caudal raphe (1.12±0.18). BP_{ND} estimates obtained *in vivo* with high resolution PET in the ROIs were correlated to ($r=0.78$, $p<0.05$) the binding density (pmol/g) values obtained *in vitro* by ARG, although values for the ventral midbrain were somewhat discrepant. Conclusions. The *in vivo* distribution of 5- HTT availability in the human brainstem measured using a template-based analysis applied to HRRT-PET data was consistent with 5-HTT quantification using post-mortem ARG. The proposed template-based methodology appears to be suitable for applied studies focused on the human brainstem.

OP557

Simplified quantification of the dopamine transporter using [18F]FE-PE2I in PD patients and control subjects

I. Sonni[1,2], P. Fazio[1], M. Schain[1], C. Halldin[1], P. Svenningsson[1], L. Farde[1], A. Varrone[1]; [1]Department of Clinical Neuroscience - Karolinska Institutet, Stockholm, SWEDEN, [2]Sapienza - University of Rome, Rome, ITALY.

Introduction: [^{18}F]FE-PE2I is a novel PET radioligand for in vivo imaging of the dopamine transporter (DAT). Validated non-invasive methods for DAT quantification using [^{18}F]FE-PE2I rely on dynamic PET acquisition, but in a clinical setting a more simplified protocol consisting in one acquisition performed after tracer injection is preferable. The aim of this study was to identify the optimal acquisition time window providing the specific binding ratio (SBR) in closest agreement with the binding potential (BP_{ND}) estimated with parametric imaging. Methods: Ten Parkinson's disease patients (PD) and ten control subjects (CS) were examined with [^{18}F]FE-PE2I. A 93-min dynamic PET measurement was performed using the high resolution research tomograph (HRRT). The measurement was smoothed to the resolution of a clinical PET system (ECAT EXACT HR) to resemble a clinical setting. ROIs for caudate (CAU), putamen (PUT), ventral striatum (VS), substantia nigra (SN) and cerebellum (CER) were drawn on co-registered MR images. SBR was computed for 8 different time windows, using CER as a reference region. Linear regression analysis was used to compare the SBR to BP_{ND} values obtained with the wavelet-aided parametric imaging (WAPI) software. The optimal acquisition time window was selected using the SBR values obtained from the HRRT dynamic measurement (HRRT-SBR). The selected acquisition time window was used to create an average lower-resolution image and to measure SBR (HR-SBR), as a clinical outcome measure. Effect sizes of SBR and BP_{ND} were calculated to assess differences between CS and PD patients. Results: SBR values obtained from the HRRT that correlated best to WAPI BP_{ND} were obtained for the time window between 16.5 and 42 min (R^2 = 0.98). A significant correlation was also observed with HR-SBR (R^2 =0.95 in CS and R^2= 0.97 in PD patients). In the striatum, HR-SBR values underestimated BP_{ND} by 37%±3% in CS and by 29%±10% in PD patients, and in the SN by 22% in CS and by 14% in PD patients. Similar effect sizes for BP_{ND} and HR-SBR were found in CAU (both 0.6), PUT (1.7 and 1.4), VS (both 0.7), and SN (0.5 and 0.4). Conclusions: The optimal acquisition time window for simplified DAT

quantification using [^{18}F]FE-PE2I is between 16.5 and 42 min. Despite underestimation of BP_{ND}, and possibly decreased sensitivity to detect nigrostriatal deficit, the SBR can be viewed as a valid quantification method for DAT using [^{18}F]FE-PE2I for diagnostic purposes, since it provides similar differentiation as BP_{ND} between CS and PD patients.

OP558

Translational Imaging Improves Diagnostic Power of FP-CIT SPECT in Parkinsonian Syndrome

C. Paschetta, F. Buttari, A. Skanjeti, D. Gned, V. Podio; San Luigi Gonzaga Hospital, Orbassano (TO), ITALY.

Aim: Neurodegenerative disease incidente is forecast to increase in next years; early diagnosis could help in slowing disease progression and in avoiding side effects from incorrect treatments. Parkinsonian Syndromes (PS) are a common degenerative disorder and their early assessment requires molecular imaging with cocaine-analogue radiopharmaceuticals (FP-CIT SPECT) since symptoms are aspecific and MR imaging can identify morphological alterations that could be related to symptoms. Our aim was to detect if integration of MR can increase sensitivity, specificity and accuracy of SPECT in assessment of PS.Materials and Methods: Sixty-three subjects with suspected PS (age 66±11, 33 M) underwent both FP-CIT SPECT and brain MR imaging in a mean time of 6 months. After at least two-years neurological follow-up, PS was confirmed in 33 patients; analysis compared findings from these patients and the 30 PS-free subjects. SPM8 was used to normalize SPECT and MR images on our home-made and built-in template respectively. For each imaging modality, SPM8 analysis defined VOIs including voxels with differences between PS patients and PS-free subjects. VOIs data were extracted by SPM8 with MarsBaR toolbox. Data were evaluated by multivariate logistic regression to identify significant relationships with diagnosis.Results: At SPECT, SPM8 identified significant difference between PS patients and PS-free subjects in basal ganglia; at logistic analysis diagnostic power was good (Se=73%, Sp=90%, Acc=81%, p<0.00001).MR analysis detected differences in thalami, anterior cingulate, posterior parietal and occipital area. In all occurrences MR shows accuracy lower than SPECT; best results ware obtained from thalami (Se=79%, Sp=57%, Acc=68%, p=0.005). The integration of MR VOIs data from thalamic region in SPECT analysis improved accuracy from 81% (SPECT alone) to 89% and halved incorrect results by increasing sensitivity to 85% and specificity to 93%. Conclusion: When movement disorders occur, semi-quantitative analysis of FP-CIT is essential but not adequate for an optimized assessment. SPECT and MR integration by automatic voxel-based morphometric analysis result in a significant accuracy improvement.Translational imaging allows the development of synergies between structural and functional methods resulting in a positive impact on quality and cost of care.

OP559

Age- and sex-related differences in 18F-FDG brain metabolism in healthy subjects using a PET-driven partial volume effect correction method

S. Bonte[1,2], P. Vandemaele[2], S. Verleden[3], K. Audenaert[3], K. Deblaere[2], I. Goethals[2], R. Van Holen[1]; [1]Ghent University: MEDISIP (Department of Electronics and Information Systems), Ghent, BELGIUM, [2]Ghent University Hospital: Department of Radiology and Nuclear Medicine, Ghent, BELGIUM, [3]Ghent University Hospital: Department of Psychiatry, Ghent, BELGIUM.

Introduction: Several authors have investigated the age- and sex-related differences in ^{18}F-FDG PET scans in healthy subjects. Most authors reported a reduced metabolism in the ageing brain, especially in the frontal regions. However, when correcting for structural atrophy using a MRI-based method, some authors reported that all age-related changes disappeared, while others observed a true decreased metabolism with increasing age. The goal of our study was to apply a purely PET-driven partial volume effect correction (PVEc) method to investigate age- and sex-related differences in the healthy brain. Materials and methods: 79 carefully selected healthy subjects were enrolled in this study. They underwent, among other investigations, a ^{18}F-FDG brain PET and MRI. PET images were corrected for the intensity diffusion caused by the point spread function of the PET-scanner using a post-reconstruction iterative deconvolution method with the use of the Huber prior for denoising, as presented by B.A. Thomas (Ph.D. dissertation, UCL 2012). Both the original and corrected image are normalised to MNI-space and smoothed using SPM12. The software is also used for a voxelwise multiple regression analysis with age and sex as covariates. Results: The analysis of all subjects with sex as a covariate yields no significant clusters with more than 100 voxels at the $p < 0.05$ significance level, both before and after PVEc. There are however negative correlations between metabolism and age, which survive PVEc, especially in the frontal lobes. When the female subgroup is investigated separately, there are no clusters that survive PVEc. In the male subgroup, there are two clusters that survive PVEc, comprising (part of) the caudate and the anterior and medial part of the superior frontal gyrus and cingulate bilaterally. Discussion: Most frequently used partial volume effect correction methods rely on a co-registered and segmented MRI-image to take structural atrophy into account. These methods are prone to registration and segmentation errors and assume a uniform uptake in various brain regions. Moreover, structural and functional information are not always directly correlated. In contrast to these methods, we have used a purely PET-

driven PVEc method. Using this method, we found decreasing metabolism with increasing age in large parts of the (medial) frontal lobes. We also documented a different ageing process in women and men. The absence of clusters after PVEc in the female brain should however be interpreted with caution, because results are only borderline significant.

OP560

Age-related changes in FDG brain uptake are more accurately assessed when applying an adaptive template to the SPM method of voxel-based quantitative analysis

A. Van Der Gucht[1], **A. Verger**[1], E. Guedj[2], G. Malandain[3], G. Hossu[4], Y. Yagdigul[1], V. Roch[1], S. Poussier[1], L. Maillard[5], G. Karcher[1], P. Marie[1]; [1]CHU Nancy, Nuclear Medecine & Nancyclotep Experimental Imaging Platform, Nancy, FRANCE, [2]AP-HM, Hospital "La Timone", Department of Nuclear Medicine, Marseille, FRANCE, [3]INRIA Sophia Antipolis-Méditerranée, Sophia Antipolis, Valbonne, FRANCE, [4]INSERM, CIC-IT 1433, Nancy, FRANCE, [5]CHU-Nancy, Department of Neurology, Nancy, FRANCE.

The impact of age is crucial and must be taken into account when applying a voxel-based quantitative analysis on brain images from [18F]-fluorodesoxyglucose Positron Emission Tomography (FDG-PET). This study aimed to determine whether age-related changes in brain FDG-PET images are more accurately assessed when the conventional Statistical Parametric Mapping (SPM) normalisation method is used with an adaptive template, obtained from analysed PET images using a Block-Matching (BM) algorithm in order to fit with the characteristics of these images. Methods. Age-related changes in FDG-PET images were computed with linear models in 84 neurologically healthy subjects (35 women, 19 to 82 y-old), and compared between results provided by the SPM normalisation algorithm applied on its dedicated conventional template or on the adaptive BM template. A threshold P-value of 0.05 was used together with a family wise error (FWE) correction. Results. The age-related changes in FDG-PET images were much more apparent when computed with the adaptive template than with the conventional template as evidenced by: 1) stronger correlation coefficients with age for the overall frontal and temporal uptake values (respective R2 values of 0.20 and 0.07) and 2) larger extents of involved areas (13% and 5% of whole brain template volume respectively), leading to reveal several age-dependent areas (especially in dorsolateral prefrontal, inferior temporal/fusiform and primary somatosensory cortices). Conclusion. Age-related changes in brain FDG uptake may be more accurately determined when applying the SPM method of voxel-based quantitative analysis on a template that best fits the characteristics of the analysed TEP images.

OP561

Head-to-head comparisons of semi-quantification tools for brain FDG-PET in diagnosis of prodromal Alzheimer's disease.

S. Morbelli[1], M. Pagani[2], F. De Carli[3], J. Öberg[4], A. Buschiazzo[1], G. Frisoni[5], A. Drzezga[6], B. N. van Berckel[7], E. Guedj[8], A. Picco[9], D. Arnaldi[9], M. Ferrara[9], A. Chincarini[10], F. Nobili[9], A. Brugnolo[9]; [1]Nuclear Medicine Unit, IRCCS San Martino - IST, University of Genoa, Genoa, ITALY, [2]Institute of Cognitive Sciences and Technologies, Consiglio Nazionale delle Ricerche (CNR), Rome, ITALY, [3]Institute of Bioimaging and Molecular Physiology, Consiglio Nazionale delle Ricerche (CNR), Genoa, Italy, Genoa, ITALY, [4]Department of Hospital Physics, Karolinska Hospital, Stockholm, SWEDEN, [5]University Hospitals and University of Geneva, Geneva, SWITZERLAND, [6]Department of Nuclear Medicine, University of Cologne, Cologne, GERMANY, [7]Department of Nuclear Medicine & PET Research, VU University Medical Center, Amsterdam, NETHERLANDS, [8]APHM, CHU Timone, Service de Médecine Nucléaire, CERIMED, INT CNRS UMR7289 , Aix-Marseille University, Marseille, FRANCE, [9]Clinical Neurology, Department of Neuroscience, Rehabilitation, Ophthalmology, Genetics, and Mother-Child health (DINOGMI), University of Genoa, IRCCS AOU, San Martino-IST, Genoa, ITALY, [10]National Institute for Nuclear Physics (INFN), Genoa, ITALY.

AIM: In the last years, several semi-quantitative automatic analysis methods have been developed to analyze brain 18Fluorodeoxyglucose Positron Emission Tomography (18F-FDG-PET) data with the aim to differentiate MCI subject due to AD (MCI-AD) from MCI due to other causes. The aim of the present work was to compare the accuracy of three different methods for the identification of MCI patients due AD. The three tested methods were 1. a ROI-based analysis within SPM8, 2.PALZ score provided by PMOD 3. a new metaROI method analyzed with the support of vector machine (SVM) METHODS: Sixty-two subjects with aMCI who during follow-up have developed AD dementia (MCI-AD, months follow-up range=6-84 mean=25.43±15.64; age=72.38±8.15; education=10.22±4.37; MMSE score = 27.0±1.58) and one hundred-nine healthy subjects (CTR; age=66.8±6.51; education=11.6±3.78; MMSE score = 29.25±1.2) were enrolled in five centers of the European Alzheimer's Disease Consortium (EADC). All subjects underwent clinical-neuropsychological evaluation, structural neuroimaging and 18F FDG-PET when they were at the aMCI stage. SPM8 was used to obtain the Regions of Interest extracted from i) the comparison between CTR and MCI-AD (ROI-1) and ii) from the correlation between brain metabolism and delayed recall in the Rey Auditory Verbal Learning Test (RAVLT) in an independent group of fifty-four elderly subjects with mild cognitive decline (ROI-2 based on a previous study of our group). In fact delayed recall

impairment is a typical feature of MCI-AD. Brain metabolism within each of the two ROIs was computed and normalized on cerebellar counts. Similarly, PALZ score and SVM were used to classify the patients as MCI-AD. ROC curves were used to evaluate the accuracy of ROI-1, ROI-2, PALZ and SVM in discriminating CTR from MCI-AD. RESULTS: The accuracy values were:; ROI-1:AUC=0.826; ROI-2:AUC=0.833PALZ score: AUC=0.867; SVM: AUC=0.947. The areas under the ROC curves (AUC) were compared between each pair of classification methods by means of the z-score (according to Hanley and McNeil, 1983). SVM method gave a significantly higher AUC than the three other methods (SVM vs ROI-1 p=0.0029; SVM vs ROI-2 p=0.0019; SVM vs PALZ p=0.0187), according to FDR criterion for multiple comparisons, while the other methods were not significantly different from each other. DISCUSSION: The study confirms the high accuracy of 18F-FDG-PET for the identification MCI due to AD and also demonstrates that different accuracy values are obtained even using the same imaging biomarker but applying different metrics. A non-linear, automatic classifier based on SVM performs better than both SPM and PALZ.

OP562

Agreement of brain amyloid PET interpretation between automated diagnosis using support vector machine and visual assessment by expert readers

I. Matsunari[1], J. Komatsu[2], M. Samuraki[2], M. Noguchi-Shinohara[2], T. Hamaguchi[2], K. Ono[2], I. Kuji[3], M. Yamada[2], S. Kinuya[2]; [1]Saitama Medical University Hospital, Iruma-gun, JAPAN, [2]Kanazawa University, Kanazawa, JAPAN, [3]Saitama Medical University International Medical Center, Hidaka, JAPAN.

Aim: In clinical practice, interpretation of brain amyloid imaging often relies on visual analysis by expert readers, which is not always available. Machine-learning based pattern recognition techniques such as support vector machine (SVM) have recently been utilized to neuroimaging modalities as an aid for automatic and objective diagnosis. The aim of this study was to assess the diagnostic performance of SVM for the detection of amyloid burden on C-11 Pib PET as compared with the visual interpretation as a reference standard. Methods: A total of 108 subjects (56 patients with cognitive disorder and 52 normal subjects) underwent C-11 Pib PET and structural MRI on a single day. Each PET image was assigned amyloid positive or negative by 2 expert readers. For SVM analysis, PET images were spatially standardized using SPM8 and co-registered MRI, followed by count normalization to cerebellum. Leave-one subject out approach was applied as a cross-validation method. Results: By visual analysis, there were 47 positive and 67 negative C-11 Pib PET scans. An excellent overall agreement (105/108 scans: 97%) was obtained between SVM and visual analysis. Using the results of visual reading as a reference standard, the SVM had sensitivity, specificity, positive predictive value, and negative predictive value of 94%, 100%, 100%, and 95%, respectively. Conclusion: Our results indicate that the machine-learning based automated analysis such as SVM may serve as an accurate diagnostic alternative to visual reading by experts for the detection of brain amyloid burden using C-11 Pib PET.

OP563

Comparison of Reference Regions to Semiquantitatively Analyse 18F-Florbetaben PET Images

H. Barthel[1], S. Bullich[2], O. Sabri[1], J. Seibyl[3], V. Villemagne[4], C. Rowe[4], N. Koglin[2], A. Stephens[2], A. M. Catafau[2]; [1]Leipzig University, Leipzig, GERMANY, [2]Piramal Imaging, Berlin, GERMANY, [3]IND, New Haven, CT, UNITED STATES, [4]University of Melbourne, Melbourne, AUSTRALIA.

Aim: Recently, amyloid β (Aβ) plaque PET imaging of Alzheimer's disease (AD) became available for clinical routine application. Binary visual interpretation is the standard assessment method in this regard. This also refers to 18F-Florbetaben (FBB). Semiquantitative PET data analysis might, however, be necessary in borderline cases or for follow-up evaluation. For relative FBB uptake quantification approaches like neocortical standardized uptake value ratio (SUVR) determination, the cerebellar grey matter (CGM) has so far consistently been used as reference region (RR). This investigation aimed at comparing CGM-FBB-SUVRs with those obtained using alternative RRs. Materials and methods: Regional and composite neocortical SUVRs were determined using CGM, whole cerebellum (WC), pons (P), and cerebral white matter (WM) as RRs in scans of three FBB PET imaging studies: (a) 271 scans of the close to clinical routine FBB Phase 2 study (composite SUVRs, standard of truth (SoT): visual assessment by 5 independent readers). (b) 88 scans of the FBB Phase 3 study (SUVRs of 4 ROIs per scan, SoT: post mortem histopathology by Bielschowsky silver staining/ immunohistochemistry for neuritic and diffuse Aβ plaques). (c) 32 scans (16 subjects) of the FBB test-retest study (composite SUVRs, endpoints: test-retest variability (TRTV) and intra-class correlation (ICC)). Results: In (a), CGM-SUVRs correlated with WC-SUVRs (ρ=0.89 (95%CI: 0.87-0.91)), P-SUVRs (ρ=0.82 (0.77-0.85)), and WM-SUVRs (ρ=0.75 (0.69-0.80)). Effect sizes which ranged from 2.41 to 3.06 in (a), as well as correlation coefficients which ranged from 0.78 to 0.84 in (a) and from 0.42 to 0.60 in (b) did not differ, with overlapping CIs, for the SUVRs as obtained by the different RRs. Likewise, no significant differences were found in TRTV which ranged from 3.17 to 4.44 in (c) or ICCs which ranged from 0.95 to 0.98 in

(c) across the different RRs. Conclusion: CGM continues to be recommended as the RR of choice to analyse FBB PET scans, due to the biological advantage of not being involved in AD-related atrophy. Regional and composite neocortical SUVRs of FBB scans are, to a large extent, robust with regard to the selection of the RR. Research support: Piramal Imaging, Berlin, Germany

1601 - Wednesday, October 14, 2015, 08:00 PM - 09:30 PM, Hall 1

CME 13 - Translational Molecular Imaging & Radiopharmacy: Image Guided Surgery in Urological Malignancies

OP564

Combined Radio- and Fluorescence Guidance during Robot-Assisted Laparoscopic Sentinel Node Procedures (ERUS Lecture)

H. van der Poel, NETHERLANDS

OP565

Combined Radio- and Fluorescence Guidance during Robot-Assisted Laparoscopic Sentinel Node Procedures (ERUS Lecture)

N. van den Berg, NETHERLANDS

OP566

Tracers for Image-Guided Surgery of Prostate Cancer

H.-J. Wester, GERMANY

OP567

Cerenkov Imaging

J. Grimm, USA

1602 - Wednesday, October 14, 2015, 08:00 PM - 09:30 PM, Hall 2

Joint Symposium 13: EANM/ESPGHAN: Paediatric Gastrointestinal Nuclear Medicine

OP568

Clinical Aspects of Neonatal Cholestasis

B. Fischler, SWEDEN

OP569

Hepatobiliary Scintigraphy in Paediatrics

R. Howman-Giles, AUSTRALIA

OP570

Scintigraphic Evaluation of Gastroesophageal Reflux and Gastric Emptying in Children

Z. Bar-Sever, ISRAEL

1603 - Wednesday, October 14, 2015, 09:30 PM - 10:45 PM, Hall 4

CTE 6: Imaging Protocols in Radionuclide Therapy

OP571

Imaging Aspects in Peptide Receptor Radionuclide Therapy

L. Bodei, ITALY

OP572

Selective Internal Therapy - Imaging and Therapy

J. de la Roche, GERMANY

OP573

Scintigraphic Evaluation of Gastroesophageal Reflux and Gastric Emptying in Children

P. A. Erba, ITALY

1605 - Wednesday, October 14, 2015, 8:00 AM - 9:30 AM, Hall G2

Do.MoRe: 90Y SIRT Dose Effects

OP574

Selective internal radiatiotherapy (SIRT) in hepatic metastases from uveal melanoma. Treatment response in comparison to transarterial chemoembolization (TACE) with Fotemustin

H. Duan[1], G. Berzaczy[2], F. Waneck[3], M. Funovics[3], C. Hoeller[4], M. Hoffmann[1]; [1]Medical University of Vienna, Department of Biomedical Imaging and Image-guided Therapy, Division of Nuclear Medicine, Vienna, AUSTRIA, [2]Medical University of Vienna, Department of Biomedical Imaging and Image-guided Therapy, Division of General Radiology, Vienna, AUSTRIA, [3]Medical University of Vienna, Department of Biomedical Imaging and Image-guided Therapy, Division of Cardiovascular Radiology, Vienna, AUSTRIA, [4]Medical University of Vienna, Department of Dermatology, Vienna, AUSTRIA.

Aim: Uveal melanoma is a rare tumor, which metastasizes primarily into the liver. Once hepatic metastases occur, the prognosis is bleak: The median survival rate 1 year after detection is <30%. SIRT with Y-90 resin microspheres is successfully used in the treatment of primary or secondary liver tumors. This study aims to evaluate the efficacy of SIRT in hepatic metastases derived from uveal melanoma. The results concerning time to progression and overall survival are compared to a cohort of similar patients treated with Fotemustin via TACE. Methods: Hitherto we included 20 patients, who received SIRT for hepatic metastases from uveal melanoma. Imaging with CT or MRI was performed before SIRT and 6 weeks after intervention to assess tumor response and afterwards every 3 months. All patients underwent Tc-99m macroaggregated albumin SPECT/CT 1 week prior to SIRT for pretreatment evaluation. Response to treatment and progression-free survival as well as overall survival was calculated and compared to a cohort of patients suffering from the same disease in similar conditions who were treated with Fotemustin via TACE. Results: After 1 SIRT, 7 patients showed partial response (PR) with a median time to progression of 7 ± 2.9 months (range: 3 to 25 mo) and 6 patients showed stable disease with a median time to progression of 8 ± 1.9 months (range 3 - 14 mo). 5 patients showed progressive disease (PD). 10 patients died within the observation period with a mean overall survival time of 8.5 ± 3.9 months (range: 1 to 32 mo). Concerning TACE with Fotemustin, the included 21 patients required up to 6 interventions and showed a mean progression free survival of 7.3 months (3.3 - 11.3 months). Comparing to 1 intervention with SIRT, the results are quite similar, but concerning safety and adverse events, with SIRT, patients showed only minor symptoms like pain and nausea during the intervention while with TACE, patients had heavier and longer lasting symptoms like fever, pain and nausea, which required medication. Additionally, multiple interventions were required. Conclusion: With these preliminary results we could show the efficacy and safety of SIRT in hepatic metastases derived from uveal melanoma in comparison to TACE with Fotemustin. Especially concerning adverse events and quality of life, the results of SIRT were superior to TACE with equal efficacy.

OP575

Comparison of different dosimetric methods for tumor and normal tissue predicted absorbed dose calculation in liver radioembolization: preliminary results

M. FINESSI[1], E. GALLIO[2], E. RICHETTA[3], M. STASI[3], R. PELLERITO[4], R. ROPOLO[2], G. BISI[1]; [1]S.C. Medicina Nucleare U, A.O.U. Città della Salute e della Scienza, Torino, ITALY, [2]S.C. Fisica Sanitaria, A.O.U. Città della Salute e della Scienza, Torino, ITALY, [3]S.C. Fisica Sanitaria, A.O. Ordine Mauriziano, Torino, ITALY, [4]S.C. Medicina Nucleare, A.O. Ordine Mauriziano, Torino, ITALY.

AIM: Radioembolization with 90Y-microspheres is an effective treatment for unresectable hepatic malignancies. Two types of 90Y-microspheres are available: resin (SIR-Spheres®) and glass (Theraspheres®). The treatment is preliminary simulated by planar and SPECT 99mTc-MAA acquisitions to avoid gastric and lung shunt and to determine the optimal 90Y therapeutic activity. Empirical (fixed-activity, body-surface-area) and multi-compartmental methods are suggested for resin microspheres. For glass microspheres only mono-compartmental is proposed. Analysing 99mTc-MAA SPECT images, it is possible to forecast tumour and normal tissue absorbed doses: multi-compartmental MIRD or voxel dosimetry are used. AAPM (American Association of Physicists in Medicine) recommendations suggest instead planar images. The aim of this study is to compare these different methods proposed to predict absorbed doses, with discrimination between tumour and normal tissue. MATERIALS AND METHODS: Four patients were treated with glass microspheres. According to the company, the prescribed dose was 120 Gy to entire lobe. Four patients were treated with resin microspheres to the aim of 120 Gy to lesion and 40 Gy to normal liver. For both groups, the predicted tumour and normal tissue doses were calculated with three different methods. For AAPM method on planar images a ROI was drawn on the anterior and posterior images encompassing the tumour; the same ROI was moved over the normal liver. For the other methods 99mTc-MAA SPECT-TC attenuation (glass) and

99mTc-MAA SPECT-TC attenuation and scatter corrected images (resin) were employed. For MIRD compartmental two VOIs, tumour and normal liver, were drawn to estimate uptakes and volumes. For voxel based calculations SPECT 3D counts matrix was exported to perform dosimetry with a MATLAB code developed at our departments. RESULTS: For glass microspheres patients average doses were significantly lower with AAPM method compared to MIRD (tumour -28%, normal liver -86%) and to voxel (tumour -41%, normal liver -89%); high discrepancies were found also for resin microspheres: MIRD (tumour -35%, normal liver -43%) and to voxel (tumour -14%, normal liver -37%). MIRD compartmental methods compared to voxel dosimetry showed instead more comparable results with a smaller range of variation: for glass microspheres(tumour -28%, normal liver +14%) and resin microspheres(tumour +25%, normal liver +19%). CONCLUSION: AAPM method seems less accurate for dose estimation. Instead, MIRD and voxel based dosimetry are more confident each other. Dose variations can be determined by non-homogenous activity distribution with only voxel approach. This preliminary results must be confirmed by further ongoing investigation with a larger patient dataset.

OP576

Reduced lymphocyte proliferation and IFN-γproduction after Selective Internal Radiotherapy

A. Domouchtsidou[1], M. Lindemann[1], J. Best[2], J. Ertle[2], S. P. Mueller[3], S. Bedreli[2], P. A. Horn[1], A. Bockisch[3], V. Barsegian[4]; [1]Institute for Transfusion Medicine, University Hospital Essen, GERMANY, [2]Department of Gastroenterology and Hepatology, University Hospital Essen, GERMANY, [3]Department of Nuclear Medicine, University Hospital Essen, GERMANY, [4]Institute of Nuclear Medicine, Helios Kliniken Schwerin, GERMANY.

Selective Internal Radiotherapy (SIRT) is an innovative therapy with yttrium-90 radioactive glass microspheres for the treatment of hepatocellular carcinoma and colorectal liver metastases. It has been described that the use of ionized radiation leads to significant lymphocytopenia. However, the data on the effect of beta rays on the immune function remain diverse. In a recent study we have shown that radioiodine therapy in patients with thyroid carcinoma does not lead to cellular immunodeficiency, but a shift from TH-2 to TH-1 response was observed. Furthermore, the use of yttrium-90-radiolabelled somatostatin analogues (Y-90 DOTATOC) in patients with neuroendocrine tumors decreases the lymphocyte proliferation and the proinflammatory immune responses causing an immunosuppression. Unlike the above two mentioned tumor radiotherapies, where the radionuclides circulate in the bloodstream, in SIRT the yttrium-90 radioactive glass microspheres become trapped in the tumor capillary bed and leave the majority of the healthy nearby tissue intact. Nevertheless, considering the high dosage administrated and the fact that approximately 12% of the total blood volume is in the liver, an unintended low dose to the immune system is possible. The aim of our study is to gain insight into the modifications that take place following a SIRT treatment at the level of the lymphocyte proliferation as well as to identify a possible antimicrobial immunological impairment. Thus, in 20 patients treated with SIRT lymphocyte proliferation and the production of pro- and anti-inflammatory cytokines (interferon-γ and interleukin-10) after stimulation with mitogens and recall antigens are tested immediately prior to therapy and at day 1, day 2, day 7 and day 28 after therapy using lymphocyte transformation test and ELISpot. Preliminary data in 16 patients indicate that from day 1 until day 28 after therapy lymphocyte proliferation and interferon-γ production are significantly ($P < 0.05$) reduced. The most prominent finding was a pronounced reduction of anti-microbial immune responses. In conclusion, according to our current results there is a severe impairment of immune function after SIRT which seems to be more intense than after radioiodine therapy or Y-90 DOTATOC treatment.

OP577

Retrospective analysis of dose-response for HCC lesions treated with 90Y resin microspheres

C. Pettinato[1], C. Mosconi[2], A. Cappelli[2], S. Civollani[1], P. Pini[3], F. Monari[4], C. Galaverni[2], B. Angelelli[5], F. Trevisani[3], R. Golfieri[2]; [1]Medical Physics Unit - AOU di Bologna, Bologna, ITALY, [2]Radiology Unit - AOU di Bologna, Bologna, ITALY, [3]Internal Medicine Unit - AOU di Bologna, Bologna, ITALY, [4]Radiotherapy Unit - AOU di Bologna, Bologna, ITALY, [5]Oncology Unit - AOU di Bologna, Bologna, ITALY.

Aim: We retrospectively analyzed 50 patients affected by HCC and treated with 90Y resin microspheres. The aim of this study was to evaluate the correlation between tumor dose and local tumor response. **Materials and Methods**: From September 2010 to October 2014 46 patients affected by HCC have been treated with 90Y resin microspheres. All patients received an intra-hepatic infusion of 150 MBq of 99mTc-MAA to calculate lung and extra-hepatic shunts and to perform lesion and whole liver dosimetry using the MIRD formalism. The activity to be injected was calculated using the BSA formula and was modulated based on tumor and normal liver doses, limiting the dose to whole normal liver to about 30 Gy. **Results**: The mean injected 90Y activity was 1.5 ± 0.5 GBq. The mean tumor volume was 288 cc ranging from 43 cc to 2566 cc, while the average dose was 258 Gy ranging from 13 to 858 Gy. Tumors with smaller volumes received

higher doses. The average doses to tumors with volumes below 100 cc, between 100-300 cc, between 300-500 cc and above 500 cc were respectively 436 Gy (95% IC: 359.2 - 795.2 Gy), 265 Gy (95% IC: 225.7 - 490.7 Gy), 135 Gy (95% IC: 127.6 - 262.6 Gy) and 108 Gy (95% IC: 92.6 - 200.6 Gy). 24/46 patients received an average tumor dose greater than 200 Gy. Among them 10 patients showed a complete response and an average survival > 12 months. 5/24 patients had a good response at 9 months follow-up, while 9/24 patients had a worsening of the disease due to progression of non treated lesions. 7/22 patients, that received less than 200 Gy, had stable or good response of treated lesions 9 months after treatment. 6 out of these 7 patients had lesion volumes greater than 300 cc. How results suggest that big tumors (>300 cc) are responsive to lower average doses because whole tumor volume, including also "non-active" or necrotic parts typical of large lesions, is considered in the average dose calculation. **Conclusions**: Average tumor dose based on ^{99m}Tc-MAA SPECT images is a good prognostic value to predict tumor response to ^{90}Y resin microspheres treatments in patients affected by HCC. Our results showed that 42% of tumors that received more than 200 Gy had complete response while 67% of tumors had stable or good response for more than one year.

OP578

PET-CT in the post-treatment evaluation of a HCC patient treated with Yttrium-90 radioembolization

R. Stoico, L. Dellavedova, M. Carletto, L. Maffioli; A.O. Ospedale Civile di Legnano, Legnano, ITALY.

The aim of the present study was to evaluate PET-CT scan method in terms of image quality and dosimetry, in a HCC patient, treated with Y90 transarterial radioembolization (TARE). The patient underwent Y90-TARE to treat a single lesion of 52.5 cm^3. Pre-treatment planning 150 MBq Tc99m-MAA SPECT-CT scan was performed in order to calculate injection activity, tumor dose and to evaluate visceral shunt. Percentage lung shunt fraction was calculated with planar whole-body acquisitions. The planned activity was calculated by the use of compartmental method. The tumor and non-tumor doses were calculated as injected activity multiplied by 50 divided by the mass. The injected activity was 3.4 GBq; the tumor and non-tumor doses were 932 Gy and 62 Gy respectively (reference values). Therasphere (Nordion, Canada) treatment was performed. No radioprotection problem during treatment angiographic procedure for health operators was recorded. The day after the treatment PET-CT (Philips Gemini TF 16 slices, CT: 120 kV, 100 mAs, Z-DOM low dose alghorithm, PET: nuclide Y90, 15 min/bed, 2 bed positions to cover the liver) scan was performed. OSEM TOF iterative algorithm (3 iterations, 33 subsets) was used. A quantitative evaluation on reconstructed images was made by the use of Philips software. The image quality was evaluated in terms of volume definition. Tumor and non-tumor thresholds ROIs were used to calculate volumes (mm^3) and activity concentration (MBq/ml). Tumor and non-tumor doses were obtained by the use of the same dosimetric planning method. Lung shunt fraction was not considered (percentage value was zero). Percentage difference between reference and scan values for image quality and dosimetric analysis was calculated. The quantitative analysis about image quality showed percentage difference in volume calculation of -5%. The dosimetric analysis showed that calculated tumor dose was 993 Gy and non-tumor dose 52 Gy. Differences between calculated and planned dose values were +6.5% to tumor, -16.5% to non-tumor. In our experience, after Y90-TARE, PET-CT was considered the optimal scan method due to high image resolution and low time consumption. The evaluation of PET-CT scan method post-Y90 radioembolization in terms of image quality showed a comparable volume definition with reference CT by the use of threshold ROI method; in terms of dosimetry a comparable evaluation of tumor dose but an underestimation of non-tumor one. This preliminary result put in evidence the importance to perform a pre-treatment dosimetric plan because the non-tumor dose is a significant parameter to evaluate liver complications post-treatment.

OP579

Comparison of Survival, Safety and Efficacy After Chemo and Radioembolization of BCLC Stage B-C Hepatocellular Cancer Patients.

C. Soydal, M. F. Arslan, N. O. Kucuk, R. Idilman, S. Bilgic; Ankara University Medical Faculty, Ankara, TURKEY.

Aim: We aimed to compare overall survival times, long-term complication and recurrence rates of chemo and radioembolization for BCLC Stage B-C hepatocellular cancer patients. Materal and Method: 80 BCLC Stage B-C hepatocellular cancer patients who received chemo or radioembolization were retrospectively included to the study. Overall survival times, long-term complication and disease recurrence rates of two groups were compared. Additionally prognostic role of gender, age, presence of underlying chronic liver disease, BCLC stage, dimension and number of liver lesions, tumor load and presence of extra-hepatic disease for each group were analyzed. Results: 40 (27M and 13F; mean age: 41.9±21.9) patients were analyzed in each group. During follow-up period, twenty-two and 30 patients were died in radio and chemoembolizations groups, respectively. Overall mean survival of whole patient group was calculated as 37.31±3.94 months (30.46-44.1, %95CI). It was 30.63±3.68 months (23.42-37.84, %95CI) for chemo and 39.24±4.62 months

(30.18-48.29, %95CI) for radioembolization groups, respectively (p=.0.014). One and two years survival rates were 72% vs 74% and 47% vs 59% for chemo and radioembolization groups. There was no significant difference between chronic complication (p=0.32) and disease recurrence (p=0.65) rates of groups. While dimension of the largest lesion was the most significant predictor (p=0.01) in radioembolization group, female gender (p=0.008), dimension of the largest lesion (p=0.03) and BCLC stage (p=0.01) were significant for chemoembolization group. Conclusion: While chemo and radioembolization for BCLC Stage B-C patients are similar in safety and efficacy, they differ in overall survival. Patients seem to live longer after radioembolization. The dimension of the largest liver lesion is predictor for both treatments. Additionally gender and BCLC stage are significant factors in chemoembolization group.

OP580

Safety of 90Y-glass microspheres therapy in hepatic malignancies, our experience.

P. Borrelli, P. Bello Arqués, P. Olivan Sasot, C. Igua Sáenz, V. Vera Pinto, J. Vercher-Conejero, J. Loaiza Góngora, C. Ruiz Llorca; Hospital Universitario y Politecnico La Fe, Valencia, SPAIN.

AIM: To follow-up clinically patients with hepatocellular carcinoma and/or unresectable liver metastasis, treated with 90Y glass microspheres using intraarterial hepatic radioembolization, and describe immediate (less then 24 hours after treatment) and later complications onset. Materials and methods: Between April 2009 and January 2015, 54 treatments were performed in 49 patients (36 men/18 women), medium age 58.22 years (28-85). 43 treatments were carried out due to hepatocellular carcinoma, 5 neuroendocrine tumor metastasis, 2 colonic carcinoma metastasis, 2 medullary thyroid carcinoma metastasis and 2 cholangiocarcinoma. Prior to treating patients a simulation study was performed using 99mTc-albumin macroagregates (99mTc-MAA), through the same tumor nurturing arterial vessel. Bremsstrahlung images were acquired in every post-treatment, to evaluate radiopharmaceutical distribution and extrahepatic leaks, if any. Since May 2013 (34 patients) were also evaluated using PET/CT. All patients received prophylactic treatment including oral steroids and proton bomb inhibitor. Results: Average follow-up was 13.65 months, during this period 30 patients (55,5%) died due to underlying disease complications. In just one case extrahepatic leak was found in the gallbladder walls, although no symptoms were shown afterwards. At the 99mTc-MAA pre-treatment test, medium pulmonary shunt was 5,58% (0.03-34.5) and gastrointestinal leak 2,12% (0-4.8). 90Y-glass microspheres medium dose administered was 2.86GBq (0.55-6.42) At the first 24 hours after radiopharmaceutical administration only 3 cases (5.55%) presented complications, two of them pain in the right hypochondrium and one cirrhotic decompensation. Eight patients (14.8%) presented asthenia and/or fever during the first month after treatment, probably due to radioembolization although it could represent symptoms associated with the underlying disease. Conclusion: Hepatic methastasic or tumoral radioembolization has proven to be a safe palliative therapy, without immediate major secondary effects. Late and non-specific secondary effects are being studied to, if feasible, identify its origin, due to the underlying progressive disease or due to late therapy effects.

OP581

Yttrium-90 Radioembolisation for Colorectal Cancer Liver Metastases: Circulating Angiogenic Factors and Treatment Response

C. E. N. M. Rosenbaum; University Medical Center Utrecht, Utrecht, NETHERLANDS.

Aim: Yttrium-90 radioembolisation (^{90}Y-RE) of liver metastases results in radiation damage and hypoxia in liver tissue, which is a powerful trigger for the systemic release of angiogenic factors that stimulate angiogenesis and may enable (extra hepatic) tumour growth. Our aim was 1) to investigate predictive value for response of baseline values of several angiogenic factors, and 2) to examine changes in serum levels of these factors following ^{90}Y-RE. Materials and Methods: A prospective cohort study was conducted in 42 patients with unresectable colorectal cancer liver metastases, refractory to systemic therapy. Blood samples were taken at baseline, and at 0, 1, 3, 7 and 30 days after treatment. Response was measured with MR and FDG-PET imaging, at baseline, one and three months after treatment and subsequently at three-month intervals until progressive disease. Angiogenic factors included vascular endothelial growth factor (VEGF), hepatocyte growth factor (HGF), angiopoietin-2, basic fibroblast growth factor (FGF-b), platelet-derived growth factor (PDGF-BB), stromal cell-derived factor 1 (SDF-1a) and thrombospondin-1. Results: Thirty patients had liver only disease and 12 patients had limited extrahepatic disease (EHD). Patients were treated with whole liver / one session resin ^{90}Y-RE (median administered activity 1.5 GBq per BSA method). Median overall survival was 9.2 month (95%-confidence interval 6.0 - 12.4 months). Median time to progressive disease of liver lesions was 3.0 months, with a significant difference between patients with versus without EHD at baseline (1.4 versus 3.5 months; p=0.001). At three months follow up, 22 patients showed progressive disease of liver lesions, which was caused by occurrence of new lesions in 19 patients and in only 3 patients by growth of baseline lesions. Baseline serum levels of several angiogenic factors varied considerably among patient groups, e.g. higher baseline levels of angiopoietin-2 and HGF were observed in patients with kRAS mutation as compared to patients without this

mutation, suggesting differences in tumour biology and behaviour. Furthermore, heterogeneity was also seen in responders versus non-responders, for example lower baseline values for serum VEGF were seen in patients with partial response at three months follow up. Several patterns of changes in angiogenic serum levels were observed, with 10/42 patients showing a distinct peak in e.g. VEGF at 7 days after treatment. Conclusion: Our findings suggest that even in this macroscopically homogenous patient group, tumour biology may vary considerably among individuals, and should be weighed carefully for individualized treatment.

1606 - Wednesday, October 14, 2015, 10:00 AM - 11:30 AM, Hall 6

M2M: Radiopharmaceuticals & Radiochemistry: Macromolecules II

OP582

The use of radiocobalt as a label improves PET imaging of EGFR using DOTA-conjugated affibody molecules.

J. Garousi[1], K. Anderson[2], J. H. Dam[3], B. B. Olsen[3], A. Orlova[4], J. Buijs[1], S. Ståhl[2], H. Thisgaard[3], V. Tolmachev[1]; [1]Department of Immunology, Genetics and Pathology, Uppsala University, Uppsala, SWEDEN, [2]Department of Protein Technology, KTH - Royal Institute of Technology, Stockholm, SWEDEN, [3]Department of Nuclear Medicine, Odense University Hospital, Odense, DENMARK, [4]Department of Medicinal Chemistry, Uppsala University, Uppsala, SWEDEN.

Aim. Epidermal growth factor receptor (EGFR) is the molecular target for monoclonal antibodies cetuximab and panitumumab, and tyrosine kinase inhibitor gefitinib. Radionuclide molecular imaging of epidermal growth factor receptor (EGFR) expression might facilitate stratification of patients for EGFR-targeting therapies. We have demonstrated earlier that 111In-labelled anti-EGFR DOTA-ZEGFR:2377 affibody molecule can image specifically EGFR-expressing xenografts. This affibody molecule has similar affinity to both murine and human EGFR. The use of PET may further improve sensitivity of EGFR imaging. We evaluated two positron-emitting nuclides, 68Ga (T½=67.7 min) and 55Co (T½=17.5 h min) as labels. The aim of this study was to evaluate influence of radiogallium and radiocobalt labels on biodistribution of DOTA-ZEGFR:2377. Materials and methods. 55Co was produced by the 54Fe(d,n)55Co nuclear reaction using isotopically enriched target and separated from target material using anion exchange on Dowex 1x8. 57Co was used as a surrogate for 55Co in some experiments. Conjugates were evaluated in vitro using EGFR-expressing A431 cells. In vivo studies were performed in BALB/C nu/nu mice bearing A431 xenografts. The injected dose of all conjugates was 40 μg/mouse. Results. DOTA-ZEGFR:2377 was labelled with 68Ga and with radiocobalt with yields >98%. Both 68Ga- and 55/57Co-labelled DOTA-ZEGFR:2377 demonstrated specific binding to A431 cells in vitro. IC50 values were 0.58±0.19, 0.70±0.15, and 0.53±0.15 pM for natGa, natIn, and natCo-loaded DOTA-ZEGFR:2377, respectively. Biodistribution of 68Ga-DOTA-ZEGFR:2377 resembled biodistribution of 111In-DOTA-ZEGFR:2377. At 3 h pi, uptake of 68Ga-DOTA-ZEGFR:2377, in tumour, blood and liver was 2.7±0.1, 0.42±0.9, and 6.2 ±0.3%ID/g, respectively. In the case of 57Co-DOTA-ZEGFR:2377, the tumour uptake was increased to 5.8±0.6%ID/g, and liver uptake decreased to 1.85±0.6%ID/g. The blood concentration was 0.48±0.02 ID/g. Tumour-to-blood and tumour-to liver rations were 7±2 and 0.44±0.03 for 68Ga-DOTA-ZEGFR:2377, and 12±2 and 3.1±0.5 for 57Co-DOTA-ZEGFR:2377. At 24 h pi, the tumour-to-blood ratio for 57Co-DOTA-ZEGFR:2377 increased to 32±7. The biodistribution data were confirmed by in vivo imaging. Conclusion. The use of radiocobalt improves targeting properties of anti-EGFR affibody molecules DOTA-ZEGFR:2377. The exact nature of this phenomenon is not quite clear for us. We can speculate that the hepatic uptake of anti-EGFR affibody depends on both EGFR expression in liver and properties of the molecule. The use of divalent cobalt instead of trivalent gallium or indium increases a negative charge at C-terminus. This might reduce hepatic uptake and makes more tracer available for tumour targeting.

OP583

223Ra-NaA-silane-PEG-SP(5-11) radiobioconjugate as a new potential radiopharmaceutical for targeted α therapy of glioblastoma multiforme

A. Majkowska-Pilip[1], P. Koźmiński[1], A. Piotrowska[1], F. Bruchertseifer[2], A. Morgenstern[2], M. Bonelli[3], M. Laurenza[3], A. Bilewicz[1]; [1]Institute of Nuclear Chemistry and Technology, Warsaw, POLAND, [2]European Commission, Joint Research Centre, Institute for Transuranium Elements, Karlsruhe, GERMANY, [3]Dept. Physiology and Pharmacology, Sapienza University of Rome, Rome, ITALY.

Aim: Despite all current forms of treatment such as advanced surgery techniques, radiation therapy and chemotherapy, the life expectancy of patients diagnosed with glioblastoma multiforme (GBM) is 12 to 15 months displaying the worst median overall survival among all human neoplasms. According to the cancer stem cell hypothesis, malignant gliomas arise from mutated, developmentally arrested multipotent progenitor cells ("glioma stem cells") that sustain tumor growth and are intrinsically resistant to radio- and chemotherapy. Targeted alpha therapy has been shown to overcome chemo- and radioresistance in vitro and thus presents a promising approach for therapy of GBM. The aim of this study is to investigate the use of radiobioconjugate - 223Ra-NaA-silane-PEG-SP(5-11) for targeted α therapy of gliomas. Materials and methods: Sodium form of an A type of nanozeolite (NaA) was

synthesized using the hydrothermal method. Size distribution and shape of NaA nanozeolite particles were characterized by dynamic light scattering analysis (DLS), scaning elektron microscopy (SEM) and transmission emission spectroscopy (TEM). PEG linker (2000 kDa) comprising the silane group at one end and N-succinimid ester (NHS) at the second was used for synthesis of silane-PEG-SP(5-11) bioconjugate. The obtained bioconjugate was characterized by thermogravimetric (TGA) and DLS analysis. Next the NaA-silane-PEG-SP(5-11) bioconjugates were labelled with 223Ra by exchange of Na+ cation and stability of obtained radiobioconjugates were tested in various biological fluids. Cell viability was assayed using the MTS colorimetric assay. Results: Nanosized zeolites were successfully prepared through hydrothermal synthesis. The TGA results has shown that silane-PEG-SP(5-11) molecules are covalently attach to the NaA nanozeolite surface. 223Ra α-particle emitting radionuclide, has been absorbed in the nanometer-sized NaA zeolite (30-70 nm) trough simple ion exchange. The 223Ra labeled nanozeolite bioconjugate successfully retain 95% fraction of the daughter products without compromising the tumoricidal properties of the radiation. It is worth to notice, that the release of the decay product from 223Ra is a negligible problem, because 75% of the α-particles energy are emitted within a 4 seconds after the 223Ra decay. Cytotoxicity assays showed a reduction of viability of GBM cells as well as GBM stem cells after incubation with 223Ra-NaA-silane-PEG-SP(5-11) in a dose dependent manner. Cell viability also decreased with increasing incubation times. Conclusion: Targeted alpha therapy with 223Ra-NaA-silane-PEG-SP(5-11) is a promising approach for treatment of GBM which is resistant for conventional therapies and warrants further investigation in vivo.

OP584

Gold Nanoparticle-Substance P(5-11) Conjugate as a Carrier for 211At in Alpha Particle Therapy

A. Bilewicz[1], &. Janiszewska[1], P. Kozminski[1], M. Lyczko[1], M. Pruszynski[1,2], J. Jastrzębski[2], J. Choinski[2], A. Stolarz[2], A. Trzcińska[2], K. Szkliniarz[3], W. Zipper[3]; [1]Institute of Nuclear Chemistry and Technology, Warsaw, POLAND, [2]Heavy Ion laboratory, University of Warsaw, Warsaw, POLAND, [3]Institute of Physics, Department of Nuclear Physics, University of Silesia, Katowice, POLAND.

Aim: The ^{211}At might be a particularly useful radionuclide in targeted radiotherapy, as it decays by the emission of short-range high-energy α-particles. However, many astatine compounds that have been synthesized are unstable *in vivo*, providing motivation for seeking other ^{211}At labeling strategies. In our work we propose to utilize formation of strong bond between metallic gold and astatine to bind the ^{211}At to biomolecules. Materials and methods: The gold nanoparticles with diameter of 2 and 20 nanometers were synthesized by Turkevich and Brust-Schiffrin methods. All types of the nanoparticles were characterized by TEM technique. The average particle size in solution and zeta potential were determined by DLS technique. The obtained gold nanoparticles were conjugated to substance P - short peptide having high affinity to NK1 receptors on the glioma cells. In first step polyethylene glicol with disulfide or thioctic acid with N-succinimidyl ester as a linkers were conjugated with substance P. After twenty four hours product was purified, lyophilized and spontaneously bound to gold nanoparticles. The synthesis of the bioconjugate was monitored by HPLC technique. The Au-PEG-SP bioconjugates were labelled with ^{211}At produced in cyclotron at the Heavy Ion Laboratory, University of Warsaw. Before labeling astatine was reduced to At^- using 0.01 M Na_2SO_3 solution. Stability of the obtained radiobioconjugates were tested in biological fluids: sodium chloride, cysteine, glutathione and human serum for 2, 4 and 19 hours. Results: The Au- PEG-SP (5-11) bioconjugates were successfully synthesized. The HPLC analysis has shown that thiol-PEG-N-Substance P bioconjugate are covalently attached to the gold surface. using the thiol approach. ^{211}At, α-particle emitting radionuclide, has been strongly absorbed in the ^{211}At-Au-PEG-SP bioconjugates. The bioconjugates nearly quantitatively retains the ^{211}At in all solutions studied. Less than 0.1% of the ^{211}At radioactivity was found in solution. Also preliminary in-vitro biological studies indicate that ^{211}At-labeled bioconjugates exhibit high cytotoxicity to glioma cells. Conclusion: We have shown that gold nanoparticles labelled with ^{211}At and functionalized with substance P presents a prospective solution for the use of the ^{211}At as a therapeutic tool for targeting glioma cells. This work was supported by National Science Center of Poland (Grant 011/01/M/ST406756).

OP585

Synergistically Enhanced Tumor Uptake via Dual-Targeting of CD105 and EGFR Using a "Click" Heterodimer

R. Hernandez, H. Luo, H. Hong, S. A. Graves, R. J. Nickles, W. Cai; University of Wisconsin-Madison, MADISON, WI, UNITED STATES.

Objective: Dual-targeting is expected to give higher targeting efficacy/specificity. Herein we designed and synthesized a heterodimer using 2 antibody Fab fragments (i.e. Cetuximab Fab and TRC105 Fab) for dual-targeting of the epidermal growth factor receptor (EGFR) and CD105. Expression of EGFR was mostly on the tumor cells, whereas expression of CD105 was primarily on the actively proliferating tumor vasculature. The synergistic dual-targeting effect of Cetuximab Fab-TRC105 Fab vs. single-targeting Fab (i.e. Cetuximab Fab or TRC105 Fab) was comprehensively compared in vitro and in vivo. Methods: Cetuximab Fab-TRC105 Fab (i.e. heterodimer) was synthesized by mixing Cetuximab Fab-tetrazines and TRC105

Fab-trans-cyclooctenes via Click chemistry. It was purified by HPLC with Sephacryl S-100 HR column, conjugated to 2-S-(4-isothiocyanatobenzyl)-1,4,7-triazacyclononane-1,4,7-triacetic acid (p-SCN-Bn-NOTA) and labeled with ^{64}Cu for positron emission tomography (PET) imaging. Dual-receptor binding studies were performed in U87MG human glioblastoma cells (expressing both EGFR and CD105) and tumor-bearing mice. Blocking experiments and ex vivo histology studies were performed to confirm the in vivo results. In addition, optical imaging using near-infrared fluorescent dye labeled heterodimer was also investigated for optical image-guided tumor resection. Results: Purified Cetuximab Fab-TRC105 Fab was confirmed by SDS-PAGE (~100 kDa band), whereas the two Fab fragments were at ~50 kDa. Flow cytometry studies showed much higher fluorescence signal for the hetorodimer when compared with each Fab alone. In U87MG mice, ^{64}Cu-NOTA-Cetuximab Fab-TRC105 Fab had significantly higher tumor uptake (32.0±6.9, 47.5±6.7, 46.0±3.3 and 44.1±9.4 %ID/g at 3, 15, 24, and 36 h post-injection, respectively; n=3) than that of ^{64}Cu-NOTA-Cetuximab Fab and ^{64}Cu-NOTA-TRC105 Fab (<15%ID/g for both). Blocking studies using either Cetuximab or TRC105 both led to significantly reduced U87MG tumor uptake of ^{64}Cu-NOTA-Cetuximab Fab-TRC105 Fab, confirming that the very high tumor uptake of ^{64}Cu-NOTA-Cetuximab Fab-TRC105 Fab was indeed due to dual-targeting of EGFR and CD105 in the tumor tissue (both tumor vasculature and tumor cells). Furthermore, low liver and kidney uptake was observed for the heterodimer (<10 %ID/g), which gave excellent tumor-to-normal tissue ratio. In addition, ^{64}Cu-NOTA-Cetuximab Fab-TRC105 Fab was able to non-invasively detect small tumor nodules of <20 mg in size by PET, and fluorescently labeled Cetuximab Fab-TRC105 Fab was successfully employed for optical image-guided tumor removal. Conclusions: Successful dual-targeting of EGFR and CD105, via a "click" heterodimer of 2 Fab fragments, leads to synergistic enhancement of tumor uptake over either Fab alone which could improve future cancer diagnosis and therapeutic efficacy.

OP586

Affibody-based bioorthogonal chemistry-mediated radionuclide pretargeting: proof-of-principle.

M. Altai[1], M. Tsourma[1], B. Mitran[2], H. Honarvar[1], A. Perols[3], M. Robillard[4], R. Rossin[4], W. ten Hoeve[5], M. Sandström[6], A. Orlova[2], A. Eriksson Karlström[3], V. Tolmachev[1]; [1]Department of Immunology, Genetics and Pathology, Uppsala, SWEDEN, [2]Preclinical PET Platform, Uppsala, SWEDEN, [3]Division of Protein Technology, KTH, Stockholm, SWEDEN, [4]Tagworks Pharmaceuticals, Eindhoven, NETHERLANDS, [5]Syncom B.V., Gröningen, NETHERLANDS, [6]Akademiska sjukhuset, Uppsala, SWEDEN.

Aim: The use of radiometal-labelled affibody molecules in targeted radionuclide therapy is hindered by the high uptake and retention of radioactivity in the kidneys. Commonly used methods for reduction of renal radioactivity were inefficient in the case of affibody molecules. Pretargeting is an efficient approach to improve biodistribution profiles. One promising approach is the use of bioorthogonal chemistry based on a reaction of trans-cyclooctene (TCO) and radiolabeled tetrazine. We propose affibody-based TCO-tetrazine mediated pretargeting for the reduction of renal uptake. Radiometal-labelled tetrazine clears rapidly from normal tissues including kidneys. The fast blood clearance and slow internalization rate of affibody molecules should allow sufficient TCO tags to be available on the surface of cancer cells at the time of tetrazine injection. If proven, the use of affibody-TCO/Tetrazine based pretargeting would give higher tumour-to-kidney uptake of radioactivity. This will permit the use of affibody molecules in radionuclide therapy. Methods: The maleimido-derivative of TCO was conjugated to the anti-HER2 affibody molecule, Z2395 through site-specific thiol directed chemistry. The conjugate was labelled with 125I. Tetrazine-DOTA was labelled with indium-111 in 0.25M acetate pH, 5.5 (n=6). Binding specificity to and cell retention by HER2-expressing cells of 125I-Z2395-TCO was studied. The feasibility of in vivo pretargeting of HER2-overexpressing SKOV-3 ovarian carcinoma xenografts in Balb/C nu/nu female mice was studied. For this mice were injected with 30μg (4.1nmol) 125I-Z2395-TCO followed by the injection of equimolar concentration of 111In-tetrazine, 4h later. Mice were then dissected at 1h p.i. of 111In-tetrazine. Control experiments included pre-saturation of HER2 in xenografts and injection of tetrazine without preinjection of Z2395-TCO. Results: Tetrazine-DOTA was labelled with indium-111 with a yield of 99.3 ±0.4% (n=5). 125I-Z2395-TCO bound specifically to HER2 (KD=45±16pM) and showed high cellular retention up to 24h. The uptake of 125I-Z2395-TCO in tumour xenografts was high (17±2 %ID/g at 5 h p.i.) and HER2-specific. Tumour uptake of 111In-tetrazine 1h after the injection was 60-fold higher for the pretargeted (9.7±1.6 %ID/g) than the non-pretargeted group (0.16 ±0.02%ID/g). The tumour uptake was reduced (2.9 ±0.4%ID/g) when mice were injected with large excess of non-labelled-tetrazine, suggesting specificity of TCO/tetrazine-reaction. Kidney uptake in pretargeted group was 57-fold lower compared to the previously studied 111In-labeled affibody molecule, 111In-DOTA-Z2395 (5 ±2 vs. 284±22%ID/g). The tumour-to-kidney ratio exceeded two. Gamma-camera imaging performed at 1h post-111In-tetrazine injection showed that the tumour is the only site with prominent accumulation of radioactivity. Conclusion: This study provides proof-of-principle for bioorthogonal chemistry mediated affibody-based pretargeting.

OP587

Technetium-99m radiolabeled aptamer as a potential agent capable of identifying tumor in vivo

L. KANG; PEKING UNIVERSITY FIRST HOSPITAL, BEIJING, CHINA.

Aim: Aptamers are small molecule DNA or RNA fragments that fold into well defined 3D structures with high specificity and affinity towards target molecules. Aptamers are emerging as a new class of molecules for radiopharmaceutical development. In this study a new tumor-targeted agent of radiolabel aptamer with technetium-99m (99mTc) was developed, and further its distribution and imaging in breast tumor bearing mice.Materials and methods: We used AS1411 in this study, a DNA aptamer specifically binding to nucleolin that is overexpressed on the plasma membrane of multiple cancer cells. The six carbon amine group was linked at the end of AS1411 so that the aptamer was radiolabeled with 99mTc via the conjugation to NHS-MAG3. Radiochemical purity and stability were evaluated by HPLC. Cellular uptake assays were carried out in the MCF-7 cell line to evaluate tumor uptake in vitro. MTT assay was used to assess the anti-cancer ability in vitro. Moreover, in vivo imaging of 99mTc radiolabeled aptamer were performed in breast cancer tumor models.Results: Aptamer AS1411 was successfully labeled with 99mTc in high radiochemical yields, showing high stability in the mixture of fresh human serum. In cellular uptake assay, the radiolabeled aptamer showed significantly higher uptake in MCF-7 cells than 99mTc-pertechnetate. 99mTc radiolabeled aptamer showed strong inhibitory ability in tumor cell lines, whereas 99mTc-pertechnetate had no inhibition by MTT assay. After the system administration, the in-vivo imaging results revealed the significant difference between radiolabeled aptamer and 99mTc-pertechnetate in MCF-7 tumor bearing mice, which suggested the specific binding and tumor detective ability of radiolabeled aptamer in vivo.Conclusion: The tumor-targeted aptamer directly labeled with 99mTc could be considered a promising agent capable of identifying tumor in vivo.

OP588

89Zr-Affibody for specific detection of EGFR expression in HNSCC

T. Burley, C. D. Martins, C. Da Pieve, R. L. Paul, D. M. Ciobota, G. Smith, K. Harrington, G. Kramer-Marek; The Institute of Cancer Research, Sutton, UNITED KINGDOM.

Aims: Although, present in normal cells, epidermal growth factor receptor (EGFR) is overexpressed in many human malignancies including head and neck squamous cell carcinoma (HNSCC). Clinical findings suggest that elevated levels of EGFR expression indicate poor prognosis and reduced survival in HNSCC patients. So far, EGFR-targeted agents have only had limited success as monotherapies. Therefore, identifying the presence of the molecular target is crucial in achieving an optimal outcome with molecularly targeted drugs. In this study, we have focused on strategies to develop and characterise a potential molecular imaging agent for *in vivo* quantification of EGFR expression.Materials and Methods: $Z_{EGFR:3115}$Affibody molecules were conjugated to desferrioxamine (DFO) and labelled with ^{89}Zr. *In vitro* radioligand binding specificity and affinity was evaluated by a panel of HNSCC cells expressing different levels of EGFR. *In vivo* studies were conducted in NCr nude mice bearing subcutaneous EGFR+ve HNSCC tumours. Mice were injected with 1-5 μg (2-5 MBq) of ^{89}Zr-$Z_{EGFR:3115}$Affibody. For biodistribution studies, mice bearing CAL27 (EGFR+++) and Detroit 562(EGFR+) tumours were sacrificed 1, 3, 24, 48hr following the administration of the radioconjugate spiked with 0 or 10 μg of nonradioactive $Z_{EGFR:3115}$Affibody. Selected organs were dissected and their radioactivity measured using a γ-counter. The i*n vivo* imaging profile of ^{89}Zr-$Z_{EGFR:3115}$Affibody was further investigated with a spiked dose at 3, 24 and 48hr post radioligand injection. The EGFR expression and distribution of the tracer was assessed *ex vivo* by IHC and autoradiography.Results: *In vitro* assay confirmed high-affinity binding of the ^{89}Zr-$Z_{EGFR:3115}$Affibody probe to CAL27 cells (K_d = 6.4±0.64 nM). Pre-incubation with non-labelled Affibody inhibited the binding of the radioconjugate to the cells in a dose-dependent manner. *In vivo* studies showed high accumulation of the radioactivity in CAL27 tumours (spiked with 10 μg) as early as 1 hr post tracer injection (%ID/g = 5.2). Tracer was eliminated quickly from the blood and normal tissues, producing high tumour-to-blood and tumour-to-muscles ratios (24hr: T/B = 8.5; T/M = 18.5). As expected, the highest normal tissue concentration of radioactivity was seen in the kidneys. Very good correlation was observed between PET and *ex vivo* estimates of tracer concentration and the receptor expression in the tumour tissue, as assessed by radioactivity accumulation and IHC respectively.Conclusion: Our results suggest that the described ^{89}Zr-$Z_{EGFR3115}$Affibody may be used to assess different levels of EGFR expression *in vivo*.

OP589

Strategies for the development of high specific activity affibody based probes for the detection of HER3 positive tumours

C. Da Pieve[1], L. Allott[1], C. D. Martins[1], L. Carroll[2], R. L. Paul[1], E. O. Aboagye[2], G. Kramer-Marek[1], G. Smith[1]; [1]Institute of Cancer Research, London, UNITED KINGDOM, [2]Imperial College London, London, UNITED KINGDOM.

Background: Human epidermal growth factor type 3 (HER3) is a transmembrane receptor of which expression in breast cancer is associated with a more resistant phenotype and poor prognosis. PET imaging of HER3 expression could aid in the identification of patients who could benefit from HER3-targeted therapy. Imaging HER3 is challenging due to modest over-expression of the receptor (typically <40,000 receptors/cell). Therefore, the development of affibody based tracers, exhibiting high target affinity and high specific activities, are necessary to image and quantify HER3 expression in vivo.Materials and Methods: An anti-HER3 affibody (ZHER3:8698, AffibodyAB, Sweden) was used as high affinity targeting molecule. Radiolabelling strategies, including the use of various radioisotopes (18F, 68Ga, and 89Zr) and chemistries, ([18F]AlF and inverse-electron demand Diels-Alder (IEDDA)), have been investigated in order to produce high specific activity products and limit thermal degradation of the protein. The stability and affinity for the HER3 receptor were tested in vitro using MCF7 breast cancer cells.Results: The affibody conjugates NOTA-ZHER3:8698 and DFO-ZHER3:8698 were synthesized, purified and radiolabelled with 18F and 89Zr respectively. The specific activity of these affibodies as [18F]AlF-NOTA and 89Zr-DFO conjugates were 0.8 MBq/μg (7.8 GBq/μmol) and 2.8 MBq/μg (22 GBq/μmol) respectively. Using the IEDDA reaction between tetrazine and trans-cyclococtyne, exemplified using 68Ga and 18F, resulted in a specific activity of 2.5 MBq/μg (20.8 GBq/μmol) for the 68Ga-DOTA-tetrazine and no labelling for the [18F]AlF-NODA-tetrazine reacted with TCO functionalized affibody. However, the reaction of [18F]AlF-NODA-TCO with the tetrazine functionalized affibody improved the specific activity of the product to 2.5 MBq/μg (20.8 GBq/μmol). All tracers were isolated with a RCP >97% and their binding affinities to HER3 were determined to be in the subnanomolar range (ca 0.44 nM).Conclusions: The labelling of the HER3 targeting affibody, using either a long lived radioisotope as 89Zr or a labelling strategy as IEDDA, could produce high specific activity tracers enabling the in vivo detection of HER3 positive tumours. Moreover, the developed IEDDA synthetic strategies can be applied to radiolabel other molecules allowing moderately expressed targets to be imaged.

1608 - Wednesday, October 14, 2015, 10:00 AM - 11:30 AM, Hall E

Clinical Oncology: Breast & Gynaecology

OP590

Identification of biomarkers including ^{18}FDG-PET/CT for early prediction of response to neoadjuvant chemotherapy in Triple Negative Breast Cancer

O. Humbert[1,2], J. Riedinger[1], C. Charon-Barra[1], A. Berriolo-Riedinger[1], I. Desmoulins[1], V. Lorgis[1], S. Kanoun[1,2], C. Coutant[1], P. Fumoleau[1], F. Brunotte[1,3,2], A. Cochet[1,2]; [1]Centre Georges-François Leclerc, DIJON, FRANCE, [2]Université de Bourgogne, UMR CNRS 6306, Dijon, FRANCE, [3]Centre Hospitalo-Universitaire, Dijon, FRANCE.

Purpose: To investigate the value of metabolic and perfusion parameters, derived from ^{18}F-fluorodeoxyglucose positron emission tomography (FDG-PET) exams, compared with clinico-biological markers to predict pathological complete response (pCR) to neoadjuvant chemotherapy (NAC) in women with triple-negative breast cancer (TNBC). Material and methods: Fifty consecutive women with TNBC and an indication for NAC were prospectively included. Different pre-treatment clinical, biological and pathological biomarkers, including SBR grade, the Ki-67 proliferation index, androgen receptor expression, epidermal growth factor receptor (EGFR) and cytokeratin 5/6 staining, were assessed. Tumor glucose metabolism at baseline and its change after the first cycle of NAC (ΔSUV) were assessed using FDG-PET. Changes in blood flow (ΔBF) were measured with FDG-PET using a dynamic first-pass model. Results: The pCR rate was 42%. In univariate analysis, a high Ki-67 proliferation index (p=0.03), negative EGFR status (p=0.04), high tumor ΔBF (p=0.02) and ΔSUV (p=0.001) were predictors of pCR. Tumor ΔSUV was the most accurate biomarker to predict pCR (threshold=-60%; PPV=80.0%; NPV=75.9%; accuracy=77.3%). In multivariate analysis, both negative EGFR status (Odds ratio=9.3; p=0.034) and high ΔSUV (Odds ratio=6.8; p=0.049) were independent predictors of pCR. Combining these two parameters could predict non-pCR with an accuracy of 92%. Conclusion: It is important to define the chemosensitivity of TNBC to NAC early. Combining EGFR status and the metabolic response assessed with FDG-PET can help the physician to predict early the probability of achieving pCR or not. Given these results, the interest of response-guided tailoring of the chemotherapy might be tested in multicenter trials.

OP591

Fusion of prone FDG PET/CT and MRI improves staging of patients with breast cancer

M. J. Ribelles, M. Rodriguez, L. Sancho, F. Guillen, L. J. Pina, M. Idoate, F. Martinez Regueira, M. Santiesteban, J. A. Richter, M. J. Garcia-Velloso; CLINICA UNIVERSIDAD DE NAVARRA, PAMPLONA, SPAIN.

Objective: To analyse the value of prone FDG-PET/CT, Magnetic Resonance Imaging (MRI), and PET/MRI fused images in preoperative staging of patients with newly diagnosed breast cancer. Material and Methods: From November 2012 to February 2015, 61 patients (mean age 52 ± 11 years) with histologically proven breast cancer were included. MRI and FDG PET/CT thoracic scans were performed with the patient in prone position using the same MRI breast array coil. FDG PET/CT was performed with point spread function (PSF) and time of flight (TOF). Both studies were reviewed independently, and fused PET/MRI images were evaluated by consensus. The quality of fused PET/MRI images was scored as excellent (full coincidence), acceptable (<10 mm displacement) or poor. The histopathology was the reference standard. Sensitivity, specificity, PPV, NPV and accuracy for each technique and for PET / MRI fusion images were calculated. Results: Lesions' mean diameter on MRI was 23±17 mm (range 3.5-84 mm). On histopathology, 102 out of 142 (75%) lesions were malignant, 5 patients had bilateral disease, 47 tumours were focal, 13 tumours were multifocal, and 6 tumours were multicentric. Clinicopathologic subtype was available in 61 patients, and luminal was the most common subtype (43 patients, 70.5%), followed by 7 HER2 (11.5%) and 11 triple negative (18%). The quality of fused PET/MRI images was excellent in 37 (61%) cases, acceptable in 16 (26%) cases, and poor in 8 (13%) cases. Sensitivity, specificity, PPV, and NPV of MRI were 95%, 55%, 84%, 81% respectively, compared to 90%, 48%, 81%, 86% for FDG-PET / CT and 98%, 75%, 91%, 94% for PET/MRI fusion. Eight lesions with luminal subtype, one lesion triple negative and one lesion HER2 positive were false-negative FDG-PET/CT. Fused PET/MRI images enabled correct diagnosis of 13 false positive MRI lesions. MRI detected axillary nodal disease in 19 patients, whereas FDG-PET/CT detected axillary nodal disease in 33 patients, internal mammary nodal disease in 3 patients, and unsuspected distant metastases in 6 patients. Conclusions: The fusion of prone MRI and 18F-FDG PET images is a feasible technique. In patients with newly diagnosed breast cancer, MRI had better sensitivity for the primary tumour. PET/MRI fusion increased the sensitivity, specificity, predictive values and accuracy, and could have avoided biopsies in benign lesions. FDG-PET/CT had added value in the detection of unsuspected lymph node and distant metastases.

OP592

Comparison of dedicated hanging breast PET and standard whole body PET/CT for primary tumour visualization in breast cancer patients

S. Teixeira[1], J. Ferrér Rebolleda[2], B. B. Koolen[1], J. Wesseling[1], R. Sánchez Jurado[1], M. P. M. Stokkel[1], M. del Puig Cózar Santiago[2], V. van de Noort[1], E. J. T. Rutgers[1], R. A. Valdés Olmos[1]; [1]Netherlands Cancer Institute - Antoni van Leeuwenhoek Hospital, Amsterdam, NETHERLANDS, [2]ERESA, General university hospital of Valencia, Valencia, SPAIN.

Purpose: Comparison of the performance of a dedicated PET for hanging breast imaging (MAMMI-PET) and whole body PET/CT for the visualization of breast cancer lesions in two European hospitals. Materials and methods: A total of 230 female patients (age: mean 52 y, range 24-82y) with ≥ 1 histologically confirmed primary breast cancer lesion (=index lesion) were included prospectively between March 2011 and March 2014. All patients were scanned with the standard whole body PET/CT (Philips, Eindhoven, Netherlands) followed by the MAMMI-PET (Oncovision, Valencia, Spain) after injection of 180-240 MBq. All index lesions were scored 0, 1 or 2 for quantity of FDG uptake. MAMMI-PET findings were further tested in relation to histological (ductal, lobular) and molecular (ER/PR/Her2) breast cancer subtype, tumour grade, breast length, maximal tumour diameter and affected breast quadrants. Results: Totally 234 affected breasts were scanned (lesion diameter 5-170 mm). Twenty-four lesions (10%) near the pectoral muscle did not reach the MAMMI-PET scanning range. Of 19 lesions that MAMMI missed comparing to PET/CT, 18 were outside its scanning range. For lesions located within its scanning range the MAMMI sensitivity was 98.6%. PET/CT missed 15 of the index lesions depicted by MAMMI (p=0.61). MAMMI-PET detected 41 additional lesions of which 16 where proven malignant (39%), 15 (36.6%) seen on other modalities, and 14 (34,2%) only visible on MAMMI-PET. Lesion visibility was influenced by tumour grade (p=0.034) but not by cancer subtype (p=0.83). Conclusion: When breast cancer is located within its scanning range MAMMI-PET is able to detect almost all

primary tumour lesions. Compared to PET/CT MAMMI-PET finds more cancer lesions provided that these are not too dorsally located in the breast.

OP593

Predictive value of dynamic and dual-phase 18 FDG PET/CT parameters in the assessment of neoadjuvant chemotherapy response in locally advanced breast cancer: A comperative study with dynamic contrast enhanced MRI.

O. Kupik, M. Tuncel, P. Kiratli, M. Akpinar, K. Altundağ, F. Demirkazık, **B. Erbas**; Hacettepe University, Ankara, TURKEY.

AIM: Several studies have shown promising results for the prediction of pathological complete response (pCR) to neoadjuvant chemotherapy (NAC) in patients with locally advanced breast cancer (LABC) using 18 FDG PET/CT. Dynamic contrast enhanced magnetic resonance imaging (dCE-MRI) can assess the response to NAC by providing information on the angiogenesis and morphology of the tumor. This study was planned to compare the predictive value of semi-quantitative paratemers obtained by dCE-MRI, dynamic and dual-phase 18FDG-PET/CT in LABC patients receiving NAC. MATERIALS and METHODS: Fortysix patients with LABC underwent dCE-MRI and 18FDG-FDG/PET at baseline and after 2-3 cycles of NAC (interim). Tumor diameter, spherical (SV), angiographic volumes (AV), peak signal intensity (PSI), rapid and medium component of initial rise, percentage of Type I, Type II, Type III curves were calculated. Dynamic 18FDG and dual phase images were recorded in the prone position. Using 18FDG dynamic data, SUVmax values for 2nd, 5th and 30th minutes were measured. In addition, SUL2peak, metabolik volume (Per2V) and total lesion glycolysis (Per2TLG) values were measured for the first 2 minutes data. For early (E) and late (L) images, SUVmax, SUVmean and SUVpeak, TLG and metabolic tumor volume (MTV) was measured using adaptive (adp) and 42% thresholding method. Baseline and interim studies were used to calculate percentage changes and compared according to the surgery results; pCR vs non-pCR. ROC curves were obtained to calculate the AUCs for the prediction of pCR. Optimal treshold values to discriminate between pCR and non-pCR were calculated. RESULTS: Late prone images had higher sensitivity and specificity to detect the residual tumor (91%, 71.4%) and residual lymph node (62.5%, 87.5%) compared to MRI (84%, 37.5%, LN: 37.5%, 57.5%) and early prone images (84.5%, 75%, LN: 50%, 83%). PET/CT parameters were significantly different between pCR and non-pCR groups, except MTV-42 values. MRI parameters were different for diameter%, SV% and PSI%. Higher AUC values were obtained for SV% (0.83), Per2V% (0.826), MTV (% 0.79), TLG% (0.785), and TTLG % (0.828). Optimal cut-off values (sens, spec.and acc.) values were -65% for SV% (80%, 73%, 75%), -67.6% for Per2V% (87%, 78%, 80.7%), -73% for MTV% (78%, 86%, 84%), -88% for TLG% (78%, 81%, 80%), and -88% for TTLG (78%, 86%, 84%), respectively. CONCLUSION: Semi-quantitavite parameters for 18 FDG PET/CT and volumetric changes obtained with dCE-MRI can predict response to NAC. Percentage changes in MTV, TLG and Per2V can identify nonresponding patients better than other parameters.

OP594

Treatment response evaluation by 18F-FLT positron emission tomography/ computed tomography after neoadjuvant chemotherapy in patients with locally advanced breast cancer

B. R. Mittal, J. Shukla, G. Singh, A. Bal, D. Kumar, M. Kumar, R. Vatsa, P. Bhusari, N. Rana, N. Khandelwal; Postgraduate Institute of Medical Education & Research, CHANDIGARH, INDIA.

OBJECTIVE: Breast cancer is a common cancer in women. 18F-fluorothymidine (FLT) is tracer for proliferation imaging. The aim of this prospective study was to assess the role of 18F-FLT PET/CT in early changes in SUVmax to NACT response and to correlate with final clinical and pathological response to NACT. Methods: 18F-FLT was synthesized and quality control was performed. 44 patients (mean age 47.5±8.54 years) of LABC were enrolled. Patients received 4 cycles of anthracycline based chemotherapy at 3 weeks interval followed by a Taxane based therapy for next 4 cycles at 3 weeks interval. 18FLT PET/CT scans were performed before therapy and was repeated after 1st, 4th and 8th chemotherapy cycles. The receptors (ER, PR, Her2) and Ki-67 expression was studied on biopsy or surgical samples after each PET/CT scan. The SUVmax of 18 patients was calculated. The correlation between 18FLT PET/CT at various time points and post therapy response was studied. Results: Of the 44 patients, only 19 patients completed NACT. Out of 19, 3 were triple negative (ER/PR/Her2), 3 with ER/PR with Her2, rest were ER/PR. The surgery was performed for 17 patients, one patient was not operated due to uncontrolled diabetes and one opted to withdraw. Out of 17 patients, 6 patients showed complete, 6 partial, 2 no response and 3 showed progression of disease on 18FLT PET/CT after end of therapy. No correlation was found with receptor expression. These results were well correlated with pathological assessment. After Ist chemocycle SUVmax in 4 patients increased. Two of the 4 showed complete response, one partial (56%) and one showed disease progression. 18F-FLT PET/CT after completion of Antracyclin therapy (4 cycles) showed complete response in 3 patients, partial in

13 patients and minimal in 2 patients (3%, 7%). However FLT scan done at the completion of Taxane therapy, showed disease progression in 2 patients, decreased response from previous therapy in 4 patients (3% to(-22%); 90 to70%, 40 to30%, 20 to(-40%), improved response in 5 (1-56%, 3-22%, 19-77%, 7-52%, 28-55%), no change was seen in 2 patients, 5 patients showed complete response on PET/CT. 4 out of 5 could be correlated with pathological response. The initial data demonstrate i) there is no correlation between type of receptor expression and outcome of therapy; ii)18F-FLT PET/CT after Ist cycle of chemotherapy does not predict response; iii)18F-FLT PET/CT after 4th cycle plays an important role in assessing the responders and non-responders.

OP595

Prognostic value of maximum standardized uptake value measured on F-18 FDG PET/CT in patients with recurrent epithelial ovarian cancer.

X. Palard; University Hospital of Brest, Brest, FRANCE.

OBJECTIVE: This study aimed to evaluate the prognostic value of maximum standardized uptake value (SUV max) measured on F-18 FDG PET/CT (FDG PET/CT) at the time of relapse in patients with epithelial ovarian cancer (EOC). METHODS: 41 consecutive relapsed EOC patients were retrospectively analysed from April 2006 to April 2014. SUV max was measured on FDG PET/CT at the time of relapse. Post-relapse overall survival (PRS) was calculated from the date of FDG PET/CT to the date of death or last follow-up. ROC analysis was used to test the statistical significance of the differences among patient characteristics. Univariate and multivariate analysis for PRS were performed using Cox proportional hazards regression model. RESULTS: Median follow-up was 20.4 months. 19 patients died during the follow-up period (median: 15.5 months). ROC analysis revealed that SUVmax > 11.7 yielded the best prediction of death (AUC = 0.761). On univariate analysis, SUVmax > 11.7, non serous carcinoma, positive macroscopic residual tumor after initial surgery, time of relapse after initial surgery < 24 months and treatment of recurrence with chemotherapy alone were all significantly associated with PRS. On multivariate analysis, SUVmax > 11.7 (HR, 7.059; 95% CI, 1.620 - 30.764; p=.009), non serous carcinoma (HR, 3.892; 95% CI, 1.377 - 11.003; p=.010) and time of relapse after initial surgery < 24 months (HR, 5.180; 95% CI, 1.280 - 20.964; p=.021) were independently and significantly prognostic factors for PRS. Patients with SUVmax > 11.7 showed significantly longer duration of PRS than patients with SUVmax ≤ 11.7 (Log rank test, χ^2 = 9, p=0.002). CONCLUSION: Our results suggest that SUV max measured on FDG PET/CT at the time of the relapse was found to be an independent predictive value for PRS in patients with recurrent epithelial ovarian cancer.

OP596

Impact of the FDG PET/CT in the primary staging of locally advanced Cervical Squamous Cell Carcinoma (CSCC).

A. Alessi[1], A. Lorenzoni[1], D. Lorusso[2], A. Cerrotta[3], V. Chiappa[2], B. Pappalardi[3], B. Padovano[1], G. Serafini[1], F. Raspagliesi[2], F. Crippa[1]; [1]Nuclear medicine PET Unit Fondazione IRCSS Istituto Nazionale Tumori, Milano, ITALY, [2]Gynecologic Oncology Unit - Fondazione IRCSS Istituto Nazionale Tumori, Milano, ITALY, [3]Radiotherapy Unit - Fondazione IRCSS Istituto Nazionale Tumori, Milano, ITALY.

Locally advanced Cervical Squamous Cell Carcinoma (CSCC) has a higher rate of recurrence and worse survival than early stage CSCC. Predictors of disease recurrence include stage and lymph node status at the time of initial diagnosis. Accurate staging is important both for selecting appropriate therapy and for prognosis. Aim The objective of this retrospective study was to evaluate the impact of FDG PET/CT in the pretreatment imaging work-up of patients with locally advanced CSCC and management change in treatment intend or radiotherapy planning. Materials and methods 35 patients with newly diagnosed locally advanced CSCC (FIGO stage IB2 to IVA) were included in the study. Each patient has been evaluated with pre-therapeutic FDG PET/CT and pelvic MRI. Patients were treated with concomitant chemoradiation and brachytherapy and/or adjuvant chemotherapy or radical surgery depending on staging results. The para-aortic region was included in RT planning in case of FDG PET evidence of disease in para-aortic lymph nodes. FDG PET findings were compared to those obtained with MRI, histopathological results or other imaging modalities in case of extra-pelvic evidence of disease on FDG PET. Results FDG PET-CT and MRI findings were concordant in 69% of patients (24/35 pts). In 20 patients FDG-PET identified only primary tumor with no evidence on lymph node involvement and in 4 patients also hypermetabolic pelvic lymph node were shown, according to MRI. In the remaining 11 patients (31%) FDG PET-CT identified extra-pelvic disease. In 5 out of 11 patients FDG PET-CT revealed retroperitoneal para-aortic (3/5) and mediastinal lymph node involvement (2/5). In 6/11 patients FDG PET-CT detected distant metastatic disease (hepatic, pulmonary, peritoneal and/or bone disease). FDG PET-CT had major clinical impact in 31% of the cases (11/35): in 3 patients with para-aortic node involvement radiotherapy field was extended and in the remaining 8 patients with metastatic disease treatment intend changed to palliative therapy instead of radically

curative. Conclusion Our results showed that FDG PET-CT has an important impact on the primary staging of locally advanced CSCC leading to a substantial changes in treatment planning in 31% of patients.

OP597

Determinants of sentinel node localization failure in gynaecological cancers: a retrospective cohort study.

E. Odouard[1], A. Tescaru[1], F. Giammarile[1], C. Bournaud[1], **S. Lancelot**[1,2]; [1]Hôpitaux de Lyon, Lyon, FRANCE, [2]Lyon Neuroscience Research Center, Université Claude Bernard Lyon 1, INSERM,CNRS, Lyon, FRANCE.

Aim: Sentinel lymph node (SLN) examination is a standard of care for patients with breast cancer and melanoma. The lack of consensus does not permit standardization of the technique in endometrial or cervical cancer. This retrospective study assessed the determinants of SLN detection failure in gynaecological indications.Material and methods:We reviewed all patients who underwent preoperative lymphoscintigraphy and peroperative SLN (Patent Blue injection followed by lymphadenectomy and SLN mapping) localization for early cervical or endometrial cancer in our center (from 2005 to 2015). SLNs were ultra-staged on final pathology.We evaluated the impact of various factors on the SLN localization : the radiopharmaceutical used ([99mTc]rhenium sulfide nanocolloid, Nanocis® or [99mTc]albumin nanocolloid, Nanocoll®), the preoperative imaging modality (planar lymphoscintigraphy or SPECT-CT), and the delay between the radiopharmaceutical injection and the peroperative SLN localization (short in one-day or long in two-day protocol).We defined SLN detection as an examination where at least one sentinel node was identified in both sides.Results: One hundred and nineteen patients with cervical cancer were included. SLNs were detected in both sides in 78 patients (65.5%) in preoperative lymphoscintigraphy, and 80 patients (67.2%) in the operating room. The SLN detection reached 83.5% (66/79) with [99mTc]rhenium sulfide nanocolloid, versus 58.3% (14/24) with [99mTc]albumin nanocolloid (p=0.009).Fifty-seven patients with endometrial cancer were included.SLNs were detected in both sides in 25 patients (44%) in preoperative lymphoscintigraphy, and 27 patients (54%) in the operating room. The SLN detection reached 57.5% (23/40) with [99mTc]rhenium sulfide nanocolloid, versus 37.5% (3/8) with [99mTc]albumin nanocolloid (not significant).For both indications, no significant differences were observed between one-day-protocol and two-day-protocol for SLN detection. The SLN detection was higher with SPECT-CT imaging compared to planar lymphoscintigraphy (not significant).Conclusion:To our knowledge, this is the first time that the role of the radiopharmaceutical and the delay of the procedure were studied. This study revealed that the radiopharmaceutical choice could be a factor influencing the success of SLN localization in cervical cancer. The SLN procedure should be performed with the [99mTc]rhenium sulfide nanocolloid in the cervical cancer.As described in the literature, preoperative SLN imaging with SPECT-CT should result in a superior overall SLN detection when compared to planar lymphoscintigraphy. These results must be confirmed by further studies.

1610 - Wednesday, October 14, 2015, 10:00 AM - 11:30 AM, Hall D

Clinical Oncology: Brain, Head & Neck

OP598

Diagnostic and prognostic value of 18F-DOPA PET and 1H-MR Spectroscopy in pediatric supratentorial infiltrative gliomas: a comparative study.

M. Massollo[1], **A. Piccardo**[1], G. Morana[2], M. Puntoni[3], C. Milanaccio[4], M. Garrè[4], A. Rossi[2], M. Cabria[1], A. Raso[5], I. Bossert[1], M. Cabria[1]; [1]Nuclear Medicine Unit E.O. Galliera Hospital, Genoa, ITALY, [2]Neuroradiology Unit, Istituto G. Gaslini, Genova, Italy, Genoa, ITALY, [3]Clinican Trial Unit, Scientific Directorate, Ospedali Galliera, Genova, Genoa, ITALY, [4]Neuro-oncology Unit, Istituto G. Gaslini, Genova, Italy, Genoa, ITALY, [5]Neurosurgery Unit, Istituto G. Gaslini, Genova, Italy, Genoa, ITALY.

AIM: 1H-MR Spectroscopy (MRS) and 18F-dihydroxyphenylalanine (DOPA) PET are noninvasive imaging techniques able to assess metabolic features of brain tumors. The aim of this study was to analyze metabolic information obtained by 18F-DOPA PET and 1H-MRS in a population of children with supratentorial infiltrative gliomas or non-neoplastic brain lesions initially suspected to be gliomas on conventional MRI. Specifically, we aimed (1) to compare sensitivity, specificity and accuracy of 1H-MRS and 18F-DOPA PET in distinguishing brain gliomas from non-neoplastic lesions, (2) to assess the ability of 1H-MRS and 18F-DOPA PET in discriminating low-grade from high-grade gliomas, and (3) to evaluate the relationship between these different metabolic biomarkers and patient's outcome in terms of progression-free survival (PFS) and overall survival (OS). MATERIALS AND METHODS: We retrospectively analyzed 27 pediatric patients with supratentorial infiltrative brain lesions on conventional MRI (21 gliomas and 6 non-neoplastic lesions) who underwent 18F-DOPA PET and 1H-MRS within 2 weeks of each other. 1H-MRS data (Choline/Nacetylaspartate, Choline/Creatine ratios, and presence of lactate) and 18F-DOPA uptake parameters (Lesion/Normal tissue and Lesion/Striatum ratios) were compared and correlated

with histology, WHO tumor grade, and patient's outcome. RESULTS: 1H-MRS and 18F-DOPA PET data were positively correlated. Sensitivity, specificity, and accuracy in distinguishing gliomas from non-neoplastic lesions were 95%, 83%, and 93% for 1H-MRS and 76%, 83%, and 78% for 18F-DOPA PET, respectively. No statistically significant differences were found between the two techniques ($p>0.05$). Significant differences regarding 18F-DOPA uptake and 1H-MRS ratios were found between low- and high-grade gliomas ($p\leq0.001$ and $p\leq0.04$, respectively). On multivariate analysis, 18F-DOPA uptake independently correlated with progression free survival ($p\leq0.05$) and overall survival ($p=0.04$), whereas 1H-MRS did not show significant association with outcome. CONCLUSION: 1H-MRS and 18F-DOPA PET provide useful complementary information for evaluating pediatric brain lesion metabolism. In view of its better availability, lower costs, and lack of radiation exposure, 1H-MRS represents the method of first choice in differentiating brain gliomas from non-neoplastic lesions. 18F-DOPA uptake better discriminates between low- and high-grade gliomas, and is an independent predictor of PFS and OS.

OP599

[18F]-fluciclovine (FACBC) PET/CT as a Supplement to MRI in Patients with Suspected Recurrent Gliomas

A. Londalen, T. Bach-Gansmo, C. Saxhaug, P. Brandal, T. V. Bogsrud; Oslo University Hospital, Oslo, NORWAY.

Aim: Early detection of recurrence or residual disease after treatment of gliomas with advanced oncological imaging techniques can positively influence the course of disease and overall survival. Post-therapeutic tissue changes which mimics tumor recurrence (pseudoprogression) and radiation necrosis are common problems. MRI has limited ability to differentiate pseudoprogression and radiation necrosis from tumor recurrence. Preliminary clinical studies demonstrated high tumor specific accumulation of the synthetic leucine analog, trans-1-amino-3-[18F]fluoro-cyclobutyl-carboxylic acid (fluciclovine, often called FACBC) in small numbers of glioblastomas. The aim of this study is to evaluate fluciclovine PET/CT as a supplement to MRI to help differentiate tumor recurrence from pseudoprogression and/or radiation necrosis. Methods: Ten consecutive patients previously treated for gliomas with suspected tumor recurrence were included in this study (4 females and 6 males) with a median age of 55 years (range 41-63 years). All patients signed a written informed consent form. Tumor diagnoses consisted of grade II in three, grade III in one and grade IV gliomas in six patients initially. The patients first underwent MRI (structural and functional imaging sequences), which were performed as part of the clinical routine; and then they underwent fluciclovine PET/CT because of suspected tumor recurrence or pseudoprogression/radiation necrosis. Tumor to background ratios (TBR) were calculated. Eight of these patients went through surgery because of suspected tumor recurrence and histological results were obtained. Results: In eight of the ten patients who underwent surgery, recurrent glioma was confirmed by histopathology. Fluciclovine PET/CT had high tracer uptake in all 8 patients preoperatively (TBRs 4,7-45 median 14,3). MRI was not conclusive in four of them and suspected tumor recurrences were noted in the other four. Two patients were followed-up. MRI showed possibly radiation necrosis in one (TBR 14,2 on PET/CT) and possible recurrence in the other (TBR=2.8 on PET/CT). Both showed clinical signs of progression, and they died 40 days and 6 months after the fluciclovine PET/CT, respectively. Conclusion: In our study fluciclovine PET/CT showed high TBRs in histopathologically confirmed tumor recurrences of gliomas. Our results indicate that fluciclovine PET/CT might be used as a supplement to MRI to differentiate tumor recurrence from treatment induced changes.

OP600

PET/MR versus PET/CT in the Initial Staging of Head and Neck Cancer

T. Sekine[1,2], F. Barbosa[1], F. Kuhn[1], I. Burger[1], G. von Schulthess[1], P. Veit-Haibach[1], M. Huellner[1]; [1]University Hospital Zurich, Zurich, SWITZERLAND, [2]Nippon Medical School, Tokyo, JAPAN.

Purpose: To compare the diagnostic accuracy of PET/MR with PET/CT for newly diagnosed head and neck cancer. Materials and Methods: This prospective study was approved by the institutional review board and by national government authorities. In this study, sequential contrast-enhanced PET/CT-MR was performed in 27 patients (median age 66, 16 males) with newly diagnosed head and neck cancer. MR sequences were: LAVA-Flex (whole body); axial T2-weighted, axial T1-weighted with and without contrast, sagittal and coronal T1-weighted with contrast, and DWI (head and neck). PET/CT and PET/MR were evaluated separately, and the TNM stage and factors that could impact on the potential resectability were assessed. Wilcoxon signed-ranks test was used. Results: The T/N/M staging by PET/CT was correct in 17 patients (63.0%) / 19 (70.4%) / 22 (81.5%), equivocal in 8 patient (29.6%) / 3 (11.1%) / 3 (11.1%), and incorrect in 2 patients (7.4%) / 5 (18.5%) / 2 (7.4%). The T/N/M staging by PET/MR was correct in 20 patients (74.1%) / 21 (77.8%) / 26 (96.3%), equivocal in 6 patients (22.2%) / 2 (7.4%) / 1 (3.7%), and incorrect in 1 patient (3.7%) / 4 (14.8%) / 0 (0%). Consistently, the TNM staging by PET/MR was comparable to PET/CT (T: $p = 0.331$, N: $p = 0.453$, M: $p = 0.034$). The sensitivity/specificity/accuracy of resectability-defining factors by PET/CT

and PET/MR were 0.68/0.93/0.97, and 0.80/1.00/0.99, respectively. Conclusion: Whole-body staging with PET/MR yields at least equal diagnostic accuracy as PET/CT in determining the stage of head and neck cancer.

OP601

11C-methionine PET-CT for contouring and response evaluation of Head and Neck Adenocystic Carcinoma treated with CIRT (Carbon Ion Radiation Therapy)

L. Olivari[1], M. Bonora[2], M. Rodari[3], M. Fiore[2], V. Vitolo[2], E. Lopci[3], F. Valvo[2], P. Fossati[2], R. Orecchia[1], A. Chiti[4]; [1]University of Milan, Milano, ITALY, [2]Division of Radiation Oncology and Radiobiology, National Center for Oncological Adrontherapy (CNAO) Foundation, Pavia, ITALY, [3]Department of Nuclear Medicine, Humanitas Research Hospital, Milano, ITALY, [4]Humanitas University, Milano, ITALY.

INTRODUCTION: Adenocystic carcinoma (ACC) is a rare radio resistant head and neck cancer that usually locates close to critical structures. CIRT, which shows some advantages to treat radio resistant tumours, needs precise target definition. Previous studies reported that 11C-methionine PET-CT (MET) could be an effective alternative to FDG, due to its low uptake in normal brain and in inflammatory tissue. METHODS: In this prospective study, 47 patients affected by ACC and treated with CIRT were investigated with MET. Pre-treatment MET, registered and fused with simulation CT, was employed as a visual aid in target contouring. MR images (T2 weighted, T1 weighted and contrast enhanced T1 weighted) were also used. Volumes with MET uptake comparable with parotid glands were included in the Clinical Target Volume (CTV); asymmetric findings with an uptake value between parotid and brain were also included, but treated with a lower dose. Pre-treatment MET failed to show abnormal uptake in 7 patients (15%). In patients with elevated initial uptake, a post treatment MET was performed one month after completion of CIRT. Semi-quantitative tumour to normal brain ratio (T/B) and volumetric change in MET uptake were evaluated in both MET exams. Dimensional response was investigated with MR every 3 months since the end of CIRT.The minimal follow up period was 5 months (range 5-22). RESULTS: Forty patients with ACC performed pre and post treatment MET. Sixteen patients had previous history of ACC (recurrent disease) while 26 had a newly diagnosed ACC. Twenty-three patient underwent surgery before CIRT. CIRT was well tolerated and none of the patient had G3-G4 toxicity three months after treatment. T/B ratio showed a mean reduction of 55% (range -100% to + 14.6%) and MET volumetric change showed a mean reduction of 72.9% (range -100% to +172%). Fifteen patients had MET complete response after CIRT, confirmed at follow-up. MET after CIRT detected progressive disease in 9/10 patients. One patient had a negative MET while MR was inconclusive. Disease was detectable six months after the end of CIRT. Fifteen patients had partial response on both MET and MR, with stable disease at follow-up. CONCLUSIONS: When used together with MR, MET demonstrated to be useful in target delineation and early response evaluation of patients affected by ACC treated with CIRT. T/B ratio and tumour volumetric changes assessed with MET, are able to increase the diagnostic accuracy of the pure qualitative image evaluation.

OP602

Value of FDG volumetric imaging parameters before radiotherapy treatment in inoperable Head and Neck cancer (HNC)

L. Olivari[1], E. Lopci[2], A. Poletti[3], R. Cavina[4], C. Arturo[5]; [1]University of Milan, Milano, ITALY, [2]Department of Nuclear Medicine, Humanitas Research Hospital, Milano, ITALY, [3]Department of Otorhinolaryngology, Humanitas Research Hospital, Milano, ITALY, [4]Department of Oncology, Humanitas Research Hospital, Milano, ITALY, [5]Humanitas University, Rozzano, Milano, ITALY.

INTRODUCTION: Inoperable head and neck cancer (HNC) are treated with concurrent chemo-radiotherapy (CCRT) alone or associated with induction chemotherapy: docetaxel, cisplatin, 5-fluorouracil (DCF). The aim of this study was to evaluate whether metabolic tumour volume (MTV) and total lesion glycolysis (TLG) of the primary tumour and nodes before CCRT and DCF-CCRT can predict outcome for patients with inoperable HNC.METHODS AND MATERIALS: Sixty-three consecutive patients with biopsy-proven, newly diagnosed, non operable HNC were included in this retrospective study. None of these patients had history of radiation therapy in head and neck district. All patients underwent FDG PET-CT before radiotherapy. An automatic algorithm, based on adaptive thresholding, delineated primary tumour and nodes. With this technique we calculated: MTV, TLG, SUVmax, SUVmean. The primary endpoint was

progression free survival (PFS). Univariate Cox regression models and Kaplan Meir with respect to PFS were performed.RESULTS: The cohort consisted of 19 female, 44 male; mean age 62,2±12.8 years. The distribution of patients by the AJCC stage of the cancers included stages I (n=3), II (n=9), III (n=15), IVa (n=34), IVb (n=1) IVc (n=1). Histology was: squamous cell carcinoma (n=49), undifferentiated carcinoma (n=12), adenocarcinoma (n=2). Tumour localization was: rhinopharynx (n=19) oropharynx (n=28), hypopharynx (n=8) and larynx (n=8). The mean follow-up was 23 months (range, 5-52 months). Six patients performed follow up in other centres. Two patients died during follow up of unrelated cancer disease. Progressive disease (PD) was demonstrated in 13 patients after a mean interval of 12.7 months (range, 7-33 months). PD occurred mainly in advanced cancer (stage IV at the diagnosis: n=8) and the primary tumour localization was mainly rhinopharynx (n=7). Cox regression demonstrated that MTV of the primary tumour value is a significant predictor with respect to PFS ($p<0.05$). Kaplan Meier analysis showed that MTV of the primary tumour less than 4.3 indicates good median PFS ($p<0.05$) with a sensitivity and specificity of 82% and 70% respectively. No correlation was found between PFS and MTV of lymph nodes. No correlation was found between PFS and SUVmax, SUVmean and TLG of the primary tumour and of the lymph nodes.CONCLUSION: In this patient population, MTV provided information of disease burden and tumour metabolic activity. High baseline primary tumour MTV (pre CCRT) was associated with worst outcomes in patients with inoperable HNC. Pre-radiotherapy MTV of primary tumours provides independent prognostic information and the threshold of 4.3 seems to predict PFS in inoperable HNC.

OP603

Predictive role of FDG-PET/CT in patients with locally advanced oropharyngeal cancer undergoing tomotherapy with dose escalation

E. Incerti[1], I. Dell'Oca[2], M. Kirienko[3], C. Fiorino[4], P. Alongi[3], S. Broggi[4], P. Mapelli[1], N. Di Muzio[2], L. Gianolli[1], M. Picchio[1]; [1]Nuclear Medicine Department, IRCCS San Raffaele Scientific Institute, Milan, ITALY, [2]Radiotherapy Department, IRCCS San Raffaele Scientific Institute, Milan, ITALY, [3]University of Milano-Bicocca, Milan, ITALY, [4]Medical Physics Department, IRCCS San Raffaele Scientific Institute, Milan, ITALY.

Aim: To evaluate the clinical outcome in patients affected by locally advanced oropharyngeal cancer undergoing intensity modulated radiation therapy, by means of helical tomotherapy (HTT), with dose escalation to FDG-PET/CT positive tumor volumes using the simultaneous integrated boost (SIB). Materials and Methods: We analyzed 38 patients studied by FDG-PET/CT and treated between 2005 and 2013 for squamocellular oropharyngeal stage III-IVB disease in our Institution. HTT was delivered with the SIB technique (HTT-SIB) in 30 fractions at different dose levels concomitantly: 69 Gy (2.3 Gy/day) to the gross tumor volume PET-positive (GTV-PET) for lymph nodes (LN) and primary tumor (T), 66 Gy (2.2 Gy/day) to the clinical target volume (CTV) for LN and T, 54 Gy (1.8 Gy/day) to the clinical negative neck region. Thirty-one patients received concurrent chemotherapy (cisplatin 75-100 mg/m^2/21 days for 23 patients, cisplatin 30-40 mg/m^2/week for 6 patients and cetuximab for 2 patients). The 2.5-year overall cancer specific (OS), local tumor disease-free (LTDFS), local node disease-free (LNDFS) and distant metastasis-free (DMFS) survivals were calculated. Correlations between PET volumetric parameters and 2.5-year OS, LTDFS, LNDFS and DMFS were assessed. The PET/CT metabolic parameters of T include GTV-T-PET, metabolic tumor volume (MTV-T), MTV thresholds 40%-50%-60% (MTV-T-40, MTV-T-50, MTV-T-60) and mean standardized uptake value (SUVmean). Results: The median follow-up was 28 months (range: 3-109 months). All patients completed the treatment as scheduled. The 2.5-year OS, LTDFS, LNDFS and DMFS were 88%, 83%, 88% and 77%, respectively. Multivariate Cox regression analyses revealed that GTV-PET and GTV-T-PET are predictors for OS with a best-cut-off value equal to 30.9 cc ($p=0.022$) and 22.4 cc ($p=0.029$) respectively; while MTV-T-40, MTV-T-60 and SUVmean are predictors for OS with a best-cut-off value equal to 21.3 ($p<0.0001$), 13.3 ($p<0.0001$) and 9.2 ($p=0.01$), respectively. Temporary treatment interruption due to acute toxicity, mainly mucosae, was observed in 8 patients. Conclusions: The use of HTT-SIB with dose escalation to FDG-PET/CT positive tumor volumes, even with concurrent chemotherapy, allows very promising 2.5-year disease control rates in patients affected by locally advanced squamocellular oropharyngeal cancer. Moreover PET/CT metabolic volumetric parameters have a predictive value for the survival outcomes, thus FDG-PET/CT may represent the basis for more personalized treatments.

OP604

Diagnostic accuracy of F18-FDG-PET/CT for the detection of perineural spread in head and neck cancer

L. Dercle, S. Ammari, L. Rozenblum, D. Deandreis, M. Terroir, M. Schlumberger, F. Bidault; GUSTAVE ROUSSY, Villejuif, FRANCE.

Background: Head and neck cancer (HNC) spread locoregionally by direct extension, lymphatic dissemination, and neurovascular spread. The accuracy of FDG-PET/CT for the diagnosis of perineural spread (PNS) remains to be determined because it could improve risk stratification, staging, treatment planning, and follow-up. Two limiting factors exist: the limited resolution of PET (partial volume effect) and the physiological FDG-uptake of the nearby brain. This report evaluates the accuracy of FDG-PET/CT and describes clinical, morphological (CT-scan), and metabolic patterns (18F-FDG-PET) attributed to neoplastic involvement along the cranial nerves (CN).Methods: Twenty-five patients were retrospectively included. MRI was used as the reference-standard. Thirty-two PNS were diagnosed. PNS was proved histologically (surgery) or suspected according to a typical evolution on long term follow-up (443±492 days). Quantitative results are expressed as mean ± SD.Results: The sensitivity of FDG-PET/CT for the detection of PNS was 88%. Two false negatives were noted and explained by a low FDG-uptake of the primary tumor due to 1/ the histological subtype, 2/ an excellent response to radiochemotherapy.They are 5 morphological and metabolic patterns observed in PNS: 1/ A typical topography of the lesion along CN: CNV1 (8%), CNV2 (50%), CNV3 (54%), and CNVII (8%). 2/ A significant enlargement along the CN (PNS: 9±5 mm, doubling size of the nerve: Se84%, ratio $CN_{abnormal/normal}$: 4.3±3.1 which is above PET-resolution and is measurable on CT-scan). 3/ An asymmetrical increased FDG-uptake (Se88%; significantly different from the physiological brain uptake; $SUVmax_{PNS:}$ 20±11; $SUVmax_{brain:}$ 17±5). 4/ An Heterogeneity Index of the SUV of the CN similar to the tumor and significantly increased in comparison with the physiological brain uptake ($HISUV_{tumor:}$ 1.5±0.2, $HISUV_{PNS:}$ 1.5±0.1, $HISUV_{brain:}$ 1.2±0.1, $HISUV_{PNS/primary:}$ 1.0±0.1, $HISUV_{PNS/brain:}$ 1.3±0.1); 5/ An enlargement of the foramina in the base of skull (doubling size of the foramen: Se64%, ratio $foramen_{abnormal/normal}$: 2.6±1.6).Conclusions: FDG-PET/CT is accurate for the detection of PNS. The diagnostic accuracy of five direct and indirect signs of PNS on FDG-PET/CT was described.

OP605

Head and neck cancer: can 18F-FDG PET/CT staging scan improve the predictive value of post-treatment 18F-FDG PET/CT assesment

I. Sandler[1], G. M. Lima[1], P. Castellucci[1], U. Caliceti[2], S. Cammelli[3], V. Allegri[1], A. Morganti[3], S. Fanti[1]; [1]Università di Bologna, Nuclear Medicine Unit, S.Orsola-Malpighi Hospital, Bologna, ITALY, [2]Università di Bologna, Head and Neck Unit , S. Orsola-Malpighi Hospital, Bologna, ITALY, [3]Università di Bologna, Radiotherapy Unit, S. Orsola-Malpighi Hospital, Bologna, ITALY.

Aims: The purpose of this retrospective study is to evaluate whether a staging or pre-treatment 18F-FDG PET/CT scan may improve the predictive value of 18F-FDG PET/CT in treatment response assessment after primary radio-chemotherapy (RT-CT) for loco-regional advanced Head and Neck squamous cell carcinoma (HNSCC). Methods: We enrolled 138 patients with a diagnosis of advanced HNSCC (96 males and 42 females, mean age 58 yo) who performed a 18F-FDG PET/CT between 2006-2013. Disease sites were oral cavity (10%), nasopharynx (14%), oropharynx (53%), hypopharynx (7%), larynx (7%), salivary glands (5%) and paranasal sinuses (4%). All patients have been treated with primary RT-CT. All patients underwent a 18F-FDG PET/CT to assess treatment response, preformed from 6 to 36 weeks (60% between 10-15 weeks) after the end of RT-CT. In 84 patients (60%) a 18F-FDG PET/CT staging or pre-treatment scan have been also performed (group A) while for the remaining 54 patients (40%) a staging 18F-FDG PET/CT was not available (group B). There were no significant differences in terms of risk stratifications between the two groups. 18F-FDG PET/CT scans were performed according to standard procedure and were visually analyzed by two expert physicians and categorized as negative or positive for residual disease. Patients were followed-up, based on clinic and radiological and/or histological findings, up to 60 months and for at least 12 months after end of therapy (median 38 months). At the end of follow-up, 18F-FDG PET/CT results were classified as true positive (TP), true negative (TN), false positive (FP) and false negative (FN). Results: - Group A (84 patients) showed: 30 TP (36%), 46 TN (54%), 3 FP (4%) and 5 FN (6%). Therefore 18F-FDG PET/CT sensitivity 86%, specificity 94%, PPV 91%, NPV 90%, accuracy 0.9. - Group B (54 patients) showed: 11 TP (20%), 38 TN (70%), 1 FP (3%) and 4 FN (7%). Therefore 18F-FDG PET/CT sensitivity 73%, specificity 97%, PPV 91%, NPV 90%, accuracy 0.9. Conclusions: According to our data, 18F-FDG PET/CT scan in staging of HNSCC does not improve significantly the Positive and Negative predictive values of post-treatment PET/CT. These results should be confirmed by larger studies.

1701 - Wednesday, October 14, 2015, 10:00 AM - 11:30 AM, Hall 1

CME 14 - Drug Development & Translational Molecular Imaging: Multimodal Imaging Agents

OP606

Exploiting Multimodal Imaging Probes for Sentinel Lymph Node Imaging in Breast Cancer/Melanoma

R.T.M. de Rosales, UK

OP607

Quantitation and Qualities: Data and Images from Multimodal Read-Outs for Preclinical Discoveries

D. Mathe, HUNGARY

OP608

Multimodality Clinical PET/MR Imaging

M. Eiber, GERMANY

1705 - Wednesday, October 14, 2015, 10:00 AM - 11:30 AM, Hall G2

Do.MoRe: Miscellaneous

OP609

3D patient absorbed dose estimation of monoclonal antibody targeting synovial sarcoma

D. Sarrut, J. Badel, A. Halty, D. Kryza, A. Giraudet; CREATIS / LUMEN, Lyon, FRANCE.

Aims: Frizzled homologue 10 (FZD10) is transmembrane receptor overexpressed in synovial sarcoma (SS). We investigated the patient absorbed dose distribution of OTSA101-DTPA-90Yttrium, a radiolabeled monoclonal antibody (mAb) targeting FZD10 developed by Oncology Therapy Science, in relapsing metastatic SS patients included in a first-in-man phase I clinical trial based on a theranostic procedure.Materials and Method: Biodistribution was analysed in 20 patients on SPECT-CT acquisitions repeated at 1, 5, 24, 48, 72 and 144 h post-injection of 185 MBq/1.5 mg OTSA101-111Indium. In case of significant tumors uptake, greater than mediastinum, and favourable biodistribution, patient was treated with OTSA101-90Y. Retrospectively, volume of interest (VOI) were drawn on H1 CT in various lesions, mainly lung metastases, and normal tissues (liver, kidneys, heart, bone marrow, spleen). Deformable image registration was performed between all CT time-points and used to warp all SPECT time-points onto the same coordinate system allowing pixel-by-pixel time-activity-curves (TAC) analysis. Time-integrated activities were computed from mono-exponential fit of TAC in all pixels and used to compute the 3D estimated absorbed doses of OTSA101-90Y with Monte-Carlo simulation (GATE) at a pixel level.Results: Tumor tracer uptake appeared to be highly heterogeneous on an inter-patient, as well as an intra-patient and inter-lesions based analysis independently of tumor size. Estimated doses to the 95 lesions ranged from [0.01;0.82] cGy by injected MBq (median 0.22). Uptake intensity was considered to be greater than mediastinum in half of the patients, observed as soon as H1 for 2 patients or only at H144 for 2. There was a trend for mAb accumulation in the tumors signing specific mAb tumor uptake. Time-integrated activities appeared to be the highest in the liver with a total estimated dose ranging from [0.34;1.19] cGy/MBq (median: 0.78) ; bone marrow and kidney estimated dose ranged from [0.02;0.19] and [0.06;0.32] cGy/MBq. Conclusion: We confirm FZD-10 antigen expression in SS metastases. OTSA101 lesions uptake is heterogeneous and appeared sufficient for radionuclide therapy for half of the patients. However, estimated dose could not reflect real received dose because of potential difference between OTSA101-111In and OTSA101-90Y. A comprehensive patient-specific absorbed dose estimation combining SPECT-CT acquisitions at several time-points, deformable registration and pixel-based 3D Monte-Carlo computation has been proposed and applied in clinical context.

OP610

Implementation and validation of a collapsed cone superposition algorithm for radiopharmaceutical dosimetry of radionuclides with photon component

M. Sanchez-Garcia[1], I. Gardin[2], R. Lebtahi[1], A. Dieudonné[1]; [1]Department of Nuclear Medicine, Beaujon Hospital, Assistance Publique-Hôpitaux de Paris (APHP) & INSERM U1149, Clichy, FRANCE, [2]Department of Nuclear Medicine, Henri Becquerel Cancer Center and Rouen University Hospital, & QuantIF – LITIS [EA 4108], Rouen, FRANCE.

Objectives: A collapsed cone (CC) superposition algorithm (CCS) has been recently implemented for radiopharmaceutical absorbed dose (AD) calculation of beta emitters (Sanchez-Garcia et al. Phys Med Biol 2014). This paper presents the implementation for radionuclides with a photon component. Methods: The superposition relies on a water dose kernel (DKw) that is linearly scaled by radiological distance between source and target voxels, taking into account tissue density heterogeneities. CC provides an acceleration of the superposition by approximating the energy transport to a finite number of directions. Our CCS implementation was extended to photons and validated on 2 radionuclides used in diagnostic nuclear medicine, F-18 and Tc-99m, and another 2 used in

therapy, I-131 and Lu-177. The DKws were generated for each radionuclide with MCNP Monte Carlo simulations (MC). The validation was done against MCNP in 6 phantoms constituted of 2 concentric (radii of 4 and 8 cm) spheres representing tissue interfaces between soft-tissue, lung and bone. The absorbed dose was scored in concentric shells of 1 mm thickness for CCS and MC, leading to a plot of AD according to the radial coordinate. The metrics used for comparison were the percentage of points in the plot satisfying the γ(3%, 3 mm) and γ(5%, 5 mm) criterions, i.e. the percentage of points satisfying a tolerance of 3% (or 5%) in dose or 3 mm (or 5 mm) in distance to agreement. Results: For F-18, γ(3%, 3 mm) was 100% for all phantoms. For Tc-99m, γ(3%, 3 mm) was between 71 and 97%, except for the bone/lung interface (7%), and γ(5%, 5 mm) was over 99% except for the bone/lung phantom too (57%). For I-131, γ(3%, 3 mm) was between 99 and 100%, except for the bone/lung phantom (92%), but γ(5%, 5 mm) was 100% for all phantoms. For Lu-177, γ(3%, 3 mm) was between 89 and 100%, except again for bone/lung phantom (59%), but γ(5%, 5 mm) was over 97% for all phantoms. Calculation times were between 3.5 and 4 minutes on a 3.2 GHz Intel Core i5 machine with 4 cores. Conclusion: Our results show that the CC superposition algorithm has a good agreement with MC simulations for various tissue interfaces and common radionuclides. This study confirms that CC superposition is a reliable alternative to MC simulations in radiopharmaceutical dosimetry.

OP611

Targeted photodynamic therapy of insulinomas and congenital hyperinsulinism by Exendin-700DX

S. Ekim[1], D. Bos[1], F. Andreae[2], M. Brom[1], M. Gotthardt[1]; [1]Radboud University Medical Centre, Nijmegen, NETHERLANDS, [2]PICHEM, Graz, AUSTRIA.

Background and aims: lnsulinomas are tumors of the pancreas that are derived from beta cells. Because the tumor produces excess amounts of insulin, it can lead to hypoglycemia. Congenital hyperinsulinism is a disease that causes high levels of insulin and hypoglicemia. Exendin is a peptide which can specifically bind to the glucagon-like peptide 1 receptor (GLP-1R) which is expressed in the beta cells in the pancreas. 700DX can create free radicals and singlet oxygen that can be fatal to the cells, when it is subjected to laser irradiation. Labeling Exendin with 700DX can be a promising way to produce a new agent for laser induced photodynamic therapy (PDT) of insulinomas and congenital hyperinsulinism, aimed at selective destruction of diseased beta cells. With this therapy, it would be possible destroy diseased beta cells in a specific area of pancreas and leave a sufficient amount of beta cells to prevent diabetes. Materials and methods: Exendin-3 (Ex-3) and Exendin-700DX (Ex-700DX) were used in the experiments. The therapeutic effect was examined on islets isolated from C3H mice, rat insulinoma cells (lNS-1E) and GLP-1R expressing CHL cells. ln vitro PDT experiments, were performed by incubating islets with 165 nM Ex-700DX, 165 nM Ex-3 and medium only (control) for 3 hours at 37°C. The islets were irradiated for 30 min at 60 Watt, with a LED laser system that emits radiation in the 690nm spectral band while the control plate was not irradiated.An hour after the PDT, cell titer glo assay was performed to detect the islet death. The effect of internalization of Ex-700DX was examined using CHL-GLP1R(+) cells by incubation at 0°C (no internalization) or 37°C (internalization). Results:Nearly 60% islet death was detected after PDT, on the Ex-700DX treated group of islets. No islet death was observed with Ex-3 and vehicle incubated groups after PDT, which proves that the compound and laser irradiation itself does not cause any islet death. The percentage of cell death after PDT was calculated as 44% when Ex-700DX internalized into the cells, while 21% cell death was observed when Ex-700DX was only bound to GLP-1R on the cells. Conclusion:First trials on mice islets and GLP-1R(+) tumor cells showed that PDT with Ex-700DX efficiently destroys the target cells. For efficient PDT, Ex-700DX should be at least bound to GLP-1R and the efficiency of the therapy increases nearly 2 times when Ex-700DX is internalized into the cells.

OP612

Integration of micro- and macro-dosimetry for calculation of radiation doses to the islets of Langerhans due to radionuclide imaging with exendin

I. van der Kroon[1], W. Woliner-van der Weg[1], M. Brom[1], L. Joosten[1], C. Frielink[1], M. W. Konijnenberg[2], E. P. Visser[1], M. Gotthardt[1]; [1]Radboud University Medical Center, Nijmegen, NETHERLANDS, [2]Erasmus Medical Center, Rotterdam, NETHERLANDS.

Aim: Radiolabeled exendin, targeting the GLP-1 receptor, is used for quantification of the insulin producing beta cells located in the islets of Langerhans. High accumulation of the radiolabeled exendin in the islets has lead to concerns about radiation-induced damage to the islets. Standard methods or models to estimate the radiation-induced damage to the islets are not yet available. Commonly used macro-dosimetry methods, such as OLINDA/EXM, do not contain the islets as a separate compartment, therefore these models are not able to provide the radiation dose to single islets. Because of the high accumulation of radiolabeled exendin in islets compared to surrounding tissue, islets need to be included as a separate compartment. In our work, a model was developed to calculate

the islet radiation dose due to the use of ^{111}In-exendin (150 MBq) and ^{68}Ga-exendin (75 MBq) in patients with differences in gender, islet size, beta cell mass and kidney uptake. Materials and Methods: The model includes the radiation dose to the islets due to accumulation of the radiotracer (i) in the kidneys, (ii) in surrounding islets and exocrine tissue in the pancreas (together: remainder of the pancreas) and (iii) in the islet (islet self-dose). The contribution of the remainder of the pancreas and the kidneys to the islet radiation dose was calculated using the standard S-value based approach as implemented in OLINDA/EXM. For the islet self-dose, Monte Carlo simulations were performed for a small sphere model (diameter 50-400 μm). As input for the model both data from a clinical study (organ distribution of the tracer) and data from a preclinical study with biobreeding diabetes prone rats (endocrine-exocrine uptake ratio), was used. Results: The islet radiation dose was found to be small ranging from 49.3 to 74.3 mGy for ^{111}In-exendin and ranging from 1.61 to 2.35 mGy for ^{68}Ga-exendin. The activity in the islets contributed up to 45% to the total islet radiation dose for ^{111}In-exendin and up to 22% for ^{68}Ga-exendin. Due to the high accumulation of radiolabeled exendin in the kidneys, the kidneys have the largest contribution to the total islet radiation dose (49-81%). Conclusion: The calculated islet radiation doses suggest that even repeated exendin imaging will not harm the islets since the maximum islet radiation dose is much smaller than the one known to cause serious islet damage (10 Gy as observed with external beam radiation).

OP613

The intrinsic absorbed dose resolution concept in voxel dosimetry - Application to 90Y microsphere radioembolization

C. Chiesa, M. Mira, M. Maccauro, E. Seregni, F. Crippa; Nuclear Medicine, Foundation IRCCS Istituto Nazionale Tumori, Milan, ITALY.

Aim & background: In radioembolization dosimetry, the analysis of uncertainties is simple, since a single acquisition of a tomographic image is sufficient. Under the local deposition hypothesis, voxel absorbed dose is simply proportional to voxel counts. Image noise (σ/N) was investigated, since it is numerically the level of uncertainty on voxel absorbed dose (intrinsic absorbed dose resolution).Methods: In uniformly filled phantoms, absorbed dose in voxels should be uniform, i.e. the DDVH should be Dirac's delta. The statistical voxel fluctuation should follow a Poissonian dependence on N , $\sigma=\sqrt{N}$. The dependence of noise on the number of iterations #IT and the number of subsets #SUBS was studied on a high statistic (N=8100) 99mTc 20 cm diameter uniform cylinder (several CT attenuation corrected OS-EM SPECT reconstruction (Siemens e.soft work station) without additional postfilter). A 2000 mL plastic bottle simulating liver, filled with a typical liver concentration of 99mTc-MAA (150 MBq/1000 mL), surrounded by non radioactive water, was acquired with clinical scan duration (15 s/projection, 900 s). Its noise was studied by varying the number of updates P=#ITx#SUBS.A TOF LYSO PET scanner was used to study an 90Y bottle in air filled with 90Y-DOTATOC solution with a concentration corresponding to a 40 Gy mean dose, with scan duration of 15 min and 60 min.Results: In 99mTc SPECT, noise was dependent on the number of updates P, and independent on different combinations giving the same P. The larger contribution to noise came from reconstruction. Fixed N=2500 in the bottle simulating liver, the evaluation showed a gaussian shaped DDVH whose width (dose uncertainty) was dependent on the square root of P (R2=0.99), with remarkable voxel dose uncertainty of 5.5%, 9%, 37% for P= 4x4, 8x8, 30x30. After optimization of reconstruction (fixed P=8x8 Chiesa et al 2015), such uncertainty could be slightly reduced increasing N (higher activity or longer acquisition time). In the 90Y PET (blob reconstruction, 3 IT, 28 subsets) reconstruction and Poisson noise were comparable. The poor N=16 cannot be improved (using LYSO), since the therapeutic activity is fixed and scan duration cannot be longer than 30 min for 2 bed positions. At a simulated dose of 32 Gy, voxel dose uncertainty is 41%. This reach an acceptable value of 11% for dose larger than 1000 Gy.Conclusion: noise from statistics and reconstruction intrinsically limit the accuracy of voxel dosimetry, which is strongly penalized in 90Y-PET with LYSO.

OP615

Improved treatment planning in radioimmunotherapy with 90Y-anti-CD66 antibody using population based modelling

C. Maaß[1], P. Kletting[2], D. Hardiansyah[1], B. Mahren[3], D. Bunjes[2], A. Beer[2], G. Glatting[1]; [1]Medical Radiation Physics/ Radiation Protection, Medical Faculty Mannheim, Heidelberg University, Mannheim, GERMANY, [2]Department of Nuclear Medicine, Ulm, GERMANY, [3]Department of Nuclear Medicine, Würzburg, GERMANY.

Aim: Accurate estimation of time-integrated activity coefficients is essential for treatment planning in radioimmunotherapy (RIT). Recently it was shown that for the estimation of these coefficients, the application of physiologically based pharmacokinetic (PBPK) models is advantageous over the standard approach (sums of exponential functions) [1, 2]. However, the prediction accuracy of therapeutic biodistributions needs to be further improved. Including knowledge about the population itself, e.g. population specific Bayesian parameters, may serve this purpose. Therefore, the aims of this work were 1) to estimate population parameters and 2) to show the effect of these

parameters on prediction accuracy of therapeutic biodistributions. Materials and Methods: Population parameters were estimated two-fold, i.e. using the standard and iterated two-stage (STS, ITS) algorithms. For each algorithm, a PBPK model was fitted to pre-therapeutic (gamma camera and serum) and therapeutic (serum) measurements simultaneously. The estimated population values (STS, ITS) were implemented as Bayesian information. The model parameters of each patient were fitted to pre-therapeutic data only, therapeutic biodistributions simulated. Prediction accuracy of the therapeutic serum curve was validated comparing the simulated and fitted time-integrated activity coefficients. Results: The relative deviations RDs between pre-therapeutic and therapeutic serum time-integrated activity coefficients are (-25 ± 16) %. When using no Bayes parameters prediction accuracy was RD = (-3 ± 20) %. Using population based parameters as Bayesian information improved RD to (8 ± 16) %) and (0 ± 10) % for the STS and ITS algorithm, respectively. Conclusion: Estimation and subsequent application of population values used as Bayesian parameters for RIT using a PBPK model for 90Y labeled anti-CD66 antibodies improves prediction accuracy substantially. Literatur: 1. Maaß C and Kletting P, Reske SN, Beer A, Glatting G. Physiologically Based Pharmacokinetic Modeling is Essential in 90Y-labeled Anti-CD66 Radioimmunotherapy. PLoS ONE, accepted, 20/04/2015. 2015; 2. Kletting P, Kull T, Bunjes D, Mahren B, Luster M, Reske SN, et al. Radioimmunotherapy with Anti-CD66 Antibody: Improving the Biodistribution Using a Physiologically Based Pharmacokinetic Model. J Nucl Med. 2010;51(3):484-91. doi: 10.2967/jnumed.109.067546.

OP616

Metrology for molecular radiotherapy: what did the MetroMRT project achieve?

V. Smyth[1], C. Bobin[2], L. Johansson[1], L. Joulaeizadeh[3], M. D'Arienzo[4], M. Capogni[4], H. Rabus[5], M. Cox[1], J. Šolc[6]; [1]National Physical Laboratory, Teddington, Middlesex, UNITED KINGDOM, [2]Laboratoire National Henri Becquerel/Commissariat à l'Energie Atomique (LNE-LNHB), Gif-sur-Yvette Cedex, FRANCE, [3]VSL, Dutch Metrology Institute, Delft, NETHERLANDS, [4]National Institute of Ionizing Radiation Metrology, ENEA-INMRI, Rome, ITALY, [5]Physikalisch-Technische Bundesanstalt (PTB), Braunschweig, GERMANY, [6]Czech Metrology Institute (CMI), Prague, CZECH REPUBLIC.

The MetroMRT project was funded through the European Metrology Research Programme (EMRP http://www.emrponline.eu/). It ran from June 2012 to May 2015, and this was the first time that the measurement of radiation absorbed dose to target and normal tissues in the modality of molecular radiotherapy (MRT) had been addressed within the discipline of metrology. The problems of standardisation of procedures, traceability to primary standards, and uncertainty in dosimetry for external beam therapy was covered in the UK by the HPA [1983] and then internationally by IAEA [1987]. This positions MRT approximately 30 years behind external beam therapy in establishing dosimetry to achieve uniformity in practice from one centre to another, or one country to another, and so that absorbed dose in MRT can become a legal quantity able to be specified in regulations.The structure of the MetroMRT project was based on the links in the measurement chain required to obtain absorbed dose within a volume of interest (VOI) in a patient undergoing a typical MRT procedure:1.Measurement of the administered activity;2.Definition and delineation of the VOI (target tissue; normal tissue);3. Quantitative imaging (QI) procedure (tracer activity, full therapy activity, surrogate) to determine activity in the VOI relative to the administered activity;4.Determination of biokinetics from a time sequence of activity measurements interpolated/extrapolated to give an activity-time curve; then obtain total disintegrations within defined VOI by integrating under the curve;5.Calculation of absorbed dose within the VOI (Gy/MBq).Workpackages in the project showed that traceability can be established within links 1, 3, and 5 to primary standards of radioactivity and radiation absorbed dose. A separate workpackage investigated the uncertainty entailed in the choice of how links 2 and 4 were carried out, and showed that by adopting best practice procedures the overall uncertainty in the measurement of absorbed dose can be evaluated.The project has therefore demonstrated that it is technically feasible to formulate a dosimetry protocol for MRT and has given strong recommendations to the relevant international bodies (IAEA, ICRP) that the process should be initiated.HPA, Revised Code of Practice for the dosimetry of 2 to 25 MV X ray, and of 137Cs and 60Co gamma-ray beams, Phys. Med. Biol. 28 (1983) 1097-1104.IAEA, Absorbed Dose Determination in Photon and Electron Beams: An International Code of Practice, Technical Reports Series No. 277, Vienna (1987).

1706 - Sunday, October 11, 2015, 4:00 PM - 4:30 PM, Hall 6
M2M: Molecular & Multimodality Imaging: PET Tracers - Preclinical Studies

---

OP617

Synthesis and evaluation of Androgen Receptor radioligand [18F]enzalutamide: comparison with [18F] FDHT

I. F. Antunes[1], R. Dost[2], A. van Waarde[1], R. Dierckx[1], D. Samplonius[3], W. Helfrich[3], D. Burg[4], E. de Vries[1], I. de Jong[2]; [1]NMMI, University Medical Center of Groningen, Groningen, NETHERLANDS, [2]Department of Urology, University

Medical Center of Groningen, Groningen, NETHERLANDS, [3]Surgical Research Laboratory, University Medical Center of Groningen, Groningen, NETHERLANDS, [4]Astellas Pharma Europe, Leiden, NETHERLANDS.

Aim: 16β-[^{18}F]fluoro-5α-dihydrotestosterone ([^{18}F]FDHT) is a PET tracer that has been investigated for the assessment of androgen receptor (AR) density in prostate cancer. Being an agonist, [^{18}F]FDHT intrinsically poses the risk pharmacological response, which is undesirable for a PET tracer. Recently, enzalutamide (formerly MDV3100) was introduced as an AR signaling inhibitor. Here we present the synthesis of [^{18}F]enzalutamide and its *in vitro* and *in vivo* behavior in comparison to [^{18}F]FDHT. Methods: The nitro-precursor was obtained by multistep synthesis starting with the nitrobenzoic acid. [^{18}F]enzalutamide was obtained by fluorination of the corresponding nitro precursor. Competition assays with [^{18}F]enzalutamide and [^{18}F]FDHT were conducted in the LnCaP (AR+) cell line to evaluate the affinity for AR. *In vitro* cellular uptake of both tracers were performed with LnCaP (AR+) and HEK293 (AR-) cells. *In vivo* PET imaging, *ex vivo* biodistribution and metabolite studies with [^{18}F]enzalutamide and [^{18}F]FDHT were conducted in athymic nude mice bearing a subcutaneous LnCaP xenograft. Results: The nitro precursor was produced with an overall yield of 2%. [^{18}F]Enzalutamide was obtained in 1.2% radiochemical yield with an apparent specific activity of 487 ± 347 GBq/mmol. [^{18}F]FDHT was obtained in 2% with a specific activity > 25.000 GBq/mmol. Co-incubation of [^{18}F]enzalutamide or [^{18}F]FDHT with an excess of DHT or enzalutamide significantly reduced cellular uptake of both tracers to about 50% in AR+ LnCaP cells, whereas co-incubation of both tracers with an excess of DHT or enzalutamide did not lead to reduction of cellular uptake in the AR- HEK293 cell line. [^{18}F]enzalutamide and [^{18}F]FDHT biodistribution studies in male mice bearing a LnCAP xenograft showed 2.5 times higher [^{18}F]Enzalutamide uptake in tumor than [^{18}F]FDHT. In addition, metabolite analysis indicated that 99% of [^{18}F]Enzalutamide remains intact versus only 3% of [^{18}F]FDHT at 60 min p.i. Conclusion: Based on our results, [^{18}F]enzalutamide seems to have more favorable properties for AR imaging than [^{18}F]FDHT. Additional evaluation in various oncological animal models is warranted to confirm its ability to monitor AR expression.Funding: Prostate Cancer Molecular Medicine 030-203.

OP618

Comparison of [11C]Choline and [18F]Galacto-RGD as pharmacodynamic biomarker for therapy response assessment of avastin therapy in a PC-3 Prostate Cancer Xenograft Model

S. Schwarzenböck[1,2], M. Souvatzoglou[1], M. Heuschkel[2], R. Nawroth[3], U. Treiber[3], T. Schuster[4], R. Senekowitsch-Schmidtke[1], M. Schwaiger[1], S. I. Ziegler[1], G. Henriksen[5], H. Wester[5], A. J. Beer[1], B. J. Krause[1,2]; [1]Technical University München, Department of Nuclear Medicine, München, GERMANY, [2]Rostock University Medical Centre, Department of Nuclear Medicine, Rostock, GERMANY, [3]Technical University München, Department of Urology, München, GERMANY, [4]Technical University München, Institution of Statistics, München, GERMANY, [5]Technical University München, Pharmaceutical Radiochemistry, Garching, GERMANY.

Introduction:In prostate cancer molecular imaging development and evaluation of new tracers with higher sensitivity and specificity for diagnosis as well as therapy response assessment is necessary. The use of 18F-labeled Galacto-RGD ([18F]RGD) - targeting the integrin alpha-v-beta-3 as a key molecule in angiogenesis and tumour metastasis - is a promising approach for prostate cancer imaging and therapy response assessment.Aim:The aim of this study was to compare the properties of [18F]RGD and [11C]Choline ([11C]CHO) as imaging biomarker and to assess response to an anti-angiogenesis avastin therapy avastin in a PC-3 human prostate cancer xenograft mouse model.Methods:We carried out a dual tracer small animal PET/CT study comparing the properties of [18F]RGD and [11C]CHO in prostate cancer imaging as well as in avastin therapy response assessment (9 untreated mice, 7 avastin therapy mice (5 i.p. injections within 10-13 days, dose of 5 mg/kg bodyweight each), 3 PBS i.p. control mice). The androgen-independent human prostate tumour cell line PC3 was implanted subcutaneously in the flanks of SCID mice. 6 weeks post xenografting all mice underwent dynamic PET/CT scanning after injection of 37 MBq [11C]CHO and 14 MBq [18F]RGD, respectively, via the tail vein on two separate days. 5x5x5 mm VOIs were placed in transaxial slices in tumour, muscle (thigh), liver, kidney and blood. Image analysis was performed calculating tumour-to-muscle (T/M) ratios based on summed images.Tumour volumes were measured using a caliper.Results:In untreated mice the mean [18F]RGD T/M ratio was significantly higher compared to [11C]CHO (4.62 +/- 2.20 vs. 1.44 +/- 0.39, mean difference +3.18, 95% CI: 2.12 - 4.25, $p<0.001$), in the PBS control group comparable results were obtained. In contrast, there was a tendency of an increase in both [18F]RGD and [11C]CHO uptake in the avastin treated group. Measurement of tumour volumes showed a decreased tumour growth in avastin treated mice compared to the control group.Conclusion:Excellent tumour visualization is possible in this PC-3 xenograft model using [18F]RGD. [18F]RGD uptake was significantly higher compared to the clinically utilized [11C]CHO. In the avastin treated group there was an increase in [11C]CHO as well as in [18F]RGD uptake (compared to untreated and PBS control mice) indicating a stimulating effect of the humanized monoclonal antibody avastin in the early stage of anti-angiogenesis therapy. Further studies using clinically relevant therapies for

prostate cancer are recommended to assess the general suitability of [18F]RGD therapy response assessment of prostate cancer.

OP619
Broadcasting the HER3 receptor status in vivo

C. D. Martins, C. Da Pieve, D. M. Ciobota, R. L. Paul, T. Spinks, G. Smith, G. Kramer-Marek; The Institute of Cancer Research, London, UNITED KINGDOM.

Background: Amongst the human epidermal growth factor receptor (HER) family, HER3 is a key node in the activation of the PI3K/AKT pathway, implicated in promoting cell survival, proliferation and metastasis. Overexpression of HER3 correlates with advanced disease stage and is involved in resistance to other anti-HER therapies. Multiple anti-HER3 mAbs are being tested in clinical trials, highlighting the potential of HER3 inhibition to improve patient care. We investigated the potential use of affibody molecules targeting HER3 ($Z_{HER3:8698}$) for PET imaging of different receptor levels in HER3+ve breast cancer models. The ultimate goal is to promote $Z_{HER3:8698}$-based imaging agents as tools for patient stratification for anti-HER3 targeted therapies. Materials and methods: $Z_{HER3:8698}$ molecules were conjugated via the C-terminus cysteine with NOTA-Maleimide and DFO-Maleimide for ^{18}F and ^{89}Zr radiolabelling respectively. The probes were characterised *in vitro* using a panel of human breast adenocarcinoma cell lines with different receptor levels (MDA-MB-231_{HER3}<MDA-MB-361_{HER3}<BT-474_{HER3}<MCF-7_{HER3}). BALB/c nu/nu mice bearing BT-474 and MDA-MB-231 xenografts were used for *in vivo* evaluation of the probes. Mice were injected via the tail vein with either of the radioconjugates (1-5 μg, 0.8-14 MBq depending on the tracer). Biodistribution as well as imaging studies were performed 1, 3 and 24 h following ^{89}Zr-DFO-$Z_{HER3:8698}$ injection, and 1, 2 h post ^{18}F-AlF-NOTA-$Z_{HER3:8698}$ administration. Results: The K_d of both ^{18}F and ^{89}Zr conjugates was determined to be within 0.44 ± 0.044 (nM). Pre-incubation with either unlabelled affibody or heregulin reduced binding of both tracers *in vitro*, confirming the specificity of the probes. There was no significant accumulation of the ^{18}F radioconjugate in BT-474 tumour bearing mice 2 h post ^{18}F-AlF-NOTA-$Z_{HER3:8698}$ injection, most likely due to low specific activity of the conjugate (SA: 0.8 MBq/μg). However, the ^{89}Zr probe (SA: 2.8 MBq/μg) specifically accumulated in BT-474 xenografts (2%ID/g) as early as 1 h post tracer injection, but not in MDA-MB-231 tumours ($T_{BT-474}/T_{MDA-MB-231}$: 3.4). Rapid clearance was observed in BT-474 bearing mice leading to high tumour to blood and muscle ratios (T_{BT-474}/Blood: 7, T_{BT-474}/Muscle: 23, $T_{MDA-MB-231}$/Blood: 0.81, $T_{MDA-MB-231}$/Muscle: 4.4). IHC and ELISA receptor evaluation showed correlation with PET signal, *ex vivo* autoradiography, and radioactivity measurements. Conclusion: Our data shows that ^{89}Zr-DFO-$Z_{HER3:8698}$ molecules accumulate with high specificity in HER3+ve tumours, providing real time information about the receptor expression. Various strategies to develop higher SA ^{18}F-radiolabelled $Z_{HER3:8698}$ molecules are being pursued.

OP620
PET Imaging of c-Met in Cancer with ^{64}Cu-Labeled Hepatocyte Growth Factor

H. Luo, H. Hong, S. Shi, S. A. Graves, R. J. Nickles, **W. Cai**; University of Wisconsin-Madison, MADISON, WI, UNITED STATES.

Objective: The hepatocyte growth factor (HGF) and its receptor, c-Met, are actively involved in tumor progression/metastasis and associated closely with poor prognostic outcome of cancer patients. Development of positron emission tomography (PET) agents for assessing c-Met expression would be extremely useful for diagnosis of cancer and subsequent monitoring of responses to c-Met-targeted therapies. Herein we report the expression and characterization of recombinant human hepatocyte growth factor (rh-HGF) as a PET tracer for non-invasive imaging of c-Met expression. Methods: rh-HGF was expressed in human embryonic kidney (HEK) 293 cells and purified by nickel-nitrilogriacetic acid (Ni-NTA) affinity chromatography. The concentrated rh-HGF was conjugated to 2-S-(4-isothiocyanatobenzyl)-1,4,7-triazacyclononane-1,4,7-triacetic acid (p-SCN-Bn-NOTA) and labeled with ^{64}Cu. c-Met binding evaluation by flow cytometry was performed in both U87MG and MDA-MB-231 cell lines, which have high and low level of c-Met, respectively. PET imaging and biodistribution studies were performed in nude mice bearing U87MG and MDA-MB-231 xenografted tumors. Ex vivo histopathology were performed to elucidate the expression patterns of c-Met in different tissues/organs and used to validate the in vivo results. Results: The rh-HGF expression yield was 150-200 μg protein per 5×10^6 cells after 48 h transfection with purity of > 85%. Flow cytometry examination confirmed strong and specific binding capacity of rh-HGF to c-Met. After labeled with ^{64}Cu, PET imaging revealed specific and prominent uptake of ^{64}Cu-NOTA-rh-HGF in c-Met positive U87MG tumors (6.7 ± 1.8 %ID/g at 9 h post-injection; n = 4) and significantly lower uptake in c-Met negative MDA-MB-231 tumors (1.8 ± 0.6 %ID/g at 9 h post-injection; n = 4). Heat-denatured rh-HGF (termed as dnrh-HGF) had significantly lower uptake in U87MG tumors, which confirmed the c-Met specificity of ^{64}Cu-NOTA-rh-HGF. Based on fluorescence staining of c-Met, c-Met expression was prominent on the U87MG tumor cells but absent on the MDA-MB-231 cells and rh-HGF can target c-Met with high specificity. c-Met staining of mouse liver and muscle gave a low signal, indicating that these tissues do not express high level of c-Met. Thus, uptake of ^{64}Cu-NOTA-rh-HGF in

the liver was mostly due to hepatic clearance of the tracer rather than c-Met binding. Conclusion: Herein we report the purification of rh-HGF, the characterization and in vitro/in vivo investigation of ^{64}Cu-NOTA-rh-HGF for in vivo PET imaging of c-Met expression. Fast, prominent and c-Met-specific uptake of ^{64}Cu-NOTA-rh-HGF in the U87MG tumors was observed, which was validated by various in vivo/ex vivo experiments.

OP621

The PET tracer [18F]-tetrafluoroborate allows reporter gene-afforded metastasis tracking.

S. Diocou[1], **G. Fruhwirth**[1], K. Chuamsaamarkkee[1], M. Jauregui-Osoro[1], L. Livieratos[1], P. Blower[1], T. Ng[1,2], G. Mullen[1]; [1]King's College London, London, UNITED KINGDOM, [2]University College London, London, UNITED KINGDOM.

Purpose: We aim to non-invasively track metastasis in a murine breast cancer model by PET/CT. The approach is based on a radionuclide-optical fusion protein as previously described (1). Metastasis tracking has not been shown before using NIS-based PET imaging. Here we compare the PET radiotracer [18F]-BF4- (2) with the SPECT radiotracer [123I]-iodide for NIS reporter gene imaging-afforded detection and monitoring of metastasis. Another goal was to compare metastasis detection and tracking of this NIS-RFP-afforded PET approach with [18F]-FDG PET in this preclinical model.Methods: Breast adenocarcinoma cells (MTLn3E) were engineered to stably express the sodium iodide symporter (NIS) fused to a fluorescent protein for multimodal multi-scale imaging. Furthermore, we transduced MTLn3E.NIS-RFP cells with full-length or truncated CXCR4 (3E.FL-NIS and 3E.Δ-NIS, respectively). The resultant cell lines served as a model for tumor xenografts that showed a low or very high propensity for spontaneous metastasis (3). Xenografts were established orthotopically in the lower mammary fat pad of female SCID/Beige mice. Dynamic radionuclide scanning using [18F]-BF4-, [123I]-iodide and/or [18F]-FDG tracers was performed by PET/CT and SPECT/CT as appropriate. Specificity and sensitivity of metastasis detection were measured by comparing radionuclide scans with confocal fluorescence microscopy of biopsied lymph node tissues.Results: Uptake of both [18F]-BF4- and [123I]-iodide in primary tumors was rapid, reaching 12.1 and 11.0 %ID/g for [18F]-BF4- and [123I]-iodide, respectively, after 12min, and 56.9 and 60.5 %ID/g, respectively, after 120min. Clearance of [18F]-BF4- from the blood was faster (falling to 0.06 %ID/g at 36 min) than clearance of [123I]-iodide (3.1 %ID/g at 36 min). 100% of lymph nodes (LN) that were detected via [18F]-BF4 PET were also confirmed positive for 3E.Δ-NIS tumor cells using confocal fluorescence microscopy of biopsied material. Furthermore, all LNs that were not detected by [18F]-BF4 PET were confirmed to be free of metastasis. LNs detected by [18F]-BF4- and confirmed to be positive for tumor metastases were not detected using [18F]-FDG in >95% of the cases.Conclusion: [18F]-BF4- PET showed more favorable tracer kinetics and signal-to-background as compared to [123I]-iodide SPECT. Furthermore, it showed much higher sensitivity and specificity for metastasis detection as compared to [18F]-FDG. This preclinical model is particularly useful for studying spontaneous cancer metastasis and for evaluating the treatment response of anti-cancer and particularly anti-metastatic therapeutics.References:(1) Fruhwirth J Nuc Med 2014; 55(4):686-94.(2) Jauregui-Osoro Eur J Nucl Med Mol Imaging, 2010; 37(11):2108-16.(3) Vermeer J Proteome Res 2012; 11(5):2996-3003.

OP622

Molecular imaging of EGFR and EGFRvIII for prediction and response monitoring of HSP90 inhibition in an in vivo squamous cell carcinoma model

D. Spiegelberg[1], A. C. Mortensen[1], R. K. Selvaraju[2], O. Eriksson[2], B. Stenerlöw[1], A. Scott[3], M. Nestor[1,4]; [1]Department of Immunology, Genetics and Pathology, Uppsala University, Uppsala, SWEDEN, [2]Preclinical PET Platform, Uppsala, SWEDEN, [3]Ludwig Institute for Cancer Research, Olivia Newton-John Cancer Research Institute, and La Trobe University, Melbourne, AUSTRALIA, [4]Department of Surgical Sciences, Academic hospital, Uppsala, SWEDEN.

Aim: The novel HSP90 targeting drug AT13387 has been shown to reduce tumor growth, angiogenesis and spreading of the disease in patients with solid cancers. Remaining challenges are to increase response rates and prolong response duration by refining treatment dose and schedules. Molecular imaging of biomarkers involved in disease progression is a useful noninvasive tool to obtain this goal. Biomarkers that are over expressed or tumor specific in several malignancies are e.g. the epidermal growth factor receptor (EGFR) and the epidermal growth factor receptor variant III (EGFRvIII). The overall goal of this study was to identify if EGFR or EGFRvIII expression monitoring in squamous cell carcinomas (SCC) could be used in order to follow the disease status during AT13387 treatment. Materials and methods: Cancer cell proliferation, cell toxicity assays and radio-immunoassays using radiolabelled monoclonal antibodies targeting EGFRvIII and EGFR, were used to quantify the effect of AT13387 on antigen expression in vitro. Inhibitor effects were then assessed in vivo in mice xenografts bearing dual SCC tumors with high or low EGFR expression, and low EGFRvIII expression. Animals were treated 5 times on 5 consecutive days with AT13387 (50 mg/kg), and were then imaged either with 18F-FDG (30 min p.i.), 124I-labelled EGFR-targeting mAb Cetuximab, or with an 111I-labeled anti-EGFRvIII antibody (48 h p.i.).

Imaging was performed with a small animal PET/CT or SPECT/CT, and was followed by ex vivo biodistribution and autoradiography measurements and immunohistochemical analysis. Results and conclusion: We could demonstrate for the first time that the HSP90 client protein EGFRvIII is downregulated, approximately by 30% in our models, by AT13387. We could also verify that EGFR is downregulated by AT13387 in SCC, approximately by 75% and 40% in our high- and low-EGFR-expressing models respectively. 18F-FDG was neither able to clearly detect nor distinguish between EGFR expression. We conclude that the 111In-labelled EGFRvIII-targeting antibody and 124I-cetuximab are promising tracers for EGFRvIII and EGFR expression analysis respectively, and could be useful tools for treatment response monitoring in combination with HSP90 inhibition in SCC patients.

OP623

Efficacy of the sequentially combined vinorelbine and gefitinib in Non-Small Cell Lung Cancer cell lines, an "in-vivo" study.

G. Bottoni[1], M. Dal Bello[2], A. Alama[2], S. Morbelli[1], C. Marini[3], F. Grossi[2], G. Sambuceti[1]; [1]1.Nuclear Medicine Unit, IRCCS-IST San Martino, University of Genoa, Genova, ITALY, [2]Lung Cancer Unit IRCCS-IST San Martino, Genova, ITALY, [3]3.Institute of Bioimaging and Molecular Physiology, CNR, Milan, Genoa Section, Genova, ITALY.

Aim: The current standard of care for advanced NSCLC is based on systemic chemotherapy or epidermal growth factor receptor tyrosine kinase inhibitors (EGFR-TKI) for patients with tumors harboring EGFR mutations. Preclinical studies suggest that EGFR-TKI may have additive effects on chemotherapy even in cancers without EGFR mutations. Our study tested, in vitro and in vivo, the anti-proliferative activity of different treatment schedules with gefitinib (GEF) and vinorelbine (VNB) in EGFR-TKI resistant NSCLCs.Methods: We studied CD1-Nude mouse subcutaneously inoculated with 3 millions H1975 cells in the dorsal hip. In each mouse, cancer growth was estimated by conventional caliper methods, while lesion glucose consumption was estimated by means of a dynamic PET scans at day 14 after tumor implantation. To this purpose, a bolus of 3-6 MBq of 18F-FDG was injected through a tail vein during a list mode acquisition lasting one hour using a dedicated microPET system. After framing rate optimization, pixelwise maps of cancer glucose consumption (MRGlc) were created using a dedicated software (PMOD) and applying Patlak graphical approach.Results: In vitro short and long-term studies demonstrated that the sequence of VNB followed by GEF was more effective than GEF followed by VNB or the concurrent administration of the two drugs. Moreover, the increased antitumor activity of the sequence VNB followed by GEF was confirmed in vivo by a significant inhibition of the H1975 tumor growth (0,13 ml vs 0,95 ml in treated and untreated lesions, respectively, $p<0.05$). This biological effect was correctly predicted by FDG-based measurement of lesion MRGlc that was 2,81±0,04 umol/min/100gr in untreated and 5.65±2.71 umol/min/100gr in treated mice, respectively ($p<0.008$).Conclusion: Our preclinical findings in NSCLC with EGFR T790M mutation showed that the sequential treatment with VNB followed by GEF can induce significant antitumor benefit to be tested in a clinical trial for TKI resistant NSCLC patients.

OP624

Oncologic Applications of High Resolution In Situ Correlations between Histopathology and FDG Tracer Uptake Obtained by Quantitative Autoradiography of Biopsy Specimens (QABS)

A. S. Kirov[1], L. M. Fanchon[1,2], S. Dogan[1], C. Czmielewski[1], E. Yorke[1], H. Schöder[1], J. O. Deasy[1], J. L. Humm[1], S. B. Solomon[1]; [1]Memorial Sloan-Kettering Cancer Center, New York, NY, UNITED STATES, [2]INSERM, UMR1101, LaTIM, Brest, FRANCE.

Purpose. To use autoradiography to determine the distribution of a PET radiotracer in biopsy specimens obtained under PET/CT guidance for correlation with histopathology and to identify the potential and the limitations of this method for different applications in oncology.Methods. Autoradiography (ARG) using imaging plates was performed on 32 core needle biopsy specimens obtained from different body locations under FDG PET/CT guidance in an interventional suite equipped with a PET/CT scanner. In this institutional review board-approved study, the specimens were extracted using 11G, 13G, 18G and 20G core needles and the response of the plates for 18G and 20G needles was calibrated using gelatin based standards with known activity prepared using the same needles. The quality of the autoradiography image, the preservation of the shape of the specimen during pathology processing, the location of the needle with respect to the PET avid region, the effect of motion on the accuracy of the fused PET/CT image, and the post biopsy management of the patient were all considered in the evaluation of the methodology for different oncologic applications.Results. Of the 32 cases, 18 were found useful for high resolution in situ correlations of tracer uptake with histopathology. Such correlations allowed separating malignant from benign liver lesions based on the activity contained in the specimens which was expressed as SUV_{ARG} (Fanchon et al, JNM, 56, p. 538, 2015). A potential application of this result is evaluating the adequacy of PET guided biopsy needle placement. Eight of the 18 cases were found adequate for calibrating the PET display window and for providing a

ground truth point for evaluation of lesion segmentation contours on the PET image. Two cases showed correlation with inflammation in a normal tissue specimens, and 1 showed uptake in the absence of histopathologic changes in the investigated slices. The percentage of specimen autoradiographs, which can be accurately correlated with histopathology has increased due to improvements of the method since implementation and further increase is expected. Thirty of the patients were treated in our institution. Investigating correlations of QABS findings with treatment outcome is possible for radiation therapy (2 cases), ablation (6 cases) and chemo or antibody therapy (14 cases).Conclusions. QABS is a promising method for providing knowledge which may have an impact on PET tracer validations for nuclear medicine, on the accuracy of interventional radiology and radiotherapy procedures, and on increasing the sensitivity of histopathology assessment of biopsy specimens.

1708 - Sunday, October 11, 2015, 4:00 PM - 4:30 PM, Hall E
Clinical Oncology: Therapy Response & External Beam RT

OP625

Textural analysis of baseline 18F-FDG PET for predicting treatment response and prognosis in patients with locally advanced esophageal cancer

X. Sun, L. Sun, L. Xing; Shandong Cancer Hospital and Institute, Jinan, CHINA.

PURPOSE: Textural features on baseline 18F-FDG PET have shown the potential role in predicting treatment response in mixed stage esophageal cancer. This study is aim to investigate the value of this new technique for locally advanced esophageal squamous cell cancer (ESCC) receiving chemoradiotherapy. METHOD AND MATERIALS: Under a waiver from institutional review board, 48 patients with newly diagnosed locally advanced ESCC who treated with concurrent chemoradiotherapy were retrospectively reviewed. Thirty-nine patients with early stage ESCC were included as control. All patients underwent pretreatment whole-body 18F-FDG PET/CT. Fifty-four texture indices describing global, local, and regional features were measured in addition to 5 conventional indices as standardized uptake values (SUVs, including maximum, peak, and mean SUV), metabolic volume (MV), and total lesion glycolysis (TLG). Patients were classified as responders (R, complete or partial response) and non-responders (NR, stable or progressive disease) according to RECIST1.1. Progression-free survival (PFS) and overall survival (OS) were recorded. The prognostic significance of parameters was examined using receiver-operating-characteristic curves, Kaplan-Meier analysis, and Cox regression analysis. RESULTS: Both intratumor heterogeneity and mean/peak intensity of FDG uptake were significantly higher in locally advanced ESCC than those in early stage. Thirty-four texture indices, MV, and TLG showed the ability to differentiate R from NR. Nine texture indices showed higher sensitivity (76.7%~86.7%) and specificity (77.8%~94.4%) than MV (76.7% and 83.3%) and TLG (73.3% and 83.3%). Ten texture indices and MV were hazard factors of PFS and OS. Large-zone emphasis, one of the regional texture indices, was the only independent predictor of survival, with hazard ratio of 4.22 (95%CI:1.83~9.72) for PFS and 3.90 (1.74~8.79) for OS. None of the SUVs could predict treatment response and survival. CONCLUSION: FDG PET texture indices provide better predictive information than conventional parameters for locally advanced ESCC. Therefore, the clinical application of FDG PET texture analysis could be an important step in personalized treatment of esophageal cancer.

OP626

The predictive value of ^{18}F-FDG PET-CT for assessing the clinical outcomes in locally advanced NSCLC patients after a new induction treatment: "low-dose" fractionated radiotherapy with concurrent chemotherapy

M. Mattoli[1], M. Massaccesi[2], V. Scolozzi[1], A. Castelluccia[2], G. Mantini[2], A. Giordano[1], M. Calcagni[1]; [1]Institute of Nuclear Medicine, Rome, ITALY, [2]Department of Radiation Oncology, Rome, ITALY.

Aim: Many patients with locally advanced non-small-cell lung cancer (NSCLC) have a poor prognosis, despite the use of two cycles of induction chemotherapy performed before the standard treatment (chemo-radiotherapy). It is emerging that the addition of "low-dose" fractionated radiotherapy (LD-RT) to the induction chemotherapy can enhance tumor cells chemo-sensitivity and improve its effects. Aim: to evaluate whether the metabolic response assessed by ^{18}F-fluoro-deoxyglucose positron emission/computed tomography (^{18}F-FDG PET-CT) after induction chemo-LD-RT can predict clinical outcomes in locally advanced NSCLC patients. Materials and methods: Forty-two consecutive locally advanced NSCLC patients (32 males, mean age 66±7.9years; 25 stage IIIA; 17 stage IIIB) underwent LD-RT (40cGy twice daily) to primary tumor and involved lymph-nodes concurrently with two cycles of induction chemotherapy, before undergoing standard chemo-radiotherapy treatment. ^{18}F-FDG PET-CT was performed before (mean 5.7±2 weeks) and after chemo-LD-RT (mean 4.6±1.5 weeks). SUVmax of primary tumor and of the most active lymph-node was evaluated in both PET-CT to obtain the metabolic changes (ΔSUV). To assess the metabolic response, PERCIST criteria were used. Patients with complete and partial metabolic response were classified as responders; patients with stable and progressive disease as non-responders. Disease free survival (loco-regional, distant

or global) and overall survival were calculated with Kaplan-Meyer method. Results: Twenty out of 42 locally advanced NSCLC patients (48%) were classified as responders: 22/42 as non-responders. Two years loco-regional failure free survival was 54%: 84.4% in responder and 24.8% in mom-responders (p=0.001). Two years distant failure free survival was 48.2%: 70.4% in responders and 22.8% in non-responders (p=0.001). Two years global failure free survival was 34%: 63.4% in responders and 0.8% in non-responders (p=0.0003). Two years overall survival was 58.2%: 73.5% in responders and 43.9% in non-responders (p=0.009). SUVmax of primary tumor and lymph-node was significantly reduced at PET-CT after chemo-LD-RT (p=0.004 and p=0.0002, respectively). No significant difference in SUVmax between stage IIIA and stage IIIB was found, either at diagnosis or after chemo-LD-RT. **Conclusion**: in patients with locally advanced NSCLC, ^{18}F-FDG PET-CT is useful for assessing metabolic response after a new induction treatment, such as" low-dose" fractionated radiotherapy with concurrent chemotherapy. Metabolic response predict clinical outcomes: patients with complete or partial metabolic response have a better prognosis than those with progressive or stable disease. These findings allow to personalize therapy, selecting patients for standard treatment or for intensified treatment.

OP627

Comparison of EORTC criteria and PERCIST for FDG PET/CT response evaluation of patients with metastatic breast cancer treated with a first line of systemic therapy.

E. Depardon[1], S. Kanoun[1,2], O. Humbert[1,2], J. Riedinger[1], M. Lasserre[1], M. Toubeau[1], A. Berriolo-Riedinger[1], I. Dygai-Cochet[1], P. Fumoleau[3], F. Brunotte[1,2], A. Cochet[1,2]; [1]Department of Nuclear Medicine, Centre Georges-Francois Leclerc, Dijon, FRANCE, [2]Le2i CNRS UMR 6306, Dijon, FRANCE, [3]Department of Medical Oncology, Centre Georges-Francois Leclerc, Dijon, FRANCE.

Aim : To compare European Organization for Research and Treatment of Cancer (EORTC) criteria with PET Response Criteria in solid Tumors (PERCIST) for response evaluation of patients with newly diagnosed metastatic breast cancer treated with a first line of systemic therapy.Methods : From December 2006 to august 2013, 57 patients who were referred to our institution for a newly diagnosed metastatic breast cancer were retrospectively included (41 HR+/HER2-, 9 HER2+, 7 triple negative). FDG-PET/CT was performed within one month before treatment and 3 to 9 months following start of a first line of systemic therapy: polychemotherapy (n=20), bevacizumab-based therapy (n=16), hormone therapy (n=12) or trastuzumab-based therapy (n=9). Response evaluation with FDG-PET/CT was retrospectively performed according to both EORTC criteria and PERCIST, classifying the patients into 4 response groups: complete metabolic response (CMR), partial metabolic response (PMR), stable metabolic disease (SMD), and progressive metabolic disease (PMD). The kappa statistic was used for agreement analysis. Overall survival (OS) within every response categories was determined by Kaplan-Meier method after a median follow up of 30 months. A multivariate analysis was also performed by Cox model to assess independent predictors of survival.Results: Average time delay between baseline and follow-up PET/CT was 5 months. With EORTC criteria, 22 patients had CMR, 17 had PMR, 6 had SMD and 12 had PMD. With PERCIST, 20 patients had CMR, 15 had PMR, 10 had SMD and 12 had PMD. There was agreement between EORTC and PERCIST in 84% of the patients, and the corresponding kappa-coefficient was 0.78. Thirty patients died during follow up (8 CMR, 12 PMR, 2 SMD, 8 PMD with EORTC; 7 CMR, 10 PMR, 4 SMD, 9PMD with PERCIST). By log-rank analysis, metabolic response evaluated with both EORTC and PERCIST was able to predict survival (p=0.028 and 0.002 respectively). Patients in the CMR group had longer median OS than patients in the combined PMR+ SMD+PMD group (60 vs 26 months; p=0.009 with EORTC; p=0.006 with PERCIST). By multivariate analysis, CMR either with EORTC or PERCIST, stratified by age and phenotype, remained an independent predictor of survival.Conclusion: In the setting of metastatic breast cancer treated with a first line of systemic therapy, metabolic response evaluation with EORTC criteria and PERCIST gave similar response and outcomes with good agreement and similar significant differences in median OS between response groups.

OP628

Monitoring Tumour Response to Neoadjuvant Chemotherapy using MRI and ^{18}F-FDG PET/CT in Breast Cancer Subtypes

A. M. T. Schmitz[1], K. E. Pengel[2], C. E. Loo[2], W. Vogel[2], J. Wesseling[2], **S. C. Teixeira**[2], E. J. T. Rutgers[2], R. A. Valdés Olmos[2], G. S. Sonke[2], S. Rodenhuis[2], M. T. F. D. Vrancken-Peeters[2], K. G. A. Gilhuijs[1]; [1]University Medical Centre Utrecht, Utrecht, NETHERLANDS, [2]Netherlands Cancer Institute - Antoni van Leeuwenhoek Hospital, Amsterdam, NETHERLANDS.

Aim: To establish a practical guideline on the use of MRI and/or PET/CT for response monitoring of the primary tumour, taking into account the breast cancer subtypes. Material & Methods: We included 188 women with stages II/III breast cancer. Baseline histology was assessed from biopsy. Primary tumours were stratified into ER-positive/HER2-negative (ER-positive), HER2-positive, and ER-negative/HER2-negative/PR-negative (triple-negative) subtypes, and treated with pre-operative neoadjuvant chemotherapy (NAC) according to subtype. MRI and ^{18}F-FDG-PET/CT were acquired before and during NAC. Primary

endpoint was pathological complete response (pCRmic) defined as no or only small numbers of scattered invasive tumour cells. Multivariate analyses assessed the association of patient, tumour and imaging characteristics with pCRmic. Using post-hoc analysis, six imaging scenarios were evaluated; MRI only, PET/CT only, and combinations of both. We used receiver operating characteristics analysis with assessment of areas under the curve (AUC) to determine optimal imaging scenarios and we selected high specificity (90%) as operating point to propose clinical guidelines per subtype. Results: A pCRmic was found in 35/46 (76.1%) of HER2-positive, 11/87 (12.6%) of ER-positive, and 31/55 (56.4%) of triple-negative tumours. Before NAC, age ($p<0.001$) and subtype ($p<0.001$) were the only predictors of response. During NAC, MRI yielded the strongest predictor for HER2-positive tumours (AUC: 0.735; sensitivity 36.2%) outperforming PET/CT (AUC: 0.543; $p=0.04$) comparable to results of combined imaging (AUC: 0.708). In ER-positive tumours, the combination of MRI and PET/CT yielded the strongest predictor (AUC: 0.818; sensitivity 55.8%) compared to MRI (AUC: 0.742) or PET/CT (AUC: 0.791) alone. For triple-negative tumours, MRI (AUC: 0.855; sensitivity 45.4%), PET/CT (AUC: 0.844) or a combination of both showed comparable results (AUC: 0.868). Conclusion: For response monitoring in ER-positive primary tumours the combination of PET/CT and MRI may be the most optimal choice. For HER2-positive and triple-negative tumours, MRI has high specificity but moderate sensitivity to monitor response. PET/CT will provide comparable results with MRI in triple-negative but not in HER2-positive breast cancer tumours.

OP629

Planning of radiotherapy with PET: Volumes only?

M. Beresova, J. Mucientes Rasilla, B. Rodriguez Alfonso, I. Zapata Paz, A. De la Torre Tomas, J. Romero Fernández, M. De Teresa Herrera, I. Plaza De Las Heras, M. Mitjavila Casanovas; HUPH Majadahonda, Madrid, SPAIN.

Aim: We assess the percentage of cases in which findings of distant disease through 18F-FDG PET/CT for radiotherapy planning lead to changes in the modality and/or intent of the treatment, or change in stage IV.Material and methods: All the studies derived from the Radiotherapy department were retrospectively analysed. Those performed for radiotherapy planning were selected. Cases with distant disease findings were assessed, investigating changes in the modality or intent of treatment and change in stage IV.One thousand four hundred seventy six studies were derived from the Radiotherapy department between April/09 and December/13. Three hundred and seventy three (25,3%) were performed for radiotherapy planning (267 males and 106 females, mean age 68.2 years). The intention of radiotherapy was for radical treatment planning.Results: In 45 of these studies (12%) there were previously not suspected findings that suggested an upstage of the patients to a clinical stage IV. The unexpected disease was located more frequently in bone (12 patients), followed by lung (9 patients), liver (10), distant adenopathy (6 patients), brain (4 patients), adrenal glands (4 patients), spleen (1 patient) and multiple progression (1 patient).In twenty-six (26/45, 7%) of these patients the findings of 18F-FDG PET/CT were confirmed as true positive for distant metastasis with complementary examinations. In sixteen (16/26) of them the modality of treatment was changed. In ten of them (10/26) the intent of treatment was changed from curative to palliative. In three patients a second primary tumour was confirmed.In remaining sixteen (16/45) patients the results of 18F-FDG PET/CT could not be initially confirmed. The confirmation was made by monitoring progression in eleven patients, one patient remained with stable disease and four patients died without being able to confirm the findings.Conclusions: 18F-FDG PET/CT studies in radiotherapy planning improve the staging of patients, leading to an upstage in a significant number of patients. Based upon the findings of 18F-FDG PET/CT, the modality or the intent of treatment may radically change, (making unnecessary radiation) or changing the intent to palliative.

OP630

Feasibility and clinical utility of 4D PET/CT for SBRT planning of liver tumors

E. Deshayes[1], L. Santoro[1], M. Eberle[1], S. Guillemard[1], F. Marre[1], N. Aillères[2], P. Fenoglietto[2], D. Azria[2], P. Kotzki[1], O. Riou[2]; [1]Nuclear Medicine Department - Institut Cancer Montpellier, Montpellier Cedex 5, FRANCE, [2]Radiotherapy Department - Institut Cancer Montpellier, Montpellier Cedex 5, FRANCE.

Aim: the aim of this study was to assess the feasibility of 4D PET/CT for patients with liver tumors, and its clinical utility for stereotactic body radiation therapy (SBRT) planning. Material and methods: we retrospectively analyzed in this study all the consecutive patients who underwent 4D PET/CT for liver SBRT radiotherapy planning in treatment position. The patients were included between January 2014 and February 2015. Patients with hepatocellular carcinoma could have undergone either FDG or F-Choline PET/CT. 4D PET/CT images were produced using a Real time Position Management system (RPM, Varian Medical System) and separated in 10 phases (bins). Each phase was then coregistered with each of the 10 phases of the radiotherapy planning 4D CT. All images were independently reviewed by a radiation oncologist and a nuclear medicine physician. Evaluation criteria were: to assess if uptake was significant on 3D PET, on 4D PET, the added

value of 4D PET over 3D PET (leading to a change in target volumes). Impact of PET/CT on treatment decision was also reported. Results: 15 patients (14 males, 1 female) were included: 10 primary tumors (3 patients with hepatocellular carcinoma performed a F-Choline PET/CT; 7 had FDG PET/CT: 5 hepatocellular carcinoma and 2 cholangiocarcinoma) and 5 metastatic liver lesions (3 from colorectal cancer, 1 from breast cancer and 1 from renal cell carcinoma). Mean age was 73.6 years (+/- 7.3). Final analysis was performed on 13 patients as PET/CT led to exclude 2 patients for SBRT (discovery of multiple unknown distant metastases). Among the 13 remaining patients, the nuclear medicine physician found a significant and useful 4D PET/CT liver uptake as compared to 3D PET/CT for 7 patients (54 %), and the radiation oncologist for 9 patients (the same 7 patients and 2 more) (69 %). Among those 9 patients, 4D PET/CT led to an effective change in radiotherapy volumes for 8 patients. For the 7 patients whose 4D PET/CT was considered as useful for both nuclear medicine physician and radiation oncologist, the mean SUVmax of the liver lesions determined on 4D acquisition was 12,4 mg/mL (+/- 2,8) versus 10,6 g/mL (+/-2,3) on 3D PET/CT. Conclusion: 4D PET/CT appears to be feasible and useful for stereotactic body radiation therapy planning of hepatic tumors.

OP631

Other than restaging phase: Serial FCH PET/CT scans can predict the response to chemotherapy in castrate-resistant prostate cancer?

L. Evangelista[1], U. Basso[1], A. Guttilla[2], F. Zattoni[2], A. Cervino[1], M. Maruzzo[1], V. Zagonel[1], F. Zattoni[2], G. Saladini[1]; [1]Istituto Oncologico Veneto I.R.C.C.S., PADOVA, ITALY, [2]University of Padua, PADOVA, ITALY.

Objectives. The present study aimed to evaluate the utility of serial FCH PET/CT scans to predict the response to chemotherapy in patients with castrate-resistant prostate cancer (CRPCa).Materials and methods. We collected FCH PET/CT data from a consecutive series of 21 CRPCa pre-treated patients (median age: 73 years) who meet the inclusion criteria (mainly, visceral and no-visceral metastasis with a clear uptake on a baseline FCH PET/CT scan and no fewer than two scans separated by at least one month and by no more than 12 months while receiving chemotherapy), in our Institute from June 2010 to October 2014. All patients had at least two FCH PET/CT scans, before and after or during chemotherapeutic treatment (taxanes in 17 patients and abiraterone acetate in 4 patients). Change in FCH uptake (SUVmax of the index lesion; ΔSUVmax) during the course of treatment was compared with clinical assessment response and PSA change (ΔPSA). The correlations were evaluated by using Kruskal-Wallis test for K independent variables, linear regression analysis and Kendall rank correlation coefficient. A $p<0.05$ value was considered statistically significant.Results. The median interval time between PET scans was 5 months (3-11 months). Median (range) PSA value and SUVmax of the index lesion were 25 (1.2-1040) ng/mL, 15.7 (5.9-30.2), 22.9 (2.3-1699) ng/mL and 5.5 (3.2-12.2) respectively at the time of baseline and 2nd PET/CT scan. The median ΔPSA and ΔSUVmax were -49.9 and 8.3, respectively. No correlation between ΔPSA and ΔSUVmax was found ($R=0.046$; $p=0.843$). In accordance with the clinical assessment, 8 (38%) patients were responders, 4 (19%) had a stable and 9 (43%) a progressive disease. A significant overlap was reported for ΔPSA and clinical categories of response ($p=0.685$). Conversely, ΔSUVmax was significantly different in patients with response to chemotherapy as compare to those with stable and progressive disease ($p=0.005$).Conclusions. The change in SUVmax, rather than ΔPSA, represents an important measure of response to chemotherapy and should be useful to stratify the prognosis of CRPCa patients. A large multicenter prospective study is necessary to confirm these findings.

OP632

Role of ^{11}C-CHOLINE PET/CT in the Radiotherapy Treatment Planning of Prostate Cancer Patients

E. Lopci, G. R. D'Agostino, C. Franzese, E. Villa, M. Rodari, M. Scorsetti, A. Chiti; Humanitas Clinical and Research Hospital, Rozzano (Milano), ITALY.

Purpose: In the era of image-guided radiotherapy (IGRT), consisting evidence demonstrates that PET imaging can play a significant role in tumour delineation for several neoplasia. However limited data are available on the use of ^{11}C-Choline PET/CT in radiotherapy (RT) planning for prostate cancer patients. The aim of this study was to verify the impact of this imaging modality in treatment planning of patients eligible for RT. Materials and Methods: For the analysis, we enrolled 37 consecutive patients (mean age 70 years, range 53-85) referred to our Institution for radiation therapy planning with a radical intent (n=7), as salvage therapy (n=15) or in order to plan a re-irradiation (n=15). Patients were submitted to a single-day protocol, including dedicated CT scan of the pelvis and ^{11}C-Choline PET/CT scan. Clinical-tumor volumes (CTV), planning-tumor volumes (PTV) and organs at risk (OAR) were outlined on CT slices with Eclipse Varian Medical System software, whereas Gross tumor volume (GTV)-PET was defined as the area of pathologic uptake and contoured with PETVCAR software on Advantage GE workstation. Results: Among the 7 patients undergoing ^{11}C-Choline PET for a radical radiation treatment, 5 (72%) pts received the planned RT, including 1 pt (14%) with a negative PET. Two (28%) pts showed evidence of positive nodes therefore a boost of dose on pathologic lymphnodes was also delivered. Of the 15 pts candidate to a

salvage RT, 4 (26%) had a negative PET and were irradiated on the prostatic bed as planned. Among the 11 pts with positive PET, 1 (9%) was irradiated only on prostatic bed as planned, 7 (64%) received also a boost on positive nodes, 3 (27%) were not submitted to RT because of the evidence of metastatic disease (2 lungs, 1 bone). Of 15 pts already submitted to RT, and undergoing ^{11}C-Choline PET/CT with a re-irradiation intent, 9 (60%) had a confirmed indication to the planned RT, 1 pt (7%) did not receive RT as planned, having the PET scan showed evidence of lung metastases, 5 (33%) because of a negative exam. Conclusion: In our experience ^{11}C-Choline PET/CT proved to have a significant impact on RT planning of prostate cancer patients, by determining a change in the therapeutic decision in up to 48% of cases, in all the therapeutic settings.

1709 - Sunday, October 11, 2015, 4:00 PM - 4:30 PM, Hall 8
Physics & Instrumentation & Data Analysis: Radiation Exposure & Protection

OP633
Initial experience in the management of radiation protection in clinical use of Ra-223

G. CICORIA[1], F. ZAGNI[1], A. INFANTINO[2], A. CORAZZA[1], D. PANCALDI[1], M. MARENGO[1]; [1]Medical Physics Department, University Hospital "S.Orsola - Malpighi", Bologna, ITALY, [2]Department of Industrial Engineering, Montecuccolino Laboratory, University of Bologna, Bologna, ITALY.

Introduction: 223Ra chloride (Xofigo®) is a novel radiopharmaceutical, currently approved for the treatment of bone metastases of prostate cancer. In this work we studied different radiation protection issues, relevant for both patients and workers, namely the emanation of gaseous 219Rn during the manipulation of the product, the calibration of surface contamination monitors and the presence of long-lived contaminants in the radiopharmaceutical solution. Materials & methods: Presence of 219Rn in the air gap of the vial containing Xofigo was quantified by carefully connecting the vial containing Xofigo and an 11 ml evacuated vial; the procedure was repeated after 5 and 15 minutes. The vial containing the sampled air was then measured in gamma-ray spectrometry. Surface contamination monitors were calibrated by uniformly contaminating three different Rad-Wipe® Smears with a mean activity of (2.18±0.12) kBq of 223Ra and evaluating counts in different positions of the sensitive windows. The investigated instruments were a Berthold LB-124 zinc-sulphide scintillator, Eberline PRM-6GM detector (HP-210 probe) and a Tema Sinergie CPS-51 (TPG46 GM detector). Radionuclidic purity was evaluated by gamma spectrometry of different batches of Xofigo® analyzed 2, 6 and 10 month after the calibration date. All the radioactivity measurements were performed with a spectrometry system equipped with a HPGe detector and multichannel analyzer. The system was properly calibrated in the 59-1836 keV range by means of a multi-radionuclide certified reference solution. Results: 219Rn emanation was 1.2% of the 223Ra activity, at the sampling time. Comparable amounts were found in the samples taken after 5 and 15 minutes. Calibration factors for the probes were (0.013±0.001), (0.09±0.02) and (4.7±0.4) Bq/cps/cm2 for LB124, PRM-6 and CPS-51 respectively. No significant activity of contaminants was detected in the measurements taken at 2 and 6 months after reference date. After 10 months only 227Th was detected (1.7±0.1 Bq). Minimum detectable activity for 226Ra and 228Th was 0.3 Bq. Conclusions: The presence of 219Rn and the quick release from liquid to air makes necessary to dispense 223Ra under ventilated hoods. Calibration of surface contamination meters provided a simple and reproducible way to usefully use these instruments to a first evaluation of surface and skin contamination. The very high radionuclidic purity found for this radiopharmaceutical avoids unjustified dose to patients and allows for easy management of both licensing and waste management issues.

OP634
Risk of Contamination and Incorporation during Preparation and Administering Radium-223-Dichlorid [XOFIGO]

L. Thomas[1], C. Scholl[2], S. Kürpig[3], R. Bundschuh[3], M. Essler[3], H. Ahmadzadehfar[3]; [1]Universitätsklinikum Bonn, Klinim für Neklearmedizin, Bonn, GERMANY, [2]Landesinstitut für Arbeitsgestaltung des Landes Nordrhein-Westfalen, FG 1.3 Strahlenschutz, Düsseldorf, GERMANY, [3]Universitätsklinikum Bonn, Klinik für Nuklearmedizin, Bonn, GERMANY.

Introduction: 223Radium-dichloride(Xofigo) is approved in the EU since November 2013 for treatment of bone metastases of prostate-carcinoma. Xofigo improves the overall survival and is the first alpha-emitter routinely used in medical-application. In most clinically used isotopes external radiation is the main source for radiation-exposure of the staff. However, Ra-223 gives most significant exposure when incorporated. Therefore the aim of this study was to estimate the risk of incorporation for medical staff handling Xofigo. Methods: During 6 month 92 applications with a total administered amount of 528MBq Ra-223 were performed. For risk-estimation of incorporation we measured the contamination in the air with aerosol filters. One in the laminar-air-flow-box(LAF) in which the preparation took place, one attached to the physician and one placed at the patient chair. The latter placed in the height of the face of the physician and the patient respectively. Two days after administration of Xofigo a stool-

sample of the physician was measured as Xofigo is secreted dominantly this way. Gloves worn in the LAF, during injection and cleaning-up were measured for contamination as well as the surgical mask which was worn all the time. At each application day all work-steps were performed by the same physician. Results: Filters from the LAF had a mean activity of 6E-4Bq/l meaning no significant aerosol concentration. The other filters did never show an activity over the quantification limit. In none of the stool samples Xofigo was found over the quantification limit of the method. Contamination measurement of the gloves showed measureable amount of Xofigo when gloves were used during preparation and cleaning-up (1E-1 to 1E4Bq). For the surgical mask in 3 cases a measureable amount of Ra-223 were found (two times 1Bq, 1 time 15Bq), this was most probably caused by cross-contamination when removing the mask. Based on the results of stool-samples and air-filters placed at the physician together with the total activity handled the incorporations factor was estimated according the ICRP model. Conclusion: Stool-samples and filters from the physician and from the application-room let conclude that there is no increased risk of incorporation of Xofigo. However, measurements of the LAF-filter indicated that this is only true for preparation in a LAF. Therefore the use of a incorporation-factor ak=10-7 is justified. Increased activity of Xofigo was found at the gloves, therefore two pairs of gloves with a change of the upper pair between all working steps is strongly recommended to avoid cross-contamination.

OP635

18F-FDG whole body PET/CT: evaluation of effective dose in pediatric patients

F. Zito[1], G. Galetta[2], L. Rossi[2], L. Florimonte[1], E. Orunesu[1], M. Castellani[1], C. Canzi[1], F. Voltini[1], R. Benti[1]; [1]FONDAZIONE IRCCS CA' GRANDA Ospedale Maggiore Policlinico, Milan, ITALY, [2]Scuola di Specializzazione in Fisica Medica Università di Milano, Milan, ITALY.

Aim: To evaluate 18F-FDG PET/CT absorbed dose in pediatric patients to optimize CT acquisition parameters and to improve protection of this high-radiation-sensitive young population.Materials and methods: Eight pediatric patients (age 1-7 years) were retrospectively evaluated. For PET examinations 18F-FDG activity was scaled according to PET scanner sensitivity and body weight of patients (on average 5 MBq/kg) but 37 MBq minimum was injected. Whole-body scans, from head to toe, were acquired after 1 h from the administration with the Biograph TruePoint system(Siemens)having 21.6 cm axial FOV. Images of 3 mm slice thickness were reconstructed with 2 iterations 8 subsets AWOSEM algorithm. All CT scans were carried out with: -automatic control of tube current by setting 60 mAs of reference current, -pitch 0.8, -24x1.2mm beam collimation and -0.5s rotation speed. For four patients CT scans were performed with 120 kV and for the other four with 100 kV. PET effective dose was assessed by multiplying the injected MBq with the ICRP 80 18F-FDG factors (mSv/MBq,interpolated factors to each patient age were used. Based on AAPM report 204, patient-specific-size CTDIvol (CTDIvol_AAPM) was calculated by correcting the scanner CTDIvol with AAPM factors relative to measured patient effective diameter on CT images. CT effective doses were estimated with ImPACT dosimetry calculator, doses referred to adult patient were scaled to pediatric by linear interpolation of Khursheed's factors. Two expert nuclear physicians scored CT image quality based on 1-3 scale, sufficient-good -excellent.Results: The four patients scanned at 100 kV kV had on average 40% reduction of CTDIvol with respect those at 120 kV, without reduction of CT image qualities. The CTDIvol_AAPM corrected for patient specific size was twofold the CTDIvol referred to the standard 32cm phantom size. The sum of PET and CT effective doses ranged from 6.4 to 8.6 mSv; the CT contribute assessed with ImPACT was for six patients on average one half that of PET and was similar to PET for two patients who had CT scans at 120 kV. CT image quality scores were good and excellent, independently on tube kV.Conclusion: This study, even if includes only 8 young patients, confirms the importance to consider the specific body size to estimate exposure dose for PET/CT examinations in young patients. The reduction of kV and then of exposure doses without affecting CT image quality has encouraged our PET/CT Unit to perform CT scans at 100 kV for patients 1-7 years old.

OP636

Efficacy of Clinical Audit on administered activities to paediatric patients undergoing dynamic renal scintigraphy

V. de Sousa[1], F. Lourenço[1], P. Pepê[2], G. Cardoso[1], A. I. Santos[1,3], J. G. Santos[1]; [1]Hospital Garcia de Orta, Almada, PORTUGAL, [2]Escola Superior de Tecnologia e Gestão – Instituto Politécnico de Portalegre, Portalegre, PORTUGAL, [3]Nova Medical School - Universidade Nova de Lisboa, Lisboa, PORTUGAL.

Introduction/Aim: In Europe, every year, more than 6 million paediatric patients, which are more radiosensitive than adults, between 2 to 10 times, undergo a Nuclear Medicine procedure. Thus, there is a need to audit administered activities, in order to evaluate its compliance with adopted Guidelines focused on radiation dose optimization. This study aims to evaluate the efficacy of awareness of technical staff to the results of a previous clinical audit on administered activities to paediatric patients. Methods: A sample of 26 ^{99m}Tc-MAG3 DRS performed to children between July 2014 and April 2015 was collected and a retrospective analysis of gender, age, weight,

administered activity (reported at the time of administration) and reference activity was performed. By reference activity we mean the activity calculated with the Paediatric EANM dosage card, adopted by the Department since its first publication. The results obtained were compared with the ones resulting from a similar analysis performed previously on a sample collected between July 2011 and June 2014 and presented to the staff. Non-parametric tests were used, considering the size of the samples and/or the Non Gaussian distribution of the values. Results: The sample collected between July 2011 and June 2014 comprised 39 females and 50 males with a median age of 36 [8, 108] months and a median weight of 15.0 [8.8, 30.5] Kg. Applying the Related-Samples Signed Rank Test (for a non Gaussian non symmetrical distribution) it was obtained a strong evidence that the statistical median of the differences between the administered and the reference activities was different from zero ($p<0.001$). The median administered activity was 39.5 [31.3, 53.2] MBq and the median reference activity was 28.0 [20.3, 43.3] MBq. These results were presented and discussed with the staff. The second sample, collected between July 2014 and April 2015 comprised 10 girls and 16 boys, with a median age of 11 [3.8, 99] months and median weight of of 9.8 [6.2, 27.2] Kg. Using the Related-Samples Wilcoxon Test (for a non Gaussian symmetrical distribution) there was a statistical evidence that the median of the differences between the administered and the reference activities is equal to zero ($p<0.07$). The median administered activity was 24.1 [18.1, 39.6] MBq and the median reference activity was 21.8 [17.8, 34.4] MBq. Conclusion: Considering the results obtained we confirm that a very simple audit procedure improves awareness and optimization of the practices, and allows acknowledging compliance to Guidelines formally adopted.

OP637

Cumulative Radiation Dose Received by Diagnostic Imaging During Staging and Treatment of Primarily Operable Ewing Sarcoma in Patients Diagnosed in Norway 2005-2012.

B. Johnsen[1], K. Fasmer[1], K. Boye[2], K. Rosendahl[3,4], M. Biermann[1,4], C. Trovik[5,4], S. M. Aukland[3,4]; [1]Centre of Nuclear Medicine and PET, Department of Radiology, Haukeland University Hospital, Bergen, NORWAY, [2]Department of Oncology, The Norwegian Radium, OSLO, NORWAY, [3]Pediatric Section, Department of Radiology, Haukeland University Hospital, Bergen, NORWAY, [4]Department of Clinical Medicine,University of Bergen, Bergen, NORWAY, [5]Ortopedic Section, Department of Surgery, Haukeland University Hospital, Bergen, NORWAY.

Objective. Ewing sarcoma is a malignant tumour mainly affecting children and young adults. Planar X-ray, Ultrasound, Computed tomography (CT), Magnetic Resonance Imaging and Skeletal Scintigraphy constitute the conventional" imaging methods. Methods reflecting the biology of the tumour, like F18 FDG PET-CT, are now emerging. During treatment, studies evaluating renal (glomerular filtration rate (GFR), radioisotope renography) and cardiac function (Multi Gated Acquisition Scan (MUGA)) is performed. There is a growing awareness of potential secondary radiation induced malignancy in children and young adults cured of their primary cancer. This national, population based study summarizes all radiological and nuclear medicine (NM) imaging including F18 FDG PET-CT in diagnostics and treatment of patients with primarily operable Ewing sarcoma. Material and methods. 61 patients below 30 years diagnosed with Ewing Sarcoma in Norway in the period 2005-2012 were identified from the Scandinavian Sarcoma registry in Malmoe. Of these, 20 patients met the inclusion criteria: primarily operable Ewing sarcoma, preoperative chemotherapy with operation in week 11, no metastasis or residual disease in a minimum follow up period of 1 year after diagnosis. The mean age was 15 years (range 4-27). The radiation doses the patients received from all radiological (planar X-ray and CT) and nuclear medicine imaging (MUGA, GFR, radioisotope renography, skeletal scintigraphy and PET-CT) 4 months prior to biopsy date to 12 months after biopsy date, was calculated for each patient using dedicated Monte Carlo based dose estimation software tools. Results. The mean (range) estimated cumulative radiation dose a patient received from all radiological and nuclear medicine imaging including PET-CT was 39 (6-86) mSv. Of this total planar X-ray imaging counted for 3 (0-16) mSv, CT imaging 13 (2 - 28) mSv, nuclear medicine imaging (excluding PET-CT) 17 (2 - 51) mSv and PET-CT 6 (0 - 23) mSv. Conclusion. In this study of children and young adults diagnosed with primarily operable Ewing Sarcoma in Norway in the period 2005-2012, the estimated cumulative radiation dose a patient received during the first year after diagnosis was 39 mSv. Compared to the total radiation burden, the contribution from nuclear medicine imaging was 59 % while PET- CT imaging alone contributed to only 15% of the total radiation dose. This study revealed a wide range, both regarding which diagnostic imaging modalities and examination that is performed on this patient group and also regarding the cumulative doses resulting from these examinations.

OP638

Practical assessment of local diagnostic reference levels for PET/CT scans with 68Ga-DOTA peptides

G. Lucconi[1,2], M. Ranaldo[2], F. Zagni[2], G. Cicoria[2], S. Fanti[3], M. Marengo[2]; [1]Alma Mater Studiorum - Bologna University, Bologna, ITALY, [2]Medical Physics Department, S.Orsola–Malpighi University Hospital, Bologna, ITALY, [3]Nuclear Medicine Department, S.Orsola-Malpighi University Hospital, Bologna, ITALY.

Aim: to establish local Diagnostic Reference Levels (DRL) for PET/CT studies with 68Ga-DOTA peptides. Materials & Methods: a sample of 50 patients undergoing 68Ga-DOTANOC PET/CT was retrospectively studied. Scans were acquired using a Discovery 710 and two Discovery STE PET/CT scanners (GE Healthcare) in a period of three months. The CT acquisition was performed following a "low dose" protocol having the following parameters: 120 kV, 80 mA, 0.8 s/tube rotation, pitch 1.75, collimation 20 mm, and 3.75 mm slice thickness; the PET acquisition lasted 3 min for each bed position, having a length of 15 cm and a superposition of 1.1 cm. Unitary patient doses were automatically dispensed by a μ DDS-A system (Tema Sinergie S.p.A.), scaled according to the weight of the patient and measured with a CAPINTEC CRC 15 PET activity meter. The accuracy of the activity meter was assessed using a NIST traceable standard source of 68Ge/68Ga. DRL for CT acquisition were assessed as the 75th percentile of the distribution of the values of CTDI and DLP. DRL for the administered activity were set as the mean activity in the patients' sample, obtained from the normal distribution fitted to observed activity values. These values were then used to estimate the effective and organ doses for a standard patient through ImPACT CT patient dosimetry calculator and the dose-activity coefficients reported in the literature. Results: since the differences in CTDI values observed among the three scanners were small, the data were pooled, giving DRL of 3.82 mGy for CTDI and 381 MBq cm for DLP. DRL for 68Ga-DOTANOC activity resulted 103 MBq and 1.5 MBq/kg, which is close to the inferior limit stated by international guidelines, revealing the capability of modern PET scanners to obtain diagnostic images with a relatively low amount of radioactive tracer. Effective doses of 5.4 mSv and 2.6 mSv were calculated for the CT and PET part respectively. The organs receiving the highest dose were thyroid, bone surface and thymus (8.5, 7.8 and 6.7 mGy) for the CT acquisition, while kidneys, urinary bladder wall and spleen (9.1, 8.5 and 7.4 mGy) for 68Ga-DOTANOC administration. Conclusions: local DRL have been assessed for 68Ga-DOTANOC PET/CT scans, according to international guidelines. These levels and the dosimetric evaluation performed may be a useful tool for optimization and comparison for other centers approaching this technique.

OP639

External radiation exposure of nuclear medicine personnel using an automatic 18F dispenser

R. Matheoudf, D. Lizio, G. Sacchetti, M. Brambilla; AOU Maggiore della Carità, novara, ITALY.

Aim. Personnel working with radiopharmaceuticals in nuclear medicine are subject to radiation exposure, and fingers are likely to receive the highest dose, especially when handling beta+ emitting radionuclides used in PET imaging. Recently, fully automated systems have been introduced to partition ^{18}F activity from the mother vial directly into syringes ready for automatic patient injection, to reduce both external irradiation and the risk of contamination. The aim of this work was to evaluate the radiation exposure of nuclear medicine personnel during the ^{18}F-fluorodeoxyglucose (FDG) loading and partition procedures performed using the automatic ^{18}F dispenser Karl100™ (TemaSinergie, SpA). Materials and Methods. Dose rate (DR) at close contact to Karl100 was monitored with the inbuilt Geiger Mueller detector (LND71210) for loading, dilution and flushing phases of ^{18}FDG transferring from mother vial into Karl100 dispensing kit and for syringe preparation, on a 4 months period. Finger dose (FD) was measured for both the technician operating on Karl100 and for physician who injected patients with the semiconductor dosimeter NED (Unfors Instruments, Inc.)worn on the finger tip of the non dominant hand and on the finger tip used for activation of automatic patient injector, by the technician and physician, respectively, on a 15 days period. Results. The highest DR were measured during ^{18}FDG mother vial loading phase (mean 25.7 μSv/h, range 9.6-37.3 μSv/h) that lasted about 1 minute. DR during syringe preparation was lower (mean 7.0 μSv/h, range 4.3-13.0 μSv/h). FD were in the range 15-87 μSv/GBq of ^{18}FDG activity (mean 42 μSv/GBq) and 33-83 μSv/GBq (mean 56 μSv/GBq) for technicians and physicians, respectively, and corresponded to the daily workload. These values resulted inferior to the lower FD ranges reported in ORAMED study in 2012.onclusion. Karl100™ guarantees a high level of radiation protection of the workers. In the cautelative hypothesis that the same technician stands at close contact to the Karl100 during both mother vial loading and ^{18}FDG partition of 12 doses per day, by using the highest DR measured, this would result in an effective dose of about 230 μSv/y. In the hypothesis of the same technician working on Karl100, he would have an extremity equivalent dose of 17 mSv/y, while for the same nuclear medicine physician injecting all the patients he would receive 3.6 mSv/y.

OP640

Skin dose saving of the staff in 90Y/177Lu PRRT therapy with the Automatic Dose-Dispenser (ADD)

F. Fioroni[1], **E. Grassi**[1], G. Cavatorta[2], S. Rubagotti[1], G. Feliciani[1], M. A. Sarti[1], A. Filice[1], A. Versari[1], M. Iori[1]; [1]IRCCS-ASMN, Reggio Emilia, ITALY, [2]University of Bologna, Bologna, ITALY.

Purpose: Labelling and administration of 90Y-DOTATOC and 177Lu-DOTATOC are very hazardous procedures because of the skin exposure to beta radiation. A variety of methods to decrease this risk has been looked for and the outcome of one of them is hereby evaluated. Aim was to investigate the equivalent dose saving of the staff working with 177Lu and 90Y in a nuclear medicine unit, when changing from an essentially

manual radiolabelling procedure to a semi automatic synthesizer ADD.Methods: Chemist and physician are the figures exposed. They were asked to wear TLDs on their fingertips, to evaluate the quantity Hp(0.07) to the skin and to replace them after each labelling and administration procedure.Data collected from 2009 to 2014 were divided into two groups: before introducing ADD (NoADD) and after introducing ADD (ADD), considering 52 procedures (177Lu) , 41 (90Y) in NoADD; 67 (177Lu) and 48 (90Y) in ADD. The mean handled activity: 23.57GBq(177Lu) and 14.31GBq(90Y) in NoADD, 30.11Gq(177Lu), 15.11GBq(90Y) in ADD.Though ADD affects only chemist work, it was considered the same division even for medical staff doses, feeling confident to identify a learning curve.Data were analysed with simple statistical tests (t-test and Wilcoxon-Mann-Whitney, p=0.05) and shown separately for chemist and physician.Results: For the chemist, Hp(0.07) mean values (95% percentile) for ADD and NoADD are 0.019(0.076) and 0.030(0.099) mSv/GBq respectively for 90Y, while 0.007(0.023) and 0.022(0.037) mSv/GBq respectively for 177Lu. T-test provided P<<0.05 for both isotopes.The relative differences before and after ADD collected for every finger and considered separately for each isotope were treated with Wilcoxon test. P-value<0.05 .For the medical staff, Hp(0.07) mean values (95% percentile) for ADD and NoADD are 0.0143(0.0565) and 0.021(0.0762) mSv/GBq respectively for 90Y, while 0.0009(0.00263) and 0.0011(0.00196) mSv/GBq respectively for 177Lu. T-test provided P<0.05 for both isotopes.The relative differences before and after ADD collected for every finger and considered separately for each isotope were treated with Wilcoxon test. P-value>0.05.ConclusionsADD affects positively the dose saving of the chemist in handling both isotopes and the dose saving depends on the isotope used, when data are analysed finger by finger.For the reason mentioned above, ADD doesn't affect strongly the medical staff dose saving. However, the mean value analysis shows a learning curve of the workers to inferior doses in more recent time. The difference in doses doesn't depend on the isotope used, when data are analysed finger by finger.

1710 - Sunday, October 11, 2015, 4:00 PM - 4:30 PM, Hall D
Neurosciences: Movement Disorders

OP641

Evaluation of nigrostriatal oxidative stress intensity in patients with Parkinson's disease using [Cu-62]ATSM PET and FP-CIT SPECT

H. Okazawa[1], M. Ikawa[1], T. Tsujikawa[1], T. Mori[1], A. Makino[1], Y. Kiyono[1], M. Yoneda[2]; [1]University of Fukui, FUKUI, JAPAN, [2]Fukui Prefectural University, FUKUI, JAPAN.

Introduction: To evaluate degree of oxidative stress and mitochondrial dysfunction in the nigrostriatal dopaminergic neurons of Parkinson's disease (PD), positron emission tomography (PET) with [Cu-62]diacetyl-bis(N4-methylthiosemicarbazone) (Cu-ATSM) and dopamine transporter (DaT) imaging were applied to patients with PD. Methods: Nine patients with PD (69 ± 5y) who showed lateral dominant symptoms at onset underwent Cu-ATSM PET. They also underwent [I-123]FP-CIT SPECT to evaluate presynaptic nigrostriatal dopaminergic deficit as well as DaT density. Dynamic PET data acquisition was performed, and standardized uptake value (SUV) images were calculated from the delayed phase data of 10-20 min frames after the injection. Multiple circular regions of interest (ROIs) were drawn on the bilateral striata and mean values from each side were used for analysis. The striatum-to-cerebellum SUV ratio (SCR) was calculated from the SUVs of the striatum and the cerebellar cortex. The same striatal ROIs were applied to the [I-123]FP-CIT SPECT images and distribution volume ratio (DVR) was calculated. Finally, SCR to DVR ratio (SDR) were obtained and used for further analysis. Results: The means of SCR, DVR and SDR of the bilateral striata in patients were 1.04 ± 0.04, 1.20 ± 0.08 and 0.88 ± 0.05, respectively. The mean values of the striatum contralateral to the initially affected body side (the dominant striatum) were lower in DVR and greater in SCR and SDR compared to the contralateral side. Although the difference in SCR was not significant, DVR and SDR showed significant difference between the bilateral striata ($P < 0.05$). The SDR of the dominant striatum showed a positive correlation with the Unified Parkinson's Disease Rating Scale (UPDRS) rating ($r = 0.67$, $P < 0.05$), indicating oxidative stress increased according to the progression of disease severity in the dominant striatum. Conclusions: Degree of oxidative stress calculated from accumulation ratios of Cu-ATSM to [I-123]FP-CIT in PD patients revealed that the dominant striatum suffered from intense oxidative stress which correlated well with the severity of symptoms. These findings indicates that oxidative stress associates with striatal neurodegeneration in PD.

OP642

FDG-PET/CT in presymptomatic and symptomatic Huntington's disease: Possible predictor of disease progression?

D. Lopez[1], V. Camacho[1], A. Fernandez[1], J. Perez Perez[2], S. Martinez-Horta[2], F. Sampedro[3], C. Achury[1], R. Jaller[1], A. Montes[1], I. Carrió[1]; [1]Nuclear Medicine department. Hospital de la Santa Creu i Sant Pau, Barcelona, SPAIN, [2]Neurology department. Movement Disorder Unit. Hospital de la Santa Creu i Sant Pau, Barcelona, SPAIN, [3]Universitat Autonoma de Barcelona, Barcelona, SPAIN.

PURPOSE: To assess metabolic changes in cerebral 18F-FDG PET/CT in presymptomatic (preHD) and symptomatic (sHD) Huntington's disease (HD) patients, to assess patterns of FDG uptake, and to correlate PET/CT findings with clinical evolution. MATERIALS AND METHODS: Thirty three patients (8 male, mean age=44, range [26-69]) carrying the HD mutation (mean CAG=43) were prospectively included. Based on the Unified Huntington's Disease Rating Scale (UHDRS) motor score and Total Functional Capacity, patients were classified as presymptomatic (preEH=16; UHDRS <4) and symptomatic (sEH=17; UHDRS>4). Subsequently, preHD patients based on Langbehn formula were classified as near (preHD-A=8) and far (preHD-B=8) to onset of clinical manifestations. A separate group of 18 healthy subjects, matched with patients by age and gender, was used as control (4 male, mean age=48 [32-69]). Brain PET/CT was performed 60 minutes after i.v. injection of 277 MBq of 18-FDG on a Philips Gemini TF. Images were initially assessed by 2 nuclear medicine physicians identifying qualitative metabolic changes in the striatum and cerebral cortex. Analysis and quantitative assessment of regional cerebral activity was performed using the Statistical Parametric Mapping (SPM8). For the regional quantitative analysis, the clusters of interest were extracted and computed to the relative standard uptake value (SUVr) of the regions of interest related to the stage of the disease. RESULTS: In the visual analysis, sHD patients presented a significant hypometabolism in striatum compared to preHD patients and controls. Quantitative analysis demonstrated a significant striatal hypometabolism in sHD respect to preHD-A and preHD-B [$p<0.05$ (FWE), EVTk=100 voxels]. Additionally, a significant decrease in metabolism of striatum in both preHD groups respect to GC was demosnstrated, showing a hypometabolic pattern in striatum that progressively declines across disease stages [$p<0.001$ uncorrected, k=10 voxels]. In addition, a significant hypermetabolism in the sHD patients was shown in the prefrontal cortex and cerebellum [$p<0.001$ uncorrected EVTk=10 voxels]. CONCLUSION: HD patients presented a significant progressive hypometabolism in striatum across the disease stages compared to controls. sHD presented a marked hypometabolism with respect to preHD. In sHD patients, a significant hypermetabolism in prefrontal cortex and cerebellum was seen probably related with movement disorder. FDG-PET/CT seems to be an early predictor for disease progression in HD.

OP643

Frequency of ^{123}I FP-CIT image characteristics differ between movement disorder and Lewy Body dementia referrals

A. Nicol[1], R. Jampana[2], C. Santosh[2], M. T. Hansen[2]; [1]South Glasgow University Hospital, Glasgow, UNITED KINGDOM, [2]Institute of Neurological Sciences, South Glasgow University Hospital, Glasgow, UNITED KINGDOM.

^{123}I FP-CI T imaging is used to evaluate the loss of functional dopaminergic neuron terminals in the striatum of patients with movement disorders (including Parkinson's disease, essential tremor, drug induced tremor) or Lewy Body dementia. The frequency of ^{123}I FP-CIT image characteristic appearances for the different referral groups will be assessed. Consecutive patients over a four month period were included (n=179). Scanning was performed on a Mediso four head scanner approximately three hours after administration of 185MBq ^{123}I FP-CIT. Referrals were divided into three categories: movement disorders, Lewy Body Dementia (DLB), clinical information including a mixture of these two categories. Scans were evaluated visually, using striatal:occipital ratio quantification as an adjunct as required. Images were categorised as follows: (a) normal (b) reduced uptake:putamen < caudate (c) balanced reduced uptake (weak comma) or (d) other (none of above). Clinical referrals were received for movement disorders in 151 of cases (84%), DLB in 17 cases (10%) and mixed referral information in 11 cases (6%). Normal image appearances were obtained in 54% of movement disorder referrals, 53% of DLB referrals and 73% of mixed clinical referrals. Of the abnormal scans, reduced uptake: putamen < caudate & balanced reduced uptake (weak comma) appearances were obtained in 38% & 3% of movement disorder referrals; 12% & 29% of DLB referrals and 0% & 9% of mixed referrals. 'Other' appearances, dominated by the presence of vascular components, occurred in 5% of movement disorder referrals, 6% of DLB referrals and 18% of mixed referral information . A chi squared test of homogeneity was performed for the movement disorders and Lewy Body Dementia referrals (n=168). This rejected the null hypothesis that the frequency of normal : putamen < caudate : balanced reduced uptake (weak comma) appearances was identical in these two patient referral groups ($p<0.01$) These results indicate that the frequency of ^{123}I FP-CIT image characteristics differ between movement disorders and Lewy Body Dementia referrals. This is critically important when clinically evaluating scans.

OP644

[11C]Donepezil PET demonstrates parasympathetic denervation in the gut of most patients with de novo Parkinson's disease (PD).

T. Fedorova[1], L. Seidelin[1], S. Jakobsen[1], E. H. Danielsen[2], D. J. Brooks[1], **P. Borghammer**[1]; [1]Department of Nuclear Medicine & PET Centre, Aarhus University Hospital, Aarhus C, DENMARK, [2]Department of Neurology, Aarhus University Hospital, Aarhus C, DENMARK.

Background: We recently demonstrated that most PD patients at a moderate disease stage display decreased [11C]donepezil PET signal in the small intestine, and 2/3 of patients displayed a similar decrease in the pancreas (Gjerløff et al, Brain 2015). It is thought that parasympathetic denervation may predate motor symptoms in PD, and parasympathetic PET imaging may therefore be a potential diagnostic marker at pre-motor stages of the disease. Objective: We used the acetylcholinesterase PET ligand [11C]donepezil to estimate the peripheral parasympathetic innervation in de novo PD. Methods: So far 17 PD patients at an early disease-stage (mean 1 year disease duration) and 10 matched control subjects were enrolled. All study participants were PET/CT scanned using [11C]donepezil. The PET signal in the myocardium, gastrointestinal tract, and pancreas was compared between groups. Results: The de novo PD patients displayed significantly decreased [11C]donepezil SUV values in the small intestine (-24%, $p<0.0001$), but not in the pancreas ($p=0.75$). A trend towards decreased signal was seen in the myocardium (-11%, $p=0.07$). Conclusions: The data implies that marked parasympathetic denervation in the gut of PD patients is established already at the time of diagnosis, whereas pancreatic denervation may be a secondary phenomenon. [11C]donepezil PET could therefore have application as a diagnostic marker in PD - maybe already at the pre-motor stage. We are currently initiating a longitudinal [11C]donepezil PET study of pro-dromal PD patients with REM sleep disorder to test this hypothesis

OP645

Brain metabolic changes in patients with Essential Tremor and progressive gait ataxia under thalamic deep brain stimulation

J. Brumberg[1], G. Marotta[2], M. Reich[3], F. Steigerwald[3], N. Pozzi[3], C. Lapa[1], S. Samnick[1], K. Herrmann[1], J. Volkmann[3], A. Buck[1], I. Isaias[3]; [1]Department of Nuclear Medicine, University Hospital Würzburg, Würzburg, GERMANY, [2]Department of Nuclear Medicine, Fondazione IRCCS Ca Granda - Ospedale Maggiore Policlinico, Milano, ITALY, [3]Department of Neurology, University Hospital Würzburg, Würzburg, GERMANY.

AIM: We investigated brain metabolic changes under different deep brain stimulation (DBS) parameters in patients with Essential Tremor (ET). We aimed to disentangle the effect of thalamic stimulation from disease progression in the evolution of gait- or limb-ataxia. MATERIALS AND METHODS: We investigated five subjects with ET (two males; median age: 74 years, range: 63-84 years) under stable bilateral thalamic DBS (no stimulation changes in the last four weeks) with progressive and severe gait-ataxia (unable to walk unassisted) by means of 18F-fluorodeoxyglucose (FDG) and two sequential cerebral positron emission tomographies (PET). PET scans were conducted stim-on and 72h after stimulation holidays (stim-off) according to a standardized protocol. Patients were fully relaxed in a lying position without any voluntary movement between the FDG injection and the scan. We performed a statistical parametric mapping voxel-by-voxel group comparison (stim-on vs. -off) applying the proportional global mean, threshold at $p<0.1$ and corrected for Family wise-error (FWE). RESULTS: At 72h stim-off, gait ataxia improved in all subjects (all were able to walk unassisted), whereas tremor reappeared with a pre-surgery severity. Compared to 72h stim-off, FDG uptake in stim-on was significantly increased selectively in the flocculonodular lobe of cerebellum ($T=6.40$, $p<0.01$) and reduced in the right medial frontal and bilateral precentral gyri (right BA 6, $p<0.001$ and left+right BA 4, $p<0.001$). CONCLUSIONS: Multiple PETs can play a relevant role in defining brain metabolic changes in different clinical or therapeutic (e.g. DBS) settings. Our findings are evocative of an antidromic effect of thalamic DBS on outflow pathways of the vestibulocerebellum in patients with ET. Accordingly, in these patients, gait-ataxia might be interpret as a stimulation side effect rather than an additional sign of this disease.

OP646

18F-FDOPA PET reveals a rostro-ventral striatal dopaminergic depletion in Parkinson's disease patients with impulse control disorder.

A. Marí Hualde, E. Prieto, L. Sancho, M. Ribelles, C. Juri, M. Rodríguez-Oroz, J. Obeso, J. Arbizu; Clinica Universidad de Navarra, Pamplona, SPAIN.

Background: Many Parkinson's disease (PD) patients experience non-motor symptomatology. Impulse control disorders (ICDs), including compulsive gambling, buying, sexual behaviour, and eating, is a severe complication difficult to diagnose that can occur in a significant number of PD population (6,1-31,2%). While these abnormal behaviours are associated with dopaminergic treatments, a differential pattern of nigrostriatal dopaminergic denervation has been suggested by findings in DAT-scan. Functional brain differences in PD patients with and without ICD remain poorly understood. Objective: To ascertain the striatal pattern of dopaminergic depletion by L-3,4-Dihydroxy-6-[18F] fluorophenylalanine (18F-FDOPA) Positron Emission Tomography (PET) in PD patients with and without ICD. Methods: 60 PD 18F-FDOPA PET scans were studied (30PD-ICD and 30 PD without a life history for ICD), as well as 16 healthy controls (HC). 12 of the PD-ICD patients had a previous basal 18F-FDOPA PET. Disease severity was ascertained with the UPDRS and the Questionnaire for Impulsive-Compulsive Disorders in PD (QUIP) and Levodopa

equivalent dose (LED) was calculated in each patient. A voxel-based-analysis (SPM) was applied to measure 18F-FDOPA uptake (Ki) between all of them. Results: PD-ICD and PD without ICD, did not differ in age or UPDRS punctuation. All PD patients showed a typical striatal denervation pattern with predominance reduction in 18F-FDOPA uptake in the caudal putamen. 18F-FDOPA uptake was significantly reduced in the anterior and ventral striatum in ICD-PD patients compared to those without ICD ($p<0,01$). But no difference was found between PD previous to ICD symptomatology scan, when compared to 12 PD without life history of ICD paired by age, LEDs and PD progression time. Total LED was higher ($p=0,006$) in ICD-PD patients (mean 957,2) compared to the non- ICD group (mean 501,27). No significant difference was found in the mean dose of dopaminergic agonist LEDs. Conclusions: This study confirms a significant reduction in ventral striatal dopaminergic activity in ICD-PD patients by 18F-FDOPA PET in advanced disease but not in basal conditions. However, the ICD-PD group received higher dose of dopaminergic agents. The interaction between denervation and treatment probably defines the origin of ICD in PD.

OP647

Correletion between 123I-FP-CIT SPECT and cognitive outcome in Parkinson's disease: 5 years of follow-up

G. Puccini[1], R. Ceravolo[2], F. Guidoccio[1], D. Frosini[2], S. Chiacchio[1], M. Gennaro[1], U. Bonuccelli[2], D. Volterrani[1]; [1]Regional Center of Nuclear Medicine, University of Pisa, PISA, ITALY, [2]Neurology Unit, Department of Clinical and Experimental Medicine, University of Pisa, PISA, ITALY.

Aim: Dopamine transporter (DAT) imaging is a common diagnostic tool for Parkinson's Disease (PD) but also evaluated as prognostic marker for both motor and non motor outcomes. The ability of coping an intersecting pentagons is considered an important clinical predictors of global cognitive decline. In this study we evaluated the prognostic role of DAT imaging and pentagon copy for cognitive outcome in a cohort of PD patients with a follow up of five years. Materials and methods: Ninety-five de novo PD patients underwent DAT imaging at baseline. Striatal semiquantitative indices were calculated with basal ganglia matching tool. All the patients were assessed with Unified Parkinson's Disease Rating Scale (UPDRS) part III for motor related impairment and Mini-Mental State Examination (MMSE) for cognitive functions at baseline and each year of the five years of follow up. The occurrence of dementia in the five years of follow up was collected. According with MMSE and pentagon test score we further divided the subjects into two sub-groups. Results: During follow up 18% of patients developed dementia. Patients developing dementia in the follow up period had lower striatal binding at baseline ($p<0.01$). The frequency of impairment in pentagon copy was significantly higher in PD patients developing dementia ($\chi2=9.9$, $p<0.001$). Rather not statistically significant, patients developing dementia showed higher level of motor impairment (UPDRS III 22 vs 18 respectively for PD with dementia and not developing dementia) and lower MMSE at baseline (MMSE 26 vs 28 respectively for PD developing dementia and not developing dementia). Binary logistic regression analysis was performed dichotomizing striatal uptake value according to striatal median uptake (2.3). The model contained two independent variables (striatal uptake and pentagon copy), the full model was statistically significant ($\chi2=20.7$, $p<0.001$) and as whole was able to predict the 35% of the variance in cognitive status. Both variable independently contribut ed to the model with an Odd Ratio respectively of 15.9 and 4.9 for low striatal baseline uptake and pentagon copy impairment. Conclusion: Our findings show that DAT imaging performed at baseline and visuospatial and constructional ability as evaluated by pentagon copy intersection performance are associated with cognitive outcome in PD patients. Multiple variables have been associated to the risk of dementia in PD. In line with previous findings our data confirm that the integration of dopaminergic deficit and the dysfunction of cortical posterior area are associated with the risk of cognitive impairment.

OP648

Initial Evaluation of [18F]GE-180 PET Imaging in Relapsing-Remitting Multiple Sclerosis Patients

S. Sridharan[1], C. Buckley[2], W. Trigg[2], W. Trigg[2], K. Heurling[2], P. Sherwin[2], D. Brooks[2], J. Crouch[3], J. Crouch[3], M. Lawler[3], R. Hinz[1], R. Paulseth[3], S. Amodeo[3], K. Gulenchyn[3]; [1]University of Manchester, Manchester, UNITED KINGDOM, [2]GE Healthcare, Amersham, UNITED KINGDOM, [3]St. Joseph's Hospital, Hamilton Health Sciences, Hamilton, ON, CANADA.

Introduction: Multiple sclerosis (MS) is characterised by demyelination, but it is known from pathology studies that inflammation, evidenced by infiltrating immune cells and activated microglia in normal appearing white matter (NAWM), is also present at different disease stages. The effects of inflammation on MS progression are not yet understood; positron emission tomography (PET) offers the opportunity to monitor these effects and thus aid patient stratification and guide therapy selection, adding to the information already available from MRI techniques.The 18 kDa translocator protein (TSPO) is upregulated in activated microglia, which are present in inflammatory lesions and NAWM in MS. [^{11}C]-(R)-PK11195 is a TSPO-PET ligand which is known to show localisation and extent of inflammation in many brain diseases, including MS[1], but suffers from a

poor signal to noise ratio (SNR) and short (20 minutes) half-life. [18F]GE-180 is a novel TSPO-PET ligand which has shown improved SNR and lower non-specific binding than [^{11}C]-(R)-PK11195 in pre-clinical models[2]. Here, we present initial results from a phase 1 study in relapsing-remitting MS (rrMS) and healthy control subjects (HVs).Methods: HVs and rrMS subjects were assessed for binding status. One non-binder in each group was included. Subjects underwent T1 pre and post gadolinium enhanced MRI scans and T2 scans additionally. 90 minute dynamic [18F]GE-180 PET scans were performed typically within 1 month. PET and T1 pre-contrast MR images were co-registered in the software package PMOD, and the Hammers atlas[3] was applied to acquire standardised uptake values (SUVs) for regions of interest (ROIs). Selected areas of T2 hyperintensity were defined manually to give MS lesion SUVs. A cortical composite grey matter (GM) region was chosen as reference for SUVRs.Results: No Gd-enhancing lesions were identifiable from T1 post-contrast MRIs. With [18F]GE-180, whole WM uptake (SUVRGM) was slightly higher in rrMS than HVs, while a lesion-rich periventricular (PV) area yielded SUVRs which were approximately 10% higher in rrMS than HVs. PET-defined lesions in rrMS showed an elevation of 20 - 40% compared to HVs.Conclusion: Preliminary results suggest that [18F]GE-180 is able to identify areas of inflammation in PET images which are non-Gd-enhancing in T1.[1] Rissanen, E. et al. 2014, J. Nucl. Med., 55: 1-6[2] Boutin, H et al. 2015, Eur. J. Nucl. Med. Mol. Imaging, 42: 503-511[3] Hammers, A. et al. 2002, Hum. Brain Mapp., 15: 165-174.

1801/1803 - Wednesday, October 14, 2015, 12:15 PM - 13:15 PM, Hall 1

Plenary 4: Highlights Lecture

OP649

Highlights Lecture

A.K. Buck, **GERMANY**
C. Decristoforo, **AUSTRIA**

Poster Walks

PW01 – Sunday, October 11, 2015, 8:30 AM - 9:30 AM, Hall 3 – Poster Exhibition

Poster Walk 1 - Radiopharmaceuticals & Radiochemistry: Radiopharmaceuticals I

PW001

18F-5-FPN, a Novel PET Imaging Probe Targeting Malignant Melanoma

X. Lan, H. Feng, X. Xia, Y. Song, C. Qin, Q. Liu, Y. Zhang; Union Hospital, Tongji Medical College, Huazhong University of Science and Technology, Wuhan, CHINA.

Aim: Melanoma is one of the most aggressive skin cancers, and early diagnosis and accurate staging are important for planning therapeutic intervention to improve patient outcomes. Radiolabeled benzamides (BZAs) are attractive candidates for targeting melanoma because they bind to melanin and exhibit high tumor uptake and retention. In this study, we synthesized a BZA analog, 5-bromo-N-(2-[diethylamino]ethyl) picolinamide, labeled it with 18F, and named it 18F-5-FPN. We evaluated its binding affinity to, and specificity for, melanin, and its in vivo pharmacokinetics, to assess its potential value in diagnosing and staging melanoma. Methods: (N-[2-Diethylamino] ethyl)-5-fluoropicolinamide and its bromo- precursors were prepared, and radiofluorination of 18F-5-FPN with a radio-synthesis module (GE TraceLab FXFN GE Healthcare, Milwaukee, WI, USA) was performed and purified. Its binding specificity was measured in vitro in two different melanoma cell lines, one pigmented (B16F10 cells) and one nonpigmented (A375m cells), and in vivo in mice xenografted with the same cell lines. Dynamic and static positron-emission tomography (PET) images using 18F-5-FPN were obtained in the tumor mice, and the static images were compared with those acquired with 18F-fluorodeoxyglucose (18F-FDG). Lung metastases mice bearing B16F10 tumor were also performed PET imaging with 18F-5-FPN. Results: 18F-5-FPN was successfully prepared with radiochemical yields of 5%-8%. Cellular uptake study revealed that binding of 18F-5-FPN to B16F10 cells was much higher than that to A375m cells. Dynamic PET images showed that B16F10 tumor could be seen about 1 min after injection of the tracer, and the uptake gradually increased over time. 18F-5-FPN was rapidly excreted by the kidneys. Static images acquired 1 and 2 h after injection revealed clearly visible B16F10 tumors, with high uptake values of 24.34 ± 6.32 and 16.63 ± 5.41 % ID/g (n=5) in the biodistribution study, and tumor-to-muscle and tumor-to-blood ratios reached to 43.90 ± 9.09 and 65.52 ± 10.76 at 2 h, respectively. In contrast, there was no visible uptake by the A375m tumors. 18F-5-FPN and 18F-FDG PET imaging were compared in B16F10 tumor xenografts, and the tumor-to-background ratio of 18F-5-FPN images were 10 times higher that of 18F-FDG (35.22 ± 7.02 vs 3.29 ± 0.53, n=5). 18F-5-FPN PET imaging also detected simulated lung metastases measuring 1-2 mm. Conclusions: 18F-5-FPN specifically targeted melanin in vitro and in vivo with higher retention, affinity and favorable pharmacokinetics. 18F-5-FPN may be an ideal molecular probe for melanoma diagnosis and staging. This work was supported by NSFC 81371626.

PW002

PET imaging of a feeding center using [11C]BU99008 with ultra-high specific activity

K. Kawamura[1], Y. Shimoda[1], J. Yui[1], Y. Zhang[1], T. Yamasaki[1], H. Wakizaka[1], M. Fujinaga[1], K. Kumata[1], L. Xie[1], A. Hatori[1], M. Ogawa[1,2], Y. Kurihara[1,2], N. Nengaki[1,2], M. Zhang[1]; [1]National Institute of Radiological Sciences, Chiba, JAPAN, [2]SHI Accelerator Service, Tokyo, JAPAN.

Aim: I2-imidazoline receptor (I2R) is involved in various central nervous systems disorders, but function associated with I2R is unknown. I2R was found throughout the brain, particularly in the arcuate nucleus of hypothalamus with a high density [1]. Nutt et al. previously reported that selective I2R ligands promoted food intake [2], which is presumed to be an effect of eating function through the arcuate nucleus of the hypothalamus known as a feeding center. We recently reported that [^{11}C]FTIMD with ultra-high specific activity (SA; mean 4470 GBq/μmol) for imaging of I2R showed higher specific binding than [^{11}C]FTIMD with conventional SA (about 100 GBq/μmol) in the hypothalamus. More recently, Kealey et al. developed [^{11}C]BU99008 as a more potent PET ligand for I2R imaging [4]. [^{11}C]BU99008 displayed a relatively high brain penetration and specific binding in the porcine and rhesus brain [4,5]. In this study, to image the feeding center, we evaluated the usefulness of PET study using [^{11}C]BU99008 with ultra-high SA. Materials and methods: [^{11}C]BU99008 was prepared by methylation of the BU-precursor and [^{11}C]methyl iodide, which was produced by iodination of [^{11}C]methane using the single-pass method [6]. Brain PET studies were conducted in SD rats and Zucker fatty rats. Results: [^{11}C]BU99008 with ultra-high SA were successfully synthesized in the range of SA at 5400~16600 GBq/μmol (n = 7) at the end of synthesis. In SD and Zucker fatty rats, the radioactivity after injection of [^{11}C]BU99008 with ultra-high SA was highly accumulated in the hypothalamus. Pretreatment with BU224 (a high affinity I2R ligand, 1 mg/kg) significantly decreased the radioactivity (AUC30-60 min) in the hypothalamus to 86% of control radioactivity. Conclusion: [^{11}C]BU99008 with ultra-high SA showed high specific binding in rat brain. PET study using [^{11}C]BU99008 with ultra-high SA would contribute to in vivo imaging of the eating function with small change.References: [1] Lione LA, et al. Eur J Pharmacol. 1998;353:123-35. [2] Nutt DJ, et al. Ann NY Acad

Sci. 1995;763:125-39. [3] Kawamura K, et al. Nucl Med Biol. 2012;39:199-206. [4] Kealey S, et al. J Nucl Med. 2013;54:139-44. [5] Parker CA, et al. J Nucl Med. 2014;55:838-44. [6] Noguchi J, et al. Nucl Med Biol. 2003;30:335-43.

PW003

Radiosynthesis of a [^{18}F]-quinuclidine 1,2,3-triazole derivative as PET radioligand for neuroimaging of the α7-nicotinic acetylcholine receptor

J. Sarasamkan[1,2], S. Fischer[1], M. Scheunemann[1], P. Brust[1], O. Vajracupta[2]; [1]Helmholz-Zentrum Dresden-Rossendorf, Leipzig, GERMANY, [2]Mahidol University, Bangkok, THAILAND.

Aim: The α7-nicotinic acetylcholine receptor (α7-nAChR) is well recognized as a key receptor involved in memory formation and cognition which implicates its involvement in the pathophysiology of neurodegenerative disorders. Currently, this receptor subtype is one of the most attractive targets for neuroimaging to monitor the etiology and progression of brain diseases such as schizophrenia and Alzheimer's disease (AD). Therefore, a new positron emission tomography (PET) radioligand selective to α7-nAChR was developed in this study. The structure of the developed ligand is based on a novel potent and selective α7-nAChR agonist, 3-(4-hydroxyphenyl-1,2,3-triazol-1-yl) quinuclidine (QND8) which demonstrated cognitive enhancement in mice. Materials and methods: The structure of the radioligand (^{18}F-QND) was modified from QND8 by replacing the hydroxyl group with fluorine. After synthesis of the starting quinuclidine azide and aryl alkyne, F-QND and its precursor were synthesized by copper-catalyzed azide-alkyne cycloaddition (CuAAC) or click chemistry. Their structures were confirmed by ^{1}H-NMR, ^{13}C-NMR and mass spectrometry (MS). ^{18}F-QND was radiolabeled by nucleophilic substitution of the nitro precursor. Altered amounts of kryptofix and various conditions (solvent and temperature) were chosen to improve the radiolabeling yield. The radiolabeled compound was separated and purified by chromatography. The radiochemical yield and radiochemical purity were analyzed by radio-thin layer chromatography and radio-high performance liquid chromatography. Non-radioactive references were used to confirm the stereochemistry of the nitro-precursor and F-QND. Results: The chemical yields of the nitro-precursor (NO_2-QND) and the reference standard (F-QND) were 21% and 11%, respectively, with purity higher than 95%. The radiolabeling yield of ^{18}F-QND was 7% with radiochemical purity > 98% and specific activity of 65 GBq/μmol. The stereochemistry study approved that both compounds were optically active. Therefore, the developed radiochemical processes can be applied for the radiosynthesis of further ^{18}F-QND-derivatives. Conclusion: Radiosynthesis of ^{18}F-QND was accomplished by nucleophilic substitution of the phenyl-nitro compound. However, at high temperature partial racemization cannot be excluded.

PW004

[11C]Me@HAPTHI - A Novel PET-ligand for the Norepinephrine Transporter: Target Affinity and Radiosynthesis

C. Rami-Mark[1], N. Berroteran-Infante[1], A. Hoepping[2], M. Hacker[1], M. Mitterhauser[1], **W. Wadsak**[1]; [1]Medical University of Vienna, Vienna, AUSTRIA, [2]ABX - Advanced Biochemical Compounds, Radeberg, GERMANY.

The norepinephrine transporter (NET) has been demonstrated to be relevant to a multitude of neuropsychiatric and cardiovascular pathologies. Due to the wide range of possible applications for PET imaging of the NET together with the limitations of currently available radioligands, novel NET-PET tracers are seriously needed.METHODS:Precursor, HAPTHI ((S)-1-(4-amino-3-hydroxybutyl)-3-phenyl-1,3-dihydrobenzo[c] [1,2,5]thiadiazole-2,2-dioxide), and reference compound, Me@HAPTHI ((S)-1-(3-hydroxy-4-(methylamino)butyl)-3-phenyl-1,3-dihydrobenzo[c][1,2,5]thiadiazole 2,2-dioxide), were custom-synthesized by ABX.For optimization of radiosynthesis conditions, small-scale reactions (<2GBq) were performed. The influence of various reaction conditions, i.e. reaction temperature, solvent and base, precursor concentration and radiomethylation agent, was investigated. The automation of the N-^{11}C-methylation reaction was done on a TRACERlab FX C Pro synthesizer (GE Healthcare).The affinity of new radiolabeled ligand was determined in a NET-expressing membrane binding protocol.RESULTS:In the radiochemical evaluation, best results were obtained with sodium hydroxide catalysis in 2-butanone(MEK) as solvent for 2min at 75°C using 2mg/mL precursor HAPTHI. Thereby, 54.0 ± 8.3% radiochemical incorporation yield was achieved. These optimum reaction parameters were subsequently used in the fully automated radiosynthesizer. So far, 9 large-scale radiosyntheses were performed, yielding 1.5 ± 0.5GBq (10.9 ± 4.9%, corrected for decay) of sterile, formulated [^{11}C]Me@HAPTHI within 36min. A mean specific activity of 71.4 ± 26.3 GBq/μmol was found. Full radiopharmaceutical quality control took 5min and showed that radiochemical purity always exceeded 98%.Affinity of reference compounds, Me@HAPTHI, using human NET membranes evinced a Kd of 0.21 ± 0.07nM (n=9). For determination of selectivity, additionally the affinity towards human DAT and SERT membranes were measured and revealed >10μM for DAT and 409 ± 43nM for SERT, respectively, (n=5). Hence, selectivity of Me@HAPTHI

towards NET was determined as DAT/NET>1947.6 and SERT/NET=9757. CONCLUSION: This study confirms an outstanding affinity and selectivity of the title compound towards human NET as well as its feasible radiochemical preparation for further preclincal evaluations ans future in-vivo applications.

PW005

Bringing radiotracing to titanium-based antineoplastics: automated synthesis, PET and ex-vivo evaluation of [45Ti](salan)Ti-derivatives

F. Zhuravlev; G. W. Severin, C.H. Nielsen, J. Fonslet, A. Ingemann, A. Kjaer,Hevesy Laboratory, Roskilde, DENMARK.

Introduction: Recent advances in titanium-stabilizing ligands have led to a new class of cytotoxic Ti-based antineoplastics. Implementation of ^{45}Ti PET (^{45}Ti: 85% positron branch, 3.1 h half-life) and radiotracing early in preclinical development could aid in determining the mechanism of action, and evaluate dosing and drug formulation. Aim: We aimed at developing a novel solid-phase based ^{45}Ti radiolabeling methodology and the implementation of ^{45}Ti-PET in titanium-based antineoplastics using hydrolytically stable [^{45}Ti](salan)Ti compounds. This development was intended to allow elucidation of the biodistribution and pharmacokinetics of promising new Ti-based therapeutics. Materials and Methods: ^{45}Ti was produced by the ^{45}Sc(p,n)^{45}Ti reaction and recovered on HypoGel 200 diol resin. A series of [^{45}Ti](salan)Ti(dipic) derivatives was synthesized by on-column complexation of resin-bound ^{45}Ti with the corresponding ligands. HPLC/radioHPLC and TLC/radio-TLC were used to confirm the identity of the radioproducts. Imaging and biodistribution studies of the parent [^{45}Ti](salan)Ti(dipic) were carried out with NMRI nude mice bearing dual-flank HT-29 xenograft tumors using intravenous (iv) and intraperitoneal (ip) injections. For the iv injection, dynamic PET data were obtained for 1h following injection. The ip injections were followed by static PET scans at 1 and 7h pi and conventional ex-vivo biodistribution studies. Results: ^{45}Ti was isolated from bulk scandium on HypoGel 200 column with 93 ± 3% recovery. The introduction of salan and dipic were performed by passing the solutions of ligands in pyridine sequentially through the HypoGel 200 column at 25oC and 100oC correspondingly giving chemically and radiochemically pure products in overall 10-20% RCY. The dynamic ^{45}Ti PET performed after iv injection demonstrated rapid (3.8 min) blood clearance. The ip injections demonstrated the biliary excretion and negligible tumor accumulation. However ex vivo biodistribution, gave a quantifiable signal in the tumors with concentration estimated at 257 pmol/g. Conclusion: The automated solid-phase radiosynthesis of [^{45}Ti](salan)Ti(dipic) derivatives was efficient and is expected to be applicable to a broad range of supporting and terminal ligands. ^{45}Ti PET and radiotracing allowed elucidation of the in vivo behavior of promising titanium compounds encouraging its adoption as a tool in Ti theranostics.

PW006

[11C]Me@HAPTHI - A Novel PET-ligand for the Norepinephrine Transporter: Preclinical Evaluation

C. Rami-Mark[1], W. Wadsak[1], C. Philippe[1], C. Vraka[1], A. Hoepping[2], M. Hacker[1], **M. Mitterhauser**[1]; [1]Medical University of Vienna, Vienna, AUSTRIA, [2]ABX - Advanced Biochemical Compounds, Radeberg, GERMANY.

The norepinephrine transporter (NET) has been demonstrated to be pivotal in many neuro-psychiatric and cardiovascular pathologies. [^{11}C]Me@HAPTHI, a novel potential NET-PET tracer, was shown to have a high target affinity and selectivity. Hence, further in vitro evaluation regarding blood-brain-barrier (BBB) penetration, stability and binding properties in autoradiography on different tissues is required. METHODS: LogD was assessed using HPLC (Donovan & Pescatore J Chrom A, 2002). Immobilized artificial membrane (IAM) chromatography was performed using a standard method (Vraka C et al. EJNMMI, 2014) to achieve Pm (permeability) values.For evaluation of stability, incubation with human liver microsomes was performed. Plasma protein binding was determined quantifying the free fraction (ff) in human pooled plasma (Huang Y et al. J Cereb Blood Flow Metab, 2002).In vitro autoradiography was performed on human brain tissue (cortex, thalamus, hippocampus, cerebellum, and hypothalamus) as well as rat heart. Non-specific binding was determined with excess Nisoxetine (10μM). For competition, non-radioactive FMeNER-D2 and Me@HAPTHI were added. After 1h at room temperature, incubation was stopped and slices were processed on phosphor imaging films. Post-autoradiographic processing of the slices was done by Nissl staining in order to facilitate morphological mapping. Immunohistochemical (IHC) staining experiments were performed on rat and human tissue cryo-slices, vicinal to the slices used for autoradiography.RESULTS:Excellent affinity (KD = 0.21±0.07nM) and selectivity (DAT/NET>1940; SERT/NET=9700) were already shown for [^{11}C]Me@HAPTHI. Both logD (2.27±0.01) and Pm

(1.15±0.25) were found to be in a range for expectable BBB penetration. After 60min incubation with human liver microsomes, 99.6±0.3% of the tracer were still intact. ff was found to be 8.2±0.3%.In the autoradiographic experiments, highest uptake of [^{11}C]Me@HAPTHI was observed in NET-rich regions identified with IHC and a concentration dependent binding displacement was seen for both competitors. CONCLUSION: Besides its high affinity & selectivity, we now demonstrated [^{11}C]Me@HAPTHI's stability, expectable BBB penetration and specific binding in autoradiography. This encourages us for in vivo application in small animal PET experiments and future clinical trials.

PW007

Preparation of 6-[18F]Anle138b: a novel PET-tracer potentially suitable for imaging of neurodegenerative and prion diseases

F. Zarrad[1,2], B. D. Zlatopolskiy[2], B. Neumaier[1,2]; [1]Institute of Neuroscience and Medicine, Nuclear chemistry (INM-5), Forschungszentrum Jülich, Jülich, Jülich, GERMANY, [2]Institute of Radiochemistry and Experimental Molecular Imaging, University Clinic Cologne, Cologne, GERMANY.

Objective: Anle138b is a novel compound that binds selectively to the deposits of aggregated proteins found in neurodegenerative diseases like Parkinson's and Alzheimer's as well as in prion disease. This work aim to prepare a 18F-labeled analog of Anle138b using 1,3-dipolar cycloaddition between the radiofluorinated phenyldiazomethane generated in situ and the appropriate terminal alkyne.Method:As a prototype reaction 1,3-dipolar cycloaddition between 4-[18F]fluorophenyldiazomethane prepared from the corresponding tosylhydrazone and 4-fluorophenylacetylene was optimized with respect to reaction time and temperature, base and solvent. 6-[18F]Fluoro-3,4-methylendioxybenzylidene tosylhydrazone ([18F]1) was prepared via the reaction of known 6-[18F]fluoropiperonal ([18F]2) with tosylhydrazide. The corresponding 18F-labeled diazomethane was generated in situ by the thermolysis of the salt of [18F]1 in the presence of base. This 1,3-dipole reacted with 3'-bromophenylacetylene to give 6-[18F]Anle138b.Results:4-[18F]Fluorobenzylidene tosylhydrazone was prepared from 18F- in 62% RCY and with 93% RCP via one-pot two-step preparation procedure using SPE purification and allowed to react with 4-fluorophenylacetylene. Under the optimized reaction conditions (LiOtBu in MeCN, 95 °C, 25 min) RCC of the appropriate 18F-labeled 3,5-disubstituted pirazole amounted to 67%. Using the same set of conditions 6-[18F]Anle138b was prepared in RCCs of 27-34%.Conclusion:An efficient method for the regioselective preparation of radiofluorinated 3,5-disubstituted pyrazoles was developed. This procedure allowed to produce 6-[18F]Anle138b, a potential tracer for protein deposition in brain, in activity amounts sufficient for preclinical studies.

PW008

Radio-synthesis and biological evaluation in animal models of [^{11}C] 1-(4-Fluorophenil)-3-(2-methoxyethyl) -2-methyl-5-(4-methyl-sulfonyl) phenil)-1*H*-pyrrole (VA 426), a highly selective Cyclooxygenase-2 inhibitor

A. Carpinelli[1], G. Di Grigoli[1], A. Di Capua[2], A. Cappelli[2], M. Biava[3], A. Coliva[4], M. C. Gilardi[1], L. Gianolli[5], M. Anzini[2], R. Moresco[6]; [1]CNR-IBFM, Milan, ITALY, [2]Università di Siena, Siena, ITALY, [3]Università La Sapienza, Rome, ITALY, [4]Università Vita-Saluta S.Raffaele, Milan, ITALY, [5]Ospedale S. Raffaele, Milan, ITALY, [6]Università Bicocca, Milan, ITALY.

Introduction: Cyclooxygenase (COX) enzymes catalyze the conversion of arachidonic acid to prostaglandins. COX-2 is considered an important target for prevention and cancer therapy, due to its major contribution in the inflammatory response and cancer progression. Non-invasive monitoring of COX-2 expression by molecular imaging techniques may provide unique opportunities to obtain information about disease progression and COX-2 potential role in pathogenesis. In this paper 1-(4-fluorophenyl)-3-(2-methoxyethyl)-2-methyl-5-(4-methylsulfonyl)phenyl) 1*H* pyrrole (VA426) has been synthesized and a preliminary in vivo brain and periphery biodistribution in healthy rats was evaluated. Materials and methods: No carrier added [^{11}C]CO_2 was produced via the $^{14}N(p,\alpha)^{11}C$ reaction using IBA Cyclone 18/9 cyclotron and transferred into a Ge Healthcare TracerlabFXc-Pro module where it was catalytically hydrogenated to form [^{11}C]CH_4. Methane was iodinated to form [^{11}C]CH_3I and then transformed in the highly reactive [^{11}C]methyl triflate by an on line flow-through process. [^{11}C]methyl triflate was bubbled into the reactor where 1-3 mg of the precursor [VA425] was dissolved in anhydrous DMSO containing 1-3 mg NaH. The crude mixture was purified by semi-preparative radio HPLC system equipped with a reversed phase column (ACE C18 250x10 mm, 10 micron, CPS). Acetonitrile/ammonium acetate 0.05M pH t.q. (60/40, v/v) was used as the mobile phase and followed by formulation through a tC18 SPE cartridge. Final solution was sterile-filtered (Millex GP, Millipore). CD rats were injected in the tail vein with 9.25 ± 1.25 MBq of [^{11}C]VA4226. At 10, 30, 60

minutes, rats (n=3 for each time point) were sacrificed and blood was collected into a heparinised tube. Plasma was separated by centrifugation and 100 μL of blood and plasma were counted in a gamma-counter (LKB Compugamma CS 1282). Immediately after sacrifice, peripheral tissues and central areas were sampled and washed with cold saline. Tissues where placed in pre-weighed tubes and counted. Radioactivity concentration was calculated as percentage of the injected dose per gram of tissue (% ID/g tissue). Results: Radiochemical yield based on triflate activity was 7 ± 3% n.d.c.. Radiochemical purity was > 99% and specific activity was 2±0.5 Ci/μmol. [^{11}C]VA4226 was progressively taken up and retained in tissues rich in COX-2 such as heart, lungs, kidneys and intestine. In the Central Nervous System [^{11}C]VA426 reached higher distribution in pons, cerebellum and cortex. Conclusion: Preliminary study encouraged us to further validate this tracer by testing it in animal models of cancer and neuroinflammation. Acknowledgements: Supported by FP7/2007-2013, agreement n° HEALTH-F2-2011-278850 (INMiND).

PW009

18F Labeling of a new naphthalene derivative as potential Alzheimer Disease PET imaging agent. Synthesis and preclinical studies.

L. Fernandez-Maza[1], S. Rivera-Marrero[2], M. Balcerzyk[1], I. Fernandez-Gomez[1], A. Parrado-Gallego[1], M. Sablon-Carrazana[2], R. Perez-Perera[2], O. Diaz-Garcia[2], A. Perera-Pintado[3], A. Prats-Capote[3], C. Rodriguez-Tanty[2]; [1]University of Seville, CSIC, Junta de Andalucía, Seville, SPAIN, [2]Centro de Neurociencias (CNEURO), La Habana, CUBA, [3]Centro de Isótopos (CENTIS), La Habana, CUBA.

Introduction: Radiotracers for β-amyloid plaques PET imaging with best results include naphthalene derivative structures. CNEURO has developed and patented some naphthalene derivative molecules for the diagnosis of Alzheimer Disease at early stages (CU/P/2009/57, CU/P/2013/27, EP 2 436 666 A20, South Africa P58243ZA00. A successful 18F-labelling of such molecules by nucleophilic substitution synthesis was developed at CNA, for β-amyloid plaques PET imaging. Matherial and methods: 3-(6-methoxy-2-naphtyl)propyl-4-methylbenzenesulphonate was used as precursor for the labelling process. 18F- was obtained from a Cyclone 18/9 MeV cyclotron (IBA, Belgium) and nucleophilic substitution took place in a modified TracerLab FXFN module (GE, USA). Azeotropic distillation was performed at 100°C in vacuum and with helium flushing. Fluorination of precursor took place at 70°C for ten minutes, with subsequent acidic hydrolysis and neutralization using NaOH 1N. The intermediate compound (before hydrolysis) was dried to avoid any presence of acetonitrile (precursor solvent). The radiotracer 2-(3-[18F]fluoropropyl)-6-methoxynaphtalene was purified by solid phase extraction cartridges (SPE), connecting two alumina Sep-Pack and a SCX Sep-Pack to retain unreacted 18F- and cationic impurities. The labeled compound was retained in a C18 Sep-Pack, and eluted in absolute ethanol. The solution of radiotracer was diluted with saline for injection. Quality controls were performed before injection to the animals; pH, absence of particles, and radiochemical purity (RCP). RCP was determined with a Dionex HPLC system and a coupled radiation detector. The stationary phase was a C18 reverse phase analytical column and acetonitrile/water (75/25) as mobile phase. Two transgenic mice APPSwe/PS1dE8 with amyloid plaques and two wild type mice for control were injected with the radiotracer for PET/CT studies. Whole body images of biodistribution were obtained, and kinetic curves of radioactivity at several cerebral regions were performed. Results: Radiochemical yield reached 49,8% (uncorrected decay), and radiochemical purity was higher than 95% in all batches. In vitro stability cromatograms demonstrated that 2-(3-[18F]fluoropropyl)-6-methoxynaphtalene is stable for more than ten hours. Comparison between transgenic and control mice was established by cortex-cerebellum SUVratio (SUVr) curve. Conclusions: Radiosynthesis of 2-(3-[18F]fluoropropyl)-6-methoxynaphtalene by nucleophilic substitution of tosyl group at the precursor gives good radiochemical yields and radiochemical purity higher than 95%, which makes the radiotracer useful for brain β-amyloid PET imaging. Its in vitro stability (more than 10h) allows several patient studies from the same batch. PET/CT studies show that 2-(3-[18F]fluoropropyl)-6-methoxynaphtalene crosses blood brain barrier, with higher brain uptake in transgenic mice, in comparison with control animals.

PW010

Efficient synthesis of [18F]FEDAC, and evaluation of non-clinical safety and stability tests for clinical application.

K. Kawamura[1], M. Ogawa[1,2], M. Takei[1], K. Kumata[1], K. Furutsuka[1,2], T. Yamasaki[1], J. Yui[1], L. Xie[1], A. Hatori[1], Y. Zhang[1], N. Nengaki[1,2], K. Hirano[3], M. R. Zhang[1]; [1]National Institute of Radiological Sciences, Chiba, JAPAN, [2]SHI Accelerator Service, Tokyo, JAPAN, [3]NMP Business Support Company, Chiba, JAPAN.

Aim: [18F]FEDAC has potent binding affinity and selectivity for translocator protein (18 kDa, TSPO) [BMCL

2009;19:1707], high signal for neuroinflammation [JNM 2010;51:1301], and high sensitivity and specificity for fatty liver diseases progression [JH 2012;57:1076]. We had previously synthesized [18F]FEDAC by 18F-fluorethylation with [18F]fluoroethyl bromide at two steps using a modified 18F-labelling synthesizer. In this study, we simplified and improved synthesis of [18F]FEDAC by direct [18F]fluorination using a 18F-labelling synthesizer, and performed non-clinical safety and stability tests for clinical study. Materials and methods: [18F]FEDAC was prepared direct fluorination by heating the tosylate precursor with [18F]F- in DMSO at 110 °C for 15 min. Evaluation experiments were performed for the radiation dose estimate in mice, the extended single-dose toxicity study in rats, and in vitro stability tests in the injection and human liver microsomes. Results: [18F]FEDAC was obtained with sufficient radioactivity and suitable quality for injection in clinical study. The radiochemical yield of [18F]FEDAC using 1 and 5 mg precursor based on 18F- was 13 ± 5% (n = 5) and 35 ± 3% (n = 3), respectively, at end of synthesis (EOS) within 65 min of an overall synthesis time. The estimated effective dose equivalent in human was 0.022 mSv/MBq, which was comparable to [18F]FDG injection (0.019 mSv/MBq). [18F]FEDAC injection was stable for 180 min after EOS (over 99% radiochemical purity). In human liver microsomes, [18F]FEDAC was metabolized gradually by CYPs (4.2% parent at 60 min after incubation). A single-dose toxicity of [18F]FEDAC injection was not observed for 14 days after injection in rats. Conclusion: We successfully synthesized [18F]FEDAC by fluorination of the tosylate-precursor with 18F-. [18F]FEDAC injection will be applicable to a clinical study with PET.

PW02 - Monday, October 12, 2015, 8:30 AM - 9:30 AM, Hall 3 – Poster Exhibition

Poster Walk 2 - Cardiovascular System: Miscellaneous

PW011

Efficacy of Gated-SPECT in Risk Stratification of Major Adverse Cardiac Events in Patients Over 60 Years with Known or Suspected Coronary Artery Disease Undergoing Noncardiac Surgery

M. Vakhromeeva, F. Chanakhchyan, E. Denisenko-Kankiya, N. Bolomatov; Pirogov National Medical Surgical Center, MOSCOW, RUSSIAN FEDERATION.

AIM: To evaluate the prognostic value of myocardial perfusion imaging with gated-SPECT (MPI/SPECT) in patients over 60 with known or suspected coronary artery disease (CAD) before noncardiac surgery. MATERIALS AND METHODS: Overall 225 patients were studied (average age of 66,1±1,1). Patients were classified into 3 groups according to age: 1) <65 years, 2) 65-74 and 3) >75. The Cardiac Risk Index was used to assess patient cardiac risk and included 6 clinical variables. All of them were referred to "stress/rest" MPI/SPECT using two-detector rotating gamma-camera ("Discovery NM/CT 670", GE) before noncardiac surgery. A 20-segment model of the LV was applied. "Summed stress score" (SSS) was used which reflects reduced perfusion in stress. Normal myocardial perfusion was considered if SSS<4; slightly abnormal: SSS=4-7; moderate and significantly abnormal: SSS≥8. The degree of ischemia was assessed by "summed difference score" (SDS): SDS<2 - no ischemia, SDS=2-7 moderate ischemia and SDS>7 - significant ischemia. RESULTS: 160 (71,1%) were proceeded to noncardiac surgery after MPI/SPECT without any additional cardiac testing. The rest 65 (28,9%) patients weren't allowed to operations due to high risk for major adverse cardiac events (MACE) in peri- and/or postoperative periods. Coronary angiography (CAG) was performed to 48 (73,8%) from them, and 46 (95, 8%) had hemodynamically significant stenosis at least in one coronary artery. Myocardial revascularization (MR) was made to 23 (47,9%) patients (15 patients-stenting, 8 patients-CABG). On the whole, SSS and SDS were statistically higher in patients, whom operations were cancelled (p<0,05). Moreover, SSS and SDS were significantly higher in patients over 75 years old (p<0,05). There was significantly reduction of SSS and SDS (p=0,009) when comparing results of MPI/SPECT before and after MR. Noncardiac surgeries were performed to all patients after MR without any MACE. However from 160 patients, whom noncardiac surgeries were performed directly after MPI/SPECT MACE occurred in 13 (8,1%). Myocardial perfusion analysis showed significantly high rates of SSS (7,77±3,79), SDS (3,38±1,68) in these patients compared with those without MACE (p<0,05). In rest 143 patients without MACE SSS and SDS were below 4 and 2, respectively. CONCLUSIONS: MPI/SPECT is an important tool in prediction of MACE in peri- and/or postoperative periods in patients with known or suspected CAD undergoing noncardiac surgery. It is also a reliable method for screening patients with stable CAD for CAG. CAG with subsequent MR should be considered in SSS>4 and SDS>2 in patients with high cardiac risk.

PW012

Hybrid PET/MR viability imaging compared with metabolism/perfusion pattern in acute myocardial infarction

I. Cho, E. Kong, K. Chun, S. Kwon; Yeungnam University Hospital, Daegu, KOREA, REPUBLIC OF.

Purpose : We evaluated simultaneous FDG and late gadolinium enhanced (LGE) PET/MR viability imaging and compared with

metabolism/perfusion patterns. Materials and Methods : Ten consecutive patients diagnosed with acute myocardial infarction were underwent hybrid FDG/LGE PET/MRI examination and Tc-99m MIBI myocardial perfusion SPECT. According to the 17-segment model, FDG uptake, LGE, and Tc-99m MIBI uptake were visually assessed for each segment. Infarcted segments were divided into transmural LGE (involving >50% wall thickness)and subendocardial LGE (involving <50% wall thickness). Results: In 170 segments, 40(23.5%) were rated as infarction on LGE images in which match, mismatch and reverse-mismatch perfusion/metabolism defects were 13(32.5%), 25(62.5%), and 2(5%)segments, respectively. 13(100%) of the match defects appeared as transmural LGE, 23(92%) of the mismatch defects did as subendocardial LGE. Two revese defects showed transmural LGE. conclusion:Perfusion/Metabolism match and mismatch defects might be well correlated with transmural and subendocardial LGE, respectively.

PW013

Metabolic scintigraphy with radiolabeled fatty acid in prognosis of cardiac resynchronization therapy in patients with dilated cardiomyopathy

Y. B. Lishmanov[1,2], M. O. Gulya[2,1], **K. W. Zavadovsky**[2,1], S. I. Sazonova[2,1], D. I. Lebedev[2], V. S. Skuridin[1], V. D. Fillimonov[1]; [1]National Research Tomsk Polytechnic University, Tomsk, RUSSIAN FEDERATION, [2]Federal State Budgetary Scientific Institution “Research Institute for Cardiology”, Tomsk, RUSSIAN FEDERATION.

Purpose of the study was to study perfusion and metabolism of the left ventricular (LV) myocardium in patients with idiopathic dilated cardiomyopathy (DCMP) and to identify the scintigraphic predictors of the efficacy of cardiac resynchronization therapy (CRT). Methods. The study comprised 63 patients with DCMP and NYHA class III-IV chronic heart failure. Before CRT, all patients received scintigraphy with 99mTc-MIBI and with 123I-BMIPP for evaluation of myocardial perfusion and metabolism, respectively. Before CRT and twelve months after, all patients underwent echocardiography study to estimate intracardiac hemodynamics. Results. Patients were divided into two groups 6 months after CRT: (1) responders - LV ESV decreased by ≥ 15% (n = 39);(2) non-responders - LV ESV decreased by < 15% (n = 24). Prior to CRT, no statistically significant differences were found between groups in hemodynamic parameters (LVEF, end-diastolic volume, end-systolic volume), intra- and interventricular dyssynchrony. Significant differences were found in the following preoperative scintigraphic parameters: myocardial perfusion defect size and metabolic defect size. Correlation analysis demonstrated the presence of significant association ($r = -0.37$, $p < 0.5$) between the sizes of metabolic defect and changes in the values of LV ESV after 6 months the implantation of CRT device. Metabolic scintigraphy showed higher diagnostic efficacy in determination of indications for CRT compared with perfusion scintigraphy (AUC 0.722 and AUC 0.612, respectively). The best metabolic defect size threshold value of 7.35% predicted CRT efficacy with the sensitivity and specificity of 77.8% and 66.7%, respectively. We also mad an analytical review of methods for obtaining of radiopharmaceuticals that are based on 99mTc -labeled fatty acids and their use in cardiology. We make conclusion about efficiency of application and investigation of 99mTc fatty acids radiopharmaceuticals that contain chelate groups EDTA or DTPA. In this study, quantum-chemical modeling of one of such conjugate is conducted and its bioavailability is thus confirmed. Conclusions. The results of myocardial metabolic scintigraphy with 123I-BMIPP may be used as the secondary criteria for selection of patients for CRT and for prediction of the efficacy of this interventional treatment modality in patients with DCMP. This work was financially supported by Federal Target Program №14.604.21.0071(project unique identifier №RFMEFI60414X0071).

PW014

Association between radiation dosimetry of the heart and the myocardial fatty acid metabolic impairment due to chemoradiation-therapy : Prospective study using I-123 BMIPP SPECT/CT

K. Takanami[1], R. Umezawa[2], N. Kadoya[2], A. Arai[1], K. Jingu[2], K. Takase[1]; [1]Department of Diagnostic Radiology, Tohoku University Hospital, Sendai, JAPAN, [2]Department of Radiation Oncology, Tohoku University Hospital, Sendai, JAPAN.

Aim: The purpose of this study was to clarify the temporal change of the myocardial fatty acid metabolic impairment due to chemoradiation-therapy (CRT). Materials and methods: This study was approval by Institutional Review Board and the informed consent was obtained from all the patients. Twelve patients (3 females, mean age of 63.4 ± 7.1 years (53-79)) who underwent radical CRT for an early esophageal cancer. At pre-CRT, pre-boost irradiation during CRT, 3 months after CRT, and 1 year after CRT, I-123 BMIPP SPECT / CT was scanned. The myocardial BMIPP uptake in each of 17 segments of the left ventricle was visually scored from 0 (normal uptake) to 4 (no uptake) and semi-quantitatively assessed using “%uptake”, which is a segmental mean uptake relative to the maximal myocardial uptake. A correlation between radiation dosimetry of the heart and the change of myocardial BMIPP

uptake after CRT was assessed. P < 0.05 was considered as statistically significant. Results: One patient died of pneumonia during the course of observation, and 11 patients were followed for 1 year after the completion of CRT. The total dose to the primary tumor was 60-70 Gy. The average dose of the left ventricle was 15.7 ± 6.9 Gy, and mean V40 (a percentage of the left ventricle that had been irradiated 40 Gy or more) was 15.9 ± 15.0. Temporal decreases of the BMIPP uptake after CRT were observed. At pre-boost irradiation during CRT, 3 months and 1 y after CRT , the changes of total visual grade of the left ventricle were 1.1 ± 1.9, 2.7 ± 2.6, and 4.5 ± 4.1, respectively, and the changes of total %uptake of the left ventricle were -22.2 ± 50.4, -38.5 ± 54.3, and -81.1 ± 69.9, respectively. At 3 months after CRT, significant correlations were observed between V40 and both the total visual grade ($r = 0.63$, $p < 0.05$) and the total %uptake ($r = -0.74$, $p < 0.01$) , while, no significant correlation was observed 1 year after CRT. At pre-boost irradiation, a significant correlation was observed between V40 and only the total %uptake ($r = -0.64$, $p < 0.05$). Conclusion: Although a myocardial metabolic impairment after CRT is associated with radiation dosimetry of the heart in the short-term, other factors are likely to affect a myocardial metabolism in the long term.

PW015

The first clinical experience with combined PET-CT myocardium in patients with multivessel coronary disease.

I. Shurupova, I. Aslanidis, A. Chernova, V. Makarenko, V. Bereznitskiy, E. Derevyanko, I. . Ekaeva; Bakoulev Scientific Center for Cardiovascular Surgery, Moscow, Moscow, RUSSIAN FEDERATION.

The aim was the comparison the perfusion abnormalities and the severity of coronary atherosclerosis in patients with established coronary heart disease based on hybrid positron emission tomography with N13-ammonia (ammonium-PET) and multidetector computed tomography with noninvasive coronary angiography (MDCT-CA). Materials: 18 patients (44 to 80 years, 62,6 ± 9,8) underwent MDCT-CA, ammonium-PET stress - rest study on hybrid scanner Biograph-64 and invasive coronary angiography (Rg-CA), which was accepted as the "gold standard". A total of 42 coronary artery (CA) segments were taken for consideration. The hybrid imaging (MDCT-CA + ammonium-PET) and MDCT-CA allow results were compared with Rg-CA. Stenosis ≥75% was considered as significant lesion for invasive and non-invasive angiography. The result of the hybrid technology is considered true-positive if significant changes was detected by at least one of the non-invasive methods, negative if in the presence of intact arteries or stenosis <75% there is no the defect of perfusion (DP). Results. According to MDCT-CA stenosis in 14/19 arteries were properly verified revealed by Rg-CA. In the group of arteries with insignificant changes according to Rg-CA coincidence of the results indicated in 31/34 cases, one artery were excluded due to the artifacts. The sensitivity of MDCT-CA in identifying functionally significant stenosis was 73%, specificity - 91%, positive predictive value (PPV) - 82%, negative PV (NPV) - 86%. A sensitivity hybrid analysis amounted to 94%, specificity- 829%, PPV - 75%, NPV - 96%. Stenotic segments with the presence and absence of stress-induced DP were analyzed individually. According to PET DP were noted in 1/16 of the arteries with stenosis <50%, in the l 5/20 arteries in the group with stenosis 50-74%, in 11/17 arteries with stenosis ≥75%. In whole group (n=18) perceptions of the hemodynamic significance changes identified in the CA, based on invasive coronary angiography and on the basis of MSCT-AG + PET, coincided in 10 patients. The presence of significant stenoses was confirmed in 4 patients, absence hemodynamic significance was confirmed in 6. The initial view of the hemodynamic significance of a stenosis, compiled only on the basis of its size, have changed in 8/18 patients (44%). Conclusions. Hybrid studies allow to increase the sensitivity of diagnosis of significant stenosis. Lower specificity of hybrid researches is due to the lack of hemodynamic significance of some stenosis more than 75%. Generally hybrid researches allowed to change the perception of the stenosis hemodynamic relevance in 44% patients.

PW016

Assessment of Right Ventricular Myocardial Perfusion and Fatty Acid Metabolism Using Planar Imaging in Patients with Chronic Thromboembolic Pulmonary Hypertension

H. Miyauchi[1], T. Iimori[2], K. Sawada[2], Y. Kuwabara[1], S. Sakao[1], K. Tatsumi[1], Y. Kobayashi[1]; [1]Chiba University Graduate School of Medicine, Chiba, JAPAN, [2]Chiba University Hospital, Chiba, JAPAN.

[Background] In patients with chronic thromboembolic pulmonary hypertension (CTEPH), right ventricular (RV) overload may result in RV enlargement and hypertrophy, which consequently increases the RV myocardial perfusion. However, there is little information on the RV myocardial fatty acid metabolism in patients with CTEPH. [Aim] The aim of this study was to quantitatively evaluate the RV myocardial perfusion and fatty acid metabolism using 201Thallium (201Tl) and 123I-labelled 15-(p-iodophenyl)-3-R, S-methylpentadecanoic acid (123I-BMIPP) planar imaging in patients with CTEPH. [Materials and Methods] The study groups included 23 patients with CTEPH and 30 healthy controls. Mean pulmonary artery pressure (mPAP) by right heart catheterization was

obtained in all CTEPH patients. 201Tl and 123I-BMIPP planar and SPECT myocardial imaging were performed in all participants. Planar acquisition was performed by obtaining the angle that best separated the RV and the left ventricle (LV) on transverse imaging. In the planar image, we measured the total counts of 201Tl and 123I-BMIPP in both the RV and LV, and calculated their relative counts of the RV to LV (abbreviated as HR/HL(Tl) and HR/HL(BMIPP) , respectively) to determine the index of myocardial perfusion and fatty acid metabolism, respectively. [Results] HR/HL(Tl) was significantly elevated in the CTEPH patients compared with control (0.60 ± 0.14 vs. 0.36 ± 0.07, p <0.01). HR/HL(BMIPP) was also elevated in the CTEPH patients (0.55 ± 0.14 vs. 0.34 ± 0.06, p <0.01). In the CTEPH patients, average mPAP was 42.0 ± 9.52 mmHg, which was significantly correlated with HR/HL(Tl) (r=0.61, p<0.01) and HR/HL(BMIPP) (r=0.65, p<0.01). [Conclusions] In patients with CTEPH, RV myocardial perfusion was increased and RV myocardial fatty acid metabolism was upregulated with the elevation of mPAP. 201Tl and 123I-BMIPP planar imaging may be useful to quantify the severity of PH.

PW017

Diagnostic performance of attenuation corrected SPECT myocardial perfusion imaging for coronary artery disease: a systemic review and meta-analysis

J. Huang[1,2], M. Cheng[1], C. Lu[1,2], Y. Wu[1,3,4], R. Yen[1], K. Tzen[1], K. Chien[3,2]; [1]Department of Nuclear Medicine, National Taiwan University Hospital and National Taiwan University College of Medicine, Taipei, TAIWAN, [2]Institute of Epidemiology and Preventive Medicine, College of Public Health, National Taiwan University, Taipei, TAIWAN, [3]Division of Cardiology, Department of Internal Medicine, National Taiwan University Hospital and National Taiwan University College of Medicine, Taipei, TAIWAN, [4]Department of Nuclear Medicine and Cardiology Division of Cardiovascular Medical Center, Far Eastern Memorial Hospital, New Taipei, TAIWAN.

PURPOSE / INTRODUCTION: Coronary artery disease(CAD) is one of the major causes of mortality and morbidity throughout the world. Single photon emission computer tomography (SPECT) myocardial perfusion imaging (MPI) is a well established diagnostic tool for CAD. However, the full clinical potential of MPI has not been realized due to many factors of artifacts. Soft tissue attenuation is one of the most common artifacts. The aim of this study is to determine and compare the diagnostic performance of AC and non-AC SPECT MPI, using coronary angiography as the reference standard. SUBJECTS & METHODS: We search Medline and Embase for English-language literature published from the earliest available date till March 20, 2015 evaluating AC SPECT MPI for diagnosis of CAD. Extraction of information including author, journal, details of study design, patient characteristics, stressor used for MPI, radiotracer, CAD definition, numbers of true positive (TP),false positive (FP), true negative (TN) and false negative (FN) was performed. Assess methodological quality using the Quality assessment of Diagnostic Accuracy Studies (QUADAS) tool. All data from each eligible study were sorted out by Cochrane's Review Manger. For each study, the sensitivity, specificity, and the diagnostic odds ratio, along with the 95% confidence interval (CI), were calculated to express the diagnostic accuracy of AC and non-AC SPECT MPI. Because methodological heterogeneity between included studies was anticipated, a random-effects (DerSimonian and Laird) model was used for pooling the data. Statistical analysis was performed using STATA and Meta-DiSc. RESULTS: Original search yielded 201 articles. On the basis of title and abstract, we exclude 158 articles. One the basis of full text, we exclude 26 articles for various reasons, such as study for rick stratification, reference standard other than coronary, etc. Seventeen studies were identified, with a total of 1763 patients; 5 studies with 582 patients used computed tomography AC (CTAC); 12 studies with 1181 patients used radionuclide source AC; 12 studies with 1605 patients reported non-AC results. Meta-analysis yielded pooled sensitivities of 0.748 [95%CI, 0.698-0.794], 0.810 [95% CI, 0.0.784-0.834] and 0.786 [95% CI, 0.757-0.812] for CTAC, all AC and non-AC, respectively, and pooled specificities of 0.82 [95% CI, 0.768-0.867], 0.817 [95% CI, 0.786-0.844] and 0.705 [95% CI, 0.668-0.739], respectively. DISCUSSION / CONCLUSION: Attenuation correction SPECT MPI with either CTAC or radionuclide source AC showed improvement in both sensitivity and specificity. Our results suggested that AC should be applied in SPECT MPI for better diagnosis of CAD.

PW018

Systematic Underestimation of High Values of Coronary Flow Reserve Provided with Multi-Detector Computed Tomography: a Comparison with SPECT Technology.

M. Bauckneht[1], G. Ferrarazzo[1], F. Fiz[1], S. Seitun[2], C. Zawaideh[3], F. Ticconi[1], I. Calamia[1], S. Morbelli[1], C. Brunelli[3], C. Ferro[2], G. Bezante[3], G. Sambuceti[1], C. Marini[4]; [1]Nuclear Medicine, IRCCS AUO San Martino IST, Genova, ITALY, [2]Department of Radiology and Interventional Radiology, IRCCS-University Hospital San Martino-IST, Genova, ITALY, Genova, ITALY, [3]Department of Internal Medicine, Chair

of Cardiology, University of Genoa, Genova, ITALY, Genova, ITALY, [4]Institute of Bioimaging and Molecular Physiology, CNR, Milan, Genoa Section, Genova, ITALY, Genova, ITALY.

Aim. Diagnostic information provided by multi-detector computed tomography (MDCT) has been recently enriched with myocardial perfusion imaging (MPI) and the possibility to assess coronary flow reserve (CFR). However, the accuracy of this method has so far poorly evaluated and reported normalcy values are markedly lower with respect to corresponding measurements with gold standard techniques. The present study was planned to compare performance of MDCT and SPECT in CFR quantification since this numeric descriptor of coronary physiology represents the theoretical basis of MPI diagnostic accuracy. Materials and Methods. Thirty-five patients (29 males, mean age 69 years) referred for chest pain and/or dyspnea to our Institute underwent dipyridamole stress/rest MPI with MDCT and SPECT. MDCT approach implied the use of a commercially available software able to diplay parametric maps of myocardial blood flow using a two-compartment model in LV myocardial tissue. SPECT measurements were instead performed, according to the validate method that implies the normalization of myocardial tracer uptake for the corresponding input function. For both approaches CFR values were compared with the anatomy of related coronary branch as depicted by CT coronary angiography. Results. Overall, CFR values at SPECT and MDCT imaging were similar (1.51±0.46 vs 1.50±0.37, respectively, p=ns) and showed a fair segment-by-segment correlation (r=0.63, p<0.001). At SPECT analysis, CFR was 1.64±0.31 in the 164 segments supplied by normal arteries (control regions), while it significantly decreased in the 114 areas supplied by vessels with intermediate stenosis (≤50%) (intermediate: 1.50±0.32, p50%) (critical: 1.33±0.22, p<0.01 vs control regions). MDCT-CFR was 1.65±0.32 in control regions and significantly decreased to similar values in intermediate (1.40±0.33 p<0.01 vs control regions) and in critical ones (1.36±0.26, p<0.01 vs control regions). At Bland-Altman analysis, a proportional bias was identified by the regression between delta (SPECT CFR - MDCT CFR) and mean CFR value that was significant (p<0.01) and displayed a positive slope of 0.288 with 95% confidence limits ranging from +0.21 to +0.31. Conclusions. MDCT-MPI and SPECT provide similar values of regional CFR in a population with suspected CAD. However, MDCT displays a limited accuracy in measuring high maximal MBF and CFR values. This limitation can be recognized even by the comparison with SPECT technology, which is known to markedly underestimate high MBF and CFR values. An accurate validation of MDCT diagnostic performance should be completed encompassing a normalcy database to optimize its diagnostic use.

PW019

Cardiac Sympathetic Innervation Assessed with 123I-MIBG Retains Prognostic Utility in Diabetic Patients with Severe Left Ventricular Dysfunction Evaluated for Primary Prevention Implantable Cardioverter-Defibrillator

M. COZAR SANTIAGO[1], P. GARCIA GONZALEZ[2], R. SANCHEZ JURADO[1], R. SANZ LLORENS[1], J. AGUILAR BARRIOS[1], F. RIDOCCI SORIANO[2], J. FERRER REBOLLEDA[1]; [1]ERESA-NUCLEAR MEDICINE DEPARTMENT. GENERAL UNIVERSITARY HOSPITAL, VALENCIA, SPAIN, [2]ERESA-CARDIOLOGY DEPARTMENT. GENERAL UNIVERSITARY HOSPITAL, VALENCIA, SPAIN.

OBJECTIVES: We analyze if the evaluation of cardiac sympathetic innervation (CSI) with iodine-123-metaiodobenzylguanidine (123I-MIBG) retains prognostic utility in diabetic patients with heart failure (HF) evaluated for primary prevention implantable cardioverter-defibrillator (ICD).BACKGROUND: Scintigraphy with 123I-MIBG is a noninvasive tool for the assessment of CSI that has proven to be an independent predictor of survival. In addition, recent studies have shown that diabetic patients with HF have a higher deterioration in CSI. It is unknown if 123I-MIBG has the same predictive value for diabetic and nondiabetic patients.METHODS: Seventy-eight consecutive HF patients (48 diabetic and 30 nondiabetic) evaluated for primary prevention ICD implantation were prospectively enrolled and underwent 123I-MIBG to assess CSI (Heart-to-mediatinum ratio (HMR), cardiac wahout rate). A Cox proportional hazards multivariate analysis was used to analyze the influence of 123I-MIBG images for prediction of cardiac events in both diabetic and non-diabetic patients. The primary end-point was a composite of arrhythmic event, cardiac death or HF hospitalization.RESULTS: During a mean follow-up of 19.5 [9.3-29.3] months, the primary end-point occurred in 24 (31%) patients. Late HMR was significantly lower in diabetic patients (1.30 vs 1.41, p=0.014). Late HMR ≤1.30 was an independent predictor of cardiac events in diabetic (hazard ratio 4.53; p = 0.012) and non-diabetic (hazard ratio 12.31; p = 0.023) patients.CONCLUSIONS: Diabetic patients with HF evaluated for primary prevention ICD show a higher deterioration in CSI than non-diabetics; nevertheless 123I-MIBG imaging retained prognostic utility for both diabetic and non-diabetic patients

PW020
18F-FDG PET-CT in the Diagnosis of Infective Endocarditis over Native and Prosthetic Valves

A. Jiménez-Ballvé[1], M. J. Pérez-Castejón[1], M. Matínez de Bourio[1], C. Sánchez-Enrique[2], I. Vilacosta[2], C. Riola Parada[1], A. Ortega Candil[1], C. Olmos[2], J. L. Carreras-Delgado[1,3]; [1]Nuclear Medicine Department, Hospital Clinico San Carlos, Madrid, SPAIN, [2]Cardiology Department, Hospital Clinico San Carlos, Madrid, SPAIN, [3]Universidad Complutense, Madrid, SPAIN.

Aim: The aim of this study was to assess the usefulness of PET-CT with 18F-FDG in the diagnosis of infective endocarditis (IE) looking for differences among native and prosthetic valves. Materials and methods: In this prospective study we included 52 patients with initial suspicion of definitive or possible IE according to Dukes criteria, from November 2012 to April 2015. PET-CT was considered positive when presented 18F-FDG uptake in the region of interest (ROI) greater than the background and persisted in the non-corrected images. On the other side, it was considered negative if there was no uptake difference between the ROI and the background or did not persist in the non-corrected images. Anatomy was the gold standard in patients who underwent cardiac surgery. In those cases without surgery, final diagnosis was done by clinical consensus of the endocarditis team (independently from the PET-CT results). Results: In the 52 PET-CT studies, we analyzed 69 foci as regions of interest, 42 prosthesis valves and 27 native valves. The suspicion of IE was 38 definitive and 31 possible. PET-CT was positive in 39 cases (57%) and negative in the other 30 (43%). 21 valve replacements were performed: 19 definitive IE (11 on prosthesis and 8 on native valves, with a PET-CT success rate of 100% and 38%, respectively) and 2 rejected IE (fibroelastoma and marantic IE, both on native valve with a PET-CT success rate of 100%). sensibility, specifity, positive predictive value (PPV), negative predictive value (NPV) and accuracy of PET-CT in global IE (prosthesic+natives) were 79%, 73%, 79%, 73% and 77%, respectively. When we just analyzed prosthesis, we achieved a very high sensibility and NPV (100%), with a specifity of 70%, PPV of 79% and an accuracy of 86%. By contrast, when we analyzed independently native valves, we obtained a sensibility of 52%, specifity of 80%, PPV of 81%, NPV of 50% and an accuracy of 63%. Conclusion: 18F-FDG PET-CT seems to be useful in the diagnosis of infective endocarditis, especially in patients with prosthesis valves, having better accuracy than in native valves.

PW03 - Tuesday, October 13, 2015, 8:30 AM - 9:30 AM, Hall 3 – Poster Exhibition
Poster Walk 3 - Neurosciences: Neuroimaging

PW021
[18F]DPA-714: peripheral metabolism in healthy volunteers and patients.

M. Peyronneau[1], C. Letaillandier[1], S. Lavisse[2], B. Kuhnast[1], C. Baron[1], B. Jego[1], P. Gervais[1], F. Dollé[1], B. Bodini[3], B. Stankoff[3], M. Sarazin[3], P. Rémy[2], M. Bottlaender[4]; [1]CEA-DSV-I2BM-SHFJ-IMIV, Orsay, FRANCE, [2]CEA-DSV-I2BM-Mircen, Orsay, FRANCE, [3]APHP, Paris, FRANCE, [4]CEA-DSV-I2BM-Neurospin-IMIV, Orsay, FRANCE.

Objectives: The translocator protein (TSPO) is weakly expressed in the healthy human brain and overexpressed in several neurodegenerative pathologies. [18F]DPA-714 is currently under clinical investigation in Alzheimer, Parkinson and Multiple Sclerosis diseases by PET. We have previously reported species differences in the metabolism of [18F]DPA-714 in rats and non-human primates and the involvement of human CYP3A4 in its biotransformation (Peyronneau et al., Drug Metab Dispos, 2013). In this study, we aimed to investigate the peripheral metabolism of [18F]DPA-714 in healthy volunteers (HV) and patients (P) and evaluate the influence of age, gender, diseases, concomitant medication and binder affinity for TSPO.Methods: Venous blood samples were collected from 145 subjects (54 HV-91 P) during PET and arterial samples in 20 HV. [18F]DPA-714 and metabolites fractions were determined by a developed solid phase extraction method and used for the correction of individual input functions. Results: As expected, [18F]DPA-714 peripheral metabolism was similar in arterial and venous plasma samples (54.8±9.7% vs 54.5±9.6% of [18F]DPA-714 at 90 min). No gender differences were observed but [18F]DPA-714 metabolism decreased with age (45±10% to 35±10% of radiometabolites; 20-90 years, $p<0.05$). No significant differences were detected between healthy volunteers and patients, except for those co-medicated with known CYP3A4 inducers/inhibitors, for whom an increase (up to 66%) or a decrease (down to 12%) of radiometabolites were observed. Finally, while no major difference in the metabolism was found whatever the TSPO affinity genetic status, the parent plasma concentration (input function) displayed a 4-fold and 1.3-fold increase in low and mixed compared to high binders.Conclusions: [18F]DPA-714 metabolism may contribute to interindividual variations of the input function used for the quantification of the tracer brain uptake.

PW022

A Novel SPECT-based Approach Reveals Early Effects of Systemic Inflammation on Brain Injury and Peripheral Organs After Cerebral Ischemia

D. Mathe[1], K. Szigeti[2], D. Veres[2], B. Martinecz[3], N. Lenart[3], N. Kovacs[1], A. Marta[2], M. Semjeni[1], A. Denes[3,4]; [1]CROmed Ltd, Budapest, HUNGARY, [2]Dept. Biophysics and Radiation Biology Semmelweis University, Budapest, HUNGARY, [3]Laboratory of Molecular Neuroendocrinology, Institute of Experimental Medicine, Budapest, HUNGARY, [4]Faculty of Life Sciences, University of Manchester, Manchester, UNITED KINGDOM.

Introduction. Inflammation that develops in the brain and peripheral organs after stroke contributes profoundly to the outcome of patients. Clinical decision making would highly benefit from rapid assessment of central and peripheral inflammatory changes after acute brain injury, but appropriate medical imaging tools are not available yet. Here we show that single-photon emission computed tomography combined with MRI (NanoSPECT/CT Plus, nanoScan MRI/SPECT) allows early visualization of blood brain barrier injury and inflammation in the brain after experimental stroke, well before signs of brain injury can be detected with magnetic resonance imaging (MRI).Materials and Methods. Whole-body 99mTc-DTPA SPECT/CT; 99mTc-HMPAO SPECT and MRI imaging was performed in groups of 5 mice with middle cerebral artery occlusion (MCAO) for 30 or 60 minutes. In one group LPS-induced systemic inflammation was present before the MCAO to model pre-existing inflammatory diseases. Imaging was done 1, 3, 6 and 24, 72 hours post MCAO and was validated by IgG, CD45 and Iba1 immunofluorescent microscopy and H&E staining in respective brains and peripheral organs.Results. Penetration of 99mTc-DTPA into the brain parenchyma overlaps with areas of brain injury and perfusion deficits after cerebral ischemia. Systemic inflammation preceding experimental stroke leads to very early perfusion deficits and increased blood brain barrier injury (within 2 h) after the onset of ischemia. Acute brain injury also leads to infectious complications in peripheral organs such as the lung. We detected that SPECT imaging reveals early (within 1-3 h) changes in perfusion, barrier function and inflammation in the lungs and the gut of all mice after experimental stroke, with good predictive value for outcome. Discussion. Our results suggest that early inflammatory changes as detected by SPECT/MRI, SPECT/CT whole-body imaging precede injury in the brain and peripheral organs. Thus these hybrid nuclear medicine imaging methods are proposed to support decision making in the clinic.

PW023

Effect of Normobaric Hyperoxia (NBO) on Hypoxic Volume and Infarct Volume Following Middle Cerebral Artery Occlusion (MCAo): An 18F-Fluoromisonidazole (FMISO) PET, MR and TTC Study

T. D. Fryer, S. Ejaz, D. J. Williamson, U. Jensen-Kondering, S. J. Sawiak, F. I. Aigbirhio, Y. T. Hong, J. Baron; University of Cambridge, Cambridge, UNITED KINGDOM.

Aim: Whether NBO is effective in reducing infarct volume in ischemic stroke remains inconclusive. NBO modestly increases arterial oxygen content, which in turn may not significantly alleviate tissue hypoxia. We determined the impact of NBO in two rat strains with different leptomeningeal collaterals. Materials and Methods: 6 Wistars and 7 SHRs underwent distal permanent MCAo (pMCAo) under either normoxic or hyperoxic conditions. Dynamic FMISO PET data were acquired for 3hrs ~5min after occlusion. Hypoxic volumes were defined on SUV2-3hrs maps. Kinetic modeling was applied to the hypoxic volume signal. Lesion volume was defined immediately after PET by T2w-MR and TTC. Additional rats were used to measure arterial PO2 (PaO2) and MCA cortex PO2 (PtO2) using an O2 probe during cycles of normoxia/NBO. Results: In SHRs, NBO increased PaO2 ~4-fold from normoxia; non-ischemic cortex PtO2 rose from mean 24 to 50mmHg in SHRs (n=5; p=0.04), and from 46 to 78mmHg in Wistars (n=4; p=0.001). During MCAo, in SHRs compared to Wistars PtO2 was lower in normoxia (2.5 vs 15mmHg) and increased less with NBO: 6mmHg (p=0.08) vs 26mmHg (p=0.09), respectively. FMISO hypoxic volume was much larger in SHRs than Wistars, but was not significantly different between normoxia and NBO in either strain (mean 207 vs 349mm3 in SHRs, and 11 vs 9mm3 in Wistars). FMISO influx rate (Ki) was significantly increased ($p<0.03$) in the hypoxic volume compared to a mirror ROI for both rat strains under both conditions, with trapping rate (k3) also increased in SHRs ($p<0.05$) with a similar trend in Wistars ($p<0.09$). However, mean SUV, Ki and k3 in the hypoxic volume were not significantly different between normoxia and NBO in either strain. A similar pattern was found for TTC (mean 136 vs 179mm3, and 18 vs 11mm3, respectively) and MR (mean 91 vs 103mm3, and 7 vs 3mm3, respectively) lesion volumes. There were strong ($p<0.001$) correlations among lesion volumes from TTC, MR and FMISO. Conclusion: Regardless of strain, there was no protective effect of NBO against tissue hypoxia and infarction. The latter is consistent with previous pMCAo studies, all in Sprague-Dawleys. However, here we directly show no effect on FMISO lesion volume and only mild effects on tissue PtO2. Early reperfusion is probably necessary for NBO to show benefit, even with good collaterals. The worse tissue hypoxia during

MCAo in SHRs is consistent with their intrinsically poorer vascular architecture, apparent from their lower non-ischemic hemisphere PtO2 under normoxia.

PW024

Regional cerebral blood flow changes after accelerated repetitive transcranial magnetic stimulation of the canine frontal cortex.

R. Dockx[1], C. Baeken[2], R. Duprat[2], F. De Vos[3], B. De Spiegeleer[3], A. Dobbeleir[1], J. H. Saunders[1], I. Polis[1], K. Audenaert[2], K. Peremans[1]; [1]Faculty of Veterinary Medicine, University Ghent, MERELBEKE, BELGIUM, [2]Faculty of Medicine, University Ghent, Ghent, BELGIUM, [3]Faculty of Pharmaceutical Sciences, University Ghent, Ghent, BELGIUM.

Repetitive transcranial magnetic stimulation (rTMS) is a non-invasive, FDA approved treatment for depression. Nevertheless, this treatment's neurobiological mechanisms remain unclear. Aim: To compare the regional cerebral bloodflow prior and after High Frequency accelerated Repetitive Transcranial Magnetic Stimulation (HF-arTMS) of the normal canine left frontal cortex. Material and Methods: Eight dogs underwent a 3 Tesla MRI scan at the Ghent University Hospital. This scan was the basis for pointer-based neuronavigation (Brainsight 2, Rogue Resolutions, LTD), a technique used to externally locate the stimulation site. Each dog's left frontal cortex was subjected to 5 consecutive stimulation sessions a day with a figure 8 coil (Magstim Company Limited, Wales, UK) at 20 Hz. The sessions consisted of 40 trains of 1.9 seconds duration, separated by a 12 second intertrain interval (1560 pulses per session). The stimulation intensity was set at 110% of the motor threshold. One day prior and after the last stimulation session, a 99mTc-HMPAO SPECT scan was acquired under general anaesthesia. SPECT data were acquired with a triple head gamma camera (Trionix, Triad) 30 minutes after tracer injection (step and shoot, 120 steps of 3 deg, 10" per step). The data were reconstructed with OSEM reconstruction and application of resolution recovery algorithms (Hybrid, Hermes, NUD, Sweden). A BW filter was applied (cut-off 1.6 cycles/cm, order 5). The perfusion indices (PI) in the frontal, parietal, temporal, rostral cingulate and caudal cingulate cortex as well as subcortical regions (thalamus, striatum) were obtained by semi quantification (normalization to total brain counts). A Wilcoxon signed rank test was used to analyze the perfusion indices. Significance level was set at $p \leq 0.05$. Results: The stimulation sessions caused a significantly increased PI in the left frontal cortex ($p = 0.01$) and a decrease in the right parietal cortex ($p = 0.03$). No significant differences were noted for the other regions compared to baseline. Conclusions: Accelerated HF-rTMS of the frontal cortex in dogs provokes an increase in rCBF at the stimulation site. This finding is line with its effects in humans and implies that rTMS may be used as a treatment for canine behavioral disorders. Further investigation is needed to evaluate the stimulation parameters and long-term effects of such stimulation.

PW025

Metabolism of the Spinal Cord in Patients With Amyotrophic Lateral Sclerosis: A FDG-PET/CT Study.

E. Pomposelli[1], G. Sambuceti[1], M. Piana[2], C. Campi[2], M. Pennone[1], A. Buschiazzo[1], A. Cistaro[3], F. Bongioanni[1], A. Chiò[4], F. Nobili[5], C. Caponnetto[6], C. Marini[7]; [1]Nuclear Medicine Unit, Department of Health Sciences, University of Genoa and IRCCS AOU San Martino-IST, Genoa, ITALY, [2]Department of Mathematics, University of Genoa, Genoa, ITALY, [3]Positron Emission Tomography Centre IRMET S.p.A., Euromedic inc, Turin, ITALY, [4]Department of Neuroscience "Rita Levi Montalcini", University of Turin, Turin, ITALY, [5]Clinical Neurology, IRCCS AOU San Martino-IST, Genoa, ITALY, [6]Department of Neuroscience, IRCCS AOU San Martino-IST, Genoa, ITALY, [7]CNR Institute of Bioimages and Molecular Physiology, Section of Genoa, Genoa, ITALY.

Aim. Amyotrophic lateral sclerosis (ALS) is a fatal late-onset neurodegenerative disorder of adult life, characterized by a progressive impairment of motor function. Its pathological feature is characterized by selective cell loss in the anterior horns of the spinal cord (SC) and in the lower motor cranial nerve nuclei as well as by cortico-spinal tract degeneration. We recently developed new software able to identify compact bone profile in PET/CT images and thus able to recognize the spinal canal and SC tracer uptake. The aim of our study was to investigate whether this method permits to identify abnormalities in SC metabolism in ALS patients. Materials and Methods. We studied 41 ASL patients at different clinical stage, submitted to FDG-PET/CT imaging. Patient population was compared with matched healthy controls, randomly selected from a published normalcy database. Image analysis was performed according to a previously validated method. The algorithm first identified the skeleton on the whole body CT images by assuming that compact bone was the structure with the highest X-ray attenuation coefficient in the human body. Once identified the skeletal border, all vertebrae were extracted from the image data set. The spinal canal was automatically identified as the non-osseous space within the spine volume. The output of the software was therefore the extraction and the 3D-representation of spinal canal volume that served as a mask to recognize SC using a segmentation algorithm based on Hough transformation. Thereafter, mean standardize uptake value (SUV) of cervical and dorsal SC, normalized to the liver, was evaluated in comparison with normal subjects. Cervical and dorsal SUV-mean normalized was considered in ASL patient both

untreated and treated with riluzole. Results. Mean SC SUV was significantly higher in ALS patients than controls in cervical (0.97±0.39 vs 0.85±0.20, p<0.05) and dorsal (0.71±0.21 vs 0.67±0.15, p<0.05) SC segments. This increase was virtually abolished in the 21 patients submitted to riluzole respect to untreated patients in both cervical (0.85±0.25 vs 1.11±0.46, p<0.05) and dorsal (0.65±0.14 vs 0.77±0.25, p<0.05) segments. By contrast no differences were found in SC volume between patients and controls or treated and untreated patients. Conclusion. This new computational FDG-PET/CT analysis provided evidence of relative increase metabolism in SC of ALS patients with respect to controls. Moreover, riluzole therapy seems to reduce SC FDG uptake. This method could improve our understanding of SC response to ALS and the effect of new possible therapeutic approaches.

PW026

Imaging of Brain TSPO Expression in a Mouse Model of Amyotrophic Lateral Sclerosis with [18F]DPA-714 and Micro-PET/CT.

S. Gargiulo[1,2], S. Anzillotti[3], A. Coda[1], M. Gramanzini[1,2], A. Greco[4,2], M. Panico[1], F. Dollé[5], G. Pignataro[6], M. Quarantelli[1], L. Annunziato[6,3], A. Brunetti[4,2], M. Salvatore[3], S. Pappatà[1]; [1]Institute of Biostructure and Bioimaging, CNR, Naples, ITALY, [2]Ceinge, Biotecnologie Avanzate s.c.a r. l., Naples, ITALY, [3]SDN IRCCS, Naples, ITALY, [4]Department of Advanced Biomedical Sciences, University Federico II, Naples, ITALY, [5]CEA, Institute for Biomedical Imaging, Orsay, FRANCE, [6]Department of Neuroscience, Reproductive and Dentistry Sciences, Naples, ITALY.

Aim: Amyotrophic lateral sclerosis (ALS) is a progressive neurodegenerative disease affecting the motor system. Transgenic SOD1G93A mice, carrying an ALS-linked mutant human superoxide dismutase gene, provide a relevant tool to investigate in vivo neuroinflammation with translocator protein (TSPO, 18 kDa) radioligands. We evaluated the feasibility of imaging microglial activation in SOD1G93A mice using [18F]DPA-714. Material and Methods: 5 non-carrier and 9 hemizygous SOD1G93A mice (aged 71-137 days) were evaluated at different symptomatic clinical stages (CS, score range: 0.5-4). High-resolution PET/CT (GE Healthcare eXplore Vista, resolution: 1.8 mm FWHM/200 μm) were performed under inhalant anesthesia (isoflurane 2%, oxygen 2 L/min). Images were acquired in dynamic mode over 30 minutes starting 20 minutes after tail vein injection of 5.55-7.00 MBq of [18F]DPA-714 (SRA: 200-800 GBq/μmol), and were processed using a 2D-OSEM iterative algorithm including random, scatter, dead time, and decay correction. Counting rates were converted to Standardized Uptake Values (SUV=Tissue activity (MBq/cc)/[Injected dose (MBq)/body weight (g)]). ROIs were defined based on PET/CT fusion images on the cerebellum, brainstem, cervical spinal cord and frontal cortex using OsiriX software. Cerebellar, brainstem and cervical spinal cord SUV were normalized to those of the frontal cortex. Statistical analysis was performed using Mann-Whitney test and Pearson's correlation. Immunostaining and confocal immunofluorescence were performed on brain and spinal cord sections using rabbit anti-TSPO and mouse anti-Iba1 antibodies. Results: In the SOD1G93A symptomatic mice the region/frontal cortex ratio was significantly increased (p=0.012) in the brainstem (2.340 ±0.784) compared to non-carriers (1.576±0.287). There was no significant correlation between [18F]DPA-714 brainstem/frontal cortex ratio and clinical scores. Preliminary results of immunofluorescence studies showed increased TSPO expression in the spinal cord, in the facial nucleus and in the nucleus ambiguus of symptomatic SOD1G93A mice that colocalizes with increased Iba1 staining. Conclusions: The preliminary results suggest that increased [18F]DPA-714 uptake can be measured with high resolution PET/CT in a mouse model of ALS in the brainstem, a region known to be the site of degeneration and increased microglial activation. Immunostaining results showed that TSPO expression is increased in brainstem nuclei and suggest that increased microglial activation might be the cellular counterpart of in vivo increased [18F]DPA-714 uptake. Acknowledgement: The research leading to these results has received funding from the European Union's Seventh Framework Programme (FP7/2007-2013) under grant agreement n° HEALTH-F2-2011-278850 (INMiND).

PW027

Positive correlation between neuromelanin accumulation in the substantia nigra and striatal dopaminergic innervation in patients with Parkinson's disease

G. Marotta[1], I. U. Isaias[2], A. Costa[1], P. Trujillo[1], P. Summers[1], G. Pezzoli[3], R. Benti[1]; [1]Fondazione IRCCS Ca' Granda Ospedale Maggiore Policlinico, Milano, ITALY, [2]Department of Neurology, University Hospital, Wurzburg, GERMANY, [3]Parkinson Institute, Istituti Clinici di Perfezionamento, Milano, ITALY.

Objectives: Parkinson's disease (PD) is a progressive neurodegenerative disorder in which the major pathologic substrate is a loss of dopaminergic neurons form the substantia nigra (SN). Our main objective was to determine in PD patients the correspondence between SN changes, evident in neuromelanin (NM)- and iron-sensitive MRI images, and dopaminergic striatal

innervation loss. Methods: The study involved 18 subjects with PD (13 males; median age: 64 years, range: 46-77 years) and a control group of 18 neurologically intact adults (HC; 11 males; median age: 58 years, range: 47-77 years). All subjects were examined at 3T MRI by means of NM-sensitive and T2*-weighted multi-echo gradient echo sequences. Using NM-MRI, we measured the volume of the SN (Volsn) and the mean contrast-to-noise-ratio (CNRsn) between SN and a background region. The susceptibility (χ) and R2* of the SN were calculated from multi-echo T2* images. Striatal dopaminergic innervation was measured as density of dopamine reuptake transporters (DAT) by means of FP-CIT SPECT, on the basis of VOIs defined by means of the Basal Ganglia Matching Tool. Results: When compared to a pre-existing group of HC, all PD patients had significantly reduced striatal DAT binding values in both putamen (PT) and caudate nucleus (CN). The reduction was greater on the side contralateral to the most affected hemibody. PD patients showed a reduced Volsn and CNRsn and both positively correlated with the corresponding striatal DAT density. R2* and χ values of SN did not differ between PD and HC. The best predictor of DAT reduction was Volsn ($p<0.001$, Press value=9.33). With reference to our HC cohort, the probability of having PD was 100% when Volsn-contra<0.35 cm3 and 32% if Volsn-contra≥0.35 cm3. Conclusions : NM-MRI is a means of quantifying SN pathology in PD patients that closely correlates with dopaminergic striatal innervation loss. It may serve as an imaging marker of PD, in particular regarding SN neuron loss, although further longitudinal multi-imaging studies, possibly involving subjects at risk of PD, are required.

PW028

Quantification of Amyloid-β Deposition Using ^{18}F-FC119S PET in Human Brains: A Phase 0-1 Study.

B. Byun[1], B. Kim[1], I. Lim[1], C. Choi[1], S. Park[2], J. Ha[2], K. Lee[3], K. Kim[3], S. Lim[1]; [1]Department of Nuclear Medicine, Korea Cancer Center Hospital, Korea Institute of Radiological and Medical Sciences, Seoul, KOREA, REPUBLIC OF, [2]Department of Neurology, Korea Cancer Center Hospital, Korea Institute of Radiological and Medical Sciences, Seoul, KOREA, REPUBLIC OF, [3]Molecular Imaging Research Center, Korea Institute of Radiological and Medical Sciences, Seoul, KOREA, REPUBLIC OF.

Aim: ^{11}C-PIB has been developed and used to measure amyloid-β deposit in the brain, which can be applied for early diagnosis and evaluation of progression of Alzheimer's disease (AD). However, several ^{18}F-labeled radiotracers with a longer half-life were introduced in clinical practice with different characteristics. The aim of the present phase 0/1 study was to obtain information about dosimetry, toxicity, pharmacokinetics, optimal dose, and optimal scan time of ^{18}F-FC119S, a new amyloid-β radiotracer.Materials and methods: Eleven control subjects (mean age = 23.0 y) and 8 clinically-diagnosed AD patients (mean age = 70.6 y) were enrolled (M: F = 9: 10). In phase 0 study, we acquired a 120 min dynamic brain PET image (3 control subjects and 3 AD patients) or 5 times of whole-body PET images during 4 hr (for dosimetry evaluation in 3 control subjects) after injection of 185 MBq of ^{18}F-FC119S. In phase 1 study, we acquired a 60 min dynamic brain PET image in 5 control subjects and 5 AD patients after injection of 370 MBq of ^{18}F-FC119S. The ratios of cerebral gray matter uptake to cerebellar uptake of ^{18}F-FC119S (C/Cbr) were automatically calculated on each PET dataset. Then, PET data acquired for 10 min, 20 min, and 30 min after the plateau of C/Cbr were respectively reconstructed. Quality of these reconstructed images was visually assessed (good/acceptable/poor) and a case with higher or equivocal gray matter uptake compared to the white matter uptake on visual analysis was considered as a PET+.Results: The estimated whole-body radiation dose was 14.7 μSv/MBq and the highest uptake was observed in the liver or gallbladder. No adverse event was observed. C/Cbr continuously increased during the first 30 min after injection of ^{18}F-119S then did not change over 120 min. The mean C/Cbr of AD patients and control subjects at plateau phase was 1.57 and 1.11, respectively. All the PET images acquired during 30-60 min irrespective of injected dose and all the PET images acquired during 30-50 min after injection of 370 MBq of ^{18}F-FC119S showed good image quality, while others showed poor or acceptable image quality. On visual analysis, 6 of 8 AD patients (75%) and 0 of 8 control subjects (0%) showed PET+.Conclusion: ^{18}F-FC119S is safe and its kinetic behavior is suitable for measuring amyloid-β in the brain. PET images acquired during 30-50 min after injection of 370 MBq of ^{18}F-119S showed good image quality.

PW029

Comparison of Visual and Quantitative 18F-Florbetaben PET Scan Assessment

J. Seibyl[1], S. Bullich[2], D. Jennings[1], M. Sabbagh[3], A. Stephens[2], H. Barthel[4], O. Sabri[4], A. Catafau[2]; [1]Molecular Neuroimaging, New Haven, CT, UNITED STATES, [2]Piramal Imaging, Berlin, GERMANY, [3]Univ of Arizona, Phoenix, AZ, UNITED STATES, [4]Univ Leipzig, Leipzig, GERMANY.

Background: Visual interrogation of 18F-Florbetaben (FBB) PET scans is currently recommended for clinical practice,

while quantification using SUVRs is a research tool which has been considered a potentially important adjunct to aid overall scan assessment. However, the added value of quantification for the clinical scan report is unknown. This study aims to compare both assessment methods for FBB PET scans to determine whether analysis of concordance/discordance between the assessments offers insight into how a visual-quantitative assessment algorithm might perform. Methods: A total of 190 FBB scans were evaluated. 109 scans were from n=70 young (27.7 ± 5.1 yrs) cognitively normal subjects (HVs) assumed to be devoid of brain beta-amyloid and n=39 subjects with Down syndrome (DS) > 40 yrs old (46.3 ± 4.7 yrs), and an additional 81 subjects scans were from a Phase 3 histopathology confirmation study. All scans were visually assessed by 3 readers using the brain amyloid plaque load (BAPL) scoring system, where negative scan=BAPL 1, and positive scan is either BAPL 2=moderate or BAPL 3= pronounced tracer uptake. Positive or negative scan agreement in ≥2 readers was considered as the result. A composite SUVR using cerebellar cortex as reference was obtained from the average SUVR in 6 cortical regions, using an automated grey/white matter MRI segmentation and PET-MRI co-registration. Composite SUVR ≥1.45 were considered positive. Results: All scans from HVs were visually assessed as negative. 91.1% of the scans were equally classified as positive or negative by both visual and quantitative approaches. Both methods were significantly and strongly related (X2 = 125, p < 0.0001; Cohen's Kappa = 0.81). In the 17 scans showing discrepancy, SUVRs range from 1.01-1.67, and readers gave divergent BAPL scores in half these cases. These challenging scans exhibited different features: poor technical quality, motion, and atrophy. In the histopathology cohort, for 6 cases with severe cortical atrophy the visual reads were more concordant with histopathology than quantitation. Conclusions: These findings support the use of either visual or quantitative assessment of FBB scans. Further investigation is required to determine the clinical utility of SUVR quantification in challenging scans.

PW030

Striatal dopamine transporter modulation after rotigotine: results from a pilot SPECT study in a group of early Parkinson's disease patients.

E. Filidei[1], C. Rossi[2], D. Genovesi[1], P. Marzullo[1], A. Giorgetti[1], G. U. Corsini[2], U. Bonuccelli[2], R. Ceravolo[2]; [1]Fondazione Toscana G. Monasterio, Pisa, ITALY, [2]Azienda Ospedaliero-Universitaria Pisana, Pisa, ITALY.

Introduction. Several in vitro data reported negative interference by dopamine-agonists on the expression of dopamine transporter (DAT) whereas from the most imaging studies nor L-dopa or dopamine-agonist resulted to interfere with DAT availability. The investigation on DAT expression by rotigotine in vivo has been not investigated yet. Methods. We evaluated presynaptic nigrostriatal function in 8 de novo Parkinson's disease (PD) patients (age 59±6.2 years; M/F 5/3) using FP-CIT SPECT before and after 3 months of treatment with rotigotine (mean dose 7.75±1.98 mg). For data analysis, specific (left and right caudate, left and right putamen) to non-specific (occipital cortex) binding ratios, putamen to caudate ratios and asymmetry indexes were calculated. Results. After rotigotine all patients improved motor symptoms (UPDRS III mean score 11.88±2.59 vs 7.63 ±1.92 on therapy, p=0.0022). Striatal FP-CIT levels showed a significant improvement in each patient at the follow-up scan. Comparisons between the whole group before and after treatment showed a significant improvement in FP-CIT uptake in both caudate and putamen ($p<0.001$ in each nucleus). Putamen to caudate ratio and asymmetry indexes did not show a significant difference before and after treatment. Discussion. We found although in a small study population a DAT overexpression after a chronic treatment with rotigotine presumably related to its pharmacological profile. The DAT upregulation by rotigotine with an opposite direction with respect to early PD compensatory mechanisms might reduce the risk of dyskinesia, but it could imply a less motor benefit because of a less stimulation by dopamine itself on dopaminergic receptors.

PW04 - Sunday, October 11, 2015, 8:30 AM - 9:30 AM, Hall 3 – Poster Exhibition

Poster Walk 4 - Clinical Oncology: Colorectal, Neuroendocrine & Lung

PW031

The role of 68Ga-DOTATATE PET/CT imaging in the decision of Peptide Receptor Radionuclide Therapy (PRRT) administration

E. Skoura[1], S. Michopoulou[1], O. M. AlMukhalid[1], E. Panagiotidis[1], M. Al Harbi[1], I. Kayani[1], R. Syed[1], P. J. Ell[1], M. E. Caplin[2], J. Bomanji[1]; [1]UCLH, London, UNITED KINGDOM, [2]Royal Free Hospital, London, UNITED KINGDOM.

Aim: Peptide receptor radionuclide therapy (PRRT) consists of the systemic administration of a synthetic peptide, labeled with a suitable β-emitting radionuclide, able to irradiate tumors and their metastases. PRRT, with either 90Y-octreotide or 177Lu-octreotate, has established to be an efficient and effective therapeutic

modality that provides objective responses in neuroendocrine tumors (NET), and is well tolerated with moderate toxicity. This study was performed to reveal if 68Ga-DOTATATE PET/CT can influence the decision of PRRT administration in NET patients.Materials ad Methods: Data from patients with NET who received PRRT or were candidate for PRRT were analyzed.Results: Between May of 2005 and August of 2013, 1246 68Ga-DOTATATE PET/CT scans were performed in patients with confirmed or suspected NET. In 13.4% of these cases (in 167 cases), radioisotope therapy, either as PRRT- 177Lutetium (177Lu)-DOTATATE and 90Yttrium (90Y)-DOTATOC- or 131I-MIBG was received after 68Ga-DOTATATE PET/CT scans. In this patient group, PRRT was decided as new treatment in 85 cases (6.8% of the total cases). In these 85 cases, 68Ga-DOTATATE PET/CT imaging showed extensive unresectable and/or metastasized disease with intense 68Ga-DOTATATE uptake. In two cases (0.2%) the PRRT was rejected as treatment because of the low tracer uptake. In detail, 177Lu-DOTATATE was administrated in 46 cases, 90Y-DOTATOC in 25 cases, while in 14 cases the given radiopharmaceutical for PRRT is not known to us (177Lu-DOTATATE or 90Y-DOTATOC). Finally, in 4 cases treatment with 131I-MIBG was decided, as the MIBG uptake in diagnostic 123I-MIBG scan, was more intense that the 68Ga-DOTATATE uptake in 68Ga-DOTATATE PET/CT scan.Conclusion: PRRT is established treatment in patients with advanced and/or progressive NET and 68Ga-DOTATATE PET/CT imaging is necessary prior PRRT to target the somatostatin receptors. Our study reveals that PRRT could be decided as new treatment in a significant percentage of NET patients, when 68Ga-DOTATATE PET/CT scan shows extensive unresectable and/or metastasized disease with intense uptake.

PW032

Radioguided laparoscopic surgery of occult colonic lesions

G. Manca[1], G. Boni[1], R. Spisni[2], S. Chiacchio[1], S. Mazzarri[1], E. Tardelli[1], M. Biricotti[2], D. Volterrani[1]; [1]Regional Center of Nuclear Medicine, Pisa, ITALY, [2]Department of Surgery, University of Pisa, Pisa, ITALY.

Introduction: intraoperative localization, during laparoscopic surgery, of small occult colonic lesions situated in particular areas and/or with concomitant inflammatory bowel disease, such as diverticulosis, perivisceritis, etc., can be problematic. We investigated the feasibility of radioguided occult colonic lesion identification during laparoscopic surgery after an adequate phase of preoperative labelling. Subjects & methods: patients presenting with colonic lesions difficult to detect for their size and location were considered eligible for our study. These patients were first submitted to coloscopy on the same day or 24 hours prior to surgery, in order to administer the radiopharmaceutical into the submucosal layer around the colonic lesion. At least two injections (each containing an activity of 20-40 MBq in a volume of 2 ml) of 99mTc-labelled albumin macroaggregates were administered through a disposable sclerosing syringe around the lesion. During surgery the search for the radiolabelling colonic lesion was carried out by a 11-mm orthogonal-view wireless laparoscopic gamma-detection probe. The site of the lesion was marked with a clip or with a suture. The pathologic features of the lesion determined the type and extension of the surgery to be adopted for each patient. Results: a total of nine colonic lesions, one for each of nine patients, were appropriately marked before surgery and were all intraoperatively detected by laparoscopic gamma-detection probe (identification rate = 100%). According to the surgeon's opinion, this method to detect the colonic lesion was technically feasible, rapid, safe and efficient, and no lengthy learning curve was necessary. Conclusion: our study demonstrates that preoperative endoscopic radiolabelling of occult colonic lesions by injecting 99mTc-labeled albumin macroaggregates followed by surgical detection with a dedicated laparoscopic gamma probe is an accurate, efficient and useful clinical approach, also safe both for the patient and the medical staff in the operating room.

PW033

Is K-ras mutation affecting 18F-FDG uptake in colorectal cancer?

A. Ozen[1], M. Tokocin[1], E. Namal[2], E. Gokmen[1], T. Vartanoglu[1], F. Celebi[1]; [1]Bagcilar Training and Research Hospital, Istanbul, TURKEY, [2]Istanbul Bilim University, Istanbul, TURKEY.

AimThe colorectal cancer (CRC) is the third most common cancer worldwide and the fourth leading cause of cancer-related mortality. Current metastatic CRC therapy uses monoclonal antibodies such as cetuximab against the epidermal growth factor receptor pathway that regulates cell survival, motility and proliferation, as well as angiogenesis and metastasis. This treatment is only useful in the absence of K-ras gene mutations. The aim of our study was whether K-ras mutation affects 18F-FDG uptake in colorectal cancer.Materials and methodsThis study included 10 male (mean age: 52.2±17.21) and 7 female (mean age: 49.14±13.88) patients with CRC. The stages of patients were I in 1(5.9%), IIA in 1(5.9%), IIIB in 1(5.9%), IVA in 9 (52.9%), and IVB in 5 patients (29.4%). The K-ras mutation status was mutant in 5 patients and wild in 12 patients. Furthermore, the patients divided two groups according to CEA level at diagnose time as high at ≥50 and low at

<50. The 18F-FDG PET/CT study was performed preoperatively in all patients. The SUVmax was calculated from images at 1-hour (SUV1) and 3-hours (SUV2) after i.v. injection of 18F-FDG. Furthermore, retention index (RI) was calculated in 11 patients following formula; RI=100 x (SUV2-SUV1) / SUV1.ResultsThe SUV1, SUV2 and RI in K-ras mutant patients were 9.448±3.247, 9.16±0.878, and 27.32%±1.56%, respectively. These values in K-ras wild patients were 13.545±6.054, 21.69±9.99, and 43.89%±16.57%, respectively. There was no statistically difference between K-ras mutant and wild patients for SUV1 (p:0.140), SUV2 (p:0.066), and RI (p:0.221). According to CEA level, There was no statistically difference between high value and low value for SUV1 (p:0.923), SUV2 (p:0.855), and RI (p:0.465).ConclusionWe found that K-ras gene mutation was not affected 18F-FDG uptake in CRC. But, our study included a small number of patients. We thought that there is need for additional research in large series of patients.

PW034

Evaluating the risk of postoperative liver failure using preoperative 99mTc-GSA SPECT/CT fused imaging

M. Yoshida[1], S. Shiraishi[2], N. Tsuda[2], F. Sakamoto[2], S. Tomiguchi[3], T. Beppu[4], H. Baba[4], Y. Yamashita[2]; [1]Amakusa Medical Center, Amakusa, JAPAN, [2]Department of Diagnostic Radiology, Graduate School of Life Sciences, Kumamoto University, Kumamoto, JAPAN, [3]Department of Diagnostic Medical Imaging, School of Health Faculty of Life Sciences, Kumamoto University, Kumamoto, JAPAN, [4]Department of Gastroenterological Surgery, Graduate School of Life Sciences, Kumamoto University, Kumamoto, JAPAN.

Aim: Evaluating the risk of postoperative liver failure is important for safe hepatectomy. Liver Uptake Value (LUV) calculated from preoperative 99mTc-GSA SPECT/CT fused imaging is useful for evaluating functional reserve of remnant liver. Therefore we compared the LUV indices with preoperative clinical risk factors of postoperative liver failure. Methods: We enrolled 560 patients (mean age 66.5±10.6 years) who were performed 99mTc-GSA SPECT/CT before hepatectomy. According to the ISGLS criteria, 27 of 560 patients showed postoperative liver failure. From 99mTc-GSA SPECT/CT, we calculated whole liver LUV and remnant LUV. The cut off value of two indices were calculated from ROC analysis. Older age (>70 years), portal vein hypertension, hepatitis, severe fibrosis, massive bleeding (>700ml), and postoperative complication (> grade 3 of Clavian Dindo classification) were decided as clinical risk factors. Results; The odds ratios of various indices were as follows; low remnant LUV (OR: 18.4; 95%CI: 3.9 - 70.5), low whole liver LUV (OR 4.7; 95%CI 2.0 - 10.9), hepatitis (OR 2.7, 95%CI 0.8 - 9.1), older age (OR 1.2, 95%CI 0.5 - 2.8), portal vein hypertension (OR 2.5, 95%CI 1.1 - 5.7), severe fibrosis (OR 4.4, 95%CI 1.7 - 11.2), massive bleeding (OR 2.7, 95%CI 1.2 - 6.1), and postoperative complication (OR 15.7, 95%CI 6.2 - 39.7). The odds ratio of combination low remnant LUV and low whole liver LUV was 19.9 (95%CI 6.8 - 58.5) and low remnant LUV and postoperative complication was 41.2 (95%CI 17.1 - 99.1). Conclusion; LUV indices calculated from 99mTc-GSA SPECT/CT fused image obtained before hepatectomy were useful for evaluating the risk of postoperative liver failure.

PW035

Can Potassium Perchlorate and Sodium Iodine influence Iodine-131 uptake in Cholangiocarcinoma?

A. F. Brito[1], T. Puga[1], R. Teixo[2,3], A. Fernandes[2,4,5], A. F. Brito[2,4,3], A. M. Abrantes[2,4,3], **L. F. Metello**[1,6], J. G. Tralhão[2,4,7], M. F. Botelho[2,4,3]; [1]Nuclear Medicine Department, High Institute for Allied Health Technologies, Polytechnic Institute of Porto, Vila Nova de Gaia, PORTUGAL, [2]Biophysics Unit, Faculty of Medicine, University of Coimbra, Coimbra, PORTUGAL, [3]CNC.IBILI, Faculty of Medicine, University of Coimbra, Coimbra, PORTUGAL, [4]Center of Investigation on Environmental, Genetics and Oncobiology (CIMAGO), Faculty of Medicine, Coimbra, PORTUGAL, [5]Gastroenterology Department, CHUC, Coimbra, PORTUGAL, [6]Nuclear Medicine Department, IsoPor SA, Ermesinde, PORTUGAL, [7]Surgical Department, Surgery A, CHUC, Coimbra, PORTUGAL.

Aim: Cholangiocarcinoma (CC) is a malignancy with poor prognostic, high mortality and limited treatment options, reason why the development of novel treatment strategies by exploiting new targets might be considered as consensually relevant. In fact, it was shown that CC expressed the sodium iodine symporter (NIS), which is responsible for iodine uptake by the cells. NIS is also the responsible for the uptake of iodine-131 (131I) in thyroid tumor and benign diseases, enabling the metabolic radiotherapy and opening possibilities of new treatment approaches for CC.Aim: This work aims to study the uptake profile of 131I mediated by NIS, in two human CC cell lines from distinct origins. The uptake specificity was tested using NIS inhibitor potassium perchlorate (KClO4) as well as the effect of sodium iodide (NaI) on 131I uptake.Material and Methods: Two human CC cell lines were used: TFK-1 from extra-hepatic CC and HuccT1 from intrahepatic CC. In order to study the

131I uptake profile, we incubated 2 x 106 cells/mL with 9.25 x 105 Bq of 131I for 120 minutes. During this period, several samples were collected and the respective counts per minute (CPM) registered. Furthermore, the NIS specificity for 131I was assessed in the presence of the inhibitor KClO4. For this purpose, the cells were pre-incubated with KClO4 (1 to 100μM) for 0, 30 and 60 minutes before adding 131I. The effect of NaI was tested using same protocol and same concentrations. The uptake of 131I was measured after 30 minutes incubation with the radiopharmaceutical.Results: It was observed 131I uptake in both cell line cell lines (TFK-1 and HuccT1). The uptake peak was between 5 and 30 minutes, remaining stable after that. Moreover, KClO4 reduced the NIS mediated 131I uptake levels, in both cell lines, when introduced in culture medium at the same time, suggesting that 131I uptake is dependent of plasma membrane functional NIS proteins. Preliminary results showed no differences in the 131I uptake, in both cell lines, when different stable iodine concentrations are present in the medium.Conclusions: Different types of human CC cell lines have the capacity to accumulate 131I, based on plasma membrane functional NIS expression. However the uptake is not influenced by the presence of NaI. These preliminary results seem to show the potential that metabolic radiotherapy with 131I could have for CC treatment.

PW036

Clinical Value of Metabolic Parameter for Evaluation of LN Metastasis in Clinical N0 Gastric Cancer

S. Choi, S. Lim, C. Na, J. Kim, Y. Han, H. Jeong, M. Sohn; Chonbuk National University Medical School and Hospital, Jeonju, Jeonbuk, KOREA, REPUBLIC OF.

Purpose: Predicting lymph node metastasis in gastric cancer has the crucial role because its possibility to changing therapeutic method either endoscopic resection or surgical gastrectomy. Preoperative CT scan has the limit to evaluate LN metastasis, which depends on size and shape, anatomically. The purpose of the study is to evaluate regional LN status by primary gastric tumor using its metabolic standardized uptake value (SUVmax) in radiologic No gastric cancer. Material and methods: We retrospectively reviewed 201 patients which were confirmed as gastric cancer from July 2012 to December 2012. All patients had done preoperative F-18 FDG PET/CT. Among the various histological gastric tumors, only adenocarcinoma showing FDG uptake evidently on PET scan is evaluated because of its accessability to measure metabolism. Among 201 patients, ninety-three patients (M : F= 61 : 32, age: 60.0 ± 12.3 yrs) show no discernible or below 0.6 cm sized regional LNs in preoperative CT scan, also having no FDG uptake which was interpreted as N negative. Dividing by two groups, 37 patients have pathologically confirmed as N positive and 56 patients have the result of N negative. Statistical analysis is performed by using student T-test and ROC curves to compare primary tumor SUVmax between two groups. Result: The mean values of SUVmax for pathologically confirmed as N positive and N negative groups are 7.39±3.4 and 5.77±2.5 each. There is significant difference between the two groups (P= 0.01). The cut-off value of SUV max in predicting LN metastasis is above 5.56. The other 69 of 201 patients, except above 93 patients, presenting FDG uptake in regional LN show high FDG uptake in primary gastric tumor, mean SUVmax= 11.91±6.7. Conclusion: The result shows higher FDG uptake in primary gastric tumor with LN metastasis than that of without LN metastasis. Furthermore, primary gastric tumor metabolism is much higher in the group which shows FDG uptake in regional lymph node. To clarify the correlation of FDG-avid LN with the other various factors, further studies should be needed. Predicting LN metastasis by means of measuring primary tumor metabolism could be the ancillary option to decide therapeutic plans in gastric cancer patients.

PW037

Comparative Analysis of Metabolic Response to Clinical Outcome in Metastatic Pancreatic Adenocarcinoma following Modified Dose Folfirinox.

A. Boustani[1], V. Patel[1], X. Cong[2], I. Doddamane[1]; [1]Yale University School of Medicine, New Haven, CT, UNITED STATES, [2]Yale University School of Public Health, New Haven, CT, UNITED STATES.

Aim: To compare early metabolic response with clinical progression free survival (PFS) and overall survival (OS) in patients with metastatic pancreatic adenocarcinoma following attenuated dose FOLFIRINOX. Methods: Of the 43 patients enrolled in the study between 11/2011 and 01/2014 29 patients were evaluated by both baseline and follow-up F18-FDG PET/CT. Medical reasons and technical issues limited accurate evaluation by F18 FDG PET/CT. 14 of the patients were excluded. A baseline PET/CT scan was obtained before treatment. It was followed by a second PET/CT after two cycles of chemotherapy with modified dose Folfirinox. Based on SUV max corrected for background, metabolic response of the lesions was categorized as stable, mild, significant, or as progression. Using Chi square test, Fisher's exact test, and Kaplan-Meier methods, PFS and OS were associated with PET response. Results: There were a total of 105 primary and metastatic lesions in 29 patients. 24 patients responded, 3 progressed, and 2 were stable. 5 patients did not respond.

Clinically, 24 of 29 patients were associated with PET response. 14 of 29 patients had significant response (48%, metabolic change by >50%). For statistical analysis, patients were also grouped as responders (83%, metabolic response by >25%) and non-responders (17%, metabolic response <25%). There was no association between PFS and OS and overall metabolic response (0.42 for both). Conclusion: An attenuated dose of Folfirinox was used for the treatment of metastatic pancreatic cancer in order to evaluate its efficacy while improving its tolerability. There was a high percentage of metabolic response at follow-up (83%). However, this did not correlate with clinical outcome. Larger sample sizes are required for further evaluation.

PW038

Role of FDG-PET/CT in predicting response to neoadjuvant therapy in esophageal cancer. Correlation with pathological response and survival. Preliminary study.

J. J. Robles-Barba[1], C. Gámez-Cenzano[1], J. L. Vercher-Conejero[1], A. Sabaté-Llobera[1], M. Cortés-Romera[1], L. Rodríguez-Bel[1], L. M. Gràcia-Sánchez[1], F. Martínez-Torrens[2], R. Mast-Vilaseca[2], M. J. Paules-Villar[3], M. Miró-Martín[4], A. M. Boladeras-Inglada[5], M. Calvo-Campos[6], M. Galán-Guzmán[6]; [1]PET-CT Unit, Institut de Diagnòstic per la Imatge (IDI). Bellvitge Hospital., L'Hospitalet de Llobregat, SPAIN, [2]Radiología. Bellvitge Hospital., L'Hospitalet de Llobregat, SPAIN, [3]Anatomía Patológica. Bellvitge Hospital., L'Hospitalet de Llobregat, SPAIN, [4]Cirugía General. Bellvitge Hospital., L'Hospitalet de Llobregat, SPAIN, [5]Oncología Radioterápica. Institut Català d'Oncologia, L'Hospitalet de Llobregat, SPAIN, [6]Oncología Médica. Institut Català d'Oncologia, L'Hospitalet de Llobregat, SPAIN.

AIM: To assess the correlation between metabolic response with FDG-PET/CT and pathological response in patients with locally advanced esophageal cancer treated with neoadjuvant chemoradiotherapy, and to study FDG-PET parameters for prediction of pathological response and outcome. MATERIAL AND METHODS: Twenty-five patients (22 male; age range 45-79 y.o) with locally advanced esophageal cancer (stage III; 10 squamous cell and 15 adenocarcinoma) underwent 2 FDG-PET/CT scans at 2 time points: 1(Initial staging and 2) 4 weeks after neoadyuvant chemoradiotherapy. FDG uptake in the primary tumor was calculated in the 2 scans with the following parameters: SUVmax, SULpeak and TLG. Metabolic response was assessed according to the reduction of PET parameters (%): complete response (mCR=100%), partial response (mPR≥50%) and no response (≤50%). Pathological response obtained after surgery, was also classified as complete (pCR), partial (pPR) or no response (pNR). Patients were followed up (range 8 - 99 months) determining free-disease interval (FDI) and overall survival (OS). RESULTS: Two patients were excluded of our study due to exitus for non-esophageal related causes. Metabolic response was observed in 18 of the 23 remaining patients (3 mCR and 15 mPR), of which 12/18 patients showed pathological response (3 pCR and 9 pPR). Major discrepancy was observed in 2 of PET non-responders patients (5) who achieved pPR. FDI and OS were apparently longer in patients with metabolic response than non-responders (18,5 and 28 months vs 12 and 20 months) but no statistical difference was found in this small group. No significant correlation was found between PET parameters (including the % of reduction) and the pathological response, FDI and OS. CONCLUSION: FDG-PET/CT is a useful technique to assess response to neoadjuvant chemoradiotherapy in esophageal cancer. Althoug in this preliminary study with a small number of patients, no correlation between metabolic and pathologic response was found and no statistical differences between responders and non-responders were observed, a tendency of a longer FDI and OS was apparently found in responders patients.

PW039

Maximum standardized uptake value on FDG PET is associated with overall survival in limited-stage small cell lung cancer

S. Lee[1], S. Kwon[1], S. Hyun[2], Y. Oh[1], J. Choi[1], K. Park[1]; [1]Ajou University School of Medicine, Suwon, KOREA, REPUBLIC OF, [2]Sungkyunkwan University School of Medicine, Seoul, KOREA, REPUBLIC OF.

Aim: We evaluated the prognostic value of ^{18}F-fluorodeoxyglucose positron emission tomography (FDG PET) parameters for limited-stage small-cell lung cancer (LS-SCLC). Materials and Methods: We enrolled 59 LS-SCLC patients who underwent pretreatment FDG PET/CT. Various PET parameters were measured in all malignant lesions, and we recorded the highest maximum standardized uptake value (SUV_{max}), and sum of metabolic tumor volume (MTV_{sum}) and total lesion glycolysis (TLG_{sum}). The relationship between SUV_{max} and volumetric PET parameters was evaluated. The prognostic significances of PET parameters and clinical variables were assessed using Cox's proportional hazard regression analysis. Overall survival (OS) and progression-free survival (PFS) were assessed by the Kaplan-Meier method. Results: The SUV_{max} of the highest metabolic lesion had a significant positive correlation with MTV_{sum} and TLG_{sum} ($P < 0.0001$). Upon multivariate analysis, SUV_{max} was an independent predictor of OS (HR: 1.133, $P = 0.003$) and MTV_{sum} was a significant prognostic factor of PFS after

adjusting for age, sex, performance status, tumor stage, and treatment modality. SUV_{max} tended to be a significant prognostic factor for PFS (HR: 1.078, $P = 0.053$). Patients with higher SUV_{max} (≥11) were also characterized by a significantly shorter median OS ($P = 0.0001$) and PFS ($P = 0.0017$) compared with patients with lower SUV_{max}. Conclusion: The highest SUV_{max} is an independent prognostic factor for survival in LS-SCLC patients.

PW040

The correlation between 18F-FDG uptake and Glut-1, Stat-1 and Stat-3 in non-small cell lung cancer patients.

H. Kaida[1], K. Azuma[2], A. Kawahara[2], S. Hattori[2], S. Takamori[2], E. Sadashima[2], K. Fujimoto[2], M. Kage[2], S. Kurata[2], Y. Hirose[2], K. Ishii[1], T. Murakami[1], M. Ishibashi[3]; [1]Kinki University Faculty of Medicine, Osakasayama City, JAPAN, [2]Kurume University School of Medicine, Kurume City, JAPAN, [3]Fukuoka Tokushukai Hospital, Kasuga City, JAPAN.

Aim. The purpose of this study was to assess the correlation between 18F-fluorodeoxyglucose (18F-FDG) uptake and glucose transporter-1 (Glut-1), signal transducer and activator of transcription-1 (Stat-1) and Stat-3 expression in completely surgically resected non-small cell cancer (NSCLC) patients. Materials and Methods. Our patients consisted of 52 patients [31 men and 21 women]. The median age of these patients was 72.5 (range, 42-91) years. The patients with tumors diameter less than 10 mm and the patients who underwent neoadjuvant chemotherapy before surgery were excluded from this study. Histopathologically, there were 38 adenocarcinomas and 14 squamous cell carcinomas. The clinical stages of all patients were as follow: stage IA (n=27), IB (n=8), IIA (n=7), IIB (n=6) and IIIA (n=4). 18F-FDG positron emission tomography (PET) was performed, and the maximum standardized uptake value (SUV max) of primary tumor was measured. Pathological tumor size was estimated by measuring the maximum diameter of the tumor, and pathological TNM staging was determined after operation. Excised tumor tissue was analyzed immunohistochemistry using monoclonal antibodies for Glut-1, Stat-1, and Stat-3. Spearman's rank correlation test and Kruskal-Wallis test were performed to assess any association between 18F-FDG uptake and each histopathlogical or immunohistochemical factor. Results. The median value of SUV max of primary tumor was 4.76 (range 0.83-15.39). The median value of immunohistochemistry staining for Glut-1, Stat-1 and Stat-3 was 30% (range, 0-80%), 1% (range, 0-15%) and25% (range, 0-70%), respectively. SUV max positively correlated with Glut-1 expression (r=0.685, P<0.001) and Stat-1 expression (r=0.295, P=0.03). SUV max inversely correlated with Stat-3 expression (r=-0.579, P<0.001). Glut-1 positively correlated with Stat-1 expression, however, inversely correlated with Stat-3 expression [r=0.35, P=0.01, Stat-1, r=-0.377, P=0.006]. Pathological tumor size positively correlated with SUV max (r=0.327, P=0.018) and Glut-1(r=0.54, P<0.001), however inversely correlated with Stat-3(r=-0.318, P=0.022). High SUV max tended to be advanced pathological T stage (P=0.01), pathological lymph node metastasis (P=0.015) positive and advanced pathological Stage (P=0.024). Conclusion. Glut-1 expression, Stat-1 and Stat-3 may be associated with SUV max of primary tumor. High Glut-1 and Stat-1 expression, low Stat-3 expression and cellularity may be related with high 18F-FDG uptake in NSCLC.

PW05 - Monday, October 12, 2015, 8:30 AM - 9:30 AM, Hall 3 – Poster Exhibition

Poster Walk 5 - Physics & Instrumentation & Data Analysis: Data Analysis & Management

PW041

Development of a new quantification method using the I-123 MIBG myocardial single photon emission tomography

Y. Kamiya[1,2], S. Okumiya[1], A. Takaki[3], K. Yamashita[3], S. Ito[1]; [1]Kumamoto University, Kumamoto, JAPAN, [2]Chibana Clinic, Okinawa, JAPAN, [3]Fujifilm RI Pharma Co.,Ltd., Tokyo, JAPAN.

[Objective]Iodine-123 metaiodobenzylguanidine (^{123}I-MIBG) myocardial scintigraphy has been used to evaluate cardiac sympathetic denervation in Lewy body disease (LBD) including Parkinson's disease (PD) and dementia with Lewy bodies (DLB). The heart-to-mediastinum ratio (H/M) in PD and DLB is significantly low compared to that in Parkinson's plus syndromes (PPS) and Alzheimer's disease (AD). The H/M is useful for distinguishing LBD from AD. However, the distinction of AD and the PPS is difficult due to narrow H/M range. Additionally, accuracy of this method is limited, as the H/M is obtained by a two-dimensional image analysis. Therefore, a new quantification method using the ^{123}I-MIBG single photon emission tomography (SPECT) image analysis is required for clinical routine study in order to guarantee repeatability and reproducibility. The purpose of this study was to develop a new quantification method with a simple determining protocol for ^{123}I-MIBG SPECT uptake measurement.[Materials and methods]The ^{123}I-MIBG input function was obtained by using integrated lung washout ratio and the input counts of the

pulmonary artery (PA). These were obtained by analyzing the time activity curve of the lung and PA. The ^{123}I-MIBG output function was obtained by using the ^{123}I-MIBG SPECT counts on the polar map. The uptake was obtained by dividing the output function by the input function.Thirty-nine patients underwent ^{123}I-MIBG SPECT at 15 min after the tracer injection and clinical features such as Hoehn and Yahr (H-Y) classification. The H/M and the uptake of ^{123}I-MIBG were calculated, and correlation with the clinical features was analyzed.[Result]The H/M of LBD (median 1.75) was significantly lower than in PPS (median 2.85, $p<0.01$). The discretion of AD (median 2.65) and PPS (median 2.85) was impossible. The uptake of LBD (median 2.09%) obtained by the new method was significantly lower than in PPS (median 7.94%, $p<0.01$). The uptake ratios of AD (median 5.62%) was significantly lower than in PPS (median 7.94%, $p<0.05$).[Conclusion]The new quantification method was developed by using ^{123}I-MIBG SPECT and integrated lung washout ratio and the input counts of the PA. The AD, LBD and PPS can be clearly distinguished by using this method. This finding indicates the possibility of clinical routine study.

PW042

Application of Novel Phase Parameters for Characterisation of Ventricular Mechanical Dyssynchrony with Radionuclide Ventriculography

K. Jones, N. E. R. Goodfield, J. Robinson, W. Martin, C. A. Paterson; NHS Greater Glasgow and Clyde, Glasgow, UNITED KINGDOM.

Aim: Assessment of left ventricular function is known to be a powerful prognostic indicator of cardiovascular disease. Synchrony (S), entropy (E) and sample approximate entropy (SampEn) are novel indices to characterise dyssynchrony, which have been shown to give additional independent prognostic information. Synchrony is a measure of ventricular contraction coherence and entropy describes the degree of randomness of ventricle phase disorder. SampEn is a measure of entropy which takes into account regional phase similarly of adjacent pixels. The aim of this study is to establish a normal range of synchrony, entropy, SampEn, the correlation of each parameter with ejection fraction (EF) and their ability to discriminate between normal studies and those with mechanical dyssynchrony. Methods: 526 clinical gated planar list-mode RNVG studies were retrospectively re-analysed using in-house software. The studies analysed consisted of 250 normal studies (QRS < 120 ms, normal myocardial perfusion scan, normal RNVG scan, normal EF), 164 with myocardial infarction (MI), 112 with left bundle branch block (LBBB). Synchrony, entropy and SampEn were calculated from phase information extracted from the first order Fourier harmonic fit to the RNVG time-activity curve. Results were analysed using receiver operating characteristic analysis (ROC) and area under the ROC curve (AUC) values were obtained. Results and Conclusion: Synchrony and entropy values were found to be significantly different when comparing normals with both MIs and LBBBs ($p < 0.005$). SampEn values were significantly different between normals and MIs but not between normals and LBBBs ($p=0.1$). Overall good diagnostic accuracy was found for detection of MIs based on dyssynchronous ventricular contraction; AUC = 0.79 for S, AUC = 0.86 for E and AUC = 0.70 for SampEn. Correlation with ejection fraction was R = 0.67 for S, R = -0.72 for E and R = -0.52 for SampEn. This study has established the normal range for synchrony, entropy and SamEn for a large cohort of normal studies and demonstrated their potential for quantifiable assessment of ventricular function. Future work will optimise and further characterise these parameters. The MI group will be further sub-categorised by size and alternative metrics for mechanical dyssynchrony will also be assessed.

PW043

Improved scatter correction applying factor analysis

P. Knoll[1], M. Ljungberg[2], S. MIrzaei[1], M. Samal[3]; [1]Wilhelminenspital, VIenna, AUSTRIA, [2]Department of Medical Radiation Physics, Clinical Sciences, Lund University, Lund, SWEDEN, [3]Department of Nuclear Medicine, First Faculty of Medicine, Charles University, Prague, CZECH REPUBLIC.

Aim: Obtaining quantitative data is a crucial task in nuclear medicine. In order to achieve this goal the various interactions of photons with matter have to be observed, modelled and considered. A problem in gamma camera imaging is the inclusion of scattered photons within the photopeak energy window used for acquisition. Many methods for scatter correction have been proposed in the past but in this work we use a novel setup applying factor analysis (FA). **Material and Methods**: Monte Carlo simulations using the SIMIND software package were used to simulate planar (99m Tc point source, 99m Tc MDP bone) and tomographic acquisitions. Furthermore a Jaszczak phantom study and patient 99m Tc MDP bone studies were performed using a large-field of view gamma camera. In order to use FA for scatter correction we subdivided the applied energy window in 28 simultaneous sub-windows which serves as input data. The Jaszczak phantom was acquired using General Electric's Infinia Hawkeye (acq. parameters: 360° SPECT, 6°/frame, 40 sec./frame) using the same number of sub-energy windows. The

tomographic data (simulation and measurement) were processed for each angular position resulting in a photopeak and a scatter data set. The reconstructed transaxial slices were quantified using an ImageJ plugin. **Results**: FA results in two factor images (photopeak, scatter) and two factor curves. The data obtained by factor analysis showed good agreement with the simulated energy spectra, photopeak and scatter images obtained by Monte Carlo simulation for all simulated data sets. The cold sphere contrast of the Jaszczak phantom applying no scatter correction ranges from -47.67 to -4.75 and with scatter correction applying FA from - 51.48 to -7.52. The cold sphere sector contrast ranges from -16.61 to -0.18 for the non-scatter corrected data and for the FA data from -16.61 to -0.23. **Conclusion**: Factor analysis can be used as a user-independent approach for scatter correction for planar and tomographic imaging.

PW044

Quantification of striatal uptake in DaTscan dopamine transporter imaging: Effect of systematically reduced count density on diagnostic accuracy

C. Paterson, J. Robinson, S. Smith, W. Martin; Glasgow Royal Infirmary, Glasgow, UNITED KINGDOM.

Outline and Aims: [^{123}I]-FP-CIT (DaTscan) is a radioligand developed for the imaging of dopamine transporters with SPECT. Its use as an in-vivo pre-synaptic imaging agent to detect degeneration of the dopaminergic nigrostriatal pathway and to characterize Parkinson's Disease (PD) has been well established. Quantification of striatal uptake has the potential to further increase diagnostic accuracy and reduce the number of equivocal reports. Increases in numbers of referrals and difficulties with subject tolerance of long imaging times has prompted consideration of reducing the administered activity and/or acquisition time. This study aims to investigate the effect that simulating a reduction in administered activity has on the quantification of the striatal specific binding ratio (SBR) and its diagnostic accuracy. Methods: 85 clinical studies (44 positive for PD based on a surrogate gold standard of previous clinical interpretation) were retrospectively re-analyzed. Reduction in administered activity to 75%, 66%, 50% and 25% of the original activity was simulated by reducing the number of counts in every pixel of the raw data projections. A Poisson noise generator was then used to add an appropriate level of statistical noise back into each image. Once the data were transformed to the reduced count densities two experienced operators independently reconstructed, processed and analysed each image for calculation of SBR.Results: The SBR technique for calculation of striatal uptake was found to have excellent inter-operator reproducibility at all count densities ($R > 0.92$; Bland-Altman bias < 1.19 and limits of agreement < 1.62) and there was excellent correlation between the SBR values calculated at the different count densities for both operators ($R > 0.94$; Bland-Altman bias < 0.47 and limits of agreement < 1.92). Furthermore, receiver operating characteristic analysis (ROC) found no significant change in the area under the ROC curve (AUC) for each count density (AUC > 0.84).Summary: Overall, the study proves the robustness of the SBR quantification technique at reduced count densities both in terms of the diagnostic accuracy of the technique and the inter-operator variability. This gives confidence that [^{123}I]-FP-CIT imaging with quantification can be performed with reduced administered activities (or reduced acquisition times). Further work will assess how visual clinical assessment of the images is affected by reduced activity, and whether or not diagnostic performance at low count densities can be improved through the use of advanced reconstruction algorithms and machine learning based interpretation.

PW045

Statistical variance in standardised striatal uptake ratio in [123I]FP-CIT SPECT imaging

A. Niñerola-Baizán[1,2], J. Gallego[2], A. Cot[1,2], F. Lomeña[3,4], D. Ros[1,2], J. Pavía[1,3]; [1]Centro de Investigación Biomédica en Red en Bioingeniería, Biomateriales y Nanomedicina (CIBER-BBN), Barcelona, SPAIN, [2]Unitat de Biofísica i Bioenginyeria, Facultat de Medicina, Universitat de Barcelona, Barcelona, SPAIN, [3]Servicio de Medicina Nuclear, Hospital Clínic, Barcelona, SPAIN, [4]Centro de Investigación Biomédica en Red de Salud Mental (CIBERSAM), Barcelona, SPAIN.

INTRODUCTION: [123I]FP-CIT SPECT is a widely used tool for the in vivo evaluation of the dopaminergic system in movement disorders including Parkinson's disease (PD). To objectively assess striatal dopamine transporter (DaT) binding, a semi-quantitative analysis including standardisation is recommended. Standardisation enables us to compare the findings from multicentre trials and to generate a comprehensive reference database. However, uptake quantification and standardisation depend on noise in projections and reconstruction parameters. AIM: To determine the reconstruction parameters and postfilters that yield the minimum variance in the standardised results. MATERIALS AND METHODS: [123I]FP-CIT SPECT studies were simulated by using the SimSET Monte Carlo code. The activity maps were obtained from 3D T1-weighted MR images corresponding to 23 subjects free of cerebral abnormalities. The FIRST segmentation tool from FSL was used to select caudate and putamen nuclei from MR images. Specific Uptake Ratio (SUR) values between 1 and 10 for caudate and putamen were selected. Three million counts in projections were simulated. Reconstruction was performed using OSEM (8 subsets and 1 to 30 iterations) with attenuation correction, PSF correction and an

ideal scatter correction with only the primary photons in the simulated projections. Reconstructed images were filtered by using a set of Gaussian post-filters with FWHM of 0 (i.e. no post-filter), 2, 4, and 6 mm. SUR values were calculated using the MRI original ROIs. Standardised SUR values were obtained by applying the inverse of the regression line relating calculated to true SUR values. The linear regression analysis allowed us to evaluate the variance of the results by calculating the standard error of the estimate (SSy) and the Root Mean Square Deviation (RMSD) between standardised and true values. RESULTS: Small differences in the minimum RMSD value were found for all post-filters. Thus, the minimum of RMSD (0.239) was achieved at 13 iterations without post-filter, whereas RMSD was 0.225 at 30 iterations when a post-filter of 6mm FWHM was applied. The number of iterations diminished to 4 and 8, respectively, if differences of 5% between actual RMSD and RMSDmin were considered. The SSy value at 8 and 30 iterations with the 6mm FWHM post-filter was 0.238 and 0.226, respectively. CONCLUSIONS: Monte Carlo simulation allowed us to estimate the variance in standardised striatal uptake ratio due to methodology. A minimum RMSD of 0.225 and a SSy of 0.226 should be considered as the methodological error to be complemented with that caused by the physiological variability.

PW046

Is a system calibration required when using a I123-FP-CIT Normal Database?

J. C. Dickson[1], L. Tossici-Bolt[2], K. Tatsch[3]; [1]University College London Hospital NHS Foundation Trust, London, UNITED KINGDOM, [2]University Hospital Southampton NHS Foundation Trust, Southampton, UNITED KINGDOM, [3]EANM EARL ENCDAT Imaging Consortium, Vienna, AUSTRIA.

Introduction: Normal databases offer the potential of improving the diagnostic performance of imaging tests such as I123-FP-CIT. It has been suggested to make best use of an I123-FP-CIT database; there should be a reference calibration of a system to allow normal range values to be tailored to that particular system. This paper studies the diagnostic performance of a normal database with and without this reference calibration, and also assesses the possibility of replacing a bespoke calibration with an existing calibration for the same system type. Methods: The ENCDAT normal database was reconstructed using iterative reconstruction with corrections for attenuation and scatter as per the ENCDAT protocol [1]. Once reconstructed age dependent normal ranges of quantitative uptake were derived for a GE Infinia system on which 44 patient studies with three year follow-up information had been acquired. Normal ranges were defined using (1) a bespoke calibration of the system (BES), (2) an existing library calibration of the same system type (LIB), (3) no calibration for the imaging system (NO). Using three-year follow-up information as the gold-standard diagnosis, sensitivity and specificity of the different calibration strategies were calculated using striatal uptake as the diagnostic marker, and using putaminal uptake as the diagnostic marker. Results: With striatal uptake as a diagnostic marker there was no significant difference in sensitivity across the three strategies 85.7% (BES & LIB), 76.2% (NO). There was also no significant difference in specificity 87.0% (BES & NO), 78.2% (LIB). Similarly, when putaminal uptake was used as a diagnostic marker, there was no significant different between calibration strategies. Sensitivity was 85.7% (BES & NO), 90.5% (LIB), and specificity 82.6% (BES), 78.3% (LIB), and 87.0% (NO). Conclusions: In our single-site sample of 44 patients there was no diagnostic advantage to be gained from calibrating the system with either a bespoke or library calibration. References: [1] Varrone A et al. European multicentre database of healthy controls for [(123I]FP-CIT SPECT (ENC-DAT): age related effects, gender differences and evaluation of different methods of analysis. Eur J Nucl Med Mol Imaging. 2013 Jan;40(2):213-27

PW047

The effect of different reconstructions algorithms on the diagnostic performance of a 123-FP-CIT SPECT database

J. C. Dickson[1], L. Tossici-Bolt[2], K. Tatsch[3]; [1]University College London Hospital NHS Foundation Trust, London, UNITED KINGDOM, [2]University Hospital Southampton NHS Foundation Trust, Southampton, UNITED KINGDOM, [3]EANM EARL ENCDAT Imaging Consortium, Vienna, AUSTRIA.

Introduction: The use of quantitative information from healthy control databases offers an improvement in the diagnostic performance of imaging tests such as I123-FP-CIT SPECT. However, it is not known how the use of different SPECT reconstructions affects the performance of these databases. The aim of this study was to explore this issue. Methods: The ENCDAT normal database [1] and patient data from 77 patients from two different centres and with three-year follow-up information were used in this study. All data was reconstructed using iterative reconstruction with corrections for attenuation and scatter (IRACSC), without corrections (IRNC), and with filtered back projection (FBP). Quantitative normal ranges using Hermes BRASS were set using the database for these reconstructions, with patient data normality assessed quantitatively on a striatal and putaminal level. Using clinical follow-up as our gold standard, sensitivity/specificity and ROC analysis were performed to assess the diagnostic accuracy of databases reconstructed in different ways. Results: Using striatal uptake as

a diagnostic marker, sensitivity was similar for different reconstructions at 83.7% (ACSC), 81.4% (IRNC) and 81.0% (FBP). Similarly specificity was not significantly different 85.3% (ACSC), 82.4% (IRNC) and 77.14% (FBP). ROC analysis confirmed that there was no significant difference in the diagnostic performance of the different reconstructions with AUC if 0.898 (ACSC), 0.913 (IRNC), and 0.880 (FBP). There were similar findings when putaminal uptake was used as a diagnostic marker with sensitivities of 81.4% (ACSC), 78.6% (IRNC), and 78.6% (FBP) and specificities of 82.4% (ACSC), 85.7% (IRNC), and 77.1% (FBP). ROC analysis derived AUC were 0.907 (ACSC), 0.917 (IRNC), and 0.893 (FBP). Conclusions: In our sample of 77 patients we found no significant difference in the diagnostic performance of a normal database using different reconstruction algorithms. References: [1] Varrone A et al. European multicentre database of healthy controls for [(123I]FP-CIT SPECT (ENC-DAT): age related effects, gender differences and evaluation of different methods of analysis. Eur J Nucl Med Mol Imaging. 2013 Jan;40(2):213-27

PW048

Investigation of the Factors Affecting Quantification of Heterogeneity derived from PET Images of the Torso NEMA Phantom

M. Tamal, C. Robinson, D. Clarke, J. Anton-Rodriguez, D. Morris, A. Jackson, M. Asselin; The University of Manchester, UK, Manchester, UNITED KINGDOM.

Introduction: Radiotracer tumour uptake is often heterogeneous and quantification of heterogeneity has the potential to be used as a biomarker of prognosis. Textural features accounting for both spatial and intensity information have recently been applied to FDG-PET images and used to predict treatment response[1]. However, textural features have been predicted to strongly depend on volume using simulated data[2] and confirmed on clinical data[2],[3]. Other factors affecting textural features such as segmentation and quantization have previously been investigated on clinical data where the actual tumour volume is unknown[4] while image contrast and noise have not been assessed systematically. This study aims to investigate the relationships between textural features and these factors using phantom data.Methods: The torso NEMA phantom was filled with 18F solutions to yield different contrasts between the six hot spheres (0.5-27ml) and the colder uniform background (2:1, 4:1, 8:1) and scanned on the TrueV PET-CT scanner for 120min. Images were reconstructed using OSEM (4 iterations, 21 subsets) for different scan durations (15-120min) and smoothed with a 4-mm Gaussian filter. Spheres were first delineated at the exact boundaries based on their known diameters and secondly using a 40% fixed threshold. Textural features were derived from the co-occurrence matrix using different quantization levels (8-256).Results: Some textural features (contrast, dissimilarity, entropy, correlation) increase while others (homogeneity, energy) decrease with quantization at different rates depending on sphere volume. When using the exact delineation, contrast and scan duration (noise) have a lesser effect on textural features than sphere volume. When applying the same exact regions on the uniform background (no partial volume), the relationships between textural features and volume are comparable to when applied to the respective spheres except for correlation. On images with very low noise (120min) and high contrast (8:1), thresholded regions underestimate sphere volumes >5ml by ≈10% and thus yield textural features similar to those using the exact delineation. However, because larger thresholded regions are segmented as contrast is lowered, textural features become contrast dependent when using a fixed threshold.Conclusion: Homogeneous regions appear heterogeneous on PET images as quantified by textural features. Since textural features differentially vary with volume, regions should be segmented using methods that are robust to variations in contrast and noise and their volume reported.References:[1]Chicklore S. et al (2013) Eur.J.Nucl.Med.Mol.Imaging 40(1):133-40[2]Brooks F.J., Grigsby P.W. (2015) PLoS One 10(2):e0116574[3]Hatt M. et al (2015) J.Nucl.Med. 56(1):38-44[4]Orlhac F. et al (2014) J.Nucl.Med. 55(3):414-22

PW049

Quantification Challenges in Dual-Time PET Scans

T. Nguyen, S. B. Christlieb, P. F. Hoeilund-Carlsen; Dept. of Nuclear Medicine, Odense University Hospital, Odense, DENMARK.

Aim: Dual-time PET to detect temporal changes in a lesion depends on a reliable comparison of region-of-interests (ROIs) between time points. Commercial software tools like ROVER (ABX, Radeberg, Germany) require the user to encircle the analysis area with a mask, based on which a background corrected peak-based threshold is estimated for subsequent ROI (lesion) segmentation within the mask. The reliance on mask placement can thus introduce observer and segmentation variability, especially in heterogeneous tissue. If the same mask is used, mask-related variation between scans is minimized, but requires that the scans are spatially aligned. Hence, inevitable inter-scan patient movement necessitates image alignment procedures that use mathematical interpolation of image intensities to transform one image to spatially match another with the risk of altering the PET data. We evaluated these aspects for lymphoma assessment. Materials and

Methods: Dual-time (1h - 3h) FDG-PET scans of 14 patients (seven with malignancy, seven benign) were analyzed retrospectively. The ROVER software was used for ROI detection with background corrected global lesion-based (LT) and local voxel-based (VT) thresholds and rigid (translation/rotation operations only) image volume alignment. ROI detection to yield ROI values of SUV_{max}, SUV_{mean}, and metabolically active volume (MAV) was performed in two analyses: 1) Separate masks and segmentations of lesions (lymph node/conglomerate) in the 1h and 3h scans. 2) Same 1h mask also used for segmentation on the 3h scan after rigid alignment of the 3h scan to the 1h scan. Results: With separate masks, SUV_{max} in the 1h (mean ± sd: 18.2 ± 10.4) and 3h scans (23 ± 12.9) was reproducible, but SUV_{mean} and MAV varied between LT and VT methods. Here, all three measures showed intra-observer variation ≦ 18%. In the 3h scans, alignment procedures resulted in consistently significant changes in SUV_{max} (8.6% -21.8%) and SUV_{mean} (LT: 6.9%-23.4%, VT: 4.7%-44.4%) and variably significant MAV increases (LT: 0.2%-60%, VT: 5.4%-71.3%). Measured with separate masks, SUV_{max} and SUV_{mean} generally increase significantly between scans ($p < 0.001$), but this increase is reduced ($p = 0.03$-0.11) when measured on the aligned scans using the same mask. Conclusion: Opting for separate masks for dual-time analysis, the observed test-retest variability and dependence on segmentation method entails doubly biased measurements that can affect temporal comparability. Using the same mask on both scans after alignment of the scans introduces unreliable scan transformation-induced measurement changes. Thus, a better analysis technique to ensure comparability is needed.

PW050

The clinical application of absolute quantification SUV SPECT 99mTc-MIBI myocardial perfusion imaging to translate myocardial viability

W. He, W. Yu, W. Zhai, J. Xi; Huadong Hospital, Shanghai, CHINA.

Objectives: To investigate the relation of SUV values between 99mTc-MIBI and PET/CT in cardac imaging to evaluate myocardial viability. Materials and Methods: 32 consecutive patients with previous MI and left ventricular (LV) dysfunction (35±6%), mean±SD, who underwent 99mTc-MIBI SPECT and FDG PET/CT. Results of the two studies were divided into two types : myocardial perfusion match (group 1 MM) and myocardial perfusion mismatch (group 2 M). The SPECT/CT images were acquired using the standard clinical acquisition protocol (1800 scan arc, 64 frames in step-and-shoot mode, 25s per frame). The raw projection data was reconstructed using the software 'SUV-SPECT™'(HERMES MEDICAL SOLUTIONS). The reconstruction parameters were set to 16 subsets and 5 iterations. Corrections were applied for CT attenuation correction, Monte Carlo-modeled scatter correction, resolution recovery, scaling for injected dose and radioactive decay. The units of counts-per-voxel were scaled to activity per unit volume (Bq/cc) based on previously performed phantom calibration work to allow for SUV measurements and scaling of different myocardial segments and compare with FGD PET/CT SUV. Results : 23 patients were mismatch , while 9 match . The value of SUV 99mTc-MIBI myocardial perfusion was Inferior (4.1±0.3), septum (2.8±0.4), anterior (4.3±0.3) lateral (3.9±0.2),apex 2.3±0.1) , SUV in 30 Mismatch segments between SPECT/CT and PET/CT was no statistical difference , but SUV in 32 match segments was 20% to 55 %difference , which has signicant difference statistically. Conclusions : Absolute quantification SUV SPECT 99mTc-MIBI myocardial perfusion imaging can be a translator to evaluate myocardial viability , The multi center study planned to be built up to explore SUV cut off in 99mTc-MIBI myocardial perfusion imaging to evaluate viable myocardium.

PW06 - Tuesday, October 13, 2015, 8:30 AM - 9:30 AM, Hall 3 – Poster Exhibition

Poster Walk 6 - Radiopharmacueticals & Radiochemistry: Radiopharmaceuticals II

PW051

One Pot Al18F Radiofluorination of GLU-UREA-LYS(AHX)-HBED-CC PSMA Ligand.

S. Boschi[1], F. Lodi[1], G. Cicoria[2], M. Marengo[2], S. Fanti[1]; [1]Nuclear Medicine, Bologna University Hospital, Bologna, ITALY, [2]Medical Physics, Bologna University Hospital, Bologna, ITALY.

Aim: Prostate cancer (PC) is the most commonly diagnosed cancer and the second leading cause of cancer death in men. Among PET radiopharmaceuticals 11C-choline and 18F-Fluorocholine have been proposed for the diagnosis, staging and restaging of PC although specificity and sensitivity of these tracers are not ideal. Recently 68Ga-labelled-PSMA ligands have been shown excellent results in detecting PC recurrence and metastases with high sensitivity and specificity. It is also well known that Fluorine-18 is the most popular and

attractive radionuclide for PET because of half-life and imaging characteristics; fluorinated tracers usually allow a higher patient throughput and the possibility of distribution of radiopharmaceutical to different users. Aim of this study was to label with Fluorine-18, via Al18F approach, the ligand Glu-Urea-Lys-(Ahx)-HBED-CC, which has been demonstrated to be of diagnostic value when labelled with Gallium-68. Results: Optimal condition for labelling Glu-Urea-Lys-(Ahx)-HBED-CC with Fluorine-18 using Al18F chemistry, in aqueous/ethanolic solution was investigated. The effect of ethanol concentration, reaction temperature, peptide amount on the labelling with Al18F as well as the effect of pH on the stability of the final product were studied. 100 μL (200-300 MBq) of 18F-fluoride in Acetate buffer 0.5M, 30 nanomoles of AlCl3 and increasing ethanol amount (30-180 μL) has been used. As demonstrated for other trivalent radiometals like 68Ga, the effect of increasing concentration of ethanol in the reaction mixture was to markedly increase the radiochemical yield (RCY). Increasing in RCY allowed a decrease in peptide concentration and in reaction temperature (30% of RCY with 90 μg of peptide at 100°C without ethanol compared to >90% labelling with 30μL of ethanol at 50°C). Increasing ethanol amount from 30μL to 180 μL in the reaction mixture led to >90% RCY at 50°C using 20 μg (21 nanomoles) of peptide. The labelled compound was further purified on SepPak C18 light cartridge, was stable for 3 hours in buffer pH 6.8 but not in saline. Two molecular forms (presumably diastereoisomers) were found, in agreement with Gallium-68 labelling data. Conclusion: These data demonstrates the feasibility of Al18F labelling of Glu-Urea-Lys-(Ahx)-HBED-CC. Radiofluorination of Glu-Urea-Lys-(Ahx)-HBED-CC was successfully obtained using the described method. The use of ethanol facilitates an efficient radiolabeling and could represent an important step toward the kit-type synthesis. Nevertheless, since automation of the synthesis is mandatory for radioprotection as well as for quality assurance issues, studies are in progress to transfer the synthesis on a fully automated cassette module.

PW052

We can do it without! Synthesis of F-18-labeled aromatic compounds without azeotropic drying, base and other additives

R. Richarz[1,2], P. Krapf[1,2], F. Zarrad[1,3], B. D. Zlatopolskiy[1,2], E. A. Urusova[1], B. Neumaier[1,3,2]; [1]Institute for Radiochemistry and Experimental Molecular Imaging, Cologne, GERMANY, [2]Max Planck Institute for Metabolic Research, Cologne, GERMANY, [3]Forschungszentrum Jülich INM-5 Short-lived radionuclides for life sciences, Jülich, GERMANY.

Aim: The classic ^{18}F labeling method via azeotropic drying of an aqueous [^{18}F]KF/cryptand system is time-consuming and error-prone. Furthermore, owing to highly basic raction conditions, base-sensitive precursors cannot be used. Published alternative labeling strategies of aromatic systems without azeotropic drying step are limitedly suitable for preparation of clinically relevant doses of PET-tracers. The aim of this work was to develop a novel radiolabeling approach using only onium precursors and [^{18}F]fluoride. Methodology: [^{18}F] fluoride is eluted from an anion exchange catridge with a solution of the appropriate onium precursor in different alcohols. After evaporation of the alcohol, a suitable solvent was added to the remaining onium (trimethylanilinium, diaryl iodonium or triarylsuilfonium, [^{18}F] fluoride) and the resulting solution was heated to provide the corresponding ^{18}F-labeled product. Results: Elution of $^{18}F^-$ with MeOH and EtOH solution of onium salt precursors proceeded almost quantitatively. Low-boiling MeOH colud be completely removed at 70 °C within 2-3 min. 2-, 3- and 4-[^{18}F]FBA were prepared in RCCs of 38-94% from the corresponding onium precursors. 28 GBq of 4-[^{18}F]FBA was prepared from 32 GBq [^{18}F] fluoride in high radiochemical purity (>98%) within 15 min. Different useful radiolabeling synthons, such as 4-[^{18}F]fluoroiodobenzene, the SFB analogue 2,3,5,6-tetrafluorophenyl 4-[^{18}F]fluorobenzoate as well as the model peptide 4-[^{18}F]fluorobenzoyl-βAla-Phe-OMe were produced from the corresponding sulfonium, anilinium and iodonium salt precursors in good RCCs in a single step. Conclusion: The minimalist ^{18}F labeling strategy is a completely new approach to the synthesis of various ^{18}F labeled compounds avoiding azeotropic drying as well as application of base and any other additives. The broad applicability of the novel procedure was demonstrated through the successful production of several useful radiolabeling synthons, as well as the one-step synthesis of a radiofluorinated model peptide. It was found, that MeOH and EtOH solutions yielded nearly quantitative [^{18}F] fluoride elution.

PW053

Microscale Radiolabelling of Antibodies with Zirconium-89 for Positron Emission Tomography

J. C. Knight[1], S. J. Paisey[2], C. Marshall[2], B. Cornelissen[1]; [1]University of Oxford, Oxford, UNITED KINGDOM, [2]Cardiff University, Cardiff, UNITED KINGDOM.

Aim: Over the last decade, several antibodies have been labelled with the radioisotope zirconium-89 (89Zr) for positron emission tomography (PET) studies. The radiochemical properties of zirconium-89 (particularly its radioactive half-life [t1/2 = 3.2 days]) make it well-suited to antibody imaging and 89Zr-labelled antibodies have been used successfully in clinical settings as tools for early detection and characterisation of certain cancers,

and as companion diagnostics during therapy. The most widely cited method for desferrioxamine (DFO)-conjugation and radiolabelling of antibodies with 89Zr requires multi-milligram (2-10 mg) quantities of protein in order to achieve adequate radiolabelling yields (>85%). During the research and development process, obtaining antibodies in such quantities can be cost-prohibitive when the antibody has to be sourced from a commercial supplier. This can also be a hindrance when the availability of the antibody in question is limited. To circumvent this limitation in the current method and aid in the preclinical evaluation of 89Zr-labelled antibodies, we sought to develop an 89Zr-radiolabelling procedure that would provide high radiochemical yields at the microscale. Materials and Methods: Tocilizumab (RoActemra®) (200-500 μg) was modified with a 10-fold molar excess of p-SCN-Bn-DFO and prepared at a concentration of 2 mg/mL in phosphate buffered saline (pH 7.4). Zirconium-89 in 1 M oxalic acid was adjusted to pH 7-8 by the addition of 1 M sodium carbonate and the resulting solution was added to the DFO-Tocilizumab solution to achieve a ratio of 0.1 MBq to 1 microgram of antibody. The reaction mixtures were incubated at room temperature for 1 h and the radiochemical yield was determined by iTLC using an eluent of 50 mM DTPA (pH 7). The reaction was performed using decreasing amounts of antibody in the range 100 to 10 μg. Results: Radiochemical yields of 96±4%, 80 ±11%, 68±27%, 71±16%, and 63±18% were obtained using 100, 75, 50, 25, and 10 μg of DFO-Tocilizumab, respectively. Conclusions: The reported method results in excellent radiochemical yields using 100 μg of DFO-antibody which compares very favourably with other methods in the literature. Using even smaller amounts of antibody provided lower, albeit still adequate radiochemical yields for preclinical research applications. Furthermore, this approach does not require access to specialised equipment and can be readily implemented in research facilities with minimal radiochemistry infrastructure. Research support: This work received financial support from Cancer Research UK.

PW054

Direct production of 99mTc with a cyclotron

M. Aboudzadeh Rovais; Nuclear Science and Technology Research Institute, Tehran, IRAN, ISLAMIC REPUBLIC OF.

Introduction: Technetium-99m (99mTc) is commonly obtained from 99Mo/99mTc generators. Recent shortages of 99Mo have led to an examination of alternative production methods that could contribute to a more robust supply. A cyclotron has been used to produce 99mTc. Production conditions such as beam and target characteristics and purification need to be optimized in order to maximize the amount of 99mTc and minimize impurities. The focus of this manuscript is on the cyclotron production of 99mTc. Method: The cross section calculations and proton project rangewere performed using the computer codes Talys-1.6 and SRIM, respectively. 99mTc was produced with newly designed and manufactured shuttle and canister target system. Essential target thickness and production yield were calculated. The 100Mo target was irradiated with 19 MeV protons for 1h at up to 50 μA. Solvent extraction method using MEK/NaOH system followed by an acidic alumina column chromatography was employed for the radiochemical separation and purifications. Results and discussion: A simple and quick procedure has been proposed and assessed for the 99mTc production with a cyclotron. Thick target calculations suggested that a large quantity of cyclotron-produced 99mTc via 100Mo(p,2n) reaction is possible. Integration of the excitation function for protons degraded from 19→9 MeV using 100% isotopic enriched 100Mo suggests the maximum production yield of 377 MBq•μA-1•h-1. The average production yield was measured to be 356 MBq•μA-1•h-1. In comparison, the practical yield obtained in this work is very close to the calculated yield. The 99mTc obtained by the combined solvent extraction and alumina column chromatography had good quality in terms of radionuclidic, radiochemical and chemical purity. It has been shown that the QC parameters were within the USP specifications. Keywords: Cyclotron • 99mTc production • targetry • simulation.

PW055

Determination of nickel in ^{64}Cu-ATSM preparations: development and validation of a colorimetric method as impurity limit test

S. Costa, C. De Nicolo, G. Cicoria, C. Malizia, S. Fanti, F. Lodi; S.Orsola-Malpighi University Hospital, Bologna, ITALY.

Aim. ^{64}CuATSM is a radio-pharmaceutical used for revealing hypoxic areas and predict treatment efficacy. ^{64}Cu is produced by (p,n) reaction on metallic ^{64}Ni. The synthesis is performed by means of a complete automatic module that allow to purify the ^{64}Cu from enriched ^{64}Ni. Due to the high amount of the target material (120 mg), traces of nickel could be found in the final formulation. Quality parameters defined in European Pharmacopoeia include Nickel maximum concentration that should not exceed 25 μg in the maximum injectable volume.

A fast colorimetric method was developed and validated as impurity limit assay. Materials and Methods. In this method a sample containing an unknown amount of nickel, and a reference standard containing 5 μg/ mL of nickel are diluted 1:20. After that they are both treated with a solution containing I^-/I_2 in order to oxidize Ni^{n+} to Ni^{4+} and then pH is bring up to 10 - 12 with a NH_3 watering solution. A dimethylglyoxime solution is added and Ni^{4+} forms a red-brown soluble complex with dimethylglyoxime (stoichiometry 1:1). The standard and the sample solutions are then compared. A commercial colorimetric kit for nickel quantification in water substrates was used as starting point; the reference method was the inductively coupled plasma mass spectrometry (ICP-MS). Specificity and limit of detection were determined according to the ICH Q2 guidelines: interferences of the whole matrix (ethanol 10%v/v, NaCl 0.9% w/v in ultra pure water) and the matrix single components at different concentrations were evaluated; interference of copper ions at different concentrations was also investigated. The lower detectable concentration was experimentally determined. Results. Matrix does not interfere with the test, while copper does at concentration higher than 0.75 mg/L. The assay limit of detection in our experimental conditions was 0.04 mg/L. The nickel limit test was then successfully applied to four different ^{64}Cu-ATSM batches. The results were in accordance with those found with ICP-MS. Conclusions. The colorimetric nickel limit test is faster and cheaper than other methods (i.e. ICP-MS) and can be well applied to the Quality Control determination of Ni in ^{64}CuATSM preparations.

PW056

Synthesis of 68Ga Radiopharmaceuticals for Cell Radiolabelling Using Anion Exchange Column

A. Socan[1], P. Kolenc Peitl[1], M. Kroselj[1], C. Rangger[2], C. Decristoforo[2]; [1]University Medical Centre Ljubljana, Ljubljana, SLOVENIA, [2]University Clinic for Nuclear Medicine, University for Medicine, Innsbruck, AUSTRIA.

AIM: 68Ga labelled radiopharmaceuticals are gaining increasing importance in the field of PET nuclear medicine imaging, due to availability of several synthesis modules and 68Ge/68Ga generators on the market enabling users to produce radiopharmaceuticals according to current pharmaceutical standards. Studies showed that although the half life of 68Ga is a limiting factor, 68Ga radiolabelled cells could be used in certain clinical indications. The aim of our study was to develop a novel, versatile approach to prepare 68Ga radiopharmaceuticals (oxine, tropolone) for cell labelling using concentration of 68Ga on an anion exchange column (SepPAK QME). MATERIALS: Column was washed with 2 ml of water. Samples of 68Ga-acetate (Na-acetate, 155mg/ml), -HEPES (1M HEPES) and -citrate (0,1M Na-citrate, pH 5) solutions, samples varying in pH (4-7) and volume, were prepared and applied on column. Activity retained on, activity washed from column and pH of solution was measured. Sample of 0,3 ml ligand solution (tropolone:1mg/ml, water; oxine:1mg/ml, 20% ethanol) was applied on column and incubated for 10 minutes. Column content was washed from column with 2 ml of PBS. Activity and pH measurements were performed as described above. 68Ga-complex formations were analyzed using extraction method into octanol. RESULTS: Yield of activity retained on column with 68Ga-citrate varied 17-96% and was pH and volume dependent. Yield decreased with volumes applied greater than 2 ml and pH bellow 4,5. Yield of 68Ga-tropolone solution was above 75% with pH between 4,4-5 and extraction into octanol above 89%. Yield of 68Ga-oxine solution was between 27-83% with pH between 5, 2-6,7 and extraction into octanol above 94%. With 68Ga-acetate yield of activity retained on column was above 95% and was not pH (3,8-5,9) and volume dependent (0,5-6ml). Yield of 68Ga-tropolone solution was above 81% with pH between 5,4-6,8 and extraction into octanol abobe 90%. Yield of 68Ga-oxine solution was between 40-65% with pH between 4,8-6,3 and extraction into octanol above 92.2%. 68Ga-HEPES yield of activity retained on column was above 89% and was not pH (3,7-7,3) and volume dependent (0,5-2, 5ml). Yield of 68Ga-oxine solution was between 43-77% with pH between 6,1-7,4 and extraction into octanol above 96%. CONCLUSIONS: Concentration of 68Ga in various buffer systems on an anion exchange column allows on-column formation of lipophilic complexes (oxine, tropolone) in very small volumes suitable for cell labelling with high yields and quality. This is a versatile and promising tool to prepare 68Ga-precursors for cell labelling potentially suitable for automated systems.

PW057

A real-time in vitro assay as a potential predictor of in vivo tumour imaging properties

D. Spiegelberg[1], **J. Stenberg**[1], A. Haylock[2], M. Nestor[1,2]; [1]Department of Immunology, Genetics & Pathology, Uppsala, SWEDEN, [2]Unit of Otolaryngology and Head & Neck Surgery, Department of Surgical Sciences, Uppsala, SWEDEN.

Aim: Predicting *in vivo* tumour binding properties of molecular imaging agents with reliable *in vitro* assays is a useful approach to increase preclinical knowledge and limit the use of laboratory animals. To our knowledge, no *in vitro* analysis methods have yet been established to accurately estimate the performance of radiolabelled binders in tumour xenografts. AbD15179 is a promising antibody fragment for molecular

imaging of CD44v6, a non-internalising antigen overexpressed in head- and neck carcinomas. In this study, we investigated if real-time *in vitro* kinetics of AbD15179 receptor binding on CD44v6-expressing tumour cells could be used to predict aspects of the *in vivo* tumour imaging properties. Materials and Methods: Antibody fragment (Fab) Abd15179 was either labelled with ^{125}I using Chloramine T or with ^{111}In using CHX-A"-DTPA. Interactions of labelled fragments with receptors *in vitro* were measured over time on high- (A431) and intermediate (H314) CD44v6 expressing tumour cells with LigandTracer. Using a dual isotope approach, the same batch of ^{111}In- or ^{125}I labelled Fab conjugates were injected in twenty mice bearing both A431 and H314 tumour xenografts. Tumour uptake as well as sensitivity and specificity of conjugates could then be measured while eliminating inter-subject variability. Simultaneous characterisation of the same conjugates *in vitro* and *in vivo* reduced potential bias from batch variability and specific activity. Results: Binding of radiolabelled AbD15179 to cells *in vitro* mainly consisted of two interactions: one high-affinity binding event with slower dissociation and one low-affinity binding event with faster dissociation. The proportion of high-affinity binders was considerably higher for ^{111}In-Fab than for ^{125}I-Fab, leading to a slower release of ^{111}In-Fab than ^{125}I-Fab from tumour cells. Clear differences in signal intensity for ^{111}In-Fab binding were present between CD44v6 high- (A431) and moderate (H314) expressing cells. In contrast, no differences between the two cell lines could be seen for ^{125}I-Fab. In accordance with *in vitro* results, ^{111}In-labeled fragments dissociated slower from tumours compared to ^{125}I-Fab and also made it possible to distinguish between A431 and H314 xenografts *in vivo*. Conclusion: Interaction properties *in vitro* correlated strongly with *in vivo* conjugate binding for CD44v6-targeting Fabs. Thus, time-resolved experiments on living cells could in this case adequately predict the performance of radiolabelled binders on mouse xenografts. If proven general, this finding may lead to a reduction of laboratory animal use in future development of tumor targeting compounds.

PW058

44Sc- and 177Lu-labeling of DKFZ-617 for dosimetry and therapy of prostate cancer

E. Eppard[1], A. de la Fuente[2], S. Kuerpig[1], F. Roesch[2], M. Essler[1]; [1]University Hospital Bonn, Bonn, GERMANY, [2]Johannes Gutenberg-University, Mainz, GERMANY.

OBJECTIVES: Radiolabeling of the prostate-specific membrane antigen (PSMA) inhibitor, Glu-NH-CO-NH-Lys (Ahx), using DOTA as chelator, a broad pool of radionuclides becomes available for labeling. These possible variations allow the visualization of the biological behavior over different periods of time depending on the half-life of the used radionuclide (68Ga t1/2 = 68 min; 44Sc t1/2= 3.9 h). Additionally, the usage of different imaging modalities or endoradiotherapies can be applied depending on the employed radionuclide. METHODS: DKFZ-PSMA-617 was obtained from ABX (Radeberg, Germany). 44Sc was obtained from a 44Ti/44Sc generator in Mainz, where 44Ti decays with a half-life of 60 d to no-carrier-added (n.c.a) 44Sc. Radiolabeling with 44Sc was performed in 3 mL 0.25 M ammonium acetate buffer with varying amount of ligand at 95°C. 177Lu was obtained from IDB Holland and labeling was performed in a gentisinic acid/sodium ascorbate solution with varying amount of ligand at 95°C. Purification (if needed) was performed using C-18 cartridges for both compounds. Quality control was performed using radioHPLC and radioTLC. Stability studies were performed at 37°C in different media (human serum, NaCl) over one half-live. RESULTS: 44Sc-DKFZ-PSMA-617 and 177Lu-DKFZ-PSMA-617 were effectively labeled at 95 °C. Subsequent cartridge-based solid-phase-extraction (C-18) resulting in a radiochemical purity of the final tracers of ≥98% can be applied for both compounds. Stability studies in different media (human serum, NaCl etc.) were successfully performed and both compounds showed high stability over a period of one half-live or longer. Radiochemical purity could be analyzed effectively using radioHPLC and radioTLC. 177Lu-DKFZ-PSMA-617 is utilized using the optimized labeling protocol for patient treatment since November 2014. CONCLUSIONS: The radiolabeling of DKFZ-PSMA-617 with the new generator-derived PET radionuclide 44Sc was investigated in detail. 44Sc-DOTA-PSMA was investigated in vitro. Further investigations including cell studies, biodistribution and small animal μPET are planned. Also radiolabeling of 177Lu-DKFZ-PSMA-617 was optimized with regard to therapeutic application and successfully integrated in clinical routine.

PW059

Development of [18F]Fluoro-sugar based prosthetic groups for the PET imaging of radiolabel peptides

C. Collet[1,2], F. Maskali[1], S. Poussier[1,2], A. Mohamadi[3,2], V. Regnault[3,2], P. Lacolley[3,2], Y. Chapleur[1,2,4], P. Marie[1,2,3], G. Karcher[1,2], S. Lamandé-Langle[4,2]; [1]Nancyclotep, Vandoeuvre les Nancy, FRANCE, [2]Université de Lorraine, Vandoeuvre les Nancy, FRANCE, [3]Inserm UMR 1116, Vandoeuvre les Nancy, FRANCE, [4]UMR 7565, Vandoeuvre les Nancy, FRANCE.

Introduction: The direct ^{18}F-labelling of biomolecules, such as proteins, peptides or oligonucleotides, is not possible under harsh conditions, but it may be obtained through a prosthetic group, a small molecule that may be labelled, with ^{18}F and

subsequently coupled in mild condition to the biomolecule. We aimed to develop sugar based prosthetic groups in this setting, a method that is likely to improve the bioavailability, pharmacokinetic and *in vivo* clearance properties of peptide/protein.Materials & Methods: The prosthetic carbohydrate derivatives should have a good leaving group allowing an easy substitution by fluorine-18. A Huisgen cycloaddition was planned for coupling the prosthetic group with the biomolecule. Some peptides containing a cysteine residue were initially tested. *S*-propargylated derivatives were easily obtained thanks to the high nucleophilicity of the thiol function. The fully automated radiosynthesis of these [^{18}F]fluoroglycopeptides was performed on an AllInOne (Trasis®) module. In the same time the biological activity of these glycopeptides was evaluated *in vitro* (platelet aggregation assay). IC_{50} values were determined from concentration-response curves fitted with an exponential decay equation. PET scans will be performed using a small-animal INVEON tomograph.Results: The synthesis of suitable precursors of these prosthetic groups and the radiolabelling of some model peptides (glutathione, RGDC, c(RGDfC)) could be successfully achieved by a two step strategy for the radiolabelling of peptides using sugar based prosthetic group[^{18}F]Fluoroglycopeptides were obtained in 10-30% radiochemical yield (dc). PET-scan images were obtained in animals. *In vitro* studies of ADP-induced platelet aggregation inhibition show that introduction of a carbohydrate moiety on linear RGD peptides strongly enhances the inhibitory activity.Discussion/Conclusion: The ^{18}F-labelling of peptides is possible in good yields by using prosthetic groups constituted of 6-fluoro sugars, equipped with an azido arm at the anomeric position. Biological evaluations are very promising.

PW060

Cyclotron production of 51Cr for clinical application

M. Aboudzadeh Rovais; Nuclear Science and Technology Research Institute, Tehran, IRAN, ISLAMIC REPUBLIC OF.

Introduction: ^{51}Cr(27.7d) is one of the attractive medical radionuclide that decays via electron capture (EC=100%). The ^{51}Cr is used to label red blood cells and quantify gastrointestinal protein loss. Sodium chromate ($Na_2{}^{51}CrO_4$) and chromium chloride ($^{51}CrCl_3$) are suitable for diagnostic applications. In this article, a selection of different reactions for production of ^{51}Cr, theoretical production yield through the excitation functions for ^{51}V(p,n)^{51}Cr, ^{51}V(d,2n)^{51}Cr, ^{48}Ti(α,n)^{51}Cr, ^{52}Cr(n,2n)^{51}Cr using TALYS 1.6, ALICE-91 and ALICE-ASH computer codes have been studied. The experimental yield as well as the production method for ^{51}V(p,n)^{51}Cr reaction are presented. Also, the essential target thickness was calculated by SRIM computer code. Method: The production of ^{51}Cr following direct ^{51}V(p,n)^{51}Cr reaction, 250mg V_2O_5(99.99% Merck) were compressed into pellets. A novel shuttle and target system was developed for the production of ^{51}Cr. The incident energy of the proton beam was 11MeV at the 20μA current for 1hr. The irradiated target was dissolved in 4N HCl(2ml) containing 10mg of ferric nitrate. The solution was added slowly to the boiling 4N NaOH(2ml). ^{51}Cr was precipitated with Fe^{3+} as a co-precipitation. The precipitate was separated from the solution by filtration and then it was dissolved in 12N HCl(10ml). The solution was passed through a chromatography column that filled with Dowex 1X8 anion exchange resin (mesh 100-200). Fe^{3+} was retained by the resin while the Cr^{3+} was passed through. Results and discussion: Different products and theoretical production yield of ^{51}Cr in different nuclear reaction were studied through the excitation functions using the previously mentioned computer codes. Although the direct ^{51}V(p,n)^{51}Cr reaction doesn't have the best ^{51}Cr production yield, this reaction is the only one that can produce no career-added ^{51}Cr and pure as the final product. The average of the experimental yields of ^{51}Cr over the optimum energy range E_p=11→3 MeV for ^{51}V(p,n)^{51}Cr reaction was 2.3MBq/μAh. The theoretical yield of ^{51}Cr was calculated as 2.7, 2.9 and 2.5 MBq/μAh for TALYS, ALICE-91 and ALICE-ASH codes, respectively. Conclusion: The ^{51}V(p,n)^{51}Cr reaction was selected because of the ^{51}Cr could be produced free of the other radionuclides. A novel targetry system was developed for this production method. The experimental production yields are close to the theoretical yields especially the one calculated from the ALICE-ASH code. Keywords: ^{51}Cr, Production yield, Pellet target, Simulation.

PW07 - Sunday, October 11, 2015, 8:30 AM - 9:30 AM, Hall 3 – Poster Exhibition

Poster Walk 7 - M2M: Molecular & Multimodality Imaging: Preclinical Imaging and Evaluation

PW061

Brown adipose tissue: Preclinical imaging beyond FDG?

M. Bauwens[1], G. Hendrikx[1], V. Schrauwen-Hinderling[1], J. Slenter[1], S. van Hoof[1], A. Vogg[2], I. Pooters[1], B. Brans[1], F. M. Mottaghy[1,2]; [1]MUMC, Maastricht, NETHERLANDS, [2]UKAachen, Aachen, GERMANY.

Introduction: The metabolic activity of brown adipose tissue (BAT) can have a significant effect on homeostasis, but is difficult to non-invasively quantify in vivo. In this study, we

performed a comparison of different non-invasive imaging techniques in a preclinical setting. Methods: 40 Wistar rats (male, 8-12 weeks old) and 42 NMRI mice (male, 6-9 weeks old) were used during the study. In rats, dynamic PET and SPECT images using [18F]-FDG, [18F]-FTHA, [123I]-MIBG, [99mTc]-MIBI and [123I]-IPA were acquired in different temperature conditions: room temperature, exposure to acute cold (4°C for 4h) or acclimatized to cold (4°C for 6h per day during 28 days). MRI/MRS was set up using a dedicated protocol to assess BAT temperature in 5 room temperature and cooled rats. In NMRI mice, static PET images were acquired using [18F]-FDG and [18F]-FTHA and using different temperature conditions (room temperature, thermoneutral conditions and 4°C) as well as a different diet (chow or high-fat diet). In addition, CT images were acquired in these mice and used as a cross-reference for the PET images. Finally, mRNA of several genes was analyzed from BAT and WAT. Results: In rats, [18F]-FDG, [18F]-FTHA, [123I]-MIBG, [99mTc]-MIBI but not [123I]-IPA allowed to visualize BAT and showed higher uptake in cold-stimulated animals. When compared to a single cold-exposure, the effect of cold-acclimatization yielded a larger volume of active BAT, indicating growth of BAT. MRI clearly showed BAT in T2 weighed images. MRS could quantify BAT temperature, but did not reveal a temperature difference between BAT and a reference region. In mice, [18F]-FDG and [18F]-FTHA could visualize BAT. However, only [18F]-FDG showed clear images and allowed a comparison between different groups, and showed the impact of the high-fat diet (lower uptake compared to chow) as well as temperature conditions (cold-stimulated animals showed more uptake). CT images clearly showed BAT, improving BAT delineation on PET images, but yielded no further additional information. mRNA confirmed the identity of BAT in all animals, and showed a clear correlation between mRNA expression and related tracer uptake. Summary: PET, SPECT, CT and MRI/MRS are all able to visualize interscapular BAT. The lack of good quantitative information from the SPECT makes it a currently suboptimal technique . In our current study, [18F]-FDG outperforms any other tracer. The combination of PET/CT and PET/MRI is nevertheless superior to only PET, due to better target delineation.

PW062

Pilot study of a novel peptide targeting GPC3 for HCC

D. Zhu[1], Y. Qin[1], L. Zhang[2], S. Zou[1], J. Wang[2], L. Zhu[2], **X. Zhu**[1]; [1]Department of Nuclear Medicine & PET, Tongji Hospital, Tongji Medical College, Huazhong University of Science and Technology, Wuhan, CHINA, [2]State Key Laboratory of Molecular Vaccinology and Molecular Diagnostics & Center for Molecular Imaging and Translational Medicine, School of Public Health, Xiamen University, Xiamen, CHINA.

Purpose: Glypican-3 (GPC3) is a heparan-sulfate proteoglycan over-expressed in most hepatocellular carcinoma (HCC). A peptide binds to GPC3 with high specificity and affinity will facilitate targeted diagnosis and/or therapy of HCC.Methods: A Ph.D.-12TM phage display library was used to screen the high affinity peptide against the human recombinant GPC3 protein. A 12-mer peptide GPC3-TJ12P1 was synthesized according to the DNA sequence of selected GPC3 binding phage. The binding affinity between GPC3-TJ12P1 and the human recombinant GPC3 protein was determined by ELISA. Specificity of GPC3-TJ12P1 to GPC3 was confirmed by western blot and cell florescent on cells with (HepG2) or without (PC3) GPC3 expression. In vivo, near-infrared fluorescent (NIRF) imaging and biodistribution studies were performed in nude mice bearing HepG2 and PC3 tumor xenografts to evaluate the target ability of Cy5.5-GPC3-TJ12P1 to GPC3. Furthermore, Cy5.5- GPC3-TJ12P1 was used to detect the GPC3 expression in patient's tumor tissues with HCC, cholangiocarcinoma (CCA) and normal adult liver tissues respectively using western blot and immunohistochemical staining.Results: The binding assay of the GPC3-TJ12P1 to GPC3 protein exhibited Kd value of 280.4 ± 33.51nM. Western blotting confirmed that GPC3-TJ12P1 was able to effectively detect GPC3 expression in HepG2 and PC3 cells. Cy5.5-GPC3-TJ12P1 mainly attached to HepG2 cells surface under confocal microscopy, while there were less fluorescent on the PC3 cells membrane. A weak signal was observed when GPC3 expressed on HepG2 cells were blocked by free GPC3-TJ12P1 before Cy5.5-GPC3-TJ12P1 labeling. In vivo NIRF study showed that HepG2 xenograft tumors had a higher accumulation of Cy5.5-GPC3-TJ12P1 than that of control group, blocking group and PC3 xenograft tumors (n=3 or 4), respectively. Tumor/muscle fluorescent intensity ratio reached 3.98 ± 0.36 at 4h post-injection in HepG2 tumor models. Ex vivo study also confirmed that an enrichment of Cy5.5-GPC3-TJ12P1 at 4h in the HepG2 dissected tumors. For patient's tissues, only GPC3 protein strip from HCC tissues was displayed with fluorescent on PVDF membrane, and there was a heavier staining in HCC slices than that of in CCA and normal adult liver slices, which confirmed using anti-GPC3 mAb simultaneously.Conclusions: A novel peptide, GPC3-TJ12P1, targeting GPC3 was obtained using phage display library and identified in vitro and in vivo. It can be applied for further studies, such as peptide mediated multifunctional molecular imaging and drug deliveries as well as a new promising molecular probe for early HCC diagnosis and intervention.[Keywords]phage display library; Peptide; GPC3; HCC; Optical imaging

PW063

A new lactam bridge 99mTc-α -melanocyte-stimulating hormone analog for diagnosis of metastatic melanoma

D. Beiki[1], D. Shamshirian[2], M. Erfani[3], B. Fallahi[1]; [1]Research Center for Nuclear Medicine, Shariati Hospital, Tehran University of Medical Sciences, Tehran, IRAN, ISLAMIC REPUBLIC OF, [2]Department of Radiopharmacy, School of Pharmacy, Tehran University of Medical Sciences, Tehran, IRAN, ISLAMIC REPUBLIC OF, [3]Radiation Application Research School, Nuclear Science and Technology Research Institute, Tehran, IRAN, ISLAMIC REPUBLIC OF.

Introduction: Over 80 % of human metastatic melanomas were reported to overexpress MC1 receptors. Since melanoma cause more than 75% of deaths from skin cancer, there is a need to develop new radiopharmaceuticals which allow diagnosing this type of tumor in an early phase. This study presents the synthesis of a new lactam bridge 99mTc-α-MSH analogue. Methods: A new [HYNIC-GABA-Nle]-CycMSHhept derivative was conveniently synthesized by solid phase peptide synthesis on sieber amide resin via Fmoc strategy. Then peptide radiolabelling was performed by 99mTc via HYNIC chelator and tricine as co-ligand. Also, stability in human serum, receptor bound internalization, protein binding, partition coefficient and tissue biodistribution in tumor bearing nude mice were thoroughly investigated. Results: The new peptide derivative was obtained in an overall yield of 35% with the purity of >98%. Radiolabeling with 99mTc was performed at high specific activities (163MBq/nmol) with an acceptable labeling yield (>98%). Also, stability studies in aqueous solution and human serum showed radiolabeled complex with no significant release of 99mTcO4− or peptide degradation up to 6 h. Protein binding and calculated partition coefficient for the radiolabeled peptide were 37% and log P=−1.31 ± 0.12 %, respectively. Also, the radioligand showed specific internalization into B16/F10 cells (13.35 ± 0.9% at 4 hours). In biodistribution studies, a receptor-specific uptake was observed in MC1 receptor positive organ so that after 4 hours the tumor uptake was 4.51±0.11 % ID/g. Predominant renal excretion pathway with a highest accumulation of activity in tumor was observed for this radiopeptide. Conclusion: This new designed labeled peptide conjugate showed high accumulation in tumor as a positive MC1 receptor targeted tissue followed by excretion via the kidney and can be a suitable candidate for diagnosis of metastatic melanomas.

PW064

Multispectral fluorescence imaging during robot-assisted laparoscopic sentinel node biopsy - a first step towards a real-time intraoperative patient-specific anatomical roadmap

N. S. van den Berg[1,2], G. H. KleinJan[1,2], T. Buckle[1], E. M. Wit[2], H. G. van der Poel[2], F. W. B. van Leeuwen[1,2]; [1]LUMC, Leiden, NETHERLANDS, [2]AVL-NKI, Amsterdam, NETHERLANDS.

Introduction:The clinical translation of hybrid tracers, e.g. the sentinel node (SN) tracer indocyanine green (ICG)-99mTc-nanocolloid, that are composed of a radioactive- and optical signal has strongly expanded the working-field of nuclear medicine by providing real-time fluorescence guidance during surgery. Limiting, however, is that surgical guidance remains restricted to a single feature such as the SN. If real-time surgical guidance can be provided for multiple parameters at once, it may help create a paradigm shift in the way surgery is performed. For this multispectral imaging concept multiple (spectrally complementary) fluorescent tracers have to be administered to a single patient. Also a fluorescence camera is required that allows for separate detection of the two signals. Following an initial evaluation in mice, in the current study we clinically evaluated this approach using ICG-99mTc-nanocolloid (SN; near-infrared (NIR)) and fluorescein (lymphangiography; visible fluorescence).Methods:For the first-in-human application, 8 prostate cancer patients with a Briganti nomogram-based risk >10% of lymph node metastases were included. Patients were scheduled for robot-assisted radical prostatectomy with extended pelvic lymph node dissection and SN biopsy. Following a transrectal ultrasound-guided intraprostatic ICG-99mTc-nanocolloid injection (2.0mL; 3h prior to surgery) preoperative lymphoscintigraphy and SPECT-CT imaging were performed. Fluorescein (2.0mL; 200mg) was injected into the prostate directly after anesthetizing the patient. Intraoperatively both fluorescent signatures were identified using a tailored multispectral fluorescence laparoscope.Results:Preoperative SPECT-CT imaging revealed on average 3.9 SNs (range 1-6) per patient. Intraoperatively, 24 of 28 SNs (85.7%) could be detected using the NIR settings. In 5 patients, the fluorescence signal of fluorescein could be used to specifically highlight the draining lymphatic ducts to 10 SNs.The accuracy and brightness with which fluorescein could be detected in vivo was remarkable. However, compared to the hybrid tracer, with fluorescein a higher background staining was seen (predominantly bowel, urine). Also this study underlined that the

guidance provided by a dedicated SN tracer is superior over the guidance provided by a lymphangiography tracer.Discussion:This study illustrated the first-in-human use of a multispectral fluorescence guidance approach using two complementary fluorescent tracers. The promising results provide a first step towards a fluorescence-based anatomical/molecular road map able to visualize multiple surgery-related anatomical structures simultaneous.

PW065

Effect of different injection routes in tumor accumulation and biodistribution of radiolabeled Pluronic P94 unimers

C. Santini[1], A. Arranja[2], A. Denkova[3], F. Schosseler[2], K. Morawska[4], P. Dubruel[4], E. Mendes[5], M. de Jong[1], M. Bernsen[1]; [1]Erasmus MC, Rotterdam, NETHERLANDS, [2]CNRS, Institute Charles Sadron, Strasbourg, FRANCE, [3]TU Delft, Radiation Science and Technology,, Delft, NETHERLANDS, [4]UGhent, Polymer Chemistry and Biomaterials Group (PBM), Gent, BELGIUM, [5]TU Delft, Department of Chemical Engineering, Delft, NETHERLANDS.

Introduction. Pluronic P94 unimers (P94) are amphiphilic block copolymers with high in vivo stability and relatively long circulation times. Due to the enhanced permeability and retention (EPR) effect, P94 can accumulate in the tumor tissue and therefore be potentially used as drug carrier. For various macromolecules it has been shown that following IV administration, limited tumor accumulation occurs versus undesired high liver uptake and clearance via the mononuclear phagocyte system (MPS). Intratumoral (IT) injection might overcome this limitation by avoiding the systemic circulation and therefore improving the retention in the tumor. In this study we compared IT versus IV administration routes of radiolabeled P94 in terms of biodistribution profiles and tumor accumulation and retention in a mouse tumor model.Materials and methods. P94 was modified with a DTPA chelator, labeled with 1In-111 and injected in tumor-bearing mice either IV (N=8, 0.2 mg/mouse, ~10 MBq/animal) or IT (N=8, 0.1 mg/mouse, ~5 MBq/animal). Molecular imaging with SPECT/CT was performed at different time points post injection (pi): 30 min, 24h, 48h and 96h pi. Ex vivo biodistribution was determined in isolated organs at 48h and 96h pi.Results. Following IV injection, accumulation in the liver was visible already 30 min pi, while tumor accumulation could be visible only starting from later time points. Ex vivo biodistribution, confirmed a reduced tumor uptake of ~1 % injected dose per gram (ID/g), whereas accumulation in the liver was ~15 %ID/g. In contrast, following IT injection most of the signal is concentrated in the tumor rim and limited liver accumulation is detected in the first hour pi. Furthermore, ex vivo biodistribution following IT injection, showed that the tumor retention increased to over 20 %ID/g, with limited uptake in off-target tissues, while liver uptake was reduced to ~10 %ID/g. The results also indicated that, independently from the injection route, the tumor could retain P94 over time, while the majority of other tissues show a significant reduction in tracer retention between 48h and 96h. The effect is however larger after IT injection.Conclusion. IV injection of radiolabeled P94 resulted in limited tumor uptake, whereas IT administration substantially increased the uptake and the retention in the tumor. The minimal involvement of off-target tissue, including liver, and the tracer retention over time especially for IT administration, confirmed the potential of P94 to be used as a carrier for therapeutic radionuclides.

PW066

A multiprobe approach to monitoring therapy response in rheumatoid arthritis

S. Y. A. Terry[1], M. I. Koenders[2], T. K. Nayak[3], A. Freimoser-Grundschober[4], C. Klein[4], W. J. Oyen[2], O. C. Boerman[2], P. Laverman[2]; [1]King's College London, London, UNITED KINGDOM, [2]Radboud UMC, Nijmegen, NETHERLANDS, [3]Roche Pharmaceutical Research and Early Development, Basel, SWITZERLAND, [4]Roche Pharmaceutical Research and Early Development, Zurich, SWITZERLAND.

Introduction: Rheumatoid arthritis (RA) is an autoimmune disease leading to chronic synovial inflammation. Monitoring therapy response by molecular imaging may allow optimization of therapy regimens and/or improve therapeutic outcome. Etanercept is a soluble fusion protein consisting of human p75 TNF-α and the Fc portion of human IgG and is often given to RA patients if methotrexate is contra-indicated or withdrawn due to adverse events. Here, we focused on imaging three different targets that play a role in arthritis, namely fibroblast activation protein (FAP), macrophages, and integrin $\alpha_v\beta_3$, and on determining whether specific imaging of these targets could monitor response to etanercept in RA mice. Methods: Male DBA/1J mice with collagen-induced arthritis were treated with anti-TNFα therapy (etanercept 10 mg/kg, 3x/week, i.p.). SPECT/CT scans were acquired of treated and untreated mice

at 1, 24 and 48 hours after injection of ^{111}In-RGD$_2$ peptide (targeting integrin $\alpha_v\beta_3$; 1 μg/mouse), ^{111}In-anti-F4/80 antibody (targeting macrophages; 10 μg/mouse), or ^{111}In-28H1 antibody (anti-FAP; 50 μg/mouse), respectively. Mice were dissected after the last scan to determine the biodistribution. Coinjection of an excess of RGD$_2$ with ^{111}In-RGD$_2$ or injection of ^{111}In-labeled control antibodies (rat IgG2b or DP47GS) served as controls to determine nonspecific tracer uptake. Results: RA was imaged with ^{111}In-28H1, ^{111}In-anti-F4/80, and ^{111}In-RGD$_2$. Treatment with etanercept was successful as macroscopic scores of RA were lower in treated mice than in untreated mice (Figure 2). At day 6 after start of therapy, average RA scores were 3.99 ± 1.67 in untreated mice and 1.84 ± 1.08 in treated mice. Tracer uptake in joints correlated with RA score in biodistribution studies and quantitative SPECT; uptake decreased from 28±15%ID/g, 8±4%ID/g, 2±1%ID/g to 11±11%ID/g, 4±4%ID/g, 1±0%ID/g in treated and untreated mice for ^{111}In-28H1, ^{111}In-anti-F4/80, and ^{111}In-RGD$_2$, respectively ($p<0.001$). Joint uptake of ^{111}In-28H1, ^{111}In-anti-F4/80, and ^{111}In-RGD$_2$ is antigen/receptor-mediated as when competing uptake of these tracers with either antibody controls or excess of peptide, joint:blood values decreased. RA-to-blood ratios (in mice with arthritis score 2) were higher for ^{111}In-28H1 (6±1, lowest population), ^{111}In-anti-F4/80 (10 ±4), and ^{111}In-RGD$_2$ (7±1) than for control ^{111}In-DP47GS (1 ±1), ^{111}In-rat IgG2b (1±0), or coinjection of excess RGD$_2$, (4 ±0). Conclusions: The three tracers can be used to specifically monitor the response to therapy in RA at the molecular level.

PW067

The imaging study of a new 99mTc-labeled PSMA inhibitor

X. Xu; J. Zhang, S. He, J. Luo, Y. Zhang *Department of Nuclear Medicine, Fudan University Shanghai Cancer Center, Shanghai, ChinaDepartment of Oncology, Shanghai Medical College, Fudan University, Shanghai, ChinaCenter for Biomedical Imaging, Fudan University, Shanghai, ChinaShanghai Engineering Research Center for Molecular Imaging Probes, Shanghai, CHINA

Aim: Prostate-specific membrane antigen (PSMA) is a well-established target for developing radiopharmaceuticals for imaging and therapy of prostate cancer (PCa). We have synthesized an amino-functionalized PSMA inhibitor(Lys-Urea-Glu) and labeled technetium-99m via HYNIC. The in vivo target capacity of the new molecular imaging pobe was evaluated in animal model and compared with ^{18}F-FDG and ^{11}C-Choline which were the mostly used in clinical.Material and method: The small-molecular inhibitor was based Lys-Urea-Glu core which linked ^{99m}Tc chelator HYNIC through 6-aminocaproic acid. We assessed the new molecular imaging probe in SCID mice bearing PC-3 and LNCaP tumor xenografts on Nano-SPECT/CT. The comparative experiment of ^{18}F-FDG and ^{11}C-Choline imaging was done in the LNCaP tumor xenografts on Micro-PET/CT. The T/B data was obtained by the analysis software accompanying with Nano-SPECT/CT and Micro-PET/CT respectively.Results and conclusion: The imaging results showed that the metabolism of the radioactive probe ^{99m}Tc-HYNIC-Acs-Lys-Urea-Glu was very fast. Kidney was the primary excretory organs and little radioactive uptake was found in intestines. There were no significant uptake in other organs. The PC-3 tumor doesn't have any radioactive uptake, the LNCaP tumor had very high radioactive uptake and the T/B (tumor to muscle) was 20.4. The blocking experiment that the probe was blocked by the excessive 2-PMPA on LNCaP tumor xenografts showed that the tumor uptake reduced significantly. This illuminated the probe exactly targeted PSMA. The T/B data obtained from the PET/CT imaging were 2.1 and 2.6 for ^{18}F-FDG and ^{11}C-Choline respectively which was much less than ^{99m}Tc-HYNIC-Acs-Lys-Urea-Glu.The probe ^{99m}Tc-HYNIC-Acs-Lys-Urea-Glu with fast metabolism and high tumor uptake was a promising molecular imaging probe targeted PSMA. It was superior to ^{18}F-FDG and ^{11}C-Choline in PCa.

PW068

Preclinical evaluation of selected 68Ga labelled peptides for glioblastoma imaging

M. Petrik[1], J. Stepankova[1], Z. Crlikova[1], R. Trojanec[1], J. Drymlova[2], M. Hajduch[1], Z. Novy[1]; [1]Faculty of Medicine and Dentistry, Palacky University Olomouc, Olomouc, CZECH REPUBLIC, [2]Department of Nuclear Medicine, University Hospital Olomouc, Olomouc, CZECH REPUBLIC.

Aim: Glioblastoma multiforme (GBM) is the most aggressive type of primary brain tumors in humans with more than 90% 5-year mortality. Early diagnosis may be the key factor for improving patient survival rates through the prevention of tumor growth. Radiolabelled regulatory peptides continue to hold promise for early diagnosis of many human diseases, including GBM. Here we report on the preclinical evaluation of two 68Ga labelled peptides as potential agents for GBM imaging and in vivo comparison with clinically used 18F labelled radiopharmaceuticals. Materials and methods: 68Ga labelling of selected peptides (NODAGA-cRGDyK dimer and DOTA-substance P) was performed in acetate buffer using fractionated method. The labelling

conditions were optimized concerning temperature, peptide amount and reaction time. For in vitro characterization, partition coefficient, protein binding properties and stability values in different media were determined. Ex vivo biodistribution and PET/CT imaging was studied in normal Balb/c and tumor (U87MG) Balb/c nude mice. Results: Both peptides were labelled with 68Ga with high radiochemical purity (>95%). 68Ga-NODAGA-cRGDyK dimer showed hydrophilic properties and was stable in vitro in human serum, concentrated iron(III) and DTPA solutions as well as at pH = 7 and in vivo. In contrast, 68Ga-DOTA-substance P displayed much lower in vitro stability, especially in concentrated iron(III) and DTPA solutions and was rapidly metabolized in vivo. Protein-bound activity of 68Ga-NODAGA-cRGDyK dimer after 120 min incubation (3.9%±1.9) was found to be 7-fold lower than for 68Ga-DOTA-substance P. In normal mice, both 68Ga labelled tracers revealed mainly renal elimination with low blood values (0.10±0.01%ID/g RGD and 0.28±0.03%ID/g S-P) 90 min p.i., while 18F-FLT and 18F-FDG showed much slower kinetics and not only renal, but also gastrointestinal excretion. Moreover 18F-FDG displayed significant radioactivity retention in metabolically active tissues (brain, brown adipose tissue and heart). In tumor mice, 68Ga-NODAGA-cRGDyK dimer was highly accumulated in tumor (5.59±2.10%ID/g, 30 min p.i. and 3.13 ±0.79%ID/g, 90 min p.i.), whereas metabolically degraded 68Ga-DOTA-substance P showed much lower accumulation in tumor (2.14±0.17%ID/g, 30 min p.i. and 0.72±0.04%ID/g, 90 min p.i.). In comparison with 18F-FLT and 18F-FDG, 68Ga-NODAGA-cRGDyK dimer revealed more favourable pharmacokinetics and comparable accumulation in tumor confirmed also by μPET/CT. Conclusion: Studied peptides bound 68Ga with high affinity, and 68Ga-NODAGA-cRGDyK dimer, especially, displayed high stability and excellent pharmacokinetics. Moreover 68Ga-NODAGA-cRGDyK dimer showed superior in vivo properties compared to 18F-FLT and 18F-FDG, while maintaining a similar uptake in tumor. 68Ga-NODAGA-cRGDyK dimer seems to be a promising agent for glioblastoma imaging.

PW069

Preclinical evaluation of two DOTA-coupled minigastrin analogues (Met and corresponding Nle congener)

M. Kroselj[1], L. Claessens Joosten[2], R. Mansi[3], J. Reubi[4], H. Maecke[3], P. Laverman[2], O. Boerman[2], P. Kolenc Peitl[1]; [1]Department of Nuclear Medicine, UMC Ljubljana, Ljubljana, SLOVENIA, [2]Department of Radiology and Nuclear Medicine, Radboud University Medical Center, Nijmegen, NETHERLANDS, [3]Department of Nuclear Medicine, University Hospital Freiburg, Freiburg, GERMANY, [4]Division of Cell Biology and Experimental Cancer Research, Institute of Pathology, University of Berne, Berne, SWITZERLAND.

Aim: The stability of the minigastrin analogues is highly influenced by the charge and the stereochemistry of the amino acid sequence constituting the spacer. It was recently shown that introduction of non-ionic (6 D-Gln) or ionic (6 D-Glu) D-amino acid spacers results in remarkable improvement in metabolic stability. The analogue with the ionic D-Glu spacer showed the best in vitro and in vivo properties and was chosen as the most suitable tracer for phase I clinical study for diagnosis and therapy of MTC patients. The aim of this work is to evaluate the properties of a new analogue, PP16(Met11), having as spacer the sequence of the mixed ionic/non-ionic amino acids $(D\text{-}Gln\text{-}D\text{-}Glu)_3$. Since it is well known that methionine is prone to oxidation that can significantly influence the binding affinity, the Nle congener PP16B(Nle11) was developed for comparison. We radiolabeled two DOTA-conjugated minigastrin analogues with ^{111}In under same reaction conditions and compared their in vitro and in vivo characteristics. Material and Methods: The minigastrin analogues (DOTA-$(D\text{-}Gln\text{-}D\text{-}Glu)_3$-Ala-Tyr-Gly-Trp-Met/Nle-Asp-Phe-NH2) were synthesized manually on solid phase. CCK-2R affinities were determined by receptor autoradiography using ^{125}I-CCK as radioligand. ^{111}In-labeled peptides were evaluated in vitro in AR4-2J cell line and in human serum. In vivo behaviour was studied using female athymic BALB/c mice with s.c. A431-CCK2R tumors. SPECT imaging was performed at 1h and 4h p.i and organs, blood and tissues of interest for biodistribution were collected 4h p.i. Results: Both peptides showed high binding affinity to the CCK-2/gastrin receptor with IC_{50} values in low nM range (0.5±0.06 Nle11 and 0.5 ±0.1 Met11). Nle11 showed higher receptor-specific internalization (15.1±0.8% vs. 10.4±0.9% at 4h), but lower enzymatic stability in human serum (85±68 vs. 141±68 h). Tumor uptake at 4h p.i. for Nle11 was 2.06±0.86%ID/g and 1.22±0.66%ID/g for Met11 (p=0.111). Tumor retention of Nle11 was 82.2% at 4h and 90.02% of Met11 (p=0.271). Conclusion: Two DOTA-coupled minigastrin analogues with the same mixed ionic/non-ionic spacer and alteration in C-terminal part (Met/Nle) were developed. Changing the natural Met for Nle had no influence on binding affinities of these molecules to CCK-2R. In addition, the replacement had no significant effect on tumor and kidney uptake. Both radiolabeled peptides demonstrate good tumor retention of radioactivity. We showed that both analogues have similar in vivo characteristics. Since Nle11 is not oxidized during the radiolabeling with radiometals, the radiolabeling step is more straightforward and thus making the Nle11 a better candidate for a possible clinical use.

PW070

Auger Electron Radioimmunotherapy with ^{111}In-Bn-DTPA-Nimotuzumab Inhibits the Growth of EGFR-Positive Human Breast Cancer Tumours in Mice at Doses that are Non-Toxic to Normal Tissues

C. Chan[1], H. Fonge[1], K. Lam[1], R. Reilly[1,2,3]; [1]Department of Pharmaceutical Sciences, University of Toronto, Toronto, ON, CANADA, [2]Department of Medical Imaging, University of Toronto, Toronto, ON, CANADA, [3]Toronto General Research Institute and Joint Department of Medical Imaging, University Health Network, Toronto, ON, CANADA.

Aim: To evaluate the tumour growth inhibition properties and normal tissue toxicity of Auger electron radioimmunotherapy (RIT) of human breast cancer xenografts overexpressing EGFR in CD1 athymic mice using ^{111}In-Bn-DTPA-nimotuzumab. Methods: Normal tissue toxicity was first evaluated in non-tumour bearing mice following i.v. injection of 8.8 or 28.2 MBq (3 mg/kg) of ^{111}In-Bn-DTPA-nimotuzumab. Control mice were treated with unlabeled Bn-DTPA-nimotuzumab or normal saline. The body weight index (BWI) was determined every few days by dividing the body weight by that prior to treatment. Complete blood cell counts (CBC), hematocrit and hemoglobin, and serum alanine aminotransferase (ALT) and creatinine (Cr) were measured at 2 weeks p.i. RIT was then performed in CD-1 athymic mice bearing s.c. MDA-MB-468 human breast cancer xenografts (1 x 10^6 EGFR/cell) by administering two doses i.v. (15.5 MBq; 3 mg/kg) of ^{111}In-Bn-DTPA-nimotuzumab separated by two weeks. Control mice were treated with unlabeled Bn-DTPA-nimotuzumab, irrelevant ^{111}In-Bn-DTPA-trastuzumab or normal saline. The tumour growth index (TGI) was determined weekly by dividing the tumour volume at selected time points by that prior to treatment. The slope of the TGI vs. time curve was calculated for each group. BWI was also measured. Results: ALT levels in non-tumour bearing mice injected with 8.8 or 28.2 MBq of ^{111}In-Bn-DTPA-nimotuzumab were 32.8±5.0 or 77.3 ±31.9 U/L, respectively, compared to 29.8±4.3 or 24.8 ±6.3 U/L in mice receiving unlabeled Bn-DTPA-nimotuzumab or saline, respectively ($p>0.05$). Cr in mice injected with 8.8 or 28.2 MBq of ^{111}In-Bn-DTPA-nimotuzumab were 63.3±33.9 or 128.6±71.7 μmol/L, respectively, compared to 22.1±14.5 or 24.5±10.0 μmol/L in mice administered unlabeled Bn-DTPA-nimotuzumab or saline, respectively ($p>0.05$). No differences in BWI were noted for any groups. There was no effect of 8.8 MBq of ^{111}In-Bn-DTPA-nimotuzumab on CBC but leukocyte counts were lower for mice administered 28.2 MBq (3.5 ±0.6 K/μL) compared to saline treated mice (8.2±0.9 K/μL; P=0.012). An intermediate dose of 15.5 MBq of ^{111}In-Bn-DTPA-nimotuzumab was selected for RIT. The slope of the TGI vs. time curve over 84 days was lower ($p<0.05$) for tumour-bearing mice treated with two doses (15.5 MBq each) of ^{111}In-Bn-DTPA-nimotuzumab (0.010 ±0.005 d^{-1}) compared to mice injected with unlabeled Bn-DTPA-nimotuzumab (0.064±0.011 d^{-1}), irrelevant ^{111}In-Bn-DTPA-trastuzumab (0.049±0.010 d^{-1}) or normal saline (0.066±0.010 d^{-1}). There was no difference in BWI among the groups. Conclusion: ^{111}In-Bn-DTPA-nimotuzumab is a promising new treatment for EGFR-overexpressing breast cancer. Supported by a grant from the Canadian Institutes of Health Research. Nimotuzumab was provided by YM Biosciences, Inc.

PW08 - Monday, October 12, 2015, 8:30 AM - 9:30 AM, Hall 3 – Poster Exhibition

Poster Walk 8 – Conventional & Specialised Nuclear Medicine: General & Miscellaneous

PW071

Bone scan and MRI in Chronic Recurrent Multifocal Osteomyelitis

L. Biassoni; Great Ormond Street Hospital for Children NHS Foundation Trust, London, UNITED KINGDOM.

Aim: Chronic Recurrent Multifocal Osteomyelitis (CRMO) is a rare inflammatory bone disorder presenting with relapsing and remitting episodes of bone pain. MRI is the imaging modality of choice; however, long waiting lists often prevent patients to have access to MRI in a timely fashion. Aim of this study was to compare the diagnostic yield of the bone scan (BS) versus MRI in CRMO and to correlate the findings with inflammatory markers and clinical symptoms/location of pain. Materials and Methods: Retrospective review of the clinical notes of children with a confirmed diagnosis of CRMO who had both bone scan and MRI between 2009 and 2014, and within 9 weeks of each other. Nine patients (7 females, 2 males, age range 7-13 years, mean 9.6) had both BS and MRI less than 9 weeks apart. We recorded for each patient: inflammatory markers at time of scans (ESR, CRP and WCC), clinical symptoms, pain location, number and location of lesions for BS and MRI. Patients were excluded if BS and MRI were done more than 9 weeks apart, or if there was any change to treatment in-between scans. BSs were acquired as a whole body sweep, with high count spot views of the areas of interest and SPECT CT when necessary. MRI scans were limited to the area of interest (only 1 patient had whole body MRI) and were acquired using T1, T2, and STIR sequences (and contrast enhanced in 6 patients). Results: Pain was always associated with a bone lesion on imaging. BS was always

positive at the site of symptoms. MRI consistently detected more lesions than BS (45 lesions versus 31 with BS), especially in the spine. However, several lesions, mainly suggestive of bone marrow oedema, were asymptomatic, and their clinical significance was questionable. BS was better at detecting rib lesions. MRI and BS were concordant in 69% of cases. The inflammatory markers were non-specific. Conclusion: MRI and BS were concordant in a high number of cases. MRI detected more lesions than BS; however, several lesions were asymptomatic and of doubtful clinical significance. BS was always positive at the site of symptoms. BS can be considered in CRMO if MRI is not readily available.

PW072

Scintigraphic functional evaluation of intrathecal drug infusion devices

G. Garraffa[1], V. Scaglione[2], F. Felice[1], R. Ricapito[1]; [1]Nuclear Medicine Unit, A.R.N.A.S. "Ospedale Civico, Di Cristina e Benfratelli", Palermo, ITALY, [2]Neurosurgery Unit, A.R.N.A.S. "Ospedale Civico, Di Cristina e Benfratelli", Palermo, ITALY.

Scintigraphic evaluation of intrathecal drug infusion devices.GARRAFFA G.1, SCAGLIONE V.2, FELICE F.1, RICAPITO R.1 AND ARNONE G.1.1 Nuclear Medicine Unit, A.R.N.A.S. "Civico, Di Cristina e Benfratelli", Palermo, Italy. 2 Neurosurgery Unit, A.R.N.A.S. "Civico, Di Cristina e Benfratelli", Palermo, Italy.Introduction and aim: intrathecal infusion devices are used for pts. with pain and spastic diseases. These are made by a pump with a reservoir for the drug allocated in the abdominal subcutaneous space and connected to a catheter ending in the spinal subaracnoid space. Malfunctioning of the infusion system or progression of pain disease causes increasing infusion rates or drug amount. Administration of a not-absorbed radionuclide (99mTc-DTPA) in the pump reservoir and sequential scanning allow to follow the progression of the radionuclide along the catheter to the spine. The images show any interruption/delay of the system radionuclide progression and, if the flow rate of the pump device is programmable, quantitative evaluation of the flow itself along system. Aim: to evaluate the effectiveness of 99mTc-DPTA infusion within the device in order to detect malfunctioning and to correlate the results with patient management and outcome.Methods: 8 patients already studied with 99mTc-DTPA scintigraphy were retrospectively reviewed. All of them had surgically implanted Medtronic® SynchroMed intrathecal (baclofen or ziconotide) infusion pump systems, because of severe spasticity (n=5) or intractable pain (n=3). About 400 MBq 99mTc-DPTA was injected into the pump reservoir, then planar serial static abdominal scans were performed every three hours for 24 hours to follow tracer progression. Once the tracer arrived in the spinal liquoral system, whole-body scans were performed.Results: no adverse effects on heat conditions correlated with 99mTc-DPTA were registered. 1 pt. showed regular device functioning without interruption of progression and with delivery flow corresponding to the programmed flow. 6 pts. showed interrupted progression along the abdominal portion of the catheter, one of which also with subcutaneous dispersion of the radionuclide. 1 pt. showed quantitative alteration of the flow rate, too slow respect to the programmed delivery flow rate. Pts. with flow stop were re-operated and operative findings confirmed the scintigraphic data. Patient with flow reduction presented pump failure, while pt. with normal flow had psychiatric disorders.Conclusions: intrathecal infusion system scintigraphy is an useful tool in non-invasive evaluation of functioning of implants with programmable pump. Use of 99mTc-DPTA radionuclide allows satisfactory and good-quality study conduction, without any adverse effects and with lower dosimetric load than 111In-DTPA.

PW073

99mTc-HDP bone SPECT with voxel-based evaluation for temporomandibular asymmetry detection in diagnosis of the idiopathic condylar hyperplasia

D. Chroustova, J. Sebek, J. Trnka, J. Kubinyi; General University Hospital and 1st Faculty of Medicine Charles University, PRAGUE 2, CZECH REPUBLIC.

Aim: Idiopathic condylar hyperplasia (ICH) is characterized by persistent or accelerated growth of the mandibular condyle, when growth should be slowing or ended. 99mTc-HDP bone SPECT and voxel-based mathematical analysis is used to verify the activity of condylar growth. The aim of the study was to verify temporomandibular asymmetry in diagnosis ICH and according the results to choose suitable surgery: condylar shaving or conventional orthognathic surgery. Treatment of patients with active condylar growth only with classical orthognathic surgery methods could lead to relapse of asymmetry. Materials and methods:106 patients (67 female a 39 male) aged 13-47 (average 21) years with laterogenia underwent bone SPECT with the right to left ratio assessment of the temporomandibular joints (TMJ) uptake using the voxel-based method. 18 patients were investigated repeatedly. Bone SPECT was performed 2-3 hours after injection of 300-700MBq 99mTc-HDP on dual-heads gamma camera Infinia GE using a low-energy, high-resolution collimator, with following acquisition parameters:120 projections, 20sec/projection, matrix 128x128. Voxel-based analysis of the right to left TMJ uptake ratio: The VOIs of the temporomandibular joints were defined using a combination of two spatial voxel masks. One mask was defined via an intensity threshold and served to

separate out the background. The other mask was defined by an origin and a radius and served to separate out objects outside the corresponding sphere. An intersection of these two masks defined desired volume of interest. Total counts from each corresponding VOI came without background correction as inputs to the default formula: L=NL/(NR+NL).100%, R=NR/(NR+NL) .100%. For the evaluation we considered 10% difference (in terms of percentage points) of 99mTc-HDP uptake between mandibular condyles as a sign of active ICH. Results: 44 subjects had uptake difference higher than 10%. These scans confirmed indication of 36 patients for condylar shaving to stop the condyle growth. Additional orthognathic surgery for fine-correction of asymmetry was needed in 7 patients and in 14 cases dental compensation of occlusion was sufficient treatment. 85 subjects had uptake difference 10% or lower. These results disproved working diagnosis of ICH in 70 patients and in 26 cases conventional orthognathic surgery was performed. No relapse was wound within 2 years postoperatively. Conclusion: 99mTc-HDP bone SPECT with voxel-based evaluation of the mandibular condyle accelerated growth is crucial in diagnosis of ICH. Finding with an asymmetrical TMJ growth is indicated to treatment with condylar shaving in the first phase and orthognathic surgery later.

PW074

Assessment of ACL Graft Viability by Dynamic FDG PET: A Phase I Study

K. Binzel[1], R. Magnussen[1], C. Kaeding[1], W. Wei[1], M. U. Knopp[2], D. C. Flanigan[1], M. V. Knopp[1]; [1]The Ohio State University Wexner Medical Center, Columbus, OH, UNITED STATES, [2]Pepperdine University, Malibu, CA, UNITED STATES.

In cases of a complete tear, injury to the anterior cruciate ligament (ACL) typically requires reconstruction with a graft. Patients having received a graft are at risk of re-injury, with no available imaging methodologies to assess ligamentization of the graft. In a first-in-human study, we demonstrate the capability of a combined imaging approach using dynamic, ultra-low dose positron emission tomography (PET) and MRI for evaluation of graft healing following reconstructive surgery. 20 patients post-ACL graft reconstruction had dynamic PET on a Gemini TF 64 and/or new digital detector PET/CT system, Vereos TF. An in-house constructed foam cushion was used to place both knees in matched positions to that of the dedicated MR knee coil during PET acquisitions. Using an ultra-low dose (<111 MBq) 18F-fluorodeoxyglucose (FDG) protocol, a single bed position centered on the knees was acquired continuously for 75 minutes. Standard of care MRI was performed on a Philips 3T Achieva (all systems Philips Healthcare, Cleveland, OH). PET images were co-registered to MRI for quantification. Standardized uptake values (SUV) were measured for regions of interest (ROI) in the proximal, middle, and distal portions of the graft, the tibial and femoral tunnels, the posterior cruciate ligament (PCL), and the quadriceps muscle for reference. Matched measurements were taken in each contralateral knee. The slope of the enhancement curve over the 75 minute acquisition was calculated for each ROI. Patients were grouped according to time since surgery, from 0-6 months, 6-12 months, 12-24 months and 24+. Dynamic PET images were readily co-registered to MRI for all patients. In the 0-6 month group the average slope of the metabolic uptake curve was 0.20 in the distal graft, 0.21 in the mid graft, 0.27 in the proximal graft, and 0.14 in the tibial tunnel. In contralateral healthy knees the average slopes were 0.06, 0.09, 0.05, and 0.05, respectively. These healthy values were similar to measurements seen in the 12-24 and 24+ month groups. Patients with longer healing times were also found to have absolute SUVs increasingly approaching healthy values as well. Quantitative evaluation of ACL graft ligamentization using an ultra-low dose PET protocol with co-registration to MRI was demonstrated. The digital PET enables even further dose reductions with improved image quality and quantitative accuracy. A combined low dose FDG PET/MRI exam to assessment of ACL graft healing appears to promising tool.

PW075

High Therapeutic Impact in New Indications of 18F-FDG PET/CT in High/Intermediate Recurrence Risk Differentiated Thyroid Carcinoma Patients

E. M. Triviño-Ibáñez[1], M. A. Muros[1], E. Torres-Vela[2], J. M. Llamas-Elvira[1]; [1]Virgen de las Nieves University Hospital, Granada, SPAIN, [2]San Cecilio University Hospital, Granada, SPAIN.

INTRODUCTION: Little is known about clinical benefits and the therapeutic impact of fluorine-18-fluorodeoxyglucose positron emission tomography/computed tomography (18F-FDG PET/CT) performed early after radioactive iodine (RAI) ablation in differentiated thyroid carcinoma (DTC). AIM: Investigate whether 18F-FDG PET/CT performed early after RAI ablation is useful in detection of disease and influence therapy in new indications of high/intermediate risk of DTC. PATIENTS and METHODS: A prospective study was carried out (June 2007 to December 2013) on 81 patients with high/intermediate risk of recurrence differentiated thyroid carcinoma, treated with surgery and radioidine ablation. Our patient selection was not based exclusively on TNM classification and included broad risk criteria (ATA guidelines 2009, etc.) [8], such as locoregional invasion, inadequate high Tg value and aggressive histological subtypes.Demographic data,

surgery and pathology report, neck ultrasound and 131I-whole body scan results and biochemical test lab report were collected. We performed 18F-FDG- PET/CT just before or inmediately after surgery. We confirmed 18F-FDG- PET/CT results with other imaging techniques, pathology report, first year whole body scan, neck ultrasound or follow-up. We used modified Hicks criteria for evaluate 18F-FDG- PET/TC results impact. RESULTS: 81 patients with high/intermediate-risk of recurrent DTC. Forty-one (50.6%) had positive uptake in 18F-FDG PET/CT, with negative 131I WBS. Sensitivity, specificity and diagnostic accuracy of PET/CT were 92.5%, 90.2% and 91.4% respectively. PET/CT results had an impact on therapy in 38.3% of patients. One year after initial therapy, 45.7% showed excellent response, 8.6% acceptable and 45.7% incomplete response. We found statistically significant relationship between negative PET/CT and excellent response (80 vs. 12.2%, p <0.001; OR: 52.8). CONCLUSIONS: 18F-FDG PET/CT performed early in surveillance of high/intermediate-risk thyroid carcinoma provides information fundamental to patients follow-up. A wide patient selection of high/intermediate risk DTC improves 18F-FDG PET/CT results and determines a high therapeutic impact.

PW076

17 years follow-up from 1998 to 2015 of 123 medium-size (2-4 x normal) EU-and Hyperthyroid (EU, HT) goitres after treatment by 131I (RIT)

C. ALS, N. LENERS; Hôpitaux Robert Schuman - Zithaklinik, Luxembourg, LUXEMBOURG.

OBJECTIVE: We present a long-time follow-up of patients (pat) with medium-size goitres (2-4x normal), (normal = ♀:18 mL, ♂:25 mL) treated by RIT in a reference centre. MATERIALS AND METHODS: (med=median, mima=min-max, ↓=decreased, <0.0005=*). Out of 673 patients treated by 131I (1998-3.2010), 123 pat (92♀, 27-90 (med 69) years (Y) and 31♂, 22-83 (med 70) Y), with a medium-size goitre by ultrasound (♀:36-72mL, ♂:50-100mL, 6 pat excluded (1 emigration/ 5 Basedow post-131I)), were followed until 03.2015, i.e., 0.9-8.8 Y post-131I (mean/med 4.1/3.9 years). Simulation was at 6h/24h/100h: calculation (MIRD, 100-300 Gy), therapeutic activity 131I (370-1295MBq, mean/med 785/800MBq). Out of 123 pat: 10 had HT Basedow (B) (med TSH 0.01 mU/L), 18 had EU goitre (med TSH 1.03 mU/L), 95 had HT functional autonomy (FA, med TSH 0.12 mU/L). RESULTS : At 4 months (mo)/1Y/endpoint, thyroid (T) vol had resp.↓ by 41.3%/55.2%/61.9% (all*), without a ♀-♂difference. Vol. normalisation 1 Y post-RIT was found in ♀41%, ♂32%. At 4 mo/1 Y, TSH: (B) 40.0/15.8 mU/l (p=0.4), EU goitre 2.52/1.88mU/L (p=0.48), FA 1.03/1.25mU/L (p=0.008). 81% pat were EU at 1Y (♀: 83%, ♂: 74%). RIT was repeated with 2 pat. Death occurred in 24 pat (survival 9-148.8 mo, med 70 mo). Clinically better subjective feeling after 12 mo in 100% pat. Hormone substitution was required in 10%/45%/61.5% of pat after 4mo/12mo/endpoint. Thyroid volumes before RIT (Mima=36-98mL, mean=55.7mL, med=52mL) were respectively at 4mo (6-78mL, 33.51mL, 30mL*), at 1Y (2-75mL, 27.31mL, 25mL*), at >1Y (2-100ml, 21.4ml, 17mL*), in ♀med respectively (50mL, 28ml*, 22ml*, 14mL*), in ♂med respectively (68.5mL, 41.5mL*, 32.5mL*, 32mL*). TSH value before RIT respectively was (0-5.4mU/L, 0.5mU/L, 0.2mU/L), at 4mo (0-89mU/L, 5.2mU/L, 1.1mU/L), at 1Y (0.1-72mU/L, 3.7mU/L, 1.5mU/L), at >1Y (0.1-36mU/L, 2.33mU/L, 1.49mU/L). Med TSH changes in ♀ and ♂ were ns. CONCLUSIONS: Compared with other thyroid pathologies, ♂ have relatively more goitres 2-4x normal than ♀. RIT is a safe and efficient method for thyroid vol ↓ and HT eradication, equally efficient with ♀ and ♂. HypoT and need for hormonal supply increases with time after RIT. Vol ↓ significantly proceeds over several years. Volume change after RIT was equally efficient in ♀ and ♂.

PW077

The Clinical Outcome and Mortality Rates in patients with Differentiated Thyroid Carcinoma with bone metastasis: Results of a 15- year clinical follow-up.

G. Ucmak, B. Demirel, **B. E. Akkas**, A. K. Fidan, N. Ercakmak; Ankara Oncology Research and Training Hospital Department of Nuclear Medicine, Ankara, TURKEY.

In this study, we evaluated the treatment response and clinical outcome of Differentiated Thyroid Carcinoma (DTC) patients with bone metastases. Method: DTC patients treated in our department from 1990 to 2014 were retrospectively evaluated, 43 patients with bone metastasis were included in this study (28 F, 15 M, mean age: 53 years). All patient records, treatment history, laboratory and clinical information were evaluated. The final status of the patients was defined according to clinical follow-up data. The total follow-up time ranged from 13 to 178 months (median: 65 months). Results: 43 patients (21 papillary, 18 follicular, 3 poorly differentiated, 1 Hurthle cell carcinoma) were included. Thirty-five patients (81%) had bone metastasis at the time of diagnosis whereas 8 patients were progressed with bone metastasis. All patients had elevated serum Thyroglobulin (Tg) levels (>500 ng/ml with TSH stimulation) at the time of diagnosis. Twenty-seven patients (63%) had multiple sites of bone metastasis. Fourteen patients had organ metastasis (33%) as well. 4 patients underwent surgical resection for metastatic foci. Inoperable iodine-

avid metastases are treated with multiple administrations of radioiodine with empirical activities of 200-250 mCi each. The cumulative doses were ranged from 200 to 1600 mCi. Twenty-six patients (60%) received external radiation therapy. The response of therapy was evaluated with serum Tg levels, anti-Tg antibody levels and radioiodine body scans. The final status of patients was defined on the basis of a long term follow-up, up to 178 months. Five patients (12%) had complete biochemical and clinical remission, 13 patients (35%) had partial remission with significant drop in serum Tg levels. Two patients had stable disease. Six patients had progressive disease, 17 patients (40%) were died of disease on follow-up. The time to exitus ranged from 1-to-11 years with a mean of 4.8 years after the diagnosis of metastatic disease. All patients with disease specific mortality had organ and multiple sites of bone metastasis mostly located on the vertebral colon. The main cause of mortality was the complications arisen from spinal cord compression due to tumoral involvement. Results: Bone metastases of DTC have poor prognosis. The mortality rate was 40% in our series. We observed that, mortality was higher in patients with vertebral colon metastasis. However, our results showed that, with combined and intensive treatment modalities, up to 12% of complete remission, 35% of good therapeutic responses and partial remission can be achieved, the quality of life can be improved.

PW078

Evaluation of a fast and a standard protocol for bone scintigraphy SPECT/CT in patients suspected for having bone metastasis

K. Knudsen, A. Bekker, S. Jentoft Kramer, P. Iversen, A. Arveschoug; Aarhus University Hospital, Noerrebrogade, AARHUS, DENMARK.

Background: Bone scintigraphy including SPECT/CT compared to wholebody scintigrams has been shown to increase the specificity, to a minor extent the sensitivity, and observer confidence in the evaluation of bone metastasis in cancer patients. Several studies have demonstrated that the proportion of indetermined bone lesions can be reduced significantly by using SPECT/CT. In order to optimize the examination time as well as the fact that many patients with bone metastasis have difficulties lying still for longer periods of time, has prompted us to optimize our bone scintigraphy SPECT/CT protocol. Aim: To evaluate whether a fast SPECT protocol could substitute the standard SPECT protocol for SPECT/CT bone scintigraphy. Methods: Thirty patients referred for bone scintigraphy, 28 suspected for having bone metastasis, were included in the study. All patients were injected with a standard dose of 99mtechnetium-labeled diphosphonate (Teceos, DPD) and had a planar wholebody scan. In each of the three regions head-neck-thorax, mid trunc and pelvic-proximal femoral area, 10 patients were scanned twice with a fast and standard SPECT/CT protocol, respectively, on a Siemens Symbia T16 SPECT/CT camera (Siemens AG, Erlangen, Germany). The fast protocol in a continuous mode and total scan time of 31 minutes for the trunc, the standard protocol in a step and shoot mode and total scan time of 50 minutes for the trunc. Three independent observers analyzed the standard and fast SPECT/CT over each region, anonymized and randomized. All foci in each region were scored on a 5-point scale as normal lesion, probably normal lesion, equivocal lesion, probably malignant lesion or malignant lesion. The wholebody scans were evaluated accordingly. Results: Independent of both observer, region and nature of foci, the total number of foci detected on the wholebody scan were considerably lower compared to both standard and fast SPECT/CT. Furthermore, the data showed a trend towards a lower total number of detected foci in the fast SPECT/CT protocol scans compared to the standard protocol scans. The difference were more pronounced in the mid trunk region, although not significant for any of the three observers in any of the three regions ($p > 0.05$). Conclusion: In this study we found no significant differences in the observers ability to detect and describe the bone pathology in a fast and a standard SPECT/CT bone scintigraphy protocol, respectively. However, the limited population size of the current study may increase the variability of the data to produce a false-negative difference.

PW079

Nephrotic Syndrome with pulmonary embolism: the role of lung scintigraphy

i. G. E. el bez, A. EZZINE, B. LTAIEF, I. SLIM, D. BEN SELLEM, l. zaabar, I. MEDDEB, I. YEDDES, b. dhaoudi, A. MHIRI, M. BEN SLIMENE; institut salah azaiez, tunis, TUNISIA.

Patients with nephrotic syndrome (NS) have an increased tendency to develop thrombosis and even to progress to pulmonary embolism (PE).This study was performed to determine the incidence of PE in NS and to evaluate the role of perfusion lung scans in these patients.Materiel and methods: Thirty-four patients with NS and risk factors for PE were studied. Eight patients had a renal failure. In all patients, the probability of PE was assessed based on the results of perfusion lung

scans (Tc-99m MAA). The perfusion scan was repeated in patients having a PE. The lung scans were judged using the modified Prospective Investigation of Pulmonary Embolism Diagnosis criteria. The patients' clinical symptoms and signs on initial examination were reported. Additional examinations included electrocardiograms, chest radiography, and biological tests such as creatinine, albuminemia.Results: Based on the findings of lung scans, 22 (64.7 %) of the patients were categorized as having a high probability of PE. 12 (35.3%) patients had a normal perfusion lung scan. CT angiography was performed in 26 patients and showed the same results that lung scan.Two weeks after the administration of intravenous heparin for anticoagulative therapy, twenty cases had a recovery or an improvement.Conclusion: The results of this study suggest that PE is not a rare complication in patients with NS. The occurrence of PE did not appear to be always correlated with the clinical or biological severity of NS. Perfusion lung scans may provide valuable clues in the evaluation of these patients.

PW080

Lung V/Q scintigraphy and perfusion SPECT in the diagnosis of chronic thromboembolic pulmonary hypertension

J. A. MARROQUÍN GÁLVEZ, D. SANCHEZ FUENTES, A. SAVIATTO, A. C. HERNANDEZ MARTINEZ, J. P. PILKINGTON WOLL, M. J. TABUENCA MATEO, S. RUIZ SOLIS, J. M. ESTENOZ ALFARO; HOSPITAL UNIVERSITARIO 12 DE OCTUBRE, MADRID, SPAIN.

AIM: To evaluate the efficacy of lung ventilation/perfusion (V/Q) scintigraphy and perfusion SPECT in the initial screening of Chronic Thromboembolic Pulmonary Hypertension (CTEPH). MATERIALS AND METHODS: Retrospective study including 32 patients (9 male and 23 female), with age ranging from 23-82 years (54.56 ± 19.12), with suspected diagnosis of CTEPH, referred by the CTEPH unit of our hospital, between April and December 2014.Lung V/Q scans were performed using 99mTc-Technegas and 99mTc-MAA (Macroaggregated Albumin) respectively, including anterior, posterior and right and left posterior oblique projections. Perfusion SPECT was also acquired in all of them.EANMMI guideline criteria (positive, negative or indeterminate) was applied when reporting the findings.CT pulmonary angiography and/or thoracic CT was also performed to all patients as part of the study.Pulmonary angiography by right heart catheterization was used as the gold standard for the final diagnosis. RESULTS: Twenty one out of 32 patients were diagnosed of CTEPH by pulmonary angiography. Planar lung V/Q scan and perfusion SPECT were positive in 23/32 patients (2 false positive for Primary Pulmonary Hypertension). The other 9/32 patients were reported as negative. We did not obtain any false negative or indeterminate result.The V/Q scan and perfusion SPECT for the diagnosis of CTEPH had a sensitivity of 100%, specificity of 81.82%, positive predictive value of 91.30%, negative predictive value of 100%, and an accuracy of 93.75%. CONCLUSION: In our study, lung V/Q scan and perfusion SPECT had a high sensitivity and negative predictive value for CTEPH diagnosis with an accuracy value around 95%, demonstrating their strong efficacy in the initial screening of CTEPH.

PW09 - Tuesday, October 13, 2015, 8:30 AM - 9:30 AM, Hall 3 – Poster Exhibition

Poster Walk 9 - Clinical Oncology: Miscellaneous

PW081

Sentinel node detection with ferromagnetic particles in breast cancer. Preliminar results

U. Granados, S. Vidal-sicart, X. Caparrós, M. Alonso, P. Fernandez, P. Perlaza, A. Tápias, F. Lomeña; Hospital Clínic, Barcelona, SPAIN.

Aim: To compare two techniques for sentinel lymph node (SLN) detection in patients with breast cancer (BC): radioactive tracer (99mTc-Nanocoll®) and ferromagnetic particles (SentiMag®) and to analyze the correlation between two different injection sites and time spent for SLN location. Material and Methods: We have studied prospectively 29 BC patients, scheduled for SLN Biopsy, with a mean age of 60.7 years. The injection of the radiotracer (111 MBq in 0.5 mL) was mainly intra / peritumoral the day before surgery. Lymphoscintigraphic images (30 min and 2 h) were subsequently performed. No external mark in SLN skin projection was drawn. In the operating room, 5 ml of ferromagnetic particles (Sienna+®) were administered by periareolar injection followed by a 5 minutes massage. The surgeon used a magnetometer and the nuclear medicine physician used the gamma radiation detection probe. The transcutaneous signal was evaluated with SentiMag (surgeon) and with gamma probe (nuclear medicine physician).The skin incision was performed after reaching a clear transcutaneous signal with SentiMag®. The correlation between the magnetic source and the radioactivity was checked. Results: In 26 patients was located at least one SLN with both techniques. In 3 patients the

detection of SLN with ferromagnetic particles was not possible (1 patient had previous surgery). In 13 cases both techniques located the same SLN (44.8%). When the injection site was the same, the correlation observed for both techniques was 63.6%; when radioactive tracer was injected intra / peritumoral this concordance droped to 33.3%. SentiMag® was faster in the location of SLN in 9 patients, in 6 patients a greater number of SLN were detected. In 13 patients the conventional gamma probe detected SLN more easily and in 3 patients was the only technique that located the SLN. The mean operating time was 44 min with SentiMag® vs 38 min with the radiotracer. Conclusions: SentiMag® detects a discrete higher number of SLN. When the injection site differs there is a major discrepancy in SLN detection between techniques. In some cases the SLN has been detected only with the conventional technique.

PW082

Gastrin-releasing peptide receptor expression is associated with estrogen receptor status in breast cancer: Findings of a PET/CT pilot study

C. Stoykow[1,2,3], T. Erbes[4], S. Bulla[1], H. Mäcke[1], V. Drendel[5], P. Bronsert[5,6], M. Werner[5,6], E. Stickeler[4], P. T. Meyer[1]; [1]University Medical Centre Freiburg, Department of Nuclear Medicine, Freiburg, GERMANY, [2]German Cancer Consortium (DKTK), Freiburg, GERMANY, [3]German Cancer Research Center (DKFZ), Heidelberg, GERMANY, [4]University Medical Centre Freiburg, Department of Gynecology and Obstetrics, Freiburg, GERMANY, [5]University Medical Centre Freiburg, Department of Clinical Pathology, Freiburg, GERMANY, [6]German Cancer Consortium (DKTK), Heidelberg, GERMANY.

The gastrin-releasing peptide receptor (GRPR) is overexpressed in several human tumors. The purpose of the present study was to evaluate GRPR imaging as a novel diagnostic approach in breast cancer. We employed positron emission tomography (PET) and the novel GRPR antagonist [68Ga]RM2, which has been developed by our group. [68Ga]RM2 possesses a low nanomolar affinity for GRPR and has already been successfully studied in prostate cancer. Fourteen female patients with histologically confirmed, locally advanced primary breast carcinoma (3 bilateral tumors) underwent PET/CT for pretreatment staging on compassionate-use basis. PET/CT was acquired 1h after injecting 150-200MBq [68Ga]RM2. In vivo GRPR binding was correlated with estrogen (ER) and progesterone (PR) expression, HER2/neu status and MiB-1 proliferation index of biopsy specimens. Normal breast tissue showed an inter-individually variable, moderate heterogeneous GRPR binding (SUVMAX 2.27±1.02), while physiological uptake of most other tissues/organs was considerably less (SUVMEAN liver, muscle and fat: 1.10±0.32, 0.38±0.10 and 0.19±0.04) except pancreas (52.7±11.6). 12/17 tumors were clearly visualized by strongly increased uptake compared to normal breast tissue (PET-positive). Noteworthy additional findings included the detection of small internal mammary lymph nodes (2-3mm) with strong GRPR binding, a contralateral axillary lymph node metastasis (n=1; verified by biopsy) and bone metastases not detected by other imaging modalities (n=1). All PET-positive tumors were ER- and PR-positive, in contrast to only 1/5 PET-negative tumors (Fisher's exact test $p=0.002$; SUVMAX 10.80 ±6.21 and 2.31±0.97 in ER-positive and ER-negative tumors, respectively). In a multivariate analysis including ER, PR, HER2/neu and MiB-1, only ER expression predicted GRPR binding ($R2=0.56$, $p<0.05$). This pilot study demonstrates that GRPR PET/CT is a promising diagnostic modality in ER-positive breast cancer. GRPR imaging may serve as a possible surrogate marker for ER expression with putative therapeutic and prognostic importance.

PW083

Measurement of early treatment response in patients with recurrent or metastatic breast cancer with 18F-FLT and 18F-FDG PET/CT: a pilot study

T. Su, S. Chan, K. Lui, J. Huang; Chang-Gung Memorial Hospital Keelung Branch, Keelung, TAIWAN.

Aim: 18F-FLT and 18F-FDG PET have been proved useful in monitoring treatment response of recurrent or metastatic carcinoma. However, combination of 18F-FLT and 18F-FDG PET in assessing treatment outcome of recurrent/metastatic breast cancer has not been reported. In this prospective study, we investigated the imaging biomarkers, 18F-FLT and 18F-FDG, to measure early treatment response in recurrent/metastatic breast cancer after the first and second cycles of taxane- or cisplatin-based chemotherapy. Materials and methods: Eleven patients with recurrent or metastatic breast cancer, who were about to commence a new pharmacological treatment regimen, were recruited. Each individual underwent 18F-FLT and 18F-FDG PET/CT at baseline, and after the first and second cycles of the new regimen. Treatment response was based on the results of 3-month post-therapy conventional work-up, with criteria of the Response Evaluation Criteria in Solid Tumors (RECIST) 1.1. Variables from 18F-FLT and 18F-FDG PET scans were correlated with the conventional imaging results. Results: Treatment response determined by RECIST 1.1 showed 5 responders and 6 non-responders. In all responders, systemic treatment had resulted in decreases in both 18F-FDG and 18F-FLT uptake

(SUVmax): -15.0±8.0% and -24.5±28.7% after one cycle; -50.6±26.0% and -37.8±39.7% after two cycles. Among non-responders, however, 5 subjects (5/6, 83%) also had decreased 18F-FDG uptake, and the changes of SUVmax were -12.3±14.4% and -24.0±14.2% after the first and second course of chemotherapy. In contrast, the corresponding 18F-FLT SUVmax uptake in non-responders showed increased tendencies compared to the baseline images (0.0±28.6% and 16.3±61.6%). In subjects with pure bony metastases (2/11), the 18F-FDG-avid bone lesions which showed no 18F-FLT uptake ended in good response to treatment, and the 18F-FDG PET could not correctly predict the good response. Conclusion: Tumor uptake assessed by 18F-FLT PET early after initiating systemic therapy appears to be a superior marker than 18F-FDG PET to predict treatment response in patients with recurrent/metastatic breast cancer. For solely bony metastasis group, presentation of 18F-FLT-photopenic lesions may be a good prognosticator.

PW084

Sentinel-node in cervical cancer patients: preoperative assessment with SPET/CT and comparison with intra-operative gamma-probe and methylene blue-dye

M. Cuzzocrea[1], F. Elisei[2], C. Crivellaro[1], C. Dolci[1], A. Buda[3], M. Signorelli[3], L. Guerra[2], D. Giuliani[4], M. Arosio[2], R. Milani[5], C. Landoni[5]; [1]University of Milan-Bicocca, Nuclear Medicine, Milan, ITALY, [2]Nuclear Medicine Department, San Gerardo Hospital, Monza, ITALY, [3]Gynaecology Department, San Gerardo Hospital, Monza, ITALY, [4]University of Milan-Bicocca, Gynaecology, Milan, ITALY, [5]University of Milan-Bicocca, Milan, ITALY.

BACKGROUND AND AIM OF THE STUDY: Lymph-node status is a major prognostic factor in cervical cancer (CC). Sentinel lymph-node (SLN) biopsy has been reported in CC, even if not yet a standard-of-care procedure. Aim of this study was to compare preoperative SPET/CT with gamma-probe and methylene blue-dye (MBD) in identification of SLN in early-stage CC. METHODS: 25 clinically early-stage CC women (66.7±9.7years, stage I-IB2) underwent preoperative lymphoscintigraphy. Tc-99m albumin nanocolloid was injected submucosally at 4 points of the cervix. After about 3 hours all patients underwent SPECT/CT study. MBD was injected into the cervix just before surgery under general anesthesia. All patients underwent hysterectomy, bilateral salpingo-oophorectomy, and radical pelvic nodal dissection. SPET/CT findings were compared to gamma-probe and MBD techniques. RESULTS: The detection rate of at least one SLN resulted 100% (25/25 patients) with SPET/CT, 92% (23/25) intra-operatively with gamma-probe and 84% (21/25) with MBD. Only in 18/25 (72%) patients a bilateral migration was obtained with all considered modalities. In particular, bilateral detection was achieved in 16 patients with SPET/CT (64%), in 11 patients with gamma-probe (44%) and in 8 patients with MBD (32%). The concordance site between SPET/CT and intra-operatively gamma probe resulted 80% (in 20/25 patients: 9 bilateral and 11 monolateral SNs); while concordance site with MBD was found in 32% (21/25 patients: 6 bilateral, 15 monolateral SNs). In the only 2/25 cases with failed SN detection by gamma probe, SPET/CT had revealed nodal uptake, however the intra-operative SN recognition was obtained with MBD. Overall 677 LNs were dissected (mean 27 LNs per patient), among which 74 SLNs (mean 3 SLNs per patient). Of 74 SLNs: 34 were "hot and blue (HB)", 15 blue only and 25 hot only. Eleven/74 SNs resulted positive for metastases in 5 patients (5 HB, 3 hot only and 3 blue only), with an incidence of LN metastases of 20%. Five positive non-SLNs were found in 2 patients, all with concomitant metastatic SLNs. False negative rate was 0%. CONCLUSIONS: Detection rate of at least one SLN was 100% with SPET/CT, 92% intra-operatively with gamma-probe and 84% with MBD. SPET/CT achieved the highest rate of optimal node mapping (bilateral migration 64%). Of 74 dissected SLNs, 34% were recognized by isotopic technique only, 20% by MBD only and 46% by both, confirming the complementary role of dual technique.

PW085

Comparison of imaging modalities (CT, FDG-PET/CT) in head and neck cancer patients

Z. Besenyi[1], S. Urbán[2], K. Hideghethy[3], T. Séra[1], Z. Lengyel[4], L. Pávics[1]; [1]University of Szeged Department of Nuclear Medicine, Szeged, HUNGARY, [2]University of Szeged,Institute of Informatics, Szeged, HUNGARY, [3]University of Szeged Department of Oncology, Szeged, HUNGARY, [4]Positron Diagnostics Ltd, Budapest, HUNGARY.

Introduction: The aim of this study was to evaluate the role of FDG-PET/CT in head and neck cancer patient treatment strategy. Gross tumor volumes delineation methods based on positron emission tomography and conventional topoCT were compared. The impact of tumor volumes were evaluated in overall and disease specific survival. Methods: 70 oncologic patients with primary head-neck cancer were enrolled in the current study. Within 3 weeks difference CT and FDG-PET/CT image acquisition were completed separately in planned irradiation position. Gross tumor volume were determined by manually contouring independently both on conventional CT based topometric slices and FDG-PET/CT images.

Radiotherapy target volume was calculated (GTV-pet GTV-ct [cm3]) using both modalities and numerical and geometrical comparisons were assesed. For a geometrical comparison manually contoured tumor shapes intersection divided by union ratio was calculated. This I/U ratio is a value between 0 and 1, where a value of 1 means full overlap and value of 0 means no overlap. Results: In regards to the total population radiotherapy target volume as assessed by FDG-PET/CT differed in 98 % (69/70) from target volumes calculated by topoCT. According to metabolic information the planned irradiation field was greater in 10 cases (14 %) and smaller in 59 cases (84 %). Significant differences were seen between CT and PET/CT based tumor volume (paired t-test $p<0.0001$). In point of geometrical view the calculated I/U ratio was average 0.37 ± 0.20 SD. Maximum value: 0.8, minimum: 0.014. The geometrical comparison showed large variation and the average ratio shows weak overlap. After average 6.4 years follow up the overall and disease specific survival showed close correlation with GTV-pet ($p=0.0001$). Conclusion: The CT and FDG-PET/CT based tumor target volumes differed significantly from each other. Differences between two modalities were even more apparent when not only tumor volume but geometric dimensions were also calculated. Our results showed that CT based morphologic information overestimates the tumor volume in larger lesions and can underestimate it in smaller target lesions in head and neck cancer. Radiotherapy planning based on the combination of structural and metabolic information with implementation of modern radiotherapy techniques may improve the efficacy of cancer therapy.

PW086

Clinical Value of FAZA-PET/CT in Head and Neck Cancer Patients

T. Saga[1], M. Inubushi[2], M. Koizumi[3], K. Yoshikawa[1], M. Zhang[1], T. Obata[1], R. Harada[4], T. Uno[4]; [1]National Institute of Radiological Sciences, Chiba, JAPAN, [2]Kawasaki Medical School, Kurashiki, JAPAN, [3]Cancer Institute Hospital, Tokyo, JAPAN, [4]Chiba University Graduate School of Medicine, Chiba, JAPAN.

Aim: The presence of hypoxia in cancer tissue is known to increase not only their refractoriness to treatment, but also their malignant potential. The information of cancer hypoxia, therefore, is important for the management of cancer patients such as prediction of treatment response and the selection of appropriate treatment strategy. The aim of the present study was to evaluate the clinical value of PET/CT with FAZA, a PET probe to detect cancer hypoxia, in head and neck cancer patients, especially on the prediction of patients' prognosis. Materials and Methods: Twenty-nine patients with head and neck cancer (stage I: 1 patient, stage II: 2 patients, stage III: 8 patients, stage IV: 18 patients; squamous cell carcinoma (SCC): 26 patients, non-SCC: 3 patients) received FAZA-PET/CT before treatment. Patients were followed to determine the treatment response and survival. Uptake parameters of FAZA (tumor-muscle ratio at 2 hours post-injection (T/M)) in primary lesion and lymph node metastasis were compared with various clinical parameters. Progression-free survival (PFS) was compared with clinical and FAZA uptake parameters in SCC patients who received chemoradiation therapy (CRT). Study protocol was approved by the institutional review board, and informed consent was obtained from all patients. Results: Among SCC cases, there was a significant correlation between FAZA primary T/M and maximal diameter of primary lesion ($P = 0.007$, $r = 0.517$). FAZA primary T/M was significantly higher in stage IV patients than in stage I ~ III patients ($P = 0.003$), and was significantly higher in T2 ~ 4 patients than in T1 patients ($P = 0.009$). Although not statistically significant, SCC patients who developed disease progression after CRT tended to show higher FAZA primary T/M than those who did not develop disease progression (1.70 ± 0.30 vs. 1.48 ± 0.36, $P = 0.095$). Kaplan-Meier analysis with Log-Rank test has shown that, among various clinical and PET parameters, only FAZA primary T/M was a significant predictor of PFS ($P = 0.010$), in which patients with FAZA primary T/M > 1.565 showed significantly worse PFS rate than those with FAZA primary T/M ≤ 1.565. Conclusion: FAZA primary T/M was a significant predictor of PFS in head and neck SCC patients receiving CRT. Pretreatment FAZA-PET/CT can afford useful information on the management of head and neck cancer patients.

PW087

Diagnostic accuracy of 18F-FDG PET/CT in primary staging of cutaneous malignant melanoma according to Breslow thickness: a preliminary study

S. Diodato[1], S. De Vivo[1], C. Baraldi[2], G. Veronesi[2], E. Dika[2], S. Fanti[2,1], A. Patrizi[2], S. Vaccari[2]; [1]Nuclear Medicine, Policlinico S.Orsola-Malpighi, University of Bologna, Bologna, ITALY, [2]Dermatology Unit, Policlinico S.Orsola-Malpighi, University of Bologna, Bologna, ITALY.

Aim: The purpose of this study was to assess sensitivity and specificity of 18F-FDG PET/CT to detect lymph node and soft tissue/visceral metastasis in the primary staging of cutaneous malignant melanoma (CMM). Materials and methods: We retrospectively evaluated 76 patients, 52 male and 24 female, mean age 62 y.o. (range 28-93), with a histological diagnosis of CMM, who underwent initial staging 18F-FDG PET/CT between april 2004 and november 2011 at Nuclear Medicine Unit, University of Bologna. Histological features of the primary tumors were available for all patients. Patients were

classified into 3 groups: group A (Breslow thickness <0,75 mm, 11 pts), group B (Breslow thickness 0,76-1,5 mm, 15 pts) and group C (Breslow thickness >1,5 mm, 50 pts). The results of the PET/CT scans were compared with those obtained by further histopathologic evaluations and/or clinical and radiological investigations, up to 3-6 months. Results: Overall sensitivity and specificity were respectively 61,5% and 93,5%. In group A and B sensitivity was 100% both for N- and M-staging. Specificity in group A was 100% for detection of lymph node metastasis and 90% for distant metastasis: the unique false positivity was observed in a patient presenting a cutaneous/subcutaneous moderately hypermetabolic lesion, that resulted a sebaceous cyst at histological examination. Specificity in group B was 100% for M-staging and 93% for N-staging. In group C sensitivity was 55,5% for N-staging and 66,7% for M-staging: a false negative result was observed in a patient with a pulmonary nodule without increased FGD uptake, that further resulted as a metastasis from CMM in the radiological follow up. Specificity was 100% for distant metastasis and 94,9% for lymph node metastasis. Diagnostic accuracy in group A, B and C were respectively 91%, 93% and 84%. Conclusion: Sensitivity and specificity of 18F-FDG PET/CT in N- and M-staging of CMM seem to be higher in patients with Breslow thickness <1,5 mm. These results are quite in contrast with the trend of studies in literature that reported a better diagnostic performance of PET/CT in high risk patients with CMM. Further studies including a larger number of patients with lower Breslow thickness are necessary to assess the potential role of PET/CT in primary staging based on Breslow's depth. Other prognostic factors , such as the number of mitoses and the presence or absence of ulceration on the histopathologic evaluation of the primary melanoma should be evaluated together with Breslow thickness.

PW088

Comparison of ^{123}I-IMP SPECT, ^{18}F-FDG PET, and ^{18}F-FDOPA PET in Detection of Uveal Malignant Melanoma

K. Kato[1], S. Tsuchiya[1], Y. Koshiba[1], T. Odagawa[1], S. Abe[2], T. Kubota[3], H. Terasaki[1], S. Naganawa[1]; [1]Nagoya University Graduate School of Medicine, Nagoya, JAPAN, [2]Nagoya University Hospital, Nagoya, JAPAN, [3]Nagoya Medical Center, National Hospital Organization, Nagoya, JAPAN.

Aim: Previously we showed that ^{123}I-IMP SPECT is a sensitive and accurate method for the detection of uveal malignant melanoma. The feasibility and usefulness of ^{18}F-FDOPA PET for detection of uveal malignant melanoma have not yet been established. The purpose of this study is to compare the usefulness of ^{123}I-IMP SPECT, ^{18}F-FDG PET, and ^{18}F-FDOPA PET for detection of uveal malignant melanoma. Materials and Methods: Forty-six patients with suspected uveal malignant melanoma were examined by ^{123}I-IMP SPECT, ^{18}F-FDG-PET/CT, and ^{18}F-FDOPA PET/CT. Results: In 29 of 46 study patients, ^{123}I-IMP SPECT showed markedly increased uptake in the site corresponding to the ocular tumor. In 26 of the 29 patients showing increased uptake of ^{123}I-IMP, the ocular tumors were confirmed histopathologically or clinically to be uveal malignant melanoma. The ocular tumors in the other 3 patients showing increased uptake of ^{123}I-IMP was diagnosed as small choroidal melanocytic lesions. The 17 ^{123}I-IMP SPECT-negative cases comprised 7 small melanocytic lesions, 1 choroidal hemangioma, 1 adenoma, and 2 melanocytoma, 2 metastases, 3 hemorrhages, and 1 unknown benign lesion. Nineteen of 20 of uveal malignant melanoma showed positive uptakes in ^{18}F-FDG PET and ^{18}F-FDOPA PET. The uptakes of both ^{18}F-FDG and ^{18}F-FDOPA were much weaker than that of ^{123}I-IMP. The range and mean ± SD of SUVmax for ^{18}F-FDG and ^{18}F-FDOPA in uveal malignant melanoma were 1.70-10.35, 3.78 ± 0.88 and 0.74-4.63, 1.18 ± 0.06, respectively. The difference between the uptakes of both tracers was statistically significant. Thus the uptake of ^{18}F-FDOPA was weaker than that of ^{18}F-FDG. Conclusion: ^{123}I-IMP SPECT is superior to ^{18}F-FDG and ^{18}F-FDOPA PET for the detection of uveal malignant melanoma. Efficacy of ^{18}F-FDOPA PET is for the detection of uveal malignant melanoma is low compared with ^{18}F-FDG PET because of its weak uptake into uveal malignant melanoma.

PW089

Potential impact of 18F-Fluorothymidine PET/CT in lymphoma patients with suspect residual disease or relapse.

L. Zanoni[1], A. Broccoli[2], C. Nanni[1], C. Pellegrini[2], F. Lodi[1], C. Fonti[1], P. Ghedini[1], S. Cambioli[1], P. Zinzani[2], S. Fanti[1]; [1]Nuclear Medicine, University Hospital S'Orsola-Malpighi, Bologna, ITALY, [2]Hematology "L. e A. Seràgnoli", University Hospital S'Orsola-Malpighi, Bologna, ITALY.

AIM: To evaluate the role of 18F-fuorothymidine (FLT) PET/CT in patients (pts) affected by lymphoma, presenting with positive or inconclusive 18F-deoxyglucose (FDG) PET/CT at end-treatment or follow-up. MATERIALS AND METHODS: Mono-centric prospective study. From May 2010 to March 2015, overall 40 pts were enrolled. They all underwent FLT PET/CT within 3 weeks from a previous positive or inconclusive FDG scan at end-treatment or follow-up and, when possible, biopsy confirmation as standard of reference to define PET results (true positive-TP; true negative-TN; false positive-FP; false negative-FN). The highest lesion SUVmax was measured with both tracers. RESULTS: Pts characteristics: mean age 55 (range 20-76); 24

males and 16 females; 30 non-Hodgkin (NHL) and 10 Hodgkin lymphoma (HL); stage at diagnosis: 8 II, 8 III, 24 IV; 6 pts were evaluated at end-treatment and 34 during follow-up/restaging. FDG-PET were judged positive in 36 out of 40 cases (mean SUVmax=10.1; range 3-31). 8/36 scans resulted also FLT positive (mean SUVmax= 7.8; range 3-16.8): 16/28 pts had the most active lesion biopsied, demonstrating 15 TP but 1 FP (HL patient presenting with FDG-SUVmax 6.9 and FLT 6.8 in cervical node: reactive follicular hyperplasia) whereas the remaining 12/28 pts could not be biopsied for ethical/practical reasons but subsequent follow-up data and final clinical evaluation (CE) confirmed 11 TP and 1 FP(reactive cervical node). 8/36 scans resulted FLT inconclusive in the light of lesion distribution and relatively lower SUVmax values (mean 4.8; range: 1.7-11.7): 5/8 were defined as TP at biopsy (2) or CE (3), whereas 3/8 represented inflammatory tissue (1 histologically-proven sarcoidosis-like reaction in mediastinal and supraclavicular nodes; 2 reactive axillary-mediastinal nodes and supraclavicular lymphadenopathy, respectively, at CE). The remaining 4/36 FDG-PET were considered inconclusive (mean SUVmax=7.2; range 4.9-8.8). 3 out of 4 were also defined inconclusive at FLT (mean SUVmax=4; range 2.6-4.9), but the final CE excluded lymphoma (1 reactive cervical node, 1 supra-diaphragmatic nodal sarcoid-like disease, 1 aspecific pericecal finding). The remaining 1/4 resulted FLT positive (SUVmax 6.9 and 6.5 for FDG and FLT, respectively) and was confirmed TP at CE. CONCLUSION: In the particular setting of residual/recurrent lymphoma, our preliminary data suggest that FLT might be complementary although not alternative to FDG. The elimination of inconclusive PET findings still represents a controversial step, therefore biopsy confirmation remains mandatory. Further lesion/semi-quantitative (i.e. target to background/mediastinal blood pool/liver ratio)/Ki67 correlation analyses are ongoing.

PW090

Comparison of 18F-FDG PET/CT and PET/MRI for the assessment of multiple myeloma

C. Sachpekidis[1], J. Hillengass[2], H. Goldschmidt[2], J. Mosebach[3], H. Schlemmer[3], U. Haberkorn[4], A. Dimitrakopoulou-Strauss[1]; [1]Clinical Cooperation Unit Nuclear Medicine, German Cancer Research Center, Heidelberg, GERMANY, [2]Medical Clinic V, University of Heidelberg, Heidelberg, GERMANY, [3]Department of Radiology, German Cancer Research Center, Heidelberg, GERMANY, [4]4Division of Nuclear Medicine, University Clinic Heidelberg, Heidelberg, GERMANY.

Objective: The aims of this prospective study are to evaluate the feasibility of 18F-FDG PET/MRI in detection of myeloma, and to investigate the reproducibility of bone marrow lesions detection and quantitative data of 18F-FDG uptake between the functional (PET) component of PET/CT and PET/MRI in MM patients. Patients and methods: The study includes 29 patients diagnosed with MM according to the International Myeloma Working Group criteria. All patients initially underwent 18F-FDG PET/CT (60 min after tracer injection), followed by PET/MRI (120 min after tracer injection). PET/CT and PET/MRI data were assessed and compared based on qualitative (lesion detection) and quantitative (SUV) evaluation. Results: The hybrid PET/MRI system provided good image quality in all cases without artefacts. PET/MRI identified 59 of the 63 lesions, which were detectable with PET/CT (93.7%). Three focal rib lesions and one lesion in os ilium in three patients were missed by PET/MRI. Quantitative PET evaluations showed the following mean values in MM lesions: SUVaverage=5.6 (median 5.1) and SUVmax=8.1 (median 7.1) for PET/CT; SUVaverage=4.1 (median 3.9) and SUVmax=6.0 (median 5.7) for PET/MRI. According to Wilcoxon matched-pairs signed rank test, both SUVaverage ($p<0.0001$) and SUVmax ($p<0.0001$) derived from MM lesions were significantly higher on PET/CT than on PET/MRI. Spearman correlation analysis demonstrated a strong correlation between both lesional SUVaverage ($r=0.755$, $p<0.0001$) and lesional SUVmax ($r=0.864$, $p<0.0001$) values derived from PET/CT and PET/MRI. Conclusion: Our study demonstrated that the PET/MRI hybrid system provides good image quality in MM and detected 93.7% of the PET/CT lesions. In terms of tracer uptake quantitation, a strong correlation between the two techniques was demonstrated, despite the statistically significant differences in lesional SUVs between PET/CT and PET/MRI.

PW10 - Sunday, October 11, 2015, 8:30 AM - 9:30 AM, Hall 3 – Poster Exhibition

Poster Walk 10 - Do.MoRe: Thyroid

PW091

The thyroid stunning effect: according to Poisson statistics, a small fraction of an ablative dose already kills a large fraction of cells.

S. Walrand, M. Hesse, F. Jamar; Université Catholique de Louvain, Brussels, BELGIUM.

Aim: The origin of the reduction in thyroid uptake after a low activity iodine scan, so-called stunning effect, is still controversial. Two explanations prevail: an individual cell stunning that reduces its capability to store iodine without altering its viability or a significant cell killing fraction that reduces the number of cells in the tissue still taking up iodine. Our aim is to analyze whether this last assumption could quantitatively explain the observed reduction. Methods: tumor (or tissue) control probability (TCP) is governed by Poisson statistics (Brahme and Agren 1987), i.e: TCP(A) = exp (-Nc x Sf(D(A))) = exp(-Nc x exp(-α D(A))) (1) where Nc is here the number of cells alive before ablation (about $4x10^7$ for 1 g of remnant tissue), Sf the survival fraction, α the cells radiosensitivity and D the mean delivered dose which is nearly proportional to the administrated activity A. Recent studies showed that a single administration of 30 mCi of I131 provides a TCP of about 75% and that a diagnostic dose of 2 mCi of I131 can induce in a following administration an uptake reduction ranging from 20 to 90%. Results: straight inversion of eq. 1 gives: Sf(A) = exp(-α D(A)) = -ln(TCP(A)) / Nc (2) Using TCP(30mCi) ≈0.75 and eq. 2, we get for 1 g of tissue: Sf(30mCi) ≈ $7x10^{-9}$ and Nc x Sf ≈ 0.3. However even if Nc x Sf < 1, due to the random nature of radiation killing, in 25% of 30 mCi-treatments there remain enough surviving cells to allow remnants relapsing. As D(2 mCi) ≈ D(30 mCi)/15, one has Sf(2 mCi) ≈ exp(-a D(30mCi)/15) = $(Sf(30mCi))^{1/15}$ ≈ 29% which is sufficient to induce a uptake reduction of 70% in a scan following a 2 mCi-diagnostic scan. Furthermore, this statistical demonstration, showing that a small fraction (1/15) of an ablative dose already kills a significant fraction of cells (≈70%), was experimentally proved in mega-colony cell assay (Kappler et al. 2007). Conclusion: The statistical analysis shows that the uptake reduction effect can be purely explained by the cell killing fraction. This supports the non-existence of an individual cell stunning effect that, if present, should induce an additional uptake reduction resulting in much larger decreases than those observed. As the β/α ratio measured in thyroid cancer cell assay is very low, this effective fractionation of the therapy should not impact the patient outcome in agreement with recent studies.

PW092

Thyroid remnant ablation in differentiated thyroid cancer: searching for the most effective radioiodine activity and stimulation strategy ina real life scenario

A. Campenni'[1], L. Giovanella[2], S. Pignata[1], M. Murè[1], M. Siracusa[1], F. Cosentino[1], L. Sturiale[1], P. Coppolino[1], M. Ruggeri[3], S. Baldari[1]; [1]Nuclear Medicine Unit of Messina, Messina, ITALY, [2]Nuclear Medicine and PET/CT centre, Oncology Institute of Southern Switzerland, Bellinzona, Switzerland., Bellinzona, SWITZERLAND, [3]Department of Clinical and Experimental Medicine and Pharmacology, Section of Endocrinology, University of Messina, Messina, Italy, Messina, ITALY.

AIM: Differentiated thyroid cancer (DTC) is rare but incidence has been increasing in the last few decades. Early treatment is based on surgery and thyroid remnant ablation (TRA) by radioiodine therapy. Despite radioiodine being widely used for decades, the choice of ablative activity is generally empirical and no consensus has been reached to date. The aim of our study was to compare the efficacy and safety of different radioiodine activities. In addition, we compared the ablation rate in patients treated in hypothyroid state or after recombinant human TSH (rhTSH) administration.MATHERIAL AND METHODS: We reviewed, retrospectively, the records of 471 patients (376 Female, 95 Male; F:M 3.9:1; mean age 46.5±10.8 years, ranges 16-74) affected by DTC and admitted to our University Hospital. Among 471 patients, 394 (83.6%) were papillary histotype (PTC), 77 (16.4%) were follicular histotype (FTC); 84 (17.8%) were pT1N0M0, 232 (49.2%) were pT2N0M0, 155 (32.9%) were pT3N0M0. Inclusion criteria were: age > 16 years, no loco-regional or distant metastases, not pregnant. All patients underwent radioiodine therapy (RAIT) after total or near-total thyroidectomy. Fifty-seven per cent of patients underwent RAIT after thyroid hormone withdrawal to achieve a serum thyrotropin (TSH) level above 30 μUI/ml. The remaining patients were treated after rhTSH-stimulation (0.9 mg daily for two consecutive days administered by intra-muscular injections). The patients were divided into three groups according to different radioiodine activity administered (A: 1110 MBq, B: 2220 MBq, C: 3700 MBq). Such activities were established by the attending physician on the basis of age, sex, TNM staging, histological variant, coexisting Hashimoto thyroiditis. All patients underwent neck-ultrasonography before RAIT, and those treated in hypothyroid state also at radioiodine uptake, obtained 24 hours after administration of radioiodine tracer activity (1.8 MBq). RESULTS: The success of TRA was evaluated twelve months later. TRA was obtained in: 62/79 (78.5%) in Group A (1110 MBq in hypothyroid state), 183/190 (96.3%) in Group B [2220 MBq in hypothyroid state or after rhTSH-administration: 87/90 (97%) and 96/100 (96%), patients respectively], 199/202 (98.5%) in Group C [3700 MBq in hypothyroid state or after rhTSH-administration:

98/100 (98%) and 101/102 (99%), patients respectively].CONCLUSIONS: Our data demonstrate that 2220 and 3700 MBq radioiodine are more effective than 1110 MBq in TRA, without significant differences between 2220 and 3700 MBq or between hypothyroidism and euthyroidism. We suggest rhTSH-aided TRA with 2220 MBq 131-radioiodine as this approach permits efficacious treatment reducing side effects, absorbed dose to body and hospital stay.

PW093

Selenium as a radiation protector of salivary glands in radioiodine remnant ablation therapy

M. Marx, S. Fastenmeier, M. Zuhayra, U. Lützen; Universitätsklinikum Schleswig-Holstein, KIEL, GERMANY.

Aim: Salivary gland impairment following high-dose radioiodine treatment is well known. This study investigates the effect of selenium to salivary glands of patients with well differentiated thyroid carcinoma receiving a radioiodine remnant ablation therapy (RAA). Furthermore the influence to remnant ablation was examined. Methods: 13 patients (group A) aged 26 - 75 years (mean 50,2 years) received 1000 µg selenium 30 minutes prior to application of 3,0 to 6,0 GBq I-131 (mean 3,4 GBq). A matched controll group (group B) aged 22 - 81 years (mean 50,9 years), received 3,0 to 6,0 GBq (mean 3,3 GBq) without selenium. The salivary gland function was investigated by salivary gland scintigraphy with Tc-99m-Pertechnetat prior to therapy and 3 months after RAA. The selenium concentration in serum was measured prior to and 72 h after therapy, also thyroglobulin (TG) before therapy as well as 3 and 6 months after therapy. Six months after RAA a radioiodine whole body scan (WBS) with I-131 was performed. Results: The patients in group A showed an average selenium concentration in serum of 75,15 mg/dl (57,0-92,0) at baseline with an significant increase to 102,0 mg/dl (73-134) 72 h after administration of selenium (p=0,00015). Prior to therapy in group A an uptake of Tc-99m in salivary glands (SG) of 0,20%±0,11% (0,10%-0,41%) was measured compared with 0,19%±0,08% (0,07%-0,33%) three months after therapy. In group B SG-uptake was determined 0,15%±0,06% (0,04%-0,24%) prior to and 0,08%±0,03% (0,05%-0,17%) after therapy. There was no significant change of salivary function in group A (p=0,85) but in the control group B (p=0, 0016). The success of ablation therapy (no measurable TG, no remnant tissue in WBS) was not affected by selenium administration. Conclusions: This first results indicate that damage to salivary glands induced by radioiodine therapy can be reduced significantly by selenium. A placebo controlled study with a greater number of patients is necessary and in planning.

PW094

Association between iodine intake and treatment outcomes of radioiodine remnant ablation in patients with intermediate risk papillary thyroid cancer

Y. Sun, W. Ouyang; Department of Nuclear Medicine, Zhujiang Hospital,Southern Medical University, Guangzhou, CHINA.

Aim To evaluate the association between iodine intake and treatment outcomes of radioiodine remnant ablation in American Thyroid Association (ATA)-intermediate papillary risk thyroid cancer(PTC) patients, and to investigate the determinants related to the ablation efficacy. Materials and Methods A total of 95 ATA-intermediate PTC patients were enrolled into the retrospective study. All patients had undergone total thyroidectomy and 2-4 weeks of low iodine diet (LID) before initial 131I therapy. According to urinary iodine excretion(UIE) of patients, they were divided into 3 groups: moderate-severe iodine deficient(UIE<50 ug/L, n=30), mild iodine deficient(UIE 50~100ug/L, n=26), adequate iodine (UIE 100~300 ug/L, n=39). Patients were followed up for 8 to 12 months after ablation, successful ablation was defined using the definition: no visible uptake in the thyroid bed on a follow-up scan and a stimulated thyroglobulin(sTg) level <2 ng/mL. Chi-square test, t-test, Mann Whitney rank-sum test and multivariate binary logistic regression analysis were performed. Results 84.2%(80/95)of patients were successfully ablated. The successful rates in the three different iodine intake groups were 96.7%(29/30), 84.6%(22/26), 74.4%(29/39), respectively, with significant difference among three groups. Besides UIE, univariate analysis revealed that TSH, sTg, remnant thyroid at ablation affected ablation efficacy. Logistic regression showed that sTg(OR=1.120) and adequate iodine intake(OR=3.473) were independent factors of ablation efficacy. Conclusion Adequate iodine intake during 131I remnant ablation is one of important factors of treatment outcomes. Thyroid remnant is more successfully ablated if we make reasonable LID protocols according to the iodine nutritional status in ATA-intermediate PTC patients before treatment.

PW095

Prognostic significance of early thyroglobulin release after radioiodine therapy under rhTSH for thyroid cancer

M. EBERLE[1], E. GALL[2], S. GUILLEMARD[1], C. ESPITALIER[1], I. RAINGEARD[2], C. CARTIER[2], M.

JARLIER[1], H. DE FORGES[1], P. KOTZKI[1], E. DESHAYES[1]; [1]ICM Val d'Aurelle, MONTPELLIER, FRANCE, [2]CHU, MONTPELLIER, FRANCE.

Aim: The main objective of our study was to determine if serum thyroglobulin values after radioiodine ablation therapy performed with recombinant human thyrotropin (rhTSH), at 3 days (TgD3) and 6 days (TgD6) post rhTSH injection, and the ratio TgD6/ TgD3, were predictive for disease free status at 6-12 months following therapy. The secondary objective was to determine if remnant tissue uptake was correlated to these thyroglobulin values, and would influence their interpretation. Patients and Methods: We included retrospectively all consecutive patients who underwent radioiodine ablation therapy under rhTSH after surgery for thyroid cancer in our department between January 1st of 2011 and June 1st of 2013. Thyroglobulin was measured at D3 (i.e. 24h after the second rhTSH injection), just before radioiodine administration, and at D5 or D6 (48h or 72h after I131 administration). Whole-body scan was performed at the same time. Remnant tissue was estimated by measurement of thyroid bed uptake on whole-body scintigraphy performed at D5 or D6. Thyroid bed uptake values were divided into 3 strata (defined by the 33th and 66th percentiles). According to current guidelines, patients were considered disease-free at 6-12 months follow-up if neck ultrasound showed no abnormalities and stimulated thyroglobulin was below 1 ng/mL (or below 0.3 ng/mL if stimulated thyroglobulin was not available). Patients with positive thyroglobulin-antibodies were excluded. Results: 102 patients were included (22 men, 80 women), with a median age 57 [17-87]. According to European guidelines for risk assessment, risk level was very low in 18, low in 62, and high in 22 patients. At 6-12 months follow-up, 86 patients were disease-free and 16 had persistent or recurrent disease (PRD). Significantly higher TgD3 levels were observed in the PRD group (3.1 ng/ml [0.2-132] vs 0.4 ng/ml [0.2-47.5]; p=0.0026) whereas TgD6 and ratio TgD6/TgD3 were not significantly different between the two groups. Radioiodine uptake in the thyroid bed (remnant tissue) was positively and significantly correlated to TgD3, TgD6 and ratio TgD6/TgD3 ($p<0.001$). TgD3 remained predictive of PRD only in strata 1 and 2 (lowest values of uptake in thyroid bed, $p<0.0001$). TgD6 was not significantly different between the 2 groups. Higher levels of ratio TgD6/TgD3 were observed in strata 3 in disease-free group (p=0.044). Conclusion: RhTSH stimulated thyroglobulin just before radioiodine ablation is predictive for disease-free status at 6-12 months. However, high values of early thyroglobulin release should not be considered of poor prognosis in patients with high thyroid remnant uptake.

PW096

Low-dose radioiodine therapy versus reoperation in patients after non-radical thyroidectomy with differentiated thyroid cancer.

E. Vasilenko, M. Karalkina, I. Lagozhina, D. Fomin; Russian Scientific Center of Roentgenoradiology, Moscow, RUSSIAN FEDERATION.

Aim: Comparative evaluation of the effectiveness of the final thyroidectomy and low radioiodine activities (1.2 to 2.0 GBq) in patients with differentiated thyroid cancer with significant thyroid remnant after non-radical primary surgery.Materials and Methods: The study included 90 patients (85 female, 5 male) of the age group 18-75 years with a mean age of 47 years. All patients diagnosed with DTC confirmed by histological tests (63 papillary carcinoma cases and 27 follicular thyroid cancer cases were identified, stage T1-T3, N0-N1, M0). According to postoperative scintigraphy, all patients had significant thyroid remnant. They were, depending on the treatment tactics, divided into 2 groups. The main group consists of 45 patients, for which radioiodine therapy with decreased activity (in the range of 1.2 to 2.0 GBq) was performed to ablate residual thyroid tissue. Repeated surgical treatment in these cases was not held due to the severe clinical state of patients, or due to the patients' refusal from surgery. The control group included 45 patients to whom was applied traditionally complete thyroidectomy as a preparation for radioiodine therapy. Then, patients in both groups were carried out a radical radioiodine activities from 3.0 to 4.5 GBq. A year after the administration of radical radioiodine, measurements of Tg, anti-Tg antibodies together and whole-body scintigraphy were performed. The success of ablation is determined by negative whole body I 123 scan and serum thyroglobulin level less than 2 ng/mL.Results: Successful ablation (negative stimulation test) achieved after low-dose radioiodine therapy in 33 patients (73%) after the complete thyroidectomy in the case of 32 patients (71%). During the first year of observation recurrences were detected respectively in 4 and 6 cases. The number of complications in the control group after reoperation increased to 44%, mainly due to permanent hypoparathyroidism, paresis of the larynx, a tracheostomy. All complications after low-dose

radioiodine therapy were transient and do not require additional appointments.Conclusions: The use of low-dose radioiodine therapy to eliminate excess volume of functioning thyroid tissue after surgery is equally effective as re-surgical treatment and is accompanied by fewer complications.

PW098

Thyroid remnant ablation of differentiated thyroid carcinoma: a comparison of ablation success with high and low doses of radioiodine (I-131)

S. A. A. Elrasad[1], Y. Abdelhafeez[2], M. A. Husseini[1], R. A. A. Amin[1], S. Elrefaei[1]; [1]Cairo university, Cairo, EGYPT, [2]Assuit University, Assuit, EGYPT.

Aim of study: To assess efficiency of low dose I131 in thyroid remnant ablation of patients with differentiated thyroid cancer after surgical treatment. Material and Method: A randomized double-armed trial comparing low-dose and high-dose radioiodine ablation. 128 patients (age 20-75 years) with differentiated thyroid cancer, tumor stage T1 to T3, with disease confined to the thyroid or cervical lymph nodes were treated with I131 after total thyroidectomy and pathologic lymph node resection, if present. Results were available for 88 cases. 39 patients received low dose [1110MBq (30mCi)] and 49 patients received high dose [2960-3700 MBq (80-100mCi)]. Six months after the administration of radioiodine, measurements of Tg, anti-Tg antibodies together with neck ultrasound exam and I131 whole-body scan were performed. The success rate of ablation is determined by negative whole body I131 scan, negative neck ultrasonography and serum thyroglobulin level less than 2 ng/mL. Results: Successful ablation reported in 23 out of 39 cases (58.9 %) in the group receiving low-dose radioiodine [1110 MBq] versus 37 out of 49 cases (75.5 %) in the group receiving the high dose [2960-3700 MBq]. (P value= 0.098). Six months later (1 year after the ablative dose) a second follow up was performed for the cases who had successive ablation from both groups. In the low dose group it was available for 12 out of 23 patients (52%), all of them didn't show disease recurrence, versus 17 cases out of 37 from the high dose group, 16 of them didn't had recurrence (43.2%), while in one case there was a recurrent disease at the thyroid bed. Conclusion: Initial results show no significant difference in successful ablation with low and high dose of 131-iodine. This is work in progress.

PW099

Theoretical model for release of patients with benign thyroid disease based on parameters obtained from EANM Standard Operational Procedures for Pre-Therapeutic Dosimetry II.

M. Salas[1], E. Mora[2]; [1]Nuclear Medicine Department, Hospital México., San Jose, COSTA RICA, [2]Nuclear Medicine Department, Hospital San Juan de Dios., San Jose, COSTA RICA.

Aim: To establish individualized restricted period for patients with benign thyroid disease treated with ^{131}I has been a topic of great importance for Radiation Protection. This work focuses on the use of dosimetry model of two compartments (blood pool and target tissue) that propose the *EANM Dosimetry Committee Series on Standard Operational Procedures for Pre-Therapeutic Dosimetry II. Dosimetry prior to Radioiodine Therapy of Benign Thyroid Diseases*, based on the biokinetic of the thyroid gland, and jointly with the model proposed by the United States Nuclear Regulatory Commission (U.S.NRC, *NUREG – 1556 Vol. 9*, *Rev. 2*) for release of patients.Materials and methods: *Calculus of residual activity that not exceed the dose constraint*: Using the equation suggested by U.S.NRC, with the parameters of two compartment model. Rewriting this equation in term of radioactivity, the residual radioactivity (activity contained in patient that not exceed that exposure dose constrain for population groups -children, pregnant women, adults, coworker-) was calculated. This equation present some disadvantages such as, it doesn't include a correction for the attenuation of the gamma emission of the blood pool, for this reason an attenuation correction

factor for ^{131}I (extrathyroidal component) was introduced, also it considers the patient like a point source, a correction to improve the calculus considering a line source distribution was introduced. To complete the parameters of the equation, an adequate exposure dose limit constraint, occupancy factor and expected distance (patient-population group) were chosen, trying to reproduce the family and working environment of the patient.*Calculus of restriction time*: Using two compartment model, a time to radioactivity contained in patient goes from the Administer Activity (t = 0) to the residual activity (t_{res}) was calculated, this difference in time gives the Restricted Period (time necessary for the patient follow instructions)Results and conclusion: Following the described procedure, restricted periods according to the population group and socioeconomic conditions can be calculated. If we consider a set of possible values k_B=0.1429h^{-1}, k_T=0.00525h^{-1}, k_t= 0.1297h^{-1}, Thyroid-Mass=20g, Administer-Activity = 247.19MBq, Maximum-Uptake$_{Thyroid}$ =80%, Dose$_{Target}$= 250Gy, Patient-Height=1.74m, Attenuation-Factor$_{Blood-pool}$=0.62, Exposure-Rate-Constant= 5.65x10^{-5}mSv m^2 h^{-1} MBq^{-1}. For a case of children up to two years old (1mSv Dose Constraint) at 0.3m distance (holding babe) and Occupancy factor of 0.25, the restriction time is 3.92 days.This work propose a model to calculate the individualized restricted period, considering all the possible correction that have been recommend in relation to the release of patient with hyperthyroidism treated with ^{131}I

PW100

Standardisation of Dosimetry for a Multicentre trial of Selumetinib Enhanced Radioiodine Therapy for Thyroid Cancer

R. Gregory[1,2], A. Fenwick[3], J. Merrett[4,3], J. Scuffham[4], J. Gear[1,2], D. Rushforth[1,2], I. Murray[1,2], G. Flux[1,2]; [1]Royal Marsden NHS Foundation Trust, Sutton, UNITED KINGDOM, [2]Institute of Cancer Research, Sutton, UNITED KINGDOM, [3]National Physical Laboratory, Teddington, UNITED KINGDOM, [4]Royal Surrey County Hospital, Guildford, UNITED KINGDOM.

The MEK inhibitor Selumetinib can enhance the uptake of ^{131}I NaI in patients with iodine refractory thyroid cancer enabling them to benefit from further radioiodine therapy. In this multicentre trial ^{123}I imaging is to be used to identify patients with uptake, for whom dosimetry using SPECT/CT scans will aim to predict the absorbed dose to tumours from the resulting ^{131}I NaI therapy. Dosimetry during therapy will allow assessment of the absorbed doses achieved following Selumetinib.To ensure the dosimetry results from all the centres are accurate and comparable the SPECT/CT systems are to be calibrated and validated for radioiodine imaging. There are currently no definitive standards for dosimetry. Therefore the aim of this work was to optimise the calibration procedures for practical accurate quantitative imaging.Methods:Seven sites are participating in the trial with 9 SPECT/CT systems in total. Six cylinders ranging from 1 cm to 5 cm in diameter and length were imaged separately and with 3 cylinders together, positioned in a 20 cm diameter 11 cm long cylinder of inactive water. The cylinders were filled with known activity concentrations (~1MBq/ml) of ^{123}I or ^{131}I, then the calibration factor to convert count concentrations to activity concentrations was calculated for each cylinder size and arrangement. Factors to correct for the dead time in ^{131}I images of a uniformly filled 20 cm diameter cylinder, filled with activities ranging from 10 MBq to 3 GBq were also measured. Doses received to the 4 members of staff performing this measurement were also assessed.Results: The factors to convert count concentrations to activity concentrations were comparable between separate images of the cylinders and images containing multiple cylinders for both ^{123}I and ^{131}I. The Siemens Intevo and GE Optima ^{131}I dead-time correction curves were similar up to 20 kcps at 1GBq. The staff performing these measurements received acombined whole body dose of 120 μSv.Conclusions: Calibration factors can be acquired from images of multiple cylinders so accurate calibration can be faster and more practical. Results from these measurements should help to establish good practice in planning and verifying molecular radiotherapy absorbed doses.

PW11 - Monday, October 12, 2015, 8:30 AM - 9:30 AM, Hall 3 – Poster Exhibition

Poster Walk 11 - Do.MoRe: Imaging, Dosimetry & Radiobiology

PW101

NTCP calculations for Selective Internal RadioTherapy (SIRT) - demonstration of the methodology

E. M. Abbott[1], A. J. Craig[2], J. M. Franklin[3], A. Denis-Bacelar[2], N. Syed[3], G. Flux[2], R. Sharma[1], K. A. Vallis[1], **N. Falzone**[1,4]; [1]MRC/CRUK Gray Institute for Radiation Oncology and Biology, Department of Oncology, University of Oxford, Oxford, UNITED KINGDOM, [2]Physics Department, Royal Marsden NHSFT, Sutton, UNITED KINGDOM, [3]Nuclear Medicine, Churchill Hospital, Oxford University Hospitals NHS Trust, Oxford, UNITED KINGDOM, [4]Tshwane University of Technology, Department of Biomedical Science, Pretoria, SOUTH AFRICA.

Aim: The aim of this study is to propose a method for applying radiobiologic models for the calculation of Tumour Control Probability (TCP) and Normal Tissue Complication Probability (NTCP), based on dosimetric and clinical data from a retrospective study. This is done to adequately interpret the local response and liver toxicity of ^{90}Y-microsphere treatment of liver metastases from colorectal cancer (CRC), hepatocellular carcinoma (HCC) and intrahepatic cholangiocarcinoma (ICC). Methods: 3-D activity distributions obtained from SPECT/CT images are combined with Monte Carlo dose voxel kernel calculations using an in-house dosimetry software package (Qrius™). Absorbed dose distribution maps (differential dose volume histograms - DDVHs) and the mean dose to healthy liver and tumour in each patient is determined using Qrius™. The Biologically Effective Dose (BED) distribution is calculated and the Equivalent Uniform Biologically Effective Dose (EUBED) is obtained from the spatial BED distribution in the volume of interest. TCP and NTCP are then calculated from the EUBED estimates. Results: Using a retrospective ^{90}Y-microsphere SPECT/CT scan, we demonstrate how a differential dose volume histogram (DDVH) generated with the Qrius™ software tool is reduced to a single dose (EUDBED) delivered to the entire volume. This functionality provides the possibility to calculate TCP and NTCP distributions. Conclusion: DVH metrics are known to correlate with patient toxicity outcomes. Adding the functionality of a convenient computational module to the Qrius™ toolkit for estimation of TCP and NTCP based on patient-specific dosimetry could facilitate patient-specific treatment planning, thus improving ^{90}Y-microsphere treatment of liver metastases.

PW102

Radiobiological Studies of Cancer Cell Using Novel External Alpha-Particle Irradiation Set-up.

J. Nilsson[1], J. Nilsson[2], M. Posaric Bauden[3], S. Strand[3], **J. H. Elgqvist**[3]; [1]Institute for Clinical Sciences, Gothenburg, SWEDEN, [2]Institute for Clinical Sciences, Malmö, SWEDEN, [3]Institute for Clinical Sciences, Lund, SWEDEN.

Aim. An external alpha-particle irradiation system was designed and constructed enabling irradiation of cells. The radiosensitivity of prostate and pancreas cancer cells after alpha-particle irradiation was investigated and compared with external Cs-137 irradiations.Materials and Methods. The irradiation system was constructed based on a circular 241-Am dish on top at which well inserts containing cells growing in monolayer were placed. The source's total radioactivity, homogeneity, and alpha spectrum were measured via HPGe-detector, digital autoradiography, and PIPS-detector measurements, respectively. Monte-Carlo simulations were used for LET (linear energy transfer) spectras and dosimetry calculations. Cell survival studies were performed for both prostate and pancreas cancer cells. The cancer cell lines LNCaP, Capan-1, and HPAF-II were irradiated using the in-house developed external alpha-particle irradiator set-up. The cells were subjected to absorbed doses equal to 0, 1, 2, or 3 Gy during the alpha-particle irradiations, or up to 10 Gy regarding the Cs-137 irradiations. For evaluation of cell survival the tetrazolium-based WST-1 assay was used. After irradiation WST-1 solution was added to each well, incubated, and then measured for level of absorbance at 450 nm, indicating the amount of viable cells.Results. Compared to Cs-137 photon irradiations, a preliminary RBE of 4-5 is observed for the alpha-particle irradiations of the LNCaP and Capan-1 cells, at 37% cell survival. These studies are still on going and additional results, including results for HPAF-II, are continuously added.Conclusion. The study shows the feasibility to construct a long-lived relatively low cost alpha-particle irradiation set-up that could be used for cell survival studies in most laboratories. The results also shows a high degree of cell inactivation after alpha-particle irradiation for all three cancer cell lines, compared to Cs-137 irradiations.

PW103

Assessing radiobiological effects of low doses of ionizing radiation on zebrafish muscle by two-dimensional gel electrophoresis

J. Lemos[1], A. Campos[2], M. Carneiro[2], T. Ribeiro[2], F. Ponte[3], P. Costa[3], L. Cunha[4], A. Carvalho[5], L. Metello[4]; [1]ICBAS.UP & ESTSP.IPP, Porto, PORTUGAL, [2]CIIMAR/CIMAR.UP, Porto, PORTUGAL, [3]Júlio Teixeira SA., Porto, PORTUGAL, [4]ESTSP.IPP & IsoPor SA., Porto, PORTUGAL, [5]FCUP.UP & CIIMAR/CIMAR.UP, Porto, PORTUGAL.

Introduction: This work relates with the application of zebrafish - Danio rerio - to the study of radiobiological effects of low doses of ionizing radiation. In recent years, the use of zebrafish has grown considerably, pointing more and more as a very interesting model in biomedical research, essentially because of the level of homology shared with the human genome, complemented by an easy and reasonably affordable practical side. The two-dimensional gel electrophoresis (2DGE) is a method used for the analysis of complex protein mixtures from biological samples. This method allows the detection of differences in protein expression under different conditions, so allowing creating relations between those differences and the irradiations that were in their basis. The present work aimed at evaluating proteome changes in the zebrafish muscle caused by low doses of X-rays exposure. Material and Methods: Animals were externally irradiated with three distinct dose protocols (100 mGy, 500 mGy and 1.000 mGy). One day after the irradiation, the animals were sacrificed and a muscle sample was collected. 2DGE was then used to identify proteins that showed a differential expression after X-rays exposure. Results: About 85 ± 21 protein spots were identified in every gel. The statistical analysis of protein expression recognized differences between the control and the irradiated groups (27 spots to 1000 mGy; 22 spots to 500 mGy; 3 spots to 100 mGy). Most differentially expressed proteins were down-regulated in irradiated groups when compared to the control group. Conclusions: The present work seems to confirm that the 2DGE based methodology might be considered as an adequate analytical tool for study radiobiological effects at the molecular level in zebrafish. It has been found that a large number of proteins were down-regulated, suggesting that a remodelling of the muscle proteome occurs after the exposition to low doses of X-rays. Mass spectrometry analysis should be performed in order to allow the identification of those proteins that were affected by exposition to ionizing radiation. This identification would most probably contribute for a deeper insight concerning the metabolic and physiological consequences of the exposition to X-ray.

PW104

Gamma Camera Calibration for SPECT Based Quantitative Imaging with LU-177:

M. D'Arienzo[1,2], M. Cazzato[3], S. Ungania[3], L. Cozzella[1], G. Iaccarino[3], M. D'Andrea[3], L. Strigari[3], A. Fenwick[4], L. Johansson[4], M. Cox[4], P. De Felice[1]; [1]National Institute of Ionizing Radiation Metrology, Via Anguillarese 301, 00123 Rome, ITALY, [2]Department of Human Anatomy, Histology, Forensic Medicine and Orthopedics, Sapienza University of Rome, Via Borelli 50, 00161 Rome, ITALY, [3]Laboratory of Medical Physics and Expert Systems, Regina Elena National Cancer Institute, Via Elio Chianesi 53, 00044 Rome, ITALY, [4]National Physical Laboratory NPL, Hampton Road, Teddington, Middlesex, TW11 0LW, UK, UNITED KINGDOM.

Over the last 15 years 177Lu has been successfully applied to peptide receptor radionuclide therapy in the form of 177Lu-DOTATATE or 177Lu-DOTATOC to treat neuroendocrine tumors and other somatostatin-receptor expressing neoplasms. The general consensus is that the collection of quantitative data is a critical step in dosimetry and treatment planning in molecular radiotherapy. In fact, inaccuracies in absolute quantification are likely to result in reduced efficacy or increased incidence of adverse side effects. Absolute gamma camera calibration procedures are currently performed either in-air or in-water using a radionuclide source with a known amount of activity concentration. However, at present there are no validated standard protocols or any established methods for calibration and verification of system performance. The aim of this work was to develop and evaluate an approach to gamma camera calibration for absolute quantification in tomographic imaging with 177Lu. Calibration studies were performed on a Philips IRIX and Philips AXIS gamma camera. For both systems the calibration coefficient was assessed using four reference geometries: a point source in air, a 16 mL Jaszczack sphere surrounded by non-radioactive water, a 16 mL Jaszczack sphere in air and a 20 cm diameter cylinder filled with water uniformly mixed with radioactive 177LuCl. Attenuation correction was performed using Chang's algorithm while scatter correction was obtained applying the triple energy window technique. We validated our method in non-reference geometry using an anthropomorphic phantom

provided with liver cavity filled with 177LuCl. Acquisitions performed with the IRIX gamma camera provided better results, with agreements within 5% for all geometries for acquisitions at 208 keV. The use of a Jaszczak sphere in water provided sensitivity values capable of recovering the activity in anthropomorphic geometry within 1% for the 208 keV peak, for both gamma cameras. However, for both systems the activity in anthropomorphic geometry was recovered with an agreement in the range -11.9%/+7.1% for acquisitions at the 208 keV photo peak. As a general rule, acquisition at the lower photopeak provided results with larger deviations from the measured activity concentration. Scatter and attenuation play a major role at 113 keV and are likely to hinder an accurate absolute quantification. In the clinical practice acquisition on the higher photopeak are therefore recommended, provided that a good counting statistic can be achieved. The research leading to these results has received funding from the European Commission, Grant Agreement N° 217257 between the EC and EURAMET under the Seventh Framework Programme.

PW105
The Impact of Registration Method on 3D Dose Distributions

E. Page[1,2], J. Tipping[1], D. Hamilton[1], A. Robinson[2], D. Cullen[2], C. Oldfield[2]; [1]The Christie NHS Foundation Trust, Manchester, UNITED KINGDOM, [2]The University of Manchester, Manchester, UNITED KINGDOM.

Aims To evaluate the impact of registration algorithm on 3D dose distributions.**Materials**Three post 177Lu Dotatate therapy SPECT - CT image series were processed using four different registration algorithms.**Methods**The effect on the dose distribution of using direct rigid body registration of SPECT images was compared to using rigid body registration of the CT images and applying the transformation to the SPECT images. The effect of registering specific organs using a VOI mask on the SPECT images rather than using the whole images was also attempted. Additionally, non - rigid registration of the SPECT images using an affine registration algorithm was evaluated. Dose calculation was performed using MATLAB scripts written in house using the Voxel S Factor method.**Results**Preliminary results demonstrate that rigid body registration of the whole SPECT image is inadequate to register all organs intra-fraction in at least one patient example (clear misalignment of the spleen at the second time point). In another patient case SPECT to SPECT registration produced an improved alignment of the SPECT activity compared to CT-CT guided SPECT registration. A comparison of direct SPECT rigid body registration to affine registration found a difference in mean organ voxel dose that ranged from -6 to + 6% for one patient, but individual voxel doses of as much as much as -61 to 330% for a particular organ. Affine registration produced a better alignment of patient organs as a whole but distorted some of the smaller tumour activity distributions (resulting in a 'stretched' appearance not apparent in the original images).**Conclusions**Rigid body registration was inadequate for aligning all organs using the whole image. The decision to align the SPECT-CT time series using the SPECT or guided by the initial registration of the CT may need to be made on a patient by patient basis. Non- rigid body registration can produce overall improvement in organ alignment but may result in activity distribution and hence dose map distortion. Differences in registration method can result in a ± 6% difference in organ mean dose, but at an individual voxel level may result in differences of up to 330%. When considering heterogeneity of dose at the voxel level, the underlying method of registration can have a significant impact.

PW106
Optimal sampling times for quantitative imaging

M. KOTZASARLIDOU[1], M. COX[2], V. SMYTH[2], V. HATZIPAVLIDOU[1]; [1]"THEAGENIO" Cancer Hospital, THESSALONIKI, GREECE, [2]National Physical Laboratory (NPL), Middlesex, London, UNITED KINGDOM.

Introduction: According to the MIRD schema, mean absorbed dose D [Gy] in a volume of interest (VOI) is D = ÃS. Ã [Bq.s] is the area under the time activity curve (TAC) and S is the mean absorbed dose per unit cumulated activity [GyBq-1s-1]. The uncertainty for an estimate of Ã depends on the time points selected for fitting the TAC. A process for determining an optimal set of time points using the criterion that this uncertainty is minimized has been developed in the European joint research project MetroMRT (http://projects.npl.co.uk/metromrt/). Aim: This study tested the process of time point optimization using blood samples from patients to be treated with 131I for differentiated thyroid cancer (DTC). Materials & Methods: A tracer dose of 15 MBq of 131I was administered orally to seven patients with DTC and a 131I standard source was prepared simultaneously. Blood samples (2ml) were taken at four or five time points post administration. Aliquots of 1 ml were prepared from each blood sample and counted in a Captus® 3000 Well Counting System. Blood activities were normalized to the administered activity and the retention per ml of blood was calculated. A data set was selected as representative of the seven data sets. A biexponential model was fitted, the area under the TAC was estimated, and optimal time points using the above criterion were obtained. Four, five and six time points were so determined, TACs formed and standard uncertainties compared. This procedure was performed for activity uncertainties either constant or proportional to activity. Results: For constant activity uncertainties, reductions

(compared with the use of the original TAC based on the prescribed five time points) in TAC area uncertainty were 14%, 27% and 36% for 4, 5 and 6 optimal time points, respectively. For uncertainties proportional to activity, corresponding reductions were 22%, 31% and 38%. The largest time point selected did not vary with the number of points. Conclusions: TAC area uncertainties decrease usefully as the number of time points increases. One time point was consistently chosen to be as large as possible to ensure that the tail of the TAC is modelled accurately. This method of determining optimal time points will be tested further to confirm whether these favourable results apply more widely.

PW107

Comparison of Sequential SPECT and CT for Targeted Radionuclide Therapy Dosimetry

T. Li, K. Leong, E. Ao, **G. S. Mok**; University of Macau, Taipa, MACAO.

Aim: Previously we showed that non-rigid registration in sequential SPECT images improved the 3D dosimetric accuracy for targeted radionuclide therapy (TRT). This study aims to investigate the potential improvement on dose estimation when co-registered sequential SPECT and CT images are both available for image segmentation and registration. Materials and methods: We modeled 3 anatomical variations each with 3 In-111 Zevalin activity distributions, i.e., a population of 9 phantoms, using the digital 4D Extended Cardiac Torso (XCAT) phantom. Local deformations of the liver, kidneys, spleen and lung were modeled of up to 5 pixels/degrees with <5% volume change, combined with whole body rigid motion of up to 5 pixels/degrees of translation/rotation among imaging at 1, 12, 24, 72 and 144 hrs post-injection. One hundred and twenty-eight realistic noisy projections for a medium energy general purpose parallel-hole collimator were generated over 360° by an analytical projector based on a system calibration factor of 1.43×10-4 counts s-1 Bq-1, modeling attenuation, scatter and collimator-detector response and then reconstructed using OS-EM with 128 updates including full compensations. The corresponding attenuation maps of the phantoms served as the CT images. Using the 24-hr time point SPECT/CT images as the reference, we performed affine + b-spline non-rigid registration on organs semi-automatically segmented from sequential SPECT and CT images respectively. For CT registration, the acquired motion vectors were later applied to register the SPECT images. Voxel-by-voxel integration was performed on registered images over 5 time points, followed by convolution with a Y-90 dose kernel to generate dose images. Organ dose, differential and cumulative dose volume histograms (DDVH & CDVH) were generated for liver, spleen, kidneys and lungs. Results: For spleen, the organ dose error and normalized absolute error of DDVH were -9.22 ±6.59% and 32.71±7.34% for SPECT registration, while they were -3.63±1.47% and 20.08±5.67% for CT registration. For liver, the organ dose error and normalized absolute error were −2.19±2.81% and 22.57±10.18% for SPECT registration, while they were -2.44±1.19% and 14.68±6.01% for CT registration. For CDVH, the CT registration method generally approached more to phantoms with no misalignment as compared to SPECT registration for all organs. Conclusion: We conclude that if both sequential SPECT/CT scans are available, organ-based CT registration method can more effectively improve the 3D dose estimation as compared to SPECT registration. Sequential low dose CT scans might be considered to be included in the standard TRT protocol.

PW108

Radiation protectio impact of radioiodine therapy for hyperthyroidism after a patient specific dosimetric study

C. Canzi, V. Longari, M. Castellani, F. Buffoni, F. Zito, F. Voltini, R. Benti; Fondazione IRCCS Ca' Granda Ospedale Maggiore Policlinico Milano, milano, ITALY.

In patients with hyperthyroidism, the treatment with ^{131}I should rapidly obtain a nonhyperthyroid status. There is an ongoing discussion on the establishment of the method to determine the activity that can be recommended for clinical practice: estimation (the so-called "fixed dose") versus calculation (based on radioiodine uptake measurements), however the optimization principle states that a patient should be given the minimum activity necessary to obtain the clinical goal. In our Nuclear Medicine Department all hyperthyroid patients are submitted to a patient specific pretreatment study to calculate the minimum activity to administer in order to achieve euthyroidism, in the case of nodular autonomies, and hypothyroidism, in the case of Graves' disease. Aim: to retrospectively evaluate the radiation protection impact of outpatients radioiodine therapies for hyperthyroidism after patient specific dosimetric studies, with respect to the standard administration of 600MBq (maximum activity allowed by Italian radiation protection law). Materials and methods: 503 patients were considered (187 Graves and 316 nodular autonomies, 364F, median age= 66y [range 17-89y], mean iodine uptake=39%). They all reached a nonhyperthyroid status within 1 year from the administration. Results: The median ^{131}I therapeutic orally administered activity was 396 MBq (10.7 mCi) with a range between 66 and 629 MBq (1.8-17.0 mCi). The total administered activity was 214 GBq (5.8 Ci). If the standard activity of 600 MBq had been administered to all patients the total activity would have been 302 GBq (8.2 Ci), an amount 41% greater than the really used one. This obviously acts also on the patient mean effective dose

equivalent and on the mean absorbed dose to the stomach wall (critical organ for ^{131}I iodide) (ICRP 53) that were 6 Sv instead of 9 Sv and 0.20 Gy instead of 0.28 Gy respectively, with a maximum of dose saving (8 times) for the patient who was given the minimum activity of 66 MBq. The reduction of ^{131}I administered activity also acts on the radiation exposure of the nuclear medicine unit staff and of population: the mean dose rate at 1 m at the dismission time is 12 μSv/h instead of 20 μSv/h. This approach involves also the environment, as in the first 24 hours the 60% of the administered activity is excreted by the body. Conclusion: the application of a patient specific pretreatment dosimetric study can reduce of more than 40% the radiation protection impact of radioiodine treatments of hyperthyroidism with optimal clinical results guaranteed.

PW109

Estimates of exposure dose to the nuclear medicine staff from inpatient 131I therapy of differentiated thyroid carcinoma

B. Liu, R. Tian; Department of Nuclear Medicine, West China Hospital, Sichuan University, Chengdu, CHINA.

Inpatient 131I therapy is still necessary for some patients with differentiated thyroid carcinoma (DTC). It is necessary to consider the potential radiation burden to the nuclear medicine staff, the present study was thus designed to estimate the radiation exposure to the nuclear medicine staff from inpatient 131I therapy of DTC on the basis of the actual measurements of patient-specific whole body dose-rates.Forty-seven patients (7 males, 40 females; age range: 23-56 years, average age: 41±13 years) with DTC were randomly and prospectively recruited in this study. At 1, 12, 24, 48, and 72 h after administration of 3.7 GBq of 131I, whole body dose-rate was serially measured with a radiation-survey meter at 1.0 m from the upright patients and the DR-time curve was fitted by exponential function. On the assumption that a nuclear medicine physician or nurse typically spends 10 min at a distance of 1.0 m per day during the first 5 days after administration, the nuclear medicine staff's exposure dose was estimated.The mean whole body dose-rate at 1.0 h after administration of 131I was 27.88 μSv/h/GBq, ranging from 15.81 to 46.48 μSv/h/GBq. The exposure dose to a nuclear medicine physician per contacting a DTC patient was predicted to be 4.02-28.35 μSv.The predicted exposure doses to the nuclear medicine staff are relatively low from short periods of contact with DTC patients undergoing 131I therapy.This work was supported by the National Natural Science Fund of China Grant No. 81401445, 81471693.

PW110

Correlation of Clinical Outcomes with Bremsstrahlung and Y-90 PET/CT Imaging Findings Following Y-90 Radiation Synovectomy

T. Barber[1,2], A. Powell[3], M. Cherk[1,2], K. Yap[1], V. Kalff[1,2]; [1]Department of Nuclear Medicine & PET Centre, The Alfred Hospital, Melbourne, AUSTRALIA, [2]Department of Medicine, Monash University, Alfred Hospital Campus, Melbourne, AUSTRALIA, [3]Department of Rheumatology, The Alfred Hospital, Melbourne, AUSTRALIA.

Aim: To correlate clinical outcomes following radiation synovectomy with bremsstrahlung and Y-90 PET/CT imaging findings.Methods: A total of 48 joints in 39 patients underwent bremsstrahlung planar and Y-90 PET/CT imaging following radiation synovectomy. The Y-90 distribution pattern on bremsstrahlung planar imaging was classified as diffuse or non-diffuse and compared with the intra or extra-articular location of activity on Y-90 PET/CT. Treatment response was assessed by patients and clinicians at 6 months using a composite change index (CCI) with a score ranging from 0-12. A successful overall response was defined as CCI > 6. In patients who underwent bremsstrahlung SPECT, side by side image comparison with PET was performed with image quality/resolution compared and scored using a five point scale.Results: Bremsstrahlung planar images were classified as diffuse in 31/48 (65%; 95% CI: 51-78%) and non-diffuse in 17/48 (35%; 95% CI: 22-49%). There was no association between overall treatment response in patients with diffuse compared to non-diffuse bremsstrahlung planar imaging patterns [8/31 (26%) vs 6/17 (35%) p = 0.49]. PET/CT confirmed an intra-articular location in all 31 diffuse scans and an extra-articular location in three non-diffuse scans. Of the three patients with extra-articular activity none had any response to treatment. Excluding these three patients, there remained no association between the bremsstrahlung planar imaging pattern and overall treatment response (p = 0.25). Of the 41 joints imaged with SPECT, PET image quality was classified as superior to SPECT in 40 and inferior in one. In one patient with extra-articular activity on PET/CT, SPECT/CT was unable to definitively localise the activity to the intra or extra-articular space.Conclusion: The distribution pattern on bremsstrahlung planar imaging did not correlate with overall clinical outcome following radiation synovectomy in our study population. However, a non-diffuse planar imaging pattern should be further assessed with Y-90 PET/CT to exclude extra-articular activity with PET providing superior image quality compared to SPECT.

PW12 - Tuesday, October 13, 2015, 8:30 AM - 9:30 AM, Hall 3 – Poster Exhibition

Poster Walk 12 - Do.MoRe: Miscellaneous Therapy

PW111

Acquisition parameters optimization for imaging with Ra-223

A. Corazza[1,2], G. Cicoria[2], F. Zagni[2], G. Lucconi[1,2], D. Pancaldi[2], M. Marengo[2]; [1]Postgraduate School in Medical Physics, University of Bologna, Bologna, ITALY, [2]Medical Physics Department, University Hospital "S.Orsola - Malpighi", Bologna, ITALY.

Introduction: Ra-223 is an alpha emitter radionuclide with an half life of 11.43 days and a reduced emission of betas and gammas (about 5%) per decay. Its chemical affinity with calcium and the high dose delivered locally make Ra-223 dichloride (Xofigo®) a relevant radiopharmaceutical for targeting areas of increased bone turnover (standard injected activity is 50 kBq/kg). This work studied acquisition parameters for post-treatment Ra-223 imaging. Material and methods: Images of Ra-223 were acquired using three windows, at 82, 154 and 269 keV with a width of 10%, 10% and 8%, and using Low Energy High Resolution (LEHR), Medium Energy Low Penetration (MELP) and High Energy (HE) collimators. The Line Spread Function (LSF) was measured by imaging for 120 minutes a 1.3 mm capillary, filled with 190 kBq of Ra-223 and placed at a distance of 10 cm from the collimator. Activity was carefully measured using a MP-DC activity meter (Mecmurphil, Italy), specifically calibrated for Ra-223. Image contrast was evaluated separately for the three windows, varying the width of the 82 keV peak from 10% to 20%. Planar images of a Jaszczak phantom, with the "rods" sector positioned at several distances on top of different collimators were acquired for > 12 hours. Static images of the rods sector were then analyzed using ImageJ. Results: Visual inspection on the three images showed that MELP collimators produce an acceptable image quality. For MELP and HE collimators, the FWHMs were 12 and 13 mm and the FWTMs were 26 and 28 mm. Quantitative evaluation of MTF was possible only for MELP (90% and 50% at 0.12 cm-1 and 0.36 cm-1), since for HE collimator the image was affected by evident artifacts. The sensitivity measured were of 2.30, 0.35 and 0.24 cps/kBq with LEHR, MELP and HE collimators respectively. Analysis on rods images showed that extending window width from 10% to 20% reduced contrast by 15% and increased counts by 79%. Adding peaks at 154 keV and 269 keV reduced contrast but increased sensitivity by 77%. Conclusions: Image quality obtained with Ra-223 is realtively poor, but sufficient to confirm the biodistribution of the radiopharmaceutical. According to our results, MELP collimators should be used; most of the information is acquired in the 82 keV window, the 154 and 269 keV contributing to total statistics but with a limited contrast modulation.

PW112

Comparison and evaluation of the effectiveness of α- [Ra-223 Dichloride] and β- particle emission treatments [combined Re-186 HEDP / Sr-89 Chloride and/or Sm-153 EDTMP/ Sr-89 Chloride] on Tc-99m-MDP scintigraphic series in pts with painful osseous metastases due to castration-resistant prostate adeno-carcinoma

G. S. Limouris[1], M. Paphiti[2], S. Synefia[1], M. Lyra[1], L. Moulopoulou[1], V. R. McCready[2]; [1]Nuclear Medicine Div - I Radiology Dept-, 'Aretaieion' Hosp, Athens Univ Medical Faculty, Athens, GREECE, [2]Nuclear Medicine Dept, Royal Sussex County Hosp, Brighton, UNITED KINGDOM.

Aim: We aimed, by the present to evaluate and highlight the efficacy of the therapeutic application of alpha radiation on follow-up [Tc-99m] MDP scintigrams and compare them with respective scans in patients after beta-emission treatments, using combined Sm-153 EDTMP / Sr-89 Chloride, since improvement in follow up [Tc-99m] MDP scintiscans after the use of beta-emission, rarely had been observed in the pastMaterial and Methods: In the last decade, approx 8000 whole-body [Tc-99m]MDP bone scintiscans have been performed on a follow up basis program. Forty-two (group A) pts with known history of hormone-resi-stant prostate adenocarcinoma were treated with combined Sm-153 EDTMP/ Sr-89 Chloride application, in a dosage of 37 MBq x kgr $^{-1}$ and 148 MBq respectively. Approx a year later, in 4(group B) out of 42 pts, Ra-223 Dichloride was additionally injected in a dosage of 50 x kgr $^{-1}$ in monthly sessions x 6, following the same MDP whole-body follow up basis program. The scintigraphic series of both groups were compared and evaluated by two independent Nuclear-Medicine-physicians. Dosimetry was performed in both cohorts from planar images on gamma energy windows of Sm-153 (27.9 %) and Ra-223 (1.1%). Absorbed doses calculations were performed using OLINDA 1.1 software. Blood samples were collected 0.30 min, 2, 4, 8 and 24hrs p.i. .Urine [24 hrs] collection was performed.Results: The visual (qualitative) comparison of the MDP follow up series [120 defects, before therapy] in the β-emission irradiated 42 pts depicted in only 2 cases an obvious reduction of the osseous defects [117/120, 32 mo post therapy, $p > 0.5$]. The comparison in the α-emission irradiated 4 pts [18 defects, before therapy] showed a marked reduction [12 defects, 8 mo post therapy, $p < 0.01$]. The dosimetric (quantitative) comparison for Sm-153/Sr-89 vs Ra-223 was

0.018 Gy/MBq and 1.16 Gy/MBq for osteogenic cells respectively, whereas for red marrow was 0,004 Gy/MBq and 0.14 Gy/MBq.Conclusion: The qualitative (visual) study of these two MDP follow up series assesses the efficacy and superiority of the effectiveness of a-particles due to marked LET differences between β- and α- treated cohorts. The use of Ra-223 Dichloride in castration-resistant prostate adeno-carcinomas in these preliminary results and the scintimaging follow-up, besides the clinical course of the disease, proved that reasonably by the use of α-emission the concept "palliative treatment" might be substituted by "curative treatment" according to the conceptual meaning of the Greek word for therapy, i.e. ίασις (iasis).

PW113

Clinical benefit of routine application of Rhenium-188-HEDP in patients with painful bone metastases from prostate or breast cancer

R. Lange[1], F. Overbeek[1], A. M. van den Berk[1], J. M. H. de Klerk[1], P. C. M. Pasker-de Jong[1], R. ter Heine[1,2], M. M. L. van der Westerlaken[1], C. J. Rodenburg[1], N. H. Hendrikse[3], H. J. Bloemendal[1]; [1]Meander Medical Center, Amersfoort, NETHERLANDS, [2]Radboud University Medical Center, Nijmegen, NETHERLANDS, [3]VU University Medical Center, Amsterdam, NETHERLANDS.

Introduction: At our hospital, the therapeutic radiopharmaceutical Re-188-HEDP has been developed for treatment of painful osteoblastic bone metastases. Since Re-188-HEDP is an unlicensed radiopharmaceutical, proper pharmacovigilance is of utmost importance. This prospective study evaluates the effect of Re-188-HEDP on pain palliation, quality of life and hematological toxicity when applied in routine clinical care. Methods: Patients were eligible for inclusion when they received Re-188-HEDP treatment for treatment of painful bone metastases of prostate or breast cancer as a part of routine clinical care in our hospital. Pain palliation was assessed using the visual analogue pain score (VAS) and measuring opioid intake before treatment and 4 and 8 weeks afterwards. A response in pain palliation was defined as a minimal decrease of two points in VAS after either 4 or 8 weeks and no increase in opioid intake. Quality of life was evaluated using the EORTC QLQ-C30 questionnaire before treatment and 4 and 8 weeks afterwards. Changes in each scale were assessed and response in quality of life was defined as a minimum increase of ten points on the global health status/QoL-scale after either 4 or 8 weeks.Nadirs from blood counts of thrombocytes and leukocytes were used to assess hematological toxicity, graded according to the CTCAE criteria. Results: Seventy-five patients with painful metastatic prostate (n=50) or breast (n=25) cancer were included in this study, of which 38 and 42 patients were evaluable for pain palliation and quality of life, respectively. Twenty-four patients received multiple injections. For this analysis only first treatments were evaluated. The response rate on pain reduction was 66%. VAS-scores decreased significantly at 4 weeks ($p<0.01$) and 8 weeks ($p=0.01$), with a mean(±SD) decrease of 2.9±3.1 and 2.3±3.6 points, respectively. For the overall quality of life the response rate was 69%. The mean(±SD) increase of the global health status/QoL was 16±21.9 ($p<0.01$) at 4 weeks and 8±25.1 ($p=0.06$) at 8 weeks, respectively. Significant improvement was seen in several symptom scales. No significant differences were observed between the responses in patients with prostate and breast cancer.The treatment was well tolerated. Hematological side effects were mild and transient. Grade III thrombocytopenia and leukopenia occurred in 2 (3.8%) and 1 (1.8%) patient(s), respectively. There were no grade IV hematological adverse effects. Conclusion: The clinically relevant response of Re-188-HEDP application on pain reduction and quality of life and the limited side effects support the use of Re-188-HEDP in routine clinical care.

PW114

Does cooling of the salivary glands reduce uptake of radiolabeled PSMA-ligands?

F. C. Gaertner, H. Ahmadzadehfar, R. A. Bundschuh, S. Kürpig, E. Eppard, M. Essler; University Hospital Bonn, Bonn, GERMANY.

Aim: One major concern of PSMA-targeted PRLT (peptide radionuclide ligand therapy, e.g. using Lu-177-labeled PSMA-binding constructs) in patients with advanced castration-resistant prostate cancer (CRPC) is xerostomia due to the high physiologic uptake of PSMA-ligands in the salivary glands. We evaluated if a physical intervention (cooling) has a significant impact on tracer uptake in the salivary glands using PET imaging with a Ga-68-labeled PSMA-ligand. Patients and Methods: 92 patients undergoing PET/CT with Ga-68-HBED-CC (PSMA-ligand) were evaluated. 44 patients started cooling the salivary glands using ice-packs (4°C) about 15 minutes before tracer injection until the start of the PET acquisition. The remaining 48 patients did not use cooling. Injected activity was approx. 2 MBq / kg body weight. SUVmean and SUVmax were measured in the salivary and lacrimal glands, as well as physiologic tracer uptake in the brain, mediastinum, liver, spleen, muscle, bone, kidneys and bladder contents. Results: 34 patients with high tumor load were excluded from analysis due to concerns of a possible tumor sink effect, reducing uptake in normal organs. Therefore, 25 patients with cooling and 33 patients without cooling could be analyzed. With cooling, SUVmean was reduced by 12% in the parotid glands (11.03 ± 2.59 vs 12.60 ± 3.06; $p <$

0.01) and by 15% in the submandibular glands (12.05 ± 2.98 vs 14.21 ± 4.24; $p < 0.01$). Regarding SUVmax, the values were 17.14 ± 4.04 vs 19.46 ± 4.36; $p < 0.01$ for the parotid glands and 18.36 ± 4.49 vs 22.42 ± 6.67; $p < 0.01$ for the submandibular glands. Also, the ratios SUVmax-to-liver-background showed significant differences for the parotid glands (4.16 ± 1.04 vs 5.01 ± 1.75; $p < 0.01$) and for the submandibular glands (4.54 ± 1.22 vs 5.33 ± 1.64; $p < 0.01$). On the other hand, no significant differences were observed for the lacrimal glands, sublingual glands, and the remaining normal organs mentioned above ($p > 0.05$). Conclusion: Cooling of the salivary glands resulted in a small, but nevertheless significant reduction of PSMA-ligand uptake in the parotid and submandibular glands. Therefore, cooling of the salivary glands seems to be a simple, non-invasive approach to achieve a slight reduction of radiation dose to the salivary glands when performing PRLT with radiolabeled PSMA-ligands.

PW115

The impact of imaging and dosimetry methodology on ^{18}F NaF PET-based molecular radiotherapy treatment planning

A. M. Denis-Bacelar[1], G. D. Flux[2]; [1]Institute of Cancer Research, London, UNITED KINGDOM, [2]Royal Marsden Hospital, London, UNITED KINGDOM.

Aim: ^{18}F NaF PET/CT scans are increasingly used for patients with bone involvement. Comparable mechanisms of uptake with radionuclide-labelled bisphosphonates and ^{223}Ra, make sodium fluoride scans suitable for dosimetry-based treatment planning in bone targeted therapies. The aims of this study were to investigate the influence of attenuation correction and dosimetry calculation methods upon the prediction of the absorbed doses to bone for typical bone-seeking radiopharmaceuticals (^{153}Sm-EDTMP, ^{177}Lu-EDTMP and ^{188}Re-HEDP).Materials and Methods: ^{18}F NaF PET/CT scans from 9 patients with prostate cancer and suspected or known bone involvement were obtained from the Cancer Imaging Archive [1]. The PET scans were reconstructed using a RAMLA iterative OSEM algorithm with 3 iterations and 33 subsets, with (CTAC) and without (NAC) CT attenuation correction. Voxel absorbed doses were predicted for the three radionuclides using convolution and full Monte Carlo (MC) methods from the NAC and CTAC scans. Decay spectra were obtained from the RADTABS/MIRD software. Dose-kernels for a uniform soft-tissue medium were generated using an in-house EGSnrc/EGS++ MC code and convolved with the PET scan normalised to 1 MBq·s. Full MC simulations were carried out in EGSnrc/EGS++ from the PET uptake distribution and the CT segmented into cortical bone, spongiosa, soft-tissue, adipose-tissue and air according to the Hounsfield units. The energy in each voxel was converted into absorbed dose assuming physical half-life and 1 GBq of activity for all radionuclides. Results: Full MC shows that 67%, 67% and 66% of the total energy was deposited in cortical bone for ^{153}Sm, ^{177}Lu and ^{188}Re respectively when the absorbed doses were predicted from attenuation-corrected scans. These were reduced to 56%, 58% and 55% when the non-attenuation-corrected scans were used. Preliminary comparisons show that the mean absorbed dose deposited in cortical bone obtained from the MC predicted distribution was underestimated by 84%, 47% and 45% for ^{153}Sm, ^{177}Lu and ^{188}Re respectively when the NAC scans were used. Ratio maps between the MC and convolution distributions show mean ratios in cortical bone of 1.04(1.4), 1.0(1.4) and 0.93(1.3) for ^{153}Sm, ^{177}Lu and ^{188}Re respectively.Conclusion: ^{18}F NaF PET/CT bone scans have the potential to be used for treatment planning in molecular radiotherapy of bone metastases. Therefore, accurate knowledge of the impact of imaging and dosimetry methods upon the prediction of absorbed doses is required. On-going work comprises the improvement of the CT segmentation to better define source and target volumes, including the metastatic lesions.[1] http://www.cancerimagingarchive.net/

PW116

Radiation Toxicity Concerning Salivary and Lachrymal Glands Caused by Peptide Radioligand Therapy Using a Lu-177 PSMA Inhibitor (I & T) in Patients with Metastasized Prostate Cancer: First in Human Studies

A. Özkan[1], C. Schuchardt[2], H. Kulkarni[2], M. Shahinfar[2], M. Sayeg[2], R. Baum[2]; [1]Yildiz Technical University, Physics Department, Istanbul, TURKEY, [2]Zentralklinik Bad Berka, Theranostics Center for Molecular Radiotherapy and Molecular Imaging (PET/CT), Bad Berka, GERMANY.

Aim: PRLT is a promising new therapy option in metastatic, castration resistant prostate cancer (mCRPC). The objective of this study was to determine the uptake, half-life (kinetics) and the mean absorbed dose in salivary and lachrymal glands during PRLT of patients with mCRPC using a Lu-177 labelled DOTAGA-PSMA inhibitor (I & T). Methods: 10 mCRPC patients (aged 74+/-8 years) were examined. The injected activity was 5.9+/-1.3 GBq Lu-177 PSMA I & T. Post-therapeutic dosimetric assessments of salivary glands and lachrymal were performed (MIRD scheme). Planar whole body scans at 0.5, 3, 24, 48 and 72 h p.i. were analyzed by region of interest (HERMES WHOLE BODY DISPLAY). Time-dependent tissue activities were determined with Microsoft EXCEL™. Half-life (based on fit to exponential function) and cumulated activity of the glands were calculated

with ORIGIN PRO 8.1G™, mean absorbed doses were estimated using the OLINDA EXM™. Uptakes were expressed as percent of injected activity (% IA). The mean target volumes were measured using a 64 slice CT scanner or taken from literature: 14 ml for the right, and 16 ml for the left parotid gland and 1.2 ml for lachrymal glands. Results: High uptake of the tracer was found in the salivary glands as well as significant uptake in the lachrymal glands in all 10 patients. The time-dependent tissue activities showed an exponential decline after 20 h p.i. Maximum uptake in the parotid glands was 1.2% IA (immediately after administration) and decreased with a mean half-life of 38+/-24 hours (11-118 hours). Based on CT volumes, the absorbed dose to parotid glands was 8+/-6 Gy (maximum 23 Gy). Lachrymal glands showed a maximum uptake of 0.2% IA and a fast wash-out with half-lives of 36+/-16 hours (12-71 hours). Assuming a mean volume of 1.2 ml, a mean absorbed dose of 9.5+/-4.9 Gy (5-25 Gy) was estimated. Clinically, no adverse effects were observed (follow-up up to 24 months) in any of the patients concerning salivary gland function (no dry-eye-dry-mouth syndrome). Conclusions: As no side effects occured, we conclude that PRLT using Lu-177 PSMA I & T exhibits no (or very low) toxicity to the salivary and lachrymal glands which is most probably due to the fast wash-out and the low beta energy of Lu-177. Further studies in a larger patient cohort as well as serial salivary gland scintigraphies are planned to confirm the safety of PRLT in mCRPC.

PW118

Response Evaluation Criteria in Solid Tumours (RECIST) in a group of patients submitted to Y-90 resin microspheres radioembolization

L. G. da Costa, J. A. M. Santos, B. Gonçalves, L. Violante, F. G. S. Lopes, O. Soares, J. P. Teixeira, I. S. Lucena, A. F. Costa, L. H. T. Duarte; Instituto Portugues de Oncologia do Porto Francisco Gentil, EPE, Porto, PORTUGAL.

Aim: One reports on eligibility, safety and response to treatment of a group of patients with primary tumours and metastatic hepatic disease treated with 90-Y resin microspheres (Sirtex Sir-Spheres). Matherial and Methods: All cases referred to our department for 90-Y resin microspheres treatment between December 2011 and January 2015 were retrospectively reviewed. All patients, except hepatocellular carcinomas, had previous 18-F:FDG PET/CT scans for disease stratification. The location of the primary tumour was accessed as well as a previous 99m-Tc:MAA distribution evaluation to envisage the possibility of gastric reflux, pulmonary shunt, and Y-90 microspheres distribution inside the liver. RECIST (Response Evaluation Criteria in Solid Tumours; version 1.1) response after 3 months was evaluated for all treated patients. Results: Thirty three (33) patients were referred for radioembolization: colorectal tumours (15 patients), hepatocellular carcinoma (12), breast cancer (3), cholangiocarcinoma (1), Hepatic Neuroendocrine Tumour (1), and medullar thyroid carcinoma (1). Eight (8) patients were excluded: metastatic disseminated disease accessed by PET/CT (2), Pulmonary shunt > 20% (2), absence of 99m-Tc:MAA in the tumour (3), and more localized disease than it was previously predicted (1). Twenty five patients were treated (18 to the two lobes and 7 to one lobe) with activities ranging from 0,7 GBq to 2,4 GBq. Pulmonary shunts were found to be between 2% and 15%. Patients were assessed by RECIST: partial response (8), stable disease (7), and disease progression (8). No patient presented a complete response. One patient had disease progression and died before evaluation could be completed. Some lateral effects were observed. Conclusion: These results showed a partial response or stable disease in two thirds of this group of patients. The evaluation result showed a reasonable agreement with those reported so far in the literature [1-3].
References: 1. Bieke Lambert, Emiel Sturm, et al. Intra-arterial treatment with 90-Y microspheres for hepatocellular carcinoma: 4 years experience at the Ghent University Hospital, Eur J Nucl Med Mol Imaging (2011) 38: 2117-2124 2. Charlotte E.N.M. Rosenbaum, Helena M. Verkooijen, et al. Radioembolization for Treatment of Salvage Patients with Colorectal Cancer Liver Metastases: A Systematic Review, The Journal of Nuclear Medicine, (2013) 54: 1890-1895. 3. Robert J. Lewandowski, Jeet Minocha, et al. Sustained safety and efficacy of extended-shelf-life 90-Y glass microspheres: long-term follow-up in 134-patient cohort, Eur J Nucl Med Mol Imaging (2014) 41: 486-493

PW119

Optimising methodologies for comparison of ^{99m}Tc-MAA and ^{90}Y-microsphere distributions

A. J. Craig[1], I. Murray[1], A. M. Denis-Bacelar[2], N. Khan[3], A. Maenhout[3], B. Rojas-Fisher[4], L. Hossen[4], G. Flux[1]; [1]Royal Marsden NHSFT & The Institute of Cancer Research, Sutton, UNITED KINGDOM, [2]The Institute of Cancer Research, Sutton, UNITED KINGDOM, [3]Chelsea & Westminster NHSFT, London, UNITED KINGDOM, [4]Royal Brompton NHSFT, London, UNITED KINGDOM.

The aim of this work is to optimise a methodology to assess the extent to which ^{90}Y-microsphere distribution can be predicted by the ^{99m}Tc-MAA study for Selective Internal Radiation Therapy (SIRT). It is postulated that differences in the pre-therapy ^{99m}Tc-MAA SPECT and post-therapy ^{90}Y-bremsstrahlung SPECT scans will either be due to inherent differences in the respective imaging processes or due to differences in the underlying distribution of the MAA and microspheres.

Therefore any comparison methodology should be independent of the differences in the imaging processes. Method: ^{99m}Tc-MAA SPECT scans were convolved with a 20mm Gaussian point spread function in order to match them with the resolution of the ^{90}Y-bremsstrahlung scans. The blurred ^{99m}Tc-MAA SPECT scans were assumed to represent a dataset of bremsstrahlung scans known to have the same underlying distribution of activity as the original ^{99m}Tc-MAA SPECT scans. The original and blurred ^{99m}Tc-MAA SPECT scans were used as a control dataset to test comparison methodologies. Spearman rank correlation and histogram intersection were tested as comparison methodologies. 12 patients with either primary liver cancer or liver metastases underwent ^{90}Y-microsphere SIRT therapy. The ^{99m}Tc-MAA and ^{90}Y-bremsstrahlung SPECT scans from these patients were then compared. Results: Spearman rank values for the control dataset with matching distributions were in the range 0.88-0.94. Control values for the histogram intersection were in the range 0.48-0.72. Histogram intersection comparisons were not undertaken for ^{99m}Tc-MAA and ^{90}Y-bremsstrahlung SPECT scans as the control measured highlighted this measure as unreliable. Spearman rank coefficients for comparing ^{99m}Tc-MAA and ^{90}Y-bremsstrahlung scans were 0.32-0.82. Conclusion: Analysis of the control dataset validated the Spearman rank correlation coefficient as a test invariant to the differences in the imaging processes. However, the control dataset showed the histogram intersection not to be independent of the imaging process and thus not appropriate for this use. Spearman rank correlation coefficients of pre and post therapy SPECT scans showed a large range in the distribution differences.

PW120

Comparison of absorbed dose calculations for non-uniform activity distributions obtained via 90Y-PET/CT after liver radioembolization

M. D'Arienzo[1,2], M. Tapner[3], E. Spezi[4], N. Patterson[5], P. Chiaramida[6], L. Filippi[7], M. Ahrens[8], T. Paulus[9], O. Bagni[7]; [1]National Institute of Ionizing Radiation Metrology, Via Anguillarese 301, 00123 Roma, ITALY, [2]Department of Human Anatomy, Histology, Forensic Medicine and Orthopedics, Sapienza University of Rome, Via Borelli 50, 00161 Rome, ITALY, [3]Research & Development at Sirtex, North Sydney 2060, NSW, Australia, AUSTRALIA, [4]Cardiff University, Cardiff CF10 3XQ, UNITED KINGDOM, [5]Department of Medical Physics, Velindre Cancer Centre, Velindre Road, Whitchurch, Cardiff, CF14 2TL, UNITED KINGDOM, [6]GE Healthcare Medical Systems, Milano, ITALY, [7]Nuclear Medicine Department, Santa Maria Goretti Hospital, Latina, ITALY, [8]Philips GmbH Innovative Technologies, Research Laboratories, Pauwelsstr. 17, 52074 Aachen, GERMANY, [9]Philips Technologie GmbH Innovative Technologies, Research Laboratories, Pauwelsstr. 17, 52074 Aachen, GERMANY.

Hepatic selective internal radiation therapy (SIRT) using either resin or glass 90Y microspheres is an established catheter-based therapy for the treatment of unresectable primary and metastatic tumors with the potential of delivering a high radiation dose directly to tumor areas meanwhile sparing healthy tissues. In the last years 90Y PET/CT has been shown to provide a superior post-administration evaluation of the treatment due to its improved spatial resolution. Furthermore activity maps obtained from quantitative PET data can be converted into absorbed dose maps, thus predicting treatment efficacy. In recent years there has been an intensifying debate revolving around the most accurate dosimetric approach for three-dimensional dosimetry in molecular radiotherapy. The aim of the present work is to evaluate the absorbed dose to lesions from 90Y-PET images using different dose calculation algorithms including: I) Direct Monte Carlo radiation transport using Raydose II) Kernel-convolution using Philips Stratos III) Local deposition algorithm IV) Monte Carlo technique (MCNP) considering a uniform activity distribution V) MIRD approach. A body-shaped anthropomorphic phantom with lung, liver and spine inserts was used in the present study. A cylindrical home-made PMMA insert was manufactured and fixed into the liver insert to simulate a hepatic lesion (17 mL, approximately). Measurements in anthropomorphic geometry were performed using a GE Discovery ST PET/CT scanner with a 6:1 tumor to background activity concentration ratio. The first scan was performed with an activity concentration of 5.5 MBq/mL for the lesion insert and 0.89 MBq/mL for the liver background. The anthropomorphic phantom was then acquired at days 4, 5, 6 and 12 (according to the scanner availability) down to an activity concentration of 0.31 MBq/mL for the lesion insert and 50 kBq/mL for the liver background. Preliminary results indicate that despite 90Y-PET is likely to provide high-resolution images, the 90Y low branch ratio may produce non-uniform activity maps, possibly leading to activity and dose underestimations when a non optimised image reconstruction protocol for 90Y is used. All dose algorithms provided satisfactory results, the worst case scenario providing an agreement between absorbed dose evaluations within 20%. Additional work is needed towards the development of 90Y specific PET reconstruction protocols to allow proper image quantification for dosimetry. The research leading to these results has received funding from the European Commission, Grant Agreement N° 217257 between the EC and EURAMET under the Seventh Framework Programme

P01 - Sunday, October 11, 2015, 4:00 PM - 4:30 PM, Hall 3 – Poster Exhibition

Physics & Instrumentation & Data Analysis: Quality Control, Performance & Standardisation

P001

Quantitative Texture Analysis on a PET-CT… With Texture Standardization in Mind!

J. Cortes-Rodicio, G. Sanchez-Merino, R. Lope-Lope, J. Ruiz-Pomar, T. Martin-Gonzalez, M. Garcia-Fidalgo; Osakidetza, Vitoria-Gasteiz, SPAIN.

INTRODUCTION AND OBJECTIVES: Texture parameters are important features commonly used for pattern recognition, image classification and, more recently in the field of "radiomics", where more useful information might be extracted from medical images. Anyway, texture quantification is affected by many technical and physiological factors. The purpose of this work is to study the textural performance of a Philips Gemini TF PET as a function of the reconstruction protocol and FDG activity concentration to set a baseline for future clinical heterogeneity studies. METHODS AND MATERIALS: Nineteen series from a cylindrical phantom filled with different FDG activity concentration (max. 23,5kBq/mL, min. 0,66kBq/mL) have been acquired in a Philips GEMINI TF PET/CT. For each acquisition the raw PET data were reconstructed using three different protocols: WB-CTAC (BLOB-OS, TOF, 4mm), HN-CTAC (BLOB-OS, TOF, 2mm) and WB-CTAC-R3D (3DRAMLA, non-TOF, 4mm). Seventy-two texture features were extracted using Chang Gung Image Texture Analysis toolbox for MatLab. Fractal dimension and lacunarity features were calculated using the free plugin FracLac of ImageJ. On the one hand, for each texture feature and reconstruction protocol, the variability with FDG activity concentration was calculated as the ratio between the mean values divided by the standard deviation. On the other hand, a Pearson correlation analysis between the fractal features and activity concentration were performed using StatGraphics Centurion XVI software. RESULTS: Only nine of the seventy-two texture features analyzed show small variability (<5%) with activity concentration. These are entropy (Haralik-1973, Sun-1983, Horng-2002); short-run-emphasis and run-percentage (Loh-1988); the homogeneity, intensity, inverse-difference-moment and code-entropy (Horng-2002); and short-zone-emphasis and zone-percentage (Thibault-2009). These features seem to be suitable for textural quantification of tumors and further classification of them. Features presenting large variations are not recommended for heterogeneity quantification. With respect the fractal dimension and lacunarity features, we find a significant statistical quadratic and linear correlation, respectively ($p<0.05$) between them and the activity concentration for all the reconstruction protocols. CONCLUSIONS: This study shows that it is feasible to apply textural and fractal analysis methods to study the heterogeneity of tumors, but taken into account the technical factors that will lead to variations on the results, in our case activity concentration and reconstruction protocol. It is mandatory to establish a reference performance of different PET in order to allow comparison of multicenter studies. Anyway, further studies should be carried out to improve the statistical power of the analysis.

P002

Performance assessment of the Albira tri-modal pre-clinical PET system

A. Attarwala[1], Y. W. Karanja[1], C. Romanó[1], M. Roscher[2], C. Maaß[1], B. Wängler[2], G. Glatting[1]; [1]Medical Radiation Physics/Radiation Protection, Universitätsmedizin Mannheim, Medical Faculty Mannheim, Heidelberg University, Mannheim, GERMANY, [2]Molecular Imaging and Radiochemistry, Institute for Clinical Radiology and Nuclear Medicine, Medical Faculty Mannheim, Heidelberg University, Mannheim, GERMANY.

Aim: Quantitative molecular imaging with a pre-clinical positron emission tomograph (PET) is a prerequisite in treatment planning, monitoring and development of new diagnostic and therapeutic radiopharmaceuticals. This study analyzes the performance characteristics of the Albira PET sub-system and measures the response of the system for the commonly used radionuclides (18F and 68Ga) in small animal imaging. Materials and Methods: The Albira tri-modal system (Bruker BioSpin MRI GmbH, Ettlingen, Germany) is a pre-clinical device with a PET, SPECT and CT. The PET sub-system is made up of single continuous crystal detectors of lutetium yttrium orthosilicate (LYSO) coupled to position-sensitive photomultipliers (PSPMTs). The detector assembly consists of three rings with each ring having 8 detector modules. The trans-axial field of view (FOV) is 80mm and the axial FOV is 148mm.Imaging was performed with the NEMA NU-4 image quality phantom (Data Spectrum Corporation, USA) having five rods with diameters 1-5mm and a uniform central region. Measurements with 18F and 68Ga were performed with a starting activity concentration of 500kBq/ml and a list mode acquisition of 10h.An energy window of 358-664keV and a coincidence time window of 5ns were selected. The data were

reconstructed with a maximum likelihood expectation maximization (MLEM) algorithm; voxel size of 0.5mm with increasing iterations from 5 to 50 (step-size 5) and corrections for randoms/scatter was included within the system. System sensitivity, count rate linearity, algorithm convergence and recovery coefficients were analysed. Convergence was assessed based on region of interest (ROI) analysis of activity concentration within the rods and uniform region. All analyses were performed with PMOD software (PMOD Technologies Ltd., Switzerland).Results: The overall sensitivities for the entire FOV were 2.79%±0.01% and 3.21%±0.01% for 68Ga and 18F, respectively. The net true coincidences with dead-time correction were linear for ≤10MBq (68Ga, R2 = 0.9999) and ≤11.5MBq (18F, R2 = 0.9999). Above these activities, system performed an overcorrection for dead-time effects. The algorithm converged after 35 iterations for both 68Ga and 18F. The recovery coefficients for the 5, 4, 3 and 2mm rods with an activity concentration of 110kBq/ml were 0.50±0.13, 0.41 ±0.09, 0.25±0.06, 0.24±0.04 for 68Ga and 0.80±0.25, 0.72 ±0.21, 0.56±0.20, 0.34±0.10 for 18F, respectively.Conclusion: The Albira pre-clinical PET system has an acceptable sensitivity range and the system linearity is suitable for the range of activity used for pre-clinical imaging. The next step would be to test the system for additional radionuclides that could be used for pre-clinical imaging.

P004

Comparison of time-of-flight PET-CT results for micro hollow spheres from 31 microliter to 8 milliliter for Fluorine-18, Gallium-68 and Yttrium-90

S. Kerschbaumer[1], L. Hofbauer[2], H. Kvaternik[1], C. Gstettner[1], R. M. Aigner[1]; [1]Medical University, Division of Nuclear Medicine, Graz, AUSTRIA, [2]University of Applied Science, Division of Radiography, Graz, AUSTRIA.

The aim of this study was to examine the positron-range-effect simulating focal nodular lesions based on micro-hollow-spheres for Fluorine-18, Gallium-68, and Yttrium-90. The varied kinetic energy of the emitted positrons influences the reconstruction, the quantitative measurement and the visual impression of the resulting sectional images. The measurement procedure uses a target/background ratio of 10:1 and 30:1. A Jaszczak-phantom-body was equipped with micro-hollow-spheres from 31 microliter (4mm diameter) to 8 milliliter (25mm diameter). The images were acquired on a Siemens Biograph-40mCT PET-CT and reconstructed respecting the CT for attenuation-correction (780mm field-of-view, 120keV, 16mA-effective, 5mm slice-thickness, pitch 1.3). Osem-3D and point-spread-function-recovery (HD-PET) were used with and without time-of-flight (TOF) with matrices 256, 400 and 512 with 3 or 4 iterations and 21 (TOF) and 24 (non-TOF) subsets. The acquisition time was altered between 1min to 10min. The maximum and average activity concentration and the threshold-based volumes were evaluated on a Siemens Syngo MMWP. The blurring contribution for different nuclides is effected by the positron-range-effect due to the different maximum positron energy (Fluorine-18 635keV, Gallium-68 1899keV, Yttrium-90 800keV). The measured volume at high contrast, HD-PET and 256-matrix with a 50% threshold was 0,81 (81%) for the 8ml sphere down to 0,50 for the 2ml sphere within 5% deviation independent from the nuclide. For 125µl the measured volume-ratio for Fluorine, Gallium and Yttrium were 1.28, 0.80 and 0.96 measured. The evaluated volume for a threshold of 10% overestimates the lesion in general. Because of the similar positron-range the factor was in a rage of 1.6 for Fluorine and Yttrium. For Gallium-68, the factor was 1.71 for the 8mm sphere and rose continuously for smaller spheres to 3.18 for 500µl, which correlates with an underestimation of the concentration in smaller spheres. The decay corrected average and maximum concentration is widely independent of the acquisition time, where the maximum value raises slightly due to counting statistics for harder reconstruction kernel, smaller voxels and also for lower contrast. For a specific reconstruction algorithm, the measured volume and concentration is not affected by time-of flight. The HD-PET-algorithm compared to the OSEM-algorithm shows higher concentrations and smaller volumes. Image blurring is nonlinear affected by the acquisition system together with the reconstruction algorithm, the lesion and the patient, the nuclide, and the tracer. While some influences can be corrected, for clinical practice it is crucial to understand the effects and characteristics close the physical limits of quantitative functional PET imaging.

P005

Conflicting measures of uniformity on a Siemens Symbia gamma camera

M. J. Memmott, I. S. Armstrong, K. J. Saint, A. Bradley, R. S. Lawson, H. A. Williams, C. M. Tonge; Central Manchester University Hospitals NHS Foundation Trust, Manchester, UNITED KINGDOM.

Gradual worsening of the uniformity of two Siemens Symbia gamma cameras (one Symbia S and one Symbia T6, installed in 2009) has been observed when using the measurement method as described in IPEM Report 86. This method uses a

point source at 5xFOV and assesses the uniformity by pixel coefficient of variation, corrected for Poisson noise, and has been used throughout the department on a variety of camera systems with consistent results. The manufacturer's recommended procedure, using a 1.0 MBq Tc-99m point source at a distance of approximately 40 cm from the detector and calculating uniformity using the NEMA NU1 standard, has failed to demonstrate similar trends over the same time interval. The closeness of the source in the manufacturer's method requires the application of a curvature correction to the image. This does not apply to the IPEM method. Both gamma cameras have recently had new energy and linearity correction maps generated. Uniformity for each method was assessed before and after new correction map generation, and differences assessed using a Mann-Whitney U test for non-parametric data. The mean (SD) uniformity value using the IPEM method prior to new correction maps for the Symbia S was 1.10 (0.05) % and 1.48 (0.09) % for detector 1 and 2 respectively. Post correction map generation, the mean value was 0.58 (0.04) % and 0.62 (0.05) % for detector 1 and 2 respectively. The difference between uniformity values pre- and post-correction map generation was significantly different, $p < 0.001$. Conversely, for the manufacturer recommended method, the mean (SD) integral uniformity value in the CFOV prior to new correction map generation was 1.75 (0.20) % and 1.66 (0.13) % for detector 1 and 2 respectively. Post correction map generation, the values were measured to be 1.74 (0.13) % and 1.58 (0.06) % respectively. There was no significant difference ($p > 0.30$) for either detector. Results for the Symbia T6 followed a similar trend. Two methods for assessing the uniformity of a Siemens Symbia gamma camera show discrepant results over time and show significantly different responses after generation of new energy and linearity correction maps. Discrepancies between the two methods implemented in this work highlight the importance of independent assessment of gamma camera performance.

P006
A Novel Method for Krypton-81m Intrinsic Uniformity Measurement

H. A. Williams, M. J. Memmott, R. S. Lawson; Nuclear Medicine, Manchester, UNITED KINGDOM.

Background: Gamma camera behaviour varies with the energy of the detected photons. Therefore, uniformity assessments and corrections derived using Tc-99m (140keV photons) may not necessarily be applicable at the higher gamma emission energy of Kr-81m (190keV), widely used for lung ventilation imaging. Kr-81m SPECT is particularly sensitive to minor uniformity variations. The rise of V/Q SPECT heightens the need to evaluate uniformity with Kr-81m, although this is challenging due to its short half-life and gaseous nature. We have designed a simple phantom to provide a point-like source for Kr-81m intrinsic uniformity measurement. Methods: A balloon was connected to a commercial Rb-81/Kr-81m generator, with reference activity 300 MBq at 12:00 CET, housed in the shielded control room adjacent to a GE Optima NM/CT 640 gamma camera, with an exhaust tube feeding into a second, adjacent shielded gamma camera room. The generator and tubing were shielded using lead bricks and pots modified for the purpose. The balloon reached an average diameter of 2cm, and was positioned more than 2 metres (~5 gamma camera fields of view) from the uncollimated detector surface, and standard 15 Mct test image acquired. For comparison, a 30 MBq Tc-99m point source (0.1ml in an LP4 tube) was positioned at the same location and another 15 Mct test image acquired. The average count-rate per head was noted. Results: The Kr-81m balloon source resulted in a average count rate of 16.1 kcps, allowing the test image to be acquired in 15.5 minutes. The Tc-99m point source resulted in a count rate of 29.8 kcps, allowing a uniformity test image to be acquired in 8.6 minutes. Image uniformity for Kr-81m was found to be acceptable and comparable with that for Tc-99m, although a slight gradient was seen across both images which infers source positioning requires further optimisation. Conclusion: The phantom which we have developed has potential to provide a quick and simple means of collecting Kr-81m uniformity data. Accurate positioning of the balloon and shielding of the generator and tubing from the uncollimated gamma camera is non-trivial, and will depend on local department layout. A series of measurements are underway to refine source positioning, and assess reproducibility, stability and correlation of Kr-81m uniformity with results for Tc-99m using a Tc-99m source in a similar geometry. Provided that this can be achieved, Kr-81m floods could become a routine QC procedure.

P007
Metrology for ^{89}Zr in the clinic

A. J. Fenwick[1,2], L. Johansson[1], E. Spezi[3,2], W. Evans[4,2], C. Marshall[4,2]; [1]National Physical Laboratory, Teddington, UNITED KINGDOM, [2]Cardiff University School of Medicine, Cardiff, UNITED KINGDOM, [3]Velindre NHS Trust, Cardiff, UNITED KINGDOM, [4]Wales Research & Diagnostic Positron Emission Tomography (PET) Imaging Centre, Cardiff, UNITED KINGDOM.

Despite an increasing number of applications under investigation using the novel PET radionuclide ^{89}Zr, no efforts have so far been made to improve measurements of absolute activity or nuclear data that are required for accurate quantification of the activity in radionuclide calibrators and imaging modalities. The determination of activity by means of a radionuclide calibrators prior to injection is essential to safeguard patients and to enable comparison of results from potential clinical trials. In addition, the determination of activity distribution within patients using quantitative imaging techniques is needed to determine doses received and ensure clinical decisions such as staging of cancer are made correctly. ^{89}Zr decays by electron capture and positron emission to both the ground state and various excited states of ^{89}Y with a half-life of 78.42 (13) hours. The electron capture decay to a metastable state of 14ms at 909 keV presents challenges in the absolute standardisation and appropriate corrections must be considered. In this work, ^{89}Zr was standardised by several liquid scintillation methods including Triple-to-Double Coincidence Ratio (TDCR), CIEMAT/NIST efficiency tracing and 4πß-γ coincidence counting with efficiency extrapolation and results were shown to be in agreement within uncertainties. Secondary standards in the form of calibration factors and dial settings for both NPL maintained and commercially used systems have also been determined for clinically relevant geometries. A new half-life value of 78.366 (78) hours was also determined and shown to be in good agreement with the currently evaluated value. These are the first measurements of the absolute activity of ^{89}Zr and further work in this area is encouraged to give confidence in these results and ensure traceability of this novel and important radionuclide.

P008

Usefulness of Mean Standardized Uptake Value for Liver as a Reference Organ on F-18 FDG PET/CT: Comparison with Standardized Uptake Values Corrected by Various Imaging and Clinical Parameters.

J. Choi[1], S. Lee[1], J. Lee[2]; [1]Soonchunhyang University Hospital Cheonan, Cheonan, KOREA, REPUBLIC OF, [2]Catholic Kwandong University International St. Mary's Hospital, Incheon Metropolitan City, KOREA, REPUBLIC OF.

Introduction/purpose: The use of liver as a reference organ for extrahepatic fluorodeoxyglucose (FDG) uptake on F-18 FDG positron emission tomographic/computed tomographic (PET/CT) scan is well known. Previous studies about relations between hepatic FDG uptake and various parameters including hepatic fat and blood glucose have been contradictory. The aim of the study is to assess the valid standardized uptake values for liver as a comparator for extrahepatic FDG uptake on F-18 FDG PET/CT scan. Materials and Methods: Consecutive F-18 FDG PET/CT scan obtained in 186 healthy subjects from October 2012 to November 2014, were retrospectively reviewed. Mean standard uptake value (SUVmean) and maximum SUV (SUVmax) were measured for liver. Other SUVs were also obtained as followings: (1) SUVLBM; SUVs were normalized by lean body mass, (2) fat-adjusted SUVmean (SUVfat); SUVmean was adjusted for hepatic fat using a formula equating percentage fat to CT density, (3) normalized glucose corrected SUVmax and SUVmean (SUVglc); SUVs were normalized for blood glucose level assuming a normal blood glucose level of 5.55 mmol/L. CT densities (in Hounsfield units) were measured in liver and spleen with identical regions of interest used for the CT and PET examinations. Fatty liver was defined as CT density of liver was less than that of spleen. Patients were divided in 5 groups on the basis of blood glucose. The correlation between hepatic FDG uptake and various clinical factors including glucose, liver function test, total cholesterol, triglyceride, erythrocyte sedimentation rate(ESR), and high sensitive C-reactive protein (hs-CRP) were also assessed. Results: SUVfat and SUVglc of fatty liver were significantly higher than those of non-fatty liver but no difference in SUVmax, SUVmean, or SUVLBM. Liver CT density significantly correlated with SUVmax before and after correcting by normalized glucose, SUVLBM, and SUVfat. Blood glucose significantly correlated positively with liver SUVmax, SUVglc, SUVLBM but not with SUVfat. Liver SUVmax also significantly correlated with BMI, AST, ALT, GGT, and TG. Liver SUVmean correlated neither CT density nor blood glucose. Conclusion: Liver SUVmean correlated neither CT density nor blood glucose while liver SUVmax is influenced by blood glucose and fatty liver. On the basis of these data, liver SUVmean is valid as a comparator for extrahepatic foci of increased FDG uptake in patients with abnormal level of blood glucose or fatty liver.

P009

Evaluation of Qualitative Expressions in Bone Scan Reports

P. Martineau, E. Saidenberg, W. Zeng; The Ottawa Hospital, Ottawa, ON, CANADA.

Background Purpose: The diagnostic report serves as the primary means of communication between nuclear medicine physicians and referring clinicians. Little is known about the variability in clinicians' interpretation of nuclear medicine

physicians' reporting terminology relating diagnostic confidence. Bone scans are the most commonly performed imaging modality in nuclear medicine; however, reporting is poorly standardized because of non-quantitative visual assessment and frequent non-specific findings. Qualitative report text, such as "likely due to" or "suspicious for" may have substantially different meanings when used by different reporting physicians, and can be understood differently by different referring physicians. These differences in interpretation may have important impacts on patient's management. In this study we propose to survey nuclear medicine and referring physicians regarding their assessment of expressions of probability in bone scan reporting. Methods: A review of bone scan reports on Ottawa Hospital cancer patients identified 12 phrases commonly used to communicate likelihood of the presence of skeletal metastases: 'consistent with', 'possible', 'suspicious for', 'cannot rule out', 'suggestive of', 'compatible with', 'in keeping with', 'likely', 'no convincing evidence', 'probably', and 'could be'. A survey regarding qualitative expressions of diagnostic confidence in bone scan reporting was used to investigate referring and reporting physicians' interpretations of these phrases commonly used in bone scintigraphy reports. The survey asked respondents to indicate the probability of disease presence implied by each of the 12 expressions on a numerical scale divided into 0.05 wide bands centred from 0.0 to 1.0 with 0.0 indicating that the condition is definitely not present and 1.0 indicating complete certainty of disease presence.Results: The results of this survey show that there exists substantial heterogeneity in the perceived meaning of standard phrases amongst both referring and reporting physicians. We believe that the results of this study may help inform the process of standardization of bone scan report findings among nuclear medicine physicians.

P010

Semi-quantitative Evaluation of Image Quality in Low Dose 18F FDG PET/CT

S. C. Kapur, Arvind K Sinha,VP Sajjith,Donald Teh and Vijay Sharma; National University Hospital, Singapore, SINGAPORE.

Aim: Quantitative evaluation of tumor metabolism by SUV is increasingly used for evaluation of therapy response of a chemotherapy or radiation treatment. In view of clinical relevance of accuracy and reproducibility of SUV max, SUV peak in PET/CT imaging, it is important to look into these variables at low dose 18 F FDG / CT protocol. This study will evaluate 18 F FDG uptakes in liver, thigh and shoulder and correlate with parameters related to PET/CT image quality. Method and Material: Cumulative radiation dose measurements were made in 150 patients who underwent whole body PET/CT examination with a low dose CT protocol and an average 18F dose of (3.51+0.8MBq/kg), ensuring optimal image quality interpretable by physician. It was optimized by quantitative measurement of SUV max / SD, SUV peak and SNR in PET and CT images of the liver, shoulder and thigh in cases with nearly same BMI and normal blood glucose. Only patients with no observed cancerous lesions were chosen. A spheroid region of interest (ROI) was placed over five selected areas of liver parenchyma in orthogonal plane. The coefficient of variation (CV) for SUV max and SNR was measured in the liver. The Image quality was evaluated by two nuclear medicine physicians in a 5 point Likert Scale Score.- Result and Discussion: This study showed substantial variations in both SUV peak and SUV max for 18F FDG distribution in liver, thigh and shoulder. The image quality at baseline was compared with dose adjusted conditions. Secondly, as a measure of image quality, we evaluated only SUV max , SUV peak and SNR in above organs and SD of the pixel values inside the ROI was used for image noise. It was noted that SUV max was uniformly distributed in the liver, shoulder and thigh in the same scale as SUV peak. The uptake ratio between shoulder and liver, thigh and liver were within same narrow range. The image quality evaluated by the physicians had a score of 4.5/5.0. Patient-specific factors influenced the accuracy and reproducibility of SUV max and SUV peak. The scan quality and diagnostic accuracy was not affected, inspite of reduction in 18F FDG dose and low dose CT parameters. The average whole body effective dose was 9.81+ 2.8mSv, which is reasonable as compared to published data.

P02 - Sunday, October 11, 2015, 4:00 PM - 4:30 PM, Hall 3 – Poster Exhibition

Physics & Instrumentation & Data Analysis: Radiation Exposure & Protection

P011

Shielding gamma-rays from nuclear medicine rooms: Monte Carlo simulations of ceiling scatter in the diagnostic and therapeutic use of ^{99m}Tc, ^{131}I and ^{18}F

R. S. Schnerr[1], A. de Jong[2], C. R. L. P. Jeukens[1], G. Landry[3], R. Wierts[1]; [1]Maastricht UMC+, Maastricht, NETHERLANDS, [2]Amphia, Breda, NETHERLANDS, [3]LMU, München, GERMANY.

Aim: In the design of diagnostic and therapeutic treatment rooms for Nuclear Medicine, an important consideration is the shielding required for blocking the ionizing radiation from the radioactive isotopes. The primary radiation, possibly with build-up correction, can be calculated analytically. However, little data is available to estimate the radiation dose contribution of ionizing radiation that travels over the (lead) shielding in the wall and scatters of the ceiling; so-called skyshine. We aim to determine the contribution of this skyshine to the radiation dose received by people outside Nuclear Medicine rooms. Materials and Methods: Monte-Carlo simulations were performed with Gate/Géant for different heights of the lead shielding in the wall, and different ceiling heights. A point source of Tc-99m (141keV), I-131 (365keV) or F-18 (511keV) was placed free in air, 1m above the floor, 3m from the wall. We used lead shielding of 2mm (Tc-99m) and 8mm (I-131 and F-18). In total 165 simulations were run; for each isotopes we varied the shielding height (1.8-5.0m) and ceiling height (3.0-5.0m). These simulations allow us to compare the contribution of the direct radiation (through the shielding), and skyshine (over the shielding). Results: We find that the skyshine contribution to the total radiation dose varies greatly (from <2% to ~100%), and strongly depends on photon energy. For low photon energies (e.g. Tc-99m) skyshine is often a dominant factor. For higher photon energies (e.g. F-18), shielding of the primary radiation is typically the most important concern.Conclusion: We have performed simulations that allow an estimation of the contribution of skyshine to the radiation dose outside a room, based on room use (occupancy, total radioactivity used for treatment), ceiling- and shielding height and the isotope used. For lower photon energies (e.g. Tc-99m) this can be a major contribution, which, if neglected, can result in insufficiently shielded rooms. This research will allow for safer and better optimized shielding designs in Nuclear Medicine departments , as the contribution of scattered radiation from the ceiling can be properly accounted for.

P012

Measurement of radioactivity in breast milk following maternal administration of ^{111}Indium-Pentetreotide

R. Bidder, C. Humphreys, S. Evans, A. Smakovs, P. Ali; ABMU Health Board, Swansea, UNITED KINGDOM.

Introduction and Aim: Radiopharmaceuticals administered to breast feeding patients may excrete into breast milk. The purpose of this study was to measure the radioactivity concentration of ^{111}Indium-Pentetreotide in breast milk and to estimate the potential effective dose to a breast feeding preterm infant. A breast feeding patient with a carcinoid tumour of the lung was referred for an ^{111}Indium-Pentetreotide investigation to assess disease extent. We report the results of measurements made on breast milk samples following ^{111}Indium-Pentetreotide administration. Methods: 101.6MBq ^{111}Indium-Pentetreotide was administered intravenously. Breast milk samples were collected on the day of ^{111}Indium-Pentetreotide administration and on days 1, 4, 5, 6, 7 and 8 days post-administration. 3ml aliquots were assayed using a 10 well automatic gamma counter (Perkin Elmer 2470 Wizard^2). Prior to counting, the responses of the 10 detectors were normalised using a standard sample of ^{111}Indium. Activity concentrations (Bq/ml) were corrected for decay between measurement and the time at which the breast milk sample was taken. The potential effective dose to our preterm infant was estimated by adjusting the ICRP value for effective dose per unit activity (mSv/MBq) by the ratio of the standard adult body weight (70kg) to the infants' body weight. Results and Discussion: Planar imaging taken at 24hrs post-injection showed that the ^{111}Indium-Pentetreotide was taken up by the carcinoid tumour of the left lung and there was increased activity within both breasts. The activity concentration in the samples measured 348Bq/ml and 3Bq/ml on day 1 and day 8 respectively. Assuming an ingestion of 180ml/kg/day of breast milk, the total potential effective dose to the preterm infant from breast milk ingestion would be 0.529mSv in the first 8 days. Three published articles have reported the level of ^{111}Indium in breast milk following intravenous administration of ^{111}Indium-labelled white cells and ^{111}Indium-Pentetreotide respectively. The range in the activity concentration (per administered activity (MBq)) in the first 24hours was 0.09-0.31Bq/ml for the ^{111}Indium-labelled white cells and 0.01-0.02Bq/ml for the ^{111}Indium-Pentetreotide. Our range was 2.03-3.42Bq/ml per administered activity (MBq). Our results are much higher than these previous studies. This difference may be related to several factors including chemical form, low numbers of patients involved in the study and the difference in breast milk intake.

P013

Patient Increase Doses From Hybrid Spect-Ct: Evaluation In Common Clinical Practice

T. Ben Ghachem, A. Mhiri; M. Ghezaiel; I. Slim; M. F. Ben Slimène; Nuclear Medicine department; Salah Azaiez Institute, Tunis, TUNISIA.

Introduction: The Single-photon emission tomography combined with computed tomography (SPECT-CT) is a hybrid imaging technique that integrates functional and anatomical data. It is a valuable complement to conventional scintigraphy. With these hybrid devices widely used, patient irradiation is not only related to the administered radiopharmaceuticals, but also to the CT component. That is why supporting physician and patient awareness in additional dosimetry is necessary.Purpose: The aim of this work is to estimate patient doses from hybrid single-photon emission computed tomography (SPECT) and computed tomography (CT) procedures.Methods: The study involved a dual-headed SPECT unit with an integrated 2-slice CT scanner (Symbia T E-Cam, Siemens Medical Systems, Erlangen, Germany) in the ISA (Salah Azaiez Institute) cancer center. Effective dose was estimated for about 146 patients. Data from 168 scans of common nuclear medicine procedures (123I-MIBG, 99mTc-MIBI parathyroid, 111 Inoctreotide,131I post therapy scan, 67 Gallium and 99mTc-MDP bone scan) were presented in this study. The CT parameters used were: tube current of 30 - 90 mAs, slice thickness of 3-5 mm, and tube voltage of 110-130 kV. For each patient the CT was acquired immediately after SPECT; the patient being kept in the same position to minimize offsets due to movement and allow proper registration on fused imaging.Results: One hundred and forty six consecutive patients and 168 SPECT/CT examinations were involved in this study. The average age of patients was 56 years (27-83), the sex ratio was 0.53. The total effective dose received by each patient for SPECT-CT examination was estimated in accordance with the recommendations of the ICRP 53 and 80.The average effective dose have ranged according to type of the exam: 1927,1 mSv for 131I-post therapeutic scans, 7,65 mSv for bone scans and 5.42 mSv for 123I-MIBG scans, and the anatomical region explored: 0.32 for Head and neck region and 4.78 for pelvis. The percentage increase of effective dose by the inclusion of the CT was about 125% for 123I-MIBG scans, 83 % for bone scans, whereas it was negligible in case of treatment with 131I (0.15%).Conclusion: In our study, the increased risk induced by the additional CT with low dose settings in line with SPECT examination, is not significant and does not exceed 0.026%. By weighing the diagnostic value of SPECT/CT examination with that of a stand-alone SPECT examination dosimetric incremental cost is justified because of its direct clinical benefit conveyed to the patient.

P014

A Different Methodology Concept For Measurements And Release Criteria In Thyroid Therapy Procedures

V. R. Mc Cready[1], M. PAPHITI[1], G. S. LIMOURIS[2]; [1]Nuclear Medicine Dept, Royal Sussex County Hosp, Brighton, UNITED KINGDOM, [2]"Aretaieion" Hospital, Athens University Medical Faculty, Athens,, GREECE.

Aim: Patients treated with I -131, are potentially a significant source of radiation hazard to their family members and public. It is aimed, by the present, to evaluate the hospital release parameters of these patients by employing a different (from the commonly adopted) methodology. Methods: Thirty five post-operative thyroid-cancer patients were included in the study and divided into two groups: Group A included patients with metastatic thyroid disease and Group B pts with no metastases. For both groups the range of administered I-131 activity was 2220-5550 MBq and dose rate levels were measured according to a 4-day basis program. Each group employed a different methodology of measurements: For those cases with metastatic disease, the exposure rate was carried out at the surface of the body, just under the mattresses at the side of the main metastases, whereas, in group B measurements were performed at a distance of 1 meter from them, in upright position. By employing the "inverse square law method" for the A group measurements, the results were in concordance with those of group B, and hence a reliable comparison could be obtained. Dose rates were plotted as a function of time and fitted using a bi-exponential model, so as to derive the teff. Since the first post uptake hours are crucial, the teff-fast part and the teff-slow one, have been tabulated. Additionally, the "retained activity" and the "isolation time" have been calculated, according to the specific data of each patient. Results: Both methods showed a difference of 0.6% between them. The variability of "isolation times" among patients indicates a strong relationship of teff on biological half-life and shows no relationship to the administered activity. In addition, the teff-fast ranges from 1 up to 11 hours and in order to avoid a possible radiation risk, thorough care of consequent measurements should be applied. Conclusion: Measurements performed at the surface of the body are reliable and suitable for metastatic disease cases, whereas for non-metastatic ones, thyroid is considered as point source and measurements should be applied at a distance of 1 meter from patient, in standing position. According to our experience, in order to ensure that the treated patient will not expose any individual or the environment to levels greater that the dose limit, a strict dose rate of < 10 μSv/hr at 1 meter and a retained activity <200 MBq should be adopted and established by the authorities.

P015

Hand Phantoms for Optimization of Radiation Protection of Nuclear Medicine Personnel

M. Fulop[1], J. Hudzietzová[2], J. Sabol[3], P. Ragan[4], P. Povinec[5]; [1]Slovak Medical University, Bratislava, SLOVAKIA, [2]Faculty of Biomedical Engineering of CTU, Kladno, CZECH REPUBLIC, [3]Faculty of Safetz management of PACR, Prague, CZECH REPUBLIC, [4]Slovak Centre of Scientific and Technical Information, Bratislava, SLOVAKIA, [5]Nuclear Medicine Clinic BIONT, Bratislava, SLOVAKIA.

AimWhen handling the radiopharmaceuticals, the skin exposure of hands is assessed based on results of routine monitoring using a ring dosimeter. However, the position of the ring dosimeter often does not correspond with the location where the exposure reaches its maximum. It is therefore necessary to determine the relationship between the response of the ring dosimeter reading in terms of the personal dose equivalent H_p (0,07) and the skin dose equivalent at the location with the maximum exposure $H_{p,max}$ (0,07). This relationship can be determined by using hand phantoms simulating specified effects of operations with radiopharmaceuticals which significantly contribute to hand exposure.**Materials and methods**-The position of $H_{p,max}$ (0,07) on hands is determined by mapping of the skin dose equivalent due to gammas and positrons using thermoluminescent dosimeters (TLDs) of type MCP-Ns placed at 11 locations on the surface of hands of workers handling the radiopharmaceuticals. The effects of radiopharmaceutical handling that significantly contribute to the hand exposure have been specified by deconvolution of integral dose equivalent map across all single operations performed during the FDG preparation and administration.The five single procedures that contributed to the dominant values $H_{p,max}$(0,07) during the preparation and administration of FDG to patients have been selected: the application by a shielded and unshielded syringe, hand holding a vial with forceps, holding a container, and hand holding an infusion tube. Physical, voxel and mathematical hand phantoms for all 5 selected operations were constructed.**Results and conclusion**The use of hand phantoms reduces personnel constraints during dose equivalent H_p(0,07) mapping on their hands. Measurement of the dose equivalent distribution for the physical, voxel and mathematical hand phantom proved good agreement with uncertainty lower than 20%. The relationship between the ring dosimeter response and the results of skin dose equivalent monitored at specific locations can be assessed by means of hand phantoms, which simulate single acts that significantly contribute to $H_{p,\ max}$ (0,07). By comparing the physical, mathematical and voxel phantoms hand, it was demonstrated the significance of physical phantoms for the determination of relationship of the ring dosimeters response and $H_{p,max}$(0,07). The results have shown advantages of the use of mathematical phantoms for optimization of radiation protection in nuclear medicine departments.Acknowledgements: This work has been carried out and support by the projects SGS15/114/OHK4/1T/17 and APVV-0241-011.

P016

Estimation of likely Radium-223 releases into the environment from filtration based sewage systems.

D. G. Morgan, A. Hallam; Oxford University Hospitals NHS Trust, OXFORD, UNITED KINGDOM.

This work developed a calculation method for estimating the activity of ^{223}Radium Chloride in a filtration based sewage system, and the likely activity that may be released into the environment from these systems. A patient was referred to our hospital for 6 treatments of ^{223}Ra Chloride as a treatment for bone metastases (from castration resistant prostate cancer). The treatment schedule was monthly injections of 3.5 MBq of ^{223}Ra. The patient had a sewage filtration system at their property with waste water leaving the system and flowing into a network of pipes under the garden of the property, where the waste water disperses into the soil. Our calculations modelled the activity entering and leaving the system during the scheduled treatments and for 3 months after. The activity entering the system was by direct excretion from the patient, in faecal matter, during the first 7 days after intravenous administration. The calculations showed that for an administered activity of 3.5 MBq (for a typical patient weighing 70 kg), the maximum concentration within the sewage tank of 0.33 kBq/l. After calculating the rate that the radioactivity enters and leaves the system per day during the week after administration, it was estimated that the waste removed from the system would lead to a maximum activity of 0.9 MBq in the soil in the patients' garden. We modelled the activity dispersed in the soil and estimated that the concentration of activity in the soil is of the order of 0.6 kBq/l. The conclusion from this calculation model is that due to the relatively long physical half-life, moderate activities of ^{223}Ra may be released into the environment from filtration based sewage systems. This will require consideration of patients' home circumstances, and specific advice must be given to ensure safety of members of the public and the patient's family, particularly if food is consumed from garden produce.

P017

Preclinical small animal PET/MRI for radiopharmaceutical dosimetry

M. Kranz[1], B. Sattler[2], M. Patt[2], W. Deuther-Conrad[1], S. Fischer[1], R. Smits[3], A. Hoepping[3], O. Sabri[2], P. Brust[1]; [1]Helmholz-Zentrum Dresden-Rossendorf, Institute of

Radiopharmaceutical Cancer Research, Leipzig, GERMANY, [2]Dept. Nuclear Medicine, University Hospital Leipzig, Leipzig, GERMANY, [3]ABX advanced biochemical compounds, Radeberg, GERMANY.

Aim:To assess the radiation risk after injection of new PET radiotracers small animal PET/MRI provides the essential whole body biodistribution data for image based dosimetry (ibD). In this study, we investigate ((S)-(-)# and (R)-(+)##-[18F]fluspidine, a PET radioligand for neuroimaging of σ1 receptors in mice. Organ doses (OD) and the effective dose (ED) were determined using PET/MR ibD to assess the radiation risk to humans. The results will be compared to those previously acquired for (-)-*and (+)-** [18F]flubatine, to proof the concept of small animal PET/MRI for incorporation dosimetry to assess the radiation exposure to humans by radiopharmaceuticals.Materials and methods: Six female CD1 mice (weight: 30.9±1.3 g) were injected i.v. with 13.2 ±3.0 MBq (#, n=3) or 12.6±1.4 MBq (##, n=3), respectively. A dynamic 2 h animal PET/MRI protocol was performed (MEDISO nanoScan®, Hungary). All relevant organs were defined by volumes of interest. Time- and mass-scales were adapted to the human anatomy; exponential curves were fitted to the time-activity-data (%ID/organ). The ODs were computed using the adult male model with OLINDA and the ED using tissue weighting factors (ICRP103). The results were compared to previously acquired data of post mortem biodistribution (PMB) studies in mice for (-)-[18F]flubatine (n=27, ∅28.2 g) and [18F]fluspidine (n=28#/n=22##, ∅29.6 g).Results:The excreting organs (kidneys, liver and urinary bladder) received the highest ODs. Subsequently, these organs provide the largest contribution to the ED. The overall radiation risk to humans based on animal biodistribution data acquired with ibD would be 12.9# and 14.0## as compared to 16.7#; 18.4## based on PMB. Comparable results were estimated for [18F]flubatine: 12.5*(PMB), 12.1**(ibD). All conversion factors in μSv/MBq.Conclusion: ibD of [18F]fluspidine reveals significant differences between the two enantiomers. Both in ibD and PMB the tracer with higher affinity and slower kinetics (##) causes a higher radiation exposure than its enantiomeric counterpart (#). Furthermore, the ibD shows lower ED values compared to the PMB due to the intrinsic methodological differences. Small animal ibB is feasible and its reliability needs to be further investigated and confirmed.

P018

Beta+ emitters: workers absorbed doses

G. Tosi[1], F. Provenzano[1], G. Testanera[1], A. Chiti[2]; [1]Istituto Clinico Humanitas, Rozzano, ITALY, [2]Humanitas University, Milano, ITALY.

Aim of this study was to measure and analyze absorbed doses for different workers operating in a nuclear medicine department starting from patient administered activity for PET examinations. In our department, radiopharmacists are in charge of synthesis and quality control of radiopharmaceuticals; nurses are in charge of collecting histories, preparing patients and administering radiopharmaceuticals; technicians are in charge of position patients, acquiring images and discharging patients. Radiation therapy technicians are involved when PET-CT is used for radiation treatment planning, where they help in positioning the patients.Material and MethodWe collected data for 3 beta+ emitters: 11C, 18F and 68Ga and we registered administered activity for 50 patients per radioisotope.For absorbed dose measurements we used an electronic dosimeters (Thermo EPD mk2) that measures equivalent doses in term of Hp(10) and Hp(0.07) and has an energy range between 15 keV and 10 MeV.ResultTable below shows data of mean administered activity for different radioisotopes.RadioisotopeMean administered activity (MBq)11C 332.618F 349.468Ga 129.2In the second table data of equivalent doses per unit of activity are shown (nSv/MBq).11C 18F 68GaHp(10)Nuclear medicine technician 2.4 6 5.8Radiotherapy technician / 5.4 /Nurse / 8.6 / Radiopharmacists 9.6 15.5 73.5Hp(0.07)Nuclear medicine technician 2.3 6.3 9.7Radiotherapy technician / 5.7 /Nurse / 5.7 /Radiopharmacists 10.819.5 439.6ConclusionDosimetric data shows that higher doses are absorbed from radiopharmacists, expecially for 68Ga manually synthesis. Moreover, for all workers, measured doses give a confortable result from radioprotection point of view as bring annual absorbed doses within law limits.

P019

Radiation protection in a veterinary nuclear medicine facility.

C. Pettinato[1], D. De Zani[2], M. Longo[2], G. Ravasio[2], M. Di Giancamillo[2], D. Zani[2]; [1]Medical Physics Unit, Bologna, ITALY, [2]DIVET, University of Milano, Milano, ITALY.

Nuclear Medicine is becoming an important imaging modality in veterinary medicine. The setup of a Veterinary Nuclear Medicine facility is quite simple but requires specific attention to radiation protection of staff and environment. The aim of this work was to describe the radiation protection issues related to a nuclear medicine facility in a veterinary hospital.The nuclear medicine facility is located in a veterinary hospital inside the Radiology Unit. A dual headed gammacamera has been refurbished as follow: one detector head was removed from the gantry and attached on a pensile on the room ceiling, the second detector head was left on the gantry and used as a single headed gammacamera. The pensile camera is used for

big animals standing in front of the detector (primarly horses), while the single head camera is used as a conventional planar and SPECT system for small animals (dogs, cats, felines, rabbits and pigs). An hot room is used for radiopharmaceutical labeling.The floor under the pensile area is equipped with a grid able to collect urine from the animals. Ionization chambers and contaminameters are used to detect surface contamination.From a radiation protection point of view there are the following majors concerns:1) Activity injected to horses is about 6-7 GBq/animal;2) Urine produced by horses can seriously contaminate surfaces and staff members;3) Horses are usually sedated but need the care of staff people that use to stay very close to the animals during scans (bone scintigraphy: 2 hours/scan);4) Small animals need general anesthesia and continuous monitoring during the scans;Staff members, usually veterinary physicians, use to wear lead aprons during scans and their personal monitoring is performed using TLD detectors for whole body and extremity dosimetry.Mobile barriers are used to monitor small animals under anesthesia during all scans.The major risks are related to horses care because of the high radiation exposure rate that they emit. Actually we measured about 25 microGy/hour, 20 microGy/hour and 18 microGy/hour respectively at one meter from the head, the thorax and the animal abdomen. A person standing very close to the animal, holding its head could receive more than 200 microGy per scan.A veterinary nuclear medicine facility is feasible and major concerns in terms of radiation protection are related to irradiation but also to possible contamination. Workers have to be very well trained on radiation protection issues.

P020

Recommended Administered Activity for Ga-68 labelled peptides in Pediatric Nuclear Medicine

J. S. Machado, **Jr**., S. Beykan, M. Lassmann; Department of Nuclear Medicine, University of Würzburg, Würzburg, GERMANY.

Aim: The aim of this study is to suggest values for calculating administered activities for Ga-68 labelled peptides based on the weight-independent effective dose model proposed by the EANM Pediatric Dosage Card for application in pediatric nuclear medicine. Methods: Time-integrated activity coefficients ("residence time") for Ga-68-DOTATATE and Ga-68-DOTATOC were taken from Sandström et al. (JNM 2013), for Ga-68-DOTATOC and Ga-68-Pentixafor from Hartmann et al. (Nuklearmedizin 2009) and Herrmann et al. (JNM 2015), respectively. With these values, the effective doses were calculated by using OLINDA/EXM for the standard series of phantoms (Adult, 15y, 10y, 5y, 1y, newborn). The weight-dependent effective dose coefficients based on these results were rescaled according to the formalism described by Jacobs et al. (EJNMMI 2004), to determine the radiopharmaceutical class of Ga-68 labelled peptides ("multiples" as defined in the EANM dosage card) and to calculate the baseline activities based on an upper limit of the administered activity (185 MBq) for an adult. With the baseline activity value and the corresponding class, the administered activity for Ga-68 peptides related to pediatric diagnostic scans can be calculated by using the EANM Pediatric Dosage Card formalism: A administered [MBq] = Baseline Activity x Multiple. Results: All calculated normalization factors of the effective doses results in the range of -0.9176 and -1.0339. These values suggest that the 68Ga labeled peptides belong to class "B" of radiopharmaceuticals. According to our analysis, the baseline activity for all compounds is 12.8 MBq. As a minimum activity, we recommend 14MBq in analogy to F-18-fluoride. For illustration, we provide the activities and the corresponding weight-dependent effective doses for Ga-68-DOTATATE for a child with 60kg (163MBq, 3.8mSv), 40kg (114MBq, 3.9mSv), 20kg (62MBq, 4.1mSv), 10kg (35MBq, 4.4mSv) and 3kg (13MBq 5.06mSv). Conclusion: For pediatric nuclear medicine with Ga-68 labelled peptides, we suggest determining the activities to administer based on the formalism proposed in this work, so that the effective dose for these procedures can be considered as almost age-independent.

P021

Whole-body Biodistribution, Dosimetry and Metabolite Correction of 11C-palmitate: A PET Tracer for Imaging of Fatty Acid Metabolism

N. L. Christensen, S. Jakobsen, O. L. Munk, S. Nielsen, L. C. Gormsen; Aarhus University Hospital, Aarhus C, DENMARK.

Aim: Positron emission tomography (PET) with fatty acid (FA) or FA analogue tracers has been used extensively to study metabolic processes. For example, 11C-palmitate is used to image FA metabolism in the myocardium, brain and liver, but despite its widespread use in human studies, no published dosimetry, biodistribution or metabolite correction data exist. Dosimetry estimates for 11C-palmitate are based on ICRP 106, where estimates for 11C tracers are listed. These estimates assume that a large proportion of the radiotracer is excreted via urine and that the bladder receives significant radiation resulting in high dosimetry estimates. Typical radiation burden often exceeds 1 mSv per injection in human experimental studies, which limits the use of 11C-palmitate for younger and healthy individuals. However, FAs are rapidly taken up by most tissues, are evenly distributed in the body and not excreted in urine. Hence, the actual radiation burden is probably of a magnitude that enables serial human studies. Our aim

was to correctly calculate 11C-palmitate dosimetry, with a secondary aim to publish population based metabolite correction data. Methods: For dosimetry and biodistribution studies, two pigs and two healthy volunteers underwent a low-dose CT scan and immediately thereafter serial whole-body PET scans (~300 MBq 11C-palmitate) with frame durations 1, 1.5, 2, 2.5 and 3 minutes per bed position. Mean effective dose and standard internal dose exposure in each organ was calculated using OLINDA/EXM software. In the human subjects, a bolus injection of 9,10-3H-palmitate was used to measure the fraction of labelled palmitate incorporated into complex lipids during a typical dynamic study. This fraction was compared to a larger patient cohort, where the fraction of 11C-palmitate in complex lipids was estimated by Sep-Pak. Results: In the pig study, mean effective dose was 3.0 μSv/MBq, with the liver (19.1 μSv/MBq) and kidneys (7.42 μSv/MBq) receiving the highest absorbed doses. In the human study, mean effective dose was 3.2 μSv/MBq, with the liver (27.5 μSv/MBq) and heart wall (10.6 μSv/MBq) receiving the highest absorbed doses. Incorporation of 9,10-3H-palmitate into complex lipids was comparable to estimates obtained by 11C-palmitate with approximate fractions at 10, 20, 30, 40 and 50 minutes reaching 92, 64, 30, 17 and 12%. Conclusion: Mean effective dose of 11C-palmitate was ~3.0 μSv/MBq, resulting in a total dose of ~1 mSv per human study, allowing multiple FA scans. In addition, little variation in free tracer was observed in the human studies allowing population based metabolite correction.

P022

Dosage in Pediatric Nuclear Medicine Diagnostics in Daily Practice

J. S. Machado, S. Beykan, M. Lassmann; Department of Nuclear Medicine, University of Würzburg, Würzburg, GERMANY.

Aim: In pediatric nuclear medicine in daily practice, it is highly recommended to review retrospectively the activities administered to patients for further optimization of the diagnostic procedures. The aim of this study, therefore, was to analyze retrospectively the administered activities and effective doses in pediatric patients undergoing nuclear medicine examinations in our department and compare the results to national and international recommendations. Methods: We collected demographic data and administered activities for the last three years and the two most frequent types of pediatric diagnostic scans in our department (F-18-FDG PET/CT scans and kidney scans with either 99mTc-MAG3 or 99mTc-DMSA). The results were compared to the weight-dependent administered activities calculated from national and international recommendations (EANM 2008 Dosage Card [EANM2008], North America Consensus Guideline [NACG], EANM/SNMMI 2014 Harmonization Document [EANM2014], and German National Recommendation [BfS2012]). In addition, we analyzed the patients' age-weight-dependent resulting effective doses taken from the corresponding ICRP data tables. Results: For F-18-FDG PET/CT scans we performed 88 exams in 44 patients (21 younger than 10 years old). The administered activity ranged from 29MBq to 345MBq; the corresponding effective doses were between 3mSv and 7.1mSv. The mean deviation of the administered activities from the values suggested by EANM2008 was +12.9%, for NACG -33%, for EANM2014 -39%, and for BfS2012 +11.4%. Related to renal scans, there were 242 exams, 216 of 99mTc-MAG3 scans (177 patients) and 26 of 99mTc-DMSA scans (24 patients). A total of 179 patients were younger than 10 years and 129 patients younger than 2 years. The administered activities ranged from 11MBq to 146MBq, the corresponding effective doses between 0.16mSv and 1.62mSv. The mean deviation of the administered activities for 99mTc-MAG3 were +6.3% (EANM2008), -51.4% (NACG), +3.7% (EANM2014), and +16.6% (BfS2012). The corresponding values for 99mTc-DSMA were -24% (EANM2008), -7% (NACG), and +3.2% (EANM2014). No values for 99mTc-DMSA are recommended in BFS2012. Conclusion: The administered activities showed good agreement with EANM2008 and BfS2012, larger differences were observed for NACG and EANM2014 for F-18-FDG PET-CT scans, because of the slightly higher recommended activities. For renal scans (99mTc-MAG3 and 99mTc-DMSA) the results show a good agreement with the EANM recommendations. The effective corresponding effective doses are low. The results of this study show that no change in daily practice is needed.

P023

Automated Dispensing and Injection of ^{18}F-FDG Decreases Personnel Radiation Burden

L. Beels, F. Lavent, D. Nicolaij, O. Gheysens, C. Van de Wiele, A. Maes; AZ Groeninge, Kortrijk, BELGIUM.

Aim: In nuclear medicine departments with a positron emission tomography (PET) system, the personnel doses have increased over the last decade due to an increasing number of PET procedures. In AZ Groeninge, the increasing personnel dose emphasized the need for optimizing the individual workload in order to keep the radiation exposure as low as possible. Therefore, an automated dispensing and injection system was

installed and an additional PET shift was implemented. The aim of our study was to evaluate the personnel whole-body and extremity doses after implementation of the extra shift and automated infusion system in comparison to historical data. *Materials and methods*: A Medrad Intego^{TM} automated dispensing and injection system was used to administer ^{18}F-fluoro-deoxy-glucose (FDG) to the patients. Personnel doses were evaluated using a breast dosimeter provided by SCK-CEN and an extremity dosimeter provided by AIB Vinçotte Controlatom. Both types of dosimeters are thermo luminescence dosimeters (TLD's), that were read out monthly. The radiation dose per PET shift was calculated because not everybody had the same number of PET shifts every month. *Results*: The reference value of the whole-body and extremity dose is respectively 38.48 μSv and 377.48 μSv per PET shift. After implementation of the extra PET shift (in casu 3 PET shifts instead of 2 shifts per day) the extremity dose decreased to 254.85 μSv per PET shift (32.5% reduction), whereas the whole-body dose remained constant (40.90 μSv per PET shift). The second optimisation consisted of using the automated dispensing and injection system. The whole-body dose decreased from 38.48 to 27.27 μSv per PET shift (29.11% reduction) and the extremity dose decreased from 377.48 to 154.66 μSv per PET shift (59.03% reduction). *Conclusion*: In AZ Groeninge, the personnel radiation burden has decreased by adding an extra shift for PET examinations and by using an automated dispensing and injection system. Optimizing radiation burden is an on-going process and further analyses are necessary to keep decreasing the personnel whole-body and extremity dose.

P024

Proposal of correction factors for the assessment of the maximum exposure to hands of workers handling radiopharmaceuticals labelled with F-18: Based on studies in CR and SR

J. Hudzietzova[1], M. Fülöp[2], J. Sabol[3], J. Doležal[4], J. Kubinyi[5], P. Povinec[6], I. Makaiová[7], A. Vondrák[8]; [1]Faculty of Biomedical Engineering, CTU Prague, Kladno, CZECH REPUBLIC, [2]Slovak Medical University, Bratislava, SLOVAKIA, [3]Faculty of Safety Management of PACR, Prague, CZECH REPUBLIC, [4]Department of Nuclear Medicine,University Hospital, Hradec Králové, CZECH REPUBLIC, [5]Institute of Nuclear Medicine of GUH, Prague, CZECH REPUBLIC, [6]Nuclear Medicine Clinic, BIONT, Bratislava, SLOVAKIA, [7]Oncology Clinic of St. Elizabeth, Bratislava, SLOVAKIA, [8]Isotope Centre, Nitra, SLOVAKIA.

Aim: The local exposure of the skin on hands averaged over 1 cm^2 constitutes a limiting factor in handling radiopharmaceuticals. In most cases, the maximum local exposure is at the tip of the index finger. The aim of this paper is to determine the correction factors (CFs) to modify the value of the personal dose equivalent $H_p(0.07)$ measured in places where finger dosimeters are worn (root index, middle or ring finger) in order to assess realistically the maximum local exposure of workers at selected PET nuclear medicine clinics in the Czech Republic (CR) and Slovak Republic (SR).**Materials and methods**: The group under investigation included the workers which were preparing or applying radiopharmaceuticals labeled with F-18 (three PET clinics in CR and SR). The quantity $H_p(0.07)$ was determined based on TLDs where altogether 12 pairs of TLDs (MCP-Ns and MCP-7) on each operator's hands were used. The results were related to the activity manipulated by the worker (about 10 GBq). Up to now, 164 measurements on 27 persons (CR) and 80 measurements on 8 persons (SR), were completed, respectively. The CFs, the ratio of maximum exposure to the result obtained from finger dosimeter monitoring (root of the index finger), were determined for each PET clinic, as well as for individual professional groups. **Results**: Based on measurements using TLDs, the maximum exposure was found on top of index fingers in about 63% of workers in CR and in 47% workers in SR. The CFs were determined taking into account not only procedure (preparation, application) but also technological equipment at the clinic (semiautomatic dispensing stations, semiautomatic applicators). The values of the CFs also differ in various groups in each clinic for right and left hand. In some cases, the CFs reached values up to 13 (CR) and 16 (SR) while average CFs were 3.2 in CR and 2.5 in SR.**Conclusion**: The experimentally obtained values of $H_p(0.07)$ have shown that the maximum local exposure was usually found in the place where finger dosimeters are not routinely worn (the tip of the index finger). Underestimation of local exposure may amount in some cases up to a factor of 13 in CR and factor 16 in SR. Therefore, it is recommended to consider the introduction of appropriate correction factors for various categories of workers who may not all handled radiopharmaceuticals the same way.Acknowledgements: This work was partially supported by the projects SGS15/114/OHK4/1T/17 and APVV-0241-011.

P025

Assessing the effect of the amount of injected 99mTC-MIBI on the calculated cardiac volume in the myocardial Gated-SPECT, A clinical survey

S. Entezarmahdi[1], A. Kamali-asl[1], M. Haghighatafshar[2], F. Gheisari[2], M. Hemmatpour[2], F. Khajerahimi[2]; [1]Radiation Medicine Engineering Department, Shahid Beheshti

University, Tehran, IRAN, ISLAMIC REPUBLIC OF, [2]Nuclear Medicine Department, Shiraz University of Medical Science, Shiraz, IRAN, ISLAMIC REPUBLIC OF.

In recent years nuclear cardiology has been rapidly extended and so many myocardial scanning perform daily. In this manner the public awareness and public concern with regard to radiation exposure in relation to this popular scanning protocol has been raised in the last decade. Accordingly with the implementation of new imaging techniques and systems, the needed dose per examining could be reduced. In this work we tried to find whether the reduction in injected dose can affect on calculated cardiac volume.Seventy five patients with the known probability of coronary artery disease who was referred to our ward enrolled in this study. To make different amount of radioactive deposited in a same myocardium, we repeated each patients' scan twice after one injection. The second Gated-SPECT scan was performed when the deposited 99mTc in the myocardium decayed up to 30 percent. Assuming that MIBI has not any significant redistribution in this time, the only parameter which has been changed is the amount of radioactivity within the myocardium. In this way we have two different images with different deposited dose in the myocardium from each patient. All the images reconstructed and processed similarly. End diastolic and end systolic volumes (EDV, ESV) was calculated by Corridor-4DM software.With reduction of radioactivity within the myocardium, as the images declare, because of partial volume effect the mid-myocardium points do not change substantially. On the other side the standard deviation of count profile decreases meaningful. Consequently, the calculated cavity volumes increased as the radioactivity decreased in the myocardium. Our results show that, with 30 percentages reduction of radioactivity within the myocardium can lead to up to 39.00 ml growth in calculated EDV (mean difference 2.84 ml, p-value=0.010) and up to 24.00 ml growth in calculated ESV (mean difference 2.35 ml, p-value=0.007).In summary we showed that, reduction in used radioactivity for myocardial perfusion scan with Gated-SPECT, could lead to statistically significant growth in calculated cavity volume both in end diastole and end systole phase.Key Words: Myocardial Perfusion Image, Gated-SPECT, Injected dose, Cavity Volume

P026

Transportation of radioactive material for Nuclear Medicine: risk assessment in the area of Bologna

S. Vichi[1], G. Cicoria[2], D. Pancaldi[2], A. Infantino[1], C. Po[3], D. Mostacci[1], M. Marengo[2]; [1]Montecuccolino Nuclear Engineering Laboratory, Department of Industrial Engineering, University of Bologna, Bologna, ITALY, [2]Medical Physics Department, "S. Orsola-Malpighi" Hospital, Bologna, ITALY, [3]Servizio Sanità Pubblica, Regione Emilia Romagna, ITALY.

IntroductionTransportation of radioactive material is regulated at International level by specific standards and procedures to ensure an adequate level of safety of people and the environment. However, no widely applicable guidelines about emergency procedures in case of accident have been approved and published by international organisms. The aim of this work is to collect statistical information on transportation of radioactive materials in the area of Bologna (Italy) and to evaluate the potential radiological risk for the population and first responders in case of accident; data were used to create a model for risk assessment as a support for the definition of an emergency protocol.**Materials & methods**An investigation of transportation of radioactive materials in the area of Bologna was conducted collecting data on authorized carriers, consignees, itineraries, type of package transported (excepted, type A / B), radioactive content of each package (radionuclide, physical form, activity), population density, vehicle traffic density and accident rate. Risk was assessed using INTERTRAN2 package, a computer code system developed by AMC Konsult AB (Bromma, Svezia) in the scope of an IAEA Coordinated Research Program. An event tree analysis was conducted to identify the most representative cases to be simulated by INTERTRAN2. To take into account the different levels of danger of an accident, severity categories were defined; the probability that an accident belonged to a defined severity category was assessed and, for each severity category, the package response was defined in terms of the release of radioactive material.**Results**More than 200 different scenarios were studied. As an example of a typical situation, we evaluated an accident involving a vehicle carrying 5 packages of ^{123}I (activity per package (a.p.p) 8.91E+08 Bq), 10 packages of ^{131}I (a.p.p. 2.92E+10 Bq), 5 packages of ^{125}I (a.p.p. 9.25E+08 Bq) and 1 package of ^{99}Mo (a.p.p. 2.25E+11 Bq). The evaluated population risk in terms of collective dose was 5.05E-10 person*Sv. On the basis of the studied cases, the average risk in transportation associate with each consignee for the S. Orsola-Malpighi Hospital was evaluated as 3.41E-10 person*Sv.**Conclusions**As a general result, risk assessment analysis of radionuclide sources in the area of Bologna showed a low risk for the population in case of accident. All information collected and results led to the implementation of a database for risk assessment, with reasonable and realistic assumptions. Moreover, this framework can be also applied to different scenarios and environment.

P027

Promotion of measures to counter radiation health concerns using the comic (manga)

k. ohno[1], T. Higashi[2], C. Okuyama[3], Y. Nakamoto[4], K. Endo[1]; [1]Kyoto Collage of Medical Science, Nantan, JAPAN, [2]Shiga Medical Center Research Institute, Moriyama, JAPAN,

[3]Image Communiation Corporation, kyoto, JAPAN, [4]Graduate School of Medicine Kyoto University, kyoto, JAPAN.

[Aim]Since the Fukushima Daiichi Nuclear Power Plant accident, four years have passed. However, Japanese people do not have most of enough opportunity to study the basic information about the radiation effect. Nuclear physicians created informative comic (manga) to promote measures to counter radiation health concerns.[Materials and Methods] All questions and answers were collected related to inquiries from the general public that were posted to reliable websites from March 2011 to November 2012.More than sixty classes and dialogs had been held at eight prefectures from October 2012 to January 2014. All the questions from participants were collected.[Results and Conclusion]The questions could be broadly classified into health effects, food safety and radiation-related knowledge. To put out accurate information about these questions, informative manga were produced, taking ideas from educational activities implemented at junior high school in Fukushima. This comic (manga) will be presented in this meeting. This comic (manga) will be useful to help people think about the issue of radiation effect.

P028

Radiation Protection Recommendations for Releasing Patients Treated with 131I for Thyroid Cancer

E. Mora Ramirez; Caja Costarricense del Seguro Social / Universidad de Costa Rica, San Jose, COSTA RICA.

The Nuclear Medicine Department at the San Juan de Dios Hospital has considered radiation protection guidelines given by the IAEA for releasing patients after 131I treatments for thyroid cancer, in the Safety Report Series No. 63, “Release of patients after radionuclide therapy”, published in 2009. However, IAEA guidelines are based on the administrated activity and it does not take into account bio-kinetics of the 131I into patient body, distance between patients and its relatives, etc. Our goal is to establish patient specific recommendations considering dose limits to relatives and caregivers, also bio-kinetics of thyroid and extra - thyroid compartments, taking into account NUREG-1556, Vol 9, Rev. 2 from USNRC considerations. For 47 patients (female 44), age range from 79 - 20 years old; effective half - life for thyroid and extra - thyroid compartments have been estimated, occupation factor, distance and effective dose have been set. Preliminary results, for average data, showed good agreement with IAEA guidelines for ablation patients in restrictions for children under 2 years old, time off work and sleep apart, however, restrictions for children from 2 to 11 years old and are not similar; on the other hand, for follow-up patients, in our case this means patients with recurrence or metastatic diseases, results are very different from the IAEA guidelines for all restrictions, our results showed that restriction times have to be increased, this means that patients specific bio-kinetics have to be take it into account. Therefore a method to establish patient specific radiation protection recommendations can be applied in a Nuclear Medicine Department taking into account bio-kinetics of 131I.

P03 - Monday, October 12, 2015, 4:00 PM - 4:30 PM, Hall 3
Poster Exhibition
Physics & Instrumentation & Data Analysis: Image Reconstruction

P029

Standard OSEM vs. Regularized PET Image Reconstruction: Qualitative and Semi-Quantitative Comparison

A. Iagaru, J. Lantos, E. Mittra, C. Levin; Stanford University School of Medicine, STANFORD, CA, UNITED STATES.

Introduction: A PET image reconstruction tool (Q.Clear®) has been recently introduced that allows more iterations of the raw PET data than the standard OSEM image reconstruction, to enable contrast recovery without amplifying noise. Here we qualitatively and semi-quantitatively compared Q.Clear® with the standard OSEM image reconstruction available on our clinical PET/CT scanners (GE Discovery 600 and 690) using patient data. Materials and methods: PET datasets from 30 previously acquired clinical research scans (16 68Ga-DOTA TATE, 11 18F-FPPRGD2, 1 18F-FLT, 2 18F-FSPG) were reconstructed using Q.Clear® (25 iterations with 3 different regularization strength or "beta" values) and compared to standard reconstruction for Discovery 600 (2 iterations and 32 subsets; with PSF modeling) and 690 (2 iterations and 24 subsets; with PSF modeling) scanners. Each of the 4 reconstructions/scan were reviewed blindly by 2 experienced nuclear medicine physicians and scored 1-5 (1 poor, 5 excellent quality). The SUVmax of the smallest lesion detected in each patient was also measured for comparison. The paired Welch t-test was used for statistical analysis. Results: Significant differences ($P < 0.01$) were noted on visual analysis for 2 beta values (350 and 450) vs. OSEM (the mean visual scores were 3.59±0.65, 3.88±0.42, 3.89 ±0.28 and 3.36±0.56 for Q.Clear® with the 3 beta values and the OSEM, respectively). SUVmax values were significantly higher ($P < 0.01$) on Q.Clear® reconstructions, resulting in increased conspicuity for some small lesions. In 2 cases, lesions were only identified on Q.Clear® reconstructions and confirmed on follow-up MRI. Conclusion: Q.Clear® with a higher number of iterations maintains image quality. Visual analysis confirmed that overall image quality is improved and may allow for improved detection of small lesions as compared to the image quality from the standard OSEM algorithm.

P030

How Does Increasing the Matrix Size / Reducing Voxel Volume Impact Quantification in FDG PET? A Detailed Analysis for Optimizing the Clinical Utility of Next Generation Digital PET/CT

K. Binzel[1], J. Zhang[1], B. Zhang[2], Z. Hu[2], P. Bardos[1], M. V. Knopp[1]; [1]The Ohio State University Wexner Medical Center, Columbus, OH, UNITED STATES, [2]Philips Healthcare, Cleveland, OH, UNITED STATES.

The introduction of solid-state PET detectors with improved count rates as well as spatial resolution facilitates the use of a larger reconstruction matrix and smaller voxel volumes. This study analyzes the impact of reduced voxel volumes on lesion quantification in whole body oncologic PET/CT independent of the visual appearance and the impact of iterative reconstruction parameters.Philips Vereos TF 64 PET/CT (Cleveland, OH) listmode data of 15 clinical patients were acquired after average injection of 480 MBq 18F-fluorodeoxyglucose (FDG). Patients were imaged from the skull to mid-thighs with 90 seconds per emission volume. Default image reconstruction used a 4 x 4 x 4 (64) mm3 voxel volume, 144x144 matrix. Additionally, data were reconstructed using a 2 x 2 x 2 (8) mm3 voxel volume, 288x288 matrix, and a 1 x 1 x 1 (1) mm3 voxel volume, 576x576 matrix. Image sets were also reconstructed using different iterative parameters. Using the 4mm images as reference, target lesions as well as physiologic uptake in background tissues were assessed by region of interest SUVmax on each image set by multiple independent readers.Utilization of a larger reconstruction matrix leads to substantially increased SUVmax's in smaller metabolically active tissues. For 8 mm3 voxel images, the average percent difference from default SUVmax was a 16% increase, with a range for target lesions from 0.2% to 48%. For 1 mm3 voxel images, the average percent difference from default SUVmax was an 86% increase, with a range for target lesions from 25% to 186%. There is an observable trend that the increase in SUVmax is most pronounced in smaller or more heterogeneous lesions. This observation concurs with a prior phantom assessment. The quantitative impact of the range of variable number of subsets per iterative reconstruction was minimal. We determined the following to be preferential: 144x144 matrix 3 iterations 15 subsets, 288x288 matrix 3 iterations 13 subsets and 576x576 matrix 3 iterations 11 subsets.Digital PET/CT appears to enable larger matrix size / reduced voxel volume reconstruction that impacts quantification especially in smaller, metabolically active lesions. This observation is consistent with improved recovery coefficients in phantom data. Larger matrix reconstruction appears to be promising in digital PET by reducing partial volume effects and thus not only improving detectability but also quantitative accuracy.

P031

Optimisation of ventilation/perfusion (V/Q) SPECT reconstruction utilising advanced reconstruction methods: a phantom study

M. J. Memmott; Central Manchester University Hospitals NHS Foundation Trust, Manchester, UNITED KINGDOM.

Introduction: Advanced image reconstruction methods implementing resolution recovery (RR) and regularisation (REG) have been exploited in various areas of nuclear medicine with the aims of improving image quality and reducing administered activity and/or acquisition time. This phantom study aimed to investigate their potential use in ventilation/perfusion (V/Q) lung SPECT. Methods: The background volume and spheres of a NEMA image quality phantom were filled with an equal Tc-99m activity concentration, equivalent to clinical ventilation SPECT. After acquisition on a GE Optima 640, using ELEGP collimators, the background activity concentration was increased by a factor of 5 to mimic perfusion SPECT, with the spheres representing mismatched defects. Reduced count SPECT datasets were also simulated via Poisson sampling to give 25 - 100% of the clinical count rate. Attenuation-corrected reconstructions were performed using variants of the GE Evolution Toolkit; implementing ordered-subset expectation-maximisation (OSEM), OSEM with RR and OSEM with RR and REG (currently reserved only for cardiac studies). The contrast for each sphere was derived from the mean voxel count in a spherical volume of interest (VOI) and mean background voxel value from 12 additional spherical VOIs. Background noise was measured using the mean coefficient of variation in background VOIs. The ratio between contrast and background noise (CNR) was calculated for each sphere. The optimal reconstruction parameters were derived through blinded interpretation of a subset of clinical reconstructions by a Consultant Nuclear Medicine Physician. Results: Reconstruction implementing OSEM with RR and REG gave highest CNR in all spheres when compared with OSEM alone, due to the noise limiting effect of regularisation. Reconstruction using OSEM with RR however gave the greater contrast overall. Optimal reconstruction parameters were found to be with 5 iterations and 10 subsets. When compared to the optimal OSEM derived data, equivalent quantitative image quality was achieved when implementing RR and RR with REG using approximately 50% of the acquired data. Conclusions: Image quality of reconstructed data acquired from a phantom mimicking a V/Q SPECT acquisition was found to be enhanced when implementing both RR and RR with REG, giving increased contrast or reduced noise respectively. Half of the clinical count-rate was required to give an equivalent image quality to OSEM, indicating that either acquisition times and/or administered activity have the potential to be reduced in clinical practice when implementing advanced reconstruction methods.

P032

Q. Freeze Software for Respiratory Motion Correction in PET/CT: A Preliminary Investigation with a Respiratory Motion Phantom

G. Havariyoun, D. Ruiz, E. Kalogianni, B. Corcoran, A. Eccles, N. Mulholland, G. Vivian; King's College Hospital, LONDON, UNITED KINGDOM.

Aim: PET/CT imaging of the lung and abdominal region can often lead to apparent increase in tumour volume, underestimation of measured standardized uptake value (SUV), and mismatched PET and CT images due to respiratory motion. GE Healthcare Q.Freeze software uses 100% of the detected events and can perform respiratory phase matching of gated PET and low-dose 4D-CT data to minimize respiratory motion artefacts. This investigation aimed to assess the effectiveness of the Q.Freeze software. **Material and methods**: The GE Discovery 710 PET/CT scanner was used to scan the Quasar® Respiratory Motion Phantom (QRMP) with two in-house constructed inserts. The QRMP inserts consisted of 4ml and 1ml ^{18}F-FDG filled spheres in air and water to model spherical lesions in lung and liver respectively. Scans were performed with a sinusoidal respiratory waveform of 20 breaths per minute (bpm) with 20mm amplitude and a single patient specific respiratory cycle pattern. Varian's Real-Time Position Management System was used to monitor the phantom's motion. Images acquired when the QRMP was motionless were used as benchmark. For each motion experiment three sets of images were reconstructed; ungated PET (UG-PET), Q.Freeze PET only gated (4D-PET) and finally Q.Freeze PET with cine CT (4D-PET/CT). Images obtained were quantitatively assessed for background variability (BV), sphere volume and SUVs. All analysis was performed on a Hermes® nuclear medicine workstation. **Results**: UG-PET images had the largest increase in volume and reduction in SUV when compared to benchmark in all images. 4D-PET and 4D-PET/CT improved accuracy by increasing SUV_{max} by a mean of 33% and 31% and decreasing volume by a mean of 216% and 211% when compared to UG-PET respectively. The improvement was greater in all cases for 4D-PET compared to 4D-PET/CT, apart from in air where 4D-PET/CT showed marginal enhancement by increasing SUV_{max} by 5% and decreasing volume by 14% compared to UG-PET. BV was largest for the 4D-PET/CT in all acquired images. **Conclusion**: Preliminary results clearly indicate that Q.Freeze largely improves SUV and volume figures when compared to UG-PET images. These results do not justify the extra radiation exposure to patients if 4D PET/CT was performed. The next step of this study will involve the construction of an insert that will replicate lesions on the liver-lung boundary.

P033

Reproducibility of quantification in F-18 FDG PET clinical application varying protocols parameters and lesions dimension

A. Zorz[1], E. De Ponti[1], L. Guerra[2], S. Morzenti[1], M. Cuzzocrea[3], C. Crivellaro[3], A. Crespi[1], M. Arosio[2], C. Landoni[3]; [1]Medical Physics, A.O. San Gerardo, Monza, ITALY, [2]Nuclear Medicine, A.O. San Gerardo, Monza, ITALY, [3]Nuclear Medicine, University of Milano Bicocca, Milano, ITALY.

Aim: Measurements of tumor metabolism is used to evaluate response to treatments using quantitative parameters as SUVmax and SUVpeak. However, they are strongly influenced by various technical features of the the scanner system, injected activity, acquisition time, reconstruction parameters and lesion's characteristics as dimension. Aim of the study was to investigate SUV variability between different size lesions and reconstructed images with a newest high sensitivity PET/CT scanner (Discovery IQ from GE Helthcare) equipped with the new Q-Clear regularised reconstruction algorithm. Q-Clear algorithm incorporates a factor (i.e. Beta parameter) able to modulate the noise allowing the algorithm to reach the full convergence of the data without excessively increasing the noise, as usually found with standard OSEM reconstruction (VPHD). Material and Methods: GE Discovery IQ scanner was used for acquisition of list data and regularised reconstruction (Q.Clear) was used with different regularization beta parameter (from 500 to 200 units). SUVmax and SUVpeak of both Q-Clear and VPHD were calculated and compared in 60 lesions. Lesions were stratified according to injected activity (standard dose 3.7 or half dose 1.8 MBq/kg) and lesion dimension (range 6-50mm, cut-off 15mm). SUVmax and SUVpeak variability was analysed as a function of the acquisition time (from 45s to 2min/FOV for standard dose and from 2min to 4min/FOV for half dose) and different beta parameters. Patients' height, weight and BMI were also balanced between compared datasets. Results: SUVmax and SUVpeak showed a complete overlap between measurements with decreasing acquisition time/FOV in both VPHD and Q-Clear reconstructions (maximum difference below 5% and linear regression model $p<0.0001$). Quantification was not affected by time of acquisition/FOV both in small and larger lesions, whereas SUVmax and SUVpeak were significantly influenced by variation of beta values and differences were higher in small lesions (37% and 15% for SUVmax and SUV peak, respectively) with respect to larger ones (14% and 6%). A maximum difference of 38.5% between VPHD and Q-Clear was measured for SUVmax quantification in smaller lesions group. Conclusion: Our data showed that SUVs were not affected by acquisition time/FOV with this new high sensitivity PET/CT system, both for small and large lesions. According to our results, quantification stability could allow the therapy response assessment with different acquisition time, condition sometime requested by patient compliance or clinical workflow.

P034

Impact of a new Bayesan penalised likelihood reconstruction algorithm on ^{68}Ga-DOTA-TOC PET/CT imaging

M. Scarlattei[1], G. Baldari[1], S. Migliari[1], C. Ghetti[2], C. Cidda[1], G. Serreli[2], L. Ruffini[1]; [1]Nuclear Medicine Dept, University Hospital of Parma, Parma, ITALY, [2]Medical Physics, University Hospital of Parma, Parma, ITALY.

In PET reconstruction standard iterative algorithms have different numbers of iterations, subsets and filters. It is now available a new Bayesian penalised likelihood reconstruction algorithm (QC, GE Healthcare, Milwaukee, USA) that requires only one input the penalisation factor (named beta).Aim of our study was to investigate clinical impact of QC algorithm compared to standard reconstruction approach (VP) in PET/CT study with ^{68}Ga-DOTA-TOC.Nineteen patients (7 men, 12 women; 13-80 years) with known or suspected NETs and tumours other than NETs underwent ^{68}Ga-DOTA-TOC PET/CT. All studies were performed on a Discovery IQ scanner (GE healthcare, Milwaukee, USA). Patients did not receive medical treatment before exam. Main indications for NETs were staging, follow-up and recurrence; for the suspected NETs increased tumor markers, clinical symptoms, and findings in conventional imaging; for non-NETs lesions indication was the SST receptor status for receptor radiotherapy with labeled SST analogues.Whole body PET/CT was performed according to the standard protocol (head-to-mid-thighs) 60 minutes after 68Ga-DOTA-TOC injection (130-220 MBq). Images were processed using QC for a range of different beta values (100-1000) and standard VP reconstruction (2 iterations, 24 subsets, 6.4mm filter).We analyzed images in a qualitative and semiquantitative way. Lesion and liver SUVmax, and liver SUV mean were measured on VP and QC images, using a VOI drawn on the PET transaxial slice presenting the highest uptake value. The maximum diameter of each lesion was measured on transaxial CT images.^{68}Ga-DOTA-TOC PET/CT was positive in 6/19 patients (31.6%). Lesions were visually localized in the meninges, lung, small bowel, lymph nodes, bone and sympathoadrenal system.A lesion-by-lesion analysis was performed and in patients with multiple foci lesion with the highest uptake was assessed. Mean lesion SUVmax was 26.3 and 32.4 in VP and QC images, respectively, Mean liver SUVmax and SUVmean were 11.03 and 11.3, 7.7 and 7.8 in VP and QC images. Mean lesion diameter was 24 mm (9-70). Micrometastases of the bone were not

completely visualized by VP images (1 patient with two bone lesions on QC images and uncertain VP; SUVmax 1.8 and 3.5 in VP and QC images)**Conclusion**: the Bayesian penalised likelihood reconstruction algorithm (QC) achieves a significant increase of SUVmax values measured in the lesions compared to the VP (32.4 vs 26.3) on 68Ga-DOTA-TOC PET/CT images. QC shows higher sensitivity in the detection of bone lesions. This new algorithm is likely to improve global cancer detection, especially for small lesions.

P035

Quantification with the new regularized reconstruction algorithm QClear in 4D and QFreeze acquisition

A. Zorz[1], S. Morzenti[1], L. Guerra[2], M. Cuzzocrea[3], E. De Ponti[1], A. Crespi[1], M. Arosio[2], C. Landoni[3]; [1]Medical Physics, A.O. San Gerardo, Monza, ITALY, [2]Nuclear Medicine, A.O. San Gerardo, Monza, ITALY, [3]Nuclear Medicine, University of Milano Bicocca, Milano, ITALY.

Aim: The aim of this study is to evaluate how the quantification of lung and hepatic lesions changes when the new regularized reconstruction algorithm QClear in different motion management protocols and 3D standard acquisition is applied. Material and Methods: The latest generation of the Discovery PET/CT family (GE Healthcare - Milwaukee; WI-US) is equipped with the new regularized reconstruction algorithm QClear, an iterative algorithm that performs 25 iterations to reach full convergence. Image noise could be optimized setting the beta parameters according to the data statistics. This preliminary evaluation is performed on 13 patients submitted to a 3D scan of 1.5minutes/FOV with a 9 minutes 4D FOV integrated into the WB scan. Data are acquired in list mode in order to perform different reconstruction: a standard 3D image of 1.5 minutes with beta 350 (WB), a 4D image of 6 phases each of 1.5 minutes with beta 350 (4D-QC350) and a 4D image of 6 phases each of 30 seconds with beta 450 (4D-QC450). These last data are also processed with the QFreeze algorithm, that performs a non rigid coregistration of all the 4D bins to obtain motion corrected static images (QFreeze). Values of SUVmax and SUVmean of 13 lesions are collected. Results: The mean values of SUVmax of WB, 4D-QC350, 4D-QC450 and QFreeze are respectively 7.30, 9.39, 9.41, 7.24. The same values for the SUV mean are 4.44, 5.80, 5.79, 4.68. For the 4D reconstructions, the highest SUV values among all bins are reported. For both parameters, the comparison of QFreeze versus 4D-QC350 is statistically significant ($p<0.0001$ for SUVmax and $p=0.0001$ for SUVmean respectively), while the differences between QFreeze and WB and between 4D-QC350 and 4D-QC450 are not statistically significant. Conclusion: Using the QClear algorithm, the same quantification is obtained both in a standard WB protocol and in a motion management protocol based on a non rigid coregistration (QFreeze). However, 4D protocol permits to measure the highest SUVmax and SUVmean values. Furthermore, no changes in quantification are observed in 4D reconstructions reducing the acquisition time from 9 minutes/bed to 3 minutes/bed and optimizing the beta parameters.

P036

Quantitative SPECT/CT imaging using a commercial software

L. D'Ambrosio[1,2], L. Aloj[1], P. Chiaramida[3], V. Cerciello[2], P. Gaballo[1], A. Prisco[1], S. Lastoria[1]; [1]SC Medicina Nucleare, Istituto Nazionale Tumori Fondazione G. Pascale - IRCCS, Napoli, ITALY, [2]UOSD Fisica Sanitaria, Istituto Nazionale Tumori Fondazione G. Pascale - IRCCS, Napoli, Italy, Napoli, ITALY, [3]GE Healthcare, Rome, ITALY.

Aim Routine SPECT imaging lacks quantitative information. The use of CT attenuation correction and lesion localization based on the fusion of diagnostic CT and SPECT datasets can improve accuracy. This work aims to validate commercially available software (Q.Metrix, GE Healthcare) that provides absolute quantification (SUV) and investigates the feasibility of applying this software in clinical practice. Materials and methods For absolute quantification Q.Metrix needs data of patients, injected activity information and camera sensitivity. This software includes tools for performing reconstruction of SPECT/CT data with attenuation, scatter and collimator depth-dependent three-dimensional resolution recovery correction. Furthermore it includes also segmentation tools both on CT and NM images. All acquisitions were performed using hybrid dual-head SPECT-CT camera (Discovery 670, GE Healthcare). Camera sensitivity was evaluated for Tc99m and I131. Accuracy of activity quantification was performed on a large homogeneous source with addition of attenuating/scattering medium. A NEMA/IEC body phantom was utilized to measure recovery coefficients. Studies of patients undergoing Tc99m MAA lung perfusion scans and I131 in post-therapy scans were analyzed. Results Tc99m (I131) sensitivity factor was 71.4 (26.1) counts/MBq*s using a source in a petri dish and planar acquisitions as recommended by the manufacturer. A simulation utilizing homogeneous phantoms containing activities yielding SUV values of 1 for the two nuclides provided measured SUVmean values of 1.08 for Tc99m and of 0.75 for I131. Recovery coefficient varied from 0.88 (26.5 ml) to 0.27 (1.15 ml) for Tc99m and from 0.53 (26.5 ml) to 0.10 (1, 15 ml) for I131. Preliminary patient studies performed show the feasibility of quantitatively assessing lobar distribution of Tc99mMAA in the lungs and absolute quantitation of lesion uptake in post-therapeutic I131 scans. Conclusions Although inferior in accuracy to PET/CT this method can be applied on

clinical SPECT-CT systems and can yield reproducible results. The possibility of performing absolute quantitation of tracer uptake in Bq/ml opens the way for novel clinical and research applications using single photon labeled radiopharmaceuticals.

P037

Optimization of acquisition time of 68Ga-PSMA-ligand PET/MRI in patients with local and metastatic prostate cancer

S. Lütje[1], S. Blex[2], B. M. Schaarschmidt[3], A. Bockisch[1], T. D. Poeppel[1], A. Wetter[2]; [1]Clinic for Nuclear Medicine, University Hospital Essen, Essen, GERMANY, [2]Department of Diagnostic and Interventional Radiology and Neuroradiology, University Hospital Essen, Essen, GERMANY, [3]Department of Diagnostic and Interventional Radiology, Medical Faculty, University Düsseldorf, Düsseldorf, GERMANY.

Aim: Prostate cancer (PCa) causes significant morbidity and still is the second leading cause of cancer-related deaths in men in the Western world. ^{68}Ga-labeled HBED-CC-PSMA is a highly promising new tracer for imaging of PCa. The aim of this study was to optimize the acquisition time of ^{68}Ga-PSMA positron emission tomography/magnetic resonance imaging (PET/MRI) in patients with local and metastatic prostate cancer. **Materials and methods**: Eleven patients were administered intravenously with the ^{68}Ga-HBED-CC-PSMA ligand (116 ± 25 MBq) and subsequently underwent PET/MRI at 159 ± 57 min after injection. PET and MR imaging data were acquired simultaneously. PET acquisition was performed in list mode and PET images were reconstructed at different time intervals (1, 2, 4, 6, 8, and 10 min). Data were analyzed at these time intervals regarding PET image quality and radiotracer uptake in tumor lesions and muscle tissue. Uptake was quantified in terms of the maximum and mean standardized uptake value (SUV_{max}, SUV_{mean}) within a spherical volume of interest (VOI). Reference VOIs were drawn in the gluteus maximus muscle on the right side. PET image quality was evaluated visually by experienced nuclear physicians/radiologists based on a 1 - 5 (excellent - insufficient) scale. **Results**: Both SUV_{max} and SUV_{mean} correlated inversely with acquisition time and reached a plateau at acquisition times of 4 min and longer. PET image quality showed a linear correlation with increasing acquisition time, reaching a plateau at 4-6 min of image acquisition. **Conclusion**: The optimal acquisition time of ^{68}Ga-PSMA-ligand PET/MRI in patients with local and metastatic PCa appears to be 4 min per bed position. At this acquisition time, PET image quality reaches its maximum while SUVs do not change significantly beyond this time point.

P038

Development of advanced data acquisition methods for quantitative single photon emission computed tomography

K. MATSUMOTO[1,2,3], Y. Takahashi[4,2], A. Takaki[5], K. Murase[2], Y. Wada[3], Y. Watanabe[3], K. Endo[1]; [1]Kyoto College of Medical Science, Kyoto, JAPAN, [2]Osaka University Graduate School of Medicine, Suita, JAPAN, [3]Center for Life Science Technologies, RIKEN, Kobe, JAPAN, [4]Gunma Prefectural College of Health Sciences, Maebashi, JAPAN, [5]Fujifilm RI Pharma Co., Ltd., Tokyo, JAPAN.

Aim: The cerebral blood flow and metabolism SPECT images require high signal to noise ratio and spatial resolution for precise evaluation of the abnormal radioactive tracer distribution in the brain. The asymmetric SPECT acquisition such as an odd number of projections is significantly improved reconstructed image quality, because for an odd number of projections the sampling interval is half of the angular step of the detector and the number of angular sampling points is doubled. The interpolated projection data estimation (IPDE) method also improve the image quality, but the spatial resolution is degraded. On the other hand, the DRAMA (Dynamic RAMLA) is an iterative algorithm similar to the RAMLA, provides fast convergence with a reasonable signal to noise ratio by updating the image with row-action by applying the subset-dependent relaxation parameter. The purpose of this study was to develop a Hybrid SPECT reconstruction method by a combination of the asymmetric SPECT acquisition, IPDE method and modified DRAMA reconstruction algorithm. Methods:A Hybrid SPECT reconstruction method was evaluated to a two-dimensional Shepp-Logan head numerical phantom with statistical noise and a Hoffman 3-D brain phantom. A gamma camera, GE Healthcare Millennium MG, were used to scan images of a Hoffman 3-D brain phantom. For 360° SPECT, we simulated 16, 32 and 64 projections with an array 128 pixel per projection. Attenuation and scatter corrections of the Hoffman 3-D brain phantom SPECT image were performed using Chang's method and a modified triple energy window, respectively. Quality of the reconstructed images was evaluated in terms of mean structural similarity (MSSIM) values and a two dimensional power spectrum analysis. Results:As for the numerical phantom, the MSSIM values of each projections were 0.9584±0.0151 (16 projections), 0.9595±0.0308 (32 projections) and 0.9511±0.0433 in the 64 projections, respectively. In the radial distribution function of a two dimensional power spectrum analysis, each phantom SPECT images quality using Hybrid SPECT reconstruction method were approximately 1.5 times better than conventional method. Conclusions:The Hybrid SPECT reconstruction method showed faster resolution

recovery with lower noise than the asymmetric SPECT acquisition and IPDE method and yielded acceptable images in 2 or 3 iteration.

P039

Effects of mis-registration of CT attenuation-corrected on myocardial perfusion images acquired using multi-focus fan beam collimator SPECT/CT and conventional SPECT

H. ONISHI[1], K. Nakamoto[2], S. Kenda[3], Y. Kangai[1], N. Yada[1], T. Saho[1], T. Sakai[3], D. Hasegawa[3], M. Fukunaga[3], H. Amijima[4]; [1]Program in Biological System Sciences, Graduate School of Comprehensive Scientific Research, Prefectural University of Hiroshima, SHOBARA, HIROSHIMA, JAPAN, [2]Department of Radiology, Hiroshima prefectural Hospital, HIROSHIMA, HIROSHIMA, JAPAN, [3]Program in Health and Welfare Sciences, Graduate School of Comprehensive Scientific Research, Prefectural University of Hiroshima, MIHARA, HIROSHIMA, JAPAN, [4]Graduate school of nursing,Hyogo University of Health Sciences, KOBE, HYOGO, JAPAN.

Aims: Algorithms for attenuation correction in SPECT/CT systems have potential for mis-registration. The present study compares mis-registration of computed tomography attenuation correction (CTAC) in IQ-SPECT and conventional (180° apart: C-mode) myocardial perfusion images (MPI). Methods: Images were acquired from seven healthy volunteers who independently underwent SPECT/CT using 740 MBq of 99m-Tc-tetrofosmin, a parallel-hole collimator (LEHR) and the same system with IQ-SPECT (IQ-mode) modification using SMARTZOOM. C-mode images were acquired over 180°-contoured orbits with 30 views/detector for 12.5 s into 64 x 64 matrices and 4.8-mm pixels. We acquired IQ-SPECT images over 208°-cardiocentric orbits with 17 views/detector for 6.25 s/view into 128 x 128 matrices and 4.8-mm pixels. Both images were attenuation-corrected using CT images. The reconstruction software was Flash3D and specific Flash3D (OSCGM) for IQ-mode. The MPI SPECT/CT registration shifted the CT data by ±1, ±2, ±3 pixels along the cephalad/caudal, dorsal/ventral and left/right axes. The % uptake in 5-wall AC-MPI polar maps was scored for each region and the direction of the shift along each axis was statistically analyzed using Student's t test. We compared regions of mismatch on non-shifted images in C- and IQ-modes. Results: The % uptake did not significantly differ between shifted and non-shifted images when mis-registration affected only 1 or 2 pixels. The most significant effects on % uptake on AC polar maps were 16.6% and 5.2% changes in the lateral wall caused by a 3-pixel ventral shift in C ($p = 0.002$) and IQ ($p = 0.29$) modes, respectively. A 3-pixel dorsal shift resulted in statistically significant 13% ($p = 0.0001$) and 3.6% ($p = 0.43$) septal changes in C and IQ-modes, respectively. The significant change in IQ-mode was caused by three ($p = 0.009$) and two-pixel ($p = 0.04$) cephalad shifts. The mismatch in IQ-mode was increased by 10% - 20% compared with that in C-mode without changes in the septum and inferior wall caused by a right shift. A 3-pixel right shift increased the mismatch of the septum and inferior wall to 49.5% in IQ-mode. However, the mismatch in IQ-mode was improved by 52.2% compared with a 3-pixel ventral shift in the lateral and inferior wall in C-mode. Conclusion: Excessive mis-registration along the dorsal/ventral axis affected the quality of AC myocardial perfusion images most significantly. These findings suggested that mis-registration affects IQ-mode less than C-mode in MPI SPECT/CT images.

P040

Optimisation and clinical impact of PSF modelling reconstruction in PET-CT

B. J. Corcoran, C. Scott, D. RUIZ, E. Kalogianni, A. Eccles; King's College Hospital, London, UNITED KINGDOM.

Aims: To quantify the impact on PET image quality of PSF modelling in the reconstruction of time-of-flight PET/CT. Method: Images of a NEMA Image Quality phantom containing 6 spherical inserts, activity ratio of 4:1 hot spheres to background, were acquired on a GE Discovery 710 PET/CT scanner. The data was reconstructed with the existing clinical protocol: VPFX (VUE point FX, 2 iterations, 24 subsets). Further reconstructions then included the SharpIR (GE Healthcare) PSF modelling: VPFX+PSF (VUE point FX + SharpIR, 1/2/3/4/5 iterations and 24 subsets). Image quality parameters were calculated: coefficient of variation (CoV), signal to noise ratio (SNR) and contrast recovery (CR). Following the phantom study 19 patients were retrospectively reconstructed using VUE point FX (2 iterations, 24 subsets) with and without SharpIR correction. SUVmax and CoV were assessed in the liver. A 60mm diameter circular region was drawn on 3 different slices in the liver for each patient and the average calculated. Changes in SUVmax were calculated for all identified lesions. Results: Visual analysis of the phantom data, contrast recovery curves and SNR curves for the 6 inserts identified the optimum image quality for the reconstruction with VPFX+PSF (2 iterations, 24 subsets). In the patient study; for the VPFX+PSF reconstruction compared to the VPFX reconstruction, the mean difference in the CoV of liver regions was -9.2% and the SUVmax was -0.7%. For the lesions identified (n=56) the measured changes in SUVmax: increased (41), no change (6), decreased (9). Conclusion: We have optimised our reconstruction for time-of-flight plus PSF corrected acquisition. As shown by other authors the signal to noise is reduced in the

image by the application of PSF correction. The uncertainty in the effect on the SUVmax presents a challenge for its routine clinical use in quantitative analysis. Further work will investigate the effect of the PSF correction on tumour detectability.

P041

Influence of SPECT reconstruction algorithm on diagnostic accuracy of parathyroid scintigraphy: comparison of iterative reconstruction with filtered backprojection

G. Kara Gedik, O. Sari; Selcuk University Faculty of Medicine, Department of Nuclear Medicine, Konya, TURKEY.

Aim:The purpose of this study was to evaluate retrospectively the value of technetium-99m (Tc-99m) methoxyisobutylisonitrile (MIBI) single photon emission computed tomography (SPECT) and to compare the diagnostic accuracy of iterative reconstruction (IR) and filtered backprojection (FBP) reconstruction algorithms about localization of parathyroid lesions. Materials and methods:Forty-four patients with primary hyperparathyroidism (37 women and 7 men, age range: 26-76 years, mean age: 53.75±12.39 years), in whom histopathological correlation could be performed and who were cured after resection of abnormal parathyroid glands were included into the study. Mean serum PTH and calcium levels were 241.97±210.7 (range: 65-940 pg/ml, reference value: 12-65 pg/ml,) and 11.30±0,88mg/dl (range: 10-14.4 mg/dl, reference value: 8.4-10.2 mg/dl), respectively. Dual phase Tc-99m parathyroid scintigraphy, in which planar views were obtained 20 and 120 minutes after injection of 740 megabecquerel(MBq) Tc-99m MIBI, was performed with a dual-headed gamma camera (Siemens, Ecam signature) in all patients. Tomographic images were acquired 120 minutes after the administration of radiopharmaceutical. The SPECT datas were evaluated using an IR (ordered subsets expectation maximation) as well as a FBP algorithm. In 23 of 44 patients SPECT acquisitions were performed in 64x64 matrix, in the remaining 21 patients, tomographic datas were collected in 128x128 matrix. The imaging results were compared to pathological findings and sensitivities of both reconstruction algorithms and planar views were calculated. Results:Using planar MIBI scans, abnormal parathyroid glands were correctly localized in 75% of the cases. Sensitivity increased to 77% using SPECT with FBP and rose to 84% with IR. When the sensitivities were further calculated according to the acquisition matrix, it is found that in patients in whom 128x128 matrix was used, the sensitivities were 95% (20/21) and 85% (18/21) for IR and FBP, respectively. The sensitivities were lower in patients who were imaged with 64x64 matrix; with IR it was calculated as 74% (17/23) whereas with FBP, the sensitivity was 70% (16/23). Conclusion:In conclusion, compared to planar scintigraphy, Tc-99m MIBI SPECT is a more sensitive diagnostic modality in the detection of abnormal parathyroid tissues. Image quality and sensitivity further improves when larger matrices with IR are used instead of FBP algorithm.

P042

Optimization of image processing for better anatomical analysis of the striatum for SPECT scans of [99mTc] TRODAT-1

A. C. Trevisan[1], L. A. Santos[2], F. A. Pitella[2], E. N. Itikawa[1], M. Kato[2], V. Tumas[2], M. M. C. M. Brito[2], L. Wichert-Ana[2]; [1]Universidade de São Paulo, São Carlos, BRAZIL, [2]Universidade de São Paulo, Ribeirão Preto, BRAZIL.

AIM: Parkinson's disease (PD) is characterized by chronic, progressive and degenerative disorder. Brain SPECT scans using 99mTc-TRODAT-1 radiotracer evidence the striatal density of Dopamine Transporters (DAT). This is particularly important in the evaluation of PD. However, there was a need for standardized protocols for image reconstruction and processing, looking for a high image quality, and the reliability of medical reports. Particularly important are the identification of striatal morphology and the use of appropriated spatial resolution, contrast and noise. This study aimed to investigate the better image processing parameters associated with high morphological identification of striatal body. MATERIALS AND METHOD: Data were acquired in the BrightView XCT - PHILIPS using an anthropomorphic striatal phantom RS-900T, and the reconstruction algorithm was the iterative algorithm OSEM (Ordered Subsets Expectation Maximization). By choosing the iterations(i) (2,0 to 60,0) and subsets(s) (4,0 - 8,0 -16,0) by one independent specialist with grades 0-5, very bad to very good. After that the projections were reconstructed by varying the cutoff (0.1 - 0.3 - 0.5 - 0.7 - 1.0 - 1.5 - 2.0) and order (0.0 - 1.0 - 2.0 - 4.0 - 6.0 - 8.0 - 10.0) of the Butterworth filter, totaling 49 images. In a descriptive analysis of 3 specialists, there was the application in 0-10 grades, also was divided to very bad to very good. RESULTS: According to the analysis, using 3i 8s, it ensures higher quality reconstruction, differentiating the putamen and head of the caudate nucleus. It also found that the greater the number of iterations, worst was the image, with a higher incidence of noise and low spatial resolution; similarly, the higher the number of subsets, also worst was the image. Through a linear regression, with the average grade of 3 experts, we found that the best cutoff independent variable was 0,5 and the best order independent variable was 0, 0. But the image built with both variables, got better. Then the proposed range to obtain a quality image was 1.2 to 1.5 cutoff and varying the order of 0.0 to 10.0. CONCLUSIONS: This study found that the variables cutoff and order are not so good when it work independent. The above proposed range of cutoff

and order assured images with high contrast, high spatial resolution and low noise. This processing protocol enable the accurate differentiation of putamen and the head of the caudate nucleus, helping specialists to better delineate the striatal body.

P04 - Sunday, October 11, 2015, 4:00 PM - 4:30 PM, Hall 3, Poster Exhibition

Physics & Instrumentation & Data Analysis: Instrumentation

P043

Continuous-spectrum Emission Tomography (CET) for quantifying the absorbed dose of in-vivo bremsstrahlung

S. Vandenberghe[1], H. W. A. De jong[2], M. Bardies[3], D. Borys[4], M. de Jong[5], S. Walrand[6]; [1]MEDISIP, Department of Electronics and Information Systems, Ghent University, iMinds Medical IT-IBiTech, Gent, BELGIUM, [2]University Medical Center Utrecht, Utrecht, NETHERLANDS, [3]Institut national de la santé et de la recherche médicale, Toulouse, FRANCE, [4] Silesian University of Technology, Comprehensive Cancer Centre, Gliwice, POLAND, [5]Department of nuclear medicine, Erasmus Medical center, Rotterdam, NETHERLANDS, [6]Department of nuclear medicine, UCL, Brussels, BELGIUM.

Introduction: Personalized dosimetry based on quantitative images of radiopharmaceutical distribution in the body can substantially improve the effectiveness of radionuclide therapy. Current nuclear medicine imaging systems are optimized for diagnostic radionuclides and suboptimal for bremsstrahlung X- rays emitted by therapeutic radionuclides.Materials and methods: We present a novel molecular imaging modality, called CET (based on elements from CT, SPECT and PET) and specifically designed for collimating and detecting the high-energy secondary body generated bremsstrahlung X-ray photons. To efficiently detect incoming high-energy X-ray photons, conventional NaI SPECT detectors are replaced with high-density scintillators from PET. A first step in the design of the complete system is the evaluation of monolithic high-resolution detectors for this modality. LYSO, the most commonly used PET scintillator, is intrinsically radioactive due to the presence of Lu-176. This leads to a continuous background in the energy spectrum, making this scintillator not suitable for CET. Therefore simulations (using the input of the continuous Spectrum of Y-90) and measurements of high-density thick PET BGO crystals are compared to the results of conventional NaI detectors. CET also combines these detectors with pinhole collimators (from small animal SPECT), with small acceptance angles and minimal penetration.These are specifically designed for a wide energy spectrum and with the primary aim to reduce scatter and collimator penetration. To efficiently construct these complex collimators with high stopping power, additive manufacturing (3D printing) of tungsten powder will be used. Since no scatter windows can be used for X-rays, quantitative reconstructions will be obtained by modeling the remaining contamination in Monte Carlo-based image reconstruction. Finally Monte Carlo or other approaches will provide the information on the absorbed radiation dose.Results. A BGO detector of 2 inch has a high stopping power of more than 70% for all energies up to 1 MeV. The conventional 3/8 inch NaI works well at low energies but has only 17 % stopping power at 1 MeV. The main advantage of BGO comes from the high amount of direct photo-electric interactions and resulting smaller amount of Compton interactions arriving in lower energy window. A disadvantage of BGO is the smaller amount of scintillation light resulting in reduced energy resolution at lower energies (>30% at 100 keV and 15 % at 1 Mev).Conclusions. All components for building a CET system with specific use in radionuclide therapy have been identified and can be combined into a new molecular multimodality imaging system.

P044

Myocardial innervation and perfusion mismatch using cardiac dual isotope (123I-MIBG/99mTc-tetrofosmin) acquisition on two different CZT cameras: a phantom study

T. Blaire[1,2], A. Bailliez[1,2], D. Legallois[3], D. Agostini[3], A. Manrique[1,3]; [1]EA 4650, Normandy University, Caen, FRANCE, [2]Nuclear Medicine Department, IRIS, Polyclinique du Bois, Lille, FRANCE, [3]Nuclear Medicine Department, CHU Cote de Nacre, Caen, FRANCE.

Purpose: New Cadmium-zinc-telluride (CZT) cameras have dramatically increased sensitivity and energy resolution. This phantom study assessed the impact of dual isotope acquisition on the assessment of 123I/99mTc mismatch using two CZT cameras (DNM 530c, GE Healthcare and DSPECT, Spectrum Dynamics). Materials and methods: We used the anthropomorphic torso phantom (Data Spectrum, Hillsborough, NC) with the cardiac insert, successively filled with a solution of 99mTc alone, 123I alone and a mixture of 123I and 99mTc. Two defects were used: one (13mL) always filled with cold water (mimicking a matched defect) and one (5,4mL) filled with 99mTc when 99mTc solution was in the cardiac insert (mimicking a mismatched defect). A total of 12 datasets on each CZT camera was acquired using both energy windows (99mTc or 123I) with increasing acquisition times (7, 11, 22 and 33 minutes). Segmental uptake (%) for 99mTc and 123I and mismatch (difference of both segmental isotope uptake) were assessed using Corridor 4DM (INVIA Michigan) and a 17-

segment model. Statistical analysis used ANOVA and a linear model including the effect of camera, acquisition type (single vs. dual isotope), isotope (123I and 99mTc) and the interaction between camera type and isotope. Results: There was a slight but significant difference between the 2 cameras (DSPECT-DNM) in assessing 123I-99mTc mismatch in segments encompassing the mismatched defect (segment #5: mean difference: -3.12%, p<0,05; and segment #11: mean difference: -2.25%, p<0,05) . There was no difference in other segments. The linear regression model showed no impact of camera type and acquisition time on the magnitude of the mismatch. Lin's concordance correlation coefficient (CCC) showed an excellent concordance for single and dual isotope acquisition for the assessment of 123I uptake between DNM and DSPECT (CCC>0,82 and 0,93 respectively) and between single and dual isotope within each camera type (CCC>0.98 in DNM and CCC>0.84 in DSPECT). Conclusion: In this phantom study, the two CZT cameras (DNM 530c and DSPECT), with higher energy resolution and sensitivity yielded no significant difference between single (successive) isotope and simultaneous dual isotope acquisition and in the evaluation of myocardial innervation and perfusion mismatch.

P045

Ultrafast Bone SPECT Imaging of the Hands Using a Solid State CZT SPECT Camera

A. Frenkel, M. Kurash, O. Israel, J. A. Kennedy; Rambam Medical Center, HAIFA, ISRAEL.

Aim: To assess the feasibility of fast bone SPECT studies of the hands using a solid state camera (CSS) dedicated for cardiac imaging. Materials and Methods: A Discovery 570c SPECT/CT device (GE Healthcare) was used for phantom simulations and clinical fast SPECT imaging of the hands. Fast SPECT studies were performed using a 350 mL hand phantom filled with 37 MBq Tc99m-pertechnetate and with a 1.5 MBq 5 μL source that simulated a focus of abnormal uptake. Four patients referred for evaluation of pain in their hands were imaged at 2 hours after injection of 925 MBq Tc-99m MDP using a standard camera (Infinia Hawkeye 4, GE Healthcare) for a 10 min spot planar scan of the hands and performed an additional fast, 3 minutes SPECT study of each hand on the CSS. Image quality and diagnostic accuracy of the SPECT studies were assessed and referenced to the standard acquisitions. Results: List mode reconstructions using default regularization in the phantom study on CSS provided images with counting statistics consistent with total activity of 46, 9, and 3 MBq in one hand. The phantom-simulated uptake was clearly visible in low-count images without a negative effect on resolution or contrast. In patient studies, fast acquisition CSS provided good quality tomographic images. Three of the eight hands evaluated in the four patients had a normal appearance on the both the planar and SPECT studies. Six sites of increased focal uptake were found in the additional five hands. Findings on planar and SPECT studies concurred in three foci in the MCPJs and three in the PIPJs. Three foci of abnormal uptake in the MCPJs and one focal uptake in the PIPJ were detected only on SPECT. Conclusions: Phantom simulation studies and clinical studies in 4 patients using the solid state CZT device suggest that bone SPECT of a small anatomical region such as the hand can be successfully achieved providing high quality images and a higher lesion detectability rate associated with a 40 % reduction in acquisition time as compared to standard planar scintigraphy.

P046

18F-Choline intravenously infusion with an automatic combined dispenser and injector system.

A. MORETTI[1], P. CAROLI[2], R. GALASSI[1], V. D'ERRICO[3], C. DONATI[4], L. FANTINI[2], V. MAUTONE[2], G. GUALTIERI[2], G. BATTARA[2], G. PAGANELLI[2], F. MATTEUCCI[2]; [1]NUCLEAR MEDICINE UNIT AUSL ROMAGNA, FORLI', ITALY, [2]NUCLEAR MEDICINE IRST, MELDOLA, ITALY, [3]MEDICAL PHYSICS UNIT tIRST, MELDOLA, ITALY, [4]PHARMACY UNIT IRST, MELDOLA, ITALY.

In nuclear medicine, the doses of radiopharmaceuticals are extracted from multidose vials, using multipurpose fractionators contained within a leaded cell and are then administered to the patient with a manual injection. All these activities cause exposure to radiations to the involved personnel: in order to reduce this exposure, while ensuring the sterility of the preparations and the precision of the administered dose, we evaluated the use of an integrated system for fractionation / injection (Intego® Bayer, Inc., Warrendale, PA, USA).METHODS:We evaluated the fractionating and injecting process of 18F-choline by comparing the automatic mode performed with the Intego® apparel with the usual manual mode of administration of the dose, simulating the above steps for 84 times in a period of two weeks . This simulation involved a total of four operators : three radiology technicians and one nurse; in order to obtain the most accurate and precise meausure of the exposure the personal was monitored by using TDL dosimeters placed on the fingertips both in the Intego® and in the manual mode.Sterility was evaluated by using media fill tests. In order to verify the correspondence between the required dose and fractionated dose, both in the automatic mode than in the manual one, it has been used the same counter properly calibrated.RESULTS:The verification with the media fill test has confirmed the sterility both in the procedure of fractionation / traditional injection than in the one that has used

INTEGO.The accuracy of the fractional dose and subsequently measured in the counter showed a difference between the traditional method and the one with INTEGO lower than the value determined by EANM guidelines (<3%).Compared to traditional methods, the administration with INTEGO showed a much lower (1 MBq than 7 MBq) residual activity in the patient administration set (PAS).From a dosimetric point of view, the comparison between the data of exposure of the involved personnel showed a 75 % reduction (2.36 +/- 0.8 mSv at 0, 6 +/- 0.3 mSv / year).CONCLUSION:Intego® is a useful tool in the operations of fractionation and injection of 18F-choline ensuring accurate and sterile doses and allowing in the same time a significant reduction in the exposure of the personnel

P047

Development of Radionebulizer Equipment for Diagnostic in Nuclear Medicine

A. F. Viana[1], P. Nabinger[1], R. Madke[1], P. Madke[1], P. R. Fereira[2], R. Anele, Filho[3]; [1]Grupo RPH, Porto Alegre, BRAZIL, [2]Bhiosupply, Porto Alegre, BRAZIL, [3]CETA/SENAI, Porto Alegre, BRAZIL.

Ventilation/perfusion (V/Q) SPECT (Single-photon emission computed tomography) of lung are indicated for the diagnostic of pulmonary embolism (PE), alveolitis, chronic obstructive pulmonary disease (COPD), among others. The combination of the ventilation and perfusion exams not only improves the diagnostic accuracy of the method but also facilitates the application of advanced image-processing techniques. In Brazil, many Nuclear Medicine Services are no longer performing the ventilation exam due to the cost of the devices necessary for the inhalation of radioaerosol. The objective of this project was to develop an affordable and easy to use radioaerossol nebulizer device for diagnostic use in nuclear medicine. The radioaerosol production technology is based on the Venturi principle, in which the apparatus is coupled to a source of compressed air producing a suitable aerosol particle (<1.5 microns) to produce pulmonary diagnostic image. The device consists of a ready-to-use blister composed of 2 chambers with isolating valves. This design allows the simple injection of the radiopharmaceutical, its nebulization and the decantation of the particles bigger than the defined size. The blister has two breathing hoses, one for the inhalation and other for exhalation. The system is also composed of a lead shield that accommodates the blisters perfectly, and protects the patient and operator from energies of 140 KeV, and a mechanism to hinder the reutilization of the blister, avoiding crossed contamination between patients. Our team was able to develop an inexpensive blister and lead shield that is reimbursed by the Brazilian Heath Care System (SUS). This project was supported by a Brazilian Federal grant from SENAI/SESI and has the patent deposit number BR 10 2014 029318 3.

P048

Monte Carlo Simulations of Beta Particle Measurement Using Cerenkov Luminescence Imaging or Beta Detection

L. Altabella, C. R. Gigliotti, A. E. Spinelli; San Raffaele Scientific Institute, Milano, ITALY.

Aim: Recently Cerenkov luminescence imaging (CLI) has been introduced as a novel tool to image in vivo the biodistribution of beta plus and beta minus emitters for both human and animal models. CLI is normally performed using a CCD detector in combination with a set of lens and filters. In this work we investigated through Monte Carlo simulations the feasibility of beta imaging of small animals with CLI or direct and indirect beta detection using beta emitters commonly used in Nuclear Medicine. CLI is based on the detection of Cerenkov photons generated in the medium when beta particles travel with a velocity greater then the speed of light in the medium. Direct and indirect beta detection are based on direct interaction with the detector or a conversion into light by means of a scintillator.Materials and methods: Monte Carlo simulations were implemented using Gamos plug-in for Geant4. We considered a slab of mouse muscle and a radioactive point sources of 32P and 90Y placed at different depth from 1 mm to 3 mm. Cerenkov photons and beta particles are collected at the exiting surface in detector direction. For indirect detection a 0.2 millimeter CsI(Tl) scintillator has been positioned at the top detector.Results: Direct beta detection show a better resolution (FWHM 2.32 mm for 32P and 2.44 mm for 90Y at 1 mm depth) with respect to CLI (FWHM 3.69 mm for 32P and 3.98 mm for 90Y at 1 mm depth) in spite of less counts. For superficial sources and direct beta detection no significant differences are found in resolution between 32P and Y90, while 32P shows a better resolution for CLI with respect to 90Y at deeper source (about 1 mm difference for 3 mm source depth). For indirect beta detection, we obtain a FWHM of 2.71 mm with 1 mm source depth.Conclusion: Direct or indirect CCD beta detection represents a good set up in terms of spatial resolution for beta radionuclide imaging however only a limited field of view (FOV) can be usually covered with this imaging setting. On the other hand CLI allow a much larger FOV (several cm) using conventional small animals optical imaging systems and is thus a more flexible approach.

P049
Attenuation Correction in Planar Scintigraphy Using Transmission Measurement with Flood Source

M. Samal, V. Sirova, D. Skibova, J. Trnka, V. Ptacnik, J. Kubinyi; Charles University Prague, Prague, CZECH REPUBLIC.

In planar scintigraphy, Tc-99m flood source is used for transmission measurement and subsequent attenuation correction (AC) in Tc-99m emission data. Alternative Co-57 flood source is faster, safer and easier to use but emits lower energy radiation. The aim of the phantom study was to test Co-57 flood source for AC in Tc-99m emission data. Methods: Two 100 ml plastic vials were attached to the rods of Jaszczak phantom and filled with 2 different activities of Tc-99m. Volume of the phantom was filled with inactive and active water backgrounds (1:8 and 1:4 with respect to a weaker vial). Emission measurements were made simultaneously by 2 camera detectors in upper and lower positions. Transmission measurements (with inactive phantom) were performed using Tc-99m and Co-57 flood sources placed below the phantom on elevated edges of lower detector. Acquisition was performed in photopeak and scatter windows. Two types of transmission images were recorded with each flood source: (a) with and without phantom by upper detector only, (b) with phantom by lower and upper detectors simultaneously. Recorded data were checked for registration and corrected for decay, table attenuation and detector sensitivity. Geometric mean (GM) of emission data was corrected for attenuation and background. Scatter was compensated using dual-energy window (DEW) or broad-beam (BB) attenuation coefficient. Recovery of total activity in both vials and relative activity in the vial with higher activity were calculated as percentage of simulated activity and percentage of total measured activity in both vials. Results: Phantom thickness calculated pixel-wise reflected well mechanical dimensions of the phantom. Tc-99m and Co-57 thickness maps were applied to correct GM data. Without AC, only 30% of simulated activity was recovered. Recovery increased to 91-92% using BB attenuation coefficient 0.12 and to 100-104% using DEW and attenuation coefficient 0.15. Best recovery (100-101%) was obtained using BB attenuation coefficient 0.13. No significant differences were found between Tc-99m and Co-57 maps and the 2 methods of transmission measurement. Regardless of AC, relative activity of stronger source (65%) was recovered accurately with mean absolute error of 0.97%. Estimated dose to the patient from 1-minute exposure to Co-57 flood source of medium activity was below 5 microSv. Conclusion: Pixel-wise maps of object thickness obtained by transmission measurements using both Tc-99m and Co-57 flood sources are sufficiently accurate to correct for attenuation in geometric-mean Tc-99m emission data. Using the simple method, planar scintigraphy can approach quantitative accuracy comparable with more sophisticated techniques.

P050
The Influence of Cardiac ROIs Contour Definition at Heart-to-Mediastinum Ratio in 123I-MIBG Scintigraphy

A. Sá Pinto, T. Vieira, S. Chaves, V. Alves, T. Faria, A. Oliveira, A. Fernandes, M. Pérez, J. Pereira; Centro Hospitalar de São João, Porto, PORTUGAL.

Aim: Metadiodobenzylguanidine labelled with 123I (123I-MIBG) is used for assessing the myocardial adrenergic system. Despite its highly independent prognostic value in heart failure, it is important to improve standardized acquisition methods and assessment criteria. We aim to study the correlations of the heart-to-mediastinum ratios (H/M) obtained through the application of different regions of interest (ROIs) at the heart, and with different acquisition methods.Methods and Material: Six patients sent to our Nuclear Medicine Department for oncological evaluation were randomly selected. Images' acquisition started 3 hours post-injection of 123I-MIBG (185-370 MBq). Twosequential thoracic static (TS) images, of 5 minutes (5M) each, were acquired (LEHR collimators; 256x256 matrix; 20% energy window set on 159 keV); immediately after, this step was repeated using ME collimators. Then, a whole body (WB) scanning was acquired (LEHR collimators; 256x1024 matrix; scan speed of 10 cm/min). Scatter Correction (SC) was applied defining a second window (130 keV +/- 10%), during the acquisition of TS and WB imaging, when using LEHR collimators. Ten minute images (10M) were obtained summing the counts in the sequential 5 minute images. Three different types of cardiac ROIs were drawn by one experienced observer (irregular manual [MAN], elliptical [ELI, 900 pixels area] and circular [CIR, 21 diameter]) while one rectangular ROI (120 pixels area) was placed at the mediastinum (M). Eight images were used to calculate H/M ratio for each patient (MAN/M, ELI/M and CIR/M): 5M/LEHR, 5M/LEHR/SC, 10M/LEHR, 10M/LEHR/SC, 5M/ME, 10M/ME, WB, WB/SC. MAN/M, ELI/M and CIR/M ratios were defined as the ratio of average counts at the heart and mediastinum. The correlations of MAN/M with ELI/M (C1), MAN/M with CIR/M (C2) and ELI/M with CIR/M (C3) were analyzed using IBM SPSS version 22.0.Results: Concerning C1, we obtained $rs = 1$ ($p < 0.001$) for the 8 images. Regarding C2, $rs = 0.943$ ($p < 0.005$) for images 5M/LEHR, 5M/LEHR/SC, 10M/LEHR and WB; for images 10M/LEHR/SC, 5M/ME, 10M/ME and WB/SC the $rs = 1$ ($p < 0.001$). C3 had a $rs = 0.943$ ($p < 0.005$) for images 5M/LEHR, 5M/LEHR/SC, 10M/LEHR and WB; for 10M/LEHR/SC, 5M/ME, 10M/ME and WB/SC the $rs = 1$

($p < 0.001$).Conclusion: H/M ratio values obtained with different methods of cardiac contour in 123I-MIBG scintigraphy seem to have excellent correlation across several methods of image acquisition. Collimation and electronic SC, as well as the duration of acquisition, may influence ROIs' definition.

P051

Performance Evaluation of a Gamma-Probe for High Energy source (131-Iodine) for Oncologic Purposes

E. N. I. Itikawa[1,2], L. A. S. Santos[1,3], D. K. S. Sonvenso[1,3], M. K. Kato[1,3], F. A. P. Pitella[1,3], C. E. P. B. Baltazar[1,4], A. C. T. Trevisan[1,2], E. R. M. Moraes[1,5], **L. W. A. Wichert-Ana**[1,2,3]; [1]Ribeirão Preto School of Medicine, Ribeirão Preto, BRAZIL, [2]Post-Graduation Program Interunits Bioengineering EESC/FMRP/IQSC-USP, São Carlos, BRAZIL, [3]Postgraduation Program in Internal Medicine, Ribeirão Preto, BRAZIL, [4]Faculty of Philosophy, Sciences and Literature of Ribeirão Preto, Ribeirão Preto, BRAZIL, [5]Faculty of Philosophy, Sciences and Literature of Ribeirão Preto, Ribeirão Preto, Ribeirão Preto, BRAZIL.

AIM: To evaluate spatial, angular and energy resolution; shielding and sensitivity of a high energy gamma-probe according to international standards for non-imaging intraoperative probes. The objective was to assure its usefulness in sentinel lymph node localization and reminiscent thyroid cancer.
MATERIAL AND METHODS: We tested the wide-range energy isotope (0.11-1 MeV) CsI-Tl probe. Low activity sources of 99m-Tc and 131-I were used in the performance tests. Spatial, angular and energy resolution were calculated in terms of FWHM. Shielding was calculated based on the intrinsic sensitivity in the probe axis. The collimator device was used to evaluate shielding; angular and spatial resolution. All the tests of this study were designed as suggested by international standards for non-imaging intraoperative probes and studies in the literature.
RESULTS: The probe was capable to solve two closely sources of 131-I and 99m-Tc only by using the collimator device in the spatial resolution test. Values of 18.3 and 10.91-FWHM(mm) were achieved, respectively. Angular resolution showed similar performance for 131-I and 99m-Tc, with better results by using the collimation. We found values of 51.4 and 29.2-FWHM(°), respectively. Energy resolution showed a value of 13.2-FWHM(%) for 131-I. Shielding test showed that the probe tip was not capable to stop high-energy photons of 131-I as desirable, even increasing lateral thickness with the collimator device. Better results were obtained with 99m-Tc. The sensitivity test showed a value of 682 and 276-cps/MBq for 131-I and 99mTc, respectively. **CONCLUSIONS**: Consistent results in the tests were achieved only by using the collimator device. Meanwhile, the use of the intraoperative probe without the collimator should not be discarded. We must consider that the tested high-energy gamma-probe needs a robust design such as a thicker lateral shielding. Furthermore, it could not be achieved without increasing the size of the crystal detector because thicker and high-density crystals tend to effectively stop high-energy photons. On the other hand, it affects geometric parameters of detection, i.e. spatial and angular resolution. Thus, the collimator was prior to improve spatial and angular resolution as it reduces the field of view of the crystal detector. Our study design is according to international standards for evaluation of non-imaging gamma probes and showed feasible results that corroborates to accurate localization in oncological intervention, i.e. melanoma, thyroid and breast cancer.

P052

Evaluation of Physical Detection Parameters of a Gamma Probe for Sentinel Lymph Node Localization in Melanoma and Breast Cancer.

E. N. I. Itikawa[1,2], L. A. S. Santos[1,3], D. K. S. Sonvenso[1,3], M. K. Kato[1,3], F. A. P. Pitella[1,3], C. E. P. B. Baltazar[1,4], A. C. T. Trevisan[1,2], E. R. M. Moraes[1,5], **L. W. A. Wichert-Ana**[1,2,3]; [1]Ribeirão Preto School of Medicine, Ribeirão Preto, BRAZIL, [2]Post-Graduation Program Interunits Bioengineering EESC/FMRP/IQSC-USP, São Carlos, BRAZIL, [3]Postgraduation Program in Internal Medicine, Ribeirão Preto, BRAZIL, [4]Faculty of Philosophy, Sciences and Literature of Ribeirão Preto, Ribeirão Preto, BRAZIL, [5]Faculty of Philosophy, Sciences and Literature of Ribeirão Preto, Ribeirão Preto, Ribeirão Preto, BRAZIL.

AIM: To evaluate angular, spatial and energy resolution, side and back shielding and the final sensitivity according to international standards of quality control for non-imaging probes. The objective in our work was to assure its usefulness in sentinel lymph node localization in patients with melanoma and breast cancer patients.
MATERIAL AND METHODS: We used a CZT probe detector EUROPROBE II ® (Eurorad, Italy) for low energy isotope (20 ~ 170 keV). The tests were performed with low activity 99m-Tc radiation sources (12 MBq upper) and also, acrylic devices for point sources and scatter medium simulators were developed to run the tests. Count acquisition was performed through time integration mode. Shielding, angular, spatial and energy resolution were also evaluated by using a collimator, a device that increases the lateral shielding and decreases the sensitive area of the detector tip, in the shielding, angular, spatial and energy resolution tests. **RESULTS**: The probe showed 31.4° and 31.6°-FWHM for 3 and 30

centimeters-distance, respectively, in the angular resolution test. Spatial resolution showed the capability of the probe to solve two closely sources of radiation through a scatter medium of 10 mm as well as the resolution test, which demonstrated a 20.5-FWHM(%) and proved to correctly discriminate the photopeak of 99m-Tc (140-keV). The gamma probe also showed good intrinsic sensitivity of 510 counts per second per unit of activity (cps/MBq), value within the suggested by its guideline in similar conditions of detection. Finally, the side and back shielding test proved that the probe tip is efficient to stop photons that come from residual or background radiation. We observed similar performance in the tests when using the collimator. As expected, the reduction of the sensitive area by the device improved the visualization of both point sources in the spatial resolution test, and reduced the FWHM values in the angular resolution test. **CONCLUSION**: The tested gamma probe showed results which are according to the international guideline for non-imaging intraoperative probes and results found in the literature. Gama probe has an important rule to access sentinel lymph nodes under difficult conditions of localization. Indeed, this tool is expected to have detection parameters consistent to this purpose and, through the results of our study, which is according to the international standard of quality criteria for non-imaging probes, we can attest its feasibility for applications in oncology.

P53

The General Idea and the Functionality Behind Real-time Handheld Emission Spot Allocator (rthESA) for Simultaneous Fusion Imaging with Ultrasound

C. Kühnel, T. Winkens, M. Freesmeyer; Jena University Hospital, Jena, GERMANY.

Objectives: First, to report on initial experiences and technical parameters of a newly developed real-time handheld emission spot allocator (rthESA), and second, to report on the simultaneous acquisition of rthESA and US data as rthESA/US fusion images. Methods: The rthESA consisted of five semiconductor-detectors made of Cd-Zn-Te arranged in alternate position in two rows. This design allowed the examination of focal activities in the same plane as US. The signals were interpreted by an ad hoc software (algorithm) and the real-time allocation of spot radiation sources within air- and water phantoms was investigated for 99mTc, 131I, and 18F. A compact intraoperative US probe (39mm transducer) was fixed in plane with the rthESA and connected to a standard US equipment. Experiments with a liver phantom were performed to verify the integration of 99mTc-rthESA data and US images. Results: The allocation proved to be successful for all radionuclides. The system showed a noticeable performance latency, most pronounced for positions far from the detector (1cm distance: 0.7 ± 0.5 sec; 4cm distance: 6.1 ± 3.2 sec). Within the liver phantom, the rthESA enabled the correct allocation of a spot radiation source within a live US image. Conclusions: The rthESA allowed an exact localization of spot radiation sources in single plane, with additional consideration of the distance from the detector, leading to real-time allocation and simultaneous overlay with US images. In spite of clear technical limitations in need of further development, this proof-of-concept study shows that this hybrid detector has the potential to provide integrated simultaneous nuclear medicine and US images.

P54

Hybrid Integration of Real-Time Ultrasound and Freehand-SPECT: First Experiences and additional informations about Radiation Exposure of the Investigator

C. Kühnel, T. Winkens, T. Opfermann, M. Freesmeyer; Jena University Hospital, Jena, GERMANY.

Objectives: Hybrid imaging has been a successful way to overcome the limitations of functional imaging. However, no integrated concept for combining ultrasound with nuclear medicine imaging has been presented up to date. We investigated the feasibility of a quasi-integrated free-hand single photon emission tomography/ultrasound (99mTcO4-fhSPECT/US) fusion imaging concept in patients with thyroid diseases. Additionally, the radiation exposure of the investigators' hand was assessed during 99mTcO4-fhSPECT/US of the thyroid. Methods: Thirty four patients were examined. After application of 75 MBq 99mTc pertechnetate intravenously, fhSPECT was performed using declipseSPECT® (SurgicEye, Munich, Germany) and navigated ultrasound using LOGIQ® E9 (GE Healthcare, Milwaukee, WI, USA). Three-dimensional SPECT data were reconstructed and transferred to the ultrasound system. The combination of two independent positioning systems enabled real-time fusion of metabolic and morphologic information during ultrasound examination. Conventional dosimetry was performed by rings with thermoluminescence detectors (TLD) and compared with the ambient dose rate, which was measured by dose rate meters (DRM), and the measurement time. Results: All examinations were technically successful. Only minor limitations in fusion offset occurred. The fhSPECT system's poor spatial resolution was the reason for further limitations. The mean

exposure per investigation was 7.53 μSv by ring dosimetry and 9.02 μSv by DRM. Conclusion: FreehandSPECT/ultrasound fusion concept proved feasible and applicable; however, technical improvements are necessary. The hand exposure in clinical routine is not expected to add a relevant risk.

P55

An integrated framework of recovering triple coincidence for enhancing PET sensitivity

H. Lin, Z. Wei, C. Chiang, K. Chuang; National Tsing Hua university, Hsin Chu, TAIWAN.

Aims: Triple events caused by simultaneously detection of three photons are usually discarded as the annihilation information being mixed with another detection induced from one of the annihilation photons scattering (inter-detector scattering triple, IDS) or from an annihilation photon from a separate decay (random triple, RnT). In addition, for non-pure positron emitter, a particular positron-gamma (β+γ) triple can be produced due to the presence of the cascade gamma ray. The majority of the triple coincidence contains the true photon pair that can be possibly recovered. To this end, we proposed an integrated framework of recovering triple coincidence events to enhance the sensitivity of PET imaging for pure and non-pure positron emitters.Materials and Methods: Multiple energy window settings were first used to classify the triple event into IDS, RnT and β+γ events. Then, different recovering strategies for IDS, RnT, and β+γ triple using combined likelihoods based on energy, temporal and double coincidence information were developed to identify the true LOR. A Biograph mCT PET scanner was modeled with a house-made GATE/MPHG Monte Carlo code. We evaluated the performance of the proposed method on a NCAT phantom at various activity levels of F-18, I-124, and Br-76.Results: Preliminary results using the simulated data show that the accuracy of recovering triple coincidence can achieve around 87% for IDS, 90% for RnT, and 82% for β+γ at 10 mCi. We found that about 15% of the triple coincidence for F-18 can be recovered using the proposed method, while increasing this ratio substantially for non-pure emitters (28% for I-124 and 43 % for Br-76).Conclusion: We conclude that the proposed integrated framework can improve the counting statistics of clinical PET imaging for pure and non-pure positron emitters, especially in high activity PET imaging.

P56

Monte Carlo Modelling and Experimental Verification of a GE Optima SPECT System: Towards Characterisation of Collimator Response

A. Grimwood[1], T. Kostou[2], P. Papadimitroulas[2], G. Loudos[2], L. Livieratos[3], J. Scuffham[1]; [1]Royal Surrey County Hospital, Guildford, UNITED KINGDOM, [2]Technological Educational Institute of Athens, Athens, GREECE, [3]King's College London, London, UNITED KINGDOM.

Aim: Monte Carlo simulations are an effective tool for characterising detector performance [1]. We employ the GATE application to model the GE Optima SPECT system. Our goal is to characterise detected photons by their interactions (direct, scattered and septal penetration) through simulation. This information can be used to optimise reconstruction of real image data [2]. To be effective, there must be good agreement between simulated and experimental results. This project is a verification between the clinical system and simulated model.
Materials and methods: The Royal Surrey County Hospital operates a GE Optima NM/CT 640 for I-131 sentinel lymph node imaging. High energy scatter and septal penetration artefacts are prevalent and can obscure features in these images. Using manufacturer specifications, the Optima system was modelled in GATE 7.0, a Monte Carlo simulation application built upon GEANT4, using a standalone PC. Simulated spectra were acquired from point sources for both Tc-99m and I-131 to characterise system performance in three configurations (intrinsic, extrinsic and in-phantom). The simulated spectra were then compared with experimental data to verify the model. Finally, spectra for direct, scatter and septal penetration detections were acquired from the simulation results and used to characterise their relative contributions to the overall spectrum. This in turn enabled us to model the collimator-detector response function.
Results: Good agreement has been achieved between the simulated and experimental spectra for both Tc-99m and I-131 sources. The separate contributions of direct, scatter and septal penetration detection events have been identified. It is demonstrated that these adequately describe features including: the characteristic lead X-ray peak, scatter peak and photopeaks. From the spectral data, collimator-detector response function was described for a simple point source planar image.
Conclusion: An effective Monte Carlo model of a clinical SPECT system has been constructed and used to characterise imaging performance using modest computing resources. Experimental verification has established the validity of the model. This sets the foundation for using the simulation as a tool in future work to optimise image acquisition and reconstruction parameters, such as energy windowing and resolution recovery.
References: [1] S. Jan, et al, GATE: a simulation toolkit for

PET and SPECT, Phys. Med. Biol., 49 (19), 2004, p4543 [2] N.G. Sakellios, et al, Monte-Carlo simulation for scatter correction compensation studies in SPECT imaging using GATE software package, Nuclear Instruments and Methods in Physics Research Section A: Accelerators, Spectrometers, Detectors and Associated Equipment, 569 (2), 2006, pp404-408

P57

Preclinical validation of automated DXA- and CT-based body composition measurements

J. Devriese[1], L. Beels[2], A. Maes[2], C. Van de Wiele[2], O. Gheysens[2], H. Pottel[1]; [1]KU Leuven campus Kulak, Kortrijk, BELGIUM, [2]Department of Nuclear Medicine, AZ Groeninge, Kortrijk, BELGIUM.

Aim: Semi-quantitative evaluation of tumor metabolic activity is possible through calculation of the standardized uptake value (SUV), defined as the ratio of measured radioactivity concentration to the injected dose per unit of volume of distribution. SUV is traditionally normalized for body weight. Lean body mass (LBM) has also been proposed as volume of distribution, since e.g. 18F-FDG distribution in fatty tissues is limited. LBM can be estimated by predictive equations, or measured by e.g. dual-energy X-ray absorptiometry (DXA) or computed tomography (CT). Accurate LBM measurements would lead to accurate and reproducible LBM-normalized SUVs. The purpose of this study is to determine and validate a set of Hounsfield unit (HU) ranges to segment CT images into tissue types and to test the validity of DXA tissue segmentation on pure, unmixed porcine tissues. Materials and methods: This preclinical prospective study was approved by the local ethical committee. Different quantities of porcine bone tissue (BT), lean tissue (LT) and adipose tissue (AT) were scanned using DXA and CT. Tissue type segmentation in two equal type DXA devices was performed via the standard clinical protocol and in CT through two different sets of Hounsfield unit (HU) ranges (Baracos et al., 2010, Clarys et al., 2010). Percent coefficients of variation (%CV) were used to assess precision while % differences of observed masses were tested against zero using the Wilcoxon signed-rank test. Results: Total mass is significantly underestimated by both DXA devices from true mass by 6.8% and 8.1% ($p = 0.016$). Total mass estimated by CT using both sets of HU ranges differ from true mass by 1.7% and 2.0% ($p = 0.69$). Both DXA devices systematically underestimate tissue type masses (BT, LT, and AT). BT mass differs from true BT mass by 78.2% and 75.8%, and for other tissue types masses are underestimated by 10.4% and 8.1% (LT) and 8.3% and 11.3% (AT). CT does not systematically over or underestimate tissue type mass. There are smaller differences from true mass, ranging from -8.8% to 10.4%. Conclusion: Automated tissue segmentation using CT images and a solid set of HU ranges is a valuable method, since these measurements were reproducible and accurate. This technique offers several possibilities in future research and clinical settings, and can become a valuable tool in quantitative nuclear medicine.

P58

Evaluation of image quality on PET/CT with Flow motion technology –Does it keep quantitative performance and uniformity ? -

K. Murakami, T. Nakahara, Y. Ogata, Y. Iwabuchi, M. Katagiri, Y. Matsusaka; Keio University, Tokyo, JAPAN.

Øbject: To compare image quality obtained by continuous table motion (Flow motion technology; FMT) to conventional method (Step and shoot; SS).This time we focused to compare quantitative performance and uniformity by analyzing SUV of liver.Materials and Methods: Biograph mCT Flow Motion(Siemens) enables us to obtain image both by using FMT and SS. After injection of FDG with 3.5MBq/kg, we acquired PET image 2 hours later using FMT and SS. To avoid influence of time difference, patients ware divided two groups at random. One group was obtained image using SS first following FMT, and another group was FMT first following SS. All patients had no abnormality in the liver. ROI was settled in right lobe of the liver with 2cm in diameter. Total number of patients were 30 cases. SUVmax and SUVstd were measured and analyzed.Results: By using SS, SUVmax=2.77±0.46, SUVstd=0.248±0.058,by using FMT, SUVmax=2.61±0.45, SUVstd=0.208±0.062. Consequently, SUVmax of FMT is lower compared to SS about 5.7%, and SUVstd also lower in FMT.Conclusion: SUVmax of FMT is a little bit lower compared to that of SS. One of the reason may improvement of uniformity in FMT to reduce SUVstd.

P05 - Sunday, October 11, 2015, 4:00 PM - 4:30 PM, Hall 3 – Poster Exhibition

Physics & Instrumentation & Data Analysis: Data Analysis

P059

18F-Fluorodeoxyglucose (18F-FDG) PET pulmonary imaging: comparative methodology in COPD patients

A. M. Fletcher[1], G. Choudhury[1], T. Clark[1], M. Connell[1], S. Fergusson[1], R. Rabinovich[1], N. Weir[1], B. Whitcher[2], I. Kilty[2], B. Vennart[2], E. J. R. van Beek[1], W. MacNee[1]; [1]University of Edinburgh, Edinburgh, UNITED KINGDOM, [2]Pfizer Worldwide Research and Development, Cambridge, MA, UNITED STATES.

Aim: To establish the optimum imaging and analysis protocol for FDG PET/CT imaging of lung inflammation in COPD patients in combination with quantitative CT analysis of emphysema. If successful the methodology could potentially be used to assess inflammation in the lungs to investigate the modulation of the FDG PET/CT signal as a biomarker of lung inflammation in drug development. Materials and Methods: Single-centre, exploratory, open-label study, of cross-sectional design to assess quantitative FDG PET-CT imaging in stable COPD patients. 20 patients with moderate-to-severe COPD underwent dynamic FDG PET imaging and high resolution CT (HRCT), combined with blood sampling to determine the localized plasma activity time curve twice 4 weeks apart. Images were analysed in the following manner: lung regions (lungs, thirds, lobes) were segmented on full inspiration HRCT and whole lung relaxed expiration attenuation correction (AC) CT using Apollo (VIDA Diagnostics, Coralville, USA). Two methods for removing emphysema were evaluated - eliminating areas below -950 HU on inspiration CT (standard for RA950) and removing the same relative area on relaxed expiration CT. Lung segmentation VOIs were transferred from full inspiration CT to PET by non-rigid registration of the full inspiration CT to the attenuation correction CT using ANTs(PICSL,UPenn). Arterial input functions (AIFs) were derived from either blood sampling or images. Finally the regional pulmonary FDG uptake was determined by SUV for 50-60 minutes. Patlak analysis of FDG time-activity curves from the lung VOIs (PMOD) generated estimates of slope (influx constant Ki) and intercept (initial volume of distribution). Results: Patlak intercept and SUV are correlated with lung density, and removing emphysema (particularly large contiguous regions) results in an increase in patlak intercept and SUV. There are issues with venous blood sampling, and image-derived AIFs when movement occurs. Conclusion: An optimum analysis protocol has now been determined. Methods of correcting for the density effect in quantitative PET lung studies require further investigation.

P060

Correlation of texture parameters with conventionally used semi quantitative parameter: standard uptake values, metabolic tumor volume and total lesion glycolysus in 18F-FDG PET/CT examination for breast cancer

N. Rana[1], K. Agrawal[1], D. Dhawan[2], A. Bhati[2], **B. Mittal**[1]; [1]Post-Grad. Inst. of Med. Education & Research, PGIMER, CHANDIGARH, INDIA, [2]Panjab University, CHANDIGARH, INDIA.

Background: Texture analysis (TA) is a set of computation methods that extract information from image on the basis of inter-relationships of pixels giving better insight of tumor heterogenity. Since metabolic heterogenity is a recognized characteristic of malignant tumor, TA is emerging as an important tool for evaluation of tumor uptake in PET studies. However, it needs to be established which indices could be of use and how they relate to conventionally used parameters. In our study we have classified texture parameters on the basis of their correlation with Standardized Uptake Values (SUVs), Metabolic Tumor Volume (MTV) and Total Lesion Glycolysis (TLG) in cases of breast tumor. Methods: Thirty-three patients with breast cancer who underwent whole-body PET/CT examination were included. TA in these patients was done using CGITA-Chang-Gung Image Texture Analysis toolbox, a software package based on MATLAB for texture analysis of molecular images having all built in functions for deriving different matrices like NGTDMs, GLRLMs, GLSZMs. PET/CT images in DICOM format of each patient were loaded on this software and sixty-nine texture parameters other than SUVs, MTV and TLG were derived by placing semi-automated ROI around active primary tumor. Conventional quantitative parameters like SUVmax, $SUV_{mean2.5}$, $MTV_{2.5}$, $TLG_{2.5}$ (threshold of SUV_{mean} = 2.5g/ml) and SUV_{mean40}, MTV_{40}, TLG_{40} (threshold of 40% of SUV_{max}) were also calculated for primary tumor using another semi-automated software for VOI placement to validate the SUVs value obtained using CGITA software. Linear correlation of each texture index with SUV_{max}, $SUV_{mean2.5}$, SUV_{mean40}, $MTV_{2.5}$, MTV_{40} and $TLG_{2.5}$, TLG_{40} was computed individually to study correlation between texture features and conventionally used quantitative parameters. Results: Texture parameters were classified as highly correlated (correlation coefficient $|r| \geq 0.90$), moderately correlated ($0.7 \geq |r| \leq 0.85$) and mildly correlated $|r| < 0.7$. Only three first order texture parameters were highly correlated to SUV_{max} and $SUV_{mean2.5}$. All texture parameters had $|r| < 0.50$ with SUV_{mean40}. Fourteen texture parameters were highly correlated and ninteen were moderately correlated

with $MTV_{2.5}$. Twenty-two were moderately correlated and none was highly correlated with MTV_{40}. Thirteen texture parameter were highly and twelve were moderately correlated with $TLG_{2.5}$. Only one texture parameter was moderately correlated with $TLG_{40.}$ Conclusion: Only few parameters had high correlation with SUV values, MTV_{40} and TLG_{40} indicating that a large number of texture parameters derived provide additional information. However level of significance of additional information provided by these texture parameters need to be tested further.

P061

Comparison of 3D texture features and metabolic parameters obtained from 18-F FDG-PET/CT images for evaluating tumor stage and subtype in non-small cell lung cancer

S. Karacavus[1], B. Yilmaz[2], O. Kayaalti[3], A. Tasdemir[4], E. Kaya[5], S. Icer[6], O. Ayyildiz[2], K. Eset[6], E. Vardareli[5], M. H. Asyali[7]; [1]Bozok University, School of Medicine, Department of Nuclear Medicine, Yozgat, TURKEY, [2]Abdullah Gul University, Department of Electrical and Electronics Engineering, Kayseri, TURKEY, [3]Erciyes University, Develi Hüseyin Şahin Vocational College, Department of Computer Technologies, Kayseri, TURKEY, [4]Kayseri Educational and Research Hospital, Department of Pathology, Kayseri, TURKEY, [5]Acıbadem University, School of Medicine, Department of Nuclear Medicine, İstanbul, TURKEY, [6]Erciyes University, Department of Biomedical Engineering, Kayseri, TURKEY, [7]7Department of Biomedical Engineering, Yıldız Technical University, İstanbul, TURKEY.

Aim: The purpose of this study was to compare three-dimensional (3D) texture features and metabolic parameters (maximum standardized uptake value (SUVmax, SUVmean), metabolic tumor volume (MTV), total lesion glycolysis (TLG) obtained from 18-F FDG-PET/CT images for evaluating tumor stage and subtype in non-small cell lung cancer (NSCLC). **Materials and methods**: Forty-two patients with NSCLC were included in this study. 3D texture features were extracted by first order statistics (FOS), gray-level co-occurrence matrix (GLCM), gray-level run-length matrix (GLRLM), and Laws' texture filters using custom MATLAB codes on 18-F FDG PET/CT images of all patients. The correlations between the 3D textural features and SUVmax, SUVmean, MTV, TLG, tumor TNM stage and subtype (adenocarcinoma (ADC) and squamous cell carcinoma (SqCCs)) were analyzed. **Results**: Significant moderate correlations were observed between MTV, TLG and GLRLM_GLN ($r=-0.5$; $p=0.002$), GLRLM_RLN ($r=0.7$; $p<0.001$) and Laws'_mean ($r=0.5$; $p=0.002$). While means of these texture features showed statistical significantly difference between TNM stage groups, there were no difference in the means of SUVmax, SUVmean, MTV and TLG values. SUVmax, SUVmean, GLCM_energy and homogeneity, GLRLM_SRLGE and LRLGE were notably different between tumor subtypes. **Conclusion**: Three-dimensional (3D) texture features of 18-F FDG images might be used as an objective tool to provide identifying tumor stage and subtype in NSCLC.

P062

The role of SUV SPECT perfusion defect quantification of the lung as a predictor of severe cardiovascular events in a cohort of patients with congestive heart failure

W. He, W. Yu, J. Xi, W. Zhai; Huadong Hospital, Shanghai, CHINA.

Objectives : The aim of this study was to investigate the use of SUV SPECT to quantify lung perfusion defects in both non-CHF and CHF patients and to explore its correlation index as an outcome predictor for CHF patients. Methods : 30 patients were enrolled in the study. 17 CHF patients were followed for 16±5 mo (mean±SD) and 13 patients were a non-CHF control group. All patients underwent a lung perfusion scan, an independent diagnostic CT plus echocardiography. The lung perfusion scan was reconstructed using the software to convert the recorded counts per voxel into activity per unit volume to allow for SUV calculations. The diagnostic CT was co-registered with the SPECT perfusion scan in order to relate the perfusion function to anatomy. Using the software 'Hybrid 3D Lung Lobe Finder'. (HERMES MEDICAL SOLUTIONS)The lungs where further split semi-automatically into individual lobes by placing 10 to 15 points along each fissure. Using the computed anatomical volumes it was possible to record the total SUV and volume of each lung and lobe. The SUV difference between the CHF group and the control group were compared. Cardiac death, acute MI, unstable angina, and late revascularization (>3 mo) experienced by the patients during follow-up were defined as cardiac events. Multivariate Cox regression analysis was applied for cardiovascular events patients and different SUV index. Results : Preliminary results showed that there were no significant differences between the total lung SUV of the two groups. There were 10 patients (33.3%) who had cardiac events, including 2 acute MI, 3 late coronary artery bypass grafting, and 5 unstable angina pectoris during the follow-up. Conclusions : SUV SPECT perfusion defect quantification of the lung is a promising method for assessing pathology, physiology state and the rate of severe cardiovascular events in CHF patients.

P063

Diagnostic accuracy of quantitative bone scintigraphy with artificial neural network in patients with breast cancer

A. Inaki, K. Nakajima, S. Watanabe, S. Kinuya; Kanazawa University Hospital, Kanazawa, JAPAN.

Bone scan index (BSI) calculated by artificial neural network (ANN) was developed as automatic and quantitative evaluation of bone metastasis. Some studies demonstrated the prognostic value of the BSI with regard to prostate cancer. The aim of this study was to assess the diagnostic value of the BSI in patients with breast cancer. MATERIALS AND METHODS We retrospectively evaluated 66 patients with breast cancer who underwent bone scintigraphy and FDG-PET with the intervals of less than 4 weeks between both examinations. RESULTS The BSI with and without bone metastasis were 1.57 ± 1.73 and 0.15 ± 0.34, and there were significant differences between 2 groups ($p < 0.001$). Mean follow-up period was 1535 ± 749 days and the number of patients of no evidence of disease (NED), alive with disease (AWD) and died of disease (DOD) were 28, 16 and 20, respectively. The sensitivity and the specificity of the BSI was 86.4% and 81.8% with a cut-off value of 0.185. The Kaplan-Meyer curve showed that the patients with higher level of the BSI had significantly lower prognosis than with lower level of the BSI. In the Cox proportional hazards model, the BSI was a good prognostic factor with a hazard ratio of 1.24 (1.13 - 1.36, 95%CI). CONCLUSION The BSI will play a important role on not only detecting bone metastasis but also predicting prognosis in patients with breast cancer.

P064

Cerenkov Radiators for Preclinical Optical Imaging

C. R. Gigliotti, L. Altabella, A. E. Spinelli; San Raffaele Scientific Institute, Milano, ITALY.

Aim: Cerenkov luminescence imaging (CLI) is a molecular imaging technique that combines nuclear and optical imaging, detecting Cerenkov radiation produced by beta-emitting radionuclides. Due to the faint emission, the use of a Cerenkov radiator (CR) can be useful to enhance the detected signal and consequently reducing the acquisition time. Since the energy threshold for Cerenkov production (CP) decreases increasing the medium refractive index (RI), the first approach is the use of high RI material to exploit the beta particles exiting from the tissue. Nevertheless, in the low energy field, other parameters have to be taken into account for the optimization of CLI. The goal of this work is to investigate the efficiency of different materials by studying the effect of their characteristics on CP. Methods: We performed MC simulations using GAMOS plug-in for GEANT4. As a proof of principle, we considered mouse muscle tissue in which, at different depths, is placed a low, medium or high energy beta-emitter used in nuclear medicine (NM) and a CR of variable thickness is superimposed to the tissue. In order to investigate the role of the material characteristics on CP, we simulated PMMA and high RI transparent ceramic. The dependence of RI and of density on CP was also investigates by slightly varying them from the true values. Results and conclusion: The higher percentage of exiting photons is observed for low density ceramic, with the same RI of the real ceramic, which shows nearly half of the efficiency, while the PMMA with a lower RI shows a halfway efficiency. The results show that the RI of a material is not the crucial parameter that affects the efficiency of CR, whereas the density seems to be the one that mainly affects the CR. We believe that such an effect is due to the way the electrons lose energy in matter that influences the change of particle velocity. Comparing the results obtained with different β-emitters, we observe the major production gain for the 32P source. We conclude that the ideal material for a CR optimized to CLI has low density and high RI and that the major enhancement of the signal is expected for medium energy β-emitter. Further investigation in order to take into account the CR effects on spatial resolution are now under implementation.

P065

Striatum specific F-18 FP-CIT analysis in Parkinson disease

J. S. Oh[1], **I. Lee**[1,2], H. Moon[1], J. Kim[2], M. Oh[1], J. Kim[1]; [1]Department of Nuclear Medicine, Asan Medical Center, University of Ulsan College of Medicine, Seoul, KOREA, REPUBLIC OF, [2]Department of Nuclear Engineering & Radiologic Science, College of Health Science, Korea University, Seoul, KOREA, REPUBLIC OF.

Aim: Conventional volume of interests (VOIs) analysis of F-18 FP-CIT PET usually employed conventional spatial normalization using whole brain PET images. Due to VOI mismatch caused by spatial normalization error, researchers needed to manually modify the VOIs for more accurate analysis, in turn, lead to labor intensiveness and inter-observer reliability issue caused by manual VOI adjustment. To better localize the VOIs, we suggest new spatial normalization method called striatum-specific SPM (SSPM) using a mask encompassing striatum and midbrain.

Materials and methods: One hundred forty subjects (23 normal controls (NC), 117 patients with Parkinson disease (PD))

underwent F-18 FP-CIT PET. Image acquisition was started 3 h after intravenous injection of 18F-FP-CIT (185 MBq). Spatial normalization was conducted using SPM8 and VOI analysis was conducted using our in-house FP-CIT PET and VOI templates. Then, we applied spherical mask with a 28 voxel (5.6cm) radius to exclude regions other than midbrain/striatum on not only FP-CIT template but also the resulting individual spatially-normalized FP-CIT PET images.An iterative spatial normalization using study specific template (SST) was conducted. Finally, mean uptake values of 12 striatal VOI templates (bilateral ventral striatum [VS], anterior caudate [AC], posterior caudate, anterior putamen, posterior putamen [PP], and ventral putamen [VP]) and that of reference region (i.e., occipital lobe) were estimated automatically by our in house software called ANTIQUE. For the ground-truth information of mean VOI uptake and VOI location, one of us (IL) manually adjusted the VOI under supervision of 20 year experiencedboard-certified nuclear medicine physician (JK). We compared FP-CIT SSPM method and conventional method in terms of VOI uptake % error and VOI location accuracy. VOI uptake % error values were calculated for each VOI using (automatic method-based uptake - manual method-based uptake)/(manual method-based uptake) x 100 (%). VOI location inaccuracy was estimated for each VOI using the mean distance between automatic VOI and manually-adjusted VOI.

Results: Except bilateral AC in NCs, the uptake % error between SSPM auto and SSPM manual is smaller than that between whole brain manual and SSPM manual ($p<0.001$) in both groups.In both group, all VOIs but VP of PD (a relatively small VOI) showed significantly decreased VOI displacement ($p<0.05$) by FP-CIT SSPM than conventional method.

Conclusion: SSPM outperform than conventional spatial normalization-based approach in terms of significantly less % error and more accurate VOI location. We suggest our SSPM may serve as a new automatic VOI analysis method of FP-CIT PET.

P066

Quantitative Evaluation of Scattered Photons in a Myocardial Pinhole SPECT Imaging

K. Ogawa, N. Aitani, Y. Hemuki; Hosei University, Tokyo, JAPAN.

Aim: Multi-pinhole collimators have been recently used in myocardial SPECT systems. Myocardial imaging with pinhole collimators may acquire many undesirable photons such as primary and scattered photons originating in the liver. This study aimed to quantify the effect of these undesirable photons. Materials and Methods: The DMCAT phantom was used in Monte Carlo simulations. The size of the phantom was 128 x 128 x 128 voxels and the size of a voxel was 2.5 x 2.5 x 2.5 mm^3. We emitted photons with an energy of 140 keV from the liver, myocardium and blood regions, and the numbers of photons were 0.8, 0.8, and 0.05 Mega/voxel, respectively. As a reference we also simulated the case without liver activity. The distance between the center of the phantom and pinhole was 18 cm and that between the pinhole and NaI detector was 9.9 cm. The diameter of a pinhole was 3 mm and the aperture angle of the pinhole collimator was 60 degrees. We rotated the pinhole detector system around the DMCAT phantom and the number of projection data was 360. The energy resolution of the detector was 10 % FWHM at 140 keV and we set an energy window with a width of 20 %. The reconstruction of an image was performed with the OS-EM method. We assumed that all regions inside the phantom except for the lungs consisted of water, and attenuation correction was performed in the process of image reconstruction. We evaluated the effect of scattered photons with a contrast ratio of the myocardial area between the conditions with and without the liver activities. Results: The myocardial images were blurred with scattered photons originating in the liver. The contrast ratios of reconstructed activities in the myocardial area to the blood area were 0.65 (without liver activities) and 0.43 (with liver activities). Conclusions: The scattered photons originating in the liver affect the quality of reconstructed myocardial images, making it very important that the scattered photons in the pinhole SPECT image be considered.

P067

Image noise estimation using sub-reconstructions of clinical Whole Body PET/CT data

A. K. Krizsan[1], A. Forgacs[2], G. K. Nagy[1], M. Szolik[1], M. Dahlbom[3], L. Balkay[1]; [1]University of Debrecen, Medical Center, Department of Nuclear Medicine, Debrecen, HUNGARY, [2]ScanoMed Nuclear Medicine Centers, Debrecen, HUNGARY, [3]University of California at Los Angeles, David Geffen School of Medicine, Department of Molecular and Medical Pharmacology, Ahmanson Biological Imaging Center, Los Angeles, CA, UNITED STATES.

Aim: The estimation of image noise defined as pixel-wise Signal-to-Noise on Whole Body PET images can be routinely performed on series of phantom scan image data. Simply Region of Interests' (ROIs) can be used to calculate the Signal (as Mean) and the Noise (as Standard Deviation) values. However, in case of a clinical patient scan the activity distribution is heterogeneous and the use of multiple scans is typically limited. A new method we propose to estimate pixel-wise noise of clinical PET images from a single raw data with series of sub-reconstructions.

Materials and Methods: A uniform cylindrical phantom set with increasing diameter and an anthropomorphic thorso phantom were scanned with 18F-FDG using clinical scanning protocols, the latter to mimic human non-uniform imaging conditions. Furthermore, Whole Body PET image data of two patients with elongated scan times were involved in the investigation. From the single list mode files sub-reconstruction series were generated with different time durations and using these image data, noise was estimated pixel-wise with linear regression interpolation. As a gold standard, we used extended PET scans in all cases and determining the image noise pixel-wise by using image sets of the clinical routine scan durations.
Results: The Standard Deviation/Mean data showed qualitative similarities in terms of image patterns. Using ROI analysis the difference between the conventional and new estimation method of image noise remained under 10% in case of the uniform cylinder and under 15% for both the anthropomorphic phantom and patient studies even in case of using post filtering on the images. This good correlation suggests further considerations on optimizations of the method and extending on a larger population of patient data.
Conclusion: The preliminary results indicate that this new method could be used for pixel-wise noise estimation of clinical PET scans without the need for repeated scans.

P068

Looking for physiological factors affecting texture analysis on clinical PET… with texture standardization in mind!

J. Cortes-Rodicio, G. Sanchez-Merino, R. Lope-Lope, J. Ruiz-Pomar, T. Martin-Gonzalez, M. Garcia-Fidalgo; Osakidetza, Vitoria-Gasteiz, SPAIN.

INTRODUCTION AND OBJETIVES: Texture parameters are important features commonly used for pattern recognition, image classification and, more recently in the field of "radiomics", where more useful information might be extracted from medical images. Anyway, texture quantification is affected by many technical and physiological factors. The purpose of this work is to study the texture features of non-pathological livers as a function of the anatomical and physiological properties of the patients undergoing PET studies.
METHODS AND MATERIALS: The data for 15 patients showing non-pathological liver were acquired on a Philips GEMINI TF PET/CT. Patients were injected with a linear FDG dose regime of 2.5MBq/kg after 6h of fasting and acquired after 60 min at rest. Raw PET data were reconstructed using a BLOB-OS reconstruction protocol with attenuation correction resulting a grid size of 4mm. Anatomical and physiological features like patient's weight, height, body mass index, liver volume and glucose level in blood, were also registered. A liver covering ROI were delineated in each patient. To avoid variability due to reconstruction protocols and activity concentration, only texture features that showed to be robust on a previous study with phantoms were analyzed using Chang Gung Image Texture Analysis toolbox for MatLab. Those were entropy (Haralik-1973, Sun-1983, Horng-2002); short-run-emphasis and run-percentage (Loh-1988); the homogeneity, intensity, inverse-difference-moment and code-entropy (Horng-2002); and short-zone-emphasis and zone-percentage (Thibault-2009). Finally, a multivariate Pearson correlation analysis was performed using StatGraphics Centurion XVI software.
RESULTS There is a high statistical correlation between liver volume and entropy (p-value<<0.05). Entropy feature is, indeed, correlated (p-value<0.05) with all patient's parameters, except body mass index. The only textural features that do not seem to be correlated (p-value>0.05) with any of the anatomical or physiological parameters are run-percentage (Loh-1988), short-zone-emphasis (Thibault-2009) and intensity (Horng-2002), making them suitable for quantitative textural analysis.
CONCLUSIONS: Textural feature analysis allow for a deeper knowledge of tumor uptake in 18F-FDG PET/CT studies but they present an intrinsic variability due to technical and physiological factors that should be taken into account. Most of the textural features analyzed are correlated with these factors and are, therefore, more prone to errors in quantifying changes or classifying patients. Only three of them seemed to be suitable for this purpose. Even though, further studies should be carried out in order to improve the statistical power of the analysis.

P069

Repeat (R)-[11C]PK11195 brain PET scans in glioma

M. Bauer[1,2], Z. Su[1], F. Roncaroli[3], A. Gerhard[1], F. Turkheimer[4], K. Herholz[1], R. Hinz[1]; [1]University of Manchester, Manchester, UNITED KINGDOM, [2]Medical University of Vienna, Vienna, AUSTRIA, [3]Imperial College London, London, UNITED KINGDOM, [4]King's College London, London, UNITED KINGDOM.

Aim: The analysis of human brain PET scans with tracers binding to the 18-kDa mitochondrial translocator protein (TSPO) is hampered by the absence of an anatomical brain region free of specific binding. We previously reported a comparison between two referencing approaches, *cerebellar* grey matter (GM) reference input function and supervised cluster analysis with six classes (SVCA6)[1], in glioma patients scanned with (*R*)-[^{11}*C*]*PK11195*[2]. Here we compare these two input functions in repeat scans. Materials and Methods: Three patients with clinically stable glioma (WHO grade: subject: 1 III, subject 2: II, subject 3: II) were

scanned twice with (*R*)-[^{11}*C*]*PK11195, at 23, 6 and 8 months after the initial PET scan. Parametric maps of binding potential* (*BPND*) *were generated with the simplified reference tissue model using either a cerebellar GM or a SVCA6 input function. Regional BPND differences* ΔBPND = $BPND_{scan2}$ - $BPND_{scan1}$ *were calculated in the following regions*: *frontal*, *temporal*, *parietal*, *occipital lobe*, *thalamus*, *hippocampus and tumour cold region. T-tests were performed to assess statistical significance*. Results: BPND with SVCA6 input function were systematically smaller than those with cerebellar GM input function (p=0.0317, paired t-test). ΔBPND derived with SVCA6 were significantly larger than those with cerebellar GM input function (p=0.0002, paired t-test). One-sample t-tests performed on the regional ΔBPND for the three patients revealed no difference with the cerebellar GM input function (p_1=0.0822, p_2=0.3595, p_3=0.6793) but statistically significant increases with SVCA6 (p_1= 0.0003, p_2=0.0055, p_3<0.0001). Conclusion: Of the two reference tissue input functions considered here, only the data-led approach SVCA6 reported statistically significant changes in BPND in the follow up scans. The cerebellum GM as an anatomically defined reference region failed to reveal changes of significance in BPND in other parts of the brain in conjunction with the simplified reference tissue model. Acknowledgments: Imaging of Neuroinflammation in Neurodegenerative Diseases (INMiND), a collaborative project in the Seventh Framework Programme of the European Union. References: [1] Turkheimer, FE et al. J Nucl Med 2007 48(1):158-67. [2] Su, Z et al. Eur J Nucl Med Mol Imaging 2013 40(9), 1406-19.

P070

Segmentation gross tumor volume on positron emission tomography by a method combined with numerical approximation and local gradient _ an animal study

Y. CHEN; Quanzhou First Hospital of Fujian Medical University, quanzhou, CHINA.

Segmentation gross tumor volume on positron emission tomography by a method combined with numerical approximation and local gradient—an animal studyPurpose: A scheme, named SUV_Shape 2.0, drawing gross tumor volume (GTV) on PET images was made by a numerical approximation method combined with maximal local gradient, and evaluated during this study.Methods: Five rabbits implanted VX2 squamous carcinomas kept fasting at least 4h before [18F]-FDG imaging. 37MBq [18F]-FDG was administrated following their blood glucose level detection. Their 3D PET data were acquired at 10min-120min after injection by a PET/CT scanner (Discovery ST8, GE Healthcare, USA). Euthanasia was done in the next 24h. Each VX2 tumors was resected, and its maximal perpendicular diameters were measured by a caliper. Its volume was computed following the equation of spheroid volume, SUV_Shape, and SUV_Shape 2.0, then labeled as GTVt, GTVs1, and GTVs2, respectively. The Spearman's rho and paired t-test among GTVt, GTVs1 and GTVs2 were done.Results: Eight VX2 tumor nodes or masses were included in this study. Their GTVt were 29.26, 0.41, 4.22, 24.15, 21.44, 1.26, 0.21, and 1.63mL. Their tumor-nontumor ratio were 16.1, 3.7, 1.63, 16,1, 4.65, 6.16, 4.58, and 1.5. The relationship between GTVt and GTVs1 was significant (Spearman's rho=0.976, P<0.01), and they were not significant difference (t=1.43, P=0.195). The correlation between GTVt and GTVs2 was significant (Spearman's rho=0.929, P<0.01), and they were not significantly different (t=0.088, P=0.933). The relation between GTVs1 and GTVs2 was significant (Spearman's rho=0.952, P<0.01), and they were not significant difference (t=-1.42, P=0.199). The GTV of VX2 tumor masses (2/3) were obviously underestimated by SUV_Shape1 (GTVs1 vs GTVt: 14.95 vs 29.26 mL, 23.52 vs 24.15mL, and 13.40 vs 21.44mL); while they were partly corrected by SUV_Shape2.0 (GTVs2 vs GTVt: 27.50 vs 29.26 mL, 31.6 vs 24.15mL, 18.5 vs 21.44 mL). However, the difference between GTVs1 and GTVt among VX2 tumor nodes were smaller than the difference between GTVs2 and GTVt.Conclusions: The SUV_Shape 2.0 scheme was good for tumor masses delineation, while SUV_Shape was good for tumor nodes outline.Key words: gross tumor volume; segmentation; positron emission tomography

P071

Computer-aided Diagnosis System to Assess Metastatic Disease Presence and Evolution

I. V. Popa[1], I. Grierosu[1,2], A. Statescu[1], M. Gutu[1,2], R. Gherasim[1], S. Bilha[1], R. Olaru[1], C. Cijevschi-Prelipcean[1,2], C. Mihai[1,2], L. Ionescu[1,2], C. Vulpoi[1,2], C. Luca[1,2], C. Stefanescu[1,2]; [1]"St. Spiridon" Hospital, Iasi, ROMANIA, [2]Medicine Faculty, "Grigore T. Popa" University of Medicine and Pharmacy, Iasi, ROMANIA.

AIMS: Our aim was to develop a computer-aided diagnosis (CAD) system able to evaluate the presence and quantitatively assess the evolution of the metastatatic disease (MTSD) on repeated radiotracer scans.MATERIAL and METHODS: We worked on ^{99m}Tc HDP whole body images of MTSD. The method was developed using Matlab® and has three steps. The first, preprocessing step, brings scan images at the same contrast level. The second, processing step, identifies areas of interest using the *watershed method* improved by a series of accessory methods. The third, postprocessing step, is about manually eliminating hyperfixing areas, automatically encircled, that are certainly not metastases (like the joints images etc.). On the final image, several descriptive quantitative parameters (both global and local) were calculated. The global parameters were: ratio between the area occupied by MTS and entire skeleton surface (RM) and the MTS number (NM). The local parameters, in order to characterize each lesion in

evolution, were: region gravity center coordinates, area, width, height, maximum intensity pixel value, mean value and standard deviation, calculated for both anterior and posterior incidences.RESULTS: We exemplified the results obtained for a MTSD patient in evolution, for the first bone scan and for the repeated bone scan, after three years. For the first image, anterior incidence, we obtained RM = 15.28% and NM = 41. For the image in evolution we got RM = 16.01% and NM = 42. Regarding the local descriptors, as an example, one hyperfixing metastasis has an area of 24 pixels at first examination and a 70 pixels area at the second. Also, it can be seen how some lesions have disappeared, some have emerged, some have grown in size and some others decreased in size. The descriptors are saved in the patient history archive, in order to compare them with the same descriptors from subsequent examinations of the same patient. The system automatically represents graphically both global and local values. CONCLUSIONS: Our CAD system proved to be efficient for quantitative assessment of MTSD in evolution on whole-body scans, but could also be applied in other scan types - for example, in the case of MTSD that uptake other radiotracers, ^{99m}Tc MIBI or ^{131}I. This system represents an automated solution capable of helping the doctor in identifying metastases and in calculating quantitative parameters in evolution, ensuring both objectivity and rapidity in the MTSD evaluation.

P072
Practical measures of dynamic 18 FDG time-activiy curves.

M. Tuncel, O. Kupik, P. Kiratli, B. Erbas; Hacettepe University, Ankara, TURKEY.

AIM: Kinetic measures of dynamic 18 FDG PET/CT studies have been proposed being superior compared to static measures such as SUVmax values. Dynamic parameters have been used in the early assessment of therapy response in oncological patients. However, complexity of kinetic analysis may limit its application in the rutine clinical studies. Therefore, this study was planned to analyze the dynamic data in an easy and practical way. MATERIALS and METHODS: Dynamic images were recorded following i.v. injection of 18 FDG. Study group had 30 patients. Time-activity curves were obtained from regions of interest drawn on the tumoral tissue and on the aortic arc as an input function. Using, lineer regression analysis of time-activity curves, slope (SL) values were calculated for several time intervals, i.e, 0-2 min (SL2), 0-5. min. (SL5), 0-10 min.(SL10), 0-30. min. (SL30), respectively. Similarly, SUVmax values for 2nd min (SUV2), 5th min (SUV5), 10th min (SUV10), and 30th min. (SUV30) were measured. For the first 2 minutes, data were added and SUVmean (SUV2mean), SULpeak (SUL2peak), perfusion volume (Per2V) and total lesion glycolysis (TLG2) values were calculated. For comparison, 2-tissue compartmental analysis was performed and K1-k4 values were measured. In addition, Ki values were calculated. Two-compartmental parameters were compared to the other measured parameters. RESULTS: SL2 had correlation with K1, whereas SL5 (r=0.64, p=0.0001), SL10 (r=0.76, p=0.0001), and SL30 (r=0.85, p=0.0001), values showed increasing correlation coeffiencient with Ki values. K3 values had correlation with SL5 (r=0.38, p=0.04), SUV10 (r=0.54, p=0.03), and SL30 (r=0.66, p=0.0001) values. SUV2 showed a good correlation with K1 (r=0.83, p=0.0001). Correlation between SUV5 (r=0.62, p=0.0001), SUV10 (r=0.44, p=0.0001), SUV30 (r=0.42, p=0.0001), and K1 was decreasing with time. SUV values were also correlated with Ki values (SUV5 r=0.65, p=0.0001, SUV10 r=0.85, p=0.0001, SUV30 r=0.88, p=0.0001), except SUV2 value. SUV2mean, SUL2peak, Per2V and TLG2 values were correlated with K1 and K2. SUL2peak and SUV2mean had highest correlation coefficient with K1 (r=0,93, p=0.0001, and r=0.88, p=0.0001, respectively). CONCLUSION: Slope and SUV measurements of dynamic curves showed good correlation with 2-compartmental analysis parameters. Those measures can be easily applied and give information about the 18FDG dynamics. Further studies are needed to explore its clinical relevance.

P073
Early X-Ray CT Radiomic Identification of Lung Tissue Harm Origins in Mice

D. Mathe[1], F. Budan[1], C. Korom[2], D. Veres[3], K. Szigeti[3]; [1]CROmed Ltd, Budapest, HUNGARY, [2]Dept. Radiology Semmelweis University Budapest, Budapest, HUNGARY, [3]Dept. Biophysics and Radiation Biology Semmelweis University, Budapest, HUNGARY.

Introduction. Lung diseases (resulting from air pollution) require a widely accessible method for risk estimation and early diagnosis to ensure proper and responsive treatment. Radiomic fractal dimension-based analysis of X-ray computed tomography (CT) attenuation pattern in chest voxels of mice exposed to different air polluting agents was performed to model disease establish differential diagnosis and discern sources of harm to lung tissue. To model different types of air pollution, the following Balb/CBYJ mouse groups were exposed: cigarette smoke combined with ozone, sulfur dioxide gas, and a control. Two weeks after exposure, the frequency distributions of image voxel attenuation data were evaluated. Specific cut-off ranges were defined to group voxels by attenuation. Each cut-off ranges were binarized and their spatial pattern was associated with calculated fractal dimension, then abstracted by the fractal dimension-cut-off range mathematical function. Each cut-off range versus fractal dimension function plot was

found to contain two distinctive Gaussian curves. The ratios of the Gaussian curve parameters distinguished the three exposure groups statistically significantly. A new radiomic evaluation method was established based on analysis of CT voxel datadistribution and fractal dimension of the resulting lung CT data segments. The resulting attenuation values of voxels corresponded to specific tissues as well as the calculatedparameters to the inflammation- and mucuspatterns to air pollution exposures. Most likely those specific attenuation patterns calculated with our method could diagnose and monitorcertain lung diseases, such as chronic obstructive pulmonary disease (COPD), asthma, tuberculosis or lung carcinomas.

P074

development of metabolic tumor volume measurement based on suvpeak

K. Koyama[1,2], T. Mitsumoto[1], K. Inoue[2], K. Tsuda[3], K. Kotaka[1], K. Yoshikawa[1], K. Hatano[1], M. Fukushi[2]; [1]Tokyo Bay Advance Imaging & Radiation Oncology Clinic-MAKUHARI, Chiba, JAPAN, [2]Tokyo Metropolitan University, Tokyo, JAPAN, [3]Tsukuba International University, Ibaraki, JAPAN.

Aim: FDG-PET/CT allows determination of metabolic tumor volume (MTV) and total lesion glycolysis(TLG) which provides prognostic and predictive value in oncology. MTV is commonly measured based on maximum standard uptake value (SUVmax). However SUVmax is affected by noise and statistical error. To achieve stabile MTV measurement we developed a new method based on peak standard uptake value (SUVpeak). Materials and methods: The Discovery 710 PET/CT device was used in this study. The participants comprised 13 patients with lung lesions (lesion size 24.5 ± 10.3 mm, lesion volume 6.6 ± 5.6 ml). A volume of interest (VOI) including the tumor threshold by 40%, 42%, 50%, 60%, 70% and 80% of SUVpeak within the VOI was used to measure MTV. MTV errors were assessed using CT tumor volume as a standard and compared with conventional methods based on SUVmax threshold by 42% and 50%. Results and conclusion: The MTV error base on SUVpeak40% was -0.54±3.0 (95% confidence interval : -2.4 - 1.3, range: 11.8) ml and the best agreement with CT volume. The MTV error based on SUVmax42% and SUVmax50%was -3.4±3.3 ml (95% confidence interval : -5.4 - -1.3, range: 12.3) and -4.3±4.0 ml (95% confidence interval : -6.9 - -1.8, range: 14.8). The MTV based on SUVpeak40%, SUVpeak42% and SUVpeak50% were significantly improved as compared with SUVmax42% (One-Way Repeated Measures ANOVA $P < 0.05$). New method based on SUVpeak reduced MTV error and statistical error. It was shown that new method based on SUVpeak reduced MTV error and was achieved stabile MTV measurement.

P075

Analysis of Inter-Detector Scattering in PET with Various Energy Window Settings

K. S. Chuang, Z. J. Wei, H. H. Lin; National Tsing-Hua University, Hsin-Chu, TAIWAN.

[**Aim**] In conventional positron emission tomography (PET) an energy window of [425 650] keV is commonly used. A large amount of useful information is lost due to the partial deposition of energy of the annihilation gamma in the detector generating inter-detector scattering (IDS) triple events in PET. These events are caused by one of the annihilation photons deposits energy in more than one detector. IDS are not recorded because the events are not in the energy window. Some of these events are recoverable, i.e. the correct line of responses (LOR) can be identified and added to the data stream. It is possible to employ a wider energy window to include and recover the IDS and increase the system sensitivity.
[**Materials and Methods**] However, several factors cause the degrading of the image quality when a lower threshold of energy window is used. (1) The number of random events increases. This can be corrected using traditional delayed window techniques but with the cost of increasing noise in the data. (2) The number of multiple scattering events becomes significant. The conventional scatter correction technique i.e. single scatter simulation (SSS) might fail. (3) The IDS events produce three ambiguous LORs. Techniques can be developed to identify correct LOR. Wrongfully recovery of the IDS events will blur the image.
[**Results**] A NURBS-based cardiac-torso (NCAT) phantom was simulated at various activity levels. Preliminary results show that IDS remains as a constant percentage at the range of activity tested while the random triple increases with the increase of activity. We will investigate the effects on image quality and sensitivity at various energy window settings based on Monte Carlo simulation. Noise equivalent count rate (NECR), spatial resolution, coefficient of variance, and

coefficient of recovery will be used to gauge the effects of energy window setting on image quality.
[**Conclusion**] A best energy window that is a tradeoff between image quality and system sensitivity can be determined from this study.

P076

Optimisation of automatic image segmentation for tumour volume determination in 18F-FDG PET/CT for patients with liver lesions

D. Ruiz, E. Kalogianni, B. Corcoran, A. Eccles, N. Mulholland, G. Vivian; King's College Hospital NHS Foundation Trust, London, UNITED KINGDOM.

Aim: There is a need for the optimisation of thresholding used for automatic PET image segmentation for lesions that lie within organs with variable background activity such as the liver. The aim of this study was to determine suitable threshold levels for use in measuring tumour volume and uptake values for assessment of respiratory gated PET for imaging liver lesions.Method: Images of a PET NEMA Image Quality phantom containing 6 spheres with volumes ranging from 0.5 - 26.5 ml were obtained using a GE Discovery 710 PET/CT scanner. The phantom was filled with 18F activity corresponding to that clinically observed in liver lesions and normal liver background. The background activity concentration was kept constant at approximately 7 kBq/ml, while the activity of the spheres was varied to obtain lesion-to-background (L/B) ratios of 1.5, 2.3, 2.7, 3.2, 3.6 and 4.4. The optimum threshold level for image segmentation was determined from phantom images by selecting that which resulted in the minimum difference between the actual and measured volume for each sphere size and L/B ratio.Results: Analysis of phantom images showed that for spheres with a volume greater than 5 ml the optimum threshold for image segmentation begins to converge for all except the lowest L/B ratios of 1.5 and 2.3. The optimum threshold was found to depend on the L/B ratio and ranged from 49 % to 95 % for the 26.6 ml sphere with L/B = 4.4 and 0.5 ml sphere with L/B = 2.3 respectively. Generally, the optimum threshold value increased with decreasing L/B ratio. The three smallest spheres were not visible in images of the phantom with the lowest L/B ratio.Conclusion: The use of appropriate threshold levels for PET image segmentation is essential for the accurate definition of lesion volume and quantitation. While more sophisticated image segmentation algorithms are required for applications such as radiotherapy treatment planning and dosimetry calculations, these results will improve the accuracy of liver lesion volume determination for evaluation of PET imaging techniques. Further work is required to validate this method for use on patient images, and implement it for assessment of respiratory gated PET.

P077

Aspects on quantification and detectability in 111In SPECT/CT and 68Ga PET/CT images of neuroendocrine tumours

A. Stenvall[1], E. Mattsson[1], E. Larsson[1], T. Ohlsson[1], C. Hindorf[1], **L. Jonsson**[2]; [1]Radiation Physics, Skane University Hospital, Lund, SWEDEN, [2]Medical Radiation Physics, Lund University, Lund, SWEDEN.

AimNuclear medicine imaging of neuroendocrine tumors (NET) is performed either by SPECT/CT imaging, using 111In-octreotide or by PET/CT imaging using 68Ga-radiolabelled somatostatin analogs. The two imaging techniques will give different image quality and thereby different detection thresholds for tumours, depending on size and activity uptake. Often a subjective evaluation is performed to compare tumour uptake with the activity uptake in the liver to decide whether the patient could be eligible for radionuclide therapy.The aim of this study was to evaluate the image quality for 111In SPECT/CT and 68Ga PET/CT imaging, i.e. the smallest volume possible to visualize for different source-to-background activity ratios. The accuracy of quantification of lesion volume and activity was also investigated to develop an objective evaluation for radionuclide therapy eligibility.Materials and methodsThe phantom study was performed using the IEC Body Phantom with six hot spheres having inner diameters of 10, 13, 17, 22, 28, and 37 mm, filled with either 68Ga or 111In with sphere-to-background (S/B) ratios of no background activity, 10:1, 5:1, 2.5:1, 1.67:1 and 1.25:1. These S/B ratios were chosen as representative values of tumour-to-background ratios in patients. Activity ratios of 1.25:1 and 2.5:1 are clinically found for lesions close to liver and spleen. Clinical acquisition and reconstruction protocols were applied. Line profiles were drawn to evaluate the smallest

detectable volume within a given S/B ratio. Recovery curves based on threshold segmentation were obtained for all combinations of S/B ratios and sphere diameters, allowing for quantification.ResultsThe line profiles showed that the 10 mm sphere was not possible to detect in SPECT images. It was detectable in PET images for S/B ratios of 2.5:1. In a background corresponding to the activity uptake in the liver (S/B 2.5:1 and 1.25:1) spheres larger than 22-37mm were detectable in the 111In-SPECT images and spheres larger than 13-22mm were detectable in the 68Ga-PET images.The maximum activity concentration was accurately quantified for spheres larger than 22mm in the PET images however the quantification was impaired by sphere size and background activity.ConclusionIt was not possible to detect the 10mm sphere in any of the SPECT images. In a background corresponding to the activity uptake in the liver, spheres larger than approximately 30mm were visible in the 111In-SPECT images and spheres larger than approximately 17mm were visible in the 68Ga-PET images. Sphere diameter and background activity strongly affect the possibility of a correct quantification.

P06 - Sunday, October 11, 2015, 4:00 PM - 4:30 PM, Hall 3 – Poster Exhibition

Physics & Instrumentation & Data Analysis: Miscellaneous

P078

Optimisation of Y-90 post-SIRT PET imaging on GE Discovery systems

L. M. Rowley, D. R. McGowan, K. M. Bradley, A. Hallam; Oxford University Hospitals NHS Trust, Oxford, UNITED KINGDOM.

Aim: To optimise image reconstruction parameters for 90Y using phantoms and patients on our GE Discovery 690 and 710 PET-CT scanners for both standard OSEM and a new Bayesian penalised likelihood reconstruction (BPL) algorithm (Q.Clear, GE Healthcare, Milwaukee, USA). Methods: Following radioembolisation for the treatment of liver tumours using 90Y, users may choose to perform either Bremsstrahlung imaging or PET-CT, to visualise the deposition of the activity and note any extra-hepatic activity. The BPL reconstruction has beta, a noise suppression term as the only user-input variable, unlike OSEM which has iterations, subsets, and filters. BPL includes point spread function (PSF) modelling (SharpIR) as part of the reconstruction. A NEMA NU-2 Image Quality (IQ) phantom was filled with 4.2GBq 90Y, with a sphere to background ratio of 8:1 in each of the six spheres. This was scanned over 9 nights on the GE Discovery 710 PET-CT scanner. Data was rebinned into 15 minute frames and reconstructed using both time of flight (ToF) BPL and ToF OSEM. For BPL this was using beta values 1-10,000. For OSEM this was using 1-5 iterations, 8-32 subsets, 0-10 mm Gaussian filter and with SharpIR both on and off. Contrast recovery (CR) and background variability (BV) were calculated as per the NEMA NU 2-2007 standard. A subset of the best performing reconstructions parameters for both BPL and OSEM were applied to ten patient images. Each set of patient images were ranked by an experienced radiologist blinded to the reconstruction parameters. Results: From the best performing phantom BPL reconstructions (beta 2,000-4,000) the patient images with a beta of 3,000 ranked highest. For this beta the CR of the 37mm sphere was 81% ±3.9% and BV 7% ± 1.5% for a total phantom activity of 2.7GBq, and CR 74% ±8% and BV 19% ±4% for a total image activity of 0.9GBq. These values were higher than the optimised OSEM reconstruction. The beta value was appropriate over the range of activities scanned (4.2GBq - 0.47GBq). Dead time was apparent at activities above 3.5GBq with contrast recoveries reduced by 23% at 4.2GBq. Clinical images using BPL with a beta of 3,000 appeared superior to optimised OSEM and Bremsstrahlung images. Conclusion: The use of BPL with 90Y post-SIRT images achieves an increase in contrast recovery and decreased background variability compared to OSEM.

P079

Analysis of Radiation-Induced Liver Disease (RILD) and Evaluation of Relationship Between Therapeutic Activity and Liver Clearance(C) Rate with Tc-99m-Mebrofenin(M) in Y-90 Microspheres Treatment(MT)

H. Tanyildizi, M. Abuqbeitah, L. Kabasakal, M. Demir; Istanbul University, Istanbul, TURKEY.

Objectives : Whole liver radiation has modest benefit in treatment of unresectable hepatic metastases but the radiation doses must keep in control. In this study, we aimed to calculate amount of max permissible activity (MPA) and critical organ doses with MIRD, to evaluate tumour doses for treatment response and whole liver doses for RILD and to find optimal liver function test additionally. Methods : This study includes 29 patients who attended our nuclear medicine department suffering from Y-90 MT. 10 mCi Tc-99m MAA was applied to patients for dosimetry. After injection, whole body SPECT/CT images were taken in one hour. The min therapeutic tumour dose is on the point of being 120 Gy1, the amount of MPAs were calculated with MIRD considering volumetric tumour/liver rate. A sub-working group was created with 11 patients randomly and liver C rate with Tc-99m-M was calculated according to Ekman formalism2. Results : The volumetric tumour/liver rates were found between 33-66% (Maksimum Tolarable Dose (MTD) 48-52Gy3) for 4 patients,

less than 33% (MTD 72Gy3) for 25 patients. According to these results the average amount of MPA, mean liver dose and mean tumour dose were found 1793.9±1.46 MBq, 32.86 ±0.19 Gy and 138.26±0.40 Gy. RILD was not observed in any patient. In sub-working group, the relationship between Bilirubin, Albumin, INR (which show presence of liver disease and its degree), liver C with Tc-99m-M and calculated MPAs were found r=0.49, r=0.27, r=0.43, r=0.57 respectively. Conclusions : The min tumour dose was found 120 Gy for positive dose-response relation. If volumetric tumour/liver rate was >66%, dose 30 Gy; if 33-66%, dose escalation 48 Gy; if <33%, dose 72 Gy. These dose limitations did not create RILD. CL measurement with M was concluded that the best method to determine the liver function. Therefore, liver CL rate with Tc-99m-M should be considered in calculation of Y-90 microspheres dosimetry.

P080

Monte Carlo simulations to evaluate dose for possible treatment of brain cancers by boron neutron capture therapy

Z. Jovanovic[1], D. Krstic[1], D. Nikezic[1], **M. Matovic**[2], R. Krstic[3]; [1]University of Kragujevac, Faculty of Science, Kragujevac, SERBIA, [2]Clin Ctr Kragujevac, Kragujevac, SERBIA, [3]KVARK Company, Kragujevac, SERBIA.

Monte Carlo simulations were performed to evaluate dose for possible treatment of cancers by boron neutron capture therapy (BNCT). The computational model of male Oak Ridge National Laboratory (ORNL phantom) was used to simulate tumour in the brain. Calculations have been performed by means of the MCNP5/X code. In this simulation, epithermal neutrons were considered. Boron neutron capture therapy (BNCT) is radio therapeutic modality, based on nuclear capture reaction that occurs when non-radioactive boron (10B) is irradiated with neutrons of the appropriate energy to yield high energy alpha particles and recoiling lithium (7Li) nuclei. Since these particles have path lengths of approximately one cell diameter, their lethality is primarily limited to boron containing cells. The selective boron uptake in the brain metastases comparing to normal tissue makes BNCT a potentially advantageous technique, especially if the whole organ has be treated. In clinical application of BNCT, 10B compounds such as BPA (Boronophenylalanine) and BSH (Sulfhydryl borane) have been widely used as short-range alpha particle-producing agents. The obtained results indicate that the brain cancer could be treated by BNCT under the assumptions of calculations.References1. Brandão F S & Campos PR T. Dosimetric analysis of BNCT - boron neutron capturetherapy - coupled to 252Cf brachytherapy. International Nuclear Atlantic Conference - INAC 2009 Rio de Janeiro,RJ, Brazil, September 27 to October 2, 2009.2. Eckerman K F, Cristy M, Ryman J C. Oak Ridge National Laboratory. Oak Ridge, TN 37831, USA; 1996. Updated 08 April (2009). http://ordose.ornl.gov/resources/Mird.pdf.3. Voyant C, Roustit R, Tatje J, Biffi K, Leschi D, Briançon J, Lantieri Markovici C. Therapeutic potential of atmospheric neutrons. Rep. Pract. Oncol. Radiother. 16:21-31, 2011.4. Verbeke J M, Vujic J, Leung K-N. Neutron beam optimization for Boron Neutron Capture Therapy using the D-D and D-T high-energy neutron sources. Nucl. Technol. 129:257-258, 2000.5. X-5 Monte Carlo Team. MCNP-a General Monte Carlo N-Particle Transport Code, Version 5 Vol. I: Overview and Theory. Los Alamos, NM: Los Alamos National Laboratory; LA- UR-03- 1987; (2003).

P081

What is the sensitivity of 90Y SPECT to microscale dose distribution?

C. Oldfield[1], D. Cullen[1], D. Hamilton[2], E. Page[2], A. P. Robinson[1], J. Tipping[2]; [1]University of Manchester, Manchester, UNITED KINGDOM, [2]The Christie NHS foundation trust, Manchester, UNITED KINGDOM.

^{90}Y microsphere treatments provide significant benefits for the therapy of some cancers, e.g. metastatic colorectal cancers. Current administration guidelines make no use of tumour dosimetry despite promising work quantifying tumour dose response for ^{90}Y microsphere therapies [1].The nature of microsphere treatments results in a unique dose distribution due to the discrete nature of the activity localisation. This allows the dose distribution to be specified down to a cellular level, far below the resolution of conventional imaging modalities.Tumour microsphere distributions based on existing data coming from analysis of histological thin slices [2] describing the statistical nature of individual microsphere distributions have been generated. Using these distributions as input to a Monte Carlo model it is possible to calculate doses throughout a tumour at a micrometre scale.This provides the basis of a Monte Carlo simulation study investigating how the microscale distribution of spheres is reflected in macroscale SPECT and PET imaging and subsequent dosimetry.Results showing the theoretical sensitivity of SPECT and PET to the underlying structure of microsphere distribution and its impact on dosimetry will be presented.Dose calculations based on observed microsphere distribution for SIR-sphere and Therasphere treatments are compared.[1] Y H Kao et al, Post-radioembolization yttrium-90 PET/CT - part 2: dose-response and tumor predictive dosimetry for resin microspheres, EJNMMI, 2013[2] A M Campbell et al, Analysis of the distribution of intea-arterial microspheres in human liver following hepatic yttrium-90 microsphere therapy, Phys. Med. Biol. 2000

P07 - Sunday, October 11, 2015, 4:00 PM - 4:30 PM, Hall 3 – Poster Exhibition

Molecular & Multimodality Imaging: PET - Clinical & Preclinical Evaluation

P082

A comparison of the utility of F18 Choline and Ga68 PSMA PET/CT in identifying distant disease in high risk prostate cancer patients being considered for radical prostatectomy

S. A. Ali[1], **L. Emmett**[1], J. Wang[1], P. Van Leeuwen[2], D. Stark[1], J. Morigi[1], P. Stricker[2]; [1]St Vincents Public Hospital, Sydney, AUSTRALIA, [2]Garvan Institute for medical research, Sydney, AUSTRALIA.

AIM:To identify the extent of metastatic prostate cancer outside the standard operative or radiotherapy field in high-risk patients undergoing pre-treatment staging with F18 Fluoromethyl-Choline (FMC) and Ga68 PSMA (Prostate specific membrane antigen).MATERIALS:All patients undergoing a pre-operative PET CT (F18 Choline or Ga68 PSMA) were analysed using a prospectively accrued ethics approved database. Gleason score, T staging, PSA and prior imaging results were documented. PSMA and FMC PET/CT plus diagnostic CT scans were undertaken and independently assessed by 2 readers blinded to clinical and imaging results. Management impact information, minor (change in delivery or site of the selected treatment) or major (change of selected treatment) change was documented. Histopathology was documented in all patients.RESULTS:27 patients with FMC and 19 patients with PSMA were included. 36/46 pre- radical prostatectomy and 10/46 pre external beam radiotherapy. Mean Gleason score 8.12 (+/-1.17 SD)(FMC) and 8.53 (+/-1.01 SD)(PSMA). PSA (ng/mL) 20.36 (+/-24.52 SD)(FMC) and 14.81 (+/-18.94 SD)(PSMA). With FMC patients (27), 15 were identified as having disease localized to within the standard operative field (9/15 prostate alone; 6/15 prostate+ local pelvic nodes). 12/27(44%), of whom 4/12 (33%) had bone and 8/12 (%66) distant nodal involvement (above common iliac). With PSMA patients, 13/19 had disease within the standard operative or radiotherapy field (10/13 prostate alone, 3/13 prostate+ pelvic lymph nodes). 6/19 (31%) PSMA had bone lesions with no distant nodes identified (PSMA). Management impact and histopathology results are in process.CONCLUSION:A significant proportion of men with high risk prostate cancer undergoing pre- treatment F18 Choline or Ga68 PSMA demonstrated disease outside of the standard surgical or radiotherapy field (particularly in bone with PSMA) leading to a significant change in management. Ga68 PSMA identified a higher proportion of men with metastatic bone disease than F18 Choline in the high risk pre-operative setting. Further large studies investigating the value of Ga68 PSMA in the high risk preoperative group is warranted.

P083

Targeting VPAC1 for Imaging Prostate Cancer

M. L. Thakur, E. J. Trabulsi, S. Tripathi, S. Kim, P. McCue, R. Birbe, A. Gandhe, P. Kumar, C. Intenzo, L. Gomella; Thomas Jefferson University, Philadelphia, PA, UNITED STATES.

Objectives: Throughout the world, prostate cancer (PC) takes hundreds of thousands of lives each year. Although a large number of minimally invasive and invasive procedures are available for detection of PC, there remains a compelling need for imaging PC and its metastatic and recurrent lesions. As a result, for PET and SPECT imaging of PC, many novel radiopharmaceuticals are being investigated. VPAC1 receptors (combined for vasoactive intestinal and pituitary adenylate cyclase active peptide) are expressed in high density on PC cells at the onset of oncogenesis and play an active role in cell proliferation, differentiation, and cell survival. On stroma, normal cells, and benign masses, only a few VPAC1 receptors are expressed. The goal here was to determine the ability of a VPAC1 receptor-specific biomolecule, ^{64}Cu-TP3805, to image biopsy-proven PC in vivo, and evaluate the findings with pathologic examination.

Methods and Materials: Twenty-five men (age 44-74 yrs, mean 63.4±7.6 yrs) scheduled for radical prostatectomy (Gleason 7) and who signed an IRB approved consent form received 148 mBq (±10%) ^{64}Cu-TP3805 preoperatively. PET images were performed at 30 min. and 2 hrs. post injection. Standardized uptake values (SUVs) were determined, malignant lesions (SUV >1.0) were counted, and data were compared with histological findings. In addition, 9 deparaffinized wholemount pathology slides from 3 benign prostatic hyperplasia (BPH) patients were incubated with ^{64}Cu-TP3805, washed with PBS, dried, and subjected to digital autoradiography (DAR). Slides were then H&E stained, read by pathology, and DAR images were compared with histological findings.

Results: By PET imaging in 25 patients, 127 malignant lesions were identified by histology, all of which were positive by imaging (SUV max range 1.1-8.8). In addition, there were 85 additional lesions with SUV max >1.1. Consistent with histology, DAR was normal for all 9 BPH slides. The pathologic nature of 85 PET lesions is being investigated.

Conclusion: PET imaging with ^{64}Cu-TP3805 accurately visualized all malignant lesions determined by histology. Consistent with histology, DAR examinations of 9 slices from 3 BPH patients showed absence of ^{64}Cu-TP3805 uptake, confirming a lack of VPAC1 receptors on non-malignant, normal cells. It is, therefore, reasonable to consider that the additional 85 PET lesions may not be false positive, but were either missed by histology or may be histologically pre-malignant, such as prostatic intraepithelial neoplasia (PIN), the precursor of PC. ^{64}Cu-TP3805 is worthy of further investigation. **Support**: NIH/NCI R01 CA157372 (MLT)

P084

The incremental value of FDG PET/CT over MDP bone scan in staging of Ewing's group of tumors

r. K. kavindran, **Sr**., s. shah; TMH, mumbai, INDIA.

Introduction: Routine staging for Ewing's group of tumors includes a Tc99m MDP bone csan, CT thorax and a MRI of the local region. FDG PET/CT scans are being increasing used for stgaing various malignancies. Aim: The evaluate the incremental value of F18 FDG PET/CT over Tc99m MDP bone scintigraphy in Ewing's group of tumors. Materials and methods: This is a retrospective analysis of 66 histological proven untreated cases of Ewing's group of tumors. A 99m Tc MDP planar bone scan and FDG PET/CTscan were done within a span of five days. Abreath hold CT chest was done after completion of the PET/CT study. Abnormalities on a MDP bone scan at primary and metastatic sites and the areas of abnormal FDG uptake in the skeletal system on a PET/CT study in all the patients were noted. A comparsion of the skeletal lesions identified by both modalities was done.Additional sites of metastases on a FDG PET/CT were also evaluated. Results: MDP bone scan identified in 4/66(6%) patients while FDG PET/CT identified skeletal disease in 12/66(18%). 50% (6/12) of the leisons identified on PET/CT were purely marrow lesions. FDG PET/CT delineated 22 (33/3) patients with non skeletal metastases (15-lung and 7 nodes),this group consisted of 19 (28.8%) patients who showed only non skeletal metastases while 3 patients had both skeletal and non skeletal metastases. Conclusion: FDG PET/CT in view of its better sensitivity (incremental value of 12%) in delineating skeletal metastses over MDP bone scan and its ability to detect non skeletal metastses (which acconted for 33% in our study) should be considered as a useful modality for stgaing Ewing's group of tumors.

P085

[18F]PR04.MZ for Dopamine Transporter Quantification in Low Density Regions - Complete Evaluation and Dosimetry in Healthy Volunteers

V. Kramer[1], R. Pruzzo[2], E. Hernandez[2], P. Chana[3], C. Juri[4], P. Riss[5], F. Rösch[6], H. Amaral[1]; [1]PositronPharma SA, Santiago de Chile, CHILE, [2]Nuclear Medicine and PET/CT Center FALP, Santiago de Chile, CHILE, [3]Universidad de Santiago de Chile, Santiago de Chile, CHILE, [4]Universidad Catolica, Santiago de Chile, CHILE, [5]University of Oslo, Oslo, NORWAY, [6]Johannes Gutenberg-Universität Mainz, Mainz, GERMANY.

Objectives: Deterioration of dopaminergic cells in the Substantia Nigra and subsequent dopaminergic deficiency in striatal regions is the main hallmark of Parkinson's Disease. Quantification of the cellbodies in this area remains difficult due to low dopamine transporter concentrations and partial volume effects. 18F-PR04.MZ is a new, high affinity radioligand for dopamine transporters, currently under investigation at our center. Aim of this study was to perform a complete evaluation and dosimetry study with 18F-PR04.MZ in healthy volunteers.Methods: 5 healthy volunteers (mean age 23 ± 2 a) underwent a dynamic PET scan (Siemens mCT) for a duration of 180 min after bolus injection of 203 ± 21 MBq (mean ± SD) [18F]PR04.MZ. PET scans were co-registrated to T1 weighted MRI scans and normalized to a brain template. Blood input function was recorded via automated online blood sampling (Twilite/Swisstrace) and plasma and parent fraction was determined by a HPLC method. Distribution volumes and binding potentials were determined by different invasive and non-invasive methods. 5 healthy volunteer underwent serial whole body PET scans for 2h to determine biodistribution and estimate internal radiation dose.Results: [18F]PR04.MZ showed a relatively fast kinetic and very high specific uptake in DAT containing brain regions. Peak uptake in putamen was reached after 25 minutes followed by slow washout. Distribution volumes were determined using 2TCM and were well correlated with non-invasive methods like SRTM. Stepwise reduction of scan duration from 180 to 90 min showed stable estimates for most binding potentials. The biodistribution study revealed urinary bladder and gastrointestinal system as main excreting organs and bone uptake was observed due to defluorination. Results from the dosimetry study are currently under evaluation but preliminary estimates showed no critical levels of radiation burden.Conclusions: [18F]PR04.MZ is a promising tool for precise quantification of striatal and extrastriatal dopamine transporters and its kinetic provides suitable and stable estimates after only 90 min of scan duration. Studies including REM sleep disorder patients and early PD patients are currently ongoing to estimate DAT density in different brain regions in early phases of PD.

P086

The potential impact of congestive heart failure (CHF) on FDG PET/CT studies

M. Ahmed[1], R. Muzaffar[1], **M. M. Osman**[1,2]; [1]Saint Louis University, Saint Louis, MO, UNITED STATES, [2]Saint Louis VA, Saint Louis, MO, UNITED STATES.

Objective:Congestive heart failure (CHF) is not uncommon among cancer patients undergoing FDG PET/CT. When present, CHF may induce reactive mediastinal adenopathy with or without cardiac cirrhosis (congestive hepatopathy). Therefore, CHF may be a source of false positive mediastinal nodes and

affect the standard uptake value (SUV) of the liver, a frequently used internal reference point in FDG PET/CT scans. We aimed to assess if CHF results into reactive mediastinal adenopathy and or affect liver SUV.Method:A retrospective study was conducted comprising of 82 patients with known CHF who had FDG PET/CT examination. Patients with malignant mediastianal lymphadenopathy, no measurable lymph nodes or completely calcified nodes were excluded resulting in a total of 31 CHF patients. They were compared with 35 age and gender matched non-CHF controls. A log was created to record the number of measurable mediastinal lymph nodes (LN), short axis size measurements, SUV max and mean Hounsfield Units (HU) of the nodes from PET/CT scans. A region of interest (ROI) was also drawn over the posterior right hepatic lobe to measure the SUV max.Results:A total of 66 cases were reviewed (31 female, 35 male, mean age of CHF group 69, mean age range of non-CHF group 70, total age range 57-90 yrs.). Mean values of the CHF vs non-CHF group are as follows:HU (mean): CHF 46.5 +/- 25.40 vs Non-CHF 47.79 +/- 24.94; p-value 0.77SUV max: CHF 1.96 +/- 0.94 vs Non-CHF 1.95 +/- 0.64; p-value 0.94LN short axis(mm): CHF 8.87 +/- 3.95 vs Non-CHF 7.67 +/- 2.66; p-value 0.04Liver SUVmax: CHF 2.79 +/- 0.62 vs Non-CHF 3.13 +/- 0.66; p-value 0.002A two tailed test of significance demonstrated a statistically significant difference in the size of LN for the 2 groups but was still below 10 mm in diameter, which is considered a cut-off in size for assessing lymphadenopathy. However, the t-test for Liver SUV was also significant with a p-value of 0.002.Conclusion:We conclude that the presence of CHF does not result in statistically significant reactive mediastinal adenopathy; however, it does result into lower liver SUV compared to age and gender matched controls without CHF. Therefore, the mediastinum may serve as a better reference point than the liver in patients with CHF. Further studies are needed to elucidate the CHF-induced hepatopathology and potential impact on FDG PET/CT exams.

P087

The Effect of Pulmonary Hypertension on Standardized Uptake Values of the Liver and Pulmonary artery in FDG PET/CT Imaging

M. Mikhayel[1], N. Parkar[1], R. Muzaffar[1], P. Kelly[1], **M. M. Osman**[1,2]; [1]Saint Louis University, Saint Louis, MO, UNITED STATES, [2]Saint Louis VA, Saint Louis, MO, UNITED STATES.

Objective: Pulmonary hypertension (PH) is not uncommon among cancer patients who routinely undergo FDG PET/CT for evaluation and follow up of their malignancy. Other risk factors for the development of PH include drugs and toxins, including chemotherapeutic drugs, as well as underlying portal hypertension. Liver and mediastinal blood pool are being used as internal reference points in FDG PET/CT examinations. The objective of this study was to evaluate potential impact of PH on standardized uptake values (SUV) within the liver and mediastinal blood pool in cancer patients undergoing PET/CT.

Materials and Methods:The study was approved by the Institutional Review Board. FDG PET/CT scans for 38 patients (2 groups) were retrospectively reviewed; 19 patients (group A) (12 male, 7 female) of which had a confirmed diagnosis of PH along with 19 control without PH (group B), matched for age and gender to group A. To define PH, the pulmonary artery diameter (PAD) was measured from the non-contrast CT from the PET/CT. A measurement of 2.9 cm was used to define pulmonary hypertension. The SUV values were also measured in the liver (right hepatic lobe) and in the main pulmonary artery within the two groups using matched volumetric regions of interest (ROI). A log was kept to record our findings. **Results**: A two-sample pooled t-test for unequal variances was used to compare SUV of the liver and pulmonary artery among the two groups. There was no significant difference in the SUV measured in the liver in group A vs. group B ($P > 0.3975$). There was also no significant difference in the SUV measured in the main pulmonary artery between group A and group B ($P > 0.5522$).

Conclusion: There is no significant difference in the SUV of the liver and pulmonary artery between patients with PH and those without PH. Therefore, the presence of PH does not preclude the use of liver and/or mediastinal blood pool as internal reference points in FDG PET/CT examination.

P088

Dynamic whole body distribution of FBPA in humans studied with 3D PET/CT

K. Isohashi[1], H. Kato[1], G. Horitsugi[1], S. Naka[1], I. Mochida[1], E. Shimosegawa[2], J. Hatazawa[1]; [1]Nuclear Medicine and Tracer Kinetics, Osaka University Graduate School of Medicine, Suita, JAPAN, [2]PET Molecular Imaging Center, Osaka University Graduate School of Medicine, Suita, JAPAN.

Objective: Boron neutron capture therapy (BNCT) is a binary cancer treatment system that requires the selective delivery of a boron-containing drug to the tumor and then irradiation with neutrons to yield high-linear-energy-transfer a particles and recoiling 7Li nuclei. Successful application of BNCT requires the selective delivery of 10B to the tumor. In order to evaluate 10B accumulation in the tumors, 4-borono-2-18 F-fluorophenylalanine (FBPA) PET has been employed. Although the indicators of T/N ratio (normal tissue 10B concentration ratio in the tumor T with respect to N) and T/B ratio (10B concentration ratio of tumor venue for blood B) are used, the

method of obtaining these are not standardized in clinical level. We examined dynamic whole body distribution of FBPA in humans by means of 3D PET/CT visually and quantitatively. Methods: Sequential whole-body FBPA PET/CT (Eminence SOPHIA SET-3000BCT/X, Shimadzu) was performed in 5 normal adults (3 males/2 females, mean age=34) after they had fasted for at least 4 h. After whole-body CT for attenuation correction and intravenous bolus injection of FBPA (3.7MBq/kg), the subjects were scanned from the parietal to the groin (data acquisition: 455 sec). The scanning was repeated seven times (interval: 48 sec). Decay of radioactivity during the PET scan was corrected to the time of initiation of the first scan. FBPA radioactivity in whole blood was measured at background, 30 sec, 1, 3, 5, 10, 20, 30 and 50 min using a PET device and a well counter corrected mutually. Spherical volume of interest with a diameter 10 mm was drawn on tomographic images within ascending aorta, aortic arch, pulmonary trunk, left and right ventricle, and inferior vena cava, and FBPA radioactivity was measured. The value of FBPA radioactivity of each site on the images and that in whole blood in the similar time was compared, respectively. This study was approved by the institutional ethics committee. Results: The FBPA uptake in the spleen, pancreas, blood (ventricle) and salivary gland peaked early after the injection and steadily decreased thereafter. The FBPA uptake in kidney and urinary radioactivity were persistently higher. There were correlations between FBPA radioactivity of each site on the images and that in whole blood in a similar time ($p < 0.001$, spearman). Conclusion: In the FBPA PET study, the scan initiation 60 min after FBPA administration provides a stable systemic image. It is possible to obtain a stable B value in T/B ratio from the image.

P089
Uptake of ^{68}Ga-DOTATATE and ^{68}Ga-DOTATOC in Primary Neuroendocrine Tumors, Metastases, and Normal Liver Tissue - is there a Significant Difference?

M. Todorovic-Tirnanic[1], M. Gajic[2], R. Baum[3]; [1]Faculty of Medicine, University of Belgrade and Center of Nuclear Medicine, Clinical Center of Serbia, Belgrade, SERBIA, [2]Institute of Statistics, Faculty of Medicine, University of Belgrade, Belgrade, SERBIA, [3]Theranostics Center for Molecular Radiotherapy and Imaging, Zentralklinik, Bad Berka, GERMANY.

Aim: I*n vivo* distribution comparison of the two ^{68}Ga-labeled somatostatin analogues [TOC and TATE; TOC exhibiting higher affinity for human somatostatin receptor 3 and 5, lower for 2 than TATE] by determining maximal standardized uptake values (SUVmax) in normal liver, primary gastroenteropancreatic neuroendocrine tumor (NET) and metastases.
Materials and methods: 76 PET/CT studies in 38 patients (1 duodenal NET, 18 pancreatic, 2 coecal, 12 ileal, 3 jejunal, 1 mesenterial, 1 in appendix) with stable disease were analyzed. ^{68}Ga-DOTATATE and ^{68}Ga-DOTATOC PET/CT were performed at consecutive controls. Injection to acquisition time was identical for both studies (±10 min). Mean SUVmax values were determined and compared.
Results: 225 metastases (98 in the liver, 67 in lymph nodes, 43 in bones, 17 in soft tissue), 18 primaries and normal liver were analyzed on both PET/CT studies. Mean SUVmax values in ^{68}Ga-DOTATATE / ^{68}Ga-DOTATOC groups were: normal liver 6.8±1.7 / 6.9±1.8, primary tumor 20.4±13.7 / 24.2±20.1, liver mets 15.4±9.4 / 17.9±11.4, soft tissue mets 15.3±16.4 / 17.3 ±18.8, lymph node mets 12.0±9.5 / 15.2±13.3, bone mets 7.5 ±5.7 / 9.9±8.0. ^{68}Ga-DOTATOC uptake was always higher: highly significantly in primaries, liver and lymph node metastases, significantly in bone metastases, not significantly in soft tissue metastases. ^{68}Ga-DOTATOC and ^{68}Ga-DOTATATE accumulated higher in primaries compared to metastases. The highest metastatic uptake was in liver and soft tissue metastases (not significantly different compared to primaries), intermediate in lymph nodes (significantly lower than in primaries) and the lowest in bone metastases. Normal liver tissue showed the lowest uptake.
Conclusion: Both radiopharmaceuticals had the highest uptake in primary tumor and three (^{68}Ga-DOTATATE) to 3.5 fold (^{68}Ga-DOTATOC) lower in the normal liver tissue. For both radiopharmaceuticals liver and soft tissue metastases had the highest uptake among metastases, lymph node intermediate and bone metastases the lower. There was no difference between ^{68}Ga-DOTATOC and ^{68}Ga-DOTATATE accumulation in the liver, which could be related to the normal peptide metabolism in the liver. Higher uptake of ^{68}Ga-DOTATOC in the primary tumor and metastases could be beneficial when theranostic approach is considered.

P090
18FDG-PET/CT Imaging in Suspected Acute Renal Allograft Rejection

P. Lovinfosse, L. Weekers, C. Bonvoisin, C. Bovy, S. Grosch, J. Krzesinski, R. Hustinx, F. Jouret; CHU of Liege, Liege, BELGIUM.

The diagnosis procedure for kidney transplant recipients (KTR) with suspected acute rejection (AR) relies on needle biopsy. Noninvasive tests to predict nonrejection would be preferable. AR is associated with a recruitment of activated leukocytes into the transplant, which are characterized by a high metabolic activity and an increased uptake of glucose analog, 18Fluoro-deoxy-glucose (18FDG). Thus, 18FDG-Positron emission tomography coupled with computed tomography (PET/CT) may help noninvasively detect renal AR. From January 2013 to February 2015, we prospectively performed 32 18FDG-PET/CT in 31 adult KTR with suspected

renal AR who underwent a biopsy. Biopsies were categorized as "normal", "borderline", "AR" or "others" according to Banff classification. PET/CT imaging was performed within 201 ± 18 minutes after i.v. administration of 3.2 ± 0.2 MBq/kg of 18FDG, before any modification of immunosuppression. The mean standard uptake values (SUV) of both upper and lower renal poles were measured, with no threshold activity. Biopsies were diagnosed as "normal", "borderline", "AR" or "others" in 8, 10, 8 and 6 (including 3 polyoma-BK nephropathies) cases. Mean SUV respectively reached 1.5 ± 0.2, 1.6 ± 0.3, 2.9 ± 0.8, 2.2 ± 1.2 in each category. Mean SUV of biopsy-proven AR was significantly higher than "normal" cases ($p<0.01$). No difference was found between "normal" vs. "borderline", or between "AR" vs. "others" histopathology. Still, a positive correlation between mean SUV and acute composite (g+i+t+v+ptc) Banff score was found, with a coefficient of 0.70 ($p<0.001$). Sensitivity and specificity of 18FDG-PET/CT in detecting pathological biospies were respectively 92.3 and 36.8, with a mean SUV threshold at 1.4. 18FDG-PET/CT imaging may help discriminate nonrejection, thereby avoiding unnecessary transplant biopsy in KTR with suspected AR.

P091

Effects of Long Acting Somatostatin Analogue Therapy on 68Ga-DOTA-Octreotate PET/CT uptake in Neuroendocrine Tumour Patients

M. H. Cherk, R. J. Hicks, **M. S. Hofman**; Centre for Cancer Imaging, Peter MacCallum Cancer Centre, Melbourne, AUSTRALIA.

Aim: To evaluate the effects of long-acting somatostatin analogue (SSA) therapy on 68Ga-DOTA-octreotate (GaTate) uptake at physiological and metastatic sites in neuroendocrine tumour (NET) patients and potential implications for peptide receptor radionuclide therapy (PRRT). Materials and Methods: Twenty-one patients (8 F; 13 M, Age 30-89) with metastatic neuroendocrine tumour (NET) who had undergone baseline and repeat imaging following long-acting SSA therapy with GaTate PET/CT scans were retrospectively reviewed. Maximum standardized uptake values (SUVmax) were measured for the thyroid, spleen, liver, pituitary, adrenals and salivary glands in all patients and for 49 metastatic lesions in 12 patients with stable disease which were then compared. Serum chromogranin-A (CgA) levels were available for correlation between scans in 17/21 patients. Results: Mean thyroid, spleen and liver SUVmax decreased significantly following SSA therapy from a baseline of 5.9 to 3.5 ($p=<0.0001$), 30.3 to 23.1 ($p=<0.0001$) and 10.3 to 8.0 ($p=<0.0001$) respectively. Mean pituitary SUVmax increased from 10.2 to 11.0 ($p=0.004$). Adrenal and salivary gland SUVmax did not change. Tumour SUVmax increased in 7 of 12 patients with stable disease; CgA was stable of decreasing in 5 of these patients.] 30/49 (61%) metastatic lesions had an increase in SUVmax and metastatic lesion:liver uptake ratio increased in 40/49 (82%) following SSA therapy. Conclusion: Long-acting SSA therapy decreases GaTate uptake in the thyroid gland, spleen and liver but in most cases increases metastatic lesion:liver uptake ratio. This has significant implications for interpretation of GaTate PET/CT as SSA therapy may thereby increase Krenning Score or other quantitative parameters resulting in apparent progression. It also increases the likelihood of a patient being deemed suitable for PRRT. Our findings also suggest pre-dosing with SSA prior to PRRT may enable higher doses to be delivered to tumour whilst decreasing dose to normal tissues, potentially reducing myelosuppression as a consequence of lower splenic irradiation.

P092

Ga-68 labelled PSMA ligand based PET/CT scan for the detection of recurrence in prostate cancer patient and comparison with F-18 choline-based PET/CT scan in a tertiary care center

B. R. Mittal, J. Shukla, R. V. Parghane, R. K. Phulsunga, R. Vatsa, P. Bhusari, N. Rana, A. Sood, A. Bhattacharya, S. K. Singh; Postgraduate Institute of Medical Education & Research, PGIMER, CHANDIGARH, INDIA.

Background: Prostate cancer (PC) is the second most frequent cancer and the sixth leading cause of cancer death in men worldwide. Detection of recurrence in prostate cancer is a major challenge for all conventional imaging. The prostate-specific membrane antigen (PSMA) is over-expressed in PC cells therefore providing a promising target for specific imaging in these patients. The aim of this study was to detect recurrence in patients with PC by using a (68)Ga-labelled PSMA ligand based PET/CT scan and compared this finding with (18)F-choline-based PET/CT scan. Material and Methods: A total of 12 confirmed cases of prostate cancer were analyzed retrospectively. All patients underwent (68)Ga-labelled PSMA PET/CT scan and (18)F-choline-PET/CT scan within 2 weeks interval. Radiotracer distributions in whole body images were assessed visually in both PET/CT scans. The semi-quantitative analysis was performed by measuring the maximum standardized uptake values (SUVmax) in prostatic bed, pelvic and abdominal lymph nodes, bone and other lesions detected on both scans. In addition, target to background ratio for all lesions detected on both scans were also analyzed. Results: The mean prostate-specific antigen (PSA) value in these patients was 9.07 ng/ml (range 0.3-38 ng/ml). A total of 19 lesions were detected in 68Ga-PSMA PET/CT while 12 lesions were detected using choline PET/CT, in 10 patients. All lesions

were confirmed on histopathological examination, MRI, bone scan and clinical follow up. All these finding on both scan were localized in four regions: prostatic bed (PSMA=8, choline=5), pelvic lymph nodes (PSMA=5, choline=4), abdominal lymph nodes (PSMA=2, choline=1), bony lesions (PSMA=4, choline=2) and were analyzed semi-quantitatively using maximum standardized uptake values (SUVmax) in these four regions. In 2 patients no lesion was found on both scans. All lesions detected by 18F-choline PET/ CT were also seen by 68Ga-PSMA PET/CT. In 68Ga-PSMA PET/CT SUVmax was clearly (>10 %) higher in 19 lesions and the tumour to background ratio was clearly (>10 %) higher in 19 lesions when compared to 18F-choline PET/CT. Conclusions: Our results indicate that 68Ga-PSMA PET/CT is better to detect recurrence in patients with PC. Moreover, more number of lesions and high SUVmax value, target to background ratio and improved contrast is achienvd as compared to 18F-choline PET/CT.

P093

Breslow thickness and 18F-FDG PET-CT result in initial staging cutaneous melanoma: can a cut-off point be established?

A. Ortega Candil, C. Rodriguez Rey, **E. Cala Zuluaga**, M. Cabrera Martin, M. Perez Castejon, A. Jimenez Ballve, A. Serrano Palacio, L. Leon Ramirez, C. Riola Parada, M. Garcia Garcia-Esquinas, L. Lapeña Gutierrez, J. Carreras Delgado; Clinico San Carlos Hospital, Madrid, SPAIN.

Aim: to establish a Breslow Thickness (BT) cut-off point for indication of PET-CT in initial staging of cutaneous melanoma and evaluate its prognostic value. Methods: retrospective analysis of 347 PET-CT studies with diagnosis of melanoma undertaken in our institution from 01/01/2011 until 31/01/2015, 108 were initial staging; 26 patients were excluded (6 metastases of unknown origin, 16 non-cutaneous melanomas and 4 cases with unknown BT) and a final sample of 82 patients remained. To establish an optimal cut-off point, we undertook a ROC curve analysis based on the Youden index (J). For evaluation of prognostic value, a survival analysis was done considering as main event death assignable to melanoma. Results: Forty nine (59.76%) of all 82 patients selected were men and 16 (19.51%) had a positive PET-CT result. Mean age was 64.89±15.61 years old. The mean BT in patients with a negative PET-CT result was 3.73±2.82mm and in the positive group 7.81±4.21mm (p=0.0016; t Student). In the ROC curve analysis (AUC 0.843, SE 0.045) we obtained an optimal value of 5 mm BT (J 0.725) with the following values: sensitivity specificity 93.8%, 78.8%, NPV 98.1%, PPV 51.7%, diagnostic OR 55.7 and accuracy 81.7%. Median follow-up was of 1.48±1.17 years detecting 2/53 (3.77%) deaths in BT<5mm group, and 9/29 (31.03%) in BT≥5mm group. Survival curves between both groups were significantly different (Log-rank, p=0.0003). Conclusions: BT average was significantly higher in patients with positive PET-CT. A 5 mm cut-off point correctly distinguishes those patients with positive PET-CT from those with negative results, reducing the number of PET-CT studies by 64.63%. Patients with BT≥5mm present a significantly worse prognosis.

P094

Positron Emission Tomography (PET) Imaging of Chemokine Receptor CXCR4 in Patients with Solid Cancers: First Results

T. Vag[1], C. Gerngross[1], U. Keller[2], H. Wester[3], M. Schwaiger[1]; [1]Clinic of Nuclear Medicine, Klinikum Rechts der Isar, Munich, GERMANY, [2]III Medical Department, Klinikum Rechts der Isar, Munich, GERMANY, [3]Institute of Pharmaceutical Radiochemistry, Munich, GERMANY.

Objective: CXCR4 is a chemokine receptor that is overexpressed in various human cancers and is involved in tumor metastasis. The aim of this feasibility study was to preliminary estimate the potential of CXCR4-targeted Positron Emission Tomography (PET) as a novel diagnostic modality in patients suffering from solid cancers. Material and Methods: 21 patients with histologically proven pancreatic cancer, laryngeal cancer, non-small cell lung cancer (NSCLC), prostate cancer, melanoma, breast cancer, hepatocellular carcinoma (HCC), glioblastoma, sarcoma or cancer of unknown primary (CUP) underwent PET imaging using the novel CXCR4 nuclear probe [68Ga]pentixafor. Maximum standardized uptake values (SUVmax) of the liver, spleen and bone marrow were measured for determination of physiological tracer distribution. For evaluation of in vivo CXCR4 expression on tumors, SUVmax and tumor-to-background ratios (T/B ratio) were determined in a total of 43 malignant lesions including 8 primary tumors, 3 local recurrent tumors and 32 metastases. When available, SUVmax of malignant lesions was compared to corresponding SUVmax measured in standard routine [18F]FDG PET. Results: Moderate tracer uptake was detectable in the liver, bone marrow and spleen with a mean SUVmax of 3.1, 3.7 and 5.6, respectively. By visual interpretation criteria, 9 of 11 primary and local recurrent tumors were detectable, exhibiting a mean SUVmax of 4.7 (range 2.1 to 10.9) and a mean T/B ratio of 2.9. 20 of 32 evaluated metastases were visually detectable (mean SUVmax of 4.5, range 3.2 to 13.8; mean T/B

ratio of 2.8). Spearman's correlation revealed a low correlation between SUVmax and number of lesions per patient (r=0.3). Compared to [18F]FDG PET additionally obtained in 10 patients, tracer uptake in [68Ga]pentixafor PET revealed a lower SUVmax in all measured malignant lesions. Conclusion: PET Imaging of CXCR4 in patients with solid cancers is feasible. Based on the experience gained within this small number of patients, SUVmax of malignant solid tumors seems to be in general lower in [68Ga]Pentixafor PET compared to [18F]-FDG PET. Moreover, CXCR4 expression in solid malignancies seems to be highly heterogeneous depending on factors, that have to be elucidated in further studies. CXCR4 expression profile could also become interesting in near future, when considering [68Ga]pentixafor as a selection marker for CXCR4 directed treatment.

P095

Colorectal pulmonary metastasis candidate to surgical resection: Preoperative prognostic value of ^{18}F-FDG PET/CT SUVmax

E. Puta[1], O. Rena[2], F. Orsini[1], L. Leva[1], E. Papalia[2], C. Casadio[2], G. Sacchetti[1]; [1]Nuclear Medicine Department, AOU "Maggiore della Carità", Novara, ITALY, [2]Thoracic Surgery Department, AOU "Maggiore della Carità", Novara, ITALY.

Aim: Surgical resection is a well established therapy in patients with lung metastases. Literature data show that patients with single metastasis and a disease-free interval (DFI)>2 years have the best survival rate. Currently there are no biological predicting factors affecting prognosis. ^{18}F-FDG-PET/CT imaging enables in-vivo visualization, characterization and measurement of biological process in tumor at the molecular and cellular level. The aim of this study was to evaluate the prognostic value of ^{18}F-FDG PET/CT SUVmax in patients with colorectal lung metastasis submitted to surgical resection.Materials and Methods: Forty-two consecutive patients (12♀, 30♂; age range 40-79 yr, mean 65) with colorectal pulmonary metastases underwent ^{18}F-FDG PET/CT from 2004 to 2012 prior to lung surgery. A total of 50 lesions were removed. All 42 scans were reviewed. SUVmax of each lung lesion was calculated. In patients with more than one lesion, the highest SUVmax of all nodules was considered. In order to identify factors affecting the long-term prognosis age, sex, ^{18}F-FDG-PET/CT SUVmax of lesions, DFI, preoperative serum CEA level, number and size of resected metastases, type of surgery and the presence of lymph nodes metastasis were retrospectively analyzed.Results: ^{18}F-FDG PET/CT SUVmax was 7.13±5.1 (range 1-22, median 5.35). DFI was 30 months (range 3-78). Preoperative CEA level>5 ng/dL occurred in 14/24 cases. Lesion mean diameter was 2.4cm (range 1-5cm). Wedge resection and lobectomy were performed in 40 and 10 lesions respectively. Mediastinal lymph nodes were sampled in 28 cases with metastasis detection in 10/28. Five-year disease free survival (DFS) and 5-year disease-correlated survival (DCS) were 48% and 55% respectively. According to univariate analysis, factors favorably affecting prognosis were single metastasis, DFI>24months, the absence of mediastinal lymph node metastases and SUVmax<5.35. According to multivariate analyses, independent prognostic factors were single metastasis, DFI>24 months and SUVmax<5.35. Patients with DFI>24 months showed 5-year DFS of 65% and 5-year DCS of 68%. Patients with SUVmax<5.35 showed 5-year DFS of 65% and 5-year DCS of 70%. Kaplan-Meier plot demonstrated a significant lower 5-year DFS in patients with preoperative SUVmax>5.35(Log-rank test P=0.018). Patients with single metastasis (n=10), DFI>24 months and SUVmax<5.35 (n=15), showed 5-year DFS of 72%.Conclusion: According to our results the preoperative value of SUVmax<5.35 in patients with colorectal lung metastases is a significant independent prognostic factor affecting favorably long-term survival. The combination of the three parameters SUVmax<5.35, DFI>24 months and single metastasis identify the subgroup of patients with the best 5-year DFS.

P096

Correlation between Proliferation Index and Metabolic Activity at the biopsy site in newly diagnosed NHL

V. Agarwal, B. SUNEETHA, S. PANDE; MEDANTA THE MEDICITY HOSPITAL, GURGAON, INDIA.

Background: In recent years, positron emission tomography (PET),particularly with [18F] fluorodeoxyglucose (FDG), has emerged as an alternative to computed tomography (CT) not only in treatment evaluation but also in the staging of lymphomas. It enables the assessment of the extent of lymphoma with a higher sensitivity than that of CT. In lymphoma, Ki-67 proliferating index (MIB-1 labeling index) indicates the proliferation potential of tumor cells, which often affects the prognosis. Although the correlation between the standardized uptake value (SUV) on PET and the proliferation potential of tumor cells has been reported in several tumors such as brain tumors, head and neck cancer, lung cancer, and bone and soft tissue tumors, only few studies have elucidated this in the case of malignant lymphoma, which is one of the most sensitive tumors to therapy. It is important to know the proliferation potential and, in turn, determine the speed of tumor growth to decide the appropriate regimen of initial chemotherapy. Method: We did a retrospective study on the 47 patients (45 were aggressive lymphomas and 02 were mantle cell) referred for initial staging of lymphoma to our nuclear medicine

department in last 1 year. Inclusion criteria were newly diagnosed biopsy proven lymphoma with complete pretreatment evaluation including history, physical examination and standard laboratory tests, Whole-body FDG PET/CT for pretreatment staging and biopsy samples evaluation using immunohistochemical staining to look for Ki-67 expression. Recurrent cases of lymphoma were excluded. Results: All the cases exhibited high SUVs at the site of biopsy (ranging from 8.8-59.43) and high Ki-67 index, ranging from 40-100%. In 17 of the 47 patients, the biopsy site was discordant with the maximum SUV site. In the remaining 30 patients, biopsy site and the site for maximum SUV were same. Bx SUVmax showed significant positive correlation with the Ki-67 proliferation index ($r=0.56$; $p < 0.01$). Significant positive correlation was also detected between the Bm SUV max and the Ki-67 proliferation index ($r=0.52$; $p < 0.01$). Conclusion: The BxSUV(max) correlated with the Ki-67 proliferation index, and a correlation was detected as well between the maximum SUV of the whole-body (BmSUV(max)) and the Ki-67 proliferation index, indicating that tumor proliferation potential might be predicted in vivo by FDG-PET/CT images and thus, PET/CT may be useful to guide biopsy by selecting sites with the BmSUV(max) when clinically appropriate.

P097

Complementary diagnostic role of Somatostatin Receptor Scintigraphy (SRS) and 18-F-FDG-PET-CT in neuroendocrine tumors management

M. Catalano, G. Annunziata, D. Scala, V. Ippolito; AORN, Naples, ITALY.

Complementary diagnostic role of Somatostatin Receptor Scintigraphy (SRS) and 18-F-FDG-PET-CT in neuroendocrine tumors management

Aim The complementary diagnostic role of Somatostatin Receptor Scintigraphy (SRS) and 18-F-FDG-PET-CT in patients (pts) affected with neuroendocrine tumors (NET) was evaluated correlating the proliferation index as determined by Ki67 to functional imaging data.

Materials and Methods We enrolled 41 pts (27 male, average age 61.2 ± 12.6) affected with NET tumors (27 GEP , 11 pulmonary NET and 3 different origin NET) from October 2013 to December 2014. Pathological data (WHO 2010 classification) identified 14 pts, 17 pts, 10 pts as G1, G2, G3 respectively . They underwent to SRS and 18F-FDG-PET-TC within about 40 days.

ResultsIn the first group SRS was positive in 9 pts (64%) and negative in 5 pts (36%) whereas 18F-FDG PET-CT was positive in 4 pts (29%) and negative in 10 pts (71%) ; in the second group SRS was positive in 14 pts (82%) and negative in 3 pts (18%) whereas 18F- FDG PET-CT was positive in 9 pts (53%) and negative in 8 pts (47%) ; in the third group SRS was positive in 4 pts (40%) and negative in 6 pts (60%) while FDG PET-CT was positive in 8 pts (80%) and negative in 2 pts (20%). According to literature data, in NET G1 SRS has a better diagnostic accuracy than 18F-FDG PET-CT. On the other hand FDG PET-TC was able to better recognize tumor and metastasis in NET G3. In the pts categorized as NET G2, we found positive SRS and sometimes unexpected positive FDG PET-CT and the number of positive and negative PET scan was the same.

Conclusion The real sensitivity of 18F-FDG PET-CT in NET management has not been enough investigated. Beyond the 18F-FDG PET-CT affirmed role in G3 NET staging and restaging, it can become a routine investigation method in G2 NET because heterogeneous phatological data are not able to characterize tumor biology and the linked therapeutic approach. Instead NET tumor characteristics can be well highlighted by 18F-FDG-PET-CT and SRS functional imaging. Furthermore FDG PET-CTscan positivity could perhaps identify more aggressive tumors.

P098

A Comparison between PET/CT and CT in Head&Neck Radiotherapy Treatment Planning

O. Ferrando[1], F. Foppiano[1], T. Scolaro[2], A. Ciarmiello[3]; [1]Medical Physics Department, St Andrea Hospital - ASL5 Spezzino, La Spezia, ITALY, [2]Radiotherapy Department, St Andrea Hospital - ASL5 Spezzino, La Spezia, ITALY, [3]Nuclear Medicine Department, St Andrea Hospital - ASL5 Spezzino, La Spezia, ITALY

Aims. The present study aims to evaluate the added value of PET/CT respect to conventional CT in radiotherapy treatment planning of head and neck tumours.

Methods and Materials. We have selected and analysed a set of 18 patients with histological diagnosis of head and neck cancer who underwent conformal-3D Radiotherapy. Patients were divided in three categories of head and neck disease: oropharyngeal, laryngeal and oral cavity cancer. PET/CT scans were performed in the treatment position. Gross tumor volumes were delineated on CT images by an expert radiation oncologist blinded to PET data. Successively another set of target volumes was defined taking into account the combined PET/CT information. The CT and PET/CT volumes were compared at the aim to validate the hypothesis of a more accurate target definition in PET/CT. The study also analysed how the therapeutic scheme in terms of total dose and irradiated volumes can be changed by PET information.

Results. In the cohort of analysed patients 4 had the nodal

stage changed from N0 to N+ when small lymph nodes identified on CT scans as insignificant were found to be FDG avid on PET/CT. 1 patient had negative PET/CT and for 1 patient PET reveals distant metastasis. For two patients gross tumour volumes should not being identified without PET information. Mean values of PET/CT gross tumour volumes were smaller than CT volumes: 109 ±110 cm^3 versus 130 ± 98 cm^3 ($p < 0.015$). The mismatching fraction between CT volumes and PET/CT volumes was 0.41. From the therapeutic point of view for 14 patients the total therapeutic dose was not changed by PET data but the irradiated volumes in PET-CT based treatment and CT-based treatment are different. Two patients had the total therapeutic dose changed by PET/CT information. BTV (biological target volume) identified by PET was boosted in 5 patients for whom a focal dose escalation was considered clinically relevant.**Conclusions**. In radiotherapy treatment planning of head and neck disease PET/CT compared with CT provide a more precise target definition and prevent exclusion of pathologic areas not detectable on CT. In our population addition of PET information to CT lead to a modification of the irradiated target in 61% of the patients analysed. The ability of PET/CT to identify the metabolic part of the tumour allows a dose escalation focused on the more aggressive part of the disease..

P099

3D Volumetric lymph node assessment based on CT versus PSMA11-PET/CT in recurrent prostate cancer

F. Giesel[1], F. Sterzing[2], H. Fiedler[1], M. Rius[3], M. Stefanova[1], A. Afshar-Oromieh[1], K. Kopka[4], J. Debus[2], U. Haberkorn[1], C. Kratochwil[1]; [1]Radiologische Klinik / Abt. für Nuklearmedizin, Heidelberg, GERMANY, [2]Radiologische Klinik / Abt. für Strahlentherapie, Heidelberg, GERMANY, [3]Joint Research Centre – Institute for Transuranium Elements, Karlsruhe, GERMANY, [4]Deutsches Krebsforschungszentrum (DKFZ) / Abteilung für Radiopharmazeutische Chemie, Heidelberg, GERMANY.

AIM: PSMA11-PET/CT is a powerful new method of detecting early nodal metastases in recurrent prostate cancer. The purpose of this retrospective investigation was to evaluate the volume and dimensions of nodes identified by Glu-urea-Lys-(Ahx)-[68Ga(HBED-CC)] (68Ga- PSMA-11) in the setting of recurrent prostate cancer. MATERIAL & METHODS: All PET/CT image acquisitions were performed 60 ± 10 minutes after i.v. injection of 68Ga- PSMA-11 (mean dose 176 MBq). Forty nine PSMA-positive lymph nodes were identified in 21 patients with recurrent prostate cancer and rising PSA. Using a semi-automated lymph node segmentation software (MeVis, Bremen, GER), node volume and short and long axis dimensions were measured and compared to the maximum standardized uptake values (SUVmax). Round nodes greater than or equal to 0.8cm were considered positive by morphologic criteria alone. The percentage of nodes identified by elevated SUVmax but not by conventional morphologic criteria was determined. RESULTS: The mean volume of 68Ga-PSMA-positive nodes was 0,5 ml (range 2,3-0,2mL); mean short axis diameter was 5,8mm (range 2,4-13,3mm). In 7 patients (33,3%) with 31 PSMA positive nodes only 11(36%) were morphologically positive based on diameters >8mm on CT. In the remaining 14 patients (66,6%) 18 (37%) of PSMA positive lymph nodes had short axis diameters <8mm with a mean short axis diameter of 5,0mm (range 2, 4-7,9). Moderate correlations of SUVmax were observed with node diameter, volume and PSA level. Thus, in this Population 68Ga-PSMA-PET/CT detected nodal recurrence in two thirds of patients who would have been missed by conventional morphologic criteria. CONCLUSION: 68Ga-PSMA-11 PET is more sensitive than CT based 3D volumetric lymph node evaluation in determining the node status of patients with recurrent prostate cancer and is a promising method of restaging prostate cancers in this setting.

P100

FDG uptake quantification: comparison of different delineation strategies and software platforms

A. de Jong[1], B. A. Blomberg[1], R. A. Nievelstein[1], V. Frings[1], G. Kramer[2], A. J. de Langen[2], O. S. Hoekstra[2], R. Boellaard[2]; [1]UMC Utrecht, Utrecht, NETHERLANDS, [2]VU Medical Center, Amsterdam, NETHERLANDS.

AimTo determine the accuracy of different tumor delineation strategies and software platforms to derive FDG uptake parameters.Materials and methodsMaximum, mean and peak standardized uptake values (SUVmax, SUVmean and SUVpeak), metabolic active tumor volume (MATV) and total lesion glycolysis (TLG) were determined in the NEMA NU 2 Image Quality phantom, and in eight FDG whole-body PET/CT scans of therapy-naïve non-small-cell lung cancer patients. The phantom study was performed according to EARL specifications, and patients were examined following the EANM FDG PET/CT guidelines (Boellaard et al EJNMMI 2015; 42: 328-54). Uptake parameters were determined using a 50% isocontour with background correction (A50%) as implemented in four different software platforms: ROVER (ABX software, Radeberg, Germany), KEOSYS (Keosys, Saint-Herblain, France) and two custom tools developed at the VU Medical Center. One of these tools attempts to enhance delineation workflow using a new approach based on initiating tumor delineation directly on the PET maximum intensity projections (MIPs).ResultsFor the phantom study there were no differences in SUVmax between the various tools. For

SUVmean and SUVpeak differences up to 15% were found, while MATV and TLG differed up to 47% and 37%, respectively. In the clinical studies, differences were found for SUVmax up to 3%, SUV mean up to 7%, SUVpeak up to 16%, MATV up to 28% and TLG up to 23%.ConclusionFor most uptake parameters large differences were found between the various software platforms, despite using a similar delineation method. This study reveals that only SUVmax can be obtained reliably in a multivendor software platform setting. There is an urgent need for standardizing software platforms before MATV and TLG can be used as quantitative imaging biomarkers in a multisoftware setting.

P101

Sequential dynamic PET and dynamic MR imaging in N-staging of lung cancer patients

P. Flechsig, D. Rath, C. Heußel, C. Kratochwil, H. Kauczor, U. Haberkorn, F. Giesel; University Hospital Heidelberg, Heidelberg, GERMANY.

Purpose:For therapy stratifications, staging of lung cancer is typically performed with FDG-PET/CT. In the context of new established integrated PET/MR-scanners, the combination of well-established dynamic contrast enhanced (DCE) MRI imaging with dynamic PET might be an upcoming imaging modality. In order to evaluate potential perfusion changes between benign and malignant lymph nodes in lung cancer patients, DCE MRI was correlated to microcirculatory and sub cellular dynamic parameters in FDG-PET/CT.Materials and Methods:According to the clinical routine, a total number of 14 patients with lung cancer were examined sequentially with FDG-PET/CT (Siemens Biograph 6) and DCE MRI (Gadovist®, Bayer, Germany; Siemens Magnetom Aera, 1,5T) prior to surgery. Findings were correlated to the histological gold standard.Results:14 lymph nodes (six malignant, eight benign) could clearly be histological analyzed and were correlated with findings in MRI and PET/CT. In DCE MRI, malignant lymph nodes showed early and generally increased perfusion values compared to benign ones, with typical signs for washout 60 seconds after contrast injection. Benign lymph node reached the typically plateau phase after 60 seconds with steady state during the first 180 seconds.This correlated well with microcirculatory and sub cellular parameters in dynamic PET according to a two compartment model, especially with changes in k3 and k4.Conclusion:The sub cellular parameters k3 and k4 in dynamic PET are correlating with changes in DCE MRI, indicating k3 and k4 as potential surrogate parameter for malignant lymph node infiltration in lung cancer patients.

P102

Development of PET in Europe

A. Stevens; Medical Options, London, UNITED KINGDOM.

AIMS: To track the development of PET in Europe. The provision of PET and PET/CT in Europe is extremely heterogeneous with a large variation in scans per head of population between countries; while within countries workload varies widely between different providers. The high level of variation between facilities, the number of new installations and the rapid growth in workload at existing sites precluded a sampling approach and required identification of all European PET providers. MATERIALS AND METHODS: Facilities with PET, PET/CT and or cyclotron(s) were identified from a number of sources including records of the IAEA, manufacturers of diagnostic equipment and sites providing nuclear medicine services. Sites were invited to describe their operation including their equipment profile, the number and types of patient studies performed and their use of radiotracers. We were able to identify over 95% of the PET, PET/CT and cyclotrons operating in Europe. Over 65% of these sites provided workload numbers for 2014. To project total workload we employed a segmentation scheme for each country or region which identified ten types of facility allowing us to estimate more accurately patient numbers at sites who did not contribute workload data. RESULTS: In 2014 there were 680 providers of PET and/or PET/CT in Europe of which 18 were mobile. PET/CT accounted for 93% of the installed systems. PET cameras were located primarily in research departments and in countries where reimbursement or replacement was regulated. PET/MR accounted for 3.6% of systems. FDG accounted for 93% of the studies. 91.0% were oncology, 4.6% neurology and 3.5% infection or inflammation. Fluorinated molecules made up the majority (51%) of other compounds and are used at ~63% of sites. F-Choline accounted for 62% of these fluorinated studies. Gallium 17%, buoyed by the introduction of PMSA, and Carbon 16% were the other significant nuclei in use. Scan numbers rose by 20.7% from the 1.27m scans estimated for 2012 versus 27.1% between 2010 and 2012. There are wide variations across Europe both in terms of scans performed and patient throughput. In some cases this is due to reimbursement and in others working practices and patient catchment.CONCLUSIONS: Across Europe there is an opportunity to double the use of FDG if the proportion of patients in regions with low adoption meets that of high adopters. The growing use of compounds other than FDG bodes well for the introduction of new molecular entities over the coming years.

P103

Feasibility of Accelerating Yttrium-90 PET by Optimizing PET Volume Overlap

J. Zhang[1], C. Wright[1], K. Binzel[1], E. J. Wuthrick[1], P. Maniawski[2], M. V. Knopp[1]; [1]The Ohio State University, Columbus, OH, UNITED STATES, [2]Philips Healthcare, Cleveland, OH, UNITED STATES.

Objectives: Yttrium-90 (90Y) microsphere radioembolization is increasingly being used as targeted treatment of unresectable liver malignancies. Nowadays while SPECT of 90Y bremsstrahlung is still the standard imaging modality for biodistribution, PET has also been utilized for post-radioembolization imaging for better spatial resolution and improved quantification however being limited by long table time due to that is predominantly a β− emitter. This study investigated the feasibility of accelerating PET by reducing and optimizing PET volume overlap to further improve patient comfort.Methods: An ongoing clinical validation trial was initiated to perform and proof the feasibility of reducing PET volume overlap for 90Y imaging. PET/CT of 5 patients in 26±2 hours post 90Y microsphere radioembolization (3.1±0.2 GBq into hepatic lobes) were performed on a Gemini TF 64 system (Philips Healthcare) with 7min/bed from diaphragm downwards to cover the entire liver under 40% and 20% PET overlaps, respectively. All coincidence events were recorded in listmode. PET data was reconstructed using a 3D TOF OSEM algorithm with a voxel size of 4 x 4 x 4 mm3 in a 144 x 144 matrix. Images were blinded reviewed by a reader panel. Quantitative assessment of volumes and total activity of 90Y microsphere biodistributions for each of the PET data sets was performed.Results: The 90Y PET data demonstrated no significant impact on the visual grade between 40% overlap and 20% overlap. The 20% overlap PET for the given FOV saved ~33% table time compared to using 40% overlap. Quantitative volume segmentation assessment resulted in equivalent volume determinations of 90Y biodistributions (variances=0.5%±5.0%). No significant counts variances were found between both PET scans (variances=0.5%±1.3%).Conclusions: 90Y PET imaging can be considerably accelerated by reducing PET volume overlap as is clinically demonstrated in this trial without degradation of image quality or significantly impact on quantification. Further validation by optimizing PET overlap together with appropriate usage of frame duration is ongoing with the goal of improving image quality with less motion artifacts and shortest patient table time.

P104

Role of 18F-FDG PET/CT and a new score system to measure the pre-test clinical risk in patients suspected of paraneoplastic neurological syndrome

F. J. Pena Pardo[1], A. Palomar Muñoz[1], A. M. García Vicente[1], C. H. Vega Caicedo[1], M. Amo Salas[2], J. F. López-Fidalgo[2], J. A. Garrido Robles[3], J. Á. de Ayala Fernández[4], P. del Saz Saucedo[5], M. Muñoz Pasadas[6], Á. M. Soriano Castrejón[1]; [1]Nuclear Medicine Sv. Hospital General Universitario, Ciudad Real, SPAIN, [2]Mathematics Dep. Universidad de Castilla La Mancha, Ciudad Real, SPAIN, [3]Neurology Sv. Complejo Hospitalario de Toledo, Toledo, SPAIN, [4]Internal Medicine Sv. Complejo Hospitalario de Albacete, Albacete, SPAIN, [5]Neurology Sv. Hospital la Mancha Centro, Alcázar de San Juan (Ciudad Real), SPAIN, [6]Neurology Sv. Hospital de Puertollano, Puertollano (Ciudad Real), SPAIN.

AIM: To assess the diagnostic impact of 18F-FDG PET/CT in patients suspected of paraneoplastic neurological syndrome (PNS) based on our own pre-test risk score (PRS) system. MATERIAL AND METHODS: A multicenter retrospective longitudinal study of patients with suspicion of PNS from 2006 to 2014 was conducted. The clinical pictures were classified into classical (CS) and non-classical syndromes (NCS). The location of nervous system disorder was recorded as central, peripheral, in the neuromuscular junction or combined. Onconeural antibodies (and their type) and tumour markers were registered, when available. We designed a seven-point scoring system using the clinical syndrome characteristics and its location, onconeural antibodies and tumour markers. Patients were classified as low (PRS 0-2), intermediate (3-4) and high (5-7) risk of PNS. FDG-PET/CT imaging assessment was performed classifying the studies as: normal, probably malignant or indeterminate (difficult to establish its correspondence with malignancy or inflammation). Final diagnosis according Graus' criteria (definite, possible or no PNS) was established after a minimal follow-up of 12 months from the PET/CT. Relation between clinical and PET/CT results was studied. RESULTS: 73 patients (47M/26F) with a mean age of 61 years (19-83) were included, with a follow-up time of 33 months (12-96). Eleven (15%) patients were finally diagnosed with neoplasm (8 invasive cancers). Ultimately, 13 (18%) and 24 (33%) subjects were diagnosed as definite or possible PNS (36 non-PNS). All the patients with final diagnosis of neoplasm had a CS (p=0.005). A significant relationship between location of neurological disorder and diagnosis of definite or possible PNS was also noticed, with a higher prevalence of central involvement with respect to non-PNS. PET/CT was helpful to diagnose 6/8 (75%) invasive cancers. PET/CT findings were associated with the final diagnosis of neoplasm (p=0.003) and the diagnosis of PNS attending to Graus' criteria (p=0.019). PRS showed significant association with final diagnosis of neoplasm. All the patients diagnosed of neoplasm had intermediate/high risk (p=0.001). There was also association with PET/CT (p<0.001) with a higher proportion of intermediate/high risk cases in probably malignant PET/CT comparing with negative or indeterminate results (6/7, 28/48 and 6/18 respectively). CONCLUSION: PET/CT detected malignancy in a

significant proportion of patients with invasive cancer. Our PRS seems to be a valid tool to select candidates for PET/CT imaging in this setting.

P105

Repeatability of Quantitative [^{18}F]Fluoromethylcholine PET/CT Measurements in Prostate Cancer

D. E. Oprea-Lager, G. M. Kramer, P. M. van de Ven, A. J. M. van den Eertwegh, R. J. A. van Moorselaar, O. S. Hoekstra, A. A. Lammertsma, R. Boellaard; VU University Medical Center, Amsterdam, NETHERLANDS.

Aim: Quantification is essential for monitoring treatment response in prostate cancer (PC) using [^{18}F]fluoromethylcholine ([^{18}F]FCH) PET/CT. Recently, it has been reported that SUV normalized to the area under the curve of the blood activity concentration (SUV_{AUC}) provides better correlation with full kinetic analysis than standard SUV (Verwer *et al*, JNM 2015). However, precision of SUV_{AUC} (and SUV) is not known yet. The purpose of this study was to assess repeatability of various quantitative [^{18}F]FCH parameters in PC.

Material and Methods: Twelve patients (64±8 years) with metastasized PC underwent 2 sets of [^{18}F]FCH PET/CT scans on two successive days. Each set consisted of a 30 minutes dynamic scan of the chest followed by a whole body (WB) PET/CT scan, 40 minutes post injection (p.i.). Patients received 200 MBq [^{18}F]FCH at the start of the dynamic scan. This scan was used to derive the AUC of the blood activity concentration. Next, lesion uptake was derived from the WB scan using various volumes of interest (VOI): maximum, peak and mean. SUVmean was obtained using a background corrected 50% of maximum isocontour. Each of these parameters was normalized to injected activity/weight, AUC of blood activity concentration and blood concentration at 40 minutes p.i. itself, resulting in SUV, SUV_{AUC} and SUV_{TBR}. Test-retest repeatability of these metrics was studied as function of VOI, VOI size, tissue type (bone/ lymph node) and anatomical localization (intrathoracically/ abdominal). Repeatability coefficients were defined as 1.96 times the standard deviation of the percent differences between test and retest data.

Results: We identified 67 choline avid metastases, 44 bone and 23 lymph node lesions, mean 4±2 per patient. 12 metastases were localized intrathoracically. In case of SUV_{max}, repeatability coefficients for SUV, SUV_{AUC} and SUV_{TBR} were 26, 30 and 45%, respectively. Similar values were obtained for SUV_{peak} and SUV_{mean}. Moreover, tissue type and tumour localization did not affect repeatability. VOIs > 5 cm^3 had comparable repeatability with the smaller ones (30 versus 40%, p=0.267). Repeatability did not differ between lesions with SUV_{max} > 10 and SUV_{max} < 10 (22 versus 28%, p=0.265). The repeatability of SUV_{AUC} for maximum, peak and mean values were comparable with those of SUV.

Conclusion: The repeatability of SUV_{AUC} was comparable to that of SUV and indicated that [^{18}F]FCH PET/CT uptake differences of 30% or more are likely to represent treatment effects. Observed repeatabilities are within the range seen with other commonly used radiotracers, such as [^{18}F]FDG and [^{18}F]FLT.

P106

Effect of motion in the quantification of lesion heterogeneity with Positron Emission Tomography

M. Carles[1], **U. Nestle**[1], A. Schaefer[2]; [1]Department of Radiation Oncology, University Medical Center, 79106 Freiburg, Germany, Freiburg, GERMANY, [2]Department of Nuclear Medicine, Saarland University Medical Center, D-66421 Homburg, Germany, Freiburg, GERMANY.

The aim of this work was to study the effect of motion on the reproducibility of heterogeneity features derived from Positron Emission Tomography (PET). For the measurements we employed four spheres with fluordeoxyglucose (FDG) solution inserted within a NEMA phantom: one commercial fillable glass insert (G) and three homemade alginate phantoms (A). The FDG concentrations (C) were C1=36kBq/ml, C2=18kBq/ml and C3= 8kBq/ml and the background was set to Bg=1.7kBq/ml. Two spheres with diameter φ=37mm presented FDG uptake of C1: glass insert (G.C1) and an alginate phantom (A.C1). Each of the other two alginate inserts was composed by two concentric spheres (ϕin=10mm, Cin and ϕout=37mm, Cout) with different activity concentrations (A.CinCout: A.C1C2 and A.C1C3). Three different measurements were carried out: 1 static and 2 dynamic with irregular breathing patterns (P1 and P2) which were generated by use of a respiratory motion platform (QUASAR by Modus). The parameters for heterogeneity quantification were derived from the volume segmented with a threshold of 40% of the maximum intensity. Heterogeneity quantification involved: coefficient of covariance(COV), Skewness(Sk), Kurtosis(Kr) and Intensity-Volume(IV90-IV10/μ), derived from the intensity histogram; and energy(E), contrast(C), local homogeneity(LH) and entropy(S), derived from the co-ocurrence matrix (with intensity levels M=32, between consecutive voxels d=1 and along the 26 connected neighborhood in 3D space). These 8 features (F) were measured on the ungated (UN-) image and each of the 10 retrospectively gated (4D-) frames resulting from each of the dynamic measurements and on the image resulting from the static measurement (ST-). The comparison of the heterogeneity quantification obtained for different target movements (UNP1 vs UNP2, 4DP1 vs 4DP2) showed reproducibility in 2/8 features with UN-image (Sk: $p<0.01$, $\Delta=100(FP1-FP2)/((FP1+FP2)/2)=37\pm8\%$ and Kr: $p<0.01$, $\Delta=7\pm3\%$) and in 6/8 with 4D-image (Sk: $p<0.05$, $\Delta=1\pm2\%$; Kr: $p<0.02$, $\Delta=0\pm1\%$; E: $p=0.02$,

Δ=4±2%; C: p<0.02, Δ=1±2%; LH: p<0.02, Δ=0±1% and S: p<0.01, Δ=1±1%). The ranking of heterogeneity (phantoms ordered from 1 to 4 based on feature values) obtained in ST-image quantification was reproduced in 4D-quantification by Sk, Kr, E and LH. The variability (SD/μ:standard deviation/mean) observed among the 4D-frames was: Sk 0.02-0.05, Kr 0.27-7.8, E 0.10-0.23 and LH 0.04-0.09. These results allow the conclusion that compared to UN-imaging the impact of motion on quantification of lesion heterogeneity is significantly minimized in 4D-imaging. Furthermore, the reproducibility obtained for Sk, Kr, E and S with 4D-images allows to recommend their use for heterogeneity quantification in lesions affected by respiratory motion.

P107

Comparison between Gallium-68 citrate PET-CT and Gallium-67 citrate scintigraphy for infection imaging

T. Segard[1], L. Morandeau[1], M. Dunne[2], O. Robinson[2], R. Murray[1], E. Geelhoed[3], R. J. Francis[3]; [1]Sir Charles Gairdner Hospital, Nedlands, AUSTRALIA, [2]Royal Perth Hospital, Perth, AUSTRALIA, [3]University of Western Australia, Crawley, AUSTRALIA.

Aim: Preliminary studies have reported promising results for the utility of Gallium (Ga)-68 citrate PET-CT for infection imaging. There are several potential benefits of Ga-68 citrate PET-CT over the current 'gold standard' nuclear imaging technique Ga-67 citrate scintigraphy: reduced radiation dose to patients, shorter time between injection and imaging and reduced time for image acquisition. The aim of this study was to prospectively evaluate Ga-68 citrate PET-CT, in a multicentre public hospital setting and to compare it with Ga-67 citrate scintigraphy to ascertain whether Ga-68 citrate PET-CT is of equivalent diagnostic efficacy for bone and joint infection or pyrexia of unknown origin (PUO) and to assess image quality and reporter confidence for the interpretation of Ga-68 citrate PET-CT compared to Ga-67 citrate scintigraphy.Materials and methods: Patients with PUO and suspected bone or joint infection were eligible for enrolment. In addition to planar wholebody and SPECT-CT images obtained 48 to 72h following Ga-67 citrate administration, patients were injected with 98MBq of Ga-68 citrate for PUO and imaged 1h after from vertex to below knees or 140MBq for bone and joint infection with localised PET-CT imaging at the site of suspected infection. Patients were followed up for 3 months post-imaging to record subsequent treatment and results: antibiotic therapy, surgery, biopsy results when performed, radiological and clinical responses to therapy.Results: Sixty patients have been recruited: thirty-two for bone and joint infection, twenty-eight for PUO. The results show an overall sensitivity of 81% for Ga-67 citrate scintigraphy and 69% for Ga-68 citrate PET-CT imaging. The specificity was 79% for Ga-67 citrate and 67% for Ga-68 citrate. The results were concordant for 76% of the participants. Analysis of reporting physician confidence scores for the diagnosis of infection demonstrated significantly lower confidence for Ga-68 citrate than Ga-67 citrate imaging (p<0.05). Reduced Ga-68 PET-CT reporter confidence was frequently due to prominent physiologic blood pool activity adjacent to the site of infection.Conclusion: In our study, the sensitivity and specificity obtained with Ga-68 citrate PET-CT for the detection of bone and joint infection or PUO was found to be consistently lower than with Ga-67 citrate scintigraphy, although this relationship did not reach significance. Additionally, due to the insufficient level of confidence of the reporting physicians for the Ga-68 citrate studies, this imaging technique could not currently be recommended to replace Ga-67 scintigraphy for routine clinical practice.*This study was supported by a WA SHRAC research grant.*

P108

Do Larger Matrix Sizes in Positron Emission Tomography always result in Increased Image Noise?

C. McKeown, G. Gillen, M. Dempsey, C. Findlay; NHS GG&C, GLASGOW, UNITED KINGDOM.

Aim: As part of a PET image quality assessment it was found that reconstructions with a 256 matrix had lower noise values, as assessed by the Coefficient of Variation (COV), than a 192 matrix - a surprising result. The aim of this study was to determine the combined effect of altering post reconstruction filter width and matrix size on image noise.

Materials and Methods: A uniform ^{68}Ge flood phantom was used to assess COV on images produced using a GE Discovery 690 PET-CT system. Post-reconstruction Gaussian filter full width half maximum (FWHM) was varied between 0mm and 10mm. Reconstructed field of view (FOV) was fixed at 700mm with 128, 192 and 256 matrices applied. Other reconstruction parameters were also examined to determine if they affected the relative noise performance of the different matrix sizes - effective iterations were varied between 18 and 540, and reconstructions were repeated with/without Time of Flight (TOF) and with/without Point Spread Function correction (PSF).

Results: Relative COV for the three matrix sizes behaved as expected at low filter widths (FWHM 0 - 2mm). The 256 matrix produced the highest COVs and the 128 matrix produced the lowest. From an example reconstruction using TOF +PSF with 54 effective iterations: COV_{256} = 13.7%, COV_{192} = 13.1% and COV_{128} = 11.4%. When the filter width was between 2mm and 4mm, the relative COV of the three matrix sizes became unpredictable - larger matrix sizes did not always produce the largest COV results. For example: FWHM =

3mm, COV_{256} (11.9%) was less than COV_{192} (12.6%). When the filter width was between 4mm and 8mm, the relative COVs of the three matrix sizes were the reverse of expected i.e. COV_{128} were highest and COV_{256} were lowest. For example: FWHM = 5mm, COV_{256} = 8.9%, COV_{192}= 9.1%. COV_{128}= 10.2%. All matrix sizes produced very similar COVs for FWHM above 8mm. All relative COV results were consistent regardless of the number of iterations or the application of TOF and/or PSF. The relative differences became more pronounced, however, as the number of iterations increased (i.e. at higher overall noise levels). **Conclusions**: The relationship between image noise and matrix size is not straightforward when post reconstruction filtering is applied. Care is therefore required when different matrix sizes are used clinically.

P109

Influence of Slice Overlap on Positron Emission Tomography Image Quality

C. McKeown, G. Gillen, M. Dempsey, C. Findlay; NHS GG&C, GLASGOW, UNITED KINGDOM.

Aim: PET scans are acquired using overlapping frames to correct for reduced sensitivity at frame edges. Some vendors have fixed overlaps while others allow operators to select overlap size. The optimum overlap for the GE Discovery 690 has not been established. This study aims to assess how image quality is affected by slice overlap. In particular it compares a 23% overlap with the maximum 49% overlap, with reference to recent EANM guidelines.
Materials and Methods: A uniform flood phantom was used to assess noise (Coefficient of Variation, COV) and voxel accuracy (activity concentrations, Bq/ml). A NEMA body phantom with hot/cold spheres in a background activity was used to assess mean Contrast Recovery Coefficients (CRCs) and Signal to Noise Ratios (SNR). Hot sphere phantoms were filled using both 4:1 and 2:1 sphere-to-background ratios.
Results: COVs for 49% and 23% overlaps were 10% and 13% respectively. This increased noise was difficult to visualise on the 23% overlap images. Mean voxel activity concentrations were not affected by overlap size. No clinically significant differences in hot or cold CRCs were observed as the overlap was altered, regardless of sphere-to-background ratio or phantom activity. Visualisation and SNR of low contrast small spheres, however, may be affected by overlap size in low count studies. The 2:1 ratio 13mm diameter sphere was visible on 5/6 acquisitions with 49% overlap (average SNR = 6.4) but was only visible on 3/6 acquisitions with 23% overlap (average SNR = 3.9). However, detectability of the 13mm sphere was only affected when the phantom background activities were below those typically observed in patient livers. EANM guidelines for weight-based FDG administrations suggest that minimum injected activities should be doubled when <30% overlap is used. This experiment demonstrated little difference in image quality either side of this 30% overlap threshold. **Conclusions**: There was minimal detectable influence on image quality in terms of noise, mean activity concentrations or mean CRCs when comparing 23% overlap with 49% overlap. Detectability of small, low contrast lesions may be affected in low count studies - however, this is a worst-case scenario. The marginal benefits of increasing overlap from 23% to 49% are likely to be offset by the disadvantages of increased patient scan times. A 23% overlap is therefore appropriate for clinical use for the GE Discovery 690. The 30% overlap threshold suggested by EANM guidelines when calculating weight-based FDG administrations may require revision.

P110

Normalized uptake fraction: a new approach for image quantification

P. Alves[1,2], A. F. Silva[3], M. F. Botelho[1]; [1]Faculty of Medicine, University of Coimbra, Coimbra, PORTUGAL, [2]IPOCFG, Coimbra, PORTUGAL, [3]IEETA, University of Aveiro, Aveiro, PORTUGAL.

Aim: Functional imaging has become a valuable tool in Oncology although quantification remains a controversial issue. SUV is affected by multiple variables, making difficult to compare exams from different patients and different labs or to use in radiotherapy planning. Our goal was the development of a new methodology for quantification that, despite remaining semi-quantitative, is less operator's dependent.Material and Methods: We studied 32 women with locally advanced cervical cancer, with 18F-FDG PET/CT pre-radiochemotherapy. PET/CT came from two different labs. Radiotherapy volumes (GTV) were obtained, using Velocity AI®, by two independent experts, in a blind study, from anatomic data and from functional imaging. Images were included in MEVISLAB® platform and we obtain parametric images of the distribution of, what we called, normalized uptake fraction (NUF).Results: Statistical analysis of GTV's showed a strong positive correlation, with statistical significance. However it seems that functional information had no impact in final volume delineation, at least for planning purposes. Our PET/CT images had great variability in acquisition methodology, as well as SUV calculations and reports, and it seems necessary to develop a new procedure of quantification. We calculate a normalized uptake fraction per voxel (NUF) and build a parametric image of its distribution. The visualization of NUF images was further conditioned by a lower bound corresponding to the average NUF values at the thigh muscles, which were excluded of the visualization. This approach allows to obtain parametric

images of NUF distribution per voxel, with visual optimization, including re-sampling with 3D reconstruction.The problem of bladder radiotracer retention was solved by a bladder mask delineated on CT images constructed from 3D interpolation of sectional contours and posterior subtraction.Besides standard planar views, a re-sampling with 3D reconstruction was performed which was the major point of interest among experts. The new visualization method allowed the observers to select the best scenarios, and it seems consistent in evaluating areas of uptake related to metabolism of tumor and lymphatics, with excellent topographic orientation.Images of NUF distribution per voxel, corresponding to tumor volume, translated heterogeneous metabolism of 18F-FDG, matching with the concept of biological conformality.Conclusions: We obtained a new approach, through visual navigation in PET/CT-mode after NUF application that allows the analysis of quantification images of PET/CT, from different patients and different equipments, without the controversial ROI or VOI definition and respective SUV calculation. For radiotherapy planning the proposed method seems to improve delineation.

P111

Influence of morphine exposure and withdrawal on the brain kinetics of [18F]DPA-714 and classical biomarkers of inflammation

S. AUVITY[1], S. GOUTAL[1], B. THEZE[1], B. KUHNAST[1], B. HOSTEN[2], W. SABA[1], R. BOISGARD[1], S. CISTERNINO[3], N. TOURNIER[1]; [1]CEA, Orsay, FRANCE, [2]INSERM U1144, PARIS, FRANCE, [3]INSERM U1144, Paris, FRANCE.

OBJECTIVES: Recently, studies have reported that morphine analgesic effects may be modulated by the brain immune response induced by morphine itself. This property was also shown to promote tolerance and dependence observed after prolonged use of morphine in the context of chronic pain or opioid abuse*. Positron Emission Tomography (PET) using radioligands of the Translocator Protein 18 kDa (TSPO) is the most advanced strategy for the non-invasive detection of glial activation in the human brain**. The aim of this study is to investigate the relevance of TSPO PET imaging for the detection of potential glial activation after chronic morphine exposure and withdrawal in rats, and the potential correlation to the expression of classical biomarkers of inflammation. METHODS: Sprague-Dawley rats (n=6) were administered escalating doses of morphine (10 mg/kg increasing to 40 mg/kg, i.p twice a day during 5 days) to achieve a withdrawal syndrome (behavioral validation) after morphine discontinuation. Control rats were administered NaCl 0.9% instead (n=6). Dynamic microPET imaging (Siemens Inveon) was performed during 68 min, 60h after the last dose of morphine using the TSPO radioligand [18F]DPA-714. Data are expressed as areas under the curve (SUV.min) obtained from the elimination phase of the time activity curves (SUV).The kinetics of glial cell activation biomarkers Iba1, GFAP and CD68 were also assessed using immunohistochemistry (IHC) on brain slices during 14 days after chronic morphine exposure. RESULTS: The brain distribution of [18F]DPA-714 was similar in the control (AUC30-68min= 9.79E-05 ± 7.31E-06 SUV.min) and morphine treated (AUC30-68min= 1.06E-04 ± 1.40E-05 SUV.min) groups ($p = 0.15$). IHC revealed the absence of modification in the Iba1, CD68 and GFAP levels of expression after chronic morphine exposure and morphine withdrawal. These glial biomarkers also remained at the same levels during 14 days after morphine discontinuation. CONCLUSION: [18F]DPA-714 TSPO PET imaging may not be a relevant approach to investigate the brain immune response to morphine exposure and withdrawal. Moreover, conventional invasive biomarkers of glial activation were not measurably impacted either. This study questions the nature of neuroimmune events that may be related to morphine tolerance and dependence. REFERENCES: * Opioid activation of Toll-Like Receptor 4 contributes to drug reinforcement. Hutchinson et al, 2012; ** Molecular imaging of microglial activation in amyotrophic lateral sclerosis. Corcia et al, 2012.

P112

Non-completed PET/CT scans - assessing its impact on service quality and patient experience

A. Nunes, G. Beynon, C. Strickland, W. Wong; Paul Strickland Scanner Centre, Mount Vernon Hospital - East and North Herts NHS Trust, London, UNITED KINGDOM.

Purpose: NHS England currently commissions around 50,000 PET/CT scans for patients in England each year.1 The non-completion of a PET/CT scan has significant repercussions. For patients, these include erosion of the patient experience and delay in vital treatment, and for service providers waste of radiopharmaceutical doses and increased waiting lists. The aims of the study was [1] to analyse the main reasons for non-completed PET/CT scans, [2] to identify causes which can be potentially minimized and [3] to determine the impact of these events in the department (both financially and operationally) and on the patient's experience and clinical pathway. Methods and Materials: PET/CT scans booked for the financial year of 2013-2014 from a single provider were analysed. The different reasons for non-completion were categorized in two groups (clinical and non-clinical) with specific sub-divisions. The financial impact of non-completion of the scans was studied. Semi-structured interviews were obtained from patients to assess the effect of the non-completions on the patient's social and clinical contexts. Results: Of the 3121 PET/CTs booked, 171 PET/CT bookings were not completed

[5.4%]. The three main reasons for non-completion were non-clinical (appointment cancellation [2.2%], scanner breakdown [1.2%] and patient not attending (DNA) [1.2%]). Other reasons were both clinical (unacceptable blood glucose levels [0.3%] and patients being unwell for the scans [0.1%]), and non-clinical (radiopharmaceutical production problems [0.2%]). A detailed analysis of the implications of the non-completed scans will be presented including documentation of its negative impact on the patient experience and the financial savings [up to £154.000 potentially for the provider in the period studied] if non-completion of scans was avoided. Conclusion: The total number of not completed PET/CTs made up only a small fraction of the total. Notwithstanding, some of the causes such as appointment cancellation, DNAs and unacceptable blood glucose levels are potentially preventable. Preventing these causes will contribute to reduce the number of non-completed PET/CT scans, improve the patient experience and lead to improvement in quality of the PET/CT service as well as some potential financial savings. 1 NHS England website (http://www.england.nhs.uk/ourwork/commissioning/spec-services/npc-crg/group-b/b02/) accessed on 26/04/2015

P113

A Hybrid random walk algorithm with spatial fuzzy C-mean clustering for segmentation of liver tumors in FDG PET imaging

M. Soufi[1], A. Kamali Asl[1], P. Geramifar[2], M. Khazaee Moghadam[1]; [1]Radiation Medicine Department, Shahid Beheshti University, Tehran, IRAN, ISLAMIC REPUBLIC OF, [2]Research Center for Nuclear Medicine, Shariati Hospital, Tehran University of Medical Sciences, Tehran, IRAN, ISLAMIC REPUBLIC OF.

Aim: Hard decision making in Random Walk image segmentation algorithm could be a source of challenge, especially in low contrast boundaries. Therefore we are going to incorporate the advantages of spatial fuzzy C-means clustering in decision making step of random walk probabilities to improve the segmentation of liver tumors in Positron Emission Tomography (PET) images.Materials and Methods: Tumor delineation in PET images is a challenging task because of statistical noisy nature. Random walk image segmentation technique has reliable noise robustness, fast computation and editing properties that makes it a strong tool in PET tumor delineation purposes.The random walk segmentation algorithm has been implemented using MATLAB. The results have been validated by 4D-NCAT phantom with different spherical lesions (20 to 80 mm diameter). For background and tumor seed localization, pixels with more than 70% maximum Standardized Uptake Value in the interested region have been considered as foreground. For background seeds, pixels with the concentration less than 35% maximum Standardized Uptake Value in eight directions around each foreground seed were searched and included. Then random walk probabilities have been calculated. In decision making step, Spatial Fuzzy C-mean clustering (SFCM) has been incorporated and its results have been compared with conventional random walk in which 50% cut-off is applied on the calculated probabilities.For quantitative performance evaluation of the proposed technique, a clinical data set containing nine liver tumors in whole body FDG-PET/CT images has been used. Manual expert delineation of lesion areas has been considered as ground truth. The results of lesion segmentation with the conventional random walk and proposed method have been compared quantitatively with the ground truth using Dice Similarity Coefficients (DSC).Results: The Hybrid Random Walk algorithm with SFCM could improve the results of conventional random walk delineation with mean DSC difference of 8% ± 11%. The large amount of Standard Deviation is mainly because of significant difference between two techniques in low contrast tumors.Conclusion: The results of this study show the combination of random walker with SFCM can improve liver lesion delineation in FDG-PET images with suitable precision and accuracy especially in low uptake tumors where the edges are not sharp and decision making of conventional random walk with 50% probability cut-off could be a challenging task.

P114

Utility of Delayed 18 FDG PET/CT Imaging for Lesions Detection Enhancement

F. Y. RISHEQ, **M. F. ALRISHEQ**, S. J. AL-SADOON, A. A. QWARIK; NUCLEAR MEDICINE, PET/CT, BMD, Dr.FARID RISHEQ CENTER, AMMAN, JORDAN.

Introduction: PET captures the level of metabolic activity of fluorine-18 fluorodeoxyglucose (18F-FDG) uptake and reported as a standardized uptake value (SUV). Delayed imaging of 18F-FDG can improve delineation of metastasis from normal tissue. Objective: Investigate improvement of lesion detection by delayed 18F-FDG imaging and decide on best imaging protocol. Subjects and Methods: Seven patients with average age 43.7±13.8y, average weight 67.7±10.3Kg undergone 18F-FDG-PET/CT scans with injection dose 240 ±50.1MBq, (7-8) bed/130sec. Early scan performed at 65.5 ±3.1min, and delayed scan at 170.4±3.9min. from 18F-FDG injection time. Thirty two lesions of different cancer diseases (HL,NHL,Ca-Breast,Ca-Colon) were investigated. Early and delayed SUVmax of each lesion were determined and retention index RI%=100*(SUVmax.delayed - SUVmax.early) / SUVmax.early was calculated. Results: A plot of SUVmax.delayed versus SUVmax.early showed linear relation with slope ~1.44 and R2~0.84. Two lesions with reduced

SUVmax.delayed (negative RI%) considered inflammatory and were excluded. Average SUVmax.early (SUVmaxAverage.early) =10.3(±7.5,1.9-30.4), and SUVmaxAverage.delayed =15.7(±10.1,4.9-43) indicating clear increase in SUVmaxAverage.delayed with RI%Average =74.4% (±66.1,2.3-239.5). For lesions with SUVmax.early ≤5.5 (11 lesions), the corresponding values were: 3.8(±1.4, 1.9-5.5), 7.8(±3.1,4.9-12) and 117.2(±77.9,25.5-239.5); and for lesions with SUVmax.early >5.5 (19 lesions), these were respectively: 14.0(±7.0,7.8-30.4), 20.3(±9.9,8.1-43.0) and 43.5(±43.5,2.3-159.6). Normal brain and liver showed significant decrease in SUVmaxAverage.delayed with negative RI%Average= -0.5±19.7 and -23.1±18.1 respectively. Lung showed increased SUVmaxAverage.delayed =0.86±0.15 compared to SUVmaxAverage.early =0.71±0.06 with RI%Average =22±22.7. No difference in behaviour was observed in relation to cancer diseases. Discussion: Delayed image RI%Average =74.4% reflects its utility in improving SUVmax of lesions. Lesions with SUVmax.early ≤5.5 have RI%Average =117.2 which is 2.7 times RI%Average =43.5 for SUVmax.early lesions >5.5. This is beneficial for the detection of lesions in their early stages (border SUVmax). Brain and liver showed negative RI%Average, being unable to retain 18F-FDG. Two patients had positive brain RI% due to anxiety. Positive RI%Average for lung is caused by breathing motion, and is within normal tissue SUVmax. Our results showed that accumulated dose of 18F-FDG is retained inside malignant lesion cells and continue for a considerable time being unable to escape to the blood stream. Radiation damage effect (energy:2γ=1.022MeV, β+=0.635MeV) could extend beyond the ten half- lives physical decay (18.3hr) and could have oncology stimulation effect. Conclusion: 18F-FDG dose of 240±50.1MBq provide high quality images as compared to 370MBq; lowering patients' radiation hazards. Delayed 18F-FDG imaging ~3hr is more helpful than ~1hr for evaluating suspicious malignant lesions with SUVmax ≤5.5. Retained 18F-FDG inside malignant cells could have oncology stimulating effect.

P115

Assessment of reconstruction parameters impact on quantification of low dose Yttrium-90 activity based on PET-CT Imaging in radioembolization

M. Khazaee Moghadam[1], A. Kamali Asl[1], P. Geramifar[2], M. soufi[1]; [1]Shahid Beheshti University, Tehran, IRAN, ISLAMIC REPUBLIC OF, [2]Research Center for Nuclear Medicine, Shariati Hospital, Tehran University of Medical Sciences, Tehran, IRAN, ISLAMIC REPUBLIC OF.

Aim: Yttrium-90 is known to have a low positron emission decay with abundance of about 32 pairs per million. This characteristic can be helpful in accurately evaluating the activity distribution of ^{90}Y particles in radioembolization of liver tumors using PET. In this study, we investigated optimal reconstruction parameters for quantifying low dose ^{90}Y pretherapy PET-CT imaging as a function of both hot-sphere size and activity concentration. Materials and Methods: The study was performed using a Siemens Biograph 6 True Point PET-CT scanner. A jaszczak phantom containing five hot syringes with different sizes and target-to-background ratio of 40:1 was imaged over 45 min. This phantom was initially imaged with a hot-sphere activity concentration of 7.2 MBq/mL and a background concentration of 0.18 MBq/mL. It was then serially imaged at multiple time points down to hot-sphere and background concentrations of about 2.53 and 0.06 MBq/mL, respectively. The attenuation and scattered corrected sinograms were reconstructed considering different iterations as well as subsets with and without resolution recovery. The assessment of noise was evaluated using multiple statistically independent region of interest (ROI). Results: For the range of applied activities, scanner linearity was confirmed. Activity was calculated in hot phantom regions based on SUV. The relative differences between calculated activities and known activity was observed between 1.36% and 11.2%. The most accurate result was achieved with 2 iterations and 21subsets, considering resolution recovery as well. The least background noise of about 8% was obtained using these parameters. Conclusion: For precise activity quantification of lesions, 2 iterations, 21 subsets and resolution recovery would give the best performance. Accuracy was improved by increasing subset size in the reconstruction. On the other hand, further increasing the number of iterations would worsen the estimated activity and the conversion from one to three iterations significantly enhanced the noise in the reconstructed images. In general assessment of ^{90}Y activity distribution based on PET-CT imaging in pre-therapy can be further improved by utilizing adapted parameter setups.

P116

Clinical utility of 18F-fluorocholine positron-emission tomography/computed tomography (PET/CT) in prostate cancer patients and comparing with18 F-FDG PET/CT and conventional imaging modality

R. K. Phulsunga, **Jr**., R. Parghane, sr, J. Shukla, Consultant, B. Mittal, Prof; PGIMER, Chandigarh, INDIA.

Aim: The aim of this study was to evaluate the clinical utility of 18F-fluorocholine positron emission tomography/computed tomography (FCH PET/CT) in detecting prostatic bed lesion, lymph nodes and skeletal involvement in prostate cancer patients and comparing these finding with 18F-FDG PET/CT and conventional imaging.Material and Methods: The study

retrospectively evaluated 32 patients who had undergone FCH PET/CT, bone scan in prostatic cancer patients. At the same time, 27 of the 32 patient's undergone 18F-FDG PET/CT, 7 of 32 patient MRI and 25 of the 32 patients had abdominal-pelvic diagnostic CT. The sensitivity, specificity and accuracy of FCH PET/CT, 18F FDG PET/CT and abdomino-pelvic CT were evaluated on a per-patient basis. Histological examination, second time PET or clinical follow-up data were used as gold standard for lesions characterization in prostatic cancer patients.Results: The overall accuracy of FCH PET/CT to detect lesion was 70%. The sensitivity and specificity of FCH was high as compared to18 F-FDG PET/CT and conventional abdominal pelvic CT scan i.e sensitivity of FCH, FDG and conventional CT was 69%, 44% and 45% and specificity was 80%, 67% and 80% respectively. Moreover, the sensitivity and specificity of FCH PET/CT were higher than 18F-FDG PET/CT to detect prostatic bed lesion, lymph nodes and skeletal lesions in prostatic cancer patients.Conclusions: Our result shown that, FCH PET/CT was very useful in detecting prostatic bed lesion, lymph-nodes and skeletal lesion in prostate cancer patients as compared to 18F-FDG PET/CT and conventional imaging modality.

P117
Qualitative evaluation of respiratory artifacts on PET/CT images

M. Shamsaie Zafarghandi, F. Gholami, B. Teimourian; Amirkabir University of Technology, tehran, IRAN, ISLAMIC REPUBLIC OF.

AimIn earlier years PET/CT has an important role for detecting tumors, planning radiation treatment and evaluating response to therapy. But difference in respiratory motion between PET and CT scans causes breathing artifacts on PET/CT images. The purpose of this paper was investigation of the qualitative error due to respiratory artifacts on tumors of the lung.Material and methodThe 4D XCAT phantom and STIR were used for all simulation in this study. Three phases of CT breathing cycle including CT image in the end exhalation (EE), end inhalation (EI) and respiration-averaged CT (ACT) image were used for PET image attenuation correction. The magnitude of induced errors in volume for different breathing phases were investigated by considering ACT as gold standard and a threshold of 50% maximum voxel intensity.ResultComparing PET/EECT and PET/EICT with PET/ACT for upper, middle and lower right and left lungs, the maximum percentage error was observed in smaller lesions with 35-mm diaphragm motion amplitude. In upper lung, volume was overestimated. Also the lesion volume error was gradually decreased with increasing the lesion size. The maximum error in the middle lobe of right lung was 95% in 10-mm lesion with 35-mm diaphragm motion and decreased with lesion size to a minimum amount of 2.1% for 25-mm lesion.The measurements showed a maximum error of 65.36% in PET/EICT for the lower lobe of right lung that causing an underestimation of lesion volume. The error reduction trend was observed with increasing lesion size from 65.36% to 57.51%. However this reduction was observed for lesion larger than 12-mm in the PET/EECT. Also in the lower lobe of left lung, the maximum error of 95% was observed in the 8-mm lesion with 35-mm diaphragm motion in PET/EICT and the error reduced to an amount of 39% for 25-mm lesion. Unlike PET/EICT, in PET/EECT the error increased with increasing the diaphragm motion amplitude.DiscussionThese results represent that respiratory motion has a minor effect on upper regions of the lung. Mismatch caused by respiratory motion has considerable effect on small tumor which placed close to diaphragm. Decreasing of errors with increasing the tumor size indicates negligible effect of respiratory motion on large tumor. Investigations show that for all upper and lower tumor of right and left lung end expiration is the best phase for attenuation correction.

P118
Serial monitoring of denervated muscle with 18F-FDG PET

K. Pak, M. Shin, I. Kim; Pusan National University Hospital, Busan, KOREA, REPUBLIC OF.

Purpose: We aimed to evaluate the serial change of glucose hypermetabolism in denervated muscle with 18F-Fluorodeoxyglucose (FDG) Positron emission tomography (PET). **Methods**: Right sciatic nerve was resected in 6 male rats (7wk old). From 1 to 10 weeks after denervation, PET scans were acquired for 5 times (1/2/5/8/10 weeks). Muscle denervation was confirmed by electrophysiologic and histologic studies. Region of interest (7mm diameter circle) were drawn in the axial section of lower legs. The ratio of right to left leg ROI weas calculated with both SUVmax and SUVmean. **Results**: Muscles of right lower leg showed hypermetabolism in 1 week after denervation (ratio: SUVmax 3.61 ±1.71, SUVmean 3.56±1.66). The ratio of FDG uptake in 2 weeks showed difference with that of 1 week (p=0.05, SUVmax 1.51±0.99, SUVmean 1.41±1.03). Until 10 weeks, the ratio of FDG uptake showed no significant difference comparing with that of 2 weeks. **Conclusions**: Hypermetabolism in denervated muscle was observed in 1 week after resection of nerve. After 1 week, the ratio decreased and showed no significant difference until 10 weeks.

P119

Usefulness of F-18 Flouromethylcholine (FCH) Positron Emission Tomography/Computed Tomography (PET/CT) in Evaluation of Bone Metastases in Suspected Recurrent Carcinoma Prostate and Comparative Role of Computed Tomography (CT) in Lesion Detection

S. Z. Ali, C. J. Tan, L. W. C. Winnie; Singapore General Hospital, Singapore, SINGAPORE.

PURPOSE: To study the usefulness of F-18 Flouromethylcholine (FCH) positron emission tomography/computed tomography (PET/CT) in detection of bone metastases in suspected carcinoma prostate with biochemical recurrence and evaluate the comparative role of computed tomography (CT) in lesion detection. METHODS: This retrospective study consisted of evaluating 70 patients with referral for F-18 Flourocholine PET/CT, between 2010 and 2014 for evaluation of suspected recurrent prostate carcinoma with rising serum prostate-specific antigen (PSA) levels. PET/CT imaging was performed with intravenous administration of F-18 FCH, with initial acquisition of the pelvis performed 2 minutes (early) followed by delayed imaging from the skull to the upper thigh at 30 minutes (delayed), after tracer administration. Non-contrast CT was performed for purpose of attenuation correction and anatomical localization. RESULTS: Among the 70 patients, there were 10 patients with 30 foci of bony uptake of F-18 FCH, suggestive of tracer-avid bone metastases. The maximum standardized uptake value (SUVmax) of the tracer-avid bone lesions measured from 3.3 to 14 with mean SUVmax=7.8 (standard deviation = 3.0). CT attenuation of such lesions ranged from 171 to 1164 Hounsfield units (HU) with mean CT HU value of 608.9 (standard deviation=293.1). The maximum CT attenuation measurement of an index lesion with FCH uptake (in skull) was 1164 HU, with corresponding SUVmax=8.4.The highest SUVmax=12.7 was noted in a lesion in lumbar vertebra with corresponding CT HU value of 286. The Pearson correlation coefficient between the FCH uptake of bone metastatic lesions and correponding CT HU values was estimated as -0.438. CONCLUSION: Due to wide variation in CT HU values, CT alone is not accurate for detection of bone metastases in prostate carcinoma. Functional imaging with F-18 FCH PET/CT is better technique for detection of skeletal metastases in suspected recurrent prostate carcinoma.

P120

PET/CT Use With Abdominal Compression Arch For Stereotactic Radiosurgery Planning With Arrested Lung And Extracorporeal Circulation

D. M. Ruiz Hernández, **J. Nogueiras Alonso**, F. Zelaya Reinquet, C. Castillo Berrio, M. Castrillón, A. Serena Puig, L. Campos Villarino, R. Guitian Iglesias; ESG36555100, Pontevedra, SPAIN.

AIM: An important number of studies have shown that the use of PET/CT when compared against the use of isolated CT, produces a statistically significant increment in the definition accuracy (GTV). This accuracy increment can be up to 42% in highly conformal radiotherapy for non-small cell lung cancer. This increment optimizes the therapeutic ratio by maximizing the dose in the tumor target whilst minimizing it in the neighboring organs. In addition, it reduces interobserver variability. MATERIAL AND METHODS: Three patients, with previously limited lung functional reserve, were diagnosed with a new NSCLC, so any suitable treatments were rejected for them. An ALART (Arrested Lung Ablative Radiotherapy) protocol was designed with the purpose of reducing as much as possible, the lung motion movement, hence, the patient was assisted with a systems of extracorporeal circulation. Aiming to reproduce to the maximum the conditions for immobilization lung, the volumes to be radiated were delineated based on 18F-FDG PET/CT images, which was acquired with a trolley with abdominal compression device ((SIHO©)) (figure 1). RESULTS: Procedure consisted of hypofractionated stereotactic radiotherapy for the first patient; original prescription for the second patient, was modified because onset of activity at hiliar node that was not previously known (figure 2), them stereotactic radiosurgery was performed in a single session (34Gy in the node and 21Gy in adenopathy); and stereotactic radiosurgery too, for the third one. First patient remains asymptomatic after 9 months, with partial metabolic response in PET/CT control, the second showed complete response in tumor and nodal partial on PET/CT control, with progression to bone metastases and died as a complication of lung infection. The third is still asymptomatic, waiting for the first PET/CT control. CONCLUTIONS: We consider interesting the description of cases to the author's knowledge, this is the first bibliographic description of the use of PET/CT 4D with arc abdominal compression in stereotactic radiotherapy planning with arresting lung and extracorporeal circulation. Although randomized controlled studies are needed, so that this procedure could be considered an alternative and effective treatment in those services that are not gating or devices for PET/CT monitoring and/or incorporated into the accelerator.

P121

Motion management in clinical practice on Discovery IQ - GE PET/CT scanner

S. Morzenti[1], **A. Zorz**[1], F. Elisei[2], E. De Ponti[1], L. Guerra[2], A. Crespi[1], M. Arosio[2], C. Landoni[3]; [1]Medical Physics, A.O. San Gerardo, Monza, ITALY, [2]Nuclear Medicine, A.O. San Gerardo, Monza, ITALY, [3]Nuclear Medicine, University of Milano Bicocca, Milano, ITALY.

Aim: The new scanner Discovery IQ provides innovative

solutions for respiratory motion management to help enhance image quality. The aim of this study is to compare different motion correction techniques available in standard clinical practice: QStatic and Motion Correct.Material and Methods: QStatic is a motion management solution fully integrated into the WB PET protocol. It permits to acquire motion free images in the thorax-abdominal region FOV selecting PET data only from the quiescent phase (end expiration) of the patient's respiratory curve registrated with a Respiratory Management System (RPM - Varian). The relative attenuation map is calculated from a total body CT performed in the end expiration phase. In order to have a statistical counts comparable to the other FOVs QStatic bed is acquired for a double time.Motion Correct is a technique that calculates the attenuation map matching a WB standard helical CT and a low dose cine CT performed in the border zone between the chest and the abdomen.Two nuclear medicine physicians compare 60 images obtained with QStatic and 30 images obtained with Motion Correct to the standard free breathing PET/CT acquisitions, giving a score from 1 (necessity to repeat the acquisition for clinically inadequate image quality) to 3 (good image quality without artefacts).Results: The comparison of the QStatic protocol to the standard PET/CT acquisition shows that in the 31% of the cases the score does not change and in the 41% of cases it increases.Moreover, the Motion Correct protocol allows to obtain a better results respect to the standard acquisition in the 48% of cases and a comparable image quality in the 50% of cases. The dose increase due to the cine CT is less than 13% of the total PET/CT effective dose.Conclusion: Both QStatic and Motion Correct protocols provide a better image quality than the standard acquisition without conditioning the clinical workflow.Nevertheless, Motion Correct should be useful for motion management in non compliant patients because this technique does not require an increased acquisition time.

P122

Optimization of Dual Time Point Delayed Regional 18F FDG PET CT Protocol With Site Specific Interventions

M. SARMA, P. SUBRAMANYAM, P. SUNDARAM; DEPT. OF NUCLEAR MEDICINE AND PET CT, AMRITA INSTITUTE OF MEDICAL SCIENCES AND RESAERCH CENTRE, AMRITA VISHWA VIDYAPEETHAM, COCHIN, INDIA.

Aims: Possible optimization of the dual time point delayed regional FDG PET/CT protocol with various site specific interventions. **Materials and Methods**: Initial WB (at ~ 60 min) and delayed regional (~2 hours post FDG injection) FDG-PET/CT images (2013 -March,2015) of 88 patients were retrospectively analysed. Interventions included (a). head/neck imaging with hands down position in TENIS patients (Group I), (b). 1 L oral contrast administration 15 min prior to delayed imaging (Group II), (c).distention of small or large bowel loops with 1-1.5 L oral contrast over a extended time of 1 hour (Group III), (d).forced diuresis with excess oral hydration and furosemide intervention 20 min prior to delayed imaging (Group IV) and (e). bladder distention with excess hydration and withholding urine (Group V). Suspected abnormalities were characterized based on (a). rising/stable dual-time point changes in SUVmax and/or (b). visualization/better characterization/disappearance of initial CT suspected abnormality. Findings were compared with subsequent HPE, other imaging /clinical follow-up. **Results**: Gr.I(n=19): 4 lymphnodes (SUVmax < 2.0 g/ml) in 3 patients showed SUVmax > 2.0 g/ml, later proven to be metastatic. Gr.II(n=11): In 4 patients, diffuse FDG uptake in the stomach wall seen initially was not appreciable on delayed scan. 2 patients showed better delineation of pyloric area thickening post distention with retained FDG uptake. Suspicious thickening of stomach wall on initial CT (with no FDG uptake) was not subsequently appreciable in 5 patients. Gr.III(n=38): Focal FDG uptake in small intestine was localized to a lymphnode (not appreciable on initial CT) in 1 patient. In 7 patients incidental focal FDG uptake was seen to retain/increase with no definite CT abnormality. Colonoscopy detected malignancy in 1 patient. 10 other patients who had suspicious thickening/abnormality of intestinal walls initially, did not show any abnormality after distention of the loops. In rest of the patients, there was significant reduction of SUVmax or disappearance of the uptake. Gr.IV(n=11): better visualisation of focal FDG uptake in kidneys in 2 patients subsequently proved to be malignant lesions. Gr.V(n=9): Better appreciation of FDG uptake in CT detected bladderwall thickening in 3 patients and subsequently lesions were proven malignant. In 2 patients suspicious wall thickening did not show FDG uptake. Patients are on follow up. In rest of the 4 patients, suspicious CT abnormality with inconclusive FDG uptake showed no CT abnormality or FDG uptake post distention. **Conclusions**: FDG-PET/CT dual time point imaging can be optimised with site based specific interventions.

P123

Performance of PET/CT for detecting the primary tumors of cervical metastases from unknown primary carcinoma: a systematic review and meta-analysis

G. Shen, Z. Jia, H. Deng; West China Hospital of Sichuan University, Chengdu, CHINA.

Aim: Growing evidence shows that 18F FDG PET or PET/CT is superior to conventional imaging methods in the detection of primary tumors in patients with cervical metastases from unknown primary carcinoma (UPC). The aim of this meta-analysis was to assess the clinical usefulness of 18F FDG

PET/CT in the detection of occult primary tumors in UPC patients with cervical metastases. Materials and methods: Studies about whole-body PET/CT for the detection of primary site in cancer patients with cervical metastases from UPC were systematically searched in PubMed, EMBASE, EBSCO, Web of Knowledge and Cochrane Library and four Chinese databases. Based on the data extracted from the included studies, we determined pooled sensitivities and specificities across studies, calculated positive and negative likelihood ratios, and constructed summary receiver operating characteristic curves with area under the curve (AUC) and Q* obtained. We also analyzed the heterogeneity between studies based on the subgroup-analysis and publication bias analysis. Results: In total, 39 studies involving 1468 patients met the inclusion criteria. PET/CT detected the primary lesion in 599, with a detection rate of 40.8%; and in these TP results, with regard to the locations of primary tumors, tumors of lung, tonsil, base of tongue, and nasopharynx were the most prevalent with rates of 24.2%, 12.9%, 10.6% and 13.1%, respectively. The pooled sensitivity and specificity were 0.90 (95% confidence interval [CI], 0.87-0.92) and 0.79 (95% CI, 0.75-0.81), respectively. Likelihood ratio syntheses yielded overall PLR of 3.50 (95% CI, 3.00-4.08) and NLR of 0.20 (95% CI, 0.15-0.26). The AUC and Q* index were 0.8930 and 0.8238, respectively. The between-study heterogeneity was only significantly observed in sensitivity, and the results of subgroup analyses showed that only the type of imaging modality did statistically significantly influence the reported sensitivities of PET/CT ($P < 0.05$), while study design, quality score, and reference standard did not ($P > 0.05$). In addition, the funnel plot seemed slightly asymmetrical with a P value of 0.001, which suggested no major publication bias. Conclusions: PET/CT is beneficial in the overall assessment of primary tumors in UPC patients with cervical metastases. Large, multicenter, and prospective studies with standard protocols are now needed to investigate the true value of PET/CT for detecting primary tumors of cervical metastases from UPC and the broad application of this method in clinical practice.

P124

Is 18F-FDG PET/CT Suitable for Selecting Lung Cancer Patients for Brain MR Under the Suspicion of Brain Metastasis?

k. hjorthaug, Sr.[1], J. Hojbjerg[1], M. Knap[1], A. Tietze[1], A. Haraldsen[1], S. Kramer[1], H. Zacho[2], P. Borghammer[1]; [1]Aarhus University Hospital, Aarhus, DENMARK, [2]Aalborg University Hospital, Aarhus, DENMARK.

Aim: Brain metastases are very common in lung cancer. Whole-body FDG PET/CT is used for general staging, but MR is the best modality for characterising brain abnormalities. We aimed to determine if PET/CT is suitable for selecting patients to MR on the suspicion of brain metastases. *Materials and methods*: FDG PET/CT was performed in 1108 consecutive patients suspected of lung cancer. The final diagnoses were extracted from medical records as lung cancer, with or without brain metastases, other kinds of cancers, or no cancer. The sensitivity, specificity and positive predictive values for detecting brain metastases were calculated. Inter-observer variation was tested in a subset of 88 PET/CT scans. *Results*: Five-hundred-and-ninety-six of 1108 referred patients had lung cancer. Sixty-six had brain metastases. One PET/CT was false positive. Thirty-one scans were true positive among the 43 patients, who were diagnosed with brain metastases in the time interval one month before to 3 months after PET/CT (metastases prevalence 7.3%). Twelve PET/CT scans were false negative. Sensitivity, specificity, and positive predictive values were 72 %, 100 %, and 97 %, respectively. Inter-observer agreement between two experienced observers was high (κ=0.83) whereas agreement between the experienced and the inexperienced observer was poor. *Conclusions*: The sensitivity of brain PET/CT for detecting brain metastases in lung cancer was above 70%, and specificity was very high. Thus, PET/CT may be suitable for selecting patients for MR in diagnostic centers, which do not perform routine MR in the pre-therapeutic staging work-up. The agreement among experienced readers was very high.

P125

Diagnostic Accuracy of 18F-FDG PET-CT for Detection of Primary Tumors in Patients with Cervical Metastases of Unknown Origin

A. Serrano Palacio[1], M. Cabrera Martín[2], C. Riola Parada[1], O. Salsidua Arroyo[1], M. Pedrera Canal[1], M. Martínez de Bourio[1], E. Cala Zuluaga[1], M. García García-Esquinas[1], J. Carreras Delgado[2]; [1]Nuclear Medicine Department. Hospital Clínico San Carlos, Madrid, SPAIN, [2]Nuclear Medicine Department. Hospital Clínico San Carlos. Universidad Complutense, Madrid, SPAIN.

Aim: To assess the ability of 18F-FDG PET-CT in the detection of primary tumors in patients with cervical metastases of unknown primary in clinical examination.Materials and methods: An observational retrospective study was performed between December 2008 and January 2015, including 63 consecutive patients who underwent 18F-FDG PET-CT studies for cervical lymph node metastases of unknown primary after clinical examination.Results: 63 patients were included, mean age 62 years (range 37-92), 48 males (76.2%). PET-CT identified the primary tumor and staged disease in 35 patients. PET-CTsuggested lymphoproliferative syndrome in 3 cases (large B-cell non-Hodgkin Lymphomas). Identification rate

of primary tumors with PET-CT was 60.3%. In 29 patients (82.8%) PET-CT suggested head and neck primary tumors, all of them with histopathological confirmation (25 squamous cells carcinomas, 2 adenocarcinomas, and 2 undifferentiated). The most frequent location was oropharynx (15 cases). Other locations were: oral cavity (2), nasopharynx (3), hypopharynx (4), larynx (3) and salivary glands (2). Primary lung tumor was diagnosed in 5 cases (3 adenocarcinomas and 2 squamous cells carcinomas) and pancreatic cancer in 1 case (adenocarcinoma). In 17 patients (27%) additional metastases were found.In 2 patients with negative PET-CT results, primary tumors were identified by randomized biopsies (floor of mouth and left amygdala).In 22 cases the primary tumor has not been identified in clinical and imaging (PET-CT, MRI) follow-up (mean follow-up 12 months, range 1-60).Conclusion: 18F-FDG PET-CT is a useful tool to locate the primary tumor in cases with cervical metastases of unknown primary after clinical examination, with high impact in clinical management. Due to the high percentage of head and neck tumors, it could be useful the performance of specific acquisitions of this anatomical region.

P126

Multiparametric Comparative Analysis of Positron Emission Tomography, Difussion Weighted Imaging and Difussion Tensor Imaging at 3T MRI: An Attempt to Provide More Accurate Data in Lung Cancer Patients Diagnosis

S. Lucic[1], I. Djan[1], M. Bjelan[1], S. Pena-Karan[2], A. Peter[1], O. Sveljo[1], D. Kozic[1], M. A. Lucic[1]; [1]Oncology Institute of Vojvodina, Sremska Kamenica, Novi Sad, SERBIA, [2]Institute of Pulmonary Diseases of Vojvodina, Sremska Kamenica, Novi Sad, SERBIA.

Aim: To explore the possible correlation and interconnection between the values of apparent diffusion coefficient (ADC), obtained by diffusion weighted imaging (DWI), mean diffusivity (MD) obtained by diffusion tensor imaging (DTI), and standardized uptake value (SUV), obtained by 18F-FDG PET/CT in the lung cancers patients.Materials and Methods: Thirty three newly diagnosed lung cancer patients with verified adenocarcinoma, and before combined radiotherapy/chemiotherapy treatment, underwent chest MRI examination on 3T MRI unit (Magnetom Trio, Siemens, Erlangen, Germany) that included DWI (3 diffusion-encoding gradient directions, with 2 b values (0 and 1000 s/mm^2), TR 5000ms/TE 80ms, slice thickness 4mm, interslice gap 0.8mm, and respiratory triggering), and DTI (30 diffusion-encoding gradient directions, with 2 b values (0 and 1000 s/mm^2), TR 4460ms/TE 80ms, and isotropic resolution of 3mm, and respiratory triggering) measurements, followed by ^{18}F-FDG PET/CT examination (Biograph 64, Siemens, Erlangen, Germany) on the very same day. A region-of-interest (ROI), covering the exactly same area of the tumour in each single patient was determined and maximal standard uptake value (SUV_{max}), mean ADC value (ADC_{mean}), and mean diffusivity value (MD_{mean}) were analyzed and measured by one independent radiologists, one nuclear medicine specialists and one both nuclear medicine specialist and radiologist, and the numerical data sets from both diagnostic modalities were obtained. The data sets were statistically analyzed by use of Pearson's correlation coefficient (r), Spearman's rank correlation coefficient (ρ), and multiple regression analysis (MANOVA) with Statistica software package (v.12.0), and the level of confidence determined at $p<0.05$.Results: We found that SUV_{max} demonstrated a statistically significant negative correlation with ADC_{mean} value in the whole group of patients (ρ=-0.339, and r=-0.286). MD_{mean} showed negative statistical significant correlation with maximal tumour diameter (ρ=-0.400 and r=-0.391). Multiple regression analysis indicated statistically significant interconnection between ADC_{mean} and SUV_{max} (b=-0.016, $p<0.05$), ADC_{mean} and MD_{mean} (b=1.580, $p<0.05$), as well as MD_{mean} and maximal tumour diameter (b=-0.002; $p<0.05$).Conclusions: Our results are indicating SUV_{max} and ADC_{mean} as two highly interconnected parameters, suggesting their importance in the lung cancer metabolism and cellularity detection. MD_{mean} value appears to be slightly less interconnected with SUV_{max} values, but still helpful. Noticed significant correlationbetween MD_{mean} and maximal tumour diameter needs further evaluation, for this correlation in our opinion might demonstrate further contribution in lung cancer monitoring and therapy response.

P127

The distribution of F-18-labeled Histone deacetylase inhibitor (HDACi) by PET/CT imaging

C. Y. Hu; Institute of Nuclear Energy Research, Taoyuan, TAIWAN.

Background and aim: Histone deacetylases (HDACs) play important roles in a wide range of cellular functions, including proliferation, apoptosis, differentiation and aging. A variety of HDAC inhibitors have been approved for anticancer therapy. The aim of this study is to identify the in vivo imaging of F18-labeled HDACi(NC109) by using molecular imaging techniques. Method: HDACi(NC109) was synthesized and F-18-labeled by the fluorination method: H-F18 pass through QMA Sep-Pak (conditioned with 0.5M K2CO3 and H2O). And eluted with Kryptofix2.2.2 solution (dissolved with K2CO3 2.7mg and Kryptofix2.2.2 15mg). Precursor (5mg) was dissolved in anhydrous DMSO (0.9 mL) and injected into the glass beaker. Reacted at 140°C for 20 minutes. And purified by Radio-HPLC using C18 semi-prepare column, elute solvent: 40% H2O/ACN isocratic and retention time was 14.7 minutes.

Bio-distribution study of F18-NC109 in male C57BL/6 mice weighing 20 ± 4 g was performed after the administration of F18-NC109 via the tail vein injection. Organs of interest and a sample of blood were collected, weighed, and counted, together with an injection standard. The PET/CT images were obtained in static mode. Mice were anesthetized under 1.5-2% isoflurane in medical-grade air for radiotracer injection and PET imaging. The static images were generated immediately following the tail vein injection of 7.4 MBq of 18F-NC109 in 0.1 mL normal saline. The residual syringe activity of F18-NC109 was measured to verify the injected dose. Then, whole-body PET/CT images were acquired and scanned for one hour. Results and Conclusion: After tail vein injection, F18-NC109 accumulated mainly in the bone. The uptake value was 0.119±0.075%ID/g at one hour after injection. Liver uptake was measured as 0.066±0.012% ID/g at one hour after injection, with the uptake being much lower than bone. The result of PET/CT imaging studies showed that F18-NC109 primarily appeared in the bone and liver, observed at one hour after injection. These results correlate well with the results of the bio-distribution study. By gathering dynamic absorption in each organ, we can obtain the very informative in vivo data, particularly on tissue distribution for clinical purpose.

P128

Value of Metabolic and Volumetric Indices of 18F-FDG PET-CT for the Prediction of Neoadjuvant Chemotherapy Outcomes in Locally Advanced Breast Cancer

O. Salsidua-Arroyo[1], M. García García-Esquinas[2], A. Jiménez-Ballvé[1], M. N. Cabrera-Martín[1,3], A. Ortega Candil[1], C. Rodriguez Rey[1], M. J. Pérez-Castejón[1,3], A. Serrano-Palacio[1], J. L. Carreras-Delgado[1,3]; [1]Nuclear Medicine Department.Hospital Clinico San Carlos, Madrid, SPAIN, [2]Nuclear Medicine Department/Radiology Department. Hospital Clinico San Carlos, Madrid, SPAIN, [3]Nuclear Medicine Department. Hospital Clínico San Carlos. Universidad Complutense, Madrid, SPAIN.

Aim:The aim of this study was to investigate metabolic and volumetric indices value of PET-CT with 18F-FDG for the evaluation of tumor and ganglionar response to neoadjuvant chemotherapy (NACT) in stages II and III breast cancer patients.Material and methods: It was a retrospective study of forty-three women with breast cancer in stages II or III. Two 18F-FDG PET-CT scans were performed to each patient, before and after NACT. To evaluate the response, the percentage difference of SUVmax (ΔSUVmax), metabolic tumor volume (MTV) and total lesion glycolisis (TLG) between the two studies were evaluated. Final histopathology following surgery after six cycles of NACT served as reference.Results: The ΔSUVmax was higher in the tumors ([P50:100; P25:95, 2-P75:100]) and when considering the locoregional disease [P50:100; P25:96,4-P75:100] in patients with pathologic complete response (pCR) ([P50:76,6; P25:53,3-P75:100] comparing with no responders [P50:76,6; P25:55,5-P75:100]) with p=0,031 and p=0,028 respectively. No significant differences in ΔMTV and ΔTLG were observed between both groups (p=0,072). No differences in the parameters on the pretreatment study (SUVmax, MTV y TLG) were detected.Conclusion: ΔSUVmax of pre and postreatment studies may be useful to predict pCR after NACT patients with locally advanced breast cancer. More sophisticated methods, such as MTV and TLG do not seem valuable in this context.

P129

Assessment of bone healing in allogenic sternal graft with 18F-Fluoride PET/CT

S. Diodato[1], I. Sandler[1], S. De Vivo[1], H. Svirydenka[1], A. Dell'Amore[2], V. Pettinato[1], P. Guidalotti[1], F. Stella[2], S. Fanti[1]; [1]Nuclear Medicine, Policlinico S.Orsola-Malpighi, University of Bologna, Bologna, ITALY, [2]Thoracic Surgery Unit, Policlinico S.Orsola-Malpighi, University of Bologna, Bologna, ITALY.

Aim The purpose of this study was to evaluate 18F-Fluoride PET/CT as an indicator of bone metabolic activity in patients who underwent allogenic sternal transplant, considering maximum standardized uptake value (SUVmax) variation as a predictor factor of bone graft healing.**Materials and methods**4 consecutive patients, 1 male and 3 females, mean age 51 y.o. (range 39-68) were included in the study. 3 patients had sternal metastasis (2 breast cancer, 1 ovarian cancer) and 1 had median sternotomy dehiscence after aortocoronary bypass surgery. All patients underwent surgical sternal excision with replacement of sternal allograft, and then performed two 18F-Fluoride PET/CT scans during follow-up to assess bone graft healing. First 18F-Fluoride PET/CT scan was performed between 8 and 15 months (mean period 11.3 months) and second 18F-Fluoride PET/CT scans from 20 to 27 months (mean period 24.5 months) after surgery. 18F-Fluoride PET/CT data were analysed by "volume of interest" (VOI) placed over the interface areas between the native bone and the graft: 1 patient had 4 VOIs (as for total sternectomy) and 3 patients had only 1 VOI (partial sternectomy). SUVmax were reported for every bone contact area and were compared between the first and second scan considering the same VOI. After the second scan the patients were followed up by clinical and radiological methods up to 19 months (mean time 12.5, range 3-19 months).**Results** 3 patients have shown significant reduction of the VOI's SUVmax between the two 18F-Fluoride PET/CT scans, in particular: SUVmax mean reduction of 42.9% in the patient with 4 VOIs (range 23.2-66.3%), 20.3% and 16.3% in the other 2 patients. These PET/CT data corresponded to uncomplicated bone healing and good clinical and radiological

outcome within the patient's follow-up. Our forth patient, female that underwent radiotherapy right after surgery, has shown increase of 13.9% in the VOI's SUVmax. She referred persisting clinical symptoms (chest pain and chills) for over 2.5 years after transplant and her radiological and clinical follow up signs indicate delayed bone healing.**Conclusions** 18F-fluoride-PET/CT imaging may be useful to assess bone healing in allogenic sternal bone graft according to SUVmax measurements of bone fluoride metabolic activity. In particular, decreasing of SUVmax over time may indicate a good incorporation of bone graft and therefore might have a prognostic value for implant fixation.

P130

The effect of urinary activity on radiation dose in patients undergoing PET/BT

s. s. gul[1], O. Dilek Ciftci[2], Z. Hasbek[3], B. Ozturk[1], T. Sahiner[2]; [1]gaziosmanpasa university medicine faculty, tokat, TURKEY, [2]The Ministry Of Health, Public Hospitals Association, Istanbul, TURKEY, [3]cumhuriyet university medicine faculty, sivas, TURKEY.

Aim: Positron Emission Tomography / Computed Tomography (PET/CT) has an increasing importance in oncological diseases. The most common clinical indications include oncologic diagnosis, staging, re-staging and evaluation of response to therapy. The aim of this study was to determine the amount of radiation to which patients undergoing PET/CT are exposed due to the activity retention accumulated in the bladder and to identify the factors affecting this process.Material-Methods: A total of 303 patients (109F and 194M; mean age 62±13 years) referred from the oncology outpatient clinic for F-18 fluorodeoxyglucose PET/CT were included in the study. The patients with at least 4 hours of fasting were examined for physical parameters including body height and weight, and blood glucose level. Patients were asked to drink 1 liter of drinking water within 45 min before the scan. Patients were divided into groups according to the oncological diagnosis. In all patients, radioactivity was measured by Geiger Muller device from a distance of 1 meter when the bladder is filled and emptied. Then, percentage of radioactivity excretion was calculated. Results were analyzed by statistical analysis program.Results: When all groups were analyzed together, the average excretion of radioactivity was 16.2±11%. Excretion of radioactivity was 17.9% vs. 7.1% in patients with head and neck cancer compared to those with bladder/urethral cancers, with a statistically significant difference between these two groups (p=0.000). The distribution of all groups is illustrated in Figure 1. There was a significantly positive correlation between body mass index and percentage of radioactivity excreation.Conclusion: Modern imaging techniques aims to achieve the most detailed images without causing any damage to the body or with the least possible harm. The radioisotopes are excreted via the urinary system in patients undergoing PET/CT scan. Therefore, in the context of biological excretion, the radioactivity concentration and dose value is high in the bladder. Moreover, the positive correlation found between body mass index and percentage of radioactivity excretion was considered to be related to the lower 18-FDG uptake in the adipose tissue. It was concluded that it is important for the control of radioactivity in patients undergoing PET/CT scan to empty their bladder frequently.

P131

Partial Volume Effect Impact On PET Preclinical Dosimetry: An Analytical Simulation Study

A. Seret[1], M. Bahri[1], C. Comtat[2,3,4], F. Bretin[1], A. Plenevaux[1]; [1]University of Liege, Liege, BELGIUM, [2]CEA, DSV, I2BM, SHFJ, Orsay, FRANCE, [3]UMR 1023 Inserm/CEA/Université Paris Sud, Orsay, FRANCE, [4]ERL 9218 CNRS, Orsay, FRANCE.

Aim. The limited spatial resolution of positron emission tomography (PET) strongly impacts preclinical dosimetry. It was proposed to combine dynamic imaging and organ harvesting in order to scale the PET time activity curve based on ex-vivo measurements. It was also suggested for the organ region of interest (ROI) to substitute centred small (3-mm diameter) spherical ROI (SROI) for the ROI based on organ anatomy (AROI). We aimed here to evaluate these two methods using an analytical PET simulator (APS) and a mouse phantom. Materials and Methods. The geometry of the microPET Focus 120 was introduced in the APS and the resolution was fine tuned in order to get recovery coefficients for the NEMA NU4 IQ phantom close to measured values. A numerical and physical mouse phantom was designed: the body was assimilated to a cylinder and the main organs (brain, heart, lungs, liver, pancreas, spleen, kidneys and bladder) were assimilated to ellipsoids. Attenuation corrected PET data were simulated and reconstructed using 3D filtered backprojection. First the activity per unit volume (A) was set identical in all organs and to zero in the lungs. Data were obtained with the microPET and APS. Moreover APS data were generated for different organ to background ratios (R) ranging from no background to R = 2. Second, A was extracted from experimental results obtained for F-DOPA, F-Tyr and UCB-H at two early and the last time points and used as APS inputs. A was measured on the reconstructed images using SROI and AROI and used to compute the recovered activity (RA) defined as the ratio between measured and expected A. Results. Experimental and simulated A matched to within 10%. For identical A simulations, RA increased with R (0.65-1.25) in a clear organ size dependent way with AROI. With SROI the dependency (0.80-

1.15) was still present for the bladder and the spleen and almost disappeared (0.95-1.05) for the other organs. For data simulating the tracers, RA depended on the time point for AROI with variations of up to 20% and more for the bladder and sometimes for one time point of one specific organ. The dependency did almost disappear for SROI. The RA clearly dependent on R with AROI but only to a very limited extend with SROI. Conclusion. SROI and post-scan organ harvesting minimize the impact of partial volume effect in preclinical PET dosimetry providing that organ harvesting could be considered as gold standard.

P132

Normal SUV values measured from Ga-68 labeled somatostatin analogue DOTATE PET/CT in patients with neuroendocrine tumors

U. Elboga[1], H. Komek[2], M. Basıbuyuk[1], S. Altındag[2], Y. Celen[1]; [1]Gaziantep University, Gaziantep, TURKEY, [2]Diyarbakır Training and Research Hospital, Nuclear Medicine Department, Diyarbakır, TURKEY.

OBJECTIVE The objective of the study was to determine the normal biodistribution of Ga-68 labeled somatostatin analogue DOTATE; to establish the range of its uptake in liver, bone and lymph node metastases in patients with neuroendocrine tumors (NET); to establish the cut-off value for differentiating between physiological uptake and tumor related somatostatin expression in the processus uncinatus of pancreas.MATERİAL AND METHODS Maximum standardized uptake values (SUVmax) of Ga-68 labeled somatostatin analogue DOTATE were determined in normal organs of 81 NET patients undergoing receptor PET/CT. In addition, SUV(max) of primary neuroendocrine tumors, liver, bone and lymph node metastases were evaluated.RESULTSSUVmax (mean + or - standard deviation) were determined in: pituitary gland 2.5 + or - 1.1, thyroid: 3.8 + or - 1.2, lung: 0.9 + or - 0.7, normal liver: 6.3 + or - 1.5 , spleen: 20 + or - 11.0, adrenal 4.9 + or - 2.2, kidney: 12.7 + or - 3.6, gastrointestinal tract 2.6 + or - 1.1, gluteal muscle:1.1 + or - 0.2, femur 0.9 + or - 0.4, blood pool 2.7 + or - 1.3 and processus uncinatus of pancreas 5.6 + or - 2.3. SUV(max) of Ga-68 labeled somatostatin analogue DOTATE was 22.4 + or - 11.2 (N=21) in liver metastases, 11.3 + or - 9.1 (N=7) in lymph nodes metastasis, 9.4 + or - 5.3 (N.=8) in bone lesions, and 18.1 + or - 9.2 (N=3) in neuroendocrine primary tumors. Target to non target (T/NT) ratios were 3.1 + or - 1.8 for liver metastases.CONCLUSION Ga-68 labeled somatostatin analogue DOTATE is an excellent tracer for the imaging of tumours expressing somatostatin receptors on the tumour cell surface, which, due to the high target to non-target ratios, allows the detection of very small lesions, especially of lymph node and bone metastases. There is a broad range of somatostatin receptor expression in metastastic lesions and in NET.

P133

Detection of gastrointestinal cancer using 4'-[methyl-11C] thiothymidine PET/CT for proliferation imaging: comparison with 18F- FDG PET/CT

Y. Fukuda[1], Y. Yamamoto[1], H. Yamamoto[2], R. Ishikawa[3], S. Akamoto[4], J. Toyohara[5], Y. Nishiyama[1]; [1]Department of Radiology, Kagawa University, Kita-gun Kagawa, JAPAN, [2]Department of Medical Physics, Kagawa University, Kita-gun Kagawa, JAPAN, [3]Department of Diagnosis Pathology, Kagawa University, Kita-gun Kagawa, JAPAN, [4]Department of Gastroenterological Surgery, Kagawa University, Kita-gun Kagawa, JAPAN, [5]Research Team for Neuroimaging, Tokyo Metropolitan Institute of Gerontology, Tokyo, JAPAN.

Aim: 4'-[methyl-11C]-thiothymidine (4DST) has been developed as an in vivo cell proliferation marker based on the DNA incorporation method. The purpose of this study was to investigate the feasibility of 4DST PET/CT for the detection of gastrointestinal cancer, in comparison with 2-deoxy-2-18F-fluoro-D-glucose (FDG) PET/CT, and determined the degree of correlation between two radiotracers and proliferative activity as indicated by the Ki-67 index. Materials and Methods: A total of 9 patients with newly diagnosed gastrointestinal cancer were examined with both 4DST and FDG PET/CT studies. Tumor lesions were identified as areas of focally increased uptake, exceeding that of surrounding normal tissue. For semi-quantitative analysis, the maximal standardized uptake value (SUV) was calculated. Proliferative activity as indicated by the Ki-67 index was estimated in tissue specimens. Immunohistochemical findings were correlated with SUVs. Results: In all 9 patients, gastrointestinal cancer were detected by both 4DST and FDG PET/CT studies. Although the mean (±SD) SUV for 4DST (6.43 ±2.13) was lower than that for FDG (16.00 ± 14.24), the difference was not statistically significant (p=0.051). A significant correlation was observed between 4DST SUV and FDG SUV (r=0.856, P<0.004). A significant correlation was observed between 4DST SUV and Ki-67 index (r=0.757, P<0.018) and for FDG SUV (r=0.717, P<0.030). Conclusion: These preliminary results indicate that 4DST PET/CT seems to be useful in detecting gastrointestinal cancer and in the noninvasive assessment of proliferation, as similar as FDG PET/CT.

P134

Lung invasive fungal infection (IFI) in acute myeloid leukemia (AML) patients: has 18-FDG-PET/CT an additional role with respect to CT scan?

L. Baratto[1], F. Elisei[2], C. Crivellaro[1,2,3], E. De Ponti[4], L. Verga[5], F. Farina[6], C. Dolci[3], C. Zarcone[1], L. Guerra[2], C. Landoni[1]; [1]Department of Nuclear Medicine, University of Milan-Bicocca, Milan, ITALY, [2]Department of Nuclear

Medicine, San Gerardo Hospital, Monza, ITALY, [3]Tecnomed Foundation, University of Milan-Bicocca, Milan, ITALY, [4]Department of Medical Physics, San Gerardo Hospital, Monza, ITALY, [5]Department of Haematology, San Gerardo Hospital, Monza, ITALY, [6]Department of Haematology, University of Milan-Bicocca, Milan, ITALY.

BACKGORUND: Combined anatomic and functional imaging with (18)F-FDG PET/CT is slowly gaining foothold in the management of various infective pathologic abnormalities. AIM: To evaluate the potential additional role of FDG PET/CT with respect to conventional CT scan, in acute myeloid leukemia (AML) patients with lung invasive fungal infection (IFI). MATERIALS AND METHODS: Twelve patients with AML and suspected lung IFI performed chest CT scan (CT1) followed by PET/CT (PET1) scan, before antimicotic treatment. CT and PET/CT were repeated 2 months after the beginning of treatment (n= 10 pts) and compared to basal evaluations to assess treatment efficacy (CT2, PET2): lesion with the highest FDG uptake was selected as "reference lesion" and SUVmax was calculated for PET1 and PET2. Metabolic response (MR) was measured as follow: complete MR (CMR, uptake ≤ than mediastinal blood-pool), partial MR (PMR, partial reduction of the lesion uptake > than mediastinal blood-pool), progressive disease (PD, increase uptake and/or new lesions). RESULTS: In 12/12 cases (100%) PET1 and CT1 were positive for IFI. The mean SUV max was 6.5 ± 2.4 (range 3.3-11.8). PET2 (n = 10) showed 4 CMR, 2 PMR, (with a mean reduction of SUVmax=53%), 2 PD and 2 with both PMR of reference lesion and concomitant new PD lung lesions with FDG uptake (PMR/PD). In the same group of 10 patients, CT2 was concordant with PET2 in 8/10 cases (80%), while in 2 cases CT2 showed partial reduction of lung lesions and a CMR on PET2. Of the 8 concordant patients, 5 died because of infections (2PMR, 2PD, 1 both PMR/PD), and 3 are alive, median follow-up 356 days from PET/CT1, (2 CR and 1 PR/PD). Of the 2 discordant patients 1 died because of sepsis, and 1 patient is on follow-up (150 days). CONCLUSION: In monitoring treatment efficacy of IFI in AML patients, CT and PET/CT were concordant in 80% of cases (8/10), while in 2 cases PET showed a complete metabolic response in a persistent lung lesion at CT. However these preliminary data cannot support a relevant additional role of PET with respect to CT scan; further follow-up and larger studies are needed.

P135

Prognostic value of post-treatment 18F-FDG PET/CT imaging in patients undergoing radio-chemotherapy for inoperable lung cancer

H. Svirydenka, S. Diodato, S. Sanfilippo, S. Cambioli, E. Tabacchi, C. Nanni, P. Castellucci, S. Fanti; Nuclear Medicine, Policlinico S.Orsola-Malpighi; University of Bologna, BOLOGNA, ITALY.

Aim: Evaluation of the prognostic value of post-treatment 18F-FDG PET/CT correlated with overall survival and progression free survival in patients with inoperable lung cancer treated with concomitant radio-chemotherapy . Material and Methods: We retrospectively studied 31 patients (pts) with stage IIB e IIIA of NSCLC lung cancer ineligible for surgery because of tumor characteristics and/or concomitant disease. All patients, 18 male and 15 female with mean age of 68 y.e. (range 58-86 y.e.), underwent definitive concurrent radio-chemotherapy between 2008 and 2014. For patients received multiple courses of radiotherapy, only the first course was included. Staging and restaging after completion of treatment 18F-FDG PET/CT scans were performed at our institution. The SUVmax in the mediastinal blood pool and the normal liver was confirmed to be stable between the pre-treatment and post-treatment scan. Response evaluation with PET/CT was performed according to the EORTC criteria. We based on PET/CT and/or clinical-radiological follow up. Progression free survival (PFS) was determined from the date of completion of therapies until the post-treatment PET/CT. Overall survival (OS) was calculated from the date of completion of treatment until the date of last follow-up. Results: The mean time after completion of therapy and post-treatment PET/CT was 3.7 months. At a mean PET follow-up of 12.1 months (range 3 - 30 months) according to criteria EORTC progression disease (PD) was observed in 14 out of 31 pts (45.2 %); CR (complete response) in 7 out of 31 pts (22.6%); PR (partial response) in 10 of 31 pts (32.2 %); no pts presented SD (stabile disease). Mean PFS was 3.4 (range 1-10) months and OS was 12.9 (range 2- 39) months. We observed the worst OS (mean OS of 7.4 months) in pts with progressive disease on post treatment PET/CT. Mean OS in pts with CR was 21.7 months. Mean OS in PR was 13.9 months. Conclusion: PD according to EORTC criteria of 18F-FDG PET/CT seems to be correlated with worst OS in lung cancer pts treated with concurrent radio-chemotherapy, suggesting a prognostic role of PET/CT scan. Because of small number of included patients further studies are necessary to confirm our findings.

P136

Comparison of C-11 Choline and C-11 Acetate PET/CT imaging for tumor detection and localization in patients with prostate cancer

R. Haloi, L. G. Jordan, III, B. J. Kemp, N. Tosakulwong, S. D. Weigand, M. Nathan, R. C. Murphy, E. D. Kwon, V. J. Lowe; Mayo Clinic, Rochester, MN, UNITED STATES.

Objective: Prostate cancer is the most prevalent type of non-skin cancer in men and the second highest cause of cancer-

related death in men. Prostate tumor cells have increased choline and acetate uptake due to elevated synthesis of phosphatidylcholine and lipids, respectively. As a result, choline and acetate labeled with the positron emitter, carbon-11 (C-11), can be used for clinical imaging of prostate cancer. Our objective was to prospectively compare image interpretation of C-11 choline and C-11 acetate PET/CT in patients with either localized prostate cancer or known metastatic prostate cancer.Methods: Eight subjects (5 with localized cancer; 3 with metastatic cancer), each having C-11 choline and a C-11 acetate PET/CT performed on the same day were evaluated. Isolated C-11 choline and C-11 acetate PET images (and corresponding unenhanced CT images) of 14 selected lesions were anonymized and randomized. Independent evaluation was performed by two experienced readers blinded to all other information, including the radiotracer identity. Each reader used a 3 point scale to independently score each lesion for conspicuity, image quality, and confidence in malignancy (5 point scale). Two weeks later, the images were permuted for re-evaluation by the same reviewers. The maximum standardized uptake value (SUV max) was calculated for the lesions and the paired differences were analyzed with a linear mixed effects model with a random intercept. Ordinal logistic regression analysis with a random subject-specific intercept was performed to model the relative odds of a higher score for C-11 Choline PET/CT readings.Results: For the lesions evaluated, the mean ± SE SUV max values were higher for C-11 choline (6.2 ± 0.7) in comparison to C-11 acetate (4.8 ± 0.7). The mean SUV difference of 1.5 ± 0.4 was significant (p=0.01). An increased odds ratio (OR) was observed in C-11 choline vs C-11 acetate for confidence in malignancy diagnosis (OR 3.8, 95% CI 1.3 to 10.7, p=0.01), lesion conspicuity (OR 4.6, 95% CI 1.1 to 19, p = 0.03), and overall image quality (OR 3.6, 95% CI 1.6 to 7.8, p = 0.001).Conclusion: In this small, prospective blinded comparison study, C-11 choline PET/CT demonstrated higher lesion-to-lesion comparison SUV max values. Reader diagnostic confidence in malignancy was higher with C-11 choline vs C-11 acetate PET/CT and enhanced overall image quality and lesion conspicuity for C-11 choline PET/CT was seen. These data support C-11 choline as the preferred PET/CT tracer agent for evaluating prostate cancer patients.

P137

Biodistribution of Ga-68 labelled PSMA ligand in normal tissues with PET/CT imaging

H. Komek[1], U. Elboga[2], C. Can[1], M. Basıbuyuk[2], Y. Celen[2]; [1]Diyarbakır Training and Research Hospital, Nuclear Medicine Department, Diyarbakır, TURKEY, [2]Gaziantep University, Department of Nuclear Medicine, Gaziantep, TURKEY.

Objective: Prostate-specific membrane antigen(PSMA) is a type II transmembrane protein with high expression in prostate carcinoma cells. Recently, Ga-68 labelled Glu-NH-CO-NH-Lys-(Ahx)-[Ga-68(HBED-CC)](Ga-68 PSMA) is a highly promising tracer for imaging recurrent prostate cancer. Our initial experience with Ga-68 PSMA suggests that this novel tracer can detect prostate carcinoma relapses and metastases with high contrast by targeting PSMA The aim of this study was to investigate its biodistribution in normal tissues. Material and Methods: A total of 43 patients with prostate carcinoma and rising prostate specific antigen levels underwent Ga-68 PSMA PET/CT. Quantitative assessment of tracer uptake was performed 1 post-injection by analysis of mean and maximum standardized uptake values (SUVmean/max) of several organs were calculated. Results: Visual evaluation revealed intense radiotracer uptake in the lacrimal and salivary glands, as well as in the spleen, liver, small intestines, kidneys and urinary tract. Some uptake was also seen in the large intestine. The highest uptake was observed in the kidneys and salivary gland. The SUVmax for the kidneys and salivary gland was 49.3 ± 16.1 and 22.2 ± 4.3, respectively. The SUVmax for the intestines, spleen, liver, lacrimal glands and prostate was 14.5 ± 5.9, 11.8 ± 5.3, 13.7 ± 3.1, 9.3 ± 4.5. and 4.8 ± 3.2, respectively. Quantitative assessment revealed excellent contrast between tumour lesions and most normal tissues. Conclusion: The biodistribution of the Ga-68 PSMA tracer was analysed in 43 patients. Within healthy organs, kidneys and salivary glands demonstrated the highest radiotracer uptake, whereas lacrimal gland, liver, spleen and bowel showed relatively moderate uptake. This study has certain limitation such as its small patient population.

P138

Metabolic Tumor Volume and Total Lesion Glycolisis in 18F-FDG PET-CT Studies. Are they Useful to Predict Recurrence in Locally Advanced Breast Cancer Patients?

O. Salsidua-Arroyo[1], A. Jiménez-Ballvé[1], M. García García-Esquinas[2], C. Rodriguez Rey[1], A. Ortega Candil[1], M. Pedrera-Canal[1], J. A. García Saenz[3], C. Riola-Parada[1], J. L. Carreras-Delgado[4]; [1]Nuclear Medicine Department. Hospital Clinico San Carlos, Madrid, SPAIN, [2]Nuclear Medicine Department/ Radiology Department. Hospital Clinico San Carlos, Madrid, SPAIN, [3]Oncology Department. Hospital Clinico San Carlos, Madrid, SPAIN, [4]Nuclear Medicine Department. Hospital Clinico San Carlos. Universidad Complutense Madrid, Madrid, SPAIN.

Aim: The aim of this study was to investigate the prognostic value of metabolic tumor volume (MTV) and total lesion glycolisis (TLG) in patients with locally advanced breast cancer (LABC). Material and methods: A retrospective study with

35 LABC patients between December 2009 and November 2010 was performed. SUVmean, MTV and TLG were calculated (cutoff 2.0). After neoadyuvant chemoterapy all patients had surgery and were followed up until January 2015. Results: 83% (29/35) of the patients were disease-free and 17% had recurrence (2 with locoregional disease and 4 with distant metastasis). No significant differences in SUVmean were found according to the recurrence status. Although differences in SUVmax were found, they were not clinically relevant. The differences in MTV and TLG where statistically significant (p=0.02 and p=0.026, respectively). Using ROC curves we calculated a cutoff of 20.9 for the MTV and 108 for the TGL, to predict recurrence with a sensibility of 83% for both values, and a specificity of 72% for the MTV and 76% for the TGL . A Cox proportional hazards model, showed that the recurrence risk was 9,6 times more when the VMT was equal or greater than 20,9 and of 11,2 times more when TGL was equal or greater than 108. A concordance between VMT and TGL was observed in all cases except one. Conclusions: The MTV and TLG could be useful to predict which patients with LABC have more probability to have a recurrence. Both parameters have a good concordance.

P139

Comparison between FDG-PET and DWIBS in Diagnosing Neuroblastoma of Child

H. Ishiguchi, S. Ito, Y. Sakurai, H. Kawai, K. Kato, S. Naganawa, A. Hama, H. Muramatsu, Y. Takahashi, S. Kojima; Nagoya University Graduate School of Medicine, Nagoya, JAPAN.

Aims: To compare the efficacy of F-18 fuluoro-2-D-glucose positron emission tomography with CT (FDG-PET/CT) and whole-body diffusion-weighted MRI called diffusion-weighted whole-body imaging with background body signal suppression (DWIBS) for the detection of lymph node metastases and bone metastases in child patients with neuroblastoma. Materials and methods: Subjects in this retrospective study comprised 16 patients (7 men, 9 women; mean age, 2.8±2.0 years old) with neuroblastoma who underwent both FDG-PET and DWIBS between January 2008 and February 2015. All patients were diagnosed as neuroblastoma based on pathological findings. Eight regions of lymph nodes and 17 segments of skeleton in all patients were evaluated. I-123 MIBG scintigraphy, bone scintigraphy and CT performed at the same time as FDG-PET and DWIBS were used for diagnosis of lymph node and bone metastasis. Two radiologists evaluated the uptake of lesions in PET-CT and the signal-intensity of lesions in DWIBS visually. The sensitivities and specificities of FDG-PET and DWIBS were calculated. McNemer test was used to compare the sensitivities and specificities of FDG-PET and DWIBS. P value less than 0.05 was considered statistically significant. Result: Lymph node metastases were confirmed in 38 of 127 regions. For detecting lymph node metastasis, the sensitivities of FDG-PET and DWIBS were 92.1%(35/38) and 81.5%(31/38), respectively, and the specificities of them were 100%(89/89) and 100%(89/89), respectively. No significant difference was observed in these values. Bone metastases were confirmed in 103 of 266 segments. For detecting bone metastasis, the sensitivities of FDG-PET and DWIBS were 75.7%(78/103) and 93.2%(96/103), respectively, and the specificities of them were 93.2%(152/163) and 84.2%(137/163), respectively. The sensitivity of DWIBS was significantly higher than that of FDG-PET (P<0.01) and the specificity of FDG-PET was higher than that of DWIBS significantly (P<0.05). Conclusion: For detecting lymph node metastasis, the sensitivities and specificities of both FDG-PET and DWIBS indicated high values. For detecting bone metastasis, DWIBS was more sensitive than FDG-PET, whereas FDG-PET was more specific than DWIBS. In patients with neuroblastoma, FDG-PET and DWIBS possibly play a complementary role each other for detecting bone metastasis.

P140

18FDG PET/CT in initial staging of lung cancer : experience of a tertiary medical center in Casablanca Morocco

S. TALEB, G. CHERKAOUI SALHI, M. AIT IDIR, S. CHOUKRY, A. GUENSI; Nuclear medicine department, CASABLANCA, MOROCCO.

Lung cancer is the most frequently diagnosed malignancy in males. It represents more than 25% of all cancer deaths. In Morocco, its incidence rates are estimated to 25.9 and 2.9/100,000 in males and females respectively. Among different imaging tools, PET/CT using 18-FDG is now described by many studies as the best imaging test for its staging and treatment monitoring. The aim of this study was to report the experience of a Moroccan tertiary medical center in 18 FDG PET/CT use in the management of patients with lung cancers. Between December 2012 and December 2014, A total of 89 patients underwent a 18 FDG PET/CT for a suspicion or a confirmed lung cancer. Sex ratio was 10. Mean age 60.2 ± 9 years. Among these patients, 56% were sent for metabolic characterization of a solitary pulmonary mass (group 1) and 44% were sent for initial staging of a biopsy-proven lung cancer (group2); epidermoid carcinoma in 37%, adenocarcinoma in 54%, and small cell lung cancer in 9%. In the group 1, PET-CT results showed a high uptake in the solitary pulmonary masse in all cases associated to distant metastases in 87% of cases. In the group 2, distant metastases were noted in 86% of

cases. Mean initial tumour SUV max was 13.4 (+/- 7). PET/CT upstaged 19% of patients showing nodal extension in 7% of cases and distant metastasis in 10% of cases which were not noted in the prior CT-scan. 18FDG PET /CT is an interesting tool in lung tumors management. Its systematic use for initial staging would allow a more precise staging and hence a more adapted treatment. Unfortunately, the lack of nuclear centers in our context retards its routine use in lung cancer patients' management.

P141

Associations between brain global hypometabolism and various clinical parameters in healthy subjects

H. Nam[1], S. Jun[2]; [1]Samsung Changwon Hospital, Sungkyunkwan University School of Medicine, Changwon, KOREA, REPUBLIC OF, [2]Kosin University Gospel Hospital, Kosin University College of Medicine, Busan, KOREA, REPUBLIC OF.

Purpose: We investigated the correlations between the degree of brain fluoro-2-deoxy-D-glucose (FDG) uptake and various physical, and laboratory parameters to define the predictors related to brain global hypometabolism. Methods: We retrospectively reviewed 188 consecutive subjects who underwent a general health check-up including F-18 FDG positron emission tomography/computed tomography (PET/CT) scan. After an overnight fast, peripheral blood was drawn to measure the levels of laboratory parameters. All measurements were conducted on the same day on which F-18 FDG PET/CT scan was performed. The 25th percentile of maximal standardized uptake value (SUVmax) of the brain in all subjects was 13.265 and we chose this value as the cut-off for dividing subjects into two groups. Results: Subjects with lower FDG uptake in the brain were older, and had higher serum triglyceride, fasting blood glucose (FBG), Hb1Ac levels than those with higher uptake. Brain FDG uptake of 32 subjects (17.0%), who were diagnosed with metabolic syndrome, was lower than that of subjects with non-metabolic syndrome (14.26 ± 2.96 vs 15.88 ± 3.17, P=0.0083). Brain FDG uptake was negatively correlated age, FBG level, Hb1Ac, mean blood pressure. No positive correlation was between brain FDG uptake and clinical parameters. Under multiple regression analysis, FBG level and age were significant predictors for brain global hypometabolism. Conclusion: the brain may show low FDG uptake without any brain disease when F-18 FDG PET-CT was performed in an older subject with diabetes mellitus or hyperglycemia.

P142

Assessment of heart injury induced by radiation therapy for esophageal cancer using FDG-PET/CT

K. Hanaoka, M. Hosono, M. Inada, K. Sakaguchi, K. Shimomura, M. Tamura, K. Matsumoto, H. Monzen, Y. Nishimura; Kinki University, Osaka Sakai-city, JAPAN.

Objectives: There have been numerous reports on radiation-induced myocardial damage after radiation therapy. The aim of this study is to evaluate the feasibility of FDG-PET/CT for the detection of radiation-induced myocardial damage. Methods: Thirty patients (5 females and 25 males, mean age: 66.7 ± 8.6 years, range: 62-81 years) with histologically confirmed esophageal cancer who underwent radiation therapy between January 2007 and November 2011 were enrolled in this retrospective study. All patients underwent pre- and post-therapeutic FDG PET/CT. The fasting period before intravenous administration of FDG was at least 4 hours. Bull's eye maps of myocardial FDG uptake were generated by Quantitative Perfusion SPECT. On radiation dose charts gererated by a 3-demensional radiation therapy planning system, the maximum dose to the left ventricle and radiation dose distribution were estimated. Changes of FDG accumulation on the left ventricle before and after radiation therapy were compared with the radiation dose distribution. Results: The proportion of the left ventricle volume receiving at least 20, 30, 40, and 50 Gy were 29.66±20.66, 16.64±16.89, 9.05±12.62, and 3.30 ±5.82%, respectively. Maximum dose in the left ventricle were 47.45±15.63 Gy (range: 14.28 - 62.63). Focal increased FDG uptake in the irradiated field of myocardium was seen in 5 patients. On the other hand, the maximum dose to the left ventricle or radiation dose distribution was not significantly correlated with the shift of FDG accumulation. Conclusions: We demonstrated the feasibility of evaluating myocardial damage by the comparison of Bull's eye map of FDG and radiation dose charts. This method could be useful in the management of patients with radiation-induced heart injury.

P143

Molecular imaging of HER2 postive tumor cell by HER2 specific 18F-labeled aptamer

h. kim, Y. Cho, J. Chae, J. Park, W. Kang; yuhs, Seoul, KOREA, REPUBLIC OF.

Receptor tyrosine-protein kinase erbB-2, or HER2, is a member of the human epidermal growth factor receptor family. HER2 regulates a variety of cell functions associated with cancer cell proliferation and opposes apoptosis through activating signal transduction pathways such as MAPK (mitogen-activated protein kinase) and/or PI3K (phosphoinositide 3-

kinase). Amplification or aberrant expression of the HER2 occurs in several breast, ovarian, gastric and other cancers. HER2-positive tumors associated with a higher rate of recurrence and poor prognosis. Thus, a variety of HER2 specific antibodies and small molecules have been assessed. Aptamer is small single-stranded oligonucleic acid that binds to a target molecule avidly and specifically. Hence, it is regarded as ideal biomarker to recognize and represent expression of the target molecule. The aim of this study is to elucidate the usefulness of HER2 specific 18F-labeled aptamer as molecular imaging prove. In this study, fluorescence-labeled HER2 specific aptamer was conjugated the HER2 positive and negative cell line for evaluate binding affinity in vitro. And we labeled radioisotope, 18F to the HER2 specific aptamer for in vivo molecular imaging. We intravenously injected 18F-labeled HER2 aptamer into mice tumor model and performed PET imaging by Siemens Inveon PET. The 18F-labeled HER2 specific aptamer microPET showed significantly increased uptake at HER2 positive than negative tumor in vivo. Uptake of HER2 in histologic sections correlated with immunohistochemistry of tumor tissue. The 18F-labeled aptamer visualized HER2 expression of breast cancer cell line and tumorigenesis in mice. And these data suggest potential use of radiolabeled aptamer as a theragnostic tool for HER2 positive cancer.

P144

F-18 FDG PET metabolic parameters in nasopharyngeal carcinoma patients with and without distal metastases

W. Huang[1], K. Lee[2], S. Li[3], Y. Kuo[4], L. Wong[1], K. Ma[4], C. Cheng[4], B. Hsieh[2], M. Chen[3]; [1]Departments of Nuclear Medicine, Changhua Christian Hospital, Changhua, TAIWAN, [2]Departments of Medical Imaging and Radiological Sciences, Central Taiwan University of Science and Technology, Taichung, TAIWAN, [3]Departments of Otorhinolaryngology, Changhua Christian Hospital, Changhua, TAIWAN, [4]Departments of Biology and Anatomy and Nuclear Medicine, National Defense Medical Center, Taipei, TAIWAN.

Aim: Nasopharyngeal carcinoma (NPC) is a common malignancy in southern Asia with different staging stratification from other cancers. About 20% of metastatic free (M0) NPC patients, however turned to distant failure (M1) in 3 years after completion of treatment resulting in patient mortality (Kam et al, 2004). We thus analyzed the relationship between metabolic parameters of F-18 FDG PET in NPC patients with and without metastases (i.e. M0 and M1). Materials: Eighty patients in all stages including 36 in stage IV were studied. They were devided into M0 vs. M1 (n=69 vs. 11 in all stages; and 25 vs. 11 in stage IV). F-18 FDG PET was performed using an integrated PET/CT (Gemini GXL). The FDG metabolic parameters including SUVmax and SUVmean, primary and total tumor volume and glycolysis (i.e. PTV, PLG, TTV and TLG) were calculated using PMOD software. A threshold of 42% of the SUVmax was applied to delineate the PTV or TTV. The PLG or TLG was calculated as mean SUV multiplied PTV or MTV. Metastases were considered by histology or various images with a clinical concordance. Results: Significant differences in PTV, PLG, TTV and TLG were found between M0 and M1 in patients covering all stages. However, only TTV and TLG revealed significant difference in the stage IV subgroup (Mo vs. M1: 26±14 vs. 88±54 and 213±160 vs. 615 ±160; $p<0.01$, each). The SUVmax and SUVmean of primary tumors showed no statistical significance between M0 and M1 in either the all stage group or the stage IV subgroup. Conclusion: TTV and TLG may play a role in evaluating metastatic status of patients with NPC, either in all stages or in stage IV subgroup.

P145

Study of game-theoretical image segmentation algorithm for PET imaging

D. Borys, D. Pierscinska, M. Danch-Wierzchowska; Silesian University of Technology, Gliwice, POLAND.

Aim: Image segmentation is very useful and not trivial step in image analysis. One example could be tissues separation or tumour delineation in medical imaging. Among broad number of segmentation algorithms, we used those, based on clustering. For segmentation purpose the notion of evolutionary games theory was used. Materials and method: Data has been obtained with Philips Gemini hybrid PET/CT device at Department of PET Diagnostics, Maria Sklodowska-Curie Memorial Cancer Center and Institute of Oncology Gliwice Branch. Used phantom was a standard cylinder with five spheres of different radius and volume (diameter from 1.3 cm up to 4 cm). Spheres have been filled with F-18 with constant concentration. For segmentation purpose, an algorithm, introduced by M.Pellilo was implemented and tested. Main idea is to represent image as edge-weighted graph, where vertices correspond to individual pixels and their weights reflect similarity between them. The clustering algorithm uses replicator dynamics. Pixels are allocated to the cluster which is removed from the graph. Described process will be repeated until all pixels are assigned to corresponding clusters. The algorithm determines number of clusters in the image. We applied the method to segment intensity images and compare it with other popular medical images processing methods (threshold based: absolute SUV 2.5 threshold, fixed and adaptive threshold range of 41-70% of maximum value and contrast-oriented method). Results obtained for each segmentation were compared to CT image based reference mask by using a Jaccard index, which has range [0,1] and 1 corresponds

to full similarity of sets. Results: The Jaccard index obtained for tested methods has mean value of 0.52 with range (0.28, 0.77). The most exact methods were SUV 2.5 threshold with accuracy value of 0.7 and proposed game theoretic based method with accuracy value of 0.77. Methods based on fixed and adaptive thresholds were far less precise. Conclusion: The highest similarity to reference mask obtained from CT images was obtained using proposed game theoretic method. However, this method is a graph based method and size of analysed images could be problematic. For bigger images inefficient graph representation causes insufficient memory problem. Further work will be concentrated on improving the efficiency of the algorithm and process automation. Acknowledgment: Grant No. UMO-2011/03/B/ST6/04384.

P146

Investigation of how the activity quantification using different blood pool volume of interests and reconstruction methods influence the absolute myocardial blood flow determined with 13N-NH3 cardiac PET

S. Akil[1], F. Hedeer[1], J. Jögi[1], H. Engblom[1], C. Hindorf[2]; [1]Dept of Clinical Physiology, Lund University, Lund University Hospital, Lund, SWEDEN, [2]Radiation Physics, Skåne University Hospital, Lund, SWEDEN.

Aim: Accurate quantification of the activity in blood is crucial for the determination of absolute myocardial blood flow (MBF) from dynamic cardiac PET. The aim of this study was to investigate quantification of absolute MBF by cardiac PET with different positions of left ventricular (LV) blood pool volume of interests (VOI), in patients and in a phantom, using two different reconstruction methods. Methods: Twelve patients diagnosed with coronary artery disease underwent cardiac PET with 13N-NH3 at rest and in stress (24 cardiac PET studies). An acquisition in dynamic mode was performed during the first 4 minutes (12x10 s, 2x30 s and 1x60 s) after administration of 550 MBq of 13N-NH3. Images were reconstructed using ordered subset expectation maximization (OSEM) and filtered back projection (FBP). The VOI to quantify the activity in the myocardial wall (epicardial and endocardial borders) was kept constant for each study while the activity in the blood was quantified within three different VOIs drawn within the LV blood pool: 1) small basal 2) small apical and 3) large extending from base to apex of the LV. The absolute MBF was determined by the deGrado compartmental model within the Carimas software (Turku, Finland) for the three different blood pool VOIs. The $MBF_{apical\ VOI}$/ $MBF_{basal\ VOI}$ and MBF_{LVVOI}/ $MBF_{basal\ VOI}$ (median; interquartile range) were calculated. For the cardiac phantom, the myocardial wall was filled with 13N-NH3 and the activity was determined with the three VOIs previously described. Results: $MBF_{apicalVOI}$/$MBF_{basalVOI}$ ratio was highest with both OSEM (1.28; 0.33) and FBP (1.34; 0.29). $MBF_{largeVOI}$/$MBF_{basalVOI}$ ratio was lowest with both OSEM (1.10; 0.11) and FBP (1.09; 0.10). The MBF determined with a basal VOI and FBP generally overlapped the MBF determined with the same VOI and OSEM. For the phantom, 16% of the activity in the myocardial wall was detected for a small apical VOI, 14% for a LV VOI and 5% for a small basal VOI despite the absence of activity in the ventricular lumen. Conclusions: The absolute myocardial blood flow determined with dynamic cardiac 13N-NH3 PET gave similar results for the two reconstruction algorithms (OSEM and FBP), but the MBF depends on the position of the blood pool VOI. The VOI should, according to the phantom study, be kept constant preferably in the basal part of the LV blood pool, to enable accurate comparisons between examinations and patients.

P08 - Sunday, October 11, 2015, 4:00 PM - 4:30 PM, Hall 3 – Poster Exhibition

Molecular & Multimodality Imaging: Preclinical Studies

P147

PET probe detecting acquired drug resistance against EGFR targeted molecular therapy

A. Makino[1,2], A. Miyazaki[2], A. Tomoike[2], H. Kimura[2], M. Hirata[3], Y. Ohmomo[3], M. Ono[2], H. Okazawa[1], Y. Kiyono[1], H. Saji[2]; [1]University of Fukui, Eiheiji-cho, Yoshida-gun, Fukui, JAPAN, [2]Kyoto University, Kyoto, JAPAN, [3]Osaka University of Pharmaceutical Sciences, Takatsuki, Osaka, JAPAN.

Aim: Epidermal growth factor receptor (EGFR) is related to tumor cell survival and proliferations, and utilized as a molecular target for tumor therapy. Gefitinib, which is a representative EGFR tyrosine kinase (EGFR-TK) inhibitor, shows curative effect against single mutated L858R EGFR-TK, and used for non-small cell lung cancer (NSCLC) treatment. However, it is reported that the following T790M mutation during the chemotherapy causes the drug resistance. Repeated evaluation of the EGFR-TK subtype expressed on tumor is important for the facile treatment, but the problem is the methodology is limited to invasive biopsy. In clinical practice, acquired drug resistance by the second EGFR-TK mutation is mainly judged by the therapeutic response. Therefore, development of a new PET tracer detecting second EGFR-TK mutation is on demanded. Materials and methods: Thienopyrimidine structure was selected as a base structure for a new PET tracer, and five compounds (FTPs1~5) were designed and synthesized. Utilizing ADP-Glo kinase assay kit (Promega, USA), inhibitory activities of these compounds against L858R and double mutated (L858R/T790M) EGFR-TKs were examined. FTP3 was radiolabeled by ^{18}F, and *in vivo* imaging was

performed by animal PET system using mice bearing human non-small cell lung cancer cells of NCI-H3255 and NCI-H1975. Results and conclusion: FTPs1~5 were synthesized by conventional organic chemical method. IC_{50} value (EGFR-TK inhibition) of Gefitinib against EGFR-TK(L858R) and EGFR-TK(L858R/T790M) was 0.021 and 7.11 mM, respectively. Importantly, IC_{50} value of FTPs1~5 against EGFR-TK(L858R/T790M) was over 10 mM, indicating FTPs1~5 could not bind to the double mutated EGFR-TK. On the other hand, IC_{50} of FTPs3~5 against EGFR-TK(L858R) was lower or comparable to that of Gefitinib. Then, [^{18}F]FTP3 was synthesized, and i.v. injected to tumor-bearing mice. In this study, NCI-H3255 (EGFR-TK(L858R)), NCI-H1975 (EGFR-TK(L858R/T790M)) were used for the model production, and PET images were acquired at 3 h post-injection. Signal intensity from H1975 was lower than that from H3255. The following *ex vivo* study indicated tumor/muscle signal intensity ratio was 6.0 (H3255) and 2.0 (H1975). In conclusion, [^{18}F]FTP3 is a promising PET tracer to detect NSCLC, which can be subjected to the EGFR targeted molecular therapy.

P148

PET with 89Zr-anti-MT1-MMP in an orthotopic mouse model of pancreatic ductal adenocarnima

M. A. Morcillo[1], A. Garcia-Lucas[1], F. Mulero[2], P. P. Lopez-Casas[2], M. Oteo[1], E. Romero[1], A. Martínez[1], A. G. Arroyo[3], M. Hidalgo[2], J. Martinez-Torrecuadrada[2]; [1]CIEMAT, Madrid, SPAIN, [2]CNIO, Madrid, SPAIN, [3]CNIC, Madrid, SPAIN.

Pancreatic Ductal Adenocarcinoma (PDAC) is associated to a high stroma (desmoplastic reaction) around the tumor. Type 1-matrix metalloproteinase (MT1-MMP) is a membrane-anchored protein overexpressed in different tumors as a mean of invasion and metastasis, including PDACs; here, MT1-MMP overexpression has been showed to be particularly prominent in areas of the tumor with intense desmoplastic reaction. The aim of the study was the in vivo validation of MT1-MMP as a biomarker for PET imaging in PDAC to assess diagnosis using an 89Zr-labeled specific monoclonal antibody (mAb). For this purpose an anti-MT1-MMP mAb was functionalized with a derivative of deferoxamine (p-SCN-Bn-Deferoxamine) as chelator to form DFO-mAb-MT1-MMP, prior to 89Zr labeling. After radiolabeling, the purification of 89Zr-mAb-MT1-MMP from small-molecule radiolabeled impurities was achieved using size-exclusion chromatography (PD-10 column). The radiolabeling yield was 91% and the specific activity was 92.5 MBq/mg (2.5 mCi/mg). Human tumor xenografts were surgically implanted in nude mice as pieces of primary tumors, coated with Matrigel. The site of implantation was in pancreas, the same organ as the original tumor (orthotopic implantation) to ensure that tumors develop in the same anatomic microenvironment. Mice bearing orthotopically implanted PDAC tumors were intravenously injected with 125 μCi (50 μg mAb; 2.5 mg/Kg body weight) of 89Zr-mAb-MT1-MMP. PET images were acquired using an Argus small-animal PET/CT at 1, 3, 6 and 8 days post-injection. Immuno-PET imaging showed high tumor uptake (SUVmax 2-7) in implanted PDAC tumors. The ratio of tumor SUVmax to the blood pool SUV increased with time and reached more than 3 at 6 days. The results suggest that 89Zr-mAb-MT1-MMP could be a promising probe for future diagnosis of PDAC tumors by immuno-PET.

P149

Evaluation on pancreatic tumor model of 68Ga-labeled somatostatin derivatives using SnCl2-based 68Ge/68Ga generator

S. Pesnel[1], D. Prince[2], C. Naidoo[2], S. Bénard[1], V. Méneyrol[1], F. Gimié[1], **E. Jestin**[1,3,4]; [1]GIP CYROI, Saint Denis, RÉUNION, [2]iThemba LABS, Somerset West, SOUTH AFRICA, [3]Inserm, UMR 1188 Diabète athérothrombose Thérapies Réunion Océan Indien (DéTROI), plateforme CYROI, Saint Denis, RÉUNION, [4]Université de La Réunion, UMR 1188, Saint Denis, RÉUNION.

Aim: The purpose of this study was to assess various 68Ga-labeled somatostatin derivatives used for the management of neuroendocrine tumors (NETs) after an elution from a SnCl2-based 68Ge/68Ga generator coupled directly with a fully automated radiosynthesis. Materials&Methods: Three DOTA-somatostatin derivatives were radiolabeled (-TATE,-TOC,-NOC) and NOTA-NOC. A 68Ge/68Ga generator (iThemba LABS, SA) was eluted with 0,6N HCl and 68Ga was directly sucked up to fully automated labeling and purifying processes on a Tracerlab FX FN. The stability was tested in buffer and in plasma during 2h. The four labeled peptides DOTA-(Tyr3)-octreotate, DOTA0-(Phe1-Tyr3)octreotide, DOTA-[Nal3]-octreotide and NOTA-[Nal3]-octreotide were injected to nude mice with AR42J pancreatic tumor xenografted. All the animals were injected intravenously with 15±3MBq. The PET acquisitions were performed during 15min using a microPET/CT system 30min post-injection. CT scans were performed right after the PET acquisitions on the same device. For all images, a ROI was drawn around the tumor and other ROIs with the same size were defined on the muscle and the liver to determine tumor-to-muscle (T/M) and tumor-to-liver (T/L) ratios. Results: After a 30min labeling process, the radiolabeling yields were up to 70% with a specific activity range from 9.5 to 13.5 GBq/μmol and radiochemical purity up to 90%. All the peptides were stable in buffer and plasma for at least 2h. The peptides were distributed in the whole mice and a renal excretion was predominantly observed after injection.

Liver uptake was significantly higher with 68Ga-DOTANOC than with 68Ga-DOTATOC, 68Ga-DOTATATE and 68Ga-NOTANOC. No significant difference between tracers was found for percentage of injected dose in muscle. No differences were found in the T/L ratio between 68Ga-DOTATATE and 68Ga-DOTATOC, both of which had a higher fraction than 68Ga-DOTANOC and 68Ga-NOTANOC. The T/M ratio was higher with 68Ga-DOTATATE than with the other peptides. Conclusion: This study shows the ability to labeled somatostatin analogues with 68Ga coming from a SnCl2-based 68Ge/68Ga generator. The imaging results are similar to the results obtained with peptides labeled with commercial generator, that is to say that the uptake was higher with 68Ga-DOTATATE in the tumor than with 68Ga-DOTANOC, 68Ga-DOTATOC and 68Ga-NOTANOC. For comparison, the tumor bearing mice were imaged after injection of 18F-FDG which is the main tracer used in clinic for oncology. The results show a very low uptake in tumor with a T/M ratio of only 1.5. This result shows the importance to have other tracers to image NETs.

P150

In vivo SPECT of neuro-endocrine tumour on chicken CAM

J. de Swart, S. J. Koelewijn, M. R. Bernsen, A. M. Bahnerth, R. S. de Bruijn, M. de Jong; Erasmus MC, Rotterdam, NETHERLANDS.

Aim: In several fields of research the chorioallantoic membrane (CAM) in chicken egg is applied as an in vivo tumour model. This model could provide a robust, rapid, low cost, and ethically preferable alternative to the mouse model, which has been the standard for in vivo oncology research, also for preclinical evaluation of novel radiopharmaceuticals. Here we investigate to feasibility of animal SPECT/CT to study tumour uptake characteristics of tracers in a CAM tumour model. Materials and methods: In normal farm chicken eggs 1.3 million CA20948 (somatostatin receptor-positive rat pancreatic tumour) cells were inoculated ten days after fertilization. One week after inoculation 12 MBq 111In-DOTA,Tyr3-octreotate (111In-octreotate) was injected into a CAM vein. 1h and 4h after injection, 30-minute and 45-minute SPECT scans were acquired respectively in list mode. Imaging was performed on a MILabs USPECT/CT system using a rat collimator with 1.0mm pinholes. SPECT was followed by a CT scan. During the scans the eggs were warmed in a foam holder in an upright position, with the air chamber on top. Anaesthesia was not used. SPECT data sets were reconstructed using the POSEM algorithm; 30 iterations, 4 subsets, and a voxel size of 0.4mm. CT was reconstructed using FBP. SPECT and CT were registered and the SPECT data were corrected for attenuation using the CT data. The resulting data was analysed using Invicro Vivoquant software. Results: In the eggs the CA20948 tumour could be clearly visualised on the SPECT scans at both time points. Uptake in the tumour could be clearly discriminated from that in the chick. The uptake of 111In-octreotate in the tumour was 1.1±0.7%IA (injected activity), uptake in the chick was 59.5±12.5%IA. The remaining injected activity was in other egg structures surrounding the chick. The chicks endured the imaging procedures well. There were no noticeable motion artefacts at the tumour site. Conclusion and discussion: It is feasible to use micro SPECT to image and quantify the uptake of radioactive compounds into a tumour inoculated in a chicken CAM, with the rigid shape of the egg and the homogeneous content facilitating robust attenuation correction. Anaesthesia does not seem to be necessary to image tumours in the CAM.The CAM tumour model is fast and inexpensive, providing in combination with SPECT a fast way to evaluate tracer tumour uptake characteristics. Because of the tiny structures in this model SPECT is preferable over PET because of the higher spatial resolution achieved.

P151

X-Ray CT Imaging of Stomach Passage of Contrast-Enhanced Floating Tablets in a New Rat Model

D. Mathe[1], F. Budan[1,2], S. Pal[3], I. Kiss[2], P. Dios[2], K. Szigeti[4]; [1]CROmed Ltd, Budapest, HUNGARY, [2]Dept. Public Health Medicine, University of Pecs, Pecs, HUNGARY, [3]Institute of Pharmaceutical Technology and Biopharmacy, University of Pecs, Pecs, HUNGARY, [4]Dept. Biophysics and Radiation Biology Semmelweis University, Budapest, HUNGARY.

Introduction. Cost-effective in vivo animal models are warranted to be developed to test modified drug delivery systems with the purpose to optimize those medical agent carriers. In this study, a novel rat model was evaluated to gain information about attributions of floating drug delivery systems (FDDS) practically in form of small sized tablets. X-ray computed tomography (CT) was performed.Materials and Methods. Sodium alginate as a biodegradable swelling polymer to create coherent frame of the tablets, sodium bicarbonate as carbon dioxide (CO2) creating agent and barium sulfate (BaSO4) contrast material to enhance X-ray CT. Partly anaesthetized rats were made to swallow tablets. In vivo imaging was performed at the following sampling times: 15 min, 1 h, 2 h, 3 h, 4 h, 6 h, 24 h and 48 h. Additionally, a maximum intensity projection (MIP) was rendered at 30 min after administration to provide fine resolution of spatial and temporal details about FDDSs in situ behavior using an adequate selected lookup table (LUT).Results. tablets with 10% BaSO4 content enabled quantitative in vivo imaging. These pharmaceutical agent

carriers formed CO2 bubbles 15 minutes after the administration and remained floating in the stomach for at least 24 hours. 48 hours after administration tablets were observed to be disintegrated mostly in the small intestine. Thus, the tablet's putative obstruction in stomach can be excluded. So the model can be considered as cheap, representative and capable to interpret results better.Conclusions.We can suppose that this newly developed rat model will be useful to provide comprehensive data about certain factors (e.g. food effect, posture, etc.) influencing gastrointestinal behavior of FDDS in future experiments by tracking their properties.

P152

Is enteral radioiodine administration the best route for radiotherapy in thyroid diseases? A preclinical study

K. Chatti[1,2], T. Pourcher[3,1,2], J. Guglielmi[1,2], J. Darcourt[4,1,2]; [1]UNS, Nice, FRANCE, [2]TIRO, Nice, FRANCE, [3]CEA, Nice, FRANCE, [4]CAL, Nice, FRANCE.

Aim: For iodine radiation therapy, the enteral route is currently used in clinical practice. Here we studied the differences in thyroid tissue uptake after eneral and parenteral administration of radio-iodine $^{123}I^-$ or $^{99m}TcO_4^-$ in mice measured by in vivo MicroSPECT/CT. Materials and methods: We used adult C57Bl6 mice under normal iodine diet (NID) or low iodine diet (LID) (8-6mice/experience) and nude mice with subcutaneous tumor expressing NIS under NID (simulating iodide avid metastasis; 3mice/experience, each mouse was its own control). Gavage (GV) with gastric tube was used for enteral administration. We used intraperitoneal (IP) administration as parenteral route (shown to be equivalent to intravenous). 3D high resolution whole body SPECT/CT (eXplorer speCZT CT 120, GE) imaging was performed using $^{123}I^-$ or $^{99m}TcO_4^-$. Dynamic SPECT/CT were acquired for the first hour with $^{99m}TcO_4^-$ or $^{123}I^-$ and 48h sequential acquisitions were added with $^{123}I^-$. Semi quantification expressed the rate of administered activity in the target organs after decay correction. T student paired test was used for statistics. Results: Thyroid uptake was significantly more intense in case of parenteral (IP) radiotracer administration than in case of enteral (GV) administration with both radiotracers, in NID and LID ($p<0.05$). In tumors expressing NIS, $^{99m}TcO_4^-$ accumulation was 1.7 fold more intense with IP administration route compared to GV. Conclusion: Thyroid uptake and accumulation was significantly higher when parenteral administration route was used in mice. These results suggest that parenteral administration could be more efficient in man for thyroid disease radio-iodine treatment.

P153

Investigation of 18FDG uptake in common carp (Cyprinus carpio) using PET/CT imaging

G. Trencsényi[1], S. Zaheri-A[2], R. Csipkés[2], A. Forgács[1], I. Komlosi[2], I. Garai[1]; [1]University of Debrecen/Scanomed Ltd., Debrecen, HUNGARY, [2]University of Debrecen, Department of Animal Husbandry, Debrecen, HUNGARY.

Aim: Positron Emission Tomography (PET) is a non-invasive diagnostic tool that provides tomographic images and quantitative parameters of glucose metabolic activity of tissues. The most important and commonly used tracer in PET is 18FDG. PET/CT is usually used in cancer studies and in these days there are many studies rely on mammals such as dogs and rodents and recently on fish. Our objectives of this survey by using 18FDG PET/CT are to optimize and determine the 18FDG uptake in common carp (Cyprinus carpio). Furthermore we investigated the effect of different fish diets on the 18FDG uptake.Materials and methods: 1.5 kg weighted common carps (Cyprinus carpio) were used in our experiments (n=3 for each group). Fish were fed with three different types of food for four weeks (basic fish meal, probiotic and vita) before the measurements. 10±1 MBq 18FDG was injected via the caudal vein under anaesthesia (10 drops of clove oil in 20 litre water). After 50 min incubation time whole body 18FDG PET/CT scans were made by using a clinical PET/CT scanner (Mediso AnyScan PET/CT) with 10 min acquisition time. The CT parameters were: 120kV, 100mA. For the quantitative analysis InterView Fusion Medical Imaging Software was used.Results: By taking the standardized uptake values (SUVmean) we found that the glucose uptake of the liver and intestines of fish were more similar to those of humans than rats or mice. The 18FDG uptake of the fish brain was significantly lower than the SUVmean values of rodent and human brain. By comparing the effect of the three different fish diet on glucose uptake we found relatively lower SUVmean values of the major organ systems in fish fed by probiotic diet than that of those fed by vita and basic fish meal.Conclusion: We found that 18FDG PET/CT is a useful tool for nutritional experiments using fish. Our results may offer us in studies of metabolism and screening for effects of nutrients to focus on body development.

P154

The role of ADAMTS-12 gene on the pathogenesis of radioiodine-induced salivary gland damage

M. SADIC[1], M. KORKMAZ[1], S. S. GÜLTEKIN[2], K. DEMIRCAN[3]; [1]Ministry of Health Ankara Training and Research Hospital, ANKARA, TURKEY, [2]Kastamonu School of Medicine, Hacettepe University and Ministry of Health

Diskapi Training and Research Hospital, ANKARA, TURKEY, [3]Turgut Ozal University, School of Medicine, Department of Molecular Biology, ANKARA, TURKEY.

Aim: A disintegrin-like and metalloproteinases with thrombospondin type-1 motif (ADAMTS)-12 is a member of a gene family with 19 subtypes. This study aims to determine effects of ADAMTS-12 gene on pathogenesis of the radioiodine I-131 (RAI)-induced salivary gland damage. Methods: Study group consists of total 30 Wistar male albino rats (260 ± 45 grams, 6-month-old) in five groups. By the polymerase chain reaction method, ADAMTS-12 gene expression levels were studied on parotid and submandibular salivary gland specimens. Quantitative analyses were carried out using 2-ΔΔct method. In control subjects (Group 1; 6/30 rats) genetic examinations were performed 24 h after removal of tissues. A 3 mCi (111 MBq) dose of RAI was administered to each rat in Groups 2,3,4 and 5 (24/30; six rats in each group) and excised salivary glands' samples obtained at respectively 4 h, 24 h, 7 d and 30 d after the RAI administration were evaluated by genetic examinations. Final data was evaluated by statistical analysis.Results: In different time periods (Group 2-5) and same time periods (Group 1 vs. 3), according to the measurements of ADAMTS-12 gene expression in the samples, reduction at the level of gene expression over time or difference was statistically significant ($p<0.05$) for the parotid gland but not statistically significant ($p>0.05$) for the submandibular gland. Mean and standard deviation values were 1,00 ± 0,00 in Group 1, 0,38 ± 0,30 in Group 2, 0,11 ± 0,05 in Group 3, 0,10 ± 0,07 in Group 4 and 0,18 ± 0,29 in Group 5 for the parotid glands and 1,00 ± 0,00 in Group 1, 1,59 ± 1,92 in Group 2, 1,57 ± 0,36 in Group 3, 1,03 ± 0,32 in Group 4 and 1,00 ± 0,67 in Group 5 for the submandibular glands.Conclusions: We thought that lower expression of ADAMTS-12 gene may have a role on mechanism of RAI-induced damage in the rat parotid gland. We didn't observe meaningful effect of ADAMTS-12 on RAI-induced damage in submandibular gland.

P155

Impact of quantification accuracy on dosimetric calculations in small animal preclinical imaging: a study in sodium/iodide symporter (NIS) radiotracers

K. Chuamsaamarkkee[1,2], P. J. Blower[1], L. Livieratos[1,3]; [1]King's College London, Division of Imaging Sciences and Biomedical Engineering, London, UNITED KINGDOM, [2]Division of Nuclear Medicine, Department of Radiology, Faculty of Medicine Ramathibodi Hospital, Mahidol University, Bangkok, THAILAND, [3]Nuclear Medicine Dept, Guy's & St Thomas' Hospitals NHS Foundation Trust, London, UNITED KINGDOM.

Background: Preliminary dosimetric data from animal studies is a basis for going forward with clinical trials in development of new radiotracers. Typically in vivo tracer kinetics are extrapolated to estimate human-equivalent dosimetry. However, quantification of small organ activities may be impaired by partial volume effects (PVE). This study aims to examine the influence of PVE in preclinical quantification of small-objects/organs and its impact on subsequent dosimetric calculations for sodium iodide symporter (NIS) radiotracers. Methods: A mouse-size equivalent micro hollow sphere (MHS) phantom was filled with different amounts of radiotracer (Tc-99m, I-123 and Re-188) and scanned with the nanoSPECT/CT preclinical system using the 3 mm. aperture collimators. Volume-of-interest (VOI) based quantification accuracy was plotted against sphere volume fitting curves with a second order polynomial equation to obtain volume-dependent correction factors (CFs). In vivo imaging of healthy controls (Scid/Beige mice, n=3 for each tracer) was performed dynamically for 4 h and also at 8 and 24 h post injection. Images were analysed and dosimetric results were calculated using OLINDA version 1.0. Organ volumes (thyroid, salivary glands, stomach and bladder) were obtained from VOIs applied to high resolution CT images and appropriate CF were defined for each organ based on volume and data from the phantom study. Dosimetric data were calculated with and without the volume-dependent PVE correction. Percentage differences of absorbed doses were compared to evaluate the impact of quantification accuracy and PVE. Results: Thyroid absorbed doses were mostly affected due to its small size. The application of applied CF increased the calculated dose by approximately 20% for Re-188, 10% for Tc-99m and 2% for I-123 compare with uncorrected PVE data. Similarly, the salivary gland absorbed doses were raised in a similar fashion. For stomach, the absorbed doses were increased by 13.60% for Re-188, 1.7% for Tc-99m whereas decreased about 2% for I-123. Similar trends were also found in urinary bladder. PVE correction had minimal impact on red-marrow absorbed doses for all isotopes. Application of CFs increased calculated effective dose values by approximately 13%, 3% and 1.5% for Re-188, Tc-99m and I-123 respectively. Conclusion: This study demonstrates the influence of PVE on the dosimetric calculations from small-animal preclinical imaging. An organ volume dependent correction based on standard geometrical phantom measurements has been proposed.

P156

Preclinical Dosimetric Comparison of 186Re- and 188Re-perrhenate versus 131I-NaI for Treatment of Non-thyroidal NIS-expressing Tumour

K. Chuamsaamarkkee[1,2], S. Diocou[1], P. J. Blower[1], L. Livieratos[1,3]; [1]King's College London, Division of Imaging

Sciences and Biomedical Engineering, London, UNITED KINGDOM, [2]Division of Nuclear Medicine, Department of Radiology, Faculty of Medicine Ramathibodi Hospital, Bangkok, THAILAND, [3]Nuclear Medicine Dept, Guy's & St Thomas' Hospitals NHS Foundation Trust, London, UNITED KINGDOM.

Background: The potential for radioiodine (131I-NaI) treatment in non-thyroidal tumour has been speculated upon following successful cloning and gene transfer of sodium iodide symporter (NIS) in a variety of cell types. However, radioiodine has practical limitations such as radiation safety restrictions to patients, the public and its therapeutic efficiency may be restricted by rapid efflux due to lack of organification in non-thyroidal tumours. Therefore, there is a window in which rhenium isotopes (186Re-, and 188Re) in the form of perrhenate (which is also a substrate of NIS) may offer greater therapeutic advantages due to shorter half-life, more energetic betas, longer soft-tissue range and lower photon abundance. This study aims to evaluate the dosimetric profile of potential isotopes for treatment of non-thyroidal NIS-expressing tumours. Methods: Rat mammary adenocarcinoma (MTLn3E) overexpressing truncated CXCR4 and hNIS were grafted at the flank of female SCID/Beige mice (n=3 for each radiotracer; 99mTc-pertechnetate, 188Re-perrhenate and 123I-NaI). Whole-body SPECT was acquired continuously for 4 h post injection (PI) with additional scanning at 8h and 24h. Percentage injected activity was derived from images and extrapolated using SUV-preserving linear-mass scaling to derive human-equivalent time-activity curves, tracer residence times and then applied to OLINDA to estimate dosimetry. Results: Percentage uptake per gram of tumour (%ID/g) in 188Re-perrhenate was 5-15 %ID/g, compared with 45-55 %ID/g of 99mTc-pertechnetate and 42-62 %ID/g of 123I-NaI at 4 h PI. Although kinetics of 188Re-perrhenate and 99mTc-pertechnetate were very similar, however based on phantom data, lesion-to-background contrast for 188Re-perrhenate might be underestimated due to scatter and elevated background from Bremsstrahlung. Due to the complexity of the proprietary multi-pinhole with multiplexed-projections, implementation of the triple-energy-window correction is not currently possible. Hence, 99mTc kinetics were used instead of rhenium isotopes and a 123I as a surrogate for 131I-NaI to achieve reasonably quantitative and accurate dosimetry estimation. Results show that tumour absorbed doses were 6.33 and 8.68 times higher for 186Re and 188Re when compared to 131I. Additionally, the therapy indexes (tumour to effective-dose and tumour to thyroid ratio) for both rhenium isotopes were greater than 131I. Red-marrow absorbed doses produced by rhenium were lower than radioiodine (0.27 and 0.50 times for 186Re and 188Re respectively). Conclusion: This work demonstrates the ability of 188Re-perrhernate for imaging and treatment of non-thyroidal NIS expressing tumour. A superior therapeutic dose ratio has been predicted for both rhenium isotopes which resulted at higher tumour absorbed dose together with lower thyroid and whole-body doses.

P157

Quantitative Imaging of ^{89}Zr on a pre-clinical PET/CT system

A. Fenwick[1,2], C. Marshall[3,1], E. Spezi[4,1], W. Evans[3,1], L. Johansson[2]; [1]Cardiff University School of Medicine, Cardiff, UNITED KINGDOM, [2]National Physical Laboratory, Teddington, UNITED KINGDOM, [3]Wales Research & Diagnostic Positron Emission Tomography (PET) Imaging Centre, Cardiff, UNITED KINGDOM, [4]Velindre NHS Trust, Cardiff, UNITED KINGDOM.

The use of the novel radionuclide ^{89}Zr in the field of mAbs and PRRT imaging has become of great investigational interest during the past few years with many publications showing the benefits of this PET radionuclide. Despite the high level of interest, no traceable measurement has yet been made of the activity either at production sites or in the clinical setting which could eventually lead to contradicting results when this product reaches clinical trials. Quantification in images is important to determine activity distribution for not only patient safety and dosimetry but to ensure staging and treatment efficacy can be accurately determined. Pre-clinical imaging is a critical step on the pathway to human trials and quantification at this stage is equally important to ensure novel radiotracers can successfully progress to future trials. A Pre-clinical PET/CT camera has been traceably calibrated in terms of activity for the first time with an associated uncertainty budget and corrections for partial volume. The calibration protocol includes measurements of various activity distributions and phantom components in order to determine an associated uncertainty and range of parameters for which the calibration is valid. The paper also describes methods for filling phantoms and reasons for the choice of phantom design used in the calibration. The results show that if care is taken to ensure traceability is maintained throughout the imaging process, an accurate and robust calibration can be made of a typical pre-clinical system and maintained during with routine practice and QA.

P158

Biodistribution study of EGFR targeting monoclonal antibody [177Lu]-Nimotuzumab

M. Kropacek, M. Tomeš, K. Kontrová, J. Zimová, M. Mirzajevová, F. Melichar; RadioMedic Ltd., REZ, CZECH REPUBLIC.

Introduction: Nimotuzumab (hR3) is a humanized monoclonal antibody (mAb) with the affinity towards the epidermal growth factor receptor (EGFR), which is overexpressed in the majority of solid tumors, including breast and ovarian cancer, colon cancer, head-and-neck cancer and non-small cell lung cancer. The aim of this work was to carry out first part of biodistribution study on healthy rats. Material and Methods: Monoclonal antibody Nimotuzumab (hR3) was purchased from Oncoscience AG (Wedel, Germany), bifunctional ligand p-SCN-Bn-DOTA was purchased from Marocyclics (Dalas, USA), Lu-177 n.c.a. was obtained from ITG (Munich, Germany). Biodistribution study was provided by Biological Testing Laboratory ÚJV Řež a.s. Native Nimotuzumab was conjugated with p-SCN-Bn-DOTA (10-fold molar excess) at pH=8.3 (0.1 M phosphate buffer) two hours at room temperature. After first hour of conjugation, reaction mixture pH was checked and readjusted, when needed. Prepared immunoconjugates were purified by ultrafiltration on Vivaspin 6. Concentration of immunoconjugate was determined by Bradford assay. Labelling with Lu-177 was carried out 0.05 M ammonium acetate buffer (pH 7.0) at 42°C for 60 minutes. Biodistribution was done on the rats (Wistar, n=52). Injected activity of Lu-177 was 3.37 MBq/animal and organs accumulation was observed 1, 24, 48, 72, 120 and 168 hours after administration. Immunoreactivity was checked using ELISA method before administration. Results: [^{177}Lu]-Nimotuzumab was obtained with specific activity 200 MBq/mg and radiochemical purity > 90%. All preparation steps met the GMP rules and conditions. Biodistribution study showed the highest activity accumulation in the liver 48 hours after injection (63.46%). Another critical organ spleen accumulated 3.61% of injected activity 48 h and the accumulation remained stable until 168 h after injection. Level of activity in the lungs reached maximum 1 hour after injection (32.29%) and then decreased to 0.55% after 24 hours. Activity in blood decreased from 43.41% (1 h) to 18.17% (24 h) and then to 7.33% (168 h) after application. Conversion, where the weight of rat blood is approximately 7% of animal's weight was applied. All activity accumulation was calculated per organ. Conclusion: First part of biodistribution study verified physiological accumulation of [^{177}Lu]-Nimotuzumab. Activity in critical organs liver and spleen indicated accumulation of product due to the biological degradation and elimination. Activity in the lung was consistent with the expectation of increased distribution due to intensive blood circulation in this organ. Biodistribution results in healthy rats were promising for next part of study carried out on immunodeficient mice with EGFR expressing tumors.

P159

Synthesis and evaluation of Gallium-68 labeled Fe3O4 - Citric acid nanoparticles for dual modality.

B. Cho[1], M. Moon[1], J. Lee[2], J. Park[2], M. Hur[2], K. Yu[1]; [1]Dongguk university-seoul, Seoul, KOREA, REPUBLIC OF, [2]Korea Atomic Energy Research Institute, Jeongeup, KOREA, REPUBLIC OF.

Aim: Dual modality imaging is powerful tools to obtain valuable information on function in biomedicine. In this present work, we report the development of nano-bio targeting composites using Fe3O4 nanoparticles and Ga-68 radioisotope for dual modality of PET and MRI applications. Materials and methods: FCNP (Fe3O4-Citric acid nanoparticles) was synthesized by one step process using citric acid as surfactant. FCNP exhibits several attractive properties such as strong magnetic, controllable particle size and stability in water. Nano-bio composites (NHFCNP and NFHFCNP) were obtained by combining the surface modified FCNP and NOTA as bi-functional chelating agent with Ga radio isotope and Folic acid by single step. The structure and morphological properties of nano-bio composites were characterized by XRD,TEM, IR and UV analysis. 68GNFHFCNPs was prepared by the reaction of NFHFCNP with Ga-68 from an in-house generator. Radio-TLC analysis confirmed the radiolabeling of 68Ga-NOTA complex. Cell viability and cellular uptake studies were performed on CT-26, SK-BR-3. Results and conclusion: The final compound, GNHFCNP (GNFHFCNP) with stable gallium isotope showed good biocompatibility and 68GNHCNPs(68GNFHCNPs) with radio gallium isotope have high uptake on CT-26 and SK-BR-3. The cellular uptake of 68GNHFCNP was maximum of 8.778 % at 120 min for CT-26 and 15.491 % at 120 min for SK-BR-3.that of 68GNFHFCNP was maximum of 9.764 % at 60 min for CT-26 and 13.591 % at 120 min for SK-BR-3. 68GNHCNPs(68GNFHCNPs) shows higher cellular uptake on the SK-BR-3 compared to CT-26. In summary, The 68GNFHFCNPs were successfully synthesized by simple chemical technique. The biological evaluation of 68GNHFCNPs confirm that as potential material for radiopharmaceuticals.

P160

High Frequency Ultrasound for the development of an Orthotopic mouse model of Human Follicular Thyroid Carcinoma

S. Albanese[1,2], L. Auletta[3], A. Zannetti[4], G. Di Maro[3], P. Mirabelli[3], C. D'Alterio[5], G. Salvatore[2,3,6], A. Soricelli[3,6], M. Salvatore[3], A. Greco[7,2]; [1]Università Parthenope, Naples, ITALY, [2]Ceinge, Biotecnologie Avanzate, Scarl, Naples,

ITALY, [3]IRCCS-SDN, Naples, ITALY, [4]Istituto di Biostrutture e Bioimmagini – CNR, Naples, ITALY, [5]Dipartimento di Immunologia Oncologica- Istituto Nazionale per lo Studio e la Cura dei Tumori "Fondazione Giovanni Pascale"- IRCCS, Naples, ITALY, [6]Dipartimento di Scienze Motorie e del Benessere, Università Parthenope, Naples, ITALY, [7]Dipartimento di Scienze Biomediche Avanzate,Università degli studi di Napoli Federico II, Naples, ITALY.

Aim: Thyroid carcinoma is the most common endocrine malignancy, with increasing incidence and mortality rate (1). High Frequency Ultrasound (HFUS) has the ability to detect structures as small as 30 μm, a property that has been exploited for thyroid visualization and analysis in mice (2). Aim of this study, was to generate a novel orthotopic mouse model of Human Follicular Thyroid Carcinoma (FTC) using HFUS-guided system and to compare this method to the orthotopic surgical model.Materials and Methods: Ten 6 weeks-old, female, balb/C nude mice underwent to a surgical orthotopic implantation of 2 x 106 FTC-133 in the right lobe of the thyroid and ten mice were injected in the right lobe of the thyroid with 2 x 106 FTC-133 using HFUS-guided system. Two weeks after injection all mice underwent HFUS imaging, HFUS and tumor volumes (TV) examinations were repeated weekly. Hematoxylin and eosin (H&E) analysis of formalin fixed paraffin embedded mouse tissues was performed at the end of the experiment. TVs were compared between the two orthotopic mouse models (surgically and HFUS-guided injected) using a Mann-Whitney's U test.Results: All the echoguided inoculated mice survived up to 40 days and cancerogenesis primarily involved the right thyroid lobe. Metastasis in salivary gland and lymph nodes were detectable. H&E analysis confirmed accurate placement of FTC-133 cells by echoguided intrathyroid injection. Mice inoculated by surgery had 100% mortality at 30 day. FTC developed in an invasive way, early metastasis were detectable, with obvious infiltrates in the muscle and salivary gland as evident from the histological images of the neck. In the surgical orthotopic model in some cases there was an evident involvement of the not injected contralateral lobe of the thyroid. A difference in TVs between the two orthotopic techniques was detected (significant at day 13, surgically 18.4 ± 1.8 vs. HFUS 32.4 ± 4.7; P=0.01).Conclusion: In our study, we develop a novel echoguided orthotopic mouse model of FTC and we compared it with the surgical orthotopic model. HFUS - guided orthotopic model is technically feasible and easily reproducible allowing prolonged monitoring of the disease, since the animals showed an increased survival rate.References1. Howlader N, et al. SEER Cancer Statistics Review, 1975-2008, National Cancer Institute.2. Mancini M, et al 2009 Morphological Ultrasound Microimaging of Thyroid in Living Mice. Endocrinol 150:4810-4815.

P161

PET and SPECT imaging of breast cancer xenografts using optimized CMKLR1-targeted DOTA-conjugated peptide tracers

S. Poenick[1], N. Beindorff[2], E. Koziolek[2], J. Castillo Gómez[2], I. Apostolova[2], R. Michel[2], S. Hallmann[1], A. Wagener[1], V. Prasad[2], S. Bandholtz[1], P. Schulz[1], B. Wiedenmann[1], W. Brenner[1], **C. Grötzinger**[1]; [1]Charité - Universitätsmedizin Berlin, Gastroenterology, Berlin, GERMANY, [2]Charité - Universitätsmedizin Berlin, Nuclear Medicine, Berlin, GERMANY.

Aim: With cancer being still one leading cause of death, there is an urgent need for personalized diagnostics and therapies. One promising target is the chemokine-like receptor 1 (CMKLR1), with its peptide ligand chemerin being an encouraging molecular entity for tracer development. Aim of this study was the utilization of our optimized and validated chemerin tracers for nuclear in vivo imaging with positron emission tomography, single photon emission computed tomography and complementary biodistribution studies. Materials and Methods: Highly specific and affine peptide ligands for the G protein coupled receptor CMKLR1 were obtained by substitution of wild type chemerin-9 and analysis of the structure-activity relationship. In consequence, we designed a panel of peptide conjugates with different linkers and chelator DOTA (1,4,7,10-tetraazacyclododecane-1,4,7,10-tetraacetic acid) to gain novel tracers for tumor targeting. The combination of radiolabeled (68Ga, 111In) peptide tracers and an established target positive tumor model in immunodeficient nude mice enabled tumor-specific imaging in vivo. Therefore, we acquired small animal PET/MR and SPECT/CT images and assessed biodistribution by ex vivo measurements. Results: Our novel chemerin peptide tracers demonstrated significantly improved properties compared to the wild type peptide concerning biological activity, affinity and metabolic stability. Their target is known to be over-expressed in different pathologies, including cancer. Beside other tumor entities like esophageal or pancreatic cancer, we could demonstrate CMKLR1 overexpression in the breast carcinoma cell line Du4475. After establishment of different target-positive cancer models along with target negative tumors, PET/MR and SPECT/CT imaging revealed a strong CMKLR1 specific uptake of the targeted radiolabeled tracers in tumor tissue within one hour (68Ga) or twenty-four hours (111In). Furthermore, the tracer conjugates cleared rapidly by predominantly renal excretion. As probe biodistribution strongly depended on hydrophilic properties as plasma protein binding, our ligand conjugates exhibited different in vivo tumor uptake. Sixty-eight hours after injection, the tumor uptake of 111In-radiolabeled tracer was about 1 % ID/g and could be blocked with a 100-fold excess of unlabeled conjugate. In addition, expression analysis of the

ex vivo tissue confirmed the target selectivity. Conclusion: We found CMKLR1 to be overexpressed in different tumor entities such as breast cancer. With the cell line Du4475, we had a model endogenously expressing our target to evaluate our optimized chemerin peptides as stable ligands with high affinity. PET and SPECT imaging using novel 68Ga- or 111In-labeled tracers revealed high and specific tumor uptake, thus we developed promising candidates for potential clinical translation.

P162

Comparison of murine and chimeric version of the anti-CD37 antibody HH1 used for antibody-radionuclide-conjugate (ARC) therapy of Non-Hodgkin Lymphoma

J. Dahle[1], A. Repetto-Llamazares[1], K. B. Melhus[1], A. O'Shea[1], R. Generalov[1], J. Andersen[2], H. Heyerdahl[1]; [1]Nordic Nanovector ASA, OSLO, NORWAY, [2]Oslo University Hospital, OSLO, NORWAY.

Introduction: The novel antibody-radionuclide-conjugate (ARC) 177Lu-DOTA-HH1 (Betalutin™) is currently in clinical phase II trial for treatment of Non-Hodgkin Lymphoma (NHL). The HH1 antibody is a murine anti-CD37 antibody and has a lower binding affinity to Fc receptors than a chimeric or humanized antibody and consequently a shorter biological half-life. A biological half-life similar to the half-life of the radionuclide will optimize irradiation of the tumor and result in lower irradiation of normal tissues. Internalization of a chimeric ARC in normal tissues expressing the neonatal Fc receptor may also result in unwanted irradiation of normal tissues. There are, however, benefits of using a chimeric antibody: 1) Reduced level and severity of human anti-drug antibody response; 2) Additional and possibly synergistic therapeutic effect from antibody dependent immunological toxicity and complement dependent cytotoxicity. This study was performed in order to investigate the similarities and differences of the murine and the chimeric version of the anti-CD37 ARC. Materials and Methods: Both the murine HH1 and the chHH1 antibodies were conjugated with p-SCN-Bn-DOTA using different DOTA:Ab ratios. Binding and internalization of the ARCs were measured using fluorescence confocal microscopy and biochemical assays. Binding to Fc-receptors and complement was measured using ELISA and recombinant Fc receptors. ADCC and CDC were measured using NK-cells and serum, respectively, from donor blood. Tissue cross reactivity (TCR) was measured by immunohistological staining of tissue sections from human and animal donors. Biodistribution of the ARCs was measured after injection in mice with NHL xenografts. The therapeutic and toxic effects of the two ARCs were compared in a NHL mouse model. Results: The two antibodies showed similar binding and internalization. TCR studies showed that both antibodies bound selectively to lymphoid tissues. The chimeric antibody bound to all the classical human Fc-receptors, while the murine antibody only bound to FcγR IIa and IIb, which is expressed on B-cells. HH1 bound weaker to human C1q than the chimeric antibody. The binding of HH1 to C1q, FcγR IIa and IIb, did, however, not result in any complement dependent cytotoxicity or antibody dependent cellular cytotoxicity, while it did for the chimeric antibody. Both ARCs had a relevant biodistribution in mouse models, however the tumor uptake of the chimeric ARC was higher than for the murine ARC. More details of the therapeutic and toxic effect of the two ARC's will be included in the presentation at the meeting.

P163

In vivo evaluation of inhibitory role of microRNA on glucose transporter by micro-PET in hepatocellular carcinoma xenografts

L. KANG; PEKING UNIVERSITY FIRST HOSPITAL, BEIJING, CHINA.

Aim: MicroRNA (miRNA) has exhibited regulatory functions in numerous cellular processes including proliferation, differentiation and apoptosis, especially in carcinogenesis. In malignant tumors, the increased glucose metabolism is due to high expression of glucose transporters (GLUTs) and phosphorylation by hexokinase. The objective is to investigate the role of miRNA in the regulation of glucose transporter and further evaluate by FDG micro-PET in hepatocellular carcinoma (HCC) xenografts. Materials and methods: The HepG2 cells stably overexpressing miRNA and empty vector were constructed by lentiviral vector transfection. The expression of insulin-like growth factor-1 receptor (IGF-1R), phosphatidylinositol-3-kinase (PI3K), AKT, and GLUT1 in HepG2 cells were evaluated by Western blotting assay. FDG cellular uptake and proliferated activity were evaluated. FDG micro-PET was performed to show the in-vivo ability of miRNA in HepG2 xenografts. Furthermore, the expression of glucose related proteins in tumor tissue were evaluated as well. Results: The hepG2 cells with stable expression of miRNA were constructed and identified by sequencing. The decreased proliferated ability was shown in miRNA over-expressed HCC cells in vitro, as well as FDG cellular uptake. Western blotting results showed the expression of IGF-1R, PI3K, AKT and GLUT1 protein were inhibited in miRNA over-expressed cells. For HepG2 tumor xenografts, small-animal PET clearly showed the significantly decreased FDG accumulation in miRNA tumors, which was verified by the suppressed FDG uptake and IGF-1R/PI3K/AKT pathway of ablated tumors. Conclusion: MiRNA exhibits a negative role in the regulation of glucose transporter via the inhibition of IGF-1R/PI3K/AKT

pathway. FDG micro-PET is useful for evaluating the role of miRNA in vivo.

P164

18F-FES and 18F-FDG micro-PET/CT imaging for the evaluation of nanovectorized radiotherapy with 188Re in a murine model of endometrial cancer.

C. Lefebvre-Lacoeuille[1,2,3], A. Genin[1,3], F. Bouchet[1,4], N. Chouin[5,6], A. Croué[1], L. Preisser[1,7], F. Hindré[2,8,1], P. Descamps[1,3], O. F. Couturier[1,2,4], **F. Lacoeuille**[1,2,4]; [1]LUNAM Université, Angers, FRANCE, [2]Inserm UMRS_1066 MINT, Angers, FRANCE, [3]Department of Obstetrics and Gynaecology, CHU Angers, Angers, FRANCE, [4]Nuclear Medicine Department, CHU Angers, Angers, FRANCE, [5]LUNAM Université, Nantes, FRANCE, [6]AMaROC, ONIRIS, Nantes, FRANCE, [7]Inserm U892, Angers, FRANCE, [8]PRIMEX Plateforme de Radiobiologie et d'Imagerie Expérimentale, Angers, FRANCE.

Aim: To evaluate changes in tumour glycolysis measured by positron emission tomography (PET) with [18F]fluorodesoxyglucose ([18F]-FDG) and in steroid hormone receptor expression measured by PET with 16α-[18F]fluoro-17β-oestradiol ([18F]-FES) following internal radiotherapy with nanoparticles loaded with rhenium-188 (LNC-188Re-SSS) in a preclinical murine model of human endometrial cancer. Materials and methods: Ishikawa endometrial carcinoma cell lines were implanted subcutaneously in nude mice (n=10). D28 after inoculation, mice (n=5) were treated with an intratumor injection of LNC-188Re-SSS. Treatment efficiency in the LNC-188Re-SSS group was compared to control group (n=5) in term of tumour growth assessed by clinical palpation and micro-PET/CT imaging. For each mouse, two [18F]-FDG and two [18F]-FES micro-PET/CT were performed on separate imaging days, at baseline before therapy, and two weeks later. Results: Fourteen days after treatment with LNC-188Re-SSS, tumour progression was significantly inhibited compared to the control group ($p<0.006$). [18F]-FDG uptake remained stable in the treated group ($p=0.9$) and was significantly lower than in control group ($p=0.03$), in which [18F]-FDG tumour uptake increased significantly ($p=0.003$). An excellent correlation was observed between [18F]-FDG tumour uptake and tumour volume ($r=0.88$, $p=0.0016$). At baseline focal [18F]-FES uptake corresponding to the known subcutaneous tumour were observed in both group of mice, and after treatment no significant [18F]-FES uptake difference was observed between the treated and untreated groups ($p=0.75$). The [18F]-FES tumor uptake was not correlated with the tumour volume ($r=0.1613$, $p=0.68$). A significant correlation was found between tumour ERα-score, measured by immunohistochemistry, and [18F]-FES uptake ($r=0.6821$, $p=0.043$). Conclusion: Because after treatment, significant changes in tumour uptake was observed only with [18F]FDG and not with [18F]-FES, [18F]-FES does not appear to be able to monitor the therapeutic effect of internal radiation with LNC-188Re-SSS.

P165

PET imaging of CD-30 positive lymphomas using radiolabelled antibodies

S. Rylova[1,2,3], C. Klingeberg[1], L. Del Pozzo[1,2,3], R. Tonnesmann[1], A. Illert[1], P. T. Meyer[1,2,3], H. Maecke[1], J. P. Holland[1,2,3]; [1]Freiburg University Hospital, Freiburg, GERMANY, [2]DKTK, Heidelberg, GERMANY, [3]DKFZ, Heidelberg, GERMANY.

Aim: The anti-human CD-30 antibody drug conjugate, brentuximab vedotin, is approved for treatment of relapsed refractory Hodgkin lymphoma and systemic anaplastic large cell lymphomas (ALCL), and has a reported overall response rate of 70%. Since CD-30 expression can vary among different types of lymphoma, and may also change during the course of the treatment, companion diagnostic imaging of CD-30 could be a valuable tool in optimizing patient-specific brentuximab vedotin treatment regimens. Material and Methods. The AC-10 mouse anti-human CD-30 antibody was conjugated with a desferrioxamine B (DFO) chelate and radiolabeled with the positron-emitting radionuclide 89Zr, the reaction was monitored using HPLC and radio ITLC. The pharmacokinetic of 89Zr-DFO-AC-10 was evaluated in Balb/c Nude mice bearing subcutaneous human ALCL tumors (CD-30 positive) or A431 tumors (CD-30 negative) using PET/CT imaging and biodistribution studies. Results and conclusion: The anti-CD-30 antibody was conjugated with DFO chelate and radiolabeled with 89Zr to give formulated 89Zr-DFO-AC-10 with a radiochemical yield (RCY) of 74.5% and radiochemical purity (RCP) of 100%. The specific activity of 89Zr-DFO-AC-10 was 99.3MBq/mg. Time activity curves (TAC) derived from longitudinal PET imaging in CD-30 positive model (100 μL i.v.; 6.9 - 7.4 MBq/mouse; imaging 24 - 144 h post-injection) demonstrated highest tissue localization in tumors with an average uptake of 21.4±2.7 %IA/g at 24 h p.i. reaching a maximum uptake 26.1±8.8 %IA/g at 120 h p.i. Among normal organs the highest uptake of radioactivity was in liver with 11.0±1.3%IA/g at 24 h, which persisted throughout the experiment (10.48±1.32 %IA/g at 144 h p.i.). The average uptake in CD-30 negative tumors was 12.6±1.2 %IA/g at 24h and remained constant throughout the imaging (10.8±1.0 %IA/g at 144 h p.i). Tumor-to-blood ratios in CD-30 positive model increased from 2.7 to 11,8 from 24 to 144 h, respectively. Tumor-to-muscle ratios increased from 2.7 to 45.1 between 24 and 144 h p.i. Biodistribution studies performed at 72 h p.i revealed 37.9±8.2 %IA/g uptake in the ALCL tumor versus

11.4±0.4 %IA/g in A431 tumors, 11.8±2.4 in liver, 8.2±0.8.1 %IA/g in spleen, 5.1±0.4%IA/g in bone and 6.4±0.5%IA/g in blood. Collectively, our data indicate that 89Zr-DFO-AC-10 can be used as a sensitive PET imaging agent for measuring CD-30 expression in tumors.

P166

Imaging of CDH17-positive gastric cancer xenografts with 64Cu-labeled anti-CDH17 IgG PET

K. Fujiwara[1], K. Koyama[1], K. Suga[2], M. Takahashi[1], O. Kusano-Arai[3], K. Mitsui[3], H. Akiba[4], H. Iwanari[3], K. Tsumoto[4], T. Hamakubo[3], T. Momose[1]; [1]Department of Radiology, Graduate School of Medicine, The University of Tokyo, Tokyo, JAPAN, [2]SANKYO LABO SERVICE Co., Ltd., Tokyo, JAPAN, [3]Department of Quantitative Biology and Medicine, Research Center for Advanced Science and Technology, The University of Tokyo, Tokyo, JAPAN, [4]Department of Bioengineering, School of Engineering, The University of Tokyo, Tokyo, JAPAN.

Aim: Cadherin 17 (CDH17) is a membrane protein that contributes cell-cell adhesion. CDH17 may have potensial as a target protein of immunotherapy or radioimmunotherapy (RIT) for gastric cancer, because CDH17 is specifically expressed at high levels in gastric cancer. In order to perform immunotherapy or radioimmunotherapy, it is necessary to identify and quantify the expression of target protein in the cancer tissues before the treatment. ImmunoPET is useful for this purpose, because PET can evaluate non-invasively and quantitatively the expression of target protein in cancer tissues. In this study, we performed PET study using 64Cu-labelled anti-CDH17 IgG monoclonal antibody against gastric cancer models. We evaluated the possibility of 64Cu-anti-CDH17 IgG as a PET agent for gastric cancer. Materials and Methods: The specificity of anti-CDH17 IgG for CDH17 antigen was evaluated by flow cytometry. CDH17-positive human gastric cancer AGS xenograft nude mice were used in this study. We conjugated anti-CDH17 MAb with 1, 4, 7-triazacyclononane-1, 4, 7-triacetic acid (NOTA), and the conjugates were labelled with 64Cu. AGS xenograft mice were injected 7 MBq of 64Cu-anti-CDH17 MAb via tail vein. PET/CT scans were performed using small animal PET scanner. Image data were reconstructed by use of OSEM2D. Region of interests were defined in tumor, mediastinum and liver. The percentage of injected dose per gram of tissue (%ID/g) was calculated for each organs. Results: Flow cytometry demonstrated the specificity of anti-CDH17 IgG for CDH17 antigen. In addition, we confirmed that NOTA conjugation and radiolabelling did not impair the affinity for anti-CDH17 IgG. In the PET study, 64Cu-anti-CDH17 IgG showed a clear image of a CDH17-positive AGS tumors. The uptake of 64Cu-anti-CDH17 IgG in tumors increased gradually over time, and the maximum uptake was 26.6 ± 4.3 %ID/g at 72 hours after injection. The uptake to mediastinum and liver decreased gradually over time. The uptake to mediastinum and liver was 5.64 ± 2.3 %ID/g and 5.53 ± 1.1 %ID/g at 72 hours after injection, respectively. Conclusion: 64Cu-anti-CDH17 IgG is a promising PET probe for evaluating the expression of CDH17 antigen in gastric cancer. This agent has the potential to facilitate the selection of appropriate patients who would benefit from anti-CDH17 IgG therapy or RIT.

P167

Preclinical evaluation of a novel bombesin peptide analog for targeting bombesin receptor expressing tumors

S. Okarvi, I. Jammaz; King Faisal Specialist Hospital & Research Centre, Riyadh, SAUDI ARABIA.

Aim: Over the last few years bombesin (BN) receptors have attracted a great clinical attention as molecular target for diagnosis and therapy as all three BN receptor subtypes are overexpressed in various human cancers. Despite substantial developments the limitations enforced by BN peptide pharmacokinetics related to binding and clearance kinetics suggest that significant improvements of these radiolabeled BN analogs are still needed. The aim of this study was to develop a BN analog having wide receptor affinity and favorable pharmacokinetics and able to be labeled both with diagnostic and therapeutic radionuclides to produce a potential theranostics for targeting BN receptor-positive tumors.*Materials and Methods*: We have designed a unique BN peptide composition consisting of a GGC sequence to facilitate complexation with ^{99m}Tc and DOTA for labeling with ^{68}Ga/^{177}Lu. A hippurate-type spacer (aminobenzoyl-Gly) was also introduced between binding and chelating site to enhance excretion through renal system. DOTA-Abz-Gly-Gly-Cys-Gln-Trp-Ala-Val-Cha-His-Nle-Met-NH_2 was synthesized by solid phase following Fmoc/HBTU chemistry. Labeling with ^{99m}Tc and ^{68}Ga was performed by stannous-tartrate and in the presence of 2.5M NaOAc buffer (pH 4-5). In vitro cell-binding was conducted on MDA-MB-231, T47D breast and PC3 prostate cancer cell lines and pharmacokinetics was evaluated in balb/c mice at 1 and 4 h p.i.*Results and Discussion*: The structure of DOTA-BN was confirmed by mass spectrometry and MALDI and its purity by HPLC. BN analog labeled efficiently with ^{99m}Tc/^{68}Ga under mild conditions (labeling efficiency ~90%) as confirmed by HPLC. Tumor cell binding indicated the high affinity and specificity of ^{99m}Tc/^{68}Ga-BN towards breast and prostate cancer cell lines with binding affinity below 25nM. Also significant internalization (~20%) into breast and prostate cancer cells was observed. In mice ^{99m}Tc/^{68}Ga-BN exhibited a rapid clearance from the blood and excretion by renal route

(~67% ID) possibly due to the presence of a hippurate-like moiety in the peptide. Likewise a low uptake and retention by the kidneys was observed (<4% ID/g). The enhanced urinary excretion and low hepatobiliary clearance suggest the pronounced effect of hippurate-like spacer on the biokinetics. The uptake in the lungs, stomach, liver, intestines and pancreas was low (<5% ID/g) both at 1 and 4 h p.i.*Conclusion*: The findings of our initial study suggest that BN peptide under investigation holds certain promising in vitro/in vivo properties as a tumor targeting agent and seems a potential candidate for further evaluation. Tumor targeting studies in xenografts models are in progress and will be reported.

P168

Monitoring of re-differentiation effect of radio-iodine refractory thyroid cancer using the new tracer F-18-TFB

J. Nagarajah, A. Boländer, C. Irwin, J. A. Fagin, W. A. Weber; MSKCC, New York, NY, UNITED STATES.

Background: Re-differentiation through inhibition of MAPK pathway is a promise attempt to treat progressive radio-iodine refractory thyroid cancer. However, it is challenging to select the optimal time window to apply I-131 to those patients. F-18-TFB is a new tracer, which binds to sodium-iodine-symporter (NIS) and can be used to image the expression of this symporter. Aim: Monitoring of the re-differentiation effect of mice with knock-in BRAFV600E thyroid cancer (TPO-Cre/LSL-BRAF-V600E mice) treated with AZD6244 (MEK-inhibition) and CKI27 (MEK and BRAF inhibition) using F-18-TFB. Method: Three groups of mice (group 1: AZD6244 50 mpk, group 2: CKI27 1.5 mpk and group 3: vehicle; each n=5) were treated for 22 days. All mice underwent ultrasound volumetry of thyroid on day 0, 5, 16 and 22, respectively. F-18-TFB was synthesized according to Jauregiu-Osoro et al. and PET scans were performed on day 0, 1, 2, 4, 9, 12 and 21, respectively using a dedicated animal PET/CT (Inveon, Siemens) about 30 minutes after injection of about 4 MBq F-18-TFB. Results: Ultrasound: Group 1 and 2 showed on average a thyroid volume reduction from day 0 to 6 (47.4 to 31.5 mm3 and 41.7 to 20.7 mm3, respectively) whereas the volume in group 3 remained rather unchanged (41.9 to 40.0 mm3). On day 22 the thyroid volume of group 1 increased to 50.6 mm3 and of group 2 to 27.3 mm3 whereas the group showed no change (42.1 mm3). F-18-TFB: The volume corrected average uptake (calculated in %ID/mm3) data showed an increase of F-18-TFB up to about 9-12 days after begin of treatment and a decrease to day 21 in both treated groups. The group 2 (CKI27) showed remarkable higher uptake values than the group 1 (AZD6244). The following numbers are given in %ID/mm3 for the seven F-18-TFB scanning time points. Group 1: 78; 100; 78; 116; 128.8; 99; 158. Group 2: 78; 206; 208; 318; 159; 214; 181. Group 3: 45; 72; 83; 80; 91; 67; 73. Conclusion: Treatment of radio-iodine refractory thyroid cancer with MEK/BRAF inhibitors show different level of NIS expression in a time dependent manner. F-18-TFB is therefore suitable to select an optimal time window to perform I-131 treatment.

P169

18F-FLT versus 18F-FDG for the assessment of therapeutic response to a BRAF inhibitor in a melanoma xenograft model

L. S. Vercellino[1], A. Martineau[1], C. Lebbé[2,3], E. Barré[1], F. Cartigny[1], S. Mourah[4,3], P. Merlet[1,3]; [1]Service de Médecine Nucléaire Hôpital Saint Louis Assistance Publique Hôpitaux de Paris, Paris, FRANCE, [2]Service d'Onco-dermatologie Hôpital Saint Louis, Paris, FRANCE, [3]Université Paris-Diderot, Paris, FRANCE, [4]Laboratoire de Pharmacologie Génétique Hôpital Saint Louis, Paris, FRANCE.

Aim: To evaluate the therapeutic response to a BRAF inhibitor of a model of a melanoma xenograft with molecular imaging. To compare the relevance of 18F-FLT and 18F-FDG micro PET/CT for this therapeutic evaluation. Materials and methods: Xenografts were obtained by injecting 5*10^6 BRAF mutated human melanoma cells A375 subcutaneously in nude mice. When tumours became palpable, baseline micro PET imaging was performed. Mice were imaged with 18F-FLT, then with 18F-FDG on the following day. 18F-FLT and 18F-FDG were injected intravenously, and a 90 minutes dynamic acquisition was performed. Mice were then treated by a BRAF inhibitor, dabrafenib, at the dose of 100mg/kg given orally once daily for 14 days. At the end of treatment a second imaging session (micro PET/CT with 18F-FLT then FDG) was perfomed. Mice were then sacrificed and tumours harvested for further histological and immnuno-hisotological analysis. Mean relative tumour volume (RTV) was calculated, by establishing a ratio between the size of tumours before onset of treatment and at the end of the treatment period. Initial image analysis was performed by determining the SUVmax within the tumours and SUVmean in the liver at 60 minutes post-injection. The ratio of SUVmaxTumour/SUVmeanliver was then calculated. Results: Mean RTV at day 15 was 2.23 in the control group, and 1.17 in the dabrafenib-treated group. In the control group mean FDG SUVmax was 1.1 and remained stable at day 15. In the treated group mean FDG SUVmax at baseline was 1.55, and 0.85 at day 15, with a mean decrease of SUVmax of 38%. The SUVmaxTumour/SUVmeanliver ratio increased by 4% in the control group, whereas it decreased of 26% in the treated group. For the FLT studies, imaging analysis yielded the following results: in the control group mean baseline SUVmax was 1.77, and

increased to a mean 2.3 at day 15, with a mean increase of 32%. The SUVmaxTumour/SUVmeanliver ratio increased of 21%. In the dafrafenib treated group mean baseline SUVmax was 1.98 and increased to a mean 2.4, corresponding to a mean increase of 16%, whereas the SUVmaxTumour/SUVmeanliver ratio increased of 6%. Conclusion: Our preliminary results show that tumours treated by dabrafenib had a slower progression than control and a decrease of FDG uptake, whereas no significant modification of FLT uptake was observed with static imaging. Further analysis of FLT dynamic imaging data and confrontation to histological data may provide additional information on this tracer relevance in this setting.

P170

Evaluation of 99mTc-duramycin for imaging conatumumab-induced tumor apoptosis: a comparative study with 18F-FDG

F. Elvas[1,2], C. Vangestel[1,2], N. Challouk[1], K. Y. Pak[3], S. Staelens[1], S. Stroobants[1,2], L. wyffels[1,2]; [1]University of Antwerp, Wilrijk, BELGIUM, [2]University Hospital Antwerp - Department of Nuclear Medicine, Edegem, BELGIUM, [3]Molecular Targeting Technologies, Inc., West Chester, PA, UNITED STATES.

Aim: Early assessment of response to cancer therapy represents one of the biggest challenges in oncology. 18F-FDG is currently the gold standard for tumor detection and therapy evaluation within clinical nuclear medicine. However, it has some limitations such as uptake in inflammatory cells and thus it lacks specificity. Imaging of cell death offers a more specific tool for treatment evaluation. Duramycin is a polypeptide that selectively binds to phosphatidylethanolamine (PE) in apoptotic and necrotic cells. Our group has recently demonstrated that 99mTc-duramycin is able to selectively detect chemotherapy-induced cell death in a mouse model of colorectal cancer(1). In the current study we further explored the potential of 99mTc-duramycin for early therapy response evaluation using conatumumab, a fully human monoclonal antibody directed against human DR5 that induces apoptosis in sensitive tumor cells.Materials and Methods: Colo205 cells (1.0E6) were injected subcutaneously in the right hind leg of female CD1 nu/nu mice aged 6-7 weeks. When the tumors reached 182 mm^3, baseline 99mTc-duramycin (37MBq) static SPECT-CT (4 h post radiotracer injection) and 18F-FDG (18.5MBq) PET-CT scans (30 min post radiotracer injection) were performed. The next day conatumumab or IgG1 control antibody (30μg; Amgen Inc., USA) were administered by intraperitoneal injection (n=4/group). Twenty-four hours after treatment, the animals underwent static 99mTc-duramycin SPECT-CT (n=4) and 18F-FDG PET-CT imaging (n=2). Radiotracer uptake in the tumors was obtained by γ-counting of the tumors (%ID/g) and will be quantified from the SPECT and PET images. Cell death in the tumors will be determined by cleaved caspase-3 (CC3) and TUNEL staining.Results: No difference was found between the volumes of treated tumors and controls. A significantly increased 99mTc-duramycin uptake was detected in conatumumab treated tumors (6.7-fold increase; p=0.002) compared to IgG1 treated tumors while 18F-FDG uptake was decreased compared to the controls (2.8 ± 0.57%ID/g vs 5.5 ± 2.0%ID/g; non-significant). The regional distribution of 99mTc-duramycin in the tumors will be determined by autoradiography and will be correlated to histology results.Conclusion: We demonstrated that 99mTc-duramycin specifically accumulates in conatumumab-responding tumors. 99mTc-duramycin is potentially a more specific alternative to 18F-FDG for early assessment of response to therapy.1.Elvas F, Vangestel C, Rapic S, Verhaeghe J, Gray B, Pak K, et al. Characterization of [99mTc]Duramycin as a SPECT Imaging Agent for Early Assessment of Tumor Apoptosis. Molecular imaging and biology : MIB. April 2015. doi: 10.1007/s11307-015-0852-6. PubMed PMID: 25896815.

P171

Development of short and specific MC1R-targeted DOTA-conjugated peptide tracers for PET imaging of melanoma xenografts

J. Körner[1], J. Castillo Gómez[2], N. Beindorff[2], E. Koziolek[2], V. Prasad[2], B. Wiedenmann[1], W. Brenner[2], **C. Grötzinger**[1]; [1]Charité - Universitätsmedizin Berlin, Gastroenterology, Berlin, GERMANY, [2]Charité - Universitätsmedizin Berlin, Nuclear Medicine, Berlin, GERMANY.

Aim: Cutaneous malignant melanoma is one of the most lethal forms of cancer. Its incidence is increasing rapidly, making it a significant public health threat. The most important approach for improvement of survival of patients still remains early diagnosis. The melanocortin receptor 1 (MC1R) is overexpressed in most melanomas making it a promising molecular target for both diagnosis and therapy. Because of their very low molecular weight, and hence their low immunogenicity and excellent tumor penetration, radiopeptides have attracted steadily increasing interest in receptor-mediated tumor targeting. Aim of this study was the development of short and specific MC1R-targeted tracers with an improved serum half-life for nuclear in vivo imaging with positron emission tomography. Materials and Methods: Structure-activity relationship of more than 80 short peptides was investigated in functional cyclic AMP and radioligand receptor binding assays. Next to an optimized specificity and affinity towards the target, an improvement of the serum half-life of the short peptides was sought-after. Therefore, stability against serum or

plasma peptidases was analyzed by HPLC. Specific and affine peptide ligands for the G protein-coupled receptor MC1R were obtained. The most promising tracers were coupled to DOTA (1,4,7,10-tetraazacyclododecane-1,4,7,10-tetraacetic acid) for later nuclear imaging applications. DOTA was conjugated to various sites of the peptide and its impact towards specificity and affinity was investigated. Several human and murine tumor cell lines were screened by using radioligand binding assays for their potential use as positive (MC1R expressing) or negative control (lack of MC1R) for in vivo PET imaging. Results: We developed several peptide tracers with a high affinity towards our target MC1R (subnanomolar Ki). These novel molecules show clear improvements over the naturally occurring α-Melanocyte stimulating hormone in terms of size (<2 kDa), stability (>2 h) and in particular specificity (>3000x towards the other 4 MC receptors). DOTA conjugation, for nuclear imaging, had virtually no negative impact on specificity or affinity. The in vitro binding of our tracers to several human and murine tumor cell lines could be shown. Next to the known MC1R-overexpressing tumor entity of cutaneous melanoma we identified several other cell lines from conjunctival melanoma and neuroendocrine tumors. Results of biodistribution and PET/MR imaging studies in mouse xenografts will be presented. Conclusion: These new molecules should enable MC1R-specific PET imaging in the future. Acknowledgement/ReferencesThis study was supported by a grant from the German Federal Ministry of Education and Research (BMBF), Unternehmen Region 03IPT614A.

P172

Evaluation of [18F]BR420 and [18F]BR351 as potential PET radiotracers for MMP-9 imaging in a colorectal cancer tumor model

N. Vazquez[1,2], S. Missault[1], C. Vangestel[1,2], D. Thomae[1,2], P. Van Der Veken[1], S. Staelens[1], S. Dedeurwaerdere[1], **w. Leonie**[2]; [1]University of Antwerp, Antwerp, BELGIUM, [2]University Hospital Antwerp, Antwerp, BELGIUM.

Aim: Matrix metalloproteinases (MMPs) are a family of Zn-dependent endopeptidases involved in the proteolytic degradation of components of the extracellular matrix. Their expression is known to increase in various inflammatory, malignant and degenerative diseases. MMP-9 is of particular interest for its potential contribution to cancer invasion and metastasis[1]. The purpose of this study was to evaluate the potential of [^{18}F]BR420[2] and [^{18}F]BR351[3] for *in vivo* visualization of MMP-9 in a Colo-205 tumor model. Materials and Methods: [^{18}F]BR420 was synthesized on a Veenstra FluorSynthon I synthesis module that was adapted for fully automated production of the radiotracer via a novel one-step synthesis strategy. [^{18}F]BR351 was synthesized following a published methodology[3]. Xenografts bearing MMP-9 expressing Colo 205 tumors were injected with [^{18}F]BR420 (150 μCi, n =4 or 1 mCi, n =1) or [^{18}F]BR351 (100-200 μCi, n =5). They underwent a 60min dynamic μPET scan followed by static scans at 2h and 4h post injection (pi). Tumor uptake was determined on PET images (SUV_{mean}) and *ex vivo* by γ-counting. MMP-9 expression was evaluated by immunohistocheistry (IHC) and in sity zymography (ISZ). Results: [^{18}F]BR420 and [^{18}F]BR351 were obtained in good radiochemical yield (15.51±3.40% and 12.4±2.6%, respectively, decay corrected to EOB), with specific activities ranging between 37 and 311 GBq/μmol (EOS) and high RCP (>98%). μPET imaging indicated the highest tumor uptake for [^{18}F]BR420 at 2h pi (SUV_{mean}=0.49g/cc) and at 11min (SUV_{mean}=0.36g/cc) pi for [^{18}F]BR351. However, metabolite analysis indicated rapid metabolism of [^{18}F]BR351 with only 19.44±6.18% intact tracer remaining in plasma at 15min pi. [^{18}F]BR420 was more stable with 79.56±3.12% intact remaining in plasma at 2h pi. IHC and ISZ confirmed MMP-9 expression in the tumors. Conclusions: Both, [^{18}F]BR420 and [^{18}F]BR351 bind to MMP-9 expressing tumor tissue and might be promising PET radiotracers for *in vivo* imaging of MMP-9 in tumors and other MMP-9 related disorders. References:[1]Mook, OR et al. Biochim. Biophys. Acta, 2004, 1705, 69-89. [2]Breyholz HJ et al. ChemMedChem. 2010, 5, 777-789. [3]Wagner S et al. J. Med. Chem. 2007, 50, 5752-5764.

P173

Estimation of tumour volumes by [11C]MeAIB and [18F] FDG PET in an orthotopic glioblastoma model

C. Aaberg-Jessen[1], B. Halle[2,3,4], H. Thisgaard[1,4], S. Hvidsten[1], J. H. Dam[1], A. S. Thykjær[4], P. F. Høilund-Carlsen[1,4], M. K. Schulz[2], C. Andersen[2], B. W. Kristensen[3,4]; [1]Odense University Hospital, Department of Nuclear Medicine, Odense, DENMARK, [2]Odense University Hospital, Department of Neurosurgery, Odense, DENMARK, [3]Odense University Hospital, Department of Pathology, Odense, DENMARK, [4]University of Southern Denmark, Institute of Clinical Research, Odense, DENMARK.

Introduction: Brain tumour volume assessment is a diagnostic challenge. Positron emission tomography (PET) may be a promising modality for this. We compared the agreement between PET- and histology-derived tumour volumes in an orthotopic glioblastoma model with a solid non-infiltrating (U87MG) and a non-solid, highly infiltrating (T87) tumour phenotype. Methods: Rats with U87MG- and T87-derived glioblastomas were continuously PET scanned for 1 hour immediately after injection of [11C]methylaminoisobutyric acid ([11C]MeAIB). One hour later, [18F]fluorodeoxyglucose

([18F]FDG) was injected followed by a 3 hour dynamic PET scan. Images were reconstructed using ordered subset expectation maximization in two dimensions (OSEM2D) and maximum a posteriori in three dimensions (MAP3D) algorithms. In addition, a parametric image, encompassing the entire tumour kinetics in one single image, was calculated based on the [11C]MeAIB images. All reconstructed images were segmented by fixed thresholding of maximum voxel intensity (VImax) and based on mean background intensity (MBI). The agreement between PET- and histology-derived tumour volumes and intra- and inter-observer agreement of the PET-derived volumes were evaluated using Bland-Altman plots. Results: By PET, the mean U87MG tumour volumes were 35.0 mm3 and 34.1 mm3 using [18F]FDG and [11C]MeAIB, respectively, and 33.7 mm3 by histology ($p<0.999$). For T87, corresponding volumes were 122.1 mm3, 118.3 mm3, and 125.4 mm3, respectively ($p<0.999$). The best agreement, between PET- and histology-derived U87MG tumour volumes was achieved with [11C]MeAIB, MAP3D reconstruction, and fixed thresholding of VImax (95% LOA -9.8-7.9, bias -1.0, SD of bias 4.5, R2 0.994). For T87 tumours, the best agreement was obtained using [18F]FDG, MAP3D reconstruction, and fixed thresholding of MBI (95% LOA -46.1-52.6, bias 3.2, SD of bias 25.2, R2 0.814). The agreement when using [11C]MeAIB, parametric imaging and fixed thresholding of VImax was slightly inferior, while the intra- and inter-observer agreement was superior. The histological intra-observer agreement was high for U87MG (95% LOA -1.7-1.0, bias 0.3, SD of bias 0.7, R2 0.998) and T87 tumours (95% LOA -16.0-14.4, bias 0.8, SD of bias 7.7, R2 0.998). The inter-observer agreement was equally high for U87MG (95% LOA -1.8-2.3, bias 0.3, SD of bias 1.0, R2 0.976) and T87 tumours (95% LOA -6.1-9.6, bias 1.7, SD of bias 4.0, R2 0.992). Conclusion: Volume estimation of solid non-infiltrating brain tumours by PET was accurate and reproducible, whereas volume estimation of non-solid infiltrating brain tumours was difficult and hard to reproduce. PET evaluation of infiltrating brain tumours should be further developed.

P174

Identification of a set of imaging procedures for the accurate assessment of tumour progression and response to treatment in a Glioma animal model

C. Martelli[1,2], S. Valtorta[3,4], L. S. Politi[5], R. Isabella[4,6], D. Cecilia[7,8], B. Sara[3,4], S. Sudati[4], G. Di Grigoli[4,3], **G. Lucignani**[9,10,2], R. M. Moresco[3,6], L. Ottobrini[7,2,3]; [1]University of Milan, Segrate, ITALY, [2]Centre of Molecular and Cellular Imaging-IMAGO, University of Milan, Segrate, ITALY, [3]IBFM-CNR, Segrate, ITALY, [4]Experimental Imaging Center, IRCCS San Raffaele Scientific Institute, Milano, ITALY, [5]Neuroradiology Department & Neuroradiology Research Group, IRCCS San Raffaele Scientific Institute, Milano, ITALY, [6]Department of Health Sciences, University of Milano-Bicocca, Milano, ITALY, [7]Department of Medical-Surgical Physiopathology and Transplants, University of Milan, Segrate, ITALY, [8]Supported by a fellowship from the Doctorate School of Molecular Medicine, University of Milan, Segrate, ITALY, [9]Department of Health Sciences, University of Milan, Milano, ITALY, [10]San Paolo Hospital, Department of Diagnostic Services, Unit of Nuclear Medicine, Milano, ITALY.

AIM: Glioma represents the most aggressive primary brain tumour characterized by wide necrotic areas, resistance to therapy, high invasiveness and a poor prognosis for the patient. Hypoxia is considered a major driving force for glioma progression and HIF-1α plays a crucial role in this context. The gold standard therapy is temozolomide (TMZ) associated to radiotherapy but the prognosis remains poor. Its efficacy relies only upon the evaluation of MGMT promoter methylation even if it is not fully predictive of patient response to treatment. Here we aimed at identifying non-invasive potentially theragnostic biomarkers involved in the regulation of tumour growth and response to treatment for early assessment of tumour sensitivity to specific therapeutic regimens using in vivo imaging strategies in a mouse model of glioma. METHODS: Orthotopic murine model was obtained by stereotaxic injection glioma cells (U251-HRE expressing Luciferase reporter gene under the control of multiple copies of an hypoxia responsive element) in female nude mice of 7-8 weeks of age (d0). Animals at 21 days from cell injection were subdivided in control (vehicle) and treated (temozolomide, 400 mg/kg o.s.) groups. Tumor growth was monitored in vivo with MRI, BLI and FLI before and after (2 and 7 days) treatment. Moreover, ex vivo preliminary studies were performed using autoradiography with [99mTc]HMPAO and [99mTc]MIBI. As regards MRI it was performed on a Bruker Pharmascan instrument equipped with a 7.0 T horizontal magnet. Images sequences of 1h of the coronal plane were acquired as follows: EPI-DTI (Diffusion Tensor), Turbo Spin Echo T2, Rare T1 Map, Dynamic Contrast Enhancement (DCE) Dynamic Susceptibility Contrast (DSC) and T1 post-contrast (0.2 μL/g of gadobutrole). All BLI/FLI acquisitions were carried out with IVIS SPECTRUM/CT instrument. HypoxiSense680 fluorescent probe and IntegriSense750 were intravenously administered to mice and after 24 h, fluorescence imaging (FLI) was performed. RESULTS: Temozolomide treatment induced a reduction of tumour volume reported by MRI and autoradiography one week after treatment. Treatment efficacy was detectable using also DWI and DCE sequences. [99mTc]MIBI uptake resulted significantly lowered after TMZ treatment allowing the identification of responsive tumours. These data correlate with those already obtained by BLI and FLI. CONCLUSIONS: This study suggests that

U251-HRE orthotopic murine model may be proposed as a predictive and reliable tool to evaluate processes involved with HIF-1α activity. Clinically translational procedures as MRI sequences and [99mTc]MIBI-SPET could be useful markers for tumour progression and early response to treatment.

P175

Longitudinal evaluation with High Frequency Ultrasound imaging of response to CXCR4 new cyclic peptide antagonist with conventional chemotherapy in colorectal cancer mice model

A. Greco[1,2], C. D'Alterio[3], L. Auletta[4], S. Albanese[5,2], M. Napolitano[3], L. Portella[3], S. Santagata[3], C. Ieranò[3], A. Brunetti[1], S. Scala[3], A. Zannetti[6]; [1]Dipartimento di Scienze Biomediche Avanzate, Università degli studi di Napoli Federico II, Napoli, ITALY, [2]CEINGE scarl, Naples, ITALY, [3]National Cancer Institute, "Fondazione G. Pascale", Napoli, ITALY, [4]IRCCS SDN, Napoli, ITALY, [5]Università degli Studi di Napoli Parthenope, Napoli, ITALY, [6]Institute of Biostructures and Bioimages of the National Council of Research, Napoli, ITALY.

Introduction CXCR4 plays a key role in the progression and metastatization of many tumors. The prognostic role of CXCL12/CXCR4–CXCR7 was previously shown in colorectal cancer (CRC) (1). Recently, a new family of CXCR4 inhibitors that showed anti-tumor activity has been developed and characterized (2). High frequency ultrasound (HFUS) is a non invasive, cost-effective, imaging modality that allow longitudinal evaluation of xenograft tumor in mice models. Aim of the present study is to evaluate the effect on tumor growth and angiogenesis of anti-CXCR4 Peptide R alone or combined with conventional chemotherapy in mice model of colorectal cancer.Materials and methodsAthymic balb/C nude mice, 5-6 weeks old (4 mice/group) were subcutaneously injected with human colorectal cancer cell lines HCT116 ($2x10^6$). Tumor volume (TV) was measured using the electronic caliper integrated on 2D ultrasonographic images. The HFUS procedure was performed under general anaesthesia with isoflurane and oxygen. The 3D integrated software associated with color doppler was used to monitor the antiangiogenic effects of the therapy. Treatment groups were: 1) Peptide R alone [5 mg/kg]; 2) 5FU [30 mg/kg] + OX [4.2 mg/kg]; 3) 5FU [30 mg/Kg] + OX [4.2 mg/kg] + Pep R [5mg/kg]; 4) PBS [100 μL/mice]. All therapies were administered i.p. daily, 5 days/week for 2 weeks.Results and discussionHFUS showed larger tumors in controls compared to all treated groups. Group 3) had smaller TV compared to both groups 1) and 2). The 3D reconstruction software showed a reduction of angiogenesis in all treated groups compared to the controls. Combination treatment of conventional chemotherapy with Peptide R determined a dramatic reduction in primary tumor growth. Nonetheless, both chemotherapy alone and Peptide R alone inhibited primary tumor growth, suggesting that the Peptide could act on all cells overexpressing CXCR4 involved in the tumor microenviroment.Conclusions: Our study showed that CXCR4 new antagonist Peptide R, alone or in combination with conventional chemotherapy, caused a reduction of CRC growth in mice model. Imaging by HFUS demonstrated to be feasible for longitudinal studies and it gave intriguing informations on tumor growth as well as on angiogenesis, in response to anticancer therapy.1)D'Alterio C. et al. 2014, Int. J. Cancer: 135, 379–3902)Portella L. et al. 2013, PLoS One 8(9): e74548

P176

Establishment of a Chinese Lung Adenocarcinoma Cell Line CPA-Yang1 with Osteolytic, Brian Metastases Properties by Molecular Imaging

C. Chang, B. Lei, C. Liu, J. Cao, G. Tao, G. Tao, W. Xie, W. Xie, S. Yang, S. Yang; Shanghai Chest Hospital, Shanghai, CHINA.

Establishment of a Chinese Lung Adenocarcinoma Cell Line CPA-Yang1 with Osteolytic, Brian Metastases Properties by Molecular ImagingCheng Chang, Bei Lei, Ciyi Liu, Jie Cao, Guangyu Tao, Wenhui Xie, Shunfang YangAim: To establish a Chinese lung adenocarcinoma cell line with complicated metastases potency.Methods: The cell came from the pericardial effusion of a fifty years old male patient with lung adenocarcinoma and diagnosis of metastasis in temporal bone and temporal lobe by CT. Primary culture the cells were obtain success after three days. Approximately 0.8 x 106 cancerous cells were injected into left cardiac ventricle or tail vein of immunodeficient mice, respectively. Combination of micro pinhole bone scintigraphy, micro SPECT/CT, micro PET/CT scanners, magnetic resonance imaging (MRI) and human conventional radiography (X ray).The gene expression was measured by cRNA microarray and real-time quantitative PCR.Result: Start to appear lower limb paralysis and spine swelling deformation in the mice after inoculation three weeks. The temporal lobe brain metastasis was appeared six weeks later. Combination of micro pinhole bone scintigraphy, micro SPECT/CT, micro PET/CT scanners, magnetic resonance imaging (MRI) and human conventional radiography (X ray) can not only sensitive to detect the lesions but also identify the type of bone metastasis (BM), osteoblastic, osteolytic or mixed BM. Affymetrix U133 plus 2.0 gene chips with 54675 probe sets and RT-PCR were used to select and confirm expression of the genes. It's important that lung cancer, especially lung adenocarcinoma, frequently develops osteoblastic and mixed BM, rare pure osteolytic and brain

metastases in immunodeficient mice. TFF1 and CDH1 maybe is a novel candidate gene involved in osteolytic and brain metastases for lung adenocarcinoma, respectively.Conclusion: Self-established Chinese lung adenocarcinoma cell line is a highly published immortalized human blood-brain barrier (BBB) and osteolytic metastases cell line. That is a suitable model of BBB physiology and osteolytic metastasis. This is a crystal of our scientific research and the precious wealth of all mankind.

P177

Development of a DOTA-conjugated peptide tracer targeted against gastric inhibitory polypeptide (GIP) receptor for PET imaging of neuroendocrine tumor xenografts

J. Körner[1], J. Castillo Gómez[2], N. Beindorff[2], E. Koziolek[2], V. Prasad[2], B. Wiedenmann[1], W. Brenner[2], **C. Grötzinger**[1]; [1]Charité - Universitätsmedizin Berlin, Gastroenterology, Berlin, GERMANY, [2]Charité - Universitätsmedizin Berlin, Nuclear Medicine, Berlin, GERMANY.

Aim: To improve the overall survival of cancer patients, an early and sensitive diagnosis is pivotal. In neuroendocrine tumor (NET) patients the finding of overexpressed somatostatin receptors and the use of somatostatin peptide analogues has led to a vast improvement in diagnosis and therapy. Unfortunately, only around two thirds of the tumors show the desired high uptake in somatostatin receptor scintigraphy. There is an urgent need for novel molecular targets in NETs. The aim of this work was to identify new target structures in neuroendocrine tumors for the use in clinical diagnostic and therapeutic applications. After validation of an overexpressed receptor, the development of a DOTA-conjugated peptide tracer was conducted for future use in positron emission tomography. Materials and Methods: A microarray-based approach was used to identify overexpressed G protein-coupled receptors in pancreatic NET samples. A high expression similar to somatostatin receptor 2 was found for the Gastric inhibitory polypeptide receptor (GIPR) and validated in real-time qPCR experiments. Neuroendocrine cell lines were investigated for their functional expression of GIPR in cyclic AMP and radioligand-receptor binding assays. The natural occurring ligand GIP1-42 was modified to enhance its size and serum- and plasma stability while maintaining its low nanomolar affinity towards GIPR. Stability was investigated by incubation in serum or plasma and analysis of the intact peptide in reverse phase HPLC. Binding constants were determined by in vitro radioligand receptor studies with GIPR expressing cells. Results: We identified gastric inhibitory polypeptide receptor (GIPR) as overexpressed in pancreatic and ileal neuroendocrine tumors (more than 30 fold compared to surrounding tissue). The mRNA expression levels were comparable to the gold standard SSTR2. In a following step, the development of tracer molecules for PET imaging was advanced. In parallel, neuroendocrine tumor cells were screened for a functional GIPR expression. We were able to identify two of six tested cell lines which react to a GIP stimulus. Results of biodistribution and imaging studies using DOTA conjugates will be presented. Conclusion: Gastric inhibitory polypeptide receptor represents a novel molecular target for neuroendocrine tumors. Development of DOTA-conjugated GIP analogues can be utilized in new diagnostic approaches for nuclear imaging and therapy such as PET and PRRT. Acknowledgement/References: This study was supported by a grant from the German Federal Ministry of Education and Research (BMBF), Unternehmen Region 03IPT614A.

P178

Biological characterisation and [^{18}F]FDG microPET/CT monitoring of relevant orthotopic preclinical models of malignant pleural mesothelioma

D. J. Colin[1], C. D'Amato-Brito[2], S. Germain[1], F. Triponez[2], Y. Seimbille[3], V. Serre-Beinier[2]; [1]Centre for Biomedical Imaging, University of Geneva, Geneva, SWITZERLAND, [2]Thoracic Surgery Unit, University Hospitals and University of Geneva, Geneva, SWITZERLAND, [3]Cyclotron Unit, University Hospitals of Geneva, Geneva, SWITZERLAND.

Aims: Malignant Pleural Mesothelioma (MPM) is an asbestos-related cancer and one of the most resistant and aggressive cancer. Its incidence is still increasing especially in countries lacking worker protection and persisting with asbestos use. Early diagnosed MPM is primarily treated by surgery, but the best current palliative treatment (cisplatin and pemetrexed) for patients with invasive MPM allows a median survival of only 9 to 18 months from diagnosis. Conversely, no relevant orthotopic models in rodent which could be non-invasively monitored have been described to date. This work describes the *in vivo* 1) tumorigenicity of four human and one mouse MPM cell lines injected subcutaneously or into the pleural cavity of immunodeficient or syngeneic mice; 2) phenotypes of the subcutaneous and or orthotopic MPM tumours; 3) growth monitoring by 2-deoxy-2-[^{18}F]fluoro-*D*-glucose ([^{18}F]FDG)-microPET and CT scans. Materials and methods: MPM human H28, H2052, MSTO-211H, JL-1 and mouse AB12 cells were cultured *in vitro* according to standard described procedures, and injected subcutaneously or orthotopically into the pleural cavity of athymic BALB/c mice (for human cells) or of syngeneic BALB/c mice (for AB12 cells). Epithelioid and sarcomatoid phenotypes, growing properties and vasculature of MPM tumours were analysed by RT-qPCR, western blotting and immunohistochemistry.

[^{18}F]FDG-microPET/CT scan was used to monitor the growth of the different models. Results: MSTO-211H and AB12 tumours grew similarly and quickly when injected subcutaneously or orthotopically; JL-1 cells produced fast growing subcutaneous tumours but slow growing orthotopic tumours; H2052 cells grew very slowly in both sites of injection; H28 cells did not generate viable tumours. Although tumorigenic-fast growing H2052-derived cells could be derived from initial orthotopic tumours, no growing models could be isolated from H28 cells even in highly immunodeficient SCID mice. Phenotypic analyses showed that all the tumours contained epithelioid and sarcomatoid malignant cells expressing calretinin and vimentin proteins. Orthotopic MPM tumours as small as 1 mm^3 could be detected by microPET/CT. The [^{18}F]FDG mean SUVs increased in a growth-dependent manner and the tumour-to-muscle ratios above 8 allowed a good visualisation of the tumours in all the models. Conclusions: Three models of relevant orthotopically xenografted human MPM models in immunodeficient mice were developed. Moreover, a syngeneic murine AB12 model which would preserve immune properties is described. These models mostly showed biphasic phenotypes *in vivo*. The use of [^{18}F]FDG-microPET/CT scan allowed the monitoring of their development and could therefore serve to non-invasively study new therapeutic strategies of MPM in preclinical settings.

P179

The impact of single or dual NEP/ACE-inhibition on the performance of 99mTc-labeled neurotensins in mice bearing human WiDr xenografts

T. Maina[1], A. Kaloudi[1], E. Lymperis[1], A. Tatsi[1], E. P. Krenning[2], M. de Jong[2,3], B. A. Nock[1]; [1]Molecular Radiopharmacy, INRASTES, NCSR Demokritos, ATHENS, GREECE, [2]Institute of Nuclear Medicine, Erasmus MC, ROTTERDAM, NETHERLANDS, [3]Instistute of Radiology, Erasmus MC, Rotterdam, NETHERLANDS.

Aim: The neurotensin (NT) radiotracers ^{99m}Tc-DT1 ([^{99m}Tc-N$_4$-Gly^7]NT(7-13)) and ^{99m}Tc-DT6 ([^{99m}Tc-N$_4$-βAla^7,Dab^8,Tle^{12}]NT(7-13)) were previously studied for potential use in the imaging of human tumors expressing the NT subtype 1 receptor (NTS1R). Despite the higher stability of double-stabilized ^{99m}Tc-DT6 in vitro, the radiotracer failed to reliably visualize NTS1R-positive lesions in patients, presumably due to rapid in vivo degradation. Neutral endopeptidase (NEP) and angiotensin converting enzyme (ACE) have been implicated in the degradation of NT analogs. In the present study, we report the effects induced by coinjection of the NEP-inhibitor phosphoramidon (PA), or the ACE-inhibitor Lisinopril (Lis), or both PA+Lis with ^{99m}Tc-DT1 or ^{99m}Tc-DT6 on radiotracer profile in mice bearing human WiDr xenografts. Materials and Methods: Either ^{99m}Tc-DT1 or ^{99m}Tc-DT6 was coinjected in mice with: a) vehicle (control), or b) PA (300 μg), or c) Lis (100 μg), or d) PA+Lis (300 μg + 100 μg, respectively). Mouse blood collected 5 min post-injection (pi) was analyzed by HPLC to measure radiotracer degradation. Biodistribution for ^{99m}Tc-DT1 and for ^{99m}Tc-DT6 was performed at 4 h pi in SCID mice bearing human WiDr xenografts; mice were coinjected with vehicle or inhibitor, as described above. Results: ^{99m}Tc-DT1 was totally consumed in mouse circulation in 5 min, while >52% of ^{99m}Tc-DT6 was detected intact. Thus, double Arg^8/Dab^8 and Leu^{12}/Tle^{12} substitution in the native NT(8-13) motif improved stability. Treatment of mice with PA led to full stabilization of ^{99m}Tc-DT6, whereas only 25% of ^{99m}Tc-DT1 remained intact. On the other hand, only ^{99m}Tc-DT1 could profit from Lis (>16% intact) or both PA+Lis coinjection (56% intact). These results are in line with the uptake of each radiotracer in WiDr xenografts at 4 h pi. Thus, tumor uptake of partially stable ^{99m}Tc-DT6 in controls (1.7 ±0.3%ID/g) significantly increased by PA (3.9±0.7%ID/g), while no further improvement was observed with PA+Lis (3.5±0.3%ID/g). On the other hand, tumor uptake of unstable ^{99m}Tc-DT1 in controls (1.2±0.2%ID/g) advantageously increased with PA (4.6±0.5%ID/g) and with the PA+Lis combination it reached outstanding values (7.7±1.2%ID/g). Interestingly, the renal uptake of ^{99m}Tc-DT6 unfavourably increased by PA (from 6%ID/g to 12%ID/g), but remained low in the case of ^{99m}Tc-DT1 (<3%ID/g). Conclusions: This study has shown that in situ NEP and/or ACE inhibition represents a powerful tool to improve the bioavailability, tumor targeting and overall pharmacokinetics of NT(8-13)-based radiotracers without requiring time-consuming compound development. This approach warrants further validation in the field of NTS1R-targeted tumor imaging and therapy.

P180

μPET as non-invasive read-out for a novel human organotypic lung tumor model

D. Fecher[1], G. Dandekar[1], S. Nietzer[1], R. A. Bundschuh[2], H. Walles[1], A. K. Buck[3], M. Steinke[1], **K. Lückerath**[3]; [1]Uniklinik Würzburg, Department of Tissue Engineering and Regenerative Medicine, Würzburg, GERMANY, [2]Uniklinik Bonn, Nuclear Medicine, Bonn, GERMANY, [3]Uniklinik Würzburg, Nuclear Medicine, Würzburg, GERMANY.

Reliable in vitro tumor models are indispensable tools for tailored drug-development and -testing. To meet this demand, we developed a complex lung tumor test system based on decellularized rat lungs. As a prerequisite we established a decellularization protocol that preserves the lung architecture, important ECM components and the basement membrane. Human tumor cells seeded on our scaffold formed clusters,

exhibited an up-regulation of the carcinoma-associated marker mucin1 and a reduced proliferation rate.Furthermore, tumor nodules were detected and could be tracked over time employing 2-deoxy-2-[18F]fluoro-D-glucose positron emission tomography (FDG-PET)-imaging, a clinically-relevant method to monitor tumor growth and metabolism. This approach enabled non-invasive monitoring of a clinically applied targeted tyrosine kinase inhibitor therapy in the lung tumor model over a 72 h treatment period. Surprisingly, single tumor clusters showed diversity in response rates to the therapy in FDG-PET, indicating heterogeneity in the lung tumor model. Using dynamic PET acquisition with simulation of FDG bolus injection and a 3-compartment model with k4 equivalent to zero, FDG-kinetics were found to resemble those observed in living rodents with optimal tumor-background intensities after 60 min.Additionally, a lung specific bioreactor was designed mimicking the biomechanical pulmonary microenvironment which allowed revascularization of the lung scaffold with human endothelial cells.Thus, our organotypic lung tumor model should allow for preclinical testing of therapeutic regimens and the development of strategies against resistant sub clones. In combination with PET-imaging, longitudinal studies regarding tumor growth, metabolism and spread as well as monitoring of response to treatment are feasible.

P181

Realistic Multi-cellular Dosimetry for 177Lu labelled Antibodies: Model and Application

S. Marcatili[1], A. Pichard[2], A. Courteau[1], R. Ladjohounlou[2], I. Navarro-Teulon[2], A. Repetto-Llamazares[3], H. Heyerdahl[3], J. Dahle[3], J. Pouget[2], M. Bardiès[1]; [1]Centre de Recherche en Cancérologie de Toulouse, UMR 1037 INSERM, Toulouse, FRANCE, [2]Institut de Recherche en Cancérologie de Montpellier, U 1194 INSERM, Montpellier, FRANCE, [3]Nordic Nanovector ASA, Kjelsåsveien 168, Oslo, NORWAY.

Aim: Current preclinical dosimetric models often fail to give account of the complex nature of energy distribution in cells. For this reason survival is often expressed as a function of added activity rather than absorbed dose delivered to the cell/cell nucleus. We propose a multi-cellular dosimetric model that takes into account realistic cell distributions, for the establishment of survival curves as a function of the absorbed dose. Materials and Methods: We developed software tools for the generation of realistic 3D cell culture geometries based on experimentally determined parameters (cell density, cluster density, average cluster size). Non-overlapping multiple clusters and isolated cells were randomly placed in a cylindrical volume whose radius is of the order of the maximum range of beta particles emitted by 177Lu. The cumulated activity in the cell was also randomized according to experimentally predetermined values. The absorbed dose to the cell was calculated considering if the radioactivity was located a) within the cell (with different hypotheses of internalization or lack thereof); b) in the culture medium; and c) from surrounding cells. The absorbed dose to the cell/cell nucleus was also averaged over a large number of geometrical configurations. A mixture of Monte Carlo and analytical approach was applied in order to achieve as accurate as possible results while reducing calculation time. The model was applied to clonogenic survival experiments carried out with and without 177Lu labelling, to compare the efficacy of a novel antibody conjugate (BetalutinTM) for the treatment of non-Hodgkin lymphoma, to those of a CD20-specific (rituximab) and an antibody that not bind to B-cells (cetuximab) on 2 different cell lines (Ramos and DOHH2). Results: Most of the absorbed dose to the target cell was due to non-internalised radiation (half of the total absorbed dose). Cross-irradiation was twice as higher than self-irradiation. Radiopharmaceutical distribution within the cell had a negligible impact on the average cell absorbed dose. In the case of Ramos cells, survival expressed per Gy in the nucleus is independent of the vector (when corrected for unlabelled antibody toxicity), demonstrating that cell death mechanism is mainly radiative. For DOHH2 cell lines, survival curves expressed per Gy in the nucleus are still well separated, thereby indicating that cell death mainly depends on cold antibody toxicity. Conclusions: Our 3D cellular model allowed a better understanding of the radiative and non-radiative processes associated to cellular death in the case of clonogenic survival experiments with 177Lu labelled antibodies.

P182

Development of 47Scandium-Bleomycin and estimation of absorbed dose as an antibiotic tumor seeking radiopharmaceutical

L. Moghaddam-Banaem; Amirkabir Technical university, Tehran, IRAN, ISLAMIC REPUBLIC OF.

Introduction: Bleomycins are tumor seeking antibiotics that are used in cancer chemotherapy. We hereby report preparation, stability tests, biodistribution and dosimetry of ^{47}Sc-BLM as a potential therapeutic complex. Scandium-47 is a moderate energy β- emitter (T1/2 = 3.42d, $E_{\beta max}$= 441 keV , %68; $E_{\beta max}$= 600 keV ,%32). Because the availability of ^{47}Sc isotope is currently extremely limited, we have performed preliminary studies using instead ^{46}Sc which is chemically identical. Material and Methods: ^{46}Sc was produced with a specific activity of 3.15 mCi/mg and radionuclide purity of 98% . The radionuclidic purity of the solution was tested for the presence of other radionuclides using beta spectroscopy as well as HPGe spectroscopy for the detection of various interfering

beta and gamma emitting radionuclides. The radiochemical purity of the 46ScCl3 was checked using 2 solvent systems for ITLC (A: 10mM DTPA pH.5 aq. solution and B: %10ammonium acetate:methanol (1:1)). Bleomycin was prepared at activity of 1.258 MBq was administered to five mice that were euthanized at 4, 24, 48, 72 h post administration. The data were analyzed to estimate the human's organs uptake and source organ residence times and cumulated activities. The dose calculation and estimation was done for a certain group of organs of human following the MIRD technique. As the S-factor is relevant to the particle energy that emitted by radionuclide and the particle energies of ^{46}Sc is different from ^{47}Sc, for dose calculation the dose S-factor of ^{47}Sc was used. Results: The biodistribution studies carried out in Wistar rats. The estimated absorbed dos as percent of injected dose (%ID) is shown on table 1. The absorbed dose by organs are also estimated and shown in table 2. The maximum cumulative activities are for liver, blood, bone, spleen, lung and kidney with 23.52, 8.65, 4.06, 2.59, 1.44, 1.22 as percent of injected activity respectively. Conclusion: In the present study 46Sc - Bleomycin complex were prepared with high radiochemical purities (>98%) under optimized reaction conditions. The radiochemical purity was >99%. The radio-labeled complex was stable for 48 hours. A significant accumulation took place in liver, spleen and kidneys which is in accordance with the biodistribution of other reported radiolabeld bleomycin compounds. The estimation of 47Sc-BLM dose in human was performed. Keywords: Bleomycin, Scandium-47, Biodistribution, Dosimetry Table 1: Extrapolation of absorbed dose(%ID) in human

P183

The effect of 1-day melatonin and pulse magnetic field administration on PET/CT scan and testicular scintigraphy in a rat model of testicular torsion-detorsion

S. S. Gul, M. Uysal, S. Gurgul, F. Erdemir; Gaziosmanpasa university medicine faculty, Tokat, TURKEY.

Aim: Testis torsion is one of the important causes of acute scrotum in childhood. It is defined as obstruction of the blood flow to the testes and accessories depending on the rotation of the spermatic cord. Testicular torsion is an emergent clinical condition in which there is a reversible damage in the spermatogenetic cells with an immediate intervention within 6 hours while the risk of irreversible damage increases when this time period is exceeded. The aim of this study was to evaluate the effectiveness of 1-day melatonin and pulse magnetic field administration on ischemic damage in a rat model of testicular torsion-detorsion. Material-Methods: Rats were divided into 4 groups of control, sham, melatonin and pulse magnetic field. In all groups except for the control group, under general anesthesia, the left testis was rotated in clockwise for 720 degrees for a total of 2 hours. Then, 10mg/kg intravenous melatonin and pulse magnetic field for 4 hours were administered to melatonin and pulse magnetic field groups, respectively. Sham rats did not receive any treatment after the torsion. Following a 4-hour period, PET/CT was performed by using 1 mCi F-18 FDG and testicular scintigraphy was performed by using 1 mCi TC-99m pertecnetate (Figure 1). After the completion of the two imaging methods, left/right testicular rates were calculated by drawing the regions of interest (ROI) in the both testicular region. Moreover, histopathological examination of both testicular tissues was performed. Results: All groups were analyzed in terms of glucose metabolism and perfusion. There was a significant scintigraphic difference between the control and sham groups ($p<0.005$). No significant difference was found between the groups in terms of glucose metabolism ($p>0.005$) (Table 1). The testicular damage was shown in histopathological examination. Conclusion: Testis torsion is one of the causes of acute scrotum in children and adolescents. The degree of testicular torsion affects the changes observed in the testis. Moreover, many of the patients with testicular torsion report a history of recurrent, sudden onset of scrotal pain, suggesting previous intermittent periods of torsion. In this study, 1-day melatonin and pulse magnetic field administration were found to have no contribution to the prevention of ischemic damage in testicular torsion. Further studies with longer periods of treatment are warranted.

P184

Enhancing the effect of radiotherapy in cultured tumour cells using p53 therapy

A. C. Mortensen[1], D. Spiegelberg[1], A. M. Scott[2], D. P. Lane[3], M. Nestor[1,4]; [1]Department of Immunology, Genetics and Pathology, Uppsala, SWEDEN, [2]Ludwig Institute for Cancer Research, Olivia Newton-John Cancer Research Institute, and La Trobe University, Melbourne, Victoria, AUSTRALIA, [3]p53Lab, Agency for Science Technology and Research (A*STAR), Singapore, SINGAPORE, [4]Department of Surgical Sciences, Uppsala, SWEDEN.

Background: Radiotherapy, external as well as radioimmunotherapy (RIT), is an established concept for cancer therapy, and the role of p53 in cancer has been extensively studied. However, the possibility of enhancing the effects of radiotherapy by targeting the p53-mdm2 interaction, using peptides such as PM2 or Nutlin, is a novel concept. Especially the combination of p53-therapy and RIT may provide an innovative and unique opportunity to utilize p53 as part of the radiation response during treatment. This could result in radiosensitized cancer cells and enhanced therapeutic effects.

Aim: To assess whether p53 therapy in combination with radiotherapy can increase the radiation sensitivity in cultured squamous cell carcinoma (SCC) cells, using both 2D- and 3D-cell cultures. Materials & Methods: A panel of SCC cell lines was first investigated regarding p53 and HPV status, as well as for colony formation abilities and spheroid forming abilities. The presence of various antigens suitable for RIT was characterized on selected cells and tumour xenografts. An EGFRvIII-targeting antibody was then optimized for labelling with e.g. ^{111}In using CHX-A"DTPA. The effects of radiation (external or RIT), p53 therapy, as well as a combination of treatments were then assessed using e.g. cell survival, cell viability, and cell growth assays. Both short-term and long-term effects were studied, and effects were assessed using both 2D and 3D cell cultures. Results: Radiolabelled RIT conjugates demonstrated an effect on cell viability and growth at selected activities, whereas negative controls did not. Furthermore, the combination of p53 therapy and radiotherapy had a greater impact on cell survival and viability than either treatment alone, with synergistic effects for some combinations. Conclusion: p53 therapy in combination with radiotherapy decreases cell survival and viability in cultured SCC cells. The combination of p53 therapy with RIT may enhance in vivo potency even further if an antibody demonstrating anti-tumour effects on its own is used.

P185

131I labelled multifunctional dendrimers for targeted SPECT imaging and radiotherapy of cancer

Y. Cheng[1], J. Zhu[2], L. Zhao[1], Y. Tang[3], X. Shi[2], J. Zhao[1]; [1]Department of Nuclear Medicine, Shanghai General Hospital, Shanghai Jiaotong University, shanghai, CHINA, [2]State Key Laboratory for Modification of Chemical Fibers and Polymer Materials, Donghua University, shanghai, CHINA, [3]Experiment Center, Shanghai General Hospital, School of Medicine, Shanghai Jiao Tong University, shanghai, CHINA.

Aim: Recent advances in nanotechnology have promoted a rapid development in building various platforms for diagnose and treat cancer. In this study, we report the utilization of ^{131}I-labelled multifunctional dendrimers conjugated chlorotoxin (CTX) for targeted cancer single-photon emission computed tomography (SPECT) imaging and radiotherapy. Materials and methods: The dendrimers were made of PEG-acetylated amine-terminated poly(amidoamine) dendrimers of generation 5 (G5.NHAc) and 3-(4'-Hydroxyphenyl)propionic Acid-OSu (HPAO). CTX, an excellent ligand targeted to matrix metalloproteinase-2 (MMP-2), was modified onto the surface of dendrimers to enable nanoparticles specifically binding to tumor cells. Followed by radiolabeling with ^{131}I and purification using PD-10 columns, ^{131}I labelled multifunctional dendrimers (^{131}I-G5.NHAc-HPAO-PEG-CTX) was synthesized and the possibilities of targeted imaging and therapeutic efficacy to cancer cells were demonstrated both in *vitro* and in *vivo*. Results: The formed nanoprobes were stable and could be completely dissolved in aqueous solution. The radioactive ^{131}I was able to be efficiently labeled onto the dendrimer platform with good stability and high radiochemical purity. The CTX-conjugated nanoprobe displayed a higher accumulation in the perinuclear region of cytoplasm than G5.NHAc in confocal assay. The radioactive signal of C6 rat glioma cells and tumor implanted in nude mice treated with CTX-modified nanoprobe was significantly stronger than that of unmodified nanoprobe. ^{131}I-G5.NHAc- HPAO-PEG-CTX was able to target selectively and display much stronger inhibitory effect on C6 cells growth than others which were unbounded CTX, while unradiolabeled nanoprobes had no cytotoxicity. Finally, tumor biopsies by histochemically staining exhibited CTX-enabled nanoprobe selectively binded to glioma tissues, and not appreciablely binded to normal tissues. Tumor reduction was achieved in vivo when using ^{131}I-G5.NHAc-HPAO-PEG-CTX. Conclusion: With the modification of CTX ligands, the efficient labeling of radioactive ^{131}I on the dendrimers exhibited an ability for targeted SPECT imaging and radiotherapy of MMP-2 receptor-overexpressing cancers. Keywords: PAMAM dendrimers, chlorotoxin, targeted imaging and radiotherapy, cancer

P187

The effect of omeprazole usage on the viability of random pattern skin flaps in rats

H. SEN[1], M. ORUC[1], V. M. ISIK[1], **M. SADIC**[2], H. SAYAR[3], M. KORKMAZ[2], U. KOCER[1]; [1]Department of Plastic and Reconstructive Surgery, Ministry of Health Ankara Training and Research Hospital, ANKARA, TURKEY, [2]Ministry of Health Ankara Training and Research Hospital, ANKARA, TURKEY, [3]Kahramanmaras Sutcu Imam University, Department of Pathology, Kahramanmaras, TURKEY.

Object: Proton pump inhibitors (PPIs) are widely used to prevent NSAIDs-induced gastrointestinal injury in surgical routine. It's well known that PPIs block the secretion of gastric acid as a result serum gastrin levels increase which might induces angiogenesis. The aim of this study was to evaluate topographically, scintigraphically, and histopathologically the effect of the omeprazole on the viability of skin flaps in rats. Material and Methods: 35 Winstar-Albino type (18 weeks old), weighing between 161-210 gr female rats were divided into 5 equal groups randomly. McFarlane random-pattern skin flaps were raised in all groups. Group I was the control group, Group II was received 10 mg/kg daily omeprazole intraperitoneally for 14 days. Group III was received 40mg/kg daily

omeprazole intraperitoneally for 14 days. Group IV was received 10mg/kg daily omeprazole and group V was received 40mg/kg daily omeprazole intraperitoneally after the seventh day for 7 days. The viability of flaps was observed by ditigal imaging and scintigraphically with use of 1 mCi of technetium-99m pertechnetate. Specimens collected from the proximal (A), middle (B) and distal part (C) of the flap and the number of vascular structures were determined by histopathologic analysis. Results: Digital imaging and radionuclide study images showed that all omeprazole recieved groups flap necrosis percentages outcome was statistically significant lower than that of the control group ($p<0.001$). There was no statistically significant diference between the omeprazole received groups ($p>0.05$). Flap necrosis percentage was evaluated with sintigraphic imaging and the value of each group was determined respectively (group I % 48,2±6,4, group II % 7,6±3,3, group III % 7,4±3,3, group IV % 6,7±1,3 and group V % 8,1 ±3,6). There was statistically significant difference between the each study group compared with the control group ($p<0.001$). Histopathologic examination showed that the mean numbers of vessels in A and C region in the study groups showed a significant increase compared with the control group ($p<0.001$). There was statistically significant difference between the each omeprazole received groups compared with the control group ($p<0.05$). There was no statistically significant diference between the omeprazole received groups ($p>0.05$). Conclusion: Our study showed that use of parenteral administration of omeprazole in skin flap surgery increases flap viability not dependent on dose and time. We believe that use of omeprazole before or at the time of flap surgery can increase flap viability and decrease flap necrosis rate.

P09 - Sunday, October 11, 2015, 4:00 PM - 4:30 PM, Hall 3 – Poster Exhibition

Molecular & Multimodality Imaging: Optical Imaging

P188

Ex Vivo Perfusion of Tumorous Kidneys with a Dual-Modality Tumor-Targeting Imaging Probe

M. Hekman, P. Mulders, M. de Weijert, D. Bos, E. Oosterwijk, H. Langenhuijsen, O. Boerman, M. Rijpkema; Radboudumc, Nijmegen, NETHERLANDS.

Introduction: Complete tumor resection might be improved by targeted intraoperative imaging techniques providing additional information about tumor localization and extent. For this purpose dual-labeled antibodies containing both a near-infrared fluorescent dye (IRdye 800CW) and a radioactive label (Indium-111) can be used. Girentuximab is an anti-CAIX antibody that can be used to target clear cell renal cancers (ccRCC), as the cell surface antigen carbonic anhydrase IX (CAIX) is expressed in 95% of these tumors. This study aimed to assess the feasibility of dual-modality imaging in ccRCC by ex vivo perfusion of tumorous kidneys using dual-labeled girentuximab. Material and Methods: Five tumorous kidneys from patients were used in the perfusion experiments. Directly after nephrectomy the renal artery was connected to a pump via a catheter. The kidney was perfused with 1.2 mg ^{111}In-DOTA-girentuximab-IRdye800CW (3.6-5.2 MBq) in 350 ml Ringer's lactate (4 °C, 10-15 h). This protein concentration is comparable to the serum concentration in patients. Next, the kidney was rinsed with Ringer's lactate (2.5-4 h) to wash out unbound antibody. Subsequently, a 5-mm thick slice of the kidney was analyzed by autoradiography and fluorescence imaging. The antibody accumulation was determined quantitatively by measuring the activity in 1 cm^3 cubes of tumorous and normal tissue in a gamma counter. The tissue cubes were subsequently analyzed (immuno)histochemically. Results: All tumors expressed CAIX and uptake of the dual-labeled tracer could be clearly visualized by autoradiography and fluorescenceimaging. There was an excellent match between the radioactive/fluorescent signal and CAIX expression. Maximum uptake of the antibody in the tumor tissue cubes was 0.33 % of the injected dose per gram (mean 0.12 %ID/g). Maximum uptake in normal kidney tissue cubes was 0.04 %ID/g (mean 0.02 %ID/g). Conclusion: Dual-labeled girentuximab accumulated preferentially in ccRCC tissue and dual-modality imaging could be used to visualize ccRCC. The concentration of dual-labeled girentuximab in vital tumor regions ex vivo was in the same range as the concentration of radiolabeled girentuximab after intravenous administration in patients. These observations warrant a clinical study to evaluate the added value of intraoperative dual-modality tumor-targeted imaging in patients with ccRCC to assess its value for intraoperative tumor visualization and radical tumor resection.

P189

Intraoperative fluorescence guidance under ambient light conditions using a new modified fluorescence camera

N. S. van den Berg[1,2], G. H. KleinJan[1,2], M. Miwa[3], T. Sato[3], Y. Maeda[3], B. Karakullukcu[2], S. Horenblas[2], F. W. B. van Leeuwen[1,2]; [1]LUMC, Leiden, NETHERLANDS, [2]AVL-NKI, Amsterdam, NETHERLANDS, [3]Hamamatsu Photonics KK, Hamamatsu, JAPAN.

Introduction: The introduction of fluorescence-labeled tracers into the operation room has revolutionized the field of image-guided surgery. Initially, fluorescence imaging (FI) was used to optically confirm lesion localization after temporarily dimming the ambient light in the operation theatre. Clearly, it would be preferable if surgical procedures can be performed

with real-time fluorescence guidance. We set out to investigate a camera that allows real-time fluorescence guidance under ambient light conditions and evaluated its value during fluorescence-guided sentinel node (SN) biopsy. Methods: 36 Patients scheduled for SN biopsy for head-and-neck melanoma (n=16), melanoma of an extremity (n=2), oral cavity carcinoma (n=7), and penile cancer (n=11) were included after obtaining written informed consent. Following a peritumoral hybrid tracer (indocyanine green (ICG)-99mTc-nanocolloid) injection, lymphoscintigraphy and SPECT-CT imaging were performed to determine the number and location of the SN s). Intraoperatively, a combination of gamma tracing and fluorescence guidance was used to localize the preoperatively defined SN. In 6 patients the modified-PhotoDynamicEye (PDE) fluorescence camera was compared to the conventional-PDE fluorescence camera for sensitivity in SN detection. In 30 additional patients the modified-PDE was further evaluated. Intraoperative fluorescence-based SN identification rates were scored and the experiences of the surgeon(s) were evaluated. Results: Preoperative SPECT-CT imaging revealed 97SNs (mean 2.7, range 1-7). Intraoperatively, FI allowed optical identification of all SNs defined on preoperative imaging. In the camera comparison, in 6 patients (20SNs evaluated), the modified-PDE was found superior in performance compared to the conventional-PDE. Even in ambient light conditions, weak SNs that could not be detected with the conventional-PDE, were picked up easily. Bright SNs could be picked up easily with both PDE-systems. Experience in the additional 30 patients underlined the modified-PDEs ability to guide SNs resection in real-time under ambient light conditions. Continuous guidance was made even more convenient by the possibility to alter between white light and FI mode. With the modified-PDE in 13 patients SNs were already visualized transcutaneously and tumor draining lymphatic ducts could be accurately visualized in 11 patients. Pseudo-coloring of the fluorescence signal to green in the modified-PDE provided better contrast with the background and increased the detectability compared to the black-and-white image in the conventional-PDE. Conclusion: The optimized FI system expands fluorescence guidance in open surgery to ambient light conditions and enables the surgeon to link fluorescence findings directly to the anatomical background information.

P190

Hybrid guidance towards the sentinel node; a comparison of fluorescence- and blue dye- based optical detection in 458 patients

G. KleinJan[1,2], N. S. Van den Berg[1,2], E. Van Werkhoven[2], J. A. Van der Hage[2], S. Horenblas[2], W. M. N. Klop[2], R. A. Valdes Olmos[2], F. W. B. Van Leeuwen[1]; [1]Leiden University Medical Centre, Leiden, NETHERLANDS, [2]NKI-AVL, Amsterdam, NETHERLANDS.

Introduction: Conventional sentinel node (SN) biopsy is performed using a combination of a radiocolloid and an intraoperative injection of blue dye. However, it has been shown that blue dye does not always stain SNs. In 2009 the hybrid tracer indocyanine green (ICG)-99mTc-nanocolloid was clinically introduced as dedicated SN tracer. This tracer is both radioactive and fluorescent, allowing preoperative SN mapping and intraoperative optical verification of the SN. This study aimed to evaluate the hybrid approach in 458 patients that underwent SN biopsy using the hybrid tracer; specifically, in a sub-analysis we compared blue dye-based SN visualization to fluorescence-based SN visualization. Materials and Methods: 458 patients scheduled for SN biopsy were included. The histopathological diagnosis were skin melanoma of the head and neck (H&N) (n=113), extremity (n=20), and trunk (n=36), or Merkel cell carcinoma of the H&N (n=6), or carcinoma of the penis (n=175), vulva (n=21) and oral cavity (n=47), or adenocarcinoma of the prostate (n=40). A median 81.8 MBq (IQR 73.5-89.8 MBq) ICG-99mTc-nanocolloid was injected in 3-4 deposits surrounding or at the primary tumor site, followed by lymphoscintigraphy and SPECT-CT imaging. The operation was carried out 3-27 hours post-tracer injection and preceded by the injection of vital blue dye. No blue dye was used in the prostate and oral cavity cancer groups. Intraoperatively SNs were initially located based on their radioactive signature; SNs were then evaluated for detection using fluorescence and/or blue dye. In a subset of our patient cohort, a recurrence rate analysis was performed using a Log-rank test. Results: In the overall group, SPECT-CT visualized 1216 SNs (median 3 SNs per patient). In the 458 patients, 1460 SNs were removed during surgery.Focusing on patients in which blue dye was used (total 797 nodes) evaluated in 273 patients, in vivo 5.4% of the removed SNs were not blue nor fluorescent, 40.4% was fluorescent but not blue, 50.7% was fluorescent and blue, and 3.5% was only blue. For the first time survival analysis of multimodal guidance during different SN biopsy procedures was obtained, showing some promising results. For example in the H&N melanoma patients, the group without blue dye showed a decreased recurrence rate with ICG-99mTc-nanocolloid (Log-rank test; p=0.0043). Conclusion: The “hybrid approach” allows for an integrated pre- and intraoperative SN biopsy procedure using a single tracer. Overall, the ability to intraoperatively identify the SN using the fluorescent signature of the hybrid tracer was superior to blue dye-based-identification.

P191

Fluorescent lectins for peripheral nerve visualization during surgery

G. H. KleinJan, D. M. Van Willigen, M. N. Van Oosterom, F. W. B. Van Leeuwen, T. Buckle; Leiden University Medical Centre, Leiden, NETHERLANDS.

Introduction: Damage to the peripheral nervous system is a surprisingly common complication during e.g. prostatectomy, colorectal surgery and the removal of head and neck tumors. In all cases such damage can lead to chronic function loss and, as such, it can negatively influence the quality of life of patients. Intraoperative visualization of these structures could potentially help decrease the level of accidental surgical damage. This preclinical study compares the nerve staining capabilities of lectin related fluorescent imaging agents. Methods: Wheat germ agglutinin (WGA), Peanut lectin (PNA), Red kidney bean (PHA-L), Tomato lectin (LEL) and Cholera Toxin subunit B (CTB) were functionalized with Cy5 (λex max 640 nm; λem max 680 nm). After local (intramuscular) injection, the migration of the individual imaging along the sciatic nerve was evaluated in Thy1-YFP mice (n = 30). Nerve staining was evaluated in vivo using an IVIS Spectrum animal fluorescence scanner. Migration distance and signal intensity were quantified by analyzing the normalized peak intensities using raw IVIS data with MATLAB software. The location of tracer uptake in the nerve was microscopically evaluated ex vivo. Results: All five lectins showed retrograde movement and staining with a signal-to-muscle ratio of around two. With an average of 0.95cm (SD 0.20cm) the longest transfer distance was obtained with CTB-Cy5 giving a migration distance along the sciatic nerve of 1.00 cm (SD 0.38cm). In a direct comparison for the peak intensities of the CTB-Cy5 and WGA-Cy5 signal, the peak intensity signal was higher for CTB-Cy5 in all cases. With confocal microscopy the Cy5 signal could be located on the epineurium of the nerve for all lectins. Conclusion: Local administration of the fluorescent CTB was shown to be a potential candidate for in vivo visualization of peripheral nerves. This said in the current setting, the migration distance along the nerve remains limited to <1cm.

P192

Evaluation of the optical and physical properties of symmetric NIR dyes towards intraoperative fluorescent markers

S. van der Wal, J. Kuil, R. R. P. M. Valentijn, F. W. B. van Leeuwen; Leiden University Medical Center, Leiden, NETHERLANDS.

Aim: Near-infra-red (NIR) dyes, most notably indocyanine green (ICG), have been used in fluorescence-guided surgical procedures that are complementary in many ways to radioguidance techniques. Similar to radiotracers, the photophysical and physical properties of the fluorescent tracer are critical to the successful application of the tracer in intraoperative settings. Moreover, the relatively larger size and thus influence of the fluorescent dye compared with radioisotopes makes validation of these properties even more critical. Another potentially limiting feature of fluorescent dyes is their tendency to interact (stack) with each other or serum proteins by Van der Waal's forces. This can lead to clusters of dye molecules with aberrant photophysical properties leading to a loss of fluorescence.The aim of this study was to evaluate the stacking properties of a set of symmetrical NIR cyanine dyes and relate this to the photophysical properties both as free dye and as monoclonal antibody (mAb) conjugate with the aim of retaining high brightness upon conjugation and limiting nonspecific protein interactions. Material and methods: A small set of negatively charged symmetrical heptacyanine dyes based on the parental ICG structure were synthesized to obtain different charge distributions and hydrophobicity. Modifications include the aromatic ring size and both location and number of the negative charge. The design of the dyes incorporated a central C-C bond that is stable in physiological conditions. The stacking behaviour and non-specific protein interactions of these dyes were evaluated by spectroscopic methods in different media and further correlated to the physical properties of the dye-mAb-conjugates. Results: Stacking, measured by an extra ~50-80 nm blueshifted peak in the absorbance spectrum was most pronounced at high concentrations and under saline conditions. This phenomenon was associated with a loss of brightness. The dye carrying indolenine rings and the highest number of negative charges (4) showed substantially reduced stacking, presumably due to coulombic repulsion of the charges. Nevertheless, stacking was still observed with the most optimal dye researched. Conjugation of these dyes to mAbs generally resulted in stacking of the dyes on the mAb, which resulted in concomitant precipitation of conjugates in the most extreme cases. Conclusions: Symmetrical centrally-C-C-bonded heptacyanine dyes are prone to stacking despite the presence of negative charges, which reduce dye-dye interactions. The molecular properties of the dye have a distinct influence on the conjugation chemistry, fluorescence brightness and non-specific protein interactions. These finding underline the potential challenges in generating fluorescent tracers for in-vivo use.

P193

(Near-infrared) fluorescence guidance during surgery: What is the detection limit?

G. H. KleinJan[1,2], A. Bunschoten[1], T. Engelen[1], N. S. van den Berg[1,2], R. A. Valdés Olmos[1,2], H. Wester[3], F. W. B. van Leeuwen[1,2]; [1]LUMC, Leiden, NETHERLANDS, [2]AVL-NKI,

Amsterdam, NETHERLANDS, [3]TUM, Munich, GERMANY.

Introduction: (Near-infrared (NIR)) fluorescence guided surgery was introduced in the clinic with the promise to allow for highly sensitive (molecular) lesion visualization. However, most studies report high doses of fluorescent tracers. As a result there has been quite some debate regarding the ability to detect fluorescent tracers at a microdose level (<100μg). Limiting herein is the ability to adequately quantify fluorescent signal intensities and thus the percentage injected dose (%ID) that ends up in tissue samples. Multimodal (or rather hybrid) imaging agents that combine a radioactive and fluorescent signature allow to quantitatively investigate that question. From our clinical trials with the hybrid tracer indocyanine green (ICG)-99mTc-nanocolloid for sentinel node (SN) biopsy we estimated the surgical detection sensitivities in relation to the %ID in the SNs.MethodsIn this retrospective analysis 47 patients were included that had undergone ICG-99mTc-nanocolloid-based SN biopsy for melanoma in the head and neck (MHH; n=21, 112SNs) and penile cancer (PenC; n=26, 58SNs). SPECT-CT images, acquired two hours post-hybrid-tracer-injection, served as golden standard for the number and location of the SNs as well as the quantification of the %ID. For this evaluation we estimated that the volume of a SN was 1mL. Percentage of tracer uptake in the SN was then correlated with intraoperative SN visualization or non-visualization via fluorescence imaging.ResultsFrom the SPECT data the ICG-99mTc-nanocolloid uptake in the SN could be divided in three categories: cat. I) 0-1%ID (0-84.8nM ICG); cat. II) 1-2%ID (84.8-169.6nM ICG); and cat. III) >2 ID (>169.6nM ICG). All these SNs could intraoperatively be identified via gamma tracing. Fluorescence-based SN detection, however, varied between the three categories. In cat. I, which had the lowest %ID, detection was 91.1% for MHH, and 89.6% for PenC. Visualization rates increased for cat II, giving 98.3% and 99.1%, respectively. For patients in cat. III all the SNs could be visualized intraoperatively using fluorescence.ConclusionBased on the approximations employed (quantifications by SPECT, each SN = 1mL), fluorescence-based detection of SNs during surgery was possible in the nM tracer range.

P194
Multimodal Optical System from Macro to Micro Bioluminescence Imaging

C. R. Gigliotti, L. Altabella, M. Crippa, A. E. Spinelli; San Raffaele Scientific Institute, Milano, ITALY.

Aim: Multimodal imaging instruments are becoming a strong demand in preclinical studies. Different combined systems are now commercially available even though they do not fully allow modifying the experimental set-up according to the specific needs. Preclinical researches include not only in vivo imaging, but also in vitro cells analysis, usually performed with dedicated microscope. We proposed a unified CCD-based approach suitable for the detection of a wide spectrum of radiation (Spinelli et al., Biomed. Opt. Exp., in press) using a system composed by a cooled EMCCD mounted on a light-tight box. In this work we demonstrate that our system, coupled with a macro lens, allows also cell bioluminescence microscopy. In particular, we focus on a method to further improve the spatial resolution, overcoming light diffusion. Methods: The method consists of acquiring several frames of few seconds, rather than only one single image with long exposure time. The sum of the signal obtained in the individual frames was used as a prior for the localization of the principal sources. A Gaussian fit for each source in each frame was performed after a smoothing of the noise with a Gaussian filter. The peak location and intensity of the corresponding fits were then used to reconstruct a high-resolution image. We performed a feasibility study with Monte Carlo simulation of bioluminescent cells, using GAMOS plug-in for GEANT4. Experimental data were acquired using our optical system, with the macro lens. As a proof of principle, a dish of luciferase-tagged mesothelioma cell line was imaged after the injection of D-luciferin in the growth medium, acquiring short frame images and long exposure image used as comparison. Results and conclusion: The post processing of the Monte Carlo simulated frames allowed halving the FWHM with respect to the image that simulates a continuous acquisition. In particular with our approach, the FWHM shrank to the physical dimension of the simulated cells (50μm). The improvement of the spatial resolution is confirmed by applying our method to experimental images. The FWHM of the signal in the long exposure image is 150 μm, while we reach a FWHM of 50 μm processing the frames. These preliminary results show the feasibility of a unified optical platform for macro and micro imaging. In particular, the acquisition method and the analysis procedure allow doubling the spatial resolution overcoming the intrinsic light diffusion.

P195
Optical Imaging of Radiation-Induced Light Emission of Luminophores

A. K. Kondakov[1], I. L. Gubskiy[1], E. Y. Prokop'eva[1], I. A. Znamenskiy[1,2]; [1]Pirogov RNRMU, Moscow, RUSSIAN FEDERATION, [2]CCH RAS, Moscow, RUSSIAN FEDERATION.

It is known that luminescence of some fluorophores, such as fluorescein, may be induced by gamma-radiation or X-rays. Aim of this study was to estimate radiation-induced luminescence of known luminophores by means of CCD-based optical

imaging device. Materials and methods. All experiments were carried out by means of CCD-based device IVIS SpectrumTM (Caliper Life Sciences, USA) that was used in bioluminescent mode. 100 MBq of 99mTc-pertechnetate (100 μL) was added in one well of black plastic microwell plate, while other wells were filled with 100 μL of double-distilled water. Image was acquired with the following parameters: f-stop=1, bining 16, time of exposition - 5 min. After that, into well with 99mTc-pertechnetate and into 3 adjacent consecutive wells 20 μL of fluorescein solution was added and image acquisition repeated. The same experiment protocol was used for investigation of luminol (20 mmol solution in DMSO). Average radiance and its change were measured on resulting images. In order to estimate spectral distribution of visible light intensity, consecutive images were acquired with use of emission filters in wavelength range of 500 to 840 nm with resolution of 20 nm. For these images, exposition time was extended for 10 min. Results. Average radiance increased after fluorescein (threefold) and luminol (by 3,7 times) addition to 99mTc-pertechnetate solution. Average radiance in wells with fluorescein decreased with increasing of squared distance from well containing 99mTc-pertechnetate. On the contrary, luminol luminescence was very weak in wells, adjacent to well containing 99mTc-pertechnetate. It is known, that luminol experiences chemiluminescence in presence of hydrogen peroxide in solution. Hydrogen peroxide is produced during gamma- and beta-irradiation of water. About 11% of 99m-technetium isotopes decay by means of isomeric transition with ejection of electrons. It was assumed that chemiluminescence of luminol is maintained by high production of hydrogen peroxide and other reactive oxygen species due to beta-irradiation. Spectral distributions in range of of 540-800 nm don't differ from usual for both luminophores. As a conclusion, we assume that different fluorophores may emit weak light in visible range. This light emission is due to direct radioluminescence (in case of fluorescein) or by irradiation-induced chemiluminescence (in case of luminol). It was noticed, that water solutions of pertechnetate are able to produce weak light emission too. Studying of these kinds of light emission by means of CCD-based optical devices may be used in wide range of biomedical research.

P10 - Sunday, October 11, 2015, 4:00 PM - 4:30 PM, Hall 3 – Poster Exhibition

Molecular & Multimodality Imaging: PET/MRI & SPECT/MRI

P196

The clinical efficacy of endometriosis diagnosis using I-123 MIBG SPECT and MRI image fusion

K. Utsunomiya[1], K. Yasuda[2], Y. Kono[3], Y. Ueno[3], S. K. HaKawa[3], A. Stundzia[4], N. Tanigawa[3]; [1]Department of Radiology, Takii hospital, Kansai Medical University, Moriguchi, JAPAN, [2]Department of Gynecology, Takii hospital, Kansai Medical University, Moriguchi, JAPAN, [3]Department of Radiology, Kansai Medical University, Hirakata, JAPAN, [4]Tomographix, Toronto, ON, CANADA.

Purpose: To determine if fusion images of I-123 metaiodobenzylguanidine (MIBG) SPECT and MRI can detect endometriosis in the pelvic cavity along with extensions. Methods: Four healthy female volunteers (mean age: 42.5 ±6.4) and four patients diagnosed with endometriosis (mean age: 45.5±4.8) were enrolled in this study. Two of the four patients were previously diagnosed, using ultrasound and MRI, with endometriotic lesions in the uterus (Group C). The other two patients had been similarly diagnosed with both endometriotic uterine lesions and bilateral ovarian lesions (Group E). In these latter cases, ovarian lesion adhesion to the intestine precluded laparoscopic resection. All patients also had findings of small to medium uterine myomas. I-123 MIBG SPECT was performed at 15 minutes (early acquisition), 3 hours (late), and 6 hours (delayed) after 167MBq I-123 MIBG injection. Same day MRI was also performed. The I-123 MIBG SPECT and MRI data were coregistered to create fusion images. (SYNAPSE VINCENT Version 4; Fuji Medical, Tokyo, Japan). Results: Healthy volunteers: Trace I-123 MIBG accumulation was observed in the uterus of one volunteer in the fused late images with no I-123 MIBG accumulation in the intestine during any time of image acquisition. No I-123 MIBG accumulation was observed in either the uterus or intestine of the other three volunteers across all image acquisition times. Endometriosis patients: Group C. I-123 MIBG uptake was observed in the uterus of both patients and in the left parametrium of one patient. The I-123 MIBG uptake peaked in early image acquisition (15min) and decreased thereafter. No intestinal uptake was found in this group at any acquisition time. Group E. I-123 MIBG uptake was observed in the fused images in the uterus, parametrium, and intestine across all image acquisition times. The I-123 MIBG was found to be time dependent, increasing with increasing post-injection time, especially in the intestine. Conclusion: Image fusion of I-123 MIBG SPECT and MRI may prove to be a clinically useful tool for the diagnosis and localization of endometriosis.

P197

Simultaneous respiratory gating in PET/MR: clinical quantification of neoplastic lesions and physiological structures

F. G. BARBOSA[1], G. DELSO[2], M. HUELLNER[1], P. STOLZMANN[1], E. TER VOERT[1], P. VEIT-HAIBACH[1]; [1]ZURICH UNIVERSITY HOSPITAL, ZUERICH, SWITZERLAND, [2]GE HEALTHCARE, ZUERICH, SWITZERLAND.

Purpose: Respiratory motion is a significant challenge for accuracy in PET images especially concerning variation of uptake measurements (SUV) and lesion mismatch in PET/MR fusion images. The aim of the study is to evaluate the impact on SUV-measurement in simultaneously respiratory gated PET/MR acquisition of the thorax in physiological structures and neoplastic lesions. Methods: Twenty seven oncological patients referred for staging/restaging were prospectively enrolled and imaged with a simultaneous PET/MRI-system (Signa PET/MR, GE Healthcare, 17 M/ 10 F; mean age 61 ± 12y). PET data were evaluated semiquantitatively (SUVmax and mean) in physiological structures and neoplastic lesions (n=45), comparing two data sets: static PET acquisition (standard shallow breathing) and respiratory gated simultaneous PET/MR acquisition. The respiratory cycle was divided in six bins, all bins were reconstructed in PET accordingly. SUVmax/mean was evaluated in both settings (static and gated). For the gated studies, the bin with the least motion was selected ("best bin") for comparison. Furthermore, PET/MR images were compared concerning artifacts and mismatch between both settings. The Wilcoxon's test was used to assess the correlation of the SUV values of tumor lesions and physiologic tissues, mismatch of PET/MR images and artifact score. Results: There is no significant statistical difference ($p>0.05$) in SUV values between static and gated PET acquision in tumoral lesion (primary, lymph node and metastase) and in most of physiologic tissue, except in lung parenchyma ($p<0.05$) where SUV values were slightly higher in static (SUVmax=0.71; SUVmean=0.43) than in gated PET (SUVmax=0.65; SUVmean=0.39). The mismatch distance in fused PET/MR images was statistically significant different ($p<0.01$) between static (mean=4.3mm;SD=2.6) and to gated PET acquisition (1.8mm;SD=1.2), predominantly in craniocaudal orientation. The artifact score in gated PET acquisition was statistically significantly superior (mean=1.14; SD=0.35) compared to static PET-images (mean=1.74; SD=0.58) ($p<0.01$). Conclusion: In simultaneous respiratory gated PET/MR no statistical significant difference in SUV value of the tumoral lesion and in most of the physiologic tissue was found. However, gated PET acquisitions had a significant lower mismatch and showed significantly less artifacts.

P198

Evaluating carotid plaque inflammation in patients with active rheumatoid arthritis (RA) using 3T magnetic resonance imaging (MRI) and Fludeoxyglucose(18F) PET (18FDG-PET) : a pilot study

S. Skeoch[1,2], **H. A. Williams**[3], P. Cristinacce[4], P. Hockings[5,6], J. James[3], Y. Alexander[7], J. Waterton[8], I. Bruce[9]; [1]Arthritis Research UK Centre for Epidemiology, University of Manchester, Manchester, UNITED KINGDOM, [2]NIHR Manchester Musculoskeletal Biomedical Research Unit, University of Manchester, Manchester, UNITED KINGDOM, [3]Nuclear Medicine, Manchester, UNITED KINGDOM, [4]Biomedical Imaging Institute, University of Manchester, Manchester, UNITED KINGDOM, [5]Drug Safety and Metabolism, Astrazeneca, Mondal, SWEDEN, [6]MedTech West, Chalmers University of Technology, Gothenburg, SWEDEN, [7]Healthcare Science Research Institute, Manchester Metropolitan University, Manchester, UNITED KINGDOM, [8]Personalised Healthcare and Biomarkers, Astrazeneca, Manchester, UNITED KINGDOM, [9]Kellgren Centre for Rheumatology, NIHR Manchester, Manchester, UNITED KINGDOM.

Emerging evidence suggests RA patients may have more inflammatory, higher risk atherosclerotic plaque. We aimed to investigate carotid plaque in RA patients using MRI and 18FDG PETCT.Patients with active RA, defined as the Disease Activity Score in 28 joints (DAS28) score of more than 3•2, were recruited to a single centre study in the UK. Patients underwent clinical and serotological evaluation, and those with carotid plaque of thickness > 2.5mm on ultrasound underwent carotid MRI, followed by 18FDG PETCT (at 2 hours p.i. of 200 MBq FDG) within 1 week. Head and neck position for MRI was replicated for PET using comparable supports, head alignment and neck extension. PET images were reconstructed using time-of-flight information and resolution recovery. PETCT scans were registered to T1-weighted MRI to co-localise plaque-specific signals, prior to volume of interest analysis around the artery sections containing plaque by a physicist (HW) who was masked to clinical information. The maximum standardised uptake values (SUVmax) in the plaque volumes were obtained and the association of SUVmax with DAS28, C-reactive protein (CRP), and CD4+CD28- T-cell frequency tested using non-parametric statistics.13 patients (9F, 4 M) underwent MRI and 18FDG PETCT, with median age 60 years (IQR 57-65), disease duration 11 years (6-25), and DAS28 score 4•52 (4•32-5•13). None had a history or symptoms of clinical cardiovascular disease or took statins. All plaques caused less than 70% stenosis, and accumulated 18FDG. Median SUVmax was 2•18 (IQR 2•00-2•65). All cases had an SUVmax greater than 1.6 (the published threshold for defining carotid plaque inflammation, although it is noted that this threshold may not be applicable to advanced PET reconstructions using time-of-flight and resolution recovery). There was a significant association with SUVmax and CRP (r=0•58, p=0•04) and quartiles of CD4+CD28- T-cell frequency (p=0•045) but not with low-density lipoprotein concentrations (r=-0•49, p=0•09) or DAS28 score (r=0•38, p=0•20). No association was found with age (r=0•13, p=0•69) or sex (p=0•64).In this small pilot study, 18FDG accumulation by carotid plaque was seen in all patients and correlated with CRP. Whether this finding represents

simultaneous joint and plaque inflammation, which might improve on treatment of joint disease, remains to be determined. CD4+CD28- T-cells are known to predict cardiovascular events in patients with angina, which suggests a possible role in cardiovascular risk prediction in RA. Larger studies are warranted to investigate these findings further.

P199

Performance of an Ultralow-Dose High-Resolution Pediatric TOF-PET Scanner Based on Monolithic Scintillators

E. Mikhaylova[1], V. Tabacchini[2], G. Borghi[2], W. Vogel[3], P. Mollet[1], E. D'Hoe[1], D. Schaart[2], S. Vandenberghe[1]; [1]University of Ghent, Ghent, BELGIUM, [2]Delft University of Technology, Delft, NETHERLANDS, [3]Netherlands Cancer Institute, Amsterdam, NETHERLANDS.

Introduction. A novel high sensitivity TOF-PET scanner will be built for multimodal in vivo molecular low dose imaging of cancer, cardiac and neurological diseases, inflammation, and hyperinsulinism in children.Materials and methods. The system was realistically modeled in the GEANT4 Application for Tomographic Emission (GATE) software and is composed of monolithic LYSO (3.2 x 3.2 x 2.2 cm) detector blocks (dual side readout, DSR) arranged in a cylindrical shape adapted to children up to the age of 12 years (54 cm diameter bore and 53 cm axial length). The simulated performance model of the detector (spatial FWHM of 1.5 mm, depth-of-interaction FWHM of 2.5 mm and TOF of 150 ps) was based on extensive measurements of LYSO blocks. The realistic child is modeled using the XCAT phantom software. A realistic FDG (40 MBq in total) distribution with 5, 10 and 20 mm hotspots (8 x higher than soft tissue value) was simulated for 3 min total acquisition time. The acquired list-mode (LM) data (without scatters) were reconstructed using the LM-OSEM algorithm with modeling of TOF kernel. The same object and distribution was simulated on the clinical reference system Philips Gemini TF (600 ps, same activity and total acquisition time).Results. The total number of counts on the pediatric PET was 15 times higher due to the increased solid angle. The new system achieves much higher image contrast and better identification of structures due to lower noise and better spatial resolution. In the pediatric PET images , we can distinguish all 5, 10 and 20 mm hot lesions in liver and lung while in the GEMINI TF scanner only 20 mm and 10 mm hot spheres in lungs can be detected.Quantitative data. The contrast recovery coefficient (CRC) is chosen as a measure of image quality. The pediatric PET shows significantly higher CRC values for all hot lesions than the GEMINI TF scanner: 28.5%, 54.6% and 86.5% for the 5, 10 and 20 mm spheres in lungs respectively for the pediatric PET versus 3.3%, 8.7% and 27.6% for the same hot lesions for GEMINI TF.Conclusions. The pediatric PET system shows the ability to obtain low-noise, high-resolution and high-contrast images with a very limited dose in a short total acquisition time.

P200

Incorporation of TOF information reduces artifacts in simultaneous TOF PET/MR scanning

E. ter Voert[1,2], H. Davison[1,3], F. de Galiza Barbosa[1,2], M. Huellner[1,2], S. Ahn[4], F. Wiesinger[5], C. Levin[6], A. Iagaru[6], G. Zaharchuk[6], G. Delso[7], P. Veit-Haibach[1,2]; [1]University Hospital Zurich, Zurich, SWITZERLAND, [2]University of Zurich, Zurich, SWITZERLAND, [3]Royal United Hospitals Bath NHS Foundation Trust, Bath, UNITED KINGDOM, [4]GE Global Research, Niskayuna, NY, UNITED STATES, [5]GE Global Research, Munchen, GERMANY, [6]Stanford University, Stanford, CA, UNITED STATES, [7]GE Healthcare, Waukesha, WI, UNITED STATES.

Introduction: In simultaneous PET/MR scanning, MR data is employed for PET attenuation correction (MR-AC). Bone or metal implants could lead to inconsistencies in the MR-AC maps, thereby affecting the PET images. Lesions close to bone or metal implants might become difficult to assess properly or might even be missed completely. A possible solution could be the inclusion of time-of-flight (TOF) information into the PET image reconstruction algorithm. This study aims to evaluate the influence of TOF information on artifact reduction and PET image quality improvement in clinical simultaneous PET/MR scanning. Methods: A total of 63 patients (median age 58 years) underwent a PET/MR examination in a new simultaneous TOF PET/MR scanner (GE SIGNA). TOF and non-TOF PET datasets were reconstructed, assessed clinically and compared by radiologists/nuclear medicine physicians. Differences in the image quality, particularly those related to (implant) artifacts, were assessed using a 5-point scale, ranging from 0 (no artifact) to 4 (severe artifact, impaired reader confidence). To quantify differences, reconstructions were repeated in 7 patients after the introduction of artificial signal voids in the attenuation map. These virtual artifacts simulated clinically relevant metal artifacts in the maxilla, humeral head, chest, sternum, thoracic spine, lumbar spine and the femoral head. Results: A total 87 image artifacts were detected and evaluated. Four patients had large and 8 patients had small implant-related artifacts, 27 patients had artifacts related to dental implants/fillings, and 48 patients had implant-unrelated artifacts. Overall, the average score was 1.14 ± 0.82 (mean ± SD) for the non-TOF PET images, and 0.53 ± 0.66 for the TOF images ($P<0.01$). In all simulated cases the magnitude of the virtual artifact was reduced (range: 20-60%) when TOF information was included in the reconstruction.

Discussion: From a clinical point of view, the use of TOF significantly improved the image quality and the reader confidence close to artifacts. TOF information reduced the impact of artifact-related errors in all metal implant cases. TOF not only improves e.g. signal-to-noise ratio, accuracy, lesion detectability and the convergence rate of the iterative algorithm, its inclusion also makes the system become better-conditioned and therefore less sensitive to errors in the attenuation map. The use of TOF in conjunction with other (MR) techniques for metal artifact correction could possibly further improve the overall image quality and clinical reader confidence. Conclusion: Our results suggest that PET imaging significantly benefits from the incorporation of TOF information in simultaneous PET/MR scanning.

P201
Brain PET/MR attenuation correction for pediatric patients

C. Ladefoged, J. B. Andersen, L. Marner, A. E. Hansen, I. Law, L. Højgaard, F. L. Andersen; Dept. of Clinical Physiology, Nuclear Medicine and PET, Rigshospitalet, Copenhagen, DENMARK.

AIM: Brain PET/MRI is challenged by inaccurate attenuation correction (MRAC). Several methods have been suggested in the literature, where the majority is based on registration to an atlas, followed by a back-warp of an average CT image, limiting the applicability to pediatric patients. The purpose of this study was to evaluate the accuracy of our new MRAC method (MR-AC_UPSTAIRS) based on the ultra-short echo time (UTE) MR sequence in pediatric patients. METHODS. Brain scans were performed on eight pediatric patients using the Siemens PET/MR scanner. Six patients with PET positive brain tumors (Group A, 4-8 years, 76±22 MBq [18F]-FET), and two healthy volunteer patients (Group B, 2-3 days, 15 MBq [15O]-labeled-water). For Group A only, a 120 kVp low-dose CT was obtained and used as reference (MRAC_CT). We compared the performance of standard MRAC_DIXON, MRAC_UTE (Siemens VB20P), and MRAC_UPSTAIRS, a fully automatic method that segments air, brain, cerebrospinal fluid and soft tissue voxels on the UTE images, and uses a mapping of R2* values to Hounsfield units to obtain a patient specific continuous bone density value. For Group A, we analyzed the effect of each MRAC method on the tumors. The tumor was defined by isocontouring as activity > 1.6 times the mean value of a background region. We measured the averaged %-deviation of SUV_MEAN and volume of the tumor, relative to PET corrected with MRAC_CT. For both groups, we measured the mean %-deviation in six consecutive homeomorphic regions extending from the cortex to the center of the image plane. RESULTS. For PET_DIXON/PET_UTE/PET_UPSTAIRS, the averaged %-deviation from PET_CT was -10%/-9%/-5% for T_MEAN and +9%/+22%/-2% for the tumor volume. The regional analysis showed a radial gradient effect when using Dixon and UTE, from -20% to -5% and -21% to -3%, respectively, from the cortex to the center. When using UPSTAIRS the radial bias is significantly reduced (-7% to -2%). For Group B, we compared Dixon to UPSTAIRS. Here, a radial bias of -14% to -6% is also present. This is similar to the Group A patients (-12% to -3%), suggesting that the performance is comparable to that measured for Group A. CONCLUSIONS. The MRAC method UPSTAIRS is able to provide continuous bone density values for brain attenuation maps in pediatric patients, which has not previously been reported. The method shows improved performance over Dixon and UTE when used for clinical purposes, and is very similar to that of CT.

P202
Combined 18F NaF/18F FDG and TOF simultaneous PET/ MRI: One-Stop Shop Staging of Patients with Breast and Prostate Cancers

R. Minamimoto, A. Loening, P. Obara, V. Taviani, S. S. Gambhir, S. Vasanawala, **A. Iagaru**; Stanford University School of Medicine, STANFORD, CA, UNITED STATES.

Introduction: We previously reported the pilot evaluation of a simultaneous PET/MRI scanner with TOF capability, as well as the use of combined 18F NaF/18F FDG PET/CT in cancer patients. Here we prospectively compared the combined 18F NaF/18F FDG PET/ MRI against 99mTc-MDP in patients with breast and prostate cancers for the detection of metastatic disease. Materials and methods: Fifteen patients referred for 99mTc-MDP bone scans were prospectively enrolled from Oct 14 - Mar 15. The cohort included 7 men with prostate cancer and 8 women with breast cancer, 41 - 85 year-old (average 61 ± 13). 18F NaF (0.7-2.2 mCi, mean: 1.2 mCi) and 18F FDG (3.8-5.2 mCi, mean: 4.2 mCi) were subsequently injected from separate syringes. The PET/MRI was done 6-30 days (average 9.3 ± 3.2) after bone scan. The whole body MRI protocol consisted of T2-weighted, DWI, and contrast-enhanced T1-weighted imaging. Lesions detected with each test were tabulated and the results were compared. Results: All patients tolerated the PET/MRI exam, and PET image quality was diagnostic despite the marked reduction in the administered dosage of radiopharmaceuticals (80% less for 18F NaF and 67% less for 18F FDG compared to standard protocols). Five patients had no bone metastases identified on either scans. Bone scintigraphy and PET/MRI showed osseous metastases in 9 patients, but more numerous bone findings were noted on PET/MRI than on bone scintigraphy in 3 patients. One patient had negative bone scan, but bone

metastases were seen on PET/MRI. Lesions outside the skeleton were identified by PET/MRI in 3 patients. Conclusion: The combined 18F NaF/18F FDG PET/MRI is superior to 99mTc-MDP scintigraphy for evaluation of skeletal disease extent. Further, it detected extra-skeletal disease that may change the management of these patients, while allowing a significant reduction in radiation exposure from lower dosages of PET radiopharmaceuticals administered. A combination of 18F NaF/18F FDG PET/MRI may provide the most accurate staging of patients with breast and prostate cancers prior to the start of treatment.

P203

68Ga-DOTATATE PET/CT vs PET/ MRI in neuroendocrine tumours: A comparative study

A. Alshammari, E. Skoura, S. Michopoulou, F. Fraioli, R. Syed, J. Bomanji; Nuclear medicine department, UCL hospital, London, UNITED KINGDOM.

Introduction: Studies are emerging about the utilization of PET/magnetic resonance imaging (PET/MRI) in NETs. From the existing studies PET/MRI is believed, to have significant advantages in body areas where MRI is better over CT, including central nervous system, upper abdominal, urogenital system and head and neck imaging. The aim of this study is to compare 68Ga-DOTATATE PET/CT with 68Ga-DOTATATE PET/MRI imaging in patients with known neuroendocrine tumours, and assess the confidence in anatomic lesion detection and localization. Furthermore, the value of each sequence of MRI was evaluated separately.Methods: We retrospectively analysed the data of 38 NET patients. Both 68Ga-DOTATE PET/CT and PET/MRI scans were performed. MR sequences undertaken were T1and T2 weighted, HASTE MR, and diffusion-weighted imaging (DWI).Results: Interobserver reliability was equally very good in both modalities. All lesions considered as malignant in PET/CT were equally depicted in PET/MRI in most of the visualized areas. Significant inter observer correlation between 68Ga-PET/CT and PET/MRI SUV max values for both primary and liver lesions was also observed. However, 68Ga-DOTATATE PET/MRI recognized more liver lesions in 3 patients. The contrast and DWI sequence of PET/MRI did not have a significant effect on final outcome, however in a selected number of cases these images confirmed and helped to further characterize and detect more lesions. There was no significant correlation between DWI mean values and SUV max for the same lesions.Conclusion: This study demonstrates the potential of 68Ga-DOTATOC PET/MRI in patients with NET, with special advantages in the characterization of liver lesions.

P204

Diagnostic accuracy of whole-body PET/MRI for tumor staging in patients with various cancers: a meta-analysis

G. Shen, A. Kuang; West China Hospital of Sichuan University, Chengdu, CHINA.

Aim: Recently published clinical studies using PET/MRI in oncological patients have confirmed its feasibility for cancer staging and have shown image quality comparable to the image quality with PET/CT for lesion detection. The aim of this study was to determine the staging accuracies of PET/MRI for different malignant diseases. Materials and methods: Relevant articles about PET/MRI for cancer staging were systematically searched in PubMed, EMBASE, EBSCO and the Cochrane Library. Two researchers independently selected studies, extracted data and assessed the quality of included studies according to the QUADAS tool. For both per-patient and per-lesion, pooled sensitivity, specificity, diagnostic odds ratio (DOR), positive likelihood ratio (PLR), and negative likelihood ratio (NLR) were calculated using STATA and Meta-Disc software. We also constructed summary receiver-operating characteristic (SROC) curves with the area under the curve (AUC) and Q* estimates obtained. In addition, with regard to the explanation of between-study heterogeneity, we performed the subgroup analysis, threshold effect analysis and publication bias analysis. Results: A total of 35 studies fulfilled the inclusion criteria, totally involving 1482 patients. On a per-patient analysis, the pooled sensitivity and specificity with 95% confidence interval (CI) were 0.92 (0.90-0.94) and 0.91 (0.88-0.94), respectively. On a per-lesion basis, the corresponding estimates were 0.80 (0.78-0.82) and 0.93 (0.92-0.94), respectively. Other estimates were presented in Table 1. Conclusions: According to our results, PET/MRI has excellent diagnostic performance for the overall assessment of cancer staging in patients with various cancers, and has the potential to be broad applied in clinical practice.

P205

Comparison of 18F-FDG-PET/MRI and 18F-FDG-PET/CT for initial staging in pulmonary carcinoma

S. Lütje[1], V. Ruhlmann[1], A. Bellendorf[1], T. D. Poeppel[1], K. Beiderwellen[2], P. Heusch[3], B. M. Schaarschmidt[3], H. H. Quick[4], J. Nagarajah[1], B. Gomez[1]; [1]Clinic for Nuclear Medicine, University Hospital Essen, Essen, GERMANY, [2]Department of Diagnostic and Interventional Radiology and Neuroradiology, University Hospital Essen, Essen, GERMANY, [3]Department of Diagnostic and Interventional Radiology, Medical Faculty, University Düsseldorf, Düsseldorf,

GERMANY, [4]High Field and Hybrid MR Imaging, University Hospital Essen, Essen, GERMANY.

Aim: At present, patients with pulmonary carcinoma are staged using whole-body low-dose ^{18}F-fluoro-deoxyglucose (FDG) positron emission tomography (PET)/computed tomography (CT) as well as cranial magnetic resonance imaging (MRI) for exclusion of cerebral metastases. So far, several clinical studies have investigated the role of whole-body ^{18}F-FDG-PET/CT compared to whole-body ^{18}F-FDG-PET/MRI in detection and quantification of tumor lesions. In these studies, ^{18}F-FDG-PET/MRI was performed first, followed by ^{18}F-FDG-PET/CT scanning. Overall, lower maximum standardized uptake values (SUV_{max}) were observed with ^{18}F-FDG-PET/MRI as compared to ^{18}F-FDG-PET/CT. In the present study, the effect of performing these techniques in reversed order on the capacity of detection and quantification of tumor lesions has been evaluated. In addition, the role of cranial MRI was evaluated. Materials and methods: Eighteen patients with pulmonary carcinoma received i.v. injection of ^{18}F-FDG (302 ± 61 MBq) and underwent PET/MRI (1h p.i.) and subsequent PET/CT (2h p.i.). Regions of interest (ROI) encompassing the entire tumor lesion were drawn into ^{18}F-FDG-PET/CT and ^{18}F-FDG-PET/MR images to determine the maximum and mean standardized uptake value. Data were analyzed quantitatively regarding the detection of tumors lesions and by SUV_{max} determination in the primary tumor as well as in metastatic lesions. In addition, cranial MRI images were evaluated upon presence of cerebral metastases. Results: Sixty-two tumor lesions were detected with both techniques (n=21 primary tumors, n=19 lymph node metastases, n=15 bone metastases, n=7 pulmonary/soft tissue metastases). Median SUV_{max} were 10.9 (range 2.3 - 39.6) and 13.0 (range 3.8 - 33.3) for ^{18}F-FDG-PET/MRI and ^{18}F-FDG-PET/CT, respectively. For both techniques, SUV_{max} derived from ^{18}F-FDG-PET/MRI and ^{18}F-FDG-PET/CT correlated well. One cranial tumor lesion was visualized in contrast-enhanced cranial MRI which was not detected using low-dose ^{18}F-FDG-PET/CT. Conclusion: In line with previous studies, lower SUV_{max} were observed for ^{18}F-FDG-PET/MRI, even when both techniques are performed in reversed order. However, ^{18}F-FDG-PET/MRI might have additional value in the detection of cranial tumor lesions as compared to low-dose ^{18}F-FDG-PET/CT.

P206

Analysis of simultaneous FDG image and DWI acquired with hybrid PET/MRI in thyroid cancer

I. Cho, E. Kong, K. Chun, S. Kwon; Yeungnam University Hospital, Daegu, KOREA, REPUBLIC OF.

Purpose: The aim of this study was to compare the detectability of thyroid cancer of simultaneous FDG images and diffusion-weighted magnetic resonance imaging (DWI) of hybrid PET/MRI system and to clarify the association between metabolic activity and restricted diffusion of thyroid cancer. Methods: Twenty nine consecutive patients diagnosed with solitary thyroid cancer were included. The size less than 1cm or more than 2cm were excluded. Simultaneous FDG image and DWI were acquired by hybrid PET/MRI before thyroidectomy. FDG uptake and apparent diffuse coefficient (ADC) values of thyroid cancer were analyzed. Results: DWI acquisition was failed in 3 patients and showed 2 false negative (n=29). FDG PET showed one false negative due to high FDG uptake in thyroid parenchyma detected in DWI (n=29). SUVmax, SUVmean and ADCmean of thyroid cancer were 6.89±4.28, 4.46±2.51 and 955.37±84.10x10^{-3} mm^2/s, respectively. The ADCmean presented a significant correlation with SUVmax ($r=-0.50$, $p<0.01$) and SUVpeak. ($r=-0.42$, $p<0.01$) Conclusion: Hybrid PET/MRI detected all thyroid cancers and made multimodality imaging for metabolic activity and restricted diffusion in thyroid cancer.

P11 - Sunday, October 11, 2015, 4:00 PM - 4:30 PM, Hall 3 – Poster Exhibition

Molecular & Multimodality Imaging: SPECT Tracers and Evaluations

P207

[123/131I](R)-1-[1-(4-Iodophenyl)ethyl] -1H-imidazole-5-carboxylic acid azetidinylamide (IMAZA) a novel radiotracer for diagnosis and treatment of adrenocortical tumours - first clinical experience

A. Schirbel[1], K. Herrmann[1], C. Bluemel[1], B. Heinze[2], H. Haenscheid[1], M. Fassnacht[2], A. K. Buck[1], B. Allolio[2], S. Hahner[2]; [1]University Hospital of Wuerzburg; Department of Nuclear Medicine, Wuerzburg, GERMANY, [2]University Hospital of Wuerzburg; Endocrinology & Diabetes Unit, Department of Internal Medicine I, Wuerzburg, GERMANY.

Aim[123/131I]Iodometomidate (IMTO), which selectively binds to the aldosterone synthase (CYP11B2) and 11ß-hydroxylase (CYP11B1), has been proven to be useful for molecular imaging in adrenal incidentalomas and radiotherapy in adrenocortical carcinoma (ACC). Due to the observation that IMTO is rapidly inactivated by endogenous esterases which may impair target tissue to background activity ratios and accordingly therapeutic efficacy, >80 new IMTO derivatives have been designed und evaluated. Here we report the first clinical experience with the best derivative, [123/131I]IMAZA, in patients with advanced ACC.Materials and MethodsIn our ongoing study we examined 17 patients with

known advanced ACC. Biodistribution and pharmacokinetics were studied by SPECT/CT and planar images up to 24 h after injection of 185 MBq [123I]IMAZA. Blood levels of tracer and metabolites were determined by radio-HPLC. Dosimetry with 40 MBq [131I]IMAZA was performed over 4 days and targeted endoradiotherapy was performed on compassionate use basis in 3 selected patients.Results[123I]IMAZA proved to be a tracer that specifically accumulates in adrenocortical tissue. As is the case with IMTO, IMAZA showed heterogenous uptake in the tumour lesions. We observed rapid clearance of unbound tracer and an up to 5-fold higher tumour uptake compared to IMTO, which significantly improved imaging quality. IMAZA enabled the visualization of very small metastasis, which could not be detected with IMTO. Analysis of blood samples by radio-HPLC demonstrated a significant higher metabolic stability of the tracer. Dosimetry showed, that the bone marrow was the critical organ; when using 2 Gy as target effective dose very high therapeutic activities of more than 60 GBq were calculated. Three patients received extremely high doses of 26-28 GBq [131I]IMAZA. Due to the high selective and long lasting uptake of [131I]IMAZA, tumour doses up to 265 Gy were reached. Treatment was well tolerated in all patients. Comparison of FDG-PET and low-dose CTs before and 9 weeks after treatment revealed SD in one patient and PD in two patients.ConclusionsWe successfully developed a new radiotracer, IMAZA, a compound with better and more selective binding properties and favourable metabolic stability than the reference iodometomidate. [123/131I]IMAZA is a highly promising radiotracer for molecular adrenal imaging and radiotherapy of adrenocortical carcinoma. The highly specific uptake in the target tissue lead to superior imaging quality and therapeutic potential compared to IMTO.

P208

Study of Novel Molecular Probe 99mTc-3PRGD2 in Diagnosis of Rheumatoid Arthritis

C. Huang, Q. Zheng, **W. Miao**; the 1st Affiliated Hospital of Fujian Medical University, Fuzhou, CHINA.

Objective: The main objective of this study is to evaluate the value of cyclic RGD (Arg-Gly-Asp) peptide conjugate with 99mTc radiolabeled, 99mTc(HYNIC-3P-RGD2)(tricine)(TPPTS) (99mTc-3P-RGD2 : HYNIC=6-hydrazinonicotinyl; RGD2=E[c(RGDfK)]2; 3P-RGD2=PEG4-E[PEG4-c(RGDfK)]2; PEG4=15-amino-4,7,10,13-tetraoxapentadecanoic acid; TPPTS= trisodium triphenylphosphine-3,3',3"-trisulfonate), in diagnosis of rheumatoid arthritis (RA). Methods: 99mTc-3PRGD2 was synthesized by HYNIC-3PRGD2 lyophilized kit with 99mTcO4-labeling. Biodistribution and planar imaging studies were performed in RA rat model. The ankles were marked by arthritis index (AI) scores (from 0 score to 3 score), according to the degree of ankle swelling, and compared the ankle uptake of 99mTc-3PRGD2. Immunohistochemical staining was used to test the expression of integrin αvβ3 in the ankle tissue, analyzing the correlation between uptake of 99mTc-3PRGD2 and receptor expression. Results: Planar imaging of arthritic ankles became visible at 30min postinjection of 99mTc-3PRGD2 and was still clear at 6 hour postinjection. AI score increased, along with the uptake of 99mTc-3PRGD2. Biodistribution study showed that 99mTc-3PRGD2 was excreted by urinary system. The uptake of ankles with different AI scores were 0.64 ±0.07%ID/g (0 score), 1.10±0.07%ID/g (1 score), 1.30 ±0.04%ID/g (2 score), and 1.73±0.05%ID/g (3 score) respectively at 1 hour postinjection, suggesting that the ankle uptake rosed with the increase of AI score. There was a linear positive correlation relationship ($r=0.852$, $P<0.05$) between the ankle uptake of 99mTc-3PRGD2 and the integrin αvβ3 expression levels in immunohistochemical study. Conclusion: 99mTc-3PRGD2 is a promising radiotracer for the diagnosis of rheumatoid arthritis.

P209

SPECT/Low Dose CT Perfusion Study in the Investigation of Suspected Pulmonary Embolism

T. Pipikos, F. Vlachou, A. Nikaki, K. Dalianis, V. Prassopoulos; Nuclear Medicine Department Hygeia SA, Athens, Marousi, GREECE.

AIM: Ventilation/Perfusion lung scintigraphy is a valuable tool in the assessment of pulmonary embolism, especially with the addition of V/Q SPECT. In some cases because of patient's general condition or even of logistic and technical reasons, ventilation study cannot be performed. Modern γ-cameras with flat panel source, give the possibility of performing SPECT/low dose CT study of the lung. In this study, we evaluate the performance of this method in the assessment of PE.Material and methods: We studied 72 patients who underwent V/Q lung planar and SPECT study and perfusion SPECT/low dose CT study. Criteria for a positive V/P planar and SPECT study were mismatch of at least one segment or two sub segments that correspond to pulmonary vascular anatomy, while the study was interpreted as non PE when the perfusion was normal and when there was a match or reverse mismatch(larger defects in ventilation). The rest of the patterns were interpreted as non-diagnostic. The perfusion SPECT/CT study was diagnosed as PE when a segmental or at least two sub segmental perfusion defects with no parenchymal lesions on the low dose CT were found.RESULTS: 21 patients were diagnosed with PE with V/P planar and SPECT method, 1 study was equivocal, while 50 patients were diagnosed as

not having PE. With the perfusion SPECT/CT study 23 patients were diagnosed with PE, 48 were normal while 1 was equivocal. Overall SPECT/CT performed quite well in the assessment of suspected PE, with two false positive findings, one regarding a patient with central located lung cancer which caused disturbance of vascular flow and pressure to the bronchi. SPECT/CT perfusion study had more over the advantage of revealing the cause of defects (emphysema, pleural effusions, atelectacis, etc.)CONCLUSION: Perfusion SPECT/low dose CT study seems to perform quite well in the diagnosis of PE. Although it can't be as accurate as V/P SPECT, it can be of great value in cases that the ventilation study cannot be performed or is unavailable.

P210

Evaluation of Cerebral Circulatory Compensation With Tc99m-HMPAO SPECT And Bilateral Transcranial Doppler Monitoring Of Middle Cerebral Artery In Patients With Chronic Carotid Artery Occlusions

I. S. Kostina, A. V. Scherbinin, D. V. Ryzhkova; North-West Federal Research Center, Saint-Petersburg, RUSSIAN FEDERATION.

Aim: to compare perfusion brain SPECT and bilateral transcranial doppler monitoring of middle cerebral artery blood flow for evaluation of the circulatory compensation capacity in patients with chronic carotid artery occlusions. Materials and methods: In 10 patients (9 man, 1 female; 61±5 years old) with the history of ischemic stroke and CT-angiographically proven chronic total carotid artery (CA) occlusions were included in the study. Six patients had complete occlusion of single internal CA at extracranial segment and 4 patients additionally showed the occlusions of single vertebral artery. All patients underwent perfusion brain single-photon emission computed tomography with 99mTc-hexamethylpropyleneamine oxime at rest and after cerebral vasodilatation by intravenous administration of adenosine (0.14 mg/kg/min body weight over 4 minutes). The cortico/cerebellar ratio (CCR) and the asymmetry index were calculated for evaluation of the regional cerebral perfusion abnormalities at resting conditions and during adenosine test. Middle cerebral artery blood flow was assessed with bilateral transcranial doppler monitoring (TCDM) during hypo- and hypercapnia tests. Results: The decrease of cerebral blood flow during hypo- and hypercapnic tests were detected in all patients by TCDM, that indicated on the abnormality of cerebral flow autoregulation. In all 10 brain rest perfusion SPECT scans the areas of moderate-to severe hypoperfusion were detected in the cortex, supplied by occluded internal CA - in 17% - parietal lobes, in 13% - frontal, 5% - temporal and 65% - both frontal and parietal lobes were affected. During adenosine test the asymmetry index increased in all cases, as well as CCR moderately reduced in the areas with lower resting cerebral perfusion compared with the normally perfused contralateral site. In 2 patients, we observed the reversible perfusion defects in hemispheres, supplied by non-occluded cerebral arteries because of steal syndrome in the territory of the artery-donor of collaterals. Conclusion: The bilateral transcranial doppler monitoring of middle cerebral artery blood flow identifies dysfunction of cerebral flow autoregulation, while brain SPECT during pharmacological test allows to assess the severity and extent of stress-induced ischemia in patients with chronic carotid artery occlusions.

P211

Comparison of SPECT/CT, SPECT, and Planar Imaging in the Management of Primary Hyperparathyroidism: A Systematic Review and Meta-analysis

W Wei, q. luo; Shanghai Sixth People's Hospital, Shanghai, CHINA.

Purpose: Successful performance of minimally invasive parathyroidectomy (MIP) is based on the reliability of preoperative parathyroid localization studies. Despite the various methodologies that are available, no consensus has been reached so far on the optimal imaging technique. The aim of our meta-analysis was to determine the accuracy of SPECT/CT, SPECT and sestamibi scintigraphy for preoperative localization of parathyroid lesions. Methods: Publications were screened by a comprehensive computer search of PubMed and EMBASE. Data were extracted from included articles and forest plots of sensitivity and positive predictive value (PPV) were calculated to investigate the diagnostic accuracy of three imaging methodologies. Results: SPECT/CT had pooled sensitivity and PPV of 84% (95% CI: 78%-90%) and 95% (95% CI: 92%-98%), respectively. SPECT had pooled sensitivity and PPV of 66% (95% CI: 57%-74%) and 82% (95% CI: 73%-89%), respectively. For the diagnostic utility of planar scintigraphy, the pooled sensitivity and PPV were 63% (95% CI: 51%-74%) and 90% (95% CI: 96%-99%), respectively. Conclusion: Our present meta-analysis suggests that with the anatomical information on CT highlighted by functional abnormalities on SPECT, SPECT/CT may be the optimal imaging methodology for patients with primary hyperparathyroidism. And we firmly believe that this technology will become more widely available and a larger number of patients will be able to benefit from combined SPECT/CT imaging.

P212

Nuclear Medicine Imagine of aseptic loosenig of joint protheses: new data

V. Soukhov[1], K. Zaplatnikov[2]; [1]Military Medical Academy, ST. PETERSBURG, RUSSIAN FEDERATION, [2]MAZ Clinic for Nuclear Medicine, Nurnberg, GERMANY.

Introduce: Implantation of joint prostheses is becoming increasingly common, especially for the hip and knee. Aseptic loosening is considered to be the most devastating of prosthesis-related complications in early time and over more than one year later. In frames of this investigation different methods was used to determine correct diagnosis: radiography, bone scan with semiquantitativ methods and, on occasion, SPECT/CT. Methods: We reviewed 59 cases of patients (38 pts with hip and 21 pts with knee protheses) admitted all examination for bone scintigraphy with a clinical suspicion of aseptical loosening in a hip/knee prostheses during the period 2006-2015. All pts were compared with a reference painless group in which scintigraphy performed related to other indications. Bone metabolism within prosthesis was uniformly assessed by zones, and was strictly different between cementfree and cemented: by hip - acetabulum, trochanter major/minor, lateral/medial site from prosthesis, by knee as well medial/lateral femoral and tibial components. Bone uptake higher as 3,3 for cementfree, and 3,5 for cement protheses was suspious for loosening. Anterior and posterior/side views of both joints with semiquantitatively performed analysis were taken and was verified by means of radiography (59 pts), SPECT/CT (14 pts), histopathological findings (7 pts), intraoperative sections (3 pts), and clinical follow-up (59 pts). RESULTS: Of 59 scintigraphies, 35 were visually negative and 24 were positive, semiquantitatively: 40 negative and 19 positive. In SPECT/CT : 9 positive, 5 negative. In radiology analysis: 40 negative, 19 positive. There were in combination 80% true positive, 92% true negative, 5% false positive, and 14% false negative outcomes. RESUME: Bone scintigraphy with additional semiquantitative methods is an effective tool for differentiation of aseptical loosening in painful pts after joints arthroplasty. Next Stepp of investigation will be assesssment of absolute uptake data for joint prostheses by means of new calibrated SPECT/CT.

P213

Evaluation of SPECT/low dose CT Imaging in the assesment of equivocal spine lesions in planar bone scintigraphy

T. Pipikos[1], F. Vlachou[1], A. Nikaki[1], K. Dalianis[2], R. Efthymiadou[3], V. Prassopoulos[1]; [1]Nuclear Medicine Department Hygeia SA, Athens, Marousi, GREECE, [2]Medical Physics Department ,Hygeia S.A., Athens, Marousi, GREECE, [3]CT- MRI Department Hygeia SA, Athens, Marousi, GREECE.

AIM: Bone scintigraphy is being used for whole body skeletal staging in the diagnosis and follow up of cancer patients. One of the main disadvantages of the modality is low specificity, with high percentage of equivocal lesions, especially in the spine. With the usage of hybrid SPECT/low dose CT devices, there is the possibility of anatomic localization and further characterization of abnormal tracer uptake foci. In this study we evaluated the effect of SPECT/low dose CT imaging in the assessment of spine scintigraphy abnormalities. MATERIAL AND METHODS: We reviewed the planar and SPECT/low dose CT images of 91 patients who underwent bone scan in our department over the last year for malignancy staging and had equivocal spine findings in planar imaging. We examined if SPECT/CT lead to confident diagnosis or diagnosis remained equivocal. Planar and SPECT/CT images were reviewed blinded to each other, by the same nuclear medicine physician. Imaging was performed with a Philips Brightview XCT system. RESULTS: With the application of SPECT/CT, confident diagnosis was established in 71/91(78%) initially equivocal on planar images cases. In 62 cases a benign cause of abnormal tracer accumulation was established, with the majority of them being of degenerative origin. In 9 cases diagnosis was changed to bone malignancy. In 20 patients SPECT/CT results did not change equivocal status. Tracer uptake in these cases did not correspond to pathological lesions in low dose CT that could help diagnosis and was not located in a joint surface. CONCLUSION: Bone imaging with SPECT/low dose CT system increases diagnostic confidence and reduces the number of equivocal spine lesions. Equivocal status was preserved in only the 22% of the scans. The majority of the lesions that caused diagnostic problem were proven to be of degenerative origin.

P214

Interpolated CT for Respiratory Gated SPECT Attenuation Correction

D. Zhang, C. Y. Ho, **G. S. Mok**; University of Macau, Taipa, MACAO.

Aim: Respiratory gated 4D SPECT with phase-matched CT improves attenuation correction (AC) and reduces respiratory artifacts in cardiac SPECT. This study aims to develop and investigate the effectiveness of the interpolated CT (ICT) method for improved cardiac SPECT AC. Materials and methods: We modeled a male patient with normal 99mTc-sestamibi activity distribution using the digital 4D Extended Cardiac Torso phantom with respiratory motion amplitude of 2 and 4 cm. The respiratory cycle was 6 s and was divided into 96 frames which were grouped to simulate 6 respiratory

phases. The average attenuation and activity maps in each phase represented gated CT (GCT) and SPECT respectively, while the 8th and 56th frame of attenuation maps represented 2 helical CTs (HCT-in and HCT-ex). The average of all attenuation maps represented the cine average CT (CACT). We used affine plus b-spline registration method combined with an empirical sinusoidal function to generate interpolated phases between HCT-in and HCT-ex. Sixty noise-free and realistic noisy projections were generated using an analytical projector over 180 degrees from RAO to LPO with attenuation modeling to model a low energy high resolution parallel-hole collimator. Projections in each gate were reconstructed with different AC maps (GCT, CACT, HCTs and ICT) using OS-EM method with up to 200 updates. Reconstructed images in each phase were registered to the end-inspiration or end-expiration phases separately and then averaged to generate the polar plots. Relative difference (RD) of the average intensity was computed for each segment using the original phantom as the reference in the 17-segment analysis. Results: For motion amplitude of 2 cm, the RDmax for AC using GCT, ICT, CACT, HCT-in and HCT-ex were 1.38%, 2.51%, 3.31%, 13.57% and 6.80% when images were registered to end-inspiration. The RDavg of 17 segments were 0.48%, 0.96%, 0.93%, 4.21%, and 2.41% respectively. For images registered to end-expiration, RDmax were 1.26%, 3.05%, 5.19%, 19.94% and 3.67%, and RDavg were 0.50%, 1.34%, 1.78%, 6.86% and 1.61% respectively. The RD of HCTs deviated from the phantom notably in the basal inferior and lateral regions especially for higher motion amplitude. Conclusion: The GCT/ICT-AC improves the image quality and quantitative accuracy for respiratory gated cardiac SPECT as compared to CACT/HCT-AC, while using ICT can potentially further reduce the radiation dose.

P215

Accuracy of Quantification Methods for Renography with 99mTc-MAG3: A Study on Virtual and Clinical Image Data

I. Ceric[1], J. Bartosik[2], M. Ljungberg[1], G. Brolin[3], M. Sydoff[4]; [1]Medical radiation physics, Lund, SWEDEN, [2]Clinical Physiology and Nuclear Medicine, Helsingborg, SWEDEN, [3]Medical Radiation physics, Lund, SWEDEN, [4]Radiation physics, Lund, SWEDEN.

P216

The application of MIBI-Tc99m SPECT/CT scintigraphy in the diagnosis of thyroid - 5 years follow-up

M. H. Listewnik, H. Piwowarska-Bilska, M. Chosia, K. Jasiakiewicz, A. Dobrowolska, **B. Birkenfeld**; Pomeranian Medical University in Szczecin, Szczecin, POLAND.

Introduction:Thyroid nodules are a relatively common problem. In 5-8% of patients with nodular goiter, a malignant neoplasm is found. Problems with not conclusive results of fine needle aspiration biopsy (FNAB), contraindications to the surgery like an advanced age or concomitant diseases, general patient's reluctance to radical treatment account quite often on an outpatient basis. In the further diagnosis of these groups of patients technetium 99m labeled metoxyisobutylisonitrile (MIBI-99mTc) is used.Aim:The aim of the study was to establish the value of double phase MIBI-Tc-99m SPECT/CT scintigraphy in the diagnosis of nodular goiter and to assess the uptake of the tracer in focal lesions in relation to normal thyroid parenchyma using available methods of scintigraphy data processing.Methods: Altogether 44 (36F, 8M, AVG. 65 years) patients were recruited to the study. The diagnosis of nodular goiter and Hashimoto disease was established in 35 (80%) and 9 (20%) patients, respectively. FNAB showed benign lesions, suspicion of follicular tumors or a non-diagnostic result in 13(30%), 15(34%) and 15(34%) of cases, respectively. In 1(2%) case, no data about the result of FNAB was obtained. They were followed-up between 2009-2013 after their scintigraphy examination. Additionally, the tumor/background ratio (TBR) based on planar scintigraphy in early and delayed phase was calculated.Results: In the initial qualitative report, the examination was assessed as positive in 23 (52%) and negative in 21 (48%) cases. Four patients from the group with a positive result had surgery and no malignancy was found. If retrospective quantitative analyze for all patients was employed, the TBR varied between 1.00-2.24 (AVG. 1.2) in the early phase and 1.02-2.17(AVG. 1.18) in the delayed phase for nodular goiter. For Hashimoto disease the TBR varied between 1.06-1.33 (AVG.1.14) in the early phase and 1.09-1.19 (AVG. 1.14) in the delayed phase, respectively.Summary: 1. Negative double phase MIBI-Tc-99m SPECT/CT scintigraphy is a suitable way to avoid unnecessary surgery.2. It was showed that quantitative approach based on planar scintigraphy allows to avoid misinterpretation in the diagnosis.

P217

Determination of functional reserve capacity with fusion SPECT-CT examination after hepatic resection

H. Papp, K. Dede, Z. Egyed, F. Salamon, A. Bursics, Z. Galler; Uzsoki Teaching Hospital, Budapest, HUNGARY.

OBJECTIVESThe goal of our study was to determine the changes of functional activity and functional volume of the liver after hepatectomy in correlation with preoperative chemotherapy.METHODS40 patients were enrolled in the study mainly with colorectal liver metastasis (36/40 pts.). The chemotherapy was terminated at least 6 weeks before the surgery. All patients had normal preoperative liver function

without any sign of obstructive hepatobiliary pathology. We performed single photon emission computed tomography (with Tc-99m Mebrofenin (BrIDA)) and computed tomography and used fusion imaging method was performed to evaluate the preoperative, residual, early postoperative (1 week after surgery) and late postoperative (6 and 12 weeks after surgery) functional reserve capacity.RESULTSPatients were separated in two groups according to the type of resection (minor: <3 segments or major ≥3 segments). The regeneration was examined in further two subgroups of patients in accordance whether they received or not preoperative chemotherapy. The residual liver volume and activity significantly increased in all patients groups one week after operation. This increase was significantly higher in the major group than in the minor (minor without chemotherapy: ΔAav=36%, minor with chemotherapy: ΔAav=45%, major without chemotherapy: ΔAav=113%, major with chemotherapy: ΔAav=120%). Significant regeneration between 1st and 6th weeks could be observed only in case of patients presenting low increment on the first week. Hasn't been experienced significant changes in the late postoperative period.CONCLUSIONIn all patients the majority of the liver functional capacity was recovered in the first postoperative week and reached the original level until the 6th week. Preoperative chemotherapy had no effect on the recovery of the functional activity and functional volume after liver resection.

P218

A Pilot Study of 99mTc-3PRGD2 in Diagnosis of Primary Hepatic Carcinoma

Z. jieling, M. weibing; Department of Nuclear Medicine, First Affiliated Hospital of Fujian Medical University, Fuzhou City, Fujian Province, CHINA.

Aim:The purpose of this study was to explore the feasibility of applying the radioactive molecular probe 99mTc-3PRGD2 in primary hepatic carcinoma, thus supplying a new method of early diagnosis of hepatic carcinoma and guiding the anti-angiogensis targeted treatment of hepatic carcinoma.Methods:The animal model was established by subcutaneous injection of 5×107/ml HepG2 cells into the shoulder flank of each mouse. Biodistribution study was performed with sixteen animals. Another twelve animals with various tumor sizes(0.056-1.0g) were injected intravenously with 10uCi of 99mTc-3PRGD2, each tumor was counted on γ-counter after 1h of the injection, integrin αvβ3 expression levels were determined by immunohistochemical staining, analyzing the correlation between the tumor uptake and receptor expression. In 8, 12, 16, 20 and 24 days after the inoculation of HepG2, two animals were injected intravenously with 1.5mCi of 99mTc-3PRGD2 and 1.0mCi of 18F-FDG, a 45-min SPECT/PET acquisition was obtained by Versatile Emission Computed Tomography System(VECT or+/CT, Milabs, Utrecht, the Netherlands), starting 50 min after injecting. The tumor uptakes of 99mTc-3PRGD2 and 18F-FDG were separately quantified, assessing the advantages and disadvantages of 99mTc-3PRGD2 and 18F-FDG for imaging diagnosis of HCC.Results:Biodistribution study showed the tumor uptakes in different time were 4.301±0.313% ID/g (0.5 h), 6.902 ±0.717%ID/g (1 h), 5.045±0.193%ID/g (2 h) and 2.099 ±0.388%ID/g (4 h) respectively, which were high and last for a long time. There was a good Linear relationship (r=0.928,P<0.05) between the tumor uptake and the integrin αvβ3 expression levels. Multimodal imaging study indicated that 99mTc-3PRGD2 SPECT/CT could sensitively detected subcutaneous tumors in 8 days after inoculation of HepG2, when the tumor size was only 0.046cm3 and the uptake of 99mTc-3PRGD2 could reach 10.67%ID/cm3. Subcutaneous tumors were visualized clearly under SPECT/CT fusion imagings, the contrast between tumor and muscle was quite good. The uptakes of 99mTc-3PRGD2 increased untill tumor tissue necrotized. On the contrary, 18F-FDG PET/CT could not accurately detected subcutaneous tumors in 8-16 days after inoculation of HepG2, the uptakes of 18F-FDG were obviously below the uptakes of 99mTc-3PRGD2 at the same time.Conclusion:99mTc-3PRGD2 is a promising radiotracer in early diagnosis of primary hepatic carcinoma, and it can offer reliable scientific basis on guiding the anti-angiogensis targeted treatment of hepatic carcinoma.

P219

Utility of 99mTc HYNIC-TOC SPECT/CT in Neuroendocrine tumors

K. Kamaleshwaran, n. sudhakar, s. paulvannan, A. shinto; Kovai medical center and hospital limited, Coimbatore, INDIA.

Aim:The objective of this study was to evaluate the use of 99mTc HYNIC-TOC SPECT/CT in the diagnosis, staging and management of gastroenteropancreatic neuroendocrine tumors (GPNETs). Methods: 40 patients (median age, 55 years) with histologically proven GPNETs underwent 99mTc HYNIC-TOC whole body scintigraphy and regional SPECT/CT as indicated. Images were evaluated by two experienced nuclear medicine physicians both qualitatively as well as semi quantitatively (tumor to background and tumor to normal liver ratios on SPECT -CT images). Results of SPECT/CT were compared with the results of conventional imaging. Histopathology results and follow-up somatostatin receptor scintigraphy with 99mTc HYNIC TOC or conventional imaging with biochemical markers were considered to be the reference standards. Results: 10 patients had pancreatic tumor with liver

metastasis,15 patients with liver and bone metastasis,8 patients had lung metastasis and other 7 patients with nodal metatsasis.99mTc HYNIC TOC showed sensitivity and specificity of 92.5% and 90.7%, respectively, for primary tumor and 98% and 89% for metastasesIt showed better results than conventional imaging modalities for the detection of both primary tumor (P<0.001) and metastases (P<0.0001). management strategy was changed in 10 patients (25%) and supported management decisions in 10 patients (25%). Conclusion: 99mTc HYNIC TOC SPECT/CT appears to be a highly sensitive and specific modality for the detection and staging of GPNETs. It is better than conventional imaging for the evaluation of GPNETs and can have a significant impact on patient management and planning further therapeutic options.

P220

Impact of hybrid imaging SPECT / CT in the first staging of children's neuroblastoma

I. Meddeb, I. Slim, I. Yeddes, H. Boudriga, A. Mhiri, M. Ben Slimène; Salah Azaiez Institute, Tunis, TUNISIA.

Aim: Neuroblastoma is a malignant tumor derived from primitive neural crest cells that normally develop into cells of the sympathic nervous system. It is the most common extracranial solid tumor of the first decade of childhood. The MIBG scintigraphy allows us, to evaluate the tumor mass and its extension. The single photon emission computed tomography/ Computed tomography (SPECT/CT) improves the sensitivity of the examination. The purpose of our work is to illustrate the contribution of SPECT/CT in addition to the planar 123-I MIBG scintigraphy in the first staging of neuroblastoma. Materials and methods: 23 children with neuroblastoma (aged 3 months - 6 years) were studied to evaluate the accurate staging at the time of diagnosis. All patients underwent whole body scintigraphy and hybrid SPECT/CT images of the involved sites, 24 h after intravenous 123-I MIBG injection. Patients were asked to discontinue any medication interfering with I-123 MIBG uptake before the study. All images were acquired with Symbia Gamma Camera fitted with a low energy general purpose collimator. The whole body images were acquired at a speed of 8 cm/min. SPECT images were acquired in 64 × 64 matrix. Following the SPECT acquisition, CT was acquired. Hybrid SPECT/CT images were examined by evaluating the individual SPECT images, CT images and the fused SPECT/CT images. Results: Planar MIBG images demonstrated primary tumors in all patients; Overall, SPECT/CT provided additional information in 18 of the 23 cases (78%): SPECT/CT images gave us most detailed information about the local tumor extent in 10 cases showing particularly an extension to the spinal canal in two cases, and showed more metastatic lymph nodes involved in primary tumor in 6 of 23 patients. Concerning metastatic lesions they showed many more foci, as to bone and bone marrow lesions in 8 cases and hepatic metastases in 3 cases. Finally, SPECT / CT allowed us to reclassify five initially considered non-metastatic patients, showing bone metastasis in 3 cases and liver metastasis in two cases. Conclusion: The MIBG scintigraphy is a simple, non invasive examination that has excellent sensitivity and specificity in detection and staging of neuroblastoma in childhood. The hybrid SPECT/CT imaging improves the performance of the planar scintigraphy as well in sensibility toward the deep and small lesions, and in specificity for foci poorly identified on planar imaging.

P221

SPECT/CT and planar bone scintigraphy in the evaluation of vascularised graft reconstruction of the mandible; our experience

S. Rodriguez Martinez de Llano, I. Candal Casado, P. Pais Silva; Centro Oncologico de Galicia, Coruña, SPAIN.

Aim.Bone scintigraphy has been used to assess revascularisation of bone,because positive uptake reflects patent anastomoses and viability of the grafted bone.Comparison of planar bone scintigraphy,SPECT and SPECT/CT in the assessment of bone grafts in mandible reconstruction. Material and methods.A three year retrospective study was conducted(2012-2015),selecting patients referred to our department to perform a bone scintigraphy to assess revascularized mandibular bone grafts.Three-phase bone scan followed by SPECT/CT imaging took place 3 hours after intravenous injection of Tc-99m MDP(740 Mbq).Results were assessed qualitatively by three experienced nuclear physicians.For the evaluation of the grafts,a six-grade scoring system was applied,based on a comparison of tracer uptake between graft and the cranium.The uptake was defined as increasing from grade 6 to grade 1.In addition,the degree of agreement among nuclear physicians was studied(Cohen's kappa).Follow-up was used as gold standard. Results.11 patients were included, all submitted from the Oral and Maxillofacial surgery department.Four women and 7 men(mean age 58.72 years).Nine with cancer(epidermoid carcinoma n= 7,osteosarcoma n=2)and 2 with osteoradionecrosis.Mandible reconstructions were performed with vascularized autogenous microvascular grafts from the fibula(n=5),cranial-parietal(n=5)and iliac crest(n=1).Three-phase bone scintigraphy and SPECT/CT were obtained in all patients,19.09 days(mean value)postoperatively.Nine of the 11 grafts had an uncomplicated clinical course.Complications in the graft occurred in 2 patients with bone necrosis(with surgical confirmation).Patients with uncomplicated healing showed in planar scintigrams increased uptake in 5 grafts(grade 1-3).Four

showed grade 5-6,with significant overlying inflammation.Follow-up studies showed in two of these patients a final grade of 1 and 4(49 and 11 days after surgery respectively).In the failed 2 grafts,decreased uptake was observed(grade 5 and 6).SPECT changed the grade in one patient(from 5 to 4)and SPECT/CT in three, from 5 to 6.There was less indeterminate ratings with SPECT/CT than with planar scintigrams and SPECT.For planar scintigrams sensitivity was 56% and 67% for SPECT and SPECT/CT,specificity was 100% for all techniques.The degree of agreement among nuclear physicians was very good(Cohen's kappa 0.88)for this grading method. Conclusions.Three-phase bone scintigraphy is useful to monitor the viability of vascularized bone grafts.SPECT/CT is also recommended.It may contribute to interpretation of the studies and to precise assessment of graft viability(helped by CT bone window),separating the overlying soft tissues with hyperemia in the recent postoperative period from the bone.Graft-cranium uptake grading method is feasable with a very good degree of agreement between physicians.Caution using early scintigraphy decrease uptake results should be taken into account in the absence of complications after surgery,follow-up studies are advisable in these cases.

P222
Complex 99mTc-PDA-DTPA for myocardial imaging

E. A. Nesterov[1], S. I. Sazonova[2], V. S. Skuridin[1], S. M. Minin[3], E. S. Stasyuk[1], N. V. Varlamova[1], E. A. Ilina[1], A. A. Nesterov[4], V. I. Otmakhov[5]; [1]Tomsk Polytechnic University, Tomsk, RUSSIAN FEDERATION, [2]Research Institute of Cardiology, Tomsk, RUSSIAN FEDERATION, [3]Novosibirsk Research Institute of Circulation Pathology, Novosibirsk, RUSSIAN FEDERATION, [4]Sibnuclon Ltd, Tomsk, RUSSIAN FEDERATION, [5]Tomsk State University, Tomsk, RUSSIAN FEDERATION.

The 123I-labeled fatty acids such as 123I-Iodophenylpentadecanoic acid and 123I-Beta-methyl iodophenylpentadecanoic acid are the agents used clinically for myocardial imaging. Fatty acids are the major source of energy for the normal myocardium. However, under ischemic conditions the myocardial cells switch to glucose metabolism for their energy needs. Fatty acids undergo prolonged metabolic stunning in patients with reversible ischemia, thereby helping in early diagnosis of coronary artery disease in high-risk patients [Anupam Mathur,a Madhava B. Mallia etc // J. Label Compd. Radiopharm 2010, 53 580-585]. High cost and limited availability of cyclotron-produced 123I, makes 99mTc-labeled fatty acids more desirable for the purpose. In diagnosis the dominant radionuclide is 99mTc. It is estimated that it is involved in about 85% of all imaging procedures in nuclear medicine. The method for preparation of new 99mTc-fatty chemical systems based on modified diethylene triamine pentaacetic acid (DTPA) molecule has been elaborated in this work . The main advantage using DTPA as chelate agent for radioactive label, is the molecule or it's derivative ability to form sufficiently stable complexes with different radioactive metals including technetium-99. Moiety of pentadecanoic acid addition gave the ability to prepare modified complex of DTPA. In a labeling procedure, freshly eluted Na99mTcO4 (20mCi) was added to a mixture of cysteine, stannous chloride, PDK-DTPA and ethanol in a vial. On keeping the reaction mixture at 90 0C for 30 min, [99mTc-PDK-DTPA] radiopharmaceutical was formed. Thereafter, the reaction mixture was cooled over ice and characterized by HPLC. The result of dynamic scintigraphic research showed, that after being injected, the substance is actively acumulated into myocardium. Eventually one can say that modified DTPA-moleculs are functionally suitable for myocardial imaging. This work was supported by the Russian Federation represented by the Ministry of Education and Science of Russia (project № RFMEFI60414X0071).

P223
Quantification of left ventricular function using gated SPECT with two different automated software packages and cardiac MRI

K. Koyama[1], K. Kubota[1], M. Mochiki[1], T. Ogura[1], H. Hoshizaki[1], S. Oshima[1], T. Higuchi[2], Y. Tsushima[2]; [1]Gunma Prefectural cardiovascular center, Maebashi, JAPAN, [2]Gunma faculity of medicine, Maebashi, JAPAN.

(Aim)We compared quantification of left ventricular function using gated SPECT with two different automated software packages and cardiac MRI(Material and Methods)Fifty patients with coronary artery disease were examined at rest SPECT and cardiac MRI. Left ventricular end-diastolic volume (EDV), end-systolic volume (ESV) and ejection fraction (LVEF) were obtained by analyzing SPECT data with two different automated software packages: Quantitative Gated SPECT (QGS) and Cardio REPO. (Results) High correlation were noted in cardiac MRI and both two SEPCT data in EDV; QGS(r:0.81), Cardio REP(r:0.84), ESV; QGS(r:0.97), Cardio REPO(r:1.12) and LVEF; QGS(r:0.87), Cardio REPO(r:0.84) Cases of smaller ESV than 50ml in MRI, ESV of Cardio REPO showed larger than that of QGS. Cases of larger ESV than 50ml in MRI, ESV of Cardio REPO showed smaller than that of QGS. And cases of smaller LVEF than 60% in MRI, LVEF of Cardio REPO appeared larger than that of QGS and larger than 60%, LVEF of Cardio REPO smaller than that of QGS.(Conclusions)It may be useful to take this information

into consideration when determining values of left ventricular function in a clinical field.

P224

Value of Hybrid Imaging with 111In-Pentethreotide in Endocrine Tumors

D. BEN SELLEM, L. ZAABAR, B. DHAOUADI, B. LETAIEF, M. F. BEN SLIMENE; Nuclear Medicine Department, Salah AZAIEZ Institute, TUNIS, TUNISIA.

Aim: Endocrine tumors are rare. The purpose is to show the value of Somatostatin Receptor Scintigraphy (SRS) with hybrid imaging in the management of endocrine tumors.Materials and methods: 111 patients (56 males and 55 female) aged 51.77+/-15.71 years (12 to 87 years, median age 54 years) underwent 119 SRS.Indications were as follows, search for a primitive and staging in 23(19.23%) cases, preoperative with known primitive in 16(13.4%) cases, post operative in 13(10.9%) cases, tumoral characterization in 33(27.7%) cases, therapeutic evaluation in 9(7.6%) cases and search for recurrence in 25%(21%) cases.Results: In search for a primitive and staging, SRS was negative in three cases, diagnosed the primitive in 12 cases in whom 10 metastases were diagnosed. It failed to determine the primitive in 8 cases but established lesions cartography among theses latter's.Among the 16 patients with primary known lesions, SRS revealed abnormal radiotracer uptake in 12 patients with 10 metastatic sites, and was negative in 4 patients, in whom 2 metastatic sites were revealed.Post operative evaluation was negative in 8 patients and positive in 5 patients (with 3 distant metastases, one lymphatic node metastasis and one residual tumor site).In post-therapeutic evaluation, SRS concluded to remission in one patient, stabilization in 7 patients and progression for the last patient.In the evaluation of recurrent disease, SRS was negative in 14 patients and established the cartography of metastases in 11 patients.In the tumor characterization, SRS was negative in 25 cases. But revealed a primary location in 8 cases associated to distant metastasis in one case and to 3 lymph node metastases.Conclusion: SRS imaging with 111In-pentetreotide plays an important role in the diagnosis, the detection of extension and the follow up of patients with endocrine tumors.

P225

SPECT/CT in metastatic skeletal lesions

O. V. Solodyannikova; Institute of Oncology AMS of Ukraine, KIEV, UKRAINE.

Background: Single-Photon Emission Tomography/ Computed Tomography (SPECT/CT) using 99mTc-methylenediphosponate (99mTc-MDP) became more useful for the diagnostic of the skeleton lesions. It created wide possibilities for simultaneous assessment of morphological, functional and molecular processes in examined tissues and could increase diagnostic accuracy of the method in comparison with separately held SPECT and CT acquisition. The determination of abundance and scintigraphic differences of the lytic and sclerotic metastatic lesions is very important, because of their metabolic features. Our aim was to determine scintigraphic accordance of different kinds of the metastatic lesions by SPECT/CT. Materials and methods: 43 patients from 36 to 82 years old (mean 60,1±8,2) with metastatic bone lesions were examined. All patients had been done SPECT/CT of the lesions. Results: There were found 55 bone metastatic lesions.We divided all lesions into 4 samples by CT: 1-sclerotic clear-cut focuses (15 lesions, 27,2%), 2-sclerotic patchy lesions (11 lesions, 20%), 3- lytic lesions without clear margins (25 lesions, 45,5%), 4- lytic focuses with clear sclerotic rim (4 lesions, 5,8%). It was analyzed correlation X-ray and scintigraphic images on the combined scans. All lesions had bigger area on the SPECT scans then on corresponding CT scans.There are correspond intensive homogeneous 99mTc-MDP uptake to 12 sclerotic clear-cut lesions, and3 lesions from the first group hadn't any uptake in it. These 3 lesions evaluated as the sponges bone condensations - "bone islets". All 11 of sclerotic patchy lesions had intensive or moderate intensity of 99mTc-MDP accumulation. All lytic lesions hadn't uptake of 99mTc-MDP in the middle of them, but they had moderate uptake near that lesions in the bone tissues. Lytic focuses with clear sclerotic rim had high intensive inhomogeneous uptake. Moreover, some zones of moderate uptake of 99mTc-MDP have not corresponding CT abnormalities. Conclusion: SPECT/CT is the useful method for size and features evaluation of bone metastatic lesions. It defined that area of metabolic abnormalities always is bigger than structural changes. Scintigraphic images of lytic and sclerotic lesions had some difference that shows divergent intensity and localization of pathologic process in them. There were benign sclerotic focuses that had not accumulate 99mTc-MDP. Metastatic lesions could be detected by Scintigraphy earlier than on the X-ray examination.

P226

The influence of age, sex and circadian rhythm on kidney function in mice measured by Tc-99m-MAG3 SPECT

K. P. Huang, I. G. Steffen, M. Lukas, C. Lange, C. Rosner, W. Brenner, **N. Beindorff**; Charite - Universitaetsmedizin Berlin, Berlin, GERMANY.

Aim: The aim of this longitudinal study was to establish standard values for the time activity curves (TAC) of Tc-99m-MAG3 for the evaluation of kidney excretion as a function of age, sex and circadian rhythm in healthy mice. Materials and methods: Six female and 6 male C57BL/6 mice were housed under standardized conditions (12 h light versus 12 h darkness). In anesthetized animals (isoflurane), a CT scan was used to position both kidneys within the 14-mm axial FOV of the dynamic semi-stationary SPECT (nanoSPECT/CTplus, Mediso). The SPECT acquisition consisting of 10 frames of 20 s followed by 25 frames of 50 s was initiated at the time of intravenous Tc-99m-MAG3 injection (23-77 MBq). Each mouse was imaged in follow-up studies up to 12 months (A: 1 month, puberty; B: 3 months, sexual mature, but not fully grown; C: 6 months, fully grown; D: 12 months). In order to monitor circadian rhythm, animals were imaged during day (sleeping phase (SP)) as well as during night conditions (awake phase (AP)). Image viewing and quantification were performed using InVivoScope 2.00 (Bioscan). Kidney excretion is expressed as time to peak (Tmax) in minutes (median [interquartile range; IQR]). Differences between groups were tested using Friedman, Mann-Whitney-U or Wilcoxon test. Results: Tmax was 1.6 [1.3-1.9] in all mice. Females showed a significantly later Tmax than males (1.6 [1.3-2.0] versus 1.3 [1.3-1.6]; P<0.001). With respect to age, this gender effect could be observed from 6 months onwards: A (female 1.5 [1.3-1.7], male 1.5 [1.0-1.9]; P=0.19), B (female 1.3 [1.3-1.4], male 1.3 [1.3-1.4] P=0.37), C (female 1.6 [1.6-2.0], male 1.3 [1.0-1.3]; P<0.001), D (female 2.0 [1.8-2.4], male 1.6 [1.4-1.9]; P<0.001). In general, mice showed an age-dependent Tmax with significantly increasing values after 6 months of age: A 1.5 [1.3-1.9], B 1.3 [1.3-1.4], C 1.6 [1.3-1.6], D 1.9 [1.6-2.2]; P<0.001). Circadian rhythm revealed a significant impact on Tmax in males (SP 1.6 [1.3-2.0], AP 1.3 [1.0-1.6]; P=0.02), while in females no significant difference could be observed so far (SP 1.6 [1.3-2.1], AP 1.7 [1.6-2.0]; P=0.13). Conclusion: This study showed a significant impact of age, sex, and partially of circadian rhythm, on kidney excretion of Tc-99m-MAG3. The limited effect of circadian rhythm might be due to the small number of animals so far. In summary, it seems essential for kidney analysis in mice to consider the impact of age, sex and circadian rhythm.

P227

Preclinical SPECT-CT imaging studies with cyclotron produced Tc-99m

G. Pupillo[1], A. Boschi[2], P. Martini[3], L. Uccelli[2], M. Pasquali[2], A. Duatti[2], G. Di Domenico[3], M. Loriggiola[1], M. Giganti[2], A. Taibi[3], M. Gambaccini[3], A. Salvini[4], L. Strada[4], M. Prata[4], M. Marengo[5], G. Lucconi[5], S. Manenti[6], F. Groppi[6], G. Cicoria[5], M. Bello[7], N. Uzunov[8], J. Esposito[1]; [1]Legnaro National Laboratories of the Italian Institute of Nuclear Physics (INFN), Legnaro (Padova), ITALY, [2]Department of Morphology, Surgery and Experimental Medicine, University of Ferrara, Ferrara, ITALY, [3]Department of Physics and Earth Science, University of Ferrara, Ferrara, ITALY, [4]Applied Nuclear Energy Laboratory and Department of Chemistry, University of Pavia, Pavia, ITALY, [5]Nuclear Medicine S. Orsola Hospital, Bologna, ITALY, [6]Accelerator and Applied Superconductivity Laboratory and Physics Department, University of Milano, Milano, ITALY, [7]Department of Physics and Astronomy, University of Padova, Padova, ITALY, [8]Faculty of Natural Sciences, Shumen University, Shumen, BULGARIA.

Aim: This work reports results of a preclinical study aimed at evaluating the diagnostic quality of radiopharmaceuticals prepared using cyclotron-produced Tc-99m as compared to generator-produced Tc-99m analogues. Material and methods: Enriched (99.05%) Mo-100 metallic targets were irradiated with a proton beam having energies within the range 19−17 MeV. Purification of Tc-99m from the irradiated targets was carried out by solvent extraction using methyl-ethyl ketone (MEK) having a well-established selective affinity for the pertechnetate ion. Further chromatographic purification afforded Tc-99m in physiological solution that was subsequently employed for the preparation of a number of Tc-99m radiopharmaceuticals for perfusion cardiac and brain imaging. Radionuclidic purity (RNP) of the Tc-eluate was measured by γ-spectrometry and radiochemical purity (RCP) of Tc-radiopharmaceuticals was checked by radio-TLC and HPLC. Anesthetized Wistar rats were injected into the jugular vein and in vivo whole-body SPECT-CT images were collected with a hybrid YAP(S)PET-CT small-animal scanner. SPECT-images were corrected for injection time and activity. Results: Radionuclidic purity of accelerator-produced Tc-99m was in the range 99.3 ± 0.2% at the end of bombardment (EOB) and 99.5 ± 0.2% at the end of chemical extraction (6 hours after EOB). Main radionuclidic impurities originated from the presence of the γ-emitting Tc-isotopes Tc-93, Tc-94g, Tc-95g and Tc-96g. This caused a detectable scatter effect on SPECT images mostly generated by the interaction of these parasite γ-rays with the high-resolution collimator of the small-animal scanner. For this reason, a scatter-correction method, based on the definition of different energy ranges, was implemented on these images. Considering the efficiency of the correction approach and the high-capacity of biological sites targeted by Tc-99m perfusion imaging agents, the impact on the image quality was negligible when compared with the same images collected with generator-produced Tc-99m. Conclusions: In vivo SPECT-CT preclinical imaging study in a rat animal model using a high-resolution small-animal scanner confirmed a superimposable biodistribution behavior of heart and brain perfusion Tc-99m radiopharmaceuticals labeled with both cyclotron- and generator-produced Tc-99m. However, it

should be noted that the effect of scattered high-energy γ-rays, generated by the decays of technetium radioisotopes impurities in cyclotron-produced Tc-99m, strongly depends on the specific imaging system and, therefore, extrapolation to images obtained with available SPECT cameras for human studies is not straightforward. This points to the need of conducting dedicated imaging tests with conventional SPECT imaging equipment employed in a clinical setting.

P228

Development of cancer-targeted Nuclear/NIRF/PTT multi-modality theranostic probe

C Peng[1], Y. Shih[1], T. Luo[1], M. Shieh[2]; [1]Institute of Nuclear Energy Research, Taoyuan, TAIWAN, [2]Institute of Biomedical Engineering, National Taiwan University, Taipei, TAIWAN.

Aim: Cancer is one of the leading death causes in the world. Cancer-targeted multifunctional probe labeled with the radionuclide has been developed to provide multi-modalities for NIR fluorescence and nuclear imaging (SPECT) and for photothermal therapy (PTT) of cancer.Materials and methods: In this study, synthesis, characterization, *in vivo* biological evaluation of a heptamethine cyanine-based SPECT/NIRF/PTT multi-modality theranostic probe were described. The NIR dye, heptamethine cyanine, allowed the probe to have multi-functions in cancer NIR imaging and photoththermal therapy (PTT).Results: The radionuclide-labeled probe enabled imaging by NIR fluorescence and by nuclear imaging (SPECT) to monitor in real-time the tumor accumulation, intra-tumoral distribution, and to guide the PTT.Conclusion: In summary, the radionuclide-labeled theranostic probe offer multi-modalities for NIR fluorescence and nuclear imaging and for PTT of cancer.

P229

Synthesis and Evaluation of a Novel Tc-99m Labeled HGK-containing Hexa-Peptide for Non-Invasive Tumor Imaging

D. Kim[1], W. Kim[2], M. Kim[1], C. Kim[1]; [1]Wonkwang University School Of Medicine, IKSAN, JEOLLABUK-DO, KOREA, REPUBLIC OF, [2]Seoul National University Hospital, Jongno-Gu, Seoul, KOREA, REPUBLIC OF.

Aim: Domain 5 of kinin-free high molecular weight kininogen inhibits the adhesion of many tumor cell lines and it has been reported that the histidine-glycine-lysine (HGK)-rich region might be responsible for inhibition of cell adhesion. Despite the good property of HGK peptide binding specifically to tumor cells, the development of imaging agent using HGK peptide had not been reported until now. The authors developed HGK-containing hexapeptide, glutamic acid-cysteine-glycine (ECG)-HGK to target tumor cells, and evaluated the feasibility of Tc-99m ECG-HGK as a molecular imaging agent. Materials and Methods: Hexapeptide, ECG-HGK was synthesized using Fmoc solid-phase peptide synthesis. Radiolabeling efficiency was evaluated using radio-high-performance liquid chromatography (radio-HPLC) and instant thin layer chromatography (ITLC). The uptake of Tc-99m ECG-HGK within HT-1080 cells was evaluated in vitro by the calculation of cellular binding affinity and confocal microscopy. In HT-1080 tumor-bearing mice, gamma images were acquired and tumor-to-muscle uptake ratio was calculated, and a biodistribution study was also performed. Results: After radiolabeling procedures with Tc-99m, the complexes Tc-99m ECG-HGK was prepared in high yield (>95%). The Kd of Tc-99m ECG-HGK determined by saturation binding was 263.7 ± 63.0 nM and the value of Bmax was 3329.0 ± 335.8 nM. Confocal microscopy images of HT-1080 cells showed strong intersperse fluorescence of FITC-ECG-HGK in cytoplasm of the tumor cells. The gamma camera imaging in the murine model showed that Tc-99m ECG-HGK was accumulated substantially in the HT-1080 tumor and the tumoral uptake was blocked by the co-injection of excess HGK. The tumor-to-normal muscle uptake ratio of Tc-99m ECG-HGK reached 5.7 ± 1.4 at 4 h (2.8 ± 0.8, 3.6 ± 0.2, 4.9 ± 0.4 and 5.7 ± 1.4 at 30 min, 1 h, 2 h and 4 h, respectively). The %ID/g value in the tumor was 1.37 ± 0.61, and tumor uptake was suppressed by co-injection of free HGK (0.37 ± 0.09). Tumor-to-normal muscle ratios of %ID/g were 4.8 ± 3.9 and it was decreased by co-injection of free HGK (1.4 ± 1.3, $p < 0.05$). Conclusion: This study successfully had developed Tc-99m ECG-HGK as a new tumor imaging agents in HT-1080 tumor. Tc-99m ECG-HGK showed a significant uptake in the tumor, and it is a good candidate for tumor imaging.

P230

SPECT/CT Imaging of Radionuclide-carrying Liposomes Predict Therapeutic Effects of Liposomal Anti-cancer Agents in Mouse Xenograft Models

I. O. Umeda[1], K. Ito[2], S. Hamamichi[1], M. Asano[2], M. Iwata[2], J. Matsui[2], Y. Hori[2], Y. Funahashi[2], H. Fujii[1]; [1]National Cancer Center, Kashiwa, JAPAN, [2]Eisai Co., Ltd., Tsukuba, JAPAN.

Objectives: Liposomal anti-cancer agents can effectively deliver drugs to tumor lesions and enhance therapeutic effects in the limited number of cancer patients. Appropriate biomarkers to identify responder are crucial for effective treatment. Here, we generated radiolabeled liposomes; i.e., liposomes encapsulating

^{111}In-DTPA, with lipid composition and size identical to Doxil®, liposomes encapsulating doxorubicin, and evaluated their usefulness to predict therapeutic effect of Doxil by SPECT/CT tumor images before the initiation of the treatment. Methods: Anti-tumor effects of Doxil to four human ovarian cancer xenograft models (Caov-3, SK-OV-3, KURAMOCHI, and TOV-112D) were evaluated though comparison of the tumor size suppression with free doxorubicin. Histopathological studies were also performed.^{111}In-labeled liposomes were prepared by using remote loading method, and their tumor accumulation after intravenous administration was determined quantitatively by measurement of their radioactivities *ex vivo* and by *in vivo* SPECT/CT imaging. Results: Anti-tumor activities of Doxil was drastically enhanced in Caov-3, moderate in SK-OV-3, and minimum in other two tumors. Doxil-perfusion assay, by observation of the autofluorescence of Doxil in the tumor, suggested that the tumor accumulation of Doxil was much higher in Caov-3 and relatively higher in SK-OV-3 than in others. The microvessel density and vascular perfusion were high in Caov-3 and SK-OV-3. The tumor accumulation of ^{111}In-labeled liposomes at 72 h after administration was high in Caov-3 and SK-OV-3 (4.0 - 4.3 % of administered dose/g of tumor, %AD/g), while it was less than 1.5 %AD/g in other two tumors. Area under the curve values over 72 h was the highest in Caov-3, followed by SK-OV-3. It was very low in other two tumors. These results were consistent with the aforementioned retention and therapeutic efficacy of Doxil in these 4 tumors. Importantly, since both Doxil effects and radiolabeled liposomal accumulation varied especially among SK-OV-3 tumor groups, we individually obtained SPECT/CT images of each SK-OV-3 bearing mouse (n=11) and then administered Doxil to them. A clear correlation between the liposome tumor accumulation and the effects of Doxil was confirmed (R^2=0.73). Discussion: These results indicated that anti-tumor activities of Doxil depended on its tumor accumulation which was closely related to the microvessel density and vascular perfusion. Tumor accumulation of radiolabeled liposomes evaluated in SPECT images should predict the anti-tumor activities. Conclusions: Radiolabeled liposomes would be a promising imaging biomarker to predict the therapeutic efficacy of liposomal anticancer drugs, such as Doxil.

P231

Imaging somatostatin receptor expression on macrophages in osteoarthritis models

S. T. van Tiel, J. de Swart, L. Utomo, M. de Jong, M. R. Bernsen; ErasmusMC, Rotterdam, NETHERLANDS.

Introduction: Macrophages are present ubiquitously in the body and they can be polarized in a dynamic way towards different physiologies (M1, M2a-d) that negatively or positively affect many different disease processes. The ability to non-invasively determine the activation type of disease-associated macrophages may therefore aid in earlier or more precise diagnostics/prognostics of disease. A variety of tracers have been suggested for this purpose. A number of studies have indicated that the somatostatin receptor subtype 2 (SSTR2) is expressed on the M1, inflammatory response inducing, macrophages. 111In-Octreoscan (111In-DTPA-octreotide) is a well-known tracer for tumour imaging, binding SSTR2 with good affinity. The aim of this study was to study the feasibility of 111In-Octreoscan for M1 macrophage SPECT imaging in two osteoarthritis (OA) mouse models, which differ in inflammation severity. Materials and methods: Male C57Bl/6 mice were used. Osteoarthritis was induced by: 1) CIA = Collagenase Induced Arthritis; injection of collagenase (10 U/ 6 µl) in the knee, causing a severe form of OA. For control purposes the contra-lateral knee was injected with 6 µl water for injection, 2) DMM = Destabilization of the Medial Meniscus, causing a milder form of OA. The contra-lateral knee underwent sham surgery for control purposes. At different time points post surgery the mice were imaged (between 1 day and 8 weeks), 2 hours after intravenous injection of 60 MBq 111In-Octreoscan. After the last scan the knees were prepared for histological staining. Results: Uptake of 111In-Octreoscan was observed in the diseased knee and almost never in the contralateral control knee. Uptake appeared to be model and time dependent. Comparing the severe form of OA with the mild form of OA the most lesion-associated uptake is seen in the severe model. Lesion-associated uptake is also seen more often when OA development progresses in time, in both models. Currently we are validating the imaging findings using histological analysis and correlating the findings to disease severity, especially the inflammatory status. Conclusions: Imaging of SSTR2 in mouse models of osteoarthritis showed lesion-associated uptake, and is therefore promising to become a relevant marker to non-invasively detect and monitor disease state.

P12 - Sunday, October 11, 2015, 4:00 PM - 4:30 PM, Hall 3 – Poster Exhibition

Molecular & Multimodality Imaging: Tumour Biology

P232

The Metabolic Role of Carbenoxolone in Cancer: a Possible Interference in Glucose Metabolism and FDG Uptake Through the Inhibition of the Endoplasmic Reticulum Hexose-6-Phosphate Deydrogenase.

A. Orengo[1], A. Buschiazzo[1], G. Sambuceti[1], S. Ravera[2], S. Bruno[3], F. Fais[3], C. Ghersi[1], G. Bianchi[4], R. Martella[4], L. Raffaghello[4], C. Marini[5]; [1]Nuclear Medicine Unit, Department of Health Sciences, University of Genoa and IRCCS AOU San Martino-IST, Genoa, ITALY, [2]Department of Pharmacy, University of Genoa, Genoa, ITALY, [3]Department of Experimental

Medicine, University of Genoa and IRCCS AOU San Martino-IST, Genoa, ITALY, [4]Laboratory of Oncology, G. Gaslini Institute, Genoa, ITALY, [5]CNR Institute of Bioimages and Molecular Physiology, Section of Genoa, Genoa, ITALY.

Aim. Hexose-6-phosphate dehydrogenase (H6PD) is a housekeeping enzyme dedicated to the redox homeostasis of the endoplasmic reticulum (ER). Differently from its cytosolic counterpart glucose-6-phosphate dehydrogenase (G6PD), H6PD recognizes the phosphorylated forms of both glucose and 2-deoxyglucose as substrates. It can thus contribute to FDG retention. To test this hypothesis, we studied the effect of carbenoxolone (CBX), a specific H6PD inhibitor, on FDG uptake and distribution in two murine cell lines of colon (CT26) and breast (4T1) carcinoma. Materials and Methods. In both cell lines, the effect of 24 hours CBX exposure was evaluated by comparing response of FDG uptake with the measurement of glucose disappearance from supernatant. Glucose concentration of administered medium was 11.1 mM and sugar disappearance was monitored for 24 hours. FDG uptake was tested through 30 minutes, using a glucose free medium and a tracer concentration of 37 kBq/mL. Western blot and spectrophotometric analysis were applied to cell lysates to study abundance of GLUT1 as well as expression and enzymatic activity of hexokinases, H6PD and its cytosolic counterpart G6PD. Results. Preliminary experiments with purified enzymes confirmed that H6PD is active on both G6P and 2DG6P. On the contrary, the unique substrate for G6PD was G6P. CBX did not alter H6PD expression while it significantly inhibited enzyme activity reducing cell lysate capability to dehydrogenate 2DG6P by 53±2% and 51±3% of control values in CT26 and 4T1 cells, respectively ($p<0001$). On the contrary, G6PD function (measured using G6P as substrate) was not affected by drug exposure in both cell lines. Moreover, with respect to untreated cells, CBX reduced to a similar degree glucose consumption (89±2% and 67 ±5%) and FDG uptake (78±2% and 61±4%) in CT26 and 4T1 cells, respectively. Finally, the role of H6PD in cancer glucose consumption and FDG retention was confirmed by the evidence that the fluorescent 2DG analogue (2NBDG) was actually sequestered within the ER. In both cell lines, CBX decreased 2NBDG colocalization with ER vital probe by more than 50%. Conclusion. H6PD enzymatic function accounts for a significant part of cancer glucose consumption and FDG uptake in cancer cells.

P233

Inhibiting hexose-6-phosphate dehydrogenase gene expression significantly reduces 18F-fluorodeoxyglucose uptake and cancer cells proliferation in two experimental models of colon and breast carcinoma.

C. Marini[1], G. Sambuceti[2], S. Bruno[3], A. Orengo[2], A. Buschiazzo[2], S. Ravera[4], A. Democrito[2], G. Bianchi[5], L. Raffaghello[5], G. Caviglia[6], F. Fais[3]; [1]CNR Institute of Bioimages and Molecular Physiology, Section of Genoa, Genoa, ITALY, [2]Nuclear Medicine Unit, Department of Health Sciences, University of Genoa and IRCCS AOU San Martino-IST, Genoa, ITALY, [3]Department of Experimental Medicine, University of Genoa and IRCCS AOU San Martino-IST, Genoa, ITALY, [4]Department of Pharmacy, University of Genoa, Genoa, ITALY, [5]Laboratory of Oncology, G. Gaslini Institute, Genoa, ITALY, [6]Department of Mathematics, University of Genoa, Genoa, ITALY.

Aim. The autosomally linked enzyme hexose-6-phosphate dehydrogenase (H6PD) catalyzes the first two reactions of pentose phosphate pathway transforming glucose-6-phosphate (G6P) to 6-phospho-gluconate within the endoplasmic reticulum (ER). Differently from its cytosolic counterpart, sex-linked G6P dehydrogenase, H6PD can process a large number of substrates beyond G6P including glucose, galactose-6P and 2-deoxyglucose-6P (2DG6P). Aim of this study was to evaluate whether this enzyme feature might contribute to 18F-fluorodeoxyglucose (FDG) retention in cancer.Materials and Methods. H6PD activity was studied in CT26 and 4T1 cell lines as models of murine colon and breast carcinoma. Gene silencing was obtained by transfection with 75 nM H6PD siRNA or SilencerTM Negative Control siRNA as a scramble. The protocol implied a validation phase measuring the response of 2DG6P dehydrogenation in lysates of treated and control cells. Once optimized siRNA administration procedure, effect on glucose consumption was evaluated by measuring glucose disappearance from culture medium with a glucose concentration set at 11 mM. FDG uptake was measured using a validated procedure with tracer administration for 30 minutes at a concentration of 37 KBq/mL in a glucose-free medium. Finally, fluorescent 2DG probe 2-[N-(7-nitrobenz-2-oxa-1,3-diazol-4-yl)amino]-2-deoxyglucose (2NBDG) was used to evaluate metabolite distribution and its co-localization with vital probes for ER detected by confocal microscopy and analyzed by a specific software (ImageJ).Results. In CT26 and 4T1 cells, gene silencing reduced H6PD enzymatic activity to 12.16% and 17.18% of control values ($p<0.001$), respectively. As a functional correlate, siRNA decreased glucose consumption (to 73%±5% and 74%±5%, $p<0.01$) and even more FDG uptake (to 54±3% and 49±2%, $p<0.001$). Scramble siRNA did not exert any effect on glucose metabolism nor on FDG retention. Fluorescent 2NBDG experiments documented a high co-localization of 2DG6P and ER signals in untreated cells (54±2% in CT26 and 58±4% in 4T1 cells). This pattern was markedly modified by H6PD silencing that decreased this match to 12±1% and 16 ±2%, respectively ($p<0.001$ vs controls). Finally, the decreased tracer uptake and the cytosolic localization of 2DG6P predicted a significant reduction of cell proliferation in the 72hours of gene silencing (to 58% in CT26 and 17% in

4T1 cells respect to controls, p<0.001).Conclusion. Taken together, our data suggest a fundamental role for H6PD enzymatic function in FDG uptake mechanism and proliferation rate of two different models of colon and breast carcinoma.

P234

The Metabolic Role of Metformin in Cancer: the Divergent Effect Between FDG Kinetic and Glucose Consumption on Cancer Aggressiveness

A. Buschiazzo[1], A. Orengo[1], S. Ravera[2], B. Salani[3], U. Pfeffer[4], F. Pastorino[5], A. Brizzolara[6], L. Raffaghello[5], G. Bianchi[5], F. Bongioanni[1], G. Sambuceti[1], C. Marini[7]; [1]Nuclear Medicine Unit, Department of Health Sciences, University of Genoa and IRCCS AOU San Martino-IST, Genoa, ITALY, [2]Department of Pharmacy, University of Genoa, Genoa, ITALY, [3]Department of Internal Medicine, University of Genoa, Genoa, ITALY, [4]Department of Integrated Molecular Pathology, IRCCS AOU San Martino-IST, Genoa, ITALY, [5]Laboratory of Oncology, G. Gaslini Institute, Genoa, ITALY, [6]Department of Experimental Medicine, University of Genoa and IRCCS-AOU San Martino-IS, Genoa, ITALY, [7]CNR Institute of Bioimages and Molecular Physiology, Section of Genoa, Genoa, ITALY.

Aim.Previous studies demonstrated a metformin effect on mitochondrial respiration through the inhibition of Complex I in different cancers. The aim of this study is to determine if the inhibition of respiratory chain causes a reduction in cancer cells energy asset. Materials and Methods.We evaluated cells culture in 5 ml of DMEM medium with a 11.1 mM glucose concentration for 48 hours. Glucose consumption was evaluated by monitoring sugar disappearance from supernatant over 24 hours under control condition and under metformin exposure (5 mM for 24 hours). FDG uptake was tested through 30 minutes using a glucose free medium and a tracer concentration of 37 kBq/mL. 5' AMP-activated protein kinase (p-AMPK) was measured by Western blotting, lactic dehydrogenase (LDH) spectrophotometrically, oxygen consumption using a thermostatically controlled oxygraph apparatus and ATP concentration by the luciferin/luciferase chemiluminescent method. Results.Metformin virtually abolished oxygen consumption through Complex I-III-IV in two murine cell lines of colon and breast carcinoma, CT26 and 4T1. Despite a preserved activity of pathway II-III-IV this action severely impaired ATP synthesis eventually leading to a fall in ATP availability and a decrease in ATP/AMP ratio. This severe energy depletion was confirmed by the expected reaction of energy sensor mechanisms, by the accelerated phosphorylation rate of p-AMPK and by marked decrease in cell proliferation rate. Metformin increased glucose consumption to 190 ±5% and 268±7% of controls in CT26 and 4T1, respectively (p<0.001). The corresponding increase in glycolytic flux was documented by the marked increase in lactate production (2.1 ±0.1 to 4±0.2 and 1.8±0.1 to 3.2±0.16 uM/106cells, p<0.01) and release (2±0.1 to 2.5±0.12 and 1.1±0.05 to 2.3±0.1 uM, p<0.01) in both cell lines, despite invariance of LDH activity. On the contrary, drug exposure decreased FDG uptake to 24 ±2% and 39±3% of baseline values in the same cell lines, respectively (p<0.001). The combined analysis of glucose consumption and FDG uptake confirmed this paradoxical divergence in broad panel of human cancer cell lines representative of NSC lung, breast and prostate carcinomas, melanoma and neuroblastoma. All these models confirmed the divergent response of glucose consumption and FDG uptake. Conclusion. Metformin directly inhibits mitochondrial respiration and depletes ATP asset of cancer cells. The consequent acceleration in glycolytic disposal faces an opposite response FDG uptake that is markedly decreased by the biguanide. Differently from glycolysis, FDG kinetic response to metformin directly predicts cancer cell proliferation, indicating a direct correlation between FDG uptake and cancer aggressiveness independent from glucose consumption.

P235

Cellular uptake and localization of a novel NSCLC penetrating peptide

H. Zhou, P. Dong, H. Cai, X. Wu, L. Li; West China Hospital, Chengdu, CHINA.

Objectives : CendR motif peptide (CRMP) has high affinity to neuropilin-1 (NRP-1), which is a widely expressed tumor marker in lung cancer, breast cancer, and colon cancer, etc. In this study, a novel NSCLC-targeting (Non-small cell lung carcinoma) peptide was designed and its penetrating capability was initially tested in vitro. This peptide was comprised with three motifs: CS motif which binds to NSCLC cells, peptidase restriction site, and cryptic CendR motif. Once CS motif has brought peptide to tumor, peptide is proteolytically cleaved and expose the CenR sequence; the truncated peptide lose its affinity for primary receptor but binds to NRP-1, and activating tissue-penetrating pathway. A tyrosine was added to N-terminal of comprised peptide for future radio-labeling. Methods : NRP-1 binding peptide CRMP-1, NSCLC binding peptide CS, and novel designed peptide YCCS were N-terminal FITC labeled. Human NSCLC cell A549 (NRP-1 +), human breast cancer cell MDA-MB-231 (NRP-1 +), normal human bronchial epithelium HBE135-E6E7 (NRP-1 -) and human liver cell HL-7702 (NRP-1 -) were used for binding test. Each one was inoculated into 96-well plate and 3 kinds of peptides were respectively added as 20μM. After 4h incubation, the cellular binding and localization of CRMP1, CS and YCCS were assessed by fluorescent microscope. Results :

CRMP-1 fluorescent signals were detected in A549 and MDA-MB-231 cells, while marginal in HBE135-E6E7 or HL-7702. Our novel multifunctional YCCS peptide showed significant fluorescent signals in A549 cells, which revealed good NSCLC binding affinity and that tyrosine addition for potential radioisotope labeling did not show influence to its binding capability. However, no captured signal of FITC-YCCS in MDA-MB-231 indicated that NSCLC binding motif blockage successfully inhibited the cryptic CRMP-1 binding unless primary motif cleavage and improved selectivity of our peptides to unexpected cells. Conclusions : The novel YCCS peptide indicated a promising strategy for improving tumor penetrating peptide with delivery capability of radiopharmaceutical drugs to NSCLC cells.

P236

Effect of Metformin on Cancer Glucose Metabolism: Correlation Between FDG Escape and Glucose-6-Phosphatase Activity in the Endoplasmatic Reticulum.

A. Buschiazzo[1], G. Sambuceti[1], A. Orengo[1], S. Ravera[2], F. Fais[3], S. Bruno[3], E. Monteverde[1], L. Garaboldi[1], G. Bottoni[1], L. Raffaghello[4], G. Bianchi[4], M. Piana[5], S. Garbarino[5], G. Caviglia[5], C. Marini[6]; [1]Nuclear Medicine Unit, Department of Health Sciences, University of Genoa and IRCCS AOU San Martino-IST, Genoa, ITALY, [2]Department of Pharmacy, University of Genoa, Genoa, ITALY, [3]Department of Experimental Medicine, University of Genoa and IRCCS AOU San Martino-IST, Genoa, ITALY, [4]Laboratory of Oncology, G. Gaslini Institute, Genoa, ITALY, [5]Department of Mathematics, University of Genoa, Genoa, ITALY, [6]CNR Institute of Bioimages and Molecular Physiology, Section of Genoa, Genoa, ITALY.

Aim. In most solid cancers the high needs of ATP result in an accelerated rate of glucose consumption. The exploitation of this glycolytic phenotype became a standard to diagnose cancer and to monitoring its aggressiveness by 18F-fluorodeoxyglucose (FDG) imaging. This glucose analogue enters the cell and is phosphorylated through the same GLUT carriers and the same hexokinases active on glucose. However, FDG-6-phosphate (FDG6P) is a false substrate for downstream enzymes triggering glycolysis and pentose phosphate pathway and is thus accumulated within the cytosol according to the overall glucose consumption. Critical to this model is the irreversible nature of FDG phosphorylation that prevents its loss from cytosol. However, most mammalian cells express different isoforms of G-6P-phosphatase (G6Pase) that might recognize FDG6P as a substrate. The present study aimed to verify whether cancer cells express G6Pase and whether this enzyme can alter FDG trapping mechanism. Materials and Methods. We studied murine colon (CT26) and breast carcinomas (4T1) cells, cultured in 5ml of DMEM medium with a 11.1 mM glucose concentration for 48 hours. To modify cell glucose consumption we used metformin (MTF, 5 mM for 24 hours) administration due to the drug capability to virtually abolish mitochondrial Complex 1 function. Glucose disappearance from extracellular medium was calculated by monitoring medium glucose concentration over 24 hours. FDG uptake was tested through 30 minutes using a glucose free medium and a tracer concentration of 37 kBq/mL. Nature of supernatant radioactivity was analyzed by using thin layer chromatography. G6Pase activity and expression were measured by spectrophotometric and Western blot techniques, respectively. Results. In all experiments, MTF significantly increased glucose consumption by more than 50%. However, this response faced a consistent reduction in FDG uptake that almost halved in both cell lines. Thin layer chromatography ruled out any breakdown of 18F- from FDG. By contrast, G6Pase activity was well represented in both CT26 and 4T1 cell lines. Enzyme affinity for G6P and 2DG6P were remarkably similar. However, MTF decreased G6Pase expression and overall activity. Conclusion. These experiments represent the first unexpected evidence of a significant G6Pase activity within murine cell lines representative of colon and breast carcinoma. This enzyme can process FDG6P and might contribute to tracer release. The mismatch between glucose consumption and tracer uptake to MTF strongly suggests the presence of a pathway downstream hexokinases sensitive to biguanide whose FDG6P processing capability contributes to ultimate tracer retention limiting tracer handling by G6Pase.

P237

Changes of glycolytic pathway and upregulation of oxidative phosphorylation in BCR-ABL-driven human leukemia cells treated with imatinib

M. Monti[1], V. De Rosa[2], F. Iommelli[2], R. Fonti[2], F. Pane[1], S. Del Vecchio[3]; [1]Hematology Division, University of Naples "Federico II", Naples, ITALY, [2]Institute of Biostructures and Bioimages, National Research Council, Naples, ITALY, [3]Department of Advanced Biomedical Sciences, University of Naples, Naples, ITALY.

Aim: Since many oncogenes including BCR-ABL may promote the acquisition of the glycolytic phenotype, we reasoned that by inhibiting BCR-ABL signaling to which tumor cells are addicted, may cause in addition to growth arrest and apoptosis, an early metabolic switch from aerobic glycolysis to mitochondrial oxidative phosphorylation. Imatinib is a potent and selective inhibitor of several tyrosine kinases including BRC-ABL and KIT and for this reason it is used for the first line therapy of patients with chronic myeloid leukemia (CML)

and gastro-intestinal stromal tumors. Here we investigated the changes of glucose metabolism in BCR-ABL-driven human leukemia cells treated with imatinib. Materials and methods: BCR-ABL-driven K562 cells were incubated with increasing concentrations of imatinib ranging between 0.01-10 μM for 48-72 h and subjected to toxicity and apoptosis assays to test drug sensitivity. Then untreated and treated cells were lysed and analyzed for levels of BCR-ABL signaling mediators and key proteins of glycolytic cascade and oxidative phosphorylation. In particular levels of GLUT1, GLUT3, Hexokinase (HK) I and II, Pyruvate Kinase (PK) M1 and M2 were determined before and after 48 h treatment with imatinib. Furthermore glucose consumption and levels of mitochondrial complexes (I-V) subunits were tested. Results: as expected BCR-ABL-driven K562 cells were highly sensitive to imatinib showing an IC50 < 1 μM. Inhibition of BCR-ABL caused a concomitant reduction of p-AKT, pSTAT3 and cyclin D1. Furthermore a strong reduction of the phosporylated form (Tyr105) of PKM2 was observed in response to imatinib treatment whereas levels of HK1 and HK2 remained substantially unchanged. Glucose consumption expressed as $\mu g/10^6$ cells was reduced after treatment in a dose-dependent manner and western blot analysis of whole cell lysates showed a strong upregulation of all mitochondrial complexes subunits in treated cells as compared to untreated controls. Conclusion: Imatinib treatment of BCR-ABL-driven human leukemia cells causes an early reduction of glucose consumption through the glycolytic cascade and an upregulation of mitocondrial complexes indicating a possible switch from aerobic glycolysis to mitochondrial oxidative phosphorylation.

P238
Glucose metabolism and lactate production in-vitro.

T. Bach-Gansmo[1], T. V. Bogsrud[1], T. A. Saga[2], E. Munthe[3]; [1]Oslo University Hospital, Oslo, NORWAY, [2]Norwegian Cyclotron Center, Oslo, NORWAY, [3]Oslo Cancer Cluster, OUS., Oslo, NORWAY.

Aim: Most cancer cells have a high glucose metabolism, the basis of fluorodeoxyglucose (FDG) positron emission tomography. The glucose metabolism is however, not primarily for the production of energy, but a substantial proportion of glucose is metabolized to pyruvate and transformed to lactate. Lactate is then excreted into the cells microenvironment, producing only 2 instead of potentially 32 ATPs if the pyruvate was metabolized through the citric acid cycle. There are two main hypothesis tenting to explain the high glucose consumption. The first hypothesis claims that glucose, being readily available, is a supply of carbon and small molecules for the *de-novo* synthesis of new biomolecules. The second hypothesis explains the high glucose metabolism as a mean for lactate production. The secreted lactate reduces the pH in the local microenvironment and hence give malignant cells, more apt to thrive in acidic environments, a proliferative advantage. It is also known that certain rapidly dividing fetal cells have a high glucose metabolism. The aim of this *in-vitro* study was to perform a comparison of the glucose metabolism and lactate production in a highly malignant and a rapidly proliferative non-malignant cell-line. *Materials and methods*: Cell cultures of the human non-tumorigenic embryonic kidney cell line 293T and a triple negative breast cancer cell-line MDA-MB-231 were incubated with FDG for one hour, washed, and the FDG content in the cell was measured in a well counter. The experiment was performed with various FDG concentrations, with 0,5 x 10*6 and 10*6 cells in culture. Three parallels were performed. Lactate, the end product of the anaerobe glycolysis was measured in the supernatant. *Results*: The FDG uptake was consistently higher in the fetal cell-line. The measurements of lactate, Ph and glucose in the supernatant gave identical results for both cultures. *Conclusion*: Fetal cells can have at least as high glucose uptake and lactate production as malignant cells. This is an argument for the high glucose consumption being instrumental in retrieving intermediates for *de-novo* biosynthesis in rapidly proliferation cells. If hypothesis two is correct, why does a benign fetal cell-line acidifies its micro environment?

P239
Papillary thyroid carcinoma tissues and clinical significance of GRIM-19

Z. Zhao, G. Shen, H. Cai; West China Hospital of Sichuan University, Chengdu, CHINA.

Aim: To investigate the expression and clinical significance of apoptosis-related genes (GRIM-19) in papillary thyroid carcinoma (PTC). Materials and methods: The expression of GRIM-19 and STAT3 in 18 specimens of PTC with corresponding adjacent normal lung tissues was examined by immunohistochemistry. In this study, immunohistochemical staining of standard criteria: in tissue sections stained nucleus or cytoplasm light yellow to brown as positive cells; each slice select five horizons, counting 100 cells per field, the percentage of positive cells derived, according to a comprehensive score and percentage of positive cells stained depth. In addition, the expression of GRIM-19 was measured by Western blotting in 18 PTC tissues and corresponding nontumorous tissues. Results: The immunohistochemical results show that the expression of GRIM-19 protein in adjacent normal tissues is mainly localized in the cytoplasm, brown particles; and GRIM-19 protein expression in thyroid carcinoma localized in the nucleus, a small amount in the cytoplasm. The positive rate of GRIM-19 in the adjacent tissues was 89% (16/18), and

that of tumor tissue was 44% (8/18), which indicated that there was significant differences (P<0.05). GRIM-19 gene expression is closely correlated with the expression of STAT3 protein. GRIM-19 gene positive, STAT3 gene tends to negative; on the contrary, GRIM-19 gene-negative, STAT3 gene tends to be positive. The positive rate of GRIM-19 was significantly related to the tumor stage, but not to age, gender, tumor size and lymph node metastasis. In addition, western-blotting results also show that GRIM-19 protein expression in thyroid carcinoma was significantly lower than that of normal tissues. Conclusion: The decline in GRIM-19 expression is the process of papillary thyroid cancer, which is an important event that may occur and progress with papillary thyroid carcinoma.

P240

Assessment of tumor IGF1- and insulin receptor expression and its linkage to anti-receptor treatment response

M. H. Vendelbo, M. Busk, D. A. Bender, A. B. Iversen, N. Jessen, J. Frøkiær, A. Morsing; Aarhus University Hospital, Aarhus, DENMARK.

Background: Insulin-like Growth Factor-1 (IGF1)- and Insulin receptors (IGF1R and IR) are increased in various cancers. Receptor stimulation leads to enhanced glucose consumption and protein synthesis and thus tumor growth through the Akt/mTOR pathway. The IGF1R and IR inhibitor OSI906 has shown promising results and is undergoing clinical testing.Aim: We set out to investigate if IGF1R and IR inhibition is associated to decreased Akt/mTOR pathway activation, glucose uptake and proliferation of cancer cells, and to develop a PET detectable probe for IGF1R and IR based on chemical modification of OSI906.Methods: OSI906 was used to detect Insulin and IGF1 sensitive cancer cells. Effect of inhibition was assessed with 18F-FDG uptake, measurements of glycolysis, proliferation and site specific phosphorylations of proteins in the Akt/mTOR pathway during receptor stimulated and non-stimulated conditions. Furthermore, OSI-906 was used as a precursor to produce [11C]-methyl-OSI906 and binding in tissue samples were assessed with autoradiography.Results: Metabolic in vitro assays based on 18F-FDG and extracellular flux analysis revealed that both insulin and IGF stimulated glucose uptake and lactic acid formation in most cell lines. These changes were effectively inhibited by OSI906. The most pronounced effect was detected in SW948 colon cancer cells. In accordance with metabolic data, site specific phosphorylations in the Akt/mTOR pathway could be stimulated by IGF1 and insulin in the SW948 cells. Furthermore, Akt/mTOR pathway activation and proliferation were effectively inhibited by OSI906 during receptor stimulated and non-stimulated conditions. Non-radioactive methyl-OSI906 (backbone for the PET tracer) was able to block receptor stimulation and OSI906 was able to block [11C]-methyl-OSI906 binding in SW948 xenograft tumor tissue.Conclusions: Present results demonstrate that IGF1R and IR inhibition reduce Akt/mTOR signaling, glycolysis, proliferation and 18F-FDG uptake in SW948 colon cancer cells. Furthermore, [11C]-methyl-OSI906 may detect cells responsive to IGF1R and IR inhibition, which could allow for rational individualized therapy.

P241

Inverse correlation between hexokinase activity and glucose-6-phosphatase activity in ovarian cancer

B. B. Olsen[1], M. H. Vilstrup[1], I. B. G. Johnsen[2], G. Neumann[3], A. Alavi[4], P. F. Høilund-Carlsen[1]; [1]Odense University Hospital, Dept. of Nuclear Medicine, Odense C, DENMARK, [2]Odense University Hospital, Dept. of Clinical Pathology, Odense C, DENMARK, [3]Odense University Hospital, Dept. Gynaecology and Obstetrics, Odense C, DENMARK, [4]University of Pennsylvania, Dept. of Radiology, Philadelphia, PA, UNITED STATES.

Aim: Increased glycolysis is considered a hallmark of rapidly growing cancer cells (i.e., the Warburg effect) and 18F-fluorodeoxyglucose (18F-FDG) PET provides clinical evidence of the Warburg effect in malignant tumours. The aim of this study was to investigate the underlying biological mechanisms of 18F-FDG uptake on PET in ovarian cancer. Materials and Methods: Fourteen patients aged 49 - 87 years (median 69 years) with ovarian cancer who had undergone an 18F-FDG-PET/CT prior to surgery, and from whom fresh frozen tissue was available, were included. The fresh frozen tumour tissue was mechanically disrupted and the proteins were extracted. The enzymatic activity of hexokinase was determined in a colorimetric assay and the enzymatic activity of glucose-6-phosphatase was determined in a spectrophotometric assay. In addition the maximum standardized uptake value (SUVmax) of 18F-FDG-PET was determined. Results: The activity of hexokinase ranged from 1.57 - 14.5 μmoles min-1mg-1 and the activity of glucose-6-phosphatase ranged from 0.07 - 0.59 μmoles min-1mg-1, whereas the SUVmax varied between 1.9 and 43.9. There was a significant inverse correlation between the activity of hexokinase and the activity of glucose-6-phosphatase (Pearson's r = -0.65; P = 0.01). However, no significant correlations were found between 18F-FDG uptake and the activity of hexokinase (r = 0.39; P = 0.16) or the activity of glucose-6-phosphatase (r = 0.20; P = 0.49). Conclusion: There was no significant correlation between 18F-FDG uptake and the activity of either hexokinase or glucose-6-phosphatase in ovarian cancer, which supports the notion that 18F-FDG uptake, is complex and that no single step

(phosphorylation or dephosphorylation) controls 18F-FDG uptake. There was, however, a significant inverse correlation between the activities of the two enzymes which warrant further investigation.

P13 - Sunday, October 11, 2015, 4:00 PM - 4:30 PM, Hall 3 – Poster Exhibition

Radiopharmaceuticals & Radiochemistry: Radiopharmaceuticals - SPECT

P242

Production and characterization of chitosan-198Au nanocomposite with high radionuclide purity: A Comparative study on activity of gold-198 and its nanoparticles

M. Aboudzadeh Rovais, M. Sadeghi, M. Sahafipour, F. Bolouri; Nuclear Science and Technology Research Institute, Tehran, IRAN, ISLAMIC REPUBLIC OF.

Aim: Gold-198 nanoparticles (^{198}AuNPs) can be engineered with precise size, shape, composition, surface chemistry and radioactivity for clinical applications of nuclear medicine. The overall objective of the current research with respect to biomedical applications of nano radioisotopes is to develop the method for production of ^{198}AuNPs@chitosan using non- radioactive precursor. Method: In the present work, chitosan-capped AuNPs were prepared by exposing $HAuCl_4$ to acidic chitosan solution under appropriate conditions and then irradiated in Tehran Research Reactor (TRR). The formation of ^{198}Au@chitosan nanocomposites were characterized by UV-vis absorption spectroscopy, FTIR spectroscopy, gamma-ray spectroscopy, scanning electron microscopy (SEM) and dynamic light scattering (DLS). The impact of the reduction process of Au^{3+} to nanoparticulate Au^0 on the activity of gold-198 was evaluated. Results and discussion: The results showed that coating of gold with chitosan can be lead to neutron scattering and decrement of activity. The SEM photograph clearly indicated that gold nanoparticles are spherical shape with an average size ~61.7 nm. FTIR studies performed for controlling of degradation effects in radiation processing of AuNPs@chitosan showed the optimum neutron flux of 3×10^{12} n cm^{-2} s^{-1} for 30 min. ^{198}AuNPs with high radionuclide purity produced using the epithermal neutron-capture reaction, ^{197}Au (n,γ) ^{198}Au, are especially useful for medical purposes. So in this study, the secondary neutron-capture reaction reduced using a cadmium foil (0.05 cm) as a thermal-neutron absorber. Key words: Gold-198 nanoparticles; Chitosan; High radionuclide purity

P243

Validation of solid phase extraction (SPE) coupled with autoradiochromatography for 99mTc-MAG3 radiochemical purity determination and comparison with traditional TLC

M. Di Franco[1], S. Tamburri[2], A. Filieri[1], V. Podio[2]; [1]Ospedale San Luigi Gonzaga, Orbassano (TO), ITALY, [2]Università degli Studi, Torino, ITALY.

AIM 99mTc-MAG3 is the most used radiopharmaceutical for nefro-urological studies. The two main analytical techniques for Radiochemical Purity (RP) control are Thin Layer Chromatography (TLC) and Solid Phase Extraction (SPE); different methods are suggested by Pharmacopoeia, technical data sheets and literature. All SPE analysis are detected by dose calibrator, often located in a high background area. We aimed to validate SPE using autoradiochromatography, a modern detection method for RP controls. We also compared the equivalence between TLC and SPE (from US kit datasheet) for analysis of MAG3 from various labeling procedures. MATERIALS AND METHODS MAG3 (1.1 GBq/10 ml and 1.5 GBq/2.5 ml) RP was checked by ITLC-SG (acetonitrile/water 60/40 and ethylacetate/butanone 60/40) and SPE (C18 cartridges with HCl 0.001 M and ethanol/saline 50/50). SPE was performed comparing wet and dried columns. Detection was by autoradiochromatography and for SPE samples also by gammacamera imaging (autoradiochromatography/gammacamera equivalence for TLC had been previously demonstrated). SPE samples volumes were 100 μl (standard), 75 and 50 μl. Statistical analysis was performed by Mann-Whitney U test (one tail, non-parametric), analysis of variance (one-way ANOVA test) and unpaired t-test with Welch's correction. RESULTS Comparison between wet and dried columns in SPE analysis evidenced higher repeatability of results from dried columns (SD 0.74% vs 4.48% from wet columns); SPE results were not influenced by detection method ($p = 0.42$); results from volume reduction (50 and 75 μl vs 100 μl) were scattered and did not show any trend. Wet columns and SPE data obtained with lower volumes were excluded from further analysis. TLC results were better than SPE data (98.04% ± 0.80% vs 93.66% ± 5.51%, $p < 0.0001$) and not influenced by labeling procedure. On the opposite, SPE analysis with Welch's correction detected difference between results of RP from the two procedures: 97.32% ± 0.27% for the lower radioactive concentration vs 92.39% ± 2.07% for the higher concentration labeling ($p < 0.05$). CONCLUSIONS SPE validation for 99mTc-MAG3 RP quality control has been performed and dried column as well as 100 μl volume have been confirmed as reference. Equivalence between gammacamera and autoradiochromatography has been demonstrated also for SPE analysis. TLC remains the reference method for repeatability and time-saving procedure despite

its unability to detect high molecular weight or lipophylic impurities except 99mTcO2. When such impurities are suspected, SPE should be used. It is still unclear which chemical factor(s) could determine low SPE repeatability (O2, Sn2+, ⋯).

P244

Production of 81Rb for the 81Rb/81mKr generator by Kr gas tar

M. Aboudzadeh Rovais; Nuclear Science and Technology Research Institute, Tehran, IRAN, ISLAMIC REPUBLIC OF.

Introduction: The $^{81}Rb/^{81m}Kr$ generator is widely used in nuclear medicine. ^{81m}Kr(13sec) is an ideal tracer for the diagnosis of any chronic obstructive lung diseases because of its ease of production, short-half life and single low-energy γ ray. In this article, a selection of different reactions for production of ^{81}Rb(4.6hr), theoretical and experimental production yield through the excitation functions for $^{nat}Kr(p,xn)^{81}Rb$ using ALICE and TALYS computer codes as well as the production method are presented. The essential target thickness was calculated by SRIM computer code. Method: The aluminum target was designed in a semi conical shape. The length of the target chamber was calculated to be 251mm with the volume of 323cm^3. It was equipped with an external water cooling circuit. The gas target was pressurized with natural krypton at 5 bars. The incident energy of the proton beam was 26.5MeV at the 20μA current for 1hr. The target gas was quantitatively recovered using liquid nitrogen. A given amount of vaporized water was abruptly transferred into the target and ^{81}Rb solution was quickly transferred to a reservoir from which dispensed into generator columns by an automated dispenser. The $^{81}Rb/^{81m}Kr$ column generator was filled with AG 50W-X8 mesh (100-200) cation exchange resins as the support for Rb. Results and discussion: The average of the experimental yields of ^{81}Rb over the optimum energy range E_p=26.5→20.8 MeV was 245 MBq/μAh. The theoretical yield of ^{81}Rb was calculated to be 271 and 315 MBq/μAh from TALYS and ALICE codes, respectively. There is relatively large difference between the predicted of yield by ALICE and experimental results. The calculated cross section by ALICE is total for ^{81}Rb that is including the cross section of ^{81m}Rb and ^{81}Rb. This is the main difference between of the results obtained from this code and the experiments. Conclusion: The reported production system for preparation of the $^{81}Rb/^{81m}Kr$ generator showed a good reliability during the irradiation. The ease of loading and unloading of the Kr gas is the advantage of this system. If the 90% enriched ^{82}Kr gas is used as the target, the production yield could be enhanced by a factor of about 4. Keywords: ^{81}Rb, Production yield, Gas target, Simulation.

P245

Labelling procedure of autologous leukocytes with 99mTc-HMPAO using Leukokit: Description of our hospital experience

A. Kolindou[1], **M. Papachristou**[2], A. Velidaki[1], A. Evagellatou[1], G. Bramis[1], I. Datseris[3], E. Kitsiou[1]; [1]Nuclear Medicine Department, GHA "LAIKO", Athens, GREECE, [2]Nuclear Medicine Department-PET/CT, GHA, Athens, GREECE, [3]Nuclear Medicine Department-PET/CT, GHA "Evaggelismos", Athens, GREECE.

Introduction: Scintigraphy with labelled autologous white blood cells (WBC) is used to detect suspected sites of acute inflammation or infection with or without localizing signs or clinical symptoms. Radiolabelling of WBCs with 99mTc is preferable over 111In due to its favourable physical characteristics, availability, cost and lower radiation burden. Aim: Description of labelling procedure of autologous leukocytes with 99mTc-HMPAO based on our hospital experience. Materials and methods: Thirty labelling procedures were performed based on the protocol of ISORBE(1). Leukokit provides all components and reagents in a closed sterile environment. Procedure lasts 2 hours including quality control of the administrated cells and includes 5 phases: - Cell plasma preparation: We collect 40 ml blood in a syringe with anticoagulant and we set reagent through a closed sterile environment for red blood cells sedimentation - We transfer WBC plasma into the separation vessel via a close sterile connection -:For WBC purification we centrifuge, aspirate supernatant and obtain a clean WBC pellet maintaining the intact sterile environment - Cell labelling for patient administration: resuspend pellet in PBS and quantitate recovered cell avoiding any microbial and radioactive contamination. Scanning takes place 2h, 4h and 24h after injection with whole body, planar and SPECT images. Results: The WBC scan was conclusive to all patients and helped detection as well as differential diagnosis between infection and inflammation. Labelling efficiency of the radiopharmaceutical was 95% - 99% and yields of radiolabelled leukocytes were 55%- 68%. The administrated dose ranged between 4 - 7 mCi. Conclusion: Based on our experience procedure of autologous leukocyte labelling using Leukokit is easy, well defined and leads to correct clinical results.

P246

The experimental study of nano-colloidal radiopharmaceuticals based on modified molecules of DTPA labeled wih technetium

S. Sazonova[1], **V. S. Skuridin**[2], E. Stasuk[3], N. V. Varlamova[3], Y. A. Nesterov[3], A. S. Rogov[3], V. L. Sadkin[3], Y. Lishmanov[1], J. N. Ilushenkova[1]; [1]Institute of Cardiology, Tomsk,

RUSSIAN FEDERATION, [2]Politechnikal University, Tomsk, RUSSIAN FEDERATION, [3]Polytechnic University, Tomsk, RUSSIAN FEDERATION.

Medical applications of radioactive nano-colloidal materials opens up opportunities for highly informative diagnostic tests in nuclear medicine. In present study we tried to perform radiolabeling of nano-colloidal substance with 99mTc by dissolving the dry residues of SnCl2 and DTPA in 99mTc solution. For this purpose preliminarily solutions of SnCl2 and DTPA were prepared separately and then evaporated. The colloidal solution of DTPA was performed by the following way: 28 mg of DTPA was transferred quantitatively into a volumetric flask of 50 ml and dissolved in 20 ml of 5% NaHCO3 solution when heated to 800S. After this volume was adjusted to the mark with the same solution (concentration 0.55 mg / ml). The particles size was determined by the optical density of the colloidal systems m using a spectrophotometer Unico 2802 (S). The average radius of the particles was 93 nm. In order to reduce the particle size up to 55 nm the suspension was heated to 70 ° C and treated with the ultrasound for 40 minutes. To prepare the feed solution of reducing agent 35 mg of Sn (II) SnCl2 2H2O was dissolved in 100 l of 1 M HCl and the solution volume was adjusted to 5 ml of distilled water (concentration 7 mg / ml). Subsequently the resulting solutions were mixed in various proportions and evaporated. Dry residues were added to vials with 99mTc, mixed and chromatographed. As mobile phases for chromatography we used different mixtures: a) chloroform: methanol: water: acetic acid (ice) = 4: 4: 0.1: 0.3 (the system number 1), the chromatography time 20 min; b) chloroform: methanol: ammonia = 5: 5: 1 (number 2 system), chromatography time 60 min; c) acetone, chromatography time 10 min. The peak of for initial 99mTc solution in all solvent systems was Rf = 0.9. The same is observed in the direct interaction of 99mTc with DTPA (Rf = 0.9). indicating the absence of interaction of DTPA with 99mTc (VII). In contrast, when the 99mTc was mixed with the reducing agent Sn (II) the main peak was Rf = 0.1, suggesting the formation of reduced 99mTc complex with Sn. Not be ruled out as a radionuclide chemisorption on the surface of colloid produced by the hydrolysis of SnCl2 2H2O. The stain of non labelled nano-colloidal substance at Rf = 0.5 was not found. This work was supported by Federal Target Program №14.604.21.0071 (project unique identifier №RFMEFI60414X0071).

P247

Preparation of 99mTc-TRODAT-1 with high specific activity for dopamine transporter imaging of brain

M. Erfani, M. Shafiei; Radiation Application Research School, Nuclear Science and Technology Research Institute (NSTRI), P.O.Box: 14395-836, Tehran, IRAN, ISLAMIC REPUBLIC OF.

Introduction: In recent years, imaging of CNS dopamine transporters using positron emission tomography (PET) and single-photon emission tomography (SPECT) has been demonstrated. In spite of the promising results reported on PET and SPECT imaging, both techniques employ radionuclides, 11C and 123I, that are produced by a cyclotron. Recent success in development of 99mTc-TRODAT-1 has opened up a new and convenient road for studing DAT in the brain. Preparation of 99mTc-TRODAT-1 previously reported as a multistep method in high temperature (120 °C) with low specific activity. To meet the requirement for a widespread clinical application of 99mTc-TRODAT-1, it is highly desirable to develop a simplified formulation which could be labeled with high specific activity in low temperature. The optimized formulation (10 μg TRODAT-1, tricine, SnCl2, mannitol) was labeled with radioactivity of 1850 MBq of 99mTc in 95° C. Radiochemical analysis involved ITLC and HPLC methods. The stability was checked in the presence of human serum at 37 °C up to 24 h. Biological evaluation of radiolabeled ligand was performed in rats. The radiochemical purity of >95% was obtained with the specific activity of 64.3 MBq/nmol. The stability of >95% was found for labeled radiopharmaceutical formulation in aqueous solution and serum even after a 24 h period. The results showed high uptake in kidney, liver, muscle, skin, lung and brain. The brain uptake was 0.51 ± 0.05% ID/g at 2 min and at 4 h after injection the ratio of ST/CB was found to be 4.25. The clinical investigation of this new formulation is under way.

P248

Validation of Multidose Protocol of ^{99m}Tc-HMPAO to Label Autologous Leukocytes

T. Scotognella[1], V. Lanni[1], I. Salvatori[2], M. Maussier[1], A. Giordano[1]; [1]Policlinico A. Gemelli - Institute of Nuclear Medicine, Rome, ITALY, [2]Catholic University of Sacred Heart, Rome, ITALY.

Aim: 99mTc-hexamethylpropyleneamine oxime (99mTc-HMPAO) is one of the most commonly used radiopharmaceutical to label autologous leukocytes for evaluation of inflammation and infection. The European Guidelines (Eur J Nucl Med Mol Imaging (2010) 37:842-848) and some scientific papers suggest to label a single kit of HMPAO with an higher technetium-99m activity than the one reported in the radiopharmaceutical package insert. We aimed at validating a multidose procedure using a single vial of HMPAO for leukocytes labelling.Materials and methods: Our procedures are based on papers dealing with high technetium-99m activity for labelling a HMPAO kit (Eur J Nucl Med (1998) 25:797-

799; Nucl Med and Biol 34 (2007) 933-938) and was validated according to the European Guidelines, performing mediafill tests. For each vial we checked the radiochemical purity (%RCP) of 99mTc-HMPAO as quality control; three consecutive RCP tests were performed for each preparation immediately after the labelling and at 15, 30 and 45 minutes after labelling. We subsequently evaluated the labelling efficiency (LE) and cells viability by the Trypan blue exclusion test. In addition, we measured technetium-99m cell efflux after 1 hour; three tests were performed for each preparation and arithmetic mean was calculated for every sample. Finally we checked the sterility and the apyrogenicity of our labelling product on three consecutive samples.Results: The results of mediafill tests demonstrated complete sterility of labelling procedure. We tested 6 vials of 99mTc-HMPAO with twelve blood samples from healthy volunteers. The radiochemical purity of 99mTc-HMPAO always resulted higher than the minimum limit reported in the radiopharmaceutical package insert (>80%). In the 91,7% of cases, the labelling efficiency was within guidelines limits (40% < LE < 80%). Also cell viability, assed by Trypan blue exclusion test, was within the regulatory limits (<4% of dead cells). In the 83,3% of cases the measurement of cell efflux of Tc-99m was within the accepted limits (release of Tc-99m < 10%). Finally, the sterility test showed no contamination from aerobic bacteria and mycetes; pyrogen levels were lower than the limits allowed by current Italian Pharmacopoeia (the endotoxin concentration limit is 175 EU/ml, per injected ml per kg).Conclusions: We obtained acceptable results by labelling two blood samples using a single HMPAO vial, in accord to European Guidelines "Guidelines for the labelling of leucocytes with 99mTc-HMPAO"; this experimental protocol, allows to optimize the working time of the operator and the costs, without reducing the efficiency of labelling procedure.

P249

One step synthesis of a radioiodinated tumor-targeted oligonucleotide and preliminary in vivo evaluation in tumor xenografts

L. KANG; PEKING UNIVERSITY FIRST HOSPITAL, BEIJING, CHINA.

Aim: Anti-miRNA oligonucleotide (AMO) has been used most widely to inhibit miRNA for loss-of-function studies and function as therapeutic agents. The application of iodine-131 radiolabeled AMO is a potential novel approach to play double therapeutic role by inhibiting the oncogenic miRNA at molecular level, however it was rarely reported previously. This study is to prepare a radioiodinated anti-microRNA oligonucleotide by one step synthesis and evaluate its role in vivo tumor xenografts. Materials and methods: A convenient strategy for iodine labeled oligonucleotide was developed without a bi-functional coupling agent here. A tyrosine was conjugated to 3' end of AMO via a C6 linker for labeling with radionuclide iodine-131. AMO was labeled with 131I by the chloramine-T method and different reaction condition was optimized. The radiolabeled product was verified by gel electrophoresis and measured its radioactive distribution. Its stability in serum was evaluated by gel electrophoresis in vitro. In vivo single photon emission computed tomography (SPECT) imaging of 131I-AMO was used to evaluate the distribution in tumor xenografts. Results: Based on the solid-phase standard Boc strategy to an amino-ON CPG method, AMO targeting miR-21 was synthesized with the conjugation of tyrosine and modification of 2'OMe and PS. It was purified by HPLC and confirmed by MOLDI-TOF. The iodine labeled yield was as high as 96%-98% within 2 min without heating. The iodine-labeled product was shown only one peak in radioactive fractions as expected. It was shown that the radioactive distribution of iodinated AMO located at exactly where the DNA band was by gel electrophoresis. Furthermore, this radiolabeled AMO presented high stability in fresh human serum during 24 h. After i.v. administration in mice, radioactivity concentration was found primary in abdomen where liver and kidneys located. Tumors were clearly visualized, especially at 24 h. Conclusions: 131I radiolabeled AMO can be prepared by one step synthesis of tyrosine conjugation. Furthermore, it provides a potential value in targeted imaging and dual therapy in vivo.

P250

Remotely controlled solvent extraction of high purity Tc-99m produced by conventional medical cyclotrons

P. Martini[1,2], A. Boschi[3], L. Uccelli[3,4], M. Pasquali[3], G. Cicoria[5], M. Marengo[5], M. Giganti[3], G. Di Domenico[1], G. Pupillo[2], A. Taibi[1], A. Duatti[6], J. Esposito[2]; [1]Department of Physics and Earth Sciences, University of Ferrara, FERRARA, ITALY, [2]Legnaro Laboratories of the Italian National Institute for Nuclear Physics (INFN), Legnaro (Padova), ITALY, [3]Department of Morphology, Surgery and Experimental Medicine, University of Ferrara, FERRARA, ITALY, [4]Nuclear Medicine S. Anna Hospital, Ferrara, ITALY, [5]Nuclear Medicine S. Orsola Hospital, Bologna, ITALY, [6]Department of Chemical and Pharmaceutical Sciences, University of Ferrara, FERRARA, ITALY.

Aim. Purpose of this work was to develop an automated module for the extraction of high-purity Tc-99m from a Mo-100 enriched target irradiated by a proton beam in a conventional medical cyclotron. The separation process was based on the well-established selective affinity of the methyl-ethyl ketone (MEK) solvent system for the pertechnetate ion. **Materials**

and methods. Enriched (99.05%) Mo-100 metallic targets were irradiated in a medical cyclotron and transferred into the reactor vial of the automated module filled with 30% v/v hydrogen peroxide and 6-N NaOH where it was dissolved under a helium stream. Addition of MEK caused the selective extraction of $[^{99m}TcO_4]^-$ into the organic phase, which was further purified by two successive passages through silica and alumina columns. Finally, $[^{99m}TcO_4]^-$ was collected from the alumina column with saline. Radionuclidic and radiochemical purity of the eluate were checked with γ-spectroscopy and chromatography (TLC, HPLC), respectively. Residual MEK was measured with gas-chromatography. **Results**. The overall separation process lasted for approximately 60 minutes and recovery of the initial activity from the target was 90.1 ± 2.5%. Radionuclidic purity of the final $[^{99m}TcO_4]^-$ was in the range 99.5 ± 0.2% at the end of chemical extraction. No significant amount of MEK was detected in the purified Tc-99m solution. Automation of the whole procedure was achieved using a simple interface resulting from the simplicity of the selected purification method. As a result, the automated module has a particularly simple and adjustable structure that could be easily adapted and further optimized through the introduction of single-use, consumable cassettes. **Conclusions**. As expected, the separation efficiency of the water/MEK solvent system was excellent due to the well-known high affinity of $[^{99m}TcO_4]^-$ for this organic phase. Radionuclidic purity of the final Tc-99m was approximately 99% and this value compares well with that of generator-eluted Tc-99m, which was set at 99.99% by Pharmacopeia standards. In conclusion, the Tc-99m obtained through cyclotron irradiation of highly enriched Mo-100 metal, and purified using the automated module described here, constitutes a valuable alternative to generator-produced Tc-99m. In particular, it could provide a convenient source of this important diagnostic radionuclide in the event of a shortage of the conventional production route based on the decay of fission Mo-99. **Acknowledgement**. This work was carried out within the Techn-OSP program supported by the Italian National Institute of Nuclear Physics (INFN).

P251

99mTc-Labeled Estradiol: Preparation and Preclinical Evaluation as an Estrogen Receptor Probe

Y. Zhang, X. Xia, H. Feng, **X. Lan**; Union Hospital, Tongji Medical College, Huazhong University of Science and Technology, Wuhan, CHINA.

Objective: Most breast cancers express estrogen receptors (ERs). Noninvasive imaging of ER expression may be helpful for therapy planning. We developed a new ER-binding probe, 99mTc labeled estradiol (EDL) with diethylenetriaminepentaacetic acid (DTPA) as a chelating ligand, named it 99mTc-DTPA-EDL, and assessed its targeting ability in vitro and in vivo. Methods: 3-aminoethyl estradiol (EDL) was synthesized by two steps from estrone, followed by 99mTc labeling. The labeling compound, 99mTc-DTPA-EDL, was purified by Sep-Pak C-18 cartridge and the labeling efficiency was calculated. Then, the radiochemical purity was determined using instant thin-layer chromatography. Western blotting and immunofluorescence staining were used to detect the expression of ER in MCF-7 and MDA-MB-231 breast cancer cells. Saturation binding and internalization experiments were performed by incubating MCF-7 cells with increasing concentrations of 99mTc-DTPA-EDL. Cell uptake, efflux, and blocking assays were also performed. To test 99mTc-DTPA-EDL in vivo, nude mice bearing either MCF-7- or MDA-MB-231-derived tumors were injected with 99mTc-DTPA-EDL, and subjected to single-photon emission-computed tomography (SPECT) imaging. Mice injected with excess unlabeled DTPA-EDL were used as specific controls. Ex vivo gamma-counting of dissected tissues from normal and tumor-bearing mice was used to evaluate the biodistribution of 99mTc-DTPA-EDL. Results: The labeling efficiency and radiochemical purity of 99mTc-DTPA-EDL were 64.5 ± 5.8% and 98.3 ± 2.3% (n=3), respectively. Western blotting and immunofluorescence staining confirmed that ERs were expressed extensively by the MCF-7 cells, and less extensively by MDA-MB-231 cells. 99mTc-DTPA-EDL displayed high binding affinity with MCF-7 cells (Kd = 15.1 ± 2.1 nM) with a > 45% specific rate of total cell uptake. SPECT images and the results of the biodistribution study showed significantly higher uptake of the tracer by MCF-7 tumors (6.06 ± 0.38 %ID/g) than by MDA-MB-231 tumors (1.57 ± 0.28 %ID/g) (n=5). Pre-injection of MCF-7 tumor-bearing nude mice with excess unlabeled DTPA-EDL significantly reduced tumor uptake of 99mTc-DTPA-EDL (2.24 ± 0.28% ID/g). These data suggest that 99mTc-DTPA-EDL specifically targets ERs in tumors. Conclusions: 99mTc-DTPA-EDL can be easily synthesized with satisfactory labeling efficiency and stability. 99mTc-DTPA-EDL specifically targeted estrogen receptors in vitro and in vivo with favorable pharmacokinetics, which allows the expression of estrogen receptors to be assessed with SPECT imaging. This work was supported by the National Natural Science Foundation of China (No. 30970853, 81071200),

P252

[^{111}In]-DOTA-anti-MUC1 for SPECT applications, the production and quality control

B. Alirezapour1, S. Abbas Abadi2, I. Kertesz3, J. Mohammadnejad4, A. Jalilian1, E. Maadi1, M. Hashemizadeh1, N. Soltani1, S. Moradkhani1; 1Department of Radiopharmacutical, Nuclear Science and Technology Institute, Tehran, IRAN, ISLAMIC REPUBLIC OF, 2Faculty of

pharmacy, University of Debrecen, Debrecen, HUNGARY, 3Department of Nuclear Medicine, University of Debrecen, Debrecen, HUNGARY, 4Department of Life Science Engineering, Faculty of New Sciences & Technologies, University of Tehran, Tehran, IRAN, ISLAMIC REPUBLIC OF.

Introduction: Radioimmunoscintigraphy (RIS) has attracted considerable clinical application in tumor detection which has greatly improves the survival rate. Underglycosylated MUC1 antigen is one ofthe early hallmarks of tumor genesis and is overexpressed in more than 80% of breast cancers. PR81 is a new murine anti-MUC1 monoclonal antibody (mAb). In this study, as the first step towards the use of this antibody for imaging purposes, we have developed an efficient indirect labeling method of PR81 with 111In ($T_{1/2}$ = 67h, gamma emitting major photo peak at 171 keV) through using DOTA-NHS bifunctional chelator and performed preliminary bio-distribution studies in rats. Methods: Anti-MUC1 was conjugated with DOTA-NHS-ester (Macrocyclics), the average number of DOTA conjugated per mAb was calculated and total concentration was determined by spectrophotometrically. DOTA-Anti-MUC1 was labeled with 111In then Radiochemical purity and immunoreactivity, internalization study by MCF7 cell line and serum stability of 111In-DOTA-Anti-MUC1 were determined. The biodistribution studies and radioimmunoscintigraphy were performed in female BALB/c mouse bearing breast carcinoma tumor (111In -DOTA-Anti-MUC1 i.v.,100 μl, 25±5 μg mAb , 12, 24, 48 and 72h). Result: 111In-DOTA-PR81 was prepared (RCP >95% ± 0.5, Specific activity 4.6 ± 1.2 μCi/μg). Conjugation reaction of chelator (50 molar excess ratio) to antibody resulted in a product with the average number of chelators attached to a mAb (c/a) of 3.4 ± 0.3. Labeling yield with 111In in 400 μg concentration of bioconjugate was 94.8% ± 1.6. immunoreaction of 111In-DOTA-PR81 complex towards MUC1 antigen was determined by RIA and the complex showed high immunoreactivity towards MUC1. *In vitro* and *in vivo* stability of radioimmunoconjugate was investigated respectively in PBS and blood serum by RTLC method. *In vitro* stability was more than 93% ± 1.23 in PBS and 84% ± 1.33 in serum over 24 h. The Immunoreactivity of the radiolabeled Anti-MUC1 towards MCF7 cell line was done by using Lindmo assay protocol. Under these conditions, the immunoreactivity of the radioimmunoconjugate was found to be 0.76. The iodistribution of 111In-DOTA- Anti-MUC1 complex in the mice with normal and breast tumor at 12, 24, 48 and 72 h after intravenous administration, expressed as percentage of injected dose per gram of tissue(%ID/g). Biodistribution and imaging studies at 12, 24, 48 and 72 h post-injection revealed the specific localization of complex at the site of tumors. Conclusion: 111In -DOTA-Anti-MUC1 is a potential compound for molecular imaging of SPECT for diagnosis and follow up of MUC1 expression in oncology.

P253
Myocardial perfusion in patients with severe hypercholesterolemia

L. Martirosyan1,2, I. Sergienko3, A. Ansheles4, A. Popova5, K. Ivanov3, V. Sergienko5; 1 Yaroslavl state medical Academy, Moskou, RUSSIAN FEDERATION, 2Russian Cardiology Research Complex., Russian Cardiology Research Complex. Moscow, RUSSIAN FEDERATION, 3 Russian Cardiology Research Complex., Russian Cardiology Research Complex. Moscow, RUSSIAN FEDERATION, 4Russian Cardiology Research Complex., Moskou, RUSSIAN FEDERATION, 5Russian Cardiology Research Complex., Russian Cardiology Research Complex. Moscow, RUSSIAN FEDERATION.

Objective: To evaluate myocardial perfusion characteristics in patients with severe hypercholesterolemia. Materials and Methods: We included 26 patients with a total cholesterol (CH) 7.5 mmol/l and LDL-CH ≥ 4.9 mmol/L, without coronary artery disease. All patients, as well as 10 healthy volunteers were examined by myocardial 99mTc-MIBI SPECT (protocol rest/stress with CT attenuation correction). In addition to the standard quantitative indicators of perfusion (rest, stress, reversibility extents, SRS, SSS, SDS) we have introduced two new parameters to assess the left ventricular perfusion heterogeneity: severity sigma and heterogeneity sigma (σ sev, σ het). σ sev and σ het calculated as standard deviations of perfusion in each of the 17 segments relative to 100% (σ sev) and relative to arithmetic mean (σ het).Results: Stress tests in all cases were negative for myocardial ischemia. According SPECT, there were no significant stability and/or reversible perfusion defects in hypercholesterolemic patients. With a qualitative assessment, inhomogeneous RFP was detected in 23 patients (88%). The difference between standard perfusion indicators in hypercholesterolemia patients and healthy volunteers were not found: Rest extent - 8.3 (5.0-11.0) and 8.0 (6.4-11.2), p = 0.67, Stress extent - 11.3 (6.5- 14.0) and 7.5 (6.5-12.5), p = 0.52, Reversibility extent - 5.0 (2.5-8.0) and 3.5 (2.9-7.1), p = 0.85, SRS - 3.5 (2.0 - 5.5) 2,9 (0.75-6.0) p = 0.94, SSS - 7.3 (4.5-9.5), and 6.5 (5.1-8.3), p = 0.87, SDS - 2.5 (2.0-6.0), and 4.0 (2.9-5.1), p = 0.42, respectively. At the same time in patients with hypercholesterolemia compared with healthy volunteers σ sev and σ het were significantly higher: σ sev - 22.6 (18.9-25.2) vs. 15.6 (15.5-21.4), respectively, p = 0.04, at the rest study. At the stress study: σ sev - 22.3 (19.2-24.4) and 17.3 (16.7-18.6), respectively, p <0.01. σ het - 7.8 (7.0-9.3) and 6.1 (5.2-7.2), p = 0.053 at the rest, σ het - 7.9 (7.0-9.3) and 5.8 (5.5-6.8), p = 0.015 at the stress. Conclusion: In patients with severe hypercholesterolemia observed initial defects of perfusion. Our proposed parameters can be useful for left ventricular perfusion heterogeneities assessment.

P254

Preparation of radionuclide labeled anti-microRNA-155 oligonucleotide and its role as a potential tumor imaging probe in multiple tumor bearing mice

L. KANG; PEKING UNIVERSITY FIRST HOSPITAL, BEIJING, CHINA.

Aim: MicroRNAs (miRNAs) have exhibited great potential for diagnosing and treating diseases as a novel type of biomarkers and therapeutic targets. MicroRNA-155 (miR-155) has been proved to overexpress in various tumors and promotes tumor growth and metastasis and considered as a biomarker of malignant tumors. Specific binding and inhibition of miR-155 using anti-miRNA antisense oligonucleotide (AAM) can be a potential imaged and therapeutic strategy for tumors in which miR-155 is overexpressed.Methods and results: 99mTc radiolabeled AAM with partial 2'-OMe and PS chemical modification was prepared via the conjugation to NHS-MAG3 for miR-155 targeted imaging. The modified AAM was revealed highly stable against degradation and radiolabeling in human serum. Western blotting results showed that the unconjugated, unlabeled and labeled AAMs up-regulated the expression of C/EBPβ protein, one of target proteins of miR-155, in tumor cells, proving a good ability in the specific binding and inhibition. Furthermore, fluorescent protein labeled AAM displayed its ability of specific distribution in tumor cells and a good stability in cellular level. After the system administration of 99mTc-AAM, the distribution and in vivo imaging revealed the significant difference between AAM and scramble control probe in multiple tumor xenograft models, which suggested the specific binding and detective ability of AAM in vivo. Conclusion: Therefore, this study supports the effectiveness of the noninvasive imaging method by radiolabeled AAM with 99mTc to track the location of miR-155 in tumors and suggests a prospective candidate for future tumor imaging.

P14 - Sunday, October 11, 2015, 4:00 PM - 4:30 PM, Hall 3 – Poster Exhibition

Radiopharmaceuticals & Radiochemistry: Antibodies & Peptides

P255

Influence of DOTA - Rituximab conjugates on their biodistribution in mice

U. Karczmarczyk, W. Wojdowska, E. Laszuk, M. Maurin, P. Garnuszek, R. Mikolajczak; Radioisotope Centre POLATOM, National Centre for Nuclear Research, Otwock, POLAND.

Introduction: Rituximab, a chimeric mAb against human CD20 antigen, which is expressed on B-cell lymphocyte and on the majority of B-cell lymphoid malignancies, was selected as model MoAb for inter-laboratory comparison under the IAEA CRP "Development and pre-clinical evaluations of therapeutic radiopharmaceuticals based on 177Lu and 90Y labelled monoclonal antibodies and peptides". Our results of Rituximab conjugation with p-SCN-DOTA and evaluation of 90Y- and 177Lu labelled conjugates obtained from the freeze-dried formulation were already described [1]. Herein we present the comparative biological evaluation of 90Y- and 177Lu-labelled DOTA-SCN and DOTA-NHS conjugated Rituximab in normal and tumour-bearing mice. Materials and methods: DOTA-SCN and DOTA-NHS (Macrocyclics) were conjugated to anti-CD20 antibody (Rituximab, MabThera) and the conjugates were used in the freeze-dried kits for radiolabelling [1]. The kits were labelled with 177LuCl3 (ca) and 90YCl3 (n.ca) after incubation at 37oC for 1 h and radiochemical purity (RCP) and stability were checked by HPLC and ITLC-SG. Biodistribution of 177Lu- and 90Y-labelled DOTA(SCN)-Rituximab and DOTA(NHS)-Rituximab was evaluated in in normal Balb/c mice in order to determine tissue localization and excretion route and in tumor-bearing (Raji s.c.) Rj:NMRI-Foxn1nu/Foxn1nu mice. Groups of 3-4 mice were injected i.v. (tail vein) with 6 MBq (10 μg) of the radioimmunoconjugates, then sacrificed at 4, 24, 48 and 72 h post-injection. Results and Conclusion: All radioimmunoconjugates were obtained with high radiolabelling yield (RCP > 98%) and specific activity at the level of 0.6 GBq/mg. The conjugates were stable in human serum and in 0.9% NaCl, however, progressive aggregation was observed with time, in particular for DOTA(SCN) conjugates. Both 177Lu- and 90Y-DOTA(SCN)-Rituximab revealed slow blood clearance (for 177Lu ca. 29, 19 and 16 %ID/g; while for 90Y ca. 41, 23 and 16 %ID/g after 1, 24 and 72 h, respectively). The highest radioactivity uptake was observed in the liver and spleen, confirming the hepatobiliary excretion route. Generally, similar distribution pattern was observed for 177Lu- and 90Y-DOTA(NHS)-Rituximab, with no statistically significant differences in radioactivity uptake in the respective tissues. For 177Lu-DOTA(SCN)-Rituximab and 177Lu-DOTA(NHS)-Rituximab a progressive accumulation of radioactivity in tumor tissue was observed (ca. 9 %ID/g and 7 %ID/g after 72 h p.i., respectively), with high tumour to muscle ratios (ca. 8-9) for both preparations. References: [1] Wojdowska W., et al. Current Radiopharmaceuticals, 2015, 8.

P256

Synthesis and radiolabeling of HYNIC-conjugated LIKKPF peptide with 18F-FDG for the detection of apoptosis

D. Beiki1, S. Khoshbakht2, S. Shahhosseini3, F. Kobarfard3, O. Sabzevari2, M. Amini4; 1Research Center for Nuclear Medicine, Tehran University of Medical Sciences, Tehran,

IRAN, ISLAMIC REPUBLIC OF, 2Dpartment of Radiopharmacy, School of Pharmacy, Tehran University of Medical Sciences, Tehran, Iran, Tehran, IRAN, ISLAMIC REPUBLIC OF, 3Dpartment of Medicinal Chemistry, School of Pharmacy, Shahid Beheshti University of Medical Sciences, Tehran, Iran, Tehran, IRAN, ISLAMIC REPUBLIC OF, 4Dpartment of Medicinal Chemistry, School of Pharmacy, Tehran University of Medical Sciences, Tehran, Iran, Tehran, IRAN, ISLAMIC REPUBLIC OF.

Aim: Apoptosis, or programmed cell death, plays important roles in the physiology and pathology of a variety of human conditions including neurodegenerative diseases, ischemic damage, autoimmune disorders and many types of cancer. LIKKPF is a hexapeptide with high phosphatidylserine (PS) binding affinity in order to visualize cell death. 18F-FDG has so far been the most utilized radiotracer in positron emission tomography (PET) imaging. We herein report the synthesis of 18F-FDG-LIKKPF as a tracer for the detection of apoptosis.Materials and Methods: The peptide was synthesized by standard Fmoc solid phase synthesis and the HYNIC-conjugated LIKKPF was considered for the radiolabeling procedure with 18F-FDG. In order to optimize labeling efficiency, a series of studies including changing the amount of HYNIC-peptide ligand, adjustment of the reaction pH and varying the reaction temperature were performed.Results: The radiochemical purity >50% was achieved for the radiolabelling procedure with 18F-FDG, in the presence of glucose (100-250 μg/mL). Also, stability studies in aqueous solution and human serum showed radiolabeled complex with no significant release of F-18 or peptide degradation up to 6 h.Conclusion: Our results showed the high potential of 18F-FDG as 18F-fluorinated prosthetic group, to be clinically accepted for the radiolabelling of peptides such as LIKKPF for the detection of apoptosis.

P257

Combined targeting of somatostatin receptor subtypes 2 and 5 with a novel 68Ga-labelled somatostatin agonist

R. Mansi1, G. P. Nicolas1, K. A. Abid2, E. Grouzmann2, J. Watson3, D. Wild1, M. Fani1; 1University of Basel Hospital, Basel, SWITZERLAND, 2University Hospital of Lausanne, Lausanne, SWITZERLAND, 3Somtheranostics, Epalinges, SWITZERLAND.

Aim: Somatostatin receptor (SSTR) targeting, specifically of subtype 2 (SSTR2), is an established method to image and treat neuroendocrine tumors. The aim of our work is to develop somatostatin analogs with affinity to more receptor subtypes than SSTR2. These analogs will potentially target a broader spectrum of tumors and/or increase the tumor uptake, as several receptor subtypes may be concomitantly present. We are presenting herein the development and preliminary evaluation of the somatostatin analog G02113, having high affinity for the subtypes 2 and 5 (SSTR2 and SSTR5), as 68Ga-PET imaging probe. Materials and methods: G02113 ((4-amino-3-iodo)-D-Phe-c[Cys-(3-iodo)-Tyr-D-Trp-Lys-Val-Cys]-Thr-NH_2) was coupled to the chelator DOTA at the N-terminus and labeled with 68Ga. The peptide-chelator conjugates DOTA-TATE and DOTA-NOC were also synthetized as reference compounds. The affinity of the three natGa-complexes for the SSTR2 and SSTR5 was determined by receptor binding assay using 125I-SS14 as radioligand. Agonistic potency of the compounds was assessed by cAMP assays. The three conjugates were labeled with 67Ga and characterized *in vitro* using the HEK cell line stably transfected with plasmids encoding the human SSTR2 and SSTR5 (HEK-SSTR2 and HEK-SSTR5) and the naturally expressing SSTR2 cell line AR4-2J. Proof-of-concept PET/CT images with 68Ga-DOTA-G02113 were acquired in HEK-SSTR2 and HEK-SSTR5 xenografts. Results: natGa-DOTA-G02113 exhibited higher affinity for the SSTR2 and SSTR5 compared to natGa-DOTA-NOC (IC_{50} = 0.32 *vs* 0.70 and 1.86 *vs* 3.38 nM, respectively). natGa-DOTA-TATE had the highest affinity among all three metallated conjugates for the SSTR2 (IC_{50} = 0.15 nM), however very low affinity for the SSTR5 (IC_{50} = 69 nM). The internalization rate of 67Ga-DOTA-G02113 was similar to 67Ga-DOTA-NOC (12.4±1.6 *vs* 16.6±2.3, at 4h), while their externalization rate was found in the same level (40-50% within 4 h). The effect on forskolin-stimulated cAMP accumulation using SS-14 as agonist control showed that natGa- DOTA-G02113 had the same potency for SSTR2 as the highest affinity compound natGa-DOTA-TATE (EC_{50} = 0.46 and 0.47 nM, respectively) and slightly better than natGa-DOTA-NOC (EC_{50} = 0.59 nM). Preliminary imaging studies illustrated the high uptake of 68Ga-DOTA-G02113 in both, SSTR2- and SSTR5-expressing tumors *in vivo*, they indicated renal excretion of the PET probe and they demonstrated an excellent tumor-to-background contrast. Conclusion: The initial evaluation of the new somatostatin analog 68Ga-DOTA-G02113 reveals its potential as PET probe for *in vivo* imaging of a broad spectrum of somatostatin receptor expressing tumours, including SSTR2 and SSTR5. Financial support: CTI Project Nr. 16403.2 PFLS-LS

P258

Adaptive self-assembling dendrimers for theranostics: a proof of concept on angiogenesis

P. GARRIGUE, A. MOYON, X. LIU, C. LIU, P. ROCCHI, L. PENG, D. TAIEB, B. GUILLET; Aix-Marseille Université, Marseille, FRANCE.

Nanoparticle-based drug delivery aims at specifically delivering therapeutic and/or diagnostic agents to the right site at the right time, in order to improve the outcome while reducing adverse effects. Many validated or experimental therapeutic drugs simulate or inhibit angiogenesis in cardiovascular or oncology applications: as companion tools, agents enabling non-invasive angiogenesis evaluation are an actual necessity. In this work, we introduced a proof of concept of 68Ga-radiolabellable adaptive self-assembling amphiphilic dendrimersomes for angiogenesis imaging on a rodent hind limb ischemia model.An αvβ3-integrin-targeting dendrimersome was designed, synthesized and radiolabelled with indium-111 for validation. The dendrimersome resulted from the self-assembly of 2 different dendrimer conjugates: one for imaging ([111In]In-NOTA conjugate, 92 MBq/100μg) and one for specific targeting (C18-PEG-RGD conjugate) or aspecific targeting (C18-PEG conjugate). 7 days after hind limb ischemia induction on Balb/c mice, long term biodistribution studies were carried out by μSPECT/CT imaging and a blood kinetic was performed: both early dynamic planar acquisitions (T+0 to T+20' post-IV injection of 5-10 MBq, 7.5s frames) and late multi-pinhole SPECT/CT (T+120', D+1 and D+2 or D+3 post-IV) were performed using a Bioscan NanoSPECT/CTplus camera. Autoradiography was also carried out on 3 other mice right after the imaging on the day of the injection. Animal experiments were carried out in accordance to Helsinki Declaration and underwent the local preclinical ethics committee agreement.We reached a radiolabeling yield >95%. The dendrimersomes were mainly eliminated through the urinary system at an early stage, with a biological half-life of 24 minutes. Late T+120' and D+1 SPECT/CT imaging showed significant ($P<0.05$) higher uptake on the ischemic site between the untargeted 111In-dendrimersomes (i/c 1.40±1.0% at the day of the injection, 2.59±0.07% one day after) and the 111In-RGD-dendrimersomes (i/c 6.29 ±0.6% at the day of the injection, 5.25±0.6% one day after) (n=3/group). Autoradiography analysis of gastrocnemius sections showed a significant uptake of the 111In-RGD-dendrimersomes in the ischemic hind limb (85573 ± 8778 DLU/mm2, n=3) compared to the contralateral hind limb (11462 ± 931 DLU/mm2, n=3) ($P<0,01$).Preliminary results with these radiolabelled nanovectors showed great promises in specific targeting to the site of interest. Additionally, dendrimers have numerous side advantages: high drug payload, stable formulation and controllable structure. Therefore, if our results are further confirmed on preclinical tumor models, these dendrimer-based nanocarriers could constitute novel and effective means for the delivery of radiopharmaceuticals and other biomedical imaging agents or therapeutic medicines, with obvious outlooks in theranostics.

P259

Radiolabeling of antibody for epitope of human carbonic anhydrase IX (IgG M75) by 61Cu and 64Cu and its biological testing

A. Čepa1,2,3, J. Rálišš2, A. Pavelka4, L. Marešová4, M. Kleinová4, D. Seifert2, I. Sieglová5, V. Král5, M. Polášek2, O. Lebeda2, M. Paurová6, M. Lázníček1; 1Faculty of Pharmacy in Hradec Kralove, Charles University in Prague, Hradec Králové, CZECH REPUBLIC, 2Nuclear Physics Institute of the CAS, v. v. i., Řež, CZECH REPUBLIC, 3Institute for Clinical and Experimental Medicine, Prague, CZECH REPUBLIC, 4ÚJV Řež a. s., Řež, CZECH REPUBLIC, 5Institute of Molecular Genetics of the CAS, v. v. i., Prague, CZECH REPUBLIC, 6Faculty of Science, Charles University in Prague, Prague, CZECH REPUBLIC.

Aim: The subject of the work was conjugating antibody IgG M75 for epitope human carbonic anhydrase IX with non-commercial new chelator denoted as "phospinate" specific for copper isotopes. Human carbonic anhydrase IX is a membrane enzyme that is significantly expressed in some types of cancer cells. The antibody IgG M75 was successfully conjugated with phosphinate, the conjugation method was optimized and is well-reproducible. The conjugate was then labeled with two positron emitting copper radioisotopes, 61Cu (3.333 h) and 64Cu (12.701 h). Labeled conjugates were tested in vivo in mice with colorectal cancer xenografts. Materials and methods: Copper radioisotopes were produced via natNi(d,x)61Cu and 64Ni(p,n)64Cu reactions (natNi, 99.999%, Goodfellow; 64Ni, 99.09%, Isoflex) on external beams of the Cyclone 18/9 and U-120M cyclotrons. Specific activity of 61Cu was 1 GBq/mg Cu and more, which was satisfactory for labeling purposes. All reagents were analytical grade that were purified prior labelling with chelex-100 in sodium form, 100-200 mesh (Sigma-Aldrich, Germany) from metals surplus. Chelator „phospinate" was synthesized and characterized in our laboratories. Antibody IgG M75 was prepared by genetic engineering methods. Immunoconjugates (IgG M75-SCN-phospinate) were separated with use of PD 10 Desalting Columns (GE Healthcare, UK) and analyzed using size exclusion chromatography column BioSep SEC-S-3000 (Phenomenex, USA). We compared positive cell line for human carbonic-anhydrase IX human colorectal adenocarcinoma (HT-29) and negative mouse standard fibroblast (NIH/3T3). Adult males of mice Nude Foxn1NU were used in the experiment. Results: The conjugate M75-SCN-phosphinate was labeled successfully with both 61Cu (96% yield) and 64Cu (97% yield). Specific activities of 61Cu-phosphinate-IgG M75 and 64Cu-phosphinate-IgG M75 were 7.4 and 1.0 MBq/μg, respectively. Biodistribution experiments revealed high uptake of both labelled compounds in tumour tissue: 61Cu-labeled conjugate showed uptake of about 10 % ID/g

after 6 hours, while 64Cu-labeled about 24 % ID/g even after 48 hours. Conclusion: The labelling resulted in the product of high specific activity (1.0 and 7.4 MBq/μg, respectively) and of high radiochemical purity (>95%). The labelled molecule has considerable potential as a radioimmunopharmaceutical suitable for imaging of tumors expressing carbonic anhydrase IX by positron emission tomography (PET). The study was supported by the Charles University Grant Agency, project no. 1752314 and by the Technology Agency of the Czech Republic, program Alfa, project no. TA02010797.

P260

Panitumumab Modified With Metal Chelating Polymers (MCPs) For Dual Labeling With 111In and 177Lu as a Potential Theranostic For Pancreatic Cancer

S. Aghevlian; University of Toronto, Toronto, ON, CANADA.

Aim: Our objective was to develop a novel "theranostic" agent that combines SPECT imaging of EGFR-positive pancreatic cancer (PnCa) with radioimmunotherapy (RIT). In order to maximize the specific activity to obtain a robust therapeutic response and improve the sensitivity for imaging, panitumumab (PmAb), a fully human anti-EGFR monoclonal antibody was modified with novel hydrazino nicotinamide metal chelating polymers (HyNic-MCP) that harbor 13 DOTA chelators for high specific activity (SA) radiolabeling with 111In and 177Lu as well as 10 polyethyleneglycol (PEG) groups to minimize liver and spleen uptake. 111In is a -emitter [$t_{1/2}$ = 2.8 days; Eγ=171, 245 keV] useful for SPECT imaging and also emits subcellular range Auger electrons for RIT of micrometastases. 177Lu is a -emitter [Eβ(max) =498, 385 and 176 keV] for RIT of millimeter-sized tumours, but also emits -photons for imaging [Eγ=113,208 keV]. Methods: PmAb was reacted with N-succinimidyl-4-formylbenzamide (S-4FB) to install aldehyde groups for derivatization with HyNic-MCP which forms a UV-measureable (354 nm) bis-arylhydrazone bond. The reaction was terminated when on average two MCPs were conjugated to PmAb. Purity and MCP conjugation were confirmed by SDS-PAGE. PmAb-HyNic-MCP was labeled with $^{111}InCl_3$ or/and $^{177}LuCl_3$ in 0.1M HEPES pH 5.5. For comparison, PmAb was modified with 4.0 ± 0.2 DOTA and labeled with 111In and 177Lu. Labeling efficiency was measured by ITLC-SG in 0.1M sodium citrate. Stability was studied in the presence of a 500-fold excess of EDTA for 1 h at 25 °C and in plasma at 37°C for 1 week by size-exclusion HPLC and ultrafiltration. EGFR binding affinity was assessed in a saturation binding assay using EGFR-overexpressing MDA-MB-468 human breast cancer cells. Results: The purity of PmAb-HyNic-MCP was >96%. PmAb-HyNic-MCP and PmAb-NHS-DOTA immunoconjugates were labeled with 111In and/or 177Lu in high labelling yield (>96%) and the maximum theoretical SA was achieved in practice. Radioimmunoconjugates were stable in plasma and to EDTA challenge. EGFR binding assays revealed a dissociation constant (K_d) of 2.2 ± 0.6 nM for 177Lu-PmAb-HyNic-MCP vs K_d of 1.0 ± 0.4 nM for 177Lu-PmAb-NHS-DOTA. Conclusions: Novel PmAb-HyNic-MCP conjugates were constructed and labeled with 111In and/or 177Lu in high labeling yield and high SA. 177Lu-PmAb-HyNic-MCP exhibited preserved EGFR binding affinity. Studies are planned to evaluate the biodistribution and imaging properties of these theranostic agents in preclinical models of PnCa. Research Support: This study was supported by a grant from the Cancer Research Society.

P261

Ga-68 NODAGA RGD: A PET radiopharmaceutical for integrin αvβ3imaging

R. Vatsa1, P. Bhusari2, S. Kumar1, G. Singh1, S. Chakraborty3, A. Dash3, D. K. Dhawan2, J. Shukla1, B. R. Mittal1; 1Postgraduate Institute of Medical Education & Research, PGIMER, CHANDIGARH, INDIA, 2Panjab University, PU, CHANDIGARH, INDIA, 3Bhabha Atomic Research Centre, BARC, Mumbai, INDIA.

AIM: Angiogenesis plays a key role in the growth and metastases of solid tumors which is strongly regulated by integrin αvβ3. Over expression of integrin αvβ3 is noted in various carcinomas including lung, prostate and breast. Radiolabeled RGD tripeptide can be used to image the over expression of this integrin non-invasively. The aim of the present study was to image αvβ3 over expression in breast and lung carcinoma patients using in-house radiolabeled Ga-68 NODAGA-RGD. Materials and Method: Radiolabeling of NODAGA-RGD was optimized in-house using Ga-68. Radiolabeling was performed at room temperature for 20 min and at 95°C for 5 min. Radiochemical yield was assessed by ITLC. Characterization of radiolabeled product was done by radio-HPLC and MALDI-TOF mass spectrometry. Patients before any definitive treatment (Chemotherapy/Surgery) were enrolled in the study after obtaining clearance from institute ethics committee and written informed consent from patients (breast n=40, lung n=5). Whole body acquisition was done 45 min post intravenous administration of 111MBq-185MBq of Ga-68-NODAGA-RGD on a dedicated hybrid PET-CT scanner with 90 sec per bed position. Attenuation correction of the emission images was done using CT. Results: The radiolabeling yield at room temperature was 50-60%. However yield was more than 90% after 5 min heating at 95°C.radio-HPLC showed good radiolabeling. Increase in molecular weight near the weight of Ga-68 on MALDI-TOF reconfirmed attachment of Ga-68 with

NODAGA-RGD. The post purification radio-ITLC showed >99% radiochemical purity. All the samples were found to be sterile on sterility test with the endotoxins content <4 EU/ml. The residual ethanol content was <2500ppm in all samples. Physiological uptake of radiotracer was seen in ventricles, salivary glands, thyroid, liver and spleen with excretion through the kidneys. Variable radiotracer uptake was with the SUVmax ranging from 2.89 to 21.12 in breast carcinoma and 1.40 to 7.82 in lung carcinoma. Metastatic lesions were also detected in patients.No adverse reactions were seen post administration of the radiopharmaceutical. Conclusion:Ga-68 labeled NODAGA-RGD synthesis is quick with good radiochemical purity. Good tumor to background ratio was observed in breast and lung carcinoma patients. Metastatic lesions were well visualized. The study indicated that Ga-68 labeled NODAGA-RGD have great potential for imaging angiogenesis.

P262

Improving EGFR imaging by use of an anti-EGFRvIII monoclonal antibody: characterizations in an in vivo squamous cell carcinoma model

D. Spiegelberg1, A. C. Mortensen1, R. K. Selvaraju2, J. Stenberg1, A. Scott3, M. Nestor1,4; 1Department of Immunology, Genetics and Pathology, Uppsala University, Uppsala, SWEDEN, 2Preclinical PET Platform, Uppsala, SWEDEN, 3Ludwig Institute for Cancer Research, Olivia Newton-John Cancer Research Institute, and La Trobe University, Melbourne, AUSTRALIA, 4Department of Surgical Sciences, Academic hospital, Uppsala, SWEDEN.

Aim: Molecular imaging of biomarkers involved in cancer progression is a valuable non-invasive tool of modern oncology and nuclear medicine. The epidermal growth factor variant III (EGFRvIII) is a truncated mutant form of EGFR. It is associated with enhanced tumourigenicity and increased chemo- and radio-resistance, and is commonly overexpressed in glioma cells. It may however also be a suitable target for molecular imaging in several solid diseases such as squamous cell carcinoma (SCC), despite the relatively sparse antigen expression, due to the tumour specific expression pattern of the antigen. For this purpose, a monoclonal antibody (mAb), targeting an epitope of EGFR only accessible in tumours that express EGFRvIII or with wild-type EGFR amplification, may be a suitable tracer. This antibody has demonstrated reduced binding and reduced toxicity to non-target tissues compared to ordinary EGFR targeting drugs. The aim of this study was to assess the feasibility of the use of 111In-labelled anti-EGFRvIII mAb to obtain high SCC tumour contrast SPECT images, even in tumour xenograft models displaying relatively low amounts of the antigen. Materials and methods: The antibody was labelled with 111In using the CHX-A"-DTPA chelator to quantify antigen expression in vitro and to evaluate tumour uptake in vivo. Radio-immunoassays and real time binding assays combined with interaction analyses were performed using 111In-mAb on SCC cancer cell lines with varying antigen expression. Mouse SCC xenografts using two SCC cell lines with low but clear antigen expression were imaged either with 111In-mAb806 (48 h p.i.), or with 18F-FDG (30 min p.i.) using a small animal SPECT/CT or PET/CT, respectively, followed by ex vivo biodistribution, autoradiography and immunohistochemical analysis.Results and conclusion: Binding studies revealed high affinity binding of the antibody on antigen expressing cells with slow off rate. Interaction map analysis demonstrated two binding interactions, one high- and one low affinity. This may correspond to the antibody binding to both EGFRvIII and wild-type EGFR amplification epitopes on the cells, or to different conformational forms of wild-type EGFR. 111In-mAb clearly imaged the SCC tumours, despite the low antigen expression, with favourable biodistribution. High and homogeneous tumour uptake was confirmed by autoradiography analysis. We conclude that 111In-mAb is a promising tracer for SCC tumour imaging, also in low antigen expressing tumours.

P263

A neurotensin derivative with increased metabolic stability labeled with 99mTc for tumors imaging

M. Erfani, M. Shafiei; Radiation Application Research School, Nuclear Science and Technology Research Institute (NSTRI), P.O.Box: 14395-836, Tehran, IRAN, ISLAMIC REPUBLIC OF.

Peptide receptors are overexpressed on various cancer cells and illustrate interesting targets for tumour imaging and therapy. Neurotensin (NT) receptors were overexpressed in a variety of human tumors such as breast, pancreatic, prostate, lung and colon. Based on this fact targeting the NT receptor with optimized analogue of neurotensin is very important for imaging of pancreatic, lung and colon tumors. In the present study, we investigated a new neurotensin derivative with increased metabolic stability also HYNIC chelator was conjugated to the N-terminus of peptide which can be labeled with a more desirable radionuclide such as 99mTc. Radioconjugate 99mTc-[HYNIC]-Neurotensin analogue was prepared and quality control tests were down via ITLC and HPLC methods. The receptor bound internalization rate was studied in neurotensin receptor expressing HT-29 cells. Biodistribution of radiconjugate was studied in C57 nude mice bearing HT-29 tumor cell. Radiochemical yield 90% was achieved, and a very low amount of 99mTc-pertechnetate and 99mTc-radiocolloid was observed. In RP-HPLC analysis we observed

a single peak which also confirms lack of any impurities. Radioconjugate was stable up to a 24 h post labeling period in the room temperature. Specific internalization (11.14 ± 1.76% up to 4 h) and metabolic stability in human serum up to 24 h after labeling and incubation were observed. High kidney uptake and accumulation in tissues like the intestines (1.21 ± 0.07% at 1 h post injection) and HT-29 tumor (1.11 ± 0.05% at 1 h post injection) was observed. The tumor and intestine accumulation and pharmacokinetic behavior such as low tendency to accumulate in liver followed by its high kidney excretion are the major advantages of this radioconjugate.

P15 - Sunday, October 11, 2015, 4:00 PM - 4:30 PM, Hall 3 – Poster Exhibition

Radiopharmaceuticals & Radiochemistry: Radiopharmaceuticals

P264

68Ga(DO3A-lysine) as a New PET Tracer for Biodistribution Study

C. YANG1, P. Chandrasekharan2, P. Padmanabhan1, J. Carlstedt-Duke1, B. Gulyás1,3, C. Halldin4,3; 1Lee Kong Chian School of Medicine, Nanyang Technological University, Singapore, SINGAPORE, 2Singapore Bioimaging Consortium, Agency for Science Technology and Research, Singapore, SINGAPORE, 3Karolinska Institutet, Department of Clinical Neuroscience, S-171 76, Stockholm, SWEDEN, 4Nanyang Technological University, Singapore, SINGAPORE.

Aim: A new ligand DO3A-lysine (DO3A conjugated with lysine derivative, see Scheme 1) has been developed as a prospective bimodal MRI/PET probe. Its Gd(III) chelate, Gd(DO3A-lysine) has demonstrated to be a useful intravascular MRI contrast agent for tumor angiography (1-3). Now we have showed that Ga-68 labeled 68Ga(DO3A-lysine) can be used as a positron emission tomography (PET) probe for biodistribution studies. Methods and materials: 68Ga(DO3A-lysine) was prepared by reaction of $^{68}GaCl_3$ in 0.05 N HCl with DO3A-lysine in Hepes Buffer (pH = 4) at 95 °C for 15 mins. The product was purified by C-18 Sep-pak column to remove unreacted 68Ga and characterized by radioHPLC, radiochemical purity >90%, radiochemcal yield: 68% (not decay corrected). The biodistribution characteristics of 68Ga(DO3A-lysine) were conducted using SCID mice bearing U87MG and HT1080 xenografts tumors. Typically 1-2 MBq of 68Ga(DO3A-lysine) was administered as a bolus injection via the tail vein. Blood was drawn by terminal cardiac puncture procedure under anesthesia. Organs were excised from euthanized animals and the radioactivity accumulated in each organ was measured using a gamma counter. Results and Discussion: Organ-to-muscle ratios for 68Ga(DO3A-lysine) were 3.86, 2.24, and 6.4 for blood, tumor and kidney, respectively, whereas for 68Ga(DOTA) they were 2.4, 2.12 and 23.67 for blood, tumor and kidney, respectively, after 30 minutes post injection. 68Ga(DO3A-lysine) demonstrated 1.6 times higher retention in blood and significantly lower accumulation in the kidneys compared to its analog 68Ga(DOTA) at 30 mins post-injection. However, 68Ga(DOTA) had a 3.7 fold increase in the kidneys compared to 68Ga(DO3A-lysine) at 30 mins post-injection. Biodistribution data of 68Ga(DO3A-lysine) showed higher tumor uptake and longer accumulation in the tumor and kidneys compared to that of 68Ga(DOTA). Conclusion: Biodistribution study of 68Ga(DO3A-lysine) in SCID mice bearing U87MG and HT1080 xenografts tumors demonstrated high retention in blood, high tumor uptake and low accumulation in the kidneys. These observations further support the desired properties of Gd(DO3A-lysine) in MRI tumor angiography study. References: [1] Yang C-T, Bates RW, et al. *ChemMedChem*.2011, 6, 781. [2] Yang C-T, Chuang K-H, et al, *Biomaterials*, 2014, 35, 327. [3] Chandrasekharan P, Yang C-T, et al, *Contrast Media & Molecular Imaging*. 2015, Accepted.

P265

A novel, specific PET-radiotracer for bacterial infections

S. M. Schneefeld1, J. Thackeray1, N. Murthy2, J. P. Bankstahl1, F. M. Bengel1, G. Meyer1, T. L. Ross1; 1Medical School Hannover, Hannover, GERMANY, 2University of California, Berkeley, CA, UNITED STATES.

Aim: The differentiation between bacterial infections and aseptic inflammation represents a great challenge in diagnostics. The objective of this work was to develop a new specific tracer for non-invasive PET imaging of bacterial infections. Maltohexaose is the major energy source for bacteria, and its cellular uptake is facilitated through the bacteria-specific maltodextrin-transporter. Since mammalian cells show no expression of this transporter, it is particularly suitable as specific target. Using optical imaging and a fluorescence labelled maltohexaose derivative, this concept has already been proved (1). Materials and Methods: An azido-maltohexaose was linked via click-chemistry to the DOTA-chelator, followed by labelling with 68Ga. The new radiotracer 68Ga-DOTA-maltohexaose was evaluated in vitro with E. coli and in vivo using healthy mice. The in vivo-biodistribution and pharmacokinetics were valued with μPET-CT and the metabolites were analyzed in blood and urine. In in vitro-studies, the uptake of the new radiotracer into bacterial cells was measured. Results and Conclusions: Excellent radiochemical yields of ≥90% were obtained under labelling conditions of 100 °C, 10 min, and 1.5 M HEPES. A specific uptake of the new

radiotracer into E. coli was found. The in vivo studies showed a fast and exclusively renal clearance without any significant unspecific background. After 50-60 min over 90 %ID/g was found in the bladder. No radiometabolites were detected in blood or urine during the first 20 min. The new 68Ga-maltohexaose shows a perfect pharmacological profile for the translation into human. The present data support further exploration of the new radiotracer for specific in vivo targeting of bacterial infections via PET imaging. References: (1) Ning X, et al. (2011) Nat. Mater., 10, 602-7

P266

A Fully Automated Procedure for the GMP-Synthesis of 68Ga-NODAGA-Exendin-4 Using a Cationic Purification Method

G. M. Franssen, M. Brom, S. M. A. Willekens, P. Laverman, C. M. van Rij, M. Gotthardt, O. C. Boerman; Radboud University Medical Center, Nijmegen, NETHERLANDS.

Aim: Our objective was to develop a safe, fast and reproducible method for the automated radiolabeling and purification of 68Ga-exendin-4-NODAGA. The procedure should result in a GMP-compliant, sterile and purified product with high yields for clinical studies. Material and methods: The synthesis of 68Ga-NODAGA-exendin-4 was performed on a Scintomics GRP module (Scintomics GmbH, Fürstenfeldbruck, Germany) connected to a GMP grade 68Ge/68Ga generator, 1850 MBq (IGG101, Eckert and Ziegler, Berlin, Germany). Elution of the generator, concentration of the 68Ga eluate, radiolabeling and purification of the 68Ga-NODAGA-exendin-4 was performed using a modified Scintomics reagent and hardware kit for synthesis of 68Ga-peptides using cationic purification (ABX, Radeberg Germany). Briefly, the 68Ge/68Ga generator was eluted with 0.1 N HCl and 68Ga was trapped on a preconditioned PS-H+ cartridge (Machery-Nagel GmbH, Düren, Germany). The concentrated and purified 68Ga, eluted with 1.3 ml 5 M NaCl/0.1 N HCl was added to 10 μg of exendin-4-NODAGA with 0.475 ml 2.5 M HEPES buffer, pH 7.0 and 50 μl 5.5 M ascorbic acid. The reaction mixture was heated for 10 min at 95 °C. After cooling down, 2.0 ml 50 mM EDTA, 0.15% Tween80 was added and the mixture was loaded onto an activated Oasis HLB Plus cartridge (Waters, Etten-Leur, The Netherlands). The purified product was eluted with 2 ml 100% ethanol, diluted with 20 ml PBS and subsequently filtered through a 0.22 μm vented filter unit into a closed sterile glass type I vial. Quality control was performed by RP-HPLC, ITLC and pH determination. 68Ge breakthrough was checked by gamma spectroscopy. Endotoxin content was determined according to Ph Eur. using Endosafe equipment (Charles River, Leiden, The Netherlands), sterility was assessed according to Ph Eur. Results and conclusion: Sterile 68Ga-NODAGA-exendin-4 was obtained in reproducible amounts of 407 ± 19 MBq (yields of 75%, decay corrected). Radiochemical purity was ≥ 95%, with 5% 68Ga colloid and < 2% unbound 68Ga. No 68Ge was detected by gamma spectroscopy after decay (<0.001%). The pH was 7.0 ± 0.5 and endotoxin levels were < 10 EU/mL. Total time of synthesis, including 68Ge/68Ga generator elution, sterile filtration and formulation, was less than 45 min. In conclusion, we developed a fully automated, GMP-compliant method to produce 68Ga-NODAGA-exendin-4 in a stable and reproducible manner with high yields for clinical use.

P267

Chelator-free 89Zr-labeling of mesoporous silica nanoparticles with superb in vivo radiostability

F. Chen, S. Goel, H. F. Valdovinos, S. Shi, T. E. Barnhart, W. Cai; University of Wisconsin-Madison, MADISON, WI, UNITED STATES.

Aim: To show that 89Zr ($t_{1/2}$=78.4 h) can be labeled to mesoporous silica nanoparticles (MSN) with superb in vivo stability in a chelator-free manner. Materials and Methods: MSN with controllable particle/pore sizes was synthesized as oxygen donor for chelator-free 89Zr-labeling, via simple mixing of 89Zr-oxalate with MSN at pH 7-8 for 2 h. Dense silica nanoparticles ($dSiO_2$) were also prepared as control. 89Zr-labeling yield of MSN and $dSiO_2$ was studied via radio-thin layer chromatography (TLC). Serum stability of 89Zr-labeled samples was studied at 37 °C for 48 h. In vivo long-term stability of 89Zr-MSN and 89Zr-$dSiO_2$ was studied by monitoring the dynamic uptake change in both liver (native tropism of 89Zr-labeled nanoparticles) and bone (detached 89Zr) with serial PET scans. Biodistribution on Day 21 (~7 $t_{1/2}$ of 89Zr) post-injection (p.i.) was studied. Results: Detailed particle size, morphology, and specific surface area characterizations confirmed successful synthesis of MSN and $dSiO_2$. We observed ~70% of 89Zr-labeling to MSN at 75 °C in only 15 min, with <30% yield for $dSiO_2$. Labeling yield was temperature dependent: higher yield at higher temperature. Serum stability testing confirmed high stability (>95%) of both 89Zr-MSN and 89Zr-$dSiO_2$ for 48 h. Surprisingly, in vivo PET scans showed superb stability of 89Zr-MSN with <1 %ID/g of 89Zr in the bone on Day 7 p.i., which remained low for 3 weeks. For 89Zr-$dSiO_2$, >10-fold higher bone uptake was observed on Day 7 p.i., indicating detachment of 89Zr from 89Zr-$dSiO_2$ hence lower stability of 89Zr on the outer surface of $dSiO_2$. As expected, liver/spleen had high uptake of 89Zr-MSN, which remained stable over 3 weeks. No obvious kidney/bladder uptake of 89Zr-MSN was observed, confirming superb in vivo stability of such chelator-free 89Zr-labeling of MSN.

Conclusion: We report the first example of chelator-free 89Zr-labeled MSN, with superb radiostability in vivo. With long $t_{1/2}$ of 89Zr and high potential of MSN for molecular imaging and drug delivery, this method offers a novel, simple, and accurate way for future PET image-guided drug delivery.

P268

Synthesis and biological evaluation of 68Ga-DOTA-capsaicin as a imaging agent for MCF-7

J. PARK1, S. LEE1, M. HUR1, S. YANG1, S. KIM2, K. YU3; 1Korea Atomic Energy Research Institute, Jeongeup-Si, KOREA, REPUBLIC OF, 2Dongguk University-Gyeongju, Gyeong-ju, KOREA, REPUBLIC OF, 3Dongguk university-Seoul, Seoul, KOREA, REPUBLIC OF.

Aim : Capsaicin (trans-8-methyl-N-vanillyl-6-nonenamide), a significant pungent ingredient in a variety of red peppers of the genus capsicum, is a type of vanilloid. It has been shown to induce apoptosis in many cell types. Especially, capsaicin is selective effect to binding with estrogen receptor.In this study, [68Ga]($t_{1/2}$=68min)-labeled capsaicin using DOTA (1,4,7,10 -tetraazocyclododecane-N,N',N",N"'-tetraacetic acid) derivative was developed for the diagnosis of estrogen receptor over-expression in MCF-7.Material and Methods : The DOTA-capsaicin, Chelated by 69Ga,was characterized by spectroscopic analysis method and mass spectrometry. [68Ga3+] was eluted from a 68Ge/68Ga generator by 0.1 N HCl and used directly for the reaction after adjusting the pH 3. The labeling of [68Ga3+](111Mbq) was performed in a 1M sodium acetate buffer with DOTA-capsaicin(4μmol) and the mixture was heated at 100°C for 10 min. The compound was purified by RP-HPLC. To determine the lipophilicity of [68Ga]DOTA-capsaicin was dissolved in a mixture of saline and 1-octanol in the E.P tube. The cellular uptake of [68Ga]DOTA-capsaicin was evaluated using MCF-7, SK-BR-3 and CT-26 cells. And then, PET imaging radioactivity was measured in MCF-7 bearing balb/c mice at 15 to 120 min.Results and Conclusions: The products were obtained in >70% radiochemical yields with a radiochemical purity of >98% as checked by radio-TLC. The partition coefficient (logP) was measured as -2.32, which is an indication of the hydrophilic nature of the agent.Cellular uptake values of [68Ga]DOTA-capsaicin was MCF-7, SK-BR-3 and CT-26 cells over incubation periods of 15, 30, 60 and 120 min. (MCF-7 : 0.16% at 15 min, 0.93% at 30 min, 0.07% at 60 min and 0.14% at 120 min, SK-BR-3 : 0.03% at 15 min, 0.46% at 30 min, 0.02% at 60 min and 0.01% at 120 min,CT-26 : 0.03% at 15 min, 0.46% at 30 min, 0.04% at 60 min and 0.04% at 120 min). PET imaging radioactivity was measured in MCF-7 uptake at 30 min. In this study, we successfully designed and synthesized a [68Ga]DOTA-capsaicin derivative as a probe for the PET detection of MCF-7 cell, and this compound was showed significant uptake in MCF-7. PET imaging of measurement result the highest uptake was observed at 30 min and rapid clearance occurred at 60minThese results suggest that this [68Ga]DOTA-capsaicin could be a potential MCF-7 targeted agent for PET imaging.

P269

Cation exchanged based post-processing of Ga-68 chloride: Comparison of three different SPE-cartridges on their suitability to DOTA-NOC, NODAGA-RGDfk and HBED-CC-PSMA.

V. Ladenbauer, J. Obermair, **P. Lam**, C. Artner; IASON GmbH, Graz, AUSTRIA.

Aim: By cation-exchanged post-processing of Ga68-generator eluate, Ga68-chloride can be concentrated and Ge68 impurities can be reduced. However, dependent on the used cation-exchanger this process is influencing the incorporation of Ga68 into its chelator in a negative way. The aim of this work was to evaluate the effect of the cation-exchange cartridges BondElut-SCX (Agilent); ChromafixPS-H+(S) (Macherey-Nagel) and StrataX-C (Phenomenex) on the incorporation-yield of the precursors DOTA-NOC; Nodaga-RGDfk and HBED-CC-PSMA and to evaluate the Ge-68 separation. **Materials and Methods**: The Ga68-generator IGG100 (Eckert&Ziegler) was eluted with 5mL 0.1M HCL by use of the Ga68-Elusynth (IASON). The activity was adsorbed on the cation-exchange cartridges. Subsequently the cartridges were eluted with a mixture of 5,0M NaCl in Water 5% 5.5 M HCL. With sodium-acetate, the pH of the reaction-solution was adjusted to 3.6 for DOTA-NOC and Nodaga-RGDfk and 4.0 for HBED-CC-PSMA. For labeling 25μg DOTA-NOC; 25μg NODAGA-RGDfk and 5μg HBED-CC-PSMA were added. After a reaction time of 7 minutes at 95°C the incorporation-yields were determined by means of iTLC. The Ge68 separation was analyzed by gamma-spectrometry. **Results**: Like described by Schultz, M.K. et al. 2012, the elution of the BondElut-SCX (Agilent) is characterized by a full desorption within 0.5mL of the eluent and a Ge68 separation of 90-95%. The incorporation-yield for HBED-CC-PSMA is up to 60%, for NODAGA-RGDfk and DOTA-NOC up to 50%. Using 0.5 mL eluent on the Strata X-C, up to 90% of Ga68 can be desorbed and 20-87% of Ge68 impurities can be removed. The incorporation-yield is up to 50% for DOTA-NOC, 60% for NODAGA-RGDfk and 45-95% for HBED-CC-PSMA. An elution-rate of up to 90% can be achieved using 1.5 mL of the eluent on the Chromafix PS-H+(S). Ge68 impurities can be reduced by 95%. No Ga68 gets eluted within the first 0.5 mL. This volume can be discarded if volume reduction is necessary. The incorporation-yield for NODAGA-RGDfk is up to 30% for DOTA-NOC 40% and

for HBED-CC-PSMA 50-80%. By increasing the precursor amount of NODAGA-RGDfk and DOTA-NOC to 50 μg yields >90% can be achieved with all cartridges. Also increasing the precursor amount of HBED-CC-PSMA to 10 μg leads to stable labeling-yields of >95%. **Conclusion**: Using fractionated synthesis methods the brought in precursor last for quantitative incorporation-yields. However, labeling with cationic post-processed Ga68-eluate requires more precursor for stable incorporation. For Ge68 reduction the cation-exchange cartridges BondElut-SCX and Chromafix PS-H+(S) are suitable. Like with fractionated methods high labeling-yields and high chemical purity can be achieved.

P270

Synthesis of Gallium-HBED-CC-EDBE-Folate available PET diagnosis agent against folate receptors overexpressed in cancel cells

P. Choi1, J. Park2, D. Chang3, T. Kim2, S. Lee4, S. Kim1; 1Dongguk University, gyeongju, KOREA, REPUBLIC OF, 2Korea Atomic Energy Reaserch, Jeongeup, KOREA, REPUBLIC OF, 3Sunchon Univerity, Sunchon, KOREA, REPUBLIC OF, 4Daegu Gyeongbuk Institute of Science and Technology, Daegu, KOREA, REPUBLIC OF.

Aim: Gallium-68 is well known positron emitting radiometal produced easily in 68Ge/68Ga generator with a half-life of 68 min, hence suitable for PET diagnosis. Trivalent Ga3+ ion is regarded as a hard acid so rapidly react with hard base donor ligards such as macrocyclic ligands DOTA and NOTA. Bifunctional acyclic chelate HBED-CC (N,N'-bis[2-hydroxy-5-(carboxyethyl)benzyl] ethylenediamine-N,N'-diacetic acid) was represented to have a high stability constant (pKf : 30) and to enable to label rapidly with DOTA or NOTA in room temperature for Ga3+ ion. Moreover, its other end can easily be linked to the biological compound such as peptides, antibodies, amino acids, and etc. In this research, we selected folic acid as a biological material because of its high affinity with folate receptors over-expressed in various cancel cells such as ovarian, breast, colorectal, renal, nesopharyngeal, cervical. Therefore we conjugated folic acid with HBED-CC attached mini-PEG lingker EDBE (2,2'-(ethylenedioxy)-bis-(ethylamine)). Before labeled 68Ga in precursor, standard compound of 69Ga-HBED-CC-EDBE-Folate was made formation to identify 68Ga labeling conditions.Materials and Methods: We synthesized standard compound 69Ga-HBED-CC-EDBE-Folate. First, precursor was synthesized by organic reactions that coupling reactions between HBED-CC and Folic acid formed amide bond using HBTU. 69Ga chelating in precursor was performed at room temperature, pH 4, RT 10 min. This complex was characterized by spectroscopic analysis as well as liquid chromatographic analysis. The stability in human serum and lipophilicity using PBS buffer and 1-octanol were also measured.Results: Synthesis of precursor was confirmed through NMR, HR-MS, reverse-HPLC. Purification was successfully performed by preparative-LC. Labeling procedure was completed within 10 min at room temperature, pH 4 for standard compound. This complex was near hydrophilic and labeling yield, thermodynamic stability was above 90%.Conclusions: We have successfully synthesized 69Ga-HBED-CC-EDBE-Folate and preparation and evaluation of 68Ga-HBED-CC-EDBE is under progress using tumor cells.Keywords : Ga-68, HBED-CC, folate receptor, Folic acid conjugate

P271

Preparation of 68Ga-DOTA peptides in a fully automated system using two generators sequentially connected

I. Vaccaro1, F. Giurgola1, S. Grugni1, G. Tarullo1, K. Marzo1, A. Chiti2; 1IRCCS Istituto Clinico Humanitas, Rozzano, ITALY, 2Humanitas University, Rozzano, ITALY.

AIM: The aim of this study was to develop a fully automated method to produce 68Ga-DOTA-peptides with a single elution from two different generators, sequentially connected. This technique was supposed to increase the starting activity as well as the final product of the synthesis. MATERIAL AND METHODS: The fully automated synthesis of 68-Gallium DOTA-peptides, made with the ModularLab™ (Eckert Ziegler, Berlin, D) requires two 68Ge/68Ga generators loaded with 1850 MBq of Germanium-68 at calibration date. 68Ge is adsorbed over a TiO2 resin and 68GaCl3 eluted with 0.1 N HCl. For the elution of the two generators connected in series, we tested an alternative fractionated technique. This method allows collecting the total activity from both generators, but increases the volume of the eluate up to 12 ml. The rather large volume of the eluate requires a pre-concentration of the activity to label the peptides, so we modified the standard elution doubling the fractioning process. This ensures to collect the total activity in 6 ml, compatible volume for the synthesis. After buffering with sodium acetate, the eluate is used directly for the radiolabeling of the DOTA-peptides. Reaction parameters such as buffer conditions, pH range, reaction temperature, time and volume of reaction solution were optimized for DOTATOC labeling. Reaction yields, pH, radiochemical purity, sterility, endotoxins, breakthrough of 68Ge and final 68Ge content were determined. RESULTS: Connecting a new generator loaded with 1850 MBq of Germanium-68 and a generator used for six months (about after 300 elution), we elute approximately 1200+/-70 MBq from the first one and 740+/-40 MBq of 68GaCl3 from the second one. Therefore, the starting activity for the synthesis was 60% more we get from a single generator. The new method allowed to produce about

1280+/-70 MBq of 68Ga-DOTA-TOC instead of 780+/-40 MBq obtained with a new single generator, before the modification. CONCLUSION:We demonstrated that after about 600 elutions the metallic impurities and 68Ge levels were in line with Ph.Eur. dossier requirements. This method allows to delay the disposal of generator extending its clinical use until one year. This double fractionated method does not contemplate a pre-purification, therefore acetone and SPE based approaches are not required. Moreover the new method guarantees high peptide bound percentage (>99%) and high specific activity.

P272

Good manufacturing practice in using an automatic module of synthesis for 68Ga-labeled molecules

S. Migliari1, G. Serreli2, O. Ortenzia2, J. Ŝimeĉek3, C. Cidda1, G. Baldari1, M. Scarlattei1, C. Ghetti2, L. Ruffini1; 1Nuclear Medicine and Molecular Imaging Department, University Hospital of Parma, Parma, ITALY, 2Medical Physics Unit, University Hospital of Parma, Parma, ITALY, 3Scintomics GmbH, Fürstenfeldbruck, Germany, Fürstenfeldbruck, Germany, GERMANY.

Generator-produced 68Ga for radiolabelling peptides used in PET applications have gained much attention due to favorable imaging characteristics. A lot of semi-automated systems connected with 68Ge/68Ga generator were born for practical routine preparation of 68Ga-radiopharmaceuticals.Moreover attention has been dedicated to the influence of metal contaminants in the $68GaCl_3$ eluate, water, buffers and hydrochloric acid that aretypical components of a labelling procedure. Besides the inevitable contaminant Zn2+, the 68Ga3+ decay product, the metals frommatrix materials (SnIV, TiIV), Fe3+, Al3+ and Cu2+are found in the eluate. Each of them is a competitor for 68Ga3+ in binding to a chelator, especially Fe3+.Our goal was to reach and validate a method to increase the radiochemical purity (RCP) and yield of the 68Ga-DOTATOC synthesis.An automated radiopharmaceutical synthesis device (SCINTOMICS GRP®) was installed in our radiopharmacy on November 2014.A TiO_2-based generator was eluted with 0.1M HCl and the $68GaCl_3$ purified using a cationic exchanger. DOTATOC could be labeled in almost quantitative yield by heating 13 nmol peptide for 10 minutes in 1.5M HEPES buffer solution and then purified with reversed-phase cartridge. RCP was measured by instant thin-layer chromatography and high-performance liquid chromatography (HPLC Ultimate 3000 Thermofisher), according to Ph. Eur. We also evaluated the reaction yield, pH, sterility, endotoxins and breakthrough of Ge-68.We collected the RCP and decay corrected yields of the synthesis from December 2014 to March 2015 (18 synthesis).The first synthesis (S_1) after the first elution in the week (E_0) showed a61.57%±0.08yield with a RCP of 98.77%±0.01. The synthesis (S_2), on the second day with a second elution (E_1)yield was 68.81%±0.05 and RCP 99.04%±0.01. The third synthesis (S_3) after third elution (E_3) showed a yield of 73.38%±0.05 and RCP 99.10%±0.01.We measured the peaks related to secondary metal impurities complexes for each synthesis: 1.33%±0.6 for S_1, 0.97%±0.6 for S_2 and 0.82%±0.12 for S_3.Our study showed a progressive increase of RCP and reaction yield related to continuous generator use, due to a decreasing amount of metal contaminants in the eluate: they compete strongly with Ga3+ to coniugate the DOTAby forming secondary complexes. Therefore it's a good practice toeluate every day 68Ga/68Ge generator to obtain an eluate poor of metal impurities and to have better results of RCP and reaction yields.The use of an automated module allows a simple and efficient preparation of 68Ga-DOTA-derivatized peptides for clinical practice.

P273

Evaluation of Zr-89 oxalate as a PET Tracer for Inflammation, Tumor and Rheumatoid Arthritis Model

J. Park, Y. Lee, J. Lee, R. Yoo, U. Shin, K. Lee, B. Kim, K. Kim, G. Ahn, **J. Kim**; Korea Institute of Radiological & Medical Sciences, Seoul, KOREA, REPUBLIC OF.

Purpose The aim of this study was to evaluate inflammation and tumor imaging with Zr-89 oxalate in comparison with [F-18]FDG and [F-18]NaF. *Methods* Human brain glioblastoma xenografts and turpentine oil-induced inflammation were inoculated in the same mouse. Cell uptake examination to mouse macrophage cell line RAW 264.7 and human brain glioblastoma cell line U87MG with Zr-89 oxalate, [F-18]FDG and [F-18]NaF were accomplished. Biodistribution, macro PET imaging, autoradiography and histological analysis of Zr-89 oxalate, [F-18]FDG and [F-18]NaF were performed. *Results* Zr-89 oxalate exhibit remarkably higher uptake macrophage cell than tumor cell. The inflammatory lesions and tumor were clearly visualized by Zr-89 oxalate and autoradiography. Compared with [F-18]FDG and [F-18]NaF, Zr-89 oxalate has high selectivity index to tumor at the early time after injection and to inflammation at the delay time (24 h p.i.). Large number of macrophage and neutrophils were found in the highest Zr-89 oxalate uptake tumor lesion demonstrating by histological examination. In the RA mouse model, Zr-89 oxalate clearly revealed high accumulation in the inflammatory lesion. *Conclusions* The Zr-89 oxalate provide a new strategy for monitor not only tumor imaging but also inflammation process.

P274

Correct Procedures for the synthesis of Ga68 radiopharmaceuticals.

I. Baldazzi, **Sr**., G. Franchi, F. Trapasso, S. Tetti, M. Martini, C. Del Mastro, P. Ragni, A. Lenza, F. Scopinaro; Az. Osp. Sant' Andrea, Roma, ITALY.

Bkg: The availability of 68Ge/68Ga generators provided with regular EMEA authorization enables the routine use of 68Ga- radiopharmaceuticals. **Aim**: To explain the actions for producing 68Ga- DOTA Peptides, e.g. 68Ga- DOTA NOC, the most used 68Ga- radiopharmaceutical for the study of neuroendocrine tumours. **Material and Methods**: As for every β+ radiopharmaceutical, for the correct synthesis of Ga68-Dotanoc we need a Category A, laminar flux hot cell. The dedicated synthesis device is located inside the hot cell. The synthesis module has to be cleaned before and after the synthesis of the radiopharmaceutical. The module is connected to the 68Ge/68Ga generator and to an Argon gas bottle for the activation of all the pneumatic process inside the device .A flux of 0.1N HCl, elutes the 68Ga from the generator; as happens in every elution, only the high specific activity part, that is the central part of the eluate, is used for the labelling process. Even if the process is automated, the technician has to pay attention to the selection of the peack eluate with high specific activity. Ethanol (EtOH), water for injection and saline are needed for the successive, labelling phase. The fraction of max activity is sent to the reaction cell, where pH, temperature and reaction time have to be regulated and optimized. After labelling the radiopharmaceutical can be purified by sterile, inverse phase tC18 column and EOTH. After the production of the tracer, the qualitity control is performed by ITLC and the Ga68- Dotanoc can be injected to patients. Sterility is continuosly monitored, so that it is possible to use the results of the preceeding sinthesis performed 24-48 h before. **Results**: The best results we obtained are: 99% labelling yield for DOTA NOC, with 60% of the initial activity in the final vial. The above results have been obtained after having set the following parameters for the reaction cell: pH 4.5, temp 95°, reaction time 7.5 min, 1.2 ml peack eluate fraction. It was possible to standardize the process by saving steps and parameters in the memory of the dedicated PC that serves the synthesis module. **Conclusion**: The Technician, thanks to standardization of the procedures, can safely perform the process of synthesis of Ga68- Dotanoc, to standardize the process and register it on manual approved by hospital ethic committee.

P275

68Ga-based radiopharmaceutical preparation using NaCl method: collected results and preliminary data on ethanol influence in labelling performances

M. Riondato, O. Ferrando, M. Gaeta, F. Montagnani, A. Ciarmiello; S. Andrea Hospital, La Spezia, ITALY.

Gallium-68 labelled peptides have been extensively used in the last decade for PET imaging as a tool to diagnose neuroendocrine tumours. More recently 68Ga PSMA-HBED-CC has gained increasing attention as a radiopharmaceutical for the detection of prostate cancer lesions. For meeting clinical and research needs several labelling strategies have been developed and applied to routine productions. Our facility has been recently implemented with an automated synthesizer for the production of Gallium-68 labelled peptides based on the "NaCl method". This work aims to present our experience with the production of some popular radiopharmaceutical for clinical use, 68Ga-DOTATOC -DOTANOC and -PSMA-HBED-CC, introducing the observed benefits by increasing ethanolcontent in the labelling reaction.DOTATOC, DOTANOC, PSMA-HBED-CC were labelled using a Modular-Lab PharmTracer module coupled with a 30 mCi 68Ge/68Ga IGG100 IPL generator (E&Z Europe). According to the NaCl method, generator eluate was first processed by the use of a SCX cartridge, facilitating activity concentration and germanium breakthrough removal. Gallium-68 was eluted with 0.5 mL (NaCl 5M plus HCl) and reacted with the precursor (45 microg for DOTATOC/DOTANOC or 10 microg of HBED-CC) in a buffered sodium acetate solution (95°C,5 min). Crude product was then processed by Sep Pak purification (C18) and the desired product was recovered from the cartridge using Ethanol/Water. The final product was ready for clinical use after dilution with saline. The original 68Ga-DOTANOC preparation protocol was sub sequentially modified increasing the ethanol content in the labelling mixture from 10% up to 50% v/v (ethanol/water). Yields were monitored in order to reduce the amount of needed precursor.68Ga-radiopharmaceuticals were produced following the standard protocols in 16 min with high yields (Ys) and radiochemical purity (RCP). 68Ga-DOTATOC (Ys dc=82.1%±4.4%, RCP=99.1%±0.7%, n=42), 68Ga-DOTANOC (Ys dc=85.1% ±3.5%, RCP=99.4% ±0.5%, n=10) and 68Ga-PSMA-HBED-CC (Ys dc=83.2% ±3.5%, RCP=95.1% ±1.3%, n=5). The best results for 68Ga-DOTANOC preparation with the modified protocol were obtained usinga labelling mixture of ethanol 40% (v/v): the required amount of precursor was 10 microg (7 nmol), ensuring high yield reproducibility (Ys dc=85.2%±2.3%, n=3) and enhancing the Specific RadioActivity up to 80 MBq/nmol.In conclusion we confirm that "NaCl method" is robust, reliable and suited for routine automated synthesis of the most used 68Ga-radiopharmaceuticals.

Furthermore the use of ethanol for 68Ga-DOTANOC preparation displayed a favourable role in reducing the precursor amount maintaining reliable yields and allowing to reach higher SRA with respect the standard applied protocol.

P276

Synthesis and Evaluation of Novel [Cu-64] Labeled Dimeric c(RGD-ACH-K) Conjugates for Tumor PET Imaging

K. Lee, J. Park, J. Lee, U. Shin, G. An, S. Lim, B. Kim, J. Kim; Korea Institute of Radiological and Medical Sciences, Seoul, KOREA, REPUBLIC OF.

Object: In a recent reports on the application of dimeric RGD peptides for detecting of angiogenesis and targeting of tumors have demonstrated that the dimeric RGD peptides is better targeting capability in vivo and enhanced receptor-binding affinity in vitro because of the increased αvβ3 integrin recognition ability as compared with the monomeric cyclic RGD peptide[1, 2]. The purpose of our study, thus, is to design and synthesis a noble 64Cu-labeled dimeric cyclic RGD Peptide conjugates for an efficient tumor imaging, with its evaluation in vitro and in vivo. Methods: The two derivatives of novel DOTA (or NOTA)-cyclic RGD-ACH-K dimer are prepared by solid-phase peptide synthesis as shown in the scheme below, applied by previously our researches [3]. After 64Cu-labeling of two conjugates, it is confirmed through Radio-TLC scanner and HPLC system. The radiochemical stability and PET imaging of these conjugates is evaluated in serum and tumor-bearing mouse for 48 h. Result: The radiochemical stability of above two conjugates was very stable over 98% for 48 h by the analysis of radio-TLC method and HPLC system, and was showed the PET tumor-imaging in mouse. Conclusion: We introduced two novel conjugates of 64Cu-labeled cyclic RGD peptides for PET diagnosis and therapy in tumor, having the highly radiochemical stability in serum and a specific tumor-uptake in vivo. Acknowledgements: This research was supported from National Reaserch foundation of Korea(NRF) grant funded by the Korean government(MEST) (2011-0030161, 2011-0030162) References: [1] Yun Wu, et al (2005) J Nucl Med, 46, 1707-1718. [2] Zi-Bo Li, et al (2008) Eur J Nucl Med Mol Imaging, 35, 1100-1108. [3] Ji-Ae Park, et al (2014) ACS Med. Chem. Lett., 5, 979-982.

P277

(68)Ga processing in the preparation of (68)Ga-citrate

H. Kvaternik, C. Barowitsch, D. Hausberger, S. Kerschbaumer, R. M. Aigner; Medical University of Graz, Graz, AUSTRIA.

Aim: Since more decades (67)Ga is established for the imaging of inflammation and infection lesions with SPECT. After (68)Ga becomes more and more available, (68)Ga-citrate is an option for inflammation imaging with PET (1). In the clinical preparation of (68)Ga-citrate, there is a challenge to concentrate the (68)Ge/(68)Ga generator eluate and to remove the (68)Ge breakthrough. Therefore, two post-processing methods were tested for feasibility.Material and Methods: The (68)Ge/(68)Ga generator (1,85 MBq)was obtained from iThemba LABS and was eluted with 10 mL 1 M HCl. The eluate was diluted to 19 mL with water and (68)Ga was collected onto an SCX cartridge (Machery Nagel). The elution of the generator was carried out semiautomatic by a GRP synthesis module (Scintomics). Using the first method, the SCX was eluted with 2 mL of a 5 M NaCl/ 0.25 M HCl mixture (2). Using the second method (3), the SCX was eluted with 2 mL 2.5 M HCl/ 50% ethanol and was directly transferred to a SAX cartridge (Machery Nagel). After purging the SAX with nitrogen to remove traces of ethanol, the purified (68)Ga was recovered from SAX by desorption with 2 mL 0.1 M HCl.Results: The first method provided a purified (68)Ga with a recovery from SCX up to 92%, well appropriate for peptide labelling. However, due to the high NaCl content, this purified (68)Ga is unsuitable for further processing to (68)Ga- citrate. Experiments for desalination by ion exchange were not effective. First results of the second method showed a combined recovery from SCX and SAX of about 60%. The purified (68)Ga, obtained in an HCl matrix, is easy to turn into an isotonic (68)Ga-citrate solution. The process is now optimized and developed to a fully automatization with respect to the good manufacturing practice (GMP) rules for hospital preparation of radiopharmaceuticals.Conclusion: Applying a new (68)Ga post-processing method by ethanolic hydrochloric acid, a production route of (68)Ga-citrate for clinical inflammation imaging is under development. The benefit of this pathway is to prevent organic solvents, were a quantitative elimination is required, in conjunction with a robust and simple process.(1)Rizzello A, et al. Nucl Med Commun 2009; 30: 542-545(2)Mueller D, et al. Bioconjugate Chem. 2012; 23: 1712−1717(3)Larenkov AA, et al. J Radioanal Nucl Chem 2015; DOI 10.1007/s10967-015-4089-2

P278

Experimental implementation and proof of principle for a Radionuclidic Purity test solely based on half life measurement

T. Jørgensen, M. Jensen; Technical University of Denmark, Roskilde, DENMARK.

Aims: The purpose of this work was to examine an experimental implementation of a new method to test the radionuclidic purity

(RNP) of F-18 compounds and find the overall limitations and possible impacts on this test. **Materials and methods**: Two different kinds of counter setups were used to collect data. One with a scintillation counter containing a NaI crystal and one with a liquid scintillation counter (LSC). The LSC was preferred over other detector systems due to the detectability of all radioisotopes. The data were obtained by measuring the decays of a number of FDG samples, that were assumed to be pure and also on samples that were contaminated manually. The counts were measured within full energy spectrum, since the test is based on a comparison of total activities of two isotopes according to the definition of RNP. The test was also carried out on simulated data. The test procedure is based on a comparison of normalized measured data with corresponding theoretical data created from the test parameters (statistical confidence of 97.5%). **Results**: We have tested several samples of FDG and found that things like background, dead time and systematic errors have crucial impacts on the test result, if not taken care of. On the other hand when these parameters are taken into account the test seems to work perfectly. The RNP = 99.9% level can be assured in less than 5 hours for all impurities with half-lives ≥ 2 times the half-life of F-18. The test cannot be used to determine, which contaminating isotope that is present. It only states whether or not the sample is pure on the basis of the test parameters with a statistical confidence of 97.5%. The production and test procedures should be planned in a way that gives as few corrections to the data set as possible in order to have the best sensitivity in the test - e.g. the correction of systematic time errors could be avoided with a better time resolution in the counting system. We have developed a GUI application written in MATLAB in order to make the RNP test easy to handle in everyday practice. **Conclusion**: We conclude that this application for the RNP test works with real data and does comply with the requirements in the European Pharmacopoeia, while other methods like direct gamma spectroscopy will not in general detect impurities to this degree.

P279

GMP compatible synthesis, dosimetry and in vivo stability of the selective αvβ6 tracer [18F]IMAFIB for clinical use

M. Onega, C. Plisson, S. Ashworth, S. Lanzarone, J. Ramada-Magalhaes, S. Moz, N. Keat, J. Passchier; Imanova Limited, London, UNITED KINGDOM.

Background/Aim: The expression levels of the epithelial-specific integrin αvβ6 may increase following injury as well as in different carcinomas and fibrosis. The peptide NAVPNLRGDLQVLAQKVART (A20FMDV2), derived from the foot and mouth disease virus, has been identified as a potent selective binder of αvβ6. Initial studies in animal models have indicated that [18F]FBA-A20FMDV2 ([18F]IMAFIB) is a promising tool compound for non-invasive imaging of αvβ6 expression in vivo.1. Herein we report the methods that were developed for the automated and GMP compliant synthesis, quality control and metabolite analysis of [18F]IMAFIB for human clinical studies, and the results from the preclinical dosimetry study. Materials and Methods: [18F]IMAFIB was labelled with fluorine-18 by conjugation of the resin bond precursor (A20FMDV2 peptide on rink amide resin) to the prosthetic group [18F]-fluorobenzoic acid ([18F]FBA), followed by acidic cleavage from the resin, purification by semi-preparative HPLC and reformulation in saline. The synthetic procedure of [18F]IMAFIB was adapted from a previously described method.1 An automated procedure was developed in-house using an Eckert and Ziegler Modular-Lab system coupled with a semi-preparative HPLC system. Quality control methods for clinical batches of [18F]IMAFIB were developed in accordance to EP guidelines. Plasma metabolite analysis was performed using the 'Hilton method'.2 Suitability of the method was determined using plasma samples from rats injected with [18F]IMAFIB. A whole body distribution of [18F]IMAFIB in healthy Sprague-Dawley rats was performed to estimate the radioactivity exposure in humans using OLINDA. Rodent tissue data were adjusted to reflect human values based on the different proportions of organ to total body mass in rat and human. Using these data, dosimetry calculations provided the individual organ doses and the whole body effective dose. Results and Conclusion: An automated GMP synthesis of [18F]IMAFIB has been successfully implemented on an Eckert & Ziegler Modular-Lab system. To our knowledge this is the first solid-phase [18F]-radiolabeling of a peptide to GMP standards. The current automated process allows reliable production of [18F]IMAFIB in suitable quantities for use in clinical PET studies. QC and metabolite analysis methods have been developed and [18F]IMAFIB routinely meets specified criteria. Finally, an estimated human effective dose of 0.026 mSv/MBq of injected activity was determined from the rodent preclinical dosimetry study. Clinical studies are ongoing and will be reported separately. References: [1] S. H. Hausner et al., Cancer Research 2007, 67, 7833. [2] J. Hilton et al., Nucl. Med. Biol., 2000, 27, 627.

P280

Effects of chemotherapeutic agents on 18F-FDG uptake in various tumour cells: Implication for 18F-FDG PET

P. Ubl, X. Gao, F. Girschele, S. Birkmann, M. Hacker, G. Hamilton, **S. Li**; Medical University of Vienna, VIENNA, AUSTRIA.

Aim: 18F-FDG positron emission tomography (PET) has been widely used for evaluation of the chemotherapy response of different tumours. However, the effect of chemotherapeutic agents on 18F-FDG uptake in tumour cells may be quite different. The purpose of this study is to investigate the 18F-FDG

incorporation in various tumour cells in response to conventional and novel chemotherapeutics. Materials and Methods: Cells derived from human small cell lung cancer (SCLC) (NCl-H417 and DMS153) and human colon cancer cell line (COLO 320DM) were incubated with different chemotherapeutic agents for 72 hours. The treatment with chemotherapeutic agents was terminated by wash the tumour cells with phosphate buffered saline (PBS) three times before 18F-FDG was added in PBS. Control cells were incubated without chemotherapeutic agents. Cell counts, viability and cell cycle distribution were also determined. Results: As compared with control cells, a significant decrease of 18F-FDG uptake was found in human SCLC (NCI-H417) cells after pre-incubation with satraplatin and in DMS153 cells after treatment with satraplatin and doxorubicin as well as 5-Fluorouracil and vinblastine. Significantly decreased uptake of 18F-FDG was also demonstrated in human colon cancer cell line (COLO 320DM) after pre-incubation with cisplatin and doxorubicin. Interestingly, the treatment with doxorubicin has led to a significant increase of 18F-FDG incorporation in NCI-H417 cells, similarly, a significant increase of 18F-FDG was also found in DMS153 cells after pre-treatment with cisplatin and dichloroacetate. Conclusion: Our results demonstrated that treatment with different chemotherapeutic agents results in diverse degrees of incorporation of 18F-FDG into tumour cells. Chemotherapeutic agents, such as cisplatin, satraplatin, 5-Fluorouracil, doxorubicin and vinblastine decrease 18F-FDG uptake in human colon cancer and human SCLC cells. Whereas, cisplatin, doxorubicin and dichloroacetate may increase 18F-FDG uptake in human SCLC cells. These results may have implications for clinical evaluation of chemotherapy response by using 18F-FDG PET.

P281

Radiosynthesis of the [18F]-FHBG and Uptake Study with Transfected Cells

M. Beaurain1, A. Salabert1, L. Vaysse1, Q. Dardonville2, V. Pottier2, M. Alonso2, I. Loubinoux1, P. Payoux3, M. Tafani2; 1Inserm UMR825, Toulouse, FRANCE, 2Radiopharmacy Department - CHU Toulouse, Toulouse, FRANCE, 3Nuclear Medicine Department, Toulouse, FRANCE.

Aim: Cell transplantation therapy is an innovative therapeutic approach particularly in neurology to compensate the neural loss after stroke. Multimodal molecular imaging enables real-time longitudinal monitoring of transplant survival. First, the cells will be transfected with a gene encoding a thymidine kinase (HSV1-tk). Then, we will use [18F]-FHBG as a reporter probe to image the expression of this enzyme. HSV1-tk phosphorylates [18F]-FHBG to its monophosphate form leading to intracellular accumulation. In order to develop this tool in our center, we worked on the [18F]-FHBG radiosynthesis optimization and we studied its capture by transfected cells. Materials and Methods: We developed an automated radiosynthesis of [18F]-FHBG using a Synchrom R&D automat (Raytest®): the first step is a nucleophilic substitution of a tosylate group with an 18F atom followed by an acid hydrolysis step. Next, we performed an HPLC purification. To maximize the synthesis efficiency, we varied the nucleophilic substitution temperature from 90°C to 100°C, 110°C and 120°C. Finally we also determined the specific activity and log D (octanol/ buffer). We developed the transfection on Neuro2a cells with a plasmid containing the HSV1-tk and a neomycin resistance gene for the selection of stably-transfected cells. Then, we measured the percentage of [18F]-FHBG captured by these cells and compared it with that of the non-transfected cells. Results: An optimal synthesis efficiency (12%) was obtained with a temperature of 110°C. The elution solvent used is a mixture of sodium acetate and ethanol (90:10) which shows compatibility when in contact with cells and in injection in vivo. The specific activity exceeds 3.2 GBq/μmoles, and the average activity synthetized is 1850 MBq. The log D is -0.88, as such, this molecule is hydrophilic. The uptake rate of transfected cells is 30 times higher than that of non-transfected cells. Conclusion: With a nucleophilic substitution temperature of 110 °C, we obtained a sufficient amount of [18 F]-FHBG to be compatible with a human or animal injection. Its uptake by transfected cells appears to be effective. In spite of its high hydrophilic character which limits its passage across the blood-brain barrier, we are planning to use it for tracking the fate of grafted cells after stroke because the BBB is disrupted. However, the long-term monitoring could be affected by the restoration of this BBB. Before evaluating this tracer in vivo in rats, we plan to perform an in vitro calibration to determine how many cells correspond to the emitted signal intensity.

P282

Promising chemical delivery system into the central nervous system of [18F]FLT for PET imaging studies of low-grade brain tumours.

F. Gourand1, A. Henry2, M. Ibazizène1, M. Dhilly1, C. Papamicaël2, V. Levacher2, L. Barré1; 1CEA/DSV/I2BM/UMR ISTCT 6301/LDM-TEP, Cyceron, Caen, FRANCE, 2Normandie Univ, COBRA, UMR 6014 et FR 3038; Univ Rouen; INSA Rouen; CNRS, IRCOF, Mont-Saint Aignan, FRANCE.

Aim: [18F]FLT (3'-deoxy-3'-18F-fluoro-L-thymidine), an analogue substrate of thymidine, has been developed as a tracer of proliferation in oncological PET studies. Low-grade brain tumours are poorly visualized and vectorisation of [18F]FLT

through the intact blood-brain barrier (BBB) could provide the opportunity to detect these tumours at an early stage. A chemical delivery system (CDS) based on Bodor's approach has been developed to enable the penetration of [18F] FLT into the brain. **Materials and Methods**: FLT has been linked to a lipophilic 1,4-dihydroquinoline carrier (CDS) that enables the transport across the BBB. The synthesis of CDS-FLT has been developed and in order to evaluate the potential of this CDS, we have undertaken its labelling with carbon-11 ($t_{1/2}$: 20.4 min). The radiolabelling was performed as a one-pot two-step procedure starting from the quaternarization of the quinoline with [11C]methyl triflate followed by a regioselective reduction with 1-benzyl-1,4-dihydronicotinamide (BNAH) to afford the corresponding [11C]CDS-FLT . The *in vivo* behaviour of [11C]CDS-FLT was carried out in healthy Sprague-Dawley rats to measure the injected dose per gram in the brain as a percentage (ID%). **Results**: The incorporation of [11C]methyl triflate to the quinoline was 85-90% and reduction with BNAH provided [11C]CDS-FLT with a conversion rate of 50-60% (based on HPLC profiles). The radiosyntheses were performed using TRACERLab FX MeI and M synthesizers. After HPLC purification and formulation, [11C]CDS-FLT was obtained in 50 min with 15% decay-corrected yields based on [11C]methyl iodide. The *in vivo* evaluation in healthy rats demonstrated that this CDS is a markedly efficient lipophilic carrier; indeed, the BBB passage was increased by a factor of 15 when compared to [18F]FLT injected alone. **Conclusion**: *In vivo* studies in healthy rats demonstrated the potential of 1,4- dihydroquinoline as a carrier to enable FLT to cross the intact BBB. These encouraging results warrant further studies into rats bearing low-grade brain tumours.

P283

Evaluation of [11C]EA10 to image GluN2B-containing NMDA receptor subunits

L. A. Wells1, S. Kealey2, O. Howes3, G. Henriksen4, J. Passchier1, E. Arstad5; 1Imanova Centre for Imaging Sciences, London, UNITED KINGDOM, 2Imperial College London, London, UNITED KINGDOM, 3Psychiatric Imaging, MRC Clinical Sciences Centre, London, UNITED KINGDOM, 4Norwegian Medical Cyclotron Centre and Institute of Basic Medical Sciences, University of Oslo, Oslo, NORWAY, 5Department of Chemistry, UCL, London, UNITED KINGDOM.

The neurotransmitter glutamate acting via the N-methyl-D-aspartate receptor (NMDAR) plays a significant role in cognitive processes and memory formation. Abnormal glutamate neurotransmission and decreased expression of the NMDAR has been reported in the pathophysiology of diseases including schizophrenia and Alzheimer's Disease1,2. Here, we evaluate [11C]EA10, a selective antagonist for the GluN2B-subtype of the NMDAR, as a potential PET radioligand. The affinity of EA10 was determined in the presence of the GluN2B antagonist [3H]Ifenprodil (8nM) and sigma-receptor block GBR12909 (3uM) with unlabelled EA10 (0.05-100nM) using radioligand binding techniques. [11C]EA10 was produced by *O*-methylation of the desmethyl precursor using [11C]methyl iodide. A rat was injected with 8 MBq [11C]EA10 prior to receiving two dynamic-PET:CT scans with and without a cold dose of EA10 (1 mg/kg). Plasma was taken and the level of radiometabolites assessed. Scans were reconstructed (2D-FBP:scatter corrected) and time activity curves (TACs) generated for the cortex and cerebellum. The central distribution of [11C]EA10 was assessed in conscious versus anesthetised animals (rats n=2 per group, mice n=4 per group) with and without 1 mg/kg EA10. Animals received 8 MBq [11C]EA10; after 60 min the activity associated with brain nuclei was assessed by a gamma counter and the standard uptake values (SUV) derived. *In vitro*, EA10 competed for the [3H]Ifenprodil binding site with a sub-nanomolar affinity compared to unlabelled Ifenprodil (EA10 Ki 0.4-0.7nM compared with Ifenprodil Ki 6.3nM). The decayed EA10 radiochemical productions competed for the [3H]Ifenprodil binding site within the same affinity range. EA10 was successfully radiolabelled resulting in good yields and specific activity (n=7, end of synthesis: activity=2006±546MBq, specific activity=67±29GBq/umol). The PET:CT image displayed a homogeneous uptake of [11C]EA10 in the CNS, no differences were observed in the TACs generated for the cortex and cerebellum during baseline conditions. No differences were observed in TACs from the baseline scan compared with the scan after administration of 1 mg/Kg EA10. The uptake of [11C]EA10 was unchanged in anesthetised compared with conscious animals with and without the administration of 1 mg/Kg EA10. EA10, a novel ligand with specific binding characteristics for GluN2B, was labelled and produced in yields relevant for clinical imaging. [11C]EA10 enters the brain however the *in vivo* distribution did not reflect the known distribution of GluN2B. Pretreatment with a high dose of cold EA10 did not lead to decreased binding. Due to the high *in vitro* affinity of EA10, the contribution of the mass dose warrants further investigation.1.Beneyto *et al*,2007. 2.Kravitz *et al*,2013. 3.Arstad *et al*,2006.

P284

Radiosynthesis and Evaluation of 2-[18F]Fluoroethyl 4-Nitrobenzyl Carbonate for Imaging Tumor Hypoxia with Positron Emission Tomography

Z. Zhang, J. Lau, N. Colpo, F. Bénard, **K. Lin**; BC Cancer Agency, Vancouver, BC, CANADA.

Objectives: 4-Nitrobenzyl carbonate derivatives of anti-cancer agents have been reported to undergo bioreductive activation specifically in hypoxic tumor tissues. Reduction of the nitro group leads to the fragmentation of prodrugs, and the subsequent

release of active anti-cancer agents. Previously, we reported the trapping of 2-[18F]fluoroethanol in mouse tissues after iv injection. The trapped radioactivity in most tissues/organs did not decrease over a 1 h period. Based on this observation, we investigated if 2-[18F]fluoroethyl 4-nitrobenzyl carbonate can undergo fragmentation under hypoxia to release 2-[18F]fluoroethanol for cancer imaging with positron emission tomography. **Methods**: 2-Fluoroethyl 4-nitrobenzyl carbonate and the radiolabeling precursor (2-bromoethyl 4-nitrobenzyl carbonate) were synthesized by coupling 4-nitrobenzyl chloroformate with 2-fluoroethanol and 2-bromoethanol, respectively, in dichloromethane with 4-dimethylaminopyridine as the base. 18F labeling was performed in acetonitrile at 60 °C for 15 min using tetrabutylammonium bicarbonate as the base. Stability of 2-[18F]fluoroethyl 4-nitrobenzyl carbonate was assessed in mouse plasma and monitored by HPLC. PET imaging and biodistribution studies were performed in NODSCID/IL2RKO mice bearing HT-29 human colon cancer xenografts. **Results**: Both 2-fluoroethyl 4-nitrobenzyl carbonate and 2-bromoethyl 4-nitrobenzyl carbonate were obtained in 69% yield. 2-[18F]Fluoroethyl 4-nitrobenzyl carbonate was obtained in 90 min synthesis time with > 99% radiochemical purity. Stability assay showed that 2-[18F]fluoroethyl 4-nitrobenzyl carbonate was metabolized extremely fast in mouse plasma with only ~ 1% remaining intact after 1 min incubation. From the biodistribution and PET imaging data, there was minimal clearance of 2-[18F]fluoroethyl 4-nitrobenzyl carbonate. At 3 h p.i., high (>5 %ID/g) and sustained uptake was observed in many tissues including blood, intestines, kidney, heart, tumor, and brain. HT-29 tumor xenografts (6.90 ± 0.27 %ID/g) were readily visualized in PET images. Despite high tumor uptake, tumor-to-blood and tumor-to-muscle ratios were suboptimal at 1.21 ± 0.03 and 1.93 ± 0.30 respectively. The highest activity was observed in bone (10.1 ± 1.54 %ID/g) suggesting a significant degree of defluorination in vivo. **Conclusion**: Although high tumor uptake was observed, 2-[18F]fluoroethyl 4-nitrobenzyl carbonate failed to clear from non-target tissues. In vivo hydrolysis of the carbonate tracer yielded 2-[18F]fluoroethanol as a radiolabeled metabolite, which contributed to high background uptake. Poor pharmacokinetics and tracer instability render 2-[18F]fluoroethyl 4-nitrobenzyl carbonate unsuitable for targeting tumor hypoxia.

P285

A Comparison of [18F]fluorotetrafluoroborate with [124I] Iodide for imaging human sodium iodide symporter

S. Samnick1, I. Israel1, M. Schiller1, M. Mix2, A. Schirbel1, A. Buck1; 1University of Wuerzburg, Wuerzburg, GERMANY, 2University of Freiburg, Freiburg, GERMANY.

Aim: The human sodium iodide symporter (hNIS) has been historically the most important target for imaging and therapy in the nuclear medicine. However, current hNIS imaging methods have severe limitations in terms of resolution and sensitivity. Therefore, there is an increased interest in developing more specific radiotracers for imaging hNIS using the more sensitive positron emission tomography (PET) technique. This study evaluates experimentally the feasibility of PET with the novel fluorinated agent [18F]Fluorotetrafluoroborate ([18F]TFB) in hNIS-expressing tumours. **Methods**: [18F]TFB was investigated in hNIS expressing tumor cells in cultures and compared with the established radioactive hNIS agents sodium [123I]iodide ([123I]NaI), and [99mTc]pertechnetate ([99mTcO_4). The specificity of the [18F]TFB uptake into hNIS-expressing cells was assessed by competitive inhibition studies using $KClO_4$ and non-radioactive sodium iodide (NaI), known as specific hNIS substrates. Furthermore, the potential of [18F]TFB for imaging hNIS-expressing tumors was tested on hNIS-expressed tumours xenografted in nude mice in comparison with sodium [124I]iodide ([124I]NaI), using μ-PET. **Results**: In vitro, [18F]TFB accumulated intensively in hNIS-expressing tumor cells. Radioactivity incorporation into cells following a 15-min incubation at 37°C was 15 ± 3% of the total loaded activity per 106 cells for hNIS-expressing cells, which was significant higher than accumulation of the clinically established [123I]NaI and [99mTcO_4 (6 ± 2% and 10 ± 3%). In comparison, the [18F]TFB uptake into non-hNIS-expressing control cells remained insignificantly low (<0.2%). The uptake of [18F]TFB into hNIS-expressing cells was inhibited up to 90% by $KClO_4$ or non-radioactive Na[127I]iodide, confirming the specificity of the [18F]TFB uptake for hNIS. Finally, PET studies using [18F]TFB and [124I]NaI in the same mice demonstrated a higher and specific accumulation of [18F]TFB in hNIS-expressing tumours xenografts, resulting to a significantly better delineation of the tumours in vivo. **Conclusions**: The specific and high-level accumulation of [18F]TFB in hNIS- transfected tumor cells in vitro and in vivo strongly indicates that [18F]TFB is a promising candidate as imaging probe for hNIS expressing tumors using PET. Our PET data suggest advantages of [18F]TFB over [124I]NaI as radiotracer for imaging hNIS-expressing tumours.

P286

Automated GMP compatible synthesis of 3-[18F] Fluoro-5-[(pyridine-2-yl)ethynyl]benzonitrile ([18F] FPEB)

S. Hader; King's College London, London, UNITED KINGDOM.

Hader, Stefan; Fortt, Robin; Twyman, Frazer; Gee, Antony* *Division of Imaging Sciences and Biomedical Engineering*,

King's College London, *UK*.**Aim**: 3-[18F]Fluoro-5-[(pyridine-2-yl)ethynyl]benzonitrile ([18F]FPEB) is a metabotropic glutamate receptor subtype 5 (mGluR5) antagonist used in preclinical and clinical PET neuroimaging of disorders of the CNS including schizophrenia and autism [1]. We describe herein a fully automated GMP compatible thermal method for the synthesis of [18F]FPEB utilising the 3-nitro-5-[(pyridin-2-yl)ethynyl]-benzonitrile precursor on an Ecker & Ziegler Modular-Lab. **Materials and Methods**: An aqueous [18F]fluoride solution (600 μl, 20 Gbq) was delivered from the cyclotron and trapped on a QMA-carbonate SPE cartridge. The [18F]fluoride was eluted with a solution of K_2CO_3 (0.7 mg) and Kryptofix 2.2.2 (12 mg) in water (200 μL) and acetonitrile (800 μL). The solution was evaporated to dryness using a combination of vacuum and nitrogen flow at a temperature of 110°C over an 8 minute period. Following evaporation, the precursor (2 mg) in DMSO (1 mL) were added and the labelling reaction was conducted at 150°C for 15 minutes. Purification was achieved by semi-preparative HPLC on a Phenomenex Luna C18 HPLC column (4.6 x 30 mm, 5 μm) with an isocratic mobile phase of 65:35 H_2O:ACN + 0.1% TFA at a flow rate of 5 ml/min. The fraction corresponding to [18F]FPEB (t_R= 18 min) was collected and reformulated by extraction onto a preconditioned Waters C18 plus SPE cartridge and eluted with 1 mL of ethanol into a sterile vial containing 9 mL of PBS and passed through a 0.22 μm sterile filter. **Results and Conclusions**: The fully automated GMP compatible synthesis of [18F]FPEB was effected in 5% EOS yield utilising the Ecker & Ziegler Modular-Lab. **Acknowledgements**: The authors acknowledge financial support from the Department of Health via the National Institute for Health Research (NIHR) comprehensive Biomedical Research Centre award to Guy's & St Thomas' NHS Foundation Trust in partnership with King's College London and King's College Hospital NHS Foundation Trust. This work was also supported by the Innovative Medicine Initiative Project EU-AIMS (115300). **References**: [1] Wang J-Q, Tueckmantel W, Zhu A, Pellegrino D, Brownell A-L, (2007), Synapse, 61, 951-961.

P287

Implementation of Routine Production of [18F]-Fallypride on the TRASIS All-in-One Universal Synthesizer.

C. Marshall, K. Drandarov, S. H. Bukhari, D. Hardwick, V. Costanza, P. Llewelyn, K. Probst, A. Dabkowski; Cardiff University, CARDIFF, UNITED KINGDOM.

[18F]-Fallypride, a high affinity dopamine D2/D3 receptor antagonist, is a useful PET tracer imaging tool for the quantitative studies of the D2/D3 receptor sites in the brain. [18F]-Fallypride is used in the diagnostics of a number of neurological and neuropsychiatric disorders. Our centre has recently acquired the Trasis All-In-One Universal Synthesizer and reports on the implementation of a routine GMP radiosynthesis of [18F]-Fallypride.The Trasis All-In-One Universal Synthesizer is an automated instrument dedicated for the labelling of PET tracers. Due to its graphical interface control it is quick and easy to programme new synthetic sequences likev 18F]-Fallypride. The synthesis sequence includes the introduction of the [18F]-label using [18F]-fluoride ions. The production of [18F]-Fallypride is performed using Tosyl-Fallyprideas starting material and prep HPLC purification. The set-up is GMP compliant as single-use cassettes were compiled specifically for this [18F]-Fallypride synthesis and [18F]-Fallypride is synthesised within 40 mins as a saline solution.At the end of the synthesis the yield varied between 40-45% (not decay corrected) with a radiochemical purity of >99% measured by HPLC. The QC is performed and according to the general guidelines of the European Pharmacopeia and the tests include appearance, pH, half-life, bacterial endotoxins, kryptofix, radiochemical purity, radionuclidic purity and residual solvent analysis, all of which meet the required standards..We have successfully implemented the[18F]-Fallypride as a new tracer on the TRASIS All In One system to the standards required by GMP.

P288

Towards nucleophilic synthesis of alpha-[18F] Fluoromethyl-p-tyrosine

R. Krasikova1, O. Kuznetsova1, V. Orlovskaja1, O. Fedorova1, V. Maleev2, Y. Belokon2, A. Geolchanyan3, A. Saghyan3, L. Mu4, S. Ametamey4, R. Schibli4; 1N.-P.Bechtereva Institute of Human Brain Russian Academy of Science, St.-Petersburg, RUSSIAN FEDERATION, 2A.N. Nesmeyanov Institute of Organoelement Compounds Russian Academy of Science, Moscow, RUSSIAN FEDERATION, 3SPC Armbiotechnology NAS, Yerevan, ARMENIA, 4BIO, Paul Scherrer Institute, Villigen-PSI, SWITZERLAND.

Aim. During the last decade considerable progress has been made to overcome difficulties in producing ring-fluorinated analogues of aromatic amino acids such as 6-[18F]fluoro-L-DOPA *via* the nucleophilic route. In this work we evaluated a nucleophilic approach to obtain 18F-labelled tyrosine derivative carrying monofluoro methyl group at the alpha position, as potential molecular probe for estimating activity of tyrosine hydroxylase, the rate-limiting enzyme in the biosynthesis of catecholamine neurotransmitters. Previous studies described ring-fluorinated 3-[18F]fluoro-α-fluoromethyl-*p*-tyrosine (Dejesus et al, 1994) and 6-[18F]fluoro-α-fluoromethyl-*m*-tyrosine (Murali et al. 2003) *via* electrophilic radiofluorination. A nucleophilic method has been recently suggested for the

synthesis of racemic α-[18F]fluoromethyl phenylalanine using cyclic sulfamidate precursor that was prepared from D, L-benzylserine (Huang et al., 2013). The present work describes an approach for the enantiomerically pure α-[18F]Fluoromethyl-*p*-tyrosine synthesis that could be performed *via* the direct nucleophilic fluorination of the NiII complex as radiolabeling precursor. **Methods**. Radiosynthesis was based on the nucleophilic displacement of the α-$MeSO_2$ (mesyl) leaving group in a labeling precursor following hydrolysis of 18F-fluorinated intermediate and deprotection of hydroxyl group of tyrosine. The precursor, NiII complex of Schiff base of (2*S*)-1-benzyl-*N*-(2-formylphenyl)pyrrolidine-2-carboxamide with (*S*)-2-amino-2-(methylsulfonyloxymethyl)-3-(4-methylsulfonyloxyphenyl)propanoic acid (Ni-(*S*)-BBA-(*S*)-MsOmethyl-TyrOMs (**I**)), was prepared in a two steps synthesis from the corresponding NiII complex of Schiff base of (2*S*)-1-benzyl-N-(2-formylphenyl)pyrrolidine-2-carboxamide with (*S*)-tyrosine (Ni-(*S*)-BBA-(*S*)-Tyr). Radiofluorination of (**I**) was performed in various solvents (acetonitrile, dichlorobenzene, DMSO, DMF, acetone) at 60-140°C in the presence of different phase transfer catalysts (kryptofix/K_2CO_3, kryptofix/KH_2PO_4, 18 crown-6/$KHCO_3$, $TBACO_3$, $TBAHCO_3$). **Results**. Despite multiple attempts to substitute the α-$MeSO_2$-group in (**I**) by [18F]fluoride under a wide variety of conditions, 18F-labeling efficiency was very poor (0.5-3% according to radioTLC of reaction mixture). The highest fluorine-18 incorporation rate of 16% was achieved by carrying out the radiofluorination in acetone (kryptofix/K_2CO_3, 60°C, 10 min). **Conclusion**. The poor fluorination efficiency of (**I**) may be caused by the steric hindrance at the α-carbon atom of the tyrosine moiety. Work is now in progress to optimize the precursor structure. **Acknowledgement**. This study was supported by the SNF grant IZ73ZO_152360/1.

P289

New Approach to Production of [18F]Flumazenil for Central Benzodiazepine Receptors Imaging by PET

N. Gomzina1, D. Vaulina1, M. Nasirzadeh2; 1N.P.Bechtereva Institute of the Human Brain Russian Academy of Sciences (IHB RAS), St. Petersburg, RUSSIAN FEDERATION, 2Saint Petersburg State University, St. Petersburg, RUSSIAN FEDERATION.

AIM[18F]flumazenil ([18F]FMZ) is a well-known radiopharmaceutical for the assessment of the central benzodiazepine receptor (cBZR) concentration by PET. These receptors are involved in many neurological and psychiatric disorders, such as epilepsy, panic disorder, acute stroke, alcoholism. Synthesis of [18F]FMZ by nucleophilic substitution of nitro group in molecule of nitromazenil with [18F]fluoride had been introduced in 2005 (*Ryzhikov N.N. et al*). The semi-preparative HPLC used to separate [18F]FMZ from precursor, because the physical-chemical properties of flumazenil are similar to those of nitromazenil. The aim was to develop the SPE purification method of [18F]FMZ instead of time-consuming HPLC.METHODS [18F]Fluoride was produced via 18O(p,n)18F nuclear reaction in [18O]H_2O water target of GE PETtrace cyclotron. [18F]FMZ was prepared by heating of 1-2 mg of nitromazenil (ABX GmbH, Germany) in DMF at 150°C in the presence of kryptofix 2.2.2/K_2CO_3. Purification step involved derivatization of nitro-precursor and following isolation of [l8F]FMZ using reversed phase cartridges. After [18F]fluorination step potassium methoxide in methanol was added to the reaction mixture. Under strong base conditions the precursor converted to less lipophilic species that easily removed by SPE, whereas [l8F]FMZ was much more stable. Then the reaction mixture was cooled and diluted with water and the activity trapped on a HLB 3cc column (Waters). The column was washed and eluted by 35 % of ethanol/water. This eluate was diluted with water and passed through a tC18 light cartridge (Waters) and finally eluted by 1-2 ml of 15% ethanol/acetic buffer.RESULTS With using of new approach [18F]FMZ was obtained with non-optimized radiochemical yield of 10 % (EOB) in less than 60 min. Radiochemical purity of [18F]FMZ was more than 97%, the amount of nitromazenil in the final product was negligible (≤1μg/mL) and otherchemicals impurities were under the limits set by the European harmacopoeia. All procedures were implemented into Tracerlab FX N Pro module (GE Healthcare).CONCLUSION The suggested approach to production of [18F]FMZhas been allowed to replace HPLC purification with more attractive for automated SPE procedure using commercially available cartridges with the efficient separation of radioligand from radiochemical and chemical impurities. Work is now in progress to optimize all the developed procedures.

P290

Use of Potassium tert-Butoxide in the Synthesis of [11C] Flumazenil, [11C]PK11195 and [11C]-(+)-DTBZ

S. F. Garcia-Arguello; Centro de Investigaciones Medico-Sanitarias (CIMES), Malaga, SPAIN.

AimAlkali metal hydroxides and sodium hydride are the preferred bases in [11C]methylations. However, they have certain limitations such as poor solubility in organic solvents and hydrolytic activity. Potassium *tert*-butoxide (KO*t*Bu) is a non-nucleophilic base that is soluble in various organic solvents. The use of this reagent in the [11C]methylation of amide or phenol moieties has not been reported. Therefore, the goal of this work was the evaluation of KO*t*Bu in the synthesis of

[11C]flumazenil, [11C]PK11195 and [11C]-(+)-DTBZ.**Materials and Methods**[11C]CO_2 was produced in a GE PET Trace cyclotron and [11C]iodomethane was synthesized in a Tracerlab FX-C module using the gas-phase method. Dry solvents, hydroxides, sodium hydride 60 % dispersion in mineral oil and potassium *tert*-butoxide solution 1M in THF were obtained from Sigma-Aldrich. Desmethyl precursors (1 mg) were purchased from ABX. Analytical radiochemical yields (decay-corrected) were analyzed using the radiochromatograms obtained in the semi-preparative HPLC purification of the labelled products. The identities of the [11C]radiopharmaceuticals were confirmed in an analytical HPLC by co-injection with the corresponding non-radioactive compounds.**Results**The synthesis of [11C]flumazenil was carried out in DMF using aqueous NaOH or KO*t*Bu as the base. Both NaOH and KOtBu gave excellent radiochemical yields (75-85 % and 65-70 % respectively), although KO*t*Bu provided somewhat inferior results due to the formation of a radioactive side product that eluted a few minutes after [11C]flumazenil.Tetrabutylammonium hydroxide (TBAOH, 1M in methanol and 1M in water), NaOH, NaH and KO*t*Bu were compared in the synthesis of [11C]PK11195. Besides that, DMF and DMSO were compared as reaction solvents. The best results were obtained using NaH suspension/DMSO, but the hydride degraded with time and blocked the tubing of the synthesis module. KO*t*Bu gave moderate but reliable radiochemical yields (30-35 % in DMF or DMSO), whereas low and irreproducible yields were obtained with TBAOH and NaOH (5-10 %).[11C]-(+)-DTBZ was produced in dry DMSO using NaOH, KOH and KO*t*Bu. In this case, the highest radiochemical yield was achieved with KO*t*Bu (75-80 %), with hydroxides giving slightly lower conversions (60-65 %).**Conclusion**The syntheses of [11C]flumazenil, [11C]PK11195 and [11C]-(+)-DTBZ were carried out with [11C]iodomethane and KO*t*Bu in DMSO or DMF using the captive solvent method. Commercially available THF solutions of KO*t*Bu were stored at room temperature and provided consistent radiochemical yields for several months. Comparison studies showed that the efficiencies of the [11C]methylation reactions with KO*t*Bu were equivalent or greater than those achieved with other bases.

P291

Direct nucleophilic synthesys of 18F-fluoroethylated arylbenzotiazole as a new potential PET probe for breast cancer imaging

C. L. Chen1, G. Y. Li1, F. C. Meng1, R. S. Liu1,2, H. E. Wang1, V. V. Orlovskaja3, D. D. Vaulina3, O. F. Kuznetsova3, O. S. Fedorova3, R. N. Krasikova3; 1Department of Biomedical Imaging and Radiological Sciences, National Yang-Ming University, Taipei, TAIWAN, 2National PET/Cyclotron Center, Veterans General Hospital, Taipei, TAIWAN, 3N.P. Bechtereva Institute of Human Brain Russian Academy of Science, St.-Petersburg, RUSSIAN FEDERATION.

Aim. The substituted arylbenzotiazoles (BT) represent a class of compounds that have shown selective and effective inhibition of tyrosine kinase overexpressed in the wide range of cancers. Among them 2-(3,4-dimethoxyphenyl)-5-fluorobenzothiazole (PMX 610) exhibited very potent (GI50 < 0.1 nM) and selective in vitro antitumor properties in human breast cancer cell lines MCF-7 and MDA-468 (Mortimer et al, 2006). Based on this BT scaffold several 11C-labelled analogues have been prepared as PET diagnostic agents (Wang et al., 2006), however their further evaluation was not reported. In this work we intend to develop corresponding 18F-fluoroethylated derivative, 2-(3,4-dimethoxyphenyl)-6-(2-[18F]fluoroethoxy) benzothiazole, to allow its preclinical evaluation as potential diagnostic agent for breast cancer imaging by PET. Methods. Radiosynthesis of 2-(3,4-dimethoxyphenyl)-6-(2-[18F]fluoroethoxy) benzothiazole was performed in one step via a Kryptofix-assisted radiofluorination of the corresponding tosyl precursor in DMF at 110-130 degC for 10-20 min. The precursor and cold reference were prepared in two synthetic approaches starting from 4-aminophenol and fully characterized by 1H NMR, 13C NMR, EI/ESI-MS and HRMS techniques. Results. After optimization of reaction conditions a fluorine-18 incorporation rate of 60% (according to radioTLC of reaction mixture) was achieved by carrying out radiofluorination at 130 degC for 20 min. This one step synthesis procedure suits well for the automation and provides radiotracer in amounts and purity sufficient for the preclinical application. Conclusion. The synthesis of 2-(3,4-dimethoxyphenyl)-6-(2-[18F]fluoroethoxy) benzothiazole has been developed via direct nucleophilic displacement of tosyl group in customized precursor. Radiopharmacological evaluation in mice bearing MDA 468 (ER-) and MCF-7 (ER+) breast tumors using small animal PET is underway. Acknowledgement. This study was supported by RFBR grant 15-54-52026/15 and MOST 104-2923-B-010 -001 -MY2

P292

F-18 Radiolabelling of Chitosan-Based Nanoparticles and its Modelling Reaction

A. LIMA OUBIÑA1, T. MIKLOVICZ1, J. VARGA1, J. BORBÉLY2, P. MIKECZ1; 1Department of Nuclear Medicine, University of Debrecen, Debrecen, HUNGARY, 2BBS NanoTech, Debrecen, HUNGARY.

AIM: The aim of this work was to label chitosan-based nanoparticles via [F-18]-4-fluorobenzaldehyde ([18F]-FBA) on

one of its amine groups. The reaction was modelled on one of its components, Glucosamine (GlcN), instead of the use of the whole polymer. Subsequently, the developed procedure was applied to chitosan radiolabeling. MATERIALS AND METHODS: [18F]-FBA was synthesized from 3 mg 4-Formyl-N,N,N-Trimethylanilinium triflate , in a 5 minutes reaction at 80°C, using SCX cartridge to remove side products. To model chitosan labelling, direct and indirect reductive amination were used, between the carbonyl group of [18F]-FBA with the amine group of GlcN and 1,3,4,6-Tetra-O-Acetyl-2-amino-GlcN (TAGlcN), at different temperatures: 110°C, 70°C, 50°C and room temperature, during 30 minutes. NaBH3CN was employed as reducing agent. To study the possible aldol side products, we performed the same experiments with N-Acetyl-GlcN and glucose. The modelling reaction concluded to use direct reductive amination at elevated temperatures (70°C and 50°C) for the labelling of the polymer. The reaction was followed by TLC analysis with samples taken at 5, 10, 20 and 30 minutes. RESULTS: [18F]-FBA radiochemical yield was 56±10%, with >95% radiochemical purity. For the reaction between FBA and TAGlcN via direct reductive amination, the HPLC-determined conversion yields were: 110°C: 7±1%, 70°C: 42±0.7%, 50°C: 41±4%, room temperature: 20±8% In case of indirect reductive amination, (with TA-GlcN), at 110°C the results are similar, 8±1%, as with direct reductive amination at the same temperature. Room temperature yield was 41±12%, but it took longer time (1h). The reactions with N-Acetyl-GlcN and glucose gave significantly different compounds of less than 5 % of activity. When radiolabeling chitosan via [18F]-FBA, using direct reductive amination, radiochemical conversion was at 50 °C: 33±3%, 46 ±2%, 60±2%, 68±1%; and at 70°C: 54±4%, 65±2%, 71±1%, 72±1% after 5, 10, 20 and 30 min, respectively. CONCLUSIONS: Modelling reaction of direct and indirect reductive amination showed that [18F]-FBA reacts mainly with the NH2 group of GlcN or TA-GlcN, with high yields at 70°C and lower temperatures. In case of absence or blocked amine group, we observed low yield aldol side reactions. These results were successfully applied to chitosan radiolabeling. Both at 50°C and 70°C, after 30 minutes approximately 70% of FBA was built in, but the reaction was faster at higher temperature. This method may be employed for radiolabeling chitosan, or other nanoparticles based on a polymer rich in amine groups. ACKNOWLEDGEMENTS: This work was supported by FP7-PEOPLE-2012-ITN (316882 RADIOMI project).

P293

An efficient radiosynthesis of [18F]Fluoro-inositol derivatives dedicated to PET imaging

C. Collet1,2, S. Schmitt3,2, S. Lamandé-Langle3,2, F. Chrétien3,2, F. Maskali1, S. Poussier1,2, P. Marie1,2, Y. Chapleur1,3,2, G. Karcher1,2; 1Nancyclotep, Vandoeuvre les Nancy, FRANCE, 2Université de Lorraine, Vandoeuvre les Nancy, FRANCE, 3UMR 7565, Vandoeuvre les Nancy, FRANCE.

Introduction: Recent results have shown that inositols derivatives could be an interesting scaffold for the preparation of new radiotracers usable for the diagnostic of cancer or inflammation but also brain diseases. However, preliminary studies demonstrated that the 1-fluoro-*scyllo*-inositol have very low brain penetration. We have therefore planed the synthesis of new *myo*- and *scyllo*-inositol derivatives radiolabelled with fluorine-18 which could be more likely to cross the Blood Brain Barrier.Two types of inositol based radiotracers were considered. The first one bearing a [18F]fluoro-arm directly branched on the cycle. In this case the six hydroxyl groups could be conserved. The second one involved an ether linkage to add the arm carrying the fluorine-18.**Materials & Methods**: Precursors of radiolabelling and cold references were synthesized using acetate as protecting group according to multistep strategies starting from *myo*-inositol. The 18F-labelling was performed using standard labelling conditions (K_{222}/K_2CO_3, ~10 µmol precursor in acetonitrile, 85-95°C, 5-15 min) on an AllInOne (Trasis®) module. The radiolabelled compounds were purified by semi preparative HPLC (conditions: 45/55 ACN/H_2O). After evaporation either a deprotection (saponification using 2M NaOH) at room temperature for 5 min or a formulation with EtOH 10% was realized. Mice-Balbc bearing a 4T1 breast cancer were used as animal models for PET imaging performed using small-animal INVEON tomograph.**Results**: Precursors were synthesized in eleven steps in ~3% yield and the fluorinated references in twelve steps in ~2% yield. Incorporation of fluorine-18 was performed in 30 to 45 % yield (dc). The corresponding hydroxylated forms were obtained after an efficient deprotection (90% yield dc). Eight injectable inositol based radiotracers (*scyllo*- and *myo*- configuration, protected and free) were so obtained in good yield and injected. PET-scan images were obtained in animals.**Discussion/Conclusion**: We developed an efficient automated strategy for inositol radiolabelling with fluorine-18. *Scyllo*- and *myo*-[18F]fluoro-inositol based radiotracers were obtained in good radiochemical yield. Their potential application as PET imaging agents is currently under investigation.

P294

18F-labeling and in vivo evaluation of PEG modified polystyrene micelles via PET imaging

J. M. Postema1, L. Jennings2, J. Thackeray3, J. Banksthal3, G. Waton2, F. Schosseler2, E. Mendes4, T. L. Ross1; 1Radiopharmaceutical Chemistry, Department of Nuclear Medicine,

Hannover Medical School, Hannover, GERMANY, 2Institute Charles Sadron, CNRS-University of Strasbourg, Strassbourg, FRANCE, 3Preclinical Molecular Imaging, Department of Nuclear Medicine, Hannover Medical School, Hannover, GERMANY, 4, Department of Chemical Engineering, Advanced Soft Matter, Delft University of Technology, Delft, NETHERLANDS.

AimMacromolecular structures as drug-delivery-systems are gaining more and more interest. Their ability to carry drugs such as chemotherapeutic agents or therapeutic radionuclides to the required site, and their unlimited modification possibilities make them perfect for a wide range of applications from non-invasive molecular imaging to targeted tumor therapy. One of the most powerful imaging techniques to study such structures in vivo is PET. In this study we have focused on the direct 18F-labeling of dimethylsilicium chloride terminated polystyrene included in PEG modified polystyrene micelles and their subsequent in vivo evaluation in rodents.Materials and MethodsDimethylsilicium chloride terminated polystyrene was labeled with [18F]fluoride in the presence of Kryptofix 2.2.2 and K2CO3 at room temperature in chloroform. Purification of the polymer was achieved by cartridge-based solid phase extraction. Stability of the purified micelles was tested against saline over 15 minutes.Micelles made out of PEG modified polystyrene / dimethylsilicium chloride terminated polystyrene (90/10) were labeled at 60 °C in chloroform in the presence of Kryptofix 2.2.2 and K2CO3. Purification was accomplished by size exclusion chromatography. The 18F-labeled micelles were applied to in vivo PET-imaging in rat and mouse.ResultsLabeling of dimethylsilicium chloride terminated polystyrene proceeded with yields of up 70 percent at room temperature within 5 minutes. After purification, the product was obtained in an excellent radiochemical purity of ≥ 98% (radio TLC). During stability testing the polymer showed no defluorination or degradation over a period of 15 minutes.The direct 18F-labeling of the provided micelles proceeded with yields of up to 35% in 15 minutes. The labeled micelles were used for preliminary in vivo PET imaging which showed a promising tumor uptake in a tumor bearing rat. Further in vivo studies with the 18F-labeled micelles in mice are currently underway.ConclusionWe have successfully labeled dimethylsilicium chloride terminated polystyrene with 18F under mild conditions. Furthermore, we have been able to label micelles in one-step with 18F. The new 18F-micelles were applied in first in vivo studies in a tumor bearing rat, which showed very promising tumor uptake with very low unspecific background in healthy tissue. Further studies are ongoing.This work was funded by the People Program (Marie Curie Actions) of the EU FP7/2007-2013 (No. PITN-GA-2012-317019 'TRACE 'n TREAT').

P295

An adapted GMP-compliant production of [18F]FAZA on a cassette based synthesis unit for the detection of hypoxia using positron emission tomography (PET)

O. C. Neels, Y. Remde, U. Hennrich, K. Kopka; German Cancer Research Center, Heidelberg, GERMANY.

Aim: [18F]FAZA ([18F]Fluoroazomycin Arabinoside) is a well-known radiopharmaceutical that has been successfully used for the detection of hypoxia using PET. Due to its usefulness for radiation therapy planning the aim of this project is to set up a quick and reliable method for the fully automated synthesis of [18F]FAZA on a cassette based synthesis unit. Materials and Methods: An aqueous solution containing [18F]fluoride was obtained by nuclear reaction (18O(p, n)18F) from a Scanditronix MC32NI cyclotron, transferred to a Trasis All in One synthesis module, trapped on and eluted from a QMA cartridge using standard procedures (Kryptofix/K2CO3 in water/acetonitrile). After azeotropic drying, 10 mg of precursor 1-(2,3-Diacetyl-5-tosyl-(-D-arabinofuranosyl)-2-nitroimidazole in 1 mL anhydrous DMSO were added and heated for 10 minutes at 120°C. The reaction mixture was cooled down to room temperature and protecting groups were removed by addition of 1 mL 1 M NaOH solution for 3 minutes. pH was adjusted with 1 mL 0.4 M NaH2PO4 solution, diluted with 2 mL 10 mM NaH2PO4/EtOH (90:10) solution and injected onto a semi-preparative HPLC column (Luna 5µ C18, 100Å, 250 x 10 mm, 10 mM NaH2PO4/EtOH (90:10), 4 ml/min). [18F]FAZA was eluted from the column after 28 minutes and sterile filtered ready for injection. Quality control and determination of specific activity was done using an Agilent HPLC system. Results and Conclusion: [18F]FAZA can be obtained in decay corrected radiochemical yields higher than 25% on a new automated cassette based synthesis module in radiochemical purities > 95% after HPLC purification and good specific activities within less than 60 minutes after end of radionuclide production and is now used for preclinical imaging experiments. Work is in progress to reduce the synthesis time using a cartridge based purification process to prepare the clinical transfer of this promising hypoxia imaging PET tracer.

P296

The role of 64CuCl2 PET/CT scan in patients with outspreaded Hodgkin Lymphoma. Is the 64CuCl2 apt to plan a rescue radionuclide therapy?

E. Capasso, **Jr**.1, S. Massidda2, C. Meleddu1; 1U.O.C. Nuclear Medicine, Cagliari, ITALY, 2U.O.C. Hematology and Bone Marrow Transplantation, Cagliari, ITALY.

INTRODUCTION AND AIM: 18F-fluorodeoxyglucose positron emission tomography (18F-FDG-PET) is performed for staging, restaging and follow up of patients with Hodgkin Lymphoma. According to new Lugano classification PET-CT can also replace the bone marrow biopsy (BMBx) for HL. The FDG-PET is although essential for the best management of patients, for instance to identify responders and non-responders, early during treatment. Infact the use of FDG-PET imaging to detect residual metabolically active disease is well validated as a surrogate biomarker for chemoresistance. Since '90s the monoclonal antibody (Lym-1) labeled with 67Cu was used for radioimmunotherapy in non Hodgkin Lymphoma patients. Nowadays also copper-64-DOTA-Rituximab is of interest in NHL. But what about Hodking Lymphoma? Is 64CuCl2 PET/CT scan apt to study patients with outspreaded Hodgkin Lymphoma? MATERIALS AND METHODS: Two patients (P1: 69y Male and P2: 70y Female) affected by refractory Hodgkin Lymphoma in progression disease neverthless chemioterapy, radiotherapy and allogenic transplantation underwent to a diagnostic 64CuCl2 PET/CT within two weeks after a FDG PET/CT. Administered activities were: P1-FDG 372 MBq and P2- FDG 230 MBq. P1 and P2- 64CuCl2 were 370 MBq. The FDG PET/CT scans were obtained from base of skull to the upper thigh of the patients with a scan/speed of 2,5 min/bed; 1 hour after the radiopharmaceutical administration. The 64CuCl2 PET/CT scans icluded also the skull vertix, were performed 3 hours after the administration with a scan/speed of 2,5 min/bed. The scans were analyzed by two different physicians. RESULTS AND CONCLUSIONS: All the avid FDG lesions showed high concentration of 64CuCl2 both in the P2 (right lung lesions) and in P1 (sovradiaphragmatic nodes, left lung and bone areas as left ribs and L1 vertebrae). The bone areas presented a lower FDG uptake, didn't shown 64CuCl2 accumulation (in the left hip for the P2).These data suggest it could be possibile use 64CuCl2 PET/CT scan in patients with outspreaded Hodgkin Lymphoma despite best-fulfilled therapy to plan out a tailored radionuclide therapy. These are preliminary data and it's necessary to increase the study population.

P16 - Sunday, October 11, 2015, 4:00 PM - 4:30 PM, Hall 3 – Poster Exhibition

Radiopharmaceuticals & Radiochemistry: Radiopharmacy

P297

A specific fluorescein-combined media fill test for validation of aseptic radiopharmaceutical preparations and assessment of good radiopharmacy practice.

A. CHANTRY1, C. FANTON D'ANDON1, A. GOUILLET1, P. GARRIGUE2,1, B. GUILLET1,2; 1AP-HM, Marseille, FRANCE, 2Aix-Marseille Université, Marseille, FRANCE.

Regularly qualifying the operators constitutes a major lead in quality management of the radiopharmaceutical unit. Simulation tests like the media fill test (MFT) have already demonstrated their usefulness and power in the field of radiopharmacy, assessing the operators' technique and the environmental adequacy to produce a sterile drug by aseptic processing, according to the current Good Radiopharmacy Practice guidelines (cGRPP). Still, no specific simulation test exists to match the radiopharmaceutical preparation routine in terms of volume sampling, specific handled materials and radioprotection. We developed a simulation test of radiopharmaceutical preparations, from the eluate sampling to the syringe conditioning. Combining fluorescein to a MFT enabled the additional assessment of the operator's ability to avoid contaminations on the working area. We intend to use this simulation protocol as an initial and periodic qualification method for the radiopharmaceutical staff. A sterile fluorescein solution was added to tryptic soy broth in strict aseptic conditions to enable a final fluorescein concentration of 10 mg/mL. The protocol consisted in 3 phases, to simulate direct sampling from the eluate, a 1-step and a 2-step radiopharmaceutical preparation process in routine conditions under a controlled environment (shielded class-A hot cell). Right at the end of each preparation, fluorescein contamination was evaluated around the working area using an UV-lamp, and photographs were taken. Prepared units were incubated following the manufacturer's instructions and the absence of turbidity was visually monitored daily. The operator's qualification was defined by the absence of microbiological contamination at day 14. In case of any microbiological contamination, germ identification would have been performed. To date, three simulation tests were carried out by a pharmacy technician, a radiopharmacist, and a pharmacy resident. No microbiological growth occurred. Discreet fluorescein traces were observed for all three operators on the working area. Though, as no hazardous handling was observed for any of the three operators, these insignificant traces seemed to be rather in relation with the use of open free needles in our preparation process, in the absence of any commercialized closed system transfer device (CSTD) adapted to the radiopharmacy practice. Hence, all three operators were successfully validated. A wider use of this simulation test is already intended in two other radiopharmacies. Still, the tests we performed highlighted the contamination risks with our current preparation process, despite working according to the cGRPP. The necessity of CSTDs should also be balanced with the quantification of this latent contamination for radioprotection matters.

P298

Comparison between two compounds of exametazime produced by different laboratories for labeling of leukocytes

A. Almarcha Gimeno1, L. Díaz Platas1, M. Romero Otero1, R. Díaz Exposito2; 1Unidad de Radiofarmacia. Hospital Clínico Universitario de Valencia, Valencia, SPAIN, 2Servicio Medicina Nuclear. Hospital Clínico Universitario de Valencia, Valencia, SPAIN.

AIM: The objective of this study was to compare two commercial compounds of exametazime used in leukocytes labeling by evaluating their radiochemical purity (RP) and stability with time, and the quality of the scintigrafic images obtained on each of them. MATERIALS AND METHODS: 26 patients with diagnosed prosthetic infection, normal body mass index, and no antibiotic treatment were selected and divided in two homogeneous groups. The diagnosis was performed by scintigraphy with 99mTc-exametazime labeled leukocytes and clinically or microbiologically confirmed. Two different commercial compounds of exametazime, Ceretec® (group A) and Exametazime-Radiopharmacy® (group B), were used for labeling leukocytes in each group of patients. In both cases the radiochemical purity, the labeling yield and cell viability were determined. In order to study the stability over time, one vial of each compound was labeled with and without cobalt stabilizer solution, and periodic determinations of the RP were performed during 7 hours after labeling. The quality of the images was quantitatively assessed by calculating the specific uptake ratio (SUR) between the regions of interest (ROI) corresponding to the lesion zone and to the contra-lateral symmetric region. The background image was also evaluated. The data analysis of the images was performed by one-way ANOVA with Bonferroni test and expressed as the mean ± SEM. The correlation index between RP and time was determined by t-test, using GraphPad Software Inc (San Diego, CA, U.S.A.). Significance was accepted when $p<0.05$. RESULTS: There were no statistical differences ($p < 0.001$) in the values obtained for the RP (A: 93.98 ± 1.12; B: 91.57 ± 3.14), the SUR (A: 1.466 ± 0.40; B: 1.427 ± 0.53), and the labeling yield (A: 69.58 ± 5.72; B: 57.33 ± 10.82). RP decreased over time in all cases, as shown by correlation indexes between RP and time (A: 0.9831, B: 0.9521, A with cobalt: 0.8903, B with cobalt 0.9397). CONCLUSION: The results show that there are no differences between both compounds (Ceretec® and Exametazime Radiopharmacy®), when used for leukocytes labelling. The stability for Exametazime Radiopharmacy® is higher than for Ceretec®, as indicated in the technical summary. The stability is also higher when using cobalt as stabilizer.

P299

Qualitative Determination of Human Antibodies Against Mouse Immunoglobulin (HAMA) Before the Administration of 99mTc-Scintimun® Using the MILLENNIA® QUIKLINE Kit

E. López, E. Ariza, F. Cuevas, M. Cardoso, Y. Santaella, P. Valderas, F. Martin; SAS, Algeciras, SPAIN.

Aim: To determine in vitro of HAMA from Millennia ®Quikline kit in a radiopharmaceutical unit before the administration of 99mTc-Scintimun. **Materials** / **Methods**: We have a kit that consists of: - Analysis device HAMA (HAMA Test Unit): membrane covered with mouse IgG combined with gold nanoparticles.-Buffer of detection (Chase Buffer): pH 7.2 buffer. Card assessment (Evaluation Cards) The method involves/is to: 1) Add 50 µl of serum on the pad dish analysis device 2) Add 1 drop of buffer. 3) Incubation: 10 minutes at room temperature (18-28°C) 4) Qualitative evaluation with the evaluation card that is included in this package. This device contains two lines: C Line control and T Line analysis. Interpretation: -If it is Positive: if the T line analysis shows the same colour or darker than the evaluation line card colour. - If it is Negative: if the T line analysis shows a lighter colour or a weaker faded shadow than the line card rating. If no line T is observed, it is also negative. The C line control should always appear (it is an operational control and cannot be used to interpret the line of analysis) **Results**: 15 tests were performed, and two tests of these were positive and the remaining two were negative. In 100% C line was obtained as an operating control. Of these 15, 8 no T line patients were obtained, and therefore we obtain the negative result of HAMA. In the remaining 6, we had to use the card rating for the result of HAMA (in our case a negative result was obtained). The 1 positive result of the two lines are clearly obtained. **Conclusion**: with this kit, we facilitate the determination of human IgG antibodies in vitro mouse, immediately in radiopharmacy unit, reducing the economic cost involved in sending it to external laboratories, such as reducing the waiting time to perform the test scintigraphy 99mTc-Scintimun and obtaining improvements for patients.

P300

Application of Molecular Modelling to Elucidate Liver Uptakes of 99mTc-Labelled Quinolone Antibiotics

M. Salahinejad, M. Aboudzadeh; Nuclear Science and Technology Research Institute, Tehran, IRAN, ISLAMIC REPUBLIC OF.

Introduction: Metal-based radiopharmaceuticals are of particular interest and play an outstanding role in both therapeutic or

diagnostic medicinal purposes. 99mTc-labeled compounds, as most commonly used radiopharmaceuticals, are highly desirable due to suitable physical properties, nuclear characteristics, and instant availability and low cost. The aim of this study was to investigate the application of three-dimensional quantitative-activity relationships (3D-QSAR) methods to elucidate the liver clearance of 99mTc-labelled quinolone antibiotics. **Material and Methods**: Experimental data of the liver uptakes of 21 99mTc-labelled quinolone antibiotics were taken from the recently published papers. The distribution data collected in rats and mice and experimentally induced infection using *Staphylococcus aureus* or *E. coli*.Comparative molecular field analysis (CoMFA), as a powerful method in 3D-QSAR approach was used for molecular modelling. The CoMFA descriptors, as independent variables correlated with the log value of liver uptakes of 99mTc-labelled quinolone antibiotics as dependent variable, employing Partial least squares (PLS) regression analysis to construct 3D-QSAR models. **Results**: The CoMFA model yielded a leave-one-out cross-validated Q2 = 0.58 with six components, non-cross-validated or calibrated, $R2_{(cal)}$ of 0.98 with standard error of estimation, SEE=0.03 and predicted $R2_{(pred)}$=0.6 with standard error of prediction SEP=0.14 for biodistribution of antibiotics in liver uptakes. The large size of the sterically unfavored yellow region around quinolone backbone indicated that the steric effects have an important impact on liver uptakes of antibiotics. Blue contours represent regions where positive charge increases liver uptakes of antibiotics, whereas red regions represent areas where the negative charge enhances it. **Conclusion**: Combining chemoinformatics and 3D molecular modeling approaches might be very useful for the development of new ligand in metal complexation. They provide alternative, robust and computationally cheap prediction of desired property in the absence of extensive experimental or computed data. These models could provide some invaluable information in the design and development of new 99mTc-labelled radiopharmaceuticals with focusing on the modification and optimization of known biologically active ligand structure.

P301

Assessment of microbiological monitoring for the evaluation of GMP-compliance at a department of Nuclear Medicine and Molecular Imaging of the University Medical Center Groningen

M. Beugeling1, F. Ekoume2, H. J. Woerdenbag3, G. Luurtsema1, M. N. Lub-de Hooge1, D. J. Touw1, S. M. Rubow4, **H. H. Boersma**1; 1University of Groningen, UMCG, Groningen, NETHERLANDS, 2Hôpital General de Yaoundé, Yaoundé, CAMEROON, 3University of Groningen, Department of Pharmaceutical Technology and Biopharmacy, Groningen, NETHERLANDS, 4University of Stellenbosch, Tygerberg Hospital, Department of Nuclear Medicine, Cape Town, SOUTH AFRICA.

Objective: The purpose of our study was to assess trends and deviations from microbiological monitoring in de cleanroom facilities at the department of Nuclear Medicine and Molecular Imaging of the University Medical Center Groningen over the past five years. This was done to evaluate the status of GMP-compliance. **Methods**: Data from active air sampling, passive air sampling, particle counting and contact prints from microbiological monitoring performed over the past five years were collected from our data bases. These tests are carried out routinely to comply with the applicable GMP-regulations. The data were retrospectively analyzed by counting the number of measurements and calculating the number of crossings of the set limit for each sampling location and each test. Statistical analysis was done by performing a Fisher's exact test ($P < 0.05$, 2 sided) to assess statistically significant differences between the years. **Results**: For evaluation, data of 40 sampling locations were analyzed. The number of measurements carried out in 2014 complied with the number of measurements indicated in the Standard Operation Procedure 'Monitoring clean rooms NMMI', except for the contact prints. This means that, when the recent data were compared to older data, many improvements were seen in the environmental monitoring results. This is particularly demonstrated by the microbiological data for one of the grade A with the grade B background hotcells. Comparing the environmental monitoring data of 2012 and 2014, most parameters (including particle counts, settle plates and active air sampling) markedly improved (>5 times decrease of limit crossings) and were statistically significant ($p<0.01$). Similar results were found in most other areas. However, in general, the results of the contact prints did not correlate with these results, indicating that the cleaning and disinfecting procedures still have to be improved. **Conclusion**: We subscribe the obtained improvements to the fact that the department demonstrated to be able to improve the premises, skills, training and attitude of the staff in the course of the period under investigation. The main weak point in environmental monitoring results for the department relates to contact prints. Both frequency and outcome need to be adjusted. Employees have to be re-trained in performing this sampling. Moreover, the cleaning and disinfecting procedures are to be improved, which can be achieved by additional training as well. In conclusion, the long-term evaluation of combined results from routine monitoring is a useful tool in continuous Quality Assurance.

P302

Labelling of leucocytes with 99mTc-HMPAO: a plasma gelled story

S. Bulcourt, E. Malek, M. Lamballais; Valenciennes Hospital, Valenciennes, FRANCE.

AimIn our Nuclear Medicine Department, the labelling of autologous white blood cells (WBCs) with 99mTc-HMPAO is a widely used method to detect sites of infection. Each step of the process are carried out in sterile conditions in a laminar flow cabinet (class A). WBCs are isolated by sedimentation of erythrocytes and centrifugation of leucocyte-rich plasma. After labelling, the radioactive WBCs suspension is infused to the patient, therefore planar scintigraphy and SPECT/CT are performed.Materials and methodsUsually, the pellet containing the labelled mixed leucocytes is resuspended in cell-free plasma. Sometimes, this last step did not go as planned.In November, it has happened that the cell-free plasma has gelled during isolation and labelling of WBCs. For this reason, it was impossible for us to use this plasma for labelled mixed leucocytes resuspension.ResultsIn absence of validated data concerning WBCs viability in pellet, we are in emergency to find a proper solution for this last step of preparation. That's why the use of 0.9% aqueous solution of sodium chloride (saline) seems to be relevant in order to proceed to a successful infusion for our patient.Our quality assurance system is based on failure modes and effects analysis. Then, we investigated this case with multidisciplinary point of view (pharmacist, radiopharmacist, biologist and physicians). The hypothesis of cold agglutinin disease was tested, therefore we incubated the cell-free plasma gelled at 37°C for one hour. As the plasma start to liquefy back, we confirmed this hypothesis.ConclusionAfter this event and this analysis, we modified our standard operation procedure for WBCs pellet resuspension. In normal condition, cell-free plasma keep to be the reference material for resuspension step. But, we formalize the use of saline solution in several situations, for example, cold agglutinin disease. Besides, we extended the saline solution use in case of hemolysis of the cell-free plasma.

P303

Bacterial Endotoxin and Sterility Testing of Active Pharmacological Ingredients used in the production of different Fluorine-18, Gallium-68 and Lutetium-177 labeled Radiopharmaceuticals

A. Mitra, S. Lad, S. Kulkarni, M. G. R. Rajan; Medical Cyclotron Facility, Radiation Medicine Centre, BARC & BRIT, TMH Annexe, Parel, Mumbai, INDIA.

AIM: The aim of the present study was to validate biological quality control tests, viz., bacterial endotoxin test (BET) and sterility test of the active radiopharmaceutical ingredients (API) viz., precursors, reagents and solvents used in the radio-synthesis of different [F-18], [Ga-68] and [Lu-177] labeled radiopharmaceuticals. The validation is a requisite as per the CGRP guidelines. MATERIALS: Acetonitrile, Acetone, DMSO, Ethanol, TBAHCO3(75mM), CH3COONa(0.2M), CH3COONH4(0.1M) NaCl(10%), NaH2PO4(1M), HCl(1N/0.1N), NaOH(0.33N), Ethanolic-water(50-8%), HCl(0.02N)/acetone(98%), Mannose-triflate, ethylene-di-tosylate, L-Tyrosine, Ni(II)-FBPB-Tyrosine-OTs, 4-nitro-benzaldehyde, Anhydro-DMTr-Thymidine, Lysate(λ:0.125/0.03EU/ml), Tris-base/HCl(0.25/0.5/0.1N). Cultures of s.aureus, p.aeruginosa, b.subtilis, c.albicans were obtained from Microbiologics Inc, Minnesota, USA. METHODS: The endotoxin limit (EL) for API's was fixed at 1EU/mg(precursor), 5EU/ml(reagents) and 2EU/ml(solvents) based on concentration, volume used and alteration limit. BET assays were performed by gel-clot method using two sensitivities of lysate. MVD was calculated considering the sensitivity of lysate, EL, concentration and volume of API's used for radiosynthesis. Sterility testing was validated by direct inoculation(DI) method using FTM and SCD media. Positive controls for s.aureus, p.aeruginosa, b.subtilis, c.albicans were set up at bacterial concentration <100CFU (serial dilution- spread plate method) and corresponding negative controls were set up with and without APIs. RESULTS: In BET, HCl, NaOH, CH3COONa, CH3COONH4, HCl/acetone exhibited inhibition due to extreme pH. However, inhibition could be resolved by neutralizing with sterile and endotoxin negative (<0.25EU/ml) Tris-base/HCl at first dilution. BET assay of organic solvents did not demonstrate any inhibition, since the test volume is 1.0/1.5ml (typical volume used in radiosynthesis). However, with the increase in test volume of organic phase, MVD was decreased resulting in inhibition in the assay, which was reversed by short evaporation step at corresponding boiling point. NaCl, NaH2PO4, TBAHCO3 and ethanolic-water (8 - 50%) did not show interferences. In sterility testing, luxuriant growth was observed for positive control culture in the presence of 1ml of any of acetonitrile, acetone, ethanol or DMSO following incubation for 24 hour (s.aureus, p.aeruginosa) and 72 hours (b.subtilis, c.albicans). Growth of all these microorganisms were partially inhibited (<100 CFU) in HCl(1N) and TBAHCO3(75mM). However, good growth were observed on neutralization with sterile and endotoxin negative Tris-buffer (0.5N) and addition of polysorbate-80(0.05%) respectively. Mannose-Triflate and other reagents exhibited no inhibition with all the above strains. No growth was seen in all APIs without the addition of above microorganisms (negative controls). CONCLUSIONS: Standardizing of sterility and BET for various APIs used in radiopharmaceuticals' production was carried out using suitable methods that are validated.

P304

In vitro stability study of 90 Yttrium-microsphere for the treatment of hepatocellular carcinoma

V. Ardisson, N. Lepareur, E. Garin; CLCC Eugène Marquis, Rennes, FRANCE.

Aim: Hepatocellular carcinoma (HCC) ranks third in cancer-related deaths worldwide. Trans-arterial radioembolization (TARE) with 90 (Y-90)-microspheres provides an opportunity for the direct deposition of radiation into malignant HCC tumors and represents a new generation of therapeutics in interventional oncology. The physical and chemical stability of the Y-90 microspheres are critical to ensure the radiation dose remains at the desired site of action, thereby minimizing the possibility of systemic Y-90 exposure and undesirable bone fixation. Therefore, the objective of this study was to characterize the stability properties of various Y-90 microsphere products by measuring their levels of in-vitro Y-90 leaching from various mediums like saline or human serum samples. Methods: Leaching was studied with resin and glass microspheres in different media: saline or human serum at 37 ° C in the presence and absence of sample stabilizers such as 1N HCL or Yttrium 89. These additive compounds were added to limit the precipitation of yttrium as the form of hydroxyl or the bounding to serum proteins. Free 90Y was determined in the medium at 37 °C for 0, 1, 24, 48 and 72 hours by gamma counting. Measurements were taken after centrifugation of an aliquot of the supernatant. Results: We found about 0.6% of free Y-90 in the product shipment medium. In 0.9% NaCl solution, 0.05% of Y-90 leached from glass microspheres and up to 1.59% from the resin microsphere. After incubation of the resin spheres in serum, leaching increases from 0.2 to 5% from 1 to 72 h. However in the presence of yttrium 89, 15 to 60% free yttrium found in the supernatant. No physical degradation of the spheres was observed by optical microscopy. After incubation of the glass spheres in the serum, leaching increases by 0.15 to 2% from 1 to 72 h. Conclusion: Yttrium-90 is directly integrated glass formulation, and showed a higher stability than the resin microspheres product, where the Y-90 is immobilized with weaker ionic interaction. Solubilization of yttrium-90 from the microspheres can depend on many parameters which can leads to a large variability in the results. The addition of yttrium 89 (or other strong cations) in the serum to saturate the serum protein causes a massive release of yttrium 90 from resin microsphere. In this situation, leaching is much more significant with resin microsphere than glass microsphere.

P305

Quality control validation of 16β-[18F] fluoro-5α-dihydrotestosterone produced with the FlexLab radiosynthesiser

J. G. Chan, K. Young, U. Ackerman, H. Tochon-Danguy, A. Scott; Austin Health, HEIDELBERG VIC, AUSTRALIA.

Background: The 18F labelled 16β-[18F]fluoro-5α-dihydrotestosterone (18F-FDHT) analog has been identified as a promising PET tracer for imaging the androgen receptor. The complex synthesis was performed using a FlexLab radiosynthesizer (iPHASE Technologies), which has proven to be reliable for the radiolabelling of other complex molecules. A fully automated and reliable synthesis for 18F-FDHT was developed with overall radiochemical yields of 18-23% (decay corrected). Aim: In this study the 18F-FDHT automated production method was validated for use in human studies. Method: Validation was performed with the usual physiochemical and biological testing which included endotoxin, sterility, residual solvents, radionuclidic identity and pH. Radiochemical purity was performed using a Shimadzu Prominence HPLC system. The stationary phase was a Phenomenex Gemini NX C18, 5μ RP column, 150 x 4.6 mm. Acetonitrile/water (55:45) was used as the mobile phase at a flow rate of 1.0 mL/min. Specific activity was measured at UV 220 nm wavelength. Stability testing was observed for 5 hours. Result: 18F-FDHT was produced with a radiochemical purity >98% and a specific activity > 55.5 GBq/μmol (1.5 Ci/μmol). The final product passed all physiochemical tests as well as endotoxin and sterility tests. The product is stable for at least 5 hours. Conclusion: The fully automated production of 18F-FDHT using the FlexLab radiosynthesizer was successfully validated for use in human studies.

P306

A Study of the Influence of Physicochemical Reaction Parameters on the Radiolabelling Efficiency and Stability of Two Types of 99mTc Radiolabelled Nanoparticles

C. Stefanescu1,2, G. Dodi3, A. Cazacu4, C. M. Uritu5, M. Pinteala5, A. Timofti2, V. Ghizdovat1,2, I. C. Grierosu1,2; 1Department of Biophysics and Medical Physics, Faculty of Medicine, "Grigore T. Popa" University of Medicine and Pharmacy, Iasi, ROMANIA, 2Department of Nuclear Medicine, "St. Spiridon" Hospital, Iasi, ROMANIA, 3Faculty of Chemical Engineering and Environmental Protection, "Gh. Asachi" Technical University, Iasi, ROMANIA, 4Department of Sciences, University of Agricultural Sciences and Veterinary Medicine, Iasi, ROMANIA, 5Advanced Research Centre in Bionanoconjugates and Biopolymers, "Petru Poni" Institute of Macromolecular Chemistry, Iasi, ROMANIA.

Aim: 99mTc radiolabelled nanoparticles are promising radiotracers both for nuclear medicine diagnosis and treatment, great efforts being made to achieve stable and effective systems. In this context, the aims of this study are to better define the relation between different physicochemical reaction parameters and the radiolabelling efficiency of two types of nanoparticles with 99mTc, in order to develop an optimal protocol for new radiopharmaceuticals obtaining.**Materials and methods**: Two types of nanoparticles were used, namely PEG

and PEI coated gold nanoparticles (AuNPs-PEG-PEI) and PEI-derivative fullerene (C60-PEI). As radioisotope for labelling, 99mTc was used. Na+ $99mTcO_4$- was eluted from a 99Mo/99mTc Drytec Generator system, supplied by GE Healthcare. The 99mTc-NPs coupling was realised by reducing, in a first step, Na+ $99mTcO_4$- with sodium borohydride ($NaBH_4$) in the NPs solutions. The radiolabelling efficiency was assessed by using instant thin layer chromatography (ITLC). The parameters taken into account for this study were: the variation of the reducing agent concentration (12.5, 25, 50, 75 and 100 mg/mL) and the variation of the Na+ $99mTcO_4$- dose used (1, 3 and 5 mCi). 99mTc-NPs coupling stability in time (0 - 4 h) was also assessed.**Results**: The radiolabelling efficiency was different for the two types of NPs used. This could be related to the functional groups existent on the NPs surface. The best radiolabelling efficiency was obtained in the case of AuNPs-PEG-PEI (92.81%). By ranging the $NaBH_4$ concentration, we found that the optimal concentration to be used is 12.5 mg/mL, the radiolabelling efficiency ranging, initially, from 77.20% (for 100 mg/mL $NaBH_4$) to 92.81% (for 12.5 mg/mL $NaBH_4$). We also found that, in the absence of active $NaBH_4$ the radiolabelling efficiency decrease dramatically (less than 5%), for both types of NPs. Regarding the coupling stability in time, was noted that the radiolabelling efficiency increased slightly, most probably because of the continuous reducing agent action. Also, our experiments showed that best radiolabelling results were obtained for the Na+ $99mTcO_4$- dose of 1 mCi, both for AuNPs-PEG-PEI and C60-PEI.**Conclusion**: These studies showed that the radiolabelling of NPs systems, as new promising radiopharmaceuticals, is greatly dependent on physicochemical reaction parameters. Optimum parameters can be established for each type of radiolabelled NPs. AuNPs-PEG-PEI seems to be more easily radiolabelled with 99mTc than C60-PEI.**Acknowledgements**: This work was financially supported by PN-II-ID-PCCE-2011-2-0028 and POSDRU/159/1.5/S/133652 projects.

P307

Evaluation of in vivo and in vitro stability of Lu-177-DKFZ-617 for systemic radionuclide therapy in patients with castration resistant prostate cancer

M. Ocak1, A. Aygun2, N. Yeyin2, E. Demirci3, E. Karayel2, A. Araman1, L. Kabasakal2; 1Department of Pharmaceutical Technology, Pharmacy Faculty, Istanbul University, istanbul, TURKEY, 2Department of Nuclear Medicine, Cerrahpasa Medical Faculty, Istanbul University, istanbul, TURKEY, 3Department of Nuclear Medicine, Sisli Etfal Training and Research Hospital, istanbul, TURKEY.

Introduction & Aim: Recently Lu-177-DKFZ-617 PSMA ligand has been shown as a promising novel radioligand for systemic radionuclide therapy in patients with castration resistant prostate cancer (1). For effective and safe targeted radionuclide therapy in vivo and in vitro stability of the radioligands is one of the most important parameters. Therefore the aim of this study was to evaluate in vivo stability of Lu-177-DKFZ-617 PSMA ligand in patients with castration resistant prostate cancer and to determine the in vitro stability in prepared patient dose. Materials and Methods: 177Lu-DKFZ-617 (~100 mci, n=4 ; ~200 mci, n=3) was applied to the patients and after application stability of 177Lu-DKFZ-617 in urine analyzed up to 24h. Stability of 177Lu-DKFZ-617 in blood analyzed 0., 30., 60., 120., and 180. min post administration. For determination of the in vitro stability of 177Lu-DKFZ-617, prepared patient dose incubated up to 48 h at 37°C in saline. Stability analysis of 177Lu-DKFZ-617 at different time points in different media was performed by using radio-reversed-phase high-performance liquid chromatography (radio-RP-HPLC). Results: We found that radioligand was always remained intact in urine, blood and saline at all testing time points, giving 99% of radiolabelling stability in all samples and excreted through urine without any damage to the compound. Conclusion: 177Lu-DKFZ-617 PSMA ligand stayed very stable at in vitro and in vivo conditions during the tested time points and no radiometabolites were detected confirming the good metabolic stability of this radioligand.

P308

Qualitative and quantitative evaluation of a single eluate from two 68Ge/68Ga generators sequentially connected, without any pre-purification

I. Vaccaro1, F. Giurgola1, S. Grugni1, G. Tarullo1, K. Marzo1, A. Chiti2; 1IRCCS Istituto Clinico Humanitas, Rozzano, ITALY, 2Humanitas University, Rozzano, ITALY.

AIM: The aim of our study is to validate the possibility to synthesize 68Ga-DOTA peptides using the elution of two Eckert-Ziegler 68Ge/68Ga generators sequentially connected avoiding prepurification methods. MATHERIAL AND METHOD: We used two 68Ge/68Ga generators loaded with 1850 MBq of Germanium-68 at calibration date. 68Ge was adsorbed over a TiO2 resin and 68GaCl3 was eluted with 0.1N HCl. For this study we connected two generators through a PTFE tubing between the outlet of the first generator and the inlet of the second one: a single mobile phase bottle is linked to the inlet line of the first generator and the eluate is collected at the outlet port of the second generator. Total activity obtained from both generators can be used for radiopharmaceutical synthesis. The elution is done with a 10 ml syringe in two different steps. The volume of 12 ml of 0.1N HCl required to remove

the total activity from both generators is aspirated in two different steps of 6 ml, using the 10ml syringe. This elution is done by an automatic system created by Eckert-Ziegler for a single generator by means of a fractionated method. Usually it allows to use only the central fraction of elution, the one witch contains the peak of radioactivity. The initial and final fractions are discarded due to the presence of impurities. For the elution of two different generators we reduced the speed of the syringe and we changed the volume of the mechanical elution. In this way, we collected the two different central fractions in a single rate containing total radioactivity available for the labeling without any pre-purification steps. RESULTS: Reducing the syringe speed we obtained a high elution reproducibility in terms of volume and activity: 12±0.1ml and 33±0.2mCi. The ability to eluate two generators sequentially connected allowed us to sum the activity from single generators and maximize the yield of elution. The Germanium-68 breakthrough is compliant with the Eu.Ph. dossier requirements. CONCLUSION: This technique allows to use the generator for a more than 300 elutions and postpone its disposal. The production of DOTA-peptides is possible because the eluate of the older generator maintains its purity characteristics even after the 300 elutions and the volumes are compatible with the synthesis.

P309

99mTc-MAA preparation for radioembolization; from just-in-time to just-in-case

J. Prince, M. G. E. H. Lam, N. de Wit, R. R. de Roos, A. D. Barten - van Rijbroek, M. A. A. J. van den Bosch, G. C. Krijger; UMC Utrecht, Utrecht, NETHERLANDS.

Aim: Macroaggregates of 99mTc-albumin (99mTc-MAA) serve as scout dose for radioembolization. In most cases, 99mTc-MAA are prepared when requested by the interventional radiologist. This preparation (30 minutes handling time) hampers logistics and increases total procedure time. The aim of this study was to evaluate the stability of 99mTc-MAA after preparation when during routine preparations. Materials and methods: The study was designed in two parts: 1) 99mTc-MAA stability was analyzed in vitro, and 2) 99mTc-MAA stability was analyzed in vivo by correlating lung shunt to time interval between preparation and administration. 99mTc-MAA (Technescan LyoMAA, Mallinckrodt Medical B.V.) stability was analyzed after 0, 0.5, 1, 2, 4, 8, and 24 hours (3 syringes per timeslot). The hypothesis was that the stability decreased over time due to disintegration and/or oxidation to pertechnetate ($99mTcO_4$-). The particle size distribution was analyzed using both the Coulter principle (Multisizer, Beckman Coulter) and the automated count of the longest diameter on 100x magnification optical microscopy (ImageJ, U.S. NIH). Both methods were calibrated using spheres with a known size of 30 μm (NIST standard reference material polystyrene spheres). The presence of pertechnetate was measured using thin layer radiochromatography (iScan, CANBERRA). In vivo, 112 patients, undergoing 139 infusions, were eligible for radioembolization between March 2011 and November 2013 and were included in the retrospective study. The lung shunt was determined on SPECT-CT. The correlation between lung shunt and time interval between preparation and administration was analyzed using Pearson's correlation coefficient. Results: More than 99% of the particles had an acceptable diameter 5-40 μm (volume-based), except for 1 out of 3 measurements on t=0.5h (97%) and 1 out of 3 measurements on t=2h (84%). Automated counting showed a mean longest diameter of 23 μm (SD 10) at t=0h. It did not increase after 24 hours (mean 21 μm, SD 11). The presence of pertechnetate fell within specifications (<7%) in all 21 syringes. The median time interval between preparation and administration was 23 minutes (range 9-91 min). The median absorbed lung dose was 1 Gy / GBq 90Y (range 0.2-18 Gy / GBq 90Y). No correlation was found; the coefficient was -0.09 (95% CI -0.26 - 0.08, p-value = 0.29). Conclusion: No significant disintegration or oxidation of 99mTc-MAA was found in vitro, nor was time interval between preparation and administration correlated to an increased lung shunt in vivo. 99mTc-MAA can be prepared during routine syringe preparations instead of on demand.

P310

Labeling and quality control of a heterocyclic nitrogen containing side chain bisphosphonate with 99mTc as a skeletal imaging agent

M. Erfani, S. Shirmardi; Radiation Application Research School, Nuclear Science and Technology Research Institute (NSTRI), P.O.Box: 14395-836, Tehran, IRAN, ISLAMIC REPUBLIC OF.

Diphosphonates are categories of drugs that used for treatment of osteoporosis and similar diseases. They have a firm tendency for calcium phosphates and for hydroxyapatite. They have been labeled with gamma emitting radionuclides to image the bone metastases. Nevertheless, it is unclear that which bisphosphonate is the best option when it is labeled with technetium-99m.A last bisphosphonate generation, 2-(3-pyridinyl)-1-hydroxyethane diphosphonic acid which has heterocyclic nitrogen containing side chain, was labeled with 99mTc. Labeling was performed at room temperature for 15 min and its radiochemical analysis included was TLC method. The stability of radiconjugate was checked in the presence of human serum at 37 °C up to 6 h. Biodistribution was studied in mice.Labeling yield of more than 98% was obtained corresponding to a specific activity of 92 MBq/μmol. The

radioconjugate showed good stability in the presence of human serum. Biodistribution studies in mice showed that radioconjugate accumulated in bone with high uptake (7.47 ± 0.25% ID/g at 4 h post injection). In addition, the bone to liver uptake ratios of radioconjugate was 11.67 at 4 h post injection.These high bone activity values, especially evident in time passage, could be due to the potent binding to hydroxyapatite crystals in bone and high stability of radioconjugate. These characteristics could be supposed as the major advantages of this radioconjugate as a candidate for skeletal imaging and tumor metastases in bone.

P17 - Monday, October 12, 2015, 4:00 PM - 4:30 PM, Hall 3 – Poster Exhibition

Radiopharmaceuticals & Radiochemistry: Miscellaneous

P311

Research to create a miniature generator of technetium-99m

A. Rogov, V. Skuridin, E. Stasyuk, E. Nestwrov, E. Ilina; National Research Tomsk Polytechnic University, Tomsk, RUSSIAN FEDERATION.

Currently, radiopharmaceuticals based on the short-lived radionuclides technetium-99m (99mTc) are used for diagnostic research in many areas of medicine. Most of the global market accounted for chromatographic 99mTc generators, which are easy to operate and can be transported over long distances. For their manufacture requires high activity 99Mo (200 Ci/g), extracted from fission products of uranium-235 by costly and environmentally dangerous technologies. An alternative possibility for production of 99Mo is its receipt by the radiative capture (n,γ) by irradiation of molybdenum-98 neutron nuclear reactor. This technology has virtually no waste, but the resulting product has a low specific activity of 99Mo at 7-9 Ci/g. In this regard, it becomes necessary to use a large amount of Mo, about 150-190mg. In world practice for the manufacture of generators sorption of technetium-99m, as a sorbent, are applied different forms of aluminum oxide. Capacitance by Mo adsorbent has a limit within 22-25mg of activated Mo per gram of sorbent. For this reason, for placement on the surface of the sorbent 190 mg of Mo is necessary to use 7.6 to 8.6g of the sorbent, which increases the size of the column and the device, respectively. To investigate the possibility of creating a sorption generator in a small version, conducted a series of studies for increasing sorption capacity of the sorbent. Depending on pretreatment aluminas becomes possible to prepare the sorbent capacity of at Mo approximately equal to 34mg/g. This is achieved by using a set of measures for the preparation of the sorbent and methods of filling sorbent containing the Mo solutions. As a result, there is a significant reduction in weight required for the application of sorbent from 8.6g before 5.6g leads to a reduction of the column and the generator frame. As a result of the research a number of proposals to create a compact design technetium generator and a number of methods by their manufacture. This work was performed on the unique scientific IRT-T equipment and financially supported by Government represented by the Ministry of Education and Science of the Russian Federation (RFMEFI59114X0001).

P312

Cost Effective and Integrated Capture Systems for Radioactive Gases Generated During Automated C-11 and F-18 Radiopharmaceutical Synthesis

D. H. R. Stimson, A. J. Pringle, D. Maillet, A. R. King, S. T. Nevin, T. K. Venkatachalam, D. C. Reutens, R. Bhalla; Centre for Advanced Imaging, the University of Queensland, St Lucia, QLD, AUSTRALIA.

Aims:The emphasis on the reduction of radioactive emissions associated with PET radiochemistry laboratories has increased due to the greater number of facilities worldwide. Historically, various radioactive gas management strategies have been reported including gas compression systems. These systems however, may be incompatible with flammable gases and can be prohibitively expensive. More recently, the use of gas sampling bags has been reported (Schweiger, 2011). This approach however, lacks any safety signal feedback putting the system at risk if overfilling occurs or if the bag is unattached.The aims of this work are to develop and implement a cost-effective gas capture strategy that is suitable for (a) multiple F-18 radiosynthesis modules and (b) use with individual C-11 radiosynthesis modules. The 2 different gas capture systems should have feedback, be integrated with the Cyclotron Safety System and have the capability of being safely emptied of radio-decayed gases without disconnection from the exhaust lines of the radiopharmaceutical synthesizers.Materials and Methods:(a) The exhaust lines of the F-18 radiosynthesis modules were connected to a large gas capture bag located in the cyclotron vault. The bag is fitted with a sensor arm to indicate the bag status. A manual 3-way valve with micro-switch is fitted to the bag inlet which allows the bag to be either filled during cyclotron target transfer/radiosynthesis or emptied.(b) A 4-port/2 way automated switching valve with position sensor was installed in the C-11 synthesizer. The synthesizer exhaust was connected to the switching valve so that gases are directed to a gas capture bag. The alternative valve position allows the bag to be emptied and directs exhaust gases to ventilation during module clean cycles. Similar to (a), the bag is fitted with a sensor arm.For (a) and (b), the valve position and bag status signals

are sent to microprocessors that are integrated with the Cyclotron Safety System. This prohibits the transfer of radioactive gas unless the bag is empty and the valve is in the correct position ("Ready to Receive" signal).A series of target transfers and radiosyntheses were conducted with exhaust stack monitoring used to detect any release of radioactive gas from the systems.Results and Conclusion:A cost-effective gas capture strategy was developed and implemented that is fully integrated with the Cyclotron Safety System. The gas capture system can be emptied without disconnection from the synthesizer. Stack monitoring data demonstrate that the system is safe and effective.

P313
A New Model of Ge-68/Ga-68 Generator

M. Li, H. Chu, C. Lee, H. Chang; Institute of Nuclear Energy Research, Taoyuan, TAIWAN.

Objectives : A Gallium-68(Ga-68) radioisotope generator includes a generating column and a citrate eluent. The generating column is at least partially filled with ion-exchange resin with glucamine groups to absorb Ge-68 and Ga-68 radioisotopes. The citrate eluent is conducted to the generating column to desorb the Ga-68 radioisotope and thereby generate an eluent containing the Ga-68 radioisotope in the form of citrate gallium. A Ga-68 radioisotope generating method is also disclosed. Conclusions : In summary, a Ga-68 radioisotope generator and a method applied in the same in accordance with the present invention are characterized by the use of an organic resin (i.e. ion-exchange resin with glucamine groups) and its selective absorption for Ga-68 in comparison with Ge-68 to generate Ga-68 nuclide. The apparatus in accordance with the present invention is simple designed, easily operated and suitable for various hospitals and research institutes to provide the public better clinic diagnosis in the field of nuclear medicine and increase social welfare. Results : As shown in FIG. 1, when the amount of the added citrate eluent is sufficient, such as 10 ml, the 0.1 or 0.2M citrate eluent (illustrated as the curves labeled with rhombuses and triangles respectively) or the 0.1 or 0.2M citrate eluent at specific pH value (pH 9, illustrated as the curves labeled with squares and crosses respectively) can perform a high level of the Ga-68 elutriation rate (at least close to 50%). Taking the 0.2M citrate eluent 10 ml as an example, its elutriation rate is 4.5×10-3%. Oppositely, the elutriation rate of the Ga-68 radioisotope is up to 75.5%. Methods: To achieve the above objective, a Ga-68 radioisotope generator in accordance with the present invention includes a generating column and a citrate eluent. The generating column is at least partially filled with an ion exchange resin with glucamine groups to absorb Ge-68 radioisotope and Ga-68 radioisotope. The citrate eluent is added into the generating column to desorb the Ga-68 radioisotope and form an eluent containing the Ga-68 radioisotope in the form of Ga-68 citrate.

P314
Determination of the pH of the Radiopharmaceutical Products in Saline

J. Laine, T. Lipponen, K. Bergström; HUS Medical Imaging Center, Helsinki, FINLAND.

Aim: In our routine production of 68Ga-Dotanoc, the pH indicator strips are used for the determination of pH of the product as it is recommended in the monograph of the gallium (68Ga) edotreotide injection in European Pharmacopoeia 8.0. The pH indicator strips are validated with NIST standard buffer solution as also recommended in Pharmacopeia. During several years of production, we have seen only a little variation in the pH and when the variation is detected, this correlates with the higher acetone content of the product. Thus the reliability of the pH strips was questioned. Materials and methods: Different pH determination methods were compared for analyzing the pH of saline, 68Ga-dotanoc and 68Ga-Citrate solutions. Two kinds of pH-indicator papers and four kinds of plastic pH-indicator strips from Merck and Macherey-Nagel were tested and compared with Thermo Scientific Orion Star 111 pH meter and two kinds of pH electrodes; standard Ag/AgCl-electrode and 8220BNWP PerpHecT ROSS microelectrode. Results and conclusion: The pH values of the solutions were measured with the pH meter, pH indicator strips and pH papers, and the results were cross-checked. Nearly all tested pH papers and plastic strips gave correct values when testing NIST standard buffer solutions pH 4, 7 and 10. Although the pH papers and plastic strips were validated correctly, they gave different pH values from the tested solutions when compared to each other. The variation of the pH of the pure saline solutions could not be seen with the tested pH papers and plastic strips, although the variation of pH was seen with the pH meter. In addition, some of the tested pH papers and pH strips gave the same result with all tested solutions. When the variation of the pH was seen with the pH meter, the variation with the pH paper and the pH strips did not correlate with the results. According to this study, reliable determination of pH can be done only with the potentiometric pH meter and the appropriate microelectrode intended for small volume. If the pH strips are used for the determination of pH of the radiopharmaceutical product, the pH strips should be validated carefully in the same solvent as the studied product and in different pH. When the commercial standard solutions in saline are not available, the reliability of the pH strips should be checked against the appropriate pH meter and the pH electrode.

P315
Labelling of leukocytes with 18F-FDG: Quantification of radiation damage

E. Miñana1, D. Ramos2, P. Campos1, T. Martinez2; 1Virgen de la Arrixaca Hospital, Murcia, SPAIN, 2Santa Lucia Hospital, Cartagena, SPAIN.

Aim: The aim of our work is to quantify the radiation damage in lymphocytes after labelling with 18F-FDG using the cytokinesis block micronucleus assay (CBMN) and to establish a correspondence between micronuclei scored and the characteristics of the radionuclide. **Materials and methods**: Blood from 5 healthy donors were taken in heparin to sedimentation for 90 minutes with 9 ml of starch; the cell-rich plasma was centrifuged at 150 g, 5 minutes resulting in a mixed leukocyte pellet. Cell suspensions of 105,5± 13,18·106 leukocytes were radiolabelled with 40,57 ± 2,46 MBq of 18F-FDG, incubated for 25 minutes in a water-bath at 37°C shaking at 5 minutes intervals. Simultaneously, 9,54 ± 2,05·106 leukocytes in 0.5 ml of cell free plasma were taken as control sample for CBNM. For the CBMN assay, lymphocytes were cultured at 37°C for 72h at an initial density of 1.53x106 / ml in a selective culture medium. Cytochalasin B of 6 μg/ml was added 44 h after the beginning of the culture. The cells were harvested, treated with a hypotonic solution and fixed with absolute ethanol:glacial acetic acid (3 : 1). Slides were stained with Giemsa at 5% and micronuclei were scored in 1000 binucleated cytokinesis-blocked cells based on the criteria summarized by Fenech et al. **For dosimetric calculations**, **homogeneity in the uptake of radiopharmaceutical by the cell suspension was assumed. The cells were considered to be spherical with radium of 10 um** (**nucleus of 5-7 um**), **and with homogeneous distribution of the radiopharmaceutical in the cytoplasm. ICRP 106 guideline was followed for absorbed dose calculations. Results and conclusion**: Lymphocytes exposed to 18F-FDG have significantly higher micronucleus frequencies than unlabelled ones (956 ±172 versus 20±13). Studies with other radiopharmaceuticals pointed out the importance of Auger electron in cellular radiation damage, but for the F-18 not Auger electron (low energy (0.52 keV)) neither 511 keV photons had a clear contribution to the absorbed dose. Our **dosimetric calculations** show 634 keV positron emission is the main source of radiation damage, with an absorbed dose in the nucleus of the cell of 0.39 Gy. As expected, 18F-FDG labelling of mixed leukocytes causes severe radiation damage to the cells, mainly related to the 634 keV positron of the F-18.

P316
Referential of radiopharmacy risks elaboration

A. VERREY, D. Martinez, C. Smadja; Hôpital Européen Georges Pompidou, Paris 15ème, FRANCE.

Aim: After the decree of 6 April 2011 about quality management of support drug and medicine in health institutions, our radiopharmacy unit decides to conduct a risk study. No specific tool is actually available, therefore our objective is to propose an evaluations risk tool called referential adapte to radiopharmacy activity. Materials and methods: A questionnaire produces by ACOMEN (Action COncertée en Médecine Nucléaire) is used as base for the referential elaboration. Furthermore, a retrospective analysis of 137 non-compliances observed between 2007 and 2013 has permit to improve the questionnaire and to adapt it on radiopharmacy. An increase critically to 3-5 is given for each question according to gravity. The questions are regrouping in different radiopharmacy topics. There are 2 types of answer: - A1: Binary responses (yes/no) - A2: Scaled answers (“disagree”, “moderately agree”, “strongly agree”, “don’t know”) For each topic, a score is calculated with positive response (Yes for A1 and “moderately agree” and “strongly agree” for A2). Results and conclusion: The elaborated referential is an auto-evaluation in 145 questions (Vs 43 in ACOMEN’s questionnaire) divided in 11 topics who reflect the radiopharmacy process based on the medication circuit. The type A1 (Yes/no answer) permit to create a risk mapping at the moment T0 (initial analysis) and to evaluate in time the risk evolution after correctives actions. When a topic score is >75%, it’s called “develop” and when a topic score is <50%, it’s called “to improve”. The action plan should make the topics “to improve” better and keep the topics “develop” on the same level or higher. The type A2 (scaled questions) estimate the feeling of the team. The risk mapping could be different between the two types (A1-A2). There are two legislations in radiopharmacy: drugs and radioelement in non-sealed source. This specificity make risk referential used in pharmacy like ArchiMed unusual. A specific referential elaboration is difficult because the radiopharmacy is linked with nuclear medicine. Therefore, the responsibility is hard to elaborate and the risk classification in process is debatable. To our knowledge no specific referential was created before this study. The referential elaborate has permit to create the radiopharmacy risk mapping. By using the non-compliance analysis, this tool is more exhaustive and pragmatic. Moreover, the comparison of two answers forms highlights the importance of communication and knowledge of the team in there activity.

P18 - Monday, October 12, 2015, 4:00 PM - 4:30 PM, Hall 3 – Poster Exhibition

Radiopharmaceuticals & Radiochemistry: Radiopharmacokinetics & Drug Development

P317

How stable is stable?

L. Nics1, A. Hahn1, O. Langer1, C. Vraka1, F. Girschele1, B. Steiner1, R. Lanzenberger1, K. H. Wagner2, M. Hacker1, W. Wadsak1, M. Mitterhauser1; 1Medical University of Vienna, Vienna, AUSTRIA, 2University of Vienna, Vienna, AUSTRIA.

Objectives: Results from preclinical experiments should be predictive for following clinical applications. In-vitro data help to explain in-vivo experiments and provide important information whether a tracer has clinical potential or not. From a pharmacokinetic point of view it is of utmost importance to learn about the metabolic fate of radioligands on their path to and at the target region. Aim of this study was to compare stability data from in-vitro experiments with data from clinical in-vivo studies for several tracers (WAY100635, DASB, Harmin, Verapamil, Tariquidar and Elacridar) in order to determine the predictive quality of these methods. Methods: Tracers were incubated with human plasma as well as human liver microsomes (CYP-450), which belong to the main locations for metabolic activity. Incubations took place under physiological conditions (37°C, pH 7.4). Time-endpoints to stop enzymatic activity were adjusted to the blood sampling timepoints of respective studies. Determination of measured values were based on an established protocol [1]. Results: Degradation of tracers in-vitro by CYP-450 (n=3): WAY100635 after 50min of incubation: 8.1%±2.8, DASB (70min): 4.7%±6.7, Harmin (80min): 85.1%±8.5, Verapamil (60min): 0%, Tariquidar (60min): 17.8%±5.6, Elacridar (60min): 0%; No degradation for all tracers in-vitro in plasma was observed (n=3). Degradation of tracers in-vivo (at the same timepoints): WAY100635: 94.2%±0.9 (n=8), DASB: 83.8%±3.4 (n=8), Harmin: 62.5%±11.8 (n=10), Verapamil: 59.3%±5.7 (n=5) [2], Tariquidar: 24.4%±12.3 (n=6) [3], Elacridar: 14.0%±5.1% (n=5) [3]. Conclusions: The degradation pattern in-vitro of the selected tracers is not comparable to respective in-vivo data. None of the investigated methods using plasma or enzymatic families generate data that correlate to in-vivo degradation in the living organism. Data of in-vitro stability as a prediction for in-vivo stability of a tracer are commonly used, but from our data this predictability seems far-fetched. The implication of the word ”stable” should therefore be questioned in that context. References: [1] Nics et al., Nuklearmedizin, 2012; [2] Wagner et al., Clin Pharmacokinet, 2011; [3] Bauer et al., J Nucl Med, 2013

P318

A stable and remote 111In-labeling of DTPA-DSPE long-circulating liposomes

T. van der Geest1, D. Gerrits1, G. M. Franssen1, J. M. Metselaar2,3, G. Storm2,4, P. Laverman1, O. C. Boerman1; 1Department of Radiology and Nuclear Medicine, Radboud university medical center, Nijmegen, NETHERLANDS, 2Department of Targeted Therapeutics, MIRA institute, University of Twente, Enschede, NETHERLANDS, 3Department of Experimental Molecular Imaging, University Clinic and Helmholtz Institute for Biomedical Engineering, RWTH-Aachen University, Aachen, GERMANY, 4Department of Pharmaceutics, Utrecht Institute for Pharmaceutical Sciences, Utrecht University, Utrecht, NETHERLANDS.

Aim:Long-circulating liposomes (LCL) are often used as a drug carrier system to improve the therapeutic index of water-soluble drugs. To track these LCL *in vivo*, they can be radiolabeled with 111In-oxine. For this labeling method, generally DTPA is incorporated in the aqueous phase of LCL, however it is still unknown whether incorporation of DTPA in the vesicles improves the loading capacity and stable retention of 111In-oxine by the vesicle. Alternatively, LCL can be labeled with $^{111}InCl_3$ by incorporating DTPA-conjugated DSPE in the lipid bilayer. Here, we compared *in vitro* properties of DTPA-DSPE LCL with those of DTPA and empty LCL. Additionally, we compared *in vivo* properties of DTPA-DSPE LCL with those of DTPA LCL. **Material and methods**:DTPA-DSPE-, DTPA- and empty LCL were prepared by injection of ethanolic lipid solution into an aqueous dispersion medium, followed by extrusion. Size distribution of resulting liposomes was determined by dynamic light scattering. DTPA- (88 nm) and empty (84 nm) LCL were labeled with 111In-oxine, and DTPA-DSPE-PEG LCL (83 nm) were labeled with $^{111}InCl_3$. Labeling efficiency at increasing specific activity was determined. *In vitro* stability of labeled LCL was determined in human serum at 37°C. *In vivo* properties of 111In-labeled LCL were examined in mice with a *S. Aureus* infection in the thigh muscle. Image acquisition, blood sampling and biodistribution studies were performed 1, 4 (only blood sampling), 24, 48 and 72 h p.i. of 111In-labeled LCL. **Results**: The DTPA-DSPE LCL could be labeled with high yields at a higher specific activity than DTPA- and empty LCL: yields were >90% at 15 GBq/mmol, >90% at 150 MBq/mmol and <65% at 150 MBq/mmol, respectively. 111In-labeled DTPA-DSPE LCL and DTPA LCL were stable in human serum for at least 48 h at 37°C (>98% radiolabel retention). In contrast, only 68% radiolabel was retained in empty LCL after 48 h. *In vivo* targeting of 111In-DTPA-DSPE LCL to the abscess was comparable with targeting of 111In-DTPA LCL (3.5 ± 0.9 %ID/g and 3.4 ± 0.9 %ID/g abscess uptake respectively, 48 h p.i.). Furthermore, 111In-

DTPA-DSPE LCL show comparable blood clearance profiles as that of 111In-DTPA LCL. **Conclusion**: *In vivo* targeting properties of 111In-labeled DTPA-DSPE LCL were comparable to those of 111In-labeled DTPA LCL. *In vitro* stability studies also revealed a similar stability for both LCL preparations. However, the maximum specific activity of the 111In-labeled DTPA-DSPE LCL was much higher, making this formulation most optimal for use in future experiments.

P319
Methotrexate labeling with 99mTc - Preclinical studies

M. Papachristou1, P. Bouziotis2, G. Kastis3, S. Xanthopoulos2, I. Datseris1; 1Nuclear Medicine Department-PET/CT, GHA "Evaggelismos", Athens, GREECE, 2Radiochemical Studies Laboratoty, INRaSTES,NCSR "Demokritos", Athens, GREECE, 3Research Center of Mathematics, Academy of Athens, Athens, GREECE.

Aim: Methotrexate is a structural analogue of folic acid and one of the most widely used antimetabolites in cancer chemotherapy.1 At low doses (up to 25 mg/ml) it is also part of the established treatment of many autoimmune disorders, like Rheumatoid Arthritis where it has nowadays became the standard of care.2 The present paper has two targets: a) Oncology: accumulation of drug in breast Ca and in skeletical lesions. b) Rheumatology: i) find the "plateau" of therapeutic dosage, ii) imaging inflammatory site of rheumatoid or/and arthritis in general, in bones and mainly in joints. Methods - Results: On microscopic level, the labelling of MTX with 99mTc was accomplished via Tc-glucoheptonate.3 The yields were 95-98%. For the radiochemical control TLC and HPLC were used. The compound was stable in vitro up to 6 h at RT, as well as in the presence of serum. Ex vivo animal experiments were performed in Swiss Albino mice (n = 3 animals per time-point). The animals were injected with 700 μCi radiotracer and sacrificed at 2 and 24 h post-injection. Apart from the kidneys, no major uptake in all analyzed tissues is observed (≤1.5 % ID/g from 2 h p.i.). The bone to blood ratio significantly increased from 2 to 24 h (0.93 and 14.8 respectively), thus leading to a pronounced differentiation between bone and non-osseous tissue. In vivo planar scintigraphy was performed with a small Anger-type camera on 2 Swiss mice injected with 700 μCi radiotracer, at 2 and 24 hours p.i.. The images illustrate increased uptake of the tracer at the bones at both 2h and 24h post injection. The increased uptake is more evident at the spinal cord and knee joints. Conclusion: The preclinical studies show that the compound accumulates in the spinal cord, in the joints and bones. The results are promising and in the future the labeling method will be transferred into macroscopic level in order for the compound to be indentified by spectroscopic methods (NMR, MS, Crystalography). Biodistribution and imaging studies in pathological breast cancer models are in progress. References 1. Rang HP, Dale MM, Ritter JM, Flower RJ, Rang & Dale's Pharmacology: with STUDENT CONSULT Online Access, 7e. Churchill Livingstone; 2011:792. 2. Weinblatt ME. Methotrexate in rheumatoid arthritis: a quarter century of development. Trans Am Clin Climatol Assoc. 2013;124:16-25. 3. Dar K.U, Khan U.I, Janed M et al, Hell J Nucl med;15 (2):120-124.

P320
Effects of erlotinib therapy on [11C]erlotinib kinetics

M. Yaqub, I. Bahce, E. F. Smit, O. S. Hoekstra, R. Boellaard, H. N. M. Hendrikse, A. A. Lammertsma; VU University Medical Center, Amsterdam, NETHERLANDS.

AIMRecently, it has been shown that [11C]erlotinib kinetics in non-small cell lung cancer (NSCLC) patients can best be quantified using the volume of distribution (VT) derived from a reversible two tissue compartment (2T4k) plasma input model. In addition, there was good correlation between the tumour to blood ratio (TBR) and VT, potentially enabling simplified analyses of clinical studies. The purpose of the present study was to assess the effects on of erlotinib therapy on kinetic simplified analyses of [11C]erlotinib kinetics.METHODSBoth full kinetic and simplified analyses of [11C]erlotinib kinetics were assessed in NSCLC patients (N=10) before and after erlotinib therapy. In 7 of these patients dynamic [15O]H2O scans were available before and after erlotinib therapy to assess the relationship between [11C]erlotinib uptake and tumour blood flow. Finally, apart from arterial blood, also venous blood samples were collected to assess possible omission of arterial cannulation.RESULTSErlotinib therapy resulted in a substantial (on average 59%) decrease in tumour VT of [11C]erlotinib. Although the reduction in TBR was smaller (on average 32%). There was no correlation ($R2 < 0.01$) between tumour VT and blood flow. TBR showed good correlation with VT both before ($R2=0.93$) and after ($R2=0.96$) erlotinib treatment. Finally, there was a reasonable correlation ($R2>0.79$) between VT values obtained using venous and arterial blood data.CONCLUSIONFurther studies are needed (1) to assess whether the reduction in VT is due to treatment response and/or to occupancy of the EGF receptor by cold erlotinib, and (2) to investigate the relationship between the initial reduction in VT and clinical response. Depending on the accuracy needed, studies can possibly be performed without arterial sampling. The good relationship between VT and TBR indicates that whole body studies might be feasible in order to investigate (interlesional) heterogeneity of response.

P321
Nanocolloid Radiopharmaceutical on the Based of Modified DTPA Labeled Technetium-99M

V. Chernov1, A. Rogov2, V. Skuridin2, E. Stasyuk2, E. Nestwrov2, N. Varlamova2, R. Zelchan3, V. Sadkin2, E. Ilina2, L. Larionova2; 1FSBI, Tomsk, RUSSIAN FEDERATION, 2National Research Tomsk Polytechnic University, Tomsk, RUSSIAN FEDERATION, 3Cancer Research Institute of Siberian Branch of the Russian Academy of Medical Sciences, Tomsk, Tomsk, RUSSIAN FEDERATION.

The use of radioactive nanocolloids in oncology based on the possibility effectively identify "sentinel" lymph nodes (SLN), which are the "trap" for the cells, so their biopsy is an objective diagnostic criterion for malignancy spread. In recent years, the best method is to use SLN identification labeled with technetium-99m (99mTc) nanoscale colloids for scintigraphy or radiometric determination of lymph node localization. Radionuclides technetium-99m is by far the most popular for such diagnostic tests. Primarily this is due to its nuclear-physical characteristics: a relatively short half-life (6.02 h) and 0.140 MeV energy of the radiation, providing a low exposure dose, and at the same time sufficient penetration to the radiometric study. As colloid-forming substance were taken based compound chemically modified molecule DTPA, showing a certain affinity with the protein molecule - the presence of an amide (peptide) bond, the existence of a zwitter-ionic form. Presupposition for use as a chelator DTPA tracer is the ability of both the molecule DTPA and its derivatives, to form sufficiently stable complexes with various metals, including the compounds of technetium-99m. The studies identified the requirements for obtaining radioactive nanopreparations on a modified molecule DTPA. It is shown that the direct interaction of the solution with a solution of 99mTc eluate mixture $DTPA_{mod}$ and $SnCl_2$ content radiochemical impurities unrestored 99mTc (VII) in the preparation of the labeled nanocolloids is 4.7%, and the yield nanocolloids with a size of 100-50 nm is about 80%. Preliminary studies on experimental animals, using scintigraphy, allowing to see that the drug enters the lymphatic system, and remains in the affected lymph node. Studies show the drug functionality of modified nanocolloids for lymphoscintigraphy and visualization "Sentinel" nodes. This work was performed on the unique scientific IRT-T equipment and financially supported by Government represented by the Ministry of Education and Science of the Russian Federation (RFMEFI59114X0001).

P19 - Monday, October 12, 2015, 4:00 PM - 4:30 PM, Hall 3 – Poster Exhibition

Radiopharmaceuticals & Radiochemistry: Radiometals & New Targets

P322
QSPR study on the Complexation of Radiometals with Bifunctional Coupling Agents for Radiopharmaceuticals Applications

M. Salahinejad, M. Aboudzadeh; Nuclear Science and Technology Research Institute, Tehran, IRAN, ISLAMIC REPUBLIC OF.

Introduction: Diagnostic metal radiopharmaceuticals are used for single photon emission computed tomography (SPECT) and positron emission tomography (PET) applications as imaging agents. Bifunctional coupling or chelating agents (BFCs) are typically used as ligands to construct, radiolabeling and target-specific delivery of radiometal-based radiopharmaceuticals.67/68Ga(III), 64Cu(II) and 111In(III) complexes have attracted great attention among metal-based PET radiopharmaceuticals. Quantitative structure-property relationships (QSPR) studies, as progressive tools in modeling and prediction of many physiochemical properties, allow cost savings by reducing the laboratory resources needed and the time required to investigate and design new compounds by desired properties The aim of the present study, is to QSPR modelling of the stability constant between a diverse set of BCFs and 64Cu(II), 67/68Ga(III) and 111In(III) radiometal ions. **Material and Methods**: Experimental data of the stability constants of a set of diverse structural BFCs containing acyclic, hetrocyclic and macrocyclic ligands were taken from the recent comprehensive published reviews. VolSurf is a computational procedure that generates useful quantitative 2D descriptors from the 3D maps of molecular interaction field (MIF) between different probes and all the atoms in a target molecule. Multi Linear regression (MLR) and support vector machine (SVM) have been utilized to construct linear and non-linear QSPR models. **Results**: As SVM analysis taking into accounts both linearity and non-linearity in model construction, therefore it yielded more predictive models than MLR analysis in prediction of complexation constant of Cu(II), Ga(III) and 111In(III) radiometal ions. **Conclusion**: Considering the variables contributed in QSPR models, it's concluded the ability of H-bonding, shape/configuration of BCFs and hydrophilicity interactions play important roles in the complexation formation of 67Ga(III), 64Cu(II) and 111In(III) radiometal ions with BCFs of diverse structure containing acyclic, hetrocyclic and macrocyclic. The obtained results could be led to the design and development of new high efficient BFC ligand with high log K_{ML} values which allow cost savings by reducing the laboratory resources needed and the time required to investigate and design new compounds by desired properties.

P323

Selecting the best buffer for 68Ga labelling: a theoretical molecular approach towards a rational choice

M. I. Prata1, S. Rodrigues2; 1IBILI and ICNAS, Coimbra, PORTUGAL, 2Coimbra Chemistry Centre UC, Coimbra, PORTUGAL.

Introduction - It is now well established that the labelling of 68Ga in medical applications involving the formation of complexes such as GaDOTA-TOC and GaDOTA-NOC is significantly enhanced by the presence of N-2-hydroxyethylpiperazine-N-2-ethanesulfonic acid (HEPES) buffer [1] and that better performance is obtained using HEPES buffer as compared with other buffers [1-2]. At the time HEPES was first used [3], this finding was not obvious, but now HEPES buffer is widely used and already accepted by the European Pharmacopeia. To explain the enhancement in labelling using HEPES it was proposed [1] the formation of weak GaHEPES complexes, which maintain gallium available in solution, prior to the formation of the much more stable, but kinetically slow forming, GaNOTA and GaDOTA complexes (as well as its derivatized moieties). As the presence of other buffers such as succinate and acetate (Ac) [2] and citrate (Cit) [4] is also considered beneficial in labelling, a similar mechanism of weaker intermediate complexes formation is expected to be involved [4]. Nevertheless, as the presence of HEPES shows to be superior in enhancing the labelling, an attempt to understand this finding seems worth to a better rationalization of the labelling process. Methods - The present work extend previous studies on GaHEPES [1] to a wider range of complexes involving Ga3+ and ligands L=HEPES, Cit, Ac, and NOTA, including complexes as GaNOTA-L, using density functional theory (DFT) and the conductor-like polarizable continuum model (C-PCM) for the water solvent. Results and Conclusions - It was found theoretically that the estimated relative energies of GaHEPES and GaNOTA-HEPES complexes in the process of forming GaNOTA appear to follow a more favourable step-like mechanism that it is followed by complexes involving Ac and Cit. This finding, that is in agreement with experimental results, provide an explanation for HEPES buffer better performance and calls the attention for the interest in using molecular modelling methods, when possible and appropriate, to complement processes of labelling development and optimization. [1] Martins, A.F.; Prata, M.I.M.; Rodrigues, S.P.J.; Geraldes, C.F.G.C.; Riss, P.J.; Coarasa, A.A.;Burchardt, C.; Kroll, C.; Roesch, Contrast Media Mol. Imaging 2012, 8, 265-273. [2] Bauwens, M.; Chekol, R.; Vanbilloen, H.; Bormans, G.; Verbruggen, Nucl. Med. Commun. 2010, 8, 753-758. [3] Eisenwiener, K.P.; Prata, M.I.M.; Han-Wen, Z.; Buschmann, I.; Santos, A.C.; Reubi, J.C.; Wenger, S.; Maecke, H.R. Bioconjugate Chem. 2002, 13, 530-541. [4] Morfin, J.F.; Toth, E. Inorg. Chem. 2011, 50, 10371-10378.

P324

Excitation function determination for 45Ti production using 45Sc(p,n)45Ti reaction in low energy cyclotrons

P. Costa1, L. F. Metello2, L. Cunha2, R. R. Johnson3, W. Gelbart4, J. Obermair5, B. Dietl5, R. Nausching5, C. Artner5, P. Lass6, G. Currie7, S. Carmo8, F. Alves8, M. D. Naia9; 1Nuclear Medicine Department, ESTSP.IPP & CEMUC®, Physics Department, ECT-UTAD, Vila Nova de Gaia & Vila Real, PORTUGAL, 2Nuclear Medicine Department, ESTSP.IPP & IsoPor SA, Vila Nova de Gaia, PORTUGAL, 3Best Cyclotron Systems Inc, Vancouver, BC, CANADA, 4Advanced Systems Design, Garden Bay, BC, CANADA, 5IASON Gmbh, Graz, AUSTRIA, 6Medical Faculty, University of Gdansk, Gdansk, POLAND, 7School of Dentistry and Health Sciences, Charles Sturt University, Wagga Wagga, AUSTRALIA, 8Institute for Nuclear Sciences Applied to Health, Univ. Coimbra, Coimbra, PORTUGAL, 9CEMUC® - Physics Department, ECT-UTAD, Vila Real, PORTUGAL.

Introduction: There are several different radioisotopes known and almost all of them may be artificially produced, however actual clinical routine applications of PET imaging are still based on 18F, 11C, 13N and 68Ga. This trend might change in the near future, since several groups worldwide are busy developing very promising new processes using unconventional radionuclides, aiming to contribute for spreading the use and efficacy of clinical diagnostic using Nuclear Medicine imaging techniques, mainly in the direction of personalized medicine. Our group is busy studying 45Ti, assuming it as a potential candidate, since it presents many interesting properties: physical half-life of 3.09h, together with relevant chemical properties, that enable radiolabelling with bifunctional chelates, ligands or even to radiolabel titanium (di)oxide nanoparticles. Aim: This work aims to disseminate the experimental results obtained during the determination of excitation function (which adequate characterization has been considered mandatory for radionuclide optimal production) of 45Sc(p,n)45Ti nuclear reaction, that is being studied as a potential route to efficiently produce 45Ti in low energy cyclotrons. Material and Methods: Excitation function of 45Sc(p,n)45Ti nuclear reaction was experimentally determined using the stacked foil technique, with 99,5% pure Sc foils mounted on an aluminum target holder and interspaced in some positions with 99,999% pure Cu foils, with short irradiations (~1μA during 100 seconds) using 16 MeV and 18 MeV cyclotrons. Results of this activation study were evaluated using HPGe

spectroscopy (always considering dead time losses ≤ 5%). Results: Results concerning the excitation function of the main route under study were collected, with the addition of some information regarding concurrent reactions leading to 44mSc and 44Sc. Experimental results were also compared with the Monte Carlo simulation results obtained before, based on TALYS code calculations, having found some discrepancies in the shape and in the overall quantitative results, suggesting that TALYS might overestimate cross-sections for this particular reaction. Conclusion: Considering our results, the production of 45Ti seems feasible in low energy cyclotrons, with the maximum yields obtained for 12-15 MeV proton beams.

P325

Synthesis and Evaluation of metal phosphate as column material for the 68Ge/68Ga generator

J. PARK1, J. Lee1, M. Hur1, S. Yang1, S. Lee2, S. kim3; 1Korea Atomic Energy Research Institute, Jeongeup-Si, KOREA, REPUBLIC OF, 2Daegu Gyeongbuk Institute of Science & Technology, Daegu, KOREA, REPUBLIC OF, 3Dongguk University-Gyeoungju, Gyeoungju-Si, KOREA, REPUBLIC OF.

Aim : 68Ge/68Ga generator provides an alternative and often more convenient sources of isotopes compared to complex facilities such as accelerators and nuclear reactors. 68Ge/68Ga generator is constructed on radiative equilibrium between a long-lived parent radionuclide ($t_{1/2}$= 271 d) and its short-lived daughter radionuclide ($t_{1/2}$= 68 min). Gallium-68 has been used in nuclear medicine diagnostic for positron emission tomography agent. In order to find much more suitable generator adsorbents, we synthesized metal phosphate. **Materials and methods** : The ability of the adsorbent to adsorb various metal phosphate {$Ti(HPO_4)_2$, $ZrTi(HPO_4)_2$, $Zr(HPO_4)_2$} was investigated in order to evaluate the possibility of its use in germanium adsorption and gallium desorption. Metal oxides were fully characterized by XRD, DLS, TEM, SEM, Zetasizer, FT-IR. The plastic syringe (5 mL, 12.46 mm) chromatographic column fitted with polyethylene frit (polyethylene, pore: 20 μm) at the bottom was packed with 200 mg of adsorbents. Germanium-68 solution (30 μCi/5 μL) containing germanium and gallium impurities were passed through the metal oxide column at a flow rate of 1 mL/min and the effluent was collected. All radio activity was measured by dosimeter. **Results and Conclusion** : A $Zr(HPO_4)_2$ based 68Ge/68Ga generator has been composed and evaluation. High purity of 68Ga elution was obtained within 1 minute as a 1.0 mL volume of 0.1 N-HCl fractions. We were successfully achieved a high radiochemical purity and low breakthrough of 68Ge using a $Zr(HPO_4)_2$ as the column material.

P326

Titanium-45 as a Candidate for PET Imaging: Cyclotron-Based Production & Functionalized-Hydroxamate Column Separation & Purification

R. I. Price1,2, R. W. Sheil1, R. K. Scharli1,2, S. Chan1, P. Gibbons1, L. Morandeau1; 1RAPID PET Labs, Sir Charles Gairdner Hospital, Perth, AUSTRALIA, 2School of Physics, University of WA, Perth, AUSTRALIA.

INTRODUCTION. Transferrin (TF) and its receptor TFR1 mediate recruitment by cancer cells of factors for their multiplication, adhesion, invasion and metastatic potential. Though primarily designed to bind iron and then be internalised into cells with its receptor, TF can also bind most transition metals including titanium. Under certain conditions TF binds Ti (IV) even more tightly than it does Fe, and this occurs at the N-lobe (as distinct from C) of apoTF. Indeed, Fe(C-lobe)Ti(N-lobe)-TF may mediate Ti cellular entry via TFR1 (Nuevo-Ordoñez et al., Metallomics **3**, pp. 1297-1303, [2011). Thus, the PET-tracer isotope 45Ti ($T_{1/2}$ =3.08hr; beta+ ratio = 85%; mean beta+ energy = 439keV) may elucidate biological mechanisms involving TF-binding and internalization, at least in preclinical (animal) models. **AIM**. Produce high-purity no-carrier-added 45Ti at sufficient specific-activity for imaging. **METHOD**. 45Ti was produced using the nuclear 45Sc(p,n)45Ti reaction by irradiating 100 micron-thick scandium (Sc) discs at 11.6MeV using an 18MeV cyclotron and in-house solid targetry, including a beam degrader (Scharli et al., AIP Conf Proc 1509, pp.101-107; [2012]). This degraded beam-energy abolishes 'contaminating' reactions 45Sc(p,n+p)44Sc and 45Sc(p,2n)44Ti. Separation and purification of product Ti, mainly from target Sc, was achieved with hydroxylamine hydrochloride-functionalised resin (Gagnon et al., AIP Conf Proc 1509, pp.211-215; [2012]). Discs were dissolved in 2mL 6M HCl, then diluted to 2M, then eluted through the column to waste-fraction-1 (w1). Then 6mL 2M HCl was eluted through the column to w2, followed by 6mL traceSELECT H_20 to w3. Finally, Ti trapped in the column was eluted into successive 1mL product-fractions (p1-4) using 5mL 1M oxalic acid; (total time~1hr). 45Ti radionuclidic purity was measured using gamma-spectroscopy. Sc elemental abundance in all vials (w1-3; p1-4) was determined using ICP-MS. **RESULTS**. Typical production (40microA proton-beam; 60min) yielded 1.8GBq, at EOB. Radionuclidic analysis revealed 44Sc (<0.19%) as the only contaminant. Only 30% of the original activity of 45Ti (EOB-corrected) was acquired in the product (p1-4) vials, with the vial of highest activity (p1) containing 14%. The elution-profile for (cold) Sc mass (ICP-MS) was negligible in all p-vials (total p1-4 <0.017%), remaining (78%) in w1 and (22%) in w2. **CONCLUSIONS**. Despite substantial 45Ti loss into waste (total 53%, EOB-corrected), 45Ti of acceptable specific

activity and radionuclidic purity was produced from 45Sc(p, n)45Ti, with separation/purification by hydroxamate-column chemistry. Two 0.100 micron-thick Sc target-discs yield isotope as the oxalate, following 40 microA-hours of beam, of adequate activity without need for concentration, for subsequent radiolabelling and preclinical imaging.

P327

Cyclotron production of 99mTc from highly enriched 100Mo

D. Pawlak, W. Wojdowska, J. L. Parus, I. Cieszykowska, T. Janiak, K. Jerzyk, M. Mielcarski, T. Barcikowski, P. Garnuszek, R. Mikołajczak; National Centre for Nuclear Research, Otwock, POLAND.

AimThe 99mTc worldwide needs are practically covered nowadays by its production from fission of 235U. Due to aging of nuclear reactors delivering it on one hand and the necessity to use low enriched uranium on the other, alternative methods of 99mTc production are being developed. One of the most promising and intensely progressing in the last few years is the use of proton accelerators and highly enriched targets of 100Mo. The biggest advantage of this method is the absence of high level active wastes, while the disadvantage is a very short processing and delivery time required. Our goal was to develop technology suitable for 99mTc production in a medical, 16 MeV cyclotron, and its further separation.Materials and methodsMolybdenum target was prepared by pressing metal powder containing 99.815% of 100Mo into pellet of 12 mm in diameter and mass of 0.723 g. After sintering in hydrogen atmosphere at 16000C for 60 min, the pellet was loaded into aluminum holder which was mounted in GE PETtrace 840 cyclotron (at HIL, University of Warsaw) proton beam and irradiated for 2 h at 2 μA current to total activity of 1.6 GBq at the EOB. The target was automatically disassembled into transportation container.Results and discussionAfter releasing from holder the target was dissolved in 30% H2O2 and alkalized with 10M NaOH (both reagents added in about 2 mL portions) to total volume of 19 mL. 99mTc was separated in 3 columns connected in series containing AnaLig, Dionex and alumina beds. The 99mTc recovery yields amounted to 76.3% and losses were 8.2%, 13.2% and 2.3% at each column respectively. The 99mTc solution was free of molybdenum. Method is further optimized to increase separation yield.AcknowledgmentsWe are thankful to the staff of the Heavy Ion Laboratory of the University of Warsaw for target irradiation. This work was supported by National Centre for Research and Development from public funds, realized within the Applied Science Program NCBiR Nr PBS1/A9/2/2012 and IAEA CRP contract 17419.

P328

Development of a cell labelling technique using zirconium-89 for inflammation imaging with positron emission tomography (PET)

M. Fairclough1, B. Ellis2, G. Brown1, H. Boutin1, A. McMahon1, A. Gennari1, A. Jones1, C. Prenant1; 1University of Manchester, Manchester, UNITED KINGDOM, 2Central Manchester University Hospitals NHS Foundation trust, Manchester, UNITED KINGDOM.

Aim: Radiolabeled leukocyte scintigraphy is a widely used clinical procedure for assessment of inflammatory diseases. However Positron Emission Tomography (PET) offers superior quantification and sensitivity and is attractive for monitoring the regional signal from migrated radiolabelled cells to pathological tissue in infectious and inflammatory diseases. The aim of this work is to develop a method for labelling white blood cells with the positron emitting isotope zirconium-89 (89Zr, $t_{1/2}$=78.41 h). Chitosan nanoparticles (CN) are used to transport 89Zr in to the cell via pinocytosis or phagocytic engulfment. Chitosan is a linear polysaccharide consisting of randomly distributed D-glucosamine and N-acetyl-D-glucosamine units with the ability to chelate metal cations. **Methods**: CN formed spontaneously upon addition of a polyanion to a chitosan solution in acetic acid via an ionotropic gelation mechanism. CN loading with 89Zr and white blood cell uptake and retention up to 24 h were studied for various CN constructs. [89Zr]-loaded CN were incubated with white blood cells at various incubation times and the labelling was terminated by the addition of cell free plasma (CFP). Next the cell pellet was collected and measured for radioactivity. To measure the rate of loss of 89Zr from white blood cells, the cell pellet was re-suspended in CFP and incubated for a set time before the pellet and supernatant were collected and measured for radioactivity. **Results**: Analysis of CN generated from 15kDa chitosan showed particles with an average size distribution of 342.7nm in diameter (polydispersity index = 0.376) and a zeta potential of 45.7±3.96mV. Cell uptake of [89Zr]-loaded CN proceeds in two-steps an initial adhesion to the cell membrane followed by cell internalisation. The second step shows a slower kinetics compared to the initial adhesion step. The fast initial loss of 89Zr from cells shows the release of [89Zr]-CN from the cell membrane with the remaining [89Zr]-CN being internalised. However the stability of the 89Zr in the cell observed after 5h up to 24h is very promising for PET imaging. These results are observed for 2-5x107 cells loaded with 6-9MBq of 89Zr. Slight cytotoxicity of [89Zr]-CN, possibly due to radiolysis, was observed (87% viable cells) . **Conclusion**: [89Zr]-CN are a simple tool for labelling mixed leukocyte cells to use as a probe for inflammation imaging with PET. [89Zr]-loaded CN uptake in to leukocyte cells is slow but stable once internalised. The imaging probe will be

eventually applied to an animal model of inflammation for PET scan.

P329

Evaluation of Layered Double Hydroxide as a Drug Delivery Carrier using Co-57

J. PARK1, J. LEE1, T. KIM2, J. OH2; 1Korea Atomic Energy Research Institute, Jeongeup-Si, KOREA, REPUBLIC OF, 2Yonsei University, Wonju, KOREA, REPUBLIC OF.

ABSTRACTAim : Layered double hydroxide (LDH) has been of great interest as cellular drug delivery carriers because of their potential applications in medical and biological fields. Especially, LDH contained the radioactive metal isotopes will be able to be used as a novel imaging agent. In this study, we have successfully incorporated either non-radioactive Co(II) and radioactive 57Co(II) into MgAl-layered double hydroxide (LDH) nanomaterials and carried out celluar uptake and biodistribution.Material and Method : Pristine MgAl-LDHs with uniform size and morphology was obtained through conventional coprecipitation followed by hydrothermal treatment. In order to substitute non-radioactive Co(II) into LDH lattice, suspension of MgAl-LDHs were added to Co(II) solution and hydrothermally treated at 150 °C. We applied the same hydrothermal reaction to incorporate radioactive [57Co](II) into LDH lattice. It was revealed that radioactive Co(II) could be successfully incorporated into LDHs. Comparision of cellular uptake using LDHs for tumor cell lines {CT-26 (Mouse colon), MCF-7 (Breast cancer), HepG2 (Liver hepatocellular carcinoma)}. CT-26 bearing balb/c mice of 7 weeks old weighing 25-30 g were used for the biostudies of [57Co]LDHs .Results and Conclusion : LDH was determined to have typical hydrotalcite-like structure, uniform 150 nm size and hexagonal plate-like morphology using X-ray diffraction patterns and electron microscopy. The incorporation saturated at 12 hours showing Mg(II)/Co(II)/Al(III) in the LDH lattice of 1/1/1 with the inductively coupled plasma-atomic emission spectroscopy. [57Co]LDHs was synthesized within 90 min at radiochemical yield (>27%). The cellular uptakes and biodisribution of [57Co]LDHs increased in a time dependent manner for cancer cell line.

P330

Radiotherapy metabolic with 131I, a new promise for cholangiocarcinoma treatment?

A. M. Abrantes1,2,3, R. Teixo1,3, A. F. Brito1,2,3, A. I. Fernandes1,2,4, A. C. Ribeiro1, M. Laranjo1,2,3, J. G. Tralhão1,2,5, **M. F. Botelho**1,2,3; 1Biophysics Unit, Faculty of Medicine, University of Coimbra, Coimbra, PORTUGAL, 2Center of Investigation on Environmental, Genetics and Oncobiology (CIMAGO), Faculty of Medicine, Coimbra, PORTUGAL, 3CNC.IBILI, Faculty of Medicine, University of Coimbra, Coimbra, PORTUGAL, 4Gastroenterology Department, CHUC, Coimbra, PORTUGAL, 5Surgical Department, Surgery A, CHUC, Coimbra, PORTUGAL.

Aim: Cholangiocarcinoma (CC) is a malignancy with poor prognosis and a reduced survival rate. It was shown that intrahepatic CC, has increased sodium-iodide symporter (NIS) expression. NIS is responsible for cellular iodine uptake and is a key molecule in the metabolic radiotherapy with iodine-131 (131I). This study aims to evaluate therapeutic efficacy of metabolic radiotherapy with 131I in two human CC cell lines (an intrahepatic cell line and an extrahepatic cell line) as well as in a human cholangiocytes cell line. Materials and methods: Two CC cell lines (TFK1 - extrahepatic CC and HuCCT1 - intrahepatic CC) and another of normal cholangiocytes (H69) were used. It was evaluated the NIS expression by immunofluorescence. Subsequently, the cells were irradiated with 131I increasing doses (0.35 to 60Gy), in order to evaluate and characterize metabolic radiotherapy effects using different techniques of molecular biology. Results: It was observed that all cell lines express NIS, however, this expression was strongest in the membrane of TFK-1 cells. Therefore, the following studies were performed only in TFK-1 cell line. 131I treatment induced cell viability decrease in a dose dependent manner only in TFK-1 cells. The predominant cell death type was apoptosis, followed by BAX/BCL2 ratio increase. A cytochrome C release and mitochondrial membrane depolarization were also observed. Two hours after irradiation, it was observed an intracellular peroxides production increase, but there were no differences in superoxide anion production. Forty-eight hours after irradiation differences were not detected in both intracellular peroxides and superoxide anion production. Nevertheless differences were observed in superoxide dismutase production, 2 and 48 hours after irradiation. Concerning glutathione a decreased production 48 hours after irradiation with higher doses was observed. It was also verified that 131I induced DNA breaks in TFK1 cells in a dose dependent manner. Conclusion: 131I treatment induces cell viability decrease in TFK1 cells followed by cell death by apoptosis. Intracellular peroxides seem to be involved. This is the first study realized in a human extrahepatic CC cell line, and proves that this therapeutic approach is also a possibility for this type of tumor.

P20 - Monday, October 12, 2015, 4:00 PM - 4:30 PM, Hall 3 – Poster Exhibition

Cardiovascular System: Basic Science

P331

Synthesis of Novel 124I-Rhodamine: a Potential PET Myocardial Imaging Agent

I. Aljammaz, B. Alotaibi, s. alyanbawi, f. alrumayan, s. okarvi; King Faisal Spec. Hosp. & Research Centre, Riyadh, SAUDI ARABIA.

Myocardial infarction is the leading cause of death in most of the countries, and myocardial perfusion imaging (MPI) is an important tool in evaluation of myocardial ischemia and infarction. Currently, MPI are usually performed using single-photon radiopharmaceuticals such as 99mTc-MIBI, 99mTc-tetrofosmin and 201Tl-chloride. Unlike SPECT, PET based imaging offers several advantages in MPI application including better sensitivity, higher spatial resolution and an improved attenuation correction. The currently used PET tracers for MPI studies ($13NH_3$, 82Rb and 15O-water) have limitations such as high cost or the need of on-site cyclotron for production. Rhodamine dyes are known to accumulate in the heart; therefore, 68Ga-NOTAGA rhodamine conjugate was prepared and demonstrated its potential as MPI agent using PET. Due to the ideal physical properties of fluorine-18, various 18F-tracers for MPI were developed. Recently, [18F]-FDG-rhodamine conjugate showed high myocardial uptake and favorable pharmacokinetics as MPI agent using PET. Thus, as part of our on-going research effort to develop novel radiotracers for MPI studies, we here report the synthesis and preclinical evaluation of new 124I-rhodamine conjugates. The synthetic approaches for the preparation of [124I]iodobenzene and pyridine rhodamine conjugates entailed sequence of reactions. The key precursors N-hydroxysuccinimide 3-tri-n-butylstannyl-benzoate and 3-tri-n-butylstannyl-pyridine carboxylate were radioiodinated using classical method involving 0.1% acetic acid/methanol, iodogen and Na124I (50 MBq) at room temperature. The N-succinimidyl-*p*-[124I]-iodobenzoate ([124I]-SIB) and N-succinimidyl-*m*-[124I]-iodopyridine carboxylates ([124I]-SIP) were purified using Sep-pak silica cartridge. EDA-rhodamine was then reacted with [124I]-SIB and [124I]-SIP to give [124I]-SIB- and [124I]-SIP-rhodamine conjugates. Radiochemical yields were quantitative and synthesis times were ranging between 30-40 min. Radiochemical purity was also greater than 98% without HPLC purification. The metabolic stability of [124I]-SIB- and [124I]-SIP-rhodamine conjugates were determined in human plasma and revealed that these radioconjugates remained stable during incubation at 37°C for at least 24 h. Initial *in vivo* characterization in normal Fischer rats at 60 min p.i., showed high myocardial uptake (~5% ID/g) and favorable pharmacokinetics. Initial cardiac imaging study using animal imaging modality, demonstrate that these radioconjugates may be useful for MPI studies using PET. However, further evaluation is warranted.

P332

Effect of dipyridamole infected for myocardial perfusion imaging on blood glucose concentration: a preliminary study

A. Khorasanchi1, M. Arabi1, A. Akhavein2, M. Eftekhari1, H. Javadi3, M. Seyedabadi4, **M. Assadi**4; 1Imam Hossein Hospital, Faculty of Medicine, Shahroud University of Medical Sciences, Shahroud, IRAN, ISLAMIC REPUBLIC OF, 2Islamic Azad University Tehran Medical Branch, TEHRAN, IRAN, ISLAMIC REPUBLIC OF, 3Golestan Research Center of Gastroenterology and Hepatology (GRCGH), Golestan University of Medical Sciences (GUOMS), Gorgan, IRAN, ISLAMIC REPUBLIC OF, 4The Persian Gulf Nuclear Medicine Research Center, Bushehr University of Medical Sciences, BUSHEHR, IRAN, ISLAMIC REPUBLIC OF.

Objective: Dipyridamole inhibits adenosine reuptake and increases cyclic adenosine monophosphate (cAMP) levels in platelets, erythrocytes and endothelial cells, all of which influence blood glucose. Acute hyperglycemia reduces endothelium-dependent vasodilation and suppresses coronary microcirculation; which, in theory, can alter the outcome of a radionuclide scan. In this study, we investigated the acute effect of dipyridamole on blood glucose. Subjects and methods: A total of 299 patients (87 men and 212 women, age: 60.52±0.60 years) were included in the study. Fasting blood glucose (FBG) was measured before and 8min after dipyridamole (0.568 mg/kg) injection during myocardial perfusion imaging. The data in different groups were analyzed by paired t-test, and are presented as mean± standard error of the mean (SEM). Results: There was not a significant difference between first (106.89 ±1.11mg/dL) and second (106.30±1.14mg/dL) FBG measurements (P= 0.587). However, when the patients were grouped based on the quartiles of first measurement, we observed an increase in FBG following dipyridamole injection in the first quartile (mean difference: 9.22 ±2.57, P<0.001); in contrast, FBG levels showed a significant decrease after dipyridamole administration in the 4th quartile (mean difference: -9.53±2.11, P<0.001). The differences in 2nd and 3rd quartiles were negligible. The patients were divided into normal, ischemic and fixed lesions based on the outcome of scans, then the possible correlation of dipyridamole-induced FBG alteration and

scan results were investigated. There were no significant difference between the FBG values before and after dipyridamole injection and the final outcome of scan 9. Conclusion: Dipyridamole may increase, decrease, or not influence blood glucose depending on its initial level. Considering the effects of acute hyperglycemia on coronary vasodilation and microcirculation, initial blood glucose must be observed in the interpretation of dipyridamole-stress scans, especially in those with FBG less than 96 or above 115 mg/dL.

P333

Measurement of concentration-dependent effect of sevoflurane on myocardial oxygen consumption using 11C acetate PET in rats

K. Matsunaga1, T. Watabe1, A. Nakae2, H. Kang2, Y. Kanai3, K. Isohashi1, H. Kato1, E. Shimosegawa1,3, J. Hatazawa1; 1Department of Nuclear Medicine and Tracer Kinetics, Osaka University Graduate School of Medicine, Suita, JAPAN, 2Department of Anesthesiology and Intensive Care, Osaka University Graduate School of Medicine, Suita, JAPAN, 3Department of Molecular Imaging in Medicine, Osaka University Graduate School of Medicine, Suita, JAPAN.

Objectives: The objective of this study is to evaluate the concentration-dependent effect of sevoflurane on myocardial oxygen metabolism using 11C acetate PET in rats. Methods : Total 18 normal male SD rats (8 weeks old, BW 244±27g) were anesthetized with different concentration of inhaled sevoflurane (1.5, 2.5 and 4.0%: n=6 in each group) in 3 L/min air. 11C-acetate 30-min dynamic PET scan was performed. As a measure of oxygen consumption, the clearance rate constant (kmono) of 11C-acetate over myocardium was calculated. The slope of the myocardial SUV time activity curve before peak was used as an index of myocardial blood flow (iMBF). Results : Kmono of 1.5, 2.5 and 4 % sevoflurane group were, 0.32±0.03, 0.33±0.05 and 0.28 ±0.08 /min, respectively. Decreasing trend of kmono against sevoflurane concentration was observed in some rats although there is no statistically significant difference. iMBF of 1.5, 2.5 and 4 % sevoflurane group were, 5.50±1.22, 6.56±0.93 and 8.17±1.83 /min, respectively. There was a statistically significant difference in iMBF between 4% and 1.5% group (p=0.01). Kmono divided by iMBF, an index of oxygen extraction fraction, of 1.5, 2.5 and 4 % sevoflurane group were, 0.061 ±0.014, 0.051±0.005 and 0.037±0.016, respectively. There was a statistically significant difference between 4% and 1.5% group (p=0.03). Conclusions: Cardiac oxygen consumption was not significantly influenced by sevoflurane concentration although some rats showed decreased kmono with higher dose. The high concentration of sevoflurane decreased oxygen extraction fraction with increased blood flow, suggesting the protecting effect against myocardial ischemia during high-dose anesthesia of sevoflurane.

P334

Myocardial Insulin Resistant under Hyperinsulinemic-Euglycemic Clamp in a Rat Model

K. Fukushima1,2, P. Arias1, H. Wakabayashi1, T. Shinaji1,3, R. Werner1,3, H. Pelzer1, **T. Higuchi**1,3; 1Würzburg Univ, Würzburg, GERMANY, 2Hyogo College of Medicine, Hyogo, JAPAN, 3Comprehensive Heart Failure Cener, Würzburg, GERMANY.

Insulin resistance, an impaired ability to invoke glucose uptake by insulin stimulation, has been suggested to be an important etiologic factor for diabetic patients. Aim of this study was to assess local cardiac insulin resistance using two-tissue compartment model kinetic analysis of 18F-FDG PET, as a surrogate maker for glucose metabolism, combining with dedicated high-resolution small animal PET system and a rat model of diabetes mellitus.Methods: Zucker diabetic fatty (ZDF) rats (n=5), a model of type 2 diabetes mellitus, and Zucker lean (ZL) control rats (n=4) were studied at age 13 weeks. Under hyperinsulinemic-euglycemic clamp, approximately 37MBq of 18F-FDG were administered via the tail vein, followed by a dynamic 35 minutes PET acquisition (8sec x 15frames, 60sec x 3frames, 300sec x 4frames, 600sec x 1frame) using dedicated small animal PET system (SIEMENS INVEON). Image derived input functions from heart ventricles and myocardial time-activity curves were obtained. Previously well described 2 tissue compartment model had been used for estimating values for individual rate constants represented as inward transport (k1), outward transport (k2), and phosphorylation (k3).Results: Systemic insulin resistant of the ZDF diabetic rats was confirmed by increased measure of insulin sensitivity (M value) compared with ZL controls. Myocardial 18F-FDG accumulations under hyperinsulinemic-euglycemic conditions decreased significantly in ZDF rats than ZL controls. Both 18F-FDG total influx constant Ki = (k1*k3/(k2+k3) (ZL vs ZDF ; 0.0057 ± 0.0022 vs 0.0029 ± 0.0010, $p<0.05$) and distribution volume of free tracer = k1/k2 (0.94 ± 0.27 vs 0.64 ± 0.06, $P<0.05$) were significantly lower in ZDF diabetic rats, while phosphorylation fraction = k3/(k2+k3) (0.077 ± 0.061 vs 0.065 ± 0.035, ns) did not show significant differences.Conclusion: We successfully estimated increased myocardial insulin resistance by dynamic 18F-FDG PET kinetic modeling in rat model of diabetes.

P21 - Monday, October 12, 2015, 4:00 PM - 4:30 PM, Hall 3 – Poster Exhibition

Cardiovascular System: Clinical Science - Perfusion, Metabolism and Receptors

P336

Higher Event Rate in Patients with Known CAD Despite a Normal Myocardial Perfusion Scan

M. u. Zaman1, N. Fatima2, U. Zaman3, A. Zaman3, R. Zaman3; 1AKUH, Karachi, PAKISTAN, 2Dr Ziauddin Hospital, Karachi, PAKISTAN, 3Dow University of Health Sciences (DUHS), Karachi, PAKISTAN.

Objective: The negative predictive value of a normal single-photon emission computed tomography (SPECT) myocardial perfusion imaging (MPI) is very high. However, prognostic implication of a normal SPECT MPI in patients with known coronary artery disease (CAD) is not clear. Objective of this study was to evaluate the cardiac event rate in patients with known CAD who had a normal stress SPECT MPI. Methods: This prospective study accrued 428 consecutive patients with a history of CAD (revascularization or previous myocardial infarction) who had a normal stress (dynamic exercise or dipyridamole intervention) and rest Tc-99m-MIBI SPECT MPI. These patients were followed for 2-5 years (median: 3.1 years) for all- cause and cardiac mortality and non-fatal myocardial infarction. Univariate and multivariate analyses were performed to identify predictors of outcome. Results: During a follow-up period, all-cause mortality was found in 60 patients (14%) and 41 (10%) died of cardiac reasons. Non-fatal myocardial infarction (MI) was found in 77 (18%) patients. Annualized cardiac mortality and non-fatal MI rates were 2% and 3.6% respectively. Smoking, CCF and failure to achieve 85% age predicted heart rate were found to be predictors for all-cause and cardiac mortality. Diabetes, dyslipidemia, smoking and limited functional capacity (<7 METS) were found to be predictors for non-fatal MI. Conclusions: Patients with known CAD had higher cardiac event rates despite a normal stress SPECT MPI. Diabetes, dyslipidemia, smoking and limited functional capacity were the predictors for fatal and non-fatal cardiac events. A cost effective but comprehensive surveillance strategy is warranted.

P337

High Negative Predictive Value of Workload ≥7 METS on Exercise Testing in Patients with Normal Gated Myocardial Perfusion Imaging: Was Imaging Really Required?

M. u. Zaman1,2, N. Fatima2,3, U. Zaman4, A. Zaman4, R. Tahseen4; 1AKUH, Karachi, PAKISTAN, 2Karachi Institute of Heart Diseases (KIHD), Karachi, PAKISTAN, 3Dr Ziauddin Hospital, Karachi, PAKISTAN, 4Dow University of Health Sciences (DUHS), Karachi, PAKISTAN.

Purpose: to evaluate negative predictive value (NPV) of functional capacity during treadmill exercise in patients with normal gated myocardial perfusion imaging (GMPI) in Pakistani population. Methods: This was a prospective study conducted at Nuclear Cardiology Department of Karachi Institute of Heart Diseases (KIHD), Karachi, Pakistan during December 2008- December 2011. It included 1318 individuals with normal exercise GMPI. On the basis of maximal age predicted heart rate (MAPHR) and metabolic equivalents (METS) achieved, these patient were divided into Group A: ≥ 85% MAPHR and ≥7 METS (714 patients), Group B: ≥85% MAPHR and <7METS (145 patients), Group C: <85% MAPHR and ≥7 METS (289 patients) and Group D: <85% MAPHR and <7 METS (170 patients). These patients were followed up on telephone (15 ±3 months) for fatal or non-fatal myocardial infarction (MI). Results: Follow-up data revealed no evidence of MI in any group and non-fatal MI in Group A and C. Non-fatal MI was reported in 2.07% in Group B and 2.35% in Group D. NPV of a normal GMPI in relation with functional capacity was found to be 100% for Group A and C (≥7METS), 97.9% and 97.6% for Group B and D (<7METS) respectively. Conclusion: We conclude that (1) patients with ≥7 METS with normal GMPI had 100% NPV for fatal and non-fatal MIs; (2)patients with <7 METS with normal GMPI had NPV of about 98% for non-fatal and 100% for fatal MIs; (3) Omitting GMPI in patients with ≥7 METS would save cost and avoid radiation exposure.

P338

Temporal Trends in Results of 9170 Myocardial Perfusion Imaging Studies (2004 to 2013)

N. Fatima1,2, M. u. Zaman3,2, U. Zaman4, A. Zaman4, R. Tahseen4; 1Department of Nuclear Medicine, Dr Ziauddin Medical University, Karachi, PAKISTAN, 2Karachi Institute of Heart Diseases (KIHD), Karachi, PAKISTAN, 3AKUH, Karachi, PAKISTAN, 4Dow University of Health Sciences (DUHS), Karachi, PAKISTAN.

Background: To assess the frequency of normal and abnormal myocardial perfusion imaging (MPI) in a consecutive cohort of patients over a period of 8.5 years from Pakistan. Material and Methods: We assessed 9170 patients who had undergone stress-rest MPI between January 2004 and June 2013. Patients were assessed for change in demographics, risk factors, and frequency of abnormal and normal MPI. Results: Overall mean age and male predominance of studied cohort was ≈ 55 year and ≈ 55:45 (M:F) respectively with no appreciable

decline or rise. Marked decline in exercise as mode of stress (from 71% to 35%, p value significant) was noted during the study period. Regarding the risk factors for CAD, only hypertension was noted to have a significant rising trend during the study period. Trend of MPI results over study period was found non-significant from 2004 till 2006 but from 2007 onward (except 2008), a marginal but significant decline in abnormal MPIs (from 45% to 42%; significant p value) and rise in normal MPI (from 55% to 58%; significant p value) was noted. Conclusions: We conclude that over the past 8.5 years, a marginal but significant decline in abnormal and a rise in normal MPIs trend have been observed. An exorbitant rise in use of vasodilator as stressor than exercise was also observed. We envisaged a follow-up study to ascertain lower negative predictive value of vasodilator as a possible reason and till than results of this and other such studies must be read cautiously.

P339

Comparison of hemodynamic effects and negative predictive value of normal adenosine gated myocardial perfusion scan with and without caffeine abstinence

N. Fatima1,2, M. u. Zaman3,2; 1Department of Nuclear Medicine, Dr Ziauddin Medical University, Karachi, PAKISTAN, 2Karachi Institute of Heart Diseases (KIHD), Karachi, PAKISTAN, 3AKUH, Karachi, PAKISTAN.

Objective: For vasodilator stress myocardial perfusion imaging (MPI) at least 12 hour caffeine is recommended as it attenuates cardiovascular hyperemic response of adenosine and dipyridamole. However, many published conflicting results have shown no significant effect upon perfusion abnormalities in MPI performed without caffeine abstinence. The aim of this study was to compare the hemodynamic changes and negative predictive value (NPV) of normal MPIs with adenosine stress performed with and without caffeine abstinence. Methods: This was a prospective study which accrued 50 patients from May 2013 till September 2013 and followed till November 2014. These patients had a normal adenosine-gated-MPI with 99mTc-MIBI after 12 hour caffeine abstinence (No-caffeine). Next day, all patients had a repeat adenosine stress within 60 minutes after ingestion of a cup of coffee (about 80 mg of caffeine) followed by no MPI in 30 patients due to concern about radiation dose (Prior-caffeine adenosine No-MPI; Group A). Twenty patients opted for a repeat MPI (Prior-caffeine adenosine-MPI; Group B). Adenosine induced hemodynamic response and NPV of normal MPI with No-caffeine and Prior-caffeine protocols were compared. Results: The mean age of the study cohort was 57 ± 09 years with a male to female ratio of 76:24% and mean body mass index (BMI) of 26.915 ± 4.121 Kg/m2. Prevalence of hypertension, diabetes, dyslipidemia and positive family history was 76%, 20%, 22% and 17% respectively. Comparison of Group A with Group B revealed no significant difference in demographic parameters, hemodynamic or ECG parameters or left ventricular function parameters during adenosine intervention with Prior-caffeine and No-caffeine protocols. During follow no fatal MI was reported but 06 non-fatal MIs based upon history of short hospitalization for chest pain but without biochemical or ECG criteria for infarction (03/30 in Group A and 03/20 Group B). Event free survival (EFS) for fatal MI was 100% for both groups while EFS for non-fatal MI was 90% for Group A and 85% for Group B (non-significant p values). Kaplan Meier's survival plot also depicted non-significant EFS for non-fatal MI. Conclusion: This study did not find any significant attenuation effect upon adenosine induced hemodynamic response and similar negative predictive value of a normal GMPI in patients with and without caffeine abstinence. We assume that better designed prospective studies are required to validate findings of our study and provide justification for revision of guidelines about caffeine abstinence.

P341

Direct Voxel-by-Voxel Comparison of Tomographic Images from Nuclear Cardiology

J. Trnka, A. Fikrle, D. Zogala; General University Hospital, Prague, CZECH REPUBLIC.

INTRODUCTION: Traditional assessment of myocardial perfusion SPECT based on polar maps and comparison against normal database suffers from several serious drawbacks: 1) normal data may have been acquired under other conditions than the study on-site, 2) manual reformatting of stress and rest data may lead to mis-registration, 3) comparison of both stress and rest data against their own normal databases may lead to artifacts in assessment. Moreover, viability assessment based on 50% rest perfusion threshold may not be robust enough regarding multimodality comparison with metabolic PET study. The aim of this work was to construct three-dimensional difference maps between rest and stress SPECT perfusion images as well as between rest SPECT and metabolic PET to overcome these limitations. MATERIAL AND METHOD: The whole procedure was performed by locally developed algorithm, which had been previously verified in clinical practice in the field of nuclear neurology. The algorithm consists of three fundamental steps: 1) automatic spatial registration, 2) intensity normalization to compensate for differences in image counts, 3) subtraction, i.e. voxel-by-voxel calculation of differences in an appropriate form. The normalization can be based either on the mean activity within a defined volume or on an arbitrarily selected mutual voxel. The system is also capable to estimate tissue volume affected by an uptake defect or another quantitative abnormality. RESULTS AND DISCUSSION: The proposed method was tested on several patients who had undergone myocardial perfusion 99mTc-

MIBI/Tetrofosmin SPECT with or without clear conclusion based on traditional assessment. It often introduced useful additional information to help clinicians make or improve the decision. The automatic spatial registration worked very well. The displayed difference maps well corresponded to visual experience and it was easy to verify their correctness. Using proper filtration and more advanced registration it was possible to match both images of the multi-modality (99mTc-SPECT/18FDG-PET) study for visual and semi-quantitative viability assessment. CONCLUSIONS: The developed method is suitable for direct comparison between rest and stress SPECT myocardial perfusion images. It may provide additional information useful for a clinician to improve the study evaluation. It is also promising for myocardial viability assessment using comparison of SPECT vs. PET images.

P342

A Useful and Easy to Develop Combined Stress Test for Myocardial Perfusion Imaging: Regadenoson and Isometric Exercise, Preliminary Results

l. janvier, **Jr**.1,2; 1CHU Bordeaux, Bordeaux, FRANCE, 2CHU Nancy, Nancy, FRANCE.

Background: Regadenoson a selective A2a receptor agonist is a vasodilator increasingly used in myocardial perfusion imaging (MPI). Adjunction of isometric exercise is a simple method that could improve side effect profile while providing better image quality. **Methods**: Patients undergoing SPECT MPI were prospectively enrolled in handgrip-Regadenoson (HG-Reg test, N= 20) and Regadenoson (Reg) stress test (N= 40). Investigator blinded to stress test analyzed clinical data and images. **Results**: Heart rate (HR) increase was statistically higher in the HG-Reg group (27±9 vs 22±15 bpm, p=0.019). Decrease in systolic blood pressure (SBP) was less frequent in the HG-Reg group than in the Reg group (55% vs 85.5%, p=0.005), there were less drops >10 mmHg (45% vs 77.7%, p=0.012). During stress testing, fewer subjects reported at least one side effect in the HG-Reg compared to Reg group (70% vs 92.5%, p=0.021). Images were more often classified as good in the HG-Reg group (75% vs 60% in the Reg group, p=0.251). **Conclusions**: Adjunction of handgrip exercise to Regadenoson administration is a well-tolerated and easy method, without loss of time. Furthermore, image quality seems to be better.

P343

Myocardial perfusion imaging pattern in patients with intermediate and significant coronary artery stenosis

K. W. Zavadovsky1,2, M. O. Gulya1,2, V. V. Saushkin1, Y. V. Saushkina1,2, Y. B. Lishmanov2,1; 1Federal State Budgetary Scientific Institution "Research Institute for Cardiology", Tomsk, RUSSIAN FEDERATION, 2National Research Tomsk Polytechnic University, Tomsk, RUSSIAN FEDERATION.

Aim. To assess the state of myocardial perfusion in patients with coronary artery disease and intermediate coronary artery stenosis. Materials and Methods: The study group consisted of 58 patients (age: 63.1±7.1 years). Inclusion criteria were the clinical signs of CAD. Excluding criteria were: acute coronary syndrome, previous myocardial infarction, any type of coronary artery revascularisation, cardiomyopathies, inflammatory cardiac diseases and contraindication for MDCT coronary angiography. All patients underwent MDCT coronary angiography and myocardial perfusion imaging at rest and in combination with pharmacological adenosine stress test. All investigations were performed on GE Discovery NM/CT 570C with cadmium-zinc-telluride detectors. According SPECT data the were analysed summed stress rest, different score, severity and extent maps. According MDCT data the were analysed the presence of coronary artery stenosis, degree of strenosis (by minimal diameter and by area). According MDCT data all patient where divided in two groups: 1) main group - with angiographically intermediate coronary artery stenosis (70%); 2) with angiographically significant coronary artery stenosis (>70%). Results. According correlation analysis we found significant correlation between stress summed score and stenosis degree by minimal diameter (r=0.28; p<0.05;) and by area (r=0.25; p=<0.05;). Also we found a correlation between stenosis degree by area and summed different score (r=0,31; p=;) and reversibility on extent maps (r=0,31; p=;). The SPECT indexes of myocardial perfusion in patients with intermediate and significant coronary artery stenosis were follows: summed stress score (6.7±4.4% and 13.7±1.8%; p<0, 05); stress extent (7.6±6.2% and 26.6±3.4%; p<0,05); stress severity (0.3±0.1SD and 1.0±0.2SD; p<0,05); summed rest score (2.7±1.2% and 3.3±0.9%; p=not significant); rest extent (9.0±4.6% and 16.3±10.2%; p<0, 05); rest severity (0.4±.2. and 0.8±0.4; p=not significant); summed different score (3.6±2.1SD and 9.8 ±2.5SD; p<0,05); reversibility extent (8.1±4.4% and 23.6±5.5%; p<0,05); different severity (1.8±1.1SD and 3.8±0.7SD; p<0,05). We established that 20±12.7% patients with intermediate coronary artery stenosis had scintigraphic pattern similar to that of patients with coronary artery stenosis more than 70%. Conclusion. In patients with intermediate coronary artery stenosis degree of coronary artery stenosis has a weak relationship with impaired myocardial perfusion. CHD patients with coronary artery stenosis greater than 70% are

characterized by a significantly more severe impaired myocardial perfusion, compared with patients with intermediate coronary artery stenosis. 20±12.7% patients with intermediate coronary artery stenosis had scintigraphic pattern similar to that of patients with coronary artery stenosis more than 70%. The study was supported by a grant from the Russian Science Foundation (№14-15-00178).

P344

A new approach to assessment of myocardial perfusion in patients with hypercholesterolemia according to the single-photon emission computed tomography

L. Martirosyan, **Doctor**, I. Sergienko, A. Ansheles, A. Popova, K. Ivanov, V. Sergienko; FGBU RC NPC MH RF, Moskou, RUSSIAN FEDERATION.

The SPECT is quantitative, reproducible, safe and affordable. Objective: the Study, using the method of SPECT, the characteristics of the perfusion of the myocardium with 99mTc-MIBI in combination with the stress test in patients with total cholesterol (TC) ≥ 7.5 mmol/l and/or cholesterol are low density lipoprotein (LDL-CH) ≥ 4.9 mmol/l, but without obvious clinical manifestations. Materials and methods: the study involved 26 patients aged 30-68 years. 14 men, 12 women. All patients underwent a SPECT of the myocardium with 99mTc-MIBI in combination with the stress test, followed by evaluation and comparison of perfusion at rest and after exercise. In addition to the standard indicators for assessing perfusion:rest, stress, reversibility extents, SDS, SRS, SSS, we used a statistic - the standard deviation - σ sev and σ het. Results: Stress tests in all cases were negative for myocardial ischemia. According SPECT, there were no significant stability and/or reversible perfusion defects in hypercholesterolemic patients. With a qualitative assessment, inhomogeneous RFP was detected in 23 patients (88%). The difference between standard perfusion indicators in hypercholesterolemia patients and healthy volunteers were not found: Rest extent - 8.3 (5.0-11.0) and 8.0 (6.4-11.2), p = 0.67, Stress extent - 11.3 (6.5-14.0) and 7.5 (6.5-12.5), p = 0.52, Reversibility extent - 5.0 (2.5-8.0) and 3.5 (2.9-7.1), p = 0.85, SRS - 3.5 (2.0 - 5.5) 2,9 (0.75-6.0) p = 0.94, SSS - 7.3 (4.5-9.5), and 6.5 (5.1-8.3), p = 0.87, SDS - 2.5 (2.0-6.0), and 4.0 (2.9-5.1), p = 0.42, respectively. At the same time in patients with hypercholesterolemia compared with healthy volunteers σ sev and σ het were significantly higher: σ sev - 22.6 (18.9-25.2) vs. 15.6 (15.5-21.4), respectively, p = 0.04, at the rest study. At the stress study: σ sev - 22.3 (19.2-24.4) and 17.3 (16.7-18.6), respectively, p <0.01. σ het - 7.8 (7.0-9.3) and 6.1 (5.2-7.2), p = 0.053 at the rest, σ het - 7.9 (7.0-9.3) and 5.8 (5.5-6.8), p = 0.015 at the stress. Conclusion: the Use of the protocols of the metric of the standard deviation compared with the standard indicators of transient ischemia allows us to have more reliable judgement of the initial processes of redistribution of blood flow in the myocardium, which is an important aspect in the diagnosis of initial pre - clinical manifestations of coronary heart disease in all its manifestations.

P345

Interchangeability of cardiac volumetric and phase analysis parameters between two software (CardioRepo and Heart Function View)

T. Kudo, R. Ideguchi, M. Uetani, Y. Koide, K. Maemura; Nagasaki University, Nagasaki, JAPAN.

Purpose: QGS (quantitative gated SPECT) is long considered as gold standard for ECG gated myocardial perfusion imaging (MPI) analysis. However, several other programs those also have phase analysis capability were on the market recently. We compare two software for ECG gated MPI named CardioRepo (CRepo: Fuji film RI pharma and Exini Diagnostics) and Heart Function View (HFV: Nihon Mediphysics).Method: Consecutive 98 patients who underwent stress/rest gated MPI were analyzed with CRepo and HFV: Nihon Mediphysics. All the MPI was performed one-day protocol using Tc-99m labeled perfusion agents (tetrofosmin or MIBI). Gated MPI was obtained using E-cam (Siemens) with 180 arc orbit, 16 frames/beat, without attenuation correction. Two phase parameters, bandwidth and phaseSD were compared between those two software. Volumetric parameters such as EDV, ESV and EF were also analyzed.Results: For functional parameters, EDV and EF showed slightly but significantly large value in CRepo (EDV; 101±42 vs 94±47 ml, p<0.01. EF; 68 ±10% vs 65±12, p<0.01 for CRepo and HFV, respectively). ESV showed slightly smaller value for CRepo (34±25 vs 37±33 ml, p<0.01) but CRepo showed larger volume in small heart subjects. For phase parameters, CRepo and HFV showed very good correlation (Bandwidth; R-square=0.65, p<0.01, PhaseSD; R-square=0.70, p<0.01) but absolute number are quite different between two software (Bandwidth; 65.4±51.3 vs 39.1±27.1, p<0.01, PhaseSD; 15.9±11.9 vs 11.2±8.3, p<0.01 for CRepo and HFV, respectively).Conclusion: Those two software showed significant difference but the difference is very minor in volumetric parameters. Thus, for volumetric parameters, those two software are considered as interchangeable. However, for phase parameters, the difference is very large. Thus, regarding phase parameters, those two software are not interchangeable.

P346

Radionuclide assessment of myocardial flow reserve in patients with multivessel coronary artery disease

K. W. Zavadovsky1,2, A. Mochula1, S. Andreev1, Y. Lishmanov2,1; 1Federal State Budgetary Scientific Institution "Research Institute for Cardiology", Tomsk, RUSSIAN FEDERATION, 2National Research Tomsk Polytechnic University, Russian Federation, Tomsk, RUSSIAN FEDERATION.

Purpose. To assess the myocardial flow reserve in patients with multivessel coronary artery disease (MVCAD) by dynamic SPECT using semiconductor (cadmium-zinc-telluride)-based gamma camera. Material and methods. This work included fifteen patients (11 males and 4 females; mean age 63.3±12.6 years) with MVCAD with the presence of stenosis greater than 50% according to invasive coronary angiography. Control group consisted of 7 men and 2 women (25±4 years) without any cardiac diseases (healthy volunteers). All patients and volunteers underwent myocardial SPECT using semiconductor (cadmium-zinc-telluride)-based gamma camera. We used 99mTc-MIBI as a radiopharmaceutical. Acquisition protocol was as follows: (1) rest radiopharmaceutical injection (volume 1 mL; dose 185 MBq); 5-min list-mode acquisition; (2) stress radiopharmaceutical injection (volume 1ml; dose 740 MBq) followed by two-minute adenosine infusion (160 mcg/kg/min); then additional two-minute adenosine infusion (160 mcg/k/min). List-mode (5-min duration) was started simultaneously with the injection of the radiopharmaceutical. All scintigraphic images were acquired on the hybrid SPECT/CT unit (GE Discovery NM/CT 570C). Using dedicated software (Dynamic Analysis Tool), we received dynamic data reflecting the passage of the radiopharmaceutical in the walls and in the cavity of the left ventricle. To assess myocardial flow reserve, we calculated the ratio of the mean counts value from the left ventricular myocardial region (apex, anterior, lateral, and septal wall) to the integral under the curve from the left ventricular cavity. The index of myocardial blood flow reserve was calculated by dividing the ratio acquired in stress test by the ratio obtained at rest. Results. The average values of the myocardial flow reserve index for the left ventricle (in general) in a MVCAD group and in a group of healthy volunteers were significantly different: 1.41±0.48 and 1.88±0.43, respectively ($p<0.05$). Regional myocardial blood flow reserve index was also significantly different in patients with MVCAD and in healthy volunteers: 1.34±0.43 and 1.88±0.38 for the apex of the left ventricle, respectively ($p<0.05$); 1.44±0.41 and 1.95±0.45 for the lateral wall, respectively ($p<0.05$); 1.32±0.44 and 1.63±0.43 for the anterior wall, respectively ($p<0.05$); and 1.44±0.77 and 2.06±0.38 for the septal wall, respectively ($p<0.05$). Conclusion. Dynamic myocardial rest-stress SPECT using semiconductor (cadmium-zinc-telluride)-based gamma camera allows for identifying low myocardial flow reserve in patients with multivessel coronary artery disease. It can be helpful in assessment of severity of myocardial perfusion abnormality in these patients. These preliminary results require verification and comparison with other modalities. The study was supported by a grant from the Russian Science Foundation (№14-15-00178).

P347

Side Effects of Adenosine as a Pharmacologic Stress Agent for Myocardial Perfusion Scan in a local setup

H. AMER; King Abdulaziz Hospital National Guards Health Affairs, Al Ahsa, SAUDI ARABIA.

Selection of the most appropriate stress method is one of the keys to success in myocardial perfusion scintigraphy. Adenosine infusion is not without side effects which may range from minor effects to major consequences. The frequency of their occurances raised the necessity of a comparative study with the international literature available. **Methods**: This was a retrospective observational registry performed in a single center in the Kingdom of Saudi Arabia. The data were collected from the nuclear medicine database identifying all the reported Gated myocardial perfusion SPECT with adenosine stress tests between January 2013 and January 2014.The adenosine dose were fixed with all patients based on body weight and was given as a continuous infusion of 140 mcg / kg / min over a 6-minute period. A shorter-duration adenosine infusion, lasting 4 minutes, was applied occasionally. Injection of cardiac radiopharmaceuticals was given at 3 minutes for a 6- minute protocol, and at 2 minutes for a 4-minute protocol. **Results**: There were 346 patients identified with cardiac nuclear scans in the pre-specified time frame who subjected to adenosine stress scan. 152 of these patients were male accounting for 44% of the total population. Average age at the time of examination was 60.82±11.29 years. Patients were presented with one or more risk factors. Most of the side effects encountered during adenosine infusion are related to ECG changes 22% (77), the other side effects are chest pain seen in 19% (66) , shortness of breath ,7% (25), flushing,2% (8), dizziness,3%, headache,2% (8), palpitation,0.7% (3),cough,0.5% (2), and sore throat,0.3% (1) , 10% (37) developed abdominal discomfort . The ECG changes were of ischemic types as ST and T-wave changes in (40) 52%. Other changes were non ischemic as 2nd degree heart block in (16) 21%, 10%, PVC's in (11), 14%, 1st degree heart block in (7) 9%, APC's,RBBB and bradycardia,1% each. No reported case of death or myocardial infarction in this study period. **Conclusion**: The frequency of side effects seen secondary to adenosine administration are matched with the international literature available and the minor differences noted could be related to the different age group in the study population and frequency of the risk factors they are carrying.

P348

Prediction of occult coronary artery disease in patients with normal myocardial perfusion scintigraphy using myocardial perfusion reserve on dynamic thallium-201 single-photon emission computed tomography with a semiconductor gamma camera

S. Shiraishi1, N. Tsuda1, F. Sakamoto1, M. Yoshida2, S. Tomiguchi1, Y. Yamashita1; 1Kumamoto University, Kumamoto City, JAPAN, 2Amakusa medical center, Hondo City, JAPAN.

Purpose: Nuclear myocardial perfusion imaging (MPI) may fail to detect balanced ischemia. We recorded the myocardial perfusion reserve (MPR) by using a 3-dimensional (3D) dynamic approach with a high sensitivity cadmium zinc telluride (CZT) camera to determine whether it could predict occult coronary artery disease (CAD) in patients without drug-induced myocardial ischemia on conventional MPI. Methods: We subjected 165 consecutive patients with suspected CAD to thallium (201Tl) chloride adenosine stress and rest MPI-dynamic single photon emission computed tomography (SPECT) and coronary angiography. We enrolled 63 patients with minimal ischemia (less than 5% ischemic myocardium) on conventional MPI. The MPR index was calculated using the standard two-compartment kinetic model. We analyzed the utility of the MPR index, other SPECT findings, and various clinical variables for predicting occult CAD. Results:Multivariate analysis showed that the MPR index and the HDL-cholesterol level were predictive. The value of the area under the receiver operating characteristic curve of the MPR index was 0.80, it was 0.65 for HDL-cholesterol, and 0.82 when the combined MPR index was added to HDL-cholesterol. We determined that a combined index value ≥ 0 yieled the highest diagnostic accuracy. Sensitivity, specificity, and accuracy were 89%, 65%, and 79%, respectively, for the combined index; these values were 76%, 81%, 78% for the MPR index, and 86%, 50%, and 71% for the HDL-cholesterol. Conclusion: Quantification of myocardial perfusion and the perfusion reserve using dynamic SPECT with a CZT camera may help to identify occult CAD in patients without drug-induced myocardial ischemia on MPI.

P349

Large myocardial injury attenuates a response to steroid therapy in patients with cardiac sarcoidosis

M. Momose1, K. Fukushima1, C. Kondo1, N. Serizawa2, A. Suzuki2, K. Abe1, N. Hagiwara2, S. Sakai1; 1Department of Diagnostic Imaging and Nuclaer Medicine, Tokyo Women's Medical University, Tokyo, JAPAN, 2Department of Cardiology, Tokyo Women's Medical University, Tokyo, JAPAN.

Aim: Steroid therapy is well known to have an anti-inflammatory effect for active cardiac sarcoidosis (CS). However its response has not been fully discussed so far because of no useful standard of a response to the therapy. FDG-PET/CT(PET) is recently reported to be useful tool to evaluate inflammation activity; therefore it may be also possible to assess a response to the steroid therapy in CS patients. The aim of the present study is to assess which imaging parameters before the therapy affect the therapeutic response. Methods: Twenty patients with CS diagnosed based on Japanese Ministry of Health and Welfare clinical criteria (JMHW), FDG-PET and/or cardiac MRI were retrospectively enrolled in the study. All patients underwent PET, 123I-BMIPP(BMIPP) and 201TL(TL) dual gated SPECT before steroid therapy. As indexes of inflammation activity by PET, SUVmax, higher metabolic activity volume in the heart (HMAV activated >2.5 in SUV) and total lesion glycolysis (TLG=HMAV x SUVmean within the activated region) were obtained using syngo.via software (Siemens). BMIPP and TL SPECT images were divided into 17 segments where each segmental defect score (0,normal; 4, absent) was graded to generate summed BMIPP and TL defect score (BMDS, TLDS). End-diastolic volume (EDV) and ejection fraction (EF) were generated by gated SPECT. All patients were treated with 30mg/day of prednisone, which was tapered to a maintenance dosage of 10-20mg/day. All the patients underwent another PET in 6-12 months to evaluate a response to the therapy, and the inflammation indexes were generated again. We classified the response to the therapy into partial (PR) and complete (CR) responses with a threshold value of 10 in TLG (CR<10). We compared the generated image parameters between PR and CR. Results: As for the PET parameters, SUVmax, HMAV and TLG were 8.34±4.31, 154±93 and 603±416 before the therapy, which were decreased to 3.16±0.88, 13.10±23.6 and 39±71 at the second scan, respectively. BMDS, TLDS, EDV(mL) and EF(%) before therapy showed 14.2±11.1, 9.6±9.1, 104 ±50 and 44±15, respectively. Seven patients were judged as PR. BMDS and TLDS were significantly higher in PR than in CR group (BMDS, 23±13 vs. 9.0±5.9, p=0.004; 16±11 vs. 5.8±4.9 p=0.013), but other imaging parameters before the therapy were not significant. Sensitivity and specificity for the detection of PR were 92 and 71% using >14 in BMDS. Conclusion: The preliminary data suggested that large myocardial injury assessed by BMIPP and TL may attenuate a response to steroid therapy in patients with cardiac sarcoidosis.

P350

Visualization of Acute Myocardial Infarction of Right Ventricle Free Wall after Cardiac Surgery by Gated SPECT with Phase Images

E. N. Ostroumov1, **E. D. Kotina**2, V. A. Ploskikh2, A. V. Babin2, A. S. Ivanov1, A. V. Rodionov1, O. M. Mas'1; 1Academician V.I. Shumakov Federal Research Center of Transplantology and Artificial Organs, Moscow, RUSSIAN FEDERATION, 2Saint-Petersburg State University, Saint-Petersburg, RUSSIAN FEDERATION.

Aim. Myocardial-like infarction ECG changes and a significant rise in the level of cardiac enzymes require the exclusion of acute myocardial focal changes. Such a situation can sometimes occur after cardiac surgery. Visualization of these changes is required to assess the prognosis. The absence of such changes in LV myocardium already shows a good prognosis, however, it does not explain the problems of clinical and instrumental signs. Material and Methods. During 5 years of research from more than 1500 patients had been undertaken a cardiac surgery we had 9 cases of changes in ECG, enzymes and clinics after cardiac surgery. Three patients underwent aortic valve replacement (one in combination with coronary anastomosis), 2 patients - multiple stenting of coronary arteries, one patient after multiple coronary artery bypass surgery, 2 patients underwent multiple stenting after heart transplantation and 1 with congenital heart defect. All patients underwent gated SPECT with the phase image not only of the left but also of the right ventricle. Results. All patients after surgery showed myocardial like infarction ECG changes and / or cardiac enzymes accompanied by clinical signs of right ventricular heart failure. In one case proximal lesion in the right coronary artery (RCA) was revealed, in the second case there was a congenital absence of RCA. In the remaining 7 cases the coronary arteries were intact. During the gated SPECT right after surgery no patient showed any focal changes in LV myocardium. However, while analyzing the images of the right ventricle in all 9 patients we identified focal reduction of perfusion and function, topographically coinciding with areas of pathological myocardial asynchrony. Conclusion. The appearance of clinical and instrumental signs of acute myocardial infarction after cardiac surgery without focal changes in LV myocardium may be associated with focal changes in the myocardium of the right ventricle even if coronary arteries are intact.

P351

Is increased septal perfusion an indicator of asymmetrical septal hypertrophy?

S. OZDEMİR1, Y. TAN1, E. GAZI2, F. CELİK1; 1Canakkale Onsekiz Mart University,Faculty of Medicine. Department of Nuclear Medicine, Canakkale, TURKEY, 2Canakkale Onsekiz Mart University,Faculty of Medicine. Department of Cardiology, Canakkale, TURKEY.

ABSTRACT: Background: In this study, we have compared scintigraphic and echocardiographic data in order to investigate whether increased septal perfusion represents asymmetrical septal hypertrophy which is a symptom followed in the scintigraphy of myocardial perfusion. As a secondary objective, we have analyzed the correlation of the size of left ventricular and dimensions obtained from echocardiography. Method: The study consists of a total of 186 patients (120 female and 66 male with an average age of 59.45 ± 11.54 years) who had normal myocardial perfusion scintigraphy and echocardiography examinations. Statistical comparison of septal wall thickness measurements obtained from echocardiography and septal-to-lateral wall ratios (S/L ratio) was performed scintigraphically. Left ventricular mass values were obtained as both scintigraphically and echocardiographically and their correlations were evaluated in order to assess the presence of left ventricular hypertrophy. Results: In statistical analyses, the values of IVSd, LVPWd, LVM and LVMI were found to be significantly higher in the Group2 (S/L ratio>1) compared to the Group1 (S/L ratio<1). In addition, S/L ratio is significantly correlated with echocardiographic IVSd, LVPWd, LVM, LVMI and scintigraphic LVM (rest) values. Furthermore, echocardiographic LVM, LVMI values were significantly correlated with LVM, LVMI values obtained from scintigraphy. Conclusion: It should be known that increased S/L wall ratio that can be monitored during scintigraphic studies can be an indicator of septal hypertrophy and/or left ventricular hypertrophy and further examination and close follow ups should be performed in necessary cases.

P353

Added value of coronary calcium scoring as part of myocardial perfusion scan

A. Notghi, S. Tomas Hernandez, J. O'Brien; Sanwell and West Birmingham Hospitals NHS Trust, Birmingham, UNITED KINGDOM.

Aim: With hybrid SPECT cameras it is now possible to perform a coronary calcium scoring (CCS) in patients undergoing myocardial perfusion scan (MPS). CCS is normally recommended for patients with low probability (<30%) coronary artery disease (CAD). Here we have looked how useful is CCS when used in conjunction with MPS in patients with intermediate probability of CAD (30-60%). Method: All patients referred for MPS with no previous angiogram were marked for CCS. GE Discovery 670 SPECT camera with 16 slice CT was used. SPECT acquisition was immediately

followed by gated CCS acquisition (2 minutes additional time). Results: In initial pilot study 45% of CCS could not be performed because of high heart rate (>70 bpm). We now administer oral beta-blocker to all patients with resting heart rate of >70 after they are stressed. This has enabled all eligible patients to have CCS. During 12 months period (2013-2014) 1713 patients had MPS. Of these 926 (54%) also had CCS with MPS. Median age was 61 (range 18 to 89 year). 394/926 (42%) had a calcium score of 0. The remaining 58% had calcium score ranging from 1 to 11800 Agatston Units (median CCS=181 AU). Discussion: Calcium score of 0 increased the confidence in reporting normal scans (MPS lesion 3% or less at stress with calcium score of 0 do not need rest study). These patients were subsequently discharged from cardiac clinics. Patients with calcium score of 0 who had >3% defects on MPS were referred for CTCA/angiogram to exclude soft plaques. Patients with CCS of ≥ 1 and normal MPS, did not come back for rest study. All patients with MPS defect had a rest study regardless of the size. A positive CCS changed the clinical management in all patients with no evidence of flow restricting disease as they were given dietary advice and aggressive control of risk factors. Those with abnormal MPS and positive CCS were referred for angiography with a view for stenting. Conclusion: CCS is a quick and easy addition to an MPS study. It can reduce the number of unnecessary rest studies (saving patient radiation and time for department), it enhances the confidence of reporting and changed the clinical management of patients leading to overall improvement in patient diagnosis and management. MPS+CCS is now part of our routine MPS study.

P354

Myocardial perfusion scintigraphy in patients undergoing cardiac rehabilitatation

S. Rizkallal Monzon1, B. Theillac2, B. Navarro Martinez2, J. Castro Beiras2, M. Martinez Gomez2; 1Hospital Universitario La Paz, Madrid, SPAIN, 2Hospital Universitario Ramon y Cajal, Madrid, SPAIN.

AIM: Cardiac Rehabilitation (CR) includes physical exercise that has proven to improve collateral recruitment. Therefore collateral circulation could be a new therapeutic target. The aim of this study is to evaluate the utility of myocardial perfusion scintigraphy (MPS) to measure ischemic change in coronary artery disease patients undergoing CR. MATERIAL AND METHODS: A total of 43 patients (6 women) were enrolled in the study (aged 59±10 years). None of them were subjected to revascularization procedures during CR. Two MPS were performed in every patient one before and the other after concluding CR. The average duration of the CR was 79 ±27 days. Quantitative perfusion and functional data were obtained in both studies. The results were expressed as mean ± standard deviation, considering them statistically relevant if $p \leq 0.05$. RESULTS: Average stress perfusion defect in the first MPS was 28.3±16 %, while in the second MPS was 22.3±15 % ($p \leq 0.01$). We did not find significant difference in poststress left ventricular ejection fraction (53.4±12 vs 54.7±1% NS) nor in rest MPS results (22.3±15 vs 20.5±14 NS). However when patients with low left ventricular dysfunction (<50%) were grouped (n: 18) the results showed improvement in their poststress ventricular function (42.0±7 % vs 45.1±9% NS ($p \leq 0.08$)). CONCLUSION: MPS has proven to be really useful evaluating changes in myocardial perfusion of patients undergoing CR. This improvement in myocardial perfusion is probably related to development of collateral circulation. Patients with previous low ventricular function showed increase in their left ventricular ejection fraction, however further studies are needed to confirm this trend.

P355

Clinical Impact of Myocardial Perfusion Scintigraphy in Patients with Previous Percutaneous Coronary Intervention

S. Czibor, M. Moravszki, K. Buga, M. Toth, R. Joba, I. Szilvasi; Hungarian Defence Forces Medical Centre, Dept. of Nuclear Medicine, Budapest, HUNGARY.

Aim: The purpose of this study was to evaluate the clinical usefulness of myocardial perfusion scintigraphy (MPS) to detect restenosis or stenosis in a new localisation in patients with previous percutaneous coronary intervention (PCI). Materials and methods: We compared the findings of MPS and invasive coronary angiography (CAG) of patients with clinically suspected restenosis. ECG-gated MPS were performed using the one-day protocol. In 142 patients MPS was followed by CAG because of stress-induced reversible perfusion defects (in 102 cases) or persistent severe clinical signs (in 40 cases) within 8±5 weeks. Age of the patients (38 women and 104 men) was 63.0±9.8 years. The median of the time interval between the last PCI and the MPS was 13,5 months. Results: Out of the 142 MPS studies, reversible perfusion defects were shown in 102 cases and were not present in 40 cases (10 with normal scans and 30 with fixed perfusion defects). Haemodynamically significant stenoses were found by CAG in 99 cases and they were absent in 43 cases. The 102 MPS studies showing ischaemia proved to be true positive in 83 (81,37%), and false positive in 19 cases (18,36%). Out of the 40 MPS examinations without ischaemia 24 were true negatives (60%) and 16 were false negatives (40%) based on CAG. An agreement in the findings of MPS and CAG was present in 107 out of 142 (75,35%) patients. The presence of ischaemia on the MPS had a considerably high positive predictive value (81,37%) for

restenosis or stenosis in a new localisation (OR: 6,55; p<0, 0001). Invasive CAG was performed significantly earlier (within an average of 7 weeks) in those who had ischaemic findings on MPS than in those without ischaemia (within an average of 12 weeks); p<0,0001. Conclusion: Our study has shown that MPS accurately predicts the presence of instent restenosis or stenosis in a new localisation in patients with clinically suspected myocardial ischaemia after previous PCI. It is a clinically useful tool in selecting patients for invasive CAG.

P356

Value of ECG-gated study during dipyridamole stress in myocardial perfusion PET

K. Nakagawa1, S. Onodera2, T. Uchida2, Y. Ozaki2, H. Henmi2, Y. Uchino2; 1Tokyo Seaside Clinic, Tokyo, JAPAN, 2Chiba Ryougo Center, Chiba, JAPAN.

[Purpose] Previous studies reported that intensive medical treatment combined with life-style modification for coronary artery disease (CAD) could improve coronary perfusion and prognosis. However, effect of treatment to cardiac function has not been reported. Thus, we measured cardiac function by ECG-gated PET and compared the values before treatment to those after treatment. [Methods] Baseline myocardial perfusion PET with N-13 ammonia was performed for 28 CAD patients at rest and during dipyridamole stress. For all the patients, intensive medical treatment combined with life-style modification was introduced for more than one year and the follow-up PET was performed after the treatment. Myocardial perfusion images were visually interpreted and its changes before and after the medical treatment were evaluated. PET data were also acquired by ECG-gated mode and ejection fraction (EF), end-diastolic volume (EDV) and end-systolic volume (ESV) were measured both at rest and during dipyridamole stress. Values before the treatment were statistically compared to those after the treatment. [Results] Of 28 patients, 13 showed improved myocardial perfusion during dipyridamole stress after the treatment (Group A), suggesting regression of coronary atherosclerosis. On the other hand, 8 patients remained unchanged (Group B) and 7 showed worsened myocardial perfusion (Group C). In the patients who showed improved myocardial perfusion (Group A), mean EF during dipyridamole was improved from 66.5% to 68.5% (p=0.005), mean EDV was changed from 92.2ml to 82.2ml (p=0.007) and mean ESV was changed from 31.5ml to 26.5ml (p=0.002). Mean EDV and ESV at rest in Group A also tended to decrease but not statistically significant (p=0.058 and 0.082, respectively). On the other hand, mean EF, EDV and ESV in Group B were similar both at rest and during dipiridamole (p>0.05). The mean values were also statistically unchanged in Group C (p>0.05). [Conclusion] ECG-gated myocardial PET is useful to evaluated cardiac function and size during dipyridamole stress in addition to myocardial perfusion. And improved cardiac function and decreased cardiac size were associated only to those who were improved in their myocardial perfusion after the medical treatment.

P357

The Value of Semiquantitative Analysis in Myocardial Perfusion Imaging using Multifocal Collimator SPECT/CT: IQ-SPECT

M. Trogrlic, M. Medvedec, S. Tezak; University Hospital Centre Zagreb, Zagreb, CROATIA.

AIM: to identify diagnostic value of semiquantitative analysis in MPI obtained with a multifocal collimator, IQ-SPECT.MATERIALS AND METHODS: 68 patients (46 males and 22 females; age group 34-90 years, mean age 65 ±10 years) with high post stress coronary artery disease probability and visually abnormal SPECT findings were included in this prospective study. All patients underwent two-day protocol perfusion scan (Gated IQ SPECT/CT) after stress test and at rest. Acquisition was performed on a Symbia T (Siemens) equipped with a dual-headed gamma camera system and with a multifocal smartzoom collimator. Acquisition was done in 128x128 matrix, 50 min after tracer injection (370 MBq Tc-99m sestamibi), 17 views per head, 20 sec/view. Flash 3D iterative reconstruction was done. Expert in nuclear cardiology qualitatively (visually) assessed all myocardial perfusion images. Using 4D-MSPECT software, stress and rest data sets of 68 patients were analyzed in fully automatic operation mode. Summed stress score (SSS), summed rest score (SRS), and resulting summed difference score (SDS) were calculated semiquantitative by comparing tracer uptake with values from gender-specific normal databases provided by manufacturer (databases with and without attenuation correction (AC)). Individual segmental scores and summed scores analysis was performed on a standardized 17-Segment model (AHA). Segment by segment comparison between qualitative, visually assessed results, and semiquantitative perfusion parameters was done. Semiquantitative parameters, with AC and without AC, were also compared and statistically analyzed.RESULTS: Agreement degree on the diagnostic accuracy between qualitative and semiquantitative analysis based on SSS parameter was: 0.76 for stress studies without AC, 0.74 for stress studies with AC, based on SDS parameter was: 0.76 for studies without AC, 0.85 for studies with AC.No significant difference was recorded between qualitative and semiquantitative results regarding total number of affected segments with perfusion abnormalities (qualitative analysis: 177 segments, semiquantitative without AC: 167, with AC:

196).SSS calculated from normal databases without and with AC were significantly different: SSS without AC 5.8±3.3; SSS with AC 6.4±4.5. SDS results were also significantly different: SDS without AC 3.4±2.2; SDS with AC 3.8 ±3.0.CONCLUSIONS: Semiquantification of MPI is often performed to assist physicians in detecting CAD and to improve diagnostic confidence levels. Semiquantitative analysis might potentially improve diagnostic accuracy of MPI when using IQ SPECT. Semiquantitative methods with AC slightly overestimated number of affected segments, while methods without AC slightly underestimated number of affected segments. Perfusion abnormalities scores obtained without AC are significantly different than scores obtained with AC.

P358

What is the impact of apparently minimal dipyridamole response to the acuracy of myocardial perfusion scintigraphy?

A. Doumas1, **I. Iakovou**1, V. Mpalaris1, D. Mpountas2, V. Athanasiou1, D. Katsaboukas1, S. Georga1, K. Badiavas1, D. Lo Presti1; 1Academic Nuclear Medicine dpt, Papageorgiou hsp, THESSALONIKI, GREECE, 2Nuclear medicine dpt "Hippokrates", THESSALONIKI, GREECE.

Aim: To investigate the accuracy of myocardial perfusion imaging (MPI) for the detection of coronary artery disease, in patients who can not increase their heart rate or lower their blood pressure after dipyridamole administration. Method: We retrospectively compared the results of MPI with the coronary angiography in 103 patients (73male, mean age 63+/-8 years), who underwent dipyridamole MPI, under no b-blockers medication. These patients were divided into two groups, depending of the mean blood pressure (BP) and heart rate (HR) that they reached at the end of dipyridamole administration. Group A consisted of 62 individuals who increased their HR at least 20% and decreased their mean BP at least 10% from their baseline values, whilst Group B (41 patients) failed to achieve at least one of the two targets. Sensitivity, specificity and accuracy was estimated in the two groups, taking as a gold standard the presence of at least 50% stenosis in one of the three main vessels in the coronary angiography. Results: There was no significant difference between the two groups, concerning age and sex. The severity of CAD, defined as the number of the diseased vessels, was similar in the two groups (70% and 71% respectively, $p>0.05$). The sensitivity and specificity of MPI for the detection of CAD was 87% and 81% in group A and 84% and 79% in group B with no statistically significant difference. The overall accuracy was also nearly identical (95% in group A and 93% in group B). Conclusion: We conclude that both BP and HR are not good predictors of adequate pharmacologic response during dipyridamole administration. The hyperemic response to the myocardium seems not to differ between patients who achieve at least 20% increase in HR and 10% fall in their mean BP and those that fail to achieve one or both of these goals. On the other hand, usually younger patients and predominantly male, are able to achieve an apparently good pharmacologic response, which however plays no role in the accuracy of the scintigraphic result.

P359

Splenic switch-off in Rb82 myocardial perfusion imaging: an indication of adequate vasodilatation?

M. J. Memmott, P. Arumugam, C. M. Tonge; Central Manchester University Hospitals NHS Foundation Trust, Manchester, UNITED KINGDOM.

Introduction: Achieving adequate stress is paramount for the interpretation of myocardial perfusion imaging. Current methods include observation of side-effects during the adenosine infusion, or analysis of the myocardial perfusion reserve via quantitative dynamic PET imaging. It has recently been reported that attenuated perfusion within the spleen at stress can provide a potential marker for adequate vasodilatation. We propose a simple method to assess efficacy of vasodilatation based on the evaluation of splenic uptake in Rb82 PET imaging. Methods: A total of 23 patients referred for a Rb82 PET myocardial perfusion study, with a low pre-test likelihood of CAD and normal patterns of perfusion, were retrospectively analysed. Of these, 17 (Group 1) demonstrated side-effects consistent with adequate adenosine vasodilatation and 6 (Group 2) did not. All patients had their myocardial blood flow (MBF) and perfusion reserve (MPR) measured as per routine protocol. Rate-pressure product (RPP) corrected MBF at stress (SMBF) and rest (RMBF) was calculated using Siemens Syngo MBF. Patients with significant motion during their dynamic acquisition were excluded. Uptake in the spleen was measured in the same location for both stress and rest studies for the 4.5 minute static acquisition, using a 2cm spherical volume of interest (VOI). The ratio between uptake in the spleen at rest and stress (Splenic Uptake Ratio, SUR) was calculated. Results: All patients in Group 1 had an SUR greater than 1.0 (median 1.58) and the majority (16/17) had a MPR of greater than 2.0 (median 2.67). In Group 2, both the median SUR and MPR were significantly lower ($p < 0.006$) than for Group 1, at 1.06 and 1.22 respectively. One patient underwent repeat imaging due to suspicion of caffeine intake, with the initial scan showing an SUR of 1.05 and MPR of 1.06. The repeated study demonstrated an increased SUR and MFR of 1.51 and 3.34 respectively. Conclusions: This small, preliminary study indicates that splenic switch-off is observed in Rb82 studies, can be evaluated using a simple ratio, and

correlates well with MPR and reported side-effects. Whilst this is an interesting observation in dynamic Rb82 PET imaging, the extension of this work to modalities where quantitative assessment of vasodilator response is not possible, such as SPECT imaging, could provide an promising indicator of adequate stress, although technical challenges remain to be overcome.

P360

One year outcome of the myocardial infarcted areas seen immediately post primary percutaneous transluminal coronary angioplasty (PTCA)

A. Doumas1, T. Christoforidis1, **I. Iakovou**1, V. Mpalaris1, D. Mpountas2, D. Katsaboukas1, V. Athanasiou1, S. Georga1, D. Lo Presti1, N. Karatzas1; 1Academic Nuclear Medicine dpt, Papageorgiou hsp, THESSALONIKI, GREECE, 2Nuclear medicine dpt "Hippokrates", THESSALONIKI, GREECE.

Aim: Areas of myocardial infarction are evident after primary PTCA in patients hospitalized due to chest pain and elevated enzymes. The extend of the existing scar seen immediately (2-3 days) post successful primary PTCA was estimated one year after the procedure. Method: Primary PTCA was performed in 64 male patients (mean age 63+/- 12 years) suffering from acute myocardial infarction (MI) due to one vessel coronary artery disease. The time interval between the onset of pain and the admission was less than 4 hours in all the patients. The area of the scar was evaluated using 99mTc-SESTAMIBI Gated-SPECT myocardial imaging (MPI), 2-3 days post PTCA and one year after. The scar area was assessed quantitatively from the rest images, using the Cedars-Sinai quantitation program and expressed as a percentage of the total myocardial mass (TMM), while the final reduction of the infarcted area was expressed as the percentage of the initial one. Depending of the infarcted area, the patients were divided into 2 groups: Group A with an area less than 20% of the TMM and in Group C with area more than 20% of the TMM. The patency of the angioplastized vessel was evaluated a year after, using either CT or invasive coronary angiography. Results: There was patency of the responsible for MI vessel in 92% of the patients. The infarcted area was reduced between 60-100% (mean value 84+/-9.8%) in group A and 20-60% in group B (mean value 34+/-22%%). Conclusion: We conclude that primary PTCA is extremely useful in patients with small to intermediate size rest perfusion defects, seen early after the procedure. The better salvage result that observed to these patients is probably due to high proportion of stunned myocardium existing during the first days after primary PTCA that is recovering thereafter. On the other hand, the extent of stunned myocardium seems to be less when infarction involves large areas of underperfused myocardium.

P361

Does observer-dependence influence the reliability of supine/prone stress-only MPI with cardiac dedicated CZT scanner?

S. Osiecki1, S. Piszczek1, P. J. Kwasiborski2, A. Mazurek1, M. Dziuk1; 1Military Institute of Medicine, Warsaw, POLAND, 2Medical University of Warsaw, Warsaw, POLAND.

Aim: Cardiac SPECT imaging is a procedure of great value in CAD diagnostics. In patients with normal stress MPI the stress-only protocol has been proven to be safe an efficient. Furthermore it allows to reduce the radiation exposure and costs. The aim of this study was to investigate how interpreter-dependent stress MPI is, especially considering stress-only protocol.Materials and Methods:203 consecutive patients having undergone cardiac SPECT with prone and supine imaging were enrolled. If possible stress only protocol was applied. Each stress MPI was assessed by 3 independent experienced physicians and assigned to one of three groups: 1- no rest MPI needed, the question of referring clinician can be answered with stress only, 2- the question of referring clinician probably can be answered with stress only protocol, but for safety rest MPI should be performed, 3- rest MPI is definitely required. In case of discrepancy between interpreters, for further clinical proceedings the consensus was established.Patients were divided in two groups: stress only (n=94) and stress-rest (n=109). In these two groups and in the whole cohort the agreement between physicians was assessed using kappa inter-rater agreement statistic. Of patients with consensus 1 (meaning no rest MPI is required) the subgroup of 20 who had although undergone rest MPI was divided and taken under more detailed analysis.Results:In the whole cohort the agreement between 3 independent physicians was substantial with 77,83%, κ=0.696546. However in the stress-only group the agreement was significantly higher with 92.55%, κ=0.202424, compared to 65.14%, κ=0.405877 in the stress-rest group.Of 95 patients whose stress MPI was assessed by consensus to be sufficient to answer the clinical question, 20 had undergone rest procedure. In this subgroup there were no significant ischemia cases (no reversible defects >10% of myocardium). 8 patients had insignificant perfusion reversibility, one of them had <10% perfusion reversibility in the inferior wall, while LAD region was to be assessed - with no abnormalities in the investigated artery area of supply.Conclusions:The study has shown that, though highly sensitive and specific, in some cases myocardial perfusion may be still observer-dependent. Thus, if any doubts appear, assessment limited to the stress-only protocol should be chosen by consensus of experienced interpreters. The higher agreement in stress-only group, and lack of significant ischemia in the consensus 1 stress-rest subgroup indicate, however, that used carefully it is a safe protocol.

P362

Myocardial blood flow quantification with 82-Rubidium PET/CT for the diagnosis of cardiac sarcoidosis

Q. Gillebert1, R. Chequer1, R. Ben Azzouna1, S. Leygnac1, N. Mikail1, F. Hyafil1, C. Chapelon-Albric2, B. Crestani3, D. Le Guludec1, F. Rouzet1; 1Department of Nuclear Medicine, Bichat University Hospital, Département Hospitalo-Universitaire FIRE, Assistance Publique-Hôpitaux de Paris, University Paris Diderot-Paris 7, Paris, FRANCE, 2Department of Internal Medicine II, CHU Pitié Salpêtrière, University Pierre et Marie Curie, Assistance Publique-Hôpitaux de Paris, Paris, FRANCE, 3Department of Pulmonology, Bichat University Hospital, Assistance Publique-Hôpitaux de Paris, University Paris Diderot-Paris 7, Paris, FRANCE.

Objectives: The early diagnosis of cardiac involvement of sarcoidosis remains challenging. The aim of the study was to evaluate the additional value of myocardial blood flow (MBF) over uptake quantification with 82-Rubidium (82-Rb) PET/CT for the diagnosis of early stage of cardiac sarcoidosis (CS).Methods : Thirty-seven patients (age: 48±12 years ; males: 60%; left ventricular ejection fraction: 51±8%) without history of cardiovascular disease were prospectively included in 5 tertiary care centres if they had a histological proven sarcoidosis and a suspicion of cardiac involvement based on symptoms, EKG or echocardiography. Patients underwent 82-Rb PET/CT in addition to routine investigations that included Holter monitoring, cardiac MRI, 18-FDG PET and myocardial perfusion SPECT. 82-Rb PET/CT (list mode acquisition after bolus injection of 10 MBq/kg over 30 sec, Discovery VCT 690, GEMS) was performed at rest and after injection of Dipyridamole (0.7 mg/kg). After reconstruction, static and EKG-gated slices were analysed both visually and automatically (FlowQuant software). Dynamic data were further processed (FlowQuant software) in order to provide rest and stress MBF and flow reserve. Absolute uptake and/or flow were considered abnormal in a segment if the mean value in this segment was <75% of the maximal value in the myocardium. The diagnosis of CS was based on the decision of a multidisciplinary team (MDT) that was allowed to review patients' medical record but was blinded to 82-Rb PET/CT result. We then compared 3 strategies for data analysis: 1/completely automated quantification of tracer uptake and MBF; 2/visual analysis alone of 82-Rb uptake (without MBF values); 3/visual analysis combined with MBF results only in equivocal segments. The results of 82-Rb PET were compared with MDT decisions.Results: Cardiac sarcoidosis was considered definite in 11 patients, excluded in 21 and possible in 5 (excluded from further analysis) according to MDT decision. Patients with and without CS had similar clinical characteristics. The sensitivity, specificity and accuracy (respectively) were: 91%, 33% and 53% for completely automated analysis; 91%, 91% and 91% for visual analysis alone, and 100%, 81% and 88% for the combined analysis.Conclusions: the present study suggests that 82-Rb PET is useful in the early diagnosis of cardiac sarcoidosis with good sensibility and specificity. The strategy combining visual analysis and MBF quantification seems to be the more relevant in order not to overlook the diagnosis with only a mild decrease of specificity compared to visual analysis alone.

P363

Impact of prone-position acquisition of 123I-MIBG cardiac imaging on heart-to-mediastinum ratio

T. Pellegrino1, V. Piscopo2, A. Boemio2, R. Carotenuto2, B. Russo2, S. Pellegrino2, G. De Matteis2, A. Cuocolo2; 1Institute of Biostructures and Bioimages, Naples, ITALY, 2University of Naples - Federico II, Naples, ITALY.

Background: Cardiac 123I-metaiodobenzylguanidine (MIBG) innervation imaging has been widely used to estimate cardiac sympathetic innervation in various forms of cardiac disorders. Although normal cardiac MIBG distribution includes a relatively low uptake in the inferior wall, the substantial uptake of the tracer in the liver could overlap the inferior left ventricular wall. Prone images might improve the relative tracer uptake in the inferior wall reducing diaphragmatic attenuation and avoiding intense uptake by the liver. This study assessed whether MIBG prone-position acquisition can change heart-to-mediastinum (H/M) values compared to supine acquisition. Methods: Forty-five patients (34 men, mean age 58±15 years) were enrolled (34 patients with heart failure and 11 with Anderson Fabry disease). All patients underwent planar 123I-MIBG cardiac imaging after intravenous administration of 111 MBq. Ten-minute planar images were acquired from an anterior thoracic view 15 minutes ("early" image) and 3 hours and 50 minutes ("late" image) after tracer administration in both supine and prone positions. Early and late H/M ratios were computed and washout rate (WR) was calculated using the standard formula background and decay corrected. Using the mean relative uptake, the inferior to anterior uptake ratios were also calculated on early and late images for both supine and prone positions. Results: Early (1.8±0.3 vs. 1.9±0.3, p=0.3) and late (1.7±0.4 vs. 1.7±0.3, p=0.8) H/M ratios, and WR (35±17.6% vs. 35±16.4%, p=0.9) were not different between supine and prone position. On early images, inferior/anterior uptake ratio in the supine position was significantly lower as compared to prone position (0.96±0.12 vs. 1.01 ±0.08; p<0.02). Conversely, on late images inferior/anterior uptake ratio was not different between supine and prone positions (0.99±0.15 vs. 1.01±0.08, p= 0.4). Conclusions: The

results of the present study show that the prone-position acquisition did not change early and late H/M ratios and WR compared to supine-position acquisition. However, the inferior to anterior uptake ratio increased using the prone-position acquisition only in early images.

P364

Preliminary report of long term follow-up with myocardial perfusion scan in breast cancer patients after external beam radiation therapy.

M. Eftekhari1, F. Kalantari1, M. Abbasi2, S. Farzanefar2, A. Fard-Esfahani1, B. Fallahi1, D. Beiki1, A. Hassanzadeh-Rad1, **A. Emami-Ardekani**1; 1research center for nuclear medicine, Tehran university of medical sciences, Tehran, IRAN, ISLAMIC REPUBLIC OF, 2Nuclear Medicine Department, Vali-asr Hospital, Tehran University of Medical Sciences, Tehran, IRAN, Tehran, IRAN, ISLAMIC REPUBLIC OF.

Aim: Radiotherapy induced myocardial injury may increase cardiovascular morbidity and mortality especially in left sided breast cancer. To evaluate the prevalence of myocardial perfusion abnormalities following radiation therapy, in left and right-sided breast cancer patients, short and long term MPI findings were compared. Materials and methods: Patients with low 10-year Framingham risk scoring of coronary artery disease were included in the study to minimize confounding factors. All patients treatment plan were modified radical mastectomy and postoperative 3D Conformal Radiation Therapy (CRT) to the surgical bed with an additional 1-cm margin, delivered by 46-50 Gy (in 2 Gy daily fractions) over a 5-week course and the same dose-adjusted chemotherapy regimen (including anthracyclines, cyclophosphamide and taxol) was given. 3 years after radiation therapy, all patients underwent cardiac SPECT for the evaluation of myocardial perfusion. These patients have been evaluated for short term effect 6 months after radiotherapy. General linear model for repeated measures was designed to assess the ischemic change over time. Results: Up to now 26 patients with a mean age of 43.7±6.9 years [13 patients with left sided breast cancer (exposed) and 13 patients with right-sided cancer (controls)] were enrolled. Dose-volume histogram (DVH) [showing the percentage of the heart exposed to >50% of radiation] was significantly higher in patients with left-sided breast cancer. The prevalence of ischemia didn't change in subjects with left mastectomy (6 out of 13 from baseline to follow-up). But this prevalence is decreased from 3 (21.3%) to 1 (7.7%) from the baseline to the second study in right sided mastectomy group. Not only the prevalence of ischemia was higher among subjects with left mastectomy in baseline study, significant interaction effect was also observed for the side of mastectomy and the result of MPI during the period of the study (partia Eta Square= 0.18, P=0.36). Conclusion: Radiation induced myocardial perfusion injury in patients treated with radiotherapy on the left hemi thorax is not low. It is advisable to apply precise radiation planning techniques to minimize the volume of the heart in the field of radiation therapy and also to screen these clinically asymptomatic patients with MPI-SPECT, as early treatment may improve cardiac outcome.

P365

Effect of Low Dose CT Attenuation Correction in the Incidence of Ischemia During Myocardial Perfusion Scintigraphy

T. Pipikos1, F. Vlachou1, A. Nikaki1, L. Koletti1, K. Gogos2, K. Dalianis2, V. Prassopoulos1; 1Nuclear Medicine Department Hygeia SA, Athens, Marousi, GREECE, 2Medical Physics Department ,Hygeia S.A., Athens, Marousi, GREECE.

AIM: Attenuation artifacts can lead to false diagnosis during the interpretation of myocardial perfusion studies. These artifacts can be corrected with the usage of SPECT/low dose CT γ-camera systems. In this study we evaluated the effect of low dose CT based attenuation correction (with the usage of flat panel x-ray source) in the performance of myocardial perfusion scintigraphy in the investigation of myocardial ischemia.Material and methods: We compared the findings of attenuation corrected and non attenuation corrected images of 93 patients who underwent myocardial perfusion scintigraphy in our department in the last 2 years and also underwent coronary angiography. Scintigraphy results of ischemia were evaluated as true positive in the patient group with coronary stenosis over 70%, while in patients with less severe stenosis, ischemia findings were evaluated as false positive. Imaging was performed with a Philips Brightview XCT γ-camera system. Interpretation of the studies was blinded between corrected and non-corrected images, as well as between scntigraphy and angiography.RESULTS: Twenty-six (26) patients had stenosis over 70% in coronary angiography. Both methods identified correctly 24/26 cases. In the group of 67 patients without severe coronary stenosis, there were 25 false positive for ischemia non attenuated scans, while with attenuation correction only 9 false positive scans were found. Sensitivity and specificity for non-attenuated images were respectively: 92% and 62%. For low dose CT attenuated images the values were: 92% and 86%. Sensitivity was high for both series of images, but diagnosis was more specific with attenuation corrected images. False positive findings of ischemia were found mainly in the inferior and inferior lateral wall, being much less in number in the corrected images.CONCLUSION: Attenuation corrected images using

low dose CT, improves the performance of myocardial perfusion scintigraphy, with less false positive findings. Diagnosis is more accurate and confident, which can lead to reduction of unnecessary cardiac catheterizations.

P366

Regadenoson safety and tolerability in myocardial perfusion imaging

M. Catalano, G. Annunziata, A. Sasso, R. Gottilla, D. Scala, V. Ippolito, I. Valenti; AORN, Naples, ITALY.

Aim: Myocardial perfusion imaging (MPI) is a widely used imaging technique for coronary artery disease diagnosis and post-revascularization follow-up. Pharmacological stress agents are used in patients (pts) unable to adequate exercise stress because of physical limitations or left bundle branch block (LBBB) at basal ECG, but the use is limited in pts with chronic obstructive pulmonary disease (COPD) or chronic kidney disease (CKD). In these pts, Regadenoson, a A2A selective coronary vasodilator, could be alternative to adenosine or dipyridamole because of greater A2A receptor affinity and lower adenosine receptor subtypes affinity with lower bronchoconstriction risk in pts with reactive airways. This study investigates regadenoson safety and tolerability in pts with COPD or CKD. Material and methods: 20 Pts, over 18 years of age (average age 70.5 ± 8.2; 80% male) affected with COPD and/or CKD, without COPD exacerbation in the last 30 days, were enrolled. Informed consent was obtained from pts. No corticosteroids, steroid combination, long-acting beta2 agonist or anticholinergic were admnistred before test. Subjects had to abstain from taking drugs, foods and beverages containing methylxanthine or theophylline within 12 hours prior MPI. Subjects received regadenoson intravenous bolus (0.4 mg/5 ml) in 10 seconds, followed by 0.9% saline 5 ml flush and 99mTc-tetrofosmin 600 MBQ . Blood pressure (BP) and ECG were monitored before test beginning, after 2 minutes and many times until BP and ECG returned to baseline. Pts were asked to report adverse symptoms or discomfort. Results: 14/20 pts were affected with COPD and the remaining with CDK. Risk factors were diabetes (10 pts), hypertension (18 pts) and cigarettes smoking (10 pts) ; many pts had more than one risk factor. A rapid increase in heart rate, about 2 minutes after regadenoson administration, that returned to baseline within 4 minutes, was observed. BP values decreased in 10 pts, remained unchanged in 4 pts and slightly increased in 6 pts. Adverse reactions were mild, transient (usually resolving within 20 minutes after the beginning of the pharmacological test), and required no medical intervention, except 2 pts that required theophylline (250mg e.v.). Adverse events were mild tachypnea (8 pts), flushing (6 pts), dry mouth (6 pts), headache (2 pts), chest pain (2 pts). Conclusions: Regadenoson is well tolerated because of low incidence of adverse events and can be safety performed in pts with COPD or CKD because of limited adverse events due to low adenosine receptor subtypes affinity.

P367

Adenosine stress Myocardial Perfusion Scintigraphy and Adenosine stress echocardiography in post arterial switch operation patients: A mid-term follow up.

K. Kumar, S. G. Roy, C. D. Patel, S. Ramakrishnan, R. Kumar, A. K. Bisoi; All India Institute of Medical Sciences, New delhi, INDIA.

Aim: To assess myocardial perfusion abnormalities by adenosine Tc99m Sestamibi (MIBI) SPECT and coronary flow reserve (CFR) by adenosine stress echocardiography in patients post arterial switch operation (ASO). Materials and Methods: In this single centre study we evaluated 14 male asymptomatic children, (mean age: 6.64+1.32 yrs, range: 5-9yrs) post ASO. All children's were operated at mean age of 81.7±114.9days (range 16-365 days). Stress echocardiography was performed during continuous intravenous adenosine infusion (140ug/kg/min) over 4 minute. In the same sitting, Tc99m MIBI (0.2mCi/kg body weight) was injected at the end of 2 minute of infusion. Coronary diastolic flow was measured in proximal Left anterior descending artery (LAD) in both resting and stress condition. CFR was calculated as the ratio of peak hyperaemic and basal mean diastolic velocities. Stress myocardial perfusion imaging (MPI) was performed 30-45 minutes after radiotracer injection. Rest images were acquired 2-3 hours after the stress images. Results:The average increase in heart rate over the basal heart rate after adenosine stress was 59.7 ± 17.0%. Adenosine infusion was terminated prematurely in two patients due to bradycardia and Atrioventricular block. Ejection fraction increased after adenosine infusion in all patients and no regional wall motion abnormality appeared during the stress. Mean coronary diastolic velocity increased to 66.2 ±18.8 cm/sec during stress from 39.9±15.6cm/sec under resting condition. Mean CFR in proximal LAD was 1.78±0.46. None of the patients demonstrated myocardial perfusion defects on Tc99m MIBI myocardial perfusion SPECT, either at rest or after adenosine stress. Conclusion: In this ongoing study of asymptomatic post ASO patients, no perfusion abnormalities were detected on Tc99m-MIBI Myocardial Perfusion Scintigraphy (MPS) and all the patients demonstrated good CFR and normal contractile reserve on echocardiography, indicating adequacy of corrective surgery and good mid-term prognosis in this group of patients.

P368

Calculation of left ventricular ejection fraction using cardiac gated parametric blood volume images from a dynamic 15O-water PET/CT scan

J. Nordström, T. Kero, C. Widström, J. Sörensen, M. Lubberink; Department of Surgical Sciences, Radiology, Uppsala, SWEDEN.

BackgroundDynamic 15O-water PET scans are considered the gold standard for myocardial blood flow measurements. However, due to the low contrast between the myocardium and the blood, calculation of left ventricular ejection (LVEF) fraction is not possible from static uptake images. If LVEF is of interest the patient has to undergo an additional PET scan with another tracer or an examination with another modality. Therefore, the aim of this study was to investigate the possibility of LVEF calculations from a single dynamic 15O-water PET/CT scan using cardiac-gated parametric blood pool images.MethodsEleven patients underwent dynamic cardiac-gated 15O-water and static cardiac-gated 11C-acetate PET/CT scans. Eight patients also underwent a cardiac MRI scan. 15O-water parametric blood pool images for each gate were constructed using a basis function implementation of the single tissue compartment model with corrections for spill-over and perfusable tissue fraction. Arterial input functions were defined on non-gated data using cluster analysis in Cardiac VUer software. LVEF from 15O-water was calculated using Cedar Sinais Blood Pool Gated SPECT application with automatic segmentation using surface, count and volume based methods. LVEF calculations from 11C-acetate-PET were performed using the Myovation application for automatic segmentation and LVEF calculations from MRI were performed using ViewForum. All LVEF calculations were performed by an experienced nuclear medicine physician. Correlation between LVEF based on 15O-water with values based on 11C-acetate and MRI were assessed using the correlation coefficient (R2) and intraclass correlation (ICC).ResultsCorrelations (R2) between LVEF for the surface, counts and volume based methods between 15O-water and 11C-acetate were 0.84, 0.91 and 0.86, respectively. R2 for the three different methods between 15O-water and MRI were 0.42, 0.61 and 0.61, respectively. ICC between LVEF based on 15O-water and 11C-acetate were 0.91, 0.94 and 0.91, and ICC between 15O-water and MRI were 0.64, 0.77 and 0.73, respectively for the three different methods. The lower R2 and ICC relative to MRI values are partly explained by the smaller range of LVEF values in the eight patients that underwent MRI (53-75) compared to the whole patient group (35-75).ConclusionThe good correlation between 15O-water-based LVEF values and more established methods shown in the present study points towards a possibility to calculate the LVEF from a single dynamic-gated 15O-water PET/CT scan. However, the method does require some hands-on work by the physician and further work is needed to make the method feasible for clinical use on daily basis.

P369

Perfusion Vector - A New Method to Quantify Myocardial Perfusion Scintigraphy Images

M. Senneby1, D. Minarik2, P. Wollmer1, L. Edenbrandt1, K. Sjöstrand3, E. Trägårdh1; 1Clinical Physiology and Nuclear Medicine, Skåne University Hospital, Lund University, Malmö, Sweden, Malmö, SWEDEN, 2Radiation Physics, Skåne University Hospital, Lund University, Malmö, Sweden, Malmö, SWEDEN, 3Informatics and Mathematical Modelling, Technical University of Denmark, Copenhagen, Denmark, Malmö, SWEDEN.

Aim: Myocardial perfusion scintigraphy (MPS) is an established imaging modality used for the diagnosis of patients with ischemic heart disease. Software packages for quantification of perfusion data and computer-aided diagnosis systems have been developed in order to make the interpretation of MPS studies more standardized but still it largely relies on visual assessment by the physician. We have previously introduced the concept of the perfusion vector as a new objective quantitative method for further assisting the visual interpretation and tested this concept using simulated images with promising results. The aim of this study was to test the concept in patient studies. Materials and methods: The perfusion vector is based on calculating the difference between the anatomical centroid and the perfusion center of gravity of the left ventricle. The centroid is the geometric center of gravity in a three-dimensional figure. The anatomical centroid of the left ventricle is calculated from MPS images setting the voxels in the myocardium of the left ventricle to 1 and the others to 0. The perfusion center of gravity is calculated by giving the voxels in the left ventricle weights corresponding to their intensity. If the perfusion in the left ventricle is homogeneous these positions will coincide. If not the perfusion center of gravity will deviate from the anatomical centroid thus creating a perfusion vector between these two positions. The size of this vector would then correspond to the severity and extent of the perfusion defect and the direction would reflect the location of the defect. 40 normal and 80 abnormal patient studies were included in the patient study. Perfusion vectors were compared between normal and abnormal (apical, inferior, anterior and lateral ischemia or infarction) studies and also correlated to defect size. Results: When comparing normal and abnormal patients there was a statistically significant difference for the stress perfusion vector on the x-axis (septal-lateral direction) for apical and lateral defects, on the y-axis

(anterior-inferior direction) for apical, inferior and lateral defects, and on the z-axis (basal-apical direction) for apical, anterior and lateral defects. A significant difference was shown for the difference vector magnitude (stress/rest) between normal and ischemic patients (p=0.001). The correlation between defect size and stress vector magnitude was also found to be significant (p<0.001). Conclusion: The concept of the perfusion vector is shown to have potential in assisting the visual interpretation in patient MPS studies. Further studies are needed to validate the concept.

P370

Is Data-Driven Cardiac Gating Possible with REGAT Software Applied to SPECT Myocardial Perfusion Imaging Acquired with Discovery NM 530c?

D. Daou1,2, R. Sabbah3, H. Bouladhour3, C. Coaguila4; 1Cochin Hospital, APHP, Paris, FRANCE, 2EA 7334 REMES, Université Paris-Diderot, Sorbonne Paris-Cité, Paris, AUSTRIA, 3CHU Jean Minjoz, Besançon, FRANCE, 4Centre Hospitalier de Bigorre, Tarbes, FRANCE.

Aim: We previously developed a data-driven respiratory-motion (RM) correction method for conventional SPECT gamma-cameras (REGAT) and adapted it to CZT multi-pinhole detector gamma camera (Discovery NM 530c). We recently reported that RM correction with REGAT applied to CZT myocardial perfusion SPECT imaging (MPI, Discovery NM 530c), is clinically feasible, easily applicable, presents interesting impact on image characteristics, and impacts substantially myocardial perfusion defects. In this preliminary evaluation, we aimed to study whether REGAT applied to MPI (Discovery NM 530c) is capable of generating a data-driven (DD) cardiac gating signal allowing the generation of valid global left ventricular (LV) function parameters (EDV: end diastolic volume; ESV: end systolic volume; EF: ejection fraction). Materials and Methods: Were included 7 patients addressed for stress/rest MPI. All patients had prone stress MPI (2 MBq/Kg 99mTc-Tetrofosmin) than prone rest MPI 3-hours later (6 MBq/Kg). All acquisitions were made on Discovery NM 530c. Each list mode acquisition was processed with REGAT to generate a dynamic SPECT acquisition study of 50 msec duration. Each dynamic SPECT study was processed to generate its corresponding DD cardiac gating signal. This DD cardiac signal curve was used to generate a mean DD cardiac GSPECT study (GSPECT-DD). In parallel, a mean ECG cardiac GSPECT study was generated using the ECG trigger signal provided by traditional ECG monitor (GSPECT-M). The 2 generated cardiac GSPECT studies were reconstructed on Xeleris workstation and processed with Emory Cardiac Toolbox (ECT). LV EDV, ESV and EF were compared between cardiac GSPECT-DD and GSPECT-M. Results: The population consisted of 5 males and 2 females with a mean age of 52±11 years. Mean body weight was 72 ±12 Kg and mean height was 1.73±0.66 m2. Stress LV EDV, ESV, and EF were 91±24 ml, 29±13 ml, and 68±10% vs 95 ±23 ml, 29±12 ml, and 70±11% with GSPECT-DD vs GSPECT-M respectively (all P: NS). Mean±SD stress heart rate was 84±16 bpm vs 84±16 bpm for GSPECT-DD vs GSPECT-M respectively. Rest LV EDV, ESV, and EF were 97±21 ml, 32±10 ml, and 67±6% vs 101±21 ml, 31±10 ml, and 69±6% with GSPECT-DD vs GSPECT-M respectively (all P: NS). Mean±SD rest heart rate was 74±16 bpm vs 74 ±16 bpm for GSPECT-DD vs GSPECT-M respectively. Conclusion: Data-driven cardiac gating of MPI with Discovery NM 530c processed with REGAT appears to be clinically feasible. It provides LV global systolic function parameters similar to those provided by the traditional clinically used ECG monitor gating.

P371

Tetrofosmin-Tc-99m Right Ventricular to Left Ventricular Uptake Ratio as a New Surrogate Marker of Subclinical Pulmonary Arterial Hypertension in Rheumatoid Arthritis

T. S. Vieira, M. Bernardes, E. Martins, V. Alves, A. Sá Pinto, A. Fernandes, A. Oliveira, T. Faria, M. Perez, J. G. Pereira; Centro Hospitalar de São João, Porto, PORTUGAL.

Aim: Cardiovascular diseases are a leading cause of death in patients with rheumatoid arthritis (RA). Pulmonary arterial hypertension (PAH) associated with rheumatic diseases carries a particularly grim prognosis, which may be explained by an underlying inflammatory component. New noninvasive parameters would be helpful to assess early subclinical PAH and direct therapeutic efforts. It was recently published that right ventricular to left ventricular uptake ratio (RV/LV) from SPECT myocardial perfusion images of an unselected population can identify patients with high pulmonary artery pressure or right ventricular hypertrophy; however that study included patients with abnormal ejection fraction. We aimed to study the usefulness of RV/LV as a new marker of subclinical PAH in a RA population with normal LV perfusion and function.Materials and Methods:Clinical caracteristics and blood samples were collected in a monitoring visit. Portuguese version of the Standford Health Assessment Questionnaire (HAQ), Disease Activity Scores (DAS28-CRP(3v), DAS28-CRP(4v), DAS28-SR(3v) and DAS28-SR(4v)), 68 tender and 66 swollen joint counts were obtained. They also performed a tetrofosmin-Tc-99m gated myocardial perfusion SPECT with adenosine. All patients had normal SPECT LV perfusion and ejection fraction. For RV/LV calculation an investigator with no knowledge of the clinical and analytical data placed 6×6

pixel ROIs in the RV and LV free walls of a mid-ventricular short-axis SPECT slice. RV/LV was calculated as the ratio of myocardial counts in each ROI. A Spearman's analysis was conducted to study the correlations of RV/LV with clinical and analytical parameters of the disease.Results and Conclusion:We evaluated 84 RA patients, 66 (79%) women, 44 (52%) under biologics, age 54±12 years, 13±10 years of disease duration, mean BMI of 26.30±4.72kg/m2, mean DAS28-CRP(4v) of 3.84±1.34 and a mean HAQ of 1.307 ±0.689. There were significant positive correlations of RV/LV with DAS28-CRP(4v) (r=0.231; p<0,05), 68 tender joint count (r=0.279; p=0,01), and patient global disease activity assessment (r=0.221; p<0,05). In a multivariate modelling (after adjusting for age, age at diagnosis, BMI, DAS28-CRP(4v), glycemia and homocystinemia), patients under methotrexate, leflunomide, bisphosphonates and folic acid supplements had lower values of RV/LV, while patients under biologic agents and NSAIDs had higher RV/LV values. Further, patients under CCB revealed higher values of RV/LV, whereas patients under diuretics, ACEIs, ARAII and BB revealed lower RV/LV values. RV/LV from tetrofosmin-Tc-99m myocardial perfusion SPECT is related with inflammatory disease activity and may be an useful new early marker of subclinical PAH in RA.

P372

Does MPI with CZT cardiac gamma camera show significant abnormalities in presence of intermediately stenosed coronaries with normal adenosine/regadenoson FFR - preliminary results

S. Piszczek, K. Tkaczewski, A. Mazurek, S. Osiecki, M. Dziuk; Military Institute of Medicine, Warsaw, Szaserów Street 128, POLAND.

Aim: Hemodynamic evaluation of intermediate stenoses in coronary arteries has recently become substantial in order to provide invasive treatment. Fractional flow reserve (FFR) assessment plays essential role in making decision of percutaneous coronary intervention. The aim of the study was to investigate, whether there are any significant perfusion abnormalities in left ventricle supplied by intermediately stenosed artery with adenosine/regadenoson FFR >0.75 regarded as normal.Materials and Methods: From the first 10 patients (median age 67) with intermediate (40-70%) stenoses in coronary angiography, normal left ventricular ejection fraction (LVEF) and adenosine/regadenoson normal FFR, seven subjects with supine and prone diagnostic MPI were analyzed. Patients with normal FFR but left bundle branch block and ventricular pacing were initially excluded. FFR was measured during adenosine infusion (140μg/kg/min) and after normalization of hemodynamic conditions, another measurement with regadenoson bolus (400 μg per patient) was done. No later than 2 months after hemodynamic assessment myocardial perfusion imaging (MPI) on CZT gamma camera was performed with two day exercise stress/rest protocol (rest imaging was performed when stress study was abnormal). Each study was estimated by two independent interpreters experienced in nuclear cardiology. Perfusion and LV motion were also assessed semiquantitatively on 20-segment polar maps in the segments corresponding with regions supplied by stenosed coronaries (the basal anteroseptal and inferoseptal segments were excluded from analysis). Perfusion abnormalities were considered true when observed in supine and prone MPI.ResultsThere was no significant perfusion abnormalities in the regions of interest (5 patients - normal perfusion in visual analysis, 2 patients - mild reversible perfusion abnormalities). Additional semiquantitative perfusion evaluation of segments corresponding with regions supplied by intermediately stenosed arteries was performed, leading to similar findings. No significant LV functional abnormalities were detected in these patients (the mean LVEF 64%, no contractility dysfunction). Intermediate stenoses were detected in left anterior descending artery in 5 patients, one stenosis in circumflex artery and one in right coronary artery.ConclusionIntermediate stenoses in coronary arteries with adenosine/regadenoson FFR >0.75 produce no significant perfusion abnormalities (defined as reversible perfusion defect greater than 10% of LV myocardium) were observed. Further studies should elucidate whether CZT MPI may serve as the surrogate for the FFR measurements.

P373

Cardiac 13N-Ammonia PET in Left Ventricular Systolic Dysfunction without Obstructive Coronary Artery Disease

A. Monroy-Gonzalez1, L. Juarez-Orozco1, E. Berrios-Barcenas2, E. Flores-Gonzalez2, R. Cruz-Mendoza2, R. Tio1, R. Slart1,3, R. Dierckx1, E. Alexanderson2,4; 1University Medical Center Groningen, Groningen, NETHERLANDS, 2Instituto Nacional de Cardiologia "Ignacio Chavez", Mexico City, MEXICO, 3University of Twente, Enschede, NETHERLANDS, 4Unidad PET/CT UNAM, Mexico City, MEXICO.

BACKGROUND: Left ventricular systolic dysfunction (LVSD) is generally divided into ischemic and non-ischemic etiology. In non-ischemic LVSD an abnormal perfusion is the result of territories with histological/dynamic changes such as myocardial fibrosis and/or abnormalities of myocardial blood flow (MBF) in the absence of obstructive coronary artery disease (CAD). Moreover, impairment of MBF in patients with LVSD is associated with an increased risk of mayor adverse cardiovascular events (MACE). The aim of this study was to analyze the role of 13N-Ammonia PET in patients with LVSD

and no obstructive CAD.METHODS: We included 124 patients without obstructive CAD, ruled out by Coronary Computed Tomography Angiography (CCTA) who underwent PET with 13N-ammonia during rest and pharmacological stress with adenosine. Detection of LVSD was performed by gated 13N-Ammonia PET. We compared the quantitative and semi-quantitative assessment of 13N-Ammonia PET among patients with LVEF <50% and preserved LVEF.RESULTS: 11 patients with LVSD (mean LVEF 40% ± 9%) and 114 with preserved LVEF (mean LVEF 69% ± 7%) composed our population. Mean age was 62 ± 11 years, 53% were male, 72% hypertensive, 16% diabetic, 64% dyslipidemic, 49% presented angina, and median BMI was 27 ± 4 kg/m2. Median SSS was 2 (min: 0, max: 27) and median SDS was 0 (min: -6, max: 22). There were no statistically significant differences in these characteristics among groups. We also did not find a static significant difference in rest MBF or myocardial flow reserve; however, hyperemic MBF was lower in patients with LVSD compared to those with normal LVEF (1.8 ± 0.6 vs. 2.3 ± 0.6 ml/g/min respectively; p=0.02). Furthermore, patients with LVSD presented an increased total perfusion deficit (TPD) when compared to those with normal LVEF, both in rest (8% [min: 6%, max: 53%] vs. 4% [min: 0%, max: 53%] respectively; p<0.001) and in stress (7% [min: 0%, max: 51%] vs. 1% [min: 0%, max: 33%] respectively; p=0.002).CONCLUSIONS: In patients with systolic dysfunction without obstructive CAD we found that hyperemic MBF was diminished and TPD was increased when measured by 13N-Ammonia PET, our results may be related to the ventricular remodeling and adaptation seen in this group of patients. We believe that hybrid imaging with 13N-Ammonia PET and CCTA represents a useful tool for the assessment of patients with LVSD as it can rule out the existence of obstructive CAD and objectify the presence and degree of microvascular or endothelial dysfunction.

P374

Long-term Follow-up in Hypertensive Patients With Normal Stress Myocardial Perfusion Imaging: a Parametric Analysis

C. Nappi1, E. Zampella1, R. Assante1, R. Green1, N. Frega1, D. D'Arienzo1, G. De Matteis1, S. Daniele2, W. Acampa2, M. Petretta3, A. Cuocolo1; 1Department of Advanced Biomedical Sciences, University of Naples Federico II, Naples, ITALY, 2Institute of Biostructure and Bioimaging, National Council of Research, Naples, ITALY, 3Department of Translational Medical Sciences, University of Naples 'Federico II', Naples, ITALY.

Aim: We assessed the relationship between arterial hypertension and temporal characteristics of cardiac risk at long-term follow-up in hypertensive patients with a normal stress myocardial perfusion single-photon emission computed tomography (MPS). Materials and Methods: We evaluated 471 consecutive hypertensive patients without known coronary artery disease (CAD) and normal perfusion at stress MPS. All patients were followed for a mean 76±21 months. End-point events were cardiac death or nonfatal myocardial infarction. The univariable and multivariable associations with cardiac events were determined by Cox proportional hazards regression analysis. A parametric survival model was used to identify how the variables influenced time to event and to estimate the risk-adjusted event rates during the follow-up. Results: Of the overall population, 299 (63%) patients underwent exercise stress test and 172 (37%) patients pharmacologic stress test with dipyridamole. At Cox analysis, age (hazard ratio 1.1, P<0.005) and stress test type (hazard ratio 2.7, P<0.005) were independent predictors of cardiac events. In patients undergoing exercise stress test, peak systolic arterial pressure (PAS) (hazard ratio 1.1, P<0.005) resulted as predictor of cardiac events. At parametric analysis, patients <60 years old who performed exercise stress test remained at low risk for the entire length of follow-up, while the highest probability of events and the major risk acceleration was observed in patients >60 years old who underwent pharmacologic stress test. In the 299 patients undergoing exercise stress test, only those who reached PAS <160 mmHg remained at low risk for the entire length of follow-up. In contrast, time to achieve a cumulative cardiac risk level of 3% was 49 months in the presence of PAS 160-180 mmHg, 35 months for PAS 180-200 and only 10 months for PAS >200 mmHg. Conclusions. In hypertensive patients without known CAD, a normal stress MPS should be considered reassuring in subjects <60 years old who performed exercise stress test and in those who reached a peak PAS <160 mmHg independently on age. On the other hand, patients who underwent exercise stress test and reached peak PAS >200 and those submitted to pharmacologic stress test should be considered for a more aggressive management.

P375

Evaluation of myocardial blood flow in patients with myocardial bridging: A 13N-ammonia PET study

A. Monroy-Gonzalez1, L. Juarez-Orozco1, E. Berrios-Barcenas2, C. Gonzalez-Padilla2, M. Martinez-Aguilar2, G. Guinto-Nishimura2, R. Dierckx1, R. Tio1, R. H. J. A. Slart1, 3, E. Alexanderson2,4; 1University Medical Center Groningen, Groningen, NETHERLANDS, 2National Institute of Cardiology, Mexico City, MEXICO, 3University of Twente, Enschede, NETHERLANDS, 4Unidad PET/CT UNAM, Mexico City, MEXICO.

BACKGROUND: Myocardial bridging (MB) is a coronary abnormality seen in up to 16% of invasive coronary angiographies. Although it is generally considered a benign condition, it has

been suggested MB can be associated to angina, arrhythmias, myocardial infarction and sudden cardiac death. Positron emission tomography with coronary computed tomography angiography (PET/CCTA) provides the reference standard for quantification of myocardial blood flow (MBF) and myocardial perfusion reserve (MPR) as well as anatomical information of the coronary artery tree. The aim of this study was to detect quantitative and semi-quantitative myocardial perfusion defects (MPD) by 13N-ammonia/PET in patients with MB. METHODS: We retrospectively included 17 patients with MB in the left anterior descending artery (LAD) and 51 controls patients without coronary artery disease who underwent hybrid PET/CCTA with 13N-ammonia during rest and adenosine stress for suspected ischemic heart disease. Semi-quantitative MPD, stress MBF, and MFR were analyzed in the vascular territory of the MB. Normal, mildly abnormal, moderately abnormal, and severely abnormal perfusion was considered if Summed Stress Score was <2, 2-3, 4-8, or >8 respectively. Normal LAD regional stress MBF and coronary flow reserve (MFR) were considered as ≥ 2.3 ml/gr/min, and ≥ 2.5 ml/gr/min values respectively. RESULTS: In our population, mean age was 62 ± 9 years, 31% were male, 65% hypertensive, 17% diabetic, 59% dyslipidemic, and 38% reported active smoking. Mean stress MBF in the LAD was 2.3 ml/g/min ± 0.8 and mean MFR in the LAD was 2.7 ml/g/min ± 1.0. We did not find a statistically significant difference among groups. However, we found an increased proportion of reduced MFR in the LAD in the presence of a MB compared to controls 53% (n=9) vs. 39% (n=20) showing a trend towards significance (p=0.054), furthermore, we found a statistically significant increase in mild reversible MPD in the territory of the LAD in the presence of a MB against controls 29% (n=5) vs. 6% (n=3) respectively, p=0.02. CONCLUSION: In this restricted population, we found an increased frequency in mild reversible MPD and a decreased MFR in patients with MB, our findings suggest that coronary vasodilator capacity impairment might be present in MB. Our results support the role of PET/CCTA in the assessment of MB as it could guide the decision-making in this scenario; nevertheless, further studies are needed to fully understand the hemodynamic impact of MB.

P22 - Monday, October 12, 2015, 4:00 PM - 4:30 PM, Hall 3 – Poster Exhibition

Cardiovascular System: Clinical Science - Plaque and Vascular Imaging

P376

Prognostic value of cardiac gated SPECT combined with coronary calcium score in patients with end-stage kidney disease

M. Kaminek1,2, M. Havel1, I. Metelkova1, M. Budikova1, L. Henzlova1, P. Koranda1, J. Zadrazil1, V. Kincl2; 1Faculty of Medicine and Dentistry, Palacky University Olomouc and University Hospital Olomouc, Olomouc, CZECH REPUBLIC, 2International Clinical Research Center, Center of Molecular Imaging, St. Anne's University Hospital, Masaryk University, Brno, CZECH REPUBLIC.

Introduction: The cardiovascular diseases are the main cause of morbidity and mortality in patients with end-stage renal disease (ESRD). Coronary artery disease (CAD) is highly prevalent in this setting, owing to clustering of traditional and uremic-specific risk factors. Asymptomatic course is common. In the current study, we assess the impact of the myocardial perfusion imaging (MPI) by gated-SPECT and added value of coronary artery calcium (CAC) score measurement for the risk stratification in ESRD patients. Materials and methods: We examined 84 ESRD subjects by gated-SPECT MPI, 69 of them underwent CAC score measurement by multi-detector computed tomography (MDCT) system. CAC scores were stratified into two groups, CAC score ≥ 1000 and < 1000. During the median follow-up period of 33 months the cardiac events (CE) defined as cardiac death or nonfatal MI or the necessity of coronary revascularization were recorded. Results: We encountered 17 CE during the follow-up, which were associated with significantly higher summed stress scores on MPI, higher percentage of ischaemic myocardium, higher occurrence of defects in multiple territories and higher CAC scores ($P = 0.0001$, $P = 0.0014$, $P < 0.0001$, $P = 0.0045$ respectively). Functional parameters as left ventricular ejection fraction and volumes did not show significant impact. CE were more frequent in subjects with severe or mild perfusion abnormality, in comparison with patients with normal perfusion findings on SPECT ($P = 0.0030$, $P < 0.0001$). There were 4 subjects with normal perfusion SPECT and encountered CE, 3 of them had CAC score values ≥ 1000 ($P = 0.0408$). There was no any CE in patients with normal perfusion, function and zero CAC score. Conclusion: Combined perfusion, function and CAC score evaluation can help to identify ESRD patients in high-risk for CAD. CAC score brings added value for future CE prediction in subjects with normal perfusion patterns.

P377

The index of the maximum accumulation 99mTc-DPD in the myocardium of patients with transthyretin (TTR) cardiac amyloidosis and of older people without known heart disease

M. Buncová, A. Čepa, M. Kubánek, A. Krebsová; Institute for Clinical and Experimental Medicine, Prague, CZECH REPUBLIC.

Aim: evaluation and comparison by using a custom quantitative index (Mc) of the local maximum accumulation of

99mTc-DPD in the myocardium in patients with TTR cardiac amyloidosis and in control group of persons over the age of 70 years without known heart disease, assessment depending Mc on the age and gender too. Materials and Methods: 3,3-diphosphono-1,2-propanedicarboxylic acid (DPD, TECEOS®, CIS Bio International, France) is kit for prepare of radiopharmaceutical which standard used for bone scintigraphy, where it delineates areas of altered osteogenesis. 99mTc-DPD was preparedby instruction for preparation of radiopharmaceuticals from SPC. In this study 1 woman and 4 men with confirmed TTR cardiac amyloidosis and the control group of 41 women and 36 men over 70 years of age, without known heart disease, in which at the same time 99mTc-DPD scintigraphy ruled out bone metastasis, were tested. For about 3-5 hours after application 99mTc-DPD (740 MBq) was done SPECT/CT of the chest. A quantitative index of local maximum accumulation 99mTc-DPD in the myocardium (Mc) consisted in the determination of the ratio of the highest count/voxel in the area of heart to the reference count density. The reference count density is the average value, calculated from the highest count/voxel values established on the 2-8. The ribs on the right side of the chest in the coronary plane identical to the localization of max. count/voxel in the myocardium. Results: the value Mc of the patients with TTR cardiac amyloidosis was 6.11-8.71 (7.17/-1.11) IE. significantly higher than in the control group, where Mc 0.81/-0.35. For women without TTR cardiac amyloidosis Mc was insignificantly higher than in men. This is because the lower the accumulation 99mTc-DPD in the bones, but also the ascendent trend of the accumulation 99mTc-DPD in myocardium in women. The dependency Mc has been not evident on the age for persons over 70 years. Conclusion: Mc may contribute to the detection, identification, determination of the degree of disability of the myocardium and development of TTR cardiac amyloidosis.

P378

The prognostic value of baseline 18F-FDG PET/CT in steroid-naïve large-vessel vasculitis: introduction of volume-based parameters

L. Dellavedova, L. S. Maffioli; AO Ospedale Civile di Legnano, Legnano, ITALY.

Aim: To analyze if a baseline 18F-FDG PET/CT scan, in large-vessel vasculitis (LVV) patients, is able to predict the course of the disease, not only in terms of presence/absence of final complications but also in terms of favourable/complicated progress (response to steroid therapy, time to steroid suspension, relapses, ⋯).Materials and Methods: 46 consecutive patients, undergone 18F-FDG PET/CT between May 2010 and March 2013 for FUO or suspected vasculitis (before starting corticosteroid therapy), were enrolled. The diagnosis of LVV was confirmed in 17 patients by temporal artery biopsy, other imaging techniques and a follow-up of at least 2 years. Considering follow-up data, positive LVV patients (17 out of 46) were divided in two groups, one characterized by favourable (9) and the other by complicated progress (8), on the basis of presence/absence of stenotic-occlusive complications, presence/absence of at least another positive PET/CT during follow-up and impossibility to comply with the tapering-schedule of the steroid, due to biochemical/symptomatic relapse. Vessel FDG uptake in subjects of the two groups was compared, not only in terms of intensity (SUVmax of the vessel wall and Vessel-to-Liver ratio) but also of extension. To evaluate the extent of active disease, we introduced the volume-based parameters metabolic "tumor" volume (MTV) and total lesion glycolysis (TLG). The threshold used to calculate MTV on vessel walls was obtained by Vessel-to-Liver ratio (the semiquantitative parameter with the highest diagnostic accuracy at ROC analysis) and was setted at 0.92 x Liver SUVmax in each patient. With this threshold, a semi-automatic ROI was drawn on thoracic and abdominal aorta, supra-aortic trunks and common iliac vessels to get the values of extension (cm3), of mean SUV and of TLG.Results: Measures of tracer uptake intensity (SUVmax of the vessel wall and Vessel-to-Liver ratio) were significantly higher in patients with complicated progress compared to those with a favourable one ($p < 0.05$). Differences in measures of disease extension were even more significant and TLG emerged as the best parameter to separate the two groups of patients ($p = 0.01$). No statistically significant differences were found in inflammatory markers.Conclusion: In LVV patients, baseline 18F-FDG PET/CT seems to be not only a diagnostic tool. The combined evaluation of the intensity and the extension of vessel involvement can predict the clinical course of the disease, separating patients with favourable or complicated progress: this information could help clinicians in the choice of personalized therapeutic approaches and follow-up planning.

P379

[18F]-FDG PET/CT imaging for detection of the inflammation in the calcified atherosclerotic plaques

D. V. Ryzhkova, D. A. Pavlova; North-Western Fedral Medical Research Centre, St.Petersburg, RUSSIAN FEDERATION.

The aim of the study was to assess how often the inflammation can be identified in calcified atherosclerotic plaque in the patients in the patients of different age. Methods: We retrospectively studied 51 patients who underwent [18F]-FDG PET/CT for detection malignancy. Whole body scan was performed 60 minutes after intravenous administration of

radiopharmaceutical. The average plaque density in Hounsfield units and maximum standardized uptake value (SUVmax) were evaluated in calcified atherosclerotic plaques in aorta. Results: The increase of [18F]-FDG uptake was observed in 95 (43%) from 220 calcified atherosclerotic plaques in aorta, that were titled FDG-positive plaques. The ratio of FDG-positive and FDG-negative calcified plaques was equal for the different parts of aorta: 50% vs 50% for the ascending aorta; 48% vs 53% for the aortic arch; 44% vs 56% for the descending thoracic aorta as well as the abdominal aorta. The all patient were divided into 3 groups in conformity with their age: younger than 40 years (16 pts.), 41-60 years (18 pts.) and older than 60 years (17 pts.). We observed only two calcified plaques (one FDG-positive and one FDG-negative) in the patients younger than 40 years. The patients, who were 40-60 years and older than 60 years had the equal ratio of FDG-positive and FDG-negative calcified plaques (29 (43%) vs 37 (57%) and 65 (43%) vs 86 (57%) respectively). We found a positive correlation between the amount of calcified plaques and patient age (R=7,83; p<00,5). The correlation between SUVmax and plaque density was not obtained. Conclusion: The increase of [18F]-FDG uptake as a marker of inflammation was visualized in 43% of aortic calcified plaques in patients older 40 years. We have not found a correlation between calcification and inflammation of atherosclerotic plaque.

P380

Influence of the peptide receptor radionuclide therapy (PRRT) on the inflammatory activity in atherosclerotic plaques based on the initial 68Ga-DOTA -TATE (DOTA) uptake

M. J. Zacherl1, A. Todica1, G. Rubinstein1, P. Bartenstein1, M. Hacker2, S. Lehner1; 1University of Munich, Munich, GERMANY, 2Medical University of Vienna, Vienna, AUSTRIA.

Aims: Previous studies suggest that PRRT has an anti-inflammatory effect on atherosclerotic plaques. The aim of this study was to investigate the influence of the initial level of DOTA uptake on the inflammatory activity after performing PRRT. Methods: Patients from an oncological cohort, who received 4 cycles of 177Lu-DOTA-TATE therapy (n = 37 , age 59 ± 10 ; 23m, 14f) were retrospectively included in the study. We performed a baseline DOTA PET/CT as well as a follow-up scan after two and four cycles of PRRT. Patients who received a DOTA PET/CT scan three times, but had no therapy with 177Lu-DOTA-TATE (n = 20, age 63 ± 12 ; 9m, 11f), served as control group. In 8 arterial segments (ascending aorta, aortic arch, thoracic aorta, abdominal aorta, right and left common iliac artery, right and left common carotid artery), the "target-to-background-ratio" (TBR) was determined. The "overall vessel uptake" (OVU) was calculated from the sum of all TBRs. Additionally, the calcium score was determined. Results: In the therapy- (TG) and the control group (CG) we found no significant change in OVU (TG : 18.5 ± 6.7 to 18.0 ± 4.1 ; P = n.s.; KG: 19.7 ± 5.7 to 20.2 ± 4.5 ; P = n.s.). Subsequently the patient groups were divided into tertiles. In the tertile with the highest initial OVU we found a decrease in OVU (23.7 ± 7.4 to 18.7 ± 3.8, P < 0.05) after 4 cycles of PRRT. In the tertile with the lowest initial OVU a stable OVU was observed after 4 cycles of PRRT (14.8 ± 1.4 and 16.0 ± 3.0, P = n.s.). There was a significant correlation of age and calcium score (R = 0.592 , P = 0.01) with only a moderate correlation of TBR with calcium score (R = 0.288 , P = 0.05). Conclusion: The reduction of the inflammatory activity by a PRTT is dependent on the initial DOTA uptake in the vascular plaque. Patients with higher inital DOTA uptake show a significant reduction in inflammatory activity after 4 cycles of PRRT. A high calcium load does not necessarily imply a high inflammatory activity.

P381

Feasibilty of Annexin A5 for ex vivo imaging of human fresh and frozen atherosclerotic plaques

S. A. de Boer1, J. van Hoek2,3, D. J. Mulder1, H. J. de Haas2, N. A. Jager4, J. G. W. Kosterink3, C. J. Zeebregts5, C. P. M. Reutelingsperger6, P. H. Elsinga2, R. H. J. A. Slart2,7, **H. H. Boersma**2,3; 1Department of Vascular Medicine, University Medical Center Groningen, University of Groningen, Groningen, NETHERLANDS, 2Department of Nuclear Medicine, University Medical Center Groningen, University of Groningen, Groningen, NETHERLANDS, 3Department of Clinical and Hospital Pharmacy, University Medical Center Groningen, University of Groningen, Groningen, NETHERLANDS, 4Department of Rheumatology and Clinical Immunology, University Medical Center Groningen, University of Groningen, Groningen, NETHERLANDS, 5Division of Vascular Surgery, Department of Surgery, University Medical Center Groningen, University of Groningen, Groningen, NETHERLANDS, 6Department of Biochemistry, University of Maastricht, Maastricht, NETHERLANDS, 7Faculty of Science and Technology, Biomedical Photonic Imaging, University of Twente, Enschede, NETHERLANDS.

Background and aim: In 2004 Kietselaar and others demonstrated the feasibility of technetium-99m-labeled annexin A5 for assessing atherosclerotic plaque instability in a clinical pilot. Annexin A5 is a plasma protein with a strong affinity for phosphatidylserine exposed on apoptotic cells. Since they evaluated only four patients (in vivo) the aim of the current study was to validate the use 99mTc-labelled Annexin A5 in ex vivo fresh and frozen human carotid endarterectomy (CEA)

specimens in order to confirm the results of the previous clinical study. Materials & methods: 15 patients with elective carotid endarterectomy because of significant symptomatic carotid artery stenosis, were included. 8 CEA specimen were used within 2 hours after CEA, and 7 specimen were used after defrosting.All CEA specimen were incubated for one hour with 99mTc-Annexin A5 and scanned with μSPECT for one hour. Tracer uptake was calculated as percentage incubated dose per gram (%inc/g) for the whole CEA specimen. A beam-shaped region of interest (ROI) was drawn around the CEA specimen and the mean and maximum tracer uptake was determined. Around the hotspot a ROI was defined as 70% of the maximum tracer uptake. Anxmax was calculated by dividing the mean tracer uptake in the hotspot by the mean tracer uptake in the whole CEA specimen. Histological immunostaining with anti-annexin was semiquantitatively evaluated. to confirm uptake. Results and conclusion:The mean weight of all CEA specimens was 0,78±0,52 g, for fresh CEA specimen 0,60±0,39 g and for frozen CEA specimen 0,99±0,59 g. In both fresh and frozen CEA specimens, significant 99mTc-Annexin A5 uptake with heterogeneous distribution was seen. The mean %inc/g for all CEA specimens was 2,9±1,6. For the fresh CEA specimens mean %inc/g was 2,9±1,8, and for frozen CEA specimen 2,8 ±1,4. No significant uptake difference in %inc/g between fresh and frozen CEA specimens ($t = 0,11$; $P > 0,05$) was demonstrated. Mean Anxmax of all CEA specimen was 6,8±1,4 for fresh CEA specimen 6,7± 1,6 and for frozen CEA specimen 6,9±1,2. Also for these uptake values, no significant difference was found ($t = -0,232$; $P > 0,05$). A congruent pattern was observed between tracer uptake and histology immunostaining. This study demonstrates that Annexin A5, as a cell death tracer, is a valid method for ex vivo imaging of atherosclerotic plaques in fresh and frozen atherosclerotic CEA specimen.

P382

Quantitative assessment of intermediate stenosis of coronary arteries by single photon emission computed tomography with attenuation correction compared fractional flow reserve

V. Solomyanyy; Russian cardiology research and production complex, Moscow, RUSSIAN FEDERATION.

Aims and objectivesFractional flow reserve (FFR) is currently used to determine the management of intermediate coronary artery stenosis. FFR more 0.80 used in clinical practice to guide revascularization. Advances in nuclear medicine single photon emission computed tomography with attenuation correction (SPECT/CT) require revaluation quantitative parameter noninvasive imaging in compared with FFR in the diagnosis of the functional significance intermediate stenosis coronary arteryMethods and materialsIn this study, 70 patients (mean age 57±5 years, 50 men, and 20 women) with ischemic heart disease and 50% to 70% coronary stenosis (target vessel). All perfusion scans were performed using a camera (BrightView XCT Philips) equipped with a low-energy, high-resolution collimator and with cardiac gating. Antianginal medication was discontinued 48 hours before the study, and patients abstained from caffeine for 24 hours prior to the study protocol one day stress (bicycle test)/rest use with 900 MBq (25 mCi) of technetium 99m-MIBI. Coronaroangiography (CAG), which was defined as angiographic moderate (50-70%), was assessed by quantitative coronary angiography (QCA) and pressure wires received FFRResultsNormal FFR > or =0.8. Summed difference scores (SDS) in the left anterior descending (LDA), right coronary artery (RCA) and ramus circumflexus (RCX) artery territory according to the 17 segment model were calculated with attenuation correction (AC) and no correction (NC). In order to evaluate the sensitivity and specificity used ROC- analysis. NC value SDS > 3 predicts the existence of a reliable, persistent perfusion defects with a sensitivity of 96.4% and a specificity of 84.2%, the images attenuation correction (AC) SDS > 4 (96.7% and 90.1%, respectively)ConclusionMethod of SPECT/CT can be used to determine the hemodynamic significance of intermediate coronary artery stenosis. Quantitative assessment of myocardial perfusion SDS determined at SPECT/CT with attenuation correction is more sensitive and specific for the coronary artery stenosis evaluation

P383

18F-FDG uptake in main arterial branches of patients with large vessel vasculitis: visual and semiquantitative analysis.

M. CASTELLANI1, M. VADRUCCI1, L. FLORIMONTE1, M. CARONNI2, E. ORUNESU1, R. BENTI1; 1FONDAZIONE IRCCS CA'GRANDA OSPEDALE MAGGIORE POLICLINICO Nuclear Medicine Department, MILAN, ITALY, 2FONDAZIONE IRCCS CA'GRANDA OSPEDALE MAGGIORE POLICLINICO Referral Center for Systemic Autoimmune Diseases, MILAN, ITALY.

Purpose: Over the last decade, the contribution of 18F-FDG (FDG) PET/CT imaging to the diagnosis of large vessel vasculitis has been widely investigated. Aim of this study was to evaluate a more extensive role for PET/CT in grading vascular inflammation in patients with different clinical stages of disease.Methods: The images of 66 PET/CT studies of 34 patients, performed at diagnosis and/or during follow-up were reviewed. FDG uptake in different regions of aorta and of its major branches was visually (regional Score: rS) and semiquantitatively (regional SUVmean: rSUV) assessed. The

global vascular uptake was also evaluated for each study by summing all rSs (summed Score; sS) and averaging rSUVs (averaged SUV; aSUV). FDG uptake in 15 PET/CT studies of control age-matched subjects without signs or symptoms of vasculitis was also analyzed.Results: Higher levels of regional and global FDG uptake were found at diagnosis in comparison with follow-up studies ($p<0.01$). In the latter group, the highest values were observed in patients with disease relapse and partial response to therapy whereas a lower uptake was found in patients fully responsive ($p<0.01$), whose FDG levels were similar to those of the control subject group. At ROC analysis, optimal cut-off levels of regional and global FDG vascular uptake provided a good discrimination between patients at diagnosis and control subjects (aSUV greater than 0.6977; PPV=92.3; NPV=92.9). A major overlap was observed between FDG levels of follow-up patients with active disease and remission (aSUV greater than 0.6532; PPV=58.3; NPV=94.1). Slight differences in the performances of visual and semiquantitative analyses were found when the corresponding areas under curves (AUCs) were compared.Conclusion: 18F-FDG PET/CT may detect different grades of inflammation in patients with large arteries vasculitis. Nevertheless, the simple analysis of FDG vascular levels may be not sufficient to separate patients with active and inactive disease.

P384

18F-FDG-PET/CT imaging in Giant Cell Arteritis: Are we still unable to "light up" temporal arteries?

Z. Rehak1, J. Vasina1, J. Ptacek2, P. Nemec3, Z. Fojtik4; 1Masaryk Memorial Cancer Inst., Brno, CZECH REPUBLIC, 2University Hospital, Olomouc, CZECH REPUBLIC, 3St. Anne's University Hospital, Brno, CZECH REPUBLIC, 4University Hospital, Brno, CZECH REPUBLIC.

Introduction: 18F-FDG (FDG)-PET/CT imaging could be useful in patients with fever of unknown origin and could detect giant cell arteritis (GCA) in extracranial large arteries. In the case of temporal arteries, it is usually assumed that they cannot be visualized with a PET/CT scanner due to their small diameter. Aim: We tried to visualize high FDG uptake in temporal arteries in patients with clinical symptoms of temporal arteritis using a hybrid PET/CT scanner in a manner that could improve detection capabilities. Methods: Three patients with clinical signs of temporal arteritis were examined using a standard whole body (WB) PET/CT protocol (skull base-mid thighs) followed by a head PET/CT scan using a brain acquisition protocol. Results: A high FDG uptake in the aorta and main arterial branches in 3/3 pts. was detected with WB PET/CT scan. Furthermore, using the brain protocol, a high FDG uptake was also detected in head arteries - temporal arteries (3/3 pts.), occipital arteries (2/3 pts.) and vertebral arteries (3/3 pts.), and even in branches of temporal arteries (3/3 pts.). All 3 patients underwent excision of temporal artery branches in 10 days after PET/CT examination with positive evidence of GCA and were treated with prednisone. Conclusions: Head imaging with brain acquisition protocol enabled us to visualize metabolically active inflammation in temporal arteries and their branches in all 3 patients with GCA. We succeeded to obtain this result probably by extending acquisition time (brain acquisition protocol) on a scanner with relatively good parameters (small reconstructed pixel size, high sensitivity and good spatial resolution).

P385

Identification of complicated carotid plaques by adding functional FDG-PET imaging to morphological characteristics on CT angiography

N. Mikail1, **F. Hyafil**1, M. Mazighi2, E. Meseguer3, C. Guidoux3, L. Cabrejo3, P. Lavallée3, K. Benali1, F. Rouzet1, D. Le Guludec1, G. Lesèche4, P. Amarenco3; 1Bichat University Hospital, Department of Nuclear Medicine, PARIS, FRANCE, 2Lariboisière University Hospital, Department of Neurology, PARIS, FRANCE, 3Bichat University Hospital, Department of Neurology, PARIS, FRANCE, 4Bichat University Hospital, Department of Vascular Surgery, PARIS, FRANCE.

Aim. Complicated plaques have specific morphological and biological characteristics. Morphological aspects associated with complicated plaques identified with CT angiography (CTA) such as hypodense areas (<30 Hounsfield units) or plaque ulceration lack sensitivity. In this study, we developed a simple semi-quantitative score for the analysis of carotid plaques with FDG-PET-CTA imaging and tested whether adding functional imaging criteria extracted from FDG-PET imaging to morphological plaque characteristics identified with CTA might improve the detection of complicated plaques.Material and methods. Twenty-eight patients scheduled for carotid endarterectomy were first imaged with PET 2 hours after injection 4 MBq/ kg of FDG followed by CTA of the supra-aortic trunks. Morphological aspects of plaques identified with CTA and metabolic activity quantified with FDG-PET (Tissue to Background ratio, TBR) were measured in the region of the operated carotid artery with the highest degree of luminal stenosis and graded using semi-quantitative CT (maximal score = 6) and PET scores (maximal score = 4). A combined score was then calculated for each carotid artery by summing CT and PET scores (maximal score = 10). After carotid endarterectomy, vascular surgeons classified carotid plaques macroscopically as complicated (presence of fresh thrombus, intra-plaque haemorrhage, plaque rupture) or non-

complicated.Results. Twenty-eight carotid arteries were operated in 26 patients (24 symptomatic patients). Sixteen plaques were classified macroscopically as complicated. CTA detected hypodense regions and ulcerations in 81 % and 25 % of complicated plaques, and in 33 % and 0% of non-complicated plaques, respectively. Hypodense areas on CTA identified complicated plaques with a sensitivity of 87 % and a specificity of 67 %. Mean TBR with FDG-PET was measured at 2.2 ± 0.4 in complicated plaques and 1.9 ± 0.3 in non-complicated plaques ($p < 0.05$). Values for the semi-quantitative score based on plaques characteristics with CTA and FDG-PET were 5.4 ± 1.7 in complicated plaques and 2.5 ± 2.4 in non-complicated plaques ($p < 0.05$). A combined PET-CT score ≥ 3 identified complicated plaques with a sensitivity of 100 % and a specificity of 67 %.Conclusions. In this study, we have developed a simple semi-quantitative score for the analysis of combined FDG-PET-CTA imaging of carotid plaques. Adding FDG-PET imaging criteria to morphological characteristics of plaques on CTA improved sensitivity to identify complicated plaques.

P386
[18F]-Sodium Fluoride Uptake in Takayasu Arteritis

E. Alexanderson1,2, **A. Monroy-Gonzalez**3, L. Juarez-Orozco3, R. Tio3, A. W. J. M. Glaudemans3, E. Estrada4, O. Garcia4, A. Meave1, R. H. J. A. Slart3,5, M. E. Soto-Lopez5; 1National Institute of Cardiology, Mexico City, MEXICO, 2Unidad PET/CT UNAM, Mexico City, MEXICO, 3University Medical Center Groningen, Groingen, NETHERLANDS, 4National Institute of Cancer, Mexico City, MEXICO, 5University of Twente, Enschede, NETHERLANDS.

BACKGROUND: Studies have shown the role of Positron Emission Tomography (PET) with 18F-fluorodeoxyglucose (18F-FDG) in diagnosing and monitoring clinical disease activity in vascular structures affected by Takayasu Arteritis (TA). Because inflammation is a serious risk factor for atherosclerosis it is necessary to prevent complications of atherosclerosis in patients with TA. 18F-sodium fluoride (18F-NaF) has already been successfully used to identify high-risk atherosclerotic plaques in patients with increased cardiovascular risk. However, the relationship of 18F-NaF/PET and TA has not yet been studied. The aim of this case series is to describe the 18F-NaF uptake in patients with TA.METHODS: We present 5 patients with confirmed diagnosis of TA by the 1990 American College of Rheumatology Classification Criteria, who were referred to our unit. All patients underwent PET whole body scan with both 18F-FDG and 18F-NaF in order to explore the localizations and correlation of 18F-NaF and 18F-FDG uptake. SUVmax of 18F-FDG (corrected for blood glucose levels) and 18F-NaF uptake along the aorta was obtained. Diagnosis of current metabolic active disease was based on increased 18F-FDG uptake. Mann-Whitney U test was used to compare difference in means of SUVmax among 18F-FDG and 18F-NaF. We performed a Spearman's Rank Order Correlation (rho) to describe the strength and direction of the linear relationship between continuous variables.RESULTS: Our population was composed of 4 female and 1 male patients, median age was 29yr (min: 19, max: 63), and all patients were non-diabetic. Median 18F-NaF SUVmax was 1.1 (min: 0.5, max: 1.5) and median 18F-FDG SUVmax was 2.5 (min: 0.1, max: 2.8); there was no statistical difference between the two tracers (p=0.69). 18F-NaF uptake showed to be increased in the aorta in all of our patients, even in patients without active metabolic disease demonstrated by 18F-FDG. One of our patients without established active disease showed increased uptake of 18F-FDG and 18F-NaF, however, increased uptake of 18F-FDG was attributed to atherosclerosis. Finally, we found a negative correlation between 18F-NaF and 18F-FDG uptake r=-0.87 (p=0.054).CONCLUSIONS: In TA patients it is possible to document active aortic micro-calcification by 18F-NaF, even in the absence of active metabolic disease measured by 18F-FDG or symptoms. We propose that 18F-NaF/PET could be a non-invasive method for the assessment of atherosclerosis and cardiovascular risk stratification in TA patients. These results may allow preventive measures, even in asymptomatic patients; however, further studies are needed to fully understand the role of 18F-NaF in TA.

P23 - Monday, October 12, 2015, 4:00 PM - 4:30 PM, Hall 3 – Poster Exhibition

Cardiovascular System: Imaging Systems

P387
Radionuclide evaluation of cardiac function and dyssynchrony in children with idiopathic ventricular tachycardia

K. W. Zavadovsky1,2, V. Saushkin1, Y. Lishmanov1,2; 1Federal State Budgetary Scientific Institution «Research Institute for Cardiology», Tomsk, RUSSIAN FEDERATION, 2National Research Tomsk Polytechnic University, Tomsk, Russian Federation, Tomsk, RUSSIAN FEDERATION.

Background: The aim of the study was to evaluate the impact of idiopathic ventricular tachycardia and premature ventricular beats on cardiac function and dyssynchrony and to elucidate relationships between data of scintigraphic and intracardiac electrophysiology studies. Methods: The study comprised 64 patients with idiopathic ventricular arrhythmias (VA) (mean age of 13.2 ± 3.14 years). Control group comprised 20 patients (mean age of 13.2 ± 3.6 years) without cardiac arrhythmias.

Electrophysiological study (EPS) and radiofrequency ablation (RFA) procedure for VA were performed in 21 children according to indications. The functional state of the right ventricle was assessed by GBP-SPECT before and after RFA in all patients. Results: Patients with VA had local areas of asynchronous myocardial contraction (AMC). Compared with control group, patients with VA had significantly higher values of the end-diastolic and end-systolic volumes, and lower indices of contractility. Negative association was found between the total number of AMC areas and cardiac contractility indices. Ectopic foci localization (based on EPS data) was associated with topography of AMC areas (based on GBP-SPECT). Radiofrequency ablation procedure significantly improved cardiac contractility indices; AMC areas completely disappeared or decreased in a number compared with the preoperative conditions. Conclusion: In patients with VA, AMC areas localized mostly in the right ventricle. Comparison of the results of GBP-SPECT and EPS studies showed a relationship between AMC localizations and ectopy topography. The fact that AMC zones disappeared after RFA supports the hypothesis stating that the presence of AMC zones is a scintigraphic symptom of ectopy. The study was supported by grant from the Russian Science Foundation (N 14-15-00178).

P388

The utility of 99mTc-Pyrophosphate SPECT in diagnosis of latent myocarditis in patients with atrial fibrillation

S. Sazonova1,2, Y. Ilyushenkova1,2, R. Batalov1, Y. Rogovskaya1, Y. Lishmanov1,2; 1Institute of Cardiology, Tomsk, RUSSIAN FEDERATION, 2National Research Tomsk Polytechnic University, Tomsk, RUSSIAN FEDERATION.

Aim: to compare results of 99mTc-Pyrophosphate myocardium SPECT with histology data in patients with isolated persistent atrial fibrillation (AF) Materials& methods: We examined 40 patients (pts) (27 males and 13 females, mean age 48.72±11,1) with isolated persistent AF. After complete clinical and instrumental examination, all patients underwent SPECT with 99mTc-Pyrophosphate (99mTc-PYP) 18 hours post injection (delayed SPECT), following by SPECT with 99mTc-MIBI at the rest condition. Both images were then combined to define more exactly the localization of 99mTc-PYP uptake in the heart and to exclude ventricles blood pool. Accumulation of 99mTc- PYP was accepted as pathological when focus localized in myocardium area, focus/background ratio exceeded 1.4. In 22 pts Cardiac Magnetic Resonance (CMR) with gadolinium was performed. Endomyocardial biopsy (EMB) samples were taken during catheter ablation of AF. Scintigraphic results were compared with the EMB and immunohistochemical findings. Results: According to histological data active lymphocytic myocarditis was verified in 5 pts (13%), the remaining 35 pts had signs of cardioscleroses in combination with myolysis, histiolymphocytic infiltration or lipomatosis. Immunohistochemical study detected the presence of viral antigens (gerpes simplex of 1 and 2 types, enterovirus) in myocardium samples of every patient with histologically confirmed myocarditis. The pathological uptake of 99mTc-PYP was found in 11 patients. The number of true-positive results was 3, true negative 28, false-positive - 6, false negative 1. The sensitivity was 80%, specificity 82%, accuracy 80%. Late gadolinium enhancement at CMR was marked at 19 of 22 pts, but neither of pts matched to «Lake Luise Criteria» of myocarditis. The sensitivity was 67%, specificity 77%, accuracy 64%. Correlation analysis according Spearman's criterion revealed a close relationship between CMR and SPECT with 99mTc-Pyrophosphate ($r=0,64$, $p<0.05$). Comparative evaluation of diagnostic efficacy of SPECT with 99mTc-Pyrophosphate and CMR by comparison of ROC curves showed lower values of AUC for CMR (0.702) than for SPECT (0.808). Conclusion: The results of our study have shown that in 13% of patients with isolated AF had latent myocarditis. Cardiac SPECT with 99mTc-PYP has a potential as an effective non-invasive tool of diagnoses of latent myocarditis in pts with isolated AF.

P389

Interpretation of myocardial perfusion SPECT with CT-based attenuation correction

A. Ansheles, L. Martirosyan, I. Sergienko, V. Sergienko; Russian Cardiology Research Center, Moscow, RUSSIAN FEDERATION.

Aim. Assessment of CT-based attenuation correction (AC) impact on cardiac perfusion images, revealing factors that increase visual difference between AC and nAC-images. Material and methods. 167 patients underwent myocardial perfusion SPECT with (AC) and without (nAC) CT-based attenuation correction. Differences between AC and nAC-images were analyzed visually, visual differences groups (VDG) were formed: group 1 - absent difference, group 2 - subtle differences, that did not change interpretation, group 3 - equivocal differences, and group 4 - reliable differences. Groups 3-4 required profound analysis of both sets to make conclusion, they were divided to "-" and "+" subgroups, relating to worse or better AC-perfusion in reference to nAC-images, and also "±"-groups, that meant presence both better and worse segments in AC-images. Factors that increase visual AC/nAC-images difference were studied from the standpoint of classifying them to a certain VDG. Results. Groups 3-4, were AC/nAC-images differed visually significantly, involved 68% of

all cases. In 80% of these cases, AC restored perfusion homogeneity, cancelling "defects" visible at nAC-images, located mostly at inferior LV wall. However, AC-images had their specific artifacts (false defects) compared to nAC-images, located mostly in apex. Factors that increased AC/nAC-images difference included: weight, large LV, male gender, patients with small focal perfusion defects and transient ischemia, insufficient activity administered (all p(s)<0.05). SRS, SSS values and transient ischemia area (reversibility extents in %) were significantly higher at AC-images than in nAC-images: 6.8 (2.5-10.6) against 4.5 (2.0-6.7), p<0.01, 8.1 (3.0-13.7) against 5.3 (2.4-7.2), p<0.01, 5.5% (3.2-7.6) against 3.3% (1.7-5.1), p<0.01, respectively. Septal perfusion defect extent was higher in AC-images: 31.1% (16.1-44.2) against 6.6% (2.6-15.3), p<0.01. In patients with transmural perfusion defects, maximum defect severity was higher in AC-images - 8.3 sigmas (5.6-11.4) against 6.3 (4.3-9.3), p=0.056. Artifacts due to bright liver/stomach appeared more often in rest AC-images (12% against 2.7%, p<0.05). Summary/discussion. CT-based AC increases myocardial perfusion SPECT diagnostic value, makes interpretation more confident, reduces number of false-positive/equivocal results. However, normal ranges of summed scores and extent parameters for AC-images require modifying, since they are higher in AC-images (perhaps due to more precise normal databases). In addition, both AC- and nAC-images showed their own artifacts patterns. In effort to minimize influence of those false perfusion "reductions" on quantitative assessments, it is discussable to take relative perfusion values for each segment as maximal numbers of both AC and nAC images, instead of using values only from one (AC or nAC) set.

P390

the efficacy of myocardial perfusion image morphing combined with computed tomography coronary angiography in the diagnosis of silent myocardial ischemia

C. Chang, W. Xie, B. Lei, L. Wang, R. Li, Z. Zheng, s. yang; Shanghai Chest Hospital, Shanghai, CHINA.

Accruate assessment of silent myocardial ischemia is the important value in the diagnosis and treatment of Coronary Artery Disease.The current study aims to compare the diagnostic efficacy of combined myocardial perfusion imaging morphing (MPI morphing) and computed tomography coronary angiography (CTCA) with MPI morphing or CTCA alone in silent myocardial ischemia (SMI). Forty-five outpatients diagnosed with ischemic ST segment abnormality (depression of ST segment larger than 0.05 mV) by ECG in the clinic or by physical examination from March 2011 to September 2014 were retrospectively studied. There were 24 males and 21 females aged 38-78 years (average age: 60.13 + 7.58 years), who were informed of the procedures and signed an informed consent prior to the examinations. All patients underwent conventional dobutamine stress/resting MPI and CTCA imaging, followed by coronary artery angiography (CAG) within a month. CAG combined with MPI morphing was used as a standard to evaluate the efficacy of MPI morphing, CTCA and MPI combined with morphing CTCA in the diagnosis of SMI.For MPI morphing combined with CTCA, MPI morphing and CTCA, the diagnostic sensitivities for SMI were 92.41%, 81.43% and 73.58%, respectively; the specificities were 92.86%, 73.85% and 71.95%, respectively; the accuracies were 92.59%, 77.78% and 72.59%, respectively; the positive predictive values were 94.81%, 77.03% and 62.90%, respectively; the negative predictive values were 89.66%, 78.69% and 80.82%, respectively. The Kappa values of MPI morphing combined with CTCA, MPI morphing, and CTCA in the diagnosis of SMI were 0.85, 0.55 and 0.44, respectively.CTCA can clearly show morphological changes in the coronary artery, while MPI morphing can determine the occurrence of myocardial ischemia in the striated coronary artery. The combination of CTCA and MPI morphing could improve the diagnostic efficacy of SMI.

P391

99mTc-HMPAO labeled leukocyte SPECT/CT in evaluation of cardiac device infection

M. Kostkiewicz, K. Holcman, W. Szot, B. Malecka; Intitute of Cardiology,Jagiellonian University, Hospital John Paul II, KRAKOW, POLAND.

Introduction. The number of device implantations has increased two- to three-fold across the last 10-15 years Unfortunately, the rate of devices infections has increased in parallel . Cardiovascular implantable electronic devices (CIED) endocarditis are associated with a poor prognosis. Imaging investigations traditionally used for diagnosis of IE and PVE are transthoracic echocardiography (TTE) and transesophageal echocardiography (TEE), with a very high sensitivity. However, the diagnostic value of echocardiography in IE diagnosis is operator-dependent and its sensitivity can decrease in presence of intracardiac devices, severe preexisting lesions, and very small or no vegetation.Aim. The aim of this study was to evaluate the accumulation of autologous radiolabeled leukocytes 99mTc-HMPAO in patients with CHED and with suspected infective endocarditis using SPECT/CT. Methods. The study group included 30 consecutive patients with suspected infective endocarditis (IE) involving a cardiac device. On all patients we performed clinical evaluation and laboratory tests (e.g. complete blood cell count, creatinine, C-reactive protein, procalcitonin, fibrinogen, blood cultures). Each patient underwent transthoracic as well as

transesophageal echocardiogram. Afterwards all patients had performed SPECT/CT with prior administration of autologous leukocytes labeled with 99mTc-hexamethylpropyleneamine oxime (99mTc-HMPAO-WBC). Images was obtained after 4-6 and 20-24 hours after reinfusion. The scintigraphic studies was classified as positive for infection when there will be observed at least one focus of abnormal uptake characterized by a time-dependent increase in radioactivity. Clinical follow-up will last 6 months. During this time patients had control transthoracic echocardiogram. Results. The very good correlations between the accumulation of 99mTc-HMPAO-WBC and exacerbation of clinical symptoms, and echocardiographic findings was found. 99mTc-HMPAO-WBC scintigraphy was totally negative in 5 patients for CIED sites of focal uptake indicating infection The SPECT/CT study, when positive, was very useful in diagnosis the region of infection in patients with cardiac device and clinical symptoms of endocarditis. There were one false positive scan with CIED. Conclusions.99mTechnetium-HMPAO-SPECT/CT, have been demonstrated to be effective imaging options in the management of IE especially in patients with high clinical suspicion of IE, in order to confirm the diagnosis in doubtful circumstances and/or to detect sites of inflammation.

P392

Dual radionuclide myocardial perfusion SPECT may be planned with much lower radiation doses on CZT cameras

V. ROCH1,2, **L. IMBERT**1,2,3, W. DJABALLAH1,2, M. PERRIN1,2, A. VERGER1,2, H. BOUTLEY1,2, G. KARCHER1,2,3, P. MARIE1,2,4; 1CHU NANCY Hopital Brabois Adultes, Vandoeuvre-lès-Nancy, FRANCE, 2Nancyclotep experimental imaging platform, Nancy, FRANCE, 3CRAN, UMR 7039, Université de Lorraine - CNRS, Vandoeuvre-lès-Nancy, FRANCE, 4INSERM, U1116, Nancy, FRANCE.

High effective doses, around 29 mSv, constitute a main limit for myocardial perfusion SPECT imaging (MPI) scheduled with a dual 99mTc/201Tl radionuclide method on conventional cameras. This study was aimed at assessing a lower dose dual radionuclide MPI method applied on a CZT camera with a stress first 99mTc-Sestamibi MPI followed only if necessary by a rest 201Tl one. **Methods**. Eighty-two patients, who had a low dose stress MPI with 99mTc-Setamibi on a CZT camera and for whom a rest 99mTc-Setamibi MPI was subsequently prescribed, also had as a part of the protocol, a rest-MPI with201Tl (36 to 63 MBq) at one hour from stress imaging. The 201Tl images were processed for spill-over and scatter corrections and uptake differences with stress-MPI were analyzed: 1) for the 201Tl (ΔTl) and 99mTc-Sestamibi (ΔTc) rest acquisitions and 2) in segments for which a definite diagnosis of ischemia or necrosis was achieved with the combined analysis of 99mTc-Sestamibi SPECT and gated-SPECT. **Results**. Mean effective dose was 13.9±1.4 mSv for the dual radionuclide procedure. ΔTl was dramatically higher in the 42 ischemic segments than in the 89 necrotic ones (14.5±10.2% vs. 6.5 ±8.9%, $p<0.001$). However, the corresponding uptake levels were much lower for ΔTc (8.4±6.4% and 2.5±7.2%, respectively, $p<0.001$ for all comparisons), presumably because of the higher background counts of 201Tl compared to 99mTc rest images (background-to-myocardium count ratio: 0.33±0.9 vs. 0.27±0.15, $p<0.001$). Finally, the best threshold to separate ischemic from necrotic segments was higher for the dual radionuclide method (ΔTl > 13%) than for the single 99mTc one (ΔTc>8%). **Conclusion**. A dual 99mTc/201Tl radionuclide method may be applied on last-generation CZT cameras with a ≥ 50% decrease in radiation doses, compared with conventional protocols (14 vs. 29 mSv). However, this stress-first 99mTc-Setamibi protocol requires adapting diagnostic criterion to the higher noise level of 201Tl rest images.

P393

Evaluation of simultaneous Tc-99m and I-123 dual-isotope SPECT imaging using cardiac CZT camera

T. Niimi1, M. Sugimoto1, M. Nanasato1, H. Maeda2; 1Nagoya Daini Red Cross Hospital, NAGOYA, JAPAN, 2Nagoya University, NAGOYA, JAPAN.

Purpose: A recently introduced, high-speed, single-photon emission computerized tomography (SPECT) device based on cadmium-zinc-telluride (CZT) detectors (D-SPECT; Spectrum Dynamics, Israel) shows high-sensitivity collimation and high-energy resolution for cardiac imaging. In particular, its high-energy resolution provides a new possibility for simultaneous dual-isotope SPECT imaging, such as using Tc-99m and I-123 (Tc-99m/I-123), which was impossible in the conventional Anger SPECT (A-SPECT). We assessed whether the simultaneous Tc-99m/I-123 dual-isotope SPECT imaging of D-SPECT was accurate using phantom experiments. Materials and Methods: We evaluated the energy resolution such as for Tc-99m, I-123, and Tl-201 of D-SPECT by phantom experiments using a simultaneous dual-isotope (SDI) phantom. Corresponding measurements of Tc-99m and I-123 were also performed on an A-SPECT. The full width at half maximum (FWHM), which is an index of energy resolution, was measured using a tube phantom (line sources) placed at the same locations in each system. Simultaneously, the Tc-99m/I-123 and Tl-201/I-123 data were acquired in energy windows centered at 140 keV for Tc-99m, 159 keV for I-123, 167 keV for the upper Tl-201 line (10%), and 69-80 keV for the main Tl-201 emission. The data from these energy windows were obtained using the CZT or Anger camera acquisition system at

the same time. Results: The energy resolution (FWHM) values of the D-SPECT system for Tc-99m/I-123 and Tl-201/I-123 were 5.5%/5.2% and 10.9%/5.2%, respectively; the corresponding values in A-SPECT for Tc-99m/I-123 were 9.1%/9.3%. The D-SPECT system with Tc-99m/I-123 had an energy resolution that was twice that of the A-SPECT. The influence of cross talk on the simultaneous dual Tc-99m/I-123 SPET imaging could not be detected by visual inspection in the SDI phantom imaging. Otherwise, the influence of cross talk on the SDI acquisition between Tl-201 and I-123 was caused by the upper peak of Tl-201 (167 keV, 10%). The influence of cross talk on the simultaneous dual Tl-201/I-123 SPECT imaging could be detected by visual inspection of the SDI phantom imaging. Conclusion: The D-SPECT system with Tc-99m/I-123 had better energy resolution than the A-SPECT. The simultaneous Tc-99m/I-123 dual-isotope SPECT imaging of D-SPECT was reliable, which showed the further potential of the CZT camera for SDI acquisition.

P394

Optimization of radioactive dose for dipyridamole and exercise myocardial perfusion Gated-SPECT.

F. Ticconi1, A. Nieri1, M. Baucknehtl, G. Ferrarazzo1, F. Fiz1, M. Pennone1, S. Morbelli1, F. Bongioanni1, C. Marini2, G. Sambuceti1; 1Nuclear Medicine, IRCCS AUO San Martino IST, Genova, ITALY, 2Institute Of Bioimaging and Molecular Physiology, CNR, Milan, Genoa Section, Genova, ITALY.

Aim: According to the fractionation principle, the ratio between myocardial uptake (Mup) of technetium labeled tracers and corresponding coronary blood flow (CBF) in each segment is directly related to the ratio between administered dose and cardiac output. Stress SPECT imaging implies tracer injection during either exercise (EX) or pharmacological vasodilation. However, while physical effort increases cardiac output, dipyridamole (DIP) selectively raises CBF. Accordingly, for any given administered dose, eventual Mup should be higher under DIP than during EX. Aim of the present study was to verify this hypothesis in order to optimize injected dose according to stress protocol. Materials and Methods: We retrospectively analyzed 60 patients with negative single day stress/rest G-SPECT myocardial perfusion imaging. Patients were divided into two groups based on the type of stress test: 30 patients underwent DIP and 30 EX stress test, respectively. For each patient sex, age, weight as well as administered doses (MBq) at stress and rest were recorded. By using a specific software (Myovation Evolution) a 3D-region of interest (ROI) was drawn on the left ventricular myocardium to estimate average and maximal counting rate as an index of Mup. Obtained values were multiplied for patient's weight and divided for administered dose. Results: Mup index significantly increased from rest to stress both in EX (0.09±0.03 to 0.14 ±0.04, $p<0.01$) and in DIP patients (0.10±0.04 to 0.13±0.04, $p<0.05$). No significant difference was observed in stress Mup index between the two groups. However, % increase of Mup index was higher in EX patients with respect to DIP ones (175 ±65% vs 129±46%, respectively, $p<0.01$). Conclusions: EX and DIP result in similar Mup values. Tracer retention increases even more during physical exercise than under DIP despite the obvious difference in cardiac output response to the two stressors. These data do not support the rationale to reduce radioactive dose in case of pharmacological vasodilation.

P395

Reference values for right ventricular and lung uptake in relation to left ventricular uptake in 99mTc-tetrofosmin myocardial perfusion SPECT/CT imaging

T. M. Laitinen1, A. Corovai1,2, H. Hämäläinen1,2, T. Laitinen1,2; 1Kuopio University Hospital, Kuopio, FINLAND, 2University of Eastern Finland, Kuopio, FINLAND.

Aim: According to current guidelines, adequate interpretation of myocardial perfusion study includes review of tomograms, left ventricular ejection fraction and volumes but also visual interpretation of lung uptake and right ventricular uptake from raw data. Increased lung uptake and right ventricular uptake are thought to reflect reduction of cardiac function, right ventricular hypertrophy or generalized reduction of left ventricular uptake. Interpretation of lung and right ventricular uptake based on inspection of raw data is just approximate and therefore additional quantitative analysis might be useful, especially in cases with borderline abnormality. The aim of this study was to define reference values for quantitative measures of lung uptake and right ventricular uptake in relation to left ventricular uptake (lung to left ventricular uptake ratio [L/LV] and right ventricular to left ventricular uptake ratio [RV/LV]).Materials and methods: We evaluated data of 384 consecutive patients who were sent to 99mTc-tetrofosmin myocardial perfusion SPECT/CT study during the year 2012 in the Department of Clinical Physiology and Nuclear Medicine, Kuopio University Hospital. Exclusion criteria were 1) previously diagnosed cardiac disease, 2) abnormal ECG at rest, 3) signs of advanced coronary artery calcification in CT, and 4) abnormal myocardial perfusion in stress/rest myocardial perfusion SPECT study. Final study population consisted of 48 subjects (38 women and 10 men) aged 42-84 years. Also 5 patients with severe heart failure were used to validate the reference values. Transverse reconstructions with attenuation and scatter compensation were made. Regional uptakes were calculated for left ventricular wall, right ventricular wall and lungs as an average of respective ROIs in two representative slices.Results: Age, gender, blood pressure and body mass index did not correlate statistically significantly with L/LV

and RV/LV. At rest an average L/LV was 0.149 and RV/LV was 0.400. According to mean + 2SD, limit of the highest normal for L/LV was 0.219 and for RV/LV 0.550. Among the 5 heart failure patients, 4 had abnormal L/LV and 2 had abnormal RV/LV. Only 1 patient had both L/LV and RV/LV within the reference limits.Conclusions: We report reference values for L/LV and RV/LV, which demonstrate quite well increased lung and right ventricular uptake in heart failure patients according to the preliminary results.

P396

Comparison of Phase analysis among three kinds of soft-ware (QGS, ETB and Heart function view) in diagnosing ischemic heart disease

S. Nagamachi, **MD**1, H. Onizuka, MD2, R. Nishii, MD1, Y. Mizutani, MD1, T. Hirai, MD1, K. Kitamura, MD3; 1Department of Radiology, MIyazaki University,, Miyazaki, JAPAN, 2Department of 1st Internal Medicine, Miyazaki University,, Miyazaki, JAPAN, 3Department of 1st Intenal Medicine, Miyazaki University,, Miyazaki, JAPAN.

(Background and Purpose) For differentiating myocardial Dyssynchrony, various software is available evaluating phase analysis. However, there are few reports addressing the compatibility of phase analysis indexes calculated by each software. In the current study, we compared the phase analysis indexes of the same patient data of Tl-201 myocardial gated SPECT using by ETB, HFV and QGS2006 retrospectively. Then we evaluated the compatibility of phase analysis indexes calculated among QGS2006, ETB, and HFV. (Methods) The patients included 97 cases (70 men, women 27, average age 71.4 years old) those gated Tl-201 myocardial SPECT were conducted for the purpose of differentiating ischemic heart disease. We calculated both Band Width (BW) and phase SD (SD) by using three kinds of software and compared each correlation, %difference and Bland-Altman plot analysis. In addition, we divided all patients into the normal group, the ischemia group, the infarction group, the infarction with ischemia group. Then we compared the phase analysis indexes among four groups both at rest and at stress condition. (Results) The correlation of the phase analysis indexes among three kinds of software at stress was moderate (from 0.49 to 0.64). However, they deteriorated at rest conditions (from 0.27 to 0.49). Around 40-50% of % differences in phase SD or BW were noted among three groups. They increased on the delayed images around 50-60%. By Bland-Altman plot analysis, both indexes tended to be higher at rest conditions, and 95% CI distributed over the range of +/-30 degrees at stress and +/-45 degrees at rest. When we compared the phase analysis indexes among ischemic patients, both values of SD and BW in the infarction and ischemia group were significantly higher than those of normal group or ischemia group. Although some differences were noted among three kinds of software, both the infarction group and the infarction with ischemia group showed highest values at stress and at rest conditions. However, any statistical significance was not noted between the ischemia and the normal group in three kinds of software. (Conclusion) In the phase analysis on Tl-201 myocardial gated SPECT, the compatibilities of phase analysis indexes were fair in ETB, HFV and QGS2006. However, we should use three kinds of software in considering the limit of their compatibilities.

P397

Assessment of left ventricular function with a fast low-dose recording protocol planned on a semi-conductor gamma-camera

M. Claudin, **Sr**., W. Djaballah, Sr., L. Imbert, Sr., N. Veran, Sr., S. Poussier, Sr., V. Roch, G. Karcher, Sr., P. Marie, Sr.; Centre hospitalo-universitaire de Nancy, Vandoeuvre-les-Nancy, FRANCE.

Introduction. New gamma cameras, equipped with Cadmium-Zinc-Telluride (CZT) semiconductor detectors, provide an enhanced image quality, as well as an enhanced count sensitivity allowing to reduce imaging time and injected doses. The purpose of this study was to compare the assessment of left ventricular function obtained through a fast low-dose recording protocol on a CZT camera (the "D-SPECT" camera) with the reference assessment obtained through cardiac MRI.Methods. We retrospectively included patients with known or suspected cardiomyopathy and who had undergone both: 1) myocardial perfusion imaging (MPI) on D-SPECT camera with a low-dose protocol (120MBq of Sestamibi-99mTc for stress and 360 MBq at rest for a body weight of 75 kg) and 2) a cardiac MRI at a < 2-months interval time from MPI. The left ventricular function was assessed at rest MPI with 8-interval-frames and by using the QGS® software.Results. Seventy-seven patients were included among whom, 43 (66%) had an history of myocardial infarction. Mean ejection fraction was 45±13% at MRI (from 12 to 69 %). For the D-SPECT recordings, on average, myocardial activity was 527±104 kcps, recording time, 3.5±2.2 min and total injected activity (stress and rest), 420±185 MBq, corresponding to an effective dose of 3.7±1.6 mSv.Correlations between D-SPECT and MRI were very good to excellent for ejection fraction (r=0.88) and for end-diastolic (r=0.90) and end-systolic (r=0.96) volumes, but with significant underestimations (-5% for ejection fraction, -16% for end-diastolic volume and -24% for end-systolic volume).Conclusion. The evaluation of left ventricular function using this CZT camera and a fast low-dose protocol correlates well with the reference assessment provided by cardiac

MRI, even if volumes and ejection fraction remain underestimated, similarly to what was previously documented with conventional Anger cameras.

P398

Long-term survival of patients with manifested coronary artery disease with and without diabetes undergoing myocardial viability assessment.

G. Rendl, P. Keinrath, K. Krommes, G. Barth, J. Holzmannhofer, C. Pirich; Department of Nuclear Medicine and Endocrinology, Paracelsus Medical University Salzburg, Salzburg, AUSTRIA.

Aim: to analyze the impact of myocardial viability assessment on survival might improve clinical decision making in patients with manifested coronary artery disease (CAD) with potential implication on survival. Material and Methods: 80 patients (9 females and 71 males) with a mean age of 71.3 ± 9.8 years were included in this study. All patients with angiographically documented coronary artery disease underwent myocardial perfusion scintigraphy using Tc99m-tetrofosmin and imaging of myocardial viability by F-18 FDG PET/CT using combination of hyperinsulinemic-euglycemic clamp protocol in combination with acipimox. 12 patients had 1 vessel disease (VD), 15 patients 2 VD and 49 patients 3 VD, respectively. Revascularization was intended when the amount of hypoperfused but viable myocardium exceeded 10 % of left ventricular area. Results: Mean follow-up was 62.4 ± 33.2 months after viability testing. Median survival was 69.3 months (95 CI: 60.1-77.9 months) in non-diabetics as compared to 46.5 months (95 CI: 32.7-60.3 months) in patients with diabetes (p=0.003). Diabetic patients had fewer percent of scar tissue (16.0 ± 12.0) as compared to non-diabetics (25.7± 18.7), while the amount of hypoperfused and viable myocardium was not significantly different (14.5 ± 12.6 vs. 9.8 ± 12.0). Patients with diabetes had significantly more commonly 3 vessel disease than patients without diabetes (83 % vs. 52 %). The number of revascularization in patients with and without diabetes was statistically not significantly different (71 % vs. 54 %). Conclusion: CAD patients with diabetes exhibited significantly shortened overall survival compared to patients without diabetes though having less scared and equal amounts of viable myocardium as indicated by PET.

P399

Is CMR reproducible enough to replace Gated Blood Pool SPECT for the follow-up of RVEF?

T. Giraudmaillet1, F. Mokrane2, C. Zadro2, H. Rousseau2, **L. DERCLE**3; 1CHU Toulouse, Toulouse, FRANCE, 2CHU TOULOUSE, TOULOUSE, FRANCE, 3Gustave Roussy, Villejuif, FRANCE.

PURPOSE: The estimation of right ventricular ejection fraction (RVEF) is crucial in order to establish the diagnosis, the risk stratification, the prognosis, and the response to treatment in a wide range of heart disease. Cardiac MagneticResonance Imaging (CMR) is the reference-standard for the evaluation of RV volumes but the manual delineation of endocardial border leads to a significant operator-dependency. This report investigates if new MRI techniques are reproducible enough to be considered as the reference-standard for the follow-up of RVEF (in 12 subgroups of heart disease), in comparison with the most reproducible technique: gated blood pool single photon emission computed tomography (GBPS). METHOD AND MATERIALS: 94 CMR and 99 GBPS were measured by two physicians. GBPS was performed using 2 automatic algorithms: BP-SPECT and QBS and a semi-automatic algorithm: TOMPOOL. Relative Inter-Observer Variability (IOV) was defined as the absolute difference between the two calculated measurements normalized to their average and expressed as a percentage. RESULTS: The overall IOV (%) was greater using semi-automatic GBPS procedure (TOMPOOL: 16 ±20%) than CMR (12±14%) or automatic GBPS algorithm (QBS: 8±12%, BP-SPECT: 6±6%). The IOV of CMR challenged GBPS in 2 subgroups of heart disease treated arrhythmia (6±5% vs 8±9%) and hyperdynamic cardiomyopathy / cirrhosis (4±3% vs 4±4%). Overall, the IOV on CMR was especially important in comparison with GBPS in dilated cardiomyopathy (20±20% vs 4±2%), LVEF<50% (17±18% vs 6 ±4%), RVEF<45% (20±18% vs 7±6%), and left or right valve dysfunction (17±20% vs 5±3%). CONCLUSION: The most reproducible procedure is automatic GBPS. Changes occurring during the follow-up should be interpreted cautiously on CMR (IOV: 12%) or semi-automatic GBPS (IOV: 16%) in case of valve regurgitation, altered ejection fraction and enlargement of the left ventricle. The reproducibility of CMR challenged GBPS in treated arrhythmia and hyperdynamic heart disease.

P400

How the change in time interval between 99mTc-sestamibi injection and image acquisition may effect on quantitative data of gated SPECT myocardial perfusion imaging at stress phases

M. Haghighatafshar1, S. Entezarmahdi2, S. Mortazavi1, F. Khajerahimi1; 1Nuclear Medicine Department, Shiraz University of Medical Science, Shiraz, IRAN, ISLAMIC REPUBLIC OF, 2Radiation Medicine Engineering Department, Shahid Beheshti University, Tehran, IRAN, ISLAMIC REPUBLIC OF.

According to several recent studies in favor of delayed 99mTc methoxy-isobutyl-isonitrile (99mTc-MIBI) redistribution, the aim of this study was to find whether different time intervals between 99mTc-MIBI injection and image acquisition could affect quantitative data of Gated-SPECT myocardial perfusion imaging (MPI). Sixty Patients with known pretest probability of coronary artery disease according to "Framingham Risk Score" enrolled in the study. Myocardial perfusion imaging with Gated-SPECT was performed on the basis of two-day protocol. The stress-phase imaging repeated four times after 15, 60, 120, and 180 minutes post injection of 99mTc-MIBI. The injected dose was 666 to 814 MBq according to the patients' weight. All the images were reconstructed and filtered in the same way. The reconstructed images were analyzed by Corridor-4DM software package. The quantitative data was extracted and compared. Results showed that the calculated end diastolic and systolic volumes (EDV, ESV) change statistically significant in an upward. As the time interval increase the calculated EDV raise 2.84 ml ($p = 0.010$) and the calculated ESV raise 2.35 ml ($p = 0.008$). As both of the EDV and ESV change almost in a same manner, their difference called stroke volume (SV) does not change significant; while the calculated ejection fraction decrease about 1.52 percentages ($p = 0.042$). The rest of quantified parameters such as sums stress score, sum motion score, and sum thickening score does not change statistically significant as the time passes from the injection point. In this work we tried to find whether delay in scanning the myocardium with Gated-SPECT at stress phase can effect on calculated quantitative parameters. According to the results, just the EDV, ESV, and EF change statistically significant, while we found that these changes are not clinically significant.Key words: Myocardial Perfusion Image, Quantitative Parameters, Redistribution

P401

Would SPECT/CT be a must for attenuation correction in gated-SPECT myocardial perfusion imaging?

L. Ali1, A. Al-Saffar1, I. Loutfi2; 1Faculty of Allied HealthSciences, Kuwait University, Kuwait, KUWAIT, 2Faculty of Medicine, Kuwait University, Kuwait, KUWAIT.

Introduction: Gated SPECT (G-SPECT) myocardial perfusion imaging (MPI) using Tc-99m lipophilic chelates is universally used for evaluation of coronary artery disease (CAD). Image interpretation can be affected by attenuation artifacts in the anterior wall of the left ventricle from the breasts in women and in the inferior wall due to diaphragm. Recently, the advent of SPECT/CT hybrid imaging has allowed localization of lesions and correction for attenuation especially in bone imaging. The objective of this study was to use the CT attenuation maps in G-SPECT/CT to allow for attenuation and to check whether it made a significant impact on the interpretation in terms of presence and severity of the lesions. Materials and Methods: Forty-five G-SPECT/CT MPI stress studies were selected retrospectively from a pool of patients referred for evaluation of CAD. G-SPECT/CT MPI acquisition was performed on a hybrid SPECT/CT dual-head gamma camera (Discovery NM/CT 670). Uncorrected (NC) and corrected (AC) SPECT images for attenuation were analyzed for presence and severity of perfusion defects. Seventeen and 20 segment polar maps were used for semi-quantitation of the lesions in terms of the summed stress score (SSS) and associated percentage count for the segments affected to the average in the total, to gauge the severity of the lesions. The abnormalities were visually scored by 2 nuclear medicine physicians using a 4-point scale (1 normal, 2 probably normal, 3 probably abnormal, and 4 abnormal).Results: The inferior wall of the left ventricle was the area most commonly affected by diaphragm attenuation. In 22 (48%) of the studies, there was a difference in the visual perfusion score. McNemar test showed that visual improvement in perfusion with attenuation correction was seen in 29 out of 45 patients (64%) in which marked difference in perfusion were seen in 20 patients (44%). Moderate agreement was seen (Kappa = 0.60). The quantitative SSS was 10.51 ± 6.89 NC and 7.38 ± 6.29 AC and the corresponding stress perfusion counts (SPC) for the affected segments, were, 59.98 ± 10.7 (NC) vs 70.76 ± 6.61 (AC) ($P<0.0005$). Conclusions: Discordance between AC and NC images in the inferior wall of the left ventricle as judged by the readers and the quantitative analysis were sufficient to consider G-SPECT/CT as a routine imaging approach leading to significant change in study interpretation.

P24 - Monday, October 12, 2015, 4:00 PM - 4:30 PM, Hall 3 – Poster Exhibition

Cardiovascular System: Miscellaneous

P402

Frequent incidental CT findings during Rubidium-82 myocardial perfusion PET

J. A. van der Heide, J. Esser, A. M. van den Berk, E. A. de Vrey, B. J. G. L. de Smet, J. M. H. de Klerk; Meander Medical Centre, Amersfoort, NETHERLANDS.

Background: We recently introduced Rubidium-82 myocardial perfusion PET as a standard procedure at our institute for myocardial perfusion imaging. We frequently observe incidental findings on low dose CT, performed during Rubidium-82 myocardial perfusion PET for attenuation correction. Methods: We prospectively reported incidental findings on low dose CT, and advised cardiologists about follow-up. Incidental findings were defined as new and unexpected findings, that were likely to require a change in patient management.

Retrospectively, we analyzed findings during follow up; minimum duration of follow up was 3 months. Results: Of 815 patients (56% males) who underwent Rubidium-82 myocardial perfusion PET from February 25th to December 31st 2014, 71 (8,7%; 54% males) showed incidental findings. Patients with incidental findings were significantly older than those without (67±10 vs 71±9 years, p=0,003). Pulmonary abnormalities were found in 50 patients (22 of whom had pulmonary nodules), liver abnormalities in 4, breast abnormalities in 6, and miscellaneous findings in 11 patients. Clinical analysis revealed malignancy in 7 patients (4 lung, 2 breast, 1 kidney), benign pulmonary nodules in 15, miscellaneous benign disease in 10,and no abnormalities in 3 patients. Follow-up remained inconclusive in 9 patients. In 4 patients, follow up is pending at the time of writing of this abstract. In 20 patients, no follow-up was pursued by the cardiologist. Of the 7 patients in whom previously undetected malignancy was diagnosed, 2 received therapy with curative intent, and 5 palliative/supportive care. Conclusions: Incidental CT findings during Rubidium-82 myocardial perfusion PET are frequent: 8,7%. Previously undiagnosed malignancy occurred in 7 patients (0, 9%), of whom 2 received therapy with curative intent. Inadequate follow-up occurred in 28%. Therefore, careful examination of the low dose CT is warranted in patients who undergo Rubidium-82 myocardial perfusion PET.

P403

The Value of Transient Ischemic Dilatation after Coronary Revascularization

S. S. Gültekin1, M. Sadic2, M. Bilgin3, E. Yeter3, G. Koca2, S. Açıkel3, M. Korkmaz2; 1Hacettepe University, Kastamonu School of Medicine and Dışkapı Yıldırım Beyazıt Training and Research Hospital, Ankara, TURKEY, 2Ankara Training and Research Hospital, Ankara, TURKEY, 3Dışkapı Yıldırım Beyazıt Training and Research Hospital, Ankara, TURKEY.

Aim: Transient ischemic dilation (TID) of the left ventricle on myocardial perfusion imaging (MPI) can be used a predictor of severe coronary artery disease (CAD) or future cardiac events. However, the meaning of elevated TID after a cardiac revascularization (CR) has not been evaluated. We investigated the value of TID as a predictor for CAD in patients undergoing CR. Methods: Study group consists of 104 (75 m, 29 f. median and range age; 60 and 37-83 y) patients retrospectively selected from a database of 2316 patients. Patients underwent a percutaneous coronary intervention (PCI) in 62/104 (60%) and a coronary artery bypass graft operation (CABG) in 42/104 (40%) for CAD. After the prior CR, they were evaluated due to new cardiac events by gated single-photon emission computed tomography (GSPECT) MPI and coronary angiography (CA). We examined on these data to determine the value of TID. Results: Mean and median TID values were 1.17 ± 0.40 and 1.15 (0.65 - 3.62). There was a strong negative correlation between TID and DLVEF values (r=0.77, p<0.01). In addition, we determined positive correlations between TID measurements with severity of CAD in GSPECT MPI (r=0.59, p<0.01) and CA (r=0.77, p<0.01). To show meaningful CAD, the best cut-off TID, sensitivity and specificity values were found to be 1.16, 82% and 64% according to GSPECT MPI and 1.21, 91% and 97% according to CA, respectively. Conclusions: In patients with CR, a high TID value was found to be well-correlated with the meaningful CAD. It may provide additional information to select the high risk patients.

P404

Usefulness and safety of adenosine stress myocardial perfusion SPECT for patients with “inactive” bronchial asthma.

T. Kasai1, M. Aiga1, Y. Iwasaki1, K. Oshima1, Y. Sasaki1, Y. Fujita1, N. Tanaka1, A. Yamashina2; 1Tokyo Medical University Hachioji Medical Center, Tokyo, JAPAN, 2Tokyo Medical University, Tokyo, JAPAN.

Aim: As elderly population grows, exercise stress testing tends to be insufficient. Although adenosine is contra indication for patients with bronchial asthma (BA) in Japan, it could be used for “inactive” BA patients safely. Materials and methods: We retrospectively investigated the frequency of insufficient stress testing, adverse effects, and sensitivity to detect coronary artery disease (CAD) in the setting of myocardial perfusion SPECT between 2011-2012 (1031 cases) and 2013-2014 (1252 cases). Invasive coronary arteriography (CAG) was recruited as a gold standard. Sensitivity was calculated from the patients’ data who underwent both SPECT and CAG within 3 months. Adenosine was never used for BA patients in the former period. On the other hand, adenosine was positively used for “inactive” BA patients in the latter period. “Inactive” was judged based on a medical history check list at stress testing laboratory. Results: As for stress methods, adenosine, exercise, and dobutamine in the former and latter periods were 925 (89.7%) vs. 1232 (98.4%); (p<0.001), 97 (9.4%) vs. 13 (1.0%); (p<0.001), and 72 (0.7%) vs. 75 (0.6%); (n.s.), respectively. Exercise has been reduced and adenosine increased in the latter period. Incidence of insufficient stress testing was frequent in the former period (20 (1.9%) vs. 6 (0.5%); p=0.001). BA patients were involved more in the latter period (19 (1.8%) vs. 60 (4.8%); p<0.001), and insufficient stress testing was also frequent in the former period (7 (36.1%) vs. 5 (8.1%); p<0.05) among BA patients. No severe adverse effects were observed. Sensitivity for detection of CAD was superior in the latter period (84.1% vs. 67.4%, p<0.001). Conclusion: Adenosine stress myocardial perfusion SPECT can be performed safely for patients with “inactive” BA and improves diagnostic sensitivity.

P405

Contraction synchronicity and work measured in patients with coronary artery disease

T. Niimi1, M. Nanasato1, H. Maeda2; 1Nagoya Daini Red Cross Hospital, NAGOYA, JAPAN, 2Nagoya University, NAGOYA, JAPAN.

Purpose: The regional contraction synchronicity and work were evaluated in patients with a reduced ejection fraction due to coronary artery disease (CAD). Materials and Methods: We evaluated 104 patients (54 with CAD and 50 normal controls) using rest electrocardiographic-gated 99mTc-tetrofosmin single-photon emission computed tomography (ECG-SPECT). The contraction amplitude, synchronous contraction index (SCI), and contraction work were evaluated using the quantification of a segmental function by solving the Poisson equation (QSFP). The cardiac wall was divided into 17 segments, and the accumulation of perfusion agents, contraction amplitude, SCI, and contraction work were calculated for each segment and plotted on polar maps. Results: The QSFP accuracy was thought to be satisfactory compared to that of quantitative gated SPECT (QGS) for the measurement of the left ventricular ejection fraction (LVEF), which had a correlation value of 0.92. The average contraction amplitude, SCI, and contraction work values in the 17 segments were 33.8% ± 4.1%, 96.6% ± 1.4%, and 6.9 ± 1.0 mJ·cm^−2/beat, respectively, in the normal individuals, and 26.1% ± 7.3%, 82.1% ± 16.8%, and 5.4 ± 1.6 mJ·cm^−2/beat, in the patients with CAD. These values were 17.9% ± 4.0%, 63.0% ± 18.4%, and 3.5 ± 1.1 mJ·cm^−2/beat in CAD patients with LVEF < 40% (n = 14). The contraction amplitude, SCI, and contraction work were significantly lower in patients with CAD than in the controls ($p < 0.005$), and were also significantly lower in the CAD patients with LVEF < 40% (n = 14) compared to the mean of the patients with CAD ($p < 0.05$). The contraction amplitude, SCI, and contraction work showed good correlation with LVEF in patients with CAD, with values of 0.91, 0.78, and 0.88, respectively. Areas of LV dyssynchrony could be visually delineated on the polar maps. Conclusion: The LV dyssynchrony associated with CAD could be detected using the contraction amplitude and SCI, and the mechanical work during dyssynchrony could be determined as the value of the contraction work. Moreover, these values could be a useful tool for the early detection of CAD, and also clarify the process for decreasing the LVEF. An assessment of myocardial viability from a mechanical perspective provides a more accurate diagnosis.

P406

Effect of Methamphetamine on perfusion and functional indices of the left ventricle using gated myocardial perfusion SPECT

V. Dabbagh, B. Dadpour, R. Afshari, S. Mohajeri; Mashhahd University of Medical Sciences, Mashhad, IRAN, ISLAMIC REPUBLIC OF.

Background: Prevalence of methamphetamine abuse increased quickly in these years. According to researches, methamphetamine abuse has adverse effects on functional statue of myocardium. Most of the studies investigate the effects of methamphetamine on nervous system and few studies assessed myocardium effects of methamphetamine. In our study we evaluated effects of methamphetamine on perfusion and functional status of myocardium of the left ventricle using gated myocardial perfusion SPECT.Method: In a cross sectional study we studied 13 abuser of methamphetamine. Inclusion criteria were: 1. one year using of methamphetamine; 2. Positive urine test; 3. Dependency to methamphetamine according to DSM IV criteria. Exclusion criteria were: 1. History of congenital heart disease; 2. History of heart disease before starting methamphetamine abuse; 3. Pregnancy. Demographic data (age and sex) and information about methamphetamine abuse (period of addiction and amount of that) was obtained and after that Two-day Dipyridamole stress/rest gated myocardial perfusion SPECT was done. Qualitative and quantitative analysis was performed using 17-segment scoring system, QPS and QGS software. Results: Thirteen abuser of methamphetamine (mean age 39.9 ± 9.5 years) participated in our study. The average use of methamphetamine was 0.9 gr and average period of addiction was 3.4 years. All participants reported daily use of methamphetamine. No evidence of ischemia and infarction was seen on gated myocardial perfusion SPECT of participants. Ejection fraction, end systolic volume and end diastolic volume of gated myocardial perfusion SPECT in all participants reported in normal range in both stress and rest steps (Stress step: respectively mean ± SD: 63.8 ± 8.9, 29.1 ± 10.9 and 78.6 ± 16.6; Rest step: respectively mean ± SD: 60.1 ± 8.1, 35.8 ± 11.8 and 88.0 ± 16.2). Also average of myocardial thickening score and myocardial motion score of gated myocardial perfusion SPECT in both steps was in normal range.Conclusion: according to our results, methamphetamine abuse can't lead to a significant perfusion abnormality on GSPECT and therefore, dilated cardiomyopathy that was reported in most of the studies may be related to other causes or longer period of methamphetamine consumption.

P407

Activity of cardiac sympathetic nervous system in patients with atrial fibrillation before and after catheter ablation

B. Chrapko, M. Pachowicz, A. Głowniak, A. Nocuń, M. Wójcik, A. Wysokiński; Medical University of Lublin, LUBLIN, POLAND.

The cardiac sympathetic dysfunction is observed in arrhythmogenic disorders. Aim: We investigated the activity of cardiac sympathetic nervous system (CSNS) by use of iodine-123 meta-iodo-benzylguanidine (123I-mIBG) before and after catheter ablation of atrial fibrillation (AF) Materials and methods: AF group consist of 10 patients (3F/7M; age 54.2 ±10.7 years). Patients in poor general condition, with diabetes mellitus, amyloidosis and neoplastic diseases were excluded from the study. In all patients cardiac sympathetic scintigraphy was performed after injection of 370 MBq 123I-mIBG. Antiarrhythmic drugs were not withdrawn before the study in AF patients. Cardiac sympathetic functions were evaluated semiquantitatively as routine heart to mediastinum ratio (H/M): 15 minute (early eH/M) and 4 hour (delayed dH/M) post administration as well as washout rate (WR). Results: Cardiac sympathetic indices before catheter ablation eH/M=1.69±0.25; dH/M=1.58±0.28, WR=49±22; after catheter ablation eH/M=1.73±0.24; dH/M=1.71±0.33, WR=36%±24. The significant differences were observed in dH/M (Wilcoxon test p=0.02) and WR (Wilcoxon test p=0,009) before and after catheter ablation. Conclusions: In patients with AF after catheter ablation in adrenergic nervous function (WR) tend to normalize as well adrenergic nervous distribution (dH/M).

P408

Usefulness of 18F-FDG PET-CT for Diagnosis of Cardiac Device Infection

A. Jiménez-Ballvé1, M. J. Pérez-Castejón1, M. Martínez de Bourio1, C. Sánchez-Enrique2, I. Vilacosta2, L. Lapeña Gutiérrez1,3, E. Cala Zuluaga1, D. Vivas2, J. L. Carreras-Delgado1,3; 1Nuclear Medicine Department, Hospital Clinico San Carlos, Madrid, SPAIN, 2Cardiology Department, Hospital Clinico San Carlos, Madrid, SPAIN, 3Universidad Complutense, Madrid, SPAIN.

Aim: The aim of this study was to assess the usefulness of PET-CT with 18F-FDG in patients with cardiac device (CD) infection, distinguishing between local device infection and cardiac device-related infective endocarditis. Materials and methods: In this prospective study we included 21 patients with suspicion of having CD infection from April 2013 to March 2015. Duke criteria were used to classify them into definitive or possible infective endocarditis (IE); and clinical criteria if there were local symptoms of infection over the pocket side. PET-CT was considered positive when presented an abnormal uptake of 18F-FDG in any portion of the CD and persisted in the non-corrected images. We differenced three locations of the uptake: pocket generator and local subcutaneous tissue, endovascular extracardiac portion and endovascular intracardiac portion of the electrode. It was considered negative when 18F-FDG uptake was not evidenced or did not persist in the non-corrected images. Anatomy was the gold standard in patients who underwent cardiac surgery. In those cases without removal of the CD, final diagnosis was done by clinical consensus of the endocarditis team (independently from the PET-CT results). Results: The initial suspicion reported 10 (48%) possible IE, 8 (38%) definitive IE and 3 (14%) cutaneus/superficial CD infection. PET-CT was positive in 12/21 (57%) patients: 6 with endovascular intracardiac electrode uptake, 1 with endovascular extracardiac electrode uptake, 4 with uptake in both pocket and endovascular extracardiac electrode and 1 with uptake over the three parts of the CD. In the other 9 (43%) cases, PET-CT was negative. In 4 patients, PET-CT also showed extracardiac findings compatible with septic emboli (3 in lung, 1 spondylodiscitis and 1 in spleen). Anatomy diagnosed 6 IE, 3 pocket infection and rejected 1 IE. Final diagnosis by clinical team was of 2 definitive EI and dismissed infection in other 2 patients. Comparing with final diagnosis, PET-CT results were true positive in 10, true negative in 9, and false positive in 2. There were no false negatives cases. Conclusion: This preliminary data suggest that PET-CT could be a good diagnostic tool in the diagnosis of CD infection and IE related to it.

P409

Cardiac 99mTc-DPD uptake in subjects with Glu89Gln transthyretin gene mutation: is it the earliest sign of disease development?

F. Minutoli1, A. Mazzeo1, G. Di Bella1, A. Sindoni2, L. Gentile1, G. Vita1, S. Baldari1; 1University of Messina, Messina, ITALY, 2AOU "Policlinico P. Giaccone", Palermo, ITALY.

AIM: Many transthyretin (TTR) gene mutations are amyloidogenic being responsible for systemic deposition of TTR variants, especially in the peripheral nervous system and heart. A considerable phenotypic variation originates from different TTR gene mutations. Presenting symptoms in patients with Glu89Gln TTR gene mutation are related to peripheral and autonomic nervous system damage; nevertheless, Glu89Gln TTR gene mutation seems to be responsible for early and severe cardiac involvement. The aim of our study was to evaluate the capability of 99mTc-3,3-diphosphono-1,2-propanodicarboxylic acid (DPD) scan to detect cardiac

amyloid deposition in asymptomatic subjects with Glu89Gln TTR gene mutation as an early sign of amyloidosis development. MATERIALS AND METHODS: Seven asymptomatic subjects (3M and 4F; mean age 42 years) with Glu89Gln TTR gene mutation, normal values of cardiac biomarkers (N-terminal pro-B-type natriuretic peptide (NT-proBNP) and troponin-I), and no electrocardiographic or echocardiographic signs of amyloidosis were enrolled in the study. Each subject underwent 99mTc-DPD scintigraphy at enrollment and was followed-up by cardiological and neurological clinical examinations, electrocardiography, echocardiography and measurement of cardiac biomarkers yearly for 5-8 years. Scintigraphic images were analyzed visually according to a routine scoring system: grade 0, no abnormal localization of the radiotracer; grade 1, myocardial radiotracer uptake lower than bone uptake; and grade 2, myocardial radiotracer uptake higher than bone uptake. RESULTS: In two patients, 99mTc-DPD scan revealed grade 2 radiotracer uptake; this finding preceded the appearance of instrumental or laboratory signs of cardiac amyloidosis and of neuropathic symptoms which developed in the following 2 years. On the other hand, five patients showed no cardiac 99mTc-DPD accumulation; instrumental or laboratory signs of cardiac amyloid deposition appeared only in 3/5 patients 4-8 years later whereas neuropathic symptoms appeared in 4/5 patients 2-6 years after normal 99mTc-DPD scan. CONCLUSION: Cardiac uptake of 99mTc-DPD may precede clinical, instrumental or laboratory signs of amyloidosis; it may represent the earliest sign of amyloidosis in subjects with Glu89Gln TTR gene mutation.

P410

The prognostic role of Fetuin-A serum levels in patients with Coronary Artery Disease. Corellation with myocardium scintigraphy.

A. Zissimopoulos1, A. Psomiadou2, L. Baloka2, E. Karathanos1, A. Thomaidou3; 1Nuclear Medicine Department,Democritus University of Thrace, Alexandroupolis, GREECE, 2School of Molecular Biology and Genetics,Democritus University of Thrace, Alexandroupolis, GREECE, 3Cardiology Clinic, Univ. Hospital of Alexandroupolis ,Democritus University of Thrace, Alexandroupolis, GREECE.

Introduction: Fetuin-A an acidic glycoprotein is produced in the liver, as an inhibitor for cysteine protease. The gene is founded in chromosome 3 (3q27). It is involved in various physiological and pathological conditions. These include vascular decalcification, bone metabolism, insulin resistance, protease function control, neurological illnesses, and multiplication of breast cancer cells. Studies on individuals with clinical cardiovascular disease supported that lower levels of fetuine-A are released with coronary artery circulation (CAC) and the function of the heart valve. Aim: The evaluation of Fetuin-A values of the patients with coronary artery disease, as a prognostic factor of the disease, in correlation with SPECT myocardium scintigraphy. Patients and Methods: We studied 40 patients, 25 male and 15 female, with a mean age 48 ± 8 years (range 36 to 69), with coronary heart disease, which were subjected to myocardium scintigraphy, in the Nuclear Medicine Dept of University Hospital of Alexandroupolis. At the same time blood samples were drawn for the determination of Fetuin-A Serum fetuin A levels were measured by a commercially available sandwich ELISA (Epitope Diagnostics, Inc., San Diego, CA). Results: The average values of Fetuin-A range between 140-297 mg/L, as it is derived from the current bibliography and our laboratory tests. In normal individuals, pathological values were considered to be under 140mg/ L. 25 patients with positive SPECT imaging for myocardium necrosis (scars) had low Fetuin values (45-148mg/ L), 10 of them passing away within 6 months, while the rest of them were showing an encumbered clinical condition ($p<0.005$). 10 patients with reversible ischemia showed relatively low values (125-302mg/L) ($p<0.005$). 5 patients with a normal myocardiac scintigraphic imaging showed normal values of Fetuin-A (165-508mg/L) ($p<0.005$). Conclusions: Patients with myocardium necrosis demonstrated very low values of Fetuin. Patients with ischemia show low amounts while patients with a negative Scintigram for ischemia showed normal results of Fetuin. The 10 patients that passed away in 6 months showed very low amounts of Fetuin. Fetuin-A is supported to be a reliable prognostic factor in monitoring patients with coronary heart disease.

P411

Continued validation of metallic artefact reduction (MAR) algorithms for reducing the likelihood of false positive cardiac implantable device infection (CIED) investigations

M. J. Memmott, J. M. James, F. Z. Ahmed; Central Manchester University Hospitals NHS Foundation Trust, Manchester, UNITED KINGDOM.

Introduction: High and low density streak artefacts in the CT data acquired for attenuation correction of [18F]-FDG PET/CT studies can cause artefactual changes in the quantification of metabolic activity around cardiac implantable electronic devices (CIEDs). Previous phantom work at our institution has shown metallic artefact reduction (MAR) algorithms cause an underestimation of SUVmax values around CIEDs, and hence reduce the impact of these effects. Here we present an initial patient series further evaluating the impact of these algorithms on quantitation. Methods: A total of 7 patients (mean age 70 years; 2/5 male/female) referred for evaluation of suspected CIED infection were included in the analysis to

date. Patients were imaged at both 90 minutes and 180 minutes post administration of [18F]-FDG on a Siemens Biograph mCT. Reconstructions were performed both with and without the manufacturer's MAR algorithm enabled using time-of-flight (TOF) with 2 iterations, 21 subsets and a 5mm Gaussian post-filter. All patients demonstrated multiple foci of uptake in various locations along the length of the device. In total, 33 foci of interest were observed and in each case the SUVmax was recorded in identical locations for both image reconstructions using a 1cm spherical volume of interest (VOI). Differences between the SUVmax values with and without MAR enabled were evaluated using the Mann-Whitney U Test for non-parametric data. Results: All foci had significantly lower SUVmax values ($p < 0.001$) for the MAR enabled reconstructions, when compared to those without MAR, and correlated well with the non-attenuation corrected (NAC) data. No foci of interest had a higher SUVmax value on the MAR enabled reconstructions. Conclusion: This growing patient series expands on previous case reports and phantom work which demonstrate that reconstructions with MAR algorithms enabled do not overestimate [18F]-FDG uptake in regions around CIEDs. The likelihood therefore of false positive results in attenuation-corrected PET images, due to CT based artefacts, is significantly reduced. Conversely, if MAR techniques are not available the likelihood of false-positive results is significantly increased; in this scenario it is imperative to use the NAC data for reporting. These implications would also extend to patients with metallic prosthetic valves.

P412

Correlation of QRS complex duration in 12-lead electrocardiography and cardiac systolic asynchrony assessed by gated SPECT myocardial perfusion imaging

M. Pachowicz, MD, K. Kosecka, A. Kocun, M. Zarobkiewicz, A. Roszkowska, L. Swierszcz, M. Belz, MD, B. Chrapko, MD PhD; Medical University of Lublin, Lublin, POLAND.

Introduction: Cardiac systolic asynchrony is a major clinical problem significantly affecting left ventricle ejection fraction and resulting in heart failure. Aim of the study: The aim of our study was to analyze correlation between the QRS complex duration and cardiac asynchrony assessed by gated SPECT myocardial perfusion imaging. Material and methods: 38 patients (all males) were enrolled into the study. 15 patients had normal stress/rest perfusion scan (excluded cardiac ischemic disease), 22 patients had various fixed perfusion defects. The left ventricle function was analyzed using Corridor 4DM software (INVIA, Ann Arbor, Michigan, USA). Rest studies were used. Cardiac asynchrony was calculated with two protocols provided by the software: time to peak thickening (TPT) and time to peak contraction (TPC) and expressed as histogram standard deviation and 95% histogram width (TPT +/-, TPT95, TPC +/-, TPC95 respectively). The patients' electrocardiograms were independently evaluated by five observers with various experience in ECG reading. The mean QRS duration was calculated for each ECG lead. The correlation was analyzed with Spearman test. Results: There was variable positive correlation between cardiac asynchrony and QRS duration in all leads. For time to peak thickening algorithm the strongest correlation was observed with QRS duration in lead I ($R = 0,82$ for TPT +/-, $R = 0,80$ for TPT95; $p<<0,001$) as well as aVR ($R = 0,66$ for both; $p<<0,001$) and aVF ($R = 0,60$ for both; $p<<0,001$). For time to peak contraction algorithm the strongest correlation was observed with QRS duration in I lead ($R = 0,82$ for TPC +/- and $R = 0,78$ for TPC95; $p<<0,001$). Conclusions: In the analyzed group of patients the strongest correlation between cardiac asynchrony and QRS complex duration was observed in lead I, followed by aVR and aVF. Increased QRS duration in these leads may be the strongest predictor of cardiac systolic asynchrony and decreased left ventricle ejection fraction.

P413

Equilibrium Isotopic Ventriculography in the Diagnosis and Follow-Up of Patients with Drugs Induced Cardiotoxicity

J. Orozco-Cortés1, I. Casáns-Tormo1, R. Díaz-Expósito1, S. Prado-Wohlwend1, H. Bowles-Antelo1, B. Bermejo-de las Heras2, M. Romero-Otero1; 1NUCLEAR MEDICINE. HOSPITAL CLINICO UNIVERSITARIO, VALENCIA, SPAIN, 2ONCOLOGY. HOSPITAL CLINICO UNIVERSITARIO., VALENCIA, SPAIN.

OBJECTIVE: Equilibrium isotopic ventriculography (EIV) is the most reproducible method to determine the left ventricular ejection fraction (EF), so it is specially indicated in the assessment of patients receiving potentially cardiotoxic chemotherapy. We have evaluated our results in diagnosis and follow-up of these patients. MATERIAL AND METHODS: We analyze 1,674 EIV from 2010 to 2012, obtained in the best septal LAO projection, all of them with the same gammacamera and the same semiautomatic processing software to determine EF. All patients had a basal EF (bEF) ≥50% before the treatment, and we considered as cardiotoxicity a decrease ≥10% of its bEF or an EF<50% during treatment. We found 85 patients (84 women), with mean age 58±13 (32-88) y/old, 51.7% of them with ≥8 performed EIV, with a total of 724 EIV. The administered treatment was trastuzumab and/or taxol (n:33-group 1) or trastuzumab, taxol and/or antraciclines (n:52-group 2). During follow-up, we assessed the first cardiotoxic EF (fcEF), the highest cardiotoxic EF (hcEF) and the last one performed EF

(lEF), establishing three groups according to the EF recovery: complete recovery 100% compared to bEF (CR) , incomplete recovery (IR) :<100% but with an EF ≥50%, and non recovery (NR):EF <50%. RESULTS: The mean bEF was 62.1 ±5.3%(50-76%), being ≥55% in 80/85(94.1%) of patients, the mean fcEF:49.8±4.9%(36-61%), with a mean decrease of 19.8±6.3% from bEF. We found an EF<50%(31-49%) during the treatment in 49/85(57%) of the patients. The mean hcEF was 47.9±5.4%(31-61%), with a mean decrease of 23.0±8.4% from bEF. We found EF recovery in 60/85 patients: CR(6)+ IR(54) and NR in 25 patients. Patients with EF recovery showed higher values of bEF comparing with NR patients (63.2±5.3 vs 59.2±3.9,p:0.001), fcEF (50.6±7 vs 47.8±4.9, p<0.02), hcEF (49.7±4.6 vs 43.6±5.0,p<0.001) and lower decrease from bEF of hcEF (21.3±5.7 vs 27.2±11.8,p:0.003) and lEF (11.4±6.8 vs 21.9±11.1,p<0.001). Between G1 and G2 there were NS differences. Patients with bEF ≥60%(n:60) showed higher fcEF (51.4±4.3 vs 46.0±4.2, p<0.001) and hcEF (49.2±5.5 vs 44.8±3.9, p:0.001) than patients with bEF<60(n:25).CONCLUSION: The assessment of the EF variations by EIV during treatment with cardiotoxic drugs could detect significant decrease of EF in subclinical phase, when the interruption of the treatment can make the recovery of the EF possible. Necessary requisites are to have always a basal determination of EF and the use of the same technical equipment to obtain and process the images during follow-up of the patients.

P414

Improvement in myocardial perfusion induced by subendocardial stem cell injection in patients with advanced heart failure

L. Lezaic1, A. Socan1, P. Kolenc Peitl1, G. Poglajen1, M. Sever1, F. Haddad2, B. Vrtovec1; 1Klinicni center Ljubljana, LJUBLJANA, SLOVENIA, 2Stanford University Medical Center, LJUBLJANA, CA, UNITED STATES.

Background: Stem cell transplantation (SCT) is an emerging treatment option in patients with advanced heart failure. Aim: To assess potential improvement in myocardial perfusion induced by subendocardial SCT. Materials, methods: In 26 patients with advanced heart failure (18 patients, nonischaemic cardiomyopathy; 8 patients, ischaemic cardiomyopathy; NYHA III-IV; LVEF<35%), hematopoietic stem cells (CD34+) were peripherally collected after G-CSF stimulation and subendocardially injected in dysfunctional, yet viable LV areas using NOGA-XP(c) system under guidance of electromechanical LV mapping and myocardial perfusion SPECT/CT (99mTc-tetrofosmin, viability protocol with nitrate enhancement). A small proportion of stem cells (20%vol) was labeled with 99mTc-HMPAO and resuspended with non-labeled portion prior to injection. Imaging of SCT was performed 1h (planar, SPECT/CT) and 18h (planar) after injection for assessment of stem cell retention and (re)distribution. Myocardial perfusion imaging was repeated 6 months after SCT; both series were quantified using 17-segment model and perfusion defect scoring (0-4). Wilcoxon signed rank test and Pearson correlation coefficient were used for data comparison and correlation, as appropriate. Results: Subendocardial injection was effective in stem cell delivery to the myocardium: myocardial retention at 1h ranged from 0,3 to 23,3 (median 4,9)%. There was significant efflux of stem cells from injection site at 18h (13,5 to 41,7%, median 32,2% of initial retention; p<0,01). Myocardial perfusion improved significantly with reduction in perfusion defect score (from pre-SCT range 2 to 30 to post-SCT range 2 to 29, median pre-SCT 10,5 to post-SCT 8,0; p<0,01). Improvement in perfusion defect score inversely correlated significantly with stem cell efflux from the myocardium (p<0,01, r=-0,57). Conclusion: Subendocardial SCT appears to improve myocardial perfusion in patients with advanced heart failure. Efflux of injected stem cells from the delivery site is inversely correlated to perfusion improvement.

P415

Evaluation of early changes in left ventricular volumes in women with breast cancer treated with adjuvant trastuzumab

C. Haase, B. Zerahn, A. Polk, D. Nielsen; Herlev Hospital, Herlev, DENMARK.

Aim: Treatment with trastuzumab is reported to be associated with cardiotoxicity. The purpose of this study was to evaluate early changes in left ventricular volumes and ejection fraction using CZT-SPECT radionuclide ventriculography during adjuvant treatment with trastuzumab in patients with primary breast cancer. Materials and methods: 77 women with primary breast cancer treated with trastuzumab as an 8 mg/kg loading dose followed by 6 mg/kg every 3 weeks were evaluated retrospectively at 6 months after initiation of treatment. The following variables were recorded: Left ventricular end systolic and end diastolic volumes (LVESV and LVEDV), left ventricular ejection fraction (LVEF) and the incidence of a reduction in LVEF to ≤ 0.5 from pre-trastuzumab therapy values. LVEF was determined by steady state 550MBq 99mTc-HSA gated (16 frames per R-R interval, 600 beats) equilibrium radionuclide ventriculography with a dedicated cardiac SPECT camera with CZT-detectors (Discovery 530c, GE). Results: One patient had a LVEF of less than 0.5 at baseline and was excluded from the study. Two patients had a decline in LVEF to ≤ 0.5 at 90 days follow up. These patients were subsequently treated for heart failure. 17 patients has not yet completed 180

days follow-up. The remaining 57 had a decline in LVEF from 66.1 % to 61.5 % (p<0.001) due to increases in LEDV (86.3 to 93.0 ml (p< 0.001)) and LESV (29.9 to 37.0 ml (p<0.001)). No significant changes in systolic or diastolic blood pressure or heart rate were recorded. Conclusions: In this retrospective study we found that the decline in LVEF during trastuzumab treatment was due to an increase in left ventricular volumes. This finding may contribute to identify the underlying pathophysiological mechanism behind trastuzumab cardiotoxicity.

P416
Effects of anthracycline and trastuzumab chemotherapy on diastolic function and mechanical synchrony

V. M. Alves, T. Vieira, A. Oliveira, A. Fernandes, A. Pinto, T. Faria, B. Perez, J. Pereira; São João Hospital Centre, Porto, PORTUGAL.

Aim: To investigate the effects of anthracycline and trastuzumab on left ventricular diastolic and systolic function, including intra- and inter-ventricular systolic synchrony. Materials and methods: Thirty-four female patients from a population with early-stage or locally advanced, HER-2 positive breast cancer were consecutively enrolled in a retrospective longitudinal study. These patients underwent systemic treatment with chemotherapy according to five different treatment schemes, three of them included anthracyclines. Patients received trastuzumab for about 11 months, concurrent with or following the chemotherapy scheme. Equilibrium radionuclide ventriculography (ERV) was performed before and after chemotherapy, and subsequently every 3 months until the end of trastuzumab (5-6 scans per patient). Informations such as: cardiovascular risk factors, chemotherapy dosage, radiotherapy, cardiac symptoms and trastuzumab discontinuation were collected from the medical records. Each ERV was processed and left ventricular ejection fraction (LVEF), heart rate (HR), right (RV) and left (LV) ventricular peak phase, RV and LV phase standard-deviation, peak filling rate (PFR) and time to peak filling rate (TPFR) were collected. Inter-ventricular synchrony was calculated. Baseline and post-treatment parameters were compared. The difference between the lowest follow-up LVEF and the baseline LVEF (Δlf-bLVEF) was determined for each patient and correlations were performed with baseline and others equivalent (Δlf-b) imaging parameters (i.e., at the same time points as the Δlf-bLVEF) as well as with clinical and treatment variables. Results: The mean age was 50 years. Eleven patients were treated with anthracyclines (doxorubicine n=6; epirubicine n=5). There was a significant decreasing of the LVEF (mean: 69.7% vs. 64.9%, p= 0.002), HR (mean: 80.3 bpm vs. 71.7 bpm, p<0.001), LV peak phase (median: 169.0° vs. 155.0°, p=0.05), VD peak phase (median: 166.0° vs. 157.0°, p=0.001) and PFR (median: 3.64 EDV/s vs. 3.18 EDV/s, p=0.001) between the baseline and the post-trastuzumab exams. No significant change was noted for intra- or inter-ventricular synchrony parameters or TPFR during the follow-up. The Δlf-bLVEF was only positively correlated with Δlf-bLV peak phase (rs=0.346, p=0.048) and Δlf-bTPFR (rs=0.413, p=0.017). Additionally, anthracycline chemotherapy was associated with interventricular dyssynchrony (p=0.028).Conclusion: Chemotherapy protocols that include trastuzumab and eventually anthracyclines were associated with impairment of systolic and diastolic ventricular function. Anthracyclines regimens were specifically associated with interventricular dyssynchrony.

P417
Association between body mass index and left ventricular mechanical dyssynchrony in patients with chronic kidney disease

V. M. Alves, A. Fernandes, T. Vieira, A. Oliveira, A. Pinto, T. Faria, B. Perez, J. Pereira; São João Hospital Centre, Porto, PORTUGAL.

Introduction: End-stage kidney disease is independently associated with left ventricular mechanical dyssynchrony (LVMD), which provides an important prognostic value in this population. LVMD has also been found in patients with metabolic syndrome (diabetic or not) or with obesity. The aim of this study was to find any association between body mass index (BMI) and LVMD in two different populations: chronic kidney disease (CKD) and non-CKD patients. Methods: We conducted a retrospective analysis of consecutive patients who performed 99mTc-tetrofosmin gated myocardial perfusion imaging (g-MPI), with adenosine stress testing, in a 2-day protocol, during 2013. We included every patient who presented with normal left ventricular perfusion and function (summed stress score=0; ejection fraction ≥45%, respectively). The exclusion criteria were heart disease, arrhythmia, conduction (namely QRS >120ms) and repolarization disorders, electrocardiographic criteria of left ventricular hypertrophy, heart transplantation and poor quality g-MPI scans. The following data were collected from the medical records: demographics, weight, height, cardiovascular history, current therapy and global and regional LV function parameters at stress (QGS/QPS® software). LVMD at stress [phase standard-deviation (PSD) and histogram bandwidth (PHB)] were obtained by reprocessing of the g-MPI on the Emory Cardiac Toolbox® software. We analyzed the association between LVMD and the variables included, before and after stratification by CKD. Results: Twenty-nine patients were included (14 females; mean age: 56±16 years; mean BMI: 25.0±5.1; 15 with CKD; 17 with hypertension; 10 with diabetes, 13 with dyslipidemia; 6 with peripheral arterial disease, and 5 smokers). Dyssynchrony parameters were similar for CKD and non-CKD groups (PSD:

10.2 vs. 11.4, p=0.278; PHB: 33.5 vs. 37.1, p=0.342; respectively). We found an association between LVMD and BMI, but only in the CKD group (PSD vs. BMI: rs=0.532; p=0.041; PHB vs. BMI: rs=0.596; p=0.019). We found no association between LVMD and the remaining cardiovascular risk factors, even after stratification by CKD. Conclusion: In a population of CKD patients without heart disease, LVMD was not increased, but we found a positive association between BMI and LVMD. Additional studies may disclose a synergic effect between overweight and CKD on the development of LVMD.

P418

Post-stress worsening of LV mechanical dyssynchrony is more frequent in CAD patients but has low diagnostic accuracy

Y. Chang, C. Hsu; Kaohsiung Chang Gung Memorial Hospital, Kaohsiung City, TAIWAN.

Aim: Previous studies showed that myocardial ischemia induces post-stress worsening of left ventricular mechanical dyssynchrony (LVMD) obtained from thallium-201 (Tl-201) gated SPECT myocardial perfusion imaging (MPI). The different dyssynchrony pattern between ischemic and normal myocardium at early post-stress may aid the diagnosis of coronary artery disease (CAD). The aim of this study is to assess the accuracy of stress-induced LVMD worsening, either global or territorial, in the diagnosis of CAD. Materials and Methods: The Tl-201 gated MPI data of 74 patients were retrospectively analyzed. All patients received coronary angiography with at least 50% luminal diameter narrowing as significance of CAD. The perfusion images were interpreted by two experienced observers in consensus. Two LVMD parameters, phase histogram bandwidth (PHB) and phase standard deviation (PSD), were calculated territorially and globally. Patients showed post-stress increasing in either PSD or PHB, were defined as post-stress worsening of LVMD.Results: Among the 74 patients, 52 patients had significant coronary artery stenoses (CAD patients) and 22 patients had no significant CAD (normal patients). In normal patients, the global post-stress LVMD parameters were significant lower as compared to LVMD parameters at rest (PSD 8.88 vs 11.52, p<0.01 and PHB 34.1 vs 45.3, p<0.01, respectively). In CAD patients, only post-stress PSD were significantly lower than rest PSD (9.73 vs 11.18, p<0.05).Global post-stress worsening of LVMD was observed in 3 of 22 normal patients (13.6%) and was more frequent in CAD patients (22 of 52, 42.3%, p<0.01). On territory-based analysis, post-stress worsening of LVMD was observed in 19 territories (19/66, 22.3%) of normal patients. There were more frequently noted in CAD patients at either coronary stenotic territories (47/102, 46.1%, p<0.01) or remote normal territories (26/54, 48.1%, p<0.01).By using perfusion defect in any one vessel territory as criteria, the sensitivity, specificity, and accuracy for CAD were 92.3%, 81.8%, and 89.2%, respectively. By using global stress-induced worsening of LVMD parameters, the sensitivity, specificity, and accuracy for CAD were 51.9%, 81.8%, and 60.8%, respectively. By territory-based analysis of LVMD parameters, the sensitivity, specificity, and accuracy for CAD were 78.8%, 54.5%, and 71.6%, respectively.Conclusion: Stress-induced worsening LV mechanical dyssynchrony, either globally or territorially, was observed more frequently in patients with CAD. However, the diagnostic accuracy of stress-induced worsening of LV mechanical dyssynchrony for coronary artery stenosis was low.

P25 - Monday, October 12, 2015, 4:00 PM - 4:30 PM, Hall 3 – Poster Exhibition

Neurosciences: Basic Science

P419

Test-retest reproducibility of adenosine A1 receptor imaging in rats, using microPET, the tracer 11C-MPDX, repeated arterial blood sampling and kinetic modeling

J. W. A. Sijbesma1, X. Zhou1, J. Doorduin1, M. Houwertjes2, C. Kwizera1, B. Maas1, P. Meerlo3, R. A. J. O. Dierckx1, R. H. J. A. Slart1, P. H. Elsinga1, A. Van Waarde1; 1University of Groningen, University Medical Center Groningen, Department of Nuclear Medicine and Molecular Imaging, GRONINGEN, NETHERLANDS, 2University of Groningen, University Medical Center Groningen, Department of Anesthesiology, GRONINGEN, NETHERLANDS, 3University of Groningen, Department of Behavioral Physiology, GRONINGEN, NETHERLANDS.

OBJECTIVES: Adenosine A1 receptors (A1AR) in the brain of experimental animals can be visualized using radiolabeled xanthines and positron emission tomography (PET). We were interested in the reproducibility of quantitative A1AR scans with the tracer 11C-MPDX, in order to evaluate whether this technique is capable of detecting subtle changes of A1AR availability. Unfortunately, a reference region without specific binding is not available in the rodent brain. For this reason, test-retest studies with 11C-MPDX demand repeated arterial cannulation and rapid arterial blood sampling. METHODS: A minimally invasive technique for arterial cannulation was developed, which can be repeatedly applied and allows longitudinal microPET studies in rodents with full kinetic modeling. A thin cannula was inserted in a superficial branch of a femoral artery and moved up through this blood vessel until the main artery was reached. After the scan, the cannula could be pulled back and the rather minor wound was surgically closed. Animals then received analgesia (subdermal bupivacaine 2.5 mg/

kg). Eight rats (healthy males, Wistar strain) were scanned twice with 11C-MPDX at an interval of 1 week, and rapid arterial blood sampling was performed in both cases. The tracer (39±18 and 26±13 MBq at scan 1 and scan 2, respectively) was administered as a slow (1 min) bolus, using an injection pump. PET images were fused with an MRI template, using the program PMOD, and regions-of-interest (ROI) for relevant brain regions were copied from MRI to PET. Tracer distribution volume (VT) in these brain regions was calculated by Logan graphical analysis, 1 tissue-compartment and 2-tissue-compartment model fitting. RESULTS: The cannulation procedure resulted in rapid wound healing and only minor discomfort to the animals. Body weight was 306±40 g at scan 1 and 325±36 g at scan 2. Test-retest reproducibility of VT was dependent on the volume and position of the ROI besides regional levels of A1AR expression, but was generally excellent. A test-retest reproducibility better than 5% was observed in cerebellum, cerebral cortex, hippocampus, striatum and thalamus. Reproducibility values between 5 and 10% were noted in amygdala, medulla, midbrain, olfactory and pons. Only in hypothalamus, variability was greater than 10%. However, if animals damaged their wound sutures and needed additional anesthesia and suturing, reproducibility suffered a little. CONCLUSIONS: Repeated arterial blood sampling in rodents is possible with this new technique, and the tracer 11C-MPDX may allow longitudinal, quantitative in vivo imaging studies aimed at detecting minor changes of apparent A1AR availability.

P420

Effect of mTOR inhibition on epileptogenesis in the rat epilepsy model

A. CULLIER1, F. MASKALI1, A. CLEMENT1, S. POUSSIER1, G. KARCHER, Pr.1, P. MARIE, Pr.1, E. RAFFO2; 1GIE-NANCYCLOTEP, VANDOEUVRE-LES-NANCY, FRANCE, 2NEUROPEDIATRY DEPARTEMENT, HOSPITAL OF BRABOIS, VANDOEUVRE-LES-NANCY, FRANCE.

The Mesial Lobe Temporal Epilepsy (mLTE) is the most drug-resistant epilepsy. Its natural history, reconstructed by the lithium-pilocarpine in rats model, starts with the SE followed by a histological restructuration within the hippocampal and para-hippocampal regions, which creates a hyper-excitable neo-circuit implementing recurring spontaneous seizures. The mTor pathway is a proteical intracellular complex that regulates synaptogenesis, neuronal plasticity, inflammation and proliferation of cerebral gliosis. This specific pathway is activated at different stages of the mLTE. The goal of the present pre-clinical study was to evaluate the impact of inhibiting the mTor pathway by Rapamycin over epileptogenesis and neuroprotection in the lithium-pilocarpine model. For this study, 44 adult rats were divided into 3 groups: treated SE (i), untreated SE (ii) and healthy witnesses (iii). Each of them received Rapamycin per os at 3 stages: H+2 at 6 mg per kg per day, then D1 and D2 at 3 mg per kg per day. The treatment was evaluated by studying metabolic modifications, using positon emission tomography and 2-[18F]-fluoro-2-deoxy-D-glucose, at H+4, D2 and D8 (1), the research for spontaneous crisis from D8 (2), and eventually by counting neurons in the interest regions after sacrifice at D60 (3). In the acute phase, we show an increase of consequences of the SE on glucose local cerebral metabolism, in the hippocampus and parahippocampal cortex, by the use of Rapamycin. However, an increased hippocampal hypometabolism at D2 suggests that Rapamycin may have a neuroprotecting potential, which has to be confirmed by histological study. We don't observe any treatment effect at D8. We don't show either any influence of Rapamycin treatment over epileptogenesis. Our results along with previous studies outcomes recommend evaluating Rapamycin administration from the beginning of SE and by the intra-peritoneal pathway, as well as treatment prolongation during the whole epileptogenesis silent phase.

P421

Are there gender differences in P-glycoprotein function at the rat blood-brain barrier ?

S. MARIE, G. POTTIER, S. GOUTAL, S. AUVITY, I. BUVAT, R. BOISGARD, F. DOLLE, F. CAILLE, N. TOURNIER; IMIV, UMR 1023 Inserm/CEA/Université Paris Sud - ERL 9218 CNRS, CEA, DSV, I2BM, Service Hospitalier Frédéric Joliot, Orsay, F-91401, FRANCE.

AIM: Many studies have reported gender differences in both toxicity and therapeutic outcome of medications, including CNS drugs, where females consistently present with greater toxicity. P-glycoprotein (P-gp) is a major efflux transporter which restricts the distribution of many compounds across the blood-brain barrier (BBB). Therefore, reduced P-gp function in females relative to males would provide a pharmacokinetic (PK) explanation for differential CNS sensitivity to drugs identified as P-gp substrates. We recently validated [11C]metoclopramide, a specific P-gp substrate with significant baseline brain uptake and no detectable radiometabolites in the brain, even in the presence of P-gp inhibition. The purpose of this study is to test the hypothesis of a functional difference in P-gp function at the BBB between male and female rats, the major animal model used for PK studies. MATERIALS AND METHODS: [11C]metoclopramide microPET imaging (37 MBq IV; 30 min scan, Siemens Inveon) was performed in male Wistar

rats in the presence (n = 4) and the absence (n=5) of P-gp inhibition (tariquidar 8 mg/kg IV, 5 min before tracer injection). Data were compared to those obtained in female Wistar rats without P-gp inhibition (n = 5). Brain time-activity curves (TACs) obtained in each condition were used to estimate the total volume of distribution (VT; mL.cm-3) using [11C]metoclopramide arterial input function corrected from radiometabolites (Logan plot analysis).RESULTS: PET data confirmed [11C]metoclopramide as a P-gp substrate at the BBB: [11C]metoclopramide brain distribution was higher ($p < 0.05$) in tariquidar-treated males (VT = 8.8 ± 1.6 mL.cm-3) compared to control males (VT = 2.6 ± 0.4 mL.cm-3). TAC shapes appeared similar in both the male and female groups. We found lower [11C]metoclopramide distribution in control females compared to control male rats, although non-significant (VT = 2.4 ± 0.3 mL.cm-3).CONCLUSION: We found no significant difference of P-glycoprotein function at the rat BBB between male and female rats. This information suggests that gender is not a confounding factor to study P-gp function at the rat BBB using PET.

P422

A [11C]preladenant PET study of Striatal adensoine A_{2A} receptor occupancy by KW-6002 in rats

X. Zhou, P. Elsinga, R. Dierckx, E. de Vries; University Medical Center Groningen, Groningen, NETHERLANDS.

Aims: The first aim of the study was to assess the suitability of [11C]preladenant-PET for studying the $A_{2A}R$ occupancy by an $A_{2A}R$ specific antagonist, using KW-6002 as a typical example. The second aim was to determine the optimal acquisition time and the reference region in a simplified reference tissue model (SRTM).Materials and methods: Eight baseline PET scans and 12 scans after *i.p*. administration of various doses (between 0.01 and 1 mg/kg) of KW-6002 were performed. Rats were *i.v.* injected with [11C]preladenant 15-25 min after KW-6002 or vehicle administration, and a 90 min dynamic PET scan was started. The binding potential (BP_{ND}) in striatum was obtained by SRTM with 90 min or 60 min acquisition, using midbrain or cerebellum as the reference tissue. Receptor occupancy was calculated by the following equation: $Occupancy(\%)=100*(BP_{ND,\ baseline}-BP_{ND,\ blocking})/BP_{ND,\ baseline}$. The in-vivo ED_{50} of KW-6002 was estimated by fitting the dose-occupancy curve with a single binding site model using the following formula: $Occupancy(\%)=100*Occ_{max}*D/(D+ED_{50})$, where Occ_{max} is the maximum occupancy, ED_{50} is the drug dose correspond to 50% occupancy, and D is the drug dose.Results: BP_{ND} estimates in striatum at baseline were slightly but significantly ($p<0.05$) higher with 60 min acquisition, compared with 90 min acquisition. BP_{ND} values were 5.96±0.62 and 6.08 ±0.52 for the 90 and 60 min acquisition, respectively, using midbrain as the reference tissue, and were 5.48±0.56 and 5.56 ±0.47 for the 90 and 60 min acquisition, respectively, using cerebellum as the reference tissue. Pretreatment of KW-6002 decreased the tracer uptake in striatum in a dose-dependent manner (10-98% occupancy correspond to 0.01-1 mg/kg blocker). The ED_{50} for *i.p*. injection of KW-6002 was estimated to be 0.056 and 0. 060 mg/kg for the 90 and 60 min acquisition, respectively, using midbrain as the reference tissue; and of 0.060 and 0.062 mg/kg for the 90 and 60 min acquisition, respectively, using cerebellum as the reference tissue. Thus, comparable estimates of occupancy and ED_{50} were obtained when either cerebellum or midbrain were used as the reference tissue. Therefore, these brain regions are equally well applicable as the reference region. Furthermore, a 60 min acquisition seems to be slightly better than a 90 min acquisition, in terms of higher BP_{ND} values with lower standard deviation obtained from a 60 min acquisition.Conclusions: [11C]Preladenant-PET is suitable to estimate striatal $A_{2A}R$ occupancy in the brain with SRTM, using cerebellum or midbrain as the reference tissue.

P423

Comparing 123I-Ioflupane (DatScan) SPECT using LEHR and Fan-Beam Collimators - an Initial Investigation into Clinical Impact

H. A. Williams, G. Al-Bahrani, J. James; Nuclear Medicine, Manchester, UNITED KINGDOM.

Methods: Patients attending for DatScan were invited to undergo additional FB SPECT following the standard 185 MBq DatScan and LEHR SPECT at 4 hours post-injection. 17 consented (7 female, 8 male), 2 withdrew after initial LEHR SPECT. All images were acquired using a dual-headed GE Millenium VG gamma camera, both SPECT procedures used 120 views over 360°but FB SPECT used 21s views compared to 30s for LEHR, reducing the overall scan time by 9 minutes.LEHR SPECT was reported as usual. The FB SPECT images were visually evaluated by the same reporting clinician, who assessed overall quality, noise, edge definition, contrast, amount of detail, and how apparent any well-defined features and hot-spots were and whether this improved with FB. Clinicians were also asked whether FB SPECT would have altered or improved confidence in the clinical conclusion from LEHR SPECT. Results: The overall quality of the FB images compared to the LEHR images was rated better in 33.3% of cases, worse in 13.3% and similar in 53.3%. Particular aspects of image quality were scored as follows:Noise - FB better, 40%; both the same 26.7%; LEHR better 33.3%Edge definition - FB better, 73.3%; both the same 13.3%; LEHR better 13.3%Contrast - FB better, 53.3%; both

the same 33.3%; LEHR better 13.3%Amount of detail visible - FB better, 93.30%; both the same 6.7%; LEHR better 0%How apparent the defects/hot-spots are - FB better, 53.3%; both the same 46.7%; LEHR better 0%How clearly defined the defects/hot-spots are - FB better, 86.7%; both the same 6.7%; LEHR better 6.7%FB images gave the reporting clinician more confidence in their diagnosis in 53.3% of cases, with confidence being similar in 26.7% and LEHR giving greater confidence in 20%. However, viewing FB images did not alter the reporting clinician's clinical conclusion in any of the 15 cases. The clinicians initially reported that the different appearance of the FB images made comparison difficult, but quickly adjusted. Conclusion: FB SPECT images were considered superior to LEHR SPECT, particularly with regard to edge and feature definition, which increased confidence in the clinical report based on the LEHR images although the clinical findings were unaltered. We are now looking to translate these findings to the gamma camera currently used for DatScan SPECT (Siemens Symbia T6).

P424

Revealing asymmetric activations in the auditory cortex in rats with FDG PET

M. Mamach1,2, G. Berding1,2, J. P. Bankstahl1, F. M. Bengel1, S. Kurt1,2; 1Medical School, Hannover, GERMANY, 2Cluster of Excellence "Hearing4All", Oldenburg, GERMANY.

Aim:Lateralization of activation in the auditory cortex in rats was previously shown using histological and electrophysiological approaches. We assessed the functional asymmetry of the auditory cortex (AC) using in-vivo FDG PET imaging in normal hearing, healthy rats.Methods:Three separated F-18-fluorodeoxyglucose (FDG, 16-20 MBq) PET (Inveon, Siemens) scans were performed in each of 12 adult female Sprague Dawley rats for three sound conditions: 55 dB background noise (BG55), 65 dB continuous white noise (WN65) and 95 dB pulsed rippled noise (RN95). These conditions were presented for 41 min, beginning 1 min before intravenous injection of FDG to trained, awake animals, which were placed into a motion restricting tube in a sound attenuated box. PET scans were acquired 1 h after tracer injection across 30 min. Data were reconstructed iteratively (OSEM) including Co-57-transmission-source-based attenuation correction. Spatial normalization and brain activity normalization were performed using a mask and FDG template of PMOD3.6. Mean normalized activities in volume of interest (VOI) were obtained based on Schwarz's VOI atlas for the AC, the inferior colliculus (IC) and a control region, the olfactory nuclei (ON). Differences of means (left - right) were analyzed using paired t-tests for each VOI and each stimulus condition. Results were compared without smoothing ([0.0mm]3) and with [2.0mm]3 Gaussian smoothing.Results:Individual left-right differences in the auditory cortex varied over all conditions from -12% to +10% without and -6% to 7% with [2.0mm]3 smoothing. Using the RN95 stimulus, the auditory cortex expressed a FDG uptake asymmetry with increased uptake in the left cortex 4.0±0.8% ($p<0.001$) for [0.0mm]3 and 3.4±0.6% ($p<0.001$) for [2.0mm]3. During WN65 stimulation, asymmetry was observed with increased left AC's uptake of 3.4±1.4% ($p<0.05$, [0.0mm]3) and 3.4±0.9% ($p<0.05$, [2.0mm]3), respectively. In BG55 environment, asymmetry amounted to 2.1±0.7% ($p<0.05$, [0.0mm]3) and 2.8±0.5% ($p<0.001$, [0.2mm]3) with increased uptake in the left AC. For IC and ON no significant asymmetry was observed.Conclusions:Statistical analyses of auditory cortex in normal hearing rats with PET revealed functional activation in AC with prevalence of the left side, but not in the IC or the ON. A tendency of larger left side prevalence in louder sound conditions was observed. The left side prevalence being a random effect is highly unlikely as the significant prevalence was observed with and without filtering. Functional asymmetry of the AC during different auditory sound conditions could be determined using FDG PET.

P425

Metabolic and Neurovascular Coupling in brain SPECT and PET of patients with epilepsy and normal 3T MRI

E. N. I. Itikawa1,2, D. K. S. Sonvenso1,3, L. A. S. Santos1,3, M. K. Kato1,3, F. A. P. Pitella1,3, C. E. P. B. Baltazar1,4, A. C. T. Trevisan1,2, V. A. J. Junior1,3,5, **L. W. A. Wichert-Ana**1,2,3; 1Ribeirão Preto School of Medicine, Ribeirão Preto, BRAZIL, 2Post-Graduation Program Interunits Bioengineering EESC/FMRP/IQSC-USP, São Carlos, BRAZIL, 3Post-graduation Program in Internal Medicine, Ribeirão Preto, BRAZIL, 4Faculty of Philosophy, Sciences and Literature of Ribeirão Preto, Ribeirão Preto, Ribeirão Preto, BRAZIL, 5Department of Neurology, Ribeirão Preto, BRAZIL.

AIM: To evaluate the neurovascular (99mTc-ECD SPECT) and metabolic (18F-FDG PET) coupling in patients with refractory epilepsy associated to normal MRI.MATERIAL AND METHODS: Twenty-seven patients with refractory epilepsy and normal MRI from the Epilepsy Surgery Center (CIREP) were screened to this study. All patients underwent interictal 99m-Tc-SPECT, 18F-FDG-PET and 3T MRI acquisition. Two nuclear medicine specialists visually evaluated functional images. Concordance inter-observer was evaluated through weighted kappa (κ_w). Brain regions were divided in frontal, temporal, parietal, occipital lobes, basal ganglia thalamus and cerebellum. Hypoperfusion and hypometabolism were scored as 0: normal uptake; 1: mild ; 2: moderate and

3: severe. Neurovascular and metabolic coupling were evaluated either through intersection of brain regions or the same level of decreased uptake using results of semiology, interictal and ictal video-EEG as a reference for seizure localization/lateralization. Fisher's exact test was used for this purpose. Posteriorly, localization hypothesis for epileptogenic zone was based on the congruence of clinical data and results of ictal and interictal video-EEG confronted with functional neuroimaging findings.RESULTS: Mean age was 34.55 years (sd = 12.25; range: 19-60 years old). Risk factor for epilepsy included encephalitis (n=1); neonatal hypoxia (n=1); obstetric complications (n=2), *status epilepticus* (n=1) and 22 showed no risk factors. Four patients showed mild mental retardation on neuropsychological examination. All patients showed abnormalities in the interictal SPECT while in 5, PET was normal. We found good concordance between the observers for interictal SPECT in temporal lobe, basal ganglia, thalamus and cerebellum. For PET images, there was no discordance in temporal and occipital lobes, thalamus and basal ganglia. Regions of hypoperfusion and hypometabolism were the same as the reported by video-EEG in 73% of the patients. The occurrence of same hypoperfusion/hypometabolic regions was not associated to a focal or diffused video-EEG profile, though. Regions of maximum neurovascular coupling were the same as the regions reported by video-EEG in 75% of the patients. Nevertheless, the occurrence of neurovascular coupling was not associated to a focal or diffuse video-EEG profile.CONCLUSION: Good concordance between the observers was achieved in the functional images evaluation. Interictal SPECT and PET showed regions of abnormal uptake and neurovascular coupling congruent to video-EEG in most of patients. Despite the qualitative approach in our study, we encourage further quantitativeanalysis of functional data such as SPM in the study of neurovascular coupling using SPECT and PET images.

P426

Quantification of GABA-A receptor binding in the auditory system of rats using F-18-Flumazenil PET

M. Mamach1,2, G. Berding1,2, J. P. Bankstahl1, T. L. Ross1, F. M. Bengel1, S. Kurt1,2; 1Medical School, Hannover, GERMANY, 2Cluster of Excellence "Hearing4All", Oldenburg, GERMANY.

Aim: The GABAergic inhibitory neurotransmitter system is known to play a major role in the auditory systems and its disorders such as hearing loss and tinnitus. F-18-Flumazenil (FMZ) PET has been used to visualize GABA-A-receptor binding. The purpose of this study was to explore the feasibility to obtain quantitative measures of GABA-A-receptor binding in small animals. Besides this, this approach might reveal new insights in auditory diseases, based on dynamic PET imaging and bio-kinetic modeling of the GABAergic system. Methods: Scans were performed in 6 normal hearing female Sprague Dawley rats using FMZ (6-20 MBq) PET (Inveon, Siemens). The tracer was injected via tail vein in isoflurane anaesthe-tized animals simultaneously with the start of dynamic scans lasting 45min. Data were reconstructed iteratively including 57Co-transmission-source-based attenuation correction for 31 time consecutive frames (5x2s, 4x5s, 3x10, 8x30s, 5x60s, 5x5min, 1x10min). Motion correction, spatial normalization and VOI-wise modelling were performed using PMOD3.6. For each scan a VOI was manually placed in the hearts left ventricle to obtain the whole blood time activity curves as input functions. Mean parametric volumes of distribution (Vt) were calculated based on the Logan plot model for auditory regions (inferior colliculus (IC), mediate geniculate body (MGB) and auditory cortex (AC)) as well as reference regions (PONS, cerebellum (CB) and somatosensory cortex (SC)) using Schwarz's VOI atlas. Binding potentials (BP) were calculated with respect to the PONS. Results: All plots showed a good agreement of model and data. FMZ revealed a high uptake in the brain. The PONS, as a reference, showed the lowest Vt 1.22±0.34. In the auditory regions, we detected higher Vts compared to the PONS: for the AC 2.58±0.47 and the IC 2.71±0.53. The corresponding mean BPs were in the AC 2.11 and in the IC 2.22. The SC showed similar values of Vt 2.63±0.54 and BN 2.16. In the thalamic MGB, values of 2.00±0.38 for Vt and 1.64 for BN were detected. The CB's means of Vt and BP were 1.76±0.33 and 1.44, respectively. Conclusions: Our data indicate that calculation of distribution volumes and binding potentials based on dynamic PET measurements of FMZ distribution in rats provides consistent results with acceptable variation. Binding in regions with specific tracer uptake clearly exceeded compared to the reference areas. We conclude from these results, that in-vivo FMZ-PET is a promising method for the evaluation of hearing disorder in small animals.

P427

Quantification of 5HT2A-Receptors in the Human Brain with [18F]MHMZ

V. Kramer1, M. Herth2, E. Hernandez3, C. Juri4, R. Pruzzo3, F. Rösch5, H. Amaral1; 1PositronPharma SA, Santiago de Chile, CHILE, 2University of Copenhagen, Copenhagen, DENMARK, 3Nuclear Medicine and PET/CT Center FALP, Santiago de Chile, CHILE, 4Universidad Catolica, Santiago de Chile, CHILE, 5Johannes Gutenberg-Universität Mainz, Mainz, GERMANY.

Objectives: PET quantification of 5HT2A-receptors is an important tool for drug occupancy studies and of major interest in

different psychiatric disorders and as biomarker for neuronal integrity. For decades 18F-Altanserin and 11C-MDL-100907 were clinically used for quantification despite their disadvantages related to extensive metabolism and half-life. 18F-MHMZ (or 18F-FE-MDL-100907) was developed as 18F-version of MDL-100907 to overcome these disadvantages and to provide the possibility of precise quantification of 5HT2A receptors in sub-cortical brain regions. We herein report the GMP compliant synthesis and a First-In-Man study in healthy volunteers. Methods: 18F-MHMZ was produced as previously described by the indirect, two step labeling approach via 18F-Fluoroethyl tosylate. The synthesis was validated on a cassette based platform under GMP conditions. 3 healthy volunteers underwent a dynamic PET scans (Siemens mCT) for a duration of 180 min after bolus injection of 185 ± 19 MBq (mean ± SD) [18F]MHMZ. T1 weighted MRI scans were acquired for each volunteer for co-registration, normalization and VOI-outlining. Blood input function was recorded by online blood sampling (Twilite/Swisstrace) and plasma and parent fraction were determined. Distribution volumes and binding potentials were determined by different invasive and non-invasive methods. Results: Starting activities of 10-40 GBq were used for labeling and 18F-MHMZ was obtained in high radiochemical puritiy (>95 %) and uncorrected RCYs of 15-30 % in 90 min. 18F-MHMZ revealed a relatively slow kinetic and high tracer uptake in cortical areas as expected. Lower uptake was observed in striatal areas, amygdala and cerebellum. The reliability of different invasive and non-invasive quantification methods is currently under evaluation. Nevertheless, first data indicate that stable estimates for binding potentials in different brain regions can be obtained after 180 min scan duration using 2TCM. Conclusions: 18F-MHMZ is a promising tool for 5HT2A receptor quantification in cortical and sub-cortical areas of the human brain.

P26 - Monday, October 12, 2015, 4:00 PM - 4:30 PM, Hall 3 – Poster Exhibition

Neurosciences: Dementia

P428

Introducing the Glucose Metabolism to Amyloid Deposition Ratio Image

K. Ishii1, R. Takahashi2, Y. Wakabyashi1, C. Hosokawa1, H. Kaida1, T. Murakami1; 1Kinki University, Osakasayama, JAPAN, 2Hyogo Prefectural Rehabilitation Hospital at Nishi-Harima, Tatsuno, JAPAN.

OBJECTIVE: Alzheimer's disease (AD) is characterized by increased cortical amyloid deposition in the prodromal stage and subsequent decrease of cerebral glucose metabolism with disease progression. The present study introduces voxel-wise metabolism into amyloid deposits ratio (MAR) imaging in order to evaluate its reliability in the diagnosis of AD. METHODS: 324 consecutive subjects with 143 AD and 181 normal subjects were included in this study from the Alzheimer's disease neuroimaging initiative (ADNI) database. The MAR image was created by dividing each FDG-PET image by corresponding AV-45 PET image using voxel-wise inter-image computation. We examined voxel wise comparison in the MAR images between AD subjects and normal subjects and compared the diagnostic performances between the MAR image and FDG-PET and AV-45 image. RESULTS: MAR images of AD subjects exhibited severe and extensive decreases compared with normal subjects in the affected region in AD. The highest t-value was equivalent to the FDG-PET and the voxel extent was much greater than the other images. The diagnostic accuracies were 82.6%, 80.7%, and 78.8% for the MAR image, FDG-PET, and AV-45, respectively. AUC for the MAR image was 0.904, and was larger than those for FDG-PET (AUC: 0.884), and AV-45 (AUC: 0.847). CONCLUSION: MAR image reflects not only amyloid deposition, but cerebral hypometabolism and can successfully classified subjects with AD. MAR imaging techniques might be a more appropriate marker for monitoring disease progression of AD.

P429

The brain SPECT perfusion rating using Neurogam program for diagnostics of early onset Alzheimer disease

R. Pichova1, A. Bartos2, O. Samokhvalova2, J. Kotoucova2, D. Ripova3; 1Charles University Prague, 3rd Medical Faculty, CZECH REPUBLIC, 2Charles University Prague, 3rd Medical Faculty, National Institute of Mental, CZECH REPUBLIC, 3Charles University Prague, National Institute of Mental Health, CZECH REPUBLIC.

Aim: To develop a simple regional semi-quantification of 3D brain SPECT perfusion using Neurogam program for early Alzheimer disease (AD) diagnostics and to assess interindividual concordance of the results. Introduction: It is hypothesised, the SPECT perfusion image changes should correspond with the anatomical cascade atrophy in AD: mediotemporal → temporoparietal → frontal area. Subjects and Methods: 35 cognitively normal controls (NC) were enrolled in the study - Mini-Mental State Examination (MMSE) 29±1 points, an average age 69 years (y), an average education 15 y. 33 patients with mild cognitive impairment (MCI) or mild dementia due to Alzheimer disease (AD) were examined - MMSE 26±3 points, an average age 77 y, an average education 14 y. 99mTc-HMPAO brain SPECT images were transformed into 3D templates using NeuroGamTMSegami software. Perfusion of parietal lobe convexity, cingulum, temporo-parietal,

mediotemporal and frontobasal regions were rated 0 (normal), 1 (border), 2 (reduced) in both hemispheres. These data were combined into a single bilateral score ranging 0 (normal), 1 (border), 2 (reduced on one side), 3 (reduced on both sides). Results: Patients with MCI and mild AD did not differ in age, gender, education, MMSE. They were merged into one AD patient group. In comparison with the NC group, these patients had significantly higher score of hypoperfusion in parietal or temporoparietal region on one side or bilaterally. All other regions including mediotemporal ones were perfused in these patients and in the controls similarly. The interindividual concordance was found in 62 out of 68 (91 %) patients. Conclusions and discussion: Semi-quantification of the visual rating of 3D Neurogam brain SPECT perfusion is a simple and convenient tool for routine clinical practice. The early onset AD patients already had incipient perfusion alterations in temporoparietal regions on one or both sides. Surprisingly, mediotemporal mild changes were common even in normal seniors and were indistinguishable from those found in AD patients. This pattern for early diagnosis needs further exploration. Assessment has satisfactory interindividual rate reliability. Supported by grant IGA NT 13183, PRVOUK 34/LF3 and DRO (PCP, 00023752).

P430

SUVratio(SUVr)-independent semiquantification of brain amyloidosis: a software-aided integration of visual and quantitative analyses

S. Morbelli1, F. Nobili2, F. Sensi3, U. Guerra4, L. Rei3, I. Bossert1, A. Chincarini for the ADNI3; 1Nuclear Medicine Unit, IRCCS AOU San Martino - IST, Genoa, ITALY, 2Department of Neurology, IRCCS AOU San Martino - IST, University of Genoa, Genoa, ITALY, 3National Institute for Nuclear Physics (INFN), Genoa, ITALY, 4Nuclear Medicine Unit, Fondazione Poliambulanza, Brescia, ITALY.

Background: In-vivo quantification of brain beta-amyloid deposition using positron emission tomography (PET) is likely to play a pivotal role in upcoming clinical trials of disease modifying agents. Because of the non trivial visual assessment, a more sophisticated approach is required in form of reliable automatic quantification methods.Aims: to compare the fundamental approaches to amyloid-PET quantification and introduce a novel, comprehensive procedure that combines visual and automatic quantification, procedural operationalization and conflict resolution.Methods: We set a reference images base of Florbetapir scans of 244 subjects from the ADNI archive. Subjects were selected to have at least two scans (at baseline and after an approximately 2 years of follow-up).Subjects clinical evaluation was taken to be the closest diagnosis to the baseline PET scan date. Cohorts are grouped by the ADNI core clinical criteria as: normal subjects (NS, N=70), early mild cognitively impaired (EMCI, N=86), mild cognitively impaired (MCI, N=26), late mild cognitively impaired (LMCI, N=51) and Alzheimer's diseases (AD, N=11).These scans were independently and blindly evaluated by three expert readers with a visual procedure according to Florbetapir guidelines and their expertise.On these scans we compare the performance, reliability and result quality of three SUVr-based quantification methods plus the novel non-SUVr based approach we developed. This method evaluates the brain as a whole and delivers a geometrical/intensity score for each image, to be used in dichotomic assessment and ranking.Results: Analyses show that the proposed SUVr independent approach has the potential to out-perform standard SUVr based methods, resulting in excellent agreement with visual rating on a single scan rating-bases(AUC ~ 0.94 / 0.98).Longitudinal analyses were though plagued by image quality and acquisition protocol consistency, requiring three or more scans to deliver a reliable trend. This effect was more pronounced on the SUVr-independent algorithm because of the inherent dependence on local image characteristics.Conclusions: The need for automatic quantification methods in amyloid-PET is dire, particularly for one that integrates visual and software assessment in a structured, procedural approach. With the delivery of procedural recommendations, we expect to significantly improve the diagnosis time and accuracy in clinical practice, where the judicious use of the quantification software will be instrumental to a more efficient decisional process and patient follow-up.

P431

18F-FDG PET/CT: A New Tool to Evaluate the Interaction between Cognitive Reserve (CR) and CSF-Biomarkers in Alzheimer Disease (AD) Patients

E. Carapelle, S. Modoni, G. Rotondo, L. Specchio; OSPEDALI RIUNITI, FOGGIA, ITALY.

Aim: To examine the effect of the correlation between CSF-biomarkers, education (a proxy of CR) on brain [18F]fluorodeoxyglucose positron emission tomography (PET) metabolism in patients with early/moderate Alzheimer Disease (AD). Methods: Twenty-seven patients with probable AD and twenty-five neurologically normal subjects (HS), matched for age and sex, were studied. CSF β-amyloid1-42 (Aβ1-42), 181p-tau and Tau concentrations were measured in AD by Innotest ELISA. 18-FDG-PET/TC was performed in AD and HS 40 minutes after i.v. administration of radiopharmaceutical (3,7 MBq/kg). Mini Mental State Examination (MMSE) was performed in AD patients. CR was measured as years of education: AD patients were classified as High Educated-AD (HE-AD) if education in years was > 5 versus

Low Educated-AD (LE-AD) if education in years was ≤ 5. By using a voxel-wise approach, we first investigated differences in the cerebral glucose uptake (GU) between AD and HS, then we assessed the correlation between education, CSF-biomarkers on FDG-PET metabolism in the patient groups. Results: No significant demographic differences were found between AD and HS. Significant clusters of low GU were observed in the posterior cingulate gyrus, in the precuneus, in the inferior and medial temporal gyrus, in the inferior parietal lobule bilaterally in AD but not in HS. No significant difference in age and MMSE was found between AD groups. By using a voxel-wise approach no significant differences in the mean values of GU were observed in HE versus LE-AD. Conversely, in the right orbital frontal cortex the mean values of GU was significantly higher in HE-AD versus LE-AD (p=0.02). A significant interaction was found between groups (HE e LE) and Aβ1-42 values in the inferior and medial temporal gyrus bilaterally. Conclusions: Decreased glucose metabolism in regions typically targeted by AD pathology (i.e., medial temporal lobes) and increased metabolism in the right orbital frontal cortex might reflect compensation mechanisms due to CR, which contrasts the neurodegeneration as assessed by CSF Aβ1-42. We hypothesized that CR could be a compensatory mechanism and it could modify the effect of Aβ plaques on cognitive activity of these regions assessed by brain metabolism.

P432

Different patterns of brain glucose consumption related to the age of onset in Alzheimer' s disease

A. Chiaravalloti1, D. Di Biagio1, R. Danieli1, B. Di Pietro1, G. Koch2, A. Martorana2, P. Abbatiello1, O. Schillaci1; 1Department of Biomedicine and Prevention, University Tor Vergata, Rome, ITALY, 2Department of Neurosciences, University Tor Vergata, Rome, ITALY.

Aim: To investigate the relationships between age of onset of Alzheimer's disease (AD) and brain glucose consumption as detectable by means of 2-deoxy-2-(18F) fluoro-D-glucose (18F-FDG) Positron Emission Tomography/Computed Tomography (PET/CT). Materials and methods: We examined 81 newly diagnosed probable AD patients according to the NINCDS-ADRDA criteria (46 women and 36 men; mean age 69 ± 7 years). All the subjects underwent a cerebrospinal fluid (CSF) assay for levels of p-Tau, t-Tau and Aβ1-42 amyloid peptide ~ 1 month before PET/CT examination. A standard Magnetic Resonance has been performed in all the subjects enrolled in the study. Relationships between age of onset of AD an brain glucose consumption have been assessed by a regression analysis in Statistical Parametric Mapping version 8 (SPM8) using gender, Mini Mental State Examination (MMSE) and CSF levels of p-Tau, t-Tau and Aβ1-42 amyloid peptide as covariates. Results: MMSE, p-Tau, t-Tau and Aβ1-42 amyloid peptide were equal to 18.52± 6, 81.29± 47, 678.8± 322 and 321.2± 127 respectively with no differences in genders. SPM8 regression analysis showed a significant decrease (with a statistical threshold of p=0.001, family wise error (FWE)-corrected) of glucose consumption in a wide portion of the left parietal lobe (BA7, BA31 and BA 40) in those patients with an early onset of the disease. No areas of significant reduction of brain glucose consumption have been found in those subjects with a late onset of the disease. Conclusions: the results of our study show that an early age of onset of AD is related to a selective metabolic pattern that involves mainly the left parietal cortex. This pattern is independent from CSF biomarkers that are commonly used in the evaluation of AD.

P433

The impact of education on FDG PET single subject analysis for Alzheimer's dementia diagnosis

I. Mainta, G. Amzalag, O. Ratib, G. B. Frisoni, **V. Garibotto**; University Hospital of Geneva, GENEVE, SWITZERLAND.

Purpose: FDG PET is a widely used biomarker of dementias, able to identify the metabolic changes associated with the regional distribution of pathology, namely in Alzheimer's Disease (AD).Education, among others, is known to increase the so-called "reserve capacity" of the brain, which modulates the association between hypometabolism and clinical expression, namely reducing the clinical severity for a given level of pathology by recruiting alternative and redundant networks. Aim of this study is to measure the impact of education on the threshold to define FDG PET abnormality and on its diagnostic accuracy.Materials and methods: We selected 45 healthy controls and 51 AD patients from the ADNI database. In order to provide an objective metric of the presence of AD type hypometabolism, we extracted mean relative glucose metabolism, within a set of regions typically affected, normalized to the activity in the cerebellar vermis and corrected for age (metaROI). We divided the AD population in two subgroups with respect to the median of years of education, thus identifying patients with a lower (23) or higher (28) reserve.We used a Receiver Operating Characteristic (ROC) curve approach.The area under the curve (AUC) of the two ROC was compared with a t-test.Results: The AUC of the metaROI values was 0.89 in patients with lower reserve, compared to controls, and 0.90 in patients with higher reserve. The difference between the two groups was not significant. The cut-off value providing a minimum sensitivity of 80% was -0.76 in subjects with lower reserve and -1.10 (indicating a more severe reduction) in subjects with higher reserve.ConclusionsFDG PET has a high diagnostic accuracy both in patients with

higher and with lower reserve. However, in order to achieve a comparable sensitivity, a different threshold for abnormality has to be used in the two groups, namely a less conservative threshold in patients with lower reserve. These results underline the importance of integrating image interpretation with patient's demographics and clinical presentation and to develop personalized analysis tools.

P434

Proposal of a Method to Estimate Normal Threshold Values of Summed Z-scores in the Specified Regions for Z Sum Analysis for Diagnosing Alzheimer's Disease with Voxel-based Control Database of I-123 IMP SPECT

N. Shuke1, C. Miyazaki1, A. Ando1, T. Onishi1, K. Saito1, J. Sato2, A. Okizaki2, K. Nishikawa3; 1Kushiro Kojinkai Memorial Hospital, Kushiro, JAPAN, 2Asahikawa Medical College, Asahikawa, JAPAN, 3Imaging Information Technology Center, Nihon Medi-Physics Co., Ltd., Osaka, JAPAN.

Objective: Using generalized extreme studentized deviate many-outlier procedure (ESD), voxel-based control database (CDB) could be generated from clinical patient's data (pts') for statistical brain SPECT analysis. The objective of this study was to propose a method for estimating normal threshold values of summed Z-scores in the specified regions (bilateral parietal, precuneus / posterior cingulate, medial occipital, and lateral occipital regions) for Z sum brain SPECT analysis (Ishii K, et. al. Computer-assisted diagnostic system for neurodegenerative dementia using brain SPECT and 3D-SSP. Eur J Nucl Med Mol Imaging. 33: 575-583, 2006) on CDB with 3D-SSP. Method: I-123 IMP SPECT data from 117 pts (70±;7 y old , M/F=50/67) were studied. CDB was generated using ESD and prior pts' data selection based on Euclidean distance to the sample mean SPECT image. To estimate normal threshold values of summed Z scores, pts' data in which all voxels in the specified regions contributed to CDB were selected. Mean and SD of Z sums for each specified region were then calculated from Z maps from CDB and selected pts' data (method 1) and from CDB and 34 normal volunteers' data as a standard reference method (method 2). Calculated mean and SD of Z sums were then compared between two methods. Results: Twenty-three pts' data were selected by the criterion and used for calculating mean and SD of Z sums in the method 1. Both mean and SD of Z sums were not significantly different ($P<0.05$) in all but bilateral medial / lateral occipital regions. Conclusion: These results indicated that proposed method (method 1) could be useful to estimate normal threshold values of summed Z-scores in the specified regions for Z sum analysis with voxel-based CDB from clinical pts' data.

P435

Correlation between brain perfusion SPECT and neuropsychological test in the diagnosis of dementia

M. J. Ibáñez Ibáñez1, **L. Mohamed Salem**1, M. V. Godoy Bravo1, L. F. Álvarez Nieto1, R. Reyes Marlés1, M. I. Castellón Sánchez1, L. Frutos Esteban1, J. L. Navarro Fernández1, J. Marín Muñoz2, C. Antúnez Almagro2, M. A. Claver Valderas1; 1Servicio de Medicina Nuclear. Hospital Clínico Universitario Virgen de la Arrixaca, Murcia, SPAIN, 2Unidad de Demencias. Hospital Clínico Universitario Virgen de la Arrixaca, Murcia, SPAIN.

AIM: To study the correlation between the results of brain perfusion SPECT and neuropsychological tests in the diagnosis of patients with clinical suspicion of neurodegenerative dementia. MATERIAL AND METHOD: We study retrospectively 100 patients with brain perfusion SPECT with 99mTc-HMPAO, with clinical suspicion of neurodegenerative dementia conducted between January and June 2014. All were referred from the Dementia Unit of our hospital where they performed neuropsychological tests. They were classified into 6 subgroups according to clinical diagnosis: 13 without dementia, 26 with mild cognitive impairment (MCI), 22 with Alzheimer's disease (AD), 7 with frontotemporal dementia (FTD), 6 with primary progressive aphasia (PPA) and 26 with other diagnoses (psychiatric illness, depression, etc). The correlation between the results of SPECT and neuropsychological test is assessed. RESULTS: We found correlation of SPECT and neuropsychological test results in 77 of the 100 patients studied (77%). The results for diagnostic subgroups are: there is a correlation between brain perfusion SPECT and neuropsychological tests findings in 13 of 13 without dementia (100%); in 19 of 26 with DCL (73%); in 19 of 22 EA (86.3%); in 4 of 7 with DFT (57.1%) and in 6 of 6 with APP (100%).CONCLUSION: The good correlation between brain perfusion SPECT and neuropsychological tests findings (besides its availability and low cost) shows a proof of high diagnostic yield and recommends his routinary use in earlier stages of neurodegenerative dementias.

P436

11C-PIB Retention Patterns in Amnestic and Nonamnestic Mild Cognitive Impairment Patients. Comparison with 18F- FDG PET/CT

Z. Bravo- Ferrer, J. Jiménez-Bonilla, M. De Arcocha-Torres, I. Banzo, I. Martínez-Rodríguez, R. Quirce, C. Lavado-Pérez, J. L. López-Defilló, M. Jiménez-Alonso, D. Meza-Escobar, F. Gómez-de la Fuente, J. M. Carril; Nuclear Medicine. Molecular Imaging Group (IDIVAL). Marqués de Valdecilla University Hospital. University of Cantabria, Santander, SPAIN.

Aim: In a preliminary study we have comparedof the PIB retention patterns and glucose metabolism in amnestic and non-amnesticMild Cognitive Impairment (MCI) patients and in the control population. Theresults were encouraging and we present here the current results in a muchlarger population of MCI patients. Methods: The study group included 81consecutive patients: 36 male and 45 female. The average age was 67.25+ 7.84years. All patients were referred from the Cognitive Impairment Unit of ourhospital, and classified according to the clinical diagnosis into non-amnesticMCI (**NA**-MCI) (n=17) andpredominantly amnestic MCI (**A**-MCI) (n=64).All patients had a 30 minutes PET/CT acquisition 60 minutes after intravenousinjection of 555MBq of 11C-PIB and 24 hours later, a 15 minutesPET/CT, 20 minutes after intravenous injection of 185 MBq of 18F-FDG wasacquired. Visual analysis of the studies was performed by two nuclear medicinephysicians with experience in brain amyloid scan. A blind interpretation of the randomlydistributed images was done. A study was considered positive when there wasuptake in Gray Matter (GM) > White Matter (WM). Regional PIBretention was classified according the following patterns: Pattern A (frontal,anterior cingulate, lateral temporal and basal ganglia) and Pattern B (retention),and compared with the FDG results. Results: 45/81 patients (55.5%) werepositive and 36/81 were negative (44.5%). Of the 64 **A**-MCI, 42 showed 11C-PIB positive scan (66%) and negativein 22 (34%) ($p<0.001$). Of the 42 PIB positive, FDG was positive only in 10patients; however in the 22 PIB negative FDG was negative in all on them. Onthe other hand of the 42 **A**-MCI PIBpositive patients, 12 showed in A-pattern and in all on them FDG was negative;however for the B-pattern only 20 of the 30 were FDG negative. Of the 17 **NA**-MCI patients, 14 were PIB negative,and all of them were also FDG negative. Conclusion: Overall, theproportion of PIB positive and PIB negative was similar. In the amnestic MCIgroup the number of PIB positive doubled the PIB negative and all the 22 PIBnegative, were also FDG negative.In non-amnestic MCI patients, PIB positive ishighly unlikely, however in the amnestic MCI patients with pattern A, FDG isexpected to be negative, and therefore FDG could not be indicated in thesepatients.

P437

Hypometabolism in posterior and temporal areas of the brain is associated with cognitive decline in Parkinson's disease

F. DEMAILLY1, C. TARD2, P. LENFANT1, F. SEMAH1, C. MOREAU3, K. DUJARDIN3; 1Service de Médecine Nucléaire, CHRU Lille, Lille, FRANCE, 2Service de Neurophysiologie, CHRU Lille, Lille, FRANCE, 3Service de Neurologie et pathologie du mouvement, CHRU Lille, Lille, FRANCE.

Objective: The primary objective was to determine whether a specific brain metabolic pattern is associated with cognitive decline in Parkinson's disease (PD).Methods: Sixteen advanced PD patients were screened for the absence of cognitive impairment (according to the Mattis dementia rating scale, MDRS) and underwent [18F]-Fluorodeoxyglucose positron emission tomography brain imaging in the "off drug" state. The MDRS was scored again about two years later, categorizing patients as having significant cognitive decline (decliners) or not (stables). The two groups were then compared in terms of their brain metabolism at inclusion.Results: There were six decliners and ten stable patients. Significant hypometabolism in the two precunei (Brodmann area (BA) 31), the left middle temporal gyrus (BA21) and the left fusiform gyrus (BA37) was found in the decliner group compared with the stables.Conclusion: In advanced PD, a particular metabolic pattern may be associated with the onset of significant cognitive decline.

P438

Role of Tc-99m HMPAO brain SPECT in the differential diagnosis of vascular and other dementias

A. T. Golubic1, R. Petrovic1, T. Samardzic1, N. Klepac2, F. Borovecki2; 1Department of Nuclear Medicine and Radiation Protection, University Hospital Center Zagreb, Zagreb, CROATIA, 2Clinical Department of Neurology, University Hospital Center Zagreb, Zagreb, CROATIA.

Aim: The aim of this study was to examine the value and importance of brain SPECT in the differential diagnosis of cognitive decline. Establishing a correct diagnosis is often challenging and is frequently dependent solely on clinical evaluation. Functional neuroimaging is emerging as an additional clinicians' aid in correctly diagnosing dementia patients and providing the appropriate therapy.Method: Sixty-nine patients (39 female)with various forms of newly reported cognitive decline were referred to our Department from November 2014 to March 2015, mostly (68%) with unspecified cognitive decline as a working diagnosis. Twelve patients (17%) were suspected to have Alzheimer's disease (AD) and eight (11.6%) were assumed to have vascular dementia. Their mean age was 71 years (range 51-89). They underwent regional cerebral blood flow (rCBF) examination with single-photon emission computerized tomography (SPECT), using standardized EANM protocol.Results: Decreased perfusion in temporoparietal cortex, usually bilaterally, characteristic for AD, was found in 12% of patients. Patchy, irregular tracer uptake with significant reductions of rCBF in majority of cerebral regions, differing in size and severity, left to right asymmetries and even globally diminished perfusion with changes in the cerebellum, characteristic for vascular dementia

(VD) was found in the majority of our patients, 52%. A third of our patients were reported to have the above mentioned AD perfusion pattern with the addition of nonuniform VD pattern, indicating a mixed dementia. Six patients had the perfusion pattern of frontotemporal and Lewy body dementia, and two had a normal finding. SPECT data were compared with clinical and psychometric data. A significant number of patients found to have mixed dementia had a positive history for high blood pressure (80%) and hyperlipoproteinemia (76%). A more specific diagnosis (AD, FTLD, LBD perfusion pattern, mixed dementia)was determined in 42% of patients. In 50 patients detailed follow-up was obtained, which indicated an altered clinical diagnosis in 23, and confirmation of the working diagnosis in additional 9 patients, with modification in patient management due to brain SPECT data in 64% of patients with follow up neurology exam.Conclusion: HMPAO brain SPECT has been presented as an immensely valuable functional neuroimaging method in differentiating patients with various cognitive decline symptoms. It presents an affordable and accessible tool which enables early and correct diagnosis and influences further patient management and therapy.

P439

Brain perfusion differences between early and late onset Alzheimer's disease

V. Valotassiou1, J. Papatriantafyllou2, N. Sifakis3, C. Tzavara1, S. Alexiou1, I. Tsougos1, D. Psimadas1, A. Ziaka1, E. Baniora1, P. Georgoulias1; 1Department of Nuclear Medicine, University Hospital of Larissa, Larissa, GREECE, 2Memory & Cognitive Disorders Clinic, Neurology Dpt., "G. Gennimatas" Hospital, Athens, GREECE, 3Nuclear Medicine Dpt, "Alexandra" University Hospital, Athens, GREECE.

Aim: Early (<65 years) onset Alzheimer's disease (EAD) differ from late (>65 years) onset AD (LAD) in clinical symptoms, genetics and neurophycological, neurochemical and neuropathological characteristics. There is limited literature with contradictory results about the influence of age onset on brain perfusion in AD patients.The aim of our study was the evaluation of brain perfusion in specific Brodmann areas (BA) in EAD and LAD patients, using an automated 3D-voxel-based processing software (Neurogam).Materials-methods:We studied 53 consecutive patients from an outpatient Memory Clinic. We used the established DSM-IV criteria for the diagnosis of dementia and the specific established criteria (NINCDS-ADRDA) for the diagnosis of AD. All the patients had a neuropsychological evaluation with a battery of tests including the mini-mental state examination (MMSE). The EAD group included 20 patients (8 men, 12 women, age±SD 63.1±5.5, MMSE±SD 18.1±6.1, education±SD 11.5±4.5 years) and the LAD group consisted of 33 patients (8 men and 25 women, age±SD 74.7±5.7 years, MMSE±SD 19.3 ±5.9, education±SD 8.4±4.5 years). All the patients underwent a brain SPECT scan 20 min after the intravenous administration of 740MBq of 99mTc-HMPAO. We applied the NeuroGamTM software on the reconstructed data, for the semi-quantitative evaluation of brain perfusion in BA in the right (R) and left (L) hemispheres. Perfusion values in BA were expressed as mean±SD percentage of mean perfusion of the cerebellum. Statistical analysis was performed using Qui-square and Mann-Whitney test.Results: Compared with EAD, LAD patients had statistically significantly lower perfusion in right anterior prefrontal cortex (BA 10R p=0.045), left orbitofrontal area (BA 11L p=0.05), inferior frontal gyrus (BA 44L p=0.029, BA 44R p=0.045, BA 45R p=0.016, BA 47L p=0.046, BA 47R p=0.014) and right dorsolateral prefrontal cortex (BA 46R p=0.014).Conclusion: We found frontal lobe hypoperfusion in LAD patients, compared with EAD patients. Our findings would be related with older age in the LAD group or with specific heterogeneities between the groups. Further brain perfusion SPECT studies with automated data analysis softwares could contribute to a better understanding of the underlying processes in EAD and LAD.

P440

FDG-PET study of psychophysiological mechanisms of aggression in patients with vascular dementia

J. Khomenko, D. Susin, G. Kataeva, T. Reznikova, N. Seliverstova, B. Lipovetsky; N.P.Bechtereva Institute of the Human Brain, RAS, St.Peterburg, RUSSIAN FEDERATION.

Introduction. It is known that patients with dementia suffer from not only cognitive but also emotional disturbances that can manifest in increase of aggression in behavior and self-aggression. It is of great importance to reveal and treat such disturbances in time because they can result in decrease of the quality of life and personal disorders. For the effective correction it is necessary to understand psychophysiological mechanisms of different types of aggression.The aim of this study was investigation of interconnections of different types of aggression (according to the Buss-Durkee method) and regional glucose metabolism rates in patients suffered from vascular dementia.Methods. PET-FDG was performed in 20 patients with vascular dementia (age 51-86) on Scanditronix scanner and standard protocol, relative estimation of regional glucose cerebral metabolic rate (rCMRglu) in regions of interest corresponding to Brodmann areas (BA) were calculated by WFU PickAtlas. Psychological examination of aggression was performed with Buss-Durkee test included subscales estimating levels of physical, verbal, displaced and total aggression,

irritancy, negativism, soreness, suspicion, sense of guilt and hostility.Results. Significant correlations between rCMRglu (p<0,05) and aggression scores were revealed. In both hemispheres rCMRglu in frontal cortex (BA 9,10,11,46) and anterior cingulate cortex (ACC) (BA 24, 32) negatively correlated with hostility, suspicion and soreness (r=-0,5-0,6), whereas verbal and total aggression positively correlated with CMRglu in ACC and amygdala (r=0,7 for left and 0,6 for right hemisphere). Also CMRglu in left BA 40 and 24 positively correlated with irritancy (r=0,6).Conclusions. Thus, injury of frontal cortex in patients with vascular dementia can result in decrease of inhibition effect and manifestation of those types of aggression in behavior and emotional state which are more related with personal feeling. Obtained results are in agreement with role of prefrontal cortex in executive control of behavior including aggression through the inhibition of the limbic system. At the same time, positive correlation of others subscale scores (as verbal and total aggression) with functional activity in ACC, amygdala and BA 40 is in agreement of finding of connection of increased rCMRglu in these structures during emotional speech and negative words encoding.Therefore, different types of aggression were associated with different brain structures that is in agreement with the results of our previous research revealed similar connections in epileptic patients.

P441

Diagnostic value of regional myocardial adrenergic imaging using 123I-MIBG compared to SPECT-HMPAO perfusion and cerebrospinal fluid biomarkers to differentiate Lowy Body Dementia and Alzheimer Disease

f. hamza1, i. jardak1, w. amouri1, f. kallel1, n. bouzidi2, s. charfeddine1, e. turki2, m. maaloul1, c. mhiri2, f. guermazi1; 1Nuclear Medicine Departement, Habib Bourguiba Hospital, Sfax, TUNISIA, 2Departement of Neurology, Habib Bourguiba Hospital, Sfax, TUNISIA.

Aim:LBD is the second leading cause of degenerative dementia after AD in the elderly population. An early differentiation of LBD from other dementias, particularly AD, is important because LBD has a different course and prognosis. The aim of this study is to determine the potential diagnostic value of regional myocardial adrenergic 123I- metaiodobenzyl guanidine (MIBG) compared to Single Photon Emission Tomography (SPECT) perfusion and cerebrospinal fluid protein (CSP) levels for differential diagnosis between Lowy Body Dementia (LBD) and Alzheimer disease (AD).Materials and methods:We report prospectively the data of 5 patients initially evaluated by a neurologist for suspicion of AD. The clinical symptoms were ambiguous; it was difficult to disentangle LBD from AD. All patients underwent SPECT-HMPAO perfusion that confirms the diagnosis of a neurodegenerative disease without discrimination AD/LBD. For that, cerebrospinal fluid protein dosage (amyloid-beta42, tau and Ptau) and cardiac 123I-MIBG scintigraphy were performed.All patients received an intravenous administration of 111 MBq of 123I-MIBG. Static images were acquired using a dual-head scintillation camera equipped with low- to energy general-purpose (LMEGP) parallel-hole collimators. A 5-min static acquisition was made in the anterior view at 15 min (early) and 3 hours (delayed) after the injection of 123I-MIBG. To assess the cardiac MIBG uptake, the delayed heart to mediastinum ratio (HMR) was calculated after manually drawing regions of interest over the entire heart and the upper mediastinum.Results:In the first case, the cardiac uptake was normal with a CSP profile of an AD (amyloid-beta42 =300 pg/ml, tau=701 pg/ml, Ptau=75 pg/ml). The HMR was significantly diminished in 3 cases in accordance with cerebrospinal fluid protein (CSP) levels, particularly a normal level of the protein amyloid-beta42 reflecting a LDB disease. However, in the last case, the reduced uptake in cardiac MIBG scintigraphy was mismatched with a reduced level of the protein amyloid-beta42 and elevated levels of the protein tau and its phosphorylated isoform suggesting the diagnosis of AD.Conclusion:Our study supports the usefulness of MIBG myocardial scintigraphy in the diagnosis of LBD. However, false positive can be observed and may be age-related because myocardial MIBG uptake has a significant age-related decrease.

P442

FDG-PET in the evaluation of brain metabolic changes induced by Cognitive stimulation in aMCI subjects

E. Giovannini, E. Borsò, F. Benso, E. Carabelli, M. Del Sette, A. Ciarmiello; Sant'Andrea Hospital, La Spezia, ITALY.

Cognitivetraining has reported to improve cognitive performance in Mild CognitiveImpairment (MCI) as well as in older healthy subjects. 18F-FDG-PET is widelyused in the diagnoses of dementia for his ability to identify early metabolicchanges. This study was aimed to assess the effect of cognitive stimulation onbrain metabolic network and clinical cognitive performance. Thirty amnestic MCI(aMCI) subjects were enrolled in the study and allocated in two groups matchedfor cognitive profile, sex and schooling and then randomly assigned to thetraining arm or to the placebo arm. All subjects underwent toneuropsychological assessment and PET imaging before and after intervention. Wefound significantassociation between brain metabolism and cognitive stimulation in treated aMCIsubjects. Brain metabolic changes include Brodmann areas reported to be involvedin

working memory and attentive processes and executive functions. Our study shows that metabolic changes occurearlier than possible clinical changes related to the intervention. 18F-FDG-PET could provide a useful biomarker of response to identify a populationof aMCI suitable to respond to treatment, according to most recent data ondefault network mode and its adaptivity to external stimuli.

P443

Graph-theoretical analysis for comparison of functional brain networks between very early Alzheimer's disease and healthy volunteers

H. Matsuda, E. Imabayashi, J. Rokicki, N. Maikusa; National Center of Neurology and Psychiatry, Kodaira, JAPAN.

Graph-theoretical analysis was applied to brain perfusion SPECT using 99mTc-ECD for comparison of functional brain networks between very early Alzheimer's disease (AD) and healthy volunteers. Sixty healthy controls (28 men and 32 women; 54-83 years of age; mean,71.5;SD,8.3) and 29 patients with very early AD (13men and16women; 57-85 years of age; mean, 70.9; SD, 7.8) at the stage of amnestic type of mild cognitive impairment (MCI), who showed progressive cognitive decline and eventually fulfilled the diagnosis of probable AD during the subsequent follow-up period of 2-6 years, were included in this study. MCI patients corresponded to 0.5 in the Clinical Dementia Rating. The Mini-Mental State Examination (MMSE) score ranged from 24 to 28 (mean, 25.8; SD, 1.5) at the initial visit. Control subjects were healthy volunteers without memory impairment or cognitive disorders whose MMSE scores ranged from 26 to 30 (mean, 28.5; SD, 1.4). They did not differ significantly in age or education from the patients with AD. Group analysis using statistical parametric mapping revealed significant perfusion decrease in bilateral posterior cingulate gyri and precunei and parietal cortices in very early AD as compared to healthy volunteers. Graph-theoretical analysis using Graph Analysis Tool(Hosseini SM, et al. PLoS One. 2012;7:e40709)running on Matlab for analyzing between-group differences in parcellated brain perfusion SPECT using automated anatomical labeling revealed significant betweenness centrality changes of decrease in left cingulate gyrus, left inferior parietal cortex, right hippocampus, left inferior frontal cortex and of increase in right middle temporal cortex, right middle frontal cortex and right inferior occipital cortex in very early AD group as compared to healthy volunteers. On the other hand, very early AD group demonstrated significant clustering changes of decrease in bilateral posterior cingulate gyri and bilateral insula and of increase in bilateral inferior parietal cortices and left precuneus as compared to healthy volunteers. Moreover, very early AD group demonstrated significant degree changes of decrease in left frontal cortex, left hippocampus, bilateral olfactory cortices, and of increase in right temporal and frontal cortex, bilateral occipital cortex and left fusiform gyrus as compared to healthy volunteers. These results revealed an alteration in small-world characteristics of the brain networks in very early AD. Compensating mechanism for damaged network in posterior cingulate gyri and hippocampus may work more prominently in right cerebral hemisphere.

P445

Pilot data on 11C-PiB PET in major depressive disorder

E. Imabayashi1, H. Baba2, H. Matsuda1, I. Kuji3; 1National Center of Neurology and Psychiatry, TOKYO, JAPAN, 2Juntendo University, TOKYO, JAPAN, 3Saitama International Center, Saitama Medical University, SAITAMA, JAPAN.

PURPOSE: Many risk factors for dementia have been epidemically investigated with the hope of preventing or delaying the onset of Alzheimer's disease (AD). Depression is one of these risk factors. In this study, the 11C-PiB slight retention in major depression in the convalescent stage was compared with that in normal controls (NC) using voxel based analysis.METHODS: Four patients (4 men, 48.5 ±4.2y.o.) with major depression and four NC (4 men, 56.3±2.5y.o.) were focused on this study. 555MBq of 11C-PIB was injected and 70 minutes acquisition was performed using PET/CT equipment with high spatial resolution (Biograph 6 Hi-Rez; Siemens Medical Systems, Inc.). Distribution volume ratio (DVR) images referenced to cerebellum were generated using noninvasive Logan graphical analysis. The CT cortical images were extracted and normalized to anatomically standardized space using DARTEL algorithm in Statistical Parametric Mapping (SPM) 12 (http://www.fil.ion.ucl.ac.uk/spm/). Individual 11C-PIB DVR images were normalized with the same parameter as the CT normalization. The normalized 11C-PIB images were then smoothed. These processed images were analyzed with SPM12, using absolute DVR value. Voxel based group analysis of DVR between the depression patients and NC was performed using t statistics. Main effects used whole-brain analyses with a threshold at a voxel level of $p<0.01$ and a cluster false discovery rate of $p<0.05$ for the multiple comparison correction. Volume of interest (VOI) analysis was also applied using Automated Anatomical Labelling (AAL) software. VOI values in each cortical areas of parcellation map on the normalized 11C-PiB DVR images are obtained. DVR values are compared with t-statistics in each area. RESULTS: In the left brain of MDD, 11C-PiB retention increased in hypothalamus, caudate, globus pallidus, putamen, uncus, insula, and superior temporal gyrus. In the right brain, it increased in anterior cingulate, subcallosal gyrus, posterior cingulate,

caudate, globus pallidus, lingual gyrus, amygdala, uncus, parahippocampal gyrus, insula, and superior temporal gyrus. No absolutely higher 11C-PiB retention in NC comparing with depression subjects. In VOI analysis of the whole brain, cortical global mean DVR of MDD and NC was 0.929 and 0.934 respectively and with no significant difference. CONCLUSION: 11C-PiB retention was increased in MDD in areas where had been reported to be damaged in MDD; Brodmann area 24 and subcallosal gyrus. It was observed both in VOI analysis and voxel based analysis. Whether this 11C-PiB retention is irreversible or not should be confirmed.

P446

Impact of PET Brain Imaging Using F18-FDG and F18-FLORBETAPIR In Patients With Cognitive Impairment

C. GAMEZ-CENZANO1, J. J. ROBLES-BARBA1, L. RODRIGUEZ-BEL1, J. GASCON-BAYARRI2, M. CORTES-ROMERA1, A. SABATE-LLOBERA1, L. M. GRACIA-SANCHEZ1, I. ROMERO-ZAYAS1, M. ROCA-ENGRONYAT1, J. L. VERCHER-CONEJERO1, C. MAJOS-TORRO1, C. SORIANO-MAS3, C. AGUILERA-GRIJALVO1, I. RICO-PONS4, R. REÑE-RAMIREZ4; 1IDI-Hospital de Bellvitge-IDIBELL, L'Hospitalet de Llobregat, SPAIN, 2Neurología-Hospital de Bellvitge-IDIBELL, L'Hospitalet de Llobregat, SPAIN, 3Hospital de Bellvitge-IDIBELL, L'Hospitalet de Llobregat, SPAIN, 4Neurologia-Hospital de Bellvitge-IDIBELL, L'Hospitalet de Llobregat, SPAIN.

Aim: To describe the impact of brain FDG-PET and Amyloid-PET scans in the differential diagnosis of patients with cognitive impairment, including the suspicion of Alzheimer's disease (AD).Materials and Methods: Prospective study including 37 patients (24 women) with mean age of 64 years (range: 51-80) with cognitive impairment (MMSEmean=23), including suspected dementias as AD. All subjects underwent FDG-PET, Florbetapir-PET, CT or MRI of the brain and a battery of neuropsychological tests. The APOE genotype was available in 10 patients.The FDG-PET brain imaging analysis was visual and quantitative (CORTEX ID. GE Healthcare). Abnormal FDG-PET brain studies were classified in 2 patterns: temporoparietal hypometabolism (AD) and other (non-AD).The Amyloid-PET images were classified as positive or negative by visual interpretation.The FDG-PET and Amyloid-PET results were compared to establish concordances and discrepancies between both types of scan and the probable clinical diagnosis. Differences in MMSE in subgroups according to PET results were calculated.Results: FDG-PET studies were abnormal in 12/37 patients (32%): 8 AD (8/8 positive Amyloid-PET) and 4 non-AD (1/4 positive and 3/4 negative Amyloid-PET, one of them with primary progressive aphasia). FDG-PET studies were normal in 25/37 (68%), but 9 of them had a positive Amyloid-PET (3 APOE of risk).Amyloid-PET studies were positive in 18/37 patients (49%); 9 of them with abnormal FDG-PET scan (8 AD; 1 non-AD).The MMSE were significantly lower in patients with abnormal FDG-PET comparing with the normal scans (mean: 19 vs 25), but there were no differences between positive Amyloid-PET and negative scans (mean: 22 vs 23).Conclusions: Brain PET is a useful diagnostic tool in patients with cognitive impairment. Brain FDG-PET (more available and cheaper) allows to identify the typical pattern of AD, especially when MMSE <20, where an additional Amyloid-PET is not needed (all positive in this study). Brain Amyloid-PET may have a major impact in patients with negative or abnormal FDG-PET with non-AD pattern.

P27 - Monday, October 12, 2015, 4:00 PM - 4:30 PM, Hall 3 – Poster Exhibition

Neurosciences: Psychiatry

P447

A comparative analysis of SERT function in neuropsychiatric disorders

S. Nikolaus, H. Müller, H. Hautzel; University Hospital Düsseldorf, DÜSSELDORF, GERMANY.

Aim: Impairment of serotonin transporter (SERT) is increasingly recognized to play a major role in the pathophysiology of neuropsychiatric diseases including anxiety disorder (AD), major depressive disorder (MDD), bipolar disorder (BD) and schizophrenia (SZ). In the present investigation, we compared SERT binding by subjecting all available in vivo binding data on AD, MDD, depressed state of BD (BDdep), manic state of BD (BDman) and SZ to a retrospective analysis. Materials & Methods: In patients with AD (n=207), MDD (n=694), BDdep (n=60), BDman (n=1) and SZ (n=46) SERT was assessed in various cortical and subcortical regions with either PET or SPECT and compared to healthy individuals. Studies were pooled and median values and interquartile ranges of percentual differences relative to controls were determined for the individual brain regions. Differences to controls were assessed with the Wilcoxon-signed-rank-test. Differences between disorders were assessed using the Mann-Whitney-U-test. Results: In AD, SERT was significantly reduced in thalamus (-10%), amygdala (-7%) and midbrain (-13%) relative to controls. In MDD, SERT was significantly decreased in straitum (-6%), thalamus (-12%), prefrontal cortex (-15%), amygdala (-15%) and midbrain (-8%), whereas in the insula (+9%), a significant elevation was observed. In BDdep, SERT was significantly elevated in cingulate (+19%) and insula (+

13%), while, in BDman, SERT was significantly elevated in the midbrain (+18%). In SZ, SERT was not significantly altered relative to controls. Comparison between disorders yielded no significant differences of SERT binding. Conclusion: The most extensive decline of SERT relative to controls was observed in MDD involving both neocortical and subcortical regions. In AD, SERT decline relative to controls was confined to midbrain, thalamus and amygdala, whereas no decline of SERT binding was observed in SZ. Moreover, in contrast to AD and SZ, increases of SERT relative to healthy individuals were detected in the insula of MDD, and in cingulate and insula of BDdep patients, while investigations on BDman yielded an elevation of midbrain SERT. Taken together, findings showed that AD, MDD, BD and SZ differ as to affected brain region(s) and extent as well as direction of SERT dysfunction, which may be related to differences in serotonin levels.

P448

Anxiety disorder, major depression, bipolar disorder and schizophrenia show different patterns of 5-HT1A receptor dysfunction

S. Nikolaus, H. Müller, H. Hautzel; University Hospital Düsseldorf, DÜSSELDORF, GERMANY.

Aim: Impairment of 5-HT1A receptor (5-HT1AR) function is increasingly implied in the pathophysiology of neuropsychiatric diseases including anxiety disorder (AD), major depressive disorder (MDD), bipolar disorder (BD) and schizophrenia (SZ). In the present investigation, we compared 5-HT1AR binding by subjecting all available in vivo binding data on AD, MDD, depressed state of BD (BDdep) and SZ to a retrospective analysis. Materials & Methods: In patients with AD (n=37), MDD (n=245), BDdep (n=95) and SZ (n=100) 5-HT1AR were assessed in various cortical and subcortical regions with either PET or SPECT and compared to healthy individuals. No investigations of 5-HT1AR were conducted in the manic state of BD. Studies were pooled, and medians and interquartile ranges of percentual differences relative to controls were determined for the individual brain regions. Differences to controls were assessed with the Wilcoxon-signed-rank-test. Differences between disorders were assessed using the Mann-Whitney-U-test. Results: In AD, 5-HT1AR were significantly reduced in frontal cortex (-13%), cingulate (-24%), hippocampus (-15%), amygdala (-22%), insula (-23%) and midbrain (-29%) relative to controls. In MDD, 5-HT1AR were significantly elevated in parahippocampal gyrus (+23%), whereas a significant reduction was observed in the midbrain (-17%). In BDdep, 5-HT1AR were significantly increased in hippocampus (+21%), amygdala (+19%) and parahippocampal gyrus (+32%). In SZ, 5-HT1AR were significantly decreased in temporal cortex (-6%), occipital cortex (-5%), amygdala (-12%) and midbrain (-5%). 5-HT1AR were significantly diminished in frontal cortex (-11%), cingulate (-8%), amygdala (-49%) and insula (-21%) of AD compared to MDD patients. Moreover, 5-HT1AR were significantly lowered in frontal cortex (-16%), cingulate (-6%) and midbrain (-19%) of AD compared to SZ patients and in the insula (-24%) of AD compared to BDdep patients. There were no significant differences of 5-HT1AR binding between MDD and SZ and between BDdep and SZ. Conclusion: Comparisons between disorders revealed that, in AD, frontal 5-HT1AR were decreased relative to controls as well as relative to MDD and SZ (where they were unaltered). Moreover, in AD, frontal, cingulate, amygdalar and mesencephalic 5-HT1AR were lowered relative to controls as well as relative to SZ. Additionally, in AD, temporal 5-HT1AR were not different from healthy individuals but elevated compared to SZ patients (where they were unaltered). From this may be inferred that frontal and limbic inhibition - as exerted via 5-HT1AR binding sites - is lower in AD relative to MDD and SZ, whereas temporal inhibition is augmented (relative to SZ).

P449

Different patterns of 5-HT2A receptor dysfunction in anxiety disorder, major depression, bipolar disorder and schizophrenia

S. Nikolaus, H. Hautzel, H. Müller; University Hospital Düsseldorf, DÜSSELDORF, GERMANY.

Aim: Impairment of 5-HT2A receptor (5-HT2AR) function is increasingly implied in the pathophysiology of neuropsychiatric diseases including anxiety disorder (AD), major depressive disorder (MDD), bipolar disorder (BD) and schizophrenia (SZ). In the present investigation, we compared 5-HT2AR binding by subjecting all available in vivo binding data on AD, MDD, manic state of BD (BDman) and SZ to a retrospective analysis. Materials & Methods: In patients with AD (n=33), MDD (n=287), BDman (n=10) and SZ (n=199) 5-HT2AR were assessed in various cortical and subcortical regions with either PET or SPECT and compared to healthy individuals. No investigations of 5-HT2AR were conducted in the depressed state of BD. Studies were pooled, and medians and interquartile ranges of percentual differences relative to controls were determined for the individual brain regions. Differences to controls were assessed with the Wilcoxon-signed-rank-test. Differences between disorders were assessed using the Mann-Whitney-U-test. Results: In AD, 5-HT2AR were significantly elevated in the temporal cortex (+8%) relative to controls. In MDD, 5-HT2AR were

significantly decreased in prefrontal (-6%), frontal (-6%) and occipital cortex (-4%) as well as cingulate (-7%). In BDman, 5-HT2AR were significantly decreased in frontal, parietal, temporal and occipital cortex as well as cingulate. insula and fusiform gyrus (-20%, each). In SZ, 5-HT2AR were significantly diminished in frontal (-25%), temporal (-19%) and occipital cortex (-5%). In AD, 5-HT2AR were significantly increased in the temporal cortex (+10%) compared to MDD patients and in the frontal (+27%) and temporal cortey (+27%) compared to SZ patients. Moreover, 5-HT2AR binding in the frontal cortex (+20%) was significantly augmented in MDD compared to SZ patients. Conclusion: In AD, temporal 5-HT2AR were elevated relative to controls as well as relative to MDD (where they were unaltered) and to SZ (where they were decreased compared to controls). Moreover, frontal 5-HT2AR were elevated in AD compared to normal subjects as well as relative to SZ (where they were decreased compared to controls). Additionally, in MDD, frontal 5-HT2AR were reduced relative to controls and elevated relative to SZ (where they were decreased compared to controls). From this may be inferred that frontal and temporal excitation - as exerted via 5-HT2AR binding sites - is higher in AD relative to MDD and SZ, and higher in MDD relative to SZ. It can be hypothesized that region-specific alterations of serotonin binding sites are related to specific disturbances in the processing of emotion and memory in the individual disorders.

P450

Brain perfusion single photon emission computed tomography (SPECT) in pateints with attention-deficit/hyperactivity disorder (ADHD) using 99mTc-ECD: a report of three cases and review of the literature

M. Taghizadeh Asl1, F. Yousefi2, R. Nemati3, **M. Assadi**2; 1Department of Nuclear Medicine, Kasra Hospital, Tehran, IRAN, ISLAMIC REPUBLIC OF, 2The Persian Gulf Nuclear Medicine Research Center, Bushehr University of Medical Sciences, BUSHEHR, IRAN, ISLAMIC REPUBLIC OF, 3Department of Neurology, Bushehr Medical University Hospital, Bushehr University of Medical Sciences, BUSHEHR, IRAN, ISLAMIC REPUBLIC OF.

Attention-deficit/hyperactivity disorder (ADHD) is one of the most prevalent developmental disorder in children. The main symptom of the disorder is inattention, hyperactivity, and impulsivity, and is among the most prevalent of childhood disorders. Only a limited number of studies have investigated cerebral metabolism or perfusion in these pateints , therefore , such indices are not fully understood yet. In this study, three cases of ADHD underwent brain perusion SPECT to evaluate cerebral perfusion. All three patients showed abnormal cerebral perfusion on brain SPECT while had normal MRI. The pateints 1 was a 5 years old girl with ADHD. The SPECT showed moderate frontal hypo perfusion and bilateral inferior temporal hypoperfusion. The patient 2 was a 14 years old girl with ADHD. The SPECT showed generalized diffuse cortical hypoperfusion more prominently on the superior pre-frontal cortex and also moderate hypo perfusion of cerebellar hemispheres. And patheint 3 was a 7 years old girl with ADHD. The SPECT showed mild hypoperfusion of the right parietal-temporal region and sub-cortical structures . In conclusion , the study showed the frontal lobe is a key structure in ADHD that another area of the brain may contribute to the disease with various severity.

P451

Our institutional pictorial essay on brain perfusion SPECT in various neuro-psychiatric disordsers and intoxication: Though practical , it is not very commonly used

M. Taghizadeh Asl1, R. Nemati2, **M. Assadi**3; 1Department of Nuclear Medicine, Kasra Hospital, Tehran, IRAN, ISLAMIC REPUBLIC OF, 2Department of Neurology, Bushehr Medical University Hospital, Bushehr University of Medical Sciences, BUSHEHR, IRAN, ISLAMIC REPUBLIC OF, 3The Persian Gulf Nuclear Medicine Research Center, Bushehr University of Medical Sciences, BUSHEHR, IRAN, ISLAMIC REPUBLIC OF.

Structural and functional images of the brain play an important role as powerful adjuncts in the management of an increasing number of neurologic and psychiatric diseases. Brain SPECT, in particular, with perfusion agents or with neuroreceptor imaging radiopharmaceuticals, is rapidly becoming a clinical tool in many places. For many neurologic and psychiatric conditions, this imaging modality has been used in diagnosis, prognosis assessment, evaluation of response to therapy, risk stratification, detection of benign or malignant viable tissue, and choice of medical or surgical therapy. We will present our institutional experience formatting a pictorial review on of brain perfusion SPECT on more than 20 types of different neurologic and psychiatry diseases such as dementias, epilepsy, cerebral palsy, head injury, brain tumor , Herpes encephalitis, hypoxic brain damage , vacuities, depression, CO poisoning , cocaine abuse and also elemental mercury poisoning.

P452

Evaluating the brain status of serotonin transporters in depression-like rat model using 4-[18F]-ADAM/animal PET

C. Cheng1, K. Ma2, S. Lu1,3, C. Shiue1, W. Huang4; 1Department of Nuclear Medicine, Tri-Service General Hospital, National Defense Medical Center, TAIPEI, TAIWAN, 2Department of Biology and Anatomy, National Defense Medical Center, TAIPEI, TAIWAN, 3Graduate Institute of Medical Sciences, National Defense Medical Center, Taipei, TAIWAN, 4Departments of nuclear medicine and medical research, Changhua Christian Hospital, CHANGHUA, TAIWAN.

Aims: Depression may lead to enormous loss of society and economy. Previous studies have demonstrated that depression may cause the decrease of brain serotonin transporter (SERT) density. The aim of this study was to assess the effects of chronic mild stress (CMS) on serotonin transporters in the depression-like rat model using the animal positron emission tomography (animal-PET) coupled with 4-[18F]-ADAM. Materials and methods: Twelve male Sprague-Dawley rats (weighted in 350±10 g) were divided into the control and CMS groups. A five weeks protocol of unpredictable CMS was applied to those rats of CMS group. The body weight measurement and depression-related behavioral test (force swimming test, FST) were used to evaluate the depression-like symptoms in CMS rat. Moreover, the concentration of corticosterone in blood was also measured with liquid chromatography-tandem mass spectrometry (LC-MS/MS). The 4-[18F]-ADAM (targeting to serotonin transporters) coupled with animal positron emission topography (animal-PET) was used to examine the status of serotonin transporters in depression-like rat model and the images were calculated and expressed as specific uptake ratios (SURs). Results: Five weeks after the operation of CMS protocol, the CMS rat showed obvious decrement of body weight than that in control rat. The data of FST showed that the CMS rats had longer immobility time than that of control rats. We also found that the concentration of corticosterone in CMS rat is higher than control value. The 4-[18F]-ADAM SURs in various brain regions of CMS rat were obviously lower than those of controls. Conclusion: These results suggest that CMS may induce the depression-like symptoms and cause the reduction of serotonin transporters in rat brain. In addition, the 4-[18F]-ADAM coupled with animal-PET may be a feasible way for evaluating the condition of serotonin transporters in depression.

P453

SPECT scanning of brainstem serotonin transporter availability reveals association with circulating inflammatory tumour necrosis factor

R. Krishnadas1, **A. Nicol**2, J. Sassarini3, N. Puri2, S. Pimlott2, D. Hadley2, I. McInnnes3, J. Cavanagh1; 1Sackler Institute of Psychobiological Research, Institute of Health and Wellbeing, University of Glasgow, Glasgow, UNITED KINGDOM, 2NHS Greater Glasgow & Clyde, Glasgow, UNITED KINGDOM, 3University of Glasgow, Glasgow, UNITED KINGDOM.

Depression is common in patients suffering from inflammatory diseases. Among the medically ill, people with inflammatory diseases are at greater risk of developing a major depressive illness compared to the general population. In patients with arthritis treated with tumour necrosis factor (TNF-α) antagonists, an antidepressant effect is seen, independent of the improvement of arthritis. In addition, pre-clinical studies in rodent models have shown that pro-inflammatory cytokines increase serotonin transporter availability and function, leading to depressive symptoms. The aim of the present study was to investigate associations between plasma TNF-α and brainstem serotonin transporter (SERT) availability using 123I-beta-CIT SPECT imaging. Healthy subjects and subjects with psoriasis (Ps) / psoriatic arthritis (PsA) undergoing treatment with TNF-α antagonist (etanercept) were included. Plasma TNF-α and brainstem SERT availability was assessed in thirteen healthy females (13 F, mean age 57 years, range 45-65 years). Twelve patients with Ps/PsA were also included in the study (6M, 6F, mean age 48 years, range 30-65 years). The Ps/PsA patients underwent investigation up to 14 days before and 6 - 8 weeks after treatment with TNF-α antagonist (etanercept 50mg once weekly). Plasma TNF-α was measured using ELISA. 123I-beta-CIT SPECT (Neurofocus 900 scanner) was used to measure brainstem SERT availability. Scanning was performed 3-4 h post 123I-beta-CIT administration (150 MBq) and specific to non-specific beta-CIT uptake ratios were computed using ROI templates drawn over the brainstem and occipital region (reference region). For the healthy subjects, plasma TNF showed a significant correlation with brainstem 5-HTT availability (corrected for age) (Spearman's rho=0.61; p=0.03).For the subjects with Ps/PsA, baseline plasma TNF-α was significantly correlated with baseline brainstem SERT availability (rho=0.76; p=0.004). TNF blockade treatment with etanercept was associated with a reduction in 123I-beta-CIT SERT binding (t=2.09; p=0.03). A relationship between brainstem SERT availability and circulating inflammatory tumour necrosis factor is indicated by these findings. These

findings support a potential mechanistic pathway that link circulating inflammatory markers to the pathophysiology underlying major depression.

P454

Resting-state Functional Connectivity in Social Anxiety Disorder Compared to Healthy Controls and the Effect of Pharmacotherapy

A. G. G. Doruyter1, C. Lochner1, P. Dupont2, D. Stein1, J. Warwick1; 1Stellenbosch University, Cape Town, SOUTH AFRICA, 2Katholieke Universiteit Leuven, Leuven, BELGIUM.

Aim: Neuroimaging research has identified differences in resting state networks between participants with Social Anxiety Disorder (SAD) and healthy controls. It has been hypothesized that network disruptions in SAD (particularly to the default mode network) may be correlated with differences in social cognition in the disorder. The effect of pharmacotherapy on these resting-state networks in SAD has thus far received little attention. Our aim is to test for effect of pharmacotherapy on resting-state functional connectivity in SAD. Materials and methods: A retrospective analysis of Tc-99m HMPAO SPECT data (obtained in previous research) of patients meeting DSM-IV criteria for SAD and healthy controls (HCs) was performed. SAD participants were scanned at baseline and after an 8-week course of pharmacotherapy (either with citalopram or moclobemide). Image data were collated and reconstructed using optimal techniques (iterative algorithms including corrections for attenuation, scatter and collimator blurring). Scans were then pre-processed using SPM12. Analyses (seed-based and using a priori regions of interest) are currently ongoing to compare resting functional connectivity in the three groups (SAD at baseline; HCs; and SAD post-treatment). Results: Twenty-seven SAD patients (of which 20 underwent follow-up scanning post-treatment) and 18 age and gender-matched HCs were included. Initial analyses indicate several differences in perfusion-based connectivity across groups. Final results of group connectivity differences, including the effect of pharmacotherapy on functional connectivity in SAD will be presented. Conclusion: The results will be discussed in the light of existing studies of functional connectivity in SAD, and in the light of emerging hypotheses about the role of the default mode network in social cognition. In particular these data will be analysed in terms of the putative role of altered social cognitive function in the aetiology of SAD.

P28 - Monday, October 12, 2015, 4:00 PM - 4:30 PM, Hall 3 – Poster Exhibition
Neurosciences: Neurodegeneration

P456

Imaging Mutant Huntingtin Aggregates: Development of Potential PET Ligands

C. J. Brown1, M. Prime1, D. Clark-Frew1, S. Schaertl2, J. Häggkvist3, C. Halldin3, V. Stepanov3, A. Varrone3, K. Varnäs3, M. Svedberg3, I. Munoz-Sanjuan4, V. Khetarpal4, J. Bard4, J. Wityak4, C. Dominguez4; 1Evotec UK Ltd, Abingdon, UNITED KINGDOM, 2Evotec AG, Hamburg, GERMANY, 3Karolinska Institutet, Stockholm, SWEDEN, 4CHDI, Los Angeles, CA, UNITED STATES.

Aim: Develop a PET ligand for mutant huntingtin (mHTT) Aggregates. Aggregates of mHTT form in some brain cells of Huntington's disease (HD) patents and can be observed by post-mortem analysis. Huntington's disease (HD) is a rare, fatal, autosomal dominant inherited disease caused by a CAG repeat expansion in the huntingtin gene which results in an expanded polyglutamine tract in the mutant huntingtin protein. Clinical manifestations of the disease include motor and cognitive impairment, psychiatric disturbances, as well as metabolic abnormalities, with disease onset typically occurring between the ages of 30 and 50, and death within 15 to 20 years. There are currently no biomarkers for mHTT aggregates in vivo. The ability to track the appearance, quantity and location of mHTT aggregates in HD patients is of critical importance. Such a biomarker may have the potential to monitor the progress of mHTT lowering therapies independently of a clinical assessment. Methods and Materials: Radioligand binding assays were used to develop novel compounds that bind to Exon1-Q46 aggregates. SAR led to compounds with good properties for autoradiography (ARG), leading to candidates for 11C-labelling. Results from micro-PET imaging of 11C-labelled lead compounds in the Q175 mouse model of HD are presented. Conclusions: Trends were identified from analysis of the ARG results that allow development of compounds with better non-specific binding and specific binding to mHTT aggregates. An 11C-labelled lead compound was identified with suitable properties for progression into human PET studies.

P457

The comparison of I-123-ioflupane dopamine transporter imaging with I-123-MIBG cardiac imaging in Parkinson's disease and Lewy body disease

M. Momose; Matsumoto Medical Center, Matsumoto, JAPAN.

Purpose; to create the flow chart of diagnosis for Parkinson's disease (PD) and Lewy body disease (LBD) by means of I-123-ioflupane dopamine transporter (DAT) imaging and/or I-123-metaiodobenzylguanidine (MIBG) cardiac imaging.

Materials and methods; 27 cases of PD and 2 cases of LBD performed DAT imaging and MIBG imaging. For DAT imaging clearly comma-shaped accumulation and specific binding ratio (SBR)≥4.5 were negative, and the others were positive. For MIBG imaging early heart to mediastinum ratio (H/M)≥2.1 and delayed H/M≥2.3 were negative, and the others were positive. Result; the positive ratio of DAT imaging was 23/29 (79.3%), and that of MIBG imaging was 17/29 (58.6%). The agreement of the both imaging findings was 19/29 (65.5%). The 2 cases of DAT negative and MIBG positive were considered to be the scan without evidence of dopaminergic deficit (SWEDD), and the 8 cases of DAT positive and MIBG negative were considered to be the Parkinson's syndrome (PS) other than PD. Conclusion; the DAT imaging has better to be performed first, and the MIBG imaging to be performed second to differentiate PD from PS.

P458

Functional correlates of cerebrospinal fluid levels of lactate dehydrogenase in Alzheimer's Disease: a 18F FDG PET/CT study

A. Chiaravalloti1, M. Pierantozzi2, C. Liguori2, C. Di Russo1, A. Fiorentini1, R. Catalano1, S. Pizzi1, O. Schillaci1; 1Department of Biomedicine and Prevention, University Tor Vergata, Rome, ITALY, 2Department of Neurosciences, University Tor Vergata, Rome, ITALY.

Aim: To investigate the relationships among cerebrospinal fluid (CSF) levels of lactate dehydrogenase (LDH) and brain glucose consumption as detectable by means of 2-deoxy-2-(18F) fluoro-D-glucose (18F-FDG) Positron Emission Tomography/Computed Tomography (PET/CT) in a population with Alzheimer's disease (AD). Materials and methods: The study included 33 newly diagnosed AD patients according to the NINCDS-ADRDA criteria (15 males and 18 females, mean age 70±7 years old) with a disease duration of 2.7 years (mean). All the subjects underwent a cerebrospinal fluid (CSF) assay for levels of LDH, p-Tau, t-Tau, Aβ1-42 amyloid peptide ~ 1 month before PET/CT examination. Moreover the Apo E phenotype of the entire population has been assessed. A standard Magnetic Resonance has been performed in all the subjects enrolled in the study. The relationships were evaluated by means of regression analysis model, Statistical Parametric Mapping (SPM8) using gender, age, disease duration, Mini Mental State Examination (MMSE) and CSF levels of p-Tau, t-Tau and, Aβ1-42 amyloid peptide and Apo E phenotype as covariates. Results: We did not find differences in the clinical and CSF parameters in genders. Low CSF levels of LDH are related to a decreased 18F-FDG uptake in left Brodmann area (BA) 10,11 and 35 while no areas of increased 18F-FDG uptake related to LDH levels have been detected. Conclusions: The results of our study suggests that increased LDH concentrations in CSF are related to a wide cortical dysfunction that involves the left frontal and temporal lobe. This pattern is independent from CSF and genetic biomarkers that are commonly used in the evaluation of AD.

P459

Is amyloid deposition related to the age of onset of Alzheimer disease?

A. Chiaravalloti1, A. Lacanfora1, R. Danieli1, A. Fiorentini1, L. Cravello2, F. Di Iulio2, C. Caltagirone2, O. Schillaci1; 1Department of Biomedicine and Prevention, University Tor Vergata, Rome, ITALY, 2IRCCS Santa Lucia, Rome, ITALY.

Aim: To investigate the relationships between age of onset of Alzheimer's disease (AD) and brain amyloid deposition as detectable by means of 18F Florbetapir Positron Emission Tomography/Computed Tomography (PET/CT).Materials and methods: We examined 55 newly diagnosed probable AD patients according to the NINCDS-ADRDA criteria (25 women and 30 men; mean age 75 ± 6 years). A standard Magnetic Resonance has been performed in all the subjects enrolled in the study before a 18F Florbetapir PET/CT scan. Relationships between age of onset of AD an brain amyloid distribution have been assessed by a regression analysis in Statistical Parametric Mapping version 8 (SPM8) using gender and Mini Mental State Examination (MMSE) as covariates.Results: MMSE resulted equal to 23±4 respectively with no differences in genders. SPM8 regression analysis (with a statistical threshold of p=0.001, family wise error (FWE)-corrected) did not show a significant relationship between age of onset and amyloid deposition in brain.Conclusions: the results of our study show that amyloid deposition in brain do not differ in those patients with an early or late onset of AD.

P460

Initial experience of the dopamine transporter SPECT in three pediatric patients with rare neurodegenerative disorder

I. Mochida, K. Matsunaga, S. Watanabe, K. Isohashi, T. Watabe, M. Tatsumi, H. Kato, E. Shimosegawa, J. Hatazawa; Osaka University Graduate School of Medicine, Suita-shi, Osaka, JAPAN.

[Introduction]Dopamine transporter imaging with I-123 FP-CIT SPECT visualizes distribution of dopamine transporter in the striatum which is the postlude of the substantia nigra-

striatum dopaminergic system nerve. I-123 FP-CIT SPECT began in January, 2014 in Japan. We experienced three children with iron deposition in the brain studied with I-123 FP-CIT. [Cases]Case 1:A 15 year-old-female. Case 2 and 3 : Both 6 year-old-boy (twin).These 3 cases had no history of severe birth trauma or ischemic condition. They had no family history of movement disorders, dementia, or psychiatric illness. They had psychomotor retardation from about 2 or 3 years old, and movement disorder was getting worse. Case 1 was diagnosed as SENDA (Static Encephalopathy of childhood with Neuro-Degeneration in Adulthood), and Case 2 and 3 were INAD(Infantile Neuro-Axonal Dystrophy)by genetic analyses. Their MRI examination of the brain was performed several times. In all cases, gradually symmetrical hypointensity was shown in the mid brain, bilaterally, on T1-, and T2-weighted MR images. All of I-123 FP-CIT SPECT findings were within normal range, but unexpected asymmetrical decrease of I-123 FP-CIT accumulation in lentiform nuclei was found in Case 2 and 3. [Discussions]The reports about the relation between ‘ iron accumulated in the midbrain and dopamine transporter in the striatum’ are not found yet. There is a report that levodopa had an effect on a patient who showed parkinsonism, regarded as SENDA, seen in the iron accumulated in substantia nigra of the brain1. Dopamine treatment may start early if we can detect a substantia nigra change in the follow-up I-123 FP-CIT SPECT. The mid brain abnormal signal area was not substantia nigra in Case 2 and 3, normal accumulation was expected in DAT scan, but recognized laterality for accumulation. The normal image data base in the growth process of child was not studied yet, as a result, the judgment was difficult, and it was necessary to accumulate knowledge continuously. 1.Gregory A, et al. J Med Genet 2009;46:73-80

P461

Investigating the co-grafted effects of porcine ventral mesencephalic tissue and mesenchymal stem cells in Parkinson’s disease rat model using [18F] -FDOPA/animal PET

K. Ma1, T. Liu1, Y. Jhao1, S. Weng1, K. Tzen2, R. Yen2, W. Huang3; 1Department of Biology and Anatomy, National Defense Medical Center, TAIPEI, TAIWAN, 2Department of Nuclear Medicine, National Taiwan University Hospital, TAIPEI, TAIWAN, 3Departments of nuclear medicine and medical research, Changhua Christian Hospital, CHANGHUA, TAIWAN.

Aim: Parkinson’s disease (PD) is a progressively neurodegenerative disease characterized by a loss of dopaminergic neurons in the nigrostriatal pathway. Transplantation of human fetal ventral mesencephalic (hfVM) tissue has been considered as an effective treatment for PD, but the ethical issues limit the clinical application. Porcine fetal ventral mesencephalic (pfVM) tissue might be an alternative source for xenografting treatment in neurodegenerative diseases. However, the immune rejection in this xenograft method needs to be resolved. Recently, mesenchymal stem cells (MSCs) have been reported to possess immunomodulatory effects that reduced attack by immune cell in animal model. MSCs can also produce growth factors and provide an appropriate micro-environment in situ. In this study, we evaluated the co-grafted effects of porcine ventral mesencephalic tissue and mesenchymal stem cells in Parkinson’s disease rat model using [18F]-FDOPA/animal PET. Materials and methods: The hemiparkinsonian rats were created by injecting the neurotoxin 6-hydroxydopamine into the median forebrain bundle. The E27 pfVM tissue and/or rat MSCs were grafted into striatum of hemiparkinsonian rat. Apomorphine-induced contralateral rotations test were performed to reflect the lesion severity at 1, 2 and 3 months after the transplantation. The [18F]-FDOPA coupled with small animal PET was used to evaluate the status of dopaminergic system. Three months after the transplantation, the immunohistochemical staining of tyrosine hydroxylase were performed and the results were compared with those of the PET images. In addition, T-cell staining was executed to clarify whether MSCs could provide immune modulation in grafted region of brain. Results: The data of rotation behavior showed that the number of rotations in pfVM-grafted group reduced after 1 month, but increased at 2 and 3 month after transplantation. In the group of co-grafted pfVM tissue with rat MSCs, the rotation numbers were reduced at all 3 months after the transplantation. The PET imaging results showed that both in pfVM group and co-graft group, the grafted area revealed obviously [18F]-FDOPA uptakes. In addition, the results of immunohistochemistry studies paralleled to those of PET imaging studies. Conclusion: Our results demonstrated that co-transplantation of pfVM and MSCs may exert beneficial effects for treatment of the Parkinson’s disease.

P462

Cerebral cortex glucose metabolism correlates with the MRS findings in white matter in HIV positive patients

E. Gromova, J. Khomenko, G. Kataeva, A. Bogdan, I. Kotomin; N.P.Bechtereva Institute of the Human Brain, RAS, St.Peterburg, RUSSIAN FEDERATION.

IntroductionIt is well known that human immunodeficiency virus (HIV) after penetrating in CNS initializes the cascade of immunological responses accompanied by inflammation that result in HIV induced white and gray matter damage and even atrophy with cognitive consequences. In our previous studies

(both with PET-FDG and MRS), metabolism reduction in anterior cingulate cortex occur early after disease onset was revealed. It is also known that significant associations between the tractography metrics and cognitive performance in HIV+ patient exists. The complex multimodal examination with neuroimaging methods could better elucidate relationship between HIV mediated CNS injury and cognitive dysfunction.The aim of this study is comparison of brain metabolic changes revealed by PET-FDG and MRS.**Methods**Two groups of HIV+ patients (age 25-40) were studied: 38 without neurological or cognitive deficit and other pathology and 17 with opportunistic infection out of brain. PET-FDG was performed on Gemini TF Base scanner and standard protocol, relative estimation of glucose cerebral metabolic rate (CMRglu) in regions of interest (ROI) corresponding to Brodman areas (BA) were calculated by WFU PickAtlas. Multivoxel MRS of brain was performed on Achieva 3T scanner, Philips (2D PRESS H-MPC, TE/TR=144/1500 ms) and included supraventricular white matter (WM) and medial cortex. Anatomical localization was taken into consideration: area of MRS study (8*9 voxels (10*10*15 mm), whole volume 80*90*15 mm) was divided into 9 ROIs: 6 in WM (3 ROIs: anterior, medium and posterior for each hemisphere) and 3 ROIs in medial cortex. NAA/Cr, (NAA - N-acethyl aspartate, Cr - creatine) were analyzed.**Results**. Significant correlations between CMRglu and NAA/Cr not only in adjacent zones in one hemisphere, but even more prominent between contralateral ROIs were revealed. In left hemisphere NAA/Cr in anterior WM ROI were correlated with CMRglu in BA 5,6 and 24 ($r=0,4$; $p<0,05$); NAA/Cr in medium WM - with BA 6,8,9,24 and 32 (r 0,4-0,5; $p<0,05$), and NAA/Cr in posterior WM - with BA 7 ($r=0,4$; $p<0,05$). Similar correlations revealed between WM of right hemisphere and CMRglu in left hemisphere, but not in ispilateral hemisphere. NAA/Cr in left anterior WM correlated with CMRglu in contralateral BA8 and 32 ($r=0,4$; $p<0,05$).**Conclusion**. Since NAA/Cr is neuronal marker, it is possible to suggest that integrity of neural tracts constituent WM coupled with the state of corresponding cortex areas, and atrophy in gray matter is associated with damage of subcortical conduction tracts.

P463

Effect of mTOR inhibition on epileptogenesis in the rat epilepsy model

A. CULLIER1,2, F. MASKALI1, **A. CLEMENT**1, S. POUSSIER1, G. KARCHER1, P. MARIE1, E. RAFFO3; 1GIE-NANCYCLOTEP, VANDOEUVRE-LES-NANCY, FRANCE, 2hospital of brabois, Vandoeuvre les nancy, FRANCE, 3hospital of brabois, VANDOEUVRE-LES-NANCY, FRANCE.

Aim: The Mesial Lobe Temporal Epilepsy (mLTE) is the most drug-resistant epilepsy. Its natural history, reconstructed by the lithium-pilocarpine in rats model, starts with the SE followed by a histological restructuration within the hippocampal and para-hippocampal regions, which creates a hyper-excitable neo-circuit implementing recurring spontaneous seizures. The mTOR pathway is a proteical intracellular complex that regulates synaptogenesis, neuronal plasticity, inflammation and proliferation of cerebral gliosis. This specific pathway is activated at different stages of the mLTE. The goal of the present pre-clinical study was to evaluate the impact of inhibiting the mTOR pathway by Rapamycin over epileptogenesis and neuroprotection in the lithium-pilocarpine model. Methods: For this study, 44 adult rats were divided into 3 groups: treated SE (i), untreated SE (ii) and healthy witnesses (iii). Each of them received Rapamycin per os at 3 stages: H+2 at 6 mg per kg per day, then D1 and D2 at 3 mg per kg per day. The treatment was evaluated by studying metabolic modifications, using positon emission tomography and 2-[18F]-fluoro-2-deoxy-D-glucose, at H+4, D2 and D8 (1), the research for spontaneous crisis from D8 (2), and eventually by counting neurons in the interest regions after sacrifice at D60 (3). Results: In the acute phase, we show an increase of consequences of the SE on glucose local cerebral metabolism, in the hippocampus and parahippocampal cortex, by the use of Rapamycin. However, an increased hippocampal hypometabolism at D2 suggests that Rapamycin may have a neuroprotecting potential, which has to be confirmed by histological study. We don't observe any treatment effect at D8. We don't show either any influence of Rapamycin treatment over epileptogenesis. Conclusion: Our results along with previous studies outcomes recommend evaluating Rapamycin administration from the beginning of SE and by the intraperitoneal pathway, as well as treatment prolongation during the whole epileptogenesis silent phase.

P464

The influence of gender on brain perfusion in patients with Alzheimer's disease.

V. Valotassiou1, J. Papatriantafyllou2, N. Sifakis3, C. Tzavara1, I. Tsougos1, S. Alexiou1, D. Psimadas1, E. Baniora1, A. Ziaka1, P. Georgoulias1; 1Department of Nuclear Medicine, University Hospital of Larissa, Larissa, GREECE, 2Memory & Cognitive Disorders Clinic, Neurology Dpt., "G. Gennimatas" Hospital, Athens, GREECE, 3Nuclear Medicine Dpt, "Alexandra" University Hospital, Athens, GREECE.

Aim: Several studies have shown sex differences in clinical symptoms in Alzheimer's disease (AD) patients, suggesting that gender may modify perfusion deficits patterns in AD.

The aim of our study was the evaluation of brain perfusion in specific Brodmann areas (BA) in men and women with AD, using an automated 3D-voxel-based processing software (Neurogam). Materials-methods: We studied 52 consecutive patients from an outpatient Memory Clinic. We used the established DSM-IV criteria for the diagnosis of dementia and the specific established criteria (NINCDS-ADRDA) for the diagnosis of AD. All the patients had a neuropsychological evaluation with a battery of tests including the mini-mental state examination (MMSE). The study group consisted of 16 men (age±SD 68.7±7.9 years, MMSE±SD 18.7±6.5, education±SD 12.5±4.6 years), and 36 women (age±SD 71±8 years, MMSE±SD 18.9±5.8, education±SD 8.3±4.2 years). All the patients underwent a brain SPECT scan 20 min after the intravenous administration of 740MBq of 99mTc-HMPAO. We applied the NeuroGamTM software on the reconstructed data, for the semi-quantitative evaluation of brain perfusion in BA in the right (R) and left (L) hemispheres. Perfusion values in BA were expressed as mean±SD percentage of mean perfusion of the cerebellum. Statistical analysis was performed using Mann-Whitney test. Results: Compared with women, men had statistically significantly lower perfusion in somatosensory association cortex bilaterally (BA 7L and 7R, p=0.016 and p=0.009, respectively), right middle temporal gyrus (BA 21R, p=0.016), anterior temporal gyrus bilaterally (BA 22L and 22R, p=0.035 and p=0.017, respectively), ventral posterior cingulated cortex bilaterally (BA 23L and 23R, p=0.002 and p=0.001, respectively), right subgenual area (BA 25R, p=0.019), right dorsal posterior cingulated cortex (BA 31R, p=0.05), fusiform gyrus bilaterally (BA 37L and 37R, p=0.034 and p=0.005, respectively), angular gyrus bilaterally (BA 39L and 39R, p=0.005 and p=0.009, respectively), supramarginal gyrus bilaterally (BA 40L and 40R, p=0.005 and p=0.011, respectively), pars opercularis bilaterally (BA 44L and 44R, p=0.012 and p=0.025, respectively) and left pars triangularis (BA 45L, p=0.05). Conclusion: More severe hypoperfusion in temporoparietal and frontal lobes in men with AD, may reflect underlying neuropathological sex differences and/or other gender-related factors. Patient gender maybe should be considered when interpreting brain perfusion SPECT studies.

P465

Application of CT based spatial normalization by DARTEL to quantitative assessment of 123I-FP-CIT SPECT.

K. Yokoyama, E. Imabayashi, H. Matsuda; National Center of Neurology and Psychiatry, Kodaira, JAPAN.

PURPOSE: 123I-FP-CIT is used for assessment of the dopamine transporter (DAT) to assess the nigrostriatal function in patients with parkinsonian syndrome (PS). In this study, to diagnose degenerative PS accurately, precise estimation of distribution of DAT, Diffeomorphic Anatomical Registration Through Exponentiated Lie Algebra (DARTEL) algorism is applied to SPECT using CT images. METHODS: Retrospective study. Eighty four patients (39 women and 45 men, 67.1 ±12.3y.o.) with PS were focused on this study. Among them 56 were clinically diagnosed as Parkinson's disease (PD) (24 women and 32 men, 68.5 ± 10.7 y.o.). The other 28 non-PD patients (13 women and 15 men, 64.3 ± 14.5 y.o.) included such as essential tremor, psychogenic disorders, drug induced PS and so forth. After injection of 167MBq of 123I-FP-CIT, SPECT images were obtained using SPECT/CT equipment (Symbia T6; Siemens Medical Systems, Inc.) with LMEGP collimator, CT based attenuation collection and without scatter collection. First, the gray matter is extracted using statistical parametric mapping 12. Spatial normalization to this gray matter images applied with the DARTEL algorism. Second, SPECT images were normalized with the same parameter as the CT normalization. Finally, 123I-FP-CIT images in Montreal Neurological Institute space are obtained. Then the volumes of interest (VOIs) were written in right, left, bilateral striatum, caudate nucleus, putamen and occipital, and the putamen was divided to anterior and posterior segments using plane rectangle to AC-PC plane (VOIs derived from a probabilistic brain atlas previously validated by Hammers et al. Hum Brain Mapp, 15:165-174, 2002). Specific binding ratios (SBR) referenced to occipital lobe were calculated. We compared the method without spatial normalization using a bilateral whole stratium VOI and whole brain as a reference, a measurement technique Tossici-Bolt, et al. suggested (Eur J Nucl Med Mol Imaging, 2006 Dec;33(12):1491-9). RESULT: Mean SBR of PD and non-PD using DARTEL algorism and Tossici-Bolt method was 1.67 ± 0.20, 3.10 ± 0.61 and 3.20 ± 1.11, 6.71 ± 1.44. Sensitivity, Specificity and Accuracy of the discrimination between PD and non-PD in each method were 98.2%, 100%, 98.8% and 90.9%, 100%, 94.0%, respectively. SBR of posterior segment of putamen was more useful to differentiate PD from the other, and had a good contrast between each disorder group than that of whole stratium. CONCLUSION: These data suggest that DARTEL normalization are useful for spatial normalization of 123I-FP-CIT images. VOI template for posterior putamen improved the sensitivity and accuracy from that of the whole stratium.

P29 - Monday, October 12, 2015, 4:00 PM - 4:30 PM, Hall 3 – Poster Exhibition

Neurosciences: Movement Disorders

P466

Is Dynamic [11C]Raclopride PET Scanning needed to Distinguish Patients from Healthy Controls?

P. Gykiere, N. Van Laeken, A. Dobbeleir, F. De Vos, I. Goethals; University Hospital Ghent, Ghent, BELGIUM.

Objective: Striatal dopamine D2 receptor PET imaging with [11C]raclopride may be helpful in the differential diagnosis of clinical parkinsonism. Dynamic [11C]raclopride acquisition allows calculating the binding potential (BP) of postsynaptic dopamine D2 receptors using a simplified reference tissue model. However, dynamic scanning requires a long acquisition time during which may be prone to movement bias of the subject. Here, the aim was to investigate whether dynamic scanning has higher diagnostic value compared to a short 10-min static PET scan obtained during transient equilibrium 30 minutes after tracer injection. Methods: [11C]raclopride PET was performed in 19 patients with clinically inconclusive parkinsonism (mean age 62.6 years, SD 12.7) and in 14 healthy volunteers (mean age 22.6 years, SD 4.1). Patients were free of dopaminergic medications that may interfere with [11C]raclopride binding. For the dynamic acquisition, the BP was calculated as the ratio of striatal activity in a VOI defined by 40% of the maximum left and right striatal activity to the reference region, namely the occipital cortex and the cerebellum. Similary, in the static scan the ratio striatal activity in a VOI defined as 40% of the maximum left or right striatal activity to the occipital cortex was calculated. Additionally, a resolution-independent specific uptake size index (SUSI) calculation was applied for measuring the specific to non-specific binding ratio, as also used in 123I-FP-CIT scans . ROC-analysis was used for all methods to investigate which method was best suited to discriminate patients from volunteers. Results: By using a 40% threshold VOI in the dynamic scan, an AUC value of 0.926 and 0.910 for respectively the occiput and cerebellum as reference region was obtained to discriminate patients from healthy volunteers. In the static scan, using 40% of striatal activity resulted in AUC value of 0.536, but SUSI calculations applied on the data provided an AUC of 0.883. Conclusion: This report suggest that a discrimination between patients and healthy volunteers is feasible by applying simple SUSI calculations on a 10-min static scan. Nevertheless, a small improvement of the diagnostic value of [11C]raclopride PET may be obtained by a dynamic scan analysis together with specific software.

P467

Relationship between dopamine deficit and the expression of depressive behavior resulting from alteration serotonin system

M. Lee1, Y. Ryu2, J. Choi2, W. Cho3, I. Hyun1; 1Inha University Hospital, Incheon, KOREA, REPUBLIC OF, 2Yonsei University, Gangnam Severance Hospital, Seoul, KOREA, REPUBLIC OF, 3Yonsei University College of Medicine, Wonju, KOREA, REPUBLIC OF.

Depression frequently accompanies in Parkinson's disease (PD). Previous research suggested that dopamine and serotonin systems are closely linked with depression in PD. However, comprehensive studies about the relationship between these two neurotransmitter systems are limited. Therefore, the purpose of this study is to evaluate the effect of dopaminergic destruction on the serotonergic system. The interconnection between motor symptoms and depression was also examined. Two PET scans were performed in the 6-hydroxydopamine (6-OHDA) lesioned and sham operated rats: [18F]FP-CIT for dopamine transporters and [18F]Mefway for serotonin 1A (5-HT_{1A}) receptors. Here, 6-OHDA is a neurotoxin for dopaminergic neurons. Behavioral tests were used to evaluate the severity of symptoms: rotational number for motor impairment and immobility time, acquired from the forced swim test for depression. Region-of-interests were drawn in the striatum and cerebellum for the dopamine system and hippocampus and cerebellum for the 5-HT system. The cerebellum was chosen as a reference region. Non-displaceable binding potential in the striatum and hippocampus were compared between 6-OHDA and sham groups. As a result, the degree of dopamine depletion was negatively correlated with rotational behavior ($R2 = 0.79$, $p = 0.003$). In 6-OHDA lesioned rats, binding values for 5-HT_{1A} receptors was 22 % lower than the sham operated group. This decrement of 5-HT_{1A} receptor binding was also correlated with the severity of depression ($R2 = 0.81$, $p = 0.006$). Taken together, this research demonstrated that the destruction of dopaminegic system causes the

reduction of the serotonergic system resulting in the expression of depressive behavior.

P468

123-I-MIBG cardiac scintigraphy quantitative analysis in Parkinson's disease (PD) and Parkinsonism (P) differential diagnosis: a classification tree (CIT) classifier additional contribute.

S. Nuvoli1, B. Palumbo2, M. L. Fravolini3, B. Piras1, G. Dachena1, S. Cascianelli2, A. Spanu1, G. Madeddu1; 1Unit of Nuclear Medicine, University of Sassari, Sassari, ITALY, 2Section of Nuclear Medicine, Dept of Surgical and Biomedical Sciences. University of Perugia, Perugia, ITALY, 3Dept of Engineering, University of Perugia, Perugia, ITALY.

AIM: Recently the usefulness of 123I-MIBG cardiac scintigraphy as diagnostic method in detecting autonomic nerve disturbances in neurodegenerative movement disorders has been reported resulting particularly important given the difficulty in discriminating between PD and P in some cases. In the present study, we performed 123I-MIBG cardiac scintigraphy in patients with movement disorders also applying the artificial neuronal network classifier CIT which consists of logical rule set organized as decision tree to product clear data classification providing numerical cut-off values able to differentiate different clinical groups. METHODS: We enrolled 106 consecutive patients,61 males and 45 females, aged 55-81 years, 35 classified as PD and 71 as P. In all patients, cardiac planar scintigraphy was performed after 111 MBq 123I-MIBG i.v. injection using a dual head gamma camera, in anterior and left anterior oblique views, in both early (15 min.) and delayed (240 min.) phases. Semiquantitative analysis was also performed calculating heart/mediastinum (H/M) ratio by mean count density measurement in manually drawn ROIs in anterior view. With regard to CIT for the 1.000 experiments, 11 patients were randomly selected as the training set, while the remaining 95 validated the trained CIT computing the validation data percentage of the correctly classified patients. The expected performance of an average performance CIT was calculated. RESULTS: The probability of a correct classification for CIT was 90 ±9.20% in PD pts and 88.35±15.26% in P patiens. The decision rule gave the early H/M ratio value of 1.56 ±0.01 for CIT. These results mean that patients with early H/M ratio values <1.56 were classified as PD, while patients with values >1.56 were classified as P. Moreover, delayed H/M ratios did not add significant information to classify the patients. CONCLUSIONS: The results of the present study demonstrated that the additional CIT use to 123I-MIBG cardiac scintigraphy quantitative analysis provided reliable and disease-specific numerical cut-off values able to differentiate PD from P patients and this is clinically remarkable for both diagnostic and therapeutic purpose. Moreover, it has also been demonstrated that the early H/M ratio values alone may be sufficient to obtain the final diagnosis avoiding further late scan necessity.

P469

Contribution of cardiac 123-I metaiodobenzylguanidine (MIBG) scintigraphy of combined whit FP-CIT SPECT in the differential diagnosis of the Parkinson disease and atypical parkinsonian syndromes.

G. Martinez Pimienta, R. Gomez Llopico, M. Bajén, A. Benitez Segura, O. Puig, J. Rojas Camacho, M. Boya-Roman, J. Rodríguez-Rubio, E. Noriega, J. Mora; Hospital Universitario de Bellvitge, Barcelona, SPAIN.

INTRODUCTION: The differential diagnosis between Parkinson's disease (PD) and atypical parkinsonian syndromes (multiple-system atrophy, MSA; progressive supranuclear palsy, PSP; Lewy body dementia, LBD) is established with clinical criteria. Imaging of the dopamine transporter with 123I-FP-CIT successfully visualizes presynaptic dopaminergic degeneration of the nigrostriatal tract in the PD and atypical parkinsonian syndrome but does not differentiate the various types of degenerative Parkinsonisms (PD, MSA, PSP, LBD). In PD and in LBD there is a cardiac sympathetic denervation, so imaging of the 123I-MIBG myocardial uptake can be helpful in the differential diagnosis of different Parkinsionian syndromes. OBJECTIVES: Evaluate the combined use FP-CIT-SPECT and cardiac 123-I MIBG Scintigraphy in the differential diagnosis of the Parkinson's disease and atypical parkinsonian syndromes. MATERIALS AND METHODS: We studied retrospectively 48 patients with parkinsonian syndrome and atypical initial presentation. A FP-CIT -SPECT and cardiac 123-I MIBG scintigraphy was performed in all patients. The FP-CIT -SPECT was assessed visually by two observers and reported as pathological or non-pathological. The cardiac 123-I MIBG uptake was evaluated by drawing standardized ROIs (heart-to-mediastinum ratio) on planar images 4 h after injection and it was considered normal if the ratio was >1.5. The FP-CIT -SPECT, cardiac 123-I MIBG and joint interpretation of both tests according to expected patterns were evaluated Diagnostic pattern expected: PD: FP-CIT -SPECT: pathological; Cardiac 123-I MIBG: pathological. LBD: FP-CIT -SPECT: pathological; Cardiac 123-I MIBG: pathological. MSA: FP-CIT -SPECT: pathological; Cardiac 123-I MIBG: non-pathological. PSP: FP-CIT -SPECT: pathological; Cardiac 123-I MIBG: non-pathological.

RESULTS: Final clinical diagnostic: PD: 31patients; LBD: 7 patients; MSA: 7 patients; PSP: 4 patients CONCLUSION: The FP-CIT -SPECT was positive in 98% of the patients with Parkinsonian syndrome but it could not differentiate between PD and atypical Parkinsonisms. The combination of FP-CIT-SPECT and Cardiac 123-I MIBG scintigraphy was concordant to the expected pattern in 85% of the patients and it helped in their differential diagnosis. The correlation of these two techniques with the expected pattern was higher in PD or LBD than in patients diagnosed of MSA or PSP.

P470

Correlation between tracer injection latency and seizure duration with the accuracy in detection of epileptogenic zone by SPECT and SISCOM

M. Suarez-Piñera1, A. Mestre-Fusco1, S. Medrano2, M. Ley3, G. Conesa4, R. Rodrigo3; 1Hospital del Mar Barcelona. Nuclear Medicine Department, Barcelona, SPAIN, 2Hospital del Mar Barcelona. Neuroradiology Department, Barcelona, SPAIN, 3Hospital del Mar Barcelona. Epilepsy Unit. Neurology Department, Barcelona, SPAIN, 4Hospital del Mar Barcelona. Neurosurgery Department, Barcelona, SPAIN.

Aims: SPECT and subtraction ictal SPECT coregistered to MRI (SISCOM) play an important role in seizure onset zone detection during the presurgical evaluation of patients with drug-refractory epilepsy. Injection latency (time between the onset of seizures and ictal tracer injection) and seizure duration have been two factors related to the accuracy in detection seizure onset area. This study has aimed to establish the correlation between injection latency and seizure duration with successfully epliptogenic zone detected by SPECT and SISCOM. Methods: Tc 99m- HMPAO SPECT ictal-interictal (dual-headed camera) and SISCOM (FocusDET) was performed in 16 refractory epilepsy patients (10 F, 38±10.8 yrs) candidates for surgical treatment. Tracer for ictal SPECT was injected manually by an expert technician in epilepsy monitoring unit. Seizure duration and injection latency was carefully noted. SPECT (visual and SISCOM) images were analyzed independently by two nuclear medicine physicians. SPECT results were compared to gold-standard; resected area localization and surgical outcome using Engel scale or with stereo-EEG (SEEG). True positive was considered SPECT results concordant with the resected area and a good clinical output (Engel I ó II) . False positive was considered spect results no concordant with resected area or suboptimal Engel (>Engel II) . Histolopathological findings of the resected areas are showed. A two-way ANOVA test was used to assess differences between injection latency and seizure duration with SPECT results. Results: Latency time ranged between (7-53 s). Seizure duration ranged between(31 and 170s). In 13/16 (81%)patients SPECT and SISCOM (together information) supported the localization of epileptogenic focus. SEEG showed multifocality in one patients and surgery was desestimated. The epileptic focus was not found in one patient. Other patient was classified as Engel III after surgery. No statistically significant differences were found between the different injection latency and seizure duration and epileptic focus localization. Our preliminary results showed the majority of the epileptic focus in temporal lobe (4 right and 3 left temporal lobe). Conclusions: SPECT and SISCOM provide a valuable diagnostic tool to localizate the epileptogenic zone in patients with medically refractory epilepsy. The findings of this study showed similar accurancy in the detection of epileptogenic zone independent of injection latency and seizure duration. These results are not in agreement with other published by other groups. A possible explications could be the homogenecity of the sample. Additional studies are needed to clarify the relationship between this factors and SPECT/SISCOM results.

P471

Importance of different modalities (SPECT/CT, MRI) in the quantitative assessment of DaTscan findings

S. Szekeres1, N. Kovacs2, G. Perlaki3, G. Orsi3, L. Papp4, B. Suha5, E. Schmidt1, K. Zambo1; 1University of Pecs Department of Nuclear Medicine, PECS, HUNGARY, 2University of Pecs Department of Neurology, PECS, HUNGARY, 3MTA-PTE Clinical Neuroscience MRI Research Group, PECS, HUNGARY, 4Mediso GmBH, Budapest, HUNGARY, 5University of Pecs Medical Faculty, PECS, HUNGARY.

Aim: The 123-I-Ioflupan as a presynaptic dopamine receptor analog molecule plays an important role in the determination of receptor density of the striatum. The method is useful to differentiate between the essential tremor (ET) and the different types of Parkinson-syndrome (Parkinson-disease (PD), Multiple System Atrophy (MSA) and Progressiv Supranuclear Palsy (PSP) and it is helpful for setting up the early and accurate diagnosis of Parkinson-disease. The aim of the present study is to compare a well-establised visual assessment and the results of different quantitative methods. Materials and methods: Examinations were performed in 40 patients with ET, with PD (in early or advanced stage and severe PD with Duodopa therapy) and in patiens with MSA and PSP. During the visual evaluation a well-establised (Ottaviani, S. et al., 2006) visual scale was applied (normal, abnormal grade I, II, III) by two independent experts. Three different methods were introduced for the quantitative evaluation: 1. on the SPECT/CT image of a patient with normal distribution of dopamine receptors 4 VOIs in the striatum and 2 VOIs in the occipital lobe (6 optimal VOIs) were circumscribed and these were applied in all patients; 2. on the SPECT/CT image of all

patients individual 6 optimal VOIs were determined; 3. after co-registration of CT and MRI pictures an MRI mask was used on the SPECT image in the different regions. Results: There was considerable agreement between the visual scores by the two observers and the visual score correlated significantly with the clinical stage of PD. We found a significant overlap between the visual scores and the automatic MRI-based evaluation. Comparing the two different types of quantitative nuclear medicine methods with each-other and the automatically determined MRI binding values presents a good choise to achieve the best suitable parameters. Conclusion: Based on our preliminary results, the quantitative methods may support the visual assessment of DAT binding. We hope that the introduction of these methods would be an excellent possibility to establish the differential diagnosis of movement disorders as well as to comfirm the diagnosis of Parkinson-disease. This work was supported by Hungarian Brain Research Program - Grant No. KTIA_13_NAP-A-II/10.

P472

Exploring the feasibility and potential advantages of applying CT-based attenuation correction in 123I-FPCIT and 123I-IBZM SPECT studies. Our first experience

K. Badiavas, I. Iakovou, V. Athanasiou, K. Mihailos; Nuclear Medicine Department, Aristotle University, "Papageorgiou" General Hospital, Thessaloniki, GREECE.

Aim. Our aim was to explore the feasibility and potential advantages of applying CT-based attenuation correction at the 123I-FPCIT and 123I-IBZM SPECT studies performed in our department, using our newly installed SPECT/CT imaging system.Materials and methods. The usual process when performing 123I-FPCIT or 123I-IBZM SPECT studies in our department is to use a dual-head γ-camera (Discovery 630 NM, Xeleris 3 workstation, GE Healthcare). After the installation of a SPECT/CT imaging system (Optima 640 NM/CT, Xeleris 3 workstation, GE Healthcare) we decided to apply CT-based attenuation correction at a limited number of 123I-FPCIT and 123I-IBZM SPECT studies who were followed by low-dose CT in order to explore the feasibility and potential advantages. For the two different approaches (CT-based AC Vs SPECT alone) we reconstructed the data (OSEM, Butterworth filtering) and applied the "manual positioning ROIs" quantification method that, according to our previous works, proved to be the best among others methods examined. ROIs were created by the same experienced user. The group of patients examined consisted of 23 patients having 123I-FPCIT SPECT scan (14 men and 9 women, aged 61.7±12.4 years) while 6 of them had also 123I-IBZM SPECT scan (5 men and 1 woman, aged 67.2±5.1 years).Results. After visual assessment, two experienced observers agreed that the resulting images after AC had better "Contrast-to-Noise ratio" leaving, though, the diagnosis that was based at the SPECT alone examination, unaltered. Data quantification produced greater values (at a mean value of 30.5%) for the specific uptake at the striatum, caudatum and putamen while leaving the Putamen-to-Caudate ratio (P/C) almost unaltered. Again, the diagnosis was not altered in any of the examined cases.Conclusion. The application of CT-based attenuation correction after a low-dose CT at 123I-FPCIT and 123I-IBZM SPECT studies definitely provides images with better "Contrast-to-Noise ratio" than SPECT alone examination. The specific uptake ratios for the striatum, caudatum and putamen against the occipital uptake (background) are all elevated but, fortunately, the Putamen-to-Caudate ratio (P/C is a ratio that we consider important) seems to be unaltered. There was no change in diagnosis for the patients we studied and considering the additional patient's radiation dose for, even a low-dose, CT scan plus the extra machine-time needed, we decided to stick to the SPECT alone examination followed by visual assessment and data quantification. Further studies are needed, so we have already programmed a series of experiments with 123I and the, well known, striatal phantom.

P473

The clinical usefulness of I-123-Ioflupane SPECT (DaTscan) in patients with equivocal diagnosis of Parkinson's disease

S. Czibor1, D. Nagy1, M. Moravszki1, L. Duffek1, E. Takacs2, E. Kalameny3, Z. Szeplaki4, A. Takats4, I. Szilvasi1; 1Hungarian Defence Forces Medical Centre, Dept. of Nuclear Medicine, Budapest, HUNGARY, 2Semmelweis University, Dept. of Nuclear Medicine, Budapest, HUNGARY, 3Hungarian Defence Forces Medical Centre, Dept. of Neurology, Budapest, HUNGARY, 4Semmelweis University, Dept. of Neurology, Budapest, HUNGARY.

Aim: Our purpose was to evaluate the clinical usefulness of the DaTscan examination in patients with equivocal diagnosis of extrapyramidal movement disorders with tremor and/or rigidity or failing response to therapy based on previous clinical diagnosis. Degeneration of the presynaptic dopaminergic neurons in the negro-striatal system can be detected by DaTscan examination.Materials and methods: Between 2009 and 2014 34 patients (9 women and 25 men, mean age 64,7±12,4 years) were studied in two large neurological departments. Patients had symptoms of either Parkinson's disease, essential tremor or extrapyramidal movement disorders but the diagnosis based on clinical-radiological findings and neurological tests was equivocal or they had insufficient response to standard therapy. Tremor was present in 26 cases (9 of those asymmetrical and 17

symmetrical), while rigidity, Negro-sign, bradykinesis and postural instability was documented in 19, 19, 8 and 3 patients, respectively. The DaTscan examinations were performed according to the guideline of the European Association of Nuclear Medicine. The visual and semiquantitative calculations were performed by two experienced independent nuclear medicine specialists.Results: The DaTscan study confirmed early-stage Parkinson's disease in 19 cases. In 6 equivocal cases essential tremor was diagnosed. 3 patients treated for Parkinson's disease with insufficient response to therapy, diagnosis changed to essential tremor. Parkinson's disease was diagnosed in 1 patient with previously assumed sleep apnoe syndrome and in 1 patient with suspected essential tremor. Diagnosis of Parkinson's disease was dismissed at 2 patients, one of them had sleep apnoe syndrome and the other had DOPA-responsive dystonia. In 2 patients, the previously suspected diagnosis of periodic limb movement disorder and Lewy-body dementia was confirmed.Conclusion: Our study has shown that the DaTscan SPECT has a clinically important role in equivocal diagnosis of Parkinson's disease and other neurological disorders with tremor. It has particular diagnostic value in early-onset Parkinson's disease and could be useful in demented patients to detect Lewy-body dementia. In patients unresponsive to therapy, DaTscan has an impact on clinical management and consequently on expenditures of the healthcare system.

P474

Diagnostic value of MIBG cardiac scintigraphy for the diagnosis of Parkinson disease.

M. Abbasi1, A. Tafakhori2; 1Department of Nuclear Medicine , Vali-e-asr Hospital, Tehran University of Medical Sciences, Tehran, IRAN, ISLAMIC REPUBLIC OF, 2Department of Neurology, Imam-komeini Hospital, Tehran University of Medical Sciences, Tehran, IRAN, ISLAMIC REPUBLIC OF.

MIBG uptake is reduced in the myocardium of patients with Parkinson disease. We intended to study the accuracy of MIBG cardiac scintigraphy for discrimination of Parkinson disease from other causes of Parkinsonism. The data of 19 patients with retractable Parkinsonism or obscure diagnosis referred for MIBG cardiac imaging were completed for this preliminary report. Planar imaging of the chest and cardiac SPECT were done 2 hours after injection of 0.7 to 1 mCi I131-MIBG. The planar and SPECT images were reviewed visually in addition to ROI analysis in planar images. The ROIs were drawn around the heart and the lung fields excluding the heart in both anterior and posterior images. The geometric means were employed and the optimal heart to lung ratios were calculated based on the shortest distance to the optimal point on the ROC curve. Patients were followed until the neurologist came to his final decision about the diagnosis of the patients based on the course of the disease, other diagnostic images and response to therapy. The diagnostic self confidences of interpreters were evaluated with the use of a 4 point visual scale from poor to optimal confidence. 10 patients (7 males) aged 66 +- 6 years had Parkinson disease and 9 patients (5 males) had other causes of Parkinsonism including ardive dyskinesia (3 cases) , essential tremor (3 cases) , multisystem atrophy (2 cases) and corticobasal degeneration (1 cases). MIBG scans were reported positive for Parkinson disease in 9 patients with Parkinson disease and negative for Parkinson disease in 8 out of patients with other diagnoses. The sensitivity, specificity and accuracy of the MIBG scan were 90%, 88.9% and 89.4% respectively. The optimal cutoff value of the heart to lung uptake ratios was about 1.3 at which the diagnosis of all non-Parkinson disease subjects were possible in addition to correct diagnosis of 9 Parkinson diseases out of 10 (accuracy of 94.7%). The interpreters evaluated the quality of planar I131 MIBG images optimal for the detection of MIBG uptake with good diagnostic confidence (mean= 3.8; median = 4). We found cardiac MIBG scan is a valuable tool for differentiation of Parkinson disease in cases with diagnostic problems. In addition we found the quality of I131 imaging acceptable for this purpose which could be used instead of I123 when unavailable.

P475

Absolute quantitative evaluation of 123I-FP-CIT: is it possible?

F. Scalorbi1, S. Bressan2, S. Favaretto3, S. Berti1, S. Pompanin3, A. Cagnin3, A. Antonini3, C. Gabelli4, P. Zucchetta1, F. Bui1, D. Cecchin1; 1Department of Nuclear Medicine of Padova, Padova, ITALY, 2Hospital of Padova, Padova, ITALY, 3Department of Neurology of Padova, Padova, ITALY, 4Centro regionale per la cura dell'invecchiamento cerebrale, Padova, ITALY.

Aim: 123I-FP-CIT (DaTSCAN) SPECT studies of the nigrostriatal pathway are a valuable tool in the diagnosis of movement disorders. Qualitative analysis of such data, however, is problematic cause it depends on the subjectivity of the operator. Semiquantification of data improve things but lacks the possibility of a reliable comparison among different centers. Aim of this study is to present an innovative open source and JAVA-based program (named SUQS: Striatal Uptake Quantification System), tested on Win, Mac and Linux, providing absolute quantitative evaluation of the striatal uptake of 123I-FP-CIT. To validate it we have tested the system on phantoms and patients. Material and Methods: The method automatically segments DICOM transaxial, filtered and attenuation corrected images then, using correction factors derived from multiple acquisitions of a fully tissue-equivalent

anthropomorphic striatal phantom (RDS) it coverts counts in MBq. Furthermore corrections for attenuation, partial volume effect and radius of percentages of the injected dose rotation, have been incorporated. It derives then the percentage of the injected dose. An RDS at different radius of rotation and at the same radius for 24 hours has been obtained to validate the system. Furthermore we tested it on 85 patients (46 males, 40 females, mean age 68.85 years, range 35-86) who underwent 123I-FP-CIT SPECT (mean activity 178.7 MBq) from 2006 to 2009 at the Nuclear Medicine Department, University Hospital of Padova (Italy). This time span has been chosen because we have a long follow-up for all this patients. At the moment of the scan 55 patients were classified as PD (Parkinson Disease), 7 as Parkinsonism (3 Cortical Basal Degeneration, 2PSP-P, 1 MSA, 1 Vascular Parkinson), 7 as Essential Tremor, 3 as Psychiatric Disorders, 11 as Extrapiramidal Syndrome, 1 as AD (Alzheimer Disease), 1 as DBL (Lewy Body Disease). Being a retrospective evaluation only the Hoehn and Yard scale was available (33 patients were classified as I, 43 as II , 8 as III, 1 as IV, none as stage V). Results and preliminary Conclusions: Although the validation is ongoing preliminary data on phantoms provided excellent results in measuring the real activity both at different radius and also considering decay over a long time (24 hrs). Preliminary data on patients seems to show that absolute quantitative evaluation is superior to qualitative and semi-quantitative evaluation in predicting the state of patients at follow-up.

P476

Cut-off values to diagnose Parkinson's disease by means of 123I-FP-CIT brain SPECT semiquantitave data as evaluated by Classification Tree algorithm

B. Palumbo1, S. Cascianelli2, I. Sabalich1, A. Santonicola1, T. Buresta1, M. L. Fravolini2, N. Tambasco3, S. Nuvoli4, A. Spanu4, G. Madeddu4; 1Department of Surgical and Biomedical Sciences- Nuclear Medicine and Health Physics-University of Perugia, PERUGIA, ITALY, 2Department of Engineering-University of Perugia, PERUGIA, ITALY, 3Unit of Neurology, Department of Medicine, Perugia University Hospital, PERUGIA, ITALY, 4Unit of Nuclear Medicine, Department of Clinical and Experimental Medicine, University of Sassari, Sassari, ITALY.

Aim: To identify cut-off values of radiopharmaceutical uptake ratios in basal ganglia able to differentiate PD and other conditions, we applied a Classification Tree algorithm (ClT) to 123I-FP-CIT brain SPECT semiquantitave data. A ClT is an automatic classifier consisting of a set of logical rules, organized as a decision tree to produce an optimised threshold based classification of data, thus providing discriminative cut-off values. **Methods**: We performed 123I-FP-CIT brain SPECT (Millenium VG, G.E.M.S.) with semiquantitative analysis with Basal Ganglia (BasGan) V2 software according to EANM guidelines in 115 patients with movement disorders; 73 were diagnosed as PD (36 M and 37 F; range of age: 60-81 yrs, Hoehn and Yahr score (HY): 0.5-1.5; Unified Parkinson Disease Rating Scale (UPDRS) score: 6-38] and 42 resulted as non-PD (Essential Tremor and drug-induced PD, 20 M and 22 F; range of age 60-80 yrs). The final diagnosis was confirmed by a clinical follow-up of at least 6 months. A 10-fold cross validation was applied by repeating 1000 random experiments. This allowed the statistical evaluation the "average performance" of ClT. **Results**: For ClT, the probability of correct classification in patients with PD was 78.97±15.62% (mean ±SD) and in non-PD patients 92.63±9.30%. For ClT, the first decision rule gave a value for the right putamen (RP) of 2.44 ±0.09, thus meaning that if RP values were lower patients were classified as PD, while if RP values were higher patients were classified as non-PD. More complex ClT structures, including caudate nuclei and left putamen values, were tested to refine the classification performance, but in our data these additional features appeared to be less significant. **Conclusion**: ClT was able to classify PD and non-PD patients by means of 123I-FP-CIT brain SPECT data; furthermore it allowed to identify reliable cut-off values able to contribute to the differential diagnosis of these categories. RP uptake values in our patients seemed to be the most discriminant for the diagnosis, probably due to a certain number of patients with initial prevalence of left clinical symptoms.

P477

Evaluation of 99mTc-TRODAT-1 SPECT in the diagnosis of Parkinson's disease and its differentiation from the other types of parkinsonism syndroms - A pilot study

D. Beiki1, A. Esmaeili1, B. Fallahi1, S. Oveisgharan2, H. Noorollahi-Moghaddam3, M. Erfani4, A. Tafakhori5, M. Rohani6, A. Fard-Esfahani1, A. Emami-Ardekani1, M. Eftekhari1; 1Research Center for Nuclear Medicine, Tehran University of Medical Sciences, Tehran, IRAN, ISLAMIC REPUBLIC OF, 2Department of Neurology, Shariati Hospital, Tehran University of Medical Sciences, Tehran, IRAN, ISLAMIC REPUBLIC OF, 3Shariati Hospital, Tehran University of Medical Sciences, Tehran, IRAN, ISLAMIC REPUBLIC OF, 4Radiation Application Research School, Nuclear Science and Technology Research Institute, Atomic Energy Organization of Iran, Tehran, Iran, Tehran, IRAN, ISLAMIC REPUBLIC OF, 5Department of Neurology, Imam Khomeini Hospital, Tehran University of Medical Sciences, Tehran, IRAN, ISLAMIC REPUBLIC OF, 6Department of Neurology, School of Medicine, Rasoul Akram Hospital, Iran University of Medical Sciences, Tehran, IRAN, ISLAMIC REPUBLIC OF.

Aim: Parkinson disease (PD) is one of the most common movement disorders. Sometimes, essential tremor (ET) and the other parkinsonian syndromes may manifest the same motor symptoms. In these cases, definite clinical diagnosis may be difficult. We conducted a study to determine the diagnostic value of 99mTc-TRODAT-1 scan to differentiate PD from ET and other cases of parkinsonism syndromes.Methods and Materials: This study was prospectively performed on 35 patients including 15 PD, 12 ET and 8 patients with other parkinsonian syndromes (PS). A new analogue of 99mTc-TRODAT-1 was used for basal ganglia (BG) imaging. A dual-head SPECT-CT was used to perform imaging for all patients following administration of at least 950 MBq 99mTc-TRODAT-1. The images were reconstructed and processed using neuroimaging software for the SPECT modality. Drawing ROIs on the BG, the uptake values were estimated and normalized to whole brain uptake. Results: Among three groups of patients, ET cases show significantly higher values of normalized BG uptake ($p<0.05$) as compared to PD and PS groups; however, no significant difference was noted between PD and PS groups. In qualitative assessment, all ET cases showed normal and symmetrical uptake in BG. From 15 PD patients, 9 cases (60%) revealed greater loss of uptake in putamen vs. cudate. On the other hand, in PS patients, 6 out of 8 patients (75%) had uniform pattern of decreased uptake in bilateral putamen and cudate and only two patients (25%) showed greater loss of uptake in putamen bilaterally, one symmetrical and the other one asymmetrical. Conclusion: The preliminary quantitative data reveals that 99mTc-TRODAT-1 scan is a very appropriate method to differentiate PD or PS vs. ET cases. However, the BG uptake values alone could not identify PD vs. PS cases. The pattern of uptake may add to diagnostic value of the test; however, the present results are equivocal and thus further investigations with more cases are needed to reach more suitable criteria for this reason.

P478

123I-MIBG cardiac scintigraphy in discriminating Parkinson's disease (PD) from vascular parkinsonism (VP) using Classification tree (CIT) classifier together with conventional quantitative analysis.

S. Nuvoli1, A. Spanu1, B. Palumbo2, M. L. Fravolini3, G. Dachena1, B. Piras1, G. Madeddu1; 1Nuclear Medicine Unit; University of Sassari, Sassari, ITALY, 2Section of Nuclear Medicine, Dept of Surgical and Biomedical Sciences. University of Perugia, Perugia, ITALY, 3Dept of Engineering University of Perugia, Perugia, ITALY.

AIM. Parkinson's disease (PD) is characterized by basal ganglia abnormalities and peripherical autonomic nerve disturbances. 123I Ioflupane SPECT represents reference diagnostic method, but basal ganglia vascular damage could reduce its specificity. In this study, we used 111I-MIBG cardiac scintigraphy to discriminate different movement disorders in patients with basal ganglia vascular abnormalities. METHODS. Among large PD patient group, we selected 25 consecutive patients clinically classified as PD, 21 stage 1 and 4 stage 2 (Hoen-Yahr scale). Three of 25 patients were never treated, while 22 were on dopamine agonist therapy, but with partial/poor response. In all cases, MRI evidenced basal ganglia vascular lesions and 123I Ioflupane SPECT had uncertain interpretation. Cardiac planar scintigraphy was performed after 111 MBq 123I-MIBG i.v. injection using dual head gammacamera, anterior and left anterior oblique views, in both early (15 min.) and delayed (240 min.) phases. Data were evaluated by qualitative and semiquantitative analyses calculating heart/mediastinum (H/M) ratio by mean count density measurement in manually drawn ROIs in anterior view. Quantitative H/M ratio evaluation was performed also applying an artificial neuronal network classifier, Classification Tree (CIT), trained in a previous our study to classify patients with movement disorders obtaining 1.56 as cut off: patients with H/M 1.56 as parkinsonism (P). RESULTS. At qualitative analysis, normal 123I MIBG cardiac uptake, in early and delayed phases, was evidenced in 7/25 cases (group A), markedly reduced in 11/25 (group B), and slightly reduced in the remaining 7/25 (group C). H/M was high in group A, being >1.56 in all cases in both early (1.72±0.15) and delayed (1.75±0.12) phases, low in group B with values < 1.3 (1.2±0.04 and 1.14±0.07, respectively) and slightly reduced in group C with values between 1.3 and 1.56 (1.41±0.18 and 1.45 ±0.07 respectively). No statistical difference was found between early and delayed H/M mean values in all groups. CIT classified groups B and C as PD and Group A as P; thus, final clinical diagnosis of this latter group patients, 6/7 of whom already on drug therapy with poor response, was VP. CONCLUSIONS.123I-MIBG cardiac scintigraphy proved reliable diagnostic method which can contribute to differentiate PD from P. In particular, in the present study, the procedure was able to obtain VP diagnosis in patients with positive MRI but uncertain 123I-Ioflupane scintigraphy interpretation. Moreover, the additional CIT employment to conventional quantitative analysis gave an useful contribute also using early phase alone.

P479

Importance of myocardial MIBG scintigraphy in differentiating idiopatic Parkinson's disease from other neurodegenerative diseases

R. Petrovic1, A. T. Golubic1, T. Samardzic1, N. Klepac2, S. Telarovic2, S. Tezak1; 1Department of Nuclear Medicine and Radiation Protection, University Hospital Center Zagreb, Zagreb, CROATIA, 2Clinical Neurology Department, University Hospital Center Zagreb, Zagreb, CROATIA.

Aim: The aim of this study was to explore and evalute the usefulness of I-131 MIBG myocardial scintigraphy in patients with idiopathic Parkinson's disease and other neurological conditions with similar symptoms. Because of common overlapping in signs and symptoms of these neurodegenerative syndromes, especially in the early stages, the differential diagnosis can be troublesome. Materials and Methods: Sixty-one patients (age from 35 to 86, mean 59) with rigidity, tremor, hypokinesia and other related symptoms, with diverse neurological working diagnoses, underwent MIBG scintigraphy. Planar chest MIBG imaging was performed 15 min, 2, 3, 4 and 24 hours after tracer injection. Myocardial MIBG activity was quantified by calculating heart to mediastinum ratio (H/M ratio). H/M value over 1.8 was considered normal, between 1.31 -1.79 decreased, and less than 1.3 severely decreased. None of the patients in this study had heart disease or any other medical condition which can influence MIBG uptake. Results: In total, H/M ratio from early and delayed MIBG scintigraphy was pathologically decreased in 42 (69%) patients. In 77% of cases of IPD suspected patients we have confirmed the main working diagnosis, thus establishing a high degree of diagnostic certainty. H/M ratios in IPD patients was not significantly correlated with disease duration and the HY scale. In 8 patients with MSA we changed initial diagnosis to IPD (73%). Three patients confirmed as MSA had normal HM ratios. In 16 patients with extrapyramidal symptoms we had 10 normal findings, and because of pathological HM ratio we changed final diagnosis to IPD in 6 patients. Of 4 other patients, 3 had pathological HM ratios, thus changing their final diagnosis to IPD. Conclusions: According to our findings, cardiac autonomic nervous system dysfunction is common in IPD, but not in other neurological conditions, especially not in MSA. We report that myocardial MIBG scintigraphy can be a powerful, yet very simple and affordable method in differential diagnosis of IPD, thus greatly assisting in diagnosing impaired peripheral adrenergic activity. Also, myocardial MIBG imaging can be of great help in establishing final diagnosis in patients with extrapyramidal symptoms, especially when nigrostriatal dopamine transporter imaging is not available. Longitudinal follow-up studies are needed in order to evaluate the effects of myocardial MIBG imaging as an indispensable method of prognostic value in routine clinical practice and management of patients with various neurological conditions.

P480

Correlation among freezing of gait , falls and dopaminergic dysfunction in Parkinson's disease: evidences of a five years follow-up.

F. Guidoccio1, R. Ceravolo2, G. Puccini1, D. Frosini2, G. Manca1, U. Bonuccelli2, I. Paglianiti1, D. Volterrani1; 1Regional Center of Nuclear Medicine, University of Pisa, PISA, ITALY, 2Neurology Unit, Department of Clinical and Experimental Medicine, University of Pisa, PISA, ITALY.

Aim:Freezing of gait (FOG) is characterized by difficulty in initiating or maintaining locomotion, frequently associated with falls in advanced disease, often related to the OFF state, and may be responsive or unresponsive to dopaminergic therapy. The role of dopamine depletion is still debated in the pathogenesis of FOG and Falls.We aimed to evaluate the role of I123-FP-CIT-SPECT imaging in predicting FOG and falls in a cohort of Parkinson Disease (PD) de-novo patients followed up for five years. Materials and Methods: Ninety-four PD de-novo patients underwent 123I-FP-CIT SPECT at baseline. Basal ganglia matching tool 2, was used to obtain semiquantitative measures of caudate and putamen uptake. Each patient was assessed with Unified Parkinson's Disease Rating Scale (UPDRS) part II and III and Mini Mental State Examination (MMSE) at baseline and each year in the follow up. FOG and falls were assessed through UPDRS III. We compared baseline clinical, demographic, and SPECT indices between patients who developed FOG and falls and subjects who did not. Results: During follow-up, 47% patients developed FOG, 15% falls. No significant statistical differences in UPDRS III and MMSE at baseline were found between patients with FOG and Falls and those without these features. Patients with FOG had a decreased uptake at baseline in putamen (right 1,42 vs. 1,86; $p < 0{,}002$, left 1,67 vs. 1,97; $p < 0{,}05$) and in caudate (right 2,77 vs. 3,32; $p < 0{,}005$; left 3,02 vs. 3,38; $p < 0{,}06$). No significant differences in baseline striatal uptake were observed in relationship with the risk of falls. Conclusion: A baseline lower uptake value of striatum seems to be predictor of FOG and this evidence might support, a link between FOG and dopamine depletion both in caudate and putamen, at least in the early stage of disease. Risk of Falls, although often associated with FOG in PD, doesn't relate to dopaminergic dysfunction, supporting the hypothesis of its complex multifactorial genesis.

P481

99mTc-TRODAT-1 SPECT in the evaluation of Parkinson's disease progression and severity

A. Damian1, C. Pascovich1, D. Muñoz1, M. Langhain1, I. Amorin2, A. Lescano2, R. Buzo2, R. Ferrando1; 1Nuclear Medicine Centre, Clinical Hospital, University of the Republic, Montevideo, URUGUAY, 2Neurology Institute, Clinical Hospital, University of the Republic, Montevideo, URUGUAY.

Parkinson's disease (PD) is a neurodegenerative disorder characterized by the loss of dopaminergic neurons in the substantia nigra pars compacta and their projections to the striatum.

99mTc-TRODAT-1 is a widely available SPECT tracer with high affinity to dopamine transporters (DATs) in dopaminergic nerve terminals in the striatum. Although some studies with limited number of patients have assessed the diagnostic performance of 99mTc-TRODAT-1 in PD, the use of this tracer to reveal disease progression and severity is still a matter of discussion. Aim: to assess the performance of 99mTc-TRODAT-1 in the evaluation of progression and severity of PD. Material and methods: Retrospective study of 92 PD patients (25-80 years old, 46 women, mean disease progression 6.2±5.0 [SD] years) and 9 controls that underwent 99mTc-TRODAT-1 SPECT scan between 2011 and 2015. Specific striatal, putaminal and caudate nucleus binding uptake ratios (SUR, striatal mean counts - occipital mean counts/occipital mean counts) and asymmetric index (2 x [(ipsilateral SUR - contralateral UR)/(ipsilateral SUR + contralateral SUR)] x 100) were calculated in all subjects and compared with clinical presentation, time of progression and Hoehn and Yahr scale (HYS) of disease severity. Spearman rank order correlation and ANOVA with Dunnett C post-hoc analysis was performed for statistical comparison. P<0,05 was considered significant. Results: Asymmetric index was higher in PD patients (31.3±28) in comparison with controls (5.1±5, p<0.001). Clinical lateralization was associated with imaging lateralization (p=0.002). Striatal SUR showed a significant negative correlation with time of progression of the disease (p<0.00001, correlation coefficient -0.43) and HYS (p<0.00001, correlation coefficient -0.48). All HYS groups had lower striatal SUR in comparison with controls (p<0.001). SUR in HYS I to IV were 0.5±0.23 (mean±SD), 0.37±0.16, 0.31±0.11, 0.24±0.12 respectively (p = 0.001). Post hoc analysis discriminated between HYS I and III (p=0.009) and beetween HYS I and IV (p=0.005). Conclusion: The SPECT tracer 99mTc-TRODAT-1 performs well in the clinical evaluation of PD patients with good correlation with disease progression and severity that support its use in clinical practice. Further prospective clinical trials with large number of patients comparing the performance of this tracer with 123I-FP-CIT are needed.

P482

Pupillometry and I-123-DaTSCAN imaging in Parkinson's disease-a comparative study.

G. Gerasimou1, E. Giza2, S. Bonstanjioloulou2, Z. Katsarou3, E. Moralidis1, E. Papanastasiou1, P. Ioannidis1, A. Gotzamani-Psarrakou1; 1AHEPA University Hospital, THESSALONIKI, GREECE, 2Papanikolaou Hospital, THESSALONIKI, GREECE, 3Hippokration Hospital, THESSALONIKI, GREECE.

Aim: The aim of this study was the evaluation of pupil light reflex (PLR) in patients with Parkinson's disease (PD) by using a modern pupillometry system and the investigation of its potential relationship with dopamine transporter imaging (DaTSCAN), which is an objective method for the evaluation of presynaptic dopaminergic system.<br Materials and Methods: PLR was evaluated using pupillometry in 35 patients with PD without clinical evidence of autonomic dysfunction and 44 healthy matched controls or individuals with essential tremor. PLR was elicited using a fully automated pupillometry system and six parameters were measured. Dopamine transporter imaging was performed using I-123 tagged ioflupane- I-123-FP-CIT (DaTSCAN). A significant increase in latency and a significant decrease in amplitude, maximum constriction velocity, as well as maximum acceleration were observed in PD patients. There was no significant difference in initial radius and minimum radius values. Investigating the relationship between pupillometry parameters and (123)I-FP-CIT binding values, we correlated values from the semiquantitative analysis of radioligand uptake with pupillometry parameters, but we found no significant correlation.<br Conclusion: This study demonstrates PLR impairment in patients with PD without overt autonomic dysfunction. This impairment does not seem to correspond to the reduction of radioligand binding in the striatum as the result of presynaptic dopaminergic dysfunction, suggesting a different deterioration rate of these systems.

P483

Difference in striatal dopamine transporter availability and psychiatric symptoms in Parkinson's disease subtypes: 123I-FP-CIT SPECT results

F. Cocciolillo1, D. Di Giuda1, S. Annunziata1, V. Scolozzi1, F. Bove2, M. G. Vita2, C. Piano2, D. Fortini1, A. R. Bentivoglio2, G. Camardese3, A. Giordano1; 1Nuclear Medicine Institute, Università Cattolica del Sacro Cuore, Roma, ITALY, 2Neurology Institute, Università Cattolica del Sacro Cuore, Roma, ITALY, 3Psychiatric and Psychology Institute, Università Cattolica del Sacro Cuore, Roma, ITALY.

Aim: Parkinson's disease (PD) subtypes may be associated with different disease progression, neuropsychiatric and neuropathological features. However, there are conflicting results on differences in pre-synaptic dopaminergic damage. We assessed dopamine transporter availability by 123I-FP-CIT SPECT in tremor-dominant type (TDT) and akinetic-rigid type (ART), using Statistical Parametic Mapping (SPM) and automatic volumes of interest (VOIs). Relationships between imaging and psychiatric findings were investigated. Material & Methods: We included 37 drug-naïve PD patients with abnormal 123I-FP-CIT SPECT scans. According to the UPDRS-III, patients were classified into 18 TDT (15 M, mean age:62±13 years; H&Y stage:1.7±0.4; UPDRS-III:17±6) and 19 ART (10

M, mean age:61±13 years; H&Y stage:1.8±0.5; UPDRS-III:19±8). At the time of SPECT, psychometric assessment included the Hamilton Depression Rating Scale (HDRS), Hamilton Anxiety Rating Scale (HARS) and Snaith Hamilton Pleasure Scale (SHAPS). A 123I-FP-CIT template was generated with parametric images of 20 healthy subjects, using a Montreal Neurological Institute template of 18F-DOPA as reference. Patient scans were spatially normalised to the 123I-FP-CIT template by SPM8. Analysis was performed using VOIs selected from a digital atlas and placed over the caudate and putamen, bilaterally, and over the occipital cortex. The mean activity concentration was obtained for VOIs and Specific Binding Ratios (SBRs) were calculated through Marsbar toolbox. Results: No differences were found in age, gender, disease duration, H&Y stage and UPDRS-III score between subtypes. In comparison with ART, TDT patients showed higher SBRs in the caudate contralateral and ipsilateral to the most affected side ($p<0.05$). SPM statistics confirmed VOI results, revealing a lower uptake in the caudate nuclei of ART patients ($p<0.01$). In the whole sample, bradykinesia and rigidity, but not tremor scores were related to SBRs ($p<0.05$). Relevant depression symptoms were found in 6 TDT (33%) and 13 ART (68%) patients ($p<0.05$); HDRS and SHAPS scores were higher in ART than TDT patients ($p<0.05$). An inverse correlation was found between SBRs in the ipsilateral caudate and HDRS or SHAPS scores in the overall sample ($p<0.05$). Conclusion: Our results indicate that ART patients have a more severe dopaminergic deficit in the caudate nuclei than TDT patients at the same disease stage. This finding is consistent with the more favourable prognosis of TDT patients, related to a less dopaminergic impairment and/or an involvement of other pathways. The association of DAT availability in the ipsilateral caudate with depression and anhedonia severity support the role of caudate dopamine function in the pathophysiology of psychopathological symptoms.

P484

The significance of the posterior part of the putamen in I-123-FP-CIT SPECT scanning and the early diagnosis of Parkinson's disease.

G. Gerasimou1, E. Papanastasiou1, E. Moralidis1, Z. Katsarou2, P. Ioannidis1, M. Arnaoutoglou1, N. Grigoriadis1, T. Tegos1, G. Liaros1, M. Gkirgkoudis1, A. Vasileiadis1, S. Bonstanjiopoulou3, A. Gotzamani-Psarrakou1; 1AHEPA University Hospital, THESSALONIKI, GREECE, 2Hippokration Hospital, THESSALONIKI, GREECE, 3Papanikolaou Hospital, THESSALONIKI, GREECE.

Aim: Parkinson's disease (PD) is a neurodegenerative disorder affecting the presynaptic dopaminergic pathway. PD starts from degeneration at the posterior part (PP) spreading to the whole of the putamen (P) and in the caudate nucleus at more advanced disease. Differential diagnosis from essential tremor (ET) is of clinical value in terms of early diagnosis and initiation of treatment or confirmation of benign tremor. We try to evaluate the significance of PP insult in the early diagnosis of PD.Methods: We studied 99 individuals with confirmed ET plus 67 patients with suspicion of PD presenting atypical and/ or unilateral symptoms. After clinical evaluation I-123-FP-CIT scan (DaTSCAN) was performed to all. ROI's were drawn over the whole of the striatum (S) plus to the CN, P and anterior plus PP. The occipital cortex was used as the background area. The PP was considered the posterior third of the whole P. The equation ROI-bg/bg was used for semi-quantitative evaluation and the Mann-Whitney test for statistical analysis.Results: A crescent-shaped S was formed n ET patients, whilst an heterogeneity was mentioned at the P and a deficit at the PP, more prominent at the contra-lateral side of the affected limb. Values derived from semi-quantitative evaluation were higher in ET than in PD individuals. A significant correlation was found between values at the PP in ET and PD patients ($p<0.0001$), as well as, at the P and whole S ($p<0.001$), even at the ipsilateral side.Conclusion: The value of DaTSCAN in the differentiation of ET and PD is indisputable and can even predict the clinical symptoms. The role of the PP is not clearly elucidated accordingly to the above mentioned data and probably more series of patients candidate for PD should be included for a clearer outcome.

P30 - Monday, October 12, 2015, 4:00 PM - 4:30 PM, Hall 3 – Poster Exhibition

Neurosciences: Data Analysis & Quantification

P485

In vivo quantification of the [11C]-DASB binding in the normal canine brain using Positron Emission Tomography

O. Taylor1, N. Van Laeken2, F. De Vos2, I. Polis1, T. Bosmans1, I. Goethals3, R. Achten3, A. Dobbeleir3, E. Vandermeulen1, C. Baeken3, J. Saunders1, K. Peremans1; 1University of Ghent (Faculty of Veterinary Medicine), Merelbeke, BELGIUM, 2University of Ghent (Faculty of Pharmaceutical Sciences), Ghent, BELGIUM, 3Ghent University Hospital, Ghent, BELGIUM.

Aims: [11C]-DASB is currently the most used radiotracer for PET quantitative studies of the serotonin transporter (SERT) in the human brain but has never been validated in dogs. The first objective was to evaluate the regional distribution of the SERT in the normal canine brain using this radiotracer. The second objective was to determine the correlation between a reference tissue method using a dynamic scan and regions to cerebellum

ratio values from a single static acquisition. Materials and Methods: The imaging was performed with a Gemini PET/CT system and a 3T MRI system on 5 healthy dogs. A PET summation image of all dynamic images was co-registered to each individual MR images with PMOD. The regional radioactivity in 20 ROIs was quantified using MRTM2 and a semi-quantitative method. The values showed least variability between 40 and 60 minutes of scanning. A semi-quantitative method measuring the ratio of the radioactivity within the ROI over the radioactivity within the cerebellum was therefore performed using the data in this time interval. The coefficient of determination R2 was calculated to estimate the correlation between the two methods. Results: For the regional analysis, the highest radioactivity concentration of [11C]DASB was observed in the hypothalamus, raphe nuclei and thalamus, intermediate levels were observed in the basal ganglia, hippocampus and frontal cortex, modest levels in the anterior and posterior cingulate gyri and temporal cortex, and low levels in the parietal cortex, occipital cortex and cerebellum. Scanning between 40 and 60 minutes was set as the optimal time interval for [11C]DASB quantification in the canine brain. The correlation (R2) between the MRTM2 and the static ratio method using the data between 40 and 60 minutes was 98.64%. Conclusion: The results from the regional analysis are consistent with the previous human and animal studies, with the highest radioactivity concentration observed in the hypothalamus, raphe nuclei and thalamus. Reference tissue models and the static scan ratio method provide a more convenient alternative to invasive arterial sampling models in the evaluation of the SERT of the normal canine brain. The optimal time interval for scanning is set at 40 to 60 minutes after tracer injection.

P486

Automated PET-only quantification of amyloid deposition with adaptive template and amyloid-specific region-of-interest

G. Akamatsu1,2, Y. Ikari1, A. Ohnishi1, T. Nishio1, H. Nishida1, K. Aita1, Y. Yamamoto3, M. Sasaki1, M. Sasaki2, M. Senda1; 1Institute of Biomedical Research and Innovation, Kobe, JAPAN, 2Kyushu University, Fukuoka, JAPAN, 3Kobe University, Kobe, JAPAN.

Purpose: Amyloid PET is useful for early and/or differential diagnosis of Alzheimer's disease (AD). Quantification of amyloid deposition has been performed to improve diagnosis and monitoring of AD, particularly in research. Although MRI is often used for segmentation of gray matter and for spatial normalization into standard Montreal Neurologic Institute (MNI) space where region-of-interest (ROI) template is defined, 3D MRI is not always available in clinical practice. The purpose of this study was to examine possibility of quantification for amyloid PET images without MRI or CT using adaptive template and amyloid-specific ROI. Materials and Methods: A total of 30 subjects (10 AD subjects; 11 MCI subjects; 9 normal control subjects) who underwent brain 11C-PiB PET were examined. A 20-minutes emission scan, starting 50 minutes after injection of 571.1±24.5 MBq was performed. The PiB images were spatially normalized to the standard MNI T1 atlas using PET-MRI coregistration and the spatial normalization for the MRI. The automatic-anatomic-labeling (AAL) template was applied to the PET images. All voxel values were normalized by the mean value of cerebellar cortex to generate the SUVR scale images. Eleven typical positive images and five typical negative images were normalized and respectively averaged to be used as the adaptive template. Positive and negative masks were created as the set of voxels with SUVR > 2.0 on each averaged image. Amyloid-specific regions were generated by subtracting negative mask from positive mask. As for the PET-only technique, all PiB images were non-rigidly normalized to both positive and negative templates and the one having higher cross-correlation was adopted. Amyloid-specific ROI was then inversely transformed to individual PET images. We evaluated correlation of SUVR between standard MR-based method and PET-only method on 20 of 30 subjects. We also compared the PET-only method with visual interpretation by qualified nuclear physician on the 30 PiB images. Results: Significant correlation was observed between the SUVRs obtained by MR-based method and PET-only method (Spearman correlation coefficient: ρ=0.97, P<0.01). All but one subject were correctly categorized into positive and negative using cutoff value of 1.5 based on either MR-method or PET-only adaptive template method. The PET-only SUVR were 2.22±0.34 and 1.35±0.06 for positive and negative images by visual interpretation. Conclusion: The PET-only amyloid quantification method with adaptive template and amyloid-specific ROI provide accurate, robust and simple amyloid quantification without MRI.

P487

Fully Parametric Imaging for Reversible Tracer of FLT within Reasonable Time

N. Kudomi, A. NIshiyama, Y. Maeda, T. Hatakeyama, Y. Yamamoto, Y. Nishiyama; Faclty Of Medicine, Kagawa University, KAGAWA, JAPAN.

Objectives: PET enables us to quantitatively image of functions such as rate constants of uptake (K1), washout (k2), phosphorylation (k3) and dephosphorylation (k4), by applying the reversible two tissue compartment model. However there are, so far, no feasible computational strategies for imaging all those rate constants within reasonable computation time. We propose a new method to compute all those rates within a

reasonable time, namely, less than 1 min. Methods: A set of differential equations for the reversible two tissue compartment model was converted to one formula which expressed as tissue and plasma curve terms involving derivative, integral and convolution terms. Feasibility was tested by applying clinical data with 18F-FLT PET (ECAT HR+) for patients with glioma (n=38). Then the images of those rates were obtained using the present developed imaging method from dynamic scan image. To test validity, regions of interest (ROI) were placed on regions with glioma on a summed image of the scan image. Parametric values of those rate constants were extracted from the obtained images. Also, time activity curve was extracted from the placed ROIs and those rate values were computed by the non-linear fitting method (Gauss-Newton method). The obtained rate values were compared between the methods. Results: Computation time was around 30 s and quality of generated images was reasonably acceptable. Obtained values for K1 were 0.15 ± 0.08 and 0.16 ± 0.08 ml/min/g for image and ROI based methods, respectively. Those were 0.18 ± 0.12 and 0.18 ± 0.11 min-1 for k2, 0.11 ± 0.08 and 0.10 ± 0.06 min-1 for k3, 0.017 ± 0.014 and 0.018 ± 0.012 min-1 for k4, respectively. Paired t-test showed no significant differences between the methods in those rate values. Regression analysis showed correlations as: r=0.94, 0.86, 0.71 and 0.52 for K1, k2, k3 and k4, respectively. Conclusion: The present results suggested that the full parametric images can be obtained within reasonable time, with reasonable accuracy and quality.

P488

Comparison with cerebral blood volume on 15Ogas-PET/CT in patients with chronic cerebrovascular disease

N. Morita, A. Shimizu, Y. Terakawa, K. Kajimoto, T. Uehara, D. Maruyama, J. Nakagawara, H. Iida; National Cerebral and Cardiovascular Center, Suita, JAPAN.

(Aim) As represented by Powers classification, increasing cerebral blood volume (CBV) suggests moderately severe ischemia and has possibility to move to severe ischemia with increasing oxygen extraction fraction (OEF). However, there has no consensus on the degree of increasing CBV by the type of disease or ischemic condition. The purpose of our study was to compare the degree of increasing CBV among patients with chronic ischemic cerebrovascular disease. (Materials and methods) Among patients who have been taken 15O-gas PET/CT study in our institution from Oct.2013-Sep.2014, 130 patients (50 female, mean age 65.0 y.o.) who fulfilled our criteria were recruited in our study. We divided into 3 groups of asymptomatic internal carotid artery (ICA) disease (asICA; n=55, 71.4±8.19y.o.), symptomatic ICA disease (sICA; n=36, 72.8±8.69 y.o.) and moya moya disease (MMD;n=39, 50.9±11.43y.o.). Also, normal database (NDB;n=10, 71.2±4.35y.o.) was applied as reference. We applied clinical PET/CT machine (Biograph-mCT; Siemens, Knoxville, USA) and original workstation (Q-view software; Research Institute, National Cerebral and Cardiovascular Center, Osaka, Japan) was used for data processing. PET examination was taken followed by dual-tracer autoradiography (DARG) method and CBV value was measured by a single inhalation of C15O. 8 ROIs were set in both MCA area (anterior and posterior), and measured mean CBV value (ml/100g/min) in affected side. Data was compared by unpaired t-test and ROC analysis was applied to evaluate the optimal cutoff value between ICA disease and MMD. (Results) Mean CBV value of NDB, asICA, sICA and MMD were 2.73±0.31, 2.97 ±0.43, 2.92±0.53 and 3.68±0.95, respectively. Mean CBV value in MMD showed statistically higher than others and there was no statistical difference between both ICA disease and NDB. In ROC analysis, the optimal CBV value was 3.21 with sensitivity of 65.4%, specificity of 72.9% between ICA disease and MMD. (Conclusion) In measuring CBV, nondiffusible tracers cannot obtain reliable values of tissue perfusion, CBV value would be mostly affected the turnover rate of the regional blood pool. We should take it into consideration of this specific feature in evaluating for CBV in chronic ischemia on 15Ogas-PET study.

P489

Evaluation of increasing cerebral blood volume on 15Ogas-PET/CT in patients with severe ischemic cerebrovascular disease

N. Morita, A. Shimizu, Y. Terakawa, K. Kajimoto, T. Uehara, D. Maruyama, J. Nakagawara, H. Iida; National Cerebral and Cardiovascular Center, Suita, JAPAN.

(Aim) As represented by Powers classification, increasing cerebral blood volume (CBV) suggests moderately severe ischemia and has possibility to move to severe ischemia with increasing oxygen extraction fraction (OEF). However, there has no consensus on the degree of increasing CBV by the type of disease. The purpose of our study was to evaluate the degree of increasing CBV in severe ischemic cerebrovascular disease with increasing OEF. (Materials and methods) 130 patients (50 female, mean age 65.0 y.o.) who fulfilled our criteria were recruited in our study. We divided into 3 groups of asymptomatic internal carotid artery (ICA) disease (asICA;n=55), symptomatic ICA disease (sICA;n=36) and moya moya disease (MMD;n=39). Normal database (NDB;n=10) was applied as reference. 8 ROIs were set in both MCA area (anterior and posterior), and measured mean CBV value (ml/100g/min) and OEF (%) in affected side. Positive OEF (increasing OEF) was

determined when OEF value was more than 2SD in NDB. We measured mean CBV value and compared the differences between positive and negative OEF group. Data was compared by unpaired t-test and ROC analysis was applied to evaluate optimal cutoff value between negative and positive OEF. Also we evaluated correlation between each quantitative CBV and OEF value. (Results)Fifty seven patients (43.8%) showed positive OEF. Regardless the OEF finding, the mean CBV value in MMD shows statistically higher than other disease ($p<0.01$). CBV value in every patient group showed higher in OEF positive groups, but the degree of increasing CBV was small and these are mostly overlapped. In ROC analysis, CBV value of 4.03 might be threshold with higher specificity of 0.925 in MMD. There was no correlation between these CBV and OEF value in every type of disease. (Conclusion) On 15Ogas PET study, CBV would be mostly affected the turnover rate of the regional blood pool, and increasing CBV in patients with chronic vessel disease indicates the long-term ischemia or collateral development. To obtain reliable values of tissue perfusion on 15Ogas-PET study, technical improvement would be expected.

P490

Deformable registration for 18F-florbetapir PET quantification

L. Sibille, C. Hutton, J. Declerck; Siemens Molecular Imaging, Oxford, UNITED KINGDOM.

Aim: The aim of this study was to compare the performance of a novel PET-based deformable registration method with PET-based affine registration and to assess the impact on 18F-florbetapir PET quantification by calculating cortex-to-cerebellum standard uptake value ratios (SUVr) following the different registration methods. Materials and methods: The PET-based deformable registration method is based on a deformable database feature matching (DFM) algorithm which matches points of interest in the patient brain against an existing database of points of interest covering a range of medical conditions and subject age. 18F-florbetapir PET and MR images were obtained from the Alzheimer's Disease Neuroimaging Initiative (ADNI). In 39 subjects, PET images were registered to MNI (Montreal Neurological Institute) atlas space (Evans et al., 1993) using DFM registration as well as PET-based affine registration which is implemented in sPAP (syngo.PET Amyloid Plaque, Peyrat et al., SNM, 2012), a previously validated PET quantification method (Hutton et al., EJNMMI, 2014). Anatomical regions of interest (ROI) were defined using an independent deformable registration method based on the subject MRI (SPM, http://www.fil.ion.ucl.ac.uk/spm/). Overlap (using Dice Coefficient) was calculated between ROIs resulting from the PET-based registration methods and those defined anatomically. The DFM method was also used to register PET images from 604 subjects to MNI space prior to calculation of cortex-to-cerebellum SUVr (Fleisher et al., 2011). The DFM registration results were visually assessed and SUVrs were compared with those calculated in a previous study using sPAP (Hutton et al., EJNMMI, 2014). Results: Dice Coefficient averaged over the anatomical ROIs was 0.7 or more in 27/39 of the cases following DFM registration, but only in 7/39 cases following affine registration. In [Hutton et al., 2014], 14 cases required manual registration adjustments following affine registration. Using DFM, only one of those cases required manual adjustment. The resulting SUVrs were correlated, with $r=0.99$ and the linear regression of DFM SUVr values on sPAP SUVr was $y = 1.0318x - 0.01$. Conclusion: The novel PET-based deformable registration resulted in improved local matching of the patient brain to MNI space. Resulting SUVrs were highly correlated and in good agreement using the different registration methods.

P491

Total Metabolic Index; Inter-Rater Variability in Quantifying Cerebral Hemispheric Glucose Metabolism in the Course of Treatment of Glioma

E. A. Segtnan1, P. Grupe1, J. O. Jarden2, S. B. Christlieb1, J. E. Pedersen1, C. Constantinescu1, O. Gerke1, S. Houshmand3, S. Hess1, A. Alavi3, P. F. Høilund-Carlsen1; 1Dept.of Nuclear Medicine, Odense University Hospital, Odense, DENMARK, 2Dept. of Neurology, Herlev University Hospital, Copenhagen, DENMARK, 3Division of Nuclear Medicine, University of Pennsylvania, Philadelphia, PA, UNITED STATES.

Aim: Maximum standardized uptake value (SUVmax) is the most used semi-quantitative parameter in cerebral FDG-PET imaging. However, it may not be ideal for characterizing gliomas due to tumour and tissue heterogeneity, limited PET resolution, and technological and biological confounders during the management course. With "Total Metabolic Index (TMI)", we aimed to establish a method to quantify the metabolically most active regions of each hemisphere using FDG-PET. Here, we present data on inter-rater variability (IRV) from five time points in the course of management of glioma patients. Material and methods: In total 49 FDG-PET scans from fourteen glioma patients followed for one year (or until death) were prospectively collected before treatment (A), after resection/biopsy (B), after radio-chemotherapy (C), during chemotherapy (D), and after treatment (E). Three independent observers applied regional 3D-masks using dedicated software to segment the hemispheres ipsilateral and contralateral to the tumour (IH and CH), and the total cerebellum (Ce) to obtain

SUVmax and partial volume corrected SUVmean (cSUVmean) of the regions with the highest metabolism (cut off 40% of max). The total volume of these high activity regions (HAV) was multiplied by cSUVmean of its own HAV to yield cSUVtotal for IH, CH and Ce, respectively. Indexed hemispheric glucose metabolism was obtained by division of hemispherical cSUVtotal by cerebellar cSUVtotal (TMI).IRV was assessed using the coefficient of variation. Results: IRV for SUVmax was 1% for both IC and HC and 1-2% for Ce at all time points. IRV for the HAV was 3%, 3%, 6%, 2%, and 4% for IH; 3%, 3%, 5%, 3%, and 3% for CH; and 7%-13% for Ce at time points A-E, respectively. IRV for cSUVmean was 3%, 3%, 6%, 2%, and 4% for IH; 3%, 3%, 5%, 3%, and 3% for CH, and 7-13% for Ce at time points A-E, respectively. IRV for cSUVtotal was 3%, 3%, 6%, 2%, and 4% for IH; 3%, 3%, 5%, 3%, and 3%, for CH, and 7-13% for Ce for time points A-E respectively. IRV for the TMI was 9%, 11%, 14%, 12%, and 13% for IH; 9%, 13%, 13%, 14% and 14% for CH at time points A-E, respectively. Conclusion: The SUVmax, cSUVmean, HAV, and cSUVtotal were highly reproducible for both the cerebral hemispheres regardless of course of management. Cerebellar values had the highest IRV. Overall, "Total metabolic index (TMI)" was reproducible and is most likely applicable for quantitative analysis in other diseases of the brain.

P493

Efficiency Changes of Cerebral Blood Flow Network in Response to Hypercapnia Show Early Abnormal Status in Mild Cognitive Impairment: a Graph Analysis Study

C. Sánchez Catsús1, G. Sanabria-Diaz2, R. Dierckx3, L. Melie-García2; 1CIREN, Havana, CUBA, 2Cuban Neuroscience Center, Havana, CUBA, 3Department of Nuclear Medicine & Molecular Imaging, Medical Imaging Center, University Medical Center, Groningen, NETHERLANDS.

There is growing support that microvascular reactivity to hypercapnia is reduced in Alzheimer's disease. However, it is less clear in patients with mild cognitive impairment (MCI). Subtle abnormal response in MCI might not be appreciated by standard metrics of cerebrovascular reactivity (CVR), especially in patients with low vascular burden. Previously, using graph analysis, we demonstrated that the cerebral blood flow (CBF) network follows 'small-world' attributes in normal cognition state at basal condition (Neuroimage. 2013 Jan 1;64:173-84), similar to other brain networks. Aim: here, using the same methodology, our aim was to investigate changes of nodal (Enod), local (Eloc) and global (Eglob) efficiencies of the CBF networks in response to hypercapnia, induced by acetazolamide (ACZ) in MCI and normal cognition states. Materials and methods: four networks were constructed: two based on CBF SPECT data at basal condition and post- ACZ, respectively, obtained from a group of 26 MCI patients with low vascular profiles; and the two corresponding networks from a group of 26 matched healthy controls. Results: we found that nodes in the temporal lobes and prefrontal cortices showed Enod decrease in the MCI CBF network in response to ACZ; while the control CBF network showed nodes with Enod decrease in temporal lobes, like MCI, but also nodes with Enod increase in prefrontal cortices and precunei. Moreover, Eloc decreased and Eglob increased in the MCI CBF network. In contrast, the control CBF network showed no changes. CVR showed no differences between groups. Conclusion: we demonstrated that changes of nodal, local and global efficiency of the CBF network in response to hypercapnia are different in the MCI state compared with the normal cognition state, which was not detected by standard CVR metrics. This suggests an early abnormal status of the reactivity of brain microvascular network in MCI, specifically in MCI patients with low vascular burden. This could help to clarify early microvascular abnormalities in MCI.

P494

Attenuation correction by CT can improve detectability of lesions by voxel based statistical analysis of brain SPECT

H. Kato1, E. Shimosegawa1, K. Fujino2, J. Hatazawa1; 1Osaka University Graduate School of Medicine, Osaka, JAPAN, 2Osaka University Medical Hospital, Osaka, JAPAN.

Objectives: SPECT-CT enables the non-uniform attenuation correction (AC) using built-in CT instead of conventional uniform AC. Although the result of the voxel-based statistical analysis based on Z-score is thought to be influenced by difference in the AC methods, the effect has not been clarified. We aimed to assess the difference in detectability for SPECT count reduction by voxel based statistical analysis depending on the AC methods. Methods: Fifteen patients with chronic cerebral infarctions and 35 healthy volunteers underwent quantitative N-isopropyl-p-(I-123) iodoamphetamine (I-123 IMP) SPECT. Image reconstruction was performed using 3D-OSEM with two different AC methods: Chang's method and CT AC method. Normal database for the analysis was constructed by the 25 randomly selected from the 35 normal SPECT data. Voxel based z-test was performed by using statistical parametric mapping 8 (SPM8) to detect significant regional reduction in the SPECT count of the remaining 10 normal volunteers or the patients. Results: The z-score indicating SPECT count decrease in the infarct lesions was significantly higher in the images reconstructed using CT AC method

than Chang's AC method (p = 0.003). As for the 10 normal volunteers, mean absolute value of the z-score in the intact brains was significantly lower in the images reconstructed using CT AC method than Chang's AC method (p = 0.005). Conclusions: Sensitivity for SPECT count reduction by voxel based statistical analysis was shown to be significantly improved, and non-specific SPECT count reduction was significantly mitigated by using CT AC instead of conventional method.

P495

Detection of Regional Cerebral Blood Flow disturbance with the assistance of statistical parametric mapping (SPM): a 99mTc-ECD brain perfusion SPECT study in Alzheimer's and Multiple Sclerosis diseases

N. Chabi1, M. Taghizadeh Asl2, **M. Assadi**1; 1The Persian Gulf Nuclear Medicine Research Center, Bushehr University of Medical Sciences, BUSHEHR, IRAN, ISLAMIC REPUBLIC OF, 2Department of Nuclear Medicine, Kasra Hospital, BUSHEHR, IRAN, ISLAMIC REPUBLIC OF.

Aim: Visual analysis is often used for rCBF SPECT images interpretation which has many limitations. So, automated methods are a necessity in this area. SPM is one of the most widely used software in quantitative assessing of functional brain imaging like PET, fMRI, SPECT that is mostly employed for comparison between groups in research analysis while is rarely used for individual assessmen. We used this software for individual assessment of brain SPECT images of different patients who suffered from various illnesses such as Multiple Sclerosis and Alzheimer disease in order to find perfusion abnormalities in cerebral SPECT examinations. Materials and methods: SPM was used to compare 17 different patient images (5 Multiple Sclerosis, 12 Alzheimer) with 12 normal brain SPECT images using statistical threshold of p < .001 . Results: Most of the obtained results are in agreement with visual assessment of a nuclear medicine physician. Also, the results were mapped onto the anatomical brain image such as T1 or T2 to better localize existing disorder. Moreover, Automated Anatomical Labelling (AAL) software in SPM provides an effective tool to better investigate the abnormalities locations. Conclusion: The automated quantification method such as SPM could be more useful in a better and more precise decision taken by physician and it could be a complementary to visual inspection of the physician in the clinical practice. Also, mapping the results on an anatomical space in addition to using AAL software can help the physician for a better recognition of the abnormalities location.

P496

Machine learning model targeting 11C-PiB PET images in diagnosis of Alzheimer's Disease

Z. Huang1, X. Shu2, J. Jiang2, Y. Guan1; 1Huashan Hospital, Fudan University, Shanghai, CHINA, 2Institute of Biomedical Engineering, School of Communication and Information Technology, Shanghai University, Shanghai, CHINA.

Aim: As one successful biological indicator for amyloid-beta peptide (Aβ), Carbon 11-labeled Pittsburgh compound B Positron Emission Tomography (11C-PiB PET) has been widely used for the diagnosis of Alzheimer's disease (AD). However, the accurate diagnosis of AD base on this technique still remains a challenge for radiologists, especially in differentiating AD, Mild Cognitive Impairment (MCI) and healthy control (HC) groups. Visual assessment (VA) is the most commonly used clinical method, which is time-consuming, and the diagnostic accuracy can be varied due to clinical experience. This paper proposed a machine learning model targeting 11C PiB PET images, trying to improve current method. Materials and Methods: The machine learning model includes four parts: (1) Aβ 3D segmentation by adapted level set method (LSM) and Lattice Boltzmann Method (LBM) based algorithms; (2) original feature decorrelations by principle component analysis (PCA); (3) feature extraction by independent component analysis (ICA); (4) classification by support vector machine (SVM). Subject: 26 groups of PiB PET images from Shanghai Huashan hospital and 120 groups of data from ADNI database. (1) All PiB PET images were smoothed and normalized; (2) 73 PCs which can represent 95% of the whole data were selected. All date were de-correlated by PCA; (3) 80 ICs were chosen as final feature to guide a classification test, and RBF kernel SVM classifiers were used; (4) The classification performance was tested in three steps: training, cross-validation and test. Cross validation was achieved by means of the leave-one-out method; (5)Two senior radiologists, with over 7-years PiB PET reading experiences from Shanghai HuaShan Hospital, were invited to provide VA results based on original DICOM images. Results: The proposed machine learning model can yield 94.34% accuracy in differentiating AD groups from HC groups; and 93.27% accuracy in differentiating MCI groups from HC groups; if both AD and MCI groups were considered as one positive group, the diagnosis accuracy was 91.67%. By comparison, the accuracy by VA was 79.3%, 68.71% and 57.45%. Conclusion: Machine learning techniques are able to aid radiologists to improve diagnostic accuracy of AD based on PiB PET images. The proposed machine learning model in this paper is effective and efficient.

P497

Quantitative comparison between different methods for measurement Dopamine Transporters (DAT): An assessment of the accuracy and precision in DAT-SPECT images

L. Alexandre-Santos1, E. N. Itikawa2, D. K. Sonvenso1, A. C. Trevisan2, M. Kato1, F. A. Pitella1, C. E. P. Baltazar1, E. R. Moraes3, O. Baffa3, L. Wichert-Ana1,2; 1Ribeirão Preto School of Medicine - University of São Paulo, Ribeirão Preto, BRAZIL, 2Bioengineering Post Graduation Programe - São Carlos School of Engineering - University of São Paulo, São Carlos, BRAZIL, 3Faculty of Philosophy, Sciences and Letters at. Ribeirão Preto, Ribeirão Preto, BRAZIL.

AIM: Molecular imaging of DAT gives differential information in research of neurodegenerative diseases, such as Parkinson's Disease (PD), when properly approached quantitatively. Yet, each method used in clinical routine may give, or not, different results when the quantifications are applied in images of several activity levels. Hence, this study assessed the accuracy and precision of DAT-SPECT quantification methods, based in ROIs.**MATERIALS AND METHODS**: Twenty three DAT-SPECT images were acquisitions of anthropomorphic striatal phantom filled with different activity concentrations of 99mTc. For each acquisition performed, the specific chambers (caudate and putamen chambers) to large chamber (simulating nonspecific background activity) was filled with solutions activity of different specific to nonspecific ratios (10, 8, 6, 4 and 2 to 1). The images were reconstructed by an iterative algorithm, corrected to attenuation effects. The extracted values were analyzed by the specific binding ratio (SBR). Five quantification DAT-SPECT methods using ROIs were assessed: Manual technique: (A) draw freehand ROIs on SPECT images. Standard size ROIs: (B) TwoBox and (C) ThreeBox Methods. VOIs using structural images: (D) MRI and (E) CT. Accuracy of methods applied were assessed by concordance correlation coefficient (CCC) and precision by Pearson's coefficient and linear regression.**RESULTS**: Quantified SBR for both individual specific chambers and striatal chamber using all methods resulted in a CCC increase, with decrease of the nominal values used. For lower SBR values, the D and E methods evidenced the maximum values of CCC in assessment of caudate (CCC_{MRI_CA} = 0.89 e CCC_{CT_CA} = 0.84) and putamen (CCC_{MRI_PU} = 0.86 e CCC_{CT_PU} = 0.82). However, striatal assessments the B method highlights a maximum accuracy between all methods applied (CCC_{TWOBOX_ST} = 0.95), for low values of SBR. A high Pearson's coefficient was found in the correlation between all methods, report thereby a good precision between them.**CONCLUSION**: The five quantification DAT-SPECT methods showed a high precision quantification even when applied in images with different activity solutions. However, investigations that need a more accurate quantification process seeking putamen evaluation and caudate nucleus separately, structural methods showed a progressive improvement in its quantification as there is a decrease of filling nominal index. To assess striatal chamber in the absence of structural information, the TwoBox method showed excellent agreement with all nominal values.

P498

Distribution of the Dopamine Transporter (DAT) in the nigro-striatal pathway examined in vivo with [18F] FE-PE2I and high-resolution PET

P. Fazio1, Z. Cselényi1,2, C. Halldin1, L. Farde1,2, A. Varrone1; 1Karolinska Institutet, Department of Clinical Neuroscience, Centre for Psychiatry Research, Stockholm, SWEDEN, 2AstraZeneca Translational Science Centre at Karolinska Institutet, Stockholm, SWEDEN.

Aim. The aim was to develop new methodology for *in vivo* quantification of dopamine transporter (DAT) availability along the nigro-striatal projections.**Methods**. High-resolution wavelet-aided parametric images (PIs) of the binding potential (BP_{ND}) in brain were generated from 11 healthy control subjects (CS) having participated in PET measurements with [18F]FE-PE2I using the HRRT system. To obtain a functional based DAT template, individual PIs were spatially normalized using a two-step normalization procedure using various tools of the FMRIB Software Library (FSL), which enables accurate normalization of the mesenchepalic and dienchepalic regions. The template enabled visualization of DAT binding along different and distinct efferent fibers projecting from the substantia nigra (SN). Template-based ROIs were delineated manually for nigro-striatal (NST), nigro-pallidal (NPT), nigro-thalamic tracts (NTT), SN and striatal regions (caudate, putamen, ventral striatum), and then applied to each parametric image to obtain individual BP_{ND} estimates. Pearson correlation analysis was used to compare the estimates obtained in the SN and the striatum with the estimates obtained for the different tracts. **Results**. The highest BP_{ND} values along the tracts were found in NST (0.49±0.07), followed by the NTT (0.35±0.13) and by the NPT (0.31±0.12). Those BP_{ND} values were lower than the values measured in the striatum (4.08±0.54) and in the SN (0.81±0.10). A positive correlation was found between BP_{ND} in NPT and BP_{ND} in SN ($r=0.648$, $p<0.02$) and striatum ($r=0.862$, $p<0.001$) and between BP_{ND} in NST and BP_{ND} in SN ($r=0.621$, $p<0.05$) and striatum ($r=0.633$, $p<0.05$). No statistically significant correlations were found for the NTT.**Conclusions**. The estimates along the tracts of interest confirmed, *in vivo*, the distribution of DAT along axons originating from the SN and the feasibility to quantify them with HRRT and [18F]FE-PE2I. The results are consistent with

previous observations *in vitro* that DAT is expressed along the axons originating from the SN. Despite the low density of DAT in these regions, its availability can be measured *in vivo* using high resolution DAT PET with [18F]FE-PE2I, providing the possibility to image the entire dopaminergic nigro-striatal pathway.

P499

Evaluation of the uniform attenuation correction in ictal SPECT images in Frontal Lobe Epilepsy: A quantitative approach through SPM

L. Alexandre-Santos1, H. T. Amaral-Silva1, E. N. Itikawa2, D. Sonvenso1, A. C. Trevisan2, T. R. Velasco1, F. A. Pitella1, V. Alexandre, Jr.1, M. Kato1, L. Wichert-Ana1,2; 1Ribeirão Preto School of Medicine - University of São Paulo, Ribeirão Preto, BRAZIL, 2Bioengineering Post Graduation Programe - São Carlos School of Engineering - University of São Paulo, São Carlos, BRAZIL.

AIM: The Attenuation Correction (AC) of gamma photons poses a clinical problem in the evaluation of ictal SPECT in Frontal Lobe Epilepsy. The main issue is that mesially located seizure focus may be underestimated. This study aimed to evaluate the impact of the AC on brain SPECT images in patients with Frontal Lobe Epilepsy (FLE). MATERIALS AND METHOD: The ictal SPECT of 10 patients diagnosed with FLE were analyzed using SPM. The brain SPECT of 12 healthy subjects were used as a control group. All SPECT images were divided in two groups: a group containing SPECT images corrected for the effects of gamma-ray photons (AC), by Chang's Method (0.12/cm), and another group without the AC (nAC). The Statistical Parametric Mapping (SPM) was used to compare the signal changes of the AC and nAC images. To the hypothesis test to this study (Two sample, t-test), two comparison models were specified: single patient (nAC) versus control group average (nAC) and single patient (AC) versus control group average (AC). Each patient was compared with the average image of the control group due to variations of epileptogenic zones locations among the ten patients. The threshold p-value used was to values $p<0.001$, with $Z>3.08$, and cluster size value $k=20$. From each selected cluster we analyzed the cluster size, pick value, and the corrected p-value for each inference level. All these clusters were evidenced in a MRI standard template for better view of the results. RESULTS: We found differences between the averaged signals of each comparison performed on both sets of images of interest, AC and nAC. Those clusters than survived the multiple comparisons test were considered. They showed that by applying the AC, the epileptogenic or propagation zones located mesially in the brain were better evidenced, either visually or quantitatively. Otherwise, the nonlinear weight in the SPECT image used by Chang's Method decreased the visualization of the seizure activated regions located in the peripheral or lateralized areas of the brain. CONCLUSIONS: We concluded that the uniform Attenuation Correction method applied in brain SPECT images is an effective tool in the investigation of FLE cases. The AC contributed to the exhibition of epileptogenic and propagation zones located mesially within the brain. However, the non AC images should also be clinically used once activated areas in the peripheral or lateralized brain regions may be underestimated with the AC techniques.

P500

Standardization of normative data as 'reference data' in a single institute for the qualitative and quantitative DaTSCAN evaluation

G. S. Limouris1, E. Konstantinidis2, N. Triantafyllou2, M. Paphiti3, I. Valais4, G. Paraskevas2, E. Kapaki2; 1Nuclear Medicine Div, I Radiology Dept, 'Aretaieion' Hosp, Athens Univ Medical Faculty, Athens, GREECE, 2Neurologic Clinic, 'Aeginiteion' Hospital, Athens Univ Medical Faculty, Athens, GREECE, 3Nuclear Medicine Dept, Royal Sussex County Hosp, Brighton, UNITED KINGDOM, 4Bioengineering Dept,TEI Athens, Athens, GREECE.

Purpose: Dopamine transporter (DAT) imaging with [123I] FP-CIT (DaTSCAN) is an established radio-molecular diagnostic tool for the evaluation of tremor-related symptoms in neuro-psychiatric disorders, and more specific in parkinsonism and dementia. Although qualitative (visual) scintigraphic criteria are used for the assessment of the diagnosis, DaTSCAN quantification is important for an accurate completion, differentiation and research of the final evaluation. For this reason the availability of normative data, obtained from studies performed in our facilities and thorough discussions, between the specialties involved [i.e. Nuclear Medicine, Neurology and Psychiatry] is more than crucial. The aim of our universitary Institutions was to create for first time in Greece a large database of [123I]FP-CIT SPECT scans to be used as reference data of normal ranges. Methods: In 113 healthy controls (67 men, 46 women; age range 38-73 years) DaTSPECT studies were performed in a single Institute ['Aretaieion' Univ Hospital'] from March 2007 to October 2014, with main pts' tank of origin the Neurology and Psychiatric Clinics of 'Aeginiteion' Univ Hospital. Brain SPECT imaging was acquired using a single-head gamma camera (Elscint Apex SPx-4) equipped with a low-energy, all-purpose, parallel-hole collimator. One hundred and twenty tomographic images, every 3 degrees in a total of 360 degrees, of 128x128 pixels matrix, on a step & shoot mode, were acquired for each patient. Images were then normalized to 64x64 pixels matrix for inter-processing compatibility. Normalized data were reconstructed

by filtered back projection and a standard Metz filter was used. Attenuation correction was performed using Chang's method with a 0.12 attenuation coefficient. Images were displayed in the transaxial, coronal and sagittal planes for interpretation. Region-of-interest analysis was performed using the CBRREC Elscint software (caudate, putamen and striatum, drown manual-ly).The outcome measure was the specific binding index (SBI). Results: Normative data according regions were as follows: stiatum (2.4 ± 0.3), caudate (2.6 ± 0.5), putamen (2.2 ± 0.4). No statistically significant ranges were found among gender and ages except a 4.8 % loss, noticed in over 68 year of age in putamen and stiatum. Conclusion: For fist time in a single Institute normative DaTSCAN data for patients of Greek origin was created. Statistically significant ranges among genders and ages were not observed. A 4.8 % decline was depicted in putamen and stiatum over the age of 68.

P501

Comparison of an Atlas-based Method of DaTscanTM Quantification to Manual Volume of Interest Definition

A. S. Nelson, A. Pilla, M. Horvat, **J. W. Piper**; MIM Software, Cleveland, OH, UNITED STATES.

Purpose: To compare an atlas-based method for volume of interest (VOI) definition to manual VOI definition in the evaluation of Parkinson's disease using DaTscan (123-I Ioflupane) SPECT. Methods: Nineteen subjects with T1W MRI and DaTscan SPECT scans were selected from the Parkinson's Progression Markers Initiative (PPMI) database (www.ppmi-info.org/data). Ten subjects were from the Parkinson's Disease (PD) cohort and nine subjects were from the Healthy Control (HC) cohort. VOIs were manually defined on all MRI scans for the: caudate, putamen, posterior putamen, anterior putamen, striatum, and occipital lobe. Manual VOIs were applied to the rigidly registered DaTscan SPECT scans and mean ratios relative to the occipital lobe were recorded. For the automated method the DaTscan SPECT scans were aligned to a template brain in a two step process. First, a global affine registration was performed followed by a separate affine for the right and left hemispheres. Once aligned to the template brain, atlas defined VOIs were applied to the subjects brain and mean ratios were recorded. Correlation of mean ratios between methods were calculated as well as the ability to classify subjects into PD vs HC using mean ratios and asymmetries (caudate/putamen, anterior putamen/posterior putamen, L/R asymmetries for all VOIs). Results: The correlation between atlas and manual methods were caudate (0.927), putamen (0.933), anterior putamen (0.906), posterior putamen(0.927), and striatum(0.930). The best method of classification for the atlas-based method was the posterior putamen mean ratio with an accuracy of 10/10 for PD and 9/9 for HC (100% overall). The best method of classification for the manual method was the posterior putamen mean ratio with an accuracy of 10/10 for PD and 9/9 for HC (100% overall). Conclusions: The atlas-based method for DaTscan quantification was found to correlate well with a manual method for VOI definition and provided the same high level of accuracy.

P31 - Monday, October 12, 2015, 4:00 PM - 4:30 PM, Hall 3 – Poster Exhibition

Neurosciences: Miscellaneous

P502

Application of PET, MRI and invasive EEG in patients with drug-resistant epilepsy

I. Kostadinova1, K. Minkin2, P. Dimova2, D. Zlatareva3, V. Hadjiiska1; 1Clinic of nuclear medicine, Medical University, Sofia, BULGARIA, 2Clinic of neurosurgery, Medical University,Sofia, BULGARIA, 3Clinic of radiology, Medical University,Sofia, BULGARIA.

Comprehensive presurgical evaluation is mandatory for patients with drug-resistant epilepsy. Presurgical work-up includes first line diagnostic methods such as long term video-EEG monitoring and MRI, but difficult cases need additional examinations to define the epileptogenic zone like PET, SPECT and invasive EEG. The aim of our study was to share our first experience in application of PET and MRI, compared to invasive EEG as methods of epileptogenic zone localization. Our study has included 22 patients with drug-resistant epilepsy who were evaluated with MRI,18FDG PET/CT / 18F-FDG activity 150-200 MBq / and invasive EEG from 2010 to 2014. Eleven of them were with temporal epilepsy and 11-with extratemporal. All patients were evaluated with dedicated MRI epilepsy protocol. PET/CT study was fused with 3D MRI study using FSL or GE software. During invasive EEG monitoring, seizures were recorded in all patients. Long term invasive video EEG monitoring has lasted from 2 days to 2 weeks. Both MRI and PET were normal in 4 patients. From the remaining 18 patients there were 5 patients with normal MRI and abnormal PET-CT demonstrating hypometabolism. There was partial or complete congruence between the zones of PET hypometabolism and the seizure onset zone defined by invasive EEG in 17/18 patients with hypometabolism on PET/CT. There was only 1 patient with discrepancy between the zone of hypometabolism on PET/CT and the seizure onset zone defined by invasive EEG. MRI was normal in 9 patients and structural lesions were identified in 13 patients. Partial or complete overlapping between the lesion and the seizure onset zone was observed in 11/13 cases with MRI lesion. In other 2 cases there was no overlapping between

the data from invasive EEG and the MRI lesion. Fourteen patients were operated on and satisfactory seizure control was achieved in 10 patients. All 10 patients with satisfactory outcome have partial or complete congruence between the invasive EEG and PET/CT hypometabolism. We could conclude, that 18FDG PET/CT is a sensitive non invasive tool for defining the epileptogenic zone in patients with drug-resistant epilepsy and according to our first experience it is more accurate than MRI. It has to be applied in all cases with normal findings on MRI.

P503

Functional/Anatomic Brain Volume Mismatch Can Serve as a Predictive Parameter for Post Stroke Patient's Candidacy for Hyperbaric Oxygen Therapy

H. Golan1, B. Makogon2, O. Volkov3, Y. Smolyakov4, E. Ben-Jacob5, R. Boussi-Gross6, S. Efrati6; 1Nuclear Medicine, Assaf Harofeh Medical Center, Beer Yaakov, ISRAEL, 2Radiology, Assaf Harofeh Medical Center, Beer Yaakov, ISRAEL, 3Assaf Harofeh Medical Center, Beer Yaakov, ISRAEL, 4Department of Medical Physics and Informatics, Chita State Medical Academy, Chita, RUSSIAN FEDERATION, 5The Raymond and Beverly Sackler Faculty of Exact Sciences, School of Physics and Astronomy, Sagol School of Neuroscience, Tel-Aviv University, Tel-Aviv, ISRAEL, 6Hyperbaric Medicine Institute, Research and Development Unit, Assaf Harofeh Medical Center, Beer Yaakov, ISRAEL.

Background: Hyperbaric oxygen treatment (HBOT) has been recently shown to induce a significant improvement in neurological status, life quality and daily functioning in post stroke patients. The purpose of this work was to determine whether the correspondence of the brain anatomical volume as demonstrated on CT scan and the brain's functional volume as obtained by rCBF-SPECT can be used as a predictive index for post stroke patients who can benefit from HBOT. Materials and methods: A retrospective review of 97 subjects with chronic ischemic cerebral stroke patients, more than 6 months from the acute event, who had HBOT with pre and post treatment brain SPECT. All subjects had pre-intervention brain CT scan ("anatomical" evaluation). Brain rCBF-SPECT (a "functional" evaluation) and Clinical evaluation including neurological assessment (NIHSS), activities of daily living check (ADL) and quality of life indices (questionnaires EQ-5D and EQ-VAS) were performed before and after HBOT. The following brain imaging parameters were analyzed: 1. Anatomical brain volume based on the pre-intervention CT scan (BVCT). 2. CT qualities of the brain infarct including: location as related to white or cortical matter (CD2-CT) and size. 3. Functional brain volume based on the pre-intervention SPECT exam, using two scales: one by a threshold of 30% (BVS30), and the other by threshold of 40% (BVS40). The statistical analysis was performed using *Statistica* (StatSoft Inc), and correlation tests were performed using the following methods: Pearson's correlation, Spearman's rank correlation, Principal component analysis, General discriminant analysis, neural network modeling and General linear models. Results: The study included 31 subjects that met the inclusion criteria (10 females and 21 males). A strong relation was found between: age, ratio of functional brain volume to anatomical brain volume (BVS40/BVCT), type of brain damage (cortical or subcortical) to the improvement in activity in daily living (ADL) after HBOT. The degree of clinical improvement in ADL after HBOT was in good correlation with smaller functional brain volume, as measured by SPECT, in relation to the anatomical volume measured by CT. Thus the degree of response to HBOT is more significant when the volume ratio of SPECT/CT is lower. Conclusions: SPECT/CT (physiology/anatomy) mismatch, marks metabolic dysfunction brain regions where neuroplasticity can be induced with HBOT even years after the acute insult. This ratio can be expressed mathematically and used as a prediction index for post stroke patient's candidate for neuroplasticity by HBOT.

P504

Calorie consumption and brain glucose metabolism in the patients with chronic severe brain injury - A study using brain 18F-FDGPET -

Y. Uchino; Chiba Ryogo Center, CHIBA CITY, JAPAN.

[Purpose]In the chronic severe brain injury (cs-TBI) patients, it is known that their requirement level of intake and consumption calories is lower as compared to healthy subjects. Their low physical activity and reduction of muscle mass has been mentioned as one reason of low calorie consumption, but a decrease in brain glucose metabolism can be considered as another important factor. In the cs-TBI patients, we compared the actual calorie intake and semi-quantitative values obtained from brain FDGPET, and examined the relationship between brain glucose metabolism and calorie intake. [Method] This study included 39cases with cs-TBI patients, age ranging 20 to 75 years (41±16yrs, mean±SD). For brain glucose metabolism measurement method by FDGPET, we placed the volume of interest (VOI) in the whole brain automatically, and the average standardized uptake value (SUV) was obtained. Then the SUVavg was multiplied by the brain volume. We defined it as the "total value of whole brain uptake" (WBu) (WBu = SUVavg×brain volume). Basal energy expenditure (BEE), considering the active factor, was calculated by the Harris Benedict Equation. Physical and psychological activities of patients were evaluated by using patients' level determination score (CHIBA score). We classified the patients into two

groups (low WBu (WBu<50): A group, 27 cases, moderate WBu (WBu≧50): B group, 12 patients). And we examined the relationship among WBu, calorie intake, activity. [Results] In 38 cases out of 39, calorie intake was below the BEE (average -330Kcal). But there was no problem in their nutritional condition. Calorie intake and activity of each group was significantly higher in the group B (calorie, A: 1093±200Kcal, B: 1390±266Kcal,(p<0.01) activity, A: 20±17, B: 53±20 (p<0.01)). Regard to calorie intake and activity level, a positive correlation was observed (R^2=0.51), and correlation was also observed between calorie intake and WBu (R^2=0.53). [Conclusion] In the chronic severe brain injury patients, there is a relationship between the calorie consumption and the degree of brain glucose metabolism. Physical activity in the patients is generally low, so the proportion of calorie consumption of the brain is high degree that cannot be ignored against that of the whole body. Therefore, by knowing the degree of cerebral glucose metabolism reduction of the patients, it is possible to estimate their proper calorie intake.

P505

99mTc-ECD brain perfusion SPECT imaging for assessment of the effect of hyperbaric oxygen therapy on secondary progressive multiple sclerosis patients with a moderate to severe stage of disease

M. Taghizadeh Asl1, R. Nemati2, **M. Assadi**3; 1Department of Nuclear Medicine, Kasra Hospital, Tehran, IRAN, ISLAMIC REPUBLIC OF, 2Department of Neurology, Bushehr Medical University Hospital, Bushehr University of Medical Sciences, BUSHEHR, IRAN, ISLAMIC REPUBLIC OF, 3The Persian Gulf Nuclear Medicine Research Center, Bushehr University of Medical Sciences, BUSHEHR, IRAN, ISLAMIC REPUBLIC OF.

Objective: The present study was performed to assess cerebral perfusion in multiple sclerosis (MS) patients with a moderate to severe stage of disease. Some patients underwent hyperbaric oxygen therapy and brain perfusion between before and after that was compared. Methods: A total of 25 secondary progressive (SP)-MS patients were enrolled in this study. In total, 16 patients underwent oxygen therapy. Before oxygen therapy and at the end of 20 sessions of oxygen treatment, 99mTc-ECD brain perfusion single photon emission computed tomography (SPECT) were performed again then the results were evaluated and compared. Results: A total of 25 SP-MS patients, 14 females (56%) and 11 males (44%) with a mean age of 38.92 ± 11.28 years participated in the study. The mean disease duration was 8.70 ± 5.30 years. Of the 25 patients, 2 (8%) had a normal SPECT and 23 (92%) had abnormal brain perfusion SPECT studies. The study showed a significant association between severity of perfusion impairment and disease duration, but did not show any significant association with Expanded Disability Status Scale score (P>0.05). There was a significant improvement in pre- and post-treatment perfusion scans (P<0.05), but this did not demonstrate a significant improvement in the clinical subjective and objective evaluation of patients (P>0.05). Conclusions: This study demonstrated decreased cerebral perfusion in SP-MS patients with a moderate to severe disability score. In addition, this study showed the effect of hyperbaric oxygen therapy in the improvement of cerebral perfusion in MS patients.

P506

Comparison of diagnostic value of brain perfusion SPECT with CT scan, EEG and MRI modalities in pediatric seizure setting

A. Shirkani1, M. Taghizadeh Asl2, F. Hafezi1, R. Nemati3, **M. Assadi**4; 1Department of Pediatrics, Faculty of Medicine, Bushehr University of Medical Sciences, BUSHEHR, IRAN, ISLAMIC REPUBLIC OF, 2Department of Nuclear Medicine, Kasra Hospital, Tehran, IRAN, ISLAMIC REPUBLIC OF, 3Department of Neurology, Bushehr Medical University Hospital, Bushehr University of Medical Sciences, BUSHEHR, IRAN, ISLAMIC REPUBLIC OF, 4The Persian Gulf Nuclear Medicine Research Center, Bushehr University of Medical Sciences, BUSHEHR, IRAN, ISLAMIC REPUBLIC OF.

Background: Seizure is the most common neurologic disorder among children. Multiple neuroimaging modalities are available to localize the eliptogenic focus. Precise localization of the eliptogenic focus is imperative before planning surgical intervention; therefore, a proper modality is strongly needed. Brain perfusion SPECT is a functional neuroimaging modality which shows the eliptogenic focus by increasing and decreasing of the of the radiopharmaceutical, substance uptake. Method: In this prospective study, the population included children with seizure (n=43) and mean age (8.76 ± 3.53)who came to the pediatric hospital affiliated university during 2010-2011.All of them were underwent EEG,CT Scan, MRI and SPECT in Intricate phase by their parents consent; All the results were documented in each code sheet. Result: Brain perfusion SPECT was abnormal in a significant higher proportion of children, 36 cases(83.7%), then either scalp EEG 12 cases(27.9%)or CT Scan and MRI in 1 cases (2.3%).In comparison with SPECT,EEG got 27.8% sensitivity(95%CI=13-41) and 71.4% specificity (95%CI=38-100); PPV of CT scan was =83.3% and negative PPV =16.1% and MRI also got 2.8% sensitivity (95%CI=o-6) and 100% specificity by a positive PPV =100% and negative PPV =16.7% compared to SPECT. Conclusion: The present study may represent that interictal SPECT indentified more focal changes in children with recurrent seizure as compare to interictal scalp EEG,CT

Scan and MRI, hence it has the best diagnostic value among other modalities.

P507

Plaque Inflammation Imaging in severe carotid stenosis and recurrent cerebral ischemia/strokes.

A. SINHA, V. sharma, S. Kapur, S. Pillai, D. Teh; National University Hospital, SINGAPORE, SINGAPORE.

OBJECTIVE: Symptomatic carotid stenosis increases the risk of early stroke recurrence compared to other stroke subtypes. Current carotid imaging techniques rely on estimating plaque-related lumen narrowing but do not evaluate intraplaque inflammation, a key mediator of plaque rupture and thromboembolism. Using combined (18) F-fluorodeoxyglucose positron-emission tomography (FDG-PET)/computed tomography, we investigated the relation between inflammation-related FDG uptake and stroke recurrence in small group of the patients. METHODS: Consecutive patients with a recent stroke and ipsilateral carotid stenosis (≥50%) were included in this study. FDG uptake was quantified as mean standardized uptake values (SUVs). Patients were followed prospectively for stroke recurrence. RESULTS: Ten patients were included. Three patients had stroke recurrence within 90 days. FDG uptake in ipsilateral carotid plaque was greater in patients with early recurrent stroke (mean SUV, 2.5; standard deviation [SD], 0.44 vs 1.58; SD, 0.32, $p = 0.02$). On life-table analysis, 90-day recurrence rates with mean SUV greater than a 2.14 threshold were 80% (95% confidence interval [CI], 41.8-99.2) versus 22.9% (95% CI, 12.3-40.3) with SUV ≤2.14 (log-rank, $p < 0.0001$). In a Cox regression model including age and degree of stenosis (50-69% or ≥70%), mean plaque FDG uptake was the only independent predictor of stroke recurrence (adjusted hazard ratio, 6.1; 95% CI, 1.3-28.8; $p = 0.02$). CONCLUSION: Inflammation in a previously stable carotid plaque is an important event that leads to local thrombosis and cerebral embolization. This phenomenon can be reliable imaged with F-18 FDG PET for better risk stratification and therapeutic strategizing in carotid stenosis.

P508

Value of the ictal and interictal Perfusion-SPECT in the localization of the epileptic focus in drug-resistant epilepsy

M. Boya-Román1, O. Puig1, R. Julio1, J. Rojas1, I. Gil1, P. Saldaña2, G. Plans1, J. Miró1, J. Mora1; 1Hospital Universitari de Bellvitge-IDIBELL, Barcelona, SPAIN, 2Institut Català d'Oncologia, Barcelona, SPAIN.

Objective:To evaluate the effectiveness of the ictal and interictal SPECT in the presurgical assessment of drug-resistant epilepsy patients.Material and method:A retrospective study of 25 patients (p) with drug resistant epilepsy who underwent an ictal and interictal SPECT and MRI.Prior to the ictal SPECT, the patients were monitored with continuous video-EEG. 740MBq 99mTc-HMPAO were injected within the first minute of the seizure onset. The interictal SPECT was performed with the same dose and radionuclide three weeks after ictal SPECT and after a minimum period of 24 hours seizure free. The SPECT were evaluated visually by at least two specialists.The SPECT scan was compared with MRI and the analysis of the surgical specimen. The minimum postoperative follow-up was 8 months and the outcome was assessed with the modified Engel scale.Results:The SPECT/MRI/ST-results agreed in 19 out of 25p(76%).The ictal/interictal SPECT correctly located the seizure focus in 21 out of 25p (84%). Among the 4p with a negative SPECT, 2 has a positive MRI and in 1 the MRI was also negative and the surgery was guided by EEG. The remaining patient had a bilateral temporal hiperperfusion in the SPECT and the MRI showed only right temporal lesions, he had a resection of the right parietal lobe and the rate of seizures was reduced by 75%.MRI detected abnormalities in 22 out of 25 patients (88%). 17 out of 25p (68%) had a mesial temporal sclerosis. In 2 out of 3 patients with negative MRI the epileptic focus was localized with the SPECT.19 out of the 21p (90%) with a positive SPECT had a surgical outcome Engel 1 whereas 2 out of 4 patients with negative SPECT were classified as Engel III-IV.Conclusion:The ictal and interictal SPECT is useful in the preoperative assessment in patients with drug-resistant epilepsy correctly locating the epileptic focus in 84% of patients. Patients whose epileptic focus was localized by SPECT showed better postoperative outcome.

P509

Three Months Follow-Up of Mild Traumatic Brain Injury in Rats: A Combined [18F]FDG and [11C]PK11195 PET Study

D. Vállez Garcia1, A. Otte2, R. A. J. O. Dierckx1, J. Doorduin1; 1University Medical Center Groningen, Groningen, NETHERLANDS, 2Offenburg University of Applied Sciences, Offenburg, GERMANY.

Aim: Mild traumatic brain injury (mTBI) is the most common cause of head trauma and it is especially relevant in adolescents and sport activities. However, the time course of its functional pathology is not well defined. In this study the consequences of mTBI were evaluated in a rat model over a period of 3 months. The presence of neuroinflammation ([11C]PK11195) and changes in brain metabolism ([18F]FDG) were determined using small animal PET

imaging. Material and Methods: A weight-drop mTBI model was used to replicate the pathological features seen in humans. Male Sprague-Dawley rats were divided into sham (n=8) and trauma (n=8) groups. PET imaging and behavioral tests (i.e. open field, object recognition and Y-maze) were performed at different time points after induction of the trauma: acute stage (9-12 days), 1 and 3 months. Differences between groups in the body weight and behavioral scores were analyzed using the Generalized Estimating Equations model and $p<0.05$ were considered significant. Differences in tracer uptake were analyzed with a voxel-based analysis. T-maps were interrogated with uncorrected $p<0.005$ and 200 threshold voxels; only clusters with FDR-corrected $p<0.05$ were considered significant. Results: Trauma induction did not result in death, skull fracture or neurological suppression of reflexes. A statistically significant decrease in gained body weight was observed in mTBI group ($p=0.003$). No statistical differences were found between groups in any of the behavioral tests. In the voxel-based analysis, a comparison between mTBI and sham groups was performed at each time point. A neuroinflammatory process was detected only in the acute phase, with significantly higher [11C]PK11195 uptake located bilaterally in the pons, medulla, cerebellum, hypothalamus, caudate, putamen, and the right amygdala. Increased regional [18F]FDG uptake in mTBI rats was detected in all time points bilaterally in the medulla, in addition to an increased uptake at 3 months in the left motor, somatosensory, visual and parietal cortices. Moreover, decreased uptake was detected during the follow-up period in the thalamus, internal capsule, amygdala, caudate, putamen, globus pallidus, hippocampus, and somatosensory cortex. Conclusion: Alterations in the regional glucose metabolism of the brain extend for a period of at least 3 months in regions that seem to present an acute neuroinflammatory response to the trauma. The presence of these long-lasting functional alterations must be considered carefully in the context of mTBI, especially in sports and recreational activities where patients may be exposed to a repeated head trauma.

P510

Baseline Right Hemispheric Metabolic Activity Predicts Improvement in Aphasia Severity and Visual Attention Tasks in Persons with Aphasia Treated with a Cholinergic Agent

A. L. Gutiérrez Cardo1, N. Roé Vellvé1, F. Alfaro Rubio1, G. Dávila2, M. J. Torres-Prioris2, M. L. Berthier2; 1Fundación General de la Universidad de Málaga, Málaga, SPAIN, 2Universidad de Málaga, Málaga, SPAIN.

Cognitive control mechanisms including attentional resources are implicated in recovery from post-stroke aphasia. It is known that cholinergic systems are engaged during visual attentional tasks and that cholinergic enhancing drugs improve language deficits in persons with aphasia (PWA). Aim: To analyse the metabolic correlates of response to the cholinergic agent donepezil in aphasia severity and visual attention tasks with brain 18F-FDG PET in PWA with chronic stroke. Methods: An 8-week open-label study of donepezil (10 mg/day) was performed in 10 PWA with chronic stroke lesions restricted to the left hemisphere identified by structural MRI. Resting 18F-FDG PET was performed in all patients at baseline (week 0) and endpoint (week 8). PET data was analysed with SPM 8. Several ROIs from the AAL atlas were examined in both hemispheres excluding lesional areas, white matter and CSF. PWA improving > 5 points on the Aphasia Quotient of the Western Aphasia Battery were considered "responders" to treatment. Visual attention was tested with the California Computerized Assessment Package. Results: Five PWA were responders to treatment. Baseline metabolic activity was increased in responders compared to 25 healthy control subjects (HCS) in the right medial occipital cortex, superior temporal cortex, medial cingulum and putamen ($p < 0.05$). By contrast, baseline metabolic activity was significantly reduced in non-responders in comparison with HCS in right caudate, posterior cingulum, and precuneus ($p < 0.05$). The whole group of PWA ($n = 10$) showed decreased metabolism compared to the HCS in right posterior cingulum, inferior parietal cortex (both $p < 0.1$) and precuneus ($p < 0.05$). Comparisons of responders versus non-responders showed that the former group had increased baseline metabolism in several right hemisphere regions (posterior cingulum, medial occipital cortex, superior temporal cortex, caudate, putamen, and whole right hemisphere) ($p < 0.05$). Significant improvements in visual sequential reaction time in the whole sample of PWA ($n = 10$) at endpoint correlated with increased metabolic activity in right cingulum (anterior and posterior), insula, posterior temporal cortex, putamen and thalamus. Conclusions: Increased baseline metabolic activity in brain areas (default mode network, basal ganglia and thalamus) innervated by the right cholinergic systems predicts improvement in visual attention tasks in PWA with chronic stroke lesions restricted to the left hemisphere. Post-treatment increases in metabolic activity in these regions correlated with gains in visual attention.

P511

99mTc-HMPAO Brain SPECT in Rabbits: Preliminary Results on CBF Variation by Different Anaestethic Drugs

M. Longo1, **C. Pettinato**2, D. De Zani1, G. Ravasio1, M. Di Giancamillo1, D. Zani1; 1DIVET, University of Milano, Milano, ITALY, 2Medical Physics Unit, Bologna, ITALY.

Aim: The aim of this study was to evaluate general brain perfusion in rabbits through a non-invasive nuclear medicine technique, before and after the administration of two different anesthetic protocols.Materials&Methods: Ten male New Zeland White rabbits were enrolled in the prospective study. All subjects underwent CT studies of the skull in order to exclude any gross malformations or lesions and to acquire images for CT/SPECT fusion. 99mTc-HMPAO brain SPECT scans were acquired with a single head gamma camera: circular orbit, continuos rotation 10 seconds/step and 120 steps. During the first session 99mTc-HMPAO was IV injected in two groups of five awake rabbits, with a randomized selection. The first one was subsequently anesthetized with propofol and the other with dexmedetomidine. The same procedure was repeated 21 days later, injecting the radiopharmaceutical after the induction of general anaesthesia. The brain perfusion uptake index (BPUi), expressed as total counts in the brain per unit of injected activity, was calculated.ResultsRabbits anesthetized with propofol showed exactly the same tracer distribution in both injection condition: awake or asleep. The radiopharmaceutical was concentrated in the brain but a generalized distribution was observed also in the facial muscles for the propofol groups and for the group of subjects administered with dexmedetomidine after 99mTc-HMPAO injection. On the contrary when dexmedetomidine was used before the 99mTc-HMPAO injection a generalized reduction of the uptake was observed especially in extracencephalic tissues.The average BPUi values were respectively 16.5 counts/KBq and 16.7 counts/KBq for rabbits anesthetized with propofol and with dexmedetomidine after the 99mTc-HMPAO injection. Animals injected with 99mTc-HMPAO after the anesthesia induction showed respectively 16.1 counts/KBq and 12.5 counts/KBq using the propofol and the dexmedetomidine protocol.Discussion and conclusions: Although the major limitation of our study is the small number of subjects analyzed, our results showed that when propofol is used as anesthetic drug, any difference in brain perfusion occurred if the radiotracer was injected prior or before anesthesia.On the contrary the vasocostriction of dexmedetomidine is responsible of a mild reduction of the radiopharmaceutical uptake in the brain and a good inhibition of tracer uptake in other tissues.These preliminary data suggest that the use of propofol in uncooperative patients, that need sedation before brain perfusion studies, could not influence the CBF. On the other hand the results of the CBF in rabbits medicated with dexmedetomidine before tracer injection, suggest a possible neuronal protective proprieties of this drug.

P512

The potential role of [18F]-FDOPA PET/CT in proton treatment planning for glioblastoma: preliminary experience

D. Donner1, D. Amelio2, S. Agostini1, G. Carbone1, A. Palucci1, S. Vennarini2, U. Rozzanigo3, M. Erini1, E. Bagatin1, M. Amichetti2, M. Recla3, F. Chierichetti1; 1Nuclear Medicine Dpt - S. Chiara Hospital - APSS, TRENTO, ITALY, 2Proton Center - APSS, TRENTO, ITALY, 3Radiology Dpt - S. Chiara Hospital - APSS, TRENTO, ITALY.

Aim of the study:Proton Therapy (PT) is an advanced external radio treatment that allows to keep low the radiation burden on the healthy tissues beyond the target.According to a joint decision with proton radiation oncologist, both high and low grade gliomas, after surgery for partial resection, were studied with 18F-DOPA PET/CT for contouring purpose in radiation treatment planning.In this study we considered only patients(pts) affected by glioblastoma (GBM) to assess the potential role of PET/CT in PT. Methods:13 GBM lesions (9pts) were studied 1 hour after i.v. injection of [18F]-FDOPA (3MBq pro Kg). Reconstructed images were visually examined and, evaluating the SUVmax tumor/normal tissue ratio, semi-quantitatively examined. The collected PET data were provided to radiation oncologist who compared them to the standard ones, established by MRI, and two dose paintings were performed and assessed. 3 months after the completion of PT, up to now, in 2(4 lesions) out of 9 pts, 18F-DOPA PET/CT was repeated, and, for each lesion, the SUV percentage change pre-treatment(tr) vs post-tr, was calculated.Results: semi-quantitative analysis on 18F-DOPA PET/CT, before PT, produced mean values of SUVmax (tumor=2.55, normal tissue =0.91) and tumor/normal tissue ratio (2.8), similar to the data of a recent pubblication (Hermann K et al, Neuro-Oncology,2014), even if with different acquisition timing.18F-DOPA PET/CT changed the expected planning, as determined just by MRI, in more than half of lesions, determinig GTV(Gross Tumor Volume) boost sub volumes in the overall planned area of treatment and showing more tumor tissue than MRI,too. About the two pts that completed PT, in spite of an enlargement of lesions, as shown by post-treatment MRI, there was a decrease in 18F-DOPA uptake: for both pts a reduction of 30% respect to basal study. Conclusions:our data confirm previous studies showing that 18F-DOPA identifies more tumor respect to MRI in GBM (Ledezma CJ et al, EurJRadiol, 2009), but, in our experience, GBM proved to be suitable to be studied by 18F-DOPA PET/CT using different acquisition protocol, without lost of sensitivity, too.PT is beneficial for a better quality of life of pts and, even if we do not have enough data about the final outcome, we can argue that a dose painting based on

functional imaging, may be more effective for a longer survival.Finally, even if few pts completed the treatment, it seems that 18F-DOPA PET/CT could be a reliable tool in the assessment of response to PT.

P513

Cisternoscintigrahy in cerebrospinal fluid fistula and intracranel hypothension syndrome

M. Castrillon; Sergas, Vigo, SPAIN.

The cisternoscintigraphy is a test that can assess the dynamics of cerebrospinal fluid from an anatomical and functional standpoint. We review those performed in our department with the suspected of cerebrospinal fluid fistula or intracranial hypopresion syndrome,to determine its usefulness to confirm / rule out its presence and its concordance with the clinical context and other complementary tests. Material and methods: Descriptive retrospective study (2006-2015). 111In- 1mCi intrathecal administration of DTPA. Planar images (tracking and static) at least at 3 and 6 hours pi, and according to findings every 24 hours until 72 hours pi. Placing cotton plugs in FN / CAE depending on clinical suspicion, renewed after each set of images obtained. Comparison of the activity at study end caps to the present in plasma. Results: 40 studies were reviewed: -11 Positive: 10 PT consistent with other tests (RM / MieloTC) and / or response to treatment performed; one discordant with MRI findings, determined as false positive after reviewing images (diagnosed as a cause of hipopresión CFS LUES). -29 Negative, all TN: 16 congruent with RM (negative) and clinical outcome (spontaneous or conservative treatment decision). 7 requested as a single test for the presence of fistula in patients with a history of TCE, which remained asymptomatic at follow-up. 3 for control asymptomatic patients with TBI who had submitted prior to discharge and positive clinical MRI, with resolution of symptoms with conservative treatment. 2 for asymptomatic control patients after surgical repair of fistula, confirming its resolution. A patient with nasal discharge on HIC lumboperitoneal shunt valve, which showed the same malfunction but not fistula. Conclusions: In our review the cisternoscintigraphy is a technique that presents an adequate diagnostic accuracy in the assessment of CSF fistula and intracranial hipopresión syndrome

P32 - Monday, October 12, 2015, 4:00 PM - 4:30 PM, Hall 3 - Poster Exhibition

Basic Oncology: Miscellaneous

P514

Characterization of 18F-DOPA-Uptake in Various Tumour Cells: Implication for the 18F-DOPA PET

M. Delivuk, P. Ubl, F. Girschele, M. Hacker, G. Hamilton, **S. Li**; Medical University of Vienna, VIENNA, AUSTRIA.

Aim: The visualization of neuroendocrine tumours (NET) by 18F-DOPA-PET based on the capability of NET to take up, decarboxylate, and store monoamine precursors such as dihydroxyphenylalanine (DOPA). In this study we have investigated the 18F-DOPA-uptake in different NET cells and in human prostate cancer as well as breast cancer cells and human embryonic kidney cells. Methods: Human small cell lung cancer (SCLC) cell lines (DMS 153, NCI H417), rat pheochromocytoma cell line (PC-12), human prostate cancer cell line (PC-3) and human breast cancer cell line (T47D) as well as human embryonic kidney cell line (HEK 293) were used in this study. 18F-DOPA was produced via the novel synthesis method. Standard 18F-DOPA accumulation assays were performed. Results: Significant accumulation of 18F-DOPA was found in PC 12 and DMS 153 cells. Moderate uptake of 18F-DOPA were shown in PC 3 and NCI H417 cells. Very low accumulation of 18F-DOPA was demonstrated in the T47D and HEK 293 cells. The rank-order of potency for 18F-DOPA uptake was PC12 cells (18.2% of total counts) > DMS 153 cells (17.9%) > PC 3 cells (5.9 %) > NCI H417 cells (4.5%) > T47D cells (2.1%) > HEK 293 (1.9%). The uptakes of 18F-DOPA in these cell lines were shown to be specific since the 18F-DOPA accumulations were inhibited by addition of unlabeled DOPA. Conclusion: Our results show that not only NET cells but also some other tumour cells such as human prostate cancer cells can accumulate specifically 18F-DOPA. Very low 18F-DOPA-uptake was also found in human breast cancer cells. Different NET cells have different capacities of accumulation of 18F-DOPA. These results may have clinical implications for the 18F-DOPA PET.

P515

Intraobserver variability in gross tumor volume delineation on PET/CT workstation and EclipseTM radiation therapy planning system of head and neck cancers

S. Sediene, I. Kulakiene, V. Rudzianskas; Lithuanian Hospital of Health science Kauno clinics, Kaunas, LITHUANIA.

Background. Precise gross tumor volume (GTV) delineation is very important for radiation therapy planning. Usually it is done by means of computed tomography. Although, there

are many different visual diagnostic procedures, it is difficult to quantify the tumor burden directly and systematically. FDG PET/CT incorporates functional criteria, therefore, it may allow systematically measure tumor burden and be more direct and reliable method. The aim of this study was to evaluate accuracy of different GTV delineation methods with FDG PET/CT images on distinct workstations, to compare and find out most precise method. Precise GTV delineation enables to plan treatment accurately and could reduce rate and severity of treatment complications.Methods. Ten patients with head and neck cancer were retrospectively chosen for the study. All patients were histologically proven squamous cell carcinoma, stage III or IV disease, without distant metastases. Patients underwent pretreatment FDG PET/CT and received neoadjuvant chemotherapy. Two weeks post neoadjuvant chemotherapy all the patients underwent follow-up FDG PET/CT, to have as low as possible inflammatory alterations. After everything all patients received definitive chemoradiotherapy. Contouring was performed by nuclear medicine specialist manually on two different workstations (GE advanced and EclipseTM treatment planning system) and semi-automatically in three dimensions by GE software. The measurements of GTV were done by visual target contouring.Results. The mean GTV volumes prior neoadjuvant chemotherapy were as follows: manually by GE ADW 18,49±17,06, manually by EclipseTM 24,93 ±20,68, semi-automatically by GE ADW 12,9±12,41. The mean GTV volumes after neoadjuvant chemotherapy were: manually by GE ADW 6,76±11,86, manually by EclipseTM 6,73±14,39, semi-automatically by GE ADW 7,79±10,52. According ANOVA repeated measurement there is statistically significant difference between GTV volumes measured manually by EclipseTM and semi-automatically by GE ADW workstations prior neoadjuvant chemotherapy (p=0,024). There are no statistically significant difference between GTV volumes measured manually by GE ADW and manually measured by EclipseTM, semi-automatically by GE ADW workstations prior neoadjuvant chemotherapy (as follows: p=0,119; p=0,441). There are no statistically significant difference between GTV volumes measured manually by GE ADW and EclipseTM and semi-automatically by GE ADW after neoadjuvant chemotherapy (p=0,872).Conclusion. All three delineation methods are reliable for gross tumor volume measurements after neoadjuvant chemotherapy. Manual GTV delineation by EclipseTM and semi-automatic three dimension delineation by GE ADW workstations are not so accurate after neoadjuvant chemotherapy while compared to manual delineation by GE advanced workstations. Prior neoadjuvant chemotherapy more reliable GTV measurement method is manual by GE ADW workstation.

P516

Development and characterization of microspheres contained with different polymers for hepatoma therapy

P. Chiang, C. Peng, Y. Chu, T. Luo; Institute of NUclear Energy Research, Taoyuan, TAIWAN.

Aim:The purpose of this study is to develop biodegradable microspheres which combined with chemotherapy to become applications such as transcatheter arterial embolization/ chemoembolization (TAE/TACE) or local injectable forms. By locally and slowly release of chemotherapeutic agents, the effect of cancer treatment can be extended. Materials and methods:In the experiment, we used biodegradable polymer Poly(D,L-lactide-co-glycolide)(PLGA) prepared amino surface modification micron particles. By double emulsion, the microspheres contain water-soluble polymers, including carboxymethylcellulose sodium salt, poly(sodium 4-styrenesulfonate), poly(4-styrenesulfonic acid) ammonium salt solution and Poly(vinylsulfonic acid, sodium salt) solution. The functional groups of those polymers will dissociate into -SO3- or -COO- in water. Doxorubincin can be loaded into the beads using an ionic exchange process between the protonated primary amine on the drug and the negatively charged groups, and it can slowly release. Results:Experimental results show that 50mg 25% PVSAS/ PLGA microspheres absorbed 2.5mg doxorubincin within an hour had the best absorption efficiency. Microspheres were labeled with 111In and performed in a rat hepatic embolization model. NanoSPECT/CT imaging and bio-distribution showed the drugs were still in the liver after 72 hours. Conclusion:The microspheres may offer the advantage of chemotherapy locally injection or embolism formulation platform. In the future, the amino surface modification micron particles can graft chelator and label therapeutic radionuclide to maximize their effects on hepatocellular carcinoma.

P33 - Monday, October 12, 2015, 4:00 PM - 4:30 PM, Hall 3 – Poster Exhibition

Clinical Oncology: Thyroid - Malignant

P517

The prognostic impact of FDG PET/CT imaging in the early postoperative work-up of differentiated thyroid carcinoma patients with elevated Thyroglobulin levels

G. Ucmak, B. Demirel, **B. E. Akkas**, A. K. Fidan; Ankara Oncology Research and Training Hospital Department of Nuclear Medicine, Ankara, TURKEY.

Introduction: The aim of this study was to evaluate the impact

of FDG PET/CT imaging in the early postoperative work-up of differentiated thyroid carcinoma patients with elevated Thyroglobulin levels out of proportion to the identified disease.**Method**: Among DTC patients who were referred to our clinic for radioiodine ablation/therapy, 35 patients (22 F, 13 M, age: 48±16 yr) with significantly elevated serum Thyroglobulin (Tg) levels which were out of proportion to the identified disease, were included in this study. FDG PET/CT was performed to define disease extent as a part of initial work-up. Patient management was planned based on clinical, laboratory and PET/CT findings. The contribution of PET/CT findings to patient management and clinical outcome was evaluated.**Results**: PET/CT detected metastatic cervical and/or mediastinal lymph nodes in 16 patients, lung metastasis in 15 patients, bone metastasis in 2 patients and multiple sites of metastasis in 2 patients. In the light of PET/CT findings, 12 patients were referred to surgery for focused neck dissection or completion compartmental neck dissection and/or metastatectomy, 4 patients received external beam radiotherapy for bone metastasis. Then, all patients received I-131 radioiodine therapy with doses of 150-250 mCi. Of these, PET/CT detected non-radioiodine avid lung and mediastinal metastasis in 5 patients. Findings of PET/CT and post-ablation radioiodine whole body scan were comparable in others. PET/CT provided a change in treatment plans for patients who were referred to surgery/radiotherapy (15/35 patients, 43%). After 36±16 months of median follow-up, 4 patients had progressive disease, 8 patients had stable disease, 22 patients had clinical/biochemical remission.**Conclusion**: As a part of initial staging algorithm, FDG PET/CT has an important role on the management of patients with high risk DTC. We consider that, especially in patients with high Tg levels out of proportion to the identified disease, PET/CT provides unique opportunity to select patients who has surgically amenable disease and help to increase therapeutic response to further radioiodine therapies which all result in an improvement of progression-free survival.

P518

The Role of Postoperative Diagnostic I123 SPECT-CT in Low and Intermediate Risk Profile Patients with Differentiated Thyroid Carcinoma

O. Bessolova, O. Perfileva, Y. Kizhaev, V. Vidioukov, N. Vyrenkova; Russian Medical Academy of Postgraduate Education, Moscow, RUSSIAN FEDERATION.

Aim: To evaluate the postoperative diagnostic I123 SPECT-CT contribution to management strategy in low and intermediate risk profile patients with differentiated thyroid carcinoma (DTC). Materials and methods: A total of 98 patients (81 women and 17 men) with mean age of 42,1 years with DTC (79 papillary, 19 follicular) were evaluated 4-8 week after thyroidectomy. Patients were subdivided retrospectively into two groups according to the histological data: group 1 of low risk profile with 38 patients included, and group 2 of intermediate risk profile with 60 patients. Whole body study (WBS) and SPECT of the neck and upper chest area were performed in all patients. In cases of increased uptake foci SPECT-CT was done (GE Infinia Hawkeye 4). The I123 studies were performed after 3 week thyroid hormone withdrawal or without medication postoperatively, 24 hour after intravenous I123 isotonic. Serum thyroglobulin (TG), anti-TG, TSH and ultrasound were evaluated. Results: We detected 83 increased uptake foci in the neck and upper mediastinum region. In group 1, 35 foci were found in 24 patients. In group 2, 48 foci were detected in 35 patients. Only SPECT study was responsible for detecting 3 foci in group 1 and 8 foci in group 2 independently and in addition to WBS. SPECT-CT accurately determined residual thyroid tissue in 34 and 39 foci of group 1 and group 2 respectively. Lymph node involvement was identified by SPECT-CT in 1 case of group 1 and in 8 cases of group 2. In 1 case of group 2 SPECT-CT revealed distant metastases in the lung. In all low and intermediate risk profile patients with residual thyroid tissue radioiodine ablation was performed. SPECT-CT data caused the change in N/M status, risk stratification status and radioiodine therapy planning with indication for surgical removal of lymph nodes in 1(3%) patient of group 1 and in 8(13%) patients of group 2. Conclusion: Low and intermediate risk profile patients with differentiated thyroid carcinoma have a need for residual thyroid tissue and lymph node involvement screening after thyroidectomy. SPECT-CT technique is a useful modality in accurate localization of the lesion and interpretation of uptake in cervical region. The unique capabilities of I123 SPECT-CT provide individual therapy and follow-up.

P519

The clinical significance of thyroid incidentaloma on FDG-PET/CT - one centre's experience

P. Martineau, M. Pelletier-Galarneau, W. Zeng, X. Pham; The Ottawa Hospital, Ottawa, ON, CANADA.

Background: Incidental thyroid uptake is not an infrequent finding in patients undergoing FDG-PET/CT for staging of a non-thyroid malignancy. Two types of pattern are typically seen: diffuse uptake, usually reported to be associated with thyroiditis, and focal uptake, which raises the suspicion of malignancy. The existing literature shows a significant heterogeneity in terms of the incidence of these findings, and their significance. Methods: We reviewed all FDG-PET/CT reports from our institution dated between 9/1/2012 and 4/2/2015 (N=4280) and identified all cases of reported abnormal thyroid

uptake. For all patients with abnormal thyroid FDG uptake, follow-up imaging, pathology, medications, medical histories, and available blood-work were reviewed. Results: 109 patients with abnormal thyroid FDG uptake (mean SUV 7.0, range 1.9-53) were identified, resulting in an overall incidence of 2.5%. A diffuse pattern of uptake was noted in 36 (33%) of these cases and follow up imaging and/or relevant clinical information was available for 19 (53%) of them. Of patients with a diffusely increased thyroid uptake, 13 (36%) were receiving thyroid hormone supplementation, another 2 (6%) were noted to have a history of hypothyroidism without evidence of thyroid hormone supplementation, and another 2 (6%) had ultrasound findings consistent with chronic thyroiditis; of note, 2 of these patients had normal thyroid function tests. In addition, 82 FDG-avid focal thyroid lesions (mean SUV 6.5, range 1.9-53) were identified in 78 patients. Of these, follow-up characterization by ultrasound was available in 34 (44%) cases, with biopsy performed in 26 cases. Pathology results revealed 10 (38%) malignancies (4 papillary thyroid carcinomas (mean SUV 13.8; range 5.0-39.1), 3 Hurthle cell carcinomas (mean SUV 3.8; range 3.3-4.5), 1 follicular neoplasm (SUV 2.9), and 2 malignancies not otherwise specified (mean SUV 10.2, range 5.8-14.5). Conclusions: Our review of abnormal FDG findings in the thyroid demonstrates that all focal thyroid lesions harbour a significant risk of malignancy which is independent of SUV. In particular, well-differentiated lesions exhibited a wide-range of FDG avidity. For patients with diffuse uptake, chronic lymphocytic thyroiditis was the most likely diagnosis in a significant proportion; however, no clear etiology could be determined for the majority of cases.

P520

Role of 18F-FDG-PET/CT Scan in the Follow-Up of Patients with Differentiated Thyroid Carcinoma. Significance of Thyroglobulin and Anti-Thyroglobulin Antibody Levels

F. S. Zelaya Reinquet, **J. M. Nogueiras Alonso**, D. Ruiz Hernández, C. Castillo Berrio, M. A. Castrillón Sánchez, A. Serena Puig, L. Campos Villarino, R. Guitián Iglesias; Hospital Do Meixoneiro, VIGO, SPAIN.

Objective/Aim:Differentiated Thyroid Carcinoma(DTC) has a good prognosis and high cure rate with 10-year survival rate of 80-90%. Recurrence may occur even late(up 20%), so that a long-term monitoring with cervical US, 131I whole body scan(I-WBS) and thyroglobulin plasma levels(TG) is mandatory. The coexistence of negative I-WBS and high TG levels suggest dedifferentiation with Na-I symporter loss a circumstance that is often associated with increased glucose metabolism. FDG-PET/CT has proved useful in these patients but criteria involving optimal use should be adequately defined.Our goal in this paper is to relate the findings of FDG-PET/CT performed in DTC patients with negative I-WBS, with serum levels of thyroglobulin and anti-thyroglobulin antibodies to determine the cut-offs that lead to increased diagnostic accuracy and performance.Material and methods:Since March 2009, 77 18F-FDG-PET/CT were performed in 43 (negative I-WBS) patients with suspected DTC recurrence by elevated levels of TG. 18F-FDG-PET/CT was performed on the third day after stimulation with rh-TSH and evaluated by two nuclear physicians. PET findings were correlated with the levels of TG-antibodies (normal value<60UI/ml) and stimulated TG (NV<0.5ng/ml). According to these two groups were defined; group A(59cases) Positive-TG stimulated levels, negative anti-TG-AB and group B(15 cases): Positive anti-TG-AB. PET findings were confirmed (true/false) by histology and/or results of other diagnostic tests or clinical follow-up.Results:43 patients with 74 scan (21♂-53♀/ age24-81years). Pathology at diagnosis: 53-papillary; 18-follicular, 3-undifferentiated histology. Confirmation of the hypermetabolic foci by pathological study in 35scan, by another method of image or follow-up in 26.Group A46PET(+): 31 True Positive(TP), 8 False Positive(FP), 7 not confirmed (NC). 13PET(-):13(TN9; FN1; 3NC). 1Deceased. Mean TG:132ng/ml (0,86-2860ng/ml). PET positive predictive value:79%; negative predictive value:90%. (considering only confirmed cases).Group BPET(+)15: 10TP; 1FP; 4NC. Average TG:94ng/ml, Mean anti-TG-AB (rank 61-2530Ul/ml): 504Ul/ml. PET positive predictive value:90%.PET performance according to TGstimulated levels.ROC analysis(AUC:0.69).15 ng/ml cut-off: S:58%; Sp:76%; PPV:75%; NPV:59%. Accuracy:66%.20 ng/ml cut-off: S:52%; Sp:88%; PPV:84%; NPV:59%. Accuracy:68%.ConclusionsFDG-PET is a procedure that is justified in patients with DTC and negative I-WBS. According to our results it modifies the therapeutic approach in 75% of cases. Its greatest value is achieved in patients with TG levels higher than 15-20ng/ml or with very high levels of antiTG even with undetectable thyroglobulin.

P521

Predictors of malignancy in thyroid incidentalomas seen on 18F-FDG PET/CT scanning in patients not known to have thyroid cancer

H. Nasr1,2; 1Prince Sultan Military Medical City, Riyadh, SAUDI ARABIA, 2Kasr El-Aini Cairo University Hospital, Nuclear Medicine Unit, Cairo, EGYPT.

Objectives: To assess the frequency of incidental thyroid abnormalities detected on 18F-FDG PET/CT and to determine the most powerful parameters that are capable to differentiate benign from malignant lesions. Methods: We retrospectively reviewed 3304 18F-FDG PET/CT scans for 1909 patients. Patients known to have thyroid malignancy were excluded. Patients who were found to have thyroid metabolic or morphologic abnormalities were further analyzed. Data analyzed included; age, sex, SUVmax, tissue density in Hounsfield units (HU) of the non-enhanced CT portion of the study, lesion size, presence of calcification and thyroid gland morphology. To differentiate benign from malignant lesions SUVmax cutoff of >4.7 and HU cutoff of >42 based on ROC analysis were used. The various parameters were compared to histopathological findings from either fine needle aspiration biopsy (FNAB) &/or thyroidectomy. Sensitivity, specificity, PPV, NPV and accuracy in detecting malignancy were calculated. Multivariate regression analysis was performed to assess the most powerful predictors for malignancy. Results: Thyroid abnormalities were detected in 120 patients of whom 78 had increased focal or diffuse FDG activity. Histopathology was available for 30/120 patients (25%). The most common primary diagnosis of these patients in descending order was lymphoma (25%), breast cancer (18%), gynecological malignancies (14%) and head & neck cancers (14%). Thyroid malignancy was confirmed in 13/30 (43.3%) (10 (77%) females) while benign thyroid lesions were noted in 15/30 (50%) (8 (32%) females). Thyroid malignancies included 10 papillary, 1 follicular, 1 Hurthle cell neoplasm and 1 lymphoma. Benign lesions were 11 benign follicular or colloid nodules and 4 autoimmune thyroiditis, while in 2/30 FNAB was undetermined or inadequate. The mean SUVmax and lesion tissue density (HU) were both significantly higher in patients with malignant versus benign lesions (7.7±6.8 Vs. 3.6±1.6, p=0.032) and (44.3±13.2 Vs. 32.5±12.6, p=0.039) respectively. None of the other factors were statistically significant. There was weak non-significant positive correlation between SUVmax and HU. The sensitivity, specificity, PPV, NPV and accuracy to predict malignancy for SUVmax>4.7 versus HU>42 were 76.9%, 86.7%, 83.3%, 81.3 & 82.1% and 75.0%, 90.9%, 90.0%, 76.9 & 82.6% respectively while the combined both parameters revealed further improvement compared to either parameter alone with sensitivity, specificity, PPV, NPV and accuracy of 92.3%, 80.0%, 92.3%, 80.0% and accuracy of 85.7% respectively. Conclusion: SUVmax and tissue density (HU) are valid parameters capable of predicting malignancy in thyroid gland insidentalomas and when combined are more powerful with risk of malignancy reaching 80-90% when criteria are fulfilled.

P522

99mTc-Methoxy-isobutyl-isonitrile (MIBI) Scintigraphy is an useful and cost-effective tool for assessing the risk of malignancy in thyroid nodules with indeterminate fine needle cytology (FNAC)

A. Campenni'1, L. Giovanella2, S. Giovinazzo3, F. Di Mauro1, S. Pignata1, M. Mure'1, M. Stipo1, M. Siracusa1, M. Ruggeri3, S. Baldari1; 1Nuclear Medicine Unit of Messina, Messina, ITALY, 2Nuclear Medicine and PET/CT Centre, Oncology Institute of Southern Switzerland - Bellinzona, Switzerland., Bellinzona, SWITZERLAND, 3Endocrinology Unit, University of Messina, Messina, ITALY.

Aim. Nodular thyroid disease is a common clinical problem. The diagnostic algorithm include laboratory test, thyroid ultrasound, thyroid scintigraphy and ultrasound-guided fine needle aspiration cytology (usFNAC), if the nodule is cold. Not rarely, the results of usFNAC are nondiagnostic (Thyr 1) or unconclusive (Thyr 3). This is a very important problem in the management of patients because the risk of under or overtreatment is high.The aim of our work was to verify if 99mTc-metossi-isobutil-isonitrile (99mTc-MIBI) scan can be employed in Thyr1-Thyr3 patients how diagnostic test to differentiate benign from malignant thyroid nodules by qualitative and quantitative analysis. Material and Methods. This prospective study was conducted on 105 patients (F= 80, M= 25; mean age 47.9 ± 12.6 years) with cold thyroid nodules at 99mTc-pertechnetate scintigraphy, greater than 1.5 cm in diameter (mean size: 26.2 mm; range 15-45). The patients had underwent FNAC, with indeterminate results: Thyr1, n= 5 and Thyr3, n= 100. sestaMIBI scintigraphy was acquired 20 and 40 minutes after tracer administration (370 MBq) by static images of the thyroid.MIBI uptake in thyroid nodules was evaluated both qualitatively (compared with that in controlateral thyroid lobe) and quantitatively, by using region of interest that were created around nodule and outside the thyroid (background activity subtraction). All patients underwent total-thyroidectomy. Results. All the cold nodules were MIBI-positive, with different intensity of MIBI uptake at qualitative analysis: low (n= 35 patients), moderate (n= 46 patients) and high (n= 24 patients). By quantitative analysis, the patients were subdivided in three groups: A (n=29) with a wash-out index (woi) ≥ -40%; Group B (n=41): woi between -20 and -40%; Group C (n=35): woi ≤ -20%. We assumed that a woi ≤ -20% was suspicious for malignancy, while a woi ≥ -40% was predictive of a benign lesion. Compared to hystopathology, all patients of the group A were negative for thyroid cancer [sensitivity and negative-predictive-value: 100%]. In

Group B were included all except seven patients affected by benign adenomas (sensitivity: 85.4%). Finally, 28 out of 35 patients of the Group C had a papillary thyroid carcinoma [specificity and positive-predictive-value: 80.0%]. All false positive patients were affected by adenoma with oxyphil cell. Conclusions. We suggest the use of MIBI-scan (by using quantitative analysis) in the work-up of cold nodule with indeterminate cytology to better stratify the risk patients' to have a malignant lesion, so reducing the number of patients refereed to surgery

P524

68Ga-DOTATATE-PET in MTC patients with elevated calcitonin but normal radiological examination

Z. Wygoda, **D. Handkiewicz-Junak**; Centre of Oncology - MSC Institue, GLIWICE, POLAND.

Early detection of medullary thyroid cancer (MTC) recurrence can results in effective cancer treatment. Biochemical follow-up with calcitonin measurements is the most sensitive method for early detection of MTC persistent disease or recurrence, but is not informative on its localisation. On the other hand radiological examination (US, CT or MR) are sometimes negative for years before biochemical recurrence turns into clinical one.**Aim**. This is a retrospective study to evaluate role of molecular imaging in MTC patients with biochemical recurrence.**Material**. Thirty eight patients diagnosed with MTC and elevated calcitonin level were included into this study. All patients were operated with radical thyroidectomy and neck limfadenectomy in case of lymph node metastases. In all patients radiological examinations (neck US and CT/MR) were negative for MTC recurrence.68Ga-DOTATATE and 18FDG were prepared on site according to GMP procedures. Acquisition was performed on PET-CT Gemini GXL16 (Philips®) PET-CT mCT (Siemens®) one hour after 107,3 - 225,7 MBq of 68Ga-DOTATATE (median: 181,3 MBq) and 136,9 - 462,5 MBq (mediana: 296 MBq of 18FDG).**Results**. 68Ga-DOTATATE-PET was performed in 38 patients diagnosed with MTC. Seven of them had also 18FDG PET/CT. In 7 (18%) patents there was an in increase in 68Ga-DOTATATE uptake in14 anatomical localisation, seven of them (50%) were also visible in 18FDG PET/CT. During 68Ga-DOTATATE examination medial calcitonin level was 546 ng/ml (range 315 to 1250). There was no correlation between calcitonin concentration and PE/CT results. During median follow up of 32 months none of the patients suffered from clinical or radiological recurrence.**Conclusions**: 68Ga-DOTATATE-PET/CT do not increase detection rate of recurrent MTC in patent with elevated calcitonin concentration and negative radiological examination.

P525

131I SPECT/CT in differentiating neck iodine fixing foci in patients with differentiated thyroid carcinoma (DTC)

A. Spanu, I. Gelo, L. Mele, S. Contu, B. Piras, S. Nuvoli, G. Madeddu; Unit of Nuclear Medicine, University of Sassari, Sassari, ITALY.

AIM. Regional lymph node spread from DTC is common particularly in papillary carcinoma, including microcarcinoma,with adverse prognostic influence mainly in older patients. In a retrospective study we investigated 131I-SPECT/CT diagnostic role in DTC patients to also evaluate whether the procedure may have an incremental value than planar. METHODS. Among 735 DTC patients, we selected 204 cases with neck iodine fixing foci; 63 patients were at high risk (H), 53 at low risk (L) and 88 at very low risk (VL). In 190 cases in chronic follow up, 48 h after diagnostic 185 MBq dose and in 56 cases after thyroidectomy (42 including in the 190 pts) 5 days after first radioiodine therapy, planar WBS followed by SPECT/CT over neck/chest and other suspect regions was performed using hybrid dual gammacamera with high energy, parallel hole collimators and with low dose x-ray tube (INFINIA-GE-Medical System), for total 294 exams. RESULTS. SPECT/CT evidenced 560 iodine fixing foci in the 204 patients,while planar 422 in 162 patients, all confirmed by SPECT/CT. Planar classified as residues 364/422 foci and unclear 59/422. SPECT/CT confirmed 356/364 residues while classified 8 foci as lymph node metastases and characterized unclear foci as 17 lymph node metastases, 23 residues, 17 physiologic structures and 2 bone metastases. Moreover, SPEC/CT evidenced 137 foci occult at planar characterizing 68 lymph node metastases, 68 residues and one physiologic uptake. Thus, SPECT/CT identified 90 lymph node metastases (24 only single) in 49 patients, while planar 25 in part wrongly classified as residues or unclear foci. According Tg levels, 18/49 patients (5H, 3L, 10 VL) had undetermined Tg levels (10 ng/ml. Furthermore, 11 VL patients, whose Tg levels were undetermined or < 2.5 ng/ml and 3 VL patients with Tg between 2.5-5.0 ng/ml were T1aN0M0. CONCLUSIONS.131I-SPECT/CT proved reliable diagnostic tool localizing and characterizing neck fixing lymph node metastases with incremental value (49.5% of cases) than planar, with more correct patient classification and management (26 % of cases) and avoiding unnecessary therapy with single physiologic foci not classified by planar (6.9 % of cases). SPECT/CT superiority than planar is particularly significant when the latter is inconclusive and Tg levels are undetermined or very low, which cannot exclude metastasis in lymph node, mainly in VL cases with T1aN0M0 and even more with single metastasis.

P526

Successful slowing of tumour growth by sequential use of different tyrosine kinase inhibitors in a patient with poorly differentiated follicular thyroid carcinoma

A. Becherer, T. G. Böhler, W. Furlan, A. A. Hofmann, F. Karakolcu, H. Wiederin; Academic Teaching Hospital Feldkirch, Feldkirch, AUSTRIA.

Case report: A male patient, 47 years old, was diagnosed with poorly differentiated follicular carcinoma (FTC) pT4 (UICC 1996), pT3 (UICC 2002) Nx, Mx. He underwent left lobectomy and subtotal resection of the right lobe, followed by radioiodine ablation with 5,5 GBq I-131. 3 Years later he had a relapse in the jugular fossa, again treated by surgery and 5.5 GBq I-131. At that time, no radioiodine avid tissue was seen. The following year he had another jugular relapse on which he was operated again with subsequent radiochemotherapy (50 Gy). His thyroglobulin (TG) level remained stable then about 4 ng/ml for 3 years. After 4 years, a slow rise in TG to 9 was noted without response to TSH stimulation. A small solitary right-sided lung lesion was diagnosed by FDG-PET, showing progression 9 months later. He underwent successful metastasectomy. 7 months later TG started to rise again and FDG-PET/CT revealed 3 new foci in the right lung and one in the left lung. The left lung was treated by hypofractionated radiotherapy (7x8 Gy) while the right lung was operated two times more within one year. 2 months after last surgery FDG-positive lesions were seen, TG 9. Another 7 months later FDG-PET/CT displayed quantitatively and qualitatively progressive disease, TG 544. Therapy with the multikinase inhibitor (MKI) sorafenib was begun. After a short drop in TG to 90 accompanied by a slight improvement of FDG-PET/CT findings 2 months after starting with sorafenib, TG started to rise again. After 4 months sorafenib, TG was 274 and a new bone lesion showed up with FDG. After one year sorafenib, TG was again 604 and therapy was switched to pazopanib. TG fell to 387 after 3 months pazopanib and increased then continuously to 1210 1.5 years later. FDG-findings deteriorated as well. Therapy was changed to the next MKI, lenvatinib. 4 months later, FDG-PET/CT was at least stable and TG was 572. Nevertheless, it continued to rise and was 753 after 6 months under lenvatinib. Discussion: This case shows that the sequential use of different MKIs is effective in slowing tumour growth in poorly differentiated FTC. Despite the tumour becomes more aggressive and escapes every new MKI over time, there is an improvement in TG-levels and sometimes even in FDG-uptake after using a new MKI. The future course will show, whether returning to the first MKI is an option when third line therapy fails.

P527

Prognostic value of CEA and Calcitonin compared to image-based monitoring of MTC patients undergoing TKI treatment

R. A. Werner1,2, C. Bluemel1, D. Muegge3, T. Higuchi1,2, J. S. Schmid1, C. Reiners1, K. Herrmann1,4, A. K. Buck1, C. Lapa1; 1Department of Nuclear Medicine, University Hospital Würzburg, Würzburg, GERMANY, 2Comprehensive Heart Failure Center, University Hospital Würzburg, Würzburg, GERMANY, 3Institute of Psychology, University of Innsbruck, Innsbruck, AUSTRIA, 4Department of Molecular and Medical Pharmacology, David Geffen School of Medicine at UCLA, Los Angeles, CA, UNITED STATES.

Objectives: Treatment options for advanced medullary thyroid cancer (MTC) remain limited. Recently, tyrosine kinase inhibitors (TKI) such as vandetanib have shown clinical effectiveness and have been recommended as standard therapy in patients with disseminated symptomatic disease. The predictive role of tumor markers (CEA, calcitonin, CTN) and tumor marker kinetics in the course of TKI treatment has not been fully eludicated yet.Methods: The study included 21 patients (male, 16, female, 5; mean age, 49±13y) with progressive MTC receiving vandetanib 300 mg orally per day. Onset of tumor progression (PD) was defined according to RECIST 1.1 criteria based on follow-up CT scans performed in intervals of 3 months (510±350 days, n=9±6 examinations). Additionally, CEA (ug/l) and CTN (pg/ml) were measured at the day of CT examination (n, 162-178 samples). A potential relationship between the findings at image-based follow-up and tumor marker levels were investigated to evaluate the predictive role of image-based PD as compared to tumor marker kinetics.Results: Both CEA and CTN showed an increase (CEA, 331±630, CTN, 6394±16383) over time indicating PD in all patients (increase compared to previous CEA, 14±67%; CTN, 3±39%). However, image-based PD did not correlate with tumor marker kinetics (CEA, r=0.006; CTN, r=0.07) whereas results of CT tended to positively correlate with CTN measurement at the same and at the following time point of blood collection (r, 0.24, r, 0.28, $p<0.01$, respectively). A CTN cut-off value of ≥40% (defined by receiver operating characteristic analysis) had a sensitivity of 70.6% and a specificity of 83.2% in predicting a CT-based PD with an accuracy of 82.0% (area under the curve, 0.76). On the other hand, alterations in CEA levels were not predictive for PD.Conclusions: A CTN cut-off value of ≥40% predicts the development of PD with an accuracy of 82% with RECIST serving as reference for PD. However assessment of CEA was not predictive and may be therefore abundant.

P528

Incremental Value of SPECT/CT Over Planar Imaging in Recombinant TSH I-131 Scanning of Follow up Patients

M. Al Janabi, **Sr**.; Mediclinic City Hospital, Dubai, UNITED ARAB EMIRATES.

OBJECTIVE: The purpose of this study was to determine the added value of SPECT/CT over planar imaging in Recombinant TSH I-131 scanning of follow up patients with differentiated thyroid carcinoma, post thyroidectomy and RAI ablation. MATERIALS AND METHODS: Fifty patients undergone whole body Iodine -131 scan as follow up, post total thyroidectomy and RAI ablation. Males (10), Females (37), Age (27-62 years; Median-41.30 years).46 patients were with Papillary Thyroid Carcinoma and 4 were with Follicular Thyroid Carcinoma. 45 patients were injected with Thyrogen and two with Thyroid Hormone Withdrawal. Blood levels of TSH, Thyroglobulin and Anti Thyroglobulin Antibodies were obtained pre and post Thyrogen injection. Whole body, Planar and SPECT/CT scans of neck & chest were obtained for all patients at 48 hours post oral administration of diagnostic dose (185 MBq) of Radio Iodine. SPECT images as well as CT images were acquired for localization purpose, from nasal region to stomach level covering the entire chest. Nuclear Medicine physician interpreted the planar scans and SPECT/CT images to assess the incremental diagnostic value with respect to localization and characterization of focal activity. Scan interpretation compared with blood values and Ultra sound scan findings. RESULTS: 39 patients had negative Iodine scan, as observed in planar and SPECT/CT and from Thyroglobulin levels, out of which one had localized pulmonary uptake, which was likely to represent underlying inflammatory or infective process. Three patients had negative Iodine scans, as shown by both planar as well as SPECT CT images but with raised thyroglobulin levels. Planar scans depicted moderate neck uptake in 5 patients, suggestive of remnant thyroid tissue. Raised Thyroglobulin level and SPECT/CT confirmed the same. Three patients had raised Thyroglobulin levels, but negative planar images. SPECT/CT images of the neck revealed foci of uptake suggestive of metastatic cervical lymph node. Because of superior lesion localization and additional anatomic information derived from the low-dose CT component, incremental diagnostic value with SPECT/CT over planar imaging was observed in three cases, where planar imaging failed to show up the lesions. CONCLUSION: Recombinant TSH Iodine 131 SPECT/CT of neck and thorax is useful for accurate evaluation of regional & distant activity localization and characterization of foci as residual thyroid tissue, nodal, pulmonary metastasis or bone metastasis, especially in follow up patients.

P529

Thyroid cancer in patients with hyperthyroidism

S. Choukry, G. Cherkaoui Salhi, s. taleb, A. Guinsi; IBN ROCHD UNIVERSITY HOSPITAL, Casablanca, MOROCCO.

The aim of this study is to describe characteristics of patients admitted for DTC and presenting a concomitant hyperthyroidism. Materials and methods: the study enrolled all patients admitted for a DTC between January 2012 and June 2013 in the Nuclear Medicine Department. Among the 700 cases included, 52 presented a concomitant clinical and biological hyperthyroidism. Results: Mean age was 43 years old (+/-11), all patients were women. Hyperthyroidism was the revealing sign in 53% of cases. It was associated to a thyroid nodule in 23% of cases, and to a nodular goitre in 19% of cases. Total thyroidectomy examination showed papillary thyroid histotype 98 % of cases and one case presented a trabecular variant of papillary carcinoma. Pathological study showed also a thyroiditis in 21% of cases and nodular dystrophy in 17%of cases. The fifth of the subjects were stages very low risk recording to the European consensus and didn't require any additional therapy. Low risk and high risk represented respectively 60% and 20% of cases, these have received adjuvant therapy by radioiodine. The follow up showed a complete remission in 96% of cases, persistent disease with lung metastases in one case, and one patient who was initially staged T4NxMx has deceased before any adjuvant treatment. Conclusion: Although its scarcity, the co-occurrence of DTC and hyperthyroidism has always to be considered.

P530

Effectiveness of aromatherapy on Physiology and Psychology in patients undergoing I-131 ablation with differentiated thyroid cancer.-Using Physiological and Sensory evaluation-

M. Nakayama1, A. Okizaki1, S. Ishitoya1, T. Uno2, T. Suzuki2, Y. Mikami2, J. Sato2, K. Takahashi1; 1Asahikawa Medical University, ASAHIKAWA, HOKKAIDO, JAPAN, 2Asahikawa Medical University Hospital, ASAHIKAWA, HOKKAIDO, JAPAN.

Objectives: The aim of this study was to investigate the physiological and psychological effects of aromatherapy in patients undergoing radioactive iodine (I-131) ablation with differentiated thyroid cancer (DTC). Methods:The subjects were 67

patients with DTC. They were divided into aromatherapy group (10 men, 24 women, age 60.5 ± 12.7 years) and a control group (7 men, 26 women, age 61.1 ± 15.6 years). We blended 1.0 ml of lemon (top note) and 0.5 ml of ginger (base note) essential oils. The patients in the inhalation aromatherapy group inhaled this blend oil and those in the control group inhaled distilled water as placebo for 10 min during admission. Some physiological and psychological indices were measured before and during I-131 ablation. Physiological effect was measured using body weight, body temperature, blood pressure, heart rate, salivary amylase activity and psychological effect was measured using the State Trait Anxiety Inventory-Form JYZ (STAI). Data analysis was performed with statistical softwarewere (XLSTAT2015, Addinsoft, Paris, France). Results: As a result, the mean activty of salivary amylase in the aromatherapy group was 42.0 ± 10.9 and in the control group was 32.0 ± 5.2 before the intervention, which changed after the intervention to 40.0 ± 10.1 and 51.0 ± 14.3, respectively.The mean State-Anxiety score in the aromatherapy group was 38.0± 1.1 and in the control group was 39.0 ± 1.3 before the intervention, which reduced to 35.0 ± 1.1 and 37.5 ± 1.4, respectively after the intervention. We found that the aromatherapy group statistically significant decreased ($P<0.03$) State-Anxiety score in STAI, and suppressed ($P<0.03$) the increase of salivary amylase activity after the intervention. There was no statistically significant difference in other physiological data between the aromatherapy and control groups. Conclusions: The aromatic effects may alleviate negative emotional stress, which, at least in part, would contribute to the suppression of sympathetic nervous system activity.

P531

Lung metastasis from differentiated thyroid carcinoma: Characteristics and prognosis factors

A. Ezzine1,2, M. Ben Fredj1,2, C. Jabeur1, S. Melki1,2, R. Sfar1, M. Guezguez1; 1Nuclear medicine department, Sousse, TUNISIA, 299/UR/08-64, faculty of Medicine Sousse, University of Sousse, Sousse, TUNISIA.

Objectives: The aim of this study was to investigate the physiological and psychological effects of aromatherapy in patients undergoing radioactive iodine (I-131) ablation with differentiated thyroid cancer (DTC). Methods:The subjects were 67 patients with DTC. They were divided into aromatherapy group (10 men, 24 women, age 60.5 ± 12.7 years) and a control group (7 men, 26 women, age 61.1 ± 15.6 years). We blended 1.0 ml of lemon (top note) and 0.5 ml of ginger (base note) essential oils. The patients in the inhalation aromatherapy group inhaled this blend oil and those in the control group inhaled distilled water as placebo for 10 min during admission. Some physiological and psychological indices were measured before and during I-131 ablation. Physiological effect was measured using body weight, body temperature, blood pressure, heart rate, salivary amylase activity and psychological effect was measured using the State Trait Anxiety Inventory-Form JYZ (STAI). Data analysis was performed with statistical softwarewere (XLSTAT2015, Addinsoft, Paris, France). Results: As a result, the mean activty of salivary amylase in the aromatherapy group was 42.0 ± 10.9 and in the control group was 32.0 ± 5.2 before the intervention, which changed after the intervention to 40.0 ± 10.1 and 51.0 ± 14.3, respectively.The mean State-Anxiety score in the aromatherapy group was 38.0± 1.1 and in the control group was 39.0 ± 1.3 before the intervention, which reduced to 35.0 ± 1.1 and 37.5 ± 1.4, respectively after the intervention. We found that the aromatherapy group statistically significant decreased ($P<0.03$) State-Anxiety score in STAI, and suppressed ($P<0.03$) the increase of salivary amylase activity after the intervention. There was no statistically significant difference in other physiological data between the aromatherapy and control groups. Conclusions: The aromatic effects may alleviate negative emotional stress, which, at least in part, would contribute to the suppression of sympathetic nervous system activity.

P532

Pre-therapy I-131 uptake value as a prediction method for metastatic lymph node status in patients with differentiated thyroid carcinoma

G. Ege Aktas, S. Soyluoglu Demir, F. Ustun, A. Sarikaya, G. Durmus Altun; Trakya University Medical Faculty Hospital Nuclear Medicine Department, Edirne, TURKEY.

Aim: Differentiated thyroid carcinoma (DTC) presents with cervical lymph node metastases (LNM) in nearly 50% of patients. Pretreatment assessment of the cervical lymph node status still remains an unsolved problem. We hypothesized that lymph node status would affect I-131 uptake due to pathophysiological behavior of benign and malign thyroidal tissue. This study was designed to assess whether 24th hour I-131 uptake value (24RIU) would predict presence of LNM in patients with DTC. Material and Methods: We reviewed the records of 121 DTC patients, aged between 16- 80 (mean: 48± 14 years), whom received postoperative I-131 ablation (mean dose: 122± 28mCi) therapy. Age, TSH, thyroglobulin (Tg), anti- thyroglobulin (Anti-Tg) level, ultrasonography, 2nd and 24th RIU, I-131 dose and post ablative I-131 scans of the patients were assessed. Patients' data were evaluated retrospectively and each group was separated into three subgroups according to exchange of 2nd and 24th RIU status: Unchanged RIU was notified as group 1(n=13), decreased was group 2

(n=49) and increased was group 3 (n=59). Results: The subgroups of patients were significantly different in respect of their mean TSH, Tg, 2nd and 24th hour RIU; mean 83.7 ±3.4, 92.6±2.9, 78.1±2.9 (p:0,04), 1.2±2.5, 11.5±4.6, 18.3 ±5.4 (p:0,001), 3.7±2.8, 2.2±2.7, 3.3±2.3 (p: 0,001), 2.2±3.1, 0.9±1.7, 11.7±1 (p:0,001) respectively. More patients had LNM in the increased uptake group (group 1=4/13, group 2=13/49, group 3=29/59; p: 0,04).There was no difference between ages, TSH, Tg, anti-Tg levels and 2 hr RIU of patients with and without LNM. 24RIU was higher in patients with LNM (8.1±1.2 vs. 4.8±6.9, p: 0,05). The ±95% confidence interval of the 24RIU for patients with LNM was 4.9 to 11.7. A 24RIU 4.9 identified 34 of 46 patients with LNM and correctly detected patients without LNM in 57 of 75 patients. When a 24RIU of 4.9 was accepted as the cut-off value, the sensitivity, specificity and overall diagnostic accuracy were, 74%, 76%, and 75% respectively. Conclusion: Our results suggest that, I-131 24 hour uptake can be helpful in predicting lymph node metastasis in patients with DTC. The mean 24RIU of the patients with LNM was significantly higher than without LNM. A cut-off value of 24RIU 4.9 yielded sensitivity of 74%, a specificity of 76%, and overall diagnostic accuracy of 75% for detecting LNM.

P533

The 18F-FDG-PET/CT for localization of tumor foci in patients with elevated thyroglobulin antibodies

J. M. Nogueiras Alonso, F. Zelaya Reinquet, D. M. Ruiz Hernández, C. Castillo Berrio, M. A. Castrillón Sánchez, L. Campos Villarino, A. Serena Puig, R. Guitián Iglesias; Hospital Do Meixoneiro, VIGO, SPAIN.

The differentiated thyroid carcinoma DTC has a good prognosis and high cure rate with survival rate at 10-year of 80-90%, but with a recurrence of 20%, it can be ruled by: negative cervical US, negative 131INa-whole body scan (I-WBS) and undetectable thyroglobulin (Tg). With a negative I-WBS, the positivity of antiTg-Ab interferes and invalidates the proper determination of Tg, knowing that if the tissue is dedifferentiated and decreased iodine uptake ability by contrast increases glucose metabolism of the tumor cell, in this sense F18-FDG/PET able to locate disease. We analyzed prospectively the use of 18F-FDG-PET/CT in follow up of patients with elevation antiTg-Ab and negative131INa-WBS.Material and methodsFrom 77 patients with DTC, negative I-WBS and detectable Tg followed since 2009, we found 15 patients with detec-table antiTg-Ab. 18F-FDG-PET/CT was made at 3rd day of stimulation with Thyrogen®, analytical (TSH, Tg and an-tiTg-Ab) basal and stimulated (3rd day), reviewed by two nuclear physicians.ResultsPatients: 15 histological types: papillary (10), follicular (4), (9♀-5♂) mean age 56,85y (31-79y).Eleven patients had metastatic lymph node involvement at initial diagnosis. After Thyrogen® all patientes showed elevated TSH (25.30 to 173.4 mIU/ml) and detectable antiTg-Ab (61-2530ul/ml), Tg(0.5-391.7ng/ml).31 Pathological hypermetabolism foci were obtained in 15 patients located in cervical region(25), supraclavicular(3), mediastinal(4), bone(1) with SUVmax of 1.5g/ml to 23.3g/ml.In 9 patients were confirmed metastatic DTC with pathological study (TP), one patient died and the result is pending in 5 patients.Conclusions18F-FDG-PET/CT shows high sensitivity (100%), detecting tumor foci susceptible to cleavage with a good diagnostic accuracy it could be considered as a suitable diagnostic method in patients with elevated antiTg-Ab and negative I-WBS. The sample is still very small, and is required a larger sample to correlate the values of antiTg-Ab with sensitivity and specificity PET/CT.

P534

Incidental Findings of Hypermetabolic Thyroid Lesions in PET-CT Studies and Their Clinical Significance

D. Villasboas-Rosciolesi, **Jr**, A. García-Burillo, MD, C. Zafón Llopis, MD, M. Salcedo-Pujantell, Jr, M. Velasco Nuño, Jr, J. Monturiol Duran, Jr, J. Castell-Conesa, MD; Hospital Universitari Vall d'Hebron, Barcelona, SPAIN.

AIM: To describe the incidence of hypermetabolic lesions in non-directed thyroid PET-CT studies and their clinical significance. MATERIAL AND METHODS: Between January 2013 and October 2014, from 4207 studies, Seventy-one studies were selected, 24 males and 47 females, 36-92 years-old (70 ± 12), who received non-directed PET-CT studies aimed to thyroid disease, in which there were uptake increments detected, both focal and diffuse ones. After intravenous administration of 3.7 MBq/kg of 18F-FDG, PET-CT acquisition (Siemens Biograph ® 64) was performed according to the standard acquisition protocol. Ultrasound-guided fine needle aspiration biopsy (FNAB) of the thyroid lesions was recommended in focal uptakes. RESULTS: Three of the seventy-one studies (4.2%, all women) showed mean SUVmax 8.11 (6.08-9.95) increased diffuse thyroid uptake. Sixty-four of the seventy-one studies (90.4%, 24 men and 40 women, 33.8% and 66.2%, respectively) showed increased focal uptake. In 19 out of 71 patients (26%) a FNAB were performed. In the men group, the mean SUVmax was 7.4 (±5.9) and 7 of them underwent ultrasound-FNAB, 2 (28.5%), of which showed Bethesda I, 2 (28.5%) Bethesda II, 1 (14.5%) Bethesda IV and 2 (28.5%) Bethesda VI. In the women group, mean SUVmax was 7.27 (±6.2) and 12 of them had ultrasound-FNAB performed. In this group 2 (16.7%) patients showed Bethesda I, 4 (33.3%) Bethesda II, 1 (8.3%) Bethesda III, 2 (16.7%) Bethesda IV, 1 (8.3%) Bethesda V and 2 (16.7%) Bethesda VI. Four out of the

seventy-one studies (5.4%, all women) showed increased diffuse and focal uptake (mean SUVmax 6.96, 4.6-11.7). Ultrasound-FNAB was performed on 2 cases, showing Bethesda I and II, respectively. Finally, thyroidectomy was performed on 4/71 (5.4%) patients (2 men and 2 women), and 2 more women (2.8%) are on waiting list for surgery. Two papillary carcinoma (one of classic and another one follicular variants) were present in men group. In two women, one corresponded to a oncocytic follicular adenoma, and the other one was papillary carcinoma. CONCLUSIONS: - The SUVmax of hyper-uptake thyroid lesions is too variable and it cannot distinguish between benign and malignant lesions. - Ultrasound-guided FNAB were performed in 26% of patients with thyroid increased uptake with a 16% of tumour prevalence.

P535

Primary mucoepidermoid carcinoma and sclerosing mucoepidermoid carcinoma with eosinophilia of the thyroid gland: a report of two cases, one with aggressive clinical course and other with good prognosis

P. Petranović Ovčariček1, M. Franceschi1, T. Jukić1, N. Dabelić1, B. Krušlin2, Z. Kusić1; 1University Hospital Center "Sestre milosrdnice", Department of Oncology and Nuclear medicine, Zagreb, CROATIA, 2University Hospital Center "Sestre milosrdnice", Department of Pathology "Ljudevit Jurak", Zagreb, CROATIA.

A 33-year old male presented with a rapidly enlarging left thyroid lobe. Neck ultrasonography (US) revealed enlarged asymmetric thyroid gland with the hypoechoic nodule 5cm x 4,7cm x 3,6cm in size, in the left thyroid lobe. The patient was euthyroid and scintigraphy with Tc 99m pertechnetate showed cold nodule in the same lobe.Fine needle aspiration cytology (FNA) revealed a poorly differentiated carcinoma. Total thyroidectomy was performed. Patohistological diagnosis was primary mucoepidermoid carcinoma of the thyroid gland. The tumor was 5,5 cm in size and was not encapsulated; it invaded the surrounding thyroid parenchyma and adjacent soft tissues.Immunohistochemically tumor was negative for thyroglobulin and calcitonin, and positive for cytokeratin.Postoperative neck US did not show suspected mass in thyroid bed or suspected lymph nodes. Four month later, US showed extensive recurrence and ipsilateral neck metastases.Six months after the initial treatment, ipsilateral radical neck dissection revealed 31 positive out of 50 lymph nodes. Computed tomography (CT) performed a month later revealed a large tumor located behind the larynx, compressing the trachea, with retrosternal spread into the mediastinum. The patient underwent radiotherapy (6000 cGy) and achieved partial tumor regression. Three months later progression was detected again and patient died soon after. This is a case, which shows the aggressive clinical course of primary thyroid mucoepidermoid carcinoma.The second case is that of a 65-year old woman who underwent regular endocrinological checkup because of lymphocytic thyroiditis and was under thyroxin therapy. US showed a mildly enlarged and diffusely changed thyroid gland with small nodules in both lobes.Fine needle aspiration cytology of a small nodule (13mm in size), in the left lobe, suggested Hashimoto thyroiditis with mesenhimal cell proliferation.Total thyroidectomy was performed. Patohistological diagnosis was sclerosing mucoepidermpid carcinoma of the left thyroid lobe with eosinophilia. It was 0,9 cm in size, infiltrating the surrounding thyroid parenchyma but not invading the thyroid capsule. Immunohistochemically, the tumor was negative for thyroglobulin and calcitonin, and positive for cytokeratin. Postoperative US have not showed any suspected lymph nodes. She is now a live and with stable disease.This case, unlike the previous one, shows good clinical prognosis of sclerosing mucoepidermoid carcinoma with eosinophilia.

P536

Evaluation of factors effecting health-related quality of life, levels of anxiety and depression in patients with thyroid cancer

G. Ucmak1, D. H. Yalvac2, **B. E. Akkas**1; 1Ankara Oncology Research and Training Hospital Department of Nuclear Medicine, Ankara, TURKEY, 2Ankara Oncology Research and Training Hospital Department of Psychiatry, Ankara, TURKEY.

The aim of this study was to evaluate the factors effecting health-related quality of life (HRQOL), in terms of anxiety and depression, on the follow-up of patients with differentiated thyroid cancer (DTC). **Method**: 518 DTC patients (446F, 72M, mean age: 46.6±11.8, 84% papillary, 16% follicular cancer) underwent total thyroidectomy and radioiodine treatment (RIT). On follow-up all patients were on L-thyroxine treatment. On interview, they were asked to take the European Organization for Research and Treatment of Cancer Quality of Life Questionnaire Core 30 (EORTC QLQ-C30) on routine control. This scale evaluated functional domains, symptom scales and a global health quality of life. Hospital Anxiety and Depression Scale (HADS) was used to measure anxiety and depression levels. Scale results were correlated with social-demographic characteristics where higher scores represented better HRQOL. **Results**: According to HADS, in 31% and 52% of patients' anxiety and depression levels were above threshold, respectively. Male patients had elevated functional-scale scores whereas symptom-scale scores were not. Patients

with a family history of cancer had lower points of physical, role, emotional, cognitive and social function scores (p:0.006), whereas they had higher HADS-A (p:0.001) and HADS-D (p:0.035) scores compared to patients without. Well-educated patients had higher physical and cognitive scores compared to under-educated patients (p:0.003). The latter had higher pain and financial difficulty scores compared to the former. Patients with social support (p:0.015) had better global health scores than single ones. The ones with anxiety and depression levels above threshold had lower global health scores and functional scale scores, higher symptom scale scores compared to others. **Conclusion**: Although disease specific survival is high in DTC, they experience a significantly decreased HRQOL. Anxiety and depression are major determinants of decreased HRQOL. The integration of supportive psychological care into management may increase the HRQOL of patients with DTC.

P537

Descriptive study of 1855 patients with differentiated thyroid carcinoma treated in the period 1998-2012 in 11 hospitals of Catalonia

A. García-Burillo1, D. Villasboas1, C. Zafón1, J. González2, M. Ysamat2, J. Castell1; 1Hospital General Universitari Vall d'Hebron, BARCELONA, SPAIN, 2Mutua de Terrassa, Terrassa, SPAIN.

OBJECTIVE: The Consortium for the Study of Thyroid Cancer (CeCAT) has been created as a working group of the Catalonian Society of Endocrinology and Nutrition (SCEN) of Catalonia. One of the first initiatives of CeCAT was to perform a retrospective descriptive study of the characteristics of patients undergoing Differentiated Thyroid Cancer (DTC) in the period 1998-2012. MATERIALS AND METHODS: To identify the centers with active databases on CDT, to update databases, to select the variables to include, to merge in the databases, and to perform statistical analyses. RESULTS: N: 1855 patients from 11 hospitals in Catalonia, 79.25% women, 20.75% male. Average age: 47.7 ± 15.7 years. Histology: 89% papillary cancer (PTC), 11% follicular cancer (FTC) 11%. Variants: 63% classical, 25% follicular, 12% others. Mean size: 21.5 ± 16 mm (20 ± 14.5 mm on women, 26.6 ± 20.3 mm on men, p = 0.000). Micro carcinomas: 30%. Multifocal: 31%. Invasion: 26%. Thyroiditis: 33%. N1: 39.4% (mean number of nodes: 12.5 ± 12 removed, 3.6 ± 5.6 infiltrated). Radioiodine treatment: 84.2% (117.4 ± 35 mCi). Mean follow-up period: 5.5 ± 3.78 years. Persistence/recurrence: 23.8%. Metastases: 5.78%. Current status: 78.6% with no evidence of disease, 17.6% with persistence/recurrence, 3.76% dead. CONCLUSIONS: This collaborative project has enabled the description of the widest series of DTC patients with follicular lineage in our country. The patient characteristics are similar to those described elsewhere in the world. The typical patient profile in the series is: female, 47 years old, with PTC of classical variant, size of 21.5 mm, treatment by total thyroidectomy plus ablation with 131I and good prognosis (80% cure rate at 5 years).

P538

Correlation Between Day 3 and Day 5 Blood Test Results After Thyrotropin Alfa (Thyrogen) Injection In Differentiated Thyroid Cancer Patients

S. Sager, **Dr**, C. Nisli, O. E. Sahin, R. Akyel, B. Rezavi, J. Nemetyazar, E. Kaymakci, B. Vatankulu, M. Halac, H. Sayman, I. Uslu, K. Sönmezoglu; Istanbul University, Cerrahpasa Medical School, Istanbul, TURKEY.

Objection and Aim:The standart treatment of differentiated thyroid cancer is total thyroidectomy, followed by radioactive iodine-131 therapy and thyroid hormone suppressive therapy. For radioactive iodine therapy TSH>30 is recommended. It is necessary to raise serum TSH levels either endogenously by thyroid hormone withdrawal (THW) or exogenously by administration of recombinant human TSH (rhTSH). Thyrotropin alfa (thyrogen) has many advantages over THW. However one of the main disadvantege of using Thyrogen is I-131 radiation dose to staff. While drawing blood for test, mostly nurses or other staff may derived radiation from the patient. Our aim is to compare day 3 and day 5, TSH, tg and anti-tg levels after thyrogen injection in differentiated thyroid cancers.Method:In this study we had 14 differentiated thyroid cancer patients with a mean age of 50.5±12.3 and Thyrogen was used in all patients. Eight patients dose was 5mCi for ablation control and for whole body imaging. Three patients dose was 150 mCi and 3 of others was 200 mCi. Blood tests were performed on day 3 and day 5 after first day injection. All patients supressed TSH, Tg, Anti-tg, Ft3 and Ft4 levels were performed 1 month before thyrotropin alfa injection. All blood tests were routinely permormed in the same labarotory standards.Results:Our preliminary data shows that day 3 TSH level is always higher than day 5 TSH level after first day thyrogen injection. The mean TSH is level 96.3 for day 3 and 27.9 for day 5. For whole body imaging and ablation control with 5 mCi I-131, Tg and anti-tg levels are nearly the same. So whole body imaging is more important than tg and anti-tg levels in these group of patients. For therapy doses with 150 or 200 mCi, day 5 thyroglobulin levels are higher than day 3. The mean tg level is 137.6 for day 3 and 320.5 for day 5.Conclusion:Exogenous stimulation with recombinant human thyrotropin (rhTSH) is approved for Tg testing or for diagnostic radioiodine scintigraphy in patients on thyroid hormone suppressive therapy. After first day thyrogen injection, day 5 blood test is not necessary. On day 3 before the

5mCi or high dose radiactive iodine application, blood test for tg, anti-tg, TSH, Ft3 and Ft4 can be done. However for ablation control with 5 mCi, if tg and anti-tg level is suspicious, blood test can be repeted on day 5 with whole body imaging.

P539

Vesicular cancer on ectopic lingual thyroid (In a case report and literature review)

S. Choukry, G. Cherkaoui Salhi, s. taleb, a. Guinsi; IBN ROCHD UNIVERSITY HOSPITAL, Casablanca, MOROCCO.

The ectopic thyroid is a result of an abnormal embryological development and/or migration of the thyroid gland. Vesicular carcinoma development within it is extremely rare. The purpose of this study was to report our first experience with vesicular carcinoma on ectopic thyroid lingual. Patient's age was 32 years old with no particular medical history, consulted for a progressive installation of dysphonia. The neck scanner showed a tumor of the epiglottis and the thyroid cartilage. Thyroid scintigraphy showed no uptake at the level of the thyroid associated to a relatively high uptake, above the thyroid lodge. The indication for surgical resection was decided, the patient underwent a tumor and hyoid bone resection. Histological examination confirmed the thyroid origin and the presence of a vesicular carcinoma within it. The tumor showed neither capsular invasion nor vascular emboli. Adjuvant treatment using radioiodine therapy (RIT) has been administered, it was dosed 3,7GBq. Whole body scan using iodine 131 six months after RIT associated to thyroglobulin's level measurement showed a complete remission.

P540

Familial Forms of Papillary Thyroid Carcinoma: a Case Report

S. Kusacic Kuna1, J. Filipovic2, G. Horvatic Herceg1, T. Samardzic1, M. Despot1, D. Huic1; 1Clin. Dept of Nucl Med, University Hospital Centre Zagreb, Zagreb, CROATIA, 2Department of Nuclear Medicine, General Hospital Pula, Croatia, Zagreb, CROATIA.

The majority of differentiated thyroid carcinomas are sporadic, but rare forms of familial tumors are also reported. The entity of familial thyroid non-medullary cancer (NMTC) is defined by the presence of follicular-cell origin tumors in three or more first-degree relatives. It seems that these tumors are often multifocal with local spreading, appear at a younger age with some more aggressive behaviour when compared with sporadic tumors. A hereditary basis for this familial NMTC is assumed, but specific genetic defect remains unknown. The aim of report is to present a case of a family with five papillary thyroid cancer affected members, with comparing the clinical and pathohistologic findings of each patient. A 30-year old women referred for ultrasound examination because of enlarged thyroid lasting one year before. An ultrasound of the neck showed hypoechogenic nodes in both lobes with suspected metastatic nodes in neck region. Fine needle-aspiration biopsy (US-FNAB) revealed papillary thyroid carcinoma in the both thyroid lobes and several metastatic neck lymph nodes. Patient underwent total thyreoidectomy with functional neck dissection of both sides of the neck, and patohistology confirmed diagnosis. During regular follow-up patient complied that her sister living abroad also operated because of same disease and after a while her second 45-year old sister admitted at the Department of nuclear medicine because of thyroid carcinoma. Bearing in mind the possibility of appearance of familial forms of papillary thyroid carcinoma in these three sisters, ultrasound of the thyroid region was suggested in family members and revealed localy advanced thyroid cancer in their 72-aged father as well as in the 24-year old son of one female patient. The extensive imaging material with a detailed demographic data, clinical history and histopathological features of the tumor are presented in this report. Processing of other close family members are in progress. In conclusion, a familial variants of papillary thyroid carcinoma are rare forms of disease that sometimes could be easily overlooked. Detailed anamnestic family data may provide earlier recognition of the familial nature of disease, with faster diagnosis and adequate treatment in family members.

P541

Correlation of perceived social support with psychological distress and the levels of anxiety and depression in differentiated thyroid cancer patients before hospitalization for radioiodine therapy

G. Ucmak1, **B. E. Akkas**1, D. H. Yalvac2, I. Ozer2, O. Yuncu2, A. Caykoylu2; 1Ankara Oncology Research and Training Hospital Department of Nuclear Medicine, Ankara, TURKEY, 2Ankara Oncology Research and Training Hospital Department of Psychiatry, Ankara, TURKEY.

The correlation of hypothyroidism and depression and/or anxiety is well established. Patients with differentiated thyroid carcinoma (DTC) experience a 2-to-4 weeks of hypothyroidism before radioiodine treatment (RIT). Anxiety and depression may exacerbate psychological distress that DTC patients may experience during the hospitalization period for RIT. The aim of this study was to evaluate the psychological status of DTC patients before hospitalization for RIT and examine the correlation of their perceived social support with

psychological distress and the levels of anxiety and depression.**Method**: 143 DTC patients were enrolled in this study. All patients had physical and psychological examinations on the day of hospitalization. We interviewed with the patients and asked them to take a questionnaire which involves social-demographic characteristics as well as patient history. Three validated questionnaires (Distress Thermometer [DT], Hospital Anxiety and Depression Scale [HADS] and The Multidimensional Scale of Perceived Social Support [MSPSS]) were used. The thresholds for validated Turkish version for anxiety and depression subscales were considered as 11 for anxiety (HADS-A) and 8 for depression (HADS-D). The DT consists of an 11-point scale with endpoints labeled 'No distress' (0) and 'Extreme distress' (10). The DT cut-off score was considered as 4 in Turkish cancer patients.Scores higher than thresholds were indicated as distress.**Results**: Depression and anxiety were diagnosed in 13% and 11 % of patients respectively. These patients had higher DT, HADS-A and HADS-D scores and lower social support scale scores compared to patients without psychological problems ($p<0.0001$). Patients with additional health problems and patients with a positive family history of malignant disease had higher DT, HADS-A and HADS-D scores. Patients with higher DT scores above threshold had more familial (p:0.001), emotional (p:0.0001) and physical distress. Patients with HADS scores below threshold had higher social support scores (p:0.002).**Conclusion**: The results of this study demonstrate that these patients have substantial levels of psychopathology at a rate of 24% and these scales used in this study play important role in recognizing risky patients for psychological distress. Higher scores for anxiety and depression and lower scores in perceived social support scales are observed in DTC with different psychological problems. Selecting DTC who are under psycho-pathological risk may demonstrate the need for psycho-oncological support during hospitalization period for RIT. Noticing psychiatric symptoms on time and arranging prompt treatment will therefore also decrease the workload of the treatment team.

P542

Not all DTC patients with N positive disease deserve the attribution "high risk".Contribution of the MSDS trial

A. Vrachimis, C. Wenning, B. Riemann; University Hospital Muenster, Muenster, GERMANY.

Background and Objectives: To investigate if patients having N1a disease are at the same risk with N1b using the collective of the well-defined European prospective Multicentre Study Differentiated Thyroid Cancer (MSDS). Methods: Overall (OS) and event free survival (EFS) were calculated.Cox multivariable regression analysis was performed in order to calculate Hazard ratios (HR). Results: EFS was significantly decreased only in patients with N1b metastasis as compared to N0 patients and became worse when N1a was concomitantly affected. A superior survival in favor of N1a patients as compared to N1b patients with regard to EFS was also observed.The patients having N1a disease showed no differences in the EFS as compared to N0. OS did not differ significantly in any of the groups. There was an increased HR for events with regards to histology,T-stage, tumor size, UICC stag and cervical lymph node metastasis. Tumor size showed a significantly increased risk for OS. Conclusion: Patients with pT3b and pT4a tumors with N1b are of higher risk for relapse, albeit not affecting overall survival. Patients with N1a are of no higher risk. The risk stratification of these patients may be adapted accordingly.

P543

"High stimulated thyroglobulin on first follow up in differentiated thyroid cancer patients is really worrisome?"

M. Gupta, **Jr**.; RAJIV GANDHI CANCER INSTITUTE AND RESEARCH CENTRE, DELHI, INDIA.

Objective: To study clinical significance of elevated stimulated thyroglobulin (sTg) with normal imaging in differentiated thyroid cancer (DTC) patients during first follow-up. Study design and methods: Retrospective analysis of DTC patients with five years follow-up or till recurrence was done. Patients were divided into group 1 (n-35) with disease free status on first follow-up and group 2 (n-29) with high sTg (>2μg/l) with normal imaging. Patients were categorized into low, intermediate and high risk based on pathological & diagnostic 131I scan findings. Statistical Analysis: Histology, stage & risk-categories of both groups were correlated with p value. Best sTg cut off for predicting recurrence was generated by ROC curve. Odd ratio for sTg trend was also analyzed for risk of recurrence in group 2. Independent T test was used for progression free survival (PFS) comparison in groups. Results: No statistical differences were seen in histology, stage and risk category distributions in groups. Group 2 patients with high sTg (Range 81-2.5 μg/ml, Mean 20.5 μg/l) on first follow-up had higher risk of recurrence (odd ratio 4.304) but p value is insignificant (p value 0.090). 86.2 % of group 2 patients showed decreasing trends and 62.1% patient's sTg become normal. Indeed, decreasing trends in sTg reduced the risk of recurrence (odd ratio 1.3939, p value 0.7912). ROC analysis showed sTg > 11μg/l was the best cutoff in predicting recurrence with sensitivity 100% & specificity 56.52%.

High sTg was not associated with lower PFS (p value 0.232), however progressive sTg had significant low PFS (p value <0.005). Conclusion: High sTg with negative DxWBS don't warrant an aggressive diagnostic and therapeutic approach. 86.2% patients showed downward trends with no higher risk of recurrence and lower PFS.

P544

Radiation dose rate of I-131 in patients with differentiated thyroid carcinoma; effect of administrated activity, admission number and TSH level on retention curve

M. Moslehi1, A. Mahmoud Pashazadeh2, **M. Assadi**2; 1Department of Nuclear Medicine, Seyedoshohada Hospital, Isfahan University of Medical Sciences, Isfahan, IRAN, ISLAMIC REPUBLIC OF, 2The Persian Gulf Nuclear Medicine Research Center, Bushehr University of Medical Sciences, BUSHEHR, IRAN, ISLAMIC REPUBLIC OF.

Background: Outcome of the radioiodine therapy of patients with Differentiated Thyroid Carcinoma [DTC] depends on the retention of the activity in the body of the patient. Several factors may influence retention time of radioiodine in the blood and body of these patients. Therefore, the aim of present study was to assess effects of administered activity, serum thyroid stimulating hormone [TSH] level and also patients' admission number, number of times they have been admitted in our nuclear medicine center to receive radioiodine therapy, on the retention of I-131 in the body of patients with DTC.Methods: This study was performed in Nuclear Medicine Department of Seyedoshohada Hospital in 2014. Number of 92 DTC patients, with different TSH levels, was treated with different I-131 activities ranged from 1850 MBq to 7400 MBq. Then post-therapy dosimetry of patients was performed immediately, 6 hours, 12 hours, 24 hours and one week after the administration of I-131.Results: Based on our findings, clearance rate of the activity was higher for those patients who had received higher amounts of I-131 in comparison to those who had received lower activities. Also, those patients who had been admitted for the third time in our nuclear medicine center had higher clearance rate as compared to those who had their first or second admission. Serum TSH level showed no effect on the amount of radioiodine retained in the body of the patients.Conclusions: Administered activity and admission number had significant effect on the retention of I-131 in the body of patients. Any correlation was not observed between serum TSH level and retention of I-131.

P545

Predictive factors for the outcome of I-131 1110MBq ablation therapy in the patients with differentiated thyroid cancer: urinary iodine, serum thyroglobulin, and uptake to thyroid bed

S. Ito1, S. Iwano1, K. Kato2, S. Naganawa1; 1Department of Radiology, Nagoya University Graduate School of Medicine, Nagoya, JAPAN, 2Deparment of Radiological and Medical Laboratory Sciences, Nagoya University Graduate School of Medicine, Nagoya, JAPAN.

Aim: In Japan, which is surrounded by sea, people take much iodine for daily meals. Low iodine diet ahead of radioiodine remnant ablation therapy (I-131 ablation) is essential for Japanese patients with differentiated thyroid cancer (DTC). The aim of this study was to evaluate the effectiveness of the measurement of urinary iodine concentration in I-131 ablation. Additionally, we evaluated the influence of the intensity of radioiodine uptake to thyroid bed and serum thyroglobulin (Tg) level on I-131 ablation. Methods: Forty-seven consecutive DTC patients (18 males, 29 females; age 55±11 years old) who underwent I-131 ablation with a dose of 1110MBq enrolled in this prospective study. Patients took low iodine diet for two weeks with two methods: self-management diet, or rigorous diet with market-sold food. Urinary iodine concentration and Tg level were measured on the day of I-131 ablation. The intensity of uptake was visually evaluated and classified into three categories: very high, high, and low. Post-therapeutic scintigraphy was performed in six to eight months after I-131 ablation, and absence or residual of I-131 accumulation to thyroid bed was determined. Results: Urinary iodine concentration before the beginning of low iodine diet was 334.5 ± 508.5 μg/L. On the day of I-131 ablation after continuation of low iodine diet, urinary iodine concentration of rigorous diet group (56.0 ± 26.3μg/L) indicated lower value than that of self-management diet group (104.90 ± 141.83μg/L), but there was no significant difference between both groups (p=0.08). Thirty-one cases (66%) showed absence of uptake (absence group), and sixteen cases (34%) showed residual of uptake (residual group) with the post-therapeutic scintigraphy. Urinary iodine concentrations of absence and residual groups were 93.4±72.7μg/L and 68.6±54.5μg/L, respectively. Tg levels of absence and residual group were 29.8±82.6 ng/mL and 38.0±81.8 ng/mL, respectively. There were no significant difference between absence and residual groups in both urinary iodine concentrations and Tg levels (p=0.25 and 0.76, respectively). Six cases (13%) showed low uptake of radioiodine to thyroid bed in scintigraphy performed in I-131 ablation, and all of them were included in absence group. However, no significant difference was observed between absence and residual groups in uptake to thyroid bed (p=0.08). Conclusion: Although strict low iodine diet is indispensable

for Japanese DTC patients in I-131 ablation, the current Japanese method of low iodine diet was shown to be sufficient to prepare for I-131 ablation. Low I-131 uptake of thyroid bed suggested the successful outcome of I-131 ablation.

P34 - Monday, October 12, 2015, 4:00 PM - 4:30 PM, Hall 3 – Poster Exhibition
Clinical Oncology: Brain

P546

Correlation of Standardized Uptake Value Derived Indices with Tumoral Aggressiveness of Gliomas in Static 18F-FDOPA PET: Use in Clinical Practice

l. Janvier, **Jr**., A. Verger; CHU Nancy, Nancy, FRANCE.

Purpose. Glioma grading is necessary for prognostic evaluation and optimal treatment decisions. The aim of this study was to establish whether a correlation between 18F-FDOPA uptakes with tumor grade was observed and to determine which of the SUV derived indices was the best correlated. Methods. Thirty-one patients were retrospectively included (aged 36.8 ± 12.1 years) including 21 proven low-grade tumors due to histology, imaging and clinical follow up and 10 histologically proven high-grade tumors. Static PET acquisitions were post-reconstructed between 10th and 30th minute after injection of 18F-FDOPA. Regions of interest (ROI) of 20 mm were applied to tumors and isocontoured volumes were defined at levels of 50 and 80% of the peak intensity voxel. Background was quantified with 30 mm diameter ROIs on contralateral striatum and centrum semi-oval. Tumoral uptake was evaluated with standardized uptake value (SUV) derived indices: SUVmax, SUVmean, SUVmean of isocontoured volume, tumor/striatum (T/S) and tumor/normal brain (T/N) SUVmax and SUVmean ratio. Results. All the SUV derived indices tested were significantly correlated with tumor grade, considering low-grade and high-grade groups ($p< 0.05$), except for the SUVmean 50%. The 2 best-correlated indices were SUVmean T/N and SUVmean T/S, with correlation coefficients of 0.561 and 0.522 respectively. Receiver-operating characteristic analysis defined optimal thresholds of 1.33 and 1 for sensitivity and specificity of 71% and 100% and 67% and 100%, respectively. Conclusions. 18F-FDOPA PET SUV derived indices are routinely available information that enables accurate discrimination of low-grade and high-grade gliomas. The best-correlated indices were SUVmean T/N and SUVmean T/S with thresholds of 1.33 and 1.

P547

Role of 11C-Methionine PET for the Molecular Characterization of Primary Brain Tumours Eligible for Surgery

E. Lopci, M. Riva, L. Bello, L. Olivari, F. Raneri, M. Rodari, A. Chiti; Humanitas Clinical and Research Hospital, Rozzano (Milano), ITALY.

Background and Aim: biological characterization of primary brain tumours is becoming increasingly relevant, thus determining the future implementation of specific molecular markers into glioma classification. The possibility to determine noninvasively these characteristics by using molecular imaging is greatly appealing. The aim of our study was to investigate the role of 11C-methionine PET imaging in molecular characterization of primary brain tumours, with as specific focus on patient outcome. Materials and Methods: for the analysis we enrolled 85 consecutive patients (M:F=57:28; mean age 46, range 17-77 years) affected by pathology proven gliomas and referred to our Institution for tumour resection. Before surgery, patients underwent 11C-methionine PET-CT, performed according to standard procedure. In all cases semi-quantitative and quantitative analyses were obtained by taking into consideration SUVmax, SUVratio, metabolic tumour volume (MTV) and tumour burden (MTB). These data were subsequently correlated to disease outcome, expressed in terms of progression-free survival (PFS), and compared to other clinical and biological information obtained from pathology. All patients were followed up for a median period of 16.8 months. Results: according to WHO classification, we analysed 34 low-grade gliomas (LGG: 3 grade I & 31 grade II), and 51 high-grade gliomas (HGG: 32 grade III & 19 grade IV). All PET parameters considered showed a statistically significant association to tumour grade, with HGG having a higher SUVmax, SUVratio, MTV and MTB compared to LGG ($p<0.01$). Based on semi-quantitative analyses, we determined a statistically significant correlation between SUVmax and SUVratio versus IDH1 mutation ($p=0.002$ and 0.001, respectively), but not versus 1p/19q co-deletion and MGMT promoter methylation. When considering disease outcome, we identified as prognostic factors to longer PFS tumour grade, MIBI%, IDH1 mutation, 1p/19q co-deletion, SUVmax and SUVratio ($p<0.05$). On multivariate analysis, the Cox regression did identify a potential independent prognostic factor IDH1 mutation ($p<0.05$). Conclusions: molecular characterization on 11C-methionine PET significantly correlates with histological grading in primary brain tumours and IDH1 mutation status. With respect to disease outcome, tumour grading, MIBI%, IDH1 mutation, 1p/19q co-deletion, SUVmax and SUVratio resulted prognostic factors to PFS, with IDH1 mutation being a potential independent predictor to outcome in this cohort of patients candidate to surgery.

P548

Comparison of PET/CT and Difusion/Perfusion Weighted Magnetic Resonance Imaging Findings in Malignant Brain Tumors

M. Sipahi; BAKIRKOY DR. SADI KONUK EDUCATION AND RESEARCH HOSPITAL, ISTANBUL, TURKEY.

In this study, our aim was to determine if there was a relationship between the metabolic activity obtained from 18F FDG PET imaging (SUVmax) and diffusion coefficient (ADC) in diffusion weighted magnetic resonance imaging (DW-MRI) and relative cerebral blood volume (rCBV) obtained from perfusion magnetic resonance imaging in malignant brain tumors; to investigate the contribution of FDG PET imaging in differentiating grade 4 glioblastoma from metastatic cerebral mass lesions. A retrospective analysis was performed in 20 cases, 9 male and 11 female, who presented to Akdeniz University Medical Faculty Hospital Neurosurgery clinic with intracranial mass lesion diagnosis/pre-diagnosis. Patients who had conventional MR and FDG PET/CT images were included in the study. Patients who were operated previously, however, had no recurrence or residual mass in subsequent examinations and patients with extra axially located mass lesions were excluded from the study. A statistically significant negative correlation between the ADC value of the primary lesion and the ratio of metabolic activity in the late images to the metabolic activity of contralateral cortex (GSUV/ GSUVK) was determined ($p<0.05$, $r=-0.52$). Also, a statistically significant negative correlation was found between the perfusion of primary tumor (rCBV) and the percentage changes in SUVmax values of the mass in the late images (GSUV- ESUV/100* ESUV) ($p<0.01$, $r=-0.63$). Besides these, it was observed that late imaging has a diagnostic value in differentiating grade 4 glioblastoma from metastatic cerebral mass lesions (100% sensitivity, 75% specifity). According to the results obtained from our study, FDG PET provides an additional contribution to intracranial mass lesion diagnosis, and we believe that specially late imaging should be performed in brain lesions.

P549

Correlation of 4'-[Methyl-11C]-Thiothymidine Uptake with Ki-67 Immunohistochemistry in Patients with Newly Diagnosed and Recurrent Gliomas: Comparison with 11C-Methionine Uptake

Y. Yamamoto1, K. Tanaka1, H. Yamamoto1, N. Kudomi1, T. Hatakeyama1, J. Toyohara2, Y. Nishiyama1; 1Kagawa University, Kagawa, JAPAN, 2Tokyo Metropolitan Institute of Gerontology, Tokyo, JAPAN.

A novel radiopharmaceutical, 4'-[methyl-11C]thiothymidine (11C-4DST), has been developed as an in vivo cell proliferation marker based on the DNA incorporation method. The purpose of this study was to evaluate 11C-4DST uptake in patients with newly diagnosed and recurrent gliomas and to correlate the results with proliferative activity, in comparison with L-[methyl-11C]-methionine (11C-MET). Methods: 11C-4DST and 11C-MET PET/CT was investigated in 36 lesions of 33 patients, including 23 with newly diagnosed gliomas and 13 with recurrent gliomas that had been treated previously. The standardized uptake value (SUV) was determined by region-of-interest analysis. The maximal SUV (SUVmax) for tumor (T) and the mean SUV for contralateral normal brain tissue (N) were calculated and T/N ratio was determined. Proliferative activity as indicated by the Ki-67 index was estimated in tissue specimens. Results: 11C-4DST and 11C-MET PET/CT detected 33 and 35 of 36 brain gliomas, respectively. In newly diagnosed gliomas, linear regression analysis indicated a significant correlation between SUVmax ($r=0.48$, $P<0.03$) and T/N ratio ($r=0.45$, $P<0.04$) using 11C-4DST and the Ki-67 index. In recurrent gliomas, no significant difference between SUVmax and T/N ratio using 11C-4DST and the Ki-67 index. In newly diagnosed and recurrent gliomas, no significant difference between SUVmax and T/N ratio using 11C-MET and the Ki-67 index. Conclusion: 11C-4DST PET/CT seems to be useful in the noninvasive assessment of tumor proliferation in newly diagnosed glioma compared with 11C-MET.

P550

PET/CT Using [11C]Methionine in Differential Diagnosis of Intramedullary Tumors from Non-neoplastic Spinal Cord Lesions

T. Skvortsova, Z. Savintseva, L. Prakhova, D. Zakhs, S. Medvedev; N. P. Bechtereva Institute of the Human Brain of Russian Academy of Sciences, Saint-Petersburg, RUSSIAN FEDERATION.

The aim of the study was to evaluate the ability of PET/CT with [11C]methionine (PET/CT-Met) to differentiate between intramedullary tumors and non-neoplastic lesions of spinal cord. Materials and methods. PET/CT-Met was performed in 20 patients (median age 39 years) with suspected intramedullary tumor according to results of previous contrast-enhanced MRI. Final diagnosis included primary or recurrent intramedullary gliomas (14), glioblastoma metastasis (1), recurrent secondary lymphomas of the brain and spinal cord (1). Other 4 patients suffered from ischemic myelopathy associated with dural spinal AVM (1), LETM (2), Sjögren's syndrome involving spinal cord (1). Diagnosis was proven histologically in 7 patients with glioma (low-grade-4, high-grade- 3) or by clinical-radiological findings (n=13).

Additionally in 7 patients diffusion-tensor imaging (DTI) was performed to assess white matter fiber tracts. The analysis of PET/CT images was based in addition to the visual assessment on semiquantitative calculations as the ratio of the SUVmean of the lesion to the that in the intact spinal cord. Results. MRI demonstrated intramedullary contrast-enhanced masses in 17 patients and nonenhancing mass-lesions in 3 patients. All tumors except 2 were well differentiated from spinal cord by visual inspection of fused PET/CT images as the lesion with increased tracer accumulation. The mean [11C] methionine uptake index was 3,3±1,2. The SUV ratio was variable in all cases without the significant difference between benign and malignant tumor type. Absolute magnitudes of SUV in unaffected spinal cord significantly differed among patients due to differences in time interval between injection and PET/CT scanning (range 10-30 min.) so SUV in the lesions had no diagnostic value. In PET-positive tumors the increased [11C] methionine accumulation was observed in the part of the lesion which was almost compatible with contrast enhancement on MRI. The nonenhancing intramedullary gliomas (n=2) were characterized by negative [11C]methionine uptake. In 3 from 4 patients with non-neoplastic myelopathy [11C]methionine accumulation did not differ from the unaffected part of the spinal cord. Only ischemic vasculopathy associated with Sjögren's syndrome demonstrated slightly increased [11C]methionine uptake (UI=1,8). Tracts of the spinal cord rounded the tumor nodules and were expanded in all other myelopathies. In tumors with negative [11C] methionine uptake MR-tractography results were crucial to confirm the neoplastic nature of the lesion. Conclusion. In cases of complicated differential diagnosis between neoplastic and non-neoplastic intramedullary spinal cord lesion PET/CT with [11C]methionine and diffusion-tensor MR imaging can provide significant additional information.

P551

FET PET in the evaluation of indeterminate brain lesions on MRI: differentiating glioma form other non-neoplastic causes

D. L. Chan, G. P. Schembri, M. Back, D. L. Bailey, P. J. Roach, H. Wheeler, R. Cook, J. Parkinson, A. Lee, D. Jayamanne, J. Drummond, **E. Hsiao**; Royal North Shore Hospital, St Leonards, AUSTRALIA.

Aim: FET PET had demonstrated excellent diagnostic performance in the assessment of cerebral gliomas. The study aims to investigate the clinical utility of FET PET in differentiating glioma from non-neoplastic lesions such as cortical dysplasia or demyelination. Methods: We reviewed 172 patients who underwent FET scanning at Royal North Shore Hospital between February 2011 and April 2014. Patients without prior histological diagnosis of CNS malignancy were identified. Histology (if available) and follow-up data were obtained. All studies were acquired on a Siemens Biograph mCT following administration of ~150MBq FET with 20-minute dynamic and 10-minute static acquisitions. Results: 20 patients had brain lesions on MR imaging (15 cerebrum, 2 corpus callosum, 2 brainstem, 1 cerebellum) which were of uncertain aetiology with differentials including glioma, demyelinating plaque or cortical dysplasia. Median age was 53 years and the clinical presentations included seizures (5), headache (4), dizziness (3) and visual changes (2). The patients were followed up for a median of 113 days. 8 out of 20 patients (40%) demonstrated increased uptake on FET PET. Five underwent surgery/biopsy which revealed three low grade gliomas, one glioblastoma multiforme and one anaplastic oligodendroglioma. The rest of FET positive patients were observed; two remained well and one commenced temozolomide for a presumed high-grade glioma (clinical and radiological progression). The 12 FET negative patients did not undergo biopsy. Of these, six had stable changes on MRI. Two had resolving changes on repeat MRI with clinical diagnoses of stroke and seizure. Three are clinically and radiologically stable. All have remained well without progression except for one patient who died after two months of progressive neurological deterioration. The patient was suspected to have high-grade glioma with neither biopsy nor autopsy confirmation. 15 patients underwent FDG PET within 28 days of FET PET. Two (13%) showed increased uptake on FDG PET. These patients were diagnosed on biopsy with anaplastic oligodendroglioma and glioblastoma multiforme respectively. All 8 patients with normal FDG and FET PET have remained clinically well with stable lesions on observation. Conclusions: FET PET demonstrates a high positive predict value for glioma in patients with indeterminate brain lesions on MRI. The combination of negative FET and negative FDG PET scans predicts an indolent clinical course. The results suggest that FET PET may have a potential role in guiding surgical management in this cohort.

P552

Use of 11C-methionine PET for the immunohistochemistry characterization of gliomas

A. Mestre-Fusco1, F. Alameda2, M. Suárez-Piñera1, S. Mojal3, M. Martínez-Garcia4, G. Conesa5, Neurooncology PSMar Group; 1Nuclear Medicine department. Hospital del Mar. Parc de Salut Mar, Barcelona, SPAIN, 2Pathology department. Hospital del Mar. Parc de Salut Mar, Barcelona, SPAIN, 3Institute of Medical Research IMIM. PRBB, Barcelona, SPAIN, 4Neurooncology department. Hospital del Mar. Parc de Salut Mar, Barcelona, SPAIN, 5Neurosurgery department. Hospital del Mar. Parc de Salut Mar, Barcelona, SPAIN.

Introduction: 11C-methionine PET (MET PET) has been used to study tumoral gradation, cell proliferation and perfusion in gliomas. **Aim**: Our aim was to compare metabolic activity of MET PET and immunohistochemical biomarker of tumor aggressiveness in glioma: Expression analysis of p53, p16, WT1, Beta-catenin, CD34, CD44 and EGFR. **Material and methods**: MET PET was performed in nineteen patients clinically and MRI (3-Tesla equipment) suggested of glioma and confirmed by surgery (n = 13 males, 29-75 years). PET MET images were analyzed visually and quantitatively (ROI) and Ratio T/N was calculated of each lesion (SUVmax tumour/SUVmax or SUVavg normal tissue on contralateral cortex regions). An immunohistochemical study of expression of tumor aggressiveness markers was calculated (%) including: p53, p16, WT1 (suppression), CD44 (activation), vascular CD34 and Beta-catenin (perfusion) and EGFR (growth). Gliomas were classified as low or high grade (WHO classification) using a cut-off point of Ratio T/N = 2.07. In case of Ratio T/N > 2.07 glioma was classified as high grade. Mean, SE and statistical significance between Ratio T/N more or less than 2.07 was estimated for each immunohistochemical variables (Mann-Whitney test, $p < 0.05$). **Results**: One patient with negative MET PET was diagnosed as gliosis. Five patients with Ratio T/N < 2.07 were diagnosed as low grade glioma (II) and one patient as high grade (III). Twelve patients diagnosed as high grade glioma showed Ratio T/N > 2.07 (one anaplastic astrocytoma and eleven glioblastomas). A significant correlation between Ratio T/N < 2.07 and low expression of suppression markers p53, p16 and WT1 of gliomas was observed. A large expression variability of these markers was observed in case of Ratio T/N > 2.07. A lineal correlation between vascular CD34 expression in case of low glioma or Ratio T/N < 2.07 was observed. No differences were found between expression of Beta-catenin, CD44 and EGFR and PET Ratio T/N. **Conclusion**: Metabolic activity of MET PET is correlated with a lower expression of immunohistochemical suppression markers in low grade gliomas.

P553

18F-fluorocholine PET/CT in the assessment of brain primary tumors

A. Montes1, A. Fernandez1, V. Camacho1, J. Craven-Bartle2, C. De Quintana3, O. Gallego4, R. Jaller1, A. Flotats1, M. Estorch1, D. Lopez1, I. Carrio1; 1Nuclear Medicine Department. Hospital de la Santa Creu i Sant Pau, Barcelona, SPAIN, 2Radiation Oncology Department. Hospital de la Santa Creu i Sant Pau, Barcelona, SPAIN, 3Neurosurgery Department. Hospital de la Santa Creu i Sant Pau, Barcelona, SPAIN, 4Oncology Department. Hospital de la Santa Creu i Sant Pau, Barcelona, SPAIN.

Purpose:Diagnosis of brain primary tumors can be challenging, and the usefulness of 18F-FDG PET/CT is limited, principally in low grade tumors. This study was aimed to evaluate the utility of 18F-fluorocholine in the assessment of different brain primary tumors.Materials and methods:Brain PET/CT with 18F-fluorocholine was performed in 13 patients. Primary brain neoplasm was suspected in 3 patients and the other 10 patients were studied in order to assess recurrence of a known brain tumor. Pathological tracer uptake was evaluated to study the benign or malignant nature of the lesions. Results were confirmed by histology (6 patients) and/or by clinical and conventional imaging follow-up (7 patients).Results:18F-fluorocholine uptake suggesting malignancy was observed in 10 of 13 patients. Three patients did not present with 18F-fluorocholine uptake.Positive PET/CT patients were histologically diagnosed with: astrocytoma grade IV (3 patients), astrocytoma grade III (1 patient), oligodendroglioma grade III (1 patient), oligodendroglioma grade II (1 patient with negative 1p/19q deletion), oligoastrocytoma grade II (1 patient), gliomatosis cerebri (1 patient), meningioma (1 patient) and brain abscess (1 patient). Significant differences in 18F-fluorocholine uptake with regard to histological tumor type were not observed.One patient without PET/CT pathological findings was finally diagnosed with oligodendroglioma grade II, with positive 1p/19q deletion. The other PET negative patients, who had a previous history of oligodendroglioma grade III and oligoastrocytoma grade II, did not show suspicion of recurrence 9 months after performing the PET studies.Conclusions:This preliminary study indicates that 18F-fluorocholine PET/CT may be helpful in the initial assessment, recurrence or progression of primary brain neoplasms, independently of histology or tumor grade. A possible association of 18F-fluorocholine PET negativity with positive 1p/19q deletion, a known genetic marker of favorable prognosis, is suggested.

P554

Differentiation of Pseudoprogress and Actual Progress in Glioblastoma Multiforme by Textural Inhomogeneity Parameters in [18F] -Fluoroethyltyrosine PET

Z. Khurshid1, S. Kebir2, U. Herrlinger2, L. Papp3, N. Zsótér3, F. Gaertner1, M. Essler1, R. Bundschuh1; 1Department of Nuclear Medicine, Uniklinikum Bonn, Bonn, GERMANY, 2Center for Neuro-oncology, Department of Neurology, Uniklinikum Bonn, Bonn, GERMANY, 3Mediso Medical Imaging Systems, Budapest, HUNGARY.

Objective: The main objective of the study was to differentiate between pseudoprogress (PSP) from actual progress in patients of glioblastoma multiforme (GBM) by studying the textural inhomogeneity parameters in [18F] -Fluoroethyltyrosine

PET (FET-PET). GBM being the commonest and one of the most aggressive primary brain tumors, often shows the phenomenon of PSP after chemoradiotherapy. For therapy decisions and therefore overall survival it is crucial to differentiate between PSP and real progress as early as possible.Materials and methods: 21 patients with histopathologically confirmed GBM and having suspected pseudoprogress were included in the study. Retrospective analysis was performed. For entire analysis InterView FUSION, Mediso system was used. 3D volumes of the lesions (VOIs) were manually delineated in FET-PET. In addition, a semiautomatic segmentation in FET-PET was performed based on background activity (estimated in 5 regions of interest (ROIs), with a fixed diameter of 15 mm placed in the normal cortex, tumor delineation cutoff was taken as 1.6 times the mean value of background ROIs). In addition to conventional PET parameters, 17 PET based heterogeneity parameters were also determined. Results obtained were then compared with clinical outcomes.Results: In differentiation of PSP versus actual progress the uptake of FET remarkably showed a negative predictive value of 100%. The positive predictive value was calculated to be 47%. In quantification several heterogeneity parameters showed statistically significant ability to differntiate PSP versus actual progress e.g., Deviation (0.001), COV (0.005), entropy (0.003), homogeneity (0.015), contrast (0.021), size and intensity variation (0.007), and complexity (0.041) in comparison to the conventional PET parameters.Conclusions: It was concluded that the FET-PET shows potential for early differentiation between PSP and real tumor progress, being a good indicator of negative predictive value. Various heterogeneity parameters showed the ability to further differentiate FET-PET uptake to improve the positive predictive potential. These results can be verified further by taking a larger patient population as study group and analyzing the delayed outcomes of patients.

P555

Usefulness of Preoperative Dual-Phase thallium-201 SPECT and Imaging Fusion with SPECT and MRI in Predicting Histopathology of Meningiomas and Hemangioblastomas

A. Abe1, S. Abe2, S. Oya1, T. Matsui1; 1Saitama Medical University, Kawagoe, JAPAN, 2Mitsui Memorial Hospital, Tokyo, JAPAN.

Background and Aim: Both meningiomas and hemangioblastomas are intracranial hypervascular tumors demonstrating tumor stains on digital subtraction angiography (DSA) with high frequency. The preoperative differential diagnosis between them is still a challenge, even after utilizing diagnostic imaging methods such as computed tomography (CT), magnetic resonance imaging (MRI) and DSA. The aim of this study is to investigate the usefulness of preoperative thallium-201 chloride brain single photon emission tomography (Tl-SPECT) in predicting the histopathology of meningiomas and hemangioblastomas. Materials and Methods: In this retrospective study, histopathologically proven 67 cases of meningiomas (3 with angiomatous, 6 with fibrous, 16 with transitional, 30 with meningothelial, 6 with atypical and 6 with unknown menigiomas) and 8 cases of hemangioblastomas were reviewed. The early-phase images at 15 minutes after the injection of 111MBq of thallium-201 chloride and the delayed-phase images at 3 hours after the injection and T2 signal weighted images (T2WIs) of MRI were obtained before neurosurgical resection. The regions of interest (ROI) were precisely placed on the uptake of the tumors (T) and contralateral normal brain parenchyma as background uptake (N) on the fusion images with Tl-SPECT and T2WIs of MRI. The thallium uptake indices of the early-phase imaging (ER) and the delayed-phase imaging (DR) were defined as follows: thallium uptake index = mean counts per pixel in T / mean counts per pixel in N. The retention indices (RI) of Tl-SPECT were calculated as follows: RI = (DR - ER) / ER. Results: ER, DR and RI values of hemangioblastomas (4.69±1.70, 1.58±0.40, -0.64±0.12) were significantly lower than those of meningiomas (12.33±7.33, 5.41±3.03, -0.49±0.21), respectively (P = 0.0064, 0.0006 and 0.0523, respectively). With the combination of ER less than 7.3 and RI between -0.8 and -0.4, the sensitivity, specificity and accuracy for diagnosing hemangioblastoma were 100%, 91% and 92%, respectively. DR and RI of angiomatous meningiomas were significantly lower than those of the other pathological types of meningiomas (P = 0.0194, 0.0069, respectively). No significant differences of ER, DR and RI were observed among the other histopathological groups of menigiomas including atypical meningiomas. Conclusion: The dual-phase imaging of Tl-SPECT and ROI analysis using imaging fusion with Tl-SPECT and MRI are useful to differentiate the hemangioblastomas from meningiomas preoperatively, thus reducing the risk of the invasive DSA.

P35 - Monday, October 12, 2015, 4:00 PM - 4:30 PM, Hall 3 – Poster Exhibition

Clinical Oncology: Head & Neck

P556

FDG PET/CT and MRI in oral cavity carcinomas: anatomical considerations

H. Munechika, T. Saginoya, Y. Miura, S. Takekawa, K. Seto, K. Watanabe; Southern Tohoku General Hospital, KORIYAMA, JAPAN.

Introduction and purpose: Anatomical structures of the oral

cavity are prone to be defective in demonstration in FDG PET/CT because of streaky artefacts caused by metals of the teeth. The oral cavity carcinomas are FDG avid. However, MRI is expected to have an additional imaging modality to FDG PET/CT for adequate evaluation of the oral cavity carcinomas. The aim of this study is to find the anatomical landmark of the oral cavity for comprehending appropriately the location and extent of carcinomas in PET/CT. Subjects and methods: In carcinomas of the tongue root, sublingual glands, retromolar trigone, gingiva, buccal mucous membrane, oral floor mucous membrane and soft palate, the anatomical structures adjacent to carcinomas are re-evaluated retrospectively in the axial, coronal and sagittal images of FDG PET/CT and MRI in order to find the useful anatomical landmark of the oral cavity. Results and discussion: The geniohyoid muscle, myohyoid muscle, genioglossus muscle, hyoid bone, submandibular glands, and sublingual glands are useful for anatomical landmarks in evaluation of carcinomas locating the inferior region of the oral cavity. The mandibular angle, buccinator muscle, medial pterygoid muscle, masseter muscle and digastric muscle are useful for anatomical landmarks in evaluation of carcinomas locating the lateral region of the oral cavity. Carcinomas of the superior or posterior region of the oral cavity can be evaluated by FDG PET/CT alone without help of MRI. Conclusion: Comprehension of the anatomical landmark in MRI is useful for evaluation of FDG PET/CT in some cases with the oral cavity carcinomas. The representative cases are presented.

P557

Semi-quantitative analysis of FDG-PET/CT images to assess residual nodal disease in patients with squamous cell carcinoma of the head and neck (HNSCC) after (chemo)radiotherapy (CRT): can it improve accuracy and prognostic value?

N. Helsen1,2, T. Van den Wyngaert1,2, L. Carp1,2, D. Van den Weyngaert1,3, S. Stroobants1,2; 1University of Antwerp, Wilrijk (Antwerp), BELGIUM, 2Antwerp University Hospital, Edegem, BELGIUM, 3Middelheim hospital, Antwerp, BELGIUM.

Background: FDG-PET/CT has been proven effective in detecting residual disease in patients with HNSCC after CRT. The aim of this study is to investigate whether the accuracy and prognostic value of this technique can be improved by using semi-quantitative parameters based on the standardized uptake value (SUV). Patients and Methods: Image data from HNSCC patients receiving whole body FDG-PET/CT for assessment of disease after completing CRT were retrospectively analyzed. The following SUV based parameters of all residual lesions on PET were measured: the maximum SUV_{max}, SUV_{peak}, and the SUV at 50% (SUV_{50}) and 90% (SUV_{90}) of the maximum. In absence of nodes on PET the paraspinal muscle uptake was used. Background region of interest (ROI) included the liver, aortic arch, and the trapezius and paraspinal muscles, and were employed to calculate relative uptake ratios. The reference standard was histological confirmation when available, otherwise 1 year negative follow-up, time of death or confirmation by subsequent imaging was used. The diagnostic accuracy of absolute and relative SUV values were compared using ROC analysis. Kaplan-Meier and multivariable Cox regression were used to study survival. Results: 129 scans from 128 patients were included (105 patients had node involvement at diagnosis). 22/129 FDG-PET/CT scans were positive for disease after therapy, while disease, according to the reference standard, was present in 25 patients. ROC analysis identified the SUV_{90} value (AUC=0.949; cutoff 2.88; SD=2.16) and the ratio of SUV_{90}/trapezius muscle(SUV_{90trap}), (AUC=0.970; cutoff 3.42; SD=3.08) as the most performant absolute and relative parameter, respectively. The sensitivity of the qualitative assessment was 76.0% (95% CI: 54.9-90.6%), compared to 88.0% (95% CI: 68.8-97.3%, p=0.25) and 92.0% (95% CI: 73.9-98.8% p=0.125) for the absolute and relative SUV parameter, respectively. Less variance was observed for the specificity (range 97.1-98.1%). All absolute and relative SUV parameters were significantly associated with disease free, disease specific, and overall survival. In contrast, none of the baseline characteristics (stage, age, therapy, lymph involvement) were prognostic. The adjusted hazard ratios of SUV_{90} and SUV_{90trap}, were 1.9 (95% CI: 1.5-2.4, p<0.001) and 2.0 (95% CI: 1.5-2.5, p<0.001) meaning that every increase of SUV_{90} or SUV_{90trap} with one standard deviation was associated with an approximate twofold increase in the hazard of death. Conclusions: The current study indicates that the use of a semi-quantitative measures could reduce the number of false negative FDG-PET/CT scans after (chemo)radiotherapy and contributes clinically meaningful prognostic information.

P558

Meta-analysis of 18F-FDG PET/CT for diagnosis of residual/recurrent nasopharyngeal carcinoma after radiotherapy

H. Zhou, Y. Zhou, L. Li; West China Hospital, Chengdu, CHINA.

Objective: To assess the diagnostic value of 18-fluoro-2-deoxyglucose positron emission tomography/computed tomography (18F-FDG PET/CT) in detecting residual/recurrent nasopharyngeal carcinoma. Method: The literatures published between January 1990 and September 2013 were searched in PubMed, EMBASE, EBSCO, Web of Science, CBM, CNKI, VIP and Wanfang databases. Two researchers

independently selected studies, extracted data and assessed the quality of included studies according to the QUADAS tool. Summary sensitivity, specificity, diagnostic odds ratios (DOR), and receiver-operating characteristic (SROC) curves were obtained using Meta-Disc software. Subgroup analysis was also conducted. Result: Twenty-six studies were included in this meta-analysis, involving 1203 patients. The pooled sensitivity, specificity and diagnostic odds ratios (DOR) were 0.92 [95% confidence interval (CI), 0.89-0.94], 0.87 (95% CI, 0.84-0.90) and 51.10 (95% CI, 34.29-76.15), respectively. The area under the curve (AUC) and Q* index estimate for PET/CT were 0.9494 and 0.8897, respectively. The results of subgroup analysis showed no significant difference between subgroups(P>0.05). Conclusion: In a word, 18F-FDG PET/CT performed well for diagnosis of residual/recurrent nasopharyngeal carcinoma, with relatively high sensitivity and specificity.

P559

Diagnostic performance of time-of-flight system to detect neck small lymph node using 18F-FDG PET/CT

H. Saito, A. Yamane, S. Imai, E. Orita, K. Hakozaki, K. Akiyama, K. Ishihara, S. Kumita; Nippon Medical School, Bunkyo-ku, Tokyo, JAPAN.

Objective:It is difficult to differentiate FDG concentration of metastatic lymph nodes from that of inflammatory lymphadenopathy, especially assessing small lymph node less than 1 cm. In head and neck cancer, it is critical for therapeutic strategy whether the presence or absence of metastatic lymph node. In head and neck cancer, 18F-FDG PET/CT has been reported to have less than 50% sensitivity to diagnose N category in the cases with missed lymph nodes by palpation. Time-of-flight (TOF) PET technology has improved signal-to-noise ratio in whole-body oncologic application. Few studies, however, have elucidated the impact of TOF on diagnostic performance to discriminate malignant uptakes from benign ones in small nodes.The purpose of this study was to compare the diagnostic performance of metastatic lymph node less than 1cm in cases with pharyngeal cancer between TOF and non-TOF (3D-RAMLA) PET systems.Materials and Methods:In this study, total 96 small neck lymph nodes consisted of 49 metastatic lymph nodes in 35 patients with pharyngeal cancer and 47 reactive lymph nodes confirmed in 29 healthy cases undergoing 18F-FDG PET/CT for self-health care. All lymph nodes were from 5mm to 10mm in long-axis diameter. The TOF and non-TOF images were reconstructed using the same PET data and the maximum of the standardized uptake value (SUVmax) was measured based on region of interest, respectively. The area under the ROC curve, sensitivity and specificity to differentiate metastasis from reactive change were compared between TOF and non-TOF images.ResultThe SUVmax of metastatic lymph nodes was 4.02±1.02 in TOF and 3.96 ±1.06 in non-TOF. On the other hand, reactive lymphadenopathy using TOF and non-TOF showed 2.62±0.48 and 2.40 ±0.43 of SUVmax, respectively. The SUVmax of metastatic lymph node was significantly greater than that of reactive lymphadenopathy in either image ($p< 0.01$). Although there were not significant differences of the AUC between TOF and non-TOF, TOF showed greater AUC than non-TOF (0.94 vs. 0.90) and thus TOF showed more excellent diagnostic performance with sensitivity of 95% and specificity of 88% than non-TOF with sensitivity of 85% and specificity of 80% .ConclusionAlthough TOF elevated both FDG uptakes of malignant and benign lesions, TOF enabled us to differentiate metastatic lymph nodes compared with non-TOF. TOF may show more power to assess tiny nodes less than 5mm.

P560

Texture analysis of pre-treatment 18F-FDG PET/CT images predicts for overall and recurrence-free survival of patients with locoregional advanced nasopharyngeal carcinoma after concurrent chemoradiotherpay

S. Chan1, K. Chang2, C. Lin2, T. Yen2; 1Keelung Chang Gung Memorial Hospital, Keelung, TAIWAN, 2Linkou Chang Gung Memorial Hospital, Taoyuan, TAIWAN.

Background: Texture analysis is a promising method of analyzing imaging data to improve diagnostic accuracy. This method involves measurement of pixel intensity variation that provides information concerning tumor heterogeneity. We assessed whether 18F-FDG PET imaging texture analysis would correctly the prognosis of patients with advanced nasopharyngeal carcinoma (NPC). Material and method: A cohort of 68 patients with primary stage III-IVb NPC was prospectively evaluated by 18F-FDG PET/CT. Overall survival (OS) and recurrence-free survival (RFS) were the main outcome measures. In an exploratory analysis, a standardized uptake value of 2.5 (SUV 2.5) was taken as the cut-off value for the detection of tumour boundaries. The textural features of pretreatment 18F-FDG PET/CT images were extracted from histogram analysis, normalized gray-level cooccurrence matrix (uniformity, entropy, dissimilarity, contrast, homogeneity, and inverse different moment), and neighborhood gray-tone difference matrix (coarseness, contrast, busyness, complexity, and strength). Result: Up to the date of analysis, 31 patients died and 27 patients experienced recurrences. The 5-year OS and RFS were 56.5% and 55.9%, respectively. Texture parameter contrast was significantly associated with T status ($p<0.0001$) and tumor stage ($p=0.007$).

Coarseness was significantly associated with T status ($p<0.0001$), N status ($p=0.039$), and tumor stage ($p=0.004$). In multivariate analysis, contrast ($p=0.021$), coarse ($p=0.036$), and complex ($p=0.02$) were independently associated with RFS. Tumor stage ($p=0.04$) and coarse (0.032) were significantly associated with OS. Conclusion: Texture parameters, contrast and coarseness, are primarily associated with clinical stage. In addition, these parameters can aid in the prediction of overall and recurrence-free survivals of advanced NPC patients.

P561

A Comparative Study of FDG PET/CT and MRI in Clinical/Pathological T4-stage Buccal Squamous Cell Carcinoma

C. Lo1, P. Kao1,2, J. Weng1; 1Chung Shan Medical Univeristy Hospital, Taichung, TAIWAN, 2Chung Shan Medical Univerisity, School of Medicine, TAIWAN.

Introduction: Buccal cancer is highly related to betel nut and tobacco use in Asia. Poor oral hygiene and dental disease with metallic implant may cause imaging interpretation difficulty. This retrospective study is to evaluate the diagnostic accuracy of FDG PET/CT and MRI in detecting surrounding soft tissue in clinical and/or pathological T4 staging buccal cancer in this area. Materials and Methods: This retrospective study has approved by IRB. We review 31 clinical and/or pathological T4 staging buccal cancer in our hospital from 2008 to 2015. All patients have MRI scan and 22 patients have FDG PET/CT within one month before surgery. Pathological results were used as gold standard. For T4-staging, the maxilla bone, mandible bone, and pterygoid muscle and masseter muscle involvement was concerned. Result and Discussion: Among them, the MRI T-staging of these patients include: 21 T4a, 8 T4b, 1 T2, and 1 T3; the FDG PET/CT T-staging include: 12 T4a, 6 T4b, 1 T1, and 3 T3; and the pathological results were 18 T4a, 2 T4b, 4 T1, 5 T2, and 2 T3. The overall T- staging accuracy of [18F]FDG PET/CT and MRI are 59% and 45%, respectively. For T4 staging, the accuracy of [18F]FDG PET/CT and MRI are 61% and 46%, respectively. Cortical bone involvement was better delineated on attenuation CT imaging of PET/CT than MRI. Review clinical history, all patients have betel nut use result in poor oral hygiene and dental problem which may cause MRI and PET/CT imaging artifact. Both imaging modalities tend to overestimate the T-staging. Conclusion: Buccal cancer as an endemic cancer in high betel nut use area, the accuracy of MRI and FDG PET/CT in diagnosis of T4 staging is affected by accompanied dental disease.

P562

Clinical value of SPECT/CT for evaluation of bone metastasis in patients with head and neck cancer

P. Arıcan, B. Okudan Tekin, R. Şefizade, S. Naldöken; Ankara Numune Education and Research Hospital, Ankara, TURKEY.

The bone metastasis is the second common side of distant metastasis in patients with head and neck cancer. The detection of bone metastasis influences the selection of treatment modality. Bone scintigraphy is higher sensitivity for the detection of suspected skeletal metastasis. But it can be difficult to distinguish between metastasis and other conditions such as postoperative, degenerative and traumatic changes, due to compact bone structure on the head and neck region. The aim of our study was evaluated the role of SPECT/CT in bone scintigraphy for the diagnosis of bone metastasis in patients with head and neck cancer.Methods and Materials:We retrospectively analysed 25 head and neck cancer patients (19 men, 6 women; mean range 55 years) who suspected bone metastasis with clinic-radiologic findings and referred to our department for bone scan between 2012 and 2014. Whole body and static images were performed at 3 hours after 740 MBq Tc-99m methylene diphosphonate (MDP) injection. Subsequently, SPECT/CT was performed from cervical and thoracic region in 22 patients, cranium in 2 patients, and pelvis in one patient. First planar bone scan was separately assessed by two nuclear medicine physicians. Second fusion images were evaluated and SPECT/CT findings were compared with the findings of planar images. The findings of planar bone scan and SPECT/CT were categorized as definitely benign, definitely malign and equivocal. The final diagnosis was verified by clinical-radiologic follow up.Results and Conclusion:There were definitely benign lesions (n=12) (%48), definitely malign lesion (n=1) (%4) and equivocal lesions (n=12) (%48) on planar bone scan, definitely benign (n=16) (64%), and definitely malign lesions (n=8) (32%), and equivocal lesion (n=1) (4%) on SPECT/CT. SPECT/CT was provided to the accurate diagnosis in 9 of the 12 patients with equivocal bone findings (2 malign, 7 benign). Sensitivity, specificity, positive predictive value (PPV), negative predictive value (NPV), and accuracy were calculated for planar bone scan, and SPECT/CT. The sensitivity of planar bone scan and SPECT/CT was 33.3%, and 100%. The specificity was 52.6%, and 88.8% respectively. PPV was 18.1%, and 75%, respectively. NPV was 71.4%, and 100%, respectively. Accuracy was 48%, and 88%, respectively.SPECT/CT is better than planar bone scan for the diagnosis of bone metastasis in patients with head and neck cancer by providing accurate anatomic localization and morphologic characteristic. SPECT/CT is superior for characterizing equivocal bone lesions on the head and neck region and can have a significant impact on patient's management.

P563

Prognostic value of pre-treatment 18F-FDG PET/CT volumetric parameters in patients with locally advanced larynx carcinoma treated with concurrent chemo-radiotherapy

G. Paone, V. Espeli, F. Martucci, L. Ceriani, A. Richetti, L. Giovanella; Oncology Institute of Southern Switzerland, Bellinzona, SWITZERLAND.

Aim: the aim of this study was to assess the prognostic value of volumetric parameters measured on 18F-FDG PET/CT determining event free survival (EFS) and overall survival (OS) in patients with locally advanced larynx carcinoma treated with concurrent chemo-radiotherapy. Material and method: we retrospectively analyzed 31 patients who performed a staging PET/CT for larynx carcinoma between 2008 and 2011. All patients had stage III-IV squamous cell carcinoma of the larynx treated with IMRT and concurrent chemotherapy. MTV, SUV max/mean and TLG were recorded. Univariate and multivariate analyses in association with Kaplan-Meier method were used to evaluate the prognostic value of these parameters considering EFS and OS. Results: In the univariate analysis, MTV (>20cm3) using a 2,5 SUV threshold had the best prognostic value than the other PET/CT parameters. We found a significant difference for predicting EFS (p<0,0001) and OS (p>0,0001) between the high MTV 2.5 (>20 cm3) and low MTV 2.5 (≤20cm3). In multivariate analysis, MTV and visual interpretation of local invasion remained significantly associated with EFS and OS (p= 0.012) while SUV max and TLG became non-significant (p=0.4 for EFS and p=0.7 for OS). At median follow up of 40 months the relapse rate was 42% (13/31 pts). Conclusion: Our data suggest that the pre-treatment 18F-FDG PET/CT MTV (>20cm3) provide better prognostic information in patients with locally advanced larynx cancer than other PET/CT parameters. 58% cure rate in this high-risk population is encouraging and confirm that chemo-radiation may be a therapeutic option.

P564

SPECT-CT in Patients with Parathyroid and Thyroid Comorbidities

O. Bessolova, O. Perfileva, Y. Kizhaev, V. Vidioukov; Russian Medical Academy of Postgraduate Education, Moscow, RUSSIAN FEDERATION.

Aim: To evaluate the role of SPECT-CT in detection and preoperative localization of parathyroid adenomas with 99mTc MIBI (dual-phase study) in patients with parathyroid and concomitant nodular thyroid pathology. Materials and methods: Our study included 37 female patients with mean age of 44 ±6.1 with laboratory features of hyperparathyroidism. Ultrasound revealed solitary/multiple 10-48 mm nodes in one/both thyroid lobes in all patients. Scintigraphy (GE Infinia Hawkeye 4) included dual-phase planar scans 15min and 2hrs after intravenous 555 MBq 99mTc MIBI respectively and SPECT after second phase study. In case of increased uptake foci on planar/SPECT images fusion SPECT-CT study was additionally performed. Results: In 21 patients increased uptake solitary foci in the thyroid lobes projection were detected independently of thyroid pathology localizations. Scintigraphically negative patients were managed according to conventional algorithms. SPECT-CT allowed precise thyroid contour delineation and increased uptake foci localization beyond it in 18 of 21 patients. These findings were solitary with typical (16) and atypical (2) location, retrosternal and paratracheal, respectively, and corresponded to parathyroid adenomas postoperatively. In 3 patients uptake foci were localized within nodular thyroid gland tissue on SPECT-CT. Fine needle biopsy (FNB) on ultrasound guidance was performed to evaluate underlying pathology in these patients. Parathyroid adenoma, follicular thyroid adenoma, follicular thyroid cancer were found respectively. Conclusion: Combined SPECT-CT can accurately localize pathological parathyroid glands and estimate their size. In case of intrathyroid uptake foci on SPECT-CT FNB should be performed to clarify underlying pathology and optimal surgery planning.

P565

Diagnostic accuracy of F-18 FDG PET/CT performed after radiation therapy in patients with head and neck cancer

W. Choi1, E. Han2, W. Lee3, Y. Park1; 1St. Vincent's Hospital, College of Medicine, The Cathoic University Of Korea, Suwon, KOREA, REPUBLIC OF, 2Deajeon St. Mary's Hospital, College of Medicine, The Catholic University of Korea, Deajeon, KOREA, REPUBLIC OF, 3Chungbuk National University Hospital, Cheongju, KOREA, REPUBLIC OF.

Purpose: To determine the diagnostic accuracy of F-18 FDG PET/CT for locoregional recurrent or residual tumor in patients with head and neck cancer who underwent previous radiotherapy.Methods and Materials: FDG PET/CT images from patients with head and neck cancer who previously underwent radiotherapy were reviewed retrospectively. Only cases with histological confirmation within 4 weeks of diagnosis by FDG PET were included. Maximum standardized uptake values were recorded and the FDG PET/CT findings were compared with the histology results.Results: Of 181 cases, 114 (63.0%) were histologically confirmed as malignant, and 67 (37.0%) as benign. The sensitivity, specificity, and accuracy of FDG PET/CT for diagnosis were 93.9%,

62.7%, and 82.3%, respectively. Of the 27 FDG PET/CT scans performed within 12 weeks after the completion of radiotherapy, there were 5 false-positive cases and there were no false-negative cases. The sensitivity, specificity, and accuracy of FDG PET/CT performed within 12 weeks were 100%, 55.6%, and 85.2%, respectively. The interval from radiation therapy to PET/CT scan of the false positive cases ranged widely from 5 days to 15 years. Of the 160 tissues with detectable FDG uptake, FDG uptake in malignant tissues was significantly higher than that observed in benign tissues ($p < 0.001$).Conclusions: FDG PET/CT could aid the diagnosis of residual or recurrent malignant tumors in patients with head and neck cancer patients who received radiotherapy, but the diagnostic accuracy might be limited, especially by false-positive results. Inflammation was the main cause of false positive results even years after radiotherapy. To ensure an accurate diagnosis for treatment planning strategies, pathologic verification of tumor status is warranted.

P566

Intra-operative lymphatic mapping and sentinel node biopsy in laryngeal carcinoma: preliminary results

R. Sadeghi1, E. Khadivi2, M. Daghighi2, K. Khazaeni2, V. Dabbagh Kakhki1, L. Zarifmahmoudi1; 1Nuclear Medicine Research Center, Mashhad University of Medical Sciences, MASHHAD, IRAN, ISLAMIC REPUBLIC OF, 2Sinus and Surgical Endoscopic Research Center, Mashhad University of Medical Sciences, MASHHAD, IRAN, ISLAMIC REPUBLIC OF.

Introduction: Sentinel node mapping has been used for laryngeal carcinoma in several studies with excellent results thus far. In the current study, we reported our preliminary results on sentinel node mapping in laryngeal carcinoma using intraoperative peri-tumoral injection of the radiotracer.Material and Methods: Ten patients with biopsy-proven squamous cell carcinoma of the larynx were included in the study. The day of surgery, after induction of anesthesia, 2 mCi/0.4 cc Tc-99m-Phytate in four aliquots was injected in the sub-mucosal peritumoral location using a suspension laryngoscopy. After waiting for 10 minutes, the sentinel nodes were searching for using a portable gamma probe. All patients underwent laryngectomy and modified radical bilateral neck dissection. All sentinel nodes and removed non-sentinel nodes were examined by H&E staining.Results: Ten patients with laryngeal carcinoma were included. At least one sentinel node could be detected in 5 patients (bilateral in four patients). One patient had pathologically involved sentinel and non-sentinel node (no false negative cases).Conclusion: Sentinel node mapping in laryngeal carcinoma is technically feasible using intraoperative radiotracer injection. In order to evaluate the relationship of T stage, and laterality of the tumor with accuracy of the technique larger studies are needed.

P567

Juvenilenasopharyngeal angiofibromas - in vitro and in vivo examinations of somatostatin receptors expression

J. Kunikowska1, W. Kukwa2, A. Cyran-Chlebicka2, D. Pawlak3, R. Matyskiel1, &. Koperski4, Z. Gronkiewicz2, B. Górnicka5, L. Królicki1; 1Nuclear Medicine Department, Medical University of Warsaw, Warsaw, POLAND, 2Department of Otorhinolaryngology, Czerniakowski Hospital, Medical University of Warsaw, Warsaw, POLAND, 3Radioisotope Centre POLATOM, National Centre for Nuclear Research, Otwock, POLAND, 4Department of Pathology, Medical University of Warsaw,, Warsaw, POLAND, 5Department of Pathology, Medical University of Warsaw, Warsaw, POLAND.

Juvenile nasopharyngeal angiofibroma (JNA) is a rare and benign disease, locally aggressive nasopharyngeal tumor, which is mainly found in adolescent male subjects. The preliminary data suggested that somatostatin receptors (SSTR) are overexpressed on JNA cells. The high density of SSTR subtype 2 on tumor cells enables the application of somatostatin (SST) analogues in diagnosis and therapy making it a promising new target for therapy of the unresectable or recurrent JNA. The aim of this study was the analysis of SSTR2 expression on JNA cells measured by the maximum Standardized Uptake Value (SUVmax) - a semiquantitative parameter derived from 68Ga DOTATATE PET/CT and correlation it with histopathological examination. METHODS: immunohistochemical examination was performed in seven male patients (age 17±7). The analysis of SSTR2 expression was done with light microscopy according to immunoreactive score (IRS) using polyclonal antibody (Sigma Aldrich). The average percentage of positive stained cells was estimated in 4 fields using 40x objective. PET/CT with 68 Ga DOTATATE PET/CT for evaluation of density of SSTR2 measured by standardized uptake value (SUVmax) was performed in all patients (Siemens Biograph 64). RESULTS: In all cases immunohistochemical examination showed presence of SSTR2 with intense reaction. The range of positive stained cells was from 73% to 100% (IRS - 8, 12). SSTR2 distribution on JNA cells was observed only in cytoplasm with increased density around nuclei and emphasis on the nuclear membrane. Reaction on cell membrane was positive only on few cells it correspond to the visual analysis on PET/CT 68Ga DOTATATE where only slightly increased uptake was observed. Semiquatitative analysis revealed SUVmax 4.6±1.5. On the other hand physiological uptake was noted, where SUVmax values were the highest in the pituitary gland 11 ±4.5, spleen18.9 ±6.6, adrenal 14.0

±5.6, and critical organ for PRRT kidneys 14.2± 3.6. CONCLUSIONS: Density of SSTR2 receptor located on surface of cells was observed only in few cells which correlated with low uptake seen in vivo examination with 68 Ga DOTATATE PET/CT. However, immunohistochemical examination showed intense reaction of SSTR2 on JNA cells, but due to mainly cytoplasmic localization these are not available for in vivo examinations.

P568

Value of 18F-FDG PET/TC in the Evaluation of Treatment Response in Head and Neck Cancer

M. Salcedo- Pujantell, C. Lorenzo-Bosquet, MD, G. Cuberas-Barrós, S. Siurana-Montilva, MD, A. Rovira-Cañellas, MD, J. Castell-Conesa, MD; Hospital Universitari de Vall d'Hebronn, Barcelona, SPAIN.

AIM: To compare 18F-FDG PET/TC and MRI in the evaluation of treatment response in Head and Neck Cancer, for more than 9-12 weeks after the end of the oncologic treatment, with histopathologic and/or clinical and imaging follow-up. MATERIAL AND METHODS: Retrospective and descriptive study of 70 patients(pts) (48 men), mean age 62.3 ± 11.1 years, with Head and Neck Cancer, who had underwent 18F-FDG PET/TC and MRI studies. 5 pts had nasopharynx tumours, 47 pts had oral cavity tumours/ oropharynx, 11 pts had hypopharynx tumours and 7 in the salivary glands. 64 pts had squamous cell carcinomas, 3 pts had adenocarcinomas and 3 pts had acinars cells carcinoma. RESULTS: 26/70 of the pts (37%) had residual primary tumour. For the detection of residual local disease, the Kappa Coefficient between PET/TC and MRI was 0.72 ($p<0.05$). PET/TC showed a sensivity of 92%, a specificity of 97%, a positive predictive value (PPV) of 96% and a negative predictive value (NPV) of 95%. For the MRI we found a sensivity of 84%, a specificity of 91%, a PPV of 85% and a NPV 90%. 27/70 of all pts included (38.5%) had residual metastatic lymph node. For the detection of them, the Kappa Coefficient between both techniques was 0.66 ($p<0.05$). PET/TC had showed a sensivity of 100%, a specificity of 97%, a PPV of 96% and NPV of 100%. For MRI we found a sensivity of 74%, a specificity of 90%, a PPV of 83% and a NPV of 85 %. 18F-FDG- PET/TC had good diagnostic performance in detecting metastases in 18/70 of all pts included and in 6/70 of the pts it was capable of detecting synchronous second primary tumour. MRI only detected perineural spread in 1/70 of all the pts included, which was not detected with PET/TC. The results were correlated with its histopathological evaluation and/or clinical and imaging follow-up (47 months ± 20m). CONCLUSION: PET/TC is superior in detecting regional lymph node metastasis and local disease. Moreover, it has a good diagnostic performance in detecting metastases and synchronous second primary tumour in patients with HNC. However, MRI seems to be superior in detecting perineural spread.

P569

Are contouring time and multimodality imaging prognostic factors for radiation therapy of advanced head and neck cancer?

M. Schmuecking1, O. Elicin2, B. Bojaxhiu2, R. Bigler2, J. Tille2, S. Fankhauser2, H. Thöny3, B. Klaeser4, A. Geretschläger5; 1Strahlenzentrum Hamburg/CyberKnife Center Hamburg, Hamburg, GERMANY, 2Inselspital Bern, Dept. of Radiation Oncology, Bern, SWITZERLAND, 3Inselspital Bern, Dept. of Radiology, Bern, SWITZERLAND, 4Inselspital Bern, Dept. of Nuclear Medicine, Bern, SWITZERLAND, 5St. Clara Spital Basel, Dept. of Radiation Oncology, Basel, SWITZERLAND.

Aim: In the DEGRO-Quiro Trials correlation of clinical outcome with contouring time in the planning process of radiation therapy and the amount of multimodality imaging has not been analyzed. To evaluate if contouring time and multimodality imaging are prognostic factors for radiation therapy of advanced head and neck cancer 207 patients were analyzed retrospectively between 2001 and 2012.Materials and Methods: Before 2007 radiation treatment planning CT was done without contrast enhancement, MR imaging and 18F-FDG PET/CT as additional imaging modalities were used only occasionally. From 2007 contrast enhanced planning CT in addition to multimodality imaging consisting of MR imaging (including DWI and ADC) and 18F-FDG PET/CT was used routinely for every head and neck cancer patient. Additionally, in unclear or equivocal imaging findings of lymph nodes a re-report was performed with a higher sensitivity at the expense of specificity to minimize geographical miss in the contouring procedure for radiation treatment and to maximize the binary decisions for each lymph node (malignant vs. benign). The re-reports were done in conjunction with radiooncologists, nuclear physicians and radiologists. Before 2007 the mean contouring time was 60 min before 2007, and 150 min after 2011 (including the time for a re-report). Clinical outcome (local, regional and locoregional control) of advanced oropharyngeal, laryngeal and hypopharyngeal cancers with lymph node metastases was assessed in two groups (group I: 2001-2007 vs. group II: 2008-2012).Results: Group I: $n = 113$, group II: $n = 94$. Regional recurrence was significantly reduced in group II (log-rank-test $p = 0.03$). Regional control after 1, 2 and 3 years was 88%, 79% and 76%, respectively as compared to 95%, 92% and 88%, retrospectively. Locoregional control for 207 patients shows no difference in survival ($p = 0.08$), inclusionof 340 patinets leads to a p-value $p < 0.05$.Conclusion: Imaging

findings of multimodality imaging and a critical re-report of these imaging findings in conjunction with a longer contouring time may have an impact on clinical outcome. However, this overtime is not reimbursed. A close collaboration of radiooncologists, nuclear physicians and radiologists in the radiation treatment planning process may have a benefit for patients with advanced head and neck cancer.

P570

Impact of 18F FDG PET CT on Initial Management of Patients Presenting with Secondaries in Neck from an Unknown Primary

M. SARMA, P. SUBRAMANYAM, P. SUNDARAM; DEPT. OF NUCLEAR MEDICINE AND PET CT, AMRITA INSTITUTE OF MEDICAL SCIENCES AND RESEARCH CENTRE (AMRITA VISHWA VIDYAPEETHAM), COCHIN, INDIA.

AIM: To assess the impact of 18F FDG PET CT on initial management of patients presenting with cervical nodal metastases from an unknown primary. MATERIALS & METHODS: 38 patients (M:F=30:8, age =32-80 years, mean age= 57.9 ± 13.39 years) with palpable histologically malignant neck node(s) were prospectively evaluated with FDG PET CT. Their initial physical examination, endoscopies and anatomical imaging to look for an unknown primary malignancy were negative. Lymphomas, haematopoietic malignancies, patients with history of previous treatments for head/neck malignancies or any other malignancy were excluded. Data of neck lymph nodal level by clinical examination, findings of FNAC/histopathology of lymphnodes, CT/MRI , FDG PET CT, FNAC or endoscopic findings from PET guided biopsies of suggested occult primaries and subsequently therapeutic decisions based on the PET CT results were analysed. RESULTS: PET CT findings changed the initial management in 12/38 patients (31.5 %). Among 11 patients who were detected with a primary malignancy, management changed in 8 patients. In 27 patients where the primary was not identified, there was change in management in 4/27 patients. The leading changes were in the radiation therapy (RT) field in 15 .7 % patients followed by initiation of palliative chemotherapy in 7.8% of patients. Patients with all N staging (AJCC 2010) had management change, except in N2a staging. Fisher Exact Test was performed to see the if there was any association between pre PET CT N staging (compared between N1/N2a and N2b, N2c, N3) and management change. P value of 0.644 (>0.05) suggested that there is no association between lower or higher pre PET CT N staging (multiplicity/ bilaterality/ large nodal size) and possibility of change of management upon investigation with FDG PET CT. 2 out of 12 (31.5%) patients presenting with supraclavicular lymphnodes had change in their subsequent Management. CONCLUSION: Management strategy gets individualised when the exact status of a possible primary (either detected or not), presence of contralateral metastatic nodes and presence/absence of distant nodal or organ metastases is accurately determined. Value of FDG PET CT in patients presenting with supraclavicular lymphnodal metastases from an adenocarcinoma or a poorly differentiated carcinoma needs to be further critically evaluated.

P571

Analysis of 18F-FDG PET/CT parameters in patients with head and neck soft tissue sarcoma

S. Baek, D. Yoon, E. Yun, Y. Seo, K. Lim, J. Kim; Kangdong Seong-Sim Hospital, Hallym University College of Medicine, Seoul, KOREA, REPUBLIC OF.

Purpose: Head and neck soft tissue sarcoma (HNSTS) is an extremely rare malignancy. The clinical use of 18F-fluorodeoxyglucose (FDG) positron emission tomography (PET) has been well demonstrated in head and neck squamous cell carcinomas (HNSCCs) but is unclear in HNSTS. The purpose of this study was to analysis quantitative parameters seen on PET/CT using 18F-FDG for understading of tumor charateristics in patients with HNSTS.Materials and Methods: 14 patients (10 males and 4 females; mean age, 45.1 ± 18.8 years; age range, 18 to 86 years) with pathologically proven HNSTSs were included in this retrospective study. PET/CT parameters_maximum standardized uptake value (SUVmax), mean standardized uptake value (SUVmean), and metabolic tumor volume (MTV), total lesion glycolysis (TLG)_were recorded. The association between the PET parameters and histologic grade and disease-free survival (DFS), were assessed.Results: The most common histologic type was Undifferentiated pleomorphic sarcoma (n = 4),i leimyosarcoma (n = 3), and angiosarcoma (n = 3). And the most common location of HNSTSs is the paranasal sinus (n = 7) in our study population. The SUVmax of primary tumors was 7.1 ± 3.7 (range, 3.4-16.7;), the SUVmean was 4.7 ± 2.8 (range, 2.2-12.1), the MTV was 18.3 ± 18.7 cm3 (range, 1.4-66.5cm3), and the TLG was 75.1 ± 64.0 g (range, 6.0-1707.8 g). All of FDG PET/CT parameters, including SUVmax, SUVmean, MTV and TLG, did not statistically correlate with the histologic grade of sarcoma ($P > 0.05$). The SUVmean (>5) of the primary tumor were significantly associated with negative effects on DFS ($P < 0.01$), where as other parameters were not.Conclusion: Our data indicate that the pretreatment PET/CT parameters may be useful for understanding of tumor and predicting prognosis in patient with HNSTSs

P572

Soft Tissue Sarcoma of the Head and Neck: CT, MRI, and FDG-PET/CT Imaging Findings

S. Baek, D. Yoon, J. Kim; Kangdong Seong-Sim Hospital, Hallym University College of Medicine, Seoul, KOREA, REPUBLIC OF.

Purpose: Head and neck soft tissue sarcoma (HNSTS) is an extremely rare malignancy. The purpose of this study was to describe the imaging features of HNSTS. Materials and Methods: Nineteen patients (11 males and 8 females; mean age, 48.4 ± 22.3 years; age range, 3 to 86 years) with pathologically proven HNSTSs were included in this retrospective study. Imaging studies including computed tomography (CT) (n = 19), magnetic resonance imaging (MRI) (n = 16), and fluorodeoxyglucose (FDG) positron emission tomography/CT (PET/CT) (n = 14) were reviewed for characteristics of tumors, such as shape, size, margin, MRI signal intensity, calcification, pattern and degree of enhancement, local tumor invasion, lymph node metastasis, and maximum standardized uptake value (SUVmax). Results: HNSTSs were most commonly located in the paranasal sinus (n = 5) and skeletal muscle (n= 3). The most common histologic type was rhabdomyosarcoma (n = 6), undifferentiated pleomorphic sarcoma (n = 3), and angiosarcoma (n = 3). Most masses had lobular shape (37%), size >5 cm (42%), well-defined margins (53%), isosignal intensity on T1-weighted image (88%), high signal intensity on T2-weighted image (63%), homogeneous (63%) and marked (58%) enhancement, local tumor invasion (63%), and SUVmax of 5.0-10.0 (50%). One (5%) patient had cervical lymph nodes metastases and distant metastases to bones. Conclusion: The imaging features for HNSTS are variable, thus are often indistinguishable from other tumors.

P36 - Monday, October 12, 2015, 4:00 PM - 4:30 PM, Hall 3 – Poster Exhibition

Clinical Oncology: Breast

P573

Diagnosis of distant recurrent breast cancer: head-to-head comparisons of FDG-PET/CT, contrast enhanced CT, and bone scintigraphy

M. G. Hildebrandt1, O. Gerke1, C. Baun1, K. Falch1, J. Ansholm1, Z. Farahani1, L. Larsen1, S. Duvnjak1, K. Soe1, A. B. Jylling1, M. Ewertz1, A. Alavi2, P. Hoilund-Carlsen1; 1Odense University Hospital, Odense, DENMARK, 2University of Pennsyalvania, Philadelphia, PA, UNITED STATES.

Aim: Recommendations for diagnostic work-up in patients with suspected recurrent breast cancer are yet undefined. The aim of this study was to investigate the diagnostic accuracy for distant recurrence of dual time point FDG-PET/CT compared to contrast enhanced CT (ceCT) and bone scintigraphy (BS) in patients with suspected recurrent breast cancer. Material and methods: In this prospective study, 100 female patients with suspected recurrent breast cancer underwent 1 hour (1h) and 3 hour (3h) FDG-PET/CT, ceCT, and BS within a median time interval of 10 days. Images were interpreted visually, and readers were blinded to other test results. Biopsy, clinicians' decision of treatment, and clinical follow-up (median 17 months, range: 0, 36) served as reference standard. Patient based accuracy results were calculated, including measures of area under the receiver operating curve (AUC-ROC, based on visually interpreted 4-point assessments, and with 95% confidence intervals (95% CI). Results: Twenty-two patients (22%) suffered distant recurrence, 18 (18%) with bone involvement. The accuracy of 1h and 3h FDG-PET/CT imaging was similar; therefore, only 1h results have been presented below. The AUC-ROC, sensitivity, specificity, and likelihood ratios for positive and negative tests were for FDG-PET/CT 0.99 (95% CI: 0.97-1), 1 (0.85-1), 0.91 (0.83-0.96), 11.1 (5.5-22.6), and 0 (N/A); for ceCT 0.84 (0.73-0.94), 0.77 (0.57-0.90), 0.83 (0.74-0.90), 4.6 (2.7-8.0), and 0.3 (0.1-0.6); and for ceCT+BS 0.86 (0.77-0.94), 0.91 (0.72-0.97), 0.72 (0.61-0.81), 3.2 (2.2-4.7), and 0.1 (0.03-0.5), respectively. Conclusion: The overall accuracy was significantly higher with FDG-PET/CT than with ceCT and ceCT+BS, and so without difference between conventional imaging at one hour than at three hours after FDG-injection. FDG-PET/CT was excellent in ruling out distant recurrence and did so with only few false positives. Thus, molecular imaging in the shape of FDG-PET/CT may be the modality of choice for imaging in suspected breast cancer recurrence.

P574

Visualization of internal mammary sentinel lymph nodes in patients with breast cancer - the corn stone for radiotherapy planning

S. N. Novikov, S. Kanaev, P. Krzhivitsky; N.N. Petrov Institute Oncology, St Petersburg, RUSSIAN FEDERATION.

Background: lymphoscintigraphy can be used as effective tool for visualization of sentinel lymph nodes (LN) localized in internal mammary (IM) region and in combination with clinical risk factors help to estimate the risk of IMLN metastatic invasion by breast cancer (BC). Objective: On the basis of scintigraphic data and known clinical risk factors to calculate probability of IMLN metastatic invasion in patient included in randomized and observation studies analyzing clinical value of radiotherapy to IMLN. To evaluate clinical value of lymphoscintigraphy as the guide for irradiation of IMLN.

Methods. Using the data of 8 published studies that analyzed lymph flow from primary BC (4541 patients) after intraperitumoral injection of nanosized 99mTc-colloids we determined probability of lymph flow from internal/central and lateral primary BC to IMLN. In 7 studies (4359 women) axillary staging was accompanied by IMLN biopsy that helps us to estimate probability of IMLN metastatic invasion in relation with the status of axillary LN. Finally we estimated probability of IMLN invasion by BC in 4 randomized and 2 observation studies that analyzed effect of IMLN irradiation on overall survival. In these pts we calculated possible additional gain survival if they would be treated according to lymph flow guided radiotherapy to IMLN. Results: Lymph-flow from internal/central BC to IMLN was detected in 16% (727/4541), from lateral lesions - in 35% (1589/4541). In women with negative axillary LN metastases in IMLN were revealed in 7.8%, in patients with positive axillary nodes - in 38.1%. Calculated probability of IMLN metastatic invasion in "high risk patients" include in all evaluated studies didnt exceed 10%. If lymphoscintigraphy would drive decision whether to irradiate IMLN or not than 72.1%-76.8% of "high risk patients" would escape RT to IMLN. In remained 23.2%-28.9% patients with lymph flow to IMLN their irradiation would improve overall survival from 1.6%-3.3% to 6.9%-14.2% Conclusion: performed analysis proves that radionuclide visualization of lymph flow from DC plays an important role in decision making about usefulness of IMLN irradiation. In patients with lymph flow to IM LN irradiation of IMLN can dramatically (6.9%-14.2%) improve 5 and 10 yeas overall survival.

P575

Role of MUGA scan in diagnosis of the effect of trastuzumab (Herceptin) on global and segmental left ventricular ejection fraction in patients with breast cancer

S. M. W. Yassin1, K. Salman1, A. Mostafa1, M. Abd El Kareem2, W. Mohamerd1, A. Abd El Samee2, Y. Mohamed2, E. Abo El-Naga1, S. Abd El Razek3; 1King Abdulla Medical City (KAMC), Jeddah, SAUDI ARABIA, 2Cairo University, Cairo, EGYPT, 3Assuit University, Assuit, EGYPT.

Intrduction: Trastuzumab (Herceptin) is a monoclonal antibody target therapy in positive HER2 breast cancer patients. Cardiac dysfunction is the side effect of greatest clinical concern of trastuzumab, probably because it blocks the HER2 receptors which protect adult cardiomyocytes. Cardiac toxicity reported to be 4% in patients on trastuzumab alone, increasing up to 13% if given with paclitaxel and up to 27% with anthracycline plus cyclophosphamide. Cardiac dysfunction was reported to be mild and asymptomatic in majority of patients. MUGA scan with evaluation of ejection fraction (EF) is the most commonly used tool for cardiac monitoring during therapy. Aim: To study effect of trastuzumab on global and segmental EF using MUGA scan. Patients and methods: 32 females with breast cancer and no history of cardiac problems and normal base line MUGA scan treated with trastuzumab, with asymptomatic reduction of global EF in follow up MUGA scan were included in the current study. Patients were followed up prior to each cycle by MUGA scan. The degree of reduction of global and segmental LVEF were calculated. Treatment was interrupted if EF is reduced below normal level(50%). Results: Reduction of global EF ranges from 1-17% with a mean value of 7.6%. Global EF reduction was below 5% in 16 patients(50%), from5-10% in 11 patients (34.4%) and from 10% to < 20% in the remaining 5 patients (15.6%). EF below normal value (50%) was reported in 3 patients (9.4%), which was reversible in follow up MUGA scanning 2-3 months post cessation of trastuzumab . The reduction of segmental EF was reported in all myocardial walls. The degree of EF diminution in anterior, anteroseptal, inferoseptal, inferior, inferolateral and superolateral left ventricular myocardial walls was reported with values of 9.03%, 5.7%,5.9, 9.6%, 9.9% and 9.8% respectively. with statistically significant less diminution of EF in septal myocardial segments compared to rest of myocardial segments. Conclusion: . Reduction of EF in patients treated with trastuzumab is below 10% in majority of patients (84.4%) and from 10- <20% in the remaining 15.6% patients, with a mean value of reduction of global EF of 7.6%. Reversible EF diminution below normal that necessitates interruption of trastuzumab therapy occurs in 9.4% of patients. Variable degrees of diminution of segmental EF in all myocardial wall segments was reported, significantly less evident reduction of segmental EF was reported in anteroseptal and inferoseptal segments, impressive of less cardiotoxic effect of trastuzumab on the thinner septum.

P576

Therapy Response Evaluation of Patients with Locally Advanced and Metastatic Breast Cancer: Comparison of Anatomic and Metabolic Criteria for Early and Accurate Response Assessment

B. Gunalp1, M. Erdogan2, S. Ince1, E. Balkan1, E. Alagoz1, A. Ayan1, N. Arslan1; 1Gulhane Military Medical Academy and Medical Faculty, ANKARA, TURKEY, 2Diskapi Yildirim Beyazit Egitim ve Arastirma Hastanesi,, ANKARA, TURKEY.

Objectives: Therapy response evaluation is important for avoiding ineffective toxic and expensive chemotherapies in early phase of treatment and changing therapy regimen to more effective ones. Anatomic (RECIST 1.1) and metabolic (EORTC and PERCIST 1.0) criteria have been proposed for

the therapy response evaluation in solid tumors. Therapy response evaluation in specific tumor types with FDG-PET/CT using both anatomic and metabolic criteria is limited in the literature. In this retrospective study, we try to determine the most applicable and accurate criteria for the therapy response evaluation in locally advanced (LABC) and metastatic breast carcinoma (MBC) patients. Methods: Twenty two LABC and 34 MBC patients underwent baseline and at least one FDG-PET/CT scans for response assessment, between 2011 and 2014 were included in this study. Baseline and follow-up PET/CT scans were analyzed measuring the dimensions on CT and SUV Max, SUL peak of up to 5 lesions on PET. These criteria were compared with clinical, pathological findings and progression free survival rates of the patients for evaluation of therapy response. Results: After neoadjuvant chemotherapy in LABC patients PET classified as complete response (CR) in 4 (18%), partial response (PR) in 5 (22%), stable disease (SD) in 6 (27%) and progressive disease (PD) in 7 (31%) patients. PET and CT sensitivity and specificity for the response evaluation were found 85%, 80% and 65%, 60% respectively. In MBC group, twelve (64%) patients had bone, six patients (17%) had liver, 5 patients (14%) had lung, 3 patients (8%) had brain metastases, 2 patients (5%) had chest wall invasion and malign pleural effusion. According to PERCIST 1.0 and EORTC criteria, there were CR in 4 (10%), PR in 8 (21%), SD in 2 (5%), PD in 12 (31%) and mixed response in 12 (33%) patients. Bone lesions in 10 patients (83%), liver lesions in 4 patients (66%) and chest wall invasions and malign pleural effusions were not measurable anatomically on CT. Conclusion: PERCIST 1.0 and EORTC criteria were found more accurate and applicable than RECIST 1.1 criteria in early response assessment and therapy response evaluation of bone metastases, chest wall invasions, malign pleural effusions and liver metastases. On the other hand RECIST 1.1 criteria were superior in response assessment of lung metastases. FDG-PET/CT overcomes limitations of both anatomic and metabolic criteria alone and gives the opportunity to revise treatment and improve outcome in breast cancer patients.

P577

Prognostic Value of Semiquantitative Tumor Uptake on Tc-99m Sestamibi Breast-Specific Gamma Imaging in Invasive Ductal Breast Cancer

S. Jang1, H. Yoon2, Y. Kim3, B. Kim2; 1Dep. nuclear medicine, Sheikh Khalifa Specialty Hospital, Ras al Khaimah, UNITED ARAB EMIRATES, 2Dep. nuclear medicine, Ewha Womans University School of Medicine, Seoul, KOREA, REPUBLIC OF, 3Ewha Womans University School of Medicine, Seoul, KOREA, REPUBLIC OF.

Objectives: This study investigated the prognostic value of preoperative breast-specific gamma imaging (BSGI) uptake measured by a semi-quantitative method in invasive ductal carcinoma (IDC). Methods: One hundred sixty-two women with IDC who underwent preoperative BSGI were retrospectively enrolled. The tumor-to-normal tissue ratio (TNR) was measured on BSGI and correlated with histologic prognostic factors. The prognostic impact of TNR was tested with regard to progression-free survival (PFS) and compared with established prognostic factors. Results: High TNR was significantly correlated with tumor size >2 cm ($p<0.001$), high nuclear grade ($p=0.04$), high histologic grade ($p=0.01$), axillary node positivity ($p=0.04$), ER negativity ($p=0.03$), HER2 positivity ($p=0.01$), and high MIB-1 index ($p=0.001$). Among 162 patients, 14 experienced recurrence during mean the follow-up time of 34.7±14.9 months. In Kaplan-Meier survival analyses, high TNR ($p<0.001$), high nuclear grade ($p=0.02$), high histologic grade ($p=0.007$), ER/PR negativity ($p=0.003$ and $p<0.001$, respectively), HER2 positivity ($p=0.01$), triple negativity ($p=0.02$), and high MIB-1 index ($p=0.02$) showed a significant relationship with poor prognosis. Among them, high TNR was an independent poor prognostic factor in a multivariate regression analysis ($p=0.01$). Conclusions: High BSGI uptake measured by a semi-quantitative method was correlated with diverse poor histologic prognostic factors and was an independent poor prognostic factor in invasive ductal cancer. (This research was supported by the National Research Foundation (NRF) of Korea (2012R1A1A1012913 and 2012M3A9B6055379)).

P578

Breast cancer patients with bone metastases reveled by FDG-PET showed worse long-term survival than those reveled only by bone scan.

Y. Huang, P. Lee, M. Liu; Koo-Foundation, Sun Yat-Sen Cancer Center, Taipei, TAIWAN.

Aim: The discrepancy between bone scan and FDG-PET in detecting bone metastasis of breast cancer had been well established. The FDG-PET showed more promising sensitivity in osteolytic lesion while the bone scan is better for osteoblastic group. This retrospective study is aim to compare the long-term survival of the patients with bone metastases reveled by FDG-PET and those with bone metastases reveled only by bone scan. Material and method: Between January 2006 and September 2010, 130 patients with advanced nodal status or locally advanced breast cancer performed both bone scan and FDG-PET performed within 7 days. The status of bone metastases were carefully reviewed and linked to the survival data base in March 2015. A total of 100 patients have sufficient information for statistical analysis. The patients were classified as three groups: A. negative for bone metastases on both

studies; B, bone metastases revealed by bone scan only; C. bone metastases revealed by FDG-PET with or without bone scan uptake. Result: Twenty out of the 100 patient (20%) were found to have bone metastases while 80 patients (group A) were free of bone metastases. In 7 out of the 20 (35%) patients, the bone metastases revealed only on the bone scan (group B), and the rest 13 (65%) patients revealed FDG-PET positive bone metastases (group C). The 10-year survival of group A, B, and C were 69.4%, 42.9% (p=0.1152; HR=2.4, 0.8-7.0), and 18.5% (p=0.0005; HR=3.6, 1.8-7.5), respectively. Conclusion: Compared to the bone metastases free patients, breast cancer patients with bone metastases revealed by FDG-PET had significant worse long-term survival than those with bone metastases revealed only by bone scan. Thus, FDG-PET may serve better prognostic value.

P579

Comparison of FDG PET/CT and bone scan for diagnosis of metastatic bone involvement in breast carcinoma patients: A retrospective analysis

B. Yazici, A. Oral, Z. Ozcan; Ege University Medical Faculty Deparment of Nuclear Medicine, Izmir, TURKEY.

Aim: In this study, the value of F-18 FDG PET/CT for the detection of bone metastasis in breast cancer (BC) was evaluated and compared with Tc-99m MDP bone scan (BS) which is a common but poor specific modality. Materials and Methods: A total of 83 patients (F/M: 79/4, mean age: 55.7) with BC in whom FDG PET/CT and BS were performed within 3 months were included. The diagnosis of bone metastasis was established by combining all imaging findings and clinical follow-up. Histopathology, Ki-67 index, CA15-3, SUVmax values were reviewed. Statistical significance was tested by Mann-Whitney U and Pearson Chi-square tests. The ability of FDG PET, FDG PET/CT and BS to detect bone metastasis was assessed by ROC analysis. As regard to area under the curve (AUC), parameters were classified as inaccurate (AUC<0.50), low (AUC=0.50-0.70), moderately (AUC=0.70-0.90) or as highly accurate (AUC>0.90). Results: A total of 267 bone lesions were detected in 83 patients. In 16 patients, 217 lesions were accepted as metastasis considering all the clinical data. In 67 patients there were no bone metastases. The frequency of elevated CA15-3 (>25 U/mL) (84.6%) was higher in metastatic patients (P<0.01). Ki-67 index difference between the groups was insignificant (P=0.64). Of the 217 metastatic bone lesions, 203 (93.5%) were FDG (P<0.01) and 132 (60.8%) were MDP avid (P=0.49). The mean value of SUVmax (7.2±5.3) in metastatic foci was significantly higher than non-metastatic bone lesions (P<0.01). In the metastatic lesions, 149 (68.7%) were osteolytic and 68 (31.3%) were sclerotic. The frequency of lytic metastasis in FDG avid and the frequency of sclerotic metastasis in MDP avid metastases were significantly high (P<0.01). Of the lytic metastases, 98.7% were FDG avid but only 49.7% were MDP avid. On the other hand, avidity of FDG and MDP in sclerotic metastasis was not very different (82.4% and 85.3% respectively). While FDG PET/CT was highly accurate (AUC>0.90) for the detection of bone metastasis, BS showed poor accuracy (AUC<0.50). Sensitivity of BS, FDG PET and FDG PET/CT were 60.8%, 93.6% and 100%; specificity were 34.0%, 93.6% and 96.0% respectively. Conclusion: It is noted that while lytic metastases showing low avidity for MDP may lead to low sensitivity on BS, those non-metastatic bone lesions with high MDP uptake cause poor specificity. The results of the current study suggest that the accuracy of FDG PET/CT is higher than BS in the detection of metastatic bone diseases in BC.

P580

Pathological Correlation of Mild Focal Uptake on the Tc-99m MIBI Breast specfic gamma camera imaging.

S. Yoon; DanKook University College of Medicine, Cheil General Hospital, Women's Cancer Center, Seoul, KOREA, REPUBLIC OF.

Purpose: In our hospital, 303 cases were pathologically confirmed by only routine early images, the sensitivity and specificity of BSGI were 90% and 60% because of many false positive lesions such as fibroadenoma, etc. BSGI using Tc-99m MIBI showed lower specificity due to many benign lesions. Images were usually categorized as score 1-5. Scores of 1, 2, and 3 were classified as negative, and scores of 4 and 5were classified as positive. In this study, we investigated the clinical significance of mild focal uptake(Score 4) on the image using breast specific gamma camera image for differentiation of benign and malignant breast lesions. Methods: Patients were injected with 925-1110 MBq of Tc-99m MIBI in the ante-cubital vein of the contralateral arm of the breast lesion. Imaging was performed 10 minutes after injection with a dedicated high-resolution, breast-specific gamma camera (Dilon 6800, Dilon Technologies, USA). Standard craniocaudal and mediolateral oblique views for each breast were obtained for five minutes each. We categorized images by visual analysis A total of 20 patients underwent pathologic confirmation with mild focal uptake on routine breast gamma camera imaging were evaluated. Results: Pathological results of malignancy and benign were then correlated with the image analysis to have mild focal uptake on the scintimammography. Nine (45%) among 20 patient underwent pathologic examination were malignant lesions, 7 of which were invasive ductal carcinoma and 2 were adenoid cystic cancer and mucinous cancer each. There were 11 false-positive lesions (55%),

defined as a BSGI examination with positive findings and 10 fibroadenomas were the most common pathologic finding showing the false positive results. Finally fibroadenomas were 50% of all mild focal uptake and 91% of false positive benign lesion. Conclusion: Although only small number of patients, mild focal uptake by degree of uptake criteria for differentiation of benign vs malignant lesion using BSGI may be causes of many false positive imaging interpretation. About half breast lesion with mild focal uptake were not malignant lesion. The most common pathologic lesions inducing many false positive interpretation were fibroadenoma. Further studies will be needed to define usefulness of BSGI in large population.

P581

Contralateral axillary sentinel lymph node in breast cancer patients: an uncommon lymphatic drainage

T. Tanaka, S. Sato, R. Inai, A. Tada, S. Kanazawa; Department of Radiology, Okayama University Hospital, Okayama, JAPAN.

[aim] For the lymphatic mapping of breast cancer, the methods using radioisotope with or without blue dye injection are superior to those using blue dye only. Sometimes we encounter the occult sentinel lymph nodes in preoperative scintigraphy that are difficult to find out in other modalities. Uncommon sentinel lymph nodes poses management dilemma for clinicians. The purpose of this study was to review atypical sentinel lymph nodes, especially contralateral axillary lymph node, in breast cancer patients. [materials and methods] We reviewed 942 breast cancer patients who performed preoperative sentinel lymph node scintigraphy at Okayama University Hospital between April 2004 and March 2015. In all patients, Tc-99m stannous phytate was injected peritumourally, and the injection sites were massaged. We evaluated lymphoscintigraphy results and patient characteristics, such as age, primary tumour location, pathological result and past medical history. [results] The contralateral sentinel lymph nodes were detected in 3 patients (0.32%). Two patients with contralateral sentinel node had lower medial tumours and the other patient had a lower lateral tumour. Bilateral lymph nodes were visualized in 2 patients, and 1 patient showed contralateral axillary lymph node only. The patients with contralateral sentinel lymph node have no previous chest or breast surgery. No local recurrence of the contralateral axillary lymph node was observed. Other atypical lymph nodes including infra- or supraclavicular were visualized in 5 patients (0.53%), and parasternal lymph nodes were detected in 21 patients (2.22%). [conclusion] Although the visualization of contralateral axillary lymph nodes was rare as previous reports, we need to pay attention for the existence of contralateral axillary lymph nodes in preoperative sentinel lymph node biopsy for precise staging.

P582

Comparison of Subareolar Injection Lymphoscintigraphy with the 1 Day and the 2 Day Protocol for the Detection of Sentinel Lymph Nodes in Patients with Breast Cancer

E. Lee, J. Seok; Department of Nuclear Medicine, Chung-Ang University, Colleage of Medicine, Seoul, KOREA, REPUBLIC OF.

Objectives: Lymphoscintigraphy and sentinel node biopsy were used for the detection of axillary lymph node metastasis in breast cancer patients. We compared the results of subareolar injections on the day of surgery (1 day protocol) with injections the day before surgery (2 day protocol). **Methods**: This study included 813 breast cancer patients who underwent surgery between 2001 and 2015. For the 1 day protocol 0.8 ml of Tc-99m Tin-Colloid (37MBq) was injected in 500 patients in the subareolar region on the morning of the surgery. For the 2 day protocol 0.8 ml of Tc-99m Tin-Colloid (185MBq) was injected in 313 patients on the afternoon before surgery. Lymphoscintigraphy was performed in the supine position and sentinel node identification was performed by hand-held gamma probe during surgery. **Results**: Among 500 patients with the 1 day protocol, 471 cases (94.2%) were identified by sentinel node lymphoscintigraphy, and 475 cases (95.0%) were identified by gamma probe. Among the 313 patients, in the 2 day protocol, 290 cases (92.7%) had the sentinel node identified by lymphoscintigraphy, and 280 cases (89.5 %) had the sentinel node identified by the gamma probe. There was no significant difference in the identification rate of the sentinel node between the 1 day and 2 day protocol by lymphoscintigraphy and the gamma probe. **Conclusions**: The results of the identification of the sentinel node according to 1 day or 2 day protocols showed no significant differences. Because the 2 day protocol allows for an adequate amount of time to perform the lymphoscintigraphy, it is a more useful protocol for the identification of sentinel nodes in patients with breast cancer.

P583

Comparison of the Efficiency for Tc-99m Tin-Colloid and Tc-99m Phytate in Sentinel Node Detection in Breast Cancer Patients

E. Lee, J. Seok; Department of Nuclear Medicine, Chung-Ang University, Colleage of Medicine, Seoul, KOREA, REPUBLIC OF.

Lymphoscintigraphy and sentinel node biopsy has become a standard method for detection of axillary lymph node metastasis in breast cancer patients, but the standard radiopharmaceutical was not prepared. About detection of axillary lymph

node metastasis by lymphoscintigraphy and sentinel node biopsy in breast cancer patient, we compared the results of Tc-99m Tin-colloid and Tc-99m Phytate by subareolar injection. **Methods**: This study included 813 breast cancer patients who were performed operation during 2001-2015. Four hundred twelve patients were injected 0.8 ml of Tc-99m Tin-colloid (37-185 MBq) by subareolar injection. Four hundred one patients were injected 0.8 ml of Tc-99m Phytate (37-185 MBq). Lymphoscintigraphy was performed in supine position and sentinel node localization was performed by hand-held gamma probe in operation. **Results**: Among 412 patients by Tc-99m Tin-colloid, 374 cases (90.8%) were localized the sentinel node by lymphoscintigraphy and 367 cases (89.1%) were localized by gamma probe. Among 401 patients by Tc-99m Phytate, 387 cases (96.5%) were localized by lymphoscintigraphy and 388 cases (96.8%) were localized by gamma probe. The detection rate by lymphoscintigraphy and gamma probe was superior for Tc-99m Phytate compared to that for Tc-99m Tin-colloid, with a statistically significant difference. ($p<0.05$, $p<0.05$) **Conclusions**: Tc-99m Phytate is a better choice for localization of sentinel node than Tc-99m Tin-colloid in breast cancer patients.

P584

The addictional value of 18F-FDG PET/CT in pre and post-operative setting in patients with locally advanced breast cancer

L. Evangelista, A. Cervino, S. Michieletto, T. Saibene, E. Bezzon, F. Pomerri, F. Bozza, C. Ghiotto, G. Saladini; Istituto Oncologico Veneto I.R.C.C.S., PADOVA, ITALY.

Purpose: the primary end-point of the present study was to determine the additional value of FDG PET/CT in patients with breast cancer at high risk of recurrence, in pre and post-operative setting. The secondary purpose was to determine the impact of FDG PET/CT on treatment planning in these patient subsets. Materials and methods: we prospectively collected data from 255 women (age: 53±12 years; range:23-85 years) with a diagnosed locally advanced breast cancer (LABC) who performed FDG PET/CT examination before (n=137, 53.7%) or after surgery (n=118; 46.3%). The mean period between surgery and PET/CT was 45±22 days. The images were visually and semiquantitatively analyzed and compared with other imaging modalities, biopsy or histology, as appropriate. The treatments were planned by a multidisciplinary team, according to the current recommendation. True positive rate (TPR) and false positive rate (FPR) were calculated by standard methods. The differences between categorical data were assessed using Yates-corrected chi-square test. Results: FDG PET/CT was positive in 36 (30.5%) and doubtful in 13 (11%) among post-operative subjects, while it resulted positive in all pre-operative patients. In this latter group, PET/CT showed an abnormal FDG-uptake in breast and breast with homolateral axillary lymph nodes in 30 (22.1%) and 55 (40.4%) patients, respectively. Moreover, additional sites of disease were depicted in 29 (21.3%) and 22 (16.2%) patients, respectively for extra-axillary lymph nodes and distant organs. Conversely, 7 (16.3%) patients of post-operative subset showed a positive PET/CT at breast level, 10 (23.3%) in homolateral axillary lymph nodes, 14 (32.6%) in extra-axillary lymph nodes and 12 (27.9%) in distant organs. TPRs and FPRs in detecting distant metastases and/or residual disease, in pre and post-operative settings were 94% and 81% vs. 6% and 19%, respectively. Finally, the change in treatment was reported in 35 (13.7%) patients, 17 in pre-operative and 18 in post-operative group (12.4% vs. 15.3%, respectively; p=0.510). Conclusions: FDG PET/CT scan in the evaluation of LABC appears necessary either before or after surgery, being associated with a high TPR in depicting extra-axillary lymph nodes and distant organ involvement. In particular, the treatment change results higher in post-operative than in pre-operative group, although not statistically significant. Anyway, a reduction in health costs could be obtained.

P585

Impact of radioguided occult lesion localization plus sentinel node biopsy after neoadyuvant chemotherapy in breast cancer.

I. Cepedello Boiso, M. Ureña Lara, J. Jiménez Anula, C. Ramírez Tortosa, J. Díaz Alarcón; Complejo Hospitalario de Jaén, Jaén, SPAIN.

AIM:. Neoadyuvant chemotherapy in breast cancer could be a valuable method to determine the efficacy of chemotherapy and potentially downsize the primary tumor, wich facilitates breast-conserving therapy. The aim of this study was to investigate the feasibility, accuracy and clinical significance of radioguided occult lesion localization plus sentinel node biopsy after neoadyuvant chemotherapy. MATERIALS AND METHODS: Prospective study performed from January 2009 to April 2015. Radioguided occult lesion localization plus sentinel node biopsy was performed after neoadyuvant chemotherapy in patients with breast cancer (tumor size > 3 cm or tumor size < 3 cm not suitable for breast-conserving surgery and axilary node negative). Axillary status was established by physical examination, ultrasound-guided core needle biopsy of any suspicious lymph node. SNOLL were carried out using standard 99mTc-colloid (activity of 3 mCi and 0,2-0,5 ml volumen) injected directly into the lesion (stereotactic or ultrasound guindance) and in the cases of no lymphatic migration, realised subdermal injection. An intraoperative macroscopic examination of the specimen with margins

evaluation was always performed. The Sentinel Lymp Node (SLN) were analysed by One-Step Nucleic Acid Amplification (OSNA). SLN was considered to be positive if macrometastases or micrometastases were found, and in such cases axillary dissection was consequently implemented. Clinic-radiological monitoring and assessment of the status of patients was conducted. RESULTS: 31 patients was recorded (all woman, 37-66 years old, mean age 49,32 years). SNOLL located all the occult breast lesions successfully. In 25 out of the 31 patients (80,6%), the breast specimen had clear and large margins. Despite intraoperative examination of the specimen, a total of 19, 4% (6 out of 31) patients required a second re-excision procedure for involved margin and in the all cases had finally clear margins. Lymphocistingraphy showed axillary drainage in every patients and 38 SLN samples (1,23 SLN/patient) were analyzed. Axillary lymph nodes were histologically negative in 25 patientes (80,6%) and positive in 6 patients (17,4%). Monitoring Period was a range from 34 to 56 months. Two out of 31 patients had metastasis: one axillary recurrence (31 month/ axillary lymph node dissection) and other pulmonary recurrence (24 month/ chemotherapy). All patients are in complete remission at present. CONCLUSION: Performing radioguided occult lesion localization plus sentinel node biopsy after neoadyuvant chemotherapy to be a successful and reliable tecnique in patients with breast cancer. However, further research taking account of larger samples an longer post-surgery monitoring time are needed.

P586

Reliable I-125 seed localization after neo-adjuvant chemotherapy to identify breast lesions in combination with sentinel node biopsy

D. Koopman1,2, D. Lots1, A. B. Francken3, H. Arkies1, P. L. Jager1, C. H. Slump2, J. A. van Dalen4; 1Isala, department of Nuclear Medicine, Zwolle, NETHERLANDS, 2MIRA Institute for Biomedical Technology and Technical Medicine, Enschede, NETHERLANDS, 3Isala, department of Surgery, Zwolle, NETHERLANDS, 4Isala, department of Medical Physics, Zwolle, NETHERLANDS.

Background: An increasing number of breast cancer patients undergo breast-conserving surgery using I-125 seeds for tumour localization, combined with sentinel node biopsy using Tc-99m. In patients who received neo-adjuvant chemotherapy, identification of the seed with a gamma probe may be hampered, as time to surgery increases and I-125 activity may be less than 10% of its original activity during surgery. The complexity gets worse for combined I-125/Tc-99m procedures due to Tc-99m Compton scatter. The aim of this study was to determine the maximum allowed ratio between Tc-99m and I-125 during surgery. Method: We performed a phantom study using 3 syringes each containing 17.4 MBq Tc-99m and one I-125 seed of 6.0 MBq, resulting in activity ratios (ARs) of 2.9, 5.8 and 8.7. To simulate breast tissue attenuation, we used perspex with varying thicknesses (T=10-50mm). Measurements were performed with a gamma probe (Neoprobe GDS). Counts per second from Tc-99m down-scatter were determined in the I-125 window ($CPS_{scatter}$). Next, the I-125 seed was added and measurements were repeated (CPS_{comb}). We hypothesized that $R=CPS_{comb}/CPS_{scatter}$ should be > 2 to successfully identify the seed. R was calculated as a function of the 3 ARs. Furthermore, we studied 10 patients who underwent combined I-125/Tc-99m surgical procedures with low activity seeds (0.3-0.6 MBq) under well-standardized conditions. At time of surgery, Tc-99m activity was approximately 23 MBq. Thereby, AR ranged from 35 to 78. Results: The phantom study showed that ratio R decreased from 5.6 (T=10mm) to 1.5 (T=50mm) for AR=8.7. These values decreased linearly with decreasing AR. Up to 40mm perspex, we could successfully identify the I-125 seed (R>2) when AR=8.7. Furthermore in 8 out of 10 patients (AR<46), it was possible to localize the I-125 seed on the skin during surgery. In 2 patients (AR>46), the seed could not be detected on the skin. However, after incision we were able to pinpoint the seed with the gamma probe. Conclusion: The phantom study suggests a maximum Tc-99m/I-125 activity ratio of 9 during surgery. In practice, combined procedures with activity ratios up to 46 were performed successfully. This discrepancy may be related to differences in the geometrical configuration of the Tc-99m deposits and I-125 seed. It is recommended to keep the activity ratio as low as possible, by reconsidering the activities that are used for Tc-99m and I-125, and if possible to shorten the time between seed placement and surgery.

P587

18F-FDG PET/CT is a prognostic bio-marker in patients affected by bone metastases from breast cancer. Comparison with 18F-NaF-PET/CT.

A. Piccardo1, M. Massollo1, V. Altrinetti1, S. Morbelli2, F. Bongioanni2, M. Iacozzi1, G. Sambuceti2, A. Gennari3, R. Gonella4, M. Puntoni5, A. Decensi3, M. Cabria1; 1Nuclear Medicine Unit E.O Ospedali Galliera, Genoa, ITALY, 2Nuclear Medicine Unit San Martino IST, Genoa, ITALY, 3Oncology Unit E.O Ospedali Galliera, Genoa, ITALY, 4Department of Internal Medicine San Martino IST, Genoa, ITALY, 5Clinical Trial Research Unit, Galliera Hospital,, Genoa, ITALY.

Abstract: Aim: To assess the association between 18F-FDG PET/CT and progression-free survival (PFS) and overall survival (OS) in patients with documented bone metastases from breast cancer (BC) and to compare the prognostic value of

18F-FDG PET/CT with that of 18F-NaF-PET/CT and of other initial prognostic parameters that influence the outcome of breast cancer patients. Methods: We retrospectively investigated 32 women with BC and documented bone metastases. All patients underwent 18F-FDG PET/CT and 18F-NaF PET/CT within 60 days of each other and no treatment was administered between the two scans. Semi-quantitative parameters were applied to 18F-FDG PET/CT and 18F-Na-PET/CT in order to evaluate disease extent and tumour metabolism. Electronic medical records were reviewed to determine known prognostic variables, including age, proliferative index Ki-67%, presence of visceral metastases, current hormone therapy, duration of bone disease and response to first-line therapy, as well as PFS and OS, which was calculated from the date of initial diagnosis scans to the date of either death or last follow-up. Results: The sensitivity of 18F-NaF-PET/CT (100%) was higher ($p<0.05$) than that of 18F-FDG-PET/CT (72% and 72%). None of the 18F-FDG-PET/CT-negative patients showed disease progression at the end of follow-up. After adjustment for age, Ki-67 levels, presence of visceral metastases, hormone therapy, duration of bone disease and response to first-line therapy, only 18F-FDG SUV mean [HR 15.7, 95% confidence interval (CI) 1.15-214.5] and 18F-FDG whole-body bone metabolic burden (WB-B-MB) (HR 16.9; 95%CI 1.87-152.2) were independently and significantly associated with OS. None of the 18F-NaF-PET/CT parameters were associated with OS. None of the conventional clinical prognostic parameters remained significantly associated with OS after the inclusion of PET/CT parameters in the model. Conclusion: our data showed that 18F-FDG PET/CT scores were highly and independently associated to PFS and OS in patients affected by bone metastases from BC. Their prognostic impact seems to be higher than that of the other clinical and biological prognostic factors included in the study. 18F-NaF PET/CT scores, despite the higher diagnostic sensitivity of this modality, are not independently associated to OS. The prognostic value of 18F-FDG seems to be similar to, or slightly higher than, the combined value of 18F-NaF and 18F-FDG.

P588

18F-Fluoroestradiol positron emission tomography in breast cancer patients: systematic review of the literature & meta-analysis

L. Evangelista1, M. Dieci1, A. Cervino1, G. Saladini1, P. Conte1,2, V. Guarneri1,2; 1Istituto Oncologico Veneto I.R.C.C.S., PADOVA, ITALY, 2University of Padua, Padova, ITALY.

Introduction: the aim of the study was to determine the correlation between 16α-18F-fluoro-17β-estradiol (18F-FES) uptake and the expression and functionality of estrogen receptors (ERs), as well as to evaluate the ability of 18F-FES PET to predict the response to hormonal therapy (HT) in patients with locally advanced or metastatic breast cancer (BC). Methods: Literature searches in the major literature databases were carried out in order to select English-language articles dealing with 18F-FES PET and BC. Studies that included patients with BC undergoing 18F-FES PET alone or in combination with other imaging modalities and included the absolute numbers of true-positive, true-negative, false-positive and false-negative test results were selected. Reviews, clinical reports and editorial articles were excluded. All journal articles were re-assessed before qualitative and quantitative analysis. Results: We found 23 journal articles, published between 1988 and December 2014, that critically evaluated the role of 18F-FES PET in BC patients. Two separate meta-analyses were carried out: the first to assess the correlation between 18F-FES uptake and ER expression and the second to determine the predictive value of FES in response to HT. For the first meta-analysis, we considered nine selected studies with a total of 238 patients. The meta-analysis provided a pooled sensitivity of 82% (95% CI: 74-88%) and a pooled specificity of 95% (95% CI: 86-99%) for the evaluation of ER functional status by 18F-FES PET. The diagnostic odds ratio (DOR) was 38.79 (95%CI: 13.0-115.4). Seven studies, with a total of 226 patients, were considered eligible for the analysis of prediction for response. The pooled sensitivities and specificities were 59.3% (95% CI: 38.8-77.6%) vs. 66.7% (95% CI: 52.1-79.2%), and 29.1% (95% CI: 17.6-42.9%) vs. 62.1% (95% CI: 48.4-74.5%), for a SUV cut-off of 1.5 and 2.0, respectively. Conclusion: from the present systematic review and meta-analysis, a good correlation between 18F-FES uptake and ER expression by immunohistochemistry emerges, while the role of 18F-FES in predicting the response to endocrine therapy in advanced BC remains undetermined.

P589

The Value of Molecular Breast Imaging in the Initial Work-up of Women with Proven Breast Cancer Scheduled for Breast Conserving Therapy

A. Collarino1,2,3, L. M. Pereira Arias-Bouda2,3, F. Smit2,3, P. Neijenhuis4, L. M. H. Wijers5, A. F. Van der Hoeven3, K. Hofkes-Fillekes5, A. Zeillemaker4, R. A. Valdés Olmos2; 1Institute of Nuclear Medicine, Università Cattolica del Sacro Cuore, Roma, ITALY, 2Department of Nuclear Medicine, Leiden University Medical Center, Leiden, NETHERLANDS, 3Department of Nuclear Medicine, Alrijne Hospital, Leiderdorp, NETHERLANDS, 4Department of Surgery, Alrijne Hospital, Leiderdorp, NETHERLANDS, 5Department of Radiology, Alrijne Hospital, Leiderdorp, NETHERLANDS.

Aim: The purpose of this retrospective study was to investigate the additional value of dedicated Molecular Breast Imaging (MBI) using 99mTc-Sestamibi as an adjunct modality to mammography (MG) and ultrasound (US) in assessing multifocal and/or multicentric disease in the clinical work-up of patients with proven breast cancer (BC) scheduled for breast conserving therapy (BCT). Materials and Methods: A total of 378 patients (mean age 60, range 30-88y) with proven BC, scheduled for BCT, were included in this analysis. All patients underwent MBI using a high-resolution small-field-of-view gamma camera (Dilon 6800, Dilon Technologies, Newport News, VA) in order to determine additional tumor lesions. After injection of 600 MBq of 99mTc-Sestamibi into an antecubital vein contralateral to the breast lesion, planar images in two standard projections (cranio-caudal and latero-oblique) of both breasts were performed, followed by an additional image (medial or lateral) of the breast with the index lesion. The scintigraphic images were directly compared with the most recent MG and interpreted according to a locally developed modified functional BI-RADS classification. In case of suspicious additional lesions on MBI, second-look US followed by US-guided biopsy was performed. If second-look US showed no substrate, follow up was agreed in these cases. Results: In 44/378 (12%) patients, MBI detected 62 additional lesions occult on MG/US. Histopathology confirmed 22 additional breast cancer lesions in 20 patients: 14 (64%) invasive ductal carcinoma, 2 (9%) lobular carcinoma, and 6 (27%) ductal carcinoma in situ. Five patients had benign lesions and in 19 patients, lesions remained unknown. In ten of 20 patients, additional malignant lesions were located in a different quadrant compared to the index lesion, in two patients both in a different quadrant and contralateral, and in one patient only contralateral. Due to the identification of additional cancer lesions, surgical management was adjusted in 13 patients. Conclusion: MBI seems to be a very useful imaging modality in revealing multifocal/multicentric lesions and bilateral disease not seen in other modalities. Incorporation of this modality to the work-up may lead to select patients who could benefit of breast conserving surgery.

P590

Diagnostic value of 99mTc-bombesin scintigraphy for differentiation of malignant from benign breast lesions

K. Aryana, F. shariati, A. Fattahi, A. Azarian; Mashhad university of medical scinences, Mashhad, IRAN, ISLAMIC REPUBLIC OF.

Objective: In this study, we evaluated the diagnostic accuracy of 99mTc-bombesin scintigraphy for differentiation of benign from malignant palpable breast lesions.99mTc-Bombesin is a tracer with high affinity for gastrin releasing peptide receptor, which is over expressed on a variety of human tumors including breast carcinoma. Materials and methods: We examined 33 consecutive women who were referred to our center with suspicious palpable breast lesions but had no definitive diagnosis in other imaging procedures. A volume of 370-444MBq of 99mTc-bombesin was injected and dynamic 1-min images were taken for 20 min immediately after injection in anterior view. Thereafter, two static images in anterior and pronelateral views were taken for 5 min. Finally, single-photon emission computed tomography images were taken for each patient. Definitive diagnosis was based on biopsy and histopathological evaluation. Results: The scan findings were positive in 19 patients and negative in 11 on visual assessment of the planar and single-photon emission computed tomography images. Pathologic examination confirmed breast carcinoma in 12 patients with positive scans and benign pathology for 18 patients. The overall sensitivity, specificity, negative and positive predictive values, and accuracy of this radiotracer for diagnosis of breast cancer were 100, 66.1,100, 63, and 76%, respectively. Semiquantitative analysis improved the specificity of the visual assessment from 66 to 84%. Conclusion: Our study showed that 99mTc-bombesin scintigraphy has a high sensitivity and negative predictive value for detecting malignant breast lesions, but the specificity and positive predictive value of this radiotracer for differentiation of malignant breast abnormalities from benign ones are relatively low

P591

Predictive and Prognostic Value of FDG-PET/CT Imaging and Different Response Evaluation Criteria after Primary Systemic Therapy of Breast Cancer

T. Tokes1, K. Kajáry2, G. Szentmártoni3, Z. Lengyel2, T. Györke4, L. Torgyík3, K. Somlai5, A. Tőkés6, J. Kulka7, M. Dank8; 1Semmelweis University, Budapest, HUNGARY, 2Pozitron PET/CT Center, Budapest, HUNGARY, 3Semmelweis University, 1st Dept. of Medicine, Oncological Division, Budapest, HUNGARY, 4Semmelweis University Department of Nuclear Medicine and Scanomed Ltd, Budapest, Budapest, HUNGARY, 5Surgical Division of the St Margaret Hospital, Budapest, HUNGARY, 6MTA-SE Tumor Progression Research Group, 2nd Department of Pathology, Budapest, HUNGARY, 7Semmelweis University 2nd Department of Pathology, Budapest, HUNGARY, 8Semmelweis University, 1st Dept. of Internal Medicine, Oncological Division, Budapest, HUNGARY.

Objective: We introduced a simplified, PET Response Criteria in Solid Tumors (PERCIST) based 18F-fluoro-deoxy-glucose positron emission tomography and computerized tomography (FDG-PET/CT) score (Method 1) and a novel, combined FDG-PET/CT score supplemented with the morphological

results of the Response Evaluation Criteria in Solid Tumors (RECIST) system (Method 2) to define clinical complete remission (CR) after primary systemic therapy (PST) in breast cancer. We assessed the accuracy of these criteria in the prediction of pathological complete remission (pCR) and evaluated their prognostic value for progression free survival (PFS) and overall survival. Methods: Seventy-one patients were enrolled in the study who underwent FDG-PET/CT imaging before and after PST. PET/CTs were evaluated by changes in maximum Standardized Uptake Value (SUVmax) and tumor size. Method 1 and 2 were applied to predict pCR and their prognostic value for survival were assessed. Because tumor metabolic behavior could vary between biological subtypes, effects of biological subtypes on tumor response and its evaluation were also analyzed. For survival analyses, Kaplan-Meier product limit methods were performed with log-rank tests. Results: A total of 23/71 patients showed pCR (32.4%). Comparing pCR/non-pCR patient groups significant differences were detected by changes in SUVmax ($p<0.001$) and tumor size ($p<0.001$) regarding the primary breast lesions. For detection of pCR, Method 2 had higher sensitivity (75% vs 43.75%) and negative predictive value (60% vs 43.75%) with lower false negativity rate (12 vs 27) than Method 1. Despite the significant differences detected between the biological subtypes regarding changes in primary tumor SUVmax and size parameters ($p=0.004$; $p=0.035$, respectively), the subtypes showed no significant impact on response evaluation with Method 1 and Method 2. In our study, neither clinical nor pathological CR was predictor of longer survival. Conclusions: Our results suggest that combined criteria are more predictive of pCR than the simplified PERCIST-based response evaluation. The effect of biological subtypes should still be taken into consideration during the response evaluation; however they had no impact on the assessment with Method 1 and Method 2.

P592

Can 18F FDG PET/CT be a new tool in the prognostic armamentarium of carcinoma breast ? Correlating 18F FDG uptake values with histopathological markers in primary breast cancer

M. Ravina1,2, M. Chauhan2, M. Jacob2, A. Pandit2, N. Sanchety2; 1Sanjay Gandhi Post Graduate Institute of Medical Sciences, Lucknow, Uttar Pradesh, INDIA, 2Army Hospital Research and Referral, New Delhi, INDIA.

Objectives: The correlation between 18F-Fluorodeoxyglucose(FDG) standardized uptake values with histopathological prognostic markers in patients with primary breast cancer was studied.Methods: 115 patients (113 females and 2 males) of biopsy proven primary breast cancer underwent 18F FDG PET/CT scan. Standardised uptake values (SUV) were compared with various clinicopathological variables.Results: In a univariate analysis 'T' stage/tumor size correlated significantly with SUV max values. T1 (n=10; median SUV, 3.8), T2 (n=49; median, 5.9), T3 (n=11; median, 8.2), T4 (n=42; median,9.1) (p=.009). Mean SUV (max) of metaplastic lesions (8.6) were higher than that of ductal (8.0) & lobular (2.9) carcinoma. Median SUV (max) of high grade tumors were 8.2 vs. 4.9 of low grade tumors. Progesterone receptor (PR) negative tumors (n=75; median, 8.3) had high SUV max values than PR receptor positive tumors (n=37; median,5.4) ($p< .001$). High uptake values were noted in estrogen recptor negative lesions (n=72;median,8.2) as compared to ER positive lesions (n=40;median,6.2)(p=.011). No significant correlation was noted between SUV max values and Her2Neu receptor status, perineural & lymphovascular invasion. Median SUV max of triple negative breast cancers (n=38;median,8.8) was higher than that of ER+/PR+/Her2- (n=31;median,4.9 , P 0.001) lesions. Multivariate analyses showed tumor size and progesterone receptor negativity were significantly correlated with SUV in primary breast cancer (P , 0.046 and ,0.009, respectively).Conclusions: High tumoral SUV levels may serve as a pretherapeutic indicator of aggressiveness of breast cancer & poor prognosis. Preoperative prediction of patient prognosis is important in a setting of neoadjuvant chemotherapy.

P593

Clinical utility of 18F-FDG PET/CT scan in younger than 40 years breast cancer patients

R. V. PARGHANE, **Sr**., R. Phulsunga, Jr, K. Agrewal, Sr., B. Mittal, Prof., A. Bhattacharya, Prof., A. Sood, Consultant; PGIMER, CHANDIGARH, INDIA.

Aim: 18F-FDG PET/CT is useful only in clinical stage III breast cancer patients as per NCCN guidelines. However, TNM staging should not be the only factor in clinical evalution of breast cancer patients and age of patient may be considered as additional factor. As young breast cancer patients often have more potential for early metastases. Younger breast cancer patients are likely to die than older patients; this is may be due to higher rate of metastatic disease undetected by conventional staging method. So, aim of this study was to evaluate the role of 18 F-FDG PET/CT in staging, restaging and changes in management of younger breast cancer patients. **Material and Methods**: Total 3100 breast cancer patients undergone PET/CT from April 2010 to December 2013, were reviewed retrospectively. Out this, only 122 breast cancer patients younger than 40 years were included in this study. Clinical staging of all younger breast cancer patients were determined based on physical examination, mammography, ultrasound and other

imaging before PET/CT. PET/CT was done within 2 weeks of clinical staging to evaluate extra-axillary lymph nodal, distant metastases and changes in patient management.**Results**: Total 122 younger diagnosed patients of breast cancer were analyzed with mean age of 30 years (range 22-40 years) and clinically stage I in 12 patients,stage II in 68 patients and stage III in 42 patients were found in this study. PET/CT was used for initial staging in 54 patients, restaging/ response evalution in 34 patients and recurrence detection in 34 patients. 40 patients were undergone second time/ follow up PET scans. PET/CT detected abnormal extra-axillary lymph nodes in 67 patients, lung lesions in 15 patients, bone lesions in 30 patients, liver lesions in 7 patients and PET/CT scan changes in clinical stage from II/III to stage III/IV in 52 patients. The lesion found on PET/CT was confirmed byhistopathologically; follow up PET / conventional imaging and clinical follow up. Based on PET/CT finding patient's management were changed in 31 patients, out this 9 patients undergone additional surgery, 3patients undergone chemo-radiotherpy and 19 patients undergone additional/changes in chemotherapy after PET/CT.**Conclusions**: Our result show, PET/CT scans detected distant metastases in 35 patients and changes management in 31 patients. Therefore our results show, usefulness of PET/CT in younger than 40 year breast cancer patients with clinical stage I/II and PET/CT can avoid unnecessary therapy and reduce morbidity and cost of patients management.

P594

[18F]FDG-PET/CT results predict outcome in breast cancer

M. Sollini1, B. Zangheri1, L. Calabrese1, M. Di Paolo2, A. Versari2, M. Gasparini1; 1IRCCS; MultiMedica, Sesto San Giovanni, ITALY, 2Santa Maria Nuova Hospital IRCCS, Reggio Emilia, Reggio Emilia, ITALY.

Aim: Breast cancer (BC) is the most commonly diagnosed cancer among women. The role of [18F]FDG-PET/CT in the management of BC patients is increasing. We aimed to assess the role of [18F]FDG-PET/CT to stage and to predict outcome in breast cancer.Materials and methods: 48 female (one bilateral) with histology proven breast cancer (ductal 46, lobular 3) were retrospectively analysed. Staging [18F]FDG-PET/CT was performed pre- (39) or post-surgery (9). [18F]FDG upatke in primary tumor (T), lymph node(s) (N) or distant (M) metastases was considered. Patients were divided in group 1 (PET/CT positive for N and/or M and any T) and group 2 (PET/CT negative for N or M and any T). Patients were followed by clinical/instrumental examinations. Disease-free survival (DFS) was calculated. P-value <0.05 was considered significant. Multivariate analysis was performed to assess the indipendent prognostic role of PET/CT along with the following factors: age at diagnosis, histology, ki-67 index and triple negative hormonal status. Kaplan-Mayer curves were analysed.Results: Mean DSF was 701±444 days. 36 patients had negative follow-up, 10 patients had progressive disease and 2 patients had stable disease. [18F]FDG-PET/CT resulted completely negative in 14/48 patients. [18F]FDG uptake was seen only in T in 16 patients, only in N in 3 cases, in T + N in 10 cases, in T + M in 1 case, in T + N + M in 4 patients, and in N + M in 1 case. Sensitivity, specificity and accuracy of PET/CT were 82%, 100%, 86% for T, 61%, 95%, 76% for N, and 100%, 95%, 95% for M parameter respectively. PET/CT changed stage of disease (all upgraded) and management in 6/48 and 4/48 patients, respectively. DFS was lower (893±110 versus 1944±173 days, p <.05) in group 1 compared to group 2. Survival analysis demonstrated a significant difference between group 1 and group 2 (Log Rank= .033). At multivariate analysis only a positive PET/CT at staging for N and/or M (any T) was independently associated with prognosis (p= .041), while other parameters were not retained.Conclusion: Our results demonstrated the potential useful role of [18F]FDG-PET/CT to stage and assess prognosis in breast cancer. Despite these preliminary data have to be confirmed by prospective larger studies, our findings support the clinical use of this approach.

P595

Quantification of Dual Time Point FDG-PET/CT in Bone Lesions in Breast Cancer Recurrence

J. A. Hansen1, M. G. Hildebrandt1, O. Gerke1, C. Baun1, K. Falch1, S. Duvnjak2, A. Alavi3, P. F. Høilund-Carlsen1; 1Department of Nuclear Medicine, Odense University Hospital, Odense C, DENMARK, 2Department of Radiology, Odense University Hospital, Odense C, DENMARK, 3Division of Nuclear Medicine, University of Pennsylvania, Philadelphia, PA, UNITED STATES.

Aim: The role of FDG-PET/CT in the diagnosis of morphologically different types of bone lesions is undefined. The aim of this study was to estimate the partial volume corrected mean standardized uptake value (cSUVmean) in different types of bone lesions using dual time point (DTP) FDG-PET/CT. Material and methods: As part of a larger prospective study in suspected recurrent breast cancer, 14 patients underwent DTP FDG-PET/CT with 1 hour (1h) and 3 hour (3h) images. All had bone recurrence verified by biopsy, clinicians' decision of treatment, and/or follow-up. An experienced radiologist categorized the bone lesions according to CT into osteolytic, osteosclerotic, mixed, or not CT-detectable metastases. Dedicated software (ROVER, ABX, Radeberg, Germany) was used to determine cSUVmean1h and cSUVmean3h. The FDG avid volumes (cm3), the difference (ΔcSUVmean)

between 1h and 3h images, and the relative change (%Change=(ΔcSUVmean /cSUVmean1h)*100) were calculated. Wilcoxon analysis was used to test for differences between 1h and 3h cSUVmean and one-way ANOVA to test for difference between bone lesion types. Results: A total of 229 lesions in 14 patients were detected with a median of 2.5 lesions per patient (range 1-98). Classification of lesions by CT showed 54 (23.6%) osteolytic, 14 (6.1%) osteosclerotic, 92 (40.2%) mixed, and 69 (30.1%) not CT-detectable. The median cSUVmean1h was 7.1 (range 0.9-13.8), 8.2 (3.5-17.0), 7.5 (2.1-19.9), and 5.7 (1.2-15.9) in osteolytic, osteosclerotic, mixed and not CT-detectable lesions, respectively, and the corresponding median volumes were 8.1 (4.9-11.4), 6.3 (2.8-9.7), 6.7 (4.8-8.7), and 4.7 (3.5-6.0). The median cSUVmean3h was 8.9 (1.1-20.1), 10.0 (4.2-14.2), 10.5 (2.9-36.3), and 6.5 (2.4-19.1) with corresponding median volumes of 9.3 (8.0-10.5), 9.7 (7.9-11.4), 11.1 (10.0-12.3), and 7.8 (6.9-8.7), respectively. There was statistically significant increase for all lesion types from cSUVmean1h to cSUVmean3h ($p<0.0001$). The median %Change was 31.4 (32.4-209.2) for osteolytic, 19.6 (-34.7-111.4) for osteosclerotic, 39.5 (-63.8-366.7) for mixed and 25.0 (-66.0-170.8) for not CT-detectable lesions. Mixed and not CT-detectable lesions were statistically different with regard to cSUVmean1h ($p= 0.003$), cSUVmean3h ($p<0.001$), and ΔcSUVmean ($p= 0.043$). No statistically significant differences were found for other groups or %Change. Conclusion: Morphologically different bone lesions had relatively high FDG uptake, all with a significant increase from 1h to 3h imaging. Our results showed only minor difference in FDG uptake between morphologically different bone lesions, hence FDG-PET/CT has proven worthy in detection of any type of bone recurrence.

P596

Effectiveness and cost-effectiveness analysis of radical axillar lymphadenectomy after a positive sentinel node in breast cancer

P. Serra-Arbeloa, Á. O. Rabines-Juárez, F. Domínguez-Cunchillos, C. de Miguel-Medina, C. Artieda-Soto; Complejo Hospitalario de Navarra, Pamplona, SPAIN.

Aim: The aim of this study was to determine the effectiveness and cost-effectiveness of the radical axillar lymphadenectomy (RAL) compared with no RAL and observation only (NRAL) in breast cancer patients after a conservative surgery and axillary sentinel node biopsy with a maximum of 2 positive sentinel nodes (SNs), over a 5 year time horizon and using the health care system perspective. Methods: A tree decision model was used to estimate the direct costs and the effectiveness measured in life years saved (LYSs), quality-adjusted life years (QALYs), and the presence of adverse events, such as lymphedema, of the two studied strategies (RAL vs. NRAL). Different costs and utility values were assigned to their respective model health states. Model input parameters, including relapse rates, mortality rates, utility values and costs, were obtained from the published literature and the government official publications. Results: Usual care (RAL) had the highest expected costs, 22,269 €/patient and the lowest effectiveness, 4.31 LYSs and 2.71 QALYs. The alternative strategy (NRAL) had lower costs, 17,597 €/patient, and higher effectiveness in both LYSs, 4.38, and QALYs, 2.81. The incremental cost effectiveness ratio for RAL was estimated to be -69, 209 €/LYs and -46,369 €/QALYs (Northwest quadrant; RAL dominated by NRAL). Taking into account adverse events, apart from the decrease in quality of life of patients following RAL, an increase of 87 € per treated patient is associated with the lymphedema. Conclusions: NRAL appears to be a more cost-effective strategy compared with RAL. NRAL allows reducing the cost with no decrease of quality of life in breast cancer patients.

P597

Defining the nodal status in the initial staging of patients with locally advanced breast cancer: Where must PET/CT stand?

B. E. Akkas, B. Demirel, G. Ucmak, S. Demirtas; Ankara Oncology Research and Training Hospital Department of Nuclear Medicine, Ankara, TURKEY.

In this study, we aimed to investigate the impact of FDG PET/CT at initial staging of patients with locally advanced breast cancer (LABC) and compared PET/CT performance with that of conventional distant work-up.Methods: 52 patients with LABC underwent FDG PET/CT for initial staging and included in this retrospective study. All patients had clinical T3-T4 or N2 disease. The performance of PET/CT was compared with that of a conventional staging approach including bone scan, chest radiography, abdominal and pelvic ultrasound or contrast-enhanced CT.Results: 47 patients had invasive ductal carcinoma, 1 had inflammatory carcinoma and 4 patients had other subtypes. Clinically; 3 patients had stage 2, 42 patients had stage 3 and 7 patients had stage 4 disease. PET/CT confirmed N2 disease in 29 patients and revealed unsuspected N3 nodes (infraclavicular, supraclavicular, or internal mammary) in 19 additional patients. PET/CT detected supraclavicular lymph nodes (LN) in 7 patients, internal mammarian LN in 4 patients, both supraclavicular and internal mammary LN in 6 patients and metastatic LN in the contralateral axilla in 2 patients. Almost all distant lesions detected by conventional imaging were depicted with PET/CT, which also showed additional lesions. In addition, PET/CT detected distant metastasis in 12 patients that were not diagnosed by conventional

techniques. The sites of metastatic disease were as follows; bones (n:7), mediastenum (n:1), contralateral breast (n:1) and multiple sites (n:3). Following PET/CT, clinical stage was upstaged in 19 patients (36.5%) of whom N3 disease was diagnosed in 7 patients and M1 disease was detected in 12 patients. Additionally, PET/CT excluded metastatic disease in 4 patients who had equivocal findings on conventional imaging modalities.Conclusion: Breast cancer stage at presentation is an important factor in prognosis and treatment. Nodal status in patients with LABC is one of the major factors that may alter treatment plan. FDG PET/CT has the advantage of scanning whole body in a single session and may change the clinical stage in a considerable percent of patient population. In our study, by providing accurate initial staging, PET/CT changed clinical management in 36.5% of patients with LABC. We conclude that PET/CT must be performed in all patients with clinical T3 and T4 tumors.

P598

Diagnosing bone metastasis in recurrent breast cancer: dual time FDG-PET/CT compared to contrast enhanced CT and bone scintigraphy

M. G. Hildebrandt1, J. Ansholm1, O. Gerke1, C. Baun1, K. Falch1, Z. Farahani1, S. Duvnjak1, L. Larsen1, I. Buskevica1, S. Bektas1, A. Alavi2, P. Hoilund-Carlsen1; 1Odense University Hospital, Odense, DENMARK, 2University of Pennsyalvania, Philadelphia, PA, UNITED STATES.

Aim: The optimal modality for diagnosing bone metastases in breast cancer has been debated in literature. The aim of this study was to investigate the role of dual time FDG-PET/CT in diagnosis of bone recurrence in breast cancer compared to contrast enhanced CT (ceCT) and bone scintigraphy (BS).Material and methods: In a prospective design, 100 female patients with suspected recurrent breast cancer underwent 1hour (1h) and 3hour (3h) FDG-PET/CT, ceCT and BS within a median time interval of 10 days. Images were interpreted visually, and readers were blinded to other test results. Biopsy, clinicians' decision of treatment, and clinical follow-up served as reference standard. Patient based accuracy results were calculated, including measures of area under the receiver operating curve (AUC-ROC), based on visually interpreted 4-point assessments, including 95% confidence intervals (CI). Further, in 14 patients with verified bone recurrence preliminary lesion based analyses were made. The bone lesions were categorized according to the CT images as osteolytic, osteosclerotic, mixed, or as not detected; hence lesion based sensitivity was obtained for stratified groups of bone lesions. Patients with a BS 'superscan' were considered positive in all lesions.Results: Eighteen patients (18%) were confirmed to have bone recurrence. Patient based analyses revealed no difference between 1h and 3h FDG-PET/CT. AUC-ROC, sensitivity, specificity, and likelihood ratios for positive and negative tests for FDG-PET/CT was 0.99 (0.98-1), 1 (0.82-1), 0.98 (0.92-0.99), 41.0 (10.4-161.0), and 0 (N/A); for ceCT, 0.82 (0.71-0.94), 0.61 (0.39-0.80), 0.99 (0.93-1), 50.1 (6.9-364.0), and 0.4 (0.2-0.7); for BS, 0.86 (0.77-0.96), 0.78 (0.55-0.91), 0.87 (0.78-0.92), 5.8 (3.2-10.6), and 0.3 (0.1-0.6); and for the combined ceCT+BS 0.89 (0.81-0.97), 0.83 (0.61-0.94), 0.85 (0.76-0.91), 5.7 (3.3-10.0), and 0.2 (0.1-0.6), respectively. A total of 229 lesions in 14 patients were detected (median number of lesions per patient: 2.5; Range: 1-98). Classification of lesions by CT showed 54 (23.6%) osteolytic, 14 (6.1%) osteosclerotic, 92 (40.2%) mixed, and 69 (30.1%) not detected by CT. The lesion based sensitivity was 99.1% (95% CI: 96.9-99.9) for FDG-PET/CT 3h, 98.3% (95.6-99.5) for FDG-PET/CT 1h, 87.8% (82.8-91.7) for BS, and 69.9% (63.5-75.7) for ceCT. BS detected significantly less of the lytic metastases (30/54) than of other bone metastatic types (171/175); $p<0.0001$.Conclusion: The overall patient based accuracy for diagnosing bone recurrence was significantly higher with FDG-PET/CT than with conventional imaging technology. With inconsiderable difference between 1h and 3h imaging, FDG-PET/CT detected significantly more metastatic bone lesions than did BS or ceCT.

P599

18F-FDG PET/CT is most cost-effective for screening distant metastases in stage II/III breast cancer patients

S. C. Teixeira, A. Miquel Cases, R. A. Valdes Olmos, E. J. T. Rutgers, W. van Harten; Netherlands Cancer Institute - Antoni van Leeuwenhoek Hospital, Amsterdam, NETHERLANDS.

Aim: 18F-FDG Positron Emission Tomography with Computed Tomography (PET/CT) has recently been shown to have a high sensitivity and specificity for detecting distant metastases in breast cancer patients before start of pre-operative systemic treatment (PST). Nevertheless PET/CT is insufficiently accepted in current medical practice, mainly due to its higher costs. Our aim is to assess the cost-effectiveness of 18F-FDG PET/CT for distant metastasis screening in stage II/III breast cancer compared to the golden standard assessment in the Netherlands (X-thorax, liver sonography and bone scan). Materials and methods: We included protectively collected data from all primary stage II/III breast cancer patients treated in the Netherlands Cancer Instiute - Antoni van Leeuwenhoek (NKI-AVL) hospital from 2007 to 2013 with PST and who received PET/CT for distant metastasis screening (n=545). We constructed four Markov decision models to compare the health-economic consequences of performing distant metastasis screening with 18F-FDG PET/CT or with the 'golden standard' in four subtypes (ER+/HER2-, HER2+/ER+, HER2+/

ER-and HER2-ER-). Sensitivity and specificity of both imaging scenarios were calculated using data from 2013 as a proxy to determine the type of systemic (neo-adjuvant & adjuvant) and local (surgery & radiotherapy) treatments administered. Costs were derived from tariffs in 2013. Epidemiological (i.e., patterns of metastasis per subtype), survival and utility data were estimated from literature or by making assumptions based on our database. Model outcomes (incremental life years (LY), quality-adjusted-life years (QALYs), costs (€), and cost-effectiveness ratio (ICER)) were calculated at a time horizon of 5-years. Cost-effectiveness was determined against the prevailing threshold of €80.000/QALY for severe diseases in the Netherlands. Results: PET/CT had a higher sensitivity (53% vs. 15%) and specificity (97% vs. 94%) than did the golden standard. Compared to the golden standard, performing distant metastasis screening with PET/CT would result in 0.02 life-years gained or 0.01 after adjusting for quality-of-life. These gains were expected similar across the subtypes. The additional costs of distant metastasis screening with PET/CT ranged between €325 and €532 (ER+/HER2-:€532; ER+/HER2+:€450; ER-HER2-:€370; ER-/HER2+:€325). In all subtypes, the increase of costs of screening with PET/CT was outweighed by the health benefits achieved thus resulting in cost-effective results (all ICERs were below €80.000/QALY; ER-/HER2+:€26.587/QALY; ER-HER2-:€31.212/QALY; ER+/HER2+:€48.587/QALY; ER+/HER2-:€59.475/QALY). Conclusion: While PET/CT does increase the costs for distant metastasis screening in stage II/III breast cancer, these seem to be outweighed by an increase on health outcomes resulting from improved diagnostic performance. Importantly, this is expected for all breast cancer subtypes.

P600

Sentinel lymph node biopsy in breast cancer in patients with previous breast surgery

J. Orozco-Cortés1, R. Díaz-Expósito1, I. Casáns-Tormo1, S. Prado-Wohlwend1, H. Bowles-Antelo1, A. Caballero-Garate2, A. Almarcha-Gimeno3; 1Hospital Clínico Universitario. Servicio de Medicina Nuclear, Valencia, SPAIN, 2Hospital Clínico Universitario. Servicio de Cirugía General, Valencia, SPAIN, 3Hospital Clínico Universitario. Unidad de Radiofarmacia, Valencia, SPAIN.

AIM: The previous breast surgery could produce changes in the lymphatic drainage. We have analyzed our results in the sentinel lymph node biopsy in patients who have had this precedent. MATERIAL AND METHODS: Retrospective study in 69 women, age 29-86(53) years old, with palpable lesions in 10 and non-palpable in 59, 49(71%) with infiltrative carcinoma. Our patients were classified in three groups. Group 1:13(18.8%) patients with breast implants; group 2: 47(68.1%) patients with previous tumorectomy for various reasons and one month to the SLNB realization; group 3: 8(11.5%) patients with breast reduction surgery. One patient had tumorectomy and breast implant. We administered 2 mCi of 99m-Tc albumin nanocolloid by intratumoral injection in 19 patients (27.5%) with periareolar reinjection in 5 (palpable lesion and ultrasound guided or stereotaxy in the non-palpable lesions) and periareolar in 50 (72.4%), at the same day of surgery, performing planar lymphoscintigraphy (PL) in different projections, intraoperative detection with hand held gammaprobe, intraoperative pathologic analysis of the SN (OSNA) and differed inmunohistochemistry. RESULTS: The global sentinel node detection was 89.9%(62/69): 92.3%, group 1, 87.2%, group 2 and 100%, group 3. The detection in the groups without tumorectomy (1 + 3) was higher (95.2%) than in the tumorectomy group (87.2%)($p<0.05$). The detection after intratumoral injection was 78.9%(15/19) against 88%(44/50) when the injection was periareolar. The axillary migration was homolateral in 61 patients, in 3 with additional internal mammary lymph nodes migration and in 1 with additional contralateral axillary migration. In one patient the migration was in the internal mammary lymph nodes exclusively. We didn't detect sentinel nodes with lymphoscintigraphy in 7 patients although there was surgical detection in 1. The characteristics of these 7 patients were: 6 with previous tumorectomy, 1 with tumorectomy and mammary implant, average age 61.2 years old, non palpable lesions in all. When the sentinel node was removed there was pathological involvement in 11/62(17.7%). The lymphadenectomy was made in 10 and showed involvement, in addition to sentinel node, in 4/10 patients. In the 7 patients without sentinel node migration only one showed lymph involvement(micrometastasis) after lymphadenectomy. CONCLUSIONS: Although the sentinel node global detection in patients with previous breast surgery was slightly lower than the optimal value (95%), it is still useful in order to avoid unnecessary lymphadenectomies. The patients with previous tumorectomy showed lower detection values because of possible alterations in the lymph drainage. We haven't found an increase in the extra axillary drainage.

P601

Combined use of portable gammacamera and mammography for the margin delimitation in Radioguided Occult Lesion Localization (ROLL) in breast cancer.

H. Rodriguez, L. Marbello, P. Abreu, M. Reyes, D. Balaguer, E. Caballero, T. Mut, C. Plancha; University Hospital Dr. Peset, Valencia, SPAIN.

Objective: Inadequate surgical margins in breast neoplasia require a reoperation. Our goal is to assess the added value the portable gammacamera images bring to mammography alone in surgical margin delimitation in non-palpable breast tumors. Material and methods: We conducted an ambispective study of 70 consecutive patients with ROLL (Radioguided Occult Lesion Localization) in non-palpable breast cancer. 37-148 MBq of 99mTc-nanocolloid albumin in 0.3 ml were injected intratumorally guided by ultrasound. After tumor resection, clear margins (CM) of the surgical specimen were determined with portable gammacamera (Sentinella®) placed 10 cm away from the sample, considering 3 images: surgical bed, excised tumor and tumor margins with the aid of an external point source; CM were considered when the images of the tumor and its contour drawn by an external point source didn't contact. Then, mammography of the tumor was done. Margins were extended during the same surgery when insufficient CM were suspected after using either of the two techniques. If histology resulted in a surgical margin of 1 mm or less, delayed reoperation was mandatory. The ability to predict positive margins using both methods was checked against histology. Tumors were classified attending to their size, morphology, localization and radiotracer placement. False negatives (FN) were considered relevant as were the discrepancies between gammacamera images and mammography and the causes of error. Results: Portable gammacamera images recommended to extend surgical margins in 37 out of 70 surgeries; mammography recommended extended surgery in 33 out of 70. There were discrepancies between both methods in 14 cases. Compared to histology, the portable gammacamera images had S: 75% E: 54% PPV: 32% NPV: 88%, and mammography S: 56% E: 55%, PPV: 27% and NPV: 81%. FN ratio (mammography/gammacamera)=7/4 = 1.75. McNemar's test was applied to paired data showing no significant difference between the two techniques (P> 0.05), but the gamma images prevented 3 out of 70 reoperations, while mammography had 3 FN. Both techniques agreed on 3 other FN: 1 microcalcifications, 1 carcinoma in situ on surgical margin and 1 after neoadjuvant therapy. 1 FN occurred solely with the portable gammacamera on a bilobed tumor. Conclusion: Portable gammacamera images combined with mammography reduce reoperation caused by positive margins. Tumors with irregular contours are more prone to insufficient resection.

P602

Analysis of the metabolic heterogeneity of breast tumors with FDG-PET/CT

B. Farkas; University of Debrecen, Debrecen, HUNGARY.

Objective: F18-FDG PET/CT examinations are part of the oncological diagnostic algorithm in the majority of malignant diseases. Judging the metabolism of tumors is not only substantial in the differentiation between benign and malignant lesions but also has prognostic importance. In clinical practice usually different standard uptake value (e.g. mean, maximum) and metabolic tumor volume based parameters are used for the characterization of tumor metabolism. The analysis of intratumoral heterogeneity is a new concept in the quantification of metabolism. We would like to examine the correlation between heterogeneity parameters and clinical stage, hormone receptor status, and other molecular pathological markers. Methods: We retrospectively evaluated the initial FDG-PET/CT scans of 32 patients examined in our institute. Exclusion criteria were tumor size smaller than 30 cm3 and previous therapy. We calculated the following heterogeneity parameters considering the segmented voxels of the lesion with SUV higher than 2.5% of SUVmax: Entropy, Contrast, Correlation, Homogeneity, and Covariance. Thereafter, we utilized Mann-Whitney U probe and Kruskal-Wallis test to find correlation between the certain heterogeneity parameter and estrogen-, progesterone-, Her2-receptor status, Ki-67 proliferation index, the number of primary lesions as well as the local and distant advance of the disease. Results: Generally, we found no correspondence between the examined heterogeneity parameters and Her2-receptor status, Ki-67 proliferation index, number of the primary lesions, and the presence of local/distant metastases. The value of Correlation as heterogeneity parameter was significantly larger (10.35->18.63; p=0.09) in progesterone-receptor positive tumors, while other heterogeneity parameters proved to be unrelated. The values of Entropy (9.89->16.95; p=0.017), Contrast (10.36->16.36; p=0.043), and Correlation (10.07->16.73; p=0.025) proved to be elevated, while the degree of Homogeneity decreased (15.57->9.73; p=0.49) in estrogen-receptor positive cases. Conclusion: In this study we found correlation between certain heterogeneity parameters and hormone-receptor status. However, further investigations are needed to clarify the clinical relevance of these findings. No obvious connection was proved between the other examined clinicopathological markers and studied heterogeneity parameters.

P603

FDG-PET/CT versus CT in local recurrent breast cancer and the standardized uptake value in local and distant recurrent breast cancer

C. B. Petersen1, M. G. Hildebrandt1, J. A. Hansen1, C. Baun1, K. Falch1, O. Gerke1, A. B. Jylling1, A. Alavi2, P. F. Høilund-Carlsen1; 1Odense University Hospital, Odense C, DENMARK, 2University of Pennsylvania, Philadelphia, PA, UNITED STATES.

Aim: This study aimed to estimate the accuracy of FDG-PET/CT versus contrast enhanced CT (ceCT), in diagnosing local recurrent breast cancer and to see if delayed FDG-PET/CT imaging improved sensitivity. Furthermore, to assess the FDG-uptake (expressed by the maximum standardized uptake value (SUVmax)) in local and distant recurrence using 1 hour (1h) and 3 hour (3h) imaging. Materials and methods: In a prospective design, 100 female patients with suspected recurrent breast cancer underwent 1h and 3h FDG-PET/CT and ceCT within a median time of 10 days. Readers were blinded to other test results, however, they were aware of the diagnosis of local recurrence from the referral text. Biopsy, choice of treatment and clinical follow up served as reference standard. Patient based accuracy results were calculated, including measures of area under the receiver operating curve (AUC-ROC), based on visual 4-point assessment. SUVmax was obtained from the most FDG-avid metastatic lesion of each patient. Four patients with local recurrence had no FDG-avid lesions and were excluded from the SUV analysis. A Wilcoxon matched-pairs signed-ranks test was applied for the differences of 1h and 3h SUVmax in patients with local and distant recurrence. A Wilcoxon rank sum test was used to test for differences in SUVmax between groups. Results: Nineteen women had local and 22 distant recurrent disease. The AUC-ROC, sensitivity and specificity for patients with local recurrence was 0.88 (95%CI: 0.78-0.99), 0.74 (0.51-0.88) and 1.00 (0.94-1.00) for FDG-PET/CT1h, 0.88 (0.78-0.99), 0.72 (0.49-0.88) and 1.00 (0.94-1.00) for FDG-PET/CT3h, and 0.59 (0.45-0.74), 0.37 (0.19-0.59) and 0.90 (0.80-0.95) for ceCT, respectively. Patients with local recurrent disease had a median SUVmax3h of 5.2 (range 0.8-12.3), which was significantly higher than the median SUVmax1h: 3.8 (range: 0.9-8.7) ($p=0.007$). Likewise, patients with distant recurrent disease had a median SUVmax3h of 15.1 (range: 7.1-29.7), which was significantly higher than SUVmax1h: 10.2 (range: 4.2-19.3) ($p=0.0001$). There was a statistically significant difference between local and distant recurrent lesions with regard to SUVmax1h ($p<0.0001$) and SUVmax3h ($p<0.0001$). Conclusion: In diagnosing local recurrent breast cancer, all diagnostic values were higher with FDG-PET/CT than ceCT, although the difference was statistically significant for the AUC-ROC only. Delayed imaging was associated with significantly higher FDG-uptake in both local and distant recurrent lesions, but did not improve sensitivity, which as expected was relatively low, yet significantly higher than with ceCT. The FDG-uptake was significantly higher in distant than local recurrent lesions suggesting change of cancer aggressiveness.

P604

Preliminary findings of our institute on initial staging of breast cancer with FDG-18 PET/CT

T. CAKIR, E. ABAMOR, A. CAKIR, P. BASIM, C. GEZEN, M. EVREN, T. ATASEVER; MEDIPOL UNIVERSITY, ISTANBUL, TURKEY.

AIM: Aim of our study is to investigate the pathology results of breast cancer patients, whom are initially evaluated using FDG-18 PET/CT. MATERIALS AND METHODS: Newly diagnosed breast cancer patients in our institute, that was founded two years ago, were evaluated in this study using FDG-18 PET/CT. Maximum Standard Uptake Values (SUVmax) of primary breast lesions and axillary lymph nodes were noted. Pathology reports were retrieved from archives if accessible. Final diagnosis of the tumors, size of the tumors, histological grades, estrogen (ER), progesterone (PR), CERB-B2 receptor expression, Ki67 values and lymph node involvements were noted. SUVmax of tumors were compared according to histological features. RESULTS AND CONCLUSION: Total number of 119 patients was retrospectively included to this study. Sixty-three of 119 have pathology reports in our system. Average ages of the patients were 49 (25-82). 46 patients were diagnosed as invasive ductal carcinoma. Only 4 patients have invasive lobular carcinoma. 6 patients have mix type carcinomas. 4 patients have triple negative breast cancer. In this 63 patients 14 was ER negative, 18 was PR negative and 29 was CERB-B2 negative. 32 patients have occult or micro metastasis to axillary lymph nodes. 8 of this 32 patient were false negative in PET/CT examination. Only two patients with mildly increased FDG uptake were negative in pathological investigation. Five patients histological grade is one, and average SUVmax is calculated as 8. Thirty patients' grade is 2 with average SUVmax of 8.5. Twenty-seven patients' grade is 3, with average SUVmax of 12.4. Ki-67 percentage and SUVmax of the primary lesions were statistically corre-

lated ($p<0.0001$), unlike Ki-67 percentage and SUVmax of the lymph nodes. Distant metastasis is present in fifteen cases. Average SUVmax of primary lesion of these patients was 12.9, while non-metastatic patients have lower average SUVmax of 9.0. Correct initial evaluation of the breast cancer is vital for the patient. FDG PET/CT have important role in the evaluation of breast cancer as well as other cancers. Further investigation of the breast cancer including subgroup analyzes with larger number of patients is planned in our institute.

P605

Is 18F-FDG uptake and apparent diffusion coefficient obtained from diffusion weighted magnetic resonance imaging correlate on the primary tumour of breast carcinoma?

A. Ozen, T. Sayin, S. Altinay, A. Celik, O. Ekmekcioglu, E. Bastug, A. Muhammedoglu, R. Albayrak; Bagcilar Training and Research Hospital, Istanbul, TURKEY.

Aim: The breast carcinoma in female population is the most common type of cancer. Diffusion-weighted magnetic resonance imaging (dw-MRI) provides additional information about microstructural characteristics of tissue and it is increasingly performed in the evaluation of tumours. Furthermore, the apparent diffusion coefficient (ADC) value obtained from dw-MRI was useful in differentiating between benign and malignant breast lesions, such as differentiating ductal carcinoma from fibroadenoma. Restricted water movement in tumors with high cellularity usually results in smaller ADC value. On the other hand, 18F-FDG uptake and cellularity in breast carcinoma are positively correlated. Therefore, SUVmax and ADC were expected to be in an inversely proportional correlation. The aim of this study was to evaluate whether 18F-FDG uptake and ADC correlate for the primary tumour of breast carcinoma. Material and methods: This retrospective study included 43 lesions in 42 female patients (mean age, 51,30 ±12,26 years; age range, 29-78 years) with breast carcinoma. Thirty eight patients had invasive ductal carcinoma, one of them with sarcomatoid differentiation, 1 invasive lobular carcinoma, 1 mixed type, 1 mucinous and 1 medullar breast carcinoma. After pre-operative staging with 18F-FDG PET/CT and dw-MRI, mastectomy or breast conserving surgery with axillary lymph node disection or sentinel lymph node biopsy was performed. The SUVmax was calculated from 18F-FDG PET/CT images at 1-hour (SUV1) and 3-hours (SUV2) after i.v. injection of 18F-FDG. Furthermore, retention index (RI) was calculated in 40 lesions following formula; RI=100 x (SUV2-SUV1) / SUV1. The ADC values from primary breast tumour were obtained automatically by measuring the intensity of the region of interest on the ADC maps. The correlation with ADC was tested by Spearman's correlation coefficient for SUVmax values, and tested by Pearson correlation coefficient for RI. Results: The mean tumour size was 2.43±0.98cm (range 1.1-5cm). The mean SUV1, SUV2, RI and ADC for the breast tumours were 6.38±5.03, 8.06±6.61, 22.78%±19.84%, and 1.092×10-3mm2/sn±0.452×10-3mm2/sn, respectively. The ADC values were not correlated with SUV1 (r:0.092, p:0.563), SUV2 (r:0.166, p:0.300) and RI (r:0.262, p:0.102). Conclusion: The correlation between SUVmax and ADC was found in some tumors such as primary cervical cancer, pancreatic adenocarcinoma, and lymph node metastasis of non-small cell lung carcinoma. Even though we found no correlation between ADC and 18F-FDG uptake in our study, these two imaging modalities might play a suplemantary role in detecting of breast carcinoma.

P606

The Contribution of FDG PET/CT in Diagnosis and Staging of Breast Cancer

E. ARSLAN1, T. ÇERMIK1, F. CAN TRABULUS2, E. KELTEN TALU3, S. TUTER BASARAN4; 1ISTANBUL RESEARCH AND EDUCATIONAL HOSPITAL CLINIC OF NUCLEAR MEDICINE, ISTANBUL, TURKEY, 2ISTANBUL RESEARCH AND EDUCATIONAL HOSPITAL CLINIC OF GENERAL SURGERY, ISTANBUL, TURKEY, 3ISTANBUL RESEARCH AND EDUCATIONAL HOSPITAL CLINIC OF PATHOLOGY, ISTANBUL, TURKEY, 4ISTANBUL HASEKI RESEARCH AND EDUCATIONAL HOSPITAL CLINIC OF PATHOLOGY, ISTANBUL, TURKEY.

Aim: In treatment selection and prediction of prognosis of the breast cancer, accurate disease staging is the most important requirement. In this study we aimed to investigate the contribution of FDG PET/CT to the initial diagnosis of breast cancer. Materials and methods: We have evaluated retrospectively 234 women (242 breast lesions, mean ± SD: 54.6±13.8 y) with breast cancer. PET/CT was performed 1 hour after the F-18 FDG injection with I.V. contrast if there were no contraindications. Primary tumor, axillary and other nodal metastatic foci and distant metastasis evaluated visually and semiquantitatively. SUV max values were calculated for T and N. Final staging was confirmed with histopathological results and/or follow-up PET/CT. Results: The

primary tumors' mean±SD SUVmax was 11.5±8.9. Uptake threshold was accepted SUVmax≥2, sensitivity of PET/CT for T was 97.1% (235/242). PET/CT was positive in 159 to 180 pathologically or clinically confirmed patients with axillary metastasis. Fifty two to 61 pathologically confirmed axillary negative patients were negative on PET/CT. With these results; Sensitivity, specificity, positive predictive value and negative predictive value of PET/CT for axillary metastasis were 88.3%, 85.2%, 94.6%, 71.2% respectively. There were 48 (20.5%) distant nodal metastatic patients, 27 of them had additional distant organ metastasis in PET/CT imaging. Fifty eight (24.7%) patients had distant organ metastasis which had 40 bone-bone marrow,14 liver, 8 lung, 6 skin, 1 brain and 1 muscular metastasis. In patient with distant metastasis, primary tumors' and axillary lesions' mean±SD SUVmax values were calculated 14.3±11.3, 10.6±5.5 respectively. However, same values were calculated 10.6±7.8 and 6.9±7.8 respectively in patients without distant metastasis. There were statistically significant differences for primary tumors (p=0.003) and axillary metastasis (p=0.001) between two groups. Conclusion: This study results show that PET/CT had very high sensitivity for primary tumor diagnosis. Although PET/CT had high sensitivity, specificity, and positive predictive value for the diagnosis of axillary metastasis, the negative predictive value was not adequate in initial staging. Because of one third of our patients had distant organ and/or nodal involvement, we suggested that PET/CT have strong impact on disease management in patient with breast cancer in initial staging.

P607

Relationship between primary tumor FDG SUVmax, histologic grade, receptor and C-erbB2 status and value in breast Cancer

E. ARSLAN1, T. ÇERMIK1, F. CAN TRABULUS2, E. KELTEN TALU3, S. TUTER BASARAN4; 1ISTANBUL RESEARCH AND EDUCATIONAL HOSPITAL CLINIC OF NUCLEAR MEDICINE, ISTANBUL, TURKEY, 2ISTANBUL RESEARCH AND EDUCATIONAL HOSPITAL CLINIC OF GENERAL SURGERY, ISTANBUL, TURKEY, 3ISTANBUL RESEARCH AND EDUCATIONAL HOSPITAL CLINIC OF PATHOLOGY, ISTANBUL, TURKEY, 4ISTANBUL HASEKI RESEARCH AND EDUCATIONAL HOSPITAL CLINIC OF PATHOLOGY, ISTANBUL, TURKEY.

Aim: Histological grade and receptor status are important criteria for the prognosis and treatment selection in breast cancer. In this study, relationship between primary tumor SUVmax value in PET/CT, histologic grade, estrogen and progesterone hormone receptors and C-erbB2 oncogene presence was investigated. Materials and methods: We have evaluated retrospectively 234 women (242 breast lesions, mean ± SD: 54.6±13.8 y) with histologically proven breast cancer. PET/CT was performed 1 hour after the F-18 FDG injection with I.V. contrast if there were no contraindications. Primary tumor evaluated visually and 235 PET positive lesions' SUVmax were calculated semi-quantitatively. The modified Scarff-Bloom-Richardson grading system was used for histological assessment (Grade 1-2-3), and also four groups were separated for the estrogen and/or progesterone hormone receptor status and the presence of C-erbB2 oncogene; Hormone(+)C-erbB2(+) (H+C+), Hormone(+) C-erbB2(-) (H+C-), Hormone(-) C-erbB2(+) (H-C+) and Hormone(-) C-erbB2(-) (H-C-). Results: One hundred thirty lesions were assessed with the modified Scarff-Bloom-Richardson grading system and 21 were grade 1, 59 were grade 2 and 50 were grade 3. These 3 groups' mean±SD SUVmax values were 6.2±3.7, 10.1 ±7.2 and 14.6±8.8 respectively. There were statistically significant differences between 3 groups (group 1 vs 2 p=0.013; group 1 vs 3 p=0.001; group 2 vs 3 p=0.002). Hormone receptor and C-erb B2 oncogene status defined for 234 lesions in which 77 were H+C+, 110 were H+C-, 23 were H-C+ and 24 were H-C. Comparison results between four subgroups were shown at table. Although there was no statistically significant difference between H-C+ versus H-C- groups, significant differences were found between other groups. Conclusion: In this study, concordance of tumor grading with SUVmax value showed that SUVmax could be used as a prognostic indicator. Also, significant differences between hormone receptor and C-erbB2 oncogene status subgroups' SUVmax values suggested that SUVmax value may contribute to the management of breast cancer.

P608

Comparison between 18F-FDG uptake patern and apparent diffusion coefficient value obtained from diffusion weighted magnetic resonance imaging on the detection of primary tumour and axillary metastases in breast carcinoma

A. Ozen, T. Sayin, O. Ekmekcioglu, S. Altinay, E. Bastug, A. Muhammedoglu, A. Celik, R. Albayrak; Bagcilar Training and Research Hospital, Istanbul, TURKEY.

Aim: Breast carcinoma (BC) is the most common type of cancer in female population. Breast magnetic resonance maging (MRI) detects increased blood flow and

tissue resolution in order to diagnose cancer, thus, being more sensitive and accurate than mammography and ultrasonography. When breast MRI findings are suspicious, diffusion-weighted magnetic resonance imaging (dw-MRI) provides additional information about microstructural characteristics of tissue and it is increasingly performed in the evaluation of tumours. Furthermore, the apparent diffusion coefficient (ADC) value obtained from dw-MRI was useful in differentiating between benign and malignant breast lesions. Our objective was to compare SUVmax patern in 18F-FDG PET/CT and ADC value of dw-MRI for the detection of primary tumour and axillary lymph node (ALN) metastases of BC. Materials and methods: This retrospective study included 42 female patients (mean age, 51,30±12,26 years; age range, 29-78 years) with BC. Thirty eight patients had invasive ductal carcinoma, one of them with sarcomatoid differentiation, 1 invasive lobular carcinoma, 1 mixed type, 1 mucinous and 1 medullar BC. After preoperative staging with 18F-FDG PET/CT and dw-MRI, mastectomy or breast conserving surgery with ALN disection or sentinel lymph node biopsy was performed. For histopathologic evaluation, Modified Bloom Richardson grading system was used. Furthermore, oestrogen (ER), progesteron (PR) receptor expression and Her-2/neu statuses were determined. SUVmax was measured from primary tumour, metastatic ALN, the normal parenchymas of breast, lung and liver. Also, ADC was measured from breast tumour and metastatic ALN. SUVmax ratios was calculated following as: •TumourSUVmax/breastSUVmax, •TumourSUVmax/lungSUVmax, •TumourSUVmax/liverSUVmax. Results: Results showed that the primary lesion detection rate for PET/CT and dw-MRI was 95.3%. The 18F-FDG PET/CT scan had lower sensitivity in detecting of ALN metastases than dw-MRI, while their specificities were equal. Higher SUVmax and/or SUVmax ratios correlated with stage T2 tumours, with histologic grade 3, and with negative ER and PR receptor status. There was no correlation between ADC and SUVmax or SUVmax ratios both primary tumour and metastatic axillary lymph node. Conclusion: Our study suggested that a) the primary lesions detection rate of both 18F-FDG PET/CT and dw-MRI was high, 95.3%. b) Both modalities had the same specificity for the detection of ALN metastases, but the 18F-FDG PET/CT scan had lower sensitivity than dw-MRI and c) SUVmax and SUVmax ratios were more compatible with pathological parameters than ADC value. These two imaging modalities might play a supplemantary role in the detection of BC and ALN metastases.

P609

Accuracy of 18F-FDG-PET/CT in staging, restaging, and treatment response in patients with male breast cancer

B. Vatankulu1, S. Kuyumcu2, P. Ç. Kocael1, E. G. Işık2, S. Asa1, S. Sağer1, M. Halaç1, C. Türkmen2, K. Sönmezoğlu1; 1İstanbul University Cerrahpaşa Medical Faculty, İstanbul, TURKEY, 2İstanbul University İstanbul Medical Faculty, İstanbul, TURKEY.

Aim: Male breast cancer, which has very different structural features than the female breast cancer, is a scarce disease. FDG PET / CT is considered to be the most important imaging methods in staging, restaging and management of female breast cancer. However there are few studies of the contribution of FDG PET / CT in management of male breast cancer. In this study we aimed to determine the significance of the FDG PET / CT findings of male breast cancer in staging, detection of recurrent disease and evaluation of response to the therapy. Materials and Methods: Between January 2008 and December 2014, patients with breast cancer who underwent FDG PET/CT were examined retrospectively. Patients were divided in 3 groups: initial staging; recurrence of the disease; to evaluate the response to treatment. FDG PET / CT findings were evaluated with histopathology and clinical outcomes of patients with at least 6 months . Results: A total of 6842 study with FDG PET/CT performed for breast cancer were examined. Male breast cancer was found in only 27(0.39%) patients. 34 FDG PET CT imaging were performed in these patients with diagnosed male breast cancer. PET/CT were performed in 10 of 27 (37%) for initial staging, 10 of 27 (37%) for restaging and 7 of 27 (26%) for evaluating to response to the therapy. 18 of 27 patients were diagnosed with invasive ductal carcinoma, 4 of 27 were diagnosed with invasive cribriform carcinoma. The histopathological results could not be found in 5 of 27 patients. Estrogen receptor was positive in all patients who had histopathology results. The progesterone receptor was positive in 20 patients and cerb - b2 gene expression was positive only in 8 patients. PET / CT imaging sensitivity , specificity , positive predictive value , negative predictive value and accuracy of detection of distant metastases were calculated as 100 %, 69% , 84 % , 100 % and 92 % respectively. Conclusion: Primary tumors and distant metastases were detected with high accuracy with FDG PET / CT in male breast cancer. FDG PET / CT was a powerful imaging technique in

initial staging, determining the presence of recurrency and response to therapy in patients with male breast cancer.

P37 - Monday, October 12, 2015, 4:00 PM - 4:30 PM, Hall 3 – Poster Exhibition
Clinical Oncology: Lung

P610

Evaluation of 18F-FDG PET/CT and low-dose CT performance in diagnosing lymph node metastases among NSCLC patients.

J. Teodorczyk1, B. Brockhuis1, G. Romanowicz1, W. Cytawa1, I. Wenzel1, J. Kozłowska1, L. Cunha2,3, A. Silva3, L. Metello2,3, P. Lass1,4; 1Department of Nuclear Medicine, Medical University of Gdansk, Gdansk, POLAND, 2Department of Nuclear Medicine, ESTSP.IPP, Porto, PORTUGAL, 3Department of Nuclear Medicine, IsoPor SA, Porto, PORTUGAL, 4Division of Molecular Spectroscopy, Institute of Experimental Physics, University of Gdansk, Gdansk, POLAND.

Objective: The aim of our study is to assess the efficacy of lymph node staging in NSCLC, with particular emphasis on operability, using 18F-FDG-PET-CT and low-dose CT. Material and methods: PET-CT and CT results were compared to pathological analysis of operatively excised material, which were used as a "gold standard". The initial part of our study included scanning and follow-up of 89 patients and 238 nodal stations diagnosed with 18F-FDG-CT in Department of Nuclear Medicine of UCC in Gdansk and treated operatively with pulmonectomy/lobectomy in the Department of Thoracic Surgery, UCC Gdansk in years 2010-2014. Our study aims to answer the following questions: what is accuracy of 18F-FDG-PET-CT and CT in defining the lymph node status; how valuable diagnostically is low-dose CT co-registered with PET study; how to modify the criteria for the evaluation of mediastinal lymph nodes in 18F-FDG-PET-CT and CT to obtain more accurate diagnosis; what is optimal SUV cutoff value to minimize false results; how strong is the need for motion correction; how strong is the need for partial volume effect correction; what are differences in diagnostic quality of PET-CT/CT between particular lymph node stations; what is the optimal algorithm for staging and operability assessment in patients with NSCLC; to what extent PET-CT modifies patient management; what is level of agreement between observers in 18F-FDG-PET-CT nodal staging; what is prognostic value of detected glucose metabolism intensity. Results: We confirmed the high specificity of 18F-FDG-PET-CT in diagnosing lymph node metastases reaching 92%. Sensitivity reached 53% and was reduced probably due to the high fraction of micrometastases in early stages of disease. Sensitivity of low-dose CT in detection of lymph node metastatic disease was only 33%, probably due to the high number of micrometastases in our group, but the specificity of low-dose CT was surprisingly high - 87%. The minimum of false (positive plus negative) results of 18F-FDG PET-CT was reached by SUVmax cutoff value 5.2. Our study confirmed high agreement between PET-CT observers - 0,885 and between observations of PET-CT and CT - 0,896. Conclusions: 18F-FDG-PET-CT has relatively high specificity but moderate sensitivity in detection of mediastinal and hilar lymph node metastases in patients with NSCLC. 18F-FDG-PET-CT was much more sensitive than CT, but only moderately more specific. Minimum of false results (FP+FN) was obtained using relatively high SUVmax cutoff value (5.2) for discrimination of benign and malignant lymph nodes. Interobserver agreement in 18F-FDG-PET-CT evaluation was high.

P611

The value of different 18F-FDG PET/CT baseline measurements in predicting response to chemo-radiotherapy in advanced NSCLC

H. N. M. Abdelwahab1, Y. G. Abdelhafez2, R. A. Amin1, A. O. Azab1, S. El-Refaei1; 1Cairo University, Cairo, EGYPT, 2South Egypt Cancer Institute, Assiut, EGYPT.

Objectives: To investigate the predictive value of the pre-treatment 18F-FDG PET/CT tumor measurements (SUVmax, SUVmean, SUVpeak, MTV and TLG) regarding response to treatment in advanced inoperable NSCLC patients receiving chemotherapy ± radiotherapy. Patients and Methods: This retrospective study included thirty patients with newly diagnosed advanced NSCLC who were referred to our center for whole body 18F FDG-PET/CT as a baseline staging method before therapy and later referred again to monitor the response to the therapy taken. For each patient, maximum, mean and peak SUVs, metabolic tumor volume (MTV) and total lesion glycolysis (TLG) of the primary tumor were determined at the pre-treatment scan. The tumor volume was measured using a semi-automatic contouring software. The selected volumes were based on the PERCIST threshold level (drawn on the right lobe of the liver). Two weeks after the end of treatment, the metabolic response of the primary tumor was evaluated using the EORTC response criteria. The correlation between each parameter and the response was done using Student's T-test. Receiver operating characteristic methodology was used to assess the performance of the different parameters to differentiate responders from non-responders (which included

progressive and stable metabolic disease). Results: ROC analysis identified SUVmax value of 8.7, MTV value of 12.18 and TLG value of 283.9 as the best predictive cut-off values for the presence of response. These values gave modest sensitivity of 67%, 42% and 67% and specifity of 56%, 78% and 62% respectively. Though not high, the accuracy of TLG (61%) was highest in predicting the tumor response to therapy, and next was the accuracy of MTV (58%), indicating that volume-based PET parameters are more accurate than SUVmax (49%) in identifying future responders from non-responders prior to treatment. Conclusion: Baseline TLG has better predictive value than SUVmax for the response to chemo-radiotherapy in advanced NSCLC, however this value is statistically non-significant.

P612

Dual-phase F-18 FDG PET diagnosis of pulmonary adenocarcinoma smaller than 3 cm

K. Hayasaka1, T. Nihashi2, H. Inoue1, T. Saitoh1, Y. Shiraishi1, K. Yoshimori1, H. Gotoh1; 1Fukujyuuji Hoaspital, Tokyo, JAPAN, 2Nagoya Graduate Scholl of Medicine, Nagoya, JAPAN.

Objective: To evaluate the applicability of SUVmax to pulmonary adenocarcinoma subtypes < 3 cm excluding variants. Materials and Methods: We used FDG-PET to evaluate 187 nodules in 185 patients (86 male, n = 86; female, n= 99; age, 68.7 y; SD, 9.9 y) with pathologically proven pulmonary adenocarcinomas (excluding variants) less than 3 cm. The nodules were classified as pre-invasive (Group 1), minimally invasive and invasive lepidic-predominant adenocarcinoma (Group 2) and invasive adenocarcinoma other than invasive lepidic-predominant adenocarcinoma (Group 3) according to the International Association for the Study of Lung Cancer (IASLC)/the American Thoracic Society (ATS)/the European Respiratory Society (ERS) (IASLC/ATS/ERS) 2011. Dual phase FDG-PET imaging proceeded one and two hours after FDG injection. The maximum standardized uptake value (SUVmax) on 1-h (E-SUVmax), 2-h (D-SUVmax) images and the ratio of changes in the SUVmax (%CR-SUVmax) were compared between the two time points. All information was obtained from a retrospective review of medical records, PET findings and other data. All data were statistically analyzed using SPSS Version 11.0 software (SPSS Inc., Chicago, IL, USA). Statistical significance was set at $p < 0.05$. Results: The mean (SD) sizes of nodules were 12.8 (5.46), 15.9 (5.35) and 18.6 (5.85) mm in Groups 1, 2 and 3, respectively. Differences in nodule size were statistically significant between Groups 1 and 3, and between Groups 2 and 3. The means (SD) of the E-SUVmax, D-SUVmax and the %CR-SUVmax in Groups 1, 2 and 3 were 1.08 (1.06), 1.09 (0.40) and 3.04 (12.5), 1.81 (1.12), 1.93 (1.37) and 8.44 (16.9), and 4.41(3.44), 5.34(4.31) and 19.1(20.3), respectively. Differences were statistically significant for D-SUVmax between Groups 1 and 2, 1 and 3, and 2 and 3, and for in E-SUVmax and %CR-SUVmax between Groups 1 and 3, and 2 and 3. Conclusions: The %CR-SUVmax was not enhanced among subtypes of pulmonary adenocarcinoma, but delayed FDG PET was more useful than early FDG PET for differentiating adenocarcinoma subtypes < 3 cm except variants. Dual-phase F-18 FDG PET imaging might offer improved diagnostic performance for each subtype of pulmonary adenocarcinoma < 3 cm excluding variants.

P613

Role of F-18 FDG PET in the differential diagnosis between mediastinal malignant lymphoma and thymic epithelial tumors

T. Yamane, A. Seto, I. Matsunari, I. Kuji; Saitama International Medicial Center, Saitama Medical University, Hidaka, JAPAN.

[Aim] Although differentiating lymphoma from other epithelial tumors are extremely important in the initial management of mediastinal tumors, there has been a limit in the conventional imaging modalities. The aim of this study is to evaluate the capability of F-18 FDG PET in the diagnosis of mediastinal tumor. [Materials and Methods] Patients with mediastinal tumors who underwent F-18 FDG PET/CT before treatment were enrolled in this study. After confirmation of histological diagnosis, patients with 4 representative diseases (49 female and 43 male, age range 17-84, median 58) were analyzed; 14 cases of thymic cyst (CY), 46 of thymoma (TM), 22 of thymic cancer (CA) and 16 of malignant lymphoma (ML). Hodgkin's lymphoma and primary mediastinal large B-cell lymphoma were included in the group of ML. Maximum standardized uptake value (SUVmax) of the tumors were measured and compared among the tumor groups. In addition, the data of patients' age was added to the analysis. Wilcoxon's test and receiver operating characteristic (ROC) analysis were used to compare each element and to determine cut off points. [Results] There were significant differences in SUVmax between the groups of CY and TM, TM and CA, and CA and ML ($P < 0.001$, respectively). In addition, there were significant differences in ages between ML and each group ($P < 0.001$, respectively). Based on the results of the ROC analysis, categorization for each group was defined as follows: CY = SUVmax < 1.45, ML = SUVmax ≥ 11.16 and age < 47.5 y, CA =

SUVmax ≥ 7.26 and age ≥ 47.5, and TM = the others. Sensitivity, specificity, positive predictive value and negative predictive value of each group were 92.0%, 100%, 100%, and 98.8% in CY, 91.3%. 88.5%, 87.5% and 92.0% in TM, 81.8%, 92.1%, 76.0% and 94.5% in CA, and 81.3%, 100%, 100% and 96.5% in ML, respectively. [Conclusions] Mediastinal tumors can be distinguished by the SUVmax of F-18 FDG PET. Information of patients' age can increase the diagnostic capability of differentiating malignant lymphoma from thymic cancer.

P614

Whole-Body Bone Scintigraphy and Serum Concentration of Bone Resorption Marker in Patients with Lung Cancer

J. Weissensteiner1, E. Babusikova2; 1Department of Nuclear Medicine, Hospital Poprad, SLOVAKIA, 2Comenius University in Bratislava, Jessenius Faculty of Medicine in Martin, Department of Medical Biochemistry, Martin, SLOVAKIA.

Introduction: Lung cancer is one of the most common and serious types of cancer. Beta-carboxyterminal cross-linking telopeptide of type I collagen (β-CTx) is marker of bone resorption and is a specific marker for the degradation of mature type I collagen in bone. The aim of this study was to correlate serum concentration of β-CTx with the presence of bone metastases detected by whole-body bone scintigraphy in patients with lung cancer. Material and methods: We estimated serum concentration of biochemical marker of bone metabolism ß-CTx and we did whole-body bone scintigraphy in 60 patients (46 men, 14 women) with lung cancer and in 10 patients without malignant disease - control group. A whole-body bone scintigraphy were obtained by using of a hybrid SPECT/CT scanner. The study populations included 50 non-small-cell lung cancers (NSCLC), 9 small-cell lung cancers (SCLC) and 1 patient with typical carcinoid of lung. Results: The bone metastases by whole-body bone scintigraphy were in 15 cases (25 %), probably bone metastases were in 11 cases (18.33 %) and 34 patients (56.67 %) were without bone metastases. We did not observed significant difference in β-CTx concentration between patients and control subjects (p=0.09). The serum concentrations of ß-CTx were above reference range in 9 cases from 60 patients (15 %) - 7 cases were patients with NSCLC (4/10 with bone metastases, 1/7 probably bone metastases, 2/33 without bone metastases), 2 cases were patients with SCLC with bone metastases. The concentrations below reference range were observed in 8 cases from 60 patients (13.33 %) - in 7 cases with NSCLC (2/10 with bone metastases, 2/7 probably bone metastases, 3/33 without bone metastases), in 1 case with SCLC (1/4 with bone metastases). We observed significant difference in β-CTx concentration between patients with bone metastases and control subjects (p=0.02). Patients with bone metastases had higher concentration of β-CTx than control subjects and slightly increased than patients without bone metastases (p=0.06). Conclusion: The serum concentration of ß-CTx correlated with bone metastases finding by bone scintigraphy in patients with lung cancer. Determination of beta-carboxyterminal cross-linking telopeptide of type I collagen could be a diagnostic marker in lung cancer patients with suspected bone metastases.

P615

NSCLC: Comparison of PET-CT and contrast enhaced CT in mediastinal staging and PET-CT diagnosis of lung cancer recurrence-impact on patient management

N. Beslic, **A. Sadija**, T. Ceric, R. Milardovic, S. Ceric, A. Beganovic, S. Kristic; University Clinical Center, Sarajevo, BOSNIA AND HERZEGOVINA.

INTRODUCTION: NSCLC is any type of epithelial lung carcinoma other than SCLC. The possibility of a surgical cure is dependent upon the extent of disease, particulary mediastinal staging. Accurate staging of mediastinal lymphnodes provides important prognostic information and is mandatory in determining treatment strategy. CT as a standard method of diagnosis and staging of lung cancer provides very good morphological data, but it has limitations in differentiating benign from malignant lesions. PET-CT based on metabolic activity has shown superiority in nodal staging and is very sensitive for diagnosis of recurrent NSCLC with a significant effect in change of management. MATERIALS AND METHODS: Total of 54 patients with NSCLC were retrospectively evaluated and divided in two groups. In I group we evaluated 26 patients in mediastinal nodal staging comparing contrast enhaced CT and PET-CT findings. Group II included 28 patients where we evaluated changes in patient management after PET-CT diagnosis of recurrent lung disease. DISCUSSION: In group I we found no differences in nodal staging in 50% patients comparing PET-CT vs CT. Other 50% of patients have been upstaged or downstaged after PET-CT study comparing to previous CT with 27% of patients who had an impact on further management. In group II we found 36% patients with no signs of recurrent disease. PET-CT detected local recurrence in 64% patients with 54% patients having qualitative change in therapy after PET-CT study. CONCLUSION: The accurate staging of NSCLC is important in planning optimal treatment strategy. Integrated PET-CT combining the benefits of both is a mandatory tool for initial nodal staging. PET-CT improved the diagnosis of recurrent NSCLC and this resulted in a significant impact and

change in further patient management in both patient groups.

P616

Prognostic Value of Early Response Assessment Using FDG PET/CT in Chemotherapy-Treated Patients with Non-Small Cell Lung Cancer

E. Han1, W. Lee2, W. Choi3, S. Kim4; 1Daejeon St. Mary's Hospital, College of Medicine, The Catholic University of Korea, Daejeon, KOREA, REPUBLIC OF, 2College of Medicine, Chungbuk National University, Cheongju, KOREA, REPUBLIC OF, 3St. Vincent Hospital, College of Medicine, The Catholic University of Korea, Suwon, KOREA, REPUBLIC OF, 4Seoul St. Mary's Hospital, College of Medicine, The Catholic University of Korea, Seoul, KOREA, REPUBLIC OF.

Purpose: To evaluate the prognostic value of early response assessment using a volumetric [18F]-fluoro-2-deoxy-glucose (FDG) positron emission tomography (PET) analysis in patients with non-small cell lung cancer (NSCLC) treated using first-line chemotherapy. Methods: We retrospectively reviewed 33 patients with NSCLC who received first-line chemotherapy and performed FDG PET/computed tomography before (baseline PET) and after 2 cycles of chemotherapy (interim PET). The maximum standardized uptake value (SUVmax) and metabolic tumor volume (MTV) of the total malignant lesion were measured in baseline (SUV1 and MTV1) and interim (SUV2 and MTV2) PET images, and percentage changes in SUVmax (ΔSUV) and MTV (ΔMTV) were calculated between the two PET images. We compared PET parameters and clinicopathologic variables such as age, sex, performance status, smoking history, histologic subtype, and TNM stage in terms of 2-year overall survival (OS). Results: The median follow-up period was 15 months and 2-year OS was 34%. In PET images, the mean SUV1, MTV1, SUV2, MTV2, ΔSUV, and ΔMTV were 13.1 ± 4.5, 307.9 ± 340.0 cm3, 9.5 ± 5.1, 180.4 ± 29.6 cm3, 27 ± 28%, and 42 ± 65%, respectively. In univariate analysis, M stage, TNM stage, and all 6 PET parameters correlated significantly with OS. Correlations with MTV1 and ΔMTV remained significant in multivariate analysis ($P < .05$). Conclusion: A smaller baseline MTV and greater decrease in MTV between baseline and interim PET images correlate statistically with a significantly prolonged OS in chemotherapy-treated patients with NSCLC. A volume-based FDG PET analysis would facilitate prediction of clinical outcome and identification of treatment-resistant patients early during chemotherapy and could thereby be applied to personalized treatment approaches for patients with NSCLC.

P617

Surprising 18F-FDG PET/CT scan findings in patient with elevated CA125

A. Mazurek1,2, M. Dziuk1,2, E. Witkowska-Patena1, S. Piszczek1,2, A. Gizewska1,2; 1Military Institute of Medicine, Department of Nuclear Medicine, Warsaw, POLAND, 2Affidea Masovian PET/CT Center., Warsaw, POLAND.

The aim of the case report is to present the utility of 18F-FDG PET/CT in a patient with elevated CA125 levels. A 51-year-old female patient was diagnosed with recurring transudate fluid in the right pleural cavity. Her medical history was negative for smoking or exposure to asbestos, without any features of cardiovascular insufficiency or infection. Transvaginal ultrasound showed cyst-like focal lesion in the right ovary. Laboratory tests revealed elevated blood CA125 levels. The patient was referred for 18FDG PET/CT scan with suspected ovarian cancer (suspected Meigs' syndrome). However, no signs of pathological accumulation of the tracer in the right ovary were observed. Surprisingly, 18FDG-PET/CT scan showed increased focal uptake of 18FDG in right pleural cavity with a significant amount of fluid. Thoracoscopy based on PET/CT findings revealed multiple nodules of right pleura. Histopathological examination of these lesions yielded the diagnosis of mesothelioma. As pleural effusion can result from many medical conditions, including cancer, finding its cause may pose a major challenge to physicians. Although elevated CA125 levels are mainly observed in ovarian malignancy, the marker is not specific for this type of cancer only. Elevated CA125 may be observed in numerous types of cancer, including pleural mesothelioma. In our case report, the medical history and performed tests results were suggestive of ovarian cancer as the cause of patient's symptoms. It was only 18F-FDG PET/CT scan that suggested the diagnosis of mesothelima, which was further confirmed by histopathological examination.

P618

The diagnostic value of 18FDG-PET/CT and DWI for the detection of mediastinal nodal metastasis in lung cancer: Which is better?

G. Shen, Z. Jia, H. Deng, A. Kuang; West China Hospital of Sichuan University, Chengdu, CHINA.

Aim: Accurate clinical staging of mediastinal lymph nodes of patients with lung cancer is important in determining therapeutic options and prognoses. We aimed to compare the diagnostic performance of diffusion-weighted magnetic resonance imaging (DWI) and 18F-fluorodeoxyglucose positron emission tomography/computed tomography (18F-FDG PET/CT) in

detecting mediastinal nodal metastasis in patients with lung cancer. Materials and methods: Relevant studies about 18FDG PET/CT and DWI for detecting mediastinal nodal metastasis in lung cancer were systematically searched in the MEDLINE, EMBASE, PUBMED and Cochrane Library databases from January 2001 to December 2014. We determined sensitivities and specificities across studies, calculated positive and negative likelihood ratios (PLR and NLR), and constructed summary receiver operating characteristic (SROC) curves with Q* index obtained. The methodologic quality was assessed using the Quality Assessment of Diagnostic Accuracy Studies tool (QUADAS 2). In addition, the publication bias was assessed by Deek's funnel plot of the asymmetry test. The potential between-study heterogeneity was explored by subgroup analyses and meta-regression analyses. Results: A total of 46 studies (39 studies for 18F-FDG PET/CT and 7 studies for DWI) met the inclusion criteria involving 6207 patients. The pooled sensitivities and specificities of PET/CT were 0.70 [95% confidence interval (CI): 0.61-0.77] and 0.92 (95% CI: 0.87-0.94), respectively. The corresponding values of DWI were 0.71 (95% CI: 0.54-0.84) and 0.94 (95% CI: 0.82-0.98), respectively. For DWI, the overall PLR was 12.38 (95% CI: 4.17-36.81) and the NLR was 0.31 (95% CI: 0.19-0.50). For PET/CT, the PLR was 8.18 (95% CI: 5.55-12.04) and the NLR was 0.33 (95% CI: 0.26-0.43). The results of the funnel plot asymmetry test for publication bias revealed no major publication bias (p=0.579, bias=-6.00 for PET/CT vs. p=0.958, bias=-2.11 for DWI). In addition, the study design (retrospective or prospective) was a potential cause for the heterogeneity. Conclusions: Both 18F-FDG PET/CT and DWI are beneficial in detecting mediastinal lymph nodes metastases in lung cancer. However, there was no significant difference of diagnostic performance between these two modalities.

P619

Correlation of [18F]FDG Uptake with Clinical and Laboratory Parameters in Patients with Lung Cancer.

M. Boudali1, **E. Skoura**2, S. Michopoulou2, I. E. Datseris1, K. N. Syrigos3; 1Evangelismos General Hospital, Athens, GREECE, 2UCLH, London, UNITED KINGDOM, 3Oncology Unit GPP, University of Athens, School of Medicine, Athens, GREECE.

Aim: This prospective study aimed to evaluate the correlation between [18F]FDG uptake in PET/CT imaging, measured by maximum standardized uptake value (SUVmax), with several tumor markers and histopathological results in patients with lung cancer. Materials and Methods: Patient demographics data, indications for [18F]FDG PET/CT and the correlation of SUVmax values with histopathological data and with several tumor markers level- CEA, Ca 125, Ca19-9, Ca15-3, AFP, NSE- were assessed. Results: During two year time, a total of 189 patients with lung cancer were included in this prospective study. The group included 137 males and 52 females with a mean age of 63.9 years old. The majority of the patients' clinical indication was the initial staging. Regarding the correlation of SUVmax with laboratory and histopathological data, there was no significant difference for SUVmax values across the histological types identified (adenocarcinoma, squamous cell carcinoma and small cell lung carcinoma). By contrast, a significant difference in CEA values, between the three different histological types, was found, with the highest values identified in adenocarcinomas ($p<0.05$). Furthermore, no significant correlation was identified between the SUVmax value and the levels of six different tumor markers-CEA, Ca 125, Ca19-9, Ca15-3, AFP, and NSE. Conclusion: This prospective study showed no significant difference regarding the SUVmax values in different histologic subtypes of lung cancer or any correlation with the levels of several tumor markers examined for lung cancer. On the contrary, there was a significant difference in CEA values for the different histopathological categories identified, with the highest values in adenocarcinomas.

P620

PET/CT imaging artifacts after talc pleurodesis - a clinical case.

Z. Dancheva, P. Bochev, B. Chaushev, T. Yordanova, A. Klisarova; St Marina University Hospital, Varna, BULGARIA.

Introduction. Talc pleurodesis is a reliable therapy, preventing recurrent pleural effusions and pneumothoraces. As it is based on local granulomatous inflammation, it is a potential source of pitfalls and artifacts on PET/CT images. Case and discussion. We present a 67 year old woman with a PET/CT positive scan seven months after talc pleurodesis, performed after metastatic effusion. The patient has held six chemotherapy courses with Paclitaxel and Carboplatin. She was in a good performance status ECOG 1, without significant pleural effusions and no computer tomography signs of progression. We performed a PET/CT scan after the last chemotherapy course for restaging. At MIP images there were many metabolically active linear, nodular and diffuse patterns of high metabolic activity in both pleurae and out of the thoracic cavity, mimicking implantation metastases. The SUVmax of the findings was up to 7.0. As the patient had a previous medical history for metastatic pleuritis, a progression was suspected at first sight. The PET positive findings were associated with CT images of high-attenuation pleural plaques, located in the left anterior and posterior costophrenic angle, and diffusely engaging the

diaphragm pleura in the left. In the right there was a band of linear radionuclide uptake in the subcutaneous tissues, forming a submuscular high attenuation deposits. A metabolically active fistula through the intercostal space was found, where some of the hyperdence deposit passes through and could be visualized in the interlobar space between lower lobes. No parenchymal metastases and enlarged and metabolically active thoracic lymph nodes were found. The high attenuation deposits raised a suspicion of a talc induced inflammation, which was confirmed after biopsy and histology exam. Conclusion. Talc pleurodesis produces increased FDG uptake on PET and high-density areas of pleural thickening on CT. When PET detects increased uptake in the pleural space, correlation with CT is recommended to detect the presence of pleural thickening of increased attenuation that suggests talc deposits rather than tumor. Key words: talc pleurodesis, metastatic pleuritis, PET/CT, arfifacts

P621

The metabolic change of dual-time-point 18F-FDG PET/CT in patients with suspected of having lung cancer

J. Lee1, S. Jang1, J. Lee2, E. Kim2, H. Jeong2, J. Rho3, S. Cho4; 1Department of Nuclear Medicine, CHA Bundang Medical Center CHA University, Seongnam, KOREA, REPUBLIC OF, 2Department of Internal Medicine, CHA Bundang Medical Center CHA University, Seongnam, KOREA, REPUBLIC OF, 3Department of Radiology, CHA Bundang Medical Center CHA University, Seongnam, KOREA, REPUBLIC OF, 4Department of Pathology, CHA Bundang Medical Center CHA University, Seongnam, KOREA, REPUBLIC OF.

The purpose of this study is to investigate the role of metabolic percentage variation in dual-time-point (DTP) (18)F-FDG PET/CT scans for differentiating diagnosis in patients diagnosed as or suspected of having lung cancer. A total 73 DTP (18)F-FDG PET/CT studies in patients suspected of having lung cancer patient were evaluated, retrospectively. The values of maximum standardized uptake (SUVmax), metabolic tumor volume (MTV), total lesion glycolysis (TLG) of lung lesion using a threshold derived mediastinal blood pool activity were obtained in early phase (early SUVmax, early MTV, early TLG) and delayed phase (delayed SUVmax, delayed MTV, delayed TLG) and the %ΔSUVmax, %ΔMTV, and %ΔTLG were calculated. These values were compared between benign and malignant tumors and between histological subtypes (adenocarcinoma (ADC), squamous cell carcinoma (SqCC), small cell lung cancer (SCLC), and inflammatory lesion) by the Mann-Whitney U test. The 64 cases were malignancy (87.6%) and histological subtype of ADC was most common (51.5%) in the cancer patient. The values of early MTV and delayed MTV were significant difference between malignant and benign tumors ($p = 0.035$, $p = 0.029$), while there were no significant differences in the values of %ΔSUVmax, %ΔMTV, and %ΔTLG. Among histological subtype groups, the %ΔSUVmax value in ADC group was significant lower than the %ΔSUVmax in SqCC group ($p = 0.016$) and SCLC group ($p = 0.025$), whereas other values were not statistically significant between histological subtypes. The metabolic change of DTP (18)F-FDG PET/CT is not useful for discriminating between benign and malignant lung masses or nodules. The SUVmax percentage variation in ADC is likely to be lower than other types of cancer.

P622

Prognostic Significance of Changes of Volumetric Metabolic Parameters in 18F-FDG PET/CT During and After Radiotherapy in Stage III Non-Small Cell Lung Cancer

N. Chiu, W. Su, H. Guo, B. Lee, H. Chen; National Cheng Kung University Hospital, Tainan, TAIWAN.

Aim: We conducted this prospective study to explore the predictive value of volumetric metabolic parameters determined by during and after radiation-based therapy 18F-FDG PET/CT in stage III non-small cell lung cancer (NSCLC) patients. Materials and methods: Patients with stage III NSCLC planned to receive definitive chemo-radiation or radiotherapy were eligible. 18F-FDG PET/CT was performed before (PET 1), during (at the 5th week, PET2) and after treatment (3 months later, PET3). Metabolic tumor volume (MTV) and tumor total lesion glycolysis (TLG) were measured and correlated with treatment response and survival. ΔMTV was calculated by subtracting the MTV of PET1 from MTV of PET2 or PET3 and dividing by MTV of PET1. ΔTLG was calculated by subtracting the TLG of PET1 from TLG of PET2 or PET3 and dividing by TLG of PET1. Univariate analysis was performed to assess the prognostic significance of ΔMTV and ΔTLG. Results: There were 30 patients enrolled initially, but 5 patients were excluded due to multiple metastases or double cancer. Twenty three received concurrent chemoradiotherapy and 2 patients received radiotherapy alone. The median radiotherapy dose was 70 Gy. During radiotherapy PET/CT and post-treatment PET/CT were performed in 25 and 19 patients, respectively. The median follow-up time was 34 months. The estimated median progression-free survival (PFS) was 8 months. Using the median of these parameters as a cut-off, during radiotherapy ΔTLG (cut-off: 65%) was a significant prognostic factor for PFS and overall survival (all $P = 0.02$). While during radiotherapy ΔMTV (cut-off: 40%), post-treatment ΔTLG (cut-off: 80%), and post-treatment ΔMTV (cut-off: 65%) were not. Conclusion: Changes of TLG determined by during

radiotherapy 18F-FDG PET is promising for predicting outcome of patients with stage III NSCLC. It has the potential to facilitate early response-adapted treatment strategies.

P623

Maximum standardized uptake value cutoff point of the lymph nodes metastases in NSCLC detected by FDG-PET/CT - a prognostic value

N. Georgieva1, Z. Dancheva2, P. Bochev2, B. Chaushev2, T. Yordanova2, A. Klisarova2, K. Peeva3; 1Department of Physics, Biophysics, Roentgenology and Radiology Medical Faculty, Trakia University, Stara Zagora, BULGARIA, 2Nuclear Medicine Department, St. Marina University Hospital, Varna, BULGARIA, 3Department of Social Medicine and Health Management, Medical Faculty, Trakia University, Stara Zagora, BULGARIA.

Aim: To determine the prognostic diagnostic value of the increased lymph nodes SUVmax in NSCLC patients and its relation to their survival. Materials and Methods: We studied 73 pre-treatment patients with NSCLC using 18FDG-PET/CT. There were 53 men (72,6%) and 20 women (27,4%), in the range of 18-79 years old. Increased pathologic SUVmax was detected in 184 lymph nodes. Patients were staged according to TNM and final diagnosis registered in Bulgarian National Cancer Registry (BNCR). Disease beginning in the BNCR was considered either the date of registration or the operation date. Patients who presented with NSCLC between July 2009 and July 2012 were included in18FDG-PET/CT pre-treatment examination and survival was followed-up until April 2014. The distribution in BNCR according to N was as follows: 18 patients had N0 (24,7%), 10 had N1 (13,7%), 21 had N2 (28,8%), 11 had N3 (15,1%) and 13 patients had Nx (17,8%). The correlations between the primary tumor SUVmax and the lymph nodes SUVmax were evaluated by Spearman correlation coefficient. A cutoff point was defined through the log-rank test and the Wilcoxon test. The survival was evaluated by the Kaplan-Meier method. Comparison between study groups was performed by the Mantel-Cox Log Rank with level of significance $P<0.05$. Results: Between the primary tumor SUVmax and the lymph nodes SUVmax there was statistically significant ($P<0,05$) positive weak correlation ($r=0,297$). Between the lymph nodes SUVmax and the survival there was statistically significant ($P=0,0001$) moderate inverse correlation ($r=-0,311$). At cutoff point equal to 4,5 for the lymph nodes SUVmax, the following NSCLC patients survival rate was estimated in months: for SUVmax<4,5, Mean=23,1, Median=16,8; for SUVmax≥4,5, Mean=10,5, Median=7,1. The studied factor lymph nodes SUVmax was considered as a dichotomous variable. It influenced statistically significant the survival of the NSCLC patients ($P=0,0001$). Statistically significant correlation was not established between the survival, the presence of lymph nodes with increased SUVmax and the histology of the primary tumor. Conclusion: The survival of the NSCLC patients is significantly dependent on the regional lymph nodes SUVmax before treatment. Regional lymph nodes SUVmax before treatment over 4,5 is a cutoff point which defines risk for worse survival and in operable patients it implies additional treatment options after the surgical intervention.

P624

Value of Tc99m-Thyrosine-Octreotide in characterization of lung masses

B. Mahmoudian1, S. D. Oskoei1, M. Nazemiyeh2, R. Javadrashid3; 1Division of Nuclear Medicine, Imam Reza Hospital, Faculty of Medicine, Tabriz University of Medical Sciences, Tabriz, IRAN, ISLAMIC REPUBLIC OF, 2Tuberculosis and Lung Research Center, Imam Reza Hospital, Faculty of Medicine, Tabriz University of Medical Sciences, Tabriz, IRAN, ISLAMIC REPUBLIC OF, 3Department of Radiology, Imam Reza Hospital, Faculty of Medicine, Tabriz University of Medical Sciences, Tabriz, IRAN, ISLAMIC REPUBLIC OF.

Aim: The aim of our study was to assess the value of Tc99m-Thyrosine-Octreotide single photon emission tomography (SPECT) in characterization of lung masses which appeared ambiguous on computerized tomography (CT). Also incremental value of fusion of SPECT images on CT slices were assessed prior to lung biopsy. Materials and Methods: Twenty five consecutive patients (15 men and 10 women; mean age 59.2±13 years) with lung mass on CT scan were referred for nuclear imaging for characterization of pulmonary mass, prior to performing trans-thoracic CT guided lung biopsy. They were prospectively allocated to undergo whole-body scintigraphy (WBS) and SPECT using Tc99m-Thyrosine-Octreotide imaging. Then fusion of reconstructed SPECT images on CT scan slices was performed using dedicated Siemens E-Cam gamma camera software. Anatomic landmarks were used for co-registration of images. Histologic findings after tissue biopsy and also one year follow-up results served as gold standard for determining diagnostic accuracy of somatostatin receptor imaging in characterization of lung masses. Qualitative visual assessment was complemented by semiquantitative analysis based on target to background count ratio on opposite side. Results: Among the 25 pulmonary lesions scanned with Tc99m-Thyrosine-Octreotide, focal uptake was increased in 17 of 19 malignancies, whereas no uptake was found in 5 of 6 benign lesions (89.5% sensitivity, 83.3% specificity, 94.5% PPV, 71.4% NPV) on SPECT. Planar scan had lower sensitivity than SPECT images (76.6% versus 89.5%, respectively),

which is more considerable in small sized lesions with diameter less than 1 centimeter. In semiquantitative study malignant lesions showed higher target to background ratios comparison to benign lesions (1.39±0.28 vs. 1.04±0.13 with p<0.01 in planar and 2.39±1.04 vs. 1.33±0.58 with p=0.01 in SPECT, respectively). Considering co-registered SPECT on CT, lung biopsy was delayed in 5 and site of biopsy was changed in 2 from 25 patients. Conclusion: This study demonstrates that Tc99m-Thyrosine-Octreotide have diagnostic value for characterizing pulmonary lesions that appear ambiguous on CT. Also co-registration of SPECT images on CT scan slices has incremental value in management of about 28% of patients with lung masses, which are candidate for lung biopsy. Key Words: Tc-99m-Thyrosine-Octreotide, SPECT/CT, lung mass, biopsy

P625

Self-pleural in culture of autologous tumor cells from human lung adenocarcinoma by 18F-FDG imaging and chemotherapy drug sensitivity

L. Chen, C. Liu, J. Cao, J. Lou, J. Jiang, W. Xie, S. Yang; Shanghai Chest Hospital, Shanghai, CHINA.

Aim: Trying to set up a new method for individualized cancer therapy. Methods: From April 2010 to July 2013, a total of 28 patients with pleural metastases diagnosed with adenocarcinoma originating in lung by 18F-FDG imaging. The pleural effusion were sterile piercing collection (250-500mL) containing 10U/mL heparin, 100U/mL Penicillin, 100μg/mL Streptomycin and 0.2% Gentamicin after blending incubated in a 37°C humidified atmosphere with 5% CO2. The effusion cells were collected by centrifugation on discontinuous Ficoll-Hypaque as Lymphocyte separation medium density gradients settings 1000g for 25 minute. Cells were inhaled to cell culture flasks with 8 mL fresh pleural per flask. After incubation, changed pleural as medium every day to remove non-adherent cells. The immunocytochemical analysis comprised of cell adhesion molecule CK7, TTF-1. Adherent cells were harvested from the flask when cells were estimated at a total amount of 3-5 × 105 cells. 3000-5000 / 0.1 mL autologous, control group cells and blank were distributed in 75, 18, 3 of 96-well plates, respectively. After incubation 24 h, preparation of drug concentration (high, middle, lower) to choose eight kinds of chemotherapy drugs commonly used lung cancer, Vinorelbine, Paclitaxel, Docetaxel, Gemcitabine, Pemetrexed, Cisplatin, Carboplatin, Ifosfamide, then added the drugs to 96-well plates respectively. Incubation 72h, CCK-8 (Dojindo, Japan) 10μL/ well was added and optical density (OD) was measured at 450 nm by a microplate reader (Bio-rad, USA) at 2 h. Results: The laboratory report showed Vinorelbine, Paclitaxel and Gemcitabine are listed in the top three preferred drugs besides Cisplatin, Carboplatin. Clinical data showed partial response (PR) NP/NC 63.15%, DP/DC 15.8%, AP 15.8%, GP 5.3%, respectively. Stable disease (SD) NP/NC 19.2%, DP/DC 42.3%, GP 15.4%, AP 15.4%, TC 7.7%, respectively. Progressive disease (PD) NP/NC 17.4%, GP/GC 34.8%, DP/DC 13%, TP/TC 13%, AP 21.7%. Time to progress (TTP) NP/NC 6-24mo, GP 0-19mo, DC/DP 6-14mo, AP 2-7mo, respectively. Overall survival (OS) NP/NC 45.57mo, GP 28.4mo, DP/DC 24mo, AP 20.2mo, respectively. Conclusion: 18F-FDG identifying imaging, self-medium and xeno-free in cell culture, short-time obtained autologous cells, appropriate drugs, good communication between laboratory and clinical is key of individualized cancer therapy. Note: NP, vinorelbine, cisplatin; NC, vinorelbine, carboplatin; DP, docetaxel, cisplatin; DC, docetaxel, carboplatin; TP, paclitaxel, cisplatin; TC, paclitaxel, carboplatin; GP, gemcitabine, cisplatin; AP, pemetrexed, cisplatin.

P626

Which factors are affecting development of the axillary metastasis in lung cancer?

F. USTUN, G. Durmuş Altun; Trakya University Medical Faculty, Edirne, TURKEY.

Aim: In lung cancer, axillary lymph node metastasis is rare and is classified as a distant lymph node metastasis. In the presence of axillary lymph node metastasis in lung cancer, are considered as the N3 in the staging system. We performed a retrospective study. The aim is this study to evaluate (i) the presence of axillary lymph node metastasis, and (ii) the effect of the primary tumours characteristics to development the metastasis of axillaries lymph node. Materials and Methods: We retrospectively reviewed F-18 FDG PET/CT images with primary lung cancer performed at our institution from October 2009 to December 2014 to identify axillary's lymph node FDG uptake. 35 patients were identified. We re-evaluated patients PET/CT parameters, medical records and pathological reports. Results: Among 35 patients with increased axillary lymph node uptake on PET/CT, 5 patients were identified by histopathologically benign. The mean age was 58.6 years (range, 32-84). In 30 patients, lymphatic metastasis to mediastinum was evident, and supraclavicular and cervical lymph nodes were involved in twenty-one. Twelve patients had direct chest wall invasion. Sixteen patients had distant metastasis other than axillary lymph node (sixteen bone, ten adrenal gland, five liver, and four soft tissue). The mean primary tumour size was 68.25 mm (range 17 to 149 mm). The mean primary tumour SUVmax was 12.46 (range 2.1 to 24.6), and axillary lymph node SUVmax was 5.77 (range 1.9 to 12.7). There was a positive correlation between primary tumour size and axillary lymph node SUVmax (R= 0.48, p=0.009), and

primary tumour SUVmax and axial lymph node SUVmax value' (R= 0.44, p=0.010). Conclusion: The different mechanisms in axillary lymph node involvement for lung cancer have been identified. According to our results, large tumours can spread by local invasion route. These tumours invaded chest wall, and then extended to the axilla. Another reason for these spread that the increased tumour SUVmax values' leads to increased tumour aggressiveness. In large lung tumours exhibiting pleural invasion and advanced lymph node involvement, should be carefully examined axillary lymph node involvement.

P627

Impact of Optimal Respiratory Gated Positron Emission Tomography on Characterisation of Intra-Tumour Heterogeneity in Lung Cancer Patients

W. Grootjans1, F. Tixier2, C. S. van der Vos1, D. Vriens3, C. Cheze-le Rest2, J. Bussink1, W. J. G. Oyen1, L. F. de Geus-Oei3, D. Visvikis4, E. P. Visser1; 1Radboud university medical center, Nijmegen, NETHERLANDS, 2University Hospital Poitiers, Poitiers, FRANCE, 3Leiden University Medical Center, Leiden, NETHERLANDS, 4INSERM, UMR1101, LaTIM, University of Brest, Brest, FRANCE.

Aim: Analysis of radiotracer uptake patterns in positron emission tomography (PET) through computation of textural features is increasingly being proposed to improve characterization of lung cancer lesions for the purpose of disease prognostication and response monitoring. However, respiratory motion artefacts cause lesion blurring that could result in loss of intra-tumour heterogeneity. In this work we have investigated the effect of respiratory gating on the recovery of intra-tumour heterogeneity. Materials and Methods: Whole body [18F]-fluorodeoxyglucose (FDG) PET/CT imaging was performed in 70 lung cancer patients from our fast-track outpatient diagnostic program. Amplitude-based optimal respiratory gating (ORG) was performed on bed positions covering the thorax. The duty cycle (percentage of the total PET data) used for image reconstruction of the ORG images was 35%. Non-gated images were reconstructed using 126 seconds of PET data, yielding similar noise characteristics as their ORG equivalents. Lesion segmentation was performed using the fuzzy locally adaptive Bayesian (FLAB) algorithm. Four heterogeneity parameters (entropy, dissimilarity, zone percentage (ZP), and high energy emphasis (HIE)), which have previously shown to be robust and associated with survival in lung cancer patients, were calculated in non-gated and ORG images. Statistical analysis was performed using the Wilcoxon signed rank test, and statistical significance was defined for $p<0.05$. Results: Considering all lung lesions, respiratory gating did not result in statistically significant differences in the heterogeneity parameters. The mean increase for entropy, dissimilarity, ZP and HIE between the non-gated and ORG images was 0.3±2.7% (p=0.5), 3.6±14.3% (p=0.2), 0.5 ±3.3% (p=0.3), 4.2±21.4% (p=0.3). Sub-group analysis revealed a significant effect of ORG on the heterogeneity parameters of lesions in the lower lung lobes. The mean increase for entropy, dissimilarity, ZP and HIE, considering lesions in the lower lobes was 1.3±1.5% (p=0.02), 11.6±11.8% (p=0.006) 2.3±2.2% (p=0.002), and 16.8%±17.2% (p=0.006) respectively. For the centrally located lesions, the mean increase for entropy, dissimilarity, ZP and HIE was 0.58±3.7% (p=0.6), 5.0 ±19.0% (p=0.4) 0.59±4.0% (p=0.9), and 4.4±27.8% (p=0.4), respectively. Lesions in the upper lobes showed a mean increase of -0.35±1.8 (p=0.3), -1.0±7.7% (p=0.3), -0.4±2.7% (p=0.5), -1.7±13.2% (p=0.4), for entropy dissimilarity, ZP and HIE, respectively. There was no significant correlation between lesion volume and the change in parameters between non-gated and ORG images. Conclusion: Results from this study indicate that ORG significantly impacts characterisation of intra-tumour heterogeneity, particularly for lesions in the lower lung lobes. This suggests that adequate management of respiratory motion artefacts is important for improving characterisation of intra-tumour heterogeneity in PET.

P628

The Diagnostic Accuracy of PET/CT in the Evaluation of Pulmonary Mass Lesions in a Tuberculosis-Endemic Area

R. du Toit, E. M. Irusen, J. A. Shaw, F. von Groote-Bidlingmaier, **J. M. Warwick**, C. F. N. Koegelenberg; Stellenbosch University, Cape Town, SOUTH AFRICA.

Background: Integrated Positron Emission Tomography/ Computed Tomography (PET-CT) is a well-validated modality for assessing pulmonary mass lesions and specifically for estimating the risk of malignant aetiology. Tuberculosis (TB) is known to cause false positive PET-CT findings. We aimed to investigate the modality of PET-CT in the evaluation of pulmonary mass lesions and nodules in a high TB prevalence setting.Methods: All patients referred for the evaluation of an apparent solitary pulmonary nodule or mass and who underwent PET-CT scanning over a 3-year period were included. The PET-CT findings, including maximum standardized uptake value (SUVmax), were compared to the gold standard (confirmed histological or microbiological diagnosis) The

sensitivity, specificity, positive and negative predictive values for malignant disease were calculated according the SUVmax cut-off of 2.5 and according to a proposed cut-off value obtained from a ROC curve.Results: Forty-nine patients (60.1+/-10.2 years, 29 males) were included, of which 30 had malignant disease. Using an SUVmax cut-off of 2.5, PET-CT had a sensitivity, specificity, positive predictive value and negative predictive value for malignancy of 93.3%, 36.8%, 70.0%, 77.8% respectively. After a ROC curve analysis, a suggested SUVmax cut-off of 5.0 improved the specificity to 78.9% with only a small reduction in sensitivity to 90.0%.Conclusion: The diagnostic accuracy of PET-CT in the evaluation of pulmonary mass lesions using the conventional SUVmax cut-off of 2.5 was reduced in a TB endemic area. An SUVmax cut-off of 5.0 has a significantly higher specificity and comparable sensitivity for malignancy compared to a cut-off of 2.5.

P629

Estimating the probability of malignancy in patients with solitary pulmonary nodules

R. Tian, C. Jiang, N. Hou, M. Su, F. Li; West China Hospital, Sichuan University, Chengdu, CHINA.

Objective 18F-FDG PET/CT has been shown to be helpful in the detection and differentiation of solitary pulmonary nodules (SPNs), however some benign lesions exhibit high uptake of 18F-FDG. The important step in the management of patients with lung nodules is to estimate the probability of malignancy. In this study, a clinical prediction model is developed using independent clinical predictors of malignancy to estimate the probability of malignancy in patients with SPN.Methods Data on age, gender, smoking , cancer history, nodule size, location, morphologic characteristics of nodules and SUV (standard uptake value of 18F-FDG) were collected retrospectively from the medical records of 251 patients with an SPN measuring 7-30 mm and a final diagnosis established by histopathology or 2-year follow-up. Multiple logistic regression analysis was used to identify independent predictors of malignancy and to develop a prediction model to estimate the probability of malignancy in patients with SPN. The accuracy of the model was assessed by calculating area under the receiver operating characteristic (ROC) curve and the model was calibrated by comparing predicted and observed rates of malignancy.Results The logistic regression analysis indicated that independent predictors of malignant SPN included being male, having a positive smoking history, older age, larger nodule diameter, and nodules exhibiting specula or high SUV. The prediction model is described by the following equation: Logit (P) = -18.408+ 2.354 (gender) + 3.581 (smoking) + 0.087 (age) + 0.101 (diameter) + 3.381 (spicula) + 0.743 (SUV). Model accuracy was very good (AUC was 0.901).ConclusionOur prediction model provided helpful information in predicting the malignant probability of SPN in Chinese patients..

P630

Is There Any Correlation Between Serum Osteopontin, CEA Levels, and FDG Uptake in Bone Metastasis in Lung Cancer?

A. K. AYAN1, B. ERDEMCI2, E. ORSAL3, Z. BAYRAKTUTAN4, E. AKPINAR5, A. TOPCU5, M. TURKELI6, B. SEVEN7; 1Ataturk University School of Medicine Department of Nuclear Medicine, Erzurum, TURKEY, 2Ataturk University School of Medicine Department of Radiation Oncology, Erzurum, TURKEY, 3Istanbul Medeniyet University School of Medicine Department of Nuclear Medicine, Istanbul, TURKEY, 4Erzurum Regional Training and Research Hospital, Department of Biochemistry, Erzurum, TURKEY, 5Ataturk University School of Medicine Department of Pharmacology, Erzurum, TURKEY, 6Ataturk University School of Medicine Department of Internal Medicine, Erzurum, TURKEY, 7Mevlana University School of Medicine Department of Nuclear Medicine, Konya, TURKEY.

Aim: Reliable blood tests for the early detection and monitoring of progression are crucial in lung cancer patients. It has been suggested that high osteopontin (OPN) and carcinoembryonic antigen (CEA) levels are significantly correlated with metastasis. This study evaluated that the serum levels of carcinoembryonic antigen (CEA) and osteopontin (OPN) levels were related to semiquantitative parameters of 18F-FDG-PET/CT or not in lung cancer patients with bone metastasis.Materials and Methods: Fourty-two non-small cell lung cancer (NSCLC) and 31 small cell lung cancer (SCLC) patients who were referred to our institution for staging by 18F-FDG PET/CT were included. The maximum standardized uptake value (SUVmax) was calculated for primary lesion. The biochemical parameters including CEA (Beckman Coulter UniCel) and OPN (Platinum ELISA kit) serum levels were measured.Results: The mean OPN levels in NSCLC patients with and without bone metastasis were 21.20±4.97 ng/ml and 13.33±4.53 ng/ml, respectively ($p<0.05$). The mean OPN levels in SCLC patients with and without bone metastasis were 23.95 ±4.78 ng/ml and 17.30±3.09 ng/ml, respectively ($p<0.05$). The mean CEA levels in NSCLC patients with and without bone metastasis were 33.79±6.49 ng/ml and

11.74±2.96 ng/ml, respectively ($p<0.05$). The mean CEA levels in SCLC patients with and without bone metastasis were 28.93±4.59 ng/ml and 13.88±4.47 ng/ml, respectively($p>0.05$).Conclusion: Bone metastasis can be detected in patients with lung cancer by measuring CEA and OPN levels. Routine PET/CT monitoring is advised when these biomarkers increased.

P631

Lung cancer versus chronic inflammation: can we differentiate the two on F-18 FDG PET/CT?

H. Kim1, I. Yoo1, H. Park1, Y. Lee1, S. Park1, H. Sohn2, S. Kim1, Y. Park3; 1Seoul St Mary's Hospital, College of Medicine, The Catholic University of Korea, Seoul, KOREA, REPUBLIC OF, 2Yeouido St. Mary's Hospital, College of Medicine, The Catholic University of Korea, Seoul, KOREA, REPUBLIC OF, 3St. Vincent's Hospital, College of Medicine, The Catholic University of Korea, Suwon, KOREA, REPUBLIC OF.

Purpose: The aim of this study is to find differentiation points between chronic inflammation and lung cancer of similar findings on F-18 FDG PET/CT. Method: FDG PET/CT images from January 2010 to October 2014, performed for evaluation of pulmonary nodule in 180 patients (mean age 62±10 years) who had irregular consolidative nodule/mass greater than 1cm in diameter with low to moderate FDG avidity were retrospectively reviewed. 174 patients (96.7%) had pathologic confirmation. 6 patients (3.3%) had what were clinically considered benign nodules as they showed decrease in size without treatment. Lesions were analyzed by component (part solid, predominantly solid, and solid only), margin (smooth, partly irregular, and irregular), location (lung lobe), other lung lesion presence, axial diameter and metabolic parameters (SUVmean, SUVmax and SUVpeak). The Student t test and Pearson's Chi-square test were used to compare continuous variables and categorical variables, respectively. Results: There were 35 (19%) benign and 155 (81%) malignant cases. The most common type of component in malignant group was part solid (80 cases, 55%) and in benign group was solid only (19 cases, 54%). There was a tendency that malignancy group had more part solid tumors than benign group (80 cases, 55% vs. 11 cases, 31%) with statistically significance ($p=0.038$). The other parameters showed no significant value in differentiating between chronic inflammation and lung cancer. Conclusion: The component of nodule provided differentiation value in differentiating chronic inflammation and lung cancer on F-18 FDG PET/CT. The pulmonary nodules with part solid feature showed higher possibility of malignancy than nodules with other component features. However, other parameters including metabolic parameters had no significant value in interpreting ambiguous pulmonary lesions.

P632

Cost-Effectiveness of 18F-FDG PET-CT for preoperative restaging in patients with non-small cells lung cancer IIIA after neoadjuvant therapy

W. Valdés, **A. Ramírez**, E. Morillo, T. Aroui, N. Testart, E. Triviño, A. Rodriguez-Fernandez, J. Llamas-Elvira; H.VIRGEN DE LAS NIEVES, GRANADA, SPAIN.

Purpose: To determine the most efficient diagnostic method, from the perspective of the Spanish National Health System, for preoperative restaging in patients with non-small cells lungs cancer IIIA after neoadjuvant therapy. Materials and methods: Three possible strategies were studied, from the perspective of the Spanish National Health System, for management of preoperative staging of patients with non-small cell lung cancer IIIA after neoadjuvant therapy. These strategies differ in the diagnostic imaging method used. The first strategy use only CT+ c (CT + contrast agent). The second one use only PET/CT. And the last one use CT+c and PET/CT. The medical literature was reviewed to obtain values of diagnostic validity of differents techniques. Costs of these were obtained from public prices of Spanish National Health System. Quality-Adjusted Life Years (QALYs) produced in each strategy were calculated, so total cost and incremental cost-effectiveness ratio (ICER). Additionally, a sensitivity analysis was performed by changing the values assigned cost both as to the factors affecting effectiveness to check the robustness of the results obtained. Results: Comparing with the strategy use only CT+c, the other two presented a higher effectiveness, although the one that use PET/CT had a higher cost. The PET/CT and CT+c strategy obtained a lower cost derivate for the reduction of almost 60% unnecessary surgeries. ICER for only PET/CT strategy was 1122.73 €/QALY and -105078.95 €/QALY for CT+c and PET/CT strategy, showing these one clearly dominant. Sensibility analysis confirmed the robustness of these

results. Discussion: The use of PET/CT for preoperative staging for patients wiht non-small cells lung cancer IIIA after neoadjuvant therapy is clearly efficient for the Spanish National Health System, further combined with CT+c.

P633

The Value of the quantitative volumetric metabolic measurements withF-18 FDG PET-CT in patients with solitary pulmonary nodules.

D. Yüksel1, **T. Şengöz**1, O. Yaylalı1, H. Aslan1, F. Bir2; 1Pamukkale University, Medical Faculty, Dept. of Nuclear Medicine, Denizli, TURKEY, 2Pamukkale University, Medical Faculty, Dept. of Pathology, Denizli, TURKEY.

Aim: We evaluated the effect of quantitative volumetric metabolic measurements to distinguish benign from malignant in solitary pulmonary nodules(SPN). Materials and methods: We retrospectively reviewed 78 patients with diagnosis of SPN who underwent F-18 FDG PET-CT. The patients were classified as benign/malignant lesions according to the results of pathology. Additionally, malign lesions were classified as primary and metastatic lung cancer. Volumetric areas of interest (VAI) were drawn with the threshold of 40% by the way that to comply with the limits of lesions on CT in PET/CT images. Metabolic volume(MV), SUVmax, SUVmean, maximum metabolic index (MImax=SUVmax X MV) and mean metabolic index(MImean=SUVmean X MV) were measured from VAI. Mean,median values and standard error of the parameters in each group were calculated. Because of the abnormal distribution, nonparametric tests were used for the comparison of each group. The $p<0.05$ was accepted statistically significant. Partial correlation analysis was used for the relation of the parameters. For all parameters, cut-off values were obtained with receiver operating characteristic (ROC) analysis for basal and 2 hr respiratory gating PET-CT images separately. Results: Of 78 lesions, 10 were benign (12.8%), 38 were primary lung carcinoma (48.7%) and 30 were metastatic lung nodules (38.5%). The SUVmax, MImax, SUVmean and MImean of the three groups were presented as mean and standard Error (SE) in Table 1. There was significant difference among the three groups for SUVmax, MImax, SUVmean and MImean parameters ($p<0.05$). There were significant difference between benign lesions and primary lung cancer, between primary cancer and metastatic groups in all parameters. There was significant difference between benign and metastatic lung lesions in SUV mean and SUVmax parameters ($p<0.05$). We determined highly significant positive correlation between SUVmax and MImax ($r=0.73;p<0.05$); moderate positive correlation between SUVmean and MImean ($r=0.56;p<0.05$). In ROC analysis, basal SUVmax and basal SUVmean were found to be most sensitive and specific methods for benign/malign discriminate. In the cut-off value=2.59, the sensitivity and specificity for SUVmax were %98.0 and %91.7,respectively. In the cut-off value=1.65, the sensitivity and spesificity for SUVmean were %94 and %91.7, respectively. The sensitivity and specificity values of respiratory gating PET-CT images was lower than basal study. Conclusion: Basal SUVmax and basal SUVmean were found to be most sensitive and specific methods for benign/malign discriminate. In addition, all of metabolic measurements may discriminate to primary lung cancer from metastatic lung cancer.

P634

FDG-PET/CT in thymic epithelial tumors: correlation with the WHO classification and the tumor stage

M. Ishibashi, Y. Tanabe, S. Fujii, Y. Ohta, T. Ogawa; Division of Radiology, Department of Pathophysiological and Therapeutic Science, Faculty of Medicine, Tottori University, Yonago, JAPAN.

The aim: The purpose of this study was to assess the usefulness of FDG-PET/CT for predicting the histological type based on the World Health Organization classification and Masaoka tumor stage of thymic epithelial tumors. Materials and Methods: Thirty-three patients (9 males and 24 females; age range, 31-95 years old) with histologically verified thymic epithelial tumors, who underwent integrated FDG-PET/CT before treatment, were enrolled in this study. The maximum standardized uptake value (SUVmax) of each tumor was measured, and the relationship between the histological types based on the World Health Organization classification and the SUVmax of the tumor was investigated. We also analyzed the relationship between the Masaoka tumor stage and the SUVmax of the tumor. Results: Tumors included low-risk thymic tumors (type A in 1, type AB in 8, and type B1 in 7) and high-risk thymic tumors (type B2 in 3, type B3 in 4 and carcinoma in 11). The SUVmax of high-risk tumors (6.43±3.45) was significantly higher than that of low-risk tumors (3.07±0.87) ($P<0.01$). The SUVmax of 3.73 emerged as the cut-off value for differentiating between low-risk and high-risk tumors with area under the curve of 0.809. The Masaoka

tumor stage was as follows: stage I in 13, stage II in 8, stage III in 10 and stage IV in 3 patients. The SUVmax of the stage III/IV (7.49±5.08) was significantly higher than that of the stage I/II (3.21±1.11) (P<0.01). Conclusions: FDG-PET/CT is a useful modality for predicting the histological type and tumor stage of thymic epithelial tumors.

P635
Solitary Pulmonary Nodule (SPN) investigation with FDG-PET/CT

F. Vlachou1, V. Filippi1, A. Nikaki1, D. Savvidou1, P. Kosmidis2, K. Iliadis3, T. Pipikos1, K. Gogos4, K. Dalianis4, I. Andreou1, R. Efthymiadou1, V. Prassopoulos1; 1PET/CT Department ,Hygeia S.A., Athens, Marousi, GREECE, 22nd Internal Medicine - Oncology Clinic Hygeia SA, Athens, Marousi, GREECE, 3Thoracic Surgery Clinic Hygeia SA, Athens, Marousi, GREECE, 4Medical Physics Department , Hygeia S.A., Athens, Marousi, GREECE.

Aim: to evaluate the role of FDG-PET/CT in discrimination of malignant/benign solitary pulmonary nodules (SPN), by co-estimating nodule's size and FDG uptake (SUVmax). Material- Method: In total, 71 patients (31 female, 40 male) who underwent FDG-PET/CT examination for investigation of SPN at a Siemens Biograph LSO 16 sections system were enrolled in the study. Nodule's size and SUVmax were co-evaluated. Statistical analysis using un-paired t-test was used for discrimination of lung adenocarcinoma from benign formations such as hamartomas and inflammation, as well as from well-differentiated malignant formations, such as carcinoids. Histologic confirmation was available for all included patients. Results: SUVmax values were statistically significantly higher (p 0.1). In a subgroup analysis, results are recorded depending on the size of SPN: a)In 20 cases, the size of the nodule was ≤1cm. 11 were lung adenocarcinomas, 1 metastatic adenocarcinoma, 7 inflammations, 1 hamartoma. The average SUVmax of adenocarcinomas was 2.6, while for inflammation was accordingly 2. There was no statistical significance in SUVmax for differentiation benign from malignant lesions (p >0.05). b)In 36 cases, the size of the nodule was >1 - ≤2cm. 23 were lung adenocarcinomas (average SUVmax 6.2), 5 metastatic carcinomas, 3 were inflammations (average SUVmax 2.1), 4 carcinoids (average SUVmax 2.3), 1 hamartoma. There was statistical significance in SUVmax values for differentiation adenocarcinomas from benign/well differentiated carcinoid lesions (p=0.003, 2 - ≤3. 9 were lung adenocarcinomas (average SUVmax 8.1), 3 hamartomas (average SUVmax 2), 2 carcinoids, 1 inflammation. There was statistical significance in SUVmax values for differentiation adenocarcinomas from benign/well differentiated carcinoid lesions (p=0.0053, <0.05) Conclusion: PET is a very useful imaging procedure in differentiation of malignant vs benign/well-differentiated carcinoid pulmonary lesions of size >1cm. For smaller SPNs, although there is tendency for higher SUVmax values in adenocarcinomas, perhaps morphologic characteristics of the nodules or complementary delayed PET acquisition could be more helpful.

P636
The evaluation of clinical usefulness of continuous bed motion scanning in positron emission tomography in diagnosis of patients with subsolid pulmonary nodule

M. Endo, K. Asakura, T. Aramaki, E. Bekku, R. Sato, K. Yoza; Shizuoka cancer center, Shizuoka, JAPAN.

Background and purpose: Recently, continuous bed motion (CBM) technology has been introduced to PET scanning in routine clinical practice, but the evaluation and/or benefits of this technique are unclear in abnormal pulmonary opacity. The purpose of this study was to access the clinical usefulness using CBM scanning of 18F-FDG PET/CT compared to conventional step and shoot (SAS) scanning in diagnosis of patients with subsolid pulmonary nodule. Materials and methods: We were retrospectively enrolled patients with abnormal pulmonary lesions smaller than 30 mm in diameter for diagnosing and/or staging lung cancer between May and August 2014 in this study approved by our institutional review board. 18F-FDG PET/CT scans were obtained with an integrated PET/CT system (Biograph mCT Flow 64-4R, Siemens, Germany). All the patients were fasted for at least 6 hour, then administered 200-210 MBq of 18F-FDG. CBM scanning was 0.4mm/sec speed w/o respiratory gating, and SAS scanning was 600 sec/frame acquisition w/o respiratory and cardiac gating at an axial sampling thickness of 4 mm/slice. Amplitude-based optimal respiratory images reconstructed with 35% of acquired PET data. Lesion localization, size and characteristics, and final diagnosis were summarized. Image quality and calculated SUV max/peak of each reconstructed images were evaluated corresponding with those of non-gated SAS image. For the evaluation of image quality of each scanning, we used 5 visual scales with consensus compared to 3 point as the score of non-gated SAS image. Kai square test and paired t-test were used for the statistical analysis. Statistical significance was assumed at a p-value <0.05. Results: 116 patients (41 females and 75 males) with 128 abnormal pulmonary lesions were enrolled. Pulmonary locations of abnormal

lesions were 28 cases in RUL, 7 in RML, 29 in RLL, 35 in LUL and 29 in LLL. There were 86 solid and 42 subsolid nodules, and mean lesion size was 16.4mm and 16.5mm, respectively. Seventy-eight patients with lung cancer, 11 in suspicious lung cancer, 22 metastatic nodules, and the rest were inflammatory lesions. Image quality and SUV max/peak values of four PET images was higher evaluated than non-gated SAS image in solid and subsolid nodules. Furthermore, SUV max/peak value of CBM with respiratory gating was significantly highest compared to the rest scanning methods in both. Conclusion: Clinical PET scanning using CBM with respiratory gating could demonstrate more accurate metabolic characteristics and high image quality even in subsolid pulmonary nodules same as solid in routine clinical setting.

P637

Efficacy of SUVmax and SUVpeak to predict distant metastasis of non-small cell lung cancer before treatment

S. Toubaru1, S. Ohashi1, Y. Tachibana1, M. Hasebe1, K. Tanimoto1, M. Zhang1, N. Yamamoto1, M. Nakajima1, M. Karube1, T. Obata1, T. Saga1, Y. Ando1, K. Yoshikawa2, T. Kamada1; 1National Institute of Radiological Sciences, Chiba, JAPAN, 2Tokyo Bay Advanced Imaging & Radiation Oncology Clinic MAKUHARI, Chiba, JAPAN.

[Introduction & purpose]SUVpeak index is now gradually being used to assess the efficacy of treatments for malignant tumors. However, its advantage over classical SUVmax is still not well discussed in various aspects of oncology. The purpose of this study is to compare the significance of SUVmax and SUVpeak regarding the prediction of future distant metastasis before treatment in non-small cell lung cancer.[Materials and methods]74 patients were selected as subjects from our local database for this retrospective study. The patients were all diagnosed as non-small cell lung cancer and were scanned by FDG-PET/CT scanner before they finally underwent charged particle radiation therapy. None of them had distant metastasis before treatment. Their outcomes were followed up for more than one year after treatment. Distant metastatic lesion appeared in 15 patients among the 74 patients in the meanwhile.For the assessment, first, SUVmax as well as SUVpeak6, SUVpeak10, and SUVpeak15 (numbers after SUVpeak indicate the diameters of VOI in mm) were obtained for each patient from their pre-treatment FDG-PET/CT. Second, cut-off value was defined for each parameter (SUVmax and SUVpeaks) by ROC analysis, respectively: the value which made the sensitivity + specificity largest for each parameter regarding the later appearance of metastasis was defined as its cut-off value. Third, the patients were divided into two groups, over and under the cut-off value for each parameter, respectively. Finally, the ratio of metastasis-appearance was compared between the groups by applying Kaplan-Meier method. The deference was analyzed by log-rank test. ($P<0.05$ was regarded significant.)[Result]Number of patients categorized to the larger SUV group and the number of patients who had metastasis later in that group were 17 and 7(SUVmax), 20 and 6 (SUVpeak6), 13 and 5 (SUVpeak10), and 5 and 3 (SUVpeak15), respectively. The ratio of metastasis was higher in the larger SUV group in all assessed parameters. Difference with significance was found in SUVmax ($P=0.017$) and SUVpeak15 ($P=0.007$). The differences in SUVpeak6 (close to the most widely used SUVpeak, $P=0.223$) and SUVpeak10 ($P=0.078$) was not significant.[Conclusion]The significant differences of SUVmax and SUVpeak15 to predict distant metastasis after charged particle radiation therapy were obtained. Considering only 3 metastases were picked up in SUBpeak15, SUVmax may be superior to any SUVpeak evaluation.

P638

Role of 18FDG-PET/CT semiquantitative parameters in the evaluation of therapy response in patients affected by recurrent pleural mesothelioma

A. Di Palo, **A. Niccoli Asabella**, C. Altini, A. Notaristefano, C. Ferrari, G. Rubini; Nuclear Medicine Unit, D.I.M., University of Bari, ITALY, Bari, ITALY.

Aim: To investigate the role of 18FDG-PET/CT semiquantitative parameters compared with mRECIST criteria for therapy response evaluation in patients (pts) with recurrent pleural mesothelioma.Materials and methods: 35 pts with recurrent pleural mesothelioma were enrolled and underwent 18F-FDG PET/CT scans twice (baseline to confirm the recurrent mesothelioma and 4-5 weeks post-therapy to evaluate the response). Volume of interest (VOIs) were drawn on both the 18F-FDG PET/CT and SUVmax, SUVav, MTV, TLG were collected. We also calculated ΔSUVmax (as difference between SUVmax1-SUVmax2), ΔSUVav (as difference between SUVav1-SUVav2), ΔMTV (MTV1-MTV2), ΔTLG (TLG1-TLG2). Response indexes (RImax% and RIav%) were also calculated as RI=[(SUV1−SUV2)/SUV1]x100). Radiologic response to therapy was evaluated using the modified RECIST criteria for mesothelioma. Responders' PET/CT patients were defined as patients with the disappearance of all lesions or as at least a 30% reduction in RImax%. No responders patients were defined as patients with stable disease, or with an increase of at least 30% in RImax%. T-student test for unpaired groups was applied. The diagnostic capability of 18F-FDG PET/CT was calculated by ROC analysis and

expressed as area under curve (AUC).Results: Based on modified RECIST criteria: responders were 12/35 (34.3%) while 23/35 (65.7%) were no responders; based on PET/CT evaluation: 11/35 (31.5%) were responders and 24/35 (68.5%) patients were no responders. According RECIST, statistical differences between responders and no-responders were significant in the analysis of MTV1 (t=-3.725, p=0.003), TLG1 (t= -3.259, p= 0.006) SUVmax2 (t=-3.994, p=0), SUVav2 (t=4.21, p=0), MTV2 (t=4.186, p=0), TLG2 (t=3.463, p=0.002), RImax% (t=-2.594, p=0.014) and RIav% (t==-2.385, p=0.023), ΔMTV (t=-5.04, p=0) ΔTLG (t=-4.783, p=0). According modified RECIST criteria, all parameters defined a good AUC but the better AUCs resulted for ΔMTV (cut-off ≤ 11.3, sensitivity 91.3%, specificity 91.7%) and ΔTLG (cut-off ≤ 59.1, sensitivity 82.6%, specificity 100%).Conclusions: It has been demonstrated that 18F-FDG PET/CT can be useful to predict treatment response in MPM patients. Among the semiquantitative parameters collectable, ΔMTV and ΔTLG resulted the best predictive value according RECIST criteria.

P639

Assessment of the infuence of several clinical, surgical and pathologic variables in bronchogenic carcinoma increasing stage from diagnostic PET/CT to reparative surgery.

E. Rodríguez Pelayo, E. Castillo Gallo, J. García Satué, B. De Olaiz Navarro, J. Aramburu González, M. Balsa Bretón, C. Paniagua Correa, M. Castillejos Rodríguez, F. Penín González; Hospital Universitario de Getafe, Madrid, SPAIN.

AIM: Assess several clinical, surgical and pathologic variables influence in bronchogenic carcinoma staging increase from 18FDG-PET/CT (cTNM) to reparative surgery (pTNM). MATERIAL AND METHOD: We retrospectively reviewed 104 patients with bronchogenic carcinoma from may/09 to june/2014, which showed a positive PET/CT for malignancy and who were surgery's candidates without neoadjuvant treatment. PET/CT staging and pathologic postoperative staging were recorded according to the 7th edition of the TNM classification. We also recorded demographic variables, pack-year, reason for consultation, mediastinoscopy (yes/no), type of surgery, tumour pathology/differentiation and the days between diagnostic PET/CT and surgery. Univariate logistic regression was performed to test for significant associations between any of variables studied with staging increase. RESULTS: In 51 of the 104 reviewed patients the diagnosis was adenocarcinoma and 27 showed final staging increase. Remaining 53 patients were diagnosed of squamous cell carcinoma, of which 22 showed staging increase. Statistical analysis showed that the only variable significantly related to staging increase in the time interval studied was smoking at diagnosis in squamous cell carcinoma (p<0.039). Remaining variables analyzed, including elapsed time, do not seem to correlate with the degree of staging increase in bronchogenic carcinoma. CONCLUSION: Statistical analysis showed that the only variable which significantly increased the final disease staging between diagnostic PET/CT and surgery was smoking at diagnosis in squamous cell carcinoma (p < 0.039).

P640

Is Molecular Remission as Detected by 18F-FDG PET/CT and Regression Grade After Neoadjuvant Treatment in the Primary Tumor and the Involved Mediastinal Lymph Nodes a Prognostic Factor in Patients With NSCLC Stage III?

M. Schmuecking1, R. P. Baum2, N. D. Klass3, E. Fritz3, S. C. Schaefer4, N. Presselt5, B. Hoksch6, K. M. Mueller7, T. G. Wendt8, B. Klaeser9, R. Bonnet10; 1Strahlenzentrum Hamburg/CyberKnife Center Hamburg, Hamburg, GERMANY, 2Zentralklinik Bad Berka, Theranostics Center for Molecular Radiotherapy and Molecular Imaging, Bad Berka, GERMANY, 3Inselspital Bern, Dept. of Radiation Oncology, Bern, SWITZERLAND, 4University of Bern, Institute of Pathology, Bern, SWITZERLAND, 5Zentralklinik Bad Berka, Dept. of Thoracic Surgery, Bad Berka, GERMANY, 6Inselspital Bern, Dept. of Thoracic Surgery, Bern, SWITZERLAND, 7University of Münster, Institute of Pathology, Münster, GERMANY, 8University of Jena, Dept. of Radiation Oncology, Jena, GERMANY, 9Inselspital Bern, Dept. of Nuclear Medicine, Bern, SWITZERLAND, 10Zentralklinik Bad Berka, Dept. of Pneumology, Bad Berka, GERMANY.

Aim: To evaluate the role of molecular remission as detected by 18F-FDG-PET/CT and regression grade after neoadjuvant treatment followed by surgical resection of pts with NSCLC stage III. Materials and Methods: For 76pts with NSCLC stage IIIA (44%) / IIIB (56%) neoadjuvant treatment consisted of 3 cycles of chemotherapy followed by concomitant chemoradiation. 15/28pts with NSCLC stage IIIA (81%) / IIIB (19%) received 3 cycles of chemotherapy followed by radiation therapy, 13/28pts only 3 cycles of chemotherapy as a sole neoadjuvant treatment. Documentation of involved lymph node stations as detected by 18F-FDG-PET/CT and lymph node sampling during surgery according to the IASLC lymph node mapping (2009). Evaluation of histological regression grade (RG) according to Junker et al. (2001) and correlation with 18F-FDG-PET/CT for primary tumor and each lymph node station. Calculation of disease free survival (Kaplan-Meier estimates, log-rank test). Results: Actuarial tumor specific survival for the 76pts with concomitant chemoradiation plus chemotherapy: complete vs incomplete metabolic remission prior to surgery after 60 months: 40% vs 24% (p = .018), RGIII/IIb

(no/less than 10% of vital tumor cells) vs RGIIa/I (more than 10% vital tumor cells) after 60 months: 46% vs 15% ($p < .006$). 42/76pts had RGIII/IIb, 20/76pts had regression grade III. In 32/76pts 18F-FDG-PET/CT was correlated with the regression grade: 1/8pts with RGIII were in the 18F-FDG-PET/CT false positive, 10pts with RGIIb (i.e. all pts with RGIIb) were in the 18F-FDG PET/CT false negative, 1pt with RGIIa was in the 18F-FDG-PET/CT false negative: Hence, the cut-off level in detecting vital tumor cells by 18F-FDG-PET/CT after neoadjuvant chemoradiation for NSCLC is about 10%. Actuarial tumor specific survival for the 28pts with sequential chemoradiation or chemotherapy as a sole neoadjuvant treatment: RGIII vs RGIIb/IIa/I after 60 months: 50% vs 16%. 05/28 pts had RGIII. Assuming a pts number of 540, the treatment regimen consisting of concomitant chemoradiation plus chemotherapy might be superior to the other neoadjuvant treatment regimens. Conclusion: Molecular remission in mediastinal lymph nodes as detected by 18F-FDG-PET correlates well with regression grade and both may predict (long-term) therapeutic outcome in pts with stage III NSCLC. The cut-off level in detecting vital tumor cells by 18F-FDG-PET after neoadjuvant chemoradiation for NSCLC is about 10%. Our preliminary data of 104pts suggest that intensification of neoadjuvant treatment may lead to a higher amount of complete remission resulting in an increased survival. However this hypothesis has to be tested in prospective trials.

P641

Study of FDG PET/CT in detecting mediastinal and hilar/interlobar lymph nodes metastases of non-small cell lung cancer

q. xue, **z. yao**; Beijing Hospital, Beijing, CHINA.

Aim: Precise mediastinal lymph nodes staging for non-small cell lung cancer(NSCLC) patients without distant metastases decides if surgery is advisable. The staging of hilar/interlobar lymph nodes affects the operational styles. The value of maximum standard uptake value (SUVmax) in mediastinal lymph nodes staging has been proven , while the value of SUVmax in hilar/interlobar lymph nodes staging has not been studied. To evaluate the value of 18F-FDG PET/CT in detecting mediastinal and hilar/interlobar lymph nodes metastases by SUVmax for NSCLC patients. To analyse the characteristics of mediastinal and hilar/intralobar lymph nodes metastases separatly. Materials and methods: 69 NSCLC patients with 18F-FDG PET/CT examination and surgery were analyzed. Preoperative 18F-FDG PET/CT was done and the lymph nodes were harvested during surgery. The SUVmax of lymph nodes were compared to histology results. The sensitivity, specificity and accuracy of SUVmax in detecting lymph nodes metastases were calculated .The optimal SUVmax cutoff value in detecting lymph nodes metastases was calculated by ROC curve. The comparison about sensitivity, specificity and accuracy in detecting lymph nodes metastases for mediastinal and hilar/intralobar lymph nodes between different cutoff values was done. The optimal SUVmax cutoff value in detecting mediastinal and hilar/intralobar lymph nodes metastases were calculated by ROC curve separately. Results: 1. The value of different SUVmax in diagnosing lymph nodes metastases: The sensitivity, specificity and accuracy of SUVmax≥2.5 in diagnosing lymph nodes metastases were 83.6%,61.9%,65.8%. The optimal cutoff value of SUVmax in diagnosing lymph nodes metastases was 3.55 got by ROC curve ,with sensitivity 75.4%,specificity 79.5% and accuracy 78.8%. Compared with SUVmax≥2.50 as standards in detecting lymph nodes metastases ,there were statistical significance in specificity and accuracy(P=0.000),with no statistical significance in sensitivity (P=0.262). 2. Lymph nodes'SUVmax in different regions: The SUVmax of hilar/intralobar lymph nodes(4.87±2.7)was significantly higher than that of mediastinal lymph nodes(2.49±2.1),P=0.000.Both SUVmax≥3.55 and SUVmax≥2.50 as standards in detecting lymph nodes metastases, The sensitivity for mediastinal lymph nodes was low and the specificity and accuracy for hilar/intralobar lymph nodes were low. 3. The cutoff value of SUVmax in different regions for detecting lymph nodes metastases: The cutoff value of SUVmax in mediastinal and hilar/intralobar lymph nodes were 2.78,4.93 separatly. The sensitivity ,specificity and accuracy were 71%, 87.1%, 84.9% for mediastinal lymph nodes by SUVmax≥2.78 and 73.3%, 77.9%, 76.6% for hilar/intralobar lymph nodes by SUVmax≥ 4.93. Conclusion: For getting better diagnostic value, different SUVmax cutoff values should be used in detecting mediastinal and hilar/intralobar lymph nodes metastases.

P642

Is there a role for 18F-FDG PET/CT to differentiate benign from malignant form of solitary fibrous tumors of the pleura?

D. Familiari1, M. Migliore2, A. Missiato3, S. Russo1, A. Ruggeri1, E. Potenza3, M. C. Fornito1; 1Nuclear Medicine Department/PET-CT center - A.R.N.A.S. Garibaldi, Catania, ITALY, 2Thoracic Sugery Department - Azienda Ospedaliera Universitaria "Policlinico- Vittorio Emanuele", Catania, ITALY, 3Thoracic Sugery Department - A.R.N.A.S. Garibaldi, Catania, ITALY.

AIM Solitary fibrous tumours of the pleura (SFTPs) is a rare neoplasm that represent less than 5% of all pleural tumors and it can occur in other extrathoracic areas. Although the majority are benign forms and STPs is discovered incidentally on chest radiographs, a 15-20% of all cases can show a malignant

behavior characterized by a less favorable outcome. Some benign form SFTP may transform into malignant after several years. A preoperative role of 18F-FDG PET/TC was suggested to indicate or exclude malignancy and, eventually reveal local recurrence or distant metastases. A SUVmax of 2.5 was generally considered as indicative of non aggressive process. The aim of this study was to evaluate the role of 18F-FDG PET/TC and to confirm if there is a real SUVmax cut-off value able to discrimi-nate benign from malignant form. MATERIALS AND METHODS Four patients (2 male and 2 female) underwent a 18F-FDG PET/TC for metabolic evaluation of an expansive process on the hemithorax suspected for SFTPs. One of this patients was already submitted to lung superior lobectomy and a local relapse was suspected. PET/TC scan was obtained an hour after intravenous injec-tion of18FDG. 18F-FDG PET and unenhanced CT images were acquired by Gemini PET/CT system (GXL Philips) with a time of acquisition of two minutes for bed. RESULTS In all the patients, PET/CT images showed the presence of voluminous, smoothly margined,lobulated extrapulmonary solid mass abutting the wall of the in-volved hemithorax without invasion of the adjacent structures. No pathologic uptake in mediastinal lymph nodes or distant metastasis were shown. On average, a value of SU-Vmax=3.5 (range 3.3-3.7) was found. Based on the literature, this uptake was interpreted as pathologic and therefore suspected for malignant form of SFTPs. After PET/CT results a thoracotomy was performed in order to remove the neoplasm. Histological examination reveal the benignant nature of the mass that was finally interpreted as benignant form of SFTPs in 3 of 4 case and as a relapse in the other one. CONCLUSIONS This study demonstrate that PET/CT is not able to differentiated be-tween malignant and benign form of SFTPs and cannot substitute histology. A SUVmax of 2.5, as reported in literature so far, is not indicative only of non aggressive forms and therefore there is not a useful FDG uptake correlated to malignant evolution.

P643

Positron Emission Tomography CT to differentiate tumour recurrence and radiation-induced pulmonary fibrosis after stereotactic body radiation therapy

G. Capriotti1, **S. Di Traglia**1, A. Covello1, P. Pizzichini1, D. Prosperi1, M. Tuccimei1, R. Maurizi Enrici2, M. Osti2, F. Scopinaro1; 1Sapienza University of Rome, Nuclear Medicine Unit, Sant'Andrea Hospital, ROME, ITALY, 2Sapienza University of Rome, Sant'Andrea Hospital, ROME, ITALY.

Aim: Changes in lung density on computed tomography CT are common after stereotactic ablative radiotherapy (SABR) and can confound to early detection of recurrence. The aim of this study was to evaluate the role of Contrast Enhanced (CT) and 18F-fluorodeoxiglucose positron emission tomography (FDG-PET/CT) in differentiating tumour recurrence from radiation fibrosis after SABR. Primary tumour maximum standardized uptake value (SUV max) on FDG-PET/CT before and after therapy has been studied as potential prognostic factor for NSCLC patients receiving SABR. Methods: 24 patients (Mean Age: 70 years; 14 male and 10 female) received SABR for stage I non-small cell lung cancer or metastatic lung cancer. Both FDG-PET/CT and CT were performed before and after treatment in different time point (<6 months, 6-12 months, 12-24 months). The FDG uptake in the lung region was assessed qualitatively using a 3-point scale (0, none or faint; 1, mild; 2 moderate to intense) ad the shape was evaluated (mass-like or non mass-like). For semi-quantitative analysis, SUV mean and SUV max were calculated and compared them to the pre-therapeutic values. Results: 7 patients had local relapse. In recurrent tumours, the combination of intensity grade 2 and mass-like shape was most common (90%). In contrast, the combination of intensity grade 0 or 1 and no-mass like shape was most common in radiation fibrosis (80%). The SUVmax of tumour relapse after 12 months was higher than of radiation fibrosis ($p<0.01$) and all tumour recurrence showed the SUVmax> 4 at diagnosis of local failure. At ≥ 12 months after SABR, the combination of intensity 2 and mass-like FDG uptake or SUVmax ≥ 4 had a high predictive value of local recurrence. Pre-RT and post-RT primary SUV can predict the outcome of patients with NSCLC treated with SABR. We observed the following pattern of changes in lung parenchyma on CT post-SABR: acute (within 6 months, corresponding to pneumonitis) and late (after 6 months, corresponding to fibrosis). Conclusion: The combination of FDG patterns and SUVmax was a useful to discern tumour relapse from radiation fibrosis. CT density changes are common post-SABR and PET scan is more sensitive than CT in detecting recurrences.

P644

Predictive value of early dynamic and static FDG PET / CT findings in evaluation of primary lung lesions

B. Vatankulu1, S. Bakan2, O. E. Şahin1, S. Sağer1, M. Halaç1, H. B. Sayman3, K. Sönmezoğlu1; 1İstanbul University Cerrahpaşa Medical Faculty Department of Nuclear Medicine, İstanbul, TURKEY, 2İstanbul University Cerrahpaşa Medical Faculty Department of Radiology, İstanbul, TURKEY, 3İstanbul University Cerrahpaşa Medical Faculty Department of Nuclear Medicineepartment of Nuclear Medicine, İstanbul, TURKEY.

Aim: Although differentiation of benign and malignant lesions of primary lung is performed with FDG PET / CT imaging, FDG which is a glucose analogue is not a specific cancer agent. To make differentiation of benign or malignant lesions

is not easy in granulomatous processes , active inflammation and infection. We aimed to find the value of dynamic and static FDG PET / CT findings in detection of malignant and benign lung lesions.Materials and method: A total of 17 patients detected primary lung lesions with histopathological results were prospectively evaluated. All patients in the study after FDG injection series displays the first 15 minutes early to receive dynamic imaging and after the injection 55-65. min in static display was made to wholebody. 50% of maximum pixel value threshold was used for VOI (volume of interest)which placed on assessment of pulmonary lesion. Arterial blood flow were evaluated with VOI's which were placed in the same size on the left ventricle and thoracic aorta. FDG phosphorylation rate (Ki) and glucose metabolic rate (MRGlu) was calculated with PATLAK analysis for each lesion. In addition to the increased activity of the lesions time activity curve (TAC slope) values were recorded . The mean and maximum standardized uptake values (SUVmax , SUVmean), total lesion glycolysis (TLG) values were calculated with static PET / CT images.Results: Malignancy were detected in 12 of 17 patients in histopathological examination. 5 patients had normal histopathology. Ki, MRGlu , the TAC slope , SUVmax , SUVmean and TLG values in evaluating for benign and malignant lung lesions were shown to be beneficial in ensuring the benign and malignant lesions with McNemar test ($p<0.05$). The sensitivity and specificity for malignant lesions of the Ki and MRGlu values obtained from dynamic studies were 92 % and 79% respectively. Although static PET / CT parameters detected malignancy, dynamic data showed benign lesions in one of the five lesions.Conclusions: The differential diagnosis of benign and malignant lung lesions may be performed with a high accuracy with the values of Ki and MRGlu obtained from dynamic FDG PET / CT imaging. The accuracy of FDG - PET / CT imaging may be increased with dynamic images in patients unable to distinguish malignant or granulomatous lung lesions.

P645

Correlation of F-18 FDG PET-CT based on metabolic volumetric parameters with survival in patients with non-small cell lung carcinoma

M. Kula1, E. Kocaagaoglu1, U. Abdulrezzak1, H. Karaca2, Ö. Onal3, A. Tutus1, Y. Kose Kurt1; 1Erciyes University, School of Medicine, Department of Nuclear Medicine, Kayseri, TURKEY, 2Erciyes University, School of Medicine, Department of Clinical Oncology, Kayseri, TURKEY, 3Erciyes University, School of Medicine, Department of Cardiovascular Surgery, Kayseri, TURKEY.

Aim: To determine the relationship between metabolic-volumetric parameters (PET-MVP) based on F-18 FDG PET-CT with survival and prognostic factors in patients with non-small cell lung carcinoma (NSCLC). Patients and Methods: Total of 215 patients with NSCLC who underwent PET-CT before any therapy between September 2009 and January 2012 were evaluated retrospectively. Univariate and multivariate analyses were performed to assess the relation of survival and PET-MVP, and the other prognostic factors. We compared ROC curves obtained by thresholds segmentation method (using thresholds of 50%/ 38% of the maximal SUV within the lesion). Results: The mean follow up time was 22 months and the estimated overall survival for cohort was 13±1, 4 months. Univariate analyses showed that age (p: 0.006), stage ($p< 0.0001$), mediastinoscopy results (p: 0.001), PMD (p: 0.004), SUVmax values of mediastinal lymph nodes ($p:<0.0001$), all of the PET-MVP (SUVmax p:0,02, others p: 0,0001) were significant prognostic factor for overall survival. On multivariate analysis, independent prognostic factors associated with overall survival were age (p:0,015, HR:1,5), stage ($p:<0,0001$) and MTV (metabolic tumour volume) %38 (p:0, 009, HR:1,58). There was no significant difference between ROC curves obtained by thresholds segmentation method. Conclusion: PET-MVP based on F-18 FDG PET-CT, especially MTV 38% are important independent prognostic factors for survival. It may be a promising tool for stratifying patients with NSCLC for risk-adapted therapies.

P38 - Monday, October 12, 2015, 4:00 PM - 4:30 PM, Hall 3 – Poster Exhibition

Clinical Oncology: Liver, Upper GI & Pancreatic Cancer

P646

Value of 18F-FDG PET/CT in the Staging of Gastric Carcinoma

L. Mena Bares, V. Gónzalez Cosano, E. Carmona Asenjo, M. Pleguezuelo Navarro, F. Maza Muret, V. Guiote Moreno, E. Moreno Ortega, J. Vallejo Casas; Hospital Universitario Reina Sofía, Córdoba, SPAIN.

Aim: The study's objetive is to analize the utility of 18F-FDG PET/CT in the gastric cancer staging comparing with the CT, the ultrasound endoscopic results and the utility in the clinical management of patients. Material and Methods: We analized retrospectively 29 patients with gastric adenocarcinoma that were diagnosed with upper endoscopy during the period between May 2012-November 2014. All patients underwent a thorax and abdomen CT study with intravenous contrast and PET/CT study with 18F-FDG from the skull base to proximal third of legs after 26 days on average compared to CT scan. With 13 patients an ultrasound endoscopic study was performed during the same study period. Results: The study consisted of 19 men and 10 women with middle ages of 67

years old. The most frequent histological subtype was de adenocarcinoma (68,2% of cases).The sensitivity values for the detection of the primary tumour were 93,1% for PET/CT, 79, 3% for CT and 100% for ultrasound endoscopic. The PET/CT study compared with CT changed the tumour stage and the clinical management in 13 patients (44, 8%). For the patients who performed CT and ultrasound endoscopic, the PET/CT changed the tumour stage in 61,5% of the cases and the clinical management in 38,5%. In the lymph stage all changes were to reduce the stage, the results were: 2 patients went from N1 to N0, 2 patients from N2 to N1 and one of them from N2 to N0. In the other side, the changes in detection of distant metastases were: one patient went from M0 to M1 and 5 patients from M1 to M0. The changes in the clinical management were: a) in patients without surgery options before performed the PET/CT: 3 patients received neoadjuvant treatment before the surgery and 2 patients surgery. b) in patients with surgery options before PET/CT: one patient became inoperable by the existence of distant metastases undetected with CT; 6 patient underwent surgery without neoadjuvant treatment and one patient surgery after neoadjuvant treatment. Conclusions: The 18F-FDG PET/CT is an useful procedure for staging of gastric carcinoma, showing higher sensitivity than CT in detecting primary tumour. The PET/CT can lead to a modification of tumour stage and therefore the clinical management of patients in up to 45% of cases.

P647

Delayed FDG image obtained 90 min after injection gives incremental information which correlates histopathological data; Analysis with surgically resected pancreatic cancer

T. Kudo1, R. Ideguchi1, M. Uetani1, A. Nanashima2, T. Nagayasu1; 1Nagasaki University, Nagasaki, JAPAN, 2University of Miyazaki, Miyazaki, JAPAN.

Purpose: Histopathological-Nuclear Medicine correlation is important issue to predict prognosis after surgical resection. Histopathogical findings of surgically resected pancreatic cancer and preoperative FDG PET parameters are correlated. Method: 16 consecutive patient who underwent surgical resection in division of surgical oncology, Nagasaki University Hospital were analyzed. FDG images were obtained 60min and 90 min after injection. SUVmax of main tumor at each time point (SUVmax-60, SUVmax-90), SUVmax normalized to normal liver average (TBR-60, TBR-90), difference between SUVmax-90min SUVmax-60 (SUVmax-diff), difference between TBR-90 and TBR-60 were calculated in each patients. Histopathological parameters such as lymphatic(ly), perineural(ne) and vascular(v) invasion were determined on resected surgical specimen. Each parameter of invasion was classified into 4 grading system (0=no invasion, 3=severe invasion). Those histopathological parameters were correlated with FDG PET parameters. Results: TBR-diff showed significant correlation between vascular invasions. “v3” showed significantly higher TBR-diff (132%) compared to all other v-grade (v0=16.9, v1=29.0, v2=34.5). TBR-90 also showed similar pattern with vascular invasion (v0=2.5, v1=2.5, v2=2.7, v3=5.3; $p<0.05$ between v3 and other 3 grades). SUVmax-90 showed similar tendency but did not reach statistical significance. TBR-60 and SUVmax-60 showed no relationship between vascular invasion grades. For perineural invasion TBR-90, SUVmax-90, TBR-diff and SUVmax-diff showed similar tendency like vascular invasion but also does not reach statistical significance. Any FDG parameters showed no correlation and tendency with lymphatic invasion. Conclusion: FDG PET image obtained 90min after injection may give us incremental information over image obtained after 60 min which was conventionally performed. However, lymphatic invasion is hard to predict.

P648

The diagnostic performance of FDG-PET/CT versus conventional imaging modalities in the evaluation of treatment response following ablation therapy for colorectal liver metastases: a meta-analysis

M. Samim1, Q. I. Molenaar1, M. F. J. Seesing1, M. A. A. J. van den Bosch1, T. J. M. Ruers2, I. H. M. Borel Rinkes1, R. van Hillegersberg1, M. G. E. H. Lam1, H. M. Verkooijen1; 1University Medical Center Utrecht, Utrecht, NETHERLANDS, 2Dutch Cancer Institute - Antoni van Leeuwenhoek, Amsterdam, NETHERLANDS.

Background: Thermal ablation therapy is increasingly applied for treatment of patients with unresectable colorectal liver metastases (CLM). Uncertainty exists on the optimal imaging modality for timely detection of local tumour progression. This systematic review and meta-analysis evaluates the diagnostic accuracy of CT, MRI and FDG-PET for detection of local tumour progression following thermal ablation therapy.Methods: A comprehensive systematic review of the literature published from inception to January 2015 was performed. Included were all English written studies that reported the diagnostic accuracy of at least FDG-PET or FDG-PET/CT for postoperative evaluation of patients with liver malignancies treated by means of ablation therapy. Studies had to report either data on the true positive, false positive, true negative and false negative results of the index test or the sensitivity and specificity. The reference standard had to be specified and was defined as histology results or clinical follow-up. Excluded from the meta-analysis were studies that reported small case series ($n<10$). The methodological quality of the studies was

assessed using a modified version of the quality assessment of diagnostic accuracy studies (QUADAS) tool. For meta-analysis, the pooled sensitivity and specificity was calculated for each imaging modality. A random effect model was chosen in case of I2 >30%.Results: The literature search resulted in 4670 hits, 13 of which were included in the systematic review. The critical appraisal showed that in the selected studies there was a risk of bias regarding the use of the reference standard and the blinding of the index tests. Based on the critical appraisal, three studies were excluded from the meta-analysis. Seven studies reported data on diagnostic performance of FDG-PET (n=328), five studies for FDG-PET/CT (n=354), eight studies for CT imaging (n=333) and three studies for MRI (n=124). Pooled sensitivity estimates were 85% (78-91%) for FDG-PET, 86% (80-91%) for FDG-PET/CT, 73% (63-81%) for CT and 69% (54-81%) for MRI. The pooled specificity estimates were 96% (91-98%) for FDG-PET, 89% (84-98%) for FDG-PET/CT, 96% (92-98%) for CT and 99% (93-100%) for MRI.Conclusion: Although the current available literature provides limited high-quality research evidence upon which to base any firm decisions, the results of this meta-analysis suggest that FDG-PET and FDG-PET/CT have the highest diagnostic accuracy for detection of incomplete ablation or local tumour progression in patients with CLM.

P649

Respiratory gated 18F-FDG-PET/CT improves quantification of metabolic parameters and their correlation with overall survival in patients with pancreatic ductal adenocarcinoma

D. Withaar, W. Grootjans, J. Hermans, K. Van Laarhoven, L. De Geus-Oei, M. Gotthardt, E. Aarntzen; Radboudumc, Nijmegen, NETHERLANDS.

Aim: Metabolic parameters, especially SUVmax, are increasingly being used to characterize tumors. Movement artifacts during respiration introduce an error in quantification of metabolic parameters, especially around the diaphragm. Previous studies in lung cancer showed that amplitude base optimal respiratory-gated (ORG) 18F-FDG-PET/CT scanning results in significant increase in metabolic parameters, except the MTV (40% threshold), which decreased [Grootjans et al. Eur Radiol 2014]. The present study investigates the additional value of ORG scanning on quantification of metabolic parameters in patients with pancreatic ductal adenocarcinoma (PDAC) in correlation with overall survival (OS). Material and Methods: A cohort of 40 patients with histologically proven PDAC underwent standard 18F-FDG-PET/CT scan and a contrast-enhanced CT (ceCT). All 18F-FDG-PET images were reconstructed according to the EANM guidelines for quantitative oncology imaging. Additionally, the ORG images were reconstructed with a duty cycle (the percentage of PET data used for image reconstruction) of 35%. Tumor lesions were identified on ceCT and two readers drew VOIs in consensus. The paired t-test was performed to compare ORG scans to their corresponding non-gated scans. The Cox proportional hazard model was performed for univariate analysis for correlation with OS. $p<0.05$ was considered significant. Results: Using non-gated reconstruction, tumor SUVmean (cut-off 3.0; HR 0.31 (95%-CI 0.10-0.94), p=0.039), metabolic tumor volume (MTV) determined at 70% SUVmax threshold (cut-off 2500; HR 0.29 (95%-CI 0.12-0.68), p=0.004) and TLG at 70% SUVmax threshold (cut-off 10000; HR 0.34 (95%-CI 0.15-0.78), p=0.011) are significantly associated with OS. However, tumor SUVmax is not. Using respiratory-gated reconstruction, these metabolic parameters changed significantly. Interestingly, SUVmean (p=0.039) and TLG (p=0.021) maintained their significant association with OS, whereas SUVmax was still not associated. In contrast to the EANM reconstructed scans, a 2.5 points difference between SUVmean in tumor lesion and normal pancreas showed significant association with OS (HR 0.34 (95%-CI 0.14-0.85), p=0.031). Conclusion: Respiratory-gated reconstruction significantly impacts the quantification of metabolic parameters in the characterization of PDAC. Particularly SUVmax does not associate with OS, irrespective of respiratory motion. SUVmean proves to be a more robust measure, and might therefore be used for prognostication. Furthermore, illustrating the improved visual discrimination of lesions on ORG scans, a difference of 2.5 points or more between SUVmean in tumor and normal pancreas is significantly associated with worse OS.

P650

18F-FDG PET/CT findings in a patient with Cowden's syndrome

K. Öksüzoğlu1, T. Öneş1, H. T. İlçe2, F. Dede1, H. T. Turoğlu1, S. İnanır1, T. Y. Erdil1; 1S.B. Marmara Universitesi Pendik Egitim ve Arastirma Hastanesi, Nükleer Tıp AD, Istanbul, TURKEY, 2Sakarya Üniversitesi Eğitim ve Araştırma Hastanesi, Nükleer Tıp AD, Sakarya, TURKEY.

Introduction: Cowden's Syndrome (CS) is a rare autosomal dominant inherited disorder (1/200.000) associated with mutations in a tumour suppressor gene called PTEN (Phosphatase and Tensin Homolog gene). CS is characterized by multiple noncancerous tumorlike growths called hamartomas and increased risk of developing cancers (breast, thyroid, uterus, kidney, colorectal mostly). CS is also often associated with macrocephaly, hamartomatous polyps (skin and mucous membranes, 60-90 % located in the gastrointestinal tract), benign skin lesions (trisilemmoma, acral keratoses) and dysplastic gangliositoma of the cerebellum etc. Purpose: In this case

report, the value of the FDG PET/CT findings evaluated in a patient who had considered CS. Case report: A 35 years-old male underwent partial small bowel resection and total gastrectomy with the diagnosis of malignant mesencymal tumour on the background of small bowel hamartomatous polyps. Postoperative histopathological examination revealed multiple benign hamartomatous polyps in the stomach too. Cowden's Syndrome was considered. The patient was referred to FDG PET/CT scan for staging. Focus of increased FDG uptake (SUVmax: 4.8 and 5.8) as compatible with postoperative changes was seen on FDG PET/CT. In addition, polypoid masses that forming filling defects on the ileocolonic segments showed intense (SUVmax: 8.9) FDG uptake and there were multiple lytic / sclerotic / destructive metastatic lesions with increased FDG uptake (SUVmax: 10.3) in the proximal part of the right humerus and the pelvic bones of the skeletal system prominently. Conclusion: Hamartamatous polyps usually have low malignancy potential and malignant transformation of adenomatous polyps in patients with CS has been reported in the literature. The distinction between adenocarcinoma and benign hamartomatous polyps in the gastrointestinal tract has not been reported in the literature yet. Intense hypermetabolic polyps in the gastrointestinal tract in patients with CS on FDG PET/CT can also be caused by benign polyps.

P651

Better accuracy of SPECT/CT in determination of liver hemangioma in patients with malignant tumor

M. PRPIC1, Z. KUSIC2; 1University Hospital Centre "Sestre Milosrdnice", ZAGREB, CROATIA, 2University Hospital Centre "Sestre Milosednice", ZAGREB, CROATIA.

AIM: to compare of Tc-99m labeled red blood cell (RBC) SPECT study combined with "low dose" CT (SPECT/CT) and contrast- enhanced CT (ceCT) concerning diagnostic accuracy in evaluation of liver lesions. METHODS:41 pts (mean age 54,9 years, range 16-76 years) with suspected liver lesions was performed RBC SPECT/CT for confirmation or exclusion of hemangioma diagnosed by ceCT in three occasions, as follows: metastasis from various primaries (endometrium, breast,colon,renis, lung,cervicis uteri, prostate); suspected liver tumors, atypical haemangioma. All pts underwent RBC SPECT at 10 min (early) and SPECT/CT at 180 min (late scan) after injection of 740 MBq (20 mCi)Tc-99m and performed within SPECT/CT system (Siemens Simbia T2). In vivo technique was used for RBC labeling. RESULTS:Overall 82 haemangiomas were detected on RBC SPECT/CT study (38 ceCT positive, 44 ceCT negative) and 10 suspected on haemangioma liver lesions (ceCT positive but RBC negative). In total, on RBC/SPECT/CT study lesions were better delineated and determined than on ceCT only, especially in case of small lesion (diameter <2cm). CONCLUSION: In our opinion, SPECT/CT allow better diagnostic confidence comparing to ceCT in characterisation of liver lesion whether it is benign or malignant.

P652

Metabolic FDG superscan in a patient with gastric adenocarcinoma: A rare finding in PET/CT imaging

B. E. Akkas, S. Demirtas, B. Demirel, G. Ucmak; Ankara Oncology Research and Training Hospital Department of Nuclear Medicine, Ankara, TURKEY.

The term "superscan" on bone scan is a well recognized phenomenon which describes increased skeletal radiotracer uptake relative to soft tissues and absent or faint genitourinary tract activity. However, the superscan on 18FDG PET/CT with increased skeletal radiotracer uptake is an uncommon finding, limited to only few case reports in the literature. In these cases, physiological FDG distribution throughout the body was relatively preserved where skeletal FDG uptake was significantly increased. The aim of this report is to present the unusual findings of a "metabolic FDG superscan "with severely altered biodistrubution of FDG throughout the whole body. There is only slight uptake in brain and significantly increased heterogeneous FDG uptake in the skeleton is seen due to widespread metastases from the primary gastric carcinoma which also demonstrates intense FDG uptake. Case Presentation: A 42 year old male patient with gastric adenocarcinoma underwent FDG PET/CT initial staging of primary gastric cancer following total gastrectomy. He had no history of bone marrow stimulating factor or corticosteroid use. On PET/CT scan, altered biodistribution of FDG was seen with significantly increased FDG uptake throughout the bones and bone marrow. In addition, multiple lytic bone lesions were detected on the corresponding CT slices. Hypermetabolic lymph nodes suggestive of metastasis were also noted in the mediastinum, supraclavicular fossa and in the abdomen. The patient had pancytopenia (white blood cell count: 3170/ μl, Hemoglobin:8.8 g/dl, platelet:30000/ μl). He died due to complications due to severe bone marrow involvement. Discussion and Conclusion: Gastric cancer is among the commonest cancers that cause superscan appearance in bone scan. However, the"metabolic superscan" is a very rare finding in the oncology practice. In this report, the altered distribution of FDG throughout the whole body caused by the gross tumoral involvement of the skeleton is presented demonstrating a

"metabolic superscan". The physiological FDG uptake is completely altered without the use of bone marrow stimulating agents.

P653

Efficacy of 18F-FDG-PET/CT for detection of suspected recurrence in post treatment follow-up of patients with carcinoma gall bladder, in a North Indian population-a pilot study.

M. Ravina, S. Gambhir, A. Prashanth, S. Barai, N. Kumar, D. Singh; Sanjay Gandhi Post Graduate Institute of Medical Sciences, Lucknow, Uttar Pradesh, INDIA.

Aims and Objectives: Carcinoma gall bladder is among the common causes of cancer related mortality in North India and Chile. Recurrent carcinoma of the gall bladder has a poor prognosis. Conventional imaging (CI) and tumour markers have limited accuracy for detecting recurrence in these patients. The aim of this study was to evaluate the efficacy of 18F-FDG-PET/CT for follow-up of patients with suspected recurrence of carcinoma of the gall bladder in a north Indian population. Methods: A total of 22 patients were evaluated with 18F-FDG-PET/CT for suspected recurrence in a north Indian population. All patients had undergone surgery with or without adjuvant therapy (chemotherapy, radiotherapy, or both) for histologically proven carcinoma of the gall bladder. Comparable CI (ultrasound or contrast-enhanced CT) was available for 14 patients. Final confirmation of recurrence was confirmed with clinical and/or imaging follow-up. Results: Patient's mean age was 53.9±9.78 years. 18F-FDG-PET/CT was positive for recurrence in 15 patients (68.1%) and negative in 7 (31.9%). Locoregional disease was observed in 5 patients, metastatic disease was observed in 5, and 5 showed both locoregional and metastatic disease. Compared to CI, 18F-FDG-PET/CT upstaged six patients, correctly characterized five patients suspected of recurrence as true negative, and concordant findings were noted in three patients. 4 of 15 recurrence positive patients detected with FDG died during follow-up period of 3.0 months and 11 are undergoing palliative radiotherapy/chemotherapy. The sensitivity, specificity, positive and negative predictive values, and accuracy of 18F-FDG PET/CT were 93.5 %, 100%, 100%, 85.7%, and 95.4%, respectively. Conclusions: Accurate detection of recurrent carcinoma of the gall bladder after intended curative surgery, radiotherapy and/or chemotherapy is imperative to select the most appropriate therapeutic strategy. 18F-FDG-PET/CT appears to be a highly specific and sensitive modality for detecting recurrence in post-therapy patients.

P654

Hepatic Epithelioid Hemangioendothelioma on FDG PET/CT

K. Oksuzoglu, R. Maleki, S. Inanir; Marmara University School of Medicine, Department of Nuclear Medicine, Istanbul, TURKEY.

Introduction: Hepatic Epithelioid Hemangioendothelioma (HEH) is an uncommon (1/1,000,000 per year) low-middle grade tumour, originating vascular endothelial cells. HEH can be multicentric and metastatic. Multifocal HEH mimics metastases radiologically and is most often confused with cholangiocarcinoma pathologically or radiologically. The prognosis of HEH is better than hepatocellular cancer and cholangiocarcinoma even at metastatic stage.Purpose: We want to report F-18 FDG PET/CT findings in a patient with a rare hepatic tumor of malignant epithelioid hemangioendothelioma.Case Report: A 49 years-old male with right upper quadrant pain and fullness complaints was referred to USG and MR which revealed multiple lesions in the liver parenchyma. Histopathological examination confirmed the diagnosis of HEH. The patient was admitted to FDG PET/CT for staging. FDG PET/CT showed multiple nodular hypodense lesions in the liver, the majority located subcapsular, causing the capsule retractions in both lobes and showed intense FDG uptake (SUV max:6.6). Also, at the lower-lobe of left lung, there was a mild hypermetabolic (SUV max:1.9) nodule with spiculated border. The patient treated with chemotherapy.Conclusion: In this case, FDG PET/CT detected HEH and showed the extent of the tumor. The diagnosis of HEH is difficult and the FDG avidity of lesions is variable. Knowing characteristic imaging findings of this rare tumor (Subcapsular localization, capsular retraction/flattening and target-like appearance on MR and CT images) helps us in differential diagnosis of hepatic multifocal lesions.

P655

Metabolic response assessment on 18F-FDG PET/CT with delta SUVmax, and its utility in predicting histological response following neoadjuvant chemoradiotherapy in patients with oesophageal cancer.

N. Ahmed, **G. Avery**, A. Razack, T. Goldstone, R. Roy, M. Hingorani, J. Cooke; Hull and East Yorkshire Hospitals NHS Trust, Hull, UNITED KINGDOM.

Aim: To assess whether metabolic response on 18F-FDG PET/CT can predict histological response in patients treated with neoadjuvant chemoradiotherapy (CRT) for oesophageal cancer (OC).Material and Methods:A retrospective audit was

conducted of 30 consecutive patients with OC. 5 patients were excluded (2 patients had no significant FDG uptake on baseline PET, whilst 3 did not undergo resection and could not be histologically graded). All patients received CRT regimen comprising of 1 cycle of induction Cisplatinum & Capecitabine followed by concurrent chemoradiation with 2 further cycles of same chemotherapy with 45 Gy of Radiotherapy over 5 weeks. A baseline 18F-FDG PET/CT was done in all patients, followed by a post-treatment study 3-5 weeks after finishing therapy. The SUVmax of the primary tumour site was recorded for both PET examinations. Resection samples were assessed and classified as per the Mandard criteria into five tumour regression grades (TRG 1-5).Results:Twenty five patients were included, mean age 62 years, of which 14 were males. They were grouped into histological responders (HR, TRG 1/2/3, n=15) and non-responders (HNR, TRG 4/5, n=10). Using median percentage reduction in SUVmax (delta SUVmax 52.2%) as threshold, metabolic response (MR) was seen in 11/15 of HR, whilst 8/10 patients in the HNR group did not show significant MR on PET (p= 0.0127, Sensitivity 73.3 %, Specificity 80%, Positive predictive value 84.6 %).Conclusion:Results of this relatively small series, suggests strong association between metabolic and histological response in this patient group. Larger studies are required to validate these results. Furthermore, correlation of metabolic response with long term survival will also help assess whether post-chemoradiotherapy PET examination is of prognostic benefit and contribute to patient selection for curative radical surgery.

P39 - Tuesday, October 13, 2015, 4:00 PM - 4:30 PM, Hall 3 – Poster Exhibition

Clinical Oncology: Neuroendocrine Tumours

P656

Additional value of the quantitative measurements of the therapeutic effect in patients with somatostatin expressing tumors using 99mTc-Tectrotyde

I. Kostadinova1, A. Demirev1, J. Mihailova2, V. Hadjiiska1; 1Clinic of nuclear medicine, Sofia, BULGARIA, 2Clinic of medical oncology, Sofia, BULGARIA.

The scintigraphy for the diagnosis of somatostatin receptor expressing (SR) neuroendocrine tumors, their staging, restaging and monitoring therapy, is known to be highly sensitive. Sometimes it is difficult to estimate visually minimal changes during therapy. The aim of our study was to introduce quantitative measurements in addition to the usual qualitative criteria for a precise evaluation of the response to the applied therapy in patients with SR-expressing tumors. During the period 2012-2014, we have performed in total 54 examinations on 22 patients (15 of them were examined twice, 7 of them triple) after 3-12 cycles of sandostatine therapy, using the somatostatin analog 99mTc-HYNIC-TOC (Tektrotyd,PL) in activity between 370-550 MBq. Whole body and hybrid imaging investigation - SPECT-CT were performed 2- 4h p.i. At presentation the average level of chromogranin was 234ng/ml and dropped during therapy to 161ng/ml and the number of pathological changes before and after therapy was respectively 65 and 60. For a quantitative measurement of the degree of activity of the radiopharmaceutical in them / compared to background /, an index of activity /IA/ was introduced, calculated in 1-5 target lesions / the number depended on the extend of the tumor /. In 19/22 of the investigated patients, it was difficult to evaluate therapeutic response, relying only on qualitative criteria, especially in those with multiple pathological lesions. In 9 of all patients, there was a partial therapeutic response with an average decrease of IA with 35.6% (calculated as a sum of IA of the all affected structures) ; in 3- complete response (without any pathological uptake); in 6 - stable disease with IA change between -12% and + 11%; in 4 of the patients -progressive disease with IA increase with 34.5%. The last group of the patients and 2 of the patients with a stable disease / all of them with Ki 67 index above 5/ were referred to PET-CT exam for eventual visualization of undifferentiated part of the tumor and further application of a common chemotherapy or surgery. In summary, we suggest that applying additional quantitative criteria to the routine qualitative one in patients SR expressing tumors, using 99mTc-HYNIC-TOC, helps in many cases for a more precise evaluation of the therapeutic effect, especially in those with an advanced disease. The therapeutic strategy could be optimized additionally applying 18F-FDG PET-CT in some of the patients.

P657

A retrospective comparison between 68Ga-DOTA-TOC and 18F-DOPA PET/CT in metastatic extra-adrenal paraganglioma

A. Kroiss1, B. L. Shulkin2, C. Uprimny1, T. Jazbec1, A. Frech1, G. M. Sprinzl3, G. Gastl1, C. Thomé1, G. Fraedrich1, I. J. Virgolini1; 1Medical University Innsbruck, Innsbruck, AUSTRIA, 2Radiological Sciences, St. Jude Children's Research Hospital, Memphis, TN, UNITED STATES, 3State Clinic St. Poelten, St. Poelten, AUSTRIA.

Purpose 18F-Fluoro-L-dihydroxyphenylalanine (18F-DOPA) PET offers high sensitivity and specificity in the imaging of nonmetastatic extraadrenal paragangliomas (PGLs) but lower sensitivity in metastatic or multifocal disease. These tumors

are of neuroendocrine origin and can be detected by 68Ga-DOTA-Tyr3-octreotide (68Ga-DOTA-TOC) PET. Therefore, we compared 68Ga-DOTA-TOC and 18F-DOPA as radiolabels for PET/CT imaging for the diagnosis and staging of malignant extraadrenal PGL. Combined crosssectional imaging was the reference standard. Methods A total of 2 men and 4 women (age range 22 to 60 years) with anatomical and/or histologically proven malignant extraadrenal PGL were included in this study. Of these patients, 2 female patients suffered from metastatic head and neck PGL disease, while the remaining 4 patients were diagnosed as extraadrenal multifocal PGL disease. Comparative evaluation included morphological imaging with CT and functional imaging with 68Ga-DOTA-TOC PET and 18F-DOPA PET. The imaging results were analyzed on a per-patient and a per-lesion basis. The maximum standardized uptake value (SUV_{max}) of each functional imaging modality in concordant tumor lesions was measured. Results Compared with anatomical imaging, 68Ga-DOTATOC PET and 18F-DOPA PET each had a per-patient detection rate of 100 % in metastatic extraadrenal PGLs. However, the per-lesion detection rate of 68GaDOTATOC was 100 % (McNemar, P<1.0), and that of 18FDOPA PET was 59.3 % (McNemar, P<0.001) in metastatic extraadrenal PGLs. Overall, 68GaDOTATOC PET identified 28 lesions; anatomical imaging identified 27 lesions, and 18FDOPA PET identified 16 lesions. The SUV_{max} (mean +/- SD) of all concordant lesions was 31.4 +/- 22.3 for 68GaDOTATOC PET and 9.2 +/ 9.0 for 18F-DOPA PET (MannWhitney U test, P<0.001). Conclusion 68Ga-DOTA-TOC PET may be superior to 18FDOPA PET and even to diagnostic CT in providing valuable information for pretherapeutic staging of metastatic paraganglioma disease.

P658

Oncogenic osteomalacia: Role of 68Ga DOTA-NOC PET/CT scan in identifying the culprit lesion and its management

S. Gambhir, D. Singh, M. Ravina, S. Barai, A. Prashanth, N. Kumar; Sanjay Gandhi Post Graduate Institute of Medical Sciences, Lucknow, Uttar Pradesh, INDIA.

Objective: Surgical removal of culprit lesion is the definitive treatment for tumor induced Osteomalacia (TIO). These patients showed multiple lesions due to fractures and other bony changes and it is confusing to identify culprit lesion. The aim of this study was to evaluate role of 68Ga-DOTA-NOC PET/CT in the detection of culprit lesion for biopsy and required intervention (surgical/ radiofrequency ablation). Methods: 15 patients (6 male & 9 female) underwent 68Ga DOTA-NOC PET/CT. The patients referred with clinical symptoms of pain, multiple fractures and biochemical evidence of hypo-phosphatemia & raised Fibroblast Growth factor-23 (FGF-23). Qualitative & semi-quantitative parameters like SUV-max and CT/MRI findings were used to identify the culprit lesions. Results: Scan revealed 41 lesions in 15 patients, 31/41 lesions were tracer avid lesions and 10/41 lesions were non tracer avid fractures. Among these 31 tracer avid lesions, 23/41 lesions were focal tracer avid (SUV max range 0.55-4.35) skeletal lesions (fracture and/or no associated CT abnormality). The 8/41 tracer avid skeletal lesions present in 6 patients (3 lesions in one patient & 1 each in rest of the 5 patients) were highly suspicious for culprit lesions in view of high SUV-max, size and associated soft tissue involvement with SUV-max (range 1.5-13.4) and size (0.9 to 5.0 cm). 2 patients were biopsied in view of suspicious lesion and both turned out to be positive phosphaturic mesenchymal tumors with SUV-max 2.2 and 8.0. 1 of the biopsy proven patient improved biochemically & symptomatically following surgical resection. The other patient underwent radiofrequency ablation (RFA) with near complete resolution of the culprit lesion. The SUV-max of lesion decreased from SUV-max 8.0 to SUV-max 3.0 with near normalization of S.FGF 23 (12000RU/ml to 180RU/ml). 1 patient with 3 lesions underwent further imaging, 02 lesions showed discordant results and 1 lesion with soft tissue component showed concordant results on MRI is planned for surgery. Two other patients with concordant results are planned for definitive treatment The patient with discordant findings (lesion SUV max- 13.4) is under further evaluation. Conclusion: There is some overlap in the SUV-max between fractures/bone associated lesions and the culprit lesion with tendency of most non-culprit lesions to have lower SUV-max. In such scenario tracer avid larger non fracture lesion with soft tissue component may lead to culprit lesion amongst multiple lesions. Following detection of culprit lesion, surgical removal or RFA (in cases of osteopenia and poor bone health) is the best treatment

P659

Utility of Ga-68 DOTANOC PET CT in evaluation of unusual or rare neuroendocrine tumors: Single institutional experience

A. Pruthi, P. Pankaj, R. Verma, A. Jain, E. S. Belho, H. Mahajan; Sir Ganga Ram Hospital and Research Centre, New Delhi, INDIA.

Ga-68 DOTANOC PET CT is an established modality for imaging gastro-entero-pancreatic neuroendocrine tumours (NETs). However, experience in evaluating unusual NETs remains limited. Purpose: To retrospectively evaluate the utility of Ga-68 DOTANOC PET CT scan in analyzing rare or unusual neuro-endocrine tumors (NETs). Methods: A total of 19 patients (10 males, 09 females; mean age 47.7 +/- 14.3 years, range 27-68 years) presenting with histopathologically proven unusual / rare neuroendocrine tumors (other than gastro-entero-pancreatic NETs & bronchial NETs), who underwent Ga-68 DOTANOC PET CT scan at our department were included for analysis. These patients were investigated retrospectively and various parameters like age, sex, sites of primary and metastatic neuroendocrine lesions, and quantitative estimation of SSTR expression in the form of maximal standardized uptake value (SUVmax) in metastatic as well as primary sites were noted. The findings were correlated with available anatomical imaging results. Results: Primary NET lesions were located in kidneys (3 patients), esophagus (3 patients) and one each in prostate, gall bladder and breast. In addition, 5 cases of paragangliomas (1 mediastinal and 4 abdominal), 2 cases of medullary thyroid carcinomas, one case each of adrenal phaeochromocytoma, thymoma and merkel cell carcinoma were also included. DOTANOC avid lesions were noted in 17 out of total 19 patients. Renal NETs showed an intense DOTANOC uptake in the primary lesion (mean SUVmax 34.3 +/- 17.9) as well as metastatic lesions in liver (mean SUVmax 23.8 +/- 8.08), lymph nodes and bones. Esophageal NETs demonstrated moderate intensity DOTANOC uptake in primary lesion (mean SUVmax 12.5 +/- 12.8) and lymph nodal metastasis (mean SUVmax 7.6 +/- 4.1). In 5 cases of paragangliomas, Ga-68 DOTANOC PET CT scans showed intense uptake in primary site (mean SUVmax 27.9 +/- 4.1) and metastatic sites (detected in 3/5 patients). DOTANOC avid local recurrence was detected in two post-operative cases of paragangliomas with raised serum chromogranin levels. In one case of merkel cell carcinoma, DOTANOC avid additional metastatic sites were detected in soft tissue, lymph nodes, bones and pancreas, which were undiagnosed before on anatomical imaging. In one case, presenting with para-rectal lymph nodes, DOTANOC avid primary site was identified in prostate gland along with additional hepatic, skeletal and lymph nodal metastasis. Conclusion: Our preliminary experience suggests that Ga-68 DOTANOC PET/CT scan is a sensitive modality for evaluation of unusual and rare neuroendocrine tumours and provides quantitative estimate of somatostatin-receptor expression, thereby guiding their overall clinical management.

P660

Comparison between 18FDG-PET/CT scan and Tc-99mHYNIC-[D-Phe1,Tyr3-Octreotide (Tektrotyd) scintigraphy in patients with neuroendocrine tumor (NET) .

I. Navales Mateu, M. Simó Perdigó, M. Salcedo Pujantell, M. Barios Profitos, A. Garcia Burillo, J. Capdevila Castillón, J. Monturiol Duran, M. Velasco Nuño, J. Castell Conesa; Hospital Universitari Vall d'Hebron, Barcelona, SPAIN.

AIM: To analyze the behavior of both techniques in patients with NET, in order to correlate the image profile with tumoral grade (G1, G2 or G3) and the eventual impact on the therapeutic decision management of the patient. MATERIAL AND METHODS: 26 patients (60median age, 11 w) with suspected/diagnosed NET were studied with Tektrotyd and FDG as part of the initial staging or in cases of recurrence. Tektrotyd scintigraphy included planar and thoraco abdominal SPECT/CT images. PET/CT scans were acquired according to EANM tumour PET procedure guideline. RESULTS: 1. -FDG- PET/CT was positive in 19 patients (73%) whereas Tektrotyd was positive in 14 cases (54%). Fifty percent of negative Tektrotyd patients (12 patients) showed a positive FDG-PET/CT study. Only one FDG-PET/CT negative patient was Tektrotyd positive. 2.- In a subgroup of 14 patients with confirmed but unresected NET tumor, FDG-PET/CT successfully localized the primary tumor in 11 cases (78%), 5 of them showed negative Tektrotyd scans (3pG2, 1pG3, 1 paraganglioma). Tektrotyd localized the primary tumor in 7 patients (50%), having only one of them a negative FDG-PET/CT (G1). 3.- Complete global agreement between both techniques was positive in 3 (16%) patients (2pG2, 1 pheocromocytoma) and negative in 6 (32%). 10 patients (53%)showed positive findings with partial concordance of both techniques (2pG1, 4pG2, 2pG3, 2pOthers). Region based analysis showed a better agreement in supradiafragmatic regions and bones, whereas higher discordance in the liver and abdomen. 4. -Regarding histologic subgroups of gastreoenteropancreatic-NET (GEP-NET): In 5 G1-NET patients, Tektrotyd detected 3 patients and FDG-PET/CT 2. The other 2 patients were negative for both tecniques. In 13 G2-G3-NET patients, FDG-PET showed a higher number of positive studies (7G2, 5G3) than Tektrotyd (6G2, 2G3). Not a single Tektrotyd positive patient was FDG-PET negative. 5.-Regading the eventual impact on the therapeutic decision , we found 13 patients with simultaneous heterogenic profile lesions (hypermetabolic and/or differentiated), identifying six of them as unexpected behavior. These includes one G1-NET patient with avid FDG lesions and one G3-NET patient with a predominantly trektrotyd positive

lesions. CONCLUSION: The combined use of FDG-PET/CT scan and Tektrotyd for the assessment of NET revealed a high rate of heterogenic profile lesions, some of them unexpected. FDG-PET/CT was better than tektrotyd in detecting the NET primary site. Our study suggests that the evaluation of NET patients with both techniques can improve lesion characterization allowing a better personalized therapeutic decision.

P661

Impact of SPECT/CT 99mTc-EDDA/ HYNIC-TOC in the diagnosis and the extension of neuroendocrine tumors

S. E. Bouyoucef, M. Habbeche, S. Rahabi, A. Talbi, B. Abdi, S. Bellabas, A. Amimour; Department of Nuclear Medicine CHU Bab El Oued, Algiers, ALGERIA.

Introduction : Incidence of neuro-endocrine tumors (NET) is increasing due to the development of diagnostic tools including nuclear medicine techniques, conventional and TEP imaging. SPECT/CT 99mTc-EDDA/ HYNIC-TOC could be available everywhere and have a great potential in the management of NET. Objective : Assess the role of SPECT/CT 99mTc-EDDA/ HYNIC-TOC in the management of NET. Methods and patients A retrospective study of 110 patients with suspected or confirmed NET had been done from 2010 to 2014 in the department of nuclear medicine. Clinical indications were, search of the primary (35%), contribution to the strategy and assessment of therapy (48%), location of the primary site (13%) and search for relapse after surgery (4%). SPECT/CT used was a dual heads gamma camera with a diagnostic CT. Double reading of reporting was done systematically for all patients. Results: In the suspected NET, SPECT/CT 99mTc-EDDA/ HYNIC-TOC has permitted to find the primary in 14/ 37 (37%) and has confirmed the diagnostic in 12 of 15 patients. All paragangliomas and pancreatic tumors were positive on SPECT/CT 99mTc-EDDA/ HYNIC-TOC. For therapy assessment, SPECT/CT 99mTc-EDDA/ HYNIC-TOC has contributed to the therapeutic strategy in 80% of patients and showed a poor response to targeted therapy in 3 patients. Conclusion: Despite the lack of Gallium peptide PET, SPECT/CT 99mTc-EDDA/ HYNIC-TOC was determinant with a great clinical impact in the management of neuro endocrine tumors.

P662

Comparison of Early and Late SUVmax Values of Somatostatin Reseptor Positive Lesions in Ga-68 DOTATATE PET/CT Images

J. Nematyazar, S. Sager, O. Erdem Sahin, B. Razavi, R. Akyel, B. Vatankulu, E. Kaymak, M. Halac, H. Sayman, I. Uslu, K. Sonmezoglu; 1Department of Nuclear Medicine, Cerrahpasa Medical Faculty, Istanbul University, istanbul, TURKEY.

Objective and Aim: Neuroendocrine tumors (NETs) are rare but have been more common over the past decade. PET/CT with Ga-68 DOTATATE achieved high sensitivity and good specificity for determining the somatostatin reseptor positive neuroendocrine tumors. The aim of the our study is to compare early and late suvmax values of lesions in Ga-68 DOTATATE PET/CT. Subjects and Method: Ten patients with age range of 52±12.9 years, and male to female ratio of 4to6 were referred for Ga-68 DOTATATE PET/CT scan for localisation of somatostain positive lesions. Seven patients were known NETs, 3 patients were carsinoid tumor, 2 patients were thyroid cancer. A mean dose of 200.54±53.28 MBq 68Ga-DOTATATE injected. Early imaging time was meanly 38.8±14.8 minutes after injection and late imaging time was meanly 101.2±6.28 minutes after injection. Positive findings were defined as areas of increased uptake other than the organs of normal distribution and were correlated with other imaging methods. Also early and late SUVmax values of normal tissue uptakes were calculated. Results: A total of 22 lesions were analysed. The early mean SUVmax values of tatol lesion were 34.94±18.16 g/ml and late mean SUVmax values were 29.87±26.02 g/ml There is no difference between early and late image quality of Ga-68 DOTATATE imaging. Also late imaging did not provide additional information according to lesion number and localisation. There is no significant difference between early and late SUVmax values of somatostatin positive lesions and early and late SUVmax values of normal liver tissue (the early mean SUVmax values were 2.89±2.19 g/ml and late mean SUVmax values were 3.16 ±3.68 g/ml). Conclusion: Ga-68 DOTATATE PET/CT is an effective tool for localising somatostatin positive lesions. There is no statistical difference between early and late SUVmax values in malign lesions in Ga-68 DOTATATE PET/CT imaging. Ga68-Dotatate PET/CT can be permormed in the diagnosis and follow-up of somatostatin positive tumors after 60-90 min injection of radiopeptides.

P663

Analysis of carbidopa premedication in patients with neuroendocrine tumors before a 18F-DOPA PET-CT study

A. Ramírez, E. Morillo, W. Valdés, N. Testart, E. Triviño, T. Aroui, A. Rodriguez-Fernandez, J. Llamas-Elvira; H.VIRGEN DE LAS NIEVES, GRANADA, SPAIN.

Purpose: Test out if carbidopa premedication before a 18F-DOPA PET/CT study in patients with neuroendocrine tumors decline the turn of the tracer in to dopamine in peripheral tissues, increasing the uptake in tumorals tissues. Patients and methods: We carry out an observational retrospective study divided in two females patient groups, that were includes in a 18F-DOPA PET/CT study. The first group was composed of 13 women in which was not indicated a previously administration of carbidopa. The second group was composed of 7 women who themeselves where given a dose of carbidopa between 100 and 150mg one hour before of radiopharmaceutical administration. The results were expressed as arithmetic mean, standard deviation and student t was calculated, comparing SUV max means in different organs in both groups. Discussion: Administrate a dose of carbidopa between 100-150mg before a 18F-DOPA study decline the uptake of the tracer in all pancreatic areas .However in other organs studied we didn't find differences in the uptake, unlike the results observed in the literature that point at greater liver a lungs uptake in those patients who were given carbidopa. This could be due to a small number of patients included in our study with carbidopa administration.

P664

Comparative evaluation of somatostatin receptor scintigraphy using Tc-99m and In-111 labelled somatostatin analogues

I. Szilvási1, Z. Varga2, R. Jóba1, K. Buga1, K. Bús2, E. Takács2, G. Dabasi2; 1Hungarian Defense Forces Medical Centre, Budapest, HUNGARY, 2Semmelweis University, Budapest, HUNGARY.

AimIn a prospective study we compared the diagnostic value of In-111-pentetreotide(OC) and Tc-99m-EDDA/HYNIC-TOC(TC) somatostatin receptor scintigraphy(SRS) in patients with neuroendocrine tumours(NET).Patients and MethodsTwo SRSs using OC and TC were performed within four weeks in 30 patients with histologically confirmed NET. Indication was staging in 15 patients and follow-up in 15 patients with suspected recidivism. The second SRS was performed, if the first results were equivocal or contradicting to clinical-data. The first radiopharmaceutical was OC in 20 and TC in 10 patients. The two scintigraphic results were compared in these selected 30 patients, mean age:47(35-80)years. Both methods were performed according to procedure guidelines. Imaging (planar and SPECT study) was performed at 4 and 24 hours (6 cases: 48 hours as well) using OC, and at 1 and 4 hours (2 cases: 24 hours as well) using TC. Images were evaluated qualitatively by two physiscians. Number of abnormal lesions were compared by regions as well. Lesions were validated by repeated SRS and/or radiological examinations during at least one year of follow-up.Results27 out of 30 patients had abnormal, 3 patients had negative SRS by both radiopharmaceuticals. 11 out of 25 patients had solitary lesion, in the other 14 patients 34 lesions were seen by at least one of the two SRS studies. Based on the follow-up examinations two of the lesions seen on TCscan and one lesion seen on OCscan proved to be false-positive, but in different regions. TcSRS had one false negative finding in the abdomen, seen by OC only. OCSRS had seven false-negative lesions: one in the thorax and six in the abdominal-pelvic region. In 26 out of 30 patients (27 with, 3 without NET) both examinations had concordant findings regarding to number of involved regions. Findings of TC and OC were partly discordant in 4 patients, because number of abnormal regions were more in 3 patients but less in 1 patient by TC.ConclusionsBased on our study, OC and TC have similar diagnostic value. Image quality of TC is better, interpretation is more reliable, sensitivity is higher. Duration of scintigraphy is shorter, however to avoid false-positive findings in the abdomen imaging at 24 hours are needed in about 1/3 of the patients. Our preliminary experience showed that this number can be reduced by SPECT/CT. Further studies are needed to define possible differences between TC and OC in SRS of tumours with various histological types.

P665

Ga-68 DOTANOC PET/CT for Neuroendocrine Tumours: Experience at Western Cape Academic PET/CT Centre

A. G. G. Doruyter, A. Ellmann, S. M. Rubow; Stellenbosch University, Cape Town, SOUTH AFRICA.

Aim: In September 2013 the Western Cape Academic PET/CT Centre began performing Ga-68 DOTANOC PET/CT for neuroendocrine tumour patients. We report our clinical experience with these scans thus far, including referral patterns; scan results and relevant clinical outcomes. Materials and methods: Referral patterns, imaging results, and laboratory and clinical data were collated for patients referred for Ga-68 DOTANOC PET/CT since September 2013. Normal biodistribution of Ga-68 DOTANOC was compared to experience with SPECT agents. Clinical follow-up allowed us to identify any

interpretative pitfalls in initial reporting. Results: Scans of 60 patients were reviewed. The majority of patients (46.7%) were referred for staging procedures. Several differences between the normal biodistribution of Ga-68 DOTANOC and SPECT agents were identified. Correlative clinical information was available in 56 of the patients, which allowed us to identify 8 false negative and 2 false positive studies. Two of the false negative studies were due to tumour dedifferentiation, and in one case the recurrent lesions were smaller than the resolution limit of the camera. In one patient an insulinoma was not detected. The reasons for the false negativity were not clear in the other 4 cases. The two false positive studies were identified after clinical follow-up and subsequent literature review, which identified an important pitfall in interpretation, namely physiological DOTANOC uptake in the uncinate process of the pancreas. Conclusion: Ga-68 DOTANOC PET/CT offers several advantages over traditional somatostatin receptor imaging methods, including improved sensitivity and shorter total scan duration. While both methods image predominantly SS2R, several notable differences exist in biodistribution. It is important that nuclear physicians be mindful of these differences as well as potential pitfalls in the interpretation of these studies. Interpreter knowledge of normal variants is important for accurate reporting. Ga-68 DOTANOC PET offers significant benefit in terms of directing clinical intervention and subsequent follow-up.

P666

GLP-1 receptor scintigraphy as a potential tool in the detection of neuroendocrine malignancies.

A. Sowa-Staszczak, A. Stefańska, M. Buziak-Bereza, M. Trofimiuk-Muldner, M. Kołodziej, A. Hubalewska-Dydejczyk; Nuclear Medicine Unit, Endocrinology Department, University Hospital Krakow, Krakow, POLAND.

It is known that a very high expression of GLP-1 receptor is seen in benign insulinoma, and scintigraphy with [Lys40(Ahx-HYNIC-99mTc/EDDA)NH2]-exendin-4 and [Lys40(Ahx-DTPA-111In)NH2]exendin-4 can be helpful in insulinoma not detected by other methods. Moreover GLP-1 receptor expression can be also found in other neoplasms e.g. gastrinomas, pulmonary NETs, paragangliomas, meningiomas, astrocytomasw, MTCs. Aim: The aim of our study was to assess the diagnostic efficiency of [Lys40(Ahx-HYNIC-99mTc/EDDA)NH2]exendin4 scintigraphy in the diagnosis the recurrence of medullary thyroid carcinoma (MTC) not detected by other available imaging methods, as well as localization of pheochromocytoma and gastrinoma. Material and methods: 15 patients were enrolled in this study: 9 with recurrent MTC with negative standard imaging results, 5 with pheochromocytoma, 1 with gastrinoma. All patients with MTC underwent a total thyroidectomy with neck lymph nodes resection, two of them - PRRT. MTC recurrence was diagnosed based on increasing values postoperative calcitonin levels. Whole-body and SPECT/CT scans with a low dose CT protocol were performed at 2 time points, between 3 - 4 h and 5 - 6 h after the injection of the 99mTc -GLP-1 analogue. Volumetric analysis was performed to assess the tumor to non-tumor ratio (T/nT ratio). Results: In 4 patients with MTC with higher level of calcitonin (median value of 631 pg/ml) and/or abnormal results of pentagastrin test an accumulation of the tracer in the location of the primary tumor or in liver metastasis was described. In 5 cases radiolabelled GLP-1 did not localize the MTC recurrence. In 3 of 5 patients with pheochromocytoma an accumulation of the tracer in adrenal tumor was found. The lesions were removed surgically and diagnosis of pheochromocytoma was confirmed histopathologically. In the case of a patient with malignant pheochromocytoma multiple foci of [Lys40(Ahx-HYNIC-99mTc/EDDA)NH2]exendin-4 accumulation in bone and soft tissues metastases was observed. In 1 patient with suspicion of recurrent gastrinoma, scintigraphy revealed focal lesions in liver and in pancreas. Conclusion: 99mTc-GLP-1 receptor imaging could be considered as a useful tool in cases of MTC, pheochromocytoma and gastrinoma, especially when other diagnostic methods are equivocal or fail.

P667

Focally increased activity in the pancreas on In-111 Octreotide scan - can it be a physiologic variant?

Z. Kováčová1, D. Zogala1, A. Pudlač2, J. Kubinyi1; 1Institute of Nuclear Medicine, First Faculty of Medicine, Charles University in Prague, Prague, CZECH REPUBLIC, 2Department of Radiology, First Faculty of Medicine, Charles University in Prague, Prague, CZECH REPUBLIC.

AIM:The aim of the study was to find out whether there could be a physiological uptake of 111-In Octreotide in the uncinate process of the pancreas. By using retrospective analysis we determined the percentage of cases where there was no explanation for the phenomenon of focal increased activity within the head of the pancreas on 111-In Octreotide scans.METHODS:We evaluated 306 111-In Octreotide scans of 287 consecutive patients examined in the 2011-2014 period. 11 scans were excluded due to incomplete data. By analyzing 295 111-In Octreotide scans and all available clinical data we determined the exact percentage of the phenomenon of focal increased activity in the head of the pancreas for which there was no explanation. The scoring system of the visual uptake on a five point scale was used (0 - no uptake, 1 - very low

uptake, 2 - clear, but faint uptake, 3 - moderate uptake, 4 - intense uptake).RESULTS:Out of 295 111-In Octreotide scans there were 69 cases (23%) with the focal increased activity within the pancreatic region. 40 cases (13.5%) were located within the head of the pancreas. For 29 cases (9.8%) there was no explanation found for the high uptake in the head of the pancreas even after the clinical research. By using our scoring system those uptakes were usually in the category 1 - very low uptake or 2 - clear, but faint uptake.CONCLUSION:The focal increased activity in the pancreatic region on 111-In Octreotide scan was interpreted as idiopathic in 29 cases (9.8%). None of those idiopathic uptakes scored higher than 2 on our five point scale scoring system. The results of the study indicated that there was a physiological uptake of 111-In Octreotide within the uncinate process of the pancreas due to higher concentration of somatostatin receptors. Therefore, nuclear medicine specialists should be careful when interpreting faint uptake within the epigastric region.

P668
Effect of I-131 MIBG Thyroid Uptake on Thyroid Function Tests

A. Hassanzadeh-Rad, S. Katal, D. Beiki, A. Fard-Esfahani, A. Emami-Ardekani, B. Fallahi, M. Eftekhari; Research Center for Nuclear Medicine, Shariati Hospital, Tehran, IRAN, ISLAMIC REPUBLIC OF.

Aim: I-131 MetaIodoBenzylGuanidine (MIBG) is used for diagnosis and treatment of neural crest tumors and in particular pheochromocytoma, neuroblastoma and ganglioneuroblastoma. Various mechanisms are responsible for thyroidal uptake of I-131 MIBG. I-131 can damage thyrocytes by beta emission, leading to decrease in thyroid hormone synthesis. Although all patients receive Lugol's solution to prevent thyroidal uptake, various amounts of 131I-MIBG are taken up by thyroid. In this study, we wanted to correlate thyroidal uptake of 131I- MIBG (both qualitatively and quantitatively) with changes in thyroid function tests by comparison between baseline and follow-up Serum levels of FT3, FT4 and TSH. Materials and Methods:34 euthyroid patients (20 males, 14 females with mean age of 11.4 years old) with documented neural crest tumors who were referred to our center for I-131 MIBG diagnostic or post therapy scans enrolled in the study. They were asked to orally take 1 drop/kg of 2 % Lugol's solution, from 2 days before to 2 weeks after \I-131 MIBG injection. 24 and 72 hours post injection of 1 mCi (for diagnostic purposes) and 5 days post injection of 100-300 mCi I-13 MIBG (for treatment purposes) whole body scans were performed with (Siemens, Biograph, T2 Series) Gamma camera. 5- minute anterior spot views from cervical region were also obtained for visualization and quantification of thyroidal uptake. Regions Of Interest (ROIs) were drawn over thyroid bed and background and background-corrected average counts were calculated for all patients. Blood samples were obtained from patients prior to and 3 months after injection of I-131 MIBG for assessment of thyroid function. Results: No significant changes in thyroid function tests were observed in the subgroup of patients without thyroid uptake of I-131 MIBG. In the subgroup with visualized thyroid uptake, mean TSH level increased significantly from baseline level of 2.59 mIU/L to follow-up level of 8.42 mIU/L (P-value <0.01). In this subgroup, mean FT3 and FT4 levels did not change significantly; however, change from euthyroid state to subclinical and clinical hypothyroidism occurred in 37.5 % and 12.5 % of these patients, respectively. Mean ROI average counts in patients converted to subclinical or clinical hypothyroidism were significantly higher than patients who remained euthyroid in follow-up tests. Conclusion: Thyroidal uptake of I-131 MIBG can result in TSH elevation and subclinical or clinical hypothyroidism. Therefore, visualization and quantification of thyroid uptake in I-131 MIBG scans are clinically informative.

P669
Contribution of Ki67 proliferation index and 111In-Pentetreotide somatostatin receptor scintigraphy in Neuroendocrine Tumors

G. Muñiz Garcia1, J. Muñoz Iglesias1, C. Penín Corderi2, R. Guitián Iglesias1; 1Nuclear Medicine Department. Complejo Hospitalario Universitario de Ourense, Ourense, SPAIN, 2Pathology Department. Complejo Hospitalario Universitario de Ourense, Ourense, SPAIN.

Aim: The aim of this study was to asses the utility of 111In-Pentetreotide somatostatin receptor scintigraphy (SSRS) and the values of Ki67 proliferation index in patients with Neuroendocrine Tumors (NETs) in the selection of candidates with somatostatin analogues therapy. Material and Methods: Twenty-seven patients with histological diagnosis of NETs were retrospectively studied with our usual protocol. SSRS and Ki67 proliferation index were performed in all patients. Ki67 proliferation index was classified according to World Health Organization (WHO). All patient with positive SSRS who had liver metastases or unresectable tumors, were treated with somatostatin analogues. Clinical, laboratory and radiological follow-up was performed (mean 12 months). Results: SSRS was positive in 17/27 patients (63%) and showed low Ki67/G1 index in 9 patients (53%), intermediate/G2 in 5 (29, 4%) and high/ G3 in 3 (17,6%). All patients with a positive SSRS received somatostatin analogues therapy. Fifteen patients showed stable disease (88,20%) and only two of them got worse (11,80%), showing a high/G3 Ki67 index. In ten

patients, SSRS was negative: two showed low/G1 Ki67 index, intermediate/G2 in 1 and high/G3 in 7. They did not receive treatment with somatostatin analogues and in the follow-up, six patients are stable, 3 have died (unresectable undifferentiated tumors with distant metastasis) and one of them had progression of local and metastatic disease (unresectable and metastatic poorly differentiated tumor). Conclusions: In our experience, SSRS is necessary for patients diagnosed with NETs, in order to select those who are candidates for treatment with somatostatin analogues for both local control of unresectable tumors and their metastases. Regardless Ki67 proliferation index, patients with positive SSRS should be included in therapy with somatostatin analogues. Patients with negative SSRS and low or intermediate Ki67 proliferation index should be individually valued the use of somatostatin analogues.

P670

The diagnostic use of a 2 day protocol in Somatostatin Receptor Scintigraphy using 99mTc-HYNIC-TOC. Preliminary Results

P. Z. Stavrou, C. Giannopoulou, E. Persakis, K. Kouvelis, M. Papachristou, E. Vlontzou, I. Datseris; Evaggelismos Hospital, Athens, GREECE.

Introduction: 99mTc-HYNIC-TOC (Tektrotyde) represents a valid Tc99m labelled compound alternative to In-111 labelled radiopharmaceuticals in the detection of lesions overexpressing somatostatin receptors. Images can be acquired up to 24 hours post injection, although the recommended time frame is between 2 and 4 hours after the radiotracer administration. The purpose of this study is to investigate the benefit of an additional delayed acquisition at 24 hours post injection. Patients and Methods: This is a retrospective study of prospectively collected data of patients with suspected or known neuroendocrine disease. All patients underwent an iv injection of 925-1110 MBq (25-30 mCi) of Tektrotyde and images were collected at 2, 4 and 24 hours post injection. Images were then processed using Segami Mirage Workstation. All studies were assessed by 2 experienced Nuclear Medicine physicians. Results: 17 studies in 16 patients, 5 females and 11 males, age 30-75 (mean 55) were assessed. Nine patients presented with known neuroendocrine disease, mainly GEP-NETs, 5 of which have been operated on the primary lesion. In 9 studies of 8 patients. foci of increased Tektrotyde uptake were observed (positive exams). In most cases the 2 and 4-hour images were adequate to perform diagnosis. In only 1 case the 24-hour acquisition was useful in excluding an ambiguous site of slightly increased uptake. In both the 2 and 4-hour acquisitions high gallbladder activity was seen, while in the 24-hour acquisitions little to no gallbladder activity was observed in all patients. Conclusion: Although in the standard 2 and 4-hour acquisitions foci of increased Tektrotyde uptake can accurately be localized, an additional 24-hour acquisition could improve specificity in ambiguous cases. This delayed acquisition can also contribute in identifying gallbladder activity that could be mistaken as a liver lesion in departments without a hybrid SPECT/CT camera.

P671

Correlation between Tumor Volume Defined by 68Ga-DOTANOC PET/CT scan and Maximum Standardized Uptake Value Variation (ΔSUVmax) after Peptide Receptor Radionuclide Therapy (PRRNT)

L. Sobral Violante1, I. Sampaio1, J. Teixeira1, A. Santos1, A. Duarte2, F. Lopes1, L. Costa1, O. Soares1, I. Paula1, H. Duarte1; 1Instituto Português de Oncologia, Porto, PORTUGAL, 2Instituto Politécnico de Bragança, Bragança, PORTUGAL.

Aim: PRRNT is a promising treatment for patients with neuroendocrine tumours (NETs) giving rise to improved survival. Literature refers that PRRT of NETs using DOTATATE labeled with beta-emitting 177Lu may be preferable for smaller tumours. The aim of this study was to evaluate the correlation between tumor volume defined by 68Ga-DOTANOC PET/CT scan and ΔSUVmax in patients who underwent PRRNT with 177Lu-DOTATATE.Material and Methods: Twelve patients with advanced well-differentiated NETs (5 women, 7 men, mean age 54 ± 9) were included: 5 pancreatic (3 non-secreting, 1 glucagonoma and 1 insulinoma), 4 small intestine (secreting), 2 pulmonary (non-secreting) and 1 rectum (secreting). Clinical evaluation (symptoms and tumour markers) and 68Ga-DOTANOC PET/CT images were reviewed at baseline and 3 to 12 months after completion of 3 cycles of PRRNT (mean activity of 5,5 GBq/cycle). A fixed threshold of 30% was used to calculate the volume of the lesions which presented highest SUVmax value in 68Ga-DOTANOC PET/CT baseline scan and a comparison of 68Ga-DOTANOC PET/CT studies was performed based on visual analysis of uptake and number of lesions and ΔSUVmax. Results were interpreted as: a) response (qualitative: visual decrease of intensity and/or number of lesions; semi-quantitative: ΔSUVmax decrease ≤ 25%), b) stable disease (qualitative: similar visual intensity and number of lesions; semi-quantitative: -25% < ΔSUVmax < + 25%) and c) progressive disease (qualitative: visual increase of intensity and/or number of lesions; semi-quantitative: ΔSUVmax increase ≥ 25%). Comparison between tumor volume and ΔSUVmax was performed using linear regression model.Results: Tumor volume of 27 lesions: 0.94 to 2113.4 cm3; average: 160.7 cm3; median: 12.13 cm3. Clinical evolution after PRRNT: improvement in 10 patients (83.3%) and stabilization in 2 patients (16.7%).

Qualitative 68Ga-DOTANOC evaluation: response in 8 patients (66.7%) and stable disease in 4 patients (33.3%). Semi-quantitative (ΔSUVmax) 68Ga-DOTANOC evaluation: response in 11 patients (91.7%) and progressive disease in 1 patient (8.3%). Qualitative and semi-quantitative (ΔSUVmax) 68Ga-DOTANOC evaluations were concordant in 8 patients (66.7%). No correlation was found between tumor volume and ΔSUVmax (R-squared= 0.01225).Conclusion: This study shows that the majority of patients responded to treatment and suggests that tumor volume in the 68Ga-DOTANOC PET/CT baseline scan has no correlation with SUVmax response to PRRNT using 177Lu-DOTATATE. A larger sample is needed to further validate this statement.

P672

[68Ga]DOTANOC PET: sex specific differences and influence of diabetes and usage of proton pump inhibitors

A. Leisser, W. Wadsak, M. Mayerhoefer, M. Mitterhauser, G. Karanikas, M. Hacker, A. R. Haug; Medical University of Vienna, Vienna, AUSTRIA.

Aims: Imaging with [68Ga]DOTANOC PET has become an important modality in patients with neuroendocrine tumors (NETs). Physiological uptake has been found to vary strongly in these patients. Some of them tend to develop type 2 diabetes or take proton pump inhibitors, which could affect the physiological uptake pattern, especially in regard to the pancreas and the stomach respectively. The objective of this study was to investigate these influencing aspects and also the significance of gender on the [68Ga]DOTANOC-uptake pattern.Methods: In 51 consecutive patients, who were examined with [68Ga]DOTANOC PET, SUVmax and SUVmean of the pancreas - subdivided into caput, corpus, and cauda -, the stomach, liver, spleen, kidneys and adrenal glands was measured. Corresponding personal data such as sex, age, history of diabetes, usage of proton pump inhibitors or oral antidiabetics and capillary blood glucose levels, were collected. For statistical analysis student's T-test was used, to determine significant differences.Results: In a study population of 51 patients, 26 were male and 25 female. Neither diabetes nor the usage of proton pump inhibitors could be proven to significantly alter the physiological uptake, in particular in the pancreas and the stomach. However, significant gender-specific (male vs female) differences were found regarding SUVmax (16.9 vs 21.4) and SUVmean (8.4 vs 11.3) of the kidneys and SUVmean (17.3 vs 21.7) of the spleen. Also, a gender-specific non-significant trend was observed, concerning SUVmax of the spleen (28.2 vs 31.9) and the liver (8.5 vs 7.5).Conclusion: Gender has a significant impact on the physiological [68Ga]DOTANOC-uptake pattern, whereas type 2 diabetes and the usage of proton pump inhibitors demonstrated no such effect.

P673

Predictors of FDG-F18 PET Positivity in Neuroendocrine Tumours

R. Silva1, L. Pires1, R. Ferreira1, A. Moreira1, P. Lapa1, G. Costa1, J. Pedroso de Lima2; 1Serviço de Medicina Nuclear do Centro Hospitalar e Universitário de Coimbra, Coimbra, PORTUGAL, 2Instituto de Ciências Nucleares Aplicadas à Saúde, Coimbra, PORTUGAL.

AIM: PET/CT with DOTANOC-Ga68 and FDG-F18 exploit different tumour characteristics of Neuroendocrine Neoplasms (NETs) for imaging. The 2 tracers may be complementary for tumour staging and response assessment, and several studies confer a strong prognostic value to FDG-F18 PET/CT. In this study we tried to predict PET/CT FDG-F18 positivity based on several tumour and DOTANOC-Ga68 PET/CT variables.MATERIAL AND METHODS: We retrospectively reviewed the findings in 18 patients (13 males, 5 females, aged:41-82 years, 1Q:53/median:62/3:70) with confirmed NETs (6 pulmonary/10 GEP/1 MEN-1 and 1 metastatic NET with unknown primary) who underwent both DOTANOC-Ga68 and FDG-F18 PET/CT imaging (time window:0-12 months, 1°Q:0/median:2/3°Q:5).Patients were scanned for initial staging (5), staging after excision of the primary tumour (5) and response assessment (8). All NETs were classified according to mitotic and Ki67 indexes (G1:2/G2:8/G3:8).Chromogranin A (CrA) and Neuron-specific Enolase (NSE) measurements were available for the majority of patients.PET/CT with DOTANOC-Ga68 and FDG-F18 studies were classified as positive or negative, and the SUVmax, SUVmean, SUVsd (Standard deviation of SUV) and SUVcv (Coefficient of variation of SUV) values of the most heterogeneous DOTANOC-68Ga avid lesion were recorded.The statistical analysis was performed using SPSSv20®. A $p<0.05$ was considered significant for all statistical tests. The Mann-Whitney test was used to test for statistically significant differences in continuous variables. A binary logistic analysis was performed to evaluate the impact of several tumour and PET/CT DOTANOC-Ga68 variables in the positivity of FDG-F18 PET/CT.RESULTS: DOTANOC-Ga68 PET/CT revealed tumour uptake in 15 of 18 patients. FDG-F18 PET/CT was positive in 11 of 18 patients. A statistical significant difference in Ki67 values was found between positive and negative FDG-F18 PET/CT patients. No statistical significant differences in CrA and NSE values between positive and negative FDG-F18 PET/CT patients were found.The SUVmax, SUVmean and SUVsd values of the most heterogeneous DOTANOC-Ga68 avid lesions were not statistically different between FDG-F18

PET/CT positive and negative patients. A statistical significant difference in SUVcv values was found between positive and negative FDG-F18 PET/CT patients.In the multivariable analysis only the SUVcv value remained as a statistically significant predictor for FDG-F18 PET/CT positivity.CONCLUSION: In this study the Ki67 and the SUVcv of the most heterogeneous DOTANOC-Ga68 avid lesions achieved a statistically significant difference between FDG-F18 PET/CT positive and negative patients. However, in the multivariable analysis, only the SUVcv value remained as a statistically significant predictor of FDG-F18 PET/CT positivity.

P674

Characterizing 68Ga-DOTA-peptide uptake in uncinate process of pancreas: normality versus Pathology

A. Kasat, C. Goh, H. Li, X. Yan; Singapore general Hospital, Singapore, SINGAPORE.

Objective: 68Ga-DOTA-peptides are somatostatin analogue tracers used for imaging neuroendocrine tumours (NET). A number of organs demonstrate normal physiological uptake of which the uncinate process of pancreas is of particular concern not only because pancreas itself is a common site for NET but also the great variability of the tracer uptake at this location that may make the interpretation difficult. Thus aim of the study is to define the characteristics of 68Ga-DOTA-peptides distribution in uncinate process of pancreas and its usefulness in distinguishing pathology from normality. Material and methods: 24 patients (each with multiple scans) with a total of 81 (68Ga-DOTATATE 68, 68Ga-DOTATOC 13) PET/CT scans performed between May 2009 and Oct. 2014 were reviewed retrospectively. 66 scans from 20 patients without tumor involvement and 15 scans from 4 patients with tumor involvement of the uncinate process were determined based on histological, clinical and radiological evaluation including at least 1 year follow-up. Visual inspection is used to determine the pattern of tracer distribution in the uncinate process by two nuclear medicine physicians. The reconstructed axial PET images were used to determine the SUV in uncinated process, body of the pancreas, spleen, pituitary and aorta. Statistical analyses including univariable Generalized Estimating Equations (GEE) was conducted. Results: There are 3 types of normal distribution in the uncinate process, diffuse (most common), focal and multifocal. The distribution pattern has nothing to do with uptake intensity. There is dramatic intrapatient and interpatients variability of the normal uptake: Average SUVmax for uncinate process is 5.88 +/- 3.34, range 1.29-14.88. There is strong positive correlation between the normal uptake intensity in uncinate process and in pituitary and spleen (both $P< 0.0001$). The uptake SUV is also negatively affected by dose of 68Ga-DOTA-peptide ($p=0.0002$). In diseased uncinate processes, NET tumor demonstrated significantly higher uptake with SUVmax of 82.49 +/- 46.32, with no correlation to uptake in any other organs. However there are only 4 patients enrolled in this study and 3 of them the histology features unknown. Conclusion: The distribution pattern and intensity of uptake in uncinate process of pancreas varies greatly between patients and between scans. Calling tumor involvement in uncinate process of the pancreas must be very cautious and cannot be made only on PET scan presentation but also correlating with other imaging and /or biopsy results. Pituitary and spleen uptake may be useful as reference in judging the nature of uncinate process uptake.

P675

The role of 68Ga-DOTA-NOC PET/CT as first step examination in cases with suspected Neuroendocrine Tumors (NET) based on clinical, biochemical and radiologic data

L. M. P. Pires, R. Silva, J. Álban, M. Silva, A. Moreira, G. Costa, J. P. Lima; Centro Hospitalário e Universitário de Coimbra, Coimbra, PORTUGAL.

Aim: Neuroendocrine tumors (NET) comprise a wide and heterogeneous group of neoplasms, historically considered rare and whose diagnosis is often challenging. 68Ga-DOTA-somatostatin analogs PET/CT is becoming the new gold standard for somatostatin receptor (SSTR) imaging of NETs. In the past few years, several studies reported the higher accuracy of this image modality for detection compared to morphological imaging procedures. The aim of this work was to assess the added value of 68Ga-DOTA-NOC PET/CT in patients with no histopathological evidence of NET, referred to our department when the presence of NET was suspected based on clinical, biochemical or radiologic data.Material and Methods: We reviewed the 298 PET/CT scans with 68Ga-DOTA-NOC performed in our department, between 2012 and 2015. Suspected NET cases (before histopathological studies) were selected, based on the presence of either clinical signs/symptoms (S), increased biomarkers (IBM) or imaging features findings (IF) suggestive of NET, as well as a combination of these conditions. PET/CT results were compared with the final diagnosis, concerning the presence of NET.Results: Fifty two patients (25 females; 27 males; 62.9±16.1 years-old) underwent 68Ga-DOTA-NOC PET/CT scans when the presence of NET was suspected on the basis of IF (12/52; 23.1%), S (6/52; 11.5%), IBM (2/52; 3.8%) or a combination of two or more of these conditions (32/52; 61.6%). The most common condition considered, was the combination of IBM plus S (13/52; 25%), followed by IF and IF plus IBM (both 12/52; 23.1%). Overall 68Ga-DOTA-NOC PET/CT was true-positive in 12 cases,

true-negative in 37, false-negative in 1 and false-positive in 2 (sensitivity=92.3%, specificity=94.8%, VPP=85.7%, VPN=97.4%, Accuracy=94.2%). The incidence of NET in the studied population was 25% (13/52) and the primary tumor was correctly identified in 12/12 cases. IBM plus IF were associated with the highest frequency of true-positive findings (7/12; 58.3%), with statistical significance regarding this parameter (chi square test, $p<0.05$), followed by IF alone (4/12; 33%). A statistical significant difference in Cromogranine-A values was found between positive and negative 68Ga-DOTA-NOC PET/CT (Mann-Whitney U test, $p<0.05$).Conclusions: Our data suggest that diagnostic accuracy of 68Ga-DOTA-NOC PET/CT is high (94.2%) even in cases wherein NET is only suspected. The association of IBM plus IF findings and IF alone are associated with a higher probability of true-positive findings.

P676

Interest of 68Ga DOTATOC-PET-CT compared to 111In-DTPA-octreotide scintigraphy to detect pancreas and duodenum neuroendocrine tumors in patients with MEN-1: preliminary results.

C. Morgat1,2,3, F. Vélayoudom-Céphise4, P. Schwartz1, M. Nunes4, J. Schulz2,3, J. Mazère1,2,3, M. Guyot1, D. Gaye4, E. Hindié1,2,3, A. Tabarin4, P. Fernandez1,2,3; 1Service de Médecine Nucléaire, CHU de Bordeaux, Pessac, FRANCE, 2Univ Bordeaux, INCIA UMR-CNRS 5287, F-33400 Talence, FRANCE, 3CNRS, INCIA UMR 5287, F-33400 Talence, FRANCE, 4Service d'Endocrinologie, CHU de Bordeaux, Pessac, FRANCE.

Introduction: Overexpression of subtypes of somatostatine receptors by neuroendocrine tumors (NET) allows imaging with 111In-DTPA-octreotide scintigraphy. However, the use of this technique to identify neuroendocrine tumors in pancreas and duodenum in patients with Multiple Endocrine Neoplasia type 1 (MEN-1) is not well defined. The somatostatin analog, 68Ga-DOTATOC, improves the detection of NET. The aim of our study was to compare PET with 68Ga-DOTATOC to 111In-DTPA-octreotide in screening pancreas or duodenal localization in MEN-1. Patients and Methods : 19 patients with MEN-1 (12 females, age: 47 ± 12 years) were included consecutively over 6 months, in the Endocrinology department and underwent a 68Ga-DOTATOC-PET-CT in addition to their annual tests. PET was performed 1 hour after injection of 68Ga-DOTATOC (97.1 ± 13.3 MBq). Metallation of the active pharmaceutical ingredient DOTATOC (Anaspec, Inc. or ABX GmbH) was performed with 68Ga obtained from a 68Ge/68Ga generator (IASON®). The gold standard was based on histology or morphological imaging (Contrast-enhanced CT or MRI). Results : 68Ga-DOTATOC and 111In-DTPA-octreotide have both detected at least one lesion in respectively 95% and 74% of patients. PET visualized 58 duodenal and pancreatic lesions in 19 patients, vs 17 lesions by 111In-DTPA-octreotide. The sensitivity of PET and 111In-DTPA-octreotide was 83% and 23% respectively for the detection of pancreas or duodenal NET. Compare to 111In-DTPA-octreotide, PET detected 41 additional lesions (pancreas, duodenum and extra-duodeno-pancreatic lesions such as lung carcinoid tumor, thymic tumor, meningioma···). Conclusion: Compare to 111In-DTPA-octreotide, sensitivity of 68Ga-DOTATOC-PET-CT is better in detecting pancreas or duodenal NET in patients with MEN-1. PET was also able to detect extra-pancreatic lesions. It could be recommended in the initial staging or monitoring of patients with MEN-1.

P40 - Tuesday, October 13, 2015, 4:00 PM - 4:30 PM, Hall 3 – Poster Exhibition

Clinical Oncology: Colorectal Cancer

P677

Added value of dual time point 18F-FDG PET/CT scanning in detection of local recurrence in rectal cancer

H. R. Farghaly1,2, **H. A. Nasr**1,3, A. Al Qarni1; 1Radiology Department, Prince Sultan Military Medical City, Riyadh, SAUDI ARABIA, 2Nuclear Medicine Unit, Assiut University, Assiut, EGYPT, 3Nuclear Medicine Unit, Cairo University, Cairo, EGYPT.

Objectives : To assess the added value of dual time point FDG PET/CT (DTP) and its associated quantitative parameters in detection of local recurrence (LR) in patients with rectal cancer (RC) Methods : Patients (n=28, 20 males and 8 females, mean age 56.43±16.68 years). All patients underwent resection ± chemotherapy and/or radiotherapy. All patients underwent whole body FDG-PET/CT scan as well as 2 hours delayed pelvic PET/CT images. To differentiate benign from malignant lesions an SUVmax cutoff of >4.0 for early images, >4.5 for delayed images and an increase in delayed SUVmax (ΔSUVmax>15%) based on ROC analysis, were used. Suspicious pelvic lesions were correlated with biopsies in 13 patients (46%) and with clinical and/or imaging follow-up (FDG-PET/CT, CT or MRI) in 15 patients (54%). Sensitivity, specificity, positive and negative predictive values, and accuracy in detection of LR using different PET/CT parameters were calculated. Results : Four patients had confirmed LR (14%). Early SUVmax, delayed SUVmax and ΔSUVmax were significantly higher in all patients with confirmed LR. The specificity, PPV and accuracy to detect LR were highest for ΔSUVmax>15% as a single parameter (83.3%, 50.0% & 85.7%) while combination of early SUVmax>4.0 or delayed SUVmax>4.5 with ΔSUVmax>15% SUVmax revealed

further improvement (87.5%, 57.1% & 89.3%) compared to single parameters. Conclusions : PET/CT has an excellent sensitivity but modest specificity and PPV for detection of local rectal cancer recurrence. Delayed PET/CT when performed is capable of improving the specificity and overall accuracy of the PET/CT.

P678

Evaluation of recurrent disease in the re-staging of colorectal cancer by 18F FDG PET/CT: can CEA and CA 19.9 help in patient selection?

A. Chiaravalloti, A. Fiorentini, D. Rinino, L. Travascio, R. Danieli, A. Lacanfora, E. Palombo, D. Di Biagio, O. Schillaci; Department of Biomedicine and Prevention, University Tor Vergata, Rome, ITALY.

Objective: The aim of our study was to evaluate the accuracy of 18F FDG positron emission tomography/computed tomography (PET/CT) in assessing the presence of recurrent colorectal cancer, in relation to carcinoembryonic antigen (CEA) and Carboidrate antigen 19.9 (CA 19.9).Methods: 18F FDG PET/CT was performed in 72 patients for re-staging colon cancer. Therapy has been discontinued at least three months before the examination. The mean CEA value (measured in 64 patients prior PET/CT examination) was 31.15 (±128.3) whereas the CA 19.9 (measured in 64 patients prior PET/CT examination) were 67.5 (±173.3). Differences in CEA and CA 19.9 values in patients with a positive and negative scans were analysed by means of ROC curve. ROC curve has been used for the calculation of sensitivity and specificity of 18F FDG PET/CT for CEA and CA 19.9 levels.Results: Results of 18F FDG PET/CT were related to CEA levels and CA19.9. PET/CT was positive for recurrence in 45/74 patients (60.8%, mean CEA and CA 19.9 were, respectively 40.97 ± 159.7 and 81.81 ± 212.3); PET/CT was negative for recurrence in 29/74 patients (39.2%, mean CEA and CA 19.9 were, ,respectively, 14.79 ± 37.29 and 43.99 ± 73.46). As expected, CEA values were higher in patients with a positive scan as compared to negative scans (p=0.027). A CEA value lower than or equal to 3.8 ng/ml was associated with a positive scan in 7/27 subjects while 31/39 subjects with a CEA cut-off value greater than or equal to 3.8 ng/ml were positive for recurrence at PET/CT (p= 0.029; sensitivity 70%; specificity 70.9%). We did not find statistically significant differences when comparing CA19.9 levels in patients with a positive or negative scan respectively.Conclusions: The possibility of detecting recurrence in patients treated for colorectal cancer with 18F FDG PET/CT is related to CEA and not to CA 19.9 serum levels. In particular, during follow up, 18F FDG PET/CT should be recommended in patients with a CEA value of at least 3.8 ng/ml.

P679

Value of FDG PET/CT in the assessment of patients with colon cancer comparing to stand-alone CT

K. Akbari1, S. Haim2, K. Emmanuel3, W. Zaglmair3, C. Pirich4, F. Fellner1, W. Langsteger2, **M. Beheshti**2; 1Radiology, General Hospital Linz, Linz, AUSTRIA, 2PET-CT Center Linz, St. Vincent's Hospital, Linz, AUSTRIA, 3GI-Cancer Center, St. Vincent's Hospital, Linz, AUSTRIA, 4Nuclear Medicine & Endocrinology, Paracelsus Medical University, Salzburg, AUSTRIA.

Purpose: To evaluate the potential of FDG PET/CT vs. contrast-enhanced CT alone in the assessment of distant metastases in primary staging, re-staging and follow up of colon cancer patients. Material & Methods: Eighty-one patients (46 men, 35 women, mean age: 70.4 ± 11.1) were included in this retrospective study: 29 (35.8%) were preoperatively (primary staging) and 52 (64.2%) postoperatively. Sixty-nine (85.2%) patients had a primary tumor stage of ≥ T3. Diagnostic contrast - enhanced CT was performed in all patients either together with FDG PET or in a separate setting (with a diagnostic protocol). Patients with a known second carcinoma, as well as patients with mucinous carcinoma of colon were excluded. All pathologic findings in both imaging modalities had to be verified with histological findings or imaging and/or clinical follow-up studies. All data were assessed based on the FDG PET/CT and ce-CT reports. In 12 patients with discordant findings between two imaging modalities, the images were reviewed again by corresponding specialists. Results: In the primary staging of pre-operative patients, FDG PET changed tumor staging and consequently the treatment approach in 10 (10/29) patients (34.5%). Nine patients were down-staged: 5 of them with suspicious organ metastases, 3 patients with suspicious lymph node (LN) metastases and 1 patient with both suspicious organ metastases and lymph nodes metastases on CT. In addition, 1 (1/29) patient (3.4%) was upstaged after FDG PET/CT. In the postoperative setting, only 2 (2/52) patients (3.8%) were down-staged. No additional findings were detected in the FDG PET comparing CT studies. In almost 25 % of follow - up patients and approx. 40 % of preoperative patients FDG PETCT was performed in addition to stand alone CT- Conclusion: The results of this study showed that in staging of colon cancer patients FDG PET/CT was able to better specify unclear lesions detected on stand-alone CT thus changing the therapy approach in 34.5% (10/29) of patients in preoperative setting. Eight of 10 patients (80%) had an advanced primary tumor (i.e. > T3). In postoperative setting FDG PET/CT may be useful in few special cases with unclear lesions on CT. Further randomized prospective studies are warranted.

P680

18F-FDG PET/CT in rectal cancer preoperative staging: improved detection of metastases and 2° unsuspected tumour

N. TESTART, A. RODRÍGUEZ-FERNÁNDEZ, T. AROUI-LUQUIN, R. SÁNCHEZ-SÁNCHEZ, M. GÓMEZ-RÍO, E. TRIVIÑO-IBÁÑEZ, A. MEDINA-BENÍTEZ, R. CONDE-MUIÑO, J. LLAMAS-ELVIRA; COMPLEJO HOSPITALARIO UNIVERSITARIO DE GRANADA, GRANADA, SPAIN.

Aim: The objective of this study is to assess the value of 18F-FDG PET/CT in the preoperative staging of rectal cancer. Methods: We analyzed a retrospective cohort including 300 patients (from January 2007 to December 2013) with pathologically confirmed rectal cancer. Preoperative staging was performed with conventional imaging techniques (colonoscopy, transrectal ultrasonography, pelvic MRi or CT), and 18F-FDG-PET/CT. All findings in 18F-FDG-PET/CT were confirmed histologically and/or by specific imaging tests and/or by clinical follow up > 1 year. Results: Following this study protocol we included 300 patients (187 males and 113 females; mean age: 67,3 ± 12,46 years), all with rectal adenocarcinoma (31 well, 258 moderately and 11 poor differentiation grade). In 66/300 patients (22%) 18F-FDG-PET/CT showed metastatic disease (M1): with a single lesion in 19 (8 pulmonary, 7 liver, 1 bone, 2 retroperitoneal lymph node and 1 mesenteric implant) and multiple location involvement in 47 patients (a total of 74 regions involved in these patients: 19 pulmonary, 33 liver, 3 bone, 16 retroperitoneal lymph node and 3 mesenteric implants). In 45/300 patients (15% of total patients, 68,2 % of metastatic patients) the 18F-FDG-PET/CT results raised the initial staging by revealing unsuspected metastases. In 23/300 patients (7,7%), 18F-FDG-PET/CT showed a second previously unsuspected malignant tumor: 16 synchronic colorectal, 2 lung, 1 prostatic, 1 thyroid, 1 endometrial, 1 gastric and 1 maxillofacial). There were 5 false negatives (FN): 3 lymph nodes, 1 mesenteric implant and 1 liver lesion, all detected by CT and confirmed after surgery by histopathological analysis; and 5 false positives (FP): 3 lymph nodes, 1 pulmonary and 1 mesenteric implant. In our study 18F-FDG-PET/CT in M1 staging showed a sensitivity of 92,4% [83,5-96,7; CI95%] and a specificity of 97,9% [95,1-99,1; CI95%], (TP: 61, TN: 229, FP: 5, FN: 5). The Global Accuracy was 96,7% [94-98,2; CI95%]. Conclusions: According to our results, the 18F-FDG-PET/CT was useful in the correct M1 preoperative staging of rectal cancer patients, mainly due to its ability to detect metastatic disease that was unsuspected by other imaging procedures. It also allowed the detection of other unsuspected tumors, leading to a better therapeutic approach in these patients.

P681

18F-FDG PET-CT Predicting Pathological Response to Neoadjuvant Therapy in Locally Advanced Rectal Cancer

D. SANCHEZ FUENTES, S. PEDRAZA FERNANDEZ, S. RUIZ SOLIS, A. HERNANDEZ MARTINEZ, P. SARANDESES FERNANDEZ, A. GOMEZ GRANDE, M. PEREZ-ESCUTIA, J. ESTENOZ ALFARO; HOSPITAL UNIVERSITARIO 12 DE OCTUBRE, MADRID, SPAIN.

PURPOSE: To assess the utility of 18F-FDG PET-CT in predicting pathological response to preoperative chemoradiotherapy (CRT) in patients with locally advanced rectal cancer. MATERIALS AND METHODS: Thirty-nine patients, 23(59%) men and 16(41%) women, mean age: 62 (range 40-83) with locally advanced rectal cancer from September 2009 to May 2014 were retrospectively included. All patients were staged with a thoracic-abdominal-pelvic CT and pelvic MRI. 18F-FDG PET-CT for staging and radiation therapy planning was also performed. Tumor location: 17(43.85%) superior, 14(35.89%) middle, 8(20.51%) inferior rectum. Histology: 37(94.87%) adenocarcinoma and 2(5.13%) mucinous adenocarcinoma. Clinical stage according to AJCC 7th: 7(17.95%) II, 31(79.48%) III and 1(2.56%) IV (liver metastases). Neoadjuvant treatment included radiotherapy (4500- 5040 cGy) over 5 weeks and concomitant chemotherapy (Capecitabine). Surgery was performed following CRT; low anterior resection was performed in 32(82.05%) and abdominoperineal resection in 7(17.95%) patients. The pathological treatment response was evaluated by the determination of the tumor regression grade (TRG) according to the Mandard criteria. Patients were divided into two groups, responders TRG 1-2 and non-responders TRG 3-5. The TRG was correlated with 18F-FDG PET-CT findings (tumor size, tumor SUVmax and nodal SUVmax). RESULTS: 7(17.94%) patients had a complete pathological response (CPR) in the resected specimens. According to the Mandard tumor regression grade (TRG), 14(35.9%) patients were responders and 25(64.10%) non-responders. Statistically significant differences between both groups were not seen when correlating metabolic findings (tumor size, tumor SUVmax and nodal SUVmax). However, were found slightly higher tumor sizes (range 2 - 15 cm, mean: 6,24) in non-responders versus tumor sizes (range 2.2 - 13.6 cm, mean: 5,84) in responders group and

slightly higher levels of tumor SUVmax (range 6.64 - 37.21, mean:21,95) in responders in comparison with non-responders (range 10.10 - 40.55, mean: 20,73). The mucinous adenocarcinomas 2(5.13%) had high levels of SUVmax (15.47 and 33.81), similar to other adenocarcinomas. There was a significant correlation between the tumor size measured by MRI and 18F-FDG PET-CT (Rho=0.49 p=0.003). Furthermore, pathological responders had better overall survival (1,6 year) compared to non-responders (0,7 year). However, this was not statistically significant (p=0.37). CONCLUSIONS: In our cohort, 18FDG PET-CT findings (tumor size, tumor SUVmax and nodal SUVmax) before neoadjuvant treatment (CRT) cannot predict the pathological response. More series are required to establish a stronger conclusion on this topic. There was a significant correlation between the tumor size measured by MRI and 18F-FDG PET-CT.

P682

Correlation Between Carcinoembryonic Antigen, Standard Uptake Value and Metabolic Volume in F-18 FDG PET/CT Positive Patients With Proven Recurrent Colorectal Carcinoma

E. G. Matovina, J. Mihailovic, D. Srbovan; Oncology institute of Vojvodina, Novi Sad, SERBIA.

Objective: To evaluate correlation between level of carcinoembryonic antigene (CEA), metabolic volume and standard uptake value (SUVmax) of the true positive lesions detected by PET/CT in patients with recurrent colorectal carcinoma. Methods: 50 18F-FDG PET/CT studies between January 2011. and January 2014 of 45 patients (14 women, 31 men; mean age: 62.93 years) with elevated CEA levels were evaluated. Measurements of serum levels of CEA were performed within 3 months of PET/CT examination. Final diagnosis of recurrence was made by histopathological findings, radiology studies or clinical follow-up. Results: Among positive scans, we chose 20 operated patients with histologically confirmed colorectal carcinoma in all lesions detected by PET/CT. In this group of patients, levels of CEA, SUVmax and summarized metabolic volume of all lesions in one patient were correlated. There was no correlation between CEA level and SUVmax in positive scans. Also there was not correlation between SUVmax and volumes of the lesions. However we have found strong positive correlation between CEA level and metabolic volume of the lesions (r=0,59).Conclusion: Our results suggest that in CRC patient with higher level of CEA we can expect higher metabolic volume of lesions, however higher level of CEA does not suggest and higher level of FDG uptake.

P683

Incidentally detected increased 11C-Choline uptake in bowel and hystopathological correlation.

E. Tabacchi, P. Ghedini, P. Castellucci, I. Grassi, S. Cambioli, S. Fanti; S. Orsola-Malpighi Hospital - University of Bologna, Bologna, ITALY.

Aim: The aim of this study is to investigate areas of unexpected increased uptake in bowel, detected during PET/CT with 11Choline in patients studied for prostate cancer. Materials and Methods: Among 2796 consecutive patients performed from January 2012 to February 2015 who underwent 11Choline-PET/CT for stage or restage prostate cancer we included in our study.21 patients in which an incidental focal Choline uptake in the bowel have been found and in which a subsequent colonoscopy and biopsy were available. We have analysed SUVmax, SUVmean and the v¬¬¬olume of the lesion and investigated relationship with biopsy results. Results: Seven-teen of 21 areas of intense focal uptake were associated with endoscopic pathological findings (positive predictive value, 81%), 4 patients resulted negative at endoscopy. Regarding endoscopic positive findings 3/17 lesions were malignant (colorectal cancer); 6/17 were pre-malignant (6 tubovillous adenoma); 8/17 lesions were benign (3 inflammatory, 2 inflamed diverticula, 1 lesion was associated with Intestinal Bowel Disease and 2 were abscess). The Mean values of SUVmax ans SUVmean were 6.4 and of 3.4 respectively in the 17 positive PET findings.Mean SUVmax of malignant lesions was 7.2 and mean value of SUVmean was 4.2. Mean Volume of the 21 lesions was 24.6 cm3. No significant difference in the SUV values was found between malignant or benign lesions (P=0.6). Volume analysis didn't show difference between malignant or benign lesion. Conclusions :Main limitation of our study is the limited number of patients enrolled. According to our retrospective study, the presence of any focal Choline uptake in the bowel justifies a subsequent endoscopic investigation. Since Pet may detect malignant e premalignant lesion in more than half of total findings. These could lead to a prompt instauration of the correct therapy and may prevent degeneration of the pre malignant lesions. Keywords: C11-Choline, PET/CT, Incidental Findings, Bowel, Colorectal Cancer

P684

Contribution of FDG PET/CT for re-staging in patients with colorectal cancer having suspicious radiological findings and/or elevated serum tm marker levels.

M. YÜKSEL, M. T. Yanmaz, H. Akyol, M. A. Aydın, E. Ziylan, T. Ipek, E. Eyüpoglu; Kemerburgaz University, Medical Faculty, ISTANBUL, TURKEY.

Aim: In patients with colorectal cancer (CRC-pts), confirmation of suspicious findings by radiological examinations and/or elevated tm markers is important to decide for patient management. Therefore, we aimed to evaluate the role of FDG PET/CT in re-staging of CRC-pts having suspicious findings by radiological examination and/or elevated serum tm markers in follow-up period. Material and Methods: A total of 189 patients with colorectal cancer having suspicious findings in radiologic examination and/or elevated serum tumour marker levels in follow-up period were evaluated with FDG PET/CT for re-staging. Medical records of the total patients were evaluated retrospectively. Results of the radiological examination and serum tumour marker levels (CEA and/or CA.19.9) were compared with FDG PET/CT findings. Results: FDG PET/CT was positive in 69/125 (55%), 43/49 (8%), and 15/17 (88%) in CRC-pts with suspicious radiological examination, elevated Tm marker (CEA and/or CA.19.9), and radiological examination+elevated Tm marker, respectively. In 23 of 189 patients (12%) with suspicious findings in radiological examination additional unknown metastatic foci were detected. Conclusion: FDG PET/CT has important contribution in evaluation of re-staging CRC-pts with suspicious findings in radiological examinations and/or elevated serum Tm marker levels. According to our findings, FDG PET/CT results were more compatible with elevated serum Tm marker levels or suspicious radiological examination+elevated Tm marker levels. Since approximately half of our CRC-pts with suspicious radiological findings were negative for recurrence and/or metastasis of the primary malignancy by FDG PET/CT, we suggest that the results of the radiological findings should be correlated with serum tm marker levels and FDG PET/CT. Further investigations with larger number of CRC-pts are needed to confirm out findings.

P41 - Tuesday, October 13, 2015, 4:00 PM - 4:30 PM, Hall 3 – Poster Exhibition

Clinical Oncology: Urogenital

P685

11C-Choline PET/CT in Prostate Cancer Patients with Biochemical Recurrence

D. M. Pursanova1, I. P. Aslanidis1, O. V. Mukhortova1, A. S. Rumyantsev1, O. B. Karyakin2, V. A. Biryukov2, V. I. Shirokorad3; 1Bakoulev Scientific Center for Cardiovascular Surgery, Moscow, RUSSIAN FEDERATION, 2A.Tsyb Medical Radiological Research Centre – branch of the National Medical Research Radiological Centre, Obninsk, RUSSIAN FEDERATION, 3Moscow City Oncology Hospital №62, Moscow, RUSSIAN FEDERATION.

Purpose: To evaluate the diagnostic impact of 11C-Choline PET/CT in the detection of recurrent prostate cancer (PCa) in patients with biochemical relapse and to assess the correlation between PET/CT diagnostic accuracy and PSA levels. Methods and materials: 11C-Choline PET/CT was performed in 83 patients (age range 50-79) with biochemical relapse after radical treatment for PCa. Imaging was performed on PET/CT scanner (Biograph-64, Siemens) 10 min after injection of 11C-Choline (700-950Mbq). The mean PSA value was 3.73 ± 4.25 (0.22-17.80) ng/ml. Patients were divided into three groups according to PSA level: ≤ 2 ng/ml, 2 to 9 ng/ml and ≥ 9 ng/ml. Results: Overall, 11C-Choline PET/CT detected PCa relapse in 38 of 83 patients (46%). The mean PSA value in PET-positive patients was 5.99 ± 5.10 (0.22-17.80) ng/ml, while in negative patients PSA value was 1.82 ± 1.82 (0.27-8.89) ng/ml. The majority - 69% (31/45) patients with PET-negative scan had low PSA levels (<2 ng/ml). Although the median PSA value was significantly higher in PET-positive than in PET-negative patients (4.34 ng/ml vs 1.2 ng/ml, $p < 0.001$), PET/CT confirmed its ability to detect relapse in patients with low PSA levels (from 0.22 ng/ml). PET/CT was positive in 8 of 39 patients (21%) with PSA of ≤ 2 ng/ml, in 21 of 35 patients (60%) with PSA of 2 to 9 ng/ml, and in 9 of 9 patients (100%) with PSA of ≥ 9 ng/ml. Local relapse was detected in 53% (20/38) patients. Both local and distant metastases were diagnosed in 29% (11/38) cases: bone lesions (7), lymph nodes (3), lymph nodes and adrenal gland (1). Distant relapse was identified in 18% (7/38) cases: bone (4), lymph nodes (2) and lungs (1). PET/CT allowed to assess the efficacy of treatment in 27% (12/45) PET-negative patients under hormone therapy at the scan time. However, PET/CT wasn't able to localize the site of PCa recurrence in these hormone-sensitive patients what might have affected the overall detection rate. Conclusion: 1) 11C-Choline PET/CT was able to detect and correctly identify the site of PCa relapse in 46% cases and therefore was useful in determining the further therapeutic approach. 2) Our data confirmed the strong correlation between the 11C-Choline PET/CT detection rate and PSA levels at restaging of PCa ($r = 0.8$). 3) 11C-Choline PET/CT might have limited utility in localizing the site of PCa recurrence in some patients under hormone therapy.

P686

Diuretic FDG PET/CT and diffusion weighted MR imaging for urothelial carcinoma: capability for prediction of pathological characteristics and prognosis

M. Nogami1, H. Iwasa2, K. Miyatake2, S. Kohsaki2, K. Ohgi2, M. Nishimori2, T. Yamagami2, D. Takenaka1, S. Adachi1; 1Hyogo Cancer Center, Akashi, JAPAN, 2Kochi Medical School, Kochi University, Nankoku, JAPAN.

PURPOSE: Diuretics yield rapid evacuation of urinary

excretion of administrated FDG and enable evaluation of urothelial carcinoma on FDG PET/CT. The purpose was to determine the association between glucose metabolism and pathological characteristics or short-term prognosis of high grade urothelial carcinoma on FDG PET/CT after diuretic (diuretic PET/CT), and to compare those with diffusion weighted (DWI) MR imaging.MATERIALS AND METHODS: Twenty-six pathologically confirmed high grade urothelial carcinomas (renal pelvis cancer, n=10; ureteral cancer, n=8; and bladder cancer, n=8) were examined by diuretic PET/CT and DWI MRI within one week before therapy. Diuretic PET/CT was performed 180 min after administration of F-18 FDG and 60 min after furosemide injection. DWI MRI was acquired at 3.0T with b-values of 0 and 1000 sec/mm2. Maximum and peak standardized uptake value (SUV max and SUV peak, respectively) and minimum and average apparent diffusion coefficient (ADC min and ADC mean, respectively) were measured. Pathological results including tumor size, depth, lymphatic and venous invasion were acquired by operations and biopsies. The prevalence of short-term recurrence and/ or metastasis after therapy was determined by follow-up studies and recorded at six months after initial treatment. To determine the relationship between glucose metabolism and restricted diffusion of the tumors, SUVs were statistically compared with ADCs by the Spearman's rank correlation coefficient. To evaluate the correlation of pathological characteristics and short-term prognosis with glucose metabolism and restricted diffusion, SUVs and ADCs were also statistically compared with pathological and prognostic status by the Mann-Whitney test.RESULTS: The histopathological results showed 21 invasive and 5 non-invasive urothelial carcinomas. Significant inverse correlation was found between SUV max and ADC min (r= -0.46, p= 0.019) and between SUVpeak and ADCmean (r= -0.44, p= 0.019), respectively. Tumor size was significantly correlated with SUVmax and SUVpeak (r= 0.74 and 0.75, p= <0.0001 and <0.0001, respectively). There was no significant correlation of the other pathological characteristics and short-term prognosis with SUVs and ADCs.CONCLUSIONS: Significant inverse correlation between SUV and ADC is found in high-grade urothelial carcinomas similar to the other cancers. SUV of high-grade urothelial carcinoma shows strong correlation with its size; however, the other histopathological characteristics and prognosis of the high-grade urothelial carcinoma are not predicted by SUVs and ADCs.

P687

68Ga-PSMA-11 dynamic PET/CT in the diagnostics of primary prostate cancer

C. Sachpekidis1, M. Eder2, K. Kopka2, W. Mier3, B. A. Hadaschik4, U. Haberkorn3, A. Dimitrakopoulou-Strauss1; 1Clinical Cooperation Unit Nuclear Medicine, German Cancer Research Center, Heidelberg, GERMANY, 2Division of Radiopharmaceutical Chemistry, German Cancer Research Center, Heidelberg, GERMANY, 3Division of Nuclear Medicine, University of Heidelberg, Heidelberg, GERMANY, 4Urology Clinic, University of Heidelberg, Heidelberg, GERMANY.

Objectives: 68Ga-PSMA-11 PET/CT is a novel imaging modality for the detection of prostate cancer (PC). Aims of the present study are to analyze the pharmacokinetics and biodistribution of the recently clinically introduced radioligand 68Ga-PSMA-11, and to study the potential correlation between tracer parameters and plasma PSA levels in patients suffering from primary PC. Methods: The study includes 22 patients with biopsy-confirmed, not previously treated PC (mean age 67.5 yrs). Their median PSA value was 54.0 ng/mL. All patients underwent dynamic PET/CT (dPET/CT) scanning (60 min) of the pelvis as well as whole body PET/CT studies with 68Ga-PSMA-11. dPET/CT assessment was based on qualitative evaluation, SUV calculation, and quantitative analysis based on a 2-tissue compartment model and a non-compartmental approach based on fractal dimension. Statistical evaluation was based on descriptive statistics and Spearman correlation analysis ($p<0.05$). Results: In 21 patients at least one lesion was detected. One patient demonstrated no tracer uptake neither in tumor nor in tissues, where physiological uptake is expected (salivary glands, lacrimal glands, liver, spleen, bowel). A total of 66 lesions were detected (21 primary PCs, 45 metastatic lesions in lymph nodes, soft tissue and bones). One patient demonstrated a diffuse metastatic disease with innumerable focal lesions. Semi-quantitative evaluations revealed the following values for the PC-associated lesions: mean SUVaverage=14.8 (median=12.0) and mean SUVmax=24.3 (median=20.9). Dynamic PET/CT studies of the pelvis revealed the following absolute 68Ga-PSMA-11 quantitative values: K1=0.26 (median=0.18), k3=0.32 (median=0.28), influx=0.16 (median=0.10) and fractal dimension (FD)=1.27 (median=1.31). Correlation analysis revealed a strong, significant correlation between PSA plasma levels and the number of lesions detected on 68Ga-PSMA-11 PET/CT (r=0.83). Moreover, PSA levels correlated significantly with the following 68Ga-PSMA-11 parameters: SUVaverage (r=0.59), SUVmax (r=0.57), K1 (r=0.31), k3 (r=0.42), influx (p=0.53) and FD (r=0.56). Conclusions: 68Ga-PSMA-11 PET/CT revealed at least one lesion per patient in 21/22 (95.0%) patients. PSA plasma levels correlated significantly with the number of 68Ga-PSMA-11 positive lesions detected on PET/CT as well as with all dynamic 68Ga-PSMA-11 PET parameters.

P688

68Ga-PSMA-11 dynamic PET/CT in biochemical relapse of prostate cancer

C. Sachpekidis1, M. Eder2, K. Kopka2, W. Mier3, B. A. Hadaschik4, A. Dimitrakopoulou-Strauss1; 1Clinical Cooperation Unit Nuclear Medicine, German Cancer Research Center, Heidelberg, GREECE, 2Division of Radiopharmaceutical Chemistry, German Cancer Research Center, Heidelberg, GREECE, 3Division of Nuclear Medicine, University of Heidelberg, Heidelberg, GREECE, 4Urology Clinic, University of Heidelberg, Heidelberg, GREECE.

Objectives: The introduction of 68Ga-PSMA-11 PET/CT is considered a promising step towards the improvement of prostate cancer (PC) diagnostics. We aim to study the pharmacokinetics and distribution of the recently clinically introduced radioligand 68Ga-PSMA-11 in recurrent PC by means of dynamic and whole body PET/CT. Methods: 32 patients with biochemical recurrence of pretreated PC (mean age 69.0 yrs) were enrolled in the study. The median PSA value was 4.8 ng/mL and the median Gleason score was 7. All patients underwent dynamic PET/CT (dPET/CT) scanning (60 min) of the pelvis as well as whole body PET/CT studies with 68Ga-PSMA-11. dPET/CT assessment was based on qualitative evaluation, SUV calculation, and quantitative analysis based on a 2-tissue compartment model and a non-compartmental approach based on fractal dimension. Results: In 25 patients at least one lesion was detected, while 7 patients were 68Ga-PSMA-negative. A total of 71 lesions were detected (7 recurrent PCs, 64 metastatic lesions in lymph nodes, soft tissue and bones). In one patient the extent of disease was very large, rendering the exact calculation of metastatic lesions practically impossible (innumerable focal lesions). Semi-quantitative evaluations revealed the following values for the PC-associated lesions: mean SUVaverage =10.9 (median =8.5) and mean SUVmax =17.0 (median =13.7). Dynamic PET/CT studies of the pelvis revealed the following absolute 68Ga-PSMA-11 quantitative values for the suspicious recurrent or metastatic lesions: K1=0.23 (median=0.18), k3=0.33 (median=0.27), influx=0.12 (median=0.11) and fractal dimension (FD)=1.25 (median=1.28). Patients with lesions on 68Ga-PSMA-11 PET/CT had a median PSA of 9.3 ng/mL and a median Gleason score of 7, while patients negative on 68Ga-PSMA-11 PET/CT had a median PSA of 0.4 ng/mL and a median Gleason score of 7. Correlation analysis revealed a significant correlation (r=0.53) between PSA levels and the number of lesions detected on 68Ga-PSMA-11PET/CT ($p<0.01$). Conclusions: 68Ga-PSMA-11 PET/CT revealed at least one lesion per patient in 25/32 (78.1%) patients. Patients positive on 68Ga-PSMA-11 PET/CT had higher PSA values than those who were 68Ga-PSMA-11 negative ($p<0.01$). PSA plasma levels correlated significantly with the number of 68Ga-PSMA-11 positive lesions on PET/CT.

P689

Radiolabeled somatostatin analogs for diagnosis and treatment of patients with advanced urothelial carcinoma

M. Rodrigues1, L. Scarpa1, D. Kendler1, C. Uprimny1, B. Nilica1, S. Buxbaum1, G. Gastl2, I. Virgolini1; 1Department of Nuclear Medicine, Medical University, Innsbruck, AUSTRIA, 2Department of Internal Medicine, Division of Haematology and Oncology, Medical University, Innsbruck, AUSTRIA.

Somatostatin receptors (SSTR) can be overexpressed in a variety of neoplasms, including neuroendocrine tumors, meningioma, mesenchymal tumors, lymphoma, and, with a low incidence and density, in renal cell carcinoma as well. Aim: to evaluate the value of radiolabeled somatostatin analogs for the diagnosis and treatment of patients with advanced urothelial carcinoma. Material and Methods: a series of six patients (3 male, 3 female; age: 57-70 years) with urothelial carcinoma (previous nephrectomy, 5 patients) was investigated with radiolabeled somatostatin analogs (68Ga-DOTA-TOC-, 3 patients; 68Ga-DOTA-lanreotide-PET/CT, 2 patients; both examinations, 1 patient) and 18F-FDG-PET/CT for staging and therapy decision-making. The time interval between PET with somatostatin analogs and 18F-FDG ranged 1-31 days. Peptide receptor radionuclide therapy (PRRT) was applied in 3 patients (cumulative activity: 177Lu-DOTA-TATE 14.4 GBq and 28.35 GBq, 90Y-DOTA-lanreotide 37.38 GBq). Follow-up (range: 3-10 years) included 68Ga-DOTA-TOC/lanreotide-PET, 18F-FDG-PET and diagnostic CT and/or MR. Results: 68Ga-DOTA-TOC/lanreotide-PET detected metastatic disease in 6 patients (liver,3; lymph nodes,3; pancreas,2; bone,1; lung, 1; stomach,1 patient). 68Ga-DOTA-TOC-PET was false negative in 1 patient. 18F-FDG-PET showed metastases in only 4 patients (liver,2; lymph nodes,2; pancreas,1; bone,1; lung,1; stomach,1 patient). Based on PET results, PRRT was indicated in 4 patients, surgery in 1 patient and chemotherapy in 1 patient. PRRT was well tolerated in all patients. Follow-up after PRRT showed stable disease in 2 patients (3 and 6 years follow-up) and complete remission in 1 patient (10 years follow-up). Conclusions: 68Ga-DOTA-TOC and 68Ga-DOTA-lanreotide-PET are valuable tools in the work-up and management of patients with urothelial carcinoma. Furthermore, our results illustrate that PRRT is a well tolerated treatment option

that can be highly effective in controlling advanced urothelial carcinoma.

P690

Correlation of serum PSA levels with 68Ga-PSMA tumor SUV in patients with primary and metastatic prostate cancer

S. Lütje1, B. Gomez1, S. Heskamp2, R. Reichel1, A. Bockisch1, O. C. Boerman2, A. Wetter3, T. D. Poeppel1; 1Clinic for Nuclear Medicine, University Hospital Essen, Essen, GERMANY, 2Department of Radiology and Nuclear Medicine, Radboud university medical center, Nijmegen, NETHERLANDS, 3Department of Diagnostic and Interventional Radiology and Neuroradiology, University Hospital Essen, Essen, GERMANY.

Aim: Prostate cancer (PCa) is the most common malignancy in men worldwide, leading to substantial morbidity and mortality. The 68Ga-labeled HBED-CC-PSMA ligand is a highly promising new tracer for imaging of PCa. The aim of this study was to evaluate the correlation between 68Ga-PSMA-PET/CT standardized uptake values (SUV) in primary and metastatic PCa lesions and serum levels of prostate-specific antigen (PSA). Materials and methods: Twenty-five patients with primary or metastatic PCa received 112 ± 30 MBq of the 68Ga-HBED-CC-PSMA ligand intravenously and underwent PET/CT (Siemens mCT) at 1 h after injection. Data were analyzed regarding the detection rate of primary tumor lesions as well as of bone and lymph node metastases, and regarding radiotracer uptake in tumor lesions. The SUV_{max}, SUV_{mean} (average SUV within a 3D isocontour thresholded at 50% of the SUV_{max}) and SUV_{peak} of 68Ga-PSMA were determined within a spheroidal volume of interest (VOI) to evaluate the correlation between SUV and serum PSA levels by calculating the Pearson correlation coefficient. As reference standard a characterization for malignancy was made in consensus taking into account the available histopathological data, and existing prior examinations. Results: In the 25 patients (mean PSA 6.8 ng/ml, range 0.1 - 16.0 ng/ml; mean SUV_{max} 10.6, range 3.3 - 27.5), a linear correlation between serum PSA levels and SUV_{max}, SUV_{mean}, and SUV_{peak} for 68Ga-PSMA-PET/CT uptake in the tumor lesions was found (r=0.53, r=0.50, and r=0.50, respectively). Strongest correlation between PSA and SUV_{max}, SUV_{mean}, and SUV_{peak} was observed for bone metastases (n=5, r=0.97, r=0.96, and r=0.98, respectively) and for metastatic lymph nodes (n=6, r=0.66, r=0.63, and r=0.59, respectively). In addition, a moderate correlation was found between the number of tumor lesions detected with 68Ga-PSMA-PET/CT and PSA serum levels in these 25 patients (r=0.45). Conclusion: Serum PSA levels of patients with PCa linearly correlate with uptake of the 68Ga-PSMA ligand in terms of SUV_{max}, SUV_{mean}, and SUV_{peak}. Strongest correlation was observed for bone metastases. In addition, the serum PSA level correlated with the number of tumor lesions detected with 68Ga-PSMA-PET/CT. In future, the observed correlation might facilitate the selection of patients for 68Ga-PSMA-PET/CT imaging.

P691

Renal cell carcinoma: clinical and prognostic value of FDG-PET/CT after surgery

P. Alongi1, M. Picchio1, M. Spallino2, L. Gianolli1, G. Saladini3, L. Evangelista3; 1IRCCS San Raffaele Scientific Institute, Milano, ITALY, 2University of Milano-Bicocca, Milano, ITALY, 3Veneto Institute of Oncology, Padova, ITALY.

AIM: Several studies, often with small cohort and divergent results, have discussed the role and possible limitations of FDG-PET/CT at staging and restaging for patients with renal cell carcinoma (RCC). However, the possible prognostic role remain still undefined. The aim of this retrospective study, through a collaboration between San Raffaele Hospital(OSR) and Veneto Institute of Oncology (IOV), was to evaluate the clinical and prognostic impact of FDG PET in the restaging process of renal cell cancer after surgery. Materials and Methods: From OSR and IOV database we reviewed restaging FDG-PET/CT scans performed in 104 patients after surgery for RCC. Diagnostic accuracy of visually interpreted FDG-PET/CT was evaluated based on final diagnoses obtained by histology, other diagnostic imaging (eCT, MRI, Bone scan) and by clinical follow-up (mean 37 months). Additional information such as, influence on treatment decisions, and impact of FDG-PET/CT findings on survival were assessed. Progression-free survival (PFS), overall survival (OS) using Kaplan-Meier method, and relative risk of progression (RRP) with Cox regression analysis were calculated in all cohort and in a second step combining PET results with TNM staging (available in 52 patients). RESULTS: Suspicious recurrence of RCC was histologically (n = 24) or by other diagnostic imaging and follow-up (n = 36) confirmed in 60/104 FDG-PET/CT scans. Overall, the sensitivity, specificity, positive predictive value, negative predictive value and diagnostic accuracy using FDG-PET/CT were 80%, 87%, 94%, 65%, 83% respectively. FDG-PET/CT findings influenced therapeutic management in 32 cases (30,7%). Cumulative survival rates over 5 years in the PET-positive vs. the PET-negative group were 19% vs. 69% respectively ($p < 0.005$). PFS rates over 3 years in the PET positive vs. the PET-negative group were 20% vs. 67% ($p < 0.005$). Cox regression analysis showed an high RRP for PET-positive compared to PET-negative patients (HR: 3.8; Chi-sq: 6.4; $p<0,005$). Conversely PET negative in comparison to PET positive patients presents a lower RRP

(HR: 0.6; Chi-sq: 1,8; p<0,005). In addition, FDG PET showed an incremental prognostic value, in terms of relative risk of progression, by comparing TNM Stage 3-4 alone (HR: 1,8; p:0.072) vs. FDG PET positivity associated with Stage 3-4 (HR: 4.3; p:0,012). Conclusion: FDG-PET/CT demonstrated to be a valuable tool in the treatment decision making and to predict the survival and risk of progression of patients affected by renal cancer, despite a possible false negativity in some subtypes. Furthermore, FDG-PET in combination with TNM staging system allowed incremental risk stratification.

P692

Optimising 18F-Choline PET-CT acquisition protocol in prostate cancer

L. Mohamed Salem, **Sr**.1, M. Ibañez Ibañez1, L. Álvarez Nieto1, V. Godoy Bravo1, R. Reyes Marles1, L. Frutos Esteban1, J. Navarro Fernandez1, M. Castellón Sanchez1, P. Nicolas Ruiz1, M. Claver Valderas1, B. Miñana López2, A. Rosino Sánchez2, P. López Cubillana1, A. Montellano Fenoy1, M. Roldan Rubio1; 1Hospital Clínico Universitario Virgen de la Arrixaca, Murcia, SPAIN, 2Hospital Universitario Morales Meseguer, Murcia, SPAIN.

Aim:In absence of an official standardised 18F-Choline PET-CT acquisition protocol, we evaluate the utility and the results of our acquisition protocols to propose an optimal acquisition protocol.Materials and methods:We study retrospectively 75 patients, 64 patients with prostate cancer (PCa) with biochemical relapse after treatment with curative intent (prostatectomy or radiotherapy), 8 patients with histological diagnosis of high risk PCa and negative conventional imaging techniques for staging, and 3 patients with Castration-refractory PCa with no previous curative intent, all patients underwent a bone scan and a new determination of PSA level (if they had not one the last month), if bone scan is positive, then PET-CT in not indicated, all patients underwent PET-CT scan (4 MBq / Kg) according to two different protocols; 55 patients had a dynamic acquisition of 8 frames (image / minute), one minute after injection, a pelvic bed at 15 and 60 minutes, and a whole body PET-CT at 30 minutes, and 20 patients dual-phase protocol, a pelvic bed one minute after injection and a whole body PET-CT at 60 minutes.In 51 of 75 patients, who had a positive PET-CT scan (68%), we analyse the mean SUVmax to assess both acquisition protocols, and the relation between the SUVmax, PSA level and the detection rate.Results:The SUVmax decreases slightly over the time in the consecutive acquisitions in all the patients with soft tissue lesions.There is a clear decreasing tendency in 8 patients with 12 soft tissue lesions with histological confirmation and an increasing tendency in 5 patients with bone lesions11 patients had positive bone scan (5 patients had PET-CT with similar findings), 19,23% PET-CT studies could be avoided with positive bone scan.The higher is the PSA level, the higher is the probability of a positive study and the higher is SUVmax.Dual-phase is more comfortable for the patient, easier to interpret, visualization of the pelvis before the arrival of radioactive urine and better management of administered activityConclusion:There is no correlation between the SUVmax at different times, the tendency is clearly decreasing in patients with histological diagnosis of high risk prostate cancer.It has a decreasing tendency in soft tissue lesions and an increasing one in bone lesions.Dual-phase protocol is more accurate, comfortable and easier.The PSA level correlates with the detection rate and the SUVmax.Practicing bone scan first can avoid PET-CT in 19,23% of the patients.

P693

Clinical efficacy of PET/CT using 68Ga-DOTATOC for restaging in renal cell carcinoma

Y. Nakamoto, K. Sano, T. Ishimori, K. Togashi; Kyoto University Graduate School of Medicine, Kyoto, JAPAN.

Objectives: Positron emission tomography / computed tomography (PET/CT) with 68Ga-labeled 1,4,7,10-tetraazacyclododecane-N,N',N",N"'-tetraacetic acid-D-Phe1-Tyr3-octreotide (DOTATOC) has been accepted as a diagnostic imaging tool especially for detecting neuroendocrine tumors, but its clinical value for restaging in renal cell carcinoma (RCC) remains unknown. The purpose of this study was to evaluate the clinical efficacy of DOTATOC-PET/CT in patients with suspected recurrent RCC after surgery. Patients and methods: A total of seven consecutive patients (M:F=5:2) who had surgery for histologically-proven renal cell carcinoma were analyzed. All patients who had been suspected of having recurrence underwent DOTATOC-PET/CT scan for restaging purpose during the follow-up period. PET/CT findings were reviewed and sensitivity was calculated in a patient-basis and lesion-basis. When patients had PET/CT with fluorodeoxyglucose (FDG), PET findings were compared. As a reference standard, histopathological findings and/or clinical data including radiological findings were used. Results: There were a total of 18 recurrent or metastatic lesions (one local recurrence, 9 lesions in bone, 2 in pancreas, 2 in soft tissue, 1 in liver, 1 in lung, 1 in parathyroid, 1 in lymph node) in seven patients. Of 18 lesions, 13 lesions in 6 patients with clear cell carcinoma were clearly depicted in DOTATOC-PET/CT, the maximal standardized uptake values of which were ranging from 2.8 to 23.3, with the average of 9.7. Excluding 2 of 13 lesions that were not assessed by FDG-PET/CT, only 3 lesions were positive in FDG-PET/CT. 4 of 18 lesions were negative in DOTATOC-PET/CT, but positive in FDG-PET/CT. Interestingly, these 4 lesions were papillary carcinomas. The remaining one lesion was a metastatic liver tumor, which

was not identified by both PET/CT. Overall, the sensitivities of DOTATOC-PET/CT and FDG-PET/CT were 86% and 67%, respectively, in patient-basis, and 72% and 56%, respectively, in lesion-basis. Conclusion: Our preliminary data indicate that DOTATOC-PET/CT could be useful for restaging in RCC. In addition, there might be differences of diagnostic performance according to histopathological types.

P694

[68Ga]PSMA-HBED uptake in sympathetic ganglia - A potential pitfall in scan interpretation

G. Kanthan, E. Hsiao, D. Chan, J. Drummond, G. Schembri; Royal North Shore Hospital, St Leonards, AUSTRALIA.

Aim: [68Ga]PSMA-HBED PET/CT imaging is a relatively new technique used to evaluate the extent of disease in patients with prostate carcinoma. A recent report suggests that PSMA uptake in coeliac ganglia is common and likely physiological. We have noted uptake in the lower neck region as a common finding. Stellate ganglia are a potential site for this physiological uptake of PSMA. In this study, we aim to determine the frequency and intensity of positive uptake in the region of coeliac and stellate ganglia on [68Ga] PSMA PET/CT imaging. Materials and Methods: The study included 50 consecutive patients with a history prostate carcinoma referred for [68Ga] PSMA-HBED PET/CT imaging to assess the extent of disease. The scans were evaluated for the presence of PSMA uptake in the region of the coeliac and stellate ganglia. Uptake was noted as either present or absent, and if present, standardized uptake values (SUV max) were recorded. SUV max:background uptake (gluteal muscle SUV mean) ratios were calculated for PSMA positive ganglia. Results: Of the 50 patients, 27 (54%) had uptake in the region of right stellate ganglion and 38 (76%) had uptake in the region of left stellate ganglion. 41 (82%) patients had positive uptake in the region of at least one stellate ganglion and 24 (50%) had uptake in the region of both stellate ganglia. The SUVmax values ranged from 1.41 to 3.61. SUVmax exceeded 3.00 in only 1 right stellate ganglia (2%) and 5 left stellate ganglia (10%). The mean SUV was 2.28 and mean SUV max:background SUV ratio was 6.24. Of the 50 patients, 13 (26%) had positive uptake in right celiac ganglion and 35 (70%) had positive uptake in left celiac ganglion. 37 (74%) had uptake in at least one celiac ganglion and 11 (22%) had uptake in both celiac ganglia. The SUVmax values ranged from 1.68 to 6.46. SUVmax exceeded 3.00 in 5 right coeliac ganglia (10%) and 9 left coeliac ganglia (18%). For PSMA positive coeliac ganglia, the mean SUV was 2.79 and mean SUV max to background SUV was 7.26. Uptake in at least one of the four ganglia is seen on 90% of patients. Conclusion: PSMA uptake in sympathetic ganglia is a common finding in PSMA PET/CT imaging. If not recognised, this can lead to false positive interpretation of the scan and incorrect staging of prostate carcinoma.

P695

Impact of 18F-choline PET-CT on management of patients with biochemical recurrence of prostate cancer

A. R. Teagle, A. Robinson, A. Nikapota, F. McKinna, S. Dizdarevic; Brighton and Sussex University Hospitals NHS Trust, Brighton, UNITED KINGDOM.

Introduction: Adenocarcinoma of the prostate is the most common cancer in men in the UK, accounting for 25% of all male cancers. Around 35% of patients will have a biochemical recurrence within 10 years after initial treatment. Detection of disseminated disease is important in order to determine the patient's suitability for local salvage versus palliative therapy. In many cases standard imaging methods such as MRI, CT and nuclear medicine bone scanning are insensitive, PSA levels needing to be over 20ng/ml in order to reliably detect disease. 18F-Choline positron-emission tomography-computed tomography (CH-PET-CT) has greater sensitivity in early detection of recurrence, even at PSA levels below 5ng/ml. The purpose of this study was to determine the impact of CH-PET-CT performed at our institution on management of patients with prostate cancer. Methods: This was a retrospective analysis of patients treated for prostate cancer who underwent CH-PET-CT at our institution between January 2014 and October 2014. Patient records, imaging and pathology results were collected. Questionnaires were sent to referring clinicians regarding the clinical indication for CH-PET-CT and its effect on subsequent management and outcome. ResultsTwenty-four CH-PET-CT scans were identified in 22 patients. After exclusions, 21 scans in 21 patients were included. Questionnaires were returned by referring clinicians in 90.5%. Fifteen scans (71.4%) were done to investigate possible recurrence in patients with rising PSA post-treatment. Four (19.0%) were done for clarification following equivocal or inconclusive conventional imaging; two (9.5%) were done for re-staging in patients with known nodal or other metastases. Positive findings of CH-PET-CT were reported in 15 patients (71.4%). In 11 cases (52.4%), CH-PET-CT confirmed findings of previous conventional imaging, and management plan was unaltered. In 10 cases (47.6%), management was altered, including beginning antihormonal therapy or chemotherapy for disseminated disease, radical radiotherapy or brachytherapy for localised disease, or observation in cases of negative CH-PET-CT. In 7 cases (33.3%), treatment intent was also changed due to CH-PET-CT result: palliative intent in 3 cases (14.3%), radical local therapy in 2 cases (9.5%), and active surveillance in 2 cases (9.5%). Conclusion: Choline-PET-CT has a significant

impact on management of patients with recurrent prostate cancer, leading to a change in therapy in almost half of our patient population. In future this may lead to more targeted treatment of such patients, with improvement in outcomes. Large prospective trials are needed to fully assess the impact of CH-PET-CT on management and subsequent patient outcomes.

P696

Preoperative Staging of Urinary Bladder Carcinoma by F-18 FDG PET/CT Using a Novel Protocol- A Prospective Study

Y. C. Lin, S. C. Tsai, J. Y. Li, W. Y. Lin; Taichung Veterans Hospital, Taichung, TAIWAN.

Aim: The use of 18F FDG PET imaging in bladder carcinoma has not been fully explored, mainly because the urinary excretion of 18F FDG interferes with visualization of the primary bladder tumor and regional lymph nodes. In this study, we established a patient-friendly 18F FDG PET/CT (PET) protocol and evaluated the diagnostic accuracy of 18F FDG PET/CT images in patients with urinary bladder carcinoma. Materials and methods: Twenty-three patients with newly diagnosed bladder cancer were enrolled in this study. PET scan was performed before operation. The PET scan was performed 40-60 minutes after the injection of 3.7 MBq/kg of 18F FDG. Immediately after the PET scanning, 10 mg of furosemide was given intravenously and the patients were encouraged to drink as much water as they can (but not compulsory) and urinate frequently after the 18F FDG injection. A delayed pelvic PET imaging was taken 3 hours after the 18F FDG injection and the patients were asked to void about 30 minutes before the end of the delayed imaging so the bladder could be refilled. Histopathologic results from the surgery were used as the gold standard. Results: Of the 23 patients, 3 patients received systemic chemotherapy instead of surgery because the PET images detected multiple metastases. 2 patients received TURBt only due to tumor in situ. 18 patients received radical cystectomy and regional lymph nodes dissection after PET images. The accuracy of PET images for primary bladder tumor and the N-stage were 100% and 83% respectively. The M-stage was correctly determined in 22/23 patients (95%) except 1 patient suspected of lung metastasis based on PET images was pathologically proved synchronous secondary lung adenocarcinoma. Overall, PET altered the TNM score in 9/23 patients (39%), the AJCC stage in 5/23 patients (22%), and treatment planning in 3/23 patients (13%). With our patient-friendly protocol, there's no patient felt urinary urgency during delayed images. Conclusion: PET/CT images proved to be more accurate in assessing the TNM-stage compared with conventional images and altered treatment planning in urinary bladder carcinoma. Our patient-friendly protocol, with drink at patients' will, low dose furosemide, and short bladder refilling time, is a feasible method of adequate urinary FDG clearance without adverse effect.

P697

First Clinical Experience Using a Cold Kit Based 68Ga-PSMA PET/CT for Recurrence Detection of Prostate Cancer

C. ARTIGAS, Z. WIMANA, G. GHANEM, B. VANDERLINDEN, P. FLAMEN; Institut Jules Bordet, Brussels, BELGIUM.

Introduction: Conventional imaging techniques are not accurate enough in order to detect prostate cancer recurrences in patients with biochemical relapse after radical treatment. 68Ga-PSMA-ligand PET/CT seems to be an excellent imaging technique to detect prostate cancer lesions in patients with biochemical relapse after radical treatment. However its use is still limited due to expensive equipment and lengthy procedures. To overcome these limitations, we used an original radiosynthesis method consisting in a kit prefilled with GMP lyophilized PSMA-ligand and additives able to chelate 68Ga3+ cathion at room temperature (ANMI S.A., Belgium). Material and methods: We present the preliminary results of the first clinical experience using a one-step cold radiosynthesis of 68Ga-PSMA-ligand. As part of an ongoing analysis, six patients with prostate cancer biochemical relapse after radical treatment and negative state of the art imaging techniques have been retrospectively analyzed [mean age 69 years (range (66-77)]. Mean PSA value was 5.1ng/ml (range 0.05-20). All patients received 68Ga- DKFZ-PSMA-11 produced using a one-step cold radiosynthesis. PET/CT images were performed under the same conditions in all patients: 2.5min/bed at 60min post-injection of 2MBq/Kg of 68Ga-PSMA-ligand. Physiological uptake was assessed by measuring SUVmean of the liver, spleen, salivary glands, parotid glands, kidneys and background activity (muscle and fatty tissue). Tumor-to-background ratios were also measured. Results: All patients showed pathological uptake in at least one lesion even with PSA values of 0.05ng/ml (100% detection rate). Two patients presented pathologic PSMA uptake in infracentimetric pelvic lymph nodes, two patients in the prostatic bed and two other patients in bone tissue. Mean tumor-to-background ratio was 24 (range 9-55.5). 68Ga-PSMA-ligand biodistribution was comparable to what has been published so far with intense uptake in kidneys and salivary glands and moderate uptake in liver, spleen, lacrimal glands and proximal small bowel. Physiological mean uptake in different organs were: liver SUVmean 4.2 (range 2.9-5.1); spleen SUVmean 6.1 (range 4.5-8.2); sub-maxillary gland SUVmean 12.2 (range 10.7-15.2); parotid gland SUVmean 11.5 (range 9-

12.5); kidney SUVmean 33 (range 27.9-41.7) and background SUVmean 0.26 (range 0.20-0.40).Conclusion:Preliminary data of the first clinical experience using a one-step radiosynthesis at room temperature of 68Ga-PSMA-ligand PET/CT in prostate cancer recurrence detection show promising results with very good detection rates and high tumor-to-background ratios. Biodistribution and physiological uptake are comparable to what has been published so far.

P698

11C-Methionine PET-CT for imaging of prostate cancer: preliminary results.

B. Padovano1, A. Lorenzoni1, A. Alessi1, N. Bedini2, S. Morlino2, C. Pascali1, C. Cucchi1, G. Serafini1, R. Valdagni2, F. Crippa1; 1Nuclear Medicine - PET Unit - Fondazione IRCSS Istituto Nazionale Tumori, Milan, ITALY, 2Radiotherapy Unit - Fondazione IRCSS Istituto Nazionale Tumori, Milan, ITALY.

Aim: 11C-Methionine (MET) PET-CT can be used for imaging of tumors with increased amino acid utilization. MET is manly used in neuro-oncology. Less frequently, other types of malignancy has been studied with this tracer and very few reports concern its utility in prostate cancer (Toth et al 2005 and Nunez et al. 2002). In this study, we present our preliminary results with MET PET/CT in patients (pts) with Prostate Cancer (Pca), most of them with radiological and/or biochemical diagnosis of cancer relapse. Materials and Methods: 24 consecutive Pca pts with Gleason score >7 (4+3), have been evaluated: 17 (71%) with biochemical recurrence (PSA mean value 7.2ng/ml), 5 (21%) with radiological diagnosis of local and/or distant metastases and 2 (8%) for staging of locally advanced disease. In fasting status, patients underwent a whole body PET/CT examination (from inguinal region to skull base; 4 min/bed), performed 30 minutes post-injections of a mean dose of 750-800 MBq of 11C-Methionine. MET PET-CT findings were correlated with other imaging modalities (CT and/or MRI), histological results of biopsied suspected lesions and/or mean clinical follow-up of 48 months. Results:MET PET-CT correctly identified the presence of disease in 16/24 pts (67%) (PSA mean value 13.3 ng/ml; range 0.74-73), detecting local recurrence in 9/16 (56%), local recurrence and distant metastatic disease in 3/16 (19%) and distant bone metastases in the remaining 4 pts (25%). MET PET-CT was negative in 7/24 (29%) pts. In 5 of them with PSA mean value of 1.1 ng/ml (range 0.6-1.8) also the other imaging tests (CT, bone scan and RM) were negative. In the other 2 pts positive biopsy of cancer relapse was obtained (PSA value 1.88 and 2.2 ng/ml).In one patient treated with radiotherapy (PSA value of 6.2 ng/ml), MET PET-CT showed an abnormal focal uptake in prostate lodge without confirmation of abnormal findings by other imaging modalities and during a follow-up of 60 months.Conclusions:According to our preliminary data, MET PET-CT might be used for imaging of prostatic cancer, as possible alternative to 11C or 18F Choline. This preliminary data have to be confirmed in a larger patient population.

P699

Cu-64 PSMA PET in Prostate Cancer

S. Mirzaei1, B. Grubmueller2, E. Capasso3, P. Knoll1, A. Floth4, C. Meleddu3, S. Shariat2, H. Klingler4; 1Institute of Nuclear Medicine with PET-Center, Wilhelminenspital, Vienna, AUSTRIA, 2Department of Urology, Medical University of Vienna, Vienna, AUSTRIA, 3U.O.C. Nuclear Medicine, Regional Oncological Hospital, Cagliari, AUSTRIA, 4Department of Urology, Wilhelminenspital, Vienna, AUSTRIA.

Aim: Prostate specific membrane antigen (PSMA) is overexpressed in most cases of prostate cancer. The aim of this study is to evaluate the possible role of Cu-64 PSMA PET in patients with prostate cancer.Patients and Methods: One patient with progressive local disease and fourteen patients (mean age 70 y, age range 51-91 y) with suspected recurrent disease were referred for PET imaging. PET images of the whole body were performed 1 and additional images of the pelvis 2 hours p.i. of mean 250 MBq Cu-64 DKFZ-PSMA-617 on a PET-scanner (Siemens, Exact, Knoxville).Results: In all, but three patient there was at least one focally enhanced Tracer accumulation suspicious for recurrent disease. The metabolic suspicious lesions were already visible in the one hour images. The patient with locally progressive disease showed only enhanced uptake in the prostate lobes and no nodal involvement.Conclusion: The preliminary results of this study demonstrate the potential of Cu-64 PSMA PET in patients with recurrent disease and in primary staging of selected patients with progressive local disease.

P700

Role of PET/CT with 18F-FDG in the staging of patients with localized or locally advanced bladder and urinary tract cancer

J. Duch, A. Montes, A. Domenech, C. Achury, G. Alfonso, G. Anguera, P. Maroto, I. Carrió; Hospital de la Santa Creu i Sant Pau, Barcelona, Barcelona, SPAIN.

Aim: Neoplasms of the urinary tract and bladder have a high rate of recurrence. Nodal and distant metastases are important prognostic factors, and abdominal CT is the standard technique for radiologic staging. The role of 18F-FDG PET/CT in these neoplasms as well as its role in the therapeutic

management are not well defined. Materials and methods: Between november 2010 and april 2015, patients with urothelial carcinoma potentially candidates for surgical treatment were retrospectively studied. All of them underwent abdominal CT as well as perioperative 18F-FDG PET/CT (before or after surgery). Staging was compared by both methods. We excluded patients with visceral metastatic involvement by CT, allowing patients in stage IV due to lymph node involvement. In our center, stage IV patients by lymph node involvement are treated with salvage surgery in case of good response to chemotherapy. Results: 48 patients were included. Median age was 68 years, 87,5% men. Location was bladder, urinary tract and urethra in 88%, 10% and 2%, respectively. Histology was transitional cell in 92%. Median follow-up was 9 months (1-30), mortality rate was 35% and median overall survival 20 months (15-25). 32 patients were operated (67%), being in these pathological stages: II (25%), III (25%) and IV (50%). Median time between abdominal CT and 18F-FDG PET/CT was 1,7 months (0,3-5,8). 3 18F-FDG PET/CT were performed after 1 cycle of chemotherapy. We found differences in staging between the 18F-FDG PET/CT and CT in 56% of cases (26). These changes implied a different strategy in 18 patients (37,5%): 10 patients (22%) considered candidates for pre-surgical chemotherapy (neoadjuvant or induction), received palliative chemotherapy because of detection of metastases in 18F-FDG PET/CT , avoiding in these cases a cystectomy which would have been indicated by the CT findings. In addition, in 8 patients who had been operated, PET detected persistent disease (3 loco-regional and 5 distance involvement). Thus, cystectomy could have been avoided in 5 cases if 18F-FDG PET/CT had been made prior to the surgery (10,4%). Conclusion: 18F-FDG PET/CT seems to provide additional information to abdominal CT, not only regarding the staging of tumors, but in terms of their prognostic and with therapeutic implications.

P701

18F-Fluorocholine PET/CT acquisition protocol in prostate cancer: the role of early acquisition of the pelvis in lesion detection rate

S. Capitanio, A. Gerali, G. Virotta, R. Rota, L. Madaschi, A. Bruno; Nuclear medicine Dept., A.O. Papa Giovanni XXIII, Bergamo, ITALY.

Aim: 18F-Fluorocholine (FCH) PET/CT is a widely used imaging technique in the evaluation of patients with prostatic cancer. However consensus concerning the best acquisition protocol has not been reached yet. Most authors propose the acquisition of early pelvic images before the standard whole body scan to better evaluate local disease. Our aim was to revise FCH PET/CT acquisition methodology, verifying whether early scan could provide additional information in staging of prostate carcinoma. Materials and Methods: We retrospectively evaluated 150 prostatic cancer patients who underwent FCH PET/CT in our centre and, among them, we selected 33 patients (mean age=70±7; mean PSA 15,72±11 ng/dl) with a biopsy proved but untreated carcinoma (mean Gleason score 7), within two months before the scan. All patients underwent a FCH PET/CT study according to the following protocol: early scan of the pelvis within two minutes after tracer injection (220±31MBq - 2 bed position of 2 min each) followed by a whole body scan 1 hour later, after bladder voiding. Early and late images were then compared in terms of detection rate of pathological findings. Semiquantitative analysis of lesions was performed by using the maximum standardized uptake value (SUV max). Results: Urinary activity appeared very quickly and was already present, at least partially, in all early images. A focal uptake within prostatic gland compatible with the presence of primary tumour was detectable in 23/33 (70%) patients at early and in 25/33 (75%) at late images. Actually, in two cases the presence of urinary activity prevented the evaluation of prostate at early scan, on the contrary the late acquisition showed a positivity. In 3 patients (9%) early scan showed an heterogeneous increased prostatic uptake in absence of an evident focus attributable to tumour site; the same pattern was confirmed at late scan.In the 23 subjects positive at both imaging, SUV didn't significantly change from early to late images (average SUV max 5.4±3.37 vs 5.08±2.43 respectively, ns).Among these 23 patients, both scans showed pathological pelvic lymph nodal uptake in 2 patients and skeletal pelvic metastasis in other two subjects, with slightly higher uptake values in delayed scans .Conclusion: These preliminary results do not support the need of early FCH scan of the pelvis in staging prostatic cancer. To this purpose, a delayed whole body imaging with an adequate bladder voiding could be sufficient and could limit radiation exposure.

P702

"Interpretation of 11C-choline PET/TC for the diagnosis of local relapse (LR) in radically treated prostate cancer (PCa)"

A. Matti1, G. M. Lima1, L. Zanoni1, C. Pultrone2, R. Schiavina2, F. Lodi1, S. Fanti1, C. Nanni1; 1S.Orsola-Malpighi Hospital, Nuclear Medicine Department, Bologna, ITALY, 2S.Orsola-Malpighi Hospital, Urology Department, Bologna, ITALY.

AIM: 11C-choline PET/CT is a widely-used tool for the diagnostic of PCa. In literature, a great variability of LR detection rate is reported. The aim of this study is to provide a positivity criteria for 11C-choline PET/CT detection of LR in patients

who had surgery for PCa and presented PSA failure. METHODS: 60 patients radically treated for PCa (radical prostatectomy ± RT ± HT after surgery) and presenting PSA failure (PSA levels at the time of the scan 0.2-16ng/ml, mean 8.1ng/ml) were retrospectively enrolled. Two of them were under HT at the time of the exam. In these patients 11C-choline PET/CT was used as the first imaging examination at the time of the detection of the PSA failure. Two Nuclear Medicine Doctors revised the 11C-choline PET/CT scans and defined by consensus if even mild focal uptake was present in the prostatic bed (PB) and bladder-urethral junction (BUJ), regardless the previous report results. The results were subsequently correlated with a clinical and radiological follow up (FU) of one to two year. TNM staging, Gleason score, PSA level at the time of the execution of the exam, RT and HT after surgery were considered as possible predictive variables. RESULTS: Overall, there have been described focal uptakes (from very low to mild) in the PB and BUJ in 22/60 patients (36,7 %). 11 of them were true positive (18.3 %), 11 false positive and 4 false negative (5.7 %) for LR, with a sensitivity of 73.3 % and a specificity of 75.6 %. Analysing the variables previously mentioned, it had been discovered a tight connection between the serum PSA level at the time of the exam and the positivity/negativity of the findings reported. In fact, most of true positive cases (10/11 patients) were associated with a PSA ≥ 1 ng/ml, while approximatly half of the false positive cases (5/11 patients) presented a lower serum level of PSA. In this evaluation the sensitivity is 66.7 % and the specificity is 86.7 %. The other variables (TNM staging, Gleason score, RT and HT after surgery) showed no influences on LR sensitivity. CONCLUSIONS: This study shows that if there is an even mild focal uptake in the PB and BUJ of patients who had surgery for PCa and presented PSArelapse ≥ 1 ng/ml, this finding must be reported, because there is a high possibility of an inital LR.

P703

The predictive value of 18F-Methilcholine PET/CT in metastatic castration-resistant prostate cancer patients treated with abiraterone acetate

P. Caroli, U. De Giorgi, L. Fantini, A. Moretti, R. Galassi, V. Conteduca, C. Lolli, G. Schepisi, E. Scarpi, D. Amadori, G. Paganelli, F. Matteucci; IRCCS IRST, Meldola, ITALY.

Aim: The role of 18F-Methilcholine positron emission tomography/computed tomography (18F-FCH-PET/CT) in patients with metastatic castration-resistant prostate cancer (mCRPC) has been demonstrated in recent years. In this study we analyzed the predictive value of functional parameters as Standard Volume Uptake (SUVmax) and total lesion activity (TLA) estimated with FCH-PET/CT in mCRPC patients treated with abiraterone therapy after chemotherapy. Methods: We prospectically studied 53 patients (mean age 73yrs; Gleason score &lt7 in 18 pts and >7 in 35 pts) with mCRPC. All patients, previously treated with docetaxel, were submitted to abiraterone acetate therapy (1,000 mg daily with prednisone 5 mg twice daily in continuous 28-day cycles). Before abiraterone treatment, 18F-FCH-PET/CT was performed in basal condition, 45 minutes after intravenous injection of 18F-Methilcholine (3,7 MBq/Kg of body weight, AAA-Advanced Application Accellerator, Ivrea, Italy). All patients were evaluated monthly for serological PSA response. For each lesion, we measured maximum standardized uptake value (SUVmax), metabolic volume activity (MV, i.e. volume of interest consisting of all spatially connected voxels within a fixed threshold of 40% of the SUVmax) and total lesion activity (TLA as the product of MV and mean standardized uptake value). We analyzed the sum of SUVmax (SSUVmax) and TLA (STLA) values up to a max of 10 lesions and, by univariate analysis, these data were correlated to PFS and OS. Results: The median value of PSA resulted 32 ng/ml (0,35-1812 ng/ml). 18F-FCH-PET/CT was positive in all pts: 29 patients with only bone lesions, 20 pts with both prostate, bone and lymphnodes, in 3 pts only lymphnodes metastasis and only 1 patients with visceral disease. The median value of SSUVmax was 68 g/ml (3,4-140,7 g/ml), while median value of STLA was 438400 (26159,4-757670,6). At univariate analysis, the median value of PSA and the absolute value of STLA showed a statistically significant correlation for both PFS and OS, while regarding to SSUVmax we found a statistically significant correlation only for PFS, considering either absolute values than median values ($p<0.013$). The analysis related to the median value of the TLA resulted statistically significant only for OS ($p<0.018$). Conclusions: Our data seemed to confirm the possible role of semiquantitative parameters of 18F-FCH-PET/CT as a prognostic tool in mCRCP pts.

P704

Incidental findings in 18F-choline PET/CT scans (FC) : an update on our series of 759 patients studied for prostate cancer (PC)

M. Rensi, F. Giacomuzzi, D. Capobianco, F. Di Gregorio, G. Ferretti, M. Povolato, **O. Geatti**; University Hospital SMM, Udine, ITALY.

Our aim is to present an overview of abnormal, unexpected sites of FC uptake, unrelated to PC, that are not rare and consequently must be kept in mind for correct scan interpretation. Methods: we analyzed 759 consecutive FC scans, done in pts with prostate cancer, in the large majority for restaging following a biochemical relapse and in few cases for staging of advanced disease. Results: we found 220 abnormal PET findings

(29 %) not corresponding to PC localizations, which were related to:1. inflammation in 165 cases and were located in:• mediastinal, cervical and inguinal lymph nodes (127 cases), of which 1 was due to sarcoidosis• pulmonary thickening (35 cases), highly suspicious for pneumonia• muscular abscesses (3 cases)2. benign nodular diseases in 32 cases, of which:• 31 adenomas (16 of the thyroid, 13 of the adrenal and 2 of the parathyroid glands)• 1 liver haemangioma3. malignant disease in 13 cases, of which:• 4 located in the lungs (3 adenocarcinomas and 1 bronchioloalveolar carcinoma),• 6 in the liver, all were HCC,• 2 were colorectal cancers,• 1 was a lymphoma4. Paget disease (4 cases), all had high bone uptake, and was correctly interpreted owing to the corresponding CT abnormalities which were not suggestive of metastases; histology confirmed later5. SNC diseases (4 cases), 3 were meningiomas and 1 had a recent cortical stroke6. miscellaneous (2 cases), 1 was a hyperplastic bone marrow in chronic myeloid leukemia and 1 had a head injury. Conclusion: FC is largely used to study PC patients, as it is more sensitive than 18F-FDG, but we must emphasize that this does not mean that the radiopharmaceutical is specific for such a neoplasm.This must be kept in mind, as in fact in almost 30% of patients, fluorocholine can concentrate in different kinds of diseases as well, which in the majority of cases are related to inflammations and benign nodular diseases, although malignant ones cannot be excluded.

P705

Correlation Between GRP Receptor Expression and Pathological and Clinical Characteristics in Radical Prostatectomy Specimens

I. L. Bakker, G. J. L. H. van Leenders, E. de Blois, M. Busstra, A. C. Fröberg, W. M. van Weerden, M. de Jong; Erasmus MC, Rotterdam, NETHERLANDS.

AIM: Prostate cancer (PC) is diagnosed by pathological evaluation of biopsy samples. Transrectal ultrasound (TRUS)-guided biopsies have disadvantages, as around 30% of the time PC is missed at the first biopsy procedure, and they provide little information about the extent of disease, a crucial parameter for patient management. MRI of PC enhances biopsy sensitivity, but only when a multi-parameter MRI is evaluated by a trained prostate MRI-expert. An alternative imaging technique to optimise the detection of PC including lymph node status, thereby supporting the selection of those patients who would benefit most of biopsy, is strongly desired. We have recently initiated a trial using Gastrin releasing peptide receptor (GRPr) targeting to detect primary PC, and the first data look very promising. GRPr is highly expressed in PC, and has low expression in benign prostate hyperplasia (BPH) and prostatic intra-epithelial neoplasia (PIN). Since detailed information on GRPr expression and its correlation to tumour localisation and volume, stage of disease, Gleason score and prostate specific antigen (PSA) levels is scarce, we initiated a site study using retrospective radical prostatectomy specimen to investigate this in more detail.MATERIALS AND METHODS: Frozen samples of 33 patients with different Gleason scores and PSA levels were selected from the Erasmus MC biobank. Iodine-125-Tyr4-bombesin autoradiography was performed on frozen prostatectomy slices. HE staining, AMACR and 34betaE12 immunostaining were performed on adjoining sections to evaluate tumour localisation and volume. AMACR is a sensitive and relatively specific staining for PC. Staining with 34betaE12 detects prostatic basal cells that are absent in PC. A pathologist evaluated all stainings. Autoradiography images were classified as high, intermediate, low or no GRPr expression compared to a standard of a cytospin of 150,000 PC3 cells with high GRPr expression.RESULTS: To date, we have obtained and evaluated full datasets of three patients, the study is still on going. PC tissue sections showed high or intermediate expression of GRPr, normal prostate and BPH showed low or no GRPr expression. Autoradiography showed good correlation with tumour demarcation as determined by classic histological staining. A clear relationship between autoradiographic classification, tumour localisation and tumour volume, could be observed.CONCLUSION: GRPr imaging is only observed in PC with no detection in BPH, PIN or normal prostate tissue. This observation suggest that GRPr imaging may be a valuable asset to detect low Gleason PC tumours, which resemble normal tissue, that might be missed on MRI or TRUS imaging.

P706

Correlation between detectability with 18F-Choline PET/CT in biochemical relapse after therapy and the risk parameters at initial diagnosis with prostate cancer

J. J. Robles-Barba1, C. Gámez-Cenzano1, J. L. Vercher-Conejero1, A. Sabaté-Llobera1, M. Cortés-Romera1, L. Rodríguez-Bel1, L. M. Gràcia-Sánchez1, I. Romero-Zayas2, M. Roca-Engronyat3, E. M. Merino-Serra4, A. M. Ferrer-Artola5, A. Ferrer-González6, J. Pera-Fábregas7, A. Arellano-Tolívar8, J. F. Suárez-Novo6; 1PET-CT Unit, Institut de Diagnòstic per la Imatge (IDI). Bellvitge Hospital., L'Hospitalet de Llobregat, SPAIN, 2Radiofarmacia, Institut de Diagnòstic per la Imatge (IDI). Bellvitge Hospital., L'Hospitalet de Llobregat, SPAIN, 3Radiofarmacia. Bellvitge Hospital., L'Hospitalet de Llobregat, SPAIN, 4Servicio de Radiología. Institut de Diagnòstic per la Imatge (IDI). Bellvitge Hospital., L'Hospitalet de Llobregat, SPAIN, 5Farnacia. Bellvitge Hospital., L'Hospitalet de Llobregat, SPAIN, 6Unidad Funcional de Próstata. Bellvitge Hospital., L'Hospitalet de Llobregat, SPAIN, 7Braquiterapia. Institut Català d'Oncología.,

L'Hospitalet de Llobregat, SPAIN, 8Oncología Radioterápica. Institut Català d'Oncología., Badalona, SPAIN.

AIM: To assess the detection rate and recurrence location with 18F-Choline PET/CT in biochemical relapse of prostate cancer, in correlation to risk parameters at initial diagnosis (TNM staging, initial PSA and D'Amico classification). MATERIAL AND METHODS: Retrospective study of 75 patients (age range 47 - 82 y.o.), previously treated of prostate adenocarcinoma with curative intention that presented biochemical relapse (PSA range: 2'5 250 ng/mL). The PET/CT protocol included one early dynamic acquisition (1min x 8) of the pelvis immediately after the e.v. administration of 370MBq of 18F-Choline, and one late whole body static acquisition. PET results were classified as "negative" or "positive"with 3 patterns of recurrence: 1) local (exclusively prostatic bed), 2) pelvic nodes and 3) distant metastasis. The positive results were correlated with TNM staging, PSA and D'Amico classification at the moment of initial diagnosis. RESULTS: The global detection rate was 79% (59/75). In positive studies the patterns of recurrence were local in 24 patients (41%), nodal in the pelvis in 22 (37%) and metastatic in 13 (22%), predominantly in retroperitoneal nodes and bones. Patients that presented metastases showed a higher incidence of T ≥3 in TNM (7/13, 54%), Gleason ≥8 (6/13, 46%) and high risk in D'Amico classification (10/13, 77%). Most patients with negative PET (75%) showed initial PSA < 10. CONCLUSIONS: The detection rate of recurrence of prostate cancer with 18F-Choline PET/CT in patients with biochemical relapse seems to correlate with the initial risk classification: a higher risk in initial parameters such as TNM staging, Gleason or D'Amico classification seems to be associated with more detection of distant metastasis.

P707

The diagnostic value of PET/CT imaging with the 68Ga-labelled PSMA ligand HBED-CC in the diagnosis of prostate cancer

E. Akdemir1, **M. Tuncel**1, M. Ç. Tuncalı1, C. Y. Bilen2, F. Akyol3, D. Baydar4, H. Özen2; 1Hacettepe University, Department of Nuclear Medicine, ANKARA, TURKEY, 2Hacettepe University, Department of Urology, ANKARA, TURKEY, 3Hacettepe University, Department of Radiation Oncology, ANKARA, TURKEY, 4Hacettepe University, Department of Pathology, ANKARA, TURKEY.

Aim: PET-CT imaging with 68Ga-PSMA-HBED-CC, has become the radiotracer of choice for detection of prostate cancer(PCa). However the diagnostic value of this method is yet to be determined in different patient populations. The aim of this study was to analyse the diagnostic value of 68Ga-PSMA-ligand PET-CT in comparison with conventional imaging(CI)& clinical dataMaterials and Methods: Thirty-two consecutive patients (age median:72±14) suffering from PCa were referred to 68Ga-PSMA-ligand PET-CT for staging(6) and restaging(26) purposes. Among these patients 6/32(19%) had no therapy prior to PETscan wheras 4/32(12%) had PSA relapse after radical prostatectomy, 5/32(16%) had hormonotherapy, 5(16%) had chemotherapy plus hormonotherapy and 12 (37%) had radiation therapy plus hormonotherapy. All patients underwent whole body 68Ga-PSMA-ligand PET/CT 1 hour after i.v injection of 129 MBq 68Ga-PSMA-HBED-CC. Delayed images were also taken from the site of involvement after 2 hours. The results of PET-CT were compared with CI(7 MRI and 25 contast enhanced CT) and correlation with clinical factors like prostate-specific antigen(PSA) level at the time of PET scan(PET-PSA), PSA doubling time(DT),PSAvelocity, PSAslope and Gleason score(GSC) were investigated. Tumor index(TI, SUV meanx volume of malign lesions) that represents whole body tumor burden was also calculated for each patient.Results In 82% of the patients at least one lesion indicative of PCa was detected. Tumor detection showed moderate positive correlation with PSAslope and moderate negative correlation with DT(Spearman's rho correlation coefficient(SCC): 0,409,p:0,019 and -0, 402 p:0,017 respectively) whereas there was no statistically significant correlation with PSAvelocity, GSC and PET-PSA (p:0,7 and 0,2 and 0,27 respectively). Altough not statistically significant there is a slight decrease in the meanSUVmax of malign lesions in the delayed phase 23±31 vs 15,9±19(p:0,18). 68Ga-PSMA-ligand PET-CT detected more malign lesions than CI. Among the 78 malign lesions (prostate: 16/78 (20%), bone metastases: 5/78 (6%) and lymph node 57/78 (73%)) not detected by CI lymph node metastases were prominent with median SUVmax of 10±22 (range:2-96) and median size of 8±2,5 (range:3-14). TI was positively correlated with detection rate of PET-CT, PET-PSA and GSC (SCC: 0,643, 0,47 and 0,48 p:0,005 respectively) but not correlated with DT, PSAvelocity and PSAslope (p>0.05)Conclusion: 68Ga-PSMA-ligand PET/CT can detect recurrent PCa in high number of patients. Tumour detection was positively correlated with PSAslope wheras negative with DT. Detection of lymph node metastases was the most prominent superiority of 68Ga-PSMA-ligand PET-CT over CI. TI is a good representative of tumor burden and better correlated with PET-PSA.

P708

Lung uptake of Fluorine-18 Fluoroethyl-Choline PET-CT in patients with recurrent prostate cancer: a first retrospective analysis.

D. A. Pizzuto1, C. Caldarella1, S. Annunziata1, F. P. Ieria1, M. A. Isgrò2, A. Del Ciello3, V. Rufini1, A. Giordano1; 1Institute of Nuclear Medicine, Department of Radiological Sciences. Catholic University of Sacred Heart, Rome, ITALY, 2Institute of General Pathology. Catholic University of Sacred Heart, Rome, ITALY, 3Institute of Radiology, Department of Radiological Sciences. Catholic University of Sacred Heart, Rome, ITALY.

Background/aim: Presence of metastatic spreading to the lungs is a well known negative prognostic factor in patients with prostate cancer (PC). Fluorine-18 Fluoroethyl-Choline (18F-FeCh) PET-CT is a reliable diagnostic tool in restaging PC patients with biochemical failure ongoing androgenic deprivation therapy (ADT). Aim of the study is to assess the role of 18F-FeCh PET-CT in the evaluation of lung lesions occurring in patients with recurrent PC and to explore the role of Gleason-Score (GS) and common biochemical markers in predicting metastatic spreading to the lungs. Materials and Methods: We retrospectively evaluated the scans of 963 patients ongoing 18F-FeCh PET-CT for PC between May 2010 and July 2014. Inclusion criteria were: histologically confirmed diagnosis of PC; finding of lung lesion with 18F-FeCh uptake. Data concerning GS at diagnosis, "trigger" PSA (PSAtr), PSA doubling time (PSAdt), PSA velocity (PSAvel) and ongoing ADT were collected when available. PET-CT findings were confirmed by histology or follow-up (FU) and classified as follows: inflammation, primary lung cancer or metastases from tumour other than PC, and metastases from PC. Results: The retrospective evaluation identified 28 patients with lung lesion with 18F-FeCh uptake; histology or FU data were available in 22/28 patients (78.5%). Inflammation, primary lung cancer or metastases from tumour other than PC, and metastases from PC were found in 4 (18.2%), 4 (18.2%) and 14 (63.6%) patients, respectively. PSAdt was found to be significantly (p=0.029) shorter in patients with lung metastases from PC (median PSAdt 1.7 months, interquartile range [IQR] 1.5 - 4.1 months) than in patients without lung PC relapse (median PSAdt 6.7 months, IQR 3.9 - 7.8); PSAvel was found to be significantly (p=0.019) higher in patients with lung metastases from PC (median PSAvel 3.2 ng/ml/month, IQR 0.65 - 6.65 ng/ml/month) than in patients without lung PC relapse (median PSAvel 0.3 ng/ml/month, IQR 0.2 - 0.5 ng/ml/month). Patients with evidence of lung metastases from PC had significantly (p=0.008) higher GS at diagnosis than patients with primary lung cancer or metastases from tumour other than PC, and inflammation. No significant differences were found in PSAtr between the three groups of patients. Conclusion: As far as we know this is the first evidence that 18F-FECh PET-CT is a useful tool in detection of lung metastases in patients with PC. GS at diagnosis and biochemical markers are good predictive factors of metastatic spreading to the lungs.

P709

18F-FACBC PET/CT for the detection of recurrence in patients radically treated for prostate cancer with biochemical relapse: preliminary accuracy data.

L. Zanoni1, R. Schiavina2, C. Pultrone2, C. Pettinato1, C. Fonti1, S. Semini1, S. Boschi1, M. Ferrari3, P. Rigatti3, E. Brunocilla2, G. Martorana2, S. Fanti1, C. Nanni1; 1Nuclear Medicine, University Hospital Sant'Orsola-Malpighi, Bologna, ITALY, 2Urology, University Hospital Sant'Orsola-Malpighi, Bologna, ITALY, 3Urology, Italian Institute for auxology, Capitanio Hospital, Milan, ITALY.

AIM: To compare the accuracy of 18F-FACBC and 11C-Choline PET/CT in patients (pts) radically treated for prostate cancer (PCa) presenting with biochemical relapse (BR). MATERIALS AND METHODS: 100 pts, radically treated for PCa and presenting with rising PSA, were consecutively and prospectively enrolled. 11 pts dropped-out. 89 pts were included in the analysis: all pts with BR after radical-prostatectomy (RP) (at least 3 months before), 11C-Choline and 18F-FACBC PET/CT performed within one week, out of hormonal therapy at the moment of the scans. SUV max and Target to Background Ratio (TBR), were used to aid the visual analysis. TBR ≥1,5 was considered significant. Sensitivity, specificity, positive-predictive-value (PPV), negative-predictive-value (NPV), accuracy were calculated for both tracers; urological follow-up of at least 1 year (PSATrend, imaging, and when possible, histo-pathology) was considered as standard of reference. RESULTS: Pts characteristics (89 pts).Age: mean 69 y, range: 55-83. PSATrigger: mean 2,95;median 1,48;range 0,20-20,72;sd 3,9. PSAdoubling-time (months): 74/89 pts;mean 8,5;median 3,9;range 0,4-120,2;sd 16,2;PSAVelocity (ng/ml/yr):mean 5;median 2;range 0-49,2;sd 8,1 (available in 74/89 pts).Treatment after RP: 23 only HT; 12 only RT; 28 RT+HT. GleasonScore: 12 pts ≤6; 33 pts 7; 32 pts 8-10; 12 pts not available (n/a). TNM: 1 T1c, 17 T2, 59 T3, 27 N0, 39 N1, 11 Nx (12 n/a). Patient-based analysis.51 pts resulted negative and 25 positive with both tracers, 8 positive with FACBC but negative with Choline, 5 positive with Choline but negative with FACBC. Overall 49 pts turned out false negative(FN), 2 true-negative(TN), 24 true-positive(TP) and none false-positive(FP) with both tracer; 1 FN Choline but FP FACBC (lymph-node, LN); 7 FN Choline but TP FACBC (5 LN; 1 BONE; 1 local relapse-LR); 1 FP Choline (LN) but TP FACBC (LR); 2 FP Choline (1 LN; 1 LR) but FN FACBC; 3

TP Choline (2 LN; 1 BONE) but FN FACBC. The sensitivity resulted 32% with Choline versus (vs) 37% with FACBC, specificity 40 vs 37, accuracy 33 vs 38, VPP 90 vs 97, VPN 3 vs 4. Psa-analysis. When pts were divided by PSA level, TP (%) were generally superior with FACBC compared to Choline: 28 pts <1 (ng/ml): 21% vs 14%; 28 pts 1≤x<2: 29% with both tracers; 11 pts 2≤x<3: 45% vs 36%; 22 pts ≥3: 59% vs 50%. CONCLUSION: FACBC can be considered an alternative tracer of Choline in the setting of pts with BR after RP. Further subgroup/region/semi-quantitative analyses are ongoing to confirm these preliminary results.

P710

18F-Choline PET/CT and prostatic gland/fossae recurrence: what can help to identify the local recurrence of disease?

L. Evangelista1, M. Cimitan2, M. Hodolic3, T. Baseric2, A. Cervino1, J. Fettich3, G. Saladini1, E. Borsatti2; 1Istituto Oncologico Veneto I.R.C.C.S., PADOVA, ITALY, 2IRCCS National Cancer Institute (CRO), Aviano, ITALY, 3University Medical Center Ljubljana, Ljubljana, SLOVENIA.

Purpose. We aimed to determine when 18F-Choline PET/CT can truly identify the presence of local prostate recurrence of disease.Materials and methods. From a multicenter collection of 1030 patients who underwent PET/CT with 18F-Choline for the recurrence of disease, we selected only with a positive 18F-Choline uptake in prostatic gland or prostatic fossae. One-hundred thirty-one patients (12.7%) had a positive uptake of 18F-Choline in the prostatic gland/fossae. Median age was 72 years (range: 48-87 years) and the median PSA level at the time of PET/CT scan was 4.41 ng/mL (0.22-18.13 ng/mL). Moreover, 45 patients (34.4%) had a gleason score (GS) >7 and the residual subjects had a GS≤7. The assessment of true or false positive findings was verified by magnetic resonance imaging and/or biopsy. A chi-square test and a Z Kolmogorov-Smirnov test were used to assess the correlation between clinical variables and PET/CT findings.Results. Positive findings at PET/CT were confirmed by MRI and/or biopsy in 75 cases (57%). In particular, PET/CT resulted truly positive (TP) in 59 patients (79%) and falsely positive (FP) in 16 subjects (21%). The median value of PSA at the time of PET/CT scan was higher in TP as compared to FP, although not statistically significant (4.76 vs. 3.04 ng/mL, p= 0.852). Similarly, median age, GS categories and the type of therapy was similar between two groups (p= 0.688, 0.689 and 0.427, respectively). However, matching GS categories and PSA values, we found that the rates of TP were higher in patients with a PSA>2 ng/mL independently from the GS (ranged between 74 and 92%). Conversely, the rates of FP were ranged between 50 and 65% in patients with a PSA≤2 ng/mL, especially in case of GS≤7, but it was around 25% in those with a GS>7 and PSA>2ng/mL.Conclusion. PET/CT with 18F-Choline has some limitation for the evaluation of prostatic gland/fossae, due to the physiological biodistribution of the radiopharmaceutical agent. However, in in 70-90% of patients with a PSA level>2 ng/mL, independently from the GS, a focal 18F-Choline uptake could be compatible with a local recurrence.

P42 - Tuesday, October 13, 2015, 4:00 PM - 4:30 PM, Hall 3 – Poster Exhibition

Clinical Oncology: Gynaecological

P711

Sentinel Node in Endometrial Cancer. Our Experience

C. Escabias del Pozo, I. Santos Gomez, M. Diestro Tejeda, S. Rodado Marina, M. Coronado Poggio, M. Orduña Diez, M. Marin Ferrer; Hospital Universitario La Paz, Madrid, SPAIN.

AIM: Detection and validation of sentinel lymph node (SLN) in patients with early stage endometrial cancer in our hospital. MATERIALS AND METHODS: Prospective study from February 2012 to October 2014, 58 patients (p) with mean age 66 (40-87), diagnosed of endometrial cáncer (50p endometrioid, 2p clear cell, 3p serous, 3p carcinosarcoma) FIGO (Federation of Gynecology and Obstetrics) stage I - II. Four cervical injections of 1 ml technetium colloid (37 MBq each) at 3 and 9 o´clock positions (superficial and deep) were given the day before surgery. Scintigraphic images were obtained 30 min and 2 hours after the injections and SPECT-CT was obtained after scintigraphic images. Patent blue was injected intracervically after induction of anesthesia and before surgery. SLN were analysed by OSNA (One Step Nucleic Acid Amplification). False negative was defined as positive non-SLN with negative SLN. RESULTS: No complications ocurred after injection of technetium colloid. The total numer of SLN visualised was 100. SLN scintigraphic detection rate was 98%. Paraortic SLN were detected in 1p (2%). The SLN was bilateral in 34p (59%). No anaphylactic reactions were noted after patient blue injection. SLN were removed laparoscopically in all patients. SLN was positive in 7p (12%). There were 3 falses negatives (5%), 2p in paraortic área and 1p in pelvic área. CONCLUSION: The cervical injection is associated with a high SLN detection rate and low detection in paraortic área. Larger prospective series are needed before considering its incorporation in the standard management of endometrial cáncer.

P713

Dual-time FDG-PET/CT imaging in suspected ovarian cancer

M. H. Vilstrup1, G. Neumann2, J. T. Asmussen3, O. Gerke1, A. Alavi4, P. Høilund-Carlsen1; 1Department of Nuclear Medicine, Odense University Hospital, Odense C, DENMARK, 2Department of Obstetrics and Gynecology, Odense University Hospital, Odense C, DENMARK, 3Department of Radiology, Odense University Hospital, Odense C, DENMARK, 4Division of Nuclear Medicine, Department of Radiology, University of Pennsylvania, Philadelphia, PA, UNITED STATES.

Aims: The clinical value of 18F-fluorodeoxyglycose (FDG) positron emission tomography (PET)/computed tomography (CT) in ovarian cancer diagnosis and/or staging has not yet been established. PET/CT has shown improved staging accuracy but also significant overlap in standardized uptake value (SUVmax) in benign and malignant lesions. We wanted to investigate if dual-time PET/CT imaging could increase the diagnostic accuracy of ovarian cancer FDG-PET/CT. Materials and methods: Thirty-four patients with suspected ovarian cancer underwent preoperative 1h and 3h 18F-FDG-PET/CT including diagnostic CT with contrast (immediately after the 3h PET). The maximum standardized uptake value (SUVmax) for both time points (SUVmax1 and SUVmax3) was determined, and the retention index (RI) was calculated as (SUVmax3 - SUVmax1)/SUVmax1. Histopathology was used as reference. Results: Fourteen had ovarian cancer (9 serous, 1 mucinous, 1 endometrioid and 3 clear cell carcinoma). Five patient cases were borderline (3 serous, 2 mucinous). Fourteen had benign lesions (fibroma, cystadenoma and endometriosis) or other non-ovarian malignancies (1 colon cancer, 1 endometrial cancer, 1 uterine sarcoma, and 1 marginal zone lymphoma). One patient was diagnosed with both ovarian cancer and a synchronous colon cancer. PET/CT clearly differentiated between malignant and benign ovarian lesions in both 1h and 3h PET. Thus, the median SUVmax1 in malignancy was 13.3 (range 4.6-22.8; [95 % CI 11.5-16.6]), the median SUVmax3 was 21.4 (5.5-29.7; [17.5-24.3]), and the median RI was 0.46 (0.15-1.16; [0.35-0.66]) compared to the following median values in benign lesions: SUVmax1 3.2 (range 1.6-8.7; [2.6-4.9]), SUVmax3 4.7 (1.3-9.3; [3.2-5.9]), and RI 0.11 (-0.48-1.00; [0.00-0.51]). The mucinous carcinoma had the lowest SUVmax1/SUVmax3/RI values (4.6/5.5/0.2) among the cancers. Borderline lesions had still lower median values: SUVmax1 3.1 (range:1.3-6.1; [1.6-4.9]), SUVmax3 4.2 (1.5-7.8; [1.6-4.9]), and RI 0.28 (0.15-1.2; [0.03-0.81]) overlapping the (above listed) values in benign lesions. Conclusion: SUVmax1, SUVmax3 and RI values obtained by 18F-FDG PET/CT in our material of suspected ovarian cancers clearly differentiated malignant from benign ovarian lesions at both 1h and 3h imaging. Though, for RI to a lesser degree than SUV measurements. However, SUVmax and RI values could not differentiate borderline from benign lesions. Adding a 3h PET/CT did not seem to add further diagnostic information in our small group of patients.

P714

Neoadjuvant treatment in advanced cervical cancer: can 18F-FDG PET/CT be predictive of response?

P. Mapelli1, F. Fallanca1, A. Bergamini2, A. Dell'Acqua2, G. Mangili2, E. Rabaiotti2, E. Incerti1, M. Candiani2, L. Gianolli1, M. Picchio1; 1Nuclear Medicine Unit, IRCCS San Raffaele Scientific Institute, Milano, ITALY, 2Gynecology Department, San Raffaele Scientific Institute, Milano, ITALY.

Aim. The aim of the present study was to evaluate the possible predictive role of 18F-FDG PET/CT in predicting response to neoadjuvant treatment in patients with advanced cervical cancer (CC). Materials and Methods. This study included 9 patients with advanced cervical cancer who underwent to 18F-FDG PET/CT before and after neoadjuvant treatment (chemotherapy: n=5; chemoradiotherapy: n=4). Semiquantitative and quantitative measurements have been performed to assess treatment response; specifically, maximum standardized uptake value (SUVmax) and metabolic tumour volume with a threshold of 60 (MTV60) of the primary tumours were measured on baseline and post-treatment scan, to investigate their possible predictive role regarding therapy response. Results. The median age at baseline PET/CT was 47 years (range: 35-68) and the median time interval between baseline and post neoadjuvant treatment scans was 2.7 months (range: 1.7-8). Comparing the baseline and the post treatment scans, 6/9 patients showed response to therapy, while 4/9 patients showed stable disease or progression after neoadjuvant treatment. The mean and median SUVmax of the primary tumour were 15.6 and 12.2 (range 3.7-35.5) and 7.9 and 11.3 (range 2.8-4.1) for the baseline and post-treatment scan, respectively. Considering all patients, the average percentage change in SUV max between baseline and post treatment scan was 21.9 (range: -102.7 - 79.4). Interestingly, baseline mean and median SUVmax of the primary tumour were higher (19.3 and 19.15; range: 3.7-35.5) in patients that experienced no response or progression after neoadjuvant treatment compared to those patients who showed response to treatment (13.1 and 11.3; range: 8.3-25.3). The mean and median MTV60 (mm3) of the primary tumour were 14 and 10.2 (range 3.1-56.4) and 7.6 and 4.7 (range 0.7-34.8) for the baseline and post-treatment scan, respectively. Considering all patients, the average percentage change in MTV60 between baseline and post treatment scan was 22.2 (range: -454.4 - 98.6). Strikingly,

baseline mean and median MTV60 of the primary tumour were lower (9.05 and 8.95; range: 3.1-15.2) in patients that experienced no response or progression after neoadjuvant treatment compared to those patients who showed response to treatment (17.3 and 10.2; range: 5.8-56.4). Conclusion. Although not reaching statistical significance, probably due to the low number of patients included in the present cohort, the reported results of this preliminary study should be taken into account because the strong difference of SUVmax values and MTV60 between responders and non-responders patients which may be relevant for patients' treatment decision-making, if confirmed in larger populations.

P715

Is multimodality, multiparametric MRI complementary or superfluous to PET-CT in the management of Pelvic malignancies?

S. Raja1,2, M. S. Qureshi2, S. George3, A. S. Aldosary2; 1Baylor College of Medicine, Bellaire, TX, UNITED STATES, 2KFMC, Riyadh, SAUDI ARABIA, 3Johns Hopkins Aramco Healthcare, Dhahran, SAUDI ARABIA.

Contemporary management of common pelvic malignancies (pelMalig) demands a multimodality (CT, MR, US) imaging approach to document tumor grade, stage and metastatic spread. However, conventional MR [(cMR): T1-W, T2-W etc.] is limited in grade prediction, evaluation of loco-regional and distant metastasis. PET is recommended for post therapeutic evaluation and restaging. Recently, advanced MR (aMR) especially Diffusion Weighted Imaging (DWI) and ADC mapping is being utilized as a complementary tool to cMR. We explored the complementary roles of multimodality FDG-PET and multiparametric MR in the workup of pelMalig.Methods: On retrospective chart review, we identified 20 pts with suspected pelMalig having concurrent (+/3 months) FDG-PET and aMR. The pt. demographics were [male=5, female=15; mean age=51 (range=27-80 yrs)]. All PET and MR were acquired with routinely accepted protocols. PET and MR images were qualitatively reviewed by experienced physicians. SUV and ADC were obtained by ROI analysis of coregistered FDG-PETand ADC maps.Results: All lesions but one, were concordantly pos. (18/20) or neg. (2/20) on PET and MR, in 1 pt. both were indeterminate. MR was pos. for pelvic lymph nodes in 14/20 pts, while only 7/14 were pos. by PET; in 6 pts. both were concordantly neg. While MR was suggestive of lympho-vascular space (mesorectal fat and parametrium) involvement in 7/20 pts., only 1/20 was pos. on PET. PET and MR were helpful in confirming suspicious lesions on MR (2) and PET (2). In 2 pts. MR was helpful in precise localization of hypermetabolic foci noted on PET-CT, while PET demonstrated more extensive lymphadenopathy outside the MR FOV in 4 pts. Correlation of lesional SUVmax and minADC revealed a modest negative correlation (higher the SUV lower the ADC), but not statistically significant.Discussion: Our study is limited by a small sample size, and includes a mixture of pelvic malignancies. FDG-PET as compared to aMR was not helpful in evaluating the lymphovascular space. MR was superior to PET for pelvic lateral wall lymphadenopathy while PET detected more extensive metastatic lymphadenopathy. Though not strong, a neg. trend of higher the SUV on PET lower the ADC on MR was observed.Conclusion: Concurrent aMR and PET appears to be complementary and not superfluous, providing incremental value. Prospective analysis in a larger series is warranted.

P716

Impact of PET-CT on the follow-up of patients with cervical and ovarian cancers

S. Carrilho Vaz, Â. Silva, R. Sousa, T. C. Ferreira, P. Ratão, A. Daniel, I. P. Carvalho, F. Brandão, L. Salgado; Portuguese Institute of Oncology – Lisbon Center, Lisbon, PORTUGAL.

AIM: To evaluate the usefulness of PET-CT in re-staging and follow-up of patients (pts) with cervical and ovarian cancers after primary treatment.MATERIALS AND METHODS: A single-center retrospective study was performed. All the pts with cervical (n=17) or ovarian (n=19) cancer who performed 18F-FDG PET-CT in our department between January-December 2014 were included. The mean age was 59 years (22-81).The histology of cervical cancers was: squamous cell carcinomas 12/17 (71%); adenocarcinoma 4/17 (23%) and glassy cell 1/17 (6%). According to FIGO (7th edition), pts staging was: stage I - 4; II - 10 and III - 3. Considering ovarian cancer (n=19), the histology was serous 15/19 (79%) and borderline tumor 4/19 (21%) and the FIGO staging was I - 3; II - 6; III - 5 and IV - 5.The mean follow-up was 8 months.We present the preliminary results of one year study.RESULTSThe reasons for asking a PET-CT in pts with cervical cancer was suspicion of loco-regional recurrence - 9/17 or distant metastasis - 8/17. In pts with ovarian cancer the reasons were increased tumor markers - 8/19, suspicion of metastases - 10/19 or chemotherapy response evaluation - 1/19.Considering PET-CT results of pts with cervical cancer we verified that it changed staging in 6/17 (35%): 12% upstaging and 23% downstaging, with consequent treatment modification. In pts with ovarian cancer, we found that PET-CT changed staging in 6/19 (32%): 11% upstaging and 21% downstaging, therefore, it had impact on therapeutic decision. Furthermore, PET-CT confirmed suspected distant metastases in 1 pt with cervical cancer and in 3 pts with ovarian cancer, confirming stage IV disease.PET-CT identified polimetastatic unknown disease in 2 pts with cervical cancer (included in

upstaged pts) and in 7 pts with ovarian cancer (not changing stage in 3 pts, upstaging in 2 pts and confirming suspected metastases in other 2 pts).In 2 pts with ovarian cancer, PET-CT identified focal breast uptake that was confirmed as breast carcinoma.The false positive rate was 6% in the examinations of pts with cervical cancer and 11% in pts with ovarian cancer.CONCLUSION: Although the analyzed group is small, this preliminary results show that PET-CT is useful in re-staging and follow-up of pts with cervical and ovarian cancers. It changed staging and had impact on therapeutic decision in 32-35% of cases.PET-CT has an important role when loco-regional disease recurrence or distant metastases are suspected.

P717

18F-FDG PET-CT in Ovarian Cancer: Can We Identify the More Aggressive Histologies?

B. González García1, M. E. Bellón Guardia2, M. P. Talavera Rubio2, A. M. Palomar Muñoz2, A. M. García Vicente2, G. A. Jiménez Londoño2, J. M. Cordero García2, V. M. Poblete García2, A. M. Soriano Castrejón2; 1HOSPITAL GENERAL UNIVERSITARIO CIUDAD REAL, Ciudad Real, SPAIN, 2SESCAM, Ciudad Real, SPAIN.

OBJECTIVE: Determine the relationship between SUVmax and the histological type, as well as with main clinico-pathologic and biochemical prognostic factors in ovarian cancer.MATERIALS AND METHODS:This is a retrospective study that included patients with epithelial ovarian cancer, who underwent pre-treatment 18F-FDG PET-CT study for staging, according to standard protocol.In all of them, the SUVmax of the primary lesion was determined.Ovarian carcinomas were classified according to the hypothesised mode of carcinogenesis and molecular characteristics into histopathological type I (indolent) or II (aggressive), and depending on the final stage as early (I-II) or advanced (III-IV) disease.Finally, we investigated the relationship between SUVmax and the histopathological type, the final stage, and the level of CA125 at diagnosis.RESULTS:Finally, 31 patients with epithelial ovarian cancer were included, with a mean age of 63,1 years (range: 33-85).The mean SUVmax of the primary lesion was 9.08 (range: 2.4-23.7).With respect to histopathological type, 12 patients (38.7%) had type I neoplasms, and the rest (19 patients) had type II ovarian cancer. The high-grade serous carcinoma was the most prevalent histology (45.2%), followed by endometrioid and clear cell carcinoma carcinoma (19.4% and16.1%, respectively).The average SUVmax in type I tumours was lower than in type II (6.66 and 10.77, respectively, $p = 0.035$). The value of SUVmax with the best statistical parameters to detect type II neoplasms was 7.65 (sensitivity 73.7%, specificity 75%; AUC 0.768, $p = 0.013$). Regarding the final stage, 9 patients had early stages, while the majority (22/31: 71%) were in advanced stages. The mean SUVmax in patients with early disease was lower than in advanced (7.99 vs 9.52), although without statistical significance.CA125 was abnormal in 26/31 patients (83.9%), with an average of 345.7. The average was slightly higher in advanced stages. No correlation between SUVmax and the level of CA125 was found. CONCLUSION: Pre-treatment 18F-FDG PET-CT identify the more aggressive ovarian cancer histologies (type II), which could have important implications for prognosis and treatment of patients with epithelial ovarian cancer.

P718

Accuracy of 18F-FDG-PET/CT in the Assessment of Incidental Suspicious Ovarian Masses. Advantages and Limitations of a Powerful Imaging Technique.

A. Marí-Hualde1, D. Zamudio1, P. Pilkinton1, T. Castellanos2, S. Alonso2, L. Chiva2, J. Alonso1; 1ITSS. MD ANDERSON CANCER CENTER MADRID, Madrid, SPAIN, 2MD ANDERSON CANCER CENTER MADRID, Madrid, SPAIN.

BACKGROUND: ovarian cancer (OC) is the second most common malignancy of the female genital system, being the leading cause of gynaecologic cancer mortality due to delay in the diagnosis.AIM: To evaluate the accuracy of 18F-FDG-PET / CT (PET/CT) in the preoperative characterization of undetermined ovarian masses.PATIENTS AND METHODS: From January 2012 to February 2014, 29 consecutive patients with non simple cystic incidentally discovered ovarian masses in other imaging techniques were recluted. A PET/CT was done to characterize them and/or to perform a possible initial staging in the cases of malignancy. A single reader classified all the lesions as malignant of benign. The results of PET/CT were compared with the histologic specimens obtained after surgery in the cases where the PET/CT was abnormal and / or follow up with serial imaging techniques (at least 1 year) . In the cases were the results were consistent with OC, FIGO staging was also performed. Sensitivity (S), Specificity (SP), Positive predictive value and (PPV) and Negative predictive Value (NPV) of PET/CT were calculated using Diagnosis test calculator. RESULTS: 22/29 cases PET / CT were classified as malignant (75.86%), presenting 2 False Positive (mature teratoma and endometriosic cyst). 7/29p were classified as benign (29.14%), with 1 false negative lesion (a borderline clear cell carcinoma). The accuracy of PET/CT was S: 95.2% (IC 95%77.3-99.2%), SP: 75% (IC 95% 40.9-92.9%), PPV: 89.4% (IC 95% 71.8-96.6%) and NPV: 87.6% (IC 95% 50.1-98%).In 21/29 cases (72.41%) (mean age: 51.9 years) tumour pathology was confirmed after surgery: 1 intestinal

GIST , 2 fallopian tube carcinomas and 18 ovarian carcinomas. PET/CT classified gynaecologic tumours according to FIGO as: 8p(40%) stage I (SUVmáx:6.4), 2p(10%) stage II (SUVmáx:5.9), 3p(15%) stage III (SUVmáx: 15.9) and 7p(35%) stage IV(SUVmáx:12.2) . These findings were histologically confirmed: 16 serous adenocarcinomas (80%), 2 clear cell carcinomas (10%), 1 mucinous carcinoma and 1endometrioid carcinoma. In 8/29p (mean age: 40.9 years and SUVmáx:3.2) malignancy was ruled out by surgery or follow up: 4 cystic endometriosis, 2 mature teratomas and 2 simple cysts. CONCLUSION: PET/CT has an excellent sensitivity and a moderate specificity for characterization of ovarian lesions, being also a useful tool for initial OC staging.

P719

F-18 FDG PET-CT in restaging of patients with cervical cancer: - experience at a tertiary care hospital

T. K. Jain, R. K. Basher, B. R. Mittal, J. Shukla, A. Bhattacharya, V. Suri, N. Kumar, S. Kumar; PGIMER, Chandigarh, INDIA, Chandigarh, INDIA, INDIA.

Objectives: To evaluate the diagnostic performance of contract enhanced F-18 FDG PET/CT in restaging of cervical carcinoma. Methods: A retrospective analysis of histopathological proven female patients of carcinoma cervix (age range 32 - 82 years; mean age 51.7 years) was done. All the patients had been treated previously (surgery, radiotherapy or chemotherapy) and referred for F-18 FDG PET/CT to rule out residual or recurrent disease. On FDG PET any abnormal tracer uptake with corresponding CECT lesion were taken as positive. Histopathological examination and clinical or imaging follow up were taken as gold standard. Results: Of the 140 patients, F-18 FDG PET/CT detected abnormal FDG uptake in 95 patients. Uptake at the primary site was detected in 45 (32%) patients and only metastatic lesions in 50(35.7%) patients. Out of 45 patients with primary lesions, 6 had only regional lymph nodes ,7 only had distant lesions, 17 had both regional and distant lesions and remaining had only primary lesion. On lesion based analyses in 64 patients with distant metastases, lymph nodes and peritoneal deposits, lung, liver, skeleton, adrenal and muscle metastases were noted in 41, 20, 7, 38, 2 and 1 patients respectively. Additionally we also detected metachronous primaries in 8 patients and confirmed on histopathology (lung-4, Rectum-2,breast,lymphoma -one each). We found F-18 FDG PET/CT sensitivity, specificity , PPV and NPV 96.4%, 67.3%, 81.6% and 92.5% respectively for residual/recurrence detection ($P < 0.05$). There was no correlation between SUV max and patient survival (Spearman's coefficient rank correlation). Conclusions: We concluded that F-18 FDG PET/CT had high diagnostic accuracy for suspected residual/recurrent disease in cervical cancer patients and also useful in detection of additional metachronous second primary.

P43 - Tuesday, October 13, 2015, 4:00 PM - 4:30 PM, Hall 3 – Poster Exhibition

Clinical Oncology: Lymphoma

P720

ΔSUV Reduction versus Deauville Visual criteria in Follicular Lymphoma evaluated with 18F-FGD PET/CT

M. COZAR SANTIAGO1, J. GARCIA GARZON2, R. SANZ LLORENS1, M. MORAGAS SOLANES2, C. VILLEGAS CARDOS3, M. SANCHEZ DELGADO3, J. AGUILAR BARRIOS1, R. SANCHEZ JURADO1, J. FERRER REBOLLEDA1; 1ERESA-GENERAL UNIVERSITARY HOSPITAL, VALENCIA, SPAIN, 2CETIR-ESPLUGUES PET/CT UNIT, BARCELONA, SPAIN, 3HEMATOLOGY GENERAL UNIVERSITARY HOSPITAL, VALENCIA, SPAIN.

AIM: in order to improve disease characterization and outcomes in Hodgkin and diffuse large cell B Lymphoma, a five-point scale to grade response is being revising recently in different workshops; at this point the objective of our work was to assess different methods (visual and semi quantitative) to evaluate response and prognosis in patients with follicular lymphomaMATERIAL AND METHODS: we have evaluated retrospectively 35 patients (18 men and 17 women with an average age of 63 years) with follicular lymphoma (bcl-2 positive; Ki67>20%).All patients underwent a baseline PET/CT (bPET) and an interim PET/CT (iPET) after first two-three cycles of chemotherapy. We used two methods of evaluation for both PET/CT: a visual method, using the Deauville criteria (5 score scale from 1 to 5; PET/CT positivity for score for score >4; liver treshhold) and a semiquantitative method (measuring SUV max in the most metabolic lesion of bPET and IPET).We calculated the concordance between these two evaluation methods according to the Kappa statistic and ROC analysis to asses the value with the semiquantitative method.We performed a follow up during fourteen months and evaluated survival curves in ΔSUV REDUCTION and Deauville score these the two valuation methods in using Kaplan-Meier plots comparing them with the log-rank test.RESULTS: with the visual analysis we found a ≥65% SUV max reduction (ΔSUVmax = baseline SUVmax - interim SUVmax/baseline SUVmax) in patients with favourable outcome with an area under the curve (AUC) of 0.875 (NPV: 83.30%).In case of Deauville criteria the area under de curve was not statistically significant and showed no potential role in

the discrimination of patients with favourable outcome.Our kappa index (K: 0.273 p <0.05) showed a low concordance between the two methods of evaluation.Log-rank test in the Kaplan-Meier plots showed statistically significant in predicting outcome only with the semiquantitative analysis (X2: 8.04, p: 0.005) but not with Deauville criteria.CONCLUSIONS: The use of iPET/CT in patients with follicular lymphoma with a semiquantitative analysis (ΔSUV REDUCTION) seems to be superior to visual analysis (Deauville criteria) to identify patients with favourable outcome and seems to have more predictive value in the follow up

P721

Could the ratio between lesion and liver SUVmax (rPET) be a prognostic factor in patients with Hodgkin Lymphoma undergoing interim FDG-PET/CT? A retrospective study

S. ANNUNZIATA1, A. Cuccaro2, M. Calcagni1, L. Indovina3, S. Hohaus2, A. Giordano1, V. Rufini1; 1Institute of Nuclear Medicine - Università Cattolica del Sacro Cuore, Rome, ITALY, 2Institute of Hematology - Università Cattolica del Sacro Cuore, Rome, ITALY, 3Institute of Medical Physics - Università Cattolica del Sacro Cuore, Rome, ITALY.

Aim. Interim FDG-PET/CT after first-line ABVD is a strong prognostic factor in patients with Hodgkin Lymphoma (HL). Recent studies demonstrated that interim target lesion SUVmax has a prognostic significance in these patients. Recently, the ratio between target lesion and liver SUV has been proposed, to convert visual qualitative scale as 5-point Deauville Score (5p-DS) in a continuous semi-quantitative scale. This ratio allows to evaluate interim FDG-PET/CT through a well-determined semi-quantitative based cut-point, and it is not dependent from administered activity and body weight. Aim of this study is to evaluate the prognostic role of the ratio between target lesion and liver SUVmax (rPET) in patients with HL undergoing interim FDG-PET/CT. Methods. Sixty-seven patients with HL undergoing interim FDG-PET/CT after two courses of ABVD were evaluated. Interim FDG-PET/CT visual interpretation was based on 5p-DS (score 4 and 5 considered as positive); we considered as semi-quantitative parameters interim target lesion SUVmax, liver SUVmax and rPET. We defined rPET as the ratio between target lesion SUVmax and liver SUVmax in each interim FDG-PET/CT exam. Primary endpoint was event-free survival (EFS). We analyzed 5p-DS, target lesion SUVmax and rPET as prognostic factors. The receiver operating characteristic (ROC) approach was applied to identify the optimal cut-point of rPET with respect to outcome, to calculate accuracy values and to define the area under the curve (AUC). Results. Interim FDG-PET/CT was positive by using 5p-DS in 11/67 patients (16%). Median target lesion SUVmax was 1.9 (range 0-15.7), median liver SUVmax 2.7 (range 1.4-4.2), median rPET 0.66 (range 0-6.54). To predict EFS, interim 5p-DS FDG-PET/CT was stronger than rPET and target lesion SUVmax as prognostic factor, with an HR of 9.3 (SE 4.87, 95% CI 3.3-26.0, p<0.001), 4.9 (SE 2.09, 95% CI 2.1-11.3, p<0.001) and 1.5 (SE 0.17, 95% CI 1.2-1.9, p<0.001), respectively. ROC analysis for rPET as prognostic factor showed an AUC of 0.81, with an optimal rPET cut-point of 1.14 (specificity 94.6%, sensitivity 53.3%). At 2 years, patients with positive 5p-DS FDG-PET/CT had an EFS of 27.3%, patients with rPET>1.14 of 15.3%. Conclusion. rPET is a prognostic factor in patients with HL undergoing interim FDG-PET/CT. 5p-DS FDG-PET/CT has confirmed to be the strongest prognostic factor. Nevertheless, patients with rPET>1.14 have a worse prognosis than patients with positive 5p-DS. Therefore, rPET could be useful to avoid unnecessary treatment intensification in patients with HL undergoing interim FDG-PET/CT.

P722

Utility of 18F-FDG-PET/CT for bone assessment in the initial staging of patients diagnosed of Hodgkin's lymphoma.

M. Fernández Rodríguez, E. Rodríguez Pelayo, M. L. Castillejos Rodríguez, C. Sandoval Moreno, M. A. Balsa Bretón, M. P. García Alonso, C. Paniagua Correa, A. Ortega Valle, F. J. Penín González; Hospital Universitario de Getafe, Getafe, SPAIN.

Aim: To confirm if 18-F-FDG-PET/CT in the staging of patients with Hodgkin's lymphoma (HL) is useful for bone evaluation in order to avoid unnecessary bone marrow biopsies (BMB). Materials and methods: We have retrospectively reviewed newly diagnosed patients with Hodgkin's lymphoma from may/09 to feb/15. A total of 19 patients with 18F-FDG-PET/CT and BMB at diagnosis. They had a mean age of 48 + 29 years (10 men and 9 women). We have reviewed clinical (B symptoms at diagnosis) and analytical factors (presence of anemia and/or increased levels of LDH). We classified PET/CT results: 1) negative-N (no bone uptake), 2) focal positive-FP (focal bone uptake) and 3) diffuse positive-DP (diffuse bone uptake). BMB were performed on left iliac crest and in 2 cases it was repeated in other locations referred in the PET/CT. It was considered to be positive when there was tumoral involvement and negative if there was not. Results: 8/19 patients (42%) had negative PET/CT and negative BMB (NPV 100%). One of them had B symptoms, anemia and increased LDH; two patients had B symptoms and another one had anemia. 4/19 patients (21%) had FP uptake, two of them had positive BMB and two, negative one. In these last 2 cases the BMB was repeated on the bone locations referred in the

PET/CT, and the result was positive. PPV was 100%. 7/19 patients (37%) had DP uptake: 6 negative BMB and another one, positive BMB. Conclusion: Although our sample is small, the results are similar to the published literature: BMB can be avoided in patients with negative PET/CT or if it shows focal bone uptake. Its utility could be questioned in those patients with diffuse bone uptake. PET/CT helps to locate lesions for biopsy sampling.

P723
FDG-PET/CT in intravascular large B-cell lymphoma: evaluation of diffuse splenic and bone marrow uptake as predictive factors of hemophagocytic syndrome

T. Kinjo, K. Nakatani, K. Yoshino, K. Kitaguchi, T. Koyama; Kurashiki Central Hospital, Kurashiki, JAPAN.

Aim: Intravascular large B-cell lymphoma (IVBCL) is a rare subtype of extranodal lymphoma characterized by the specific proliferation of lymphoma cells within the lumina of microvasculature. Classical IVLBCL (Western form) usually has several neurologic and skin symptoms, whereas Asian variant of IVLBCL often lacks these signs and is rather associated with hemophagocytic syndrome (HPS). The aim of this study was to investigate the role of FDG-PET/CT as a predictor for HPS in patients with IVLBCL. Materials and methods: 10 patients with histologically proven IVLBCL who underwent FDG-PET/CT between 2009 and 2014 were analyzed. Their histological specimens were obtained by biopsy prior to chemotherapy from bone marrow, skin, lung, liver, stomach, or adrenal gland. One patient was excluded since he had already started chemotherapy before this study. Based upon the hemophagocytic lymphohistiocytosis diagnostic criteria 2009, the patients were divided into HPS and non-HPS group by their physical examination and laboratory tests. FDG uptake in the following organs: brain, spleen, liver, bone marrow, and ascending aorta, of each group was compared by measuring SUVmax. For spleen and bone marrow, visual assessment in comparison with liver uptake was also made. Mann-Whitney's U test and Fisher's exact test were used for the statistical analyses. Results: Among the 9 IVLBCL patients, 5 patients had HPS. HPS group showed significantly higher splenic SUVmax than non-HPS group (8.33 ± 5.86 vs. 2.89 ± 0.51; p=0.032). The difference in SUVmax between each group was not significant for brain (5.48 ± 2.41 vs. 6.79 ± 2.37; p=0.91), liver (4.00 ± 1.39 vs. 2.45 ± 0.63; p=0.063), bone marrow (3.46 ± 0.53 vs. 2.88 ± 0.77; p=0.19), and ascending aorta (1.76 ± 0.31 vs. 1.40 ± 0.20; p=0.19). For the visual assessment, diffuse increased splenic uptake relative to liver was seen in 4 of 5 HPS patients and in 3 of 4 non-HPS patients (p=1.00), and diffuse increased bone marrow uptake was seen in 2 of 5 HPS patients and in 4 of 4 non-HPS patients (p=0.17); neither were statistically significant difference. Conclusion: Increased splenic FDG uptake would be helpful as a predictor of HPS in IVLBCL patients. Increased hepatic FDG uptake might also be helpful, though not significant.

P724
[18F]FDG-PET/CT in extranodal lymphoma

M. Sollini, B. Zangheri, L. Calabrese, M. Gasparini; IRCCS MultiMedica, Sesto San Giovanni, ITALY.

Aim: Although lymphoma generally originates from lymph nodes, in up to 40% of HD/NHL (especially NHL), arises at extranodal sites along the gastrointestinal tract, head and neck, orbit, central/peripheral nervous system, thorax, bone, skin, breast, testis, thyroid, and genitourinary tract. We aim to evaluate the role of [18F]FDG-PET/CT in extranodal manifestations of lymphoma. Materials and methods: we retrospectively evaluate 28 patients (M=14; F=14) who performed from 04/2011 to 03/2015 a [18F]FDG-PET/CT for a total of 63 examinations. Lymphoma originated from gastrointestinal tract in 10 cases (stomach=7; bowel=3), head and neck in 5 cases (orbit=1; pharynx=1; parotid=1; cheek=1; tongue=1), breast in 6 cases, skin in 4 cases, heart in 2 cases and brain in 1 case. PET/CT was acquired 1 hour after [18F]FDG injection (median activity=304 MBq; range 245-644 MBq). [18F]FDG-PET/CT was performed to stage (n=17), to evaluate treatment response (n=5) or during follow-up (n=41) patients. [18F]FDG-PET/CT results were compared to final diagnosis obtained by follow-up (clinical-radiological, [18F]FDG-PET/CT or histology). We excluded from the present analysis 3 patients affected by cardiac, ileum and orbital NHL respectively (for a total of 4 scans), due to the lack of final diagnosis. Results: Out of the 59 scans performed (staging=17, treatment response evaluation=5, follow-up=37), [18F]FDG-PET/CT resulted positive in 26 cases and negative in 33 cases. Based on final diagnosis was classified as true positive (TP), true negative (TN), false positive (FP) and false negative (FN) in 23, 32, 3, and 1 cases, respectively. FP results were observed during the follow-up period of a gastric and a rectum NHL patients in which focal [18F]FDG uptake (SUVmax > 3.0) was present in stomach (2 scans) and rectum (1 case). The only case resulted FN was a patient with gastric NHL in which biopsy performed after PET/CT confirmed microscopic residual disease. Considering the clinical purpose, sensitivity and specificity of PET/CT were 93% and 100% in the staging setting and 100% and 90% in the follow-up. Seven patients who performed PET/CT to stage disease performed additional PET/CT during follow-up which diagnosed disease recurrence in 2/7 and residual disease in 1/7 case. In the only 5 scans performed to evaluate treatment response PET/CT was TP in 1 case and TN in the remaining 4 patients. PET/CT revealed additional site(s) of

disease in 14 cases (lymph nodes=13, bone=1, spleen=1, adrenal=1, pharynx=1). Conclusion: as for nodal lymphoma, [18F]FDG-PET/CT presents high diagnostic performances also in extranodal lymphoma (sensitivity=96%, specificity=91%, accuracy=93%).

P725

FDG PET/CT Can Reliably Determine Bone Marrow Involvement in Diffuse Large B Cell Lymphoma but not in Follicular Lymphoma

A. R. Teagle1, **H. Barton**1, E. Charles-Edwards1, S. Dizdarevic1, T. Chevassut2,1; 1Brighton and Sussex University Hospitals NHS Trust, Brighton, East Sussex, UNITED KINGDOM, 2Brighton and Sussex Medical School, Brighton, East Sussex, UNITED KINGDOM.

Non-Hodgkins lymphoma (NHL) is a common malignancy, accounting for an estimated 4% of all new cancer cases annually. It is important to identify bone marrow involvement as it affects staging and management. Bone marrow biopsy (BMB) is considered the gold standard for detecting marrow involvement in NHL but the use of FDG PET/CT to provide additional information for staging is becoming increasingly widespread. BMB has a non-negligible complication rate and it is unpleasant for patients to undergo. This study compares determination of bone marrow involvement by FDG PET/CT against BMB in Diffuse Large B-cell Lymphoma (DLBCL) and Follicular Lymphoma (FL).Methods: This was a retrospective study of patients with histologically confirmed NHL treated at a single UK Cancer Centre, who had had a baseline (pre-treatment/staging) FDG PET/CT and baseline BMB in the period from June 2010 to February 2013. Information was collected from patient notes and the local cancer register, plus histological and imaging reports. All FDG PET/CT scans were dual-reported by consultants in Nuclear Medicine and Radionuclide Imaging. Results were compared between BMB and FDG PET/CT to determine diagnostic accuracy of FDG PET/CT using BMB as the reference standard. Results: In total, 24 patients with DLBCL and 12 patients with FL were included in the study. 5 patients with DLBCL had bone marrow involvement on FDG PET/CT, which was confirmed in all cases on BMB. 3 patients with FL had bone marrow involvement on FDG PET/CT but not on BMB; 1 patient with FL had bone marrow involvement on BMB but not on FDG PET/CT. Using BMB as the reference standard, the sensitivity and specificity of FDG PET/CT in detecting bone marrow involvement were 100% and 100%, respectively, in DLBCL, and 0% and 72.7% in FL, respectively. Conclusion: When compared to BMB, FDG PET/CT is highly accurate for detection of bone marrow involvement in our group of patients with newly diagnosed Diffuse Large B-cell Lymphoma, but not in those with Follicular Lymphoma. This study adds to the literature suggesting that FDG PET/CT may be able to safely rule out bone marrow involvement in DLBCL without the need for confirmatory BMB.

P726

The Liver as Reference Organ for Quantification of 18F-FDG Uptake in Lymphoma

C. N. Strandholdt1, O. Gerke1, J. T. Friis1, T. S. Larsen2, K. J. Mylam3, P. F. Høilund-Carlsen1; 1Dept. of Nuclear Medicine, Odense University Hospital, Odense C, DENMARK, 2Dept. of Haematology, Odense University Hospital, Odense C, DENMARK, 3Dept. of Medicine, Vejle Hospital, Vejle, DENMARK.

Aim: It is widely accepted to use a reference organ when quantitative PET methods are applied in the evaluation of various diseases. This study examined the applicability of the liver as a reference organ in disease assessment in lymphoma patients using 18F-FDG PET/CT and dedicated software. Materials and methods: Partial volume corrected standard uptake values (cSUVmean) were obtained in the liver of ten patients, aged 61-71 years, with diffuse large B-cell lymphoma, at baseline and at interim PET/CT scans. Two interim scans were excluded due to technical artefacts in the liver. 18F-FDG PET/CT scans performed at 2-year follow-up in 10 survivors of upper GI-cancer, aged 56-68 years, served as reference. All patients in the latter group were still alive and recurrence free. The FDG uptake was measured in three different regions (Reg 1,2,3) in the liver, using for each of them a small volume ROI of about 25-35 cm3 and at a large volume ROI of approximately 95-115 cm3. A dedicated software, ROVER (ABX, Radeberg, Germany), providing segmentation by a voxel based adaptive threshold method and correction for partial volume effect was used for the analysis. Mixed-effects regression was applied to test for differences between regions, small and large volume sizes, time points, and patient groups. Results: For the 60 ROIs in lymphoma patients at baseline, the mean cSUVmean was 2.53, range 2.0-3.4. For the 48 ROIs in lymphoma patients at interim, the mean cSUVmean was 2.69, range 2.1-3.3. For the 60 ROIs in the reference group, the mean cSUVmean was 2.17, range 1.7-2.7. cSUVmean was statistically significantly higher in lymphoma patients versus reference ($p<0.0001$), whereas cSUVmean increase over time was not. The mean difference in cSUVmean between Reg 1 ROI and Reg 2 ROI was -0.05 (95% CI: -0.07 to -0.02; $p<0.0001$). The mean difference in cSUVmean between Reg 1 ROI and Reg 3 ROI was 0.01 (95% CI: -0.04 to 0.06; $p=0.71$).The mean difference in cSUVmean in small volume ROIs versus large volume ROIs was 0.01 (95% CI: 0.004 to 0.02; $p=0.003$).Conclusion: The differences between

measured cSUVmean values were small and clinically insignificant independent of ROI size and the location in the liver demonstrating that in these categories of patients the liver uptake of FDG is in fact very homogeneous. Therefore, it may be feasible to use just a part of the liver as a reference, when assessing disease activity in patients with diffuse large B-cell lymphoma.

P727

The Utility Of 18F-FDG PET/CT In Evaluation Of Bone Marrow Involvement In Non-Hodgkin's Lymphoma Patients

D. Vassileva1, B. Spassov1, I. Kostadinova2, M. Guenova1; 1Specialized Hospital for Active Treatment of Hematological Diseases, Sofia, BULGARIA, 2University Hospital Alexandrovska, Sofia, BULGARIA.

Background: Bone marrow biopsy (BMB) is a standard method for the evaluation of bone marrow infiltration in non-Hodgkin's lymphoma (NHL) patients although it is an invasive and painful procedure. Since BMB allows analysis of very limited area, false negative results can be observed. FDG-PET/CT has been used for follow-up examinations in patients with aggressive NHL. However few data are available regarding utility of FDG-PET/CT in NHL patients with bone marrow involvement in comparison with BMB. Aims: To evaluate the value of 18-F FDG PET/CT and its concordance with BMB in determining post-treatment bone marrow involvement (BMI) in NHL patients. Methods: Data from 70 NHL patients (39 men and 31 women), aged 21-69 years, were analyzed retrospectively. All patients were examined by FDG PET-CT and iliac crest bone marrow biopsy. BMB results were used as reference standard. FDG-PET/CT results were compared with the BMB results in order to evaluate BMI. Results: Both FDG-PET/CT and BMB were negative in 52 (74.3%) patients after the cytotoxic therapy. Eighteen patients (25.7%) were considered positive lymphomatous infiltration by FDG-PET/CT (PET-CT/BM+). Focal and diffuse bone marrow 18 F-FDG uptake were detected in 10 and 8 patients, respectively, and bone marrow SUV max values ranged 2, 8-9,6. Five patients (7.1%) were identified positive by BMB (BMB/BM+). There was a discordant result in thirteen patients (72.2%) who were PET-CT/BM+ but BMB/BM- due to focal pattern of BMI. Conclusion: FDG-PET/CT findings can complementally detect positive BMI patients missed by BMB due to focal pattern of infiltration in NHL patients at follow-ups. Additional clinical trials are needed to define the prognostic value of positive BMI detected by FDG-PET/CT.

P728

Recognition of Graft-Versus-Host-Disease by Semi-Quantitative Analysis of Lung Parenchyma at FDG PET/CT images.

F. Fiz1, F. Bongioanni1, M. Pennone2, I. Calamia1, A. Bacigalupo3, C. Marini4, S. Morbelli2, G. Sambuceti1; 1Nuclear Medicine Unit, Department of Health Sciences, University of Genoa, Genoa, ITALY, 2Nuclear Medicine Unit, IRCCS San Martino - IST, Genoa, ITALY, 3Hematology and Bone Marrow Transplantation Unit, IRCCS San Martino - IST, Genoa, ITALY, 4CNR-IBFM, Milano, ITALY.

Background and Aims: Graft-Versus-Host-Disease (GVHD) is a frequent complication of Heterologous Hematopoietic Stem Cell Transplantation (HSCT), in which donor T-Lymphocytes recognize the foreign antigens and mount an inflammatory reaction towards the donor's tissues. It can be acute or chronic, it generally affects multiple organs, including the liver, the gut, the skin and the lungs and can severely impact short-term survival or long-term quality of life. Recongnizing GVHD at its early stages is important for treatment planning and subsequent clinical outcome. In this study, we retrospectively analyzed the FDG PET/CT images of patients submitted to HSCT to assess differences in tracer distribution within the lung parenchyma. This tissue was chosen because the very low baseline uptake might allow detecting even subtle changes in glucose metabolism. Patients and methods: 30 patients (11 women, mean age 32 years), with relapsed Hodgkin Lymphoma, underwent FDG PET/CT for response assessment 30 days after Heterologous HSCT between 2009 and 2013. Volumes of Interest (VOI) were manually drawn bilaterally on the whole lung parenchyma, carefully excluding the mediastinal structures and pleura. SUVmax and SUVmean were then normalized for blood-pool, obtained from a 10-slice thick VOI in the inferior vena cava. Any evidence of pulmonary infection was a criterion of exclusion. 30 sex- and age-matched controls from a published normalcy database were used as reference. Results: Average SUVmean was increased in the patients' group when compared to controls (0.6±0.32 vs 0.39±0.1, $p<0.01$); SUVmax was similarly increased ($p<0.05$). This difference can be largely attributed to immune mechanisms, as patients who subsequently had a Grade-2 or greater GVHD (7/30, 23%) had a greatly increased SUVmean with respect to the remaining ones (0.87±0.33 vs 0.47±0.18, $p<0.001$), as well as a marked increase in SUVmax ($p<0.01$). Conversely, patients with no subsequent acute or chronic GVHD didn't show a definite increase in metabolic indexes when compared to controls. Conclusions: Semi-quantitative analysis of FDG PET/CT is a sensitive modality, able to grasp minimal metabolic changes that are associated with an ongoing GVHD.

P729

Revised Criteria for 18F-FDG-PET Bone-marrow Evaluation in Lymphoma-staging: High Diagnostic Accuracy in selected patients

E. Orunesu1, M. Longo2, L. Florimonte1, M. Castellani1, F. Zito1, C. Canzi1, F. Voltini1, M. Goldaniga3, R. Benti1, A. Cortelezzi1; 1Department of Nuclear Medicine, Fondazione IRCCS Cà Granda Ospedale Maggiore Policlinico, MILAN, ITALY, 2Nuclear Medicine Residency, University of Milan, Unit of Nuclear Medicine, San Paolo Hospital, MILAN, ITALY, 3Oncohaematology Division, Fondazione IRCCS Cà Granda Ospedale Maggiore Policlinico, MILAN, ITALY.

Background:For evaluation of bone-marrow-involvement in staging of Hodgkin (HL) and Non-Hodgkin Lymphoma (NHL), international recommendations (Lugano Classification) state that bone-marrow-biopsy (BMB) is no longer mandatory in all HL and high-grade-NHL, based on superior sensitivity of 18F-FDG-PET/CT versus bone-marrow-biopsy (BMB) in this setting. However, the lack of well-established criteria for grading FDG bone-marrow-uptake, renders difficult a proper assessment of the bone-marrow-infiltration in clinical practice. The aforementioned recommendations rely on studies in which the presence of focal FDG-bone-uptake, was considered as a proof of bone-marrow-involvement, ignoring the possibility of concomitant absent bone-marrow tumor-spread. To improve our understanding of the effective accuracy of PET in the evaluation of bone-marrow, we performed a separate evaluation of bone marrow-involvement in patients with focal bone-lesions. After evaluating our patients with this method and with the previously adopted, we compared the results, using BMB as gold-standard.Methods:We evalutated 18F-FDG-PET/CT studies, performed for staging of 51 NHL-patients (aggressive N=27; indolent N=24; M:F ratio= 1.5:1; median age= 61). For evaluation of bone-marrow uptake we adopted a 5-point scale, consisting in: 1= no uptake; 2= uptake ≤ mediastinum; 3= uptake >mediastinum but < than liver; 4= uptake moderately higher than liver; 5= uptake markedly higher than liver.Results:Overall accuracy was best when setting the threshold for positivity, above or equal to 3. When comparing results using our criteria with previous criteria, the specificity for bone-marrow involvement in high-grade NHL increased from 53% to 75% (for all NHL: from 66% to 80%).Nevertheless the overall accuracy of 18F-FDG-PET/CT with our criteria was 70% versus 61% for aggressive NHL (and 70% vs. 68% for all NHL), showing equally low values for low- and high-grade NHL. Furthermore, we observed that by setting a cut-off at level 4, the specificity of bone-marrow-uptake reached a value of 93%, meaning that most cases of high bone-marrow-uptake are BMB positive. In patients with evidence of bone-lesions (N=9), the positive-predictive-value for bone-marrow involvement was 100% for all NHL, but further data is needed to confirm this observation.Conclusion:Based on our results, despite the high accuracy of FDG-PET in staging of NHL, the diagnostic performance in detecting bone-marrow involvement seems poor and in most cases we think that BMB would bring additional value. Despite this, our preliminary data show high accuracy of FDG-PET-bone-marrow evaluation in patients with concomitant FDG-avid bone-lesions. Further data will establish if BMB might be reliably avoided in this subset of patients.

P730

18F-FDG-PET/CT in the evaluation of patients with follicular lymphoma

R. Fonti1, B. Salvatore1, A. De Renzo2, S. Pellegrino3, C. Cerchione2, M. Monti2, C. Cimmino2, F. Pane2, L. Pace4, S. Del Vecchio3; 1Institute of Biostructures and Bioimages-CNR, NAPLES, ITALY, 2Haematology Division, University "Federico II", NAPLES, ITALY, 3Department of Advanced Biomedical Sciences, University "Federico II", NAPLES, ITALY, 4Department of Medicine and Surgery, University of Salerno, SALERNO, ITALY.

Follicular lymphoma is characterized by slowly progressive adenopathy showing variable FDG avidity. Recent studies support the use of functional imaging by 18F-FDG-PET/CT at diagnosis in order to identify patients with indolent or more aggressive disease according to tumor metabolic behavior. Aim. The aim of our study was to evaluate lymph node involvement in patients with follicular lymphoma by 18F-FDG-PET/CT and to correlate the imaging parameters derived by this methodology with standardized clinical, biochemical and haematological variables used in the staging and prognosis of this lymphoproliferative disease. Methods. We evaluated retrospectively 24 patients (9 males, 15 females; mean age±SD, 57±8.7 years) with follicular lymphoma who had undergone whole-body 18F-FDG-PET/CT and contrast-enhanced CT alone or as part of 18F-FDG-PET/CT examination at the time of diagnosis. Patients were staged according to standard criteria including the evaluation of parameters belonging to the Follicular Lymphoma International Prognostic Index (FLIPI) 1 such as age, stage, lactate dehydrogenase (LDH), haemoglobin and number of pathological nodal sites or FLIPI 2 such as the diameter of the largest lymph node involved. Results. In the 24 patients studied, the number of pathological lymph node basins at 18F-FDG-PET/CT ranged between 1 and 33 and the SUVmax of the lymph node with the highest metabolic rate varied from 2.9 to 14.6 while at CT the number of pathological lymph node basins ranged between 1 and 28 and the maximum diameter of the largest involved lymph node varied from 17 to 75 mm. The number of pathological lymph nodes at 18F-FDG-PET/CT was significantly correlated with

stage and FLIPI1 score (Spearman rank correlation coefficient r=0.76, P=0.0002 and r=0.56, P=0.0068, respectively). Likewise, the number of pathological lymph nodes at CT was significantly correlated with stage and FLIPI1 score (Spearman rank correlation coefficient r=0.65, P=0.0016 and r=0.64, P=0.0022, respectively). Moreover, a statistically significant direct correlation was found between the maximum diameter of the largest pathological lymph node at CT and the SUVmax of the lymph node with the highest tracer uptake (r=0.55 P=0.0075). The largest lymph node size showed a significant correlation with stage (Spearman rank correlation coefficient r=0.48, P=0.0252) while the highest SUVmax value was directly correlated with LDH levels (r=0.42 P=0.0464). Conclusion. In patients with follicular lymphoma 18F-FDG-PET/CT provides a useful contribution in evaluating lymph node involvement and therefore can be of aid in the prognostic assessment of these patients.

P731

Staging and Indices measured with 18F-FDG PET/CT as a predictor of survival in Non-hodgkin's lymphoma

B. DIRLIK SERIM1, E. UMIT2, F. USTUN3, B. TOKUÇ4, M. DEMIR2, G. DURMUS ALTUN3; 1Istanbul Medicine Faculty, Nuclear Nedicine Department, Istanbul, TURKEY, 2Trakya Universty Medicine Faculty, Hematology Department, Edirne, TURKEY, 3Trakya Universty Medicine Faculty, Nuclear Medicine Department, Edirne, TURKEY, 4Trakya Universty Medicine Faculty, Department of Public Health, Edirne, TURKEY.

Purpose: We aimed to evaluate the value of initial [18F]2-fluoro-2-deoxyglucose (FDG)-positron emission tomography (PET) scan for prediction of survival in patients with Non-hodgkin's lymphoma (NHL). We also aimed to assess the role of other quantitative parameters such as mediastinum,liver and brain indices measured at baseline and interim PET/CT for prediction of survival.Methods: Data from 18F-FDG PET/CT scans of 31 patients with NHL at the initial, after two cycles and after the completion of treatment were evaluated in a retrospective review (2015-2009). The ratio of SUVmax value of primary lesion to SUVmean values of mediastinum, liver and brain obtained from PET/CT scan were defined as mediastinum, liver and brain indices. Indices were determined at baseline and interim PET/CT. Treatment outcomes were compared between groups according to metabolic parameters and the International Prognostic Index (IPI). Relation between quantitative parameters and overall survival (OS) was analyzed.Results: After a median follow-up of 54 months (range, 30-72 months) of 31 patients (F/M: 18/13, range: 58 ±13 years), seven patients developed recurrence after chemotherapy while three patients never reached a remission. Relation between quantitative parameters and OS was statistically analyzed using Mann Whitney U test, Fischer Exact Test and Kaplan Meier survival analyis. Among quantitative metabolic parameters, there was a statistically significant relation between initial mediastinum (p=0.008), liver (p=0.02), brain (p=0.022) indices and pre-treatment staging. Additionally interim PET/CT indices was negatively associated with treatment outcomes. (mediastinum index r= -,642, p=0.00, liver index r= -,641, p=0.00, brain index r=-,652, p=0.00) Furthermore initial PET staging was significantly associated with OS. Advanced stages in initial PET/CT significantly reduced OS (stage 1 versus stage 0 , 8.1 times reduces, 95% CI 1.82 - 36.85 and stage 2 versus stage 0 , 8.3 times reduces 95% CI 1.36 - 51.06)Conclusion: The significant relation of initial PET/CT staging with OS improves the importance of PET scan in NHL. Likewise, interim PET/CT indices give direction to the decision about tailoring the treatment according to individual response. Interim PET/CT indices may be useful to identify patients with NHL who are at increased risk for relapse after conventional therapy. Multicentral further studies with larger patients groups are needed to identify quantitative parameters contributing prognosis prediction in NHL.

P732

Delayed-time-point [18F]-FDG-PET in MALT lymphoma: is [18F]-FDG-PET better than its reputation?

M. Mayerhoefer, C. Giraudo, D. Senn, M. Hartenbach, M. Raderer; Medical University of Vienna, Vienna, AUSTRIA.

AIM: Current guidelines do not recommend [18F]-FDG-PET for imaging of MALT lymphoma, because this lymphoma subtype has shown a variable FDG avidity in previous studies. It was thus the aim of this prospective study to determine whether, in patients with MALT lymphoma, delayed-time-point 2-[18F]-fluoro-2-deoxy-D-glucose-positron emission tomography ([18F]-FDG-PET) performs better than standard-time-point [18F]-FDG-PET. METHODS: Patients with untreated, histologically verified MALT lymphoma, who were undergoing pre-therapeutic [18F]-FDG-PET/CT (computed tomography) and consecutive [18F]-FDG-PET/MR (magnetic resonance imaging), using integrated hybrid PET/CT and PET/MR systems, and using a single [18F]-FDG injection (250-300 Mbq), were included in this prospective, Institutional Review Board-approved study. Region-based and patient-based rates of agreement of the respective [18F]-FDG-PET scans at time points 1 (45-60 min after tracer injection, TP1) and 2 (100-150 min after tracer injection, TP2) with the histology-based reference standard were calculated, and lesion-to-liver and lesion-to-blood SUVmax and SUVmean (maximum and mean standardized uptake values) ratios were assessed. Paired t-tests were used for group comparisons.

RESULTS: Ten patients (six females and four males; mean age, 65.4±16.1 years) with 5 nodal and 15 extranodal lymphoma manifestations met our criteria for participation in the study. [18F]-FDG-PET at TP1 agreed with the reference standard in 14/20 involved regions, and 6/10 patients. [18F]-FDG-PET at TP2 agreed with the reference standard in 18/20 involved regions, and 8/10 patients. Lesion-to-liver and lesion-to-blood SUVmax ratios were significantly lower at TP1 (ratios, 1.12±0.42 and 1.67±0.63) than at TP2 (ratios, 1.85±0.76 and 2.82±1.11) (P=.006 and P=.003). Similarly, lesion-to-liver and lesion-to-blood SUVmean ratios differed significantly between [18F]-FDG-PET at TP1 (ratios, 1.23±0.38 and 1.53 ±0.52) and [18F]-FDG-PET at TP2 (ratios, 1.99±1.32 and 2.58±1.33) (P=.06 and P=.017). CONCLUSION: Delayed-time-point imaging may improve the performance of [18F]-FDG-PET in MALT lymphoma. Thus, [18F]-FDG-PET may, after all, have a role in the clinical workup of MALT lymphoma patients.

P733
FDG-PET in aggressive non Hodgkin lymphoma: the prognostic value of interim evaluation

L. Aloj1, F. Frigeri2, C. Caracò1, S. Crisci2, R. Farese3, F. Ibello1, A. Morisco3, G. Capobianco2, F. Volzone2, A. Pinto2, S. Lastoria1; 1SC Medicina Nucleare, Istituto Nazionale Tumori Fondazione G. Pascale - IRCCS, Napoli, ITALY, 2SC Ematologia, Istituto Nazionale Tumori Fondazione G. Pascale - IRCCS, Napoli, ITALY, 3Centro Ricerche Oncologiche Mercogliano, Istituto Nazionale Tumori Fondazione G. Pascale - IRCCS, Mercogliano (AV), ITALY.

Aim FDG-PET is growingly recognized as a very important tool to assess early response to therapy in patients with lymphoma. We are evaluating the prognostic value of interim PET in patients with aggressive non Hodgkin lymphoma (NHL) treated at our institution. Materials and Methods We have reviewed the charts of 125 patients (pts) undergoing first line treatment for aggressive NHL between January 2006 and September 2013 (41% DLBCL, 33% DLBCL-ABC, 12% BCLU, 10% PMBCL, 4% other). Patients included in the analysis had performed PET at baseline, interim (median of 4 cycles, range 2-5 from start of treatment) and at least 35 days following the end of therapy (EOT). Deauville criteria were utilized to assess the interim PET (iPET) studies. A score ≥ 3 was considered positive. Findings were correlated with event free and overall survival (EFS and OS). Results Forty of the 125 patients (32%) had a positive iPET, the remaining 85 were negative (iPET-). A complete response (CR) at EOT based on PET and CT was obtained in 21 iPET+ pts (53%) and 77 iPET- pts (91%). Relapses were observed in 5/21 (27%) of iPET+ pts but only in 11/77 (14%) of iPET- patients. Of note in this latter group 7/11 patients had a diagnosis of very aggressive NHL (6 DLBCL-ABC and 1 BCLU). With a median follow-up of 30 months, EFS was 68% vs 35% for iPET- vs iPET+ pts ($p<0.0001$) and OS 71% vs 57% ($p=0.006$). EFS and OS rates in pts who were CR at EOT were not statistically different in the iPET- and iPET+ groups (EFS 75% vs 66%, OS 78% vs 74%, respectively p=ns). Conclusions Our data confirm that a negative iPET is an important predictor of prolonged response and overall survival in aggressive NHL. iPET may be utilized to select patients requiring treatment intensification with the aim of increasing the EOT CR rates and consequently long term outcome.

P734
Prolonged effect of chemotherapy on FDG uptake of the noraml bone marrow in patients with malignant lymphoma

G. S. Alobthani1, T. Morita1, K. Isohashi1, H. Kato1, M. Tatsumi1, E. Shimosegawa2, J. Hatazawa1; 1Department of Nuclear Medicine and Tracer kinetic ,Graduate School of Medicine, Osaka University, Osaka, JAPAN, 2Department of Molcular Imaging in Medicine,Graduate School of Medicine, Osaka University, Osaka, JAPAN.

Aim : 1-To evaluate the prolonged effect of chemotherapy on FDG uptake in the normal bone marrow. 2- The possibility of using PET-CT as good , quantitative and noninvasive technique for the evaluation of the condition of bone marrow. Methods : 56 lymphoma patients without proven bone marrow involvement , the median age was 58.5 +/- 13.5 years . 26 patients were treated with CHOP regimen , 15 patients with THP-COP regimen , 10 patients with Rituximab , 5 patients with ABVD. Granulocytes colony stimulating (GCS) factor was not given to any case. The mean time interval between the end of chemotherapy and scanning by PET-CT was 94 +/- 79 days . The bone marrow uptake of FDG was calculated by measuring the maximum standardized uptake value (SUV max) with setting of the region of interest (ROI) over the lumbar vertebrae 1-5 . The sagittal , coronal and transaxial planes of FDG PET- CT scan were used. We use SUV max rather than SUV mean , to avoid the calculation of the FDG uptake of intervertebral discs and cortical bone of the vertebral bodies during the process of calculation of the bone marrow FDG uptake. P value set as significant if less than 0.05. Results : There was a statistically significant difference (P value 0.0001) between Pre and Post chemotherapy bone marrow FDG uptake , the mean of pre chemotherapy SUVmax was 1.97 +/- 0.45 and the mean of post chemotherapy SUVmax was 1.67 +/- 0.37 , So There was 15 % reduction in post chemotherapy bone marrow FDG uptake This study gives us good idea about the normal FDG uptake of bone marrow (pre

chemotherapy) which was about 1.97 +/- 0.45. Conclusion : 94 days, a relatively long period to see the effect of chemotherapy in the bone marrow by an imaging method but a statistically significant difference between pre and post chemotherapy bone marrow FDG uptake can be still found, so PET-CT may be a good noninvasive method to quantify and visualize the activity of bone marrow. Bone marrow FDG uptake at about 3 months post chemotherapy still less than the pre chemotherapy level , so any case at 3 months post chemotherapy with SUVmax level same as pre chemotherapy level, bone marrow infiltration may be considered , although this post chemotherapy SUV max level is still within normal range.

P735

Predictive value of F-18 FDG PET/CT quantification parameters for progression-free survival in patients with B-cell lymphoma

W. He, W. Zhai, W. Yu; Huadong Hospital, Shanghai, CHINA.

Purpose: To evaluate the predictive significance of F-18 FDG PET/CT quantification parameters for progression-free survival in patients with B-cell lymphoma before chemotherapy. Methods: We conducted a retrospective study including 54 patients with B-cell lymphoma between January 2010 and July 2014 and underwent FDG PET/CT prior to first-line treatment. Mean liver SUV was measured by placing a 14 ml cubic volume of interest in the liver,a smoothing filter to segmented bones from CT to create a bone mask was applied. For each patient,all lesions were segmented by using an Tumor Finder Application with automatic 3D region-growing algorithm with a defined minimum SUV threshold [LiverSUVmean+ SD*2.00]. This computation, after removal of physiologic activity above the measured threshold, defined the metabolic tumor volume (MTV),and the total lesion glycolysis (TLG) was then calculated as [TLG=SUVmean*MTV]. Results: At Spearman analysis, the values of cumulative MTV and TLG were positively related to Ann Arbor Stage, IPI Score and LDH level. The number of enlarged lymph nodes was only positively related to LDH level. There were no relationship between the value of SUVmax and clinical characteristics. At univariate Cox regression analysis, the values of total MTV, cumulative TLG and number of enlarged lymph nodes were predictive (HR=1.027, 1.059, 1.098 respectively; P=0.001, 0.006, 0.046 respectively). The value of SUVmax was not suitable for predicting PFS. According to cut-off of ROC analysis, the lower values of total MTV and cumulative TLG were highly predictive of favorable outcomes in PFS. Conclusion: The quantitative method is a friendly-user independent ,much faster repeatable and reliable . The F-18 FDG PET/CT scan has great value for predicting the prognosis. Total MTV and cumulative TLG may be significant prognostic markers for PFS in B-cell lymphoma, in contrast to SUVmax.

P44 - Tuesday, October 13, 2015, 4:00 PM - 4:30 PM, Hall 3 – Poster Exhibition

Clinical Oncology: Leukaemia & Myeloma

P736

Is there any complomentary role of F-18 NaF PET/CT in detecting of osseous involvement of Multiple Myeloma?: A comperative study for F-18 FDG PET/CT and F-18 FDG NaF PET/CT

I. AK SIVRIKOZ1, H. ONNER1, O. AKAY2; 1ESOGU SCHOOL OF MEDICINE, DEPARTMENT OF NUCLEAR MEDICINE, ESKISEHIR, TURKEY, 2ESOGU SCHOOL OF MEDICINE, DEPARTMENT OFHEMATOLOGY, ESKISEHIR, TURKEY.

Multiple myeloma (MM) is a disease characterized by a monoclonal plasma cell population in the bone marrow whereby osseous involvement is a predominant feature. F-18 FDG PET/CT is an accurate and dependable technique in detecting MM osteolytic lesions in a higher number of patients. There is limited information in the literature regarding the diagnostic utility of F-18 NaF PET/CT in the assessment of bone involvement in MM. The aim of this prospective study was to investigate the combined use of F-18 FDG and F-18 NaF PET/CT in the skeletal assessment of patients with MM and to compare the efficacy of these two PET tracers regarding detection of myeloma-indicative osseous lesions. A total of 26 patients (14 females and 12 males, mean age 61.8±1.8 years (range 40-81 years) with MM diagnosed according to standard criteria. All patients underwent both F-18 FDG PET/CT and F-18 NaF PET/CT scans within one week after the completion of the usual staging workup for MM. In total, approximately 128 focal F-18 FDG avid skeletal lesions were detected; the stage I (n=5) pts had 10 bone lesions, the stage II (n=11) pts had 43 lesions, and the stage III (n=10) pts demonstrated 75 focal bone lesions. F-18 NaF PET/CTs demonstrated fewer myeloma indicative lesions than F-18 FDG PET/CTs. Totally, 57 focal bone lesions were detected with whole body F-18 NaF PET/CT (mean 2.19±0.34, between 1-9 lesions); the five stage I pts had 6 bone lesions, the eleven stage II pts had 18 lesions, and the ten stage III pts demonstrated 33 focal bone lesions. On the other hand, F-18 NaF PET/CT demonstrated additionl 135 bone lesions defined as rib fractures, and other findings due to degenerative changes. In conclusion, our study implies that F-18 NaF PET/CT scan didn't actually aid for assessing the myelomatous bone lesions in patients with MM. Therefore, F-18 NaF PET/CT can contribute to the detection of

minor and unexpected fractures and give a general view of the bone remodelling of the whole skeleton in a single exam.

P737

Bone marrow plasma cell infiltration rate is higher in multiple myeloma patients with pathological 18F-FDG PET/CT than in patients with normal scans

C. Sachpekidis1, E. K. Mai2, J. Hillengass2, H. Goldschmidt2, U. Haberkorn3, A. Dimitrakopoulou-Strauss1; 1Clinical Cooperation Unit Nuclear Medicine, German Cancer Research Center, Heidelberg, GERMANY, 2Medical Clinic V, University of Heidelberg, Heidelberg, GERMANY, 33Division of Nuclear Medicine, University of Heidelberg, Heidelberg, GERMANY.

Purpose: We aim to compare the degree of bone marrow malignant plasma cell infiltration in patients suffering from primary multiple myeloma (MM) according to their 18F-FDG PET/CT distribution pattern. Procedures: The study included 67 patients with primary, previously untreated MM (mean age: 59.5 years; 43 male, 24 female). Whole body PET/CT studies from the skull to the knees were performed. PET/CT evaluations were based on visual/qualitative analysis and patients were initially classified in two groups: those with normal tracer distribution (negative) and those with pathological findings (positive). Furthermore, the 18F-FDG PET/CT positive patients were classified in three groups: patients with foci of increased tracer uptake (focal), patients with intense, diffuse bone marrow 18F-FDG accumulation (diffuse) and patients with a mixed pattern (diffuse bone marrow uptake with focal osseous lesions). Bone marrow aspirates/biopsies were performed within four weeks around the 18F-FDG PET/CT examinations. Percentage of bone marrow infiltration was assessed via light microscope from Giemsa-stained bone-marrow smears. Wilcoxon rank-sum test was performed in order to assess potential significant differences in terms of bone marrow infiltration rate between the different groups of tracer uptake ($p<0.01$). Results: PET/CT negative patients demonstrated a mean infiltration rate of 21.2% (median 12%, n=15 patients), while PET/CT positive patients had a mean infiltration of 38.9% (median 35%, n=52 patients) ($p<0.01$). Among PET/CT positive patients, those who presented with a focal pattern had a 31.1% mean infiltration rate (median 20%, n=19 patients), those with diffuse 18F-FDG bone marrow uptake had a 36.5% mean bone marrow plasma cell infiltration rate (median 38%, n=12 patients) and, finally, patients with a mixed pattern of tracer uptake demonstrated the highest mean infiltration rate of 47.3% (median 50%, n=21 patients). Conclusions: MM patients with pathological findings on 18F-FDG PET/CT demonstrated higher bone marrow infiltration by malignant plasma cells than patients with negative PET/CTs. Patients with a mixed pattern of tracer uptake had the highest infiltration rate.

P738

Correlation of 18F-FDG SUVs derived from reference bone marrow with recognized prognostic laboratory parameters in multiple myeloma

C. Sachpekidis1, E. K. Mai2, J. Hillengass2, H. Goldschmidt2, U. Haberkorn3, A. Dimitrakopoulou-Strauss1; 1Clinical Cooperation Unit Nuclear Medicine, German Cancer Research Center, Heidelberg, GERMANY, 2Medical Clinic V, University of Heidelberg, Heidelberg, GERMANY, 3Division of Nuclear Medicine, University of Heidelberg, Heidelberg, GERMANY.

Purpose: Our aim was to study 18F-FDG uptake derived from reference bone marrow of the os ilium in correlation with some standard laboratory variables of recognized prognostic significance in multiple myeloma (MM). Procedures: 67 patients with primary, previously untreated MM (mean age: 59.5 years; 43 male, 24 female) were enrolled in the study. All patients underwent dynamic PET/CT studies of the pelvis and lower lumbar spine. SUVs evaluation was based on volumes of interest (VOIs), drawn with a 50% isocontour, placed over the bone marrow of os ilium that didn't demonstrate any focal tracer enhancement. 18F-FDG SUVs were studied in correlation with the following laboratory recognized prognostic MM factors parameters: β2-microglobulin, thrombocytes, serum albumin, Hb, LDH, CRP and κ/λ ratio. The statistical evaluation was based on Wilcoxon rank-sum test and Spearman´s rank correlation analysis. The results were considered significant for p less than 0.05 ($p<0.05$). Results: SUVaverage correlated positively with the levels of β2-microglobulin ($r=0.22$) and negatively with the levels of thrombocytes ($r=-0.18$), albumin ($r=-0.21$) and Hb ($r=-0.45$). SUVmax also correlated significantly with β2-microglobulin ($r=0.22$), albumin ($r=-0.25$) and Hb ($r=-0.47$). Patients with hypoalbuminemia had a higher SUVmax than patients with normal albumin levels. Anaemic patients had higher SUVaverage and SUVmax than patients with normal haemoglobin levels. Furthermore, patients with pathologically elevated CRP and pathological κ/λ ratio demonstrated higher values of both SUVaverage and SUVmax than those with normal values of these indices. Conclusions: Correlation analysis revealed significant but weak - moderate correlations between 18F-FDG SUV derived from the bone marrow of the os ilium, and levels of the established prognostic MM factors β2-microglobulin, thrombocytes, albumin and Hb. SUVs were higher in patients with hypoalbuminemia, anemia, pathologically elevated CRP and pathological κ/λ ratio.

P739
Italian Interpretation Criteria for FDG PET/CT in Multiple Myeloma(MM)

C. NANNI1, A. VERSARI2, A. BIANCHI3, M. RENSI4, M. BELLO'5, S. CHAUVIE3, E. ZAMAGNI1, M. CAVO1, S. FANTI1; 1AOU S.ORSOLA-MALPIGHI, BOLOGNA, ITALY, 2S.MARIA NUOVA IRCCS, REGGIO EMILIA, ITALY, 3ASO S. CROCE E CARLE, CUNEO, ITALY, 4AOU S.MARIA DELLA MISERICORDIA, UDINE, ITALY, 5AO CITTA' DELLA SALUTE E DELLA SCIENZA, TORINO, ITALY.

FDG PET/CT is able to detect active disease in MM pts.An Italian group of physicians defined new visual interpretation criteria to standardize FDG PET/CT evaluation in MM and tested their reproducibility. This Italian multicenter protocol is a sub-protocol of EMN02, an international prospective multicenter trial of the European Myeloma Network.The criteria were written in multidisciplinary consensus meetings. They include the description of: bone marrow metabolic state(BM), nr and site of focal PET positive lesions(Fx), osteolysis(Lx), extramedullary disease(EM), paramedullary disease(PM), fractures(Fr). The uptake is defined for the target lesion and EM lesions according to modified Deauville Criteria.MM pts who had performed an FDG PET/CT at baseline(PET0), after induction(PET-AI) and the end of treatment(PET-EoT) were enrolled. The PET scans were interpreted in a blinded independent central review process managed by WIDEN®. 4 expert nuclear medicine reviewers scored the scans according to the new criteria. Concordances on different metrics were calculated using alpha Krippendorf's coefficient.17 consecutive pts were enrolled. PET0: Alpha for BM score(BMs) and F score(Fs) was 0.33 and 0.47, respectively. Alpha for Fx and Lx was 0.40 and 0.32. Skull, spine and extra-spinal involvements were demonstrated in 2, 14 and 12 pts with a mean concordance of 37%, 78% and 71%. 4 pts had a fracture for 1 reviewer and 1 pt had fractures for two. 2 pts had a PM lesion for 1 reviewer and 2 had PM lesions for all. 4 pts had EM-nodal and EM-extranodal lesions. PET-AI: Alpha for BMs and Fs was 0.09 and 0.43. Alpha for Fx and Lx were 0.22 and 0.21. Skull, spine and extra-spinal involvements were demonstrated in 1, 13 and 5 pts with a mean concordance of 25%, 67% and 79%. 4 pts had a fracture for 1 reviewer and 1 pt had fractures for all. 4 pts had a PM lesion for 1 reviewer and 2 had PM lesions for all. No pts had EM disease. PET-EoT: Alpha for BMs and Fs was 0.07 and 0.28. Alpha for Fx and Lx was 0.25 and 0.21. Skull, spine and extra-spinal involvements were demonstrated in 1, 9 and 5 patients with a mean concordance of 25%, 47% and 70%. 5 pts had a fracture for 1 reviewer. Agreement on focal lesions' score turned out to be good, as well as the number of focal lesions.New visual interpretation criteria in MM pts are therefore feasible in the clinical practice.

P740
Application of PET-CT for Evaluation of the Therapeutic Effect in Patients with Multiple Myeloma

M. B. Garcheva-Tsacheva1, B. Spassov2, D. Vassileva3; 1Medical University, Sofia, BULGARIA, 2Department of Clinical Hematology, Specialized Hospital for Active Therapy of Haematological diseases, Sofia, BULGARIA, 3Department of Nuclear Medicine, Specialized Hospital for Active Therapy of Haematological diseases, Sofia, BULGARIA.

The aim of the study is to assess utility of PET/CT findings and serum β2M levels and correlate them with therapeutic response in multiple myeloma patients (MM) treated with chemotherapy with or without autologous stem cell transplantation (ASCT). Material and methods: Thirteen MM patients were evaluated. Eleven patients were assessed after chemoradiotherapy and two - after chemoradiotherapy and ASCT. Two of them had vertebroplasty, and other 2 - endoprostheses of the fractured bones. PET/CT was performed according to standard protocol. Serum β2M levels were measured by radioimmunoassay.Results: Complete remission (CR) was detected in 53.8% (7/13) of the patients - no residual metabolic focuses was registered in five patients, whereas in two patients with vertebroplasty, areas around surgery were detected with moderate metabolic activity, which was attributed to the procedure and to some hardening effect due to the used material. The serum β2M levels of these MM patients were near to the normal range of 1.2 - 2.4 mg/l. In one patient with multiple lesions according to the baseline scan, only one of the previous lesions had metabolic activity and new fracture was detected on the follow-up. The serum β2M level was 3.28 and the therapeutic effect was evaluated as a partial response (PR). The remaining 38.5% (5/13) of the patients were evaluated to have significant residual disease activity detected by PET/CT. One of these patients had metabolic active lesion in just one bone, whereas four patients had multibone infiltration. The median serum β2M level was 8.58 mg/l and all of these patients need to continue the treatment due to the active metabolic disease. The correlation with serum β2M levels in these patients was very important for the confidence in the therapeutic response evaluation. Conclusion. PET/CT was very useful for the evaluation of MM patients after treatment by determining those with CR, PR or lack of response. It was also valuable for planning further consolidation chemo- and/or radiotherapy. The serum β2M level determination correlated well with PET/CT evaluation of the therapeutic effect.

P741

FDG PET/CT correlates better than the percent bone marrow infiltration with the status of active disease in patients with Multiple Myeloma

G. Ucmak, **B. E. Akkas**, B. B. Demirel, S. Demirtas; Ankara Oncology Research and Training Hospital Department of Nuclear Medicine, Ankara, TURKEY.

The aim of this study was to compare FDG PET/CT findings with the percentage of atypical plasma cell infiltration in bone marrow and to evaluate the importance of PET/CT results on follow-up of patients with multiple myeloma (MM) . Method: 17 patients (10M, 7 F, mean age:56.5± 12.3) with multiple myeloma underwent FDG PET/CT imaging for staging and re staging. The percentage of plasma cell infiltration (CD38 /CD138) in bone marrow on initial staging and after therapy were correlated with FDG uptake in bone and soft tissue/plasmocytoma lesions on staging and follow-up PET/CT studies. The results of PET/CT and bone marrow biopsy were evaluated for correlated with the activation of disease prognosis and on follow-up. Results: PET/CT showed hypermetabolic bone lesions in all patients. PET/CT detected extramedullary disease in addition to bone/bone marrow disease in 9 patients. All patients had standard therapy according to NCCN guidelines. On follow up (11-72 months;mean 30 months), 9 patients had remission, 2 patients had stable disease and 6 patients had progressive disease. In 9 patients with remission, the percentages of atypical plasma cell infiltration on bone marrow as well as FDG uptake of lesions were significantly decreased and patients had no evidence of disease clinically. In 6 patients with progressive disease, despite a significant decrease in the percentage of atypical plasma cell infiltration in bone marrow, FDG uptake of lesions were significantly elevated compared to initial study and/or new FDG-positive lesions were detected. These patients had biochemical signs of disease (eg. high M-protein production rates, increased β2microglobulin levels). Patients with stable disease still had FDG-positive lesions. Conclusion: The preliminary findings of this study showed that PET/CT findings correlates better with active disease in patients with MM than the percentage of atypical plasma cell infiltration in bone marrow. PET/CT offers the perfect advantage to detect extramedullary disease and to scan whole-body at one session as well. PET/CT may provide important prognostic information regarding metabolically active disease even if bone marrow biopsy may fail to demonstrate the existence of disease in patients with MM. In conclusion, we considered that further prospective studies with larger patient population are needed to support the findings of this study.

P742

Combined Use Of PET/CT And Serum Beta-2-Microglobulin In Patients With Multiple Myeloma

D. Vassileva1, B. Spassov1, M. Garcheva2; 1Specialized Hospital for Active Treatment of Hematological Diseases, Sofia, BULGARIA, 2University Hospital Alexandrovska, Sofia, BULGARIA.

Background: Multiple myeloma (MM) is a malignant haematologic disorder characterized by bone marrow infiltration with neoplastic plasma cells, paraproteinemia and osteolytic bone destruction. Standard diagnostic imaging methods, such as radiography and bone scan, have certain limitations for the early evaluation of bone and bone marrow lesions in MM patients (pts). PET/CT is a metabolic imaging technique useful to detect lesions in malignant diseases. Serum beta-2-microglobulin (β_2M) levels had been used to detect tumour burden in MM pts. However data regarding correlations between PET/CT findings with serum β_2M levels in MM pts are limited.The aim of the study was to correlate PET/CT findings with serum β_2M levels in MM patients.Material and methods: Twenty-two MM pts were evaluated (14 males and 8 females; a median age of 56.8 years (range 31-76). 18F-FDG-PET/CT scan was performed according to the standard protocol. Serum β_2M levels were measured by radioimmunoassay.Results: Different patterns of 18F-FDG-PET/CT uptake were described in 22 MM pts. Diffuse 18F-FDG-PET/CT uptake was detected in the bone marrow before other visual methods in 2 patients without bone lesions. The metabolic activity correlated with the percentage of bone marrow plasmocytes. The median serum β_2M levels was 4,3 mg/l.In one patient bone lesions showed focally increased FDG uptake. Nineteen pts had a multifocal pattern of FDG-PET/CT uptake. A total of 76 bone lesions were detected in the calvaria, spine, ribs, pelvis and long bones. The pts with advanced disease had median serum β_2M levels of 9,2 mg/l.The extramedullary lesion in the soft tissues was detected in 18.2% (4/22) pts. The potential of PET/CT to detect medullary and extramedullary lesions in a single examination is important advantage over other visualization methods.18 F-FDG PET revealed 3 previously unknown additional lesions in two patients. The diagnosis was confirmed by bone and bone marrow biopsy. The median SUV max value of PET/CT scans of the pathological foci was 5.8.Conclusion: The results showed the effectiveness of the PET/CT in detection of skeletal involvement and bone marrow infiltration in patients with MM. Our data showed that 18 F-FDG PET uptake correlated significantly with increased serum β_2M levels.

P743

Diagnostics of multiple myeloma using FET PET/CT - fesibility study

B. Malkowski1, A. Jurczyszyn2, R. Lopatto1, M. Wrobel1, M. Olejniczak1, J. Czyz3; 1Oncology Centre, Bydgoszcz, POLAND, 2Hematology Clinic, JU, Krakow, POLAND, 3University Hospital, Bydgoszcz, POLAND.

Aim: Precision of FDG PET/CT scans in diagnostics of myeloma is not certain, but is better than conventional methods of imaging. Publications give us conflicting results. Due to reactions in bone marrow and post-terapeutic changes, assessment and adequate conclusions using FDG could be difficult. There are some reports about possibility of using amino-acid tracers in this type of cancer. Positive experiences with 11C-methionine confirm possibility of apply this group of radiopharmaceutics in myeloma. Because the methionine's transport and metabolism is similar to another aminoacid like thyrosine, we are trying to use 18-fluoro-ethyl-thyrosine (FET) to diagnose myeloma level of advance. Materials: 31 patients from 34 to 72 years old (mean 59,6) with myeloma. They were referred from Hematology Clinic to differentiate changes which were detected with different methods like CT, X-ray or MRI, in which there were doubts of possibility of the active disease or the place of disease was unknown. Methods: FET PET/CT were performed before start of treatment. FET were produced in our Laboratory in Oncology Centre in Bydgoszcz using module Syncrom R&D (Raytest). The acquisition was made 60 minutes after injection of 350±10 MBq FET. The acquisition were performed on Biograph mCT128 or Biograph mCT20 scanners. Foci of higher metabolism FET than background with coexistence or not myeloma changes in CT scans was stated as pathological. The background activity in the brain, spleen, gluteus muscle, Th10 and L4 and was assessed. Results of PET were compared with clinical stage and background activity. Results:23 patients had active disease and 8 were in remission(not active) FET-PET was negative in 8 patients in remission , positive in 23 patients with active disease. FET PET/CT results were in the agreement with clinical state of the patients. In FET-PET/CT scans SUV values in the pathological foci (103) were 1,850-6,02 (average 3,57). There were lesions characteristic for myeloma in CT scans without metabolic activity in FET . We found five FET foci, which haven't been discovered by other examinations in four from the group of FET-PET positive patients. Mean background activity (SUV max) was : brain - 1,1, spleen - 2,3, muscle - 1,74, Th10 - 2,14, L4 - 1,82. In individual patients background activity (apart from spleen) was clearly lower than in pathological foci. Conclusion: FET could be the tracer used in diagnostics of multiple myeloma.

P744

Possibility of the early assessment of treatment effectiveness in multiple myeloma by FET PET/CT - initial results

B. Małkowski1, R. Lopatto1, M. Wróbel1, M. Olejniczak1, A. Jurczyszyn2, J. Czyz3; 1Oncology Centre Bydgoszcz, Bydgoszcz, POLAND, 2Haematology Clinic Jagiellonian University, Kraków, POLAND, 3Haematology Clinic CM NC University, Bydgoszcz, POLAND.

Aim: There are experiences with 18-fluoro-ethyl-thyrosine (FET) to diagnose activity of disease multiple myeloma. The aim of the study was to use this amino-acid tracer to assess early treatment efficacy in this disease.Materials: 6 patients from 56 to 65 years old (mean 62) with newly diagnosed of multiple myeloma. They were referred from Hematology and Clinical Oncology Clinics to treatment efficacy.Methods: First FET PET/CT were performed before start of treatment. Second FET PET/CT were performed after the second course of chemotherapy just before the third course. FET were produced in our Laboratory in Oncology Centre in Bydgoszcz using module Syncrom R&D (Raytest). The acquisitions were made 60 minutes after injection of 350 ±10 MBq FET. The acquisition were performed on Biograph mCT128 or Biograph mCT20 scanners. Foci of higher uptake of FET than background with coexistence or not myeloma changes in CT scans were stated as pathological. We compared individual uptake in all pathological foci (SUVmax) in these two examinations.Results: All 6 patients had active disease in first examination FET-PET. In first FET-PET/CT scans SUVmax values in the pathological foci were 3,85-8,2 (average 5,24). In second examination, after second course of chemotherapy, SUVmax values in the pathological foci were 1,5-2,7 (average 2,31). In second FET PET/CT scans SUV values were clearly lower than in the first examination.We were noticed significant decline of SUVmax in average 53% (from 34% to 74%).Conclusion: FET could be the tracer used in diagnostics and assessment of treatment effectiveness in multiple myeloma.

P745

Diagnostic value of F-18 FDG PET-CT imaging in multiple myeloma

F. CANBAZ1, Y. USTA1, O. YAPICI1, M. TURGUT2; 1Ondokuz Mayis University Hospital, Faculty of Medicine, Nuclear Medicine Dept., KURUPELIT / SAMSUN, TURKEY, 2Ondokuz Mayis University Hospital, Faculty of Medicine, Hematology Dept., KURUPELIT / SAMSUN, TURKEY.

Aim:Multiple myeloma(MM) is a malignant neoplasm of plasma cells producing a monoclonal immunoglobulin that accumulate in bone marrow(BM) leading to bone destruction and marrow failure.According to The IMWG, diagnosis of MM requires the fulfillment of the following criteria:Clonal bone marrow plasma cells ≥10% or biopsy-proven bony/soft tissue plasmacytoma PLUS one of related organ/tissue impairment(Anemia,Hypercalcemia,Renal insufficiency and bone lesions).The skeleton is involved in more than 80% of patients at the time of initial diagnosis.Conventional imaging may miss bone lesions related to the disease.The value of F18-FDG PET in the diagnostic approach of MM remains incompletely elicited.The aim of this study was to evaluate the diagnostic value of FDG-PET CT imaging in MM. Material and Methods:Thirty patients, clinically suspected of MM and who underwent FDG PET-CT imaging were retrospectively analyzed.According to the diagnostic criteria, findings of bone BM biopsy, presence of plasmasitoma with monoclonal gammopathy and tissue impairment parameters were examined. Results:The mean age of the patients was 60.51 ±11.43(20 Male;10 Females).Considering the diagnostic criteria of MM, 18/30 patients were fulfilled the diagnostic MM criteria and of these, 7/18 patients showed multiple hypo-hypermetabolic lytic lessons, 5/18 patients showed increased heterogenic BM activity.In 2 patients with biopsy-proven skeletal plasmacytoma, multiple hypermetabolic lesions were detected;in 4/18 patient, no abnormality could be found on PET/CT imaging.PET/CT scan provided the diagnosis of MM in three patients with >10% plasma cells (without any other organ impairment parameters) by showing hypermetabolic lytic lesions.Patients with <10 % plasma cells in BM, had negative findings or increased minimal heterogen BM metabolic activity.Of 10 patients with %10-60 plasma cells in BM, 4 had negative findings, 2 had heterogenic metabolic activity in BM and 4 had multiple lytic lesions on FDG PET/CT scan.All of the 3 patients with >60% plasma cells in BM, had multiple lytic lesions FDG PET/CT scan. Conclusion:It is important to distinguish MM from other causes of the clinical presentations for prognosis and treatment.To discriminate MM patients in a timely fashion is also crucial since a major delay in diagnosis leads to a negative impact on the disease course.Patients with negative PET/CT demonstrated the lowest bone BM plasma cell infiltration, whereas those with multiple lytic lesions in different metabolic activity showed the highest BM infiltration rate.Our results supported that FDG PET CT imaging is useful in the diagnostic workup of MM and it can provide to make correct diagnosis or help to exclude other clinical presentations mimicking MM.

P746

Discrepancies in detection of Myeloma's bone lesions between PET and CT components in 18F-FDG PET/CT studies.

L. F. León Ramírez, C. González Roiz, A. Ortega Candil, C. Rodriguez Rey, A. Serrano Palacio, C. Riola Parada, R. Couto Caro, J. L. Carreras Delgado; Hospital Clinico San Carlos, Madrid, SPAIN.

AIM: To detect bone lesions by using PET/CT technique in patients with diagnosis of Multiple Myeloma (MM). Material and Methods: We retrospectively reviewed 29 studies performed in our Nuclear Medicine Department from November 2008 to January 2015 and we correlated these findings with MR results. Lesions detected with CT were independently evaluated from FDG uptakes suggestive of malignancy in PET. We established a scale to evaluate CT findings according to the number of lytic/sclerotic bone lesions, considering as an independent lesion the presence of diffuse bone involvement, in the form of osteopenia or myelomatosis. To evaluate PET results, the number of focal pathological FDG uptakes was considered and diffuse bone marrow involvement was also considered an independent lesion. Results: 29 studies were analyzed. There were 14 women and 15 men (mean age 62.9 years old) with diagnosis of MM. 55% of them were heavy chains (45% IgG, 10% IgA). The remaining (45%) were Bence Jones or not secreting (46% Kappa, 17% Lambda and the remaining non-secretory). In 9/29 studies the same number of lesions were detected with both techniques. In 16/29 studies the CT detected more lesions than PET and in 4/29 the PET detected no visible lesions in CT, with a moderate index of agreement (kappa 0.46). From the total number of lesions detected with the CT component, PET detected 67% of them (Rho Spearman Index 0.66). It was taken into account if the patient received systemic therapy at the time of the test, and no statistically significant differences in the detection of lesions were found. Conclusions: PET has a lower detection rate of bone lesions in multiple myeloma, possibly because it is unable to detect low-grade lesions, which makes imperative the combined use with CT.

P45 - Tuesday, October 13, 2015, 4:00 PM - 4:30 PM, Hall 3 – Poster Exhibition

Clinical Oncology: Bone

P747

Bone scintigraphy as a new imaging biomarker: the relationship between bone scan index and PSA in prostate cancer patients receiving radium-223 dichloride therapy.

Y. Nakagami, D. Kano, M. Kusumoto; National Cancer Center, Chiba, JAPAN.

Aim: A computer-aided diagnosis system for bone scintigraphy with a semiquantitative index from the Bone Scan Index (BSI) has been used to quantify the spread of bone metastases. However, few papers have made clear associations among BSI, bone metabolic markers, and prostate-specific antigen (PSA). And the estrangement between the progression of cancer and a value of the PSA may become for the castration-resistant prostate cancer. On the other hand, radium-223 dichloride, a targeted α-emitter, improved overall survival and was well tolerated in patients with castration-resistant prostate cancer and symptomatic bone metastases. The objective of this study was to explore the prognostic value of the Bone Scan Index (BSI) obtained at the time of diagnosis in a group of high-risk prostate cancer patients receiving radium-223 dichloride therapy. Materials and Methods: This was a retrospective study based on consecutive prostate cancer patients at high risk, based on clinical stage (T2c/T3/T4), Gleason score (8 to 10) and prostate-specific antigen (PSA) (>20 ng/mL), who had undergone whole-body bone scans < 3 months after diagnosis and who received radium-223 dichloride therapy. The intervals between bone scans and blood examinations were 0-16 days (median 0 day). The serum markers of PSA were examined. Subjects were divided into 4 groups according to BSI; Group A: 0 to <2, Group B: 2 to <4, Group C: 4 to <8, and Group D: over 8. BSI was calculated using an automated method. BSI, which corresponded to the amount of metastatic lesion, was automatically calculated by BONENAVI software (FUJIFILM RI Pharma, Co. Ltd., Tokyo, Japan; Exini Bone, Exini Diagnostics, Sweden). Results and Conclusions: In a multivariate analysis, Gleason score and BSI were associated with survival, but clinical stage and PSA were not prognostic. The 5-year probability of survival was 52% for patients without metastases, 41% for patients with BSI < 1, 30% for patients with BSI = 1 to 5, and 0% for patients with BSI > 5. All bone scans showed high uptake with bone metastases. BSI did not correlate significantly with the serum PSA. The changes in BSI did not show a close relationship with the serum PSA. The BSI can be used as a complement to PSA to risk-stratify high-risk prostate cancer patients at the time of diagnosis. This imaging biomarker, reflecting the extent of metastatic disease, can be of value in patient management when deciding on radium-223 dichloride therapy.

P748

Automatic bone scan index for therapy response assessment of radium-223-dichloride (Ra-223) therapy in advanced prostate cancer

M. Sakretz, J. Kurth, S. M. Schwarzenböck, B. J. Krause, M. Heuschkel; Rostock University Medical Center, Department of Nuclear Medicine, Rostock, GERMANY.

Aim: Evaluation of progression and therapy response is needed to improve and optimize individualized therapy management of patients suffering from metastatic castration resistant prostate cancer (mCRPC). However, there is a lack of consistent data for therapy response assessment to optimize treatment. Treatment decisions based on PSA-value alone are inadequate, therefore other clinical and radiologic criteria indicating disease progression should be taken into account. Therefore we evaluated the utility of an automatic bone scan index (aBSI) to assess response to Ra-223-therapy in patients with mCRPS with bone metastases, in comparison to established response markers, e.g. number of lesions or PSA. Materials and Methods: Nine patients with clinical progress of bone metastases from mCRPC, who underwent 6 cycles of Ra-223-therapy were retrospectively included in this pilot study. Whole-body bone scans with Tc-99m-DPD were performed and blood samples were taken approximately four weeks before and after 6 cylces of Ra-223-therapy. The aBSI was calculated using EXINIboneBSI (EXINI Diagnostics AB, Sweden). Changes of aBSI, number of lesions, levels of PSA and alkaline phosphatase (AP) were compared pre- and post-therapy. Correlation between aBSI and PSA as well as AP was evaluated by calculation of Pearson's correlation coefficient. Results: Therapy response / progress was defined as decreasing / increasing aBSI, less / more than two new lesions in whole-body bone scan and lower / higher PSA level compared to baseline. Response was found in 2/9 (22 %), stable disease in 1/9 (11%) and progress in 6/9 (67%) of the patients. The median aBSI was 2,67±2,62 at baseline scan and 2, 71±2,73 at control scan after 6 cycles of therapy. The median number of lesions was 18±40 and 22±42, respectively. The median PSA level was 38,5±339,19 and 46,7±364,63, respectively. Median alkaline phosphatase level was 1,28±1,87 and 1,23±2,18, respectively. The ΔaBSI (mean 0,04±0,86) showed a statistically significant correlation with ΔPSA (mean 60,79±117,2; r = 0,76, p = 0,014) and weaker one with ΔAP (mean -0,28±1,86; r=0,59, p = 0,093). Limitations are the small patient sample-size, the retrospective analysis and high inter-individual variability. Conclusions: The aBSI might be a useful and promising data analysis tool for the assessment of therapy response to Ra-223. Studies in larger cohorts are needed.

P46 - Tuesday, October 13, 2015, 4:00 PM - 4:30 PM, Hall 3 – Poster Exhibition

Clinical Oncology: Melanoma

P749

Benefits of performing ultrasound and US-guided FNAC in melanoma patient scheduled for sentinel lymph node biopsy

G. Horvatic Herceg1, I. Bracic1, M. Kralik2, D. Herceg3, S. Kusacic-Kuna1, J. Antulov4; 1Clinical department of nuclear

medicine and radiation protection, University Hospital Center Zagreb, Zagreb, CROATIA, 2Department of radiology, University Hospital Center Zagreb, Zagreb, CROATIA, 3Department of Medical Oncology, University Hospital Center Zagreb,, Zagreb, CROATIA, 4Clinical department of histopathology, University Hospital Center Zagreb, Zagreb, CROATIA.

Lymph node status is the most meaningful prognostic indicator for overall survival of patients with stage I/II melanoma. Sentinel lymph node biopsy (SLNB) has become a common procedure in melanoma and it is considered to be a highly accurate procedure that allows appropriate regional nodal staging and identification of patients without nodal metastases. However, this method brings also some disadvantages: certain degree of invasiveness, possible risk of unnecessary surgery and the high cost of the procedure. Therefore, high-frequency ultrasonography (US), with fine needle aspiration cytology (FNAC) of suspicious lymph nodes, was investigated as a tool to identify or exclude nodal disease in melanoma patients. Methods: 136 consecutive patients with cutaneous melanoma (75 females and 61 males; mean age 59 years, range: 19-81 years) planned for SLNB between August 2008 and April 2015 were included in the study. The preoperative US of the regional lymph node basins was carried out in 136 SNB candidates with FNAC of suspicious lymph nodes (LN). In cases of malignant findings, patients were submitted to complete lymph node dissection (CLND). The findings were correlated with histopathology after CLND. Results: In 23 SNB candidates, the US-guided FNAB was positive for metastases and they proceeded directly to CLND. All FNAC findings were confirmed by histopathology, with no false positive results. There were 9 false negative results out of 113 patients with negative echographic findings. In those patients histopathology revealed metastases, mostly in form of small foci of tumor cells or individual atypical cells. The sensitivity, specificity, positive predictive value, and negative predictive value of US combined with FNAC were 71.87%, 100%, 100% and 92.04%. Conclusion: Patients with US suspicious regional lymphadenopathy confirmed to be of metastatic nature by preoperative FNAC, should undergo a therapeutic LND. However, in such patients, especially those with primary melanoma of the trunk or head and neck, lymphoscintigraphy should be considered to identify other nodal basins at risk, and SLNB in these areas may be performed in conjunction with therapeutic lymphadenectomy of the clinically involved nodal basin. More advanced US probes should allow better spatial resolution and assessment of lymph node vascularization, enabling diagnosis of metastasis measuring less than 2 mm in diameter.

P750
Sentinel Lymph Node Biopsy for Melanoma: our Experience

E. M. Triviño-Ibáñez, N. Testart, J. M. Ruiz-López, R. Sánchez-Sánchez, J. M. Llamas-Elvira; Virgen de las Nieves University Hospital, Granada, SPAIN.

Objective: to analyze our experience in the use of SLNB in melanoma and identify the predictive factors of positive SLNB and poor prognosis. Patients and methods: Retrospective study of 109 patients who underwent SLNB for melanoma between December 1999 and November 2013. Demographic, topographic characteristics of MM were collected, histologic features of the tumor (Breslow thickness, presence of ulceration, mitotic index, regression), distribution and drainage of the sentinel node (SN), result histogycal, development of distant metastasis and survival time. Results: 109 patients (mean age of 51.69 ± 15.05 years, women 56%). The most common tumor location was the trunk with 50 cases (45.9%), followed by the lower limbs with 36 (33%), upper limbs 20 (18.3%) and head and neck in 3 cases (2.8%). The median Breslow thickness was 2.43 ± 1.92 mm, with the presence of tumor ulceration in 23 (21.1%) cases. SN number of isolates was between 1 and 4, being in 80 cases (73.4%) of single location. The definitive study of the SN was positive in 26 (23.9%) patients. Related factors statistically significant, with a positive result of SN were: age at diagnosis (49.10±14.79 vs 59.96±12.93 years, p= 0.01), Breslow thickness (1.98 ±1.57 vs 3.82±2.22 mm; p <0.01), male sex (32/83 vs 16/26, p= 0.039, OR: 2.55) and tumor ulceration (12/44 vs 11/19, p= 0.021). The average follow-up was 60.08 ±47.47 months. 10 patients have died (9.2%) and 21 (19.3%) developed metastases. Of the 21 patients who developed distant metastases, 12 (57.1%) had a positive result in the SLNB, while it was negative in 9/21 (42.8%). The comparative analysis between patients who developed metastases and those without, showed statistically significant differences in age at diagnosis (50.16±14.61 vs 57.71±15.95 years, p= 0.042), Breslow thickness (2.20±1.85 vs 3.6±1.94 mm; p< 0.01), presence of ulceration (13/50 vs 10/13 cases; p<0.01) and positive SN (14/87 vs 12/21 cases; p<0.01). Survival analysis shows statistically significant differences in age at diagnosis (50.8±15.1 vs 60.5±12.3 years, p= 0.039), Breslow

thickness (2.28±1.89 vs 3.93±1.83 mm, p= 0.009), tumor ulceration (18/57 vs 5/6 patients; p= 0.012), positive SN (20/99 vs 6/10 patients, p<0.01) and development of metastases (12/98 vs 9/10 patients, p<0.01). Conclusions: In our study, age at diagnosis, Breslow thickness, ulceration of the tumor and the positive outcome of the SN are the main factors related to the development of metastases in the MM determining decreased survival.

P47 - Tuesday, October 13, 2015, 4:00 PM - 4:30 PM, Hall 3 – Poster Exhibition

Clinical Oncology: Imaging Guided Surgery (including Sentinal Lymph Node)

P751

"SPECTacles" for surgeons: SECT-CT visualization of axillary sentinel lymph nodes in patients with breast cancer - obligatory step of surgery planning

P. Krzhivitskiy, S. Kanaev, **S. N. Novikov**, P. Krivorotko, L. Jukova; N.N. Petrov Institute Oncology, St Petersburg, RUSSIAN FEDERATION.

Purpose: to determine individual variability of axillary sentinel lymph nodes (SLN) localization in patient with breast cancer (BC) and to evaluate clinical value of SPECT-CT for surgery planning in patients with breast cancer. Material and methods: Individual topography of axillary SLN was determined in 127 patients with early BC. All women were candidates for breast conserving surgery with SLN biopsy. SPECT-CT visualization of SLN started 120-240 min after intratumoral injection of 74-150MBq of 99mTc-macrocolloids (200-1000nm). Taking into account large particle size all visualized LN were considered as sentinel. Distribution of SLN in axillary region was allocated to following subregions: central (C), anterior pectoral (AP), sub-(SP) intrapectoral (IP), lateral (L), subscapular (SSc), LN "lying on the ribs" (Th). According to routine practice in our surgical departments surgeons take for evaluation SLN localized in C and AP subregions. In patients with positive SLN axillary dissection obligatory cover IP and SP nodes. Results: SPECT-CT visualization of SLN demonstrated large variability in their localization. In most cases they were detected in C (64 observations, 50.5%) and AP (34 women, 26.8%) subregions. In 19 (14.9%) cases SLN were revealed in Th and in another 10 (7.8%) patients -in L or SSc subregions. In 17 (13.4%) women SLN were localized both on I and II (IP, SP) levels. Analysis of surgery practice demonstrated that SLN "lying on the ribs" were effectively biopsied only after introduction of SPECT-CT technology. Biopsy of SLN localized in IP, SP, L and SSc regions become more accurate. Finally we find that in 14.9%-22.7% cases SPECT-CT visualization of SLN can improve accuracy of this surgical procedure. Conclusion: SPECT-CT localization of SLN is an important part of surgery planning because in 14%-23% patients SPECT-CT data can improve accuracy of SLN biopsy

P752

Sentinel node biopsy in head and neck tumors. Validation results

M. Bellón Guardia1, M. Talavera Rubio1, A. Palomar Muñoz1, R. Galan Hernandez2, L. Gonzalez Lopez3, B. González García1, V. Poblete Garcia1, F. Pena Pardo1, A. Soriano Castrejon1; 1Servicio de Medicina Nuclear. Hospital General Universitario, Ciudad Real, SPAIN, 2Servicio de Cirugía maxilofacial. Hospital General Universitario, Ciudad Real, SPAIN, 3Servicio de Anatomia Patológica. Hospital General Universitario, Ciudad Real, SPAIN.

OBJECTIVE. Compare selective sentinel node biopsy (SLNB) with conventional lymphadenectomy in patients with head and neck tumor (HNT) and evaluate parameters of clinical applicability. MATERIAL We have included patients with HNT prospectively (PI 2010/63), clinical and radiological T1-2N0 stage, diagnosed by FNA and scheduled for elective resection and uni or bilateral lymphadenectomy between 2010 and 2014. METHOD Preoperative lymphoscintigraphy was performed 2-3 hours before surgery. Four doses of 9MBq of radiocolloid were injected perilesionary. Planar and tomographic images were obtained, identifying the number and anatomical location of the sentinel nodes (SN). The SN was studied by staining H/E. RESULTS 29 patients were recruited (22males) with HNT. The most common location was floor of the mouth (10p) and tongue (10p). In all patients evidenced at least 1 SN. In 11 patients bilateral lymphadenectomy was the optimal treatment, analyzing a total of 40 procedures. We found positive lymphadenectomy in 9 patients. We obtained two false negative results, both in patients with floor of mouth tumor. Regarding the 40 procedures, the detection rate of SN in lymphoscintigraphy was 92.5%. In our series SLNB showed a sensitivity of 80%, specificity of 100% and NPV of 93.1% for the detection of disease. CONCLUSION To date, these results allow the validation process of SLNB technique in patients with HNT and implementation in our environment, taking special care in floor of mouth tumors.

P753

The clinical impact of selective axillary dissection after lymphoscintigraphy axillary reverse mapping to reduce breast-cancer related lymphedema : long term results of a preliminary study

M. Maccauro1, M. Gennaro2, A. Lorenzoni1, G. Aliberti1, C. Sigari3, L. Bedodi3, M. Castellani1, E. Seregni1, R. Agresti2, A. Caraceni3, M. Greco2, F. Crippa1; 1Nuclear Medicine Unit, Department of Diagnostic Imaging and Radioterapy, Fondazione IRCCS Istituto Nazionale dei Tumori, Milan, Italy, Milan, ITALY, 2Breast Unit, Department of Oncological Surgery, Fondazione IRCCS Istituto Nazionale dei Tumori, Milan, Italy, Milan, ITALY, 3Department of Rehabilitation and Palliative Care, Fondazione IRCCS Istituto Nazionale dei Tumori, Milan, Italy, Milan, ITALY.

Aim: Axillary reverse mapping (ARM) is a technique to distinguish the lymphatic pathway of the arm from that of the breast allowing the sparing of the draining nodes and/or lymphatic ducts from the arm during axillary dissection. The use of ARM may preserve upper extremity drainage preventing breast-cancer-related lymphedema (BCRL) in patient with indication for axillary lymph node dissection (ALND). The aim of this study was to assess the feasibility of selective axillary dissection (SAD) after ARM and to evaluate the rate of related lymphedema. Materials and methods: From 06-2009 to 02-2012 sixty patients (pts) stage with II-III breast cancer and positive sentinel lymph node (SLNB) were enrolled in the study. ARM procedure included lymphoscintigraphy that was performed 4-6 hours prior SAD by three subcutaneous injection of 99mTc-nanocolloid (15 MBq, 0.3 ml) into the dorsum of hand. SAD was performed up to Berg's level III with the gamma probe to identify and preserve the arm's lymphatic hot spot. Breast-cancer-related lymphedema was evaluated by physiatric assessment (increase > 2 cm of the arm circumference) and lymphoscintigraphy of the upper extremities during follow-up. Results: SAD was performed in all pts patients who underwent to ARM (60/60). The draining lymph nodes were located medially to where the thoracodorsal merged with the axillary vein in 40/60 pts or laterally to the thoracodorsal vein in 5/60 pts. In 15/60 (25%) patients hot nodes were removed during surgery because located below the second intercostobrachial nerve, where metastatic spread from breast carcinoma is most likely to occur. At a mean follow-up of 39 months (range 19-59) 5/15 pts (33%) in who hot node was removed developed BRCL. Only 2/45 pts in who the draining nodes from the arm during were spared developed BRCL (4%). One of these 2 pts was previously treated with the extend mantle field radiation therapy for Hodgkin's Disease. None of the patients had nodal relapses during considered follow-up. Conclusion: Selective axillary dissection using axillary reverse mapping is a feasible and safe procedure to markedly reduce BCRL (33% pts with ALND vs 4% pts with SAD).

P754

Contribution of SPECT/CT imaging to radioguided sentinel lymph node biopsy in melanoma

J. Villanueva Curto, A. Cobo Rodriguez, A. Sainz-Esteban, C. Gamazo Laherrán, M. González Selma, M. Ruíz Gómez, M. Alonso Rodríguez, R. Olmos García; HOSPITAL CLÍNICO UNIVERSITARIO DE VALLADOLID, Valladolid, SPAIN.

Aim: To assess the contribution of SPECT/CT to planar images in radioguided sentinel lymph node biopsy (SNLB) in patients with melanoma in terms of diagnostic accuracy and anatomic localization of sentinel node (SN). Methods: We include 40 patients (21 women, mean age: 57) with melanoma located in head and neck (6), trunk (13) and limbs (21). Acquisition of dynamic and static planar images was performed after the intradermal administration (peritumoral/pericitricial) of 148 MBq of 99mTc-nanocoloidal albumin the day before surgery. A SPECT/CT was performed in all patients. Detection of SN was marked on skin. During the surgical procedure a hand-held gammaprobe was used to identify hot nodes. When SN showed metastasic disease, lymph node dissection was performed. Results: Seventy three SN were detected in planar images in our 40 patients (detection index: 100%). SN were located in head and neck (15), truck (53) and limbs (4). SPECT/CT did not detected additional SN, but prevented misinterpretation of false positive no-nodal site of uptake (in 3 patients) that corresponded to contamination (3) and a canalicule (1). SPECT/CT detected the exact anatomical localization of all the SN but was specially useful in 15 patients (37.5% of patients) in which the SN were located in auricular (5) and cervical region (4), face (5) and thorax (1). Besides, SPECT/CT changed the anatomical localization of 5 SN in 4 patients (10% of patients), which were located in axilar region on planar images and were correctly located in periscapular region on SPECT/CT. Finally, in one patient SPECT/CT confirm one suspicious uptake detected in the planar study that resulted a SN in the inguinal region. Conclusion: SPECT/CT detected the exact anatomical localization of all the SN and improved the anatomical localization of SN already visualized on planar images in almost a third of the patients. Besides, it improved the characterization of no-nodal site of uptakes, dismissing false positives findings and confirmed a suspicious

uptake detected on planar images. However, SPECT/CT did not detect additional SN.

P755

Review of breast cancer sentinel node scintigraphy at Hospital da Luz - 2009-2013

V. Sousa, T. Cunha, C. Loewenthal, M. Vieira; Hospital da Luz, 1500-650, PORTUGAL.

Aim- The aim of this study was to review our population of breast cancer scintigraphy patients (pts) and determine if there is any predictive factor in our cohort of patients related to: a positive sentinel lymph node biopsy (SLNB), a positive axillary lymph node clearance (ALNC) and recurrence rate after treatment. Materials and methods- A retrospective analysis of 317 breast cancer sentinel node scintigraphies performed between January 2009 and May 2013 was undertaken. It included a cohort of 313 patients (4 patients were bilateral tumours) with clinical follow-up in our breast cancer unit (average 38 months). Statistical data analysis was processed with SPSS. Results- All the patients were females with a median age of 56 years (range 27-88y). The histological types most often seen were invasive ductal carcinoma (82%), in situ ductal carcinoma (8%) and invasive lobular carcinoma (5%). Seventy-three percent of carcinomas were G2 Elston-Ellis, 25% G1 and 2% G3. The average size was 15mm (median 13mm) (pT1 size frequency of 76%). Of 317 SLNB performed, 47 (15%) had metastases of which 40 (82%) were macrometastases and 9 (18%) micrometastases. Of 47 positive SLNB, 44 patients underwent axillary dissection (average 16 nodes excised) and 18 (41%) had additional lymph node disease. The rate of sentinel node identification by lymph node scintigraphy was 98% (310/317). Of 7 lymph node scintigraphies in which the sentinel node was not identified, due to non-drainage, 6 (86%) underwent ALNC. Of these 6 ALNC performed, 3 (50%) had axillary metastatic disease. One of 7 pts (14%) later presented with disease recurrence. The disease-free survival rate was 97.5%, with a recurrence rate of 2.5%. The median time to recurrence was 24 months. Using statistical analysis, lymphovascular invasion (p~0,000) and size (p=0,002) were significant predictors for positive sentinel node, whereas non-drainage (p=0,044) was a significant predictor for recurrence. In this population we were not able to demonstrate a correlation between positive sentinel lymph node and disease recurrence. Conclusion- Our study confirms a high breast cancer sentinel node identification rate with lymphoscintigraphy and suggests not only a correlation between lymphovascular invasion, size and a positive sentinel node, but also, a correlation between non-drainage on scintigraphy and recurrence.

P756

Utility of sentinel lymph node biopsy in vulvar cancer.

A. SAINZ-ESTEBAN, A. Cobo Rodríguez, J. Villanueva Curto, C. Gamazo Laherrán, M. González Selma, M. Ruiz Gómez, M. Alonso Rodríguez, R. Olmos García; Hospital Clínico Universitario de Valladolid, VALLADOLID, SPAIN.

Aim: the aim of the study was to determine the detection rate and negative predictive value (NPV) of sentinel lymph node biopsy (SLNB) in vulvar cancer (VC). Material y methods: A retrospective study from 2007 and 2014 has been performed in women with VC who underwent SLNB in our service. A total of 8 women were studied: one with melanoma, one with adenocarcinoma of the bartholino gland, 5 with epidermoid carcinoma and one with sebaceous carcinoma. Seven patients presented a stage I and the patient with the melanoma presented a stage IIb. Three patients had tumours in the midline. None of the patients had clinically suspicious inguinofemoral lymph nodes or previous treatment with surgery, chemotherapy or radiotherapy. Acquisition of dynamic and static planar images was performed after the intradermal administration of 37-148 MBq of 99mTc-nanocoloidal albumin. A SPECT/CT was performed in 6 the patients. In 5 patients excision of sentinel lymph nodes (SLN) was followed by an inguinofemoral lymphadenectomy (IFL) (bilateral or unilateral depending on tumour localization) because the SLNB in this centre was under the validation period. All patients were observed with follow-up for at least 9 months. Results: Eleven were identified in planar images detected 11 SLN in the 8 patients (detection rate: 100%). SPECT/TC did not detect additional SLN but improved the anatomical localization of all the SLN. Unilateral drainage was obtained in 7 patients and one patient with a midline tumour presented bilateral drainage. SLN was positive for metastasis in 2 patients and negative in 6. Of the 6 patients with negative SLN, the IFL was negative in three and the follow-up in 2. The last patient with a midline tumour presented a SLN in the right groin that was negative for metastasis and did not show other lymph node affected. However, the left IFL showed several metastatic lymph nodes (false positive) (NPV: 5/6). Conclusion: SLNB seems to be a useful technique for the detection of nodal involvement in early stages vulvar malignancies.

P757

Comparative evaluation of 99mTc-Al2O3 and 99mTc-fitat nanocolloids for sentinel lymph nodes visualization in patients with cervical cancer

I. Sinilkin1,2, V. Chernov1,2, A. Chernyshova1, L. Kolomiets1, A. Titskaya1,2, R. Zeltchan1,2, O. Bragina2, A. Lyapunov1, V. Skuridin2; 1Tomsk Cancer Research Institute, Tomsk, RUSSIAN FEDERATION, 2Tomsk Polytechnic University, Tomsk, RUSSIAN FEDERATION.

Purpose: To study the feasibility of using of 99mTc-Al2O3 and 99mTc-fitat nanocolloids for sentinel lymph nodes (SLN) visualization in patients with cervical cancer. Materials and methods: Nanocolloid 99mTc-Al2O3 with size of nanoparticles 80-100 nm coated with organic covering was studied. During passage through the lymphatic way nanoparticles lose organic coating and strongly accumulate in the sentinel lymph nodes without redistribution. Nanocolloid 99mTc-fitat has size of nanoparticles 50-100 nm. The study included 35 patients with cervical cancer of stage I. To identify sentinel lymph nodes a 99mTc-Al2O3 was administered to 15 patients (first group) and 99mTc-fitat was injected to 20 patients (second group). Nanocolloid was injected peritumoral in four points to 40 MBq one day prior to the planned operation. SPECT study was performed at 18 hours after injection, intraoperative detection was executed by gamma probe at 20 hours after injection. Results: In the first group in all patients 19 SLN were identified in by SPECT and 24 SLN by gamma probe. Accumulation of 99mTc- Al2O3 in SLN was 7-11% by SPECT and 17-31% by gamma probe (in compare to spot of injection). In the second group by SPECT in 17 patients 23 SLN were identified and by gamma probe in 19 patients 27 SLN were visualized. Accumulation of 99mTc-fitat in SLN was 1,5-2% by SPECT and 3-7% by gamma probe (in compare to spot of injection). Conclusion: The clinical study of 99mTc-Al2O3, a new radiopharmaceutical agent, have shown that the studied nanocolloid has high uptake level in SLN and can be successfully used for visualization of SLN in patients with cervical cancer.

P758

Comparative evaluation of 99mTc-Al2O3 and 99mTc-fitat nanocolloids for sentinel lymph nodes visualization in patients with cancer of larynx and hypopharynx

V. Chernov1,2, I. Sinilkin1,2, E. Choynzonov1,2, S. Chijevskaya1, A. Titskaya1,2, R. Zeltchan1,2, O. Bragina2, A. Lyapunov1, V. Skuridin2; 1Tomsk Cancer Research Institute, Tomsk, RUSSIAN FEDERATION, 2Tomsk Polytechnic University, Tomsk, RUSSIAN FEDERATION.

Purpose: To study the feasibility of using of 99mTc-Al2O3 and 99mTc-fitat nanocolloids for sentinel lymph nodes (SLN) visualization in patients with cancer of larynx and hypopharynx.Materials and methods: Nanocolloid 99mTc-Al2O3 with size of nanoparticles 80-100 nm coated with organic covering was studied. During passage through the lymphatic way nanoparticles lose organic coating and strongly accumulate in the sentinel lymph nodes without redistribution. Nanocolloid 99mTc-fitat has size of nanoparticles 50-100 nm. The study included 28 patients with cancer of larynx and hypopharynx (T1-3NxM0). To identify sentinel lymph nodes a 99mTc-Al2O3 was administered to 10 patients (first group) and 99mTc-fitat was injected to 18 patients (second group). Nanocolloid was injected peritumoral submucous in four points to 40 MBq one day prior to the planned operation. SPECT study was performed at 18 hours after injection, intraoperative detection was executed by gamma probe at 20 hours after injection.Results: In the first group in all patients 12 SLN were identified in by SPECT and 14 SLN by gamma probe. Accumulation of 99mTc-Al2O3 in SLN was 5-10% by SPECT and 18-33% by gamma probe (in compare to spot of injection). In the second group by SPECT in 16 patients 18 SLN were identified and by gamma probe in 17 patients 23 SLN were visualized. Accumulation of 99mTc-fitat in SLN was 1,2-1,9% by SPECT and 3-6% by gamma probe (in compare to spot of injection).Conclusion: the clinical study of 99mTc-Al2O3, a new radiopharmaceutical agent, have shown that the studied nanocolloid has high uptake level in SLN and can be successfully used for visualization of SLN in patients with cancer of larynx and hypopharynx.

P759

Axillary lymph node biopsy: standard radioisotopic technique with 99mTc-nanocolloid versus new magnetic tracers.

C. Castillo-Berrio, M. Castrillón, F. Zelaya, D. Ruiz, F. Loira, J. M. Nogueiras, A. Lopéz, A. Serena, L. Campos; Meixoeiro University Hospital., Vigo, SPAIN.

Objective: Asses radioisotopic SLNB versus with magnetic tracer, in patients with breast cancer. Material and methods: Prospective descriptive study (March-April / 2014): 22 patients, mean age 57.7 (41-78 years), axilla clinically and radiological negative.Lymphoscintigraphy (24 hours before surgery): peritumoral /subareolar injection, 4 doses of 37MBq/ 0.5ml of 99mTc-nanocolloid. Images: 30 min and 2 hours; SPECT-CT. Skin label in hot spots site.Surgery: post-anesthesia, subareolar injection of magnetic tracer (2ml-Sienna + in 3ml /SSN). Breast massage for 5 minutes. Verification counting on skin marks and after incision, alternatively with radioactive and magnetic detector probes. Removing lymph

activity (threshold 10% maximum, for both) and / or palpable. Detection rate and number of sentinel lymph node extracted by both techniques were compared. Results: Overall removed 58 (sentinel lymph nodes) in 22 Patient (2.64 nodes per patient).Detection rate: 100% isotopic technique; 95.4% (21 / 22Patients) magnetic technique.Number of nodes identified: 39 (67.2%) radioactive, 45 (77.5%) magnetic, 11 (18.9%) exclusively palpation.-Same Number of nodes with both techniques (15 patients):• 11 Patients: negative.1 Patient: 2 nodes excised both positive (macrometastasis and micrometastasis).1 Patient: 2 nodes excised 1 positive (micrometastasis).1 Patient: 4 nodes excised 1 positive (micrometastasis).1 Patient: 2 nodes excised, 2 positive (micrometastasis).-Different Number of nodes (7 patients):• 5 patients, negative sentinel: magnetic technique detected one or two additional nodes per patient, compared to radioisotopic technique.• 1 Patient with 4 nodes excised: two palpables (macrometastasis) not detected by any method. Two sentinel nodes negatives (localized by magnetic), only 1 by isotopic.• 1 Patient with the excision of 2 nodes: the first (macrometastasis) detected with both, the second (negative) only by magnetic. Conclusions: Although the radioisotope technique was slightly more sensitive in our series, both methods were equivalent in identifying sentinel location, however magnetic tracer showed more lymph nodes number. The diagnostic accuracy was similar with both tracers. When radioisotopic technique is used, the possibility of lymphoscintigraphy for infrequent drains detection, the number of sentinel nodes displayed, its economy and minimal risk, supports the isotopic technique as the method of choice in Centers with Nuclear Medicine Services availables.

P760

Clinical Impact of the Implementation of Radioguided Localization of Non-Palpable Breast Tumors

C. SANDOVAL MORENO, M. A. BALSA BRETON, P. GARCIA ALONSO, E. RODRIGUEZ PELAYO, M. FERNANDEZ RODRIGUEZ, L. CASTILLEJOS RODRIGUEZ, A. ORTEGA VALLE, C. PANIAGUA CORREA, F. J. PENIN GONZALEZ; HOSPITAL UNIVERSITARIO DE GETAFE, MADRID, SPAIN.

Aim: To evaluate our experience after implementation of ROLL and SNOLL techniques in our hospital, comparing the results between radioguide surgery and wire localization in non- palpable breast tumours. Material and methods: We have reviewed 31 cases of non-palpable breast tumours marked with ROLL or SNOLL (ultrasound guide) and 29 cases with wire localization (ultrasound guide too), performed in our hospital along a year. A single 11-148 MBq dose of a 99mTc -colloid radiopharmaceutical in 0.3-0.4 ml was injected for both, radioguided localization and sentinel lymph node biopsy. Imaging guidance was achieved with sonography. Inmediately, the patients were submitted frontal and lateral view planar scintigraphic images and localization of the area of highest radioactivity was performed with a hand-held gamma probe on the breast. In the SNOL group more scintigraphic images were performed at least 2 hours after the injection to localize sentinel nodes. The next day the handheld gamma probe was used to remove the non-palpable breast tumours and sentinel nodes. We collected information about surgical margins and reexcision performed the same day or in a second procedure (depending on pathology results). Results: - 21/31 patients (67.7%) in the radioguided surgery and 24/29 (82.7%) in the wire localization of non-palpable of non-palpable lesions needed intraoperative extending edges. - Reexcision was performed in a second procedure only on 1 of the 31 patients undergoing radioguided surgery (3.22%). By contrast it was necessary on 7 of the 29 undergoing wire localization (24.14%). Conclusion: According to our experience, we can conclude that radioguided surgery reduces the number of intraoperative extending edges and reexcision in a second procedure which benefits patients and decreased costs.

P761

Validation of selective sentinel node biopsy in patients with adenocarcinoma of the prostate with high-intermediate and high-risk

V. Vera Pinto, P. Bello Arques, C. Igua Sáenz, P. Borrelli, P. Olivan Sasot, J. Vercher Conejero, J. Loaiza Góngora, P. Sopena Novales, C. Ruiz-Llorca; Hospital Universitario y Politécnico La Fe, Valencia, SPAIN.

OBJECTIVE: To determine the effectiveness of Selective Sentinel Node Biopsy (SLNB) in patients with adenocarcinoma of the prostate with high-intermediate and high-risk. MATERIAL AND METHODS: Descriptive study of 27 patients (50-73 years old) in which SLNB was performed between August 2012 to March 2015 after ruling out distant metastases. All patients were diagnosed with prostate adenocarcinoma in high-intermediate or high-risk stages. Prior to surgery day, 10 mCi (370 MBq) of nanocolloids labelled with 99mTc were injected within the prostate guided by transrectal ultrasound. Simultaneously, abdominopelvic acquisitions were made with portable gamma camera to ensure intraprostatic deposit of the tracer. 2 hours later, planar abdominopelvic acquisitions were performed, followed by SPECT / CT. In all cases, laparoscopic technique was done, using portable gamma camera and scintigraphic probe to identify radioactive lymph nodes and lymphatic drainage chains involved. Systematically, pelvic lymphadenectomy was performed, which will become extended in cases where migration of the tracer reaches unusual lymphatic territories. Abdominopelvic acquisitions with portable gamma

camera pre and post lymphadenectomy were also done. All sentinel lymph nodes (SLNs) were removed and examined with haematoxylin and eosin staining and immunohistochemical techniques. RESULTS: In 100% of cases there was migration of the radiotracer with positive scintigraphy. 26% (7/27) of patients presented metastatic SLN infiltration. 74% of patients (20/27) were true negatives, obtaining negative predictive value of 100%. In 48% (13/27) of patients there was migration of the radiopharmaceutical to paraaortic chain, and 40% (11/27) to presacral chains. CONCLUSIONS: SLNB in prostate cancer is a reliable and useful tool, capable to identify first landing lymphatic chains of the prostate, therefore allowing properly assessing lymph node involvement in prostate cancer. It is also useful and able to detect patients with atypical prostate lymphatic drainage, in which extended lymphadenectomy should be indicated.

P762

Sentinel lymph node biopsy after neoadjuvant chemotherapy in breast cancer patients with initial axillary node metastasis

N. Testart, A. C. Rebollo-Aguirre, R. Sánchez-Sánchez, T. Aroui, E. M. Triviño-Ibáñez, J. García-García, S. Menjón-Beltrán, J. M. Llamas-Elvira; Hospital Universitario Virgen de las Nieves, Granada, SPAIN.

Aim: To analyze our experience in sentinel lymph node biopsy (SLNB) in patients with operable breast cancer treated with neoadjuvant chemotherapy (NAC) with axillary involvement at diagnosis. Materials and methods. Prospective study (2008-2014) including 77 patients with infiltrating breast carcinoma T1-3/N1 treated with epirubicin/cyclophosphamide, docetaxel and trastuzumab in Her2/neu positive patients, in which was performed SLNB. Axillary status at diagnosis was evaluated by physical examination, MRi and/or mammary ultrasound, with guided core needle biopsy and histopathological confirmation of lymph nodes involvement (n=69, 89.6%). After NAC, reevaluation of axillary status was performed by MRi (n=64) and ultrasound (n=41). Sensitivity and specificity of both imaging techniques was calculated. After the NAC, the day before surgery, an experienced nuclear medicine physician performed the SLN identification and radiolabelling following the periareolar administration of 99mTc-albumin nanocolloid (4 intradermical/subdermical injections, total dose: 74-111MBq), acquiring static imaging (minimum 2 projections) and marking the skin guided by a gamma probe. In the surgery room, patients underwent SLNB performed by an experienced radiosurgery team and subsequently axillary lymph node dissection (ALND). SLN were examined by hematoxylin-eosin staining and immunohistochemical analysis or OSNA (one-step nucleic acid amplification). Identification rate (IR), false-negative rates (FNR) and global accuracy (GA) were determined. Histopathological analysis of both, breast tumor and axillary status was set down at diagnosis and after the NAC to determine the cases with pathologically complete response (pCR). Results. The SLNB IR was 83.1% (95%CI: 73.2-89.8%) with a FNR of 8.3% (95%CI: 2.9-21.8) and a GA of 95.3% (95%CI: 87.1-98.4%). In the axillary status after the NAC, the ultrasound showed sensitivity: 55.6% (95%CI: 33.7-75.4%), specificity: 91.7% (95%CI: 74.2-97.7%), GA: 76.2% (95%CI: 61.5-86.5%) and MRi showed sensitivity: 60.0% (95%CI: 44.6-73.7%), specificity: 75.0% (95%CI: 55.1-88.0%), GA: 65.6% (95%CI: 53.4-76.1%). The molecular subtypes: Luminal-A (n=12, 15.6%) showed pCR in breast (n=2), axilla (n=0), breast-axilla (n=3); Luminal-B/HER2- (n=28, 36.4%) had pCR in: breast (n=2), axilla (n=1), breast-axilla (n=6); Luminal-B/HER2+ (n=15, 19.5%) exhibited pCR in breast (n=1), axilla (n=1), breast-axilla (n=7); HER2+ (n=8, 10.4%) revealed pCR in: breast (n=1), axilla (n=5), breast-axilla (n=2); and Triple negative (n=14, 18.2%) showed pCR in: breast (n=3), axilla (n=2), breast-axilla (n=7).Conclusions. SLN biopsy after NAC is a feasible and accurate staging tool in patients with operable breast cancer T1-3,N1 and clinically node-negative after therapy. Patients with HER2+ and triple negative subtypes are potential candidates for avoiding unnecessary ALND due to its higher axillary node negative status after NAC.

P763

Sentinel lymph node biopsy in vulvar cancer. Our experience after five years

J. Muñoz Iglesias1, G. Muñiz García1, B. Couso Cambeiro2, J. Doval Conde2, R. Guitián Iglesias1; 1Nuclear Medicine Department. Complejo Hospitalario Universitario de Ourense, Ourense, SPAIN, 2Gynecology and Obstetrics Department. Complejo Hospitalario Universitario de Ourense, Ourense, SPAIN.

Purpose: To assess the reliability of sentinel lymph node biopsy (SLNB) in the inguinal lymph node staging of vulvar cancer and describe the technique and the results obtained after the validation stage. Material and Methods: A retrospective study from November 2009 to Febrary 2015 was performed in thirty-one patients with vulvar cancer (94% squamous cancer, mean age 71.24 years), who underwent SNLB. In all cases, local anesthetic cream was applied 90-120 minutes before the lymphscintigraphy (perilesional/pericicatricial injections, 0.1 ml of 99mTc-nanocolloidal albumin per injection; total

activity was 74 MBq). Dinamic study and static planar images were acquired sixty minutes post-injection (256x256 matrix, zoom 1 and cobalt source). It was regarded as SLN any increased focal uptake with drainage path and / or near the injection site. The SLNs detected were marked on skin.SLNs were removed during surgery guided by a gamma probe, with or without dye. Histological analysis with hematoxylin / eosin was made.Clinical and imaging follow-up was performed. Results: Fifty-four SLNs were identified in planar images in the 31 patients (detection rate 94%; 29/31), mean 1,75 nodes/patient: unilateral lymphatic drainage was obtained in 21/31 (72%) and bilateral drainage in 28%. The radiotracer did not migrate in two patients but in one of them, the dye did it.Histological grades: G1 19 (61.3%), G2 11 (35.5%) and G3 1 (3.2%). Eighteen patients had lesions ≤ 2 cm and 13 patients had lesions> 2 cm.FIGO staging: IA 6 patients (19.3%), IB 16 patients (51.6%), IIIA 7 patients (22.6%) IIIB 1 patient (3.2%) and IV 1 patient (3.2%).The SLN was negative in 22 patients (71%), 91% of them showed no recurrence at follow-up.The most common postoperative complication was wound dehiscence (22%). Conclusion: In our experience, SLNB in patients with vulvar carcinoma is safe and accurate, achieves suitable nodal staging and avoids lymphadenectomy in patients with negative sentinel node.

P764

Sentinel lymph node biopsy and neoadjuvant chemotherapy in breast cancer patients: a single institution experience.

A. C. Rebollo-Aguirre, **N. Testart**, R. Sánchez-Sánchez, T. Aroui, E. Triviño-Ibáñez, J. García-García, S. Menjón-Beltrán, J. M. Llamas-Elvira; Hospital Universitario Virgen de las Nieves, Granada, SPAIN.

Aim: To analyze our experience in sentinel lymph node biopsy (SLNB) in patients with operable breast cancer treated with neoadjuvant chemotherapy (NAC). Materials and methods. Prospective study, from january 2008 to december 2014, including 235 SLNB in patients with infiltrating breast carcinoma T1-3/N0-1 treated with epirubicin/cyclophosphamide, docetaxel and trastuzumab in Her2/neu positive patients, in which was performed SLNB. Exclusion criteria: inflammatory carcinoma, previous breast treatment with surgery or radiotherapy, multicentric tumors, metastatic disease, 2nd malignancy, progression of disease during NAC, pregnancy or breastfeeding and age <18y. Axillary status at diagnosis was evaluated by physical examination, MRi and/or mammary ultrasound, with guided core needle biopsy of any suspicious lymph node and histopathological analysis. After NAC, reevaluation of axillary status was performed by the same imaging procedures. The day before surgery, an experienced nuclear medicine physician performed the SLN identification and radiolabelling following the periareolar administration of 99mTc-albumin nanocolloid (4 intradermical/subdermical injections, total dose: 74-111MBq), acquiring static imaging (at least 2 projections) and marking the skin guided by a gamma probe. In the surgery room, patients underwent SLNB performed by an experienced team of surgeons and a nuclear medicine physician, guided by a gamma probe and subsequently axillary lymph node dissection (ALND). SLN were examined performing hematoxylin-eosin staining and immunohistochemical analysis (n=92) or OSNA, one-step nucleic acid amplification (n=114). Identification rate (IR), false-negative rates (FNR) and global accuracy (GA) were determined. Results. Patients were divided into 4 groups according to their clinical and pathological caracteristics and the intended management: i) Group I-SLNB-preNAC in patients cN0 at diagnosis: n=73, IR: 97.2% (95%CI: 90.5-99.2%); ii) Group II-2thSLNB-posNAC in patients pN1(sn) at diagnosis: n=31, IR: 61.3% (95%CI: 43.8-76.3%), FNR: 18.2% (95%CI: 5.1-47.7%), GA: 89.5% (95%CI: 68.6-97.1%); iii) Group III-SLNB-posNAC in patients cN0 at diagnosis: n=54, IR: 96.3% (95%CI: 87.5-99.0%), FNR: 9.5% (95%CI: 2.7-28.9%), GA: 96.2% (95%CI: 87.0-98.9%); and iv) Group IV-SLNB-posNAC in patients cN1 at diagnosis and ycN0 postreatment: n=77, IR: 83.1% (95%CI: 73.2-89.8%), FNR: 8.3% (95%CI: 2.9-21.8%), GA: 95.3% (95%CI: 87.1-98.4%). Conclusions. The detection rate for the SLNB is excellent prior NAC. A second SLNB after NAC in women with a positive SLN at diagnosis is not a useful option. SLNB after NAC is feasible in cN0 and cN1 patients at diagnosis, clinically axillary node-negative after therapy (ycN0), with posterior ALND if positive SLNB or not migration, when it is performed by an experimented multidisciplinary team.

P765

Cervix Cancer: our Experience Using Lymphatic Mapping and Sentinel Node Biopsy

P. Olivan Sasot, P. Borrelli, C. Igua Sáenz, V. Vera Pinto, P. Bello Argués, J. Loaiza Góngora, C. Ruiz Llorca, A. Repetto; Hospital La Fe, Valencia, SPAIN.

AIM: To correlate the images obtained using lymphatic mapping and sentinel node biopsy (SLNB) with anatomopathologic results from pelvic lymph node dissection in patients with cervix cancer refered to nuclear medicine department prior to surgery intervention. MATERIALS AND METHODS: 25 patients were included, with an average age 51,2 years (31-80), from November/2009

to January/2015. Three injections were performed peritumorally using 6mCi of 99mTc-albumin nanocolloid in a volume of 0.4ml x 3 injections. After injection static pelvic imaging was obtained using Philips BrightView XCT gamma camera, to visualize radiofarmaceutical migration. In 16 patients, SPECT/CT was added to improve lymph node anatomical location. RESULTS: Location rate was 88% (22 patients), in the remaining 12% no migration was detected and in lymph node dissection, lymph node metastasis was found. Para-aortic sentinel lymph node was found in 2 of our patients. Surgery average lymph node was 2,27 per patient. 4 patients had SLNB positive for metastasis. The remaining 18 were negative, and pelvic lymph node dissection didn't shown any metastatic infiltration. Later monitoring, one patient presented tumoral relapse with-in 4 mesenteric lymph nodes metastatic, and colonic infiltration. Another one, presented tumoral relapse in suture stitches. After global evaluation of these results, 100% negative predictive value was established to the technic for pelvic lymphatic node affection in this patient series. CONCLUSION: A negative result in the anatomopathologic sentinel node biopsy, would be reasonable motive to limit pelvic lymph node ressection extension to the sentinel node, and it would avoid associated comorbidity. Rare lymph node chain drainage like para-aortic was found.

P766

Feasibility of 3D-image guided resection of neuroendocrine tumours

C. Bluemel, M. Gasser, M. Fassnacht, R. A. Werner, A. K. Buck, K. Herrmann; Universitätsklinikum Würzburg, Würzburg, GERMANY.

Aim: The aim of this study was to evaluate the feasibility and advantages of 3-D image guided resection of gastro-enteropancreatic neuroendocrine tumours (GEP-NET) and their metastases. Methods:4 patients with initial diagnosis of a GEP-NET and scheduled for tumour resection were included in this prospective study. All patients underwent somatostatin-receptor (SSTR) scintigraphy (111-In-octreotide; mean, 114 MBq (98-148 MBq)) on the day prior to surgery to localize the primary tumour and metastases. On the following day intraoperative tumour localization was guided by palpation, ultrasound and radioguided procedure with freehand SPECT allowing for intraoperative imaging SSTR-positive tumour lesions and dedicated 3-D navigation to tumour lesions. Results: 2 patients had a pancreatic NET (insulinoma) and 2 patients suffered from a metastasized (both lymph node metastases, one patient additional liver metastases) ileum NET. In all patients localization and visualization of tumour lesions using freehand SPECT was feasible. However, also with conventional localization techniques (preoperative imaging as road map, palpation and ultrasound) all lesions could be successfully localized. Conclusions: These preliminary data show for the first time that 3-D image guided intraoperative localization of GEP-NETs using freehand SPECT is feasible; however, advantages over conventional localization techniques could not be demonstrated.

P767

Sentinel lymph node biopsy in patients with locally advanced breast cancer with negative axilla after chemotherapy

P. Olivan Sasot, P. Borrelli, C. Igua Sáenz, V. Vera Pinto, P. Bello Arqués, J. Loaiza Góngora, C. Ruiz Llorca, P. Sopena; Hospital La Fe, Valencia, SPAIN.

Aim: To demonstrate (sentinel lymph node biopsy) SLNB validity in patients with locally advanced breast cancer after neoadjuvant chemotherapy in negative axilla pre-chemotherapy and cases that became negative after chemotherapy. Materials and methods: SLNB was performed after chemotherapy to 88 women (March 2007-March 2015), aged from 27-73 years , with mean age 47,36 years . At 68 first patients, axillary lymphadenectomy was made to validate SLNB technique, after that, 20 routine SLNB was made and LN was studied by OSNA technic and exclusively in SLNB positive cases or in those cases without radiopharmaceutical axillary migration, lymphadenectomy was performed. Axillary staging was made by fine-needle aspiration biopsy and/or ultrasound, 45 patients had negative axilla and 43 had positive axilla previous chemotherapy. Histology types were infiltrating ductal carcinoma in 93,2% cases, and infiltrating lobular carcinoma in 6,8%. Results: Lymph node (LN) location rate was 74% (65/88). Medium LN removed per procedure was 1,52. In the 45 patients with negative axilla before chemotherapy: 29 patients had negative SLNB, 6 positive and 10 had no migration. In the 43 patients with positive axilla before chemotherapy: 13 patients had negative SLNB, 17 positive and 13 had no migration. No radiopharmaceutical migration was found in 23 patients (26%): anatomopathology results were positive in 14 cases and were negative in 9. Conclusion: In women with locally advanced breast tumor is safe to use SLNB after chemotherapy, also in cases of negative axilla clinically and radiologically before chemotherapy and in women who converted positive axilla before chemotherapy to negative after treatment. Unnecessary lymphadenectomy its morbidity could be avoided using this technic. High no radiopharmaceutical migration rate could be attributed to: metastasis in 61% of cases (14/23) and fibrosis produced by chemotherapy 39% of cases (9/23).

P768

Differences in clinical-biological characteristics and SLN detectability in different age-groups of breast cancer patients

S. M. Nieves Maldonado, S. Argibay Vazquez, M. Garrido Pumar, V. Pubul Nuñez, J. Cortes Hernandez, A. Ruibal Morell; Hospital Clínico Universitario de Santiago de Compostela, Santiago de Compostela, SPAIN.

AIMS: Our goal is to evaluate the differences in clinical-biological characteristics and sentinel node detectability in different age- groups of patients diagnosed with breast cancer.MATERIALS AND METHODS: Our study Involved 828 consecutive breast cancer patients who underwent isotopic detection of SLN in our department, without known palpable or ecographic lymph node invasion. lymphoscintigraphy images were acquired after the injection of 111 MBq of tc99m nanocolloid for SLN mapping. SLN localization at surgery was performed using a hand-held gamma probe. Conventional Histopathological study was used in 439 patients for SLN analysis, and molecular examination (OSNA) was performed in 387 patients. Axillary lymphadenectomy was indicated in SLN positive cases. Mean age of patients was 58 (range 28-88), and they were divided into four age groups: <40 years old (n = 56), 40-54 (n = 272), 55-69 (n = 326), and > 70 (n = 174).RESULTS: The most frequent type of tumor was the ductal infiltrating carcinoma (84%), the most common tumor site was the upper outer quadrant (35%), and the left breast was the most commonly affected (53%) for all groups. The molecular diagnosis was predominantly negative Her2 Luminal B (36%) in the younger group, and for the other age groups it was the Luminal A type (40%). The group of patients between 40 and 54 years had a higher proportion of tumor multifocality (6%) than other groups. Most groups presented an average of 2 focal deposits in lymphoscintigraphy, and in the older than 70 years group a higher proportion of patients showed absence of migration of the tracer (19.5%) compared to younger groups. Patients under 40 presented with increased detectability of intraoperative sentinel lymph nodes (94.6%), this group of patients showed a greater positivity of the SLN (52%), and the same age group had fewer positive nodes at the lymphadenectomy (mean 1, range 0-13).CONCLUSIONS: In our population there are no differences between age groups respect to histological type, or location, however with regard to molecular type there is a tendency towards Luminal A type at older ages. Mamography screening in middle-age groups helps the detection of non-palpable lesions in this age group; this is not the case for younger and older women. As expected the higher prevalence of absence of scintigraphic visualization of SNL was found in the population older than 70 years.

P769

ROLL technique application for Minimally-Invasive Radioguided Parathyroidectomy (MIRP) in Hyperparathyroidism (HPT)

I. Santi1, P. Carcoforo2, G. Trasforini3, S. Panareo1, C. Cittanti1, C. Peterle1, V. de Cristofaro1, E. Degli Uberti3, L. Feggi1; 1Sant'Anna University Hospital, Nuclear Medicine Unit, Department of Diagnostic Imaging and Laboratory Medicine, Ferrara, ITALY, 2Sant'Anna University Hospital, Breast and Radioguided Surgery Unit, Surgical Department, Ferrara, ITALY, 3Sant'Anna University Hospital, Endocrinology Unit, Department of Medical Sciences, Ferrara, ITALY.

Aim: In HPT patients (pts) requiring surgery, MIRP is usually associated to MIBI imaging for preoperative parathyroid localization and intraoperative guidance.Aim of our study was to evaluate the feasibility and reliability of MIRP performed through ROLL technique for enlarged parathyroid gland (epg) localization, likewise the established method in non-palpable breast lesions.Materials and Methods: HPT pts addressed to parathyroidectomy for at least 1epg detected by ultrasound and confirmed by dual-tracer parathyroid scintigraphy (PS) and/or FNA, were considered eligible.All pts underwent ultrasound-guided injection of 99mTc-nanocolloid inside the epg for scintigraphic localization on the day before surgery (not MAA because colloid was already prepared for scheduled breast cancer procedures).MIRPs were performed using a gamma-probe to identify the pge and verify complete excision that was further assessed through intraoperative quick PTH assay (ioPTH). Histologic examination of surgical specimens was carried out.Results: 28pts were studied (21F, 7M, median age 56.5±21.5y), 27 had a single epg and one had 2epg.Sintigraphy at 75±45' median time from injection (median activity 60±23MBq in 0.2ml) depicted 1active spot in the anterior neck region in 27pts and 2spots in 1 (uptake was also found in 1laterocervical lymph node in 3pts).The same surgeon performed all MIRPs: 1active pge was identified and removed in 27pts and 2glands in 1case, without residual activity in the surgical field (no interference with MIRP occurred in the 3pts with concurrent laterocervical lymph node uptake); ioPTH confirmed complete removal (level reduction>50%) in all pts.Histology demonstrated pge in all specimens: adenoma in 18pts (64%), hyperplasia in 10 (36%) - single gland in 9 and 2glands in 1case.Prior to enrollment 26/28pts underwent PS: 5negative (19.2% - 4small adenoma cases and the 2-gland hyperplasia case), 21positive (80.8%).Conclusions: Despite our limited series, ROLL procedure for MIRP resulted feasible, reliable and reproducible with 100% surgical success rate in HTP pts.Advantages are: no background activity that makes it easier for surgeons to identify the active pge and check its complete removal without looking for >20% greater counts then background established

for MIBI-based guidance; low activity of 37-74MBq injected the day before surgery vs. 37-740MBq injected 1-3hours prior to surgery, tying surgical timing, reported in literature for MIBI; preoperative localization even in cases of negative PS.However, highly skilled operators are needed to ensure valid injection and thorough surgical removal.Further studies are needed to better define pts that may benefit from this approach.

P770

Improving the sensitivity of sentinel node biopsies in malignant melanoma of the head and neck using a handheld gamma camera

S. Schneider-Burrus, A. Pokrywka; Charité Universitätsmedizin, Berlin, GERMANY.

Objective: Sentinel lymph node biopsy (SLNB) is a very important tool for precise staging of patients with malignant melanoma. Identification of sentinel lymph nodes (SLN) can be difficult, especially when they are located in proximity to high radiotracer activity or in challenging anatomic regions. This is particularly true in tumors of the head and neck. The purpose of this study was to evaluate the sensitivity of a handheld gamma camera when used in combination with a conventional gamma probe in SLNB in melanoma of the head and neck. Methods: From October 2014 to April 2015, we conducted SLNB in 15 patients with malignant melanoma of the head and neck. Lymphoscintigraphy with 99mTc-nanocolloid was done with a conventional fixed gamma camera (FGC). The following day, SLNB was performed using a handheld gamma camera (HGC, CrystalCam, Crystal Photonics) in combination with a gamma probe (GP, Navigator, Auto Suture). Results: Before surgery, a total of 26 SLN were identified in 19 lymph node basins in 14 out of 15 patients by FGC imaging. In one case, due to the proximity of the injection site to the draining lymph node basin, lymphoscintigraphy did not reveal any SLN. During surgery, a total of 44 SLN were removed in 26 lymph node basins. SLNB was successfully performed in all 15 patients. In 6 lymph node basins, the detection of the SLN was only possible by HGC. Sensitivity for detecting SLN basins was 82% for FGC and 100% for intraoperative use of HGC. The histology report revealed in 4 out of 15 patients lymph node metastases, one of the metastatic SLN was only detected using the HGC. Conclusions: Intraoperative HGC imaging in combination with a gamma probe has a high sensitivity for detection of SLN in the head and neck. Especially for SLNB in challenging locations like the head and neck, the use of a HGC can improve the detection rate for SLN in malignant melanoma.

P48 - Tuesday, October 13, 2015, 4:00 PM - 4:30 PM, Hall 3 – Poster Exhibition

Clinical Oncology: External Beam Radiation Therapy Planning

P771

An Automatic Method for PET Delineation of Cervical Tumors

A. Stefano1,2, S. Vitabile3, G. Russo1, F. Marletta4, C. D'Arrigo4, D. D'Urso1, O. Gambino2, R. Pirrone2, E. Ardizzone2, M. C. Gilardi1, **M. Ippolito**4; 1IBFM-CNR, Cefalù, ITALY, 2DICGIM, University of Palermo, Palermo, ITALY, 3DIBIMED, Palermo, ITALY, 4Cannizzaro Hospital, Catania, ITALY.

Aim: PET imaging is increasingly utilized for radiation treatment planning. Nevertheless, accurate segmentation of PET images is a complex and unresolved problem. Aim of this work is the development of an automatic segmentation method of Biological Target Volume (BTV) in patients with cervical cancer. Materials and methods: Random walks (RW) is a graph-based method that represents a DICOM (Digital Imaging and COmmunications in Medicine) image as a graph. The voxels are its nodes and the edges are defined by a cost function which maps a change in image intensity to edge weights. Then, RW partitions the nodes into target and background subsets. To create an automatic method starting from previous work (A. Stefano, et al. A Graph-Based Method for PET Image Segmentation in Radiotherapy Planning: A Pilot Study, in A. Petrosino, ed., Image Analysis and Processing - ICIAP 2013: LNCS, v. 8157, Springer Berlin Heidelberg, p. 711-720), we propose an automated RW seed localization approach. The algorithm identifies the PET slice with the highest SUVmax and a maximum of 10 target and 8 background seeds for each volume slice. The voxels with a SUV>95% of SUVmax are marked as target seeds. Then, the method explores the hottest voxel neighborhood through searching in 8 directions to identify the background voxels with a SUV<30% of the average SUV of target seeds. Once the target and background seeds are localized, RW performs a 3D lesion delineation. BTV is manually defined by two nuclear medicine physicians in 18 patients with cervical metastases undergoing a 11C-labeled Methionine PET/CT examinations before the radiotherapy treatment. The accuracy of the proposed method is evaluated making a comparison with manual delineation by the dice similarity coefficient (DSC) and median Hausdorff distance (HD). Results: The BTV delineation is not subject to both intra and inter-operator variability. An analysis of the time performance shows that the segmentation time for single slice is around 0.3 seconds. The DSC range of PET delineation is found to be from 81.7% up to 92.6% with a mean of 88.57

±3.22%. The HD range is found to be from 1.00mm up to 3.67mm with a mean of 1.96±0.62mm. Conclusion: A slice-by-slice manual PET segmentation is a time expensive method because dozens of slices must be delineated. Results show that our algorithm is automatic and fast, satisfying critical requirements in a clinical environment. In addition, high DSC and low HD values confirm the accuracy of delineation method.

P772

The usefulness of intratumoral metabolic heterogeneity in selecting patients for radiotherapy dose-escalation

S. Kang1, H. Kim1, K. Park2, G. Jeong1, H. Park1, J. Kim2, J. Min1, H. Song2, H. Bom1, S. Kwon1; 1Chonnam National Unuversity Hwasun Hospital, Hwasun-Gun, KOREA, REPUBLIC OF, 2Chonnam National Unuversity Hospital, Gwang-ju, KOREA, REPUBLIC OF.

Purpose:We evaluated the value of intratumoral metabolic heterogeneity assessed using area under curve of cumulative SUV-volume histogram (AUC-CSH) in FDG PET/CT to select patients for radiotherapy dose-escalation in patients with stage III non-small cell lung cancer.Materials and methods:Fifty-nine patients with stage III non-small cell lung cancer, who underwent pretreatment FDG PET/CT before starting concurrent chemoradiotherapy (CCRT) were retrospectively reviewed (60 Gy: 27; 66 or 70 Gy: 32). For the classification of metabolic heterogeneity of primary tumor, median value of AUC-CSH calculated using P-mode software was used. Progression-free survival (PFS), locoregional recurrence-free survival (LRFS), and distant metastasis-free survival (DMFS) curves were produced using Kaplan-Meier methods and survival difference between groups was assessed by Wilcoxon test.Results:Twenty-seven patients had metabolic homogeneous primary tumor (AUC-CSH>4489) and 32 patients had heterogeneous tumor (AUC-CSH≤4489). In Kaplan-Meier analysis, high-dose RT (66 or 70 Gy) was associated with improved PFS (p=0.032), but not in LRFS (p=0.112) and DMFS (p=0.183). In metabolic homogeneous group, high-dose radiotherapy was strongly associated with improved PFS (p=0.003) and LRFS (p=0.026). However, in metabolic heterogeneous group, high-dose RT was not associated with improved PFS (p=0.952) and LRFS (p=0.949).Conclusion:This preliminary study suggests that radiotherapy dose-escalation can improve progression-free survival (PFS) and locoregional failure survival (LRFS) not in patients with metabolically heterogeneous stage III lung cancer but in patients with homogeneous lung cancer.

P49 - Tuesday, October 13, 2015, 4:00 PM - 4:30 PM, Hall 3 – Poster Exhibition

Clinical Oncology: Therapy Response Assessment

P773

Tumor FDG-Metabolic Values to Predict Pathological Response After Neoadjuvant Chemoradiotherapy in Patients with Resectable Locally Advanced Esophageal Cancer

K. Itoh1, T. Kitsukawa2, H. Takahashi3, M. Myoujin4, T. Oishi5, T. Takenouchi5, S. Watanabe1, K. Kanegae1, M. Hosokawa2; 1Keiyukai Sapporo Hospital, Radiological Imaging Center, Sapporo, JAPAN, 2Keiyukai Sapporo Hospital, Department of Digestive Surgery, Sapporo, JAPAN, 3Keiyukai Sapporo 2nd Hospital, Department of Internal Medicine, Sapporo, JAPAN, 4Keiyukai Sapporo Hospital, Deparrtment of Radiotherapy, Sapporo, JAPAN, 5Keiyukai Sapporo Hospital, Department of Clinical Pathology, Sapporo, JAPAN.

[Background and Objectives] Neoadjuvant chemoradiotherapy (NACRT) followed by esophagectomy is a widely accepted treatment options for patients with resectable locally advanced esophageal cancer (LAEC). The value of [F-18] FDG PET/CT (PET/CT) to predict response of LAEC to NACRT and to aid in subsequent treatment decisions is still controversial. We sought to clarify the role of PET/CT in these tumors. [Materials and Methods] We reviewed the cases of 52 patients (44 male, median age: 64 years) with LAEC (clinically staged T3−4, N0−3 and M0). Prior to NACRT, patients were staged with different modalities, including endoscopic ultrasonography, CT, MRI, barium swallow, and PET/CT. PET/CT was repeated 2−4 weeks after the completion of NACRT. The complete treatment plan included NACRT (cisplatin + 5-FU, two courses)/50.4 Gy (28 fractions of 1.8Gy) followed 3 to 6 weeks later by transthoracic en bloc esophagectomy. For PET/CT (Gemini GXL®, Philips Medical Systems Inc. Eindhoven, the Netherlands), whole body images were obtained 1 hour after IV administration of 185 MBq to fasting patients. The maximum standardized uptake value (SUVmax), metabolic tumor volume (MTV), and total lesion glycolysis (TLG) were calculated using a workstation (Syngo.via®, Siemens Healthcare. Erlangen, Germany). The pre- and post-NACRT SUVmax were compared in order to calculate the response rate (RR). [Results] There were 50 patients with squamous cell carcinoma and two patients with adenocarcinoma. Most resected specimens showed down-staging compared with pre-treatment stage. The pre-treatment SUVmax values (mean 16.85, 95%CI 14.30−18.13) were significantly higher than the post-treatment values (mean 4.81, 95%CI 4.29−5.23) (p<0.0001). A metabolically complete response (CR) (post-treatment SUVmax < 3.0) was observed in 13 patients. However, there was no correlation between metabolic and pathologic responses (p=0.842). Pre- and post-treatment SUVmax, MTV, TLG, and RR were not significantly different between 18 patients (35%) with a pathologic CR and 34 patients with

pathologic partial response. ROC curve analysis also did not reveal sufficiently high AUC values. [Conclusions] Metabolic and morphologic changes in esophageal carcinoma on PET/CT 2−4 weeks after NACRT did not correlate with pathological response, and cannot be used to guide decisions regarding surgery.

P774

PET/CT Reconstruction and Its Impact on Quantitative Image Analysis

G. Kuhnert1, R. Boellaard2, D. Kahramann1, M. Scheffler1, J. Wolf1, M. Dietlein1, A. Drzezga1, C. Kobe1; 1University Hospital of Cologne, Cologne, GERMANY, 2VU University Medical Centre, Amsterdam, NETHERLANDS.

Background: In oncological imaging using PET/CT the standardized uptake value (SUV) has become the most common parameter used to measure tracer accumulation. The aim of this analysis was to evaluate Ultra High Definition (UHD) and Ordered Subset Expectation Maximization (OSEM) PET/CT reconstructions for their potential impact on quantification. Patients and Methods: We analyzed 10 PET/CT scans of lung cancer patients who had undergone PET/CT. The maximal SUV (SUVmax) and the peak SUV (SUVpeak) were determined in the single hottest lesion in the lung and normalized to a reference region for UHD and OSEM reconstruction. SUVmax, SUVpeak and their normalized ratios for the two reconstruction settings were compared using the paired sample t-test. The distribution of SUVmax and SUVratio in relation to the reconstruction method was demonstrated in the form of histograms, box-plots and frequency distribution curves. Assessment of the agreement between OSEM and UHD reconstructions was performed with Bland-Altman analysis. Results: A significant difference was observed after OSEM and UHD reconstruction for SUVmax (8.6 vs. 12.9, p=0.000) and for SUVpeak (6.8 vs. 8.5, p=0.000). The mean values of the ratios after OSEM and UHD reconstruction showed equally significant differences for SUVmax (4.0 vs. 6.1, p=0.001) and SUVpeak (4.0 vs. 6.1, p=0.003). Bland-Altman analysis showed that SUVmax and its ratio were about 55% higher while SUVpeak and its ratio were about 33% and 31% higher after UHD reconstruction as compared to OSEM reconstruction. Conclusion: OSEM and HD reconstruction brought a significant difference of over 30 % for SUVmax, SUVpeak, and their normalized ratios, indicating that standardization of reconstruction and the use of comparable SUV measurements are crucial when using PET/CT for response evaluation.

P775

Texture analysis for tumor hypoxia visualized by FMISO PET/CT during radiation therapy

M. Hosono, I. Tachibana, Y. NIshimura, K. Hanaoka, S. Kanamori, K. Nakamatsu, K. Ishikawa, K. Sakaguchi; Kinki University Faculty of Medicine, Osaka-Sayama, JAPAN.

Aim: F-18-fluoromisonidazole (FMISO) PET/CT is one of the useful tools that have been investigated to visualize hypoxic status in tumors. The aim of this study was to clarify the feasibility of texture analysis of tumor hypoxia as well as absolute levels of FMISO uptake on FMISO PET/CT in association with local control by radiation therapy (RT). Materials and methods: This study involved 18 patients (pts) with neoplasms (head and neck 8, esophagus 5, anus 2, lung 2, uterus 1) who underwent RT and FMISO PET/CT. FMISO PET/CT scans were conducted at the baseline and at 20 Gy of RT; each patient received iv injection of FMISO (7.4 MBq/kg) and underwent PET/CT at 180 min. Regions of interest were placed on tumors to measure SUVs of FMISO. Additionally, texture analyses dealt with the heterogeneity indices of skewness, kurtosis, and another heterogeneity index of area under curve of cumulative SUV histogram (AUC-CSH). And a larger skewness, a larger kurtosis, and a smaller AUC-CSH were considered to indicate a higher heterogeneity. Pts were categorized into CR and non-CR (PR+NC+PD) groups, and the parameters were compared between the two groups by Mann-Whitney's U test. Results: Pts received chemoradiation therapy (n=17, 42-70 Gy) or RT alone (n=1, 64 Gy). Nine pts reached CR, while 9 did not. Reduced FMISO SUVs were observed at 20Gy as compared to before RT, which might correspond to reoxygenation. CR group showed statistically significant lower SUVmax and kurtosis and a tendency of lower skewness and higher AUC-CSH. Conclusion: Texture analysis of intratumoral FMISO distribution was feasible. Correlation of heterogeneity and therapeutic response should be clarified in further studies. A lower absolute level of FMISO accumulation before RT might be predictive of a better therapeutic response.

P776

PERCIST versus RECIST versus Visual PET assessment for the evaluation of response by PET/c.e.CT to chemoradiation neoadjuvant therapy in patients with locally advanced esophageal cancer

A. Cervino1, L. Evangelista1, E. Scagliori1, R. Alfieri1, V. Sileni Chiarion1, S. Galuppo1, A. Ruol2, F. Pomerri3, G. Saladini1; 1Istituto Oncologico Veneto I.R.C.C.S., PADOVA, ITALY, 2Hospital of Padua, PADOVA, ITALY, 3University of Padua, PADOVA, ITALY.

Purpose. The aims of the present study were 1) to assess the utility of PET/CT scan before and after neoadjuvant therapy and 2) to evaluate the therapeutic response in locally advanced esophageal cancer with comparing PET response criteria (PERCIST), to visual PET/CT analysis and to response evaluation criteria in solid tumours (RECIST 1.1).Materials and methods. 38 patients with locally advanced esophageal cancer receiving neoadjuvant chemoradiation therapy (NCRT) were prospectively enrolled. Chemo-radiation responses were evaluated by using FDG PET/CT and c.e.CT performed in a single-session, according to visual PET assessment, RECIST 1.1. and PERCIST 1.0. PET/c.e.CT was performed after at least 4-5 weeks from the end of NCRT. In accordance with PERCIST and RECIST, the response to therapy was categorized in four levels: CR (CMR)=1; PR (PMR)=2; SD (SMD)=3; PD (PMD)=4. For visual PET analysis, the readers identified three different categories on PET/CT scan on the basis of FDG-uptake [no evidence, residual (near or superior to surrounding tissue) and increase or new appearance]. Surgery or histopathology was used for the final definition of the response to therapy. Person chi-square was used to compare the proportion of four levels in RECIST/PERCIST and of three subsets in the visual PET analysis.Results. The body weight of patients resulted significantly lower after NCRT (75 vs. 71 kg, respectively before and after therapy; p=0.025). Semiquantitative PET data (such as SUVmax, SULpeak, metabolic tumour volume-MTV and tumour lesion glycolysis-TLG) were significantly higher before than after therapy (all $p<0.05$), independently from the final response. After NCRT, SUVmax of primary tumor, MTV and TLG resulted significantly lower in responder patients as the counterpart (all $p<0.05$). Moreover, the change in SUVmax and in TLG were significantly higher in responder than non-responder patients. The difference of evaluation results between RECIST and PERCIST and between RECIST and visual PET analysis were not significant (p=0.863 and p=0.527, respectively). Conversely, a significant difference for the evaluation of response to NAC between the visual PET analysis and PERCIST was found (p=0.001). A complete and partial response to therapy was better discriminate by visual PET analysis and by PERCIST as compared to RECIST.Conclusions. The change in SUVmax and in TLG can be helpful to distinguish between responder and non-responder subjects. Both visual PET assessment and PERCIST are more sensitive than RECIST in detecting complete and partial remission of esophageal cancer after NAC.

P777

Heterogeneity of Metabolic Parameters and Impact on Early Response Evaluation with FDG PET/CT in Patients with Metastatic Colorectal Cancer treated with Cetuximab Monotherapy

E. J. van Helden, O. S. Hoekstra, R. Boellaard, H. M. W. Verheul, C. W. Menke-van der Houven van Oordt; VU Medical Center, Amsterdam, NETHERLANDS.

Aim.The aim of this study was to explore the level of intrapatient heterogeneity in metabolic responses as defined with 18F-FDG-based quantitative metrics, in patients with metastasized KRAS wild-type colorectal adenocarcinoma (mCRC), treated with third line cetuximab monotherapy.Methods.We performed 18F-FDG PET at baseline and after four weeks (2 cycles) of cetuximab in 10 patients with mCRC. Quantitative analysis of target lesions (≥2 cm and above background determined in liver or aorta) was done for all lesions, ≤ 5 lesions (≤2 per organ) and for the metabolically most active lesion per PET (cf. PERCIST guidelines). In addition, the effects of different quantification units (SULmax, SULpeak and Total Lesion Glycolysis (TLG)) on response prediction were evaluated. Metabolic response was categorised with a threshold of 30% for SUL and 45% for TLG. Quantitative data were correlated with clinical benefit, defined as SD, PR or CR according to Response Evaluation Criteria In Solid Tumors version 1.1 (RECIST) after two months of treatment. Intrapatient differences with respect to metabolic response between lesions were analysed.Results.In nine evaluable patients the total number of target lesions was 36 (1 - 8 per patient). Evaluating individual lesions using SULpeak, two patients had a mixed metabolic response (metabolically progressive, stable or responding lesions). Using SULmax and TLG, mixed metabolic response was observed in three patients. The overall concordance between dichotomised metabolic data of the metabolically most active lesion (i.e. progressive and stable metabolic disease versus metabolic response) and clinical benefit was 89% for all three quantification units. Evaluating metabolic response using SULmax or SULpeak summed over maximally five or all target lesions, demonstrated no improved concordance with clinical benefit. However, using TLG (summed over the lesions) concordance was 100%.Conclusion.Mixed metabolic response was observed in 38% of all patients with multiple lesions treated with cetuximab. However, using PERCIST guidelines only one patient was miscategorised. A

100% correlation with clinical benefit was observed if response prediction was done using TLG summed over multiple lesions. Validation of these promising preliminary results in a larger patient cohort is currently ongoing.

P778

Therapeutic response assessment of bone metastatic prostate carcinoma treated by abiraterone using x-SPECT QUANT® : a feasibility study.

R. de Laroche, P. Robin, P. Le Roux, J. Malhaire, D. Bourhis, P. Salaun, R. Abgral; University Hospital of Brest, Brest, FRANCE.

Aim: The therapeutic response assessment is a major challenge in patients with bone metastatic prostate carcinoma (BMPC). BMPC progression criteria (PCWG 2, 2007) take into account serum PSA level changes or appearance of 2 or more new bone scan lesions. Interpretation of SPECT-CT with a visual analysis limits its performance, making difficult an objective response evaluation. The aim of this prospective study is to assess the feasibility to use a SPECT-CT quantification method for BMPC response evaluation. Materials and Methods: Patients with castrate-resistant BMPC treated by abiraterone (Zytiga®) were included. All patients underwent 3 SPECT-CT (Symbia, Intevo, Siemens®): baseline (M0), at 3 (M3) and 6 months of treatment (M6). SUVmax and SUVpeak quantification were performed using the xSPECT-QUANT® tool on the highest uptake target lesions (maximum of 5). Criteria used for response evaluation were arbitrarily the same used in PET-CT for solid cancers (EORTC99 and PERCIST1.0). Results were compared with serum PSA level changes. Results: Eight patients aged of 73.4 +/- 8.5 years were included from April 2014 to March 2015. Two patients died before M6. The mean delay between M0 and M6 was 6.6 +/- 0.8 months. The mean SUVmax and SUVpeak on target lesions were respectively 30.7 and 25.6 on M0 and 16.1 and 14.0 on M6. Two, 2 and 2 patients were respectively in partial response (PR), stable disease (SD) and progressive disease (PD) according to EORTC99. Two, 2 and 2 patients were respectively in PR, SD and PD according to PERCIST1.0. Four and 4 response evaluations according to EORTC99 and PERCIST1.0 respectively matched with serum PSA level changes. Conclusion: These preliminary results show the feasibility to use the xSPECT QUANT® tool in bone scan for the response assessment of BMPC treated by Zytiga®. To the best of our knowledge, it is the first study evaluating this first marked SPECT-CT quantification tool in a clinical series.

P779

Evaluation of Platinum-based Therapy Response in Non-Small Cell Lung Cancer

M. Ippolito1, A. Stefano2,3, G. Russo2, S. Gieri2, S. Cosentino1, G. Murè1, S. Baldari1, M. G. Sabini1, F. Fraggetta1, S. Vitabile4, M. C. Gilardi2, G. Banna1; 1Cannizzaro Hospital, CATANIA, ITALY, 2IBFM CNR - LATO, Cefalù, ITALY, 3DICGIM, University of Palermo, Palermo, ITALY, 4DIBIMED, Palermo, ITALY.

Aim: To evaluate the clinical value of PET imaging for an early prediction of tumor response to platinum-based therapy in patients with non-small cell lung cancer (NSCLC). In order to avoid unnecessary toxicity of ineffective chemotherapy treatment, an early identification of NSCLC patients who benefit from this therapy is mandatory.Materials and methods: Seventeen patients are enrolled prospectively: 18F-FDG-PET examinations are carried out before treatment and after the first course. The lesions with the highest uptake in each patient are evaluated according to EORTC, PERCIST and RECIST classifications to discriminate between patients who respond (complete and partial response) from those who do not respond (stable and progressive disease) to treatment. Metabolic Tumor Volume (MTV) and Total Lesion Glycolysis (TLG) are also used to evaluate therapeutic response. MTV indicates the volume of metabolically active tumors; TLG is the product between SUV mean and MTV. In literature, there are no cut-off points for therapy evaluation based on TLG or MTV variations (Δ) in sequential scans. In order to estimate cut-off values for these parameters, receiver operating characteristic (ROC) curves are used. RECIST classification is used as the outcome for the ROC analysis. Kaplan-Meier test is used to calculate Overall Survival (OS) time. OS is compared between responders and non-responders using a log-rank test. The level of statistical significance is defined as a p-value (p) of less than 0.05.Results: The ROC analysis indicates a cut-off point of -36% for ΔTLG, and -8% for ΔMTV. The Kaplan-Meier analysis shows that RECIST, ΔTLG, and ΔMTV prove to be a significant prognostic factor for predicting OS. For RECIST responder patients median OS is 595 days whereas for non-responder patients median OS is 238 days. ΔTLG shows a median OS of 492 days for responders and 238 days for non-responders. ΔMTV shows a median of 423 days for responders versus 188 days for non-responders. Conversely, EORTC and PERCIST classifications are inadequate to discriminate between responder and non-responder patients ($p>0.13$). For this reason, we use ROC analysis to propose an alternative PERCIST threshold of 17% for an early therapy monitoring.Conclusion: PET examinations provide an early

identification of patients who benefit from platinum-based treatment. Results confirm that TLG proves a strong early prognostic factor in patients with NSCLC and could play a significant role in the field of personalized medicine, avoiding the unnecessary administration of non-curative and toxic drugs to preserve the patient's quality of life.

P780

18F-FLT PET/CT as a surrogate biomarker for synergy quantification in EGFR targeted combination therapy of NSCLC

F. Iommelli1, V. De Rosa1, M. Monti2, M. Panico1, R. Fonti1, S. Del Vecchio2; 1Institute of Biostructures and Bioimages, National Research Council, Naples, ITALY, 2Department of Advanced Biomedical Sciences, University "Federico II", Naples, ITALY.

Aim: A poor clinical response of non-small cell lung cancer (NSCLC) to treatment with EGFR tyrosine kinase inhibitors is often the results of concurrent mechanisms of resistance and combination therapy is an emerging strategy to improve the outcome of NSCLC patients treated with these agents. Previous studies indicated that the combined treatment with EGFR and MET inhibitors of tumors bearing MET amplification and mutant or wild type EGFR is more effective than single agent alone in reducing the rate of proliferation. Here we tested whether 18F-FLT uptake can be used as a surrogate biomarker for synergy quantification in EGFR targeted combination therapy of NSCLC. Materials and Methods: NSCLC H1993 cells with MET amplification and wild type EGFR, H820 cells with MET amplification and EGFR T790M and H1975 cells with EGFR T790M and MET expression, were selected and tested for the effects of EGFR and MET inhibitors, alone or in combination (at 1:1 constant ratio) on cell viability, proliferation and levels of signaling mediators. Then, tumor-bearing mice underwent 18F-FLT PET/CT scan before and after treatment with EGFR and MET inhibitors alone or in combination and post-treatment changes of 18F-FLT uptake in tumors were determined on images. Dose-effect curves were generated for each set of in vitro and in vivo data using the Chou and Talalay method and CompuSyn software. The combination index (CI) was then calculated for each effect level and total doses of combined drugs. A CI <1, CI =1 or CI >1 indicates synergism, additivity or antagonism, respectively. Results: In the selected cell lines, data analysis of cell viability assays showed that the CI at the total dose causing 50% of the effect ranged between 0.3 and 0.7 for H1993 cells, between 0.1 and 0.3 for H820 cells and between 0.7 and 0.85 for H1975 cells indicating synergism, strong synergism and moderate synergism, respectively. Similar results were obtained from cell cycle and signaling mediators analysis. In agreement with in vitro data, the CI corresponding to the mean reduction of 18F-FLT uptake in response to escalating doses of combined inhibitors in H1993 xenografts varied between 0.5 and 0.7 indicating in vivo synergism. Finally, the analysis of cell proliferation in tumor sections confirmed the imaging results. Conclusion: Our findings indicate that 18F-FLT uptake may be used as a surrogate biomarker for synergy quantification in combination therapy of refractory NSCLC patients.

P781

The role of 18F-FDG PET-CT for evaluation of radiotherapy response in lumbar and sacrococcygeal spine chordoma

S. Cambioli1, C. Nanni1, P. Ghedini1, L. Zanoni1, E. Tabacchi1, A. Svirydenka1, S. Diodato1, S. Bandiera2, S. Fanti1; 1Nuclear Medicine Department, University Hospital S.Orsola-Malpighi,, Bologna, ITALY, 2Department of Oncological and Degenerative Spine Surgery, Rizzoli Orthopedic Institute, Bologna, ITALY.

Aim: Chordoma is an uncommon primary bone tumour characterized by a slow growth, often localized at the sacrococcygeal level. The standard treatment consists in an en-bloc excision with wide margins. In case of unresectable chordoma, carbon-ion therapy is also considered as a new experimental option. Current standard diagnosis are performed by means of magnetic resonance and biopsy. In this context, the scientific literature lack of a comprehensive study of positron emission tomography (PET) for the detection of primary lesions and for the post therapy response. To this aim, the present work reports a first attempt of using 18FDG-PET/CT in the study of chordoma.Materials and Method: Nine patients (4 female; mean-age 56) were enrolled in this study with a diagnosis of primary chordoma of the lumbar (2 patients) and sacrococcygeal (7 patients) spine. All patients underwent a 18FDG-PET/CT at baseline and a second scan 5-12 months (8 months average) after carbon-ion radiation therapy (one patient underwent also surgery). The diagnostic results of the subsequent 18FDG-PET/CT were validated through comparison with post-therapy histological reports.The SUV of both scans (SUV1,SUV2) and its variations (SUV1-SUV2/SUV1) were analyzed. The volume of the lesion, named "metabolic tumor volume" (MTV), of both scans (MTV1,MTV2) was also evaluated. A threshold of 42% of the lesion SUV for the definition of MTV was used. The variations of MTV (MTV1-MTV2/MTV1) were then compared with SUV changes.Results: Baseline PET/CT scans resulted positive for 8 of 9 patients. The measured SUV1 at diagnosis was moderately low and equals to 5.2 in average (from 2.2 to 10.4). After the radiotherapy, 18FDG-PET/CT scan was still positive for the same 8 of 9 patients while the biopsy was positive for all

the 9 patients. The mean of SUV2 was 3.7 (from 2 to 5.5) and the corresponding variation with the baseline scan was found to be around 30%. The mean MTV at diagnosis was 39.7 cm3 while after therapy is 23.9 cm3 leading to a mean variation around 40% roughly in agreement with the variation of SUV.Conclusions: This study, based on 18FDG-PET/CT result, shows that carbon-ion therapy does not completely dump the glucidic metabolic activity of the lesions. In fact, the post-therapy 18FDG-PET/CT scans here reported show a minimum residual FDG-uptake which is explained by a persistence of disease confirmed by histological exams. These results highlight the need of an extended follow-up in order to evaluate the stability of disease.

P782

The response of metastatic lesions in renal cell carcinoma to tyrosine kinase inhibitors evaluated by F-18 FDG PET/CT

O. Yaylali, D. Yuksel, G. G. Dogu, T. Sengoz, A. Yaren; Pamukkale University, Denizli, TURKEY.

BACKGROUND / AIM: Tyrosine kinase inhibitors (TKIs) have been used quite a while for advanced renal cell carcinoma (RCC), but it is not known exactly whether the antitumor effect of TKIs depends on various areas of metastasis. In this study we retrospectively investigated the metabolic F[18]-2-fluoro-2-deoxyglucose (FDG) response of various metastatic lesions to tyrosine kinase inhibitors (TKIs) treatment as assessed by positron emission tomography/ computed tomography (PET/CT) in renal cell carcinoma (RCC) patients. METHODS: A total of 18 patients with advanced RCC treated with a TKI and no prior anti-VEGF exposure were evaluated by FDG PET/CT before and and at 3 to 12 months after the onset of TKI treatment initiation. The maximum standardized uptake value (SUVmax) of all metastatic RCC lesions were measured and analyzed. RESULTS: Eighteen patients with mRCC were retrospectively enrolled in this study. The primary lesions were surgically removed in all patients before TKI treatment. We evaluated 55 RCC metastatic lesions. The metabolic response was evaluated from the PET/CT images. The pretreatment and after treatment SUVmax values (mean ± SD) were as follows: in the 9 lung metastases, 3.88 ± 1.37 and 2.10 ± 1.38 ($p = 0.004$); in the 12 bone metastases, 3.60 ± 2.05 and 3.76 ± 1.42 ($p = 0.853$); in the 17 lymph node metastases, 2.98 ± 2.26 and 1.86 ± 1.47 ($p = 0.179$); in the 17 abdominal parenchymal organ/ other soft tissue metastases, 4.75 ± 1.67 and 3.21 ± 1.87 ($p = 0.01$), respectively. The SUVmax values of the metastatic lesions after treatment were significantly decreased in the lung and abdominal parenchymal organ / other soft tissue metastases. There was no significant difference after treatment in bone lesions and lymph nodes ($p > 0.05$). The SUVmax change ratios after TKI treatment (mean ± SE) were -11.6±47.8 % in the lung metastases, 30.5±48.4 % in the bone metastases, 31.8±19.2 % in the lymph node metastases, -8.3 ±31.7 % in the abdominal parenchymal organ metastases. CONCLUSIONS: In patients with mRCC, the significant decrease of FDG SUVmax value of lung and abdominal parenchymal organ / other soft tissue metastases evaluated by PET/CT at 3-12 months after TKI treatment initiation. However, significant changes were not observed in bone and lymph node metastases after TKI treatment. The degree of reduction in 18F-FDG uptake after TKI treatment in patients with aggressive mRCC, may provide valuable prognostic information. Larger studies are needed to confirm these findings.

P50 - Tuesday, October 13, 2015, 4:00 PM - 4:30 PM, Hall 3 – Poster Exhibition

Clinical Oncology: Miscellaneous

P783

The clinical value of FDG-PET/CT in common cancers: Actual use compared with literature-based recommendations

P. F. Høilund-Carlsen1, H. Petersen1, P. C. Holdgaard2, P. H. Madsen3, L. M. Knudsen4, D. Gad5, A. E. Gravergaard5, M. Rohde6, B. Engelmann7, D. Theilmann-Jørgensen8, J. B. Christensen9, A. Johansen1; 1Dept. of Nuclear Medicine, Odense University Hospital, Odense C, DENMARK, 2Dept. of Nuclear Medicine, Vejle Hospital, Vejle, DENMARK, 3Dept. of Medicine, Vejle Hospital, Vejle, DENMARK, 4Dept. of Haematology, Odense University Hospital, Odense C, DENMARK, 5Dept. of Plastic Surgery, Odense University Hospital, Odense C, DENMARK, 6Dept. of ORL Head & Neck Surgery, Odense University Hospital, Odense C, DENMARK, 7Dept. of Internal Medicine, Næstved Hospital, Næstved, DENMARK, 8Dept. of Gynaecology and Obstetrics, Aabenraa Hospital, Aabenraa, DENMARK, 9Dept. of Quality and Research, Odense University Hospital, Odense C, DENMARK.

Aim: The Region of Southern Denmark (RSD), one of Denmark's five administrative regions holding about 1/5 of the country's population of about 6 million inhabitants, appointed a task force to (1) search evidence in the literature for the clinical usefulness of PET/CT, (2) establish consequent recommendations for the use of PET/CT, (3) compare the actual use with established recommendations, and (4) identify areas of future development and growth. Material and methods: A professional Subgroup should coordinate and present the results. It made six Clinician Groups conduct literature reviews on six selected cancers responsible for 61% out

of 9,213 PET/CT scans in the RSD in 2012. Applying the method of Rapid Evidence Assessment which uses the methodology of systematic reviews with predefined limitations, a structured search of relevant literature was conducted in PubMed, EMBASE, and the Cochrane Library. Included were only articles published in English/ Danish/ Swedish/ Norwegian after 2002. PICO questions were defined (where P stands for patients/problem; I for intervention; C for comparison; O for outcome), and data were recorded, quality checked and rated with regard to strength and evidence level. Following that, the Subgroup compared the actual 2012 use of PET/CT with the literature-based recommendations and suggested areas of future development and growth of PET/CT. Results: Out of 11,729 citations, 1,729 were eligible for review, and 204 were included. The retrieved evidence suggested that PET/CT was a useful method in lung, lymphoma, melanoma, head-and-neck, and colorectal cancers, whereas results were less clear-cut and sparser in gynaecologic cancers. There was a good agreement between the actual use of PET/CT in the first five of the aforementioned cancers in that 96.2% of scans performed in these were made for 'established' or 'useful' indications, while 0.6% were made for 'potentially useful' indications, 1.4% for non-recommendable indications and 1.8% for indications lacking literature documentation. In gynaecologic cancers, 22.2% of scans were made for 'established', none for 'useful', 77.2% for 'potentially useful' indications, and 0.6% for indications not addressed in this literature review. Development and growth were foreseen in cancer, inflammatory/infectious conditions, heart and neurologic diseases. Conclusion: This task force found evidence for the clinical usefulness of PET/CT in five of the six selected cancer types, and sparse documentation in the sixth type, gynaecologic cancers. The actual clinical use of PET/CT agreed well with the evidence-based recommendations. Development and growth was foreseen in many cancers and in other major types of disease.

P784

Diagnostic value of 18F-FDG PET/CT in whole body cancer screening

Y. Sone1, M. Abe1, C. Arakawa1, I. Kato2, A. Sobajima2, T. Kawachi2, I. Takeda3, T. Kumada3; 1Department of Radiology, Ogaki Municipal Hospital, Ogaki, JAPAN, 2Department of Radiological Technology, Ogaki Municipal Hospital, Ogaki, JAPAN, 3Health Management Center, Ogaki Municipal Hospital, Ogaki, JAPAN.

Aim: One remarkable advantage of whole-body 18F-FDG PET/CT is the ability to detect cancer from healthy population. This prospective study determined the prevalence and clinical features of pathologically confirmed cancer detected by PET/CT for cancer screening. Materials and Methods: Between June 2008 and March 2015, a total of 318 participants (male 201, female 117, mean age: 60.6 years) underwent whole-body 18F-FDG PET/CT for cancer screening. PET/CT findings were interpreted, and divided among 4 groups as described below, A: no abnormal findings, B: minor abnormal findings (follow-up unnecessary), C: abnormal findings (follow-up necessary), D: abnormal findings suspicious for malignancy (further examination necessary). Medical records of participants were reviewed to clarify pathological or clinical diagnoses and the clinical courses. Results: The participants were classified into group A: 148 (46.5%) , B: 86 (27.0%) , C: 36 (11.3%), D: 48 (15.1%). The major sites of abnormal findings in group D were colorectum 11, genitourinary 11, head and neck 10, chest 6, hepatobiliary and pancreas 6. Among 48 participants, 38 (79.2%) received further examination. Cancer was pathologically confirmed in 6 participants (sigmoid colon 2, rectum 1, pancreas 1, thymus 1, thyroid 1). Positive rate was 15.1% (48/318), and detection rate was 1.89% (6/318). Curative resection was performed at 5, chemotherapy at 1 (pancreatic cancer with liver metastases). Follow-up records were available in 166 participants. During follow-up period, urogenital cancers (kidney 1, bladder 1, prostate 1) were revealed. The interval from PET/CT to pathological diagnosis was 2, 14, 42 months, respectively. Conclusion: PET/CT is a valuable tool for detecting a wide variety of curable cancers, but showed poor detectability of urogenital cancer.

P785

Cost-Utility Analysis for Improved Decision Making in Method Comparison PET Studies: an Example in Lymph Node Staging of Prostate Cancer

O. Gerke, M. H. Poulsen, P. Høilund-Carlsen; Odense University Hospital, Odense C, DENMARK.

Aim: To examine to which extent paired diagnostic studies of accuracy can be also used to estimate economic implications of introducing a new diagnostic test. Cost-effectiveness and cost-utility analyses are commonly done directly in connection with randomized controlled trials (RCTs) or indirectly by stochastic modeling based on RCTs. However, in our rapidly developing environment, RCTs are difficult to conduct and their use in PET/CT imaging is sparse. We propose a simple decision tree model-based cost-utility analysis comparing a new test and its chosen reference standard and exemplify this with local data from lymph node staging of prostate cancer. Materials and Methods: Average procedure costs were taken from the Danish Diagnosis Related 2013 Groups Tariff, and life expectancy was estimated for an ideal 60-year old patient based on prostate cancer stage and curative versus palliative treatment. Quality-adjusted life-years (QALYs) were deduced

from the literature, and the incremental cost-effectiveness ratio (ICER) was used to compare staging by 18F-fluoromethylcholine PET/CT (FCH-PET/CT) with lymph node dissection and histopathological examination as reference standard. Sensitivity and specificity of FCH-PET/CT for the detection of lymph node metastases were estimated previously to be 0.73 (95% CI: 0.58-0.84) and 0.88 (95% CI: 0.82-0.92), respectively. Results: The ICER was -1,444 € per QALY as FCH-PET/CT was both more costly (1,495 €) and less effective in terms of QALYs than the reference standard (-1.0351 QALYs). However, lower bounds of sensitivity and specificity of FCH-PET/CT were established at which the replacement of the reference standard by FCH-PET/CT came with a trade-off between worse effectiveness and lower costs (e.g. 0.78 and 0.92, respectively, resulting in an ICER of 11 € per QALY). Conclusion: Compared to a true reference standard, any imperfections in accuracy means that replacing the reference standard by the new test generates a loss in effectiveness. So, a trade-off between (lower) cost and (decreased) effectiveness is the best outcome in this situation. In the chosen example, there was no benefit of FCH-PET/CT, which, however, is not the point. It is that similar assessments will prove especially fruitful when comparing several imaging modalities or the same PET modality using different tracers with a common independent reference standard. This will provide useful additional information by ranking the different imaging techniques by their economic benefit (or lack thereof).

P786

18-F-FDG-PET/CT Value in the Therapeutic Management of Unknown Primary

M. B. Garcheva-Tsacheva, **Sr**.1, V. Hadzhiyska1, Z. Mihaylova2; 1Medical University, Sofia, BULGARIA, 2Military Medical Academy, Sofia, BULGARIA.

The aim of the study is to evaluate the place of 18F-FDG-PET/CT in the diagnostic algorithm of unknown primary for shortening the decision for further management of patients.Matherial and methods. Forty three patients (aged from 33 to 79 years) were evaluated and followed up during a two years period by FDG-PET/CT on GE Discovery 16T, using the weight adjusted activity, 60 minutes delay between injection and registration, hydration of patients with diuretic stimulation by furosemide and oral contrast intake. The inclusion criteria were patients with proved malignant histology by lymph node biopsy (gr. LN, n= 23), patients with histological proof of malignancy from brain surgery (gr.BS, n=7), patients with imaging proofs of malignancy by other imaging methods (gr. Im, n= 13). Results. Fifty eight percents (25/43 patients) had positive PET results. Five patients from gr. LN with proved by PET advanced disease were directed for chemotherapy, 2 patients with proved lung and ovarian carcinoma needed operation, and 2 - with head and neck tumors were sent for radiotherapy. From gr. BS all 5 positive cases were with lung carcinoma. Three of them were sent for fibrobronchoscopy (FBS) and radiotherapy planning, 2- with advanced disease - for chemotherapy. From gr. Im: 3 (cholangio- and pancreatic carcinoma) without dissemination were sent for surgery, and 2 - to SRS (somatostatin receptor scintigraphy) , because of suspicion for NET (neuroendocrine tumors). Five patients with data of advanced disease were sent for chemotherapy. As a whole PET/CT directed for treatment 9 patients from gr. LN, 2 from BS, 8 from gr.Im. Three pts were sent for FBS, 2 patients needed additional imaging examinations, besides the group with PET negative studies (2+18 patients, 46%). Conclusion. PET/CT was positive in the majority of patients (58%) sent for the detection of unknown primary. It reduced the need of additional imaging examinations in 54% of patients and directed to therapy 19 (44%) of patients (unfortunately the majority of them with advanced disease). In 4.5 % (H&N tumors with regional spread) PET/CT examination seems able to improve the patients' prognosis and survival. FDG-PET/CT may contribute to the management of patients with CUP tumors and especially those with cervical adenopathies and single metastases (IV,B)

P787

Barriers and Facilitators to Doctors' Engagement with the National PET CT Clinical Audit Programme

P. Ross1, J. Hubert2, M. Saunders3, **W. L. Wong**4; 1Birkbeck University of London, London, UNITED KINGDOM, 2NHS South West Commissioning Group Englang, Bristol, UNITED KINGDOM, 3Alliance Medical Molecular Imaging, London, UNITED KINGDOM, 4Mount Vernon Hospital, Northwood, UNITED KINGDOM.

Aim: The NHS England PET-CT Clinical Audit Programme [Audit Programme] represents a significant change initiative and is one of the major national clinical audit programmes in the NHS. To implement change effectively healthcare professionals need to be fully engaged. The purpose of the study was to 1] identify the barriers and facilitators of doctors' engagement and 2] explore how and why levels of engagement varied between doctors reporting on the Audit Programme. Materials and Methods: A single embedded case study centred on the Audit Programme. A mixed methods approach was adopted using qualitative and quantitative data to investigate the factors which influence medical engagement. A pilot study of 13 purposefully selected in-depth semi-structured interviews with consultant doctors was undertaken over a six month period and informed an on-line survey to all 59 doctors reporting on the Audit Programme. 58/59 doctors responded to the survey.

The interview data and free text was coded and analysed using directed thematic content analysis with the themes compared against the study's propositions. The numeric survey data was transferred to an excel spread sheet and statistical tests were run to produce descriptive charts and graphs to summarise the factors to affect the medical engagement of doctors. Data triangulation techniques were used to corroborate and validate the findings across the different methodological techniques. Results: The main barriers to engagement with the Audit Programme were lack of a common vision, poor communication and poor inter-professional relationships. The factors to facilitate engagement centred on the adoption of a collaborative non-judgemental culture within which audit was re-framed as a process of learning and professional validation. Survey responses showed: doctors initially found audit threatening 76%; doctors nevertheless found audit reassuring 85%; audit helped validate professional competence 92%; participation in audit improved reporting skills 76%. The factors which influenced doctors' engagement most were: perception of audit's usefulness; trust and the dissemination of clinical performance data. Conclusion: The study makes use of a unique data set and to the best of our knowledge is one of the first studies to document how the dissemination of doctors' performance data positively influences engagement with clinical audit. The study also shows that a supportive audit environment is associated with increased levels of engagement and learning, reduced levels of professional anxiety and can provide a framework for the validation of professional competence.

P788

Does 18F-FDG PET-CT field of view that includes vertex have an impact on oncological patients management

Y. E. Ramirez, I. Santos, A. Martinez, S. Rodado, I. Hernandez, C. Escabias, M. Coronado; Hospital Universitario La Paz, Madrid, SPAIN.

The field of view (FOV) in oncological PET/CT is not standardized therefore many centers perform limited scans (base of skull to thigh) but often do not performed other image studies (CT/MR) to detect brain/skull metastases. To determine whether performing 18F-FDG-PET/CT FOV from the vertex of skull to mid thigh is clinically useful. This is a retrospective review of 566 consecutive patients (from January to August2013) who had performed 18F-FDG PET/CT for oncological purpose: hemathologic 112 (98lymphoma), lung cancer 100 (6 small cell and 80 non small cell), breast 55, head-neck 54, colorectal 48, gynaecological 35, esophagus-gastric 21, tumor unknown origin 14, melanoma 16, and other 117. Patients (250 female; mean-age 60; 11pediatric) fasted at least 6h, blood glucose test was obtained (≤180mG/dL) and after 60min 18F-FDG injected underwent PET/CT without intravenous contrast on same scanner (DiscoveryLS, GEMedical Systems). FOV included acquisition from vertex to mid thigh with patient's head locked. Head abnormalities (PET and/or CT) were classified by location (brain, skull or soft tissue) and whether known or not based on previous (image studies or medical record) available data. Findings were correlated with imaging studies, pathology and/or clinical follow-up. Twenty six of the 566 (4.6%) scans showed head abnormalities (30lesions were found: 23CT, 12PET uptake) that were unknown in 15 cases. Lesions were localized: brain (19/26), bone (5/26), both (1/26) and soft tissue (1/26). In 13/26 patients were metastases (9brain and 4skull), one patient soft tissue inflammatory lesion, 8vascular lesions (1/8 unknown), 1trauma and 3other lesions (arachnoid cyst, meningiom). According to primary tumors, brain-skull metastases: (1/98) lymphoma, (1/55) breast, (1/48) colorectal, (1/35) gynaecological, (2/54)3.7%head-neck (6/86) 6.9% lung cancer (6.25% of non small cell lung cancer) and (1/14) 7.14% unknown primary tumor. Despite these new metastases were detected stage only changed in 7/13 patients and modified management/treatment in 8/13head metastases patients. Eight patients (1.4%,8/556) changed their clinical management. Altought FOV (vertex to thigh) 18F-FDG-PET/CT has shown little benefit to detect additional metastases in oncological patients these metastases have an outstanding potential to significantly impact clinical management. Out of these data and within the constrains we had evaluated a small number of patients use limited FOV in order to reduce scanning time it is not cost-effectiveness, especially with new PET/CT equipments (considering scan time and exposure radiations) and in some tumors (unknown primary tumor, head and neck and lung cancer) with higher incidence of head metastases.

P789

The Evaluation of Dual-time-point F-18 FDG PET/CT and chest CT for the prediction of the WHO grade in thymic epithelial neoplasms

T. Shinya1, Y. Otomi1, T. Tanaka2, R. Inai2, S. Kanazawa2, M. Harada1; 1Tokushima university graduate school, Tokushima-city, JAPAN, 2Okayama university hospital, Okayama-city, JAPAN.

Objectives: The purposes of the present study were to assess dual-time-point (DTP) 18-fluorine fluorodeoxyglucose (F-18 FDG) positron emission tomography/ computed tomography (PET/CT) findings of thymic epithelial neoplasms (TEN) and to investigate the diagnostic capacity of PET/CT comparing chest computed tomography (CT) features for differentiating thymic carcinoma from thymoma with receiver operating characteristic (ROC) analyses.Methods: We performed a retrospective study of data from August 2006 to September 2014,

on 56 patients with pathologically proven TEN. The patients were categorized into three groups according to World Health Organization classification (low-risk: 9 A, 7 AB, 11 B1; high-risk: 9 B2, 5 B3; 15 C). For semiquantitative analyses of FDG uptake, we calculated the ratio between standardized uptake value of the tumour and aortic arch (T/M ratio) on both 90-min early and 2-h delayed scans. Multivariate logistic regression analysis was used to estimate the CT features of thymic carcinoma. We compared the diagnostic capacities between PET/CT and chest CT using ROC analyses.Results: T/M ratio of thymic carcinomas was significantly higher than thymoma on both early and delayed scans (p=0.002 for early scan; p=0.003 for delayed scan). No significant difference were found in T/M ratio between early and delayed scans between three groups. The ROC curve for diagnosing thymic carcinoma revealed that the appropriate cut-off value of T/M ratio for the highest accuracy was 2.39, with a sensitivity of 86.7%, specificity of 73.2%, and accuracy of 75.0%. The area under the curve (AUC) was 0.855. The statistical analyses for DTP scans with 35 TEN demonstrated the accuracy and AUC were the accuracy of 74.3% and AUC of 0.838 for early scan and the accuracy of 82.9% and AUC of 0.825 for delayed scan. The multivariate logistic regression indicated increased pericardial effusion (p=0.018) and mediastinal fat infiltration (p=0.026) were the predictors of thymic carcinoma. Obtained ROC curve for the model showed that AUC 0.899.Conclusions: Delayed scans with T/M ratio calculation may have the potential to improve the diagnostic capacity for thymic carcinoma. For chest CT features, increased pericardial effusion and mediastinal fat infiltration were the predictors of thymic carcinoma with moderate diagnostic capacity.

P790

Physiological joint pitfall and misinterpration of PET/CT DOPA Scan

A. Cervino, L. Evangelista, M. Burei, P. Reccia, G. Saladini; Istituto Oncologico Veneto I.R.C.C.S., PADOVA, ITALY.

Introduction. 18F-DOPA PET/CT is increasingly being used in the evaluation of neuroendocrine tumors, although the standardization of protocol acquisition is still missed. The aim of this study was to retrospectively determine the rate of false positive DOPA uptake at bone level, in a cohort of 148 patients. Materials and methods. Between December 2012 and July 2014, we retrospectively re-viewed 148 18F-DOPA PET/CT scan in patients with known or suspected neuroendocrine tumors. PET/CT was performed after the injection of 3 MBq/Kg of 18F-DOPA, and the acquisition was started 60 minutes later. All images were interpreted by an expert nuclear medicine physician and later re-analyzed by a second physician. Co-registrated CT images were used for assessing the presence of a malignant or a benign bone lesion. Results. Out of 148 PET/CT scans, 67 were negative while the residual 81 resulted positive (45.2% and 54.7%, respectively). In 31 patients (21%), PET/CT showed an abnormal uptake in the joints. Eleven out of 67 (16.4%) patients with a negative scan had a significant uptake in the joints versus 20/81 (24.7%) subjects with a positive scan. In 10/31 cases (32.3%), DOPA-uptake was reported in acromion-clavicular joints; whereas in 26/31 (83.4%), it was seen in the vertebral joints, mostly at cervical and thoracic levels (n=12; 46%). In the selected patients, the clinical indications were known or suspected pheocromocytoma (n=5; 16.1%), medullary thyroid cancer (n=13; 41.9%), multi-endocrine familiar syndromes (n=5; 16.1%) and known or suspected neuroendocrine neoplasia (n=8; 25.8%). Finally, in these 31 patients, a malignant bone involvement was depicted in only 5 cases. Conclusions. The interpretation of 18F-DOPA PET/CT appears extremely important, because the rate of false positive findings can be high, both in negative and in positive scans, ranging between 15% and 25%. A misinterpretation can be avoided by a careful lecture of co-registrated CT images.

P791

FDGPET/CT for Pseudomyxoma Peritonei (PMP) and other peritoneal malignancies: Diagnostic features and prognostic consideration

K. Kubota, M. Morooka, M. Okasaki, M. Kameyama, Y. Miyata, R. Minamimoto, Y. Goda, H. Yano; National Center for Global Health and Medicine, TOKYO, JAPAN.

PMP is a rare pathology characterized by mucinous peritoneal effusion mostly associated with appendiceal adenocarcinoma, and some with ovarian cancer or others. Previously FDG-PET had been said not useful because of low FDG uptake by PMP. Recent advances in combined therapy of radical surgery and intra-operative hyper-thermic chemotherapy dramatically improved survival. It prompted us to re-evaluate the possible role of FDGPET/CT for the diagnosis of PMP in comparing to other peritoneal malignancy.Purpose: To find diagnostic characteristics and prognostic potential of FDGPET/CT for PMP.Method: From Jan. 2013 to Dec.2014, 64 FDG-PET/CT studies (48 PMP, 8 peritoneal mesothelioma and 8 peritoneal dissemination of colon cancer patients) were analyzed retrospectively. PMP patients were divided into two groups based on the amount of ascites.Results:22 patients (group A) having larger amount of peritoneal effusion including both mutinous and serous tended to have moderate FDG uptake in the disseminated nodular foci of abdominal and pelvic wall, also have larger swollen ometum with moderate FDG uptake, 26 patients (group B) having smaller amount of ascites, little nodules on abdominal wall and low FDG uptake by

omentum.Definite mass lesions with high FDG uptake (SUV>3.0) in the appendix or peritoneum were observed in 13/22 of Goup A and in 12/26 of Goup B. The incidences were similar in both groups despite the differences of the ascites.Mesothelioma and colon cancer tended to have definite mass lesion with higher FDG uptake in peritoneum with higher incidence, little effusion and lower omentum FDG uptake than PMP.Conclusion: Large amount of ascites and moderate FDG uptake by swollen omentum and peritoneal wall are characteristic findings of PMP, however, incidence of high FDG uptake by definite mass lesion (known prognostic factor) may not directory correlated to such characteristics. These findings can be derived only by FDGPET/CT not by CT. Appropriate evaluation of FDGPET/CT of PMP may help to search best therapeutic strategy.

P792

The utility of 18F-FDG PET/CT in patients with carcinoma of unknown primary.

A. Sowa-Staszczak, M. Kołodziej, M. Buziak-Bereza, M. Trofimiuk-Muldner, A. Stefańska, A. Hubalewska-Dydejczyk; Nuclear Medicine Unit, Endocrinology Department, University Hospital Krakow, Krakow, POLAND.

INTRODUCTION: Patients with carcinoma of unknown primary (CUP) are a diverse and heterogenous group. There are various clinical manifestations and some of the patients could be asymptomatic and diagnosed incidentally. An adequate diagnostic and primary focus finding seem to be essential for the proper treatment of the patient. Among numerous imagining techniques, PET/CT seems to be the most suitable for localizing the primary tumor. The sensitivity of PET/CT in detecting primary tumor is 29%-69% according different authors and it is higher comparing to contrast enhanced CT. AIM: The aim of our study was to evaluate the utility of 18F-FDG PET/CT for localizing the primary tumor. METHODS: We analyzed 144 patients (73 males, 71 females, the median age 64y) in whom 18F-FDG PET/CT imaging was performed in a standard protocol in Nuclear Medicine Department University Hospital Krakow, Poland between October 2012 and September 2014. All of the patients were diagnosed with metastases and other diagnostic methods hadn't revealed a primary tumor. RESULTS: FDG PET/CT suggested a primary tumor in 105 cases. Among them, the most common site of primary tumor detected was gastrointestinal tract, including pancreas (n = 25), which was followed by lung (n = 14), liver (n = 14), head and neck including thyroid (n=11), lymphoproliferation (n = 9), prostate (n = 2) and others (n=30) e.g. ovary, kidney, uterus, bladder. In 14 cases the result of PET/CT confirmed metastases but the primary tumor remained unidentified. In 25 patients PET/CT didn't confirm the presence of metastases and allowed to exclude previously suspected malignancy with high glucose metabolism. CONLUSION: Our study suggests that 18F-FDG PET/CT may be an effective diagnostic tool in patients with carcinoma of unknown primary.

P793

(18) F-FDG PET-TC imaging in the detection of primary tumors in patients with metastatic carcinoma of unknown primary origin: a multicentric study

M. Rossi1, A. Romeo2, M. Della Porta1, F. Malvaldi1, D. Bacciardi1, S. Stefanini1, R. Pratali1, N. Mazzuca1; 1U.O. medicina nucleare, USL 6 di Livorno, Livorno, ITALY, 2U.O. medicina nucleare, Ospedale Maggiore, Bologna, ITALY.

Aim: to assess the value of 2-[fluorine-18]-fluoro-2-deoxy-D-glucose (18F-FDG) positron emission tomography/computed tomography (PET/CT) in the detecting of cancer of unknown primary (CUP) in patients with histologically proven tumor metastasis and/or with a high clinical suspicion of metastatic diffusion.Methods: 172 patients with cancer of unknown primary, unsuccessfully investigated with extensive conventional diagnostic procedures (including CT/MRI/endoscopy) and laboratory investigation, were enrolled for 18 F-FDG PET-CT whole body imaging. Patients received 370 MBq FDG (10 mCi) intravenously, and whole-body images were acquired at 60 min after injection. The images obtained were analyzed with visual and semi-quantitative methods. Histopathology and/or cytology were used to evaluate the PET/CT results.Results: the primary tumor site was correctly identified by 18 F-FDG PET/CT in 25 patients (56/172; 32.5%): lung (n=11), rino/oro-pharynx (n=9), lymphatic system (n=6), colon (n=6), ovary (n=4) liver (n=4), pancreas (n=3), mammary gland (n=3) muscles-endothelium (n=2), stomach (n=2), testicle (n=1), mesothelium (n=1), prostate gland (n=1), thyroid (n=1), parotid gland (n=1) and kidney (n=1). 18 F-FDG PET/TC results were proved false positive in 17/172 patients (19.8%), in which 18 F-FDG focal uptake were located in the lung (n= 10), the rino/oro-pharynx (n=6) and ileocolonic junctional region (n=1). In 77 patients 18 F-FDG PET/CT scans were negative (77/172; 44.7%) and in 12 of them histopathology revealed a primary localization (false negative 15.5%). In 95 patients (95/172; 55.2%), the primary tumor was not localized, although in 21 of them (21/95; 22.1%), 18 F-FDG-PET/CT detected newly unexpected metastases. And globally, in 48 patients of the whole enrolled population (48/172; 27,9%), 18 F-FDG-PET/CT depicted new metastatic sites modifying the stage of the disease and the subsequent management.Conclusion: our results showed that 18F-FDG PET/CT correctly revealed the primary tumor site in 32.5% of patients and in 27.9% of subjects detected further

localization of metastasis providing a relevant value in the clinical and therapeutic management of patients with cancer of unknown primary.

P794

Time-dependent reduction of liver 18 FDG activity in the dual-phase 18 FDG PET/CT study.

O. Kupik, M. Tuncel, P. Kiratli, **B. Erbas**; Hacettepe University, Ankara, TURKEY.

AIM: Liver SUVmean value corrected for lean body mass has been used as a quality measure in the PERCIST. There is visual interpretation scales comparing tumoral tissue 18FDG uptake with liver 18FDG activity which have been used in the response assessment. However, time-dependent reduction of liver 18FDG activity has been reported, and because of time-differences between pre and post-therapy studies might result in discrepancies. Therefore, the change of liver SUVmean values were studied in a dual-phase 18 FDG PET/CT study.MATERIALS AND METHODS: Early and late 18 FDG PET/CT studies were performed in 37 patients who had normal liver functions. 118 FDG PET/CT images were obtained before the therapy and after 2. cycles of chemoterapy. SUVmean values were measured using volumetric region of interests drawn on the right lobe of the liver and corrected for lean body mass values. Early and late SULmean values were compared with wilcoxon analysis. Percentage change was calculated.RESULTS: At baseline study, late SULmean values were significantly lower than early values [1.01 (0.57-1.5) vs 1.29 (0.82-2.04), p=0.0001]. At interim period, similar difference between late and early images was observed [1.18 (64-1.39) vs 1.39 (0.91-1.97)]. SULmean values were not different between baseline and interim studies. Median value of the time difference between early and late studies for baseline and interim period were 70 min (39-114) and 79 min (43-157), respectively. Median percentage change of SULmean was -29% for baseline and -16% for interim period. Percentage changes were correlated with elapsed time (r= 0.57, p=0.0001).CONCLUSION: Liver 18 FDG activity is dependent on the elapsed time. Time-dependent reduction of liver 18 FDG activity should be kept in mind in the interpretation of dual-phase stuies and response assesment, especially in the studies in which liver activity has been used as reference point.

P51 - Tuesday, October 13, 2015, 4:00 PM - 4:30 PM, Hall 3 – Poster Exhibition

Radionuclide Therapy & Dosimetry: MIBG & Peptides Therapy

P795

Peptide Receptor Radionuclide Therapy with Lu-177 DOTATATE in patients with somatostatin receptor positive tumours

K. Kamaleshwaran, n. sudhakar, s. paulvannan, m. vysakh, A. shinto; Kovai medical center and hospital limited, Coimbatore, INDIA.

Aim: Aim is to assess the therapeutic efficacy of 177Lu-DOTATATE in therapy of Neuroendocrine tumours. Methods: 30 patients (age 45±15 years) with Neuroendocrine tumors were included The study was approved by institutional ethics committee.Pre-treatment 99mTc-HYNICTOC SPECT/CT study was performed to confirm the presence of somatostatin receptors. Transfusion of reno-protective amino-acids and anti-emetics were done before and during the treatment. 100-150 mCi of 177-Lu-DOTATATE was administered over 30 minutes and cycles were repeated at intervals of 3 months. Response assessment was done by comparing serum biochemical markers and 99mTc-HYNICTOC SPECT/CT. Results: 20 patients each of medullary carcinoma thyroid (MTC), pancreatic NET (PNET), and gastro-intestinal NET (GI-NET), 1 of mediastinal teratoma with NET component, 3 paragangliomas and 6 NET with unknown primary. There was history of prior surgery in 15, sandostatin treatment in 18, chemotherapy in 17 and radiotherapy in 2 cases. There were lymph node metastases in 19 patients, liver metastasis in 10 , primary in 15, skeletal mets in 7 and pulmonary lesions in 4 cases.10 patients have been administered more than two therapeutic administrations and assessed for treatment efficacy. Biochemical response measured using tumour markers and serum Chromogranin A demonstrated a significant decrease of >50% in 20 (66%) patients and stabilization of the same in 10 (33%) cases. Partial remission, stable disease and progressive disease was observed in 20 (66%), 5 (17%) and 5 (17%) patients, respectively using RECIST criteria. There was a significant improvement in quality of life in 24 (80%) and moderate improvement in 6 (20%) cases. The median overall survival of the patients was found to be 18 months. Conclusions:177Lu-DOTATATE in Neuroendocrine tumours is a safe treatment with significant clinical response and reduction tumour size and biochemical markers.

P796

Early side effects of radio ligand therapy with 177-Lutetium-PSMA of metastatic castrate-resistant prostate cancer

H. Ahmadzadehfar1, A. Yordanova1, S. Kürpig1, E. Eppard1, F. Gärtner1, S. Rogenhofer2, M. Essler1; 1University Hospital Bonn, Department of Nuclear Medicine, Bonn, GERMANY, 2University Hospital Bonn, Department of Urology, Bonn, GERMANY.

Objectives: Peptide radionuclide ligand therapy (PRLT) with 177Lu-PSMA-DKFZ 617 (LU-PSMA) (prostate-specific membrane antigen) is a novel targeted therapy of metastatic prostate cancer. We present the first clinical experiences assessing early possible side effects of this therapy. Methods: 25 PRLT were performed in 16 hormone and/or chemo refractory patients with distant metastases and progressive disease (mean age: 74 y/o). 68Ga-PSMA PET/CT was performed in all patients 1-2 weeks prior to and 7 weeks after PRLT. Median PSA was 376 ng/ml (range: 20-1650). We tried to protect the salivary glands with ice packs during therapy. All patients received CBC, renal and liver function tests on the day before and two days after application (median administered activity 6.2 GBq, range 4.1 - 7.2 GBq), followed by further tests every two weeks. All patients were contacted by telephone every week regarding side effects or any positive and negative changes. Results: All patients showed in Ga-PSMA-PET bone and lymph node metastases, of whom six patients also had residual/locally recurrent tumor. All lesions detected by PET/CT exhibited high Lu-PSMA uptake on post-therapy planar and SPECT/CT scan performed two days after application. Although the treatment was well tolerated by all patients without any significant adverse effects, four patients complained 6-9 hours after the application of mild nausea. A mild dry mouth and fatigue in the first 4 weeks after the application in 3 and 4 patients, respectively, were the most important complaints of the patients. Majority of patients experienced no hematotoxicity and nephrotoxicity. A PSA response were observed in about 70 % of patients. Conclusions: Our initial results indicate that PRLT with Lu-PSMA is safe and seems to have low early side effects profile. A significant PSA decline was observed in the majority of patients.

P797

The clinical efficacy and effectiveness of the Lu-177 DOTATATE therapy

E. Acar, H. Durak, G. Çapa Kaya; Dokuz Eylül University, School of Medicine, Department of Nuclear Medicine, İzmir, TURKEY.

Aim: The purpose of this study was to compare disease state before-and-after Lu-177 DOTATATE therapy in patients with metastatic well-differentiated neuroendocrine tumor/carcinoma.Material and Method: We retrospectively evaluated the total of 15 patients who received 50 courses of (1-6 courses/patient) Lu-177 DOTATATE therapy in the Department of Nuclear Medicine between October 2013-January 2015. There were 10 women and 5 men (mean age: 50, range: 36-78); 3 with pancreatic, 1 with stomach, 1 with bowel, 10 with unknown primary neuroendocrine tumor/carcinoma. CT and Ga-68 DOTANOC PET/CT were performed to all patients before-and-after treatment. Therapy responses were determined based on RECIST (Response Evaluation Criteria In Solid Tumors) and PERCIST (PET Response Criteria In Solid Tumors) criteria.Results: 4 patients were excluded from study due to recent therapy administration which was too early to assess response to treatment. Among the 11 patients evaluated; 6 patients had regression (54.5%), 3 patients had progression (27,5%), 1 patient had regression after first-two treatments but after the following two treatment courses; the patient had regression with RECIST criteria, progression with PERCIST criteria (9%) and 1 patient had progression with RECIST criteria, stable disease with PERCIST criteria (9%). 1 patient died 7 months after the second treatment. She had poorly differentiated pancreatic neuroendocrine tumor (Ki-67 >30%, grade 3), she received Lu-177 DOTATATE therapy because of negative F-18 FDG PET/CT but positive Ga-68 DOTANOC PET/CT. She had regression after two treatment courses, so the treatment was discontinued. Other 2 patients with progression and 1 patient with progression with RECIST criteria, stable disease with PERCIST criteria, did not have Ki-67 indices reported by pathology.Conclusion: Approximately in 50% of patients with well-differentiated neuroendocrine tumors, regression/stable disease was observed after Lu-177 DOTATATE therapy have. Ki-67/mitotic index has a prognostic value.Key words: neuroendocrine carcinoma, metastasis, Lu 177 DOTATATE therapy

P798

Peptide Receptor Radionuclide Therapy with 177Lu-dotatate is an active treatment in advanced bronchial carcinoids: prognostic role of TTF1 and FDG-PET.

A. Ianniello, M. Sansovini, S. Severi, S. Nicolini, V. Lanzetta, K. Massri, F. Matteucci, P. Caroli, A. Bongiovanni, M. Monti, V. D' Errico, G. Paganelli; IRCCS IRST of Meldola, Meldola, ITALY.

Aim: Bronchial carcinoids, Typical carcinoids (TCs) and Atypical carcinoids (ACs), represent 20-25% of all neuroendocrine tumors. Their incidence is increasing and in advanced disease new therapeutic options are still needed. We prospectively investigated the efficacy and safety profile of Peptide Receptor Radionuclide Therapy with 177Lu-dotatate (Lu-PRRT) in advanced TCs and ACs patients (pts) treated at two different dosages. We also investigated the role of TTF-1 and FDG-PET as prognostic factors for pts treated with Lu-PRRT. Methods: Thirty-four consecutive pts with documented radiological progression were treated with Lu-PRRT at two different therapeutic cumulative activity (CA) of 18.5 GBq or 27.8 GBq in four or five cycles. CA was choosen according to the patient's kidney function and bone marrow reserve

(IRST protocol n°100.01). TTF-1 was available in all pts. FDG-PET was available in 29/34 pts at baseline. Results: All patients received at least 4 cycles of Lu PRRT with a median cumulative dosage of 21.5 GBq (12.9-27.8). Median follow up was 29 months (range 7-69). Regardless the CA received, pts with TCs showed a Disease Control Rate (DCR) equal to 80% with 6% of CR, 27% of PR and 47% of SD. Median progression-free survival (PFS) was 20.1 months (range 11.8-26.8). In ACs pts we obtained SD in 47% whereas 53% continued PD. PFS was 15.7 months (range 10.6-25.9). Remarkably, none of the pts had major acute or delayed toxicity, including pts with reduced kidney's function and bone marrow reserve. Of note, PFS in TCs TTF1 negative showed a median value of 26.3 months (range 12.9-45.2), while in TCs TTF1 positive the PFS was 7.2 months (4.2-14.0); p=0.0009. FDG-PET was negative 13 pts: 10 in TCs and 3 in ACs. FDG-PET was positive in 16 pts: 4 in TCs and 12 in ACs. The median PFS in negative FDG-PET pts was 26.4 months (range 14.2-48.9) and it was 15.3 months (range 11.7-31.1) in pts with increased glucose metabolism at baseline FDG-PET; p 0.201. Conclusion: Lu-PRRT has an antitumor activity in bronchial carcinoids in terms of DCR and PFS. According to the IRST protocol, Lu-PRRT is safe in all patients including those at higher risk of side effect. TTF1 seems to be an important prognostic factor in bronchial carcinoids. As for GEP-NET, FDG-PET positivity is a hallmark of more aggressive tumors and is more frequent in ACs compared to TCs.

P799

The clinical efficacy and effectiveness of the Y-90 radioembolization therapy for the treatment of liver malignancies

E. Acar1, G. Çapa Kaya1, A. Gülcü2, H. Durak1; 1Dokuz Eylül University, School of Medicine, Department of Nuclear Medicine, İzmir, TURKEY, 2Dokuz Eylül University, School of Medicine, Department of Radiology, İzmir, TURKEY.

Aim: The purpose of this study was to compare disease state before-and-after Y-90 radioembolization therapy in patients with primary or metastatic liver carcinomas. Material and Method: We retrospectively evaluated the total of 32 patients who received 43 courses of (1-3 courses/patient) Y-90 radioembolization therapy in the Department of Nuclear Medicine between April 2009-December 2014. There were 15 women and 17 men (mean age: 56, range: 40-77); 12 with colorectal cancer, 8 with HCC, 7 with neuroendocrine tumor/carcinoma, 2 with gastric cancer, 1 with breast cancer, 1 with pancreas cancer, 1 with unknown primary/metastatic liver cancer. CT, MR and F-18 FDG/Ga-68 DOTATATE PET/CT were performed to all patients before-and-after treatment. Therapy responses were determined based on RECIST (Response Evaluation Criteria In Solid Tumors) and PERCIST (PET Response Criteria In Solid Tumors) criteria. Results: 6 patients were excluded from study, 4 of them had a recent therapy administration which was too early to assess response to treatment and 2 patients with very poor general condition so they were unable to undergo therapy response imaging. Among the 26 patients evaluated; 7 patients had regression (27%), 1 patient had regression with RECIST criteria, stable disease with PERCIST criteria (3.8%), 2 patients had regression in therapy field but had progression in the other part of the body (7.7%), 5 patients had initial regression but had progression after 5.2 (1-11) months (19.2%), 2 patients had regression in some liver lesions and progression in other liver lesions (7.7%), and 9 patients had progression (34.6%). 12 patients died in an average of 9 (2-22) months after the therapy. There was no significant difference compared to disease progression or regression with localizations of primary disease. Conclusion: Approximately in 1/4 of patients with primary/metastatic liver cancer, regression was observed after Y-90 radioembolization therapy. 62% of patients are still alive. This suggests that the treatment is partially successful. Key words: liver, metastasis, radioembolization, Y-90

P800

Assessment of Response with Evaluation of Renal Toxicity in Patients Receiving 177Lu-DOTA-(Tyr3)-octreotate Therapy in a Tertiary Care Centre in Mumbai, India

T. BHARADWAJ1, H. Rathore1, H. Shah1, P. Aland1, B. Jois KS1, S. Ghosh1, P. Singh2, P. Chandrak3, P. Chaudhuri1, L. Reddy1, P. Kumar1, S. Patro1, V. Lele1; 1Jaslok Hospital and Research Centre, Mumbai, INDIA, 2K.E.M Hospital, Mumbai, INDIA, 3Tata Memorial Hospital, Mumbai, INDIA.

Introduction: Peptide receptor radionuclide therapy is an established modality of treatment for metastatic or inoperable somatostatin receptor expressing tumours. Indigenously synthesised 177Lutetium Chloride in BARC, India has added to both its cost effectiveness and easy availability. However,literature pertaining to clinical and radiological response assessment, and related toxicities in Indian scenario is sparse. Aim: The primary objective is to assess the clinicaland radiological response following repeated cycles of therapy in patients, among those primarily failed to respond conventional modalities. Studying the effect on findings of serial renograms was a secondary objective. Materials and Methods: A cohort of 23 patients who had 1. Received cumulative dose of 29.6 GBq (+/-10%) 177Lu-DOTA-(Tyr3)-octreotate (four cycles of 200mci each at 6-8 weeks interval) 2. Baseline and post therapy Somatostatin receptor PET -CT scan.3. Baseline and post therapy clinical status recorded through subjective interview and Karnofsky's Performance Score. Radiologic response was

evaluated through RECIST 1.1 criteria. Patients were grouped into subgroups according to site of primary (Gastroenteropncreatic, thyroid, paraganglioma or others), sites of metastases (liver, bones or lymphnodes). Clinical and radiological response was assessed for each subgroup individually and in combination with site of primary. Mean percentage reduction in clearances was calculated. Results: Out of 23 patients 15 had gastroenteropancreatic (GEP), 2- thyroid, 2-paraganglioma ,4- others. Most of them were failures to conventional therapy(16). Subgroups (based on site of metastasis): A- 6/23 (liver+ bone + lymphnodes), B-5/23 (bone + lymphnodes), C- 4/23(liver + lymphnodes), D- 5/23 (liver), E- 2/23(lymphnodes), F- 1/23 (bone). Symptoms subsided in 56.5%, unchanged in 26.1% and new symptoms in 17.4% of which 2 died. KPS improved by 10% in 65%, unchanged in 26.1% and decreased by >= 10% in 8.7% who died. Radiologically, 26.1% showed response, 34.8% stable disease, 39.1% progression. Poor response was seen with patients having liver metastasis(r=-0.44) and good response with bone metastasis(r=0.93). Mean percentage reduction in 99mTc-EC clearance was 16.1%(+/-12.2%), more so in patients with prior chemotherapy. Conclusion: 177Lu-DOTA-(Tyr3)-octreotate can be used as a viable treatment option in inoperable cases of somatostatin receptor expressing tumours with good response and tolerable renal side effects.

P801

Peptide receptor radionuclide therapy of neuroendocrine tumours with 177Lu-octreotate: first experience in a French Canadian centre

M. Del Prete, F. A. Buteau, J. M. Beauregard; Université Laval, Quebec City, QC, CANADA.

Aim: Peptide receptor radionuclide therapy (PRRT) with radiolabeled somatostatin analogues is currently a promising targeted palliative treatment against advanced/metastatic gastroenteropancreatic neuroendocrine tumours (NETs). We report initial data of a retrospective study in metastatic NET patients treated with PRRT at CHU de Québec.Materials and methods: Files of patients with NET treated with 177Lu-octreotate between November 2012 and March 2015 were reviewed. Four induction cycles of approximately 7.4 GBq (lowered to 5.5 GBq in cases of impaired renal function or widespread bone metastasis) were administered at 8-10 week intervals, with concurrent amino acids infusion. Maintenance cycles were administered to responders. Overall response was assessed at 3 months following 4th cycle. Radiological response was evaluated according to RECIST 1.1 and SWOG criteria, while biochemical response was evaluated by the analysis of chromogranin-A (CgA). Haematological, hepatic and renal function tests were performed before, and at 2 and 4 weeks after each cycle, and 3 months after the 4th cycle. Treatment toxicity was evaluated according to the National Cancer Institute Common Toxicity Criteria (CTCAE) version 4.0.Results: Twenty-two patients (median age 61; range: 43-82) were treated and 79 treatments (75 induction and 4 maintenance cycles) were given. Nine patients were assessable 3 months after the 4th induction cycle. According to RECIST criteria, all patients (100%) had stable disease (SD), while according to SWOG criteria, 8 (88.9%) patients had SD and 1 (11.1%) had minor response. Six patients were evaluable for biochemical response at 3 months, with a stabilization of CgA levels in 4 (66.7%) and a biochemical progression in the other 2 (33.3%). Symptomatic response was observed in 6 (66.7%) patients, 1 (11.1%) patient had stabilization of symptoms and 2 (22.2%) patients had aggravation of symptoms (pain, fatigue, flushing and diarrhea). Most common toxicities were haematological or renal, of grade 1 or 2 (20% of all cycles). No patients experienced any grade 4 toxicity, while subacute grade 3 haematological toxicity occurred in 2 (2.7%) cycles and in 2 (9.1%) patients. No patient experienced chronic toxicity grade 3 or 4 or death due to PRRT.Conclusion: Our preliminary results indicate that 177Lu-octreotate PRRT appears to be a safe and effective palliative treatment for metastatic NET patients. The low rate of minor or partial radiological responses we observed may be due to an initial referral bias towards patients with more advanced disease.

P802

Peptide Receptor Radionuclide Therapy (PRRT) in Patients with Metastatic Neuroendocrine Tumors: How Effective and Safe Are They?

T. Liotsou, A. P. Stefanoyiannis, S. N. Chatziioannou; 2nd Department of Radiology, Nuclear Medicine Section, National and Kapodistrian University of Athen, Athens, GREECE.

Aim: Neuroendocrine tumors (NETs) are well-differentiated tumors, the majority of which express peptide receptors in the surface of their cells. Peptide receptor radionuclide therapy (PRRT) is based on the systemic administration of a synthetic peptide, labeled with β-emitting radionuclides 90Y or 177Lu. This study aimed to evaluate the efficacy and safety of this therapy. Material and Methods: Twenty (20) patients were treated with 90Y-DOTATOC (total dose of 13.3 GBq) or 177Lu-DOTATATE (total dose of 29.6GBq). These patients were presented with histologically proven well-differentiated, metastatic or unresectable NETs (15 patients with gastroenteropangreatic tumors, GEP-NETs, 3 patients with lung carcinoid and 2 patients with medullary thyroid carcinoma). In all patients, somatostatin receptor scintigraphy was positive before treatment and the burden of their disease was determined via CT or MRI imaging. Patients were followed up

for 3-36 months after the end of the PRRT. Co-administration of amino acid solution was carried out in all patients in order to avoid nephrotoxicity. RECIST criteria were used to evaluate radiological response, WHO criteria for biochemical response evaluation, whereas clinical response was based on the reduction of the symptoms' frequency. Toxicity was estimated using Common Toxicity Criteria version 4.0. Results: Radiological partial response was observed in 40%, biochemical partial response in 35% and clinical partial response in 60%. Concerning toxicity, it appeared only in some patients who received 90Y-DOTATOC treatment (1 patient with transient liver toxicity grade II and 3 patients with renal toxicity of grade I). Other side effects during therapy were nausea, vomiting and headache due to administration of amino acids, with complete remission few hours after therapy. Conclusion: The efficacy of this treatment is very important based on tumor response rates. On the other hand, the few side effects and the clinical improvement makes this treatment a important tool for the therapy of NETs.

P803

Efficacy and and long-term tolerability of 177Lu-DOTATATE treatment

J. Svensson1, A. Elf2, R. Rossi Norrlund3, V. Johansson2, B. Wängberg2, P. Bernhardt4; 1Department of Oncology, The Sahlgrenska Academy, Sahlgrenska University Hospital, Göteborg, SWEDEN, 2Department of Surgery, The Sahlgrenska Academy, Sahlgrenska University Hospital, Göteborg, SWEDEN, 3Department of Radiology, The Sahlgrenska Academy, Sahlgrenska University Hospital, Göteborg, SWEDEN, 4Department of Radiation Physics, The Sahlgrenska Academy, Sahlgrenska University Hospital, Göteborg, SWEDEN.

Aim: Peptide receptor radionuclide therapy is a valuable option for patients with neuroendocrine tumours overexpressing somatostatin receptors. Durable disease control is reported, though randomised data is still lacking. Tolerability is generally reported as very good, though renal and hematologic toxicity exist. More recent reports on this therapy have focused on potential prognostic factors for effect and toxicity, to improve the selection of patients. Both toxicity during treatment and long term tolerability is relevant for these patients who have a relatively long life expectancy and later often are candidates for further therapy. The aim of this study was to evaluate renal and bone marrow function at late follow up.Material & Methods: 51 patients were treated with in average 24.6 GBq (range 8.0-44.8) 177Lu-DOTATATE on 1 to 6 occasions during 2006-2011 at Sahlgrenska University Hospital, Gothenburg. Kidney protecting amino acids were co-infused at treatment. Responses were monitored radiologically with RECIST criteria, and biochemically. To evaluate treatment tolerance, hemoglobine, leucocytes, platelets, serum creatinine and glomerular filtration rate (GFR) was monitored during treatment and follow up. Results: 40 patients were radiologically evaluable according to RECIST 1.1. Of these patients 6 had PR, 32 SD and 2 PD, with a mean time to progression of 37 months. Of 40 patients biochemically followed, 31 had elevated Chromogranin A in serum or tU-5HIIA in urine. 21 of these patients responded with a reduction to less than 75 % of base line values after treatment. Mean values for leukocytes, platelets, serum creatinine (n=49) and GFR (n=36) did not differ significantly from baseline values after a mean follow up time of 45 months (36 months for GFR). Hemoglobine values had decreased from 129 to 117 g/L ($p<0.01$). 23 patients are still alive, with a mean follow up time of 74 months. Conclusion: Disease control rate (PR+SD) was 95 % for radiologically evaluable patients with a response time comparable to what has been reported by other groups. Renal and bone marrow function seems preserved at long term follow up.

P52 - Tuesday, October 13, 2015, 4:00 PM - 4:30 PM, Hall 3 – Poster Exhibition

Radionuclide Therapy & Dosimetry: Thyroid

P804

Effect of application of prophylactic central compartment lymph node dissection to radioiodine ablation doses in patients with papillary thyroid carcinoma.

C. Soydal, E. Ozkan, N. O. Kucuk, K. M. Kir; Tip Fakultesi, Ankara, TURKEY.

Aim: We aimed to document the effect of application of prophylactic central compartment dissection to radioiodine ablation doses for papillary thyroid carcinoma. Material and Method: 452 (382F, 69M, mean age: 46.69, min-max: 13-71) patients who received ablative doses of radioiodine between April 2010 and December 2014 were included retrospectively. Histopathological reports of thyroidectomy and given radioiodine doses were evaluated. Frequencies of prophylactic central compartment dissection according to T stage of primary tumor, detection rate of lymph node metastases and its effect to given radioiodine ablation dose were calculated. Results: Totally 252 (56%) of patients had undergone prophylactic central compartment dissection. T stages of these patients were T1a, T1b, T2 and T3 in 85 (34%), 106 (42%), 41(16%) and 20 (8%). Given radioiodine ablation doses was affected from central compartment lymph node metastases 112 (44%) patients. While 32 (29%) of these patients had papillary microcarcinoma (T1a), 48 (43%), 20 (18%) and 12 (11%) of them had T1b, T2 and T3 tumors. Conclusion: Application of prophylactic central compartment dissection affects

radioiodine ablation dose in approximately half of patients. This effect comes forward in T1 stage tumors.

P805

Radioiodine therapy outcome in older patients with thyreotoxicosis caused by Graves' disease : our experience

M. Yaneva; UMBAL St.George Plovdiv, PLOVDIV, BULGARIA.

Older patients have fear or some contraindications for operative treatment. In the last years the endocrinologists try, sometimes for a very long time and unsuccessfully, to treat them with antithyroid drugs. Some of these collegues discovered that in practice radionuclide treatment with 131-I still exists. Aim: We wanted to evaluate the effectiveness of 131-I therapy in older patients with thyreotoxicosis caused by Grave's disease in 10 years time. Material and method: We made a retrospective assessment of 187 patients with thyreotoxicosis, 151 women and 36 men at median age 67 ± 7,5. All of them were treated with thyreostatics for 3-5 years with data of relapse. The hormonal tests showed higher values than normal, they did not accept operative treatment and their possibility for treatment remained 131-I.The applied doses of 131-I were 5-6 mCi .The patients were treated as outpatients for the clinic. Results: After a follow up on the sixth month 57% (107 pts) did not need treatment, 19 % (36 pts) still accepted Laevothyroxin, but in a lower dosage and only 1 patient had no effect after the application of 131-I. Patients that did not respond to the first dosage of 5 mCi got another 5 mCi on the next year. Then the response was good and they had no need of thyrostatics. Our results show favourable influence of 131-treatment on hyperthyroidism. Patients felt much better after the iodine treatment and they remember the radionuclide treatment with131-I with satisfaction.No side effects were observed in all patients. Conclusion: We strongly suggest that 131-I therapy should be applied to patients who had undergone unsuccessful treatment with thyreostatics, those that have relapse after operation and contraindications or unwillingness for operative treatment.

P806

99mTc-HYNIC Octreotide and F-18 FDG PET -CT in differentiated thyroid cancer patients with raised thyroglobulin levels and negative 131I whole-body scans

K. Kamaleshwaran, n. sudhakar, m. vysakh, A. shinto; Kovai medical center and hospital limited, Coimbatore, INDIA.

Objectives: Thyroid cancer is the most common endocrine tumor and its incidence is increasing. Nuclear medicine plays an important role in the clinical management of the disease. It has been described the use of 99mTc labeled somatostatin analogues for thyroid cancer patient evaluation after surgery and iodine treatment in those who persist with high thyroglobulin levels and a negative iodine whole body scan. The aim of our work was to perform an intrapatient comparison of F-18 FDG PET-CT with 99mTc HYNIC Octreotide scans in 20 patients of thyroid cancer and follow up them for one year. Methods: FDG PET/CT examinations were performed to 20 patients bearing differentiated thyroid cancer (15 papillary and 5 follicular) post-thyroidectomized with raised thyroglobulins (21 to 67 ng-ml; mean 35 ng-ml), negative antithyroglobulins and negative I 131whole body scans (15 women, age 29-55 yr, 5 men, age 45-75) that already had a positive 99mTc HYNIC Octreotide scintigraphy. Studies were performed after obtaining informed consent and our Ethics Committee approval. Results: 99mTc HYNIC Octreotide scintigraphy showed focal thyroid bed (n=10), node (n=3) and lung (n=7) uptake . F-18 FDG PET-CT studies showed discordant matches with 99mTc HYNIC Octreotide scans in most of the patients. The patients with somatostatin receptor uptake does not show glucose uptake.those patients which showed HYNICTOC positivity underwent LU-177 DOTATATE therapy and with FDG uptake underwent retinoic acid redifferentiation therapy. Conclusions: These results may reflect the different somatostatin receptor and glucose receptor expression in thyroid cancer associated to different affinities of these two radiolabeled analogues . This information may path the way to new insights to in vivo molecular understanding of somatostatin receptor expression in thyroid cancer and used in peptide receptor therapy..

P807

Thymic involution after radioiodine therapy for Graves' disease

M. Jinguji1, M. Nakajo1, M. Nakajo1, Y. Nakabeppu1, C. Koriyama2, T. Yoshiura1; 1Department of Radiology, Kagoshima University Graduate School of Medical and Dental Sciences, Kagoshima, JAPAN, 2Department of Epidemiology and Preventive Medicine, Kagoshima University Graduate School of Medical and Dental Sciences, Kagoshima, JAPAN.

Aim: Graves' disease is an autoimmune condition characterized by the presence of circulating thyroid stimulating hormone receptor antibody (TRAb). Thymic hyperplasia in patients with Graves' disease is well documented. However, the underlying mechanism of thymic hyperplasia in patients with Graves' disease is not understood. The aims of this study were to examine whether the volume and CT attenuation of the thymus in patients with Graves' disease will change after

radioiodine therapy, and to elucidate factors that affect these changes. Materials and Methods: The subjects were 40 consecutive patients with Graves' disease (7 males and 33 females; mean age, 49.6 years; age range, 20-73 years) who underwent neck and chest CT before and 6 months after radioiodine I-131 therapy. Thymic and thyroid volumes were measured on CT, and thymic CT attenuation value (thymic density) was measured at the level where the thymus appeared most prominently. We examined the associations between thymic volume or density and the following factors: age, serum triiodothyronine (T3), thyroxin (T4) and TRAb levels and thyroid volume before radioiodine therapy using the Spearman rank correlation test. Thymic volume, density and TRAb were compared between before and after the therapy using the Wilcoxon signed-rank test. Furthermore, we examined the associations between thymic volume reduction ratio and the following factors: age, serum T3, T4 and TRAb decline and thyroid volume reduction ratios using the Spearman rank correlation test. Results: A significant correlation was observed only between thymic density and age (ρ=-0.650, P<0.001) before radioiodine therapy. Thymic volume and density were significantly decreased after radioiodine therapy (P <0.001 for both). There were significant correlations between thymic and thyroid volume reduction ratios (ρ=0.422, P=0.007), and thymic volume reduction and T3 decline ratios (ρ=0.345, P=0.029), respectively. Six months after radioiodine therapy, serum TRAb levels were significantly increased (P =0.003). No significant correlation was found between thymic volume reduction and TRAb decline ratio (ρ=0.052, P=0.772). Conclusion: Significant thymic involution occurs after radioiodine therapy in patients with Graves' disease. Serum T3, but not TRAb may be related to thymic hyperplasia and involution following radioiodine therapy.

P808

First experience of treatment of thyroid cancer with high-ablative dose of I-131

R. Alimanovic-Alagic1, A. Skopljak-Beganovic2, E. Elma Kucukalic-Selimovic1; 1University Clinical Centre Sarajevo, Clinic of Nuclear Medicine, Sarajevo, BOSNIA AND HERZEGOVINA, 2University Clinical Centre Sarajevo, Department of Medical Physics and Radiation Safety, Sarajevo, BOSNIA AND HERZEGOVINA.

Introduction: Radioactive iodine treatment is a type of internal radiotherapy and has been used for over 60 years in the treatment of patients. After total thyroidectomy, a patient is treated with I-131 targeted treatment. Main types of cancer for I-131 treatment are follicular and papillary thyroid cancer. This study represents our own experiences with ablation therapy at thyroid cancer over a period of 12 months. Materials and methods: The study included 91 patients after total thyroidectomy. We have analyzed 67 patients with papillary thyroid carcinoma iand 24 patients with follicular thyroid carcinoma. All subjects were assessed prior to treatment: personal history and physical status, laboratories, appropriate blood tests, EKG exam, internal medicine specialist examination, ultrasound examination residual part of the thyroid gland. There was a TSH hormone, Titer Antibodies: Tg and ATGL. Then certain ablative dose doses of 1,85 GBq to 7,4 GBq (50 to 200 mCi) of I-131 in the form of a capsule is administered to the patient. 72 hours after the treatment of the patient, the whole body scintigraphy is performed. 2-3 months after discharge from the hospital, the patient is ordered to come back and check the hormone status. Results of Investigation: After total thyroidectomy and without therapy levotiroxine all patients has high TSH. A total of 91 patients with papillary and follicular carcinoma were treated with I-131 for ablation of a postoperative thyroid remnant. In the both therapeutic groups blood test showed decreased TSH values (from 46,5 to >100 mIU/ml), Tg (from < 0,1 to > 500 ng/ml), and elevated ATGL (from 1,3 to 2509 IU/ml). With this study we demonstrated that the dose (specific activity of I-131 administered) required to achieve ablation is a high dose of approximately 100 mCi, and, in terms of successful remnant ablation, lower doses are not as beneficial as the conventional doses of 1,85 GBq to 7,4 GBq (50 to 200 mCi). Conclusion: In the both therapeutic groups there was normalization of the hormonal status, subjective and objectives parameters, at the control examinations, already after three months and six months follow-up. The side effects did not appear in the any of therapeutic groups, what demonstrates safe application. We conclude that after increasingly meticulous near-total surgery and careful patient selection, the available data continue to favor higher doses of radioiodine (1, 85 GBq to 7,4 GBq (50 to 200 mCi) for remnant ablation, especially after near-total thyroidectomy.

P809

Radioioeine Retreatment or Wait for a Limited Time in Patients with Differentiated Thyroid Carcinoma with Negative Thyroglobulin and Antithyroglobulin, but Remained Thyroid Residue after Post-Surgery Radioiodine Ablative Therapy?

A. Fard-Esfahani, B. Fallahi, A. Emami-Ardekani, S. Sahari, D. Beiki, M. Abedi, A. Hassanzadeh-Rad, M. Eftekhari; Tehran University of Medical Sciences, Research Center for Nuclear Medicine, Tehran, IRAN, ISLAMIC REPUBLIC OF.

Thyroid cancer follow-up after total thyroidectomy and radioiodine ablation therapy is performed mainly by assessment of radioiodine whole body scan (131I-WBS), thyroglobulin (Tg), anti-thyroglobulin antibody (Anti-TgAb) levels and

sonography. Considering there are a number of patients with negative Tg, Anti-TgAb and sonography, but with a remained thyroid residue, and there is a concern about prolonged therapeutic effect of radioiodine, the best therapeutic approach as to give another therapeutic I-131 dose, or wait for a limited time to get more I-131 therapeutic effect from the first dose, is evaluated in this paper. Materials and Methods: In this study, we enrolled the DTC patients with only thyroid remnant in 131I-WBS six months after first ablative therapy. Patients with detectable Tg, high Anti-TgAb, evidence of neck mass in sonography and evidence of local or distant metastasis were excluded. The patients were randomly placed in two groups: A group who received I-131 retreatment and those who did not (follow-up group). Then after six months, the clinical results of these two groups were compared by evaluating 131I-WBS, Tg, Anti-TgAb and sonography. Results: From 94 enrolled patients, 36 patients were in retreatment group and 58 patients were in follow-up group without retreatment. Both groups matched by the variables including age, sex, pathology, tumor size, capsular, vascular and lymphatic invasion. In 47.2% of the retreatment group 131I-WBS still showed thyroid remnant, while in 52.8% 131I-WBS became negative. These values for the follow-up group without retreatment were 65.5% and 34.5%, respectively (p=0.08). In retreatment group, six months after retreatment, 97.2% of patients still had Tg<1ng/ml and 2.8% showed Tg elevation (Tg>1ng/ml). In the follow-up group, after six months 96.6% of patients still had Tg<1ng/ml and 3.4% showed Tg elevation (Tg>1ng/ml) (p=0.857). In 94.4% of retreatment and 98.3% of follow-up group Anti-TgAb six months after retreatment was <100mIU/ml (p=0.304). Sonography results were also insignificant (p=0.403). Conclusion: In patients with undetectable Tg/Anti-TgAb and only thyroid remnant in the six- month post-ablation 131I-WBS, delay in prompt radioiodine retreatment may be considered, as due to continued ablative effect of radioiodine, about one-third of these patients may have a negative 131I-WBS in the next six-month study, consequently less patient and society radiation burden and less economical loss, with same clinical results will be achieved.

P810

Risk Factors for Persistent Disease in Papillary Thyroid Carcinoma with Lymph Node Metastasis

A. Oral1, B. Yazici1, A. Akgun1, H. Hassoy2, Z. Ozcan1; 1Ege University, Faculty of Medicine, Department of Nuclear Medicine, Izmir, TURKEY, 2Ege University, Faculty of Medicine, Department of Public Health, Izmir, TURKEY.

Aim: It is known that the presence of neck lymph node (LN) metastasis is correlated with persistent and recurrent disease in papillary thyroid carcinoma (PTC) patients. Cervical LN metastasis in PTC is present in an average of 60 % of the patients. After surgery and radioiodine treatment most of the patients become disease-free. But some of the patients have persistent disease. In the present study it was aimed to determine the factors affecting persistent disease in PTC patients with histopathologically confirmed LN metastasis. Materials and Methods: In this study, patients with non-papillary thyroid carcinoma, without LN metastasis, having less than 2 years of follow-up or initial distant metastasis and patients with high serum thyroglobulin antibodies were excluded. We analyzed 130 (F/M: 93/37, median age: 40.5 years) consecutive PTC patients with histopathologically proven LN metastasis. In 94 of the patients LN metastasis were detected on histologic examination of initial surgical material. In 36 patients LN metastasis were surgically removed during the follow-up after radioiodine therapy. Clinicopathological characteristics and persistent disease after treatment were examined. Univariate and multivariate analysis were performed to identify risk factors for persistent disease. Results: At the end of a median follow-up of 84 months, 90 (69 %) of the patients became disease free, and 40 (31 %) patients had persistent disease. Univariate analysis showed that male gender, older age at initial diagnose (≥45 years), larger tumor size (>4 cm), presence of lateral cervical LN metastasis, extrathyroidal invasion and higher number of metastatic LN (≥10) were significant predictors for persistent disease. Multivariate analysis showed that extrathyroidal involvement, presence of lateral cervical LN metastasis and older age at initial diagnose (≥45 years) were independent predictors for persistent disease. Conclusion: Despite the presence of LN involvement, most of patients may become disease free with therapy. Patients with extrathyroidal invasion, presence of lateral cervical LN metastasis and older age at initial diagnose (≥45 years) are more likely to have persistent disease. However disease control can be achieved with close follow-up and therapy.

P811

Clinical impact of circulating anti-thyroglobulin autoantibodies on the prediction of recurrence in patients with differentiated thyroid cancer after first remnant ablation

G. Shen, S. Hu, A. Kuang; West China Hospital of Sichuan University, Chengdu, CHINA.

Aim: The aim of the study was to evaluate the clinical impact of circulating anti-thyroglobulin antibody (TgAb) titers after remnant ablation on the prediction and management of differentiated thyroid carcinoma patients who had undetectable thyroglobulin (Tg) values. Materials and methods: Patients with differentiated thyroid carcinoma who underwent total thyroidectomy followed by 131I remnant ablation between 2007 and

2011 were enrolled. Of these, three hundred and seventeen consecutive DTC patients with undetectable Tg were the subjects of this study, which consisted of positive-TgAb and negative-TgAb patients. All the patients had been followed for 2 years. Recurrence was assessed by 131I scan, 18F-fluorodeoxyglucose positron emission tomography, sonography, computed tomography, or by surgical operation. The tumor characteristics and final outcomes were compared between these two groups. In addition, the mean ablation courses of each group were also counted. Results: Ninety-seven patients (30.6%) of the Tg-undetectable patients showed positive TgAb, and the prevalence rate of high-risk patients in TgAb-positive patients was significantly higher than that of TgAb-negative controls (12.2% vs. 3.1%, $p<0.05$). Forty eight of these TgAb-positive patients were confirmed with recurrence, and the recurrence rate of TgAb-positive patients was significantly higher than that of TgAb-negative patients (49.4% vs. 11.7%, $p<0.001$). During the two-year follow-up, 64.7% of the disease-free patients showed spontaneously decreased TgAb levels. A total of 59.4% of patients with recurrent cancer, who showed responses to surgical operation or radio-iodine treatment, also showed a decreased TgAb level. In addition, the TgAb-positive cohort had more 131I therapy courses than TgAb-negative group (mean 2.7 vs. 1.0, $p<0.05$). Conclusions: Positive serum TgAb titer after first thyroid remnant ablation appears to be a useful marker for recurrence in DTC patients with undetectable serum Tg results.

P812

J - 131 Therapy of Autonomously Functioning Thyroid Adenoma: the Outcome of Our 20 Years Experience

Z. PETROVSKI; DEPARTMENT OF NUCLEAR MEDICINE CLINICAL HOSPITAL - BITOLA, BITOLA, MACEDONIA, THE FORMER YUGOSLAV REPUBLIC OF.

Objective: To investigate the results of J - 131 treatments in patients (pts) with autonomous thyroid adenomas in long period of follow up. Material and Methods: We enrolled 68 consecutive pts with Plummer's disease (50 females, 18 males, mean age 54,7 yrs, range 21 - 79 yrs) for period 1994 - 2014. 87%(59/68) pts had a unifocal nodule, while 13% (9/68) pts had multifocal toxic autonomous nodules.Pts stopped antithyroid drugs for at least one month prior to the radioiodine therapy and than we administered a J- 131 activity of 740 -+ 180 MBq (range 550 - 1150 MBq), based of size and weight of "hot" nodules and the value of radiiodine uptake.Volumetry was done by ultrasound.The mean duration of follow up was 7,84 yrs.Results: In 65/68 (95%) pts was administered a single dose, while 3/68(5%) pts needed two doses. 62/68 (91,3%) pts who received a single dose were euthyroid with scintigraphic normalization.The percentage of euthyroid did not significantly change in long term of 20 yrs observation.The recurrent hyperthyroidism was 2,9% (2/68) pts.The cumulative incidence of hypothyroidism was 11,8% (8/68) pts withing 1 - 6,2 yrs.The nodular volume was statistically higher in pts who had recurrent hyperthyroidism over hypothyroidism ($p<0,01$) and euthyroidism ($p<0,02$).The development of hypothyroidism was higher in pts who showed extranodular uptake and after TSH suppression.No differences were observed in the results between unifocal and multifocal nodules.Conclusion:J - 131 therapy is a simple, safe and 97% effective treatment of autonomous functioning thyroid adenoma after one or more radioiodine doses.

P813

Evaluation of ablation of thyroid remnants with 1850MBq iodine-131 in patients with thyroid cancer

J. Kawabe, S. Higashiyama, K. Kotani, A. Yoshida, S. Shiomi; Graduate School of Medicine, Osaka City University, Osaka City, JAPAN.

Aim: Radioiodine remnant ablation (RRA) with I-131 is recommended for differentiated thyroid cancer patients without residual macroscopic metastases post-thyroidectomy. The administered iodine activity necessary for ablation is controversial. We have been performing RRA with 1850 MBq at our facility since 2011, and evaluated the outcome retrospectively. Materials and methods: Of the postoperative thyroid papillary carcinoma patients without macroscopic metastases, 61 patients who underwent ablation at our facility from November 2011 to December 2014 (17 men, 44 women; mean age, 59.5 years) were evaluated. TSH, thyroglobulin (Tg), and anti-Tg antibody levels were measured in pretereatment status, just before RRA after a 2-week low iodine diet combined either with thyroxine withdrawal (THW) (n=16) or recombinant human TSH (rhTSH) stimulation (n=45). All patients received I-131 (1850MBq) treatment, followed by I-131 scintigraphy after 10 days. Three months later, 2-week low iodine diet combined with either THW (n=51) or rhTSH stimulation (n=10) was restarted, followed by measurement of TSH, Tg and anti-Tg antibody levels and I-131 scintigraphy. Successful RRA was defined as follows: visually negative thyroid bed uptake (TBU) and a Tg level 3 months after RRA < 2 ng/mL. Results: Visually, negative TBU shown in 55 patients (90.16%) of 61 patients. Quantitatively, the averages of pretreatment Tg levels, just before RRA and 3 months after RRA of 53 patients excluding 8 patients with anti-Tg antibody was 2.87 +/- 5.80 ng/mL, 27.92 +/- 70.88 ng/mL and 21.50 +/- 41.27 ng/mL, respectively. In 50 patients excluding 11 patients both with positive anti-Tg antibody and positive TBU from all 61 patients, patients with the Tg levels below 2 ng/mL 3 moths after RRA were 28 patients (56%). In five characteristics such as:

Body weight (p=0.0016), BMI (p=0.0035), body surface area (p=0.0031), Pretreatment Tg levels (p<0.0001) and Tg levels just before RRA (p<0.0001) of 14 characteristics, significant differences were shown. Of them, Pretreatment Tg levels (p = 0.0065) and Tg levels just before RRA (p = 0.03) were significant predictive factors for success of RRA with univariate logistic regression analysis. Conclusion: Ablation with 1850MBq I-131 effectively destroyed the thyroid bed. Measurements of pretreatment Tg levels and Tg levels just before RRA are useful for prognoses of success of RRA.

P814

Radioiodine scan feature [multifocal versus unifocal pattern] as the determinant for radioiodine ablative treatment dose in patients of Differentiated Thyroid Carcinoma

P. Singh1,2, S. Basu2, R. Asopa2, M. Rajan2; 1Seth G.S. and K.E.M. Hospital, Mumbai, INDIA, 2Radiation Medicine Centre, BARC, Mumbai, INDIA.

Aim: To evaluate and compare the appropriate effective dose of 131I therapy for successful ablation in differentiated thyroid cancer patients demonstrating multifocal radioiodine uptake/uptake outside thyroid bed and thus proposing this factor as an important determinant in justifying higher dose for successful radioiodine ablation in neck as compared to that administered for standard unifocal radioiodine uptake in neck after total thyroidectomyMaterials and Methods: Patients of differentiated carcinoma of thyroid (post-thyroidectomy and considered for radioiodine remnant ablative therapy) including aggressive histological variants were included in the study (n=125). A preablative scan with 3.7 MBq 131I, post-treatment scan before discharge and follow-up scan after 6 months of therapy with 0.111-0.136 GBq 131I were part of regular protocol. Scans were done on gamma camera and interpreted by two independent Nuclear Medicine Physicians. In case of discordance, opinion of a third Nuclear Medicine Physician was taken. Patients with multifocal uptake in neck/uptake outside thyroid bed in preablative and/or post ablative scintigraphy were included in the study group (84/125). Unifocal uptake in neck in both preablative and postablative scintigraphy comprised the control group (41/125). Patients with distant metastasis were excluded. 49/84 patients with multifocal neck uptake received low ablative dose (1.85GBq) and 35/84 received high dose 3.7-7.4 GBq. 7/84 patient's scan had discordant findings and were dropped in favor of multifocality restricted to thyroid bed. 20/41 patients with unifocal neck uptake in scintigraphy received low ablative dose (1.85GBq) and 21 received high ablative dose (3.7-7.4 GBq). The objective ablation parameters were Scintigraphy, biochemical markers (Thyroglobulin), relevant radiological investigations and SPECT-CT when available.Results: 44.44 % (20/45) of patients demonstrating multifocal uptake outside thyroid bed in pre/post-treatment dose scan treated with initial low dose (1.85 GBq) required a second higher dose of radioiodine (total 3.7-7.4 GBq). 95% (19/20) had either papillary or its follicular variant as histopathology. 5% (1/20) had follicular carcinoma of thyroid. 100% (32/32) curative rate was noted in patients with multifocal uptake in and outside thyroid bed treated with initial higher radioiodine ablative dose. 2/32 patients had aggressive histopathology. 31.25% (10/32) of patients with multifocal uptake outside thyroid bed were missed on 3.7 MBq preablative scan.Conclusion: Multifocality outside thyroid bed in pre / post-ablative scans required second high dose treatment in significant number of patients who were treated with low ablative radioiodine dose. The preablative diagnostic scan can play a major role in the risk stratification and dose determination.

P815

Radioiodine treatment of Grave's disease despite history of iodine allergy

i. G. E. el bez, n. bechir, I. MEDDEB, I. YEDDES, k. trabelsi, h. boutruigua, l. zaabar, D. BEN SELLEM, B. letaief, I. SLIM, A. MHIRI, M. BEN SLIMENE, M. BEN SLIMENE; institut salah azaiez, tunis, TUNISIA.

Graves's disease is the most common cause of hyperthyroidism. There are three current therapeutic options: anti-thyroid medication, surgery, and radioactive iodine (I 131). There are few data in the literature regarding the effects of radioiodine therapy.We describe a 47-year-old patient who had Grave's disease and has a history of an anaphylactic reaction to computed tomography (CT) contrast agent. She came to our institute for further management of her hyperthyroidism.We considered her normal salt-containing diet and advised radioactive iodine treatment, which did not carry any reaction in the patient. It makes us question whether radioiodine treatment is harmful for patients with a history not only of 'iodine allergy' but also of the existence of an allergy to iodine itself.The patient agreed with this analysis and successfully underwent treatment with 12 mCi (444 MBq) radioactive iodine.The patient was followed up for 2 weeks after radioactive iodine treatment. The patient reported no problems during or after the treatment.

P816

Evaluation of the expression of ADAMTS-3, -4 and -15 genes in parotid and submandibular salivary glands after RAI therapy

M. SADIC1, H. I. ATILGAN2, S. O. HALACLI3, K. DEMIRCAN4, M. KORKMAZ1; 1Ministry of Health Ankara Training and Research Hospital, ANKARA, TURKEY, 2Division of Nuclear Medicine,Ministry of Health, Kahramanmaras Necip Fazıl City Hospital, Kahramanmaras, TURKEY, 3Hacettepe University, School of Medicine, Department of Molecular Biology, ANKARA, TURKEY, 4Turgut Ozal University, School of Medicine, Department of Molecular Biology, ANKARA, TURKEY.

Aim: The genetic changes of salivary glands are not well described in the literature after radioactive iodine (RAI) administration. A disintegrin-like and metalloproteinase with thrombospondin type-1 motif (ADAMTS) proteases might play role in damage of salivary glands after high dose RAI administration as well as their critical roles in matrix degradation and repair. The aim of this study which is the first in this area is to investigate the expression of ADAMTS-3, -4, and -15 genes in acute and subacute salivary gland damage after high dose RAI. Materials andMethods: Sixty four male Wistar albino rats were divided into six groups. Group 1 was the unexposed control group (n=20), group 2 (n=6) four hours after RAI administration, group 3 (n=20) 24 hours after RAI administration, group 4 (n=6) 48 hours after RAI administration, group 5 (n=6) 7 days after RAI administration, group 6 (n=6) 30 days after RAI administration. RAI was administered 100 MBq (~3 mCi, 12 mCi/kg) via orogastric route. We evaluated the mRNA expression of ADAMTS genes with quantitative real time PCR. In addition, histopathological evaluation (sialadenitis, interstitial, cellular and nuclear changes) was performed with the samples obtained from right parotid and submandibular salivary glands according to the designated time courses. Results: There was not statistically significant increase in the expression of ADAMTS-3, -4 and -15 with quantitative real time PCR after high dose RAI administration at the designated time courses defined as group 2, 3, 4, 5 and 6 compared to unexposed control group. Histologic examinations of salivary glands in the RAI administered groups showed the extensive nuclear coarsening, binucleolization and focal subnuclear vacuolization while normal nuclear properties have been demonstrated in the control group. Other histopathologic parameters were not different between RAI and control groups in acute and subacute periods. Conclusion: We could not generate a convincing data supporting our hypothesis that ADAMTS-3, -4 and -15 genes are substantial proteases for radiation-damaged rat salivary glands as no gene expression was evaluated.

P817

Treatment of hyperthyroidism with iodine-131: Experience of nuclear medicine department at the salah azaiez Institute in Tunis

i. G. E. el bez, n. bechir, k. trabelsi, h. boutruigua, I. SLIM, I. YEDDES, l. zaabar, I. MEDDEB, D. BEN SELLEM, B. LTAIEF, A. MHIRI, M. BEN SLIMENE; institut salah azaiez, tunis, TUNISIA.

Aim : We report through this work the experience of nuclear medicine department at Salah Azaiez Institute, in the treatment of hyperthyroidism with iodine-131. Materiel and methods : We retrospectively studied a cohort of 300 patients with hyperthyroidism, from several regions of tunisia between January 2006 and december 2012. A clinical examination and a serum assessment of TSHus, FT4 and anti thyroid antibodies, have been made at baseline and at 3, 6 and 12 months after radioiodine therapy. Results : The activity of iodine-131 administered ranged from 444 to 925 MBq and depended on the pathology being treated, age, thyroid volume, intensity of clinical and biological hyperthyroidism and socioeconomic situation. Radioiodine therapy has often been proposed as a treatment for second intention, after failure of medical treatment. Graves' disease was the most common etiology (80%), followed by toxic adenoma (15%), and multinodular toxic goiter (5%). The therapeutic efficacy of a fixed single dose of radioiodine evaluated after a 6-months follow-up was 95% in Graves' disease, 98% in toxic adenomas and 96% in toxic multinodular goiter. No acute complication was observed. Conclusion : Taking into account our socioeconomic context, radioiodine therapy remains the preferred treatment of hyperthyroidism in our country with good value vs price and excellent tolerance.

P818

Comparison between low and high radioactive iodine (131I) ablation dose in patients with low risk of papillary thyroid cancer

i. G. E. el bez, I. SLIM, T. BEN GHACHEM, I. YEDDES, I. MEDDEB, l. zaabar, D. BEN SELLEM, B. LTAIEF, A. MHIRI, M. BEN SLIMENE; institut salah azaiez, tunis, TUNISIA.

AIM:The aim of this study was to compare the ablation rate after low and high ablation doses of iodine-131 dose in patients with low risk of papillary thyroid cancer.PATIENTS AND METHODS:The study included 50 patients with low risk of papillary thyroid cancer. The patients received an ablation dose, which was low (1110 MBq) in 25 patients and high in the remaining 25 patients (3700 MBq). A whole-body scan

and Tg level assessment were carried out. The criteria for complete ablation included absence of residual functioning thyroid tissue and a Tg level lower than 1 ng/ml.RESULTS: The overall successful complete ablation was achieved in 18 of 25 patients who received a low ablation dose and in 19 of 25 patients who received a high reablation dose; no statistically significant difference was found between the two groups (P>0.05).CONCLUSION: The overall complete ablation rate after both a low and a high dose was no statistically significant difference. An activity of 30 mCi 131I is effective in patients with a low risk of papillary thyroid.

P819

Hürthle cell Carcinoma of the thyroid gland presenting a favorable outcome (about 2 cases)

S. TALEB, G. CHERKAOUI SALHI, S. CHOUKRY, M. AIT IDIR, A. GUENSI; Nuclear medicine department, CASABLANCA, MOROCCO.

Hürthle cell Carcinoma (HCC) is a rare and aggressive thyroid cancer histotype. It is considered by the World Health Organisation as a variant of the conventional follicular derived neoplastic subtypes. Local invasion and distant metastasis are frequent making its treatment difficult and worsening its prognosis. The aim of this study was to report the clinical and histological features and outcome of HCC patients treated at a nuclear medicine institution in Morocco. Among 1239 thyroid carcinoma treated at Nuclear Medicine Department - Ibn Rochd University Hospital - Morocco between January 2011 and December 2013, two patients were diagnosed HCC. Treated by total thyroidectomy and radioiodine, these two cases had a favorable outcome with undetectable stimulated serum Thyroglobulin and negative Whole Body Scan. These two cases will exemplify an unusual outcome of HCC.

P820

Effectiveness of total remnant ablation with single therapeutic dose of radioiodine in patients with thyroid cancer after initial surgery

E. Takacsova, R. Králik, J. Kausitz; St. Elisabeth Cancer Institute, BRATISLAVA, SLOVAKIA.

AIM: The aim of our study was to evaluate the effectiveness of total remnant ablation with therapeutic dose of radioiodine (> than 30 mCi) in patients with differentiated thyroid cancer after initial surgery and thyreoelimination radioiodine dose. METHODS: We analysed 108 patients after total thyroidectomy for papillary or follicular thyroid cancer who were treated with radioiodine (131I) in our hospital from January2012 to December 2012. There were 50 (46%) low risk and 58 (54%) high risk patients. We investigated the effectiveness of total remnant ablation after initial surgery and thyreoelimination 131I dose (activity 42 - 120 mCi, average 78 mCi) with the use of therapeutic dose (activity 36 - 200 mCi, average 114 mCi) administered 6 months after the thyreoelimination dose, aside from the level of corresponding serumthyroglobulin. Persistence of remnant thyroid tissue was evaluated using scintigraphy after therapeutic 131I dose. Included were also patients with active disease, but investigated was only scintigraphic persistence of remnant thyroid tissue. Patients with pre-thyreoelimination radioiodine uptake in the thyroid bed higher than 10% were excluded from the study. RESULTS: We achieved complete ablation ofremnant thyroid tissue with the use of therapeutic 131I dose only in 49 (45%) of 108 patients - in 24 (48%) of 50 low risk patients and in 25 (43%) of 58 high risk patients. Neck ultrasonography before the second dose of radioiodine showed persistent remnant tissue in 14 (13%) of 108 patients - in 8 (16%) of 50 low risk patients and in 6 (10%) of 58 high risk patients. CONCLUSION: We found complete ablation of remnant thyroid tissue after thyreoelimination 131I dose only in **45**% of all patients. Persistence of remnant thyroid tissue was evaluated using scintigraphy after therapeutic 131I dose (> than 30 mCi)administered 6 months after thyreoelimination dose. Neck ultrasonography was not useful method for detecting persistent remnant thyroid tissue after thyreoelimination dose of radioiodine.

P821

Patients (Pts) with Differentiated Cancer Thyroid (DTC): prognostic value of Serum Thyroglobulin (Tg0) at the time of the first Ablative Radioiodine Treatment (RAI) and follow up with 131I Whole Body Scan (WBS)

L. Bertolazzi, V. Barbetti, L. Di Ciolo, C. Cananzi, M. Gaffuri, G. Agnese, C. Motta, E. Piccardo, P. Moresco; Azienda Ospedaliera Santa Corona, PIETRA LIGURE (SV), ITALY.

Aim. The purpose of this review is twofold. To assess retrospectively the initial prognostic factors for treatment efficacy and the relevant cut off of Tg0 in a large cohort of consecutive patients (Pts) submitted to RAI. To evaluate, in the follow up, which is the best factor to detect functioning recurrence: diagnostic thyroglobuline (Tgl) or WBS. Materials and Methods. The study included 278 Pts who had had total thyroidectomy and RAI between 2007 and march 2015. Tg0 was measured off L-T4 and just before RAI (131I mean dose 2,5 GBq, range 2,2-3,0 GBq). Tg values were the result of duplicate measurements done with RIA in our laboratories (Thyroglobuline IRMA Radim, detection limit <0,5 ng/ml). 15 Pts were

excluded for positive anti-Tg antibodies. The 263 Pts enrolled (192 females and 71 males, age 18-84, mean age 47) were affected by papillary cancer (221 Pts = 84%) and by follicular cancer (42 Pts = 16%). 108 Pts (A Group)) had Tg0 <1,5 ng/ml and 155 Pts >1,5 ng/ml (B Group): we have considered only Pts of A Group (41% of all Pts). After 6-12 months A Group, which followed a low iodine diet and off L-T4 (TSH > 40 uU/ml), underwent diagnostic assessment with WBS (185 MBq of 131I) and Tg1. Results. WBS after RAI in 90/108 Pts 83 % (C Group) was positive for thyroid remnants (R); in the remaining 18 Pts 17 % (D Group) WBS was positive for R and for lymph nodes metastases (N). In 61/90 Pts of C Group Tg0 was undetectable (<0,5 ng/ml), while in D Group 9 Pts Tg0 was >0,6 ng/ml. At diagnostic assessment after 6-12 months from RAI in C Group (90 Pts) WBS and TG1 were negative for R and N. In D Group 9 Pts had WBS and Tg1 negative for R and N while 9 Pts had WBS positive for lymph nodes and Tg1 was detectable between 0,6 and 1,5 ng/ml. Conclusion. In 90/108 Pts (83 %) with Tg0 undetectable is not necessary to perform a second RAI. In 18/108 Pts (17 %) WBS diagnostic assessment allowed the identification of positive lymph nodes while Tg0 and Tg1 are < 1,5 ng/ml. In 9/18 Pts (50 %) with Tg0 undetectable and with positive lymph nodes only first ablative therapy was sufficient. On the basis of these findings we recommend the complementary diagnostic use of 131I WBS.

P822

Assessment of prognosis in differentiated thyroid carcinoma patients showing detectable thyroglobulin level 6 months after therapy based on radioactive iodine whole body scan results (A preliminary report)

B. Fallahi, A. Fard-Esfahani, N. Ahmadpour, D. Beiki, A. Emami-Ardekani, M. Eftekhari, S. Farzanefar, S. Izadyar; Research Center for Nuclear Medicine, Tehran University of Medical Sciences, Tehran, IRAN, ISLAMIC REPUBLIC OF.

Aim: Differentiated thyroid carcinoma is a highly treatable and usually curable cancer with excellent survival rate; however, as to the possibility of recurrence, the management of this cancer is a lifelong process. Furthermore, the prognosis may be variable from case to case and the disease-free survival may be affected by many factors. The effectiveness of the first radioactive iodine (RAI) therapy, as defined by off-T4 thyroglobulin (TG) level and the results of RAI whole body scan (WBS) following a 6-month post-treatment interval, may play an important role in the enduring prognosis of these patients. The aim of this study was to compare the patient' prognosis in four subgroups of cases showing detectable TG levels 6-months following RAI therapy, defined by serum off-T4 TG levels, i.e. 10>TG>2ng/dl vs. TG≥10ng/dl combined with WBS results, i.e. negative vs. positive. Materials and Methods: Totally 450 patients were enrolled in our retrospective study. These patients had TG more than 2 ng/dl, 6 months after the first RAI therapy. On the basis of the first 6-month follow-up evaluations, the patients were divided in 4 subgroups, G1 were consisted of cases with TG<10 and negative WBS, G2 consisted of patients with TG=10 and negative WBS and finally the patients with TG >=10 and positive WBS were included in G4 subgroup. All patients were followed for at least 5 years (up to 15 years) and lab data, clinical examinations and the results of WBS were reviewed. Results: Median follow-up duration was 99 months. Number of repeated surgeries, the rate of recurrences based on histopathological findings, the frequency and cumulative doses of repeated RAI therapies as well as the frequency of disease progression defined by the new findings on WBS images were different between subgroups ($p<0.001$). The risk of recurrence or disease progression was estimated as 0% for G1, 29% for G2, 8% for G3 and 33% for G4 ($p=0.10$). Conclusion: We concluded that patients with higher TG level (>=10) 6 months after the first RAI therapy reveal higher rate of hospital admissions, higher frequency of repeated neck surgeries, higher cumulative RAI dosage and higher rate of disease progression. Positive whole body RAI scan 6 months after the first RAI therapy also show additive prognostic value for these patients.

P823

Epidemiological analysis of patients referred to nuclear medicine consultation for therapeutic evaluation

M. J. Ibáñez Ibáñez, M. V. Godoy Bravo, L. F. Álvarez Nieto, R. Reyes Marlés, M. I. Castellón Sánchez, F. Nicolás Ruiz, L. Mohamed Salem, L. Frutos Esteban, J. L. Navarro Fernández, M. A. Claver Valderas; Servicio de Medicina Nuclear. Hospital Clínico Universitario Virgen de la Arrixaca, Murcia, SPAIN.

AIM: Perform a descriptive epidemiological analysis of patients referred to Nuclear Medicine department in 2014. MATERIAL AND METHOD: We study 526 patients retrospectively analyzing the following variables: age, sex, pathology, pathology results, scintigraphic findings and metabolic treatment given to each of them. With all this, we build a database that would allow us to group patients by diseases and analyze the different variables. RESULTS: Of the total of 526 patients (77% women, aged between 15 and 94 years), 329 patients (62.5%) were referred for differentiated thyroid carcinoma (DTC), 194 patients (36.9%) for hyperthyroidism, 2 for evaluation pre-adrenocortical scintigraphy and 1 for previous assessment to treatment with Samarium-153. Among the 329 patients seen by DTC (77% women; mean age 50 years; 61.4% with over 45 years of age), 44.1% are post-thyroidectomy ablation of thyroid remnants (of which 80.7%

were papillary carcinomas, 22.7% folicular carcinomas and 4.5% micropapillary carcinomas, and 28.3% had lymph node involvement), 47.4% are diagnostics whole body scans, 6.7% therapeutic doses and 1.8% empirical I-131 doses. Of the 194 patients with hyperthyroidism (78% women; mean age 58 years), 20.1% is due to Graves' disease and the patterns observed in thyroid scintigraphy are: diffuse pattern in 17.5%, plurimicronodular in 23.2%, plurinodular in 43.8% and toxic adenoma in 15.5%. CONCLUSION: In the Region of Murcia, with a high incidence and prevalence of thyroid disease in both malignant and benign, we emphasize the importance in treatment and monitoring of these patients by Nuclear Medicine, and the high workload it generates in our service.

P824

Revaluation of risk of recurrence in patients with differentiated thyroid cancer depending on their initial response to treatment

L. F. Cáncer Garza, M. Delgado, A. Andrés, L. Tardin, S. Ayala, P. Razola, M. López, V. Cardona, E. Prats; Hospital Clínico Universitario Lozano Blesa, Zaragoza, SPAIN.

AIM: To analyze the usefulness of revaluation risk criteria based on response to initial treatment (RIT), total thyroidectomy and radioactive iodine remnant ablation, in patients with Differentiated Thyroid Cancer (DTC).MATERIAL AND METHODS: We retrospectively reviewed 108 patients diagnosed of DTC, 94 (87%) papillary and 14 (13%) follicular, after total thyroidectomy and radioactive iodine remnant ablation. 78.7% were women and 21.3% men, 17 - 77 years old (mean age 46.8 y.o.) with a median follow-up period of 7'5 years. *According* to modified Tuttle criteria, we revaluated the patients depending on their initial response to treatment based on stimulated thyroglobulin, antithyroglobulin antibodies levels and structural imaging into three groups: Excellent, Acceptable and Incomplete Response. Each patient was also stratified using European Thyroid Association (ETA) and American Thyroid Association (ATA) criteria. Then, we have correlated the three risk criteria systems with the status at final follow-up: no evidence of disease or persistent/recurrent disease.RESULTS: Following ATA criteria, 8 patients (7.4%) were considered as high risk, 44 (40.7%) intermediate and 56 (51.9%) low risk. According to ETA criteria, 46 (42.6%) were of high risk and 62 (57.4%) low risk. When we use the modified RIT system, 18 (16'7%) patients presented incomplete response, 12 (11'1%) acceptable and 78 (72.2%) excellent. At the end of the follow-up 96 patients (88.9%) had no evidence of disease and 12 (11.1%) had persistent or recurrent disease. With the proposed RIT criteria, 100% of patients with excellent response had no evidence of disease at final follow-up, while this rate decreased to 75% with acceptable and 50% with an incomplete response. With the modified RIT criteria the NPV was 100%. Comparing to ATA and ETA risk stratification systems: 53.8% of patients with high/intermediate risk (ATA) and 52'17% of high risk criteria (ETA) were considered as excellent response using modified RIT criteria. All of them were free of disease at the end of follow-up.CONCLUSIONS: The modified risk stratification criteria based on the response to initial therapy in patients with DTC predicts the long-term follow-up, especially in patients with an excellent response to initial treatment.

P825

Follicular thyroid carcinoma in Morocco : predictive factors of distant metastasis

S. TALEB, G. CHERKAOUI SALHI, S. CHOUKRY, M. AIT IDIR, A. GUENSI; Nuclear medicine department, CASABLANCA, MOROCCO.

The aim of this study was to determine predictive factors of distant metastasis in patients with FTC in a tertiary medical center in Morocco.METHODS: This is a retrospective study. It included all patients with a histological diagnosis of FTC treated in Nuclear Medicine Department in IBN ROCHD University Hospital in Casablanca between January 2005 and December 2013. Patient's files were reviewed for clinico-pathological characteristics, treatment and outcome compared with a papillary carcinoma sample treated during the same study period. Univariate analysis of patients' features was performed using IBM SPSS Software.RESULTS: Among 3400 patients treated during the study period for a thyroid malignancy, 82 patients (2.4%) were included. Mean age was 51 years old (+/- 14), sex ratio (M/F) was 0,17. Bone metastases at presentation were noted in 10% of cases. More than half patients lived in non coastal regions, known for their iodine deficiency. On univariate analysis, age > 45 years ($p = 0.003$), tumor multifocality ($p = 0.01$), capsular invasion ($p = 0.07$), vascular emboli ($p=0.03$) and serum thyroglobulin concentration over 300 ng/ml ($p<0,001$) were independent predictors of distant metastasis.Compared to a papillary carcinoma, FTC histotype correlates with higher risk of metastasis ($p <0.001$).All patients underwent a total thyroidectomy followed by radioiodine therapy. External beam radiation therapy and metastasis surgery was indicated in 7% and 11% of cases respectively,

depending on each subject. Mean follow-up period was 6 years. It showed a persistent disease in 27 % of cases, a progressive disease in 5% of cases, a complete remission in 60% of cases whereas one patient died of the disease (1.1%)CONCLUSION: Older age, multifocality, capsular invasion, vascular emboli and high thyroglobulin concentration seem to be independent risk factors for predicting distant metastases in patients with FTC. Prospective study with more patients is needed to confirm these results.

P826

Influence of coexistence of Hashimoto's disease on the prognosis of patients with differentiated thyroid cancer. A retrospective study

D. PAPADOULI, L. Iordanidou, E. Doika, C. Petropoulos, E. Matselas, E. Trivizaki; METAXA CANCER HOSPITAL, PIRAEUS, GREECE.

Aim: The association between Hashimoto's thyroiditis (HT) and differentiated thyroid carcinoma (DTC) remains controversial. The aim of this study is to investigate the difference of the prognostic outcome between patients with DTC with and without HT. Methods: We studied the records of 87 patients (72 females and 15 males) who were treated for DTC (all with papillary carcinoma) in the department of Nuclear Medicine at Metaxa's Hospital. The mean follow-up was 40 months (range 12 to 50 months). The patients were classified into 2 groups according to the existence or not of HT. All patients were analyzed according to the stage of the disease and the radioiodine treatments. Complete/partial response or persistent disease, was assessed within 1 year from ablative dose. Results: This preliminary study included 87 pts, 55 /87 had DTC without HT (control group) and 31/87 (35.6%) had DTC with HT (DTC-HT group). There were 63 pts with stage I disease, 41 (65%) from the control group and 22 (35%) from the DTC- HT group, 4 pts with stage II, 3 pts from control group and 1 from DTC- H, 16pts with stage III, 7 from the control group and 3 from the DTC-HT group and 4 pts with stage IV, 3 from control group and 1 from the DTC-HT group. From the total number of pts, 54 (62%) had complete response with one ablative dose. In the stage I, 19/41pts (46%) from the control group and 6/22 pts (27%) from DTC- HT group received additional I131 therapies and in the stage II, 1/3 pts from the control group. In the stage III, 3/10 pts from the control group and 3/6 from the DTC-HT group had additional treatments and in the stage IV 1/2 pts from the DTC-HT group. Conclusion: According to our preliminary results although there is no significant difference in the prognostic outcome between the two groups, it seems that the DTC-HT patients need less radioiodine treatments to achieve remission, indicating a less aggressive behavior.

P827

Iodine 131 uptake in lactating breasts

P. Martineau, W. Zeng; The Ottawa Hospital, Ottawa, ON, CANADA.

Iodine accumulation in the lactating breast has been recognized for 60 years. Radioiodine in lactating breast and milk results in increased radiation to the mother's breasts and damage to the nursing baby's thyroid gland. Patients are routinely instructed on discontinuation of breastfeeding prior to high dose radioiodine therapy; however, failure to communicate this effectively to patients occasionally occurs, as illustrated in the case.A 39 year old female status post total thyroidectomy was treated with 3700 MBq (100 mCi) I-131 sodium iodine for T3N0M0 papillary thyroid carcinoma. The patient had given birth to a daughter two years prior and was diagnosed with thyroid cancer shortly after the birth. A nuclear medicine consultation took place 14 months after the birth of her daughter. Instructions on radiation safety precaution were provided to the patient. However, the instruction to discontinue breastfeeding was not documented, and presumably not reinforced by the referring physician. The patient unfortunately delayed the treatment due to personal reasons. Consequently her radioiodine ablation therapy was given approximately 10 months after the initial consultation. At the time of therapy only radiation exposure precaution to her 2 year old daughter and other family members was discussed and the issue of breastfeeding had never been raised with the treating physician.On the post therapy whole body scan, significantly increased activity was noted in the anterior chest. The findings of bilateral breast uptake were confirmed on SPECT/CT images. On questioning the patient it became clear that she only stopped breastfeeding on the day of radioiodine therapy. The patient was instructed to continue pumping her breast milk frequently to reduce radiation exposure to her breasts.It is critical to emphasize the importance of communication to thyroid cancer patients. The problems leading to breast uptake in this patient will be reviewed. Steps to ensure that lactating patients be well informed on breastfeeding issue and changes to improve our service will be discussed. The current guidelines by SNM and American Thyroid Association on discontinuing breastfeeding prior to treatment will be reviewed. The

absorbed dose to the breasts and the probability for induction of fatal breast cancer will be estimated based on the available literature.

P828

Feasibility of Blood Dosimetry Estimation by Remote-Measurement System in DTC Patients with High Dose Radioiodine Therapy.

Y. Chen, Y. Lai, Q. Chang, M. Chung, P. Hsiao, H. Chen, F. Chiang; Kaohsiung Medical University Hospital; Kaohsiung Medical University, Kaohsiung, TAIWAN.

Practically individual blood dosimetry assessment of DTC patients with high dose radioiodine therapy is an important issue in clinic. Herein, we introduce remote- measurement method to estimate blood dosimetry during hospitalization. Patients and Methods: Among our hospital data, we collect forty-two and seventeen DTC patients (female to male ratio as 3:1; age over 45 y/o as 59.3%) with 100 mCi and 200 mCi radioiodine therapy, respectively after bilateral total thyroidectomy or recurrence. Patient after high dose radioiodine intake are allowed to release based on 70 uSv/ hr/ M (by regulation) when administration in radiation protection ward. Serial time-dependant dose measurements are acquired as one-meter away by remote- monitor system (GM counter). Blood dosimetry calculation is based on formulation as rad/ mCi by ERC 2009. The weighting clearance time of radioiodine is compared between patients with rh TSH preparation or thyroxin-withdraw method. Results: The estimated rad/mCi is 0.92 in the patient with 100 mCi and 200 mCi radioiodine intake, respectively. The calculated blood dosimetry is 0.92 Sv and 1.97 Sv in patient with 100mCi and 200m Ci radioiodine intake, respectively. In 100mCi radioiodine intake group, the weighting clearance time of radioiodine is faster (14.4 3.4 hr) in patient with rh TSH preparation. However, there is no significant difference of weighting clearance time (around sixteen to eighteen hr) by meaning of rh TSH preparation or thyroxin-withdraw method in patient with 200 mCi radioiodine intake. Conclusion: The average of rad/ mCi among 59 patients with 100mCi and 200 mCi radioiodine intakes is around 0.96. The practically individual blood dosimetry assessment is feasible and convenient by means of remote measurement system.

P829

Advantages of thyroidal therapy uptake calculation with 2D-diagnostic imaging

R. Ringler, M. Stich, K. Schuller; Technische Hochschule Amberg-Weiden, Weiden, GERMANY.

Introduction:For the determination of thyriodal uptake is usually either a thyroid uptake counter (TUC) or a gamma camera (GC) to choose from. The recommendations of the guidelines of the German Society of Nuclear Medicine (DGN) are to use a TUC-device. The aim of the study was to compare the two methods with the use of phantoms either with Tc-99m or I-131.Methods:The study was performed using a TCU-ISOMED 2162 and two gamma cameras - e.cam and Multicam 1000. The I-131 (3-5MBq) uptake was simulated with a cylindrical neck phantom which was used at the two GC and TCU. The evaluation of the count rates was carried out under different intervals and distances. The evaluation of the count rates was carried out under different distances of phantom to the detector surface to determine the optimal patient-gamma camera distance. The influence of the deviations from the center line in the thyroid uptake counter was also tested.Results:The results support the recommendation of the minimum distance of 25cm to the guideline of DGN. Taking into account the optimized distance, the ROI analysis in the 2D-diagnostics improves the uptake calculation and the resulting dose for therapy. The ROI in the 2D image reduces the scattered radiation from neck and salivary glands by a mean of 28% (24.9% to 33.54%). The uptake calculation depends on the depth of the I-131 test activity inserted in the neck phantom - differences of about 17% (compared with / without ROI) were determinde.Conclusion:The results show that a ROI technique in 2D imaging with a gamma camera for determining the thyroidal uptake is superior to TUC devices. The correct depth of the hot node in the thyroid is important for a optimized I-131 uptake calculation. By using a TUC device the correct placement along the center line of the system is important.

P830

Thyroidal diagnostics need optimized collimation and segmentation within 2D-imaging

R. Ringler, J. Vogt, S. Seemann, M. Stich; Technische Hochschule Amberg-Weiden, Weiden, GERMANY.

Introduction:Two setups of gamma cameras for thyroidal imaging are used. The user can either choose from a thyroid collimator or a high resolution collimator. The aim of our study was to characterize the resolution and detectability of cold and hot nodes in a thyroidal phantom with a high resolution of a gamma camera. A correct segmentation of the thyroid lobule is essential for the uptake value in the diagnostic. To evaluate the influence on the uptake different algorithms for segmentation were tested by Tc-99m and I-131.MethodsThe study was performed using a gamma camera - Multicam 1000 (Intermedical) with a Low Energy High Resolution collimator (LEHR) and a thyroidal collimator (TC) for Tc99m (5 - 15

MBq). The Multicam 1000 was used with a High Energy collimator (HEC) for the I-131 (3 - 37 MBq). The optimized collimation with Tc-99m was evaluated with a standard 2D thyroid phantom. The measurements to determine the resolution and detectability of cold and hot nodes in a thyroidal phantom a variable background activity was used (0-5 MBq. To validate the Uptake in the thyroid different algorithm were tested (Canny, LOG, Prewitt, Sobel, Roberts and an intensity filter).ResultsThe comparisons of the thyroid collimator to the LEHR collimator show significant differences in favor of the resolution to TC collimator but a much better sensitivity in LEHR collimator. The results support also the recommendation of the guideline of DGN. The automated segmentation of the thyroid lobes with Canny and LOG detect the outlines of the thyroid in a closed outer contour. Using the modified 1/e-intensity filter the two lobes are automatically segmented. The ROI's for I-131 in a thyroid phantom can outline the contours of the thyroid with the above mentioned segmentation algorithm.ConclusionThe results of the studies show that a automated ROI-segmentation-technique in 2D imaging with a gamma camera for determining the thyroidal uptake is possible. The choice of the collimator shows that with a LEHR collimator even at low signal-to-background a good contrasts and results can be achieved. The uptake by using a thyroid phantom with I-131 can be calculated whereas the resolution of the nodes is to be considered using a HEC-collimator.

P831

Exposition Rates of Thyroid Cancer Patients Treated with Radioiodine. Differences Between Endogenous and Exogenous Stimulation

J. Rodríguez-Rubio Corona1, E. Noriega Álvarez1, O. Puig1, G. Martinez Pimienta1, J. Rojas Camacho1, M. Boya-Román1, P. Saldaña Gutiérrez2, I. Romero-Zayas3, A. Rodríguez-Gasén1; 1Hospital Universitari de Bellvitge, Barcelona, SPAIN, 2Medical Physiscs and Radiation Protection Department, Instituto Catalán de Oncología, L'Hospitalet de Llobregat, SPAIN, 3IDI-PET Unit, Hospital Universitari de Bellvitge-IDIBELL, Barcelona, SPAIN.

AIM: To compare exposure rates (ER) after administration of 3700 MBq of 131I in thyroid cancer patients stimulated with recombinant human thyrotropin (rhTSH) or levothyroxine withdrawal during 4 weeks (T4W). MATERIAL AND METHODS: 80 thyroid cancer patients who underwent total thyroidectomy and who received a remnant ablation dose of 3700 MBq of 131I were studied and divided in two groups according to their TSH stimulation method (rhTSH group: 40p and T4W group: 40p), with similar age and gender features (average age: rhTSH group: 53.5 years old and T4W: 50 years old; and gender: rhTSH: 27 women and T4W: 30 women). None of the patients had renal failure. They were measured immediately after the dose administration (ERi), and after 2h, 4h, 24h and 48h, with an ionization camera (Nardeux, Babyline 81) focusing 1m away on the cervicothoracic region of the patient. We analyzed the data with the t-Student test. RESULTS: The mean values obtained at each time of measurement (ERi, 2h, 4h, 24h, 48h), expressed in mRad/h (with a confidence interval at 95% for each average value) were those shown below: A. rhTSH group: ERi=28,6(25,9-31,2), ER2h=20,5(19,3-21,8), ER4h=16,8(15,6-17,9), ER24h=5,1(4,2-6,1), ER48h=1,7(1,2-2,1) B. T4W group: ERi=23,5(22,1-24,9), ER2h=19,9(19-20,8), ER4h=17,2(15,8-18,5), ER24h=6,4(5,6-7,1), ER48h=2,2(1,9-2,6) The means values showed the following p for comparisons between each group at each measurement time: o ERi: significant (95%, p=0.001) o ER 2h: not significant (95%, p=0.43) o ER 4h: not significant (95%, p=0.64) o ER 24h: inconclusive (95%, p=0.04) o ER 48h: inconclusive (95%, p=0.05) CONCLUSIONS: These data show that the ERi is greater with rhTSH stimulation than with T4W, being this statistically different (p=0.001). The decrease of the ER along time seems to be faster with rhTSH than with T4W, but the differences between both groups are not statistically significant, probably due to the wide variability of the values of the measurements

P53 - Tuesday, October 13, 2015, 4:00 PM - 4:30 PM, Hall 3 – Poster Exhibition

Radionuclide Therapy & Dosimetry: Bone Metastases - Pain Palliation

P832

Hematotoxicityand non-hematological adverse events of Ra-223 dichloride (Ra-223) in patients with castration-resistant prostate cancer (CRPC) and bone metastases

H. Ahmadzadehfar1, K. Azgomi1, S. Rogenhofer2, R. Bundschuh1, S. Kürpig1, L. Thomas1, M. Essler1; 1University Hospital Bonn, Department of Nuclear Medicine, Bonn, GERMANY, 2University Hospital Bonn, Department of Urology, Bonn, GERMANY.

Objectives:Ra-223 is a first-in-class alpha-emitting pharmaceutical recently Food and Drug Administration approved for treatment of CRPC patients with bone metastases.The aim of this study was to investigate the incidence and severity of hematotoxicity and other non-hematological adverse events (AE) of this therapy. Methods: Eligible patients had progressive hormone and/or chemo refractory PC with bone metastasesand no known visceral involvement. Bone scintigraphy was performed in all patients 1-2 weeks prior to Ra-223 Therapy. All patients received CBC and renal tests as well as

measurements of PSA and alkaline phosphatase (ALP) on the therapy days and at least 4 weeks after the last therapy. Results: a total of 140 treatments (range: 1-6 (median: 4)) were performed for 35 patients (mean age: 74 (range: 56-86)) with a mean PSA-Value of 545 ng/ml (0.5-4710) and a mean ALP of 203 U/l (43-517). 17 patients had a history of chemotherapy. No hematological toxicity more than grade 2 was observed until 8 weeks after the last cycle. There was not any significant correlation between the cumulative activity and the level of hematotoxicity in this time period. 67 treatments were not associated with any subjective side effects. The most important non-hematological AE were mild diarrhea for 2-3 days in about 7-10 days after 13 therapies and severer generalized pain in 2 patients began3 h after application, which lasted 1day.No renal toxicity was observed. Conclusions: Ra-223 is a well-tolerated tx for CRPC with bone metastases.

P833

Therapeutic response of Sm-153 EDTMP treatment in breast cancer with painful bone metastases

M. Elzahry1, H. Sinzinger2, B. Palumbo3; 1Faculty of Medicine-Department of Clinical Oncology and Nuclear Medicine, South Valley University, EGYPT, 2Faculty of Medicine, ISOTOPIX- Institute for Nuclear Medicine, Vienna, AUSTRIA, 33Department of Surgical, Radiological and Odontostomatological Sciences, Nuclear Medicine Section, University of Perugia, ITALY.

Bone metastases from breast cancer are associated with significant morbidity including immobility and the development of pathological fractures, spinal cord compression and the need for surgery and radiotherapy to bone. An improved understanding of the pathophysiology of bone metastases from breast cancer has encourged the development and clinical use of bone-targeted agents in this area. Systemic therapy with radionuclides as Sm-153 EDTMP is used in patients with painful skeletal metastases owing to its efficacy, low cost and low toxicity. Aim of this study was to assess if there is a difference in uptake and therapeutic response of Sm-153 EDTMP in 164 female patients suffering from recurrent breast cancer who received single dose of therapy for painful metastatic bone lesions (osteoblastic(BL), osteolytic(LY) or mixed(MI). Patients &methods, 164 female patients suffering from breast cancer were included in this study. Their age ranged from 35-77 years. Their tumor histology was the following: 116 (70.03%) ductal, 37(22.56%) lobular, 10 (6.09%) mixed and 1(0.61%) medullar. All the patients had metastatic bone pain and lesions number varied from 1 up to ≤ 5 judged intially by sequential x-ray and/or MRI to be verified later by bone scintigraphy. Results, among the different types of bone recurrences, there was no significant difference in uptake (mean: 55.2%, 53.6% and 54.9%) respectively. While there was a decline in pain response rate with time (91.8% vs 77.9% and 96.3% vs 81.5%, with more pronounced decline at mixed type 87.5% vs 66.7%), respectively at 7 and 12 weeks. Number and extent of bone lesions had no influence on the findings. Females on long-term statin therapy (n=61) showed a significantly more pronounced decrease in adhesion molecules ($p<0.05$) being comparable for all histological types of breast cancer. In conclusion, there was no significant difference of bone uptake and pain response rate between the different types of bone recurrences either BL, LY or MI in breast cancer patients on single dose of 153Sm-EDTMP. Therefore, Sm-153 EDTMP can be used as the most effective palliative treatment in painful metastatic skeletal lesions irrespective of the type of bone recurrences on scintigraphy. Wherever, the effect of statins on adhesion molecules is a direct drug effect or reflect an antitumoral action as well as, the influence on the extent of recurrences should be examined in prospective studies.

P834

Radium-223 therapy in metastatic castration resistant prostate cancer: South Central England single centre early experience

h. chorfi, F. sundram; Southampton general hospital, southampton, UNITED KINGDOM.

Aim: Majority of metastatic castration resistant prostate cancer (mCRPC) patients experience painful bone metastases, resulting in death, disability and decreased quality of life. Radium-223 is a novel bone-targeted α-emitter associated with a survival benefit. We present our early experience and outcomes in mCRPC patients undergoing Ra-223 treatment.Material and methods: Retrospective study over 1 year (March 2014 - February 2015) of mCRPC patients referred for Ra-223 treatment. Information obtained included age, prior treatments, bone symptoms, analgesic requirements, imaging and blood results. Ra-223 (50 kBq/kg) was administered every 4 weeks, up to the recommended 6 therapy cycles. Endpoints assessed included pain patterns, side effects, skeletal related events (SREs), disease biomarkers (PSA & ALP levels) and haematological parameters. Results: 32 patients were referred. Median age was 74 yr (range 54-91 yr). Median follow-up was 5.3 months (range 1-11 months). All patients received on average, three previous lines of treatment. All bone scans showed foci of abnormal uptake. CT scans revealed malignant lymphadenopathy in 7 patients, with absence of visceral involvement. 22 commenced Ra-223 therapy. 10 were unable to commence treatment for the following reasons:• 5 were affected by radiopharmaceutical unavailability• 4 deceased before treatment commencement• 1 unsuitable due to liver metastases22 patients had Ra-223 therapy:• 18 (82%)

were symptomatic, 17 (94%) required analgesics (9 opioids, 8 non-opioids)• 4 (18%) had no bony pain• 7 completed the recommended 6 cycles, of whom:¦ 3 had bony pain reduction¦ 1 had worsening¦ 3 had absence of bony pain, remaining stable, not requiring analgesia• 10 are currently undergoing treatment• 5 discontinued treatment :¦ 3 developed extra skeletal disease¦ 1 deteriorated clinically¦ 1 experienced significant side effectsOf 7 patients who completed 6 therapy cycles, side effects were mostly mild gastrointestinal symptoms. No patients developed SREs during follow-up. A marked decrease in median blood count parameters was noted after cycle 1, remaining broadly stable after cycle 3. There was a significant post treatment reduction in ALP levels, however, mean PSA levels increased from baseline. Conclusion: Ra-223 improves bony symptoms, with mild side effects encountered. Myelosuppression is significant after the first cycle. Ra-223 has a major impact on serum ALP levels, with negligible effect on PSA levels. Therefore ALP appears to be a useful biomarker of therapy response.

P835

Radiopharmaceutical therapy for palliation of bone pain from osseous Metastases: what about beta Therapy in prostate cancer?

T. Ben Ghachem1, A. Mhiri1, I. Slim1, I. Yeddes1, I. Elbez1, I. Meddeb1, A. Sellem2, H. Hammami2, M. F. Ben Slimène1; 1Nuclear Medicine department; Salah Azaiez Institute, Tunis, TUNISIA, 2Nuclear Medicine department; Military Hospital, Tunis, TUNISIA.

Introduction: Bone pain from metastatic prostate cancer is the most common symptom and the most difficult to support. Its treatment aims to improve the quality of life of patients. It has been treated historically by palliative external beam radiation therapy and pharmacological analgesics. Bone-seeking targeting radiopharmaceuticals have entered the therapeutic armamentarium for the treatment of multiple painful osseous lesions: Beta-emitting agents, such as Strontium-89 and Samarium-153 and recently Alpha-emitting radiopharmaceutical Radium-223. Our study will focus on metabolic radiotherapy with Samarium 153-ethylenediaminetetramethylenephosphonic acid (153Sm-EDTMP; Quadramet) which is a beta-particles emitter that concentrates in the areas of enhanced osteoblastic activity. Purpose: Our aim was to evaluate the value of this therapy in prostate cancer. Methods: A retrospective, descriptive longitudinal and multicentric study was carried about 15 years on 74 patients with prostate adenocarcinoma with bone metastases, in the nuclear medicine department of Salah Azaiez Institute (ISA) and Military Hospital. All these patients were treated with at least one cure 153Samarium-EDTMP (37 MBq/kg). All patients had painful bone metastases to more than one anatomical region. For assessment of therapy effectiveness, three parameters were evaluated before and after treatment: motor activity, pain relief and reduction in analgesic requirements with a receding of 35 months. Toxicity of 153Samarium-EDTMP was also estimated. Results: Treatment response was positive in 86.1% of cases: complete in 33.78% and partial in 52.32%. The administration of successive cures of 153Samarium-EDTMP, with 3 months interval between treatments showed that the cures could be repeated with similar response as in the first cure. Neither status of the patients before treatment nor treatment previously received had influence on this metabolic radiotherapy response. The therapeutic effectiveness was at least equivalent to those of other therapeutic modalities, with almost no side effects. The only observed toxicity was hematologic; usually mild and reversible. Besides, the effect on the pain came with an improvement of the quality of life of the patients treaties. Conclusion: Due to its half-life of 46 hours and its beta emissions, a high dose rate of 153Samarium-EDTMP can be delivered to regions adjacent to enhanced osteoblastic activity over a short period of time with little residual long term activity being left in the bone marrow. It should no longer be a solution of last resort thanks to its efficiency and low toxicity. Its early introduction in the management of patients with prostate cancer and painful bone metastases could greatly improve their quality of life.

P836

Bone metastases in patients with differentiated thyroid carcinoma: clinical features and outcome (medullary carcinoma excluded)

G. CHERKAOUI SALHI1, S. TALEB1, S. CHOUKRY1, M. AITIDIR2, A. GUENSI1; 1IBN ROCHD UNIVERSITY HOSPITAL, CASABLANCA, MOROCCO, 2MOHAMED IV UNIVERSITY HOSPITAL, MARRAKECH, MOROCCO.

Bone metastases are the second most common metastasis site in differentiated thyroid carcinoma (DTC). Its occurrence makes the treatment difficult and worsens the prognosis. The aim of this study was to report the clinical features and outcome of patients with bone metastases of DTC treated in a Nuclear Medicine department in Morocco. Patients and Methods: Retrospective study selecting all patients with bone metastases of DTC treated in Nuclear Medicine Department in Ibn Rochd University Hospital in Casablanca between January 2005 and December 2013. Patient's files were reviewed for background data, clinico-pathological characteristics, treatment and outcome. Results: Among 3077 patients treated for DTC during the study period, 32 were included in the study

(1%). Patient's average age was 59 years old [29-75], sex ratio (M/F) was 0.14. Bone metastasis was recorded as the revealing sign of the disease in 34 % of cases. All patients underwent a total thyroidectomy, it was completed by cervical lymph node dissection in 12% of cases. Half of cases had a follicular carcinoma. Mean primary tumour size was 4cm [1 - 11cm]. Patients were staged pT3 and pT4 respectively in 48% and 10% of cases. Lymph node extension was noted in 9% of cases and lung metastasis in 34% of cases. Bone metastases were often multiple and located at the axial skeleton. All tumours showed radioiodine avidity. Repeated radioiodine therapy was completed by external beam therapy in 28% of cases and metastases surgery in 31% of cases. Median follow-up period was 6 years. It showed a complete remission in 15% of cases, persistent disease in 55% of cases and a progressive disease in 9% of cases with a local recurrence. To date, the survival rate is 84%. Bone metastases are synonym of pejorative prognosis in DTC. However, a multidisciplinary care adapted to each case remains the best way to insure an optimal treatment and hence, a better outcome.

P837

Roll of different XCAT phantom BMIs in dosimetery for 153Sm-EDTMP bone pain palliation

M. Fallahpoor, **S. Farzanefar**, S. Heydarinejad, M. Abbasi; Department of Nuclear Medicine , Vali-e-asr Hospital, Tehran University of Medical Sciences, Tehran, IRAN, ISLAMIC REPUBLIC OF.

For internal dosimetry either patient's CT scan or the attenuation maps of available phantoms are used. The most accurate way is to use patient CT scan which needs organ segmentation. XCAT is one of the most flexible data bases which may eliminate the need for time consuming and operator dependent organ segmentation procedures. Nevertheless the phantom is different in the body shape and composition including the BMI from the patient's reality. Recently different BMIs for the XCAT phantom were generated which may solve this obstacle. In this study we examine the effect of different BMIs on the dosimetry for a bone pain palliation agent, 153Sm EDTMP.The simulation was done by the GATE Monte Carlo code. S-factor (mGy/MBq-s) and SAFs (kg-1) were calculated for the dosimetry of the radiation from the spine as source organ into the whole body. Female XCAT phantoms with the following different BMIs were employed: 18.6, 20.8,22.1, 26.8, 30.3 and 34.7. The difference of the whole body dosimetry from the phantom with BMI 26.8 were calculated for both gamma and beta radiations.The differences of the SAFs of the dosimetry in phantoms with lowest to highest BMI from the referral phantom (i.e. BMI=26.8) were 16.4%, 8.2%, 4.1%, -9.5% and -1.4%. All these difference fit well within the 10% acceptable dosimetry calculation error. The differences of the S-factor for the phantoms from the BMIs equal to 18.6, 20.8, 22.1, 30.3 and 34.7 from the phantom with BMI of 26.8 were 40.2%, 20.1%, 9.0%, -7.9% and -4.9%.The dosimetry of the gamma photons do not change with the use of phantoms with unfitted BMI but the dosimetry of the beta particle which results in the therapeutic effect of 153Sm-EDTMP and is important for dose calculation changes remarkably with employing the phantom with wrong BMI.

P838

Role of EDTMP-Samarium in the management of Bone metastasis:

S. E. Bouyoucef, B. Abdi, R. Drahmoune, A. Talbi, S. Rahabi, M. Habbeche; Department of Nuclear Medicine CHU Bab El Oued, Algiers, ALGERIA.

Introduction: Radionuclide therapy is an important tool in the management of painful bone metastasis. The strategy of its use depdends on a certain parameters including local medical protocols of chemotherapy. Objective: To determine the best response to radionuclide therapy according the stage and the extension to the bone of cancer disease Patients and Methods 70 patients with prostate and breast cancer and bone metastases have been referred to the department of nuclear medicine for radionuclide therapy of painful bone metastasis from 2009 to 2012. All patients have had multiple lesions on bone scan and normal blood and kidney tests. Incontinent patients, patients with medullar compression and fractures have been excluded from the study. Average activity of 153Sm-EDTMP used was 37MBq/kg for all patients and injection was done slowly during 3 minutes with glucose line. Assessment of response was done each 6 weeks according clinical symptoms, dose of morphine and Eva and Karnofsky score. Results: Clinical Improvement was observed in 85% of patients including decrease of the dose of morphine or drugs. The drugs and morphine were totally stopped in 13% after 3months of radionuclide therapy. The response to treatment was much better when the number of lesions is limited and widespread. The rate of response was little bit higher in patients with prostate cancer. Only one case had had bone marrow suppression after 6 months. 15% of patients relapsed and needed a second or a third cycle of radionuclide therapy. Most patients (89%) survived at 3 months and 13% at 2 years. Conclusion: Radionuclide therapy of painful bone metastasis of Prostate and breast is efficient in most cases. However, selection of patients is absolutely required to avoid bone marrow complications and better efficiency of treatment. Despite the new Alpha therapeutic agent (Radium 223), 153Sm-EDTMP will remain an excellent alternative for controlling pain in metastatic cancer patients.

P839
223Ra Therapy: A Successful Patient Outcome

K. Gannon, R. Cornhill, R. Gunasekera, K. Tarver; Barking, Havering and Redbridge University Hospitals Trust, Romford, UNITED KINGDOM.

Introduction: 223Ra dichloride (Xofigo®) has been available in the UK for the treatment of advanced castration-resistant prostate cancer since Jan 2014. Its success follows the positive outcome of the ALSYMPCA phase III clinical study[1] which generated results for 921 patients (614 study drug patients, 307 placebo patients), with an overall survival improvement of 3.6 months in the study drug group. Queen's Hospital has provided a therapy service for patients since Sept 2014 and recently completed a full treatment cycle for the first patients recruited. Materials and Methods: Patients DS (77yr male) was identified as a candidate for treatment in September 2014 after meeting a strict set of recruitment criteria. The patient began 6 cycles of injection spaced approximately 28 days apart, with a treatment interruption after the first administration due to drug availability. Patient weight was obtained prior to each administration and the activity of each injection was determined using a 50kBq /kg calculation. Prior to commencing treatment the patient underwent a 99mTc Whole Body Bone scan to determine the extent of skeletal metasteses. Upon completion of the treatment the patient underwent a follow up bone scan to determine disease progression. Throughout the course of treatment the patient underwent regular blood testing to check Hb, PLT, ALP and PSA levels. Results: Initially the patient's PSA (409.1 μg/L) and ALP (554 iu/L) values were very high and the patient complained of poorly controlled bone pain in the left hip. A 99mTc whole body bone scan was obtained 3 months prior to treatment following a course of chemotherapy. This revealed multiple skeletal lesions and prominent activity in the spine and pelvis, potentially due to disease progression. By the end of the 6 cycles of treatment, the patient's PSA (363.5 μg/L) and ALP (233 iu/L) had improved and the subsequent bone scan revealed improvement in previously suppressed activity in the ribs, pelvis and long bones. Previously noted focal abnormal activity in the skull was no longer visible. Stable Hb and PLT levels throughout treatment also suggest it was well tolerated. Conclusions: In patients with castration resistant prostate cancer and multiple bone metasteses, the use of 223Ra therapy can provide marked improvement in PSA and ALP, whilst reducing the number and intensity of existing bone lesions. References: 1. Parker C et al "Alpha Emitter Radium-223 and Survival in Metastatic Prostate Cancer" N Engl J Med. 2013; 369: 213-223

P840
Early experience with 223Ra-dichloride treatment of prostate cancer patients with multiple bone metastases

O. Sántha, J. Szegedi, I. Garai; Scanomed Ltd., Debrecen, HUNGARY.

Aim: Presenting our experience in the alpha-radiating 223Ra-dichloride treatment of prostate cancer patients with multiple bone metastases by the overview of the medical history of the patient and relevant literature.Method:Castration resistent prostate cancer patients with symptomatic multiple bone metastases without the involvement of any other organ can be treated with 223Ra-dichloride. So far 15 patients have been under treatment at our institute. The treatment consists of 6 intravenous injections, 4 weeks between each. Every time 50 kBq/kg of activity is administered. A known side effect of the radiopharmaceutical is bone marrow suppression, so a week before each treatment the hematological status of the patient is checked to insure patient safety. On the day of the treatment a pain scale is used to determine the level of pain the patient suffers from. The radiopharmaceutical is administered by using an intravenous cannula. Approximately 30 minutes after the injection the patients can go home. The medical history and the examination results of these patients were reviewed.Results:At our institute, 2 of the 15 patients completed the whole 6 cycle treatment. By the end of the treatment their bone pain decreased significantly according to the pain scale data. The treatment had to be aborted in 5 cases: 2 patients had increased risk of pathological fracture, 3 patients had severe hematological blood test anomalies. At present 8 patients are under treatment, 4 of them have received 4 injections so far, their bone pain has been reduced according to the pain scale.Discussion:According to our results the 223Ra-dichloride treatment reduces patients' bone pain. We are planning to compare the AP, PSA and bone scintigraphy results before and after treatment.

P54 - Tuesday, October 13, 2015, 4:00 PM - 4:30 PM, Hall 3 – Poster Exhibition

Radionuclide Therapy & Dosimetry: Local Radionuclide Treatment

P841
Biological Therapy and Radiosynoviorthesis in Patients with Rheumatoid Arthritis

M. Szentesi, Z. Nagy, P. Géher, I. Nagy; Budai Irgalmasrendi Kórház, BUDAPEST, HUNGARY.

The treatment of patients with rheumatoid arthritis (RA) has been spectaculary changed since the 1950's. Introduction of

the steroid compounds and their local application, the chemical and radionuclide synovectomy, surgical synovectomy, use of non steroid drugs, the basic treatment and the spread of biological therapy are the most important steps. Introduction of the biological therapy has changed the quality of life for these patients. Objectives: During biological therapy sometimes 1 or 2 joints could be affected by inflammation. In this cases always the question is how to solve the problem. Change of the biological or basic therapy, use surgical synovectomy or radiosynovectomy (RSO)? Patients and Methods: In our reumatological department 1500 patients with RA were treated with biological therapy between 2002 and 2014. In 100 patients we applied RSO because of the inflammation of the knee joint during biological therapy. We made a long term follow-up in 62 patient. All participants provided written informed consent. In all participants inflammatory knee joint disease was diagnosed on the basis of the American College of Rheumatology. 55 of 62 patients with rheumatoid arthritis were seropositive, 7 seronegative. Mean age of 8 male and 56 female patients was 51.4 years (range 24-79) years. In 32 patients the right knee, in 30 the left knee was treated by radiosynovectomy. Steinbrocker functional stadium II was observed in 52, stadium III in 10. Mean duration of disease was 7.3 years (range 0.5-25), of synovitis (6.3month (range 3-8) Mean number of punctions of the treated joint prior to radiosynovectomy was 4,2 per patient and of steroid administrations prior to radiosynovectomy 3,0. In 12 patients a systemic steroid therapy has been performed. Results: During the study period, inflammation decreased. In the first two years excellent and good results were recorded in 82,2%. Two years after radiosynoviorthesis 83.3% of patients did not need another punction. Before the knee inflammation patients were in complete remission which status has been achieved after RSO as well. DAS: 2,4+-0,4. Conclusions: 1. RSO is an effective method to treat the inflammation of the knes. 2. The RSO performed during biological tehrapy is as effective as in the case of patients without biological therapy.

P842

Trans Arterial Radio Embolization (TARE) In The Management Of Intractable Hypoglycemia In Malignant Insulinoma

M. Menga1, M. Zotta2, A. Codegone1, E. Richetta1, A. Piovesan3, E. Arvat3, R. E. Pellerito1; 1Nuclear Medicine - A.O. Ordine Mauriziano, Turin, ITALY, 2Nuclear Medicine - A.O.U. Città della Salute e della Scienza, Turin, ITALY, 3Oncological Endocrinology - A.O.U. Città della Salute e della Scienza, Turin, ITALY.

Insulinoma is a rare islet cell tumor with an incidence of 4 cases per million per year, presenting usually with recurrent episodes of symptomatic hypoglycemia. Recently has been reported efficacy of selective hepatic artery radioembolization with radioisotope Yttrium-90 (Y-90) in patients with malignant neuroendocrine tumors. Materials and methods: Male patient 37 years-old presented in 2011 with episodes of hypoglycemia and hyperinsulinemia. Imaging demonstrated a lesion of the pancreatic body, multiple hepatic metastasis and a small nodule in the right lung. Patient began therapy with Diazoxide (up to 600 mg/die) and Octreotide (0,6 mg/die). Fine needle agobiopsy of the dominant hepatic lesion was performed highlighting neuroendocrine origin (Ki67 30%). January 2012 spleno-distal pancreasectomy and enucleoresection of hepatic lesions followed by Thermoablation on several hepatic lesions (S6, S7 e S8). March 2012 PET-CT with 68Ga DOTATATE uptake only on a hepatic lesion, no indication to the Peptide Radio Receptor Therapy. May 2012 hepatic progression of disease (PD), persistence of hypoglycemia and aggravation of the general conditions; initiated therapy with Everolimus 10 mg/die. July 2013 recurrence of disease, multiple Trans Arterial Chemo Embolization (TACE) with DC-Beads, treating both right and left liver. February 2014 evidence of PD (increase of the well known hepatic lesions, new hepatic lesion in S5 and left adrenal node suggestive for secondary localization). September 2014 further PD (increase of the adrenal node and hepatic lesion in S4; enlargement of abdominal lymph nodes). In consideration of failure of conventional standard multiagent medical treatment and hepatic chemoembolization, it has been proposed TARE with 90-Y resin-based microspheres as palliative treatment. Results and conclusions: Patient underwent radioembolization after scintigraphic assessment of the presence of pulmonary and gastrointestinal shunts and dosimetric evaluation of the optimal therapeutic activity. On 5 November 2014 patient underwent preliminary scintigraphy with 99mTc-MAA and TARE at the confluence of right and left hepatic artery (1.4 GBq) experiencing only mild pain. Post-procedural imaging (bremsstrahlung and PET-CT) confirmed the correct localization of the microspheres in the hepatic tumoral lesions. Clinical improvement was seen in the subsequent days after the procedure indeed dextrose infusion was rapidly discontinued and patient was discharged from hospital. Despite few studies on the use of TARE in hepatic metastases of neuroendocrine tumors and experience with malignant insulinoma is even more limited because of the very low incidence, nevertheless, as demonstrated by our case, management of malignant hypoglycemia seems safe and feasible by means of 90-Y microspheres TARE.

P843

Radioembolization with Y-90 resin microspheres for intrahepatic cholangiocellular carcinoma: Prognostic factors

C. Soydal, N. O. Kucuk, S. Bilgic, E. Ibis; Tip Fakultesi, Ankara, TURKEY.

Aim: We have investigated prognostic factors to predict overall survival after radioembolization in patients with cholangiocellular carcinoma. Material and Method: 16 patients who received radioembolization with Y-90 resin microspheres for cholangiocarcinoma were included to the study. Statistical relationship between overall survival after radioembolization and age, serum AST, ALT, total bilirubin levels, presence of extrahepatic metastases, number, dimension and FDG avidity of liver lesions have been analyzed. Results: Mean 1.7± 0.1 GBq Y-90 microspheres were administered total 16 patients (mean age: 55.37±17.7; 8 Male, 8 Female). Mean AST, ALT, total bilirubin levels were calculated as 35±15 IU/L, 40±37 IU/L and 0.77±0.37 mG/dl patients had extrahepatic metastases before treatment. Number of liver lesions was 1, equal or less than 5 and multiple in 6, 2 and 8 patients and their dimensions varied between 12-120 mm. Liver lesions of 13 patients were FDG avid (mean SUVmax: 7.4±2.2). Extrahepatic metastases were demonstrated in 5 patients. 12 patients were died during 243±229 days follow-up period. In Cox-regression analysis, serum AST (p=0.035) and ALT (p=0.020) levels, FDG avidity (p=0.018) and dimension (p=0.019) of liver lesions have been found statistically significant parameters to predict overall survival after radioembolization (p=0.007). Conclusion: Serum AST and ALT level, FDG avidity and dimension of liver lesion are prognostic factors in patients who received radioembolization for cholangiocellular carcinoma. Patients with good liver reserve, FDG negative and smaller tumors seem to survive longer after radioembolization.

P844

177Lu-labeled hydroxyapatite (Lu-177 HA) in Radiosynovectomy of knee joints due to Rheumatoid arthritis.

K. Kamaleshwaran, S. Thirumalaisamy, V. Rajamani, E. Radhakrishnan, A. shinto; Kovai medical center and hospital limited, Coimbatore, INDIA.

Aim: To evaluate the use of radiosynovectomy (RS) using Lu-177 labeled hydroxyapatite (Lu-177 HA) in the treatment of knee joints in rheumatoid arthritis(RA). Methods: 22 patients, diagnosed with RA and suffering from synovitis of the knee joints were referred for RS and were followed up for period of 1 year.The duration of the disease was 11.2± 10 months.15/22 knees had pain during the night and 10/22 had abnormal flexibility. Three-phase bone scintigraphy(BS3) of knee joint was performed to confirm active synovitis and RS was performed according to the EANM guidelines.All were treated with 333 ± 46 MBq of Lu-177 HA administered intra-articularly. Monitoring of activity distribution was performed by static imaging of knee joint. They were evaluated clinically at 1 year after the treatment by considering the pain improvement from baseline values in terms of 100-point visual analogue scale(VAS), the improvement of knee flexibility and the pain remission during the night.RS response was classified as poor (VAS < 25), fair (≥25 - 50), good (≥50 - 75) and excellent (≥75),with excellent and good results considered as success,while fair and poor as failure.BS3 was repeated after 1 year and Changes in the 2nd phase of BS3 were assessed visually,using a 4-degree scale and in the 3rd phase, semiquantitatively with J/B ratio to see the response. Results: 1 year after treatment, the VAS% improvement from baseline was 90% ± 5.2% and found to be significantly related to patients age (P = 0.01), duration of the disease(P = 0.03).The overall success rate (VAS ≥ 50) was 90%.Remission of pain during the night achieved in 100% and knee flexibility improved in 80%.The changes in blood pool phase before RSV were 3.8 ± 0.5 and after 0.8 ± 0.4 ($P <$ 0.001).The J/B ratio was: before RSV 2.8 ± 0.5; after treatment 1.0 ± 0.3 ($P < 0.05$).RS side effects were minor and not significant. Conclusion:RSV with Lu-177 HA was safe and effective in patients with knee joint synovitis of rheumatoid origin. They show significant therapeutic effect after 1 year follow- up period with no significant side effects.Controlled clinical trials are necessary to evaluate therapeutic efficacy and safety compared to treatment with other radionuclides and steroids.

P846

Evaluation of the delivered activity of yttrium-90 resin microspheres with sterile water and 5% dextrose (D5W) as application agents

H. Ahmadzadehfar1, C. Meyer2, C. Pieper2, R. Bundschuh3, M. Muckle3, F. Gärtner3, H. Schild2, M. Essler3; 1University Hospital Bonn, BONN, GERMANY, 2University Hospital Bonn Department of Radiology, BONN, GERMANY, 3University Hospital Bonn Department of Nuclear Medicine, BONN, GERMANY.

Purpose: To evaluate impact of switching from sterile water to 5% dextrose (D5W) as the application agent for yttrium-90 (90Y)-resin microspheres on: total activity of 90Y administered (expressed as a proportion of the prescribed/calculated activity), as well as the number of cases of stasis and the reported incidence of discomfort during the Selective Internal

Radiation Therapy (SIRT) procedure. Methods: In December 2013, we switched from sterile water to D5W for the application of SIRT in all patients. This retrospective observational single-center case series describes our experience in the months preceding and after the switch. Apart from the change in application agent, the protocol for SIRT was otherwise identical. Results: One hundred and four SIRT procedures were performed on 78 patients (45 male, mean age: 63 years, range: 31-87 years) with either unresectable hepatocellular carcinoma, cholangiocarcinoma or chemorefractory liver-dominant metastatic cancer. Compared with sterile water, the whole prescribed activity was administered in significantly more procedures with D5W: 85% vs. 22%; $p<0.0001$. A significantly higher proportion of the calculated activity was administered with D5W: 96.1% ± 11.0 vs. 77.4% ± 24.3 ($p<0.0001$). D5W procedures were also associated with a lower incidence of stasis or flow reduction (20% vs. 56 % procedures; $p<0.0001$) and mild-to-moderate upper abdominal pain during the procedure (1.8% vs. 44% procedures; $p<0.0001$). Conclusions: Replacing sterile water with isotonic D5W as the application agent favorably impacts on the safety of SIRT, eliminates and/or minimizes flow reductions/reflux during administration of 90Y-resin microspheres and improves percentage activity delivered and ease of delivery.

P847

First ever use of Peptide Receptor Radionuclide Therapy (PRRT) with the Radiolabeled Somatostatin Analog (177Lu-DOTATATE) in metastasized neuroendocrine tumors (NETs) in a Spanish Public Hospital. Our experience in the first year.

I. Plaza de las Heras, C. Field Galán, R. de Teresa Herrera, A. Prieto Soriano, B. Rodriguez Alfonso, J. Cardona Arboniés, J. Aller Pardo, M. Mitjavila Casanovas; University Hospital Puerta de Hierro, Majadahonda, SPAIN.

Aim: Describe the first ever use of metabolic treatment with 177Lu-DOTATATE in metastasized NETs in progress in our hospital in the first year. Materials and methods: Treatment approval is needed as "individualized use" by the Spanish Agency for Medicines and Health Products (AEMPS). From February 2014 until May 2015, 12 treatments with 177Lu-DOTATATE were given to 7 patients (4 men and 3 women) with metastasized NETs in progress, 6 of them were diagnosed with gastroenteropancreatic tumours (2 insulinomas, 1 vipoma, 3 small mid intestine) and 1 of them a bronchial carcinoid. All patients had a positive OctreoScan preceding the treatment and they had previously received another alternative treatment modalities whithout response. 6 of the 7 patients met the inclusion criteria according to the guideline of the EANM. They had received 1-4 cycles of 200 mCi (7.4 GBq of 177Lu-DOTATATE) with intervals of 6 to 12 weeks. In one case, the treatment was terminated before because of the poor physical condition of the patient. All patients received premedication against nausea and steroids. The treatment started with a dual infusion of a solution containing amino-acids (VAMIN®) through an intravenous three-step cannula (to protect the kidneys from radiation) from 30 minutes before and during 6 hours. The infusion of radioactive premedication was given 30 minutes after the start of the amino-acids and took 30 min. Finally we washed the cannula and the drip was removed. It was well tolerated in all cases. Images were acquired after 24 hours (wholebody scintigraphy and thoracoabdominal SPECT/CT) to determine whether the radioactivity had been well absorbed by the tumors. To asses response we monitorize renal, hepatic and hematologic function with blood samples and imaging (ECO, CT-scan or MRI).Results: All patients showed stable disease on the Octreoscan and improvement in quality of life. They have not submitted short term renal, hepatic or hematologic toxicity. Six of them are still alive and 1 deseaced. Conclusion: The literature shows very promising results with treatment with 177Lu-DOTATATE in metastasized NETs which supports it's general approval for individual use by AEMPS. In our Hospital with a long experience in metabolic treatment and a multidisciplinary team it's easily administered, well tolerated, has few adverse short term effects and requires a 24 hour hospitalization. Our results show disease stability in all the patients and improved quality of life.

P848

Radioembolization of primary and / or metastatic hepatic tumors with 90-yttrium microspheres: our experience.

R. DE TERESA HERRERA, I. PLAZA DE LAS HERAS, C. FIELD GALAN, M. BERESOVA, J. CARDONA ARBORIES, A. PRIETO SORIANO, S. MENDEZ ALONSO, S. MENDEZ ALONSO, M. MITJAVILA CASANOVAS; HOSPITAL UNIVERSITARIO PUERTA DE HIERRO, MAJADAHONDA, MADRID, SPAIN.

Objective: To analize the results after radioembolization (RE) with 90Y microspheres in our hospital. Material and methods: From 10/2012 to 02/2015 we evaluated 35 patients, of which we treated 27 (11 women, 17 men, mean age 63.1 years) ,11 hepatocellular carcinoma, 1 cholangiocarcinoma and 15 liver metastatic tumors (13 colorectal 1 neuroendocrine tumor, 1 adenoid cystic tumor). In 22 we used resin radiolabelled microspheres and in 5 of them we used glass microspheres. All patients had previously received at least two lines of treatment. Before radioembolization treatment, hepatic arteriography and scintigraphy 99mTc-MAA were performed. According to the results obtained in these tests it was decided which patients were candidates for therapy with 90-Y (four patients were

excluded, one because of vascularization problems, one due to > 20% hepatic-pulmonary shunt, one because of difficult hepatic surgery access, and the last one because of extensive infiltration of the rigth hepatic lobe with extense thrombosis of the rigth portal vein). The 90Y activity was calculated according to the instructions of use of the microspheres. In the patients treated with resins we used the body surface method. To assess response to treatment we used modified RECIST criteria, tumor viability (EASL) and liver tests. Results: Of the 27 patients treated, 10 are still alive, with an overall average survival after RE of 10.5 months and progression-free survival average of 4 months. Eight of the 27 patients presented secondary complications of RE (3 liver radiotoxicity, 2 ulcers due to radiation, 1 intrahepatic hemorrhage, 1 febrile syndrome, 1 hydropic decompensation), six of those eight had a metastatic liver disease. Conclusions: in our experience , we found similar results to those reported in the literature , with particular emphasis on liver toxicity in the treatment of metastatic disease , which forces to reconsider the hepatic reserve in these patients.

P849

Resin-Based 90 Yttrium Radioembolization Of Liver Tumors: The Three First Cases Performed In Lebanon.

F. CHEHADE, J. DAHER, F. KAMAR, C. TAYAR, M. GHOSN, B. MOURANI, K. YAMMINE; CLEMENCEAU MEDICAL CENTER, BEIRUT, LEBANON.

INTRODUCTION: Resin-based 90 Yttrium radioembolization (RYRE) is a complex procedure that requires multidisciplinary management for safety and success. The published literature suggests that there is sufficient evidence to support the safety and effectiveness of RYRE in selected patients with non-resectable primary or secondary liver tumors. MATERIAL AND METHODS: Three patients with non-resectable liver tumors were hospitalized in our institution within a period of 24 hours and underwent RYRE for their liver tumors. A 65 years-old and a 68 years-old female patients have cholangiocarcinoma and recurrent cholangiocarcinoma respectively, and an 88 years-old male has hepato-cellular carcionoma. The patients received 0.65 MBq, 1.4 MBq and 1.2 MBq of the radiopharmaceutical respectively. The pretreatment work up included: 1) whole body 18FDG PETC; 2) catheterization to delineate arteries irrigating tumors selectively according to the individual anatomy of each patient; 3) instillation in the selected artery of 148 MBq of 99mTc-human albumin aggregates in order to assess by planar and tomographic scintigraphy the lungs shunt, the tumor to non-tumor activity ratio, and the possibility of inadvertent spread of the microspheres to non-target organs such as stomach and small bowels; 4) measurement of the tumor volume using 3-dimensional CT Scan reconstruction; 5) calculation of the therapeutic activity dose according to tumors volume, BSA, percentage of lung shunts, and liver laboratory tests. RYRE was monitored by cross sectional and metabolic imaging modalities including 18F-FDG PET CT. RESULTS: RYRE was tolerated in all patients, there were no major post therapeutics complications and 90Y Bremsstrahlung scintigraphy revealed preferential tracer accumulation in diseased liver parenchyma. This treatment was efficient since two months later, radioembolized tumor masses showed decrease in number, size and activity. Moreover, the female patient with recurrent cholangiocarcinoma had no active liver tumor after RYRE. Liver tumors that are still active or newly appeared, are programed for a second session of RYRE at 4 months interval. CONCLUSION: Our initial clinical experiences with RYRE has led to encouraging response of the liver tumors with survival potential.

P850

Clinical efficacy of radiosynoviorthesis in finger joint systemic arthritis.

I. Iakovou, K. Badiavas, A. Doumas, V. Mpalaris, S. Tosounoglou, D. Kotrotsios, V. Athanasiou, D. Katsaboukas, S. Georga, D. Lo Presti, G. Arsos; Academic Nuclear Medicine dpt, Papageorgiou hsp, THESSALONIKI, GREECE.

PURPOSE:To retrospectively evaluate the long-term efficacy of radiosyniviorthesis (RS) in patients with systemic arthritis (rheumatoid or psoriatic arthritis) of the finger joints.METHODS:Thirty-six painful despite pharmacotherapy finger joints of 29 patients (28 females, 67.4 ± 7years) were treated by intra-articular injection of 169Er citrate. All joints presented a positive blood pool pattern in a pretherapeutic bone scan, suggestive for local synovitis. Success rate was determined by a change composite index (CCI, from 1-> total disability to 10 -> lack of any impairment, with CCI≥6 -> success) calculated taking into account functional disability, a ten-step visual analog scale (VAS) for pain, joint tenderness and swelling, patients and physician's total assessment prior to and after treatment, with a mean follow-up of 12 months.RESULTS:Twenty-nine (83.4%) joints reported a pronounced improvement (19 good and 10 moderate response) proved by a CCI≥6 at the end of the year's follow up vs. 72.3% at 6 months, $p<0.05$ (18 good and 7 moderate response). Interphalangeal joints were more frequently resistant to therapy whereas best results were obtained in the thumb base joints.CONCLUSION:RS is highly effective in finger joint systemic arthritis with concomitant local synovitis.

P851

The impact of isotope intra-articular distribution and extra-articular leakage on the clinical outcome of radiosynoviorthesis (RS) of the knee.

I. Iakovou, A. Doumas, K. Badiavas, V. Mpalaris, S. Tosounoglou, D. Kotrotsios, V. Athanasiou, D. Katsaboukas, S. Georga, D. Lo Presti, G. Arsos; Academic Nuclear Medicine dpt, Papageorgiou hsp, THESSALONIKI, GREECE.

AIM: To assess the impact of extra-articular leakage and the intra-articular distribution of 90Y on the clinical outcome of RS in patients with knee activated osteoarthritis (aOA) and rheumatoid arthritis (RA) in a 18 months follow-up period. METHODS: We prospectively evaluated 52 patients, 26 with aOA resistant to conventional therapy and 26 with RA referred for RSO due to synovial inflammation, as demonstrated by early-phase bone scintigraphy, for a 18 months' period of time. They were all treated with 185 MBq 90Y combined with a glucocorticoid intra-articular injection. Success rate was determined by a change composite index (CCI, from 1-> total disability to 10 -> lack of any impairment, with CCI≥6 -> success) calculated taking into account functional disability, a ten-step visual analog scale (VAS) for pain, joint tenderness and swelling, patients and physician's total assessment prior to and after treatment. Yttrium-90's intra-articular distribution (IAD) was assessed by planar imaging 20 minutes after RS (scored as mainly diffuse or mainly focal). Leakage to regional lymph nodes, the liver and spleen was assessed with a dual-head gamma-camera after 24 hours. RESULTS: The overall response rate (RR) for all treated joints was 65% at 6 months and 60% at 18 months (P = ns). The mean improvement rate for the treated joints in RA was higher than aOA in total. IAD was mainly diffuse in 84% with RR of 67% versus 65% in cases with focal distribution, p> 0.05. 90Y leakage was found only to the liver and the spleen (0.3% vs. 1%, respectively) being significantly less in case of diffuse IAD. Neither IAD nor 90Y leakage were correlated with CCI. CONCLUSION: Yttrium-90 radiation synovectomy exerts a beneficial therapeutic effect in patients suffering of knee synovial inflammation, providing better results in rheumatoid arthritis than in osteoarthritis. Isotope IAD and leakage do not influence its clinical effect

P852

Radioisotope synoviorthesis in paediatric and adolescent patients with haemophilia

A. Martínez-Esteve, R. Álvarez-Pérez, J. Tirado-Hospital, R. García-Jiménez, R. Núñez-Vázquez, I. Borrego-Dorado; Virgen del Rocío Universitary Hospital, Seville, SPAIN.

Objective: To assess the outcome and adverse-effects of the radioisotope synoviorthesis in paediatric and adolescent patients with haemophilia.Methods: Prospective study of historical cohort was conducted in our department between June 2005 and July 2014. A total of 21 consecutive haemophiliac boys with a mean age of 12.42 years (range 4-17) were included. The diagnosis of synovitis was established on the basis of clinical follow-up including radiological images (radiography and / or MRI). For evaluation, the classification proposed by Fernandez-Palazzi was used. Inclusion criteria: patients aged less than 18 years old with hemophilia and more than one haemarthrosis in less than three months remaining a chronic synovitis despite prophylactic therapy intensification. All the patients underwent 28 radioisotope synoviorthesis with 90Y-citrate-colloid and/or 186Re-sulphide-colloid. The effectiveness of the procedure was assessed through pre and post treatment clinical comparison at 6 months after radioisotope synoviorthesis. The mean follow-up was 66.05 months (range 18-109).Results: Twenty-seven of the 28 synoviorthesis (96.4%) had a good response (13 procedures) or excellent response (14 procedures), and only 1 (3.5%) had partial response. No patient had no response to the procedure. It was necessary to repeat the procedure in 3 joints of 3 different patients, due to haemarthrosis at 6 months after treatment and at a late stage at 20 and 23 months, obtaining in all cases a good or excellent response with disappearance of haemarthrosis, and subsequent recovery of the joint range of motion. We appreciated inflammatory reaction after procedure in 4 cases (14.3%), which improved with analgesics and nonsteroidal anti-inflamatory drugs. None of the patients presented malignant or premalignant lesions during the follow-up.Conclusion: The radionuclide synoviorthesis is a very effective procedure in paediatric and adolescent patients with hemophilia, being a minimally invasive procedure, easy to perform, safe and with minimal side effects.

P853

Safety and efficacy of transarterial Y-90 radioembolisation for liver metastases of neuroendocrine tumours

G. Boni1, I. Bargellini2, M. Tredici3, s. mazzarri3, A. Farnesi4, S. Chiacchio3, A. C. Traino5, G. Manca1, F. Guidoccio3, R. Cioni2, C. Bartolozzi2, S. Ricci6, D. Volterrani3; 1Regional Center Of Nuclear Medicine,University Hospital Of Pisa, pisa, ITALY, 2Department of Radiology, Vascular and Interventional Radiology,University Hospital Of Pisa, pisa, ITALY, 3Regional Center Of Nuclear Medicine, University Hospital Of Pisa, pisa, ITALY, 4Division of Oncology, Hospital of Pisa, pisa, ITALY, 5Health Physics Unit, Section of Medical Physics, University Hospital, Pisa, Italy, pisa, ITALY, 6Division of Oncology, University Hospital of Pisa, pisa, ITALY.

AIMTo present the preliminary data about transarterial radioembolisation (TARE) with Y-90 microspheres in patients (pts) with liver metastases of neuroendocrine tumors (NETs). METHOD: Since 2012 up to now 11 patients (3 male and 8 female) with a mean age of 62±11.7 yrs (range 40-77) affected by unresectable liver neuroendocrine metastases underwent Y-90 TARE with resin microspheres (Sirtex). Primary site of the NETs was ileum (3 pts), lung (3 pts) and pancreas (5 pts). We didn't treat with TARE those pts with high bilirubin level (>1.8 mg/dl). Pts with minor extrahepatic metastases were included, because it didn't affect the prognosis. All pts previously selected by MRI or CT scans had pre-TARE planning angiography and Tc-99m-MAA SPECT/CT in order to detect possible shunting into gastrointestinal vasculature, to assess the lung shunt and to simulate the distribution of the microspheres within the tumoral and the non-tumoral liver.Y-90 TARE was performed 7-14 days later followed by PET/CT imaging within 24 hrs. The estimated activity was determined using the standard BSA method. Response to TARE was evaluated with morphological criteria measured at 4-6 weeks and then every 3 months on CT or MRI scan. RESULTS: We totally perform 17 treatments for 11 pts, because 6 patients were submitted to the TARE twice (bi-lobar treatment), and 14 diagnostic SPECT/CT with 99Tc-MAA, because 3 of the "double treatment" were performed within a month by the first diagnostic scan. The mean injected activity of resin microspheres was 0.96±0.33 GBq and the mean target volume was 326±321 mL (range 5-1180 mL).In 10/11 evaluable pts at a mean follow-up of 9±5.5 months, we obtained after the first TARE a partial response in 3/10 pts (33%) and a stable disease in the remaining 7 pts. In 4/6 evaluable pts ,who were submitted to second TARE, we observed a partial response in 3 pts, and a stable disease in 1 pt. No significant side effects and TARE related complications were observed in our series. Hepatic toxicity occurred at grade G1 in 3 pts and at grade G2 in 1 pt. CONCLUSIONS: Y-90 TARE is a feasible and safe method to treat liver metastases of NETs with an acceptable level of complications, a low percentage of toxicity, a good response rate and high clinical benefit.

P854

Safety and efficacy of selective internal radiotherapy with Y-90 glass-microspheres in patients with progressive hepatocellular carcinoma (HCC) after failure of transarterial chemoembolization (TACE)

A. P. Bellendorf1, S. P. Müller1, A. Bockisch1, S. Ezziddin2, J. Nagarajah3, J. Best4, J. Schelhorn5, T. D. Poeppel1, A. Sabet1; 1University Hospital Essen, Germany, Department of Nuclear Medicine, Essen, GERMANY, 2Saarland University Homburg, Germany, Department of Nuclear Medicine, Homburg, GERMANY, 3Memorial Sloan Kettering Cancer Center, New York, NY, UNITED STATES, 4University Hospital Essen, Germany, Department of Internal Medicine and Gastroenterology, Essen, GERMANY, 5University Hospital Essen, Germany, Institute for Diagnostic and Interventional Radiology and Neuroradiology, Essen, GERMANY.

Aim: Transarterial chemoembolization (TACE) is currently the standard of care in patients with non-resectable, locally advanced hepatocellular carcinoma (HCC). Selective internal radiotherapy (SIRT) is mostly used as an alternative modality in patients considered poor candidates for TACE. Data on SIRT in TACE-refractory patients are sparse. This study aims to evaluate the safety and efficacy of SIRT with glass microspheres in patients with progressive HCC after failure of TACE.Methods:47 patients with progressive HCC after a median of 2 (range 1-13) TACE sessions received SIRT with Y-90 microspheres (3.5±1.5 GBq; liver target dose 110-120 Gy). Toxicity was recorded 4 and 12 weeks after the treatment and reported according to Common Terminology Criteria for Adverse Events v.4. Treatment response was assessed 1 and 3 mo after treatment using modified response criteria in solid tumors (mRECIST) and survival analyses were performed with the Kaplan-Meier method (log-rank test, $P < 0.05$). Results: Reversible hepatotoxicity (≥ grade 3) occurred in 15 of 47 patients (32%). Treatment response consisted of partial response in 26 (55%), stable disease in 12 (26%), and progressive disease in 9 (19%) patients. Median overall survival (OS) was 14 months (95%CI: 12-16) and objective response to SIRT was associated with longer OS ($p=0.006$). Conclusion:Selective internal radiotherapy is a safe and effective salvage treatment option in HCC patients refractory to TACE.

P855

Radiosynovectomy application after arthroscopic surgery on the hip joint

H. I. ATILGAN1, **M. SADIC**2, H. OZSOY3, G. KOCA2, A. OZSOY4, M. KORKMAZ2; 1Kahramanmaras Necip Fazıl City Hospital, Department of Nuclear Medicine, Kahramanmaras, TURKEY, 2Ministry of Health Ankara Training and Research Hospital, ANKARA, TURKEY, 3Memorial Ankara Hospital, Department of Orthopedics and Traumatology, ANKARA, TURKEY, 4Ministry of Health Ankara Numune Training and Research Hospital, Clinic of Radiology, ANKARA, TURKEY.

Aim: Pigmented villonodular synovitis (PVNS) is

characterized as the proliferation of synovial tissue of the joint, tendon sheath and bursa. It is usually seen in middle-aged women and the most common joints are knee, hip and ankle. Recurrence is common and recurrent tumors cause more destruction and invasion. Besides wide surgical excision, radiosynovectomy (RS) increases local control. In the literature, RS performed after open surgery to the hip joint in almost all of the cases. In this case, we present the efficacy of RS after arthroscopic surgery of the hip joint with PVNS. Case Presentation: Synovial hypertrophy and effusion compatible with PVNS was observed in contrast enhanced magnetic resonance imaging (MRI) of a 32-year-old patient that had administered to orthopedic clinic with right hip pain. The patient underwent arthroscopic synovectomy for the lesion in the hip joint. Six weeks after surgery, RS was performed with yttrium-90 (Y-90) colloid (CIS Bio International, France) to the hip joint. Three phase bone scintigraphy was taken before RS. Minimal increased perfusion in blood flow phase, minimal hyperemia in blood pool phase and relatively increased activity accumulation in late images were seen in right hip joint. 3 mCi (111 MBq) Y-90 colloid was applied to right hip joint under fluoroscopy. Bremsstrahlung imaging was made for the evaluation of distribution of Y-90 colloid in fourth hour after RS with gamma camera (Siemens, ECAM, Hoffman Estates, IL, USA) equipped with low energy general purpose collimator. Distribution of Y-90 colloid was normal with no extraarticular leakage (Figure). Hip joint was stabilized for 72 hours after RS. Patient did not have any complaints in sixth and ninth month controls. MRI and three phase bone scintigrapy were taken in ninth month control. There was no pathological activity accumulation in bone scintigraphy and no residual or recurrent tumour was detected in MRI. Conclusion: As an alternative to RS applied to the hip joint after open surgery, RS application after arthoscopic surgery is effective in achieving local control. Key words: radiosynovectomy, yttrium-90 (Y-90), pigmented villonodular synovitis (PVNS). Figure: Good intraarticular distribution is seen in anterior whole body (a) and static (b) images four hours after Y-90 colloid injection to right hip joint. There was no extraarticular leakage.

P856

Phase I Clinical Experience of Post-Radioembolization Yttrium-90 Imaging Using Next Generation Digital PET/CT

C. L. Wright1, J. Zhang1, K. Binzel1, E. J. Wuthrick1, P. Maniawski2, M. V. Knopp1; 1The Ohio State University, Columbus, OH, UNITED STATES, 2Philips Healthcare, Cleveland, OH, UNITED STATES.

AIM: Targeted intraarterial delivery of Yttrium-90 (90Y) microspheres into unresectable hepatic malignancies and metastases allows for embolization of the tumor-associated neovascularity and local deposition of high therapeutic doses of radioactivity. Bremsstrahlung scintigraphy of 90Y radioactivity using planar and SPECT/CT approaches is the current imaging standard for immediate post-therapy assessment. Alternatively, there is a small fraction of 90Y internal pair production which can be readily imaged using conventional photomultiplier-based PET systems but its clinical use is limited due to long image acquisition times which can disrupt routine clinical workflows. The solid-state digital photon counting PET detector (i.e., digital PET or dPET) is the fundamental innovation to advance clinical PET imaging of 90Y. The purpose of this ongoing Phase I clinical trial is to assess the feasibility and clinical capability of next-generation dPET/CT to accurately and more efficiently image post-therapy 90Y biodistribution. MATERIALS AND METHODS: A next-generation dPET/CT system (Philips Vereos 64 ToF) was used to image patients following 90Y radioembolization for malignant/metastatic liver lesions in an ongoing Phase I clinical trial. Qualitative and volumetric dPET/CT assessment of 90Y activity within the liver was compared with standard bremsstrahlung SPECT/CT images (Siemens Symbia T16). In order to determine minimum acquisition times per bed position, segmented reconstruction of list mode acquired data was obtained from 1 to 7 min. Matched pair comparison of dPET/CT image characteristics with standard bremsstrahlung SPECT/CT imaging were also performed and assessed by multi-reader review. RESULTS: 90Y dPET imaging is clinically feasible and produces evaluable images with improved quality when compared with standard bremsstrahlung SPECT/CT. Digital PET images demonstrate markedly improved 90Y-to-background contrast and enable more accurate volumetric assessment of 90Y activity. Faster image acquisition times are attainable with dPET/CT which appears to be become robust around 5 min per bed position. CONCLUSION: At present, there is an unmet clinical need to more accurately and efficiently assess 90Y biodistribution in post-radioembolization patients. The current results demonstrate that dPET/CT technology is capable of imaging 90Y with improved image quality and volumetric assessment. Faster acquisition times are also attainable with dPET/CT without significant impact on image quality. Continued refinement of 90Y dPET image acquisition strategies and image reconstruction will enable more accurate and even faster evaluation of 90Y patients.

P55 - Tuesday, October 13, 2015, 4:00 PM - 4:30 PM, Hall 3 – Poster Exhibition

Radionuclide Therapy & Dosimetry: Data Collection Methods & Pharmacokinetics

P857

Image Quality Parameters and Quantification Issues with Y-90 Bremsstrahlung SPECT/CT

S. Beykan, M. Lassmann, S. Schlögl; Department of Nuclear Medicine, University of Würzburg, Würzburg, GERMANY.

OBJECTIVES: The aim is to investigate the influence of various parameters on the reliability of quantitative bremsstrahlung SPECT/CT. A phantom study was performed for studying the influence of collimators, energy windows and reconstruction-settings on image-contrast, image-noise, contrast-recovery-coefficient, coefficient of variation, visibility and calibration. METHODS: For measuring the image-quality a torso-based-phantom containing 6 spheres (diameters: 10-37mm) was used. Each sphere was filled with 1.59MBq/ml Y-90. A 50ml bottle (~80MBq) was used for calibration in air. SPECT/CT data were acquired (SIEMENS Symbia T2) by using several acquisition-parameters, two reconstruction protocols (2D-OSEM and 3D-FLASH), collimator-sets ('HEGP' and 'MEGP') and CT-based attenuation correction. As image quality parameters; the results of contrast (C [%]), contrast-recovery-coefficient (QH), coefficient of variation (CV), visibility (VH) and signal-noise-ratio (SNR) of the spheres and the bottle in Y-90 SPECT-CT images were calculated and compared for both collimators and reconstruction-algorithms in each energy windows setting. >For 11 different energy window ranges, collimators and reconstruction algorithms, the total and specific number of counts-to-activity concentration ratios (CA-Ratio) were calculated for each sphere and the bottle. Moreover, the difference between a calibration in air and water was investigated. RESULTS: The best energy window for CV was determined as 50-195keV while the best energy window for C [%], QH, VH and SNR was established as 86-106keV. The measurements based on 2D-OSEM with HEGP showed better results. The best results of CA-Ratios per spheres (which also show the lowest partial volume effect) were observed in the energy-window 86-106keV for the HEGP-collimator. Changing the order of processing for the combined energy-windows has no influence on the image quality parameters. Higher count rates per MBq were observed in MEGP-collimator. The calibration factors obtained in air as compared to those in water were inconsistent most likely caused by material-dependent variable bremsstrahlung yields. CONCLUSIONS: Collimation, applied energy window range and reconstruction algorithm have substantial effects on Y-90 bremsstrahlung image quality. For the best image quality based on determined parameters, the 86-106keV energy window in conjunction-with the 2D-OSEM reconstruction algorithm using a HEGP collimator is recommended.

P858

Radiation dose estimate from patients undergoing 18F-FDG scanning: implications for the general public and nuclear medicine technicians

B. Liu, R. Tian; Department of Nuclear Medicine, West China Hospital, Sichuan University, Chengdu, CHINA.

As 18F-FDG PET/CT is increasingly applied in clinical practice and patients will contact with the general public after completing the scanning. It is necessary to consider the potential exposure burden to the general public and nuclear staff. This study was to estimate the exposure dose to the general public and nuclear medicine technicians from patients undergoing 18F-FDG PET/CT scanning. Methods Fifty-seven patients (38 males,19 females; age range: 19-72 years, average age: 43±16 years) with different malignancies undergoing 18F-FDG PET/CT scanning were randomly and prospectively recruited. Approximately at 5 minutes after intravenous injection of 18F-FDG , whole-body initial dose rate was measured with a radiation-survey meter at 0.3 and 1.0 m from the patients. On the basis of human 18F-FDG metabolic rate proposed by the International Commission of Radiological Protection and human social contact model proposed by the National Council on Radiation Protection and Measurements, the total effective dose equivalent (TEDE) to the general public from exposure to patients who have completed 18F-FDG PET/CT scanning and left nuclear medicine department were calculated. On the assumption that a nuclear medicine technician typically spends 5 minutes at a distance of 0.3m for positioning the patient, the technician's TEDE was also estimated. Results The whole-body initial dose rates at 0.3m and 1.0 m were 100.5-156.4 μSv/h and 16.8-46.8 μSv/h, respectively. The TEDE to a family member sleeping with the patient at night was predicted to be 32.49-58.01 μSv, to a family member contacting the patient at daytime 4.59-13.48 μSv, to a colleague 6.06-17.79 μSv and to a passenger 98.43-175.77 μSv. The TEDE to a technician per 18F-FDG PET/CT scanning procedure was predicted to be 4.05-7.24 μSv. Conclusion The predicted doses to the general public and nuclear medicine technicians from exposure to patients undergoing 18F-FDG PET/CT scanning are significantly lower than the regulatory dose limits. The general public should not be afraid of contacting with the patients who have undergone 18F-FDG

PET/CT scanning. This work was supported by the National Natural Science Fund of China Grant No. 81401445, 81471693.

P859

The Importance of Treatment Planning in Radiopharmaceutical Therapy According to Human Data of 153Sm-EDTMP

M. Meftahi1,2, A. Bahrami Samani2, I. Jabbari1, T. Hoseinnejad3; 1University of Isfahan, Isfahan, IRAN, ISLAMIC REPUBLIC OF, 2Nuclear Science and Technology Research Institute, Tehran, IRAN, ISLAMIC REPUBLIC OF, 3Mashhad University of Medical Science, Mashhad, IRAN, ISLAMIC REPUBLIC OF.

Aim: to Show that different patients have various physiologic responses in treatment by 153Sm-EDTMP as a therapeutic agent by means of comparing of patient by patient data obtained from the routine method of fixed value injection.Material and method: 7 patients (6 males and 1 female) were injected with the radiopharmaceutical (manufactured by PARSISOTOPE Company) and each one received a dose of 1mCi/kg and was scanned at intervals of 15min, 3, and 24h post injection. Planar imaging was performed at anterior posterior direction. Then total counts of whole body were calculated as geometric mean of counts in anterior and posterior states. Results were analyzed in order to evaluation of absorption and excretion of the agent for each patient. Regarding that the first image was performed before urinary excretion of the patients, it was considered to be a reference of total activity for each patient.Results: the results indicated obvious variation in physiologic behavior among patients. The minimum, maximum, and mean values of excretion were 57%, 12%, and 30%, respectively at 3h post injection. More than 50% of administered total activity remained in bone in 5 patients at 24h post injection. The maximum, minimum, and mean values of absorption were 60%, 25%, and 47% at this time interval.Conclusion: Consideration of the results demonstrates an egregious fluctuation in physiologic response among the patients. It can be problematic in many cases. Because some patients may be overdosed and suffer from the common side effects or vice versa may receive ineffective dose and not have suitable response to the therapy. Therefore the fixed value injection cannot be suitable for all cases and optimization and treatment planning for each patient is a matter of great concern.

P860

Absolute SPECT/CT calibration for dosimetry in 177Lu targeted radionuclide therapy

F. Fioroni, E. Grassi, V. Ferri, S. Marco Antonio, F. Angelina, A. Versari, M. Iori; IRCCS-ASMN, Reggio Emilia, ITALY.

Purpose: Peptide Radionuclide Radiation Therapy (PRRT) with somatostatin analogues labelled with 90Y and 177Lu is increasingly used for the treatment of NETs. An accurate evaluation of tumour and organs at risk doses is mandatory for a personalized therapy. The purpose of this study is to develop a SPECT/CT quantitative protocol to generate an accurate 177Lu activity quantification for dosimetry assessment. Methods: First of all, the calibration factor (CF) for the absolute quantification was obtained by a cylindrical uniform phantom filled with 177Lu (0.187 MBq/ml; volume 5640 ml), unaffected by partial volume effect. In order to evaluate the count rate effect, several acquisitions of the phantom were performed in about one month. Images were obtained with a SPECT-CT system (Symbia T2, Siemens) with a clinical acquisition protocol and reconstructed using a commercial 3DOSEM algorithm (Flash3D) with CT-based attenuation correction, energy window-based scatter correction and full collimator-detector response compensation.In order to validate the calculated CF, we acquired a cylindrical phantom with hot inserts and an antropomorphic torso phantom with organs and added lesion inserts [2.5÷1200 ml], filled with known activity concentration of 177Lu [0.07÷2.25 MBq/ml]. Volumes and concentrations were chosen as close as possible to the clinical data, thus mainly simulating the volume of tumours and organs at risk. Recovery coefficients and noise dependence as function of OSEM iterations and subsets for different volumes were evaluated. Results: We obtained a CF (15.8cps/MBq) with a coefficient of variation of 5%; the CF doesn't depend on count-rate in the evaluated activity range. The system is capable of recovering the activity in a 280 ml sphere by an accuracy of ±4%. The linear dependence of noise on the number of subsets and iterations is visible as for fixing the number of subsets, varying the number of iterations and viceversa. This dependence is also confirmed by the ANOVA two factor factorial model (<10-7).SPECT-CT was been calibrated in sensitivity taking into account the insert volume to consider Partial Volume Effect, for body and brain protocols. We found out the optimum combination of the iterations and subsets employed in our commercial algorithm (10 iter-8 subsets), in order to establish the quantitative accuracy of our clinical SPECT patient imaging studies. Conclusions: The 177Lu SPECT/CT reconstruction algorithm settings for dosimetry purpose were evaluated. Clinical absolute quantification for SPECT/CT dosimetry is feasible, though further efforts to improve physics modelling are wished to enhance accuracy and reproducibility.

P8610

Comparison of Geant4 and MCNPX Monte Carlo systems in the calculation of voxel S values for the therapeutic radionuclides 90Y, 111In, 177Lu and 131I

L. Auditore1, **E. Amato**1, A. Italiano2, F. Minutoli1, A. Campennì1, S. Baldari1; 1University of Messina, MESSINA, ITALY, 2Istituto Nazionale di Fisica Nucleare, MESSINA, ITALY.

This work was aimed to compare the differences in voxel S values in soft tissue calculated through two Monte Carlo codes for four radionuclides commonly used in nuclear medicine therapies.We developed two Monte Carlo simulations, in Geant4 and in MCNPX, of tissue regions divided into 11x11x11 cubic voxels of 3 mm side. The different physics models available for low-energy electromagnetic processes were tested.The decay of each radionuclide (90Y, 111In, 177Lu, 131I) was simulated as homogeneously distributed within the central voxel (0,0,0), and the energy deposited in it and in the surrounding voxels was properly scored.The results obtained with the two Monte Carlo codes were compared each others and with the ones calculated by means of a previously published analytical method. Voxel S factors were represented as a function of the "normalized radius", defined as the ratio between the source-target voxel distance and the voxel side. MC simulations show a good agreement each other and with the analytical calculation method. Main differences are probably due to the different implementation of the decay spectra for the considered nuclides. The analytical model provides results which differ up to 50% from MCNPX data. These differences can be explained by the approximations introduced by the analytical approach which, however, do not influence significantly the accuracy of the dosimetric calculation.

P56 - Tuesday, October 13, 2015, 4:00 PM - 4:30 PM, Hall 3 – Poster Exhibition

Radionuclide Therapy & Dosimetry: Preclinical and Clinical Dosimetry & Radiobiology

P862

Pre-therapy Initial Dosimetry Results of Lu-177 -DOTA-617-PSMA In Castration Resistant Prostate Cancer

M. M. Abuqbeitah, N. Yeyin, A. Aygün, E. Demirci, M. Ocak, M. Demir, L. Kabasakal; Istanbul University, İstanbul, TURKEY.

Aim: Targeted radionuclide therapy (TRT) is an increasingly used in treatment of wide Types of cancer. Presently dosimetry is highly required either to plan treatment or to estimate the absorbed dose delivered to critical organs during treatment. Methods and materials : The study comprised 7 patients suffered from prostat cancer with progressive disease and candidated to undergo Lu-177-DOTA-617 therapy following to Ga-68-PSMA PET/CT imaging for all patients. 192.4±11.1 Mbq (5.2±0.3 mCi) was intravenously injected and to evaluate bone marrow absorbed dose 2 cc blood samples were withdrawn in short variable times (3, 15, 30, 60, 180. Minutes and 24, 48, 120. hours) after injection .further more whole body scans were performed using scintillation gama camera in 4, 24, 48 and 120 hour after injection and in order to quantify the activity taken up in the body, kidneys, liver, right parotid and left parotid, the geometric mean of anterior and posterior counts were determined through ROI analysis, after that background subtraction and attenuation correction were applied using patients Ga-68-PSMA PET/CT images taking in a consideration; organ thickness ,body thickness and Hounsfield unites from Computed Tomography scan. OLINDA/EXM dosimetry program was used for curve fitting, residence time calculation and absorbed dose calculations. Results: Calculated absorbed dose of bone marrow, left kidney, right kidney, liver, left parotid, right parotid and total body. 1.28±0.52, 32.36±16. 36,32.7±13.68, 10.35±3.45, 38.67±21.29, 37.55 ±19.77, 2.25±0.95 (mGy/mCi) respectively. Conclusions : Our first results clarify that Lu-177-DOTA-617 is safe and reliable therapy as there was no complications seen.İn the other hand the observable variation in the absorbed dose of the critical organs among the patients necessitate patient- specific dosimetry approach to save body organs and particularly highly exposed kidneys and parotid gland.

P863

Influence of syringe residual activity (SRA) on effective dose (ED) estimates from myocardial perfusion imaging (MPI) exams

F. A. A. de Jonge, S. Valente, T. C. Ferreira; Hospital Lusíadas Lisboa, Lisbon, PORTUGAL.

Aim: To estimate the effect of syringe residual activity on ED from MPI exams. Methods: MPI was done with a one-day low-dose stress, high-dose rest protocol with 99m-Tc-tetrofosmin. Stress (S) and rest (R) dose activity (DA in MBq) was measured in a dose calibrator (Veenstra); for S a 1 ml syringe was used; for R a 2,5 or 3ml syringe was used (with occasional use of 5ml syringe); measured residual activity (RA) after injection was available for three different cohorts: C1= 148 MPI consecutive exams, period FEB-MAR 2014, RA for all S, only for 16 R exams. C2= 27 MPI consecutive exams APR 2015, RA for 27 S and 26 R exams. C3= 88 MPI non-consecutive exams, executed in 2014, for which RA

for S and R exams were available (not included in C1). All data processing was done in R: A Language and Environment for Statistical Computing (http://www.R-project.org). Data are presented as median (minimum - maximum). ED was calculated with the ICRU voxel phantom / ICRP 103 values, as cited for tetrofosmin S and R exams in Andersson et al (EJNMMI Physics 2014), using either the uncorrected dose activity DA or the DA, corrected for RA (CDA). Results: Stress RA for the three cohorts (263 exams) was 21.2 MBq (8 - 67); as a percentage of DA: 5.9 % (2.3% - 17.8%) at a median S DA of 364 MBq. Rest RA, availbale for 130 exams, was 35 MBq (5 - 65); as a percentage of DA: 3.8% (0.58% - 7.0%) at a median R DA of 900 MBq. ED for S exams (263 exams) was 2.1 mSv (1.7 - 2.7) and using S CDA, 1.97 mSv (1.6 - 2.6). ED corrected as percent of non-corrected was 94.1 % (82.3% - 97.7%), mean 93.6% ED for R exams (130 exams) , was 5.6 mSv (4.7 - 6.3) and, using R CDA, 5.4 mSv (4.5 - 6.3). ED corrected as percent of non-corrected was 96.2 % (93% - 99.4%), mean 96.1%. For 130 S+R exams, ED corrected for RA as percent of non-corrected was 95.2 % (92.6% - 98.3%), mean 95.2%. Conclusion: Taking into account syringe residual activity, lower ED estimates will be obtained, both for stress (by median 94.1%) and rest exams (by median 96.2%). For a combined stress and rest exam, on average a 95.2% lower ED estimate is obtained.

P864

Revised dose calculations for 99mTc-pertechnetate used for diagnostic nuclear medicine procedures in adults

M. ANDERSSON1, L. JOHANSSON2, D. MINARIK1, S. MATTSSON1, S. LEIDE SVEGBORN1; 1Medical Radiation Physics, Malmö, SWEDEN, 2Department of Radiation Sciences, Umeå, SWEDEN.

Aim and background: Technetium-99m is the most commonly used radionuclide at nuclear medicine investigations. The radionuclide is eluted as 99mTc-sodium pertechnetate from a 99Mo/99mTc generator and is then used for labelling a variety of pharmaceuticals. There are also some examinations where 99mTc-pertechnetate is used directly. Moreover for substances labelled with 99mTc there is always a risk that 99mTc get loss from the specific molecules and therefore dosimetrically has to be treated as free pertechnetate. Recently a detailed review of the biokinetics of pertechnetate in adult humans was published (Legget and Giussani, 2015). In 2009, ICRP/ICRU published new adult reference computational voxel phantoms. These two updates have created a possibility to perform new risk estimations for intravenously and orally administered 99mTc-pertechnetate. Materials and methods: Absorbed dose and effective dose estimation were performed with the internal dose computer program IDAC 2.0 and based on the new biokinetic model referred to above. IDAC 2.0 uses the ICRP/ICRU reference adult voxel phantom and the tissue weighting factors from ICRP publication 103 to calculate the effective dose. Nuclear data were gathered from the ICRP publication 107. Dose calculations were performed for both intravenous and oral administrations. In both calculations the urinary bladder was assumed to have a voiding time of 3.5 h. Results and conclusion: The effective dose for intravenously and orally administered 99mTc-pertechnetate was estimated to 0.027 and 0.024 mSv/MBq, respectively. For intravenous administration the effective dose is a factor of 0.6 of that obtained with calculations based on the biokinetic model given in ICRP publication 53 with the adult reference voxel phantom and the ICRP publication 103 organ weighting factors. For orally administered activity the effective dose was a factor of 2.6 higher using the new biokinetic model than the ICRP Publication 53 biokinetic data. In conclusion, new biokinetic data have increased the accuracy for new estimations of patient doses at diagnostic examinations with 99mTc-pertechnetat, or with Tc-labelled substances from which technetium is released.

P865

Partial volume effect restoration in dose volume histograms for Y-90 dosimetry: a proof of concept

M. Sanchez-Garcia1, P. Buyssens2, I. Gardin3, R. Lebtahi1, A. Dieudonné1; 1Department of Nuclear Medicine, Beaujon Hospital, Assistance Publique-Hôpitaux de Paris (APHP) & INSERM U1149, Clichy, FRANCE, 2QuantIF – LITIS [EA 4108], Rouen, FRANCE, 3Department of Nuclear Medicine, Henri Becquerel Cancer Center and Rouen University Hospital, & QuantIF – LITIS [EA 4108], Rouen, FRANCE.

Objective: 3D dosimetry of Y-90-radioembolization is based on Dose Volume Histograms (DVH) which are degraded by partial volume effect (PVE). A PVE correction has been develop to improve 3D dosimetry, using a semi-automated segmentation of sub-regions and the geometric transfer matrix (GTM) method. Material and Methods: A phantom consisting of an ellipsoid with radii 4x4x5 cm and a 2 cm radius sphere close to its center was analytically modeled to simulate an heterogeneous distribution. The sphere-to-background ratio took values of 1.1, 1.2, 1.3, 1.5 and 2.0. Projections were generated using the STIR software (stir.sourceforge.net) with a 3D modeling of the system PSF with depth dependent FWHM tuned to simulate a Symbia T2 camera. Poisson noise was added to projections. The reconstruction was done with STIR using the OSMAPOSL algorithm with 3D PSF. For each data set, the ellipsoid was subdivided into uniform sub-regions using an eikonal-based region growing algorithm (Buyssens et al. Image Vision Comput 2014). Then, partial volume correction was performed using the GTM algorithm. The DVHs

were calculated on the ideal, measured and corrected distributions using dose-point kernel convolution. The number of subregions was chosen by the user to reproduce the degraded DVH. The absorbed doses values covering 95%, 50% and 5% of the tumor where calculated for the simulated and corrected activity distributions and the results compared to the ideal one. The corresponding relative deviations were noted ΔD95, ΔD50 and ΔD5 respectively. Results: For 1.1 and 1.2 datasets, the segmentation algorithm failed to find the heterogeneity with the worst results found for a ratio of 1.2 where ΔD95, ΔD50 and ΔD5 were -10.8%, 0.8% and -2.4% for the simulated distribution and 2.0%, 2.1% and -14.7% for the corrected one. For ratios 1.3, 1.5 and 2.0 the segmentation algorithm identified the heterogeneity. Maximum deviation in D95, D50 and D5 were -10.7%, 0.6% and -5.7% for the simulated distributions and below 1% for the corrected ones. Conclusion: A PVE correction based on sub-region segmentation with a region growing algorithm and GTM method has been developed. This method showed promising results on an analytical phantom in the cases where the concentration ratio is higher than 1.3.

P866

Automatic image segmentation for 3D dosimetry in Lu177-DOTATATE PRRT using a robust cluster algorithm on dynamic SPECT data

L. Vomacka, A. Delker, A. Gosewisch, E. Mille, H. Ilhan, F. J. Gildehaus, P. Bartenstein, G. Böning; Ludwig-Maximilian-University of Munich, Munich, GERMANY.

Aim: In Lu-177-DOTATATE PRRT the estimation of dosimetric values for tumours and radiation sensitive organs such as the kidneys supports individualized therapies. For this purpose a volume-of-interest (VOI) for each entity has to be defined in image data, acquired at days 1, 2 and 3 p.i.. We have studied a method to automatically segment tumour and kidney VOIs in 4D SPECT data compared to manually defined VOIs. Material and methods: Three patients (mean 70.7y) with neuroendocrine tumours who received 7.4GBq of Lu-177 DOTATATE were imaged with a Dual-head SPECT/CT (Siemens Symbia T2) with 20s/step in 64 steps/head. The CT image taken at day 1 was coregistered to each SPECT dataset and utilized for attenuation correction in penalized OSEM reconstruction employing compensation for distance dependent detector blur and photon scatter. The three SPECT volumes were synthesized to form a 4D SPECT study. A robust k-means cluster algorithm was used to automatically detect eight clusters in these dynamic image data, followed by a labeller to segment each individual connected VOI. For comparison, three to five tumours and two kidney VOIs were manually defined for each patient and an auto contour at the 40% of maximum value was applied. Based on the mean time-activity curves of each selected VOI a 3D dose map was calculated using S-value convolution kernels (Monte Carlo simulation in soft tissue). Results: The automatic segmentation successfully found 11 out of 12 tumour VOIs and three out of six kidney cortex VOIs. The missed entities can be addressed to overlapping with surrounding high-activity VOIs, mainly tumours and spleen. The mean dose values of the 11 tumours were 17.2±9.1Gy with the automatic and 16.5±9.1Gy with the manual method. The estimated dose to the cortex of the three successfully segmented kidneys was 9.7±1.7Gy with the automatic and 8.7±1.1Gy with the manual method. We found a strong correlation (ρ=0.8) and no significant difference (paired t-test) between the dose estimates of both methods. Conclusion: The automatic segmentation is a promising approach to reduce the effort to generate dose estimates in PRRT. Nevertheless we observed that the position of kidneys can significantly change between measurement days, hindering an accurate coregistration on the voxel or organ boundary level. These misregistered boundaries can result in false segmentation and dosimetric results. Furthermore the inclusion of structural information such as the CT image into the automatic segmentation algorithm could be a promising improvement.

P867

Estimation of local photon dose to active bone marrow in Lu-177 PSMA PRRT therapy using patient-specific Monte Carlo simulations

A. Gosewisch1, A. Delker1, L. Vomacka1, W. P. Fendler1, A. Brunegraf1, F. J. Gildehaus1, A. Mairani2, K. Parodi3, P. A. Bartenstein1, G. Böning1; 1University Hospital Munich, Munich, GERMANY, 2National Centre for Oncological Treatment, Pavia, ITALY, 3Ludwig-Maximilians University Munich, Munich, GERMANY.

Aim: Active bone marrow is a main critical organ in targeted radionuclide therapy. Particularly in Lu-177 DKFZ-PSMA-617 for treatment of metastasizing prostate cancer high radioactivity accumulations are observed close to active marrow bearing regions due to a high activity uptake in the bone metastasis. Further for dosimetry especially the long-range photon dose contribution cannot be predicted by simple standard models accurately. Thus the aim of our work was to determine the photon absorbed dose to regions which contain a high amount of active marrow (thoracic and lumbar vertebrae, pelvis) and show bone metastasis at the same time by means of patient-specific Monte Carlo (MC) simulations.Material and methods: Accumulated activity maps for three source regions (bone metastasis, kidneys, rest of body (ROB)) were generated for 2 patients using quantitative SPECT images acquired approximately 1h, 24h, 48h and 72h after administration of

3.7 GBq Lu-177 DKFZ-PSMA-617 on a Siemens Symbia SPECT/CT. Thereby the fitting of the activity-time points was done with a combination of a linear and an exponential fit. For dose calculation 200 million photons were simulated using the FLUKA MC code in combination with the accumulated activity maps and the patient CT data as patient-specific simulation input. To generate weighting factors for the energy deposition specifically in active marrow during simulation for each interaction in an active marrow region of interest the ratios of the mass energy absorption coefficients for active marrow and total bone were scored according to the energy of the interacting photon and the site-specific total bone composition.Results: The averaged active marrow doses to the lumbar, thoracic and pelvis regions are, respectively, 21.3, 23.0 and 20.0 mGy. Thereby the tumour doses make up 26.4, 36.8 and 42.4 % of the lumbar, thoracic and pelvis mean active marrow doses while the largest dose contribution comes from the ROB with 62.2, 54.7 and 55.7 %. The relative uncertainty of all MC simulations was below 6.5 % (mean 3.2 ± 1.3 %).Conclusions: In this study we developed a simple model to study the local photon dose to bone marrow in selected regions bearing a high amount of active marrow and activity using patient-specific MC simulations. Preliminary results show that bone metastasis contribute notably to the marrow dose although the magnitude of the estimated dose values in general is below commonly applied dose constraints.

P868

Partition model for accurate radiation therapy with yttrium-90 Glass microspheres in hepatocellular carcinoma.

S. Adib, M. Monteiro, S. Gnesin, P. Bize, A. Denys, J. Prior, A. Boubaker; CHUV, Lausanne, SWITZERLAND.

Aim: To evaluate the impact of individualized dosimetry using partition model for radioembolisation of hepatocellular carcinoma with yttrium-90 glass microspheres. Materials and methods: We performed a selective internal radiation therapy with yttrium-90 glass microspheres for patients with hepatocellular carcinoma, between February 2013 and July 2014, using a partition model analysis for accurate dose prescription to tumoral and non tumoral liver. The child score was A5 in 9 cases, A6 in 4 cases and B6 in 2 cases. Results: In total, 15 patients (aged 67±8y) were followed for an average of 10±15 [range 1-20] months. They were treated with 254±135 [110-548] Gy in the tumoral volume. Progression was observed in 6/15 patients (40%). Progression-free survival at 6, 12 and 18 months was 87%, 49% and 49%, while overall survival was 92%, 69% and 69%, respectively. Median progression-free survival time was 11.7m and not reached for overall survival. No unexpected events were recorded and all desired activity could be injected to the patient. These numbers compare advantageously with historical survival in published cohorts (Hepatology 2010;52:1741-1749; OS@6/12m=75%/59% with a 16.4m median survival rate and PFS=10m). Conclusions: Using partition model to compute dosimetry using Tc-99m-MAA is feasible and safe. Overall survival and progression-free survival seems to be comparable to historical cohorts.

P57 - Tuesday, October 13, 2015, 4:00 PM - 4:30 PM, Hall 3 – Poster Exhibition

Radionuclide Therapy & Dosimetry: Miscellaneous

P870

Radiation Protection Challenges When Treating Dialysis Patients With I-131

S. Gould, R. Fernandez, J. Robinson, P. Geraghty, C. Mills, H. Mohan; Guy's and St Thomas' NHS Foundation Trust, London, UNITED KINGDOM.

Aim: Three patients in renal failure undergoing haemodialysis have been treated with radioiodine (I-131) at our centre recently. For such patients, removal of radioactivity following administration occurs only with dialysis. Patient management therefore requires careful consideration of various issues related to radiation protection of the patient, their family and healthcare staff. Materials and Methods: The three haemodialysis patients were administered with 3849 MBq (thyroid ablation), 818 MBq and 770 MBq (thyrotoxicosis). All patients underwent dialysis immediately prior to radioiodine administration and were then admitted to a dedicated therapy isolation suite. Subsequently, each patient underwent at least two dialysis sessions in a side room (designated a radiation controlled area) in a dialysis unit within the hospital. Staff members caring for the patients in the dialysis unit were issued with electronic personal dosimeters (EPDs) to measure whole body doses. EPDs and dose rate meters were used to measure radiation dose to patients undergoing dialysis in adjacent rooms. Disposable tubing and clinical waste generated during each dialysis session was collected and disposed of via the usual hospital radioactive waste stream. Patients were permitted to resume their usual arrangements for dialysis when the activity in the solid waste collected from a dialysis session was below the 40 kBq threshold for very low level waste. The patients presented challenging radiation protection issues upon hospital discharge. One patient required a carer to assist her at home whilst another patient was blind. For the latter, her husband was designated a ‘comforter and carer’ and was issued with a whole body dosimeter which was worn for one month following hospital discharge. Results: All radiation

doses received by staff were well below permitted limits. A maximum of 66 μSv and 30 μSv were received by nurses caring for the thyroid cancer and thyrotoxic patients respectively. Over a four hour dialysis session, a maximum of 19 μSv was recorded by an EPD placed in an adjacent room. Solid waste collected from the dialysis procedure contained low levels of radioactivity (maximum 10 MBq). There was no evidence of radioactive contamination of the dialysis machine. The comforter and carer radiation dose recorded was not significant. Conclusion: Treatment of haemodialysis patients with radioiodine is complex and challenging but not impossible. Control of radioactive contamination, staff doses and appropriate waste disposal can all be effectively managed with hospital admission and appropriate input from the dedicated multidisciplinary team members before discharge back into the community.

P871

Single-cell dosimetry: effect of cell geometry on cellular S-values

N. Falzone1,2, J. M. Fernández-Varea3, G. Flux4, K. A. Vallis1; 1University of Oxford, Oxford, UNITED KINGDOM, 2Tshwane University of Technology, Department of Biomedical Science, Pretoria, SOUTH AFRICA, 3Universitat de Barcelona, Facultat de Física (ECM and ICC), Barcelona, SPAIN, 4Royal Marsden NHSFT, Physics Department, UNITED KINGDOM.

Aim: Several radionuclides used in medical imaging emit a significant number of Auger electrons (AE) which, depending on the targeting strategy, could either be exploited for therapeutic purposes or may contribute to an unintentional mean absorbed dose. The virtues of twelve AE emitting radionuclides are evaluated in terms of cellular *S*-values in concentric and eccentric cell/nucleus arrangements and by comparing their dose point kernels (DPKs). Materials and Methods: The Monte Carlo code PENELOPE was used to transport the full particulate spectrum of 67Ga, 80mBr, 89Zr, 90Nb, 99mTc, 111In, 117mSn, 119Sb, 123I, 125I, 195mPt and 201Tl by means of event-by-event simulations. Cellular *S*-values were calculated for varying cell and nucleus radii and the effects of cell eccentricity on *S*-values were evaluated. DPKs were determined up to 30 μm. Energy deposition at DNA scales are also compared to an emitter, 223Ra. Results: PENELOPE determined *S*-values were generally within 10% of MIRD values when the source and target regions strongly overlap, i.e. *S*(NN) configurations, but greater differences were noted for *S*(NCy) and *S*(NCS) configurations. Cell eccentricity has the greatest effect when the nucleus is small compared with the cell size and for cases where the radiation sources are located on the cell surface. DPKs taken together with the energy spectra of the radionuclides can account for some of the differences noted in energy-deposition patterns between the radionuclides. The relative dose of 119Sb, 125I, 195mPt and 201Tl are higher compared to 223Ra over dimensions 2 nm. Conclusion: A single-cell dosimetric approach is required to evaluate the efficacy of individual radionuclides for theragnostic purposes, taking cell geometry into account with internalizing and non-internalizing targeting strategies.

P872

A 3D Printed Anthropomorphic Phantom for Validating Quantitative SIRT Imaging in Multicentre Trials

J. Gear1, C. Cummings2, M. Tapner3, G. Flux1; 1Royal Marsden NHSFT, Sutton, UNITED KINGDOM, 2Institute of Cancer Research, Sutton, UNITED KINGDOM, 3SIRTEX, North Sydney, AUSTRALIA.

The use of selective internal radiation therapy (SIRT) is rapidly increasing and dosimetry for SIRT is very appealing with a number of large scale clinical trials currently underway. The aim of this project was to develop an anthropomorphic phantom that can be used for validating SIRT imaging in multicentre clinical trials. Anatomical data was obtained from a 24 second T1 weighted volume interpolated breath hold examination (VIBE) on a Siemens Aera 1.5 T MRI scanner, giving an in-plane pixel size of 0.7 mm and 2.8 mm contiguous slices. The liver, lungs and abdominal trunk were segmented using the Hermes image processing workstation. Organ volumes were then uploaded to the Delft Visualization and Image processing Development Environment for smoothing and surface rendering. Triangular meshes defining the isosurfaces were saved as STL files and imported into the Autodesk® meshmixer software, The organ volumes were subtracted from the abdomen and a removable base designed to allow access into the liver cavity. Connection points for placing lesion inserts and filling holes were also added in the design stage. A 50% scale model of the phantom was printed using an Objet EDEN 300V 3D printer. The printer uses stereolithography technology combined with ink jet printing. A 16 micron layer of liquid ultraviolet curable photopolymer is printed and cured using an ultraviolet laser. This process is repeated printing each layer of photopolymer on to the last and curing with the laser. Final print material is an opaque solid acrylic plastic, with reasonable tensile strength, low water absorption and density similar to water (1.09g/cm3). Total print time for the phantom was dependant on size, with the scale model taking 27 hours and the full size torso estimated at 76 hours. Smaller tumour inserts, for placement inside the liver cavity are printed with a transparent photopolymer and take under 2 hours to print. Initial scans of the phantom have been performed with Tc99m SPECT/CT, the organ shape showed

good correspondence with anatomical references. After these initial tests with the scale model a full size phantom will be printed shortly.

P58 - Tuesday, October 13, 2015, 4:00 PM - 4:30 PM, Hall 3 – Poster Exhibition

Conventional & Specialised Nuclear Medicine: Uronephrology

P873

Application of a dual nuclear medicine protocol in patients with urolithiasis.

V. Hadzhiyska1, T. Petrov1, I. Kostadinova1, V. Marianovski2, B. Mladenov2, Y. Asenov3; 1University Hospital Alexandrovska, Sofia, BULGARIA, 2University Multiprofile Hospital for Active Treatment and Emergency Medicine "N.I.Pirogov", Sofia, BULGARIA, 3University Hospital "Tsaritsa Yoanna", Sofia, BULGARIA.

The aim of this study was to apply a dual nuclear medicine protocol, using dynamic renal scintigraphy (DRS) and single photon emission tomography/computed tomography (SPET/CT) and to determine its additional value in patients with known or suspected urolithiasis. Subjects and methods: We have examined 50 patients by dual nuclear medicine protocol, including dynamic renal scintigraphy (DRS) and single photon emission tomography/computed tomography (SPET/CT). Thirty of the patients had known urolithiasis, while twenty were suspected for urolithiasis in the emergency department. Results: By our dual protocol we detected pathological findings in 78 (78%) of 100 investigated kidneys, while by DRS alone in 53 (53%) and by SPET/CT alone in 36 (36%) of them. The proposed dual imaging protocol have better results in the diagnosis of obstructive uropathy and in the evaluation of its functional impact on the renal parenchyma. The estimated accuracy for the diagnosis of urolithiasis and the obstructive uropathy was 96% and 92%, respectively. When interpreting the obstructive uropathy we found a significant correlation ($R=0.612$, $p<0.00010$) between the results, obtained by the DRS (drainage impairments) and those, obtained by the CT-part of the imaging protocol (secondary signs of obstruction). However, the use of the combined imaging protocol gave 35 % change in the final interpretation (respectively in 27 out of 78 kidneys with detected pathological changes), compared to DRS (27 %, in 21 kidneys) or to the low dose CT alone (8%, in 6 kidneys).The most frequently encountered functional and morphological findings in the kidneys with calculous pyelonephrits were inhomogeneous and/or diminished fixation of the tracer (18 out of 26 kidneys - 69%), reduced parenchymal thickness (8 out of 26 kidneys - 31%), and irregular renal contours (9 out of 26 kidneys - 34%). Impaired drainage function was detected by scintigraphy in 17 (85%) out of 20 patients with suspected renal colic. Secondary CT signs of obstruction in this patient group were reported in 6 (60%) of the cases with total obstruction by scintigraphy and in 2 (40%) of those with partial obstruction. SPET procedure alone could be helpful for better visualization and identification of a late accumulation of the tracer in the collecting system and in some cases for recognizing the level of the obstruction. Conclusion: The proposed dual nuclear medicine protocol can be applied not only for establishing the diagnosis of urolithiasis but also for determining its complications even in patients from the emergency department.

P874

Extracellular volume (ECV) assessment by Cr-51-EDTA plasma clearance and bioimpedance spectrometry (BIS) : a comparison study

G. Arsos1, D. Katsampoukas1, C. Sachpekidis2, E. Manou3, K. Lazaridis1, E. Mitsopoulos3; 13rd Dept of Nuclear Medicine, Aristotle University of Thessaloniki Medical School, Papageorgiou Hospital, Thessaloniki, GREECE, 2Clinical Cooperation Unit Nuclear Medicine, German Cancer Research Center, Heidelberg, GERMANY, 3Dept of Nephrology, Papageorgiou Hospital, Thessaloniki, GREECE.

Aim : ECV measurement by exogenous tracer plasma clearance kinetics during the bolus injection-multiple sample technique of glomerular filtration rate (GFR) measurement has been recently reported. ECV may be useful for both body fluid balance assessment in a variety of clinical situations and for a physiologically meaningful GFR indexation. Although ECV values in health and disease have been reported using Cr-51-EDTA as the tracer (ECV-Cr), validation against an established ECV assessment method like bromide dilution is lacking. Moreover, ECV-tracer values are influenced by the molecular size of the tracer, the duration of the procedure and the magnitude of the ECV itself. BIS, based on Hanai mixture theory, is a simple, non-invasive, higly reproducible method for ECV assessment (ECV-BIS), extensively validated against and showing negligible bias and excellent precision compared to bromide dilution. Hence, we aim to evaluate ECV-Cr using ECV-BIS as the reference in a number of individuals submitted to GFR measurement for clinical purposes. Subjects and methods : A total of 156 Caucasian adult patients (33.3% F), aged 55.6±16.8 years, including 142 patients with chronic kidney disease and 14 prospective kidney donors were evaluated. GFR and ECV were measured by bolus injection of 3.7 MBq Cr-51-EDTA, 10 plasma samples at 5, 10, 15, 30, 45, 60, 90, 120, 180 and 240 min p.i. and tracer plasma kinetics data analysis. ECV-Cr was expressed in l and GFR, after normalization by body surface area (GFRn), in ml/min/1.73 m2.

ECV-BIS (in l) was also assessed by four-electrode multifreequency impedance measurement using a Body Composition Monitor (Fresenius Medical Care). Proper statistics were applied for the between-variable differences and correlations assessment. Agreement between ECV-Cr and ECV-BIS was assessed by Blant-Altman statistics. Results : ECV-BIS and ECV-Cr were (mean±SD, 17.7±3.2 vs 15.7±3.2 l respectively, $p<0.05$), significantly different and their correlation was moderate ($r = 0.737$, $p<0.001$). The difference ECV-BIS - ECV-Cr (DECV) was 2.0±2.3 l with a 95% confidence interval of -2.6 - 6.6 l. DECV was correlated positively with ECV-BIS ($r=0.366$, $p<0.001$) and negatively with ECV-Cr ($r=-0.359$, $p<0.001$). DECV was not correlated with GFRn ($r=0.06$, $p=0.481$). Conclusions : ECV determined by Cr-51-EDTA plasma kinetic analysis during radionuclide GFR measurement does not reliably represents true ECV because it significantly underestimates the later. Predictably, the underestimation is higher as true ECV increases. The present findings question the validity of ECV-Cr for both the clinical assessment of the body fluid balance and the GFR indexing.

P875

Extracellular volume (ECV) may not represent a major improvement in glomerular filtration rate (GFR) normalization compared to body surface area (BSA)

G. Arsos1, C. Sachpekidis2, D. Katsampoukas1, E. Manou3, K. Lazaridis1, E. Mitsopoulos3; 13rd Dept of Nuclear Medicine, Aristotle University of Thessaloniki Medical School, Papageorgiou Hospital, THESSALONIKI, GREECE, 2Clinical Cooperation Unit Nuclear Medicine, German Cancer Research Center, Heidelberg, GERMANY, 3Dept of Nephrology, Papageorgiou Hospital, THESSALONIKI, GREECE.

Aim : GFR normalisation remains an open issue with considerable criticism exerted on the traditional but unreasonable GFR indexation by BSA (GFR/BSA). Given the central role of kidneys in body fluid balance, ECV and total body water (TBW) have been proposed as more suitable “physiological” indexes for GFR normalisation compared to BSA, lacking substantial supporting evidence however. ECV derivation from exogenous tracer plasma clearance kinetics (PCK) during bolus injection-multiple sample techniques of GFR measurement (ECV-Cr) has been recently shown but not validated against bromide dilution, the established reference. Bioimpedance spectroscopy (BIS), a convenient, non-invasive method for both ECV (ECV-BIS) and TBW (TBW-BIS) assessment, is successfully validated against bromide and deuterised water dilution methods respectively. In order to test for additional value of GFR indexing by parameters beyond BSA, we first explored the correlations between BSA and TBW-BIS, ECV-Cr and ECV-BIS and then between GFR/BSA and GFR normalized by TBW-BIS, ECV-Cr and ECV-BIS (GFR/TBW-BIS, GFR/ECV-Cr and GFR/ECV-BIS respectively) in a number of individuals submitted to GFR measurement for clinical purposes. Subjects and methods : One hundred fifty-six Caucasian adult individuals (33.3% F), aged 55.6±16.8 years including 142 patients with chronic kidney disease and 14 prospective kidney donors were evaluated. GFR and ECV were measured by bolus injection of 3.7 MBq Cr-51-EDTA, 10 plasma samples at 5, 10, 15, 30, 45, 60, 90, 120, 180 and 240 min p.i. and PCK analysis. BSA was calculated according to Haycock formula. ECV-Cr was expressed in l and GFR, after normalization by BSA (GFRn), in ml/min/1.73 m2. ECV-BIS and TBW-BIS (both in l) were also assessed by four-electrode multifreequency impedance measurement using a Body Composition Monitor (Fresenius Medical Care). Between-variable correlations were assessed by linear regression analysis. Results : TBW-BIS, ECV-Cr, ECV-BIS were (mean±SD) 38.1±7.9, 15.7±3.2, 17.7±3.2 l respectively. BSA was moderately correlated with ECV-Cr (r 0.617, $p<0.001$) and well with TBW-BIS and ECW-BIS (r 0.824 and 0.879 respectively, $p<0.0001$ for both). GFR/BSA was strongly correlated with all of the GFR/ECV-Cr, GFR/TBW-BIS and GFR/ECV-BIS (r 0.930, 0,917 and 0.977 respectively, $p<0.0001$ for all). Conclusions : GFR normalised by body fluid volumes derived either during GFR measurement (ECV-Cr) or by BIS (TBW-BIS, ECV-BIS) are closely correlated with BSA normalised GFR values, body size being the probable link connecting BSA and body fluid volumes. Our findings question the additional utility of ECV or TBW as GFR indexing parameters in a clinical setting.

P876

Diuretic Renography in Seated Position F+10(sp) for Post-Emergency Clinical Management in PerCutaneous Nephrostomy.

G. Tartaglione1, M. Vittori2, A. Cina3, M. Pagan1, A. D'Addessi2, P. F. Bassi2; 1Nuclear Medicine, Cristo Re Hospital, Rome, ITALY, 2Urology, Catholic University of the Sacred Heart, Rome, ITALY, 3Radiology, Catholic University of the Sacred Heart, Rome, ITALY.

Aim: PerCutaneous Nephrostomy (PCN) is an emergency procedure to relieve an obstructed or infected collecting renal system. A catheter perforates the skin and terminates in the renal pelvis providing a temporary drainage. Before planning surgery, it is recommended to evaluate renal function and drainage. In order to test function and drainage, we performed a diuresis renography, with PCN clamped, in a seated position using the procedure F+10(sp). Material and Methods: We enrolled 51 consecutive Patients (26 m, 25 f. with a PCN. 7 pts had a bilateral PCN. A total of 58 renal units with PCN were

studied. The test was deferred for 3-4 weeks after positioning PCN, to enable the urinary system to decompress. Renograms were performed in posterior view, using a dual detector system with rectangular large view (Infinia II-Xeleris, GE), with a single-head flexibility allowing scan in seated position. After consulting with a urologist the PCN was clamped during the study. A dose of 99mTc-MAG3, 150 MBq was injected using a 22G peripheral IV catheter with injection port. A 20-min dynamic phase was acquired, 60 frames x 2" and 108 frames x10", ,128x128 matrix, zoom 1. At 5th min after tracer injection, the pt drank 400-500 mL of water. A dose of 20 mg of Furosemide was injected IV at 10th min, during dynamic acquisition, using procedure F+10(sp). Later images at 20'-60' were acquired post voiding. The clamp was removed at end of study, or during the test in the event of obstruction signs or symptoms. The serum Creatinine levels were ranging from 0.68 to 4.12 mg/dL. Results: 28 kidneys with PCN clamped had a complete obstruction, 7 kidneys had a partial obstruction (ratio 20min/peak >0.25), 10 kidneys had a normal drainage (Tmax< 6mins; ratio 20min/peak <0.25), 12 kidneys showed a poorly function (split renal function <10%), 1 kidney had a complete failure. Conclusion: Due to the gravity effect, the test F+10(sp) in seated position may allow a better discrimination between obstruction and a normal drainage, reducing equivocal results. Diuretic renography is well tolerated also in pts with Creatinine level >2 mg/dL.This test may be an useful alternative to antegrade or retrograde pyelography before planning surgery in PCN kidney, especially in patients at risk of infection or contrast allergy.

P877

A new quantitative index for baseline renal transplant scintigraphy with Tc-99m DTPA in evaluation of delayed graft function and prediction of 1-year graft function

B. Yazici1, A. Oral1, C. Gokalp2, A. Akgün1, H. Toz2; 1Ege University Medical Faculty Department of Nuclear Medicine, Izmir, TURKEY, 2Ege University Medical Faculty Department of Internal Medicine Division of Nephrology, Izmir, TURKEY.

Aim: The aim of this study was to assess the value of a single renal transplant scintigraphy (RTS) with Tc-99m DTPA performed in the first two days after transplantation for evaluation of delayed graft function (DGF) and prediction of 1-year graft function. Quantitative indices were compared between each other and a new index for baseline RTS was described. **Materials and Methods**: A total of 165 patients to whom RTS with Tc-99m DTPA was performed within 2-days after transplantation were analyzed retrospectively. Hilson's perfusion index (HI), time between peak perfusion of graft and iliac artery (ΔP), peak-to-plateau ratio (P:Pl), ratio of peak graft perfusion to peak iliac artery (P:A), T½ of perfusion curve downslope (GW½), peak perfusion to peak uptake ratio (P:U), ratio of peak perfusion to uptake at 3 minutes ($P:U_3$) and ratio of uptake at 20 to 3 minutes (R20/3) were obtained. In addition, we first described the following formula called as Graft Index (GI) or Yazici's index (YI) for assessment of graft function: $GI=(\Delta PxAxPl)/(PxU_3)$. A sCr of >1.5 mg/dl at 1-year follow-up was considered to be abnormal. Mann-Whitney U, Spearman's coefficient of correlation tests and receiver-operating characteristic (ROC) curve analysis were used for statistical analysis. $P<0.05$ was accepted significant. Sensitivity, specificity and predictive values of the tests were calculated. **Results**: Mean values of the all indices were significant between the patients with and without needing dialysis and the patients with 1-year sCr of >1.5 and ≤1.5 mg/dl. Among the all indices, GI had the strongest correlation ($r=0.67$) with 1-week sCr and only GI and P:A had a correlation coefficient of ≥0.40 or ≤-0.40 ($r=0.40$ for GI, $r=-0.42$ for P:A) with 1-year sCr. Using the ROC curve analysis, the most accurate index for both evaluation of DGF and prediction of 1-year graft function was GI. Area under the curve (AUC) for GI was 0.94 in evaluating DGF and 0.79 in predicting 1-year graft function. Additionally, the most sensitive and specific index was also GI not only for DGF (sensitivity of 86.1%, specificity of 86.2%) but also for prediction of 1-year graft function (sensitivity of 74.1%, specificity of 76.0%). **Conclusion**: Several methods of quantifying RTS have been suggested. The question is which index is the best indicator. This study demonstrated that the parameters of baseline RTS should be assessed together by the formula of GI which provides more accurate information to diagnose DGF and predict 1-year graft function.

P878

Correction of Differential Renal Function for Asymmetric Renal Area Ratio in Unilateral Hydronephrosis

G. Ege Aktas, A. Sarikaya; Trakya University Medical Faculty Department of Nuclear Medicine, Edirne, TURKEY.

Objective: Children with unilateral hydronephrosis are followed up with anterior posterior pelvic diameter (APD), hydronephrosis grade, MAG-3 drainage pattern and differential renal function (DRF). İndeterminate drainage, preserved DRF in higher grade of hydroneprosis, in some situations complicates the decision making proses. False negative DRF estimations, due to asymmetric renal area ratio, can cause missing optimal surgery timing. This study was designed to assess whether correcting the DRF estimation according to kidney area could reflect the clinical situation of hydronephrotic kidney better than classical DRF calculation; concurrently with hydronephrosis grade, APD and MAG-3 drainage pattern. Material & methods: We reviewed MAG-3,

DMSA scans and ultrasonography (US) of 23 children (6 girls, 17 boys, mean age: 29±50 months) with unilateral hydronephrosis. MAG-3 and DMSA scans were performed within 3 months (mean 25.4±30.7 days). Closest US (mean 41.5±28.2 days) findings were used in evaluation. DMSA DRF estimations were obtained using geometric mean method. Second calculation was done correcting the counts (total counts divided by the number of pixels in ROI) according to kidney area. Renogram patterns of patients were evaluated retrospectively and separated into four subgroups. Visual assessment of DMSA scan was also noted and the hydronephrotic kidney was classified (compared to the normal contralateral kidney's uptake) as normal, slightly decreased and decreased. Correlations of DRF values of classical and area corrected methods with MAG-3 renogram patterns, visual classification of DMSA scan, hydronephrosis grade and APD were assessed. Results: DRF estimations of two methods were statistically different (p: 0.001). 11 hydronephrotic kidney changed category. There were no correlations between classical DRF estimations and hydronephrosis grade, APD, MAG-3 drainage patterns, visual DMSA uptake evaluation. DRF estimations with corrected method correlated with all: With the increasing hydronephrosis grade and APD, DRF estimations were decreasing, MAG-3 drainage patterns were worsening (c: -.649, -.675, -.745, -.873, p: 0.001, 0.001, 0.001, 0.001 respectively). Decrease in DRF (<45%) was determined when APD was ≥10 mm. When APD was ≥26 mm, reduction of DRF below 40% was determined. Conclussion: We found a good correlation between area corrected DRF estimations and widely accepted clinical parameters that are taken into consideration in follow up of persistent hydronephrosis. Our results suggest that, correcting DRF estimation for asymmetric renal area ratio in unilateral hydronephrosis can be more robust than classical DRF estimations, in defining the clinical situation of the kidney; especially in higher grades of hydronephrotic kidneys, under equivocal circumstances

P879

The evaluation of inter- and intraobserver variability of 99mTc-Dimercaptosuccinic acid SPECT renal scintigraphy

U. Can, **G. DURMUS ALTUN**; Trakya University Medical Faculty, Edirne, TURKEY.

99mTc-Dimercaptosuccinic acid (DMSA) scintigraphy is a frequently used diagnostic test to assess the presence and severity of cortical damage. The aim of this study is to investigate the variability in the interpretation of 99mTc-DMSA SPECT scans by using of the standart criterions. The study consisted 106 patients amog 4-81 years old (the mean age: 30±21 years). After 2-6 hours later from the injection of 99mTc-DMSA, in addition to the standart planar projection posterior 180 degrees SPECT imaging were obtained simultaneously using a dual head camera. Two experienced nuclear medicine physicians independently interpreted 106 DMSA scans (206 kidneys). While first observer was evaluating the only SPECT images,during his fist and second readings, and evaluating SPECT and planar images together in his third reading, the second observer evaluated only the SPECT images. In the calculation of the agreement rates, the analysis of kappa statistics (κ), Spearmann correlation (rs) and Kendall corrrelation (rk tau-b) and total agreement rates (%) were used. In the localization of the kidneys, the place of the prevalent lesions with the contour disorder and the evaluation of the defect severity, it was found that there are agreements among all three agreements highly and about excellent. Highly agreement rates in the spheric lesions place and in the evaluation of defect severity were obtained. In the evaluation of the 54 agreement in the normal, scar, inflammation in commentary/interpretation, in the variability of intra-oberserver, highly agreement (right rs=0.767, 72,7%; left rs=0.664, 55,6%) was found. As a result, the SPECT imaging can be used alonly and trustly in the finding of the place of the kidneys, in the existence of the contour disorder, in the place of the prevalent lesions and in the evaluation of the defect severity. Each observer, as general impression, states that only SPECT images can not be enough for certain diagnosis in the evalution of the kidneys as normal, scar/inflammation/scar+inflammation and states that they should be evluated with their planar images.

P880

Clinical Value of Cystatin C and Beta-trace Protein in Glomerular Filtration Rate in Chronic Renal Disease Adult Cases With Different Degree Renal Function Disorder: Comparison by The 99mTc-DTPA Plasma Sample Method

F. AYDIN, E. Surer BUDAK, S. DEMIRELLI, A. ONER, G. SULEYMANLAR, H. AKBAS, F. DAVRAN, S. BOZKURT, F. GUNGOR; Akdeniz University, Antalya, TURKEY.

Glomerular filtration rate (GFR) is the best indicator of the renal function. Gold standard for GFR measurement is inulin clearance (Cin). However, its measurement is inconvenient, time-consuming, and non-economic. Thus, in both scientific studies and routine clinical practice Nuclear Medicine methods (99mTc DTPA, 51Cr EDTA) are preferred, which are highly correlated with Cin. In addition, recently cystatin C (Cys) and beta trace protein (BTP) are also used for this purpose. In literature, however, data are limited about the clinical value of Cys and BTP in GFR measurement in CKD cases and the results have been inconclusive. In this study, we aimed to determine the efficiency of Cys and BTP in determination of

GFR in CKD patients. A total of 84 (59 males, 25 females) CKD patients aged 21 to 88 years (mean 61 years) were included criteria. GFR was calculated with three different methods: 1) using the gold standard DTPA two plasma sample method (TPSM); 2) using formula containing Cys to calculate GFR ; 3) using formula containing BTP. Correlation of GFR values calculated with Cys and BTP with that obtained with DTPA TPSM was assessed. GFRs calculated with both methods were significantly correlated with that calculated with gold standard method. However, GFR values obtained with Cys had a better correlation com-pared to those of BTP. Using Bland Altman analysis, scatter graphics of the differences between GFR values calculated using DTPA TPSM and those calculated with Cys, BTP at a confidence interval of 95% (mean ± 1.96SD). The GFR values obtained with Cys and BTP did not have reliable consistency. As a conclusion, we showed that GFR values calculated with Cys and BTP failed to show GFR of the CKD. Based on these results, our study demonstrated that Cys and BTP is not sufficient in reflecting GFR.

P881
"Hot Kidney" Artifact on Bone Scan: Incidence and Approach to Quantification

A. K. Kondakov1, D. S. Kharina1,2, E. A. Servuli1,2, I. A. Znamenskiy2,1; 1Pirogov RNRMU, Moscow, RUSSIAN FEDERATION, 2CCH RAS, Moscow, RUSSIAN FEDERATION.

Aim. It is well known that intense renal hyperfixation, or "hot kidney" artifact, appears in 0.5 - 2% of bone scintigraphy, though cause of this phenomenon is not clear. Hypercalcemia, acute kidney injury and chemotherapy are main predisposing factors of this condition. Aim of this study is to analyze incidence of the "hot kidney" artifact and propose the method of its quantification. Materials and methods. 1080 bone scans of adult patients (1 : 1.02 male-to female ratio) were retrospectively analyzed. All patients underwent whole-body bone scintigraphy in 2.5 - 3 hours after intravenous injection of 99mTc-pyrophosphate (53%), 99mTc-EDTMP (42%) or 99mTc-zoledronic acid (5%). In order to quantify severity of artifact, kidney-to-lumbar index (KLI) was determined as ratio between counts in equal regions of interest (ROIs) above kidney and lumbar spine on posterior views. There were three degrees of "hot kidney" severity: mild (1<=KLI<1.5), moderate (1.5<=KLI<=2) and severe (KLI more then 2), while KLI<1 was treated as absence of artifact. Results. Analysis revealed 15 cases of "hot kidney" artifact that corresponds to incidence about 1.4%. Most of cases (11 cases, 73%) were mild, two cases were moderate (13.5%) and two cases were severe (13.5%). In cases of severe "hot kidney" artifact, there was virtually no bone uptake of bone-seeking radiopharmaceutical. Both cases were performed with 99mTc-pyrophosphate. Repeated bone scans with 99mTc-zoledronic acid 5 days later showed increase in bone accumulation (KLI<1 in first case, KLI=1.6 in second). In first case (male, 58 years old), medical history was unremarkable, except prostatectomy for a prostate cancer. In the second case (male, 69 years old, prostate cancer) there was found that patient underwent MDCT with intravenous contrast a day before first scan, so it was suggested, that contrast-induced nephropathy (a form of acute kidney injury) was primary cause of artifact. Conclusion. "Hot kidney" appearance is relatively common artifact that affects about 1.4% of bone scans. Mild and moderate forms, defined by kidney-to-lumbar index, are prevalent and usually have little influence on interpretation. Severe form of artifact complicates the interpretation of bone scan results and it may be necessary to repeat bone scan few days later. If possible, contrast radiographic studies should be avoided before bone scintigraphy in order to prevent contrast-induced nephropathy. Radioactive tracer distribution should be studied for all forms of increased renal parenchymal uptake for correct effective dose estimation in patients.

P883
Diagnostic and Prediction Accuracy of GFR Prediction Equations in Comparison with 51Cr-EDTA

V. Ptacnik, J. Kubinyi, H. Jiskrova, D. Skibova, R. Rysava, V. Tesar, M. Samal; Charles University Prague, Prague, CZECH REPUBLIC.

Prediction of glomerular filtration rate (GFR) by regression equations from the patient serum creatinine and anthropometric data is simple, cheap but inaccurate. Measurement of GFR by 51Cr-EDTA, 99mTc-DTPA, or iohexol is accurate but more costly and not readilly available. The aim of our study was to compare diagnostic and prediction accuracy of GFR prediction equations and 51Cr-EDTA. Methods: In 49 adult patients with creatinine clearance (CC) 3 - 153 ml/min/1.73m2, serum creatinine level (SC) and EDTA clearance were measured with 1 day median interval between laboratory and radionuclide examinations. Reference EDTA GFR was calculated from 2 blood samples obtained 2 and 4 hrs post-injection. Mean absolute (MAE) and relative (MRE) errors of predicting reference GFR were calculated for single-sample EDTA (4 hrs), reciprocal SC, CC, and several prediction equations (Cockcroft-Gault, MDRD, CKD-EPI, Lund-Malmö, Mayo). Diagnostic accuracy of identifying the patients with GFR<30 and GFR<60 ml/min was assessed by ROC curves. Results: In the range of GFR<30 ml/min, MAE (~3.6 ml/min) and MRE (~23%) of prediction equations were similar to those of CC and reciprocal SC while the error of single-sample

EDTA was greater (5 ml/min, 34%). In the range of GFR≥30 ml, the lowest error was found with single-sample EDTA (2.4 ml/min, 5%); CC reflected reference GFR with error 9 ml/min or 16%, prediction equations 14-17 ml/min or 23-28%, and reciprocal SC 19 ml/min or 31%. In population with high prevalence, prediction equations identified the patients with GFR<30 ml/min with diagnostic accuracy 93-95%, in comparison with 95% using CC, 92% using reciprocal SC, and 99% using single-sample EDTA. Patients with GFR<60 ml/min were identified with diagnostic accuracy 97-100% by all methods. Conclusion: In agreement with previous reports, prediction equations performed best in the range of lower GFR values (but not better than CC and only slightly better than reciprocal SC). Despite large prediction errors in the range of GFR≥30 ml/min, prediction equations identified the patients with GFR<30 and GFR<60 ml/min with good diagnostic accuracy comparable with that of CC and EDTA. Except Mayo-clinic equation with lower accuracy, no significant differences were found between respective prediction equations. Diagnostic accuracy of prediction equations is sufficient to identify the patients with GFR below certain level. However, they should not be used to assess quantitative changes in GFR and wherever accurate GFR value is required to assess true renal function. In the latter applications, measurement with radionuclides or iohexol remains standard.

P59 - Tuesday, October 13, 2015, 4:00 PM - 4:30 PM, Hall 3 – Poster Exhibition

Conventional & Specialised Nuclear Medicine: Thyroid - Benign

P884

Recombinant Human Thyrotropin Stimulation Before 131I Therapy in Toxic Multinodular Goiter with Low Radioactive Iodine Uptake

M. Azorín-Belda, A. Martínez-Caballero, G. C. Figueroa-Ardila, C. A. Gómez-Jaramillo, J. Verdú-Rico, J. I. Dolado-Ardid, M. Antón-Leal, M. Martínez-Ramírez; Hospital Universitario San Juan de Alicante, Alicante, SPAIN.

AIM: To evaluate the efficacy of recombinant human thyrotropin (rhTSH) stimulation prior to 131I therapy in patients with a large toxic multinodular goiter and low radioiodine uptake. We have studied its effect on hyperthyroidism and thyroid volume reduction. MATERIALS AND METHODS: In a prospective trial from March-2012 through July-2014, 32 patients (26 women) with a goiter bigger than 50 g, radioactive iodine uptake (RAIU) at 24 hours <18% and surgery excluded, were treated with 800 MBq of 131I. 16 patients received a single 0,3 mg dose of rhTSH 24 hours before (Group I), and 16 patients were treated without stimulation (Group II). The follow-up period was 9 months and included evaluation of thyroid size reduction by scintigraphy, clinical assessment of compression complaints and serum TSH and FT4 levels. Complete response was considered when there was compressive clinical improvement and cure of hyperthyroidism, partial response if only improved one of the two factors and null if no response was observed. RESULTS: There were no statistically significant differences between the 2 groups for age, sex, goiter volume, RAIU at 24 hours and estimated absorbed dose. At 9 month, size reduction in group I was 36,6 ± 13,2% vs 28,3 ± 20,6% in group II ($p<0,05$). In group I 92,3% of patients showed compressive clinical improvement vs 63,6% in group II ($p<0,05$). Regarding hyperthyroidism, a cure of 93,8% and 68,8% was observed respectively in groups I and II ($p<0,05$).Full response was observed in 14/16 patients (87,5%) in group I and 9/16 (56,3%) in group II, partial response in 2/16 (12,5%) in group I and 4/16 (25%) in group II and null response 3/16 (18,8%) in group II ($p<0,05$). CONCLUSION: In patients with toxic multinodular goiter and low RAIU, rhTSH stimulation prior to radioiodine therapy achieved functional and clinical improvement, representing a treatment option in patients who previously would have been discarded.

P885

Correlation between auotimmunthyroid diseases and Vitamin D deficiency in a German population

C. Körber, N. Körber-Hafner; Nuclear Medicine Fulda, Fulda, GERMANY.

AIM OF STUDY: Vitamin D deficiency is considered to be a predictor for chronic diseases (1). Here the correlation to thyroid autoimmune disorders should be evaluated. METHOD: In blood samples of 880 patients with autoimmune thyroid diseases we measured TSH-level (BRAHMS Hennigsdorf, TSH 1), parathyroid hormone levels (IBL, parathyroid hormone total intact IRMA) and 25-hydroxyvitamin-D (IBL, 25 OH-Vit D3-RIA CT). These data were correlated to gender, age, thyroid volume diagnosed by ultrasound (ESAOTE my lab seven), thyroid hormone, thyroid medication and the influence of these parameters according to the level of D3 was statistically analysed. Also TPO-levels (each BRAHMS, anti TPOn), TRAK (TRAK human) and fT4-levels (FT4 RIA) were correlated. Patients under Vitamin D medication werde excluded. Statistical analyses were conducted with Statistica 10.0 (StatSoft). Two-tailed P values of less than 0,05 were considered to indicate statistical significance using student t-test and multiple regression analysis. Hashimoto thyreoiditis (H) and Graves disease (GD) were analysed as different patient groups. RESULTS: 790 females and 90 males each younger than 35 years participated in the study. The age of the patients was 31,5±4,2 (mean ±SE) years, TSH-level (H) 2,1±3,5 (GD under antithyroid medication) 1,3±2,5, parathyroid hormone

concentration 27,1±16,7 pg/ml (normal range 10-57), 25-hydroxyvitamin- D 17,8±11,8 ng per ml (normal range 8 - 60). The statistical analysis revealed a very high significane for the study population between vitamin D and parathyroid hormone level (p<0,001) in the student t-test, often seen in vitamin D deficiency. The table shows the significance levels of the parameters in the multiple regression analysis, the tests itself reached the significance level with H p< 0,03 and GD p<0,0059. DISCUSSION: In both diseases the Vitamin D concentration was influenced significantly by only few parameter. Thus a significant influence of Viatmin D deficiency on the disease development and progession can be excluded. Literature: Table of Contents (1) Bioavailability of Vitamin D and Its Metabolites in Black and White Adults (1) Bioavailability of Vitamin D and Its Metabolites in Black and White Adults Michael F. Holick, M.D., Ph.D. N Engl J Med 2013; 369:2047-2048November 21, 2013DOI: 10.1056/NEJMe1312291

P886

Comparison of planar and tomographic methods for calculating thyroid volumes in cats and dogs

R. P. Jóba1, G. Dabasi1, A. Polyák2, Z. Pösténvi2, J. Thuroczy3, K. Bús1, L. Jorgov1, L. Balogh2; 1Dept. of Nuclear Medicine, Semmelweis University, Budapest, HUNGARY, 2National "F.J.C." Research Institute for Radiobiology and Radiohygiene (NRIRR), Budapest, HUNGARY, 3Veterinary Faculty, Szent Istvan University, Budapest, HUNGARY.

Aim: Our aim was to compare several well established planar, and three dimensional SPECT methods for calculating thyroid volumes in cats and dogs. In addition we goaled to adopt the human volumetric procedures to be more accurate in therapeutc 131-iodine dose applications for feline and canine thyroid patients. Materials And Methods: More than twenty animals, referred feline and canine thyroid patients were sent for SPECT/CT examination from the early of december 2011. The suspected cases were uni- and bilateral hyperthyroidisms, benign and malignant thyroid tumors (adenomas and carcinomas). The intravenously applied radiopharmaceuticals were 99mTc-pertechnetate and 131I-iodine both 15 MBq/bwkgs. Data collection was carried-out in intravenous anaesthesia within 8-14 minutes per case in planar images, we calculated the thyroid volumen using some different standard methods from the human diagnostic: A: [(π/6) × L × H × W], B: [(π / 2)× L × W2], C: [0.33 × (area cm2)3/2], D: [1.08 × (π /6) × L × W2], E: (area × H), F: (0.27 × area × L), G: (π × L × W2) and H: [π × (4/3) × W3]. In SPECT images we selected the thyroid volumens with the help of automatic isocount VOIs.We used diagnostic dose CT images as a gold standard. CT measurements were made by selecting the thyroid VOI manually on each slices. Results: Compared to the golden standard CT volumetric data the only SPECT method proved to be the most similar. Planar method "D" resulted also non-significant alterations from the golden standard and SPECT method while data from planar methods "A" and "B" slightly differ and methods "C, E, F, G and H" provide significatly differing data from CT volumes.Conclusion: Based on our preliminary data SPECT/CT thyroid calculations seems to be the most accurate volumetric estimation however planar method "D" might be also applicable especially when hybrid instrumentation is not available. Authors believe that SPECT/CT thyroid imaging and volumetric estimation methods will be also applied into veterinary diagnostics within soon.

P887

Detection of papillary carcinoma in patients with chronic nodular autoimmunothyroiditis

K. Zaplatnikov1, **V. Soukhov**2; 1MAZ Clinic for Nuclear Medicine, Nürnberg, GERMANY, 2Military Medical Academy, ST. PETERSBURG, RUSSIAN FEDERATION.

OBJECTIVE: Multinodulary goiter as a consequence of autoimmune immunothyroiditis (AIT) Hashimoto type (HT) often associated with autonomous thyroid nodules (ATNs). Unfortunately it is not fully examined at a time and we have no even background understanding. Increased thyroid dysfunction in regions with low iodine supply and additional radiation exposure (eg., North Kazahstan Nuclear-weapon-tests region) led to increased incidence of AIT, papillary carcinoma (PC) and ATNs. This study exploited multimodal approach as combination of nuclear medicine data and laboratory characteristics of AIT and ATNs. MATERIALS AND METHODS: 411 patients - immigrants from North Kazakhstan that were lived in Germany between 2005 and 2013, with US-diagnosed goiter and thyroid nodules, and RIA-evidenced AIT, underwent full in-vitro examination, US with Doppler and scintigraphy. AIT patients with coexisting suspicious hypo functional nodes goiter was evaluated by FAB or histologically and verified (39 pts - Gr. A), pts with ATN and AIT (Gr. B, 23 pts) were compared with patients with group ATNs alone (group C, n=112) and typical AIT only (Gr. D - 237 pts). RESULTS: From the whole cohort of 411 patients 17 (11/6 F:M ratio; age 43±15 yrs) had multifocal papillary carcinoma (PC) and coexisting AIT HT, remaining in euthyreo/hypothyreosis state wiyh levels of TSH 1,0-12,00EU and TU 0,3-3,2%. There were only 6 PC patients in Gr. B with suppressed TSH (<0.01 mU/L) and typical scintgraphic signs of AIT. Hyperthyroidism/or subclinical hyperthyroidism signs not considered as AIT evidence were noticed in 37 pts of Gr. C. There were no histological confirmation of PC in any pts in Grs C and D. In group A there was shift to subclinical hyperthyroidism (76 vs. 24%), opposite to group

B (56 vs. 44%) (P=0.005). Maximal diameter of the ATNs was down to 8% smaller in group A as compared with group B. A positive correlation between nodule size and age was found only in group B (P=0.015). RESUME: Besides of very small difference in the size of nodules (non-statistic significance between groups A and B) chronic thyroid lymphocytic infiltration in presence of HT AIT may decrease the growth tendency of ATNs and reduce their functionality.

P888

Factors Influencing the Length of Remission Period in Patients with Graves' Disease

D. Šfiligoj1, S. Gaberšček1, P. Jaki Mekjavič2, K. Zaletel1, E. Pirnat1; 1University Medical Centre Ljubljana, Department of Nuclear Medicine, Ljubljana, SLOVENIA, 2University Medical Centre Ljubljana, Eye Hospital, Ljubljana, SLOVENIA.

AIM. Most patients with Graves' disease (GD) are initially treated with antithyroid drugs (ATD). In case of prolonged or recurrent disease, a definite treatment with radioiodine (RAI) usually follows. The reported relapse rate after the cessation of treatment with ATD is 51-68%. The aim of our study was to evaluate factors influencing the length of remission period in patients with GD, previously treated with ATD. MATERIALS AND METHODS. We reviewed medical records of 724 patients, first diagnosed with GD between 2005 and 2009, and later on treated with RAI. Patients failing to achieve remission during treatment with ATD were not included in the analysis. Patients with a period of GD remission after the cessation of ATD were empirically divided into two groups. Group 1 included patients in whom remission period lasted for 6 months or less and Group 2 included patients in whom remission period lasted for more than 6 months. RESULTS. We included 261 patients, 212 females and 49 males. In Group 1 we established 147/261 patients (56.3%) and in Group 2 114/261 patients (43.7%). With respect to age, patients in Group 1 were significantly older than in Group 2 (46.1±15.1 years, range 18-85 years and 41.0±13.1 years, range 18-75 years, respectively, p=0.003). Patients in Group 1 were initially treated with ATD for a significantly longer period of time than patients in Group 2 (12.0±3.7 months and 11.1±2.9 months, respectively, p=0.021), and had a larger thyroid volume at the onset of GD (20.5±11.9 mL and 17.2±9.6 mL, respectively, p=0.036). Regarding the level of thyroid hormones at the onset of GD, patients in Group 1 had significantly higher levels of free thyroxine (fT4) (57.0±26.6 pmol/L and 49.8±23.2 pmol/L, respectively, p=0.029) and free triiodothyronine (fT3) (22.0±8.0 pmol/L and 19.4±8.1 pmol/L, respectively, p=0.011), while the initial fT4/fT3 ratio did not differ between the two groups (p=0.430). Patients in Group 1 also had significantly higher levels of TSH receptor antibodies than patients in Group 2 (13.9±11.3 U/L and 9.5±7.0 U/L, respectively, p=0.005). CONCLUSION. Patients with the shorter remission period after the cessation of treatment with ATD were older, they have been initially treated with ATD for a longer period of time, had a larger thyroid volume, they were more severly hyperthyroid, and had higher levels of TSH receptor antibodies at the onset of GD as compared to patients with the longer remission period.

P889

Late single uptake measurement for accurate absorbed dose calculations in I-131 treatments of hyperthyroidism

K. S. Andreasson1, J. Svensson2,3, F. Henriksson2,3, P. Bernhardt4,3; 1Sahlgrenska University Hospital, Departments of Medical Physics & Biomedical Engineering, Gothenburg, SWEDEN, 2Sahlgrenska University Hospital, Department of Oncology, Gothenburg, SWEDEN, 3The Sahlgrenska Academy, University of Gothenburg, Gothenburg, SWEDEN, 4Sahlgrenska University Hospital, Department of Radiation Physics, Gothenburg, SWEDEN.

The administrated activity in I-131 treatment of hyperthyroidism is often based on individual dosimetry, where the estimated biologic half-life is calculated from two or more uptake measurements of a given test activity. However, from patient data a relationship between the measurement time (t) and the product of initial uptake and effective half times could be used for determine a linear coefficient (kt), sufficient for estimation of the absorbed dose by a single uptake measurement (Jönsson and Mattsson, 2003). This method seems to be reliable for one late uptake measurement, but more data are needed to confirm this statement. The aim of this study was to evaluate the precision of the single uptake measurement method. Method: This retrospective study is based on 300 patients with Graves' disease (n=100), multinodular goiter (n=100), and autonomous noduli (n=100). The percentage of women in all three groups is equivalent to the ratio of women with hyperthyroidism in the population (80 %). The treatment of these patients was based on individual dosimetry with two uptake measurements at 24h (n=300) and 4 days (n=156) or 6 days (n=144) after administration of 0.3 MBq I-131. For these measurement times the kt factor was estimated by linear regression. Results: The value and precision of the linear coefficient increased with measurement time points; k(24h)= 6.27 (r2=0.58), k(4d)=6.92 (r2=0.88), and k(6d)=7.38 (r2=0.97). No statistical significant difference in kt between sex and diagnosis was observed. Conclusion: We confirm the earlier statement that a late single uptake measurement is sufficient for accurate dosimetry, and preferably the uptake measurement should be performed as late as 6 days after the injection of the test activity. A single late uptake measurement can simplify the I-131 treatment for

patients and reducing the cost for the health care insurances, and could therefore be considered as an alternative approach for I-131 dosimetry.

P890

Patients with Different Types of Hypothyroidism have Different Biochemical Characteristics in Spite of Normal Thyrotropin Levels and Similar Weekly Dose of L-Thyroxine

S. Gaberscek1,2, B. Samec2, G. Setnikar2, E. Pirnat1, K. Zaletel1; 1Department of Nuclear Medicine, University Medical Centre Ljubljana, Ljubljana, SLOVENIA, 2Faculty of Medicine, University of Ljubljana, Ljubljana, SLOVENIA.

AIM. Most frequent causes of hypothyroidism are Hashimoto's thyroiditis (HT), treatment with radioactive iodine 131 (I-131), and thyroidectomy. For decades, monotherapy with L-thyroxine (L-T4) has represented the mainstay of treatment of hypothyroidism. However, little is known about the effectiveness and characteristics of this treatment in different types of hypothyroidism. MATERIALS AND METHODS. We reviewed records of all patients with most frequent causes of hypothyroidism treated with L-T4 between 2011 and 2013. In this study we only included patients with thyrotropin (TSH) levels inside the reference range (0.35-5.5 mU/L). Cumulative weekly dose of L-T4, levels of TSH, free thyroxine (fT4), and free triiodothyronine (fT3) were evaluated. The fT4/fT3 ratio was calculated. RESULTS. We included 498 patients with HT (Group 1), 24 patients after I-131 treatment (Group 2) and 34 patients after thyroidectomy (Group 3). According to ANOVA analysis, patients in the three groups significantly differed with respect to age (median (range), 53 (16-91), 48 (20-77), and 65 (38-87) years, respectively, p=019). However, they did not differ with respect to weekly dose of L-T4 (median (range), 350 (125-1050), 700 (175-1400) and 750 (175-1275) mcg, respectively, p=0.053). Patients in the three groups had significantly different TSH levels (median (range), 2.06 (0.35-5.48), 2.17 (0.36-5.44), and 1.61 (0.45-5.21) mU/L, respectively, p<0.001). Levels of fT4 were not significantly different (median (range), 16.2 (11-24.8), 19.1 (14.4-28.8), and 18.7 (13.8-25.5) pmol/L, respectively, p=0.597). Patients in the three groups had different levels of fT3 (median (range), 4.6 (2.1-6.5), 4.3 (3.5-4.8), 4.4 (2.9-5.5) pmol/L, respectively, p<0.001). Accordingly, patients in the three groups had different fT4/fT3 ratio (median (range), 3.5 (2.5-8.1), 4.5 (3.2-7.6), and 4.4 (2.5-6.1), respectively, p=0.011). Patients after I-131 treatment and patients after thyroidectomy had similar levels of fT4 and fT3 as well as similar fT4/fT3 ratio (p=0.658, p=0.137, p=0.775, respectively). Patients with HT and patients after I-131 had similar levels of fT4 (p=0.797), different levels of fT3 (p<0.001), and different fT4/fT3 ratio (p=0.037). Patients with HT and patients after thyroidectomy had similar levels of fT4 (p=0.497), different levels of fT3 (p<0.001), and different fT4/fT3 ratio (p<0.001). CONCLUSION. Patients with HT have different TSH and fT3 levels as well as different fT4/fT3 ratio in spite of TSH level within the reference range and similar weekly dose of L-T4 as compared to patients after I-131 treatment and patients after thyroidectomy. The difference is probably caused by the remaining thyroid function in HT patients.

P891

Patients Treated for Central Hypothyroidism have Different Biochemical Characteristics than Patients Adequately Treated for Hypothyroid Hashimoto's Thyroiditis

S. Gaberscek1,2, G. Setnikar2, B. Samec2, T. Kocjan3,2, E. Pirnat1, K. Zaletel1; 1Department of Nuclear Medicine, University Medical Centre Ljubljana, Ljubljana, SLOVENIA, 2Faculty of Medicine, University of Ljubljana, Ljubljana, SLOVENIA, 3Department of Endocrinology, Diabetes and Metabolic Diseases, University Medical Centre Ljubljana, Ljubljana, SLOVENIA.

AIM. In contrast to the widespread Hashimoto's thyroiditis (HT), central hypothyroidism (CH) is a rare condition. Patients with CH have otherwise normal thyroid gland, which is not sufficiently stimulated by thyrotropin (TSH. Unlike in patients with HT, in those having CH treatment with L-thyroxine (L-T4) cannot rely on TSH levels. Therefore, treatment of CH still represents a challenge. Our aim was to establish the adequacy of L-T4 treatment in CH.MATERIALS AND METHODS. In this retrospective study we included age-matched groups of consecutive patients treated with L-T4 because of HT or CT and compared them with healthy subjects (HS). Patients with HT and HS had TSH within the reference range (0.35-5.5 mU/L). Cumulative weekly dose of L-T4, levels of free thyroxine (fT4), and free triiodothyronine (fT3) were evaluated. The fT4/fT3 ratio was calculated.RESULTS. We included 40 patients with HT (Group 1), 40 patients with CH (Group 2) and 40 HS (Group 3). According to ANOVA analysis, subjects in the three groups did not differ with respect to age (median (range), 64 (26-86), 64 (26-87), and 65 (26-86) years, respectively, p=0.883). Subjects in the three groups had significantly different levels of fT4 (median (range), 18.1 (12.4-22.0), 15.6 (12.7-21.3), and 14.2 (11.0-18.9), respectively, p<0.001). Levels of fT3 were also different (median (range), 4.8 (2.1-5.7), 4.5 (2.7-5.9), and 4.9 (3.5-6.7), respectively, p=0.004). Subjects in the three groups had significantly different fT4/fT3 ratio (median (range), 3.7 (2.5-8.1), 3.7 (2.5-5.2), and 2.9 (2.0-5.2), respectively, p<0.001). In patients with HT, the weekly dose of L-T4 was significantly lower than in patients with CH (median

(range), 525 (175-1050) and 700 (350-1252), respectively, p=0.002). In spite of that, patients with HT had higher levels of fT4 (p=0.002), higher levels of fT3 (p=0.007), while the fT4/FT3 ratio was similar (p=0.747). In both treated groups of patients, levels of fT4 were significantly higher than in HS (p=0.003 and p<0.001, respectively). In CH but not in HT, levels of fT3 were lower than in HS (p=0.001 and p=0.245, respectively). In both treated groups of patients, the fT4/fT3 ratio was significantly higher than in HS (p<0.001 for both).CONCLUSION. Patients with CH have lower fT4 and fT3 levels in spite of higher weekly dose of L-T4 as compared to adequately treated patients with HT. The difference is probably caused by the remaining thyroid function in HT patients and by the inability to rely on TSH levels in patients with CH.

P892

The Role of Colour Flow Doppler Sonography in the Evaluation of Autonomous Thyroid Nodule Activity

K. Zaletel1, M. Jakič2, M. Jager2, E. Pirnat1, S. Gaberščeк1, 2; 1University Medical Centre Ljubljana, Ljubljana, SLOVENIA, 2University of Ljubljana, Ljubljana, SLOVENIA.

AIM. Colour flow Doppler sonography (CFDS) provides useful information on thyroid vascularity and activity in different thyroid diseases. The data in the literature on autonomous thyroid nodule vascularity before and after the treatment with radioactive iodine 131 (I-131) are scarce. Therefore, our aim was to evaluate the role of CFDS in the evaluation of autonomous nodule activity. MATERIALS AND METHODS. In our prospective clinical study, which was performed between October 2013 and April 2014, we enrolled 37 consecutive newly diagnosed hyperthyroid patients with autonomous thyroid nodule (29 females and 8 males), aged between 17 and 90 years (mean, 60.8±18.6 years). They were treated with activity between 737 and 979 MBq of I-131 (median, 920 MBq) without any concomitant treatment with antithyroid drugs. A day before I-131 treatment, we measured thyroid uptake of I-123. One day before and 3 months after I-131 treatment, we determined thyroid function and we ultrasonographically measured the volume of autonomous nodule. Additionally, we estimated the CFDS pattern value and measured the peak systolic velocity (PSV) of autonomous nodule and paranodular tissue at the level of intrathyroid arteries. We compared the measurements before and after I-131 treatment and determined associations between variables. RESULTS. Autonomous thyroid nodule had higher CFDS pattern value (p<0.001) and higher PSV (14.44±4.87 cm/s and 9.24±2.53 cm/s, respectively, p<0.001) than paranodular tissue. A correlation between autonomous nodule PSV and paranodular tissue PSV was positive (R=0.779, p<0.001). Thyroid uptake of I-123 varied between 9.37 and 46.85% (mean, 23.63±9.59%). PSV of autonomous nodule was positively associated with I-123 uptake (Beta=0.651, p=0.007), but not with age, thyroid hormones or nodule volume. After I-131 treatment, thyroid function significantly improved (TSH 1.66 mU/L compared with 0.045 mU/L before treatment, p<0.001), and nodule volume significantly reduced (4.82±5.81 mL compared with 10.35 ±9.95 mL before treatment, p=0.003). A significant decrease in both CFDS pattern (p<0.001) and PSV (9.38±3.29 cm/s compared with 14.44±4.87 cm/s before treatment, p<0.001) of autonomous nodule was observed. In paranodular tissue, we found a significant increase in both CFDS pattern (p<0.001) and PSV (11.13±2.67 cm/s compared with 9.24 ±2.53 cm/s before treatment, p=0.003). We determined a negative correlation between PSV and the applied activity of I-131 (R=-0.496, p=0.003). CONCLUSION. On the basis of our findings we may assume that CFDS provides additional useful information in the evaluation of autonomous nodule activity and effectiveness of I-131 therapy.

P893

Predictors of outcome in radioiodine treatment of Graves' disease

M. Silva1, L. Cardoso2, R. Silva1, L. Pires1, F. Rodríguez1, N. Vicente2, P. Lapa1, G. Costa1, F. Carrilho2, J. Pedroso de Lima1; 1Serviço de Medicina Nuclear do Centro Hospitalar e Universitário de Coimbra, Coimbra, PORTUGAL, 2Serviço de Endocrinologia, Diabetes e Metabolismo do Centro Hospitalar e Universitário de Coimbra, Coimbra, PORTUGAL.

Aim: Graves' disease (GD) is a common thyroid disorder. Radioiodine is a reliable and cost-effective therapy choice. However, there are several factors that can influence the clinical outcome. The aim of this study is to identify predictors of therapeutic outcomes.Material and methods: Patients with GD, submitted to radioiodine therapy between October/2002 and April/2014 and with a follow-up longer than 12 months were selected. We found 143 patients (116 females, 27 males; age: mean 42.5±15.3yr, range 13-81yr). All patients were assessed before (laboratorial and ultrassonographic thyroid status), and at 3, 6 and 12 months after radioiodine treatment (laboratorial thyroid status). Antithyroid drugs (ATD) were routinely discontinued at least 1 week before radioiodine and therapeutic activity was calculated based on 24h radioiodine uptake (24h-RIU) and thyroid mass (TM). Several variables were recorded: age, gender, type of ATD used, antithyrotrophin-receptor antibody (TRAb), nodules larger than 10mm, 24h-RIU, functioning TM, heterogeneity in radioiodine distribution and administered therapeutic activity. Therapy success was defined as a euthyroid or hypothyroid status without the need for additional radioiodine or ATD.

Variables were analyzed to identify the potential predictive factors for therapeutic failure. Influence of those variables on the rate of hypothyroidism at 3, 6 and 12 month after treatment was also evaluated. All statistical analyses were carried out using SPSS-version-22. A $p<0.05$ was considered significant for all statistical tests. A multivariable analysis, including all previous statistical significant variables, was performed.Results: Overall success rate (euthyroidism or hypothyroidism) was 80.4 % (115/143). Herein, 43.2% (48/115) developed hypothyroidism at 3 months, 72.4% (84/115) at 6 months and 87.0% (100/115) at 12 months. The 19.6% (28/143) unsuccessful cases showed a significantly higher TRAb values, TM and radioiodine activity than successful ones (respectively: 48.2U/L vs. 20.0U/L; 77.8g vs. 48.1g; 517MBq vs. 398MBq). Age, gender, type of ATD, nodules >10mm, 24h-RIU, radioiodine heterogeneity distribution and therapeutic activity were not statistically significant. We found a statistical significant relationship between age and hypothyroidism development at 3 months. The rate of hypothyroidism in the first 3 months after radioiodine therapy was significantly higher in younger patients ($p=0.018$). In the multivariable analysis only TM remained as statistically significant.Conclusions: Radioiodine is very effective in GD, even in patients previously submitted to ATD. Patients with higher TRAb titres and larger thyroid glands have a lower probability of remission with just one radioiodine course. On the other hand, hypothyroidism shortly after treatment often develops in the youngest.

P894

Prevalence of normal TSH levels in patients with thyroid autonomy detected by thyroid scintigraphy.

G. Treglia1, P. Trimboli2, F. Verburg3, M. Luster4, L. Giovanella1,2; 1Department of Nuclear Medicine, Oncology Institute of Southern Switzerland, Bellinzona and Lugano, SWITZERLAND, 2Thyroid Center, Ente Ospedaliero Cantonale, Bellinzona and Lugano, SWITZERLAND, 3Department of Nuclear Medicine, University Hospital of Aachen, Aachen, GERMANY, 4Department of Nuclear Medicine, University Hospital of Marburg, Marburg, GERMANY.

Background: International guidelines diverge significantly about the usefulness of thyroid scintigraphy (TS) in patients with nodular goiter. Particularly its role in detecting/excluding autonomously functioning thyroid nodules (AFTN) in patients with normal serum thyrotropin (TSH) is widely debated. Therefore we assessed the prevalence of normal TSH values among patients with AFTN detected by TS performed in our Center. Furthermore we carried out a meta-analysis of the literature to evaluate the usefulness of TS in European patients with AFTN and normal TSH values. Methods: We included patients with AFTN detected by TS and enrolled at the Thyroid Center of Southern Switzerland. Prevalence of AFTN with normal TSH values was calculated. Furthermore a comprehensive literature search of European studies published until 2014 on AFTN detected by TS was performed and a meta-analysis on the prevalence of patients with AFTN and normal TSH values was carried out. Results: 110 patients with AFTN enrolled at our Center and 2662 European patients with AFTN described by six articles were selected for the meta-analysis. Prevalence of patients with AFTN and normal TSH was 35% in our Center. Pooled prevalence of AFTN detected by TS with normal TSH was 45% (95% confidence interval: 27-64%) on a per patient-based analysis. Conclusions: Serum TSH measurement is not an effective screening test to diagnose AFTN, at least in Europe, as a significant proportion of patients with AFTN detected by TS had a normal TSH value. TS remains the only technique that permits the diagnosis of thyroid autonomy which does not require invasive procedures.

P895

The role of combined single-isotope dual-phase scintigraphy with 99mTc -tetrofosmin with SPECT technique in minimal invasive parathyreoidecomy

M. Yaneva, A. Botushanowa; UMBAL St.George Plovdiv, PLOVDIV, BULGARIA.

Preoperative parathyroid scintigraphy is highly beneficial for reduction of the duration and extent of surgery in the commonly used nowadays minimal invasive parathyroidectomy. Aim: To evaluate the diagnostic value of combining single isotope dual-phase scintigraphy with 99mTc -tetrofosmin with SPECT technique in preoperative evaluation of patients with hyperparathyreodism. Materials and methods: 26 patients from 38 to 62 years of age were included in the study. Of these 22 were women and 4 men. Elevated levels of serum calcium and parathyroid hormone were registered in all of them. The examination was conducted on a dual-headed SPECT gamma camera SIMBIA using protocol for single-isotope dual-phase technique with 99mTc -tetrofosmin. Patients were injected with 740 MBq 99mTc -tetrofosmin, after which planar images were taken at an early phase / 20 min / and late phase / 120 min /. SPECT registration of the neck and upper thorax was performed after the early phase. Results: Hyperfunctioning parathyroid glands were registered in 14 patients in both phases and on the SPECT images as well. Areas suspicious for abnormal parathyroid glands were visualized in the early SPECT images in 5 patients, which were not registered in the late phase. This may be due to early washout of the radionucleotide.All 19 patients undergone surgical exploration. In 18 of them a parathyroid adenoma was found. Conclusions: Combining both techniques provides complementary information for the localization of abnormal parathyroid

glands, does not expose the patients with additional radiation and is easy to perform technically and increase sensitivity.

P896

Subacute Thyroiditis Management and Follow-up with use dual scintigraphy modality

V. Soukhov1, K. Zaplatnikov2; 1Military Medical Academy, ST. PETERSBURG, RUSSIAN FEDERATION, 2MAZ Clinic for Nuclear Medicine, Nürnberg, GERMANY.

Aim: This study was the next step evaluation of relationship between accumulation of Technetium-99m (Tc-99m) tetrofosmin (TF) in thyroid gland for staging of subacute thyroiditis (SAT) as well as assessment of response to therapy. Material and methods: We performed 747 studies in 266 patients with SAT using 99mTc-pertechnetate scintigraphy and 99mTc-tetrofosmin imaging before prescribing of therapy, during treatment and follow-up. Tc-99m-TF scans were interpreted both visually and quantitatively before treatment, within therapy course (2-6 weeks) and in early and delayed follow-up. Results: Clinical signs of thyrotoxicosis: fever, tremor of extremities, unexplainable fears and painful goitre - were seen in all cases. That first stage of SAT was concordant with significantly poorer uptake of 99mTc-pertechnetate in thyroid (close to background). At the same time 99mTc-TF thyroid images showed diffuse increased uptake at 10 min and 1,5-2 hours p.i. The thyroid-to-background uptake ratio of tetrofosmin was associated with the stage of SAT: slope of clearance curves in the acute stage and in the recovery differed appr. twice. The uptake ratio assessed as thyroid-to-background uptake correlated with the serum concentrations of biochemical substances and immunological data. Resume: Use of Tc-99m-TF thyroid scan procedures in patients with SAT is significantly diagnostically and prognostically helpful for staging and treatment of inflammatory process in a glabd. 99mTc-TF uptake may serve as an indicator of SAT's activity and help to manipulate with therapy strategy according to states severity of the inflammation process.

P897

Clinical Value of I-131 SPECT/CT over planar imaging in Detecting Metastases in Patients with Differentiated Thyroid Carcinoma

W. Yao, Y. Wang, N. Chiu, C. Hung; College of Medicine, National Cheng Kung University, TAINAN, TAIWAN.

Aim: I-131 planar whole body scan (WBS) is routinely used for detecting metastases of differentiated thyroid carcinoma (DTC). However, the WBS is limited by lacking anatomic landmark and characteristic findings. We investigated whether a hybrid SPECT/CT may have additional value over planar imaging in detecting metastases in DTC patients. Materials and methods: In a two-year period, 319 thyroidectomized DTC patients (65 men and 254 Women, aged 20-83 years) received I-131 WBS a week after an ablative or therapeutic dose of I-131. Patients with focal uptakes on WBS had additional focal SPECT/CT. The final diagnosis was proved by pathology and diagnostic images. Results: Among 319 WBSs, 104 foci of uptake were detected in 60 patients. All 104 focal uptake and additional 21 uptakes were localized by SPECT/CT. Eighteen uptakes were regarded as physiological uptake: 7 in GI tract, 2 in urinary bladder, 3 in endometrium, 1 in lacrimal gland and 5 contaminations. Thirty-three uptakes represented benign lesions, including: 17 uterine cervix, 3 renal cysts, 3 thymus, 2 sinusitis, 2 myomas, 1 parotid sialoadenitis, 1 bronchiectasia, 1 prostate, 1 cystic teratoma, 1 ovarian cyst, and 1 benign bone lesion. The remaining 74 uptakes were characterized as metastases, including: 57 in lung, 15 in bone, and 2 in abdominal wall. In addition, patients with metastases had higher serum TG levels than with physiologic uptake and benign lesions (117.8 vs. 4.6 and 2.2 ng/mL, $p<0.001$). Conclusion: SPECT/CT may correctly localize and characterize focal uptake on I-131 WBS, detect more lesions, help to differentiating between physiologic uptake, benign lesions and metastases, and permits appropriate therapeutic approach for DTC patients.

P898

Evaluation of Radioiodine Therapy with an Adapted Dosimetric Approach in Patients with Hyperthyroidism

A. Fernandes1, T. Faria1, P. Coelho1, J. Casalta-Lopes2,3, A. Oliveira1, V. Alves1, A. Pinto1, M. Pérez1, T. Vieira1, J. Pereira1; 1Centro Hospitalar São João, Porto, PORTUGAL, 2Centro Hospitalar e Universitário de Coimbra, Coimbra, PORTUGAL, 3Faculdade de Medicina da Universidade de Coimbra, Coimbra, PORTUGAL.

Aim: The recommended activities for the treatment of hyperthyroidism associated with benign thyroid disorders are subject to discussion, as is the use of a fixed approach over a dosimetric one. We aim to evaluate the 1-year-treatment success rate at our department using a dosimetric approach that considers 24-hour radioiodine uptake, and thyroid mass estimation, as well as 2 and 4h radioiodine uptake, diagnosis, gender, age, and clinical history. We also evaluated success rates differences between lower and higher activities. Materials and Methods: We reviewed data from all patients (n=133) treated with radioiodine therapy (RIT) for hyperthyroidism at our department, from January 2008 to March 2014, including 74 patients with Graves Disease (62.2%), 23 with

toxic multinodular goiter (19.3%), 15 with solitary hyperfunctioning thyroid nodules (12.6%), 5 with toxic adenomas (4.2%) and 2 with toxic diffuse goiter (1.7%). Patients without follow-up in our institution (n=18) were excluded. RIT was considered successful if euthyroidism or hypothyroidism were achieved. All statistical analyses were carried out using IBM SPSS version 20.0 for Mac. A type I error 0.05 was considered. Results: 115 patients were included. 102 (87.4%) were submitted to only one therapy, and 13 (12.6%) to two. From the latter, only two remained with hyperthyroidism. Regarding treatment response, 91 (79.1%) succeeded, while 24 (20.9%) remained hyperthyroid after one RIT. The activities used varied between 148 MBq and 703 MBq, (388.5 ± 135.1 MBq). There were no significant differences between the lower and higher activities used (p=0.879). Conclusion: Our results confirm RIT effectiveness in hyperthyroidism treatment, with success rates of 79.1% with only one treatment. Mean activities used in our department were inferior to those generally prescribed, irrespective of the method used (200-800 MBq, with the majority of patients receiving 400-600 MBq). Though we used inferior activities, we achieved high success rates one year after treatment, comparable to the best in literature. There were no significant outcome differences between the lower and the higher activities used. These results suggest we should take into careful consideration each patient singularities to warrant the best therapeutic outcome, avoiding unnecessary exposure.

P899

Middle-Term Outcome and safety of hyperthyroid patients treated with calculated activity of radioiodine

A. Campenni'1, E. Amato1, M. Murè1, F. Di Mauro1, M. Stipo1, G. Cabbanè1, V. Gangemi1, M. Bertia1, M. Cucinotta1, M. Ruggeri2, S. Baldari1; 1Nuclear Medicine Unit of Messina, Messina, ITALY, 2Department of Clinical and Experimental Medicine, Endocrinology Section, University of Messina, Italy, Messina, ITALY.

Aim: Radio-iodine-treatment (RaIT) is a well-established method for treatment of hyperthyroidism due to Graves' disease (GD), toxic adenoma (TA), toxic multinodular goiter (TMG).The optimal 131-Iodine (131I) activity to be administered is still debated.We report our experience with calculated activity of 131I.Materials and Methods: Sixty-nine (16 GD, 39 TA, 14 TMG) patients [44 females and 25 men; mean age 64.2 ±12.6 years] were enrolled. All but 17 patients (24.6%) were overtly hyperthyroid and 41 (59.4%) had received anti-thyroid drugs, withdrawn 5-10 days before RaIT. Twenty patients were anti-thyroid antibody positive. All patients underwent: a) Thyroid Scintigraphy (TS) and Radioiodine-Thyroid-Uptake (RTU) measurements from 3 to 168 hours after 131I administration (1.8 MBq); b) thyroid ultrasonography (TU), to calculate the volume of "hot" thyroid nodule(s) or of the whole gland. In TMG and TA patients, the "effective" volume of the hot nodule(s) was calculated subtracting the volume of involution area(s).Mean RTU was 49.1±13.8%. Therapeutic activity was calculated by Snyder formula modified according to "effective" volume. In 11 patients with TMG the activity was calculated for all "hot" nodules. Mean administrated activity was 303±135.4 MBq and mean adsorbed dose was 223±48.6 Gy. Mean follow-up was 47.4±16.9 months.Results: Fifty patients became euthyroid within a mean of 3.2±2 months after RaIT. Fourteen patients developed overt hypothyroidism within a mean of 5.6±5.0 months. Two women (TMG and GD) developed sub-clinical hypothyroidism respectively 12 and 16 months after RaIT. Other 3 patients with GD showed recurrence of hyperthyroidism after 2 months and underwent a second RaIT (with standard activity). TS was performed in 34 TMG or TA patients about 3 months after RaIT, demonstrating partial (22 patients) or total (12 patients) ablation of the "hot" area(s). In 15 patients with TA, the TU performed 4 months after RaIT showed a significant reduction of the nodule volume (p 0.03). No side effects were observed during follow-up.Conclusions: Calculated activity of 131I permitted to obtain euthyroidism in 50/69 (72.5%) patients [in 48/53 (90.6%) patients considering only TA and TMG cases]. The cure-rate was higher (95.6%) if we consider hypothyroidism as a successful outcome. In an our previous experience with standard activity of 131I we found a lower cure-rate, despite a significantly higher administered activity (mean 541 MBq *vs* 303 MBq; p<0,05). It follows that calculated activity will correspondingly reduce both the dose absorbed by "critical organs" (stomach, bladder) and the radiation exposure to other people.

P900

Predictive value of pyramidal lobe, % thyroid uptake and age for ablation outcome after 15mCi fixed dose of radioiodine-131 in Graves' disease

M. u. Zaman1, N. Fatima2, U. Zaman3, Z. Sajjad1, A. Zaman3, R. Tahseen3; 1AKUH, Karachi, PAKISTAN, 2Dr Ziauddin Hospital, Karachi, PAKISTAN, 3Dow University of Health Sciences (DUHS), Karachi, PAKISTAN.

Objective: Aim was to find out efficacy of a fixed 15 mCi radioactive iodine-131 (RAI) dose and predictive values of various factors for inducing hypothyroidism in patients with Graves' disease (GD). Methods: This was a retrospective study conducted from January 2012 till August 2014. Records of all patients with GD treated with RAI were evaluated. Patients who had a Tc-99m thyroid scan, thyroid antibodies, received fixed 15 mCi RAI and did follow endocrine clinics for at least 6 months were selected. Patients with GD who did

not meet these criteria were excluded. RAI was considered successful if within 06 months of RAI therapy patients developed hypothyroidism. Results: Out of 370 patients with GD who had RAI during study period, 210 (57%) qualified study criteria. Mean age of patients was 48 ± 15 years with female: male ratio of 69:31, positive thyroid antibodies in 61%, means thyroid uptake of 15.09 ± 11.23% and presence of pyramidal lobe in 40% of total population. Within 06 months after RAI therapy, 161 (77%) patients developed hypothyroidism while 49 (23%) patients failed to achieve it (remained hyperthyroid or euthyroid on antithyroid medication). Patients who became hypothyroid were significantly younger with higher proportion of presence of thyroid antibodies and pyramidal lobe and lower % thyroid uptake on thyroid scan than those who failed. Multiple logistic regression analysis revealed that age (odd ratio; OR= 2.074), pyramidal lobe (OR = 3.317), thyroid antibodies (OR = 8.198) and % thyroid uptake (OR = 3.043) were found to be significant prognostic risk factors for post-RAI hypothyroidism within 06 month. Gender was not found to have any significant association with the development of post-RAI hypothyroidism. Receiver operating characteristic (ROC) analysis revealed age <42 years and thyroid uptake <15% as threshold values for the development of post-RAI hypothyroidism. Conclusion: We conclude that fixed (15 mCi) RAI dose is highly effective in rendering hypothyroidism in patients with GD. Age (≤42 years), thyroid uptake (≤15%) and presence of pyramidal lobe are strong predictors of hypothyroidism and must be considered for selecting optimal RAI dose.

P901

99mTc-MIBI SPECT/CT in patients with hyperparathyroidism and the relationship between uptake ratio and serum PTH, calcium as well as volume of lesion

Z. Cheng, S. Zou, **X. Zhu**; Department of Nuclear Medicine & PET, Tongji Hospital, Tongji Medical College, Huazhong University of Science and Technology, Wuhan, CHINA.

Objectives: This study aimed to compare the diagnostic efficiency among of ultrasound, 99mTc-MIBI scintigraphy and SPECT/CT for hyperparathyroidism, investigate the relationship between 99mTc-MIBI uptake and biochemical features, including preoperative serum PTH, calcium levels as well as volume of lesion in patients with hyperparathyroidism. Patients and Methods: 60 patients with hyperparathyroidism were retrospectively enrolled. A Dual-phase 99mTc-MIBI planar scintigraphy and delayed SPECT/CT, ultrasonography were performed after calcitonin treatment. The pathologic volume (Vp) of the lesion was measured after parathyroidectomy. Then 34 primary hyperparathyroidism patients were selected with scintigraphy positive but ultrasonography showing no sign of thyroid nodule. Mean uptakes of surgery confirmed parathyroid lesion and mean uptakes of contralateral thyroid tissue were measured to calculate the parathyroid lesion-to-background ratio (T/NT) on dual-phase 99mTc-MIBI planar scintigraphy and SPECT/CT images. The biochemical features, including preoperative serum PTH and calcium levels before and after calcitonin treatment were also evaluated. Results: Surgery confirmed 63 lesions of 58 patients including 87.30%(55/63) parathyroid adenoma, 11.11%(7/63) parathyroid hyperplasia and 1 parathyroid carcinoma, 2 patients with nodular goiter and normal parathyroid tissue. All 3 ectopia parathyroid adenomas were displayed by parathyroid scintigraphy, but only one of them was detected by ultrasonography. The sensitivity and positive predictive value of the ultrasonography, dual-phase 99mTc-MIBI planar scintigraphy and delayed SPECT/CT for preoperative localization of hyperparathyroidism lesion were 68.97%(40/58), 79.31%(46/58), 86.21%(50/58) and 95.24%(40/42), 97.87%(46/47), 96.15%(50/52), respectively. Serum calcium significantly decreased after calcitonin treatment ($p<0.01$). T/NT in delayed phase was significantly higher than that of early phase ($p<0.01$). T/NT in both early and delayed phase and SPECT/CT significantly correlated with Vp, serum PTH and initial calcium ($p<0.05$), but not correlated with the calcium after calcitonin treatment. Vp significantly correlated with serum PTH and initial calcium ($p<0.05$). Conclusions: The sensitivity of dual-phase 99mTc-MIBI planar scintigraphy and delayed SPECT/CT for preoperative localization of hyperparathyroidism lesion are higher than ultrasonography, especially in the cases of ectopia parathyroid adenoma. Uptake ratio of hyperparathyroidism lesion significantly correlated with volume of lesion, serum PTH and calcium so that preoperative 99mTc-MIBI SPECT/CT can be a good image modality to evaluate disease severity quantitatively. Calcitonin treatment may not affect the uptake ratio of hyperparathyroidism lesion.

P60 - Tuesday, October 13, 2015, 4:00 PM - 4:30 PM, Hall 3 – Poster Exhibition

Conventional & Specialised Nuclear Medicine: Paediatric Uronephrology

P902

Contribution of diuretic renal scintigraphy with 99mTc-MAG-2 to surgical indication in infants with antenatal hydronephrosis.

C. Gamazo Laherrán, J. Villanueva Curto, A. Cobo Rodriguez, A. Sainz-Esteban, M. González Selma, M. Ruiz Gómez, R. Olmos García; HOSPITAL CLINICO UNIVERSITARIO DE VALLADOLID, VALLADOLID, SPAIN.

AIM: To assess the contribution of diuretic renal scintigraphy with 99mTc -MAG-2 to surgical indication for treatment in infants with antenatal hydronephrosis. METHODS: We include 36 infants referred to our department (24 male and 12 female, mean age: 4,4 months) who had been diagnosed by ultrasound of antenatal hydronephrosis (unilateral in 25 and bilateral in 11, a total of 47 pathological kidneys). All patients underwent a 40 minutes diuretic renal scintigraphy after the intravenous administration of 3,7 MBq/kg of 99mTc -MAG-2 and the later diuretic furosemide stimulation. Prenatal and postnatal ultrasound were indicated in all cases, characterizing as causes of hydronephrosis ureteropelvic junction stenosis in 20 cases, megaureter in 8, ureterocele in 4 and 15 from other causes. Renographic curve pattern was classified after images evaluation in obstructive, partially obstructive and non-obstructive. RESULTS: Twenty-three out of 47 hydronephrotic kidneys confirmed by postnatal ultrasound in different degrees according to renal pelvis dilatation, presented in the scintigraphy an obstructive pattern, 9 a partially obstructive and a 15 non-obstructive pattern. Three kidneys presented duplex collecting system associated (2 of them within the obstructive group and the other one within the non-obstructive group). Eighteen out of 23 obstructive kidneys, underwent surgery (78%) and 5 are currently pending intervention. Of the 9 kidneys with partial obstructive pattern, 5 had surgery. Only one out of 15 kidneys with non-obstructive pattern had a surgical treatment due to severe renal hypofunction and 4 resolved spontaneously. The surgical technique used in the 24 kidneys depended on the etiology of hydronephrosis in each case, performing 15 pyeloplasties, 3 expansions, 3 heminephrectomies (corresponding to duplex collecting system) and 3 interventions by other techniques. CONCLUSION: Diuretic renal scintigraphy is a simple protocol that provides both functional and anatomic information with relatively low radiation dose to the patient. When combined with ultrasound study, diuretic renal scintigraphy can be used to determine the need for surgery especially in patients with an obstructive pattern due to an ureteropelvic junction stenosis.

P903
Preliminary Validation of Blood-Pool Compensation Method for Assessment of Relative Renal Uptake in Children

M. Samal1, A. Brink2, M. J. Wesolowski3, C. A. Wesolowski3; 1Charles University Prague, Prague, CZECH REPUBLIC, 2Red Cross War Memorial Children's Hospital, Cape Town, SOUTH AFRICA, 3University of Saskatchewan, Saskatoon, SK, CANADA.

In dynamic renal scintigraphy, relative renal uptake is measured by several techniques with recent dominance of integral and Patlak-Rutland (PR) methods. In 2013, Wesolowski et al introduced the new method for determining split renal function based on a simple plot of the renal curve against the curve measured over blood-pooling organs such as the heart, liver, or spleen. During uptake interval, the plot demonstrates a linear segment that is back extrapolated to zero counts in the blood-pooling organ (intercept with vertical axis). The intercept is proportional to single-kidney function and is used to calculate split renal uptake. Compensation for vascular background is intrinsic to the method. The method was recently validated in adults with good results. The aim of our study was to test performance of the method in children. Methods: 172 dynamic renal studies (128x128 images recorded in 15s intervals for 40 minutes) with 99mTc-MAG3 in children of various age and renal function collected for inclusion into the database www.dynamicrenalstudy.org were analyzed. Relative renal function was measured by PR as a reference. Blood-pool compensation (BPC) method was applied with the heart (BPC-H) and the liver (BPC-L) ROI curves. No background was subtracted prior to analysis. The results of all three methods (PR, BPC-H, BPC-L) were highly correlated (0.9986 - 0.9995). Mean absolute difference between PR and BPC-H was 0.5 ± 0.6 % ($p > 0.05$) and between PR and BPC-L 1.0 ± 1.0 % ($p > 0.05$). Mean absolute difference between BPC-H and BPC-L was 0.9 ± 1.1 % ($p > 0.05$). Maximum absolute difference between PR and BPC-H was 3.9 %, between PR and BPC-L 4.7 % and between BPC-H and BPC-L 7.2 % (all in the patients with poor unilateral or total renal function). Conclusion: Preliminary results in children confirm previous good results in adults. The new, technically simple method provides the values of relative renal function that are practically identical to those provided by Patlak-Rutland plot. One of the advantages of the new method is freedom of choice of blood pooling organ in case the heart is outside the field of view while preserving intrinsic subtraction of vascular background. It can be also used in parallel with other techniques as simple but efficient quality control tool.

P904
Importance of Vesicoureteral Reflux Detected During Routine 99mTc-MAG3 Renal Scintigraphy in Pediatric Patients

N. C. M. Gulaldi, N. Altun Yologlu, S. Ozyurt; Department of Nuclear Medicine, Dr. Sami Ulus Maternity and Children's Health and Diseases Training and Research Hospital, ANKARA, TURKEY.

Aim: The aim of the study is to investigate the importance of vesicoureteral reflux (VUR) detected on routine 99mTc-MAG3 renal scintigraphy compared to VCUG (voiding cystourethrography) in pediatric patients. Methods: Eighteen

patients (5 female, 13 male) in whom VUR episodes were detected on routine renal scintigraphy were included into the study (1-113 months, mean=16,5±31 months) Dynamic 99mTc-MAG3 renal scintigraphies were performed in all patients to reveal any obstruction at collecting systems or to measure renal functions because of antenatally detected hydronephrosis. All patients had VCUG within 3 months of renal scan. Indirect VUR episodes were detected on scintigraphy from cine display and from ROI's drawn over ureter and pelvicalyceal systems. Spontaneous micturation during the study into the diaper was used as a triggering event for detecting VUR with cine display or quantitative approach. Results: Ten patients with VUR detected on dynamic renal scintigraphy were also diagnosed as VUR on VCUG. While 9 of these patients had Gr III-IV reflux, only 1 patient had Gr I-II reflux on VCUG. Lateralization of the VUR was exactly the same in concordant patients (3 left side, 2 right side and 2 bilateral) (positive predictive value is 100%), while VCUG also revealed VUR in contraletal side in 3 patients. 2 patients didn't make micturation during the study and showed VUR during the filling phase of bladder. Rest of 8 patients with VUR episodes detected on scintigraphy did not reveal any reflux sign in VCUG. These patients were between 1-6 months old and all VCUG examinations were done after the renal scintigraphy. This situation gave rise the suspicion of naturally resolving reflux between the exams which are predicted within this age group especially in low-grade reflux. Conclusions: Our study suggested that careful examination of late part of 99mTc-MAG3 renal scintigraphy can give complimentary and valuable information to the refering physician if it reveals any unknown high-grade VUR in patients with hydronephrosis. If there is backward activity to ureters and to renal collecting systems, it should be included into the scintigraphy report to alert physician for the possibility of VUR to prevent further renal function deterioration. VCUG is the gold standard for the first diagnosis and indirect and direct radionuclide cystography should be used for the follow-up of patients. VUR detected on routine renal scintigraphy should only be regarded as a varrant for the further evaluation.

P905

Invalidity of Gates method to assess renal function in children

V. Markovic1,2, **D. Eterovic**1,2, A. Punda1,2, Z. Antunovic3; 1University Hospital Split, Split, CROATIA, 2School of Medicine, University of Split, Split, CROATIA, 3Department of Physics, Faculty of Science, University of Split, Split, CROATIA.

AIM: The gamma camera early kidney uptake of Tc-99m-DTPA- the Gates method of measuring glomerular filtration rate (GFR) demonstrated limited value in majority of evaluation reports. Still, owing to its simplicity, the method is offered in many commercial gamma camera software packages. We noticed that the problems with the method may be especially exacerbated in children and addressed the issue systematically. MATERIALS AND METHODS: In the consecutive group of 102 patients (51 were females) with wide range of age (2 months-87 years) and renal function (14-155 ml/min/1.73 m2) GFR was concurrently assessed by the Gates method (GFRG) and the single sample Tc-99m-DTPA plasma clearance method (GFRss; reference method). The primary descriptors were systematic error-bias (mean percentage difference between GFRG and GFRss) and random error-precision (standard deviation of those percentage differences). The percentages were used to account for proportional error (errors in GFRG increased with increasing GFR). The secondary descriptors were the outputs of the regression analyses, both linear (correlation coefficient (r) and root-mean squared error (RMSE)) and non-linear. RESULTS AND CONCLUSION: With respect to age the error of the Gates method sharply increased for children aged 13 years or less. In the older group the Gates method underestimated GFR (bias = -29.4%) with substantial variability (precision = 18.2%). In this group the relation between GFRss and GFRG was apparently bilinear (the percentage underestimation error increased at the cut-off point of 60 ml/min; overall $r = 0.83$, $p<10\text{-}6$). Therefore, slightly better than linear, was the following regression equation: GFRss = -96.9 + 106 x log (GFRG). This rescaling reduces the bias, but not the random error (RMSE = 15.4%). In case of children younger than 13 years the Gates GFR estimates were both large and variable overestimations (bias = 77%, precision = 87%) in poor correlation with the reference standard ($r = 0.15$, $p=0.29$). Thus, for patients over 13 years of age the Gates method has some, but limited validity (comparable performances were reported for serum creatinine-based GFR estimations) and is completely unreliable for younger children.

P906

Impact of 99mTc-DMSA scan during acute phase of pyelonephritis

S. E. Bouyoucef, M. Habbeche, S. Benadda, A. Bellabes, B. Abdi, K. Chentli, A. Khelifa; Department of Nuclear Medicine CHU Bab El Oued, Algiers, ALGERIA.

Objectives: To evaluate the role of 99mTc-DMSA scan vs Ultrasonography during the acute phase of pyelonephritis. Patients and methods: 197 children aged from 1 month to 14 years underwent 99mTc-DMSA scan for assessment of an acute pyelonephritis (PNA). 68% were under 5 years and 60% were girls. Diagnostic of PNA has been made on clinical

signs, biological parameters and positive urine bacterias. Results: In 91 children (46%), 99mTc-DMSA scan was positive showing kidney scars meanwhile US was totally normal. Both 99mTc-DMSA scan and US were negative in 53 children (26%). US was positive in 55 children by showing parenchyma reduction patterns of hydronephrosis, ureterohydronephrosis, horse kidner or kidney duplicity. In those children, 99mTc-DMSA scan showed scars only in 33 children. In a sub group of 21 children with a vesico-ureteral reflux, 99mTc-DMSA scan showed evidence of kidney infection in 18 of them meanwhile US was positive only in 7. During the follow up of 45 patients with positive 99mTc-DMSA scan, a new 99mTc-DMSA scan showed a critical improvement in 22, slight improvement or stabilization in 23. In this group of children, US showed no changes. Discussion: 99mTc-DMSA scan is more performed during the assessment of the initial stage of PNA. The role of US is to assess the morphological features of the urinary tract but has a little impact in the management of PNA.

P907

The Four Year Experience of Congenital Hydronephrosis in the Single Centre of Nuclear Medicine from the North-Eastern Region of Romania

I. C. Grierosu, **Sr**.1,2, M. Starcea3,2, M. Munteanu3, R. Russu3, A. Rotaru3, A. Statescu1, R. Gherasim1, S. Atudosie2, V. Ghizdovat1,2, I. Miron3,2, C. Stefanescu1,2; 1Emergency Clinical Hospital Sf. Spiridon, Iasi, ROMANIA, 2Faculty of Medicine, Iasi, ROMANIA, 3Emergency Hospital for Children Sf. Maria, Iasi, ROMANIA.

Aim: We wish to share our experience and results of the collaboration between two departments (Nuclear Medicine and Pediatric Nephrology Department), from two major Public Hospitals of North-Eastern region of Romania, Moldavia region, regarding congenital hydronephrosis. Materials and methods: The study is a retrospective one and was realized on a four year period of time (2011 - 2014), meaning 158 cases of congenital hydronephrosis at children (under 18). From these, we counted only 137 cases for which there was maximum two days between the creatinine dosage and the DTPA scintigraphy. The patients were classified according with age, sex and urban/rural provenience. 99mTc DTPA dynamic scintigraphy with diuretic administration (according to EANM guidelines) at 20th minute was performed to determine the type of obstruction and to calculate the GFR. There were practiced two methods to estimate the GFR: the scintigraphic acquired images processing through a standard Siemens protocol and Schwartz equation. We calculated both formulas and we compared them ussing statistical correlations. Results: Related to the age, we found: group 1 (1 to 12 months old) = 24 cases (17.5%), group 2 (1-3 years) = 31 cases (22.6%), group 3 (3-7 years) = 35 cases (25.5%), group 4 (7-18 years) = 47 cases (34.3%). In the first group, 83.33% were diagnosed antenatally by ultrasonography. The main diagnostics were: congenital ureteropelvic junction obstruction (51.82%), vesicoureteral reflux (25.55%), megaureter uni- or bilaterally (9.49%) and reno-ureteral duplication (13,14%). 99mTc DTPA renal dynamic scintigraphy parameters were correlated to Schwartz equation. We found a medium correlation (r = Pearson correlation) in group 2, children aged 1 to 3 years (r2 = 0.3291, with p value = 0.07064), and low correlation in other groups: r1 = 0.1683, r3 = 0.1758, r4 = 0.1760. Conclusion: Our experience, certified by this retrospective study, recommend the use of GFR value results from radioisotopic investigations for the management of congenital hydronephrosis and for follow up after conservative or surgery treatment.

P908

Study of association of lesion and ambulation level with kidney dysfunction in spina bifida

E. Ozgonenel1, L. Ozgonenel2, I. Karalok3; 1Istanbul Bilim University Department of Nuclear Medicine, Istanbul, TURKEY, 2Istanbul Bilim University Department of Physical Theraphy and Rehabilitation, Istanbul, TURKEY, 3Istanbul Bilim University Department of Radiology, Istanbul, TURKEY.

Introduction:This is a pilot study to investigate the association of lesion and ambulation level with kidney dysfunction in children with spina bifida.Functional Mobility Scale(FMS)is a simple assessment tool used for measuring ambulation abilities in children with cerebral palsy.Tc-99m-DMSA(Tc-99m dimercaptosuccinic acid)scintigraphy was performed to evaluate kidney function. Methods-results:In this study 42 children(25boys,17 girls) with myelomeningocele(MMC) were enrolled.Mean age of the patients was 5.1±2.6(2-14) years.31 patients had thoracic and upper lumbar lesion(73.8%),11 had mid-lumbar(26.1%) .Functional Mobility Scale(FMS)was used for measuring ambulation abilities in children with spina bifida.Total sum of FMS score was calculated for each patient.Mean score of FMS was 7(5-26).Significant loss of renal function was scored if there was >10% functional difference between two kidneys in Tc-99m-DMSA scintigraphy.There was not a statistically significant difference in FMS scores between patients with kidney dysfunction and patients without kidney dysfunction(p=0.23). Conclusion:Children with spina bifida should be evaluated for kidney function even they have low FMS score and ambulation level.

P909

Diagnostic Accuracy of Tc-99m DMSA Scintigraphy and Renal Ultrasonography in Children with Spina Bifida During Long Term Follow up

E. Ozgonenel1, I. Karalok2, &. Alatas3, E. Ceylan Günay1, L. Özgönenel4, P. Gün Atak5, B. Yazıcı6, K. Özel7; 1Istanbul Bilim University Department of Nuclear Medicine, Istanbul, TURKEY, 2Istanbul Bilim University Department of Radiology, Istanbul, TURKEY, 3Istanbul Bilim University Department of Neurosurgery, Istanbul, TURKEY, 4Istanbul Bilim University Department of Physical Theraphy and Rehabilitation, Istanbul, TURKEY, 5Istanbul Bilim University Department of Biochemistry, Istanbul, TURKEY, 6Istanbul Bilim University Department of Peadiatrics, Istanbul, TURKEY, 7Istanbul Bilim University Department of Peadiatric Surgery, Istanbul, TURKEY.

Introduction:As part of the follow up of children with Spina Bifida(SB) we compared Tc-99m dimercaptosuccinic acid(Tc-99m-DMSA)scintigraphy with renal ultrasonography in identification of renal scarring. Methods:We reviewed data on all children with SB referred to our specialized outpatient clinic between April 2014 and April 2015.DMSA scan and renal ultrasonography have been performed to check for the status of the upper urinary tract and due to complications such as febrile urinary tract infection and chronic renal failure. Data of 100 children of 135 could be evaluated by the end of the study.Outcomes of both modalities were compared with focus on renal scarring. Results: In total 100 patients with 198 renal units underwent both scintigraphy and ultrasonography. More scars were seen on DMSA scintigraphy than on ultrasonography:5% vs. 1,5% of renal units; $p<0$, 05.Conclusion:In children with SB,renal ultrasonography is used to demonstrate dilatation,presumed function and renal scarring but renal scars are often missed, especially when the interpretation of ultrasound is impaired by body shape(e.g. scoliosis,obesity).

P61 - Tuesday, October 13, 2015, 4:00 PM - 4:30 PM, Hall 3 – Poster Exhibition

Conventional & Specialised Nuclear Medicine: Bone & Joint

P910

Title: Does the Differences in Hydration Influence the Image Quality in 99mTc-MDP Bone Scintigraphy?

N. Hosseinifar1, M. Hosntalab1, **M. Eftekhari**2, F. Babapour Mofrad1, P. Geramifar2; 1Islamic Azad University Science and Research Branch, Faculty of Engineering, Tehran, Iran, Tehran, IRAN, ISLAMIC REPUBLIC OF, 2Research Center For Nuclear Medcine, Tehran University of Medical Sciences, Tehran, IRAN, ISLAMIC REPUBLIC OF.

Aim: Drinking large volume of water is cumbersome specially in patients suffering from renal disease, GI cancer or heart failure. In this study we evaluated the effects of different levels of hydration on quality of images as evidenced by the bone-to-soft tissue ratio (B: ST), contrast-to-noise ratio (CNR) and overall image quality following 99mTc-MDP skeletal scintigraphy. Materials and Methods: Forty patients were divided into four groups with various levels of hydration (water intake) in liters equal to 0.5, 1, 1.5 and 2.5 liters respectively. Qualitative and quantitative methods were applied for evaluation of image quality. For qualitative measurements, three nuclear medicine physicians without knowledge of the hydration history of the patients were asked to visually rate and characterize the following indices: bone-to-soft tissue contrast, differentiation of single ribs in anterior and posterior projections, lateral processes of vertebrae, visibility of bony details of the pelvis and filling of the bladder. For quantitative evaluation, we calculated bone-to-soft tissue and contrast-to-noise ratios. For B: ST, we drew equal regions of interest over the femoral diaphysis and the contralateral adductor area. The total number of counts from bone region of interest (ROI) and soft tissue ROI was expressed as a ratio and mean values were calculated in anterior and posterior projections. Pelvic CNR was measured by drawing ROIs over the hip region to determine the number of counts in the bone as well as the soft tissue and background noise. We also investigated possible relation of image quality score to patient's age, body mass index (BMI), and/or post injection time interval. Results: No statistically significant difference was found between the mean B: ST ratios [P=1] and the semi quantitative scores [P =0.98] or CNR [P= 0.58] in our four groups of patients. Conclusion: In conclusion the effect of hydration on bone-to-soft tissue ratio and image quality is negligible. Instead other factors namely age, BMI and post injection time interval play important role in overall bone image quality. Post injection time interval being the most important direct factor while age and BMI inversely affect the image quality.

P911

Improved therapy response assessment in patients with bone metastases of prostate cancer using an expert system for bone scan interpretation

F. Päsler1, G. Berding1, A. Namazian1, F. Wilke2, A. Böker3, L. Geworski2, M. Kuczyk3, F. Bengel1, I. Peters3; 1Dpt. for Nuclear Medicine, MHH, Hannover, GERMANY, 2Dpt. of Medical Physics and Radiation Protection, MHH, Hannover, GERMANY, 3Dpt. for Urology, MHH, Hannover, GERMANY.

Aim: For the evaluation of treatment response in bone metastases of prostate cancer, biomarkers like prostate specific antigen (PSA) and visually interpreted bone scans have limitations in early and accurate assessment of the further course of disease. Hence we investigated if a semi-quantitative parameter of systemic bone involvement - the bone scan index (BSI) - enables an improved response assessment. Methods: In 43 patients with prostate cancer (73±6yrs; median Gleason score: 8, range 5-10) 157 bone scan pairs with a median interval of 3 months were performed for the assessment of response to chemotherapy. Whole body bone scanning was acquired 2-3 hours after injection of 7 MBq Tc-99m-MDP per kg body weight with a large field dual-head gamma-camera. Scans were evaluated (i) visually by an experienced nuclear medicine specialist and (ii) by the artificial neural network based determination of the BSI using the expert system EXINI bone (EXINI, Lund, Sweden). Progression of metastatic bone involvement was defined by (i) occurrence of two new lesions in the visual interpretation (VI) by a nuclear medicine specialist and (ii) different thresholds for the relative increase of the BSI by 5, 10 or 25% (BSI-5%, BSI-10%; BSI-25%) between two scans. Finally, assessments according to bone scanning were compared to changes of prostate specific antigen (PSA) in serum. Results: Based on VI and BSI-25% progression was detected in a similar magnitude (28 vs. 27%, p=0.7440). Though, PSA increases suggested progression significantly more frequently (50%, p<0.0001). Using BSI-5% and BSI-10% significantly higher rates of progression compared to VI (49 and 43 vs. 27%, p<0.0001) were detected - not significantly different to the rate of PSA increase. However, assessment of progression diverged between PSA and BSI changes in 38% of the cases (for BSI-5%) and 39% (for BSI10%), respectively. Conclusion: A relative increase of 5 - 10% in the BSI - in a frequency comparable to PSA - is superior to the visual interpretation of scintigraphy in the assessment of bone metastatic progression. Thus bone scintigraphy in conjunction with expert system evaluation holds potential for more accurate response monitoring in these patients. Nevertheless, results have to be correlated to longer follow up, in order to explain differences in progression assessment between BSI and PSA in a considerable number of cases.

P912

Validation of the Imaging Biomarker Bone Scan Index - Influence of Image Quality on Reproducibility

R. Kaboteh1, A. Anand2, L. Bath1, A. Bjartell2, L. Edenbrandt1; 1Sahlgrenska University Hospital, Gothenburg, SWEDEN, 2Division of Urological Cancer, Lund University, Malmo, SWEDEN.

Objective: Bone Scan Index (BSI) represents the tumor burden as percentage of total skeletal mass. In several studies, BSI has shown to be associated with survival in prostate cancer patients. To clinically qualify BSI as an imaging biomarker a comprehensive analytical validation is required. In this study, we assessed the reproducibility of BSI in assessing bone scans with varying image quality, measured as total number of Counts. Method: Two repeat whole-body bone scans were obtained from each of 48 patients with prostate cancer. Both bone scans were done within four hours after a single intravenous injection of 600 MBq 99mTc MDP. In 21 patients the same scan speed was used in both scans, adjusted so that routine bone scans were in accordance with the EANM procedure guidelines (anterior and posterior images each contain >1.5 million counts). In 27 patients, the second scan was acquired with double scan speed, resulting in a reduction of counts in the images by 50%. The BSI values were generated automatically using the software EXINI boneBSI. A reproducibility threshold of automated BSI for consistent measurement of change in bone scan was defined as 95th percentile of the absolute difference. Result: The mean BSI was 2.29 in the "same scan speed" group and the mean absolute difference between the two BSI values was 0.16 (SD 0.28), the reproducibility threshold was observed at 0.37. In the group with one double speed scan the mean BSI was 1.98. The mean differences between the low counts scan and standard counts scan were 0.08 (SD 0.29) (p=0.17). Five of the 27 patients (19%) showed differences greater than the reproducibility threshold of 0.37. Conclusion: Bone scans with low counts are less reproducible and it is important that EANM procedure guidelines are followed for this type of quantitative analysis. Within reproducibility threshold of 0.37, BSI can be used to produce a consistent quantitative analysis of bone scans in patients with prostate cancer.

P913

Feasibility of bone scan index for the diagnosis and follow-up of medication-related osteonecrosis of the jaw

S. Watanabe, K. Nakajima, H. Yaegashi, A. Mizokami, N. Noguchi, S. Kawashiri, M. Inokuchi, S. Kinuya; Kanazawa University Hospital, Kanazawa-city, JAPAN.

Aim: A computer-aided diagnosis using a bone scan index (BSI) has been shown to enhance diagnostic accuracy of bone metastases. However, no study has applied BSI to the detection and quantification of osteonecrosis of the jaw. Bisphosphonate (BP)-related osteonecrosis of the jaw was recently renamed to medication-related osteonecrosis of the jaw (MRONJ). The aim of this study was to determine optimal methodology for detecting MRONJ and validate the usefulness of BSI. Methods: A total of 26 patients (32 lesions) diagnosed with MRONJ were selected. Median age was 68 years

(range 45-82 years). The primary disease was prostate cancer (69%), breast cancer (12%), renal cancer (12%), lung cancer (4%), and osteoporosis (4%). Regarding the treatment, 89% of the patients had BP, 4% denosumab, and both in 8%. The median duration of medication was 36.5 months (range 7-82 months) by the time of MRONJ diagnosis. All patients underwent Tc-99m methylene diphosphonate bone scintigraphy. Bone uptake in the jaw was analyzed using BSI, which was calculated by BONENAVI (FUJIFILM RI Pharma, Japan; EXINIbone, EXINI Diagnostics, Sweden). Significant hot spots were manually selected according to both serial scintigraphic images and dental records, and the fraction of them to the entire skeleton was referred as BSI of the jaw (BSIJ). The BSIJ was compared with conventional semiquantitative methods, uptake ratios (URs), which were determined as lesion-to-opposite jaw or forehead count ratios. Relationship between BSIJ and URs was evaluated in comparison with various clinical parameters. Results: The median BSIJ of lesions was 0.14% (range 0.0-0.47) at the time of MRONJ diagnosis. When patients were classified according to their clinical stages of MRONJ, BSIJ was significantly higher in the higher stage. Correlation with the clinical stage was better evaluated by BSIJ than URs. The reproducibility of BSIJ was superior to URs. Of 4 inflammatory clinical parameters including pus discharge, pain, swelling and C-reactive protein (CRP), patients with ≥2 parameters showed the significantly higher BSIJ ($p < 0.01$). The median CRP was 1.3 (range 0.0-9.5), and BSIJ was significantly correlated with CRP ($r = 0.62$, $p = 0.0015$). Conclusion: To detect the inflammatory reaction due to MRONJ, this study indicated that BSIJ approach was promising. BSIJ is highly reproducible and well correlated with the clinical stage and the inflammatory reaction of MRONJ. Therefore, BSIJ could be a good parameter to evaluate the occurrence and follow up of MRONJ.

P914

Are the patients who observed as definitely benign in planar bone scintigraphy actually benign? The value of SPECT/CT

P. Arıcan, B. Okudan Tekin, R. Şefizade, S. Naldöken; Ankara Numune Education and Research Hospital, Ankara, TURKEY.

Aim: Bone scintigraphy is higher sensitivity for the diagnosis of bone metastasis in patients with known malignancies. But it can be difficult to distinguish between metastasis and other conditions such as postoperative, degenerative and traumatic changes, especially in compact bone structures. The aim of our study was evaluated the role of SPECT/CT for the diagnosis of bone metastasis in patients with known malignancies who were interpreted as definitely benign by planar bone scintigraphy. Methods ve Materials: One thousand patients who known cancer and referred to our department for performing planar bone scintigraphy and SPECT/CT between 2010 and 2014 were analysed retrospectively. Five hundred ten patients (250 women, 260 men; mean age 50 years) who had definitely benign lesions on planar bone scintigraphy were included in this study. Whole body and static images were performed at 3 hours after 740 MBq Tc-99m methylene diphosphonate (MDP) injection. After the planar bone scan, SPECT/CT was performed to the region of equivocal lesions in all patients. First planar bone scan was separately assessed by two nuclear medicine physicians. Second fusion images were evaluated. The results of planar bone scan and SPECT/CT were compared. Follow up clinical information, radiological studies and/or PET/CT were used as a gold standard. Results: SPECT/CT was determined bone metastasis in 24 of 510 patients (4.7%). The final diagnosis was malign in these patients. There were breast cancer in 8 patients, unknown primary in 3 patients, nasopharynx cancer in 2 patients, malign melanoma in 2 patients, primer bone cancer in 2 patients, and others in 7 patients (bladder cancer, soft tissue tumour, hepatocellular cancer, over cancer, gastric cancer, prostate cancer, spinal mass). The localisation of bone metastasis was vertebral column (n=18), pelvis (n=7), sternum (n=4), rib (n=1), and femur (n=1). These metastatic lesions were lytic (n=14), sclerotic (n=4), and lytic-sclerotic (n=6). Conclusion: SPECT/CT is better than planar bone scan for the diagnosis of bone metastasis in patients with known malignancies, by providing accurate anatomic localization and morphologic characteristic, especially in compact bone structures as cranium, vertebral column, and pelvis. Even though bone sintigraphy is interpreted as definitely benign, SPECT/CT should be performed in the patients who suspected bone metastasis with clinic and radiological findings.

P915

Sacral Insufficiency Fractures in Oncologic Patients Revealed by Bone Scan and SPECT/CT

O. Lapina, S. Tiskecivius, **M. Stalnionis**; National Cacner Institute, Vilnius, LITHUANIA.

Aim: Sacral insufficiency fracture (SIF) is a type of fracture which occurs within normal stress on weakened bone matrix due to conditions such as osteoporosis, previous radiotherapy or chemotherapy. Although, relatively common in the elderly and patients with structurally weakened bones and low back pain, SIF often remains underdiagnosed. SIF can also get misinterpreted as bone metastases in oncologic patients. In this case series we aim to emphasize the awareness of this condition and to demonstrate the importance of SPECT/CT imaging in patients with

SIF seeking to avoid misinterpretation in the setting of concomitant oncologic disease.

Materials and Methods: From July 2013 to January 2015, 14 oncologic patients (12 female and 2 male; mean age 67.5) diagnosed with SIF after the 99mTc-MDP bone scan were retrospectively reviewed. Those patients were referred to the NM department after the initial radiological assessment due to onset low back pain and suspected bone metastases. Patient data and NM images were analyzed and evaluated for SIF features, localization of fracture lines and associated pelvic fractures.

Results: Bone scans revealed increased osteoblastic activity in lateral parts of sacrum which makes typical "Honda" sign in 71.4% of the cases. SPECT/CT images showed obvious fracture lines with mottled sclerosis in 92.9%, cortical break in 85.7% of the cases. Bilateral SIF occurred in 71.4%, whereas unilateral in 28.6% of the cases. In 85.7% of the cases the fracture lines were located in zone 1, according to Denis classification, whereas in 14.3% in zone 2 and 3. Associated pelvic fractures were found in 46.1% of the cases. 50% of these fractures were located in pubis, 25% in acetabulum, 12.5% in ischium and 12.5% in transverse process of L5 vertebra. 64.3% of the patients underwent previous pelvic radiotherapy and 42.9% had previous chemotherapy.

Conclusion: "Honda" sign on the bone scan, fracture lines with adjacent bone sclerosis and cortical break on the CT images are considered diagnostic features for SIF and occurred in up to 93% of the cases. In most cases fracture lines occurred in zone 1. SIFs were more common in elderly women. Precise review of the whole pelvic ring is advisable due to high incidence of associated fractures. SPECT/CT proved to be the determining modality in SIF diagnosis.

P916

Role of bone scintigraphy in the early detection of fatigue fractures

H. Boudriga, **I. Yeddes**, I. Meddeb, I. El Bez, A. Mhiri, M. Ben Slimène; Salah Azaiez Institut, Tunis, TUNISIA.

Introduction :Fatigue fractures (FF) or stress fractures (SF) occur on healthy bone when subjected to constant loading, which the normal carrying range capacity is exceeded. With high load-bearing activities, active people tend to be more prone to such bone lesions. Bone scintigraphy facilitates the early detection of abnormalities in bone prior to the development of cortical disruption, thereby preventing increased morbidity and possible disabling sequelae.The aim of our study is to demonstrate the role of bone scintigraphy in the early detection of fatigue fractures.Materials and methods :We retrospectively reviewed a series of 10 patients (7 women and 3 men) with a mean age of 42 years (75-20 years) from 1999 to 2015, all suspected to have had a fatigue fracture. They all presented with bone pain while all having negative standard X-rays.They were submitted to technetium-99m-hydroxy methylene diphosphonate (99mTc-HMDP) intravenous injection. Two hours later a whole body scan was performed along with selected planar spot views.Results :Of 10 patients, fractures were demonstrated within three. Whereas in the rest they were excluded. Three of which were normal, while osteitis was confirmed in one patient, periostitis was found in one patient, and algodystrophy was confirmed in two patients.Positive planar scintigraphies showed an increased uptake fractures in the second left metatarsal bone in one patient, in the first right metatarsal bone in the second patient and in the lower third of the left tibia with the third patient.Conclusion :Scintigraphy with a bone-seeking radiopharmaceutical is suitable for the early detection of stress lesions and its follow up It may lead to an early and a timely management of the fracture especially with athletes.

P917

A new area for F-18 NaF PET/CT: Avascular Necrosis of the Femoral Head as a benign disease

I. AK SIVRIKOZ1, H. ONNER1, N. KOSE2; 1ESOGU SCHOOL OF MEDICINE DEPARTMENT OF NUCLEAR MEDICINE, ESKISEHIR, TURKEY, 2ESOGU SCHOOL OF MEDICINE DEPARTMENT OF ORTHOPEDIC SURGERY, ESKISEHIR, TURKEY.

Avascular necrosis (AVN) of the femoral head is an increasingly common cause of musculoskeletal disability, and it poses a major diagnostic and therapeutic challenge. Although patients are initially asymptomatic, AVN of the femoral head usually progresses to joint destruction, requiring total hip replacement. The widespread availability of positron emission tomography (PET) and PET/computed tomography (PET/CT) cameras has led to renewed interest in F-18 Na Fluoride (NaF) bone scanning. It provides highly sensitive, 3-dimensional imaging of the skeleton, with demonstrable utility in a growing range of benign and malignant bone disorders.The authors present an interesting image of bilateral AVN of the femoral heads diagnosed on F-18 NaF positron emission tomography/computed tomography. An 45-year-old female patient with a history of long termed steroid use presented with pain in both hips (more on the left side) for 1 year. PET/CT images were acquired in 3D mode 60 minutes after intravenous injection of 370 MBq of F-18 NaF. Photopenic areas were detected in both femoral heads, with surrounding margins of increased tracer

uptake in the axial, sagittal and coronal MIP PET images. Intense F-18 NaF uptake was also noted in both acetabular margins. The photopenic areas in the femoral heads corresponded to sclerotic changes on the CT (bone window) image and likely represent microvascular occlusion. A diagnosis of bilateral avascular necrosis of the femoral heads was made. While magnetic resonance imaging (MRI) is considered the most sensitive and specific technique in the early diagnosis of AVN, 3-phase bone scan with single photon emission computed tomography/computed tomography (SPECT/CT) has also shown comparable diagnostic accuracy. F-18 Fluoride uptake depends on regional blood flow and osteoblastic activity similar to Tc-99m Methylene Diphosphonate. However, the better spatial resolution of PET and the favorable pharmacokinetic characteristics of F-18 Fluoride make this a more sensitive modality. The present case suggests that F-18 NaF PET has the advantages of high spatial resolution, attenuation correction, 3-dimensional tomographic images, and hybrid PET/CT imaging. In addition, it may be an effective alternative for the diagnosis of femoral head AVN in patients with contraindications to MRI like cardiac pacemakers, intracranial clips, or claustrophobia.

P918

Evaluation of sternoclavicular hyperosteosis in 20 patients: preliminary study

B. Celik1, **F. Canbaz**2, Y. Bilgin Büyükkarabacak1, A. Taslak Sengul1, Z. Pelin Sürücü1, A. Başoğlu1; 1Ondokuz Mayis University Hospital, Faculty of Medicine, Thoracic Surgery Dept., KURUPELIT / SAMSUN, TURKEY, 2Ondokuz Mayis University Hospital, Faculty of Medicine, Nuclear Medicine Dept., KURUPELIT / SAMSUN, TURKEY.

Aim: Sternocostoclavicular hyperostosis(SCCH) is a chronic inflammatory disorder, characterized by erythema, swelling and pain of the sternoclavicular joint. Palmoplantaris pustulosis may develop at any stage of the disease in approximately 50% of patients. Trauma, degenerative or infections should be considered in the differential diagnosis. Bullhorn sign is a characteristic, highly sensitive pattern on bone scan. The diagnosis of SCCH is confirmed radiologically by hyperostosis and sclerosis of the sternum with involvement of the first rib on computed tomography (CT). In this study we aimed to evaluate clinical and imaging characteristics of patients diagnosed with SCCH. Methods: Twenty patients presented with swelling of sternoclavicular junction (SCJ) with or without pain and diagnosed with SCCH scintigraphically were retrospectively studied. Their clinical, laboratory and scintigraphic findings were analyzed. Results: Of twenty patients, sixteen were female and four were men. The mean age was 51 ±13 (21-68). Eight patients had only swelling and eight had swelling with pain on SCJ. Four patients had only pain on SCJ. The mean duration of complaints was 6 (2-18) months. None of our patients had skin manifestations of the disease. All patients were advised anti-inflammatory medicine in the beginning of the diagnosis. Laboratory findings including hemogram, sedimentation rate and C-reactive protein were all normal. Eight / 20 patients had bilateral and 12/20 patients had unilateral increased osteoblastic activity on bone scan which was typical for SCCH. 11/20 patients showed increased sclerosis of SCJ on computed tomography 5/ 20 patients had arthritis in other joints. Three patients were biopsied because of the detriment of complaints and the suspicious of malignancy. All of the histopathological results were benign. On follow up, of 14 patients whom we could be informed, seven had near to completely remission and seven had persistent swelling in the sternoclavicular joint. Conclusion: Sternocostoclavicular hyperostosis is a chronic sterile osteomyelitis of the sternum, the medial end of the clavicle, and the upper ribs. Restricted mobility of the adjacent shoulder joint may also be the sole presenting symptom. Patients often undergo multiple serologic, imaging and also unnecessary invasive examinations before a correct diagnosis is made. Greater awareness of SCCH among nuclear medicine physicians as well as rheumatologists and other clinicians needed to prevent irreversible physical, psychological impairment associated with the delay in the diagnosis and the treatment of the disease.

P919

Semiquantitative analysis of bone SPECT studies in the detection of active sacroiliitis

A. Kokkini, G. Koniaris, A. Zafirakis, K. Athanasiou, D. Kassimos, **J. Koutsikos**; 401 General Military Hospital, ATHENS, GREECE.

INTRODUCTION: Bone SPECT has progressively become an excellent diagnostic imaging modality in the detection of active sacroilitis in patients with spondyloarthropathies. Although visual evaluation appears to be quite efficient in most nuclear medicine studies, semi-quantitative (SQ) analysis is also applied in order to standardise the quality of the procedures. Our aim was to assess accuracy and inter-operator reproducibility of bone SPECT, analyzed by a SQ method.MATERIALS AND METHODS: Bone SPECT studies of 45 patients suffering from spondyloarthropathies, were retrospectively analyzed for detecting active sacroilitis. Two experienced nuclear medicine physicians were asked to evaluate each SPECT study, using the same default processing procedure. The algorithm consisted of the following steps:1. Review of projection data in cine mode for an initial determination of scan quality, patient motion, and artifacts2. Use of ReSPECT iterative reconstruction software.3. Reconstruction

of images into slices in 3 axes (frontal, vertical and sagittal)4. Reorientation of images5. Selection of 5 images of interest using the frontal axis reconstructed data, in order to create one summed static image6. SQ analysis of sacroiliac joints (SIJ), applying ROIs to both SIJ and L4.SQ data were analyzed by Receiver Operating Characteristic (ROC) analysis to establish the accuracy; the inter-class correlation coefficient (ICC) was used to evaluate the inter-observer reproducibility. The later was evaluated also for the visual assessment; focally increased radiotracer uptake at the base of the SIJ was evaluated as positive. The diagnosis of sacroilitis was established according to ASAS criteria.RESULTS: Area under the curve, estimated by ROC analysis, regarding SQ method was 0.266 (p=ns) and ICC demonstrated no significant correlation among the operators (p=ns). On the contrary, regarding the visual analysis, inter-observer reproducibility was very good, with correlation coefficient 0.89-0.96 ($p<0.0001$).CONCLUSION: Estimation of SIJ ratios in bone SPECT studies by a semi-quantitative analysis shows neither accuracy, nor significant reproducibility among different operators, and can therefore not be used as a solid method. These results were mainly attributed to the subjective selection of static image sequence. The qualitative assessment of radiopharmaceutical uptake in the SIJ of the reconstructed tomographic images is highly accurate and reliable.

P920

Bone scintigraphy, DAS 28 score and biochemical parameters in patients with Rheumatoid Arthritis

S. Karacavus1, M. Ucar2, M. F. Gecer3, O. Balbaloglu2, O. Nas4, U. Sarp4; 1Bozok University, School of Medicine, Department of Nuclear Medicine, Yozgat, TURKEY, 2Bozok University, School of Medicine, Department of Physical Medicine and Rehabilitation, Yozgat, TURKEY, 3Yozgat State Hospital, Department of Nuclear Medicine, Yozgat, TURKEY, 4Yozgat State Hospital, Department of Physical Medicine and Rehabilitation, Yozgat, TURKEY.

Aim: Rheumatoid arthritis (RA) is a chronic inflammatory and autoimmune disease characterized by progressive damage of joints. In this study, we investigated the relationship between the disease activity scores and bone scan findings and biochemical parameters in patients with RA. Material and Method: Sixty two patients (F/M: 44/8, age 51,8±11,1; range 31-77) diagnosed with RA according to the American College of Rheumatology (ACR) criteria were included in the study. All patients were divided to two groups regarding their DAS28 score; Group 1 was DAS28 score≥3,2 and Group 1 was DAS28 score<3,2. The whole body bone scintigraphy with Tc99m-MDP (TVKS) was performed all subject. A increased uptake on any joint in blood pool phase and late static phase of bone scan was evaluated as a positive result. Laboratory data including the erythrocyte sedimentation rate and C-reactive protein were recorded. The clinical parameters were assessed by the Health Assessment Questionnaire (HAQ) and Ritchie articular index (RAİ). Results: The mean number of peripheral joint involvement was higher in Group 1 than in Group 2 (11/8; $p<0.05$). Number of joint involvement ($r=0.5$,$p=0.019$) and biochemical parameters ($r=0.7$,$p<0.001$) were increased with clinical score in Higher disease activity score group. In 6 of 13 patients of lower DAS28 group, number of peripheral joint involvement were similar to high DAS28 group. Conclusion: Whole body bone scintigraphy is a cheap and easy method, that contributes a lot to the clinical approach in patients with rheumatoid arthritis, in the evaluation of peripheral joints in a single session and determining the joints those not expressing significant clinical findings yet.

P921

Interest of SPECT/CT hybrid imaging in the management of McCune-Albright syndrome

A. Matrane, M. Bsiss, S. Hiroual, S. Bennani Doubli; Mohammed VI University Hospital, Marrakech, MOROCCO.

Introduction. McCune-Albright syndrome is a genetical disease with a mosaïc distribution. It is characterized by skin pigmentations, fibrous dysplasia and sexual precosity but can also include others endocrinopathies (hyperthyroidism, Cushing's syndrome and acromegaly). Fibrous dysplasia may involve one or more skeletal sites and it is manifested by lameness, pain and sometimes by a pathological fracture. The aim of our work is to elucidate the contribution of SPECT/CT in the diagnosis and management of osteo-articular complications of McCune-Albright syndrome about a clinical case. Case report. A 41 years-old patient, with McCune-Albright syndrome, presents a painful limp progressively worsening. Clinical examination shows skin pigmentations with facial dysmorphia combining prognathism, hypertelorism and frontal bossing. The standard radiological assessment shows fibrous dysplasia interesting long bones, skull, maxilla and the mandible. The SPECT / CT showed a Polyostotic achievement of fibrous dysplasia. The lesions involve all the bones of the axial and peripheral skeleton. Discussion. McCune-Albright syndrome is a genetical disease characterized by skin pigmentations, fibrous dysplasia and sexual precosity. Fibrous dysplasia is classified among benign bone tumors. It can be monostotic or polyostotic. The craniofacial localization occurs in 10%-25% of cases in monostotic forms and in 50% of cases in polyostotic forms. Fibrous dysplasia essentially affects children and young adults, with no sex preference. Its diagnosis is not always straightforward because the functional symptomology is often absent or not specific. Medical

imagery is necessary and in difficult cases a bone biopsy. The major complication of the illness remains sarcomatous degeneration. The SPECT/CT can increase the sensitivity and specificity of planar bone scintigraphy. It confirms the location of Fibrous dysplasia and defines its anatomical relationships in order to optimize surgical management. Conclusion. The SPECT/CT has an important role in the management of patients with McCune-Albright syndrome. It provides better anatomical localization and improves the diagnosis value in the assessment of Fibrous dysplasia.

P922

Value of quantitative 3 - phase bone scintigraphy in the assessment of hip and knee endoprosthesis

C. C. Schiller, F. Fitz, S. Haim, H. Söser, J. Hochreiter, W. Langsteger, M. Beheshti; Nuclear Medicine & Endocrinology, St. Vincent's Hospital, LINZ, AUSTRIA.

Aim: This study evaluates the impact of quantitative 3-phase bone scintigraphy in patients with clinically suspicious knee- or hip- prosthesis loosening and equivocal findings on the visual assessment of bone scanning. Methods: A total of 196 patients with knee - and / or hip- total endoprosthesis (TEP) [70 H-TEP (hip) and 126 K-TEP (knee)] with equivocal findings in the visual assessment who underwent quantitative 3-phase scintigraphy and 6 months follow-up study were included in this study. A region of interest (ROI) was defined over the pathologic peri-prosthetic uptake as well as normal ipsilateral and/or contralateral bone. Counts per ROI were measured and the ratio of pathologic to normal bone was calculated in various segments of prosthesis. All patients have been followed - up with quantitative 3-phase bone scintigraphy. Increasing pattern of uptake was considered as prosthesis loosening. The imaging findings have been correlated with clinical follow-up and/or surgical results within 2 years as standard of truth. Results: Quantitative analysis improves the predictive value for the diagnosis of prosthesis loosening in the Tibia plateau. A cut-off ratio of 1.26 was suggestive of loosening with a sensitivity of 100% and specificity of 33% (AUC = 0.614, p = n.s.). Increasing target to normal bone ratio in the 6 months follow-up quantitative scans improves the predictive value for loosening process with a cut-off of 3.45% on the Tibia plateau (sensitivity 71%, specificity 73%, AUC = 0.692, p = 0.056) and 16.5% on the Femoral condyle (sensitivity 67%, specificity 90%, AUC = 0.733, p = 0.129).No meaningful data could be extracted in the H-TEP region. Conclusion: Quantitative 3-phase bone scintigraphy seems to improve the diagnostic accuracy of the knee - TEP loosening. However, it providess no additional value to visual assessment of the Hip - TEP. Further research with a homogeneous patient's population and a higher number of cases are needed to draw an accurate conclusion.

P923

Scintigraphy studies for the evaluation of painful hip and knee prosthetic joints

J. A. Sequeira1, J. G. Santos1, A. Prata1, S. Carmona1, J. Salreta2, M. Tapadinhas2, A. I. Santos1; 1Hospital Garcia de Orta - Serviço de Medicina Nuclear, Almada, PORTUGAL, 2Hospital Garcia de Orta - Serviço de Ortopedia, Almada, PORTUGAL.

Aim: To retrospectively evaluate the triple scintigraphic approach - three-phase 99mTc-HMDP bone scintigraphy (BS) in conjunction with 99mTc-antigranulocyte monoclonal antibody BW 250/183 scintigraphy (AGS) and 99mTc-albumine-colloid bone marrow scintigraphy (BMS) - for the diagnosis of infected hip and knee prosthetic joints. Materials and Methods: 56 patients with painful hip and knee prostheses and suspected prosthetic joints infection (20 prosthetic hips and 36 prosthetic knees) who underwent BS, AGS and BMS, were selected. AGS images were acquired 2 and 4-6 hours post radiopharmaceutical administration in all studies; in 11 studies an additional image at 24 hours was also performed. Images were interpreted in conjunction with the ones obtained through BS and BMS, according to the following criteria considered positive for infection: a) Increased periprosthetic AGS uptake with congruent pattern with BS. b) AGS increased uptake or extension over time. c) Incongruent AGS/BMS images. In addition to visual interpretation of the images, semiquantitative analysis was also employed, calculating early and late ratios between uptake on the area of suspected infection and a contralateral area. Final diagnosis was based on surgical, histological and bacteriological data (33 patients submitted to surgery) or clinical follow-up at 12 months as proof of absence of infection (the remaining 23 patients). Results: Among the 56 hip and knee prostheses investigated, the final diagnoses were: infection in 20; non-infection in 33; and inconclusive in 3. The overall sensitivity, specificity and accuracy of combined BS, AGS and BMS for the diagnosis of periprosthetic infection were 83%, 86% and 85%, respectively. Positive and negative predictive values were 75% and 91%, respectively. All five infected hip prostheses and 10 of the 13 infected knee prostheses were correctly diagnosed with this triple scintigraphic evaluation. There were 5 false positive findings (3 with massive loosening without infection, 1 with allergic reaction and 1 with arthrofibrosis) and 3 false negative (in one of these the studies were performed on antibiotic therapy). Negative studies (33/56 cases) were very helpful for the exclusion of infection. In 18/20 patients with positive studies reoperation was performed, motivated by the scintigraphic results.

Conclusions: Our results suggest that the conjunction of bone scintigraphy with antigranulocyte and bone marrow scintigraphies has a role on the diagnostic workup of infected hip and knee prostheses, its greatest strength being a high negative predictive value. Further analysis should be performed to evaluate the additional value of bone marrow scintigraphy over bone and granulocyte scintigraphies.

P924
Does bone scintigraphy keeps a place in para-articular osteoma?

D. BEN SELLEM, L. ZAABAR, B. DHAOUADI, B. LETAIEF, M. F. BEN SLIMENE; Nuclear Medicine Department, Salah AZAIEZ Institute, TUNIS, TUNISIA.

Aim: Para-articular osteomas (PAO) are ossifications occurring around articulations and muscles limiting their functions. They occur in situations like hemophilia, cerebral vascular accidents but especially on cranial traumatized patients and those with medullary injuries. They occur early during intensive care hospitalization. The removal of these PAO permits at least the recuperation of functional articular amplitudes. The risk of recurrence with then the possibility of deterioration is possible after this surgery, especially if it is done early on osteoma still evolving. The purpose is to evaluate the indication and usefulness of bone scintigraphy in PAO. Materials and methods: 32 patients confined to bed for a long period (24 males and 8 females mean age 33.45 years) were referred to our department for suspicion of PAO. Thirty seven bone scintigraphies with 99mTc-HMDP were performed (32 for initial evaluation and 5 for follow up). Results: We evaluated 60 articulations with suspicion of PAO to the hip in 28 patients (44%), to elbow in 16 cases (27%), to knees in 14 cases (23%) and to the hip shoulder in 2 cases (3%). Bilateral localization was diagnosed in 20 articulations among 12 patients (12 for the hips, 6 to knees and 2 for elbows). The bone scintigraphy was positive in 61 times, with the following respective results, 27 (44%), 17 (28%), 14 (23%) and 2 (3%) for hip, elbow, knees and shoulder. An anterior tarsal infra clinical and radiological localization was diagnosed (2%). In fact bone scintigraphy confirmed the 57 suspected articulations 26 (46%) for hip, 15 (26%) for elbow, 14 (25%) for knees and 2 (3%) for shoulders, infirmed 3 localizations and revealed 4 unknown localizations. Bilateral localization occurred in 13 cases. Among PAO diagnosed, 55 were immature. During follow up, 3 immature PAO passed to maturation, the first one at 5 months, the second at 7 months and the third, 13 months later. Conclusion: Three phase bone scintigraphy with HMDP technetium 99m remains the exam of choice for the diagnosis, cartography and especially the evaluation of maturation of PAO to indicate the adequate moment for surgical remove of theses PAO.

P925
FDG-PET/CT of bone lesions

Y. Otomi1, H. Otsuka2, T. Shinya1, K. Terazawa1, M. Kubo1, M. Harada1; 1Tokushima University Hospital, Tokushima, JAPAN, 2Tokushima University, Tokushima, JAPAN.

Objectives: The aim of this study was to evaluate the usefulness of 18F -2-fluoro-2-deoxyglucose positron emission tomography/computed tomography (FDG-PET/CT) in detecting malignancy arising from a variety of bone lesions. Methods: Data were retrospectively analyzed for 25 consecutive patients (13 men, 12 women; mean age: 57.4 years, range: 16-86 years) with bone lesions examined using FDG-PET/CT prior to therapy between May 2008 and July 2014. Twenty-four cases were pathologically proven to involve bone lesions and one case was diagnosed during follow-up. We performed a semi-quantitative analysis to assess the FDG uptake of the lesions by measuring the maximum standardized uptake value (SUVmax). There were 16 malignant lesions (5 plasmacytomas, 4 diffuse large B cell lymphomas, 2 chondrosarcomas, 2 metastatic bone tumors, 1 bone sarcoma, 1 fibrosarcoma, 1 spindle cell sarcoma) and nine benign lesions (3 cases of osteomyelitis, 2 cases of Langerhans cell histiocytosis, 1 hemangioma, 1 simple bone cyst, 1 chordoma, 1 case of pyogenic spondylitis). The cutoff value for balancing the sensitivity and specificity was obtained according to a ROC analysis. The sensitivity, specificity, positive predictive value (PPV), negative predictive value (NPV) and accuracy of FDG-PET/CT in detecting malignant lesions of the bone were evaluated. Results: The results of the semi-quantitative analysis were as follows. The SUVmax of the malignant lesions was 8.9 ± 7.3 and that of the benign lesions was 6.6 ± 3.4; the difference between the SUVmax values of the malignant and benign lesions was not statistically significant. The cutoff value for the SUVmax obtained using the ROC analysis was 10. The sensitivity, specificity, PPV, NPV and accuracy of FDG-PET/CT were 31.3%, 88.9%, 83.3%, 42.1% and 48.0%, respectively. Conclusions: The average SUVmax of malignant lesions is higher than that of benign lesions, although the range for malignant and benign lesions overlaps. Differentiating between malignant and benign bone lesions is difficult. In particular, the possibility of malignancy is considerably high for bone lesions showing high accumulation with a SUVmax of more than 10.

P926

Role of F18 Bone Scan in metastatic workup of Primary Bone tumors

H. B, **Sr**., V. Pawar, S. C H; BGS Global Hospital, Bangalore, INDIA.

Primary bone tumours constitute less than 1% of all cancers. They mainly metastasize by haematogenous route. Lungs and bones form most common areas of metastases. During metastasis workup we require to do MDP bone scan and CT chest to rule out metastases to bone and lung respectively. However since F18 bone scan produced cross sectional images we will have better anatomical correlation for bone lesions and in addition due to presence of whole body CT scan, lung evaluation is also done together. Lung metastases in primary bone tumors are in the form of soft tissue density/calcified nodules which are usually less than 6 mm. FDG PET CT will not show uptake in these nodules due to partial volume effect. Since F18 bone scan provide both information about metastases to lungs and bone, we tried to assess impact of bone scan in management of primary bone tumors. AIM : To evaluate role of F18 bone scan in metastatic workup of primary bone tumors. MATERIAL AND METHODS: It is an observational study done in Dept of Nuclear medicine in collaboration with Dept of Orthoonco at BGS Global Hospital, Bangalore between June 2013 to Feb 2015. 48 consecutive patients with biopsy proven primary bone tumors (osteosarcoma -34, Ewing's sarcoma- 8, Condrosarcoma-5 and fibrosarcoma-1) were enroled. Male: female ratio is 1. Age ranged between 6 -60 years. Out of 48 patients 16 patient had lung nodules (4 had solitary and rest had multiple) and 19 patient had F18 avid skeletal lesions of which 1 was histological proven osteochondroma and other was osteoid osteoma . Rest 17 were metastases. CONCLUSIONS: F18 bone scan plays an important role in the evaluation of primary bone tumors. It is more specific for extra primary skeletal lesions as it has anatomical correlation with CT scan. Attenuation correction of PET images by CT images can be used for assessing lung metastases. Since bone tumors metastases predominantly to lungs and bones, F18 bone scan can be cost effective one stop shop for metastatic workup from primary bone tumors. LIMITATIONS: Pure marrow metastases can be picked up by FDG PET CT and may be missed by F18 bone scan. This can happen in Ewing's Sarcoma than in other primary bone tumors. Hence it is advantageous to do metastatic workup by FDG PET CT for Ewing's Sarcoma and F18 bone scan for others.

P927

SPECT-CT with 99mTc-MIBI in patients with recurrent malignant soft tissue sarcomas: is it important for radiotherapy planning and monitoring of its efficacy.

S. Kanaev, S. N. Novikov, P. Krzhivitskiy, G. Gafton; N.N. Petrov Institute Oncology, St Petersburg, RUSSIAN FEDERATION.

Purpose: to evaluate clinical value of SPECT-CT with 99mTc-MIBI in radiotherapy planning and monitoring of treatment efficacy. Material and methods: the study group consisted of 9 patients with recurrent malignant soft tissue sarcomas (RMSTS) that were inoperable (2 patients with pelvic tumours) or considered as candidates for amputation (7 patients with RMSTS of extremities). High dose rate (HDR) brachytherapy was performed in order to reduce tumor volume and to decrease invasive potential of RMSTS during non-compartmental surgery. After CT guided insertion of plastic needles and HDR therapy planning 3 fractions of 7 Gy (with at least 4-6 hours of interfractional interval) were delivered in first 4 patients and 3 fractions of 8Gy - in last 5 cases. SPECT-CT with 99mTc-MIBI was performed before treatment in order to visualize viable tumour subregions and areas with reduced tracer uptake. Posttreatment SPECT-CT was performed 3-4 and 6-8 weeks after the end of brachytherapy for monitoring of its efficacy and in order to determine optimal time for surgical intervention. Results: SPECT-CT with 99mTc-MIBI effectively visualized viable and hypoxic-necrotic subregions of RMSTS. This helps us to perform dose painting with obligatory irradiation of all viable tumor regions and if possible to increase radiation dose to areas with decreased tracer uptake. After treatment SPECT-CT correctly determine tumour regression in all 2 patients with pathomorphological complete or nearly complete (>90%) response, all 2 cases with partial pathologic response and 3 observation with stabilization or tumour progression. All 4 patients with complete or partial SPECT-CT response underwent limb saving surgery and are in remission. Conclusion: SPECT-CT with 99mTc-MIBI can accurately determine response of RMSTS to HDR brachytherapy and can be considered as a promising tool for monitoring of radiotherapy efficacy in this patient group.

P928

Follow-up in patients with Ewing sarcoma: value of an imaging protocol including FDG-PET(-CT) and MRI for recurrence detection

M. Heinemann1, A. Ranft1, H. Jürgens1, T. Langer2, V. Vieth1, M. Schäfers1, M. Weckesser1, L. Stegger1, U. Dirksen1; 1University Hospital Münster, Münster, GERMANY,

2University Hospital Schleswig-Holstein, Campus Lübeck, Lübeck, GERMANY.

Aim: To evaluate a prospectively defined imaging protocol with regular FDG-PET(-CT), MRI, bone scintigraphy, thoracic CT/-x-ray and x-ray at the site of primary tumour for the detection of recurrence in patients with Ewing sarcoma and to compare detection rates with those for recurrence detection by clinical symptoms. To additionally assess the influence of detection mode on survival.Methods:After achieving complete remission, eighty patients with Ewing sarcoma treated at one institution underwent regular follow-up examinations with tomographic and conventional imaging methods according to a prospectively defined protocol over a duration of 5 years. In case of clinical symptoms additional non-protocol imaging was performed. The number of recurrences and the modes of recurrence detection (imaging method, clinical symptom) were determined from the imaging reports and patient files. Additionally, the influence of the mode of recurrence detection on 3-year survival was investigated.Results:From the eighty patients included in this study thirty had tumour recurrence within the first five years of follow-up; 14 (47%) relapsed during the first year. Recurrent tumour was detected by protocol imaging studies in 19 patients (63%) and by clinical symptoms in 11 patients (37%). Detection rate of protocol imaging was: 8/164 investigations for FDG-PET(-CT), 1/309 for MRI, 2/151 for thoracic CT, 2/318 for bone scan, 6/1052 for X-ray.FDG-PET-CT and thoracic CT detected significantly more frequently pulmonary metastases <1cm than chest X-ray (P=0.002). Most frequent clinical symptom of recurrence was pain (n=9), followed by sensomotor dysfunction, swelling/oedema and dyspnoea. Osseous metastases were significantly more frequently symptomatic than pulmonary metastases (P=0.036).Nine patients achieved 3-year survival (2 additional patients still alive <3 years after recurrence detection), all of them after relapse detection by protocol imaging (P=0.026).Conclusion:Most recurrences of Ewing sarcoma were detected by protocol imaging studies, among these many with FDG-PET(-CT). Diagnosis of recurrence by protocol seems to be associated with advantage for survival.

P929

Disappearing Bone Disease (Gorham's Disease) demonstrated on SPECT/CT imaging

A. Atabaki1,2, R. Mansberg2; 1Westmead Hospital, Sydney, NSW, AUSTRALIA, 2Concord Hospital, Sydney, NSW, AUSTRALIA.

BACKGROUND: Gorham's disease (vanishing bone disease) is a very rare skeletal condition of uncertain aetiology, characterised by the uncontrolled proliferation of distended, thin walled vascular or lymphatic channels within bone, which leads to resorption and replacement of bone with angiomas and/or fibrosis. AIMS: To assess the patient case study of a lytic bone lesion due to a rare diagnosis of "vanishing bone disease" (Gorham's disease). METHODS: A 55-year-old male with nonspecific headache was referred for a CT scan, which demonstrated a lytic lesion in the left parietal skull. A bone scan with SPECT/CT and MRI were performed to further evaluate the lesion and assess for the presence of occult lesions elsewhere in the skeleton for malignancy. RESULTS: The imaging investigations revealed a large solitary lytic lesion in the left parietal bone with pseudo-herniation of the brain into the defect. No other occult lesion was demonstrated elsewhere in the skeleton. The patient subsequently underwent left parietal craniectomy, reduction of encephalocoele and reconstructive duraplasty/cranioplasty. The histopathology showed osteolysis and thin walled blood vessels (occasionally cyst-like) without evidence of malignancy consistent with Gorham's disease. CONCLUSION: The evaluation of a lytic lesion is a common indication for performing skeletal scintigraphy, in order to assess for the presence of primary or metastatic neoplasm. Due to the rarity of this condition, it is important for imaging doctors to consider Gorham's disease in the differential diagnosis of a lytic lesion as demonstrated in this case with multi-modality imaging and histological confirmation.

P930

Prominent thallium-201 uptake of giant cell tumor of bone : comparison with osteosarcoma

R. Inai1, S. Takayoshi2, T. Tanaka1, Y. Tsuboi1, S. Norikane1, K. Kojima1, A. Tada1, T. Kunisada1, S. Sato1, T. Ozaki1, S. Kanazawa1; 1Okayama university hospital, Okayama, JAPAN, 2Tokushima university hospital, Tokushima, JAPAN.

Aim: Giant cell tumor of bone (GCT) is a local aggressive benign tumor. This tumor shows the lytic lesion without sclerosis around it on radiography and low signal intensity on T2-weighted MRI. These findings are often similar to osteosarcoma, especially in the case of osteoblastic calcification's absence. GCT has also been reported to show the prominent uptake in thallium-201 (201-Tl) scintigraphy. We hypothesized GCT showed higher 201-Tl uptake than osteosarcoma. This study aims to compare with 201-Tl uptake between GCT and osteosarcoma. Materials and Methods: Between January 2006 and December 2012, 19 patients with GCT and 24 patients with osteosarcoma underwent 201-Tl scintigraphy before treatment. We used the tumor-to-background contrast (TBC) and washout rate (WR) to evaluate the 201-Tl uptake. The differences of TBC on the early and delayed imaging and

WR were estimated by the Mann-Whitney U test. Results: This retrospective study included 19 patients with GCT (12 men, 7 women; mean age, 38.5 years; range, 20-61 years) and 24 patients with osteosarcomas (12 men, 12 women; mean age, 32.4 years; range, 9-69 years). The median TBC of GCT was higher than that of osteosarcoma on delayed imaging (236 vs. 119, $p < 0.05$) in 201-Tl scintigraphy. However, there were not statistically significant differences in the median TBC on early imaging (331 vs. 230, NS) and WR (0.49% vs. 0.46%, NS). Conclusion: Giant cell tumor of bone showed higher uptake than osteosarcoma only on the delayed imaging in 201-Tl scintigraphy.

P931

Inclusion of Trabecular Bone Score (TBS) in Risk Assement of Fragility Fracture in Postmenopausal Women

B. PEREZ LOPEZ, R. RUANO PEREZ, L. G. DIAZ GONZALEZ, M. E. MARTIN GOMEZ, E. MARTIN GOMEZ, M. P. TAMAYO ALONSO, F. GOMEZ CAMINERO LOPEZ, P. GARCIA-TALAVERA SAN MIGUEL, J. DEL PINO MONTES, T. CARRANCO; HOSPITAL UNIVERSITARIO CLINICO DE SALAMANCA, SALAMANCA, SPAIN.

TBS is a measure of gray-level texture used to evaluate pixel measurements from a two-dimensional DXA image of the lumbar spine. TBS provides information about bone microarchitecture and has the potential to discern differences between DXA scans that show similar BMD measurements, in such a way an elevated TBS value correlates with better skeletal microstructure.OBJECTIVEEvaluate if TBS provides complementary information to T-scores of lumbar spine from DXA scans.PATIENTS AND METHODS174 postmenopausal women were included, the mean age was 66 years old (range 50-89), without previous fragility fracture or medical treatment for osteoporosis. 55 of them had normal BMI (<25), 85 overweight (BMI 25-30) and 34 obesity (BMI >30). According to bone mineral density were classified in: normal ($T > -1.0$), osteopenia ($-2.5 < T < -1.0$) and osteopososis ($T \leq -2.5$). Bone structure was classified in: normal ($TBS < 1.300$), partially degradated ($1.200 < TBS < 1.300$), degradated ($TBS \leq 1.200$). Mayor fragility fracture risk using both parameters was defined as: low (<5/1000/year), moderated (5-10/1000/year) and high (>10/1000/year).RESULTSIn the whole sample 68 women (39.1%) showed normal T-score, 81 (46.6%) osteopenia, and 25 (14.4%) osteoporosis. Osteoporosis detection was 18.2% if normal BMI, 16.5% if overweight, and only 2.9% if obesity was associated. This difference was statistically significant ($x2$, $p<0.05$).When combining T-score and TBS, mayor fracture risk was low in 75 women (43.1%), moderated in 65 (37.4%) and high in 34 (19.5%). TBS rised up 27/81 (33.3%) osteopenic women to high risk. Biggest modification was found in obesity group, 56% women were re-classified as high risk, liable to treatment.CONCLUSIONInclusion of TBS in DXA scans of lumbar spine allows to classify osteopenic women in a higher fracture risk. Obesity underestimates osteoporosis detection that can be solved by evaluating bone structure with TBS.

P932

Bone Mineral Density in Patients Treated with Antipsychotics

A. Cengiz1, V. Altınyazar2, B. G. Manoğlu2, F. Vahapoğlu2, O. Kocabaş2, I. Kurt Ömürlü3, Y. Yürekli1; 1Adnan Menderes University, Medical School, Department of Nuclear Medicine, Aydin, TURKEY, 2Adnan Menderes University, Medical School, Department of Psychiatry, Aydin, TURKEY, 3Adnan Menderes University, Medical School, Department of Biostatistics, Aydin, TURKEY.

Purpose: Antipsychotic drugs may reduce the bone mineral density (BMD). In this study we investigated the effect of prolactin levels, duration of disease, metabolic syndrome, use of mood stabilizer drug, smoking and exercise on BMD in schizophrenia and bipolar disorder patients treated with antipsychotics. Methods: 130 patients (54 females and 76 males, mean 40±12 years old) were included in the study. All patiens with diagnosis of bipolar affective disorder (30 patients) and schizophrenia (100 patients) were being treated with antipsychotic drugs. BMD was measured at the lumbar spine L1-L4, the femoral neck, the trochanteric regions of the left hip using dual energy x-ray absorptiometry (DEXA). Blood sampling was performed for prolactin levels. Arterial blood pressure, waist circumference, fasting glucose, HDL cholesterol, triglyceride levels of the patients were measured for diagnosis of metabolic syndrome. Age, weight, height, smoking habit, regular physical exercise (with a minimum duration of 30 minutes a day, three days per week) and additional mood stabilizer drugs administered were recorded. Results: In lomber region, 57 patient's BMD were normal, osteopenia was found in 45 patient and osteoporosis was found in 28 patient in terms of T score derivation. Prolactin level was high in 60 patients (normal range: 2.58-18.12). In patients evaluated for metabolic syndrome, 49 of 113 (%43) were suffering from metabolic syndrome. There was no statistically significant relationship between BMD and plasma prolactin level, using additional mood stabilizer drug, dose of antipsychotic drug and metabolic syndrome ($p>0.05$). Negative correlations between duration of illness, duration of antipsychotic drug use and BMD of femoral neck were found ($r=-0.248$ ve -0.232). Lomber BMD was significantly higher in patients who don't smoke and make exercise regularly than those of patients who smoke

and don't make regular physical exercise ($p<0.05$). Conclusion: Due to sedantary lifestyle, prolonged use of antipsychotic drugs and smoking, risk of osteoporosis can increase in patients with schizophrenia and bipolar affective disorder. BMD measurement should be performed before starting treatment with antipsychotics and BMD of these patients should be followed-up with regular intervals.

P933
Knowledge Challange: Garlet Sign on DXA Scan

N. Fatima1, M. u. Zaman2; 1Department of Nuclear Medicine, Dr Ziauddin Medical University, Karachi, PAKISTAN, 2AKUH, Karachi, PAKISTAN.

This is a 55 years old postmenopausal lady, being worked up for left sided breast cancer. On first to Radiology department she had a contrast enhanced abdomen chest CT studies and then had a Dual Energy X-ray Absorptiometry (DXA) scan (Figure 1). However, after reviewing the scan, the nuclear physician requested a repeat study after 3 days. Figure 1: DXA scan of lumbar spine on first visit. Question 1: Why a repeat study was suggested? Answer: a. Patient was not positioned properly b. Error in energy window of X-ray c. Computer error in calculating T and Z-scores d. Optimal study but with abnormally high T and Z scores Figure 2: DXA scan of lumbar spine on subsequent visit. After 3 days a repeat DXA scan done and this time exam was found satisfactory. Q2: Why abnormally high T and Z-scores got normalized? Answer a. Patient was positioned properly b. Technical error in DXA machine was rectified c. Oral contrast has been washed out d. Patient has received some treatment to bring her T and Z score into normal limits.

Comment: Correct answers are 1d and 2 c. One her first visit she had a contrast enhanced CT study which was followed by a DXA scan. Due to presence of oral gastrografin in transverse colon (visible in Figure 1 as a "Garlet Sign") this has resulted in higher photon attenuation over the lumbar spine. This attributes to falsely elevated bone mineral density (BMD), T and Z-scores for her age. Repeat scan after 3 days shows absent "Garlet Sign" due to clearance of gastrografin and correct measurement of BMD and other scores over lumbar spine. It is important to defer a DXA scan for at least 2 weeks after an intravenous contrast, 3-7 days after an oral contrast and 1-2 days after a nuclear medicine procedure performed with Tc-99m to avoid falsely high BMD, T and Z-score values.

P62 - Tuesday, October 13, 2015, 4:00 PM - 4:30 PM, Hall 3 – Poster Exhibition

Conventional & Specialised Nuclear Medicine: Infection & Inflammation

P934
FDG PET/CT in left ventricular assist device infection

D. Grigolato, M. Zuffante, E. Carmagnani, M. Cucca, E. Concia, M. Ferdeghini; Azienda Ospedaliera di Verona, VERONA, ITALY.

Aim: To evaluate the utility of FDG PET/CT in confirming or excluding the presence of left ventricular assist device infection (LVADI), defining the extent of the involvement and guiding the most appropriate therapy. Methods: Between 2013 and 2014 ten consecutive patients, all males (age 51-69, mean 60.8), with Heartmate II and infections of the skin at the exit of the driveline, underwent 16 FDG PET/CT. A whole body scan (head to feet) was performed after 1 hour from FDG injection in fasting condition. Four sites of increased FDG uptake in LVADI were recognized: of the driveline (DL), of the prosthetic device (PD), of the inflow valve housing (IV) and outflow valve housing (OV); the tracer uptake was described as focal or extensive, the grade of involvement with SUV max values and SUV ratio between infection site and liver (mild, moderate and severe) was depicted. Every site of increased uptake of FDG was checked in non-attenuation corrected images (NAC). Results: Microbiology cultures from percutaneous DL and blood mainly isolated Staphylococcus Aureus in 5 patients, coagulase-negative Staphylococci in three men and Burkholderia Cepacia in one case. Fourteen PET were positive and infectious sites were attributed to the DL in 13, IV in 8, PD in 4, OV in 7. The grade of infection was mild in 9 PET, moderate in 2 and severe in 3 scans. All patients were treated with the most suitable antibiotics according to the pathogens and the extension of the LVADI. Two patients with severe and one patient with moderate but extensive involvement at PET, who did not respond to antibiotic treatment, underwent transplantation with confirmation of the sites of infection. All patients with mild grade and focal uptake of LVADI had their personalized antibiotic treatments and they are in good life conditions at follow-up. One patient died for non-infectious reasons. In our study we did not see any changes in the OV tracer uptake during different antibiotic treatments, the SUV values and the extension of the uptake were always mild and focal respectively, suggesting a chronic inflammatory response to the prosthetic graft material rather than a site of infection. None of these patients revealed the presence of septic embolism at PET imaging. Conclusion: In this small sample of patients, FDG PET/CT was helpful to the clinicians in recognizing the sites, the extension and grade of LVADI, which had important implications on patient management.

P935

Diagnosis value of 18F-FDG PET/CT with myocardial suppression in the deteccion of cardiovascular implantable electronic device infections

U. Granados, D. Fuster, J. Pericas, S. Ninot, J. Tolosana, A. Moreno, C. Falces, J. Miro, F. Lomeña; Hospital Clínic, Barcelona, SPAIN.

Aim: To asses the usefulness of 18F-Flurodeoxyglucose positron emission tomography/computed tomography (18F-FDG PET/CT) with myocardial suppression in patients with suspected infection of cardiovascular implantable electronic device (CIED). Material and Methods: A total of 19 consecutive patients (mean age 68±18.0 years) with suspected CIED infection (11 pacemakers and 8 implantable cardiac defibrillators) were prospectively included. All patients underwent whole-body 18F-FDG PET/CT with myocardial suppression protocol (Heparin 50 UI/Kg). The results were interpreted by two experienced nuclear medicine physicians. All of the patients were subjected to clinical, microbiological, and echocardiographic evaluation. Diagnosis of infection was made by microbiological documentation of explanted devices or clinical follow-up for 12 months. Results: 7/19 patients (37%) were diagnosed of CIED infection (4 implantable cardiac defibrillators and 3 pacemakers). Sensitivity, specificity, NPV and PPV of 18F-FDG PET/CT were 84%, 92%, 91% and 83%, respectively. The overall accuracy of 18F-FDG PET/CT in the detection of CEID infection was 84%. In two patients 18F-FDG PET/CT was the only technique to identify infection. As and additional contribution 18F-FDG PET/CT imaging revealed 5 unexpected extracardiac findings in 4 patients diagnosed of pulmonary embolism (n=2), splenic embolism (n=1), spondylodiscitis (n=1) and high grade villous colon adenoma (n=1). Conclusions: This study suggests that 18F-FDG PET/CT may be relevant in the evaluation of patients with a suspected CIED infection. 18F-FDG PET/CT can detect unexpected embolic infection which influence in the therapeutic management of the patients.

P936

Diagnostic value of 18FDG PET imaging patients with clinical suspicion of vasculitis

E. Piekarski, F. Hyafil, N. Mikail, B. Mahida, J. Slama, E. Blanchet, J. Calais, H. Regaieg, R. De Paola Chequer, F. Rouzet, D. Le Guludec, K. BenAli; Bichat's hospital, Paris, FRANCE.

Introduction: The diagnosis of large vessel vasculitis relies on the association of clinical, biological and histological criteria but can sometimes be difficult. In this study, we evaluated the diagnostic performances of 18FDG-PET imaging in a large monocentric cohort of patients with a clinical suspicion of active vasculitis. Material and methods: A total of 152 patients with a clinical suspicion of vasculitis were sent in our department for 18FDG-PET imaging. Patients were imaged with PET 90 minutes after injection of 4 MBq/kg. 18FDG-PET imaging was found positive (1) for active vasculitis in presence of high 18FDG uptake in the aorta and supra-aortic trunks wall using a semi-quantitative visual scale; (2) for polymyalgia rheumatic (PR) in presence of high 18FDG uptake in proximal joints (pelvic and scapular girdle) and in spinous processes of cervical and lumbar spine. Clinical outcome of all patients was collected one year after 18FDG-PET imaging. Patients were considered as presenting active vasculitis and/or PR based on validated clinical criteria either at time of the scanning or during FU. Results: From the 152 patients imaged with 18FDG-PET imaging, 34 patients (22,4%) were considered as presenting an active vasculitis or PR. Twenty patients (13,1%) presented isolated giant cell arteritis (GCA), 4 combined GCA and PR (2,6%), 1 patient Takayasu arteritis (0,6%), 9 patients isolated PR (5,9%). From the 34 patients, active vasculitis or PR was confirmed in 25 patients. In the remaining 9 patients with positive 18FDG-PET, diagnosis of active vasculitis or PR was not clinically confirmed (atheromatous disease was considered in 4, 1 had CADASIL associated with atheromatous disease, 2 had ankylosing spondylitis and psoriatic arthritis). In the 118 patients with negative 18FDG-PET imaging, only three patients had a confirmed GCA on histology. These 3 patients had all been treated by corticotherapy before the imaging. The remaining 115 patients did not present any sign of vasculitis during a 1-year follow-up. 18FDG-PET imaging demonstrated sensitivity of 89,2%, specificity of 92,7%, predictive positive and negative value of 73,5% and 97,4% for the diagnostic of active vasculitis or PR. Conclusions: In this monocentric cohort of 152 patients with a clinical suspicion of active vasculitis, 18FDG-PET imaging demonstrated good diagnostic performances for the detection for active vasculitis and PR. This confirms that 18FDG-PET imaging has an incremental role over usual criteria for the early identification of active vasculitis.

P937

FDG-PET in suspected infection versus loosening of Orthopedic Fixation Device (rods, plates, screws, and wire loops) - correlation with cultures.

S. Raja1,2, N. Alnakshabandi2, S. George3, M. AlHarbi2, R. Sergey2; 1Baylor College of Medicine, Bellaire, TX, UNITED STATES, 2KFMC, Riyadh, SAUDI ARABIA, 3Johns Hopkins Aramco Healthcare, Dhaharan, SAUDI ARABIA.

Objectives: Orthopedic devices (ODev) including rods, plates, screws, chains, and wire loops etc. (RO, PL, SC, CH, WL) are

increasingly used for fracture fixation. Despite the deployment of conventional multimodality imaging, the diagnosis of infected ODev/ underlying osteomyelitis (Uost) in traumatized bone continues to be challenging. Recently, FDG-PET has been found to be encouraging in the evaluation of MSK infections. We explored the utility of PET in evaluating suspected ODev infections/Uost - post hardware placement. Methods: Retrospective review of all PET scans from 2012 to current revealed 15 pts (male=9, female=6, mean age=41.5 yrs) scanned for suspected infected ODev/Uost post hardware placement. The PET-CT fusion images were reviewed interactively on a dedicated workstation, findings on PET were correlated with cultures (when available), and clinical follow-up. Results: Out of total 160 ODev, 7 (6/128 SC, and 1/9 WL) were infected in 6/21 pts. The remaining 8/8 RO, 12/12 PL and 3/3 CH were not infected. In all 6 pts with infected ODev, concurrent 3-Phase Bone Scan (3PhBS) was +ve on blood pool and delayed phases. In discordant 3-PhBS +ve on delayed phase only and -ve on PET, cultures/followup were -ve for infection/Uost. In 1 pt. two SC were +ve for infection by concurrent PET and 3PhBS, however, repeated biopsies showed nonspecific granulating tissue. Correlative multimodality imaging i.e. plain films, MRI, diagnostic CT, routine 3PhBS and Ga-67 were complementary to PET. Not documented observations suggest that concurrently negative PET and bone scans essentially rule out infected ODev and/or Uost in traumatized bone, while increasing the confidence in interpretation of PET. MRI was not efficacious in evaluating ODev, and was falsely suspicious for Uost in 2 cases. In 4/5 cultures from extracted Odev PET was true positive. Conclusions: Findings in our series suggest that FDG may be superior to contemporary multimodality imaging for evaluating suspected infections complicating orthopedic fixation devices. Literature search suggests that our group is the 1st to present comprehensive utility of PET-CT in infected hardware.

P938
FDG PET/CT and WBC scan in vascular graft infection

M. Pacilio, C. Lauri, F. Trapasso, I. Baldazzi, D. Prosperi, A. Lenza, C. Tirotti, M. Taurino, F. Scopinaro, A. Signore; Università Sapienza Roma, Rome, ITALY.

Introduction: there are few studies comparing [18F]FDG-PET/CT and scintigraphy with 99mTc-HMPAO-WBC in the diagnosis of vascular prostheses infections. Moreover, the distribution patterns of FDG and of radiobelled-WBC in patients with endoprosthesis, in relation to the type of stent and time from surgery, is not know. Aim: to compare [18F]FDG and 99mTc-HMPAO-WBC in patients operated with vascular endoprosthesis Endurant® and to define the patterns of normality and abnormality for both radiopharmaceuticals. Materials & Methods: 16 patients, that underwent an endovascular exclusion of abdominal aneurysm with Endurant® endoprostheses, were retrospectively enrolled in the study. Half of patients had suspicion of infection (based on CT, ESR, GB, PCR, fever), half were clinically and biochemically infection free and were operated 8-41 months before. Each patient performed both scans. For WBC: dynamic images were acquired on the abdomen in the anterior-posterior from time 0 to 2.5 minutes (one frame every 4 seconds for 40 frames). Planar images were acquired on the abdomen in antero-posterior and oblique front left and right. The first set of images was acquired 10 minutes after administration of WBC (100 seconds acquisition time), the second set at 3h (141 seconds acquisition), the third set at 20h (1040 seconds acquisition). For PET: images were acquired 1h after administration of 185 MBq [18F]FDG. All images were examined by 2 independent physicians. Qualitative analysis was performed for WBC scans and both qualitative and semi-quantitative analysis (SUV_{max} and $SUV_{maxT}/SUV_{meanBKG}$) was performed for PET scans. Final diagnosis was made by clinical-surgical follow-up. Results: no patients of first group had an infection but 5 of second group were infected. All patients but 1 were correctly identified using the following interpretation criteria: for WBC scan, positivity for infection is represented by the accumulation of radioactivity with time in the peri-prosthetic tissue; negativity for infection was consistent with no uptake in peri-prosthetic tissues; for FDG-PET/CT, positivity was characterized by an inhomogeneous intra- and extra-vascular uptake with a $SUV_{max} \geq 3.6$ and a $SUV_{maxT}/SUV_{meanBKG} > 3.0$; negativity was considered an homogeneous uptake with an $SUV_{max} < 3.6$ and a $SUV_{maxT}/SUV_{meanBKG} \leq 2.0$. The only discordant case (FDG positive and WBC negative) had no infection. Conclusions: PET/CT with FDG seems to be equally sensitive than WBC but less specific using the above mentioned interpretation criteria. Patients with an Endurant® type of endoprostheses and no infection, have a negative FDG and WBC scan from 8 months after surgery.

P939
Assessment of the Diagnostic Performance of Quantitative FDG-PET/CT Parameters in the Detection of Vascular Graft Infection

S. Houshmand1, A. Salavati1, M. Sadic2, K. T. Pedersen3, A. Alavi1, P. F. Høilund-Carlsen3, **S. Hess**3; 1University of Pennsylvania, Philadelphia, PA, UNITED STATES, 2Ankara Training and Research Hospital, Ankara, TURKEY, 3Odense University Hospital, Odense, DENMARK.

AIM: Vascular graft infections are associated with significant morbidity and mortality. The diagnosis may be difficult and

accurate and precise diagnostic tools are pivotal to improve patient management and outcome. Visually assessed FDG-PET/CT has been suggested as a reliable modality in this setting, albeit with relatively poor specificity especially infections early after surgery. In this study, we explored the potential of novel quantitative parameters derived from FDG-PET/CT in suspected vascular graft infections. MATERIAL AND METHODS: Thirty-one patients with suspected vascular graft infections were retrospectively included in this study. Comprehensive data on all diagnostic procedures, results of cultures, events during follow-up, and treatment regimens were obtained through reviews of the patients' medical charts. Final diagnoses were based on all available clinical information including results of surgical revisions, cultures, and/or follow-up. Quantitative analyses were obtained by dedicated software using an adaptive contrast-oriented thresholding algorithm. Three-dimensional regions of interest were placed around the sites of suspected infection by an experienced physician and metabolically active volume (MAV; i.e. a volume with an uptake above a specified threshold), maximum standard uptake values (SUVmax), mean SUV (SUVmean), total lesion glycolysis (TLG=MAV*SUVmean), and SUVpeak (i.e. the average SUV within a 1 cubic cm volume of the lesion with the highest uptake) were calculated. Receiver operating curve (ROC) was performed for assessment of diagnostic performance of the volumetric FDG-PET/CT parameters. RESULTS: Eleven female and 20 male patients aged 37-82 years old (median age 70) were included. Median graft age was 11 months (range 1-144 months). Several graft types were represented, i.e. aorto-bifemoral (n=16), aortic (n=7), femoro-femoral (n=5), axillo-bifemoral (n=2), femoro-popliteal bypass (n=1). Infection was the final diagnosis in 19 patients (61%). The areas under the ROC curves were 0.883 for TLG, 0.876 for SUVpeak, 0.849 for SUVmax and 0.823 for MAV and SUVmean ($p<0.001$). TLG > 54.6, SUVmax > 4.5, and SUVmean > 2.6 all yielded 94.7% sensitivity, 72.7% specificity with positive predictive values (PPV) of 84%, and negative predictive values (NPV) of 89%. SUVpeak > 3.6 had a sensitivity of 94.7% and a specificity of 81.8% with PPV and NPV of 89% and 90%, respectively. MTV > 18.6 was 84% sensitive and 72.7% specific with PPV=82% and NPV=74%. CONCLUSION: In suspected vascular graft infection, quantitative parameters obtained from FDG-PET/CT seem feasible with relatively high sensitivity, specificity, and predictive values. However, larger scale prospective studies are needed to conclude further on the potential of this technique.

P940

Usefulness of (18)F-FDG PET/CT in the infections of peritoneal catheter

S. SANFILIPPO, A. Svirydenka, P. Ghedini, P. Castellucci, R. Bonfiglioli, S. Diodato, S. Cambioli, S. Fanti; Azienda ospedaliero-universitaria S.Orsola-Malpighi, Bologna, ITALY.

Aim: The aim of our study was to evaluate the diagnostic role of (18)F-FDGPET/CT in the detection of the site of infection in patients with peritoneal catheter during peritoneal dialysis (PD). Material and Methods: we enrolled 20 patients (10 women; 10 men; mean age 61y; range 31-87y) between October 2010 and January 2015, with the clinical suspicious of infection in the peritoneal catheter. All the enrolled patients were treated with peritoneal dialysis due to chronic kidney failure. All patients underwent (18)F-FDGPET/CT scan, performed according to standard procedure. We evaluated 18F-FDG uptake in the soft tissue contouring the peritoneal catheter. Any uptake higher than the liver has been considered positive. (18)F-FDG PET/CT findings were validated by clinical and/or cytological and biochemical findings during follow up. Thirteen out of 20 enrolled patients were symptomatic (fever of unknown origin (FUO), asthenia, clinical observation like heat and redness of the skin); 5/20 patients had positive laboratory findings; 2/20 had suspicious US findings. Results: (18)F-FDG PET/CT resulted positive in 12/20 patients. Among these: 8 pts were confirmed to be positive by cytological analysis (Staphylococcus Aureus and Pseudomonas Aeruginosa). The remaining 4 pts were referred to (18)F-FDG PET/CT for FUO and/or positive laboratory tests. In these patients cytological analysis performed in the site of peritoneal catheter resulted to be negative. Among the 8/20 negative (18)F-FDG PET/CT, one was false-negative, as shown by the result of cytological analysis (Staphilococcus). The remaining 7 patients were (18)F-FDG PET/CT true negatives, according to normalization of inflammatory markers in subsequent clinical and laboratory follow-up without any kind of therapy. According to our results (18)F-FDG PET/CT showed: Sensitivity: 88%, Specificity: 64%. and Accuracy 75%. Conclusions: main limitations of our study is the small number of patients enrolled. According to our preliminary data however, (18)F-FDG PET/CT could have an effective role in establishing the presence and the extent of the infections of peritoneal catheter. Keywords: (18)F-FDG PET/CT; infection; peritoneal catheter; FUO.

P941

Fever of Unknown Origin (FUO). Utility of 18F-FDG PET-CT.

C. Riola-Parada1, M. N. Cabrera-Martín2, O. Salsidua-Arroyo1, M. Pedrera-Canal1, M. Martínez-de-Bourio1, E. Cala-Zuluaga1, L. Lapeña-Gutierrez2, R. Couto-Caro1, J. L. Carreras-Delgado2; 1Nuclear Medicine Department. Hospital Clínico San Carlos, Madrid, SPAIN, 2Nuclear Medicine Department. Hospital Clínico San Carlos. Universidad Complutense, Madrid, SPAIN.

Objectives: The aim of this study was to evaluate the utility of 18F-FDG PET-CT in the identification of the causes of

FUO.Material and methods:A retrospective study was performed in 51 consecutive patients with FUO (34 men and 17 women, mean age 61years, range 21-89) who received 18F-FDG PET-CT examination from December 2008 to December 2014.All patients met the Durack and Street criteria for FUO and signed informed consent form.Final diagnosis was obtained through microbiological and histopathological examination and clinico- radiological follow-up.Mean follow-up was 7,02 months (range 0,17-23,30).Results:30 of 51 studies (59%) showed abnormal findings.Among the true positive studies (29), the cause of fever was infection in 17 patients, inflammatory process in 7, malignancy in 4 and miscellanea (ischemic colitis) in one patient.The only one false positive case showed increased FDG uptake in bone marrow suspicious for lymphoproliferative syndrome. Bone marrow biopsy was negative, and final diagnosis was mesenteric panniculitis and febrile neutropenia, without evidence of localized infection.8 studies were considered true negative because etiology was not identified despite diagnostic procedures and clinico-radiological follow-up (mean 6.74 months).Among the false negative studies (13), the cause of fever was infection in 7 patients, inflammatory process in 5 and miscellanea (dysautonomia in the setting of degenerative neurologic disease) in one patient.Accuracy was 72%, sensitivity 69%, specificity 89%, positive predictive value 97% and negative predictive value 38%.Conclusion:18F-FDG PET-CT contributes significantly in the etiologic diagnosis of FUO. 18F-FDG PET-CT should be included in diagnostic protocols of FUO.

P942
The Clinical Value of FDG-PET/CT in Bacteraemia of Unknown Origin: A Retrospective Study

M. B. Brøndserud1, S. Hess1, A. H. D. Johansen1, C. Pedersen2, P. F. Høilund-Carlsen1; 1Dept. of Nuclear Medicine, Odense University Hospital, Odense, DENMARK, 2Dept. of Infectious Diseases, Odense University Hospital, Odense, DENMARK.

AIM: Gram-positive bacteraemia without a known focus of infection (i.e. bacteraemia of unknown origin; BUO) is a serious condition associated with high morbidity and high mortality. A fast and reliable diagnosis is imperative to institute targeted treatment at an early stage and avoid delay in diagnosing clinically "silent" foci of infection, which may otherwise give rise to complicated and prolonged disease courses. The diagnostic process relies traditionally on extensive clinical, microbiological, and serological testing, and a variety of sometimes futile diagnostic and imaging procedures, including invasive ones. We investigated the clinical value of FDG-PET/CT in BUO. MATERIAL AND METHOD: Our retrospective study population comprised patients admitted to Odense University Hospital in 2013 with gram-positive BUO who subsequently underwent FDG-PET/CT. Patients were excluded if they had active cancer and no baseline FDG-PET/CT scan. Clinical data was collected from the patients' medical records. A final decision about the origin of bacteraemia was based on the entire patient course and included all available data. This served as a composite reference standard for comparison with the result of the FDG-PET/CT scan. FDG-PET/CT was considered of high clinical impact if it correctly revealed sites of bacteraemia (in agreement with the composite reference standard) in areas not assessed by other imaging modalities, or if other imaging modalities where negative or equivocal in these areas, if it established a new diagnosis, and/or changed the antimicrobial treatment. All other results were considered of low clinical impact. RESULTS: A total of 67 patients were evaluated, 4 were excluded. The remaining 63 patients were 29 females and 34 males with a mean age of 69.3 years (range 23-94). The median time span from BUO was suspected to FDG-PET/CT was performed was 6 days (range 2-21). FDG-PET/CT located the source of bacteraemia in 62% (95% CI: 49-74) of patients, and had a high clinical impact in 56% (95% CI: 43-68). Patients underwent in median 5 (range 2-19) examinations prior to FDG-PET/CT, and 2 (range 0-19) examinations afterwards. CONCLUSION: FDG-PET/CT appears to be a reasonable first-line modality in BUO with high clinical impact in more than half of the patients and a potential to obviate a substantial number of futile examinations. Our results were limited by their retrospective nature, but highlight the need for prospective studies of FDG-PET/CT in BUO.

P943
Comparison of 18F-FDG-PET/CT and 99mTc-HMPAO-labelled-leukocyte SPECT/CT in the evaluation of patients with fever

G. Cusato1, P. Ferro1, S. Fiorino1, M. Spallino1, C. E. Popescu2, R. Sara2, M. Milella2, G. Cabrini2, C. Rossetti2; 1Università Milano-Bicocca, Milano, ITALY, 2Ospedale Niguarda, Milano, ITALY.

Aim: Inflammatory and infectious processes are a heterogeneuos class of diseases with a wide setting of presentation, including fever. Early diagnosis is crucial and involve CT, blood cultures, serological tests and Nuclear Medicine tecniques such as PET/CT with 18-F-FDG and SPECT/CT with 99mTC-HMPAO labelled leukocyte. The aim of our preliminary study was to compare the clinical value of the two techniques in localizing infection loci in patients with fever. Methods: we retrospectively analysed 24 consecutive patients (10 women and 14 men, age range 5-85 years) with fever and no other significative symptoms undergoing both 18F-FDG-PET/CT and 99mTc-HMPAO-SPECT/CT for precise

anatomical mapping . Patients were under investigations for: fever of unknown origin (FUO) (9), endocarditis (4), vascular prosthetis infection (3), heart device infection (1), identification of unknown septical foci (3), evaluation of surgical wounds (3), cerebral aracnoiditis(1). Both methods were considered "positive" or "negative" on agreement of 3 independent observers on qualitative analysis of the images. Final diagnosis was based on biopsy/microbiological findings, and/or clinical/serological/imaging follow up. Results: In FUO, concordance was observed in 5/9 patients : 4 both negative (in 3/4 no cause of FUO was found on further investigations, 1/4 had a hodontegenous sepsis) and 1 both positive (pace-maker). There was discordance in 4/9 patients, with positive 18F-FDG-PET/CT and negative 99mTc-HMPAO-SPECT/CT. In these 4 patients the diagnosis of inflammation was confirmed by further investigations, in particular the final diagnosis were pericarditis, aortititis, inflammation of hepatic cysti and inflammatory paravertebral expance. In suspected endocarditis, SPECT/CT and PET/CT showed concordance in 2/4 patients: 1 positive (increasing levels of PCR and no antibiotic therapy), 1 negative (diagnosis of endocarditis later rejected). In 2/4 patients there was discordance: both positive on PET/CT and negative on SPECT/CT (endocarditis confirmed by further follow up). Discordance was found also in identification of unknown septical foci (1/3), evaluation of surgical wounds (3/3). PET/CT showed an overall higher lesion detection rate (22vs5). Conclusion: PET/CT detected more lesions, whereas SPECT/CT added value was to exclude an ongoing infection mainly in FUO. Even in this limited group of patients, PET/CT seems to be a better tool in the evaluation of suspected endocarditis. Hybrid imaging allows better anatomical correlation and may improve the inflammatory/infection disease management. Signs of acute infection (especially PCR levels and fever) should be considered in choosing 99mTC-HMPAO-SPECT/CT over 18F-FDG-PET/CT, even if influenced by the ongoing antibiotic therapy.

P944

Complementary roles of retrospectively co-registered PET and MR in evaluation of suspected osteomyelitis of foot.

S. Raja1,2, N. Alnakshabandi2, S. George3, M. AlHarbi2, S. Rumyantsev2; 1Baylor College of Medicine, Bellaire, TX, UNITED STATES, 2KFMC, Riyadh, SAUDI ARABIA, 3Johns Hopkins Aramco Healthcare, Dhahran, SAUDI ARABIA.

Accurate diagnosis of Osteomyelitis (Osteo) often necessitates multimodality imaging including MR and scintigraphy. Though MR is very sensitive, it is limited in its specificity; especially in post-surgical settings, post hardware placement, and in violated bone. FDG-PET is emerging as an important tool in MSK infections. We exhibit difficult/complicated cases of Osteo, wherein PET has been helpful. Furthermore the complementary roles of PET and multiparametric MR in comparison with conventional imaging (plain films, CT and scintigraphy) will be illustrated. Materials: Retrospective review of radiology archives revealed 12 pts. (Male = 9, Female = 3; mean age= 38.3 yrs). All PET and MR scans were acquired per accepted protocols. The case mix was as follows: suspected Osteo in foot 6, pelvis 2, skull base 2, chest 1, and spine 1. Teaching points: 1. Unique findings on both MR and PET in Madura Foot. 2. Utility of 3D rendered PET, and PET-CT/MR fused images to track the sinuous sinus tracts in 2 pts (1 pt. with infected cardiac pacemaker wire sinus formation tunneling parallel to the sternum from pericardium to subcutaneous tissue, and draining pus. 3. Superior efficacy of PET as compared to MR in complicated Osteo, such as infected hardware. 4. Utility of functional MR (DWI-ADC) and PET-SUV in quantitating response to antibiotic therapy utilizing maxSUV and ADC estimates derived from PET and MR. 5.Resolving indeterminate findings on either MR or PET with the help of its coadjutor PET or MR respectively. 6. Use of Novel coregistration algorithm (MIMsoft, Cleveland Ohio, USA) in accurately co-registering often technically difficult to coregister and fuse feet and ankle 3D PET and MR datasets. Conclusion: Our unique series will illustrate the need for coregistering PET and MR images, and interactively review the fused datasets for an accurate diagnosis. Findings in our series concur that PET and MR are complementary in pts. with complicated Osteo.

P945

SPECT/CT value in the diagnosis of diabetic foot infections by 99mTc-HMPAO-labeled leucocyte scan

S. Georga1, C. Manes2, D. Lo-Presti1, V. Mpalaris1, I. Tsavdaridis2, I. Iakovou1, D. Katsaboukas1, V. Athanasiou1, K. Badiavas1, A. Doumas1, G. Arsos1; 13rd Dept of Nuclear Medicine, Aristotle University Medical School, Papageorgiou Hospital, THESSALONIKI, GREECE, 2Diabetes Center, Papageorgiou Hospital, THESSALONIKI, GREECE.

Introduction-Aim: Scintigraphy with in vitro labeled leucocytes is a well established method for diagnosing diabetic foot osteomyelitis (DFO). However, poor spatial resolution and lack of anatomic landmarks often limit the ability of labeled leucocyte scan to discriminate bone from soft tissue infection, especially in areas with small bone structures as in the foot. The aim of the study was to evaluate the contribution of SPECT/CT as an adjunct to planar images of 99mTc-HMPAO-labeled leucocyte scan (LS) for diagnosing and localizing infection in the diabetic foot. Patients and methods:

Thirty-one consecutive patients with clinical suspicion of DFO or under antibiotic treatment for proven DFO were included in the study. Totally 40 pedal sites suspected for DFO were investigated. Planar images were acquired 1 and 4 hours post injection of in vitro labeled autologous leucocytes followed by a SPECT/CT scan at the end of the study. LS images were interpreted alone and in conjunction with SPECT/CT scans and were considered to be positive for DFO when focally increased persistent leucocyte bone uptake was observed. Final diagnosis was based on clinical and radiological follow-up or surgical findings. Results: Among the 40 pedal sites investigated, 7 cases of DFO, 5 cases with Charcot arthropathy without osteomyelitis, 14 sites with simple soft tissue infection and 14 sites of cured DFO were finally diagnosed. LS planar images showed increased leucocyte accumulation compatible with active infection in 26 of 40 sites, and were negative for active infection in 14 of 40 sites. In patients with positive scans, the addition of SPECT/CT correctly localized infection to bone in 7/7 sites with DFO and to soft tissues in 32 sites, changing the interpretation of planar images in 12 of 26 patients (46%) with positive scans. On the contrary, the addition of SPECT/CT did not significantly altered the evaluation of patients with negative LS planar scans as it changed the interpretation of planar images in only 1 patient. Totally, the addition of SPECT/CT improved the diagnostic accuracy of LS for DFO from 85.0% to 97.5%. Conclusion: SPECT/CT enhances the diagnostic performance of 99mTc-HMPAO-labelled leucocyte scan for diabetic foot infections. The CT component of SPECT/CT provides accurate anatomical localization of increased leucocyte uptake, enabling discrimination of bone from soft tissue infection and better assessment of the extent of infection.

P946

99mTc-HMPAO white blood cell labelled scintigraphy in patient with osteosynthesis material and inter-observer reproducibility

E. Noriega, M. Bajén Lázaro, A. Benítez Segura, A. Rodríguez-Gasén, P. Saldaña, O. Puig Calvo, G. Martínez Pimienta, M. Boya Román, J. Mora Salvadó; Hospital Universitari de Bellvitge-IDIBELL, L'Hospitalet de Llobregat (BARCELONA), SPAIN.

Aim: Scintigraphies with 99mTc-HMPAO labelled white blood cells (SWBC) in patients with osteosynthesis material and suspected bone infection are not easy to interpret and, because of this, often inter-observer discrepancies exist. The aim of this study is to evaluate the inter-observer reproducibility when interpreting the SWBC planar images in patients with osteosynthesis material and suspicion of bone infection. Materials and methods: Prospective study of 41 patients (29 women, age between 40 and 86 years old) with osteosynthesis material and suspected bone infection (25 patients had a knee prosthesis, 11 had a hip prosthesis, one had a shoulder prosthesis and 4 had other osteosynthesis material). Planar images with 99mTc-HMPAO labelled white blood cells were acquired at 30 minutes, 4, 8 and 24 hours with acquisition times of 5, 8, 12 and 20 minutes respectively (acquisition time corrected for decay). The unprocessed images were reviewed by 4 nuclear medicine specialists (with more than 10 years of experience) independently and blinded to other diagnostic tests and/or clinical course. The scintigraphy was considered negative when there was no leukocyte accumulation, and positive, when there was leukocyte accumulation that increased over time (in extension or intensity). The definitive diagnostic was obtained by culture/biopsy or after six months of follow up. Statistical calculation was done using the kappa coefficient (κ), the interpretation of which is done by correlating its value with a qualitative scale that includes six levels of strength agreement: 0 (Poor); from 0.01 to 0.20 (Mild); from 0.21 to 0.40 (Acceptable); from 0.41 to 0.60 (Moderate); from 0.61 to 0.80 (Considerable) and from 0.81 to 1.00 (Almost perfect). Results: The overall inter-observer κ value was $\kappa = 0.739$, indicating a considerable agreement between the observers. The agreement in the studies that were considered negatives was considerable ($\kappa = 0{,}758$), but in those considered positive it was just acceptable ($\kappa = 0{,}444$). Conclusion: This study has demonstrated considerable inter-observer agreement in the interpretation of the planar images of SWBC in patients with osteosynthesis material and suspicion of bone infection. The agreement in negative studies is higher than in positive studies.

P947

Contribution of labelled leukocytes scintigraphy with decay correction at 8 or 24 hours in the diagnosis of osteoarticular infection

J. Rodríguez-Rubio Corona1, E. Noriega Álvarez1, I. Gil Viciano1, A. Rodríguez-Gasén1, A. Benítez-Segura1, I. Romero-Zayas2, G. Martínez-Pimienta1, M. Boya-Román1, M. Roca Engronyat1; 1Nuclear Medicine Department, Hospital Universitari de Bellvitge-IDIBELL, L'Hospitalet de Llobregat (Barcelona), SPAIN, 2IDI-PET Unit, Hospital Universitari de Bellvitge-IDIBELL, L'Hospitalet de Llobregat (Barcelona), SPAIN.

AIM: In bone infection diagnosis by labelled leukocyte scintigraphy (LLS) it is important to perform delayed images, at 8 or 24h, although in clinical guidelines they are optional registrations. The objective of this study is to demonstrate that delayed images are essentials in bone infection diagnosis. MATERIAL AND METHODS: - 70 patients were studied (43 women, 22-83 years old) with suspected osteoarticular

infection. - The labelling of leukocytes with 99mTc-HMPAO was based on EANM guideline (2010). - Planar images with 99mTc-HMPAO labelled with white blood cells (WBC) were acquired (with high resolution and low energy collimator) at 30 minutes, 3, 8 and 24 hours after reinjection of labelled WBC with acquisition times of 5, 8, 12 and 20 minutes respectively (acquisition time corrected for decay). - Three groups of images have been evaluated by two expert nuclear physicians: A: 30 minutes and 3 hours images; B: 30 minutes, 3 hours and 8 hours images; and C: 30 minutes, 3 hours and 24 hours images. - The scintigraphy was considered negative when there was no leukocyte accumulation, and positive, when there was WBC accumulation that increased over time (in extension or intensivity). The definitive diagnostic was obtained by culture/biopsy or after six months of follow up. - Sensitivity (SE), specificity (SP), positive predictive value (PPV), negative predictive value (NPV) and accuracy (ACC) have been analysed. RESULTS: - Definitive clinical diagnosis: 19 patients with bone infection and 51 patients without bone infection. - Scintigraphy diagnosis: A. (30 min-3h): 45 patients with scintigraphy suggestive of infection (LLS +) and 25 with negative scintigraphy (LLS-) (29 false positives). B. (30 min-3h-8h): 20 with LLS+ and 50 with LLS- (4 false positives). C. (30 min-3h-24h): 16 with LLS + and 54 with LLS- (2 falses positives). The values of SE, SP, PPV, NPV and ACC were the following for the different groups: A. SE=84.2%, SP=43.1%, PPV=35.6%, NPV=88%, ACC=54.3%. B. SE=84.2%, SP=92.2%, PPV=80%, NPV=94%, ACC=90%. C. SE=73.7%, SP=96.1%, PPV=87.5%, NPV=90.7%, ACC=90%. CONCLUSION: The implementation of delayed images with 99mTc-HMPAO labelled WBC in bone infection diagnosis is essential because it decreases significantly the rate of false positives and, therefore, increases the specificity and positive predictive value.

P948

Effectiveness of 18F-FDG PET/CT in patients with suspected residual spinal infection, with or without surgical device : a prospective 30 case study.

A. DUTERTRE; CHU Bordeaux, BORDEAUX, FRANCE.

Aim of the study : Evaluate the predictive value of 18F-fluorodeoxyglucose Positron Emission Computed Tomography (18F-FDG PET/CT) in patients with suspected residual spinal infection (SI), after antibiotic treatment, compared to magnetic resonance imaging (MRI).Materials & Methods : From March 2010 to June 2013, 30 patients with suspected residual SI were involved in a prospective monocentric study after well conducted treatment. They all underwent a 18F-FDG PET/CT and an MRI. Each modality was blindly interpretated by 2 physicians in a qualitative way. For 18F-FDG PET/CT, we added a combined "qualitative-quantitative" analysis with a ratio of maximum standard uptake value (SUV) (SUVmax) compared to reference (healthy vertebral body). A 1-year follow-up examination was performed.Results : Among the thirty patients, only 7 presented a residual SI at the 1-year follow-up examination : 1 patient underwent a biopsy and 6 patients presented a clinical or biological unfavorable outcome. For qualitative and combined "qualitative-quantitative" (with a threshold of SUVmax ratio = 2,3), the sensitivity, specificity, positive (VPP) and negative (VPN) predictive values were respectively 85,7%, 73,9%, 50%, 94,4% and 85,7%, 82,6%, 60%, 95%. Out of 27 MRI, the values were respectively of 66,6%, 61,9%, 33,3% and 86, 6%. Diagnosis performances of 18F-FDG PET/CT were higher than those of MRI but non significantly (p=0.295). FDG uptake patterns were determined to differenciate infected from non-infected patients.Conclusion : Our results suggest that 18F-FDG PET/CT may be useful for evaluating patients with suspected residual SI after treatment, moreover in post-operative cases where F-18 FDG PET/CT seems to be more effective than MRI with a high VPN.

P949

The role of 18F-FDG PET / CT in HIV positive patients.

R. BONFIGLIOLI, T. Graziani, F. Ceci, S. Sanfilippo, L. Zanoni, C. Pettinato, M. Bartoletti, P. Viale, C. Nanni, P. Castellucci, S. Fanti; Azienda ospedaliero-universitaria S.Orsola-Malpighi, BOLOGNA, ITALY.

AIM: to investigate the role of 18F-FDG-PET/CT in detecting eventual co-morbidity in patients with HIV positive serology and to evaluate the added value of 18F-FDG-PET/CT to change the therapeutic approach.MATERIALS AND METHODS:Inclusion criteria were: a) HIV positive serology; b) suspected or already known tumors (lymphoma or other tumors HIV-related) or suspected infections; c) 18F-FDG-PET/CT performed for clinical/diagnostic suspicious of co-morbidity d) histological validation of 18F-FDG-PET/CT positive findings.We retrospectively analyzed 79 HIV patients studied with PET/CT from 2008 to 2013. Twenty seven out of 79 fulfilled the inclusion criteria of a full clinical profile and histological diagnosis of the 18F-FDG-PET/CT positive findings.RESULTS:In 4/27 of patients 18F-FDG-PET/CT revealed 2 progressions (lymphoma) and 2 relapse (Kaposi Sarcoma of the face and hepatocellular carcinoma) of the known malignant disease. These findings were later confirmed by biopsy and the management was changed according to 18F-FDG-PET/CT results. In 4/27 patients 18F-FDG-PET/CT showed new malignancy not previously diagnosed (2 lymphoma:1 hepatic,1 diffused with bone involvement; 2 cancer-HIV related: 1 Bartolini gland cancer, 1 mesenchymal

sarcoma) and confirmed to be as true positive by biopsy on 18F-FDG PET/CT findings.In 7/27 18F-FDG-PET/CT resulted negative, but in one patient autopsy revealed the presence of a malignancy (penis cancer). Two out of 7 patients, had inflammation described by 18F-FDG PET/CT and not suspected before in which 18F-FDG PET/CT has been able to guided biopsy and the subsequent therapy (1 was consistent with RCU, 1 was an infected ascitis).In 3/27 patients unexpected lung infections have been diagnosed by 18F-FDG-PET/CT, and later confirmed by bronchoscopy.Finally in 13/27 (48%) 18F-FDG PET/CT changed the clinical management and in 14/27 patients no significant changes of the therapeutic approach have been performed on the basis of 18F-FDG PET results.CONCLUSIONS:Main limitation of our study is the small number of patients investigated. In our series 18F-FDG-PET/CT proved to be a useful imaging technique to investigate HIV patients proving an added value to change the therapeutic strategy in almost the half of the patients.

P950
FDG PET/CT in pulmonary aspergillosis

D. Grigolato, M. Zuffante, M. Cucca, E. Carmagnani, E. Concia, M. Ferdeghini; Azienda Ospedaliera di Verona, VERONA, ITALY.

Aim: to evaluate if functional metabolic image findings with FDG PET/CT in the patients with suspected pulmonary aspergillosis (PA) or during their antifungal treatment may help the clinicians in their work-flow.Methods: We retrospectively evaluated 20 consecutive patients from our Nuclear Medicine database who underwent 18F-FDG PET/CT for suspected PA (number 12) or during their treatment between March 2011 and February 2015 (11 men, 9 women, mean age 52 years). Half of them had underlying predisposing condition or comorbidity (in transplantation, previous chemotherapy or radiotherapy, previous TBC, diabetes mellitus). Chest radiography and CT were performed in all patients. We analysed the patterns of FDG uptake, both visually and with maximum standardized uptake value (SUV max) of the pulmonary lesions on PET/CT, together with the number and shape of the lesions.Results: the diagnosis of PA was confirmed with the histological identification of Aspergilus spp in biopsies or positive sputum cultures or positive galactomannan assay of bronchoalveolar lavage specimens. All patients had positive results on Chest radiography and CT with excavated pulmonary thickening in 17 patients and fibrosis with bronchiectasis in 3 cases. Twentyfive FDG-PET/CT were performed in 20 patients. Twelve patients underwent FDG-PET/CT for suspected PA and in 7/12 (58.3%) were positive and PA was confirmed. In this group of patients the SUVmax values were 1.5-8.4 The remaining 3/5 patients had other features with increased uptake in PET which guided further biopsies and a definitive diagnosis (sarcoidosis and lymphoma). Among the nine patients who performed 12 FDG PET for the control of therapy or for the follow-up we registered 8 positive PET/CT in 4 patients (44%), they had higher FDG values in the lesions and in three of them the antifungal therapy was not discontinued. Five patients were considered negative at PET/CT with very low FDG uptake (<1.5) and they are in follow-up.Conclusions: FDG PET/CT could help to determine suitable treatment plans, particularly in immunocompromised patients to guide the timing for the antifungeal treatment and in the follow-up

P951
FDG-PET/CT in ANCA Associated Vasculitis: An Exploratory Pilot Study

S. Hess1,2, M. J. Velander3, P. F. Høilund-Carlsen1,2, H. Laustrup4; 1Dept. of Nuclear Medicine, Odense University Hospital, Odense, DENMARK, 2Institute of Clinical Research, University of Southern Denmark, Odense, DENMARK, 3Department of Internal Medicine, Section of Rheumatology, Odense University Hospital - Svendborg Hospital, Odense, DENMARK, 4Dept. of Rheumatology, Odense University Hospital, Odense, DENMARK.

INTRODUCTION: FDG-PET/CT is useful in large vessel vasculitis, but virtually unexplored in ANCA associated vasculitides (AAV), i.e., a heterogeneous group of small-medium vessel vasculitides. Initial diagnosis is difficult, especially in early and clinically quiescent lesions. Furthermore, during the course of disease, flares, indistinguishable from infection and cancer, may occur. We aimed to explore the potential of FDG-PET/CT in prevalent and incident AAV. METHODS: FDG-PET/CT was performed in 35 patients in 2009-2012. Eighteen patients had known AVV (prevalent cases) with suspected cancer or infection versus flare of disease, while 17 turned out to have AAV following FDG-PET/CT (incident cases). Clinical data was collected from patient records. FDG-PET/CT data were obtained from routine scan interpretations (prevalent cases) or after re-interpretation (incident cases). RESULTS: In prevalent cases, FDG-PET/CT was undertaken for suspected cancer (10/18; 56%) or infection (8/18; 44%). In the former subgroup, 4/10 had areas of increased FDG uptake; biopsy confirmed novel malignancies in 3 of these, AAV-flare in 1. The remaining 6 did not develop cancer during 38-65 months of follow-up. In the latter subgroup, 5/8 had areas of increased FDG-uptake. Four had pneumonia (verified clinically or by diagnostic imaging) and one had clinically verified flare. One of the remaining three recovered spontaneously, while two had clinical AAV-flare. Recurrence of infection did not occur during follow up. In incident cases, FDG-

PET/CT was originally performed on the suspicion of cancer (9/17; 53%), infection (3/17; 29%), vasculitis (2/17; 12%), or other (1/17; 6%). In total, 15/17 (88%) had areas of increased FDG uptake. Six received glucocorticoids at the time of scan, including the two with negative FDG-PET/CTs. Compared to the clinically established organ involvement, FDG uptake was present in the lungs in 10/11, kidneys in 6/7, upper respiratory tract in 2/4, eyes in 1/4, and joints in 2/5. Seven patients had possible occult organ involvement (aorta, pericardium, lung, shoulder, or kidneys). There was no correlation between SUVmax and clinical disease score. CONCLUSIONS: In prevalent AAV, FDG-PET/CT is a promising modality in patients with suspected malignancy or infections as the site of malignancy or infection was correctly identified in all cases and reliably ruled out in the remainder. The clinical value of FDG-PET/CT in incident AAV is debatable, although PET may have a role in identifying sites of occult inflammation allowing tailored treatment. There was no association between disease activity and SUVmax suggesting that there is need of novel quantitative PET approaches.

P952

The role of 18F-FDG PET/CT combined with MRI in the diagnosis and follow-up of the retroperitoneal fibrosis and vasculitis in a 14year-old girl

D. Chroustova1, J. Jahoda1, M. Kyncl2, J. Trnka1, P. Dolezalova1, J. Kubinyi1; 1General University Hospital and 1st Faculty of Medicine Charles University, PRAGUE 2, CZECH REPUBLIC, 2Hospital Motol and 2nd Faculty of Medicine Charles University, PRAGUE 5, CZECH REPUBLIC.

Aim: Retroperitoneal fibrosis (RPF) is characterized by the development of extensive fibrosis throughout the retroperitoneum, which results in entrapment retroperitoneal structures. We present a case of an adolescent girl with RPF, where severe fibro-inflammatory process involved right kidney, abdominal aorta and other arteries. 18F-FDG PET/CT and MRI determined accurately the extent of pathological changes and served as the main follow-up tool. Patient and methods: Retrospective case analysis of a 14 year-old girl is presented with clinical and laboratory assessments and serial imaging using FDG-PET/CT and MRI/MRA. Both PET/CT whole body scans were started 70 minutes after i.v. administration of 155 MBq 18F-FDG on PET/CT GE Discovery 690 immediately after injection of 55 ml Iomeron 400 with the following acquisition parameters 3min/bed, and CT parameters: Helical, 80kV, 100mA, Pitch 0,948:1.The PET images were reconstructed using CT transmission data for attenuation correction including TOF and PSF reconstruction options. Within year 2014 abdomen MRI and MRA angiography were repeatedly performed to patient follow -up during therapy. The examination was done in the basal plane T1W, T2W, DW after i.v. 10ml Gd-DTPA application. Results: The first signs of disease started at the age of 13 years with fever, high inflammatory parameters and back pain. Abdominal ultrasound showed retroperitoneal mass. Initial PET/CT scan confirmed the presence of extensive inflammatory lymphadenopathy. The biopsy of cervical lymph node did not confirm the presence of malignancy In August 2013 her back pain returned with hypertension. The follow-up PET/CT imaging showed the high 18F-FDG accumulation in abdominal aorta and renal arteries with amputation of the right renal artery. After hypertensive crisis due to ischaemic and nonfunctional right kidney the patient underwent nephrectomy. Histopathological findings from retroperitoneum confirmed the presence of granulomatous inflammation and vessel vasculitis affecting the spectrum of blood vessels. The girl was treated with corticosteroids and a course of pulse intravenous cyclophosphamide with no significant effect on MRI imaging. B-cell depleting therapy with rituximab was then commenced and the next follow-up PET/CT scan demonstrated complete metabolic and partial morphologic regression of the retroperitoneal lymphadenopathy. However there was found aortitis progression with new vasculitis changes on both iliac and pulmonary arteries, which were confirmed on MRA Methotrexate has been added. Conclusion: Our case report demonstrates the essential role of both 18F-FDG PET/CT and MRI imaging not only in the diagnosis of RPF and vasculitis, but more importantly in the patient follow-up during therapy.

P953

Long fasting with HNF is effective in inhibiting myocardial 18FDG uptake for evaluating cardiac sarcoidosis or endocarditis

P. VIAU, G. Nivaggioni, R. Capet, M. Razzouk-Cadet; University Hospital Archet, Nice, FRANCE.

Aim: To evaluate the effectiveness in inhibiting physiological myocardial 18FDG uptake of a complete preparation (CP) including long fasting over than 15 hours, carbohydrate restriction regimen the previous day and non-fractioned heparin loading 15 minutes before 18FDG injection to study cardiac sarcoidosis or endocarditis in Mediterranean population. Material and method: We analysed 32 ptts (15 male; mean age 52y±18; BMI 25±5 kg/m2; fasting period 16,9h ±1,1, glycaemia 0,97±0,35 g/L) suspected of cardiac sarcoidosis (25) or endocarditis (7) had a CP before 18FDG injection When cardiac sarcoidosis was confirmed, the lower 18FDG uptake was evaluated. A visual four-point scale was used to assess myocardial 18FDG uptake in comparison with hepatic uptake (1 no uptake, 2 lower, 3 moderate heterogeneous, 4

higher diffuse). Most of them (28) had serum free fatty acid and glycaemia blood test before heparin. CP's patients were compared to 34 ptts control (20 male; mean age 62±14; BMI 26±4 kg/m2; fasting period 15±4,4h; glyc 1,05±0,24 g/L) with only a long fasting over 12h (LF) before 18FDG injection. Results: Myocardial 18FDG uptake was 1,44 ± 0,84 in CP with heparin and 2,68 ± 1,07 in LF ($p < 0,05$). In CP, free fatty acid immediately before heparin load was above the normal threshold in 25/28 ptts. Myocardiac analysis was considered as interpretable in 27/32 ptts (84,4%) with no (75%) or low physiological uptake (9,4%). In LF, myocardiac analysis was confident in 12/34 ptts (35,3%) with no uptake (20,6%) or low uptake (14,7%). Conclusion: In our study we found that a complete preparation before myocardiac analysis (carbohydrate restriction, long fasting >15h and non-fractioned heparin) was better than long fasting alone for inhibiting physiological myocardial 18FDG uptake.

P954

The role of 18F-FDG PET/CT in clinical management of patient with spondylodiscitis

N. Prandini1, L. Massi1, A. Bedini2, S. Taralli1, A. Franceschetto1, A. Casolo1, S. Zona2, C. Mussini2; 1Nuclear Medicine University Hospital, Modena, ITALY, 2Infectious Disease Clinic, University, Modena, ITALY.

Introduction: Diskitis is an inflammatory process that involve vertebral column. The most common way is the haematogenous spread but direct contamination of the intervertebral disc or vertebral body can occur during surgery or after surgical procedures. 18F-FDG PET/CT is being used to examine and manage patients with infectious disorders. Aim of our study was to evaluate the potential role of 18F-FDG PET/CT in clinical management of spondylodiscitis. Methods: We retrospectively evaluated 88 18F-FDG PET/CT scans performed in 33 patients (21 males; mean age 63.6±17.5 years) with histopathological, laboratoristic and/or clinical diagnosis of spondylodiscitis. For each patient a visual and semiquantitative image analysis (SUVmax) were performed after a baseline PET/CT (PET/CT1). A second PET/CT (PET/CT2) was performed for therapy response assessment (median after 30 days). Nineteen patients underwent to a third PET/CT and three patients to a fourth PET/CT because of clinical complications. The final diagnosis about the status of the patients at the end of therapy was assessed by clinical/radiological follow-up of more than 4 months. Results: A single vertebral body was involved in 26/33 cases: cervical (n=1), dorsal (n=5), lumbar (n=16), sacral (n=4); 7/33 patients presented a multifocal spondylodiscitis. A causative microorganism was identified in 24/33 patients: S. aureus (n=6), M. tuberculosis (n=5), E. coli (n=3), Streptococcus (n=3), Candida albicans (n=2), Aspergillus (n=1), Pseudomonas aeruginosa (n=1), Klebsiella pneumoniae (n=1), Proteus mirabilis (n=1), Enterococcus (n=1). Histopathology or microbiological test resulted not-diagnostic in the remaining 9 cases. In most cases etiopathogenesis was hematogenous (n=31), contiguous tissue (n=1) or post-spinal surgical (n=1) spread. At initial evalution (PET/CT1), 24/33 patients (72.7%) presented with adjacent tissue involvement and a mean SUVmax of 7.2±3.3, and 9/33 showed only vertebral involvement and a lower SUVmax of 5.5±0.8. According to final disease status, 29/33 patients (87.9%) were classified as responders and 4/33 (12.1%) as no responders. Responder patients showed a decreased uptake at early therapy response evaluation (PET/CT2). No responder patients showed a mean SUVmax of 6.2±3 at PET/CT1, similarly to responders, and an increased uptake at PET/CT2 (mean SUVmax: 7.3±3.1), conversely to responder ones. Moreover, all no responder patients had multifocal disease and 3/4 showed adjacent tissue involvement. Conclusions: The highest metabolic activity ad baseline PET/TC, the multifocal disease, the adjacent tissue involvement are different metabolic findings observed in no responder patients. A post-therapy 18F-FDG PET/CT assessment is able to predict the prognosis of patients with spondylodiscitis and suggest a potential impact on therapeutic strategy planning.

P63 - Tuesday, October 13, 2015, 4:00 PM - 4:30 PM, Hall 3 – Poster Exhibition

Conventional & Specialised Nuclear Medicine: General & Miscellaneous

---

P955

Comparison of Prognostic Value Between NP-59 Adrenal Scintigraphy and Adrenal Venous Sampling in Primary Aldosteronism Patients After Adrenalectomy

C. Lu, V. Wu, C. Chang, K. Wu, TAIPAI Study Group, R. Yen; National Taiwan University Hospital, Taipei, TAIWAN.

Purpose: Adrenal venous sampling (AVS) is the gold standard for lateralization in primary aldosteronism (PA). NP-59 single photon emission tomography/computed tomography (NP-59 SPECT/CT) is an alternative method for lateralization with good prognostic value of post-surgical outcome. This study is aimed to compare the prognostic ability according to the post-surgical outcome between AVS and NP-59 SPECT/CT. Methods: From March 2010 to April 2014, 22 PA patients were included with AVS and NP-59 adrenal scintigraphy results before adrenalectomy. Four-point blood pressure (BP) scale (0-3), serum aldosterone to renin ratio (ARR, 0 or 1) and a 5-point score (0-4) combining BP and ARR were used to evaluate the prognostic ability after adrenalectomy. Serum potassium is normalized in all patients and is not included for

outcome assessment. Lateralization results of AVS and NP-59 SPECT/CT were compared according to two outcome parameters, BP scale of 2 and 5-point score of 3, to evaluate the prognostic value after adrenalectomy. Results: Taking BP scale of 2 as the outcome parameter, NP-59 SPECT/CT showed slightly better sensitivity (92%) than AVS (69%) with p value of 0.08, while both of them had similar specificity (78% and 33%, respectively, p=0.10). Considering 5-point score of 3 as the outcome parameter, NP-59 SPECT/CT also had better sensitivity (100%) than AVS (70%) with p value of 0.08, and both of them had similar specificity (67% and 33%, respectively, p=0.10). The concordance rate between AVS and NP-59 SPECT/CT was 59% (13/22). Conclusion: As a non-invasive procedure, NP-59 SPECT/CT has slightly better sensitivity and equal specificity compared to AVS in post-surgical outcome prediction, mainly on significant outcome improvement such as large scale of BP improvement and overall normalization. NP-59 SPECT/CT may stand for a trustable study as AVS to predict clinical outcome after adrenalectomy.

P956

Transport capacity of lymphatic system of lower extremities in patients with diabetes

O. Lang1,2, V. Prymkova2, I. Kunikova1, H. Krizova1, H. Balon1; 1Charles Univ, Prague 10, CZECH REPUBLIC, 2District Hosp, Pribram, CZECH REPUBLIC.

Introduction: Lymphatic system can play an important role in the development of some pathological processes in diabetic foot syndrome. It is associated with neurological abnormalities and various degree of peripheral vascular disease in the lower limbs which can increase the amount of interstitial fluid. We, therefore, tested function of lymphatic system of lower extremities in diabetic patients. Material and methods: We evaluated 13 diabetic patients (4 male, 9 female, average age 64 years) with undefined feeling in lower limbs. We selected control group (13 paired patients without diabetes) from our historical database. Lymphoscintigraphy was performed after subcutaneous injection of radio-colloid in the web spaces of the feet. Static images were performed immediately post injection, 30 minutes post injection at rest and after 30 minutes of walking. The transport capacity (percentage of the injected dose accumulated in the regional lymph nodes) was then calculated. Paired t-test was used for comparison. Results: Mean transport capacity in diabetic and non-diabetic pts on the right and left side at rest and after stress was 4.4%, 18.6%, 4.8%, 19.5%, 0.4%, 4.8%, 0.3%, and 2.9%, respectively (p=0.000-0.007). Rest transport capacity in diabetics was at the level of stress transport capacity in non-diabetics while transport capacity reserve in non-diabetic pts was twice as higher as in diabetics - see table. Conclusion: Transport capacity of lymphatic system of both lower extremities at rest is much higher in diabetic patients comparing to patients without diabetes while their transport capacity reserve is much lower. We believe this is a sign of overload of lymphatics due to increased amount of interstitial fluid which can contribute to development of diabetic foot syndrome.

P957

The effect of age on indices of quantitative lymphoscintigraphy (LS)

G. Arsos1, D. Dionyssiou2, C. Sachpekidis3, K. Michailos1, E. Demiri2; 13rd Dept of Nuclear Medicine, Aristotle University of Thessaloniki Medical School, Papageorgiou Hospital, THESSALONIKI, GREECE, 2Plastic Surgery Clinic, Aristotle University of Thessaloniki Medical School, Papageorgiou Hospital, THESSALONIKI, GREECE, 3Clinical Cooperation Unit Nuclear Medicine, German Cancer Research Center, Heidelberg, GERMANY.

Aim : LS quantitation has been shown to enhance diagnostic sensitivity in lymphedema investigation. However, lymph flow dynamics may be altered by body habitus or age thus rendering the derivation of normal ranges of the quantitative LS indices complicate. In order to test the hypothesis that age-related relative lymphatics dysfunction can be reflected in the "normal" quantitative LS indices, we examined the relationship between age and some LS indices in lower limbs (LL) with clinically intact lymph drainage. Subjects and methods : All of the 31 adult patients (5 men) enrolled in the study were submitted to LL quantitative LS. By the age cut off value of 45 years patients were allocated in two age groups, A1 (10) and A2 (21 patients). Sixteen of them, without signs of LL oedema, were examined in the context of donor area evaluation before vascularised inguinal lymph nodes transplants harvesting for the treatment of secondary upper limb lymphedema and contributed one randomly selected LL per patient for analysis. The rest 15 of the patients were investigated for contralateral LL oedema. Body mass index (BMI) and body surface area (BSA) were calculated according to Quetelet and Haycock formulas respectively. For quantitative LS, 55 MBq of Tc-99m-nanocolloid were subcutaneously injected in the first interdigital web of both foot. Spot images over the injection sites at 0, 45 and 180 min p.i. and over inguinal-pelvic area at 45 and 180 min p.i. were obtained. Tracer clearance from the injection site (CIS) and uptake by the inguinal lymph nodes (INU) at 180 min p.i., both in % of injected dose (%ID), were calculated. Differences between A1 and A2 groups were assessed by the Mann-Whitney U test and correlation between age and CIS and INU by linear regression analysis. Results : Age significantly differed between A1 and A2 groups (34.1 ±8.6 vs 62.0±10.0 years, p<0.05). BSA and BMI did not

significantly differ between the groups. CIS and INU significantly differed between the groups (30.5±16.9 vs 20.8±11.1 %ID and 15.8±6.6 vs 9.0±5.0 %ID respectively, $p<0.05$ for both). Significant negative correlations were found between CIS and age and INU and age ($r = -0.351$ and $r = -0.461$ respectively, $p<0.05$ for both). Conclusions : Normal lymph drainage deteriorates with advancing age and indices of quantitative LS are similarly affected . This fact should be taken into consideration when normal values of quantitative LS indices are to be determined.

P958

Accuracy of 99mTc-Sestamibi Molecular Breast Imaging Guided Needle Biopsy Using a Stereotactic Lesion Localisation System

A. Collarino1,2,3, L. M. Pereira Arias-Bouda2,3, F. Smit2, P. Neijenhuis4, L. M. H. Wijers5, A. F. Van der Hoeven3, K. Hofkes-Fillekes5, A. Zeillemaker4, R. A. Valdés Olmos2; 1Institute of Nuclear Medicine, Università Cattolica del Sacro Cuore, Roma, ITALY, 2Department of Nuclear Medicine, Leiden University Medical Center, Leiden, NETHERLANDS, 3Department of Nuclear Medicine, Alrijne Hospital, Leiderdorp, NETHERLANDS, 4Department of Surgery, Alrijne Hospital, Leiderdorp, NETHERLANDS, 5Department of Radiology, Alrijne Hospital, Leiderdorp, NETHERLANDS.

Aim: Molecular Breast Imaging (MBI), also called BSGI, is useful to detect radiologically occult lesions suspicious of cancer. Using slant-hole collimation, the device is able to determine lesion depth enabling radio-guided biopsy. The present study evaluates both workability and accuracy of this novel biopsy modality in patients with non-palpable breast lesions in whom radiological image-guided biopsy was not possible. Materials and Methods: In 27 patients (mean age 60, range 41-77y) with breast lesions occult on second-look ultrasound or in whom radiological image-guided biopsy failed, an average of 600 MBq 99mTc-Sestamibi was administered and two stereotactic images were performed with a breast-dedicated gamma camera (Dilon 6800®, Dilon Technologies, USA) equipped with slant-hole collimators to determine X, Y, Z coordinates of the lesion. After lesion localisation using an MBI-based system (GammaLōc®, Dilon Technologies, USA) equipped with a vacuum-assisted device (VAD), a trocar needle was placed into the lesion followed by verification using a radioactive Cerium source to ensure correct position. Subsequently, biopsies were taken and a radiological marker was left behind at the biopsy site to enable further lesion excision or follow-up. Tissue sample activity was measured ex-vivo, followed by histopathological analysis. Finally, mammography was performed to verify marker position. Results: The mean procedure duration was 75 minutes. In all patients, samples were found to be radioactive and contained enough tissue for histopathological analysis. In 16/27 patients, histopathology revealed malignancy. In 11/27 patients, lesions were benign, histopathology revealed fibrocystic mastopathy or adenosis; four of these patients were followed for at least one year and no malignancy was found. Mammography confirmed correct marker position in 25 patients, in two patients the marker had migrated directly after placement. Conclusion: MBI-guided breast lesion needle biopsy using 99mTc-Sestamibi and a stereotactic lesion localisation device appears to be highly accurate with good patient acceptability. The modality appears to be a helpful alternative in patients with occult breast lesions not possible to be sampled by conventional radiological image-guided biopsy.

P959

The hidden sentinel node in breast cancer: reevaluating the role of SPECT/CT and tracer reinjection

B. Pouw, D. Hellingman, M. Kieft, W. V. Vogel, E. J. T. Rutgers, M. P. M. Stokkel, R. A. Valdés Olmos; Netherlands Cancer Institute, Amsterdam, NETHERLANDS.

Introduction: Lymphoscintigraphy with planar imaging is considered a helpful tool to depict lymph node drainage in patients with invasive breast cancer. Single Photon Emission Computed Tomography with integrated CT (SPECT/CT) is usually performed to detect sentinel nodes (SN) in breast cancer patients showing non-visualisation on planar images. In our institution, the incorporation of new SN indications (N0 patients with previous breast surgery and/or radiotherapy, neo-adjuvant chemotherapy) has led to an increase of non-visualisation on lymphoscintigraphy. The present study (re)evaluates the overall contribution of SPECT/CT and tracer reinjection in patients showing no drainage on planar lymphoscintigraphy in terms of SN visualisation and surgical identification rate. Materials and Methods: Between 1st of July 2008 and 6th of November 2014 in total 1982 breast cancer patients underwent a SN procedure after intra-tumoural tracer administration. SPECT/CT was performed in 298 patients (15%) who showed non-visualisation on planar lymphoscintigraphy. Ninety-one (30.5%) of these patients had previous surgery or radiation therapy at the same breast prior to the SN procedure and 40 (13.4%) were scheduled for neo-adjuvant chemotherapy. If SN non-visualisation persisted on the SPECT/CT images, a second radiotracer injection with repeated scintigraphy was performed when logistics allowed this. Univariate analysis was performed to examine if specific subgroups, such as age, BMI, T-stage or previous treatment, have influence on visualisation rates of SPECT/CT. Results: SPECT/CT visualised one or more SN in 22.8% (68/298) of the patients with no drainage

on planar images. Univariate analysis of subgroups revealed no significant factors influencing SPECT/CT visualisation. In patients with persistent non-visualisation on SPECT/CT and having a reinjection, the SN visualisation rate reached 60.3% (38/63). The overall visualisation rate including planar imaging, SPECT/CT and reinjection was 90.3% (1790/1982). In the operating room the combination of gamma-probe detection and blue dye led to identify SN in 87.1% (175/201) of the patients with a primary tumour after non-visualisation on planar imaging. Conclusion: The visualisation rate of SPECT/CT after non-visualisation on planar imaging was lower than the SN visualisation after reinjection, in an evaluation including all new breast cancer SN indications. Therefore, our institutional protocol for non-visualisation on planar lymphoscintigraphy has been adjusted reserving SPECT/CT imaging only for patients with persistent absence of drainage after reinjection.

P960

SPECT/CT Imaging: Clinical Utility in Lymphoscintigraphy for Sentinel Node Mapping in Patients with Melanoma .

J. RODRIGUEZ ALBAN, A. ALBUQUERQUE, M. SILVA, L. PIRES, P. LAPA, A. MOREIRA, R. VIEIRA, A. FIGUEIREDO, G. COSTA, J. PEDROSO DE LIMA; CHUC, Coimbra, PORTUGAL.

Introduction: To evaluate the added value of an integrated SPECT/CT system, over conventional planar lymphoscintigraphy, for anatomic mapping of the sentinel lymph nodes (SLN) in patients with operable melanomas. Materials and Methods: Between April 2009 and April 2015, one hundred fifty four patients (80 male and 74 female, age range 29-82 years, mean 65.4 years) with malignant melanomas of the skin were evaluated for detection and localization of SLN, by using both planar lymphoscintigraphy and SPECT/CT. Planar and SPECT/CT images were interpreted in separate and later compared to surgical information for a correct anatomic localization. Results: Melanoma was located on the head (25 patients), trunk (70), upper extremities (18) and lower extremities (41). Eighteen melanomas of the head drained to postmandibular nodes, two to occipital nodes and five to parotid gland, all localized by SPECT/CT. Of the trunk melanomas SPECT/CT localized the SLN as superficial or deep in the nodal basin; 1 patient with melanoma of abdominal wall showed a subcutaneous sentinel node underneath the injection site that is not visible on the conventional images and only visualized by SPECT/CT; 4 patients showed also drainage to SLN in the iliac-obturator region, 2 to the para-aortic and intercostal nodes, anatomical information only provided by SPECT/CT. Of the 18 upper extremity lesions, SPECT/CT showed anatomical information not restricted to axilla and in 2 recognized the precise location of interval nodes in middle humeral level. In the lower extremity melanoma, SPECT/CT helped the surgical approach, with enhanced superiority in overweight patients. Conclusions: On a patient basis, SPECT/CT had an overall added value in addition to conventional dynamic and static lymphoscintigraphy in 90% of the cases. SPECT/CT is a useful imaging tool in melanoma patients, with an added value over planar lymphoscintigraphy for the detection of SLN and the anatomical mapping of lymph drainage. It provides more precise information to the surgeon about the anatomic location and depth of SLN and shows the relationship between sentinel nodes and other anatomic structures facilitating sentinel node biopsy.

P961

Potential role of Lymphangioscintigraphy in anticipating results of Lymphatic-Venous Anastomoses: Clinical and Imaging Patterns

E. Cracco1, A. Busetto2, A. Bonazza1, F. Dei Rossi1, M. Gallan1, R. Mameli1, M. Rizzo2, M. Sicolo2; 1Division of Nuclear Medicine, Ospedale dell'Angelo, Mestre, ITALY, 2Division of Surgery, Ospedale dell'Angelo, Mestre, ITALY.

Aim: Modified radical mastectomy, performed in patients with clinically detected axillary lymphadenopathy, bears a significantly high risk of upper limb lymphedema, because of regional lymph drainage impairment, with an estimated frequency of 5-30%. Microsurgical Multiple Lymphatic-Venous Anastomoses (MLVA) can correct lymph drainage and prevent or cure upper limb lymphedema when performed before or after surgery, respectively. We used interstitial lymphangioscintigraphy to assess regional lymph drainage changes induced by clinical axillary lymphadenopathies and to evaluate if lymphoscintigraphic pattern may anticipate the result of micro-surgical MLVA. Materials and methods: Ten consecutive patients underwent lymphoscintigraphy: 4 before radical mastectomy, 6 after surgery and before MLVA. In two cases lymphoscintigraphy was performed after MLVA. For all patients a transport kinetics score was designed (Transport Index, TI) based on: radionuclide temporal and spatial distribution, lymph nodes appearance time, intensitv of lymph nodes and vessels uptake, ranging from 0 to 9. Thus, the resulting TI ranged from 0 (normal) to 36 (pathological). MLVA was performed by injecting a blue dye in the skin and subcutaneus tissue of the medial region of the arm to trace regional lymphatic vessels and inserting the “blue lymphatics” coming from the upper limb into one of the small collateral branches of the axillary vein (telescopic end-to-end anastomosis). Results: Lymphatic-venous anastomoses allowed an effective lymphatic drainage of the affected areas in 9 cases.

Only 1 patient had a lymphangitis during radiotherapy. Lymphangioscintigraphic results showed a total mean transport index of 39.5 and 4.5 (n.v. < 9) before and after MLVA, respectively, showing the patency of microvascular anastomoses.None of the patients had nodal relapses during the follow-up time. Clinical outcomes were measured by pre- and post- microsurgical MLVA volumetry. Conclusions: MLVA has been shown to be a safe procedure for patients in order to prevent or cure the upper limb breast-cancer related lymphedema. Microsurgical lymphatic derivative and reconstructive techniques can yield positive results in the treatment of peripheral lymphedema, mostly in early stages, when there are only slight tissular changes and a complete restore of lymphatic drainage is feasible. Lymphangioscintigraphy appears to be a promising technique in identifying upper arm lymphatic pattern before and after modified radical mastectomy procedure. Transport index is a simple, operator-independent semiquantitative parameter, which allows a correct assessment of limphatic drainage and of the patency of microvascular anastomoses.

P963

Scintigraphy is a Validated Method for in vivo Evaluation of Drug Delivery to Gastrointestinal System

B. E. Akkas1, L. Guner2, A. Celkan3, F. Acarturk3, F. Tugcu Demiroz3, N. Gokcora4; 1Ankara Oncology Research and Training Hospital Department of Nuclear Medicine, Ankara, TURKEY, 2Acibadem Hospital Department of Nuclear Medicine, Istanbul, TURKEY, 3Gazi University Faculty of Pharmacy, Department of Pharmaceutical Technology, Ankara, TURKEY, 4Gazi University Faculty of Medicine, Department of Nuclear Medicine, Ankara, TURKEY.

PURPOSE: The purpose of the present study was the development and in vitro/in vivo evaluation of the guar gum-based colon-specific compression-coated tablet formulation of theophylline which can be used for the treatment of nocturnal asthma. METHODS: The core tablets containing 100 mg of theophylline were compression coated with various amount of guar gum. The physical properties of tablets were tested and in vitro release studies were performed by a USP Apparatus I in simulated gastric juice at a pH of 1.2 followed by simulated intestinal juice at a pH of 6.8 with and without galactomannanase enzyme. Samarium oxide (152-Sm) was added to the core tablet as the tracer. After the conversion of non-radioactive 152-Sm to 153-Sm via neutron bombardment, scintigraphy was used to monitor the tablet's movement and distribution throughout the GI system on 6 healthy volunteers. Comparative dissolution test of tablets containing samarium oxide was also carried out in the same conditions. RESULTS: The drug release from these tablets was found to be 0.318-3.29% for the first 2 hours, 27-54% during the 12 hours and 82-104% at 24 hours. Addition of the galactomannase enzyme increased the teophylline release. The physicopharmaceutical properties of the tablets which were used in in vivo studies met the compendial requirements. Addition of samarium oxide to the core tablets (Formulation T2-S) did not affect the release of the drug. In vivo scintigraphy studies showed that the gastric emptying time for the tablets varied between 1-2 hours. The tablets reached the colon at 5, 6 and 8 hours in three of the six subjects. CONCLUSION: Theophylline delivery to terminal ileum or colon could be achieved and theophylline-guar gum compression coated tablet formulation may be a promising system for the treatment nocturnal asthma. Scintigraphy is a validated method to monitor the passage and behaviour of drug delivery to gastrointestinal system.

P964

Scintigraphic evaluation of pyloroplasty role in Ivor-Lewis esofagectomy

M. Zuffante, L. Gobbi, L. Pavanello, S. Giacopuzzi, J. Weindelmayer, F. Longo, E. Carmagnani, M. Cucca, D. Grigolato, G. de Manzoni, M. Ferdeghini; AOUI, Verona, ITALY.

BACKGROUND-AIM: The neoadjuvant treatment has increased patients (pts) survival with esophageal cancer. In our recently published experience (155 pts) we have achieved an overall survival of 43%. After surgery quality of life become our main goal. Routinely, pyloroplasty (PP) is used to improve gastric emptying and to reduce ab-ingestis pneumonia and anastomotic leakage. We analyzed the importance of the scintigraphic data for the decision making of a routinely performing PP during Ivor-Lewis esophagectomy in a bigger study on a group of pts underwent to a complete functional analysis for liquid and solid emptying, acid reflux and quality of life. METHODS: The whole study includes 63 pts.with locally advanced carcinoma, R0 resections, at least 6 months of follow-up, no recurrence or anastomotic stricture. Pts enrolled to scintigraphic study were 26: in 15 PP was performed, in 11 was not done (NPP). A semisolid balanced meal labeled with 40 MBq of 99mTc-nanocolloid was given to pts seated close to gamma-camera. To study gastric emptying first we acquired dynamic images of 60 sec/frame for 30 minutes, then we acquired static images of 60 sec/frame every 10 min until 120 min. RESULTS: The study evidences that the mean percentage of radioactivity in the gastric conduit at 30 and 120 minutes were 43±30.19 and 10.63±9.08 in PP group and 41.09 ±29.5 and 16.08±17.7 in NPP group (p-value>0.05). Mean half-life (T1/2) was lower in PP group (29.03±22.32 minutes) than in NPP group (40.64±51.48 minutes), but the difference was not statistically relevant (p-value=0.5). Nevertheless

analyzing the T1/2 box and whisker plot of the 11 NPP pts is notable a great dispersion with a large 25-75 percentile box. This was due to 3 pts that had a mean T1/2 of 106 min compared to a mean T1/2 of 6.5 min for the other 8. CONCLUSIONS: Scintigraphyc study has discriminated between a good or a delayed emptying of gastric conduit and demonstrated a non-inferiority of the NPP group compared to the PP. There wasn't a statistically relevant difference between the two groups. Nevertheless 3 NPP pts had a longer T1/2. They could be defined as a potentially "high risk pneumonia" in the early post-operative period. Our interpretation of this study is that, in the majority of pts, PP is an overtreatment with possible post-operative morbility and increasing of biliary reflux and dumping syndrome. Even if we would like to identify the "high risk group" treatable.with PP.

P965

Gastric Motility SPECT/CT with Tc99m labelled standard quality food (SQF)

I. Garai1, A. Forgács1, K. Kukuts1, S. Barna1, G. Opposits2, S. A. Kiss2, M. Emri2, Z. Csiki3; 1ScanoMed Ltd,, Debrecen, HUNGARY, 2Institute of Nuclear Medicine, University of Debrecen, Debrecen, HUNGARY, 3Institute of Internal Medicine, University of Debrecen, Debrecen, HUNGARY.

Dyspepsia is a common disease in all ages. In about 50-70% of patients with dyspepsia, no definite organic changes can be revelaed. This functional dyspepsia is estimated to affect about 15% of the general population in developed countries causing severe discomfort for the patients. Aim of our study was to assess the changes of the volume of gas and solid food after comsuption of radiolabelled standard quality food (SQF) and emptying dinamics using SPECT/CT. Method: We investigated 6 patients suffering from dyspepsia. All was undergone on prior gastroscopy to exclude organic disorders of the stomach. The examination was performed in fasting state. 22 g standard quality food (Gastroscint, Mediradiopharma) was labelled with 70MBq Tc99m and we provided 4.8 g extruded bread (Abonett) and 200 ml nutritional supplements(Nutri-Drink., Nutricia) with known contents. QC of radiolabelled food was also made to check in vitro radiochemical stability. The examinations were performed with 3 head SPECT/CT (Anyscan, Mediso) with LEHR collimator. The acquisition was the following: Early and late SPECT: 128x128 matrix, 20sec/frame, 32 view, Total SPECT acquisition was 10 min 40 sec. Dynamic images: 60x1 min. Low dose CT (20mAs,120kV) was made of the abdominal region before the early and after the late SPECT. The total time of collimation was 90 min. Evaluation: Low-dose CT images were segmented by an in-house developed automatic classification software using mathematical morphology and dedicated clustering algorithms. Using reconstructed SPECT data the volume of Tc99m SQF were calculated by a threshold-based (20% of maximum value) segmentation procedure. The speed of digestion was estimated from the dynamic gamma-camera scan by nonlinear weighted least-squares estimation algorithms implemented in R software. A complex image processing pipeline was developed to integrate the analysis of repeated measurements of CT, SPECT and the dynamic planar data. Results: Increased volume of total gas calculated from CT was revealed 5 cases from 6. Decrease of solid volume calculated from SPECT was presented 4 cases from 6. The rate of gastric emptying was significantly low only in one patient, (emptying fraction: 17% versus 30-41% in other cases) The emptying fraction of stomach calculated from dynamic images showed correlation with the emptying rate. However the correlation was weaker with changes in volume of total abdominal gas. Conclusion:This newly developed method seems promising in investigation of functional dyspepsia providing additional sensitive parameters of gastric motility. However further studies are needed to define population based normal values.

P966

Diagnostic accuracy of 123I-MIBG SPECT-CT using semi-quantitative analysis in patients with adrenal pheochromocytoma

Y. Sugihara, Y. Fukushima, S. Kumita; Nippon Medical School Hospital, Tokyo, JAPAN.

Background: 123I-metaiodobenzylguanidine (MIBG) SPECT-CT plays an important role in the diagnosis of pheochromocytoma. However, the diagnostic accuracy of MIBG SPECT-CT is reported to be insufficient up to now (both sensitivity and specificity are 82%). Increased physiological uptake in adrenal glands may be mistaken for pheochromocytoma and impair its diagnostic accuracy. The purpose of this study was to examine the diagnostic accuracy of MIBG SPECT-CT using semi-quantitative analysis in patients with adrenal pheochromocytoma. Materials and methods: Nineteen consecutive patients from January 2011 with adrenal tumors, suspected as pheochromocytoma, were included in this study. All patients underwent MIBG SPECT-CT, and a total of 38 adrenal glands were examined. In the visual analysis of MIBG SPECT-CT, the diagnosis of adrenal tumor type was confirmed with the consensus of two experienced nuclear medicine specialists. By contrast, in the semi-quantitative analysis of MIBG SPECT-CT, adrenal-gland-to-blood ratio (AAR) was calculated to estimate the amount of MIBG accumulation in adrenal glands. Two-dimensional regions of interest were drawn on both affected and unaffected adrenal glands, and also placed in the lower portion of abdominal aorta. AAR was calculated by dividing adrenal maximal counts by mean blood

pool counts in the abdominal aorta. In all participants, definitive diagnosis was confirmed according to the pathological findings after surgical resection or various clinical examinations, including hormone tests. The cut-off value of AAR between pheochromocytoma and normal adrenal gland or other kinds of tumor was determined using an receiver-operating-curve (ROC) analysis. Furthermore, diagnostic accuracy of MIBG SPECT-CT using semi-quantitative analysis was evaluated and compared with visual analysis alone. Results: In all 38 examined adrenal glands, definitive diagnoses were 9 pheochromocytomas, 17 normal adrenal glands, 10 adenomas and 2 metastatic tumors. In the visual analysis of MIBG SPECT-CT, the sensitivity, specificity and accuracy were 80%, 73% and 82% respectively. In the semi-quantitative analysis, AAR were 24.1 (16.4-48.8) in pheochromocytomas and 6.5 (4.6-8.3) in non-pheochromocytoma sites ($p<0.001$). As a result of ROC analysis, the cut-off value of AAR for the diagnosis of pheochromocytoma was calculated as 14.00. Using this cut-off value, its sensitivity, specificity and accuracy were 89%, 100% and 97% respectively. Namely, the true negative rate was 100%, and adrenal physiological uptake was completely differentiated from pheochromocytoma.Conclusions: The diagnostic performance of MIBG SPECT-CT for pheochromocytoma can improve under semi-quantitative analysis and avoid its pseudo positive results.

P967

The value of parathyroid hormon determination in fine needle aspiration washout fluid in patients with negative or equivocal scintigraphic findings

S. INCE, H. SAN, M. O. EMER, E. ALAGOZ, A. AYAN, K. OKUYUCU, B. GUNALP, A. O. KARACALIOGLU, N. ARSLAN; GÜLHANE MILITARY MEDICAL ACADEMY, ANKARA, TURKEY.

Aim: Tc-99m MIBI parathyroid scintigraphy (PS) could be negative or equivocal in some cases with highly suspicious clinical and biochemical results for parathyroid adenoma (PA). Some of the patients referred for PS have concomitant diseases such as nodular guatr or Hashimato thyroiditis with perithyroidal lymph nodes which may cause difficulty in differantial diagnosis with ultrasound (US). The aim of this study was to evaluate the role of parathyroid hormon (PTH) determination in the fine needle aspiration (FNA) washout fluid in order to distinguish PA from other concomitant lesions in patients with negative or equivocal scintigraphic findings. Materials and Methods: One hundred-eight patients with primary hyperparathyroidism were referred to our clinic for PS. A detailed neck US was performed to all patients in order to document any intra or extrathyroidal lesion. 24 (22.2%) of them had scintigraphic and ultrasonographic findings concordant with PA. 45 (41.6%) of them had no finding both in PS and US. The remaining 39 (36.1%) patients (10 male, 29 female, mean age±SD: 53±15) were included in the study. In all 39 cases, there were hypoechoic lesions, adjacent or outside the thyroid capsule, suspected to be PA in US, although their PS was negative or equivocal. PTH assay in FNA washout fluid was performed in these patients. PTH washout levels at least two times higher than blood PTH levels were considered as concordant with PA. Results: The mean serum PTH and calcium levels were 204.4±237.7 pg/ml and 10.8±1.04 mg/dl, respectively in the study group. The values of PTH in the aspirates ranged from 4.0 to 23604 pg/ml. 35 patients (89.7%) had elevated PTH concentrations in FNA washout fluid and 15 (42.8%) of them underwent surgery. Final histopathologic examination showed PA in these 15 patients with a positive predictive value of %100. The postoperative serum PTH (55.5 ±36.2 pg/ml) and calcium (9.3±0.8 mg/dl) levels decreased significantly. 4 patients (10.3%) had low levels of PTH in the aspirate (<10 pg/m) and FNA biopsy revealed 2 nodular goiters and 2 benign lymph nodes. The sensitivity and specificity of the PTH assay in FNA washout fluid were both found %100 in the group of patients underwent surgery. Conclusion: Our results showed that elevated PTH concentration in FNA washout fluid has high accuracy in differential diagnosis of PA from thyroid nodules and lymph nodes before surgery, especially in patients with negative or equivocal scintigraphic findings.

P969

PSYCHIATRIC SYMPTOMS IN A PATIENT WITH PARATHYROID ADENOMA: diagnostic role of sestamibi scintigraphy.

M. FINESSI1, A. Pia2, V. Podio1, A. Barberi3, P. Moretto4, V. Marci5, T. Angusti1; 1Nuclear Medicine, San Luigi Hospital, University of Turin, Orbassano, ITALY, 2Internal Medicine, San Luigi Hospital, University of Turin, Orbassano, ITALY, 3Psychiatry, San Luigi Hospital, University of Turin, Orbassano, ITALY, 4Radiology, San Luigi Hospital, University of Turin, Orbassano, ITALY, 5Division of Pathology, San Luigi Hospital, University of Turin, Orbassano, ITALY.

AIM. Primary hyperparathyroidism (PHPT) is the most common cause of hypercalcemia in patients over 50y with a female:male ratio 4:1. PHPT is diagnosed by laboratory test; afterwards, patients undergo cervical ultrasound (US) and scintigraphy in order to localize the affected gland/s, sestamibi parathyroid scintigraphy is the most accurate approach for detection of enlarged parathyroid glands. Psychic manifestations of PHPT are usually understimated, however often we can observe a large number of patients report symptoms like depression, fatigue, sleep disturbance, personality changes,

anxiety and, in advanced cases, psychosis. Our report describes a case of PHPT with dominant psychiatric symptoms where the scintigraphy had a diagnostic rather than localizing role, and resulted crucial also in the therapeutic workup of the patient. MATERIAL AND METHODS. A 63y male, with depression, fatigue, personality changes and psychosis was referred to our institution for an episode of attempted suicide. Laboratory tests did not show a typical PHPT biohumoral pattern: hypercalcemia (calcium 2.84 mmol/L, normal value 2.10-2.55 mmol/L) was associated with normal range PTH value; in order to reduce hypercalcemia and to verify if PTH value was "inappropriately low", hydratation and medical therapy with diuretic, glucocorticoids and bisphosphonates was administered. It provided an increase of PTH value to highly abnormal levels and a reduction of hypercalcemia (2.47 mmol/L), suggesting hyperparathyroidism. The patient was referred to sestamibi scintigrahy which detected an "hot spot" in left cervical region and ultrasound confirmed the presence of an enlarged gland posterior to thyroid. The patient underwent minimally invasive parathyroidectomy (MIP): at surgery a parathyroid adenoma was found. One month later the patient was free from both psychiatric symptoms and biohumural sign of HPT. CONCLUSION. 1) Although the association between PHPT and psychiatric symptoms is reported in the literature, psychiatric specialists rarely refer to endocrinologists these patients; serum calcium screening test appears to be very important not only in the monitoring lithium-treated patients, but also in patients with severe psychotic episodes to verify a possible PHPT. 2) Usually parathyroid scintigraphy is used for lesion(s) localization, according to EANM guidelines; in this case, scintigraphy led to diagnosis in spite of equivocal laboratory test: sestamibi scintigraphy seems indicated in cases of inappropriately normal iPTH in relation to the calcium value. This case supports other evidences that suggest a possible extended use of parathyroid scintigraphy for diagnostic purposes, at least in selected clinical situations.

P970

99mTc-MIBI dual phase planar and SPECT CT scanning in diagnosis of hyperparathyroidism in patients with MEN 1

M. Castellon Sanchez, M. Godoy Bravo, M. Balsalobre Salmeron, L. Alvarez Nieto, M. Ibáñez Ibáñez, J. Rodriguez Gonzalez, F. Nicolás Ruiz, L. Mohamed Salem, R. Reyes Marlés, M. Claver Valderas; Nuclear Medicine department, Hospital universitario clínico Virgen de la Arrixaca, Murcia, SPAIN.

AIM: The aim is to evaluate the performance and to discuss the value of preoperative 99mTc-MIBI parathyroid dual phase planar, PinHole and SPECT CT scanning in hyperparathyroidism diagnosis in patients with MEN1 and in recurrent hyperparathyroidism after surgery. MATERIAL AND METHODS: A retrospective study of 82 patients with MEN 1, of which 57 (74%) had hyperparathyroidism, we studied 54 (29 women and 25 men, aged between 17-70, mean age 38.3 years). 32 (59.2%) were asymptomatic and 22 (40.8%) had hyperparathyroidism symptoms. Calcium, phosphorus and PTHi levels were measured and genotype and mutations in the MEN1 gene were studied. 50 patients underwent a preoperative 99mTc-MIBI parathyroid dual phase planar, PinHole and SPECT CT scanning to detect and localize parathyroid glands. After surgery, a 65.2 months (6-180) follow up, we found 86.3% cure rate and 10 (18.5%) patients (7 women and 3 men, mean age 36.4 years) presented recurrent hyperparathyroidism. The recurrent hyperparathyroidism mean time after surgery was 85.8 (6-124) months. All patients underwent 99mTc-MIBI parathyroid dual phase planar, PinHole and SPECT CT scanning. RESULTS: Preoperative 99mTc-MIBI parathyroid dual phase planar, PinHole and SPECT CT scanning found 1 gland in 18 patients, 2 glands in 21 patients, 3 glands in 2 patients and 4 glands in 3 patients and was negative/uncertain in 6 patients. 2 ectopic glands were found. In 100% of patients with recurrent hyperparathyroidism the localization diagnosis was made with 99mTc-MIBI parathyroid dual phase planar, PinHole and SPECT CT scanning, finding 1 gland in 8 patients, 2 glands in 2 patients and 4 ectopic glands. No genotype was associated with higher hyperparathyroidism incidence. Calcium, phosphorus and PTHi levels were 11.6mg/dl (10.2-14), 2.6mg/dl (1.1-4) and 146.1(23-610) respectively. Mean age of asymptomatic patients was lower than symptomatic ones (33.2 vs 45.9 years) $p<0.001$ and the mutation in MEN 1 gene presented in 80% of recurrent hyperparathyroidism was 1650delC-ter558exon10. CONCLUSIONS: Although surgical bilateral neck exploration is required in patients with MEN 1 and hyperparathyroidism, preoperative 99mTc-MIBI parathyroid dual phase planar, PinHole and SPECT CT scanning detected 2 ectopic glands before surgery improving the success of the procedure.In recurrent hyperparathyroidism, 99mTc-MIBI parathyroid dual phase planar, PinHole and SPECT CT scanning is the first line imaging technique for detection and localizing parathyroid glands and SPECT CT allows a better anatomical correlation which is especially useful in ectopic glands.We didn't found correlation between PTHi, calcium and phosphorus levels and scintigraphics findings.

P971

Lung Ventilation/Perfusion SPECT feasibility and interobserver concordance in patients with suspected pulmonary embolism

D. Balaguer, L. Marbello, H. Rodríguez, P. Abreu, D. Reyes, T. Mut, C. Plancha, E. Caballero; Dr. Peset Hospital, Valencia, SPAIN.

Aim: Several studies have assessed the feasibility of the Ventilation/Perfusion SPECT (V/P SPECT) and its improvement in diagnosis compared to Ventilation/Perfusion planar scintigraphy (V/P PLANAR). After implementing this technique as a clinical routine in Dr.Peset Hospital, this study aims to: 1. Assess the feasibility of the process. 2. Assess the interobserver concordance (κ value) of the V/P PLANAR and V/P SPECT in patients where both tests were performed. 3. Evaluate when the V/P PLANAR diagnosis was changed by the V/P SPECT. Materials and methods: Sixty-three consecutive patients with suspected pulmonary embolism (PE) were included between May 14th 2014 and January 31st 2015. The V/P test was performed using Technegas (20mCi) for ventilation and 99mTc-MAA (6mCi) for perfusion. The exploration was done in the sequence: V-PLANAR, V-SPECT, P-PLANAR, P-SPECT, without moving the patient. A minimum 1:4 ratio for V:P was sought. The study was processed with subtraction software to avoid false negative diagnoses. The ventilation and the subtracted perfusion images were merged. The image evaluation was done separately by two observers and the diagnosis was reached using trinary interpretation (PE present / PE absent / Non-diagnostic) as EANM recommends. The feasibility was then calculated, as well as the interobserver concordance and the percentage of cases where the V/P SPECT changed the diagnosis. Results: 1. V/P SPECT test was done to 25 patients. The other 38 patients did not undergo the complete exploration. Thus the feasibility is of 39.7%. Analysing the causes of non-performance of the V/P SPECT, more than half of the cases were due to logistic problems (mainly the long duration of the exploration). To a lesser degree it was due to the patient's clinical status. 2. The interobserver concordance (κ) for the 25 patients was of 0.82 for the V/P PLANAR and 0.80 for the V/P SPECT, indicating a very good concordance in both tests. 3. The main advantage of the V/P SPECT over the V/P PLANAR was the reduction of non-diagnostic explorations (0% versus 8%). Conclusions: The feasibility of V/P SPECT in our department is low. It is limited by logistical problems and to a lesser degree by the clinical status of the patient. Given that V/P SPECT has a high degree of interobserver concordance and fewer non-diagnostic cases than V/P PLANAR, we propose V/P SPECT as the standard technique, and the option of not performing the V/P PLANAR test.

P972

Body fat changes in HIV patients on highly active antiretroviral therapy (HAART): a longitudinal DEXA study.

G. Madeddu1, A. Spanu2, P. Solinas2, G. M. Calia1, C. Lovigu1, M. Mannazzu1, P. Bagella1, S. Nuvoli2, M. S. Mura1, G. Madeddu2; 1Unit of Infection Disease, University of Sassari, Sassari, ITALY, 2Unit of Nuclear Medicine, University of Sassari, Sassari, ITALY.

AIM.HIV patients receiving HAART may develop metabolic and morphologic abnormalities including body fat changes despite virologic control and pathogenetic mechanism is still unclear. In a long follow-up we monitored quantitative body fat composition in HIV patients treated with HAART to also identify possible therapeutic and host related associated risk factors. METHODS.We studied 180 HIV patients on HAART, of whom in 72 CDC stage A, 60 stage B, 48 stage C; 86 had protease inhibitors (PI) + non nucleoside reverse transcriptase inhibitors (NRTI) and 94 non nucleoside reverse transcriptase inhibitors (NNRTI) + NRTI in their therapeutic protocol. Fat changes were clinically present in 78 patients (Group 1) and absent in 102 patients (Group 2). In each patient, in basal conditions and during follow up, we measured by DEXA fat mass (FM) in whole body (WBF), trunk (TF) and peripheral (PF) regions such as arms (A) and legs (L), calculating trunk/peripheral (T/P) ratio, total weight (TW) and BMI. CD4 count by cytometry and HIV viral load by Nuclisens NASBA were also determined. RESULTS. At the first observation, WBF, FP, L values were significantly lower in Group 1 than in Group 2 ($p<0.01$, $p<0.001$, $p<0.001$, respectively), while A were lower in Group 1, but not significantly. Group 1 patients had higher TF and FT/FP ratio than in Group 2, but significantly only for the latter parameter. No TW and BMI difference was present between the two patient groups. CD4 count and CD4 rise from nadir were significant higher in Group 1 than Group 2. WBF, PF and L negatively correlated, while FT/TP positively, with PI and NRTI therapy duration, but not with NNRTI. At 5 year follow up, we could monitor 84 (39 receiving PI and 45 NNRTI) patients who continued the same therapy remaining with stable disease. In these patients, TF further increased and A and L further decreased, especially in patients receiving PI.CONCLUSIONS. Fat changes can occur in HIV patients on HAART with fat loss higher in the cases with clinical signs, mainly involving peripheral regions, with central fat accumulation tendency and with significantly higher rise in CD4 cell count from nadir, thus suggesting proinflammatory cytokine mediated role of immune recovery and peripherical fat loss dysfunction. These changes seem to worsen over time and should be considered in HIV patient in order to optimize treatment management in clinical practice and a DEXA study is suggested during follow up.

P973

Extravasation of Radiopharmaceuticals: Which Action Is Required? A Systematic Review

J. A. J. van der Pol, F. M. Mottaghy, S. Vöö; Maastricht University Medical Center, Maastricht, NETHERLANDS.

Background and aim: Extravasation of radiopharmaceuticals is rare, but can potentially have serious consequences, such as tissue necrosis. Nevertheless, little is known about preventive measures that can be taken to limit its complications and, to our knowledge, no specific recommendations are being proposed to date.The aim of the current study is to determine the incidence of radiopharmaceutical extravasation, subsequent clinical consequences, clinical management, and efficacy of applied medical treatments suggested in the available literature.Materials and methods: A comprehensive computer literature search of studies and cases published in Pubmed/MEDLINE and Embase databases through April 2015 was carried out. Inclusion criteria was extravasation of a diagnostic radiopharmaceutical (EDR) and/or a therapeutic radiopharmaceutical (ETR) in patients (search keywords included 'misadministration', 'extravasation', 'paravascular infiltration', combined with 'tracer', 'radionuclide', 'radiopharmaceutical', and a list of keywords referring to clinically used tracers (i.e. 'Technetium 99m', 'Yttrium 90')). The search included also guidelines on diagnostic and therapeutic radiopharmaceutical procedures of EANM, SNM, and the Dutch Society of Nuclear Medicine (NVNG). Included publications were systematically reviewed, data was pooled and a per patient analysis was performed.Results: Twenty-one articles comprising of in total 68 patients with radiopharmaceutical extravasation were found. Despite low incidence of ETR (4/68), all cases resulted in severe radiotoxic lesions such as wet desquamation and tissue necrosis within 7 weeks following the extravasation event. In contrast, the majority of EDR cases (61/64) described no or only limited and short-lasting skin lesions (i.e. erythema) with spontaneous recovery within days after the extravasation event. However, wet desquamation and tissue necrosis were reported in three EDR cases (3/64), involving Thallium 201 and Iodine 131 radionuclides. Only 4 out of 13 EANM/SNM/NVNG guidelines on therapeutic radiopharmaceuticals refer to the risk of extravasation but give no clear indications on its clinical management. In addition, specific measures taking into account the radiotoxicity of the radionuclide and the type of radiopharmaceutical were summarized from literature. Advised clinical management included immediate cessation of injection, fluid aspiration, and local tissue drainage.Conclusion: Cases of radionuclide extravasation are scarcely reported in the literature and are insufficiently taken in consideration in current guidelines. Reported events did result in severe skin lesions in all reported therapeutic cases, as well as in a minority of diagnostic cases. An advice on standard medical procedures is provided, based on experience in existing literature.

P974
Nuclear medicine in veterinary practice: preliminary experiences at Az. Polo Veterinario di Lodi

D. De Zani1, **C. Pettinato**2, M. Longo1, G. Ravasio1, M. Di Giancamillo1, D. Zani1; 1DIVET, University of Milano, Milano, ITALY, 2Medical Physics Unit, Bologna, ITALY.

Introduction and aimThe aim of this report was to describe the preliminary clinical and experimental experience in our veterinary nuclear medicine department in oncology, internal medicine and orthopaedics applications.Material and methodsIn our centre we study primarly horses but also small animals (dogs and cats) as clinical subjects, as well as pigs and rabbits for experimental protocols.In our Nuclear Medicine facility we have a single head gammacamera, performing SPECT and planar scintigraphy, and a stand alone gammacamera head, mounted on a pensile, to investigate big animals like horses.Equine scintigraphic scans were performed using 99mTc-labelled methylene diphosphonate, (99mTc-MDP 1 Gbq/100 kg) and both pool and bone phase have been acquired with the horse standing.Bone scan were also acquired in dogs in order to investigate lameness localized to the elbow (planar acquisition) and shoulder regions (planar acquisition and SPECT).Thyroid scans (both planar and SPECT) were performed in dogs injecting 99mTc-Pertecnetate.Feline injection-site sarcoma (FISS) has been investigated using 99mTc-sestaMIBI.For experimental purposes gated myocardial perfusion SPECT with 99mTc-sestaMIBI was performed in piglets affected by induced myocardial infarction.ResultsA total of 26 horses underwent bone scintigraphy. In 24 lame horses bone scan allowed to recognize the site of injuries while in 2 cases, referred for poor performance, no lesions were detected.In two lame dogs a focal and intense uptake of the radiotracer was observed in planar or SPECT images at level of elbow or shoulder.Thyroid scintigraphy allowed identification of a mass in two dogs. In one case, the mass showed a focal and severe IRU while in the other case, no IRU was observed.In the cat with a diagnosis of FISS a very intense and well-defined uptake was observed in the mass localized on the back. No uptake was visible in other sites suspected of metastases as lung or satellite lymph nodes. Gated myocardial perfusion SPECT allowed the exact localization of myocardial lesions in 2 piglets.ConclusionNuclear medicine has high potentiality in veterinary medicine.In our preliminary experience we can assert that, in both equine and small animal practice, nuclear medicine could be a very useful diagnostic tool, especially in association with other diagnostic techniques as CT or MRI. Furthermore, experimental studies could be helpful in veterinary like human medicine not only for research purposes but also as pre-clinical experiences for future development of new clinical approaches.

P975
18F-FDG PET/CT Contribution in Characterization of Malignancy of Brain Tumors

L. F. León Ramírez, M. Martinez de Bourio, M. N. Cabrera Martin, C. Gonzalez Roiz, A. Ortega Candil, M. J. Pérez

Castejón, E. Cala Zuluaga, M. Pedrera Canal, A. Jiménez Ballvé, J. L. Carreras Delgado; Hospital Clinico San Carlos, Madrid, SPAIN.

AIM: To determine the utility of 18F-FDG PET-CT in the differentiation of low-grade from high-grade cerebral tumors and to correlate with hystopathological analysis (HA). Material and Methods: We retrospectively evaluated 56 consecutive 18F-FDG PET-TC studies performed in our department from December 2008 to January 2015 (27 women, 29 men, mean age 63.7 years) in order to characterize and stage brain lesions. All lesion were corregistered with MRI studies. We use cutoff levels of FDG uptake ratios described by Delbeke in the differentiation of high-grade from low-grade tumors: 1.5 for tumor-to-white matter (T/WM) ratios and 0.6 for tumor-to-cortex (T/C) ratios.RESULTS37/56 studies were compared with histopathological analysis. 32 PET-CT studies suggested high grade malignancy (true positive results) and 3 were suggestive of benign lesions (true negative results). We had two false positive results, who corresponded to Erdheim-Chester Disease and tuberculosis. CONCLUSION: 18F-FDG PET-TC is a useful diagnostic tool in metabolic characterization of brain tumors, and could be helpful to guide the best area for biopsy.

P976

Added value of SPECT/CT to Technetium 99m-labeled red blood cells scintigraphy in small bowel bleeding

W. Amouri, F. Hamza, I. Jardak, H. Charfi, M. Maaloul, F. Kallel, S. Charfeddine, F. Guermazi; Habib Bourguiba Hospital, Sfax, TUNISIA.

AIM: to underline the role of Tc-99m-labeled red blood cells (RBC) spect/ct in localizing and guiding management of small bowel bleeding. MATERIALS AND METHODS: We present two cases of intestinal bleeding in whom planar dynamic images were performed after injection of 20 mci in vivo Tc-99m-labeled RBC, followed by serial static abdominal images. A fused image composed of those from Tc-99m-labeled RBC SPECT and from x-ray CT revealed small intestinal bleeding with specific anatomic information. RESULTS: The two patients were hospitalized with anaemia from recurrent gastrointestinal bleeding. Endoscopic explorations have failed to locate the bleeding. Planar 99mTc-tagged RBC bleeding scan suggested an active site of bleeding in the lower abdomen, but it could not conclusively define the bleeding as originating in small versus large bowel. The SPECT / CT allowed specifying the exact site of bleeding at the small intestine. Surgical resection of the bleeding site was performed successfully and the pathological examination showed angiodysplasia. CONCLUSION: RBC scintigraphy is an effective imaging modality in localizing lower gastrointestinal bleeding in patients for whom other diagnostic tests have failed to locate the bleeding. We conclude that spect/ct is useful for anatomic localization of bleeding sites in the small intestine and helpful for surgical intervention.

P977

Lung perfusion scintigraphy with SPECT-CT for diagnosis of pulmonary embolism.

A. Tzonevska1, M. Shindov1, M. Yaneva2; 1National Center of Oncology, SOFIA, BULGARIA, 2University Hospital "St.Georgi", PLOVDIV, BULGARIA.

The aim of the study is to compare the results of planar lung perfusion scintigraphy and SPECT-CT in patients with suspected pulmonary embolism(PE) and to assess the impact of SPECT-CT in the diagnosis. Material and methods: We included 39 patients in the study. All patients passed clinical assessment, planar lung perfusion scintigraphy combined with SPECT-CT. PISA-PED criteria for interpretation were applied. Results: All of the included patients were with pretest clinical probability of PE (Wells score>4). All of the patients had abnormal perfusion scan. In 24(62%) patients the results confirmed PE with abnormal (PE+) scan: 59 segmental and subsegmental defects were registered, SPECT-CT identified 17(29%) defects additionally. In 9(23%) patients with perfusion defects in planar scintigraphy, but inconclusive for PE, SPECT-CT identified abnormal (PE-) results with nonsegmental hypoperfusion defects and assessed the concomitant disease (COPD, emphysema, CHD), in 6(15%) patients SPECT-CT identified abnormal (PE+) results with subsegmental hypoperfusion defects. Conclusion: The study results show that using SPECT-CT in patients with suspected PE, it is possible to precise localization of perfusion defects, the false negative results decrease, the diagnostic accuracy increases. The PE diagnosis should be performed by team including pulmologist and nuclear medicine specialist who interpret clinical and nuclear medicine results all together. Key wards: PE, planar lung perfusion scintigraphy, SPECT-CT

P978

Impact of Fluorodeoxyglucose-PET scan in characterizing pleural effusions (massive/submassive) in non-oncologic patients

M. SIMO, J. MONTURIOL, M. VELASCO, I. NAVALES, M. BARIOS, J. CASTELL; HOSPITAL UNIVERSITARIO VALL HEBRON BARCELONA, BARCELONA, SPAIN.

AIM: Determined the ability of 18F-fluorodeoxyglucose (FDG) positron emission tomography (PET) to differentiate

benign and malignant pleural effusions (massive/submassive) in non-oncologic patients. MATERIALS AND METHODS: We included 38 consecutive patients (29men/8 women, median age: 67 years old) with massive/submassive pleural effusion. None of them had history of cancer and showed non-diagnostic paracentesis. The diagnostic approach in our institution included a diagnostic Chest computed tomography (CT), a PET-scan and talc pleurodesis. CT findings which were suggestive of malignancy was pleural nodularity, pleural rind, mediastinal pleural involvement, and pleural thickening. FDG PET revealed positive findings if pleural activity was greater than background mediastinal activity; FDG PET revealed negative findings if pleural activity was the same as or less than background mediastinal activity. All the results of PET-scan and Chest CT were correlated with pathologic diagnosis determined with thoracentesis. RESULTS: FDG PET revealed positive findings in 19 patients (1 False positive), negative findings in 17 (1 False negative) and indeterminate result in 2 patients (1 was true positive). The mean SUV value in PET positive patients was 9.6 compared to SUV max of 2.3 in the PET negative group. The definitive histological examination showed benign condition in 18 patients (acute, chronic or fibrous pleuritis), malignant in 19 (mesothelioma n=8 or pulmonary adenocarcinoma, intestinal adenocarcinoma, unknown primary site n=11) and non diagnostic in one patient. Sensitivity, specificity, PPV, NPV values for PET were 95%, 94%, 95% and 94% respectively, with a unique false negative result. The PET-scan located the primary en 5 patients (4 lung cancers and 1 gastric cancer). CONCLUSION: This study suggests that FDG PET may be useful in this group of non-oncologic patients with massive/submassive pleural effusions. PET scan showed high sensitivity and PPV to detect malignancy. The inclusion of this technique in the work-up of pleural effusions help to select patients to aggressive therapeutic approach.

P979

Determining prognosis using lower limb perfusion SPECT-CT in patients with arteriosclerosis obliterans

H. Hashimoto; Department of Radiology, Nippon Medical School, Tokyo, JAPAN.

Aims: Patients with arteriosclerosis obliterans (ASO), especially with critical limb ischemia, have high morbidity of cardiovascular disease and mortality. Whereas the diagnostic accuracy of lower-limb perfusion scintigraphy was previously reported, the prognostic value of lower-limb perfusion SPECT-CT using quantitative analysis has not been demonstrated up to now. The purpose of this study was to estimate lower-limb-muscle-perfusion abnormality using lower-limb perfusion SPECT-CT, and to determine the prognostic value of lower-limb perfusion SPECT-CT in patients with ASO. Materials and methods: A total of 29 patients, who were clinically diagnosed with arteriosclerosis obliterans, were included in this study (23 men and 6 women, 71 ± 13 years). The clinical diagnosis was based on clinical symptoms, a treadmill exercise test, ankle-brachial indices, and lower-extremity angiography findings. Patients with collagen disease, Behçet disease, Buerger disease, diabetic foot and other types of vasculitis were excluded from this study. All enrolled patients underwent lower-limb perfusion SPECT-CT using SPECT-CT combined system, Symbia T2. SPECT acquisition was started from 15 min following the administration of 99mTc-tetrofosmin 740 MBq. In all images, 3D volumes of interest were drawn on each lower-extremity muscle, and lower-limb-muscle-to-blood ratio (LMBR) was calculated by dividing lower-limb-muscular mean counts/volume by blood-pool mean counts/volume in unaffected distal-femur bone marrow. In order to estimate the clinical importance of LMBR, all participants were divided into two groups based on their LMBR value. All patients were followed up over one year from the initial test and observed for the occurrence of major adverse events; defined as amputations of ischemic leg, cardiovascular events, cerebrovascular events, or all-cause mortality. The relationships between the occurrence of major adverse events and various clinical parameters including LMBR were also analyzed. Results: High and low LMBR groups included 23 and 6 patients respectively. LMBR in the high group was 8.43 ± 3.23 and was 3.68 ± 0.27 in the low LMBR group. The proportion of patients that adverse events occurred was significantly higher in the low LMBR group than in the high LMBR group (5 of 6 versus 1 of 23, $p < 0.001$). Conclusions: The amount of lower-limb-muscle perfusion was estimated by calculating LMBR using lower-limb perfusion SPECT-CT. LMBR was proved to have a high prognostic value for the occurrence of major adverse events in patients with ASO.

P980

Is diffuse increased FDG uptake in renal parenchyma associated with impaired renal disfunction?

N. Hayakawa, Y. Nakamoto, T. Ishimori, K. Togashi; Kyoto University Graduate School of Medicine, Kyoto, JAPAN.

Aim: The aim of this study was to evaluate the association between diffuse increased FDG uptake in renal parenchyma and impaired renal function. Materials and Methods: 25 patients who showed diffuse increased renal uptake (higher than liver) pattern in FDG PET/CT (DRU group) was compared with age- and gender-matched 25 patients with normal renal uptake (control group), regarding parameters related to renal function as follows: (i) estimated glomerular filtration rate (eGFR), (ii) Cr ratio = serum creatinine level within two days

before or after the PET/CT scan / the lowest creatinine level in one month before or after the PET/CT scan (minimal Cr), and (iii) maximal Cr ratio = the highest serum creatinine level during the past one month before PET/CT scan / minimal Cr. In DRU group, we also assessed the correlation between these parameters and the SUVmax in renal parenchyma. Results: Underlying disease in DRU group is malignant tumor (n = 16), collagen disease (n = 4), and other diseases (n = 5). No significant difference was observed between DRU group and control group in eGFR (83.5 ± 50.4 vs. 92.0 ± 40.8, p = 0.23) and Cr ratio (1.52 ± 0.76 vs. 1.21 ± 0.19, p = 0.30). On the other hand, maximal Cr ratio in DRU group was significantly higher than that in control group (1.81 ± 0.78 vs. 1.39 ± 0.45, p = 0.04). The ratio of patients whose maximal Cr ratio equal to or greater than 1.5 is 56% (14/25) in DRU group and 20% (5/25) in control group (p = 0.01). In DRU group, no apparent correlation was observed between SUVmax in renal parenchyma and each parameter. Conclusion: Diffuse FDG uptake in renal parenchyma may indicate recent impaired renal function even when renal function is normal at PET/CT scan.

P981

Evaluation of preventive effect of dexpanthenol in radiation injury by lung perfusion scintigraphy

Z. Koç1, E. In1, Ö. Üçer1, I. Karslıoğlu2, S. Canpolat3; 1Fırat University Hospital, Elazig, TURKEY, 2Medical Park Hospital, Elazig, TURKEY, 3Fırat University, Elazig, TURKEY.

Aim: The aim of this study was to demonstrate the preventive effect of dexpanthenol from radiation injury caused by radiotherapy using lung perfusion scintigraphy in preradiotherapy and postradiotherapy period. Materials and Methods: Six male New Zaelland rabbits (5-6 month old, approximately 2,5-3 kg in weight) were subjects of this study. The animals were subjected to Tc-99m MAA lung perfusion scintgraphy in the preradiotherapy and postradiotherapy (after two weeks period). The scintigraphies were performed by the same dose and methodology by the same acquisition parameters and by same staff. The rabbits were divided into two groups; Group 1 (only administering RT) and Group 2 (administering Im 500mg dexpanthenol injections for consecutive 14 days after RT). Quantification was performed in order to compare groups and quantification variables were compared using Paired Samples T Test, $p<0,05$ considered statistically significant. Additional pathological analysis was performed to all rabbit's lungs. Results: The postradiotherapy scintigraphies contained demonstrative decrease in counts in both lungs indicating early postradiotherapy injury. The difference between counts obtained from both lungs in Group 1 and 2 was significantly different favoring the Group 2. Pathological analysis showed findings of severe injury in the lungs of rabbits in Group 1 and milder injury in Group 2. Conclusion: It is possible to estimate postradiotherapy changes in early period (in contrary to previous data) by lung perfusion scintgraphy. Dexpanthenol may prevent the effects of RT in a degree. Although this is the first study indicating preventive effect of Dexpanthenol from RT injury, further studies are warranted in this area.

P982

Application of combined nuclear medicine protocol including Whole Body Bone Scintigraphy and Single Photon Emission Computed Tomography/Computed Tomography (SPECT/CT) of the pelvis for the initial staging of prostate cancer

V. Hadzhiyska1, T. Petrov1, I. Kostadinova1, V. Mariyanovski2, D. Zlatareva1, M. Garcheva-Tsacheva1; 1University Hospital Alexandrovska, Sofia, BULGARIA, 2Pirogov Hospital, Sofia, BULGARIA.

The aim of the study was to apply a combined nuclear medicine protocol, including Whole Body Bone Scintigraphy and Single Photon Emission Computed Tomography/Computed Tomography (SPECT/CT) for the initial staging of patients with prostate cancer. Material and Methods: We have examined 23 patients with newly diagnosed prostate cancer by using a combined nuclear medicine protocol including Whole Body Bone Scintigraphy (WBS) and Single Photon Emission Computed Tomography/Computed Tomography (SPECT/CT) of the pelvis. According to the NCCN Guidelines (version 2.2014) the patients were divided in to three risk groups, respectively low risk group (5 patients, 22%), intermediate risk group (6 patients, 26%) and high risk group (12 patients, 52%). Results: Pathological findings detected by WBS were reported in 16 (67%) of the patients. In 7 (30%) of them they were suspicious for metastases.After the SPECT /CT of the pelvis all suspicious foci from the WBS were confirmed to be osteosclerotic metastatic leasons. In addition, the CT scan visualized enlarged regional lymph nodes in 7 patients (30%), respectively presacral lymph nodes (N=5) and parailiac lymph nodes (N=9). Additional findings from the CT were also seminal vesicles with altered morphology suspected for infiltration in 5 patients (22%) and unexpected extracapsular extension of the primary in 2 patients (9%). In four out of 7 patients with enlareged lymph nodes we found simultaneous bone metastases, while in the rest of them the lymphadenopathy was an isolated finding. As a result from the application of the combined nuclear medicine protocol in one of the patients from the low risk group and in one of those with intermediate risk, as well as in six high-risk patients the opportunity for surgery was rejected because of bone metastases and/or regional lymphadenopathy. In the remaining 15 patients, including also those with high risk, decision for radical prostatectomy was made.

Conclusion: Our first experience with the application of the combined nuclear medicine protocol, including WBS and SPECT/CT of the pelvis demonstrated that the procedure allows for right initial staging of patients with prostate cancer as well as for choosing an appropriate treatment by performing a one-stop complex imaging examination.

P984

Tc99m tagged RBCs venography with additional abdominal/pelvic SPECTCT in diagnosis of Iliac venous compression (May-Thurner syndrome).

Y. Chen, C. Lin, D. Wu, C. Chiu; Kaohsiung Medical University Hospital, Kaohsiung, TAIWAN.

May Thurner syndrome is status of iliac venous compression, due to small space between bifurcation and the 5th lumbar spine. Tc99m tagged RBCs venography (CNM, 2001) is a highly sensitive routine method to evaluate lower leg swelling and differentiate deep venous thrombosis. Among those leg swelling patients with susp deep venous thrombosis, high-level venous flow deficiency, as iliac/ femoral portion is common findings on Tc99m RBCs venography. In this article, we introduce additional abdominal/pelvic SPECTCT during Tc99m RBCs venography to elucidate pathophysiology of potential May-Thurner syndrome. Patients and Methods: We collect leg-swelling patients with high-level venous flow deficiency in Tc99m RBCs venography and applying additional abdominal/ pelvic SPECTCT process, retrospectively. There are thirty two patients (male to female ratio as 19:13; age range 34-82 y/o as 63.2±13.1 y/o) during one year. All of them have bilateral or unilateral leg swelling in clinic. In vivo RBCs tagged technique is applied. Then, each 8 mCi pertechnetate is subcutaneous injection around digital- space of feet. Two phase half-body imagings are acquired with/ without tourniquet compression applied, consequently. The additional abdominal SPECTCT (Philips Bright-views X CT) is needed when patients with asymmetrical reduction of iliac/ femoral venous radioactivity. Results: Based on imaging interpretation, twenty-one patients (66%) are suspicion of iliac venous compression, mostly involved left iliac vessel. The average age in this group is 54.9 y/o. The other eleven (34%) cases, with high-level venous flow deficiency are not identified as iliac venous compression on SPECTCT imaging. However, several findings are still seen on SPECTCT imaging, as large osteophyte formation, psoas abscess and abdominal aneurysm adjacent abdominal bifurcation , also have risk of venous hemodynamic disturbance and potential thrombosis formation. The average age is 72.3 y/o in the non iliac venous compression group. We have two patients with malignant history as rectal and breast cancer. Conclusion: Tc99m RBCs venoscintigraphy is a convenient and high sensitive method for evaluate status of deep venous flow from calf to iliac portion and diagnosis of deep venous thrombosis. Additional abdominal/ pelvic SPECTCT provides function and anatomy to elucidate risk of iliac venous compression in subgroup patients.

P985

Prognostic impact of deep-inspiratory breath-hold pulmonary perfusion SPECT-CT in patients with pulmonary thromboembolism

Y. Fukushima, S. Kumita, H. Hashimoto, Y. Sugihara; Nippon Medical School Hospital, Tokyo, JAPAN.

Introduction: Pulmonary perfusion SPECT is commonly used for the assessment of pulmonary perfusion abnormality in patients with pulmonary thromboembolism (PTE). However, in conventional non-breath-hold SPECT, respiratory lung motion during image acquisition deteriorates its image quality and smears perfusion defects. Conversely, pulmonary perfusion SPECT-CT, using deep-inspiration breath-hold (DIBH) acquisition, can obtain each static image and estimate the severity of pulmonary perfusion defect with a high degree of accuracy. The aims of this study were to calculate the percentage of pulmonary perfusion defect (%PPD) using DIBH pulmonary perfusion SPECT-CT, and to evaluate its prognostic value in patients with PTE.Materials and methods: A total of 97 patients (47 men and 50 women, 67 ± 15 y) with respiratory failure and suspected PTE were included in this study. All patients underwent DIBH pulmonary perfusion SPECT-CT. Clinical diagnosis of PTE was confirmed based on the combination of CT pulmonary angiography, DIBH pulmonary perfusion SPECT-CT and serum D-dimer level. The DIBH method required patients to hold their breath for 10 seconds during each continuous 360 degrees image acquisition. It was performed 12 times with 10 second intervals between each acquisition. These data were combined to create SPECT images. SPECT data were reconstructed using CT attenuation correction, and SPECT-CT images were built by hardware fusion. In pulmonary perfusion SPECT-CT images, %PPD was calculated by dividing perfusion defect volume in SPECT image by lung volume in CT image. In order to evaluate the clinical importance of %PPD, all patients were divided into two groups based on the value of %PPD using receiver-operating-curve analysis. All patients were followed up over two years from the onset of PTE and observed for the occurrence of major adverse events, defined as all-cause mortality, non-fatal symptomatic recurrent PTE, hospitalization due to deterioration of respiratory failure and hospitalization due to deterioration of heart failure.Results: This study contained 38 PTE patients, with low and high %PPD groups consisting of 17 and 21 participants respectively. Median %PPD in the low

%PPD group was 19 (15-28) and 63 (50-81) in the high %PPD group. The proportion of patients that occurred major adverse events was significantly higher in the high %PPD group than in the low %PPD group (p = 0.022).Conclusions: The severity of pulmonary perfusion defect was estimated by calculating %PPD using DIBH pulmonary perfusion SPECT-CT. %PPD was proved to have a high prognostic value for the occurrence of major adverse events.

P986

Physiological uptake of the uncinate process of the pancreas: incidence of this potential pitfall in a retrospective study fo 220 patients.

J. Pinaquy, **Sr**., P. Schwartz, L. Bordenave; CHU BORDEAUX, Bordeaux, FRANCE.

Whereas the ability to tag somatostatin analogs with Gallium-68 has significantly improved the diagnosis and staging of patients with neuroendocrine tumors (NETs), the gold standard and most used for detection and staging of most of the NETs is always 111Indium-DTPA-octreotide (SRS). Most of the pitfalls are well known but some remains few described. The aim of our study was to retrospectively evaluate the incidence and the intensity of physiological uncinate process of the pancreas. Materials and methods : 246 patients (124 women, mean age 57 years [15-92]) who underwent SRS were retrospectivelyincluded from June 2012 to March 2015. 229 abdominal SPECT-CT were performed. 9 patients with a prooved uncinate process tumor were excluded. The intensity of the uptake uncal was evaluated based on Rotterdam visual scale. The clinical, radiological, or surgical follow-up was used as gold standard. Results: 42.3% (93/220) of the patients had an uncinate process uptake. Of these 93 patients, 39.8% (37/93) had an uptake greater than or equal to the liver. No significant lesion were highlighted. Conclusion : These study shows that significant uncinate process uptake is not uncommon and must be known. Mistaking exaggerated physiologic pancreatic uptake for pancreatic tumor can result in harmful consequences for the patient, especially if a whipple procedure is performed on the basis of these findings. Close correlation with findings at MRI imaging and thin-section multiphase CT can be helpful in further assessing equivocal findings.

P987

IMP and MIBG scintigraphy as an index comparable to the core symptoms for a diagnosis of dementia with Lewy bodies?

F. Sakamoto1, S. Shiraishi1, N. Tsuda1, H. Yuki1, T. Namimoto1, M. Kitajima1, M. Hashimoto2, S. Tomiguchi3, M. Ikeda2, Y. Yamashita4; 1Diagnostic Radiology Graduate School of Life Sciences Kumamoto University, kumamoto, JAPAN, 2Department of Neuropsychiatry, Graduate School of Life Sciences, Kumamoto University, Kumamoto, Japan, kumamoto, JAPAN, 3Department of Diagnostic Medical Imaging, School of Health Faculty of Life Sciences, Kumamoto University, Kumamoto, Japan, kumamoto, JAPAN, 4Department of Diagnostic Radiology, Graduate School of Life Sciences, Kumamoto University, kumamoto, JAPAN.

Aim: As the clinical symptoms of different types of dementia overlap, it is difficult to distinguish dementia with Lewy bodies (DLB) from other neurodegenerative dementias based on clinical manifestations alone. Nuclear medicine may yield a high-value index for the objective evaluation and diagnosis of DLB. We attempted to develop a nuclear medicine index that used factors other than clinical core symptoms for the diagnosis of DLB. Materials and Methods: We enrolled 332 patients with suspected DLB; all underwent 123I-MIBG myocardial scintigraphy. The diagnosis was probable DLB in 92patients (39 males, 52 females; mean age ± SD, 78.0 ± 8.9 years; range, 56 - 89 years), and no DLB in 240 (98 males, 142 females; mean age, 75.2 ± 4.8 years; range, 70 - 87 years). The clinical evaluation index was primarily based on fluctuating cognition, visual hallucinations, and Parkinsonism. The nuclear medicine index used the cerebral blood flow on IMP scintigraphs of the posterior cingulate, precuneus, and occipital lobe, the MIBG washout rate, and the early and delayed heart to mediastinum (H/M) ratio. Results: Univariate and multivariate analysis of fluctuating cognition, visual hallucinations, Parkinsonism, and the early H/M ratio in patients with probable and without DLB revealed significant differences. The area under the curve (AUC) in receiver operating characteristic (ROC) analysis was 0.693, 0.760, 0.611, and 0.918. The diagnostic value of the highest 123I-MIBG uptake on the AUC was 82.4% for sensitivity, 96.3% for specificity, and 92.5% for accuracy. Conclusion: 123I-MIBG myocardial scintigraphy can serve as a diagnostic index equal to the core clinical features of DLB. The diagnostic value of the objective nuclear medicine index is high. We expect that 123I-MIBG scinitigraphy will be valuable for the early diagnosis and early treatment of DLB.

P988

Assessment of vascular reserve state with brain SPECT in asymptomatic patients with steno-occlusive lesion in Brain MRA

S. OH1, J. Han2, M. Cha3, S. Pyun3, J. Lee1; 1Department of Nuclear Medicine, National Police Hospital, Seoul, KOREA, REPUBLIC OF, 2Department of Nuclear Medicine, National Police HospitalGapyeong Public Health Center, Gapyeong, KOREA, REPUBLIC OF, 3Department of Neurology, National Police Hospital, Seoul, KOREA, REPUBLIC OF.

Objectives : This study is to assess the vascular reserve state with Brain SPECT in asymptomatic patients with stenoocclusive lesion on Brain MRA. Methods : Fourteen asymptomatic patients who were identified as steno-occlusive lesion on their MRA performed for general medical examination underwent brain SPECT. On MRA, the lesion was classified into 4 grades (mild, moderate, severe, total occlusion). Brain SPECT was visually analyzed by two nuclear medicine physician. Location, severity of the lesions were compared between two modalities. Statistical analysis using Chi-square test was performed to compare the frequency of perfusion or vascular reserve decrease between the subgroups by the severity of stenosis. Results : On MRA, 6, 4, 2, 2, patients had the lesion in MCA, ICA, carotid bulb and ACA, respectively. Five patients were identified as total occlusion, 4, 2, 3 patients were severe, moderate and mild stenosis. On SPECT, 5 cases were normal, otherwise, 9 showed perfusion or reserve decrease. No patients with mild stenosis on MRA showed abnormal finding on SPECT. Four Of 5 cases with total occlusion showed perfusion and reserve decrease on SPECT. All of 4 patients with severe stenosis showed concordant perfusion and reserve decrease. One of 2 moderate stenosis cases was normal on SPECT. By location of lesions, 1 of 2 ACA lesion, 1 of 2 carotid bulb, all of 4 ICA lesion, 3 of 6 MCA lesion showed concordant perfusion or reserve decrease. In group with severe stenosis or total occlusion on MRA, reserve decrease was more frequent as compared with the group with mild to moderate stenosis ($p<0.05$) Conclusions : Even in asymptomatic patients with steno-occlusive lesion on MRA, vascular reserve might be decreased. Brain SPECT could give additional valuable information in asymptomatic patients with steno-occlusive lesion on Brain MRA.

Technologist Posters

TP01 - Tuesday, October 13, 2015, 8:00 AM - 9:30 AM, Hall 3 –Poster Exhibition
Technologist Poster Session 1

TP001

Radiosynovectomy as a Primary Modality of Treatment for Diffuse Pigmented Villonodular Synovitis of Elbow joint treated with Rhenium-188 labelled Tin-Colloid.

K. Kamaleshwaran, L. Babu, b. krishnan, m. mallia, A. shinto; Kovai medical center and hospital limited, Coimbatore, INDIA.

Aim: Diffuse Pigmented villonodular synovitis (DPVNS) is a rare, relatively benign, intra-articular lesion characterized by a slowly progressive proliferation of synovial tissue. The knee is the most frequently involved joint, but elbow joint can be also involved. There are previous reports which used Re-188 tin colloid in knee joint synovitis but use of Re- 188 tin colloid in elbow joint DPVNS is not yet reported. We describe the use of Re-188 tin colloid in a 30 year old male who presented with DPVNS of left elbow joint. Methods: A 30 year-old male patient presented with left elbow joint swelling and pain for duration of 4 months.X ray of elbow was done which showed soft tissue swelling with no bone involvement. Magnetic resonance imaging(MRI)of elbow joint was done which showed synovial thickening and enhancement with mild joint effusion noted ,suggesting DPVNS .He was referred for RSV due to high rate recurrence with surgery.Three phase bone scintigraphy showed increased blood pooling in left elbow joint consistent with synovitis.Whole body image showed increased uptake in left elbow joint Results: RSV was performed with precise intra-articular injection under sterile conditions and fluroscopic guidance.Before joint puncture, local anesthesia was administered with 2% lidocaine- hydrochloride.Prior to the injection of Re 188 tin colloid , Depomedrol (10 mg in 0.2 mL) was injected into the joint in order to reduce the risk of acute radiation induced synovitis and to avoid skin radiation necrosis.Subsequently, 370 MBq dispersed in 0.5 mL of sterile, apyrogenic normal saline was administered intra-articularly into left elbow joint and then the needle was flushed with 0.3 ml of normal saline.An orthopedic bandage was applied as a semi rigid splint was immobilised for 48 hours. Images were acquired in an dual head gamma camera in high energy general purpose collimator with 155±20 Kev window. Re-188 tin colloid SPECT/CT images showed good distribution of tracer in the left elbow joint inside the synovium. On follow up after 3 months,there was significant decrease in pain and swelling of elbow joint. Conclusion: In our case, RSV was useful as primary modality of treatment with DPVNS of elbow joint . We suggest that Re- 186 tin colloid can be used safely for the elbow involvement of DPVNS.

TP002

Comparison Between Left Ventricular Function Parameters as Measured on 8- Versus 16-Frame ECG-Gated $13NH_3$ Myocardial Perfusion PET Studies

N. J. Hoogvorst; Medical Center Alkmaar, Alkmaar, NETHERLANDS.

Aim: The purpose of the present study was to validate the accuracy of the 8-frame gated reconstruction for assessing left ventricular ejection fraction (LVEF), end diastolic volume (EDV) and end systolic volume (ESV) from gated $13NH_3$ PET using 16-frame reconstruction as a reference. By implementing the 8-frame gated reconstruction it would be possible to reduce the reconstruction time and eventually decrease injected dose. Methods: 35 patiënts underwent rest and stress myocardial perfusion PET using a Siemens Biograph 16 TruePoint PET/CT scanner in listmode format after the intravenous injection of 300 and 400 MBq $13NH_3$, respectively. Datasets were reconstructed in a 168x168 matrix and ECG-gated in either 8 or 16 intervals per cardiac cycle. Left ventricular ejection fraction (LVEF), end diastolic volume (EDV) and end systolic volume (ESV) were determined using the QGS software package (2012 Cedars Sinai Medical Center) for all datasets, and differences were tested for significance and correlation between both groups, for rest and stress studies. Results: A significantly lower LVEF was obtained from the 8-frame reconstructed rest $13NH_3$ PET dataset as compared to the 16-frame reconstructed data (60.7%±13.2% vs 64.3%±13.5%, respectively, $P<0.001$), but measurements correlated strongly ($r=0.996$). The 8-frame reconstruction of the rest study produced a significantly higher ESV (48.9±38.7 ml vs 44.7 ±38.6 ml for 16 frames, $P<0.001$ and $r=0.999$) and EDV was not significantly different (113.1±42.3 ml vs 113.7 ±42.4 ml, $P=0.133$ and $r=0.998$). The stress data also revealed a significantly lower LVEF in the 8-frame vs the 16-frame gated study (60.3%±12.6% vs 64.2%±12.9%, $P<0.001$ and $r=0.993$), a higher ESV (53.0±39.6 ml vs 48.6±4.3 ml, $P<0.001$ and $r=0.997$) and not significantly different EDV (123.3±43.0 ml vs 123.7±44.1 ml, $P=0.485$ and $r=0.997$). Conclusions: Reconstruction of $13NH_3$ gated PET studies using 8 frames per cardiac cycle leads to significantly lower LVEF, significantly higher ESV and not significantly different EDV as compared to those obtained from 16-frame gated studies, but correlation is very strong for all values.

TP003

Renal Parenchymal Analysis: 99mTc-MAG3 'v' 99mTc-DMSA

T. De Sousa, D. Bailey; Guy's and St. Thomas' NHS Foundation Trust, London, UNITED KINGDOM.

Background: 99mTc-DMSA scan is currently used for the analysis of renal parenchymal defects, particularly in paediatric patients. Diuretic 99mTc-MAG3 dynamic scintigraphy has been used in the evaluation of kidney function and to exclude obstruction. However, 99mTc-MAG3 provides visualisation of parenchyma with high object/background ratio at 2-4 min post injection and can be considered in the analysis of parenchymal disorders. Aim: To evaluate the reliability of the parenchymal analysis using 99mTc-MAG3 instead of 99mTc-DMSA for paediatrics patients, allowing simultaneous information on parenchymal evaluation, split kidney function and drainage. Method:Paediatric patients referred for both scans were considered for the study. Patients had 99mTc-MAG3 scan done first followed by 99mTc-DMSA 3 hours later as per local protocol. Administrated activities were consistent for EANM paediatric recommendations. Data Analysis: Images from three different patients were displayed on the same grey scale and blinded with respect to radiopharmaceutical used. Images analysed by 3 observers for evidence of renal parenchymal defects. Confidence level when reporting scored on a 1 to 5 scale.Results:Confidence level is higher when reporting 99mTc-DMSA than 99mTc-Mag3 images: 4.5 vs. 2.9, on a scale from 1 to 5.88.9% concordance was achieved between both reports.No false negatives reported on 99mTc-Mag3 images.One false positive for focal parenchymal lesion was reported by one observer on a 99mTc-Mag3 image. Conclusion:99mTc-MAG3 could be used as a stand alone study for the assessment of suspected renal damage and would offer the following advantages of providing simultaneous additional information on renal drainage, reduce the total attendance time for patients and their carer and reduce radiation exposure in the paediatric population;The use of LEHR collimators may improve resolution and increase reporting confidence.

TP004

Influence of attenuation correction in the MPI image reconstructed by the Evolution for Cardiac™ software

D. F. F. Ribeiro1, J. Vilaça1, C. Nunes1, L. Freire1, M. Pinheiro1, G. Cantinho2, E. Carolino1, E. Sousa1; 1Escola Superior de Tecnologia da Saúde de Lisboa, Lisbon, PORTUGAL, 2Atomedical, Laboratório de Medicina Nuclear, Lisbon, PORTUGAL.

Introduction - The acquisition of a Myocardial Perfusion image (MPI) has great importance for the diagnosis of coronary artery disease, since it allows evaluating which areas of the heart are not being properly perfused, in rest and stress situations. This exam is greatly influenced by photon attenuation which creates image artifacts and affects quantification. Aim - To evaluate the influence of incorporating an attenuation correction map in the analysis of MPI and the outcome in perfusion quantification and imaging quality. Methods - The population comprised two sets of individuals (ten male and ten female, with a body mass index (BMI) above 30Kg/m2). A MPI study was acquired after the Computed Tomography (CT), using EANM guidelines and reconstructed with the Evolution for Cardiac software. Studies were reconstructed twice, the first time relying uniquely on the MPI and the second time relying on the MPI and on the attenuation correction map given by the CT image. For perfusion quantification purposes, images were segmented by vascular territories. For imaging quality, the location of each wall in the short axis was identified. Each study was processed three times by the same operator, and average values were computed and compared between studies with and without attenuation correction . Results - The level of significance for all comparisons was 1%. Significant differences were found in female rest studies for the right coronary ($p=0.004$) and the circumflex artery ($p=0.0$), and in stress for the right coronary ($p=0.0$). For the male rest set these were found for the right coronary ($p=0.0$) and the circumflex artery ($p=0.002$), and in stress for the right coronary ($p=0.0$) and the circumflex artery ($p=0.002$). The data acquired for noise in female rest studies revealed, significant differences for the inferior ($p=0.003$) and septum ($p=0.0$) walls and in stress for the inferior wall ($p=0.005$). In the male rest set these were found for the inferior ($p=0.001$) and septum ($p=0.0$) walls, in stress for the lateral ($p=0.007$) and inferior ($p=0.005$) walls. When evaluating the contrast, significant differences were found in all walls for both sets, except for the inferior wall in male stress studies ($p=0.049$). Conclusion - Results show that performing attenuation correction with CT attenuation maps, produces differences in perfusion and image quality. The study showed that contrast is greatly influenced by attenuation correction. Differences between the male and female sets, correlate with the ones described in literature.

TP005

Influence of geometry on the measurement of an alpha emitter radionuclide, Ra-233.

K. Thongklam, P. Charoenphun; Division of Nuclear Medicine, Ramathibodi hospital, Mahidol University, Bangkok, THAILAND.

Aim: Alpha-emitting radionuclide therapy has been used for treating cancer with metastasis such as Radium-223 dichloride for the recent years. Alpha particles are highly efficient to kill the target tumour cells with minimum damage to surrounding normal cells. Regarding the dose calibrator measurement, geometry is very important to measure activity accurately. Aim of this work is to evaluate the influence of geometry and obtain an appropriate dial factor for Ra-223. Materials and Methods: The dial setting for Ra-223 was initially applied in dose calibrator according to manufacturer recommendation using Ra-223 dichloride solution in a vial. Decay correction was applied for activity readings at the time of measurements. Radium-223 solution was exactly dispensed 1.0 ml into 5.0 ml syringe. Actual activity of 1.0 ml Ra-223 solution was calculated. First, radioactivity was measured with the initial factor. Consequently, dial setting was adjusted until activity reading of Ra-223 was the same as calculated activity before repeating measurements. Ra-223 solution was additionally withdrawn to get the final volume of 2.0, 3.0, 4.0 and 5.0 ml in the same syringe. The measurements were sequentially performed in the same manner for each volume (using either initial factor or adjusted factors corresponding to each volume). Measurements with initial factor were compared to those measurements with adjusted factors to get the percentage of differences. Statistical significances between reading activities from initial factor and adjusted factors were analysed using pair T-test. Results and conclusions: Initial dial factor of Ra-223 in the vial was 16.9 while dial factors for 1.0, 2.0, 3.0, 4.0 and 5.0 ml were respectively 13.5, 15.6, 15.7, 16.1 and 17.0. Differences between measured activities of Ra-223 solutions (with initial factor and adjusted factors) ranging between 1.0 and 4.0 ml were respectively 25.23% and 4.87%. On the other hand when measuring 5.0 ml Ra-223 in syringe, the difference was only -0.33% ($p = 0.01$). In conclusion measurement of Ra-223 is increasingly influenced with geometry at lower volumes. Inaccurate measurements of Ra-223 activity was obtained when initial factor is used to measure less than 5.0 ml Ra-223 in syringe. We suggest that appropriate dial factor should be applied in order to administer accurate doses to patients.

TP006

Patient satisfaction in The Department of Nuclear Medicine and PET-Centre, Aarhus University Hospital, Denmark

A. Dysterdich, V. Larsen, L. Pedersen; Aarhus Universitetshospital, Aarhus, DENMARK.

Aim: This study was preformed to evaluate patient satisfaction with The Department of Nuclear Medicine and PET-Centre. Our main aims were to examine the quality of the information to be given prior to the examination and the patients' satisfaction and experience on the day of examination.Materials and methods: Validated patients feedback questionnaires were collected prospectively from 454 patients who attended NUK-PET over a period of 2 weeks (December 8 to December 19 2014)This study was conducted at one of the largest departments in Denmark with 140 employees and an average survey data of 16000 per year.The study questionnaire included 17 questions based on an ordinal scale. Descriptive and analytical statistics were preformed in SurveyXact.Results527 patients was handed the questionnaire and a collection of 454 questionnaires gave a response rate of 86%. The information to be given prior to the survey was oral (66%) and written (77%). Almost all of the patients (>95%) felt they had received all the necessary information and were satisfied with the content and quality. Only 8% of patients had visited the department website.98% of patients thought that the number of staff they met was adequate. 100% of the patients thought that the staff was friendly and had the necessary time fore them.15% of the patient experienced waiting time but 86% were informed accordingly. In deepening their answers the maximum of waiting time were 35 minutes. Half of the patients were not aware of the complaints system or that they could report unintended events. 5% of patients did not think that there were possibilities to exchange confidential information. The patients' comments have been prepared in a prioritization diagram divided into major / minor and low satisfaction / high satisfaction. Conclusion: The study findings indicated that there is great satisfaction with the information patients receive before they show up for examination. The number of patients who receive both written and verbal information prior to examination can be improved. Not many have visited the department's website. The study findings indicated that there is great satisfaction with the examination and with the number of staff they meet. The study also shows that the staff are welcoming and accommodating. Patient awareness of reporting unintended events and complaints can be improved. Efforts should focus on the patients' comments and improving patients' experiences during waiting.

TP007

Technologist radiation exposure performing PET/CT using F18-FDG automatic dispenser

M. I. Larg, C. Pestean, M. Crisan, E. Barbus, D. Piciu; Ion Chiricuta Institute of Oncology, Cluj-Napoca, ROMANIA.

AIM. PET/CT using F18-FDG needs specific radiation protection due to the high energy photons produced by positron annihilation: strong shielding devices, appropriate working conditions and strict rules. The aim of this study is to evaluate the efficiency of radiation protection devices from the

department such as FDG automatic dispenser, and also the efficiency ofthe procedures performed by the nuclear medicine technologist. MATERIAL AND METHODS. The study was conducted over a period of one month on 50 patients (10 patients/day), an average daily activity of 187mCi (6919MBq) was manipulated, with a mean+/-SD of 187+/-12.79mCi (6919+/-473.23MBq). The administrated activity/patient had mean+/-SD of 7.85+/-1.24mCi (290,45+/-45, 88MBq). The dose rate measurements were taken during the F18-FDG loadingin the dispenser (5 minutes/procedure) and syringe dispensing procedures (4 minutes/procedure). The dose rate has been measured with a Radiagem 2000 Portable Dose Rate Meter.For the F18-FDG loading and dispensing was used a Karl 100 system where the lead pot containing the multi dose vial with F18-FDG is automatically uncapped by the system. Automated infusions were performed using the tungsten shielded infusion device. RESULTS. The average dose rate at a distance of 30cm from the loading system was 70.1μSv/h with a mean+/-SD of 69.8+/-3.93μSv/h, which means an exposure dose of 29.2μSv. Using aWi-Fi remote control system the average dose decreased at 0.034μSv/h with a mean+/-SD of 0.04+/-0.0089μSv/h which means an exposure dose of 0.014μSv/month resulting from this procedure. During the dispensing syringes procedures in the automated injector for F18-FDG the average dose rate at a distance of 30cm was 7.008μSv/h with a mean+/-SD of 7+/-1.17μSv/h which means an exposure dose of 23.36μSv. By increasing the distance using the Wi-Fi remote control system the average dose rate decreased at 0.035μSv/h with a mean+/-SD of 0.04+/- 0.01μSv/h, which means an exposure dose of 0, 11μSv/month/procedure.CONCLUSIONS. Besides shielding devices the increasing of the distance by using an F18-FDG autodispenser could be the most useful method to optimize radiation protection in PET/CT practice. Extrapolation of these results from these procedures to an annual dose revealed that the annual extrapolated exposure values remained under the authorized limits for workers classified to work in a radioactivity-controlled area.

TP008

Studies on measurement of thyroid uptake rate on I-131 scintigraphy images

Y. Koshiba1, S. Abe2, S. Tsuchiya1, N. Fujita2, T. Odagawa1, K. Kato1; 1Nagoya University Graduate School of Medicine, Nagoya-shi, JAPAN, 2Nagoya University Hospital, Nagoya-shi, JAPAN.

Aim: Measurement of I-131 thyroid uptake rate (TUR) is usually performed before the internal I-131 therapy for patients with Graves' disease, and the dose of I-131 to be administered is determined from the data of TUR. TUR values before and after I-131 therapy are not necessarily the same. In the previous study using a thyroid phantom, we found that TUR could be measured on the planar and SPECT/CT images with less than 5% of errors. In this study, we compared TUR values before and after I-131 therapy using clinical data. Materials and Methods: Thirty-seven patients with Graves' disease treated with I-131 therapy between August 2013 and March 2015 in Nagoya University Hospital, 13 patients of whom underwent SPECT/CT scans, were enrolled in this study. First, using the planar and SPECT/CT images acquired with the I-131 capsule, the equation for indicating the relationship between the I-131 radioactivity and the counts on the planar and SPECT/CT images was established. Using the equation, the counts on the planar and SPECT/CT images corresponding to the I-131 dose administered were determined. TUR values were calculated with the clinical data acquired from the planar and SPECT/CT images and compared with those measured by the TUR measurement system (AZ-800, Anzai Medical) before I-131 therapy. Results and Conclusion: TUR values measured on the planar and SPECT/CT images after I-131 therapy closely correlated with those measured by the TUR measurement system before I-131 therapy. The difference between TUR values measured on the planar images and those before the therapy were about 25%, whereas the difference between those measured on the SPECT/CT images after the therapy and those before the therapy was less than 20%. Results suggest that TUR values measured on SPECT/CT images after the therapy more closely approximate those measured before the therapy than those measured on the planar images.

TP009

Semi-quantitative 18F-NaF PET/CT in the assessment of bone mineral density (BMD): Comparison with dual-energy X-Ray Absorptiometry (DXA)

S. Haim1, F. Fitzal2, B. Saboury3, A. Alavi3, C. Schiller1, W. Langsteger1, M. Beheshti1; 1Nuclear Medicine & Endocrinology, St. Vincent's Hospital, Linz, AUSTRIA, 2Breast Cancer Center, St. Vincent's Hospital, Linz, AUSTRIA, 3Division of Nuclear Medicine, University of Pennsylvania, Philadelphia, PA, UNITED STATES.

Aim: To examine the value of semi-quantitative 18F-NaF PET/CT by means of standardized uptake value (SUV) in the assessment of bone mineral density (BMD) correlating with DXA BMD scanning, aging and various therapies. Material & Methods: Seventy patients (mean age of 56.6±12.3 years) in the context of initial staging of breast cancer (64 pts) and prostatic cancer (6 pts) without known bone metastases were included. The maximum time interval between 18F-NaF PET/CT and DXA scan was 9 months. Patients with recent chemo- and/or radiotherapy (less than 3 months) were

excluded. Semi-quantitative analysis was performed using volume of interest (VOI) which was manually drawn on the medullary part of L1, L2, and L3 as well as left femoral neck excluding the vertebral cortex. DXA measurements in the same regions were used for comparative analysis. Results: SUVmean showed a significant correlation with T and Z score in L1 and L2 (P = 0.01). However, there was no significant correlation between SUVmean and BMD (g/cm2) in L1 and L3. Using linear regression, the possibility for prediction of bone mineral deficit by means of SUVmean was very low. No significant differences were noted in the bone density of patients with or without calcium supplementation, bisphosphonates, hormonal and chemotherapy. However, patients with bisphosphonates therapy had significantly lower SUV in lumbar spine compared to patients without bisphosphonate treatment. In addition, there was no significant correlation between age and SUVmean ($p > 0.6$), while statistically significant negative correlation was seen between age and DXA BMD. Conclusion: In osteoporotic patients a significant correlation was found between semi-quantitative 18F-NaF PET/CT analysis and DXA BMD T and Z scores in the lumbar spine. However, its potential for prediction of bone mineral deficit should be evaluated in future prospective studies focusing on volume-based apparent bone mineral density assessment an approximation of the volumetric density of bone calculated on different sites.

TP010

Implementation of new Hidex automatic gamma counter

S. M. Virtaniemi, J. Laine, K. Bergström; Helsinki University Central Hospital, HUS, FINLAND.

Aim: A new Hidex automatic gamma counter was acquired to measure Cr-51, Ge-68 and Ga-68 for GFR-studies, Ge-68 breakthrough from Ge-68/Ga-68 generator and Ga-68 tracers' quality control, respectively, in our Nuclear medicine unit. The Hidex gamma counter has a 3 inch NaI crystal, and optimized 55-80mm lead shielding to minimize the background and interference from samples on the conveyor. Hidex gamma counter is equipped with a multichannel analyzer for gamma spectrum analysis and software which will enable automatic reporting of results. The implementation of the new gamma counter conforms to the requirements of the Finnish Radiation and Nuclear Safety Authority (STUK). Materials and methods: The linearity, sensitivity, stability, repeatability and background of the Hidex gamma counter was tested with Cr-51 and Ge-68 samples. Suitability of the gamma counter for PET tracer application was tested by analyzing the distribution of the Ga-68 on the TLC plate. These results were used to determine the radiochemical purity of the Ga-68-Dotanoc. All the results were cross-checked with the results achieved with the Wallac/Perkin Elmer Wizard 3" 1480 Automatic gamma counter. Results and conclusion: The linearity was measured with a Ge-68 standard solution series of 8 triplicated samples with count rates between 1 900 and 244 000 CPM. The achieved calibration line was linear (R2=0,9997) and the relative standard deviation between triplicated samples was ≤1, 3%. Stability of the gamma counter was studied weekly with two Ge-68 standard solution samples activities approx. 10000 and 30000 CPM. Measured activity differed always less than 1% from the calculated activity. Dilution series of Cr-51-EDTA standard solution gave linear (R2=0,9999) results from triplicated samples measured four times. The shift of the sample takes about 33 sec. Therefore, half-life correction should be done especially for PET-radioisotopes with a short half-life. The linearity, sensitivity, stability and repeatability of the Hidex gamma counter was shown to be comparable with the Perkin Elmer Wizard gamma counter. The user friendly software interface with a touch screen made the Hidex gamma counter pleasant to use.

TP011

Enhanced Myocardial Glucose Uptake During Viability Assessment Using Modified Niacin Induced Protocol 2-[18F] Fluoro-2-Deoxy-D-Glucose (18F-FDG) Positron Emission Tomography/Computed Tomography (PET/CT)

M. Che Nordin1, A. Nordin1, F. Ahmad Saad1, H. Abdul Razak2; 1Universiti Putra Malaysia (UPM), Serdang, MALAYSIA, 2Universiti Teknologi Mara (UiTM), Puncak Alam, MALAYSIA.

There are several established protocols available in the clinical assessment of myocardial viability using 18F-FDG PET/CT. This study was aimed to assess the intensity of 18F-FDG uptake in the wall of left ventricle (LV) using a modified protocol in a total of 33 subjects who had been equally divided into three groups; Group A for normal volunteers, Group B for oncology patients, and Group C for ischemic heart disease patients. The 18F-FDG uptake in the wall of LV was qualitatively and quantitatively evaluated. The mean age for group A, B and C were 35.00 ± 11.91, 45.91 ± 14.58 and 51.36 ± 9.97 respectively. The results showed that there was an increment on 18F-FDG uptake in LV of group A subjects, in which significant differences of mean SUVmax had been noticed at mid (5.32 ± 3.48 vs 3.71 ± 2.16 vs 4.92 ± 3.99, p=0.04), basal (8.28 ± 3.88 vs 3.79 ± 2.92 vs 6.94 ± 3.63, p=0.015) and apex (7.39 ± 3.57 vs 3.84 ± 2.82 vs 6.17 ± 3.48, p=0.023) regions. The mean normalized 18F-FDG distribution in 20-segment polar map expressed in percentage for group B was the lowest in comparison with the other two groups; A and C (61.02% vs 72.28% vs 61.64%, p=0.04). The outcome of this study may postulate that niacin can be utilized together with modified glucose loading protocol to enhance 18F-FDG uptake in routine clinical assessment of myocardial viability study using

PET/CT. Keywords: myocardial viability, niacin, PET/CT, glucose uptake

TP012

Possible sources of artificial focal 18F-FDG accumulations in the lung tissue without corresponding morphological CT changes

T. K. Lehnskov, T. A. Roholm, U. Talleruphuus; Bispebjerg and Frederiksberg Hospital, Copenhagen, DENMARK.

Aim: To investigate the source and possible physiological reason for a number of lung foci in whole body 18F-FDG PET scans not visible as co-existing lesions on the simultaneously performed CT scans. Materials & Methods:In eleven patients a whole body 18F-FDG PET/CT scan revealed focal FDG accumulations in the lung tissue without corresponding morphological changes in the concomitant diagnostic CT scan. All artefacts occurred within a three month period. Details concerning dispensing and administration of 18F-FDG, study acquisition were noted, and the technologists involved in the examinations were interviewed. We registered time of dispensing, weekday of examination, external supplier of tracer, order of patients, total tracer activity, volume administered to the patient, residual activity in syringe and administering technologist. Finally we noted the volume of x-ray contrast and flushing saline administered. Results: The 18F-FDG was administered between 8:55 AM and 11:36 AM. Six patients received FDG tracer from one external supplier and five from another external supplier. Three patients received the first dose of the day, while the remaining patients received doses ranging from number three to eight. Mean injected dose was 202 MBq ±1.84 (SD), residual activity was 2.55 MBq ±1.05 (SD). All CT scans were diagnostic and intravenously contrast-enhanced (iohexol) . The volume of contrast was weight-adjusted (1 mg/kg) and varied from 70 to 128 ml. The subsequent volume of saline was 50ml for all patients. The artefacts were seen at least once on any given weekday, but only when the 18F-FDG was administered by one of the same two technologists. The interviews revealed that these 2 out of 11 technologists didn't follow proper guidelines by not flushing the catheter with 10 ml saline after administration of tracer. The two technologists were retrained and re-certified. After this intervention we have not seen additional foci for three months.Conclusion:Since the 18F-FDG PET foci only appeared in patients where the catheter was not flushed immediately after administration of tracer, and because they received contrast in conjunction with the scan, we speculate that not properly flushing the catheter allowed small clots to form in the presence of 18F-FDG, which were subsequently flushed into the lungs of the patients while administering contrast intravenously at high flow rate.

TP013

Evaluation of therapeutic response to 131I in the treatment of hyperthyroidism

A. C. C. Caetano1, A. P. S. Leite1, J. I. R. Madrid2, J. S. Vicente2, E. Carolino1, L. Vieira1; 1Escola Superior de Tecnologia da Saúde de Lisboa, IPL, Lisboa, PORTUGAL, 2Hospital Infanta Cristina, Badajoz, SPAIN.

Introduction: Thyroid disorders are the most common form of endocrine disorders, and Nuclear Medicine has contributed significantly to the handling thereof, binding together the 131I therapy, which aims to reach a normal state of hormonal levels. Hyperthyroidism is mainly caused by Graves' disease, Toxic Adenoma (TA), Multi Nodular Goiter (MNG) and Toxic Nodular Goiter (TNG). Objective: To evaluate the therapeutic response to 131I in the treatment of benign hyperthyroidism caused by different etiologies, taking into consideration the age and 131I administered dose. Methodology: Retrospective study, using non-probability convenience sample of 90 female patients with benign etiology of hyperthyroidism, submitted by clinical indication to therapy with 131I at the Nuclear Medicine Service of Infanta Cristina Hospital, from 2005 to 2009, with activities between 370MBq and 740MBq. After treatment, the sample was divided by three categories - Hypothyroidism, Normal, and Hyperthyroidism - depending on the outcome of therapy for each patient. To determine the presence of statistically significant differences in age and dose depending on the outcome of therapy, and depending on the initial type of hyperthyroidism, we used the non-parametric Kruskal-Wallis Test. To study the association of the outcome of therapy with the initial type of hyperthyroidism, we used the Chi-Square Test for the Monte Carlo Simulation. Results: From the sample of 90 patients with an average age of 51 years, 43 had hyperthyroidism caused by Graves' disease (42 years ± 13) 25 by MNG (64 years ± 8), 10 by TNG (56 years ± 14) and 12 by TA (53 years ± 20). It was determined that 4% (4) of patients continued to have hyperthyroidism, 30% (27) reached a normal hormonal levels and 66% (59) acquired post-therapeutic hypothyroidism. It was also found that the patients with hyperthyroidism derived from Graves' disease had a higher incidence of hypothyroidism post-therapy. In contrast, patients with hyperthyroidism derived from NMR reached a state of normal hormonal levels after therapy. Conclusions: In this sample, treatment with 131I was found effective at treating hyperthyroidism. It was in hyperthyroidism associated with NMR that the therapy with 131I showed higher efficacy, since the patients had hormonal values within normal limits. Patients with hyperthyroidism primarily associated with Graves' disease responded well to therapy with 131I, but had major side effects such as post-therapeutic hypothyroidism. In hyperthyroidism associated with NBT and TAA, the final result of the therapy was shown partitioned between post-therapy hyperthyroidism and normal state.

TP014

Standardization analysis protocol proposal for isotopic ventriculography

P. Borrelli1, J. Loaiza Góngora1, J. Vercher-Conejero1, C. Ruiz Llorca1, C. Igua Sáenz1, D. Hervás Marín2, C. Olivas Arroyo1, V. Vera Pinto1, P. Olivan Sasot1, P. Bello Arqués1; 1Hospital Universitario y Politecnico La Fe, Valencia, SPAIN, 2Instituto Investigación del Hospital Universitario y Politecnico La Fe, Valencia, SPAIN.

Aim: To establish the post-processed analysis method for determining left ventricular ejection fraction (LVEF) in isotopic ventriculography, that presents the minimum interobserver variability and a consistent reproducibility. Material and methods: During 2014, 50 isotopic ventriculographies were aleatorized and anonymized and then selected to analysis. Five nuclear specialists then performed 4 different analysis methods, totalizing 1000 studies performed. After aleatorization patients selected were, 32 female and 18 males, mean age 59 years. Referring clinical departments were oncology in 96%, neurology 2% and neurology 2%. All studies were performed at the Philips Extended Brilliance Workstation. The first three analysis were performed using manual left ventricular multi unit gated analysis (LV-MUGA), with the following color schemes: method A (inversegray), method B (gray) and method C (smart). The forth and last anaylisis, method D, was performed using semi-automatic LV-MUGA. Patients were injected with 296 MBq (8mCi) of 99mTc- autologous erythrocytes. Images were acquired using a double-headed gamma camera (BrightView XCT, Philips Healthcare) using standard acquisition parameters. Interobsever variability was estimated among the different methods, calculating intraclass correlation coefficient (ICC) for each of them. Comparison P-values between distinct ICC was estimated using bootstrapping analysis. Statistical analysis was made using R software (3.1.2 version). Results: ICC for method A (inversegray manual MUGA) was 0,58, 95% confidence interval (CI) 0,45 - 0,70, for method B (gray manual MUGA) ICC was 0,53, CI 0,40 - 0,66, method C (smart manual MUGA) the ICC was 0,58, 95% CI 0,45 - 0,71. For method D (semi-automatic muga) ICC was 0,84, with 95% CI 0,77 - 0, 90. Due to the high ICC presented by method D, all other methods were compared with it. P-values for the comparison among the three with method D were < 0,001 for all of them. Conclusion: Semi-automatic LV MUGA was proven to have the best intraclass correlation coefficient at the Philips Extended Brilliance Worstation, and it is safe to recommend its use in the routine daily practice for the Philips Brighview XCT gamma-camera, due to its reproducibility among observers. Further studies among different gamma-camera brands would be necessary to establish which analysis protocol could present the best ICC for the different analysis software.

TP015

Surface contamination from 99mTc -Technegas aerosols in the SPECT/CT room after lung ventilation.

S. D. Lind, R. S. Olsen, I. L. Rasmussen, M. Lonsdale; Department of Clinical Physiology & Nuclear Medicine, Bispebjerg and Frederiksberg University Hospital, København NV, DENMARK.

Aim: We want to examine the surface contamination from 99mTc -Technegas aerosols on different sites of interest in the SPECT/CT room when used in lung aerosol ventilation studies. Airborne 99mTc-Technegas is known to adhere to surfaces, due to the chemical and physical character of the aerosol particles. This may lead to an unknown contamination of the room. Materials and methods: Seven sites, specifically marked in the SPECT/CT room, were wiped down with alcoholic swaps (82% ethanol, 0.5% chlorhexidine). The swaps were put in different test tubes, immediately after the ventilation but before the initiation of image acquisition, and measured in a gamma counter to estimate the 99mTc surface contamination. The chosen areas were located on top of the TechnegasPlus Generator (Cyclomedica), on the front of the generator, on the backside of the generator acrylic lead shield, on one detector arm, on the measuring detector head, on the non-measuring detector and on the door for patient entry. Prior to any isotope handling, a background measurement was obtained for all seven sites. All measurements, found in counts per minute (CPM) by the gamma counter, were corrected for decay and background and reported as activity per area (Bq/cm2). Results: A total of 14 day series (with 1 – 3 patients/day) were studied, in which we observe a clear overall increase in the surface contamination after each patient scanning. Initially, we measure an average background level of 0.22 (between 0.1 and 0.4) Bq/cm2 from all seven sites in the room. This level increases up to an average of 0.34 (between 0.1 - 0.7) Bq/cm2 after the initial patients of the day and further to an average of 0.60 (range 0.2 - 1) Bq/cm2 after the second patients. Finally, an average of 0.62 (range 0.2 - 1.2) Bq/cm2 is detected after the third patients. The seven different sites studied also show different levels of contamination with a clear tendency of the generator sites being in the low end (around 0.2 Bq/cm2) of the measurement scale and the detector sites in the high end of the scale, i.e. between 0.4 and 1.0 Bq/cm2.ConclusionWe do measure a room surface contamination, but with values below safety threshold. In general, we observe an increase in the surface contamination level during the day – after each patient scanning. Also, the different sites show different contamination levels naturally due to the nature of the sites studied in the room.

TP016

Clinical classification versus semiquantification with adapted reference values for 123I-FP-CIT SPECT in a Nuclear Medicine Department

D. Silva1, M. Queiroga1, M. Elias1, J. Serrano2, J. Madrid2, E. Carolino1, E. Sousa1; 1Escola Superior de Tecnologia da Saúde de Lisboa, Instituto Politécnico de Lisboa, Lisbon, PORTUGAL, 2Nuclear Medicine Department, Hospital Infanta Cristina, Badajoz, Spain, Badajoz, SPAIN.

Introduction: Although semiquantification in 123I-FP-CIT SPECT (DaTScanTM) is used in clinic daily basis, sometimes there is a suspicious about discriminative capability and concordance with the diagnostic classification for Parkinson Syndromes performed by a physician.Aim: The aim of this study is to test the capability of reference values obtaind from an adapted database of healthy controls - named DBRV. This Database was previously created and validated for 60 to 75 years old population of Hospital Infanta Cristina, located in Badajoz.Methods: In previously studies the DBRV was created and validated. For creation proposes, a group of 30 healthy controls (GI) was submitted to semiquantification used semiautomatic method of segmentation. Average and standard deviation ($x \pm \delta$) values were calculated for the following ratios: left and right Caudate nucleus/ Occipital respectively (A) and (B); left and right Putamen/Occipital respectively (C) and (D); striatum/Occipital (E); left striatum/occipital (F), right striatum/occipital (G), Putamen/ nucleus caudate (H).). These values were calculated and stablished DBRV. For validation process DBRV was compared with two different groups of 30 patients each, of same age group: database of healthy controls (DBVGIIH), and database of subjects with diagnosed Parkinsonian Syndromes (DBVGIIIP). Control Chards and ROC (Receiver operating characteristic) Curves were calculated.In this segment of study, for test de capability of DBRV in Parkinson Syndromes diagnostics, a random Group of 30 patients was also submitted to semiquantification by the same method and calculi of Rations A to H. Ratios C to H are the ones with higher sensibility for early stages of Parkinson Syndromes. The values obtained for these ratios were compared with DBRV. If one of the Ratios was below of the respective reference value ($x - \delta$) the exam was considered Pathological. The physician reports based on visual assessment were compared with diagnostics based on DBRV. Specificity, Sensibility, Positive (PPV) and Negative (NPV) predictive values were calculated.Results: For comparison between DBRV and physician confirmation for Parkinson Syndromes it was obtained PPV=0.466; NPV=1; Sensibility=1 and Specificity=0.65.Discussion/Conclusion: From these concordance results is possible to confirm that DBRV have high sensibility and consequently high NPV in diagnostic of Parkinson Syndromes, so has high capability to predict heathy studies. From the value of Specificity and PPV is possible to conclude that sometimes, obtained values below of the respective reference value, essentially in early stages of Parkinson Syndromes, cannot match Pathological studies.

TP017

Elution features of sorptive generators technetium-99m.

A. Rogov, V. Skuridin, E. Stasyuk, N. Varlamova, E. Nestwrov, V. Sadkin, L. Larionova, E. Ilina; National Research Tomsk Polytechnic University, Tomsk, RUSSIAN FEDERATION.

Short lived isotopes technetium-99m is widely used for diagnostic studies in medicine. To date, up to 83% all radionuclide procedures performed using radiopharmaceuticals based 99mTc. For obtaining isotope technetium-99m is used generator technetium. Greatest distribution has received sorption generators. World production of sorption technetium-99m generators based on using highly active 99Mo. Its production is based on the fission products of uranium-235. The technology of obtaining poses risks to the environment. Alternative possibility for production of 99Mo is its getting by radiation capture reaction (n, γ) by irradiating the of molybdenum-98 with neutrons nuclear reactor. This technology has virtually no of waste, but the resulting product has a low specific activity of 99Mo at a level 6-10 Ci/g. Use of such materials for the production of generators requires the use of oversized columns. This leads to a decrease in the volume of activity of the resulting preparation of technetium-99m. The aim of the work was to study the factors influencing the elution features generators of technetium-99m, made of neutron irradiation of enriched molybdenum-98. The objectives of the research was to determine elution profiles generators with different adsorbed mass of molybdenum. The objectives of the research was to determine elution profiles generators with different adsorbed mass of molybdenum. Subsequent study of the nature of the distribution of molybdenum over the length of the sorption columns. The experiments show that with increasing mass of the adsorbed molybdenum elution profile generators narrowed. Reaching a minimum at certain limiting mass corresponding to the maximum sorption capabilities of the selected sorbent. When studying the distribution in columns of the generator is set that the value of maximum adsorption of molybdenum (maximum concentration) immediately upstream of entrance columns depends on the total mass of molybdenum introduced. Indicating that the initial decomposition of complex polyanions and subsequent redistribution of the tracks on the free active centers oxide. The degree of polymerization n within the mass of molybdenum changes from 180 to 70 mg in a 0.6 times decrease, which leads to a nonlinear change of the degree of filling columns molybdenum. Based on this

suggested that the active centers of the vacant sorbent present in the outlet portion columns hinders elution of 99mTc generator. Their number to achieve the desired output 99mTc should be strictly regulated conditions predsorbtsionnoy training oxides Al_2O_3. This work was financially supported by Ministry of Education and Science of the Russian Federation (RFMEFI57514X0034).

TP018

The Evaluation of External Dose Measurements in Children and Adolescent Patients Receiving Radioiodine Therapy for Well-Differentiated Thyroid Cancer

N. Edis, A. Ogretici, M. O. Tamam, M. Mulazimoglu; Okmeydanı Training and Research Hospital, Istanbul, TURKEY.

Background: In Turkey, the dose rate of discharge limits for the patients treated with 131I at the end of hospitalization is, under 30 μSv/h (3mR/h) at 1meter (m) or the activity in the body is under 600 MBq. The aim of this study was to evaluate the changes in external dose measurements (EDM) according to patient age, administrated dose and hospitalization time in children and adolescent well-differentiated thyroid cancer patients during the discharge. Materials and Methods: Between 3-19ages (16 ± 3.5 years), 67 patients' (15M, 52F) 87 EDM were evaluated retrospectively. Patients were divided into two groups according to their ages: under the age of 10 (4 patients) and above 10 (63 patients). Radioactive 131I doses were evaluated in 4 groups as follows: (a) Less than 3700 MBq, (b) 3700 MBq, (c) 5550 MBq and (d) 7400 MBq. Hospitalization time comparisons were done in 3 groups as 2 days, 3 days and 4 days. EDM were done at 1m distance from the patient in abdominal level using a portable Geiger-Müller survey meter in μSv/h units. Results: All the EDM were below the threshold of 30 μSv/h. EDM of patients under the age of 10 and above 10 were 1-25μSv /h (mean 9.71 ± 9.52 μSv/h), and 1-30 μSv/h (mean 8.87 ± 7.89 μSv/h), respectively. External dose measurements according to the dose for groups a, b, c, d were measured as; 2 -18 μSv/h (mean 10.38 ± 9.35 μSv/h), 1-30 μSv/h (mean 9.17 ± 7.68 μSv/h), 1 -20 μSv/h (mean 7.93 ± 5.70 μSv/h) and 1 - 25 μSv/h (mean 9.00 ± 8.99 μSv/h), respectively. External dose measurements according to hospitalization time groups were measured as; 1 -30 μSv/h (mean 10 ± 9,53 μSv/h) for 2 days group,1 -27 μSv/h (mean 11.15 ± 7.47 μSv/h) for 3 days group, 1 -20 μSv/h (mean 5.61 ± 4.39 μSv/h) for 4 days group. Conclusion: The external dose measurements are reduced as the day of hospitalization is increased. Dose measurement average value is considered to be within the permissible limits when evaluated according to given doses. In particular, parents of children under the age of 10, receive more radiation due to staying closer to the children for a longer period. The results of this study will provide more information about radiation exposure, thus children with thyroid cancer treated with radioactive 131I and their family members will benefit in terms of radiation protection.

TP019

Radiotherapy Planning in PET/CT: The Process and Challenges

S. A. Summers, A. Ribeiro; The Royal Marsden NHS Hospital, Sutton, UNITED KINGDOM.

Aims: Accurate imaging is vital for treatment planning process for most malignancies managed with curative intent. Positron Emission Tomography scanning has brought about a revolution in the imaging of many common cancers and has it becomes widely available in developed countries, is increasingly being incorporated into routine radiation therapy planning. Materials and Methods: Radiotherapy planning is a multistep process which requires the appropriate selection and delineation of target volumes (TV) and Organs at Risk (OAR) is of paramount importance. It requires the proper use of both extremely sensitive and specific imaging modalities. PET/CT offers Radiotherapy Planning numerous advantages, however it does present us with a few limitations and challenges which need to be addressed before the service is installed. The most important precondition for successful integration of functional imaging in Radiotherapy treatment planning is the goal orientated as well as close and thorough communication between PET/CT and Radiotherapy/Oncology departments on all levels of interaction; careful planning is required. All roles from receiving requests and booking patients to scanning and reporting of the images need to be established at the outset of the process. The essential resources need to be in place to run the service, including appropriate training of all staff and important quality control procedures and protocols established. Resources include: PET/CT Camera, Carbon Fibre table top, Laser lights, Immobilisation devices, contrast media, computer network and trained staff. Last but not least the patient needs to be considered; this will include a decision as to which patients would be appropriate for PET/CT Radiotherapy planning and what is required to ensure the patient receives optimal patient care. Results: The challenges a department will face setting up this service will vary. These could depend on the timing of the PET/CT scan, camera availability and increased radiation dose to staff and other practical installation issues. Conclusion: With the successful planning and set up, the inclusion of PET allows functional imaging to be incorporated in the localization and planning process giving a further level of accuracy to the definition of the tumour volume and the individualisation of treatment.

TP020

Comparative study on recovery coefficients of SPECT-CT

S. Tsuchiya1, S. Abe2, N. Fujita2, Y. Sakuragi2, Y. Koshiba1, T. Odagawa1, K. Kato1; 1Nagoya University Graduate School of Medicine, Nagoya, JAPAN, 2Nagoya University Hospital, Nagoya, JAPAN.

Aim: Calculation of the recovery coefficients (RCs) are usually conducted for assessment of the quantitativity of nuclear medicine imaging. RCs of hot spots change due to the difference in shapes and reconstruction methods even if their volumes are the same. In this study, we compared RCs of hot spots having the same volume but different shapes. Materials and Methods: A solution of Tc-99m was enclosed into the spherical phantom including 6 spheres and the irregularly shaped phantom including 5 containers having the same volume but different shapes. SPECT-CT data of the phantoms were acquired and reconstructed using 3D-OSEM. Varied conditions on the subsets×iterations (SI) and FWHM of the Gaussian filter were used for the reconstruction of images. ROIs were drawn on the reconstructed images, average counts per pixel were measured, and the radioactivity of the Tc-99m solution was calculated. RCs were aquired using the calculated values and the actually measured activities. RCs of the spherical and the irregularly shaped phantom were compared and the differences in the RCs (D values) were obtained. Results: Slopes of the recovery curves were increased at the range of SI≦120 and fixed at the range of SI>120. The quantitativity of images became worse with an increase of the FWHM of the Gaussian filter. RCs of each container of the irregularly shaped phantom did not depend on SI, but became lower with an increase of FWHM of the Gaussian filter. D values were high at the range of SI≦60 and fixed at a relatively low value at the range of SI>60. D values could be lowered when FWHM of the Gaussian filter≦4mm or non-filter. Conclusions: The reconstruction parameters capable of improving the quantitativity of SPECT-CT images and lowering their D values are as follows: the SI>60 and FWHM of the Gaussian filter≦4mm or non-filter. Further studies will be needed to improve physical and visual qualities of SPECT-CT images.

TP021

Practical consequences of new indications for sentinel node procedures in breast cancer: evaluating the role of SPECT/CT and tracer reinjection

M. Kieft, B. Pouw, D. Hellingman, W. V. Vogel, M. P. M. Stokkel; NKI-AVL, Amsterdam, NETHERLANDS.

Introduction: Sentinel Node (SN) procedures for breast cancer is now common practice in many countries. Planar lymphoscintigraphic imaging with Single Photon Emission Computed Tomography with integrated CT (SPECT/CT) for particular indications can be used for preoperative imaging. However, together with the incorporation of SPECT/CT, indications for the SN procedure were extended to patients with more locally advanced breast cancer receiving neo-adjuvant chemotherapy, multicentric/multifocal breast cancer, and patients with local breast cancer recurrence after surgery and/or radiotherapy. In our institution, we experienced increasing numbers of non-visualisation on planar imaging since the introduction of these new breast cancer SN indications. The present study evaluates the practical consequences in terms of the additional workload at the nuclear medicine department required for patients with non-visualisation on planar imaging scheduled for a breast cancer SN procedure. Materials and Methods: Between 1st of July 2008 and 6th of November 2014 in total 1982 breast cancer patients underwent a SN procedure after intra-tumoural tracer administration. SPECT/CT was performed in 298 patients (15%) who showed non-visualisation on planar lymphoscintigraphy. Ninety-one (30.5%) of these patients had previous surgery or radiation therapy at the same breast prior to the SN procedure and 40 (13.4%) were scheduled for neo-adjuvant chemotherapy. If SN non-visualisation persisted on the SPECT/CT images, a second radiotracer injection with repeated lymphoscintigraphy was performed when logistics allowed this. All information about additional time on the SPECT/CT scanner and the additional time required to perform a reinjection was collected. Results: SPECT/CT and reinjection visualised respectively in 22.8% (68/298) and 60.3% (38/63) of the patients SNs on the preoperative imaging. All 298 SPECT/CT scans took approximately 30-40 minutes including examination of the images by the nuclear physician. The 63 reinjections of the Tc-99m tracer took approximately 5-30 minutes preparation and 10 minutes administration with 15 minutes additional scanning after a resting period of an hour. This all required considerable flexibility and rescheduling for technologist, nuclear physicians, and the surgical department. Conclusion: The new breast cancer SN indications caused an increase in the non-visualisation rate and therefore demands more time for the preoperative SN imaging at the nuclear medicine department. Flexibility is required to allow additional SPECT/CT scans and tracer reinjections in case of non-visualisation and should be considered for these new indications in breast cancer SN procedures.

TP022

Non-invasive quantification of the regional cerebral blood flow using I-123 IMP SPECT and phase contrast MRA; preliminary study of combination and revisit of the matured technologies.

S. Mano, M. Tadokoro, S. Shirakawa, M. Ishiguro, H. Toyama; Fujita Health University, Toyoake City, JAPAN.

Background: SPECT is now widely used for the patients who need regional cerebral blood flow evaluation. But most of the cerebral blood flow (CBF) SPECT are performed without quantification, because of the difficulties in quantification technique and the invasiveness. Phase contrast (PC) MRA can stably measure the velocity and amount of blood flow at cervical vessels; internal carotid arteries, vertebral arteries and basilar artery. The flow measurements of these arteries give accurate quantification of whole brain blood flow without invasiveness. Combined use of both techniques could non-invasively make quantitative regional CBF images, theoretically. This idea was already proposed by several investigators, almost twenty years ago. But, we have never seen this technique in clinical practice of CBF evaluation. Aim: In this paper, we would like to present preliminary study of non-invasive quantification of regional CBF with combination of SPECT and PC-MRA in a few subjects, and discuss on the possibility of this method in daily clinical practice.Methods: Two patients who were ordered both CBF-SPECT and MRI on the same day for the evaluation of mild memory impairment were hired. The CBF-SPECT were performed after injection of 167 MBq of I-123-N-isopropyl iodoamphetamine (IMP). MR studies were performed by 1.5T MR scanner. PC-MRA were performed at the level of just above the carotid bifurcation, and the velocity and flow were measured in bilateral internal carotid and vertebral arteries. ImageJ (NIH) was used for image calculations. Results: Quantitative CBF-SPECT images were easily produced by simple calculation. Total brain CBF measured by PC-MRA were just divided by whole brain counts of the CBF-SPECT to produce pixel-by-pixel images of quantitative CBF. Measured CBF of the gray matter were within the range of 35 to 55ml/min/100g.Discussion: Preliminary study of the combined use of SPECT and PC-MRA showed the possibility of easy and non-invasive quantification of regional CBF, which can be used in daily clinical practice of cerebral diseases. But this study only showed the possibility. Comparative assessments with other methods of CBF quantification are essential for the validation.

TP023

Dynamic F18-FDG studies with a dedicated breast-PET: Preliminary results.

R. Sanchez Jurado1, J. Ferrer Rebolleda1, B. Kundu2, S. Majewski2, X. Zhang3, Y. Li3, A. González4, M. Garcia1; 1ERESA, VALENCIA, SPAIN, 2Radiology and Medical Imaging, University of Virginia, Virginia, VA, UNITED STATES, 3Beijing Institute of Technology, Beijing, CHINA, 4Institute for Instrumentation in Molecular Imaging, VALENCIA, SPAIN.

PURPOSE: To develope an image segmentation method for dynamic F18-FDG MAMMI-PET. METHOD AND MATERIALS: Prone dynamic F18-FDG PET studies were performed on five patients covering affected breast region (40 mm only). Training database was established with some typical pixels to different features (tumor and non-tumor region) using back-propagation (BP) Artificial Neural Network (ANN) combined with time activity curves (TAC) features of 18F-FDG uptake of breast in vivo using a dedicated breast-PET (MAMMI-PET; Oncovision). Results were correlated with biopsy and histology. RESULTS: The TAC and uptake rate of tumor and non-tumor region were clearly distinguished. The TACs of tumor region had higher value of FDG uptake as time passes and the curves had steep slopes. However in non-tumor región TACs had a gentle slope and a downward trend. We stablished a clear differentiation between tumor and non-tumor region around 12-15 minutes after injection. CONCLUSION: An innovative approach for image segmentation of breast cancer has been proposed. ANN with BP algorithm in F18-FDG breast PET images had a good performance in the segmentation of breast tumor and background. Here we shown preliminary data that, despite being very encouraging, further studies are needed to validate them.

TP024

A Case Report: Suitability of Measuring Kidney Depth with Assessment of GFR Using 99mTc-DTPA in Ectopic Kidney and Pediatric Patients.

J. CHOI; Asan Medical Center, SEOUL, KOREA, REPUBLIC OF.

Aim: This case report is to share three specific cases regarding glomerular filtration rate(GFR) study. Furthermore, this report verifies significant differences among five different methods for kidney depth measurement. Case 1: 49-y-old woman had a GFR study for kidney donation. Due to the misplacement of her kidney, depth correction was conducted. For depth correction, CT images were evaluated.Depth was determined by averaging the anterior and posterior depth at the CT images.The two CT images that show the most superficial anterior kidney surface and the deepest posterior kidney surface were chosen. There was a gap more than twice between Tonnesen and manual method. Case 2: 69-y-old man had a GFR study for kidney donation. The patient had GFR studies twice at intervals since right kidney's GFR was below normal. GFR slightly fell short of the normal value while other pathologic results indicated normal. Similar to the first case, the two CT images were selected. It showed a remarkable difference between the kidney depth and GFR. Case 3: 3-y-old toddler had a GFR study. GFR slightly fell short of the normal value while other pathologic results indicated normal. The problem here was that we applied the Tonnesen in a young patient. Tonnesen's method was quiet underestimated while others stay in normal. How

serious are these differences especially in young patients? Materials and methods: Along with this case report, we made comparison between kidney depth of 57 adults kidney donors (26 male and 31 female; mean age, 42.6 y) who took GFR study. One way anova test was performed with SPSS 13.0 to analyze and compare kidney depth, GFR and normalized GFR derived from 5 methods including Tonnesen, Taylor, Itoh, T-Itho and manual method. Results: It showed significant differences between Tonnesen and other 4 methods in kidney depth, GFR and normalized GFR($p< 0.05$). Otherwise, there was no significant differences among Taylor, Itoh, T-itoh and manual method. Conclusion: It is essential for technologists to measure exact kidney depth. In case of a follow up study, consistency of the method must be observed. The importance of measuring for skin to kidney distance has been well recognized in adults. However, similar corrections have not generally been incorporated into algorithms which evaluate renal function in children. As one of the study performers, we should contemplate what the best option for pediatric patients would be.

TP025

Planar Scintigraphy vs SPECT/CT in The Visualisation of Sentinel Node(s) for Patients with Vulvar Carcinoma

M. Brom-Attard, E. Mijnheere, M. Janssen; Radboud University Nijmegen Medical Centre, Nijmegen, NETHERLANDS.

Aim: Vulvar carcinoma is a demoralising disease involving older women. Women diagnosed with primary cancer of the vulva go through complicated surgery to remove the tumour with the possibility of distressing complications, in addition to the removal of lymph nodes. The removal of lymph nodes adds to the complications of the surgery. Sentinel node imaging has been developed to remove the affected lymph nodes that receive drainage from the tumour thereby keeping the removal of lymph nodes to a minimum and reduces the possibility of developing complications from having a total lymph node dissection. Planar scintigraphy is the routine procedure performed but might introduce some problems, such as non-visualisation of sentinel nodes, contamination, and a misleading location of sentinel nodes. This pilot study has been carried out to determine whether SPECT/CT is better than planar scintigraphy in the detection of sentinel nodes. Materials and Methods: In this pilot study, ten patients were included, who underwent the routine sentinel node procedure with the addition of the SPECT/CT four hours post-injection of 99mTc-labelled Nanocolloid. Four nuclear medicine physicians and five nuclear medicine practitioners were asked to document the number of sentinel nodes seen on planar scintigraphy and SPECT/CT. The inter-observer agreement was determined by Cohen's Kappa agreement. Results: The results of the study showed that there was no significant difference in the detection of sentinel nodes by SPECT/CT when compared to planar scintigraphy. SPECT/CT was useful in determining the exact depth and location of the sentinel node(s), especially if found in an unexpected location, and in incidents of contamination. The inter-observer agreement was higher between nuclear medicine practitioners (K=0.468) when compared to that of physicians (K=0.256). Conclusion: In this pilot study, SPECT/CT is only better than planar scintigraphy in the visualisation of depth of the sentinel node(s) and displaying their exact location. SPECT/CT has shown the same number of sentinel node(s) as planar scintigraphy and will only be performed adjacent to the routine procedure if needed.

TP026

Evaluation of a rhodamine-angiotensin conjugate as a potential breast cancer imaging agent

S. Okarvi, I. Jammaz; King Faisal Specialist Hospital & Research Centre, Riyadh, SAUDI ARABIA.

Aim: Rhodamine (Rh) is a positively charged lipophilic fluorescent dye that accumulates specifically in mitochondria of living cells. Rh dyes are known to accumulate in the heart and share several properties with 99mTc-sestamibi. Additionally mitochondrial-specific Rh dye has been evaluated as a potential anticancer agent because of its high uptake and prolonged retention in most cancer cells and rapid release from normal cells. Change in mitochondrial potential is an important feature in tumor cells. It is believed that cancerous cells as compared to normal epithelial cells may have higher mitochondrial or plasma trans membrane potential and Rh crosses these barriers because of net positive charge on the molecule. The high specificity for mitochondria and low toxicity to normal cells coupled with selective accumulation in carcinoma cells suggest that 99mTc-Rh-AngII may prove to be an effective tumor imaging agent. It is therefore of great interest to evaluate the potential of 99mTc-Rh-AngII as breast cancer targeting agent. Materials and Methods: Rh-angiotensin (Rh-AngII) Rh-Lys-Gly-Gly-Cys-βAla-Asp-Arg-Val-Tyr-Ile-His-Pro-Phe-NH_2 was synthesized by Fmoc/HBTU based solid-phase peptide synthesis. Carboxytetramethylrhodamine (TAMRA) was linked to AngII peptide via the free amino group of Lys residue by manual synthesis. Rh-AngII was radiolabeled with 99mTc via GGC chelating moiety by tartrate ligand exchange method. *In vitro* cell binding was determined on MDA-MB-231 and MCF7 breast cancer cell lines and *in vivo* biokinetics was studied in balb/c mice at 1 and 4 h p.i. Results: Rh-AngII conjugate was prepared conveniently by solid-phase synthesis and its structure was confirmed by mass spectrometry and

purity by HPLC. The conjugate was radiolabeled efficiently with 99mTc. In vitro tumor cell-binding demonstrated high affinity and specificity of 99mTc-Rh-AngII towards human breast cancer cells (binding affinities below 20 nM). The tumor cells binding characteristics of 99mTc-Rh-AngII was found to be comparable with 99mTc-sestamibi. In vivo biodistribution and clearance kinetics in mice displayed a rapid clearance from the blood and other tissues and organs both at 1 and 4 h p.i. 99mTc-Rh-AngII was excreted mainly by the renal pathway with some elimination via the hepatobiliary system.Conclusion: The results of this initial study towards the development of a breast cancer imaging agent indicate some similarities of 99mTc-Rh-AngII with 99mTc-MIBI highlighting the potential of hybrid conjugate for targeting of breast cancer. The use of hybrid conjugate appears to hold a great promise as a new and attractive approach for tumor targeting. More tumor targeting studies are in progress and will be reported.

TP02 - Tuesday, October 13, 2015, 8:00 AM - 9:30 AM, Hall 3 – Poster Exhibition

Technologist Poster Session 2

TP027

A new amyloid imaging probe 125I-EISB in PET/SPECT imaging of amyloid was developed for both brain and whole body for clinical use

S. Tsukimoto; Kumamoto University, Kumamoto, JAPAN.

[purpose] We developed a new radio-compound 125I-EISB (1-(2-125I-ethoxy)-2,5bis (styryl) benzene) which is amyloid imaging probe to detect β-amyloid plaques both in human brain and the whole body using PET/SPECT. The aim of this study is to evaluate in vivo bio-distribution of 125I-EISB and accumulation to amyloid in mice. We performed bio-distribution studies in mice to examine in vivo distribution of 125I-EISB and find an affinity of the compound to amyloid plaques in amyloid deposition. [method] In bio-distribution studies, 0.3 ml of 125I-EISB was injected by tail vein to normal and amyloid deposition mice. After 1, 3, 15, 30 and 60 minutes, brain, heart, spleen, liver, stomach, the small intestine, large intestine, kidney and muscle were taken out and the weight and radioactivity of the organs are measured and obtained %Dose/ g. Following bio-distribution studies, autoradiographs of mouse brain and SPECT/CT imagings of whole body were measured. [result] In bio-distribution studies of the normal mice, 125I-EISB was accumulated mainly to liver (40.1±3.6%) and kidney (15.1±2.2%). With the amyloid deposition mice, 125I-EISB was accumulated mainly to liver (40.1±4.8%) and spleen (15.1±1.6%). The images of the brain were obtained using imaging plate (IP) detector and 125I-EISB of the amyloid mouse was observed a high brain uptake in IP. In SPECT imaging of normal mouse, 125I-EISB was accumulated mainly to liver and kidney as obtained in bio-distribution. On the other hand, 125I-EISB was accumulated mainly to liver and spleen in amyloid mice. [conclusion] In bio-distribution and SPECT imaging, it was found that 125I-EISB were accumulated to β-amyloid. 125I-EISB was promising for the detection of the amyloid plaques for clinical use.

TP028

Influence of Nuclear Medicine Technologists' professional experience and visual function in the Myocardial Perfusion Gated-SPECT semi-automatic processing

A. S. Reimão1, F. Nascimento2, E. Carolino3, J. Pereira4, M. Nobre2, I. Poças2, L. Vieira5; 1Nuclear Medicine Scientific Area, Lisbon School of Health Technology – Lisbon Polytechnic Institute (ESTeSL-IPL), Lisbon, PORTUGAL & Brighton and Sussex University Hospitals NHS Trust, Brighton, UNITED KINGDOM, 2Orthoptics Scientific Area, ESTeSL-IPL, Lisbon, PORTUGAL, 3Mathematics Scientific Area, ESTeSL-IPL, Lisbon, PORTUGAL, 4Nuclear Medicine Scientific Area, ESTeSL-IPL, Lisbon, PORTUGAL, 5Nuclear Medicine Scientific Area, ESTeSL-IPL & Instituto de Biofísica e Engenharia Biomédica, Faculdade de Ciências da Universidade de Lisboa, Lisbon, PORTUGAL.

Aim: Myocardial Perfusion Gated-SPECT (MPS) plays an important role in the diagnosis, evaluation and follow-up of patients with Coronary Artery Disease. Its processing can be performed manually, semi-automatically or automatically, however the semi-automatic is the most widely used for routine clinical practice. Since the Nuclear Medicine Technologists (NMT) performance might be affected by individual and environmental factors, the aim of this study was to evaluate the influence of NMT professional experience and visual function on the MPS semi-automatic processing, and therefore in the determination of function and perfusion quantitative parameters (QP) measured. Materials and Methods: 20 NMT were selected and categorized into two groups according to their experience on the Quantitative Gated SPECTTM software: Group A (GA) - NMT ≥ 600 h and Group B (GB) - NMT without experience. All NMT underwent an orthoptic evaluation for assessment of visual function and processed 21 MPS five times in a non-consecutive way. It was assumed to be an altered vision when at least one visual function parameter was found abnormal. Friedman's and Wilcoxon Tests were applied to compare the QP between operators and to analyse GA and GB performance respectively. To compare the NMT with normal vs. altered vision, the Mann-Whitney Test was used and the ETA association coefficient was performed to

evaluate the visual function influence in each QP. Statistically significant differences at a significance level of 5% were assumed. Results: A greater discrepancy in GB was noted when compared with GA, and the Septal Wall (SW) was the only statistical difference (zw=-2,051, P=0.040). Regarding the influence of visual function, significant statistical differences in Left Ventricle Ejection Fraction (LVEF) (U=11.5, P=0.012) were observed, contributing the vision 33.99% for its variation. It was denoted more differences between NMT that have a greater incidence of ocular symptomology and a diminished Binocular Vision. Conclusion: On MPS semi-automatic processing, it was verified that professional experience and visual function influence the SW and LVEF QP respectively. This work was supported in part by Fundação para a Ciência e a Tecnologia - Portugal (UID/BIO/00645/2013).

TP029

I131 Effective Half-Life in Well Differentiated Thyroid Cancer Patients

S. Saengsuda; Rajavithi hospital, Bangkok, THAILAND.

Background: Oral administration of radioiodine (131I) has been used in treatment of well differentiated thyroid cancer (DTC) after surgery to decrease recurrence and mortality. Patients with high dose 131I administration (>2.96 GBq) requires hospitalization with isolation ward for radiation precaution to limit the radiation dose to family members and member of the public. The advised precautions are generally based on radiation dose rate and effective half-life for clearance of radioactive body burden. Objective: To assess the effective half-life of 131I in DTC patients who had been administered high-dose 131I (>2.96 GBq). Material and method: From January 2009 to Febuary 2012, a retrospective review of total 200 DTC patients with age range 8-80 years, mean age 41.98±15.57 years, 173 women and 27 men treated postoperatively with high dose 131I administration were collected for this study. The range of 131I administered activity was 3.18-8.51 GBq with the mean activity was 4.82±1.0GBq. Two measurements of exposure at t time (1-3 days later, E_t) were used for calculation of effective half-life of clearance of administered activity. Result: The range of 131I administered activity was 3.18-8.51 GBq with the mean activity was 4.82±1.0GBq. The mean initial exposure rates of total patients 81.65±32.36 (E_0) and 17.55±15.94 (E_t) μSv/h were shown with the mean duration time between E_0 and E_t 61.68±24.48 h. The mean effective half-life of 131I clearance was 13.2±12.96 h and the median effective half-life was 9.60 h. Conclusion: In DTC patients receiving 131I administration after surgery, the value of effective half-life is in accordance with the previous reports in literature. Patient release planning should be differentiated on the basis of individual measurements of exposure rate and calculation of effective half-life.

TP030

Optimizing the azeotropic drying of 18F- way to improve 18F-Fluorocholine radiochemical yields!

H. Hassan1, S. Abu Bakar2, K. Che A. Halim2, J. Idris2, A. Nordin1; 1Universiti Putra Malaysia, Serdang, Selangor, MALAYSIA, 2National Cancer Institute, Putrajaya, MALAYSIA.

Aim: 18F-Fluorocholine has been suggested as one of the reputable imaging agents for detection of prostate cancer in Positron Emission Tomography / Computed Tomography (PET/CT) modality. Nevertheless, it has never been synthesized in Malaysia. Thus, there was no available data on 18F-Fluorocholine synthesis was reported. We acknowledged the major problem with 18F-Fluorocholine is due to its relatively low radiochemical yield at the end of synthesis. Therefore, we reported improved 18F-Fluorocholine radiochemical yields before and after we had optimized the azeotropic drying of 18F-Fluorine. Materials and methods: Syntheses were performed using a modified GE TracerLab MX_{FDG} module (n = 6). 18F-Fluorocholine was synthesized via N-alkylation of dimethylethanolamine (DMEA) with 18F-fluorobromomethane ($BrCH_2F$), followed by purification on the CM cartridge with ethanol and water. Prior to addition of dibromomethane (100 ul) in acetonitrile (3 ml) to reactor vial, an aqueous 18F-Fluorine solution (25 - 75 GBq) delivered from cyclotron was subjected to azeotropic drying (with acetonitrile in the reactor vial). We investigated the effect of duration time during azeotropic drying phase and pressure inside the reactor vial on the radiochemical yield. Radiochemical yield of 18F-Fluorocholine synthesized in shorter duration time of azeotropic drying at atmospheric pressure (0 atm) (Condition 1; n = 3) was compared to radiochemical yield of 18F-Fluorocholine synthesized in longer duration time of azeotropic drying at high vacuum pressure (-0.65 to - 0.85 bar) (Condition 2; n = 3). In the end, the mean radiochemical yield was statistically compared between two azeotropic drying conditions to observe whether the improvement made was significant to the radiochemical yield. Results: After six consecutive runs, the 18F-Fluorocholine was obtained in 9 - 25% radiochemical yields (decay not corrected), with more than 95% radiochemical purity. In Condition 1, the 18F-Fluorocholine mean radiochemical yield obtained was 10.4 ± 0.8% (decay not corrected) whereas in Condition 2 was 21.3 ± 2.6% (decay not corrected). We observed 18F-Fluorocholine radiochemical yield increased at one fold, when the duration time of azeotropic drying was made longer at high vacuum pressure inside the reactor vial, regardless on the initial amount

of 18F-Fluorine activity. Conclusion: An improved 18F-Fluorocholine radiochemical yields were obtained after we had optimized the azeotropic drying of 18F-Fluorine. From the paired sample t-test analysis, it reveals that the improvement made was statistically significant difference in the mean of 18F-Fluorocholine radiochemical yield ($p < 0.05$).

TP031

The Radiation Dose Received by the Staff Responsible for the Collection and Transport of the Radioactive Waste

N. Edis, **A. Ogretici**, M. O. Tamam, M. Mulazimoglu; Okmeydanı Training and Research Hospital, Istanbul, TURKEY.

Objective: Radioactive waste arising after the imaging and treatment in nuclear medicine clinic are considered to be low-level. However, according to intensity of the work in the clinic and variety of imaging modalities effect the amount and the variety of the radioactive waste. The aim of current study was to assess the radiation dose received by the staff responsible for the collection and transport of the radioactive waste. Material and Method: In our clinic, the radioactivity used monthly are approximately 296 GBq activity of Tc-99m, 249GBq of I-131, 166GBq of FDG. We evaluated the 3 years thermoluminescent dosimeter data (TLD) whole body dose of 4 staff responsible for the collection and transport of the radioactive waste. One staff was responsible of I-131 and Tc-99m waste, 2 staff were responsible of FDG waste and one staff for removing the waste from waste processing center. The staff responsible of I-131 and Tc-99m waste was also followed up daily for 1-month with a digital dosimeter. These data were analyzed according to monthly activity amount, daily external dose measurement, and the variety of radioactivity. For the measurements Chest type thermoluminescent dosimeter is (TLD) and ÇNAEM NEB-236-C brand digital dosimeter was used and reading of TLDs is a two-month period. Surface dose measurements of waste were performed with the device ÇNAEM brands NEB211 Geiger Müller. Results:The annual measurement of the staff collecting I-131 ve Tc-99m wastes showed a sum of 0,49mSv/year. The Daily measurement of this staff with digital dosimetry showed a mean value of 4,79 ±0,36 μSv at the day collecting I-131 and a mean value of 3,95 ± 0,06 μSv/h at the day collecting Tc-99m wastes. Digital dosimeter recorded daily average operating time was found to be 425 minutes. I-131 surface dose measurements of monthly average of 13.5±24.6 μSv/h waste, whereas the Tc-99m waste 28.9±38.8 μSv/h was calculated. The other 3 personnel have been found under the average annual dose of 0.1 mSv. Discussion: The measured annual dose was far below than the dose limit, which is 20 mSv / year, permitted for workers responsible of collection and transport of radioactive waste. Maximum exposure dose measurements of the staff observed, was even 1/40 of the allowed annual dose limit. The reason lower dosimetry measurement of the staff responsible for the of FDG waste than other staff is that FDG has very short half-life and the FDG waste is collected the next day.

TP032

Additional findings above skull base on 18F-FDG PETCT: the usefulness of imaging from vertex

N. Gulliver, A. Almeida, N. Mulholland, G. Vivian, A. Eccles; King's College Hospital, London, UNITED KINGDOM.

Background: Recently updated EANM guidelines for 18F-FDG PETCT in tumour imaging (2015) state that for most oncology indications covering the range from the base of the skull to the mid-thigh (half-body) is sufficient. In patients with tumours with a high risk of head and brain metastasis but not metastasis in the lower extremities (e.g. lung cancer), it may be appropriate to perform an extended half-body scan from vertex to include the brain. Imaging from vertex on FDG PETCT has been demonstrated to be of use in assessment of patients with myeloma or melanoma, and in investigating paraneoplastic syndrome and pyrexia of unknown origin. Standardisation of image acquisition technique can be difficult to maintain with a rotating technologist workforce with varying experience of interpreting clinical indications. Methods: We conducted a retrospective audit of all half-body FDG PETCTs carried out in our department March 2014-March 2015. In our centre, conflicting methodology over the length of scan required clear & concise streamlining. PET and low dose CT for attenuation correction and localisation were performed with a GE Discovery 710 PETCT. In order to simplify departmental protocol we introduced vertex to mid-thigh scan length for all FDG PETCT scan indications that previously started at skull-base. Discussion: Instances where abnormal clinically-significant intra-cranial FDG uptake was demonstrated coincidental to the primary indication were recorded (<5% of cases) and four cases are presented here: (i) a staging scan for lung cancer revealing a photopenic parietal brain lesion alongside avid lung primary and bone metastases; (ii) a staging scan for lung cancer showing a recent extensive hypometabolism through the right temporal lobe, a likely recent ischaemic event; (iii) a staging scan for Hodgkin's lymphoma patient demonstrating paraneoplastic cerebrallitis; (iv) a scan for assessing extent of metastases prior to local resection on a patient with breast cancer which demonstrated posterior parietal hypometabolism consistent with a dementia diagnosis. CT acquisition from vertex instead of skull-base increased average effective dose by ~0.15mSv. Conclusion: Although additional intra-cranial findings were relatively uncommon, retrospective review of cases

has underlined the usefulness of imaging from vertex. All FDG PETCT patients in our department are now scanned from vertex with an extra 3 minute PET bed position acquired compared to imaging from skull-base. This has had no impact on the smooth running of patient worklists with minimal additional CT dose.

TP033

Technologist Radiation Exposure in Routine Clinical Practice with I-131 Administration for Ablation of Thyroid Cancer

A. Ergulen, F. Ustun, O. N. Yigitbası, G. Durmus-Altun; Trakya University Medical Faculty, EDIRNE, TURKEY.

Objective: In many countries, patients treated with therapeutic amounts of radioactive iodine (I-131) is hospitalized because of radiation safety considerations. The use of radioactive iodine for clinical thyroid cancer ablation therapy increases technologist radiation dose exposure because of the higher γ-radiation energy of this isotope than of other conventional medical γ-radiation-emitting isotopes. Therefore, I-131 therapy necessitates stronger radiation protection requirements. The aims of this study were to assess technologist whole-body exposure in our radionuclide department and to evaluate the efficiency of our radiation protection devices. Methods: In 119 patients with DTC, I-131 ablation of thyroid cancer was monitored for technologist radiation exposure in routine clinical practice. Radiation dose assessment was performed for single as well as for multidose application with both LiF thermoluminescence dosimeters (TLD) and electronic personal dosimeters (ED). Results: The mean dose of I-131 treatment was 122 ±28 mCi (range 75-200 mCi). The mean ± SD total effective doses received by technologists (n=119) during all of the working steps were 1.12 ± 2.38 μSv and dose rate 31.2 ± 22.8 μSv/hr, respectively, as measured with ED. These values were confirmed by daily TLD technologist whole-body dose measurements. There was a faint correlation between I-131 dose and technologist radiation dose rate (r=0.21, p: 0.01). In our department four technologists were working routine clinical practice. The mean ± SD total effective doses received by each technologist were 0.68 ±0.55, 1.65±3.62, 0.54±0.57, 1.61±2.99, respectively; p>0.05). Conclusion: These results showed that technologist radiation doses in our radionuclide therapy department were lower than those reported in the literature. Extrapolation of these results to an annual dose (2 patients per day per technologist) revealed that the annual extrapolated exposure values remained under the authorized limits for workers classified to work in a radioactivity-controlled area

TP034

Comparison of capability of diagnosis supporting system between two deifferent gamma cameras for bone scintigraphic images in diagnosing bone metastasis of cancer

K. Shimizu1, M. Hino1, K. Matsumoto2, S. Yamamoto3; 1Kobe City Medical Center General Hospital, Kobe, JAPAN, 2Kyoto College of Medical Science, Nantan, JAPAN, 3Nagoya University Graduate School of Medicine, Nagoya, JAPAN.

Aim: BONENAVI, a diagnosis supporting system for evaluating bone scintigraphic images with a computer, was developed and less variance among interpreters and improved diagnostic accuracy have been reported. Clinical trials with diagnosis supporting systems have been carried out and it is important to compare capability of diagnosing bone metastasis with different gamma cameras in a multi-center study. However, capability of diagnosing the bone scintigraphic images obtained with different gamma cameras remains unclear. This study aimed to investigate the difference in diagnostic capability of bone metastasis between different gamma cameras for bone scintigraphic images. Materials and Methods: The subjects comprised 181 cases examined by bone scintigraphy with 99mTc-MDP. They were cancer cases with a pathologically confirmed primary lesion, in which presence or absence of bone metastasis had been clinically diagnosed. Exclusion criteria were patients that could not be analyzed due to abnormal body posture and extraskeletal accumulation and contraindications for the employed drugs. Bone scintigraphic images obtained with two different gamma cameras, GE SPECT/CT Discovery 670NM and Infinia Hawkeye, were subjected to analysis with diagnosis supporting system software BONEVAVI. According to the obtained results (ANN values) and the results of interpreters, sensitivity, specificity, positive predictive value, negative predictive value, and AUC by ROC analysis were calculated to compare capability of diagnosing bone metastasis. Results: Discovery 670NM and Infinia Hawkeye provided sensitivity at 83% and 85%, specificity at 85% and 92%, positive predictive value at 86% and 65%, negative predictive value at 82% and 97%, and AUC at 0.893 and 0.948 (p = 0.175), respectively. Conclusion: There was no significant difference in diagnostic capability with bone scintigraphic images obtained with two different gamma cameras. It was elucidated that different diagnosis supporting systems could be used in a multi-center study as long as accuracy of the systems had been confirmed in advance.

TP035

Dosimetric analysis of Lu-177-DOTA-Rituximab in patients of relapsed/refractory Non-Hodgkin's Lymphoma

M. P. Yadav, S. Singla, P. Thakral, S. Ballal, S. K. Gupta, C. Bal, A. Malhotra; All India Institute of Medical Sciences, New Delhi, INDIA.

Aim: Radioimmunotherapy (RIT) targeting CD20 receptors in lymphoma using radiolabelled chimeric antibodies may demonstrate better therapeutic responses than radiolabeled chimeric antibodies or cold anti-CD20 antibodies. The study was designed to assess the biodistribution and give reasonable estimates of normal organ doses, including red marrow using 177Lu-DOTA-Rituximab. Materials & Methods: Patients with relapsed/ refractory CD20+ B-cell NHL were recruited in the prospective study. In house labeling of 177Lu-DOTA-Rituximab was performed and administered after quality assurance. Rituximab (375 mg/m2) followed by 50 mCi (1850 MBq) of 177Lu-DOTA-Rituximab was administered as slow intravenous infusion and emission images were acquired. Region of interest (ROI) were drawn for kidney, liver, heart, bladder, spleen and tumor lesions on both anterior and posterior images. Internal dose estimation was made using OLINDA v1.0 software. Results: The mean age of the ten patients (8 males and 2 females) was 52 ± 1 years. The uptake of radiolabeled antibody was visualized within 30 minutes of administration in liver, kidneys, heart, spleen and bladder. The coefficient of determination (R2) was greater than 0.95 for organs and whole body in all patients. The effective half-life of radioimmunoconjugate was 100 ± 28 hours (42 - 126 hrs). The critical organ in our study was the red marrow. Conclusion: There may be considerable inter-individual differences in absorbed doses of organs and generalization or extrapolation of doses in clinical setting at present does not seem feasible with 177Lu-DOTA-Rituximab in NHL patients.

TP036

Validation of an in-house media-fill on radiopharmaceuticals compared to ready-to-use kits: a cost-effective procedure fitted on each nuclear medicine needs

M. Di Franco1, S. Valfre2, T. Scotognella3, T. Angusti1, D. Ielo1, V. Podio1; 1Ospedale San Luigi Gonzaga, Orbassano (TO), ITALY, 2Università degli Studi, Torino, ITALY, 3Policlinico Agostino Gemelli, Roma, ITALY.

AIM: Most radiopharmaceuticals are designed for parenteral admninistration and for this reason must be produced by asepting processing; asepsys has to be continuously assessed in order to guarantee drug safety. Media-fill tests (recommended by Pharmacopoeias) are designed to simulate normal labeling procedures but with microbiological growth medium in place of drug solutions. Many producers make available expensive ready-to-use kits (vacuum vials, colture medium or vials containing colture medium, labels) that do not always fit specific nuclear medicine needs. In our institution, we aimed to develop and test media-fill from raw materials to final data analysis. MATERIALS AND METHODS: All materials are certified as sterile and apyrogenic; tryptic soy broth (TSB) is certified by producer also for fertility. Vial types and sizes were chosen to properly match the single procedure, avoiding large vials (not fitting shields or labeling devices). Operating in a class A laminar flow cell, TSB was transferred into vials (fitted with bromobutyl rubber closures and aluminium cap seals) by 0.22 μm syringe filters; sterility and apyrogenicity were checked after filling. Vacuum and TSB-filled vials were used to simulate the different steps of routine procedures. Similarly to ready-to-use kit procedures, also in our laboratory four main steps were identified: elution (if appropriate), labeling, fractioning and dispensing. In addition, samples subjected to heating, cooling under cold water and mixing were analyzed as single-steps using fresh culture medium for every elementary procedure. All TSB samples were incubated for 7+7 days (25 °C and 35 °C respectively) in a stove for microbiological studies and visually assessed each day; all results were recorded on appropriate worksheet. RESULTS: All materials were already in use in our hospital or readily available on the market. In-house media-fill achieved a perfect match with all elements of standard procedures of radiopharmaceutical synthesis and manipulation; this match was not possible with ready-to-use kits. Moreover, despite the larger number of steps involved (with 33 vs 21 vials to be tested), the total expense was much lower than costs of commercially available kits. CONCLUSIONS: Despite various operating procedures and different radiopharmaceuticals, in-house media-fill could match each single nuclear medicine department needs; it is versatile, easily designed by the quality assurance supervisor and prepared in any hospital with available vials and TSB. In our experience, no test was positive, but a positive test would exactly identify the single step involved: no uncertainty would be possible.

TP037

Myocardial Perfusion Radiopharmaceuticals and Imaging in SPECT and PET

R. Adães1, E. Pereira2, M. Fernandes2, **E. Sousa**1; 1Escola Superior de Tecnologia da Saúde de Lisboa, Instituto Politécnico de Lisboa, Lisbon, PORTUGAL, 2Nuclearmed - Instituto de Medicina Nuclear, Lisbon, PORTUGAL.

Purpose/Introduction: Myocardial perfusion imaging (MPI) has an effective role and are well implemented in detecting

disorders of left ventricle myocardial perfusion and function, yet it is a major subject of research. The development of new radiopharmaceuticals in this field allows increasingly more sensitive and specific for the diagnosis and monitoring of heart diseases along with the development of more specific radiopharmaceuticals. This work aims to conduct a review of the inherent examinations that use radiopharmaceuticals in clinical practice in studies of myocardial perfusion tomography by single photon emission tomography (SPECT) and Positron Emission Tomography (PET). Is also intended to focus radiopharmaceuticals that are under investigation or in clinical trials with great potential for cardiac imaging in conventional Nuclear Medicine and PET, proceeding to a comparative analysis of both techniques. Subjects/Methods: Literature search was undertaken through the portal b-on and in scientific journals, where the search words SPECT, myocardial perfusion imaging, PET radiopharmaceuticals and SPECT radiopharmaceuticals, which were subsequently revised. Results/Discussion: In clinical use for SPECT applications technetium labelled agents are the ones now available and in clinic utilization: 99mTc-Tetrafosmine and 99mTc-Sestamibi, the most used. 99mTc-Teboroxime is approved and in clinic use in United States, and 99mTc-N-NOET has good characteristics for MPI but at this point is still not approved in USA. 201Talium Chloride it was a popular myocardial perfusion agent but is now of very little importance and use in clinical practice. In clinical use for MPI PET applications the semi-disintegration time is one of the major concerns, it can be used 13N-Amonia, Rubidium-82 (82Rb), Oxigenium-15 (H215O), 18F-FDG (Fluordesoxiglucose). Rubídium-82 (82Rb), is the mostly used radiopharmaceutical for its availability due to the generator of 82Stroncium/82 Rubidium. Conclusion: MPI by PET has great advantages of imaging resolution and several radiopharmaceuticals available. SPECT MPI are still very used due to their financial cost and availability in most of countries.

TP038

Evaluation of the quality of neuroimaging features as Alzheimer's Disease biomarkers

F. Lucena1, T. F. Vaz1, J. Pé-Leve2, A. S. Ribeiro3, L. Lacerda4, N. Silva5, D. Nutt3, J. McGonigle3, H. A. Ferreira2; 1Institute of Biophysics and Biomedical Engineering of the Faculty of Sciences of the University of Lisbon / Lisbon School of Health Technology of the Polytechnic Institute of Lisbon, Lisbon, PORTUGAL, 2Institute of Biophysics and Biomedical Engineering of the Faculty of Sciences of the University of Lisbon, Lisbon, PORTUGAL, 3Centre for Neuropsychopharmacology, Division of Brain Sciences, Department of Medicine, Imperial College London, London, UNITED KINGDOM, 4Centre for Neuroimaging Sciences, Institute of Psychiatry, King's College London, London, UNITED KINGDOM, 5Institute of Neuroscience and Medicine 4, Forschungszentrum Jülich GmbH, Jülich, GERMANY.

The main challenges in Alzheimer's Disease (AD) are earlier diagnosis and classification of different stages, being neuroimaging an important tool. This work aims to evaluate the quality of neuroimaging features as AD biomarkers.T1-weighted magnetic resonance imaging (MRI), diffusion tensor imaging (DTI) and 18F-AV-45 positron emission tomography (PET) data were processed and analyzed using the Multimodal Imaging Brain Connectivity Analysis (MIBCA) toolbox. Data from 45 individuals, obtained from the Alzheimer's Disease Neuroimaging Initiative database, were divided in: 12 healthy controls (CTRL); and 11 early mild cognitive impairment (EMCI), 11 late mild cognitive impairment (LMCI), and 11 AD patients.The metrics evaluated were: gray-matter-volume (GMV); cortical thickness (CThk); mean diffusivity (MD); fractional anisotropy (FA); fiber count (FiberConn), structural connectivity node degree (Deg) and clustering coefficient (ClusC); and relative standard-uptake-values (rSUV). Receiver operating characteristic curves were used to evaluate and compare the diagnostic accuracy of the most significant neuroimaging metrics and brain regions, expressed as the area under the curve (AUC). Comparisons were performed between CTRL-EMCI, CTRL-LMCI and CTRL-AD, based on biomarkers showing AUC>70% and intervals of confidence >0.5.Our results suggest that cortical atrophy begins in confined areas of the temporal region and mainly in the left hemisphere. The atrophy gradually involves other parts of the cerebral cortex from both hemispheres at later stages of MCI and AD, indicating an increased spread of cortical atrophy characteristic of AD progression, which can be the result of the accumulation of neurofibrillary tangles.Regarding CTRL-EMCI comparison, several brain regions act as potential biomarkers when assessed by PET and DTI, supporting the evidence that metabolic and microstructural alterations, respectively, might precede atrophy. The elevated MD and decreased FA in temporal regions are consistently found in MCI stages, and are thought to reflect progressive loss of the barriers restricting the motion of water molecules in tissue compartments associated with the neuronal loss and disruption of myelin sheaths in AD.Temporal lobe regions were highlighted in CTRL-LMCI, being more related with structural changes and connectivity metrics due to progression to AD. Other regions from the parietal and frontal lobes were identified as having high AUC regarding rSUV (AUC=99%), corroborating the literature.In this study, several potential biomarkers (brain regions/neuroimaging metrics) were studied and the best candidates for differentiating between healthy controls and patients groups identified. Nonetheless, results must be taken with caution as the study sample was small and consequently further studies are warranted with larger samples.

TP039

Qualitative and quantitative analysis of 123I-DaTSCAN SPECT in the diagnosis of Parkinson's diseases: body-contouring versus circular orbit acquisition

A. PALMIERI1, A. ZOCCO2; 1SANTA MARIA NUOVA HOSPITAL, REGGIO EMILIA, ITALY, 2UNIVERSITA' DI MODENA E REGGIO EMILIA, MODENA, ITALY.

BACKGROUND: SPECT (single photon emission computed tomography) with N-u-fluoropropyl-2a-carbomethoxy-3a-(4-iodophenyl) nortropane, also called FP-CIT, labelled with 123Iodine (commercially known as DaTSCAN) has been proven to be useful in the diagnosis of Parkinson's diseases. DaTSCAN-SPECT provides qualitative and quantitative information to confirm dopaminergic degeneration in patients with parkinsonism. AIM: SPECT data acquisition can be performed using a circular orbit or a body-contouring system. The aim of this study is to investigate whether circular orbit offers different information about qualitative and quantitative analysis than body-contouring orbit in cerebral SPECT with 123I-DaTSCAN. MATERIALS AND METHODS: To acquire data we used a Symbia T2 SPECT-CT scanner (Siemens Medical Solutions). Acquisitions were performed on three patients, 3 hours after receiving 185 MBq of 123I-DaTSCAN. Each study was acquired using the same standard acquisition's parameters provided for a cerebral SPECT. Scans were performed using LEHR parallel hole collimators, over 360 degrees at 120 angles, 30 seconds/angle, 128x128 matrix, zoom 1.23. Every patient was scanned twice: for the first study we used a body-contouring orbit and patient's head was placed at the center of FOV; for the second we selected a circular orbit with fixed radius and patient's head was decentralized. Images were processed using data management system "Syngo". SPECT projections were reconstructed with filtered backprojection algorithm, butterworh filter (cutoff: 0.45, order: 8). We analyzed qualitative transaxial images and we performed ROI on basal ganglia and background for quantitative analysis. RESULTS Qualitative analysis: Images obtained using circular orbit have a worse quality, lower resolution and they appear more smoothed and noisy than images acquired with body-contouring. Quantitative analysis revealed a decrease of absolute counts in SPECT data acquired with circular orbit SPECT, because distance between detector and patient was more than in the acquisition with body-contouring orbit. On the other hand, relative counts (ratio: basal ganglia-background/background) were very similar in both acquisitions. CONCLUSION This study demonstrates that using body-contouring in SPECT we can obtain better results from a qualitative point of view, because the image's resolution worsens with increasing distance to the camera. Instead, semi-quantitative analysis doesn't reveal important differences between two acquisitions.

TP040

Influence of disposable materials in 99mTc-MAG3 radiolabelling

M. Menzaghi, R. Lucianini; Ospedale di Circolo, VARESE, ITALY.

AIM: The evidence of the reduction of MAG3 Radiochemical Purity during routine workload has led a systematic analysis of the whole "in situ" product process. Our evaluation has revealed a correlation between the loss in product quality and medical devices recently introduced such as disposable syringes. MATHERIAL AND METHOD: The MAG3 compound is radiolabelled with dual-step process, the first one introduces a known 99mTcO4- saline radioactivity volume in the lyophilized vial and the second step is the boiling phase which gets the metal complex 99mTc-MAG3 binding reaction. Traceability introduced by the Rules of Good Manufactoring Practice in radiopharmaceuticals (NBP-RF) highlighted a significant loss of the radiochemical purity in a two-month period, by relating the syringe used in the process with Radiochemical Purity and pH value of the RF MAG3. The entire process systematic analysis has suggested the likely lossy factor the use of new 10 ml syringes during labelling. The comparative analysis of the disposable material data-sheets (Artsana, Farmac-Zabban, BD) and the available literature prompted the conclusion that the only factor responsible is the oil lubricant of the three parts syringe plunger (body, piston, elastomer). The amount of silicone oil used in the syringe can determine interference in the labeling reaction of 99mTc-MAG3. RESULTS: The comparative analysis showed that all manufacturers use the same medical lubricant and the specific oil amounts refer to the Rule limits therefore they don't indicate the exact quantity. This assumption suggests that the problem is pretty quantitative: the silicone material released from the syringe to the lyophilized kit defines alterations in the Red-Ox reactions during the complex formation. A gold standard analytical method, such as mass spectrometry, is desiderable to measure the amount of silicone oil in the suspension. This method could indicate new reference limits for lubricants used in disposable devices for the 99mTc-MAG3 labelling. CONCLUSIONS: The quality of Radiopharmaceuticals prepared in the Radiopharmacy Laboratory must be guaranteed by the careful choice of used disposable materials. The continuous check of the more significant qualitative indicators for 99mTcMAG3, such as RadioChemical Purity and pH values, can help a Nuclear Medicine Department to guarantee the necessary product quality and help to define a quality improvement strategy.

TP041

Intraobserver and interobserver variation of myocardial perfusion SPECT results related to repeated reconsructions

M. Kraft, T. Koivumäki, M. Hakulinen, M. Kokkonen, A. Leinonen, T. Laitinen; Kuopio University Hospital, Kuopio, FINLAND.

Aim: The myocardial perfusion SPECT is used to detect and assess obstructive coronary artery desease. During image reconstruction process maching the attenuation map and SPECT-image, orientation of myocardium and exclusion of extracardiac activity is done manually by the technologists, which can potentially lead to variation in results. The aim of this work was to study intra- and interobserver variation in myocardial perfusion results from reconstruction point of view. Material and methods: Data of eleven patients (7 male, 4 female, age 50-86 years) were collected. Images were acquired with Siemens Symbia SPECT-CT camera (Tc99m-tetrofosmin, matrix 128*128, 64 angles, time per view 25-30s, 16 ECG frames). Images were reconstructed iteratively (OSEM, 5 iteration, 16 subsets, 3D Gaussian 14mm FWHM). Perfusion parameters, that are Summed stress score (SSS), Summed rest score (SRS), Summed difference score (SDS), Stress Extent%, Rest Extent% and Ischemia%, were calculated using Quantitative Perfusion SPECT 2012 software (QPS, Cedars-Sinai Medical Center, Los Angeles, CA). If the QPS program told about mask failure, experienced doctor verified the contours. The reconstructions and analyses were performed three times with four weeks separation by three technologists. Intra- and interobserver variations were evaluated by calculating intraclass correlation (ICC), Cronbach's alpha and coefficient of variation (CV%, root mean square). Results: The reproducibility results were practically similar in intra- and interobserver variations. Intraobserver ICC was lowest in SDS 0,268 and highest in SRS 0,986. Mean CV% varied between 24,4 (Ischemia) and 76,1 (Rest Extent). Lowest Cronbach's alpha was 0,51 (SDS) and highest 1,0 (SRS). Interobserver reproducibility (ICC) was lowest in SDS 0,290 and highest in SRS 0,98. Mean CV% varied between 33 (Ischkemia) and 80,8 (SRS). Lowest Cronbach's alpha was 0,51 (SDS) and highest 0,99 (extent stress and extent rest). In cases with disagreement between analyses of different reconstructions, slight changes in contour detection had significant impact on results. Conclusions: The intra- and interobserver reproducibility (ICC) was good in SSS, SRS, stress extent and rest extent.The rebroducibility of SDS was poor in both, intra- and interobserver variation. Ischemia had moderate reproducibility, in intra- and interobserver variation. In addition to effect of variation in reconstructions, also variation in contour detection is responsible for poor reproducibility in SDS.

TP042

Influence of Reconstruction Parameters for FBP in Semiquantification of Brain Studies with 123I-FPCIT

F. Alves1, R. Adães2, C. Fortes2, **E. V. Sousa**2; 1Alliance Medical, London, UNITED KINGDOM, 2Escola Superior de Tecnologia da Saúde de Lisboa, Instituto Politécnico de Lisboa, Lisbon, PORTUGAL.

Aim: Brain dopamine transporters imaging by Single Photon Emission Tomography (SPECT) with 123I-FP-CIT has become an important tool in the diagnosis and evaluation of parkinsonian syndromes. However, Ordered Subset Expectation Maximization (OSEM) is the method recommended in the literature for imaging reconstruction Filtered Back Projection (FBP) and is still used due to its fast processing. The aim of this work is to investigate the Influence of reconstruction parameters for FBP in semiquantification of Brain Studies with 123I-FPCIT compared with those obtained with OSEM recommended reconstruction. Material and methods: 16 exams of Brain Studies with 123I-FPCIT were processed by using Butterworth filter in FBP, with the cutoff frequencies (Cf) 0.4, 0 .5, and 0.6 cycles per pixel combined with the orders of 6 , 8, 10 and 15. For OSEM reconstruction it was used 3 iterations with 8 subsets. Chang's attenuation correction (μ=0.11cm-1) was applied for both reconstruction methods, and each exam was reconstructed three times. The outcome measure was the specific binding ratio (SBR). For statistical analysis it was used the Friedman's test, a non-parametric approach for paired samples. Results: OSEM and FBP methods were compared, and for the last one with the orders 8 and 10 with 0.5Cf it wasn't found out any significant differences (pvalue=0.16). Those combinations of orders and cutoff frequencies produce an image with a compromise between resolution and noise reduction similar, This led to conclude that both methods of reconstruction allow to identify the regions in study in a reliable way, permitting the identification of the SBR of the pathology independently of the reconstruction method. However FBP Cf 0.6 and order 6 are the parameters where FBP rates more differently from OSEM; Cf 0.5 and order 8 are the ones that rates closest. A significance level of 5% was used. Conclusion: Both reconstruction methods can identify the regions to study, allowing identifying and classifying in similar way the SBR. FBP method with Cf 0.5 and order 8 shows closer values to the ones from OSEM, and it can be used as a reliable alternative in clinical practice for the SBR calculation

TP043

Half-time oncologic bone scintigraphy imaging in patients with prostate and breast cancer

S. J. C. Serém1, M. I. Gomes1, W. Grootjans2, W. J. M. van den Broek2, E. P. Mijnheere2, B. F. Bulten2, L. Heijmen2, R. Hermsen2; 1Coimbra Health School, Polytechnic Institute of Coimbra, Coimbra, PORTUGAL, 2Radboud University Medical Center, Nijmegen, NETHERLANDS.

Aim: Bone scintigraphy has an established role in the management of patients diagnosed with breast and prostate cancer. However, the noisy character of the images either requires a sufficient amount of radiotracer to be administered or sufficiently long image acquisition times, resulting in considerable radiation exposure or reduced patient comfort. In this study, the performance of a Pixon enhanced planar processing (EPP) algorithm was investigated with the purpose of reducing image acquisition time in bone scintigraphy of breast and prostate cancer patients. Materials and Methods: Standardized phantom experiments were conducted to access the performance of the EPP software. For this purpose, the sphere insert of the National Electrical Manufacturers Association (NEMA) phantom was placed in the cylindrical casing of the Jaszczak phantom. Images were acquired with different sphere-to-background ratios (4:1, 8:1, 17:1, 22:1, 32:1 and 71:1) and scan speeds (8, 12, 16 and 20 cm/min). Image quality was determined by calculation of signal-to-noise ratio (SNR) and contrast-to-noise ratio (CNR) of the spheres, and coefficient of variation of the background ROIs. Furthermore, 51 patients diagnosed with breast and prostate carcinomas were included for clinical investigation. Each patient was scanned using a standard protocol, in concordance with the EANM guidelines for bone scintigraphy, and a shortened acquisition protocol. Three nuclear medicine physicians performed independent reading of standard, half-time, and half-time processed (EPP) images, scoring image quality, and providing a final diagnosis. Results: Image noise, as reflected by the coefficient of variation, was considerably reduced in EPP images. Based on the phantom experiments, it was determined that EPP images acquired with half-time protocol (16 cm/min) had similar image quality as standard images (8 cm/min). Subjective and objective image quality in the clinical EPP images improved, being comparable to the standard images. There was substantial agreement with respect to diagnosis and diagnostic confidence based on all three image types between observers. Moreover, the number of lesions or affected anatomical areas was not considerably different based on all three image types. Conclusion: It was shown in this study that half-time imaging in oncologic bone scintigraphy is feasible with the current clinical protocol. Although EPP improved image quality, the diagnosis provided was not different in all three image types. These results emphasize that there may be the possibility to further reduce image acquisition time, certainly with the availability of EPP tools, eventually contributing to improving clinical workflow and patient comfort.

TP044

Albumin macroagregates (MAA) kit fractionation for labeling with 99mTc: temperature and storage time influence in quality parameters

S. F. C. Mendes, B. F. Oliveira, A. G. F. Ramos, F. Lucena; Escola Superior de Tecnologias da Saúde, IPL, Lisboa, PORTUGAL.

Albumin macroagregates (MAA) kit-fractionation for 99mTc-labeling is a procedure that can be used as strategy to maximize resources and reduce costs. Therefore, quality parameters [percentage of 99mTcO4- (%99mTcO4-), pH and size of particles] should be accurately controlled. It is necessary to optimize the procedures assuring the quality of the radiopharmaceutical and not compromising the diagnostic procedure. The aim of this work is to evaluate the influence of fractionation, temperature and storage time on the quality parameters of 99mTc-MAA.Two fractions were obtained from each MAA-kit provided by the manufacturer which were evaluated immediately after fractioning (G1) and after 1 week in the freezer (G2). Each fraction was radiolabelled with 99mTc (740MBq / 6mL) and the variables pH (10 min), size of the particles (2h) and %99mTcO4- (10 min and hourly from 1-6h) were determined. Also residual activity in the syringe was measured with different incubation times (0, 10 and 20 min), with (Sh) and without shaking (n-Sh). Descriptive and inferential statistics were applied (IBM-SPSS software, version22). Significance was considered for p-value<0.05.Preliminary results: there were no significant differences in %99mTcO4, pH and size of particles between groups; significant differences in % 99mTcO4- over time were found for G1 (p-value=0.000) and G2 (p-value=0.001) with a decreasing pattern from 1-4h (G1) and 1-5h (G2); freezing produced %99mTcO4- (1h) above the 10% limit of the manufacturer; there were differences in residual activity at 0 min (p-value = 0,000) and 20 min (p-value = 0,000) of incubation, with syringe shake between groups; residual activity ranged between 11% (0 min-Sh) and 85% (20 min-n-Sh) for G1 and between 12% (10 min-Sh) and 88% (20 min-n-Sh) for G2; in each group, differences related with residual activity were found between 0, 10 and 20 minutes of incubation, except in the Sh-syringes of G2; significant differences were found in G1 and G2 between Sh vs n-Sh syringes, except in G2 syringes with 0 minutes of incubation.Based on our results, fractioning of MAA should be used carefully and further research should be developed. Incubation time and shaking of syringe affect considerably the residual activity and procedures should be managed accordingly while handling 99mTc-MAA.

TP045

The Study on Effect of the Image Applying to Breast Implants in Breast Specific Gamma Imaging

J. Lee1, H. Lee2, J. Kim3, H. Park4; 1Graduate school of Public Health, Yonsei University, Seoul, KOREA, REPUBLIC OF, 2Department of Nuclear Medicine, Konkuk University Medical Center,, Seoul, KOREA, REPUBLIC OF, 3Department of Nuclear Medicine, Seoul Medical Center, Seoul, KOREA, REPUBLIC OF, 4Shingu College, Seongnam, KOREA, REPUBLIC OF.

There are limits to check the lesion as inserting a breast implant patients. So the application of BSGI based on Nuclear Medicine examination has increased. In this study, therefore we confirmed the effect of the image applying to breast implants in Breast Specific Gamma Imaging. We utilized Dilon 6800 BSGI scanner and developed the phantom. The self-development phantom was a rectangular shape of 230 × 190 × 80 mm size and had 5 spheres which consisted of diameters of 10, 13, 17, 22, 28 mm in central part. We injected $99mTcO_4$ into the self-development phantom in the proportion of four to one and made each additional phantom filled with 0.9% sodium chloride, silicon and paraffin. Each additional phantom was placed between detector and self-development phantom. Each image was acquired five times depending on the type and thickness of the additional phantom. Statistical analysis with SPSS ver.18 was applied. In the test of variation according to the thickness of all additional phantoms, as the phantoms which 0.9% sodium chloride, silicon and paraffin increased, the attenuation variation was higher($P<0.005$). The attenuation variation was not significant difference for each material of additional phantom. The attenuation variation was similar in 10, 20 and 30 mm of the variation according to each additional phantom($P<0.005$). In the study, as the thickness increased, the attenuation variation got higher, and the quality of image declined. Therefore, if the effect of the image applying to breast implants in Breast Specific Gamma Imaging is confirmed, the higher diagnostic value can be achieved.

TP046

Biodistribution Assessment of Sodium Pamidronate and Methylene Diphosphonate for Rats Bone Scintigraphy Images

T. S. C. Camozzato, **Sr**.1, A. Z. P. De Souza2, M. Tizon1, S. J. Garcia1, V. F. Dutra1, T. G. Costa1; 1Instituto Federal de Educação, Ciência e Tecnologia de Santa Catarina, Florianópolis, BRAZIL, 2Universidade Federal de Santa Catarina, Florianópolis, BRAZIL.

Once there are more studies on radiopharmaceuticals interaction in nuclear medicine (NM) examinations with standard pharmaceuticals, it will be possible to trace strategies in order to enable the least possible interactions between them during clinical NM testing on patients. This study aims to develop a research to assessment drugs biodistribution and interaction with radiopharmaceuticals used in NM protocols. Sixteen Wistar rats were randomly divided into 2 groups, weighing between 200 and 250 grams. Group #1 was injected with 1 mCi (99m)Tc-methylene diphosphonate (MDP) intravenously. Group #2 was administered 0.1 ml Sodium pamidronate intravenously and after 10 minutes was administered 1 mCi (99m)Tc-MDP intravenously. Each rat syringes was imaged and activities were recorded prior and post injection. After 60 minutes, scintigraphic images were acquired using a Philips SPECT gamma camera with multiplane formatting and a 60 seconds acquisition time, with unleaded shield on rat`s tail. We acquired images during 10 minutes with rat's tail lead shielded. Image acquisition were similar for both groups. The images analysis of Group 1 showed a normal bone structure, with increased osteoblastic activity similar on both sides joints, and face. Four out of 8 rats in group #1 had radiopharmaceutical renal retention. Most animals presented detailed bone definition. the rats on group #1 no showed increased uptake in soft tissues. On group #2, all images showed a normal appearance bone structure with an increase in osteoblast activity similar on both sides joints, and face. Three of 8 rats in group #1 showed a radiopharmaceutical kidney retention. The majority of rats showed little detail in bone definition, and 2 animals showed soft tissue uptake. The study showed that in group #1 there were no cases of soft tissue uptake, except for renal retention, which is common for (99m)Tc-MDP is mainly excreted by urinary tract. On the other hand, group #2 showed 2 cases of soft tissues uptake. Another fact is bone definition: in group #2 they presented very detailed bone definition, while in group #2, they presented few details in bone definition. One can concluded that both groups had common outcomes such as renal retention and bony structures, but also showed different results. Difference in bone definition and the uptake occurred in group #2 are examples of this, establishing the idea that Pamidronate Sodium can alter normal biodistribution of (99m)Tc-MDP.

TP047

Implementation of a New Reference values's Database for Semiquantification in 123I-FP-CIT Brain Single Photon Emission Tomography

M. Queiroga1, D. Silva1, M. Elias1, J. Serrano2, J. Madrid2, E. Carolino1, E. Sousa1; 1Escola Superior de Tecnologia da Saúde de Lisboa, Instituto Politécnico de Lisboa, Lisbon, PORTUGAL, 2Nuclear Medicine Department, Hospital Infanta Cristina, Badajoz, Spain, Badajoz, SPAIN.

Purpose/Introduction: Brain dopamine transporters imaging by Single Photon Emission Tomography with 123I-FP-CIT has become an important tool in the diagnosis and evaluation of

parkinsonian syndromes, in this exam semiquantification can improve the diagnosis and is useful to have adapted reference values for a specific protocol and clinic's population. Aim: To create and validate a database of healthy controls for the Dopamine transporters (DAT) with 123I - FP-CIT named DBRV. The created database is adapted to Nuclear Medicine Department's protocol and population of Infanta Cristina's Hospital located in Badajoz. Subjects/Methods: It was used a semiautomatic method for segmentation and posterior calculi of binding potential in dopamine transporters (DAT) in striatum structures and in a nonspecific binding region, of the 30 healthy controls of the DBRV. All exams where acquired by EANM's Guidelines protocol, and processed three times for one operator, average values were used. Average and standard deviation ($x \pm \delta$) values were calculated for the following ratios: left and right Caudate nucleus/ Occipital respectively (A) and (B); left and right Putamen/Occipital respectively (C) and (D); striatum/Occipital (E); left striatum/occipital (F), right striatum/occipital (G), Putamen/ nucleus caudate (H). These values where calculated and stablished new reference values for this hospital's population between 60 and 75 years. For validation purposes two database of thirty patients each: database of healthy controls (DBVGIIH), and database of subjects with diagnosed Parkinsonian Syndromes (DBVGIIIP), where processed using the same protocol, and its results where compared with the ones of DBRV. Assessment control charts where calculated. Results: The reference values ($x \pm \delta$) obtained were for the following ratios: A (2.60 ± 0.40); B (2.57±0.36); C (2.29± 0.36); D (2.31±0.35); E (2.44±0.35); F (4.89±0.74); G (4.88 ±0.68); H (0.89±0.07). The DBVGIIH results were within the new reference values for healthy subjects; the DBVGIIIP results were below the new reference values for healthy subjects. Discussion: It was considered that all values for all ratios that were above negative value of stand deviation (-δ) were healthy, it was considered that all values for all ratios that were below negative value of stand deviation (-δ) were classified as pathological positive for Parkinson syndromes. Conclusion: The new created database and reference values for of Infanta Cristina's Hospital located in Badajoz agreed with the external classification of patients as healthy and as pathological for Parkinson Syndromes classification. The new database is an adapted and improved tool for clinical use assessment.

TP048

ASTRIM® Software Implementation - Complying with the Italian Current Regulations - for the Radiolabelling of Therapeutic Radiopharmaceuticals: the Role of Nuclear Medicine Technicians

N. Bartolini, G. Di Guilmi, G. Marchi, M. Casi, F. De Lauro, M. Bartolomei; Nuclear Medicine Unit M.Bufalini Hospital, Cesena, ITALY.

INTRODUCTION AND PURPOSE: Since the beginning of 2013 a novel software ASTRIM® has being employed in the Nuclear Medicine Unit of M. Bufalini Hospital in Cesena. This computer tool was created by the computing company - and currently used in many Nuclear Medicine Centers - to manage, control and register all the phases regarding the diagnostic use of radioparmaceuticals. This modality of work is required by Italian Current Regulations, which include also specific issues and recommendations regarding the therapeutic use of radiopharmaceuticals. Unfortunately, the basic version of the software ASTRIM® was not able to manage the therapeutic activities, which were carried on using an ordinary approach, not computerized and based on hand-written papers. The Nuclear Medicine Technicians (NMTs) of our Unit have an important role in the organization of therapeutic procedures: in particular, NMTs take part in the radiolabelling of somatostatin analogues with the high energy beta-emitting isotope Yttrium-90 for PRRT. After a formal agreement with the ASTRIM® Company, the NMTs began collaborating with the Application Technologists of ASTRIM® in order to develop the software, making it suitable for therapeutic applications. METHODS: The specific procedure regarding the radiolabelling of 90Y-DOTATOC was taken into account and splitted in seven subsequent phases, as follows: 1) storage and registration of devices, peptide, isotope and any other reagent for radiolabelling; 2) preparations of devices for radiolabelling; 3) preparations of peptide, isotope and other reagents for radiolabelling; 4) radiolabelling of 90Y-DOTATOC; 5) quality control of 90Y-DOTATOC; 6) dilution and ultrafiltration of 90Y-DOTATOC; 7) fractionation of 90Y-DOTATATE into single rates for patients. Therefore, new modules were included in the software. In particular, for each of the seven above listed phases, new pages and specific schemes were created and then integrated with the other software parts, as well. RESULTS: In particular, the NMTs and the other operators are guided in any single phase of the work process, and all the main data and parameters concerning the procedure (radiopharmaceuticals' total activity and expiration time, efficacy of radiolabelling assessed by a specific control quality test, amount of activity injected in any patient) are registered in the software archive. CONCLUSIONS: The specific role and knowledge of the Nuclear Medicine Technicians was fundamental for improving the ASTRIM® software. These modifications made the software able to manage, control and register all the diagnostic and therapeutic activities in our Nuclear Medicine Unit, saving time and lowing the risk of mistakes.

TP049

5-HT1A agonist and antagonist PET radiopharmaceuticals bind differently to receptors in Alzheimer 's disease: a postmortem study

B. VIDAL1, J. SEBTI1, M. VERDURAND1, S. FIEUX1, N. STREICHENBERGER1, T. BILLARD2, A. NEWMAN-

TANCREDI3, **L. ZIMMER**1; 1Université Claude Bernard Lyon 1, Lyon, FRANCE, 2CNRS, Lyon, FRANCE, 3Neurolixis, Dana Point, CA, UNITED STATES.

Aim: PET studies revealed a decreased density of 5-HT1A receptors in hippocampi of Alzheimer's disease (AD) patients at advanced stages. A limitation of this approach is that PET 5-HT1A radiopharmaceuticals are antagonists, thought to bind to the high-affinity state of 5-HT1A receptors (functional) and to the low-affinity state of these receptors (decoupled from G proteins and non-functional). Comparing the PET images obtained using a new agonist radiopharmaceutical, which binds selectively to functional receptors, with the PET imaging obtained using an antagonist radiopharmaceutical would therefore provide original information on 5-HT1A receptor impairment during AD. Materials and Methods: Quantitative autoradiography using [18F]F13640 or [18F]MPPF, a 5-HT1A agonist and antagonist, respectively, was performed in hippocampi of AD patients (n=25, at different Braak's stages) and control subjects (n=10). The coronal sections were incubated in a saline buffer containing 37 kBq/mL of [18F]F13640 or [18F]MPPF. Hippocampal subregions were drawn according to a brain atlas and binding quantification was performed with extemporaneous fluorine-18 scales. The specific binding of both radiotracers was determined by addition of WAY-100635 and the agonist binding of [18F]F13640 was revealed by addition of Gpp(NH)p. The neuronal density in ROIs was quantified in adjacent brain sections by NeuN immunohistochemistry. Results: The highest binding density of both 5-HT1A PET radiotracers was in the pyramidal layer of CA1. The incubation with Gpp(NH)p reduced significantly [18F]F13640 binding, confirming its specific binding to G-coupled receptors. In the same conditions, no significant modification of [18F]MPPF binding was measured after decoupling of receptors. Whereas total 5-HT1A receptor sites measured by the antagonist, [18F]MPPF, were unchanged in CA1 area at all AD stages (except for the more advanced stage), there was a significant decrease in the density of binding sites labeled by the 5-HT1A agonist, [18F]F13640, at the early and advanced Braak's stages (from I to VI). There was a significant correlation between the neuronal density (NeuN) and the [18F]F13640 agonist binding sites, but not with the [18F]MPPF antagonist binding sites, suggesting that 5-HT1A non-functional receptors could have a non-neuronal overexpression at AD advanced stages. Conclusion: The present results support a new concept consisting in comparing the binding profiles of a PET agonist and antagonist in patients to determine the extent of G-protein coupling of 5-HT1A receptors and to follow their functional modifications during the neurodegenerative process. A first-in-man study of [18F]F13640 is therefore scheduled to prepare the transposition of this paradigm to in vivo PET neuroimaging.

TP050

Introduction of a new Gallium-68 (Ga-68) DOTATATE synthesis module: a retrospective evaluation of GMP qualification and validation, radiation hygiene and organizational planning.

S. Baank, L. de Wit-van Veen, M. Jonker, E. Aalbersberg; Antoni van Leeuwenhoek Hospital, Amsterdam, NETHERLANDS.

Introduction: Since 2012 the department of Nuclear Medicine of the Antoni van Leeuwenhoek hospital (AVL) has started with the production of Gallium-68 (Ga-68) DOTATATE for the localization of Neuroendocrine Tumors (NET). Although initially a semi-automatic module was used, the continuity of the synthesis could not be assured resulting in unacceptable waiting periods for patients. These issues have led to the purchase of a commercially available automatic production module (Scintomics GmbH, Germany). With the purchase of this module the following issues needed to be addressed: qualification and validation according to good manufacturing practice (GMP), radiation hygiene, organizational planning and personnel. Aim: To enumerate the advantages and disadvantages of the implementation process, which can be used as future starting point for the production of other radiopharmaceuticals in a clinical setting with this module. Methods and materials: A retrospective evaluation of the implementation and initial production of Ga-68 DOTATATE within the department nuclear medicine was performed. This included a qualitative and retrospective review of all the used documents, interviews with the personnel involved with the implementation and/or production and assessment of the first clinical usage of the Ga-68 DOTATATE radiotracer within the department of nuclear medicine of the AVL. Results: The validation and qualification by GMP standards was successful and the production of Ga-68 DOTATATE using the commercial module for clinical use is nowadays a fact. The findings of this study indicate a learning curve when using the system. Furthermore, future improvements can be made in education of personnel, organizational planning and logistics regarding both patients and personnel. Conclusion: Based on the results of this retrospective study, a generalized checklist and a thorough implementation and evaluation plan were constructed, which includes factors from GMP qualification of the product to organizational planning.

TP051

Nuclear Medicine/PET/CT Research: The role of a technologist/radiographer

A. S. F. Ribeiro, S. Summers; Royal Marsden Hospital, Sutton, UNITED KINGDOM.

Aims: Nuclear Medicine/PET/CT is an area of constant evolution. New tracers combined with equipment and software development have seen the role of Nuclear Medicine (NM) technologists and radiographers evolve over the past years. Research has become one of the "new roles" for technologists/radiographers. Materials and Methods: The role of a research NM technologist/radiographer however is not standardized across the board. Different countries, different areas in the same country and just different hospitals have very different practices. We are seeing more jobs advertised for "research NM technologists/radiographers", mainly in centres who have strong foundations in research. In our centre we have a dedicated team to research; composed of consultants, trial coordinators, research fellows, physicists and NM research technologists/radiographers, who all work as a team and oversee all aspects of research within the department. Results: The input a research NM technologist/radiographer can have in research is as fundamental as it is diverse. In our experience there are clear advantages; setting up scanning protocols for different studies; dealing with data queries from sponsors, being a point of contact; relieving other members of staff from having to perform extra tasks that are purely research such as dynamic scans and/or blood tests; reviewing protocols and having a direct input in setting up imaging studies. But there are some disadvantages, which can arise from sparsely clinical exposure where some skills can become rudimental. Conclusion: Nuclear Medicine/PET/CT can perhaps be defined as unstable as its isotopes. Particularly with the availability and widespread of PET/CT scanners who have urged for new and improved tracers and with that comes research. The role of technologists/radiographers in research is crucial and should be deep-rooted, starting in universities, post graduate programmes and by managers and nuclear medicine consultants. However a balance between research and clinical is fundamental for achieving excellence.

TP03 - Tuesday, October 13, 2015, 8:00 AM - 9:30 AM, Hall 3 – Poster Exhibition
Technologist Poster Session 3

TP052

The use of non-attenuation corrected PET images in the assessment of cardiac implantable electronic device infections

C. Abreu1, J. O'Doherty1, A. Corrigan2, S. Barrington1, J. John1; 1PET Imaging Centre, King's College London, King's Health Partners, St Thomas' Hospital, London, UNITED KINGDOM, 2Department of Radiology, Maidstone Hospital, Maidstone and Tunbridge Wells NHS Trust, Kent, UNITED KINGDOM.

Aim: This study assessed the need for interrogation of the non-attenuation corrected images (non-AC) in patients with clinical suspicion of cardiovascular implantable electronic devices (CIED) infection investigated with 18FDG-PET/CT.Introduction: 18FDG-PET/CT has a role in the assessment of potential CIED infection. CT artefacts induced by metallic components of CIEDs may cause inappropriate CT-based attenuation correction (CTAC) maps. This can result in overestimation of local tracer accumulation on attenuation corrected (AC) images.Method: We retrospectively reviewed AC and non-AC images of 43 patients referred for assessment of potential CIED infection with 18F-FDG PET/CT. An experienced clinician scored as 'positive' or 'negative', uptake at both the lead and at the CIED.Results: Difference in uptake occurred between AC and non-AC images in 7/43 (16.2%) cases; 7 positive scores were observed in AC images when the non-AC did not show uptake. From the 7 devices with different uptake, 4 were pacemakers, 2 implantable cardioverter defibrillator and one Cardiac Resynchronization Therapy Defibrillator. This supports the suggestion that artefactual CTAC occurs in AC images, which potentially overestimate the level of 18F-FDG uptake around the CIED.Conclusion: Positive uptake at CIED or lead raises concern for local infection. We have shown that significant uptake may be related to CTAC artefact and that the non-AC images should routinely be used in conjunction with the AC images in the clinical reporting of suspected CIED infection to avoid false-positive results.

TP053

Performance of image evaluation due to the difference in the acquisition time using multifocal collimator with 99mTc myocardial SPECT: Evidence from a phantom study

Y. Banno1, M. Onoguchi1, K. Nakajima2, S. Matsuo2; 1Department of Quantum Medical Technology, Kanazawa University Graduate School of Medical Sciences, Kanazawa, JAPAN, 2Department of Nuclear Medicine, Kanazawa University Hospital, Kanazawa, JAPAN.

The goal of this study was to compare image quality and detectability of defects due to difference in the acquisition time using a myocardial phantom with normal or defects. Method: SPECT/CT (Symbia T6, Siemens) equipped with SMARTZOOM collimator (SZC) and torso phantom (Data Spectrum) were used to simulate a normal myocardium and a inferior wall defect. The radioactive concentration of Tc-99m in the normal myocardium (120mL) was 4.17μCi/mL, SPECT was performed with an acquisition time of 3, 6, 9 and 15 sec/view. Acquisition parameters were set as 4.8 mm/pixel, 1282 matrix, 34 views over 208°arc. Reconstruction was performed with no correction (NoAC), attenuation correction (AC) and both attenuation and scatter corrections (ACSC). Visual

evaluation (with 5 grade scores,1=poor to 5=excellent) and quantitative evaluations (%count) were done. Results: Acquisition time of 3, 6, 9 and 15 sec resulted in 8, 16, 24 and 40 counts/pixel respectively. Percent count of the normal myocardium did not depend on acquisition time and was approximately 90% in the anterior wall after each correction. The uniformity score showed a low score (3.0) with < 6-sec acquisition before correction. The acquisition time of > 9-sec improved uniformity scores (≥4) in each condition. A false defect was seen in four o'clock direction with NoAC regardless of acquisition time, which was improved after correction. Defect detectability score was high (4.0) independent of the acquisition time. Improvement of uniformity was not observed with a 3-sec acquisition even after each correction. Conclusion: The image qualities and defect detectability of ≥6-sec was nearly equivalent to a 9-sec acquisition. Image quality, however, was not improved even with 15-sec acquisition. We therefore suggest that ≥16 counts/pixel for average counts were needed for stable image evaluation.

TP054

64Cu-ATSM PET studies: Are radiation protection restrictions required for patients after scan?

S. Pereira, E. Woods, J. John, A. Jacob, C. Abreu, L. Alves, L. Pike; PET Imaging Centre, St Thomas' Hospital, King's College London, London, UNITED KINGDOM.

Aims: 64Cu-ATSM is used in our department as a marker for hypoxic tissue for head and neck cancers. The long half-life of 64Cu (T1/2 =12.7 hours), in comparison with other PET tracers, means that restrictions on patients following discharge may be required. No data currently exists on measured dose-rates from 64Cu patients. The aim of the study was to estimate the radiation doses to family members, ward staff and the general public deriving from patients undergoing 64Cu-ATSM PET studies. Materials and Methods: Radiation dose-rates were measured from 15 patients who were administered with 64Cu-ATSM (activity = 546 ± 51 MBq). Measurements were performed at 0.1, 0.5, 1.0 and 2.0m from patient prior to discharge. Patient contact with critical groups was modelled and combined with the 95th percentile measured dose-rates. The biological half-life was not taken into account to provide the worst-case estimates. The total doses received were calculated for approximately four half-lives of 64Cu. Results: The mean dose-rate coefficient for 64Cu at 1m was (0.020 ± 0.008) μSv/MBq/hr, with the highest dose rate measurements from the right torso, corresponding to location of liver. Calculated doses to all groups for different contact scenarios were less than the recommended dose limit of 1mSv. The maximum calculated dose was 0.9mSv for contact with partner and children <2 years old. Conclusion: The dose-rates at discharge do not result in any legal dose limits being breached. However as best practice, radiation protection advice may be prudent regarding contact with partner, especially if pregnant, and children under 5 years old.

TP055

The Comparison of Lesion Localization Methods in Breast Lymphoscintigraphy

Y. Joonho, H. Gunchul; Samsung Medical Center, Seoul, KOREA, REPUBLIC OF.

Purpose: Breast lymphoscintigraphy is an important technique to present for body surface precisely. In this study, we evaluated several methods of body outline imaging to present exact location of lesions, as well as compared respective exposure doses. Methods: RANDO phantom and SYMBIA T-16 were used. A lesion and an injection site were created by inserting a point source of 0.33 MBq on the axillary sentinel lymph node and 37 MBq on the right breast. The first method for acquiring the image was used by drawing the body surface of phantom for 30 sec using $Na^{99m}TcO_4$ as a point source. The second, the image was acquired with Co-57 flood source for 30 sec on the rear and left side of the phantom, the image as the third method was obtained using a syringe filled with 37 MBq of $Na^{99m}TcO_4$ in 10 mL of saline, and as the fourth, we used a photon and scatter energy of Technesium emitting from phantom. Finally, the image was fused the scout image and the basal image of SPECT/CT using MATLAB® program. We measured radiation exposure and conducted preference of 10 images from nuclear medicine doctors by the survey. Results: TBR values of anterior and right image in the first to fifth method were 334.9 and 117.2 (1st), 266.1 and 124.4 (2nd), 117.4 and 99.6 (3rd), 3.2 and 7.6 (4th), and 565.6 and 141.8 (5th) respectively. And also exposure doses of these method were 2, 2, 2, 0, and 30 μSv. Among five methods, the fifth method showed the highest TBR value as well as exposure dose, whereas the fourth method showed the lowest TBR value and exposure dose. And the fifth method showed the highest score in the survey result. Conclusion: Scout method of SPECT/CT can be useful that provides the best values of TBR and the best score of survey result. Even though personal exposure dose when patients take scout of SPECT/CT was higher than another scan, it was slight level comparison to 1 mSv as the dose limit to non-radiation workers. If the scout is possible to less than 80 kV, exposure dose can be reduced, and also useful lesion localization provided.

TP056

Clinical application of breath-hold PET/CT to improve quantitation of the NSCLC

W. Huang1, S. Tasi1, T. Pan2, J. Tseng1, K. Lin1, T. Yen1; 1Molecular Imaging Center and Department of Nuclear Medicine, Chang Gung Memorial Hospital, Taoyuan, TAIWAN, 2Department of Imaging Physics, The University of Texas M.D. Anderson Cancer Center, Houston, TX, UNITED STATES.

Aim: Impact of respiratory motion to quantitation of the NSCLC has been reported. However, most studies proposed a 30 to 40 sec deep-inspiration breath-hold (DIBH), difficult for patients to comply. Some suggested a single DIBH of 20 sec, which lacked the statistics for quality PET images. In this study, we designed a clinically practical protocol of breath-hold PET/CT to improve quantitation of the NSCLC based on multiple 15-sec DIBHs, and compared the quantitation results with the baseline free-breathing data. Materials and Methods: We recruited a cohort of 16 NSCLC patients in this study. Each patient was injected with 370 MBq 18F-FDG and whole-body PET/CT scanned with free-breathing (FB)1 hour post-injection. The same patient was scanned following the whole-body PET/CT for a series of three DIBH of 15-sec to reduce the impact of tumor motion. The three DIBH scan data were summed to increase the statistics of the study. All scans were conducted on the Siemens Biography mCT scanner. The respiratory monitoring device was the AZ-733V (Anzai Medical) to ensure the breath-hold position was maintained during the DIBH scan by the patient. Comparison of the SUVmax from breath-hold with the baseline free-breathing PET was made. Results: The study included 17 lesions from 16 patients.There were mis-alignments between the CT and the PET images on nine lesions for the FB PET, and one lesion for the DIBH PET. The SUVmax values of the DIBH images were significantly higher than the SUVmax values of the FB whole-body PET/CT scans (4.72 vs. 3.33, P=0.043) Conclusions: Using a series of three 15-second DIBH PET scans can improve the quantitation of NSCLC. The average SUVmax increase was 50.8%.

TP057

The Correlation of PSA and PSA kinetics to 11C-Choline Positron Emission Tomography/Computerized Tomography for recurrent Prostate Cancer after Radical Prostatectomy

L. G. Jordan, III, G. Dimonte, M. L. Burton, R. Haloi, L. J. Rangel, J. C. Hung, B. J. Davis, M. A. Nathan, E. D. Kwon, R. J. Karnes; Mayo Clinic, Rochester, MN, UNITED STATES.

Purpose: We examined the correlation of PSA and PSA kinetics with serial 11C-Choline positron emission tomography/computerized tomography (PET/CT) to detect recurrent prostate cancer (PC) after radical prostatectomy (RP). Methods: Sequential PSA records were analyzed for Mayo Clinic patients (N = 54) who underwent salvage lymph node dissection (sLND) for PC detected by 11C-Choline PET/CT scans (N = 124). Some patients had 2 or more scans (maximum of 7 serial scans). In patients that had serial scans, the scan just prior to (sLND) surgery was used for analysis. The probability of a positive PET/CT scan was ascertained as a function of PSA and PSA velocity (PSAV). For positive lesions, the standardized uptake value (SUV) and tumor volume (TV), as measured on the PET image, were used to calculate a total uptake activity (TUA) as their aggregated product and was then compared with PSA and PSAV. In addition, PET/CT TV was compared to TV as seen on sLND Results: The probability of a positive PET/CT (P+PET/CT) scan was found to increase with PSA to 100% for PSA > 3 ng/mL. For PSA ≤ 3 ng/mL, P+PET/CT increased from 0 to 62% to > 90% for PSAV < 0.5, 0.5-1 and > 1 ng/mL/Yr, respectively. The TUA of the PC lesions was found to increase linearly with PSAV with a correlation coefficient of R = 0.68. Furthermore, the TV's from the PET/CT and the subsequent sLND correlated well (R = 0.68). Conclusion: In this small select group of patients, the five-year experience at the Mayo Clinic showed 11C-Choline PET/CT scans with a 100% detection rate for patients with PSA > 3 ng/mL. The PC detection rate increases with increasing PSAV to P+ PET/CT > 90% for PSAV ≥ 1 ng/mL/Yr. These results suggest that PSA and PSAV are useful correlative markers for tumor size and disease progression as seen on 11C-Choline PET/CT scans. TV as predicted by 11C-Choline PET/CT correlates well with sLND TV measurements. Performing this analysis in the future using a larger number of 11C-Choline PET/CT scans will help to decrease statistical variation and possibly substantiate these findings.

TP058

FCH for detection of parathyroid adenomas in Tc-99m-sestamibi negative patients

B. M. de Jong, M. Postma, S. J. Eelkman Rooda, J. P. Esser, J. M. H. de Klerk; Meander Medisch Centrum, Amersfoort, NETHERLANDS.

Introduction: Preoperative ultrasonography and 123I-sodiumiodide/Tc-99m-sestamibi dual phase subtraction scintigraphy and SPECT/CT are commonly used to localize parathyroid adenomas in patients with hyperparathyroidism (HPT). In some patients both of these imaging techniques turn out to be a false negative. 18F-fluoromethylcholine (FCH) PET/CT is used for the detection of metastases of prostate cancer. Thus far few studies report the use of FCH for detecting parathyroid adenomas. We report six cases showing a

negative (ultrasound and) dual phase subtraction scintigraphy and SPECT/CT with positive FCH PET/CT. Methods: FCH-PET/CT was performed in six patients, five females and one male with a mean age of 64 (range, 54-68 years), clinically presenting with hyperparathyroidism were retrospectively evaluated, with histopathologic examination as the golden standard. All patients underwent ultrasound and dual phase subtraction scintigraphy and SPECT/CT prior to FCH-PET/CT. In patients where dual phase scintigraphy and SPECT/CT were negative patients were referred for FCH-PET/CT. First phase of dual phase subtraction scintigraphy consisted of a dynamic series acquired directly post 750 MBq Tc-99m-sestamibi injection. 35 MBq I-123-sodiumiodide was administered directly after the dynamic series. Second phase started 60 minutes post I-123-sodiumiodide injection with a dual-isotope static series. SPECT/CT was acquired adjacent to the second phase in dual-head 180° configuration, 25 seconds per frame for 64 frames. Patients are scanned up from medulla auris externa (MAE) down to and including the heart, positioned feet-first supine arms down. PET/CT acquisition was performed 30 minutes after the administration of 150 to 300 MBq FCH. Two bed positions of 5 minutes each were made, up from MAE down to and including the liver. Patients are positioned headfirst supine arms down. Results: All six patients showed marked FCH uptake in parathyroid adenomas. Patients were referred for surgery. Five out of six patients have had surgery. Post-surgery histopathologic examination confirmed parathyroid adenoma in these five patients. Conclusion: This study shows that FCH is both highly sensitive and specific for the detection of parathyroid adenomas and can be recommended for patients presenting with a HPT while ultrasound and dual phase subtraction scintigraphy including SPECT/CT are negative.

TP059

Positioning of the arms is essential in reducing artefacts in PET/CT-scans

B. Christensen, P. C. Holdgaard, MD; Vejle Hospital, part of Lillebaelt Hospital, Vejle, DENMARK.

AIM: Investigate the implications of scanning patients who are unable to hold their arms above the head during a PET/CT-scan and to determine which arm position gives least artefacts. Materials and Methods: Retrospective study of all patients PET/CT-scanned with arms down in a recent 2 month period in our department. Arm position was recorded: Alongside of the patient or in front of the patient, and if there were a pillow or blanket in between for comfort. A physician in Nuclear medicine evaluated the studies and scored PET attenuation artefacts and CT-streak-artefacts on a scale from 0 to 5 and location was determined to be in the abdomen or in the spine. Patients were scanned on Philips Gemini 16/64 PET/CT scanners with mainly(89%) a dose modulated low-dose CT (Doseright ACS-Z-dom, 120kV, 50mAs). CT-doses were recorded and compared with arms up. Results: 9% of patients were scanned with their arms down(=55 scans). 24(44%) with the arms alongside, 31(56%) in front and 24(77%) of these had a pillow/blanket in between. Artefacts were visible on 53 scans(96%). Arms alongside the body showed 17 scans(71%) with moderate to severe CT-artefacts compared to 13(42%) with the arms in front($p=0,055$). The localisation of the artefacts depended on the position of the arms($p<0,001$). Arms alongside: 18(75%) showed artefacts in the spine. Arms in front: 5(16%) showed artefacts in the spine, instead artefacts were shown in the abdomen. Only the 4 patients(7%) with elbows outside CT field of view had PET-artefacts($p<0,001$) and arm misalignment alone had no influence. CT-artefacts increased with patient weight($p<0,01$). Men had more CT-artefacts($p=0.017$) compared to women. Patient CT-doses(DLP) increased 34 percent($p<0,001$) with arms down (from 280 to 376 mGy*cm on average in sex matched group) Conclusion: It is important to try and position arms over the head whenever possible to reduce artefacts and patient CT-dose. If arms are kept down CT-artefacts are unavoidable no matter how arms are positioned when using only a low-dose CT. PET attenuation artefacts will always appear if elbows are not in CT field of view and is not dependent on misalignment of arms. It is advisable to take notice of the positioning of the arms if there is a special region of interest e.g. above the thighs on a blanket if the vertebral column is of special interest.

TP060

Fast or Food: a Study on Cardiac FDG Preparation Effectiveness

A. Almeida, N. Gulliver, G. Vivian, A. Eccles, N. Mulholland, B. Corcoran; King's College Hospital NHS Foundation Trust, London, UNITED KINGDOM.

Background and Aim: We recently started cardiac sarcoidosis PET-CT imaging service, and decided to apply the prolonged fasting preparation method to reduce the normal physiological myocardial 18F-FDG uptake, as suggested in the EANM guidelines. We initiated this service evaluation with the aim to assess the effectiveness of the method and patient compliance. Materials and Methods: Eighteen patients referred for a standard PET-CT scan, within an age range from 24 to 79 years old, were included in the study and divided in three groups. The selection occurred from November 2014 to April 2015, with exclusion criteria of diabetes mellitus, known cardiac conditions, dementia, and concurrent steroid medication. The first 10 patients were asked to follow the standard 6h fasting preparation. From these, 5 patients fasted for less than 10h and

were included in the first group. The other 5 patients fasted for between 10 and 15h and were included in the second group. The last 8 patients were asked to follow the prolonged 18h fasting preparation. These patients were included in the third group if they fasted for over 15hours. All patients were administered 4.5MBq/kg ±10% 18F-FDG (max 400MBq), with an average uptake period of 67.5min. A low dose CT and a standard half-body PET acquisition were performed using the GE Discovery 710TOF PET-CT scanner. A quantitative assessment of the SUVmax of background mediastinal blood pool (MBP), background liver and myocardium was carried out using Hermes Hybrid Viewer. We compared the myocardial activity against liver and MBP for each of the three groups of patients, using a method we based using Deauville philosophy (D-score).Results:The average value of the BGL was lowest in the longest fasting group, but there is no statistically significant difference between the groups (P>0.05).The mean SUVmax of the three areas was higher in the 3rd group, although it also is not statistically significant (P>0.05).Observing the D-score values, 4/5 patients with the shortest fast and 4/8 patients with the longest fasting period scored 5 (myocardium uptake much higher than liver). However, 3/8 patients that fasted longer scored 1 (no cardiac uptake), which averages as the lowest D-score, although not statistically significant (P>0.05). Conclusion: The novel D-scores are proposed to measure cardiac FDG uptake.Prolonged fasting as a method of eliminating cardiac activity for dedicated cardiac PET/CT studies is insufficient for reliable imaging.

TP061

Evaluation on Artifacts by Bone Cement of PVP Performed Patients and Usefulness of CT Correction in SPECT/CT Examinations

J. Kim1, H. Park2, J. Lee3, H. Son1, S. Park1; 1Seoul Medical Center, Seoul, KOREA, REPUBLIC OF, 2Shingu College, Seongnam-si, KOREA, REPUBLIC OF, 3Graduate School of Public Health, Yonsei University, Seoul, KOREA, REPUBLIC OF.

Aim: The most commonly performed percutaneous vertebroplasty(PVP) to treat compression fracture is in the increasing trend. But, the bone cement material used in the PVP influences the image quality by forming an artifact in the CT image. Therefore, the objective of the research lies on evaluating the effect the bone cement gives to SPECT/CT image. Materials and methods: The images were acquired by inserting model cement to each cylinder, after setting the background, hot cylinder and cold cylinder to the NEMA-1994 phantom. Non-attenuation correction(NAC), attenuation correction(AC+SC-) and attenuation & scatter correction(AC+SC+) were used for the CT correction method. The mean count by each correction method and the count change ratio by the existence of the cement material were compared and the contrast recovery coefficient(CRC) was obtained. Additionally, the bone/soft tissue(B/S) ratio was obtained by 20 patients who had the PVP. Results : AC+SC- for the quantitative count and AC+SC+ for the contrast ratio were analyzed to be the highest. The rate of mean count increase of NAC, AC+SC- and AC+SC+ when cement existed showed 12.4%, 6.5%, 1.5% at the hot cylinder, 75.2%, 85.4%, 102.9% at the cold cylinder about phantom and 33.1%, 41.4%, 63.5% at the fracture region, 53.1%, 61.6%, 67.7% at the normal region about clinical image. CRC and B/S ratio implying the contrast ratio were improved in the order of NAC, AC+SC-, AC+SC+ when cement existed showed 6.4, 6.8, 8.0 at the hot cylinder, 0.9, 0.8, 0.9 at cold cylinder, 20.5, 38.0, 70.0 at the fracture region and 6.6, 13.3, 21.2 at the normal region. Conclusions : The use of AC+SC- in the spine SPECT/CT examination of PVP performed patients drastically increases the image count and enables a high density image of the lesion. But it also increases the noise count of the soft tissue and the scatter area as well along with the effect of the bone cement. Therefore, it is considered to be useful in a clinical diagnosis if the application of AC+SC+ that improves the contrast ratio is combined.

TP062

Whole body bone SPECT: aspects of methodology

K. Kukuts, I. Fordzyun, A. Forgács, S. Barna, I. Garai; Scanomed Ltd., Debrecen, HUNGARY.

Aim: The basic limitations of diagnostic imaging with radionuclides are the amount of radioactivity administered to the patient, the physical and biological half time of the radionuclide and the duration of the examination. With these conditions the primary aim is to maximize the information content and to increase the diagnostic value. As a large number of bone scintigraphies are performed, the duration of the examination and the availability of the radionuclide are both critical points of the management of these examinations. Routinely a bone scintigraphy has a 15 minute acquisition time, followed by one or multiple regions multi-FOV SPECT/CT if necessary for the exact localisation with a 16 minute additional acquisition time. Making decision to require further SPECT/CT takes at least 5-10 minutes additionally, depending on the availability of the specialist. Our aim is to define a whole body bone SPECT acquisition protocol on a 3-headed SPECT/CT camera to reduce the total acquisition time and the radionuclide demand compared to conventional bone scintigraphy. Method: In case of 30 patients after the conventional bone scintigraphy we performed a whole body SPECT acquisition on a 3-headed Mediso AnyScan SC camera. Usually the examination contains 5-6 FOVs depending on the height of the patient, 5 minute acquisiton time per bed position, so the total examination

time is 25-30 minutes, which is the same as the acquisiton time of a whole body bone scintigraphy and a SPECT/CT of one region. The iterative image reconstruction was performed by using the Interview XP software. A nuclear medicine specialist identified the lesions on both the anonimized bone scintigraphy and the 3D whole body SPECT images. Results: The acquisition time on a 3-headed camera is comparable to the acquisition time of a common conventional bone scintigraphy, with increased diagnostic value. After the optimalization of the reconstruction there was no significant difference between the two methods regarding the number of the bone lesions identified. There is the possibility of performing an additional low-dose CT to gain more diagnostic information in equivocal cases. Discussion: Whole body SPECT examination can be a good alternative of whole body bone scintigraphy. At nuclear medicine departments with a large number of patients this examination method is able to reduce the daily total acquisition time and radionuclide demand.

TP063

Evaluation of 68Ge-68Ga Generator and Synthesis Module efficiency in the procedure of 68Ga-DOTATOC labelling

L. Pavanello, F. Sciume', M. Zuffante, D. Grigolato, E. Carmagnani, M. Ferdeghini; Nuclear Medicine AOUI, Verona, ITALY.

AIM: To evaluate efficiency of 68Ge-68Ga Generator and Synthesis Module in the procedure of peptide DOTATOC labelling. The evaluation was carried by comparing the radiation activity between expecteds and obtained values in 38 synthesis. MATERIALS AND METHODS: 68Ge-68Ga Generator calibrated 1110MBq to 4 April 2014 (IDB Holland), Synthesis Module (Scintomics GRP), cassettes for peptide labelling (ABX) and peptide DOTATOC (ABX) are used. It was considered the time from 1 April 2014 and 30 March 2015. The comparison of radiation activity between expected and obtained values considering that synthesis procedure has a duration of 36 min, elution is performed 6 min after the start of the procedure, the measurement of 68Ga radiation activity is performed 34 min after the elution. Comparative tables are created considering that the radiation activity at the time calibration of the 68Ge-68Ga Generator (with half-life of 288 days for 68Ge) has a linear decay and radiation activity in the Synthesis procedure has a loss to 25% compared to the expected value because it is measured 34 min after the elution of the Generator. Synthesis procedure was performed every seven days for two consecutive days. 68Ge-68Ga Generator has not eluted daily and only one elution was made 24 hours before the first procedure of the week. The activity was measured using always the same calibrator and vials size. In 37 cases the synthesis performed 24 hours after the first procedure. RESULTS: Activity obtained in the synthesis procedure showed gradually decreased than expected during the 52 weeks. Values decreased of 95% after the 2nd week reaching 65% of values in 52th weeks. 68Ge-68Ga Generator inactivity for periods over than seven days, resulted in a loss of radiation activity in synthesis (10-15% greater than expected). In the 37 cases of second synthesis, was measured a higher radiation activity of 3-5% compared to the value of the first synthesis obtained the day before. CONCLUSION: Due to non-elution daily of 68Ge-68Ga Generator showed that the decrease of radiation activity obtained was higher than expected. This work demonstrated the importance of a periodic and constant elution of the Generator independently of the number of synthesis. It was also showed the importance of synthesis execution every 24 hours to increase the quantity of radio-labeled product.

TP064

The devil is in the details…. Radioactive Waste disposal changes

C. Vroonland, M. Sonneborn, L. Janssen-Pinkse; Antonie van Leeuwenhoek Hospital, Amsterdam, NETHERLANDS.

Aim: Two years ago several of our waste bins were returned to us by the Waste Disposal Facility as they were “still radioactive”. The facility had upgraded their radiation detectors and now maintained a zero tolerance limit instead of the National exemption limit. Our department maintains an even lower exemption limit of < 2x background. We were thus required to review and adjust our radioactive waste procedures or be forced to dispose of these (and future) bins as radioactive waste at a much higher cost. Our aim was to clarify and optimise our radioactive waste procedures to ensure that our waste will not be returned to us again. Method and Materials: Our Radiation Safety officers determined that the returned waste bins were indeed very mildly radioactive and below the National exemption limit. Radiation measurements within our hospital’s radioactive waste storage area revealed that the background measurements were not above normal. The only abnormality was the fact that the waste bins were still radioactive despite having been sealed more than 6 months previously. It became clear that a long-lived isotope was present. Additional examination (spectrometry) showed that the bins were emitting radiation consistent with 154Europium which is now known to be a manufacturing impurity in the production of 153Sm-EDTMP. Results: A separate disposal procedure was set up for 153Sm-EDTMP vials, injection waste and possible contaminated items. To ensure no other impurities are discovered this way, all new radiopharmaceuticals are now left to decay separately. These are then measured at periodic intervals for radioactive impurities. This led to a complete overhaul of our radioactive waste

management procedures, including periodic wipe testing within the department to check for contamination in unexpected area's (such as keyboards, light- and door switches, dictaphones etc). Also a new radioactive waste procedure has been implemented for long lived radiopharmaceuticals (154Eu and now also 68Ge) in the form of COVRA waste bins. This company collects, processes and stores radioactive waste with a long half-life. Conclusion: The waste procedures within our department have been mapped and altered to ensure that even mildly radioactive waste is no longer sent to the Waste disposal facility.

TP065

Static Myocardial Perfusion Imaging using denoised dynamic Rb-82 PET/CT scans

M. N. M. Petersen, C. M. Hoff, H. J. Harms, K. Bouchelouche, J. Sørensen, L. P. Tolbod; Dept. Nuclear Medicine & PET-Centre, Aarhus University Hospital, Aarhus N, DENMARK.

Introduction: Relative and absolute measures of myocardial perfusion are derived from a single 82Rb PET/CT scan. However, images are inherently noising due to the short half-life of 82Rb. We have previously shown that denoising techniques can be applied to dynamic 82Rb series with excellent quantitative accuracy. In this study, we examine static images created by summing late frames of denoised dynamic series. Method: 47 random clinical 82Rb stress and rest scans (27 male, age 68+/- 12 y., BMI 27.9 +/- 5.5 kg/m2) performed on a GE Discovery 690 PET/CT scanner were included in the study. Administered 82Rb dose was 1110 MBq. Denoising using HYPR-LR or Hotelling 3D algorithms was performed as post-processing on the dynamic images series. Static series were created by summing frames from 2.5-5 min. The image data was analysed in QPET (Cedars-Sinai). Relative segmental perfusion (normalized to the hottest pixel) was compared in order to assess whether a correlation between original image data and denoised image data could be found. In addition to this, correlations for TPD, Extent of defect and summed defect scores (SSS, SRS and SDS) were investigated. The data was analysed using linear regression and Bland-Altman analysis. Results: For HYPR-LR, a good correlation was found for relative segmental perfusion for both stress (y=1.007x+0.313, R2=0.98) and rest (y=1.007x+ 0.421, R2=0.96) scans with negative bias of -0.79±1.44 and -0.90±1.63, respectively. Correlations for SSS (R2=0.94), SRS (R2=0.92), SDS (R2=0.89), TPD (stress, R2=0.99; rest, R2=0.97) and Extent (stress, R2=0.99; rest, R2=0.96) were likewise excellent. For Hotelling 3D, correlations were slightly lower than for HYPR-LR: relative perfusion (rest, y=1.016x-0.131, R2=0.95; stress, y=0.982x+3.165, R2=0.87), SSS (R2=0.90), SRS (R2=0.88), SDS (R2=0.75), TPD (stress, R2=0.98; rest, R2=0.93) and Extent (stress, R2=0.97; rest, R2=0.90).Conclusion: Static 82Rb series for quantifying relative myocardial perfusion can be created by summing denoised late frames of dynamic 82Rb series. Excellent quantitative accuracy was found for both HYPR-LR and Hotelling 3D algorithms. This enables either an improvement in image quality or a reduction in administered dose. Further studies are required to define the optimal tradeoff between administered dose and image quality.

TP066

RubiShort: Reducing scan time in 82Rb heart scans to minimize movements artifacts

J. Madsen, K. J. Vraa, H. J. Harms, K. Bouchelouche, J. Frøkiær, J. Sørensen, L. P. Tolbod; Dept. Nuclear Medicine & PET-Centre, Aarhus University Hospital, Aarhus N, DENMARK.

Aim: Relative and absolute myocardial blood flow (MBF) can derived from a single 82Rb PET/CT scan using list mode data to extract both static and dynamic PET series. However, patient movement and changes in breathing pattern, especially during pharmacological stress, reduce the quality of the scans and are known to introduce artifacts in 10-15% of all scans. By reducing scan time from 7 min. to 5 min, we expect to reduce the frequency of motion artifacts. This is, however, at the cost of information used for MBF calculation and count statistics in the relative blood flow images. We set out to examine if a reduction of scan time would affect the accuracy of the examination. Method: Both stress and rest 82Rb scans from 11 random clinical patients without motion artifacts were selected. Using list mode data, dynamic series from 0-7 min (standard) and 0-5 min (short) after 82Rb infusion as well as static series from 2.5-7 min (standard) and 2.5-5 min (short) after 82Rb infusion were reconstructed. Data was analyzed using QPET (Cedar Sinai). Absolute (MBF, 17-segment AHA-model) and relative (%Extend, %Reversible and Total Perfusion Deficit (TPD), 5 segments) parameters were compared by using scatter plots and linear regression. Results: Excellent correlation between the 7 min. and 5 min. data was found for absolute MBF (y=1.014x, R2=0.98). For all relative parameters obtained from the static reconstructions, excellent correlation was likewise observed between 7 min. and 5 min. reconstructions (%Extent: y=1.013x, R2=0.98; %Reversible: y=1.008x, R2=0.95; TPD: y=1.000x, R2=0.99). Conclusion:, Scan time of myocardial perfusion scans using 82Rb can be reduced from 7 min. to 5 min. without loss of quantitative accuracy. Since patient motion is frequent in the last minutes of the scans, scan time reduction is likely to reduce motion artifacts.

TP067

Comparison of absolute myocardial blood flow with 13N-NH3 cardiac PET determined by different compartmental models and softwares

B. Olsson1, S. Akil1, F. Hedeer1, H. Engblom1, C. Hindorf2; 1Clinical Physiology and Nuclear medicine, LUND, SWEDEN, 2Radiation Physics, LUND, SWEDEN.

Aim: The absolute myocardial blood flow (MBF) can be determined from a dynamic acquisition that starts simultaneously with the injection of 13N-NH3. Activity in blood and in the myocardium as a function of time after injection serve as input functions to the compartmental model applied for the calculation of the MBF. Several softwares and compartmental models have previously been developed for the calculation. The aim of this study was to compare the MBFs from different softwares and compartmental models. The intraobserver variability was also evaluated. Methods: Five patients diagnosed with coronary artery disease were examined with 13N-NH3 at rest and in stress (10 cardiac PET studies). A listmode acquisition was performed after injection of 555 MBq 13N-NH3. A dynamic study with a duration of 10 minutes (12 images for 10s, 6 images for 30s, 2 images for 60s and 1 image for 180s) were reconstructed with OSEM from the listmode acquisition. The global MBF was determined by the deGrado, Hutchins and Krikovapich compartmental models in the Carimas software (Turku, Finland) and with the Hutchins compartmental model in the syngoMBF software (Siemens). Each evaluation was performed three times to assess the intraobserver variability (determined as (max-min)/mean for each cardiac PET study). Results: The mean value for the first of three evaluations of all patient studies was MBFdeGrado,Carimas=1.8ml/min-g, MBFHutchins, Carimas=1.9 ml/ml-g, MBFKrivokapich,Carimas= 2.3 ml/min-g and MBFHutchins,syngo =1.7ml/min-g. The intraobserver variability, reported as the mean of the percentual deviation, was 9% for deGrado,Carimas; 15% for Hutchins,Carimas; 7% for Krivokapich,Carimas and 8% for Hutchins,syngo.ConclusionsThe mean of the global myocardial blood flow varied between 1.7 and 2.3 ml/min-g for the compartmental models and softwares that were evaluated. The Krivokapich compartmental model in Carimas showed the smallest intraobserver variability but the mean myocardial blood flow deviated from the results from the other methods. The Hutchins compartmental model in syngo showed a smaller intraobserver variability than the same model in Carimas, whichmight be explained by a more automatic image processing in the syngo software.

TP068

Assessing left ventricular dysfunction by the use of three distinct molecular imaging techniques

J. Reis1, **L. Cunha**1, P. Costa1, D. Neves2, T. Oliveira2, A. Ferrer-Antunes2, M. Faria Joao2, L. Metello1; 1Nuclear Medicine Department, ESTSP.IPP, Porto, PORTUGAL, 2Nuclear Medicine Department, DIATON SA, Leiria, PORTUGAL.

AIMS: Left ventricular dysfunction might be assessed using distinct molecular imaging modalities. The most relevant are first pass radionuclide ventriculography (FPRV), multigated radionuclide angiography (MUGA) and gated blood-pool SPECT (GBPS) and are very often used for monitoring chemotherapy-related cardiomyopathy. This work aims to correlate these three molecular imaging techniques. METHODS: 400mg of potassium perchlorate and 20 μg/kg of stannous agent were administered to a group of 30 patients (35-65 years old) 20 minutes before the iv bolus injection of 740-925 MBq of 99mTc. First pass images were acquired in anterior projection immediately after 99mTc injection, in a total of 1.500 frames with 25 msec/frame each. Fifteen minutes later, MUGA images were acquired in left anterior oblique projection for a minimum of 600 cardiac cycles using 24 bins/cycle. Finally, GBPS images were obtained using 24 bins/cycle and 20 cycles/projection in a total of 60 projections acquired over 180° in step-and-shoot mode. All images were acquired with a double-headed gamma camera, equipped with LEHR collimator. Left and right ventricular ejection fraction (LVEF and RVEF) as well as ventricular volumes were calculated. RESULTS: The first subgroup of 14 patients were analyzed. Global LVEF assessed by GBPS showed a good correlation with conventional planar methods (correlation coefficient = 0.87). The average LVEF obtained by planar techniques was 59.7 ± 9.7%, whereas for GBPS was 66.2 ± 10.4%. The correlation coefficient between MUGA and FPRV was 0.92. The average LVEF obtained by FPRV was 56.3 ± 7.5%. The correlation coefficient between FPRV and GBPS was 0.81. CONCLUSION: Results obtained so far suggest a better correlation for LVEF between FPRV and MUGA techniques in comparison to GBPS. Moreover, GBPS provides additional information, since it allows the assessment of RVEF and wall motion, which can be of value in patients with congestive heart failure. The work is still ongoing and the final subjects will be evaluated shortly, with their contribution for the results being added subsequently. Final results will be presented and discussed using the adequate statistical tools.

TP069

Strategies to reduce Radiation Dose from Myocardial Perfusion Imaging:

A. Ghilardi, G. Medolago, L. Pozzi, M. Caloiero, C. Bianchi, E. Iampietro, A. Bruno; Papa Giovanni XXIII, BERGAMO, ITALY.

Aim: Nuclear Cardiology plays an essential role in the evaluation, management in coronary artery disease[CAD]. Indeed it demands ongoing re-evaluation of myocardial perfusion imaging[MPI] to improve patient care: accurate definition of candidates [appropriateness], optimization of MPI protocol and upgraded technologies to give the lowest possible radiation dose upholding high accuracy. Great challenge is to choose the proper radiotracer, acquisition-processing procedures for each patient to provide accurate and clinically meaningful information to physician. Methods: Patient selection is the primary and most relevant issue of handling radiation exposure from MPI and needs appropriate use criteria[AUC]. When MPI is clinically appropriate the benefits in terms of advance clinical decision making and care are greater than any potential risk from radiation exposure. Once MPI is considered the best diagnostic procedure next step is choosing the best protocol-stressor test to be used. Tc99m-perfusion tracers are preferable for availability, imaging quality, lower radiation dose: anyway injected dose must be adjusted for patient weight. Normal Stress imaging as first step allows to avoid rest perfusion: the accuracy of single stress protocol is unequivocally high. IQSPECT, using cardiac-focusing collimator, offers increased sensitivity with similar resolution, compared to LEHR collimator, resulting in reduced administered dose, shorter acquisition time. With CZT detectors, having the greatest sensitivity, energetic and spatial resolution, dosimetry is further reduced: dynamic studies can also be acquired to obtain quantification of blood-flow and coronary reserve. Iterative reconstruction filtering [with resolution recovery] allows to obtain very good quality images also with lower count density, demonstrating to be a valid tool to use low-dose protocol. Current-generation PET 3D-scanners are equipped with advanced hardware-software capabilities of high resolution[2mm], low dose imaging [time-of-flight, high-definition iterative reconstruction and motion-frozen imaging]. Single-Stress PET MPI [NH13, Rb82] with myocardial blood flow and coronary reserve assessment can be performed with less than a 1-mSv radiation dose. With the availability of F18 perfusion agents PET is going to be MPI procedure of choice. In our laboratory of Nuclear Cardiology since July-2012 we've been using IQSPECT with excellent results, obtaining significant reduction of radiation dose to patient, acquisition time, maintaining very good quality images and not least appropriate selection of patients to be studied. Conclusions: MPI studies should be performed in appropriate patients using short-lived perfusion tracers and using all possible and available measures to minimize radiation exposure, so that the benefits of the diagnostic and prognostic information outweigh the risk of radiation exposure.

TP070

Impact of attenuation and scatter corrections in the quantification of SPECT brain images

S. Chaves1, T. S. Vieira1, J. G. Pereira1, F. Caramelo2, N. C. Ferreira2; 1Centro Hospitalar S. João, Porto, PORTUGAL, 2Instituto Biomédico de Investigação de Luz e Imagem (IBILI – FMUC), Coimbra, PORTUGAL.

Aim: One of the most challenging tasks in Nuclear Medicine (NM) is to quantify the activity concentration of a radiopharmaceutical in acquired images. The emergence of multi-modal equipment combined with the evolution of fully 3D image reconstruction algorithms, that demand correction techniques of different physical phenomena, have been contributing to derive better solutions for the quantification problem.Our purpose is to evaluate the effect of attenuation correction (AC) and scatter correction (SC) in SPECT quantification of brain images. Materials and Methods: We determined the system calibration factor using a cylindrical phantom filled with a uniform concentration of activity, for two isotopes: 123I and 99mTc.To quantify the activity concentration, two phantom experiments were performed. The first trial was carried out using a Jaszczak phantom with six spheres of different diameters (4.2 - 47mm) filled with the same activity (0.5 MBq/cm3 for 123I and 0.8 MBq/cm3 for 99mTc). The second test was performed using an anthropomorphic striatal brain phantom filled with water: the striatal nuclei with a concentration of 0.2 MBq/cm3 for the two isotopes and without background. For the SPECT/CT (Infinia-Hawkeye 4, GE®) were used LEHR collimators; rotation of 360°; 120 projections, 40 seconds/projection; 128x128 matrix; 20% energy window centred on the isotope photopeak. OSEM reconstruction method was adopted and all images were submitted to CT-based AC and SC by dual energy window (defining a second window - 130 keV +/- 10% for 123I, 120 keV +/- 5% for 99mTc). After image reconstruction, VOI's were drawn around spheres and basal nuclei (AMIDE®), guided by CT, to obtain the total counts (decay corrected). The concentration of the corresponding activity was calculated using the calibration factor. It was determined the relative error between real concentration and calculated activity. Results and Conclusion: The activity was underestimated by at least 65% if no correction was applied, in both phantom experiments.In the

brain phantom, when applying AC and SC, the mean relative error in quantifying radioactivity concentration in absolute terms was 45% for 123I and 35% for 99mTc. Otherwise, for the Jaszczak phantom, the mean relative error of estimated spheres activity was 4% for 123I and 1% for 99mTc, for spheres with higher volumes. For both isotopes, we observed an increase in the quantification error with decreasing sphere volumes. Attenuation and scatter corrections are important to SPECT absolute quantification, and for small structures other additional corrections might be needed to achieve better results.

TP071

Validation of a New Reference Values's Database for Semiquantification of 123I-FP-CIT SPECT scans in one Nuclear Medicine Department

M. Elias1, M. Queiroga1, D. Silva1, J. Serrano2, J. Madrid2, E. Carolino1, E. Sousa1; 1Escola Superior de Tecnologia da Saúde de Lisboa, Instituto Politécnico de Lisboa, Lisbon, PORTUGAL, 2Nuclear Medicine Department, Hospital Infanta Cristina, Badajoz, Spain, Badajoz, SPAIN.

Introduction: Reference adaptaded values of healthy and pathological controls for quantification the Dopamine Transporters (DAT) with 123I - FP-CIT have become an important tool in the diagnosis and evaluation of parkinsonian syndromes. Aim: The aim of this study was evaluate the discriminate capability of a department's adapted database reference's values of healthy controls for DAT with 123I - FP-CIT, this database is named DBRV. The reference values are adapted to Nuclear Medicine Department's protocol and population of Infanta Cristina's Hospital located in Badajoz. Subjects/Methods: It was used a semiautomatic method for segmentation and posterior calculi of binding potential in dopamine transporters (DAT) in striatum structures and in a nonspecific binding region, of the 30 healthy controls of the DBRV. All exams were acquired by EANM's Guidelines protocol, and processed three times for one operator, average values were used. Average and standard deviation ($x \pm \delta$) values were calculated for the following ratios: left and right Caudate nucleus/ Occipital respectively (A) and (B); left and right Putamen/ Occipital respectively (C) and (D); striatum/Occipital (E); left striatum/occipital (F), right striatum/occipital (G), Putamen/ nucleus caudate (H). These values where calculated and stablished new reference values for infanta Cristina's Hospital population between 60 and 75 years. For validation purposes two database of thirty patients each: database of healthy controls (DBVGIIH), and database of subjects with diagnosed Parkinsonian Syndromes (DBVGIIIP), were processed using the same protocol, and its results where compared with the ones of DBRV. Assessment Control Charts and Receiver Operating Characteristic Curves (ROCC) were calculated.Results: The DBVGIIH results were within the new reference values for healthy subjects; the DBVGIIIP results were below the new reference values for healthy subjects. By the ROCC assessment for each ratio the values of area under the curve (AUC) it was obtained the following values: A (AUC= 0.81); B (AUC= 0.79); C (AUC= 0.91); D (AUC= 0.93); E (AUC= 0.88); F (AUC= 0.86); G (AUC= 0.87); H (AUC= 0.87), the ROCC curve discriminate well, AUC significantly different from 0.5, $p<0.0001$. Discussion/Conclusion: From the ROCC analysis it's possible to conclude that the DBRV and its reference values newly created have good discriminative capability between healthy controls and subjects with Parkinsonian Syndromes. The new database is an adapted and improved tool for clinical use assessment.

TP072

PET- CT Determinants of Achievement Experience

C. D. R. Oliveira1, C. Pacheco1, A. Grilo1, L. Vieira1, L. Vieira2, D. Faria3, D. Faria4, J. C. A. Farto5, M. C. Vázquez5; 1Escola Superior de Tecnologia da Saúde de Lisboa, Lisboa, PORTUGAL, 2Faculdade de Ciências da Universidade de Lisboa, Lisboa, PORTUGAL, 3Hospital Lusíadas do Porto, Porto, PORTUGAL, 4Faculdade de Engenharia da Universidade do Porto, Porto, PORTUGAL, 5Instituto Tecnológico de Serviços Sanitários, MD Anderson Cancer Center, Madrid, SPAIN.

An inadequate provision of information on diagnostic tests in daily practice of a Nuclear Medicine Service, can generate the feeling of fear of the unknown on the patient, and thereby increase the anxiety level of the same. Nuclear Medicine Technologist has to develop the gift of perceiving when a patient is anxious in his daily life, if anxiety is inherent to his medical situation, or if it's related to a pathologic diagnosis. Many factors can induce anxiety on the patient, e.g. contact with radiation.Injection of the radiopharmaceutical is one of the main causes of anxiety because of everything that is involved, as the patient has to be kept away within a certain distance from his family and people who surround him during the day, especially pregnancy women and children.High levels of anxiety can also result in a low image quality as a result of patient motion during acquisition or as a result of muscular uptake of the radiopharmaceutical. On the other hand, it can decrease the global comfort of the patient as he may feel dissatisfied with the health care which he received during his exam.The aims of this study are to evaluate the subjective perception of patients about the exam, understand if the information given to the patient was adequate and identify the factors that decrease or increase the anxiety state.Material and methods: 60 patients of both genders, grouped by age groups 18-39, 40-59 and 60-79 and 80+. The study will exclude patients with significant communication impairments that would affect their ability to respond to the interviewer's questions, patients with a history of psychiatric illness , patients in poor condition who were unable to cooperate, patients who were illiterate and had neurological

problems. Evaluation of the state of anxiety before and after the examination, based on the results of a questionnaire and STAI forms [State Anxiety Inventory (STAI-S): evaluating how the patient feels in that particular situation or moment, and Trait Anxiety Inventory (STAI-T): evaluating how the patient feels independently of the situation or condition at that moment].Results/Conclusions: An appropriated communication between the Nuclear Medicine Technologist and the patient helps to decrease anxiety levels on the patient. Informed patients on the procedures related to the exam itself are quiet and are more cooperative.Note: This work was supported in part by Fundação para a Ciência e a Tecnologia - Portugal (project UID/BIO/00645/2013)

TP073

Comparison of GFR estimation methods in chemotherapy Monitoring

V. Rangarajan, V. Kumar, N. Purandare, S. Shah, A. Agrawal, J. Bajpai; Tata Memorial centre, Mumbai, INDIA.

INTRODUCTION: Simple and accurate determination of the Glomerular filtration rate (GFR) in chemotherapy monitoring still poses a challenge. Our goal was to compare various methods and find out a simple, cost effective, precise and accurate method for GFR estimation. OBJECTIVES OF STUDY: Primary objective: Comparison of standard two sample plasma sampling method (PS2) to gamma camera Gates method (GT) by retrospective analysis of data of patients receiving chemotherapy. Secondary objective: - Comparison of other serum creatinine based formulae methods with PS2 method for estimation of GFR. METHODS: GFR estimation was done in patients diagnosed of Osteogenic sarcoma at baseline (prechemotherapy) and post 4 cycles of Cisplatin based chemotherapy using PS2, GT (with 99mTC DTPA) and other serum creatinine based methods like Cockcroft-Gault (CCG), MDRD, Schwartz (SHW), and Counahan-Barrat (CB). Gold standard PS2 was compared with all the other methods using paired T test, linear regression and coefficient of correlation. RESULTS: 37 patients had pre and post 4 cycle chemotherapy GFR data, which met all the inclusion and exclusion criteria with a median age of 18 years. There was statistically no significant change in the mean difference between the PRE (PR) and POST (PO) 4 cycles of GFR values either by standard PS2 or by test GT method. The mean difference and p values are PR PS2 - PO PS2 = 1.438, (p= 0.819), and PR GT - PO GT=-2.13, (p= 0.575). Whereas the other test methods based on serum creatinine, body weight and height, (CCG, MDRD, SHW, and CB) showed significant change (increase) in GFR. The mean difference and p values are - PR CG - PO CG = -17.7, (p=0.00), PR MDRD - PO MDRD= -33.54, (p=0.00) PR SHW - PO SHW= -23.14, (p=0.00), PR CB - PO CB= -19.94, (p=0.00). Similar results were also observed in individual pediatric and adult groups. CONCLUSION: GT can be used as a reliable substitute for PS2 in estimating the change in GFR as its results are similar to that of PS2 in adults as well as in pediatric age group. The formula methods based on serum creatinine are not as reliable as PS2 in accurately estimating the change in GFR.

TP074

Therapy planning and dose prescription in radioiodine-131 therapy for hyperthyroidism using radioiodine-123 SPECT/CT imaging

K. Hanaoka, M. Hosono, M. Otsuka, Y. Asai, M. Okumura, K. Ishii, T. Murakami; Kinki University, Osaka Sakai-city, JAPAN.

Objectives: Functional thyroid weight is one of the most important factors for prescribing radioiodine doses in iodine-131 (I-131) therapy for hyperthyroidism. Thyroid weights are usually determined with planar scintigraphic methods such as Allen's method, which may include statistical deviations especially in case of atypical thyroid morphology. In this study, we assessed the usefulness of SPECT/CT in the measurement of functional thyroid weight for radioiodine therapy. Methods: Forty patients with Graves' disease who underwent I-131 therapy along with preceding radioiodine-123 (I-123) planar scintigraphy and SPECT/CT scan between February 2010 and November 2014 were enrolled in this retrospective study. On planar images, thyroid weight was measured using Okubo's (2D) method, a modified Allen's method for Japanese population. On SPECT/CT images, volumetric regions of interest (VOI) were placed over the thyroid on SPECT images by referring to CT images. These measurements were performed by 4 operators. Thyroid weights estimated by these methods were analyzed and compared by regression analysis and Bland-Altman Plot. Results: Variations among 4 operators were 4.50% and 11.22% for the SPECT/CT and 2D methods, respectively. In the patients, a good correlation was observed between the two methods ($r=0.98$, $p<0.01$) with a difference of 4.69±16.1%. Bland-Altman Plot revealed no systematic errors between the SPECT/CT and 2D methods. However, 7 patients showed differences of over 20% in the estimated thyroid weights between the two methods, and peculiar findings such as a heterogeneous uptake, an ectopic uptake and a non-functional mass were identified on SPECT/CT fusion images and were thought to be one of the causes of the discrepancy. In terms of change in dose prescription, the prescribed I-131 dose in capsules was increased in 6 patients and was decreased in 4 using the SPECT/CT method. Conclusions: Our method using SPECT/CT is one of the optimal ways to determine functional thyroid weight. This method navigates an operator-

reproducible measurement by adding morphological information to functional images.

TP075

Emerging role of Bremsstrahlung SPECT/CT imaging in yttrium-90 radiosynovectomy

A. Atabaki, R. Mansberg, R. Russo, S. Gunaratne; Concord Hospital, Sydney, NSW, AUSTRALIA.

BackgroundYttrium-90 radiosynovectomy has been a therapeutic option in the management of monoarticular proliferative arthropathy for decades. Post therapy imaging has been used to confirm successful administration of tracer to the affected joint and to image extravasation at the joint, draining lymph nodes and the liver, however the benefit has been limited by the poor imaging characteristics of yttrium-90AimsTo evaluate the role of Bremsstrahlung SPECT/CT imaging in yttrium-90 radiosynovectomy in confirming successful therapeutic administration and assessment of extravasation.MethodsPatients referred for radiosynovectomy were assessed and treated in the conventional manner. Following intra-articular in administration of yttrium-90 patients were arrested in the supine position for 72 hours. Regular planar images were performed of the treated joint, draining lymph nodes and the liver. In addition Bremsstrahlung SPECT/CT of the treated joint was performed and the images were compared with the planar images.ConclusionBremsstrahlung SPECT/CT imaging in yttrium-90 radiosynovectomy may benefit patients undergoing this therapy by more accurate imaging of treated joints. This may result in better and more specific localisation of extravasation which could benefit patients by instituting earlier and more specific therapy.

TP076

Nuclear Medicine therapies applied to small animals

D. F. F. Ribeiro, F. Lucena; Escola Superior de Tecnologia da Saúde de Lisboa, Lisbon, PORTUGAL.

Introduction - Nuclear Medicine (NM) procedures have been used in the field of Veterinary Medicine (VM) for some years, with a recent increasing interest in Radionuclide Therapy (RNT), especially in hyperthyroidism and bone metastasis. Aims - Describe RNT applications in VM, with focus on well established procedures for small animals. A new therapeutic approach with 177Lu-DOTMP will also be included. Methods - A systematic review was conducted based on key-words, “Radioactive iodine therapy”, “Iodine 131 therapy”, “Radioiodine treatment”, “hyperthyroidism", "therapies with radiopharmaceuticals", "Palliation treatment with radiopharmaceuticals", "radionuclide therapy”, “veterinary”, “153Sm-EDTMP”, “dogs”, "177Lu-DOTMP”, “animals” and “small animals", and relevance of the content. Twenty articles were included and the analysis was focused on precautions prior and post therapy, therapeutic procedures and adverse effects of therapies with 131I, 153Sm-EDTMP and 177Lu-DOTMP. Results - The research included review articles (N=2; 15.38%), experimental articles (N=6; 46.15%), official documents (N=3; 23.08%) and official webpages (N=2; 15.38%). 131I therapy represents the most common treatment in VM due to its effectiveness and less disadvantages. Prior to the therapy it is advisable to determine thyroxine blood concentration, blood pressure and renal and cardiac function. Animals should by isolated no less then 7 days, in a quiet environment with shielded cages. The administered activity may be determined by: fixed activity; based on a scoring system; or by kinetic models. After the therapy renal function should be monitored. Regarding bone metastasis, 153Sm-EDTMP and 177Lu-DOTMP are being used as they represent attractive therapies although 177Lu-DOTMP seems to be more effective since it doesn’t deteriorate the urinary tract. Prior to the therapy, erythrocytes, leucocytes and platelets levels should be evaluated and a bone scintigraphy is also advisable. The activities for each radiopharmaceutical should be determined based on the animal’s weight, and motorization should be provided until 14 days post therapy. Although none of these two therapies are considered for the first therapeutic approach, they are often used as palliative treatment and might potentiate the effects of radiotherapy. Conclusion - RNT allied with simple therapeutic procedures provides an effective therapeutic approach in VM, giving the animals better chances of survival, with low incidence of adverse effects. Although 131I is the better established RNT, both the 153Sm-EDTMP and 177Lu-DOTMP appear promising and are slowly gaining their way into the VM community.

TP04 - Tuesday, October 13, 2015, 8:00 AM - 9:30 AM, Hall 3 – Poster Exhibition

Technologist Poster Session 4

TP077

Comparative retrospective study of peptide receptor radionuclide therapy (PRRT) with Y-90-DOTATOC and Y-90-DOTATATE in neuroendocrine tumours (NET)

M. Marx, H. Plagge, C. Winkler, Y. Zhao, U. Lützen, M. Zuhayra; Universitätsklinikum Schleswig-Holstein, KIEL, GERMANY.

Aim: Peptide receptor radionuclide therapy (PRRT) for treatment of metastasized neuroendocrine tumours (NET) can be performed with Y-90- or Lu-177-labelled DOTA-peptides.

Usually DOTATOC is used for labelling Y-90, while DOTATATE is used for labelling with Lu-177. In this study we compared the outcome and side effects of Y-90-DOTATATE compared with Y-90-DOTATOC in patients with NET. Materials and Methods: 83 consecutive patients with NET were treated with Y-90-DOTATOC (27 patients, 6 women, 21 men, aged median 68 years (47-81 years); 10 CUP, 8 foregut , 7 midgut und 2 hindgut tumours; median 7,0 GBq) or Y-90-DOTATATE (56 patients, 21 women, 35 men; aged median 69 years (41-81 years); 18 CUP, 24 foregut, 10 midgut, 4 hindgut tumours; median 6,8 GBq). We compared response rates (clinical and morphological), progressive free survival (PFS), overall survival (OS), as well as side effects to bone marrow (blood cells) and kidney function. Results: Response rates showed no significant differences in both groups (DOTATOC: remission 34,8%, stable disease 43,5%, progressive disease 21,7%, DOTATATE: remission 22,4%, stable disease 57,1%, progressive disease 20,4%). Furthermore, no significant differences were seen concerning PFS: DOTATOC 5 months (KI95 % 3,5-6,5), DOTATATE 6 months (KI95% 4,2-7,7) and OS: DOTATOC median 23 months (KI95% 0-50,5), DOTATATE median 32 months (KI95% 22,8-51,2). Effects on blood cells were pronounced in the DOTATATE group for red blood cells (p=0,011), white blood cells (p=0,012) and platelets (p=0,04). Severe side effects (infections, bleeding, blood transfusion necessary) were more seen in the DOTATOC group (p=0,018). No significant differences were shown between the pre- and post therapeutic creatinine concentrations in plasma in both groups, whereas (until now) renal failure occurred only in 4 patients(14,8%) following Y-90-DOTATOC therapy after a period of mean 35,5 months (14 - 59 months). Conclusions: Peptide receptor radionuclide therapy with Y-90-DOTATOC and Y-90-DOTATATE lead to similar results concerning response rates, progressive free survival and overall survival. Severe side effects were more often seen after Y-90-DOTATOC.

TP078

Development of a new quantification method of dopamine transporter density with 123I-ioflupane

S. Okumiya, A. Ofuji, S. Ito; Kumamoto University, Kumamoto, JAPAN.

[Objective]123I-ioflupane has a high affinity for dopamine transporters (DAT) in the corpus striatum, and the single photon emission tomography (SPECT) imaging provides distribution density of DAT in brain. Quantifying specific binding ratio (SBR) of 123I-ioflupane's signal at the striatal region is a common brain imaging method to confirm the diagnosis of the Parkinson's disease. Generally, SBRs are calculated by comparing the activity in the structure of interest with the activity in a reference region (with a very low DAT concentration) by the semi-quantification method. However, the SBR by the semi-quantification method depends on the system performance of the SPECT camera.Therefore, quantification is important for research and for completion of a diagnostic evaluation.The purpose of this study is to develop a new quantification method for obtaining the true-SBR.[Materials and methods]A striatal phantom filled with 123I solution (1.4~123 kBq/ml) using striatal to background (BG) ratios between 4:1 (left side: BG) of and 8:1 (right side : BG) was imaged on two different SPECT systems with two different collimators (low-energy high resolution (LEHR) and low and medium energy general purpose(LMEGP)). Data from each system were reconstructed using 2-dimensional ordered subset expectation maximization method (subsets:10, iterations:10). Attenuation and scatter corrections were performed. After fusion of SPECT and CT data, left and right side region of interest (ROI) of striatum were obtained by tracing the striatal outline of the CT images. These ROIs and a rectangular ROI of the BG were set on the SPECT images. The activity in each ROI was obtained by using a count-activity conversion coefficient (CC). The CC was obtained by analyzing the count-activity curve of each ROI. The activity in each ROI was calculated by multiplying the SPECT counts by the CC. The true-SBR was determined by using these activities. [Result]Linear regression equations of the count-activity curves were obtained for the phantom study in all SPECT systems. The CC of the left side striatum was approximately equal to that of the right side. The true-SBRs of the four SPECT systems were approximately equal to the theoretical values. The lower detection limit of the striatum was 7.2 kBq/ml.[Conclusion]A new quantification method was developed using the individual CC of the striatum and BG. Clinical study is necessary to confirm the feasibility of this method.

TP079

To Manual Handle, or to NOT Manual Handle?

C. Vroonland, S. Baank, M. Stokkel; Antonie van Leeuwenhoek Hospital, Amsterdam, NETHERLANDS.

Aim It is widely known that nursing staff has one of the highest incidences of musculoskeletal pain and injuries, which has resulted in the development of Patient and Manual Handling strategies and equipment. Employees in other departments can also benefit from these strategies and equipment.Our aim is to raise awareness of the necessity and to stimulate the implementation of patient/manual handling techniques and equipment within Nuclear Medicine departments, not only due to heavier patients but also especially due to the lead shielding we are required to work with.Method and MaterialsI n the Netherlands there are currently only

guidelines, no legal legislation requiring the use of Patient/Manual Handling techniques and equipment. As a result, such equipment is often only scarcely available within imaging departments. Several years ago a Risk Analysis was performed in our department in which the staff indicated which areas of their activities were physically demanding. These activities included patient handling (transfer of the patient from chair-bed or bed-bed), collimator exchanging, and Hotlab activities mainly due to the use of lead shielding.With the help of a Nuclear Medicine Technologist experienced in Manual Handling, a newly appointed Health and Safety advisor and the Risk Analysis, we were able to pinpoint specific areas where Manual Handling strategies and equipment could be implemented and training provided at a relatively low cost.Results Simple and low cost equipment has been installed benefitting both staff and patients. Manual Handling coaches have been appointed and trained through the Health & Safety department. These coaches are able to train their own colleagues and oversee the use of Manual Handling techniques and equipment.The Risk Analysis was a key tool in the decision making process for a ceiling mounted patient hoist during the purchase of the new big bore PET camera.Conclusion Despite the lack of legal legislation we have been able to implement several improvements, the results of which we hope will be reflected in the Risk Analysis due to take place later this year.Possible new improvements and/or strategies are often evaluated and implemented as the raised awareness stimulates staff to think of new solutions to Manual Handling problems.

TP080

Evaluation of CZT-SPECT system for nuclear cardiology: comparison with conventional Anger SPECT

T. Niimi1, M. Sugimoto1, M. Nanasato1, H. Maeda2; 1Nagoya Daini Red Cross Hospital, NAGOYA, JAPAN, 2Nagoya University, NAGOYA, JAPAN.

Purpose: Recently, the D-SPECT (D-SPECT; Spectrum Dynamics, Israel) system, based on cadmium-zinc-telluride (CZT) detectors, has been commercialized for myocardial single-photon emission computerized tomography (SPECT). However, the most of the differences in the performance of the CZT camera or collimation systems remain unclear, except for evaluations by some research organizations. We evaluated the performance of the D-SPECT system to understand the differences in the performance of the CZT camera or collimation systems in comparison with a conventional Anger SPECT (A-SPECT).Materials and Methods: We evaluated the performance of the D-SPECT system in terms of its energy resolution, detector sensitivity, uniformity, spatial resolution, and collimator resolution compared with an A-SPECT (BrightView; Philips, Japan). The energy resolution was measured for Co-57, Tc-99m, I-123, and Tl-201 using line sources placed at the same locations in each system. Corresponding measurements were also done on an A-SPECT. The full width at half maximum (FWHM), which is an index of energy resolution and spatial resolution, was separately estimated for each pixel by fitting the sum of a Gaussian function, reporting the Gaussian FWHM. The detector sensitivity and uniformity were also determined using the same phantom data as the energy resolution. The spatial resolution was evaluated using a NEMA phantom and the reported FWHM. The collimator resolution was calculated based on the material and geometry (the collimator of A-SPECT was LEGP.).Results: The energy resolution (FWHM) values of the D-SPECT system for Co-57, Tc-99m, I-123, and Tl-201 were 5.8%, 5.5%, 5.2%, and 10.9%, respectively; the corresponding values in A-SPECT for Tc-99m and I-123 were 9.1% and 9.3%, respectively. The D-SPECT system with Tc-99m and I-123 had an energy resolution that was twice that of the A-SPECT. Tc-99m and Tl-201 had detector sensitivities that were respectively 6.4 and 11.7 times higher than that of the A-SPECT. The uniformity was equal, and the spatial resolution was twice that of the A-SPECT. The collimator resolution (FWHM at a distance of 10 cm) of the D-SPECT system was 13.3 mm, where as that of A-SPECT was 7.6 mm, which was superior to that of the D-SPECT.Conclusion: The energy resolution and detector sensitivity of the D-SPECT were superior to those of a conventional A-SPECT system, with similar uniformity. However, the quality of the D-SPECT image is still unclear because the collimator resolution, which is an index of image quality, showed a value that was 1.75 times lower than that of the A-SPECT.

TP081

Post therapeutic 131I Scan Total Body after a successive therapy (WBS) in Patients (Pts) affected by metastases of thyroid cancer (DTC) and 18F-FDG PET/CT (PET): usefulness of PET for staging and evolution recurrence in Pts with elevated Thyroglobulin (Tg)

L. Bertolazzi, L. Di Ciolo, V. Barbetti, C. Cananzi, M. Gaffuri, E. Piccardo, C. Motta, G. Agnese, P. Moresco; Azienda Ospedaliera Santa Corona, PIETRA LIGURE (SV), ITALY.

Aim. The purpose of this study is to investigate the possible role of PET in Pts with DTC and positive WBS in which was planned a successive 131I-radiomethabolic therapy (RAI) for metastases. Meanwhile the study tries to evaluate PET's possible utility and helpful for staging and evolution recurrence and maybe skip a successive diagnostic 131I-scan (TB). Materials and Methods. This retrospective review comprised 113 Pts that, after total thyroidectomy and more RAI between 2007 and march 2015 (80 females and 33 males, age 34 - 83 years,

mean age 48 years), were affected by papillary cancer (83 Pts=73%) and by follicular cancer (30 Pts=27%) undergoing in already a second RAI in off L-T4 (TSH > 40 uU/ml). All 133 Pts had elevated Tg (range 5 - 600 ng/ml, mean range 133 ng/ml) and performed PET and Tg just before RAI and after 5 days post therapeutic WBS. Results. WBS after a second RAI in all 113 Pts showed lymph nodes and-or lung or bones metastases. In 44 Pts (39%) PET was positive (A group). In 69 Pts (61%) PET was negative (B group). PET in A group has showed in 24 Pts more metastases than WBS. Tg values in A group (44 Pts) were very elevated (mean range 255 ng/ml). In B group (69 Pts) Tg values were lower (mean range 56 ng/ml). Conclusion. PET is a well-established method in the follow up of Pts with DTC with elevated Tg and negative WBS: high FDG uptake in large tumor masses may have an unfavorable prognostic significance. In our research, PET detected all or more metastases in about 1/3 of Pts who had positive WBS with most elevated Tg (range 143 - 600 ng/ml). In these clinical cases PET is a valuable tool in investigating Pts and it seems reasonable to omit a successive TB to evaluate outcome after RAI, achieving real clinical managerial vs in off LT4 Pts and valuable economic advantages vs recombinant human thyrotropin (rhTSH) method. TB with 185MBq of 131I decreases thyroid uptake for several weeks and can impair immediate subsequent RAI (stunning effect). 44 Pts of A group with the most elevated Tg levels (over 143 ng/ml) have positive PET and follow up may be with PET; in B group Pts with lower levels of Tg could leave out to perform PET.

TP082

One pot synthesis of [18F]labelled benzyl chloride for asymmetric nucleophilic synthesis of 6-[18F] fluoro-L-DOPA

V. Orlovskaja1, O. Fedorova1, E. Studentsov2, A. Golovina2, R. Krasikova1; 1N.P.Bechtereva Institute of Human Brain Russian Academy of Science, St.-Petersburg, RUSSIAN FEDERATION, 2Saint-Petersburg State Institute of Technology, St.-Petersburg, RUSSIAN FEDERATION.

Aim: In the past two decades many efforts were directed to develop or optimize nucleophilic production methods for 6-[18F]fluoro-L-DOPA starting from easy available aqueous [18F]fluoride. Suggested approaches were based on multistage “built-up” procedures and asymmetric synthesis strategies (Lemaire et al, 2004; Krasikova et al., 2004), affording 6-[18F]fluoro-L-DOPA in a high enantiomeric purity. Substituted [18F]fluorobenzyl halides employed at the key chiral alkylation step were usually prepared in a three steps synthesis. It comprised nucleophilic displacement of the leaving group in a labeling precursor (substituted benzaldehyde (BZ)); reduction of 18F-labelled BZ into alcohol and halogenation. This procedure involved intermediate purifications and associated with the radioactivity losses and longer synthesis time. Here we report simple one-pot three steps synthesis procedure for a substituted [18F]fluorobenzyl chloride using novel labeling precursor, 4,5-dibutoxy-2-nitrobenzaldehyde (I). Methods: 18F-fluorination of (I) was performed in DMF at 150°C for 5-10 min in the presence of kryptofix/K_2CO_3. After cooling reaction mixture, the solution of $NaBH_4$ (0.8 mg in 0.2 mL of DMF) was added, the reduction was carried out at r.t. for 3 min. The following halogenation step was accomplished by adding $SOCl_2$/DMF (12 μL in 0.3 mL) and keeping reaction mixture at r.t. for 3 min. All the three synthesis steps were performed in a standard closed 5 mL conic reaction vial. The courses of radiofluorination, reduction and halogenation steps were monitored by radio TLC with minimal amounts of reagents. Results: 18F-incorporation rate into (I) was 83±5%, n=15. Extremely high (up to 100%) conversion rates were observed at the following reduction and halogenation steps. The synthesis lasts 11 min and avoids intermediate purifications. Noteworthy, the protecting 4,5-dibutoxy groups in a new labeling precursor (I) can be cleaved under mild reaction conditions that facilitates final hydrolysis/deprotection step in the synthesis of 6-[18F]fluoro-L-DOPA. Conclusions: One pot three step synthesis has been developed for the preparation of 4,5-dibutoxy-2-[18F]fluoro benzylchloride, a useful radiolabeled alkylating agent for asymmetric synthesis of 6-[18F]fluoro-L-DOPA or other applications. The feasibility of this approach was confirmed in the test experiments for asymmetric synthesis of 6-[18F]fluoro-L-DOPA using NiII Schiff base complex of glycine as a chiral inductor. This study was supported by RFBR grant 14-03-31492.

TP083

Comparison of 2 Methods for Reduction of Infra-Cardiac Activity in Myocardial Perfusion Imaging

M. Schalken1, I. Rutten - Vermeltfoort1, J. de Jong1, M. Brink-Wieringa2; 1Institute Verbeeten, Tilburg, NETHERLANDS, 2Elisabeth-TweeSteden Ziekenhuis, Tilburg, NETHERLANDS.

Aim: In technetium (Tc)-99m myocardial perfusion imaging (MPI), abdominal activity often interferes with the evaluation of the perfusion of the inferior wall. Because of a reduction of the diagnostic accuracy in these cases, repetition of the imaging is often necessary. The aim of the study was to compare the efficacy of 2 different types of patient preparation in reducing infra-cardiac activity. In order to improve the image quality of MPI studies we also examined the effect of other risk factors for infra-cardiac activity. Methods: Data of 454 consecutive MPI studies in Institute Verbeeten Tilburg (NL) were

prospectively collected. This includes all studies with exercise, pharmacological stress (adenosine and regadenoson) and rest. Patients were randomized to receive either conventional preparation (water, fatty meal and exercise) or conventional preparation with the addition of chocolate milk prior to myocardial SPECT imaging. The frequency of intestinal activity adjacent to the inferior myocardial wall resulting in the need for a repeated scan, was evaluated by observers on SPECT images. Results: For all rest studies, the need for rescan due to abdominal activity was 16% (35/219) in the conventional group versus 12% (28/235) in the chocolate milk group, (p=0.21); in pharmacological stress these were resp. 14% (22/158) versus 11% (19/173), (p=0.42). There was no significant difference between the groups. Univariate-analysis for gender, diabetes mellitus, age, gastrointestinal medication and body mass index showed no significant difference except age in the pharmacological stress group (p=0.04). A multivariate-analysis logistic regression model using above mentioned risk factors also showed no significant difference. Conclusion: This study shows no significant improvement in the reduction of infracardiac activity in MPI using chocolate milk in addition to our conventional preparation. With the exception of age, no other risk factors were found to have a significant impact on the risk of repeated scan.During exercise abdominal activity is a far less frequent problem and is in this respect the preferred modality.

TP084

DMSA scintigraphy: Do we really need to perform geometric mean assessment?

i. G. E. el bez, h. boutruigua, n. bechir, k. trabelsi, l. zaabar, I. YEDDES, I. MEDDEB, D. BEN SELLEM, B. LTAIEF, I. SLIM, A. MHIRI, M. BEN SLIMENE; institut salah azaiez, tunis, TUNISIA.

The aim of this study is to validate the use of Geometric mean (GM) method, in the calculation of relative renal function (RRF) in paediatric patients with various renal problems compared to aritmethical mean (AM) method. Material and Methods: one hundred Tc99m DMSA scans were studied retrospectively. The patients were divided into five age groups: group I : patients aged under 10 years; group II, patients aged betewen 10 and18 years; and group III : patients ageded upper 18 years. The RRF of the right and left kidney was calculated using the posterior images for AM and anterior and posterior images for GM. The differences between AM and GM were calculated for all patients according to age groups and renal pathologies. A difference more than 5% was accepted significant. Results: Out of 100 patients, 60 had normal kidneys, 40 had abnormal findings on the DMSA scans as parenchymal damages, cortical scarring and atrophy due to urinary tract infection while 6 of them had malrotated or malpositioned kidneys. The AM of the kidneys were calculated as 0.49 for the right kidney and 0.51 for the left kidney, while the GM was 0.50 for both kidneys, respectively (p>0.05). When the patients were analysed according to the age groups, the difference was not significant (p>0.05), except group III. Interestingly, no statistical difference was observed between the patients when they were evaluated according to their renal pathologies. However in the 6 malrotated or malpositioned kidneys the RRF change 15% for right and 12% for left kidney when GM method is used. Conclusions: The calculation of RRF using the GM method revealed no significant difference from that using posterior images except in group III. Therefore, it is unnecessary to performanterior imaging in young patients unless they have malrotated or malpositioned kidneys for RRF.

TP085

The technologist role in 177Lu dosimetry for PRRT (Peptide Receptor Radionuclide Therapy)

E. Leoni, A. Filice, A. Palmieri, G. Ghiraldini, F. Fioroni, E. Grassi, S. Cola, A. Versari; ASMN, Reggio Emilia, ITALY.

Background: Neuroendocrine cancers are neoplasms that generate from the diffuse neuroendocrine system (DNES). This kind of neoplasms can express somatostatin receptors (SSTR2, SSTR3, SSTR5). Treatment consists in using the specific high affinity of receptor-peptide interactions in order to convey radioactivity to tissues that show this kind of receptors through a specific radionuclide (68Ga, 90Y, 177Lu).Aim: The dosimetric analysis allows evaluating the patient's radiopharmaceutical distribution in order to calculate the dose absorbed by the cancer and healthy tissues. The aim is to prescribe the maximum radiopharmaceutical quantity, establish a dose-response relation for toxicity to healthy organs and evaluate treatment's effectiveness. Matherials and Methods: Patients are injected with 177Lu-DOTATOC (equivalent to somatostatin). The activity is specifically calculated on single patients (depending on weight, age, kidney and marrow dosimetry, risk factors, lesions size). After therapeutical administration, the dosimetry protocol requires: 5 SPECT/CT image acquisitions of abdomen to be executed 1, 4, 20, 40 and 70 hours after administrating 177Lu-DOTATOC, in order to evaluate the dose absorbed by the kidney, liver, spleen and cancer lesions of the abdomen zone. Whether there should be cancer lesions in other zones than abdomen, more SPECT/CT image acquisitions must be carried out in the second zone of interest (e.g. cranium or thorax) 4, 40 and 70 hours after administration. Every SPECT/CT image acquisition is carried out by following the same image acquisition protocol. The dose assessment for organs and lesions will not be affected by any change due to a patient's different set-up or different acquisition parameters. The equipment consists of a SPECT/CT hybrid machine

with variable geometry double-headed gamma ray demodulator and a spiral CT (Siemens Symbia T). Dose re-elaborations and assessments are carried out through the OLINDA software (Organ Level International Dose Assessment).Conclusion: After the first treatment session, the dosimetric analysis allows establishing the toxicity degree of undamaged organs and the correct dose for the lesion, in order to prescribe an effective and personalised treatment cycle.

TP086

18F-Fluoride PET for quantification of axial and peripheral lesions in adjuvant-induced arthritis in Lewis rats.

R. OUICHKA1, A. DERRIEN1, C. HENRIONNET1, F. MASKALI2, G. KARCHER2, P. GILLET1, D. LOEUILLE3, A. PINZANO1; 1University of lorraine, VANDOEUVRE-LES-NANCY, FRANCE, 2NANCYCLOTEP, VANDOEUVRE-LES-NANCY, FRANCE, 3DEPARTEMENT OF RHEUMATOLOGY, HOSPITAL OF BRABOIS, VANDOEUVRE-LES-NANCY, FRANCE.

Aim: Evaluation of disease severity in experimental arthritis is inevitably associated with assessment of structural bone damage. A non-invasive imaging technology allowing objective quantification of pathophysiological alterations of bone structure in rodents could substantially extend the methods used to date in preclinical arthritis research, for staging of autoimmune disease severity or efficacy of therapeutical intervention. 18F-fluoride (18F-FNa) is a bone-seeking tracer well suited for molecular imaging. Therefore, we examined the use of 18FNa positron emission tomography (PET) in Lewis rats with adjuvant-induced arthritis for cross-sectional quantification of pathological bone metabolism. Methods: 18F-FNa was injected in rats before disease onset and at various time points of progressing experimental arthritis (Days 4, 12, 21, 30, 60, 90). Naive age-matched rats were used as controls. Radioisotope accumulation in joints of hind paws and proximal tail was analyzed by PET measurements. For validation of bone metabolism quantified by 18F-FNa PET, high-resolution radiographs scoring and clinical parameters were used. Results: Before clinical arthritis onset, no distinct accumulation of 18FNa was detectable in hind limbs of rats immunized with complete adjuvant. In the course of experimental autoimmune disease, 18FNa bone uptake was increased at sites of enhanced bone metabolism caused by arthritic process and cicatricial bone remodeling at both peripheral and axial (tail) locations. Moreover, 18F-FNa uptake at different stages of adjuvant arthritis was significantly correlated with the degree of radiological bone sdestruction/remodeling, rather than inflammatory parameters. Conclusions: The results from this study suggest that small animal PET using 18F-FNa as tracer is a feasible method for quantitative assessment of pathophysiological bone metabolism in rat adjuvant-induced arthritis. Furthermore, the possibility to perform repeated non-invasive measurements in vivo should allow longitudinal studies monitoring therapeutical intervention.

TP087

Our experiences with reinjections for non-visualisation in sentinel lymph node procedures for penile cancer

G. A. Ebbens, B. Pouw, D. Hellingman, M. L. Donswijk, M. P. M. Stokkel; Antoni van Leeuwenhoek, Amsterdam, NETHERLANDS.

Aim: Currently there are several methods to visualise and identify sentinel lymph nodes (SLN) in penile cancer preoperatively or during surgery. Unfortunately in a subgroup of patients non-visualisation on preoperative imaging is observed. In such cases, we perform a reinjection of the radioactive tracer and repeat additional lymphoscintigraphy to improve the visualisation rate. The aim of this study is to assess the value of a preoperative reinjection for SLN imaging in penile cancer. Method and materials: In total, 193 patients were scheduled for a penile SLN procedure within a period of 3 years (02-03-2012 till 05-03-2015). Preoperative imaging, lymphoscintigraphy and Single Photon Emission Computed Tomography with integrated CT (SPECT/CT), was performed after 99mTc-nanocolloid or Indocyanine green (ICG)-99mTc-nanocolloid injection. During surgery, SLN were initially approached using a gamma probe, followed by patentblue dye and/or fluorescence imaging. A portable gamma camera was used to confirm excision of all SLN. In this group, 22/193 patients had unilateral visualisation of SLN. We assessed if a reinjection was performed and if bilateral drainage was visualised. Furthermore, we searched for all relevant parameters about the preoperative visualisation, surgical identification, and pathological outcomes of SLN and non-SLN. Results: In 171/193 patients (88.6%) bilateral SLN were visualised and in 22/193 patients (11.4%) unilateral SLN on preoperative imaging. A reinjection was performed in 19/22 patients, and in 3/22 patients a reinjection was not possible due to logistics. After reinjection, bilateral SLN were visualised in 7/19 patients, unilateral SLN were visualised in 10/19 patients, and no further imaging was performed in 2/19 patients. Intraoperatively, bilateral SLNs were found in 7/15 (46.7%) patients who did not show bilateral lymphatic drainage on preoperative imaging. Pathologic analyses of all excised non-SLN and SLN revealed metastases in 3/22 patients (13.6%), of which 1 patient had metastases in a groin without lymphatic drainage on preoperative imaging and during surgery. Conclusion: In penile carcinoma patients, preoperative lymphoscintigraphy visualises bilateral SLN in 88.6% and after reinjection in 92.2% (178/193 patients). Combined with the intraoperative results bilateral SLN identification rises up to 95.9% (185/193 patients).

TP088

Prone versus supine breast F18-FDG PET acquisition in breast cancer

R. SANCHEZ-JURADO1, J. Ferrer Rebolleda1, M. Cózar Santiago1, R. Sanz Llorens1, J. Aguilar Barrios1, E. Blanco Pérez1, C. Fuster Diana2; 1ERESA, VALENCIA, SPAIN, 2UNIVERSITY GENERAL HOSPITAL, VALENCIA, SPAIN.

PURPOSE: Retrospective evaluation of positioning in patients with breast cancer who underwent a 18FDG-PET. Benefits of prone position for locorregional diagnosis.METHOD AND MATERIALSIn an internal data review we selected 50 female patients (55 ± 15 years-old) histologically confirmed breast cancer who were performed a FDG PET-CT in prone and supine position at the same or not scanning session. All patients were scanned with PET-CT system (Gemini TF16; Philips) and with a dedicated breast-PET (MAMMI-PET; Oncovision) 60-80 min and 90-120 min after injection, respectively.Locorregional staging, maximal tumor diameter and affected breast quadrants were evaluated in prone versus supine breast-PET positioning and compared to previous reports of mammography, ultrasound and breast-MRI studies that had been performed previously.RESULTSTotally 68 affected breasts were scanned. The sensitivity was 96,8% for lesions located within the scanning range of dedicated breast-PET (prone position); 87,3% for supine breast PET-CT and 92, 8% for prone breast PET-CT. Similar maximal tumor diameter were registered between PET-positioning but a clear correlation was shown in the register of the affected breast quadrants comparing with previous studies: 99,3% db-PET, 78% prone PET-CT and 56% supine PET-CT.CONCLUSIONThe implementation of prone position for the locoregional PET imaging results provides a more correct definition of T and N-stage than standard supine PET-positioning. Also, affected breast quadrants can't be evaluated clearly by supine method and therefore it demonstrated that prone positioning was more accurate for tumor localization. Finally T-stage and affected breast quadrants were better diagnosed (rinsed) by MAMMI-PET than Whole Body prone PET-CT.

TP089

The effectiveness of dopamine transporter volume estimated by C-11 PE-2I PET in diagnosing Parkinsonism-Novel parameter for quantifying the total amount of dopamine transporter-

S. Nagamachi1, R. Nishii1, Y. Mizutani1, Y. Umemura2, R. Ohkubo2, H. Takashima3, T. Hirai1; 1MIyazaki University, Miyazaki, JAPAN, 2Fujimoto Hayasuzu Hospital, Miyakonojou, JAPAN, 3Kagoshima University, Kagoshima, JAPAN.

(Objective) In the diagnosis of Parkinsonism, C-11 PE2I (N- (3-iodoprop -2E-enyl)-2β-carbomethoxy-3β-(4-methyl-phenyl) nortropane) is useful radiopharmaceutical for its high binding selectivity and specificity to dopamine transporter (DAT) . The current study was done to evaluate the effectiveness of novel parameter, dopamine transporter volume (DTV) that was calculated with C-11 PE-2I PET/CT, in diagnosing Parkinsonism. (Materials and Methods) Twenty-three patients with Parkinsonism, 16 idiopathic Parkinson diseases (PD) and 7 Parkinsonism of other cause (PS) were evaluated. All patients were done two kinds of examination, C-11 PE-2I PET/CT, I-123-metaiodobenzylguanidine (123I-MIBG) myocardial scintigraphy and I-123 DAT SPECT. Three dimensional VOI (volume of interest) was automatically drawn around striatum respectively on C-11 PE-2I PET/CT images using workstation (syngo.via, Siemens). Both sided maximum standardized uptake value (SUVmax) and dopamine transporter volume (DTV) were obtained. The threshold value for calculating DTV was 40% of SUVmax. On MIBG scintigraphy, Heart to mediastinum ratio (H/M) and washout ratio (WR) were calculated from early (E) and delayed (D) chest planar images. On I-123 DAT SPECT, Specific binding ratio (SBR) was calculated. Correlation analysis among all C-11 PE-2I PET/CT parameters, MIBG parameters and SBR on I-123 DAT SPECT were done. In addition, all parameters were compared between PD and PS. (Results) Both sides DTV showed weak positive correlation with both the early and delayed H/M (correlation coefficients were from 0.29 to 0.39). In addition, mean value of both sided DTV in PD were significantly lower compared with those of PS (Right DTV: 7.81ml vs. 10.28ml, Left DTV: 7.26ml vs. 9.85ml). However, SUVmax showed no statistical significance. (Conclusion) Novel parameter, dopamine transporter volume (DTV), calculated from C-11 PE-2I PET/CT was useful for quantifying conditions of dopamine transporters in Parkinsonism. In addition, it was also useful parameter in differentiating PD from PS.

TP090

Simplified and reliable quality control analysis method of 18F-Fluorocholine for a small scale hot lab

H. Hassan1, S. Abu Bakar2, K. Che A. Halim2, J. Idris2, A. Nordin1; 1Universiti Putra Malaysia, Serdang, Selangor, MALAYSIA, 2National Cancer Institute, Putrajaya, MALAYSIA.

Aim: 18F-Fluorocholine has never been synthesized in Malaysia. Thus, there was no available data or guideline for quality control analysis of 18F-Fluorocholine was documented. The study aims to present simplified and reliable method of quality control analysis for 18F-Fluorocholine in order to assist small

scale hot laboratory and local authority in Malaysia.Materials and methods: 18F-Fluorocholine was synthesized via N-alkylation of dimethylethanolamine (DMEA) with 18F-fluorobromomethane ($BrCH_2F$), followed by purification on the CM cartridge with ethanol and water. Prior to synthesis, quality control analysis method for 18F-Fluorocholine was developed and validated, by adapting the equipment set-up used in 18F-Fluorodeoxyglucose (18F-FDG) routine production. Quality control on the 18F-Fluorocholine was performed by means of pH, radionuclidic identity, radio-high performance liquid chromatography equipped with ultraviolet, radio-thin layer chromatography and gas chromatography. Results: Post-synthesis; the pH of 18F-Fluorocholine was 6.42 ± 0.04, with half-life of 109.5 minutes (*n* y *12*). This affirmed the labelling of Fluorocholine tracer with radioisotope Fluorine-18 was successful. The radiochemical purity was consistently higher than 99%, both in radio-high performance liquid chromatography equipped with ultraviolet (r-HPLC; SCX column, 0.25 M NaH_2PO4: acetonitrile) and radio-thin layer chromatography method (r-TLC). The calculated relative retention time (RRT) in r-HPLC was 1.02, whereas the retention factor (Rf) in r-TLC was 0.64. Potential impurities from 18F-Fluorocholine synthesis such as ethanol, acetonitrile, dimethylethanolamine and dibromomethane were determined in gas chromatography. Using our parameters, (capillary column: DB-200, 30 m x 0.53 mm x 1 um) and oven temperature of 35°C (isothermal), all compounds were well resolved and eluted within 3 minutes. Level of ethanol and acetonitrile in 18F-Fluorocholine were detected below threshold limit; less than 5 mg/ml and 0.41 mg/ml respectively. Meanwhile, dimethylethanolamine and dibromomethane were undetectable. Conclusion: A simplified and reliable quality control analysis method for 18F-Fluorocholine has been developed and validated for a small scale hot laboratory, which in compliance to release criteria. This simplified method may provide a guideline to local GMP radiopharmaceuticals laboratory and local authority in Malaysia.

TP091

Histopathological correlation of 123-I Metaiodobenzylguanidine (MIBG) scintigraphy findings in pediatric patiens with suspected neuroblastoma

S. M. Nieves Maldonado, J. Lopez Urdaneta, P. Fierro Alanis, S. Argibay Vazquez, I. Dominguez Prado, M. C. Pombo Passin, A. Ruibal Morell; Hospital Clínico Universitario de Santiago de Compostela, Santiago de Compostela, SPAIN.

AIM: Our purpose was to determine the diagnostic value of the study with 123-I MIBG and evaluate the correlation of the scintigraphic findings with pathology results in pediatric patients with suspected diagnosis of neuroblastoma. MATERIALS AND METHODS: We have evaluated 58 pediatric patients with suspected diagnosis of neuroblastoma, not receiving medication that could block radiotracer uptake mechanism, which underwent a 123-I MIBG scintigraphy in our department between 1997 and 2013. The imaging findings were assessed taking into account the 123-I MIBG tumor uptake and histopathology results (incisional or escisional biopsy), and other parameters as age at diagnosis, sex, location of the mass, and tumor dissemination. RESULTS: The evaluated population was 55% male, with an average age of 2 years (range 0-13 years). The location of 48% of the masses was on the right side (n = 20/58), and 50% were located at the abdomen. 52% (n = 30/58) of the scintigraphic studies showed abnormal uptake, histopathological results were compatible with neuroblastoma in 77% (n = 23/30) of cases. Metastases were found in 40% (n = 12/30) of patients with positive imaging, bone metastases represented a 42% (n: 12.5) of these findings. There were 7 positive studies with different pathologic results from clinical suspicion, they were listed as nephroblastoma, sarcoma and bleeding. Studies without pathological uptake, 82% (23/28) presented results corresponding to other tumor histopathological groups, and 17% (n = 5/28) was compatible with poorly differentiated / undifferentiated neuroblastoma (n = 4) and well differentiated witha high degree of necrosis neuroblastoma (n = 1). CONCLUSIONS: The 123-I MIBG scintigraphy is still an useful tool in the diagnosis and staging of neuroblastomas. The correlation of the scintigraphic findings with the degree of tumor differentiation in pathology is possible. Some undifferentiated neuroblastomas and other well differentiated with necrosis may show and absence of uptake.

TP092

Nodal Visualisation in Sentinel Node Imaging

A. Vaz; St Barts Hospital, London, UNITED KINGDOM.

Histological evaluation of the first draining lymph node (sentinel node) in the axilla of patients with breast cancer has dramatically altered the surgical approach to these patients, with sparing of the axilla if no tumour cells are identified. In a fraction of patients imaged after injection of radiocolloids, there is no visualisation of the sentinel node. A retrospective study including patients with successful and unsuccessful nodal identification was performed to assess the variables associated with failure to identify a node. 1023 patients were imaged following subcutaneuos injection of 99mTc-Nanocolloid, immediately and up to 5.5h post injection. The scintigraphic data were analysed with reference to patient's age, tumour location, volume injected and radiopharmaceutical's labelling concentration, using univariate analysis and a logistic regression model. A sentinel node was visualised in 990 of 1023 patients (97.2%). Comparison of patients with non-visualised sentinel

nodes disclosed no statistically significant relation to tumour location (quadrant, p=0.338 and side, p=0.581). Age (p=0.032), radioactive labelling concentration (p=0.002), volume of injection (p=0.023) and concentration of particles (p=0.010) were statistically significant at interfering with nodal visualisation. The results show that increasing age, high labelling concentration, low particle concentration and small volume of injection decrease nodal visualisation. **Key-words**: Breast Cancer, Sentinel lymph node, lymphoscintigraphy, nodal non-visualisation.

TP093

Preliminary Study of Multicenter Nuclear Medicine Imaging Quality Assurance by ACR Phantom in Taiwan

C. Lo, **Esq**., P. Kao; Chnug-Shan University Hospital, Taichung, TAIWAN.

Introduction: To improve nuclear medicine practice and to advance scientific initiatives as well as clinical research projects, a phantom study is to subjectively evaluate image quality of routine SPECT/CT and PET/CT acquisition with Jaszczak Deluxe Flangeless ECT (ACR) phantom at 4 different nuclear medicine sites in Taiwan. Materials and Methods: Phantom preparation for this study at 4 different sites were done by a team members for the research. Radioactivity concentrations in different parts of the phantom were predetermined by the team. Imaging acquisition parameters were standardized for each brand name of the imaging modalities simulating routine clinical practice. These imaging were centralized for interpretation by 7 experienced nuclear medicine physicians. Five items of the phantom studies were to assess, including PET-CT and SPECT-CT alignment, hot spheres resolution and deformity, and overall satisfaction. All level for five parts: 5=excellent, 4=good, 3=acceptable, 2=poor, 1=non-diagnostic. Result: The results of SPECT-CT and PET-CT alignment were 2.8±0.8 and 3.8±0.6 respectively; hot spheres resolution level were 2.2±1.1 and 3.4±0.8; deformity rate represent 2.6±0.9 and 3.8±1.2; overall satisfaction were 2.7±1.2 and 3.5±1.3. Conclusion: The results of this preliminary study make us feel confidence for a future study as a standardized procedure for accreditation in nuclear medicine practice. The study is still in progress, we will conduct 4 more nuclear medicine sites in the next 3 months to conclude the standards for accreditation in the future.

TP094

Influence of the application of post-filter, variation of the number of iterations and attenuation correction in the tomographic image quality.

A. A. Santos1, A. F. Fernandes2, H. R. Martins1, E. Pereira3, L. Vieira4; 1Escola Superior de Tecnologia da Saúde de Lisboa - IPL, Lisboa, PORTUGAL, 2Escola Superior de Tecnologia da Saúde de Lisboa- IPL, Lisboa, PORTUGAL, 3Hospital Particular de Almada / Escola Superior De Tecnologia Da Saúde de Lisboa - Instituto Politécnico de Lisboa, Lisboa, PORTUGAL, 4Área Científica de Medicina Nuclear, Escola Superior de Tecnologia da Saúde de Lisbo-IPL/ Instituto de Biofísica e Engenharia Biomédica, Faculdade de Ciências da Universidade de Lisboa, Lisboa, PORTUGAL.

Abstract: Tomographic image reconstruction can be done with analytic and iterative algorithms. The iterative reconstruction methods appeared as a solution to the limitations of the analytic methods and its application in Nuclear Medicine Center has been growing. The purpose of this study consist in evaluating the effects of the application of post-filter (Butterworth), the variation of the number of iterations (2 and 4) and the application of attenuation correction (Chang's uniform method) in Single Photon Emission Computed Tomography (SPECT) image quality. Methods: Experimental study using a GE™ Healthcare Discovery NM630 and a Jaszczak phantom filled with 740MBq of Sodium Pertechnetate (99mTcO4-). A tomographic study was obtained with a low energy high resolution collimator, with an acquisition angle of 360.°, in step-and-shoot mode, with a matrix of 128x128pixels, zoom of 1.33, 120 projections, and 30 seconds per projection. The image was reconstructed with FBP and OSEM with and without the application of attenuation correction with Chang's method and the application of post-filter Butterworth and ranging the number of iterations, 2 to 4, during reconstruction. Results: The study is still ongoing however it is already possible, through the statistical analysis of the results so far, verify that as the number of iterations increases so does the contrast and special resolution as well as image noise. The application of a post-filter is useful to diminish image noise and this effect is more significant than the increase of the number of iterations. The attenuation correction has effect on noise, diminishing it, and improves qualitatively special resolution. However, attenuation correction does not have a significant influence on contrast. Conclusions: It is envisaged that the application of the post-filter and the application of 4 iterations in OSEM has a positive contribute to the global image quality, even though the reconstruction time is longer

TP095

Reference Range in Blood-Pool and Liver SUV for 18F-FDG PET/CT

Y. Parlak, D. Goksoy, G. Gumuser, E. Bilgin; Celal Bayar University, MANISA, TURKEY.

Aim: The aim of this study was to document the normal range in blood-pool SUV and liver SUV for 18F-FDG PET/CT.

Material and Methods: Five hundred oncology patients (mean age: 60±5 years; 255 female, 245 male) had PET/CT scans using a Philips True Flight Select 16 PET/CT scanner. Patient preparation, acquisition parameters and reconstruction protocols for all patients were standardized. All patients were divided into ten cancer groups, including 50 patients (esophagus, stomach, colon, rectum, larynx, lung, breast, endometrial, ovarian and lymphoma cancer) in each group. Mean SUV values were obtained from 2-dimensional regions of interest in the aortic arch blood pool and in the right lobe of the liver. Results: The group's mean serum glucose level was 6.0 mmol/L. The variation in blood-pool and liver SUVs had gaussian distributions. The group's mean blood-pool and liver SUV were 1.57, with an SD of 0.14; 2.34, with an SD of 0.16, respectively. The variation in blood-pool SUV had a mean of 0.12 and SD of 0.35. The variation in liver SUV had a mean of 0.18 and SD of 0.43. Conclusion: These ranges are applicable in clinical practice as they indicate a practical limitation on qualitative tumor response assessment or tumor to background ratios in comparisions using 18F-FDG PET/CT.

TP096

Appropriate time interval of dynamic 201Tl SPECT-MPI data acquisition for quantitative myocardial blood flow analysis on cardiac dedicated ultrafast SPECT camera

G. Ogushi, S. Kudo, R. Matsuda, S. Tomiguchi, S. Shiraishi, Y. Yamashita; Kumamoto University, Kumamoto, JAPAN.

[Aim/Purpose] Single photon emission computed tomography myocardial perfusion imaging (SPECT-MPI) is useful and important to evaluate coronary artery disease (CAD). Recently, cardiac dedicated ultrafast SPECT camera is has been developed and enables to shorten the SPECT data acquisition time. Thus, dynamic SPECT-MPI for the quantitative assessment of myocardial blood flow (MBF) and flow reserve (MFR) is available in clinical use. It is important to obtain an accurate input function for the quantitative MBF analysis. The input function is defined by analyzing the time-activity curve (TAC) made to set a ROI on the left ventricular cavity. Time interval of dynamic SPECT-MPI data acquisition affects to the shape of TAC. The aim of this study is to clarify the optimal time interval for making the accurate input function from the TAC by phantom study. [Material and Methods] An anthropomorphic torso phantom with cardiac insert filled with 201Tl water solution in the myocardial part was used. 201Tl radioactivity concentration in the myocardium was regulated to the equivalent radioactive concentration to 111MBq injection (full dose). List-mode SPECT data acquisition (list-mode SPECT) was performed in the phantom for 30 minutes with dedicated ultrafast SPECT camera (Discovery NM 530c:GE). List-mode SPECT was also performed in the phantom with 201Tl radioactivity concentration(RC) corresponding to 1/2, 1/4 and 1/8 injection dose. Five set of images with 5 different time intervals (1,2,3,4 and 5 second) for making the TAC were reconstructed by using Maximum a Posteriori Expectation maximization (MAP-EM) algorithm. The appropriate time interval was assessed by linearity between RC in the myocardium and the calculated SPECT counts (SC) in each time interval. Area under the curve (AUC) value of TAC made every time interval was defined As AC. [Result] Linear correlation with high correlation coefficients from 0.986 to 0.988 was observed between RC and SC in time interval of more than 3 second on full dose phantom study. Good liner correlation between RC and SC was also demonstrated on 1/2 dose phantom in time interval of more than 3 second. [Conclusion] Appropriate time interval of dynamic SPECT data acquisition is considered to be more than 3 second in case of both full dose and half dose 201Tl injection. Therefore, 201Tl dynamic SPECT-MPI with half-dose injection is considered an useful method for the quantitative analysis of MBF and MFR.

TP097

Analysis and discussion of CT attenuation correction on apical muscular of in myocardial perfusion imaging

Y. Wang; Nuclear Medicine, Huashan Hospital, Fudan University, Shanghai, CHINA.

Objective: To study the influence of CT attenuation correction on cardiac apex in SPECT myocardial perfusion imaging. Methods: All the patients did SPECT resting myocardial perfusion imaging in my hospital from September to November 2014. Coronary angiography was carried out before and after SPECT examination, and the results of DSA showed that all the plunger of three major blood vessels were less than 10%. Do a comparison of the apex changes before and after CT attenuation correction at a non-gated condition. A 17 - segment model were used to divde the myocardium. 13 to 17 area represented respectively apical segments, apical anterior, apical septal, apical inferior, apical lateral apex. Results: There were 7 cases of data for discussion. Normalized Map statistics data were analyzed by using software Corridor4DM. T test results of 13 to 17 areas for: (t=-2.485, p=0.047; t=-0.117 p=0.911; t=-2.848 p=0.029; t=0.915, p=0.395; t=-5.365, p=0.002). The blood perfusion of the apical segments, apical anterior, apical septal were reduced after CT attenuation correction. Conclusion: CT attenuation correction will reduce the blood perfusion of apical segments, apical septal, apical lateral apex area in SPECT resting myocardial perfusion.

TP098

Investigation of Methods to Reduce Staff Whole Body Radiation Exposure in a PET-CT Department

L. Alves, E. Woods, A. Jacob, C. Abreu, S. Pereira, R. Cabral, J. John; King's College London and Guy's and St Thomas' NHS Fundation Trust, London, UNITED KINGDOM.

Aim: Due to the risk of high radiation exposure in a PET-CT facility, department design and working procedures should be optimised to ensure staff radiation doses are as low as reasonably practicable. The purpose of this study was to evaluate the dose-saving efficiency of various simple dose reduction techniques currently used in the PET Centre. Materials and Methods: Four dose reduction methods were analysed: explanation of the procedure to patient pre-injection, use of an intercom to communicate with patient post-injection, use of colour-coded system to assist with patient navigation, and use of whole-body shields when positioning the patient on the scanner. Radiation doses received by staff at each stage of the patient pathway were measured using calibrated dosimeters, and doses estimated with and without use of the above dose reduction techniques. Only patients referred for half body scans with 18F-FDG were considered. Results: Assuming a single technologist deals with 5 patients per day, the techniques investigated can result in a daily dose-saving of 5.2 μSv. The highest dose reduction was recorded for full explanation of procedure pre-injection (62% of the measured dose-saving). The use of whole body shielding reduced dose during patient set-up by 47%. Conclusion: Use of simple radiation protection methods in a PET-CT department can result in a decrease in technologist mean daily dose of 47%. This corresponds to a potential whole body dose saving of 1.3 mSv per year.

TP099

Occupational radiation exposure of nursing staff in PET facility in association with performance status of patients

M. Hosono, N. Takahara, Y. Yakushiji, K. Sakaguchi, Y. Yamada, C. Hosokawa, K. Ishii; Kinki University Faculty of Medicine, Osaka-Sayama, JAPAN.

Aim: Radiation protection is an important issue for nurses who take care of patients in PET facilities. Radiation exposure of nurses may be increased when patients have problems in activities of daily living (ADL) and need intensive nursing care. We measured individual dose of nurses in consideration of performance status of patients. Materials and methods: Individual dose of nurses was measured during PET examination through injection of FDG, nursing care, to patients' discharge from the facility. Each nurse wore 2 individual dosimeters (MYDOSE PDM-111, Hitachi Aloka Medical, Ltd.) on the chest and abdomen. Performance status of patients was recorded using Katz index of independence in ADL (Katz S et al. N Engl J Med 1983;309:1218), which is a standard method to assess ADL by categorizing into 7 grades from Index 6 (good ADL, needs no special care) to Index 0 (poor ADL, needs extensive care). Radiation doses and contact time were recorded and analyzed. Results: Nurses cared overall 902 consecutive patients, who were grouped into Index 6 of 825 patients (91.5%), Index 5 of 41 (4.5%), Index 4 of 13 (1.4%), Index 3 of 7 (0.8%), Index 2 of 6 (0.7%), Index 1 of 3 (0.3%), and Index 0 of 7 (0.8%). Mean contact time of nurses to patients was 1 min to 10 min for Indices 6 to 0. Radiation doses of nurses were correlated with ADL of patients. The difference in radiation doses between the chest and abdomen of nurses may be attributable to the geometry of shielding materials. On the basis of these results, the weighted average of exposure of a nurse was 0.25 μSv/patient. Conclusion: This approach of considering ADL of patients for dose evaluation of nursing staff was useful to optimize radiation protection countermeasures. In our facility, patients with poor ADL account for a small fraction of patients, then, how to reduce radiation exposure from good ADL patients is an important issue for reducing overall radiation exposure.

TP100

Obtaining medical isotope 99mTc by extracting and chromatography.

A. Rogov1, V. Skuridin1, E. Stasyuk1, E. Nestwrov1, E. Ilina1, V. Sadkin1, V. Chernov2, R. Zelchan3, L. Larionova1; 1National Research Tomsk Polytechnic University, Tomsk, RUSSIAN FEDERATION, 2FSBI "RI Cardiology" SB RAMS, Tomsk, Tomsk, RUSSIAN FEDERATION, 3Cancer Research Institute of Siberian Branch of the Russian Academy of Medical Sciences, Tomsk, Tomsk, RUSSIAN FEDERATION.

Radiopharmaceuticals based on the radionuclide (99mTc) are used for diagnostic studies in oncology, cardiology, endocrinology, and other areas of medicine. They can spend more than 80% of the total number of radiodiagnostic procedures. Technetium-99m has a half-life of 6.02 hours, and is a daughter product β-decay of the isotope 99Mo. To separate it from the isotope 99Mo in a medical laboratory use devices called 99Mo/99mTc generators. The basis is the chromatographic column filled with aluminum oxide adsorbed thereon 99Mo. In contrast, sorption, extraction method for separating a pair of 99Mo/99mTc is concentrated and produces highly active preparation of 99mTc low-level (5-8 Ci/g) 99Mo produced by waste-free nuclear reaction of radiative capture (n,γ) of molybdenum (trioxide) natural composition or enriched in the

isotope 98Mo. Such materials are prepared by srednepotochnyh nuclear reactors, which are widespread in Russia and in the world. The aim of this work was to study the method of separation of 99mTc from the extractant express method using a sorbent. As such sorbent investigated in gamma alumina. The objectives of the research was to study the effect of pH form of aluminum oxide on the value of their sorption capacity of 99mTc in static and dynamic modes of adsorption, as well as the determination of the distribution coefficients of 99mTc-ethyl ketone in the 99mTc-alumina. In this work a study was conducted adsorption extracted with methyl ethyl ketone 99mTc on gamma-alumina with different pH in the form of static and dynamic conditions of the process. The coefficients of distribution of 99mTc in the methyl ethyl ketone - 99mTc - alumina. The parameters of pH at which the maximum adsorption capacity of an oxide of radionuclides, and the highest yield of 99mTc (over 98%) for its subsequent allocation in the form of sodium pertechnetate 99mTc. The total duration of the separation of 99mTc from the extractant, 20 minutes, which is comparable with the time of receipt of 99mTc eluate from traditional sorption generators, and, ultimately, provides the ability to create resource-efficient environmentally friendly production of radiopharmaceuticals 99mTc. This work was financially supported by Ministry of Education and Science of the Russian Federation (RFMEFI57514X0034).

TP101

New system for production of reactor medical radionuclides tested with Lu-176

D. Seifert, M. Kropáček, M. Tomeš, J. Kučera, O. Lebeda; Nuclear Physics Institute of the CAS, v. v. i., Řež, CZECH REPUBLIC.

Aim: Development and testing of a new system for irradiation and subsequent processing of Lu-176 target. Material and Methods: A new type of an irradiation vessel consisting of external aluminum alloy cover and inner quartz tube for sample placement was designed and tested. The system is waterproof. The ampoule was designed as disposable and has been tested for He leak - achieved leakage level was in order of 2E-09 mbar.l/s and in a real irradiation conditions.Results: Experiments performed under the highest available neutron flux density have shown reproducible behaviour of the systems regarding leakage, target processing and activity recovery.Conclusion: The designed system demonstrated suitability for high-level activities production of reactor medical radionuclides, in particular of Lu-177.

TP102

First Danish experiences of Radium-223 treatment to patients with prostate cancer and bone metastases. Is it safe for the staff?

A. K. Cortsen, **A. K. Cortsen**; Rigshospitalet, Copenhagen, DENMARK.

Introduction: Ra-223 dicloride is an alfa-emitting radionuclide therapy approved for treatment of patients with castration-resistant prostate cancer and symptomatic bone metastases. In a large randomised placebo-controlled study, prolonged survival and time to bone-related complications and improved quality-of-life was demonstrated. As a calcium mimick Ra-223 binds into newly formed bone tissue, and accumulates in bone metastases. Ra-223 emits alpha-radiation with a high linear energy transfer.This radiation, which accounts for 95% of the emitted energy, kills the cells of the bone metastases, with relatively little damage to the surrounding tissues. Less than 5% of the radiation is in the form of X-ray and gamma radiation. Method: It is essential during the staffs´ handling of the Ra-223, that there is no internal contamination either from inhalation, ingestion, injection or adsorption. Therefore, we apply special safety precautions when handling the Ra-223. The staff, which participate in the direct handling of Ra-223, are measured in our whole-body-counter in the morning before, and in the afternoon immediately after handling (dispensing, administration, clean up) the Ra-223 to the patients, so we can demonstrate, that any internal contamination has been avoided. To avoid this a special protective dress is used and control measurement of gloves/hands are performed after each handling of the therapy dose. The treatment itself is simple. A dose based on the patient's weight is injected slowly over 1 minute via an intravenous cannula. After 15 minutes of observation the patient can go home. Results: As yet, Rigshospitalet is the only center in Denmark approved for the Ra-223 treatment. From May 2014 to May 2015, we have administered a total of 200 Ra-223 treatments to 60 patients on 25 different days (1-15 patients at each treatment day). The WBC measurements have demonstrated no internal contamination to any staff member. Table of Contents. Conclusion: When special radiation safety precausions are used Ra-223 is a safe treatment both for the staff and the patients. In the majority of the prostate cancer patients with symptomatic bone metastases Ra-223 reduces pain without serious side effects. On-going studies may show whether Ra-223 treatment also will be beneficial in other types of bone metastases e.g. from breast cancer.

Authors' Index

Aaberg-Jessen, C. P173
Aalbersberg, E. TP050
Aalbersberg, E. A. OP223
Aarntzen, E. OP106, P649
Abamor, E. P604
Abbas, K. OP478
Abbas Abadi, S. P252
Abbasi, M. P364, P474, P837
Abbatiello, P. P432
Abbott, E. M. PW101
Abdelhafeez, Y. PW098
Abdelhafez, Y. G. P611
Abd El Kareem, M. P575
Abd El Razek, S. P575
Abdel-Rehim, M. OP332
Abd El Samee, A. P575
Abdelwahab, H. N. M. P611
Abdi, B. P661, P838, P906
Abdul Razak, H. TP011
Abdulrezzak, U. P645
Abe, A. P555
Abe, K. OP171, OP437, P349
Abe, M. P784
Abe, S. PW088, TP008, TP020
Abe, S. P555
Abedi, M. OP477, P809
Abella Tarazona, A. OP260
Abgral, R. P778
Abid, K. A. P257
Abi-Dargham, A. OP509
Able, S. OP281
Aboagye, E. O. OP589
Abo El-Naga, E. P575
Aboudzadeh, M. P300, P322
Aboudzadeh Rovais, M. P242, P244, PW054, PW060
Abrantes, A. M. P330, PW035
Abreu, C. OP411, TP052, TP054, TP098
Abreu, P. P601, P971
Abualhaj, B. OP117
Abu Bakar, S. TP030, TP090
Abuqbeitah, M. P079
Abuqbeitah, M. M. OP529, P862
Acampa, W. OP120, OP167, OP174, P374
Acar, E. P797, P799
Acarturk, F. P963
Achten, R. P485
Achury, C. OP456, OP642
Achury, C. P700
Açıkel, S. P403
Ackerman, U. P305
Adachi, S. P686
Adães, R. TP037, TP042
Addolorato, G. OP511
Adib, S. OP361, P868
Aerts, J. OP096
Afshari, R. P406
Afshar-Oromieh, A. OP308, OP428, OP429, P099
Agarwal, V. P096
Aghevlian, S. P260
Agnese, G. P821, TP081
Agostini, D. OP505, P044
Agostini, E. OP251
Agostini, S. P512
Agrawal, A. OP149, TP073
Agrawal, K. P060
Agresti, R. P753
Agrewal, K. P593
Aguiar, B. OP327
Aguilar Barrios, J. P720, PW019, TP088
Aguilera-Grijalvo, C. P446
Ahmadpour, N. P822
Ahmad Saad, F. TP011
Ahmadzadehfar, H. OP457, OP634, P796, P832, P846, PW114
Ahmed, F. Z. P411
Ahmed, M. P086
Ahmed, N. P655
Ahn, G. P273
Ahn, S. P200
Ahrens, M. PW120
Aiga, M. OP187, P404
Aigbirhio, F. I. PW023
Aigner, R. M. P004, P277
Aillères, N. OP630
Aita, K. P486
Aitani, N. P066
Aitidir, M. P140, P819, P825, P836
Ajani, J. A. OP056
Akamatsu, G. P486
Akamoto, S. P133
Akay, O. P736
Akbari, K. P679
Akbas, H. P880
Akdemir, E. OP550, P523, P707
Akgun, A. P810, P877
Akhavein, A. P332
Akhlaghpoor, S. P845
Akhurst, T. OP293
Akiba, H. P166
Akil, S. P146, TP067
Akiyama, K. P559
Akkas, B. E. P517, P536, P541, P597, P652, P741, P963, PW077

Akpinar, E. P630
Akpinar, M. OP593
Ak Sivrikoz, I. P736, P917
Akyel, R. OP535, P538, P662
Akyol, F. P707
Akyol, H. P684
Akyuz, C. OP495, OP496, OP498
Alagoz, E. P576, P967
Alama, A. OP147, OP623
Alameda, F. P552
Aland, P. OP164, P800
Alatas, P909
Alavi, A. P241, P491, P573, P595, P598, P603, P713, P939, TP009
Al-Bahrani, G. P423
Álban, J. P675
Albanese, S. P160, P175
Albanus, D. OP549
Albayrak, R. P605, P608
Albuquerque, A. P960
Aldosary, A. S. P715
Alekseev, B. OP083
Alessi, A. OP596, P698
Alessio, M. OP445
Alexander, Y. P198
Alexanderson, E. OP124, OP173, P373, P375, P386
Alexandre, V. P499
Alexandre-Santos, L. P497, P499
Alexiou, S. P439, P464
Alfaro Rubio, F. P510
Alfieri, R. P776
Alfonso, G. P700
Algalarrondo, V. OP434
Al Ghuzlan, A. OP091
Al Harbi, M. OP548, P944, P937, PW031
Alhussieny, M. A. OP500
Ali, L. P401
Ali, M. OP259
Ali, P. OP222, P012
Ali, S. A. P082
Ali, S. Z. P119
Alibegovic, V. OP154
Aliberti, G. P753
Alimanovic-Alagic, R. P808
Alirezapour, B. P252
Aljammaz, I. P331
Al Janabi, M. OP444, P528
Allaart, C. P. OP067
Allan, S. OP343
Allegri, V. OP605
Aller Pardo, J. P847
Allolio, B. OP534, P207
Allott, L. OP589
Allsop, D. OP343
Almarcha Gimeno, A. P298, P600
Almeida, A. TP032, TP060
Al-Mohammad, A. OP113
AlMukhalid, O. M. OP548, PW031
Alnakshabandi, N. P937, P944
Alobthani, G. S. P734
Aloj, L. P36, P733
Alongi, P. OP252, OP253, OP300, OP302, OP603, P691
Alonso, J. P718
Alonso, M. P281, PW081
Alonso, O. OP296
Alonso, S. P718
Alonso Rodríguez, M. OP158, P754, P756
Alotaibi, B. P331
Al Qarni, A. P677
Alrisheq, M. F. P114
Alrumayan, f. P331
Als, C. PW076
Al-Sadoon, S. J. P114
Al-Saffar, A. P401
Alsey, K. OP257
Alshammari, A. P203
Al Shoukr, F. OP476
Altabella, L. OP112, P048, P064, P194
Altai, M. OP244, OP586
Altinay, S. P605, P608
Altini, C. OP459, P638
Altındag, S. P132
Altınyazar, V. P932
Altrinetti, V. P587
Altundağ, K. OP593
Altun Yologlu, N. P904
Álvarez Nieto, L. F. P435, P823, OP260, P692, P970
Álvarez-Pérez, R.-P. P852
Álvarez-Ruiz, S. OP370, OP371
Alves, F. OP480, P324, TP042
Alves, L. OP411, TP054, TP098
Alves, P. P110
Alves, V. OP418, P050, P371, P898
Alves, V. M. P416, P417
Alyanbawi, S. P331
Amadori, D. P703
Amaral, H. P085, P427
Amaral-Silva, H. T. P499
Amarenco, P. P385
Amaro, A. OP184
Amato, E. OP237, P861, P899
Ambrosini, V. OP552
Amelio, D. P512
Amer, H. P347
Ametamey, S. OP285, OP288, P288

Amichetti, M. P512
Amijima, H. P39
Amimour, A. P661
Amin, R. A. P611, PW098
Amini, M. P256
Amini, N. OP287
Ammari, S. OP369, OP604
Amodeo, S. OP648
Amor-Coarasa, A. OP482, OP483
Amorin, I. P481
Amo Salas, M. P104
Amoui, M. P845
Amouri, w. P441, P976
Amthauer, H. OP163
Amzalag, G. P433
An, G. P276
An, R. OP203
Anagnostopoulos, C. D. OP450
Anand, A. P912
Andersen, C. P173
Andersen, F. L. P201
Andersen, J. P162
Andersen, J. B. OP050, P003, P201
Anderson, K. OP582
Anderson, T. OP489, P335
Andersson, M. P864
Ando, A. P434
Ando, Y. P637
Andreae, F. OP611
Andreasson, K. S. P889
Andreev, S. P346
Andreou, I. P635
Andrés, A. P824
Anele, R. P047
Angarita, E. OP516
Angelelli, B. OP577
Angelides, S. OP259
Angelina, F. P860
Angelini, A. OP454
Anguera, G. P700
Angusti, T. P969, TP036
Anizan, N. OP476
Ankrah, A. O. OP111
Annunziata, G. P097, P366
Annunziata, S. P483, P708, P721
Annunziato, L. PW026
Ansheles, A. P253, P344, P389
Ansholm, J. P573, P598
Antonacci, L. OP136
Antonelli, M. OP511
Antonini, A. P475
Antón-Leal, M. P884
Anton-Rodriguez, J. PW048
Antulov, J. P749
Antúnez Almagro, C. P435
Antunovic, Z. P905
Anzillotti, S. PW026
Anzini, M. PW008
Ao, E. PW107
Apitzsch, J. OP549
Aplin, M. OP415
Apostolidis, C. OP197, OP089
Apostolova, I. OP163, P161
Appelman, Y. OP122
Arabi, M. P332
Arai, A. PW014
Arakawa, C. P784
Arakawa, Y. OP162
Aramaki, H. OP284
Aramaki, T. P636
Araman, A. OP535, P307
Aramburu González, J. P639
Araujo, J. OP238, OP309
Arbizu, J. OP646
Arıcan, P. P562, P914
Archer, J. K. J. OP448
Archibald, S. J. OP102
Ardisson, V. P304
Ardizzone, E. P771
Ardizzoni, A. OP254
Arellano-Tolívar, A. P706
Argibay Vazquez, S. P768, TP091
Arias, P. P334
Arias-Camison, I. OP157
Ariza, E. P299
Arkies, H. P586
Armor, T. OP040, OP083
Armstrong, I. S. P005
Arnaldi, D. OP561
Arnaoutoglou, M. P484
Arnberg, F. OP053
Arnoldo, V. OP414
Arora, A. OP323
Arosio, M. OP366, P121, P33, P35, PW084
Aroui, T. P632, P663, P762, P764
Aroui-Luquin, T. P680
Arques Aguilo, H. OP333
Arranja, A. PW065
Arroyo, A. G. P148
Arslan, E. P606, P607
Arslan, M. F. OP579
Arslan, N. P576, P967
Arsos, G. P850, P851, P874, P875, P945, P957
Arstad, E. P283
Artieda-Soto, C. P596
Artigas, C. OP425, P697

Artiko, V. OP349, OP350, OP442, P882
Artner, C. OP480, P269, P324
Arturo, C. OP602
Arumugam, P. OP120, OP174, P359
Arvat, E. P842
Arveschoug, A. PW078
Aryana, K. P590
Asa, S. P609
Asai, Y. TP074
Asakura, K. P636
Asano, M. P230
Asenov, Y. P873
Ashworth, S. P279
Aslan, H. P633
Aslani, A. OP196
Aslanidis, I. P. P685
Aslanidis, I. PW015
Asmussen, J. T. P713
Asopa, R. P814
Assadi, M. P332, P450, P451, P495, P505, P506, P544
Assante, R. OP120, OP174, P374
Asselin, M.-C. PW048
Åstrand, M. OP242
Asyali, M. H. P061
Atabaki, A. P929, TP075
Atasever, T. P604
Atcher, R. W. OP489
Athanasiou, K. P919
Athanasiou, V. P358, P360, P850, P851, P472, P945
Atilgan, H. I. P816, P855
Attarwala, A. A. OP010, OP015, OP117, P002
Atudosie, S. P907
Audenaert, K. OP559, PW024
Auditore, L. OP237, P861
Aukland, S. M. OP637
Auletta, L. P160, P175
Auvity, S. P111, P421
Avelar Rivas, J. OP117
Avery, G. P655
Ayala, S. P824
Ayala-German, A. OP173
Ayan, A. P630, P576, P967
Aydin, B. OP495
Aydin, F. P880
Aydın, B. G. OP498
Aydın, M. A. P684
Aygun, A. OP084, OP087, OP139, OP535, P307
Aygün, A. P862
Ayyildiz, O. P061
Azab, A. O. P611
Azarian, A. P590
Azgomi, K. P832
Azorín-Belda, M. P884
Azria, D. OP630
Azuma, K. PW040

Baank, S. TP050, TP079
Baas, F. OP064
Baba, H. P445, PW034
Babapour Mofrad, F. P910
Babich, J. W. OP482, OP483
Babin, A. V. P350
Babu, L. TP001
Babusikova, E. P614
Bacciardi, D. P793
Bach-Gansmo, T. OP039, OP295, OP599, P238
Bacigalupo, A. P728
Back, M. P551
Backer, T. OP152
Badel, J.-N. OP609
Badiavas, K. P358, P850, P472, P851, P945
Baechler, S. OP361
Baek, S. P571, P572
Baeken, C. P485, PW024
Baffa, O. P497
Bagatin, E. P512
Bagella, P. P972
Bagnasco, M. OP525
Bagni, O. PW120
Bahce, I. P320
Bahnerth, A. M. P150
Bahrami Samani, A. OP477, P859
Bahri, M.-A. P131
Bailey, D. OP086, OP196, P551, TP003
Bailey, E. A. OP086, OP228
Bailliez, A. OP189, OP505, P044
Bajén, M. P469
Bajén Lázaro, M. P946
Bajpai, J. TP073
Bakan, S. P644
Bakker, I. L. OP200, OP299, P705
Bakshi, S. OP537
Bal, A. OP594
Bal, C. OP537, TP035
Bal, J. OP063
Balaguer, D. P601, P971
Balbaloglu, O. P920
Balbi, T. OP233
Balcerzyk, M. PW009
Balci, T. OP150
Baldari, G. P272, P34
Baldari, S. OP237, OP256, P409, P522, P779, P861, P899, PW092
Baldassarre, L. OP337
Baldazzi, I. P274, P938
Balink, H. OP060

Balkan, E. P576
Balkay, L. P067
Balkin, E. R. OP479
Ballal, S. TP035
Ballinger, J. R. OP481
Balm, A. J. OP234
Balogh, L. OP205, OP342, P886
Baloka, L. P410
Balon, H. P956
Balsa Bretón, M. A. P639, P722, P760
Balsalobre Salmeron, M. P970
Baltazar, C. E. P. B. P051, P052, P425, P497
Bandholtz, S. P161
Bandiera, S. P781
Baniora, E. P439, P464
Bankstahl, J. P. OP055, P265, P424, P426
Banksthal, J. P294
Banna, G. P779
Banno, Y. TP053
Banzo, I. OP438, P436
Başoğlu, A. P918
Barai, S. OP232, P653, P658
Baraldi, C. PW087
Baratto, L. OP366, P134
Barber, D. C. OP113
Barber, T. PW110
Barberi, A. P969
Barbetti, V. TP081, P821
Barbiaux, J. OP189
Barbier, B. OP506
Barbosa, F. OP600, P197
Barbus, E. TP007
Barcikowski, T. P327
Bard, J. P456
Bardiès, M. OP422, OP487, P043, P181
Bardos, P. OP118, OP453, P30
Bargellini, I. P853
Barios, M. P978
Barios Profitos, M. P660
Barkhodari, A. OP047
Barletta, G. OP147
Barna, S. P965, TP062
Barnett, S. A. OP351
Barnhart, T. E. OP247, P267
Baron, C. PW021, PW023
Baron, T. OP052
Barowitsch, C. P277
Barré, E. P169
Barré, L. P282
Barrington, S. OP411, TP052
Barsegian, V. OP576
Bartenstein, P. OP051, OP070, OP326, OP384, P380, P866, P867
Barten - van Rijbroek, A. D. P309
Barth, G. P398
Barthel, H. OP324, OP325, OP326, OP563, PW029
Bartoletti, M. P949
Bartolini, N. TP048
Bartolomei, M. TP048
Bartolozzi, C. P853
Barton, H. P725
Bartos, A. P429
Bartosik, J. P215
Basıbuyuk, M. P132, P137
Baseric, T. P710
Basher, R. K. P719
Basim, P. P604
Bassi, P. F. P876
Basso, U. OP631
Bastien, J. B. OP455
Bastug, E. P605, P608
Basu, S. P814
Batalov, R. P388
Bath, L. P912
Battara, G. P046
Bauckneht, M. OP472, OP540, P394, PW018
Bauder-Wüst, U. OP337, OP426
Baudin, E. OP091
Bauer, M. P069
Bauer, W. R. OP433
Bauersachs, J. OP475
Baum, R. P. OP037, OP140, OP141, OP192, OP239, OP430, OP533, P089, P640, PW116
Baumgartner, C. OP474
Baun, C. OP190, OP417, P573, P595, P598, P603
Bauwens, M. PW061
Baydar, D. P707
Byaraktutan, Z. P630
Beatovic, S. OP349, OP350, P882
Beaurain, M. P281
Beauregard, J. M. OP093, P801
Bebbington, N. A. OP451
Becavin, S. OP276
Becherer, A. P526
Bechir, N. P815, P817, TP084
Bedini, A. P954
Bedini, N. P698
Bedodi, L. P753
Bedreli, S. OP576
Beek, A. M. OP067, OP123
Beekman, F. J. OP501
Beels, L. P023, P57
Beer, A. OP141, OP615
Beer, A. J. OP618
Beerens, C. OP388, OP391
Beganovic, A. P615

Beheshti, M. OP154, P679, P922, TP009
Behrendt, F. OP549
Beiderwellen, K. P205
Beijst, C. OP357, PW097
Beiki, D. P256, P364, P477, P668, P809, P822, PW063
Beindorff, N. P161, P171, P177, P226
Bekker, A. PW078
Bekku, E. P636
Bektas, S. P598
Belho, E. S. OP554, P659
Bellabas, S. P661
Bellabes, A. P906
Bellendorf, A. OP013, OP043, P205, P854
Bello, L. P547
Bello, M. P227, P739
Bello Arqués, P. OP580, P761, P765, P767, TP014
Bellón Guardia, M. E. OP461, P717, P752
Bellusci, A. OP301
Belokon, Y. P288
Beltramo, G. OP249
Belz, M. P412
Benabdallah, N. OP134
Benadda, S. P906
Benali, K. P385, P936
Bénard, F. P284
Bénard, S. OP104, P149
Ben Azzouna, R. OP434, P362
Bender, D. OP294
Bender, D. A. P240
Benesova, K. OP368
Benesova, M. OP308, OP426, OP429
Ben Fredj, M. P531
Bengel, F. OP055, OP513, OP546, P265, P424, P426, P911
Ben Ghachem, T. P013, P818, P835
Benitez Segura, A. P469, P946, P947
Ben-Jacob, E. P503
Benjaminsen, C. P003
Bennani Doubli, S. P921
Bennedbæk, F. N. OP152
Bennink, R. J. OP060
Ben-Reguiga, M. OP332
Ben Sellem, D. P224, P815, P817, P818, P924, PW079, TP084
Ben Slimene, M. P220, P224, P815, P817 P818, P835, P916, P924, PW079, TP084
Benso, F. P442, P444
Benti, R. OP635, P383, P729, PW027, PW108
Bentivoglio, A. R. P483
Benz, D. OP188
Beppu, T. PW034
Bera, G. OP538
Berardi, G. OP252
Berdelou, A. OP091
Berding, G. OP055, OP513, P424, P426, P911
Beresova, M. OP629, P848
Bereznitskiy, V. PW015
Bergamini, A. P714
Bergantin, A. OP249
Bergmann, R. OP138
Bergström, K. P314, TP010
Bermejo-de las Heras, B. P413
Bernardes, M. P371
Bernardini, M. OP134, OP335
Bernasconi, S. OP421
Berndt, M. OP341
Bernhardt, P. OP014, OP334, P803, P889
Bernsen, M. PW065
Bernsen, M. R. OP200, P150, P231
Berriolo-Riedinger, A. OP590, OP627
Berrios-Barcenas, E. P373, P375
Berroteran-Infante, N. PW004
Berthier, M. L. P510
Berthold, C. OP335
Berti, S. P475
Berti, V. OP126
Bertia, M. P899
Bertolazzi, L. P821, TP081
Bertolini, A. OP367
Berzaczy, G. OP574
Besenyi, Z. PW085
Beslic, N. P615
Bessolova, O. P518, P564
Best, J. OP576, P854
Betti, F. OP136
Betzel, T. OP288
Beugeling, M. P301
Beuthien-Baumann, B. OP046, OP363
Beyer, T. OP044, OP416, OP449
Beykan, S. OP194, OP491, P020, P022, P857
Beynon, G. P112
Bezante, G. PW018
Bezzon, E. P584
Bhalla, R. P312
Bharadwaj, T. OP164, P800
Bhati, A. P060
Bhattacharya, A. P092, P593, P719
Bhayana, R. OP537
Bhoori, S. OP424
Bhusari, P. OP041, OP594, P092, P261
Bhutani, M. S. OP056
Bianchi, A. P739
Bianchi, C. TP069
Bianchi, G. P232, P233, P234, P236
Bianchi, L. OP249, OP439, PW071
Biava, M. PW008
Bidault, F. OP091, OP604

Bidder, R. P012
Biello, F. OP147
Biermann, M. OP637
Bigler, R. P569
Bilen, C. Y. P707
Bilewicz, A. OP478, OP583, OP584
Bilgic, S. OP579, P843
Bilgin, E. TP095
Bilgin, M. P403
Bilgin Büyükkarabacak, Y. P918
Bilha, S. P071
Billard, T. TP049
Binse, I. OP013
Binzel, K. OP118, OP453, P103, P30, P856, PW074
Bir, F. P633
Birbe, R. P083
Bird, N. OP508
Biricotti, M. PW032
Birkenfeld, B. P216
Birkmann, S. P280
Birnbaum, E. R. OP479
Biryukov, V. A. P685
Bisi, G. OP575
Bisoi, A. K. P367
Biterlich, N. OP192
Bize, P. P868
Bjartell, A. P912
Bjelan, M. P126
Bjerring, O. S. OP059
Blagic, M. OP350
Blaire, T. OP189, OP505, P044
Blakkisrud, J. OP039
Blanchet, E. P936
Blanco Pérez, E. TP088
Blex, S. P37
Bloemendal, H. J. PW113
Blomberg, B. A. OP362, P100
Blower, P. J. OP481, OP621, P155, P156
Bluemel, C. OP194, OP277, OP534, P207, P527, P766
Blum, M. A. OP056
Blykers, A. OP343
Bobin, C. OP616
Bochev, P. P620, P623
Bockisch, A. OP013, OP043, OP156, OP536, OP576, P037, P690, P854
Bodei, L. OP193
Bodini, B. PW021
Boellaard, R. OP362, OP419, P100, P105, P320 P774, P777
Boemio, A. OP071, P363
Boér, K. OP062
Boerman, O. OP106, OP198, OP394, P188, PW069
Boerman, O. C. OP105, OP202, OP204, OP420, OP485, OP488, P266, P318, P690, PW066
Boersma, H. H. OP124, OP173, P301, P381
Boers-Sonderen, M. J. OP420
Bogdan, A. P462
Bøgeskov, L. OP494
Bogsrud, T. V. OP295, OP599, P238
Böhler, T. G. P526
Božinović, M. OP441
Boisgard, R. OP104
Boisgard, R. P111, P421
Bojaxhiu, B. P569
Böker, A. P911
Boladeras-Inglada, A. M. PW038
Boländer, A. P168
Bolis, S. OP366
Bolomatov, N. PW011
Bolouri, F. P242
Bolstad, B. OP039
Bom, H.-S. P772
Bomanji, J. OP548, P203, PW031
Bonazza, A. P961
Bonelli, M. OP583
Bonfiglioli, R. OP454, P940, P949
Bongarzone, S. OP099
Bongioanni, F. OP147, OP540, P234, P394, P587, P728, PW025
Bongiovanni, A. P798
Boni, G. OP136, OP421, P853, PW032
Böning, G. OP384, P866, P867
Bonnet, R. P640
Bonora, M. OP601
Bonstanjiopoulou, S. P482, P484
Bonte, S. OP559
Bonuccelli, U. OP647, P480, PW030
Bonvoisin, C. P090
Booij, J. OP069
Boot, E. OP069
Borbely, J. P292
Borbély, K. OP062
Bordenave, L. P986
Borel Rinkes, I. H. M. P648
Borget, I. OP091
Borghammer, P. OP109, OP292, OP294, OP644, P124
Borghi, G. OP502, P199
Borgwardt, L. OP494
Borovecki, F. P438
Borre, M. OP292, OP294
Borrego-Dorado, I. P852
Borrelli, P. OP580, P761, P765, P767, TP014
Borsatti, E. P710
Borsò, E. OP136, OP421, P442, P444
Borys, D. P043, P145
Bos, D. OP198, OP202, OP395, OP611, P188

Boschi, A. P227, P250
Boschi, F. OP112, OP484
Boschi, S. P709, PW051
Bosmans, T. P485
Bossert, I. OP598, P430
Bossi Zanetti, I. OP249
Botelho, M. F. P110, P330, PW035
Botello, M. OP480
Botta, F. OP330
Bottlaender, M. PW021
Bottoni, G. OP525, OP623, P236
Botushanowa, A. P895
Boubaker, A. OP361, P868
Bouchelouche, K. OP121, OP292, OP541 TP065, TP066
Bouchet, F. OP038, P164
Boudali, M. P619
Boudousq, V. OP280, OP487
Boudriga, H. P220, P916
Bouillot, C. OP052
Bouladhour, H. OP547, P370
Bourgeois, M. OP276
Bourhis, D. P778
Bourhis, J. OP298
Bournaud, C. OP597
Boussi-Gross, R. P503
Boustani, A. PW037
Bouter, C. OP297, OP393
Bouterfa, H. OP307, OP491
Boutin, H. OP343, P328
Boutley, H. P392
Boutruigua, h. P815, P817, TP084
Bouyoucef, S. E. P661, P838, P906
Bouzidi, n. P441
Bouziotis, P. OP450, P319
Bove, F. P483
Bovy, C. P090
Bowles-Antelo, H. P413, P600
Boya-Román, M. P469, P508, P831, P946, P947
Boye, K. OP637
Bozkurt, M. P340
Bozkurt, S. P880
Bozza, F. P584
Braat, M. N. G. J. OP329, OP423
Bracic, I. P749
Bradley, A. P005
Bradley, K. M. P078
Brændgaard, H. OP322
Bragina, O. P757, P758
Brambilla, M. OP639
Bramis, G. P245
Brandal, P. OP599
Brandão, F. P716
Brandl, J. OP474
Brans, B. OP092, OP263, PW061
Bravo-Ferrer, Z. OP438, P436
Breeman, W. A. P. OP489
Brendel, M. OP051, OP326
Brenner, W. P161, P171, P177, P226
Bressan, S. P475
Bretin, F. P131
Brink, A. P903
Brinks, P. OP524
Brink-Wieringa, M. TP083
Brito, A. F. P330, PW035, PW035
Brito, M. M. C. M. P42
Brizzolara, A. P234
Broccoli, A. PW089
Brock, B. OP322
Brockhuis, B. P610
Broggi, S. OP603
Broholm, H. OP494
Brolin, G. OP383, P215
Brom, M. OP198, OP202, OP395, OP611 OP612, P266
Brom-Attard, M. TP025
Brøndserud, M. B. P942
Bronsert, P. PW082
Brooks, D. OP648
Brooks, D. J. OP644
Broos, W. OP263
Brown, C. J. P456
Brown, G. P328
Bruce, I. P198
Bruchertseifer, F. OP197, OP280, OP394, OP485, OP488, OP489, OP583
Bruchertseifert, F. OP089
Brugnolo, A. OP561
Bruijnen, R. C. G. OP423
Brumberg, J. OP645
Brunegraf, A. OP384, P867
Brunelli, C. PW018
Brunetti, A. P175, PW026
Brunetti, V. OP356
Bruno, A. P701, TP069
Bruno, I. OP511
Bruno, S. P232, P233, P236
Brunocilla, E. P709
Brunotte, F. OP506, OP590, OP627
Brusasco, G. OP544
Brust, P. P017, PW003
Bsiss, M. P921
Buccino, P. OP327
Buchegger, F. OP298
Buck, A. OP035, OP194, OP277, OP433, OP475, OP534, OP645, P180, P207, P285, P527, P766

Buckle, T. OP234, P191, PW064
Buckley, C. OP648
Buda, A. PW084
Budan, F. P073, P151
Budikova, M. P376
Buffoni, F. PW108
Buga, K. P355, P664
Bui, C. OP168
Bui, F. OP440, P475
Buijs, J. OP582
Bukhari, S. H. P287
Bulcourt, S. P302
Bulla, S. PW082
Bullich, S. OP324, OP325, OP563, PW029
Bulten, B. F. TP043
Buncová, M. P377
Bundschuh, R. OP634, OP457, P180, P554, P832, P846, PW114
Bunjes, D. OP615
Bunko, H. OP169
Bunschoten, A. P193
Burei, M. P790
Buresta, T. P476
Burg, D. OP617
Burger, C. P492
Burger, I. OP116, OP600
Burgos, N. OP160
Burke, B. P. OP102
Burley, T. OP588
Bursics, A. P217
Burton, M. L. TP057
Bús, K. P664, P886
Buschiazzo, A. OP561, P232, P233, P234 P236, PW025
Buscombe, J. R. OP193
Busetto, A. P961
Busk, M. P240
Buskevica, I. P598
Busnardo, E. OP252
Bussink, J. P627
Busstra, M. OP299, P705
Buteau, F. A. OP093, P801
Buttari, F. OP558
Buvat, I. OP387, P421
Buxbaum, S. P689
Buyssens, P. P865
Buziak-Bereza, M. P666, P792
Buzo, R. P481
Buzogány, I. OP083
Byun, B. OP614, PW028

Caballero, E. P601, P971
Caballero-Garate, A. P600
Cabbanè, G. P899
Cabral, R. TP098
Cabrejo, L. P385
Cabrera Martin, M. P093, P125, P128, P941, P975
Cabria, M. OP472, OP598, OP598, P587
Cabrini, G. P943
Cacciari, G. OP552
Caetano, A. C. C. TP013
Caglar, M. OP413, OP495, P340, P523, P968, P983
Cagnin, A. P475
Cai, H. P235, P239
Cai, W. OP247, OP394, OP585, OP620, P267
Caille, F. P421
Cakir, A. P604
Cakir, T. P604
Calabrese, L. P594, P724
Calabretta, R. OP125
Calais, J. P936
Calamia, I. OP472, OP525, P728, PW018
Calandrino, R. OP252
Cala Zuluaga, E. P093, P125, P408, P941, P975
Calcagni, M. OP626, P721
Caldarella, C. P708
Cal-Gonzalez, J. OP449
Calia, G. M. P972
Caliceti, U. OP301, OP605
Callahan, J. OP351
Caloiero, M. TP069
Caltagirone, C. P459
Calvo-Campos, M. PW038
Camacho, A. OP506
Camacho, V. OP642, P553
Camardese, G. P483
Cambioli, S. OP108, OP310, OP532, P135, P683, P781, P940, PW089
Camden, B. OP259
Cammelli, S. OP301, OP605
Camozzato, T. S. C. TP046
Campana, D. OP552
Campbell, S. OP337
Campen, M. P335
Campenni', A. P522, P861, P899, PW092
Campi, C. PW025
Campos, A. PW103
Campos, L. P759
Campos, P. P315
Campos Villarino, L. P120, P520, P533
Can, C. P137
Can, U. P879
Cananzi, C. P821, TP081
Canbaz, F. P745, P918
Cáncer Garza, L. F. P824
Candal Casado, I. P221

Candiani, M. P714
Cano, F. OP327
Canpolat, S. P981
Cantinho, G. TP004
Cantoni, V. OP167
Can Trabulus, F. P606, P607
Canzi, C. OP635, P729, PW108
Cao, J. P176, P625
Caobelli, F. OP302, OP546
Çapa Kaya, G. P797, P799
Caparrós, X. PW081
Capasso, E. OP036, P296, P699
Capdevila Castillón, J. P660
Capet, R. P953
Capitanio, S. P701
Caplin, M. E. OP548, PW031
Capobianco, D. P704
Capobianco, G. P733
Capogni, M. OP616
Caponnetto, C. PW025
Cappelli, A. OP233, OP577, PW008
Caprio, M. G. OP445
Capriotti, G. P643
Carabelli, E. P442
Caraceni, A. P753
Caracò, C. P733
Caramelo, F. TP070
Carapelle, E. P431
Carbone, G. P512
Carcoforo, P. OP353, P769
Cardinale, J. OP426
Cardona, V. P824
Cardona Arboniés, J. P847, P848
Cardoso, G. OP636
Cardoso, L. P893
Cardoso, M. P299
Carles, M. P106
Carletto, M. OP578
Carlsen, J. OP051
Carlstedt-Duke, J. P264
Carmagnani, E. P934, P950, P964, TP063
Carmo, S. OP480, P324
Carmona, S. OP159, P923
Carmona Asenjo, E. P646
Carneiro, M. PW103
Caroli, P. P046, P703, P798
Carolino, E. OP184, TP004, TP013, TP016, TP028, TP047, TP071
Caronni, M. P383
Carotenuto, R. OP071, P363
Carp, L. P557
Carpinelli, A. PW008
Carranco, T. P931
Carraro, A. OP414
Carreras Delgado, J. P093, P125, P128, P138, P408, P746, P941, P975, PW020
Carril, J. M. OP438, P436
Carrilho, F. P893
Carrilho Vaz, S. P716
Carrió, I. OP456, OP642, P553, P700
Carroll, L. OP589
Carroll, M. J. OP448
Cartier, C. PW095
Cartigny, F. P169
Cartron, G. OP422
Carvalho, A. PW103
Carvalho, P. I. P716
Casadio, C. P095
Casali, M. OP012
Casalta-Lopes, J. P898
Casanova, R. OP116
Casanova Martins, M. OP222
Casáns-Tormo, I. P413, P600
Casazza, G. OP421
Cascianelli, S. P468, P476
Casi, M. TP048
Casolo, A. P954
Cassano, B. OP236
Cassidy, C. OP509
Castagnoli, H. OP125
Castell, J. P537, P978
Castellani, M. OP635, P383, P729, P753, PW108
Castellano, G. OP327
Castellanos, T. P718
Castell-Conesa, J. P534, P568, P660
Castello, A. OP302
Castellón Sanchez, M. OP260, P692, P435, P823, P970
Castellucci, P. OP254, OP301, OP454, OP605, P135, P683, P940, P949
Castelluccia, A. OP626
Castillejos Rodríguez, M. P639, P722, P760
Castillo Berrio, C. P120, P520, P533, P759
Castillo Gallo, E. P639
Castillo Gómez, J. P161, P171, P177
Castrillón, M. P120, P513, P759
Castrillón Sánchez, M. A. P520, P533
Castro Beiras, J. P354
Catafau, A. M. OP324, OP325, OP563, PW029
Catalano, M. P097, P366
Catalano, R. P458
Cavanagh, J. P453
Cavatorta, G. OP640
Çavdar, I. OP529
Caviglia, G. P233, P236
Cavina, R. OP602
Cavo, M. P739

Cawthorne, C. OP102
Caykoylu, A. P541
Cazacu, A. P306
Cazzato, M. PW104
Cecchin, D. OP440, P475
Ceci, F. OP254, OP454, P949
Cecilia, D. P174
Celebi, F. PW033
Celen, Y. P132, P137
Celik, A. P605, P608
Celik, B. P918
Celik, F. P351
Celkan, A. P963
Celler, A. OP385
Cengiz, A. P932
Cengiz, M. OP150
Čepa, A. P259, P377
Cepedello Boiso, I. P585
Ceravolo, R. OP647, P480, PW030
Cerchione, C. P730
Cerciello, V. P36
Ceriani, L. P563
Ceric, I. P215
Ceric, S. P615
Ceric, T. P615
Çermik, T. P606, P607
Cerrotta, A. OP596
Cervino, A. OP251, OP631, P584, P588, P710
P776, P790
Ceylan Günay, E. P909
Cha, M.-J. P988
Chabi, N. P495
Chae, J. P143
Chakraborty, S. P261
Challouk, N. P170
Chambron, J. OP231
Champiat, S. OP369
Champion, C. OP279
Chan, C. PW070
Chan, D. P694
Chan, D. L. OP196, P551
Chan, H. S. OP489
Chan, J. G. P305
Chan, S.-C. P560, PW083
Chan, S. P326
Chana, P. P085
Chanakhchyan, F. PW011
Chandrak, P. OP164, P800
Chandrasekharan, P. P264
Chang, C.-J. OP460
Chang, C. P176, P390
Chang, C.-C. P955
Chang, D. P270
Chang, H.-C. P313
Chang, K.-P. P560
Chang, Q.-L. P828
Chang, Y.-H. P418
Chang, Y.-C. OP460
Chantry, A.-S. P297
Chao, A. OP460
Chapelon-Albric, C. P362
Chapleur, Y. P293, PW059
Charalampakis, N. OP056
Charfeddine, s. P441, P976
Charfi, H. P976
Charles-Edwards, E. P725
Charoenphun, P. TP005
Charon-Barra, C. OP590
Chatalic, K. L. S. OP488
Chatti, K. P152
Chatziioannou, S. N. P802
Chatzioannou, A. OP195
Chaudhuri, P. OP164, P800
Chauhan, M. P592
Chaumet-Riffaud, P. OP538
Chaushev, B. P620, P623
Chauvie, S. P739
Chauvierre, C. OP476
Chaves, S. OP418, P050, TP070
Che A. Halim, K. TP030, TP090
Chehade, F. P849
Chen, C. L. P291
Chen, F. OP247, P267
Chen, H.-W. P828
Chen, H. P622
Chen, L. OP507, P625
Chen, M.-K. P144
Chen, Y. P070
Chen, Y.-W. P828, P984
Cheng, C.-Y. P144, P452
Cheng, M.-F. PW017
Cheng, Y. P185
Cheng, Z. P901
Che Nordin, M. TP011
Chentli, K. P906
Chequer, R. P362
Cherk, M. PW110
Cherk, M. H. P091
Cherkaoui Salhi, G. P140, P529, P539, P819
P825, P836
Chernov, V. P321, P757, P758, TP100
Chernova, A. PW015
Chernyshova, A. P757
Chevassut, T. P725
Chevrette, A. OP323
Cheze-le Rest, C. OP305, P627

Chiacchio, S. OP647, P853, PW032
Chiam, Q. OP168
Chiang, C.-C. P55
Chiang, F.-Y. P828
Chiang, P.-F. P516
Chiappa, V. OP596
Chiaramida, P. P36, PW120
Chiaravalloti, A. P432, P458, P459, P678
Chien, K.-L. PW017
Chierichetti, F. P512
Chiesa, C. OP330, OP424, OP613
Chijevskaya, S. P758
Chin, B. OP040
Chincarini, A. OP561
Chiò, A. PW025
Chiti, A. OP146, OP532, OP601, OP632, P018, P271, P308, P547
Chittenden, S. OP137, OP235
Chiu, C.-C. P984
Chiu, N. P622, P897
Chiva, L. P718
Chnina, C. OP189
Cho, B.-B. P159
Cho, I. P206, PW012
Cho, S.-H. P621
Cho, W. P467
Cho, Y. P143
Choi, C. OP614, PW028
Choi, J. OP245, P008, P467, PW039, TP024
Choi, K.-H. OP100
Choi, P.-S. P270
Choi, S. PW036
Choi, W. P565, P616
Choi, Y. OP258
Choinski, J. OP478, OP584
Chorfi, h. P834
Chosia, M. P216
Chou, H.-H. OP460
Choudhury, G. P059
Choudhury, P. S. OP058
Chouin, N. OP038, OP276, OP280, OP487, P164
Choukry, S. P140, P529, P539, P819, P825, P836
Choynzonov, E. P758
Chrapko, B. P407, P412
Chrétien, F. P293
Christensen, B. TP059
Christensen, J. B. P783
Christensen, N. L. P021
Christlieb, S. B. P491, PW049
Christoforidis, T. P360
Chroustova, D. P952, PW073
Chu, H.-H. P313
Chu, Y.-H. P516
Chuamsaamarkkee, K. OP621, P155, P156
Chuang, K. S. P075, P055
Chun, K. P206, PW012
Chung, M.-L. P828
Ciarmiello, A. P098, P275, P442
Cicoria, G. OP310, OP452, OP532, OP633, OP638, P026, P227, P250, PW051, PW055, PW111
Cidda, C. P272, P34
Cieszykowska, I. P327
Cijevschi-Prelipcean, C. P071
Cillero Etxebeste, I. OP157
Cimitan, M. P710
Cimmino, C. P730
Cina, A. P876
Ciobota, D. M. OP588, OP619
Cioni, R. P853
Cipollini, F. OP125
Ciprotti, M. OP293
Cistaro, A. PW025
Cisternino, S. P111
Cittanti, C. OP353, P769
Civollani, S. OP577
Claessens Joosten, L. PW069
Claesson, K. OP240
Clark, T. P059
Clarke, D. PW048
Clarke, M. OP415
Clark-Frew, D. P456
Claudin, M. P397
Claver Valderas, M. OP260, P435, P692, P823, P970
Clement, A. P420, P463
Clemente, G. S. OP102
Cmunt, E. OP368
Coaguila, C. OP547, P370
Cobo Rodríguez, A. OP158, P754, P756, P902
Cocciolillo, F. OP511, P483
Cochet, A. OP255, OP590, OP627
Coco, S. OP147
Coda, A. PW026
Codegone, A. P842
Coelho, P. P898
Cohen, F. OP538
Cohnen, J. OP536
Cohrs, S. OP243
Cola, S. TP085
Colabufo, N. OP286
Colin, D. J. P178
Coliva, A. PW008
Collarino, A. OP229, P589, P958
Collet, C. P293, PW059
Collin, B. OP506
Colombo, C. B. OP367
Colombo, E. S. P335

Colpo, N. P284
Comtat, C. P131
Concia, E. P934, P950
Conde-Muino, R. P680
Conesa, G. P470, P552
Cong, X. PW037
Connell, M. P059
Constantinescu, C. P491
Conte, P. P588
Conteduca, V. P703
Contu, S. P525
Conversano, L. OP110
Cook, R. P551
Cooke, J. P655
Cooper, M. S. OP481
Coppolino, P. PW092
Corazza, A. OP633, PW111
Corcoran, B. P076, P032, TP060
Corcoran, B. J. P40
Cordero García, J. M. OP461, P717
Cornelissen, B. PW053
Cornhill, R. P839
Coronado, M. P788
Coronado Poggio, M. P711
Corovai, A. P395
Corrigan, A. TP052
Corsini, G. U. PW030
Cortelezzi, A. P729
Cortese, N. OP146
Cortes Hernandez, J. P768
Cortes-Rodicio, J. P001, P068
Cortés-Romera, M. P446, P706, PW038
Cortsen, A. K. TP102, TP102
Cosentino, F. PW092
Cosentino, S. P779
Costa, A. F. PW118
Costa, A. PW027
Costa, G. OP553, OP553, P673, P675, P893, P960
Costa, L. P671
Costa, P. OP185, OP480, P324, PW103, TP068
Costa, S. OP452, PW055
Costa, T. G. TP046
Costanza, V. P287
Cot, A. PW045
Courbon, F. OP255
Courteau, A. OP422, P181
Couso Cambeiro, B. P763
Coutant, C. OP590
Couto Caro, R. P746, P941
Couturier, O. F. OP038, P164
Covello, A. P643
Cox, M. OP383, OP616, PW104, PW106
Cozar Santiago, M. P720, PW019, TP088
Cozzella, L. PW104
Cracco, E. P961
Craciun, L. OP480
Craig, A. J. OP382, PW101, PW119
Cravello, L. P459
Craven-Bartle, J. P553
Cremonesi, M. OP330
Crespi, A. P121, P33, P35
Crestani, B. P362
Crippa, F. OP424, OP596, OP613, P698, P753
Crippa, M. P194
Crisan, M. TP007
Crisci, S. P733
Cristinacce, P. P198
Crivellaro, C. OP366, P134, P33, PW084
Crlikova, Z. PW068
Crouch, J. OP648, OP648
Croué, A. P164
Cruz-Mendoza, R. P373
Cselényi, Z. P498
Csiki, Z. P965
Csipkés, R. P153
Cuberas-Barrós, G. P568
Cucca, M. P934, P950, P964
Cuccaro, A. P721
Cucchi, C. P698
Cucinotta, M. P899
Cuevas, F. P299
Cullen, D. P081, P869, PW105
Cullier, A. P420, P463
Cullinane, C. OP481
Cummings, C. P872
Cunha, L. OP185, OP480, P324, P610, PW103, TP068
Cunha, T. P755
Cuocolo, A. OP071, OP120, OP167, OP174, OP445, P363, P374
Currie, G. OP480, P324
Cusato, G. OP110, P943
Cutaia, C. OP528, OP544
Cutler, C. S. OP479
Cuzzocrea, M. OP366, P33, P35, PW084
Cwikla, J. B. OP193
Cydzik, I. OP478
Cyran-Chlebicka, A. P567
Cytawa, W. P610
Czepczyński, R. OP497
Czibor, S. P355, P473
Czmielewski, C. OP624
Czyz, J. P743, P744

Dabasi, G. OP083, P664, P886
Dabbagh, V. P406

Dabbagh Kakhki, V. P566
Dabelić, N. P535
Dabkowski, A. P287
Dabli, D. OP038
Dachena, G. P468, P478
da Costa, L. G. PW118
D'Addessi, A. P876
Dadpour, B. P406
Daerr, S. OP326
Daghighi, M. P566
D'Agostino, G. R. OP632
Daher, J. P849
Dahlbom, M. P067
Dahle, J. OP039, OP422, P162, P181
Dal Bello, M. OP623
Dalianis, K. P209, P213, P365, P635
Dalm, S. OP392, OP490
D'Alterio, C. P160, P175
Dam, J. S. OP491
Dam, J. H. OP582, P173
D'Amato-Brito, C. P178
D'Ambrosio, L. P36
Damian, A. OP327, OP516, P481
Damle, N. OP537
Danad, I. OP123, OP126
Dancheva, Z. P620, P623
Danch-Wierzchowska, M. P145
Dandekar, G. P180
D'Andrea, M. PW104
Danek, A. OP326
Daniel, A. P716
Daniele, S. OP120, P374
Danieli, R. P432, P459, P678
Danielsen, E. H. OP644
Dank, M. P591
Dansilio, S. OP327
Daou, D. OP547, P370
Da Pieve, C. OP588, OP589, OP619
Darcourt, J. P152
Dardonville, Q. P281
D'Arienzo, D. P374
D'Arienzo, M. OP616, PW104, PW120
D'Arrigo, C. P771
Dash, A. P261
Datseris, I. P245, P319, P670
Datseris, I. E. P619
Dávila, G. P510
Davis, B. J. TP057
Davis, I. OP293
Davison, H. P200
Davran, F. P880
Day, K. OP415
Dazzi, C. OP310
Deandreis, D. OP091, OP369, OP604
Deantoni, C. OP256
De Arcocha-Torres, M. OP438, P436
Deasy, J. O. OP624
de Ayala Fernández, J. Á. P104
Deberdt, W. OP323
Deblaere, K. OP559
de Blois, E. OP299, OP489, P705
de Boer, S. A. OP473, P381
de Bruijn, R. S. P150
Debus, J. OP428, P099
De Carli, F. OP561
DeCastro, P. OP352
Decensi, A. P587
Declerck, J. P490
de Costa, R. OP259
de Cristoforo, V. OP353, P769
Decristoforo, C. OP101, OP530, PW056
Dede, F. P650
Dede, K. P217
Dedeurwaerdere, S. P172
De Fazio, L. OP367
De Felice, P. PW104
De Forges, H. PW095
de Galiza Barbosa, F. P200
De Geus-Oei, L.-F. P627, P649
De Giorgi, U. P703
Degli Uberti, E. P769
De Haan, S. OP067
de Haas, H. J. P381
Dei Rossi, F. P961
de Jong, A. OP362, P011, P100
de Jong, B. M. TP058
De Jong, D. OP106
de Jong, H. W. A. M. OP357, P043, PW097
de Jong, I. OP617
de Jong, J. TP083
de Jong, M. OP200, OP299, OP336, OP388, OP391, OP392, OP488, OP489, OP490, P043, P150, P179, P231, P705, PW065
de Jonge, F. A. A. P863
de Keizer, B. PW097
de Klerk, J. M. H. P402, TP058, PW113
de Labriolle Vaylet, C. OP134
de la Fuente, A. OP327, PW058
Delage, J. OP298
de Langen, A. J. OP362, P100
de Laroche, R. P778
De la Torre Tomas, A. OP629
De Lauro, F. TP048
Del Ciello, A. P708
De Leonardis, F. OP499
Delgado, M. P824

Delivuk, M. P514
Delker, A. OP384, P866, P867
Dell'Acqua, A. P714
Dell'Agnello, G. OP323
Dell'Amore, A. P129
Della Porta, M. P793
Dellavedova, L. OP578, P378
Dell'Oca, I. OP603
Del Mastro, C. P274
Del Pino Montes, J. P931
Delpon, G. OP305
Del Pozzo, L. P165
Del Prete, M. OP093, P801
del Puig Cózar Santiago, M. OP592
del Saz Saucedo, P. P104
del Sette, M. P442
Delso, G. P197, P200
Del Vecchio, S. OP303, P237, P730, P780
Demailly, F. P437
de Manzoni, G. P964
De Matteis, G. OP071, OP167, P363, P374
de Miguel-Medina, C. P596
Demir, M. OP529, P079, P731, P862
Demircan, K. P154, P816
Demirci, E. OP084, OP087, OP139, OP535, P307, P862
Demirel, B. P517, P597, P652, P741, PW077
Demirelli, S. P880
Demirev, A. P656
Demiri, E. P957
Demirkazık, F. OP593
Demirtas, S. P597, P652, P741
Demmery, A. OP261
Democrito, A. P233
Dempsey, M. P108, P109
Denat, F. OP427
Denes, A. PW022
Deng, H. P123, P618
De Nicolo, C. PW055
Denis-Bacelar, A. M. OP137, PW115, PW101, PW119
Denisenko-Kankiya, E. PW011
Denkova, A. PW065
Dennler, P. OP199
Denys, A. P868
De Olaiz Navarro, B. P639
De Paola Chequer, R. OP434, P936
Depardon, E. OP627
De Ponti, E. OP366, P121, P134, P33, P35
Deprez, K. OP504
De Quintana, C. P553
Dercle, L. OP091, OP369, OP604, P399
De Renzo, A. P730
Derevyanko, E. PW015
de Roos, R. R. P309
De Rosa, V. OP303, P237, P780
D' Errico, V. P046, P798
Derrien, A. TP086
de Ruiter, M. OP234
Desai, A. OP486
Desar, I. M. E. OP420
Desbordes, P. OP161
Desbrée, A. OP134, OP335
Descamps, P. OP038, P164
Deshayes, E. OP630, PW095
de Smet, B. J. G. L. P402
Desmoulins, I. OP590
De Sousa, T. TP003
de Sousa, V. OP636
De Souza, A. Z. P. TP046
De Spiegeleer, B. PW024
Despot, M. P540
Després, P. OP093
de Swart, J. OP200, P150, P231
De Teresa Herrera, M. OP629
de Teresa Herrera, R. P847, P848
Deuther-Conrad, W. P017
De Vincentis, G. OP066, OP236
De Vivo, S. P129, PW087
De Vos, F. P466, P485, PW024
Devous Sr, M. D. OP323
de Vries, E. OP048, OP054, OP111, OP283, OP510, OP617, P420, P422
Devriese, J. P57
Dewaraja, Y. K. OP380
de Weijert, M. P188
de Wit, N. OP329, P309
de Wit-van der Veen, L. J. OP230
de Wit-van Veen, L. TP050
De Zani, D. P019, P511, P974
Dhaouadi, B. P224, P924, PW079
Dhawan, D. P060, P261
Dhilly, M. P282
D'Hoe, E. P199
Díaz Alarcón, J. P585
Díaz Exposito, R. P298, P413, P600
Diaz-Garcia, O. PW009
Diaz Gonzalez, L. G. P931
Díaz Platas, L. P298
Di Bella, G. P409
Di Biagio, D. P432, P678
Di Capua, A. PW008
Dichgans, M. OP471
Di Ciolo, L. P821, TP081
Dickerscheid, D. B. M. OP524
Dickson, J. C. OP114, OP160, PW046, PW047
Di Domenico, G. P227, P250
Dieci, M. P588

Dierckx, R. OP048, OP617, P373, P375, P422, P493
Dierckx, R. A. OP124, OP173
Dierckx, R. A. J. O. OP049, OP054, OP111, OP205, OP283, OP510, OP514, P419, P509
Diestro Tejeda, M. P711
Dietl, B. P324
Dietlein, M. OP155, P774
Dieudonné, A. OP332, OP381, OP610, P865
Di Franco, M. OP044, P243, TP036
Di Giancamillo, M. P019, P511, P974
Di Giuda, D. OP511, P483
Di Gregorio, F. P704
Di Grigoli, G. P174, PW008
Di Guilmi, G. TP048
Di Iulio, F. P459
Dika, E. PW087
Dilek Ciftci, O. P130
Di Maro, G. P160
Di Mauro, F. P522, P899
Dimcheva, M. OP360
Dimitrakopoulou-Strauss, A. P687, P688, P737, P738, PW090
Dimonte, G. TP057
Dimova, P. P502
Di Muzio, N. OP252, OP256, OP300, OP603
Diocou, S. OP621, P156
Diodato, S. OP552, P129, P135, P781, P940, PW087
Dionyssiou, D. P957
Dios, P. P151
Di Palo, A. OP459, P638
Di Paolo, M. P594
Di Pietro, B. P432
Dirksen, U. P928
Dirlik Serim, B. P731
Di Russo, C. P458
Di Traglia, S. P643
Dittmann, H. OP358
Divoli, A. OP137, OP382
Dixson, H. OP168
Dizdarevic, S. OP415, P695, P725
Djaballah, W. P392, P397
Djan, I. P126
Djelbani S. OP436
Dobbeleir, A. P466, P485, PW024
Dobrowolska, A. P216
Dockx, R. PW024
Doddamane, I. PW037
Džodić, R. OP151
Dodi, G. P306
Doeswijk, G. OP490
Dogan, S. OP624
Dogu, G. G. P782
Doika, E. P826
Dolado-Ardid, J. I. P884
Dolci, C. OP302, P134, PW084
Doležal, J. P024
Dolezalova, P. P952
Dollé, F. OP104, P421, PW021, PW026
Dolstra, H. OP204
Domenech, A. OP456, P700
Domingos, R. OP159
Dominguez, C. P456
Domínguez-Cunchillos, F. P596
Dominguez Prado, I. TP091
Domouchtsidou, A. OP576
Donati, C. P046
Dong, P. P235
Donner, D. P512
Donswijk, M. L. OP229, TP087
Doorduin, J. OP054, OP283, OP510, OP514, P419, P509
Dore, M. OP305
Doruyter, A. G. G. P454, P665
Dos Santos, G. OP296
Dost, R. OP617
Doumas, A. P358, P360, P850, P851, P945
Doval Conde, J. P763
Dowell, N. G. OP227
Drahmoune, R. P838
Drandarov, K. P287
Drendel, V. PW082
Drenth, J. OP106
Driessen, R. OP122, OP123
Drummond, J. P551, P694
Drymlova, J. PW068
Drzezga, A. OP155, OP561, P774
Du, Y. OP137
Duan, H. OP574
Duarte, A. P671
Duarte, H. P671
Duarte, L. H. T. PW118
Duatti, A. P227, P250
Dubois, B. OP323
Dubruel, P. PW065
Duch, J. OP456, P700
Dudek, A. OP323
Duffek, L. P473
Dujardin, K. P437
Dul, E. OP121
Dunn, R. OP168
Dunne, M. P107
Dupont, P. P454
Duprat, R. PW024
Durak, H. P797, P799
During, H. OP501
Durmus Altun, G. P532, P626, P731, P879, TP033

D'Urso, D. P771
Dutertre, A. P948
du Toit, R. P628
Dutra, V. F. TP046
Duvnjak, S. P573, P595, P598
Dygai-Cochet, I. OP627
Dysterdich, A. TP006
Dziuk, M. P361, P372, P617

Ebbens, G. A. TP087
Eberle, M. OP630, PW095
Eberlein, U. OP194, OP277, OP491
Eccles, A. P076, P32, P40, TP032, TP060
Edenbrandt, L. OP169, P369, P912
Eder, M. OP308, OP337, OP426, OP429, P687, P688
Eder, V. OP436
Edis, N. TP018, TP031
Eelkman Rooda, S. J. TP058
Efrati, S. P503
Eftekhari, M. P332, P364, P477, P668, P809, P822, P910
Efthymiadou, R. P213, P635
Ege Aktas, G. P532, P878
Egejord, L. OP322
Ego, K. OP163
Egyed, Z. P217
Einsele, H. OP035
Ejaz, S. PW023
Ekaeva, I. PW015
Ekim, S. OP395, OP611
Ekmekcioglu, O. P605, P608
Ekoume, F. P301
El Bez, I. P815, P817, P818, P835, P916, PW079, TP084
Elboga, U. P132, P137
Elf, A.-K. P803
Elgqvist, J. OP240, PW102
Elias, M. TP016, TP047, TP071
Elicin, O. P569
Elimova, E. OP056
Elisei, F. OP366, P121, P134, PW084
Elison, B. OP168
Ell, P. J. OP548, PW031
Ellis, B. P328
Ellis, W. OP083
Ellmann, A. P665
Elrasad, S. A. A. PW098
El-Refaei, S. P611, PW098
Elschot, M. PW097
Elsinga, P. OP048, OP049, OP286, P381, P419, P422
Elvas, F. OP339, P170
Elzahry, M. P833
Emami-Ardekani, A. P364, P477, P668, P809, P822
Emer, M. O. P967
Emmanuel, K. OP154, P679
Emmett, L. OP088, P082
Emri, M. P965
Endepols, H. OP103
Endo, K. P027, P38
Endo, M. P636
Engberg, A. M. E. OP042
Engblom, H. P146, TP067
Engelen, T. P193
Engelmann, B. P783
Engle, J. W. OP479
Engler, H. OP296, OP327
Entezarmahdi, S. P025, P400
Eppard, E. P796, PW058, PW114
Erba, P. OP530
Erbaş, B. OP496, OP498, OP593, P072, P794
Erbes, T. PW082
Ercakmak, N. PW077
Erdem, O. OP549
Erdem, Z. OP549
Erdemci, B. P630
Erdemir, F. P183
Erdem Sahin, O. P662
Erdil, T. Y. P650
Erdogan, M. P576
Erfani, M. P247, P263, P310, P477, PW063
Ergen, B. OP495
Ergulen, A. TP033
Eriksson, O. OP622
Eriksson Karlström, A. OP244, OP246, OP586
Erini, M. P512
Erlandsson, K. OP114, OP160
Ertl, G. OP433
Ertle, J. OP576
Escabias, C. P711, P788
Eset, K. P061
Eshghi, P. P845
Esmaeili, A. P477
Espeli, V. P563
Espitalier, C. PW095
Esposito, J. P227, P250
Esquinas, P. L. OP385
Esser, J. P. P402, TP058
Essler, M. OP457, OP485, OP634, P554, P796, P832, P846, PW058, PW114
Estenoz Alfaro, J. P681, PW080
Estorch, M. OP456, P553
Estrada, E. P386
Etchebehere, E. OP056, OP238, OP309
Eterovic, D. P905
Eu, P. OP351
Evagellatou, A. P245
Evandri, A. OP452
Evangelista, L. OP251, OP302, OP414, OP631

P584, P588, P691, P710, P776, P790
Evans, S. P012
Evans, W. P007, P157
Evren, M. P604
Ewertz, M. P573
Exner, S. OP282
Eyüpoglu, E. P684
Ezziddin, S. OP013, P854
Ezzine, A. P531, PW079

Facciorusso, A. OP424
Fagin, J. A. P168
Fairclough, M. P328
Fais, F. P232, P233, P236
Falces, C. P935
Falch, K. OP190, OP417, P573, P595, P598, P603
Fallahi, B. P364, P477, P668, P809, P822, PW063
Fallahpoor, M. P837
Fallanca, F. P714
Falzone, N. OP281, P871, PW101
Familiari, D. P642
Fanchon, L. M. OP624
Fanelli, M. OP459, OP499
Fani, M. OP307, P257
Fankhauser, S. P569
Fanti, S. OP088, OP108, OP146, OP233, OP254, OP301
OP310, OP454, OP532, OP552, OP605, OP638
P129, P135, P683, P702, P709, P739, P781
P940, P949, PW051, PW055, PW087, PW089
Fantini, L. P046, P703
Fanton D'Andon, C. P297
F. Antunes, I. OP617
Farahani, Z. P573, P598
Farahati, J. OP156
Farcomeni, A. OP066
Farde, L. OP556, OP557, P498
Fard-Esfahani, A. P364, P477, P668, P809, P822
Farese, R. P733
Fddddddddarghaly, H. R. P677
Faria, D. OP183, TP072, TP072
Faria, T. P050, P371, P416, P417, P898
Faria Joao, M. TP068
Farina, F. P134
Farkas, B. P602
Farnesi, A. OP136, P853
Farto, J. C. A. TP072
Farzanefar, S. P364, P822, P837
Fasmer, K. OP637
Fassbender, M. E. OP479
Fassnacht, M. OP534, P207, P766
Fastenmeier, S. PW093
Fatima, N. P336, P337, P338, P339, P900, P933
Fattahi, A. P590
Favaretto, S. P475
Favre, C. OP421
Fazio, P. OP556, OP557, P498
Fecher, D. P180
Fedele, F. OP066
Fedorova, O. P288, P291, TP082
Fedorova, T. OP644
Feggi, L. OP353, P769
Feliciani, G. OP640
Felício, P. OP227
Fellner, F. P679
Fendler, W. OP070, OP384, P867
Feng, H. P251, PW001
Feng, M. U. OP380
Fenner, J. W. OP113
Fenoglietto, P. OP630
Fenwick, A. OP094, OP447, P007
P157, PW100, PW104
Ferdeghini, M. P934, P950, P964, TP063
Fereira, P. R. P047
Fergusson, S. P059
Fernandes, A. OP418, P050, P330, P371
P416, P417, P898, PW035, TP094
Fernandes, M. TP037
Fernandez, A. OP642, P553
Fernandez, P. P676, PW081
Fernandez, R. P870
Fernandez-Gomez, I. PW009
Fernandez-Maza, L. PW009
Fernández Rodríguez, M. P722, P760
Fernández-Varea, J. M. OP281, P871
Ferrando, O. P098, P275
Ferrando, R. OP516, P481
Ferrara, M. OP561
Ferrarazzo, G. OP147, OP472, OP525
OP540, P394, PW018
Ferrari, C. OP459, OP499, P638
Ferrari, M. OP330, P709
Ferreira, H. A. TP038
Ferreira, N. C. TP070
Ferreira, R. OP553, P673
Ferreira, T. C. P863
Ferrer, L. OP305
Ferrer-Antunes, A. TP068
Ferrer-Artola, A. M. P706
Ferrer-González, A. P706
Ferrér Rebolleda, J. OP592, P720, PW019, TP023, TP088
Ferretti, G. P704
Ferri, V. OP012, OP191, P860
Ferro, C. PW018
Ferro, P. OP110, P943
Ferrulli, A. OP511
Fessler, J. A. OP380

Fettich, J. P710
Fidan, A. K. P517, PW077
Fiedler, H. OP428, P099
Field Galán, C. P847, P848
Fierro Alanis, P. TP091
Fieux, S. TP049
Figueiredo, A. P960
Figueroa-Ardila, G. C. P884
Fikrle, A. P341
Filice, A. OP012, OP191, OP640, TP085
Filidei, E. PW030
Filieri, A. P243
Filip, T. OP290
Filipovic, J. P540
Filippi, L. PW120
Filippi, V. P635
Fillimonov, V. D. PW013
Findlay, C. P108, P109
Finessi, M. OP575, P969
Finnema, S. J. OP289
Finocchiaro, G. OP146
Fiore, M. OP601
Fiorentini, A. P458, P459, P678
Fiorenzo, D. OP108
Fiorino, C. OP252, OP603
Fiorino, S. OP110, P943
Fioroni, F. OP012, OP191, OP640, P860, TP085
Fischer, A. OP335
Fischer, B. M. OP042
Fischer, E. OP199, OP243
Fischer, S. P017, PW003
Fitz, F. P922
Fitzal, F. TP009
Fiz, F. OP472, OP525, OP540, P394, P728, PW018
Flamen, P. OP386, OP425, P697
Flanigan, D. C. PW074
Flechsig, P. OP148, P101
Fletcher, A. M. P059
Flitter, M. OP323
Flores-Gonzalez, E. P373
Florimonte, L. OP635, P383, P729
Flotats, A. OP456, P553
Floth, A. P699
Flux, G. OP137, OP235, OP382, P871, P872, PW100, PW101, PW115, PW119
Foa, P. OP367
Fodor, A. OP252, OP256
Foekens, J. OP392
Fojtik, Z. P384
Follacchio, G. A. OP066, OP236
Fomin, D. PW096
Fonge, H. PW070
Fonseca, G. OP183
Fonti, C. P709, PW089
Fonti, R. OP303, P237, P730, P780
Foppiano, F. P098
Fordzyun, I. TP062
Forgács, A. OP119, P067, P153, P965, TP062
Fornito, M. C. P642
Forsting, M. OP250
Fortes, C. TP042
Fortini, D. P483
Fossati, P. OP601
Fosse, P. OP038
Fraccarollo, D. OP475
Fraedrich, G. P657
Fraggetta, F. P779
Fraioli, F. P203
Frakulli, R. OP301
Franceschetto, A. P954
Franceschi, D. OP356
Franceschi, M. P535
Franchi, G. P274
Francis, R. J. P107
Franck, D. OP134
Francken, A. B. P586
Frank, P. OP148
Franklin, J. M. PW101
Franssen, G. M. P266, P318
Frantellizzi, V. OP066, OP236
Franzese, C. OP632
Frasoldati, A. OP012, OP191
Frauenstein, L. OP385
Fravolini, M. L. P468, P476, P478
Frech, A. P657
Freesmeyer, M. P53, P54
Frega, N. P374
Frehland, B. OP288
Freimoser-Grundschober, A. OP105, PW066
Freire, L. TP004
Frenkel, A. P045
Frey, E. C. OP387
Frielink, C. OP198, OP202, OP612
Frigeri, F. P733
Friis, J. T. OP059, P726
Frings, V. OP362, P100
Frisoni, G. OP561, P433
Fritz, E. P640
Fröberg, A. C. OP299, P705
Froberg, L. OP530
Frøkiær, J. OP121, OP292, OP294, P240, TP066
Frosini, D. OP647, P480
Fruhwirth, G. OP621
Frutos Esteban, L. OP260, P435, P692, P823
Fryer, T. D. PW023
Fujii, H. P230

Fujii, S. P634
Fujimoto, K. PW040
Fujinaga, M. PW002
Fujino, K. P494
Fujita, N. TP008, TP020
Fujita, W. OP224
Fujita, Y. OP187, P404
Fujiwara, K. P166
Fukuchi, K. OP224
Fukuda, Y. P133
Fukunaga, M. P39
Fukushi, M. P074
Fukushima, K. OP171, OP431, OP437
OP432, OP542, P334, P349
Fukushima, Y. P966, P985
Fukuzawa, S. OP170
Fülöp, M. P015, P024
Fumoleau, P. OP590, OP627
Funahashi, Y. P230
Funovics, M. OP574
Furlan, W. P526
Furumoto, S. OP162
Furutsuka, K. PW010
Fuster, D. P935, TP088

Gaballo, P. P36
Gabelli, C. P475
Gaberšček, S. P888, P890, P891, P892
Gad, D. P783
Gaertner, F. OP457, P554, PW114
Gaeta, M. P275
Gaffuri, M. TP081
Gafton, G. P927
Gaitanis, A. OP450
Gajic, M. P089
Galán-Guzmán, M. PW038
Galan Hernandez, R. P752
Galassi, R. P046, P703
Galaverni, C. OP577
Galetta, G. OP635
Gall, E. PW095
Gallan, M. P961
Gallego, J. PW045
Gallego, O. P553
Galler, Z. P217
Galli, F. OP205
Galli, L. OP136
Gallio, E. OP575
Galuppo, S. OP251, P776
Gamazo Laherrán, C. OP158, P754, P756, P902
Gambaccini, M. P227
Gambhir, S. P202, OP232, P653, P658
Gambino, O. P771
Gamboni, A. OP310
Gámez-Cenzano, C. P446, P706, PW038
Gan, H. OP293
Gandhe, A. P083
Gandolfo, P. OP249
Gangemi, V. OP256, OP300, P899
Gannon, K. P839
Gao, X.-O. P280
Garaboldi, L. P236
Garai, I. P153, P840, P965, TP062
Garbarino, S. P236
Garcheva-Tsacheva, M. P740, P742, P786, P982
Garcia, M. TP023
Garcia, O. P386
García, R. OP516
Garcia, S. J. TP046
García Alonso, M. P. P722, P760
Garcia-Arguello, S. F. P290
Garcia Burillo, A. P534, P537, P660
Garcia-Fidalgo, M. P001, P068
Garcia-Fontes, M. OP296
Garcia-Garcia, B. OP352
García-García, J. P762, P764
Garcia Garcia-Esquinas, M. P093, P125, P128, P138
Garcia-Garzon, J. P720
Garcia Gonzalez, P. PW019
García-Jiménez, R. P852
Garcia-Lucas, A. P148
García Saenz, J. A. P138
García Satué, J. P639
Garcia-Talavera San Miguel, P. P931
García-Velloso, M. J. OP352, OP591
García Vicente, A. M. P104, P717
Gardin, I. OP161, OP610, P865
Gargiulo, S. PW026
Garibotto, V. P433
Garin, E. P304
Garkavaya, T. OP236
Garnuszek, P. OP530, P255, P327
Garousi, J. OP242, OP582
Garraffa, G. PW072
Garrè, M. OP598
Garrido Pumar, M. P768
Garrido Robles, J. A. P104
Garrigue, P. P258, P297
Garske-Román, U. OP011
Gärtner, F. P796, P846
Gasbarrini, A. OP233
Gascon-Bayarri, J. P446
Gasparini, M. P594, P724
Gasser, M. P766
Gastl, G. P657, P689
Gaudieri, V. OP120, OP174

Gaudin, E. O. OP093
Gaye, D. P676
Gazi, E. P351
Gear, J. OP382, P872, PW100
Geatti, O. P704
Gecer, M. F. P920
Gee, A. D. OP099
Geelhoed, E. P107
Géher, P. P841
Geist, B. K. OP221
Gejl, M. OP322, OP541
Gelbart, W. OP480, P324
Gelo, I. P525
Generalov, R. P162
Genin, A. OP038, P164
Gennari, A. P328, P587
Gennaro, M. OP647, P753
Genova, C. OP147
Genovesi, D. PW030
Gentile, L. P409
Gentile, R. OP237
Geobel, G. OP530
Geolchanyan, A. P288
Georga, S. P358, P360, P715, P850
P851, P937, P944, P945
Georgieva, N. P623
Georgoulias, P. P439, P464
Geraghty, P. P870
Gerali, A. P701
Geramifar, P. P113, P115, P910
Gerasimou, G. P482, P484
Geretschläger, A. P569
Gerhard, A. P069
Gerke, O. OP059, OP190, OP417, P491, P573
P595, P598, P603, P713, P726, P785
Germain, S. P178
Gerngross, C. P094
Gerrits, D. OP105, P318
Gervais, P. PW021
Geurts, J. OP263
Geworski, L. OP055, OP513, P911
Gezen, C. P604
Ghanem, G. OP425, P697
Ghazzar, N. OP335
Ghedini, P. OP108, OP454, P683, P781, P940, PW089
Gheisari, F. P025
Gherasim, R. P071, P907
Ghersi, C. P232
Ghetti, B. OP324, OP325
Ghetti, C. P272, P34
Gheysens, O. P023, P57
Ghilardi, A. TP069
Ghione, P. OP540
Ghiotto, C. P584
Ghiraldini, G. TP085
Ghizdovat, V. P306, P907
Gholami, F. P117
Ghosh, S. OP164, P800
Ghosn, M. P849
Giacomuzzi, F. P704
Giacopuzzi, S. P964
Giammarile, F. OP597
Giannopoulou, C. P670
Gianolli, L. OP252, OP253, OP256, OP300
OP603, P691, P714, PW008
Gibbons, P. P326
Gieri, S. P779
Giesel, F. OP089, OP148, OP226, OP308
OP428, OP429, P099, P101
Giganti, M. P227, P250
Gigliotti, C. R. OP112, OP484, P048, P064, P194
Gil, I. P508
Gilardi, M. C. P771, P779, PW008
Gildehaus, F. OP384, P866, P867
Gilhuijs, K. G. A. OP628
Gillebert, Q. OP255, P362
Gillen, G. P108, P109
Gillet, P. TP086
Gillett, D. OP508
Gil Viciano, I. P947
Gimié, F. OP104, P149
Giordano, A. OP511, OP626, P248, P483, P708, P721
Giorgetti, A. PW030
Giorgio, S. M. d. A. OP445
Giostra, A. OP528
Giovacchini, G. OP252, OP256
Giovanella, L. P522, P563, P894, PW092
Giovannini, E. P442, P444
Giovenzana, G. B. OP101
Giovinazzo, S. P522
Giraudet, A.-L. OP609
Giraudmaillet, T. P399
Giraudo, C. P732
Girschele, F. P280, P317, P514
Giuliani, D. PW084
Giurgola, F. P271, P308
Giusti, M. OP525
Giza, E. P482
Gizewska, A. P617
Gjedde, A. OP322
Gjertsson, P. OP334
Gkirgkoudis, M. P484
Glatting, G. OP009, OP010, OP015, OP016
OP090, OP117, OP615, P002
Glaudemans, A. W. J. M. OP111, OP473, P386
Gned, D. OP558

Gnesin, S. OP359, OP361, P868
Gobbi, L. P964
Goda, Y. P791
Godoy Bravo, M. OP260, P435, P692, P823, P970
Goel, S. P267
Goethals, I. OP559, P466, P485
Goffin, K. OP083
Gogos, K. P365, P635
Gokalp, C. P877
Gokcora, N. P963
Gokmen, E. PW033
Goksoy, D. TP095
Golan, H. P503
Goldaniga, M. P729
Goldenberg, D. M. OP394, OP485
Goldschmidt, H. P737, P738, PW090
Goldstone, T. P655
Golfieri, R. OP233, OP577
Golovina, A. TP082
Golubic, A. T. OP512, OP555, P438, P479
Gomella, L. P083
Gomes, M. I. TP043
Gomez, B. OP043, OP536, P205, P690
Gomez-Caminero Lopez, F. P931
Gómez de la Fuente, F. OP438, P436
Gomez-Grande, A. P681
Gómez-Jaramillo, C. A. P884
Gomez Llopico, R. P469
Gómez-Rió, M. P680
Gomzina, N. P289
Goncalves, V. OP427
Gonçalves, B. PW118
Gonda, K. OP162
Gonella, R. P587
Gong, S. OP293
González, A. TP023
González, J. P537
Gonzalez, M. OP327, OP385
Gónzalez Cosano, V. P646
González García, B. OP461, P717, P752
Gonzalez Lopez, L. P752
Gonzalez-Monroy, A. OP124
Gonzalez-Padilla, C. P375
González Roiz, C. P746, P975
Gónzalez Selma, M. OP158, P754, P756, P902
Goodfield, N. E. R. PW042
Goorden, M. C. OP501
Görges, R. OP156
Gormsen, L. C. OP109, OP541, P021
Górnicka, B. P567
Gosewisch, A. OP384, P866, P867
Gotoh, H. P612
Gott, M. D. OP479
Gotthardt, M. OP198, OP202, OP395
OP611, OP612, P266, P649
Gottilla, R. P366
Gottrup, H. OP322
Gotzamani-Psarrakou, A. P482, P484
Gouillet, A. P297
Gould, S.-M. P870
Gourand, F. P282
Gourni, E. OP427
Goutal, S. P111, P421
Głowniak, A. P407
Gràcia-Sánchez, L. M. P446, P706, PW038
Gramanzini, M. PW026
Granados, U. P935, PW081
Granberg, D. OP011
Grassi, E. OP012, OP191, OP640, P860, TP085
Grassi, I. OP108, OP310, P683
Grasso, I. OP532
Gravergaard, A. E. P783
Graves, S. A. OP585, OP620
Gray, M. OP382
Graziani, T. OP233, OP254, OP454, P949
Greco, A. P160, P175, PW026
Greco, M. P753
Green, A. J. OP278, OP387
Green, R. OP167, P374
Gregory, J. OP343
Gregory, R. PW100
Greisen, G. OP050
Grierosu, I. P071, P306, P907
Grigolato, D. P934, P950, P964, TP063
Grigoriadis, N. P484
Grilo, A. TP072
Grimwood, A. P56
Grizzi, F. OP146, OP532
Grošev, D. OP387
Gromova, E. P462
Gronkiewicz, Z. P567
Grønnemark, L. F. OP412
Grootjans, W. P627, P649, TP043
Groppi, F. P227
Grosch, S. P090
Grossi, F. OP147, OP623
Grötzinger, C. OP282, P161, P171, P177
Grouzmann, E. P257
Groves, A. OP114, OP160
Grubmueller, B. P699
Grugni, S. P271, P308
Grünberg, J. OP243
Grundman, M. OP323
Grupe, P. P491
Gstettner, C. P004
Gualtieri, G. P046

Guan, Y. P496
Guarneri, V. P588
Gubskiy, I. L. P195
Guedj, E. OP560, OP561
Guenova, M. P727
Guensi, A. P140, P819, P825, P836
Guerif, S. OP305
Guérin, B. OP446
Guermazi, F. P441, P976
Guerra, L. OP366, P121, P134, P33, P35, PW084
Guerra, U. OP546, P430
Guezguez, M. P531
Guglielmi, J. P152
Guida, A. OP544
Guidalotti, P. P129
Guidoccio, F. OP647, P480, P853
Guidoux, C. P385
Guillemard, S. OP630, PW095
Guillén, E. F. OP352
Guillen, F. OP591
Guillén-Grima, F. OP370, OP371
Guillet, B. P258, P297
Guinsi, A. P529, P539
Guinto-Nishimura, G. P375
Guiot, T. OP386
Guiote Moreno, V. P646
Guitián Iglesias, R. P120, P520, P533, P669, P763
Gul, S. S. P130, P183
Gulaldi, N. C. M. P904
Gülcü, A. P799
Gulenchyn, K. OP648
Gulliver, N. TP032, TP060
Gültekin, S. S. P154, P403
Gulya, M. O. P343, PW013
Gulyás, B. OP053, P264
Gumuser, G. TP095
Gunalp, B. P576, P967
Gunaratne, S. TP075
Gunasekera, R. P839
Gün Atak, P. P909
Gunchul, H. TP055
Guner, L. P963
Gungor, F. P880
Guo, H.-R. P622
Guo, N. OP293
Guo, W. OP009, OP010, OP016
Gupta, M. P543
Gupta, R. K. OP537
Gupta, S. K. TP035
Gurgul, S. P183
Gustafsson, J. OP383
Gutiérrez Cardo, A. L. P510
Guttilla, A. OP631
Gutu, M. P071
Guyot, M. P676
Gykiere, P. P466
Györke, T. P591

Ha, J. PW028
Ha, S. OP145
Haase, C. P415
Habbeche, M. P661, P838, P906
Haberkorn, U. OP089, OP148, OP226, OP308
OP337, OP428, OP429, P099
P101, P687, P737, P738, PW090
Habraken, J. B. A. OP524
Hacker, M. OP070, OP365, P280, P317
P380, P514, P672, PW004, PW006
Hadaschik, B. A. P687, P688
Haddad, F. P414
Hader, S. P286
Hadjiiska, V. P502, P656
Hadley, D. P453
Hadzhiyska, V. P786, P873, P982
Haeck, J. C. OP200
Haenscheid, H. P207
Hafezi, F. P506
Häggkvist, J. OP053, OP289, P456
Haghighatafshar, M. P025, P400
Hagiwara, N. OP171, OP437, P349
Hahn, A. P317
Hahner, S. OP534, P207
Haidinger, I. OP416
Haim, S. P679, P922, TP009
Hajduch, M. PW068
Haji Dheere, A. OP099
Ha-Kawa, S. K. P196
Hakozaki, K. P559
Hakulinen, M. TP041
Halaç, M. OP535, P538, P609, P644, P662
Halacli, S. O. P816
Halders, S. G. E. A. OP092
Hall, D. O. OP143, OP261
Hallam, A. P016, P078
Halldin, C. OP053, OP287, OP289, OP556
OP557, P264, P456, P498
Halle, B. OP275, P173
Hallmann, S. P161
Haloi, R. P136, TP057
Halty, A. OP609
Hama, A. P139
Hamaguchi, T. OP562
Hamakubo, T. P166
Hämäläinen, H. P395
Hamamichi, S. P230
Hamilton, D. P081, P869, PW105

Hamilton, G. P280, P514
Hammami, H. P835
Hamza, F. P441, P976
Han, C. OP126, OP127
Han, E. P565, P616
Han, J. P988
Han, Y.-H. PW036
Hanaoka, K. P142, P775, TP074
Handkiewicz-Junak, D. P524
Haney, M. OP509
Hanneke, P. OP198
Hanney, M. B. OP113
Hänscheid, H. OP035, OP194
Hansen, A. E. OP042, P201
Hansen, A. K. OP541
Hansen, J. A. P595, P603
Hansen, M. T. OP643
Hansen, S. B. OP322
Harada, M. P789, P925
Harada, R. PW086
Haraldsen, A. OP109, P124
Hardiansyah, D. OP009, OP010, OP015 OP016, OP090, OP615
Hardwick, D. P287
Harms, H. J. OP067, OP121, OP123 OP292, TP065, TP066
Haroche, J. OP538
Harrington, K. OP588
Harrison, H. OP337
Hartenbach, M. OP044, OP416, P732
Hartl, D. OP091
Hasbek, Z. P130
Hasbroucq, C. OP189
Hasche, E. OP168
Hasebe, M. P637
Hasegawa, D. P39
Hashemizadeh, M. P252
Hashimoto, H. P979, P985
Hashimoto, M. P987
Hassan, H. TP030, TP090
Hassanzadeh-Rad, A. P364, P668, P809
Hassoy, H. P810
Hatakeyama, T. P487, P549
Hatano, K. P074
Hatazawa, J. OP515, P088, P333, P460, P494, P734
Hatori, A. PW002, PW010
Hatt, M. OP305
Hattori, S. PW040
Hatzipavlidou, V. PW106
Haug, A. R. P672
Hausberger, D. P277
Hautzel, H. P447, P448, P449
Havariyoun, G. P32
Havekes, B. OP092
Havel, M. P376
Hayakawa, N. P980
Hayasaka, K. P612
Haylock, A.-K. PW057
He, W. OP165, P062, P735, PW050
Hedeer, F. P146, TP067
Heijmen, L. TP043
Heinemann, M. P928
Heinze, B. OP534, P207
Heinzel, A. OP549
Hekman, M. P188
Helfrich, W. OP617
Hellingman, D. P959, TP021, TP087
Helsen, M. M. OP105
Helsen, N. P557
Hemmatpour, M. P025
Hemuki, Y. P066
Hendriks-deJong, M. OP530
Hendrikse, H. N. M. P320
Hendrikse, N. H. OP531, PW113
Hendrikx, G. PW061
Henmi, H. P356
Hennessy, T. M. OP196
Henning, W. OP050
Hennrich, U. P295
Henriksen, G. OP618, P283
Henrikson, O. OP334
Henriksson, F. P889
Henrionnet, C. TP086
Henry, A. P282
Henzlova, L. P376
Heo, D. OP145
Herceg, D. P749
Herde Müller, A. OP285
Herholz, K. P069
Hermans, J. P649
Herms, J. OP051
Hermsen, R. OP106, TP043
Hernandez, E. P085, P427
Hernandez, I. P788
Hernandez, R. OP394, OP485, OP585
Hernandez Martinez, A. C. P681, PW080
Herrlinger, U. P554
Herrmann, K. OP035, OP194, OP534, OP542 OP645, P207, P527, P766
Herth, M. P427
Hervás Marín, D. TP014
Heskamp, S. OP204, OP394, OP485, OP488, P690
Hess, S. OP059, OP061, P491, P939, P942, P951
Hesse, M. OP503, OP523, PW091
Hetzheim, H. OP429
Heurling, K. OP648

Heusch, P. P205
Heuschkel, M. OP618, P748
Heußel, C.-P. P101
Heydarinejad, S. P837
Heyerdahl, H. OP422, P162, P181
Hickey, A. OP088
Hicks, R. OP293, OP351, OP481, P091
Hidalgo, M. P148
Hideghethy, K. PW085
Higashi, T. P027
Higashiyama, S. P813
Higuchi, T. OP194, OP431, OP432 OP542, P223, P334, P527
Hijazi, S. OP297, OP393
Hildebrandt, M. G. OP059, P573, P595, P598, P603
Hillengass, J. P737, P738, PW090
Hindié, E. OP279, P676
Hindorf, C. P077, P146, TP067
Hindré, F. OP038, P164
Hingorani, M. P655
Hino, M. TP034
Hinz, R. OP648, P069
Hirai, T. P396, TP089
Hirano, K. PW010
Hirata, K. OP144
Hirata, M. P147
Hirose, Y. PW040
Hiroual, S. P921
Hirschmann, M. T. OP262
Hitre, E. OP062
Hjorthaug, K. P124
Ho, B. OP088
Ho, C. Y. P214
Hober, S. OP242
Hobo, W. OP204
Hochreiter, J. P922
Hockings, P. P198
Hodolic, M. P710
Hoeilund-Carlsen, P. OP061, OP190, OP417, PW049
Hoekstra, O. S. OP362, OP531, P100, P105, P320, P777
Hoeller, C. OP574
Hoepping, A. P017, PW004, PW006
Hofbauer, L. P004
Hoff, C. M. OP121, TP065
Hoffman, I. OP443
Hoffmann, A. OP324, OP325
Hoffmann, M. OP574
Hofheinz, F. OP046, OP163, OP363
Hofkes-Fillekes, K. P589, P958
Hofman, M. S. OP351, P091
Hofmann, A. A. P526
Hofmann, F. OP338
Hofstetter, W. OP056
Högberg, J. OP334
Hohaus, S. P721
Höhn, S. OP471
Høilund-Carlsen, P. OP059, OP390, P173, OP275, P241 P491, P573, P595, P598, P603, P726 P713, P783, P785, P939, P942, P951
Hojbjerg, J. P124
Højgaard, L. OP042, OP050, OP494, P003, P201
Hoksch, B. P640
Holcman, K. P391
Holdgaard, P. C. OP412, P783, TP059
Holland, J. P. P165
Holley, D. OP047
Holmin, S. OP053
Holte, H. OP039
Holtedahl, J. OP039
Holzmannhofer, J. P398
Honarvar, H. OP242, OP244, OP246, OP586
Honeywell, R. J. OP531
Hong, H. OP247, OP585, OP620
Hong, J.-H. OP460
Hong, Y. T. PW023
Hoogvorst, N. J. OP186, TP002
Hooper, C. E. OP143
Hoppela, E. OP166
Horenblas, S. OP231, P189, P190
Hori, Y. P230
Horitsugi, G. P088
Horn, P. A. OP576
Horvat, M. P501
Horvatic Herceg, G. P540, P749
Hoseinnejad, T. P859
Hoshizaki, H. P223
Hosntalab, M. P910
Hosokawa, C. P428, TP099
Hosokawa, M. P773
Hosokawa, S. OP284
Hosono, M. P142, P775, TP074, TP099
Hosseinifar, N. P910
Hossen, L. PW119
Hossu, G. OP560
Hostege, G. OP514
Hosten, B. P111
Hou, N. P629
Houshmand, S. P491, P939
Houwertjes, M. P419
Hovinga - de Boer, M. C. OP473
Howes, O. P283
Høyer, S. OP294
Hsiao, E. OP086, OP228, P551, P694
Hsiao, P.-J. P828
Hsieh, B.-T. P144
Hsu, C.-C. P418

Hu, C. Y. P127
Hu, S. P811
Hu, Z. P30
Huang, C. P208
Huang, J.-Y. PW017
Huang, J.-S. PW083
Huang, K. P. P226
Huang, S.-H. OP460
Huang, W.-C. TP056
Huang, W.-S. P144, P452, P461
Huang, Y.-E. OP460
Huang, Y.-Y. P578
Huang, Z. P496
Hubalewska-Dydejczyk, A. OP530, P666, P792
Hubert, J. P787
Huchet, V. OP255
Hudson, P. OP293
Hudzietzová, J. P015, P024
Huellner, M. OP116, OP600, P197, P200
Huic, D. P540, OP555
Huisman, M. C. OP067, OP123, OP419
Hultborn, R. OP334
Humbert, O. OP590, OP627
Humm, J. L. OP624
Humphreys, C. OP222, P012
Hung, C. P897
Hung, J. C. TP057
Hunter, J. OP227
Hur, M. P159, P268, P325
Husseini, M. A. PW098
Hustinx, R. P090
Hutton, C. P490
Hvidsten, S. P173
Hyafil, F. OP471, OP474, P362, P385, P936
Hyun, I. P467
Hyun, S. PW039

Iaccarino, G. PW104
Iacozzi, M. P587
Iagaru, A. OP045, OP047, P029, P200, P202
Iakovou, I. P358, P360, P472, P850, P851, P945
Iampietro, E. TP069
Ianniello, A. P798
Ibáñez Ibáñez, M. OP260, P435, P692, P823, P970
Ibazizène, M. P282
Ibello, F. P733
Ibis, E. P843
Icer, S. P061
Ichikawa, S. OP170
Ideguchi, R. P345, P647
Idilman, R. OP579
Idoate, M. OP591
Idris, J. TP030, TP090
Ielo, D. TP036
Ieranò, C. P175
Ieria, F. P. P708
Igarashi, T. OP170
Igua Sáenz, C. OP580, P761, P765, P767, TP014
Iida, H. P488, P489
Iimori, T. PW016
Işık, E. G. P609
İlçe, H. T. P650
Ikari, Y. P486
Ikawa, M. OP641
Ikeda, M. P987
Ilan, E. OP551
Ilhan, H. P866
Ilić, S. OP441
Iliadis, K. P635
Ilina, E. P222, P311, P321, TP017, TP100
Illert, A.-L. P165
Ilushenkova, J. N. P246
Ilyushenkova, Y. P388
Imabayashi, E. P443, P445, P465
Imai, S. P559
Imamovic, L. OP154
Imbert, L. P392, P397
Imberti, C. OP481
In, E. P981
Inada, M. P142
Inagaki, M. OP170
Inai, R. P581, P789, P930
Inaki, A. P063
Inanir, S. P650, P654
Iñarra-Talboy, F. OP124
Ince, S. P576, P967
Incerti, E. OP252, OP253, OP256, OP300, OP603, P714
Indovina, L. P721
Infantino, A. OP452, OP633, P026
Inokuchi, M. P913
Inoue, H. P612
Inoue, K. P074
Inoue, T. OP144
Intenzo, C. P083
Inubushi, M. PW086
Invernizzi, M. OP249
Ioannidis, P. P482, P484
Iommelli, F. OP303, P237, P780
Ionescu, L. P071
Iordanidou, L. P826
Iori, M. OP640, P860
Ipek, T. P684
Ippolito, M. P771, P779
Ippolito, V. P097, P366
Ironside, J. W. OP324, OP325
Irusen, E. M. P628

Irwin, C. P168
Isabella, R. P174
Isaias, I. OP645, PW027
Isgrò, M. A. P708
Ishibashi, M. P634, PW040
Ishiguchi, H. P139
Ishiguro, M. TP022
Ishihara, K. P559
Ishii, K. P428, PW040, TP074, TP099
Ishikawa, K. P775
Ishikawa, R. P133
Ishimori, T. P693, P980
Ishitoya, S. P530
Ishiwata, K. OP048, OP284
Isik, V. M. P187
Isohashi, K. P088, P333, P460, P734
Israel, I. P285
Israel, O. P045
Israel, S. OP454
Italiano, A. OP237, P861
Itikawa, E. N. P042, P051, P052, P425, P497, P499
Ito, K. P230
Ito, S. P139, P545, PW041, TP078
Itoh, K. P773
Iuele, F. OP107
Ivanov, A. S. P350
Ivanov, K. P253, P344
Iversen, A. B. P240
Iversen, P. PW078
Iwabuchi, Y. P58
Iwanari, H. P166
Iwano, S. P545
Iwasa, H. P686
Iwasaki, Y. OP187, P404
Iwata, M. P230
Izadyar, S. P822

Jabbari, I. P859
Jabeur, C. P531
Jackson, A. PW048
Jacob, A. TP054, TP098
Jacob, M. P592
Jager, M. P892
Jager, N. A. P381
Jager, P. L. OP543, P586
Jahns, R. OP431, OP432, OP433
Jahns, V. OP431, OP432
Jahoda, J. P952
Jain, A. OP554, P659
Jain, N. OP063
Jain, T. K. P719
Jakič, M. P892
Jaki Mekjavič, P. P888
Jakobsen, S. OP294, OP644, P021
Jaksic, E. OP349, OP350, P882
Jakubowski, A. OP478
Jakuciński, M. OP197
Jalilian, A. OP492, P252
Jaller, R. OP456, OP642, P553
Jamali, M. OP047
Jamar, F. OP503, OP523, PW091
James, J. P198, P411, P423
Jammaz, I. P167, TP026
Jampana, R. OP643
Jang, S. P577, P621
Janiak, T. P327
Janiszewska, &. OP584
Jankovic, M. OP151, OP349, OP350, P882
Janse van Rensburg, V. OP225
Janssen, M. TP025
Janssen-Pinkse, L. TP064
Janvier, l. P342, P546
Jardak, I. P441, P976
Jarden, J. O. P491
Jaritz, L. OP457
Jarlier, M. PW095
Jasiakiewicz, K. P216
Jaskiewicz, L. OP193
Jastrzębski, J. OP478, OP584
Jaukovic, L. OP372
Jauregui-Osoro, M. OP621
Javadi, H. P332
Javadi, M. OP431
Javadrashid, R. P624
Jaworska, A. OP051
Jayamanne, D. P551
Jazbec, T. P657
Jego, B. PW021
Jenkins, L. C. OP451
Jennings, D. PW029
Jennings, L. P294
Jensen, J. D. OP040
Jensen, M. P278
Jensen, R. R. P003
Jensen, S. B. OP491
Jensen-Kondering, U. PW023
Jentoft Kramer, S. PW078
Jentzen, W. OP092
Jeong, G.-C. P772
Jeong, H.-J. PW036
Jeong, H.-C. P621
Jerzyk, K. P327
Jessen, N. P240
Jessop, M. OP415
Jestin, E. OP104, P149
Jeukens, C. R. L. P. P011

Jhao, Y.-T. P461
Jia, Z. P123, P618
Jiang, C. P629
Jiang, J. P496, P625
Jieling, Z. P218
Jimenez, C. OP040
Jiménez-Alonso, M. OP438, P436
Jiménez Anula, J. P585
Jiménez-Ballvé, A. P093, P128, P138, P408, P975, PW020
Jiménez-Bonilla, J. OP438, P436
Jiménez Londoño, G. A. OP461, P717
Jin, X. OP203
Jingu, K. PW014
Jinguji, M. OP057, P807
Jiskrova, H. P883
Joba, R. P355, P664, P886
Jødal, L. OP491
Jodłowska, E. OP497
Jögi, J. P146
Johannesen, H. H. OP042
Johansen, A. P783, P942
Johansson, L. OP094, OP383, OP447, OP616 P007, P157, P864, PW104
Johansson, V. P803
John, J. OP411, TP052, TP054, TP098
John, K. D. OP479
Johnsen, B. OP637
Johnsen, I. B. G. P241
Johnson, R. R. P324
Jois KS, B. OP164, P800
Jones, A. P328
Jones, K. PW042
Jonhson, R. OP480
Joniau, S. OP083
Jonker, M. TP050
Jonsson, L. P077
Joo, Y. OP258
Joonho, Y. TP055
Joosten, L. OP198, OP202, OP612
Jordan, L. G. P136, TP057
Jørgensen, M. OP494
Jørgensen, T. P278
Jorgov, L. P886
Joulaeizadeh, L. OP616
Jouret, F. P090
Jovanovic, Z. P080
Jovanovska, A. OP360
Juárez-Orozco, L. OP124, OP172, OP173 P373, P375, P386
Juhler, M. OP494
Jukić, T. P535
Jukova, L. P751
Julio, R.-R. P508
Jun, S. P141
Jung, K. OP355
Junior, V. A. J. P425
Jurczyszyn, A. P743, P744
Jürgens, H. P928
Juri, C. OP646, P085, P427
Jurisson, S. S. OP479
Jylling, A. B. P573, P603

Kabala, J. OP261
Kabasakal, L. OP084, OP087, OP139, OP529 OP535, P079, P307, P862
Kaboteh, R. P912
Kadoya, N. PW014
Kaeding, C. PW074
Kage, M. PW040
Kahramann, D. P774
Kaida, H. P428, PW040
Kajáry, K. P591
Kajimoto, K. P488, P489
Kajiya, Y. OP057
Kalameny, E. P473
Kalantari, F. P364
Kalff, V. PW110
Kallel, F. P441, P976
Kalogianni, E. P076, P32, P40
Kaloudi, A. OP336, P179
Kamada, T. P637
Kamaleshwaran, K. P219, P795, P806, P844, TP001
Kamali Asl, A. P025, P113, P115
Kamar, F. P849
Kameyama, M. P791
Kaminek, M. P376
Kamiya, Y. PW041
Kan, H. OP186
Kanaev, S. P574, P751, P927
Kanai, Y. P333
Kanamori, S. P775
Kanazawa, S. P581, P789, P930
Kandeel, A. A. OP500
Kandler, R. OP097
Kandolf-Sekulovic, L. OP372
Kanegae, K. P773
Kang, H. OP614, P333
Kang, L. OP201, OP587, P163, P249, P254
Kang, S.-R. P772
Kang, W. P143
Kangai, Y. P39
Kano, D. P747
Kanoun, S. OP590, OP627
Kanthan, G. P694
Kao, P.-F. P561, TP093
Kapaki, E. P500

Kapp, T. OP338
Kappadath, S. C. OP115, OP328
Kapur, S. P010, P507
Karabulut, E. OP413, OP495, P523, P968
Karaca, H. P645
Karacalioglu, A. O. P967
Karacavus, S. P061, P920
Kara Gedik, G. P041
Karakaya, J. P983
Karakolcu, F. P526
Karakullukcu, B. P189
Karalis, G. OP147
Karalkina, M. PW096
Karalok, I. P908, P909
Karanikas, G. OP365, P672
Karanja, Y. W. P002
Karathanos, E. P410
Karatzas, N. P360
Karayel, E. P307
Karcher, G. OP560, P293, P392, P397
P420, P463, PW059, TP086
Karczmarczyk, U. P255
Karfis, I. OP195, OP386
Karnes, R. J. TP057
Karslıoğlu, I. P981
Karube, M. P637
Karyakin, O. B. P685
Kasai, T. OP187, P404
Kasat, A. P674
Kassimos, D. P919
Kastis, G. OP450, P319
Kataeva, G. P440, P462
Katagiri, M. P58
Katal, S. P668
Kataoka, S. OP437
Kato, H. OP515, P088, P333, P460, P494, P734
Kato, I. P784
Kato, K. P139, P545, PW088, TP008, TP020
Kato, M. P042, P051, P052, P425,P497, P499
Katsaboukas, D. P358, P360, P850, P851, P945
Katsampoukas, D. P874, P875
Katsarou, Z. P482, P484
Kauczor, H.-U. OP148, P101
Kaufmann, J. OP307, OP491
Kaul, F. OP307
Kausitz, J. P820
Kavindran, R. K. P084
Kawabe, J. P813
Kawachi, T. P784
Kawahara, A. PW040
Kawai, H. P139
Kawai, K. OP224
Kawamura, K. PW002, PW010
Kawashiri, S. P913
Kaya, E. P061
Kaya, H. OP150
Kayaalti, O. P061
Kayani, I. OP548, PW031
Kaymak, E. P662
Kaymakci, E. P538
Kealey, S. P283
Keam, B. OP145
Keat, N. P279
Kebir, S. P554
Keinrath, P. P398
Keller, S. H. OP042
Keller, U. OP035, P094
Kelly, J. OP482, OP483
Kelly, P. P087
Kelten Talu, E. P606, P607
Kemp, B. J. P136
Kenda, S. P39
Kendler, D. P689
Kennedy, J. A. P045
Kero, T. P368
Kerschbaumer, S. P004, P277
Kertesz, I. P252
Kessler, H. OP338
Ketring, A. R. OP479
Khadivi, E. P566
Khajerahimi, F. P400
Khan, N. PW119
Khandelwal, N. OP594
Kharina, D. S. P881
Khazaee Moghadam, M. P113, P115
Khazaeni, K. P566
Khelifa, A. P906
Khetarpal, V. P456
Khomenko, J. P440, P462
Khorasanchi, A. P332
Khoshbakht, S. P256
Khurshid, Z. P554
Kieft, M. OP223, P959, TP021
Kiesewetter, B. OP365
Kilian, J. OP168
Kilty, I. P059
Kim, B. OP614, P273, P276, P577, PW028
Kim, C. P229
Kim, D.-W. OP145, P229
Kim, E.-K. P621
Kim, H. P143, P631, P772
Kim, I. P118
Kim, J. OP258, P065, P273, P276
P572, P571, P772, PW036
Kim, J.-H. TP045, TP061
Kim, K. P273, PW028

Kim, M. P229
Kim, S. P083, P268, P270, P325, P616, P631
Kim, T. OP145, P329
Kim, T.-H. OP258
Kim, T.-S. P270
Kim, W. OP109, P229
Kim, Y. P577
Kimura, H. OP287, P147
Kincl, V. P376
King, A. R. P312
Kinjo, T. P723
Kinuya, S. OP065, OP169, OP435, OP562, P063, P913
Kir, K. M. P804
Kiratli, P. OP593, P072, P794
Kirienko, M. OP252, OP603
Kirov, A. S. OP624
Kiss, I. P151
Kiss, S. A. P965
Kist, J. W. PW097
Kisteneva, I. OP068
Kitaguchi, K. P723
Kitajima, M. P987
Kitamura, K. P396
Kitsiou, E. P245
Kitsukawa, T. P773
Kiyono, Y. OP641, P147
Kizhaev, Y. P518, P564
Kjær, A. OP042
Kjærgaard, B. OP491
Klaeser, B. P569, P640
Klass, N. D. P640
Kılıçkap, S. OP550
Klein, C. OP105, PW066
Klein, E. OP083
Klein, H. C. OP111
KleinJan, G. H. OP231, OP234, OP306, P189 P190, P191, P193, PW064
Kleinová, M. P259
Klén, R. OP166
Klepac, N. P438, P479
Klette, I. OP037, OP140, OP533
Kletting, P. OP009, OP015, OP016, OP090, OP141, OP615
Klicov, N. OP526
Klingeberg, C. P165
Klingler, H.-C. P699
Klisarova, A. P620, P623
Klop, W. M. N. P190
Kluge, A. W. OP192
Kmaid, A. OP327
Knaapen, P. OP067, OP122, OP123
Knap, M. P124
Knappen, P. OP126
Knesaurek, K. P492
Knight, J. C. PW053
Knol, R. J. J. OP172, OP186
Knoll, P. OP036, P699, PW043
Knollema, S. OP543
Knop, S. OP035
Knopp, M. U. PW074
Knopp, M. V. OP118, OP453, P103, P30, P856, PW074
Knudsen, K. PW078
Knudsen, L. M. P783
Knuuti, J. OP126, OP166
Kobarfard, F. P256
Kobayashi, M. OP224
Kobayashi, Y. PW016
Kobe, C. OP155, P774
Koç, Z. P981
Koca, G. P403, P855
Kocaagaoglu, E. P645
Kocabaş, O. P932
Kocael, P. Ç. P609
Kocer, U. P187
Koch, G. P432
Kocjan, T. P891
Kocovski, P. OP293
Kocun, A. P412
Koegelenberg, C. F. N. P628
Koelewijn, S. OP489, OP490, P150
Koenders, M. I. OP105, PW066
Koglin, N. OP563
Kohsaki, S. P686
Koide, Y. P345
Koikkalainen, J. OP166
Koivumäki, T. TP041
Koizumi, M. PW086
Kojima, K. P930
Kojima, S. P139
Kokki, T. OP166
Kokkini, A. P919
Kokkonen, M. TP041
Kolenc Peitl, P. OP530, P414, PW056, PW069
Koletti, L. P365
Kolindou, A. P245
Koljevic Markovic, A. V. OP151
Kolomiets, L. P757
Kolstad, A. OP039
Komatsu, J. OP562
Komek, H. OP150, P132, P137
Koźmiński, P. OP583
Komljenovic, D. OP426
Komlosi, I. P153
Kondakov, A. K. P195, P881
Kondo, C. OP171, OP437, P349
Kong, E. P206, PW012

Koniaris, G. P919
Konijnenberg, M. W. OP489, OP530, OP612
Kono, Y. P196
Konsek, S. J. OP193
Konstantinidis, E. P500
Kontrová, K. P158
Kołodziej, M. P666, P792
Koolen, B. B. OP592
Koopman, D. P586
Koperski, &. P567
Kopka, K. OP308, OP337, OP426, OP428 OP429, P099, P295, P687, P688
Kopschina Feltes, P. OP283, OP510
Koranda, P. OP083, P376
Körber, C. OP135, P885
Körber-Hafner, N. OP135, P885
Kordys, E. OP103
Koriyama, C. P807
Korkmaz, M. P154, P187, P403, P816, P855
Körner, J. P171, P177
Korom, C. P073
Kose, N. P917
Kosecka, K. P412
Kose Kurt, Y. P645
Koshiba, Y. PW088, TP008, TP020
Kosinski, M. OP298, OP361
Kosmidis, P. P635
Kostadinova, I. P502, P656, P727, P873, P982
Kosterink, J. G. W. P381
Kostina, I. S. P210
Kostkiewicz, M. P391
Kostou, T. P56
Kotaka, K. P074
Kotani, K. P813
Kotina, E. D. P350
Kotomin, I. P462
Kotoucova, J. P429
Kotrotsios, D. P850, P851
Kotzasarkidou, M. PW106
Kotzerke, J. OP046
Kotzki, P. OP630, PW095
Koumarianou, E. OP245
Koutsikos, J. P919
Kouvelis, K. P670
Kovács, M. OP200
Kovacs, N. P471, PW022
Kováčová, Z. P667
Koyama, K. P074, P166, P223
Koyama, T. P723
Koziara, H. OP197, OP389
Kozic, D. P126
Koziolek, E. P161, P171, P177
Kozminski, P. OP584
Kozłowska, J. P610
Kraft, M. TP041
Krajewski, S. OP478
Krakauer, M. OP152
Král, V. P259
Kralik, M. P749
Králik, R. P820
Kramer, G. OP362, P100, P105
Krämer, S. D. OP199, OP285, OP288
Kramer, S. OP109, P124
Kramer, V. P085, P427
Kramer-Marek, G. OP588, OP589, OP619
Kranenborg, E. OP524
Kranz, M. P017
Krapf, P. OP097, OP098, OP103, PW052
Krasikova, R. OP289, P288, P291, TP082
Kıratlı, P. Ö. OP496, OP498
Kratochwil, C. OP089, OP148, OP226, OP308 OP428, OP429, P099, P101
Krause, B. J. OP618, P748
Krebsová, A. P377
Krenning, E. P. OP336, P179
Krijger, G. C. OP329, OP423, P309
Krishnadas, R. P453
Krishnan, b. TP001
Kristensen, B. W. P173
Kristic, S. P615
Krivorotko, P. P751
Krizova, H. P956
Krizsan, A. K. P067
Kroiss, A. P657
Królicki, B. OP197, OP389
Królicki, L. OP197, OP389, P567
Krommes, K. P398
Kropáček, M. P158, TP101
Kropf, S. OP035, OP534
Kroselj, M. PW056, PW069
Krstic, D. P080
Krstic, R. P080
Kruger, T. H. C. OP513
Krušlin, B. P535
Kryza, D. OP609
Krzesinski, J.-M. P090
Krzhivitskiy, P. P574, P751, P927
Kuang, A. P204, P618, P811
Kubánek, M. P377
Kubinyi, J. OP368, P024, P049, P667, P883, P952, PW073
Kübler, W. OP429
Kubo, M. P925
Kubota, K. P223, P791
Kubota, T. PW088
Kucuk, N. O. OP579, P804, P843

Kuczyk, M. P911
Kudo, S. TP096
Kudo, T. P345, P647
Kudo, Y. OP162
Kudomi, N. P487, P549
Kuenzel, L. OP358
Kučera, J. TP101
Kuerpig, S. PW058
Kuge, Y. OP144
Kuhn, F. OP600
Kuhnast, B. P111, PW021
Kühnel, C. P53, P54
Kuhnert, G. P774
Kuil, J. P192
Kuji, I. OP562, P445, P613
Kucukalic-Selimovic, E. P808
Kukuts, K. P965, TP062
Kukwa, W. P567
Kula, M. P645
Kulakiene, I. P515
Kulka, J. P591
Kulkarni, H. OP037, OP140, OP141, OP192, OP239, OP430; PW116
Kulkarni, S. P303
Kumada, T. P784
Kumar, D. OP594
Kumar, K. OP537, P367
Kumar, M. OP594
Kumar, N. OP232, P653, P658, P719
Kumar, P. OP164, P083, P800
Kumar, R. P367
Kumar, S. P261, P719
Kumar, V. TP073
Kumata, K. PW002, PW010
Kumita, S.-I. P559, P966, P985
Kundu, B. TP023
Kunikova, I. P956
Kunikowska, J. OP197, P567
Kunisada, T. P930
Kuntner, C. OP290
Kunze, K. OP226
Kuo, Y.-Y. P144
Kupferschlaeger, J. OP358
Kupik, O. OP593, P072, P794
Kural, A. R. OP087
Kurash, M. P045
Kurata, S. PW040
Kurihara, Y. PW002
Kuroiwa, N. OP170
Kürpig, S. OP634, P796, P832, PW114
Kurt, S. OP055, P424, P426
Kurth, J. P748
Kurt Ömürlü, I. P932
Kurtys, E. OP510
Kurucu, N. OP496
Kusacic Kuna, S. P540, P749
Kusano-Arai, O. P166
Kusić, Z. P535, P651
Kusumoto, M. P747
Kutluk, T. M. OP498
Kuwabara, Y. PW016
Kuwert, T. OP331, OP364
Kuyumcu, S. P609
Kuznetsova, O. P288, P291
Kvaternik, H. P004, P277
Kwasiborski, P. J. P361
Kwee, R. OP263
Kwizera, C. OP049, P419
Kwon, E. D. P136, TP057
Kwon, S. P206, P772, PW012, PW039
Kyncl, M. P952

Lacanfora, A. P459, P678
Lacerda, L. TP038
Lacoeuille, F. OP038, P164
Lacolley, P. PW059
Lad, S. P303
Ladd, M. E. OP426
Ladefoged, C. OP050, P201
Ladenbauer, V. P269
Ladjohounlou, R. OP280, OP422, OP487, P181
La Fougère, C. OP358
Laghai, I. OP302
Lagozhina, I. PW096
Lahner, H. OP013
Lahoutte, T. OP245
Lai, C.-H. OP460
Lai, Y.-C. P828
Laine, J. P314, TP010
Laitinen, I. OP474
Laitinen, T. P395, TP041
Lal, H. OP232
Lam, K. PW070
Lam, M. G. E. H. OP329, OP423, P309, P648
Lam, P. P269
Lamandé-Langle, S. P293, PW059
Lamballais, M. P302
Lambers Heerspink, H. J. OP473
Lammertsma, A. OP067, OP122, OP123 OP419, OP531, P105, P320
Lan, X. OP203, P251, PW001
Lancelot, S. OP052, OP597
Landoni, C. OP366, P121, P134, P33, P35, PW084
Landry, G. P011
Lane, D. P. P184
Lang, J. OP203

Lang, O. P956
Lange, C. P226
Lange, R. PW113
Langendijk, J. A. OP054
Langenhuijsen, H. P188
Langenhuijsen, J. F. OP420
Langer, N. H. OP042
Langer, O. OP290, P317
Langer, S. W. OP042
Langer, T. P928
Langhain, M. OP516, P481
Langsteger, W. OP154, P679, P922, TP009
Lanni, V. P248
Lanoy, E. OP369
Lantos, J. P29
Lanzarone, S. P279
Lanzenberger, R. P317
Lanzetta, V. P798
Lapa, C. OP035, OP194, OP277, OP433 OP534, OP542, OP645, P527
Lapa, P. OP553, OP553, P673, P893, P960
Lapeña Gutierrez, L. P093, P408, P941
Lapina, O. P915
Laranjo, M. P330
Larg, M. I. TP007
Larhed, M. OP340
Larionova, L. P321, TP017, TP100
Larobina, M. OP174
Larsen, H. C. OP412
Larsen, L. P573, P598
Larsen, T. S. P726
Larsen, V. TP006
Larsson, E. OP240, P077
Lass, P. OP480, P324, P610
Lassen, M. OP044
Lasserre, M. OP627
Lassmann, M. OP194, OP277, OP387 OP491, P020, P022, P857
Lastoria, S. P36, P733
Laszuk, E. P255
Lau, J. P284
Lauenstein, T. OP250
Laurenza, M. OP583
Lauri, C. P938
Laustrup, H. P951
Lavado-Pérez, C. OP438, P436
Lavalaye, J. OP524
Lavallée, É. OP446
Lavallée, P. P385
Lavent, F. P023
Laverman, P. OP105, P266, P318, PW066, PW069
Lavisse, S. PW021
Law, I. OP050, OP494, P003, P201
Lawler, M. OP648
Lawson, R. S. P005, P006
Lazarenko, S. OP186, OP172
Lazaridis, K. P874, P875
Lázníček, M. P259
Lebbé, C. P169
Lebeda, O. P259, TP101
Lebedev, D. I. PW013
Le Blay, M. OP487
Leboulleux, S. OP091
Lebtahi, R. OP332, OP610, P865
Lecomte, R. OP446
Lee, A. P551
Lee, B.-F. P622
Lee, C.-T. P313
Lee, D.-E. OP100
Lee, E. P582, P583
Lee, F.-T. OP293
Lee, H.-J. TP045
Lee, I. P065
Lee, J. OP056; P008, P273, P276 P325, P329, P621, TP045, TP061
Lee, J.-G. P988
Lee, J.-Y. P159
Lee, K. OP168, OP355, P144, P273, P276, PW028
Lee, M. P467
Lee, P.-I. P578
Lee, S. OP258, OP293, P008, P268, PW039
Lee, S.-H. OP145
Lee, S.-K. P270, P325
Lee, W. P565, P616
Lee, Y. P273, P631
Lefebvre-Lacoeuille, C. OP038, P164
Lefrandt, J. D. OP473
Legallois, D. OP505, P044
Legendre, S. OP332
Le Guludec, D. OP434, OP476, P362, P385, P936
Lehmann, M. OP160
Lehner, S. OP070, P380
Lehnskov, T. K. TP012
Lei, B. P176, P390
Leicht, M. OP333
Leide Svegborn, S. P864
Leinonen, A. TP041
Leisser, A. P672
Leite, A. P. S. TP013
Leite Ferreira, P. OP359
Lele, V. OP164, P800
Lemaire, C. OP096
Lemkes, J. OP122
Lemos, J. PW103
Lenart, N. PW022
Lenda-Tracz, W. OP530

Leners, N. PW076
Lenfant, P. P437
Lengyel, Z. OP062, P591, PW085
Lenz, J. W. OP479
Lenza, A. P274, P938
Leong, K. PW107
Leong, T. OP351
Leoni, E. TP085
Leonie, W. P172
León Ramírez, L. P746, P093, P975
Leotta, K. OP337
Leotta, S. OP237
Lepareur, N. OP038, P304
Le Roux, P.-Y. OP351, P778
Lescano, A. P481
Lesèche, G. P385
Letaief, B. P224, P815, P924
Letaillandier, C. PW021
Letourneur, D. OP476
Leva, L. P095
Levacher, V. P282
Leverenz, J. OP324, OP325
Levigoureux, E. OP052
Levillain, H. OP381
Levin, C. OP047, P200, P29
Ley, M. P470
Leygnac, S. P362
Lezaic, L. P414
Lhommel, R. OP503
Li, F. P629
Li, G. Y. P291
Li, H. P674
Li, J. Y. P696
Li, L. P235, P558
Li, M.-H. P313
Li, R. P390
Li, S.-Y. P144
Li, S. P280, P514
Li, T. PW107
Li, X. OP433
Li, Y. TP023
Liaros, G. P484
Libani, I. OP367
Liberatore, M. OP066, OP236
Liguori, C. P458
Lim, I. OP614, PW028
Lim, K. P571
Lim, S. OP614, P276, PW028, PW036
Lima, G. M. OP254, OP301, OP605, P702
Lima, J. OP553, P675
Lima Oubiña, A. P292
Limouris, G. S. OP195, P014, P500, PW112
Lin, C.-Y. P560, P984
Lin, G. OP460
Lin, H. H. P055, P075
Lin, K.-J. TP056
Lin, K.-S. P284
Lin, W. Y. P696
Lin, Y. C. P696
Lind, S. D. TP015
Lindberg, U. OP050
Lindbo, S. OP242
Lindeberg, G. OP340
Lindemann, M. OP576
Lindenblatt, D. OP243
Lindner, S. OP051
Liotsou, T. P802
Lipovetsky, B. P440
Lipponen, T. P314
Lishmanov, Y. OP068, P246, P343
P346, P387, P388, PW013
Listewnik, M. H. P216
Little, P. OP053
Liu, B. OP527, P858, PW109
Liu, C. P176, P258, P625
Liu, F.-Y. OP460
Liu, J. OP168
Liu, M.-C. P578
Liu, Q. PW001
Liu, R. S. P291
Liu, T.-T. P461
Liu, X. P258
Livieratos, L. OP621, P155, P156, P56
Lizio, D. OP639
Ljungberg, M. OP330, OP380, OP383
OP387, P215, PW043
Llamas-Elvira, J. M. P632, P750, P762
P663, P764, P680, PW075
Llewelyn, P. P287
Lo, C.-C. P561, TP093
Loaiza Góngora, J. OP580, P761, P765, P767, TP014
Locantore, L. OP300
Lochner, C. P454
Lodi, F. OP254, OP310, OP532
P702, PW051, PW055, PW089
Loeffen, D. OP304
Loening, A. P202
Loeuille, D. TP086
Loewenthal, C. P755
Löfgren, J. OP042
Loira, F. P759
Lolli, C. P703
Lomeña, F. P935, PW045, PW081
Løndalen, A. OP039; OP295, OP599
Longari, V. PW108
Longo, F. P964

Longo, M. P019, P511, P729, P974
Lonsdale, M. TP015
Loo, C. E. OP628
Look, M. OP392
Lopatto, R. P743, P744
Lopci, E. OP146, OP310, OP532 OP601, OP602, OP632, P547
Lope-Lope, R. P001, P068
Lopes, F. P671, PW118
Lopéz, A. P759
Lopez, D. OP456, OP642, P553
López, E. P299
López, M. P824
Lopez-Casas, P. P. P148
López Cubillana, P. P692
López-Defilló, J. L. OP438, P436
López-Fidalgo, J. F. P104
Lopez Urdaneta, J. TP091
Lo Presti, D. P358, P360, P850, P851, P945
Lorenzo-Bosquet, C. P568
Lorenzon, L. OP330
Lorenzoni, A. OP596, P698, P753
Lorgis, V. OP590
Loriggiola, M. P227
Lorusso, D. OP596
Lötjönen, J. OP166
Lots, D. P586
Lott, J. OP358
Lotz, J. OP297
Lou, J. P625
Loubinoux, I. P281
Loudos, G. P56
Louedec, L. OP476
Lougovski, A. OP046, OP163, OP363
Lourenço, F. OP636
Loutfi, I. P401
Lovigu, C. P972
Lovinfosse, P. P090
Lowe, V. J. P136
Lowrey, M. OP323
Lozza, C. OP487
Ltaief, B. P817, P818, PW079, TP084
Lu, C.-C. P955, PW017
Lu, S.-W. P452
Lubberink, M. OP011, OP551, P368
Lub-de Hooge, M. N. P301
Luca, C. P071
Lucconi, G. OP638, P227, PW111
Lucena, F. OP227, TP038, TP044, TP076
Lucena, I. S. PW118
Lucianini, R. TP040
Lucic, M. A. P126
Lucic, S. P126
Lucignani, G. OP367, P174
Lückerath, K. OP534, P180
Lui, K.-W. PW083
Lukas, M. P226
Lumbroso, J. OP091
Lundstrøm, A. OP152
Luo, H. OP585, OP620
Luo, Q. P211
Luo, T.-Y. P228, P516
Luster, M. P894
Lütje, S. OP250, OP536, P205, P37, P690
Lützen, U. PW093, TP077
Luurtsema, G. OP286, P301
Luxen, A. OP096
Lyapunov, A. P757, P758
Lyburn, I. D. OP143
Lyczko, M. OP584
Lyerly, H. OP245
Lymperis, E. OP336, P179
Lyra, M. OP195, PW112

Ma, K.-H. P144, P452, P461
Ma, M. T. OP481
Maadi, E. P252
Maaloul, M. P441, P976
Maas, B. OP049, P419
Maaß, C. OP010, OP015, OP090, OP117, OP615, P002
Maassen, J. R. OP479
Macapinlac, H. OP056, OP238, OP309
Maccauro, M. OP424, OP613, P753
Machado, J. S. P020, P022
Mäcke, H. PW082
MacNee, W. P059
Madaschi, L. P701
Madeddu, G. P468, P476, P478, P525, P972
Madke, P. P047
Madke, R. P047
Madrid, J. TP013, TP016, TP047, TP071
Madsen, J. TP066
Madsen, K. L. OP390
Madsen, P. H. P783
Maecke, H. OP298, OP427, OP490, OP530, P165, PW069
Maeda, H. P393, P405, TP080
Maeda, Y. P189, P487
Maekawa, J. OP170
Maemura, K. P345
Maenhout, A. PW119
Maes, A. P023, P57
Maffioli, L. OP578, P378
Magnander, T. OP014
Magnen, M. OP276

Magnussen, R. PW074
Magota, K. OP144
Mahajan, H. OP554, P659
Mahida, B. OP434, P936
Mahmoudian, B. P624
Mahmoud Pashazadeh, A. P544
Mahren, B. OP615
Mahvash, A. OP328
Mai, E. K. P737, P738
Maikusa, N. P443
Maillard, L. OP560
Maillet, D. P312
Maina, T. OP299, OP336, OP530, P179
Mainolfi, C. OP303
Mainta, I. P433
Mairani, A. P867
Mairinger, S. OP290
Majewski, S. TP023
Majkowska-Pilip, A. OP583
Majos-Torro, C. P446
Makaiová, I. P024
Makarenko, V. PW015
Makino, A. OP641, P147
Makogon, B. P503
Małkowski, B. P744
Makris, N. E. OP419
Maksud, P. OP538
Malandain, G. OP560
Malaroda, A. OP278
Malecka, B. P391
Maleev, V. P288
Malek, E. P302
Maleki, R. P654
Malhaire, J.-P. P778
Malhotra, A. TP035
Malizia, C. PW055
Malkowski, B. P743
Mallia, M. TP001
Malterre, J. OP359
Malvaldi, F. P793
Mamach, M. OP055, P424, P426
Mameli, R. P961
Mammatas, L. H. OP531
Manca, G. P480, P853, PW032
Manenti, S. P227
Manes, C. P945
Mangiacotti, F. OP233
Mangili, G. P714
Mango, L. OP236
Maniawski, P. OP118, OP453, P103, P856
Mannarino, T. OP120, OP167, OP174
Mannazzu, M. P972
Manni, I. OP205
Mano, S. TP022
Manolios, N. OP259
Manoğlu, B. G. P932
Manou, E. P874, P875
Manrique, A. OP505, P044
Mansberg, R. P929, TP075
Manser, R. OP351
Mansi, R. OP298, OP307, P257, PW069
Mantini, G. OP626
Mapelli, P. OP252, OP256, OP300, OP603, P714
Marabelle, A. OP369
Marbello, L. P601, P971
Marcatili, S. OP422, OP487, P181
Marchesi, F. OP146
Marchi, G. TP048
Marchiano', A. OP424
Marci, V. P969
Marco Antonio, S. P860
Marcotte, M. E. OP093
Marengo, M. OP452, OP633, OP638, P026
P227, P250, PW051, PW111
Marešová, L. P259
Marianovski, V. P873
Marie, P.-Y. OP560, P293, P392
P397, P420, P463, PW059
Marie, S. P421
Marí Hualde, A. OP646, P718
Marin, G. OP386
Marin Ferrer, M. P711
Marini, C. OP472, OP540, OP623
P232, P233, P234, P236
P394, P728, PW018, PW025
Marini, I. OP511
Marín Muñoz, J. P435
Mariyanovski, V. P982
Markewycz, A. OP259
Markovic, V. P905
Marletta, F. P771
Marner, L. OP494, P003, P201
Maron, L. OP333
Maroto, P. P700
Marotta, G. OP645, PW027
Marre, F. OP630
Marroquín-Gálvez, J. A. PW080
Marshall, C. P007, P157, P287, PW053
Marshall, J. OP486
Marta, A. PW022
Martella, R. P232
Martelli, C. P174
Martens, J. OP392
Martin, B. OP356
Martin, F. P299
Martin, W. PW042, PW044

Martineau, A. P169
Martineau, P. OP264, P009, P519, P827
Martinecz, B. PW022
Martinez, A. P148, P788
Martinez, D. P316
Martinez, T. P315
Martinez-Aguilar, M. P375
Martínez-Caballero, A. P884
Martínez de Bourio, M. P125, P408, P941, P975
Martínez-Esteve, A. P852
Martínez-Garcia, M. P552
Martinez Gomez, M. P354
Martinez-Horta, S. OP642
Martinez Pimienta, G. P469, P831, P946, P947
Martínez-Ramírez, M. P884
Martinez Regueira, F. OP591
Martínez-Rodríguez, I. OP438, P436
Martinez-Torrecuadrada, J. P148
Martínez-Torrens, F. PW038
Martin Gomez, E. P931
Martin-Gonzalez, T. P001, P068
Martini, M. P274
Martini, P. P227, P250
Martinotti, A. S. OP249
Martins, A. OP159
Martins, C. D. OP588, OP589, OP619
Martins, E. P371
Martins, H. R. TP094
Martinsen, A. OP039
Martirosyan, L. P253, P344, P389
Martorana, A. P432
Martorana, G. P709
Martucci, F. P563
Maruyama, D. P488, P489
Maruzzo, M. OP631
Marx, M. PW093, TP077
Marzo, K. P271, P308
Marzullo, P. PW030
Mas', O. M. P350
Maskali, F. P293, P420, P463, PW059, TP086
Maskell, N. A. OP143
Massaccesi, M. OP626
Massi, L. P954
Massidda, S. P296
Massollo, M. OP147, OP598, P587
Massri, K. P798
Mast-Vilaseca, R. PW038
Matei, L. OP480
Mathe, D. P073, P151, PW022
Matheoud, R. OP639
Mathiasen, R. OP494
Matínez de Bourio, M. PW020
Matović, M. OP441, P080
Matovina, E. OP526, P682
Matrane, A. P921
Matselas, E. P826
Matsuda, H. P443, P445, P465
Matsuda, R. TP096
Matsui, J. P230
Matsui, T. P555
Matsumoto, K. P38, P142, TP034
Matsunaga, K. P333, P460
Matsunari, I. OP224, OP562, P613
Matsuo, S. OP065, OP169, OP435, TP053
Matsusaka, Y. P58
Matteucci, F. P046, P703, P798
Matthews, R. OP356
Matti, A. P702
Mattioli, S. OP146, OP310, OP532
Mattoli, M. OP626
Mattsson, E. P077
Mattsson, S. P864
Matveev, V. OP083
Matyskiel, R. OP389, P567
Maurin, M. P255
Maurizi Enrici, R. P643
Maus, J. OP046, OP363
Maussier, M. P248
Mautone, V. P046
Maya, Y. OP431, OP432, OP542
Mayerhoefer, M. OP044, OP365, OP416, P672, P732
Maza Muret, F. P646
Mazère, J. P676
Mazighi, M. P385
Mazurek, A. P361, P372, P617
Mazzaferro, V. OP424
Mazzarri, s. OP136, OP421, P853, PW032
Mazzeo, A. P409
Mazzuca, N. P793
McBride, W. OP394, OP485
McCready, V. R. OP195, P014, PW112
McCue, P. P083
McDonald, J. P335
McDougald, D. OP245
McGeehan, A. OP323
McGonigle, J. TP038
McGowan, D. R. P078
McInnnes, I. P453
McKeown, C. P108, P109
McKinna, F. P695
McMahon, A. OP343, P328
Meave, A. P386
Meckel, M. OP138, OP276
Medaer, E. OP443
Meddeb, I. P220, P815, P817, P818
P835, P916, PW079, TP084

Medina-Benítez, A. P680
Medolago, G. TP069
Medrano, S. P470
Medvedec, M. P357
Medvedev, S. P550
Meerlo, P. OP286, P419
Meftahi, M. P859
Meijerink, M. OP531
Mele, L. P525
Meleddu, C. OP036, P296, P699
Meletta, R. OP199
Melhus, K. B. P162
Melichar, F. P158
Melie-García, L. P493
Melis, M. OP392
Melki, S. P531
Meller, B. OP297, OP393
Meller, J. OP297, OP393
Memmott, M. J. P005, P006, P31, P359, P411
Memo, L. OP414
Mena Bares, L. P646
Menconi, M. OP421
Mendes, E. P294, PW065
Mendes, S. F. C. TP044
Mendez-Alonso, S. P848, P848
Mendiola, A. OP157
Meneyrol, V. OP104, P149
Meng, F. C. P291
Menga, M. P842
Menjón-Beltrán, S. P762, P764
Menke-van der Houven van Oordt, C. W. OP419
OP531, P777
Menzaghi, M. TP040
Mercier, J. OP096
Merenda, N. OP499
Merino-Serra, E. M. P706
Merlet, P. P169
Merrett, J. OP094, OP447, PW100
Meseguer, E. P385
Mestre-Fusco, A. P470, P552
Meszaros, L. OP481
Metelkova, I. P376
Metello, L. F. OP185, OP480, P324, P610
PW035, PW103, TP068
Metselaar, J. M. OP105, P318
Meyer, C. P846
Meyer, G.-J. P265
Meyer, P. T. OP427, P165, PW082
Meza-Escobar, D. OP438, P436
M. Gaffuri, P821
Mhiri, A. P220, P815, P817, P818,
P835, P916, PW079, TP084
Mhiri, C. P441
Miao, W. P208
Michailos, K. P957
Michalaki, V. OP195
Michel, J. OP476
Michel, P. OP510
Michel, R. P161
Michieletto, S. P584
Michopoulou, S. OP548, P203, P619, PW031
Miederer, M. OP138
Mielcarski, M. P327
Mier, W. OP226, OP308, OP429, P687, P688
Migliari, S. P272, P34
Migliore, M. P642
Migliorisi, M. OP424
Mihai, C. P071
Mihailos, K. P472
Mihailova, J. P656
Mihailovic, J. OP526, P682
Mihaylova, Z. P786
Mijnheere, E. TP025, TP043
Mikail, N. OP476, P362, P385, P936
Mikami, Y. P530
Mikecz, P. P292
Mikell, J. OP115, OP328
Mikhayel, M. P087
Mikhaylova, E. P199
Miklovicz, T. P292
Mikolajczak, R. OP193, OP342, OP530, P255, P327
Milanaccio, C. OP598
Milani, R. PW084
Milardovic, R. P615
Milella, M. OP110, P943
Mille, E. P866
Mills, C. P870
Milton, D. OP238, OP309
Min, J.-J. P772
Minamimoto, R. OP045, OP047, P202, P791
Miñana, E. P315
Miñana López, B. P692
Minarik, D. P369, P864
Minazzi, P. OP101
Minear, G. OP449
Minin, S. M. P222
Minkin, K. P502
Mintun, M. OP323
Minutoli, F. P409, P861
Miorin, E. OP440
Miquel Cases, A. P599
Mira, M. OP330, OP424, OP613
Mirabelli, P. P160
Miralbell, R. OP298
Mirijello, A. OP511
Miró, J. P508, P935

Miró-Martín, M. PW038
Miron, I. P907
Mirzaei, S. OP036, P699, PW043
Mirzajevová, M. P158
Mishugin, S. OP083
Missault, S. P172
Missiato, A. P642
Mitjavila Casanovas, M. OP629, P847, P848
Mitra, A. P303
Mitran, B. OP246, OP340, OP586
Mitsakis, P. OP298
Mitsopoulos, E. P874, P875
Mitsui, K. P166
Mitsumoto, T. P074
Mittal, B. OP041, OP594, P060, P092
P116, P261, P593, P719
Mitterhauser, M. OP365, P317, P672, PW004, PW006
Mittra, E. OP045, P29
Mitxelena, M. OP157
Miura, Y. P556
Miwa, M. P189
Mix, M. P285
Miyata, Y. P791
Miyatake, K. P686
Miyauchi, H. PW016
Miyazaki, A. P147
Miyazaki, C. P434
Mizokami, A. P913
Mizutani, A. OP224
Mizutani, Y. P396, TP089
Mladenov, B. P873
Mochida, I. P088, P460
Mochiki, M. P223
Mochula, A. P346
Modat, M. OP160
Modoni, S. P431
Modzelewski, R. OP161
Moghaddam-Banaem, L. OP492, P182
Mohajeri, S. P406
Mohamadi, A. PW059
Mohamed, Y. P575
Mohamed Salem, L. OP260, P435, P692, P823, P970
Mohamerd, W. P575
Mohammad, A. OP139
Mohammadnejad, J. P252
Mohan, H. P870
Mohnike, W. OP138
Mohring, M. OP474
Mojal, S. P552
Mok, G. S. OP507, P214, PW107
Mokrane, F. P399
Mol, M. OP193
Molenaar, Q. I. P648
Molkenboer-Kuenen, J. D. M. OP204, OP485, OP488
Møller, A. OP322
Møller, N. OP322
Mollet, P. P199
Mölne, J. OP334
Momose, M. OP171, OP437, P349, P457
Momose, T. P166
Monari, F. OP577
Monroy-Gonzalez, A. P373, P375, P386
Montagnani, F. P275
Monteiro, M. P868
Monteleone, F. OP066, OP236
Montellano Fenoy, A. OP260, P692
Montes, A. OP642, P553, P700
Monteverde, E. P236
Monti, M. OP303, P237, P730, P780, P798
Montini, G. OP552
Monturiol, J. P534, P660, P978
Monzen, H. P142
Moon, H. P065
Moon, M. P159
Mora, E. PW099
Mora, J. P469, P508
Moradkhani, S. P252
Moraes, E. R. P051, P052, P497
Morahas Solanes, M. P720
Moralidis, E. P482, P484
Morana, G. OP598
Morandeau, L. P107, P326
Mora Ramirez, E. P028
Mora Salvadó, J. P946
Moravszki, M. P355, P473
Morawska, K. PW065
Morbelli, S. OP147, OP472, OP525, OP540
OP561, OP623, P394, P430
P587, P728, PW018
Morcillo, M. A. P148
Moreau, C. P437
Moreira, A. OP553, P673, P675, P969
Moreno, A. P935
Moreno Ortega, 0E. P646
Moresco, P. P821, TP081
Moresco, R. P174, PW008
Moretti, A. P046, P703
Moretto, P. P969
Morgan, D. G. P016
Morganti, A. OP605
Morgat, C. OP279, P676
Morgenstern, A. OP089, OP197, OP280, OP394
OP485, OP488, OP489, OP583
Mori, T. OP641
Morigi, J. J. OP088, OP254, OP301, P082
Moriguchi Jeckel, C. M. OP283, OP510

Morillo, E. P632, P663
Morisco, A. P733
Morita, N. P488, P489
Morita, T. P734
Morlino, S. P698
Moro, A. OP367
Morooka, M. P791
Morosi, C. OP424
Morris, D. PW048
Morris, O. OP343
Morsing, A. P240
Mortazavi, S. P400
Mortensen, A. C. OP622, P184, P262
Morzenti, S. P121, P33, P35
Mosconi, C. OP577
Mosebach, J. PW090
Moslehi, M. P544
Mostacci, D. P026
Mostafa, A. P575
Mota, R. P335
Motta, C. TP081
Mottaghy, F. OP009, OP015, OP016, OP085, OP090 OP092, OP304, OP549, P973, PW061
Mouden, M. OP543
Moulopoulou, L.-E. OP195, PW112
Mourah, S. P169
Mourani, B. P849
Mourtada, F. OP115, OP328
Moyon, A. P258
Moz, S. P279
Mpalaris, V. P358, P360, P850, P851, P945
Mpountas, D. P358, P360
Mu, L. OP285, OP288, P288
Mucientes Rasilla, J. OP629
Muckle, M. P846
Muegge, D. P527
Mueller, C. OP533
Mueller, K. M. P640
Mueller, S. P. OP576
Muggeo, P. OP499
Muhammedoglu, A. P605, P608
Mukhortova, O. V. P685
Mulazimoglu, M. TP018, TP031
Mulder, D. J. OP473, P381
Mulder, J. OP053
Mulder, S. F. OP420
Mulders, P. OP420, P188
Mulero, F. P148
Mulholland, N. P076, P32, TP032, TP060
Mullen, G. OP481, OP621
Müller, A. OP341
Müller, B. OP009, OP015, OP016
Müller, E. OP188
Müller, H.-W. P447, P448, P449
Müller, M. OP290
Müller, S. P. OP043, P854
Müller Herde, A. OP199
Munck af Rosenschöld, P. OP494
Munechika, H. P556
Muñiz Garcia, G. P669, P763
Munk, O. L. P021
Muñoz, D. P481
Muñoz Iglesias, J. P669, P763
Muñoz Pasadas, M. P104
Munoz-Sanjuan, I. P456
Munteanu, M. P907
Munthe, E. P238
Mura, M. S. P972
Murakami, K. P58
Murakami, T. P428, PW040, TP074
Muramatsu, H. P139
Murase, K. P38
Murcia Durendez, M. OP260
Murè, G. P779
Murè, M. P522, P899, PW092
Murer, L. OP440
Muros, M. A. PW075
Murphy, D. OP293
Murphy, R. C. P136
Murray, I. OP235, OP382, PW100, PW119
Murray, R. P107
Murthy, N. P265
Muselaers, C. H. J. OP420
Mussini, C. P954
Mut, T. P601, P971
Mutvar, A. OP555
Muzaffar, R. P086, P087
Mylam, K. J. P726
Myoujin, M. P773
Myschetzky, P. S. OP152

Na, C. PW036
Nabid, M. OP477
Nabinger, P. P047
Nag, S. OP149
Nagamachi, S. P396, TP089
Naganawa, S. P139, P545, PW088
Nagar, V. OP118, OP453
Nagarajah, J. OP156, P168, P205, P854
Nagayasu, T. P647
Naghshine, R. P845
Nagpal, C. OP063
Nagy, D. P473
Nagy, G. K. P067
Nagy, I. P841
Nagy, Z. P841

Nai, Y. OP162
Naia, M. D. P324
Naidoo, C. P149
Naka, S. P088
Nakabeppu, Y. OP057, P807
Nakae, A. P333
Nakagami, Y. P747
Nakagawa, K. P356
Nakagawara, J. P488, P489
Nakahara, T. P58
Nakajima, K. OP065, OP169, OP435, P063, P913, TP053
Nakajima, M. P637
Nakajo, M. OP057, OP431, OP432, OP542, P807
Nakamatsu, K. P775
Nakamoto, K. P39
Nakamoto, Y. P027, P693, P980
Nakao, R. OP287
Nakata, T. OP065
Nakatani, K. P723
Nakayama, M. P530
Naldöken, S. P562, P914
Nam, H.-Y. P141
Namal, E. PW033
Namazian, A. P911
Namimoto, T. P987
Nanasato, M. P393, P405, TP080
Nanashima, A. P647
Nanni, C. OP108, OP233, OP552, P135, P702 P709, P739, P781, P949, PW089
Napolitano, M. P175
Nappi, C. OP120, OP174, P374
Nas, O. P920
Nascimento, F. TP028
Nasirzadeh, M. P289
Nasr, H. P521, P677
Nataf, V. OP255
Nath, A. OP232
Nathan, M. OP257, P136, TP057
Nausching, R. P324
Navales, I. P978
Navales Mateu, I. P660
Navarro Fernandez, J. OP260, P435, P692, P823
Navarro Martinez, B. P354
Navarro-Teulon, I. OP280, OP422, OP487, P181
Nawroth, R. OP618
Nayak, T. K. OP105, PW066
Nazemiyeh, M. P624
Neels, O. OP429, P295
Negri, A. OP251
Neijenhuis, P. P589, P958
Nekolla, S. OP224, OP471, OP474
Nelson, A. S. P501
Nelson, R. OP380
Nemati, R. P450, P451, P505, P506
Nematyazar, J. OP084, OP087, OP535, P662
Nemec, P. P384
Nemeth, Z. OP062
Nemetyazar, J. P538
Nengaki, N. PW002, PW010
Neshandar Asli, I. P845
Nesterov, A. A. P222
Nesterov, E. A. P222
Nesterov, S. V. OP126
Nesterov, Y. A. P246
Nestle, U. P106
Nestor, M. OP622, P184, P262, PW057
Nestwrov, E. P311, P321, TP017, TP100
Neumaier, B. OP097, OP098, OP103, PW007, PW052
Neumann, G. P241, P713
Neumeyer, J. L. OP289
Neves, D. TP068
Nevin, S. T. P312
Newman-Tancredi, A. TP049
Ng, T. OP621
Ngo, H. V. OP013, OP043
Nguyen, F. OP276
Nguyen, Q. OP088
Nguyen, T. OP061, PW049
Niccoli Asabella, A. OP107, OP459, OP499, P638
Nickles, R. J. OP585, OP620
Nicol, A. OP643, P453
Nicolaij, D. P023
Nicolas, G. P. OP307, P257
Nicolás Ruiz, F. P823, P970
Nicolas Ruiz, P. OP260, P692
Nicolini, S. P798
Nics, L. P317
Niculae, D. OP480
Niedermoser, S. OP117
Nielsen, D. P415
Nielsen, K. D. OP190
Nielsen, M. M. OP292
Nielsen, S. P021
Niepsch, K. OP192
Nieri, A. OP540, P394
Nietzer, S. P180
Nievelstein, R. A. OP362, P100
Nieves Maldonado, S. M. P768, TP091
Nigam, S. OP102
Nihara, T. OP057
Nihashi, T. P612
Niimi, T. P393, P405, TP080
Nijsen, J. F. W. OP423
Nikaki, A. P209, P213, P365, P635
Nikapota, A. P695

Nikezic, D. P080
Nikolajsen, M. OP417
Nikolaus, S. P447, P448, P449
Nikou, G. OP195
Nilica, B. P689
Nilsson, J. PW102
Niñerola-Baizán, A. PW045
Ninot, S. P935
Nisbet, A. OP447
Nishi, K. OP224
Nishida, H. P486
Nishii, R. P396, TP089
Nishijima, K.-I. OP144
Nishikawa, K. P434
Nishimori, M. P686
Nishimura, Y. P142, P775
Nishio, T. P486
NIshiyama, A. P487
Nishiyama, S. OP048
Nishiyama, Y. P133, P487, P549
Nisli, C. P538
Nivaggioni, G. P953
Nobili, F. OP323, OP561, P430, PW025
Nobre, M. TP028
Nock, B. OP299, OP336, P179
Nocuń, A. P407
Nogami, M. P686
Noguchi, N. P913
Noguchi-Shinohara, M. OP562
Nogueiras, J. P120, P520, P533, P759
Nonnekens, J. OP388, OP391, OP488
Noorollahi-Moghaddam, H. P477
Noponen, T. OP166
Nordin, A. TP011, TP030, TP090
Nordström, J. P368
Norenberg, J. OP489, P335
Nørgaard, M. OP042
Noriega, E. P469, P831, P946, P947
Norikane, S. P930
Nortier, F. M. OP479
Notaristefano, A. OP107, OP459, P638
Notghi, A. P353
Notni, J. OP338
Novelli, P. M. OP380
Novikov, S. N. P574, P751, P927
Novy, Z. PW068
Nowak, C. OP277
Nowicki, M. L. OP193
Nunes, A. P112
Nunes, C. TP004
Nunes, H. OP436
Nunes, M.-L. P676
Núñez-Vázquez, R. P852
Nutt, D. TP038
Nuvoli, S. P468, P476, P478, P525, P972
Nygaard, B. OP152
Nysom, K. OP494
Nysus, M. OP489

Obara, P. P202
Obata, T. P637, PW086
Obek, C. OP087
Obenhuber, T. OP471
Öberg, J. OP561
Obermair, J. OP480, P269, P324
Obeso, J. OP646
O'Brien, J. P353
OcakK, M. OP084, OP087, OP139, OP535, P307, P862
Odagawa, T. PW088, TP008, TP020
O'Doherty, J. OP411, TP052
Odouard, E. OP597
Oehme, L. OP046, OP363
Ofuji, A. TP078
Ogata, Y. P58
Ogawa, K. P066
Ogawa, M. PW002, PW010
Ogawa, T. P634
Ogretici, A. TP018, TP031
Ogura, T. P223
Ogushi, G. TP096
Oh, J.-M. P329
Oh, J. S. P065
Oh, M. P065
Oh, S. P988
Oh, Y.-T. PW039
Ohashi, S. P637
Ohgi, K. P686
Ohkubo, R. TP089
Ohlsson, T. P077
Ohmomo, Y. P147
Ohnishi, A. P486
Ohno, K. P027
Ohta, Y. P634
Oishi, T. P773
Okamoto, M. OP284
Okamoto, S. OP144
Okamura, N. OP051, OP162
Okarvi, S. P167, P331, TP026
Okasaki, M. P791
Okazawa, H. OP641, P147
O'Keefe, G. OP293
Okino, S. OP170
Okizaki, A. P434, P530
Öksüzoğlu, K. P650, P654
Okuda, K. OP065, OP169

Okudan Tekin, B. P562, P914
Okumiya, S. PW041, TP078
Okumura, M. TP074
Okuyama, C. P027
Okuyucu, K. P967
Olaru, R. P071
Oldfield, C. P081, P869, PW105
Olejniczak, M. P743, P744
Olesen, O. V. P003
Olivan Sasot, P. OP580, P761, P765, P767, TP014
Olivari, L. OP146, OP601, OP602, P547
Olivas Arroyo, C. TP014
Olive, D. OP204
Oliveira, A. P050, P371, P416, P417, P898
Oliveira, B. F. TP044
Oliveira, C. D. R. TP072
Oliveira, L. OP159
Oliveira, T. TP068
Olivier, P. OP255
Olivotto, I. OP125
Olmos, C. PW020
Olmos García, R. OP158, P754, P756, P902
Olsen, B. B. OP275, OP390, OP582, P241
Olsen, J. R. OP040
Olsen, R. S. TP015
Olsson, B. TP067
Omrane, M. A. OP098
Onal, Ö. P645
Öneş, T. P650
Onega, M. P279
Oner, A. P880
Onishi, H. P39
Onishi, T. P434
Onizuka, H. P396
Onner, H. P736, P917
Ono, K. OP562
Ono, M. P147
Onodera, S. P356
Onoguchi, M. TP053
Oosterwijk, E. OP420, P188
Opfermann, T. P54
Opposits, G. P965
Oprea-Lager, D. E. P105
Oral, A. P579, P810, P877
Orduña Diez, M. P711
Orecchia, R. OP601
Oredsson, S. OP240
Orengo, A. P232, P233, P234, P236
Orita, E. P559
Orlova, A. OP242, OP244, OP246
OP340, OP582, OP586
Orlovskaja, V. P288, P291, TP082
Ornilla, E. OP352
Orozco-Cortés, J. P413, P600
Orsal, E. P630
Orsi, G. P471
Orsini, F. P095
Ortega Candil, A. P093, P128, P138, P746,
P975, PW020
Ortega Valle, A. P722, P760
Ortenzia, O. P272
Oruc, M. P187
Orunesu, E. OP635, P383, P729
Osada, T. OP245
O'Shea, A. P162
Oshima, K. OP187, P404
Oshima, S. P223
Osiecki, S. P361, P372
Oskoei, S. D. P624
Osman, M. M. P086, P087
Osterkamp, F. OP037
Osti, M. P643
Ostroumov, E. N. P350
Oteo, M. P148
Otmakhov, V. I. P222
Otomi, Y. P789, P925
Otsuka, H. P925
Otsuka, M. TP074
Otte, A. OP514, P509
Ottervanger, J. OP543
Ottobrini, L. OP367, P174
Oudot, A. OP506
Ouichka, R. TP086
Ouyang, W. PW094
Oveisgharan, S. P477
Overbeek, F. PW113
Overhoff, F. OP051
Oya, S. P555
Oyen, W. OP106, OP204, OP420, OP485,
P627, PW066
Ozaki, T. P930
Ozaki, Y. P356
Ozcan, Z. P579, P810
Ozdemir, S. P351
Özel, K. P909
Ozen, A. P605, P608, PW033
Özen, H. P707
Ozer, I. P541
Ozgonenel, E. P908, P909
Ozgonenel, L. P908, P909
Özkan, A. OP239, PW116
Ozkan, E. P804
Ozsoy, A. P855
Ozsoy, H. P855
Ozturk, B. P130
Ozyurt, S. P904

Pace, L. P730
Pacella, S. OP366
Pacheco, C. TP072
Pachowicz, M. P407, P412
Pacilio, M. OP236, OP330, P938
Padmanabhan, P. P264
Padovano, B. OP424, OP596, P698
Paeng, J. OP145
Paesler, F. OP513
Pagan, M. P876
Paganelli, G. P046, P703, P798
Pagani, M. OP561
Page, E. P081, P869, PW105
Paglianiti, I. P480
Pahnke, J. OP290
Paik, J. OP355
Paillas, S. OP486, OP487
Paisey, S. J. PW053
Pais Silva, P. P221
Paiusco, M. OP251
Pak, K. OP339, P118, P170
Pal, S. P151
Palard, X. OP595
Palmieri, A. TP039, TP085
Palomar Muñoz, A. OP461, P104, P717, P752
Palombo, E. P678
Palucci, A. P512
Palumbo, B. P468, P476, P478, P833
Pampaloni, M. H. OP040
Pan, T. TP056
Panagiotidis, E. OP448, OP548, PW031
Panareo, S. OP353, P769
Pancaldi, D. OP633, P026, PW111
Pande, S. P096
Pandit, A. P592
Pane, F. P237, P730
Pani, R. OP236
Paniagua Correa, C. P639, P722, P760
Panico, M. OP120, P780, PW026
Pankaj, P. OP554, P659
Paolillo, S. OP071
Paone, G. P563
Papachristou, M. P245, P319, P670
Papadimitroulas, P. P56
Papadouli, D. P826
Papalia, E. P095
Papamicaël, C. P282
Papanastasiou, E. P482, P484
Papatriantafyllou, J. P439, P464
Paphiti, M. OP195, P014, P500, PW112
Papp, H. P217
Papp, L. OP457, P471, P554
Pappalardi, B. OP596
Pappatà, S. PW026
Pappon, M. OP361
Paraskevas, G. P500
Parente, A. OP054, OP283
Parghane, R. P092, P116, P593
Park, H. P631, P772
Park, H.-H. TP045, TP061
Park, J. OP355, P143, P159, P268, P276, P325, P329
Park, J.-A. P273
Park, J.-H. P270
Park, K. P772, PW039
Park, S.-R. TP061
Park, S. OP145, P631, PW028
Park, Y. P565, P631
Parkar, N. P087
Parker, C. C. OP235
Parkinson, J. P551
Parlak, Y. TP095
Parmar, M. OP041
Parodi, K. P867
Parrado-Gallego, A. PW009
Parus, J. L. P327
Pascali, C. P698
Paschetta, C. OP558
Pascovich, C. OP516, P481
Pasker-de Jong, P. C. M. PW113
Päsler, F. P911
Pasquali, M. P227, P250
Pasquino, M. OP528, OP544
Passantino, S. OP125
Passchier, J. P279, P283
Passoni, P. OP300
Pastorino, F. P234
Patel, B. OP222
Patel, C. D. P367
Patel, V. PW037
Paterne, L. OP361
Paterson, B. OP481
Paterson, C. PW044
Paterson, C. A. PW042
Patrizi, A. PW087
Patro, S. P800
Patt, M. P017
Patterson, N. PW120
Paul, R. L. OP588, OP589, OP619
Paula, I. P671
Paules-Villar, M. J. PW038
Paulseth, R. OP648
Paulus, T. PW120
Paulvannan, S. P219, P795
Paurová, M. P259
Pavan, S. OP337

Pavanello, L. P964, TP063
Pavelka, A. P259
Pavía, J. PW045
Pavic, K. OP259
Pávics, L. PW085
Pavlakis, N. OP196
Pavlova, D. A. P379
Pawar, V. P926
Pawlak, D. OP197, P327, OP342, P567
Payoux, P. P281
Pedersen, B. G. OP292
Pedersen, C. P942
Pedersen, J. E. P491
Pedersen, K. T. P939
Pedersen, L. TP006
Pedraza-Fernandez, S. P681
Pedrera Canal, M. P125, P138, P941, P975
Pedroso de Lima, J. P673, P893, P960
Peet, B. J. OP502
Peeva, K. P623
Pé-Leve, J. TP038
Pelin Sürücü, Z. P918
Pelisek, J. OP474
Pellegrini, C. PW089
Pellegrini, G. OP243
Pellegrini, R. OP236
Pellegrino, S. OP071, P363, P730
Pellegrino, T. OP071, P363
Pellerito, R. OP528, OP544, OP575, P842
Pelletier-Galarneau, M. OP264, P519
Pelzer, H.-T. P334
Pena-Karan, S. P126
Pena Pardo, F. P104, P752
Peng, C.-L. P228, P516
Peng, L. P258
Peng, N.-J. OP460
Pengel, K. E. OP628
Penín Corderi, C. P669
PENIN GONZALEZ, F. J. P760
Penín González, F. P639, P722, P760
Pennone, M. OP540, P394, P728, PW025
Pepê, P. OP636
Peper, M. OP277
Pera-Fábregas, J. P706
Pereira, E. TP037, TP094
Pereira, J. OP159, OP418, P050, P371
P416, P417, P898, TP028, TP070
Pereira, S. OP411, TP054, TP098
Pereira Arias-Bouda, L. M. P589, P958
Peremans, K. P485, PW024
Perera-Pintado, A. PW009
Perez, B. P416, P417
Pérez, M. P050, P371, P898
Pérez Castejón, M. P093, P128, P408, P975, PW020
Perez-Escutia, M. P681
Perez Lopez, B. P931
Perez-Perera, R. PW009
Perez Perez, J. OP642
Perfileva, O. P518, P564
Pericas, J. P935
Perlaki, G. P471
Perlaza, P. PW081
Perols, A. OP586
Perrillo, T. OP499
Perrin, M. P392
Perrone Filardi, P. OP071
Perry, L. OP225
Persakis, E. P670
Pesce, G. OP525
Pesnel, S. OP104, P149
Pestarino, E. OP472
Pestean, C. TP007
Peter, A. P126
Peterle, C. OP353, OP552, P769
Peters, G. J. OP531
Peters, I. P911
Petersen, C. B. P603
Petersen, H. OP061, P783
Petersen, M. N. M. TP065
Petit, S. OP189
Petitguillaume, A. OP335
Petr, J. OP046, OP363
Petranović Ovčariček, P. P535
Petretta, M. OP120, OP167, OP174, P374
Petri, I. OP108
Petrik, M. OP101, PW068
Petropoulos, C. P826
Petrov, T. P873, P982
Petrovic, R. OP512, P438, P479
Petrovski, Z. P812
Pettinato, C. OP577, P019, P511, P709, P949, P974
Pettinato, V. P129
Peyronneau, M.-A. PW021
Pezzoli, G. PW027
Pfeffer, U. P234
Pfister, J. OP101
Pham, X. OP264, P519
Philippe, C. PW006
Phulsunga, R. P092, P116, P593
Pia, A. P969
Piaggio, G. OP205
Piana, M. P236, PW025
Piano, C. P483
Piccardo, A. OP472, OP598, P587
Piccardo, E. P821, TP081
Picchio, M. OP252, OP253, OP256

OP300, OP603, P691, P714
Picco, A. OP561
Pichard, A. OP280, OP422, OP487, P181
Pichova, R. P429
Piciu, D. TP007
Piekarski, E. P936
Pieper, C. P846
Pierantozzi, M. P458
Pierie, J. P. E. N. OP060
Pierscinska, D. P145
Pignata, S. P522, PW092
Pignataro, G. PW026
Pike, L. TP054
Pilkington Woll, J. P. PW080
Pilkinton, P. P718
Pilla, A. P501
Pillai, S. P507
Pimlott, S. P453
Pina, L. J. OP591
Pinaquy, J.-B. P986
Pinheiro, M. TP004
Pini, P. OP577
Pinteala, M. P306
Pinto, A. P416, P417, P733, P898
Pinto, J. OP183
Pinzano, A. TP086
Piotrowska, A. OP583
Piovesan, A. P842
Piper, J. W. P501
Pipikos, T. P209, P213, P365, P635
Piras, B. P468, P478, P525
Pires, L. P673, P675, P893, P960
Pirich, C. OP154, P398, P679
Pirnat, E. P888, P890, P891, P892
Pirrone, R. P771
Piscopo, V. OP071, P363
Piszczek, S. P361, P372, P617
Pitella, F. A. P042, P051, P052, P425, P497, P499
Piwowarska-Bilska, H. P216
Pizzi, S. P458
Pizzichini, P. P643
Pizzocaro, C. OP546
Pizzuto, D. A. P708
Plagge, H. TP077
Plancha, C. P601, P971
Planjery, V. OP056
Plans, G. P508
Platzek, I. OP046
Plaza De Las Heras, I. OP629, P847, P848
Pleguezuelo Navarro, M. P646
Plenevaux, A. OP096, P131
Plisson, C. P279
Ploskikh, V. A. P350
Po, C. P026
Poblete Garcia, V. OP461, P717, P752
Poças, I. TP028
Podio, V. OP558, P243, P969, TP036
Poenick, S. OP282, P161
Poeppel, T. D. OP013, OP043, OP536
P205, P37, P690, P854
Poglajen, G. P414
Pokrywka, A. P770
Polášek, M. P259
Poletti, A. OP602
Poli, G. OP387
Polis, I. P485, PW024
Politi, L. S. P174
Polk, A. P415
Pollmann, J. OP338
Polverari, G. OP552
Polverini, M. OP454
Polyák, A. P886
Pombo Passin, M. C. TP091
Pomerri, F. P584, P776
Pompanin, S. P475
Pomposelli, E. OP525, PW025
Ponte, F. PW103
Pontecorvo, M. OP323
Pooters, I. PW061
Pop, G. OP436
Popa, I. V. P071
Popescu, C. E. OP110, OP302, P943
Popov, S. OP068
Popova, A. P253, P344
Pöppel, T. OP250
Poppert, H. OP471
Portella, L. P175
Portinari, M. OP353
Posaric Bauden, M. PW102
Poschenrieder, A. OP035, OP474
Postema, J. M. P294
Pöstényi, Z. OP342, P886
Postma, M. TP058
Potenza, E. P642
Pottel, H. P57
Pottier, G. OP104, P421
Pottier, V. P281
Pouget, J.-P. OP280, OP422, OP486, OP487, P181
Poulantzas, V. OP195
Poulsen, M. H. P785
Pourcher, T. P152
Poussier, S. OP560, P293, P397, P420, P463, PW059
Pouw, B. OP230, P959, TP021, TP087
Povinec, P. P015, P024
Povolato, M. P704

Powell, A. PW110
Pozzi, L. TP069
Pozzi, N. OP645
Prabhu, M. OP164
Prado-Wohlwend, S. P413, P600
Prakhova, L. P550
Pramesh, C. S. OP149
Prandini, N. P954
Prasad, V. OP282, P161, P171, P177
Prashanth, A. OP232, P653, P658
Prassopoulos, V. P209, P213, P365, P635
Prata, A. P923
Prata, M. P227, P323
Pratali, R. P793
Prats, E. P824
Prats-Capote, A. PW009
Preisser, L. P164
Prenant, C. OP343, P328
Presselt, N. P640
Price, R. I. P326
Prieto, E. OP646
Prieto Soriano, A. P847, P848
Prigent, A. OP538
Prime, M. P456
Prince, D. P149
Prince, J. OP329, OP423, P309
Pringle, A. J. P312
Prior, J. OP298, OP359, OP361, P868
Prisco, A. P36
Probst, F. OP051
Probst, K. P287
Prokop'eva, E. Y. P195
Prosperi, D. P643, P938
Provenzano, F. P018
Prpic, M. P651
Pruszynski, M. OP245, OP584
Pruthi, A. OP058, OP554, P659
Pruzzo, R. P085, P427
Pryma, D. A. OP040
Prymkova, V. P956
Psimadas, D. P439, P464
Psomiadou, A. P410
Ptacek, J. P384
Ptacnik, V. OP368, P049, P883
Pubul Nuñez, V. P768
Puccini, G. OP647, P480
Pudlač, A. P667
Puga, T. PW035
Puig, O. P469, P508, P831, P946
Pultrone, C. P702, P709
Punda, A. P905
Puntoni, M. OP598, P587
Pupić, G. OP151
Pupillo, G. P227, P250
Pupo, F. OP525
Purandare, N. OP149, TP073
Puri, N. P453
Pursanova, D. M. P685
Puskas, C. OP333
Puta, E. P095
Pyun, S. P988
Qehajaj, D. OP146
Qin, C. PW001
Qin, Y. PW062
Quagliata, A. OP327
Quarantelli, M. PW026
Queiroga, M. TP016, TP047, TP071
Quetier, I. OP486
Quick, H. H. P205
Quinto, M. A. OP279
Quirce, R. OP438, P436
Quon, A. OP045
Qureshi, M. S. P715
Qwarik, A. A. P114

Rabaiotti, E. P714
Rabines-Juárez, Á. O. OP370, OP371, P596
Rabinovich, R. P059
Rabus, H. OP616
Raderer, M. OP365, P732
Radhakrishnan, E. P844
Radulovic, M. OP349, OP350, OP372
Raffaghello, L. P232, P233, P234, P236
Raffo, E. P420, P463
Ragan, P. P015
Ragni, P. P274
Rahabi, S. P661, P838
Rahal, D. OP146
Raijmakers, P. OP122, OP123
Raingeard, I. PW095
Raja, S. P715, P937, P944
Rajamani, V. P844
Rajan, M. P303, P814
Rajashekharrao, B. OP063
Rajić, M. OP441
Rajović, M. OP372
Ráliš, J. P259
Ramada-Magalhaes, J. P279
Ramakrishnan, N. K. OP049
Ramakrishnan, S. P367
Rami-Mark, C. PW004, PW006
Ramírez, A. P632, P663
Ramirez, Y. E. P788
Ramírez Tortosa, C. P585
Ramos, A. G. F. TP044
Ramos, D. P315

Rana, N. OP594, P060, P092
Ranaldo, M. OP638
Raneri, F. P547
Ranft, A. P928
Ranganathan, P. OP149
Rangarajan, V. OP149, TP073
Rangel, L. J. TP057
Rangger, C. OP101, OP342, PW056
Rasch, H. OP262
Rasmussen, I. L. TP015
Raso, A. OP598
Raspagliesi, F. OP596
Ratão, P. P716
Rath, D. OP148, P101
Rathore, H. OP164, P800
Ratib, O. P433
Rausch, I. OP044, OP416, OP449
Ravasio, G. P019, P511, P974
Ravera, S. P232, P233, P234, P236
Ravina, M. OP232, P592, P653, P658
Ray, G. OP309
Razack, A. P655
Razav, B. OP084, OP087, OP535, P662
Razola, P. P824
Razzouk-Cadet, M. P953
Rebollo-Aguirre, A. C. P762, P764
Reccia, P. P790
Rechenmacher, F. OP338
Recla, M. P512
Redaelli, I. OP249
Reddy, L. OP164, P800
Redgate, S. OP113
Regaieg, H. OP434, P936
Regnault, V. PW059
Rehak, Z. P384
Rei, L. P430
Reich, D. OP338
Reich, M. OP645
Reichel, R. OP536, P690
Reilly, R. PW070
Reimão, A. S. TP028
Reineke, U. OP037
Reiners, C. P527
Reis, J. TP068
Reiter, T. OP433
Remde, Y. P295
Rémy, P. PW021
Rena, O. P095
Rendl, G. P398
Reñe-Ramirez, R. P446
Rensi, M. OP302, P704, P739
Renzi, R. OP254
Repetto, A. P765
Repetto-Llamazares, A. OP422, P162, P181
Reubi, J. PW069
Reutelingsperger, C. P. M. P381
Reutens, D. C. P312
Reyes, D. P971
Reyes, M. P601
Reyes Marlés, R. OP260, P435, P692, P823, P970
Rezavi, B. P538
Reznikova, T. P440
Rho, J. P621
Ria, F. OP249
Ribeiro, A. P330, TP019
Ribeiro, A. S. TP038, TP051
Ribeiro, D. F. F. TP004, TP076
Ribeiro, T. PW103
Ribelles, M. J. OP352, OP591, OP646
Ricard, M. OP091
Ricci, S. OP136, P853
Richarz, R. OP098, PW052
Richetta, E. OP528, OP544, OP575, P842
Richetti, A. P563
Richter, J. Á. OP352, OP591
Rico-Pons, I. P446
Ridocci Soriano, F. PW019
Riedinger, J.-M. OP590, OP627
Riemann, B. P542
Rigatti, P. P709
Rijavec, E. OP147
Rijnierse, M. T. OP067, OP123
Rijpkema, M. OP394, P188
Ringler, R. P829, P830
Rinino, D. P678
Riola Parada, C. P093, P125, P138, P746, P941, PW020
Riondato, M. P275
Rios, G. OP157
Riou, O. OP630
Ripova, D. P429
Risheq, F. Y. P114
Riss, P. P085
Ritt, P. OP331, OP364
Ritter, C. O. OP297
Rius, M. P099
Riva, M. P547
Rivera-Marrero, S. PW009
Rizell, M. OP334
Rizkallal Monzon, S. P354
Rizzo, M. P961
Roach, P. J. OP086, P551
Roberson, P. L. OP380
Robertson, S. P335
Robillard, M. OP586
Robin, P. P778

Robinson, A. P081, P659, P869, PW105
Robinson, C. PW048
Robinson, J. P870, PW042, PW044
Robinson, O. P107
Robles-Barba, J. J. P446, P706, PW038
Roca Engronyat, M. P446, P706, P947
Rocchi, P. P258
Roch, V. OP560, P392, P397
Rodado, S. P711, P788
Rodari, M. OP601, OP632, P547
Rodell, A. OP322
Rodenburg, C. J. PW113
Rodenhuis, S. OP628
Rodionov, A. V. P350
Rodrigo, R. P470
Rodrigues, I. OP159
Rodrigues, M. P689
Rodrigues, S. P323
Rodríguez, F. OP157, P893
Rodriguez, H. P601, P971
Rodriguez, M. OP352, OP591
Rodriguez Alban, J. P960
Rodriguez Alfonso, B. OP629, P847
Rodríguez-Bel, L. P446, P706, PW038
Rodriguez-Fernandez, A. P632, P663, P680
Rodríguez-Gasén, A. P831, P946, P947
Rodriguez Gonzalez, J. P970
Rodriguez Martinez de Llano, S. P221
Rodríguez-Oroz, M. OP646
Rodríguez Pelayo, E. P639, P722, P760
Rodriguez Rey, C. P093, P128, P138, P746
Rodríguez-Rubio, J. P469, P831, P947
Rodriguez-Tanty, C. PW009
Roesch, F. OP138, OP276, PW058
Roé Vellvé, N. P510
Rogenhofer, S. P796, P832
Rogov, A. P246, P311, P321, TP017, TP100
Rogovskaya, Y. P388
Rohani, M. P477
Rohde, M. P783
Roholm, T. A. TP012
Rohren, E. OP238, OP309
Rojas, J. P508
Rojas Camacho, J. P469, P831
Rojas-Fisher, B. PW119
Rojnic, M. OP512
Rokicki, J. P443
Roldan Rubio, M. OP260, P692
Romano, A. OP445
Romanó, C. P002
Romanowicz, G. P610
Romeo, A. P793
Romero, E. P148
Romero Fernández, J. OP629
Romero Otero, M. P298, P413
Romero-Zayas, I. P446, P706, P831, P947
Rominger, A. OP051, OP326
Romito, R. OP424
Roncali, M. OP012,
Roncalli, M. OP146
Roncaroli, F. P069
Ropolo, R. OP575
Ros, D. PW045
Rosário, D. S. OP545
Rösch, F. P085, P427
Roscher, M. P002
Rösel, K. OP155
Roselt, P. OP481
Rosenbaum, C. E. N. M. OP581
Rosenbaum-Krumme, S. OP156, OP536
Rosendahl, K. OP637
Rosenfeld, A. B. OP278
Rosenström, U. OP340
Rosiak, E. OP389
Rosino Sánchez, A. P692
Rosner, C. P226
Ross, P. P787
Ross, T. L. P265, P294, P426
Rossetti, C. OP110, P943
Rossi, A. OP598
Rossi, C. PW030
Rossi, L. OP635
Rossi, M. P793
Rossin, R. OP586
Rossi Norrlund, R. P803
Roszkowska, A. P412
Rota, R. P701
Rotaru, A. P907
Rothley, J. OP380
Rotondo, G. P431
Rousseau, C. OP255, OP305
Rousseau, H. P399
Rousseau, J. OP038, OP276
Rouzet, F. OP434, OP476, P362, P385, P936
Rovira-Cañellas, A. P568
Rowe, C. OP563
Rowley, L. M. P078
Roy, R. P655
Roy, S. G. P367
Rozenblum, L. OP604
Rozzanigo, U. P512
Ruano Perez, R. P931
Rubagotti, S. OP640
Rübben, H. OP250
Rubini, D. OP107, OP459
Rubini, G. OP107, OP459, OP499, P638

Rubinstein, G. P380
Rubow, S. M. P301, P665
Ruchała, M. OP497
Rudzianskas, V. P515
Ruers, T. J. M. P648
Ruffini, L. P272, P34
Rufini, V. P708, P721
Ruggeri, A. P642
Ruggeri, M. P522, P899, PW092
Ruggieri, P. OP454
Ruhlmann, M. OP156
Ruhlmann, V. P205
Ruibal Morell, A. P768, TP091
Ruiz, D. P032, P040, P076, P759
Ruíz Gómez, M. OP158, P754
Ruiz Gómez, M. OP158, P754, P756, P902
Ruiz Hernández, D. P120, P520, P533
Ruiz Llorca, C. OP580, P761, P765, P767, TP014
Ruiz-López, J. M. P750
Ruiz-Pomar, J. P001, P068
Ruiz Solis, S. P681, PW080
Rumyantsev, A. S. P685
Rumyantsev, S. P944
Rungby, J. OP322
Ruol, A. P776
Rushforth, D. PW100
Russo, B. OP071, OP167, OP174, P363
Russo, C. OP532
Russo, G. OP445, P771, P779
Russo, R. TP075
Russo, S. P642
Russu, R. P907
Rust, P. OP044
Rutgers, E. J. T. OP230, OP592, OP628, P599, P959
Rutten - Vermeltfoort, I. TP083
Rylova, S. P165
Rysava, R. P883
Ryu, Y. P467
Ryzhkova, D. V. P210, P379

Saam, T. OP471
Saba, W. P111
Sabalich, I. P476
Sabaté-Llobera, A. P446, P706, PW038
Sabbagh, M. PW029
Sabbah, R. OP547, P370
Sabet, A. OP013, OP043, P854
Sabini, M. G. P779
Sablon-Carrazana, M. PW009
Sabol, J. P015, P024
Saboury, B. TP009
Sabri, O. OP324, OP325, OP326, OP563, P017, PW029
Sabzevari, O. P256
Sacchetti, G. OP639, P095
Sachpekidis, C. P687, P688, P737, P738 P874, P875, P957, PW090
Sachs, J. OP090
Sadashima, E. PW040
Sadeghi, M. P242
Sadeghi, R. P566
Sadic, M. P154, P187, P403, P816, P855, P939
Sadija, A. P615
Sadkin, V. P246, P321, TP017, TP100
Sadowsky, C. OP323
Saengsuda, S. TP029
Saga, T. P246, P637, PW086
Sager, S. P538, P609, P644, P662
Saghyan, A. P288
Saginoya, T. P556
Sahafipour, M. P242
Sahari, S. P809
Sahin, O. E. OP084, OP087, P538, P644
Sahine, L. P340
Sahiner, T. P130
Sahlholm, K. OP049
Sahlmann, C. O. OP297, OP393
Saho, T. P39
Saibene, T. P584
Saidenberg, E. P009
Saint, K. J. P005
Sainz-Esteban, A. OP158, P754, P756, P902
Saito, H. P559
Saito, K. P434
Saitoh, T. P612
Saji, H. P147
Sajjad, Z. P900
Sakaguchi, K. P142, P775, TP099
Sakai, S. OP171, OP437, P349
Sakai, T. P039
Sakamoto, F. P348, P987, PW034
Sakao, S. PW016
Sakretz, M. P748
Sakuragi, Y. TP020
Sakurai, Y. P139
Salabert, A.-S. P281
Saladini, G. OP251, OP631, P584, P588 P691, P710, P776, P790
Salahinejad, M. P300, P322
Salamon, F. P217
Salani, B. P234
Salas, M. PW099
Salaun, P.-Y. P778
Salavati, A. P939
Salcedo Pujantell, M. P534, P568, P660
Saldaña, P. P508, P946

Saldaña Gutiérrez, P. P831
Salgado, L. P716
Salman, K. P575
Salreta, J. P923
Salsidua-Arroyo, O. P125, P128, P138, P941
Salvatore, B. P730
Salvatore, G. P160
Salvatore, M. OP167, P160, PW026
Salvatori, I. P248
Salvi, F. OP310
Salvi, N. OP066
Salvini, A. P227
Samal, M. P049, P883, P903, PW043
Samardzic, T. OP512, P438, P479, P540
Sambuceti, G. OP147, OP472, OP525, OP540
OP623, P232, P233, P234, P236
P394, P587, P728, PW018, PW025
Samec, B. P890, P891
Samim, M. P648
Samnick, S. OP433, OP475, OP645, P285
Samokhvalova, O. P429
Sampaio, I. P671
Sampedro, F. OP642
Samplonius, D. OP617
Samuraki, M. OP562
San, H. P967
Sanabria-Diaz, G. P493
Sanchety, N. P592
Sánchez Catsús, C. P493
Sanchez Delgado, M. P720
Sánchez-Enrique, C. P408, PW020
Sanchez Fuentes, D. P681, PW080
Sanchez-Garcia, M. OP381, OP610, P865
Sánchez Jurado, R. OP592, P720, PW019,
TP023, TP088
Sanchez-Merino, G. P001, P068
Sánchez-Sánchez, R. P680, P750, P762, P764
Sancho, L. OP352, OP591, OP646
Sanco, R. OP414
Sanders, J. C. OP331
Sanderson, T. OP382
Sandhu, P. OP225
Sandler, I. OP233, OP301, OP605, P129
Sandoval Moreno, C. P722, P760
Sandström, M. OP011, OP244, OP551, OP586
Sanfilippo, S. P135, P940, P949
Sankar, G. OP232
Sankowski, A. OP193
Sano, K. P693
Sansovini, M. P798
Santaella, Y. P299
Santagata, S. P175
Santesteban, P. OP157
Sántha, O. P840
Santi, I. OP353, P769
Santiesteban, M. OP591
Santini, C. PW065
Santonicola, A. P476
Santopolo, G. OP544
Santoro, A. OP146
Santoro, L. OP630
Santoro, N. OP499
Santos, A. P671
Santos, A. I. OP184, OP636, P923
Santos, A. A. TP094
Santos, I. P788
Santos, J. A. M. PW118
Santos, J. G. OP636, P923
Santos, L. A. P042, P051, P052, P425
Santos Gomez, I. P711
Santosh, C. OP643
Sanz Llorens, R. P720, PW019, TP088
Sá Pinto, A. OP418, P050, P371
Sara, B. P174
Sara, R. OP110, P943
Sarandeses Fernandez, P. P681
Sarasamkan, J. PW003
Sarazin, M. PW021
Sari, H. OP114
Sari, O. P41
Sarikaya, A. P532, P878
Sarma, M. P122, P570
Sarp, U. P920
Sarrihni, O. OP446
Sarrut, D. OP609
Sarti, M. A. OP640
Sas, N. OP276
Sasaki, M. P486
Sasaki, Y. OP187, P404
Sassarini, J. P453
Sasso, A. P366
Sathekge, M. M. OP111
Sato, J. P434, P530
Sato, R. P636
Sato, S. P581, P930
Sato, T. P189
Sattler, B. P017
Sauberer, M. OP290
Saunders, J. P485, PW024
Saunders, M. P787
Saushkin, V. P343, P387
Saushkina, Y. OP068, P343
Saviatto, A. PW080
Savintseva, Z. P550
Savio, E. OP296, OP327
Savio, I. OP327

Savolainen, H. OP286
Savvidou, D. P635
Sawada, K. PW016
Sawiak, S. J. PW023
Saxhaug, C. OP599
Sayar, H. P187
Sayeg, M. OP037, OP141, OP192, OP239, PW116
Sayin, T. P605, P608
Sayman, H. P538, P644, P662
Sazonova, S. P222, P246, P388, PW013
Scaggion, A. OP251
Scagliori, E. P776
Scala, D. P097, P366
Scala, S. P175
Scalorbi, F. P475
Scarlattei, M. P272, P34
Scarpa, L. P689
Scarparo, P. OP066
Scarpi, E. P703
Schaarschmidt, B. M. OP250, OP536, P205, P37
Schaart, D. OP502, P199
Schacht, A. OP322
Schaefer, A. P106
Schaefer, S. C. P640
Schaertl, S. P456
Schäfer, M. OP426
Schäfers, M. P928
Schain, M. OP556, OP557
Schalken, M. TP083
Scharli, R. K. P326
Scheffler, M. P774
Scheie, D. OP494
Schelhorn, J. OP043, P854
Schembri, G. OP086, OP196, OP228, P551, P694
Schenck, M. OP250
Schepisi, G. P703
Schepmann, D. OP288
Scherbinin, A. V. P210
Scherthan, H. OP277
Scheunemann, M. PW003
Schiavina, R. OP254, P702, P709
Schibli, R. OP199, OP243, OP285, OP288, OP533, P288
Schierbaum, U. OP337
Schild, H. P846
Schillaci, O. P432, P458, P459, P678
Schiller, C. P922, TP009
Schiller, J. OP070
Schiller, M. P285
Schindler, A. OP471
Schirbel, A. OP035, OP534, P207, P285
Schlemmer, H.-P. PW090
Schleyer, P. OP411
Schlögl, S. P857
Schlumberger, M. OP091, OP369, OP604
Schmid, J. S. P527
Schmidt, E. P471
Schmidt, M. C. OP155
Schmidtlein, C. R. OP116
Schmitt, S. P293
Schmitz, A. M. T. OP628
Schmuecking, M. P569, P640
Schneefeld, S. M. P265
Schneider, C. OP155
Schneider, M. OP475
Schneider-Burrus, S. P770
Schnerr, R. S. P011
Schöder, H. OP624
Scholl, C. OP634
Schoots, I. OP299
Schorr-Neufing, U. OP192
Schosseler, F. P294, PW065
Schott, J. OP160
Schottelius, M. OP035, OP474, OP534
Schramm, G. OP046, OP363
Schrauwen-Hinderling, V. PW061
Schuchardt, C. OP037, OP140, OP141, OP239, PW116
Schuller, K. P829
Schulz, J. P676
Schulz, M. K. P173
Schulz, P. P161
Schulz-Schaeffer, W. OP324, OP325
Schuster, T. OP618
Schwaiger, M. OP471, OP474, OP618, P094
Schwarte, L. A. OP531
Schwartz, P. P676, P986
Schwarzenböck, S. OP618, P748
Sciagra, R. OP125, OP126
Sciume, F. TP063
Scolaro, T. P098
Scolozzi, V. OP626, P483
Scopinaro, F. P274, P643, P938
Scorsetti, M. OP632
Scotognella, T. P248, TP036
Scott, A. OP293, OP622, P184, P262, P305
Scott, C. P40
Scuffham, J. OP447, P56, PW100
Searle, J. OP143
Sebahoun, S. OP332
Sebek, J. PW073
Sebti, J. TP049
Sediene, S. P515
Seemann, S. P830
Seesing, M. F. J. P648
Şefizade, R. P562, P914

Segard, T. P107
Segarra Fenoll, D. OP260
Segbers, M. OP200
Seghezzi, S. OP302, OP367
Segtnan, E. A. P491
Sehested, A. OP494
Seibert, O. OP337
Seibyl, J. OP324, OP325, OP563, PW029
Seidelin, L. OP644
Seidl, C. OP485
Seifert, D. P259, TP101
Seimbille, Y. P178
Seitun, S. PW018
Sekhar, C. OP164
Seki, C. OP162
Sekine, T. OP600
Selcuk, N. OP139
Selivanova, S. V. OP446
Seliverstova, N. P440
Sellem, A. P835
Selvaraju, R. K. OP622, P262
Semah, F. P437
Semini, S. P709
Semjeni, M. PW022
Sen, H. P187
Senda, M. P486
Senekowitsch-Schmidtke, R. OP618
Şengöz, T. P633, P782
Senn, D. P732
Senneby, M. P369
Sensi, F. P430
Seo, Y. P571
Seok, J. P582, P583
Sepp, D. OP471
Seppänen, M. OP153
Sepulcri, M. OP251
Sequeira, J. A. P923
Séra, T. PW085
Serafini, G. OP596, P698
Seregni, E. OP424, OP613, P753
Serém, S. J. C. TP043
Serena, A. P120, P520, P533, P759
Seret, A. P131
Sergey, R. P937
Sergienko, I. P253, P344, P389
Sergienko, V. P253, P344, P389
Sergieva, S. OP360
Serizawa, N. OP437, P349
Serra-Arbeloa, P. OP370, OP371, P596
Serrano, J. TP016, TP047, TP071
Serrano Palacio, A. P093, P125, P128, P746
Serre-Beinier, V. P178
Serreli, G. P272, P34
Serry, O. M. OP500
Servuli, E. A. P881
Setnikar, G. P890, P891
Seto, A. P613
Seto, K. P556
Seven, B. P630
Sever, M. P414
Severi, S. P798
Seyedabadi, M. P332
Sfar, R. P531
Šfiligoj, D. P888
Sgard, B. OP436
Shafiei, M. P247, P263
Shah, H. OP164, P800
Shah, S. OP149, P084, TP073
Shahhosseini, S. P256
Shahinfar, M. OP239, PW116
Shamsaie Zafarghandi, M. P117
Shamshirian, D. PW063
Shanmuganathan, S. OP190, OP417
Shariat, S. P699
Shariati, F. P590
Sharma, R. PW101
Sharma, V. P507
Shaw, J. A. P628
Sheikh, A. OP264
Sheil, R. W. P326
Shen, G. P123, P204, P239, P618, P811
Sherwin, P. OP648
Shi, S. OP247, OP620, P267
Shi, X. P185
Shidahara, M. OP162
Shieh, M.-J. P228
Shiga, T. OP144
Shih, Y.-H. P228
Shimaoka, S. OP057
Shimizu, A. P488, P489
Shimizu, I. OP284
Shimizu, K. TP034
Shimoda, Y. PW002
Shimodaira, Y. OP056
Shimomura, K. P142
Shimosegawa, E. OP515, P088, P333, P460, P494, P734
Shin, D. OP614
Shin, M. P118
Shin, U. P273, P276
Shinaji, T. P334
Shindov, M. P977
Shinto, A. P219, P795, P806, P844, TP001
Shinya, T. P789, P925
Shiomi, S. P813
Shiozaki, H. OP056
Shiraishi, S. P348, P987, PW034, TP096

Shiraishi, Y. P612
Shirakawa, S. TP022
Shirato, H. OP144
Shirkani, A. P506
Shirmardi, S. P310
Shirokorad, V. I. P685
Shirvani Arani, S. OP477
Shiue, C.-Y. P452
Shraddha, S. OP164
Shu, X. P496
Shuke, N. P434
Shukla, J. OP041, OP594, P092, P116, P261, P719
Shulkin, B. L. P657
Shurupova, I. PW015
Sibille, L. P490
Sicolo, M. P961
Siebermair, J. OP070
Siebert, A. OP332
Sieglová, I. P259
Sieuwerts, A. OP392
Sifakis, N. P439, P464
Sigari, C. P753
Signore, A. OP205, P938
Signorelli, M. PW084
Sijbesma, J. W. A. OP049, OP283, P419
Sileni Chiarion, V. P776
Silva, A. P110, P610, P716
Silva, D. TP016, TP047, TP071
Silva, H. OP184
Silva, M. P675, P893, P960
Silva, N. TP038
Silva, R. OP553, P673, P675, P893
Siman, W. OP328
Ŝimeĉek, J. P272
Simo, M. P978
Simon, D. OP156
Simon, H. OP231
Simone, F. OP107
Simó Perdigó, M. P660
Sindoni, A. P409
Singh, A. OP037, OP140, OP141, OP430, OP533
Singh, D. P653, P658
Singh, G. OP041, OP594, P261
Singh, N. OP415
Singh, P. P800, P814
Singh, S. K. P092
Singla, S. TP035
Sinha, A. P507
Sinilkin, I. P757, P758
Sinzinger, H. P833
Sipahi, M. P548
Sipilä, H. OP166
Siracusa, M. P522, PW092
Sirova, V. P049
Sitarz, M. OP478
Siurana-Montilva, S. P568
Sjögreen Gleisner, K. OP383
Sjöstrand, K. P369
Skanjeti, A. OP558
Skeoch, S. P198
Skibova, D. P049, P883
Skopljak-Beganovic, A. P808
Skoura, E. OP548, P203, P619, PW031
Skudlinski, M. W. OP205
Skuridin, V. P222, P246, P757, P758, PW013
Skvortsova, T. P550
Slama, J. P936
Slama, M. OP434
Slart, R. H. J. A. OP111, OP124, OP172, OP173
OP473, P373, P375, P381, P386, P419
Slavik, R. OP285
Slawin, K. OP083
Slenter, J. PW061
Sletten, H. OP295
Slifstein, M. OP509
Slim, I. P220, P815, P817, P818, P835, PW079, TP084
Slim, N. OP300
Slump, C. H. OP543, P586
Smadja, C. OP335, P316
Smakovs, A. P012
Småstuen, M. C. OP295
Smerling, C. OP037
Smillie, C. OP168
Smit, E. F. P320
Smit, F. P589, P958
Smith, G. OP588, OP589, OP619
Smith, S. PW044
Smits, M. L. J. OP423
Smits, R. P017
Smolyakov, Y. P503
Smyth, V. OP616, PW106
Soares, O. P671, PW118
Sobajima, A. P784
Sobic Saranovic, D. OP349, OP350, OP442, P882
Sobral Violante, L. P671
Socan, A. P414, PW056
Söderström, J. OP014
Soe, K. P573
Soffientini, A. OP546
Sohn, H. P631
Sohn, M.-H. PW036
Šolc, J. OP616
Soliman, W. O. OP500
Solinas, P. P972
Sollaku, S. OP066
Sollini, M. OP012, OP191, P594, P724

Solnes, L. B. OP040
Solodyannikova, O. ,. V. P225
Solomon, S. B. OP624
Solomyanyy, V. P382
Soltani, N. P252
Soltermann, A. OP116
Somlai, K. P591
Somsen, G. A. OP064, OP069
Son, H.-S. TP061
Sone, Y. P784
Song, H.-C. P772
Song, Y. PW001
Sonke, G. S. OP628
Sönmezoglu, K. P538, P609, P644, P662
Sonneborn, M. TP064
Sonni, I. OP557
Sonvenso, D. P051, P052, P425, P497, P499
Sood, A. P092, P593
Sopena, P. P761, P767
Sørensen, C. H. OP152
Sørensen, J. OP121, OP292, P368, TP065, TP066
Soriano Castrejón, Á. OP461, P104, P717, P752
Soriano-Mas, C. P446
Soricelli, A. P160
Sosabowski, J. OP486
Söser, H. P922
Soto-Lopez, M. E. P386
Soufi, M. P113, P115
Soukhov, V. P212, P887, P896
Sousa, E. OP415, TP004, TP016
TP037, TP042, TP047, TP071
Sousa, R. P716
Sousa, V. P755
Soussan, M. OP436
Souvatzoglou, M. OP618
Souza, E. OP225
Sowa-Staszczak, A. P666, P792
Soydal, C. OP579, P804, P843
Soyluoglu Demir, S. P532
Spallarossa, P. OP540
Spallino, M. OP110, OP253, P691, P943
Spanu, A. P468, P476, P478, P525, P972
Spassov, B. P727, P740, P742
Spaun, G. OP154
Specchio, L. P431
Spezi, E. P007, P157, PW120
Spiegelberg, D. OP622, P184, P262, PW057
Spinelli, A. E. OP112, OP484, P048, P064, P194
Spinks, T. OP619
Spisni, R. PW032
Spohn, F. O. OP226
Sposito, C. OP424
Spreafico, C. OP424
Sprinzl, G. M. P657
Spycher, P. R. OP243
Srbovan, D. P682
Sridharan, S. OP648
Sromek, A. W. OP289
Stace, C. OP337
Stadlbauer, A. OP044
Staelens, S. OP339, P170, P172
Ståhl, S. OP582
Stakhiv, O. OP415
Stalnionis, M. P915
Stanek, J. OP290
Stankoff, B. PW021
Starcea, M. P907
Stark, D. OP088, P082
Stasi, M. OP528, OP544, OP575
Stasyuk, E. P222, P246, P311, P321, TP017, TP100
Statescu, A.-M. P071, P907
Staudenherz, A. OP221
Stavrou, P. Z. P670
Stebner, V. OP156
Stefanescu, C. P071, P306, P907
Stefanini, S. P793
Stefano, A. P771, P779
Stefanova, M. OP428, P099
Stefanoyiannis, A. P. P802
Stefańska, A. P666, P792
Steffen, I. G. P226
Stegger, L. P928
Steiger, S. OP116
Steigerwald, F. OP645
Stein, D. P454
Steinbach, J. OP046
Steinberg, J. OP354
Steiner, B. P317
Steinke, M. P180
Steinmair, M. OP154
Stella, F. P129
Stenberg, J. P262, PW057
Stenerlöw, B. OP622
Stenvall, A. P077
Stepankova, J. PW068
Stepanov, V. OP287, OP289, P456
Stephens, A. OP563, PW029
Sterzing, F. OP428, P099
Stevens, A. P102
Stević, M. OP441
Stich, M. P829, P830
Stickeler, E. PW082
Stillebroer, A. B. OP420
Stimson, D. H. R. P312
Stipo, M. P522, P899
Stoico, R. OP578

Stokholm, M. OP294
Stokke, C. OP039
Stokkel, M. OP223, P229, OP230, OP592 P959, TP021, TP079, TP087
Stolarz, A. OP478, OP584
Stolz, J. OP083
Stolzmann, P. OP116, P197
Storm, G. OP105, P318
Stoykow, C. PW082
Strada, L. P227
Strand, J. OP246
Strand, S.-E. OP240, PW102
Strandholdt, C. N. P726
Streichenberger, N. TP049
Stricker, P. OP088, P082
Strickland, C. P112
Strigari, L. PW104
Stroobants, S. OP339, P170, P557
Stubbs, J. OP040
Student, V. OP083
Studentsov, E. TP082
Stuijfzand, W. OP122, OP123
Stundzia, A. P196
Sturiale, L. PW092
Su, M. P629
Su, T.-P. PW083
Su, W.-C. P622
Su, Z. P069
Suárez-Novo, J. F. P706
Suarez-Piñera, M. P470, P552
Subramanyam, P. P122, P570
Sudati, S. P174
Sudhakar, N. P219, P795, P806
Suga, K. P166
Sugihara, Y. P966, P985
Sugimoto, M. P393, TP080
Suha, B. P471
Suleymanlar, G. P880
Summer, D. OP101
Summers, P. PW027
Summers, S. TP019, TP051
Sun, L. OP625
Sun, X. OP625
Sun, Y. PW094
Sundaram, P. P122, P570
Sundin, A. OP011, OP551
Sundram, F. P834
Suneetha, B. P096
Supiot, S. OP305
Surer Budak, E. P880
Suri, V. P719
Sкuridin, V. P311, P321, TP017, TP100
Susin, D. P440
Suzuki, A. OP437, P349
Suzuki, T. P530
Svedberg, M. OP289, P456
Sveljo, O. P126
Svenningsson, P. OP557
Svensson, J. OP014, OP334, P803, P889
Svirydenka, A. P781, P940
Svirydenka, H. P129, P135
Swanston, N. OP238, OP309
Swierszcz, L. P412
Sydoff, M. P215
Syed, N. PW101
Syed, R. OP548, P203, PW031
Synefia, S. PW112
Syrigos, K. N. P619
Szegedi, J. P840
Szekeres, S. P471
Szentesi, M. P841
Szentmártoni, G. P591
Szeplaki, Z. P473
Szigeti, K. P073, P151, PW022
Szilvasi, I. P355, P473, P664
Szkliniarz, K. OP478, OP584
Szolik, M. P067
Szot, W. P391

Tabacchi, E. P135, P683, P781
Tabacchini, V. OP502, P199
Tabarin, A. P676
Tabuenca Mateo, M. J. PW080
Tachibana, I. P775
Tachibana, Y. P637
Tada, A. P581, P930
Taddei, C. OP099
Tadokoro, M. TP022
Tafakhori, A. P474, P477
Tafani, M. P281
Taghizadeh Asl, M. P450, P451, P495, P505, P506
Tagliabue, L. OP367
Tahseen, R. P337, P338, P900
Taibi, A. P227, P250
Taieb, D. P258
Takacs, E. P473, P664
Takacsova, E. P820
Takahara, K. OP435
Takahara, N. TP099
Takahashi, H. P773
Takahashi, K. P530
Takahashi, M. P166
Takahashi, R. P428
Takahashi, Y. P038, P139
Takaki, A. P038, PW041
Takamori, S. PW040

Takanami, K. PW014
Takano, A. OP287
Takase, K. PW014
Takashima, H. TP089
Takats, A. P473
Takayoshi, S. P930
Takeda, I. P784
Takei, M. PW010
Takekawa, S. P556
Takenaka, D. P686
Takenouchi, T. P773
Talavera Rubio, M. OP461, P717, P752
Talbi, A. P661, P838
Talbot, J. OP255
Taleb, S. P140, P529, P539, P819, P825, P836
Talleruphuus, U. TP012
Tam, H. OP225
Tamaki, N. OP144
Tamal, M. PW048
Tamam, M. O. TP018, TP031
Tamayo Alonso, M. P. P931
Tambasco, N. P476
Tamburri, S. P243
Tamura, M. P142
Tan, Y. P351
Tanabe, Y. P634
Tanaka, K. P549
Tanaka, N. OP187, P404
Tanaka, S. OP057
Tanaka, T. P581, P789, P930
Tang, C. OP257
Tang, R. OP088
Tang, Y. P185
Tanguay, J. OP385
Tani, A. OP057
Tanigawa, N. P196
Tanimoto, K. P637
Tanyildizi, H. OP139, OP529, P079
Tao, G. P176, P176
Tapadinhas, M. P923
Tápias, A. PW081
Tapner, M. P872, PW120
Taralli, S. P954
Tard, C. P437
Tardelli, E. PW032
Tardin, L. P824
Tarlinton, L. OP088
Tartaglione, G. P876
Tarullo, G. P271, P308
Tarver, K. P839
Tasdemir, A. P061
Tashiro, M. OP162, OP162
Tasi, S.-F. TP056
Taslak Sengul, A. P918
Tatsch, K. OP333, PW046, PW047
Tatsi, A. P179
Tatsumi, K. PW016
Tatsumi, M. P460, P734
Taurino, M. P938
Taviani, V. P202
Tayar, C. P849
Taylor, J. C. OP113
Taylor, M. OP343
Taylor, O. P485
Taywade, S. OP058
Teagle, A. R. P695, P725
Tegos, T. P484
Teh, D. P507
Teimourian, B. P117
Teixeira, J. P671, PW118
Teixeira, S. OP592, OP628, P599
Teixo, R. P330, PW035
Telarovic, S. P479
Tenbergen, G. OP513
ten Hoeve, W. OP586
Tenke, P. OP083
Teodorczyk, J. P610
Terakawa, Y. P488, P489
Teräs, M. OP166
Terasaki, H. PW088
Terazawa, K. P925
Terroir, M. OP091, OP369, OP604
Terry, S. OP281, OP481, PW066
Ter Voert, E. P197, P200
Tesar, V. P883
Tescaru, A. OP597
Testanera, G. P018
Testart, N. P632, P663, P680, P750, P762, P764
Tetti, S. P274
Teufel, D. P. OP337
Teuho, J. OP166
Tewes, B. OP288
Texier, M. OP369
Tezak, S. P357, P479
Thackeray, J. OP546, P265, P294
Thakral, P. TP035
Thakur, M. L. P083
Theillac, B. P354
Theilmann-Jørgensen, D. P783
Thelen, P. OP393
Thelu, M. OP189
Therkelsen, A. OP275
Thevenet, H. OP335
Theze, B. P111
Thielemans, K. OP166
Thimister, W. OP443

Thirumalaisamy, S. P844
Thisgaard, H. OP275, OP582, P173
Thomae, D. P172
Thomaidou, A. P410
Thomas, L. OP457, OP634, P832
Thomé, C. P657
Thomsen, C. OP494
Thongklam, K. TP005
Thöny, H. P569
Thuroczy, J. P886
Thykjær, A. S. P173
Tian, R. OP527, P629, P858, PW109
Ticconi, F. P394, PW018
Tie, H. OP168
Tietze, A. P124
Tijink, B. M. OP231
Tille, J. P569
Tillmanns, J. OP475
Timofti, A. P306
Tindale, W. B. OP113
Tio, R. OP124, OP172, OP173, P373, P375, P386
Tipping, J. P081, P869, PW105
Tirado-Hospital, J. P852
Tirotti, C. P938
Tiskecivius, S. P915
Titskaya, A. P757, P758
Tixier, F. P627
Tizon, M. TP046
Tkaczewski, K. P372
Tőkés, A.-M. P591
Tochon-Danguy, H. P305
Todica, A. OP070, P380
Todorovic-Tirnanic, M. OP442, P089
Togashi, K. P693, P980
Tokes, T. P591
Toklu, T. OP139
Tokocin, M. PW033
Tokuc, B. P731
Tolbod, L. P. OP121, OP292, OP541, TP065, TP066
Tolmachev, V. OP242, OP244, OP246
OP340, OP582, OP586
Tolosana, J. P935
Tomas Hernandez, S. P353
Tomassetti, P. OP552
Tomeš, M. P158, TP101
Tomiguchi, S. P348, P987, PW034, TP096
Tomiyama, Y. OP126
Tomoike, A. P147
Tonge, C. OP120, OP174, P005, P359
Tonnesmann, R. P165
Topcu, A. P630
Tordjmann, J. OP436
Torgue, J. OP487
Torgyík, L. P591
Torres-Prioris, M. J. P510
Torres-Vela, E. PW075
Tosakulwong, N. P136
Toschi, L. OP146
Tosi, G. P018
Tosounoglou, S. P850, P851
Tossici-Bolt, L. PW046, PW047
Toth, M. OP053, P355
Touati, J. OP333
Toubaru, S. P637
Toubeau, M. OP627
Tournier, N. P111, P421
Tout, D. OP120, OP174
Touw, D. J. P301
Toyama, H. TP022
Toyohara, J. OP284, P133, P549
Toz, H. P877
Trabelsi, k. P815, P817, TP084
Trabucco, I. OP544
Trabulsi, E. J. P083
Trägårdh, E. P369
Traino, A. OP136, OP421, P853
Tralhão, J. G. P330, PW035
Tran, T. OP240
Trapasso, F. P274, P938
Trasforini, G. P769
Traub-Weidinger, T. OP365
Travascio, L. P678
Traxl, A. OP290
Tredici, M. P853
Treglia, G. P894
Treiber, U. OP618
Trencsényi, G. P153
Trevisan, A. C. P042, P051, P052, P425, P497, P499
Trevisani, F. OP577
Triantafyllou, N. OP195, P500
Trigg, W. OP648, OP648
Trimboli, P. P894
Trinckauf, J. OP188
Tripathi, M. OP537
Tripathi, S. P083
Triponez, F. P178
Triviño, E. P632, P663
Triviño-Ibáñez, E. M. P680, P750, P762, PW075
Trivizaki, E. P826
Trneny, M. OP368
Trnka, J. P049, P341, P952, PW073
Trofimiuk-Muldner, M. P666, P792
Trogrlic, M. P357
Trojan, L. OP393
Trojanec, R. PW068
Trolle, W. OP152

Trompoukis, N. OP195
Trovik, C. OP637
Truini, A. OP147
Trujillo, P. PW027
Trzcińska, A. OP478, OP584
Tsai, S. C. P696
Tsavdaridis, I. P945
Tseng, J.-R. TP056
Tsougos, I. P439, P464
Tsourma, M. OP586
Tsuboi, Y. P930
Tsuchiya, S. PW088, TP008, TP020
Tsuda, K. P074
Tsuda, N. P348, P987, PW034
Tsujikawa, T. OP641
Tsukada, H. OP048
Tsukimoto, S. TP027
Tsumoto, K. P166
Tsushima, Y. P223
Tuccimei, M. P643
Tuerler, A. OP533
Tugcu Demiroz, F. P963
Tumas, V. P42
Tuncalı, M. Ç. P707
Tuncel, M. OP496, OP498, OP550, OP593 P072, P707, P794, P983
Tunninen, V. OP153
Turcotte, É. OP446
Turgut, M. P745
Turkeli, M. P630
Turkheimer, F. P069
Turki, e. P441
Türkmen, C. P609
Turoğlu, H. T. P650
Tuter Basaran, S. P606, P607
Tutus, A. P645
Tzavara, C. P439, P464
Tzen, K.-Y. P461, PW017
Tzonevska, A. P977

Ubl, P. P280, P514
Ucar, M. P920
Uccelli, L. P227, P250
Üçer, Ö. P981
Uchida, T. P356
Uchino, Y. P356, P504
Ucmak, G. P517, P536, P541, P597, P652, P741, PW077
Uehara, T. P488, P489
Ueno, Y. P196
Uetani, M. P345, P647
Umeda, I. O. P230
Umemura, Y. TP089
Umezawa, R. PW014
Umit, E. P731
Ungania, S. PW104
Unger, N. OP013
Unlu, M. OP413, P340
Uno, T. P530, PW086
Uprimny, C. P657, P689
Urbán, S. PW085
Ureña Lara, M. P585
Uribe, C. F. OP385
Uritu, C. M. P306
Urusova, E. A. OP098, OP103, PW052
Uslu, I. P538, P662
Usta, Y. P745
Ustun, F. P532, P626, P731, TP033
Utomo, L. P231
Utsunomiya, K. P196
Uysal, M. P183
Uzunov, N. P227

Vaccari, S. PW087
Vaccaro, I. P271, P308
Vadrucci, M. P383
Vag, T. P094
Vahapoğlu, F. P932
Vai, A. OP249
Vaidyanathan, G. OP245
Vaissier, P. E. B. OP501
Vajracupta, O. PW003
Vakhromeeva, M. PW011
Valais, I. P500
Valdagni, R. P698
Valderas, P. P299
Valdés, W. P632, P663
Valdés Olmos, R. A. OP229, OP230, OP592, OP628 P190, P193, P589, P599, P958, P959
Valdovinos, H. F. OP247, P267
Vale, J. OP183
Valente, S. P863
Valenti, I. P366
Valentijn, R. R. P. M. P192
Valentini, M. C. OP036
Valeyre, D. OP436
Valfre, S. TP036
Vallejo Casas, J. P646
Vallez Garcia, D. OP054, OP283, OP514, P509
Vallis, K. A. OP281, P871, PW101
Valotassiou, V. P439, P464
Valtorta, S. P174
Valvo, F. OP601
van Amelsvoort, T. A. OP069
van Beek, E. J. R. P059
van Berckel, B. N. OP561

van Buchem, M. A. OP234
van Dalen, J. A. OP543, P586
Vandeghinste, B. OP504
van de Giessen, E. OP509
Vandemaele, P. OP559
van den Berg, N. S. OP231, OP306, P189, P190, P193, PW064
Vandenberghe, S. OP504, P043, P199
van den Berk, A. M. P402, PW113
van den Bosch, M. A. A. J. OP329, OP423, P309, P648
van den Broek, W. J. M. TP043
van den Eertwegh, A. J. M. P105
van den Hoff, J. OP046, OP163, OP363
van den Hoven, A. F. OP329, OP423
van de Noort, V. OP592
Van den Weyngaert, D. P557
Van den Wyngaert, T. P557
van der Geest, T. OP105, P318
Van Der Gucht, A. OP560
Van der Hage, J. A. P190
van der Have, F. OP501
van der Heide, J. A. P402
Van der Hoeven, A. F. P589, P958
van der Kroon, I. OP202, OP612
Vanderlinden, B. OP386, P697
van der Meulen, N. P. OP533
Vandermeulen, E. P485
Van der Poel, H. G. OP306, PW064
van der Pol, J. A. J. P973
Van Der Veken, P. P172
van der Vos, C. S. P627
van der Wal, S. P192
van der Westerlaken, M. M. L. PW113
van der Zant, F. M. OP172, OP186
van der Zee, E. OP060
van Deurzen, C. OP392
van de Ven, P. M. P105
Van de Wiele, C. P023, P57
van Dijk, J. D. OP543
van Driel, W. J. OP229
van Duijnhoven, F. OP230
van Echteld, C. OP192
van Eck - Smit, B. L. F. OP064, OP069
Vang, K. OP322
van Gent, D. OP488
van Gent, D. C. OP388, OP391
Vangestel, C. OP339, P170, P172
van Gils, C. A. J. OP357
van Harten, W. P599
van Helden, E. J. P777
van Herpen, C. M. L. OP420
van Hillegersberg, R. P648
van Hoek, J. P381
Van Holen, R. OP504, OP559
van Hoof, S. PW061
vankadari, k. PW117
van Kranenburg, M. OP388
van Kroonenburgh, A. OP085
Van Laarhoven, K. P649
Van Laeken, N. P466, P485
van Leenders, G. J. L. H. OP299, P705
van Leeuwen, F. W. B. OP231, OP234, OP306, P189 P190, P191, P192, P193, PW064
van Leeuwen, M. OP122
van Leeuwen, P. OP088, P082
van Luijk, P. OP054
van Moorselaar, R. J. A. P105
Vanni, I. OP147
van Nierop, B. J. OP329
van Oostenbrugge, T. J. OP420
Van Oosterom, M. N. P191
van Rietschoten, K. OP337
van Rij, C. M. P266
van Rooij, R. OP357
van Roosmalen, J. OP501
van Rossum, A. OP067, OP122, OP123
van Royen, N. OP122
van Tiel, S. T. P231
Van Timmeren, J. OP123
Van Waarde, A. OP049, OP286, OP617, P419
van Weerden, W. M. OP299, OP488, P705
Van Werkhoven, E. P190
Van Willigen, D. M. P191
Varasteh, Z. OP340
Vardareli, E. P061
Varga, J. OP119, P292
Varga, Z. P664
Vargol, S. E. P968
Varjo, P. OP153
Varlamova, N. P222, P246, P321, TP017
Varnäs, K. OP556, P456
Varrone, A. OP053, OP556, OP557, P456, P498
Vartanoglu, T. PW033
Vasanawala, S. P202
Vasileiadis, A. P484
Vasilenko, E. PW096
Vasina, J. P384
Vassallo, G. OP511
Vassileva, D. P727, P740, P742
Vastenhouw, B. OP501
Vatankulu, B. OP529, P538, P609, P644, P662
Vatsa, R. OP041, OP594, P092, P261
Vauclin, S. OP161
Vaulina, D. P289, P291
Vaysse, L. P281
Vaz, A. TP092

Vaz, T. F TP038, OP184, OP227
Vázquez, M. C. TP072
Vazquez, N. P172
Veenland, J. OP299
Vega Caicedo, C. H. P104
Vegt, E. OP306, OP354
Veit-Haibach, P. OP116, OP600, P197, P200
Velander, M. J. P951
Velasco, M. P978
Velasco, T. R. P499
Velasco Nuño, M. P534, P660
Vélayoudom-Céphise, F.-L. P676
Velidaki, A. P245
Velikyan, I. OP551
Velipasaoglu, Z. P983
Velumani, A. OP063
Vendelbo, M. H. P240
Venkatachalam, T. K. P312
Vennarini, S. P512
Vennart, B. P059
Ventroni, G. OP236
Vera, P. OP161
Veran, N. P397
Vera Pinto, V. OP580, P761, P765, P767, TP014
Verberne, H. J. OP060, OP064, OP069
Verbist, B. M. OP234
Verburg, F. OP549, P894
Vercellino, L. S. P169
Vercher Conejero, J. OP580, P446, P706
P761, PW038, TP014
Verdun, F. OP359, OP361
Verdurand, M. TP049
Verdú-Rico, J. P884
Veres, D. P073, PW022
Verga, L. P134
Vergara, E. OP445
Verger, A. OP560, P392, P546
Verheul, H. M. W. OP531, P777
Verkooijen, H. M. OP329, P648
Verleden, S. OP559
Verma, R. OP554, P659
Veronesi, G. PW087
Verrey, A.-S. P316
Versari, A. OP012, OP191, OP640
P594, P739, P860, TP085
Verschure, D. O. OP064, OP069
Viale, P. P949
Viana, A. F. P047
Viau, P. P953
Vicente, J. S. TP013
Vicente, N. P893
Vichi, S. OP452, P026
Vidal, B. TP049
Vidal, E. OP440
Vidal-sicart, S. PW081
Vidioukov, V. P518, P564
Vieira, L. OP183, OP184, TP013
TP028, TP072, TP072, TP094
Vieira, M. P755
Vieira, R. P960
Vieira, T. OP418, P050, P371, P416, P417, P898,
TP070
Viergever, M. A. PW097
Vieth, V. P928
Vija, A. H. OP331
Vija, L. M. OP538
Vilaça, J. TP004
Vilacosta, I. P408, PW020
Vilgrain, V. OP332
Vilhelmsson-Timmermand, O. OP240
Villa, E. OP632
Villanueva Curto, J. OP158, P754, P756, P902
Villasboas, D. P534, P537
Villavecchia, G. OP472
Villegas Cardos, C. P720
Villemagne, V. OP563
Vilstrup, M. H. P241, P713
Vinjamuri, S. OP448
Violante, L. PW118
Violati, M. OP367
Virgolini, I. OP530, P657, P689
Virotta, G. P701
Virtaniemi, S. M. TP010
Visser, E. P. OP612, P627
Visvikis, D. OP305, P627
Vita, G. P409
Vita, M. G. P483
Vitabile, S. P771, P779
Vitolo, V. OP601
Vittori, M. P876
Vivas, D. P408
Vivian, G. P032, P076, TP032, TP060
Vlachou, F. P209, P213, P365, P635
Vlajković, M. OP441
Vlastou, E. OP450
Vlontzou, E. P670
Vogel, W. OP628, P199, P959, TP021
Vogg, A. PW061
Vogt, J. P830
Volkmann, J. OP645
Volkov, O. P503
Volterrani, D. OP136, OP421, OP647,
P480, P853, PW032
Voltini, F. OP635, P729, PW108
Volzone, F. P733
Vomacka, L. P866, P867

Vomstein, S. OP307
Vondrák, A. P024
von Gall, C. OP364
von Groote-Bidlingmaier, F. P628
von Guggenberg, E. OP101, OP342
von Schulthess, G. OP600
Vöö, S. OP085, OP263, OP304, P973
Vraa, K. J. TP066
Vrachimis, A. P542
Vraka, C. P317, PW006
Vrancken Peeters, M.-J.T. F. D. OP230, OP628
Vriens, D. P627
Vrigneaud, J.-M.M. OP506
Vroonland, C. TP064, TP079
Vrtovec, B. P414
Vukovic, D. OP243
Vulpoi, C. P071
Vyrenkova, N. P518
Vysakh, M. P795, P806

Wachowiak, J. OP497
Wada, Y. P38
Wadhwa, R. OP056
Wadsak, W. P317, P672, PW004, PW006
Wagener, A. P161
Wagner, K.-H.H. P317
Wakabayashi, H. OP194, OP431, OP432, OP542, P334
Wakabyashi, Y. P428
Wakili, R. OP070
Wakizaka, H. PW002
Walczak, R. OP478
Walgreen, B. OP105
Walker, E. OP337
Walker, P. M. OP506
Walles, H. P180
Walls-Laguarda, L. OP173
Walrand, S. OP503, OP523, P043, PW091
Wan, S. OP114
Waneck, F. OP574
Wanek, T. OP290
Wang, C.-C. OP460
Wang, H. E. P291
Wang, J.-T. P082
Wang, J. PW062
Wang, L. P390
Wang, X. OP056
Wang, Y.-C. P897
Wang, Y. TP097
Wängberg, B. OP014, P803
Wängler, B. P002
Wängler, C. OP117
Wareing, T. OP115
Warnier, C. OP096
Warnock, G. P492
Warwick, J. P454, P628
Watabe, H. OP162
Watabe, T. P333, P460
Watanabe, E. OP171
Watanabe, K. P556
Watanabe, S. OP144, OP515, P063, P460, P773, P913
Watanabe, Y. P38
Waterton, J. P198
Waton, G. P294
Watson, J. P257
Weber, M. OP285, OP365
Weber, W. A. P168
Weckesser, M. P928
Weekers, L. P090
Wehner, P. S. OP494
Wei, W. P211, PW074
Wei, Z. J. P055, P075
Weibing, M. P218
Weichselbaumer, V. OP188
Weickhardt, A. OP293
Weigand, S. D. P136
Weijers, R. OP263, OP304
Weijers, R. OP304
Weindelmayer, J. P964
Weineisen, M. OP239, OP338, OP488
Weinmann, P. OP335
Weinstein, J. OP509
Weintraub, B. D. OP205
Weir, N. P059
Weissensteiner, J. P614
Wells, L. A. P283
Wendt, T. G. P640
Weng, D. OP203
Weng, J.-H. P561
Weng, S.-J. P461
Wenning, C. P542
Wenzel, I. P610
Werner, M. PW082
Werner, R. OP194, OP277, OP431, OP432 OP433, OP542, P334, P527, P766
Wesolowski, C. A. P903
Wesolowski, M. J. P903
Wesseling, J. OP592, OP628
Wessels, F. J. OP423
Wester, H.-J. OP035, OP140, OP239, OP338 OP430, OP474, OP488, OP534 OP618, P094, P193
Westerlund, K. OP244, OP246
Weston, B. R. OP056
Wetter, A. OP250, OP536, P37, P690
Wheeler, H. P551

Whitcher, B. P059
Wichert-Ana, L. P042, P051, P052, P425, P497, P499
Widström, C. P368
Wiedenmann, B. P161, P171, P177
Wiederin, H. P526
Wierts, R. OP092, P011
Wiesalla, S. OP141
Wiesinger, F. P200
Wieslander, B. OP152
Wiessalla, S. OP037, OP239
Wijers, L. M. H. P589, P958
Wikberg, E. OP014
Wild, D. OP307, OP479, P257
Wilderman, S. J. OP380
Wilke, F. OP055, OP513, P911
Willekens, S. M. A. OP202, P266
Willemsen, A. T. M. OP514
Williams, H. A. P005, P006, P198, P423
Williamson, D. J. PW023
Willowson, K. P. OP196
Wimana, Z. OP386, OP425, P697
Win, Z. OP225
Windhorst, A. D. OP286
Winkens, T. P53, P54
Winkler, C. TP077
Winnie, L. W. C. P119
Winter, G. OP141
Wit, E. OP306, PW064
Withaar, D. P649
Witkowska-Patena, E. P617
Wityak, J. P456
Woerdenbag, H. J. P301
Wójcik, M. P407
Wojcik, R. OP503
Wojdowska, W. P255, P327
Wolf, J. P774
Woliner-van der Weg, W. OP612
Wollmer, P. P369
Wondergem, M. OP186
Wong, L.-Y. P144
Wong, V. OP040
Wong, W. L. P112, P787
Woods, E. TP054, TP098
Wright, C. OP118, OP453, P103, P856
Wrobel, M. P743, P744
Wu, D.-K. P984
Wu, K.-D. P955
Wu, V.-C. P955
Wu, X. P235
Wu, Y.-W. PW017
Wünsch, B. OP288
Wuthrick, E. J. P103, P856
Wyffels, L. OP339, P170
Wygoda, Z. P524
Wysokiński, A. P407
Xanthopoulos, S. P319
Xi, J. P062, PW050
Xia, X. P251, PW001
Xie, L. PW002, PW010
Xie, W. P176, P176, P390, P625
Xing, L. OP625
Xu, G. OP045
Xu, X. PW067
Xue, Q. P641

Yada, N. P39
Yadav, M. P. TP035
Yaddanapudi, K. OP356
Yaegashi, H. P913
Yagdigul, Y. OP560
Yakushiji, Y. TP099
Yalvac, D. H. P536, P541
Yamada, M. OP562
Yamada, Y. TP099
Yamagami, T. P686
Yamamoto, H. P133, P549
Yamamoto, N. P637
Yamamoto, S. TP034
Yamamoto, Y. P133, P486, P487, P549
Yamanaka, K. OP170
Yamane, A. P559
Yamane, T. P613
Yamasaki, T. PW002, PW010
Yamashina, A. OP187, P404
Yamashita, K. PW041
Yamashita, Y. P348, P987, PW034, TP096
Yammine, K. P849
Yan, X. P674
Yanagisawa, T. OP431, OP432
Yanai, K. OP162
Yaneva, M. P805, P895, P977
Yang, C.-T. P264
Yang, L.-Y. OP460
Yang, S. P176, P176, P268, P325, P390, P625
Yanmaz, M. T. P684
Yano, H. P791
Yao, W.-J. P897
Yao, z. P641
Yap, K. PW110
Yapici, O. P745
Yaqub, M. OP531, P320
Yaren, A. P782
Yassin, S. M. W. P575
Yasuda, K. P196
Yaylalı, O. P633, P782
Yazici, B. P579, P810, P877, P909

Yeddes, I. P220, P815, P817, P818 P835, P916, PW079, TP084
Yen, R.-F. P461, P955, PW017
Yen, T.-C. OP460, P560, TP056
Yeter, E. P403
Yeyin, N. OP084, OP139, OP529, P307, P862
Yigitbası, O. N. TP033
Yilmaz, B. P061
Yokoyama, K. OP169, P465
Yoneda, M. OP641
Yoo, I. P631
Yoo, R. P273
Yoon, D. P571, P572
Yoon, H.-J. P577
Yoon, S.-N. P580, P712, P962
Yordanova, A. P796
Yordanova, T. P620, P623
Yorke, E. OP624
Yoshida, A. P813
Yoshida, M. P348, PW034
Yoshikawa, K. P074, P637, PW086
Yoshimori, K. P612
Yoshinaga, K. OP126
Yoshino, K. P723
Yoshiura, T. OP057, P807
Young, A. OP088
Young, J. D. OP481
Young, K. P305
Yousefi, F. P450
Yoza, K. P636
Ysamat, M. P537
Yu, K. P159, P268
Yu, W. OP165, P062, P735, PW050
Yui, J. PW002, PW010
Yuki, H. P987
Yüksel, D. P633, P782
YükselL, M. P684
Yun, E. P571
Yuncu, O. P541
Yurekli, E. OP413
Yürekli, Y. P932

ZAABAR, L. P224, P815, P817, P818, P924, PW079, TP084
Zach, C. OP326
Zacherl, M. OP070, P380
Zacho, H. P124
Zadrazil, J. P376
Zadro, C. P399
Zafirakis, A. P919
Zafón, C. P534, P537
Zaglmair, W. P679
Zagni, F. OP452, OP633, OP638, PW111
Zagonel, V. OP631
Zaharchuk, G. OP047, P200
Zaheri-A, S. P153
Zaitsu, Y. OP284
Zając-Spychała, O. OP497
Zakhs, D. P550
Zaletel, K. OP530, P888, P890, P891, P892
Zalutsky, M. R. OP245
Zamagni, E. P739
Zaman, A. P336, P337, P338, P900
Zaman, M. P336, P337, P338, P339, P900, P933
Zaman, R. P336
Zaman, U. P336, P337, P338, P900
Zambo, K. P471
Zampella, E. OP120, OP174, P374
Zamudio, D. P718
Zangheri, B. P594, P724
Zani, D. P019, P511, P974
Zannetti, A. P160, P175
Zanoni, L. OP108, P702, P709, P781, P949, PW089
Zanotti-Fregonara, P. OP279
Zapata Paz, I. OP629
Zaplatnikov, K. P212, P887, P896
Zappalà, M. OP414
Zaramella, E. OP414
Zarcone, C. P134
Zarifmahmoudi, L. P566
Zarobkiewicz, M. P412
Zarrad, F. OP103, PW007, PW052
Zattoni, F. OP631
Zavadovsky, K. W. P343, P346, P387, PW013
Zaw, H. OP257
Zawaideh, C. PW018
Zeebregts, C. J. P381
Zeillemaker, A. P589, P958
Zelaya, F. P759
Zelaya Reinquet, F. P120, P520, P533
Zelchan, R. P321, TP100
Zeltchan, R. P757, P758
Zeng, W. P009, P519, P827
Zerahn, B. P415
Zerna, M. OP341
Zhai, W. OP165, P062, P735, PW050
Zhang, B. P30
Zhang, D. P214
Zhang, J. OP118, OP453, P103, P30, P856
Zhang, L. PW062
Zhang, M.-R. P637, PW002, PW010, PW086
Zhang, X. TP023
Zhang, Y. P251, PW001, PW002, PW010
Zhang, Z. P284
Zhao, J. P185
Zhao, L. P185

Zhao, Y. TP077
Zhao, Z. P239
Zheng, Q. P208
Zheng, Z. P390
Zhou, H. P235, P558
Zhou, K. OP458
Zhou, X. OP048, P419, P422
Zhou, Y. P558
Zhu, D. PW062
Zhu, J. P185
Zhu, L. PW062
Zhu, X. P901, PW062
Zhuravlev, F. PW005
Ziaka, A. P439, P464
Ziegler, S. I. OP618
Zilli, T. OP298
Zimmer, L. OP052, TP049
Zimmerman, B. E. OP387
Zimová, J. P158
Zinzani, P. PW089
Zipper, W. OP478, OP584
Zischler, J. OP103
Zissimopoulos, A. P410
Zito, F. OP635, P729, PW108
Živković, V. OP441
Ziylan, E. P684
Zlatareva, D. P502, P982
Zlatopolskiy, B. D. OP097, OP098, OP103, PW007, PW052
Znamenskiy, I. A. P195, P881
Zocco, A. TP039
Zogala, D. P341, P667
Zollino, M. OP511
Zona, S. P954
Zonnenberg, B. A. OP423
Zorz, A. P121, P33, P35
Zotta, M. P842
Zou, S. P901, PW062
Zsótér, N. OP457, P554
Zucchetta, P. OP440, P475
Zuffante, M. P934, P950, P964, TP063
Zuhayra, M. PW093, TP077
Zuvic, M. OP555

ESNM

Clinical Partner Courses 2016

European School of Nuclear Medicine

ESNM/ESO Learning Course on ^{18}FDG PET/CT in Lymphoma

April 15–16, 2016 | *Vienna, Austria*

An initiative of ESNM in cooperation with

ESNM/ESTRO Course on Molecular Imaging and Radiation Oncology

May 19–22, 2016 | *Lisbon, Portugal*

An initiative of ESNM in cooperation with ESTRO School

More Clinical Partner Courses will be announced soon. Find more information at **www.eanm.org**

EANM'16

EANM® European Association of Nuclear Medicine

BIOMEDICAL IMAGING AND THERAPY FOR PERSONALIZED HEALTHCARE

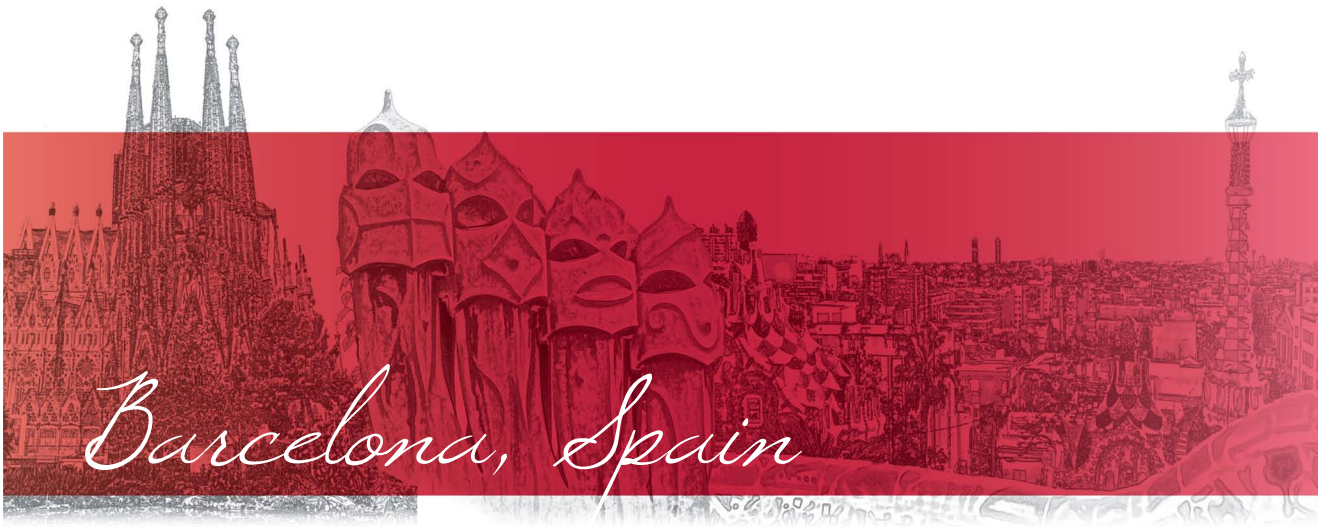

Annual Congress of the European Association of Nuclear Medicine

October 15–19, 2016
Barcelona, Spain

www.eanm.org

Visit us on .com/officialEANM